NASA SP-327

SYMPOSIUM ON SIGNIFICANT RESULTS OBTAINED FROM THE EARTH RESOURCES TECHNOLOGY SATELLITE–1

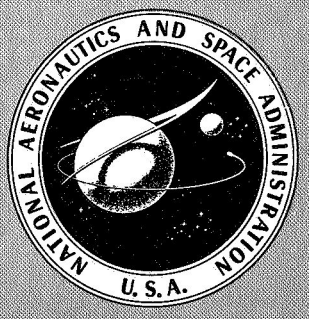
Volume I: Technical Presentations
Section A

A symposium held by

GODDARD SPACE FLIGHT CENTER

New Carrollton, Maryland

March 5–9, 1973



NATIONAL AERONAUTICS AND SPACE ADMINISTRATION

NASA SP-327

SYMPOSIUM ON SIGNIFICANT RESULTS OBTAINED FROM THE EARTH RESOURCES TECHNOLOGY SATELLITE-1

Volume I: Technical Presentations
Section A

The proceedings of a symposium held by
Goddard Space Flight Center
at New Carrollton, Maryland
on March 5–9, 1973

Compiled and Edited by

Stanley C. Freden
Enrico P. Mercanti
Laboratory for Meteorology and Earth Sciences
and

Margaret A. Becker
Technical Information Division
Goddard Space Flight Center



Scientific and Technical Information Office 1973
NATIONAL AERONAUTICS AND SPACE ADMINISTRATION
Washington, D.C.

This document is "made available under NASA sponsorship in the interest of early and wide dissemination of Earth Resources Survey information and without liability for any use made thereof." (NPD 8000.2A March 16, 1973)

For sale by the Superintendent of Documents
U.S. Government Printing Office, Washington, D.C. 20402
Price $13.65 domestic postpaid or $12.50 GPO Bookstore per set (Sections A and B)
Stock No. 3300-00515; GPO Catalog No. NAS 1.21:327
Library of Congress Catalog Card No. 73-600115

PREFACE

The first Earth Resources Technology Satellite (ERTS-1) was launched on July 23, 1972. In the seven months since it was activated over 34,000 scenes of the earth have been obtained covering all major land masses and about 75% of the world's land area. Some areas, such as the United States, have been imaged at least twelve times. The purpose of this program is to provide an assessment of remote sensing from a satellite as a technique for inventorying and monitoring the earth's resources to provide for better management of these resources.

This Symposium provided the first open forum where the users of the ERTS data had the opportunity to present the significant accomplishments from their investigations. It also provided the first opportunity for representatives of federal, state and local organizations to present their views on how ERTS data are being used and will be used for solving operational resource management problems.

In order to provide maximum visibility for both the scientific/technological results as well as for the applications results from ERTS, and to provide these results in a relatively concise manner to those who could not be in attendance all week, the Symposium was structured into three parts:

1. The first three days, after an opening introductory session on Monday morning, were devoted to contributed papers in the various disciplines. A total of 184 papers were presented. These papers are contained in this publication as Volume I; they are numbered and presented in the order that they were listed in the Abstracts. Several papers not listed in the Abstracts are contained at the end of this Volume. A summary paper pertaining to ERTS-1 Data Product Performance, which was given as the first paper because of its general interest to all participants, is contained as the first paper in this Volume.

2. The Thursday Summary Session of the Symposium was designed to summarize the significant results presented during the first three days and also to present some typical examples of how ERTS results are being applied to solving operational resource management problems primarily at the federal and state levels. Highlighting this Summary Session were addresses by Dr. James C. Fletcher (Administrator, National Aeronautics and Space Administration), the Hon. James Symington (Representative, U. S. Congress, State of Missouri) and the Hon. Ed Reinecke (Lieutenant Governor, State of California). These were followed by a summary paper on the ERTS-1 status and then by four key papers selected from the presentations made during the first three days. On Thursday afternoon, four papers were presented which summarized the significant results from the first three days in selected disciplines. Five papers exemplifying the applications of ERTS results to meeting selected federal and state program objectives and resource management objectives in several disciplines were then presented. The proceedings of the Thursday Summary Session are contained in Volume II.

3. Volume III contains the reports of the Working Groups which were convened on Friday to summarize and critique the ERTS results in the various disciplines. These working groups were chaired by the respective discipline session chairmen and were composed of selected specialists in the disciplines. Opinions and recommendations expressed in these reports are those of the panel members and do not necessarily reflect an official position of NASA.

Stanley C. Freden
Symposium Chairman

TABLE OF CONTENTS

VOLUME I

TECHNICAL PRESENTATIONS

Paper No.		Page
	ERTS-1 DATA PRODUCT PERFORMANCE, B. T. Bachofer	1
	AGRICULTURE, FORESTRY, RANGE RESOURCES	
A 1	IDENTIFICATION OF WINTER WHEAT FROM ERTS-1 IMAGERY, Donald L. Williams, Stanley A. Morain, Bonnie Barker and Jerry C. Coiner	11
A 2	SEMI-AUTOMATIC CROP INVENTORY FROM SEQUENTIAL ERTS-1 IMAGERY, Claude W. Johnson and Virginia B. Coleman	19
A 3	CROP IDENTIFICATION USING ERTS IMAGERY, Maurice L. Horton and James L. Heilman	27
A 4	IDENTIFICATION OF LARGE MASSES OF CITRUS FRUIT AND RICE FIELDS IN EASTERN SPAIN, Fernando López de Sagredo and Francisco G. Salinas	35
A 5	ENGINEERING ANALYSIS OF ERTS DATA FOR SOUTHEAST ASIAN AGRICULTURE, Howard L. Heydt and Arthur J. McNair	37
A 6	AN INTERREGIONAL ANALYSIS OF NATURAL VEGETATION ANALOGUES USING ERTS-1 IMAGERY, Charles E. Poulton and Robin I. Welch	53
A 7	NATURAL VEGETATION INVENTORY, Barry J. Schrumpf	59
A 8	VEGETATIVE AND GEOLOGIC MAPPING OF THE WESTERN SEWARD PENINSULA, ALASKA, BASED ON ERTS-1 IMAGERY, James H. Anderson, Lewis Shapiro and Albert E. Belon	67
A 9	ERTS-1 EVALUATIONS OF NATURAL RESOURCES MANAGEMENT APPLICATIONS IN THE GREAT BASIN, Paul T. Tueller and Garwin Lorain	77
A 10	EVALUATION OF ERTS-1 IMAGERY IN MAPPING AND MANAGING SOIL AND RANGE RESOURCES IN THE SAND HILLS REGION OF NEBRASKA, Paul M. Seevers and James V. Drew	87
A 11	MONITORING CALIFORNIA'S FORAGE RESOURCE USING ERTS-1 AND SUPPORTING AIRCRAFT DATA, David M. Carneggie and Stephen D. DeGloria	91
A 12	TESTING THE USEFULNESS OF ERTS-1 IMAGERY FOR INVENTORYING WILDLAND RESOURCES IN NORTHERN CALIFORNIA, Donald T. Lauer and Paul F. Krumpe	97
A 13	INTERPRETATION OF ERTS-MSS IMAGES OF A SAVANNA AREA IN EASTERN COLUMBIA, G. W. W. Elbersen	105
A 14	DELINEATION OF MAJOR SOIL ASSOCIATIONS USING ERTS-1 IMAGERY, W. L. Parks and R. E. Bodenheimer	121

TABLE OF CONTENTS (Continued)

Paper No.		Page
A 15	EVALUATION OF REMOTE SENSING IN CONTROL OF PINK BOLLWORM IN COTTON, Virginia B. Coleman, Claude W. Johnson and Lowell N. Lewis	127
A 16	APPLICATION OF ERTS-1 IMAGERY & UNDERFLIGHT PHOTOGRAPHY IN THE DETECTION AND MONITORING OF FOREST INSECT INFESTATIONS IN THE SIERRA NEVADA MOUNTAINS OF CALIFORNIA, Ralph C. Hall	135
A 17	IMPACT OF ERTS IMAGES ON SURVEYS OF FOREST INSECT INFESTATIONS IN COOK INLET BASIN, ALASKA, James H. Anderson, F. Philip Weber, John M. Miller, Enzo Becia and Roy C. Beckwith	143
A 18	ERTS-1 IMAGERY AND HIGH FLIGHT PHOTOGRAPHS AS AIDS TO FIRE HAZARD APPRAISAL AT THE NASA SAN PABLO RESERVOIR TEST SITE, Robert N. Colwell	145
A 19	PHENOLOGY SATELLITE EXPERIMENT, Bernard E. Dethier, Marshall D. Ashley, Byron Blair and Richard J. Hopp	157
A 20	FOREST AND RANGE MAPPING IN THE HOUSTON AREA WITH ERTS-1 DATA, G. R. Heath and H. D. Parker	167
A 21	APPLICATION OF ERTS-1 DATA TO ANALYSIS OF AGRICULTURAL CROPS AND FORESTS IN MICHIGAN, Gene R. Safir, Wayne L. Myers, William A. Malila and James P. Morgenstern	173
A 22	CROP SPECIES RECOGNITION AND MENSURATION IN THE SACRAMENTO VALLEY, Frederick J. Thomson	181
A 23	THE RESULTS OF AN AGRICULTURAL ANALYSIS OF THE ERTS-1 MSS DATA AT THE JOHNSON SPACE CENTER, R. M. Bizzell, L. C. Wade, H. L. Prior and B. Spiers	189
A 24	AGRICULTURAL APPLICATIONS OF ERTS-1 DATA, William C. Draeger	197
A 25	IDENTIFICATION OF AGRICULTURAL CROPS BY COMPUTER PROCESSING OF ERTS MSS DATA, Marvin E. Bauer and Jan E. Cipra	205
A 26	IDENTIFICATION AND MAPPING OF SOILS, VEGETATION, AND WATER RESOURCES OF LYNN COUNTY, TEXAS BY COMPUTER ANALYSIS OF ERTS MSS DATA, Marion F. Baumgardner, Steven J. Kristof and James A. Henderson	213
	MINERAL RESOURCES, GEOLOGICAL STRUCTURE AND LANDFORM SURVEYS	
G 1	EVALUATION OF ERTS-1 IMAGERY FOR GEOLOGICAL SENSING OVER THE DIVERSE GEOLOGICAL TERRANES OF NEW YORK STATE, Yngvar W. Isachsen, Robert H. Fakundiny and Stephen W. Forster	223
G 2	ANALYSIS AND APPLICATION OF ERTS-1 DATA FOR REGIONAL GEOLOGICAL MAPPING, D. P. Gold, R. R. Parizek, and S. A. Alexander	231
G 3	GEOLOGY OF UTAH AND NEVADA BY ERTS-1 IMAGERY, Mead LeRoy Jensen	247

TABLE OF CONTENTS (Continued)

Paper No.		Page
G 4	PRELIMINARY GEOLOGIC APPLICATION OF ERTS-1 IMAGERY IN ALASKA Ernest H. Lathram, I. L. Tailleur, W. W. Patton, Jr.	257
G 5	A COMPARISON OF GEMINI AND ERTS IMAGERY OBTAINED OVER SOUTHERN MOROCCO, Herbert W. Blodget and Arthur T. Anderson	265
G 6	CAPABILITY OF ERTS-1 IMAGERY TO INVESTIGATE GEOLOGICAL AND STRUCTURAL FEATURES IN A SEDIMENTARY BASIN (BASSIN PARISIEN – FRANCE), Claude Cavelier, Jean-Yves Scanvic, Guy Weecksteen and Alain Ziserman	273
G 7	APPLICATION OF ERTS-1 MULTISPECTRAL IMAGERY TO MONITORING THE PRESENT EPISODE OF ACCELERATED EROSION IN SOUTHERN ARIZONA, Roger B. Morrison and Maurice E. Cooley	283
G 8	A STUDY OF MORPHOLOGY, PROVENANCE, AND MOVEMENT OF DESERT SAND SEAS IN AFRICA, ASIA, AND AUSTRALIA, Edwin D. McKee, Carol S. Breed and Lawrence F. Harris	291
G 9	ESTABLISHMENT, TEST, AND EVALUATION OF A PROTOTYPE VOLCANO-SURVEILLANCE SYSTEM, Peter L. Ward, Jerry P. Eaton, Elliot Endo, David Harlow, Daniel Marquez and Rex Allen	305
G 10	SATELLITE GEOLOGICAL AND GEOPHYSICAL REMOTE SENSING OF ICELAND – PRELIMINARY RESULTS FROM ANALYSIS OF MSS IMAGERY, Richard S. Williams, Jr., Agúst Bödvarsson, Sturla Frídriksson, Gudmundur Pálmason, Sigurjón Rist, Hylnur Sigtryggsson, Sigurdur Thórarinsson and Ingvi Thórsteinsson	317
G 11	PRELIMINARY ASSESSMENT OF GEOLOGICAL APPLICATIONS OF ERTS-1 IMAGERY FROM SELECTED AREAS OF THE CANADIAN ARCTIC, Alan F. Gregory	329
G 12	EXPLOITATION OF ERTS-1 IMAGERY UTILIZING SNOW ENHANCEMENT TECHNIQUES, Frank J. Wobber and Kenneth R. Martin	345
G 13	MAPPING QUATERNARY LANDFORMS AND DEPOSITS IN THE MIDWEST AND GREAT PLAINS BY MEANS OF ERTS-1 MULTISPECTRAL IMAGERY, Roger B. Morrison and George R. Hallberg	353
G 14	GLACIATION OF NORTHWESTERN WYOMING INTERPRETED FROM ERTS-1, Roy M. Breckenridge	363
G 15	FIRST-LOOK ANALYSIS OF GEOLOGIC GROUND PATTERNS ON ERTS-1 IMAGERY OF MISSOURI, William H. Allen, James A. Martin, and David L. Rath	371
G 16	RATIO MAPS OF IRON ORE DEPOSITS ATLANTIC CITY DISTRICT, WYOMING, Robert K. Vincent	379
G 17	USE OF ERTS-1 IMAGES IN THE SEARCH FOR PORPHYRY COPPER DEPOSITS IN PAKISTANI BALUCHISTAN, Robert G. Schmidt	387
G 18	RELATION OF ERTS-1 DETECTED GEOLOGIC STRUCTURE TO KNOWN ECONOMIC ORE DEPOSITS, Ernest I. Rich	395

TABLE OF CONTENTS (Continued)

Paper No.		Page
G 19	PRELIMINARY GEOLOGIC INVESTIGATIONS IN THE COLORADO PLATEAU USING ENHANCED ERTS IMAGES, Alexander F. H. Goetz, Fred C. Billingsley, Donald Elston, Ivo Lucchitta and Eugene M. Shoemaker	403
G 20	STRUCTURAL GEOLOGIC ANALYSIS OF NEVADA USING ERTS-1 IMAGES: A PRELIMINARY REPORT, Lawrence C. Rowan and Pamela H. Wetlaufer	413
G 21	REGIONAL TECTONIC CONTROL OF TERTIARY MINERALIZATION AND RECENT FAULTING IN THE SOUTHERN BASIN-RANGE PROVINCE, AN APPLICATION OF ERTS-1 DATA, I. C. Bechtold, M. A. Liggett and J. F. Childs	425
G 22	ERTS APPLICATIONS IN EARTHQUAKE RESEARCH AND MINERAL EXPLORATION IN CALIFORNIA, Monem Abdel-Gawad and Joel Silverstein	433
G 23	SOME ASPECTS OF ACTIVE TECTONISM IN ALASKA AS SEEN ON ERTS-1 IMAGERY, Larry D. Gedney and James D. VanWormer	451
G 24	ERTS-1 IMAGE CONTRIBUTES TO UNDERSTANDING OF GEOLOGIC STRUCTURES RELATED TO MANAGUA EARTHQUAKE, 1972, W. D. Carter and G. P. Eaton	459
G 25	RECOGNITION OF SURFACE LITHOLOGIC AND TOPOGRAPHIC PATTERNS IN SOUTHWEST COLORADO WITH ADP TECHNIQUES, Wilton N. Melhorn and Scott Sinnock	473
G 26	ERTS-1 IMAGERY AS AN AID TO THE DEFINITION OF THE GEOTECTONIC DOMAINS OF THE SOUTHERN AFRICAN CRYSTALLINE SHIELD, Morris J. Viljoen and Richard P. Viljoen	483
G 27	NEW ASPECTS ON THE TECTONIC OF THE ALPS AND THE APENNINES REVEALED BY ERTS-1 DATA, J. Bodechtel and B. Lammerer	493
G 28	STRUCTURAL LINEAMENTS OF GASPE FROM ERTS IMAGERY, Roberto Steffensen	501
G 29	LINEAMENTS IN COASTAL PLAIN SEDIMENTS AS SEEN IN ERTS IMAGERY, Charles F. Withington	517
G 30	EVALUATION OF COMMERCIAL UTILITY OF ERTS-A IMAGERY IN STRUCTURAL RECONNAISSANCE FOR MINERALS AND PETROLEUM, Donald F. Saunders and Gilbert E. Thomas	523
G 31	STRUCTURAL INTERPRETATIONS BASED ON ERTS-1 IMAGERY, BIGHORN REGION, WYOMING-MONTANA, Richard A. Hoppin	531
G 32	APPLICABILITY OF ERTS-1 TO LINEAMENT AND PHOTOGEOLOGIC MAPPING IN MONTANA – PRELIMINARY REPORT, Robert M. Weidman, David D. Alt, Raymond E. Flood, Jr., Katharine T. Hawley, Linda K. Wackwitz, Richard B. Berg and Willis M. Johns	539
G 33	A NEW FAULT LINEAMENT IN SOUTHERN CALIFORNIA, Robert W. Pease and Claude W. Johnson	547

TABLE OF CONTENTS (Continued)

Paper No.		Page
	ENVIRONMENT SURVEYS	
E 1	FRACTURE MAPPING AND STRIP MINE INVENTORY IN THE MIDWEST BY USING ERTS-1 IMAGERY, Charles W. Wier, Frank J. Wobber, Orville R. Russell and Roger V. Amato	553
E 2	ERTS-1 INVESTIGATION OF ECOLOGICAL EFFECTS OF STRIP MINING IN EASTERN OHIO, Phillip E. Chase and Wayne Pettyjohn	561
E 3	THE USE OF ERTS-1 MSS DATA FOR MAPPING STRIP MINES AND ACID MINE DRAINAGE IN PENNSYLVANIA, S. S. Alexander, J. Dein and D. P. Gold	569
E 4	MONITORING VEGETATION COVER ON MINE DUMPS WITH ERTS-1 IMAGERY: SOME INITIAL RESULTS, Brian Gilbertson	577
E 5	REMOTE DETECTION OF AEROSOL POLLUTION BY ERTS, G. E. Copeland, A. R. Bandy, E. C. Kindle, R. N. Blais and G. M. Hilton	585
E 6	DETECTION, MAPPING AND ESTIMATION OF RATE OF SPREAD OF GRASS FIRES FROM SOUTHERN AFRICAN ERTS-1 IMAGERY, J. M. Wightman	593
E 7	MAPPING ATLANTIC COASTAL MARSHLANDS, MARYLAND, GEORGIA, USING ERTS-1 IMAGERY, Richard R. Anderson, Virginia Carter and John McGinness	603
E 8	IDENTIFICATION OF MARSH VEGETATION AND COASTAL LAND USE IN ERTS-1 IMAGERY, V. Klemas, F. Daiber and D. Bartlett	615
E 9	APPLICATION OF ERTS-1 DATA TO THE PROTECTION AND MANAGEMENT OF NEW JERSEY'S COASTAL ENVIRONMENT, Robert L. Mairs, Frank J. Wobber, Donald Garofalo and Roland Yunghans	629
E 10	MONITORING OCEAN DUMPING WITH ERTS-1 DATA, C. T. Wezernak and N. Roller	635
E 11	ENVIRONMENTAL STUDY OF ERTS-1 IMAGERY: LAKE CHAMPLAIN AND VERMONT, Aulis O. Lind, E. Bennette Henson and James Pelton	643
E 12	WATER TURBIDITY DETECTION USING ERTS-1 IMAGERY, Harold L. Yarger, James R. McCauley, Gerard W. James, Larry M. Magnuson and G. Richard Marzolf	651
E 13	DIGITAL ANALYSIS OF POTOMAC RIVER BASIN ERTS IMAGERY: SEDIMENTATION LEVELS AT THE POTOMAC-ANACOSTIA CONFLUENCE AND STRIP MINING IN ALLEGHENY COUNTY, MARYLAND, J. S. Schubert and N. H. MacLeod	659
E 14A	A STUDY ON THE EROSION OF NIIGATA BEACH FROM ERTS-A IMAGERY, Takakazu Maruyasu	665
E 14B	APPLICATION OF ERTS DATA TO THE DETECTION OF THIN CIRRUS AND CLEAR AIR TURBULENCE, Kiyoshi Tsuchiya and Toshiro Kamiko	673

Paper No.		Page
E 14C	POLLUTED AND TURBID WATER MASSES IN OSAKA BAY AND ITS VICINITY REVEALED WITH ERTS-A IMAGERIES, Kantaro Watanabe	681
E 14 D	RED TIDE IN ISE BAY, Hiroaki Ochiai	689
	WATER RESOURCES	
W 1	HYDROGEOLOGY OF CLOSED BASINS AND DESERTS OF SOUTH AMERICA, ERTS-1 INTERPRETATIONS, George E. Stoertz and William D. Carter	695
W 2	DETECTION OF MAJOR RIVER BED CHANGES IN THE RIVER EBRO (NORTH-EASTERN SPAIN), R. Espejo, J. Torrent and C. Roquero	707
W 3	APPLICATIONS OF MULTISPECTRAL IMAGERY TO WATER RESOURCES DEVELOPMENT PLANNING IN THE LOWER MEKONG BASIN (KHMER REPUBLIC, LAOS, THAILAND AND VIET-NAM), Willem J. van Liere	713
W 4	PRELIMINARY TEST OF ERTS-1 IMAGERY FOR IMPROVING DEFINITION OF NATURAL STREAMFLOW, Este F. Hollyday	743
W 5	APPLICATION OF ERTS-1 IMAGERY TO FLOOD INUNDATION MAPPING, George R. Hallberg, Bernard E. Hoyer and Albert Rango	745
W 6	ASSESSMENT OF FLOOD DAMAGE IN ARIZONA BY MEANS OF ERTS-1 IMAGERY, Roger B. Morrison and Maurice E. Cooley	755
W 7	USE OF THE SRI ELECTRONIC SATELLITE IMAGE ANALYSIS CONSOLE FOR MAPPING SOUTHERN ARIZONA PLANT COMMUNITIES FROM ERTS-1 IMAGERY, Raymond M. Turner	761
W 8	MONITORING OF STREAMFLOW IN THE VERDE RIVER BY ERTS-1 DATA COLLECTION SYSTEM (DCS), Herbert H. Schumann	769
W 9	PRELIMINARY ANALYSIS OF ERTS-RELAYED WATER-RESOURCES DATA IN THE DELAWARE RIVER BASIN, Richard W. Paulson	777
W 10	MODELING SUBTROPICAL WATER-LEVEL DYNAMICS DISTRIBUTION, A. L. Higer, E. A. Cordes and A. E. Coker	793
W 11	AN EVALUATION OF SPACE ACQUIRED DATA AS A TOOL FOR MANAGEMENT OF WILDLIFE HABITAT IN ALASKA, Bill J. Van Tries	795
W 12	PRELIMINARY EVALUATION OF ERTS-1 FOR DETERMINING NUMBERS AND DISTRIBUTION OF PRAIRIE PONDS AND LAKES, Edgar A. Work, Jr., David S. Gilmer and A. T. Klett	801
W 13	DYNAMICS OF PLAYA LAKES IN THE TEXAS HIGH PLAINS, C. C. Reeves, Jr.	809

TABLE OF CONTENTS (Continued)

Paper No.		Page
W 14	STUDIES IN THE LAKE ONTARIO BASIN USING ERTS-1 AND HIGH ALTITUDE DATA, A. Falconer, S. H. Collins, W. T. Dickison, R. Protz, R. P. Bukata, K. P. B. Thomson, G. P. Harris and P. J. Howarth	819
W 15	PROGRESS OF AN ERTS-1 PROGRAM FOR LAKE ONTARIO AND ITS BASIN, Thomas W. Wagner and Fabian C. Polcyn	829
W 16	REMOTE SENSING OF TURBIDITY PLUMES IN LAKE ONTARIO, Edward J. Pluhowski	837
W 17	ERTS-1 VIEWS THE GREAT LAKES, Walter A. Lyons, Steven R. Pease	847
W 18	USE OF ERTS DATA FOR MAPPING SNOW COVER IN THE WESTERN UNITED STATES, James C. Barnes and Clinton J. Bowley	855
W 19	EVALUATION OF ERTS IMAGERY FOR MAPPING AND DETECTION OF CHANGES OF SNOWCOVER ON LAND AND ON GLACIERS, Mark F. Meier	863
W 20	DETECTION OF TURBIDITY DYNAMICS IN TAMPA BAY, FLORIDA USING MULTI-SPECTRAL IMAGERY FROM ERTS-1, A. E. Coker, Aaron Higer and Carl R. Goodwin	1715
	LAND USE AND MAPPING	
L 1	CARTOGRAPHIC QUALITY OF ERTS-1 IMAGES, R. Welch	879
L 2	PROGRESS IN CARTOGRAPHY, EROS PROGRAM, Alden P. Colvocoresses and Robert B. McEwen	887
L 3	CHANGE IN LAND USE IN THE PHOENIX (1:250,000) QUADRANGLE, ARIZONA BETWEEN 1970 AND 1972: SUCCESSFUL USE OF A PROPOSED LAND USE CLASSIFICATION SYSTEM, John L. Place	899
L 4	LAND USE INVESTIGATIONS IN THE CENTRAL VALLEY AND CENTRAL COASTAL TEST SITES, CALIFORNIA, Dr. John E. Estes	907
L 5	LAND USE IN THE NORTHERN COACHELLA VALLEY, Jack B. Bale and Leonard W. Bowden	915
L 6	LAND USE CLASSIFICATION AND CHANGE ANALYSIS USING ERTS-1 IMAGERY IN CARETS, Robert H. Alexander	923
L 7	ERTS REGIONAL-SCALE OVERVIEW LINKING LAND USE AND ENVIRONMENTAL PROCESSES IN CARETS, Robert H. Alexander	931
L 8	EVALUATION OF LAND USE MAPPING FROM ERTS IN THE SHORE ZONE OF CARETS, Robert Dolan and Linwood Vincent	939

TABLE OF CONTENTS (Continued)

Paper No.		Page
L 9	INVESTIGATIONS USING DATA FROM EARTH RESOURCES TECHNOLOGY SATELLITE IN THE FIELDS OF AGRICULTURE/GEOGRAPHY. (TIMBER INVENTORY – LAND USE) IN THE PROVINCE OF HUELVA-SPAIN, Emilio de Benito, Serafin López-Cuervo and Joaquin Rodriguez	949
L 10	GEOGRAPHIC APPLICATIONS OF ERTS-1 DATA TO LANDSCAPE CHANGE, John B. Rehder	955
L 11	IDENTIFICATION OF SOIL ASSOCIATIONS IN WESTERN SOUTH DAKOTA ON ERTS-1 IMAGERY, Frederick C. Westin and V. I. Myers	965
L 12	LAND USE OF NORTHERN MEGALOPOLIS, Robert B. Simpson and David T. Lindgren	973
L 13	REMOTE SENSING APPLIED TO LAND-USE STUDIES IN WYOMING, Roy M. Breckenridge, Ronald W. Marrs and Donald J. Murphy	981
L 14	ERTS-1 APPLICATIONS TO MINNESOTA LAND USE MAPPING, Dwight Brown, James Gamble, Steven Prestin, Dale Trippler, Merle Meyer, Joseph Ulliman and Ralph Eller	991
L 15	A MULTIDISCIPLINARY SURVEY FOR THE MANAGEMENT OF ALASKAN RESOURCES UTILIZING ERTS IMAGERY, John M. Miller and Albert E. Belon	999
L 16	THE USE OF ERTS-1 DATA FOR THE INVENTORY OF CRITICAL LAND RESOURCES FOR REGIONAL LAND USE PLANNING, J. L. Clapp, R. W. Kiefer, M. M. McCarthy and B. J. Niemann, Jr.	1007
L 17	INVESTIGATIONS OF AN URBAN AREA AND ITS LOCALE USING ERTS-1 DATA SUPPORTED BY U-"PHOTOGRAPHY," H. A. Weeden, F. Y. Borden, D. N. Applegate, and N. Bolling	1015
L 18	'FIRST LOOK' ANALYSES OF FIVE CYCLES OF ERTS-1 IMAGERY OVER COUNTY OF LOS ANGELES: ASSESSMENT OF DATA UTILITY FOR URBAN DEVELOPMENT AND REGIONAL PLANNING, S. Raje, R. Economy and J. McKnight	1023
L 19	PREPARATION OF URBAN LAND USE INVENTORIES BY MACHINE-PROCESSING OF ERTS MSS DATA, William Todd, Paul Mausel and Kenneth Wenner	1031
L 20	A COMPARISON OF LAND-USE DETERMINATIONS USING DATA FROM ERTS-1 AND HIGH ALTITUDE AIRCRAFT, M. Ann Lundelius, C. Mark Chesnutwood, Joe G. Garcia and R. Bryan Erb	1041
L 21	DIGITAL LAND USE MAPPING IN OAKLAND COUNTY, MICHIGAN, Irvin J. Sattinger and Robert D. Dillman	1047
L 22	MAPPING OF AGRICULTURAL LAND USE FROM ERTS-1 DIGITAL DATA, A. D. Wilson, G. A. May and G. W. Peterson	1055
L 23	THE USE OF THE TEMPORAL DIMENSION IN CLASSIFYING AND MAPPING ERTS-1 MSS DATA, F. Y. Borden and D. N. Applegate	1059

Paper No.		Page
L 24	IDENTIFICATION AND MAPPING OF COAL REFUSE BANKS AND OTHER TARGETS IN THE ANTHRACITE REGION, F. Y. Borden, D. N. Thompson and H. M. Lachowski .	1067
L 25	AUTOMATIC INTERPRETATION OF ERTS DATA FOR FOREST MANAGEMENT, Leonard Kirvida and Greg R. Johnson	1075
L 26	LAND RESOURCES SURVEY FQR THE STATE OF MICHIGAN, Buzz Sellman	1083
L 27	TERRAIN CLASSIFICATION MAPS OF YELLOWSTONE NATIONAL PARK, Frederick J. Thomson and Normal E. G. Roller	1091
	INTERPRETATION TECHNIQUES DEVELOPMENT	
I 1	ATMOSPHERIC EFFECTS IN ERTS-1 DATA, AND ADVANCED INFORMATION EXTRACTION TECHNIQUES, William A. Malila and Richard F. Nalepka	1097
I 2	DETERMINATION OF AEROSOL CONTENT IN THE ATMOSPHERE, Michael Griggs	1105
I 3	A TECHNIQUE FOR CORRECTING ERTS DATA FOR SOLAR AND ATMOSPHERIC EFFECTS, Robert H. Rogers and Keith Peacock	1115
I 4	EXPERIMENTAL MASKING OF RBV IMAGES TO REDUCE STATIONARY RESIDUAL INACCURACIES IN RADIOMETRIC CORRECTION, Donald S. Ross	1123
I 5	GEOMETRIC QUALITY OF ERTS-1 IMAGES, Robert B. McEwen	1129
I 6	DIGITAL RECTIFICATION OF ERTS MULTISPECTRAL IMAGERY, Samuel S. Rifman	1131
I 7	RESULTS OF PRECISION PROCESSING (SCENE CORRECTION) OF ERTS-1 IMAGES USING DIGITAL IMAGE PROCESSING TECHNIQUES, Ralph Bernstein	1143
I 8	SIGNIFICANT TECHNIQUES IN THE PROCESSING AND INTERPRETATION OF ERTS-1 DATA, S. B. Cousin, A. C. Anderson, J. F. Paris and J. F. Potter	1151
I 9	COMPUTER TECHNIQUES USED FOR SOME ENHANCEMENTS OF ERTS IMAGES, Fred C. Billingsley and Alex F. H. Goetz	1159
I 10	DIGITAL ENHANCEMENT OF MULTISPECTRAL MSS DATA FOR MAXIMUM IMAGE VISIBILITY, Vidal Raphael Algazi	1169
I 11	ERTS-1 IMAGE ENHANCEMENT BY OPTICALLY COMBINING DENSITY SLICES, Gerald O. Tapper and Robert W. Pease	1179
I 12	PSEUDOCOLOR TRANSFORMATION OF ERTS IMAGERY, Jeannine Lamar and Paul M. Merifield	1187
I 13	DIGITAL INTERACTIVE IMAGE ANALYSIS BY ARRAY PROCESSING, Bruno E. Sabels and Jerry D. Jennings	1199

TABLE OF CONTENTS (Continued)

Paper No.		Page
I 14	COMBINING HUMAN AND COMPUTER INTERPRETATION CAPABILITIES TO ANALYZE ERTS IMAGERY, J. D. Nichols	1205
I 15	ANALYSIS OF ERTS IMAGERY USING SPECIAL ELECTRONIC VIEWING/MEASURING EQUIPMENT, Wm. E. Evans and Sidney M. Serebreny	1211
I 16	COMBINED SPECTRAL AND SPATIAL PROCESSING OF ERTS IMAGERY DATA, Robert M. Haralick and K. Sam Shanmugam	1219
I 17	TERRAIN TYPE RECOGNITION USING ERTS-1 MSS IMAGES, Nicholas Gramenopoulos	1229
I 18	CLASSIFICATION OF ERTS-1 MSS DATA BY CANONICAL ANALYSIS, H. M. Lachowski and F. Y. Borden	1243
I 19	IN SITU SPECTRORADIOMETRIC QUANTIFICATION OF ERTS DATA, Edward F. Yost	1253
	MARINE RESOURCES AND OCEAN SURVEYS	
M 1	SEASONAL CHANGES OF LITTORAL TRANSPORT AND BEACH WIDTH AND RESULTING EFFECT ON PROTECTIVE STRUCTURES, Turbit H. Slaughter,	1259
M 2	RECOGNITION OF BEACH AND NEARSHORE DEPOSITIONAL FEATURES OF CHESAPEAKE BAY, Randall T. Kerhin,	1269
M 3	APPLICABILITY OF ERTS-1 IMAGERY TO THE STUDY OF SUSPENDED SEDIMENT AND AQUATIC FRONTS, V. Klemas, R. Srna, W. Treasure and M. Otley	1275
M 4	CORRELATION OF ERTS MULTISPECTRAL IMAGERY WITH SUSPENDED MATTER AND CHLOROPHYLL IN LOWER CHESAPEAKE BAY, D. E. Bowker, P. Fleischer, T. A. Gosink, W. J. Hanna and J. Ludwick	1291
M 5	PLUME DEVELOPMENT IN LONG ISLAND SOUND OBSERVED BY REMOTE SENSING (ERTS-1), Frederick H. Ruggles, Jr.	1299
M 6	OBSERVATIONS OF SUSPENDED PARTICLE PATTERNS IN NEARSHORE NORTH-EASTERN PACIFIC OCEAN WATERS BY ERTS-1 IMAGERY, Paul R. Carlson, Richard J. Janda and T. John Conomos	1305
M 7	NEW INSIGHTS INTO THE INFLUENCE OF ICE ON THE COASTAL MARINE ENVIRONMENT OF THE BEAUFORT SEA, ALASKA, Peter W. Barnes and Erk Reimnitz	1307
M 8	ERTS-1 OBSERVATIONS OF SEA SURFACE CIRCULATION AND SEDIMENT TRANSPORT, COOK INLET, ALASKA, F. F. Wright, G. D. Sharma and D. C. Burbank	1315
M 9	SEDIMENT DISTRIBUTION AND COASTAL PROCESSES IN COOK INLET, ALASKA, Duwayne M. Anderson, Lawrence W. Gatto, Harlan L. McKim and Anthony Petrone	1323
M 10	DISTRIBUTION AND MOVEMENT OF SUSPENDED SEDIMENT IN THE GULF OF MEXICO OFF THE TEXAS COAST, Ralph E. Hunter	1341

Paper No.		Page
M 11	OCEANOGRAPHIC MAPPING OF STRUCTURE AND DYNAMICS OF THE NORTHERN GULF OF CALIFORNIA BY THE USE OF SPECTRAL MODELING AND ERTS-1, L. K. Lepley, Gustavo Calderon, and J. R. Hendrickson	1349
M 12	OCEANOGRAPHIC FEATURES IN THE LEE OF THE WINDWARD AND LEEWARD ISLANDS: ERTS AND SHIP DATA, Kirby J. Hanson, Frank Hebard and Richard Cram	1357
M 13	REMOTE SENSING OF OCEAN CURRENTS USING ERTS IMAGERY, George A. Maul	1365
M 14	USE OF ERTS DATA FOR MAPPING ARCTIC SEA ICE, James C. Barnes and Clinton J. Bowley	1377
M 15	BIOMASS IN THE UPWELLING AREAS ALONG THE NORTHWEST COAST OF AFRICA AS VIEWED WITH ERTS-1, Karl-Heinz Szekielda and Robert J. Curran	1385
M 16	ERTS IMAGERY AS AN AID TO FISHERIES MANAGEMENT IN THE NORTHERN GULF OF CALIFORNIA, J. R. Hendrickson, Alfredo Cota, Gustavo Calderon and L. K. Lepley	1403
M 17	APPLICATION OF ERTS-1 IMAGERY TO THE HARVEST MODEL OF THE U. S. MENHADEN FISHERY, Paul M. Maughan, Allan D. Marmelstein and O. Ray Temple	1405
M 18	COASTAL AND SUBMARINE FEATURES ON MSS IMAGERY OF SOUTHEASTERN MASSACHUSETTS: COMPARISON WITH CONVENTIONAL MAPS, Richard S. Williams, Jr.	1413
M 19	WATER DEPTH ESTIMATION WITH ERTS-1 IMAGERY, D. S. Ross	1423
M 20	CALCULATIONS OF WATER DEPTH FROM ERTS-MSS DATA, Fabian C. Polcyn and David R. Lyzenga	1433
	MULTIDISCIPLINARY/REGIONAL RESOURCE SURVEYS	
R 1	MULTIDISCIPLINARY APPLICATION OF ERTS-1 DATA TO NORTH CAROLINA NATURAL RESOURCE MANAGEMENT, Charles W. Welby, J. O. Lammi and Robert J. Carson	1443
R 2	NATURAL RESOURCE INVENTORY AND MONITORING IN OREGON WITH ERTS IMAGERY, G. H. Simonson, D. P. Paine, C. E. Poulton, R. D. Lawrence, J. H. Herzog, and R. J. Murray	1451
R 3	RESOURCE MANAGEMENT IMPLICATIONS OF ERTS-1 DATA TO OHIO, David C. Sweet, Terry L. Wells and George E. Wukelic	1459
R 4	ASSESSMENT OF SOUTHERN CALIFORNIA ENVIRONMENT FROM ERTS-1, Leonard W. Bowden and James H. Vieilenave	1467
R 5	APPLICATIONS OF REMOTE SENSING (ERTS) TO RESOURCE MANAGEMENT AND DEVELOPMENT IN SAHELIEN AFRICA (REPUBLIC OF MALI), N. H. MacLeod	1475

Paper No.		Page
R 6	FIRST ERTS-1 RESULTS IN SOUTHEASTERN FRANCE: GEOLOGY, SEDIMENTOLOGY, POLLUTION AT SEA, A. Fontanel, J. Guillemot and M. Guy	1483

PAPERS NOT LISTED IN THE ABSTRACTS OF THE SYMPOSIUM

	DCP-COLLECTED ABSOLUTE TARGET REFLECTANCE SIGNATURES ASSIST ACCURATE INTERPRETATION OF ERTS-1 IMAGERY, Frederick P. Weber	1513
	UNIQUE CHARACTERISTICS OF ERTS, Alden P. Colvocoresses	1523
	ERTS-1 APPLIED FOR STRUCTURAL AND MORPHOLOGICAL INVESTIGATIONS CASE STUDIES: (1) LOS ANGELES, CALIFORNIA AND (2) COASTAL PLAIN, NEW JERSEY, Ervin Y. Kedar	1527
	A PRELIMINARY EVALUATION OF ERTS-1 IMAGES ON THE VOLCANIC AREAS OF SOUTHERN ITALY (NASA CONTRACT FO-013), R. Cassinis and G. M. Lechi	1539
	THERMAL SURVEILLANCE OF CASCADE RANGE VOLCANOES USING ERTS-1 MULTISPECTRAL SCANNER, AIRCRAFT IMAGING SYSTEMS, AND GROUND-BASED DATA COMMUNICATION PLATFORMS, Jules D. Friedman, David G. Frank, Duane Preble and J. Earle Painter	1549
	INITIAL EVALUATION OF THE GEOLOGIC APPLICATIONS OF ERTS-1 IMAGERY FOR NEW MEXICO, Karl Vonder Linden and Frank E. Kottlowski	1561
	COMPUTED ATMOSPHERIC EFFECTS ON ERTS OBSERVATIONS, Robert S. Fraser	1567
	MAPPING OF SPOIL BANKS USING ERTS-1 PICTURES, Professor Moid U. Ahmad David A. Kantner and John W. Antalovich	1575
	AIR QUALITY INDICES FROM ERTS-1 MSS INFORMATION, PR 568, Ellen L. Riley, Steven Stryker, and Edward A. Ward	1583
	SNOW COVER SURVEYS IN ALASKA FROM ERTS-1 DATA, Carl S. Benson	1593
	UTILIZATION OF ERTS-1 DATA TO MONITOR AND CLASSIFY EUTROPHICATION OF INLAND LAKES, Phillip E. Chase, Larry Reed and V. Elliott Smith	1597
	ERTS-1 OBSERVES ALGAL BLOOMS IN LAKE ERIE AND UTAH LAKE, Alan E. Strong.	1605
	USE ERTS-1 DATA FOR REGIONAL PLANNING IN THE METROPOLITAN WASHINGTON COUNCIL OF GOVERNMENTS – A SHORT BRIEF, Harry J. Mallon	1613
	LAND USE MAPPING AND CHANGE DETECTION USING ERTS IMAGERY IN MONTGOMERY COUNTY, ALABAMA, Richard Paul Wilms	1625
	DETERMINATION OF LAND USE IN MINNESOTA BY AUTOMATIC INTERPRETATION OF ERTS MSS DATA, Raymond E. Zirkle and Deborah R. Pile	1635

Page

DIGITAL DATA PROCESSING OF ERTS-1 IMAGERY OF DELAWARE BAY, Alfred C. Conrod 1641

THE USE OF PHOTOGRAPHIC METHODS IN CONTRAST ENHANCEMENT OF ERTS-1 IMAGES, Lawrence F. Harris 1649

PRECISION ANNOTATION OF PREDETERMINED PRIMARY SAMPLING UNITS ON ERTS-1 MSS IMAGES, Jan W. van Roessel and Philip G. Langley 1661

UNSUPERVISED CLASSIFICATION AND AREAL MEASUREMENT OF LAND AND WATER COASTAL FEATURES ON THE TEXAS COAST, L. M. Flores, C. A. Reeves, S. B. Hixon and J. F. Paris 1675

USE OF ERTS-1 PICTURES IN COASTAL OCEANOGRAPHY IN BRITISH COLUMBIA, J. F. R. Gower 1683

RELATIONSHIPS BETWEEN REMOTELY SENSED FISHERIES DISTRIBUTION INFORMATION AND SELECTED OCEANOGRAPHIC PARAMETERS IN THE MISSISSIPPI SOUND, Andrew J. Kemmerer and Joseph A. Benigno 1685

APPLICATION OF ERTS-1 IMAGERY IN COASTAL STUDIES, Orville T. Magoon, Dennis W. Berg and Robert J. Hallermeier 1697

APPLICATION OF ERTS-1 IMAGERY IN THE FIELDS OF GEOLOGY, AGRICULTURE, FORESTRY, AND HYDROLOGY TO SELECTED TEST SITES IN IRAN, Khosro Ebtehadj 1699

AUTHOR'S INDEX 1727

VOLUME II

SUMMARY SESSION

INTRODUCTION TO SUMMARY SESSION	Dr. James C. Fletcher, Administrator National Aeronautics and Space Administration
GENERAL REMARKS	Hon. James W. Symington, Representative, U. S. Congress, State of Missouri
KEYNOTE ADDRESS	Hon. Ed Reinecke, Lt. Governor State of California
REVIEW OF ERTS-1 STATUS	Dr. William Nordberg, Chief Laboratory for Meteorology and Earth Sciences NASA, Goddard Space Flight Center

KEY FINDINGS FROM SELECTED INVESTIGATIONS

IDENTIFICATION AND MAPPING OF SOILS, VEGETATION, AND WATER RESOURCES OF LYNN COUNTY, TEXAS, BY COMPUTER ANALYSIS OF ERTS MSS DATA, Marion F. Baumgardner, Steven J. Kristof and James A. Henderson, Jr.

PRELIMINARY GEOLOGIC APPLICATION OF ERTS-1 IMAGERY IN ALASKA, Ernest H. Lathram, Irvin L. Tailleur, William W. Patton, Jr. and William A. Fischer

A MULTIDISCIPLINARY SURVEY FOR THE MANAGEMENT OF ALASKAN RESOURCES UTILIZING ERTS IMAGERY, John M. Miller and Albert E. Belon

APPLICATION OF ERTS-1 IMAGERY TO FLOOD INUNDATION MAPPING, George R. Hallberg and Bernard E. Hoyer and Albert Rango

INVITED SUMMARIES IN SELECTED DISCIPLINES

AGRICULTURE, FORESTRY, RANGE RESOURCES, Charles E. Poulton

LAND USE AND MAPPING, David T. Lindgren and Robert B. Simpson

MINERAL RESOURCES, GEOLOGICAL STRUCTURE AND LANDFORM SURVEYS, Laurence H. Lattman

WATER RESOURCES, Vincent V. Salomonson and Albert Rango

INVITED PRESENTATIONS ON APPLICATIONS OF ERTS-1 RESULTS

THE EARTH RESOURCES PROGRAM OF THE CORPS OF ENGINEERS, John W. Jarman

APPLICATION OF ERTS-1 RESULTS TO USDI PROGRAMS, John M. DeNoyer

A PRELIMINARY ASSESSMENT OF ERTS IMAGERY FOR MARINE RESOURCES, Gifford C. Ewing

THE USE OF ERTS-1 DATA TO AID IN SOLVING WATER RESOURCES MANAGEMENT PROBLEMS IN THE STATE OF CALIFORNIA, Robert H. Burgy

APPLICATION OF ERTS RESULTS TO LAND AND RESOURCE MANAGEMENT IN THE STATE OF MISSISSIPPI, Preston T. Bankston

TABLE OF CONTENTS (Continued)

VOLUME III

DISCIPLINE SUMMARY REPORTS

AGRICULTURE, FORESTRY, RANGE RESOURCES, Chairman—W. J. Crea

LAND USE AND MAPPING, Chairman—D. W. Mooneyhan

MINERAL RESOURCES, GEOLOGICAL STRUCTURE AND LANDFORM SURVEYS, Chairman—N. M. Short

ENVIRONMENT SURVEYS, Chairman—L. S. Walter

WATER RESOURCES, Chairman—V. V. Salomonson

MARINE RESOURCES AND OCEAN SURVEYS, Chairman—J. R. Greaves

INTERPRETATION TECHNIQUES DEVELOPMENT, Chairman—W. L. Alford

MULTIDISCIPLINARY/REGIONAL RESOURCE SURVEYS, Chairman—G. Trafford

ERTS-1 DATA PRODUCT PERFORMANCE

B. T. Bachofer, *General Electric Company, Space Systems, Philadelphia, Pennsylvania*

ABSTRACT

The quality of the ERTS-1 data products produced during the initial months of system operation are evaluated. Quantitative performance data - principally geometric and radiometric accuracy and resolution - are determined for these data products. A comparison of these measurements with prelaunch predictions is also made.

INTRODUCTION

This paper is an assessment of the overall quality of the data products collected, produced and distributed by the ERTS-1 system during its initial period of sustained operation. This assessment is intended to quantify the inherent characteristics of the data products for investigators and experimenters involved in its scientific interpretation and analysis.

The period of evaluation covers the first three to six months of ERTS operation. Most of the data evaluated was collected during the first five eighteen day coverage cycles (the first three months) with more selectivity during the fourth through sixth months of operation. In order to keep the amount of data evaluated to a reasonable quantity while still maintaining a good sampling throughout the successive coverage cycles, test sites were selected which provided imagery suitable for making quantitative measurements (i.e. sufficient ground truth, urban detail, fairly constant atmosphere, large scale inert areas, etc.). System corrected imagery from each site in both 70 mm and 9.5 inch formats were ordered from the NDPF using the normal "standing order" procedure. This data was supplemented as required with system corrected imagery from other test sites.

The data was analyzed to determine its quality in terms of geometric accuracy, resolution and radiometric accuracy. For reference these measured results were compared to the prelaunch estimates published in the ERTS Data Users Handbook. By repetitive analysis of data taken at different times performance indicative of sustained operation was possible and allowed short term or start up type anomalies to be differentiated from normal performance or legitimate trends.

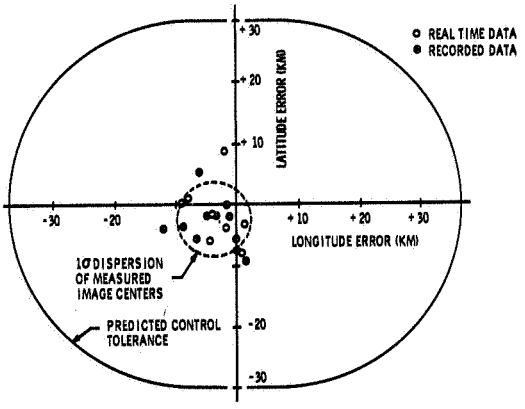
GEOMETRIC ACCURACY

The geometric quality of system corrected photographic data was evaluated and measured over a broad set of parameters ranging from the degree of control over the geographic areas imaged by the ERTS sensors to the precision with which a picture element in one spectral image can be related to that in another.

Image Center Control. Initial program goals were established to control the spacecraft orbit and attitude, compute the ephemerides from tracking data, command the sensors and frame the imagery so that nearly the same geographical area on the earth would be contained in imagery collected on successive coverage cycles. Prelaunch tolerances on the control of image centers was predicted to be within 30 km in the in-track direction and 37 km in the cross-track direction of a predefined matrix of "nominal" image center locations. Figure 1 shows the difference between measured and the corresponding "nominal" image centers for test sites in the U.S. (real time) and abroad (recorded). Data Collected during a one month period following discontinued use of the RBV cameras on 6 August 1972 are excluded from the data set since during this period a new image framing technique had to be developed and unusually large errors were experienced. Thd dispersion of the data is quite small (> 6 km 1σ) with a slight offset from nominal to the south and west, due to spacecraft attitude. Since spacecraft attitude will vary principally with spacecraft position in orbit and sensor duty cycles, this bias will vary for test sites at different latitudes, but at a latitude, well within the overall tolerance limits. The latitude of the U.S. and most of the foreign test sites selected for this evaluation were approximately the same.

Figure 1

IMAGE CENTER CONTROL
(VARIATION FROM NOMINAL CENTER)



Absolute Location. Images are annotated with alphanumeric data and latitude and longitude tick marks to relate the image content to an earth reference. Absolute location is a measure of the accuracy with which the true latitude and longitude of points in an image can be determined using the tick marks at the edge of the image. Figure 2 shows the trends in location errors versus time. The large errors following launch are attributable to several "bugs" in the annotation software. After the

correction of these, errors ranged in the one to three kilometer region as additional refinements in the annotation processing were instituted. Periodic measurements made during the early months of 1973 show these errors to range from 500 to 1100 meters, comparing reasonably well with prelaunch predictions of 800 meters.

Figure 2
LOCATION ACCURACY
(SYSTEM CORRECTED DATA)

2000 - 7000 METERS	LAUNCH THROUGH MID-OCTOBER
1000 - 3000 METERS	MID-OCTOBER THROUGH DECEMBER
500 - 1100 METERS	1973
~800 METERS	PREDICTED

Band-to-Band (Spectral) Registration. Band-to-band or spectral registration is the measure of how well points in an image from one spectral band overlay the corresponding points in another band from a single observation of a ground scene. Table 1 shows that registration errors are about three times smaller than prelaunch predictions, and, in the case of the MSS, approach the resolution limit of the sensor. This performance is attributable to better than expected stability at the sensors and ground processing equipment as well as accurate calibrational/correction data.

Table 1
BAND-TO-BAND (SPECTRAL) REGISTRATION (METERS, RMS)

	MEASURED	PREDICTED
MSS	60	159
RBV	110	336

Temporal Registration. Temporal registration is the measure of how well points in one spectral band overlay the corresponding points in that same spectral band from different observations of the same scene. The "best fit" is determined by translating and rotating one image with respect to the other so that the RMS value of the distance between corresponding pairs of points is minimized. MSS temporal registration errors are shown in Table 2. Again, the results indicate actual performance to be significantly better than predicted. Since repetitive RBV data was not available, no measurement could be made.

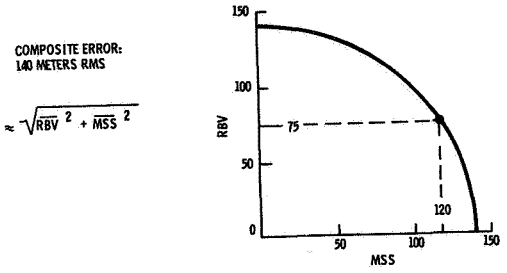
Table 2
TEMPORAL REGISTRATION (METERS, RMS)

	MEASURED	PREDICTED
MSS	185	~ 275
RBV	NOT MEASURED	~ 350

Relative Mapping Accuracy. Relative mapping accuracy is the measure of how well points in an image can be located with respect to other points in that image; that is, it is the measure of how well the internal distortions within an image are corrected. An excellent, and rather easy to obtain, indirect measure of the combined relative mapping accuracy of both MSS and RBV images can be made by comparing images of the same scene from both sensors. That is, by translating, rotating and

scaling points in one band of an MSS image (usually the visible red) with the corresponding points in the RBV image, a measure of the combined errors of both images is made. This composite error is 140 meters. It is not possible, using this method, to separate the total into the contribution from the individual sensors. (See Figure 3) If we assume RBV and MSS relative mapping errors to be roughly equal, each would be just under 100 meters RMS. A distribution of RBV and MSS errors of 75 meters and 120 meters respectively is probably a more realistic estimate.

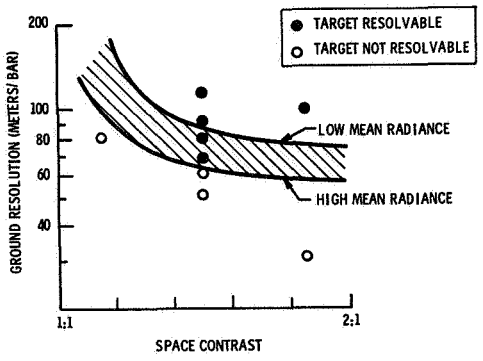
Figure 3
RELATIVE MAPPING ACCURACY



RESOLUTION

Image Resolution. The predicted resolution of ERTS products is based on analysis using standard tribar targets. Since proper targets of this type are not available in ERTS images, natural patterns of grossly equivalent form were used. These were identified and located using high resolution aircraft imagery. The ERTS images were then examined to determine whether these patterns could or could not be resolved. Pier structures in harbors proved particularly useful. Contrast was a subjective estimate. Figure 4 shows a comparison of this type measurement with predicted resolution curves for one band of the MSS. Plotted as solid circles are patterns that could be resolved. Open circles are patterns that could not be resolved. Agreement with predicted resolution is quite good. Similar results were obtained for other MSS bands and for RBV data.

Figure 4
PREDICTED VS MEASURED MSS RESOLUTION (BAND 2)



Resolution of Computer Compatible Tape (CCT) Data. The inherent resolution of system corrected CCT data is better than that of standard photographic image products since it is not degraded in any way by the image generation and photographic copying processes. A measure of CCT resolution, albeit subjective, can be made from examination of an enlargement of a portion of a scene from a CCT. For reference purposes Figure 5A is a high resolution aircraft image of a portion of the downtown Washington D.C. area. Figure 5B is an enlargement of a small portion (about one-four-hundredth) of a single ERTS frame. The enlargement was done digitally



Figure 5A High Resolution Aircraft Image



Figure 5B Enlarged Filtered CCT Image

and then filtered and displayed on a TY type monitor at a scale such that the resolution of the TV monitor does not substantially affect image quality. Features as small as the Jefferson, Lincoln and Roosevelt Memorials and Washington Monument are detectable.

RADIOMETRIC ACCURACY

Radiometric Transfer Function. The radiometric transfer function relates film transmission to sensor output and, therefore, also to input radiance. The nominal transfer function is linear between the minimum transmission of 0.4% to the maximum transmission of 40%. During the first five coverage cycles, periodic adjustments were made to improve the slope and linearity of this transfer characteristic.

Figure 6

EXAMPLE OF POOR RADIOMETRIC TRANSFER FUNCTION

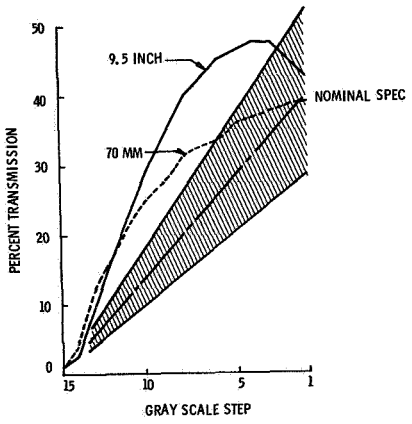
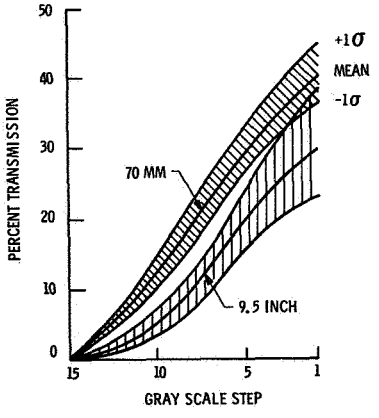


Figure 6 shows one of the poorer transfer characteristics measured on an image obtained during the second coverage cycle. The high slope and bow have the effect of causing positives to be generally lighter and negatives generally darker, than the nominal. Further, for the 9.5 inch imager, there is a portion of the dynamic range which is double valued, which renders this part of the range useless for radiometric purposes; fortunately, however, measurements show that little image data (except for clouds) fall into the upper part of the dynamic range.

Figure 7 shows the average transfer function as it now exists, measured over ten differnet days of the first months of '73. The mean and one sigma dispersion in the transfer characteristics are shown. The linearity, average slope and dispersion for the 70 mm imagery is excellent. For 9.5 inch imagery, the transfer characteristic is somewhat below nominal, but double valued regions have been eliminated.

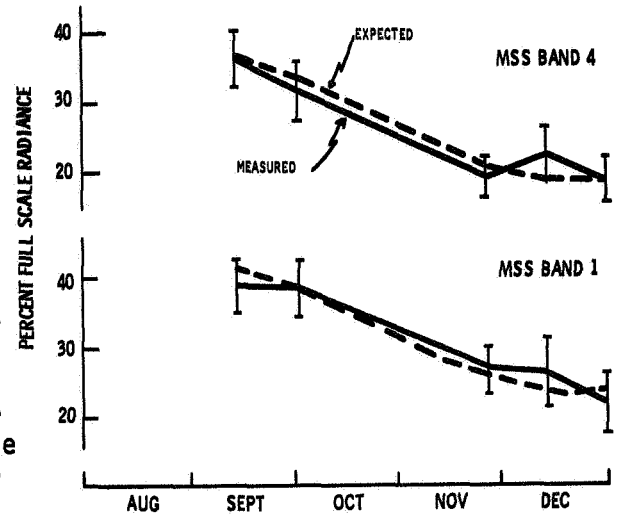
Figure 7

CURRENT RADIOMETRIC TRANSFER FUNCTION
(MEAN AND STANDARD DEVIATION FOR MEASUREMENTS ON 10 DIFFERENT DAYS)



Radiometric Accuracy and Stability. Because of the intervening effects of the atmosphere, a good direct measure of the absolute radiometric accuracy or its stability is not available. Two approaches toward indirectly measuring stability of the system radiometric calibration for MSS data were investigated -- one using repetitive observations of the same areas; the other by monitoring the sun calibration data periodically taken.

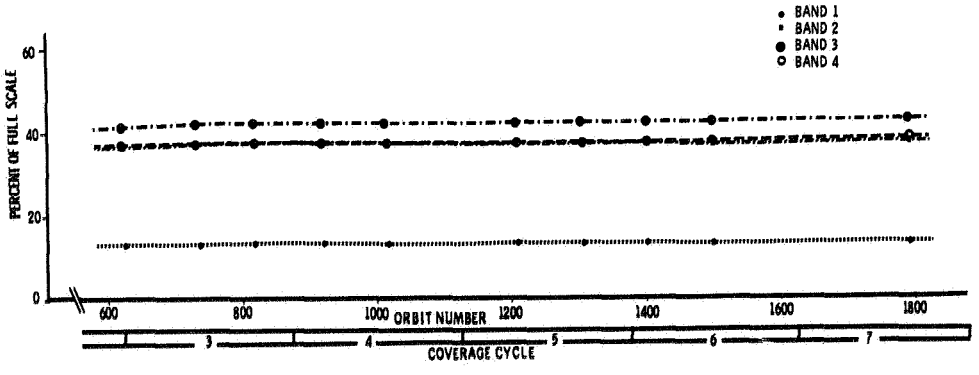
Figure 8
RADIANCE HISTORY
(DEATH VALLEY AREA)



Imagery of relatively inert areas (in the vicinity of Death Valley, California) where surface reflectivity is assumed to be homogenous and constant, were observed on successive coverage cycles. The mean radiance from many targets in each observation was computed and plotted. The solid lines of Figure 8 connect these points for band 1 and band 4. The dashed lines show the expected change in radiance caused by seasonal illumination changes. Agreement is reasonable and within the uncertainty of the individual measurements; however, the number of sets of cloud free images and the time periods over which repetitive imagery was available was sufficiently short that quantitative conclusions are not warranted.

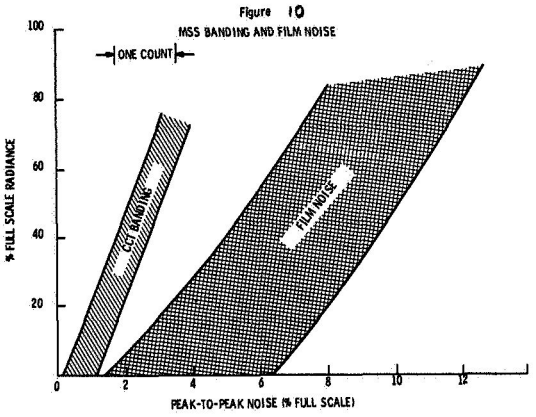
One each orbit the MSS can image the solar disk through a small aperture and reflecting mirror. Periodic observations of the sun calibration data for the MSS are shown in Figure 9. The calibrated sun data in all bands remains relatively flat, indicating stable system radiometric calibration within a few percent.

Figure 9
MSS SUN CAL HISTORY



MSS Banding. MSS computer compatible tapes were analyzed to determine the effectiveness of the relative detector-to-detector calibration. That is, to determine how much variation from scan-line to scan-line (detector-to-detector) exists over a uniform portion of an image. Data was evaluated at different radiance levels, in all spectral bands, and from CCT's obtained at different times. The results are plotted as the broad shaded curve in the left part of Figure 10. This plot is the peak-to-peak difference between any of the detectors in a band versus the mean level in that band.

Figure 10
MSS BANDING AND FILM NOISE



It is interesting to note that at low radiance levels the peak-to-peak banding amounts to only about 1% (half a quantum level) and increases with increasing radiance. In film images, however, banding is visible to the eye principally at low radiance levels and not at the higher levels. This is because of the eye's sensitivity to the higher contrast ratio at these low levels and because of other sources of "banding" in film images.

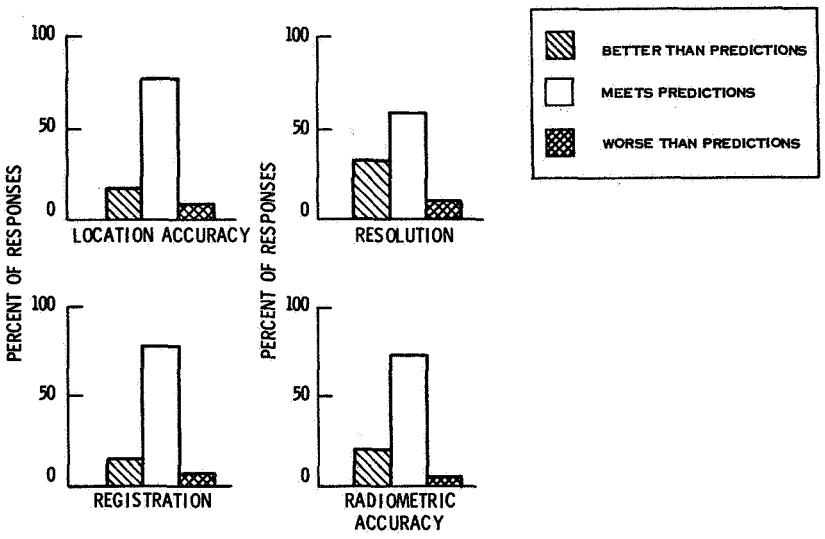
The right hand portion of Figure 10 represents the peak-to-peak value of all "system noise" as measured on film with a microdensitometer. Since the microdensitometer scans were made with a narrow but long slit with the long dimension parallel to the scan lines, this noise will include nonuniformities produced in film image generation, certain photographic nonuniformities as well as the inherent detector banding of the MSS. Note that Figure 10 is plotted in terms of peak-to-peak noise; RMS noise would be about four times smaller.

SUMMARY COMMENTS

The foregoing analyses leads to the general conclusion that the quality of the system corrected products produced by the ERTS-1 system during its initial period of operations is, from a resolution and radiometric accuracy viewpoint, quite consistent with prelaunch estimates. In the geometric sense, these data products are somewhat better (and in a few cases considerably better) than prelaunch estimates.

Another independent, but perhaps more subjective, measure of data quality was obtained from a questionnaire mailed to all principle investigators. The investigators were asked to give their evaluation of the data products with respect to the prelaunch estimates they were provided. The responses are plotted in Figure 11 and show, perhaps, and even better report card than the more quantitative evaluation of this paper.

Figure 11
USER QUESTIONNAIRE RESULTS



AGRICULTURE, FORESTRY, RANGE RESOURCES

Paper A 1

IDENTIFICATION OF WINTER WHEAT FROM ERTS-1 IMAGERY

Donald L. Williams, Stanley A. Morain, Bonnie Barker, and Jerry C. Coiner,
The University of Kansas Center of Research, Inc., The University of Kansas, Lawrence, Kansas 66044

ABSTRACT: Continuing interpretation of the test area in Finney County, Kansas, has revealed that winter wheat can be successfully identified. This successful identification is based on human recognition of tonal signatures on MSS images. Several different but highly successful interpretation strategies have been employed. These strategies involve the use of both spectral and temporal inputs. Good results have been obtained from a single MSS-5 image acquired at a critical time in the crop cycle (planting). On a test sample of 54,612 acres (22,101 hectares), 89 percent of the acreage was correctly classified as wheat or non-wheat and the estimated wheat acreage (19,516 acres, 7,898 ha.) was 99 percent of the actual acreage of wheat in the sample area.

****

Continuing interpretation of ERTS-1 MSS images of Finney County, Kansas, has established that hard red winter wheat may be successfully distinguished from all other crops and cropping conditions by a simple human interpretation technique. This technique was initially developed for irrigated wheat, but has proven applicable to non-irrigated wheat as well. On a test sample of 54,612 acres (22,101 hectares) for which surface observations were available, 89 percent of the acreage was correctly classified as wheat or non-wheat. The error terms conformed to the Central Limit Theorem. The estimate of wheat in this test was 19,516 acres (7,898 ha.), 99 percent of the actual amount of wheat (19,674 A., 7,962 ha.) in the sample. This estimate was based on a single band/time-frame image, MSS-5, acquired September 21 and September 22, 1972. The estimate is therefore based on imagery acquired during the planting period.

The sample analyzed for this report represents 6.5 percent of the land area of Finney County and includes all environmental and agricultural types in the county except for the intensive irrigation area in the northwestern part of the county, where wheat is not a significant component of the landscape. Finney County (Figure 1) was originally selected as a test area because of the magnitude and diversity of agriculture in the county. Most of the 1308 square mile (3,388 sq. km.) area is typical of the large field agricultural system of the winter wheat belt of the Great Plains. However, large areas of rangeland exist in the county and extensive and intensive irrigation is widely practiced. The single most important crop in the county is wheat. In 1971, Finney County ranked third among Kansas counties with wheat production of 6,921,000

bushels (188,326 metric tons). In the same year, the county was among the ten most productive counties in Kansas for sorghum for grain, corn for grain, corn for silage, alfalfa hay, and sugar beets while ranking seventh in number of cattle on farms (Kansas State Board of Agriculture, 1972).

Five sample areas were selected in Finney County in such a way that the areas are readily located on ERTS-1 imagery and all environmental and agricultural types in the county have been included. Surface observations of crop type and condition have been obtained for each field in these test areas. Environmental parameters, principally soil type and topography, have been obtained from the standard soil survey map (USDA, Soil Conservation Service, 1965) and available topographic maps.

Four of the five sample areas were used in this analysis (Figure 1). The fifth sample is located in the small field irrigated area of northwestern Finney County and contains a limited amount of wheat. Samples 1 and 2 represent the part of the county with sandy soils. Most of this area is composed of large irrigated fields. Samples 3A and 3B represent the area with nearly level loamy soils. Most of this area is composed of large non-irrigated fields. Sample 4A represents the area of rolling lands with mostly loamy soils. All cultivation in this area is large-field dryland. Sample 4B represents the area of nearly level clayey soils. Most of this area is large-field dryland cultivation.

To obtain ERTS-1 data for analysis of these samples, a simple human image interpretation technique was employed. The gray scale tablet along the bottom of the image was divided into five steps which the three interpreters, Williams, Coiner and Barker, agreed were distinct and detectable in the image context (Figure 2). A map showing field boundaries and field numbers for each sample area had been previously prepared. The interpreter recorded the apparent tone of each field as perceived by comparison to gray scale tablet. All interpretations were replicated, by all three interpreters in most instances. However, Williams performed the data analysis. To avoid possible bias, after he began the analysis for a given sample area, he took no further image data for that area.

The initial wheat detection experiment was designed on a multi-image basis (Williams, et al, 1973). Tonal data had been taken from four images for sample areas 1 and 2. These images were MSS-5 acquired August 16, September 21, and December 2, and MSS-7 acquired December 2. A decision matrix (scattergram) was constructed for the data from sample area 1 and a wheat/non-wheat boundary was drawn through the decision matrix. This boundary resulted in 93 percent separation of wheat fields from non-wheat fields. Due to partially offsetting errors, the estimated number of wheat fields (47) was 98 percent of the actual number. When this decision boundary was applied to the data from sample area 2, 86 percent of the fields were correctly classified and the estimated number of wheat fields (14) equaled the actual number. However, the method (1) did not appear applicable to the data from Sample Area 4, (2) was cumbersome, and (3) seemed unsuitable for application to large areas. Further analysis of the decision matrix revealed that the MSS-7 image had not contributed to the successful discrimination of any field.

This fact led to the concept of monitoring temporal change as a method of identification. The MSS-5 image acquired December 21, 1972, was added to the data set at this time. Although this method of observing tonal change through time also successfully discriminated wheat, the method was plagued by the same shortcomings as the other multi-image approach.

While the temporal change analysis was in progress, further study of the original decision matrix revealed that most of the wheat/non-wheat separation had been due to a single image, MSS-5 acquired September 21, 1972. Part of the county was cloud covered on that date. However, all cloud covered sample areas were clear on September 22. The cloud free coverage for each test area was used for the interpretation.

The hypothesis under which any binary discrimination is achieved is that the two conditions are more or less distinct in the data space (Figure 3). In the case under consideration, the hypothesis is that wheat fields have lighter tones than non-wheat fields. This conclusion may be confirmed by inspection of the graphs in Figure 3. However, the significant degree of overlap in tone level 3 is obvious. This overlap constitutes a serious error if the tone is assigend to either wheat or non-wheat.

Inspection of the data subdivided according to environmental area (Figure 4) reveals that this serious overlap does not exist in the individual areas. Instead, most fields assigned to tone level 3 are wheat in sample areas 1, 2, and 4B, while most fields assigned to tone level 3 are non-wheat in sample areas 3 and 4A. That is, error is spatially distributed as a function of the spatial distribution of environmental variables.

Based on these spatial results, the following optimum rule for wheat indentification in Finney County, Kansas, was devised: on MSS-5 imagery acquired during the wheat planting period in 1972, all fields with light and medium tones (tone levels 1, 2, and 3) on sandy soils and nearly level clays are wheat and all fields with light tones on nearly level to rolling loamy soils are wheat.

This rule was initially developed for and applied to all fields 80 acres (32 ha.) or larger, because these fields were consistently detectable as discrete entities in the image. The four sample areas contained 377 fields 80 acres or greater in size. These 377 fields contained 54,612 acres (22,101 ha.), for an average size of 145 acres (59 ha.). The accuracies (Table 1) of classification and estimation of wheat were identical for both number of fields and acreage. Eighty-nine percent of all fields and acreages were correctly classified as wheat or non-wheat. The estimated number and acreage of wheat fields was 99 percent of the actual number and acreage. Use of a single classification rule for all sample areas results in slightly decreased accuracy of classification and serious errors in the estimation of wheat acreage. For example, if only fields having tones 1 and 2 are assigned to wheat, the accuracy of the classification is 86 percent but wheat acreage is underestimated by 26 percent. On the other hand, if all fields having tones 1, 2 and 3 are assigned to wheat, the classification accuracy drops to 82 percent and wheat acreage is overestimated by 35 percent.

Fields smaller than 80 acres had been omitted from the initial analysis because (1) they were often hard to separate from adjacent fields, and (2) most of the resolution cells contain boundaries and are, therefore, averages of often disparate tones. However, tones were also assigned for smaller fields in areas 1, 2, and 3A. These areas contained 202 large and 78 small fields. The large fields contained 23,896 acres (9,670 ha.). This acreage was classified with 91 percent accuracy and the wheat acreage estimate was 100 percent correct. The 78 small fields contained only 2,925 acres (1184 ha.). Only 74 percent of this acreage was correctly classified and wheat acreage was overestimated by 13 percent. But when this modest acreage was added to that of the large fields, the resulting acreage classification was still 89 percent accurate and the overestimation of wheat acreage was 2 percent.

Although temporal data were not required for the identification of winter wheat, these data may serve two important roles. The estimates of wheat acreage presented here are estimates of acreage planted and are, therefore, significantly larger than the acreage harvested. In the fall of 1970, 192,000 acres (77,702 ha.) were seeded in Finney County. In June 1971, 189,000 acres (76,488 ha.) were harvested. Although this difference was small, the amount of wheat destroyed is quite variable from year to year and must be removed from the original acreage estimate. Furthermore, temporal data may provide information on the state of the crop. For example, tones of wheat fields are highly variable on MSS-5 images acquired in December. This variability is an indication of the degree of fall growth, which varies greatly from one field to another. This tonal variability makes identification of wheat very difficult, but, if a field has already been identified as wheat, the variability provides useful data on the state of the crop in that field.

The results presented here demonstrate that a simple method for winter wheat identification may be developed given an adequate prior knowledge of local environment and crop cycle. The method appears to be applicable to other crops if suitable distinct crop cycle events may be defined. Knowledge of the local environment is critical if the interpretation is to be successfully conducted. Components of the local environment data set can be taken directly from the ERTS-1 imagery (Williams and Coiner, 1973) but other components are best developed at the local level. Furthermore, surface observations for a small number of fields from each environmental area would be a necessity. The necessity for (1) surface observation, (2) knowledge of the local environment, (3) knowledge of local crop cycles, and (4) the modest amount of equipment and training required to perform these interpretations make this method suitable for implementation at the local (county) level.

REFERENCES:

ERTS-1 Imagery

DATE	FRAME NUMBER	SCALE	QUALITY
8-16-72	1024-16511-5	1:1,000,000	Excellent
9-21-72	1060-16512-5	1:1,000,000	Good, partial haze cover
9-22-72	1061-16564-5	1:3,300,000	Good
9-22-72	1061-16570-5	1:3,300,000	Good
12-2-72	1132-16514-5	1:1,000,000	Good
12-2-72	1132-16514-7	1:1,000,000	Good
12-21-72	1151-16572-5	1:1,000,000	Good
12-21-72	1151-16575-5	1:1,000,000	Good

Reports:

Kansas State Board of Agriculture. 1972. Farm Facts, 1971-1972. Topeka, Kansas: Kansas State Printer.

U.S.D.A., Soil Conservation Service. 1965. Soil Survey, Finney County, Kansas. Washington: Government Printing Office.

Williams, Donald L., and Jerry C. Coiner. 1973. Land Use Map, Finney County, Kansas. Center for Research, Inc. CRINC - DIIR 2264-3.

Williams, Donald L., Bonnie Barker, and Jerry C. Coiner. 1973. Discrimination of winter wheat on irrigated land in southern Finney County, Kansas. Center for Research, Inc. CRINC - DIIR 2264-4

TABLE 1: Contigency table for discrimination of wheat from non-wheat fields ≥ 80 acres, all test areas, Finney County, Kansas, September 21, 22, 1972.

Rule: Field is wheat (areas 1, 2, 4B) if tone is ≤ 3
Field is wheat (areas 3, 4A) if tone is ≤ 2

	Number of fields assigned		Acres assigned	
	wheat	non-wheat	wheat	non-wheat
Actual wheat	140	22	16,710	2,964
Actual non-wheat	20	195	2,806	32,132

Total = 377 fields
Accuracy of Assignment = 89%
Accuracy of estimation wheat = 99%

Total = 54,612 acres
Accuracy of Assignment = 89%
Accuracy of estimation of wheat acreage = 99%

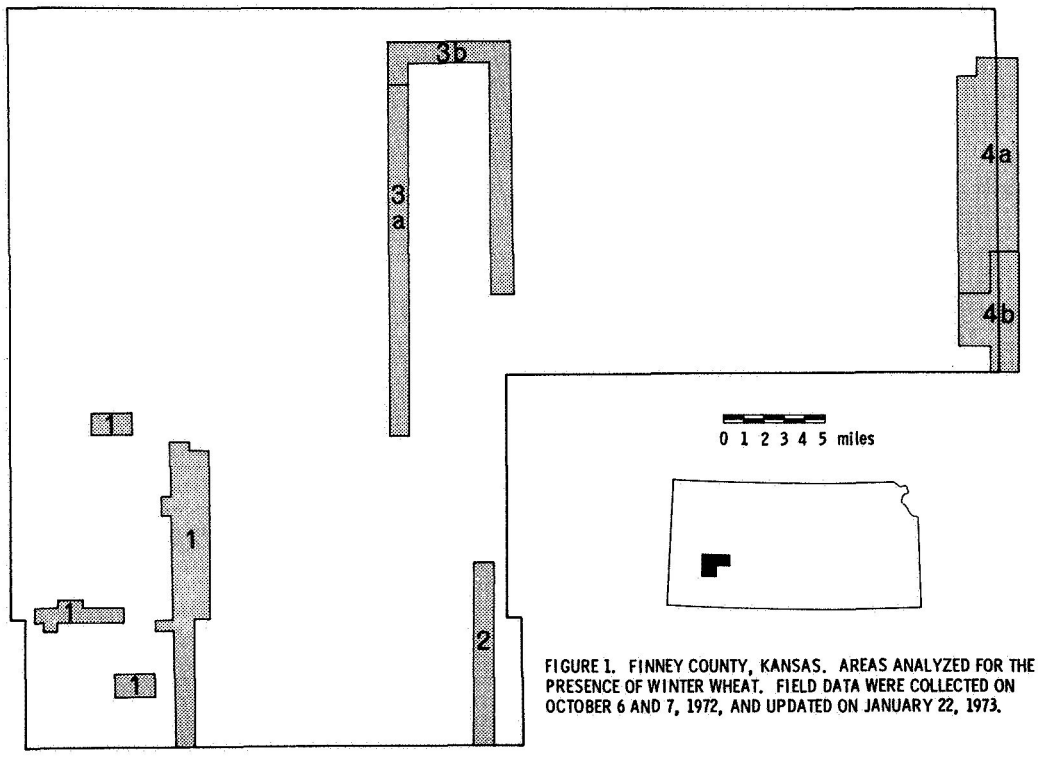


FIGURE 1. FINNEY COUNTY, KANSAS. AREAS ANALYZED FOR THE PRESENCE OF WINTER WHEAT. FIELD DATA WERE COLLECTED ON OCTOBER 6 AND 7, 1972, AND UPDATED ON JANUARY 22, 1973.

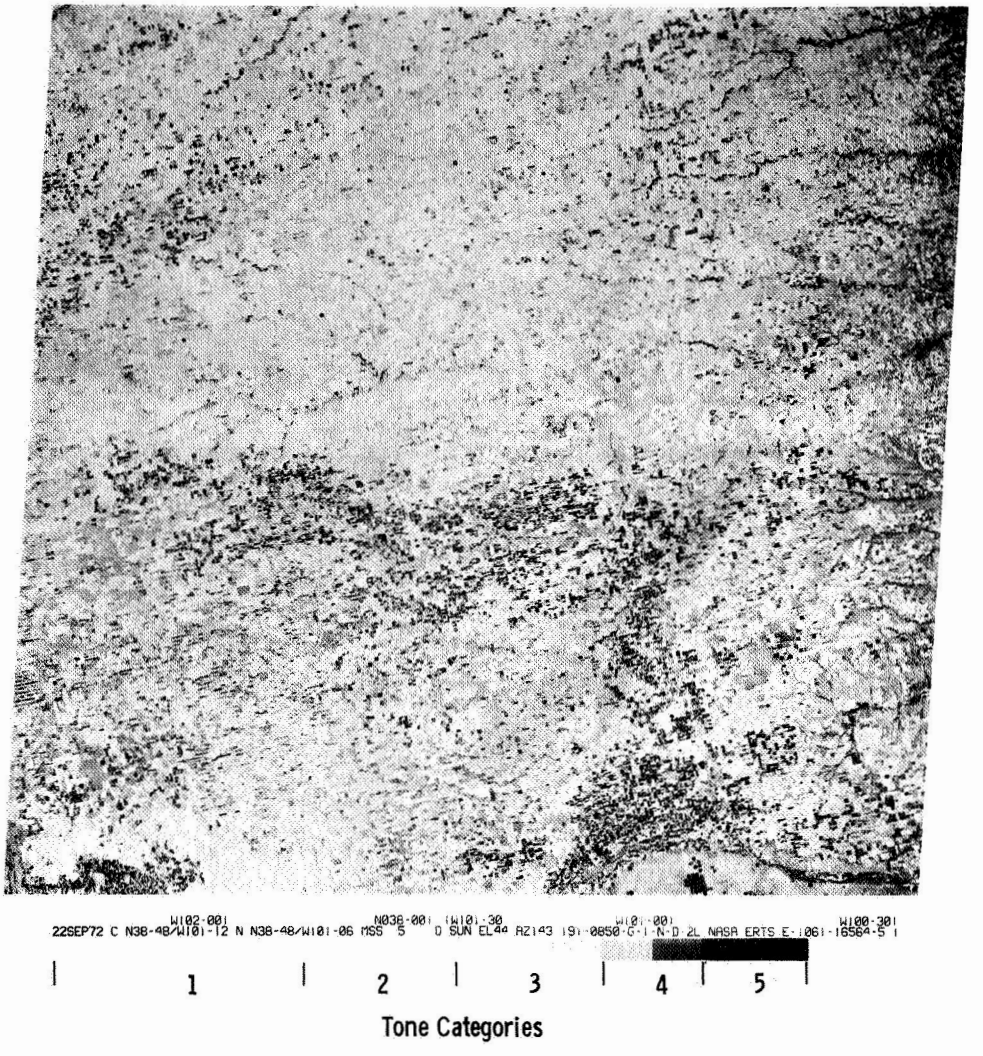


Figure 2. ERTS-1 MSS-5 image acquired September 22, 1972. Part of Finney County, Kansas, is in the southeast corner of this image.

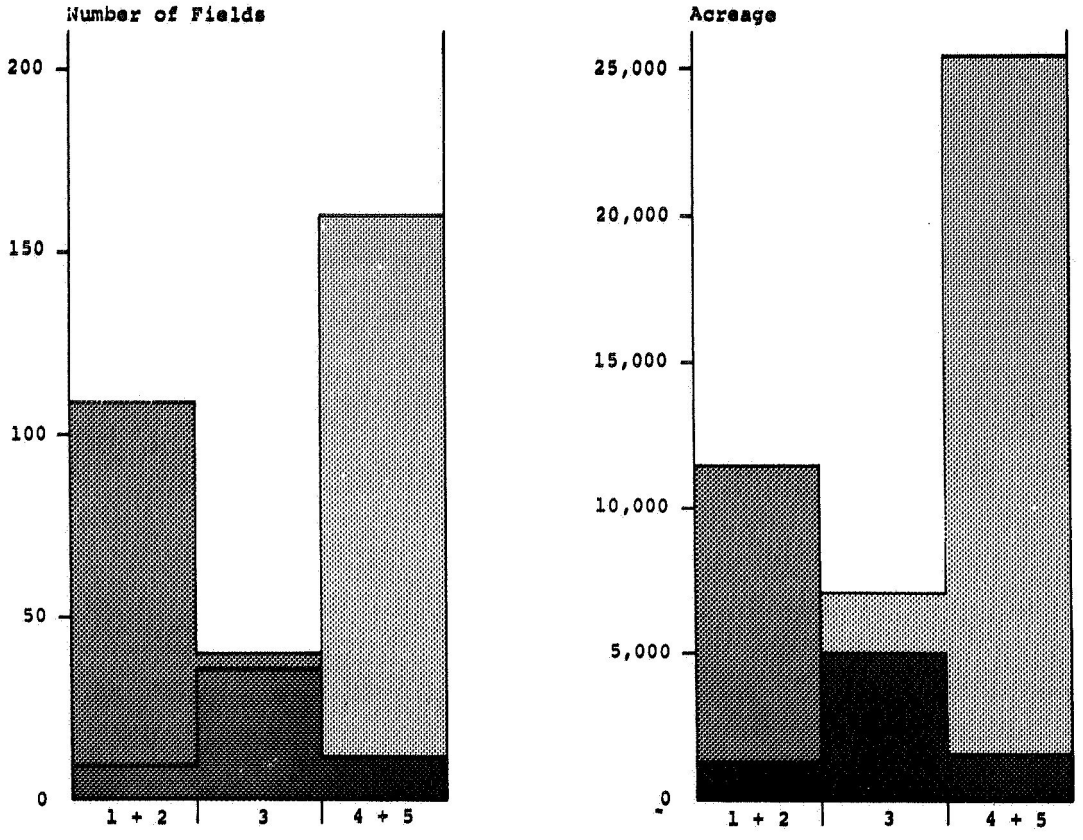


Figure 3. Frequency with which MSS-5 image tones were associated with wheat and non-wheat field conditions in Finney County, Kansas, September 21 and 22, 1972.

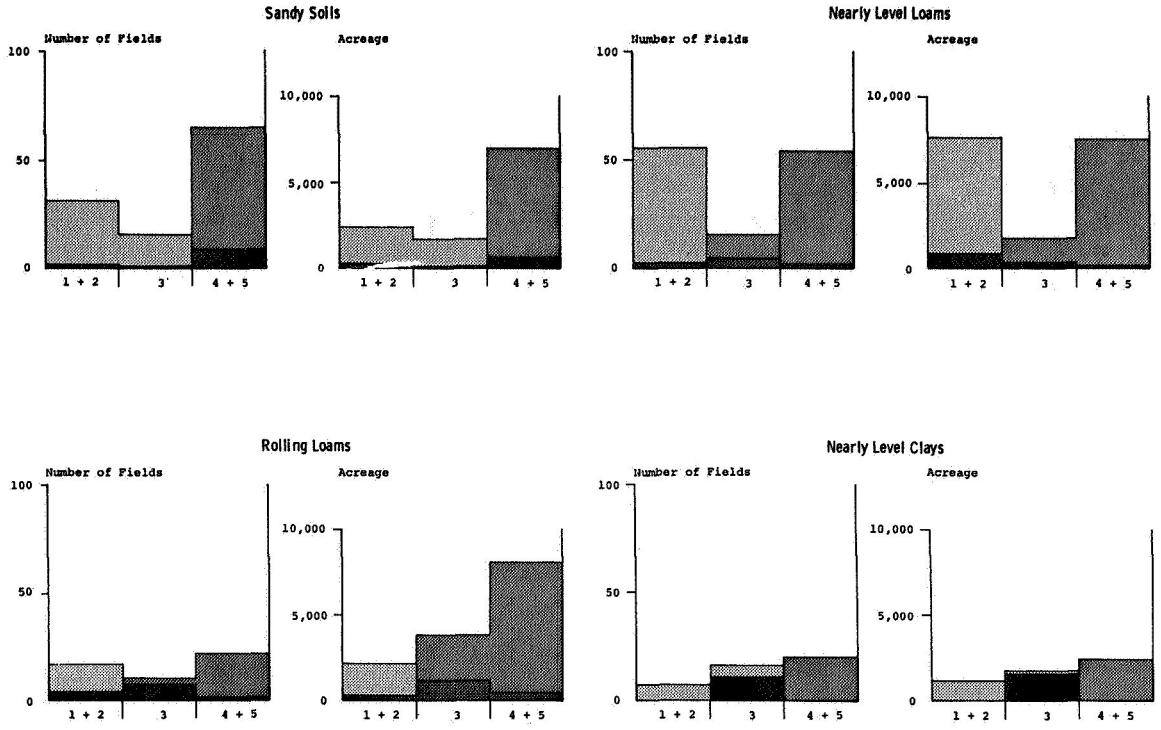


Figure 4. Frequency with which MSS-5 image tones were associated with wheat and non-wheat field conditions in Finney County, Kansas, September 21 and 22, 1972, as a function of soil and landform types.

Paper A 2

SEMI-AUTOMATIC CROP INVENTORY FROM SEQUENTIAL ERTS-1 IMAGERY

Claude W. Johnson and Virginia B. Coleman, *Department of Geography, University of California, Riverside, California 92502*

ABSTRACT

The detection of a newly introduced crop into the Imperial (California) Valley by sequential ERTS-1 imagery is proving that individual crop types can be identified by remote sensing techniques. Initial results have provided an extremely useful product for water agencies. A system for the identification of field conditions enables the production of a statistical summary within two to three days of receipt of the ERTS-1 imagery. The summary indicates the total acreage of producing crops and irrigated planted crops currently demanding water and further indicates freshly plowed fields that will be demanding water in the near future. Relating the field conditions to the crop calendar of the region by means of computer techniques will provide specific crop identification for the 8000 plus fields.

1. INTRODUCTION

At the conclusion of the first named authors report on Crop Inventory of the Imperial Valley from Apollo IX it was stated that the identification of specific crops could be greatly improved over the 60% accuracy attained, if sequential imagery from satellites could be obtained. ERTS-1 has provided such imagery! Each successive image is supplying additional proof that in the laboratory environment of the Imperial Valley automatic crop identification is possible.

The objective of the current investigation is to develop a semi-automatic system that will identify the specific crop being produced in each of the 8000 plus fields in the Imperial Valley. Time is of the essence if data interpreted from ERTS is going to be useful to the water managers, the packers, the shippers, the market specialists, the loan bankers, ad infinitum. Therefore, any system must produce results in the shortest possible time, and certainly no longer than one week after the instant inventory is obtained.

Initial results from ERTS-1 indicate that the data can be interpreted, analyzed, and produced within two to three days with less than 40 man hours and a few minutes computer time. A "spin off" result

of the procedure provides an immediate assessment of irrigation demands that will hold for the entire 18 days between ERTS-1 cycles.

2. ANALYSIS AND METHODOLOGY

The system adopted for the research is somewhat unique from several other types of crop identification systems. It combines the best talents of man and machine to produce rapid results. More unique is the lack of dependence on the variability of the color infrared response as the prime differentiation factor between crop types. The system does depend upon both: (1) the ability to detect individual field conditions from ERTS-1, and (2) the ability to relate sequential field conditions to the regional crop calendar. The key to rapid analysis in the current study is the use of the multi-spectral response to detect only the presence or absence of a producing crop in a field.

The quality of resolution from ERTS-1 imagery has proven to be better than that experienced with Apollo IX imagery. Superimposition of the imagery onto a 1:62,500 scale base map enables the detection of field conditions of fields as small as 10 acres (4 hectares) and a few even smaller 5 acre (2 hectares) plots. However, because of the uncertainty of detection (or identification) of all fields below 20 acres (8 hectares) the project is being limited to the monitoring of fields of 20 acres and greater. Less than 2% of the total farmable acres are affected by this decision. The resolution will permit the first dependent criteria of individual field detection to be met, but can the field condition be identified?

The first thing noted on the ERTS-1 imagery of the Imperial Valley was four distinct colors within the agricultural fields - red, purple, lavender or brown, and white. Certainly the red from false color multi-spectral infrared imagery relates to vegetation which we can identify as growing crops. The white color easily relates to dry bare fields in the arid desert climate. The bare fields can be either fallow fields awaiting the next crop rotation or they can be fields which have been abandoned because of uneconomical production due to salinity problems. The other two colors proved to be the transition activity from fallow field to producing field. The moisture content revealed by a freshly plowed field produces a light brown or lavender color on the ERTS-1 color combined image. Likewise, the moisture response of a freshly irrigated field in which the seed has not yet germinated will produce a deep purple or dark blue response on the color combined ERTS-1 image. The difference between purple and blue is in the quality control factor of the color combined image produced from bands 4, 5, and 7 of the multi-spectral scanner images. The detection of four simple colors enables us to follow the farming cycle from fallow, to plowed, to irrigated seed, to growing crop, and in the case of grain crops to the harvest cycle. The latter case occurs when the maturing crop turns to yellow or golden brown or

even when only the yellow stubble remains in the field. A yellow response on the ERTS imagery thus indicates a mature or harvested grain crop. A color that has not yet occurred in Imperial Valley, but has been seen in the Central Valley of California is the black resulting from the burning of the grain stubble fields. Again we have seen that the detection of the individual field condition is possible from ERTS imagery and our first dependent identification factor can be satisfied. What about relating the field condition to the crop calendar?

Table 1 relates the Imperial Valley Crop Calendar to ERTS-1 cycles 2, 4, 6, and 8. For the purposes of computer manipulation the five field conditions detectable on ERTS have been coded 1 for growing crops, 2 for wet planted fields, 3 for plowed fields, 4 for bare fields, and 5 for harvested fields. Reference to the specialized calendar indicates how a crop such as sugar beets will change from bare soil to a growing crop over the four 36 day cycles of ERTS-1. A computer program that will examine the cyclic record of each of the 8000 plus fields and establish the most likely specific identification based upon the crop calendar is presently being written. Previous experience with a similar type computer program suggests that 93 to 97% accuracy can be anticipated.

The use of the variation in the red hues to assist in differentation of crop types has not been completely discarded by the authors, but previous experience has produced serious reservations about the effectiveness of the color variation factor. Uncontrollable factors of variation are introduced into color infrared imagery by initial film production, physical factors occurring at the time the image is obtained, phenelogical and maturation factors in the vegetation itself, even reproduction factors in the color combining process, and variations in the final film processing. Time restraints have made us decide that we should not rely too heavily on the red color variations for crop identification at this time.

The current timing for production of statistics for one ERTS-1 cycle is 5-6 hours of field condition interpretation from a superimposed image onto the base map. Approximately 25-30 hours of coding and keypunching the data from the base map to computer cards are required. To complete the statistical summaries shown in Table 2 about 30 seconds of IBM 360 computer time is required.

3. RESULTS

The detection on the December 12 (cycle 8) ERTS-1 imagery of a newly introduced crop into the Imperial Valley and subsequent reference to previous sequential imagery provides strong indications that the crop calendar system will be successful. On the December image eight fields totaling 900 acres (364 hectares) appeared as a very distinctive orange-yellow. Located in the northeast area of the valley, to the east of

Wiest Lake, the field conditions did not fit the crop calendar pattern for a harvested crop. These fields then became the first crops that did not fit into the 97% identifiable category. Reference to the 1972 Crop Report of the Imperial Irrigation District revealed a new crop under production. In 1971 80 acres (32 hectares) of a new crop (Alicia Grass) was tested. In 1972 over 1000 acres (405 hectares) of Alicia Grass was planted. Alicia Grass is a variety of Bermuda Grass and is grown to provide a high protein fresh hay that will produce in mid-winter. The calendar for Alicia Grass indicates that it should be ready for harvest in mid-December and will thus provide the only yellow response for this time of year in the Imperial Valley.

Table 2 summarizes the statistical "spin-off" generated by the investigation to date. The 460,000 farmable acres (186,155 hectares) can easily be monitored for field conditions as previously described. The decline of growing crop acreage from 33% down to 31% in the early fall is to be anticipated. Unlike many other areas of the United States the crop production begins to increase in November (43%) and will be expected to rise to a peak in late March or early April. The cyclic demands for irrigation water can be readily determined by both immediate crop demands and future needs. Future needs are indicated by the freshly plowed fields. Completion of the initial phase of the ERTS-1 project will provide the State Water agency and the Imperial Irrigation District a very definitive cyclic record of water demand throughout the year.

4. CONCLUSION

The ability to detect and identify individual field condition has been proven without question. The ability to automatically relate the field conditions to the crop calendar remains to be determined. The compilation of field condition data from four 36 day cycles from ERTS-1 provides the necessary input to test a computer program that will examine each of these cycles for each of the 8000 plus individual fields and predict what crop each of the fields is producing. The remaining months of the contract will be devoted to the completion and testing of the computer program.



Figure 1. ERTS-1 December 12, 1972 MSS Band 5 image of Imperial Valley. Dark fields are growing crops. Note the lack of growth in the Mexicalli Valley in Baja California at this time of year.

TABLE 1

IMPERIAL VALLEY CROP CALENDAR FOR ERTS-1 DETECTED FIELD CONDITIONS

CROP TYPE	FIELD CONDITION CODE BY DATE			
	AUGUST 26	OCTOBER 1	NOVEMBER 6	DECEMBER 12
FIELD CROPS				
Barley (Pasture)	4	2	1	1
Barley (Grain)		4	3	2
Sorghum	1	5	5	
Oats		4	3	2
Wheat		4	4	3
Corn (Grain)			4	3
Grass (Bermuda & Alicia)	2	2/1	1	1/5
Grass (Rye)	4/3	3/2	2	1
Grass (Sudan)	1/5			
Alfalfa	1/4	1/2	1/2	1/2
Sugar Beets	3	2/1	2/1	1
Cotton	1	1	5/4	5/4
Rape	3	2	1	1
VEGETABLE CROPS				
Lettuce	3	2	2/1	1
Mustard	3	2	1	1
Cabbage	4	2	1	1
Cantaloupe (Fall)	1	1/5		
Cantaloupe (Spring)		4	3	2
Cucumbers (Fall)	2	1/5		
Cucumbers (Spring)		4	3	2
Watermelon			4	3
Tomatoes			4	3
Carrots	3	2	2/1	1/2/5
Onions (Bunching)	2	1	1	1/5
Onions (Dry)	4	4	2	2
Squash (Summer)	2	1/5		

(FIELD CONDITION CODE LEGEND: 1-(Red) growing crops; 2-(Purple) wet soil seeded crops; 3-(Lavender) plowed soil; 4-(White) bare soil; 5-(Yellow) harvested stubble)

TABLE 2

SUMMARY OF IMPERIAL VALLEY FIELD CONDITIONS DETECTED FROM ERTS-1

Field Condition / ERTS Color Code	GROWING CROPS (Red) (1)	WET PLANTED (Purple) (2)	DAMP PLOWED (Lavender) (3)	DRY BARE (White) (4)	HARVESTED STUBBLE (Yellow) (5)	PERMENENT AGRICULTURAL (8)	NO DATA (0)
	(Acres) (%)	(Acres) (%)	(Acres) (%)	(Acres) (%)	(Acres) (%)	(Acres) (%)	(Acres) (%)
August 26	153,528 (33.3)	40,374 (8.8)	128,219 (27.8)	123,025 (26.7)	2,636 (0.6)	3,640 (0.8)	9,599 (2.1)
October 1	142,047 (30.9)	69,115 (15.0)	150,351 (32.7)	83,642 (18.2)	787 (0.2)	3,640 (0.8)	10,470 (2.3)
November 6	199,197 (43.3)	120,330 (26.2)	48,736 (10.6)	80,221 (17.4)	315 (0.1)	3,640 (0.8)	7,627 (1.7)

	TOTAL PRODUCING ACRES	FEED LOTS	FARM ASSOCIATED	OFFSITES (Roads,Canals)	TOTAL AGRICULTURAL	URBAN	TOTAL ACRES
	(Acres)	(Acres)	(Acres)	(Acres)	(Acres)	(Acres)	(Acres)
August 26	461,021	2,698	180	51,508	515,407	14,640	530,047
October 1	460,052	2,703	184	51,467	514,406	15,140	520,546
November 6	460,066	2,747	463	51,442	514,718	15,350	530,068
December 12							

Paper A 3

CROP IDENTIFICATION USING ERTS IMAGERY[1]

Maurice L. Horton and James L. Heilman,[2] *Remote Sensing Institute, Water Resources Institute, and Plant Science Department, South Dakota State University, Brookings, South Dakota*

ABSTRACT

Digital analysis of August 15 ERTS-I imagery for southeastern South Dakota was performed to determine the feasibility of conducting crop surveys from satellites. Selected areas of bands 4, 5, 6, and 7 positive transparencies were converted to digital form utilizing Signal Analysis and Dissemination Equipment (SADE). The optical transmission values were printed out in a spatial format. Visual analysis of the printouts indicated that cultivated areas were readily distinguished from non-cultivated areas in all four bands. Bare soil was easily recognized in all four bands. Corn and soybeans, the two major crops in the area, were treated as separate classes rather than as a single class called row crops. Bands 6 and 7 provided good results in distinguishing between corn and soybeans.

1. INTRODUCTION

Crop resources are the food and fiber which we use every day. Satellite surveillance of crops planted, crop condition, yield and harvest offers significant advance in the management and reporting of crop resources.

SDSU-RSI-J-02 Contract #NAS 5-21774

[1] Contribution from the Remote Sensing Institute, the Water Resources Institute, and the Plant Science Department, South Dakota State University. Approved for publication by the Director of the South Dakota Agricultural Experiment Station as Journal Paper No. 1173.

[2] Associate Professor of Plant Science, South Dakota State University, and Graduate Research Assistant, South Dakota State University, Brookings, South Dakota 57006.

Considerable background has already been developed for interpretation of remote multispectral imagery of agricultural crops (Hoffer, 1967) and in crop species discrimination from Apollo 9 imagery (Wiegand et. al. 1969). Mapping of crop, soil, and geological features using digitized multispectral satellite photography has been discussed by Anuta et. al. 1971.

Recent studies on the use of nonparametric methods for pattern recognition (Hahn and Nelson, 1972) show considerable promise for machine classification of crops.

The study reported here utilized ERTS-I imagery, ground truth, and K-classification using SADE (Signal Analysis and Dissemination Equipment).

2. PROCEDURE

The study area investigated was a 3.2 km by 14.5 km strip located south of Centerville, South Dakota. The major crops grown in the area were corn, soybeans, and oats. During the month of June, 1972, the study area was surveyed and mapped to determine field sizes and crop species planted in the various fields. Ground truth information was gathered during the time of the first ERTS overpass on August 15, 1972.

The initial analysis was performed on August 15 ERTS-I imagery. An area corresponding to the study area was masked off for bands 4, 5, 6, and 7 on nine inch positive transparencies. The mask was prepared by applying opaque photographic tape directly to the transparencies.

Each of the four transparencies was digitized at a resolution of 36 data points per mm using Signal Analysis and Dissemination Equipment (SADE). The coded outputs proportional to optical transmission for each band were printed out in a spatial format. The format divided the 0 to 255 range of coded outputs into 55 increments of five values each. A specific character was assigned to each increment.

Three classes consisting of corn, soybeans, and fallow were selected for the initial analysis. Oats were not used because all oats had been harvested by August 15. Three corn fields, two soybean fields, and two fallow fields representative of the three classes in the study area were located on the printouts. An 8 point by 8 point matrix inside each field boundary was used as the statistical sample of data points for the field. Since the data points on the printouts were in terms of characters assigned to the various output increments, the points had to be converted to actual output values. This was accomplished using a computer program with inputs being the initial x and y coordinates of the matrix along with the size of the matrix. The coordinates were

only measured on the band 6 printout under the assumption that errors in the masking operation would not be great enough to cause some of the sampled points to be outside the field boundaries in bands 4, 6, and 7. Nonparametric K-class classification (Zagalsky, 1968 and Hahn and Nelson, 1972) was performed on the data.

3. RESULTS

Results obtained with the K-classifier are shown in Table 1. Using one feature the highest percent correct classification was obtained using band 6. Using two features, best results were obtained using bands 4 and 6 or bands 5 and 6. Using three features, good results were obtained using bands 4, 5, and 6; bands 4, 6, and 7; and bands 5, 6, and 7. Results obtained using all four features were also satisfactory.

TABLE 1. Percent total correct classification of the training samples

Feature in terms of ERTS bands	Percent total correct classification
4	46.65
5	47.10
6	87.28
7	42.86
45	61.38
46	83.04
47	46.65
56	93.75
57	45.10
67	90.40
456	81.92
457	63.84
467	82.59
567	93.53
4567	81.47

Figures 1, 2, 3, and 4 show the probability density functions of each class in bands 4, 5, 6, and 7 respectively. The peaks and valleys in the curves are due to the small number of data points that were sampled. It is assumed that a larger sample of data points would result in smoother curves.

Little separation of classes was achieved in band 4 except for one corn field represented by the curve in the left hand portion of figure 1. The difference between this corn field and the other corn fields does not appear to be related to soil differences. No explanation of the differences between the corn fields has been found. The sharp fallow peaks indicate that some discrimination of bare soil was achieved. Also, some separation of soybeans was achieved.

Figure 2 shows some separability of corn for lower output values. It also shows significant overlap of the three classes. Some discrimination of fallow and little discrimination of soybeans was obtained in band 5.

Figure 3 shows that almost complete separation of classes was obtained in band 6. The excellent separation of classes achieved in band 6 is reflected in K-classifier results where this band is included.

An analysis of the band 7 printout indicated that discrimination of the three classes was possible in band 7. This does not completely agree with figure 4. The reason for the discrepancy lies in the masking operation on the band 7 transparency. When the matrix coordinates based on band 6 measurements were fed into the computer, the masking error caused some of the data points in band 7 to be sampled outside the field boundaries.

4. SUMMARY

The ERTS-I imagery selected for detailed processing has been of excellent quality. Imagery from band 6 (0.7-0.8 μm) has given greater than 90% accuracy in nonparametric K-classification of three classes - fallow, corn, and soybeans. The number of fields classified to date have been limited due to development of techniques.

One of the greatest difficulties encountered has been in accurately locating field boundaries and in masking off the appropriate area of the transparencies for digitization.

It appears that through the use of sequential ERTS imagery, machine processing (SADE), and limited ground truth a timely and accurate picture of crop resources can be prepared.

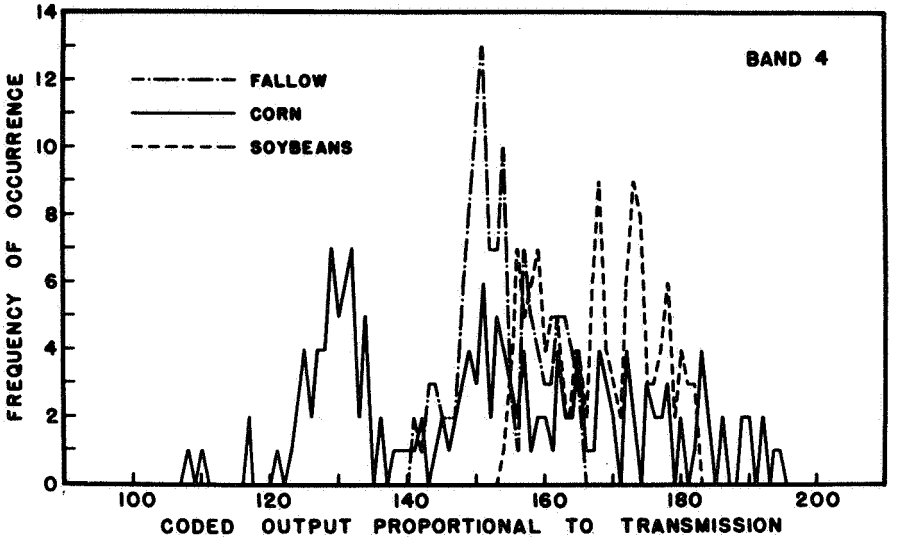


Figure 1. Probability density functions of corn, soybeans, and fallow in band 4 (0.5-0.6 μm)

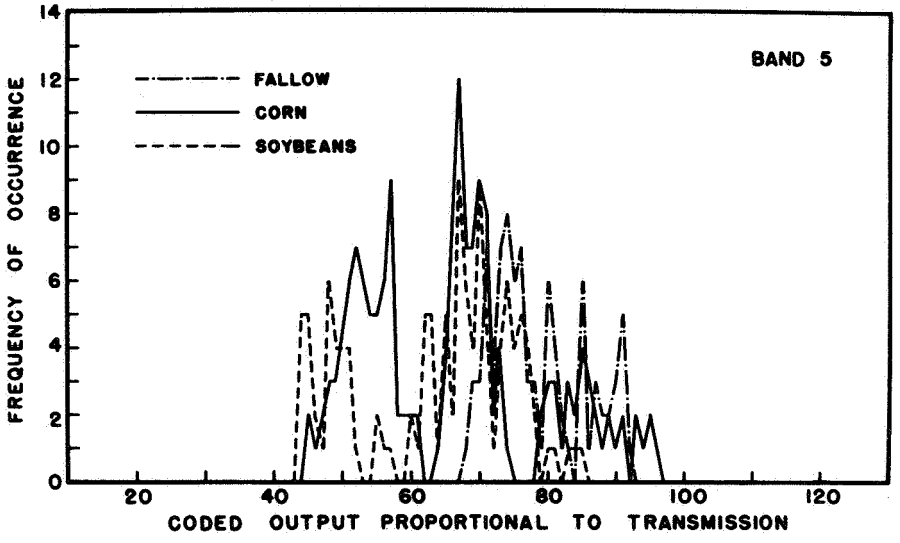


Figure 2. Probability density functions of corn, soybeans, and fallow in band 5 (0.6–0.7 μm)

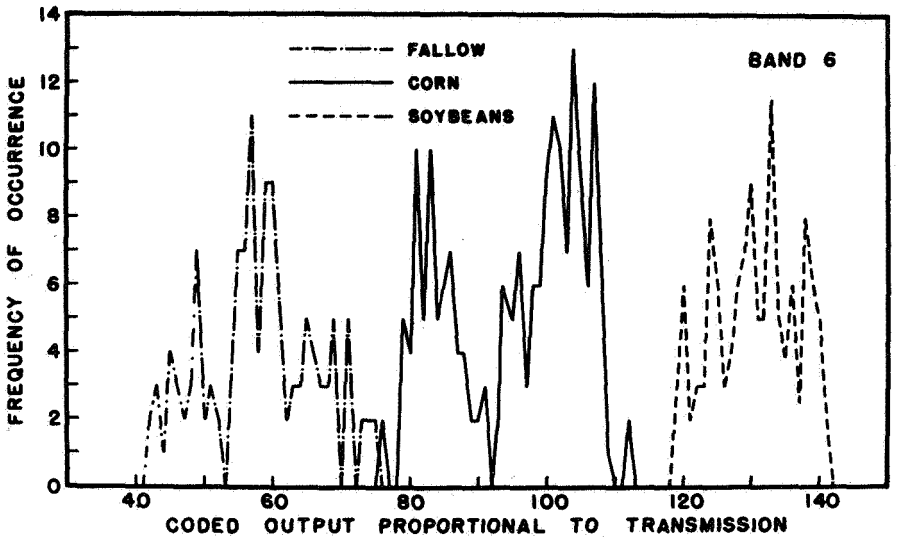


Figure 3. Probability density functions of corn, soybeans, and fallow in band 6 (0.7-0.8 μm)

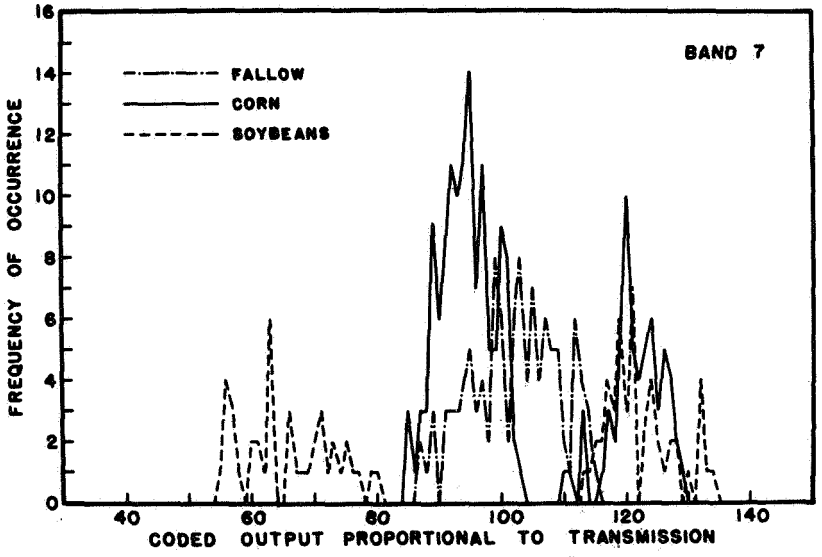


Figure 4. Probability density functions of corn, soybeans, and fallow in band 7 (0.8-1.1 μm)

5. REFERENCES

Anuta, P. E., S. J. Kristof, D. W. Levandowski, T. L. Phillips, and R. B. MacDonald. 1971. Crop, soil, and geological mapping from digitized multispectral satellite photography. LARS Information Note #061371. 33 pages. Laboratory for Agricultural Remote Sensing, Purdue University, Lafayette, Indiana.

Hahn, S. F. and G. D. Nelson, 1972. A comparative study of nonparametric methods for pattern recognition. Interim Technical Report SDSU-RSI-72-19 to NASA. 88 pages. Remote Sensing Institute, South Dakota State University, Brookings, South Dakota.

Hoffer, R. M. 1967. Interpretation of remote multispectral imagery of agricultural crops. LARS Research Bulletin No. 831, 36 pages. Laboratory for Agricultural Remote Sensing, Purdue University, Lafayette, Indiana.

Wiegand, C. L., R. W. Leamer, and A. H. Gerbermann. 1969. Crop species and soil condition discrimination on Ectachrome Infrared Apollo 9 imagery. USDA, Weslaco, Texas.

Zagalsky, N. 1968. A new formulation of a classification procedure. M. S. Thesis, University of Minnesota, St. Paul, Minnesota.

Paper A 4

IDENTIFICATION OF LARGE MASSES OF CITRUS FRUIT AND RICE FIELDS IN EASTERN SPAIN

Fernando Lopez de Sagredo and Francisco G. Salinas, *E. T. S. de Ingenieros Agrónomos, (Universidad Politécnia de Madrid)*

ABSTRACT

ERTS-1 imagery has been succesfully used for the identification of large areas of citrus groves and rice fields in the Valencia region of Eastern Spain. Results are encouraging and will facilitate the elaboration of a Land Use Map with a fair degree of definition once methods prove to be fully operational.

1. GROUND TRUTH DATA ADQUISITION

Before receiving ERTS-1 imagery a survey was made so as to obtain all available aerial photographs of the study zone. In the same way meteorological data such as temperature, rainfall, atmospheric pressure, humidity etc. were carefully examinad for all stations of the area. A report about meteorological conditions is, at present, being produced every day.

Part of the ground truth data about vegetative vigour, blooming periods, ripening etc. of the citrus trees are supplied by the Centro Regional de Burjasot, dependant on the Instituto Nacional de Investigaciones Agrarias and the Botany and Photointerpretation Departments of the Universidad Politécnica de Valencia. In addition three test sites have been selected at Nules, Sagunto and La Albufera in which terrrestrial photographs are periodically taken. These

include black and white panchromatic, colour, black and white infrared, colour infrared. Collections of leafs and soil samples are made periodically and subsequently analyzed and their spectrograms taken in the 450 to 2150 nm. region.

2. ERTS-1 IMAGERY HANDLING

With the arrival of the ERTS-1 imagery the following methodology was used :Based on flights USAF-B (1957) and Citrus Trees Census (1971) all citrus groves and rice fields of model areas were delimitated and their boundaries drawn on the National Topographic Map scale 1 : 50,000. Reductions were made to different scales ranging from 1 : 100,000 to 1 : 400,000 and they were subsequently compared to the enlarged MSS 4 to 7 bands.

3. RESULTS

Tonal response for the studied areas was distinctive for either citrus trees or rice fields. Bands MSS 5 and 7 were more useful than either 4 or 6 which were discarded in a first approach to the experiment.

From the preliminary results a draft general map was obtained which showed citrus groves or rice fields areas. This was drawn on a ERTS-1 image, scale 1 : 300,000. This map has been used recently in the field so as to asses the degree of correct identification.

So far results are encouraging and it is expected that they will serve as an important basis for the elaboration of a Land Use Map that will supersede the existing one published in 1958.

False colour products have not been used so far but it is hoped that, in a near future, a three-lantern system will be made operational thus improving apreciably the actual results.

Paper A 5

ENGINEERING ANALYSIS OF ERTS DATA FOR SOUTHEAST ASIAN AGRICULTURE

Howard L. Heydt, *General Electric Company, Re-entry and Environmental Systems Division.* Prof. Arthur J. McNair, *Cornell University, School of Civil and Environmental Engineering*

The present program focuses on rice because of its importance world-wide as a food. Specifically, the focus is on rice fields in the Philippines. Two primary program objectives are (Figure 1) to establish the feasibility of extracting from ERTS imagery the areas where rice is grown, and to determine those measurements on the imagery which enable the assessment of crop condition (moisture vigor, maturity, etc.). Achieving these objectives with procedures which can be cost-effective can lead the way toward yield prediction, irrigation system management, and similar functions which are known to be important needs in Southeast Asia.

The program team is comprised of specialists in several disciplines from (Figure 1) Cornell University, General Electric Company, and two groups in the Philippines concerned with ground truth information functioning under the auspices of the Philippine national program in remote sensing. We particularly wish to acknowledge the efforts of Prof. S. M. Miranda, University of the Philippines, Los Baños and Dr. Thomas Wickham, International Rice Research Institute, Los Baños.

There are a few special aspects of the investigation which should be noted (Figure 2). First, we have an adequate number of test sites where good ground truth data can be acquired. The sites span a range of plant varieties, irrigation and fertilization conditions, and they are dispersed geographically. Some of the sites can be used for signature training, others for recognition algorithm testing. When some sites are cloud-covered in a frame of imagery others may be clear. However, these sites, while located in areas where considerable rice is grown,

are each very small and quite difficult to recognize precisely in ERTS imagery. It is still possible to carry out the planned program in this situation, but the problem is probably more acute than for most sites in the U. S.

Indications are that the observed signatures for rice fields will vary rather rapidly with time through the growing cycles. This should be an asset; use will be made of temporal variations in spectral signatures. There will be need, however, to communicate interim results of the imagery analysis process to ground truth personnel in the Philippines for their specific comments relative to particular situations. This will involve certain time delays but, again, is not an overwhelming obstacle.

Figure 3 is the color composite imagery for a portion of the island of Luzon for October 31, 1972. Two of our test site areas, each with several individual test sites, are contained in this frame. The individual sites often have areas of 200 hectares or less and their linear dimensions are less than one percent of the field-of-view of the ERTS imagery frame. In order to achieve the objectives of this investigation it is our plan to extract reliable spectral signatures from test site areas, carefully correlate signatures with ground truth, and use the correlation results to develop recognition algorithms. Procedures for recognition of the locations where rice is grown will be developed first. Then, attention will be focused on procedures for assessing crop conditions. But for this approach, a considerable amount of signature extraction and correlation with ground truth will be involved in the first part of the program.

We are using color composites as the principal form of imagery input in the analysis process. The composite transparencies are analyzed at General Electric using a three-color man-machine analysis system (GEMS) operating in near-real-time with a digital computer tied in. The GEMS will not be described here, but prior to presenting results to date it is necessary to describe the color space framework used.

We acquire spectral signature data in three-dimensional color space as illustrated in Figure 4. The bounds to the rectangular volume in 3-space are set by the analyst to cover the spectral-radiometric range for the test site with which he is concerned.

We have found it adequate to sub-divide this volume into 5 x 5 x 5 = 125 individual color cells. The significant items to note here are that the overall 5 x 5 x 5 volume can be positioned repeatably to its proper location in the 3-D color space, and, further, it is referenced in each color channel to the gray steps in the step-wedge for that color composite. Thus, the 5 x 5 x 5 volume can be referenced to the spectral radiation in the scene.

The San Nicolas test site area is shown in Figure 5, which is a photograph of the analysis system color TV monitor displaying an optically zoomed portion of the overall color composite. The rectangular cursor, set to include the test site, is positioned by the analyst. The cursor dimensions in the scene are approximately 9000 ft. x 4000 ft.. In the color composite the region within the cursor contains considerable deep blues plus a little red and some light pinks or beiges. (The imagery was obtained at harvest time and it is suspected that the blues pertain to moist soil exposed as a result of harvesting). The analysis system is asked to indicate where the picture cells within the cursor (there are about 650 such pixels) fall in the 5 x 5 x 5 color space. The result is shown in Figure 6.

To show the results quantitatively the 5 x 5 x 5 volume in Figure 6 is broken into five layers each containing 5 x 5 = 25 color cells. The numbers in the color cells indicate the percentage of the total number of pixels within the cursor which pertain to each color cell. It is noted that 33 of the 125 color cells are occupied, but of these only about a dozen cells are significantly populated. In 3-space it would be found that the populated color cells are in clusters with a few regions of high population corresponding to the blues, reds and light pinks or beiges in the cursor area. These cluster locations are found to be quite repeatable with successive analyses on different days.

To continue the analysis, it is now necessary to reverse the process. That is, go to particular color cells and ask the analysis system to indicate where the picture cells are located in the scene (within the cursor) which populate those color cells. This is illustrated for a second test site shown in Figure 7 - the Malimba site. Note that within the cursor (includes the test site) there are regions of deep blue, pink-light beige - whitish regions, and areas of red.

In Figure 8 twelve of the most populated color cells are indicated for the pixels within the cursor. For each of these color cells the analysis system determined and produced a computer printout showing the locations of the picture elements corresponding to these color cells. The printouts are reproduced and superimposed in the figure with different types of cross-hatching for groups of color cells. The combined printout results shown in the figure correspond quite well to the scene features within the cursor as shown in Figure 7. Presumably these features are related to conditions in the scene at the time of the overflight. That is, they presumably relate to areas of recent harvesting where moist soil is exposed, to areas of growing rice, to areas of less vigorously growing rice, to harvested areas where there are weeds or drier soil, etc. Detailed ground truth, available to the ground truth team for the precise time of the overflight, is to be examined by that team to provide the correlation. Once that correlation is made, then spectral signatures in the 5 x 5 x 5 color space may be assigned to particular features or crop conditions.

The dashed line in Figure 8 outlines our best estimate of the location of the test site area. The exact location (to an accuracy better than 500 feet) is difficult to determine because of the lack of good spatial reference points in the scene. Precise test site location may have to be determined in the imagery by relating it to the observed feature patterns and their correlation with ground truth.

The scene in Figure 9, the color TV display of a zoomed portion of the color composite, includes a third test site area - Mahipon. The analysis system has once again related the key color cells with the locations of the picture elements which populate these color cells. Results of this analysis, analogous to that for the Malimba site, are shown in Figure 10. The estimated location of the test site relative to the cursor boundaries is shown with the dashed line. Once again there is the difficulty in establishing its exact location, and correlations of observed feature patterns with ground truth may be the necessary approach. In any event some questions arise concerning the results as shown in Figure 10. Ground truth indicates that the site is at least 27 percent harvested. Yet none of the picture cells within the test site boundary fall into color cells corresponding to the blue in the color composite (color cells indicated by the horizontal-vertical cross-hatch). Thus, either the location of the test site in the imagery is slightly in error, or the harvested areas involve a drier soil or perhaps weeds which are represented by picture cells which fall in some of

the other color cells. This question is to be examined and answered by the ground truth team.

Once questions such as that just described are answered, then it is a relatively simple matter to establish the spectral signatures for the test site as a whole and for the features within it. For example, if the horizontal-vertical cross-hatched areas in Figure 8 actually represent harvested fields with exposed moist soil, the data now exist to show where the picture cells fall in 5 x 5 x 5 color space for just those harvested fields which are within the site boundary. Figure 11 illustrates what such results would be like for the Malimba and Mahipon sites assuming the site boundaries have been properly located in the imagery. In this illustrative case it is seen that there are differences in site signatures. There are more occupied color cells corresponding to deep blue for the Malimba site than for Mahipon, and conversely Mahipon has more color cells occupied which correspond to pink, light beige and whitish tones. The numbers in the color cells represent cell population in percent of total picture cells involved.

Thus, the techniques are in hand to extract the desired feature signatures, and the necessary ground truth correlations are underway. Because test site areas are small and not readily recognizable in the imagery, a clustering approach in color space with corresponding picture cells correlated with ground truth is used as the basis for determining signatures for features or conditions within the site boundaries. It would have been virtually impossible to proceed directly to a test site feature for signature extraction since there is no apparent direct way to assure the location of that feature in the imagery.

Signatures vs. time for several test area rice fields with a variety of associated conditions will be extracted from ERTS imagery throughout the growing cycle. These will form the basis for recognition procedures to be tested and applied to larger areas later in the program. Expected results at that time can be in the form illustrated in Figure 12. The Mahipon site area is shown once again with analysis system enhancement of rice fields within the site which have a certain set of characteristics. Rice fields external to the test site having a similar signature and presumably having similar field characteristics are also enhanced. Ideally, a recognition process is illustrated. But its accuracy is not known at this time. That is to be established

during the program. Once accuracy is known and is acceptable, then area measurements, position locations, and statistical analyses for the enhanced areas in the scene are readily obtained from the digital data producing the enhancement. This, in turn, will assist government agencies in yield predictions and in improved irrigation and crop management. The thrust of our effort is toward achieving that capability cost-effectively.

Program Objectives

- Establish the feasibility of extracting from the imagery the areas where rice is grown.
- Determine those measurements on the imagery enabling assessment of the crop condition.

Program Team

- Cornell University, Civil and Environmental Engineering, Agricultural Engineering.
- University of the Philippines, Los Baños.
- International Rice Research Institute, Los Baños.
- General Electric Company.

Figure 1

Special Aspects of the Investigation

- Adequate and diverse number of test sites.
- Test sites are small and difficult to recognize.
- Rice signatures can be expected to vary fairly rapidly with time.
- Long communication link to the ground truth team.

Figure 2

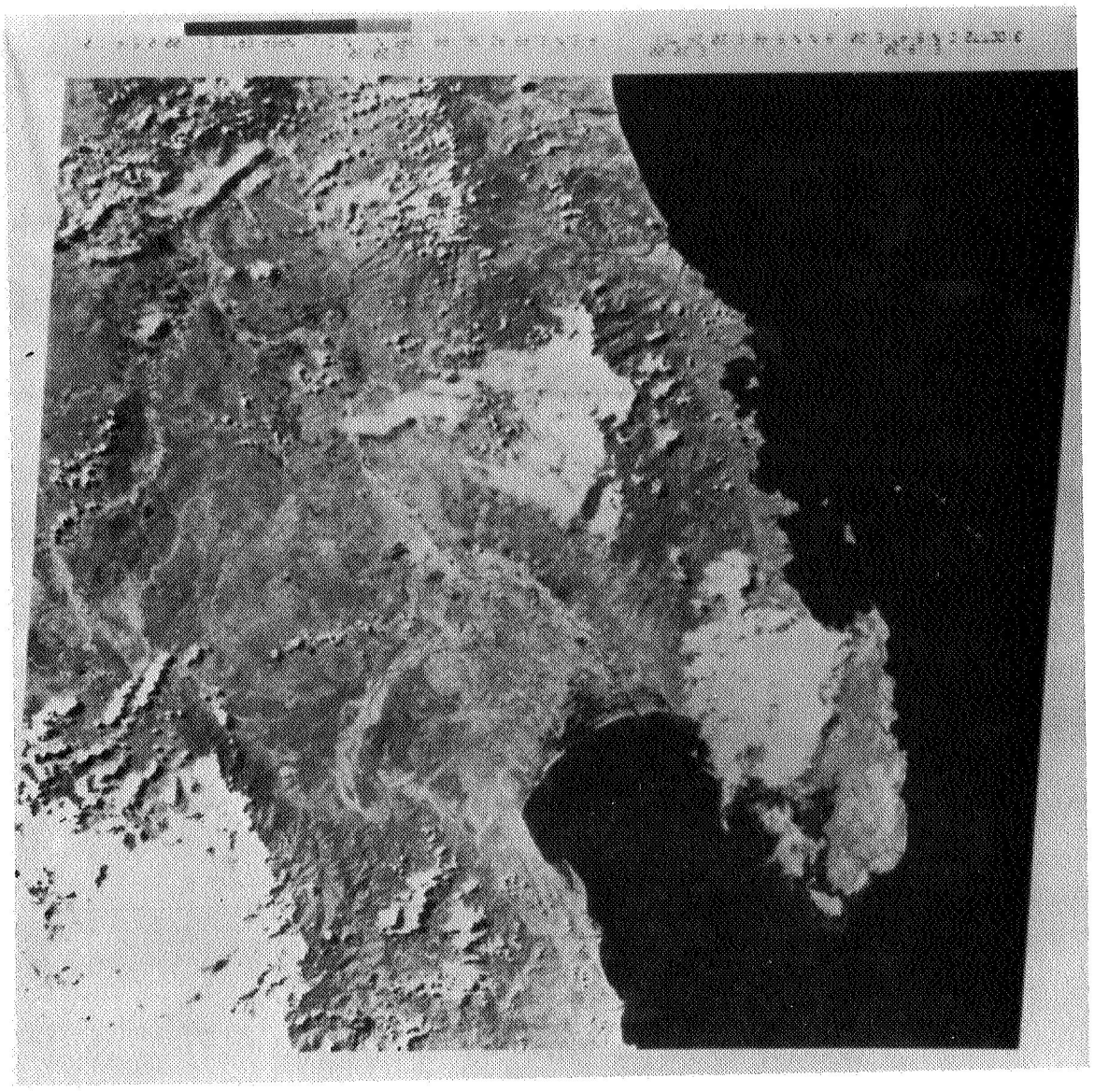


Figure 3

3 - D COLOR SPACE

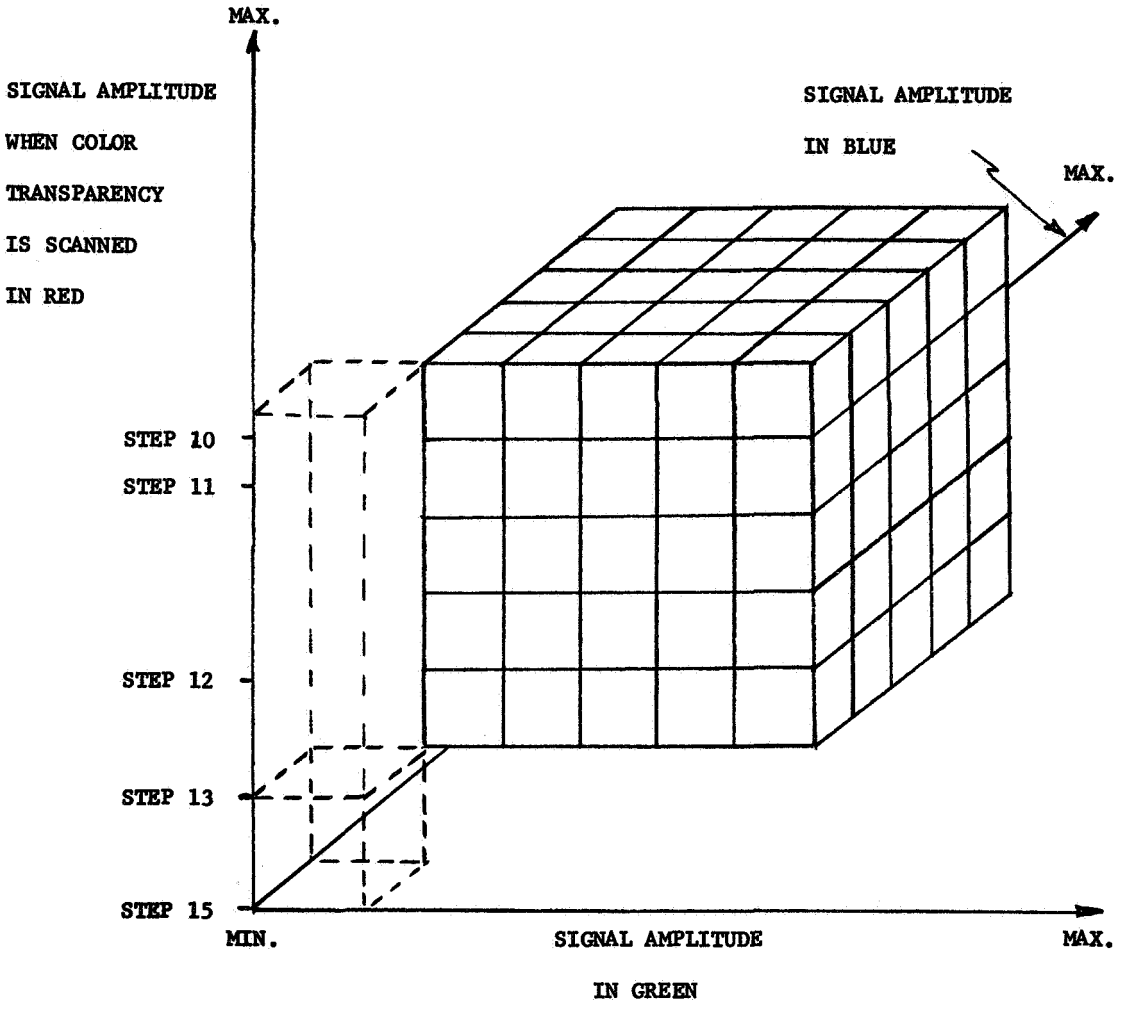


Figure 4

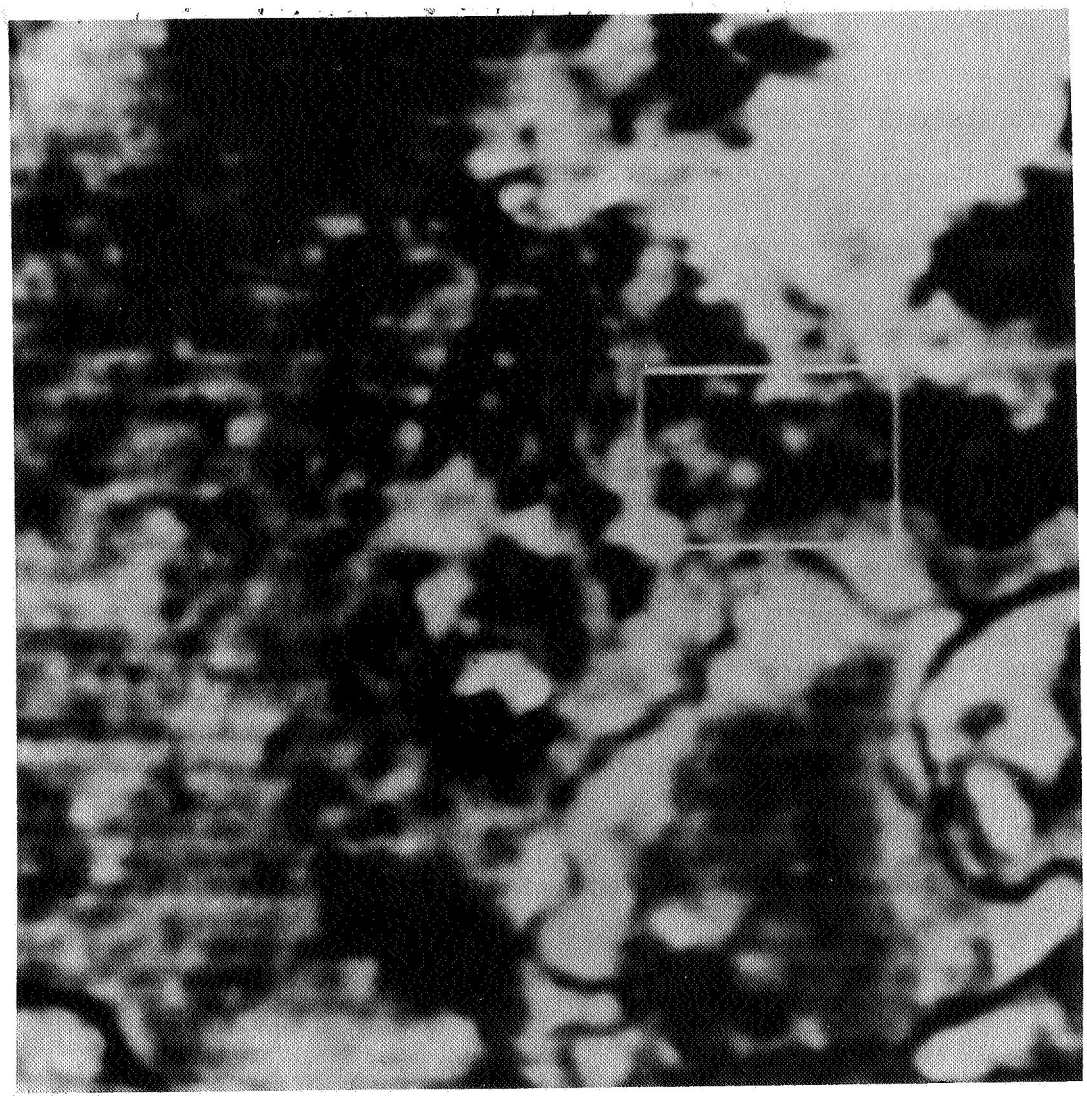


Figure 5

POPULATION OF 125 3 - D COLOR CELLS

IN PERCENT OF TOTAL PICTURE ELEMENTS*

WITHIN CURSOR (SAN NICOLAS SITE)

*APPROXIMATELY 650 ELEMENTS

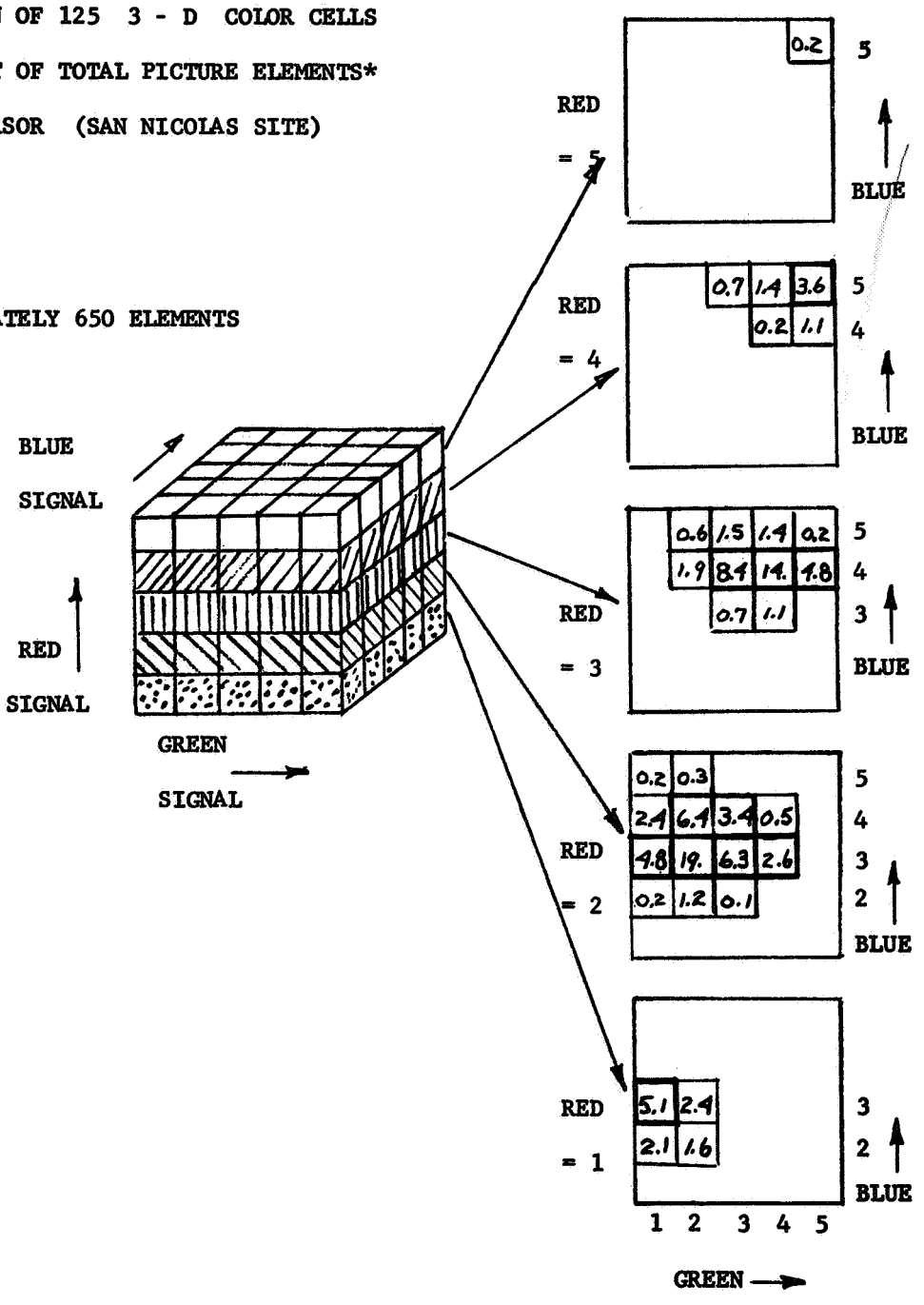


Figure 6

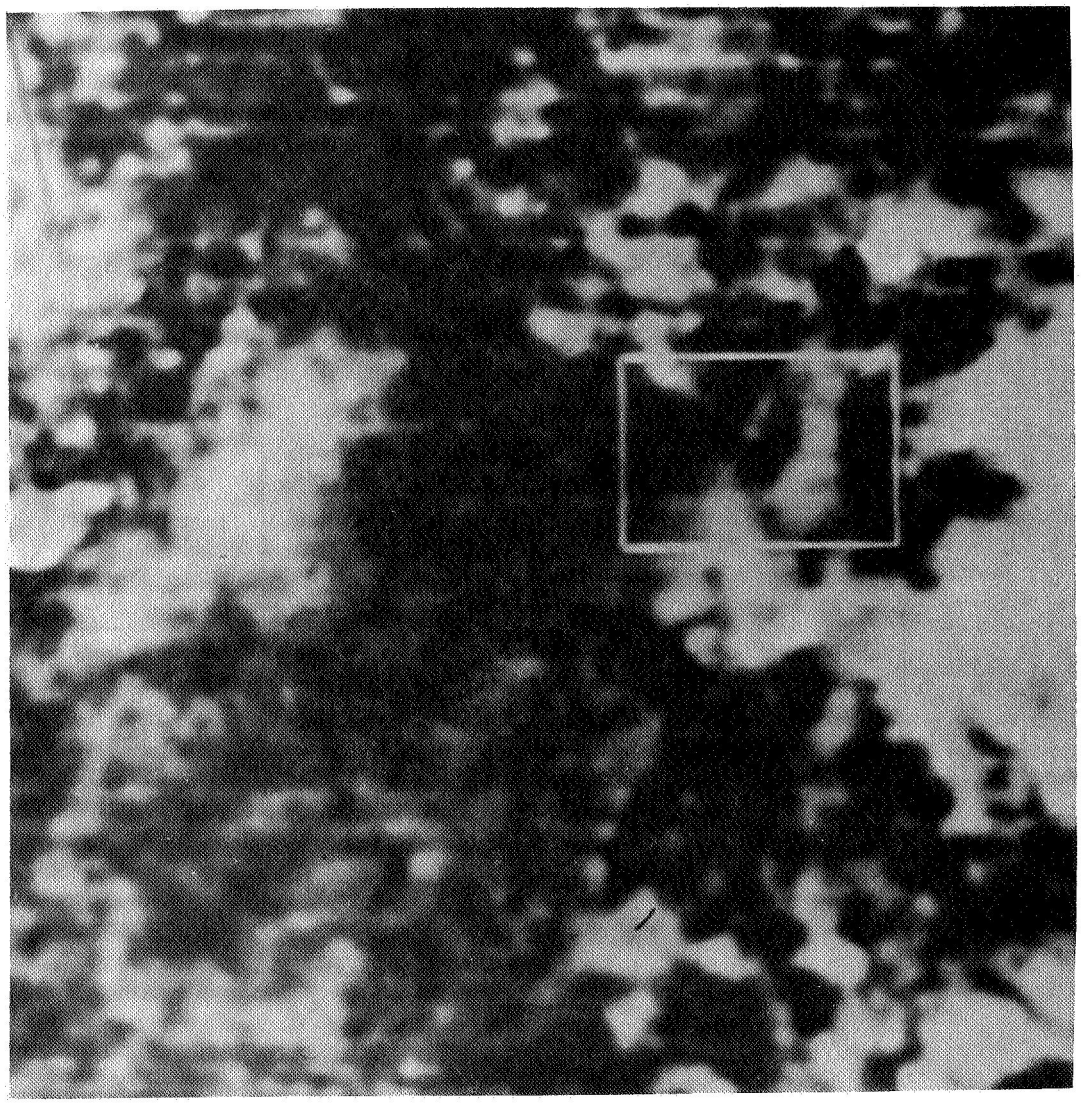
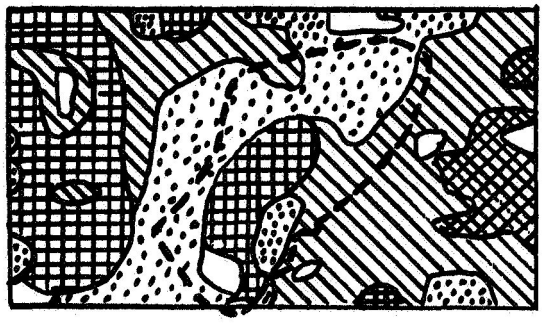


Figure 7

MALIMBA TEST SITE

AREAS CORRESPONDING TO

COLOR CELL CLUSTERS



GROUND TRUTH:

52% HARVESTED

5% FLOODED

FERTILIZER - 41.6 kg N/ ha

YIELD 3.09 T/ ha

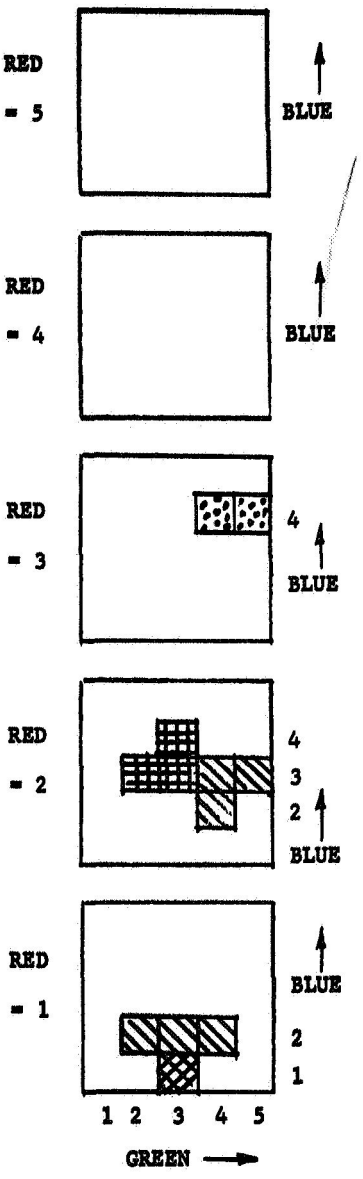


Figure 8

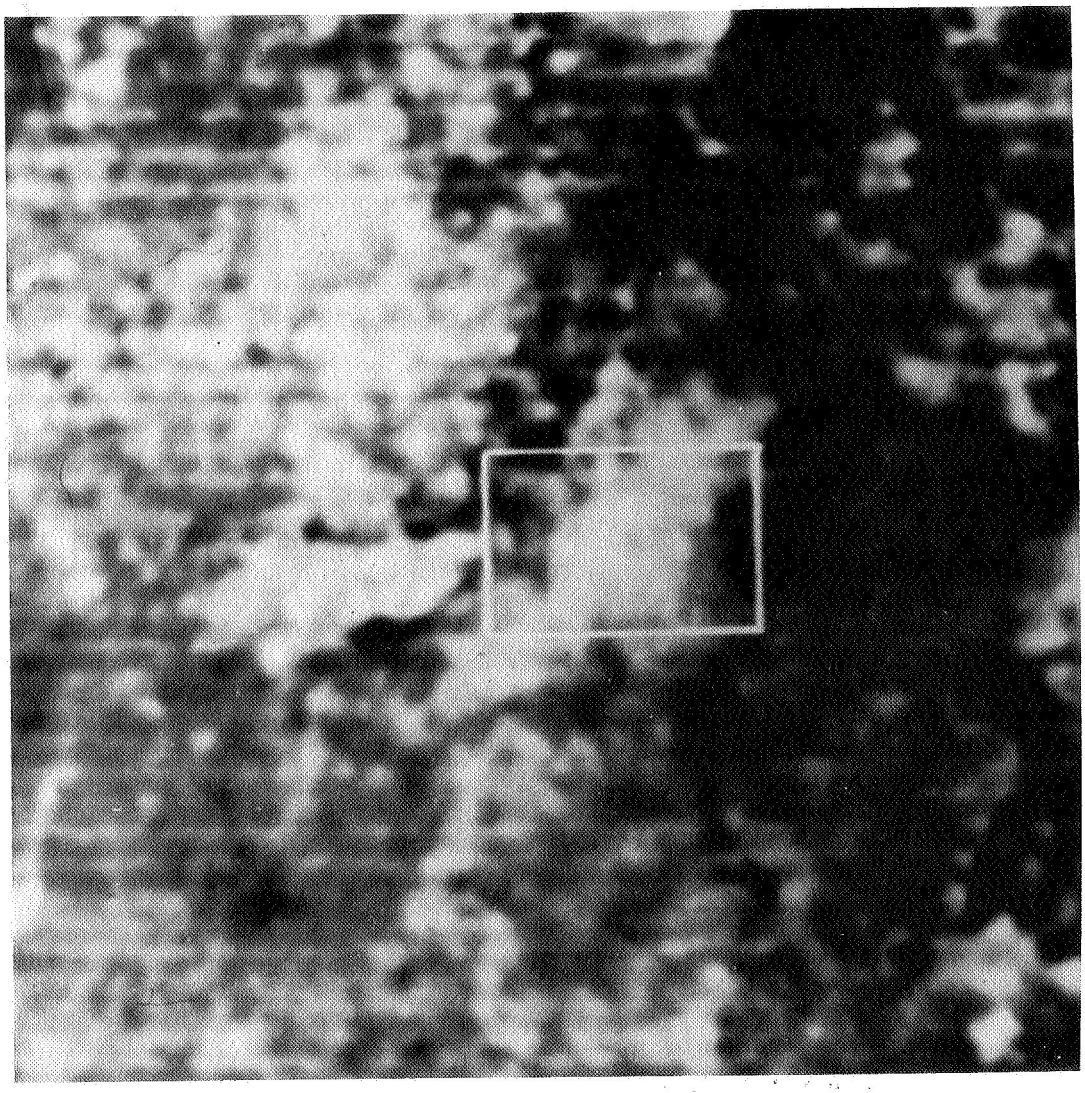
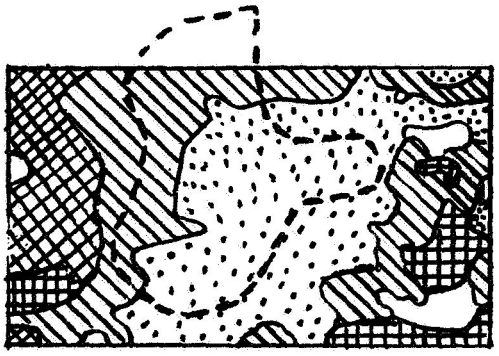


Figure 9

MAHIPON TEST SITE

AREAS CORRESPONDING TO

COLOR CELL CLUSTERS



GROUND TRUTH:

27% HARVESTED

14% FLOODED

FERTILIZER - 29.8 kg N/ ha

YIELD 1.95 T/ ha

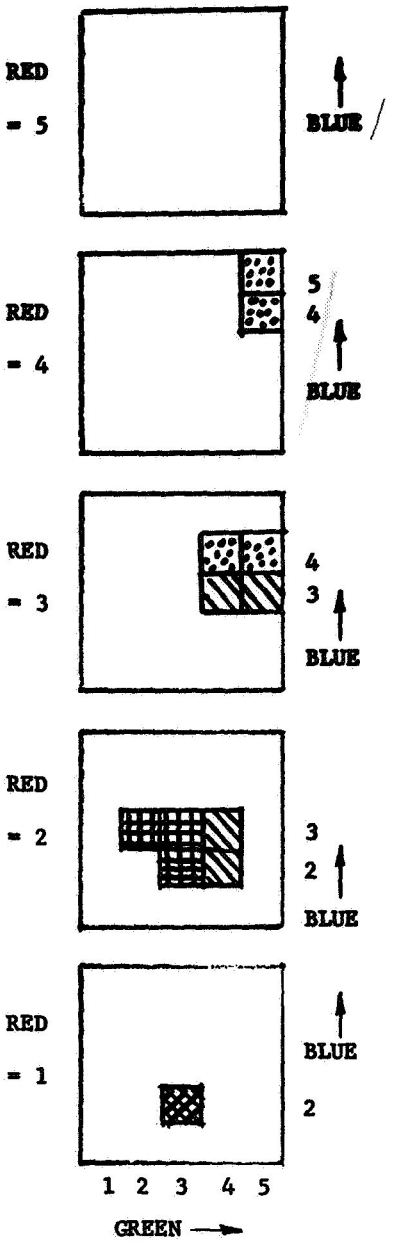


Figure 10

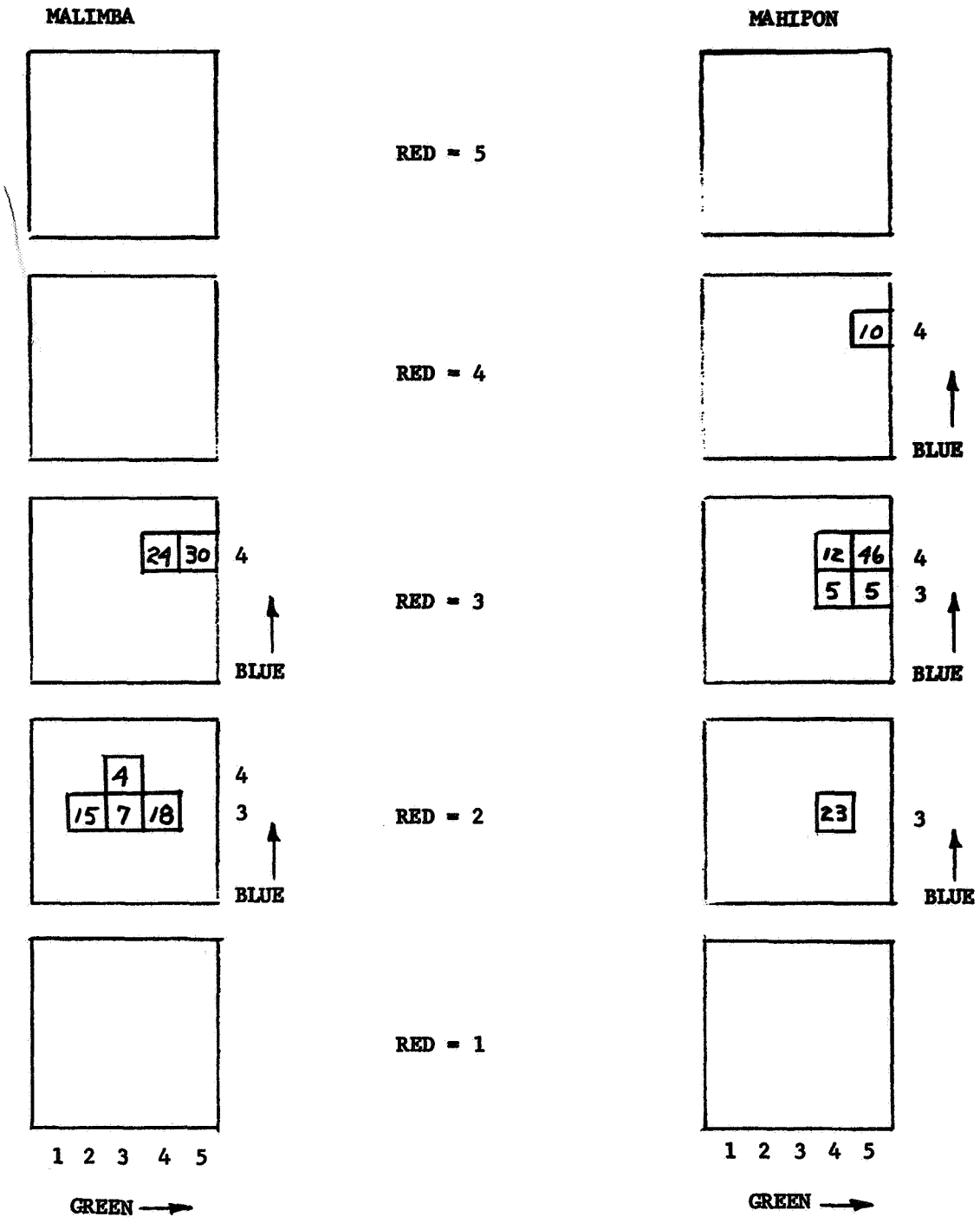


Figure 11. Signature Comparison for Two Test Sites

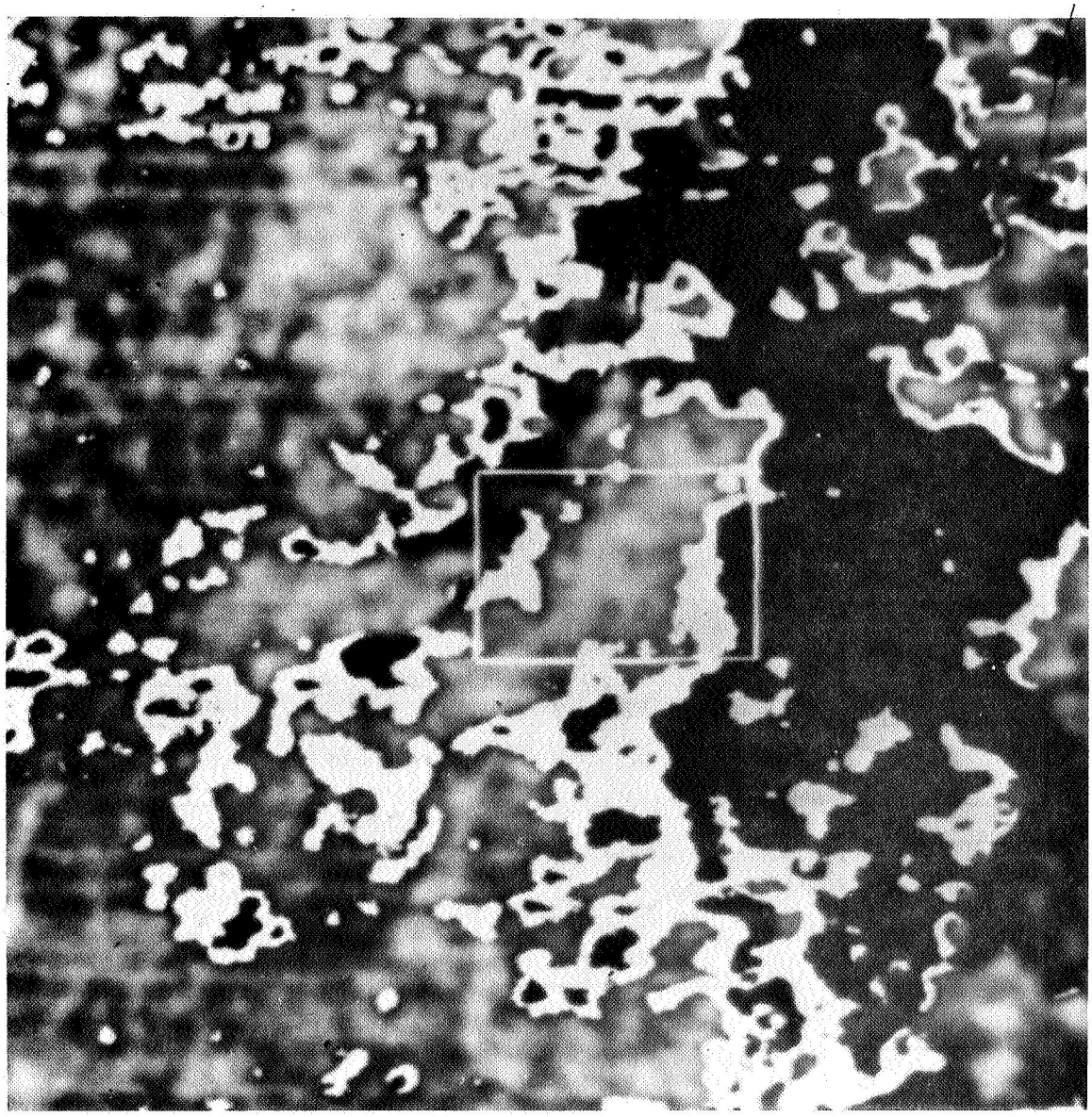


Figure 12

Paper A 6

AN INTERREGIONAL ANALYSIS OF NATURAL VEGETATION ANALOGUES USING ERTS-1 IMAGERY

Charles E. Poulton and Robin I. Welch, *Earth Satellite Corporation, 2150 Shattuck Avenue, Berkeley, California 94704*

ABSTRACT

We are seeking to determine if ecological analogues of natural vegetation and a key food crop, rice, have sufficiently analogous signatures to be interregionally and, potentially, globally identifiable from ERTS-1 imagery. In the proper seasons, rice does have a unique signature in one of our test sites and we have identified within-field variation that is production related. We have also demonstrated unique signatures for four natural vegetation analogues from color prints and are developing some promising color additive analytical techniques to support this and other projects. Even this limited progress is encouraging with respect to feasibility of a uniform ecological inventory of vegetational resources from ERTS imagery.

Space-acquired imagery has made it possible and practical to inventory and monitor vegetational resources in the global context. Full realization of this potentiality requires three things in addition to the imaging capability. First is a vegetational resources classification concept that is logical and that can be maintained in synoptic treatment across political and jurisdictional boundaries. In contrast to established classifications of the plant geographer and plant ecologist, a usable classification must also be compatible with the requirements for interpretation of remotely sensed images, including the concept of multistage inventory. Second is the determination of the interregionally applicable vegetational signatures that can be used to identify image areas in this context. This requires identification of the characteristics of the signatures of each analogue and determination of the extent to which each signature can be extrapolated for application in regional, interregional, and eventually global inventories. This knowledge should permit optimum use and maximum benefit from interpretation criteria

developed in one region of the globe as it is used in image analysis of agroclimatologically analogous regions elsewhere. The third requirement is the determination of image interpretation procedures essential to the recognition and mapping of vegetational analogues by use of the interactive system of space and aircraft imagery with human knowledge and skills.

To help meet these requirements, we have selected two pairs of interregional test sites in the United States. One pair (Southern Louisiana and Interior Valley California) is for the study of a key food crop analogue and the other pair (Colorado Plateau and Sierra-Lahontan) for natural vegetational analogues. In this ERTS-1 Symposium, we are reporting preliminary results relating to requirements one and two above. Our concern with requirement three is minimal to this point in time.

One of our analogues is the world-important food crop, rice. Definitive work on this analogue will start with the 1973 growing season. From ERTS-1 imagery in July and September, 1972, we have made some meaningful observations in the California test area. Among crops in this area, rice does have a highly unique, pre-ripening signature in the color reconstituted ERTS-1 data. It appears that highly accurate identification will be possible. We have also determined that some within-field variation can be detected directly from the ERTS imagery at operationally feasible, color reconstituted scales. In this instance, we are seeing the ground-confirmed influence of soil salinity. This is an example of one of the negative production factors that will be used in a procedure we have developed for yield prediction.

Aircraft photography is an integral part of these predictions. Highflight provides the second stage in multistage sampling. The higher resolution enables both refinement of delineation and identification of other more elusive yield-influencing environmental factors as evidenced in plant growth.

Now turning to the natural vegetation component of our investigation, in theory and in fact, no two stands of vegetation are identical; but in spite of this seeming dilemma, we have an operational legend system that meets previously mentioned requirements one and two. If one concentrates attention on the similarities instead of the differences and considers the plant community as a whole rather than as individual economic species, highly useful classifications are possible. It is well established by plant sociologists and plant geographers that the concept of vegetational analogues is valid. Demonstration of the degree of analogy is dependent on the classification criteria used and on the recognition of hierarchically comparable levels in the classification scheme. With special attention to the needs of ERTS interpretation, we have adapted a uniform ecological legend system initially devised by my graduate students and me at Oregon State University to the needs of this

project. It is a devisive system in which the three broadest hierarchical levels are based on physiognomic and structural characteristics of the vegetation. The fourth level is based on floristic criteria, generally at generic level. The more refined hierarchical levels below this are based on plant sociological criteria and are best developed by agglomerative classification methods (Poulton, 1972).

In this study, we are not considering these latter, highly refined classes because they are generally not identifiable from space imagery except through associated and convergent evidence. In general, as one moves from the local to the regional, to the continental, and to the global scene, ecological analogues are demonstrable only by moving up the hierarchical classification to broader generalizations. The problem of interpreting analogous vegetations from remotely sensed imagery requires that we first determine the level in the hierarchical legend that is appropriate to the scale, resolution, and discriminating power of each system. Our work on interregional analogues is helping to define these legend levels for the ERTS-1 system.

We have been approaching the study of natural vegetation analogues by working with the black and white photo images until as recently as last week. We have identified a group of analogues that are candidates for interregional comparison (See Type II Report, Poulton and Welch, 31 January 1973). We have just made a first analysis of intra-regional repeatability of some of these signatures in the color reconstituted product from an I^2S Addcol. By carefully setting the lamp intensity dials to the same setting for each separate scene, fidelity of the color reconstituted signature for many vegetational analogues was very good among scenes and upon resetting of identical scenes.

In studying these image areas, it is immediately obvious that many of us who are concerned about interpretation of natural vegetation will face two contrasting situations, each with its own unique solution. These situations are:

1) In subhumid and humid areas, vegetation density is sufficient to primarily determine image characteristics.

2) In some semi-arid conditions and particularly in arid environments, sparsity of vegetation produces an image that is overridden by the nonvegetational features of the subject--by the exposed soil surface.

In the first instance, the vegetation analogues are directly interpretable to the extent that their images are consistent within and different among analogues. In the second case, photo-identification of vegetational subjects can be done only from associated and convergent evidence rather than by image features that are related directly to vegetation

reflectance. We have so far been concerned with situations where vegetation features override the soil background in determining image characteristics.

We have made one set of intra-regional comparisons between two scenes for analogues of dense Douglas fir/spruce-fir, oakbrush/aspen, juniper, ponderosa pine, sagebrush and saltsage. The consistency of these images between scenes encourages us to expect some interregional applicability of the signatures. The sharpness of color image separations of all these analogues except the oakbrush/aspen and the sagebrush/saltsage also suggests that our experimental hypothesis is sound and that benefits will, therefore, accrue from the characterization and identification of analogous signatures in one region for use in another if the regions are in fact vegetationally analogous. Our work plan now calls for quantification and a more systematic comparison of photo image characteristics for ecological analogues and study of image consistency and identifiability among scenes between regions and over time. It may be that some analogues not identifiable in these single, late-summer scenes will have a unique multidate signature.

Especially to investigate these kinds of phenomena as well as changes in the resource over time, Phil Langley of our Berkeley Office has been experimenting with special optical enhancement techniques by color combining both positive and negative for the same scene and date and by successfully registering among dates. By combining positives of bands 5 and 7 for July with a positive and a negative of band 7 of the same scene for October, he has been able to produce strong color contrasts in areas of change. These included generation of a unique color for changes in agricultural crops between the two dates, detection of areas of deciduous hardwoods, separation of north-slopes supporting Douglas fir/Sugar pine vegetation, and the vivid detection of changes in the areas of lakes. We expect that techniques like these will find usefulness in all of our participating projects where vegetation is the subject of concern.

Aircraft photography is an integral part of our data base. The procedure is to plot aircraft highflight lines on the 1:1,000,000 ERTS imagery and then strive to locate all calibration sites in these strips. The designation or mapping of unique images on the highflight serves as an intermediate "ground truth" for ERTS interpretation and will be an essential component of the system where the analogue signatures are to be used in a multistage inventory of natural vegetation or food crop resources. The aircraft photography often helps to explain anomalies in the ERTS imagery where vegetation patterns are intricate. In addition, we have taken low oblique photos over all test areas as an additional aid to image identification and subject characterization.

The following is our assessment of benefit from project activity to date: We have confirmed the advantages of interpreting the ERTS in stereo wherever side-lap permits. This is particularly helpful when relating vegetation to landforms, especially in semi-arid and arid environments or where confirmation of major elevational relationships is important to the identification decision.

From preliminary work with the rice identification problem, we feel that use of ERTS imagery together with aircraft subsampling will lead to efficiencies attributable to the space imagery in estimating acreage and production of this key world food crop.

The capability to provide a uniform synoptic treatment of vegetational resources irrespective of ownerships, agency jurisdiction, and political boundaries brings within our grasp a nation-wide system of uniform ecological inventory and monitoring of our entire vegetational resource base. Because of ERTS, this could now be nearing feasibility in a context not attainable from the myriad of use- and product-biased legend systems and inventory methods used by the many Federal and state agencies concerned with vegetational resources of our country.

To the extent that interregional, and eventually global, vegetation analogues can be demonstrated and their differentiating image features defined and characterized, we will greatly enhance the value and interpretability of ERTS imagery. Our work to date has encouraged us in the feeling that the approach we are using will significantly reduce the eventual cost of ground-truth work as progress on the national, continental, and global assessment of vegetational resources and key food crops is carried out--hopefully with a fully operational satellite imaging system.

LITERATURE CITED

Poulton, Charles E. 1972. A comprehensive remote sensing legend system for the ecological characterization and annotation of natural and altered landscapes. Oregon Agricultural Experiment Station Technical Paper No. 3435. In: Proceedings, 8th International Symposium on Remote Sensing of Environment, Ann Arbor, Michigan, October 2-6, 1972.

Paper A 7

NATURAL VEGETATION INVENTORY

Barry J. Schrumpf, *Rangeland Resources Program, Oregon State University, Corvallis, Oregon*

ABSTRACT

Unique characteristics of ERTS imagery can be used to inventory natural vegetation. While satellite images can seldom be interpreted and identified directly in terms of vegetation types, such types can be inferred by interpretation of physical terrain features and through an understanding of the ecology of the vegetation.

The concept of utilizing recognition of natural vegetation as indicators of environments having similar biological potential is not new. This approach has been extensively applied in Europe and somewhat in Australia. However, application in the United States has amounted to little more than some small percent of the potential. The indicator values of some plant species and vegetations are known and have enabled land managers to recognize environmental characteristics which impact management schemes. For example, some species indicate soils conditions which result in plant toxicity to grazing animals, others are susceptible to frosts and, therefore, indicate areas that may have climatic conditions suitable for frost intolerant crops, and some vegetation is indicative of soil suitable for rangeland reseeding.

Personnel of the Rangeland Resources Program, Oregon State University, conducted studies of natural vegetation in southern Arizona utilizing S065 photography from Apollo 9 and NASA high altitude aircraft photography. That work concluded with a vegetation resource inventory for the Phoenix vicinity. This set the stage for demonstrating the utility of such an inventory in an analysis showing the lands most likely to have potential for agricultural and/or urban development. The significant result was that most of the land potentially suitable for agricultural development was also suited to urbanization. The converse of this was not true. This work can be reviewed in Pettinger and Poulton, 1970; Poulton, Johnson, and Mouat, 1970; and Poulton, et al.,

1971. One solution to the conflict is to seek out new agricultural lands and delay the direct conflict between the two land uses by shifting the location of one. Receipt of ERTS-1 imagery provided the opportunity to search for other areas which appear to fulfill the criteria of potential agricultural lands. Extensive, broad, minimally dissected valleys are present south-southwest of the Phoenix area and can be identified on ERTS-1 imagery by visual interpretation. NASA ERTS E-1068-17382 recorded on 29 September 1972 shows these areas as the lighter toned valley fill having a braided drainage network supporting enough vegetation to make the network darker toned and contrasting with the lighter toned interfluves. A check of land ownership patterns (U.S.D.I., BLM, 1964) in the region reveals that the lands which appear to have agricultural potential are parts of military ranges and wildlife refuges, a situation which presumably precludes the possibility of agricultural development. In conclusion, it would appear that the land use conflict between agricultural development and urbanization that is currently existing in this region will have to be settled primarily on those lands which are currently in agricultural use or available for development.

Having once recognized the appearance on ERTS-1 imagery of the vegetation/landform unit indicative of potential agricultural land (MSS Band 5 was the most useful), a photo interpreter can quickly review hundreds of square miles of the southern Arizona terrain in search of similar images. ERTS not only greatly facilitates that task, but also provides for a very quick review of current and potential agricultural activities in relation to land ownership patterns. In this manner, the land use conflict in the region is drawn into sharper focus and better perspective. While the conclusion must be considered as tentative, it does provide a more complete background to contribute to the directing of regional planning.

The analysis briefly mentioned above began with, and depended upon a classification and inventory of the natural vegetation. Our strong belief in the value of vegetation classification and inventory as a starting point for solving many natural resource management problems guided the formulation of our current research with ERTS data. That data is being used in the development of inventory approaches which make use of multistage sampling, plant phenology pattern recognition, computer classification of apparent radiance data, and relationships among physical features of the terrain and vegetation. To date, our efforts have produced results primarily with the last approach.

A test site, 3200 square miles in size, was selected with Tucson, Arizona in the northwest corner and Willcox Playa, Arizona in the northeast. The test area contains a great diversity and complexity of vegetation and therefore provides a good opportunity to develop and apply the approaches listed in the preceding paragraph. The vegetation

of the area includes representatives of the Sonoran and Chihuahuan Desert shrub, grassland, savannah, chaparral, woodland, and forest. Images of this landscape obtained from a satellite seldom contain characteristics that can be interpreted directly in terms of the vegetation. However, those same images provide a considerable amount of detail pertaining to the physical terrain features. In fact, these features are some of the more salient characteristics of the ERTS images. A broad range of elevation, all classes of macrorelief, drainage densities, soil parent materials, aspects, slopes, etc., are present and depicted in the images. These variables were sampled at 250 locations in the test site (Mouat, 1972). At each location, data was collected pertaining to the physical terrain features and the plant species. The species present were recorded and assigned prominence ratings (these ratings are explained in Poulton, Faulkner, and Martin, 1971). This information was supplemented by ground photographs. The plant species information was also collected at an additional 250 locations. A vegetation classification resulting in 31 broad types was produced from analysis of the field data. The classification is based primarily upon the presence or absence of the more common plant species and, secondarily, on the prominence of those species.

A step-wise discriminant analysis (SWDA) was used to detect the relationships existing among vegetation types and the physical terrain features sampled. This analysis had already been conducted to relate plant species and terrain features (Mouat, 1972). A detailed explanation can be found there.

Results from the vegetation type-terrain feature analysis indicate that the terrain features which appear to be the better discriminants of vegetation are elevation, macrorelief class, solar radiation class (a function of aspect and slope), drainage density, and parent material, in that order. No one feature can be used to successfully discriminate all vegetation types. Table I includes the means and the 95% confidence interval for elevation data for 25 vegetation types used in the SWDA. Elevation proved to be the best discriminant of vegetation types. This table shows that the range for each vegetation type, as defined by the mean elevation plus and minus one standard deviation, overlaps those of other vegetation types. These tendencies to overlap reflect a degree of ecological similarity among groups. However, when several terrain features are considered, vegetation types that showed similarity in one case may show dissimilarity in others.

Figure 1 depicts such a consideration. The three vegetation types are referred to as: *Hilaria mutica* and *Prosopis juliflora* (Himu), *Prosopis juliflora* and *Bouteloua* without *Quercus* and *Juniperus* (Prju), and *Cercocarpus brevifolius* with *Juniperus deppeana* and/or *Pinus cembroides* and usually with *Quercus* (Cebr). In this case, the terrain feature, macrorelief, is sufficient for discriminating the three types.

The three types are also discriminated by considering the terrain features: elevation and drainage density. This example oversimplifies the real world, however, the possibility is suggested for an ERTS image interpretation key. It would make use of the interpretability of terrain features and the ability to narrow down the likely possibilities for vegetation types on the basis of the terrain feature characteristics of a given portion of the landscape.

The following is given as an example. A location chosen from within the test site has these terrain feature values: elevation, 5320 feet; macrorelief class, 5; solar radiation class, 1; drainage density, 71 miles/square mile; and parent material, 2 (sandstone). By SWDA, the following vegetation types are likely to occur where each of the above terrain features prevail.

Elevation, 5320': vegetation types 17, 18, 23, 24, 25, 26, and 30

Macrorelief class, 5: vegetation types 12, 17, 23, 25, 27, and 30

Solar radiation class, 1: vegetation types 14, 16, 17, 23, 24, 26, 27, and 30

Drainage density, 71: vegetation types 9, 10, 11, 12, 15, 16, 17, 18, 19, 23, 25, 26, 27, 29, and 31

Parent material, 2: vegetation types 3, 8, 9, 15, 16, 17, 19, 23, 25, 26, 27, 29, 30, and 31

From the above vegetation type possibilities, it is easy to determine by a process of elimination that vegetation types 17 and 23 are the types most likely to occur at this site because they are the only types included as likely possibilities in the case of the five terrain features considered.

Step-wise discriminant analysis does appear to be able to suggest a small number of vegetation types which would most likely be expected to occur in a given area. However, SWDA may not be able to provide a means for 100% accuracy of vegetation type identification from interpretation of terrain feature variables on ERTS imagery.

Utilizing natural vegetation types for recognizing analogous areas of the landscape having similar biological potentials has been an approach proven useful to land managers. High altitude and space imagery have been used in a corollary approach to inventory areas appearing to have agricultural and/or urban development potential. With ERTS-1 imagery, a reconnaissance was rapidly conducted over a much more extensive region. A detailed study utilizing ERTS-1 imagery in vegetation inventories has been initiated. Several approaches are being

explored including one which utilizes the interpretability of physical terrain features on ERTS imagery as a basis for inferring vegetation types. A vegetation classification and some relationships among vegetation types and terrain features have been established.

Contributions to the research reported in this paper have been made by James R. Johnson, David A. Mouat, and other personnel of the Rangeland Resources Program, in addition to the author. The work effort is defined as Task I (Inventory and Monitoring of Natural Vegetation and Related Resources in an Arid Environment by the Use of ERTS-A Imagery) of contract NAS5-21831 between National Aeronautics and Space Administration, Goddard Space Flight Center, and Oregon State University.

TABLE 1. Elevation means and 95% confidence intervals of elevation data for 25 vegetation types used in the step-wise discriminant analysis. Vegetation types are identified by number only.

Vegetation Type	Mean Elevation (feet)	95% Confidence Interval (feet)
2	2913	2614-3212
3	3360	3082-3638
9	3587	3322-3851
6	3663	3336-3990
22	3978	3621-4334
21 (Himu)	4071	3754-4388
8	4081	3664-4498
10	4243	4109-4377
15 (Prju)	4284	4051-4517
31	4340	4076-4604
14	4435	3629-5241
29	4471	3818-5124
11	4531	4257-4805
7	4535	4397-4673
12	4546	4242-4850
27	4773	4436-5110
16	4785	4449-5121
19	4811	4545-5077
18	4879	4287-5471
25	4961	4566-5357
17	5077	4537-5616
24	5126	4834-5418
26	5244	5090-5398
30	5321	4963-5679
23 (Cebr)	5406	5230-5582

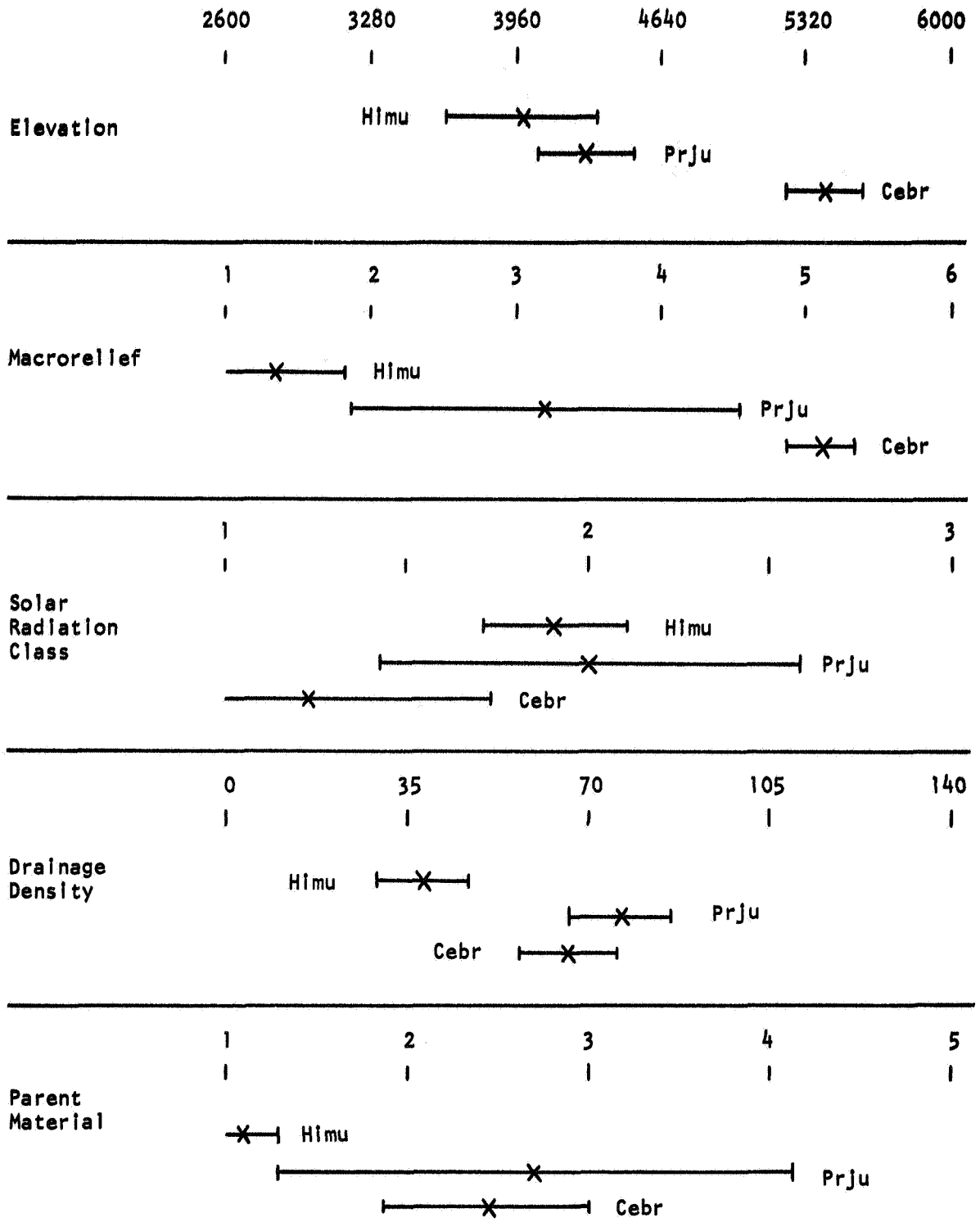


FIGURE 1. SELECTED VEGETATION TYPE-TERRAIN FEATURE RELATIONSHIPS (With 95% confidence interval; x = group mean)

BIBLIOGRAPHY

Mouat, D. A. 1972. Vegetation-terrain feature relationships in southeast Arizona. In: Proceedings, 3rd Annual ARETS Symposium, International Conference on Remote Sensing in Arid Lands, November 8, 9, and 10, 1972, University of Arizona, Tucson. 19 pp. (Available from U.S. Dept. of Commerce, National Technical Information Service, microfiche item E72-10228)

Pettinger, L. R. and C. E. Poulton. 1970. The application of high altitude photography for vegetation resource inventories in southeastern Arizona. Final Report on Contract NAS9:9577 for Earth Observations Division, MSC/NASA, by Forestry Remote Sensing Laboratory, University of California, Berkeley. 147 pp.

Poulton, C. E., J. R. Johnson, and D. A. Mouat. 1970. Inventory of native vegetation and related resources from space photography. Annual Progress Report, Remote Sensing Applications in Forestry for Earth Resources Survey Program, OSSA/NASA by Range Management staff, Oregon State University, Corvallis. 32 pp.

Poulton, C. E., et al. 1971. Inventory and analysis of natural vegetation and related resources from space and high altitude photography. Annual Progress Report, Remote Sensing Applications in Forestry for Earth Resources Survey Program, OSSA/NASA by Range Management staff, Oregon State University, Corvallis. 59 pp.

Poulton, C. E., D. P. Faulkner, and N. L. Martin. 1971. A procedural manual for resource analysis--Application of ecology and remote sensing in the analysis of range watersheds. Final Project Report to Bureau of Land Management, U.S.D.I. Range Management Program, Agricultural Experiment Station, Oregon State University, Corvallis. 133 pp.

U. S. Department of Interior, Bureau of Land Management. 1964. Areas of administrative responsibility of federal lands. Arizona. (Map)

Paper A 8

VEGETATIVE AND GEOLOGIC MAPPING OF THE WESTERN SEWARD PENINSULA, ALASKA, BASED ON ERTS-1 IMAGERY

James H. Anderson, Lewis Shapiro and Albert E. Belon, *University of Alaska, Fairbanks, Alaska 99701*

ABSTRACT

ERTS-1 scene 1009-22095 (Western Seward Peninsula, Alaska) has been studied, partly as a training exercise, to evaluate whether direct visual examination of individual and custom color-composite prints can provide new information on the vegetation and geology of this relatively well known area of Alaska.

The vegetation analysis reveals seven major vegetation types, only four of which are described on existing vegetation maps. In addition, the ERTS analysis provides greater detail than the existing maps on the areal distribution of vegetation types.

The geologic analysis demonstrates that most of the major rock units and geomorphic boundaries shown on the available geologic maps could also be identified on the ERTS data. Several major high-angle faults were observed, but the zones of thrust faults which dominate the structure of the area are much less obvious. All of the previously mapped granitic intrusive rocks in the area were identifiable on the images; however, a radial drainage pattern about 7 km in diameter, probably indicative of a buried intrusive, was recognized for the first time on the ERTS images. The known association of tin deposits with granitic rocks on the Seward Peninsula suggests that the area of this pattern be investigated further.

Background and definition of problem

Vegetation is a primary component of most landscapes and ecosystems and it is one of the most important land resources. Knowledge of the composition, structure, distribution and environmental relationships of vegetation or vegetation types is therefore a key requisite in approaching land resource problems. Similarly, geologic data indicating provinces of potential importance for the development of metallic or non-metallic mineral deposits, or fossil fuel resources, is an important element in consideration of these problems. In Alaska, data regarding vegetation is sparse and, for much of the state, geologic data, in the form of geologic maps at scales of 1:250,000 or larger, is lacking. However, there is currently major activity in land-use planning and development of resource

management techniques. Important decisions must be made in the near future, in spite of the noted lack of much vital information. Among the goals of the University of Alaska ERTS-1 project is the development of image interpretation techniques to increase knowledge in these areas, and, as a corollary, to perform land resource analyses and to open lines of communication to potential data users. In particular, an immediate objective has been to assess the potential contribution which the ERTS imagery can make to rapidly providing the necessary data so that informed land-use planning decisions can be made.

It is anticipated that many potential ERTS imagery users will have no means for image analysis other than direct visual examination of photographic prints or transparencies, possibly aided by a magnifying glass. It was decided therefore that in the early stages of the present project, prior to the availability of analytical equipment, an exercise would be conducted with one of the first ERTS images to determine the extent to which interpretations could be made by direct visual examination. As a result, no enhancement techniques were employed in this study, other than the preparation of a reconstituted, simulated color-infrared photographic print prepared from bands 4, 5 and 7 of the ERTS-1 multi-spectral scanner (MSS). This print was used exclusively for the vegetation study. For the geologic analysis, the 9-1/2 x 9-1/2 NASA supplied paper prints of bands 4, 5, 6 and 7 were also employed.

Ground truth used in this study was limited to references readily available in the literature. For the vegetation study, this consisted of four small-scale vegetation maps and a few published reports (see reference list), supplemented by fire records of the U. S. Bureau of Land Management. A recent 1:250,000 scale geologic map of part of the area (Sainsbury, 1972) provided the ground truth for the geologic analysis.

Approach

The studies were done separately and followed the concepts of aerial photographic interpretation standard in each discipline. However, some modifications were required by the nature of the ERTS images.

For the vegetation analysis, interpretations were based on the following assumptions: (1) Most of the western Seward Peninsula is covered by vegetation and this is therefore chiefly responsible for the spectral reflectance registered on the image. (2) Different vegetation types have different spectral characteristics, and color, color intensity and textural patterns on the image therefore depict different vegetation types and their distributions. (3) Positive identification of spectral signatures according to vegetation type depends on one or more of the following forms of ground truth: aerial photography; field observations, including low overflights in light aircraft; and information in the literature, including vegetation maps. (4) The resolution of ERTS imagery permits definition of vegetation types at a level useful for the plant ecological and resource analysis questions addressed.

In the case of geologic investigations, the synoptic aspect, resolution and scale of the ERTS imagery, and the availability of multiband data, require some changes in the objectives of the study of the images from those which might be sought through the use of conventional aerial photographs. As examples, details of bedding altitude, effects of subtle changes in rock

texture or composition, and the presence of minor structural features would generally not be discernable on the ERTS images. However, structural trends, drainage patterns and geological provinces of regional extent become evident. Thus, for geologic studies, the ERTS images provide information not previously obtainable except possibly from detailed study of many large-scale aerial photographs. Simultaneously, information which would have been available from the study of conventional aerial photographs cannot be extracted from the ERTS images. As a result, the present study was primarily concerned with examining the applicability of the ERTS images to small-scale reconnaissance mapping and other investigations utilizing the synoptic and multiband features of the data.

Results of vegetation studies

Seven distinct colors were recognized on the image. Four were identified through matching of their general distribution patterns with those of vegetation types on the existing maps: Bright red - shrub thicket; light gray-red - upland tundra; medium gray-red - wet tundra; gray - alpine barrens. In the bright red color two phases, violet and orange, were recognized and tentatively ascribed to differences in species composition in the shrub thicket type. Significantly more detail in the distribution of these types, particularly of small units or stands, could be seen on the image than could feasibly have been depicted on the maps at the scales used. Some of this detail is shown on the new map presented here, which was drawn at the same scale as the ERTS image (Figure 1). The three colors having no map unit equivalents were tentatively interpreted through reference to the literature and general plant ecological knowledge as follows: Pink - grassland tundra; dark gray-red - burn scars; light orange-red - senescent vegetation. The interpretation of dark gray-red as indicating areas of former vegetation fires was subsequently confirmed by records of the U.S. Bureau of Land Management.

Figure 1 is the new vegetation map of the western Seward Peninsula, drawn by tracing on an acetate overlay of the image. Besides the seven colors discussed above, five additional map units are shown. These represent mosaics of color units too small feasibly to map individually at the scale of the unenlarged ERTS image. Figure 2 is a tracing of part of an existing vegetation map (Spetzman, 1963), enlarged to the same scale, which may be compared with the new map to emphasize the increase in mappable information derived from the image. The new map required only about ten man-hours to draw and label. It is believed that considerably more detailed and accurate maps than this one will be possible using the various image enhancement and digital data processing techniques which are becoming possible with ERTS imagery.

Besides the promise this exercise shows for delineating and mapping vegetation types with ERTS imagery, promise is also shown for surveying phenological developments and vegetation fires using sequential imagery.

Knowledge of the distribution and relative areal importance of vegetation types, particularly as shown on the new map, may be applicable

in the areas listed below. In each case, the broad geographic or synoptic coverage is of primary importance.

1) Hydrology. Stream patterns may be examined through the recognition of riparian vegetation types, i.e., the shrub thicket type in part, and areas of poor drainage or standing water and of excessive drainage may be recognized, at least in a general way, from the occurrence of certain vegetation types.

2) Soil science. The close relationship between soil and vegetation development could permit study of the distribution of soil types through examination of the vegetation map.

3) Plant ecology. Besides the immediate, scientific plant ecological interest of the knowledge resulting from this exercise, a basis for further study of relationships between vegetation and environmental factors is provided.

4) Meteorology. Vegetation is responsive to meteorological and climatological conditions. Therefore, study of the image and the map from this standpoint could provide an indication of conditions over broad and more or less remote areas where no weather stations are located.

5) Wildlife biology and management. Study of the distribution of vegetation types is essentially a study of the availability and distribution of habitat and food materials for wildlife. Knowledge of species preferences could enable an analysis of the distribution of animal populations and to some extent the estimation of their abundances. Insight into the nature of migration patterns may also be obtained, particularly through the study of sequential imagery and the determination of a vegetation phenology schedule.

6) Land use planning. A land use planning team could use knowledge of the presence and distribution of vegetation types (a) to help in locating areas containing representative ecosystems for preservation, (b) for identifying and delineating, for example, caribou (upland tundra), moose (shrub thicket) and waterfowl (wet tundra) ranges and determining areas to be managed primarily for sustaining populations of these animals, (c) for delineating areas suitable for certain recreational activities, including mechanized and non-mechanized forms, (d) for delineating areas with agricultural potential which might be opened to homesteading, or areas supporting substantial populations of fur bearers which should be managed to include trapping, and (e) similarly, for identifying and delineating areas for use in meeting various other human needs or desires.

Results of geologic studies

A total of about six-man hours were spent examining the prints of the four bands of the image. The results of the investigation were recorded on overlays for comparison with the geologic map.

The most striking result is that almost every important boundary shown on the geologic map could also be identified on the ERTS images. Particularly outstanding features are the part of the map area under-

lain by limestones of various ages, the metamorphic belt of the Kigluaik Mountains, several granite stocks, beach deposits and zones of thaw ponds along coastal areas. Boundaries of these units were obvious at first glance and were easily mapped over the entire image area. Further study was required to locate other, more subtly expressed boundaries. High-angle faults were easily identified on the images by their generally straight traces, but the important zones of low-angle thrust faults, which dominate the structure in some areas, were not generally recognizable. In general, however, there is no doubt that an acceptable 1:250,000 scale reconnaissance geologic map of the area could have been produced from the ERTS data with only minimal ground truth to identify rock types.

The ease with which boundaries were recognized on these images is primarily a result of the close association between rock units and vegetation patterns in the area. Many of the boundaries between vegetation types shown on Figure 1 are also geologically significant.

Two features of interest which do not appear on the geologic map were noted on the ERTS images. The first is a zone of parallel or sub-parallel lineaments which can be traced for about 60 km in an east-west direction from 65°30'N, 166°W to 65°30'N, 167°W (Figure 3). The geologic map shows small faults with this trend near the ends of the zone, but does not indicate continuity between these. It is possible that the zone was recognized during mapping and thought not to be significant, but its clarity on the ERTS images shows that it is indeed real. The second feature of interest occurs at about 65°66'N, 166°30'W. Just east of this point, a granitic stock, with associated tin deposits, is exposed in the cone of a structural dome upon which a radial drainage pattern is developed. Examination of the ERTS image shows that, at the point indicated, this drainage pattern is distorted by a second, smaller radial drainage pattern about 7 km in diameter (Figure 3). This implies the presence of a second structural dome, also probably resulting from emplacement of a smaller granitic stock which is still buried. The known association of tin deposits with granitic rocks in the area suggests that the area of the second, previously unknown, dome may have economic implications.

Conclusions

The results of this study show that reconnaissance maps of vegetative and geologic features can be produced rapidly from ERTS images, and at scales useful for resource studies, and land-use planning in Alaska.

References

Anderson, D. M., R. K. Haugen, C. W. Slaughter, C. W. Marlar and H. L. McKim. 1972. Arctic and subarctic environmental analyses utilizing ERTS-1 imagery. Cold regions environmental analysis based on ERTS-1 imagery. Cold Regions Research and Engineering Laboratory, Hanover. 19 p.

Anderson, J. H. and A. E. Belon. 1973. A new vegetation map of the western Seward Peninsula, Alaska, based on ERTS-1 imagery. Scientific Report on NASA Contract NAS 5-21833, Institute of Arctic Biology and Geophysical Institute, University of Alaska.

Hanson, H. C. 1953. Vegetation types in northwestern Alaska and comparisons with communities in other arctic regions. Ecology 34:111-140.

Hopkins, D. M. and R. S. Sigafoos. 1951. Frost action and vegetation patterns on Seward Peninsula, Alaska. U.S. Geological Survey Bulletin 974-C:51-101.

Kuchler, A. W. 1966. Potential natural vegetation of Alaska, U. S. Geological Survey, Washington. Map.

Sainsbury, C. L.. 1972. Geologic map of the Teller Quadrangle, Western Seward Peninsula, Alaska. U.S. Geol. Survey Misc. Geol. Inv. Map I-685.

Sigafoos, R. S. 1951. Soil instability in tundra vegetation. Ohio Journal of Science 51:281-298.

Sigafoos, R. S. 1958. Vegetation of northwestern North America, as an aid in interpretation of geological data. U.S. Geological Survey Bulletin 1061-E:165-185. Includes map.

Spetzman, L. A. 1963. Terrain study of Alaska, Part V: Vegetation. U.S. Geological Survey, Military Geology Branch. Department of the Army, Office, Chief of Engineers, Washington. Map.

Viereck, L. A. and E. L. Little Jr. 1972. Alaska trees and shrubs. U.S. Forest Service Agriculture Handbook No. 410. 265 p. Includes map.

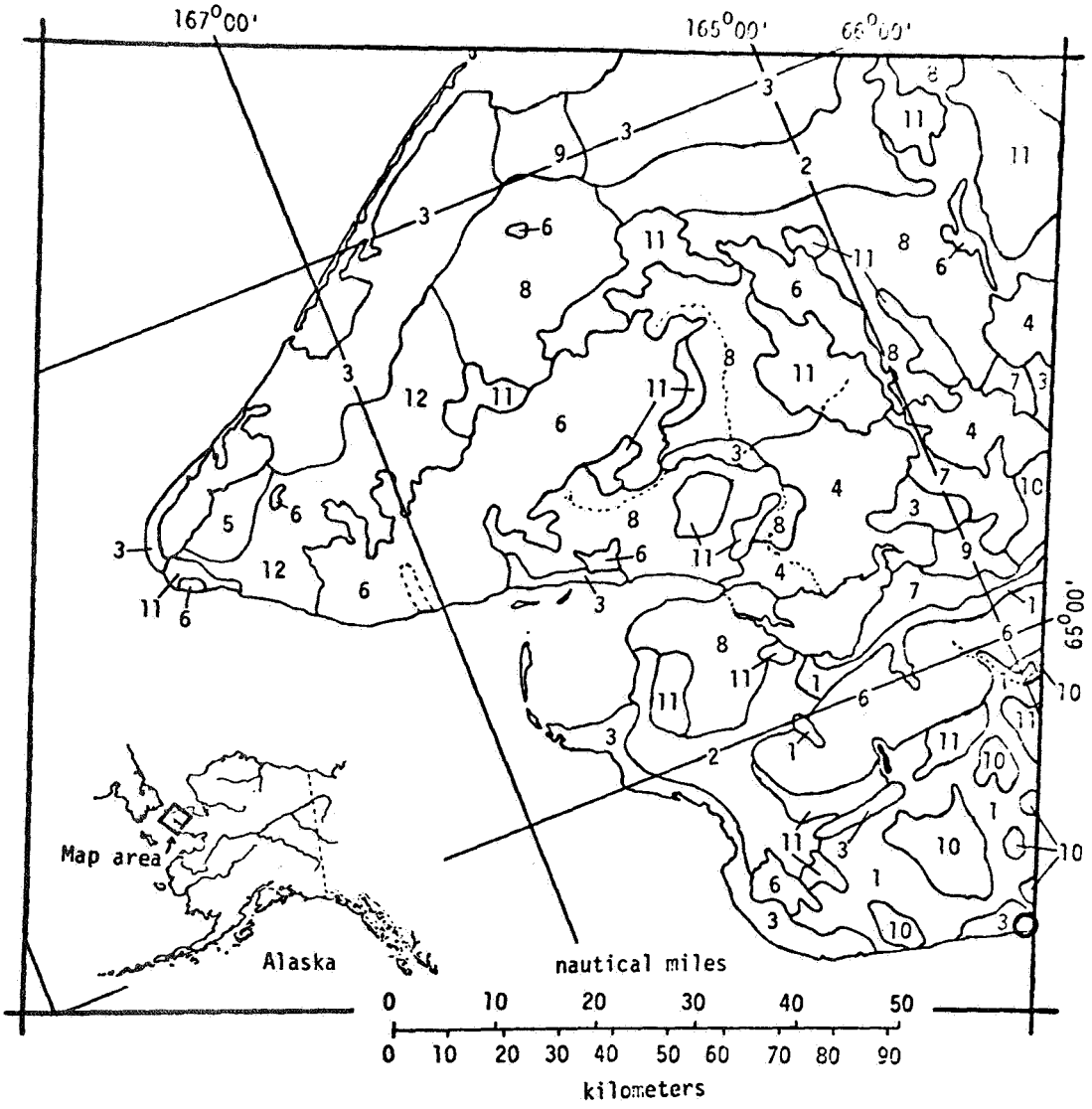


Figure 1. Vegetation map of the western Seward Peninsula, Alaska

Traced from an ERTS-1 image

1. Shrub thicket
2. Upland tundra
3. Wet tundra
4. Fire scar
5. Senescent vegetation (?)
6. Alpine barrens
7. Grassland tundra (?).
8. Shrub thicket/Upland tundra mosaic
9. Shrub thicket/Wet tundra mosaic
10. Shrub thicket/Alpine barrens mosaic
11. Shrub thicket/Upland tundra/Alpine barrens mosaic
12. Upland tundra with some senescent vegetation

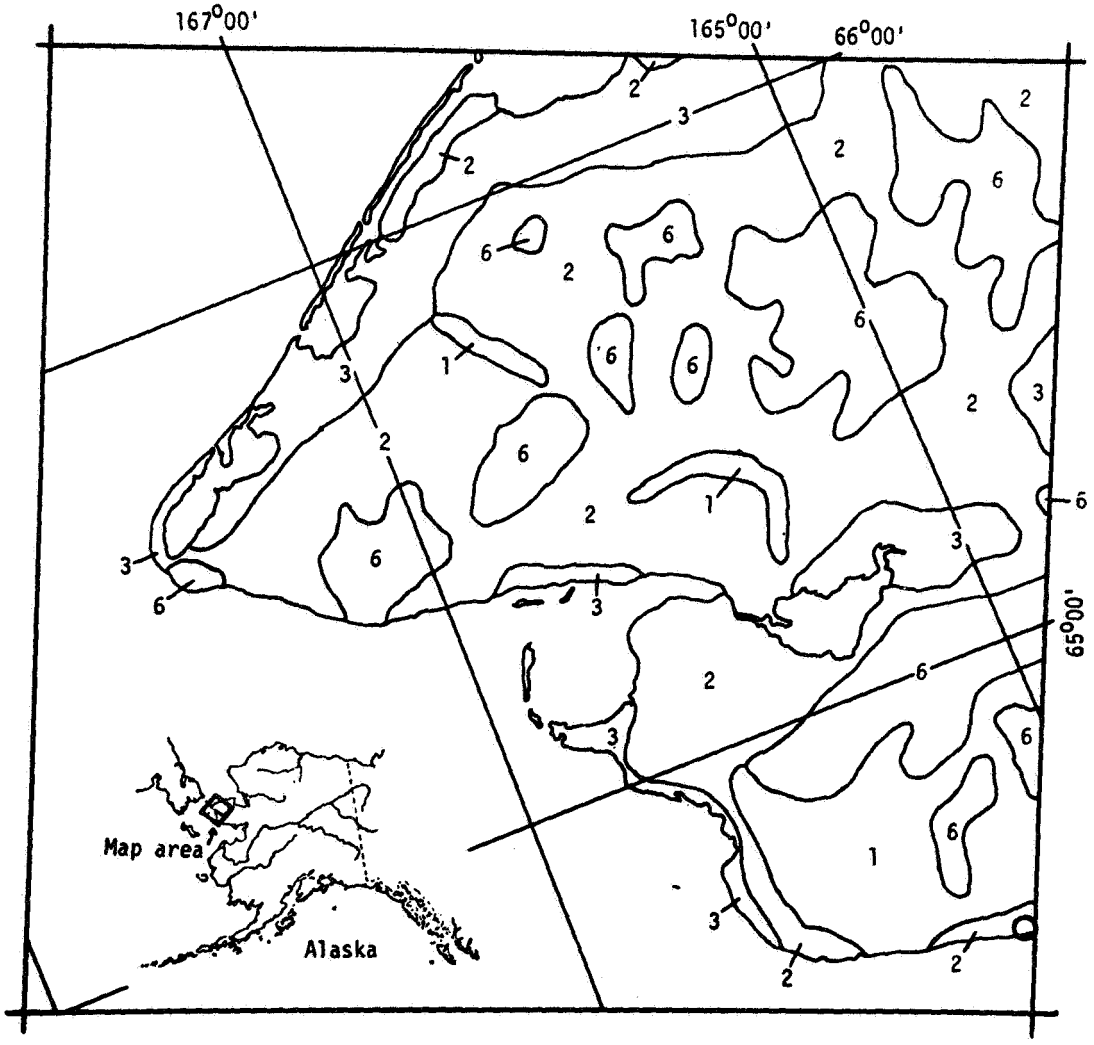


Figure 2. Vegetation map of the western Seward Peninsula traced and enlarged from Spetzman's (1963) map of Alaskan vegetation. This is provided for comparison with Figure 3. The map units designated by Spetzman and their approximate equivalents as termed in this paper are: 1. High brush - Shrub thicket; 2. Moist tundra - Upland tundra; 3. Wet tundra and coastal marsh - Wet tundra; 6. Barren and sparse dry tundra - Alpine barrens.

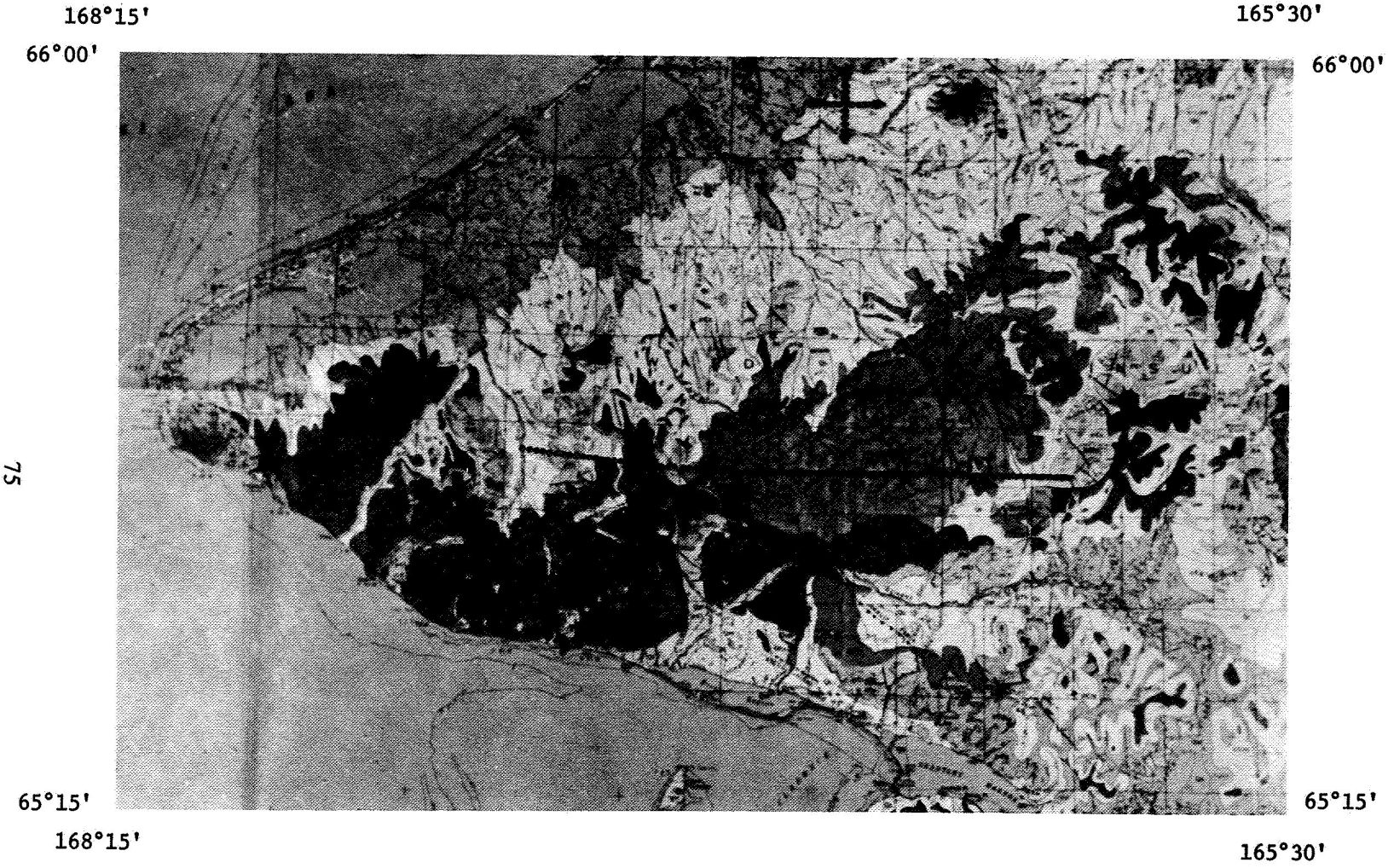


Figure 3: Geologic map of part of the Seward Peninsula (after Sainsbury, 1972). Lineament zone and site of possible buried intrusive indicated by dotted symobls (see text).

Paper A 9

ERTS-1 EVALUATIONS OF NATURAL RESOURCES MANAGEMENT APPLICATIONS IN THE GREAT BASIN

Paul T. Tueller, Garwin Lorain, *Remote Sensing Laboratory, Renewable Resources Center, University of Nevada Reno, Reno, Nevada*

ABSTRACT:

The relatively cloud free weather in the Great Basin has allowed the accumulation of several dates of excellent ERTS-1 imagery. Mountains, valleys, playas, stream courses, canyons, alluvial fans, and other landforms are readily delineated on ERTS-1 imagery, particularly with MSS-5. Each band is useful for identifying and studying one or more natural resource features. For example, crested wheatgrass seedings were most easily identified and measured on MSS-7. Color enhancements simulating CIR were useful for depicting meadow and phreatophytic vegetation along water bodies and stream courses.

A lack of sequential ERTS-1 coverage during the growing season has precluded an evaluation of vegetation phenology changes. However, significant phenology comparisons have been made with U-2 data and offer promise of usefulness in making resource management decisions. Work is underway to inventory and monitor wildfire areas by age and successional status. Inventories have been completed on crested wheatgrass seedings over the entire State of Nevada, and inventories of playa surfaces, water surfaces, phreatophytic vegetation, snow cover, meadows, and other features is continuing. Most of this data is unavailable from conventional sources and would not be available without the possibility of rapid inventory on ERTS-1 imagery.

Vegetation ecotones are being delineated for vegetation mapping. The pinyon/juniper-northern desert shrub ecotone has been identified with considerable success. Phenology changes can be used to describe vegetation changes for management.

INTRODUCTION:

Cloud free weather in the Great Basin has allowed complete coverage of Nevada. Many areas are covered by several dates. A mosaic of the state has recently been constructed using 21 black and white prints at a scale of 1:1 million (24 by 36 inch sheet) and 1:2 million (12 by 18 inch sheet). The red band (MSS 5) was used to construct the mosaic because landform features appeared more striking. This mosaic is being used as a base to map resource features and compare changes on other imagery types and dates.

Ground coverage for single ERTS-1 frames is approximately 12,500 square miles. Resolution of MSS data was found to be excellent, although exposure problems have been encountered. One reservoir 275 feet across was identifiable on MSS 7. The cities of Reno and Las Vegas are easily distinguishable

on all bands. Smaller towns like Elko and Battle Mountain were easily identifiable only on snow covered frames.

Limited numbers of roads and railroads are visible. Four lane paved roads and freeways were visible only when they were in high contrast with the adjacent terrain, as was true with two lane paved roads. Many wide dirt roads traversing valley bottoms were visible due to their high reflectance. MSS 7 was superior for identification of all roads.

USES:

Our initial evaluations of ERTS-1 were directed to identification and determination of resolution. Secondly, we have been studying uses. The first of these has been inventory of natural resource features. Thirdly, we are studying change detection, which goes a step beyond inventory and provides systematic time dependent data useful to resource managers. Examples of inventory and change detection are described below.

Mountains, valleys and playas, stream courses, canyons, and alluvial fans can be easily delineated on ERTS imagery. MSS 5 was found to be the most useful for identification of these general landform features. Steep canyons were identified easily on MSS 7 where thick phreatophytic vegetation occurred. The large valleys and playas were easily identified on all bands. Mapping of land use and of other natural resources features is not difficult. Early in our studies, we evaluated a single frame of 12,500 square miles in Central Nevada (Table 1). These data were extracted successfully in 3 man days.

Native vegetation has been plowed and planted to introduced grasses to increase grazing potential. These seedings have been quantified using a mid-September ERTS date (Table 2). The MSS 7 band was the most useful. Seedings were delineated by county and their acreage computed from dot grids, millimeter squares and a grid corresponding to sections (1 square mile). Acreage was determined by ownership or administration: public, private, county, Forest Service, Bureau of Land Management, Indian Reservations and other. This was derived by comparing locations on a newly published 1:500,000 scale land status map of Nevada. Intermediate scale photography over selected portions of the state and field checking by aircraft flights have confirmed identifications. We expect to update this data and possibly identify dates which are more interpretable. A recently received winter date with complete snow cover tended to make the seedings more obvious and additional ones were identified.

Numerous variations in reflectance were noticed among seedings and are attributed to condition (secondary successional patterns), age, recent precipitation, or grazing intensity. These factors will be further evaluated by analyzing sequential imagery during the growing season.

A major objective has been to map the natural vegetation of Nevada. The valleys are sparsely vegetated with shrubby, desert vegetation (Fig. 1). These areas appear fine textured on the ERTS imagery, and usually have a light gray tone on all bands, depending on soil type. Separations have not yet been possible for the northern desert shrub, southern desert shrub, or salt desert shrub vegetation except for geographical location and landform position. Soil surface colors produce more tonal differences than do the vegetation.

Table 1. Area in square miles of identifiable features for one frame of ERTS imagery (12,500 sq. mi.)* of Central Nevada.

Feature	Area (sq. mi.)	% Total Area
low or flat lying areas	1,852	14.6
alluvial fans	4,465	51.1
mountains	4,333	34.3
Total	12,650	100.0

Feature	Area (sq. mi.)	% Total Area
seedings	1,078	8.5
meadows	222	1.8
playas	1,284	10.2
irrigated fields	134	1.1

* Frame I.D. number 1018-17592-M

Table 2. Seedings within the state of Nevada broken down by county and land status.*

	Land Status					
	Public Land		Private Land		Acres	% of State
County	Acres	%	Acres	%	Total	Total
Churchill	1,235	100.0	-	-	1,235	.1
Douglas	494	100.0	-	-	494	-
Elko	317,983	63.5	182,464	36.5	500,447	50.4
Eureka	42,344	85.5	7,200	14.5	49,544	5.0
Humboldt	83,492	69.6	36,427	30.4	119,919	12.1
Lander	42,849	94.7	2,400	5.3	45,249	4.6
Lincoln	63,585	97.1	1,920	2.9	65,505	6.6
Lyon	7,343	79.3	1,920	10.7	9,263	.9
Mineral	1,309	48.2	1,408	51.8	2,717	.3
Nye	36,810	86.8	5,600	13.2	42,410	4.3
Washoe	4,693	100.0	-	-	4,693	.5
White Pine	141,270	93.2	10,240	6.8	151,510	15.2
Total	743,407	74.9	249,579	25.1	992,986	100.0

* Only those counties which have seedings are included.



Fig. 1. Diamond Valley Frame (MSS 5). Vegetation mapping is possible on this frame. Crested wheatgrass (1) seedings and wildfire scars (2) are easy to delineate.

This task has been very difficult without the aid of color composites. Some images have been enhanced on the I^2S Corporation's Addcol viewer, and more recently, we have used color composites made from diazochrome transparencies. We found that pinyon/juniper can be mapped on winter color infrared composites because it is the only vegetation type exhibiting IR reflectance at this date. Aircraft photography is being used to compute different pinyon/juniper densities which are checked to determine if they can be identified on ERTS data. Plant communities will generally have to be larger than the 300 feet resolution due to low contrast between stands of different communities.

Chaparral and mountain brush communities were identified on late

summer/fall imagery before it had lost its infrared reflectance due to leaf fall. Other types will be identified on spring and enhanced imagery. Salt desert shrub and sagebrush types are being identified by correlating with landform and soil types. Meadows larger than 300 feet in one dimension are readily visible on late summer imagery. For example, a 50 acre meadow at the base of the Ruby Mountains was readily visible on ERTS. Fence line contrasts were visible in this same area where a differential grazing intensity has caused a deterioration in meadow condition across the fence line. The color composite was required for this observation.

The pinyon/juniper-northern desert shrub ecotone is being evaluated by identifying individual ecotones of varying length. The success of accurately defining these ecotones on ERTS-1 imagery has been determined (Table 3). Color infrared has proven superior and was not as susceptable to error caused by the appearance of landforms as was the black and white imagery. Small amounts of infrared reflectance caused by the presence of pinyon/juniper is detectable with the Color IR imagery, thus preventing possible confusion with other features. Larger scale (1:110,000) RB57F photography and aerial reconnaissance have been used to verify the true locations of the ecotones.

With the use of a dot grid and RB57F photography, the minimum density of pinyon/juniper that can be recognized on ERTS-1 Color IR has also been determined. It was found that a density as low as 16.4 trees per acre could be seen on ERTS-1 Color IR imagery if the trees were close and continuous. Areas of pinyon/juniper as small as 55 acres could be seen with a density of 29.5 trees per acre. A discontinuous area of pinyon/juniper with a broken pattern having trees only on the lower slopes of many close ridges showed sufficient reflectance to be identified only when the density exceeded 43.9 trees per acre. Generally, a pinyon/juniper community with a density of 30 trees per acre and larger than 55-60 acres can be identified on ERTS-1 Color IR imagery.

Green, healthy fields reflect strongly in the infrared and are identified easily on color composites. Fallow fields appeared highly reflective on all bands and were therefore identifiable. Irrigated fields were separated from the non-irrigated fields and phreatophytic types by their constant tone and their characteristic straight line borders. Numerous variations in reflectance were noted from date to date on ERTS imagery corresponding to harvesting, watering, fertilizing, plowing, etc.

Wildfire scars, both recent and old, are being inventoried and monitored. A quantitative estimate of the number of acres burned may be obtained easily. We are identifying these burns by relative age: less than one year, 1-10 years, and over 10 years. These are fairly rough estimates and are based on secondary succession textural changes.

Phreatophytic vegetation has been cursorily quantified along the Truckee River and the Las Vegas Wash, using ERTS imagery. A more precise inventory of this vegetation will be made in the future and feasability has been established. Similar data are being obtained for meadow vegetation.

Standing water surfaces were inventoried using mid-September imagery as a base. Reservoirs, lakes and ponds were identified on MSS 7 images (Table 4; Fig. 2) and named from existing topographic maps. The surface

Table 3. Success of identifying the pinyon/juniper-northern desert shrub ecotones in the Great Basin.

Imagery	% Success	% Closure	% Failure	Total no. Evaluated
ERTS 1-Fall	39.4	45.5	15.1	33
ERTS 1-Fall (Color IR)	81.8	9.1	9.1	11
ERTS 1-Winter	54.5	33.3	12.2	33
RB57F - 1:110,000	100.0	0.0	0.0	33
Total (ex.RB57F)	51.9	35.1	13.0	77

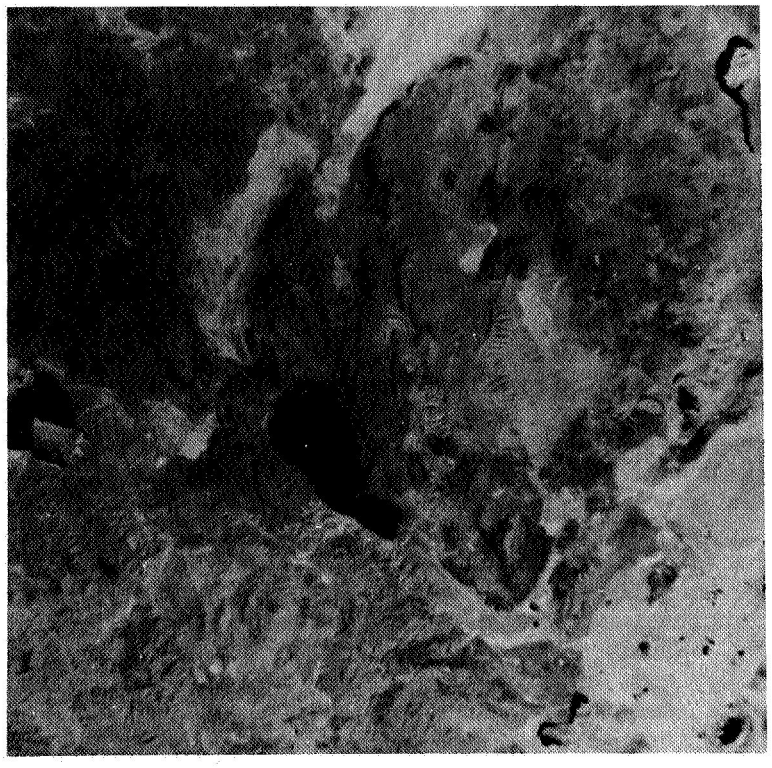


Fig. 2. Pyramid Lake Frame (MSS 7). The ease of inventorying water surfaces is strongly enhanced. Honey Lake in the center left was difficult to evaluate on MSS 5.

Table 4. Standing water resources inventory from selected Nevada Counties.

Counties	Acres	%
Washoe	128,488	43.4
Mineral	37,890	12.8
Clark	65,842	22.1
Douglas	18,949	6.4
Churchill	10,579	3.6
Pershing	9,657	3.3
Total	271,405	91.6
Total in Nevada	295,872	100.0

area was quantified by acreage using a system similar to that described earlier. Each water surface is being analyzed for area changes on new imagery as it becomes available. These changes can be related to water consumption, evaporation, climatic conditions, and amount of potential irrigation water available, all of which are important considerations in the arid Great Basin. Freezing and thawing are also being evaluated. A technique is currently being developed to assign a gray scale value to each water body on each MSS band to correlate with water turbidity.

Playas, numerous in Nevada, are interior drainage basins in which water drains into and stands until it evaporates. These playas are apparent on ERTS imagery whether dry or partially full. The MSS 7 band detects the water even though it may be only one inch deep. The MSS 4 and 5 bands tell us something about the quality of the water in these playas, which is often poor. The presence or absence of water in these playas gives a good indication of recent precipitation in and near the local watersheds.

Inputs on a few lakes or reservoirs that are being monitored can provide correlative data that can be extrapolated to remote water surfaces. For example, the thawing date of a reservoir will affect the type of recreation potential. The freezing date of another pond may limit its value for waterfowl use.

A lack of sequential ERTS-1 coverage during the growing season has precluded an evaluation of vegetation phenology changes. However, significant phenology comparisons have been made with U-2 data and offer promise of usefulness in making resource management decisions.

We have related plant phenology to signatures seen on pre-ERTS multispectral and color infrared U-2 photography flown by NASA. This photography covered our study sites on three to six dates between April 3,1972 and June 14, 1972.

The black and white multispectral U-2 bands were analyzed by assigning standard Munsell shades of gray to each vegetation type on each date. The infrared band was found to be most valuable in the detection of the various vegetation growth stages. Annual grassland (cheatgrass) and brushland areas

in the Reno area showed a general increase in infrared reflectivity with increased vegetative growth. No imagery was available for the late summer dormant period for these areas to determine if the reflectance decreased as the plants became completely dry. Problems with exposure and insufficient sequential dates led to an incomplete analysis. Exposure differences may have masked the true values of date to date variations in gray scale.

The color infrared U-2 photography was also compared to the vegetation phenology. The annual grasses (cheatgrass) in the Reno area were identified on the sequential photography as green and healthy from April 19 to May 5 (the best time for cattle grazing). The May 31 photography revealed that this grass was completely dry (past optimum period for cattle grazing). Field observations supported this conclusion.

In the Ruby Marsh study site (Northern Nevada), several management units occur in which the water levels have been manipulated for control of the heavy stands of bulrush (for interspersion to promote duck nesting). On the April 20, U-2 black and white IR imagery, three of these units appeared identical. Later photo dates revealed higher infrared reflectance in one of the three management areas. Ground notes showed the water level to be equal in the three areas on April 20. Later, one area was dropped to a very low water level for bulrush control. On this area, the phenology was advanced with a corresponding increase in infrared reflectance.

A mountain brush community occurring in eastern Nevada was also studied on the ground and with U-2 color infrared photography. This important cattle and mule deer range was covered with 1 foot of snow on April 20. By May 3, the area was free of snow, but showed no infrared reflectance (showing a lack of spring growth). The June 14 imagery showed this area to be growing vigorously (high infrared reflectance). A practical use for these data would be to govern the date that cattle would be turned onto the range. Good range management requires that stock be kept off the range until the desirable plants have had time to start their spring growth.

Seasonal changes during the early part of the 1972 growing season were not significant. Late season reflectance might have provided significant changes in gray scale if they were available. Gray scales varied considerably among vegetation types (Table 5). Exposure variations confound gray scale site comparisons among dates for a single plant community.

Summary of Significant Results:

Accurate identification and delineation of crested wheatgrass seedings has enabled a broad but detailed inventory of these resources in Nevada. The wide coverage of ERTS-1 is extremely useful for putting these seeded areas into proper perspective for inventory. This constituted the first total inventory of this resource in the state and was accomplished in only 2 man weeks of labor. Automatic techniques can reduce this requirement. Irrigated fields, pastures, meadows, wildfire scars, water bodies, playas, land forms, and other resource features can be similarly inventoried. These total inventories, we feel, are not economically feasible with any known ground or aircraft inventory methods.

Table 5. "Gray Scale"* variations by date, area, and vegetation community on U-2 imagery (0.69 - 0.76 micrometers) in 1972.

	April 20	May 3	June 14
1. Big Sagebrush . . .	4.0	5.5	6.0
2. Low Sagebrush . . .	6.5	7.0	8.5
3. Mountain Brush . .	3.0	4.0	5.0
4. Cheatgrass	4.5	6.0	4.5
5. Marsh-drained . . .	4.0	6.5	4.5
6. Marsh-low water . .	4.5	6.5	3.5
7. Marsh - full . . .	2.5	3.5	2.0
8. Cattail	6.0	6.0	8.5

* Gray scale from 0.5-9.5 on the Munsell Scale.

ERTS-1 imagery is well adapted for a 1:1,000,000 scale base map or mosaic for mapping vegetation over large land areas. Even though all vegetation ecotones are not visible on the photography, the ERTS-1 base map is extremely valuable in and of itself. Field notes, reconnaissance flights, and larger scale photography can be used to map vegetation that cannot be distinguished on ERTS-1 imagery. Sequential dates, summer to winter, significantly increase the capacity for vegetation mapping in the Great Basin.

Phenological changes can be quantitatively described on ERTS-1 imagery. This provides the opportunity to exploit the sequential aspects of ERTS-1 to study the dynamics of natural resources features of wild lands and thus provide input to intial resource management decisions.

Paper A 10

EVALUATION OF ERTS-1 IMAGERY IN MAPPING AND MANAGING SOIL AND RANGE RESOURCES IN THE SAND HILLS REGION OF NEBRASKA

Paul M. Seevers and James V. Drew, *Department of Agronomy, University of Nebraska-Lincoln, Lincoln, Nebraska 68503*

ABSTRACT

Interpretations of high altitude photography of test sites in the Sandhills of Nebraska permitted identification of subirrigated range sites as well as complexes of choppy sands and sands range sites, units composing approximately 85% of the Sandhills rangeland. These range sites form the basic units necessary for the interpretation of range condition classes used in grazing management. Analysis of ERTS-1 imagery acquired during August, September and October, 1972 indicated potential for the identification of gross differences in forage density within given range sites identified on early season aerial photography.

1. INTRODUCTION

The major purpose of this investigation is to evaluate MSS imagery acquired by ERTS-1 of the Sand Hills region of Nebraska for application in: (1) delineating major soil mapping units and associated range sites. (2) estimating forage density and forage utilization on specific range sites, and (3) monitoring the development of center-pivot irrigation.

The Sand Hills region of Nebraska occupies the north-central one-third of the state and is centrally located in the Great Plains. The region is composed of approximately 20,000 square miles of eolian sand dunes interspersed with nearly level valleys, and is stabilized by native grasses or grasslike plants.

2. RESULTS

The project was specifically designed to utilize imagery acquired early during the growing season for the delineation of range sites and associated soil mapping units. High altitude, color infrared aerial photography obtained in early June, 1972 shows the unique dune patterns and the intense infrared reflectance of the sub-

irrigated valleys. Thus, aerial photography or satellite imagery obtained early during the growing season is of maximum value in interpreting soil patterns and range sites. Estimates of forage density were possible utilizing data obtained throughout the growing season.

Range sites for evaluation were selected along four major north-south transects established across the Sand Hills region. High altitude, color infrared aerial photography was first evaluated for recognition of range sites and associated soil patterns. Range sites are basic landscape units used in range management. Each site is a unique combination of soils and plant communities, and its management is based on current forage production relative to optimum forage production. Thus, site recognition is the first step in proper range management.

On the color infrared photography, three major range sites could be recognized. The choppy sands and sands sites make up 76% of the Sandhills and appeared as bluish-gray and white mottled patterns. Subirrigated sites, making up 11% of the Sandhills, appeared as predominantly red areas. Sandy sites, making up 7% of the Sandhills, appeared as predominantly blue areas.

Differences in forage density could also be recognized on the color infrared photography. Comparison of the first sandy site with a second sandy site which produces 50% less total biomass indicates an increase in photo density relative to an increase in forage density on the sites. Fenceline contrasts can also be seen, indicating forage density differences on the same site where a fence divides management practices.

Comparison of reflectance patterns of plant communities with soil mapping units defined in the field was accomplished by photographically reducing existing soil maps to the same scale as the photography. Soil mapping units associated with sands sites were combined on an overlay and superimposed over the color infrared photography. The overlay separates sands range sites and associated soils classified as Typic Ustipsamments from subirrigated range sites and associated soils classified as Aquic Haplustolls and Typic Haplaquolls.

Our success with high altitude color infrared photography suggested that a similar approach would apply to ERTS imagery, especially color composites. Band 5 of the multispectral scanner provided an initial indication in imagery obtained on August 17, 1972 that range sites could be recognized and forage density differences could be qualitatively distinguished on the sandy sites.

Our initial color composites using MSS bands 4,5 and 7 of the same area show very much the same information as band 5 with regard to site recognition and forage density. Color composites provide the added

dimension of infrared contrast in the red color of the subirrigated areas and in the ease of distinction of water bodies. Based on experience with high altitude aircraft color infrared photography, early season ERTS-1 imagery should be superior to August imagery for interpretations of range sites and associated soils. Soil-vegetation relationships appear the same in color composites of ERTS imagery as on the high altitude altitude aircraft color infrared photography.

An unexpected interpretation of ERTS-1 MSS imagery was discovered shortly after delivery of the first imagery for the Sand Hills region. Range fires which occurred in the spring of 1972 could be detected, but only with band 7 of the multispectral scanner. High altitude color infrared imagery detected the fire pattern which occurred on March 6, 1972 and destroyed forage, livestock, buildings and equipment valued at one million dollars, but color composites did not.

The area burned was approximately 30 miles long, 10 miles wide at its widest point and involved 76,460 acres. Utilizing the ERTS imagery, it was possible to locate the burned area and to rapidly and accurately measure the acreage burned. Wind erosion resulting in blowouts is evident on ERTS imagery. Thus, the imagery will provide a means for monitoring erosion problems in areas that are overgrazed or burned by range fires.

Center pivot irrigation has been developed recently in the Sandhills where topography and water supply permit. Individual systems are installed on sands or sandy sites to provide additional pasture or hay sources for the rancher. Unsuccessful systems indicate that careful selection of sites for development is necessary. ERTS-1 imagery provides data for the selection of sites for irrigation and for monitoring the development of center-pivot systems within the region.

The economic prosperity and ecological stability of the Nebraska Sand Hills region are related primarily to cow-calf operations which depend on proper management of the 20,000 square miles of grazing and hay land. It has been estimated that improved range management could provide a twenty percent increase in animal productivity, reflecting an approximate $10 million increase in return to ranchers. Interpretations of ERTS-1 imagery will be significant in developing this increase in productivity.

Paper A 11

MONITORING CALIFORNIA'S FORAGE RESOURCE USING ERTS-1 AND SUPPORTING AIRCRAFT DATA

David M. Carneggie and Stephen D. DeGloria, *Forestry Remote Sensing Laboratory, University of California, Berkeley, California 94720*

Throughout the western United States, large livestock operators, livestock associations, county farm advisors, state statistical reporting services and federal land resource managers have expressed the need for improved techniques for regional monitoring of the forage resources associated with rangelands and wildlife habitats. The new techniques they desire should provide more accurate and timely information regarding the distribution and availability of forage, the health or condition of the forage, the duration of the green-feed period (the time period the forage plants are green), and the amount of forage produced. This information is essential for determining: (a) the animal carrying capacity for the range; (b) the time when grazing animals can begin grazing and the time when they should be removed from the range to minimize damage to the forage plants; (c) the location and condition of alternative sources of forage once the forage at a given range site has been fully utilized; and (d) the fire hazard created by unutilized forage once it has dried and become combustible.

NASA's Earth Resource Technology Satellite (ERTS-1) launched July 23, 1972, offers for the first time the unique capabilities for regional monitoring of forage plant conditions. The repetitive coverage every 18 days, the synoptic view and the real-time recovery of the imagery for immediate analysis, combine to make the ERTS satellite a valuable tool for improving the evaluation of our rangeland resources. Studies presently underway at the University of California, Berkeley (sponsored jointly by NASA and the Bureau of Land Management), seek to determine if imagery obtained from high altitude aircraft and spacecraft (ERTS) can provide: (1) a means for monitoring the growth and development of annual and perennial range plants in California, and for determining the time and the rate of initial plant growth (germination) and terminal plant growth (maturation and senescence; (2) a means for determining or predicting the relative amount of forage that is produced; and (3) a means for mapping rangeland areas having different forage producing capabilities.

Relatively cloud free ERTS imagery for much of California was obtained during the first six cycles: July through October. This imagery has provided an excellent opportunity to monitor the changes associated with the termination of the green-feed period in the perennial rangelands,

and the initiation of the green-feed period in the annual grassland ranges. The perennial rangelands in California are located primarily in the extreme northeastern portion of the state and throughout and east of the Sierra Nevada Mountains. Forage plants associated with the perennial rangelands generally commence growth in late spring or early summer and mature and dry in late summer or early autumn. Thus only the last half of the 1972 growth season of perennial forage plants was monitored during the period of July through October. The annual rangelands in California are located primarily in the foothills of the Coast and Sierra Nevada Mountains. Forage plants associated with the annual ranges generally commence growth during the autumn in response to sufficient rainfall to cause germination of the seeds. Usually a half-inch of rain is required. The first rains of the 1972-73 season fell on September 26 and 27 causing germination of the annuals throughout the northern half of the annual grassland range. The second rains occurred between October 7 and 14 causing further germination to the south over approximately half of the remaining range where germination had not occurred. Finally, during the first and second weeks of November, rainfall caused germination of the remaining annual grassland areas. This southern progression of germination was monitored by the ERTS pass during the first week of October and by the subsequent passes 18 days later.

Analysis of range condition and change has been performed on diazochrome composites of MSS imagery (bands 4, 5 and 7). The diazochrome composites are comprised of a yellow transparency of band 4, a magenta transparency of band 5 and a cyan transparency of band 7. Each of the colored transparencies are made by exposing the 9 x 9 inch black-and-white positive ERTS transparency on the appropriately colored diazochrome film using ultraviolet light. The three colored transparencies are registered (sandwiched) to make the composite which simulates the color renditions of color infrared film. Diazochrome composites were made for each of the first six passes providing a medium on which to compare changes in the vegetation and surface features.

Change detection was also facilitated by employing "positive-negative" masking techniques. This method of detecting change involves superimposing in registration the negative image from one band on one date with the positive image of the same band at a second date. If the two possible composites are made (negative image from the early date with positive image from the later date and vice versa) those features which appear light or white in tone on the composite should depict features which have changed. Because the negative and positive images can also be reproduced on diazochrome colored film transparencies, many combinations of color composites can be created which both show changed features while enhancing feature classification. In any event features which have changed during the interim between passes of the ERTS vehicle can be monitored and their significance evaluated in relation to rangeland environments.

High altitude aircraft data obtained in association with certain of the ERTS overpasses provide verification of many of the conditions of features analyzed. In addition, aircraft data from previous years provide a means for comparing conditions during this growth cycle with previous growth cycles. A network of sample sites located throughout California's rangelands provide ground truth data regarding species composition, growth stage and condition, plant height, degree of utilization, and forage produced. Observations are made at approximately monthly intervals to document the changing forage conditions and provide accurate verification of the conditions analyzed on the ERTS imagery for corresponding areas. Rainfall and temperature data are also collected to correlate with plant development and production.

Significant Results

1. Detailed mapping within rangeland environments is not possible from ERTS data. Gross vegetation types such as forestland, rangeland and meadow land can be discriminated, but the resolution of ERTS imagery does not permit detailed mapping needed for evaluating management problems or making management decisions. This result should be qualified by indicating that the level of information mapped from ERTS imagery would not be useful to the local or district manager of rangelands. Further qualification should emphasize that it is the mapping performed by humans which is not sufficiently detailed to be useful. Automatic classification using the magnetic tape data of ERTS will be tested to determine if refined mapping from ERTS data can be performed.

Vegetation-soil maps derived from high altitude aircraft data generally are detailed enough to be useful to local or district range managers. The comparison of the supporting high altitude aircraft data with ERTS imagery of the same area demonstrates the limiting resolution of ERTS data for detailed vegetation-soil mapping.

2. Most ephemeral lakes within the perennial rangeland can be detected and mapped. Their presence and/or size on a given date provide clues to the climatic variables that directly affect forage production and condition. The ephemeral lakes are best observed on bands 6 and 7.

3. The most important use of the ERTS imagery for evaluating rangelands is for monitoring changes in forage plant condition and development. Annual rangeland containing recently germinated forage species could be differentiated from rangeland where germination had not occurred. Thus the approximate time of germination and the extent of the range where germination has occurred can be determined from analysis of ERTS data. It follows from these observations that the cessation of plant growth in response to insufficient rainfall and soil moisture depletion can also be monitored by ERTS data. A comparison of ERTS images obtained on October 5 and 6, with images obtained 18 days later confirms the

southward spread of germination in the annual grassland of California resulting from the rains during the interim period. From the information obtained through analysis of ERTS data it is possible: to predict when grazing could commence and when it should be terminated at the end of the growth season due to a reduction in nutritive value associated with the drying of range forage species, or to the absence of sufficient forage to maintain the grazing animals; and to determine the length of the green-feed period which is correlated with the amount of forage produced. When the growth season is short forage production will be below normal and the animals will leave the range much earlier and lighter than normal (more supplemental feed or alternative sources of feed will be required). When the growth season is long, forage production will be above normal and the animals will leave the range at a later date and be considerably heavier than normal. They will require less feed supplements.

4. Analysis of the ERTS imagery should reveal the location and size of ranges affected by favorable or unfavorable climatic variables that cause above- or below-normal (respectively) forage condition and production.

5. ERTS imagery can provide the bases for determining the location and extent of rangelands where potential fire hazard exists either by virtue of early drying or by virtue of the presence of abundant forage which when dry creates the flash fuel for spreading fire to more valuable vegetation types.

6. ERTS data does not provide sufficient resolution to determine the cover or condition of forage plants in most perennial range plant communities. A noteworthy exception is that of meadow sites which have a dense cover of vegetation in contrast to the generally sparse cover of plants in other perennial plant communities. Moreover, the drying trend of the meadow vegetation could be monitored from one pass to the next in the perennial rangeland between August and October. Thus meadows and ephemeral lakes can be monitored using ERTS data, and provide indicators to the climatic variables governing forage production and condition throughout the perennial rangelands. It is envisaged that ERTS data will also prove valuable for determining conditions early in the growth season which indicate when grazing can commence without doing damage to the perennial forage plants.

7. ERTS data provide a permanent record of range conditions at a given date and for a given year. A comparison of ERTS images with aircraft data obtained on previous years reveal the relative difference in range condition between years. ERTS data acquired on a year-to-year basis can provide the first and most effective means for comparing changes in range condition from year-to-year for large rangeland areas.

Specific users who stand to benefit from the information obtained

through analysis of ERTS data include: (a) the Bureau of Land Management and the U.S. Forest Service -- both agencies are required to regulate the time and duration of grazing on lands that they administer; (b) the California Crop and Livestock Reporting Service -- an example of a state agency that can use ERTS derived information to account for animal movements, the need for feed supplements, and the determination of range conditions; (c) the California Division of Forestry and other fire control agencies (BLM and USFS) -- these are vitally concerned with acquiring information which permits more accurate and timely allocation of manpower and equipment to prevent potential wild fires; and (d) ranchers, feedlot operators, and others involved in using or supplying feed supplements -- they need timely information regarding availability of green forage, the time of animal movements to and from rangelands, and the availability and demand for alternative sources of feed supplements.

In summary, the data provided by ERTS and high altitude aircraft enables range managers to monitor the development of range lands throughout California. By providing timely and accurate data regarding the availability, distribution and condition of forage, the ERTS satellite can contribute greatly to more effective utilization and management of California's rangelands. To the extent that predictions of forage production can be made from ERTS data (in conjunction with ground and climatic data), range managers, feedlot operators and suppliers of feed supplements can more efficiently predict the time, direction and numbers of animals moving to and from rangelands, and determine the need for feed supplements which will sustain the animals until they are converted to consumable meat products.

Paper A 12

TESTING THE USEFULNESS OF ERTS-1 IMAGERY FOR INVENTORYING WILDLAND RESOURCES IN NORTHERN CALIFORNIA

Donald T. Lauer and Paul F. Krumpe, *Forestry Remote Sensing Laboratory, University of California, Berkeley, California 94720*

INTRODUCTION

The Forestry Remote Sensing Laboratory at the University of California is in the process of testing the usefulness of ERTS-1 imagery for inventorying wildland resources in northern California. Studies are being conducted in two large wildland areas, namely, the Feather River Watershed and the Northern Coastal Zone.

The 2.5 million-acre Feather River headwaters area in northern California is the keystone watershed for the California Water Project, one of the most extensive and ambitious water resource developments ever attempted. Consequently, accurate and timely information on the quantity, quality and distribution of timber, forage, water and recreational resources is of immediate importance to each public agency and private group managing this vast, but inaccessible, wildland area.

Likewise, the Northern Coastal Zone (consisting of the counties of Marin, Sonoma, Mendicino, Humbolt and Del Norte) is relatively rural, with an economy based on agriculture, timber, commercial fishing and tourism. However, it is expected that intensive resource use resulting from increasing population will soon become a serious problem unless wise land use planning is undertaken. Thus, this coastal region is particularly well suited to investigations of the ways in which ERTS-1 imagery and other supporting data may be used in conducting land use evaluations.

OBJECTIVES

Research being performed within wildland areas in northern California stresses both the applications of ERTS-1 imagery and the benefits derived from these applications. Specific objectives are to (1) evaluate the feasibility of mapping vegetation/terrain resources with the aid of ERTS-1 imagery, (2) evaluate the cost/effectiveness of resource mapping using various types of data, including ERTS-1 and aircraft imagery, (3) develop suitable aids for training image interpreters (4) test quantitatively selected ERTS-1 images for detailed wildland resource information, (5) compare -- in terms of accuracy of boundary placement, accuracy of type identification and degree of interpretation efficiency -- information

derived from ERTS-1 imagery with that derived from conventional and/or high flight photography, (6) compare ERTS-1 and high flight interpretation results with existing regional mapping capabilities that employ conventional techniques, and (7) evaluate the interpretability of multiband-multidate ERTS-1 image color composites.

Several types of color composite imagery are being analyzed, including those made by diazo overlay, optical projection, direct photo reproduction (multiple exposure), and electronic display (direct from ERTS-1 digital tapes). Emphasis in the results reported below has been placed on documenting levels of accuracy, degree of timeliness, and costs associated with utilizing ERTS-1 imagery for inventorying wildland vegetation/terrain resources.

SIGNIFICANT RESULTS

It is well understood that possibly the most useful characteristic of the ERTS-1 system is its ability to acquire data for the same point on the earth on a repetitive cycle. At the time of preparing this paper, most investigators have had little opportunity to study ERTS-1 data taken sequentially of the same area. However, our preliminary research results derived primarily from ERTS-1 data procured during the first few orbital passes made last July, are extremely encouraging.

Significant conclusions resulting from work done within the Feather River Watershed region are summarized below:

1. Numerous user agency groups have been identified which are keenly interested in the ERTS-1 investigations being conducted in northern California. For each of these agencies, resource management specialists have been contacted by FRSL personnel and avenues of communication and interchange have been established (see Figure 1).

2. Regional analysis of over thirty important wildland resource features within the Feather River Watershed, as seen on ERTS-1 imagery, have resulted in the development of a feasibility table which indicates the general degree of feature detection and identification.

3. A projected cost ratio of 7 to 1 was calculated for interpretation of high flight photography versus ERTS-1 imagery, respectively (see Figure 2).

4. An image interpretation key to 19 resource features occurring within the Davis Lake intensive study area was developed.

5. A quantitative image interpretation test of ERTS-1 imagery showed that within the Davis Lake study area specific resource type identification could be done at a level of accuracy of 65 percent and broad resource type identification at 70 percent (see Figure 3).

6. The Forestry Remote Sensing Laboratory automatic data processing hardware and software systems are now operating efficiently, and ERTS-1 digital magnetic tape data can be displayed on a color TV monitor, and CALSCAN and RECLASS classification procedures can be applied.

7. Within the Bucks Lake study area, boundaries between contrasting forest types were properly mapped by image interpretation on ERTS-1 imagery and subtle boundaries between less contrasting types (and, therefore, the less important boundaries) were the ones which were most often misplaced (see Figure 4).

8. The ERTS-1 imagery yielded less detailed information than conventional aerial photographs at the Bucks Lake study area, but the image interpretation was done much more cheaply (e.g., type delineations were drawn nearly 20 times faster on the ERTS-1 image than on black-and-white photographs, scale 1:15,840). (See Figure 5.)

9. A quantitative interpretation test was performed on several single observation ERTS-1 color composite images and one single band (#5) image. In no case were interpretation results derived from one image type significantly different than from those derived from another for the three vegetation types identified (conifers, brush and dry site hardwoods).

10. Initial vegetation/terrain type computerized classification results within the Bucks Lake study area using CALSCAN showed that three out of six types are reliably separated; these types were meadows, brush fields and barren areas.

Likewise, significant conclusions resulting from the work done within the Northern Coastal Zone Test Site are summarized below:

1. Contacts were made and interviews conducted with environmental planners throughout the north coast counties of California, resulting in the definition of parameters which are important for determining the potential of an area in terms of land use.

2. Within the southern portion of the Northern Coastal Zone Test Site, 23 mapping units were delineated by image interpretation on an ERTS-1 color composite image. However, when working with only single-date ERTS-1 imagery, an interpreter could consistently identify only five mapping unit categories.

3. A quantitative image interpretation test was performed within the San Pablo Reservoir study area using 300 ground controlled points. Differentiation on ERTS-1 imagery between various types of woody vegetation (i.e., Monterey pine, mixed hardwoods, eucalyptus, and chaparral) was difficult -- Monterey pine was identified correctly 78 percent of the

time, but all other types were identified correctly less than 50 percent of the time.

4. The quantitative image interpretation test performed at the San Pablo Reservoir area, however, showed that a skilled image analyst could identify woody vegetation, versus everything else, with better than 86 percent accuracy.

5. The perimeter around a large burned area and damage levels within the perimeter were mapped on ERTS-1 imagery taken over the Pocket Gulch fire ten days after suppression. The burned area was accurately mapped on the ERTS-1 image as 13,340 acres while California Division of Forestry personnel estimated the burned area at 10,340 acres (see Figure 6). Low altitude oblique photography indicated that the estimate obtained from the ERTS-1 imagery is accurate.

6. The costs associated with mapping burned areas using conventional methods are 10 times greater than by using the ERTS-1 image.

CONCLUSIONS

In summary, it is much too early to reach definitive conclusions regarding the feasibility of using ERTS-1 for detecting, inventorying and monitoring wildland resource features and conditions in northern California. However, the preliminary results reported upon above have been surprisingly good. There appears to be every indication that many kinds of regional resource information can be obtained more quickly, more reliably and at lower costs through the use of ERTS-1 imagery in comparison to conventional data gathering techniques. Likewise, intensive area resource information, such as forest land classification, major vegetation type identification and post fire maps, can be easily and accurately obtained from ERTS-1 imagery by applying manual and/or automatic data extraction techniques which are currently operational. It must be remembered that (1) most of the case studies reported upon herein were done with the aid of the very first ERTS-1 images, taken in July over California, and (2) the unique characteristics of ERTS-1 lie in its synoptic view, sequential capabilities. Consequently one can expect that as ERTS-1 continues to procure high quality imagery on an 18-day cycle, the relatively high accuracy and low cost figures associated with each study done to date will be improved -- and results derived from other experiments currently in progress will be equally as impressive.

USER GROUP AGENCY	PERSONNEL CONTACTS	REMOTE SENSING RESEARCH APPLICATION
CALIFORNIA REGION FRAMEWORK STUDY COMMISSION FOR SOUTHWEST INTER-AGENCY COMMITTEE: WATER RESOURCES COUNCIL	MR. JIM COOK (USFS) MR. LYLE KLUBBEN (USFS) MR. WILLIAM FRANK	REGIONAL VEGETATION/TERRAIN MAPPING LAND USE PRACTICES AND CHANGES LANDSLIDE AND STREAM SEDIMENTATION DETECTION
REDWOODS NATIONAL PARK, U.S. NATIONAL PARK SERVICE	MR. H. T. HATZIMANOLIS RESOURCES MANAGEMENT SPECIALIST	CHANGE DETECTION ANALYSIS LAND USE PATTERNS ON ADJACENT LANDS VEGETATION INVENTORY REGENERATION ANALYSIS
DEPARTMENT OF WATER RESOURCES, STATE OF CALIFORNIA	MR. G. SAWYER MR. A. DE RUTTE	SNOWPACK DETECTION HYDROLOGIC OUTPUT PREDICTIONS
CALIFORNIA COOPERATIVE SNOW SURVEY	MR. V. LEMMONS	SNOWPACK DETECTION AND HYDROLOGIC PREDICTIONS
CALIFORNIA DEPARTMENT OF CONSERVATION DIVISION OF FORESTRY	MR. T. ARVOLA MR. C. PHILLIPS	VEGETATION-SOILS INVENTORY FIRE DAMAGE APPRAISAL RANGELAND CONTROL BURNING MONITORING COMPLIANCE WITH FOREST PRACTICE ACT
U.S. FOREST SERVICE	MR. JIM MC LAUGHLIN	SOILS-TERRAIN ANALYSES
TAHOE REGIONAL PLANNING AGENCY	MR. JIM BRUNER	ENVIRONMENTAL CHANGE DETECTION SEDIMENT POLLUTION ANALYSIS LAND USE INVENTORY
CALIFORNIA STATE DEPARTMENT OF PARKS AND RECREATION	MR. GEORGE RACKELMANN MR. JOHN HAYNES MR. SANDY RABINOWITCH MR. KEN COLLIER MR. ED POPE	LANDSCAPE INVENTORY SITE LOCATION AND PLANNING

Figure 1. Cooperating user agency personnel who have shown a keen interest in the ERTS-1 experiments being conducted within wildland areas in northern California.

TASK	SMALL SCALE CIR TRANSPARENCY (9 x 9 in.)	ERTS-1 COLOR COMPOSITE PRINT (16 x 16 in.)
DELINEATION OF WATERSHED BOUNDARY (2.5 MILLION ACRES)	3.0 HOURS	0.5 HOURS
PLOTTING EFFECTIVE AREAS	5.0 HOURS	0.0 HOURS
DELINEATION OF HOMOGENEOUS AREAS	48.0 HOURS	3.0 HOURS
PHOTO INTERPRETATION TRAINING & TESTING	6.0 HOURS	2.0 HOURS
RESOURCE TYPE CLASSIFICATION	210.0 HOURS	30.5 HOURS
TOTAL INTERPRETATION TIME REQUIRED	272.0 HOURS	35.5 HOURS
HOURLY WAGE	$7.00/HOUR	$7.00/HOUR
TOTAL INTERPRETATION COSTS (TIME)	$1,904.00	$248.50
TOTAL COST/ACRE	0.07¢	0.0098¢
COST RATIO	7	1

Figure 2. Projected time and costs associated with mapping vegetation/terrain resources throughout the entire 2.5 million-acre Feather River Watershed using high flight photographs or ERTS-1 imagery.

COMPONENTS	A,BB,C,E		F,H		KK,K		N,N(V)		Q		R,P		L,S		V,W,WB		X		
COMPREHENSIVE RESOURCE	CONIFEROUS FOREST		HARDWOOD FOREST		MOUNTAIN CHAPARRAL		XERIC GRASSLAND		CULTIVATED CROPS		MESIC RANGELAND		SAGEBRUSH SCRUB		EXPOSED SOIL		STANDING WATER		TOTALS
NO. TEST CELLS	71		4		31		17		4		23		44		10		6		210
INTERPRETER ID	A[a]	B[b]	A	B	A	B	A	B	A	B	A	B	A	B	A	B	A	B	A	B
NO. CORRECT	57	60	0	0	23	19	0	4	4	3	22	17	36	32	7	4	6	6	155	145
NO. COMMISSION	6	15	1	0	9	5	0	3	0	0	4	4	7	8	5	3	0	0	32	38
NO. INDICATED	63	75	1	0	32	24	0	7	4	3	26	21	43	40	12	7	6	6	187	183
NO. OMITTED	14	11	4	4	8	12	17	13	0	1	1	6	8	12	3	6	0	0	55	65
PERCENT OMITTED	19	15	100	100	25	38	100	76	0	25	4	26	18	27	40	60	0	0	26	30
PERCENT COMMITTED[c]	8	21	25	0	29	16	0	17	0	0	17	23	15	18	50	30	0	0	15	18
PERCENT COMMITTED[d]	9	20	100	0	28	20	0	42	0	0	15	19	16	20	41	42	0	0	17	20
PERCENT CORRECT	80	84	0	0	74	61	0	23	100	75	95	73	81	72	70	40	100	100	73	69

[a]Results for Interpreter A

[b]Results for Interpreter B

[c]Error based on number of type present

[d]Error based on number of a type indicated

Figure 3. Results of a quantitative image interpretation test of broad vegetation/terrain type identification using ERTS-1 imagery.

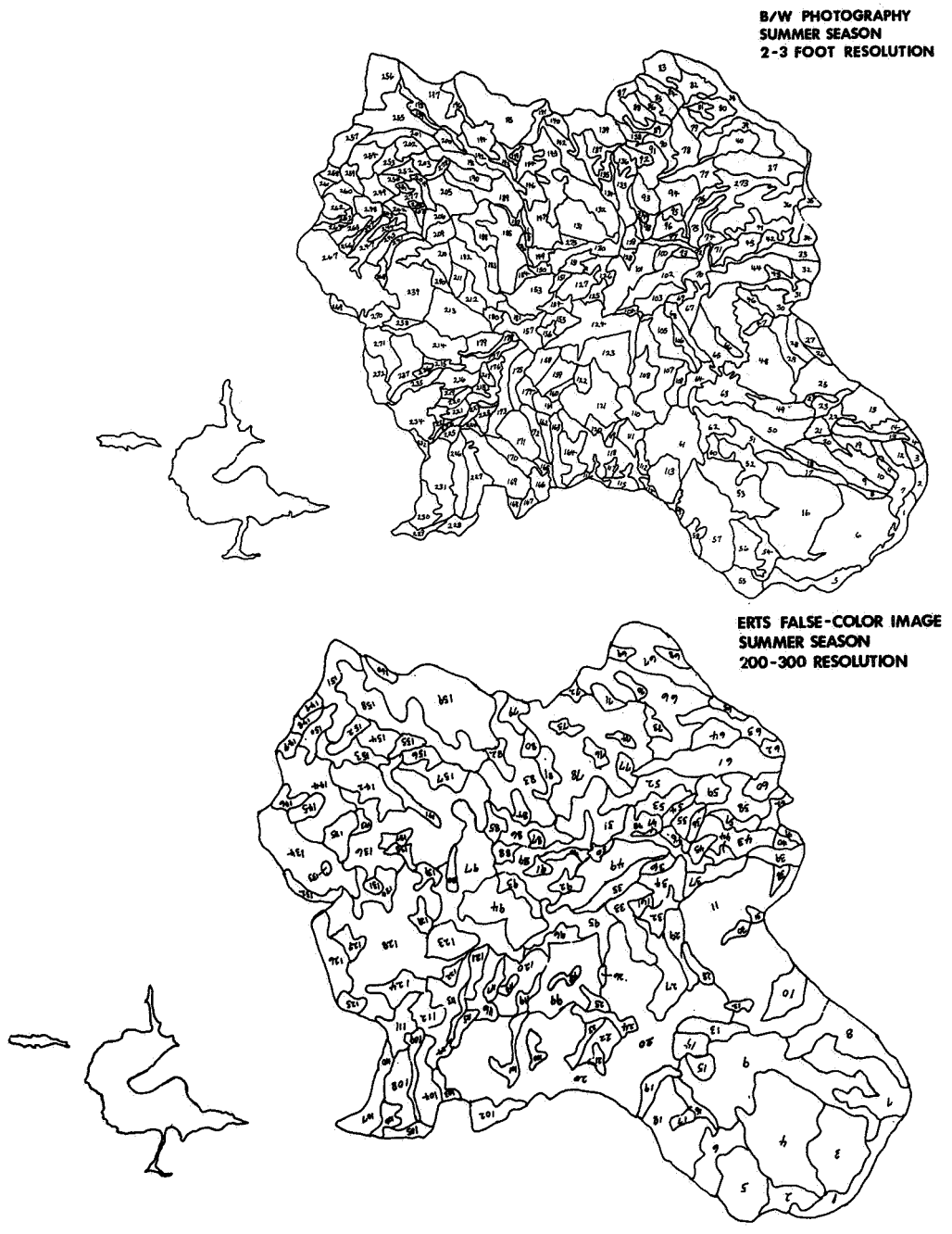


Figure 4. Forestland stratification boundaries made from 78 conventional black-and-white photographs, original scale 1:15,840, at the top and a small portion of an ERTS-1 image, original scale 1:1,000,000 at the bottom.

Task	B/W Photography	High Flight CIR Photo	ERTS False-Color Image
Delineation of watershed boundary	6 hours	1 hour	.5 hour
Plotting effective areas on photos	5 hours	0 hours	0 hours
Interpreter training and testing	3 hours	3 hours	.5 hour
Type delineation and classification	30.5 hours	17 hours	1.25 hours
Total time required	44.5 hours	21 hours	2.25 hours
Hourly wage	$7.00/hour	$7.00/hour	$7.00/hour
Total interpretation costs (time)	$311.50	$147.00	$15.75
Total cost per acre	.622¢	.294¢	.032¢
Cost ratio	19.8	9.3	1

Figure 5. Time and costs associated with mapping vegetation/terrain resources within the 50,000 acre Bucks Lake study area using conventional black-and-white photographs, high flight photographs and an ERTS-1 image.

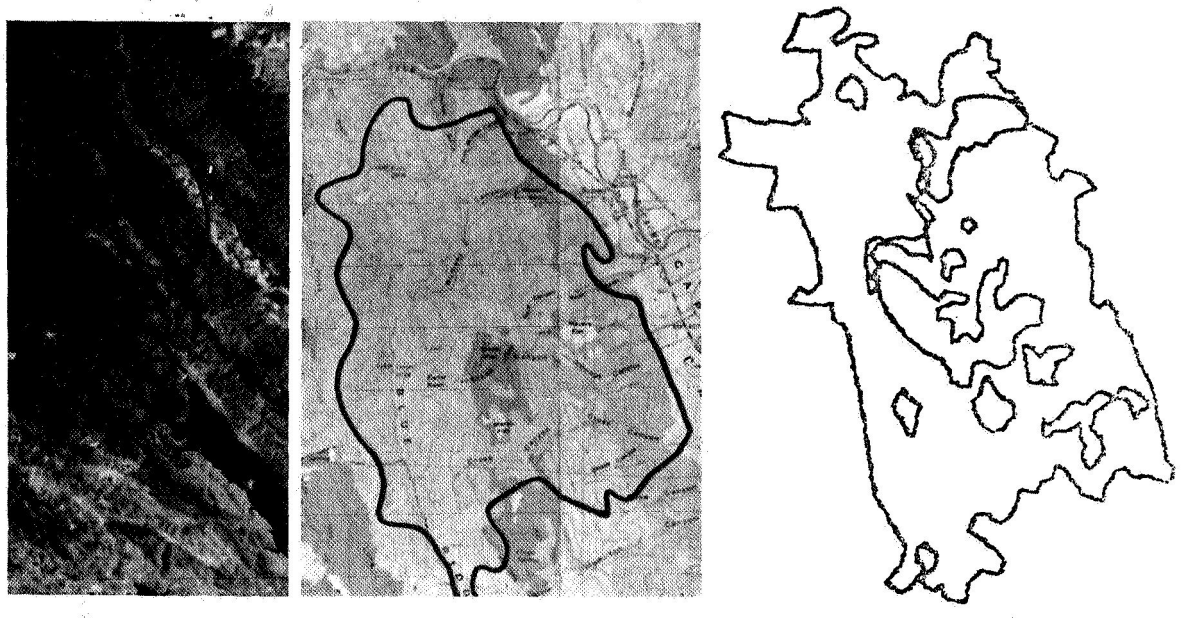


Figure 6. A portion of an ERTS-1 MSS band 7 image showing the Pocket Gulch burn is on the left. The California Division of Forestry map of the burn is in the middle (estimated acreage = 10,340). A map derived from the ERTS-1 image is on the right (estimated acreage = 13,340).

Paper A 13

INTERPRETATION OF ERTS-MSS IMAGES OF A SAVANNA AREA IN EASTERN COLUMBIA

G. W. W. Elbersen, *Centro Interamericano de Fotointerpretacion, Apartado Nal. 762/2 Bogota, D. E. Colombia*

Introduction

One of the objectives of CIAF's ERTS proposal nr SR 305 was to make an extrapolation of existing soil maps into unmapped areas, of the Llanos Orientales of Colombia. The first image received (nr 1086-14201 - 4, 5, 6 and 7) had no recovery with the area for which ground truth exists. It had recovery with the area requested but only with the part intended for extrapolation. Nevertheless interpretation of the image was started and while the investigation was in progress, we received new images which did cover the sample area requested (nr 1088-14320 - 4, 5, 6 and 7). Interpretation of these new images and confrontation of this interpretation with groundtruth confirmed the validity of most of the delineations made in the preliminary interpretation.

Interpretations were made according to the conventional photointerpretation technique called "Physiographic analysis" developed by Buringh, 1960 and in use at ITC and CIAF. Most usefull were the green and infrared images, the information from which was pooled. Samples of 1/60000 aereal photographs were interpreted from both areas. Extrapolation of information was done via existing soil map to ERTS image and photoimage. The interpretation of the unknown area on ERTS was verified by the interpretation of aerial photo samples. (see methods) and applying the knowledge gained by interpreting AP's of the existing soil map.

Most units delineated in the existing reconnaissance soil map at a scale of 1:250000 could be recognized and delineated in the ERTS image. With repetitive coverage the results would no doubt have been even better.

Methods

The interpretation of the ERTS images was carried out on blow ups at a scale of app. 1:500.000 of the green and infrared channels. (The blue channel was of a much lower quality due to haze, while the red channel did not supply any information not available with better contrast on the infrared, for our purposes).

We tried two methods for pooling the information of both channels. The images were fused by means of the mirrorstereoscope and delineations were made according to patterns visible in the joint image. In the second approach an interpretation was made on the green channel image transferring the transparent overlay to the infrared one, in order to bring infrared derived detail into the map.

It was found that the use of a stereoscope though accurate, was very tiresome mainly due to the difficulty of fusing images which show the same objects in very contrasting tones.

The interpretations were carried out notwithstanding the fact that no real stereoscopy is to be obtained according to the conventional photointerpretation technique called "Physiographic analysis" described by Buringh (1960) and in use at ITC and CIAF. Applying this technique, one tries to establish which processes like alluvial sedimentation, aeolian sedimentation, etc., have formed or are forming the landsurface under consideration. Subsequently an interpretation is made which is based on knowledge concerning the relation between soil formation and the abovementioned processes. Some lines are very obvious, others can only be drawn when there is additional local knowledge.

Of both the area with and without groundtruth a strip of aerial photographs of 1:60.000 scale was interpreted. For the data flow in the extrapolation see scheme.

The derived maps were consequently enlarged to a scale of 1:320.000 with the sole purpose of facilitating comparison with the existing soil map at 1:250.000. It is recognized that enlargement of interpretation beyond the scale of the original base is generally unsatisfactory since errors are magnified.

Description of Units

General

Since the Meta river flows in a fault line there is a strong contrast between the area studied S. of the Meta river and the landscapes N. of this river which have not been object of intensive study on ERTS so far. The main object was the high plain (A) a very old alluvial surface with some aeolian influence divided into various units: the well drained level part (Aa), the poorly drained part (As), the undulating part (Ao) the dissected part (Ac) the minor drainageways (Ae) and the major drainageways (Av). Most of these units could be distinguished.

Of the floodplain of the Meta river (V) the main subdivision (Vb) with the high inundation hazard was present, occasionally including remnants of terraces (T) with a very low position (Tv). Relatively cumbersome proved some minor patches of aeolian influence within the flood plain related to extensive aeolian plain N. of the Meta river (E). On this landscape the subdivisions (Em)dunes, (Es) poorly drained aeolian plain and(Er) better drainaged patches within the level aeolian plain, occurred. Of these only (Em) could be identified with certainty especially if the influence transgressed into the high plains.

Unit: Aa

Occurrence: Anywhere in the level high plains S. of the Meta river wherever these plains are neither poorly drained, nor dissected.

Aspect: In the ERTS images both in the 5 and 7 channels a rather uniform grey if not disturbed by human influence or by burn patterns in various stages of regrowth. The unit is identified in this analysis more by its position around its characteristic drainage pattern and by the lack of those characteristics that identify adjacent contrasting units of the same or other landscapes.

On AP's the same aforementioned criteria apply, but in addition a typical pattern known as "rizamiento" occurs which consists of parallel erosion features on the long slopes toward the drainageways and a reticular pattern in the centres of the interfluves.

Soils: Well drained oxisols (1)* (typic subgroup) in the high parts of the landscape, fine silty in the N. fine loamy and clayey in the S. The slopes are characterized by oxic haplorthents of course loamy textures.

Reliability: Though the drainage pattern of these units is rather characteristic transitions towards the Ao and Ac units, which are more dissected, are rather gradual. Often a slight difference in grey tone on the 7 channel image shows, but this is not uniformly so, especially since old burn patterns spoil this contrast. For the present interpretation the inclusion of a certain amount of Ao and Ac within Aa has to be taken for granted. Limits with the unit As are thought to be highly confiable due to its easy identification in channel 7, while the occurrence of small units of Em along rivers and streams is rather easily detected in the 5 channel, so that only minor contamination with these units is to be expected

Remarks: Repetitive ERTS coverage will facilitate a better separation of Aa from Ao and Ac. Images from the end of the dry season are expected to show maximum vegetation differences due to drainage conditions between the level and dissected areas.

---

(1)* Under this heading we give the literal translation of the description of these units taken from pages 66, 67 and 68 of Vol. II of FAO,1966. No attempt has been made to update the classifications made according to Soil Classification 7th App., 1960. It may be mentioned that many authors consider the soils of this area to be Ultisols rather than Oxisols (Guerrero, 1971). This is probably due to the rejuvenation by volcanic ashes (Elbersen, 1972).

Unit: As

Occurrence: In the level high plains S. of the Meta river. In the larger interfluves wherever drainage is insufficient.

Aspect: On ERTS imagery channel 7 these areas are easily identified especially due to the peculiar aspect of the adjacent drainage ways. Since these courses grow into the poorly drained areas by a process of mass movement (as described by Goosen, 1972) the tips are very much enlarged in comparison to the gully downstream. These broad poorly drained tips devoid of arboreal vegetation show in a striking way on the infrared channel. The classification of the drainagesystem drawn on channel 5 into poorly drained tips and normal "esteros" on evidence from channel 7 forms the basis for the delineation of the As areas.

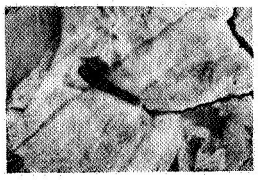
Other factors which aid in their identification are a slightly darker tone of the poorly drained interfluves as a whole and a higher incidence of burn patterns (the latter due to the fact that more dead vegetation is available for burns in these areas)

On AP's the same factors aforementioned occur but in addition the identification is greatly facilitated by the occurrence of solifluction rills locally called "escarceos".

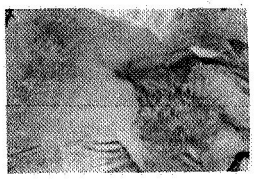
Soils: Association of albaquox in the depressional parts with aeric and typic normaquox and the plinthic subgroup of the well drained oxisols in the higher parts.

Reliability: Taking into consideration the generalization due to the scale of the images, we may state that the mostly inferred limits of these areas are generally reliable. Within the poorly drained areas patches of better drained soils may occur (as indicated on the existing soil map and in the interpretation of the AP's) where according to Goosen (1972) whole blocks have moved in a catastrophic way over distances of hundred of meters due to instant liquifaction of the the subsurface layers, probably triggered by quakes. These inclusions cannot be predicted on the ERTS imagery and remain as impurities in the units.

Remarks: Repetitive coverage could include maximal contrast for the poorly drained zones if taken in extreme situations (dry and wet) Now boundaries are mostly inferred from the characteristics of the drainage pattern, only locally did tone differences help in the establishment of these limits.



Enlarged Gully head on AP



Solifluction rills of As contrast with "riza miento" of Aa on AP.

Unit Ae

Occurrence: As minor drainageways in the high plains S. of the Meta river.

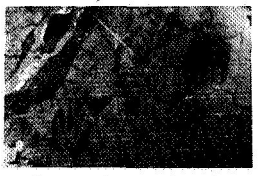
Aspect: On ERTS imagery the 5 channel gives the most complete picture of the drainage pattern since both the gallery forest and the non arboreal vegetation of the poorly drained tips show up in contrasting dark tones. For the separation between poorly drained tips, essential for the delineation of As, and normal forested tips, we have to resort to the 7 channel where this difference shows in a very marked way (see description of Unit As): the gallery forest appears light grey while the poorly drained tips appear in a dark grey tone.

On AP's presence of absence of forest vegetation is the main basis for distinction of the two parts of the drainage system.

Soils: Humic normaquox or clayey or fine silty texture occupy the lowest parts of the esteros surrounded by albaquox especially in the N. part of the area surveyed.

Reliability: Due to the limitations of the scale of the material these areas could not be delineated. The interpretation had to be restricted to the representation of this unit as a symbol (drawn line for the normal esteros and dotted line for the poorly drained tips.) This representation is thought to be highly accurate. Check with AP's showed that only some very minor secondary gullies were missed.







Trident shapped "Estero" on AP, ERTS 5 and ERTS 7 respectively. Note that forested part is distinguishable in ERTS 7 as white line, ERTS 5 does not permit this distinction.

Unit: Ao and Ac

Occurrence: In the level high plains S. of the Meta river where an intricate drainage pattern has dissected the landscape.

Aspect: On ERTS these two units representing two fases of dissection could not be separated while limits of this combined unit with the unit Aa are difficult to trace exactly. Locally the Ao and Ac units show a lighter tone on both 5 and 7 channels which may be due to scarcer vegetation. In other areas however it has been observed that Ao/Ac shows a darker tone on the 7 channel than in adjacent Aa areas; in this case the darker color may be due to the presence of laterite crust fragments on the surface of the dissected areas This matter needs further investigation.
On AP's the units are easily separated in the stereoimage due to their different relief. In addition the absence of the "rizamiento" pattern characteristic of Aa serves as an easy guide for distinction,.

Soils: For Ao there is a dominance of oxic haplorthents on the slopes that grade through sapric tropepts to the typic well drained oxisols of the hillocks. Entic and sapric tropepts occur around the outcrops of indurated plintite gravel.

In Ac sapric tropepts with a hardened plintite gravel layer close to the surface are dominant alternating with oxic haplorthents. Depressions may have aeric plintic normaquepts.

Reliability: Since most limits are inferred from characteristics of the drainagepattern which in turn does change gradually, a lot of inclusions of Aa will occur. Tone differences of these areas with Aa though locally helpfull are not consistent and need further investigation.

Remarks: Here too repetitive coverage may turn out to be usefull since in extreme situations of drought vegetation differences between these areas and Aa will be more marked

Unit Av

Occurrence: As major drainageways in the high plains S. of the Meta river.

Aspect: On ERTS imagery these show up very clearly both in the 5 and 7 channels. The gallery forest shows, just as for the unit Ae, dark on channel 5 and light on channel 7. The watercourses meandering within these small floodplains show well on the 7 channel. The major ones show their complete streambed while the minor ones, the channel of which is partly obscured by vegetation show as a "string of pearls". The latter probably due to the fact that the small units of water are less than the minimum picture element and consequently show up enlarged. Most streambeds could probable be reconstructed completely, within this unit Av, but for cartographic reasons no attempt was made, to show them.

On AP's these units are identified by their level topography and characteristic galery forest.

Soils: Humic normaquox of clayey textures that limit with aquic tropepts and with well drained psammentic oxisols.

Reliability: Comparing AP's we may conclude that this unit is accurately delineated. Since the vegetation is the factor on which the galery forest-boundary has been shifted slightly due to burns.

Unit Vb

Occurrence: In the valleys of the main rivers along the streambed.

Aspect: On ERTS imagery this unit shows a rather light tone on the channel 7 and a rather dark one on channel 5. On the latter channel the tone is variable according to the occurrence of forest or shrub. A difference which does not show up in the 7 channel.

On aerial photographs this unit is easily separated in the stereoimage due to its position, flat topography and the ocurrence of numerous small streamchannels. The color tone and texture indicative of shrub and forest respectively serve as an added guide.

Soils: Entisols and entic tropepts on point bars and levees; aeric normaquepts are dominant in the low parts with humic subgroups in the depressions.

Reliability: At certain places in the alluvial plain there exists a certain aeolian influence (Es and Er). These units were not detected on the ERTS imagery so that the unit indicated as Vb on the map may contain units of Es and Er.

In the aforementioned areas with aeolian influence the escarpment separating the unit from adjacent better drained areas is poorly expressed resulting in low contrast on the images and consequently inaccurate boundaries.

Remarks: With repeated ERTS coverage it is quite well possible that the delineation of Vb from Er can be improved especially if coverage includes high flood situations.

Unit Tv

Occurrence: As small units (terrace remnants) within the Meta floodplain mostly adjacent to the escarpment of the high plain.

Aspect: On ERTS imagery of channel 7 these units show up as dark colored patches within the light grey tones of the galery forest of unit Vb. They contain many open waterbodies. In the channel 5 they cannot be distinguished.

The dark color of these units is probably due to the poor internal drainage of its soils which are mostly of a heavy texture.
On AP's these terrace remains are characterized by a lower probably denser shrub vegetation which contrasts with the higher gallery forest of unit Vb.

Soils: The lagoons of this unit are surrounded by typic normaquepts and aeric humaquepts of clayey textures; aeric plinthic normaquepts characterize some levees and borders of escarpments, while the albaquox ocupy those parts of the terrace that suffered aeolian influence.

Reliability Comparison with the existing soil map shows that some units appear strikingly clear in the ERTS image while others can only be inferred with difficulty from the open waterbodies. The aforementioned aeolian influence which is difficult to distinguish from Vb makes errors in delineation of certain units probable.

Remarks: ERTS coverage from a high flood situation would probably make the delineation of these units more accurate.

Unit Em

Occurrence: Small patches of longitudinal dunes, blown out from the major rivers and occurring on the S. river shores either in the floodplain or invading the high plain.

Aspect: On ERTS imagery especially in the 5 channel these dunes show up as light colored elongated patterns with a clear NE-SW orientation. The poorly drained areas between the dunes are easily identified on the 7 channel, where they show up as dark colored streaks. The 5 channel shows the depressions as well due to vegetation differences though with less contrast. On AP's the same features outlined above together with the characteristic relief visible in the stereoimage serve to identify this unit.

Soils: Ultic and typic quarzipsamments on the dunes that grade through aquic haplorthents to humic normaquepts of coarse loamy texture in the depressions.

The transitions towards the solifluction rills have aeric plinthic normaquepts.

Reliability: Though one unit identified in the sample strip of AP's was missed in the ERTS interpretation, we are rather confident that most major units have been identified and properly delineated, since the units generally have a strong contrast with their surroundings and a predictable position.

Unit Er

Occurrence: Within the eolian plain mainly N. of the river Meta in better drainage positions along drainageways and escarpments.

Aspect: In the eolian plain N. of the river Meta these units show up as light colored strips along drainageways on the 7 channel ERTS image. In the small patches S. of the Meta river this unit could not be identified in the Es patches which as a whole are difficult to recognize within the floodplain.

On AP's they are identified by their position within the aeolian plain and by their lack of solifluction rills.

Soils: Typic tropepts of fine silty texture that change towards the drainage ways into the typic subgroups of the well drained oxisols of fine loamy texture. Towards the aeolian plain aeric plinthic normaquepts appear.

Reliability: For the area S. of the Meta very low. The area N. of the Meta where these units have a major extension looks more promising as far as the identification and delimitation of these units is concerned.

Unit: Es

Occurrence: As level poorly drained plains mainly N. of the Meta river.

Aspect: On ERTS imagery N. of the Meta river these areas are distinguished by a dark mottled tone in the 7 channel to a lesser extent this mottling can be observed in the 5 channel too. The small patches that occur S. from the Meta river mainly within the floodplain are not easy to identify and very difficult to separate from unit Tv. After consulting the existing soil map, identification is possible but delineation of minor patches without this aid seems troublesome. In the AP's these units are easily recognized due to the occurrence of "escarceos" (solifluction rills). Confusion between Es and As does not occur since both units have very different positions.

Soils: Dominance of albaquox with fine loamy and clayey textures in the level parts; transitions towards dunes include oxic haplorthents. In areas with a slight slope towards drainage ways aeric and aeric plinthic normaquepts are found. Very seldomly found are the plinthic subgroups of the well drained oxisols.

Reliability: The small patches occurring S. of the Meta river cannot easily be identified and consequently occur as inclusions in unit Vb. Confusion with Tv is also possible.

Remark: ERTS coverage for high flood situations could help in solving the identification problems.

Conclusion

Resuming we may state that most of the important units of an existing 1:250,000 reconnaissance soil map could be extrapolated successfully into an unknown similar area using ERTS imagery in conjunction with sample strips of aerial photography. In those cases where delineations were insatisfactory it is to be expected that repeated ERTS coverage could improve the results. The resulting map shows sufficient detail to justify a publication scale of 1:500.000. It can be classified as a soil map which is in between exploratory and schematic. With repeated ERTS coverage and some field work it may be improved to a soil map which classifies in between exploratory and reconnaissance. Since these maps are usefull in the first stages of planning in remote undeveloped areas it is stressed that the application of conventional photointerpretation techniques (physiographic analysis) on ERTS imagery can yield significant practical results especially in the developing countries.

Bibliography

1. Buringh, P. The application of aerial photographs in soil surveys. In: Manual of photographic interpretation. Washington, American Society of Photogrammetry, 1960. pp. 633-666.

2. Elbersen, G. W. Influencias volcánicas en los Llanos Orientales de Colombia. In: Cuarto Congreso Latinoamericano de la Ciencia del Suelo, Maracay, Venezuela, Noviembre, 1972.

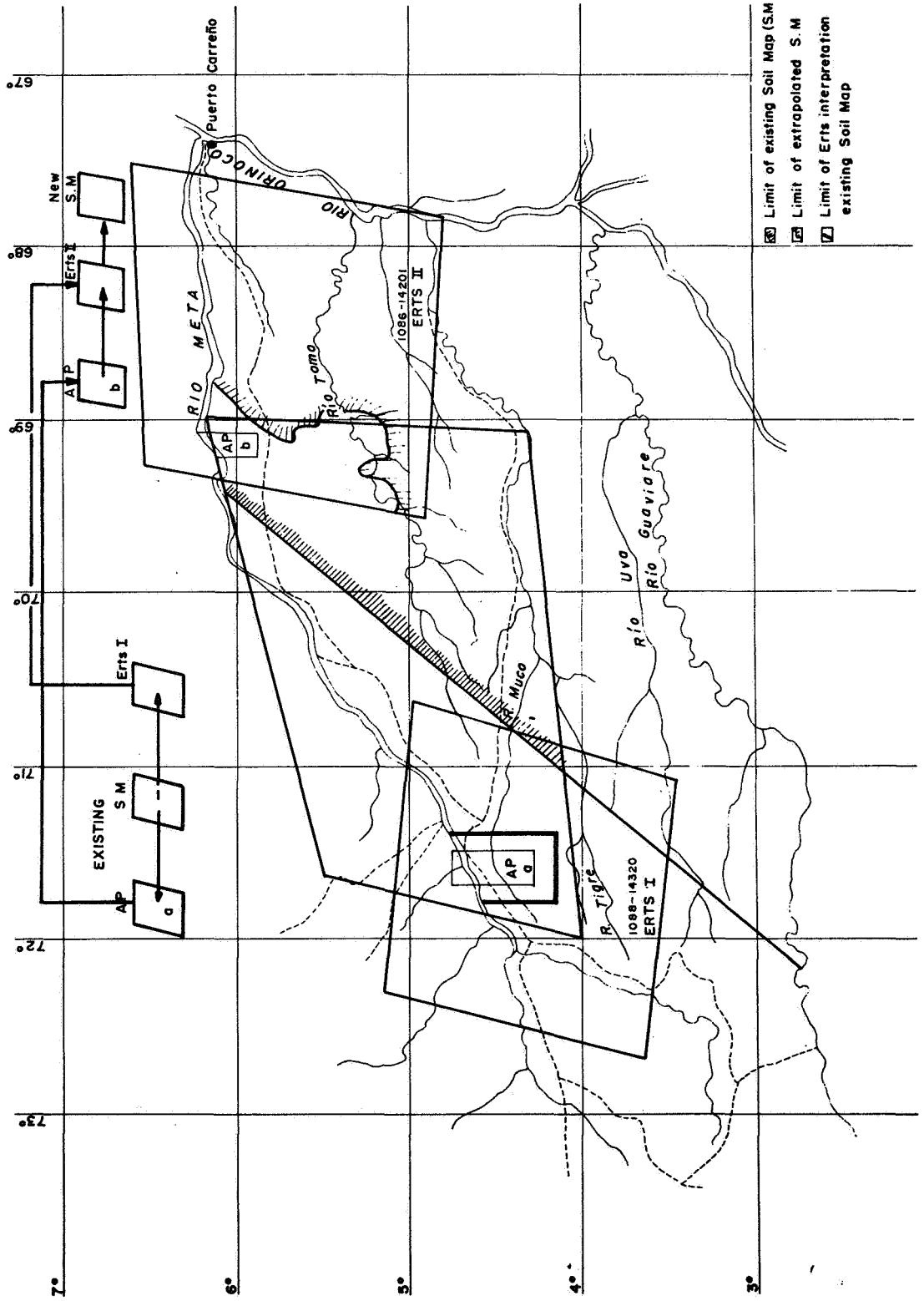
3. Goosen, D. Algunos fenómenos de inestabilidad física en suelos planos de América Latina. In: Cuarto Congreso Latinoamericano de la Ciencia del Suelo, Maracay, Venezuela, Noviembre, 1972.

4. Goosen, D. Physiography and soils of the Llanos Orientales de Colombia. Enschede, International Training Centre for Aerial Survey and Earth Sciences Series B 64. 1971.

5. Guerrero R. Soils of the Colombian Llanos Orientales. Composition and Classification of selected soil profiles. Thesis Ph.D. Agr. Raleigh, North Caroline State University, 1971.

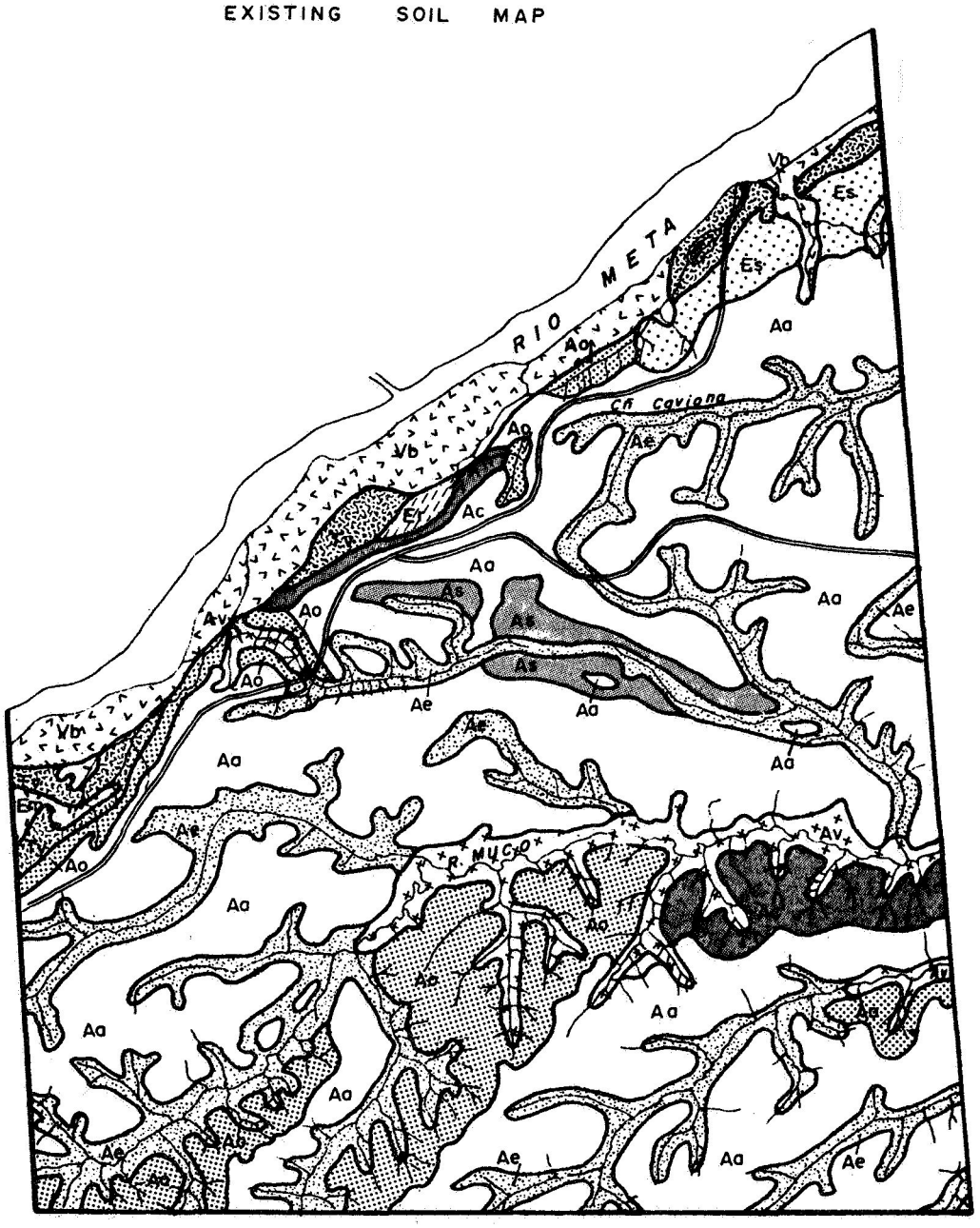
6. ORGANIZACION DE LAS NACIONES UNIDAS PARA LA AGRICULTURA Y LA ALIMENTACION (FAO). Reconocimiento edafológico de los Llanos Orientales de Colombia. Roma. FAO/SF 11/COL. 1966.

* * * * * *


Limit of existing Soil Map (S.M
Limit of extrapolated S.M
Limit of Erts interpretation existing Soil Map
Puerto Carreño
ORINOCO
RIO
RIO META
Río Tomo
1088-14201
ERTS II
Río Uva
Río Guaviare
Río Muco
R. Tigre
1088-14320
ERTS I
AP
a
b
New S.M
Erts II
Erts I
EXISTING S M
67°
68°
69°
70°
71°
72°
73°
7°
6°
5°
4°
3°

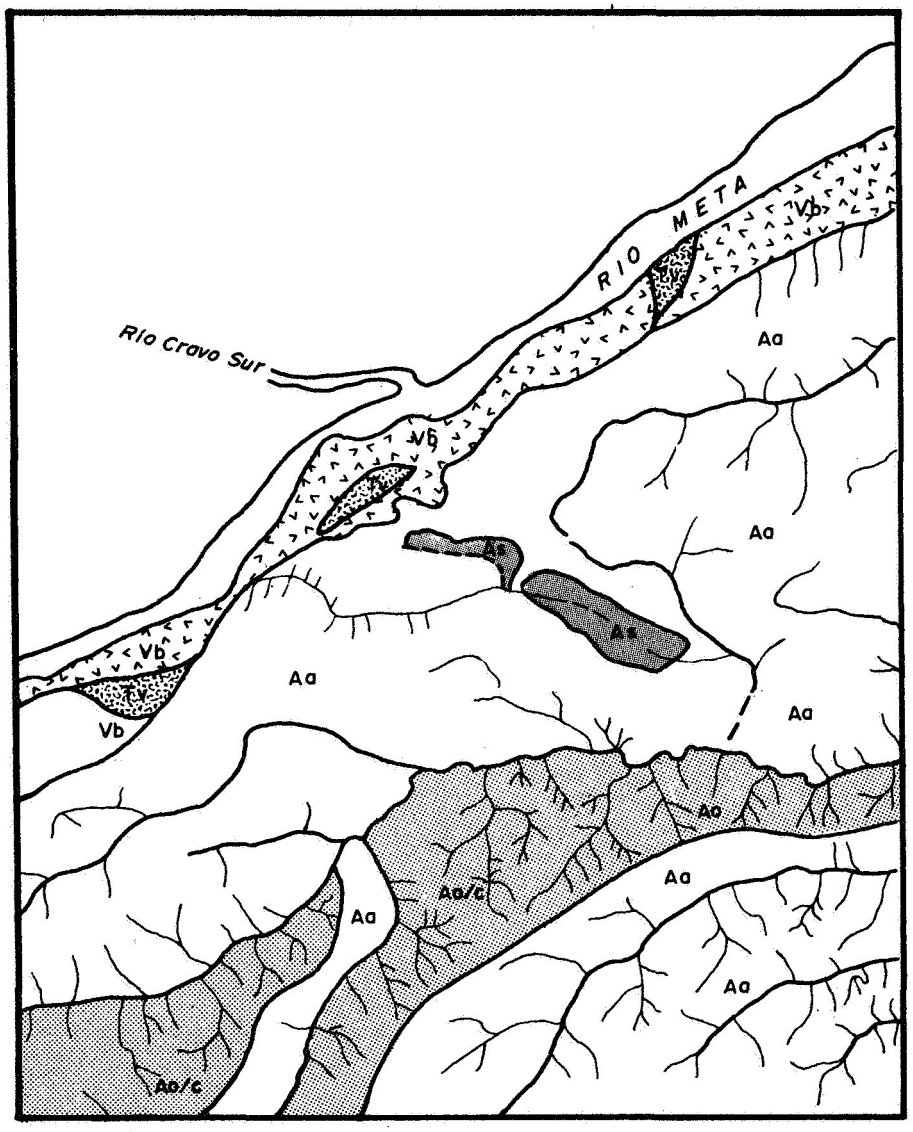
LEYENDA	LEGEND
Terrazas Aluviales	**Alluvial Terraces**
Tv Terrazas Bajas	Low Terraces
Llanura Eolica	**Aeolian Plain**
Em Medanos	Dunes
Es Llanura Eolica con "Escarceos" pobremente drenada	Aeolian Plain with "Escarceos" poorly drained
Er Rebordes de Caños y Barrancos bien a imperfectamente drenados	Borders of Streams and Escarpments well to imperfectly drained
Aluviones Recientes	**Recent Alluvium**
Vb Vegas bien a pobremente drenados con alto peligro de inundación	Floodplains well to poorly drained with a high inundation hazard
Altillanuras	**High Plains**
Aa Altillanura Plana bien y moderadamente bien drenada	Level High Plain well and moderately well drained
As Altillanura Plana moderadamente bien a pobremente drenada	Level High Plain moderately well to poorly drained
Ao Altillanura Ondulada	Undulating High Plain
Ac Altillanura Fuertemente Disectada	Strongly Dissected High Plain
Av Valles Coluvio Aluviales	Colluvial-Alluvial Valleys
Ae "Esteros" muy pobremente a imperfectamente drenados	"Esteros" very poorly to imperfectly drained
Rio o Caño	River or Stream
Límite de unidad	Unit boundary
Bancos	Banks
N Nubes y sombras de nubes	Clouds and cloud shadows

EXISTING SOIL MAP



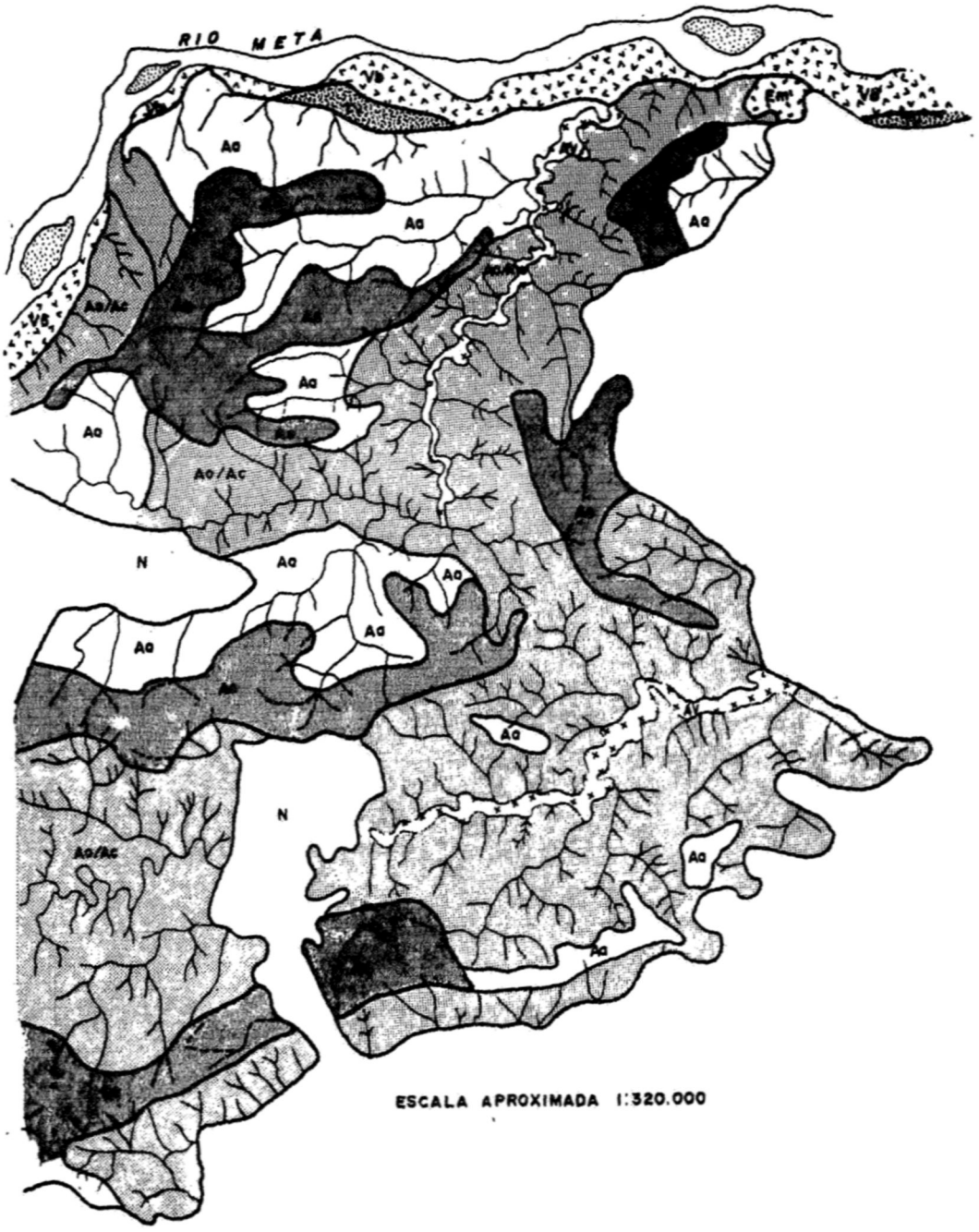
ESCALA 1:250.000

ERTS INTERPRETACION EXISTING SOIL MAP



ESCALA APROXIMADA 1:320.000

EXTRAPOLATED SOIL MAP



Paper A 14

DELINEATION OF MAJOR SOIL ASSOCIATIONS USING ERTS-1 IMAGERY

W. L. Parks and R. E. Bodenheimer, *Departments of Soil Science and Electrical Engineering, University of Tennessee, Knoxville, Tennessee*

ABSTRACT

The delineation of a major soil association in the loess region of Obion County has been accomplished using ERTS-1 imagery. Channel 7 provides the clearest differentiation. The separation of other smaller soil associations in an intensive row crop agricultural area is somewhat more difficult. Soil differentiation has been accomplished visually as well as electronically using a scanning microdensitometer. Lower altitude aircraft imagery permits a more refined soil association identification and where imagery is of sufficient scale, even individual soils may be identified.

INTRODUCTION

The reflectance characteristics of soils are conditioned by many factors. The soil color and soil moisture content are two factors that greatly influence soil reflectance. The medium textured soils of the southeast generally have a reddish or yellowish hue. The reflectance from these soils generally reaches a minimum at a moisture content of 16 to 18 percent by weight (about 2 bars tension). As the moisture content increases or decreases, the soil reflectance increases. Maximum soil reflectance is obtained at a moisture level near or slightly below field capacity (1/3 bar tension).

If soils are to be delineated through the use of aircraft or ERTS imagery, the best conditions are when the soil is void of vegetation and preferably in a freshly tilled state. This condition is generally found only in areas of intensive row crop agriculture or areas where all vegetation is removed from the land each year as in sections of developing countries with extremes in yearly rainfall distribution.

Another means for soil identification is where the soil is covered with a vegetative cover characteristic to a particular soil association or soil group. This characteristic occurs in many forested areas but may also be found in other types of vegetative cover. In such cases the soil associations are delineated through the reflectance characteristics of a reasonably uniform type of vegetation possessing the same boundaries as the soil associations. The identification of vegetation types through reflectance characteristics is quite widely known and used.

METHODS OF IMAGERY ANALYSIS

Channel 7 ERTS-1 imagery in 9½ inch transparencies was used in these studies. After visual analysis, selected areas are analyzed through the use of a high speed digital scanning microdensitometer and an IBM 360/65 computer with the appropriate software developed for this type of analysis. A 25 micrometer raster was used for scanning.

RESULTS AND DISCUSSION

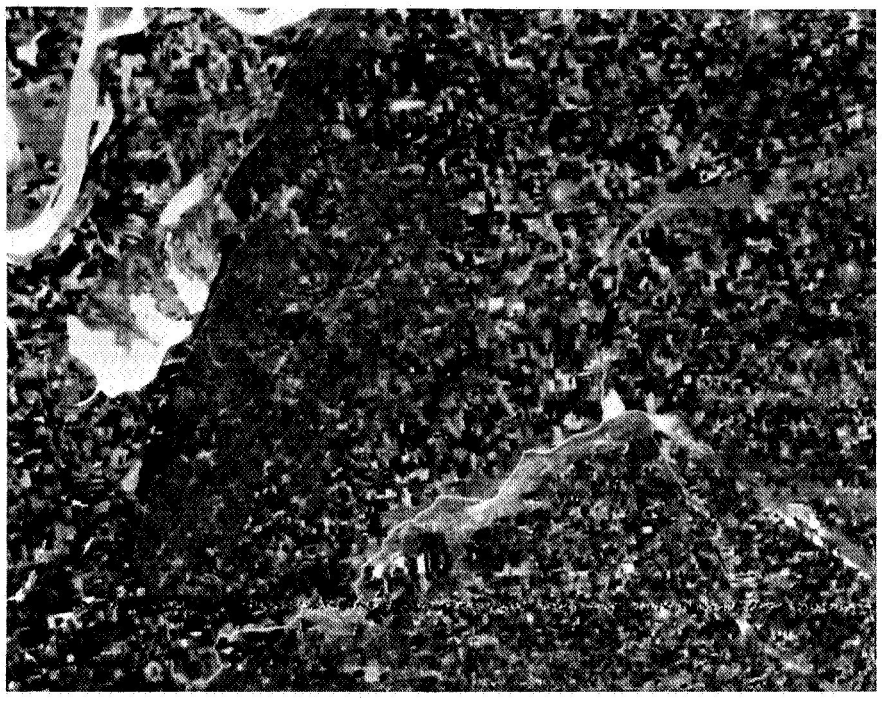
The example reported herein is a case of soil association delineation through the reflective characteristics of a fairly uniform cover of vegetation. In this particular case the Memphis soil association may be identified in Obion County using ERTS imagery. This Memphis soil association occurs in the western edge of the loess that covers most of West Tennessee. It is known as the "bluffs" and occurs at the break between the loess soils and the delta soils of the Mississippi floodplain.

Figure 1 shows a photograph from Channel 7, ERTS-1 imagery of 1, October, 1972 and a soil association map of Obion County. The orientation features in the photograph are Reelfoot Lake and the Mississippi River in northwest corner and the Obion River that crosses the county from northeast to the southwest. The map and picture scale is 1 inch equals about 8.5 miles.

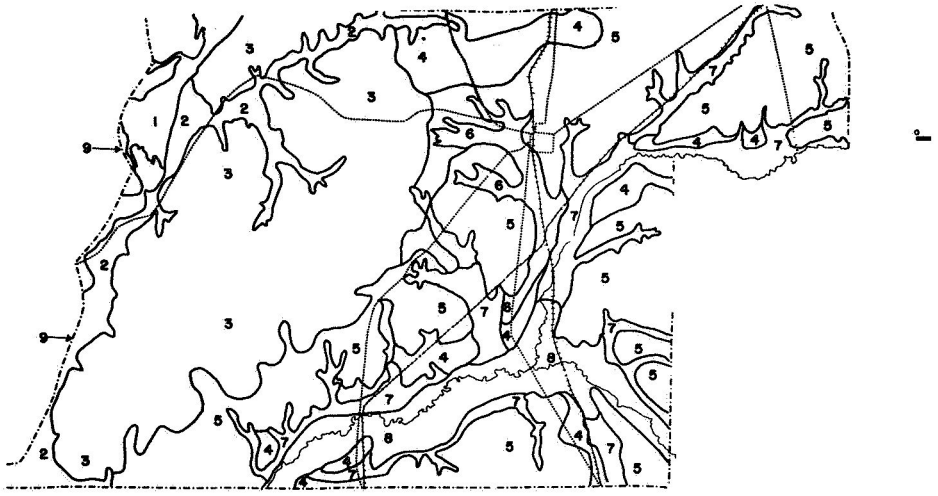
The Memphis soil association is the large block (No. 3) in the western portion of the county. A small block of the Memphis association is found in the northwest portion of the county and extends across the state line into Kentucky. The area has a fairly uniform vegetative cover of pasture grasses and this characteristic permits its delineation through ERTS-1 imagery. Small cultivation and wooded areas are found throughout the area but most of these are not of sufficient size to be detected. The areas east of the large Memphis block is one of intensive row crop agriculture.

The computer printout of the large block of the Memphis association is too large to be adequately shown in one photograph. Figure 2 shows a small portion of the computer printout that separates Reelfoot Lake, the Adler-Convent-Falaya, and the Memphis soil associations. Figure 3 shows the computer printout of the Obion River and the adjacent Waverly-Swamp association.

These findings demonstrate the feasibility of delineating major soils through vegetative cover characteristics common to the soils in question. Channel 7 provides the most information for studies of this type.



From ERTS-1, Obion County, Tennessee, 1, October, 1972



Obion County soil associations: 1. Bowdre-Sharkey, 2. Adler-Convent-Falaya, 3. Memphis, 4. Routon-Calloway-Center, 5. Grenada-Loring-Center, 6. Fountain-Dekoven, 7. Falaya-Waverly-Collins, 8. Waverly-Falaya-Swamp, 9. Iberia-Sharkey.

Figure 1. ERTS-1 imagery and soil association map of Obion County, Tennessee showing delineation of the Memphis soil association.

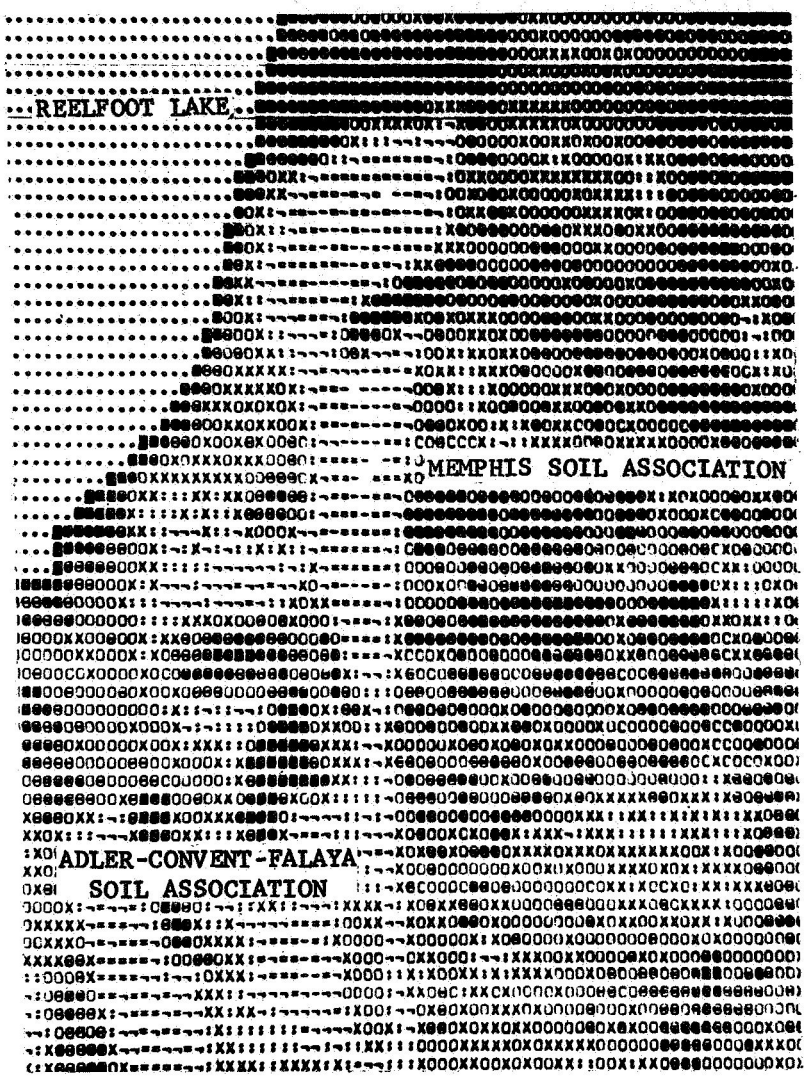


Figure 2. Computer printout from ERTS-1 imagery evaluation separating Reelfoot Lake, the Adler-Convent-Falaya, and the Memphis soil associations.

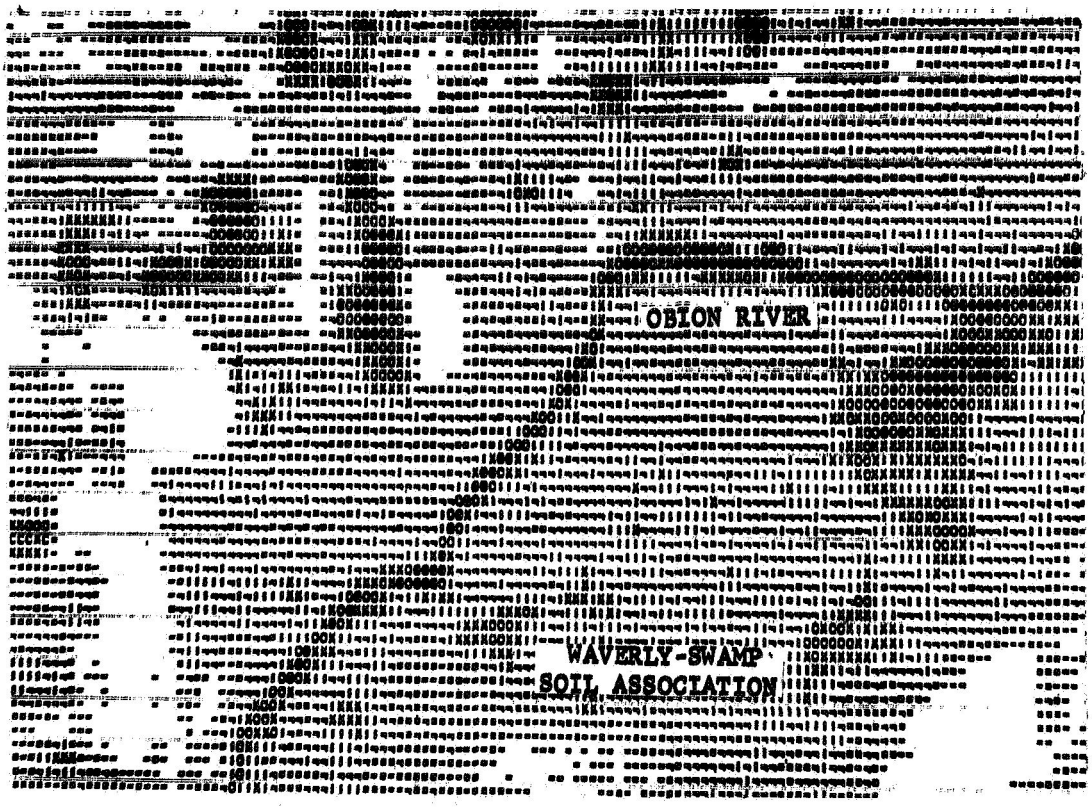


Figure 3. Computer printout from ERTS-1 imagery evaluation showing the Obion River and the adjacent Waverly-Swamp area.

Paper A 15

EVALUATION OF REMOTE SENSING IN CONTROL OF PINK BOLLWORM IN COTTON[1]

Virginia B. Coleman, Claude W. Johnson and Lowell N. Lewis, *Citrus Research Center/ Agricultural Experiment Station, Department of Geography, and Citrus Research Center/ Agricultural Experiment Station, University of California, Riverside, California 92502*

ABSTRACT

The purpose of our project is to identify and map cotton fields in the southern deserts of California. Cotton in the Imperial, Coachella, and Palo Verde Valleys is heavily infested by the pink bollworm which affects both the quantity and quality of the cotton produced. The California State Department of Agriculture, therefore, has regulated the growing season of cotton by establishing planting and plowdown dates. These procedures ensure that the larvae, whose diapause or resting period occurs during the winter months, will have no plant material on which to feed, thus inhibiting spring moth emergence.

There are approximately 800,000 acres of cotton in California and they are mapped yearly by ground survey teams. A more practical means of accomplishing that objective seemed necessary and satellite data from ERTS-1 was considered a viable alternative.

The underflight data from the U-2 aircraft has shown that we can detect the differences between a growing, a defoliated, and a plowed down field providing that we know where the fields are. The ERTS-1 multispectral scanner (MSS) data are being analyzed using an I^2S (International Imaging Systems) optical color combiner to determine which combinations of dates and colors will identify cotton fields and thus provide the data needed to produce maps of the fields for the forthcoming cotton season.

1. BACKGROUND

Our study sites, the Imperial, Coachella, and Palo Verde Valleys, are heavily infested with pink bollworm (Fig. 1 and 2). The pest affects both the quantity and quality of cotton produced by boring into the cotton boll and consuming the cotton seed, thus allowing other pests and diseases to enter the boll and either destroy the cotton fiber or prevent the boll from opening. Research is continuing on chemical and biological controls, but a satisfactory system has not been found. At present, the



Fig. 1. The Coachella Valley north of the Salton Sea, and the Imperial Valley south of the Salton Sea in southern California.



Fig. 2. The Palo Verde Valley along the Colorado River in southern California.

only effective means of control appears to be the plowdown procedure. This method provides that the pink bollworm larvae are allowed no plant material on which to feed during the diapause or resting period in the winter months. The California State Department of Agriculture has, therefore, established host-free periods for all the cotton districts in California. Cotton may not be planted until a given date and it must be picked, the remaining plant material shredded and plowed underground, and all gin trash disposed of by a certain date. Thus, the pink bollworm larvae are deprived of food during the diapause stage and spring moth emergence should be greatly reduced.

There are approximately 800,000 acres of cotton grown annually in the State of California. All the fields are mapped by ground survey teams and then monitored throughout the season to ensure compliance with state law. This procedure is extremely time consuming and therefore restricts or prevents the performance of other tasks vital to the rest of California's agriculture.

The pink bollworm has not yet become a problem in the San Joaquin Valley where 90% of California's cotton is grown, but there are indications that the pest may soon become a major problem. A more efficient means of monitoring cotton fields than ground survey is needed in order to prevent the spread of the pink bollworm. The use of satellite data appears to be the only feasible alternative at this time.

2. METHODS OF INVESTIGATION

Two methods of investigation are being employed to identify and map cotton fields. The first method involves the use of the crop calendar. Claude Johnson (Department of Geography, University of California at Riverside) is using this procedure to identify and map all crops in the Imperial Valley.

Essentially, the procedure is to map the status of each field, i.e., bare, wet, cropped, plowed, or harvested, from ERTS-1 imagery. A statistical analysis is then performed by computer to establish the probability of a given crop in a given field at a given time. For example, fields that are bare in August, in vegetative crop by September and October, and are not harvested until June and July are sugar beet fields. Cotton, because of its state regulated season which is coincident with no other crop, is considered to be easily identifiable.

The second method, which is being used for the Coachella and Palo Verde Valleys, relies principally on all bare fields evident in January and February photography. All fields which are bare at these times could potentially be cotton fields (Fig. 3). Cotton cannot be planted in the Coachella or Palo Verde Valleys until February 28, thus any crops appearing prior to that date in any of the bare fields are not likely to be cotton. Bare fields which begin to show crops in late March and early

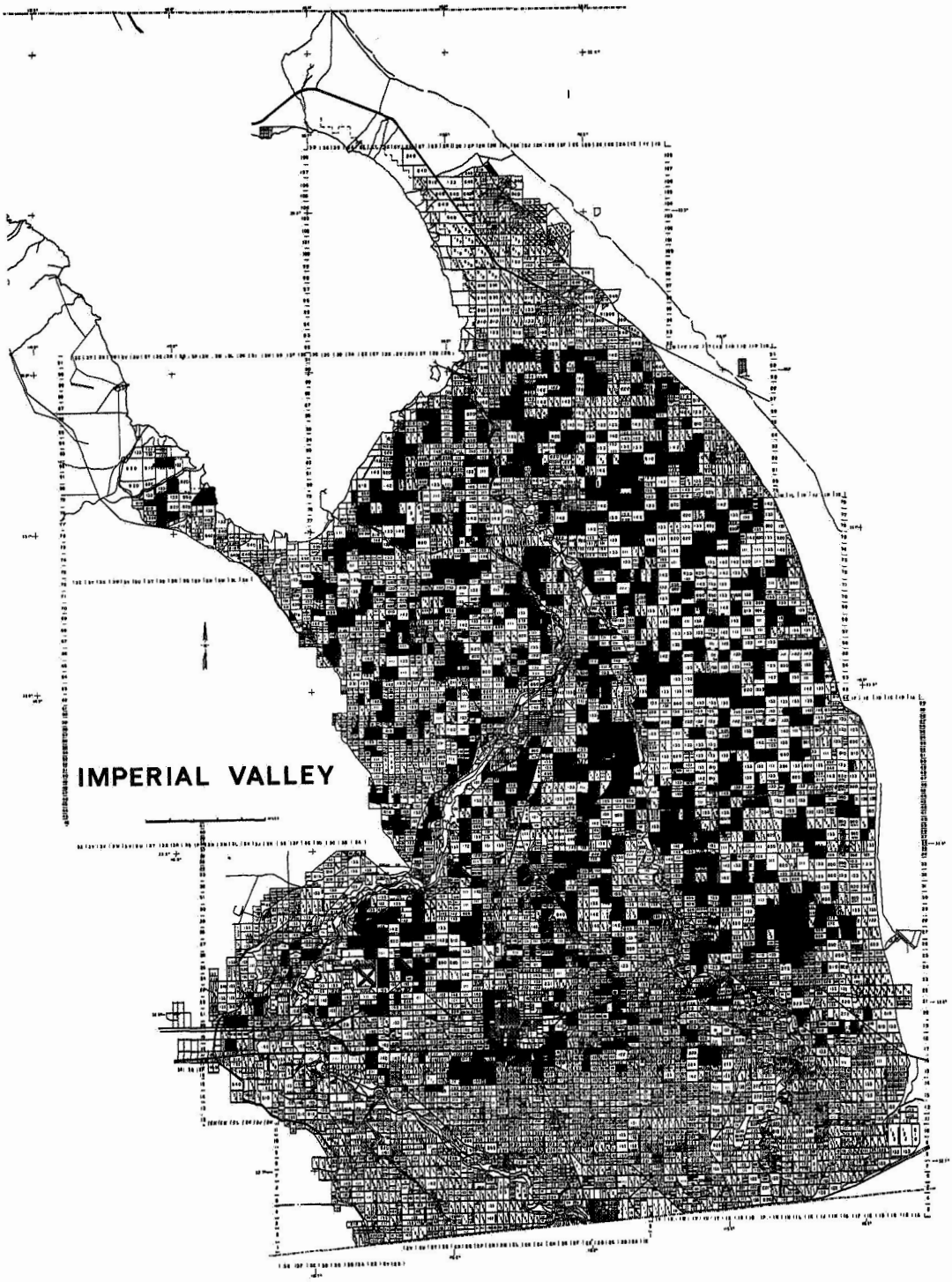


Fig. 3. Potential cotton fields mapped from ERTS-1 imagery, Dec. 30, 1972.

April are most likely to be cotton. Only minimal field checking would be necessary for fields less than forty acres since cotton is not usually planted in smaller acreages.

The plowdown date, December 15 in all three valleys, is, of course, the most critical date. The various stages of cotton harvesting, defoliation, picking, and shredding, are discernible on the U-2 underflight photography but are not identifiable on ERTS-1 imagery. However, once the location of all cotton fields is known, it is possible to tell whether or not a field is bare on December 15 because a plowed field can be easily identified on ERTS-1 imagery.

3. IMAGERY

The U-2 underflight photography and the ERTS-1 data have been very complementary. The U-2 color infrared (CIR) photography taken from the RC-10 camera has been particularly useful for updating base maps and for identifying the various stages of cotton harvesting: lavendar for defoliated and picked fields, pinkish brown for shredded fields, and dark grey for plowed fields. The photography also provides a check on ERTS-1 imagery interpretation to ensure accuracy of the status of a given field.

Color combining of ERTS-1 data is considered essential to this project. The 9" x 9" positive transparencies are color conbined using the Diazochrome process. In this method, bands 4, 5, and 7 are exposed respectively to yellow, magenta, and cyan Diazochrome acetate sheets, then developed in ammonia vapor. The sheets are then superimposed and a simulated CIR transparency is produced. The second method uses the I^2S (Internation Imaging Systems) optical color combiner. Bands 4, 5, and 7 from the 70 mm positive transparencies are superimposed optically to provide simulated color infrared.

The ERTS-1 data in addition to being color combined to simulate CIR can also be combined in other ways to give additional information. For instance, if the percentage of change from cropped to harvested fields between one month and another is needed, the following procedure can be used. Band 7 from two different months, in this case September and December, are color combined in green and red, respectively. The combined product gives the following results: bright green fields has crops in September, but not in December; bright red fields - crops in December but not September; light colored fields indicate a crop in the field at both times, but there has been a change in status, i.e., a crop is beginning to emerge or has recently been harvested; dark colored fields indicate either no change in the status of a crop or that a field has been fallow for the entire period.

4. RESULTS

Although complete results will not be available until the March and April imagery have been analyzed, we are expecting to achieve 80-90% accuracy in identifying cotton fields for the coming season. Maps showing the location of cotton fields in each of the three valleys will be produced in late April or early May and distributed to each agricultural commissioner. The reliability of the satellite maps will be tested by their ground survey teams and if the accuracy is considered tolerable, the commissioners will consider satellite mapping to be an efficient alternative to their present methods and would consider using this method on a regular basis.

The real test of these techniques will come when they are tested in an area such as the San Joaquin Valley which, like many places in the world, is not uniquely cloud-free as are the deserts of southern California. If these techniques, the use of satellite data with minimal underflight and ground survey support, can be used reliably in the San Joaquin Valley, then the use of satellite data for agricultural management programs becomes a practical tool for the user and releases a great deal of manpower needed for other tasks.

[1]The authors gratefully acknowledge the support provided by NASA for Contract No. NAS5-21771 awarded to Lowell N. Lewis.

Paper A 16

APPLICATION OF ERTS-1 IMAGERY & UNDERFLIGHT PHOTOGRAPHY IN THE DETECTION AND MONITORING OF FOREST INSECT INFESTATIONS IN THE SIERRA NEVADA MOUNTAINS OF CALIFORNIA

Ralph C. Hall, *Natural Resources Management Corporation, 2150 Shattuck Avenue, Berkeley, California*

ABSTRACT

Preliminary analysis of ERTS-1 imagery in a rugged mountain area in the Sierra Nevada Mountains of California indicates some promising possibilities of detecting two types of insect infestations as our primary objective and secondary detecting and mapping other features such as timber or untimbered areas; timber stand density; principal stream courses, mountain meadows, lakes, massive rock outcrop and domes, riparian vegetation, grazing land and possible glaciers. We have used and found exceedingly useful, NASA underflight RC-10 imagery.

1. INTRODUCTION

In the general field of pest management early detection and monitoring of insect outbreaks are of paramount importance in the protection and management of our natural resources. If an insect pest reaches outbreak proportions before it is detected, supression measures become very costly, and even if effective, are applied only after the host crop has been severely damaged. This is particularly true of forest insect outbreaks in remote areas.

The longtime, overall objective of our study was to develop space data acquisition methodology which would permit rapid, accurate and comprehensive detection and monitoring of insect infestations and other causes of physiological stress and morbidity in vegetative ecosystems, through the use of ERTS-1 imagery alone, and when supplemented by underflight photography. It was hoped that this methodology, when fully developed, would eliminate the present need for expensive, patchwork aerial and ground surveys and would provide a continuously up-dated basis for operational programs of control and salvage, and would permit frequent evaluation of economic and ecological impact of existing and impending infestations as a basis for determining broad research and control strategies.

In addition to ERTS-1 imagery we also had available, through contract with Earth Satellite Corporation, color infrared, for the total test sites at a scale of 1/18,500, and sample coverage of about 10 percent of the area in color and color infrared at a scale of 1/5,000 in

9" x 9" transparencies, as well as U-2 support covering the entire target area. Earth Satellite Corporation also subcontracted on some of the photo interpretation and multistage sampling technique.

2. THE TEST SITE

The test site selected was in the Sierra Nevada Mountains of California where we had long standing research evidence of the existence of heavy damage by the mountain pine beetle, Dendroctnus ponderosa, (Fig. 1) and reasonable expectations of an outbreak of the lodgepole needle miner, Recurvaria miller, (Fig. 2), developing during the course of the study.

The area is centered in the Yosemite National Park and represents some of the most rugged mountainous terrain in the West; with high elevations ranging from about 7,500 to more than 12,000 feet, and subalpine coniferous forests in which lodgepole, the host species, was the dominant tree species. (Fig. 2).

Because of the wide range in sizes of the infested timber blocks, it should offer opportunity to determine the smallest area consistently identifiable from, (a) ERTS-1 imagery, (b) from conventional aerial photography, and (c) from a combination of both.

3. PEST CHARACTERISTICS

The two dominant pest species were the lodgepole needle miner and the mountain pine beetle. The lodgepole needle miner is one of the most destructive defoliators of some of California's most scenic mountain forests, and its feeding causes the foliage to turn brown. The caterpillars of this inconspicuous moth feed within the pine needles, and have a two-year life cycle, with maximum damage and discoloration of the needles occurring at the end of the second year. In this study, maximum brown discoloration is expected to be late spring, 1973.

The mountain pine beetle is one of the most destructive bark beetles in the West, particularly in lodgepole pine. The trees are killed by the feeding of the larvae in the cambial area, causing the foliage to change from green to red. The second year after death, the bark beetle trees change to a gray color with most of the foliage gone.

4. PROCEDURE PRIOR TO THE RECEIPT OF ERTS-1 IMAGERY

Aerial photos in color and color infrared were obtained, processed and interpreted at scales of 1/18,500 for the whole area and at 1/5,000 for sample areas representing differing degrees of damage. Ground truth was then obtained by careful analysis and classification of each tree as to its condition, on a series of four-acre plots selected at random.

Analysis of these data permitted the target area to be classified into damage units as light, medium, and heavy for both needle miner and



FIGURE 1

An example of almost total kill of mature lodgepole pine (Ghost Forest) in Yosemite National Park as a result of a combination of needle miner and the mountain pine beetle. This would represent our designated heavy damaged area.



FIGURE 2

An example of heavy damage to lodgepole pine from the needle miner in an earlier outbreak in the Tenaya Gap Area. Light colored trees in the foreground damaged; darker ones in the background are non-host mountain hemlock. Note the rugged topography and foreground which is almost solid rock.

the bark beetle. Due to an early snow storm, only about 90 percent of the ground truth was collected and analyzed prior to the receipt of the ERTS-1 imagery.

5. INTERPRETATION OF U-2 SUPPORT

We had U-2 photo coverage in 70mm black and white, April, May and June, 1972, but found this of little use for detecting insect damage. We received our first RC-10 aerochrome infrared photos on December 3, which were flown on July 27, 1972, and made a comparison of these with our own 1/18,500. We found that using the original 1/120,000 scale we could detect many, but not all of the areas of heavy and medium damage. We found by enlarging the U-2 photos to approximately the same scale as our 1/18,500, that in this particular test area, we were able to detect all degrees of damage detectable on our original 1/18,500. The main contrast in this test was between a heavily damaged area and one with little or no damage. We need to run further tests with the enlarged U-2 under stereo to determine if we can identify individual trees, which is possible on our original 1/18,500 color infrared, and to explore other areas of different degrees of damage. We feel encouraged by these preliminary tests and are hopeful that the U-2 by itself will prove to be an important tool in forest insect detection and monitoring.

Our only criticism of the RC-10 was that the images were generally dark, and we failed to get good detail in deep canyons and shaded northern slopes. We would suggest in future U-2 support in mountainous country that the exposure be changed to compensate for the generally darker target areas.

We ran some tests on the same film strip in the Bay Area, and the exposure appeared to be extremely good. Our tentative conclusion is that black and white is of little value in detecting forest insect damage under the conditions of our test.

6. ERTS-1 IMAGERY INTERPRETATION

Because we were delayed in receiving our ERTS-1 color infrared transparencies until December and had difficulty getting enlarged prints of our target area, we have only partially analyzed our data. For this reason, our conclusions must be considered as tentative. We have had four men interpreting the imagery including: Dr. Thomas Koerber, from the Pacific Southwest Forest & Range Experiment Station; Dr. B. H. Wilford and Dr. R. C. Hall, from Natural Resources Management Corporation, and Stephen Daus, from Earth Satellite Corporation. The first three named are all experienced forest entomologists with considerable experience in interpretation of insect damaged areas from conventional aerial photos. Daus is a forestry graduate and an experienced photogrammetrist. We also had the close cooperation of Ralph S. Mac Farland, the Chief Photographer from the Pacific Southwest Forest & Range Experiment Station who aided greatly in image enhancement.

Interpretation was done partly in stereo in the original NASA positive transparencies, but we were unable to cover the whole area in stereo. We worked with enlarged color prints from these ranging in scale of one inch = 4.5 statute miles to one inch = 1.25 statute miles.

The concensus of all interpretors was that our scale of one inch = 1.25 statute miles was the best of the series, and we were able to identify three degrees of tree mortality, light, medium, and heavy (Fig. 3) with a reasonable degree of certainty. It should be pointed out, however, that this test represented only one time phase, September 16, 1972, with optimum cloud free conditions. We are scheduled for ERTS-1 imagery in late June and again in August. We expect little change in color rendition in our tree mortality areas, but do expect more contrast in our defoliated areas, as well as drastic changes in mountain meadows and grassy areas interspersed in the timber. At the time of our September imagery, our mountain meadows were light brown, and we expect these areas to be dark green by June.

Time did not permit the planned differentiations of defoliated areas where we are able to classify these into light, medium, and heavy damage.

We were able to differentiate the bark beetle damage areas principally on the basis of color differences. We have classified these colors as follows:

Imagery: ERTS-1 NASA Original Color Transparancy
September 16, 1972, Yosemite Frame

Classification	Color by Eye	From Munsell Book of Color
Light Mortality	Cherry-red	5R - 5-8
Heavy Mortality	Milk Chocolate Brown	10RP - 4-4
Mountain Meadows	Light Yellow	10YR - 8-8
Lakes	Dark Blue	10B - 2-4
Dome Shadows (resembling lakes)	Black	10B - 2-1

Imagery: Enlargement to scale 1" = 1.25 S.mi.

Heavy Mortality	Moldy-yellow	5YR - 6-4
Medium Mortality	Chocolate Brown	10R - 5-4
Light Mortality	Blood-red	5R - 4-8
Grassy Areas in Timber	Cherry-red	5R - 5-8

7. SIGNIFICANT RESULTS

In our preliminary tests, we are reasonably sure that we can do the following: differentiate areas of heavy damage from those with little or no damage in the lodgepole pine type; non-timbered vs timbered areas; lakes;



Figure 3: YOSEMITE NATIONAL PARK TEST SITE
ERTS-1 Imagery, September 16, 1972
Illustrating bark beetle damage: Upper left, medium; middle, light; and lower right, heavy. Mono Lake, upper left; Tuolumne Canyon, running from top to bottom in center; Tuolumne Meadows, upper center.

Scale: 0 5 10
Statute Miles

rock domes and rock dome shadows, which closely resemble lakes; mountain meadows; pasture and agricultural land; and desert, from the ERTS-1, NASA prepared color transparencies.

We are more confidant of our work with the enlargements of the above imagery to a scale of 1" = 1.25 statute miles, where we believe that we can definitely differentiate between heavy, medium and light damage in a sample area selected where we knew these three conditions existed. U-2, RC-10 compares quite favorably with conventional infrared color photography except in deep canyons and shaded northern slopes.

8. COST BENEFIT ANALYSIS

We have done no significant work on this phase of the problem, but we hope to do so in the near future. We have been experimenting with an in-house system in cooperation with the Pacific Southwest Forest & Range Experiment Station; where we believe that we can speed up the enhancement of ERTS-1 imagery where it can be rapidly interpreted and screened for any suspected massive areas of damage. We will also attempt a comparison of cost with that of the conventional Regional Aerial Survey System.

9. CONCLUSIONS

As a result of our research to date, we can arrive at the following conclusions: (1) If we develop a system which can be expected to replace the aerial survey method we are going to need the same type of experienced observors we are now using in the airplane, particularly if the job is to be done on a visual basis; (2) A photo interpretor with previous experience in detecting insect damage from conventional aerial photos has a definite advantage over a straight photogrammetrist. In other words, he knows better what to look for. We also feel that the U-2 underflight support greatly improves efficiency of detection and except for rare instances, can eliminate the need for any other underflight photography.

We are still a long way from achieving our original objective, but we feel that we are making progress even though it is slow.

Paper A 17

IMPACT OF ERTS IMAGES ON SURVEYS OF FOREST INSECT INFESTATIONS IN COOK INLET BASIN, ALASKA

James H. Anderson*, F. Philip Weber**, John M. Miller*, Enzo Becia† and Roy C. Beckwith††

ABSTRACT

Aerial surveys conducted during the past three summers by the U.S. Forest Service have identified a severe spruce beetle (Dendroctonus obesus (Mann.)) infestation to a 200,000 acre region west of Cook Inlet near the Tyonek Indian Reservation, and additional acreages identified on the Kenai Peninsula in the Kenai Moose Range and adjacent state and private lands. Estimates have been made of two billion board feet of white spruce killed or damaged by the spruce beetle; however, the large areal extent of the spreading infestation presents a difficult task for maintaining surveillance of the extent of the affected trees.

Techniques have been implemented using November 1972 ERTS-1 imagery of the Cook Inlet Basin to stratify damage to White spruce into three levels - healthy, newly killed, and old killed. The three step analysis was performed on the ERTS imagery. A color composite was created using color recombining of the bulk 70-mm transparencies, an optimum color composite was chosen for display and interpretation at 28 times enlargement on a Variscan scanner, and scene radiance differences were analyzed from microdensitometer scans.

As of now we have been able to map the pure spruce stands as being different from the mixed spruce - hardwood stands, and we have been able to map the extent of old killed spruce stands. Work is continuing with other ERTS scenes taken earlier in the growing season where snow was not a problem for the purpose of further stratification of damage in spruce.

*University of Alaska, Fairbanks, Alaska 99701

**USDA Pacific SW Forestry Experiment Station, Box 245, Berkeley, California 94701

†Alaska Department of Natural Resources, Division of Lands, 323 E 4th Avenue, Anchorage, Alaska 99501

††USFS, Institute of Northern Forestry, Fairbanks, Alaska 99701

(PAPER NOT PRESENTED)

Paper A 18

ERTS-1 IMAGERY AND HIGH FLIGHT PHOTOGRAPHS AS AIDS TO FIRE HAZARD APPRAISAL AT THE NASA SAN PABLO RESERVOIR TEST SITE

Robert N. Colwell, *Associate Director, Space Sciences Laboratory, University of California*

INTRODUCTION

Some unusual circumstances currently are combining to produce a condition of critical fire hazard in many parts of California. The hazard is especially great in a very hilly portion of the NASA San Pablo Reservoir Test Site, immediately east of the Oakland-Berkeley metropolitan complex in which nearly 1 million people currently are living and working.

Part of the circumstances which are now of concern had their origins more than 200 years ago with the accidental importation from Spain of various herbaceous annual plants -- especially "wild oats" (Avena fatua). These plants probably were introduced accidentally by the Spanish explorers and missionaries and soon became well established. In fact they now comprise the bulk of the vegetation in most of California's foothill country. In the summer time these annual plants turn from green to golden brown (we never admit that they die) and constitute a great fire hazard.

Another part of the circumstances which currently are contributing to California's fire hazard originated a little over 100 years ago with the intentional importation from Australia of eucalyptus trees (mainly Eucalyptus globulus or "blue gum"). Some say they were introduced by the Australian prospectors who came all the way from "down under" to join California's gold rush. Others point out that the first formal planting of eucalyptus in California was in 1856 and that the main planting was during the period 1910-1913. During that brief period more than 8 million trees were planted by one group alone in the Oakland-Berkeley hills along a 25-mile ridgeline. As will presently be seen these trees can constitute a very real hazard even under normal climatic conditions and an extreme fire hazard under certain abnormal climatic conditions.

The circumstances which have just been described would constitute no greater cause for alarm this year than at any time in the past several years were it not for two remarkable abnormalities of climate which have developed during the past few months in many parts of California and especially in and around the NASA San Pablo Reservoir Test Site.

One of these abnormalities pertains to precipitation. The test site

area, like much of the rest of California, currently is experiencing what has already been termed the "wettest rainy season in history". Consequently the wild oats and other herbaceous annuals are growing more luxuriantly there now than ever before. By the summer of 1973, when such vegetation will have turned brown and become tinder dry, it probably will constitute the largest volume of "flash fuels" that the rangelands in this area have ever known.

The other abnormal climatic factor pertains to temperature. During a 9-day period in mid-December of 1972 the test site area experienced the coldest temperatures in recorded history. Even at the semi-sheltered botanical gardens of the University of California the temperature hovered around 10°C below zero for most of this period. Consequently the frost-susceptible eucalyptus trees, most of them for the first time in their 60- to 100-year old lives, were severely damaged by frost. In fact one estimate indicates that more than 2 million of these trees were killed during the December cold snap. The tall dense eucalyptus timber stands, with their tremendous crown canopies of tinder dry foliage that is loaded with volatile oils, are so flammable as to be regarded by some authorities as virtual "funeral pyres" for the whole Oakland-Berkeley metropolitan complex. With reference to the height of these stands, some of them in the test site area exceed 200 feet. They are reportedly the tallest hardwood trees in the North American continent and perhaps in the entire Northern Hemisphere. The fact that long strips of shaggy bark hang from the trunks and larger branches of these trees adds to the likelihood that fire brands could spread spot fires over great distances. The fire hazard is further increased by the presence beneath these eucalyptus stands of very large amounts of flammable forest litter. In fact in some portions of the area the amount of this litter exceeds 100,000 pounds per acre. The threat to homes that have been built either within or near the eucalyptus stands is obvious enough because of the possibility that fires might start next summer either directly within these stands or in surrounding grasslands from which such fires could readily spread to the timber stands, themselves, and then to the shake-roofed wooden houses.

The threat is believed by some, however, to be even greater than the above facts might indicate, because eucalyptus is a notorious fire type. In its native Australia it has been known to develop "fire storms" capable of producing spot fires at distances of more than 10 miles from the main fire. Among the notable topographic characteristics of the Oakland-Berkeley hills are their steep slopes, deeply incised canyons and elevations in excess of 2,000 feet, all of which make them unusually favorable for the development of such storms. Furthermore, there are times during the summer months when hot dry winds, coming all the way from the Nevada deserts via the hot Central Valley of California, make the situation even more critical. Such winds blow strongly past the Oakland-Berkeley hills and directly from there toward the nearby cities of Oakland and Berkeley. It is in this regard that the high concentration of wooden-roofed houses

in the Oakland-Berkeley metropolitan complex is of great concern. Still fresh in the memory of many of the older residents of the area is the great Berkeley fire of 1923 which, aided by such winds, burned 625 homes, even though the area then was only sparsely settled. There are even some residents who can recall the great San Francisco fire of 1906, which occurred a scant 10 miles across the Bay from the presently threatened area. As for the possible consequences of a "firestorm" which might develop next summer, some authorities consider them to be potentially far more serious than those which occurred in Hamburg, Germany during World War II, snuffing out the lives of 30,000 people.

A series of hearings recently has been held leading to the conclusion that most of the dead trees will have to be removed promptly, but there is a considerable amount of uncertainty as to the magnitude and cost of that undertaking. Estimates range from $4 million upward and there is general agreement that state and federal emergency funds must be obtained. This, in turn, has created the requirement for a quick assessment of the enormity of the problem and has raised the question of whether ERTS-1 imagery or high flight aerial photography might facilitate the task.

TYPES OF IMAGERY USED IN THE PRESENT STUDY

During the past 8 years NASA has flown large amounts of aerial photography of the NASA San Pablo Reservoir Test Site, of which the present area of concern is a part. This photography has included all of the black-and-white film-filter combinations and all of the color films which investigators have considered for possible use in making earth resource surveys. Furthermore it has been obtained at various seasons of the year and at altitudes ranging from less than 1,000 feet to more than 65,000 feet. In addition, side-looking airborne radar (SLAR) images and thermal infrared images (by day and by night) have been obtained of this same area. In fact there is a strong possibility that this area has been the most thoroughly remotely-sensed spot on the surface of the earth.

Since the launch of ERTS-1 in July, 1972, cloud-free coverage of this same area has been obtained on at least 8 different occasions by the ERTS-1 multispectral scanner system and on at least one occasion by its return beam vidicon system.

Perhaps the most useful imagery of all in relation to the present study is that which was obtained almost simultaneously on January 4, and again on January 22, 1973, by both ERTS-1 and a NASA "high flight" aircraft based at the NASA Ames Research Center and covering the entire NASA San Pablo Reservoir Test Site and its environs.

The report which follows incorporates the result of the author's first-look analysis of the most useful of the above-mentioned types of

imagery and of the associated terrestrial photos and low altitude oblique aerial photos which he has taken of the study area.

RESULTS OBTAINED TO DATE FROM A STUDY OF THE AVAILABLE IMAGERY

One benefit accruing to anyone who writes reports on the usefulness and limitations of photography is that the photographs usually "speak for themselves". That certainly is the case with respect to the photographs comprising Figures 1 through 8, even though the black-and-white reproductions are less interpretable than the color originals from which they were made. However, the reader usually can benefit from an explanation of certain specific points which the author has found to be valid during the course of his photo interpretation and associated field work. Such explanations appear, where appropriate, in the captions which accompany the above-mentioned figures and hence need not be repeated here.

The main value of the ERTS imagery relates to the fact that both the annual grasses and the eucalyptus plantations are scattered very widely throughout the state of California. Merely from an examination of ERTS imagery it has been possible to select areas in which vegetation stress was developing to the point where a closer look with aerial photography was warranted. For other areas no aerial photography was needed.

It also is evident from the accompanying photographs that much can be told, on both ERTS-type imagery and high altitude aerial photography, about topographic conditions and about the density and location of housing and other structures which are of primary concern in relation to fire hazard appraisal. These particular factors are better assessed on the high altitude aerial photos than on the ERTS imagery, however.

Obviously, to the extent that smaller areas can be resolved on aerial photos, more detailed mapping of areas exhibiting plant stress can be made on such photos than on space photos. Of greater significance, however, is the fact that the evidence of plant stress can be detected at as early a date on ERTS-1 photos as on aerial photos. This fact can be of great value in those instances where early warning relative to the loss of vigor in plants can permit both timely and effective remedial measures to be taken at a fraction of the cost that would be entailed if the condition of vegetation stress were not to be discovered until a later date by which time it had reached a more advanced stage and/or affected a much larger number of plants.

As evidenced by the accompanying image examples and the interpretations of them indicated in the captions, it seems quite rational to conclude from this study that ERTS-type imagery, when used in concert with limited amounts of aerial photography and direct on-site observation, can greatly facilitate the making of fire hazard appraisals of the type dealt with in this paper.

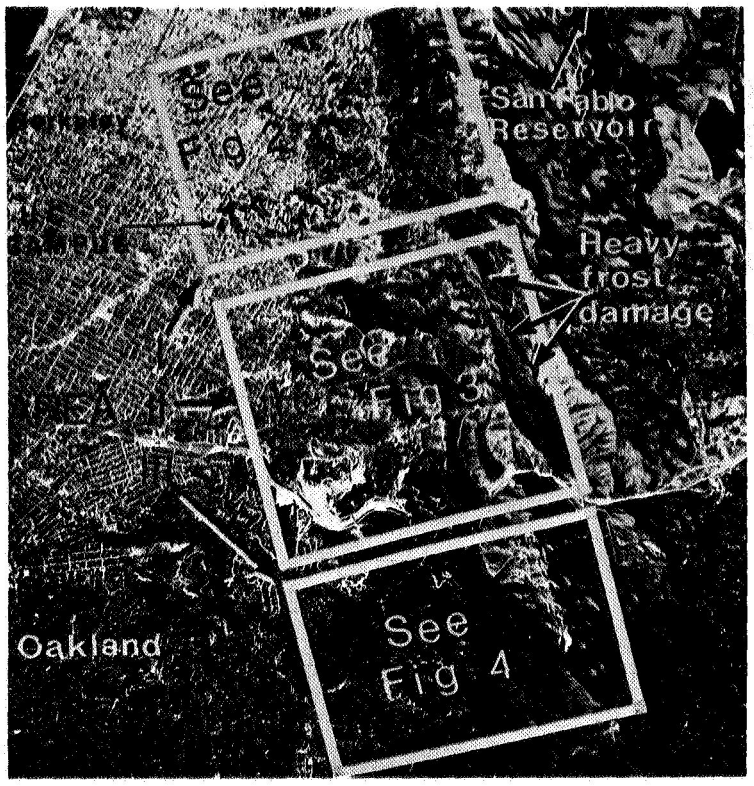


Figure 1. Black-and-white reproduction of part of an infrared Ektachrome "high flight" photo of the NASA San Pablo Reservoir Test Site. This photo was taken by one of NASA's U-2 aircraft from an altitude of 65,000 feet on January 22, 1973, approximately six weeks after the area experienced a killing frost. This is part of the photographic coverage which routinely is being obtained of the test site in support of the NASA-funded ERTS-1 studies that are being conducted there by personnel of the Forestry Remote Sensing Laboratory of the University of California. The fact that frost-damaged stands of eucalyptus trees can be discerned on this photograph is quite apparent if one compares the 3 rectangular areas with large scale photos of the same areas as shown in Figures 2, 3 and 4, respectively.



Figure 2. Black-and-white reproduction of part of an Infrared Ektachrome photo of the NASA San Pablo Reservoir Test Site, taken from an altitude of 25,000 feet on January 22, 1973. Compare with Area I, as outlined on Figure 1, and also with Figures 5a b c d.

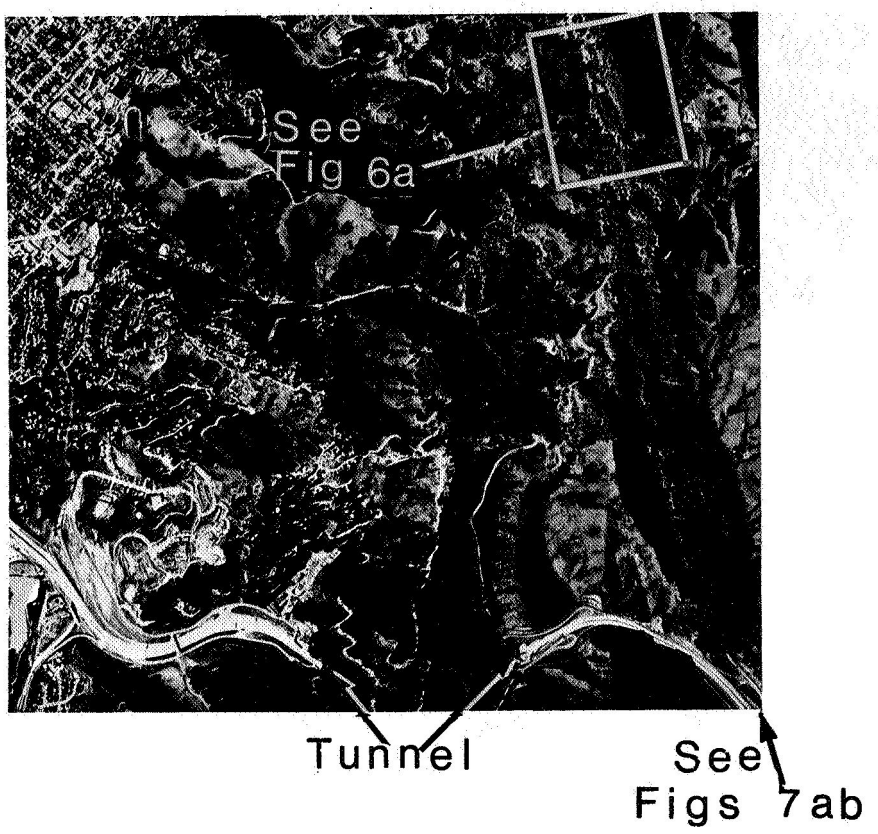


Figure 3. Black-and-white reproduction of part of an Infrared Ektachrome photo of the NASA San Pablo Reservoir Test Site, taken from an altitude of 25,000 feet on January 22, 1973. Compare with Area II, as outlined on Figure 1, and also with Figures 6a, b, c, d and 7a, b.

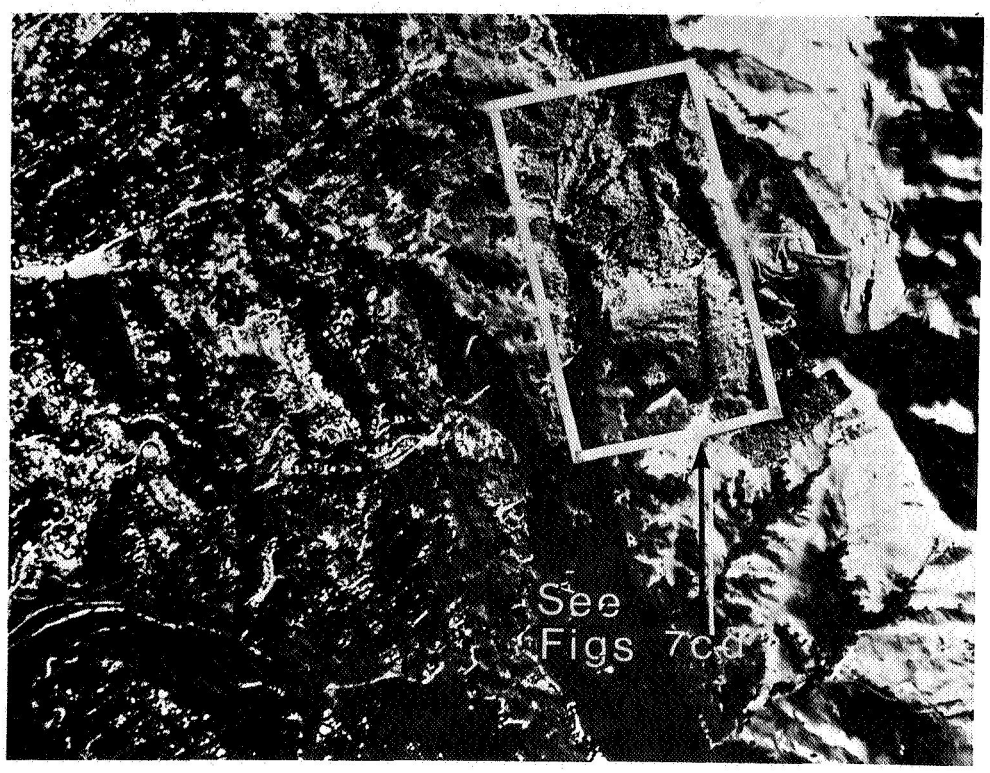


Figure 4. Black-and-white reproduction of part of an infrared Ektachrome photo of the NASA San Pablo Reservoir Test Site, taken on January 22, 1973. Compare with Area III, as outlined on Figure 1, and also with Figures 7c, d.



Figure 5. a: The light-toned trees on the golf course are frost-damaged eucalyptus. The dark-toned trees are healthy conifers. b, c and d: Three aerial oblique views of the NASA-built Space Sciences Laboratory of the University of California. Note frost-damaged eucalyptus trees.

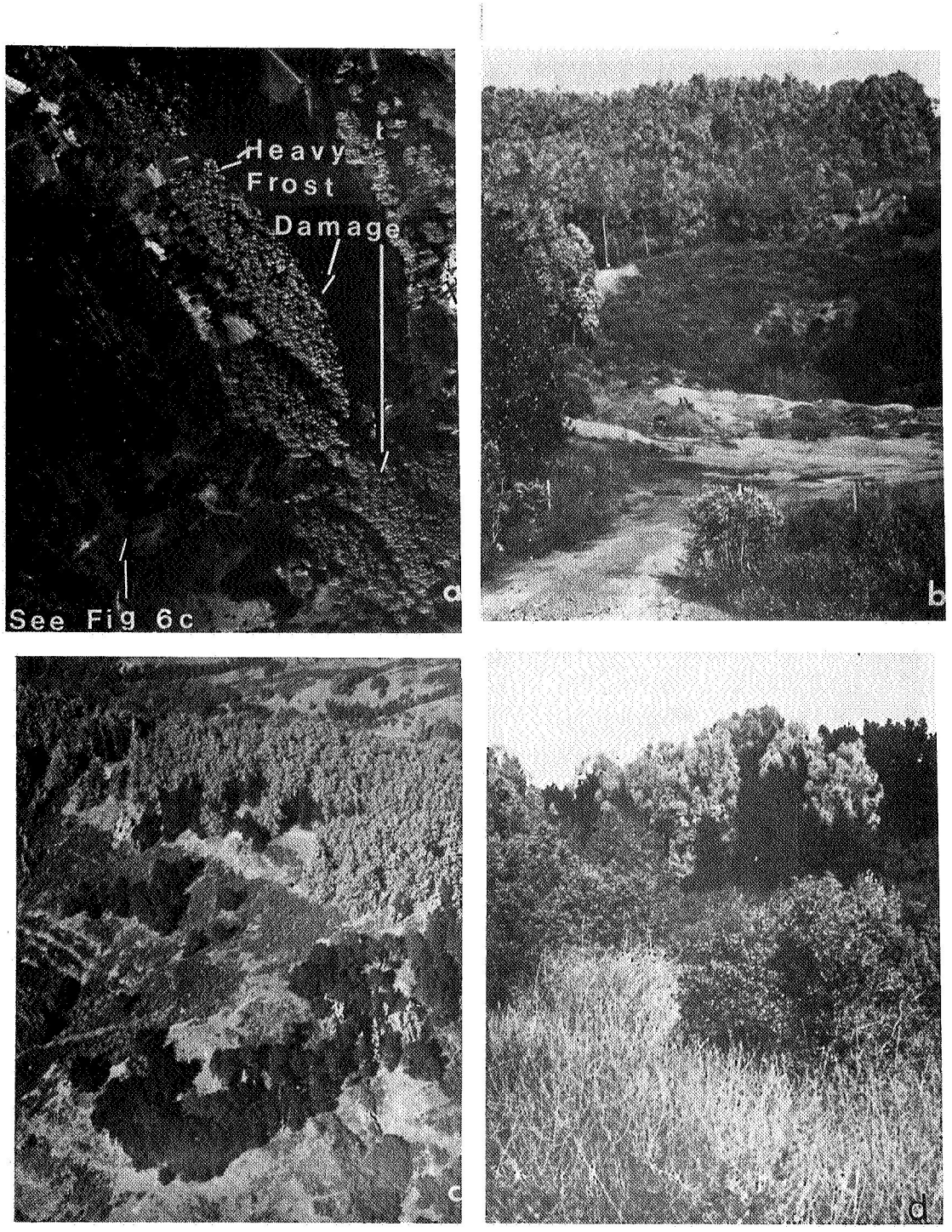


Figure 6. Compare areas shown here with same areas as annotated in Figures 1 and 3.

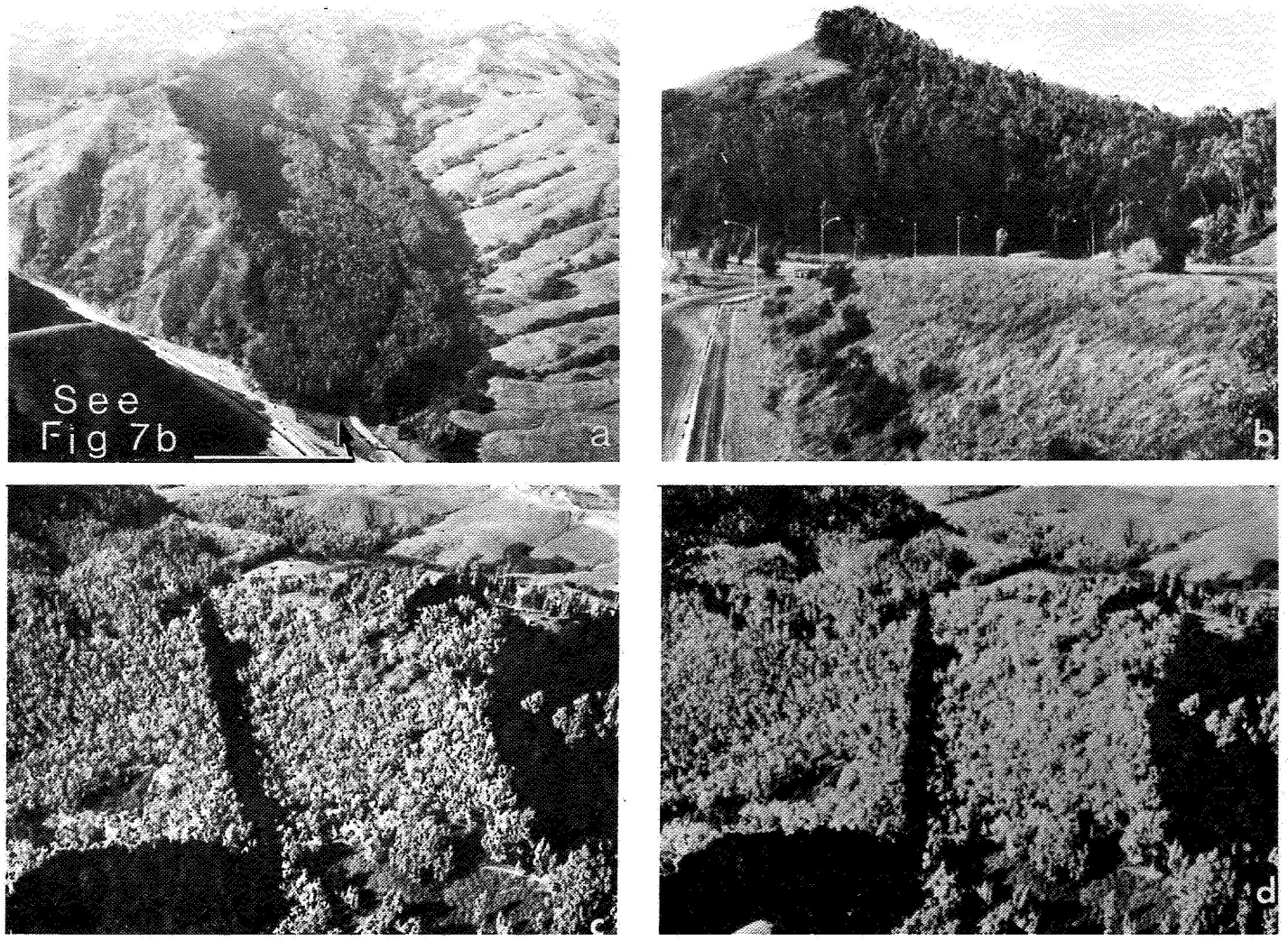


Figure 7. a & b: Some area as labeled on Figure 3, showing moderate frost damage in foreground and heavier damage in background, at higher elevation. c and d: Prints from Ektachrome and Infrared Ektachrome photos, respectively, showing area outlined in Figure 4.

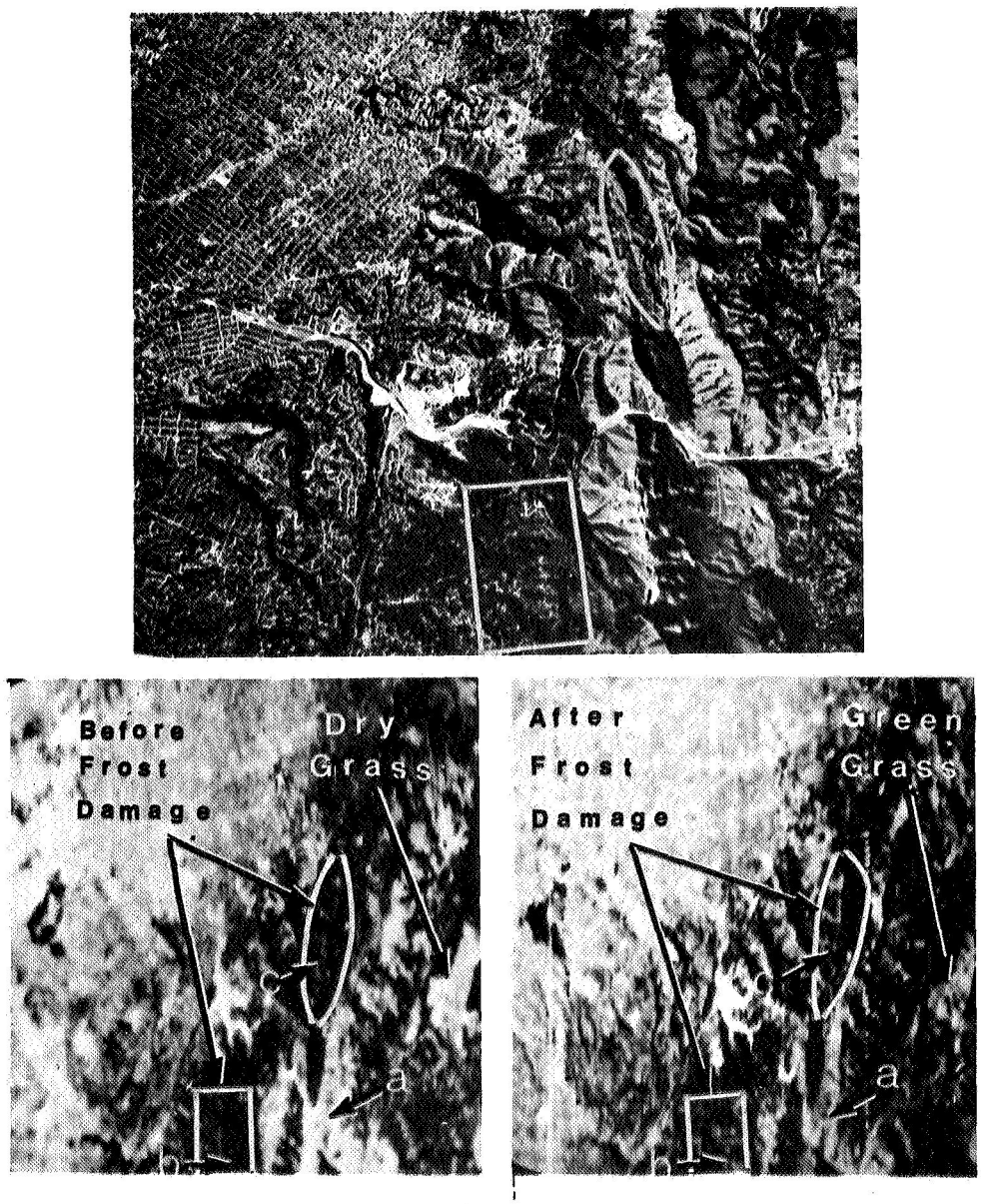


Figure 8. a. January 1973 high flight imagery of essentially the same area as shown in Figure 1. b. July 1972 ERTS imagery (band 5 of same area), taken before frost damage. c. January 1973 ERTS imagery (band 5 of same area), taken after frost damage. Note that grasslands labeled "a" are lighter in tone in July when they are brown than in January when they are green. Conversely, note that eucalyptus stands labeled "b" and "c" are darker in tone in July when they are green than in January when they are brown, due to frost damage. (Enhancements by Ralph Algazi and Jeff Schriebman, University of California).

Paper A 19

PHENOLOGY SATELLITE EXPERIMENT[1]

Bernard E. Dethier, Marshall D. Ashley, Byron Blair and Richard J. Hopp[2]

ABSTRACT

The detection of a phenological event (the brown wave-vegetation senescence) for specific forest and crop types using ERTS-1 imagery is described. Data handling techniques included computer analysis and photo interpretation procedures. Computer analysis of ERTS-1 multi-spectral scanner digital tapes in all bands was used to give the relative changes of spectral reflectance with time of forests and specified crops. These data were obtained for a number of the study's twenty-four sites located within four north-south corridors across the Unites States.

Analysis of ground observation photography and ERTS-1 imagery for sites in the Appalachian Corridor and Mississippi Valley Corridor indicates that the recession of vegetation development can be detected very well. Tentative conclusions are that specific phenological events such as crop maturity or leaf fall can be mapped for specific sites and possibly for entire regions.

Preliminary analysis based on a number of samples in mixed deciduous hardwood stands indicate that as senescence proceeds both the rate of change and differences in color among species can be detected. This will permit timber surveys by species over large areas and the determination of conditions of wildlife habitats.

The roles of the State Agricultural Experiment Station and the cooperative state extension agent and specialist in disseminating methods of applying ERTS data to agricultural, forestry and wildlife management practices are also discussed.

---

[1]Project co-investigators: J. A. Asleson, Montana State Univ.; M. F. Baumgardner, Purdue Univ.; N. L. Canfield, NOAA; J. M. Caprio, Montana State Univ.; W. C. Kennard, Univ. of Conn.; M. D. Magnuson, NOAA; J. W. Rouse, Jr., Tex. A & M Univ.; and M. T. Vittum, Geneva Exp. Sta., Geneva, N.Y.

[2]Atmospheric Sciences, Cornell Univ., Ithaca, N.Y.; Forest Resources, Univ. of Maine, Orono, Me.; Agronomy, Purdue Univ., Lafayette, Ind.; and Plant and Soil Science, Univ. of Vermont, Burlington, Vt.

I. INTRODUCTION

The term "phenology" appears to have been first applied in 1853 by the Belgian botanist, Charles Morren, to that branch of science which studies periodic phenomena in the plant and animal world insofar as they depend upon the climate of any locality. The word phenology itself is derived from the Greek word "phaino", meaning to show. Plants can be used as indicators of climatic differences because the times of occurrence of phenological events of many plants is to a large degree controlled by the weather. Thus, phenology represents a merging of the meteorological and biological sciences, each contributing something to the other.

Scientists have known for many decades that plant species are excellent indicators of environmental conditions. Some phenological indicator plants reflect climatic contrasts between locations through their differential rate of seasonal development; other species indicate soil moisture conditions, depth to water table, and nutrient status of soils. Two phenological sequences are observed in the Phenology Satellite Experiment:

1. The Green Wave: A record of the geographical progression with time of foliage development over wide areas. This is the first step that must be taken toward a real time inventory of the yield potential, yield realization and crop management over extended crop and timber producing areas of the nation.

2. The Brown Wave: A record of the geographical progression with time of vegetation senescence (maturation of crops, leaf coloration, and leaf abscission). It plays the analogous role in the autumn as the Green Wave phenomenon does in the spring in terms of phenological predictors for vegetation management.

This report describes the phenological changes during the fall season (Brown Wave) detectable through satellite scanner systems.

The research was conducted at 24 sites within four corridors: (1) the Appalachian Corridor from Maine to North Carolina, (2) the Mississippi Valley Corridor from Michigan to Texas, (3) the Rocky Mountain Corridor from Montana to Arizona, and (4) the Columbia Valley Corridor in Washington and Oregon (Fig. 1). Multispectral scanner data from selected segments in each corridor were analyzed and correlated with ground site photography from corresponding segments.

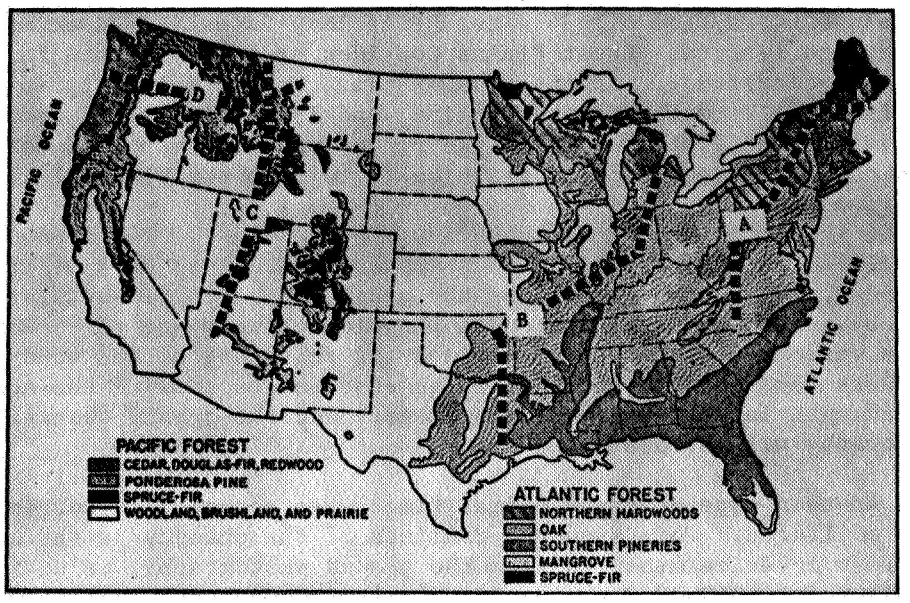


Figure 1. A - Appalachian Corridor, B - Mississippi Valley Corridor, C - Rocky Mountain Corridor, D - Columbia Valley Corridor.

The photographic analysis of the Rocky Mountain and Columbia Valley Corridors is being performed by Dr. Joseph Caprio, Montana State University. Dr. John Rouse, Texas A & M, is processing the MSS data for these corridors and correlating similar data from 10 sites in a Great Plains Corridor for an associated ERTS-1 project.

The ERTS satellite provides the only reasonable means of making synoptic phenological measurements over the interregional areas described in a time frame which will allow operational use of the results. The results described here are derived from analysis of MSS data from the Appalachian and Mississippi Corridors.

II. DATA SOURCES AND METHODS OF ANALYSIS

Imagery from all four multispectral scanner (MSS) bands is being evaluated. Standard products used are 70 millimeter and 9x9 inch positive transparencies, 9x9 inch color infrared composite transparencies from bands 4, 5, and 7, and computer compatable tapes from all bands. On-site photographs of the forest, crop, and range sites is being taken on a six day cycle at each site so that the date of every third set of photos coincides with an ERTS overpass. This photography provides a basis for comparison in the ERTS data analysis.

Computer analysis and photo interpretation procedures are being used to determine phenological changes. Computer programs have been written by the Laboratory for Applications of Remote Sensing (LARS), Purdue University, and the Remote Sensing Center (RSC), Texas A & M University, to express the relative reflectance in each band.

Analysis of data from all 34 sites (Phenology Satellite Experiment project and 10 sites Great Plains Corridor project) for the fall season is continuing. At the present time, sequential analysis of data from the Vermont, North Carolina, and Indiana sites is complete. The average and distribution of the reflectance in each band for a given date have been plotted graphically to show the spectral changes with time.

Photo interpretation methods are used to construct similar time sequences. Gray tone changes on the black and white products are being evaluated as an indicator of phenological change. ERTS imagery of the Vermont test site was examined for this part of the study. As more data becomes available, time lapse sequences showing the coincident changes in vegetation on the imagery and the ground observation photography will be assembled.

Another type of phenological time lapse sequence is currently being collected. This sequence consists of the changes in the amount of forest cover as measured from the ground photography, using a Digicol model 4010-32 density slicer. The Digicol has an electronic planimeter attachment which evaluates the percent area of different density levels (e.g. sky versus foliage) within a photo. The changing percentages between sets of photography of the same scene result from foliage development or recession.

III. RESULTS AND DISCUSSION

The relative differences in reflectances for an Indiana forest site are illustrated in Figure 2A. Reflectance in both bands 6 and 7 decreased with each succeeding overpass. The ground observation photography also shows a significant change during this eight week period. The leaves in mid-September were fully developed and green while by the October 19 overpass fall coloration was well under way. Leaf fall was complete by November 24. A similar analysis for two successive passes over the North Carolina site before leaf senescence had started shows, as would be expected, little change in reflectance (Fig.2B). These correlations indicate that phenological changes (Brown Wave) can be readily detected from ERTS-1 data.

The photo interpretation analysis also has shown substantive results. On site photography has documented the fall phenological changes at the corridors' sites. By evaluating the complete sets of photos, the time of crop development and maturity, leaf coloration, and leaf fall can be determined for the different geographical locations. Digicol measurements quantify these events.

The timing of vegetation senescence is not strictly a function of latitude. In the Appalachian corridor the northern hardwood leaves at the Vermont site, 44°25'N lat. (Nov. 4) fell before those at the Orono,

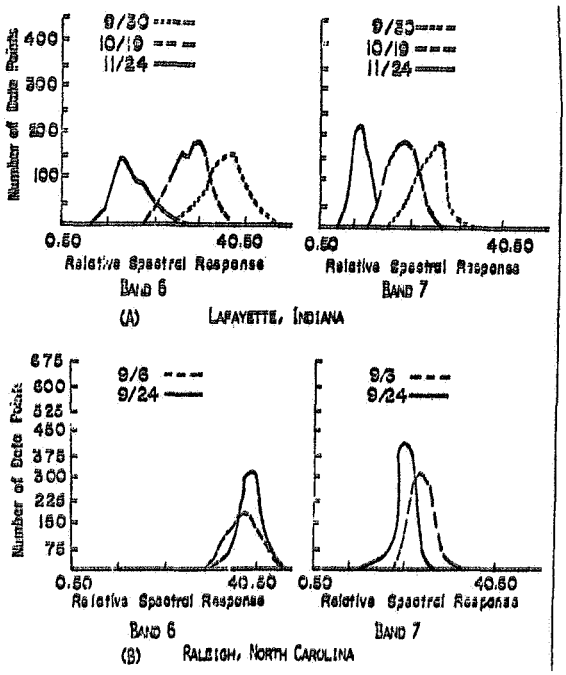


Figure 2. Histograms of the comparative spectral response of forest test sites, (A) Lafayette, Indiana; (B) Raleigh, North Carolina.

Maine site, 44°55'N lat. (Nov. 12). In the Mississippi Corridor, oak leaves in Missouri, 38°46'N lat. completed coloration (Nov. 15) before those at Lafayette, Indiana, 40°26'N lat. (Nov. 24). Elevation, soil type, moisture, and other environmental factors also influence the timing of phenological events.

ERTS-1 imagery used in conjunction with the ground observation photography sequences provides evidence of the geographical progression of vegetation development. Figures 3 and 4 show how some phenological changes in crops and forest appear when correlated in this way. ERTS frames E-1079-15063 (October 10) and E-1096-15115 (October 27) in bands 5 and 7 are presented along with ground observation photography of the test site near Richmond, Vermont. The ground photos were taken on October 10 and November 4, 1972, the dates nearest ERTS-1 overpasses. The terrestrial photos on October 10 are of standing mature corn and a forested area containing northern hardwood species. The forest leaves were near the height of fall coloration. The later set of ground photos shows that the corn has been harvested with only stubble remaining in the fields and the leaves at the forest site have nearly all fallen. Examination of the corn field and the forested site on the imagery verifies these events.

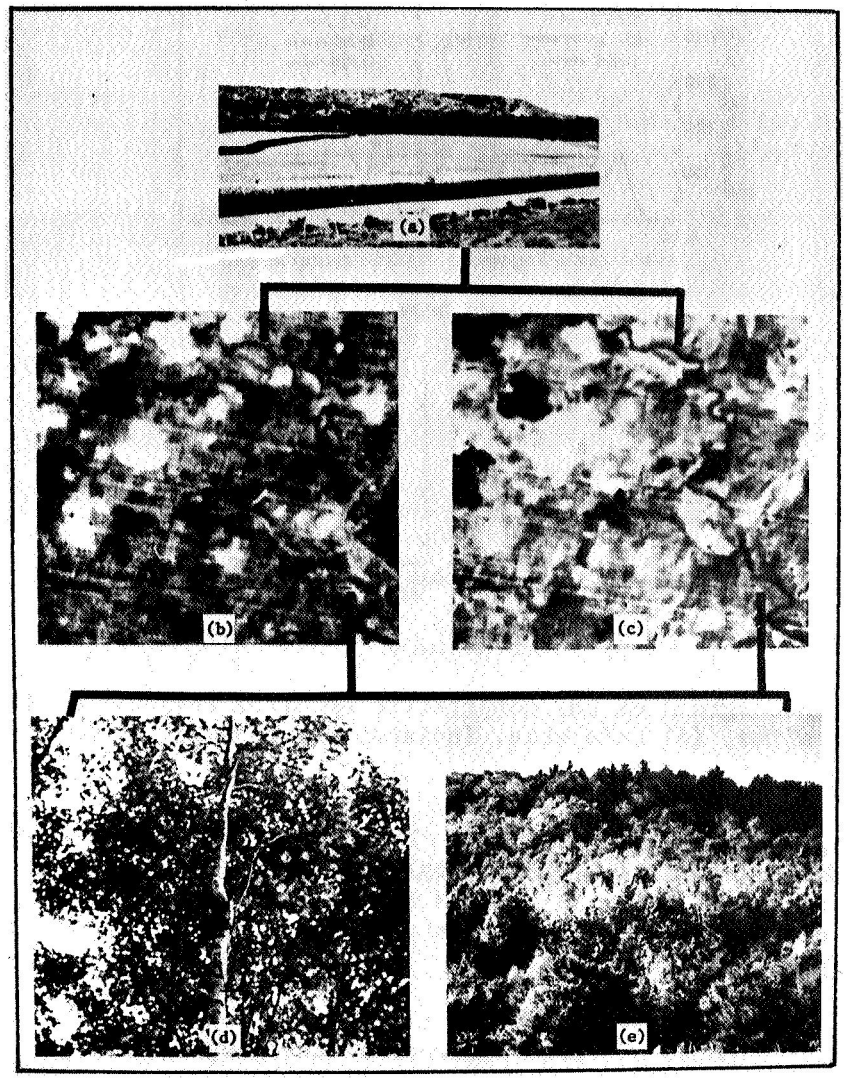


Figure 3. Ground observation photography and ERTS-1 imagery showing stages of vegetational development on 10 Oct 1972 at the Vermont Test Site: a) partially harvested corn, b) MSS Band 5 (scale 1: 125000), c) MSS Band 7 (scale 1:125000), d) forest canopy, and e) forest site.

The phenological progression can be detected using either band 5 or 7. When compared with the October 10 imagery (Fig. 3) the corn field appears lighter in tone on the October 27 (Fig. 4) imagery in the red band and about the same tone or a little darker in the infrared band. Perhaps this can be explained by the soil and stubble having relatively higher reflectance in the red wavelength than standing mature corn, while the infrared reflectance remained about the same or was slightly less for the stubble and soil. The red band also shows a general increase in reflectance throughout the Winooski River Valley and hardwood forest areas. The change is not as pronounced in band 7 imagery.

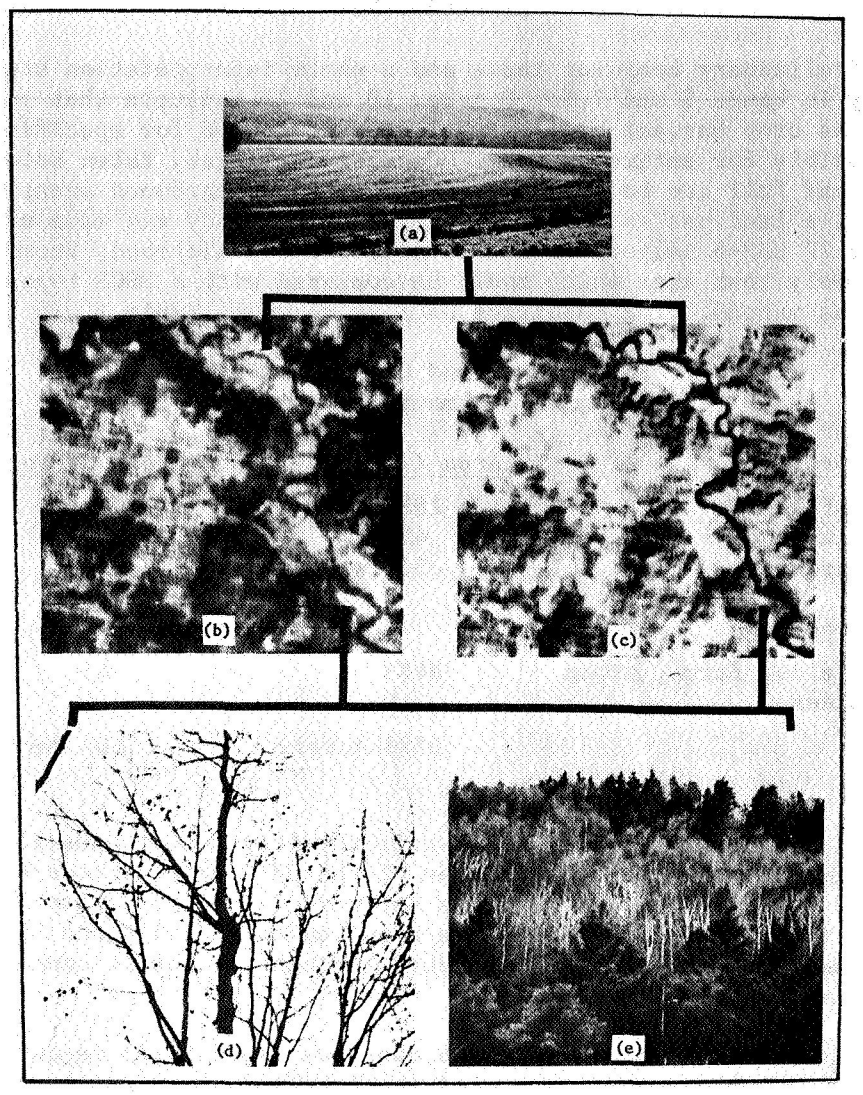


Figure 4 Ground observation photography (4 Nov 1972) and ERTS-1 imagery (27 Oct 1972) showing stage of vegetational development at the Vermont Test Site: a) corn stubble, b) MSS Band 5 (scale 1:125000), c) MSS Band 7 (scale 1:125000), d) forest canopy, and e) forest site.

While the evidence from analysis of band 7 is not conclusive, the analysis of band 5 does indicate a relationship between vegetative cover, reflectance, and phenological change. The depletion of chlorophyll in the vegetative cover due to leaf fall and senescence of lower vegetation results in a higher reflectance of solar energy in the red wave lengths. The potential for mapping such changes over large areas is evident.

IV. APPLICATIONS

Preliminary computer tests and a photo interpretation study of imagery in bands 5 and 7 for October 10 and 27 indicate that such events as crop harvest and leaf fall can be mapped for specific areas and possibly for entire regions. Comparison imagery taken before and after leaf fall can be used to map softwood and hardwood areas. For example, a land use and forest classification study was made using the October 27 MSS-5 imagery of the area around the Richmond, Vermont test site. Only that area which could be compared with a USGS topographic sheet was mapped. The resulting data is shown in Table 1.

Table 1. Forest and Land Use Classification
Richmond, Vermont test site.

Forest	Area (Acres)	Percent of Total
Softwood	1883	34
Mixedwood	415	7
Hardwood	532	10
Other		
Fields, farms, urban	2483	45
Water	210	4
	5523 Acres	100 Percent

These figures were obtained by tracing the gray tone boundaries of the land uses as seen from a projection of the ERTS frame onto a base map (scale 1:125,000) and then using a dot grid to get the areas in each class. Only 20 to 30 minutes were required to classify the 5500 acres. This time can be considerably reduced through the use of computer techniques.

Another application of the Brown Wave (leaf fall) is in the study of wildlife habitat conditions and availability.

Results to date from the Phenology Satellite Experiment shows the feasibility of the development and refinement of phenoclimatic models similar to the one illustrated in Figure 5 .

The model presented is a world map showing isolines for the greening of grass in spring in the northern hemisphere. The lines are based on a number of reference points and data calculated from a mathematical model.

Satellite data, such as that received from ERTS-1, will make worldwide phenological monitoring possible. This is necessary to develop universally applicable phenoclimatic models.

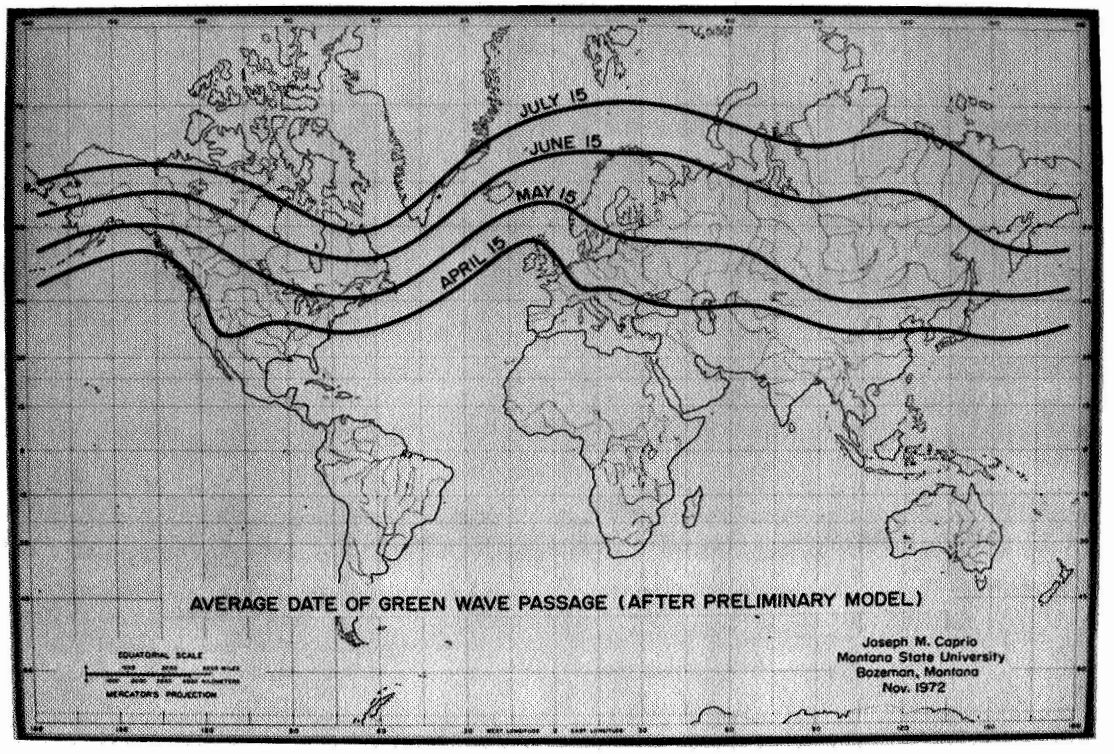


Figure 5. Average date of the Green Wave (greening of grass) passage in the northern hemosphere.

For countries with highly developed agriculture, such information would be useful in characterization of crop status, yield prediction, and management planning. Phenological data in less-developed countries could be useful for agricultural land use planning and for determining site suitability.

In the final analysis, the success of Earth Resources Technology Satellites will depend on the ultimate use of interpreted data. In the agricultural, forestry, and related segments of the economy these data will contribute to decision-making of economic significance in management, provide more accurate estimates of acreage and yield forecasts of many commodities. The means of disseminating the interpreted data to the user is available through Cooperative State Extension Service. Working with the scientists from the State Agricultural Experiment Stations, extension specialists could be trained to incorporate satellite derived information into their state advisory programs.

Paper A 20

FOREST AND RANGE MAPPING IN THE HOUSTON AREA WITH ERTS-1 DATA

G. R. Heath and H. D. Parker, *Lockheed Electronics Company, Inc., Houston Aerospace Systems Division*

ABSTRACT

ERTS-1 data acquired over the Houston area has been analyzed for applications to forest and range mapping. In the field of forestry the Sam Houston National Forest (Texas) was chosen as a test site, (Scene ID 1037-16244). Conventional imagery interpretation as well as computer processing methods were used to make classification maps of timber species, condition and land-use. The results were compared with timber stand maps which were obtained from aircraft imagery and checked in the field. The preliminary investigations show that conventional interpretation techniques indicated an accuracy in classification of 63 percent. The computer-aided interpretations made by a clustering technique gave 70 percent accuracy.

Computer-aided and conventional multispectral analysis techniques were applied to range vegetation type mapping in the gulf coast marsh. Two species of salt marsh grasses were mapped. Aside from their importance for grazing and wildlife habitat, the separation of marshhay cordgrass *(Spartina patens)* and gulf cordgrass *(Spartina spartinae)* locations may be significant in coastal zone management since the natural boundary between the two species approximately marks a change in elevation as small as three inches above sea level. Preliminary results indicate the two types are separable in ERTS-1 MSS data, (Scene ID 1073-16251), both manually and automatically.

1. INTRODUCTION

The ERTS-1 Forest and Range Analysis Teams at the Johnson Space Center (JSC) are investigating the utility of ERTS-1 data for mapping forest and range vegetation types for four study areas in the Houston Area Test Site. This report summarizes preliminary results from two of the study areas, the Sam Houston National Forest Study Site, and the San Bernard Range Study Site.

The authors acknowledge aid and cooperation from personnel of the USDA Forest Service and the U.S. Fish and Wildlife Service in these investigations. Team leaders were G. R. Heath (Forest) and H. D. Parker (Range). Other contributing members of the two analysis teams were: Forest Team - W. A. Kinkel and J. E. Weaver; Range Team - J. M. Disler, E. P. Kan, D. T. Pendleton, A. Simon, and R. S. Trejo.

2. THE FOREST INVESTIGATION

The U.S. Forest Service has a need for forest resource inventory techniques which can be applied over large areas rapidly and with greater efficiency than procedures now used. The ERTS-1 Forest Analysis Team is applying conventional and computerized processing to ERTS-1 data to investigate its potential for forest inventory applications.

For this investigation, an area approximately 7 × 9 kilometers in the Sam Houston National Forest was chosen as the primary study area, because a large amount of data concerning it was available. A secondary area, composed of the west unit of the Raven District, partially surrounds the primary area. The objectives of the study are to determine data, and to learn how the data can be used to make classification maps. The data being used are multispectral scanner (MSS) tapes and imagery from the coverage of August 29, 1973, (Frame 1037-16244).

Ground truth was a broad classification map of the vegetative cover, and related forest features in the study area. It was constructed from aerial photos and ground inspection

2.1 CONVENTIONAL PROCESSING

To determine the size of areas detected by the sensors, representative features were selected on the ground truth map. Criteria were established for the minimum size of each feature to be evaluated, based on Forest Service management needs. These criteria were 8 hectares (20 acres) for timber types, 15 meters (50 feet) width for streams and right-of-way, and 2 hectares (5 acres) for water impoundments and rural settlements. Features of these minimum sizes, and larger features, were selected for study, and ERTS-1 imagery was analyzed for detection quality. Results were tabulated for all MSS bands, for the Goddard type C color composite, and for a composite made at the Johnson Space Center.

Band 4 (green) was the poorest of the four bands; it provided very little information. Band 5 (red) was the best band for some vegetation types, but it was poor for detecting hardwoods and water bodies. One pine stand for four hectares (10 acres) was observed. In band 6 (IR) hardwoods began to appear and water bodies stood out well, but pine stands were less visible. Band 7 (IR) had similar characteristic showing hardwoods best, but was slightly poorer in general than band 6. However, it revealed the smallest feature seen on ERTS-1 imagery by the Forest Team, a group of one hectare (2 acre) lakes. The composite made at JSC produced the best detection results of all the media examined; the Goddard composite rated midway between bands 6 and 7 (table 1).

Table 1

Media	Features Detected
JSC Composite	21 of 30
Band 5	20 of 30
Band 6	16 of 30
Type C Composite	15 of 30
Band 7	11 of 30
Band 4	4 of 30

Classification mapping by several multispectral enhancement methods is planned but this work is still incomplete. An ocular comparison was performed between ERTS-1 band 7 imagery and aircraft photos. A 9×9 transparency was placed in a rear projection viewer and enlarged to 25X. Then, the various gray levels were delineated onto a transparent medium placed on the screen. These gray levels were compared with ground truth and classifications were assigned which most closely matched the known class. By placing a grid over both maps and by counting points of agreement vs. disagreement, it was determined that the ERTS imagery matched 63 percent of the ground truth classifications.

2.2 COMPUTER PROCESSING

The team plans to classify the study area using a clustering program and a maximum likelihood pattern recognition program. To date, only the clustering analysis is complete.

As shown in figure 1, which illustrates the printout of a 24-cluster map, the symbol 1 is most prevalent. It forms a pattern which most closely approximates the pine category in the ground truth. The pattern produced by the symbol 7 appears most often where hardwoods are found. It was observed that certain combinations of symbols seemed to fall in patterns which represented other classifications. For example, wherever there was a site prepared for pine regeneration the symbols 2, 4, 7, and 8 appeared together, with the 2's predominating. Using this method, the team worked up a code of symbols and combinations of symbols which represented the ground truth classes, and provided a set of symbol signatures for each class. Others have used this technique of interpreting cluster combinations and are finding it useful.

The resulting printout map was then converted to the base map scale and made into a line drawing. A computation of the agreement between the clusters and ground truth yielded 70 percent agreement. It must be emphasized that for

forest classification, clustering analysis is an experimental technique that is still under study; its analysis role is not yet defined.

The tape produced from the clustering program was then film-recorded on a Data Analysis Station and subjected to the same comparative analysis as the printer map. Since combinations of symbols could not be represented by a single color on the film map, agreement was only 60 percent, 10 percent less than the results of the printout map analysis.

The team's next step will be to attempt extension of these analyses to a secondary study area, with less ground truth.

2.3 SUMMARY

The preliminary results in this report may be summarized as follows: (1) forest feature visibility in ERTS-1 imagery was very good, (2) the ocular imagery interpretation technique was not an efficient method for analyzing ERTS data on forest classification, becuase of its low (63%) agreement with ground truth, and the time it required, and (3) the clustering technique appears promising, but it needs further testing and refinement.

3. THE RANGE INVESTIGATION

The ERTS-1 Range Analysis Team is investigating the utility of ERTS-1 data for mapping range vegetation types on the San Bernard Site, west of the San Bernard River outlet on the Texas Gulf Coast. Conventional and computer-aided processing techniques are being applied to the data set acquired by the satellite on October 4, 1972 (Scene 1073-16251).

The San Bernard Site, about 370 km^2 in area, is typical of much of the gulf coastal marsh in Texas and Louisiana. The objective of this investigation is to determine the accuracy with which the two major vegetation zones in the marsh could be distinguished with ERTS-1 data. The zone nearest the water, at about 0-2 inches above mean sea level is characterized by marshhay cordgrass *(Spartina patens)*. Frequently inundated by gulf water, it is often referred to as "wetlands". Adjacent and slightly higher is the gulf cordgrass *(Spartina spartinae)* zone. Both types produce large amounts of livestock forage and provide unique habitat for numerous wildlife forms.

The likelihood of future increases in the demand for both grazing and recreation in the marsh creates a need for information on the amount and distribution of vegetation resources which has heretofore been unavailable over large areas. If ERTS-1 data can provide such inventory information, it may be a valuable tool for the high intensity management of the resource which this increased demand will require in the future. Another potential benefit which may drive from separation of the two marshgrass zones, is the mapping of boundaries between the lower (wetland) areas normally subject to inundation, and the drier portions of the marsh. This type of information would be valuable for planning any development in the marsh.

Ground truth for the investigation was a vegetation type map, constructed from aircraft photography and ground inspection of the area. The boundary between the two vegetation types was clearly visible in late Spring color infrared aircraft photos. The San Bernard Site was divided into two areas, one for training and reference, the other for testing. All image enhancements and computer training were done by reference to imagery of the training area; later ERTS data evaluations will be based on results in the test area.

3.1 CONVENTIONAL PROCESSING

Conventional processing involved construction of color composites, enhanced by reference to the training area, to display the boundaries between the two zones.

Two examples of the color composites from conventional processing are shown in figures 2 and 3. Figure 2 was constructed on a multi-channel film viewer from portions of 9.5 inch ERTS-1 images in bands 4, 5, and 7. Figure 3 was generated from the same imagery on an additive color viewer/printer. In both images, the dotted lines indicate vegetation boundaries from ground truth.

A quantitative measure of the precision with which the type boundaries were located will be obtained by planimetering the areas interpreted in each type.

3.2 COMPUTER PROCESSING

As in the forest study, initial computer classification of the San Bernard data was done by clustering. By reference to a vegetation type map of the training area, the clusters were combined such that the boundary between the two vegetation zones was approximated in the output cluster map, which was color-coded and filmed, (fig. 4). The cluster combinations were:

water - 3 shades of blue - 3 clusters
woodland - brown - 1 cluster
marshhay cordgrass zone - yellow - 2 clusters
gulf cordgrass zone - green - 3 clusters
unclassified - white - 3 clusters

The clusters coded white (unclassified) were found to be non-vegetated features including beaches, spoil banks from dredging, and urban areas, including the city of Freeport, Texas.

In recent work to correlate individual clusters with specific ground phenomena, confusion was observed between vegetation in the marshhay cordgrass zone, and burned portions of the gulf cordgrass zone; both were included in the same cluster. In a subsequent clustering run, this confusion was eliminated, but the burned areas were clustered with water (see fig. 5). Apparently, water, burned gulf cordgrass areas, and the marshhay cordgrass zone were multispectrally quite similar. Additional data, acquired after regrowth has occurred on the burns, is expected to reduce or eliminate this confusion.

The cluster statistics generated by the clustering program were input to a maximum likelihood classification program, to obtain a supervised classification with a classification threshold of 0.95 (fig. 5). The map produced was generally very similar to the cluster map, as expected. However, the large number of unclassified (white) data points suggests that the cluster distributions were not as tight as they may appear in the cluster map. Additional classifications, using other threshold values and statistics of conventional training fields, have produced classifications very similar to the map in figure 5. That result, and the similarity of the cluster map to the vegetation zone boundaries from ground truth, indicates that the groups of clusters constructed did provide a reasonable match with the vegetation zones.

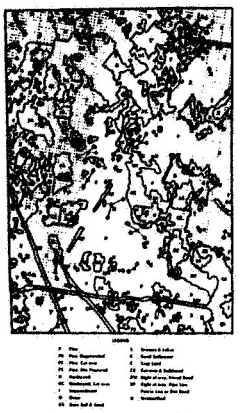
4. DISCUSSION

Both the forest and range investigators encountered difficulty in relating clusters to specific ground features. With the exception of large, homogeneous features such as water and tree stands, the vegetation types did not occur in single clusters when the clustering program was allowed to run to stable conditions (i.e., when all splitting and re-combining was complete). Two approaches were taken, and are continuing, to solve this problem.

The first approach, illustrated in these results (fig. 4) was to let the program run to stability, but then combine clusters such that one or more are represented by the same symbol (color). The other approach was to constrain the program to generation of only a few clusters with the expectation that only those features of greatest multispectral contrast will be clustered, and further, that those few clusters will coincide with vegetation type boundaries. The first trial of this technique on the San Bernard Site appeared to work well (fig. 5). The program successfully made the distinction between the two vegetation zones without manipulation by the investigators.

Although quantitative evaluations of all techniques must yet be completed, it appears the computer classifications were superior to the conventional image enhancements for delineating the boundaries. This difference is not believed due to more accurate classifications, however. Rather, the superior resolution achieved in the final analysis products from computer classification rendered the vegetation type boundaries more distinct.

In summary, both conventional and computer-aided processing techniques have been used successfully to distinguish between the two marsh vegetation zones. Although a quantitative comparison of the precision of each technique must yet be made, it appears that ERTS-1 data is capable of providing the needed vegetation inventory information in wetland areas along the Texas coast.



COMPUTER PRINTOUT -
CLUSTER CLASSIFICATION - FOREST STUDY AREA

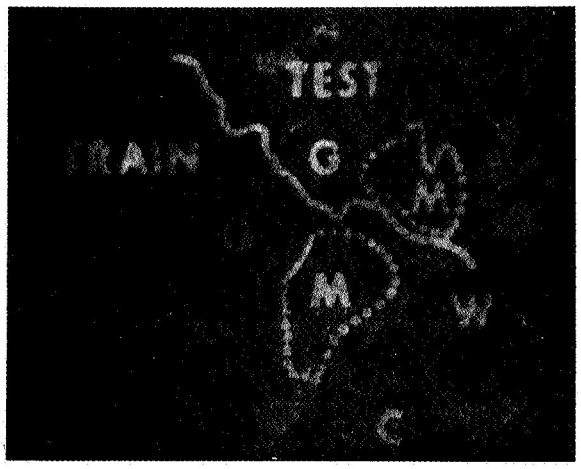


Figure 2 - Multichannel film viewer (electronic) enhancement showing marshhay cordgrass zone (M) and the Gulf cordgrass zone (G), in the training and testing areas. Dotted lines indicate zone boundaries from ground truth. Water areas (W) and offshore clouds (C) are also indicated.



Figure 3 - Additive color viewer (optical) enhancement. (See legend in Figure 2.)

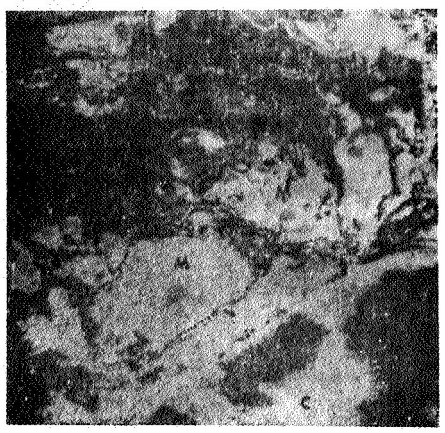


Figure 4 - Cluster map constructed by combining clusters manually. (See legend in Figure 2.)



Figure 5 - Cluster map generated entirely automatically. (See legend in Figure 2.)



Figure 6 - Supervised classification map; threshold level was 0.95 for all classes. (See legend in figure 2.)

Paper A 21

APPLICATION OF ERTS-1 DATA TO ANALYSIS OF AGRICULTURAL CROPS AND FORESTS IN MICHIGAN

Gene R. Safir, Wayne L. Myers, *Michigan Agricultural Experiment Station, Michigan State University, East Lansing, Michigan;* William A. Malila, James P. Morgenstern, *Environmental Research Institute of Michigan, Ann Arbor, Michigan*

ABSTRACT

The results reported are based on analysis of ERTS Frame 1033-15580 collected over southwestern Lower Michigan on August 25, 1972. Major agricultural crops such as corn and soybeans were approaching maturity at this data and forest canopies were dense.

Extensive ground truth information was gathered by detailed field study of test strips. This detailed information was supplemented over larger areas by interpretation of RB-57 and C-47 photography and MSS imagery. The U.S.D.A.-A.S.C.S. also cooperated by providing information on crops from their records.

Recognition processing of ERTS-1 MSS data was carried out on a digital computer. Fields and forest stands were selected as training sets and test areas. Aerial imagery was essential for locating the positions of these selected areas on ERTS digital tapes.

The recognition process was successful for each type of vegetation which had a dense green canopy such as forests, corn, and soybeans. Bare soil was also recognizable as a category. However, recognition of species was difficult in senescing or senescent vegetation. Since the accuracy of recognition depends on stage of growth, optimum times for collecting data will vary from one crop to the next.

Accurate computer recognition of crops from satellite data will be useful in operational surveys as the first stage in a multistage sampling process.

Michigan Agricultural Experiment Station, Journal Article 6315

Introduction

Michigan State University (MSU) in cooperation with the Environmental Research Institute of Michigan (ERIM) began a program in the summer of 1972 to test the usefulness of ERTS-1 satellite data for monitoring and managing crops and forests in Michigan. Specifically, the objectives included: (1) verification that major agricultural crops and forest types can be identified from ERTS-1 data; (2) development, application, and testing for accuracy of multispectral techniques for crop and forest acreage estimation in Michigan; (3) correlation of variations in signatures from space with ground truth data.

In addition to the scientists directly involved in analysis of the data, a team of cooperators has been assembled to evaluate the operational utility of the results which emanate from the project. This team includes members of state, federal, and local agricultural and natural resource agencies.

Data analysis to date has been confined to ERTS frame E-1033-15580 (August 25, 1972) as a result of the inclement weather conditions which prevailed throughout most of Michigan's 1972 growing season following the launch of ERTS-1.

Ground Truth Information

Direct field observation and 35-mm photography were the main sources of ground truth information for the analysis of agricultural crops. Specifically, biological parameters such as plant height, row direction and width, percent ground cover, stage of growth, corn tassel color, and disease incidence were estimated and recorded for numerous selected fields in the test area. Since forest cover changes less rapidly than agricultural crops, the primary source of information for forests was photointerpretation of RB-57 and C-47 underflight imagery. The photointerpretive work was supplemented by collection of data on the ground as necessary. The RB-57 and C-47 imagery was also extremely useful for analysis of agricultural crops. In addition to the field and underflight data, cooperators in both the United States Department of Agriculture, Agricultural Stabilization and Conservation Service (U. S. D. A. -A. S. C. S.) and the Forest Service have contributed to the pool of ground truth information. The A. S. C. S. efforts produced a set of annotated copies of enlarged airphotos showing the location and nature of vegetation types on the holdings of landowners who subscribe to A. S. C. S. programs.

M. S. S. Digital Analysis - Methods

Digital tape data for frame 1033-15580, were screened for quality by preliminary processing on the ERIM digital computers. They were found to exhibit the same problem present in a set of tapes for the same frame received by ERIM under another contract. The problem is that reproduced signals from one of six detector elements which generate the MSS data in ERTS band 6 (0.7-0.8 μm) are faulty. Thus, anomalous data are present for band 6 in every sixth line of data; otherwise, the data appear to be satisfactory. This problem complicates signature extraction and data analysis. In particular, recognition processing for the work described here was restricted to three channels.

The primary test sites (in Eaton Co., Michigan) were located within the digital data, and line-printer gray maps were produced for all ERTS bands. The gray maps for ERTS band 5 were used to locate selected training and test plots of known ground cover. The RB-57 and C-47 underflight imagery was essential for correctly locating these plots, which were then designated by line and point number to the computer for extraction of signal statistics. In the selection of training sets, care was taken to avoid boundary points. Fifty-eight plots were designated and ERTS signal statistics were extracted for eight types of ground cover. These statistics were subjected to cluster analysis, and the results were used to select several plots for combination to form recognition signatures. The plots which were not used directly for specifying signatures became "test" sets for evaluating the accuracy of recognition. Eighteen additional test plots were then selected and included in the analysis.

Recognition maps were produced for an intensive test area in Eaton Co., Michigan. Recognition runs were based on the three good ERTS channels using several different sets of parameters. First, twelve recognition signatures were used and maps were produced with different rejection threshold levels. That is, each observation was classified as belonging to one of the recognition signatures and then tested to see if it was unlikely enough to be rejected and categorized as belonging to none of the classes considered. Next, seven recognition signatures were used; the seven recognition signatures included combinations of the pairs of signatures used for several classes in the twelve-signature runs.

MSS Digital Analysis - Results

Recognition results were analyzed for the 76 identified plots. The overall results of the first-look analysis of recognition are summarized

in Table 1 for five cover classes (corn, soybeans, trees, senescent vegetation, and soils). As noted earlier, only three ERTS channels were used (4, 5 and 7). The values in Table 1 represent averages of percentages computed separately for each plot analyzed. The overall average percentage of correct classification (for test sets) is over 83%. The average percentage error is 10%, with 16% being Type 1 (i. e., missed classification, including not classified) errors and 4% being Type II (i. e., incorrect classification) errors. If "not classified" points are excluded from the computation, the overall average is nearly 85% correct.

Recognition percentages are high for those vegetation classes that had mature and uniform canopies at the time the data were collected (Aug. 25th). Corn, soybeans, and trees (forest) met this criterion, and were classified accurately. The class of senescent or senescing vegetation included observations from field beans, wheat stubble, and grass. These canopies were characterized by non-uniform distributions of dead and dying vegetation along with patches of more healthy vegetation. For example, field beans had matured and had begun senescing, while soybeans and corn were more vigorous. Also, wheat stubble fields were dry and brown except for some that had been seeded to alfalfa or red clover; the latter fields had patches of green growth among the stubble. The wide variability within these vegetation types at this time of year makes it difficult to classify them accurately. Alfalfa is a crop that is harvested repeatedly at irregular intervals throughout the growing season, and plots of it can appear very different, depending on their conditions at the time of observation. One vigorous alfalfa was included initially and accurately recognized. A lack of test plots, for which the exact condition at the time of the ERTS-1 pass is known, caused us to omit alfalfa as a class from the reported analysis. Bare soil was distinctive and accurately recognized.

Thus, the first-look analysis for computer recognition within boundaries of selected plots shows a good capability for differentiating each type of vegetation that has a dense green canopy, with bare soil also being recognizable as a category. The next step in the analysis of computer recognition is a more critical evaluation of accuracy by cover type for all resolution elements in selected portions of the frame.

Element-by-Element Analysis for Forest Cover

Figure 1 is a portion of the gray map for ERTS band 5 in Chester and Roxand Townships of Eaton County, Michigan with major roads

delineated. An RB-57 color infrared photo was used to transfer the locations of the forests to the gray map, and the elements that fall within the forest area are shown by heavy dots in Figure 1. Figure 1 is conservative in that most doubtful border elements were not designated as "forest". Figure 2 is a computer recognition map for the same area. Heavy dots have been superimposed on the elements which were correctly classified as "trees" (forest). The forest elements which were not recognized as such by the computer (Type 1 error) are indicated with a heavy square having a white center. Type II errors (incorrectly classified as "trees") are indicated by triangles. The Type I error for forests on this portion of the frame is approximately 40%. An examination of Figure 2 shows that most of these errors take place in border elements. For the most part, these border elements were classified as corn. The remaining Type I errors are mostly accounted for by areas in which the forest canopy is sparse. The Type II errors are only about 3%.

Since the original "trees" training sets were located in the center of dense woodlots, the misclassification of sparsely stocked areas is not too surprising. An examination of the likelihood for the misclassified elements showed a very low probability of classification under the "trees" signature. Use of separate training sets and subresolution element analysis are being investigated as possible means of improving recognition in sparse forests. The current classification would give a reasonable estimate of the acreage that is suitable for woodlot management, but would give an underestimate for total acreage of forest.

Summary

Computer analysis of ERTS-1 data provided good recognition of vegetation classes that had mature and uniform canopies at the time when the data were collected. Bare soil was also recognized accurately. Classification was extremely difficult for senescent vegetation which was characterized by non-uniform distribution of dead and dying vegetation along with patches of more healthy vegetation. Since the accuracy of classification depends on the stage of growth, optimum times for collecting data will vary from one crop to the next. However, the optimum for recognizing each crop is yet to be determined. This bears further study, especially for field beans since Michigan is the leading producer of this crop in the United States.

TABLE I. SUMMARY OF RECOGNITION RESULTS ON A PLOT-BY-PLOT BASIS FOR 76 PLOTS, ERTS FRAME 1033-15580, 3 CHANNELS (ERTS 6 EXCLUDED), 0.001 PROBABILITY OF REJECTION

A.

Class	No. Plots	No. Points	Average Percentage of Class'Plots Assigned to Listed Recognition Signature						
			Corn	Soy	Alf	Tree	Senesc Bean	Grass	Soil
Corn	21	481	84.27	0.55	0.13	9.85	3.85	1.35	0
Soy	10	115	1.00	89.40	2.30	2.59	2.61	0	0
Trees	12	358	11.00	3.80	0	84.50	0.20	0.50	0
Senesc	16	306	16.30	6.55	7.15	0	54.30	8.23	6.53
Soils	4	56	0	0	0	0	0	0	97.62
TOTALS	76	1416							

B. Summary of Percentages (Averaged Over Plots)

Class	No. Plots	No. Points	Not Clas'd	Correctly Assigned To Class	Incorrect. Assigned To Class	Average Error	Correct Excluding Not Clas'd
Corn	21	481	0	84.27	7.29	11.51	84.27
Soy	10	115	2.10	89.40	.50	6.55	91.31
Trees	12	358	0	84.50	3.66	9.58	84.66
Senesc	19	340	0.94	62.53	2.59	20.03	63.12
Soils	14	122	2.38	97.62	2.00	2.19	100.00
Averaged Over Five Classes			1.08	83.66	0.61	9.97	84.67



Figure 1. Channel 5 gray map for portions of Chester and Roxand Townships in Eaton County, Michigan showing actual locations of woodlots (●) and roads (←→).



Figure 2. Computer recognition map showing correctly and incorrectly classified elements associated with forest cover; ● indicates correctly classified forest areas, ◘ indicates forest areas misclassified, and ▼ indicates non-forest areas classified as forests.

Paper A 22

CROP SPECIES RECOGNITION AND MENSURATION IN THE SACRAMENTO VALLEY

Frederick J. Thomson, *Environmental Research Institute of Michigan, Ann Arbor, Michigan*

ABSTRACT

An earlier paper, presented at the 28 September meeting at Goddard, dealt with agricultural recognition maps of a portion of the "San Francisco" frame (1003-18175). The recognition maps were generated by applying multispectral pattern recognition techniques to ERTS-MSS digital taped data. The earlier results have been improved and extended as a result of field studies to check the accuracy of the original recognition. The goal of the second recognition map prepared from these data was to delineate various crop species in a portion of the Sacramento Valley, and at the same time to determine how accurately each could be classified and measured from ERTS-1 data.

The new recognition map, a new and concise display of the old map, and classification and mensuration accuracy data will be presented and discussed. The mensuration accuracy, in particular, is affected by the presence of an edge effect one resolution wide surrounding nearly all fields. Points on the edge are misclassified because they contain a mixture of e.g., crop and bare soil. Using a processing technique to estimate the proportions of unresolved objects in this edge region, a much improved mensuration capability will be demonstrated.

1. INTRODUCTION

Shortly after the launch of the ERTS satellite, the Environmental Research Institute of Michigan (then Willow Run Laboratories of the University of Michigan) obtained digital tapes of the "San Francisco" ERTS frame, designated 1003-18175. The request for these tapes was made

so that existing multispectral data analysis software could be tested on ERTS data. To verify the software performance, it was decided to generate a recognition map of a portion of the data. The area selected for analysis was northwest of Sacramento. This 375 sq mi area of intensive, irrigated agriculture was classified into eight categories. The identity of these categories was later verified by ground visits to the site and to Bureau of Reclamation offices.

The initial maps produced were discussed at the Goddard symposium of 29 September, 1972 and have been further analysed by the ERIM staff (Refs. 1, 2). While the original maps were good and accurate classifications of the data, two questions remained.

1. It was clear that conventional digital computer page printer displays of ERTS data were cumbersome because of the large quantity of data displayed. While the use of computer page printer data for initial analysis was acceptable, could a more concise display be found for the final classified results?

2. While several economically important crops were classified in the first effort, there were several "salad" categories (categories consisting of several crop species). While this was unavoidable in the first map because of lack of ground information, could a crop species map be generated given training sets for the important crop species in the area?

Because the answers to these questions were felt to be significant to the ERTS data analysis in general, processing of this data set was pursued.

2. CONCISE DISPLAY OF ERTS DATA

ERTS data are delivered in digital tape and film form. For many ERIM analyses, digital tape data are processed for wide area surveys. The concise display of such processed results is clearly important. A conventional page printer display of all the data in one ERTS frame covers a 27 ft x 24 ft area!! While the utility of computer page printer outputs for initial analysis is acceptable, some more concise display of final processed outputs is essential if these processed outputs are to be accepted by users.

Two solutions to the problem exist. First, at ERIM we have good 70 mm filmstrip printers developed for producing aircraft scanner imagery. Through the development of digital to analog (D/A) conversion facilities, we are now able to produce high resolution images of ERTS raw data or processed results on the same printers used for printing aircraft multispectral data. Data from each digital tape of ERTS data may be printed

separately and results mosaiced to provide a 9" x 9" display quite comparable to a typical 9" x 9" transparency from Goddard.

Second, we have obtained through the courtesy of Data Corporation, Dayton, Ohio, a color coded recognition map of the Sacramento data presented at the earlier Goddard meeting. This is shown in Figure 1. (Unfortunately, the black and white figure cannot do justice to the vivid colors present in the original). This display was produced from digital tape using a special display device developed by Data Corporation. While the cost of the device was too high for us to buy a printer,Data Corporation agreed to make maps at a reasonable price for us. Display sizes up to 40" x 60" are available, and the basic resolution element size is 1/72". The device directs different colored inks at paper to produce an effective color display.

3. CROP SPECIES RECOGNITION AND MENSURATION

After obtaining ground information from the Sacramento Valley area, we were convinced that our first map was an accurate map of agricultural categories in the area. However, we wanted to determine whether the economically important species could be recognized in such an agricultural area. Also we wished to determine how accurately crop acreages could be determined from ERTS data.

First, we attempted to classify the crops of the area, using training sets selected from fields of different crop species as determined from ground information. The results, shown only for the area for which ground information was readily available, are shown in Figure 2.

We determined that crop species could be discriminated on the basis of signatures. The criterion was the probability of misclassification computed from the signature information. Typical probabilities of misclassification are shown in Table 1 below. We were unable to discriminate between wheat and barley stubble because the wheat had been harvested and was stubble at the time. Also, tomatoes and sugar beets could not be discriminated, probably because both have dark green foliage and were relatively immature at the time of ERTS coverage.

The probabilities of misclassification are useful for defining separable classes but do not tell the whole story because of the limited training set areas used to calculate these probabilities. So to further test the ability to classify crops, we made a recognition map. (See Figure 2). The signatures for the recognition map were derived from three fields of each class of vegetation.

TABLE I

SELECTED PROBABILITIES OF MISCLASSIFICATION
FOR SACRAMENTO VALLEY CROP SPECIES

CATEGORIES	PROBABILITY OF MISCLASSIFICATION
Stubble-Wheat*	0.204
Tomatoes-Sugarbeets*	0.157
Melons-Sugarbeets	0.075
Milo-Sudan	0.059
Tomatoes-Sudan	0.038
Corn-Orchard	0.032
Corn-Milo	0.032
Tomatoes-Melons	0.030

*Combined in Recognition Map

3.1 Analysis of the Recognition Map

We analysed the recognition map of Figure 2 to determine the classification accuracy of the various crops on a per field basis.

Rice was well recognized. Of 30 rice fields (other than the training set) examined, all were correctly classified. A field was assumed to be correctly classified if more than 50% of the points (exclusive of the boundary points) were rice. Boundary elements were recognized as corn and occasionally milo.

About half of the dozen safflower fields were correctly recognized. The remainder were called stubble. Examination of the color IR simulated imagery reveals a subtle destination between the pale yellow tone of safflowers and the white tone of stubble. Apparently, safflowers were mature at the time and some may have been harvested.

Stubble recognition was correct in all 20 areas examined. As previously mentioned, wheat and barley stubble could not be distinguished, and the stubble training set also solidly recognized some safflower fields.

Tomatoes and sugarbeets were correctly classified in each of the ten fields examined. There was a tendency for scattered sugarbeet and tomato recognition to occur in other areas, particularly in melon fields.

Melons were poorly recognized in the three fields examined. Closer examination of one of these fields on the CIR simulation reveals a varied

planting pattern with some areas in melons and some bare areas. Since the recognition map classifies melons in those areas which are planted; and bare soil recognition elsewhere, the map is felt to be more indicative of the true situation than the ground information.

Water was consistently well recognized, with rivers, large irrigation canals, lakes and some flooded fields all recognized. A fallow field signature obtained from one of the flooded fields proved very specific, recognizing that field and one or two others. The combination of the recognition of these two training sets is felt to accurately portray all water in the scene.

Alfalfa, orchard, corn, and milo recognition was disappointing. Areas of these crops were correctly classified, but a great amount of recognition showed up in other areas. Alfalfa and orchard signatures were derived from areas of sparse cover and probably represent only a subtle departure from bare soil. This fact may account for the appearance of so much orchard and alfalfa recognition outside orchards and alfalfa fields.

Bare soil was consistently correctly classified. Sudan grass was also correctly classified in the three areas examined.

3.2 Mensuration

Since we had good success recognizing rice, we addressed the problem of acreage estimation. We had acreages of some fields available from ground information and concentrated on these fields for a test of rice acreage recognition.

At the outset we knew that the boundary elements being misclassified would impair our acreage estimation accuracy. So we estimated the percentage of rice in the boundary elements using special techniques developed by Nalepka (Ref. 3). We found that about 75% of a typical boundary element was rice and 25% bare soil and water. This value is in good agreement with the ground measured 50-60 ft irrigation canal width. A canal of this size would occupy about 1/4 of an ERTS digital tape sample point.

The results of acreage estimates for the seven rice fields studied are shown in Table II. Notice that all fields are greater than 100 acres in size. Acreage estimates taking only samples recognized as rice are consistently low, even though solid recognition was obtained in each field. Using a revised estimate based on recognition and mixtures, much better acreage estimates are obtained. (Mixtures analysis was used to estimate the amount of rice in the boundary elements. Boundary elements separating two rice fields were assigned equally to both fields.) The improvement in acreage estimation using the mixtures technique is felt to be significant.

TABLE II

COMPARISON OF RICE FIELD ACREAGES ESTIMATED BY RECOGNITION AND BY RECOGNITION PLUS CONVEX MIXTURES

RICE FIELD	TRUE ACREAGE	RECOGNITION ESTIMATE	RECOGNITION PLUS CONMIXED
1	150	119	144
2	212	174	205
3	106	71	95
4	159	130	163
5	176	149	179
6	194	173	196
7	224	214	236
TOTAL	1221	1030	1218

4. SIGNIFICANT RESULTS

Several significant results have accrued from this investigation.

1. Concise display of ERTS digital tape video or recognition data can be obtained by D/A conversion of data and printing on 70 mm filmstrip printers developed for the airborne scanner program. Alternatively, special purpose color digital displays may be generated by devices which print in colored inks directly on paper using 0.014" resolution cell size.

2. Accurate crop species recognition can be done in areas of large field agriculture under relatively clear atmospheric conditions. Crops most accurately recognized are those which are green and substantially completely cover the underlying soil. Mature or harvested crops can be discriminated with lesser degrees of accuracy. Crops with incomplete cover can be recognized inside their field boundaries, but recognition also occurs outside agricultural fields yielding a large number of false alarm detections.

3. Accurate acreage estimation of crops in fields 100 acres in size or smaller requires that some estimate be made of the amount of crop contained in possibly misclassified boundary elements. Without this estimate, acreage determined from pattern recognition results will be biased low. The amount of bias increases with decreasing field size, and is also dependent on field shape.

5. REFERENCES

1. Thomson, F. J., Gordon, M. and Morgenstern, J., "Environmental Research Institute of Michigan Computer Processing of ERTS-1 MSS Data from the "San Francisco" Frame (1003-18175), Environmental Research Institute of Michigan, Ann Arbor, Michigan, Report No. 011229-4-S.

2. Thomson, F. J., Gordon, M. Morgenstern, J., Sadowski, F., Environmental Research Institute of Michigan Computer Processing of ERTS-1 MSS Data from the "San Francisco" Frame (1003-18175), Environmental Research Institute of Michigan, Ann Arbor, Michigan, Report No. 011229-8-L.

3. Nalpeka, R. F., Horwitz, H. M., and Thomson, N. S., "Investigation of Multispectral Sensing of Crops", Infrared and Optics Laboratory Willow Run Laboratories, Institute of Science and Technology, The University of Michigan, Technical Report No. 31650-30-T, May 1971.

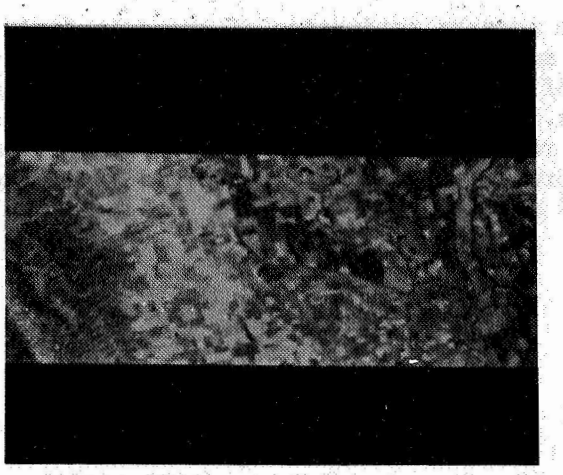


Figure 1a
Imagery of Sacramento Valley Test Area
(original in color)

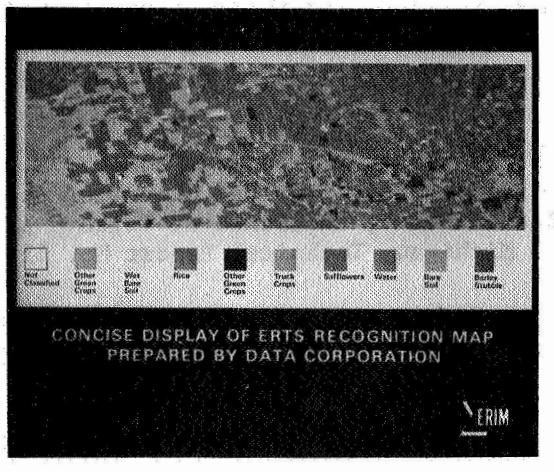


Figure 1b.



Figure 2
Crop Species Map of Sacramento Valley ERTS Data
(Original in color)

Paper A 23

THE RESULTS OF AN AGRICULTURAL ANALYSIS OF THE ERTS-1 MSS DATA AT THE JOHNSON SPACE CENTER

R. M. Bizzell, L. C. Wade, H. L. Prior and B. Spiers*, *Earth Observations Division, NASA, Johnson Space Center, Houston, Texas*

ABSTRACT

This report describes the initial analysis of the ERTS-1 multispectral scanner (MSS) data at the Johnson Space Center (JSC), Houston, Texas. The primary data set utilized was the scene over Monterey Bay, California, on July 25, 1972, NASA ERTS ID No. 1002-18134. It was submitted to both computerized and image interpretative processing.

An area in the San Joaquin Valley was submitted to an intensive evaluation of the ability of the data to (1) discriminate between crop types and (2) to provide a reasonably accurate area measurement of agricultural features of interest.

The results indicate that the ERTS-1 MSS data is capable of providing the identifications and area extent of agricultural lands and field crop types. Later data sets of Hardin Co., Iowa, and Holt Co., Nebraska, have undergone preliminary analyses as a portion of a joint USDA/ASCS-NASA/JSC ERTS-1 data evaluation project. These preliminary results using the same techniques as those carried out on the Monterey data show an ability to discriminate major crops which are representative of different agricultural practices.

1. INTRODUCTION

The Earth Observations Division (EOD) at JSC is involved in an extensive program related to the evaluation of the utility of the Earth Resources Technology Satellite (ERTS) in terms of applications related objectives. This report is intended to describe some of the early results achieved from the analysis of System Corrected MSS data over agricultural target areas.

---

*Agricultural Stabilization and Conservation Service.

Two separate but interrelated efforts related to agricultural applications are described here. The first is a general investigation directed to familiarization and feasibility type objectives. The second is a more specific investigation directly intended to determine the utility of the ERTS-1 MSS data to meet defined functional requirements of the Agricultural Stabilization and Conservation Service (ASCS).

The initial data set received at JSC of Monterey Bay, California, of July 25, 1972, was utilized to accomplish our first general objectives: 1) to obtain a cursory evaluation of the potential of satellite acquired multispectral data to provide information which would support applications related objectives; 2) to checkout existing, and initiate the development of necessary additions to the earth resources data processing facilities; and, 3) to develop and define the initial analysis techniques and operational procedures necessary to support the subsequent activities related to the EOD ERTS-1 Project. The area selected for the initial analysis lies in the San Joaquin Valley, a major agricultural region in the Monterey Bay frame which is representative of farmlands developed due to the application of irrigation systems. The area is approximately 23 x 38 km in size or 218, 352 acres. "Ground truth" information for approximately 5 percent of the area was available through the courtesy of the Anderson, Clayton and Co. They maintain an extensive farming operation in the San Joaquin Valley and utilize monthly aerial photographic missions over their fields as operations management tools. The specific information supplied to us was an annotated map and a related aerial photograph depicting crop types for several fields in the Delta Mendota region on July 13, 1972.

In order to accomplish our overall objective in a reasonably short period of time, the following specific objectives were defined at the completion of our initial examination of the ground truth information and associated crop calendars: (1) Crop type discrimination – to obtain some measure of the ability to discriminate between crop types using the ERTS data, it was decided to concentrate our efforts on rice because it is one of the major crop types within the Delta-Mendota, and several ground truth fields were available. It is a warm weather crop with a 120 to 175 day growing season, and, thus, being July 25 it is basically at its mid-stage of growth and should be fairly uniform between fields. Both computerized and image interpretative techniques were evaluated. (2) Detection of cultivation practices – the ground truth information revealed that one crop, barley, was in the processes of undergoing change as related to the local farming practices. Although there were no known mature barley fields in the study area, there were fields in three distinct phases which were selected for further analyses and performance evaluation investigations: (a) barley stubble – the remains of a mature barley field after undergoing harvesting operations, (b) burned barley stubble, and (c) barley fields which have been plowed under in preparation for the next season's crop. In the above objective, it is obvious that in the case of the burned fields, it would be highly improbable to discriminate between a plowed under barley field and a plowed under wheat field, and it is not the objective of this exercise to do so. What we are attempting to do is merely to detect what the field condition of the known fields are at the time of the ERTS overpass, July 25, 1972. And for a few fields compare

them with what their respective conditions were at the time of the ground truth acquisition, July 13, 1972. This should give us an indication in crop growth of the utility of the repeat coverage from ERTS-1 to monitor temporal changes and farming practices. (3) Mensuration accuracy – for a few selected fields of various dimensions an exercise was conducted to determine how well one may be able to obtain a measure of the area extent of a crop type after it has been detected and identified. The baseline or control data was generated in-house utilizing the best available rectified high resolution aerial photographs.

The first image interpretation analysis performed was of a black and white image of MSS 5 (the red band). Using a known, triangular-shaped rice field as a key, the entire study area was searched for fields having a similar characteristics. Within the study area nineteen (19) fields or groups of contiguous fields were identified as rice. The two known rice fields, in addition to the training field, were correctly identified using this one black and white image. No attempt was made to identify the barley crop using this imagery.

The second task was to analyze an optically enhanced color IR image composited from B/W MSS System Corrected images of bands 4, 5, and 7, on an additive color viewer printer (ACVP). This viewer permits individual filter densities to be selected and enlarges the original image approximately eight times. Because of this enlargement factor only a part of the study area is covered on this image. Only rice was interpreted using this imagery. Ths same field indicated earlier was used as a key, and a total of seventeen fields or contiguous areas were identified as rice. The results using this technique were not as reliable as the preceding or subsequent technique.

The third task was to identify the crops (rice, barley stubble, and burnt barley stubble) using two images generated from the digital computer compatible tapes (CCT) with an electron beam film writer. One image was a pseudo- or false-color composite of MSS bands 4, 5, and 6 and the other was a color IR composite of MSS bands 4, 5, and 7. Due to the saturation of other highly vegetative fields in the IR band (MSS 7), the rice fields could not be uniquely identified on the color IR image. However, using the false-color image 18 contiguous rice fields were identified with all of the known or ground truth fields readily detected. Also, for the barley stubble fields the false-color image appeared to provide better distinction characteristics and a total of 22 fields were identified. However, when trying to identify the burnt barley stubble fields the color IR image exhibited the best visual discrimination characteristics. Twelve fields in this category were identified using the color IR imagery.

The accuracies achieved from this analysis is currently being evaluated. In all cases, the known fields were correctly identified, however, information on the other fields identified at the time of the ERTS-1 overpass is not complete. This may point out one of the benefits of a cyclic data acquisition system such as ERTS, i.e., as a source of information for hisforical reference which heretofore was nonexistent on a regional basis.

The results of this analysis of the ERTS-1 MSS data satisfactorily achieved our objectives. Using only the images produced in this analysis, additional crop species could have been discriminated and we are confident

that with the proper application of existing enhancement techniques most of the major crop types in the study area could be identified.

In the computerized processing phase the known fields for rice, barley, stubble, etc., were defined to an automatic pattern recognition routine, the statistics for the required classes were computed, then each data point in the entire set was classified according to their spectral "signature" as defined by the 4 MSS bands and the generated statistical parameters. The results are shown in the following table:

CLASSIFICATION SUMMARY REPORT FOR KNOWN FIELDS IN DELTA MENDOTA

Classes	Rice	Stubble	Burned	Turned	Other	Overall
No. Pixels	13,528	6,483	4,155	22,820	153,915	200,901
% Total	6.7	3.2	2.1	11.4	78.6	100%
Equivalent Acreages	14,703	7,046	4,516	24,802	167,285	218,352
Training Field Accuracy	92%	97%	90%	98%	93%	94%
Test Field Accuracy	97%	98%	76%	94%	95%	93%

In addition to these, other major crop types in the study area were identified, e.g., safflower, alfalfa, cotton, etc., as a result of the computer processing operations. Also, the utilization of image interpretation analysis of the computer generated images yielded additional information related to crop condition and/or farming practices, e.g., areas depicted as water in curiously familiar rectangular shapes were deduced and later confirmed to be, flooded rice fields.

The results achieved from the computerized processing far exceeded our original expectations. In fact, for the purpose of detecting and identifying crop species in fields of 10 acres or more over large areas (10 miles square or more), our experiences here and with airborne multispectral data would at this time dictate a preference for the ERTS-1 MSS data for accomplishing an application objective of that scope. This observation assumes a reasonable requirement for accuracy of the results, e.g., does not require location or area measurement within 1 percent.

Upon completion of the classification of the identified crop species, the mensuration investigation was initiated. The objective here was to obtain a preliminary quantitative measure of the digital ERTS-1 ability to provide reasonably accurate area measurements. For this investigation three rice fields of known dimension were located on rectified, high resolution, aerial photography, and the ground equivalent units or acreages were determined. Then the acreages for these fields were extracted from outputs acquired as a result of the computerized and image interpretative classification schemes. For the computerized this was a simple count of the picture elements (pixels) which were classified in the three known rice fields and applying a conversion factor of 1.1 acres/pixel to this count (Note: The 1.1 value was determined from an evaluation of known distances in this particular study area and may not necessarily apply to other areas.)

The following table lists the results achieved from this cursory investigation:

RESULTS OF THE MENSURATION ACCURACY INVESTIGATION

(Results in Acres)

Field	A/C Ground Truth	Image Interpretation	Converted Pix. Counts
R1	164	150	144
R2	190	170	176
R3	161	161	150

The significance of the converted pixel count discrepancy with the aerial photograph measurement lies not only in the 15 acre average difference but the fact that it is in all cases smaller. This could be attributable to two effects: (1) the aerial photographic measurements are not absolute but relative based on the accuracy of actual registration especially in scale to the map positions used for the initial control, i.e., the values derived from the aerial photo is in all cases larger than the true ground measurements and (2) the only pixels converted were those which were actually classified as rice. Post-analysis communications with Anderson, Clayton and Co., revealed that although the field size of one of the ground truth fields (R3) was listed at 160 acres, that included a fringe area, outside the actual growing rice boundary, which extended to the center of the road adjacent to the field. Thus, the acreage as determined by the converted pixel count of actual rice should in reality be less than the listed field size. Although an attempt to rectify the classification images to remove the known geometric distortions was not conducted, it is expected based on past experience that these accuracies could be improved. Additional studies in mensuration are being conducted in order to obtain a verification of the accuracies which may be achieved. In any case, the simple study described here indicates that accuracies in the order of 90-95 percent or approximately 15 acres of error in a 160 acre field, is not unrealistic.

Utilizing basically the techniques developed during the Monterey Bay analysis, a separate analysis is being conducted as part of a joint project whereby NASA through JSC and the USDA through the ASCS will jointly evaluate the feasibility of using ERTS type data to meet the ASCS functional requirements for crop identification/land use classification, acreage measurements, and correlation of crop and land use data to ground position. For the purpose of the overall JSC/ASCS analysis, six agricultural study areas of 12 square miles each were selected for intensive study. These study areas were selected to provide a manageable size working area while retaining a variety of crop types, geographical conditions, and varying problem complexity levels.

Within the selected study area for each county, ASCS personnel have made a very thorough one-time ground truthing of every field. In addition, ground truth was collected for selected fields in the study area on the day of each ERTS overflight during the agricultural growing season.

With the ground truth information the study areas may now be used as controlled test, training, and evaluation sites in regard to the objectives of crop species identification, acreage measurement, and tract registration.

The six counties selected for this overall analysis at JSC were: (1) Hill County, Montana with strip-fallow farming practices and wheat/barley as major crops; (2) Hardin County, Iowa with typical corn belt farming practices and primary crops of corn, soybeans, oats, and smaller field sizes; (3) Butte County, California, with a combination of rice, fruits, and nut crops and larger irregular shaped fields; (4) Imperial County, California, with its larger size fields, complex variety of winter and summer crops, and abundant historical ground truth; (5) Worth County, Georgia, with cotton and tobacco crops in small size fields of irregular shapes, and (6) Holt County, Nebraska, with a small number of crop types and large known size fields in a unique pattern. The emphasis at this time will be to present some preliminary results from two of these study areas: Holt County, Nebraska, and Hardin County, Iowa, as obtained primarily from a clustering technique.

Holt County is located in the upland sand on the eastern edge of the Nebraska sand hills and bordered to the north by the Niobrara River. Holt County comprises an area of 2,400 square miles of which 1,500,000 acres are in agricultural use. The crop variety of Holt County is limited with corn being by far the major crop type, with alfalfa hay ranking second and in lesser amounts, popcorn, sun flowers, christmas trees, oats, grain sorghum, and irrigated pasture lands. This area was made a priority study area because of its unique and relatively high contrast targets of a known acreage and its small variety of major crop types. The higher contrast targets are provided as a result of the development of the center pivot irrigation systems to convert the low productivity, sandy, shallow profile soil to productive cropland. These uniform circular field patterns of irrigation are clearly visible from ERTS-1 altitude and comprise a target of an accurately known dimension and area (135 acres).

Due to an ERTS launch relatively late in the growing season, it was highly desirable to make use of the earliest possible clear coverage of the area. The earliest data pass over Holt County occurred on July 30, 1972, and was found to be cloud free. This data was contained in a digital form as a portion of a MSS CCT as produced by NDPF and GSFC and designated by NASA identification number 1007-16551MB-4 of 4.

After screening and reformatting the data to a form compatible with our analyses systems, the next step was to utilize the clustering algorithm to cluster the data measurements into unique groupings which could be correlated to actual ground truth information. The necessary ground truth information was collected for each study area by the ASCS County Executive Director's Office.

The results of the clustering analyses were displayed on the DAS and color coded for correlation to the ground truth data. These results are shown to be correlated reasonably well with the known ground data.

As represented by the DAS output, the cultivated land is fairly well separated from the noncultivated farmland and the sand hills to the north. Within the noncultivated area three major groupings are clearly

detectable: short grasses and active grazing areas represented by one cluster, ungrazed thick grasslands represented by a second cluster, and bare sandy soil areas represented by a third cluster. Of interest in the bare soil areas are a 1/2 circle of fallow land in the southwest corner of the study area and a quarter mile wide strip of fallow in the south center of the study area, which are well correlated with the ground truth map. The remainder of the bare soil areas are primarily representative of a Dune sand area between Big Sandy Creek and Brush Creek in northern Holt County and correlates well with existing soil maps. Within the cultivated portion of the study area, 32 separate fields of field corn are shown in the ground truth map, of this number 30 are partially or fully represented by the information within several clusters. The second major cluster grouping within the study area is representative of the remaining cultivated area. This clustering distinctly defines two popcorn fields of the three in the ground truthed area, the one known sun flower field and the remaining two fields of field corn. The discrepancies noted within this grouping appear to be tied to either a differing maturity stage or possibly a difference in irrigation practices, which will require further analysis. Additional analysis using temporal data separated by 18 days and color additive techniques has shown an ability to differentiate between the popcorn and sun flower fields of this same data set and is being evaluated at this time.

The statistical data developed as a part of the cluster analysis will as a next step be input into one of the automatic pattern recognition routines implemented in the Monterey Bay analysis for further refinement and development of a classification map.

The second county to be discussed at this time is Hardin County, Iowa, with results again being of a preliminary nature using the clustering algorithms. Hardin County is located in the North Central portion of the state and bisected by the Iowa River. The area is in the heart of the fertile, gently rolling, north central glacial till plain. Hardin County covers an area of 574 square miles, of which 350,000 acres, or 95 percent, is in farm land, with about 75 percent being cultivated cropland. Corn, soybeans, oats, and other feed grains are the most extensively grown. Crops with a small portion of the crop land are in hay, permanent pasture, tame and native grasses. The selected study area is representative of typical corn belt farming practices, and as opposed to Holt County, nonirrigated crops.

The earliest useable data pass over this area occurred on August 13, 1972, with some limited amount of cloud cover to both the north and south of the study area. This data is contained in a digital form on MSS CCT designated by the NASA identification number 1021-16324MB-4 of 4.

Again as with Holt County, the data was submitted to be processed only with the clustering algorithm and color coded on the DAS for correlation with the ground truth. Being typical corn belt, the major crop types in Hardin County are the corn, soybeans, and oats. At this maturity stage it is expected that those three crops could be reasonably well separated. For corn and soybeans the clustering results seem to indicate this as being true; however, the oats being harvested in July

now have a strong cover of secondary growth and appear mixed with other grasses and legumes. The corn is represented by the major cluster output from the clustering and is fairly well defined. A total of 76 corn fields are represented on the ground truth tabulation, and of these 73 are partially or wholly clustered uniquely by the clustering algorithm. Those three fields unaccounted for are small individual fields that are beyond the expected resolution limit and the larger fields are all fairly well defined with very little extraneous data. A thin scattered cloud to the south of the study area casts a weak shadow along the northern edge of the area and causes a lumping of other crop types with the corn in this area. A later date separation indicates that the soybeans are also uniquely clustered and separable from the corn and oats; however, further analysis of these crop types is required.

2. CONCLUSIONS

In conclusion, in order to meet agricultural applications related objectives, these analyses concerning the utility of ERTS-1 multispectral scanner data have yielded the following significant findings: (1) most important, with existing technology, we are right now able to extract information from the ERTS-1 data which satisfy certain agricultural related objectives. Specifically, we were able to detect and identify major crop species over large geographical regions and to determine the location and areal extent of the associated fields; however, additional analysis and evaluation must be made to determine which and to what extent specific requirements of ASCS can be accomplished. With the development of new techniques and improved application of the existing ones, we hope to meet the more stringent requirements; (2) The greater radiometric fidelity of the system corrected digital data and the subsequent flexibility available for the application of enhancement techniques to this data suggests a preference of this data for the detection and identification processes; (3) The discrimination capability of the data is good and in some cases better for crop species identification activities, as compared to similar experiences with low altitude airborne multispectral data; and (4) This investigation revealed that significant results could be achieved with limited ground truth information or, at most, utilize merely aerial photography to provide most of the control information required for training, test and verification purposes.

In summary, these preliminary results achieved here indicate that with proper selection of data based on crop calendars, and ground truth information, and the utilization of enhancement and pattern recognition systems currently available, major crop types can be detected, identified, and their area extent determined from the ERTS-1 multispectral scanner data.

Paper A 24

AGRICULTURAL APPLICATIONS OF ERTS-1 DATA

William C. Draeger, *Forestry Remote Sensing Laboratory, University of California, Berkeley, California 94720*

INTRODUCTION

Considering the present needs for regional, national, and worldwide inventory and evalution data, coupled with the particular capabilities of the ERTS system, agricultural applications appear to be especially promising as an area in which important benefits might be realized from the use of such technology. In the United States, the Department of Agriculture presently conducts an enumerative program in which virtually all agricultural land is inventoried annually. In addition numerous other federal, state and local agencies conduct extensive crop inventories, land use surveys, and soils mapping projects of varying magnitude. On a worldwide basis it would seem that the principal obstacles to providing enough food for all persons are those of allocation and distribution. What is needed is knowledge as to where and how much food is now being produced, and how crop production is changing with time.

Up to the present time agricultural inventories have required a tremendous effort on the part of on-the-ground enumerators, and have presented a formidable data compilation task. However, a satellite sensing system, with which large areas of land can be surveyed in their entirety on one image, and which can provide uniform worldwide coverage with a relatively small number of images offers great promise as a data collection tool for alleviating these problems. Furthermore, the dynamic nature of agriculture requires not a single evaluation in most cases, but rather a continual updating of conditions. In fact, it has been shown that desired information about agricultural crops can often be obtained only by capitalizing on a knowledge of the patterns of change of particular crop types of conditions. Again, this suggests that a satellite sensing system such as ERTS, which makes possible regular, frequent observations of each spot on the earth's surface, can provide a service which would be totally infeasible using conventional techniques.

Based on these facts, plus the encouraging results achieved using both high altitude aircraft and spacecraft imagery for crop inventory experiments over the past several years, the Forestry Remote Sensing Laboratory at the University of California has undertaken the experiment described in this paper. The experiment is designed to evaluate the feasibility of using satellite data regionally to provide needed agricultural information on an operational basis. The experiment is being performed in Maricopa County, Arizona and San Joaquin County, California in cooperation with a number of state and federal agencies.

In an effort to accurately determine the degree of detail which can be extracted from ERTS-1 data, and the optimum use of "subsampling" in the form of aerial photography and ground truth data for various agricultural-related tasks, the investigation is being carried out in a step-wise fashion beginning with gross land use mapping, and progressing to very detailed crop inventories. In all cases, emphasis is being placed on obtaining a quantitative expression of the accuracy of estimates obtained by the use of remote sensing for the county as a whole, and where possible, a comparison of these results with those obtained using conventional techniques. Investigations entail the use of both human interpreters and automatic classification and data handling techniques, and an evaluation of the optimum mix of human and machine techniques for each analysis problem. In each case, an attempt is made to ensure that the types of information compiled (e.g., maps, tabular data, crop acreages, etc.) conform to actual requirements or desires as expressed by those persons currently involved in resource evaluations and planning in the test site.

In the area of agricultural land stratification, initial stratifications have been performed in the San Joaquin area on ERTS-1 imagery which was obtained on July 26, 1972. Plans call for similar stratifications on later dates of imagery, and for comparisons of delineations made at different dates and seasonal states. Preliminary analyses of the stratifications to ascertain the extent to which they do provide meaningful crop type and condition information already have been carried out. Finally, a study is under way to analyze the usefulness of stratification information in improving crop classification accuracy using automated techniques.

Crop classification and inventory studies are progressing concurrently with the stratification investigation, as it seems likely that any operational inventory procedures will be heavily dependent on an initial stratification of agriculture on ERTS or other small scale imagery. At the present time an automatic "CALSCAN" classification has been completed for a single stratum using ERTS data acquired in July, 1972. Subsequent work will include an extension of these techniques to the entire San Joaquin test site, and the use of multidate imagery for crop classification. Little crop inventory work using human interpreters has been done to date due to the dependence of the interpreter on the selection of optimum dates of imagery for specific crop categories. This factor seems to be more critical in the case of human interpreters than with automatic classification. Therefore most non-automated crop inventory work will be done next spring. In the meantime, however, studies are under way to ascertain optimum methods for point sampling in the interpretation process on ERTS imagery of large areas for crop inventory purposes. This work is based on the assumption that if crop inventory techniques using ERTS and other remote sensing data are ever to be adopted on an operational basis, efficient statistical sampling methods must be developed concurrent with the actual interpretation methods in order to adequately demonstrate the practicality of using space-acquired data.

Agricultural land use change detection studies are being conducted primarily in the Maricopa County test site, where MAPIT techniques will be used to analyze both long-term and short-term additions to and depletions of agricultural land using both Apollo 9 and earlier conventional aerial photographs as well as the ERTS imagery as data inputs.

Finally, efforts to develop a computer storage and compilation capability for the handling of the large amounts of ground data gathered in the two test sites is progressing well, and it is planned that this work should be completed soon.

RESULTS

a. Agricultural Land Use Stratification

In an attempt to evaluate the usefulness of ERTS imagery for the production of land use stratifications as a preliminary step in the crop inventory process, all land within San Joaquin County was delineated into broad land use and crop category classes based on their appearance on the ERTS-1 color composite image. The stratification of the agricultural land use categories proved to be a relatively simple task, taking each of three interpreters approximately 30 minutes to complete. The three interpretations were quite similar, requiring only minor revisions to produce a "consensus" stratification. A total of 13 different agricultural strata were recognized, differing both in general field size and relative proportions of crop types and degree of irrigation. Upon comparing these interpretations, it was concluded that nearly all boundaries were truly representative of differing cropping practices. In a number of cases, the stratifications agreed almost exactly with soil type boundaries as drawn by earlier soils surveys, and in many cases probably represent a refinement of those earlier boundaries drawn "in the field".

Certainly a much more detailed and up-to-date stratification was produced from the ERTS image than is currently used by the Statistical Reporting Service of the USDA for their inventory work. The obvious questions arise, however, as to: (1) whether the strata as drawn on the image are meaningful in terms of actual land use conditions, and (2) whether such a detailed delineation could enable the SRS to more efficiently and accurately estimate the parameters of interest on a statewide basis.

The capability has been developed to digitize stratification boundaries as drawn by the interpreters and to store these data for future retrieval. The resulting data bank can then be used to accomplish the following:

1. Provide area information for individual strata from an analysis of the digitized boundary coordinates.
2. Monitor the degree to which strata boundaries change as delineated on imagery acquired at different times throughout the year.
3. Compare stratification boundaries with data from other sources.

In order to quantitatively evaluate the correlation between land use/

crop type as delineated on ERTS-1 imagery and actual ground conditions, a sampling system using transects flown by a light aircraft was developed. As the transects are flown, an observer records the land use/crop type that appears below the aircraft at 10 second intervals. Six such sample transects, with about 130 observations per line, were flown over the San Joaquin test site, and a statistical analysis performed to test the relationship between the proportion of each land use/crop type appearing in each stratum. It was concluded that the delineations as drawn by the interpreters were indeed meaningful on a quantitative basis. Furthermore, the method of data collection proved to be quite efficient, and will be utilized for future aspects of this study.

b. Monitoring Agricultural Land Use Change

The use of satellite imagery in monitoring the shift of land use in agricultural areas has been investigated using coverage of the Maricopa County test site acquired both from Apollo 9 and from ERTS-1.

An ERTS-1 color composite of the area taken on August 23, 1972 was interpreted and delineations were made of the agricultural, wildland and urban areas. These delineations were transferred onto acetate material which was directly overlaid on the Apollo 9 enlargement such that shifts in land use could be quickly identified. Since the prime interest in this study was to monitor land use shifts, either to or from agricultural use, only changes involving agricultural usage were quantified. With the use of a dot grid the acreages of land shifts were calculated.

For the Salt River Valley region of the county there were no apparent significant shifts of wildlands into agriculture during the period in question. All of the agricultural land shifts were to urban uses of various kinds, mostly urban residential usage. The total agricultural acreage shift into urban usage was computed to be approximately 28,160 acres, indicating an average annual shift of approximately 9,400 acres of agricultural land converted to urban use each year. In a recently published report of the Economic Research Service, it was estimated that for the period from 1949 to 1964, Maricopa County had an average annual shift of all land into the urban category of 9,010 acres. Eighty percent of this figure was agricultural land being urbanized, and thus the average annual shift of agricultural land to urban usage for the period of their study was 3,208 acres per year. Thus it can be seen that the rate of urbanization of agricultural land in Maricopa County has tripled in recent years.

c. Crop Identification and Inventory -- Manual Interpretation

In a study designed to evaluate the potential for manually identifying crop types on the ERTS-1 imagery, a survey of safflower fields in a portion of the San Joaquin County, California test site was carried out using human photo interpreters. Approximately sixty fields were interpreted, of which thirty were safflower as ascertained by ground surveys. In a selected portion of the test area the interpreter was asked

to delineate all safflower fields, thus necessitating not only an identification of the crop, but a determination of the field boundaries as well. Safflower was chosen as the subject crop for this test because it was the only crop that was passing through an "optimum" phenological stage for discrimination on the single date for which ERTS-1 data were available.

The identification test produced an 83 percent correct identification, while in the area where both detection and delineation were required, the results were as follows:

$$\% \text{ Correct} = \frac{\text{\# of fields correctly delineated as safflower}}{\text{total \# of safflower fields in the test area}} \times 100 = 79\%$$

$$\% \text{ Commission Error} = \frac{\text{\# of fields incorrectly delineated as safflower}}{\text{total \# of safflower fields in the test area}} \times 100 = 4.6\%$$

Considering the fact that in this initial test the interpreters were unable to exploit the advantage of sequential coverage which ERTS-1 will provide, and that perhaps more nearly "optimum" dates for crop discrimination can be found at other times of the year, these results were quite encouraging. Certainly they show that an interpreter can detect and delineate individual fields on the imagery. It was the general consensus of persons interpreting the ERTS-1 color composite that ground resolution for non-linear objects of medium contrast was on the order of 250 to 350 feet, and that it was possible to observe generally reliable signatures for fields down to 20 acres in size on the color composite.

d. Crop Identification and Inventory -- Automated Interpretation

During the initial phase of the study, considerable effort has been directed toward: (1) The creation of a computer system and programs which will accept the varied inputs derived from the ERTS-1 images, tapes, supporting training and ground data (and also the subsequent data produced in the steps leading to an operational output), and which will provide output in a format that is both efficient for the operator and useful for the consumer. (2) The implementation of techniques for utilization of ground data, spectral information and imagery stratification to facilitate classification of ERTS-1 data into useful information.

Four major classes of computer programs have been assembled for use on the Forestry Remote Sensing Laboratory computer and the associated large scale computers: (1) Digital image handling and display, (2) Statistical spatial and spectral pattern recognition, (3) General statistical, and (4) Multilevel data bank. These programs are being used to process the data obtained from ERTS-1 aircraft, and ground data collections. Their use allows the selection and reformatting of areas of the state that are being analyzed intensively for correlation with ground data, mapping of features of interest based on their spatial and spectral characteristics, selection of optimum dates and spectral band(s) for classification, and comparison with existing data, both mapped and point. They are also being used to compare manually mapped

boundaries and computer generated boundaries with ground data. The FRSL system has been applied to the problem of crop classification in San Joaquin County with very good results.

The first quantitative evaluation of the CALSCAN process for classifying ERTS-1 data was performed using black-and-white MSS bulk transparencies acquired of the San Joaquin test site on July 26, 1972.

Of the forty-eight ground data cells in San Joaquin County, eleven cells in the field crop strata (as delineated by photo interpreters in the stratification study described previously) were selected for intensive analysis.

Each cell was scanned on each of the four MSS transparencies to a common scale and registration such that each data point represented a 250 x 250 foot spot on the ground. To accomplish this, the map coordinates of the cells were entered in a program that computed the translation, rotation, and scale change necessary to place the map coordinates over the MSS images. This transformed coordinate information was then used by the scanner program to locate and scan the cells. Twenty-seven representative training areas were selected from the data to train the classification algorithm on the ten land use categories considered.

After the point-by-point classification was completed, each point was reclassified by an algorithm that considers the classification assigned to neighboring points. This technique improved the point-by-point classification between ten and thirty percent, depending on the homogeneity of the field. A field map of the ground truth was then laid over the final automatic classification results. Each field was then assigned by an interpreter to the class that had the maximum data point count within the field on the overlaid map.

A total of 201 fields were classified in the test area, with an overall correct identification of eighty-four percent. Again, these results are based on a field-by-field rather than a point-by-point identification, and are the result of an analysis of data from all four MSS bands. Use of the scanned photo data and pre-mapped field boundaries allowed classification down to a twenty-acre field size.

The classification of a large agricultural block on the west side of the San Joaquin County test site was next undertaken (1) as the natural subsequent step in an effort to show the capability of an automated data processing approach in producing accurate and timely agricultural inventories of larger areas and (2) as the next step in the automated analysis of human stratification of agricultural areas and of the relation of these strata to further automatic classification.

The area classified comprises approximately 340 square miles or 220,000 acres, and, at the time of image acquisition, contained primarily field crops of which asparagus, corn, alfalfa and sugar beets comprised the majority. The study was accomplished by training on 1,340 acres, and testing on 11,000 acres. The total area of the inventory was 219,872 acres.

Ten agricultural categories which comprised the majority of crops

in the test area were included in twenty-five training fields. After training of the statistical models, each point in the area was classified using an algorithm that computes a likelihood factor that the point is statistically similar to each training model and then assigns to the point the name of the category for which its factor is the highest. The area was then run through "reclassification" as described earlier. Quantitative evaluations were made of the point-by-point results in the training areas by a routine in the CALSCAN program and of the field-by-field results in the test cells by manually overlaying field maps and assigning to each field the crop indicated by a majority of its points.

The point-by-point evaluation of the training fields showed a class average of 87.8 percent correct for the "classified" results and 96.1 percent after "reclassification". Overall, 88.3 percent of the fields in the test areas were correctly identified, some of which were smaller than ten acres in size. The major crops in the test area were asparagus and corn which scored 89.4 and 92.2 percent correct, respectively.

With the results from the test area as an indicator of the accuracy obtained, the classification of the entire test area was undertaken. The results of the total area classification in terms of acreage and percentage of crop type are shown in Table 1. The data presented there are essentially a quantitative description of the study area. The table lists the number of elements or points classified by CALSCAN as each crop type in the (1) "classified", (2) "reclassified", and (3) "reclassified with weights" versions of the display routine. Also shown are acreages and the percent of the total area occupied by each crop type, according to the "classified" results. In addition, the number of points, corresponding acreages and percent of total area or areas extracted on which the test fields were scored are listed. Comparison of the "% of total" columns shows that the ground data cells are quite representative of the area as a whole.

CONCLUSIONS

Certainly the results described here demonstrate the potential usefulness of data acquired from satellites such as ERTS-1 for agricultural applications. Particularly when the ability of the human interpreter to delineate meaningful land use strata is combined with the demonstrated ability of computerized systems to produce fast and accurate crop classifications, a potentially powerful tool is provided for the collection of agricultural information on a regional basis.

TABLE 1
POINT-BY-POINT RESULTS OF CLASSIFICATION OF ERTS-1 TAPE DATA
SAN JOAQUIN COUNTY, CALIFORNIA

	STUDY AREA					TEST EXTRACTIONS		
CROP TYPE	CLASSIFIED POINTS	RECLASSIFIED POINTS	RECLASSIFIED W/WEIGHTS	ACRES	% OF TOTAL	CLASSIFIED POINTS	ACRES	% OF TOTAL
ASPARAGUS	56,371	56,833	57,857	62,070	28.23	17,446	19,190	33.21
HARVESTED	32,103	31,282	30,416	35,377	16.09	5,159	5,675	9.83
CORN	26,662	31,320	31,290	29,375	13.36	8,720	9,592	16.60
SUGARBEET	15,646	14,689	15,046	17,238	7.84	4,309	4,740	8.20
SAFFLOWER	11,089	9,127	9,513	12,225	5.56	2,945	3,240	5.61
WATER	10,189	12,188	10,189	11,235	5.11	2,404	2,644	4.58
POTATO	5,749	3,022	3,137	6,332	2.88	1,866	2,053	3.55
BARE SOIL	1,450	973	1,450	1,583	.72	647	712	1.23
TOMATO	30,409	29,584	30,059	33,487	15.23	7,019	7,721	13.37
ALFALFA	9,932	10,582	10,643	10,950	4.98	1,994	2,193	3.80
TOTALS	199,600	199,600	199,600	219,872	100.00	52,509	57,760	99.98

Paper A 25

IDENTIFICATION OF AGRICULTURAL CROPS BY COMPUTER PROCESSING OF ERTS MSS DATA

Marvin E. Bauer and Jan E. Cipra, *Laboratory for Applications of Remote Sensing, Purdue University, West Lafayette, Indiana 47907*

ABSTRACT

Quantitative evaluation of computer-processed ERTS MSS data classifications has shown that major crop species (corn and soybeans) can be accurately identified. The classifications of satellite data over a 2000 square mile area not only covered more than 100 times the area previously covered using aircraft, but also yielded improved results through the use of temporal and spatial data in addition to the spectral information. Furthermore, training sets could be extended over far larger areas than was ever possible with aircraft scanner data. And, preliminary comparisons of acreage estimates from ERTS data and ground-based systems agreed well. The results demonstrate the potential utility of this technology for obtaining crop production information.

1. INTRODUCTION

Crop identification has long been recognized as one of the potential applications of remote sensing. In fact, accurate identification of crop species is a prerequisite to deriving crop production estimates (acres x yield per acre) from remotely sensed multispectral measurements, and the value of this type of information is substantial. It is used in managing production, storage, and transportation and in determining the market price of crops. Additionally, the USDA uses crop production information in designing national farm programs and establishing import/export policies.

Any improvement in the quality of this vital information could have far-reaching benefits. Eisgruber, ("Potential Benefits of Remote Sensing: The Actual Framework and Empirical Estimate", LARS Information Note 030872) shows that reduction from three to two percent in the error of estimate for corn, soybean, and wheat production estimates would result in 14 million dollars net social benefit to the country. Reduction to one percent would add another nine million dol-

lars. More frequent and timely estimates alone, even without an accompanying improvement in accuracy, would result in additional benefits (Ewart, "Effect of Information on Market Behavior", Ph.D. dissertation, Purdue Univ., 1972).

The wide area coverage of ERTS, combined with the capabilities of computer data processing, offers a unique opportunity to reduce the above-mentioned error of estimate through reduction in sampling error. Furthermore, the sequential coverage capabilities of ERTS may lead to benefits arising from improvements in the frequency and timeliness of estimates.

Because of these potential benefits, the overall objective of this research has been to quantitatively evaluate the utility of the machine analysis of ERTS MSS data in identifying crop species. Future investigations will verify the utility of ERTS MSS data in identifying crops over a wide range of environments with differing soils, climates, and cultural practices and make crop acreage estimates for larger geographic areas.

2. PROCEDURES

The area which was classified on the basis of ERTS data (Dekalb, Lee and Ogle Counties in northern Illinois) contains highly productive, level to gently rolling prairie soils and is intensively cropped. In 1972, about two-thirds of the total farm land was planted to corn and soybeans (Table 1). ERTS data analyzed came from Frame 1017-16093, which was acquired on August 9, 1972.

Ground truth data used to support the analysis consisted of identification of the crop or use of over 500 fields in four different areas of the three counties. Crops identified were corn and soybeans, sorghum and alfalfa, and other cover types or land used identified were hay, pasture, and small grain stubble. However, for the purposes of this analysis, only three classes were considered: corn, soybeans, and "other" (all cover other than corn and soybeans, including towns and highways). These 500 fields were used for training the maximum likelihood classifier and testing the accuracy of classifications.

Most fields could be accurately located in the ERTS data using a computer printout image generated on the basis of statistics from the nonsupervised classifier. Following the locating procedure, a random selection of training fields was made from each crop or cover type (all available fields not used for training were included in the test set). The number

of corn and soybean training fields varied from 3 to 12 in order to allow evaluation of the number of training fields on classification performance. For the "other" classes, two to four fields of each cover type were included in the training set.

Statistics for the selected set of spectral training fields were then computed and evaluated. The "other" class displayed much more variation than either the corn and soybeans which were found to be uniform spectrally (as indicated by their small variances). Additionally, the feature selection program that was run indicated that bands 5 and 6 should give results as good as either a band 5, 6, and 7 combination or all four MSS channels. Classification results subsequently confirmed this.

Classifications of each of the three counties were next carried out utilizing a training set comprised of fields from that county. This led up to a classification of the entire three-county area which was made using a subset of training fields previously used for classifying the individual counties. Several different analyses were also conducted in order to answer basic questions concerning the utility of the machine-processing of ERTS MSS for crop species identification.

3. RESULTS

The Dekalb County area was classified first, using a training set with 12 corn fields, 12 soybean fields and two to three fields for each of the "other" classes. An overall test performance (total test points correctly classified/ total test points classified) of 83 percent was achieved for the three classes of corn, soybeans, and "other". Quantitative results from this classification are shown in Table 2 (results in the other two counties were similar.)

A classification map of corn, soybeans, and "other" present in part of the three-county area is shown in Figure 1. While useful in qualitatively evaluating a classification, such maps are not necessary to successfully determine crop acreages. Nor will it be necessary to classify entire areas since estimates with very small sampling error can be obtained from classifying a random selection of sample units.

To test extendability of training sets, the training set from each county was used to classify the other two counties also. Results (Figure 2) show that equally good performance was achieved by using any of the three training sets for classifying the three, which are 15 to 25 miles apart. In further tests, there was little difference in classification

performance for two different training sets selected in the same manner (Table 3).

The next test was designed to determine if a reduction in the number of fields in the training set would bring about a decrease in classification accuracy. This test, carried out with the Dekalb County data, evaluated training sets composed of 12, nine, six, and three fields each of corn and soybeans. Although there was a decrease in the accuracy of corn identification in the reduction from 12 to nine fields, the remainder of the training sets for corn and the three-, six-, and nine-soybean training field-sets performed as well as the 12 (Figure 3).

The extendability, variability, and size limitations of training sets required to achieve accurate classifications have a large impact on the design and requirements of a ground observation system to use with remote sensing.

Preliminary comparisons between estimates from ERTS data and estimates by USDA of the percentage of the area in the three counties covered by corn and soybeans show that the estimates agree well, particularly for corn (Table 4). It should be noted that the estimates from ERTS data have been corrected for classification bias, (non-corn called corn, etc.) using information from test class performance tables such as in Table 1. There has not yet, however, been any adjustment for the highways, which are over-represented and included in the tabulation of "other".

Through use of a sample classifier which includes spatial information in the classification process, recognition accuracy of corn and soybeans went up about five percent (Table 5). This classifier requires input of field coordinates which would make it difficult to use for making acreage estimates.

One of the important advantages of computer processing of multispectral scanner data is that data from two or more dates can be included in the same analysis. This is accomplished by spatially registering (overlaying) the data. In many instances the addition of temporal information in this manner can be expected to improve classification performance. And, the capability to register data for successive dates also means that field coordinates need be manually located. Temporal analyses with August, September, and October data have been conducted. Recognition of "other" was markedly improved, while corn and soybean recognition was unchanged. These preliminary results, however, do not represent the full potential of temporal information. Data from earlier

in the growing season should give greater improvement in crop recognition.

4. SUMMARY AND CONCLUSIONS

Computer analysis of ERTS MSS data was shown to be an effective method for identifying agricultural crops over large areas. When fully developed, this capability should lead to improvements in the precision and timeliness of crop production estimates.

5. ACKNOWLEDGEMENTS

The contribution of the LARS staff to this work is gratefully acknowledged. The research was sponsored under NASA Contract NAS5-21773 and NASA Grant #NGL 15-005-112.

Table 1. Crop acreages and percent agricultural land in three-county test site.

Area	Total Area (000 Acres)	1971 Corn Acreage (000)	1971 Soybean Acreage (000)	Percent Farmland in 1971
Dekalb Co.	415	194	80	90
Ogle Co.	487	206	47	93
Lee Co.	437	185	90	97
Total	1339	585	217	93



black: Corn gray: Soybeans white: "Other"

Figure 1. Computer classification map of corn, soybeans, and "other" for Dekalb, Ogle, and Lee Counties, Illinois.

Table 2. Classification of corn, soybean, and "other" test fields by computer analysis of MSS data.

Crop	No. Points	No. Points Classified As Corn	Soybeans	"Other"	Percent Correctly Classified
Corn	3968	3367	357	244	85
Soybeans	1113	115	855	133	77
"Other"	295	16	50	234	79
Total	5376	3498	1262	611	

Overall Performance: 83 percent

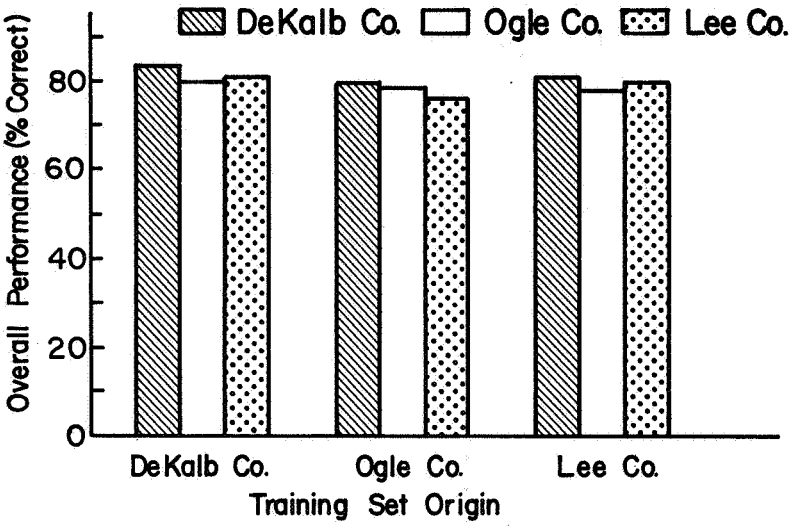


Figure 2. Test of the extendability of training sets.

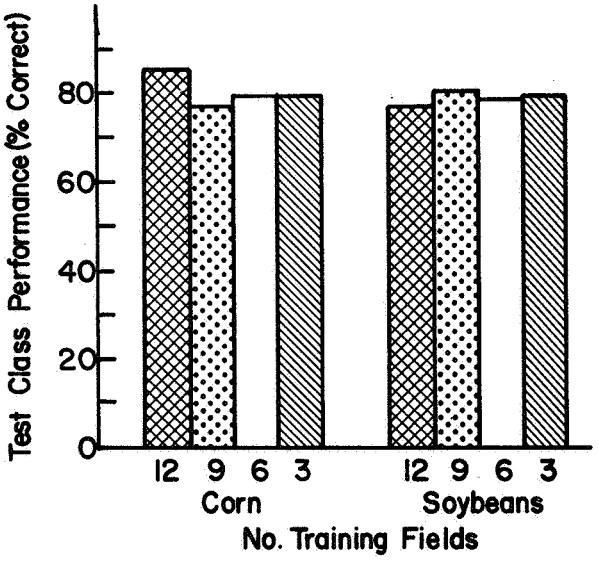


Figure 3. Influence of training set size on classification performance.

Table 3. Comparison of test field classification accuracy for two random selections of training fields

Area Classified	Overall Classification Performance (% Correct) Training Set 1	Training Set 2
Dekalb Co.	83	81
Ogle Co.	79	78
Lee Co.	81	75

Table 4. Comparison of USDA acreage estimates with estimates derived from computer analysis of ERTS data (Dekalb, Ogle, and Lee Counties, Illinois)

	USDA	ERTS
	(Percent of Total Area)	
Corn	40	40
Soybeans	17	23
"Other"	43	37

Table 5. Use of spatial information (sample classifier) in addition to only spectral information (point classifier)

	Point Classifier	Sample Classifier
	% Correct	
Corn	85	90
Soybeans	77	81
"Other"	79	71
Overall	83	84

Paper A 26

IDENTIFICATION AND MAPPING OF SOILS, VEGETATION, AND WATER RESOURCES OF LYNN COUNTY, TEXAS BY COMPUTER ANALYSIS OF ERTS MSS DATA

Marion F. Baumgardner, Steven J. Kristof, James A. Henderson, *Laboratory for Applications of Remote Sensing, Purdue University, West Lafayette, Indiana 47907*

ABSTRACT

A 2,360 km^2 test site was selected to assess the utility of ERTS MSS data for mapping and monitoring soil, vegetation, and water resources. Using computer-implemented overlay techniques, ERTS MSS data obtained on three different dates were analyzed. Temporal changes in vegetation and water supply in Lynn County were identified and mapped. Ground observation and aircraft underflight data were used as training and test sets for the computer-implemented analysis of the ERTS data.

Features which were identified include row crops, unimproved and improved rangelands, bare soils, hydrologic features, and gross geologic and soils features. Results suggest that these techniques may be used to identify drought and other crop stress conditions, crops damaged by hailstorms, areas of active wind erosion, crops species, and soils patterns. The ultimate goal is to provide better yield predictions and more efficient management of agricultural resources.

1. INTRODUCTION

This paper presents the results of the analysis and interpretation of ERTS MSS data obtained over Lynn County, Texas. The test site was chosen because it embodies a variety of problems associated with the development and management of agricultural resources in the Southern Great Plains. It is one of ten counties in a larger ERTS test site centering around Lubbock, Texas.

Description of Test Site

Lynn County is a part of the High Plains lying south of the Canadian River. Known as the Llano Estacado, it is

essentially a plateau, bounded on the north, east, and west by prominent escarpments rising from stream-eroded lower lands. On the south it merges physiographically with the Edwards Plateau.

The plains surface is quite flat and, except for a few canyons, is devoid of topographic features. The surface slope is southeast averaging 1 1/2 to 2 meters per kilometer. Canyon erosion is gradually reducing the total area of the Llano by slow retreat of the bounding escarpments. Stream drainage of the Llano surface is imperfectly developed. There are only a few widely-spaced minor valleys. These valleys typically have alluviated and unchanneled floors and are almost devoid of tributaries. Only during rare periods of excessive rainfall does water flow through the Llano valleys.

The most remarkable topographic and hydrologic characteristics of the Llano are the great number of shallow depressions, ranging in size from a few hectares to more than 15 km^2. These "prairie potholes", "playas", or "salinas" accumulate drainage from local watershed areas that range in area from less than 100 hectares to several hundreds of hectares. Most of the playas contain ephemeral, fresh to alkaline water during part of the year. The form of the depressions varies, with topography of the bottom and sides depending on the character of the formations in which the depressions are formed. Water loss from the playas is by evaporation and seepage towards recharge of the water table.

The principal income of Lynn County is derived from agriculture and ranching. The major problems associated with the development and management of the agricultural and rangeland resources of the county are drought, wind erosion, hailstorms, soil productivity, and invasion of rangelands by mesquite (Prosopis glandulosa and Strombocarpa odorata). The purpose of this study is to examine the utility of ERTS MSS data in identifying, characterizing and mapping the soil, vegetation and water resources in this semiarid region. Successful application of remote sensing and machine-processing techniques to arid and semiarid land management problems will provide valuable new tools for the one-third of the world's lands lying in arid-semiarid regions.

2. DATA ACQUISITION AND ANALYSIS

Ground Observation Data Collection

Ground observation data for Lynn County were collected by residents of the area. Six Lynn County farmers who were interested in cooperating in this experiment were requested

to make ground observations along segments (6-10 kilometers) of county roads at the time of each ERTS overpass. Fields along each segment were numbered and information on crop type, crop conditions, soil conditions, planting pattern, row direction, and ground cover were recorded. These data from segments well distributed over the county were used in selecting training and test areas for the supervised classifications.

Aircraft Underflight Data

On 12 September 1972 an aircraft mission obtained data over the center of Lynn County on a single north-south pass at an altitude of 6,000 m. Color infrared photographs from this mission were very useful in the interpretation of patterns of rangelands shown in the classification from the computer-analysis of ERTS MSS data.

ERTS Data Analyzed

Multispectral scanner data from ERTS passes over Lynn County on 9 October, 14 November, and 2 December 1972 were used in this study.

Analysis Procedure

The LARSYS software system is a package of computer programs which have been designed to analyze and display remotely sensed multispectral data. Five major processing algorithms were used in this study: (1) CLUSTER, (2) STATISTICS, (3) CLASSIFYPOINTS, (4) PRINTRESULTS, and (5) NEWPHOTO. The CLUSTER processor is an unsupervised classifier that groups data vectors into spectrally distinct classes. Mean vectors and covariance matrices are calculated by the STATISTICS processor and are then used in the CLASSIFYPOINTS processor which performs a maximum likelihood Gaussian classification on a point-by-point basis over the entire area. Results from the analysis are then displayed using: (1) the PRINTRESULTS processor to make alphanumeric maps; and (2) the NEWPHOTO processor to display the results on the Digital Image Display System.

The Digital Image Display System receives an image from a System/360 computer, stores these data in a video buffer, and displays the image in a raster scanning mode on a standard television screen. An interactive capability to edit, annotate, or modify the image is provided through a light pen and a program function keyboard. An additional photographic copying capability is also provided.

3. RESULTS AND DISCUSSION

Ground observation data and aircraft underflight photography were used in the analysis and interpretation of the ERTS measurements. Ground observations were made by six cooperating farmers. Each farmer identified crops and described soil and crop conditions in fields on each side of a 10-13 kilometer segment of a county road. Figure 1 (a classification of ERTS data) represents one of the observation segments. "A" is an area of cultivated fields. "B" is an area of rangeland in which the mesquite has been successfully eradicated. Projection of the observation segments on the Digital Image Display System made it possible to identify and locate the address of each ground observation site on the digital MSS data tapes.

A. Soils Resources

Although a large percentage of the land surface of Lynn County was covered with natural vegetation and crop residues at the time of the ERTS overpasses reported herein, broad soils patterns are revealed in the ERTS multispectral data. Figure 2 is an MSS band 2 (0.6-0.7μm) gray scale image of the test site on 14 November. The dark areas along the north and east of the image (A) represent deep moderately permeable loams and clay loams; the small, highly reflective area (B) contains deep permeable fine sands. The highly reflective soils in the southwest and west of the county (C) are deep, moderately permeable fine sandy loams. Results to date suggest that well chosen training sets for the analysis of ERTS MSS data obtained at a time when a maximum percentage of soil is without cover could greatly refine and improve the capability to delineate the soils boundaries of Lynn County.

B. Vegetation Resources

The two major land uses in Lynn County are agriculture and ranching. Of the total agricultural land there is little under irrigation. Approximately 58% of the county was in cotton in 1972. Other cultivated crops include grain sorghum and forage sorghum. Vegetation of rangelands consists primarily of natural grasses and mesquite.

Ground observation data obtained on 9 October were used for training and test sets for the computer-implemented analysis of 9 Oct., 14 Nov., and 2 Dec. ERTS data. Classifications of row crops, pasture, fallow, and water were obtained for each of these dates (Figures 3, 4, and 5). Examination

of these classifications reveals that field boundaries and homogeneity of fields are much better for 9 October. With the use of temporal overlay techniques a classification was obtained using the best combination of four MSS bands from the three dates (9 Oct., 14 Nov., 2 Dec.). The four bands selected to give the best classification of row crops, pasture, fallow, and water were bands 5 (0.6-0.7μm) and 7 (0.8-1.1μm) for 9 Oct. and 14 Nov. (Figure 6).

The highest percent correct recognition was 89.6% for the 9 Oct. classification. The accuracy declined for the 14 Nov. and 2 Dec. data. For the temporal overlay classification (Figure 6) the accuracy approached that of the classification accuracy for the 9 Oct. data.

It was not expected that this late in the growing season temporal overlay would improve classification results. A killing frost early in November, excessive autumn rains, and late summer weed growth contributed to much confusion in classification results from the November and December data. Experience in identification of summer annuals indicates that the most significant contributions of temporal overlay will be made during the active growing season prior to senescence.

C. Water Resources

Since water has very low reflectance in the near infrared wavelengths (ERTS spectral bands 6 and 7), it was easy to separate and map playas and reservoirs containing water. Water was separated spectrally from all other categories for three ERTS overpass dates. It was found that many of the playas containing water on 9 October contained no water on 14 November; many with no water on 14 November had water on 2 December.

Examination of the precipitation records revealed a record high rainfall for August and September. At the time of the 9 October ERTS overpass essentially all playas were full (Figure 7). During the three weeks prior to the 14 November overpass very little rain had fallen in Lynn County. Water in the playas had been partially or completely depleted by evaporation and/or seepage to groundwater recharge. The period from 12 November to 2 December (ERTS overpass) was characterized by cloudy days, high humidity and several light rains. The ERTS data for 2 December reveals water in many playas which had no water in mid-November (Table 1).

D. Temporal Overlay

Temporal overlay capabilities provide a significant

advance in the machine-processing of multispectral scanner data. It is no longer necessary to go through the tedious exercise of locating ground observation sites on the digital data from each ERTS overpass. Once the address of a ground observation site has been located on a digital tape from any ERTS overpass, the overlay technique can be used to locate the same address on a digital tape of MSS data from any other ERTS pass over the same area.

The temporal overlay technique also adds a valuable dimension for identifying and mapping changes in vegetation, water, and other dynamic surface features.



Figure 1. Classification of area around a ground observation site.

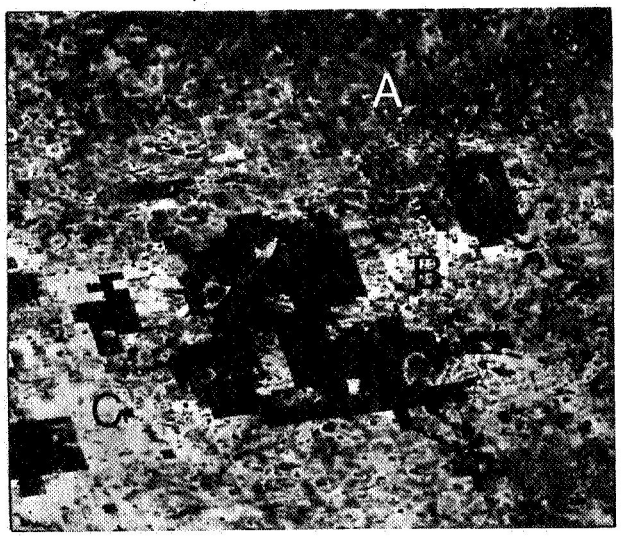


Figure 2. Gray scale image of Lynn County, Texas. ERTS MSS band 5 (o.6-0.7μm),]4 Nov 72.

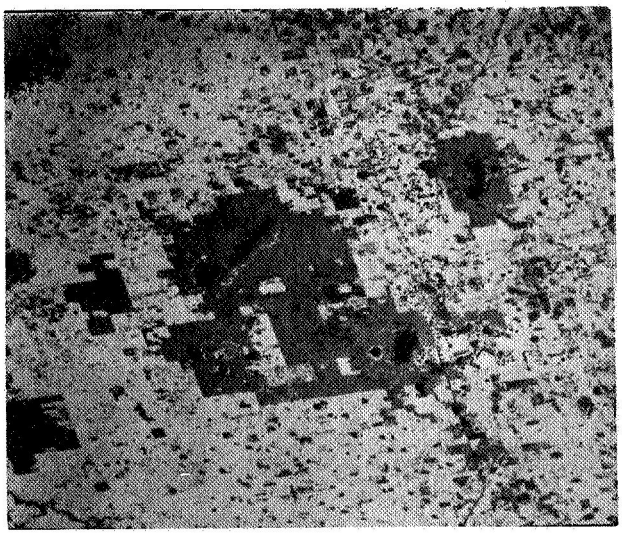


Figure 3. Four spectral classes representing row crops, pasture, fallow, and water. ERTS data-- 9 Oct 72.



Figure 4. Four spectral classes representing row crops, pasture, fallow and water. ERTS data--14 Nov 72.



Figure 5. Four spectral classes representing row crops, pasture, fallow, and water. ERTS data--2 Dec 72.

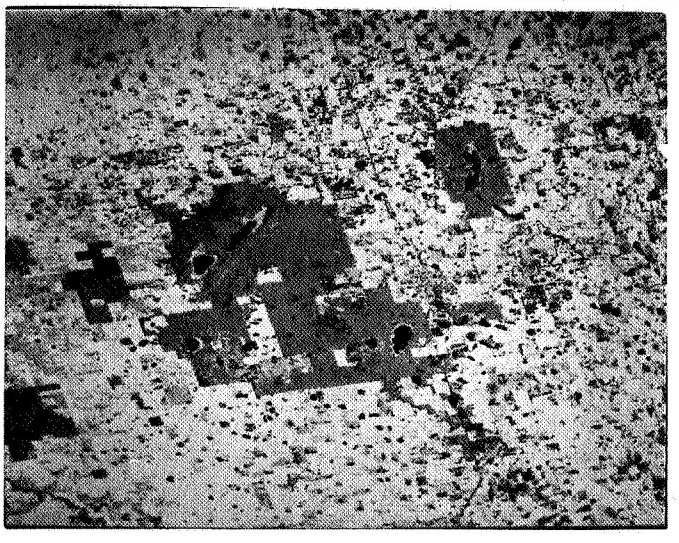


Figure 6. Four spectral classes representing row crops, pasture, fallow, and water. From overlay of ERTS MSS bands 5 and 7 on 9 Oct and 14 Nov 72.

Table 1. Estimated Changes in Water Surface Area.

Date	Points	Hectares
9 Oct.	4374	1924
14 Nov.	3735	1643
2 Dec.	5120	2252

Total Area 197683 Hectares



Figure 7. Two spectral classes representing water and other in Lynn County, Texas. ERTS data--9 Oct 72.

MINERAL RESOURCES, GEOLOGICAL STRUCTURE AND LANDFORM SURVEYS

Paper G 1

EVALUATION OF ERTS-1 IMAGERY FOR GEOLOGICAL SENSING OVER THE DIVERSE GEOLOGICAL TERRANES OF NEW YORK STATE

Yngvar W. Isachsen, Robert H. Fakundiny and Stephen W. Forster, *Geological Survey, New York State Museum and Science Service, Albany, New York*

ABSTRACT

Film positives of ERTS-I imagery, both as received from NASA and photographically reprocessed, are being analysed by conventional and color additive viewing methods. The imagery reveals bedrock and surficial geological information at various scales. Features which can be identified to varying degrees include boundaries between major tectonic provinces, lithological contacts, foliation trends within massive gneisses, faults, and topographic lineaments.

In the present imagery the greatest amount of spectral geology is displayed in the Adirondack region where bedrock geology is strongly linked to topography. Within this basement complex, the most prominantly displayed features are numerous north-northeast trending faults and topographic lineaments, and arcuate east-west valleys developed in some of the weaker metasedimentary rocks. The majority of the faults and lineaments shown on the Geologic Map of New York at 1:250,000 appear in the ERTS imagery. In addition, many new linears were detected, as well as a number of anomalous curvilinear elements, some circular in plan and measuring up to 25 km in diameter which do not bear any strong relationship to mapped geological contacts. One of these, centered on Cranberry Lake, has a radial pattern of linears and resembles a spoked wheel. The possibility that this spectral feature is an astrobleme will be investigated on the ground when snow conditions permit, and earlier by observation from small aircraft.

Surficial features observed in the imagery include the following: Harbor Hill and Ronkonkama moraines, in part, revealed by cultural enhancement, Tully moraine revealed by land-use discontinuity, glaciated valleys and cross channels south of Syracuse, glacial streamline forms atop Tug Hill Plateau, ice marginal channels in the Watertown quadrangle, and tonally distinguished glacial lake deposits south of Plattsburgh and northeast of Black Lake. Tonal variations in ERTS imagery taken September 6 and 7 in western New York, however, show no obvious correlation with glacial deposits, but a poor correlation with the mapped distribution of major soil groups.

1. INTRODUCTION

This report summarizes results to date of a project to evaluate the usefulness of ERTS-I imagery as a spectral geological tool in the diverse geological terranes on New York State. The study concentrates on the

geologically useable (i.e. sufficiently cloud-free) imagery obtained over New York, although major new structural elements will be studied where they extend into adjacent regions.

New York State lies astride five tectonic provinces (Fisher and others, 1971). A major platform of essentially undeformed Lower and Middle Paleozoic strata on Proterozoic basement underlies most of the state. A second platform, of Cretaceous strata on Paleozoic basement, forms the substrate of Long Island. Between these platforms lies the Appalachian Orogen or Foldbelt, with subdivisions including reactivated Proterozoic rocks of the Hudson Highlands, and major thrust sheets and submarine gravity slides of the Taconics. South of the Hudson Highlands is the Triassic Basin. Lastly, the Adirondack Dome in the northern part of the state exposes Proterozoic basement rocks as an extension of the Grenville Province of the Canadian Shield. As would be expected, the amount and kind of spectral geological information varies considerably from province to province.

2. ERTS-I DATA AND ANALYSIS

ERTS-I imagery received to date totals 125 frames covering 32 scene areas over New York State as well as portions of adjacent states and Canada. It has been catalogued and categorized in terms of geological usefulness as a function of cloud distribution. An inventory of imagery on hand through Feb 73, in terms of geological usefulness, is as follows: useful (0-50 percent cloud cover), 50 percent; marginally useful (50-70 percent cloud cover), 10 percent; useless (70-100 percent cloud cover), 40 percent.

The entire state is now covered by at least one image having greater than 70 percent cloud-free area (figure 1), and all except the three scenes in the western part of the state are 100 percent cloud-free.

For all useable imagery covering New York State, film positives have been analyzed in transmitted white light for spectral signatures which may have a geological linkage. These data are traced onto clear mylar and combined into a state-wide "spectral geological map" at 1:1,000,000 (figure 2), which is updated as new imagery arrives. For the late summer and fall imagery, bands 5 and 7 compliment each other and contain all the spectral signatures which appear to be geologically-linked; no additional data were found on bands 4 and 6.

After the more obvious spectral geological features were extracted from the standard black and white film positives, it was decided to experiment with other methods as follows:

1. Multispectral color-additive viewing of 70 mm positives of bands 4, 5, 6 and 7, as received from NASA, using a Spectral Data Corporation Model 64 Viewer-Projector. Despite considerable experimentation with a variety of scenes, no information was added to that obtained by conventional viewing in transmitted light.

2. Experimentation to determine what effect photographic reprocessing to produce higher contrast prints might have on the identifiability of linears in ERTS-I, band 5, using transmitted white light. Image 1079-15122-5 (orbit 192) was chosen for the experiment because it includes a portion of several structural provinces, namely: the Adirondack Mountains crystalline rocks, the Alleghany Plateau consisting of Silurian and Devonian strata, the Mohawk and Hudson Valleys underlain by variably faulted and folded Cambrian and Ordovician sedimentary rocks, and the Taconic Mountains which consist of allocthonous Cambrian clastic rocks.

The photographic reprocessing method used was as follows: convert, by contact printing, a 70 mm ERTS-I negative to a 70 mm Kodalith film positive. Convert this high-contrast product by contact printing, to a high contrast negative using Kodak Professional Copy film, and develop in D-72.

Paper enlargements were then made of both the 1:1,000,000 reprocessed and unreprocessed 70 mm negatives, and identifiable linears were scribed on clear mylar overlays. A comparison showed that all linears identifiable on one image were clearly recognizable on the other, although the expression of linears was greater on the high-contrast reprocessed image.

3. Pre-formatting of ERTS-I 70 mm film positives for multispectral viewing to avoid the time-consuming task of separately registering each map in the Viewer every time a scene is to be viewed. A successful method was devised as follows: on a 9.5 x 12 inch piece of 0.005 inch clear mylar, roughly locate the position of the four viewer windows in the 9.5 inch roll film holder and draw two perfectly parallel horizontal lines to guide the placement of the upper edge of the 70 mm film positives. Using these lines, tape the images in perfect parallelism. This pre-formatted array will permit rapid registration, requiring only limited x-y adjustment, the need for rotational adjustment having been eliminated.

4. Multispectral color additive projection of the photographically reprocessed imagery has been initiated. The resulting photographic products are striking in appearance, but additional analysis will be required before their usefulness can be evaluated.

3. ERTS-I AND BEDROCK GEOLOGY

A variety of known bedrock geological features visible to varying degrees in ERTS-I imagery include the following: 1. boundaries between major tectonic provinces; 2. lithological contacts within tectonic provinces; 3. foliation trends within massive gneisses; 4. faults and topographic lineaments; and 5. mine dumps and tailings ponds. In addition, numerous new linear and curvilinear features are discernible, as well as some highly speculative linears. (The word "linear" rather than "lineament" is used in the sense of Dennis, 1967, p. 103, to designate "lines of unsure origin on areal photographs"). Several examples of each of the above bedrock geological categories are itemized below, and may be referred to in figures 1 and/or 2:

1. Boundaries between major tectonic provinces: the contact between the Adirondack basement and onlapping Cambrian rocks is well defined along the southwest border of the Adirondacks, along the north-central border, and along part of the southeastern border. In the southeastern part of the State, the angular unconformity separating Silurian-Devonian strata from the more deformed Ordovician rocks is clearly defined. The same holds for the parallel contact to the west which marks the western limit of Acadian folding. Further to the southeast, the contact between the Hudson Highlands and the Triassic Basin is visible.

2. Lithological contacts within tectonic provinces: north of the Adirondacks, the contact between the Cambrian Potsdam sandstone and the overlying Theresa arenaceous dolostone is marked by a fairly sharp transition from light to dark tone. The broad arcuate valleys crossing the Adirondacks reflect lithological variations within the crystalline rocks. South and southwest of the Adirondacks, the arcuate lines result from lithological variations in the Devonian stratigraphic section.

3. Foliation trends within massive gneisses: some of the arcuate spectral trends in the Adirondacks occur within single map units of massive gneisses.

4. Faults and topographic lineaments: these are indicated by the solid lines in figure 2.

5. Mine dumps and tailings ponds: these are shown by the heavier dots and line in the northwest Adirondacks (figure 2).

6. New linear and curvilinear elements, and highly speculative linears: numerous examples are shown on figure 2. A numerical summary of the Adirondack linear information shown on figures 1 and 2 is tabulated below:

Category	Number	Combined length, km
Known lineaments and faults seen on ERTS-I imagery	232	1890
New and anomalous linears seen on ERTS-I imagery	329	3060
Total linears seen on ERTS-I imagery	561	4950
Known lineaments and faults not discernible on ERTS-I imagery	297	1750

Bearing in mind that the numbers in categories 2 and 3 will be modified as analysis of anomalies progresses, the above numbers should be regarded as approximations.

It may be noteworthy that the known lineaments and faults missed on the ERTS-I imagery tend to be concentrated in the eastern Adirondacks where the film positives received from NASA are abnormally dense. It is therefore possible that the ERTS-I multispectral scanner actually sensed more than 50 percent of Adirondack lineaments and faults.

7. Curvilinears. This term is applied to broadly curved spectral line data, and numerous examples can be seen in figure 2. Most of these have not yet been evaluated. One, however, is of particular interest; namely, the "spoked wheel" or Cranberry Lake anomaly which centers on Cranberry Lake in the west-central Adirondacks. A comparison of this feature with mapped geological contacts (Buddington and Leonard, 1962; Fisher and others, 1971) shows only a partial correspondence; in part the "wheel" cuts directly across the trend of resistant crystalline rock units. The possibility that this structure is an eroded astrobleme remains to be field-checked.

4. ERTS-I AND SURFICIAL GEOLOGY

The available late summer and early fall imagery was examined for surficial geological features of two kinds: essentially two-dimensional features, such as end moraines, glacial lake shorelines and glacial drainage channels; and features having some areal extent, such as glacial lake deposits.

End moraines searched for were the Harbor Hill and Ronkonkama moraines of Long Island, the Fort Covington moraine of the St. Lawrence Valley, the Valley Heads moraine of the Finger Lakes region, and the series of moraines south and east of Lake Erie in western New York State. Of these, only a short segment of the Valley Heads moraine south of Syracuse and portions of the Harbor Hill and Ronkonkama moraines were detectable on the imagery (images 1080-15180-5 and 1096-15074-5); these segments were visible only where enhanced by land use differences.

Glacial drainage channels occur in several areas, but are particularly well shown in the Syracuse area and on the northern flank of the Tug Hill Plateau (image 1080-15180-7).

Glacial lake shorelines were searched for throughout the State, as was the shoreline of the Champlain Sea in the St. Lawrence Lowland. None were seen.

Glacial deposits recognized on the imagery to date are limited to two. Sand deposits of glacial Lake Vermont mapped by Denny (1967) show up on image 1079-15115-7 south of Plattsburgh as an area of dark tone. The same applies to a sand area mapped by MacClintock and Stewart (1965) which extends from the village of Malone westward to the St. Lawrence River (image 1080-15174-7).

South of Lake Ontario an extensive area of drumlins is spectrally enhanced by land use patterns (scenes 1080-15180 and 1046-15292-5).

Because one of us (Fakundiny) has a particular familiarity with the surficial geology of the western part of the State, it was decided, despite the inferiority of the present imagery (images 1080-15180-5 and 1046-15292-5), to attempt an evaluation of tonal variations. Comparisons made with generalized soils maps at 1:1,000,000 of Arnold and others

(1967) and of the Genesee/Finger Lakes Region Planning Board (1970) show only a 10 percent correspondence of soils contacts and tonal boundaries, and that correspondence applies mainly to valley bottoms; it thus appears to be principally a correlation with topography.

5. CONCLUSIONS

As anticipated in our original research proposal, ERTS-I imagery has revealed a number of hitherto unknown spectral linears which may turn out to be geologically-linked. It is therefore very likely that ERTS-I imagery will prove useful in regional fracture analysis. A number of unsuspected and intriguing curvilinear anomalies have also been recognized in the imagery and will be investigated further.

The paucity of spectral evidence for geological contacts (both bedrock and surficial) in the central and western parts of the State may be due to accentuated land-use camouflage during the growing season. Spring imagery which pre-dates the growing season will be carefully scrutinized with this in mind.

Financial support for this research was provided under NASA Contract NAS5-21764.

REFERENCES

Arnold, R.W., and eleven others, 1967. General soils map of Five-County area around City of Syracuse in New York State. Extension Publications of the New York State College of Agriculture at Cornell University, Ithaca, New York.

Buddington, A.F. and Leonard, B.F., 1962. Regional geology of the St. Lawrence County magnetite district northwest Adirondacks, New York. U.S. Geol. Survey Prof. Paper 376, 145 pp.

Dennis, J.G., ed., 1967. International Tectonic dictionary - English terminology. Am. Assoc. Petroleum Geologists Mem. 7, 196 pp.

Denny, C.S., 1967, Surficial geologic map of the Dannemora quadrangle, and part of the Plattsburgh quadrangle, New York. U.S. Geol. Survey Map GQ-635.

Fisher, D.W., Isachsen, Y.W., and Rickard, L.V., 1971, Geologic Map of New York, 1970, and Generalized Tectonic-Metamorphic Map of New York, 1971, N.Y. State Mus. and Sci. Service Map and Chart Series No. 15.

Genesee/Finger Lakes Regional Planning Board, 1970, Regional soils inventory: classification and analysis; Genesee/Finger Lakes Regional Planning Board Technical Studies Series, Rept. No. 6, 39 pp.

MacClintock, P., and Stewart, D., 1965. Pleistocene geology of the St. Lawrence Lowland, N.Y.S. Mus. and Sci. Service Bull. 394, 152 pp.

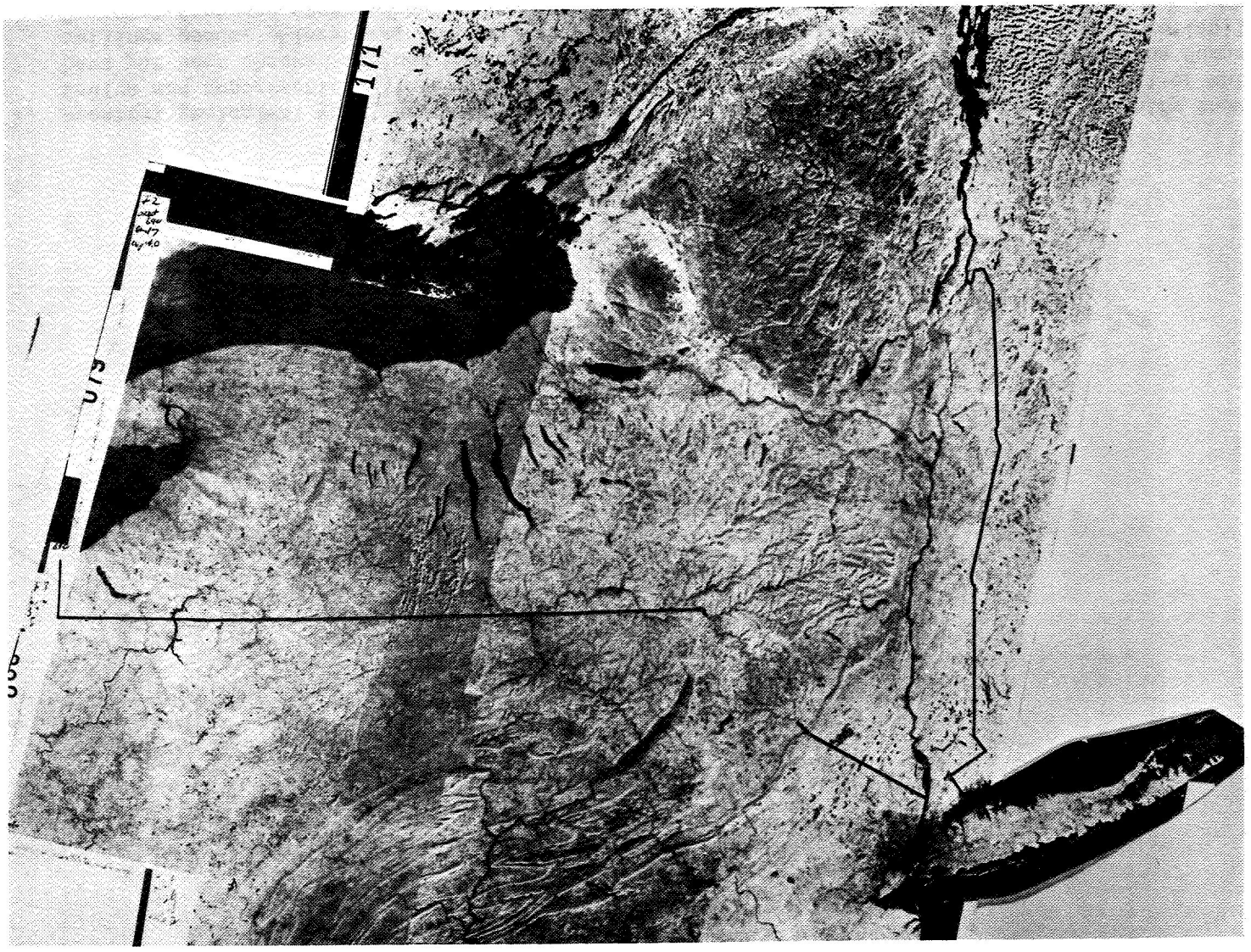


Figure 1. ERTS-I mosaic of New York State made from Bruning prints of 9.5 inch multispectral scanner film positives of band 7. Images used in this mosaic are 1027-15231, 1027-15233, 1027-15240, 1046-15292, 1046-15295, 1077-15014, 1079-15115, 1079-15122, 1079-15124, 1079-15131, 1080-15174, 1080-15180, 1080-15183, 1096-15072, 1096-15074. SCALE: 1mm = 3.5 km.



Figure 2. Spectral geological work map of New York State. In the Adirondacks, solid lines signify known faults and topographical lineaments; dotted lines represent spectral anomalies not all of which have yet been checked against cultural features; the heavy dots and line represent mine dumps and tailings ponds. Elsewhere, the range from solid to dotted lines is a rough index of reliability. Spectral features produced by known lithological variations are omitted. SCALE: 1 mm = 3.5 km.

Paper G 2

ANALYSIS AND APPLICATION OF ERTS-1 DATA FOR REGIONAL GEOLOGICAL MAPPING

D. P. Gold, R. R. Parizek, and S. A. Alexander, *Department of Geosciences, The Pennsylvania State University, University Park, Pennsylvania 16802*

ABSTRACT

Combined visual and digital techniques of analysing ERTS-I data for geologic information have been tried on selected areas in Pennsylvania. The major physiographic and structural provinces show up well. Supervised mapping, i.e. following the imaged expression of known geologic features on ERTS band 5 enlargements (1:250,000) of parts of eastern Pennsylvania, delimited the Diabase Sills and the Precambrian rocks of the Reading Prong with remarkable accuracy.

From unsupervised mapping, transgressive linear features are apparent in unexpected density, and exhibit strong control over river valley and stream channel directions. They are unaffected by bedrock type, age, or primary structural boundaries, which suggests they are either rejuvenated basement "joint" directions on different scales, or they are a recently impressed structure possibly associated with a drifting North American plate. With ground mapping and underflight data, 6 scales of linear features have been recognized, viz., joints (10's of feet), fracture traces (several 100's feet to 1 mile), short lineaments (1 to 5 miles), intermediate lineaments (5 to 50 miles), long lineaments (>50 miles) and megalineaments (several 100's of miles). Their numbers decrease with increase length, suggesting they are related in mechanism through 1st, 2nd, 3rd and possibly higher order shears. The smaller linear features are important economically in terms of foundation engineering projects, ground water exploitation, mining, tunneling, etc., while the larger lineaments appear to exert some control over the emplacement of some base metal deposits.

1. INTRODUCTION

Although the association of scale to structural elements and geologic features is implicit in the detailed, regional, or compiled geologic maps, and in the division of some disciplines (Structural Geology versus Tectonics) only in Structural Analysis is there a conscious interplay between scales of the fabric or structural elements characteristic of each scale (Turner and Weiss, 1963). Apart from the direct measurements and observations made in man-size scale (mesoscopic), most of

the data gathered on other scales is sensed remotely and integrated into a composite or mosaic for viewing in the mesoscopic scale.

Painstaking synthesis or the integration of data on one scale to provide information on the next smaller scale over many years has provided our regional, State, National, and Global maps. However, the synthesis of features on one scale does not guarantee that a larger feature will necessarily be apparent on the smaller scale map generated, because of artifacts in mosaicing, poorly known scaling laws, and the inconsistent conditions (variable sun angle, albedo, seasons, etc), of data collection, are more likely to obscure than enhance subtle features. Hence the value of the ERTS imagery.

Unfortunately, most remote sensed data are surficial in nature, and the features displayed are but the trace on the surface exposed of 3-dimensional structural elements. Interpretation and correlation of subsurface features and parameters requires a background knowledge of the geometry and nature of the parameter sought. Proving utility and production from a remotely sensed class of feature may take years of detailed "ground truth" data gathering by drill holes, geophysical probes, and pumping tests (Parizek, 1971a).

2. OBJECTIVES

Although our goals are broader based we have concentrated on (a) testing the utility of Regional Geological Mapping by studying a few well known areas in detail, and (b) in classifying the linear transgressive features apparent on all scales of overflight imagery. We feel that the latter study will have the best and quickest economic pay-off (hydrogeology, engineering geology, ore deposits) because we have considerable ground data for establishing correlations, and because there is a theoretical base for possibly linking linear features through scale (McKinstry, 1953; Moody and Hill, 1956; Price, 1966).

3. METHODOLOGY

The methodology, is continually developing as we gain experience in interpreting the imagery and learn to recognize the real signals. The criteria used in mapping like areas (visual similarity in tone, spatial patterns, or texture) are classified according to whether they represent a direct or indirect manifestation of the bedrock condition. In forested areas such as in Pennsylvania a knowledge of the indirect indicators is important for geologic interpretations even though their relationship to the bedrock conditions may not be understood.

The main parameters (criteria) used are:

(a) Boundaries or interfaces that seperate areas of different tone, texture, or pattern. Whereas irregular boundaries generally result from differences in land use (arable land versus forests), smooth and regular boundaries commonly reflect geologic control, expecially where layered rocks are involved. Combinations of these two habits, e.g., forest cover over untillable rocky areas, enhance the contrast and the interpretability if the correlation can be made and the cause identified from the ground truth data. The diabase sills in eastern Pennsylvania show up best on band 5 because of their overlaying forest cover in contrast with the surrounding cultivated fields.

(b) Linear transgressive features (lineaments) that shows as a narrow band contrasting in tone, topography, or displacing areas of like tone or pattern. These are generally long features (5 to several hundred miles) and some morphologically represent the alignment of wind and water gaps: others represent the surface expression of dikes, faults, zones of fracture concentrations, etc., without any apparent displacement.

The main stages in analysing ERTS data are:

(a) Primary correlation with the available ground truth geologic boundaries on $1:1X10^6$ scale and enlargements (1~250,000) of ERTS imagery using combinations of channels.

(b) Mapping and classification of anomalous features.

(c) Computerized mapping of selected areas using cluster analysis on digital data, with the parameters controlled (supervised) from training areas.

(d) Unsupervised computer mapping, to bring out any latent features that might have geologic significance.

4. RESULTS OF MAPPING PRIMARY STRUCTURES

Although the necessary programs have been developed for stages (c) and (d), we have not yet progressed beyond the basic correlations and classifications. The contacts of some lithologic boundaries in eastern Pennsylvania, e.g., the Conestoga Formation, the Diabase Sills, and the Precambrian inliers of the Reading Prong, can be placed, using band 5 imagery at a scale of 1;250,000 with an accuracy of 400m(1/4 mile) with respect to the Geological Map of Pennsylvania(Figure 1). Much of this error may be in transferring boundaries from the ERTS imagery to the base map.

The physiographic provinces in Pennsylvania show up well, particularly the "Folded Appalachian Belt" in bands 5 and 7. However, little new geology can be added to the existing geological maps, but the remarkable correlation between the imaged and the ground truth boundaries demonstrates the feasibility of locating geologic contacts in unmapped areas. An example of the combined use of tone, boundary shape, vegetal cover, and characteristic spectral response is in the mapping of the diabase sills and flows in eastern Pennsylvania (Fig. 1). Some of the ore deposits associated with the diabase are aligned along a possible transgressive linear zone that is not apparent on the images.

5. LINEAR FEATURES (see Figure 2a, b, c, and d).

Introduction

Perhaps the most encouraging and unexpected features on the ERTS imagery are the number, distribution and patterns of unspecified linear features. Geologists have long recognized the presence of straight to slightly curved linear features on the earth's surface. These vary in size from 10's to 100's of feet for the systematic and non-systematic joints to "lineations" 10's of miles long that commonly had no obvious field expression and were visible on aerial airphoto mosaics. To distinguish among features recognizable on aerial photographs, Lattman (1958) defined a "fracture trace" as a "natural linear feature consisting of topographic (including straight stream segments), vegetation, or soil tonal alignments, visible primarily on aerial photographs, and expressed continuously for less than one mile". Those greater than one mile he termed "lineaments". Wise (1968) termed these regional and sub-continental sized fracture systems "linears", and noted their independence of regional structure. A considerable amount of work has been done with joint traces, and joint orientation studies in the field, and more recently (since 1957) with fracture traces. Including ground based and aircraft overflight data we now recognize at least 6 scales of linear features, and while there is a link between joints and fracture traces, theory suggests(McKinstry, 1953; Badgley, 1965; Moody and Hill, 1956; Price, 1966) that the same mechanism may link all scales.

Recognition and Characteristics

In addition to the criteria listed above, fracture traces may be revealed by straight valley segments, abrupt changes in valley alignment, gaps in ridges, gulley development, aligned sink holes and swallow holes, localized springs and diffuse seepage areas, localized vegetational differences, etc.,(Fig. 2a, 2b),(Parizek, 1971a and b). Fracture traces and lineaments are commonly straight, unaffected by topography, and hence are considered surface manifestations of vertical to near-vertical zones of fracture concentration (Mollard, 1957a and 1957b; Hough, 1960; Lattman and Parizek, 1964; Parizek and Voight, 1970, Parizek 1971a and 1971b). In carbonate terranes, surface

sags and depressions 2-10 ft. deep may develop along fracture traces or open sinkholes 10 to 50 ft. deep may occur. The width of these depression appears to vary with the thickness of weathered mantle above bedrock and the width of the zone of fracture concentration. Calkins (1966) found that fracture traces in granite represent linear depression 2-8 ft. deep and 15 to 200 ft. wide. Parizek (1971b) has measured zones from 10 to over 100 ft. wide in various rock types in the United States, and locally in Pennsylvania, has found zones 20 to 40 ft. wide in folded and faulted carbonate rocks. In silt-stones and shales of northeastern Pennsylvania they varied from 15 to over 60 ft. wide, and average 39 ft. There, zones of fracture concentration maybe inclined only 2 tp 3 degrees from vertical (Parizek, 1971a). Individual joints may be closely spaced, 5 to over 60 in number, sub parallel to parallel, and cut all beds equally well, or be concentrated in selected bedrock units without vertical continuity.

Relationship to Structure

Parallelism has been recognized between fracture traces orientation and joints in relatively undeformed bedrock of Pennsylvanian age of the Appalachian Plateau (Lattman and Nickelson, 1958) and flat-lying rocks elsewhere (Hough, 1960; Boyer and McQueen, 1964). In folded rocks fracture traces and joints have been found to have different trends (Lattman and Matzke, 1961; Keim, 1961). These authors found that joint sets are parallel and perpendicular to the strike of bedding in Nittany Valley, and that fracture traces are unrelated to local fold and fault structures. Dominant trends of fracture traces and joints differ; fracture traces appear to be unaffected by tight folds and tend to lie at a constant (52°) angle to regional structure in Central Pennsylvania. (Fig. 2b). This work, together with that of Calkins (1966) and Lattman and Segovia (1961), supports the conclusion that fracture traces are not controlled by local structure but rather by regional features.

Application to Hyrogeologic and Engineering Studies

Lattman and Parizek (1964) established the important relationship between the occurence of ground water and fracture traces for carbonate aquifers, and in particular that fracture traces are underlain by zones of localized weathering, increased permeabilityand porosity, Highly productive wells used in their study were intentionally located by Parizek on one fracture trace or at fracture-trace intersections; the low producing wells more commonly proved to be off fractures traces. Siddiqui (1969), Siddiqui and Parizek (1969, 1971a, and 1971b) further demonstrated that fracture traces are the surface expression of zones of increased permeability and porosity. Moreover fracture zones form an interlaced network in most terranes (Fig.2b) serve as local ground-water feeder routes from more massive blocks of rock in inter-fracture

areas; and supply water to regional conduits, which inturn may be localized by these same features.

Incorrect location of fracture traces probably accounts for the lack of correlation between well yields and fractures traces (Meisler, 1963) for carbonate rocks in the Lebanon Valley, near Harrisburg (Parizek, 1971b). Favorable relationships between well yields and fracture traces have been reported from as far afield as Sao Paulo, Brazil (Setzer, 1966). Wobber (1967) suggested that fracture traces may be useful in locating zones of increased permeability in bedrock in Illnois, overlain by glacial drift. He found an association between fracture trace orientations, and that of bedrock joints buried by up to 150 ft. of drift.

Parizek and Voight (1970) showed that fracture traces could be used in geotechnical investigations to predict zones of increased weathering in advance of foundation exploration; areas of potential roof collapse and excess water in mining and tunneling operations; and leakage beneath dams and into excavations within bedrock. Zones of fracture concentration also could be mapped to account for seepage pressure variation, risk of blowouts and piping, and strength variations within bedrock. Detailed knowledge of the significance and distribution of zones of fracture concentration also is useful in planning, designing, and conducting grout or cut-off wall operations, and in locating highly-effective pressure and drainage wells. Parizek, (1971a); and Parizek and Tarr, (1972); Koppe and Thompson, (1972), showed how they can be employed in acid mine drainage abatement projects.

Faults

High angle faults and fault zones are common in the Appalachian folded rocks. Stratigraphic separations of only a few feet are generally sufficient to concentrate ground water flow, and hence solution and weathering. Exposures in caves and quarries reveal that other fault zones are tight and do not facilitate weathering. In Nittany Valley the presence of major springs on fault zones indicates their regional influence in the valley hydrogeology (Parizek, 1971b). Thrust faults in the Appalachian folded rocks tend to be several miles to tens of miles in length. They have the potential of exerting regional controls on permeability and may localize ground-water drains. Warman and Causey (1962) indicate that thrust faults in Alabama form the principal reservoirs and conduits along which ground water from deep and distant sources reaches the surface.

Lineaments (linears)

Much less is known about linear features a mile or more in length. Hobbs, (1905, 1911), and more recently Lattman, Parizek, Wise and others have noted their presence in Pennsylvania,(see figure 2 e and d).

Several lineaments that transgress regional structural grain and also physiographic province boundaries have been discovered from visual examination of the ERTS MSS images. Four tentative scales of lineaments have been recognized, viz., 1 to 5 miles long features, 5 to 50 features, 50 to a few hundred miles, and megalineaments on a subcontinental scale. Little is known about the length, frequency, and relationship to fracture traces and joints, but there appears to be an inverse relationship of length to abundance and density. Lineament mapping from ERTS tapes is cumbersome because of their variability in length, and unreliable because of their variation in expression along strike (e.g., between ridges and valleys, or even from one valley to another), and the difficulty of distinguishing man-made effects (roads, field boundaries, etc.), and machine artifacts.

Lineaments have the same morohological characteristics as fracture traces except in that they are wider, longer, are not at all obvious in the field, and exert a major influence on topography. Years of airphoto mapping and field work in central Pennsylvania did not reveal many of the lineaments so obvious on the ERTS images, although it was known that the wind gaps and water gaps in the ridges may be aligned.

Although most of the lineaments are straight, some are gently curved and appear to be independent of regional structural trends. However, some of the long lineaments, spaced about 10 miles apart are approximately perpendicular to the Appalachian trend, and fan with the Appalachian orocline. Offsets and drag features are associated with the east-west striking line lineaments, e.g., north of Harrisburg, and through the South Mountains near Gettysburg, and must represent the trace of faults. In the test area east of Harrisburg, the intermediate and short lineaments appear to be conjugate with an angle of about 30° to a northwesterly trending axis. Likewise these shorter lineaments cut across regional primary structure and even the major physiographic province boundaries. Generally, they are spaced less than a mile apart. Except for lineaments coincident with known faults, their physical nature in 3 dimensions is not known, but by analogy with the fracture traces we speculate they are underlain by zones of fractured and joined rocks and represent zones of deformation or movement between "jostling" blocks. They transgress rocks

from Precambrian to Triassic age in Pennsylvania, and though they are blanketed by the Pleistocene glacial drift in part of the State they are not obscured by it. They must be either a rejuvinated crustal fracture system impressed on the younger rocks and in a sense are a reflection through the cover rocks of active crustal "joints", or they represent the deformation in response to a wide-spread and pervasively imposed stress field as would be expected from a drifting North American plate.

Potential Applications; Research Directions

There is urgent need for a genetic classification of "linears" and the development of an appropriate descriptive terminology. Lineaments with associated offsets most probably are the trace of faults or fault zones; others are the trace of dikes. For the majority of lineaments, displacements are not apparent, but because of a correlation in mines to zones of poorer rock condition and increased density of joints (broken ground), and also an increase in density of joints in the wind and water gaps that define the longer lineaments, we predict they are surface manifestations of imposed mechanical breaks with little or no displacement, i.e., scaled up fracture traces.

It is obvious from a comparison of figures 2a, b, c, and d, that the density of linear features (fractures) is related to scale, but this relationship has yet to be quantified. By analogy with fracture traces and joints (Parizek, 1971a,1971b; Parizek and Voight, 1970) it is reasoned that most lineaments are approximately vertical zones of joint concentration. Although the relationship of joint frequency to (a) residual stress after faulting, (b) strain energy of lithology, (c) thickness of beds, and (d) degree of tectonic deformation, are recognized (Price, 1966), no model has yet been proposed linking "joints" and fractures on different scales.

Because most joint and fracture traces are essentially vertical, the intermediate principal stress axis of the associated stress field should also be vertical. We suggest that the 2nd order shear mechanism (McKinstry, 1953) applied to a wrench fault model (Moody and Hill, 1956; Badgley, 1965) as a working hypothesis for genetically relating certain "linears" of different size and density. Anderson (1951) showed that under these conditions (σ 2 vertical), the stresses near the center of the fault were relieved by fault movement but that the original level of stress is equalled or exceeded at a distance of 0.4 times the length of the fault, perpendicular to the fault plane. This gives a theoretical distribution of faults or zones of fracture, for stress can also be relieved by the

development of joints (Price, 1966).

For a very simple model that assumes fractures (joints) to develop along the planes of maximum shear stress oriented symmetrically at 30° to each successive order of normal stress and that each order "shear" will be separated by a distance of 0.5 the length of its associated higher order shear, then the number of joint bounded blocks per unit area increases by 2^{2n-1}, where n is the order number. The unit area chosen may vary in size, but for each area the longest "fracture" is assigned to order 1. This model neglects the asymmetry of the (n+1)th "shears" to the normal of the nth "shear" (McKinstry, 1953) and yields only 3 directions of fracture instead of 8 (Moody and Hill, 1956). However, this should affect the pattern and not the size of the resulting "fracture" blocks.

This model at least predicts fracture density, which should be ameanable to testing using ERTS, underflight, and ground mapping data. If the thickness to joint interval relationship (Price, 1966) holds for the larger lineaments, then the roots to the lineaments must be deep and represent a neglected element in Global tectonics.

There can be little doubt that lineaments must have a subsurface control similar to that of fracture traces, because in out study areathey exhibit a similar strong control over the position and direction of river valleys. Streams once established may be trapped in their present position controlled by these vertical "zones of weakness", and underscores the role of lineaments in the evolution of river valleys and topography.

We are on the verge of many exciting discoveries which is inevitable whenever a new research tool improves on the resolution of features that were previously rather obscure. Hardware of the ERTS program provides us with such a tool.

REFERENCES CITED

Anderson, E.M., 1951. The Dynamics of Faulting. Oliver and Boyd, Edinburgh

Badgley, P.C., 1965. Structural and Tectonic Principles. Harper and Row Pub., New York.

Boyer, R.E. and J.E. McQueen, 1964. Comparison of mapped rock fractures and airphoto linear features: Photogramm. Eng. Vol. 30, p. 630-635.

Calkins, J.A., 1966. The geology of the west limb of the Hazara-Kashmir Syntaxis, West Pakistan and Kashmir; Unpublished Ph.D. thesis, The Pennsylvania State Univ.,142 p.

Hobbs, W.H., 1911. Repeating Patterns in the relief and the Structure of the Land. Bull. Geol. Soc. Amer.,v.22p.123-176.

_____, 1905, Examples of joint controlled drainage from Wisconsin and New York, Jour. Geol. v. 13, p. 363-

Hough, V.N.D., 1960. Joint orientation of the Appalachian Plateau in southwestern Pa.; Unpublished M.S. thesis, The Pennsylvania State University, 82 p.

Keim, J., 1962. A study of photogeologic fracture traces over the Bisbee quadrangle, Cochise County, Ariz. Unpub. M.S. thesis, The Pennsylvania State University, 42 p.

Koppe. E.F. and D.R. Thompson, 1972. Progress in the recognition of fractured rock zones in prevention and abatement of mine drainage, 4th Symposium on Coal Mine Drainage Res, Mellon Institute, Pittsburgh, Pa. p. 41-47.

Lattman, L.H., and R.P. Nickelson, 1958. Photographic fracture trace mapping in Appalachian Plateau, Bull. Am. Assoc. Petrol. Geol., Vol. 42, No. 9, p. 2238-2245.

Lattman, L.H., 1958. Technique of mapping fracture traces and lineaments on aerial photographs, Photogramm. Eng., Vol. 24, p. 568-576.

Lattman, L.H., and R.H. Matzke, 1961. Geological significance of fracture traces; Photogramm. Eng. Vol. 27, No. 5 p. 635-638.

Lattman, L.H. and A.V. Segovia, 1961. Analysis of fracture trace pattern of Adak and Kagalaska Islands, Alaska; Bull, Am. Assoc. Petrol. Geol. Vol. 45, No. 2, p. 249-263.

Lattman, L.H., and R.R. Parizek, 1964. Relationship between fracture traces and the occurence of ground-water in carbonate rocks, Jour. Hydrol, Vol. 2, p. 73-91.

McKinstry, H.E., 1953. Shears of the Second Order. A,er. Journ. Science, Vol. 251, p. 401-414.

Meisler, H., 1963. Hydrogeology of the carbonate rocks of the Lebanon Valley, Pennsylvania, Pa. Geol. Survey, 4th Series, Ground-Water Rept., W17, 81 p.

Mollard, J.D., 1957a. Aerial photographs aid petroleum search, Canada Oil and Gas, Inc. Vol. 10, p. 89-96.

Mollard, J.D., 1957b. A study of aerial mosaics in southern Saskatchewan and Manitoba, Oil of Canada, Winnipeg, Issue August 5.

Moody, J.D., and M.J. Hill, 1956. Wrench Fault Tectonics. Bull. Geol. Soc. Amer., Vol. 67, p. 1207-1248.

Parizek, R.R., 1969. An environmental approach to land use in a folded and faulted carbonate terrane. Environmental Planning and Geology, U.S. Dept. of Housing and Urban Development and U.S. Dept. of Interior, p. 122-143.

Parizek, R.R., and B. Voight, 1970. Question 37: on remote sensing investigations for dam and resrvoir construction in karst terranes: Commission Internationale des Grands Barranges, Montreal, G.R.Q. 37, Trans. 10th Internat'l Congress on Large Dams, Vol. VI, p. 538-546.

Parizek, R.R., 1971a. Prevention of coal mine drainage formation by well dewatering, Special Research Report, SR-82, Coal Research Section, The Penn State University, 73 p.

Parizek, R.R., 1971b. Hydrogeologic Framework of Folded and Faulted Carbonates - Influence of structure; In Hyrdrogeology and Geochemistry of Folded and Faulted Carbonate Rocks of the Central Appalachian Type and Related Land Use Problems, Circular 82, Mineral Conservation Section Series, The Pennsylvania State University, p. 28-38.

Parizek, R.R., and E.G. Tarr, 1972. Mine drainage pollution prevention and abatement using hydrogeological and geochemical systems, 4th Symposium on Coal Mine Drainage Research, Mellon Institute, Pittsburgh, Pa. p. 56-83.

Parizek, R.R. and L.H. Drew, 1967. "Random drilling for water in carbonate rocks", in Proceedings of a Symposium and Short Course on Computer and Operators Research in Mineral Industries; Min. Ind. Experiment Stat, Vol. 3, Special Pub. 2-65.

Price, N.J., 1966. Fault and Joint Development in Brittle and SemiBrittle Rock. The Commonwealth and International Library, Pergamon Press, Oxford.

Setzer, J., 1966. Hydrologic significance of tectonic fractures detectable on air photos, Ground Water, Vol. 4, No. 4, p. 23-27.

Siddiqui, S.H., 1969. Hydrogeologic factors influencing well yields and aquifer hydraulic properties of folded and faulted carbonate rocks of central Pennsylvnia, Ph.D. dissertation, The Pennsylvania State University, 502 p.

Siddiqui, S.H., and R.R. Parizek, 1969. Hydrogeologic features influencing well-yields in folded and faulted carbonate rocks, Central Pennsylvania (Abstract), Trans. A. Geophy. Union, Vol. 50, No. 4 p. 154.

Siddiqui, S.H. and R.R. Parizek, 1971b. Hydrogeologic factors influencing well yields in folded and faulted carbonate rocks in central Pennsylvania, Water Resources Res., Vol. 7, No.5.

Siddiqui, S.H.,and R.R. Parizek, 1971b. Variations in well yields and controlling hydrogeologic factors; In Hydrogeology and Geochemistry of Folded and Faulted Carbonate Rocks of the Central Appalachian Type and Related Land Use Problems, Mineral Conservation Section, Circular Series 82, The Pennsylvania State University, p. 87-95.

Turner, F.J., and L.E. Weiss, 1963. Structural Analysis of Metamorphic Tectonites, McGraw-Hill Book Co., Inc. New York.

Wobber, F.J., 1967. Fracture traces in Illinois; Photogrammetric Eng., Vol. 33, No.5, p. 499-506.

Warman, J.C., and L.V. Causey, 1962. Geology and ground-water resources of Calhoun County Alabama; Geological Survey of Alabama, County Report 7, 77 p.

Wise, D.U., 1968. Regional and Sub-Continental Sized Fracture Systems Detectable by Topographic Shadow Techniques. Geol. Surv. Canada Paper 68-52, p. 175-199.



Figure 1. ERTS image of an area east of Harrisburg, Pa. showing boundaries of the Precambrian rocks of the Reading Prong (1), the Traissic Basin (in dashed lines), the Diabase Sills (2), and the Conestoga Formation (3) and Martic Line (4) in the Piedmont province. (Enlargement of ERTS image 1080-15185 band 5; October 11, 1972).

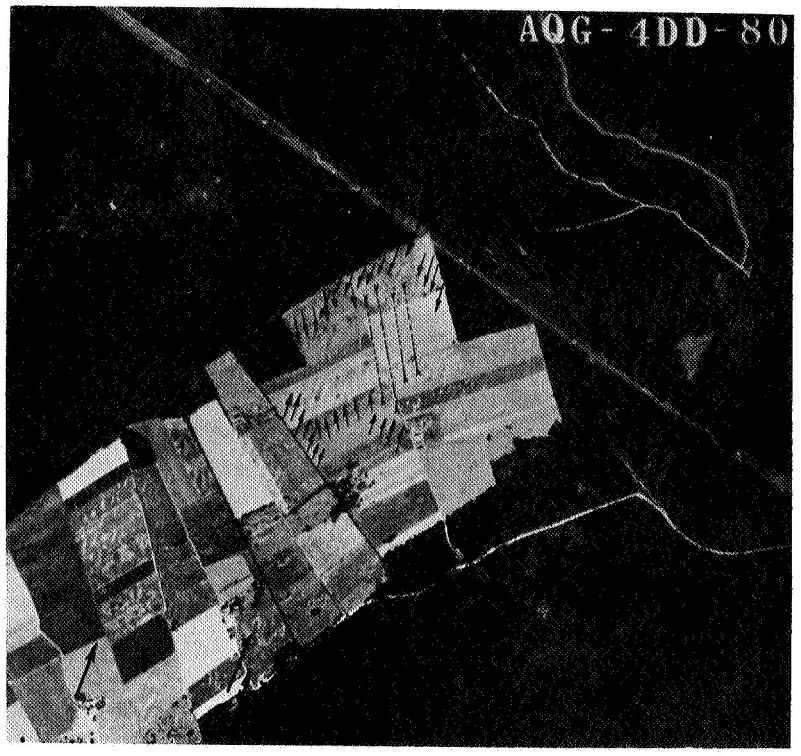


Figure 2(a). Fracture traces (large arrows) faintly visible in cultivated fields and forest in Pennsylvania, underlain by 5 to more than 100 feet of residual soils derived from folded limestone, dolomite, and sandy dolomite. Systematic joint sets account for the mottled tonal patterns in the cultivated areas (small arrows). (Modified after Parizek, 1969. USDA aerial photograph AQG-4DD-80).

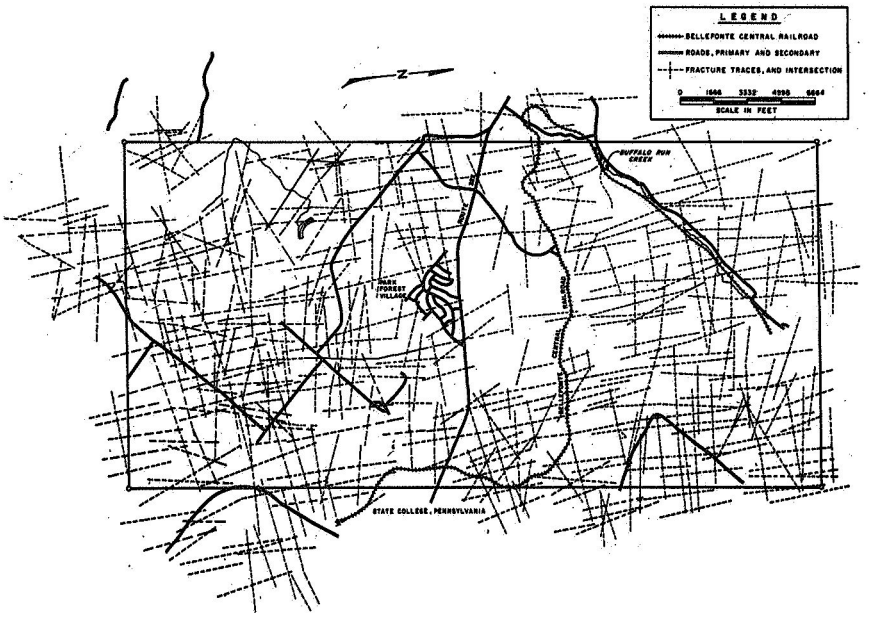


Figure 2(b). Distribution of fracture traces near State College, Pennsylvania. Note that the fracture traces are generally less than 1 mile long, are straight even in folded rocks, are not necessarily uniformily distributed, and may display two or more prominent orientations. (After Parizek and Drew, 1966).

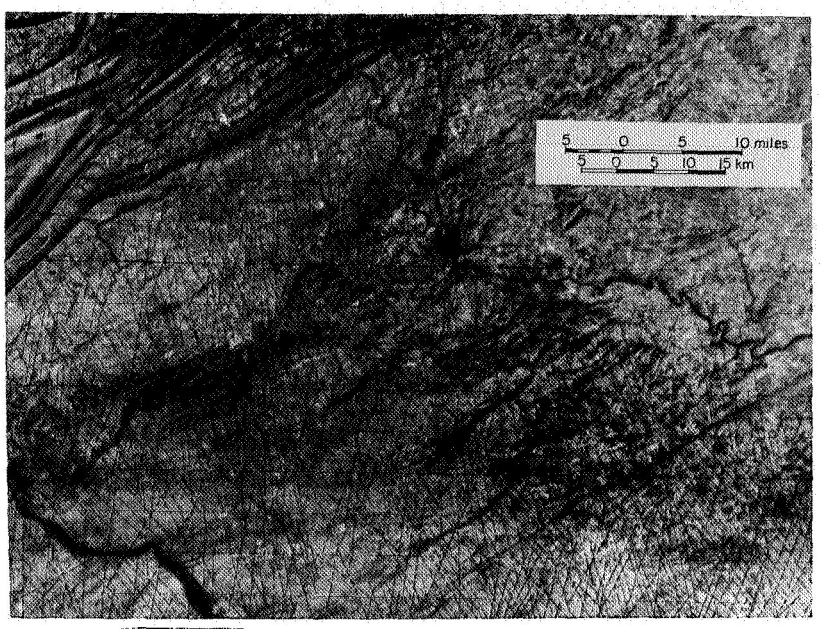


Figure 2(c). "Short" to "intermediate" lineaments crossing the Valley and Ridge, Great Valley, Triassic Basin, and Piedmont structural provinces east of Harrisburg, Pa. The Susquehanna River appears in the lower left, and the Schuykill River in the northeast half of the figure. Reading is located on the Schuykill near the center of the figure. (Enlargements of ERTS image 1116-15192 band 7, November 16, 1972).

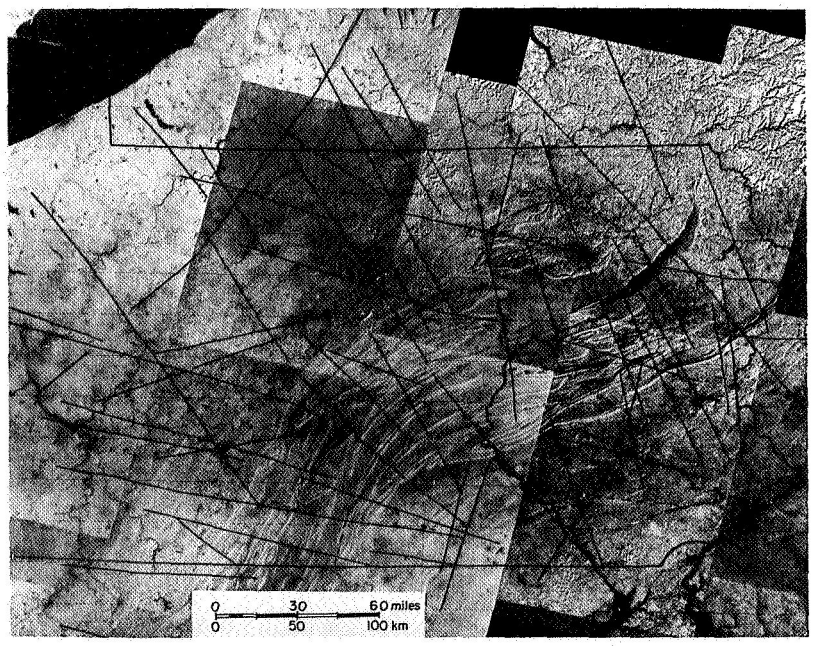


Figure 2(d). "Longer" Lineaments in Pennsylvania. Dashed lines represent known faults that exhibit displacements on this scale of the ERTS imagery: solid lines are lineaments (without genetic implications). The physiographic provinces, the Allegheny plateau to the north and west, the curved Appalachian folded belt through the central section, and the Piedmont to the southeast, show up well. The dark crescentric area in the northeast part of the State in the "anthracite basin" around Scranton and Wilkes-barre.

Paper G 3

GEOLOGY OF UTAH AND NEVADA BY ERTS-1 IMAGERY

Mead LeRoy Jensen, *Department of Geological and Geophysical Sciences, University of Utah, Salt Lake City, Utah 84112*

Abstract

Repetative ERTS-1 imagery covering Utah and Nevada is being studied as an aid in structural geology, mineral exploration, and limnological and hydrological aspects.

Limnological features of algal blooms and varying biological activities in Utah Lake and the Great Salt Lake are grossly evident on the imagery with more subtle details detected on the different bands.

Major structural breaks, lineages, or trends are abundant throughout the area of study. The correlation of positive aeromagnetic anomalies with the trends suggests near surface intrusive bodies, not yet exposed at the surface, that can be tested for possible associated mineralization by collecting soil-gas at the surface which is analyzed for mercury that is (1) apparently associated with mineralization, (2) escapes as a vapor, and (3) can be readily measured in extremely low amounts of less than 1 ppb by absorbtion.

Initial studies are proving that the ERTS images show lineament trends and some of these lineaments do release anomalous Hg contents and are prime zones for further mineral exploration study.

Introduction

The prime objectives of NASA ERTS-1 Contract UN 113, of which I am the Principal Investigator, pertain to mineral resources and exploration, and structural geology. Limnological observations are also proving to be interesting. The area of coverage is large extending over all of Utah, most of Nevada, and portions of California and Wymoning. The boundaries of this rectangular area are from 37° to 42° N latitude and from 109° to 119° W longitude.

Geologically and physiographically, the area includes diverse provinces, viz., Colorado Plateau, Uintah Mountains, Wasatch Mountains, Green River and Uintah basins, a portion of the Sierra Nevada and all of the northern portion of the Basin and Range province. The diversity of mineral and oil deposits, ages of formations and igneous rocks, and the variation in structural features provide a vast potential for the practical application of multispectral imagery to the study of this area. Specific areas of more detailed study are indicated.

Imagery

Only bulk MSS imagery is being used in all four bands. The initial study is greatly enhanced by viewing with a Nikkon binocular microscope mounted over a light table and used to view the positive transparent films at 10X to 80X. The former magnifications is best as it offers a larger area of study but still with retention of details on the imagery.

Those images that provide areas or features of greatest initial interest are further enhanced when printed in B & W but enlarged four times to a scale of about 1/250,000. Interestingly enough, little detail is lost with

the enlargement and numerous geological maps of the area are available at the same scale. A prime example is Humbolt County, Nevada, where regional structural trends, basin and range normal faults, transverse (essentially E-W) faults and specific lithologic types can be recognized on the imagery while some are not noted on the geological map. The enlarged ERTS-1 image is perfectly adequate as a base map and could have served readily as a field base map for mapping.

A simple method of producing color composites and single-color band-images is being used. This involves the use of Diazochrome color films in an Ozalid contact copier. The method is rapid, simple, and relatively inexpensive. The superposed films result in a color transparency which can be re-photographed by 35 mm or other cameras to produce excellent projection materials. The superposed films can be used directly on overhead projectors or viewed with light tables. We find that some experimenting is required with this technique because of the variations in the density of the imagery and the need to use the proper color of diazochrome with specific bands. Generally, the lighter pastel colors provide far better false color enhanced imagery. Examples will be shown with 35 mm colored slides.

Hydrologic Features

Two ancient watercourses have been observed on ERTS-1 imagery. These lie in the Waterpocket Fold area, north of the Marble Canyon section of the Colorado River, in Arizona and Utah. The old watercourse appears to have been northward flowing, following the Waterpocket Fold west of the Henry Mountains, across the present Fremont River and other drainages have captured portions

of the system. The watercourse can be observed on image No. 1032-17370. A cutoff meander on the Colorado River, still above the present level of Lake Powell, appears to be of similar age and possibly related to the ancient watercourse. The major part of the path of the watercourse appears to be structurally controlled. The tributaries generally flow northwestward and northeastward and intersect the major rivers with the acute angle as if the major streams still flowed northward rather than southward.

A second old watercourse can best be seen in the vicinity of Long Ridge and the San Juan River on image No. 1031-17313.

A remarkable correlation of the annual precipitation on the Uintah Basin is evident by comparing image No. E 1121-17312-4 with a computer generated shaded map (Fig. 1) of the same area. The remarkable similarity of the boundaries of the lowest precipitation are evident.

Limnological Features

Image No. 1051-17414 contains some very useful information concerning the hydrology, sedimentology, and biology of Great Salt Lake and Bear Lake in Utah. The greater penetration of wavelengths in band 4 of the MSS imagery yields much information about sediment plumes and water depth. Band 5, with lesser penetration, gives more information about surface phenomena, including algal populations, etc. The infrared bands provide information about shallow water in marsh areas where the water is hidden from shorter-wavelength bands by vegetation. In Great Salt Lake, there is a sharp line between the portion of the lake north of the railroad causeway, which is essentially a rock and earthern dam, and that south of the causeway (Fig. 2). There is a marked difference in salinity across the causeway, and this is reflected in different

algal species, plainly visible in band 5. A reddish algae occupy the north limb, while blue-green varieties occupy the south limb. The negative water budget in the north limb causes brine concentration in that area, accompanied by northward surface flow through the two narrow openings in the causeway. This flow can be seen in band 5. The high density in the northern limb results in density-current counterflow at depths, and this can be seen in band 4. The sediment plumes from inflowing rivers are plainly visible on bands 4 and 5. These features are enhanced in the false color images as shown by 35 mm studies.

Image No. 1051-17420 contains part of Great Salt Lake and all of Utah Lake. The latter displays a very interesting surface pattern which is probably due to an algal bloom which has been swirled into a spiral by the circulation of the lake. This was a short-lived phenomenon observed on the September 12 overpass only which has not been observed on other imagery to date. The algal nature of the phenomenon is not yet proven but is to be studied in cooperation with ERTS-1 limnologists of the National Oceanic and Atmospheric Administration who first noted this feature as shown in Fig. 3.

Geological Features

The prime geological features that are most obvious in the area are major structural trends, lineaments, or structural breaks. These are most prevalent in the Wasatch and Basin and Range provinces. The majority have never been recognized before ERTS-1 imagery and they provide an exploration potential of major significance. This is the application of geochemical and geophysical study over trends that extend into alluvial or volcanic areas that are post-mineralization in age and hide evidence of potentially mineralized areas below the overburden.

As there is significant evidence that mercury vapor escapes from mineralized zones, soil-gas samples are collected in the post-ore blankets over the inferred extension of mineralized trends using a hood equipped with a fan that forces the air through 80 mesh silver screen. The amalgon is later heated in the laboratory and the quantity of released Hg is measured by an atomic absorption instrument. Such studies have been done over known mineralized zones with significant Hg amounts of about 400 ppb to > 1000 ppb have been measured while samples collected over presumably mineral barren zones assay generally in the range of < 300 ppb of Hg.

It is our desire to locate Hg soil-gas anomalies in post-ore covered zones and perform cursory induced polarization surveys over the amonalies with the hope of detecting sulfide mineralization at depth. The practical significance of this application of ERTS-1 imagery in correlative studies with known geotechnics is quite obvious.

Interestingly enough, besides the evident mineralization exposed in bed rock adjacent to the alluvial filled valleys, aeromagnetic maps are also used as additional ground truth and are of aid in correlating the lineages and trends with positive aeromagnetic anomalies. This is especially true in north central Nevada where intrusives have presumably given rise to mineral deposits in favorable carbonate rocks underlying major thrust faults. The overlying rocks of the thrusts consist of essentially siliceous and volcanic formations that are comparatively non-reactive to mineralizing fluids.

In conclusion, therefore, structural breaks detected on ERTS imagery may target trends that correlate with positive aeromagnetic anomalies where anomalous Hg content in soil-gas further delineate where induced polarization surveys should be done with the hope of detecting sulfide deposits for which there is no surface evidence other than the evidence on the ERTS imagery.

CLASS INTERVAL	CATEGORY	SYMBOL
0 - 6 inches	1	.
6 - 10	2	-
10 - 14	3	+
14 - 18	4	=
18 - 22	5	0
22 - 26	6	θ
26 - 30	7	Ø
30 - 34	8	⊕
34 and above	9	⊠

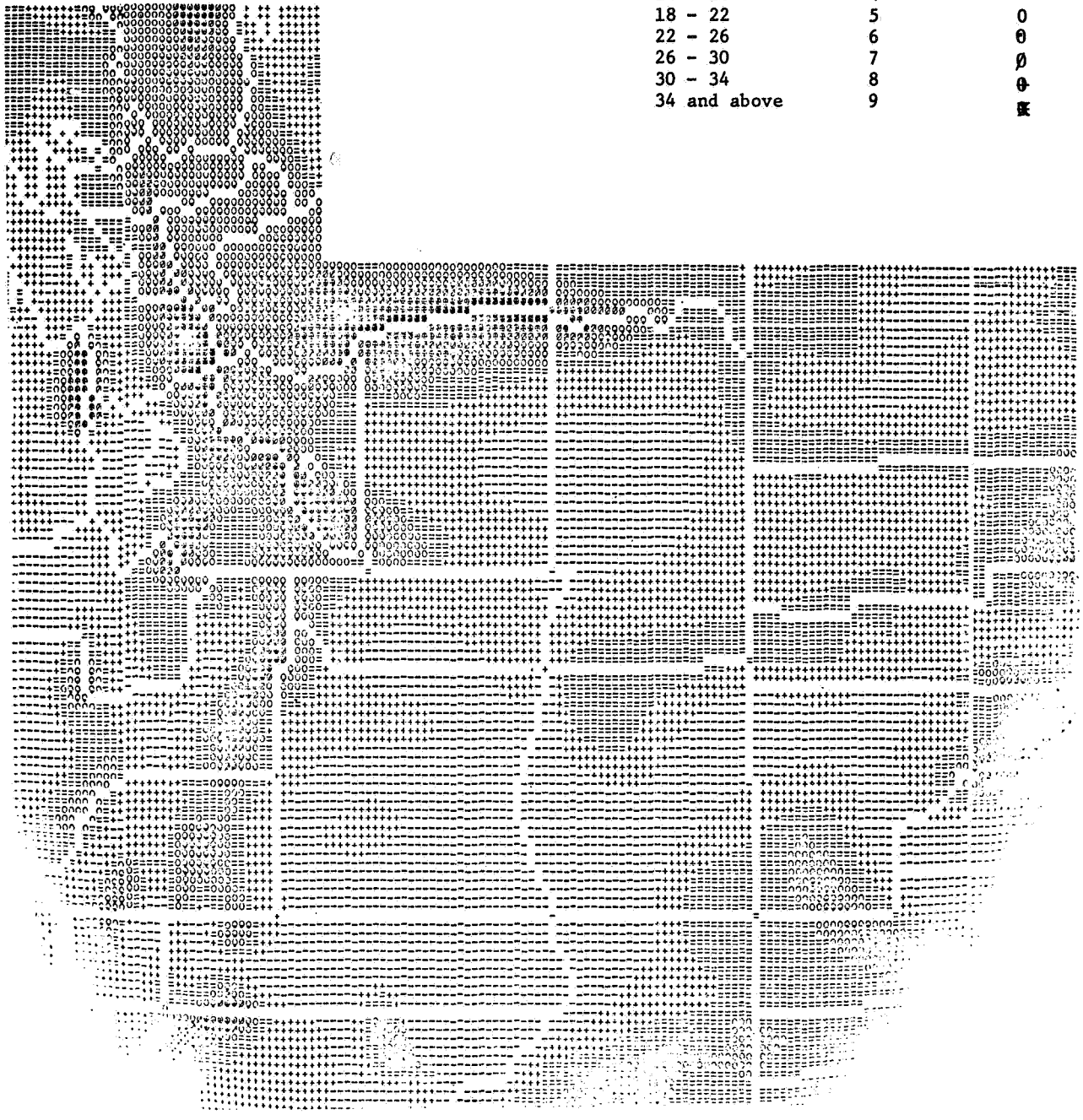


Figure 1


W114-001
W113-301
W113-001
W112-301
13SEP72 C N41-41/W113-10 N N41-40/W113-02 MSS 6 D SUN EL45 AZ142 191-0725-G-1-N-D-2L NASA ERTS E-1052-17472-6 01

Figure 2


W113-001
N039-301
W112-30
7108001X
12SEP72 6 N40-17/W112-12 N N40-17/W112-05 MSS 7 D SUN EL46 AZ140 191-0711-0-1-N-D-IL NASA ERTS E-1051-17428-7 01

Figure 3

Paper G 4

PRELIMINARY GEOLOGIC APPLICATION OF ERTS-1 IMAGERY IN ALASKA[1]

Ernest H. Lathram, I. L. Tailleur, W. W. Patton, Jr., *U. S. Geological Survey, Menlo Park, California;* W. A. Fischer, *U. S. Geological Survey, Washington, D. C.*

ABSTRACT

Linears and faults on ERTS-1 images corroborate the existence of possible deep-seated structures first noted on Nimbus IV images. These structures may have influenced location of mineralization. ERTS images also display more comprehensively and explicitly than heretofore possible the thrust-faulted, complexly folded and open-folded terranes and strongly contrasting lithologies in northwestern Alaska, provide new data on faults in central Alaska, and display previously unknown lineations that suggest concealed folds in northern Alaska. The concealed folds are verifiable only by geophysical techniques and may be significant to petroleum exploration.

INTRODUCTION

The objectives of ERTS-1 Investigation SR 180, "Identification of geostructures of the continental crust particularly as they relate to evaluation of mineral resources," are:

1. To improve existing regional analyses and develop new regional analyses and concepts of geologic history and mineral resource potential employing the unique capability of ERTS images to portray regional relations of fundamental geologic structures, and to depict features and relations whose regional extent is too large to be recognized in conventional field or aerial photographic study.

2. To enhance medium- and small-scale geologic mapping through the synoptic and orthographic view of structural relations afforded by ERTS images and through detection of lithologic differences by ERTS multi-band sensing, and to extend geologic mapping into unmapped areas using these characteristics.

Studies to date have yielded positive results in both categories.

---

[1] Publication authorized by the Director, U.S. Geological Survey.

PRECURSORY INVESTIGATIONS

Prior to the launch of ERTS-1, an unusual cloud-free image of Alaska was obtained by the Nimbus IV IDCS (Image Dissector Camera System). In addition to the major known faults and folded mountain ranges of Alaska and western Canada, this image showed a set of northwest- and northeast-trending linears that suggest previously unrecognized geologic structures deep in the earth's crust (Lathram, 1972). This finding added support to the growing recognition that satellite images show gross geologic features recognizable in no other way (Shapiro, 1971; Segerstrom, 1970; Carter, 1972).

Subsequently the relation of these linears to the distribution of mineral deposits in Alaska was studied and compared to the relation of mineral deposits and fundamental fractures in the Canadian Cordillera as presented by Sutherland-Brown and others (1971). Results of this study suggest general, but inconclusive spatial relation of the distribution of mineralized belts in Alaska to these deep-seated features rather than to the north-convex arcuate distribution of lithologic belts (fig. 1; Lathram and Gryc, 1972) and thus provide an alternative concept to guide mineral resource exploration.

ERTS-1 INVESTIGATIONS

Linears and faults on numerous ERTS-1 images examined to date have the same trends as the northwest- and northeast-trending set identified on the Nimbus IV image, corroborating its existence and extensive distribution. Several linears on ERTS images support the interpretation that this set represents fundamental crustal structures. A northwest-trending linear on image 1003-21355 in the Shungnak area is strongly expressed in topography and in the course of the Kobuk River. However, rocks on either side of the linear are the same age and lithology and do not appear to have been significantly deformed along it, suggesting that the linear represents a structural break at some depth beneath the volcanic rocks at the surface. On image 1009-22090 in the western Brooks Range, another northwest-trending linear is displayed. Southwest of this linear, Jurassic and Cretaceous strata are intricately folded; to the northeast, Cretaceous rocks are less complexly deformed. The linear also coincides with a southward deflection of structural trends in the De Long Mountains (fig. 2). In the Fairbanks area, linears of both trends of the set are well expressed on image 1030-20442, and several have been previously mapped as faults. A study of microseismic activity in central Alaska (Gedney and others, 1972) shows that shallow epicenters lie along these linears and are concentrated at their intersections. The regionally dominant linear is northwest-trending, lies along the Tanana River, is locally marked by mapped faults, and coincides with a major northwest linear identified on the Nimbus image. Southeast of Fairbanks, this linear marks a significant geologic boundary, which suggests that it is a fundamental feature.

An understanding of these features and their significance in the regional geologic framework is essential in analyzing the mineral potential of Alaska.

Other features whose understanding is critical to evaluating the petroleum potential of the northern Alaska and Yukon-Koyukuk petroleum provinces are displayed on ERTS-1 images. Images 1009-22090, 1046-22143 and 1046-22145 give a unique perspective of geologic structures of northwestern Alaska. Folded flat thrust plates in the De Long Mountains are clearly shown, several marked by limestone (image of Band 5, not illustrated) and one by remnants of an ultramafic layer (image of Band 7, fig. 2). The intricate nature of complex folds in the foothills northwest of the De Long Mountains is portrayed comprehensively for the first time and contrasts markedly with broad folds in younger rocks to the north (fig. 2). In the Alatna Hills of west-central Alaska a previously unknown series of closely spaced northeast-trending fractures identified on ERTS-1 image 1072-21180 (fig. 3) supports the conjecture that the Kobuk fault zone is a major east-trending zone of strike-slip faulting. The fractures have the trend and pattern of closely spaced shears expected in areas within such strike-slip fault zones.

The most significant result with respect to regional analysis of mineral resource potential was achieved in the study of an image of northern Alaska (Fischer and Lathram, unpub. data). Lakes in the Arctic Coastal Plain are dominantly elongate, with their long axes parallel and trending about N 9° W. On ERTS-1 image 1004-21395, an additional strong east-trending regional lineation, not previously recognized on aerial photographs or in field study, is expressed by elongation of some lakes, alignment of others, and by linear interlake areas (fig. 4). The trend of this lineation is parallel to the trend of deflections in contours of the magnetic and gravity fields in the area and parallel to westerly deflections in the northwest ends of northwest-trending folds mapped to the south. In addition, the alignment of many small lakes forms a large and a small ellipse superimposed on the regional lineation. Sparse seismic profiles show periodic reversals in dip and regional arching in shallow strata beneath the lineated area. These data suggest that heretofore unsuspected structures may be concealed beneath the Quaternary mantling Gubik Formation in the area of the image. The strata in shallow folds are younger than those tapped by the oil wells of the Umiat field to the south, and favorable reservoir beds may occur in the area. Furthermore, the folds in the shallow rocks in this area may reflect structural conditions conducive to oil accumulation in older strata at or near basement.

The scale of 1:250,000 has been adopted as the standard of the U.S. Geological Survey for geologic mapping in Alaska. To date, structural complexity and sparsity of field data have hampered preparation of geologic maps at this scale in northwestern Alaska. ERTS-1 images 1009-22090, 1046-22143 and 1046-22145, enlarged to 1:250,000 scale, provide portrayals of the earth's surface that aid significantly in solving these problems by serving not only as excellent base maps, but also as a means of

extrapolating field observations of lithology and structure into unmapped areas. Geologic maps at 1:250,000 scale are currently being prepared, using these enlargements. The comprehensive and orthophotographic portrayal of the structure in this area will provide maps that are significantly more useful to petroleum exploration than using conventional planimetric or topographic bases.

ERTS-1 images at scale of 1:1,000,000 are also being used operationally in the completion of a new 1:1,000,000-scale geologic map of northern Alaska, and a new 1:2,500,000-scale geologic map of the entire state, as they provide additional information in areas where field geologic mapping is sparse or lacking.

CONCLUSION

ERTS-1 images provide both a new perspective of geologic conditions and new geologic information of great benefit in determining the geologic framework and mineral resource potential of Alaska. They also provide new and excellent operational tools for representing the geology of areas already mapped and for extrapolating geologic knowledge into unmapped areas.

REFERENCES

Carter, W. D., 1972, Geologic questions and significant results provided by early ERTS-1 data [abs.]: U.S. Dept. Commerce Natl. Tech. Inf. Service, NASA-CR-128121, 1 p.

Gedney, L., Shapiro, L., Van Wormer, D., and Weber, F., 1972, Correlation of epicenters with mapped faults, east-central Alaska, 1968-1971: U.S. Geol. Survey open-file report.

Lathram, E. H., 1972, Nimbus IV view of the major structural features of Alaska: Science, v. 175, p. 1423-1427.

Lathram, E. H., and Gryc, George, (in press), Metallogenic significance of Alaskan geostructures seen from space: Internat. Symposium on Remote Sensing of Environment, 8th, Ann Arbor, Mich., Oct. 1972, Proc.

Segerstrom, K., 1970, Apollo 7 photography in Antofagasta Province, Chile--An interpretation, in Geological Survey research 1970: U.S. Geol. Survey Prof. Paper 700-D, p. D10-D17.

Shapiro, L. H., 1971, Comparison of information content of space photography and low altitude aerial photography: U.S. Geol. Survey Inter-agency Rept. USGS-229, 40 p.

Sutherland-Brown, A., Cathro, R. J., Panteleyev, A., and Ney, C. S., 1971, Metallogeny of the Canadian Cordillera: Canadian Inst. Mining and Metallurgy Trans., v. 74, p. 121-145.

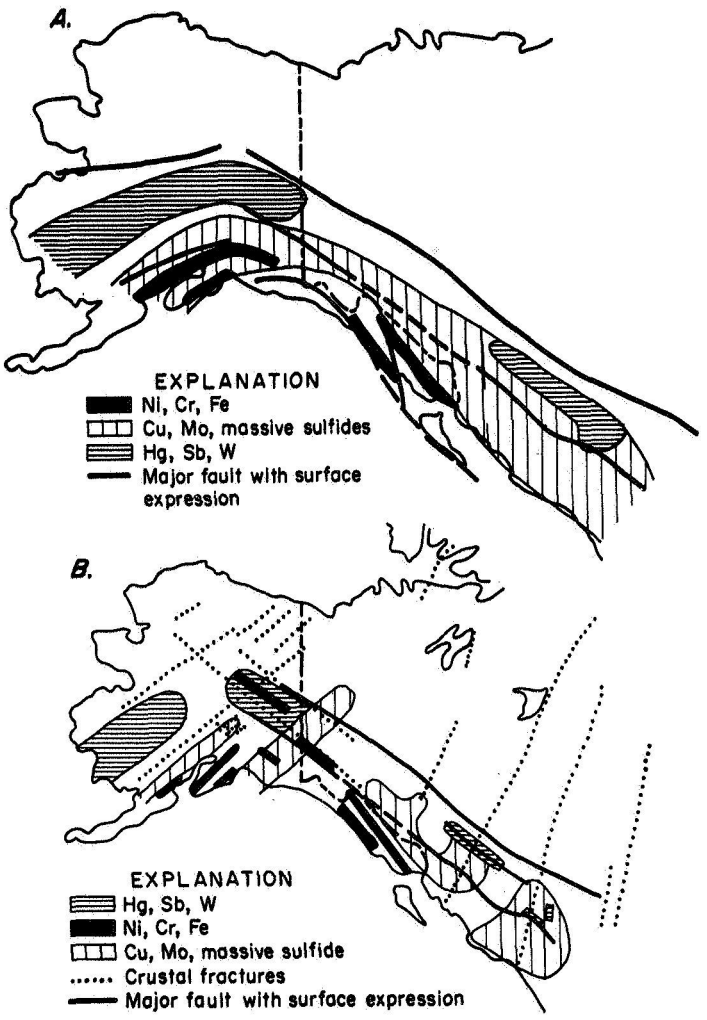


Figure 1. Areas of Alaska and western Canada considered favorable for location of deposits of selected metals based on extrapolation of geologic conditions at known occurrences. A) Conventional concept guided by north-convex arcuate distribution of lithologic belts. B) Postulated alternative assuming lineaments seen on Nimbus IV image are crustal fractures and have influenced mineralization.

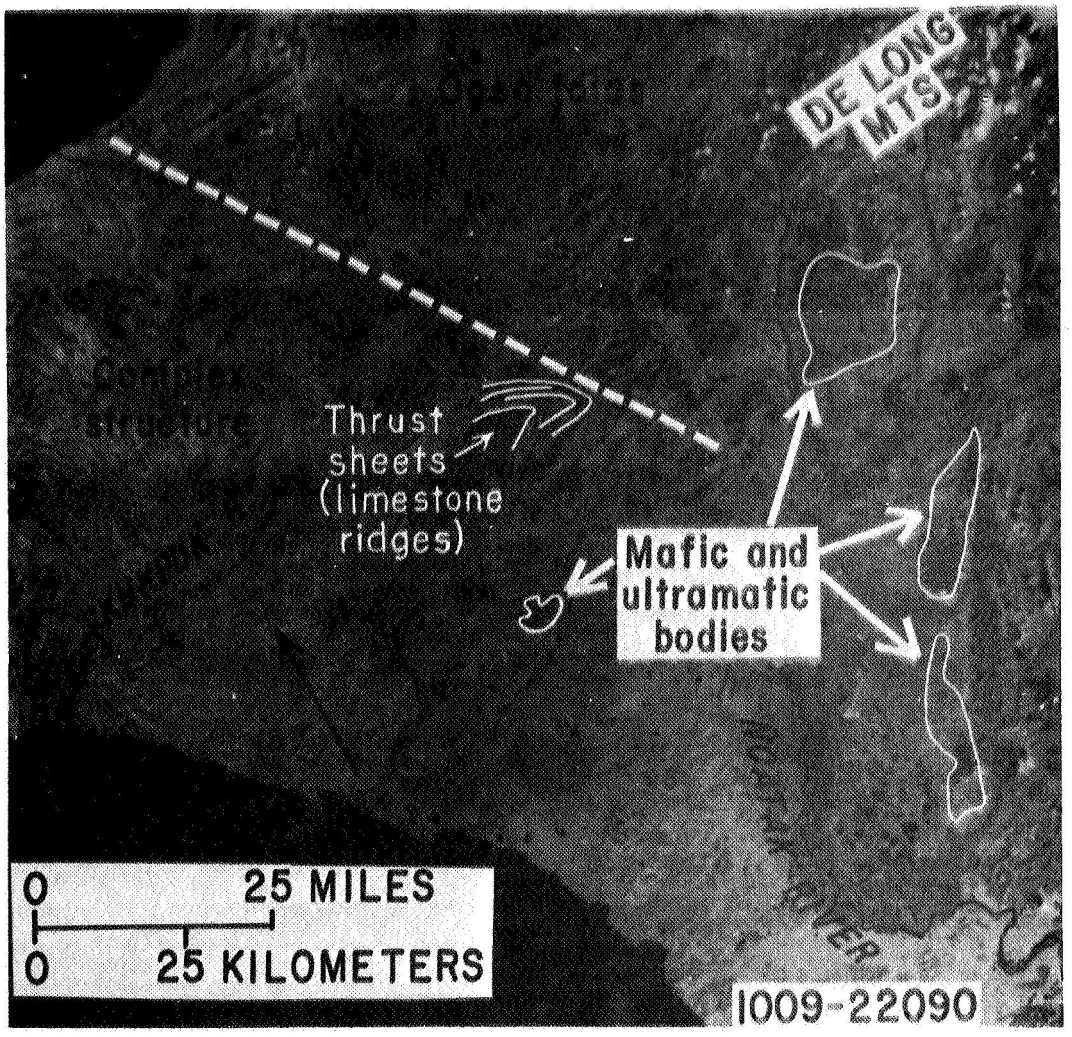


Figure 2. ERTS-1 image (Band 7) showing differing structures and the aspect of some known lithologic types in the western De Long Mountains.

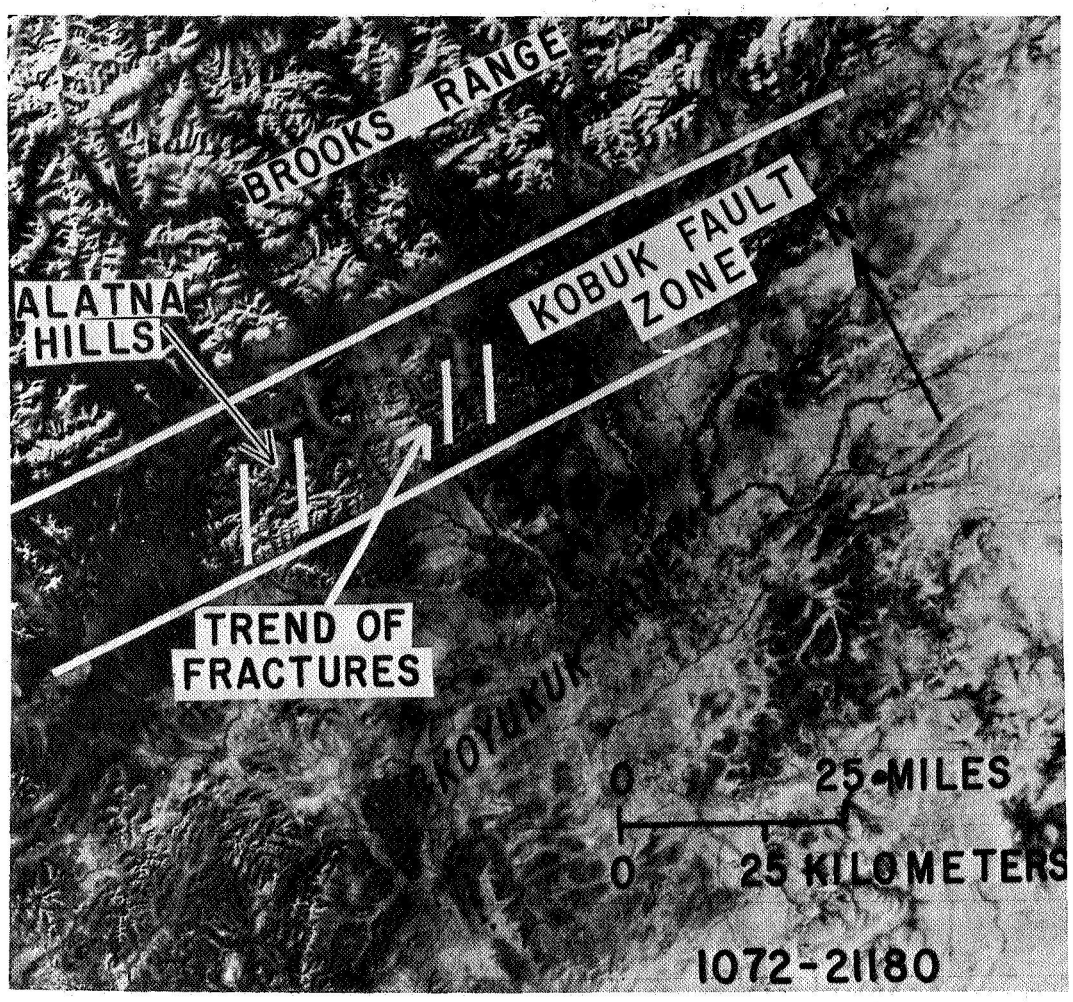


Figure 3. ERTS-1 image (Band 5) showing closely-spaced fractures in the Kobuk fault zone.

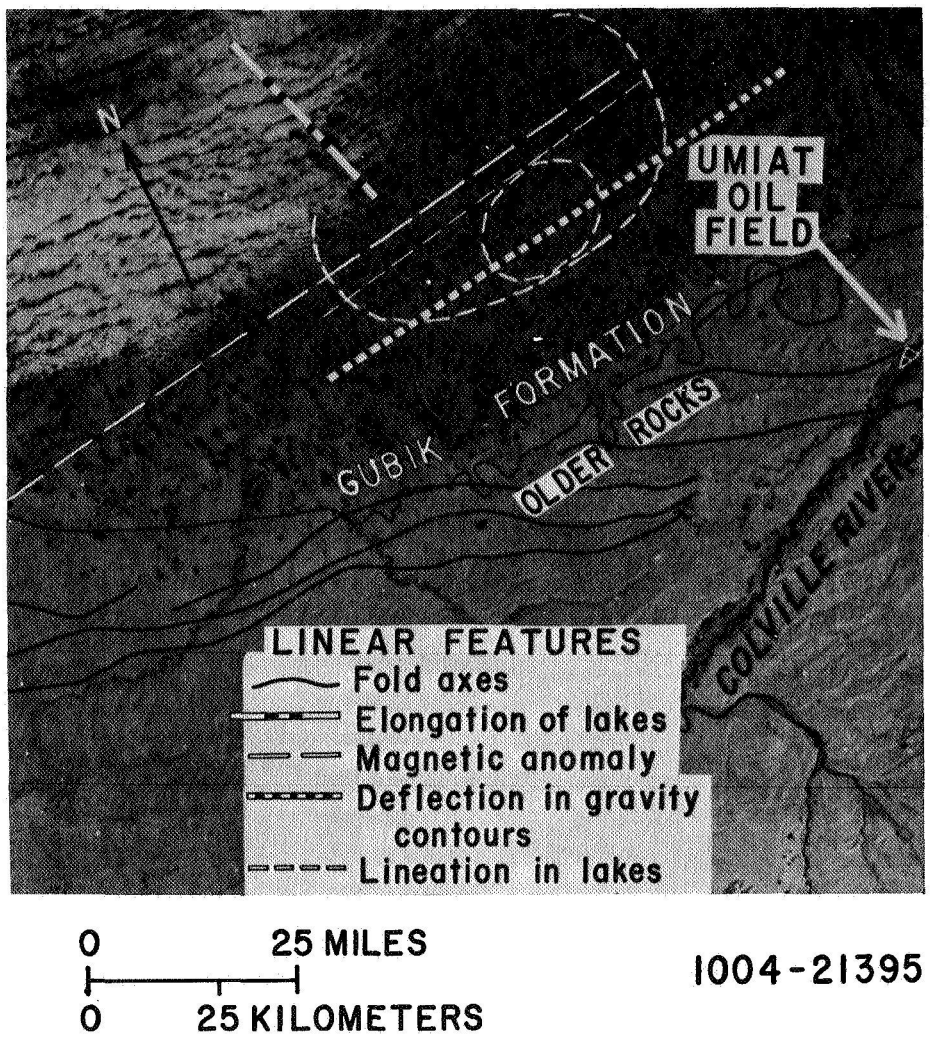


Figure 4. ERTS-1 image 1004-21395 showing lineation in lakes, trends in magnetic anomalies and deflections in gravity contours, trends of previously mapped folds, and generalized contact between Gubik Formation and older rocks.

Paper G 5

A COMPARISON OF GEMINI AND ERTS IMAGERY OBTAINED OVER SOUTHERN MOROCCO

Herbert W. Blodget and Arthur T. Anderson, *Earth Survey Science Office, NASA, Goddard Space Flight Center, Greenbelt, Maryland 20771*

ABSTRACT

A mosaic constructed from three ERTS MSS band 5 images enlarged to 1:500,000 compares favorably with a similar scale geologic map of southern Morocco, and a near-similar scale Gemini 5 photo pair. A comparative plot of lineations and generalized geology on the three formats show that a significantly greater number of probable fractures are visible on the ERTS imagery than on the Gemini photography, and that both orbital formats show several times more lineaments than were previously mapped. A plot of mineral occurrences on the structural overlays indicates that definite structure-mineralization relationships exist; this finding is used to define underdeveloped areas which are prospective for mineralization.

More detailed mapping is possible using MSS imagery than on Gemini 5 photographs, and in addition, the ERTS format is not restricted to limited coverage.

Studies in the various earth science disciplines using data from orbiting spacecraft have been conducted for over a decade now. These investigations have utilized data from numerous satellite-instrument combinations. However, the most effective pre-ERTS studies have utilized photographs obtained for the S-05 Synoptic Terrain Photography Experiment, for which Dr. Paul Lowman of the Goddard Space Flight Center was Principal Investigator (Lowman, 1969). We are all now involved in conducting our separate discipline studies using ERTS data, so this would be a good time to see how this really does improve our resource evaluation capability.

One geologically interesting area where investigations have been conducted using both Gemini and ERTS imagery is northwest Africa, or more specifically, the southern-most part of Morocco (Figure 1).

This area as seen on ERTS imagery is shown on Figure 2. On the right is a photo mosaic constructed from 3 MSS band 5 frames enlarged to a scale of 1:500,000 on the original. This band was selected be-

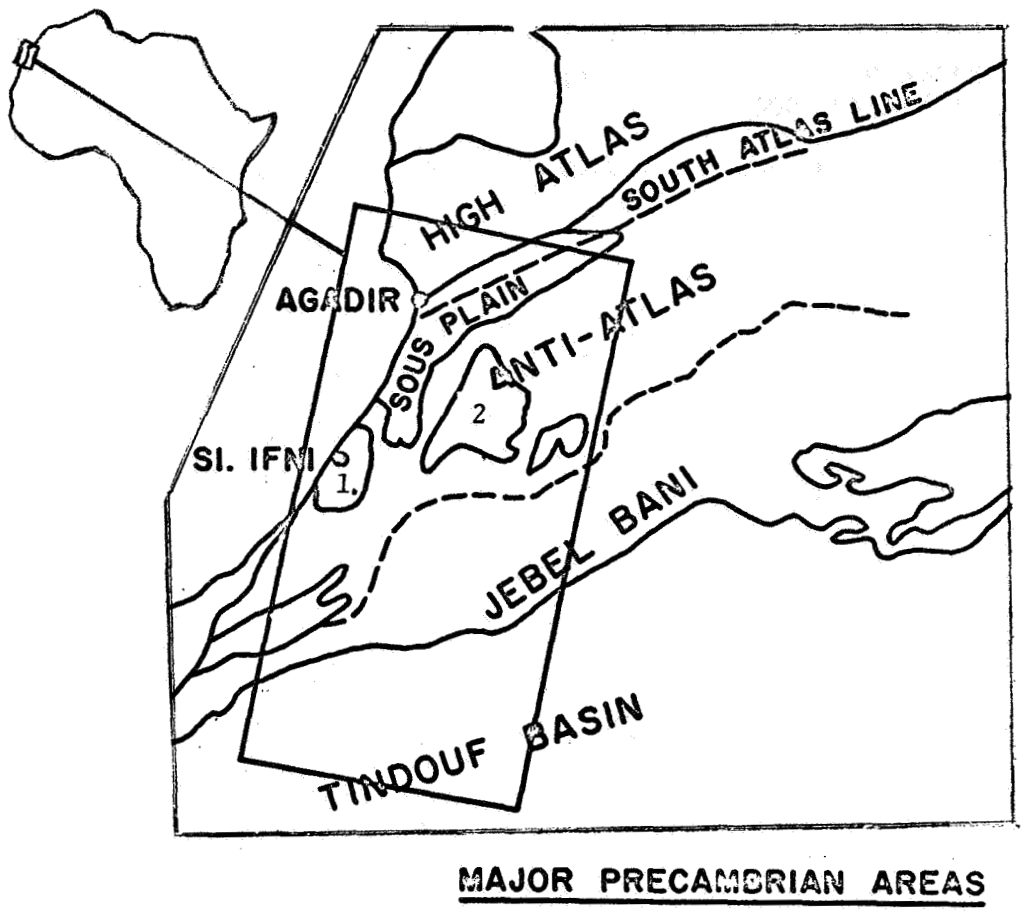


Figure 1. Location Map: ERTS-1 Coverage.

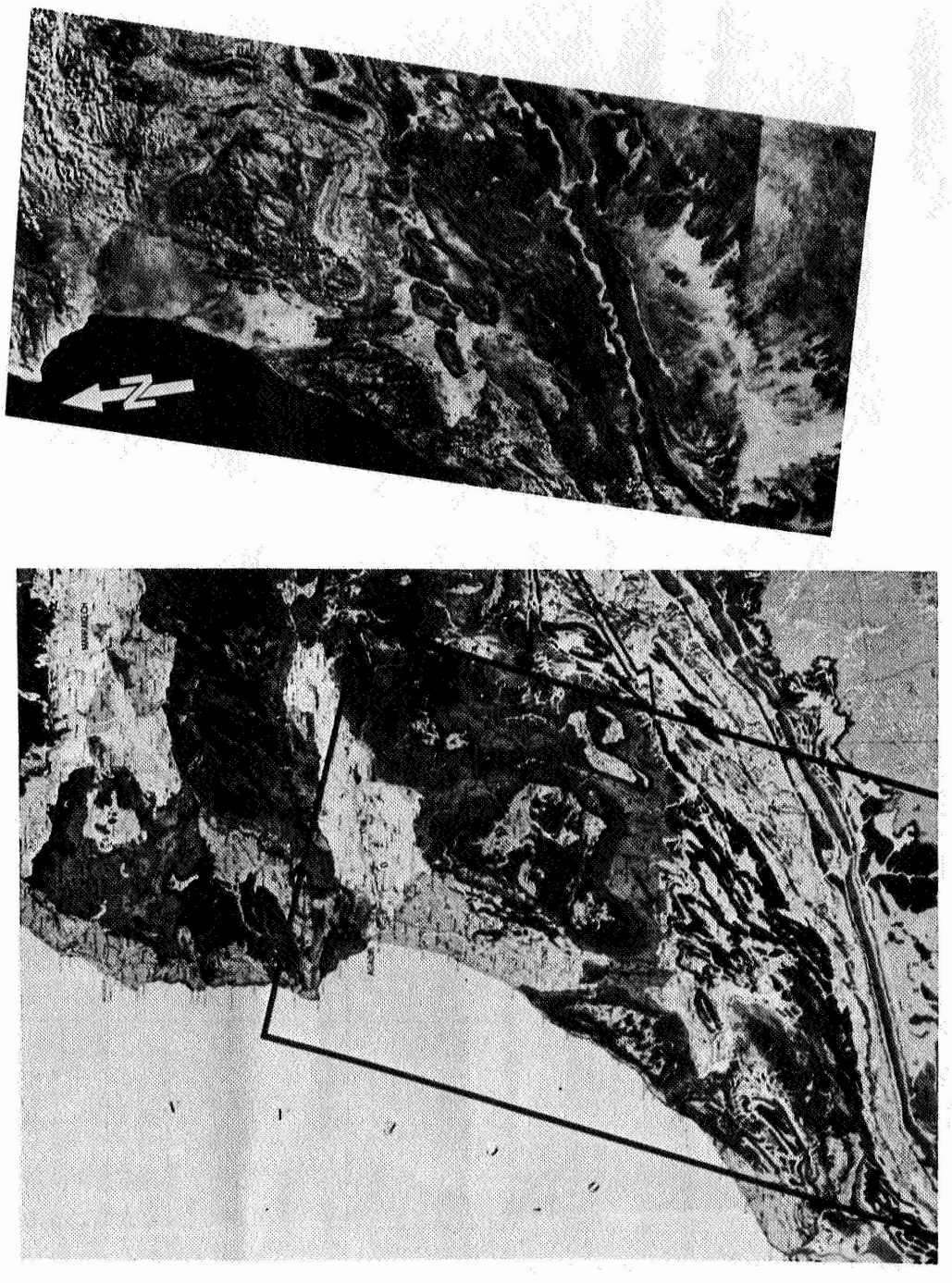


Figure 2. Geologic map and comparable scale ERTS MSS-5 mosaic.

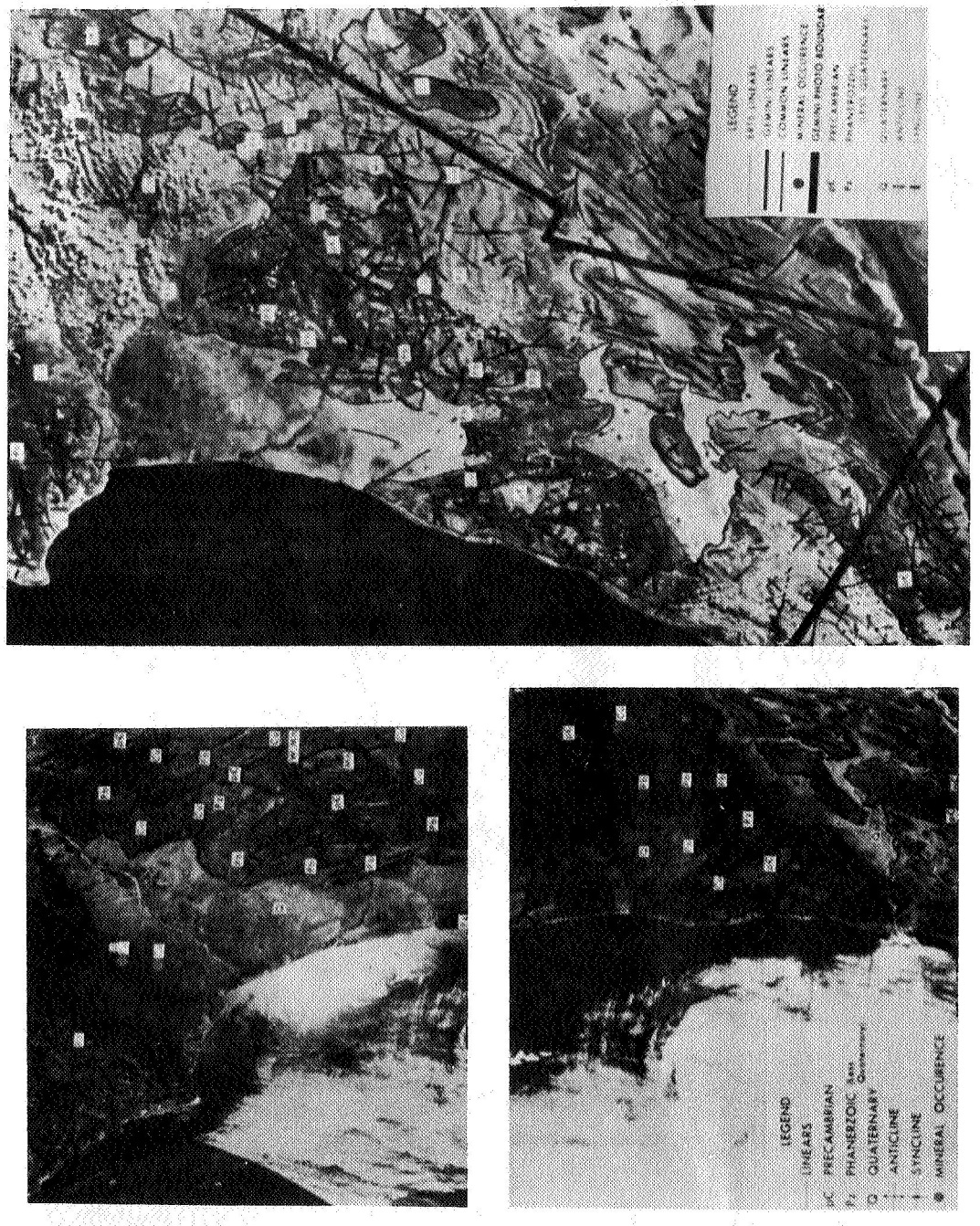


Figure 3. Gemini 5 and ERTS MSS-5 imagery with plotted lineations and mineral occurrences.

cause it exhibited the highest resolution in this area. The imagery was obtained November 3, 1972, and includes frames 1103-10411, 13 and 15. A similar scale geologic map (1956), includes the outlined area of the top 2 ERTS frames and is shown on the left side of Figure 2.

All the major geologic structures shown on the published map and described by Furon (1963, p. 78, 106-116) are clearly visible on the ERTS imagery. The east-northeast trending High Atlas mountains are separated from the geology to the south by the South Atlas line or Agadir fault. On the generalized geologic maps of Africa, it is shown as extending east-northeast from Agadir to the Mediterranean Sea, and is considered by De Sitter (1959, p. 179) as one of the great fundamental faults. Although a fault of the proper magnitude is not indicated on the geologic map, the major Agadir fracture probably lies below the Quaternary sediments of the Sous Plain and may account for the general straightness of the Wadi Sous. South of this major fault, the Sous Plain separates the High Atlas from the subdued Anti-Atlas mountains; this is the western-most link of a discontinuous chain of troughs trending parallel to the south Atlas line. The broadly uplifted, eroded domes of the Anti-Atlas mountains, extend northeastward from the Ifni Enclave, and are flanked on the southeast by the plunging foreland folds which form the Jebel Bani mountains. Further south, the margin of the Tindouf basin is outlined. Figure 3 shows the same area compared with Gemini 5 coverage taken in 1965.

The domal uplift of the Anti-Atlas mountains was accompanied by a complex system of structural fracturing which can, in part, be recognized on the orbital imagery as a series of lineaments. These are particularly prominent across the Precambrian-Cambrian contacts. Most of the tranverse faults shown on the geologic map can be recognized and have been plotted on both the Gemini and ERTS imagery. In addition, numerous lineations, which are probably in large part also structural fractures, are clearly defined on the orbital formats, but do not show up on the published maps. Many of the published strike-slip faults, however, cannot be identified from orbital altitudes. In particular, the faulting developed in the saddle between the Ba Amran and Oulite Precambrian domal areas cannot be recognized in contrast to the strike of the beds.

Lineations visible on the orbital imagery were plotted on acetate overlays, using near-1:500,000 image enlargements for the bases; this scale was selected to maintain maximum continuity with the published map. The 3 easily recognizable lithologic units were also outlined; these include dark massive Precambrian basement, light-toned Quaternary sediments and an all-inclusive Phanerozoic unit in between. Plots on the Gemini base are shown on the left, while on the right, is a composite overlay made on MSS band 5 imagery. All the linears visible on ERTS imagery were first plotted on the composite as thin black lines. This overlay was then compared with the Gemini overlay, and lineaments which were identified on both imagery types are shown here as lines of

intermediate width. Finally, the lineaments which were seen on the Gemini photos and not observed on the MSS images were extrapolated and are designated by the widest lines. These plots show that the southern, more vertical Gemini photo compares quite favorably to the band-5 imagery in the areas of major domal uplift. Fractures mapped in the folded foreland area, however, are only marginally identifiable at best on the Gemini print, so were notgenerally delineated. The upper Gemini photo, however, is more oblique, and exhibits several linears which were not recognized on the ERTS data. Many of these approach the direction of the scan lines, so they may thereby be masked on the MSS image. The few remaining linears are somewhat aligned with the Gemini spacecraft tilt and have probably been enhanced by viewing down the lineament strike. The overlays without the base are shown on Figure 4.

To get a general numerical feel for the respective linears mapped, the lineaments for each of the three defined groupings were counted. In total there are 257 seen on the MSS imagery only, 38 seen on the Gemini image only, 115 that were delineated on both Gemini and ERTS. This indicates that about three times as many linears can be seen on ERTS imagery than are visible on the Gemini photos. This comparison, however, is probably too strongly weighted by inclusion of linears mapped in the southeast folded areas. If this group is discounted, a more realistic comparison emerges, with approximately 25 percent more linears seen on the ERTS pictures. There are several possible explanations for the increased lineament recognition capability: a. The imageries were obtained under different sun angle, (Gemini taken at 11:38 and ERTS during mid-morning, b. the viewing angle was different (vertical for ERTS and differing for each of the oblique Gemini photographs), c. there may be important seasonal differences (ERTS was taken November 3 while Gemini 5 was flown in August 22), or d. atmospheric differences may have influenced visibility on the different dates. The affect of each of these individual parameters is not certain. However, one thing that can be seen here empirically is the degradation of resolution in the direction of Gemini obliquity, as evidenced in the decrease of Gemini-mappable linears in the northeasterly direction.

After the linear plots were drawn, known mineral occurrences were superposed to determine possible relationships between mineral deposits and structure, and are shown on Figures 3 and 4 as large dots; a total of 25 ore deposits were located and plotted on the overlay. Of the 25, thirteen (13) fall on or very close to the Precambrian-Phanerozoic contact. This would be expected if one considers that mineralizing fluids related to the domal uplift will generally solidify in fractures near their genetic source, as described by Wisser (1960, p. 99). In addition, 7 of these 13 deposits appear to be on or near visible lineations on the ERTS imagery (only 5 of these 7 fractures were visible on the Gemini photos) and these are most commonly oriented in a east-northeasterly fault direction.

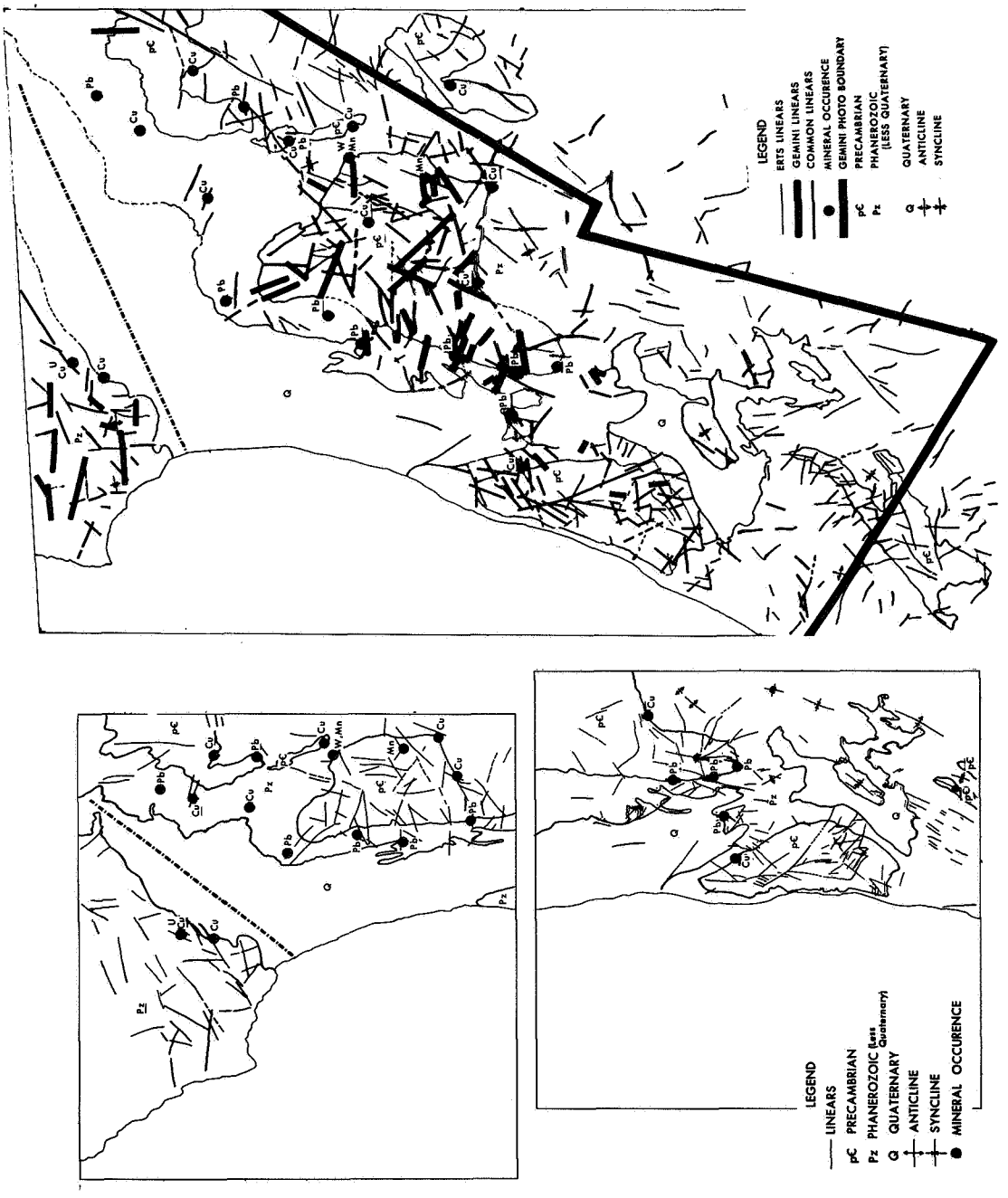


Figure 4. Lineations and mineral occurrences from Figure 3 without the photographic base.

Having once determined these general structure-mineralization relationships, it would be advantageous to use the synoptic view to identify other areas having similar relationships; the objective, of course, being to isolate additional areas which appear to be mineral prospective.

One such area which is strikingly evident is the Precambrian-Phanerozoic contact near the former Morocco-Ifni border. Ifni was only ceded to Morocco in 1969 so mineral exploration prior to that time was not practical along a poorly-defined political border. The area thus, is relatively virgin for prospecting. Of the total lithology contact area, those locations associated with east-northeast "Agadir-trend" faulting seem especially attractive, and should be investigated in the field.

This study, it should be stressed, does not claim ro replace currently used mapping and exploration techniques, but rather, it permits delineation of the more prospective areas, and thus can permit standard field techniques to be utilized in the most efficient manner.

In conclusion, both Gemini and ERTS imagery provide significant data for regional studies, and this can aid in the evaluation of mineral resources. In our immediate study area, however, the vertical ERTS format provides some additional detail which is not visible on the slightly oblique Gemini photos. In addition, it can be seen that the resource studies using photography obtained from previous manned orbital flights are limited to those relatively small areas where imagery is available, while ERTS imagery, on the other hand, has the capability of world wide coverage.

REFERENCES

de Sitter, L.U., 1959, Structure Geology: McGraw-Hill Book Co. Inc., New York, 552 p.

Furon, R., 1963, The Geology of Africa; Hafner Publishing Co., New York, 277 p.

Lowman, P.D., 1969, Geologic Orbital Photography: Experience From The Gemini Program - Photogrammetria, v. 24, 77-106 p.

Ovazzani, M.T., Eyssautier, M.L. Marcais, M.J., Coubert, M.R. and Fallot, M.P. 1956, Empire Cherifien, Marrekech Sheet: Ministere de la Geologie, Service de la Carte Geoloique, Scale 1:500,000.

Wisser, E., 1960, Relation of Ore Deposition to Doming in the North American Cordillera: Geol. Soc. of America, Memior 77.

Paper G 6

CAPABILITY OF ERTS-1 IMAGERY TO INVESTIGATE GEOLOGICAL AND STRUCTURAL FEATURES IN A SEDIMENTARY BASIN (BASSIN PARISIEN - FRANCE)

Claude Cavelier, Jean-Yves Scanvic, Guy Weecksteen and Alain Ziserman, *Bureau de recherches géologiques et minières, Orléans - France*

ABSTRACT

A preliminary study of the MSS imagery is in progress on a sedimentary basin whose structure is regular. Crops and natural vegetation are distributed all over the site located under temperate climate. Ground data available concern plant species geology and tectonic and are correlated with results from ERTS 1 imagery.

This comparison shows a good correlation.

The main geological units are detected or enhanced by way of agricultural land use and/or natural vegetation. Alluvial deposits are outlined by vegetation grass land and poplar trees.

Some spatial relationship of geostructures, suspected until now, are identified or extended in associating results from different spectral bands.

I/ INTRODUCTION

The MSS images which form the subject matter of this communication (1) are situated outside the test-site we proposed for NASA, i.e. the Massif Central. However they do partially resolve a problem which we brought up in our proposals, that of the possible prolongation of the important Sillon Houiller fault towards the North-East outside the Massif Central and particularly its possible relation to the Metz fault.

The work was realised by visual study of Bulk black and white 9"1/2 positive paper prints with an enlargement system. The interpretation made on overlay was renewed for each spectral band and then compared with existing cartographic documents.

II/ GEOLOGICAL AND PHYSICAL BACKGROUND

The MSS images examined cover an eastern sector of the Parisian Basin between the towns of Laon in the NW, Briey in the NE, Langres in the SE and Sens in the SW. The town of Vitry-le-François is approximately central halfway between Paris and Nancy.

The region in question has a very regular relief of shelving plateaux bounded one from the other by erosion "cuestas". The highest section (average altitude 400-500 m) is in the SE angle (Langres Plateau) ; the lowest point (about 50 m) in the NW (the Aisne valley). The general orientation of surface drainage is in direct relationship with the hypsometry : all the important rivers : Meuse, Marne, Aube, Seine, etc., have their sources in the SE and flow towards the N, NW or W.

The formations represented are of sedimentary origin. The oldest, being of the Liassic Age, outcrops in the SE ; the most recent except for Quaternary formations, are of the Oligocene and are found in the western sector. From the SE or NE towards the W the succession of outcropping formations is regular at the scade considered and shows concentric strata of the Jurassic, Cretacious, and Paleogene.

This arrangement has no relation to a progressive recession of the Triassic and Oligocene marine water towards the center of the basin and on the contrary is essentially due to the Tertiary and Quaternary erosion in relation with Pyreneo-Alpine tectonics and climatic variations. The parisian basin's great natural unity at present is the result of a very complex geological history beginning at the Paleozoic and continuing still.

The sector under consideration shows a general dip of the eastern peripheral beds towards the West, this being in relation with the slightly subsident synclinal basin, practically centred on Paris, which was laid down during the Cretaceous Age and received its individual character essentially during the Paleogene. This monoclinal structure is complicated in its details by folds and faults among which may be distinguished those of Armoricain (NW-SE) and Variscian (SW-NE) orientation on the one hand and radiating and concentric faults on the other hand, linked to the Pyreneo-Alpine orogenesis. The former are generally interpreted as superficial reappearance of the great Hercynian faults affecting the Paleozoic foundation of the basin. The latter are put in relation with the architectural model of the Cretaceo-Tertiary Parisian Basin.

III/ CONTRIBUTION OF THE STUDY OF MSS IMAGES

3.1. Land Use

In a region such as the Parisian Basin land use is the most accessible parameter at the orbital scale. Consequently it is necessary to analyse rapidly the vegetation signal in the different spectral

bands before evaluating the contribution of MSS images to geology.

Band 4 - important scattering effects and the image is hazy
Band 5 - gives an excellent view of land use repartition.

The distinctions below are made possible by the strong absorption of the vegetation in this spectral band :

gray scale 14:forests

gray scale step 12:association of cultivation and grassland over humid grounds, of grassland and poplar trees along the water courses, Champagne vinyards.

gray scale step 10:cereal cultivation and pine woods on Chalky soils.

Band 6 - the increase of reflectance leads to a leveling of the cereal cultivation and grasslands signal, making possible a good discrimination of the forests.

Band 7 - the principal difference with Band 6 is the disappearance of the forests.

3.2. Geological Mapping

The region covered by the MSS images has the benefit of complete geological mapping at the scale of 1/80 000, 1/320 000 and 1 1 000 000 revised several times over the last century. The geological map at 1/50 000, is in course of preparation, the published sheets concerning essentially the western third and the angles NW and SW.

Talking this into account the MSS images do not add anything new of importance concerning outcropping formations in the sector under consideration. However the comparison of the images and the existing geological maps, particularly the one at the scale of a millonth, produces important information of two winds :

. First, a good correspondance is seen between the large units distinguished at first sight on the images (in particular band 5) and the concentric strata of the Jurassic, Lower Cretaceous, Upper Cretaceous and Paleogene on the map. The extension of the modern alluvia of the valleys is also easily seen on the images. Obviously, in view of the result of this comparison, such images contribute a great deal to geological mapping at a large scale of regions whose geology is not so well known as that of the Parisian Basin. In particular these images seems to be suitable for resolving problems faced by the geologist when preparing large research expeditions (the preliminary photo interpretation and the choice of itineraies can only be made easier).

. Secondly, the comparison of MSS images with the geological map at a millionth shows, in some sectors, notable differences linked to the very conception of the geological map considered which introduces exclusively stratigraphic distinctions, ignores the representation of covering deposits and does not express lithological variations.

Thus in the sector between Troyes and Sens the map only shows the Upper Cretaceous (chalk) formations and parts of the lower Eocene (sands, shingles) purposely omitting the flinty clay covering, the result of surface alteration of chalky grounds during the Tertiary. These covering grounds which do not exist further North, support a forest vegetation similar to that of the Tertiary deposits, at the beginning of the apparent continuity shown by the MSS images.

In another respect the very dark and palpably median formation on the MSS images (particulary band 5) corresponds perceptibly to the South of Vitry-le-François to the outcropping of the sandy and argillaceous grounds of the Lower Cretaceous to the exclusion of the Cenomanian chalk. To the North of Vitry-le-François this encloses Cenomanian grounds represented by sands and marls which support a vegetation comparable with that of the Lower Cretaceous grounds. In these particular cases there is only an apparent contradiction between the image which expresses lithological differences and the geological map with the conventional stratigraphic limitations.

The comparison of MSS images and the hydrogeological map of the Parisian Basin at 1/500 000 which shows the great lithological formations, removes all ambiguity (fig.1).

3.3. Analysis of geostructures

Amongst the many faults revealed by the study of the MSS images we shall consider only three (successively those of Metz, Juranzé and the double fault of the Marne).

3.3.1. The Metz Fault

Revealed by G. GUERRIER and P. PRUVOST the Metz fault represents the southern boundary of the "bassin houiller lorrain". A south-west extension of this fault has been discovered by drilling up to Saint-Mihiel Commercy (on the river Meuse). These drill hole carboniferous show the existance of an important Hercynian Tectonic rift valley with a carboniferous filling of 4 000 m (2 000 m at Metz).

From the Meuse - the orbital images not covering the zone further to the East - we have noticed a conspicuous alignment unknown until now, passing by Bar-le-Duc, Vitry-le-François, merging at its western end with the linear course of the Seine revealed by spectral band 7. It ends in the West at Montereau against the group of North-South faults extending those of Limagne and the sillon houiller.

The aero-magnetic map of France, 1/1 000 000 scale, confirms the existence of such a fault but slightly more to the South than that traced by the MSS images (and one may deduce that this fault is not vertical). According to these same geophysical methods the North-South faults cut the principal fracture.

The gravimetric data (scale at 1/1 000 000) express more differences but J. GOGUEL emphasizes the Vitry-le-François anomaly and

formulates hypotheses which, up to Arcis-sur-Aube, agree with our interpretation.

Finally to the West of Arcis-sur-Aube he situates a possible continuation of the fault, but more to the North, near to Provins.

The isopach curves of the Permian Age, established by J. LIENHARDT, show that the fracture we are considering could form the southern boundary of the Courgiveau - Trois Fontaine - Saint-Michel (50 m of the Permian) high, whose NE-SW direction corresponds with the direction of the Metz fault.

Finally, Claude MEGNIEN points out NE-SW undulations of the subsurface at the base of the Tertiary, to the South of the Marne (Villier St Georges - Provins), which correspond to structures situated immediately to the North of the Seine. The fracture seen on the MSS images is parallel to these structures and could mark out a flexure.

We come to the conclusion, following J. LIENHARDT that the Permian comes to fill in the paleo-relief sculpted by the Hercynian Tectonic and that this Tectonic imposes its style over the whole basin: the epicretacèous fractures would be traced on these movements. We may think that the fault emphasired by the MSS images reflects, at the level of the Cretaceous, a deep structure of Ante Permian and Variscian direction. The knowledge of these faults is important in trying to understand the Hercynian paleogeography which could guide research for new coal-bearing structures ; and all new discoveries in the sphere of tectonics could start up again research for petroleum which up to now has only happened on the Dogger. Thus MSS images may be considered as an extra tool for the geologist and may certainly have economic influence.

In conlusion the continuity of the fault interpreted on the MSS images is corroborated by complementary and fragmentary information from numerous methods of geological investigation. Without entirely proving the relation between this fault and the sillon houiller faults and those of Limagne - at least in its northern extensions - it shows clearly enough that the phenomena presented by J. GROLIER and J. LETOURNEUR may very probably exist.

3.3.2. The Jurenzé fault

The Jurenzé fault revealed by gravimetric and aeromagnetic surveys is a south-eastern continuationof the large Pays de Bray fracture. This fracture is seen on MSS images from Brienne-le-Chateau towards the East. The satellite image is particularly interesting in that by means of complementary spectral bands - phenomenum already noted for the Metz fault - we observe that this fault divides beyard Brienne into two branches of equal importance. The first, in the North and already known, follows an East-West course and represents an extension of the Vittel fault. The second, further South, follows a North West-South East direction, passes through Bar-sur-Aube and was

unknown until now. The convergence of these two faults constitutes a tectonic trap which had been suspected during research for petroleum but which was not proved because localisation of the phenomenum was inexact. This therefore constitutes an interesting contribution of the MSS images.

The non-visibility of the Juranzé fault's extension towards Bray in the NW is explained in that we know, thanks to F. HERITIER and J. VILLEMIN, that the Upper Cretaceous is not faulted here , a compensation of thickness being produced at the level of the Albian. Consequently it is difficult for us to study on MSS images the interactions of the two most important faults of the Parisian Basin, the Metz fault's extension, and that of Bray-Jurenzé (J. GOGUEL notes that this interaction could be situated at different depths and could cross each other).

3.3.3. The double fault of the Marne

This was first described by R. ABRARD and G. CORROY who ascribed to it a total length of 50 km. Gravimetric interpretations confirm its importance. The MSS images make it possible not only to find again the trace already known but also to suggest a prolongation towards the SE which would bring its length to 110 km. It would seem, according to the interpretation of the MSS images that this fault system cuts again the Metz fault.

3.3.4. General tectonics

In general, without going into detail concerning the many other fractures discerned on MSS images which may be compared with faults on the geological map at the same scale, the following may be concluded :

- it is band 5 which gives the most information concerning the fracturation. It shows features emphasized by boundaries of cultivation associations, or natural vegetation, as well as by poplar trees which show the trace of water courses of an average importance,

- bands 6 and 7 show the fractures emphasized by the forest boundaries and by the linear trace of water courses where the alluvial zones occupied by poplar trees are very developed. In the case of the Metz fault's extension towards the South West bands 6 and 7 are most important in that in this way the course of the Seine can be observed, blotting out the poplar trees. As for the scale this makes it possible to disregard the numerous meanders which characterize the Seine and to retain just the straightness of its course, particularly conspicuous at the scale under consideration.

- bands 5, 6 and 7 are therefore complementary.

IV/ CONCLUSIONS

The example described shows that within sedimentary basin known for its regular disposition in a region where vegetal cultiva-

tion takes up almost all the surface, MSS images at a small scale can give very interesting information concerning :

- the lithology which is cultivated areas is represented by the associations of different cultures and a specific division in land use and in regions of natural vegetation by the associations of forests and grasslands closely linked to the lithology,

- lineaments for which the contribution of the scale is of major importance. Indeed, in this way, elements which appear discontinuous at conventional scales of observation can be integrated into one same alignment.

Certainly one of the most remarkable lessons we may draw from ERTS 1 images is that deep structural elements under a thick sedimentary cover can be translated on the surface by indirect criteria.

BIBLIOGRAPHICAL REFERENCES AND MAPS

- Carte géologique de France - B.R.G.M. - 1/1 000 000
- Carte de la végétation - Comité national de géographie - 1/ 1 000 000
- Carte aéromagnétique B.R.G.M. 1/1 000 000
- Carte gravimétrique 1/1 000 000, publiée par le B.R.G.G.M.
- Carte métallogénique B.R.G.M. 1/ 2 500 000 UNESCO-B.R.GM.
- Carte hydrogéologique du Bassin de Paris - B.R.G.M. - 1/500 000

R. ABRARD et G. CORROY - Etude de la double faille de la Marne Bull. Service de la carte géologique -France- N°165, 1926-27

J. GOGUEL - Levé gravimétrique détaillé du Bassin de Paris, 1954, B.R.G.G.M.

J. GROLIER et J. LETOURNEUR - Evolution tectonique du grand sillon houiller du Massif central français - XXIII - International geological congress - Vol.1 - 1968

R. GUERRIER et P. PRUVOST - La limite septentrionale du bassin houiller de Lorraine - C.R. Académie des Sciences de Paris - 1965 -

F. HERITIER, J. VILLEMIN et C. MEGNIEN - La tectonique du Bassin de Paris Bull. B.R.G.M. Section 1 (n°2) - 1971 -

M. J. LIENHARDT - Etude stratigraphique, pétrographique et structurale du socle ante-Permien du Bassin de Paris. Annales Soc. géologique du Nord - 1961 -

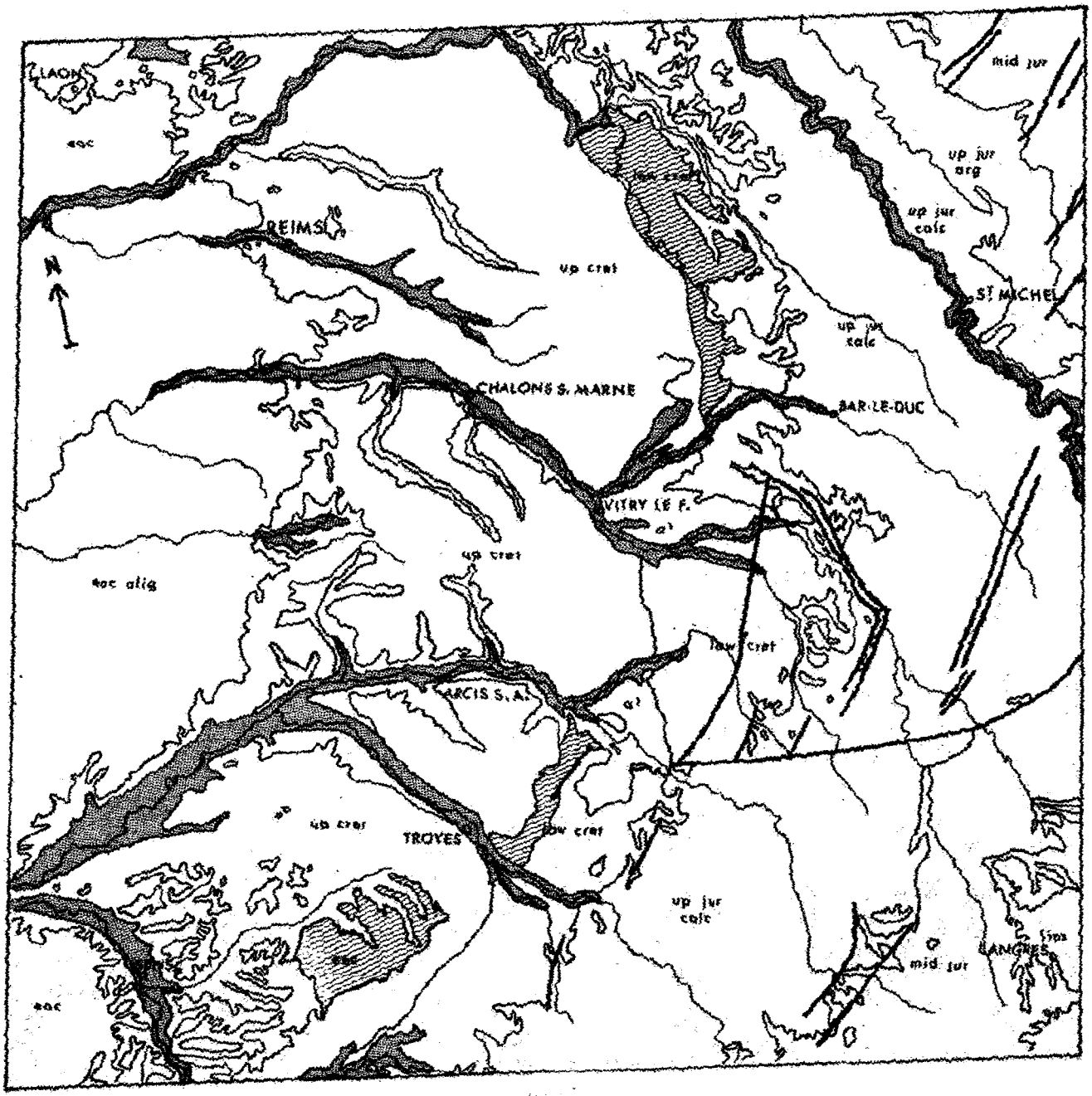

LAON
eoc
REIMS
N
up cret
CHALONS S. MARNE
mid jur
up jur org
up jur calc
ST MICHEL
up jur calc
BAR-LE-DUC
VITRY LE F.
up cret
eoc alig
low cret
ARCIS S. A.
up cret
TROYES
low cret
up jur calc
mid jur
LANGRES
eoc
Geological map Scale 1/1,000,000
completed with shading for lithology
Modern alluvium

Figure 1

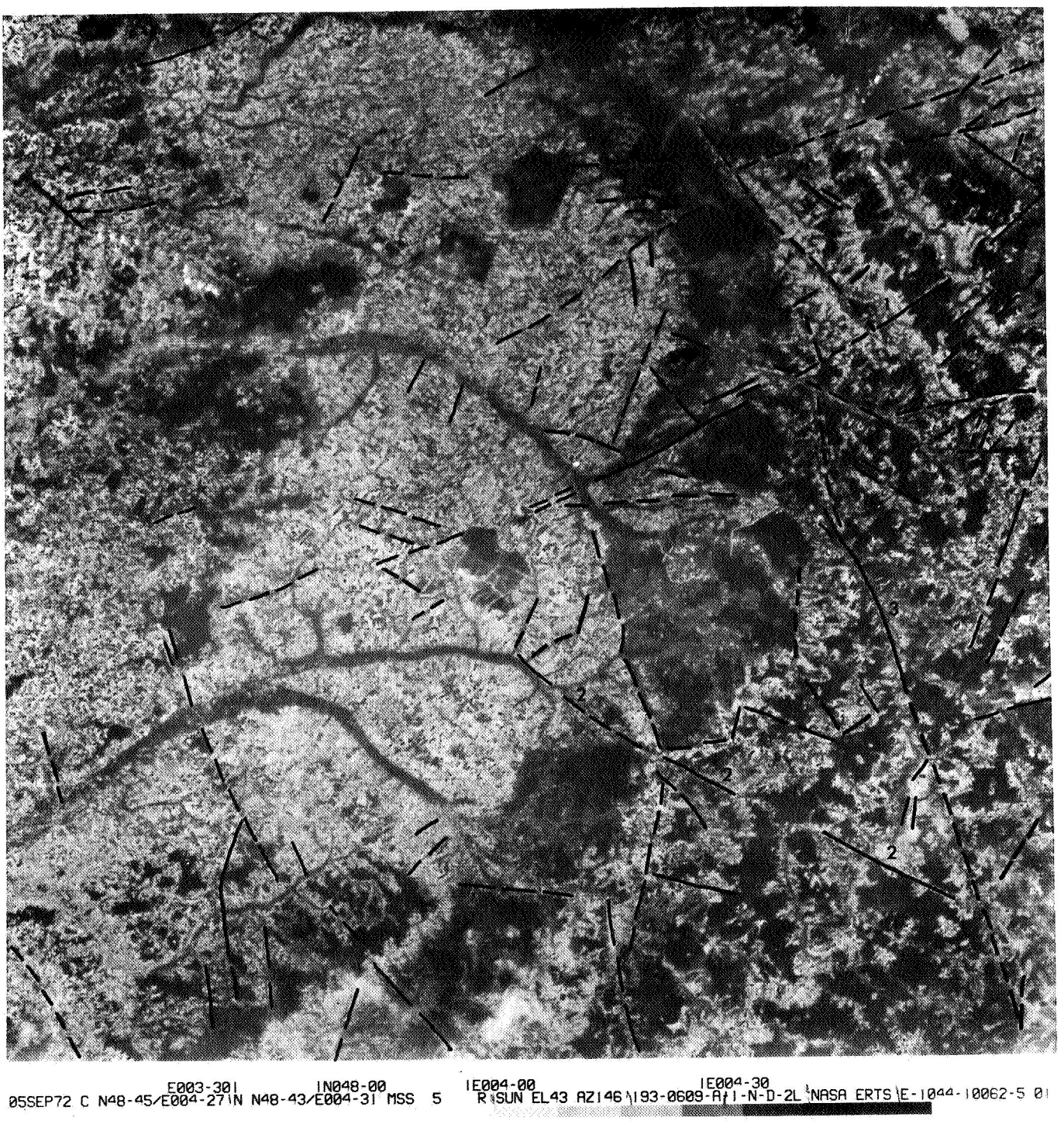

3
2
2
2
E003-301 N048-00 E004-00 E004-30
05SEP72 C N48-45/E004-27\N N48-43/E004-31 MSS 5 R\SUN EL43 AZ146\193-0609-A\1-N-D-2L\NASA ERTS\E-1044-10062-5 01

Figure 2

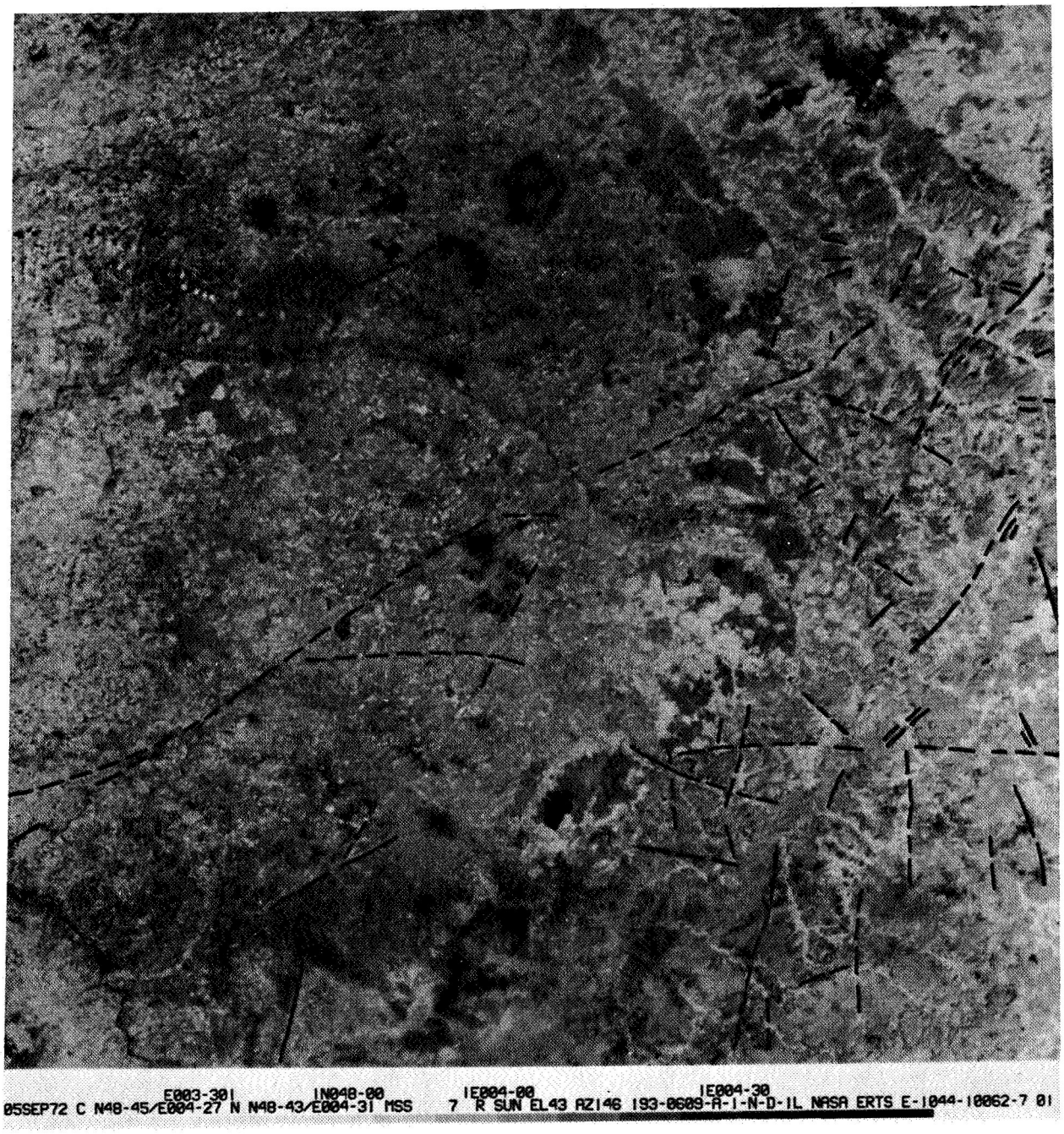

E003-30| |N048-00 |E004-00 |E004-30
05SEP72 C N48-45/E004-27 N N48-43/E004-31 MSS 7 R SUN EL43 AZ146 193-0609-R-1-N-D-IL NASA ERTS E-1044-10062-7 01

Figure 3

Paper G 7

APPLICATION OF ERTS-1 MULTISPECTRAL IMAGERY TO MONITORING THE PRESENT EPISODE OF ACCELERATED EROSION IN SOUTHERN ARIZONA

Roger B. Morrison and Maurice E. Cooley, *U. S. Geological Survey, Denver, Colorado, and Tucson, Arizona*

Abstract

An episode of accelerated arroyo-cutting and sheet erosion commenced about 1890 in southern Arizona, following several thousand years of generally sluggish erosion. For a 17,000-square-mile study area, ERTS-1 images, supplemented by ultrahigh-altitude (U-2 and RB-57) airphotos, are proving effective for producing the first comprehensive maps showing the distribution and seriousness of the post-1890 erosion features, for monitoring new erosion changes, and for assessing the effectiveness of ameliorative measures. Such data are essential for understanding and controlling the accelerated erosion, a key environmental problem in this region.

ERTS-1 project 182 is evaluating the usefulness of ERTS-1 imagery of southern Arizona for identifying and mapping the effects of an episode of accelerated erosion that began about 80 years ago. This project is under the EROS Program of the Department of the Interior and is funded by NASA.

Before I tell you about the results from the ERTS imagery, let me explain what the modern erosion is like and why it is a serious problem.

Before the Civil War, the larger streams in southern Arizona and their main tributaries flowed sluggishly in shallow channels through grass-choked flood plains dotted with pools. Archeologic and geologic data indicate that this situation had existed for at least two thousand years, broken only by relatively brief and minor erosional episodes. After the Civil War, a boom in ranching led to a dramatic increase in the numbers of cattle and sheep. Within a few years, floods began to be much larger than formerly. By about 1890, severe entrenchment, catastrophic in places, was underway on all the main streams. Arroyo-cutting subsequently worked its way far upstream and back along the various tributaries, stopping the former natural irrigation of the grassy flood plains and causing much of the grass to die. The most productive parts of the rangelands were thereby ruined, as was much irrigated farmland.

Publication authorized by the Director, U. S. Geological Survey.



Figure 1. View of a typical post-1890 arroyo (Railroad Wash, near Duncan, Arizona about 36 miles east of Safford) showing headcuts on a moderately well-grassed and nearly level flood plain. As headcutting continues upstream, excellent pastureland will be converted into a barren badland.

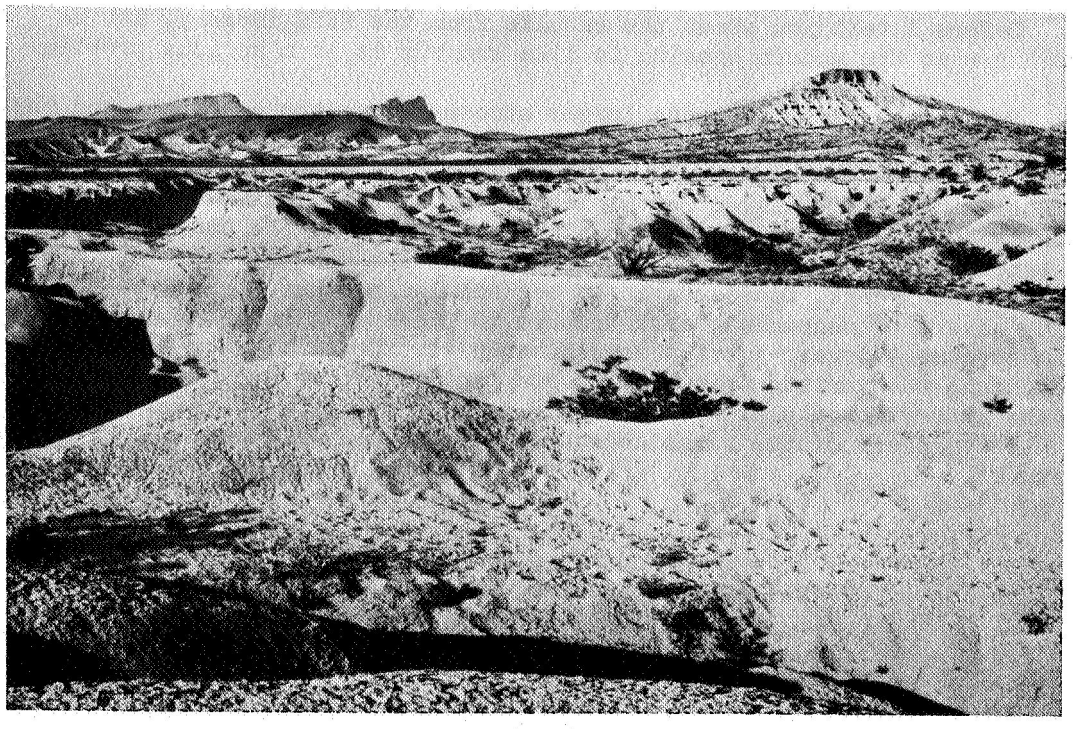


Figure 2. View several miles downstream along the same wash, showing the type of badland that has resulted from the modern trenching of this wash. Sixty years ago this area was a lush pasture and was regularly cut for hay.

The causes of the post-1890 erosion are not fully understood. Four principal causes have been considered: overgrazing, climatic change, control of range fires, and increase in rodents and jack rabbits. Researchers generally agree that overgrazing and climatic change are the the two chief factors, probably acting together to trigger the modern erosion episode. Furthermore, photographs and other records show that these factors have produced a fundamental change in the vegetation balance of the whole region: grass has steadily declined in abundance and shrubs have markedly increased on the desert plains and foothills.

The geologic result of this drastic vegetational change is of great human significance because the geologic consequences are practically irreversible. The former condition of "landscape stability," without much stream erosion or deposition, which had lasted several thousand years, has been replaced by an episode of accelerated erosion whose end is not in sight. The areas now undergoing the most erosion are the valley lowlands whose fine-textured alluvium was deposited during the last 10,000 radiocarbon years or so. This young alluvium is a legacy of a delicate balance between rainfall and runoff that was maintained by a vigorous desert grassland ecosystem in both uplands and lowlands. The well-grassed uplands held most of the rainfall and released the runoff slowly and so flood peaks and stream erosive powers were lower than today. The stream channels were narrower and shallower than now, and the seasonal floods regularly overflowed them, inundating the flood plains, irrigating the grass and depositing fine sediment. Now the whole system has changed -- the grassland has deteriorated, runoff is less retarded, flood crests are higher, and erosive powers of the streams have become much greater. The former flood plains are especially vulnerable because, with loss of much of their grass cover, conditions have been reversed from those favoring accumulation of fine sediment to those in which such sediment is actively eroding.

The erosion progresses in three stages. The first is vegetative stress, as a result of overgrazing and/or adverse climatic change. Deterioration of grass cover is especially significant because grass is the most effective type of vegetation for retarding runoff, preventing erosion, and trapping sediment. The second stage is sheet erosion of areas with little or no grass cover. The third stage, gullying or arroyo-cutting, is the spectacular one.

A step toward highlighting the seriousness of the erosion problem is to inventory the modern gullies, arroyos, and sheet-eroded areas. Although they have been mapped in a few small areas, the modern erosion features have not been mapped comprehensively and extensively in southern Arizona. Our project is attempting to do this for a 17,000-square-mile area that represents all the important environments in the region in terms of topography, geology, climate, soils, and vegetation (Fig. 3). For this mapping, we are utilizing both the broad overview capabilities of the ERTS-1 images and the closer looks provided by U-2 and RB-57 aerial photographs. We are using the ultrahigh airphotos to map representative parts of the study area in considerable detail, combined with some fieldwork, in order to have a basis for assessing the mapping done from the ERTS images.

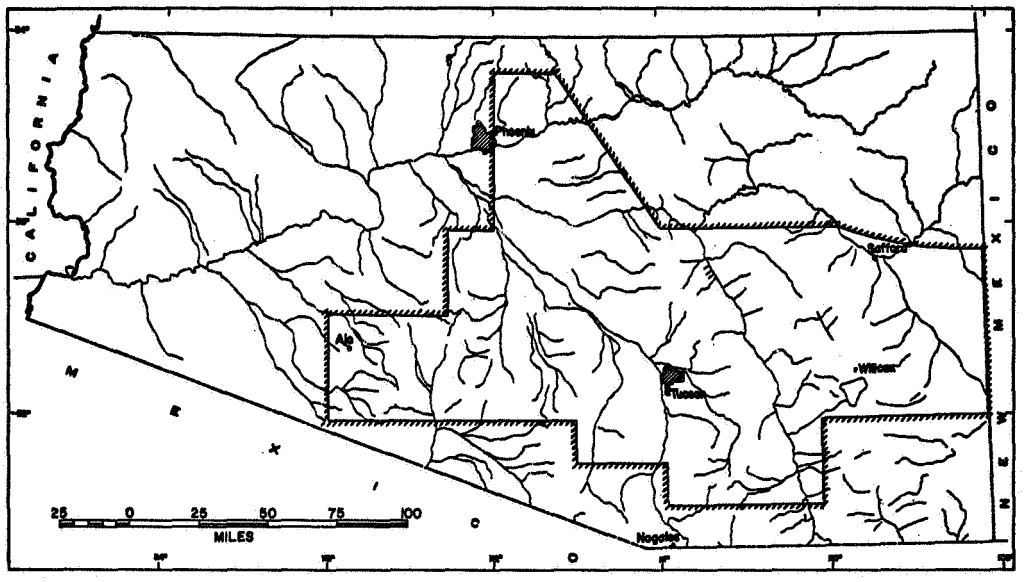


Figure 3. Outline map of the study area in southern Arizona

In addition to the gullies, arroyos, and sheet-eroded areas that have developed since 1890, we also map the areas of modern wind erosion and deposition (which are tiny in this region), and other data pertinent to the erosion problem, such as the distribution of the more erodible types of soil.

We view the 70-mm and 9 x 9-inch positive transparencies of the MSS images under various magnifying devices. We received full coverage of the study area by 9 x 9-inch transparencies during late February (before that we had only one of them), therefore, most of our interpretations have been made from the 70-mm transparencies. For viewing these, a binocular microscope, using 9 times magnification, has been very convenient. To reduce glare and improve contrast, we commonly insert colored Diazochrome sheets between the light source and the image. The multispectral bands of a few frames have been viewed using an I^2S Mini-Addcol additive color viewer. We also have used negative enlargement prints at about 1:1,000,000 scale, made from positive 70-mm transparencies. We have ordered 1:250,000 scale enlarged prints but have not yet received them. We believe it will be most efficient and productive to view the 9 x 9-inch transparencies under a zoom transferscope and plot our interpretations onto either USGS 1° x 2° maps or onto the 1:250,000 scale enlargements of the ERTS images.

Figure 4 shows all the arroyos within the study area that have been identified from the ERTS images. We find that the "red" MSS band 5 gives the sharpest definition of modern arroyos. As linear features, the arroyos can be distinguished when their width is about a tenth of the minimum width for recognition of equidimensional features. On the best images that we have received, we can distinguish modern arroyos as narrow as 150 to 200 feet in reaches where their contrast with adjacent areas is only moderate, and as narrow as 60 to 75 feet in reaches where their contrast is high. High contrast is produced by dark riparian vegetation against light-toned arroyo beds and soils of former flood plains that now are bare of vegetation. Both the red and infrared bands (bands 5, 6, and 7) show differences in soils and vegetation. In the late fall and winter images, band 7 generally is the most useful for mapping the more erodible soils.

The resolution of many images is degraded by atmospheric haze (including smog and smelter smoke haze), especially in the lower parts of the intermontane basins and near Phoenix and Tucson. All bands of the images taken in summer were overexposed in the desert areas because of the high reflectivity of the light-toned soils. This seriously hampered interpretation. The late fall and winter images are correctly exposed for the desert areas because the lower sun-elevation angle has reduced the reflectance. In these images, shadowing also has improved the contrast of some reaches of the deeper arroyos. Dark shadows begin to be distinguishable in arroyos deeper than about 30 feet when sun elevation angles are less than 30°. Near the winter solstice, sun-elevation angles in the study area are around 27°.

Figure 5 is an example of the more detailed mapping possible with the ultrahigh airphotos. In this case, we used 9 1/2 x 9 1/2-inch color infrared positive transparencies (EK 2334 film) taken last August by NASA's U-2 aircraft

with a Wild RC 10 metric aerial camera at about 62,500 feet above ground, giving a photo scale of about 1:125,000. We are extremely pleased with the resolution-detectability and spectral sensitivity characteristics of these photographs; they are proving to be valuable research tools. This map shows a 50-mile belt along San Simon Creek, between the towns of San Simon and Solomon in southeastern Arizona, that has been affected considerably by post-1890 erosion. This wash is 75 miles long and has a drainage area of about 2,200 square miles. It has trenched its channel commonly 20 feet and, in places, 40 feet since 1905. The solid black lines show the channels and narrow flood plains that have formed since 1905, and the three types of patterns show the areas that are severely gullied, severely sheet-eroded, and moderately sheet-eroded. We plan to prepare similar maps for sizable parts of the study area to represent all the important soil, climatic, vegetational, and geomorphic-topographic conditions, and also the areas most affected by post-1890 erosion.

As the investigation progresses, we will utilize the repetitive ERTS-1 imagery and ultrahigh aerial photography to monitor erosional changes. We also are utilizing aerial photography back to 1935, to prepare detailed maps of the evolution of the modern erosional features. Thus, we hope to determine the rates of headward growth, widening, deepening, or aggradation of the gullies and arroyos. We will also monitor the erosional effects of highway construction, stream channelization, and urban and suburban developments. An ultimate objective is to develop a quantitative understanding of the factors that have caused the modern episode of accelerated erosion, as an aid to planning and implementing ameliorative measures.

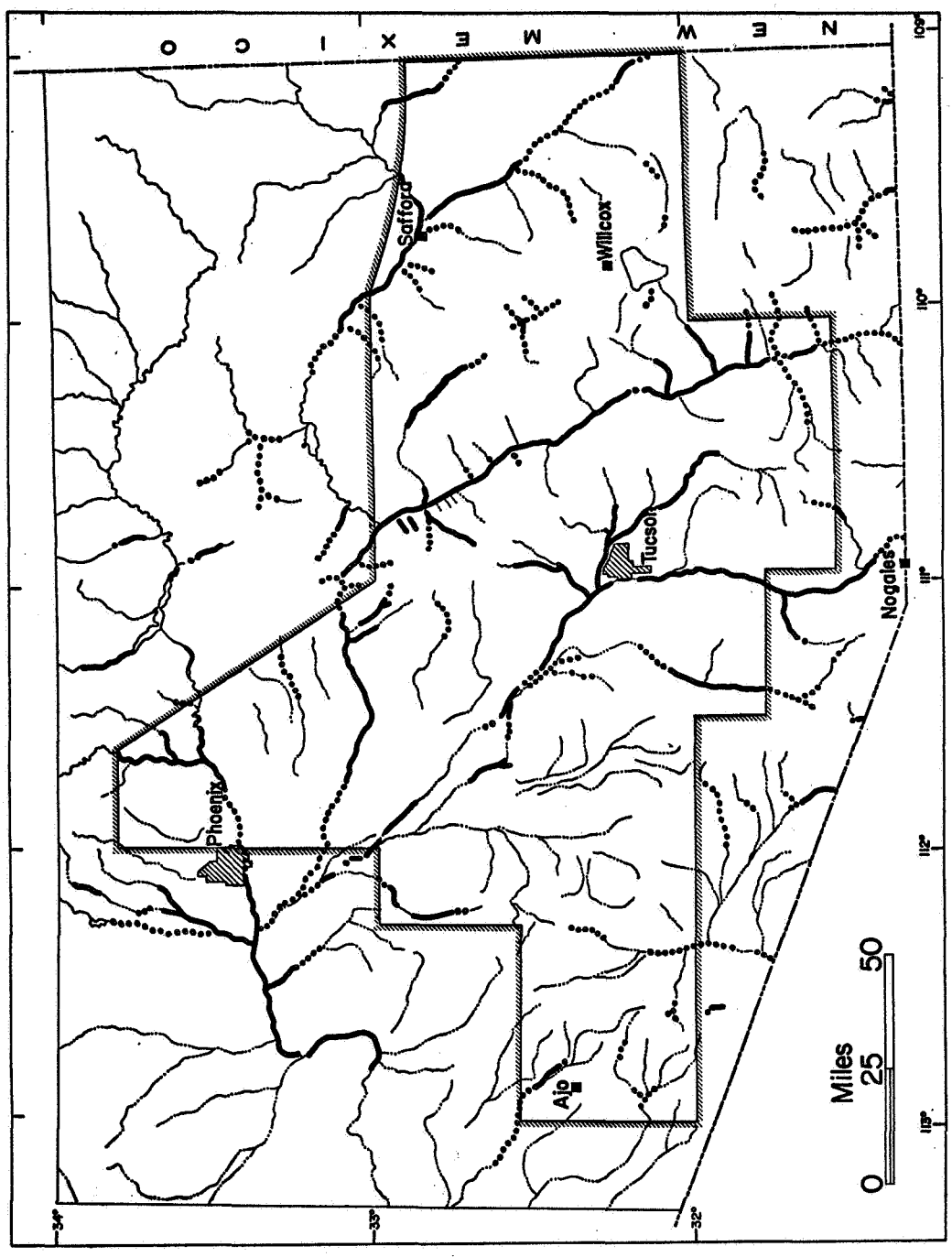


Figure 4. Modern arroyos in south central and southeastern Arizona that are detectable from ERTS-1 imagery (shown as heavy lines where continuously detectable, dotted lines where intermittently detectable).

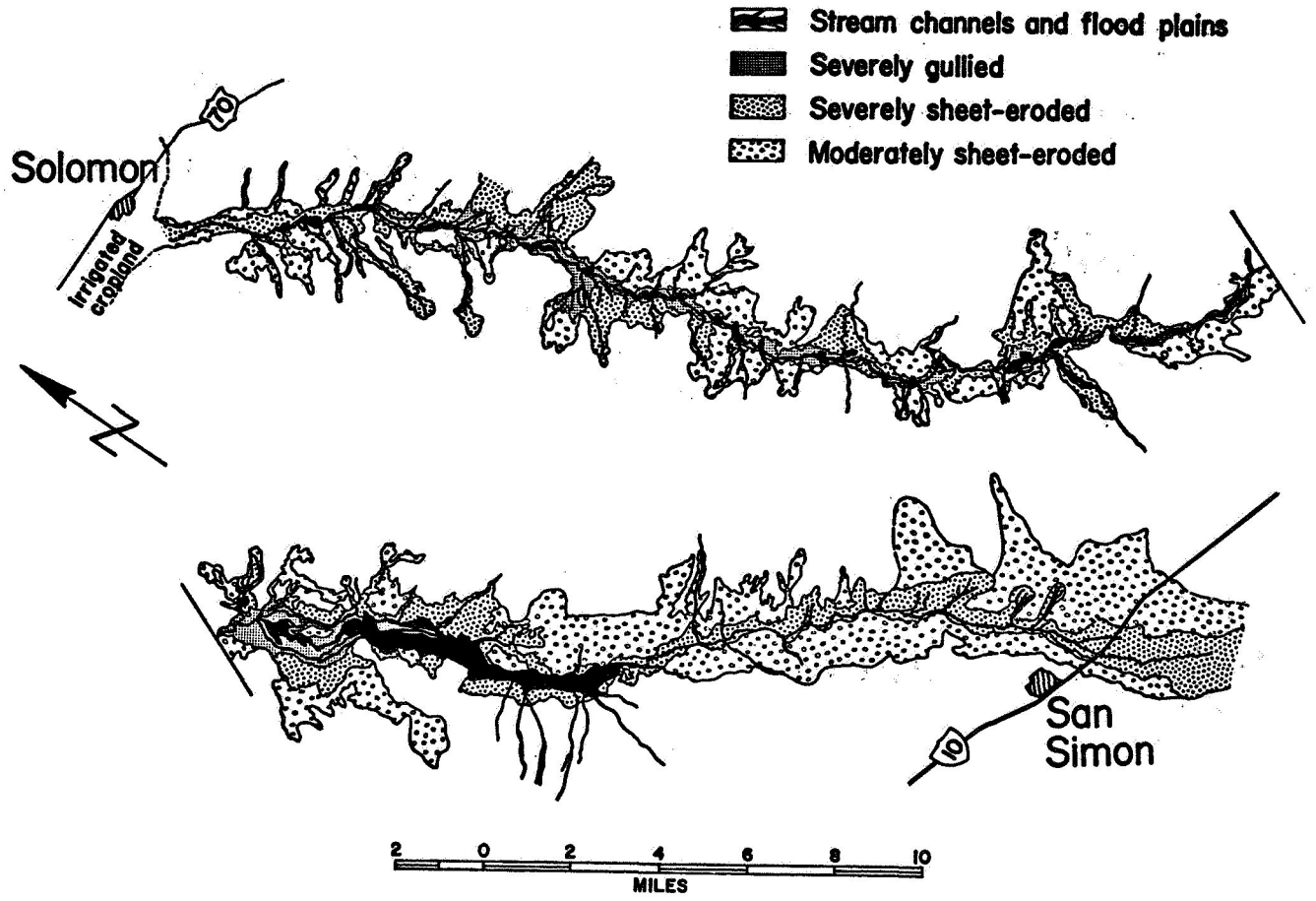


Figure 5. Map of modern erosion features along a 50-mile reach of San Simon Creek, southeastern Arizona. Solomon is 5 miles east of Safford.

Paper G 8

A STUDY OF MORPHOLOGY, PROVENANCE, AND MOVEMENT OF DESERT SAND SEAS* IN AFRICA, ASIA, AND AUSTRALIA

Edwin D. McKee, *U. S. Geological Survey, Federal Center, Building 25, Denver, Colorado 80225;* Carol S. Breed, Lawrence F. Harris, *U. S. Geological Survey, Museum of Northern Arizona, Flagstaff, Arizona 86001*

ABSTRACT

This study is designed to describe and classify major types of sand seas on the basis of morphologic pattern and lineation. For analyzing patterns of deposits on ERTS images, where the visible forms are mostly dune complexes rather than individual dunes, several steps are being used:

A. Enhancement of ERTS imagery by rephotographing 70mm transparencies using (1) different types of negative film, (2) overdevelopment of films in high-energy developers, and (3) printing on high-contrast papers. These methods can enhance the contrast between light and shadow to provide sharper pictures of the patterns under study.

B. Differentiation of dune sand from other objects within a sand sea by comparing images in all four spectral bands and composite color for each test site.

C. Recognition of atmospheric conditions, the effect of varying sun angles, and possible other seasonal influences upon interpretation of ERTS imagery by comparing images from numerous passes that show differing conditions on different dates.

Further analyses and final checks are made by comparative studies of air photos or ground data available for each site. After completion of thematic maps portraying the pattern and lineation of sand bodies, data on directions and intensity of prevailing and other winds are plotted on corresponding bases, as a preliminary to determination of internal structures through ground truth.

*Publication authorized by the Director, U.S. Geological Survey

1. INTRODUCTION

Principal objectives of this investigation are to compare the major sand seas of the world by recording types of geomorphic forms and trends developed in these sand bodies, to determine relations of their trends to wind and other meteorological controls, to vegetation, water, and topographic influences and, finally, to show the type of internal structure (stratification) characteristic of each geomorphic form. The structures may ultimately be used in determining the genesis and geometry of ancient eolian sandstones.

Development of a classification of large sand-desert deposits of the world is the initial step of the investigation. ERTS imagery is uniquely valuable for this purpose, providing coverage and revealing patterns of landform development on a scale heretofore unavailable. ERTS images are being studied from repeated passes over sixteen selected areas--eleven large foreign test sites and five small areas in the U.S.A., included largely to provide ground truth. The areas under study are:

1. Western North Africa including Algeria, Spanish Sahara, and Mauritania.
2. The Sahara Desert of Libya, Niger, and Chad.
3. The Kalahari and Namib Deserts of South Africa, Bechuanaland, and South-West Africa.
4. The Takla-Makan Desert of Sinkiang, China.
5. The western Inner Gobi Desert of China-Mongolia.
6. The Thar Desert of India-Pakistan.
7. The Kyzylkum ("Red Sands") and Karakum ("Black Sands") of the U.S.S.R.
8. The Great Sandy Desert of Australia.
9. The Great Victoria and Simpson Deserts of Australia.
10. The An Nafud of northern Saudi Arabia.
11. The Empty Quarter of southern Saudi Arabia.
12. White Sands, New Mexico.
13. Great Sand Dunes, Colorado.
14. Little Colorado Valley, Arizona.
15. Yuma Desert, California and Mexico.
16. Henry Mountains area, Utah.

2. INITIAL PROCEDURE

Upon receipt of ERTS imagery, data for each image are compiled on a worksheet (fig. 1) devised by Carol Breed of this project for cataloguing primary information about each test site. Tabulated for each image are the ERTS number of the image, its center point coordinates, the type of retrospective data requests to be made, and some initial observations on the quality of the image and the significance of observed geomorphic features and patterns, as well as the date of accession of the image.

Next, each image center point is plotted on an index map of the appropriate test site (fig. 2). These small index maps provide quick reference to the type of coverage obtained. On these maps all ERTS images that show features pertinent to the study (with adequate resolution) are indicated in red, whereas other images that seem not to have significance to the project, or whose quality is not adequate, are marked in blue and probably will be eliminated from further consideration.

In the preparation of some ERTS images for study an additional step is taken. It consists of the enhancement of images (figs. 3, 4, 5) that show features considered of key importance to the investigation. This enhancement involves rephotographing of the 70mm ERTS transparencies using (1) various types of negative film, (2) overdevelopment of films in high-energy developers, and (3) printing on high-contrast papers. A detailed description of these procedures is given in a paper entitled "The use of photographic methods in contrast enhancement of ERTS images" prepared for the symposium by Lawrence F. Harris (1973).

As scanning of the transparencies continues, retrospective data requests are sent to Goddard Space Flight Center for black-and-white and color prints (fig. 6) of images in key areas marked for further study. One complete set of prints covering each test site will ultimately be assembled into a photomosaic using as a base the U.S. Coast and Geodetic Survey/U.S. Air Force Operational Navigation Charts (ONC) which are at the same scale (1:1,000,000) as the ERTS images. At thisscale, as suggested in the recent abstract of A. P. Colvocoresses (1973), the ERTS MSS bulk imagery matches the ground control reasonably well. From the photomosaics, thematic maps of desert geomorphic trends will be derived. These maps will, we hope, help us to develop and illustrate a classification of dune array types in the sand seas of the world.

3. INTERPRETATION OF BAND DIFFERENCES ON BLACK AND WHITE ERTS IMAGERY

Commonly, significant differences in appearance of desert landforms and water bodies occur from spectral band to spectral band of the same image. For example, figure 7 shows marked difference in the appearance of several lakes in the Simpson Desert of Australia, which could affect interpretation. The near-infrared band 7, which shows water as black, reveals that the lakes all contain water rather than being dry, which might be assumed from observation of the same features on band 4 (green). The light tone of the lakes on band 4 is therefore interpreted as sediment in water, rather than being a salt pan or other reflective, dry material. Vegetation is apparent on band 4. Band 6, near-infrared, (middle picture) gives probably the most valid picture of any one band, for this area.

Another example of the importance of comparing images in all bands is given by figure 8, the Rann of Cutch area in Pakistan. The Indus River is on the west, the great dune area is in the east center and the partly water-covered Rann itself lies to the southeast. Figure 9 shows a lake clearly defined in band 7, whereas sediment in the water appears as light tones in the lake in other bands. Band 4 characteristically shows vegetation along the river course, whereas band 7 clearly defines the wet river. In figure 10 channels in the Rann are well defined in band 6, but are very weak in bands 4 and 5, probably because of sediment. Sand dune areas to the north are uniformly visible in all bands; this uniformly bright appearance of the sand is evident in all bands.

An unusual example of band differences in a sand area occurs in the Empty Quarter of Saudi Arabia (fig. 11). In band 4 the interdune areas are dark and the dunes are light, whereas in band 7, the dunes are dark and the interdune areas are light. The reasons for these differences are not definitely known, but probably can be determined from low-altitude photography or other form of ground truth.

4. USE OF BULK COLOR COMPOSITE PRINTS

The value of bulk composite color prints furnished by Goddard Space Flight Center is apparent. In figure 6 (ERTS number 1057-06193) in the Empty Quarter of Saudi Arabia, a color composite print shows the sand dunes bright yellow, and the interdune areas blue-green. The same area is illustrated in each of the three parts of figure 5, where the left picture is an ERTS positive print, the center picture is an enhanced photograph of the same image, and the right picture is a photocopy (by xerography) of the enhanced photograph. The purpose of this enhancement is to define more sharply the patterns that reveal the geomorphic forms of the various sand bodies, and to aid in measurements of these bodies. The color composite print (fig. 6) of the same image confirms that the patterns were formed by moving sand.

The yellow color of sand bodies in general seems to be consistently characteristic of all of the deserts for which we now have some color coverage, i.e. western North Africa, Saudi Arabia, and Australia. This consistency may mean that color prints of key areas can solve some problems of interpretation, where black-and-white imagery may be ambiguous. Two examples are noteworthy:

(1) Where the nature of some linear features is not certain from black-and-white prints, a color print of the same image may show these linear features to have the characteristic yellow of sand bodies. Illustrations were observed on color composite prints from near the Senegal River, southern Mauritania.

(2) Sand bodies are sometimes confused with cloud formations, drifting snow, or salt deposits, all of which appear similarly bright on black-and-white images. On color composite prints, sand appears as yellow, whereas those other features are clearly white.

5. CLASSIFICATION

After the distribution of principal sand areas has been established for each study area under investigation, and methods have been perfected for distinguishing between modern active dunes on the one hand, and stabilized old dunes or erosional (nondepositional) sand bodies, on the other, this study will concentrate on tabulating and analyzing the principal patterns represented in the various areas. Six dune patterns (fig. 12), from six areas indicated by number below, are at the same scale and show marked morphologic differences. The areas represented (fig. 12) are: (6) Takla-Makan, China, (1) Mauritania, (15) Empty Quarter, Saudi Arabia, (3) Libya, (2) Algeria, and (14) An Nafud, Saudi Arabia.

Patterns of sand areas are being recorded and plotted as a basis for developing a classification and will be used in preparing thematic maps of the areas being compared. They will ultimately be given designations for reference purposes and attempts will be made to analyze each. Interpretation of many patterns can be made through the use of low-altitude air photography, in which individual dune forms can be recognized even though at the same places, at the scale of ERTS imagery, only sand complexes can be detected. Illustrations from the Algerian desert show linear patterns in an ERTS image (fig. 13) that are seen in an aerial photograph kindly furnished by Dr. H.T.U. Smith as strings of star dunes (fig. 14); likewise, a reticulate pattern in an ERTS image (fig. 15) appears as clusters of star dunes (fig. 16) in another aerial photograph by Dr. Smith.

6. GROUND TRUTH

A future part of this project is to determine, where possible, the causes of particular dune-complex patterns and of lineation. Meteorological data are currently being compiled to establish probable relationships of wind direction and wind velocity to dune form and trends. Finally, an attempt will be made to gather ground truth on internal structures of sand bodies in relation to their form and pattern in order to establish their genesis and to recognize their presence in the geologic record.

7. REFERENCES CITED

Colvocoresses, A. P., 1973, Overall evaluation of ERTS imagery for cartographic application /abs./, in NASA Earth Resources Survey Program weekly abstracts: U.S. Dept. Commerce Natl. Tech. Inf. Service, p. 7-8 (Jan. 22, 1973).

Harris, L. F., 1973, The use of photographic methods in contrast enhancement of ERTS images: ERTS-1 Symposium Proc.

E10 (ERTS #)	Center Point Coordinates	IF ORDER ED	Test Site: Sahara (1) Order Type + Comments	
64-10234	N28-47/ W005-17	✓ C7	Few dunes - east - Order for mosaic	
64-10254	N21-35/ W007-12	✓ BW4	Linear dunes	1/17
64-10240	N27-20/ W005-41	BW4 ✓ C7	Same as 10271 Dunes in north. Oriented reference	1/17
64-10272	N15-49/ W008-10	✓ BW 7	Order for mosaic - No dunes but some linear streaks	"
64-10270	N17-15/ W008-19	BW4 ✓	Also entire pass over Order in	"
64-10263	N18-41/ W007-57	BW 1 ✓	Order for mosaic Order later cycle	"
64-10245	N24-28/ W006-27	BW4 C7	Dunes + sand streaks & ergs. Clouds left center. See 38-10245	"
64-10243	N25-55/ W006-04	BW4 C7	Sand streaks in north.	"
64-10270	N17-15/ W008-19	✓ BW4	dunes	"
59-09550	N21 E001	—	No dunes	1/21
59-09552	"	—	"	"
102-10370	N24-24/ W009-24	-	No dunes	1/21

Figure 1.--Sample copy of worksheet

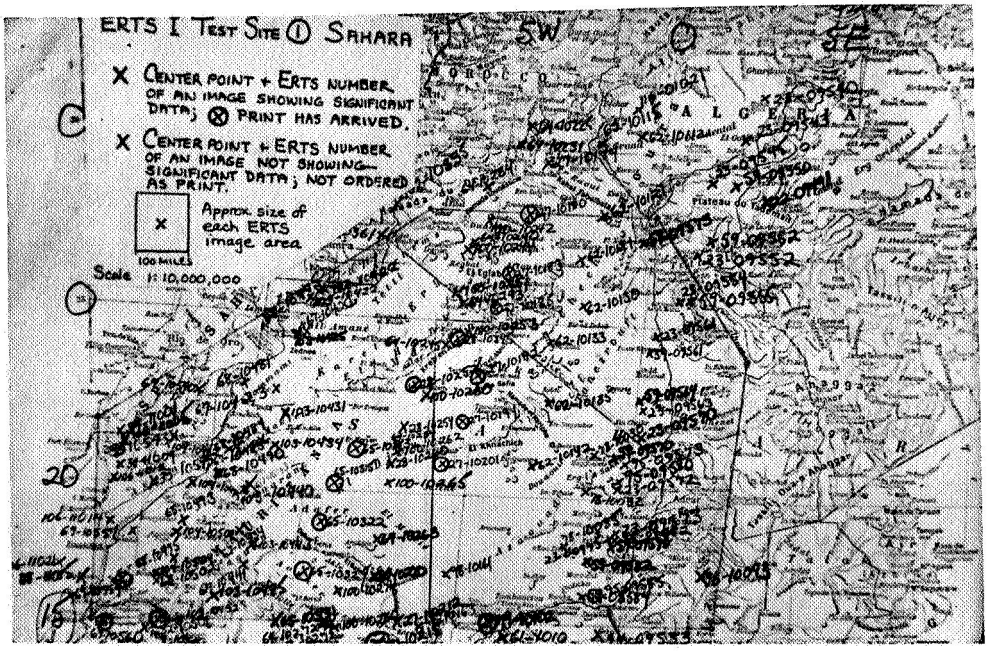


Figure 2.--Sample of test-site plots on base map from Air Force Operational Navigation Chart; sites to be studied are shown in red; those probably to be eliminated in blue.

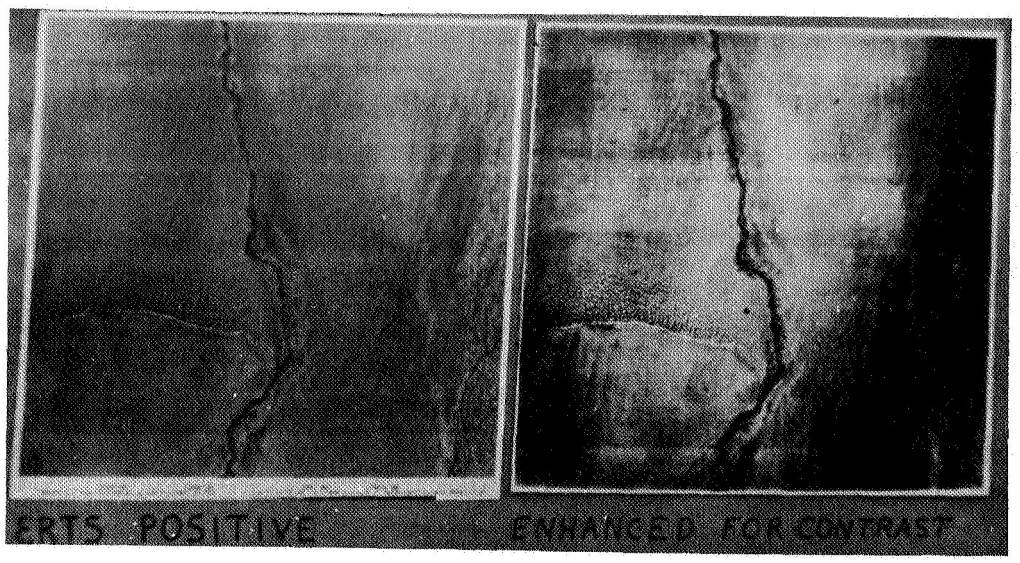


Figure 3.--Test site in Takla Makan desert, China. Illustrates results of contrast enhancement from ERTS positive. ERTS #1078-04481

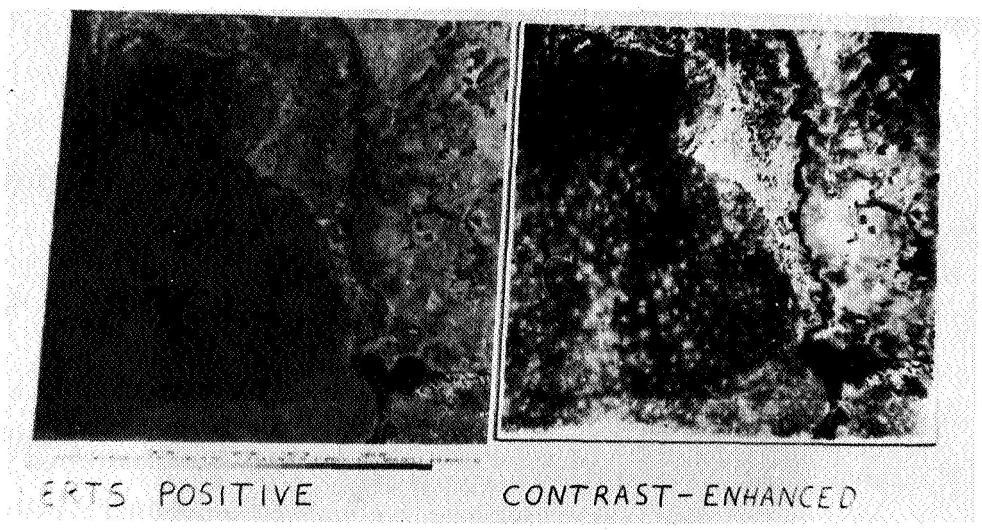


Figure 4.--Test site in Tashkent area, Uzbekistan, U.S.S.R. Illustrates results of contrast enhancement from ERTS positive. ERTS #1070-05443

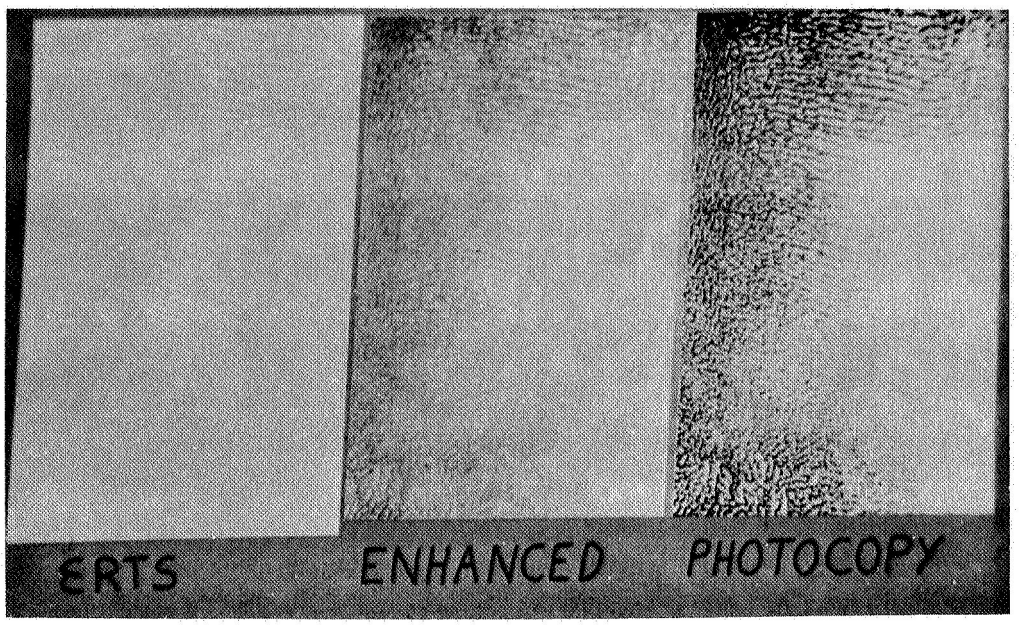


Figure 5.--Test site in the Empty Quarter, Saudi Arabia. Comparison between ERTS positive, contrast enhanced print and photocopy of enhanced print. ERTS #1057-06193



Figure 6.--Test site in the Empty Quarter, Saudi Arabia. Black and white print of color composite print by Goddard Space Flight Center in which sand appears yellow and interdune space blue green. ERTS #1057-06193

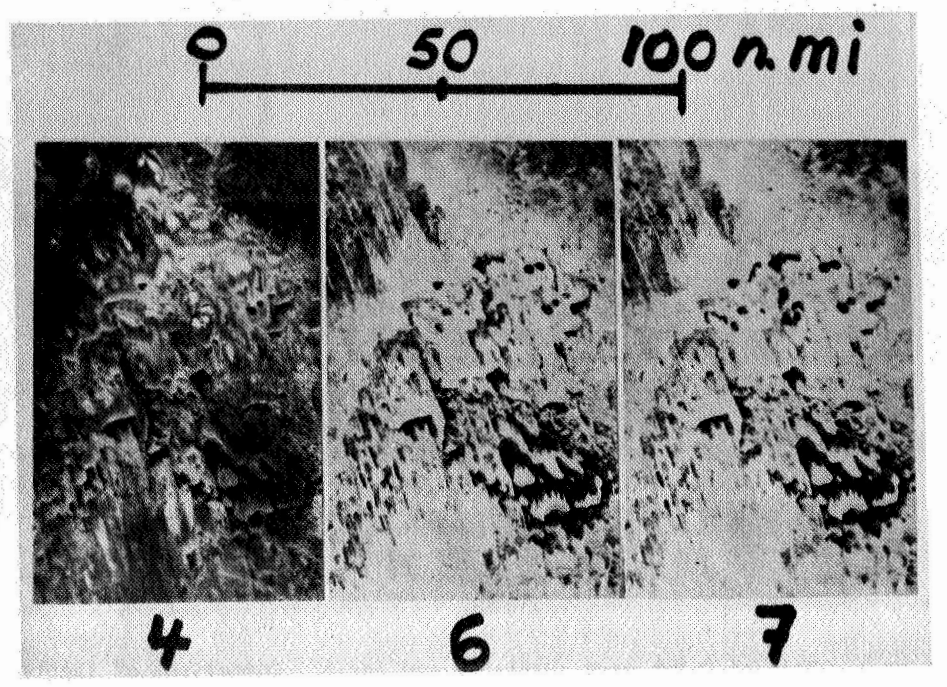


Figure 7.--Test site in Simpson Desert, Australia. Comparison of bands 4, 5, and 6. ERTS #1097-00034.

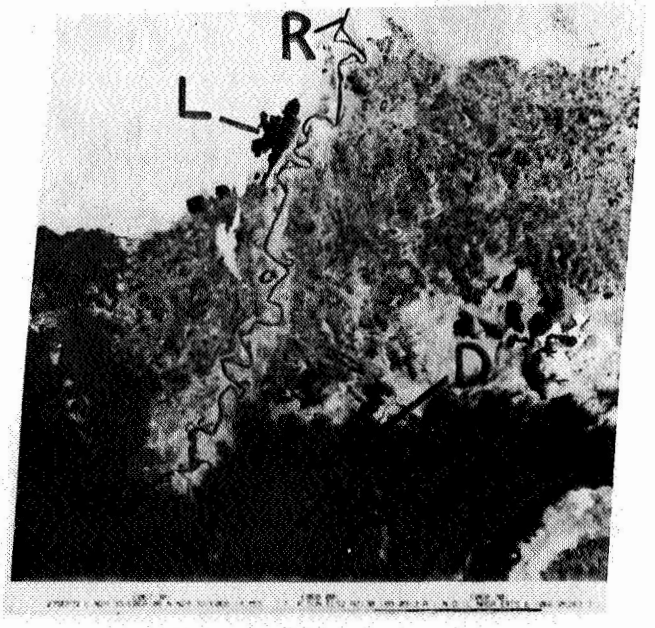


Figure 8.--Test site in the Rann of Cutch area, Pakistan and India. R, Indus River; L, lake; D, dunes; and the Rann (lower one third). ERTS #1066-05263

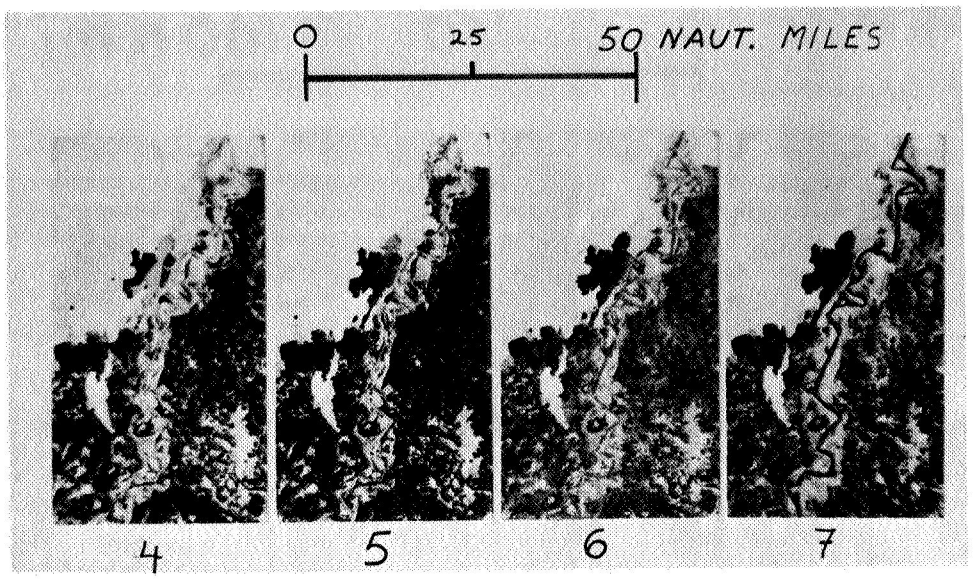


Figure 9.--Rann of Cutch area, Pakistan and India. Comparison of spectral bands 4, 5, 6, and 7 in vicinity of Indus River. ERTS #1066-05263, NW part.

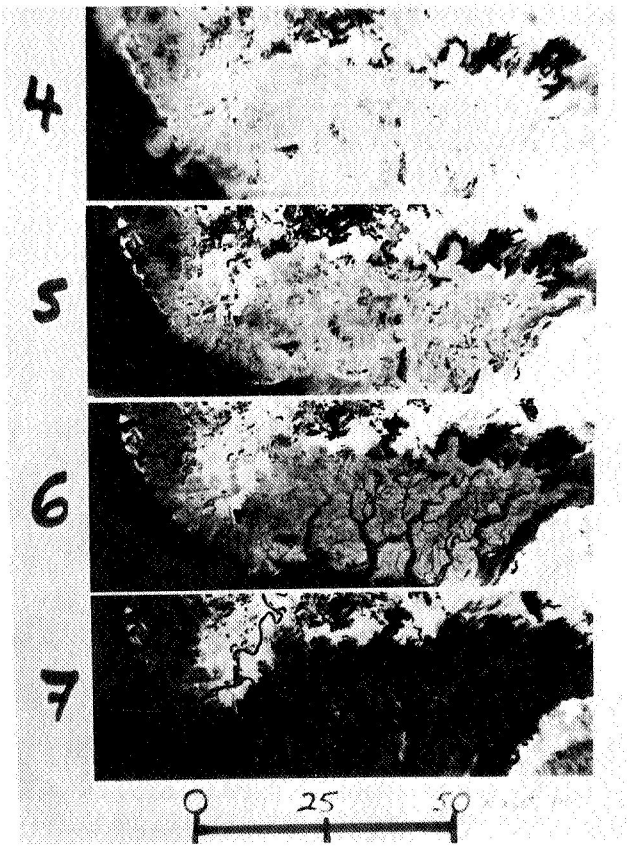


Figure 10.--Rann of Cutch area, Pakistan and India. Comparison of spectral bands 4, 5, 6, and 7 in vicinity of the Rann. ERTS #1066-05263, south part.

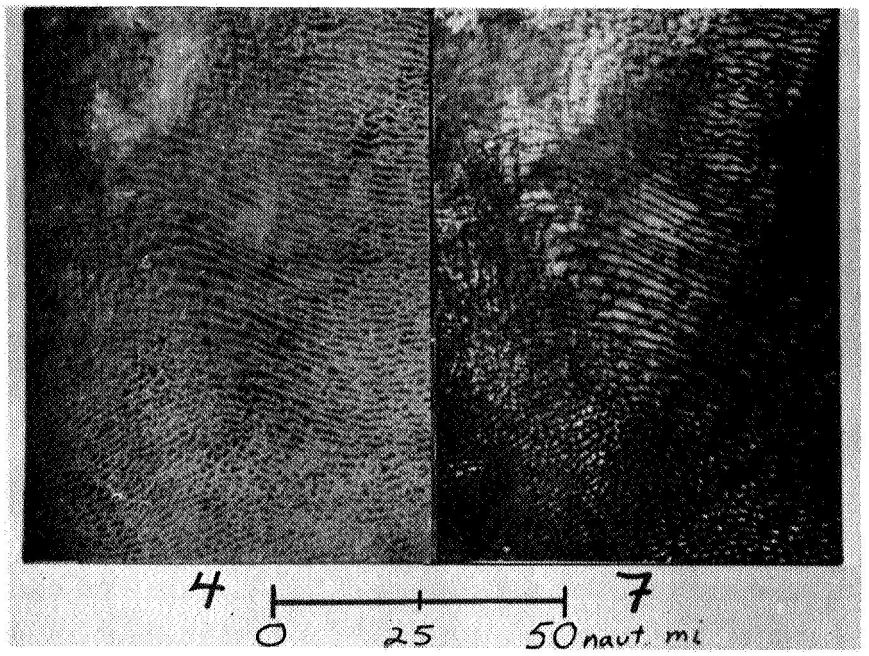


Figure 11.--Test site in the Empty Quarter of Saudi Arabia. Comparison of bands 4 and 7. ERTS #1057-06190

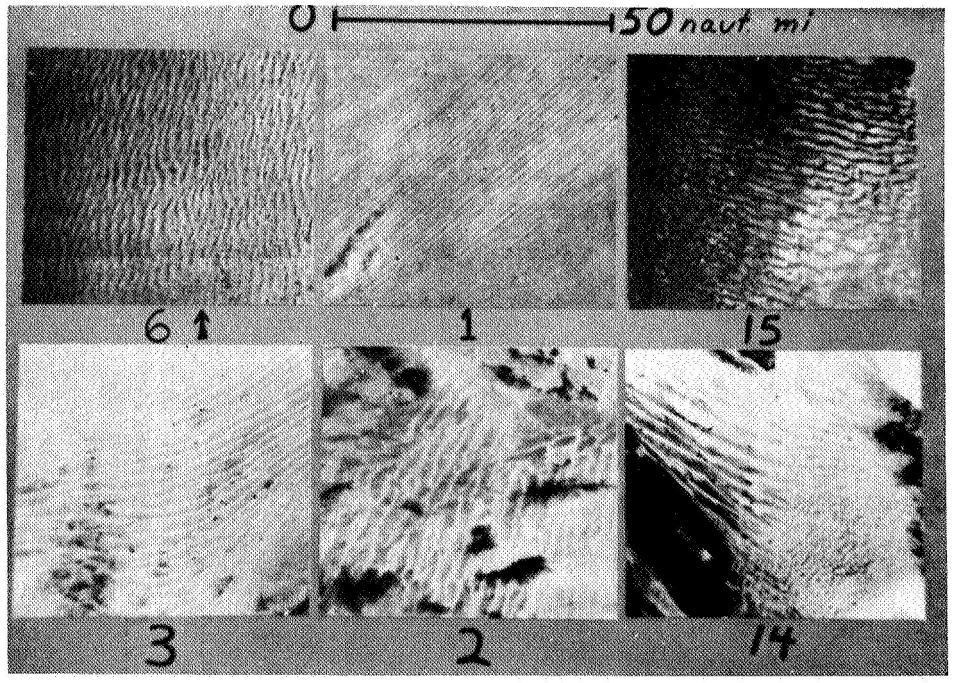


Figure 12.--Varieties of patterns in various sand seas: Takla Makan, China (6), Mauritania (1), Empty Quarter, Saudi Arabia (15), Libya (3), Algeria (2), An Nafud, Saudi Arabia (14).

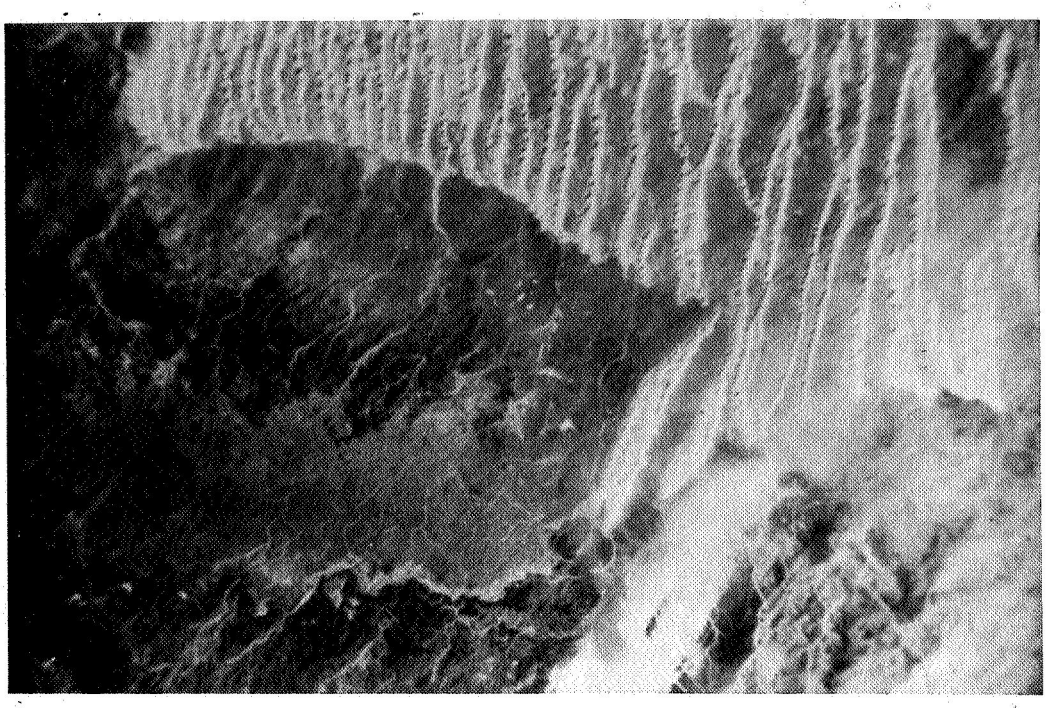


Figure 13.--Linear pattern in sand of Algerian desert shown in ERTS image. Formed by rows of star dunes. ERTS #1111-09442

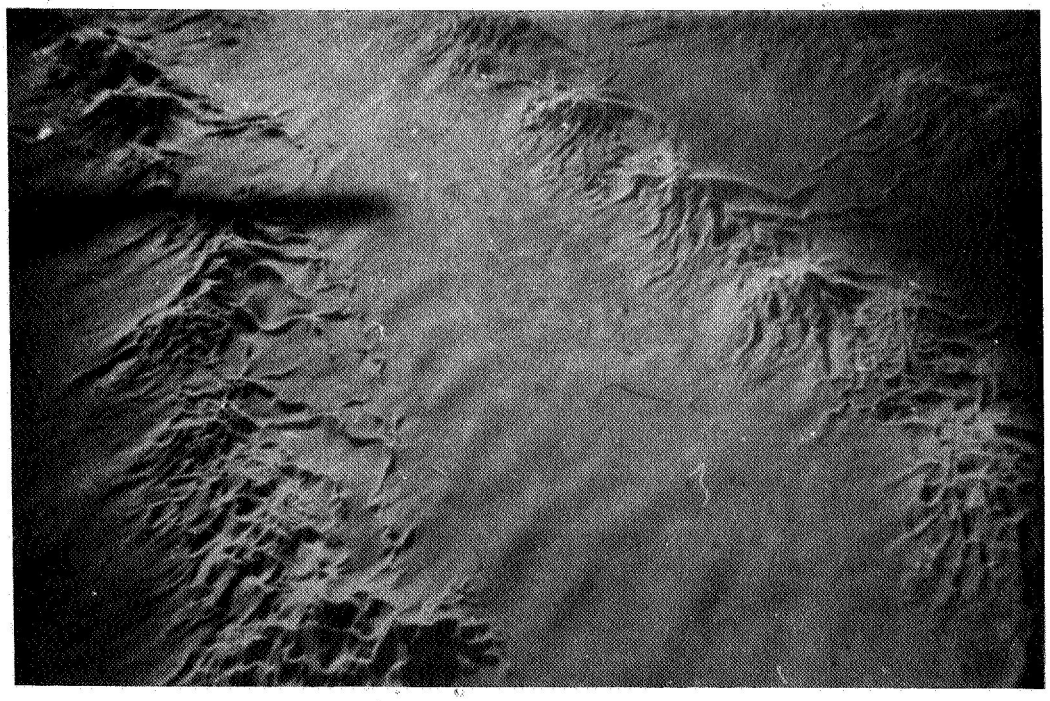


Figure 14.--Rows of star dunes in Algerian desert as seen in aerial photograph. Photo by H.T.U. Smith.

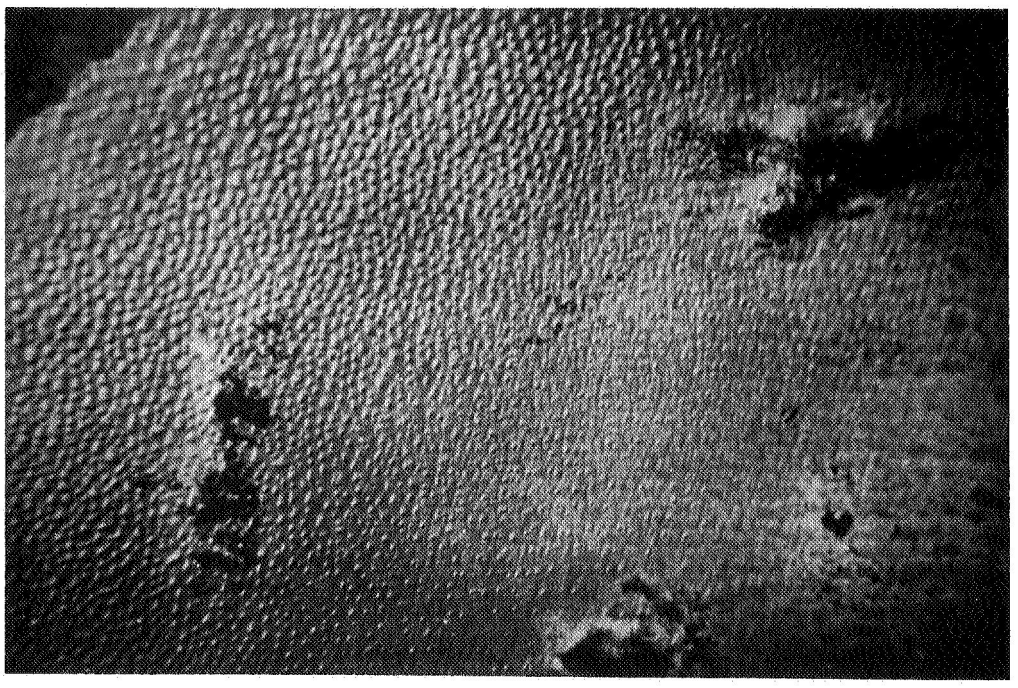


Figure 15.--Reticulate pattern in sand of Algerian desert shown in ERTS image. Formed by clusters of star dunes. ERTS #1109-09322

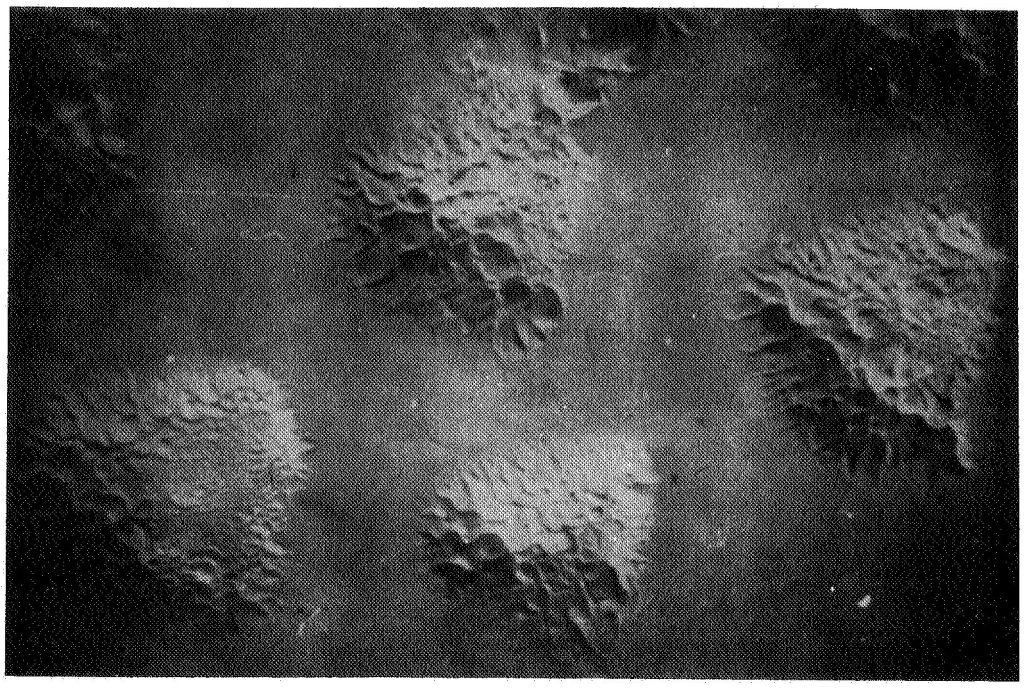


Figure 16.--Cluster of star dunes in Algerian desert as seen in aerial photograph. Photo by H.T.U. Smith.

Paper G 9

ESTABLISHMENT, TEST, AND EVALUATION OF A PROTOTYPE VOLCANO-SURVEILLANCE SYSTEM_/

Peter L. Ward, Jerry P. Eaton, Elliot Endo, David Harlow, Daniel Marquez and Rex Allen, *National Center for Earthquake Research, United States Geological Survey, Menlo Park, California*

ABSTRACT

A volcano-surveillance system utilizing 23 multilevel earthquake counters and 6 biaxial borehole tiltmeters is being installed and tested on 15 volcanoes in 4 States and 4 foreign countries. The purpose of this system is to give early warning when apparently dormant volcanoes are becoming active. The data are relayed through the ERTS-Data Collection System to Menlo Park for analysis. Installation was completed in 1972 on the volcanoes St. Augustine and Iliamna in Alaska, Kilauea in Hawaii, Baker, Rainier and St. Helens in Washington, Lassen in California, and at a site near Reykjavik, Iceland. Installation continues and should be completed in April 1973 on the volcanoes Santiaguito, Fuego, Agua and Pacaya in Guatemala, Izalco in El Salvador and San Cristobal, Telica and Cerro Negro in Nicaragua.

The event counters developed for this use count earthquakes of four different amplitudes. An earthquake is assumed if 10 peaks of a full-wave rectified seismic signal exceed a given threshold in 1.2 seconds and no peaks had exceeded the threshold in the previous 15 seconds. This latter criterion inhibits the counters if the ground noise is high for long periods of time. Inhibit times are counted on separate counters. All data are printed on a unique printer in the counter that provides a check on the reliability of the DCS. The average power consumption is only 2 milliwatts, and the counters are now operating reliably in a wide range of environments. Standard seismometers are being placed near most event counters in this initial program in order to verify that the counters are discriminating earthquakes as anticipated. Local earthquakes are being recorded at nearly all sites.

The biaxial tiltmeters are 2 inches in diameter and fit in a hole 5 feet deep. They are proving easy to install and are operating stably with a sensitivity of about one microradian.

Since this project was not funded until one month before the launch of ERTS-A, much of the first year of satellite life has been

---

_/Publication authorized by the Director, U.S. Geological Survey

spent building and deploying equipment. The data available to date show that the instruments are working quite reliably and show how the system can be tuned to improve the data and reliability. The primary objective--evaluating the effectiveness of the system--must await more data.

1. INTRODUCTION

A prototype volcano-surveillance system consisting of 23 multi-level earthquake counters and 6 biaxial tiltmeters is being installed and tested on 15 volcanoes in Alaska, Hawaii, the Cascades, Iceland and Central America. The data from the instruments are relayed via the ERTS Data Collection System to Menlo Park for analysis. Such rapid and routine collection of data from a variety of widely spaced volcanoes is a major breakthrough in the surveillance of potentially hazardous volcanoes. There are more than 500 historically active volcanoes scattered throughout the world, but only a few may be erupting at one time. Some volcanoes emit fume for years with no explosive eruptions, while other seemingly dormant volcanoes suddenly become violently active. Although visual evidence of an impending eruption may be detected too late to allow proper study, there are usually much earlier indications that an apparently dormant volcanic center is becoming active, such as increases in earthquake activity and the rate of ground tilting. Until now, routine observations have been logistically and financially feasible at only a few volcanoes. Very few volcano observatories exist, primarily because of the long-term financial commitment necessary. A devastating eruption may arouse interest in establishing an observatory, but by the time one can be developed, the volcanoes it was designed to study may have become inactive. Thus, there is a great need in volcanology for a method of monitoring large numbers of volcanoes with relatively simple instruments and with a minimum of manpower and other resources, for the purpose of identifying the most dangerous volcanoes. Once these are identified, studies aimed at predicting devastating eruptions can be started.

The ERTS Data Collection System offers an excellent opportunity to collect data from widely scattered instruments and to make them rapidly available for analysis at a central facility with minimal logistical expense. It eliminates the need to send observers in many different countries up the sides of rugged volcanoes, often in bad weather, to collect data routinely. It also permits rapid, simultaneous evaluation and comparison of observations from a large number of similar volcanoes by a single group of volcano specialists; thus new results from any volcano that does erupt are immediately available to aid in interpreting data from many others.

Two relatively easily measurable phenomena that have been observed to change most consistently prior to volcanic eruptions are the occurrences of large numbers of small earthquakes and small changes in the ground tilt, which are typically related to the swelling of the volcano (e.g. Eaton and Murata, 1960; Minakami et al., 1969; Minakami, 1960; Tokarev, 1971). Tokarev (1971) has even used the rate of increase in

numbers of small earthquakes to predict the eruption of andesitic volcanoes in Kamchatka and Japan. The recent eruption of Helgafell volcano in Iceland, for example, was preceded by an intense swarm of small earthquakes on the previous day (Páll Einarsson, oral communication, 1973).

For these reasons, we have chosen to develop multilevel earthquake counters and biaxial tiltmeters for use with the satellite data relay system and are presently evaluating and testing the reliability and utility of the instruments under a wide variety of conditions.

2. DEVELOPMENT OF THE EARTHQUAKE COUNTERS

Standard methods for recording earthquakes produce data at the rate of about 4 million digital bits per 12-hour period. Yet the ERTS Data Collection System can only relay approximately 64 bits in a 12-hour period. Other satellite relay systems would not significantly increase this data rate and still keep the system economical enough to operate on a wide scale. Thus, substantial data compression is necessary.

Since the most important aspect of volcanic earthquakes to be monitored is a large increase in the rate of occurrence of local earthquakes, a multilevel earthquake counter was developed and tested in 1971 (Figure 1). This experience led to the development of a new counter in 1972 for the ERTS-A experiment. Twenty-three of these counters were built and are proving to operate very reliably in a wide variety of climates (Figure 2). The principal criteria for an event to be counted are as follows: 1) 10 peaks of the full-wave rectified seismic signal must be above a given threshold level during an interval of 1.2 seconds, and 2) there must have been no signal above the threshold during the previous 15 seconds. Each instrument contains four counters separated in threshold level by factors of four. This multilevel feature is an important improvement over the single level event counters used earlier by Decker (1968) because it allows the reliability of the data to be tested and gives a greater dynamic range. Each earthquake counter channel is inhibited by continuous high ground noise. The inhibit times are counted on separate counters. All counts are recorded on a small printer, as well as being relayed to the satellite. The printer has only one moving part, a solenoid, and records the data in a compact binary matrix. In this way 75 bits of information can be printed every 6 hours for 2 years on a reel of tape only 0.25 inches wide and 3 inches in diameter.

The design of the new event counters appears quite suitable and reliable for this use. One principal question to be answered is whether these criteria for data compression are indeed satisfactory. Thus, in the present experiment, standard seismometers have been set up near most of the event counters so that the compressed data can be compared directly with the more usual types of seismic recordings (Figure 3).

Other methods of compressing seismic data, but using digital computers and complex analog circuits, have been under development at the National Center for Earthquake Research for some time (e.g. Stewart et al., 1971). Such methods are still too complex to be used in a widespread system and are not yet sufficiently well developed and reliable for use in a volcano-surveillance network, although they hold considerable promise for the future.

3. DEVELOPMENT OF THE TILTMETERS

Eaton (1959), building on earlier work in Japan (Hagiwara, 1947; Hagiwara et al., 1951), developed extensively the use of watertube tiltmeters in Hawaii and demonstrated their great value in studying volcanoes. Since that time he and others have searched for ways to measure tilt more routinely and simply. This search culminated in the development of a pendulum-type borehole tiltmeter by Allen (1972) and others at the National Center for Earthquake Research. During 1972 an entirely different type of borehole tiltmeter was developed by suitably packaging an electronically monitored level bubble developed by North American Rockwell for use in the Minuteman Missile. The new instrument is a very low power biaxial tiltmeter only 2 inches in diameter and about 3 feet long (Figure 4). In tests alongside other types of tiltmeters operated by the USGS, this new tiltmeter has proved to be stable and sensitive enough to record earth tides. Furthermore, it is substantially cheaper and easier to install than the other tiltmeters tested.

Under the ERTS-A program one of these meters was installed in welded tuff on Mt. Lassen in California and one in sand in Hawaii, and two will be installed in Guatemala. Two others have been installed in Hawaii under a related program. We have found methods for installation in rock (Figure 5) and all types of soil using only tools that can be easily backpacked. Different designs of installations and different types of sites still need to be tried, however, to develop simple and reliable methods of placing these new meters in regions of maximum tilt changes on andesitic volcanoes.

4. ESTABLISHMENT OF A PROTOTYPE VOLCANO-SURVEILLANCE SYSTEM

The distribution of earthquake counters, standard seismometers, and tiltmeters installed or planned as part of this prototype surveillance system is summarized in Table 1. This program was funded less than a month before the launch of the satellite. As NASA continued to delay the start of this program, we realized that it was becoming impossible to develop the earthquake counters and install them in Alaska and the Cascades before winter. Thus, we began designing the counters in January 1972, and with the help of a loan from the EROS program, we were able to issue a subcontract in May to build the 23 counters. The first counters were delivered in late August 1972, and by late Septem-

ber the system was integrated and tested. The sites had already been selected where possible, and despite early snowfalls, installation in the Cascades was completed by late October. In Alaska, however, we could only install instruments at St. Augustine in September before winter set in. Owing to subfreezing temperatures, a second instrument was placed near Iliamna Volcano, rather than the planned sites on the volcanoes Redoubt and Spurr.

In December 1972, event counters and DCP's were installed in Hawaii and at a site near Reykjavik, Iceland, to test whether the range of the ERTS data transmission system is sufficient to reach these important volcanic regions. The Icelandic instrument will be moved to a volcano next summer when weather allows. During November and December, sites were selected in Central America, and the necessary permits were obtained. Installation was begun in Guatemala in February and should be completed in Nicaragua by April. An average of about 10 messages per day are being received from stations in the Cascades and 6 per day from Alaska, with all transmitters adjusted to transmit once every 3 minutes. In Hawaii and Iceland the transmitters send data every 90 seconds, and an average of about 6 and 10 messages per day, respectively, are received. These data rates are quite sufficient.

The final key link in the system will be a teletype from Goddard Spaceflight Center to Menlo Park for rapid data analysis. We hope this will be installed by April 1973.

5. SIGNIFICANT RESULTS

By February 1973, over 13,000 messages had been received from the satellite and analyzed. These data show clearly that the event counters and tiltmeters are working quite reliably and with incredibly few problems, considering the complexity of the system and the speed with which the instruments were designed, built, and installed. The only instruments to stop altogether are those on Mt. Baker, where a storm in January either destroyed the antennas or buried them too deeply in snow. Thus, we have succeeded in designing and building equipment that is reliable and stable at least over a short time period. We have also shown that the ERTS Data Collection System will operate satisfactorily over nearly twice the anticipated range. Naturally, our experience has led to many ideas for minor adjustments and improvements to tune up the system. These changes will be incorporated where feasible, but the main object now is to evaluate and test this volcano-surveillance system. Although too few data have been recorded so far to support a meaningful detailed analysis, it is clear that the event counters are discriminating earthquakes from most other seismic noises and that many small earthquakes are occurring at nearly every volcano studied, including Mts. Baker and Rainier in the Cascades.

Now we need to establish the background level of seismicity and tilt at these volcanoes so that abnormal activity can be rapidly identified.

The long-range objective of this project is to develop an automated global volcano-surveillance system utilizing relatively simple and inexpensive earthquake counters and tiltmeters on many volcanoes in order to detect which volcanoes are undergoing the most rapid internal changes and should be studied in detail to assess the danger of devastating eruptions. Thus, the most important objective is to observe the performance of these instruments before, during and after various stages of volcanic activity at a wide variety of volcanoes to prove whether the event counters, tiltmeters and data relay system do indeed work as planned to provide accurate, economical and timely information about the eruptive state of volcanoes. Now that the major hurdle of design and deployment has nearly been successfully passed, we feel the appropriate data can be collected in the next few years to meet this objective. The odds of observing eruptions seem quite good. The volcanoes Kilauea, Pacaya and the Fuego-Acatenango complex have been erupting in the past few months. The odds could be substantially increased, now that the range of the Data Collection System has been proven, by extending this surveillance system into Costa Rica, where there are several very active volcanoes. Otherwise this program as now formulated gives a good test of the event counters, provided the system functions for many years.

More tiltmeters, however, should be installed to give them a proper test. Only a few were included in this original program because during the planning stage inexpensive borehole tiltmeters were not proven. Now that we have shown the feasibility and practicality of these tiltmeters, we need to test their long-term reliability and stability under a wide range of conditions and to further develop techniques for deploying them on the many types of volcanoes.

In summary, installation of the prototype volcano-surveillance system being developed and tested by the U.S. Geological Survey under the ERTS-1 program is nearly finished. The equipment is working well. As the data begin to accumulate and evaluation begins, it should become more and more apparent that this network will make a major breakthrough in the surveillance of potentially hazardous volcanoes made possible primarily by the data-collection capability of the ERTS-1 satellite.

TABLE 1: PROTOTYPE VOLCANO-SURVEILLANCE NETWORK

COUNTRY OR STATE	VOLCANO	EVENT COUNTER + DCP	VISIBLY RECORDING SEISMIC SYSTEMS	TILTMETER + DCP	INSTALLED 1972-1973
ALASKA	ST. AUGUSTINE	1	1 existing		SEPTEMBER
	ILIAMNA	1	U.S.G.S. network		SEPTEMBER
WASHINGTON	BAKER	1	1		OCTOBER
	RAINIER	1	1		OCTOBER
	ST. HELENS	1	1		OCTOBER
CALIFORNIA	LASSEN	1	1	1	OCTOBER
HAWAII	KILAUEA	2	U.S.G.S. network	3	JANUARY
ICELAND	NEAR REYKJAVIK	1	1 existing		DECEMBER
GUATEMALA	PACAYA	1	1	1	FEBRUARY
	AGUA	1	-	-	FEBRUARY
	FUEGO	1	1	1	FEBRUARY
	OFF VOLCANIC AXIS	1	1	-	FEBRUARY
	SANTIAGUITO	2	1	-	MARCH*
EL SALVADOR	IZALCO	1	1		MARCH*
NICARAGUA	SAN CRISTOBAL	1	1		MARCH*
	TELICA	1	-		MARCH*
	CERRO NEGRO	1	1		MARCH*
	OFF VOLCANIC AXIS	1	1		MARCH*
		20	12 new		*planned

References Cited

Allen, R. V., 1972, A borehole tiltmeter for measurements at tidal sensitivity, Bull. Seism. Soc. Amer., 62, 815-821.

Decker, R. W., 1968, A seismic event counter for active volcanoes, Bull. Seism. Soc. Amer., 58, 1353-1358.

Eaton, J. P., 1959, A portable water-tube tiltmeter, Bull. Seism. Soc. Amer., 49, 301-316.

Eaton, J. P., and K. J. Murata, 1960, How volcanoes grow, Science, 132 (3432), 925-938.

Hagiwara, T., 1947, Observations of changes in the inclination of the earth's surface at Mt. Tsukuba, Bull. Earthq. Res. Inst., 25, 27-32.

Hagiwara, T., K. Kasahara, J. Yamada, and S. Saito, 1951, Observation of the deformation of the earth's surface at Aburatsubo, Miura Peninsula, Bull. Earthq. Res. Inst., 29, 455-468.

Minakami, T., 1960, Fundamental research for predicting volcanic eruptions (Part 1) earthquakes and crustal deformations originating from volcanic activities, Bull. Earthq. Res. Inst., 38, 497-544.

Minakami, T., S. Hiraga, T. Miyazaki and S. Utibori, 1969, Fundamental research for predicting volcanic eruptions (Part 2), seismometrical surveys of volcanoes in Japan and volcano Sotara in Colombia, Bull. Earthq. Res. Inst., 47, 893-949.

Stewart, S. W., W. H. K. Lee, and J. P. Eaton, 1971, Location and realtime detection of microearthquakes along the San Andreas Fault System in Central California, Bull. Roy. Soc. New Zealand, 9, 205-209.

Tokarev, P. I., 1971, Forecasting volcanic eruptions from seismic data, Bull. Volcanol., 35(1), 243-250.



Figure 1: The multilevel earthquake counter with the satellite transmitter on the left and batteries for operation for one year on the right. The seismic sensor is in the foreground. The event counter weighs 25 pounds and measures 10 by 14 by 12 inches.

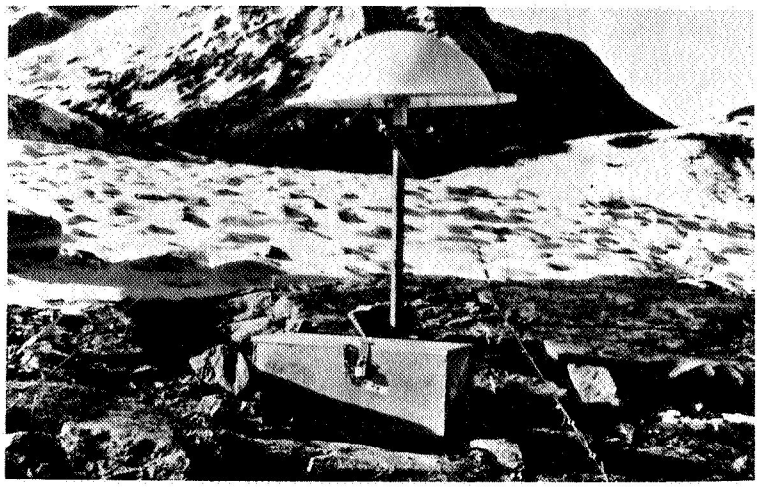


Figure 2: A typical field installation of the seismic event counter. The dome on the antenna is to insulate the antenna's active elements from snow. This instrument is located in Alaska on the flank of Mt. Iliamna.

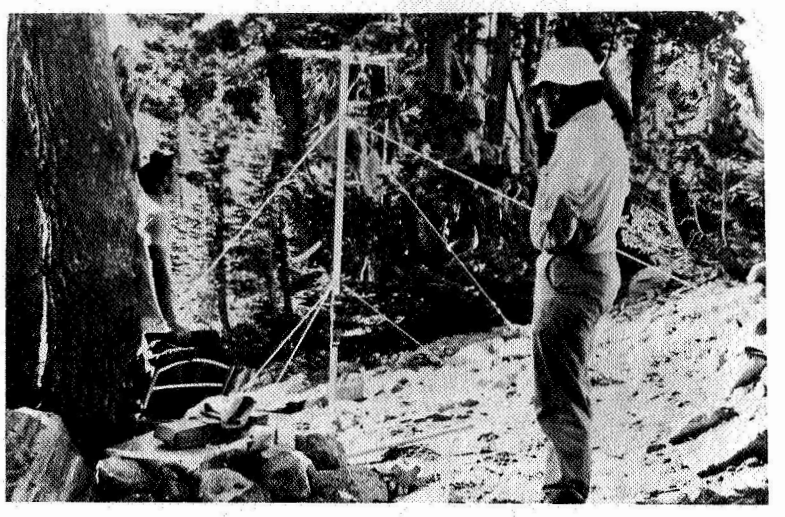


Figure 3: The standard seismic station on Mt. Lassen. The electronics and batteries are in the box in the left foreground. The signal is transmitted in the FM mode to Menlo Park for recording using the VHF antenna shown.

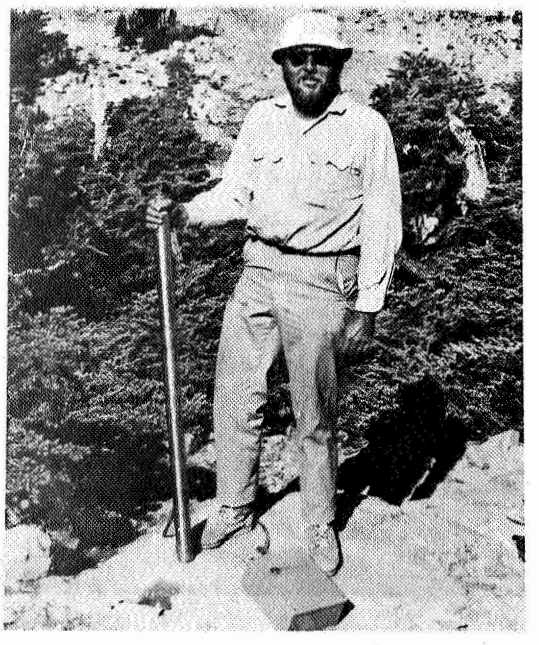


Figure 4: The biaxial borehole tiltmeter used in this project.

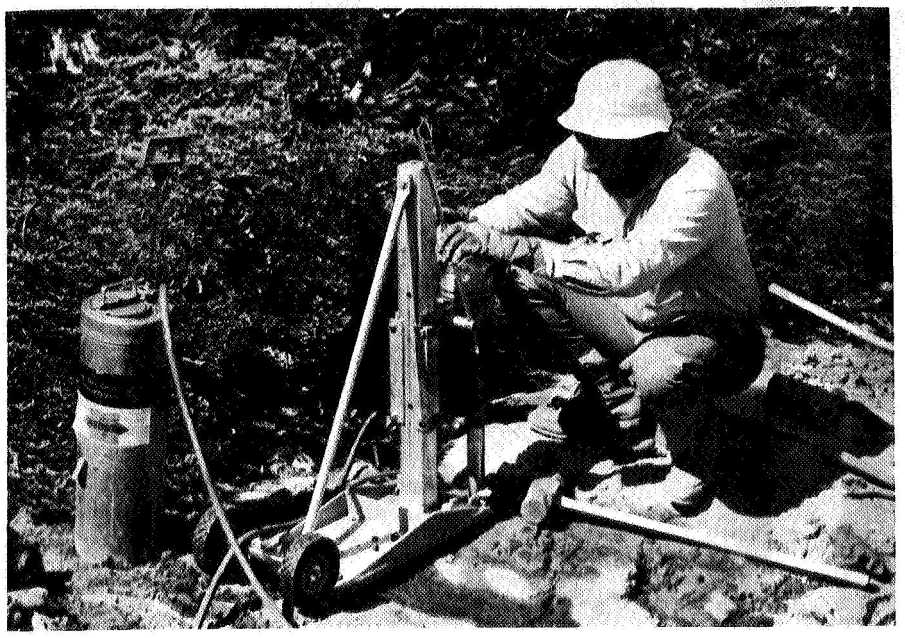


Figure 5: Drilling a four inch in diameter hole in welded tuff on Mt. Lassen. The drill frame is bolted to the rock.

Paper G 10

SATELLITE GEOLOGICAL AND GEOPHYSICAL REMOTE SENSING OF ICELAND - PRELIMINARY RESULTS FROM ANALYSIS OF MSS IMAGERY*

Richard S. Williams, Jr., *U.S. Geological Survey, EROS Program Office, Washington, D.C. 20244;* Agúst Bödvarsson, *Icelandic Surveying Dept., Reykjavik, Iceland;* Sturla Fridriksson, *Agricultural Institute, Reykjavik, Iceland;* Gudmundur Pálmason, *National Energy Authority, Reykjavik, Iceland;* Sigurjón Rist, *National Energy Authority, Reykjavik, Iceland;* Hlynur Sigtryggsson, *Icelandic Meteorological Service, Reykjavik, Iceland;* Sigurdur Thórarinsson, *University of Iceland, Reykjavik, Iceland;* Ingvi Thórsteinsson, *Agricultural Institute, Reykjavik, Iceland.*

ABSTRACT

A binational, multidisciplinary research effort in Iceland is directed at an analysis of MSS imagery from ERTS-1 to study a variety of geologic, hydrologic, oceanographic, and agricultural phenomena. A preliminary evaluation of available MSS imagery of Iceland has yielded several significant results - some of which may have direct importance to the Icelandic economy. Initial findings can be summarized as follows: (1) recent lava flows can be delineated from older flows at Askja and Hekla; (2) MSS imagery from ERTS-1 and VHRR visible and infrared imagery from NOAA-2 recorded the volcanic eruption on Heimaey, Vestmann Islands; (3) coastline changes, particularly changes in the position of bars and beaches along the south coast (e.g., north and west of Ingólfhöfdi), are mappable; (4) areas covered with

*Publication authorized by Director, U. S. Geological Survey

new and residual snow can be mapped, and the appearance of newly fallen snow on ERTS-1, MSS band 7 appears dark where it is melting; (5) sediment plumes from the discharge of glacial rivers along the south coast can be delineated; (6) the area encompassed by glacial ice (ice caps, valley and outlet glaciers, etc.) can be mapped, including the new position of a surging glacier, Eyjabakkajökull, and such related phenomena as nunataks and moraines; (7) the plotting of changes in position of rivers, changes in size of lakes, and the occurrence of new lakes are feasible; (8) low sun-angle imagery, particularly of snow-covered terrain, markedly enhances the morphologic expression of constructional glacial and volcanic landforms, thus permitting the mapping of previously unrecognized structural features such as central or subglacial volcanoes; (9) the MSS color composites will permit the regional mapping of the gross distribution of vegetation in Iceland; and (10) at least at 1:250,000 map scale and smaller, ERTS-1 imagery provides a means of updating various types of maps of Iceland and will permit the compilation of special maps specifically aimed at those dynamic environmental phenomena which impact on the Icelandic economy.

1. INTRODUCTION

Iceland (Figure 1) is an island republic with a relatively small population of 206,818 (1 Dec. 1971) but with an area of 103,000km^2, resulting in a population density of 2 persons per km^2. Approximately 12,000km^2 of the area is covered by glaciers and 67,000km^2 is lakes, lava, sands, or non-productive land. Only 1,000km^2 is cultivated; the remaining 23,000km^2 is used for grazing, principally by 736,000 sheep, 53,000 cattle, and 33,000 Icelandic ponies. Living as the Icelanders do in the far north, dependent on the surrounding seas for fish and the land for agricultural products, their economic well-being is heavily influenced by the natural environment, and how effectively they use the limited resources available to them. Much of the Icelandic scientific effort is directed at an understanding of their environment because of its importance to the Icelandic economy. The effect of volcanic activity, the impact of frequent changes in climate, the condition of the rangelands (particularly phenological considerations), the hydrology of the country, and distribution and persistence of snow cover, are just some of the dynamic environmental data which

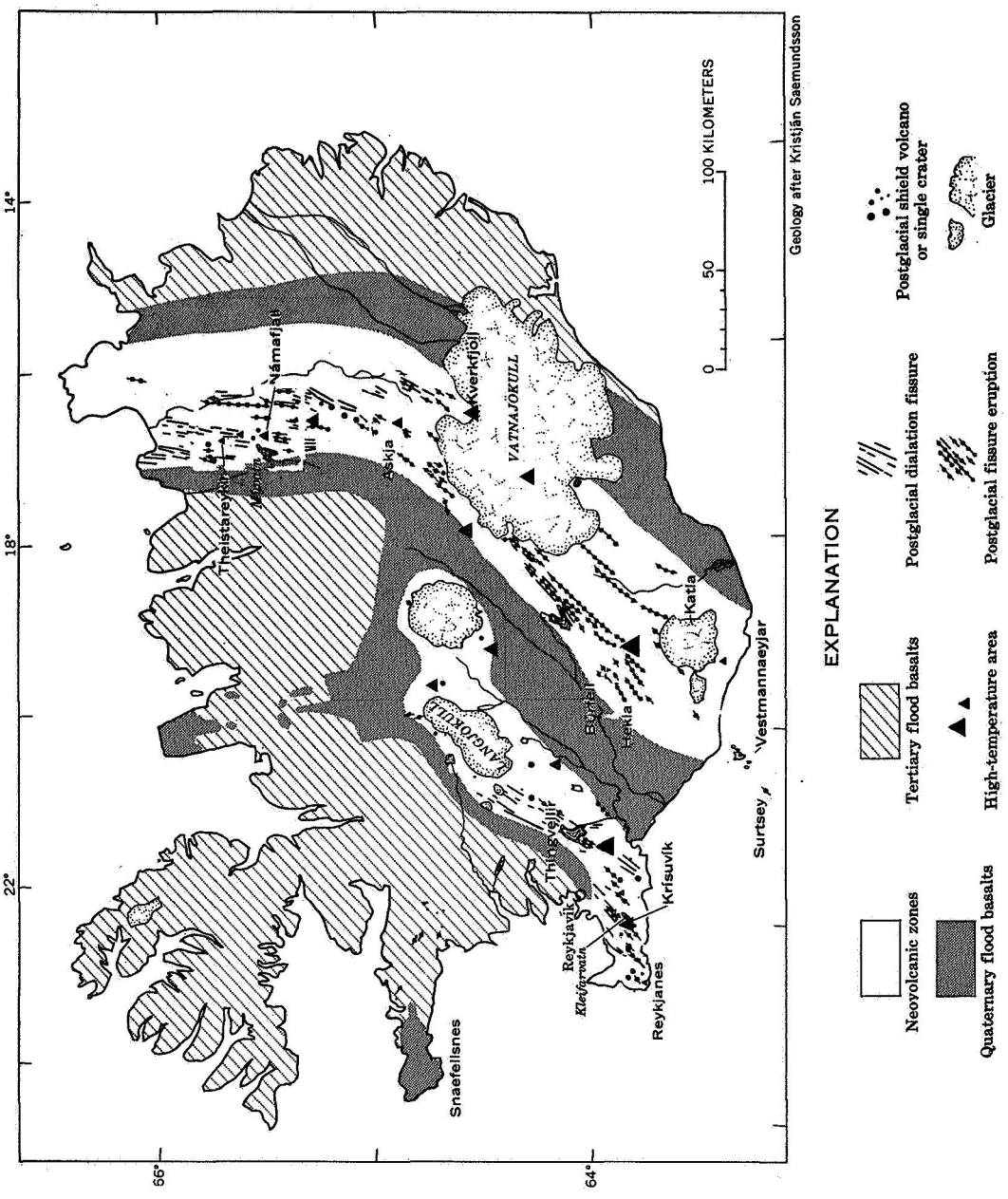


Figure 1. - Index map of Iceland

have a strong economic justification for acquisition. The limited number of scientists, the amount and type of environmental data needed to make effective and accurate decisions on the management of limited resources, and the lack of financial resources limit the acquisition of certain types of environmental data. From the very limited analysis of available ERTS-1, MSS imagery of Iceland, it can be stated that this imagery, when available on a timely basis and in a repetitive manner, can provide, at low cost, the environmental data necessary for resource management decisions. The remainder of the paper will be devoted to a more detailed discussion of the initial results from the series of experiments collectively entitled, Satellite Geological and Geophysical Remote Sensing of Iceland (Williams, 1973).

2. VOLCANIC ERUPTIVE PRODUCTS

Figure 2 shows the Vikrahraun lava flows which flowed out of a fissure in the Askja caldera (45km^2) during the period October-December 1961. The lavas encompass an area of 11km^2 and reach a length of 7.5km. Some of the flows from the 1921-1924 effusive volcanic eruptions appear to be distinguishable southwest and southeast of the lake (Öskjuvatn). There is also the possibility that thermal emission, as recorded on aerial thermographs in 1966 (Friedman, Williams, and Pálmason, 1968) is reflected on the ERTS-1 MSS image as snow-free areas on the eastern shore of Öskjuvatn. Comparison of the ERTS-1 MSS image of the Vikrahraun with the maps published by Thórarinsson and Sigvaldason (1962) and Thórarinsson (1963) and the 1969, 1:100,000 map (Blad 84., Herdubreid) published by the Icelandic Surveying Department shows that the ERTS-1 image provides better detail as to the areal extent of the Vikrahraun than any of the other three maps.

The 1970 lava flows from Hekla (Thórarinsson, 1970) particularly the flows which emanated from Sudurgigar and flowed south and southwest for 5.5km, can be delineated. The Skjólkvíar flows to the north, and the flows to the northwest from an area southwest of Axlargígur are in shadow. It also appears possible that the 1947-48 lava flows on the southeast flank of Hekla can be mapped. The progression of lichen colonization since the cooling of lava flows may be represented in a different spectral reflectance, thus appearing as a different tone on the

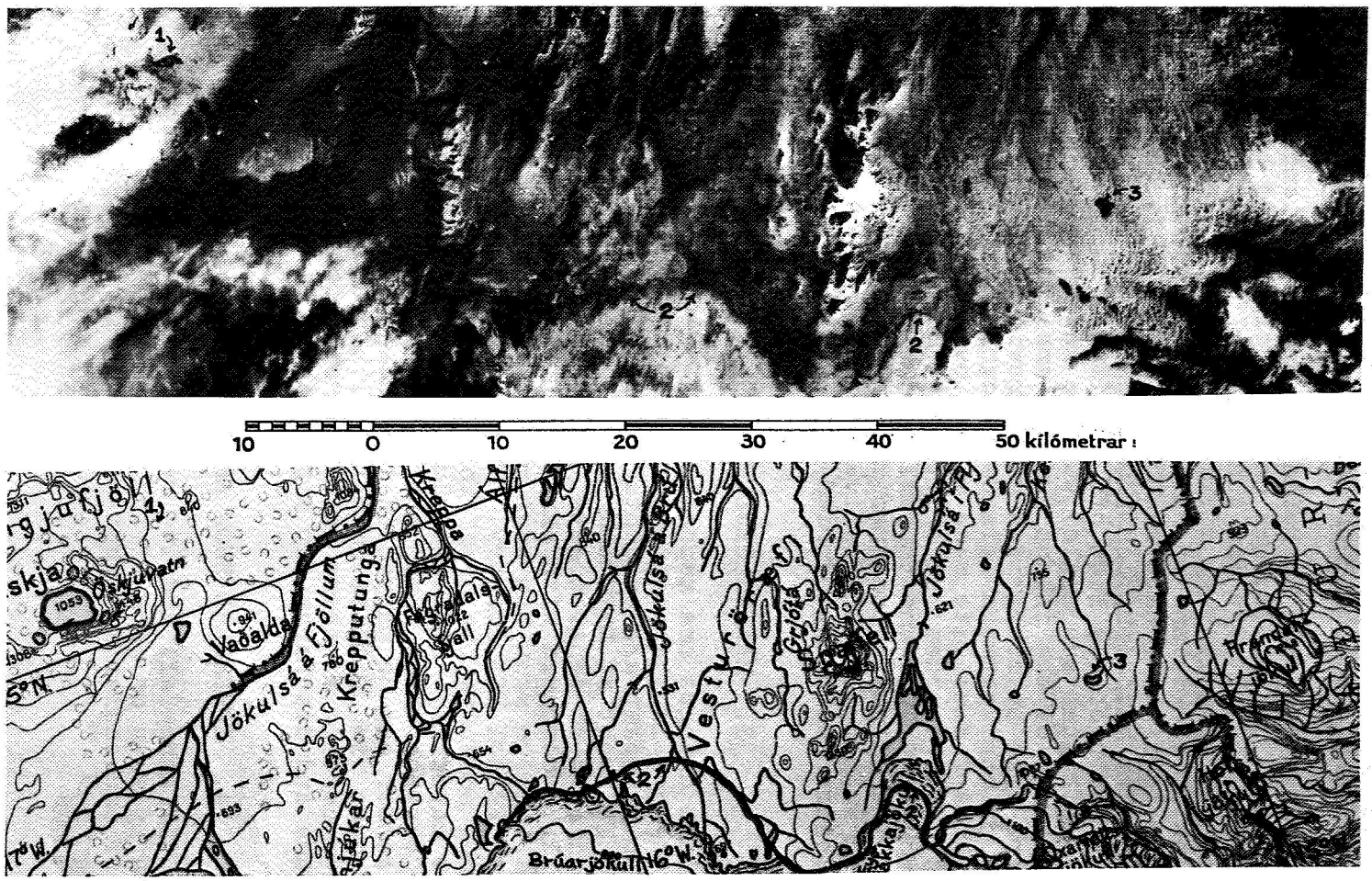


Figure 2. - Comparison of ERTS-1, MSS image (14 Oct. 1972, E-1083-12021-5) of a part of northwest Iceland with a 1:500,000 scale map (Geodaetisk Institut, Copenhagen, 1945) of the identical area. Of particular interest are the geologic and hydrologic changes evident and mappable from the ERTS-1 image: (1) Vikrahraun lava flows (1961) 6km northwest of Öskjuvatn, (2) new position of the snouts of Brúarjökull and the surging glacier, Eyjabakkajökull, and (3) appearance, disappearance, and changes of lakes.

ERTS-1 MSS imagery. The position of Toppgígur (Summit Crater) and Axlargígur (Shoulder Crater) can be mapped.

The volcanic eruption on Heimaey, Vestmann Islands, which began on 23 Jan. 1973, was only faintly imaged by ERTS-1 on 3 Feb. 1973. The low sun angle (7°), black lava and tephra, make it very difficult to see all but a faint outline of the island of Heimaey. White steam clouds, where lava flows have reached the sea, apparently can be seen. The main eruption plume can be seen only indistinctly and probably lies off the image to the east. Later imagery (higher sun angle) will be necessary to map the new coastline of the island and the areal distribution of the tephra fall by comparison with previously acquired MSS imagery of the Vestmann Islands volcanic archipelago. (Note: The NOAA-2 satellite made a pass over Heimaey on 25 Jan. 1973 and recorded the eruption plume on both the visible band 0.6-0.7μm) and thermal band (10.5-12.5μm) imagery and thermal emission from the lava flows on the thermal band imagery. Quantitative measurements of radiant emission are being carried out.)

3. MARINE GEOLOGY

Coastline changes are mappable from the ERTS-1 imagery. Changes in the position of bars and beaches along the south coast are evident, particularly along the coast north and west of Ingólfhöfdi. As more imagery becomes available of other coastal areas of Iceland, the imagery will be compared with existing 1:250,000 to 1:1,000,000 maps to show how such maps can be readily updated with ERTS-1 MSS imagery. The image of the Ingolfhöfdi area provides the proof that such coastal changes are mappable. Sediment plumes from the discharge of glacial streams which cross the Skeidarársandur and Medallandssandur can be mapped in the ocean. The size of the plumes over time will be compared with hydrograph records to ascertain if there is any correlation between size of plume and discharge for a particular river.

4. EPHEMERAL SNOW AND ICE

Early fall snowfall and its relationship to elevation can be clearly seen on many of the ERTS-1 images of Iceland. Of particular interest, however, is the

appearance of a light (?) snowfall in the Stórisandur area (Figure 3) which appears differently on MSS bands 4 (0.5-0.6μm) and 7 (0.8-1.1μm). On band 4 the snow cover is more extensive than is portrayed on band 7. This is because melting snow appears very dark at infrared wavelengths because of absorption due to free water. Similar dark areas of melted snow can be seen in the highland areas around Eiríksjökull and Okjökull. The mid-winter snow cover and its absence on the low-lying coastal areas (e.g., Skeidarársandur) is mappable. Snow-covered and frozen Lake Graenalón (approx. 3km x 5km) can be delineated.

5. GLACIOLOGICAL FEATURES

Glaciological features are exceptionally well portrayed on the ERTS-1 MSS imagery. Figure 2 shows (black line on 1:500,000 scale map) the current position of part of Brúarjökull and the new position of the snout of the surging glacier, Eyjabakkajökull. It should be noted that MSS band 5 was better than the other 3 bands in plotting the position of the glacier, but that the MSS color composite was mandatory in obtaining the necessary map precision in distinguishing the terminal moraine from the non-glacier covered terrain. The black and white images were difficult to work with because the morainal material of the terminal moraine is composed of the same material as the terrain in front of the glacier, making only a slight reflectance difference between the two. On the 14 Oct. 1972 MSS image the advancing front of Eyjabakkajökull is very steep; a shadow cast by the 15° sun angle enhances the steep front and is clearly delineated from the terrain which it has overridden. The last known surge of Eyjabakkajökull was in 1890 (Thórarinsson, 1964). The current surge of unknown magnitude [0.5 km (?), Thórarinsson, personal communication] still puts the present snout on the MSS image at a recession of 3.5km from the position in 1890.

Comparison of the position of glacial rivers on the MSS imagery with maps at scales as large as 1:250,000 shows many changes. The same is true of ice margin lakes and other lakes in Iceland. ERTS imagery will likely lead to greatly improved maps of such features and provide the capability for periodic revisions.

Early fall MSS imagery of glaciological features of Iceland was best. The best image of Mýrdalsjökull and Eyjafallajökull, with exceptional detail of two of the glaciers of Mýrdalsjökull, Sólheimajökull and Höfdabrekkujökull (Kötlujökull), is from early Sept. 1972. August

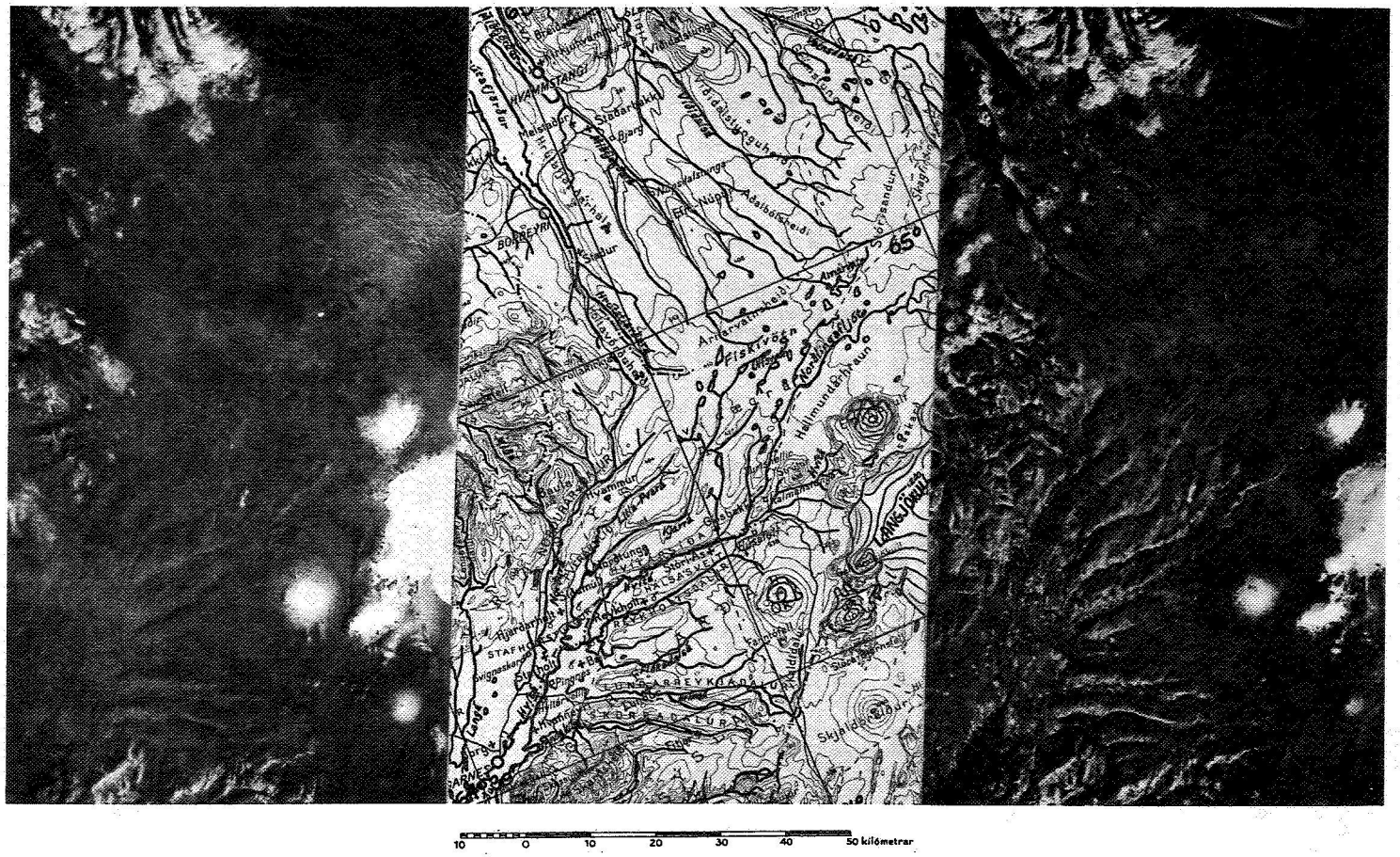


Figure 3. - Comparison of ERTS-1, MSS images (Left: 19 Oct. 1972, E-1088-12305-4; Right: 19 Oct. 1972, E-1088-12305-7) of a part of northeast Iceland with a 1:1,000,000 scale map (Geodaetisk Institut, Copenhagen, 1963) of the identical area. Of particular interest are the geologic and hydrologic phenomena recorded on the ERTS-1 image: (1) changing appearance of light snowfall in the highlands area north of Langjökull (Stórisandur) on band 4 and band 7 and around the ice caps, (2) changes evident in position of ice caps, and (3) circular structural feature at **Saudafell** which is a central volcano in the Tertiary volcanic rocks.

imagery would be optimum because of time of minimum snow cover, however.

6. STRUCTURAL AND MORPHOLOGIC FEATURES

A mid-winter image of the snow-covered Vatnajökull and the area west and south of this huge icecap in which the sun angle was at 7° shows incredibly fine morphologic and structural details of constructional volcanic and glacial landforms. The crater rows, Laka Gígar in particular, fissures, grabens, etc., are starkly portrayed. Old end moraines around outlet glaciers of Vatnajökull and Hofsjökull are mappable. Considerable detail exists on the snow-covered surface of Vatnajökull some of which definitely reflects the underlying geologic structure. The outline of the Grímsvötn caldera and the summit area of Öraefajökull are striking. Of great interest are at least four other circular features within the icecap. Two of them in the Kverkfjöll area almost certainly mark the position of subglacial volcanoes. Thórarinsson (1950) shows a possible eruption center in the upper part of the Dyngjujökull area, but the MSS image clearly shows that the suspected eruption center is not correctly located. The Hveradalur thermal area (Friedman, Williams, Thórarinsson, and Pálmason, 1972) appears to be structurally related to the second circular feature on the ERTS image. Two other circular or elliptical features on Vatnajökull, one at Bárdarbunga and the other near Hamarinn, may also have a volcanogenetic cause.

In the Torfajökull geothermal area, the largest geothermal area in Iceland (100km^2), the circularity of the structure, recently reported by Saemundsson (1969 and 1972) is portrayed. West of Langjökull, in the Tröllakirkja area, a pronounced circular structure may represent the position of a previously unrecognized central volcano in Tertiary volcanic rocks.

7. GRASSLANDS AND FORESTS

Knowledge of the areal distribution, health, and growth rate of the grasslands of Iceland is vitally important to the economic well-being of the agriculture industry. The vagaries of the climate in Iceland (Eythórsson and Sigtryggsson, 1971), deposition of tephra after

volcanic eruptions (e.g., after the 1970 Hekla eruption and the 1973 Kirkjufell eruption on Heimaey), and presence and persistence of sea ice off the Icelandic coast all impact on the state of the grasslands. Considerable reclamation work is directed at reseeding of barren areas (Fridriksson and Pálsson, 1970) and reforestation of suitable sites to halt the rate of soil erosion and to provide additional grazing lands for sheep, cattle, and horses. A vegetation mapping program is currently underway to plot the vegetation of Iceland (Thórsteinsson, 1972), but additional, timely data on the health (e.g., lack of winter kill) and growth characteristics of the grasslands is needed for resource management decisions leading to the most effective utilization of the rangelands. A preliminary evaluation of ERTS-1 MSS color composites shows that vegetation distribution can be mapped. Seasonal imagery is needed before changes in the rangelands can be mapped and evaluated. It appears, however, that MSS color composites will provide Iceland with a powerful tool to map the seasonally changing condition of its grasslands, condition of reseeded and reforested areas, and - with an operational satellite - provide the timely data necessary for accurate resource management decisions.

8. REFERENCES

Eythórsson, J., and Sigtryggsson, H., 1971, The climate and weather of Iceland: in The Zoology of Iceland, v. I, pt. 3, p. 1-62.

Fridriksson, S., and Pálsson, J., 1970, Landgraedslutilraun á Sprengisandi: Islenzkar Landbúnadar Rannsóknir, v. 2, no. 2, p. 34-49.

Friedman, J. D., Williams, R. S., Jr., and Pálmason, G., 1968, Infrared sensing of active geologic processes: in Proc. Fifth Symp. on Remote Sensing of Environment, Univ. of Mich., Ann Arbor, Mich., p. 787-820.

Friedman, J. D., Johansson, C. E., Oskarsson, N., Svensson, H., Thórarinsson, S., and Williams, R. S., Jr., 1971, Observations on Icelandic Polygon Surfaces and Palsa Areas. Photo interpretation and field studies: Geografiska Annaler, v. 53, ser. A, no. 3-4, p. 115-145.

Friedman, J. D., Williams, R. S., Jr., Thórarinsson, S., and Pálmason, G., 1972, Infrared emission from Kverkfjöll subglacial volcanic and geothermal area, Iceland: Jökull, v. 22, p. 27-43.

Saemundsson, K., 1969, Infrared imagery of Torfajökull thermal area: National Energy Authority Rept., Jan., Reykjavík, 22 p. (mimeo.)

Saemundsson, K., 1972, Jarðfraediglefsur um Torfajökulssvaedid: Náttúrufraedingurinn, v. 42, p. 81-99.

Thórarinsson, S., 1950, Jökulhlaup og eldgos á jökulvatnasvaedi Jökulsár á Fjöllum: Náttúrufraedingurinn, v. 20, p. 113-133.

Thórarinsson, S., 1963, Eldur í Öskju: Reykjavík, Almenna Bókafélagid, 101 p.

Thórarinsson, S., 1964, Sudden advance of Vatnajökull outlet glaciers 1930-1964: Jökull, v. 14, p. 76-89.

Thórarinsson, S., 1970, Hekla - A notorious volcano: Reykjavík, Almenna Bókafélagid, 62 p.

Thórarinsson, S., and Sigvaldason, G. E., 1962, The eruption in Askja, 1961 - A preliminary report: Amer. Jour. Sci., v. 260, p. 641-651.

Thórsteinsson, I., 1972, Gródurvernd: Reykjavík, Rit Landverndar 2, Reykjavík, 128 p.

Williams, R. S., Jr., 1972, Satellite geological and geophysical remote sensing of Iceland: in Proc. Eighth Intl. Symp. on Remote Sensing of Environment, Univ. of Mich., Ann Arbor, Mich., p. 1465-1466.

Paper G 11

PRELIMINARY ASSESSMENT OF GEOLOGICAL APPLICATIONS OF ERTS-1 IMAGERY FROM SELECTED AREAS OF THE CANADIAN ARCTIC

Alan F. Gregory, *Gregory Geoscience Ltd., 909 Richmond Road, Ottawa K2A OG8 Canada*

1. Use vs Practical Application of ERTS Data:

ERTS-1 data are surrogates for information about the environment and its resources. Interpretation gives meaning to such remotely-sensed data and thus is crucial to understanding the benefits that may accrue from the whole activity.

Three levels of interpretation may be recognized and often may be employed to derive information from a single image or data format:

(1) rapid recognition, or interpretation of obvious or self-explanatory information. This level of interpretation may be undertaken by anyone who has an appreciation of scale, maps and regional geography.

(2) skilled interpretation. This level is discipline-oriented and may be carried out by a specialist or team of specialists. The interpretation is still relatively simple, often comprising only visual analysis, but it may include machine enhancement of major contrasts in spectral, spatial or temporal aspects of the data. Skilled interpretation depends upon local expertise and specialized knowledge about resources and the environment. It need not require geometric correction or special equipment and training, other than that normally received by specialists in their disciplines and in the methodologies of air-photo interpretation.

(3) automated interpretation, or spectral, spatial and temporal analysis. This level of interpretation is machine-assisted, complex and relatively expensive. The products are tables, print-outs, classifications and other data formats that must be validated by human knowledge and experience in order to provide useful information. The relevant methodologies are still largely experimental but they hold promise for providing much new information.

Interpretation per se is not an application, although it may use ERTS data. This is less a problem of semantics and more a problem of understanding. For example, anyone can use ERTS data by simply looking at an image, or other format, as an aesthetic exercise in art appreciation. On the other hand, when the observer begins to derive practical information from patterns and contrasts, such a "use" becomes a "potential application". It becomes a "practical

application" when the data are systematically acquired in order to meet recognized economic and social goals. Thus, research to see whether ERTS-data can be used for a certain purpose is not really an application, although obviously the data are being used. Accordingly, the criterion for practical application is an imminent return on society's investment rather than an addition to scientific knowledge. Obviously the cut-off point, if not the definition, is controversial.

In this practical context, the reality of applications for ERTS-data is determined by three factors: the timeliness of interpretation, the need for the derived information and the cost-effectiveness compared to other methods for acquiring comparable information. Of these three factors, the need for derived information can be assessed now in terms of current information systems that are being used to manage the environment and resources. Need, however, is a very imprecise concept and will, unfortunately, vary from user to user. The timeliness of simple levels of interpretation is readily apparent, especially when compared with interpretation of more voluminous data, for example from aerial surveys. Moreover, the needs for new data, new information and more sophisticated interpretation will develop more slowly. Cost-effectiveness may be unreliable at this early stage in the development of orbital sensing systems; but where else can one obtain myriad data for an area of 31,000 square kilometres at the cost of a few dollars?

In the last analysis, the practicality of any application depends on the user's need for some or all of the ERTS-data. Undoubtedly, the most immediate benefits will result from the simple methods of interpretation. However, in no way does this imply that the best applications or the greatest benefits will also accrue from those methods. Such judgements are best made in the light of history.

Within this framework of immediate practical application, there is much evidence that one immediate benefit from ERTS will be improved efficiency in planning for and operation of programs of regional geological mapping. The following results, which should be considered as tentative, were obtained by simple interpretation at the skilled level using MSS band 6 only. Images were acquired under both summer and early winter conditions in two areas of the Canadian Arctic for which geological and geomorphological mapping had been completed. No field work or other calibrative studies have been conducted specifically in support of this interpretation.

2. ERTS-1 Images for Northern Yukon

In the winter image of the Richardson Mountains (Figure 1), the patterns of infrared reflectance can be readily grouped into 5 classes (A to E on



2/OCT 9 C N66-39/W134-55 N N66-40/W134-55 MSS- 6 -D SUN EL17 AZ170 203-1089-P-2-A-P-0 CCRS E-1078-20092- 6

Figure 1. ERTS-1 image of Richardson Mountains area; early winter, Oct. 9/72; sun elevation, 17°; no geometric correction; MSS band 6.

Figure 1). B & D may be equivalent classes. By comparison with the preliminary geological map (Norris et. al., 1963); it is apparent that the class A reflectance pattern represents Cretaceous shales (crosshatched unit 13 on Figure 2), class B represents a group of upper Paleozoic and Mesozoic clastics (units 8, 9 & 12 on Figure 2), class C represents two Paleozoic carbonates (units 3 & 6 on Figure 2) and class D represents the same units as class B. Class E reflectance patterns represent poorly-drained alluvium overlying Cretaceous, and lesser Devonian, clastics. The A/B, B/C and C/D boundaries are fairly sharp and they coincide with geological boundaries of certain formations or groups of formations (c.f. Figures 1 & 2). The D/E boundary is not readily defined and no correlation with mapped features is apparent. Except in this latter case, the coincidence of boundaries is remarkable as may be demonstrated by superimposing a transparency of the ERTS image on the map at the same scale. There are several noticeable discrepancies; however, their causes have not yet been established. Such discrepancies may well represent geological features that were not indicated on the preliminary map. For example, sharp contrasts along the B/C and C/D boundaries (as indicated in green on Figure 2) suggest that these boundaries may be faulted contacts.

In the more highly folded rocks of the Ogilvy Mountains area (Figure 3), similar contrasts in lighology are not as clearly indicated by MSS band 6. The high reflectance patterns at F (Figure 3) represent three Paleozoic carbonates (units 5, 6 & 7 on Figure 2) similar to those represented by class C reflectances (Figure 1). However the high reflectances at G (Figure 3) also represent Precambrian quartizites, clastics and associated rocks. The Paleozoic and Mesozoic clastics are separable from the above rocks on the basis of reflectance (compare H and I with F and G on Figure 3). Indeed, with further experience the separation of Paleozoic clastics (at H, Figure 3) from Mesozoic (at I, Figure 3) may be feasible. South of the map area (Figure 2), the highly reflective classes appear to comprise a wide variety of rocks (c.f. Green, 1972). Investigation of the multispectral characteristics of these rocks has not yet been undertaken. The characteristic patterns used in classifying the reflectances for MSS band 6 are also present on the summer images, although they are much less apparent (compare "a" on each of Figures 3 & 4).

Structural elements for all of these rocks are clearly portrayed on the early winter imagery (compare Figures 2 & 3). In particular, note the folds and faults (such as indicated in green on Figure 2) which were not recorded on the preliminary geological map. Many of these structural elements are also visible on summer imagery although commonly with less clarity (compare Figures 3 & 4). Also note that the incised valleys of the lower Peel River (at "b" on Figure 1) are emphasized on the early winter imagery. On other ERTS-images of Arctic terrain, such features as drumlins, eskers and glacial flutings

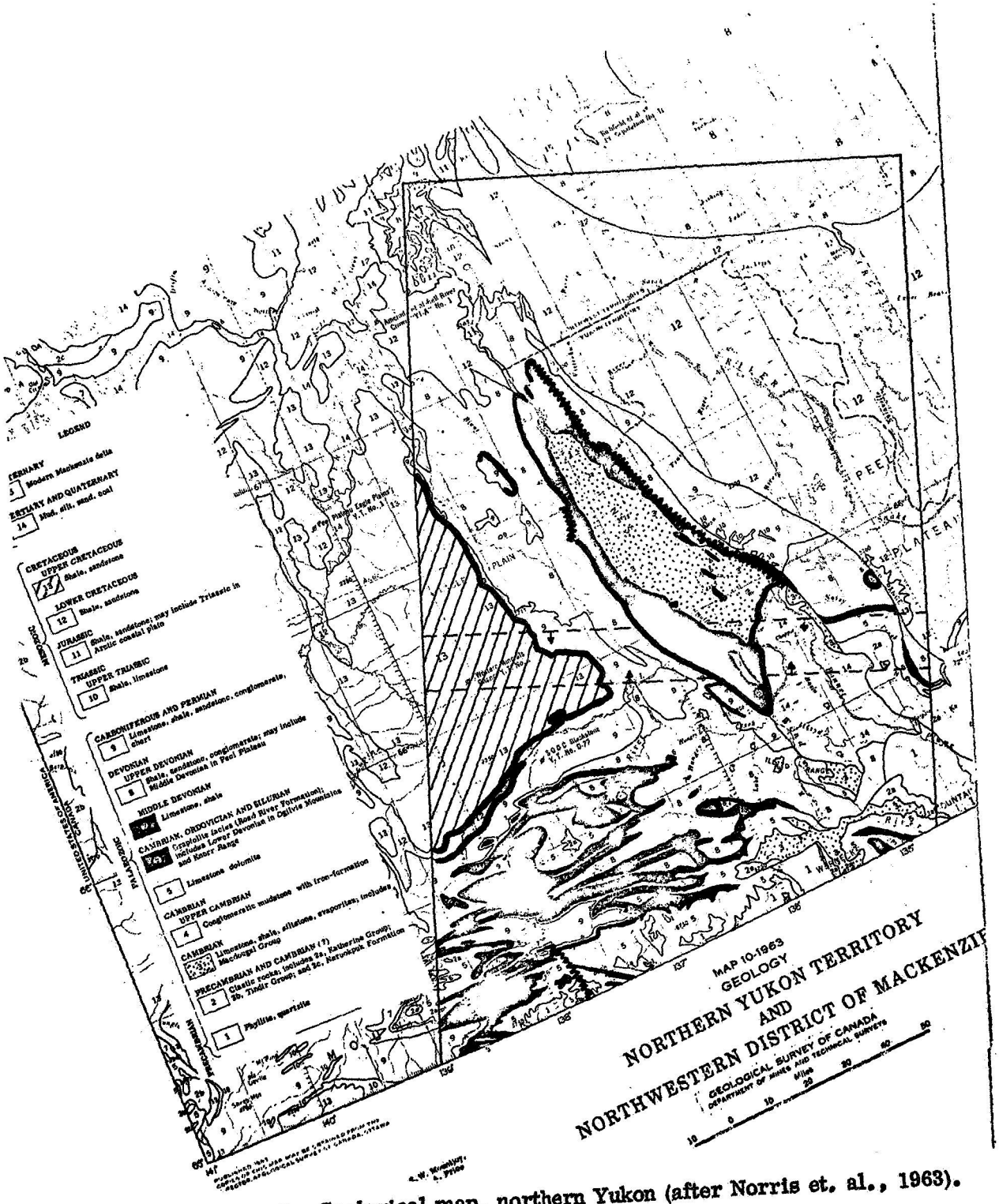
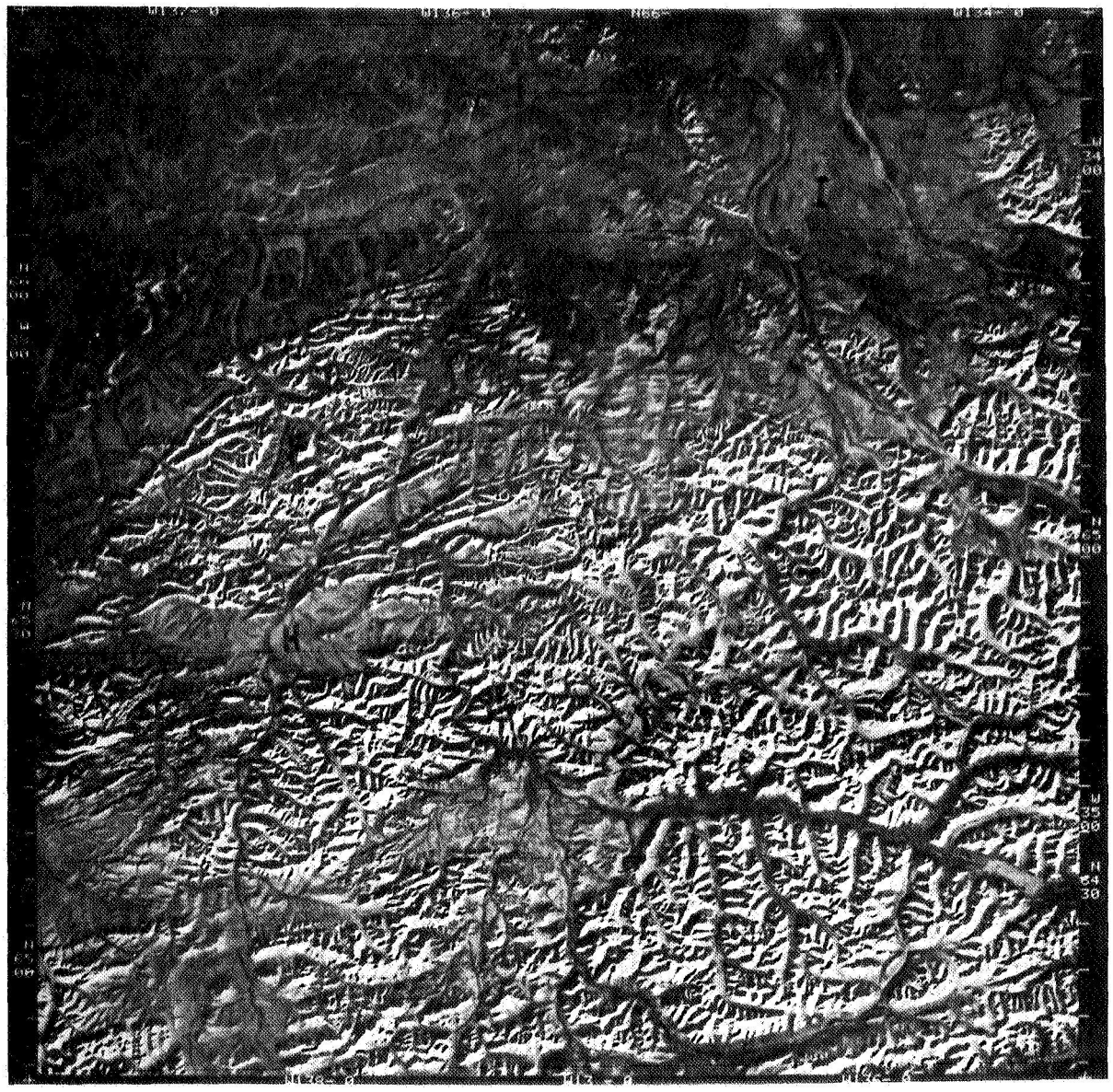


Figure 2. Geological map, northern Yukon (after Norris et. al., 1963).



72/OCT/ 9 C N65-18/W136-24 N N65-19/W136-24 MSS- 6 -D SUN EL18 AZ169 202-1089-P-1-A-P-0 CCRS E-1078-20894- 6

Figure 3. ERTS-1 image of Ogilvie Mountains area; early winter, Oct. 9/72; sun elevation, 18°; no geometric correction; MSS band 6

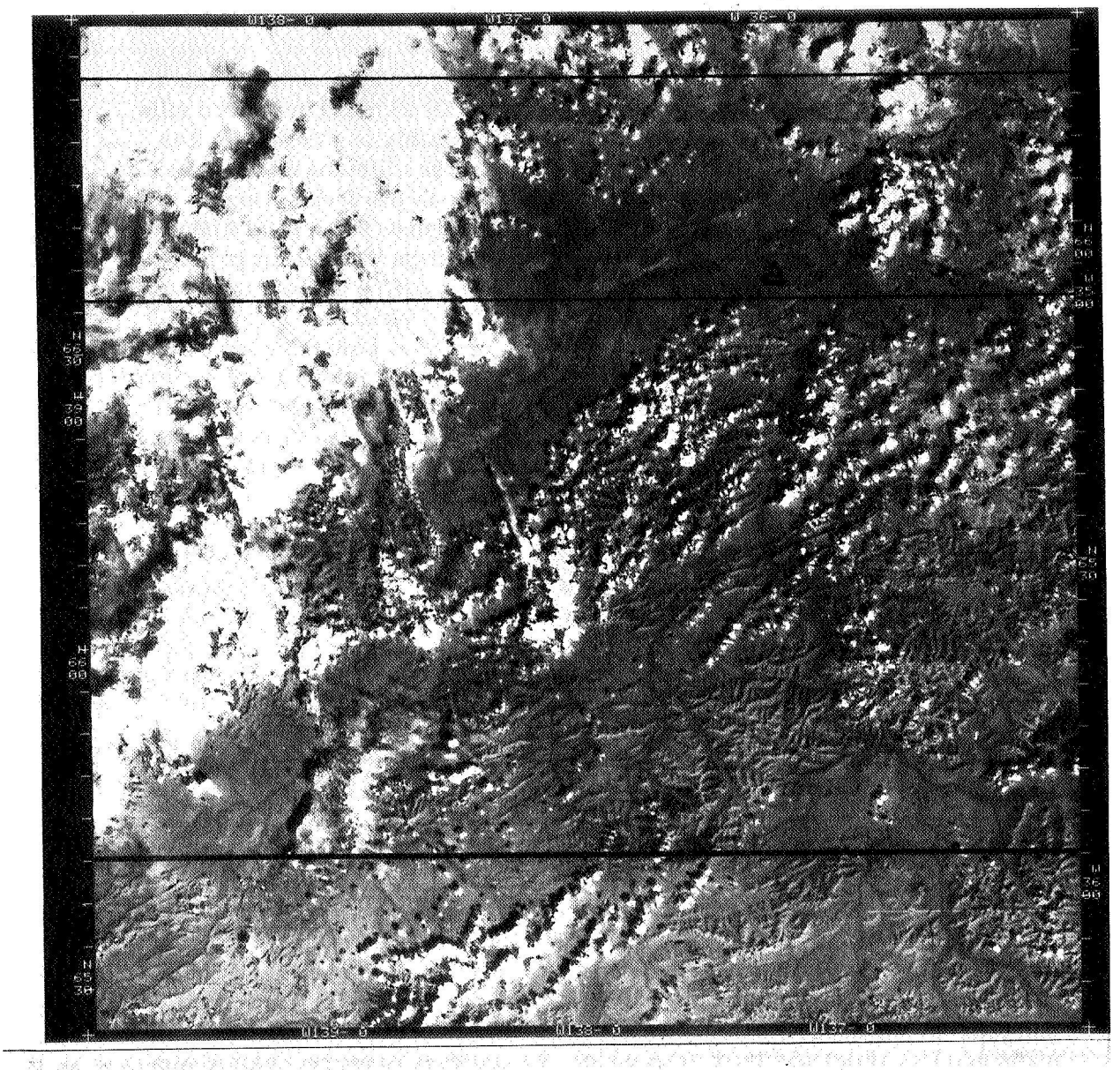


Figure 4. Image of Ogilvie Mountains area; summer, July 30/72; sun elevation, 42°; no geometric correction; MSS band 6.

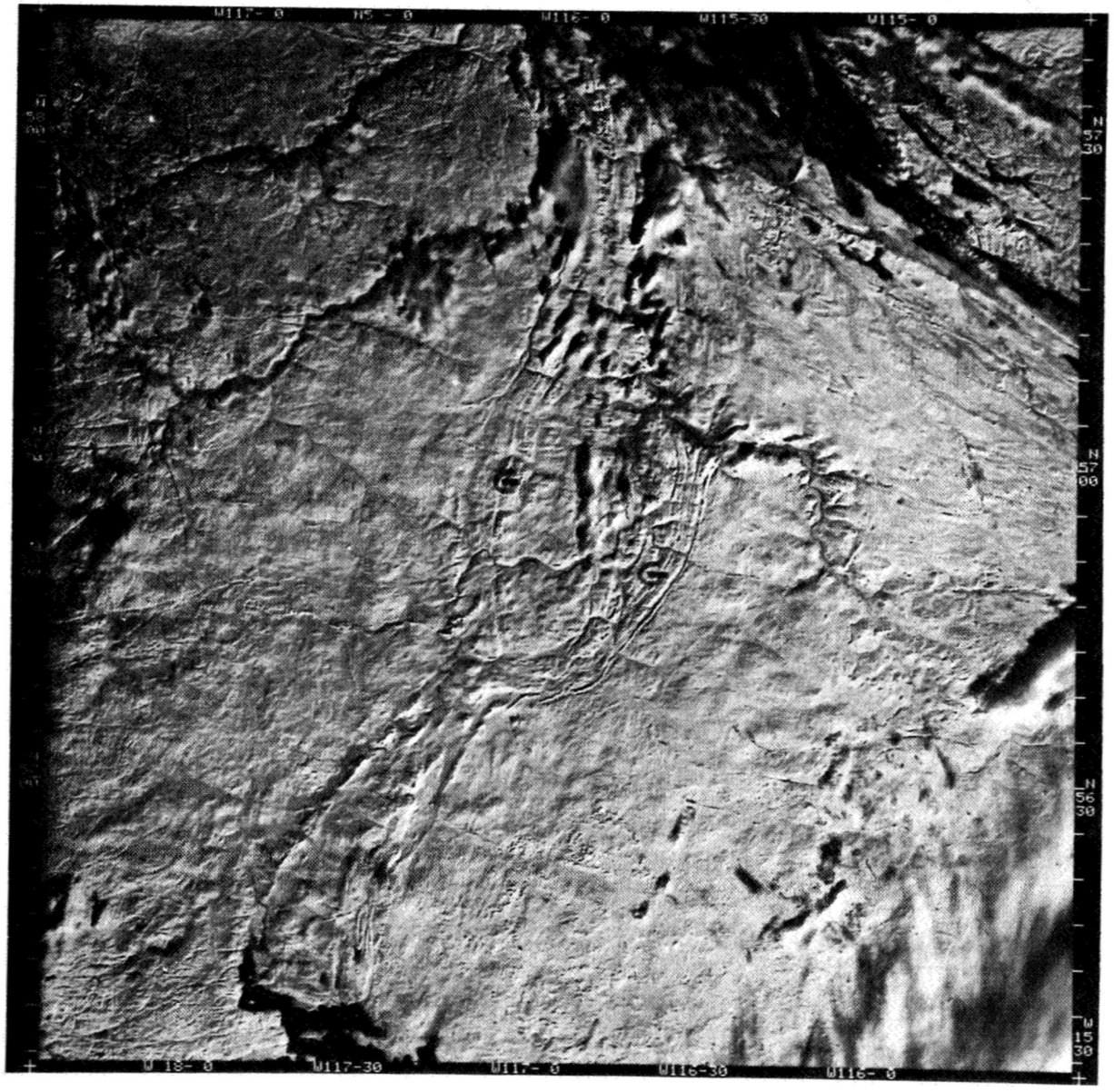
also appear to be best displayed on early winter images. On the other hand, morainic topography and oriented lakes are most clearly seen on summer images.

3. ERTS-1 Images for Bathurst Inlet area, N. W. T.

The winter image of the Bathurst Inlet area (Figure 5) clearly reveals the folded basin of Proterozoic sediments which is partly rimmed by gabbro sills (Figure 6). These Proterozoic rocks lie uncomformably on steeply dipping Archean gneisses, granites and metasediments. The sills commonly have a relief of 100-200 feet but occasionally form hills up to 800 feet in height. Note that stratification of the Goulborn quartzite (G in Figures 5 and 6) is well displayed and that the direction of dip can be inferred from the outcrop patterns of marker horizons. A number of folds and faults are visible in the Proterozoic, especially the major scarp of the Bathurst Fault zone which has relief of 300 to 1000 feet. Several interpreted and previously unmapped faults are indicated (in green on Figure 6). Many other linear features are also visible in the Archean rocks. Some of these coincide with mapped faults; others probably represent faults and joints that are not indicated on the preliminary map. These features are best displayed where associated relief is of the order of 100 feet or more. Several gabbro dykes with relief of about 100 feet are also visible on the image (compare Figures 5 and 6) although most dykes are not apparent. Pleistocene deposits are also evident, particularly eskers which rarely exceed 100 feet in height. Most of these features are not visible on the summer image (compare common areas south-west of Bathurst Inlet on Figures 6 and 7).

The high infrared reflectance (A on Figures 7 & 8) of areas within the Coronation Gulf Lowlands (Bird & Bird, 1961) is the most prominent contrast in terrain reflectance of the summer image from Bathurst Inlet. Several areas outside the lowlands have similar reflectances (e.g. B and C on Figures 7 & 8). As outlined below, these contrasts are interpreted as the consequence of major differences in vegetative cover between the abundant vegetation in the lowlands and the sparsely covered to bare uplands.

The Mackenzie Uplands (Bird & Bird, 1961) comprise bedrock with a thin and discontinuous veneer of boulder-till. The well-drained surface supports only scattered tussocks of grass, patches of lichen and occasional marshy tundra. On the other hand, the Coronation Gulf Lowlands comprise clay-till and bedrock which are largely covered by marine silts at elevations less than about 400 feet above sea level (Figure 8). The surface is poorly drained and is covered by a relatively luxurious growth of vegetation (Bird & Bird, 1961). Grasses, sedge tussocks, marshy tundra and flowering plants are abundant. Woody shrub thickets are common, especially on the west side of Bathurst Inlet.



72/OCT/ 9 C N57-07/W116-30 N N57-08/W116-30 MSS- 6 -D SUN EL25 AZ162 197-1088-P-2-A-P-0 CCRS E-1078-18260- 6

Figure 5. ERTS-1 image; early winter, Oct. 9/72; sun elevation 25°; no geometric correction; MSS band 6

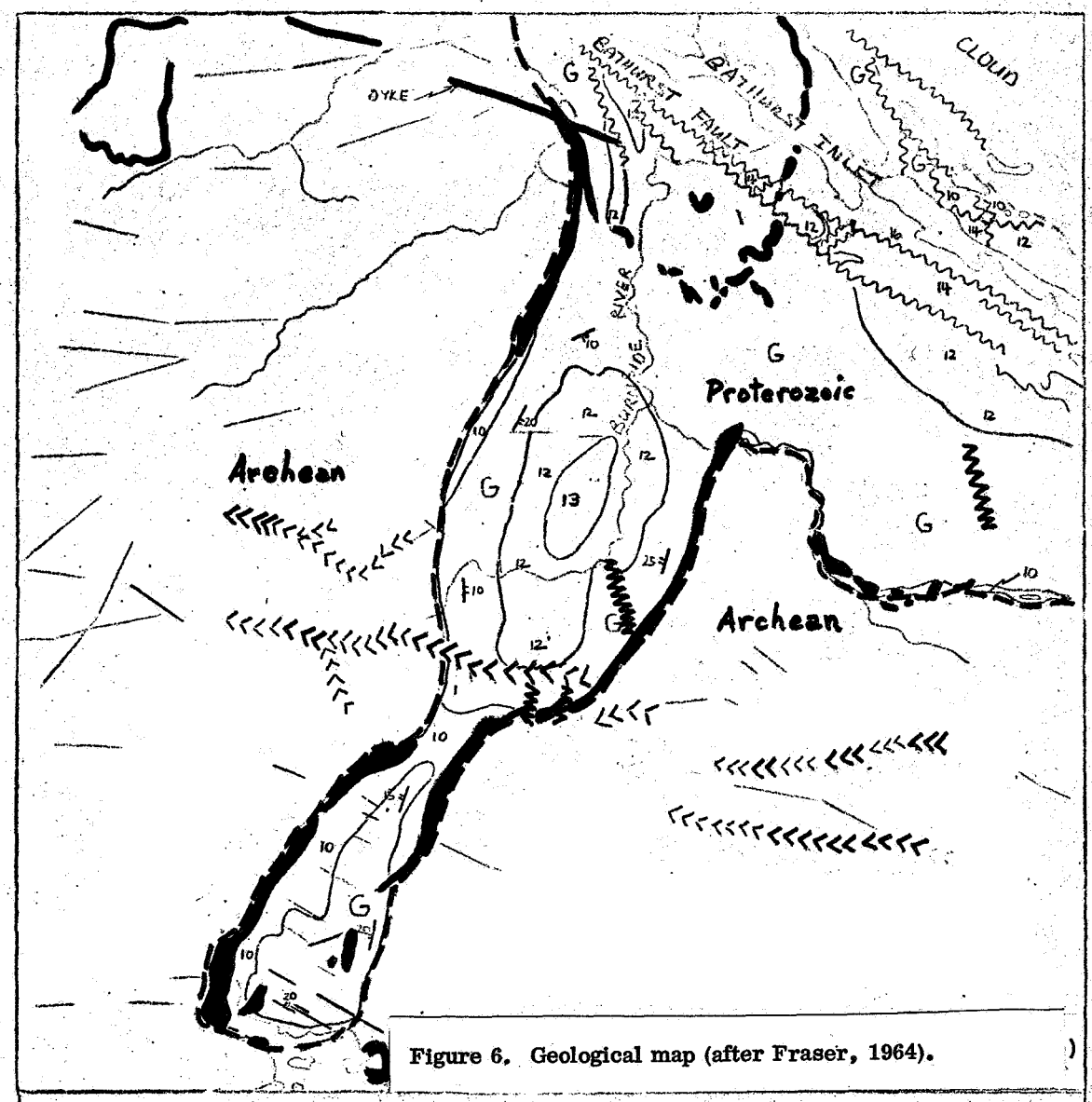


Figure 6. Geological map (after Fraser, 1964).

GABBRO SILLS & DYKES

16 SANDSTONE

14 SILTSTONE • ARGILLITE

13 DOLOMITE LIMESTONE

12 ARGILLITE

G GOULBOURN QUARTZITE

10 ARGILLITE

FAULT (MAPPED, **INTERPRETED**)

BEDDING

UNCONFORMITY AT BASE OF PROTEROZOIC

ESKER (MAPPED, **INTERPRETED**)

LINEARS JOINTS FAULTS (MAPPED, INTERPRETED)

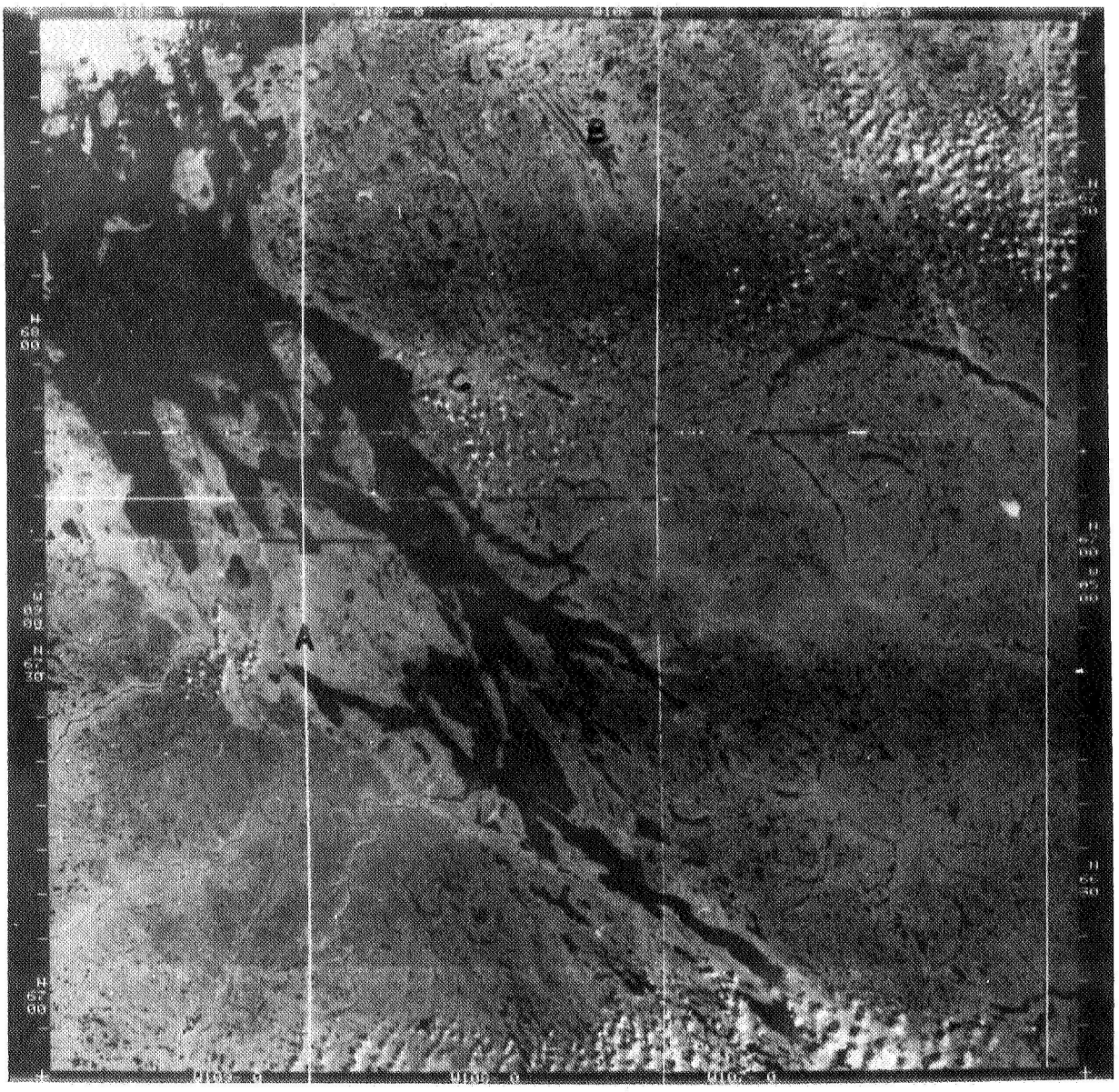


Figure 7. ERTS-1 image; summer, July 28/72; sun elevation 41°; no geometric correction; MSS band 6

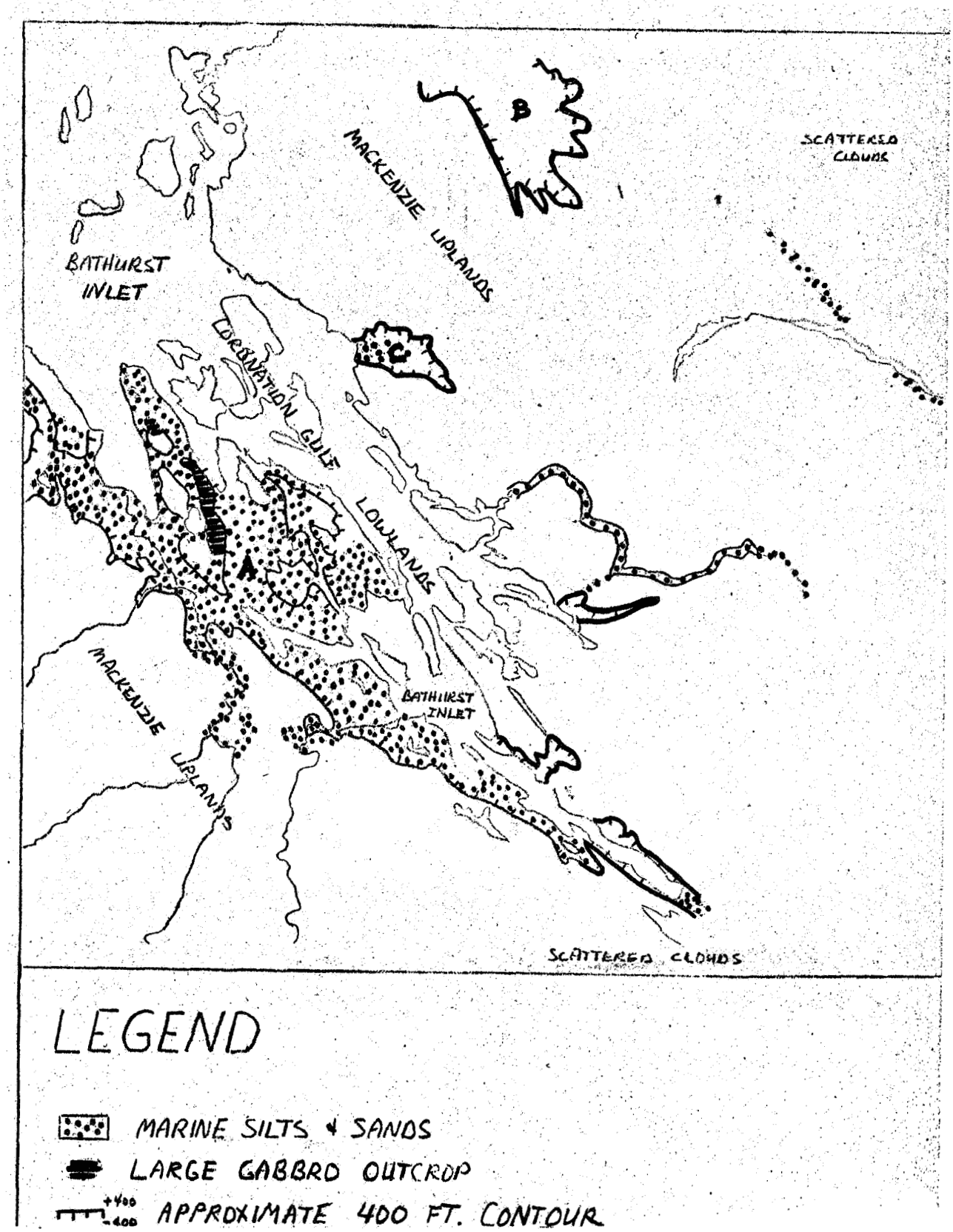


Figure 8. Map of selected surficial features (after Bird & Bird, 1961, & Fraser, 1964).

The highly reflective area at B (Figure 8) coincides with a greenstone belt surrounded by granitic gneisses. In view of the prevalent surficial deposits and low elevation, both at B and at other similar locations (in green, Figure 8), the high reflectances are interpreted as similar lowlands covered by marine silts and abundant vegetation. Several areas of low reflectance in the lowlands (north of A in Figure 7) correlate with large outcrops of gabbro.

4. Summary of Results

These preliminary interpretations indicate that early winter conditions are advantageous for observing some geological features in the Arctic because:

(1) the thin snow cover suppresses terrain "noise" from vegetation, soils, rocks and water and thus presents a uniformly reflective surface with irregularities that have geological and geomorphological significance;

(2) the low inclination of the sun accentuates textural patterns and surface irregularities with shadowing analogous to side-looking radar.

In conjunction, these two conditions of early winter serve to emphasize structure, relief and texture of the terrain surface. Where such features reflect rock-type, geological formations may be broadly classified and their boundaries delineated.

On the other hand, the summer imagery serves to delineate soil-vegetation complexes and the boundaries of water bodies more precisely than winter imagery.

In brief, both summer and early winter images provide common information useful to the geologist, but in addition each set of seasonal images provides equally useful information that is not readily derived from the other set.

5. Benefits from ERTS-1 Data

Programs of geological and geomorphological mapping for northern Canada are commonly planned in the winter and completed in about 3 months during the summer. For large areas, such rapid mapping usually requires a team of 5 or 6 professionals, support staff and several helicopters to assure representative sampling of all the rock formations. Gross structure may be outlined from aerial photos before field operations but is refined, augmented and corrected by field observations. Rock classifications depend on essential field and laboratory studies.

Had ERTS-1 images been available for the areas discussed in this paper, a significant saving in time and a more efficient mapping program might have been effected because the gross distribution of many geological and geomorphological features is readily apparent on a relatively few images. Thus ground traverses could have been more effectively organized to sample the area and to provide essential details that cannot be derived from ERTS-images. It is difficult to assess how much time might have been saved and used for other purposes. Accordingly, a realistic benefit/cost ratio is equally difficult to evaluate. However, the practicality of applying ERTS-data to assist regional mapping of both bedrock and surficial deposits seems assured despite the experimental nature of ERTS. Once a full set of seasonal coverages has been acquired for an area, that set will suffice for most geological purposes except dynamic phenomena (e.g. erosion, landslides, volcanism).

A further benefit to such mapping may accrue from enlargements of ERTS images. Preliminary assessment of enlargements to 1/250,000 and 1/100,000 suggest that they will comprise useful base maps for plotting data. Enlargements to 1/30,000 have been prepared to test their use as base maps for flying aerial surveys. Cartographic quality is not expected and the size of the geometric errors is currently being assessed.

6. Conclusions:

6.1 Immediate benefits can be achieved by simple interpretation of ERTS images to provide information about the structure and disposition of geological formations.

6.2 Simple interpretation of MSS band 6 provides no information about rock composition but, under certain limited conditions, it may assist in the broad classification of rocks.

6.3 Practical applications of ERTS-data will develop most readily where the underlying philosophy "goes beyond finding how to do things right in order to find the right things to do" (after Peter Drucker).

7. References

Bird, J. B. & Bird, M. B. (1961): "Bathurst Inlet, Northwest Territories", Memoir #7, Geographical Branch, Dept. of Energy, Mines and Resources, Ottawa

Fraser, J. A.: (1964) "Geological Notes on Northeastern District of Mackenzie, Northwest Territories", Paper #63-40, Geological Survey of Canada, Dept. of Energy, Mines and Resources, Ottawa

Green, L. H.: (1972) "Geology of Nash Creek, Larsen Creek and Dawson Map-areas, Yukon Territory", Memoir #364, Geological Survey of Canada, Dept. of Energy, Mines and Resources, Ottawa

Norris, D. K. et. al.: (1963) "Geology, Northern Yukon Territory and Northwestern District of Mackenzie", Map 10-1963, Geological Survey of Canada, Dept. of Energy, Mines and Resources, Ottawa

Norris, K. K.: (1963) "Light Helicopter Reconnaissance-Operation Porcupine, 1962", Canadian Mining Journal, vol. 84, #11, (November) pp. 45-50

Paper G 12

EXPLOITATION OF ERTS-1 IMAGERY UTILIZING SNOW ENHANCEMENT TECHNIQUES

Frank J. Wobber and Kenneth R. Martin, *Earth Satellite Corporation, Washington, D. C. 20006*

ABSTRACT

Photogeological analysis of ERTS-simulation and ERTS-1 imagery of snow-covered terrain within the ERAP Feather River site and within the New England (ERTS) test area provided new fracture detail which does not appear on available geological maps. Comparative analysis of snow-free ERTS-1 images has demonstrated that MSS Bands 5 and 7 supply the greatest amount of geological fracture detail.

Interpretation of the first snow-covered ERTS-1 images in correlation with ground snow depth data indicates that a heavy "blanket" of snow (e.g., > 9 inches) accentuates major structural features while a light "dusting", (e.g., < 1 inch) accentuates more subtle topographic expressions.

An effective mail-based method for acquiring timely ground-truth (snow-depth) information was established and provides a ready correlation of fracture detail with snow depth so as to establish the working limits of the technique. The method is both efficient and inexpensive compared with the cost of similarly scaled direct field observations.

The technique of snow enhancement appears to afford a simple [and no-cost] means of edge enhancement during the snow-covered periods. Increased tonal contrasts along the snow-covered/snow-free interface provide a form of natural edge enhancement for low resolution imagery. The investigators suggest that monitoring variation in snow melting and accumulation can supply unique fracture data unavailable during other seasons.

INTRODUCTION

Photogeological analysis has traditionally been conducted, whenever possible, using snow-free imagery on the assumption that snow-cover obscures geological features. This apparently results from a "no leaves and no snow" philosophy which has served as a criterion for successful aerial data acquisition and which may be extended to analysis of ERTS-2 imagery.

The principal investigator recently suggested that imagery of snow-covered terrain was a much under-utilized source of photogeological data. This report is an up-to-date review of the value and application of the technique for small-scale low resolution image analysis. It describes the spectral bands most useful for enhancing geological features in snow-covered terrain, presents a preliminary evaluation of supplemental image enhancement techniques and demonstrates snow enhancement as a photogeological technique.

It is anticipated that the early reporting of these results will both introduce scientists to a usable photogeological technique, and provide a useful forum for an interchange of ideas on the phenomena of snow enhancement.

BACKGROUND

That snow cover may actually be utilized as a photogeological tool to identify fracture traces and faults (particularly under conditions of low solar illumination) was proposed by the Principal Investigator following analysis of Gemini, Apollo and Nimbus photography. He suggested that monitoring snow cover variations in combination with low angle solar illumination may serve to accentuate subtle fracture traces and increase the detectability of topographically - expressed but subtle geological structure.

Seasonal snow cover served as a photogeological tool for Woloshin (1965) and Lowman (1967) to detect the extension of a fault in the East Sayan Mountains of the USSR. Recently, several previously unmapped fractures and faults in Alaska and western Canada were discovered utilizing heavily snow-covered Nimbus imagery.

The investigators noted from analysis of Apollo photography that fracture lineaments were frequently accentuated by the marked black and white tonal contrasts, i.e., between the dark-toned lineaments and the bright white tones of adjacent snow-capped rocks. Snow enhancement served as an especially useful technique for exploiting low resolution imagery. The technique has been made available to the

mineral industry as a step leading to cost-benefit analysis of ERTS-1 technology.

Geological structure and lithology exert a strong influence on surface relief. Fractures (joints and faults) are usually more easily eroded than surrounding rock, producing linear to curvilinear surface depressions which are frequently imaged with dark-tones. Utilizing imagery with snow cover, fractures stand out in contrast to surrounding terrain because of (a) an absence of snow cover, (b) accentuaton of variations in vegetative cover, and/or (c) shadowing. The apparent absence of snow cover is attributed to accelerated melting rates induced by the higher moisture content of subsurface materials in fracture zones or, the obscuration of snow cover by vegetative overstory. Low angle solar illumination provides a pseudo-radar effect and produces shadows which emphasize subtle relief differences.

Gray scale variances introduce unnecessary background detail which slows the photogeologist during his interpretive process. Snow-covered terrain tends to reduce background "noise", thereby simplifying the interpretation process. For example, grass covered areas present a uniform and homogeneous appearance when the ground is thickly snow-covered. The accompanying reduction in overall gray scale variance with snow cover reduces the threshold of lineament detection, increases the total number of identifiable lineaments, and reduces the number of "decisions" necessary for automated machine processing. Additionally, increased tonal contrasts along a given snow-covered/snow-free interface provide a form of natural edge enhancement for low resolution imagery.

New snowfall patterns or differential snow melting patterns within unfrozen materials are diagnostic of variations in the moisture content (and hence thermal properties) of surface and subsurface materials. This is significant in that fracture zones commonly have higher moisture contents than surrounding materials.

DESIGN AND ANALYSIS

The investigators are employing a low cost method for obtaining ground truth information. A somewhat low density snow depth reporting network was organized within western Massachusetts and Connecticut with assistance from the National Weather Service. A higher density newwork was subsequently developed by contacting newspapers within both the primary New England test area (Massachusetts and Connecticut) and the secondary test area in Maryland and Virginia to enlist public support. Newspapers in areas lacking snow depth observers were selected to feature an article briefly describing the ERTS Program, the Snow Enhancement Experiment and appeal for public support.

Significant public interest in the experiment and ERTS Program was found to exist. Readers have written to express a desire to participate as snow depth observers. These observers have supplemented the existing network (coordinated by EarthSat) which continues to report snow depth data on a weekly basis. Compilation of snow depth data on 1:250,000 scale photo base maps facilitates comparison of fracture data yield with snow depth for the purpose of defining the optimum conditions for snow enhancement.

In addition to manual analysis of snow-covered imagery, several viewing techniques are being utilized to speed acquisition of fracture data from ERTS-1 imagery of snow covered areas. The techniques include additive color presentations, film sandwiching, Ronchi grating and optical edge enhancement. Oblique imaging from light aircraft under integrated conditions of snow cover and low angle solar illumination, provided additional opportunities to detect subtle lineaments. Preliminary evaluations of these techniques are discussed in the following section.

RESULTS

Photogeologic analysis ERTS-simulation and ERTS-1 imagery of snow-covered terrain with the ERAP Feather River Site and within the New England (ERTS) test area provided new fracture detail which did not appear on available geological maps. Analysis of snow-free ERTS-1 images (1096-15065 and 1096-15072) indicates that numerous lineaments can be mapped; analysis of comparative ERTS-1 imagery during snow-covered periods allows for more rapid fracture analysis and provides additional fracture detail (Figure 1).

ERTS MSS/Bands 5 and 7 were determined (by comparative analytical tests) to supply the greatest quantity of fracture detail. MSS Band 4 supplied the least detail; MSS Band 6 closely approximated the data yield of Band 7. Considering these results in conjunction with analysis of ERTS-simulation imagery, it is suggested that the red region (approximately 580-700nm) is the optimum visible spectral region for fracture analysis. The infrared portion of the spectrum best suited for fracture mapping was the 800-1100nm (Band 7) spectral region which provided greater tonal contrast than the 700-800nm (band 6) region.

Additive (false) color viewing yielded unique information on fracture-related vegetative cover. Optical edge enhancement (Digicol), film sandwiching and use of a Ronchi grating have all been found to

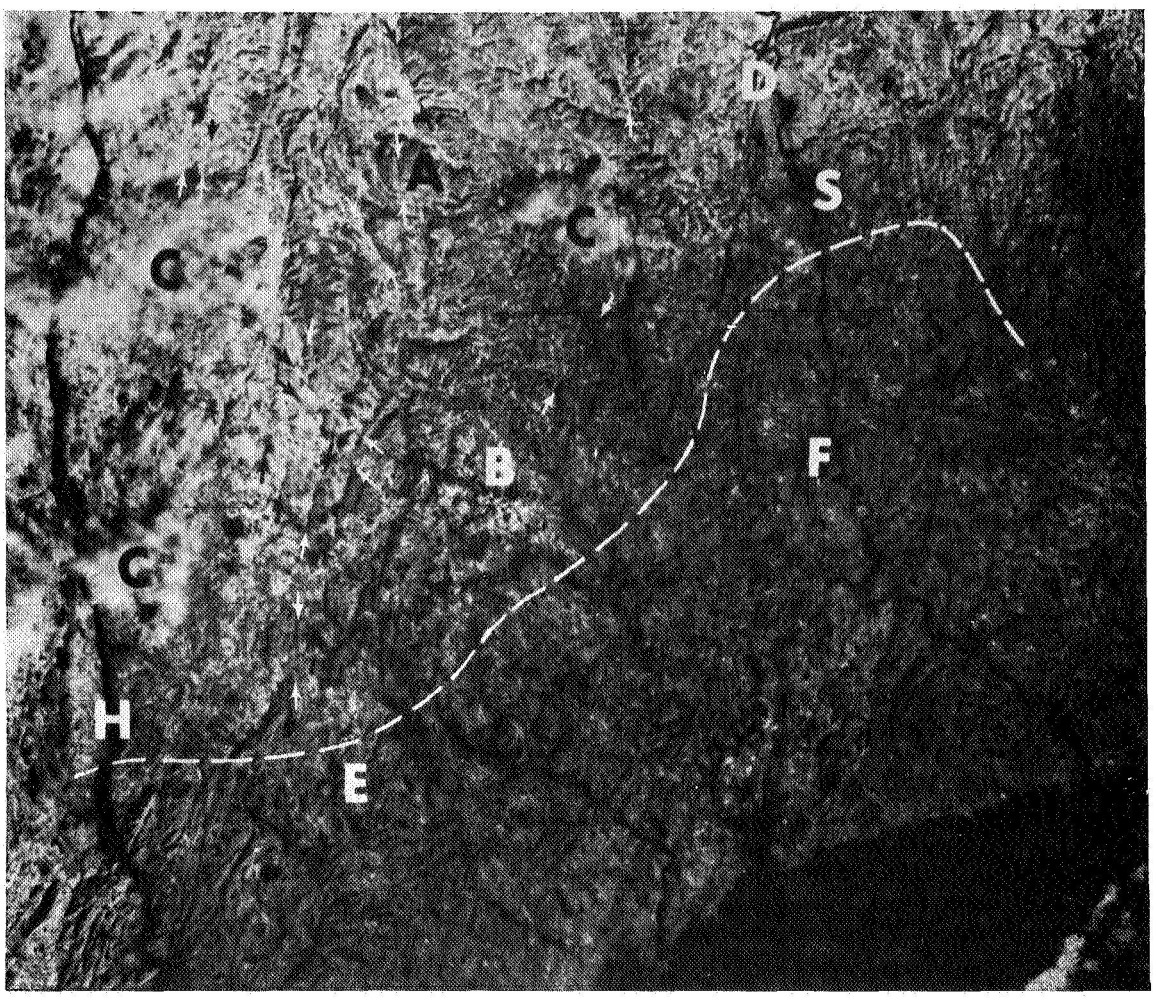


FIGURE 1: ERTS-1 image (1132-15074-7) at 1:1,000,000 scale acquired on December 2, 1972. The imaged area is partially snow-covered and includes Connecticut, southwestern Massachusetts and the eastern edge of New York. The southern limitation of snow cover is indicated by a dashed line. Geographic reference points include Hartford, Connecticut (F), Springfield, Massachusetts (S), the Hudson River (H) and Mount Tom (D). Partial cloud cover (C) obscures ground detail, but can be distinguished from snow cover following careful image analysis. Based on field observations, snow depths vary from <1 inch just north of the line to 9 inches in the northwestern corner of the photo. Low angle solar illumination (22 degrees) accentuates subtle topographically expressed features (E) not as easily detected with a higher sun angle. Northwesterly trending thrust fault blocks (A) are accentuated by a thick (approximately 9 inches) snow cover. Light-toned (snow-enhanced) lineaments (B) approximate the direction of recorded glacial striations and are probably of glacial origin. Dark-toned (snow-free) lineaments (arrows) represent a small sampling of mappable lineaments within the snow-covered areas. A complete analysis is now in progress. Lineaments will be confirmed through subsequent geological validation procedures. Analysis was confined to the area of greatest snow visibility within the western portions of Connecticut and Massachusetts.

conditionally yield additional fracture information, but further study is needed to more completely define the utility of these techniques for fracture discrimination.

Preliminary correlation of selected fractures with snow depth ground data indicates that snow depth greater than was anticipated by the investigators (e.g. $>$ 9 inches) provides significant topographic enhancement. It now appears that thick cover of snow (e.g. $>$ 9 inches) accentuates major topographically expressed geological features e.g., thrust faults (Figure 1), while a light "dusting" (e.g., $<$1 inch) accentuates subtle fracture trends. The importance of snow depth in controlling the detectability of geological structures will be more fully defined following receipt and analysis of additional ERTS-1 data.

Low angle solar illumination produced topographic shadowing which emphasized subtle relief differences not as apparent on snow-free imagery collected during autumn. Factors such as density and type of vegetative cover and texture and permeability of surface materials influence the enhancement capabilities of snow cover and have yet to be studied in detail.

ANTICIPATED BENEFITS

The investigators are testing benefits that may be realized through practical application of snow enhancement techniques. For example, commercial flying firms may extend the period (from snow-free into snow-covered periods) during which satisfactory images for selected photogeological studies can be acquired. In geological reconaissance, bedrock outcrops may be more readily located under conditions of differential snow cover, i.e. increased snow free/snow cover tonal contrasts. Fracture data derived from the experiment will be provided to the Boston office of the U.S. Geological Survey who have been mapping the area for over 8 years.

The Principal Investigator suggests that snow enhancement is a simple and no-cost form of edge enhancement, i.e., it can be useful in place of costly electronic edge enhancement in some cases. It is also suggested (but not adequately tested) that snow enhancement will simplify automated recognition of other geological features. For example, the density (or absence) of overstory controls the amount of ground snow cover which can be aerially sensed and therefore the spectral return of geobotanical indicators of mineralization. Certain cultural features such as airport runways and highways could be identified on snow-cover imagery, but not on snow-free imagery of comparable resolution. This was attributed to the high contrast of the dark-toned snow free surfaces with the adjacent light-toned snow piles.

Navigational benefits have already been realized by the investigators in ERTS field checking.

Extension of snow enhancement techniques from temperate areas to areas of permanent snow cover for acquisition of geological data is likely. This seems particularly true since relatively deep snow (e.g.> 9 inches) was found to enhance certain topographic features indicative of geologic structure.

ACKNOWLEDGEMENTS

The Principal and Co-Investigator acknowledge the contributions of Dr. Paul Lowman, Scientific Monitor, and Mr. Arthur Fihelly, Technical Monitor for their continuing interest in the study. Mr. Roger Amato, Ms. Marge Kolar, and Mr. Luis DeMendoza of EarthSat are contributors to the study.

REFERENCES

Lowman, P., 1967. "Geologic Applications of Orbital Photography." NASA Technical Note D-4155. Goddard Space Flight Center. 25pp.

Wobber, F. J., 1969. "Environmental Studies using Earth Orbital Photography," Photogrammetria. Vol. 24, No 3/4, pp. 107-165.

Wobber, F. J., and Martin, K., 1972a. "Exploitation of Aircraft and Satellite Imagery Using Snow Enhancement Techniques." Presented to the International Geological Congress, Montreal, Canada. August, 1972.

Wobber, F. J., and Martin, K., 1972b. "Utilizing Snow Cover for Accentuating Geological Fracture Systems: A New Photogeological Technique," World Mining. Vol. 25, No 12. p. 55-89

Woloshin, A., 1965. "Notes on Geologic Interpretation of Nimbus AVCS Image of Southern California," in Multisensor Imagery Collection, U. S. Army Corps of Engineers for NASA Earth Resources Survey Program, pp. 189-191.

Paper G 13

MAPPING QUATERNARY LANDFORMS AND DEPOSITS IN THE MIDWEST AND GREAT PLAINS BY MEANS OF ERTS-1 MULTISPECTRAL IMAGERY[1]

Roger B. Morrison, *U. S. Geological Survey, Denver, Colorado;* George R. Hallberg, *Iowa Geological Survey, Iowa City, Iowa*

Abstract

ERTS-1 multispectral images are proving effective for differentiating many kinds of Quaternary surficial deposits and landforms units in Illinois, Iowa, Missouri, Kansas, Nebraska, and South Dakota. Examples of features that have been distinguished are: the more prominent end moraines of the last glaciation; certain possible "palimpsests" of older moraines mantled by younger deposits; various abandoned river valleys, including suspected ones deeply filled by deposits; river terraces; and some known faults and a few previously unmapped lineaments that may be faults. The ERTS images are being used for systematic mapping of Quaternary landforms and deposits in about 20 potential study areas (mostly 1° x 2° in size) within the project area. Some study areas, already well mapped, provide checks on the reliability of mapping from the images. For other study areas, previously mapped only partly or not at all, our maps will be the first comprehensive, synoptic ones, and should be useful for regional land-use planning and ground-water, engineering-geology, and other environmental applications.

This project is testing the applicability of ERTS-1 images for identifying and mapping Quaternary surficial deposits and landforms in six Great Plains-Midwest States - Illinois, Iowa, Missouri, Kansas, Nebraska, and South Dakota. Among the features we are looking for are end moraines of the last glaciation, terrace sequences along the main rivers, and middle or early Pleistocene glacial moraines and valleys that have been buried beneath younger glacial drift, loess, or eolian sand.

[1]Publication authorized by the Director, U.S. Geological Survey.

The geological surveys of the six States are collaborating on the project and the State geologists are coinvestigators. Twenty-four potential study areas, mostly 1° x 2° in size and covering a total of 155,000 square miles, have been selected for intensive study (Fig. 1). Each study area is of current interest to the respective State's geological survey. Those areas that are already well mapped will provide checks on the reliability of our mapping from the ERTS images. For other study areas, previously mapped only partly or not at all, ours will be the first, comprehensive maps; they should be useful for regional land-use planning and for groundwater and other environmental applications.

The investigation of each area progresses through six phases. Phase 1 consists of preliminary mapping of geologic and geomorphic features using only ERTS imagery. Higher phases involve published and unpublished ground truth data, and, from repetitive ERTS imagery, additional data revealed by changes in time-variant phenomena such as vegetative cover, soil-moisture conditions, plowing of croplands, and snow cover. Phase 6 is the delineation of the new information detected from the ERTS imagery.

To date, we have received only 70 mm positive transparencies and some 70 mm negatives that are mostly too dense to produce satisfactory enlargements with the equipment we have. We examine the positive transparencies under 8X to 10X magnification, and in some cases with an I^2S Mini-Addcol additive color viewer. In order to provide a photographic base for mapping

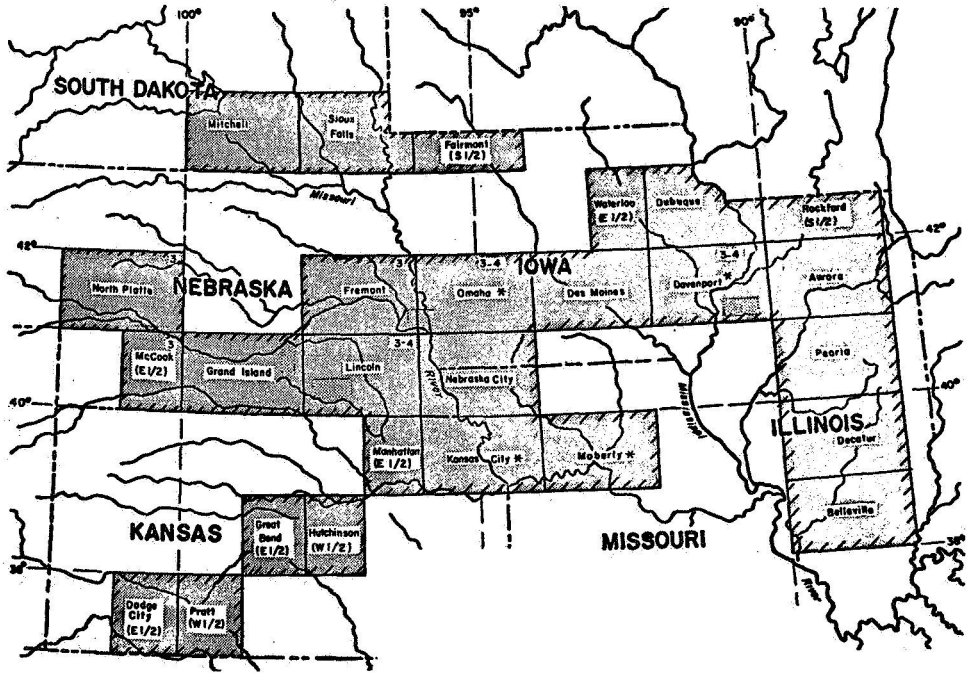


Fig. 1. Map showing the potential study areas in the Great Plains-Midwest regi

geologic-terrain features, we originally prepared negative enlargement prints from the 70 mm positives, at scales ranging from 1:1,000,000 to 1:250,000. Now, however, we are using internegatives prepared from the 70 mm positives to make enlarged positive prints. We believe that it would be more efficient and productive if we use 9" x 9" positive transparencies under a zoom transferscope and mapped our interpretations directly onto our base maps, but to date we have received very few of the large transparencies.

Problems that have hampered this investigation are the ubiquitous vegetative cover during the growing season throughout the Great Plains-Midwest, the exceptionally rainy and cloudy summer and fall, and attendant commonly poor atmospheric conditions. During the summer growing season, crops and natural foliage in the pastures and woodlands greatly obscure information about the geology, soils and even the smaller topographic features. In the summer images, the "red" MSS band 5 was the most useful for interpreting geologic-terrain units. In the fall images, the infrared bands have become more important because the total infrared response from crops and natural vegetation has decreased. Spring imagery should yield the most information about soils, surficial deposits and landforms

We are quite pleased with the potential afforded by ERTS images for differentiating and mapping geologic-terrain units at scales of 1:250,000 and smaller. Resolution and detectibility are surprisingly good. Rural "section line" roads, typically 60 to 80 feet wide (including roadbed, shoulder, ditches, and backslope) generally can be identified, thus enabling precise location of features. We find that the main landform associations and larger landforms generally are quite distinct on the better ERTS images, and commonly the gross associations of Quaternary surficial deposits also can be differentiated. It is appropriate to point out that for the interpretation of geologic-terrain features from small-scale images like these, rarely are there "unique signals"; instead, we must deal with differences that commonly involve small, subtle changes in several components of an image, for example, in tone, texture, pattern, hue, and chroma. We interpret landform types by analyzing stream dissection and drainage patterns, stream-divide relations, and land-use patterns. Interpretation of surficial materials is more difficult than that of landforms and generally involves secondary and tertiary levels of inference. Thus, a considerable input of "ground truth" is essential to control the inferences if a reliable map is to be produced. The ground truth may come from published geologic maps, unpublished maps and file data, subsurface data (drill-hole logs), and from field studies by ourselves and our collaborators in the State geological survey.

Among the features that have been identified are the major outwash channels and moraines formed during the last galciation, such as the Bloomington and Shelbyville moraine systems in Illinois and the Bemis and Altamont moraine systems in Iowa and South Dakota. Much less evident are moraines of earlier glaciations. These invariably are severely eroded and buried beneath variable thicknesses of loess and other sediments. Synoptic analysis

of drainage and stream-divide patterns and degrees of stream dissection is helpful in detecting anomalies that may signal buried moraines. This analysis is greatly facilitated by the comprehensive mega-views provided by the ERTS images. From analysis of drainage and stream-divide patterns in Nebraska, Kansas, Iowa, and Missouri, we have been able to identify several pre-Wisconsin moraine systems that already are fairly well known, mainly from borehole data. Also, several other similar anomalies that have been found in these States may indicate previously unrecognized pre-Wisconsin moraine systems.

Similar analysis has proved useful for detecting abandoned river valleys, especially ancient filled ones which are hard to identify. Several known filled valleys and a few possible ones have been found.

Figure 2 is typical of the preliminary maps prepared during the earlier phases of our program of investigations. The map, a composite of two of our study areas (the North Platte 1° x 2° quadrangle and the eastern half of the McCook quadrangle), is representative of both the Sand Hills and the High Plains of western Nebraska. Although coverage by satisfactory ERTS images still is incomplete, and limited mostly to images obtained during the growing season, vegetative cover in this semiarid region is less of an impediment than in the more humid region to the east. Analysis of both land-use patterns and stream-dissection/stream-divide patterns has enabled mapping the major geologic-terrain units. On the best image of the Sand Hills portion, the larger dunes and interdune depressions can be distinguished clearly. The infrared bands afford a synoptic register of the water-level status of the myriad ponds and marshes in this area, and thereby an up-to-date inventory of ground water conditions. Hydrologists lately have become concerned about possible depletion of ground-water by overpumping in some parts of the Sand Hills.

Figure 3 is a reduction and generalization of a preliminary map of the Lincoln, Nebraska, 1° x 2° study area. This area is typical of the transition zone between the unglaciated eastern Great Plains and the Central Plains that were glaciated during the middle and early Pleistocene. This map shows not only the major classes of geologic-terrain units that can be differentiated from the ERTS images but also several of the rather obscure buried features that we are trying to find. The trend-lines of three ancient moraine systmes are revealed by anomalous drainage and stream-divide relations. The moraines, of Kansan and perhaps greater age, were much eroded before being covered by loess; thus, they are not very obvious. An aberrant stream pattern near Lincoln also reveals a buried valley. These features have been substantiated by surface and drill-hole data collected by the Nebraska Geological Survey.

A 10,000 square-mile area extending from Des Moines to 30 miles west of Omaha has received the most study to date (Fig. 4). Only a few of the more significant features are shown. The most prominent boundary in the north-eastern part is that between the area covered by ice as recently as 14,000 to 13,000 years ago (the Des Moines glacial lobe) and the older landscape in

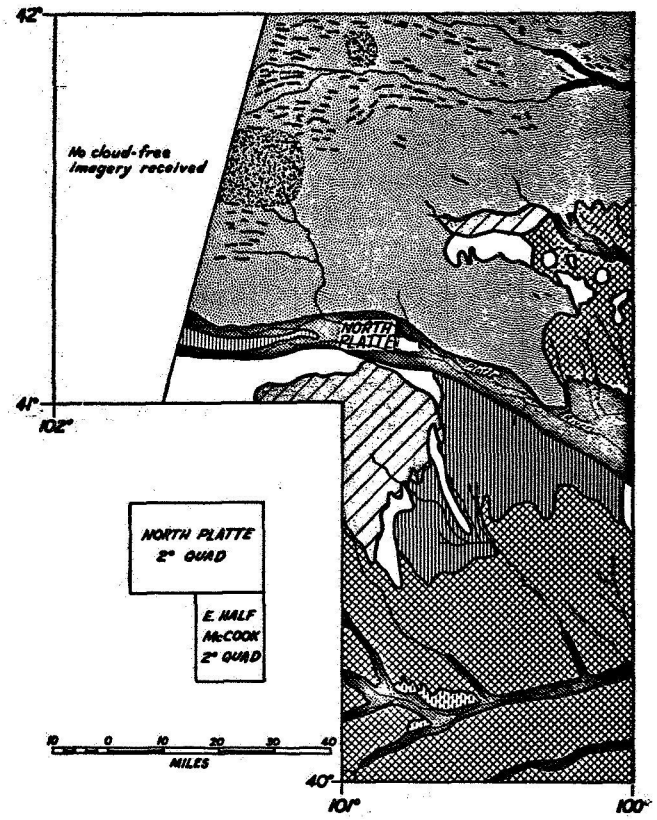
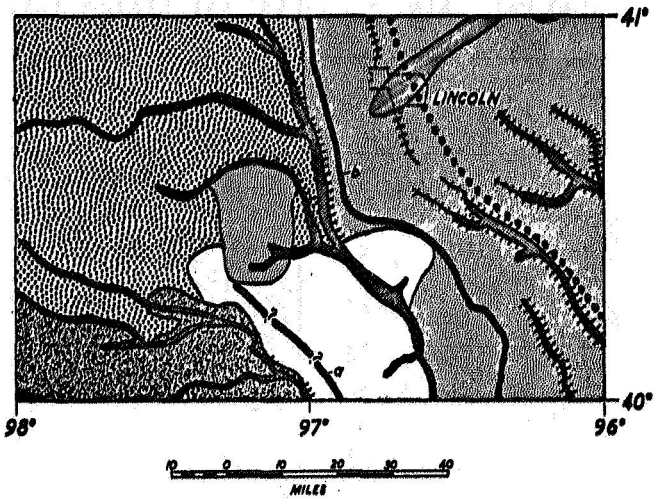


Fig. 2

PRELIMINARY MAP OF THE NORTH PLATTE AND EASTERN MCCOOK, NEBRASKA, STUDY AREAS

EXPLANATION

Map unit		Landform characteristics	Surficial geologic materials
		Valley lowlands--flood plains and lower alluvial terraces	Alluvium of late Quaternary (Wisconsin and Holocene) age
	Sand Hills units	Higher, most extensive and continuous sand dunes. Local relief commonly 100 to 250 ft. Transverse and longitudinal dunes alternate with narrow interdune lowlands that have ponds and marshes locally; very few streams. Heavy dashed lines indicate trends of the larger elongate dunes. Heavy stipple shows areas with many active sand blowouts.	Eolian sand, 50 to more than 250 ft thick, over middle Pleistocene alluvium, loess, and other deposits.
	Sand Hills units	Lower sand dunes and sand plains with isolated dunes; local relief generally less than 75 ft; very few streams.	Eolian sand, 5 to rarely more than 75 ft thick, over middle Pleistocene alluvium, loess, and other deposits.
		Plains, nearly level, with local relief generally less than 50 ft, rarely 100 ft; few, widely spaced streams.	Loess and local eolian sand over middle Pleistocene alluvium and loess.
		Moderately dissected plains (local relief generally less than 200 ft), moderately wide to narrow, relatively level interstream uplands; stream valleys moderately spaced.	Uplands have thick loess mantle of late Quaternary age over middle Pleistocene alluvium and loess, and in the S ½ half of the E ½ McCook quadrangle, over bedrock (mainly Ogallala Formation).
		Moderately dissected plain (local relief generally less than 100 ft).	Uplands have loess mantle of late Quaternary age over possibly either middle Pleistocene alluvium of bedrock.
		Highly dissected plains (local relief commonly about 200 ft), with closely spaced valleys and narrow interstream divides.	Uplands have thin loess mantle of late Quaternary age over middle Pleistocene alluvium and loess.



EXPLANATION

Compiled from ERTS-1 images 1022-16384-5; 1095-16451-5,7; 1076-16391-5,7

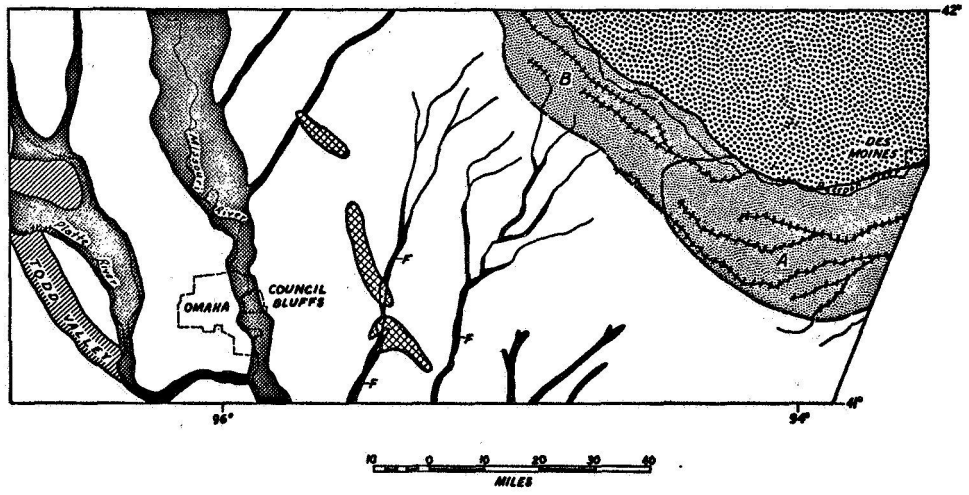
Map unit	Landform characteristics	Surficial geologic materials
	Plains with widely spaced streams and wide, nearly level interstream uplands. Main streams are entrenched generally less than 100 ft.	Uplands have thick loess mantle of late Quaternary age, overlying middle and early Pleistocene alluvium and loess, and till locally in eastern portion.
	Moderately dissected plains. Moderately wide to narrow, relatively level interstream uplands; stream valleys moderately spaced. Main streams are entrenched 100 to about 200 ft.	
	Moderately dissected plains like above.	Uplands have thin to thick loess mantle of late Quaternary age, over till, alluvium, and other deposits of middle and early Pleistocene age.
	Intricately dissected plains with closely spaced valleys and narrow interstream uplands. Main streams are entrenched 100 to rarely more than 200 ft.	
	Valley lowlands distinguishable on the ERTS images: flood plains and lower alluvial terraces, hachured where alignment possibly was controlled by moraines of middle or early Pleistocene age.	Alluvium and local loess of late Quaternary (Wisconsinan and Holocene) age.
	Ancient (middle Pleistocene) valley	

Streams without lowlands distinguishable on ERTS images, whose alignment possibly was controlled by moraines of middle or early Pleistocene age.

Drainage divide controlled by known morainic system of middle Pleistocene ("Kansan") age. a = moraine of the Nickerson Till; b = moraine of the Cedar Bluffs Till.

Trend-line of drainage anomaly, possibly due to moraine system of middle or early Pleistocene age.

Fig. 3. Preliminary map of the Lincoln, Nebraska, study area



EXPLANATION

Map unit	Landform characteristics	Surficial geologic materials
	Valley lowlands. Flood plains and lower terraces. "F" denotes inundated zones along the East and West Nishnabotna Rivers, detected from ERTS imagery.	Alluvium of late Quaternary (Wisconsin and Holocene) age.
	Plains, moderately to intricately dissected.	Uplands are mantled with loess of late Quaternary age, over till and other deposits of middle and early Quaternary age.
	Intermediate terrace of the Platte River, and Todd Valley, an abandoned channel of the Platte River.	Alluvium of Wisconsin age.
	Moraines (Bemis end moraine system) and till plain of the Des Moines glacial lobe.	Till of late Wisconsin (Cary/late Woodfordian) age, locally over older Pleistocene deposits.
	"Tonally anomalous" area with arcuate entrenched drainage paralleling the Bemis moraine system. Area A is delineated from image 1003-16334-5; area B is a possible extension, from image 1076-16384-7.	Uplands are mantled with rarely more than 20 ft of late Quaternary loess, over till of middle and possibly early Pleistocene age.
	Anomalously dark areas (with low infrared reflectance) on image 1003-16334-7.	Like unit 2. Significance of the infrared anomalies is uncertain.

Streams whose alignment possibly was controlled by moraines of middle or early Pleistocene age.

Fig. 4. Preliminary map of the Omaha and parts of the Des Moines and Fremont study areas, Nebraska and Iowa

the south that was glaciated in middle Pleistocene time and is now deeply dissected by streams. This boundary is fairly obvious (from land-use patterns) on the "red" MSS band 5 in images taken during the growing season, but is indistinct on the infrared bands. On an October 7 frame, however, this boundary is best defined on infrared band 7.

Extending 15 to 24 miles south of this boundary is an interesting area to which we have given considerable attention. It is "tonally anomalous" (in photointerpretive terms) in that it has tone and texture more like the young glaciated terrain within the Des Moines lobe than like the older dissected Kansan till plain of southern Iowa. Moreover, both its overall plan and its stream pattern are arcuate, parallel with the outer edge of the Des Moines glacial lobe. This arcuate parallelism suggests that the streams may have been alined before their entrenchment by a set of previously unrecognized moraines of an ancient ancestor of the Des Moines lobe, at least Kansan in age, perhaps early Pleistocene. Supporting this hypothesis is evidence that the arcuate drainage pattern is not controlled by bedrock lithology or structure. The valleys cut across several structural trends and across the boundaries of formations having considerable difference in lithology and resistance to erosion. They also cross a buried "preglacial" bedrock valley that is concordant with the bedrock structure.

This map also shows the zones inundated by a major flood, as mapped from the ERTS imagery. These zones are the "valley lowlands" designated by "F" in the south-central part of Figure 4. From September 11 through 13, the East Nishnabotna River, in southwestern Iowa, had a flood of probably greater than 50-year-recurrence-interval magnitude. The West Nishnabotna River also flooded, to somewhat lesser degree. The inundated zones show as clearly anomalous dark zones on the infrared bands (especially band 7) of ERTS images taken 6 and 7 days after the flood. The reduced infrared reflectance appears to result from excess soil moisture and plant stress. The Remote Sensing Laboratory of the Iowa Geological Survey, under the direction of James Taranik, mapped the inundated zones from multispectral and color-infrared aerial photographs taken 3 days after the flood. The inundation limits mapped from the airphotos agree well with those mapped from the ERTS images.

In conclusion, the ERTS multiband images have both limitations and certain strong advantages. Their chief limitation are their moderate degree of resolution-detectability and their very limited stereoscopic capability. Even where lateral variations in orbital tracks have resulted in considerable overlap between repetitive images of the same area, the high orbital altitude results in such limited parallax that small differences in relief cannot be seen.

Their chief advantage, in our opinion, is that they provide instantaneous mega-views of very large regions. Another important advantage is that they pinpoint the areas where field and/or subsurface studies are needed. Their multispectral and repetitive coverage is an additional strong asset.

These images, the first space images of the Great Plains and Midwest, already show great potential as important new research tools for synoptic geologic-terrain mapping and related studies. For small-scale mapping they are far superior to conventional aerial photographs and airphoto mosaics. The ERTS-1 images bring out relationships that never before were so evident. We must point out, however, that extracting some kinds of information, or detecting anomalies from the images of the Great Plains and Midwest is more difficult than in areas of higher relief, less vegetative cover, and less atmospheric haze. Owing to the small relief in this region, considerable study and repeated viewing of the images are required to detect anomalies that may indicate such less obvious features as buried valleys and moraines.

Paper G 14

GLACIATION OF NORTHWESTERN WYOMING INTERPRETED FROM ERTS-1

Roy M. Breckenridge, *Department of Geology, University of Wyoming, Laramie, Wyoming 82070*

ABSTRACT

Analysis of ERTS imagery has shown a number of alpine glacial features can be recognized and mapped successfully. Although the Wyoming mountains are generally regarded as the type locality for Rocky Mountain glaciation some areas have not been studied from a glacial standpoint because of inaccessibility or lack of topographic control. ERTS imagery provides an excellent base for this type of regional geomorphic study. A map of maximum extent of Wisconsin ice, flow directions and major glacial features was compiled from interpretation of the ERTS imagery. Features which can be mapped are large moraines, outwash fans and terraces. Erosional ice features including cirques, large scale "grooves", U-shaped valleys and glacial lakes are useful in delineating glaciated areas. Present-day glaciers and snowfields are easily discriminated and mapped. Glaciers and glacial deposits which serve as aquifers play a significant role in the hydrologic cycle and are important because of the increasing demand placed on our water resources. ERTS provides a quick and effective method for change detection and inventory of these vital resources.

TEXT

During the Pleistocene epoch the largest mass of glacial ice outside of the continuous ice sheet in North America formed in northwestern Wyoming leaving a profound effect on the present-day topography and scenery. In addition the sand and gravel deposits formed by glacial erosion are important sources of construction materials as well as being excellent aquifers. Glaciation also provided numerous natural reservoirs in the form of tarns and moraine-dammed lakes. Rocky Mountain glacial chronology is based on type deposits found in the Wind River Mountains of Wyoming. Although glaciation has locally been studied in detail, the region as a whole has not been studied from a glacial standpoint. The large area involved, rugged topography, lack of control and general inaccessibility have discouraged regional investigations. ERTS-1 appeared to provide an excellent base for broad-scale geomorphic studies of this type. This paper presents preliminary

results of an effort to map glacial geology from satellite imagery using simple techniques and limited ground truth.

Figure 1 is a small scale photomosaic of ERTS-1 MSS-5 imagery in the area studied. The darker area with moderate relief and the prominent lake in the northwest corner of the image is the Yellowstone Plateau. It is bordered on the east by the rugged Absaroka Range and on the south by the Teton and Gros Ventre Mountains. The large northwest-striking structure in the south-center of the mosaic is the Wind River Range. The north-trending ridges and valleys on the southwest margin of the image are the Wyoming Overthrust Belt. All of the images were taken in early fall (1972) and are cloud-free. The imagery was analyzed using basic photo interpretive techniques together with color-additive and stereo viewing.

Overlay maps were compiled outlining the extent of ice at glacial maximum. A simplified and reduced glacial map is presented in Figure 2. Glaciated areas as shown are based on the recognition of one or more glacial features. Glacial landforms can be grouped into erosional and depositional features both which could be recognized on the imagery. Moraines are considered the most diagnostic depositional glacial landform. The Bull Lake and Pinedale type deposits (Wisconsin) were easily outlined on the imagery although they could not be separated where in close contact. These massive looping terminal moraines impound large glacial lakes on the flanks of the Wind River Range (Fig. 1, location A). The Bull Lake and Pinedale tills are not suited for agricultural use because of relief, rocky character and permeability. On the other hand, glacial outwash, fans and valley trains (stratified drift) beyond the former ice margin often contain sufficient matrix to support field crops such as hay and alfalfa. Thus glacial drift could be categorized as till or stratified drift using false-color infrared composites to enhance the vegetation difference. This technique was only successful in the Wind River and Teton Ranges where glaciers advanced out of the mountains onto the basins where vegetation contrasts occur. Terminal and lateral moraines in mountain valleys could neither be reliably distinguished from stratified drift nor from other valleyside surficial deposits except in a few cases where characteristic geomorphic features were recognized. Most of the pre-Wisconsin glacial features have been subsequently destroyed by erosion or covered by later deposits. Remaining exposures are too small to recognize on the imagery. Large gravel-capped mesas or pediments at the mountain flanks and in the basins probably represent erosional cycles of these early glaciations. These pediments or benches appear dark on all bands but are best recognized using a composite of MSS 5 and 7 (Fig. 1, location B).



0 50 miles

Figure 1

ERTS MSS 5 MOSAIC OF NORTHWESTERN WYOMING

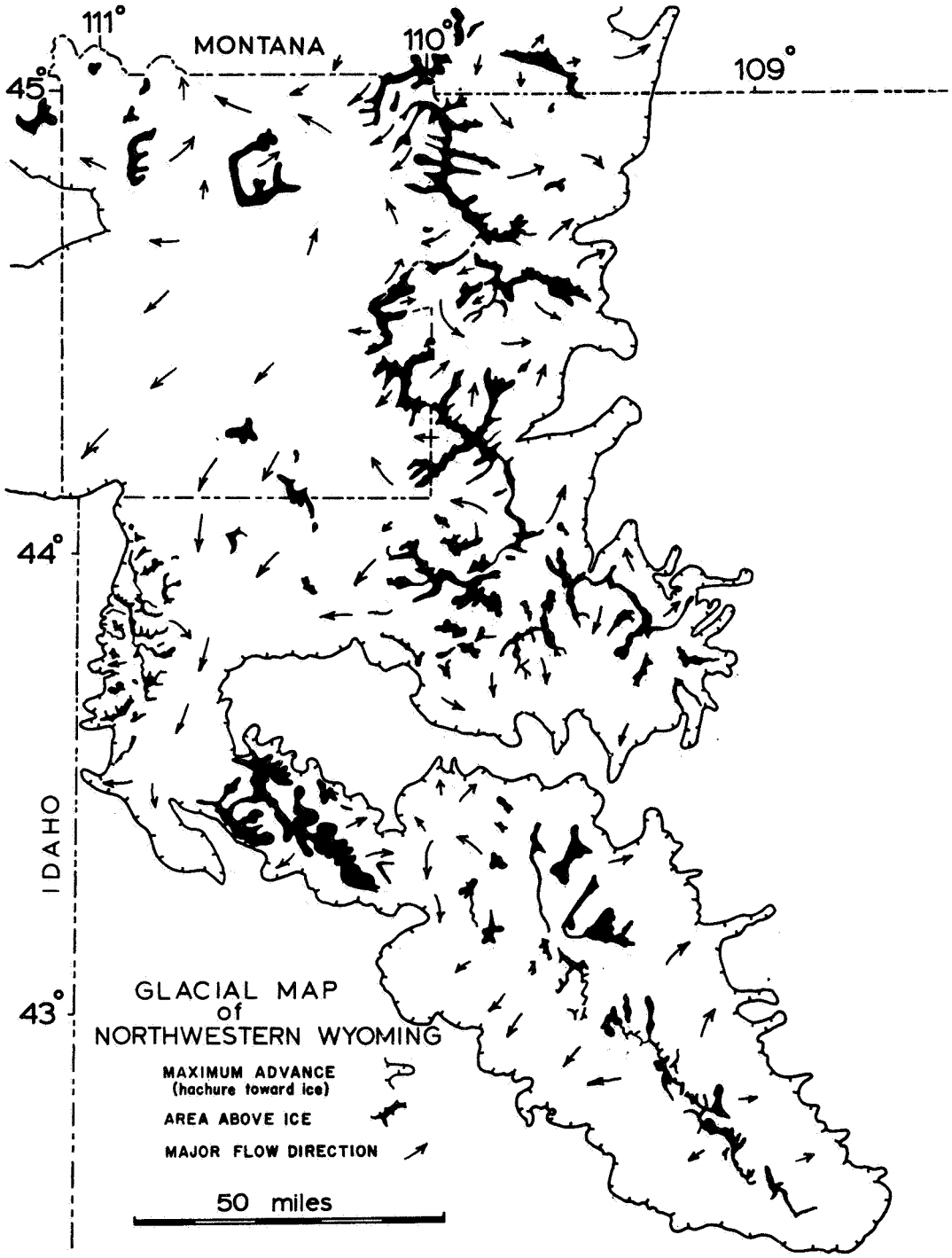

111°
MONTANA
110°
109°
45°
44°
IDAHO
43°
GLACIAL MAP
of
NORTHWESTERN WYOMING
MAXIMUM ADVANCE
(hachure toward ice)
AREA ABOVE ICE
MAJOR FLOW DIRECTION
50 miles

Figure 2

Where massive terminal moraines were absent or not recognizable, glaciated areas were outlined on the basis of glacial topography. Alpine glacial erosion is distinctive and stereoscopic viewing of adjacent ERTS passes facilitated the recognition of U-shaped troughs, cirques, horns, aretes, cols and truncated spurs. Ice limits can be located approximately where valleys change from a U to V shape in cross valley profile. Most of the crests of Wyoming mountain ranges culminate in flat uplands often referred to as high-level erosion surfaces which bevel across the rock structure. Glacial dissection of these surfaces results in the classic biscuit-board topography. Morphology and topography recognized using stereo pairs allowed distinction of the unglaciated areas above the ice (Fig. 2). Color composites enhanced the contrast between tundra vegetation on the erosion surfaces and the bare cirque walls. Glacial tarns distinguished on MSS-7 were useful as indicators of glaciated bedrock.

The glaciated volcanic terrane of the Absaroka Range posed several special problems. Alpine glacial features in the Absarokas are not well-preserved as in the crystalline terrane of the Wind River, Teton or Beartooth Ranges and the glacial cycle is manifest in different forms of mass movements such as landslides and rock glaciers. Because of the absence of moraines and tarns, cirque development and valley morphology were used as indicators of glacial boundaries. Although the Yellowstone Plateau is also a volcanic province, the lower relief has resulted in less intensive mass wasting and more glacial indicators are preserved including moraines, outwash and lacustrine deposits.

Major flow directions (Fig. 2) were mapped using directional criteria such as slope direction and orientation of glacial troughs, U-shaped valleys, and cirque headwalls. Scoured bedrock served as an excellent indicator in some areas. Flow directions in the high Wind River Range were indirectly controlled by the large-scale joint pattern in the Precambrian rocks. These linear joint concentrations represent zones of weakness which were selectively eroded by ice leaving many parallel sets of straight glacial valleys. An excellent example of flow direction recognizable on ERTS imagery is in northern Yellowstone Park (Fig. 1, location C), where ice moving from the Buffalo Plateau can be traced down the valley of the Yellowstone River to Gardiner, Montana. A combination of drumlins, lateral moraines together with scoured bedrock in the form of large grooves and oriented tarns show on the imagery as parallel lines. Linear features are especially well developed on Mt. Everts near Mammoth where ice must have been over 2000 feet deep in order to cover the top of the mountain. Another area where flow direction can be dramatically observed is at the northern end of the Wind River Range where the Green River glacier flowed north out of a huge Yosemite-like valley and made a 120° turn into the Green River Basin after encountering the Gros Ventre Range (Figure 1, location D). The flow indicators in this instance are medial and lateral moraines.

Large glacial outwash channels are visible in the southwest corner of Yellowstone where cascading meltwater scoured many parallel channels (Fig. 1, location E).

Comparison of maximum advance and flow directions interpreted from the imagery indicates there were two major centers of ice accumulation, the Wind River and Yellowstone-Absaroka ice caps. Most of the Wind River ice sheet was restricted to the Precambrian highlands except in perhaps a dozen places where valley glaciers breeched the hogback belt and flowed out onto the basins. Ice from the Yellowstone-Absaroka source area flowed in locally complex patterns but generally radiated north down the Yellowstone valley, east to the Bighorn Basin, south into Jackson Hole and west toward the Snake River Plain. The Teton and Gros Ventre glaciers were generally incorporated into the flow of the two major sheets. The Beartooth ice cap was north of Wyoming although south-flowing ice merged with the Yellowstone- Absaroka mass.

In addition to glacial features a number of related or periglacial phenomena were successfully mapped. Large recent mass movements were sometimes recognized. Most often the scar was first detected where the mass separated from the surrounding rock, soil and vegetation. Commonly mass movements exhibit characteristic arcuate fronts and hummocky surfaces depending on the nature and speed of the movement. This characteristic shape was of considerable utility in recognizing these mass movements. Large landslide complexes at Gardiner, Mammoth, Carter Mountain and Togwotee Pass were readily distinguished on color composite images. Slide scars and debris at the famous Gros Ventre and Hebgen Lake rockslides were also apparent. Masses of slow-moving rock debris (rock glaciers) were mapped by using MSS 5 and 7. The largest and most numerous rock glaciers were identified in the cirques of the Absaroka Range. Other periglacial features (with the exception of dune fields) are only distinguishable from low level aircraft imagery. A large belt of dunes south of the Wind River Range may represent glacial eolian deposits. These dunes were mapped and active dunes distinguished from vegetated stabilized dunes by their characteristically high reflectance in all bands.

All of the Wyoming basins depend on the runoff from the mountains for water supply. Permanent snowfields and small glaciers remaining from the Neoglacial stades or "little ice age" are an important part of the hydrologic cycle. Preliminary results indicate snow and ice covered areas can be mapped and monitored using the ERTS imagery. Late summer imagery was successfully used to locate permanent snowfields and small glaciers. Snow is best mapped on MSS 4 while MSS 7 allows better distinction of glaciers from snow cover. The ancient glacial and alluvial deposits serve as important aquifers that retain the meltwater and release it slowly through the summer months. False-color composites were used to map these valley-train or alluvial deposits which in the basins

support crops or exhibit greater density of vegetation than the surrounding Cretaceous and Tertiary rocks.

Results of the ERTS investigation were compared with aircraft data and the available glacial maps compiled by conventional techniques. The ERTS map agreed well with the work of Love (1961), Richmond (1964), Richmond and others (1965, 1972), Waldrop and Hyden (1963), and Pierce (1968). Many glacial features visible on ERTS imagery were not recognized until comparisons were made with conventional maps or aircraft imagery. Low-level aircraft imagery was more useful than the satellite imagery where detail was important. In some cases aircraft photointerpretations were superior to field maps. In most cases imagery interpretation was hampered by vegetation. Subtle topographic differences are generally better mapped from imagery than on the ground.

The success of this study demonstrates the utility of ERTS imagery in regional geomorphic studies, especially when inaccessibility is a major factor. Detailed stratigraphy and discrimination of similar tills is not possible but some gross distinctions can be made where units form wide exposures. Snow and ice cover can be easily and quickly mapped and monitored for change using ERTS.

REFERENCES CITED

Love, J. D., 1961, Reconnaissance study of Quaternary faults in and south of Yellowstone National Park, Wyoming: Geol. Soc. America Bull., v. 72, p. 1753.

Pierce, W. G., 1968, The Carter Mountain landslide area, northwest Wyoming: U.S. Geol. Survey Prof. Paper 600-D, p. D235-D241.

Richmond, G. M., 1964, Glacial geology of the West Yellowstone Basin and adjacent parts of Yellowstone National Park: U.S. Geol. Survey Prof. Paper 435, p. 223-236.

Richmond, G. M., and others, 1965, Glacial chronology of the Wind River Mountains, in Internatl. Assoc. for Quaternary Res., VIIth Congress, Guidebook for field conference E, Northern and Middle Rocky Mountains. Nebraska Academy of Sciences, Lincoln. p. 28-37.

Richmond, G. M., Pierce, K. L., and Waldrop, H. A., 1972, Surficial geologic map of Yellowstone National Park: U.S. Geol. Survey Miscellaneous Geologic Investigations Map I-710.

Waldrop, H. A., and Hyden, H. J., 1963, Landslides near Gardiner, Montana: U.S. Geol. Survey Prof. Paper 450-E, p. E11-E14.

Paper G 15

FIRST-LOOK ANALYSIS OF GEOLOGIC GROUND PATTERNS ON ERTS-1 IMAGERY OF MISSOURI*

William H. Allen, James A. Martin, and David L. Rath, *Missouri Geological Survey, Box 250, Rolla, Missouri 65401*

ABSTRACT

Examination of ERTS-1 data for selected areas of Missouri revealed not only many of the known geologic features but also a number of unknown linear, circular and arcuate ground patterns. The number of new geologic elements that have been brought to light as well as the sharp definition and probable extensions of several known geologic features point out the importance of multispectral imagery via satellite and the synoptic views which they provide. To date, analysis and interpretations have been a "first-look" visual examination of the unenhanced projected images.

1. INTRODUCTION

The Missouri Geological Survey has received ERTS imagery through involvement in two ERTS-1 projects: (1) An Application and Evaluation of ERTS-1 Data in Environmental Geology and Land-Use Planning in the St. Louis-Kansas City Corridor, Missouri (SR-168) and (2) An Evaluation of ERTS-1 for Mapping Pleistocene Deposits and Landforms in the Midwest and Great Plains (SR-238). This paper is not a progress report for either of these projects but rather an evaluation of the imagery by the Mineral Resources and Stratigraphy Sections of the Survey as to how it may relate to present and future projects. Admittedly, we were somewhat skeptical as to the potential usefulness of ERTS imagery other than providing a synoptic view of major waterways and gross structural features. However, examination of early pictures covering the southeast and northeast part of the state greatly changed this view and generated much enthusiasm.

The ERTS coverage for three areas of Missouri is discussed -- southeast, northeast and central. The frames analyzed are: E-1071-16111 (SE), E-1036-16162 (NE) and E-1073-16221 (C). The principal references used for comparison of imagery features to known geologic data were the Geologic Map of Missouri (McCracken, et al., 1961) and Structural Features of Missouri, map & report (McCracken, 1971). The geologic setting of the areas ranges from Ordovician through Pleistocene in the central and northeast areas and from Precambrian through Mississippian, with a large area of Cretaceous, Tertiary and Quaternary deposits in the southeast. Multispectral enhancement plus the synoptic view has allowed in some cases the tracing of certain structural linear elements across several of these geologic boundaries.

---

*Publication authorized by the Director, Missouri Geological Survey

2. SOUTHEAST MISSOURI (NASA-E-1071-16111)

Evaluation of this imagery resulted in the identification of many geologic features, some of which are suspected to be part of the basic structural framework of the Midcontinent Platform. Three factors led to the examination of this area: (1) Southeast Missouri is a major North American lead-zinc-copper, iron Metallogenic Province; (2) the St. Francois Mountains are the principal Precambrian outcrop in central United States; and (3) the imagery received for this area was very sharp and free of cloud cover. Features noted and described are shown on Figure 1.

Ozark Escarpment: This prominent physiographic feature forms the boundary between the Ozark uplift (McCracken, 1971) and the Mississippi embayment. Its trace on the imagery is primarily defined by a change in vegetation and topography and is not distinct everywhere along its extent. A short distance south of the escarpment and rising above the level terrain of the embayment are two physiographic highs, Crowleys Ridge and Benton Hills. The bedrock of Benton Hills is Ordovician, Cretaceous and Tertiary and its boundaries are exceptionally well defined. Crowleys Ridge is underlain mainly by Tertiary and Quaternary deposits, and its outline is only weakly suggested. An abandoned channelway (K) is thought to be an Ohio River drainageway (stage B) shown by Fisk (1944).

Farmington Anticline: This northwest-trending fold is the most prominent structural feature on this image. A disturbed area with some 75 diatremes present at the south end of the fold is not readily apparent. From the imagery, an anticlinal structure plunging toward or with closure at the south end would be suspected.

Ste. Genevieve Fault System: One of the major fault zones in Missouri, this complex structure is part of a major east-west continental fracture pattern, the 38th Parallel Lineament (Brock & Heyl 1961; Snyder & Gerdemann, 1965; and Heyl, 1972). The fault is most prominent on the Illinois side and for a short distance after it changes direction from northwest to west in Missouri. A second directional change back to the northwest is not apparent.

Unknown Feature A-A: Among the more prominent linears on the image, this feature extends about 50 miles in a slightly east-northeast direction crossing two major fault systems, the Palmer and Simms Mountain, plus the Farmington anticline without any apparent break in the trace. It appears to terminate just west of the Ste. Genevieve fault system, but a faint suggestion of its continuation is present in Illinois. The Dent Branch volcanic structure lies on the trace. Extending the trace westward beyond the frame, it lies 5 miles south of the Crooked Creek cryptoexplosive structure. The lineament has not been field checked nor compared with available subsurface data; however, the initial assumption is to relate it to the 38th Parallel lineament and attribute it to the Precambrian expression of this continental fracture.

Simms Mountain Fault System: A major and complex fault zone in the St. Francois Mountains area, it is poorly defined on the imagery. A weak,

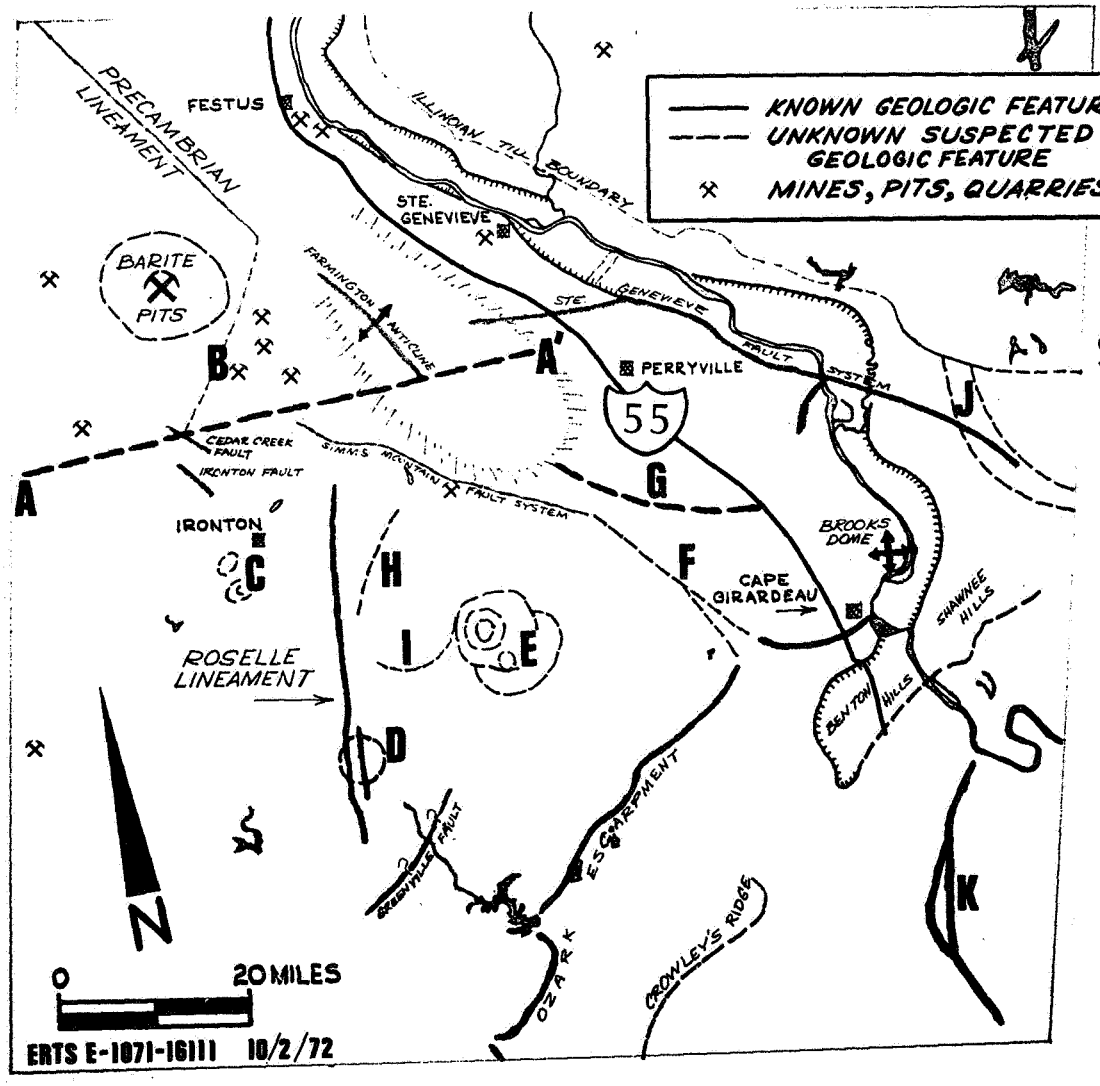


FIGURE 1

S.E. MISSOURI

relatively straight trace only roughly follows the major trend of the system. From the imagery, a linear would be suspect but not a major fault system.

Precambrian Lineament: A weak but recognizable linear, it extends for 30 miles on a northwest trend and coincides with a possible Precambrian lineament proposed by Hayes (1962) which recent drilling tends to confirm (Eva Kisvarsanyi, personal communication, 1973). A lineament would be postulated from the imagery.

Feature F: This linear might be a continuation of the Simms Mountain fault system or possibly an extension of the previously described Precambrian lineament. The trace is prominent but the bifurcation at the southern end is weak and suspect.

Roselle Lineament: The feature is clearly shown on the ERTS imagery and lies along three parallel faults mapped by Amos & Desborough (1960). Gillerman (1968) recognized it on SLAR imagery and named it the Roselle lineament. The short double trace and circular pattern (D) at the south reflects a Precambrian igneous knob (Mudlick Mtn.) and drainage pattern. Extension north of the Simms Mountain fault system was not indicated on the ERTS imagery examined. The curved line (H) can be attributed to the course of the St. Francis River for most of its extent.

Circular Features C & E: A number of circular patterns, some superimposed, are discernible on the imagery for this area. Feature C is one of the largest and coincides with one described by Gillerman (1968). Their origin is unknown but could range from volcanic calderas to astroblemes. Many of these suggest a reflection of a structural attitude in the Precambrian.

Feature B: This linear extends from the Precambrian lineament to the linear (A-A') and roughly follows the strike of the Big River fault. It separates the "Old" Lead Belt from the Washington County Barite District.

Ironton and Cedar Creek Faults: The imagery traces of these structures show only a small portion of their total extent. The Ironton portion is a questionable fault along the southwest flank of a Precambrian high (Buford Mtn.). Neither trace is exceptionally strong.

Brooks Dome: This structure, which has been verified by drilling, is accentuated by drainage, vegetation and relief. From imagery alone, a dome would be suspected.

Greenville Fault: This fault, in an area of thick residuum, has been postulated from drill hole records (McCracken, 1971). The linear on the imagery is weak and lies about 5 miles southeast of the fault trace. That the offset may exist has been suggested by several Precambrian drill holes (Eva Kisvarsanyi, personal communication, 1973).

Feature G: A semi-arcuate line which extends a distance of about 25 miles, it lies some 5 miles northeast of the Simms Mountain fault system. There are no known structures in the area.

Feature I: A strong arcuate trace that reflects a portion of the drainage pattern of Twelve Mile Creek, this feature is in part along the contact between Precambrian igneous rocks and Cambrian sediments.

Illinoian Till Boundary: On the imagery this boundary is weak but could be placed tentatively in the area shown by Weller (1945). The significance of lines J is not known.

3. CENTRAL (ERTS-E-1073-16221) & NORTHEAST (ERTS-E-1036-16162)

Northern Missouri is covered by till, which would be expected to hide evidence of the underlying structural features. However, certain linear traces are recognized and mapped in spite of the surficial cover. Information obtained on the Pleistocene deposits is not specifically verified; however, the ERTS-1 coverage does provide a rational base for defining a study of the surficial deposits north of the Missouri River. Figure 2 shows and identifies the features discussed for this area.

Lincoln Fold: The most prominent feature on the northeastern imagery, it was initially thought that the trace reflected the steep southwestern flank. Comparison with Precambrian test holes indicates that the imagery trace is on the crest (Kisvarsanyi, personal communication, 1973). In the area of its intersection with the Cap au Gres fault, the fold swings to the east. Its relationship to the fault is hazy, as the Cap au Gres itself is poorly expressed.

Mexico Anticline: Normal to the majority of structural trends in north-central Missouri, the imagery indicates the structure extends beyond the presently recognized limit to the northeast and appears to merge with the Sangamon arch in Illinois (Whiting & Stevenson, 1965). It is intersected by an east-west arcuate trace (B-B') which is a probable recessional moraine.

Mineola Structure: Originally described as a domal structure, it is shown on the imagery as a northwest-southeast trace that intersects the Mexico anticline at right angles. Further north it intersects the arcuate features (E) a reflection of the Middle Salt Fork drainage and possibly a Nebraskan Till boundary. The southern extension of this feature (D-D') is indicated by a light trace on the imagery. It is paralleled by the line C-C' which cannot be seen when the till cover thickens. Line D-D' is approximately 90 miles long and crosses Ordovician, Devonian, Mississippian, Pennsylvanian, and Quaternary deposits.

Stratigraphic Boundaries: Several stratigraphic boundaries are quite obvious. The most prominent is between the lower Ordovician Roubidoux (Or) sandstone and dolomite and the Jefferson City-Cotter (Ojc) dolomite. The trace closely approximates the mapped boundary and is enhanced by a topographic break and change in vegetation from timber to pasture and cropland. The Ordovician (Ojc)-Mississippian (Mk-o) boundary is less distinct. Enhancement of this contact is caused by a change in rock types and soils.

Postulated Pleistocene features: Lines shown on Figure 2 as B, E, F, and G are thought to be related to moraine features of early Pleistocene age. West of the Missouri River, the southernmost line of B-B' defines the boundary between loess-covered till and Pennsylvanian shales. Further east till of suspected Kansan age is recognized south of the line. Due to highly dissected terrain the southern limit of the till sheet has not been recognized on the imagery. In this area the line represents a suspected recessional moraine. At least two till units are recognized north of the line, whereas to the south there is only one till unit that has been presently verified. Extension of line B-B' east of the Lincoln fold was not considered feasible because of a dubious interpretation of imagery data; however, it terminates directly west of the Kansan till border in Illinois (Willman & Frye, 1970). Along Line B-B', in the center of Figure 2 there are two minor flexures which reflect the Mexico anticline to the east. Features indicated by E lie just south of the Nebraskan Till boundary (Heim 1963). The Salt Fork River has an arcuate pattern that may be an expression of a terminal moraine of Nebraskan age. No significance can be attached to the faint lines indicated by letters F and G.

4. CONCLUSIONS

The analysis of the imagery is preliminary; however, the following summary is offered:

(1) ERTS-1 MSS coverage provides a valuable recon tool for geologic investigations; however, it demands a rather wide knowledge of field data and exhaustive image review.

(2) There are indications that certain structures may be relocated or extended beyond their presently known limits. Linears may reflect deeply buried structural elements.

(3) Review of the imagery provides an effective method for planning and defining areas for concentrated field investigations.

(4) Utilization of satellite imagery can play a major part in studies of mineralization and mineral resource potential.

(5) Repetitive coverage is mandatory for more comprehensive evaluation of structural, stratigraphic, geomorphic, and cultural features.

(6) Geologists at the Missouri Geological Survey as well as those from mining companies and the University of Missouri - Rolla are enthusiastic about the geologic details that can be delineated on the imagery.

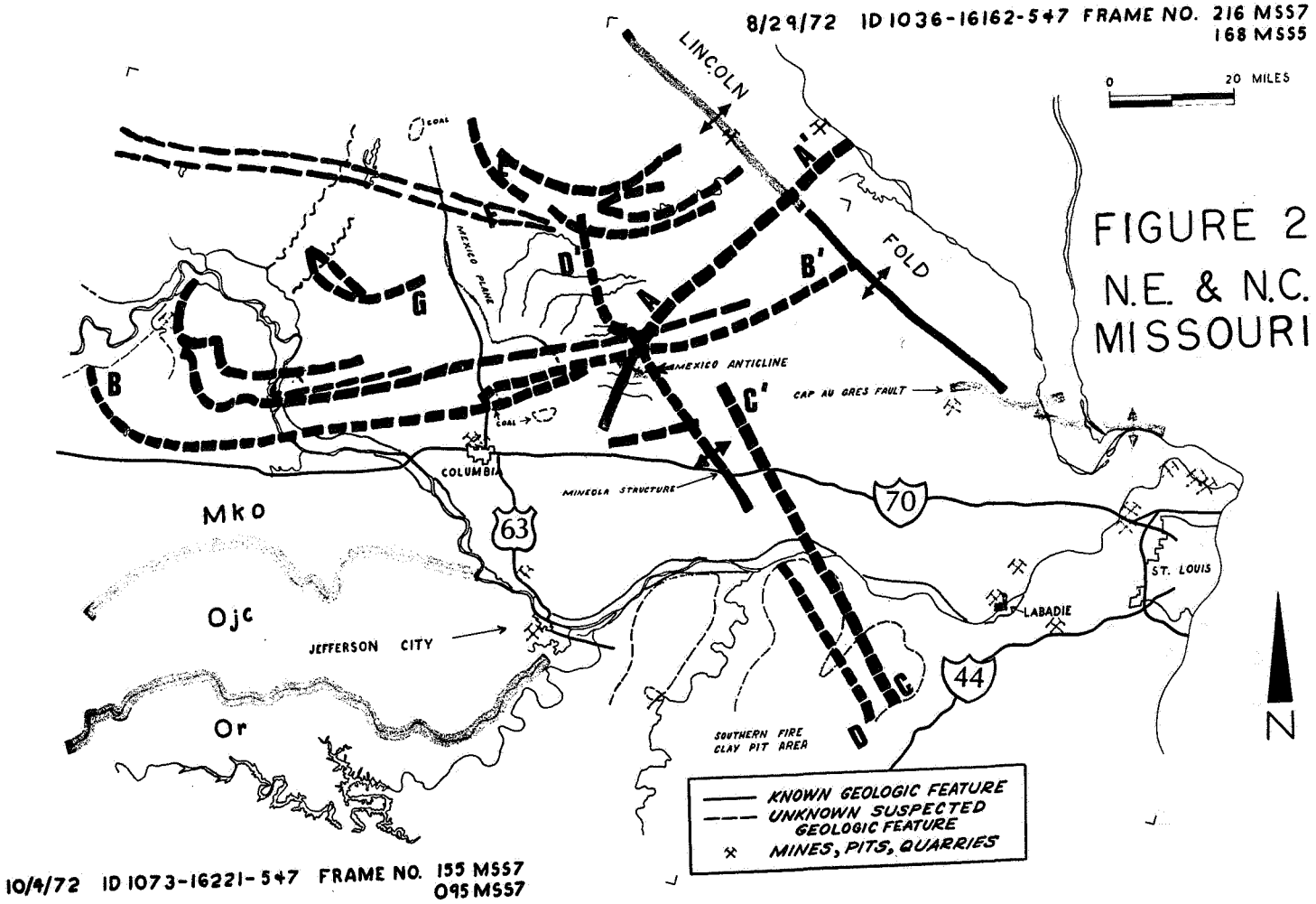


FIGURE 2
N.E. & N.C.
MISSOURI

REFERENCES

Amos, Dewey H. & Desborough, George A., 1962, Geologic map of parts of the Ironton and Fredericktown areas, Missouri: unpubl. ms., Mo. Geol. Surv. (publ. as Mo. Geol. Surv. Rept. Inv. 47, 1970)

Fisk, Harold N., 1944, Geological investigation of the alluvial valley of the lower Mississippi delta: Miss. River Comm., War Dept., U. S. Army Corps of Eng.

Gillerman, Elliot, 1968, Major lineaments and possible calderas defined by side-looking airborne radar imagery, St. Francois Mtns., Mo.: CRES Technical Report 118-12, Nat'l. Aeronautics & Space Admin.

Hayes, W. C., Jr., 1962, Map showing configuration of the Precambrian surface and major structural lineaments: Mo. Geol. Surv.

Heim, George E., 1963, The Pleistocene and engineering geology of the Hannibal-Canton area, Missouri: unpubl. thesis, Dept. of Geol., University of Ill.

Heyl, Allen V., 1972, The 38th parallel lineament and its relationship to ore deposits: Econ. Geology, vol. 67, p. 879-894.

Kisvarsanyi, Eva B., 1973, personal communication on Precambrian drill hole data: Geologist, Mo. Geol. Surv.

McCracken, Mary H., et al., 1961, Geologic map of Missouri: Mo. Geol. Surv.

_____, 1971, Structural features map of Missouri: Mo. Geol. Surv.

_____, 1971, Structural features of Missouri: Mo. Geol. Surv. Rept. Inv. 49.

Snyder, F. G., & Gerdemann, Paul E., 1965, Explosive igneous activity along an Illinois-Missouri-Kansas axis: Am. Jour. Sci., vol. 263.

Weller, J. Marvin, et al., 1945, Geologic map of Illinois: Ill. Geol. Surv.

Whiting, L. L. & Stevenson, D. L., 1965, The Sangamon arch: Ill. Geol. Surv., Circ. 383.

Willman, H. B., et al., 1967, Geologic map of Illinois: Ill. Geol. Surv.

_____ and Frye, J. C., 1970, Pleistocene stratigraphy of Illinois: Ill. Geol. Surv., Bull. 94.

Paper G 16

RATIO MAPS OF IRON ORE DEPOSITS ATLANTIC CITY DISTRICT, WYOMING

Robert K. Vincent, *Environmental Research Institute of Michigan, Ann Arbor, Michigan*

ABSTRACT

Preliminary results of a spectral ratioing technique are shown for a region at the southern end of the Wind River Range, Wyoming. Digital ratio graymaps and analog ratio images have been produced for the test site, but ground truth is not yet available for thorough interpretation of these products. ERTS analog ratio images were found generally better than either ERTS single-channel images or high altitude aerial photos for the discrimination of vegetation from non-vegetation in the test site region. Some linear geological features smaller than the ERTS spatial resolution are seen as well in ERTS ratio and single-channel images as in high altitude aerial photography. Geochemical information appears to be extractable from ERTS data. Good preliminary quantitative agreement between ERTS-derived ratios and laboratory-derived reflectance ratios of rocks and minerals encourage plans to use lab data as training sets for a simple ratio gating logic approach to automatic recognition maps. Empirical atmospheric corrections indicate that atmospheric corrections are needed to make the ratio method, and possibly other types of data processing, consistent over large geographical and temporal displacements. The ratio method, designed for geochemical prospecting and geologic mapping, should also be useful for other scientific applications from satellite data as well.

1. BACKGROUND

The primary objectives of this ERTS investigation are to develop a generally applicable method for mapping large exposures of iron compounds, to use this method for mapping iron compounds in the Wind River Range, Wyoming vicinity, and to estimate the usefulness of this method for limited geochemical prospecting from ERTS data in this and other (geologically well-exposed) regions of the world. The method involves empirical corrections for atmospheric effects, spectral ratioing of reflected radiances of selected pairs of ERTS multispectral channels, production of analog ratio images, and production of automatic recognition maps of as many rock classes as possible, using laboratory data as training sets whenever possible.

The data processing steps used to correct for atmospheric and illumination effects in this ratio method have been described in an earlier paper [1]. In brief, the radiance detected for the darkest object (usually shadow or water) in a given scene is subtracted from the detected radiance of all other points for each MSS channel. The resulting radiances in two of the MSS channels are ratioed. The ratio for all points is then divided by the ratio of a known point in the scene (ratio normalized) and multiplied by the reflectance ratio (determined from laboratory data) of the known point. This yields a ratio of reflectances in the two selected spectral channels for every point in the scene. To a first approximation, it is hypothesized that most atmospheric and illumination effects are removed from this ratio of reflectances by this procedure. As a qualitative example, typical reddish rocks (high reflectance in channel 5 and lower reflectance in channel 7) will have an $R_{\frac{5}{7}}$ ratio less than 1.0; vegetation, which exhibits the opposite spectral behavior, will have an $R_{\frac{5}{7}}$ ratio much greater than 1.0. Further processing involves inputting the ratio of reflectance into digital and analog computers to produce digital ratio graymaps and analog ratio images, respectively. Later processing is planned in which automatic recognition maps of various rock classes will be produced, using two to four of the above reflectance ratios as a basis for automatic decision making.

The four months since ERTS data were first obtained have been spent primarily on development of the data processing techniques to be used, some of which are presented here. Initial interpretative efforts have been based on comparisons of aerial photography, geologic maps, and expected ratio values calculated from laboratory data. All of the data processing to date has been done on parts of ERTS frame E-1013-17294, collected on 5 August 1972. Once satisfactory results have been obtained for the primary test site, the rest of the ERTS frame will be "prospected" for unusual concentrations of iron oxides. A field trip to Wyoming to check anomalies and to collect samples for laboratory spectral measurements will be made this coming summer.

2. GEOLOGIC DESCRIPTION OF THE TEST SITE

The primary test site chosen for this investigation is the Atlantic City District, at the southern end of the Wind River Range, Wyoming. In this district, which has been mapped by R.W. Bayley [2], the Goldman Meadows Formation consists of schist, quartzite, and metasedimentary iron-formation. The iron-formation member, which contains on the average of 35% iron, is composed mainly of magnetite and quartz, with small amounts of chlorite, garnet, and amphibole. It is in this region that the U.S. Steel Corporation has an operating iron mine.

Just south and east of the Goldman Meadows Formation is the Roundtop Mountain Greenstone Formation, consisting of ellipsoidal greenstone (derived from basalt) and green schist. Just southeast of that formation is the Miners Delight Formation, composed primarily of graywacke (turbidites), schist, conglomerate, and ellipsoidal greenstone (derived from andesite). To the west

of the iron mine is the Louis Lake batholith, which is primarily biotite-hornblende quartz diorite and granodiorite, bordered by migmatite and gray gneiss. Interlaced within the batholith are diabasic gabbro dikes of widths on the order of 60 to 100 meters and lengths up to 10 kilometers. All formations previously listed are Precambrian in age. Due north of the Goldman Meadows Formation lies a sedimentary series of beds from Precambrian to Mesozoic in age. These beds lie unconformably on the metamorphic and igneous rocks previously mentioned and dip northeastward, exposing Precambrian sandstone adjacent to the metamorphics.

3. AIR PHOTOS AND ERTS SINGLE-CHANNEL IMAGES OF THE TEST SITE

Figure 1 shows an aerial photo taken from a high-altitude, October, 1971 flight of the NASA U-2 aircraft [3] and a MSS channel 5 ERTS image of the test site. Both photo and image encompass the red portion of the visible spectrum and are the same scale, although the ERTS image is inadvertently shifted slightly northward in comparison of the aerial photo. The iron mine, which is the one-km-wide bright region (shaped somewhat like an extracted molar) in the lower right of the ERTS image, seems more distinct in the ERTS image, probably due to film-saturation of the image for even moderately bright targets. On both photo and ERTS image, intersecting diabasic gabbro dikes (on the order of one ERTS spatial resolution element) are visible west of the iron mine in the Louis Lake batholith. For future reference,note three things: (1) the iron mine does not appear unique, or even distinctive, from other areas in the scene; (2) the sedimentary strata in the upper right corner of the ERTS image appear similar to one another; and (3) vegetation (dark) in the channel-5 ERTS image is easier to distinguish from non-vegetation than in the aerial photo (probably because of the time of year). Dark shadows (in the northeast trending valley) appear similar to vegetation in both ERTS image and photo.

Figure 2 shows the same scene as in the previous figure. The aerial photo was taken in the 0.51 - 0.90μm wavelength range and the ERTS image is for MSS channel 7(0.8 - 1.1μm wavelength region). Although the iron mine is darker than its surroundings, in contrast to a brighter-than-average reflectance in the visible red region, it is not distinct from the surrounding terrain in the reflective infrared region of either the aerial photo or the ERTS channel 7 image. Note further that the diabasic gabbro dikes in the Louis Lake batholith are virtually undetectable in the ERTS channel 7 image, the sedimentary strata in the upper right corner appear similar to one another in both photo and image, and vegetation (bright) in the upper right corner of the channel 7 ERTS image is more discriminable from non-vegetation than in the false color aerial photo, again possibly because of time of year differences between the data collections.

4. RATIO MAPS OF THE TEST SITE

Two forms of ratio maps have been produced thus far for the test site; one is a digital ratio graymap and the other form is an analog ratio image.

The digital graymap is used as a research tool for quantitative analysis, to examine the accuracy of the ratio method. Figure 3 shows an R_{75} (ERTS channel 7 divided by channel 5) digital ratio graymap. (Note: This figure and figure 4 were originally in color. See Figure 4 for color interpretations). Green represents vegetation, violet is primarily a mixture of rock and vegetation, blue is rock outcrop, and red represents magnetite, possibly some greenstone, and other possible iron-rich outcrops. The darkest red occurs only in the iron mine and along pond edges, where muds or tailings may be present.

The atmospheric path radiances obtained from the dark object subtraction were about 12% of the mean signal level in channel 5 and less than 4% of the mean level in channel 7 in the hilly Atlantic City District, which is approximately 2.5 km above sea level. At two other points, approximately one-half and three-fourths of the ERTS frame to the east, in flat, open plains that are about 0.3 km lower in elevation, path radiance percentages determined by dark object subtraction in channels 5 and 7 were 22% and 4%, respectively, of the mean signal levels. Without these corrections large errors in the ratio would have been made for objects which are dark in channel 5 within a given scene, and the errors would have been substantially different in the two parts of the ERTS frame. Since this ERTS frame was collected on a clear, dry day for a high mean elevation test site, atmospheric corrections would appear to be more necessary for less favorable observing conditions over lower test sites, if consistent data processing results are desired.

Figure 4 shows some R_{75} reflectance ratios calculated from a subset of laboratory data contained in the NASA Earth Resources Spectral Information System at the Johnson Spacecraft Center in Houston, Texas. Not all of the categories displayed here are represented in the test site. The values corresponding to the graylevels of the ratio graymap in figure 3 are also shown here. For calculation of these laboratory spectra reflectance ratios, square filters were assumed for the ERTS MMS channels; this assumption makes the calculated vegetative R_{75} ratio lower than that calculated from ERTS data because of the rapidly rising reflectance of vegetation longward of 0.67μm. The other ratios should be close to the ERTS-drived ratios, and they are to the best of our current estimation. All of the obviously exposed rocks (granite, limestone, greenstone, magnetite, hematite, gray sand) in the Atlantic City District have ERTS-derived R_{75} ratios that are within the R_{75} ratio ranges calculated from corresponding lab samples. However, only lab spectra of rock samples from the test area will yield a final answer as to the absolute accuracy of the ratio method.

There are two comments concerning figure 4 that should be made here. First, the lab-derived ratio ranges represent the extreme (highest and lowest) in R_{75} for each given rock category, and most categories include specimens as small as 0 - 5μm in particle diameter. This is a worst case. Secondly, this is only one ratio, and final decisions concerning rock classifications will be made on the basis of two to four ratios. Further

work using laboratory data to derive ratio limits for these rock categories is planned, such that a ratio gating logic can be derived for the production of automatic recognition maps with an AND gate for each of the two to four ratios.

The other form of ratio map produced thus far is an analog ratio image. This yields a continuous display of ratio values, as if the ratio were a single channel of information. Figure 5 is an R_{75} analog ratio image which includes the whole Atlantic City District and more of the surrounding region. Note the enhanced iron mine (dark) discrimination from most of the immediately surrounding background. Note also that the sedimentary strata in the upper right of the R_{75} ratio image (not as near the corner as in Figures 1 and 2) are still indistinct. The diabasic gabbro dikes in the Louis Lake batholith are distinctive, however. Finally, note that the discrimination between vegetation (brighter) and non-vegetation (darker) is better in this ratio image than in either aerial photos or single-channel ERTS images.

An analog R_{74} ratio image of the same area (Fig.6) shows the iron mine (dark, but brighter than water) to be unique from all other points in the scene. The Jurassic sediments (relatively bright) and thin, dark beds of some sedimentary origin are discriminated from adjacent sedimentary strata in the upper right of the R_{74} ratio image. In no other photos or images shown in Figures 1 through 5 are there sediments discriminated this well. Vegetation is easily discriminated from non-vegetation; shadows, which are minimized, are not mistaken for vegetation here, as they were in the channel 5 ERTS imagery of Figure 1.

These analog ratio images focus the attention of the geologist or other scientist on areas in the scene where chemical properties of a target are different from its surroundings. The ratio images contain information which, when interpreted by the human eye, is either not available or difficult to distinquish in aerial photos or single channels of ERTS imagery. Furthermore, the ratios are dimensionless numbers with which laboratory data and points in the scene of interest can be compared. The data shown here only prove that geochemical data exist in ERTS data. Further data processing and ground truth investigations are necessary to permit the organization of these data into as many meaningful classifications as it possible.

5. CONCLUSIONS

The following general conclusions are made from the foregoing discussions:

1. Ratio images of ERTS data appear to be better than either aerial photos or ERTS single channel images for discrimination between vegetation and non-vegetation.
2. Some geological features smaller than the publicized spatial resolution of ERTS, such as the diabasic gabbro dikes in the

Louis Lake batholith, are seen as well in ERTS single-channel images and ERTS ratio images as in high altitude aerial photos.

3. Geochemical information definitely is contained in ERTS images and ratio images, which are generally superior to aerial photos because of the limited spectral range of the latter. Iron oxides are more easily discriminated from ERTS ratio images than from ERTS single-channel images or from high altitude aerial photography. This is useful in mineralogical exploration because exposures of several types of metallic ores are often associated with iron oxides. The differing relationships between rock type and iron-bearing minerals may also be useful in general geologic reconnaissance mapping, due to the resultant variability of ferric and ferrous compounds present. Satellite geologic reconnaissance would be much cheaper than aerial data collection over most large, remote sites.

4. On the basis of the ERTS ratio images, it seems plausible that an automatic recognition map can be made on the basis of selected spectral ratios of ERTS data which will distinguish rock and soil exposures from all other materials in the scene (within the limits of the ERTS spatial resolution) and discriminate two to four meaningful rock groups (each consisting of one or more rock types).

5. The agreement observed thus far on absolute ratio numbers between ERTS ratio maps and laboratory spectra encourages efforts to use laboratory data as training sets for geologic targets, which if successful, would enable the same automatic discrimination over unknown geologic terrain throughout the world, with reasonable atmospheric conditions.

6. Early quantitative analysis indicates that consistent results for this or other data processing techniques over large geographical distances or large time periods over a given test site will require some type of atmospheric corrections. The empirical atmospheric corrections used in this ratio method appear to be effective for high-elevation test sites, but have yet to be tested with areas near sea level.

7. The method being developed for this investigation would appear to be useful for scientific applications other than geology. Soil mapping and biomass estimation are two such applications.

REFERENCES

R.K. Vincent, "An ERTS Multispectral Scanner Experiment Mapping Iron Compounds," Proceedings of the Eighth International Symposium on Remote Sensing of Environment, Ann Arbor, Michigan, to be published in 1973. Also ERTS-1 Report No. E72-10181.

R.W. Bayley, "A Preliminary Report on the Precambrian Iron Deposits hear Atlantic City, Wyoming," USGS Bulletin 1142-C, 1963, pp.C1-C23.

J.A. Dorr, Private Communication, Dept.of Geology and Mineralogy, University of Michigan, 1973.

ACKNOWLEDGMENTS

I am grateful to Bette Salmon, William Pillars, and Fred Mauk of ERIM for their invaluable assistance. I also thank Dr. John Dorr of the University of Michigan for the aerial photos. This work was supported by NASA contract NAS-5-21783.

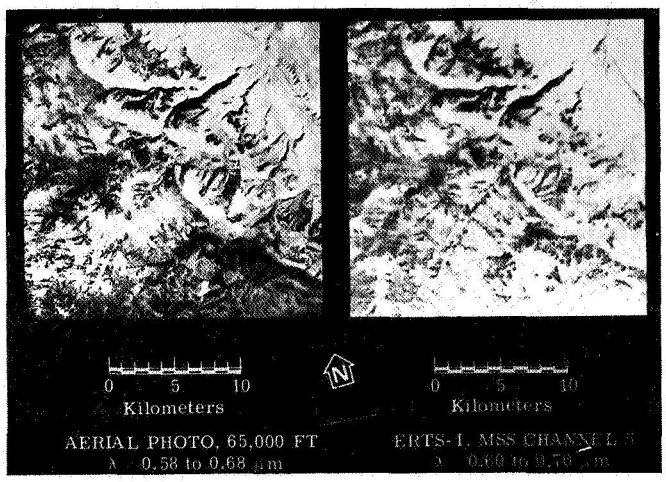


Figure 1. Aerial Photo and ERTS Image in the Visible Red of the Southern Wind River Range, Wyoming

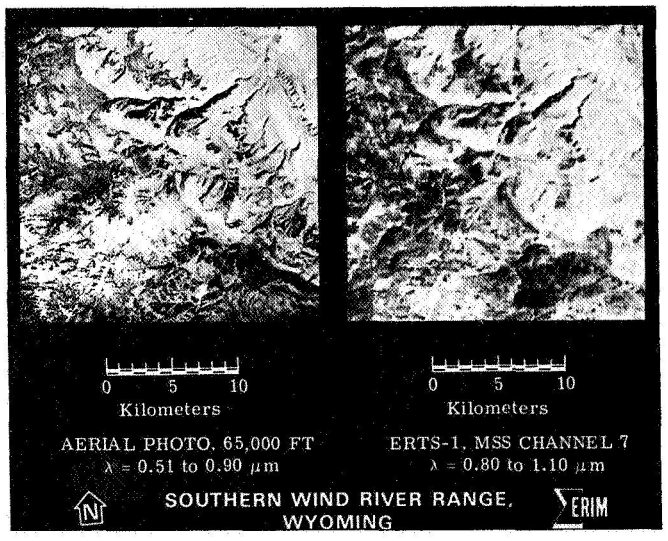


Figure 2. Aerial Photo and ERTS Image in the Reflective Infrared of the Southern Wind River Range, Wyoming



Figure 3. ERTS Digital R_{75} Ratio Graymap of Southern Wind River, Wyoming

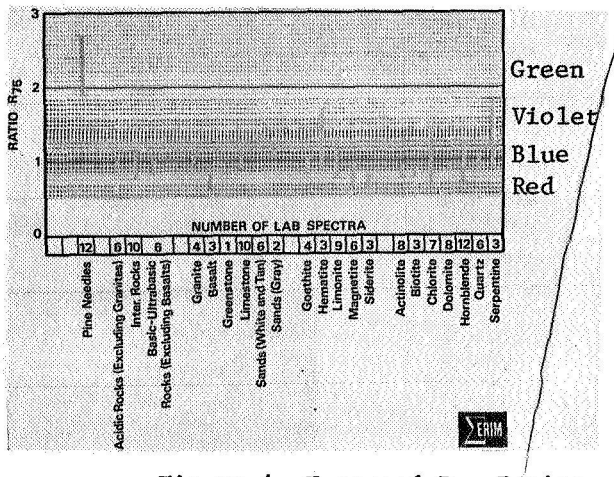


Figure 4. Expected R_{75} Ratios Calculated from Laboratory Data

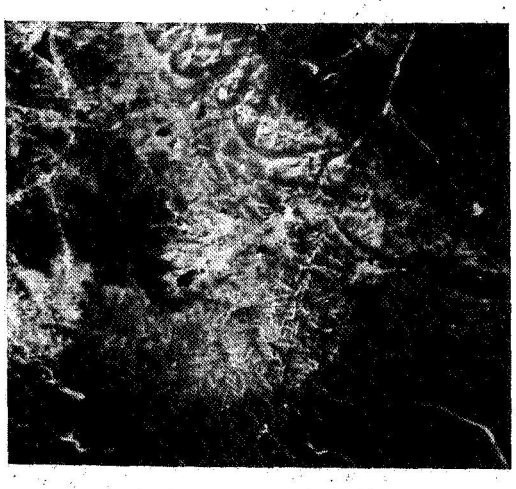


Figure 5. ERTS Analog R_{75} Ratio Image of Southern Wind River Range, Wyoming

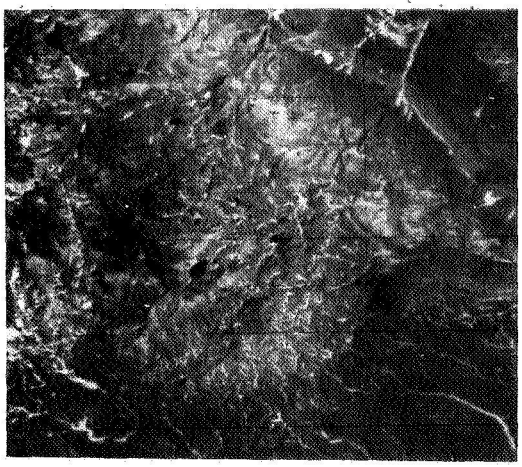


Figure 6. ERTS Analog R_{74} Ratio Image of Southern Wind River Range, Wyoming

Paper G 17

USE OF ERTS-1 IMAGES IN THE SEARCH FOR PORPHYRY COPPER DEPOSITS IN PAKISTANI BALUCHISTAN*

Robert G. Schmidt, *U.S. Geological Survey, Washington, D.C. 20244*

ABSTRACT

Geomorphic features related to a known porphyry copper deposit at Saindak, western Chagai District, Pakistan, are easily distinguished on ERTS-1 images. New geologic information from the images was used in conjunction with known geology to evaluate one previously known prospect area and to suggest two additional ones, but no new prospects were recognized on the basis of the images alone. The study also showed that Saindak-type deposits are not likely to be present in some extensive areas of the Chagai District.

The Saindak deposit is in an area of relatively easily eroded folded sedimentary and volcanic rocks. The deposit is characterized by an elongate zone of easily eroded sulfide-rich rock surrounded by a resistant rim of hornfels and propylitically altered rock. Both this rim and the central sulfide-rich valley are conspicuous features on the images. Swarms of dikes are probably useful for distinguishing real rims from other resistant rock types, but there is no expression of them on the image, although they are easily seen on aerial photographs of the Saindak rim.

During field mapping, patches of strong red and yellow hue related to the mineral natrojarosite were noted in the central valley. Attempts to detect a color anomaly using simple false color composites were not successful.

The investigation showed that a rim like that at Saindak does not form if regional metamorphism has increased the resistance of the country rock to erosion, as in the Pakistan-Iran border region northwest of Saindak.

---

* Publication authorized by the Director, U.S. Geological Survey.

INTRODUCTION

This investigation is based on the premise that the large low-grade copper sulfide orebody at Saindak in the Baluchistan desert (Figure 1) could be recognized on an ERTS-1 image, that other similar deposits may reasonably be expected in the region, and that ERTS-1 imagery offers a unique and convenient means of evaluating nearby areas for such deposits.

Mapping was undertaken at Saindak in 1962 because the locality was thought to have some economic mineral potential, and the complete results of this study were reported by Ahmed, Khan, and Schmidt (1972). In 1962, after discovery of the copper sulfide orebody, we noted several features of the deposit that lent themselves to optical remote sensing, and colored aerial photography was suggested as the most practical method (Schmidt, 1968, p. 60).

The discovery in 1967 of a major porphyry copper deposit at Sar Cheshmeh, near Kerman in Iran (Figure 1), and the subsequent discovery of several more deposits including those in the vicinity of Kuh-e-Hanza, to the southeast, as well as some to the northwest of Sar Cheshmeh has increased interest in this region as a potential source of minable copper. Examination of the deposit at Saindak was recently resumed by the Geological Survey of Pakistan (Khan, 1972).

All of the western part of Pakistan is covered by 1/253,440 photogeologic reconnaissance maps (Hunting Survey Corporation, Ltd., 1960), but probably less than 1 percent of the Chagai District has been mapped in detail. Mineral reconnaissance has been spotty and mainly for high-grade deposits; if a porphyry copper deposit had been noticed, it might have been passed over as too low grade for consideration at this time. Very little detailed topographic mapping is available for the region.

Studies on this project were made mostly on one bulk 9.5 inch positive transparency photographic image, ID 1125-05545. Comparisons were made with image ID 1143-05545 to determine that certain white patches were probably not snow cover. False color composites were prepared by printing multispectral scanner bands 4, 5 and 7 on yellow, magenta, and cyan transparent foils. Foils of various color densities were made and one set was then selected to give both optimum differentiation of geologic units and enhancement of the difference between eolian sand and other near-white geologic features. Areas of interest were examined in conjunction with photogeologic reconnaissance maps, and recognition of mapped geologic units on the image was generally easy. An excellent impression of relative topographic relief from the images, combined with the photogeologic maps, is a powerful interpretive tool. No study was made of the adjacent part of the image in Iran.

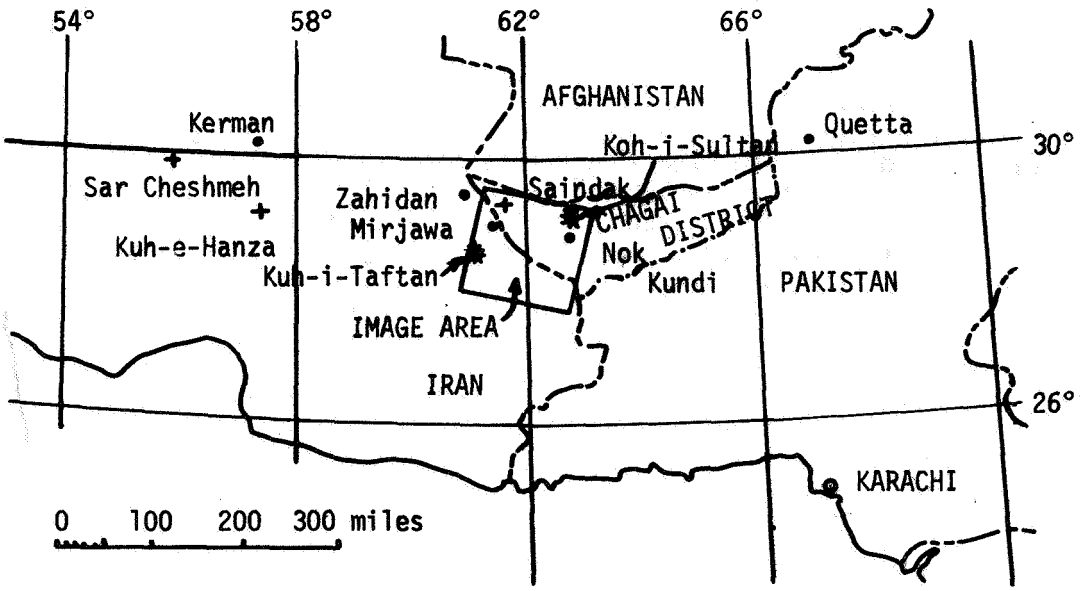


Figure 1: Index map of the Saindak area.

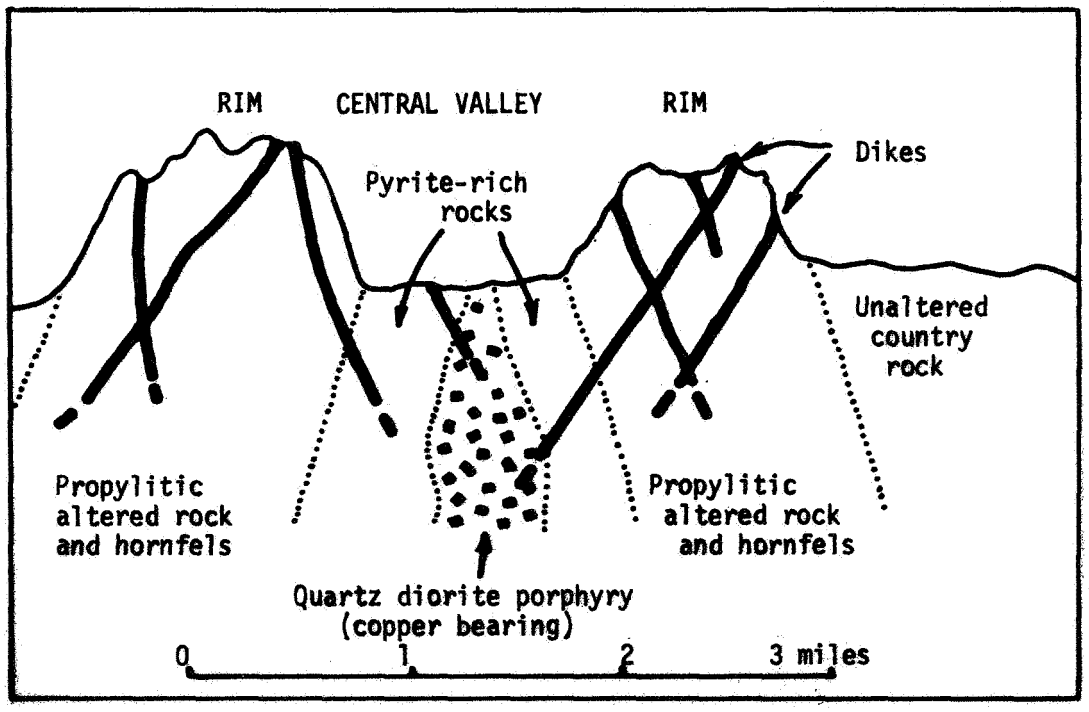


Figure 2: Hypothetical cross section of Saindak-type porphyry copper deposit. Vertical scale is exaggerated.

REGIONAL GEOLOGY

The areas of interest in the Mirjawa range --the folded mountains along the Pakistan-Iran border (Hunting Survey Corporation, 1960, plate 1)-- and in the Nok Kundi region have somewhat different regional geology. The rocks of both areas are of Cretaceous to Quaternary age, with the proportion of the area covered by Cretaceous to Tertiary strata possibly considerably less than is shown on Hunting Survey Corporation, Ltd., maps (1960).

The Mirjawa range area, which includes the Saindak deposits, has mostly folded and much faulted sedimentary and volcanic-sedimentary strata with relatively small amounts of intrusive and extrusive igneous rock. The detailed description of the Saindak area (Ahmed, Khan, and Schmidt, 1972) is fairly representative of the geology of this border region. Cretaceous sedimentary rocks represent a wide variety of marine and continental depositional environments; lower Tertiary rocks are mostly shallow marine, and upper Tertiary-Quaternary strata are from continental sites.

Regional metamorphism, probably related to granitic intrusives 25 miles west of Saindak in Iran, has been noted on the ground a few miles west of Saindak, and at many places northwestward from Saindak along the Mirjawa range.

In the Nok Kundi region, a western section of the northern Chagai hills, folding and faulting are also present but without a strong linear pattern. Intrusive rocks are more abundant, several volcanic necks are conspicuous, and there are volcanic cones and probably plug domes, as well as the dormant or extinct volcano Koh-i-Sultan.

ECONOMIC GEOLOGY

At Saindak several small copper-bearing porphyritic quartz diorite stocks cut northward across the entire folded lower Tertiary stratigraphic section. The stocks are perhaps cupolas on a single unexposed granitic body 5 miles long and less than half a mile wide. The group of stocks or larger body are surrounded by zones of contact metamorphism and hydrothermal alteration, simplified in cross section in Figure 2. The stocks are enclosed in a sulfide-rich envelope that contains as much as 15 percent pyrite; the envelope in turn is surrounded by a zone of propylitic alteration in which pyroclastic rocks in particular are altered to a hard, dark epidote-rich hornfels. Because the intrusive trend cuts several formational units, the hornfels is derived from conglomeratic sandstone, siltstone, mudstone, and these same rocks with various proportions of incorporated pyroclastic material. Limestone in the zone of alteration has been changed to marble and tactite, some hematite rich and some sulfide rich. Many dikes cut

these alteration zones and are easily identified on aerial photographs, and within the limits of the alteration, veins containing sparse lead and copper minerals are common.

The sulfide-rich central core including both the intrusive porphyry stocks and the adjacent pyrite rich rock (of several primary sedimentary types) has been eroded out to form a light-toned valley (Figure 2). Desert soils associated with many porphyry deposits the world over have distinct red and orange color anomalies, and this is true at Saindak as well, where the mineral natrojarosite has been identified in the pigmented material. Windblown and alluvial grains considerably dilute or cover much of the colored soil in the central valley at Saindak however. In plan this valley is encircled by a symmetrical rim of hills more rugged than the surrounding region. Large-volume low-grade porphyry copper ores can be a normal association of the sulfide-rich central zone, but only detailed field examination can determine this.

On the image (Figure 3) the linear central valley and surrounding rim of hills at Saindak are cut off at the north end, perhaps by a basin-range type border fault. Abundant dikes easily seen on aerial photographs, and perhaps helpful in identification of alteration centers, are too small for recognition at this scale. The interior valley is of light tone, but no color anomaly could be seen on the color composites that I made.

Both the central valley and rim are displaced left-laterally by a major east-trending fault. The fault was mapped in 1961-62, but the displacement of the sulfide-rich zone was noted first in 1972 by Khan. Both the fault and the displacement of rim and central valley are easily identified on the ERTS-1 image.

The gradual increase in topographic relief westward from Saindak is caused by an increase in regional metamorphism, probably related to large granitic intrusives in Iran. The metamorphism was known in a very general way but had not been mapped: the affected area can easily be delimited on the image. This metamorphism is important because the increased resistance to erosion may preclude the formation of a rim of the Saindak-type in the border ranges northwest of Saindak.

EVALUATION OF PORPHYRY COPPER PROSPECTS USING ERTS-1 IMAGE DATA

Several possible prospect areas were evaluated using old data from reconnaissance maps, prospect descriptions, and personal experience together with new information from the image, and some adjustments of prospect priorities were made. Two new prospect areas resulted from using the old and new data together, although no new prospects were

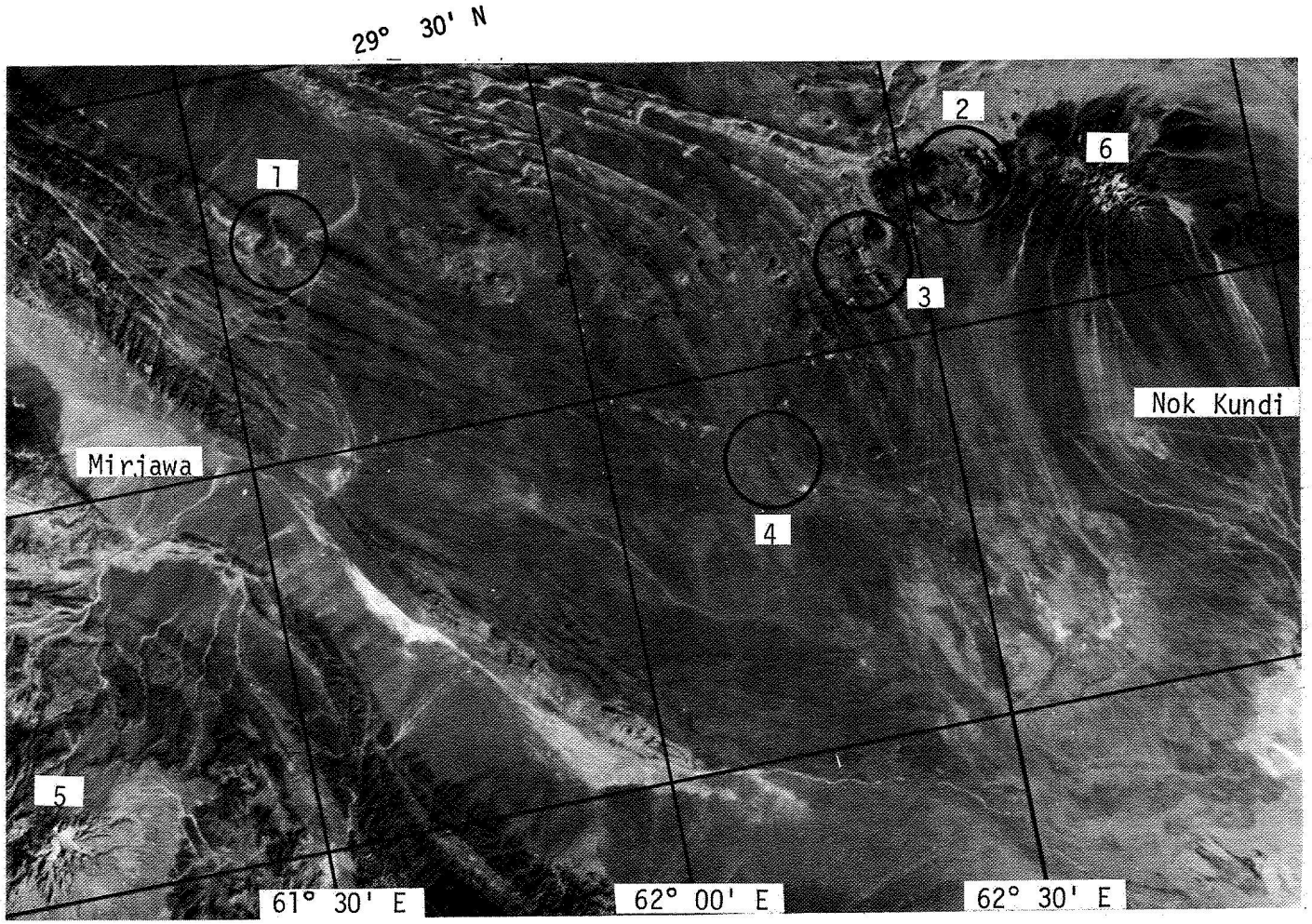


Figure 3: Annotated northern part of ERTS-1 image ID 1125-05545, MSS band 7. Numbered localities are: 1/ Saindak copper porphyry prospect 2/ Amir Chah copper prospect 3/ new prospect near Mashki Chah 4/ new prospect near Koh-i-Dalil railway station 5/ volcano Kuh-i-Taftan 6/ volcano Koh-i-Sultan. The circles are eight miles in diameter.

found on the basis of image data alone. The study showed that certain extensive areas are not likely to be mineral bearing and ground surveys there for copper porphyry deposits can be placed on a lowest priority basis.

Evaluation of old prospect areas:

Amir Chah locality - 29°08' to 11' N., 62°32' to 35' E. (Figure 3) -- Disseminated weak copper mineralization is present in a granodiorite(?) stock (Schmidt, 1968, p. 60), and there are small lean copper-bearing veins in hills a short distance to the west. The image shows that the central area of intrusive rock is topographically low and though partly mantled by dune sand, I think enough bedrock is exposed to indicate it has a light tone. Except rocks to the east which are younger volcanics, the surrounding dark more rugged areas, especially to the southwest and northwest, are interpreted to be hornfelsic zones of alteration, perhaps forming a fairly complete rim of hills; in contrast, hornfels was formerly known at only one locality on the northwest side. A hematite skarn with stains of malachite is also known on the northwest side (Hunting Survey Corporation, Ltd., 1960, p. 449.)

Although examination of the image did not add much new information, it helped reinforce my interpretation that the Amir Chah pluton may fit the general Saindak-type model, and this should be regarded as a fairly high priority prospect.

New potential prospects:

Mashki Chah locality -- 29°06' N., 62°24' to 28' E. (Figure 3) -- This is an area 6 miles north of Mashki Chah where a small intrusive is shown on the photogeologic map (Hunting Survey Corporation Ltd., map 22). Unfortunately this is also an area partly mantled by dune sand. The image shows that the intrusive forms a northeast-trending topographic depression, with a good suggestion of hornfelsic zones to the northwest and southeast. The whole feature is about the same size as the one at Saindak. This I regard as a relatively high priority prospect that deserves careful field inspection.

Koh-i-Dalil railway station area -- 28°53' N., 62°14' E. (Figure 3) -- This site was studied because the localized dike swarm suggests an intrusive center like that at Saindak. The only intrusive stocks mapped here are shown as diorites of the Tanki-sill type, but the image shows that the outcrop areas are not at all like the Tanki sills farther west, and are more likely to be quartz diorite type stocks. Slightly more rugged topography near the northernmost intrusive may be part of a hornfelsic rim. The entire feature occupies about the same area as that at Saindak. Because of its proximity to the highway and railway, this site deserves field examination prior to more remote localities.

Other possibilities in the Mirjawa Range -- Inspection of the image and photogeologic map indicate no other likely sites in the unmetamorphosed border range area besides Saindak and the Koh-i-Dalil railway station locality, and I would give other prospecting here a low priority. The metamorphosed area west and northwest of Saindak is not susceptible to this evaluation method and this study has not changed exploration priorities for porphyry-type copper deposits there.

REFERENCES CITED

Ahmed, Waheeduddin, Khan, S. N. and Schmidt R. G., 1972, Geology and copper mineralization of the Saindak quadrangle, Chagai District, West Pakistan: U.S. Geol. Survey Prof. Paper 716-A, 21 p.

Hunting Survey Corporation, Ltd., 1960, Reconnaissance geology of part of West Pakistan; a Colombo Plan Cooperative Project: Toronto, 550 p. (Report published by Government of Canada for the Government of Pakistan).

Khan, S. N., 1972, Interim report on copper deposit of Saindak, Chagai District (Baluchistan), Pakistan: Geol. Survey of Pakistan, Saindak copper report no. 1.

Schmidt, R. G., 1968, Exploration possibilities in the western Chagai District, West Pakistan: Econ. Geology, v. 63, no. 1, p. 51-60.

Paper G 18

RELATION OF ERTS-1 DETECTED GEOLOGIC STRUCTURE TO KNOWN ECONOMIC ORE DEPOSITS

Ernest I. Rich, *Department of Geology, Stanford University, Stanford, California*

ABSTRACT

A preliminary analysis of ERTS-1 imagery of the Northern Coast Ranges and Sacramento Valley, California, has disclosed a potentially important fracture system which may be one of the controlling factors in the location of known mercury deposits in the Coast Ranges and which appears to be associated with some of the oil and gas fields within the Sacramento Valley. Recognition of this fracture system may prove to be an extremely useful exploration tool, hence careful analysis of subsequent ERTS imagery might delineate areas for field evaluation.

INTRODUCTION

The intent of this report is to summarize, in a preliminary way, the regional geologic structure of the Northern Coast Range and Sacramento Valley, California and to suggest a possible relation between the geologic structure and known occurrences of mercury, hot springs (geothermally active areas), and some of the oil and gas fields of northern California. The area covered by the study includes all of northwestern California, extending from the latitude of San Francisco Bay on the south, to the California-Oregon border on the north, and the Pacific Ocean on the west, to the western foothills of the Sierra Nevada on the east (figure 1).

The original objective for examining the ERTS imagery was to determine the feasibility of detecting gross lithologic and structural data from satellite imagery. In preparation for the examination of the satellite imagery, ERTS-compatible photographs were obtained from NASA, U-2 aircraft underflights, which were flown in conjunction with an on-going environmental study of the San Francisco Bay Region by the U.S. Geological Survey. These photos were taken at varying time intervals during 1970 to 1972 and under various climatic conditions. In addition, the photographs from a single stereo-strip along the 39th parallel, extending from the Pacific Ocean to the crest of the Sierras, a distance of about 320 km (200 miles), were flown for another ERTS investigator and copies were made available to the project. From these various sets of photographs, visual interpretive criteria were developed for each multispectral bandwidth and,

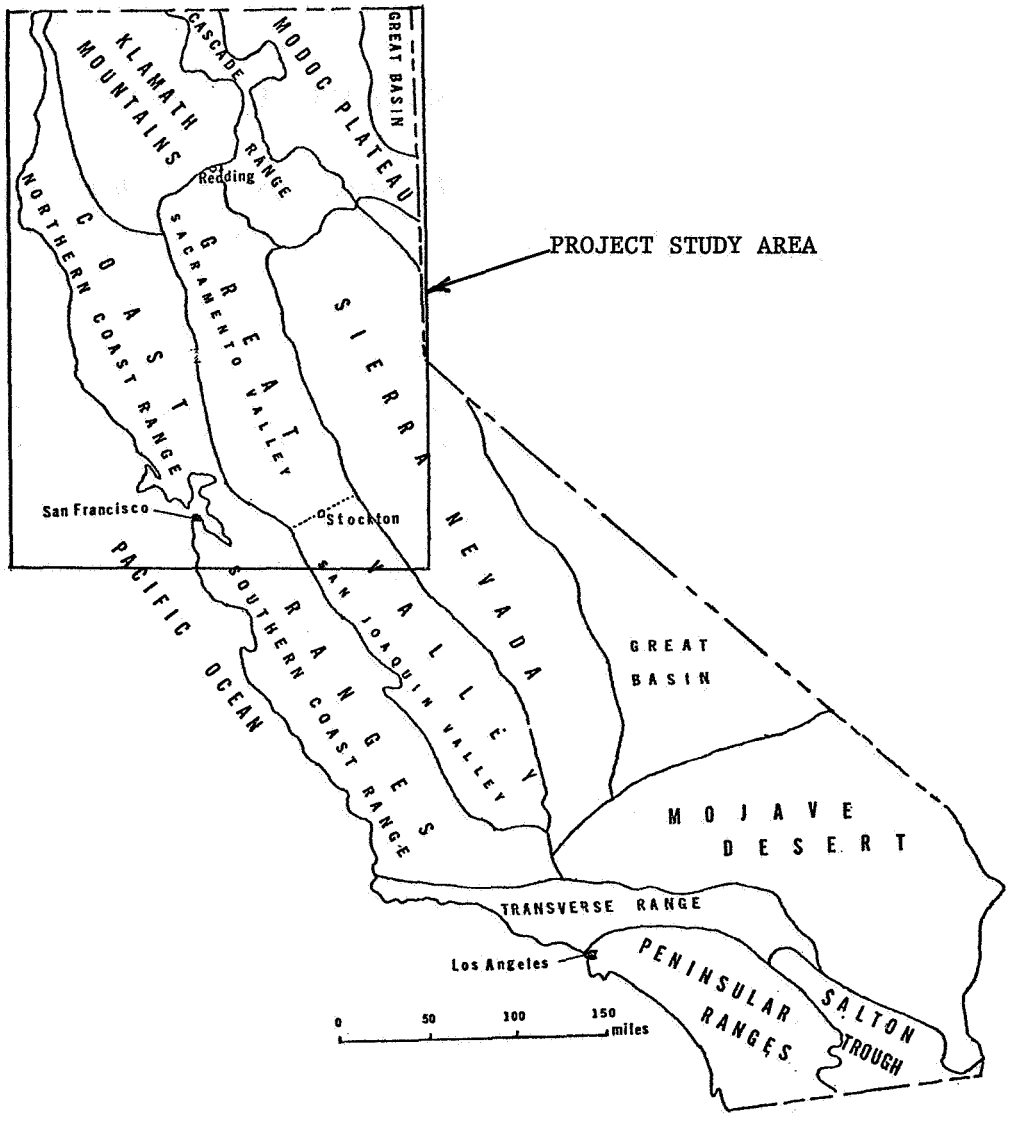


FIGURE I

OUTLINE MAP OF CALIFORNIA SHOWING PHYSIOGRAPHIC PROVINCES

within the limits of the available photography, the photo-characteristics of the various rock types under seasonally different climatic conditions were evaluated and recorded for later use. Data from these underflights suggested that the objective of the project could be best served by grouping the wide variety of lithologic types within the area into three broadly defined lithologic groups: 1) ultramafic igneous rock, including peridotite, serpentinized peridotite, and serpentinite; 2) extrusive volcanic rocks, including andesitic-basalt contained within the late Mesozoic Franciscan assemblage, rhyo-dacitic flows of the Pliocene to Recent Sonoma-Clear Lake volcanic fields, and Pliocene to recent basaltic volcanic flows of the Modoc Plateau (northeastern California); and 3) sedimentary rocks, including the late Mesozoic marine sedimentary rocks of the Great Valley sequence, Tertiary marine and nonmarine sedimentary rocks along the margins of the Sacramento Valley and parts of the coastal belt, and recent unconsolidated sediments, such as the alluvium within the Sacramento Valley and along the major drainages.

Reliable lithologic identification depends, to a large extent, on relating the photogeologic criteria to vegetation changes, which occur on the various lithologic groups, during the annual seasonal changes (wet to dry season and/or dry to wet season). ERTS data for all of these time periods are not presently available. A regional geologic structural interpretation has been made from the available ERTS imagery, independent of the lithologic data, and is presented here. Undoubtedly the structural interpretations will need to be modified when the lithologic groups can be more clearly identified.

The regional geologic structure was not studied in detail during the preliminary preparatory stage of the project as it was believed that the structural features could be independently evaluated. After receipt of the first ERTS-1 imagery, the frames were carefully analyzed and the chief geologic structural elements were recorded. Each frame was enlarged and the geologic data transferred to a topographic base map of northern California (1:500,000 scale). Data on the locations of mineral and fuel deposits were obtained from resource maps published by the California Division of Mines and Geology.

GEOLOGIC STRUCTURES

The geologic structure of the Coast Ranges is extremely complex and poorly understood. Recent ideas based on plate tectonics, or seafloor spreading, attribute the structural complexity (mélange-style deformation) to the piling-up of oceanic-plate material along a subduction zone associated with a late Mesozoic trench (Ernst, 1970). The coeval marine sedimentary rocks of the Great Valley sequence are little deformed and are thought to have been derived from a Sierran arc and to have been deposited in a late Mesozoic "arch-trench gap" which probably existed between the Coast Range Trench and the Sierran Arc (Dickinson and Rich, 1972).

A preliminary examination of ERTS imagery disclosed three potentially important systems of linear features within the Coast Ranges which may represent fault systems or shear zones inasmuch as topographic offset and stratigraphic disruption can be seen along some of the lineations (figure 2). Some of the linear features shown on figure 2 represent bedding traces, or unusual alignment of topographic features, and still others have no presently known explanation.

One of the systems is subparallel to the San Andreas fault and is confined to the Pacific coastal belt (Coastal System). Another set of lineations (the Central System), which at their northern terminus acutely join but do not transect the Coastal System, is confined to the core of the Coast Ranges. It is less well defined but it appears to be the chief control for the structural and topographic grain of the terrain. These two systems can be seen on figure 3 (ERTS-1, Frame No. 1094-18231-MSS-6). The third set of linear features (the Valley System) has not been clearly recognized heretofore. It trends north or northeasterly, at obtuse angles to the Central System, and one or two lineations within this system can be discontinuously traced from the core of the Coast Range across the alluviated part of the Sacramento Valley into the foothills of the Sierra Nevada, figure 4 (ERTS-1, Frame No. 1075-1870-MSS-5). Stratigraphic disruption of the late Mesozoic Great Valley sequence along the western margin of the Sacramento Valley (figure 4), is, in part, associated with the Valley System. Linear elements subparallel to the Valley System, can be detected in the Coast Ranges and the alluviated part of the Sacramento Valley. Within the Sacramento Valley, they may reflect the continuation of the Valley System within the bedrock that floors the Valley. In the northern part of the area the Valley System is roughly parallel to the off-shore Mendocino Escarpment and its landward extension.

The ERTS imagery of the Klamath Mountains and Modoc Plateau of northern California and southern Oregon have not been completely evaluated at this time; hence, some of the trends of the linear features in the northern part of the California Coast Ranges, shown on figure 2, may reflect the influence of these two large geologic features.

The locations of known mercury deposits and northern California oil and gas fields have been plotted on the map (figure 2). Some of the mercury deposits, recent volcanism, as well as some of the geothermally active areas near Clear Lake, in the Coast Ranges, are along the Valley System or at the intersection of the Central and Valley systems; however, other mercury deposits seem to be more clearly related to the Central System, or appear to show no direct relation to the linear systems. This preliminary review suggests, however, that recognition of the linear systems may prove to be an extremely valuable exploration tool.

All of the oil and gas fields in northern California are beneath the alluviated part of the Sacramento Valley. The locations of some of these fields are closely associated with some of the linear elements in the Valley System and others with the linear elements of the Central System. A thorough analysis of the published data is underway in order to determine the subsurface control in each of the fields. If the relations reported here prove reliable, the analysis of ERTS imagery may suggest other areas for mineral fuel exploration.

REFERENCES CITED

California Division of Mines and Geology, 1955, Economic Minerals Maps of California, Special Bull. 45.

Dickinson, W.R., and Rich, E.I., 1972, Petrologic Ingervals and Petrofacies in the Great Valley sequence, Sacramento Valley, California: Geol. Soc. American Bull. v. 83, p. 3007-3024.

Ernst, W.G., 1970, Tectonic contact between the Franciscan mélange and the Great Valley sequence, crustal expression of a late Mesozoic Benioff zone: Jour. Geophys. Research, v. 75, p. 886-902.

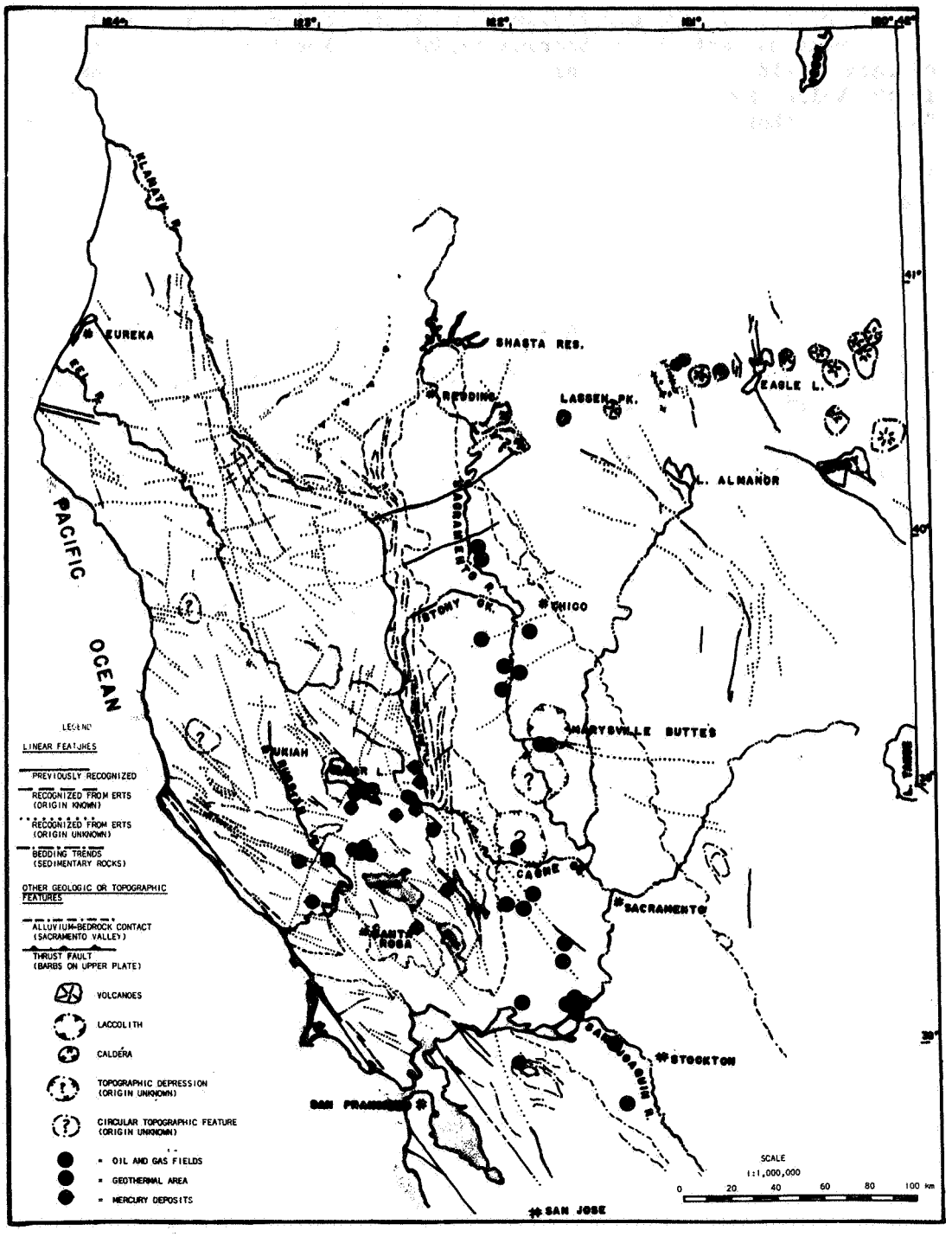


FIG. 2. MAP OF NORTHERN COAST RANGES AND SACRAMENTO VALLEY, CALIFORNIA SHOWING ERTS-RECOGNIZED GEOLOGIC STRUCTURES.

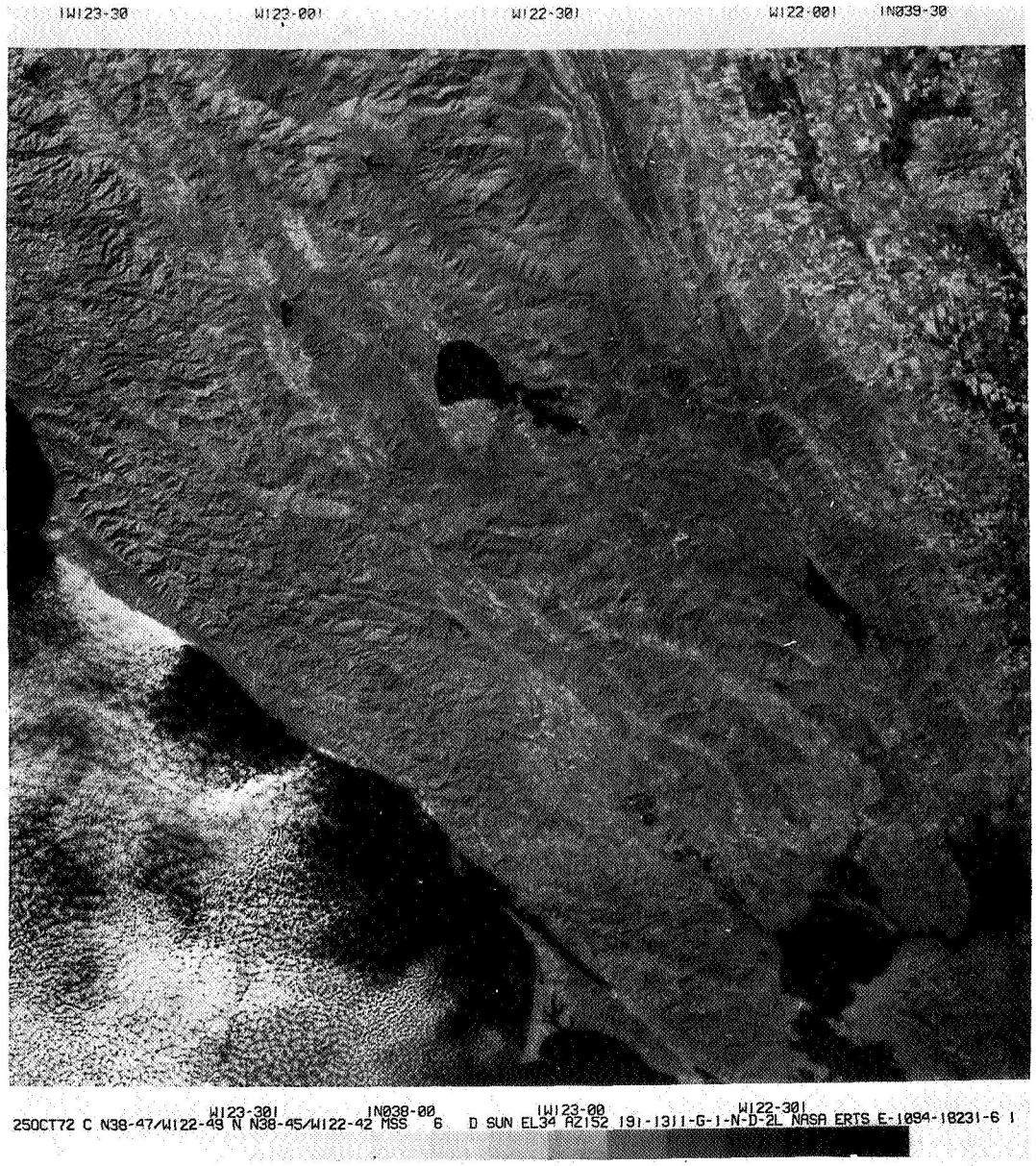


Figure 3. Part of Northern California Coast Ranges showing prominent linear systems: Coastal System including the San Andreas and related faults, near coast between Point Reyes (1) and Point Arena (2); Central System between San Francisco Bay (3) and northwestern part of image; and a prominent linear of the Valley System trends northeasterly through Clear Lake (4). Marysville Butte laccolith (5) and topographic depression (6) within Sacramento Valley (ERTS-1 Frame, 1094-18231-6).

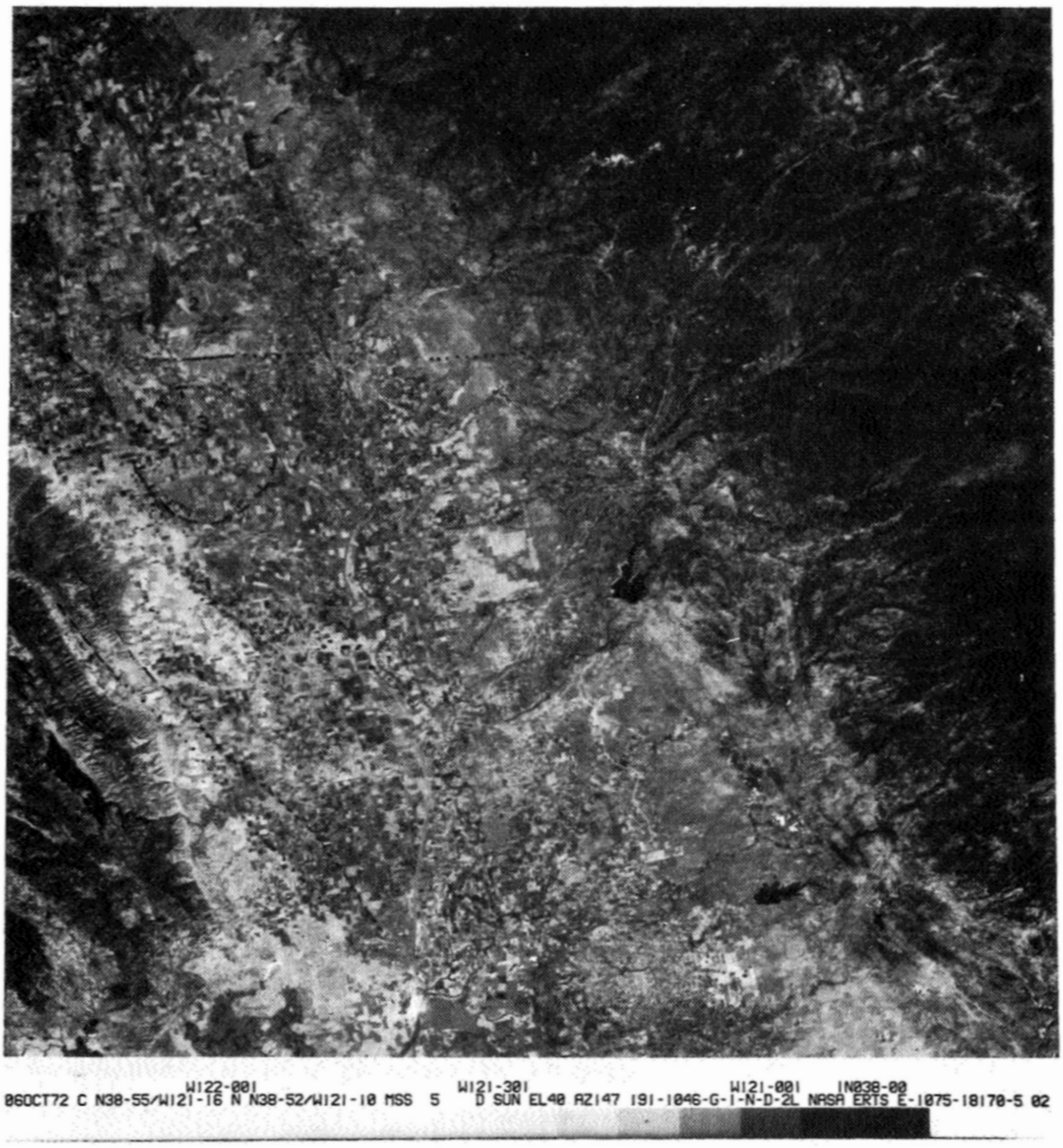


Figure 4. Part of Sacramento Valley and Sierra Nevada foothill belt showing extension of the Central System into the Valley alluvium near Lake Berryessa (1) and a prominent linear of the Valley System through Marysville Buttes laccolith (2). Circular topographic depression-caldera? (3). See figure 2 for details (ERTS-1 Frame, 1075-18170-5).

Paper G 19

PRELIMINARY GEOLOGIC INVESTIGATIONS IN THE COLORADO PLATEAU USING ENHANCED ERTS IMAGES

Alexander F. H. Goetz, Fred C. Billingsley, *Jet Propulsion Laboratory, Pasadena, California*
Donald Elston, Ivo Lucchitta, *U. S. Geological Survey, Flagstaff, Arizona*
Eugene M. Shoemaker, *California Institute of Technology, Pasadena, California*

ABSTRACT

Bulk and computer enhanced frames of the Verde Valley region of Central Arizona, an area which has been well mapped, have been analyzed for structural information and rock unit identification. Most major rock units in areas of sparse ground cover are identifiable on enhanced false-color composites. Regional structural patterns are strikingly visible on the ERTS images. New features have been identified which will aid in the search for ground water near Flagstaff, Sedona and Stewart Ranch.

1. INFORMATION

The purpose of our study in Central and Northwestern Arizona is to marry the techniques of computer image processing and field geologic mapping to attack some regional geologic problems of special interest. Work in only one of the three areas under study is discussed in this paper. This area is situated in north-central Arizona (Fig. 1) and is about 70 miles in north-south extent and 50 miles wide, and includes parts of the Colorado Plateau and the adjacent "Mountain Region" to the south. The area is centered on the Verde Valley, and on the west includes part of the Chino Valley. Flagstaff is on the northeast boundary and Prescott lies near the western boundary.

II. GEOLOGIC SETTING

In the Colorado Plateau area, Tertiary basaltic flows less than a hundred to a few hundred feet thick, derived from scattered eruptive centers during the past ~15 m.y., mantle nearly flat-lying sedimentary strata of Paleozoic age (Fig. 2). The Paleozoic beds aggregate several thousand feet in thickness. In the Verde Valley area, the Paleozoic strata rise structurally in a southerly direction, and the basaltic flows

rest on successively older beds to the south. The southwestern most extent of preservation of Paleozoic strata in central Arizona occurs in the southern part of the map area (Fig. 2). In the western and southwestern parts of the area, the Tertiary basalts overlie a variety of Precambrian igneous and metamorphic rocks. A great deal of the area has been mapped geologically in detail, at scales of 1:62,500 and 1:48,000 (see references). The generalized geologic units shown in Figure 2, and the faults shown in Figure 3, were drawn principally from this published information.

Non-metallic deposits currently being exploited are limestone for cement, gypsum for plasterboard, volcanic cinder deposits and gravel deposits for road metal. Copper is the principal metallic mineral that has been mined. Production has come mainly from the Serome area and from south of Humboldt.

III. PRELIMINARY FINDINGS

The simple color composites of bands 4,5 and 7, computer stretched to increase contrast, show remarkably good correlation with the generalized geologic map shown in Figure 2. Areas not covered by Ponderosa pine exhibit color tones diagnostic of the individual geologic units, in spite of moderate vegetation cover in the form of Juniper bushes, sagebrush and grass. In the areas of sparse vegetation all major geologic units are identifiable. Areas mapped as Qg, gravel and sediment deposits, cannot be differentiated from the units from which they were derived. For instance in the northern Verde Valley the deposits derived from the Paleozoic Supai Formation have the same characteristic color as the original unit.

The major copper workings, as well as the tailings leach ponds, are highly visible down to one resolution element in size, because of the characteristic low sulfide reflectivity in the near IR compared to the visible. These areas appear bright blue on a false-color IR composite.

IV. FAULTS AND LINEATIONS

Well-developed regional structural patterns are strikingly visible on the ERTS images, particularly where Precambrian metasedimentary and metavolcanic rocks are at the surface (e.g. southern part of area; Figs. 2 and 3). The ancient structural grain trends predominantly northeast and north, and includes subordinate widely spaced east-trending lineations. Northwest-trending structures and lineations reflect comparatively recent structural adjustments and the development of the present geomorphologic form of the region. The northwest-trending linear features, for the most part, are less conspicuous than the north and northeast-trending lineations. ERTS images show that most of the eruptive centers for the basaltic volcanism on the Colorado Plateau are clearly localized along northeast and north-trending lineaments. This suggests that Precambrian structures were responsible for the localization of the eruptive centers, and that structural adjustments along the ancient trends occurred during the Tertiary volcanism. The Oak Creek Fault, for example, is inferred to overlie a north-trending fault system in the basement that is en echelon to the Shylock Fault Zone north of Humboldt.

The lineaments mapped photogeologically from the ERTS images locally supplement, and generally complement, the pattern of known mapped faults. In unmapped areas, the lineaments constitute the only structural information, information which provides an overall sense as to the nature of the crackling of the crust. The lineaments range from very strongly developed sets of joints, to vaguely developed, almost indefinite groups of short linear features which together portray a possible structural grain. In some cases, the well defined lineations reflect stratification in metamorphosed rocks (south of Humboldt); in other cases, they reflect strong zones of fracture (in Paleozoic rocks near Sedona). It should be noted that northwest-trending fractures in the Sedona area are extremely abundant and closely spaced, and in images from low altitude are the overriding structural characteristic. The ERTS images of this area, however, display some very strongly developed northeast- and east-trending lineations which previously were unrecognized. Similarly, a strong north-trending lineament which parallels and lies east of the Oak Creek Fault was recognized as an element of the Oak Creek Fault system in light of the ERTS images. The ERTS images appear to provide a method for "seeing" important structural grain in sedimentary rocks beneath the basalt cap in the Flagstaff area. Structural discontinuities in the basement also may be traced even where concealed by thick valley-fill deposits. An example occurs in the Chino Valley where one or more lineations may be traced northwestward from Humboldt to past Stewart Ranch.

An example of directional filtering to remove horizontal banding and enhance small oriented features is shown in Figure 4. Several orientations of structural grain are visible over a wide area of the image. Such enhancements are useful to attract the attention of the viewer to subtle, oriented features. However the subjective evaluation of the mapper is necessary to exclude possible artifacts. A more detailed account of the various methods of image processing is given elsewhere in this volume (Billingsley and Goetz, 1973).

V. APPLICATION TO GROUND WATER RESOURCE PROBLEMS

The City of Flagstaff is presently in the process of developing a source of subsurface water from the Coconino Sandstone at two localities: (1) in the Woody Mountain area, where several wells have been drilled, and (2) in the lower Lake Mary area where one well has been drilled. The Coconino Sandstone appears to be saturated at these places and reliable producing wells depend on fractured ground. Areas marked by the intersection of differently oriented sets of fractures will be important for guiding the location of wells that are to be drilled this summer into the Coconino Sandstone, and the location of a planned deep well that is to test the stratigraphically much lower Redwall Limestone. Long range plans for the development of a large supply of water will require the structural evaluation of ground extending some 60 miles southeast of Flagstaff.

The lineaments shown on Figure 3 in the area of the Oak Creek Fault and Lake Mary have been informally provided to the City of Flagstaff and have been transferred to the city's working map of the Woody Mountain area.

Figure 3 shows that an area immediately southeast of Woody Mountain may be structurally favorable for subsurface water. Strongly developed northwest-trending lineaments impinge and appear to intersect north-trending lineaments of the Oak Creek Fault system. The utility of the minor lineaments and their relation to a regional fracture pattern remains to be demonstrated. A lineament map is to be made employing normal aerial photographs in an analytic stereo plotter to supplement the lineaments derived from ERTS images. RB-57 photography has been ordered to allow the compilation of lineaments for a more extended area at a scale of 1:62,500, which is compatible with anticipated drilling target areas. The latter will cover the area of intermediate and long range planning for the development of Flagstaff's water resources.

Sedona area: The State Geologist of Arizona and Water Resources Division of the U. S. Geological Survey, are concerned with discovering a new and extensive supply of water to serve the scenic and rapidly developing Sedona area of the Verde Valley. The potential aquifer is the Redwall Limestone, which underlies Sedona and the cliffs of Supai Formation and Coconino Limestone that bound Sedona on the north and east. Information needed includes elevation control on key horizons in exposed beds, which will provide data on the structural attitude and spatial position of the potential aquifer. Also needed is the distribution of fracture zones that would permit the interconnection of karst or cavernous ground anticipated in the lower part of the Redwall. In such cases, one can encounter virtual underground "rivers".

Existing ERTS images (Fig. 3) and high altitude RB-57 color photographs display the character of fracturing in the Sedona area. A few very well developed east-west-trending lineaments transect the more common NE-, NW- and north-trending sets of lineaments. We interpret that the scenic embayment in the Colorado Plateau margin in which Sedona is located resulted from erosion in an area that is somewhat more fractured than adjoining areas. The greater fracturing presumably reflects the existence of the fourth (E-W) set of fractures. Development of water resources will depend on the location of a favorable structural position for the potential aquifer and the existence of suitably fractured ground. We have begun discussions which may lead to the establishment of a cooperative effort toward the solution of this problem.

Chino Valley, Stewart Ranch area: Another area of interest to the State Geologist and Water Resources Division is in Chino Valley, near the Stewart Ranch. Here, substantial quantities of ground water occur near the surface, and flowing wells have been drilled. Control, source, and recharge areas for the water are not really known, although the existence of outcrops of Precambrian Mazatzal Quartzite in low hills nearby (Fig. 2) suggests some form of structural control on the aquifer (Redwall Limestone).

The ERTS images have revealed the existence of lineaments of Chino Valley which extend northwestward from Humboldt. These can be traced to and well beyond the Stewart Ranch area. They are provisionally interpreted to reflect structure in bedrock beneath the valley fill. Their

existence suggests that the near-surface ground water is controlled by the existence of a heretofore unrecognized "dam" in the subsurface.

A structural evaluation of this area is needed to allow the proper development of ground water resources. ERTS images, and high altitude photographs, need to be analyzed for the distribution and character of lineaments. These, interpreted in light of structure to be obtained from surface and subsurface studies, should shed light on water resources in this part of the Chino Valley. We tentatively plan to carry out the required structural studies as part of a cooperative investigation with the appropriate federal and state agencies.

REFERENCES

Anderson, C. A., and Blacet, P. M., 1972, Precambrian Geology of the Northern Bradshaw Mountains, Yavapai County, Arizona: U. S. Geol. Survey Bulletin 1336, 82 p., 2 pl.

Anderson, C. A., Blacet, P. M., Silver, L. T., and Stern, T. W., 1971, Revision of Precambrian Stratigraphy in the Prescott-Jerome Area, Yavapai County, Arizona: U. S. Geol. Survey Bulletin 1324-C, p. C1-C16.

Anderson, C. A. and Creasey, S. C., 1958, Geology and Ore Deposits of the Jerome Area, Yavapai County, Arizona: U. S. Geol. Survey Bulletin 1230-F, p. F1-F19, 1 pl.

Billingsley, F. C. and Goetz, A. F. H., 1973, Computer Techniques Used for Some Enhancements of ERTS Images, ERTS Investigator Symposium March 5-9. Goddard Space Flight Center.

Huff, Lyman C., Santos, Elmer, and Raabe, R G., 1966, Mineral Resources of the Sycamore Canyon Primitive Area, Arizona: U. S. Geol. Survey Bulletin 1230-F, p. F1-F19, 1 pl.

Krieger, Medora H., 1965, Geology of the Prescott and Paulden Quadrangles, Arizona: U. S. Geol. Survey Prof. Paper 467, 127 p., 5 pl.

Lehner, Robert E., 1958, Geology of the Clarkdale Quadrangle, Arizona: U. S. Geol. Survey Sulletin 1021-N, p. N511-N592, 3 pl.

Twenter, R. F., and Metzger, D. G., 1963, Geology and Ground Water in Verde Valley--the Mogollon Rim Region, Arizona: U. S. Geol. Survey Bulletin 1177, 129 p., 1 pl.

Wilson, Eldred D., Moore, Richard T., and Cooper, John R., 1969, Geologic map of Arizona (scale 1:500,000): Arizona Bureau of Mines and U. S. Geological Survey.



Figure 1. A portion of ERTS frame 1014-17375-7 showing the area under study.

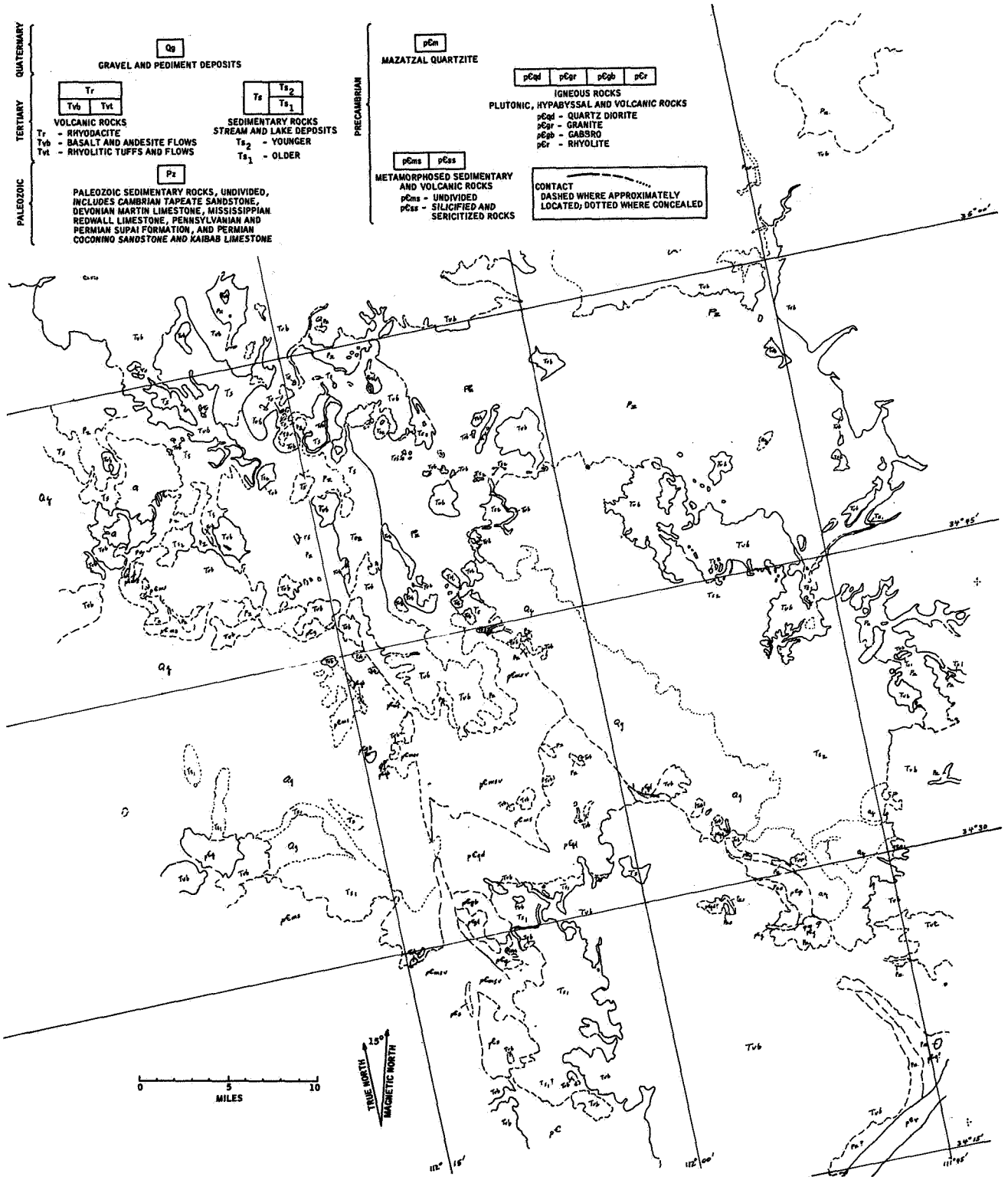


Figure 2. Generalized Geologic Map Compiled from the Listed References

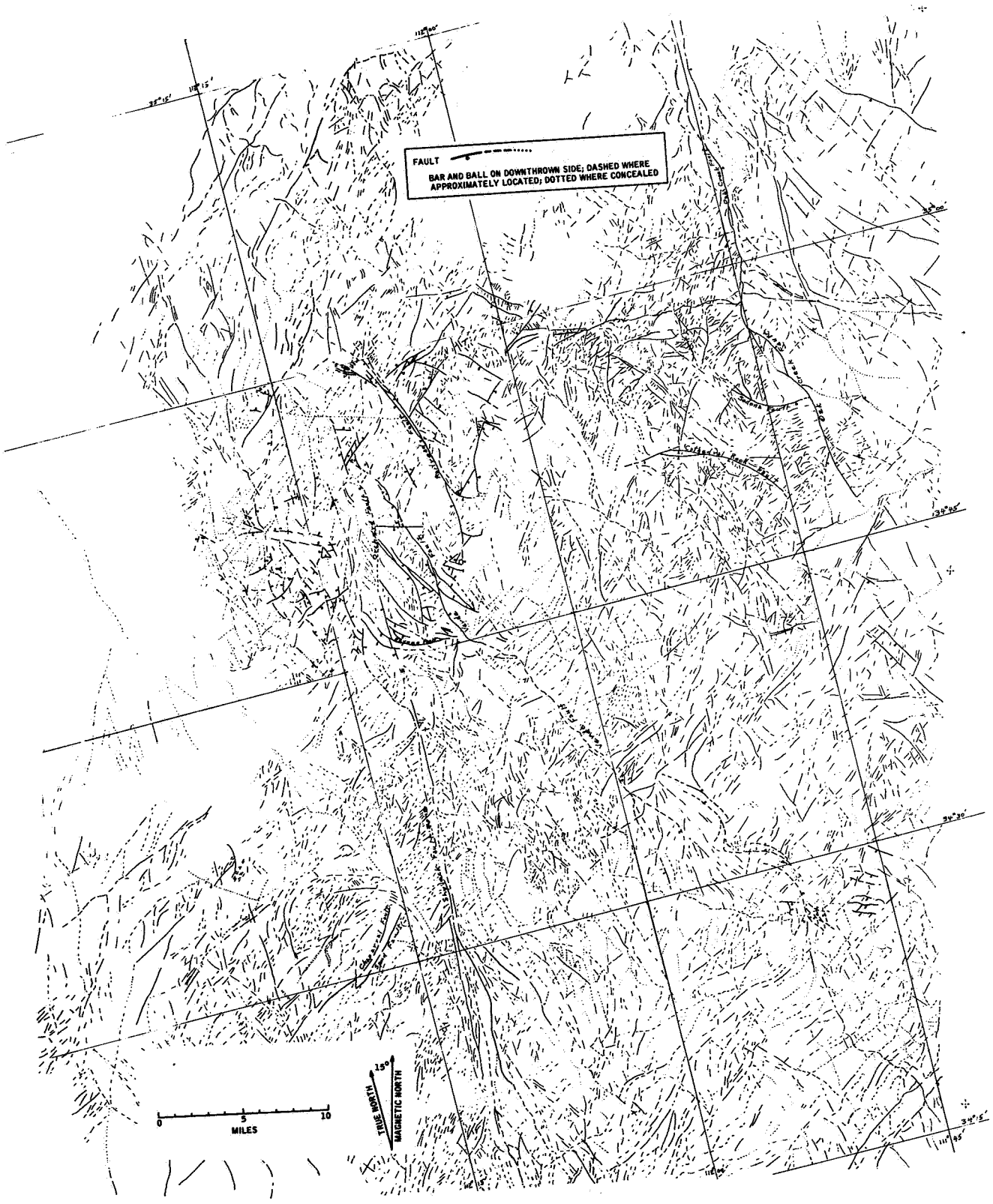


Figure 3. Lineament map of the Verde Valley Region. Heaviest lines denote mapped faults, other lineaments derived from ERTS photos.



Figure 4. Computer enhanced product of Figure 1. The horizontal bar filter removes banding and enhances small linear features in other directions.

Paper G 20

STRUCTURAL GEOLOGIC ANALYSIS OF NEVADA USING ERTS-1 IMAGES: A PRELIMINARY REPORT

Lawrence C. Rowan and Pamela H. Wetlaufer, *U.S. Geological Survey, Washington, D.C.*

ABSTRACT

Structural analysis of Nevada using ERTS-I images shows several previously unrecognized lineaments which may be the surface manifestations of major fault or fracture zones. Principle trends are NE, NW, NNE-NNW, and ENE. Two lineament zones, the Walker Lane and Midas Trench lineament system, transect the predominantly NNE-NNW trending mountain ranges for more than 500 km. 50 circular features have been delineated. Comparison with known Tertiary volcanic centers and reference to geologic maps suggest 8 new centers.

Preferred distribution of mines and Tertiary volcanic centers along some of the major lineaments suggests a genetic relationship. The intersection of three previously unmapped lineaments in northwestern Nevada is the location of a highly productive metallogenic district. In the Walker Lane, ENE-trending lineaments appear to be related to the occurrence of productive ore deposits.

INTRODUCTION

ERTS images provide information which is pertinent to several aspects of geologic exploration, but structural analysis is benefited particularly by these synoptic views of complex terrain. Lineaments indicative of zones of weakness and circular features suggestive of volcanic or intrusive activity can be delineated efficiently and analyzed in regional context. These types of data are important for understanding the geologic evolution of large regions and are directly applicable to mineral exploration.

This report briefly describes preliminary results of an evaluation of ERTS images of part of Nevada. The main objective of this experiment (NASA SR 9648) is to develop structural and radiometric analysis techniques for geologic exploration from satellite platforms. Radiometric analysis has been limited thus far to visual comparison of the Multispectral Scanner (MSS) bands, mainly to identify areas for detailed analysis. Because some of these results are reported elsewhere (Rowan, 1972), this paper is restricted to the structural analysis aspects of the experiment.

Structural Analysis

The topography of Nevada is characterized by north-northeast- to north-northwest-trending block-faulted mountain ranges and intermontane basins, typical of the Basin and Range physiographic province. In many places the ranges are transected and bounded by escarpments which, along with linear zones of rock and soil contrast and many elements of the drainage system, form an intricate lineament pattern. Alinement of these lineaments over great distances is known to be the surficial manifestation of fracture and fault zones which form part of the tectonic framework of this geologically and economically important region.

To the north and along the southwestern border of the state, the Basin and Range pattern gives way to volcanic landforms. Volcanic activity has also been very important throughout the remainder of the study area. Volcanic features are commonly marked by circular or eliptical topography and radial drainage.

Because ore deposits are commonly localized by fault and fracture zones and volcanic centers, our structural studies have concentrated thus far on delineation and initial analysis of lineaments and circular (and elliptical) features. Review of published geologic maps and reports shows that several of these structural features have not been previously recognized. Comparison of the areal distributions of the major lineaments and circular features with mining areas in Nevada suggests a genetic relationship. The preliminary nature of this work must be emphasized, however, as statistical analysis and field studies have not been conducted and many aspects of this experiment have not been integrated into this evaluation.

Lineaments

Lineament analysis of the study area (fig. 1) was initiated on individual images and then expanded areally by the use of mosaics at the 1:1,000,000 scale. Although lineaments as short as 2-3 km have been mapped in considerable detail for most of the area, only those longer than 75 km are discussed here. The major lineament pattern is dominated by four general directions: NNE-NNW; NW; NE; and ENE (fig. 1). Although all of these directions are represented throughout the study area, the densities and magnitudes vary geographically. In the southwest, generally NW-trending lineaments mark the Walker Lane along the Nevada-California border. ENE-trending lineaments which are continuous for more than 100 km occur almost exclusively in this area. NE-trending lineaments are subordinate in the southern part of the study area. In marked contrast, the pattern in the north is dominated by a zone of NE-trending lineaments which is continuous for approximately 500 km. We refer to this prominent feature as the "Midas Trench lineament" because of its apparent association

with the topographic depression (A, fig. 1) near Midas, Nev. The fourth prevalent lineament direction in the study area, NNE-NNW, represents faults which most commonly bound, but locally transect, the mountain ranges. The geographic distribution of these lineaments is reasonably uniform. In addition to these four prominent trends, four WNW-trending lineaments are equally spaced, some 200 km apart, between the Walker Lane and the northern boundary of the area.

The Walker Lane is a major northwest-trending zone of right-lateral transcurrent faulting, known to extend through southern Nevada from Pyramid Lake to Las Vegas (Shawe, 1965; Stewart and others, 1968). Gianella and Callaghan (1934) first recognized this zone from right-lateral displacements in the Cedar Mountains caused by the earthquake of December 20, 1932. Billingsley and Locke (1941) named the regional lineament the "Walker Line," later changed to the "Walker Lane" by Locke and others (1940).

Most evident on the ERTS-I imagery of Nevada is the NW-trending topographic discontinuity across southern Nevada, marking a distinct change in trend of mountain ranges. North of the break, the ranges trend NNW-NNE, whereas south of the break, the ranges trend predominantly northwest. Lineaments mapped by eye on the imagery suggest a zone of faulting along this discontinuity.

The two NW-trending lineaments lying south and southwest of Pyramid Lake (B, fig. 1) are mapped by Bonham (1969), and Gimlett (1967), respectively, as right-lateral strike-slip faults. We propose that these faults are part of the Walker Lane system. Continuing southeast of Pyramid Lake, two parallel NW-striking lineaments on the order of 65 km in length pass east of Walker Lake (C, fig. 1). The northeasterly one is documented as the Battle's Wells fault and the southwesterly one as the Soda Springs Valley fault (Nielson, 1965), both right-lateral strike-slip faults. Albers and Stewart (1965) propose three NW-trending right-lateral faults continuing southeast into Esmeralda County. In addition, they map another right-lateral fault (E, fig. 1) trending ENE across the northwestern part of the county; we extend this lineament approximately 175 km eastward. Right-lateral strike-slip faulting along the more northerly trending lineament south of Goldfield (D, fig. 1) is suggested by Gianella and Callaghan (1939), Locke and others (1940) and Ekren and others (1971).

The Midas Trench lineament zone is much more poorly known than the Walker Lane mainly because only small parts of the area have been mapped in detail. The most conspicuous segments of the Midas Trench lineament are linear topographic depressions near Midas (A, fig. 1) and the escarpment to the northwest (F, fig. 1) which separates the Owyhee Desert on the northwest from the mountain ranges to the southeast. Northeastward projection of this escarpment falls along straight segments of streams in the high mountains.

Geologic maps are available for only relatively small parts of the northeastern area transected by this lineament. In the Rowland quadrangle, one of the main structural features is the N.40°-70°E.-striking Trail Gulch fault which Bushnell (1967) believes has right-lateral displacement. Coats (1964) maps ENE-trending normal faults in the adjacent Jarbidge quadrangle, and a major ENE-trending normal fault is described by Decker (1962, pl. 1) in the Bull Run quadrangle to the southwest of the Rowland and Jarbidge quadrangles. In summary, NE-trending faults are major tectonic features in this part of the area, but the sense of movement is not clear.

To the southwest, this lineament assumes a slightly less distinct character. The alinement of steep-sided canyon and ridges, however, strongly suggests continuation of this zone to the vicinity of Pyramid Lake and Carson City where it intersects the Walker Lane.

Reconnaissance geologic maps covering the southwestern extension of the Midas Trench lineament zone neither deny nor support the significance attached herein to the feature. Although NE- and ENE-trending faults are mapped along this projected segment (Tatlock, 1969), intensity and magnitude and sense of displacement are difficult to assess. Shawe (1965) suggests on the basis of topographic map patterns a major transverse lineament which approximates the location of the Midas Trench lineament. He believes that this lineament represents a first-order left-lateral strike-slip fault.

Other lines of evidence suggest that this lineament may represent a major crustal feature. Projection northeast beyond the present study area results in coincidence with the southeast border of the somewhat anomalous Snake River Plains; continued projection intersects the volcanic area of Yellowstone National Park. Magnetic data compiled at the 1:1,000,000 scale show a NE-trending total intensity anomaly which extends from north-central Nevada through Yellowstone National Park and beyond (Isidore Zietz, oral communication). The Midas Trench lineament is the southeastern boundary of this anomaly in northern Nevada and along the Snake River Plains.

Two other lineaments are noteworthy. Several topographic escarpments 10-20 km long aline to form a major lineament (G, fig. 1) which is orthogonal to the Midas Trench lineament. This lineament is marked by a distinct positive magnetic anomaly for approximately 200 km (Mabey, 1966; Robinson, 1970). Mafic dikes intruded along a zone of structural weakness apparently account for this anomaly (Robinson, 1970). In the northwestern part of the state, two slightly offset NW-trending lineaments (H, fig. 1) transect the generally N-trending ranges for approximately 200 km. The area of offset is near the probable intersection with the projected Midas Trench lineament.

Circular Features

Visual analysis of ERTS images has resulted in delineation of 50 circular or elliptical features (fig. 2) which are presumed to be volcanic or intrusive centers. Most of these features occur along the Walker Lane and in the north-central part of the state near the Basin and Range-Snake River Plains boundary. A comparison with the 78 Tertiary volcanic centers mapped in the study area by Albers and Kleinhampl (1970) indicates some good agreement between the proposed and known volcanic centers (fig. 2). Although this comparison is complicated by several factors, such as scale and topographic expression versus actual vent areas, it is useful for locating previously unrecognized centers. Thirty of the known Tertiary centers fall within or on the edge of the proposed centers. On the other hand, 21 do not correlate at all with the Tertiary data of Albers and Kleinhampl. Although 7 of these 21 proposed volcanic centers are, according to available geologic maps, not composed of Tertiary volcanic rocks, the remaining 14 have significant areas underlain by Tertiary extrusive rocks (fig. 2). Judging from the diameter and structural relations indicated at the 14 proposed Tertiary volcanic centers, 8 appear to be major centers. These possible major centers are designated by the letter "T" in figure 2.

Structural control of Tertiary volcanism in the Walker Lane is suggested by the coincidence of centers with this NW-trending fault zone and by the alinement of centers along (NW) and across (ENE) this zone (fig. 2). Alinement of centers along the northeastern part of Midas Trench lineament is reasonably convincing. Many centers, however, seem to have no obvious relationship with the main lineaments.

Distribution of Ore Deposits

The existence of metallogenic belts in the western United States has been debated vigorously for many years. Considerable disagreement still exists concerning the relative importance of various geological variables (such as host rocks, depositional environment, tectonic and volcanic activity), but most workers emphasize the spatial and temporal relationship of ore deposits and structural and igneous activity. Although the structural significance of the lineaments mapped here is not clear, a genetic relationship is implied by the coincidence of productive ore bodies and some major lineaments.

The distribution of productive silver, gold, copper, lead, and zinc mining areas as compiled by Jerome and Cook (1967) appears at first glance to be nearly random, except perhaps for a concentration along the Walker Lane (fig. 3). However, comparison of major lineaments delineated on ERTS images with mining districts (fig. 3) shows that several important districts are located at lineament intersections (fig. 3). Productive districts occur preferentially along the northeastern part of the Midas Trench lineament zone, and numerous highly productive areas are concentrated where this lineament intersects the NW-trending lineament designated "H" in figure 1.

Mineralized areas in the Walker Lane occur chiefly as vein deposits along faults in Tertiary rocks (Roberts, 1966). Although the Walker Lane is basically a zone of NW-trending wrench faults, correlations shown in figure 3 strongly suggest that ENE-trending lineaments also played a role in localizing productive deposits. For example, along the lineament designated "I" in fig. 3 there are 14 productive mines; many other areas are situated along similarly oriented lineaments in this part of the area. Numerous volcanic centers are also located along this lineament.

A genetic relationship between Tertiary volcanic activity and segregation of ore deposits is indicated reasonably clearly where productive mines occur in the proximity of isolated proposed centers (fig. 3). Assessment of the role of Tertiary volcanism is more difficult where centers are situated along lineaments because of the strong correlation of mines and lineaments. Some of these centers appear to localize the ore deposits particularly where the mines occur exclusively at the volcanic center. A few of the alined centers however have no associated productive mines.

SUMMARY

Although tentative, the results of this study demonstrate the potential of ERTS images for regional structural analysis. Most of the major lineaments mapped in this study were either previously unrecognized or known only locally. Concentration of known ore bodies along some of the lineaments and at intersections strongly suggests a genetic relationship. Tertiary volcanic centers are alined similarly but seem to be less important in the segregation of these metallic ore deposits. Careful geologic analyses using geophysical, geochemical, and structural techniques are needed to evaluate the full significance of these preliminary results.

REFERENCES

Albers, J. P., and Kleinhampl, F. J., 1970, Spatial relations of mineral deposits to Tertiary volcanic centers in Nevada, in Geological Survey Research 1970: U.S. Geol. Survey Prof. Paper 700-C, p. C1-C10.

Albers, J. P., and Stewart, J. H., 1965, Preliminary geologic map of Esmeralda County, Nevada: U.S. Geol. Survey Mineral. Inv. Field Studies Map MF-298.

Billingsley, P. R., and Locke, Augustus, 1941, Structure of ore districts in the continental framework: Am. Inst. Mining Metall. Eng. Trans., v. 144, p. 9-59.

Bonham, H. F., 1969, Geology and mineral resources of Washoe and Storey Counties, Nevada: Nevada Bur. Mines Bull. 70, 140 p.

Bushnell, Kent, 1967, Geology of the Rowland quadrangle, Elko County, Nevada: Nevada Bur. Mines Bull. 67, 38 p.

Coats, R. R., 1964, Geology of the Jarbidge quadrangle, Nevada-Idaho: U.S. Geol. Survey Bull. 1141-M, 24 p.

Decker, Robert W., 1962, Geology of the Bull Run quadrangle, Elko County, Nevada: Nevada Bur. Mines Bull. 60, 65 p.

Ekren, E. B., Anderson, R. E., Rogers, C. L., and Noble, D. C., 1971, Geology of the northern Nellis Air Force Bombing and Gunnery Range, Nye County, Nevada: U.S. Geol. Survey Prof. Paper 651, 91 p.

Gianella, V. P., and Callaghan, Eugene, 1934, The earthquake of December 20, 1932, at Cedar Mountain, Nevada, and its bearing on the genesis of Basin and Range structure: Jour. Geology, v. 42, no. 1, p. 1-22.

Gimlett, J. I., 1967, Gravity study of Warm Springs Valley, Washoe County, Nevada: Nevada Bur. Mines, Rept. 15, 31 p..

Jerome, S. E., and Cook, D. R., 1967, Relation of some metal mining districts in the western United States to regional tectonic environment and igneous activity: Nevada Bur. Mines Bull. 69, 35 p.

Locke, Augustus, Billingsley, P. R., and Mayo, E. B., 1940, Sierra Nevada tectonic patterns: Geol. Soc. America Bull., v. 51, p. 513-540.

Mabey, D. R., 1966, Regional gravity and magnetic anomalies in part of Eureka County, Nevada, in Mining Geophysics, v. 1, Case Histories: Tulsa, Okla., Soc. Exploration Geophysicists, p. 77-83.

Nielsen, R. L., 1965, Right-lateral strike-slip faulting in the Walker Lane, west-central Nevada: Geol. Soc. America Bull., v. 76, p. 1301-1308.

Roberts, R. J., 1966, Metallogenic provinces and mineral belts in Nevada, in AIME Pacific Southwest Mineral Industry Conf., Sparks, Nevada, 1965; Papers, Pt. A: Nevada Bur. Mines Report 13, pt. A, p. 47-72.

Robinson, E. S., 1970, Relations between geological structure and aeromagnetic anomalies in central Nevada: Geol. Soc. America Bull., v. 81, p. 2045-2060.

Rowan, L. C., 1972, Iron-absorption analysis for the discrimination of iron-rich zones: USGS ERTS-I Type 1 Progress Report, 1 Sept. - 31 Oct., 1972, NASA CR 129286: U.S. Dept. Commerce, Natl. Tech. Inf. Service, no. E72-10294, 3 p.

Shawe, D. R., 1965, Strike-slip control of Basin-Range structure indicated by historical faults in western Nevada: Geol. Soc. America Bull., v. 76, p. 1361-1378.

Stewart, J. H., Albers, J. P., and Poole, F. G., 1968, Summary of the regional evidence for right-lateral displacement in the western Great Basin: Geol. Soc. America Bull., v. 79, p. 1407-1414.

Tatlock, D. B., 1969, Preliminary geologic map of Pershing County, Nevada: U.S. Geol. Survey open-file map, scale 1:200,000.

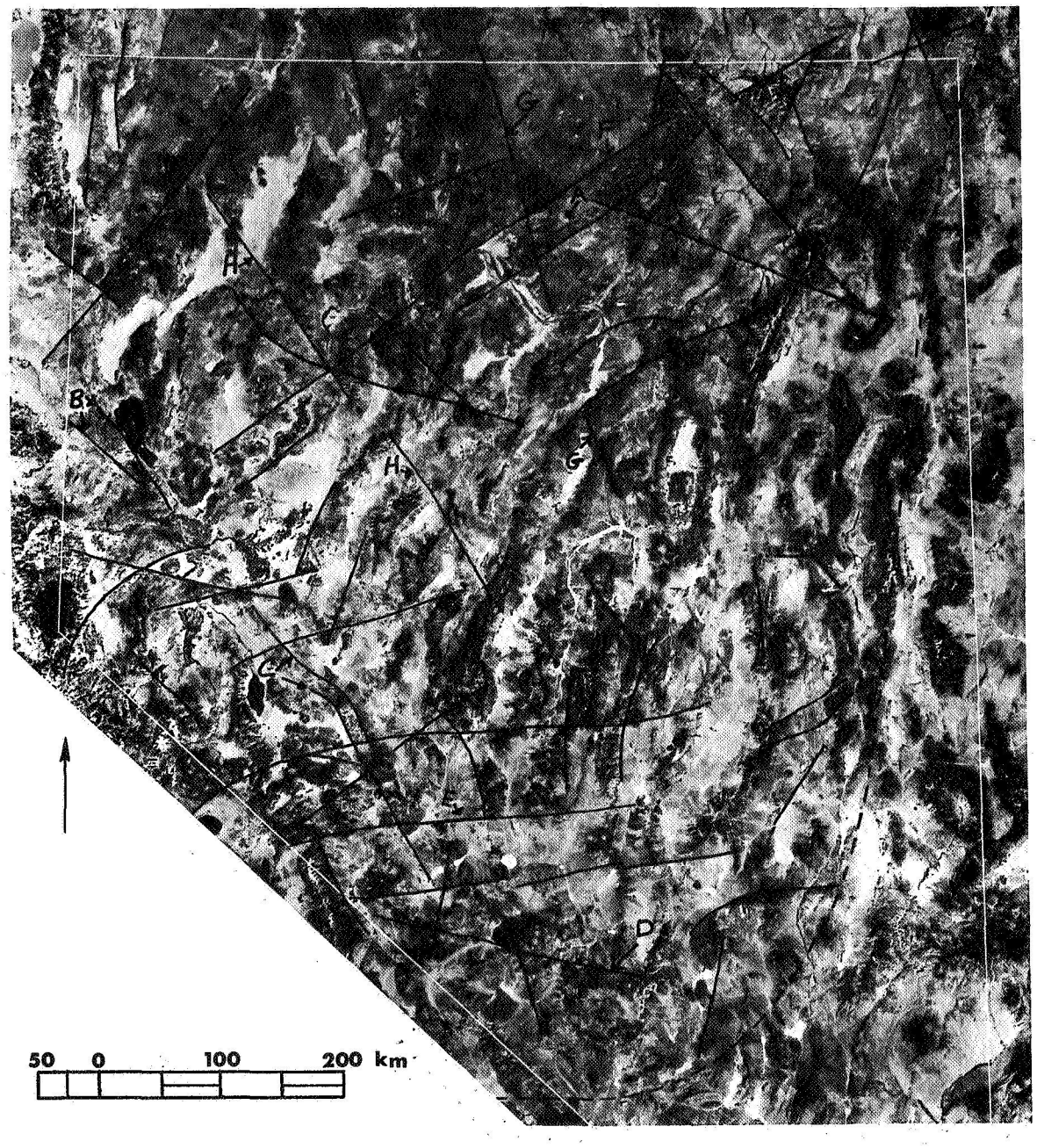


Fig. 1 - ERTS-I mosaic of MSS-5 images obtained in Sept. 1972 showing major lineaments in Nevada, the study area; dashed line shows eastern limit of the area. (Mosaic prepared by Aerial Photographers of Nevada for the University of Nevada, Reno.)

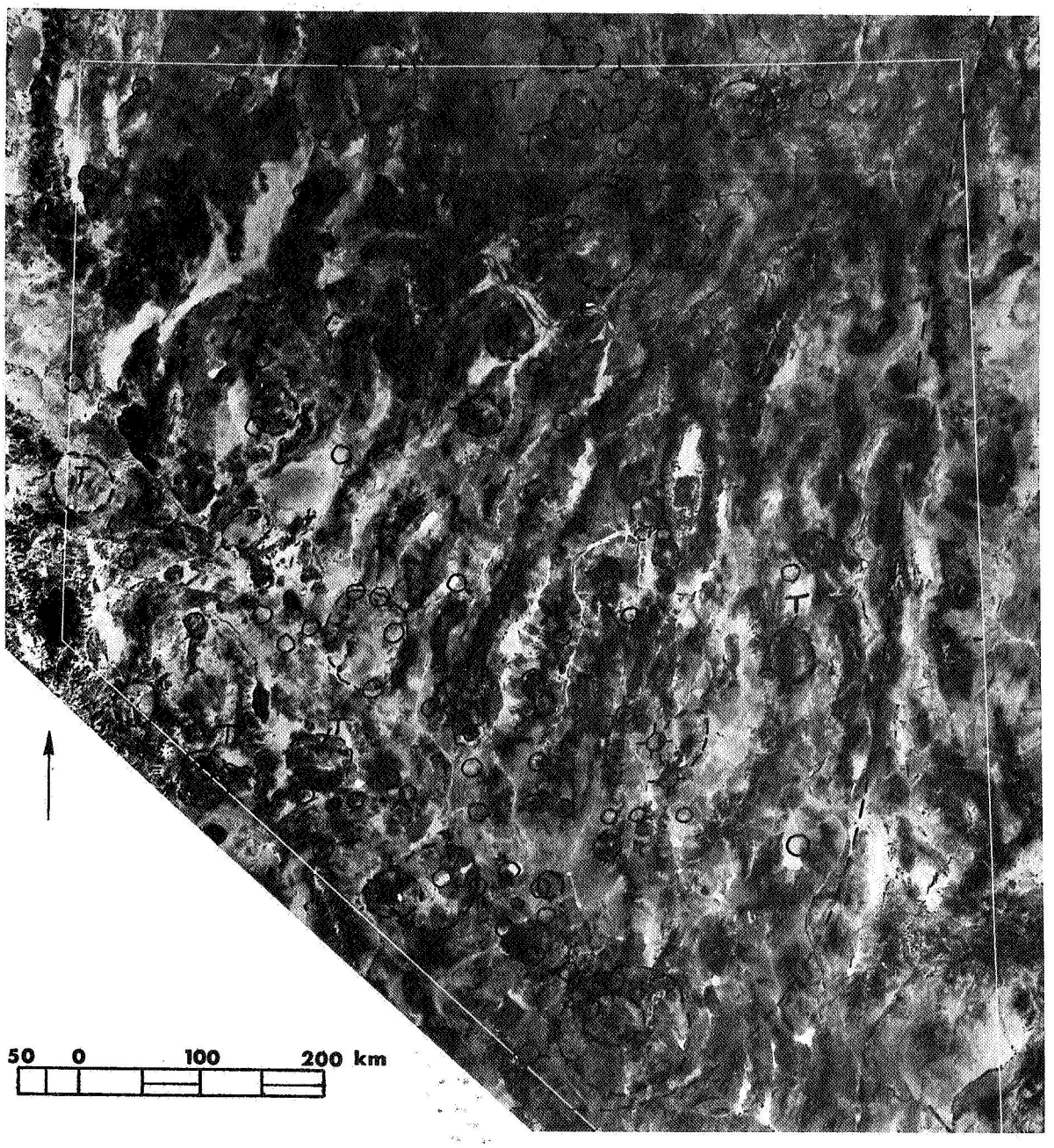


Fig. 2 - Sept. 1972 ERTS-I image mosaic of Nevada showing circular and elliptical features (dashed lines) and Tertiary volcanic centers of Albers and Kleinhampl (1970) (solid lines, ⊙ for calderas). Proposed major Tertiary volcanic centers are designated by "T."

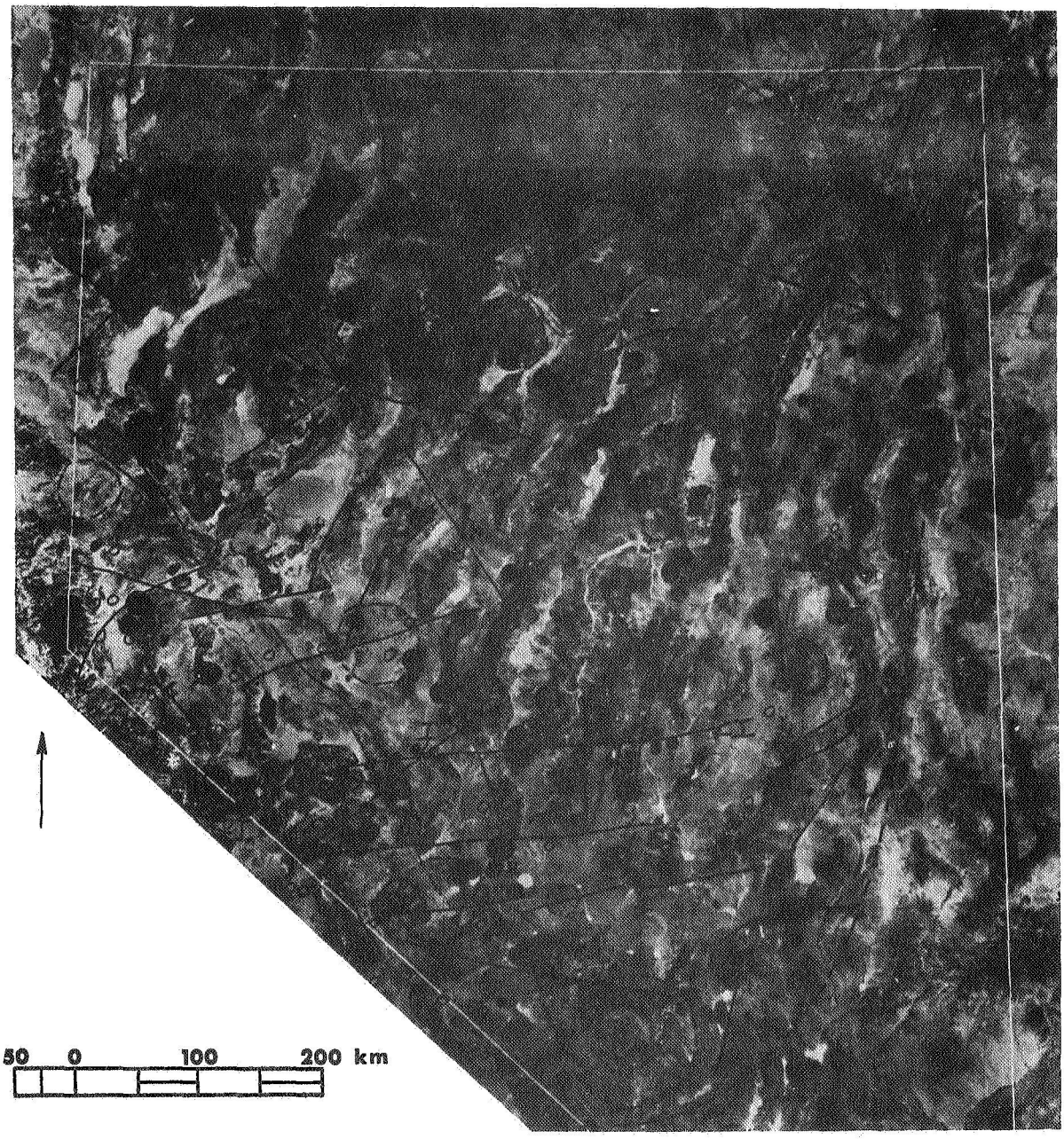


Fig. 3 - Sept. 1972 ERTS-I image mosaic of Nevada showing major lineaments, circular and elliptical features, and silver, gold, copper, lead, and zinc mines. Production levels of mines (Jerome and Cook, 1967): ○ - less than $100 thousand; ● - $100 thousand to $1 million; ● - $1 million to $100 million; ● - more than $1 billion.

Paper G 21

REGIONAL TECTONIC CONTROL OF TERTIARY MINERALIZATION AND RECENT FAULTING IN THE SOUTHERN BASIN-RANGE PROVINCE, AN APPLICATION OF ERTS-1 DATA

I. C. Bechtold, M. A. Liggett and J. F. Childs, *Argus Exploration Company, Newport Beach, California*

ABSTRACT

Research based on ERTS-1 MSS imagery and field work in the southern Basin-Range Province of California, Nevada and Arizona has shown regional tectonic control of volcanism, plutonism, mineralization and faulting. This paper covers an area centered on the Colorado River between 34°15' N and 36°45' N. During the mid-Tertiary, the area was the site of plutonism and genetically related volcanism fed by fissure systems now exposed as dike swarms. Dikes, elongate plutons, and coeval normal faults trend generally northward and are believed to have resulted from east-west crustal extension. In the extensional province, gold and silver mineralization is closely related to Tertiary igneous activity. Similarities in ore, structural setting, and rock types define a metallogenic district of high potential for exploration. The ERTS imagery also provides a basis for regional inventory of small faults which cut alluvium. This capability for efficient regional surveys of Recent faulting should be considered in land use planning, geologic hazards study, civil engineering and hydrology.

INTRODUCTION: This report summarizes a portion of a NASA funded investigation intended to test the application of ERTS-1 imagery to studies of regional tectonics. The region discussed in this paper occupies a belt approximately 25 miles wide and 125 miles long aligned along the Colorado River between 34°15' and 36°34' N latitude in the Basin-Range province of southern Nevada, southeastern California and northwestern Arizona. This area is shown in Figure 1.

The primary tool used in the investigation is additive color enhancement of ERTS-1 MSS imagery. The synoptic perspective gained in ERTS imagery permits investigation of regional geologic phenomena at a scale not feasible using conventional aerial photography. As a complement to ERTS data, intermediate scale remote sensing imagery and low altitude aerial reconnaissance has proven valuable in guiding efficient and economical ground based geologic reconnaissance. The primary data used in this study includes:

NASA ERTS-1 MSS	12 September 1972, Frame 1069-17432
	5 November 1972, Frame 1105-17443
	6 November 1972, Frame 1106-17495

NASA Apollo 9 Ektachrome Frames AS9-20-3135; 3136

NASA SLAR AN/APQ 97, 5 November 1965 Mission 103

USAF-USGS U-2 Black and White Photography

10 July 1968	Mission 018
17 July 1968	Mission 059
6 Sept. 1968	Mission 374

NASA U-2 Color Infrared Photography

11 Oct. 1971	Mission 189

REGIONAL TECTONICS: In the ERTS-1 image of Figure 1, a belt of anomalous north-south topographic, textural and color expression is visible along the Colorado River. Structural analysis of this imagery and related literature research and ground based reconnaissance has led to a hypothesis integrating many aspects of the regional geology previously considered as isolated phenomena.

We believe the anomalous north-south structural pattern is the result of east-west crustal extension of at least 30 km which occurred during an episode of Miocene plutonism and genetically related volcanism. The bulk of igneous activity occurred in an interval from 10 to 15 million years B.P. (Anderson & Others, 1972) and was synchronous with major strike-slip displacement on the Las Vegas Shear Zone (Fleck, 1970). We believe the Las Vegas Shear Zone extends eastward just north of Lake Mead, and forms the northern boundary of the extensional province. This tectonic relationship is illustrated in the simplified model of Figure 2. Here the strike-slip fault zone (X-Y) is a transform fault bounding two areas of crustal extension (braided patterns). The southern extensional province corresponds to the area described in this paper; a sister province is believed to exist in the vicinity of the AEC Nevada test site, 75 miles north-west of Lake Mead.

A diagrammatic section across an area of crustal extension is shown in Figure 3. Normal faults related to extension, shown in Figure 3, are believed to decrease in dip downward and give way at depth to a zone of plastic deformation (Stewart, 1971). Extension by low dipping normal faults in a thick Tertiary volcanic sequence near Nelson, Nevada has been described by Anderson (1971). Another mechanism of crustal extension is the addition of new crust by plutonism and related volcanism; in part along extensional fault zones (Bechtold et al, 1972). Figure 4 shows the distribution of Tertiary granitic plutons and related dike swarms in the area of investigation. Dings (1951) describes numerous large rhyolite dikes in the Wallapai Mining District north of Kingman, Arizona. Petrographic and chemical similarities among the volcanics, dikes and larger plutonic bodies have been demonstrated by Volborth (personal communication, 1972) for the Newberry Mountains area, Nevada. Temporal and genetic relationships between plutonic and volcanic rocks within the area have been cited by Volborth (personal correspondence 1972), Lausen (1931), Ransome (1923), Bechtold et al, (1972), Callaghan (1939), and Anderson et al, (1972).

MINERALIZATION: The shallow granitic plutons and dike swarms of Figure 4 are closely related to extensive gold, silver and lesser copper-molybdenum mineralization. Figure 5 shows the distribution of known mining areas in the region. Longwell et al (1965) briefly discuss many Nevada mining districts, and Ransome (1923), Callaghan (1939) and others describe some of the larger mining areas in detail. Review of the literature and geologic reconnaissance has revealed marked similarities in the structural setting, ore and gangue mineral assemblages, and rock type associations among mining areas. The gold-silver deposits along the Colorado River are part of a north-trending metallogenic province genetically related to the Tertiary extensional deformation. This regional structural control of mineralization has not been previously reported. The value of ore recovered in this province (based upon 1973 metal prices) exceeds 100 million dollars. Although mining activity is largely inactive at present, the new understanding of the area made possible by ERTS data merits consideration in future mineral exploration programs.

RECENT FAULTING: In addition to regional tectonic syntheses, ERTS data has provided a basis for efficient geological reconnaissance of relatively small faults which cut alluvium. Most of the faults cut alluvium of probable Recent age.

Figure 6 shows the distribution of these faults identified in ERTS and intermediate scale imagery and confirmed during subsequent reconnaissance and detailed field mapping. Faults previously reported (Longwell, 1963) and confirmed by our imagery analysis are distinguished from newly recognized faults. Displacement is mainly dip slip, and in several instances the faults form small grabens (Bechtold et al, 1973). Many of the faults occur out from the range fronts in intermontane alluvial sediments where they are difficult to recognize in ground-based mapping. The faults trend generally northward and probably represent late-Tertiary to Recent east-west extension similar to that recognized elsewhere in the Basin-Range Province. (Thompson, 1967).

The use of ERTS-1 imagery for efficient reconnaissance of Recent faulting over large areas of semi-arid terrain can have important applications in the planning and design of engineering projects such as dams, highways and nuclear power generating stations. Related applications can also be made in regional geologic hazard studies and in the search for increasingly valuable ground water sources.

CONCLUSIONS: ERTS-1 MSS imagery is a unique tool for a broad range of geologic investigations, some of which are discussed above. Analysis of ERTS data coordinated with the use of other remote sensing techniques has permitted efficient and economical ground-based reconnaissance. At a regional scale, the application of ERTS to tectonics shows promise in reconnaissance mineral exploration. In addition, the resolution of the ERTS-MSS imagery is sufficient for surveys of relatively small faults which cut alluvium. This capability should be considered in land-use planning, geologic hazards study, and civil engineering.

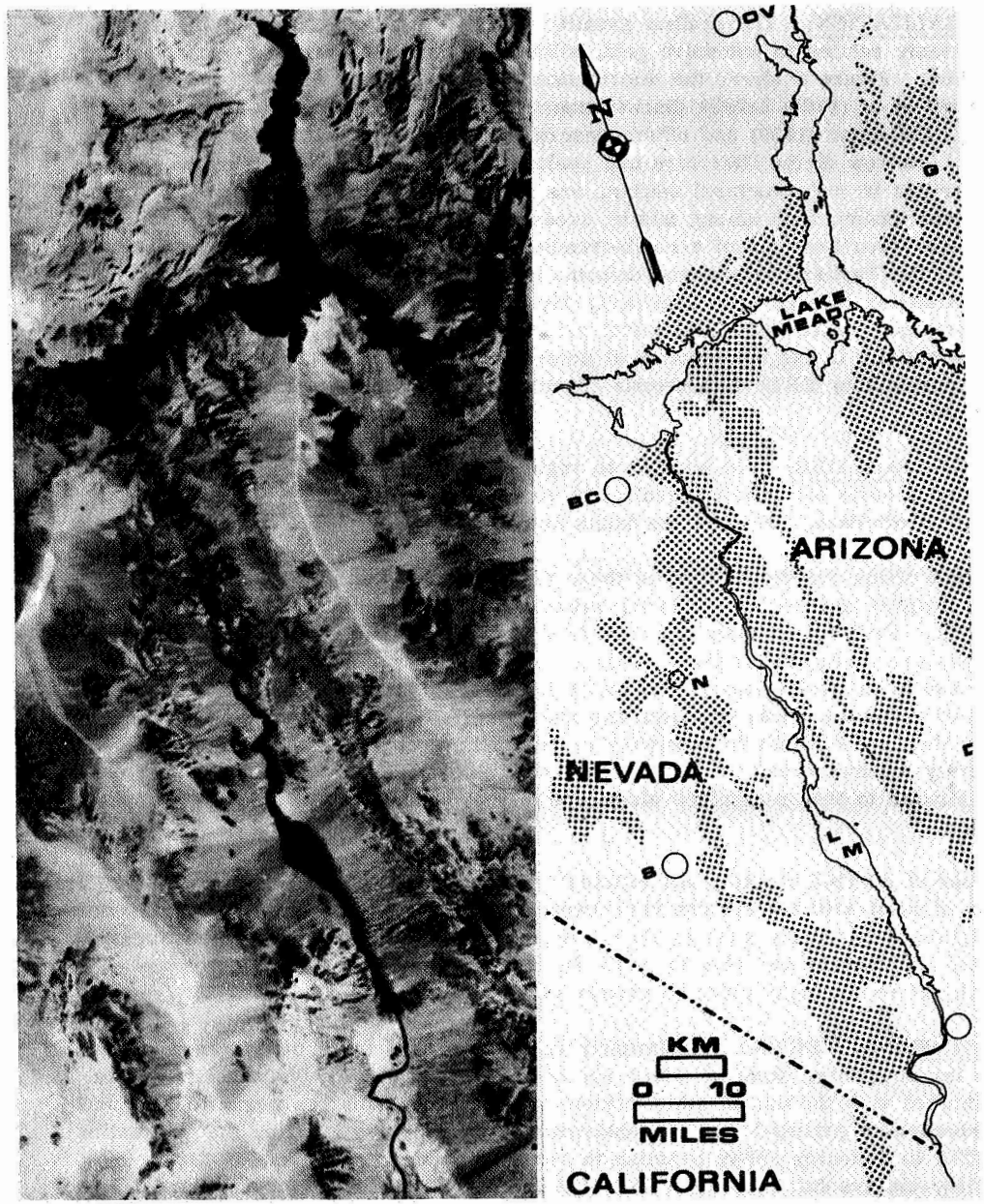


Figure 1: Portion of ERTS-1 MSS image 1106-17495-7 and index map of the study area. Location names are as follows:

B	-	Bullhead City, Ariz.	LM	-	Lake Mojave
BC	-	Boulder City, Nev.	N	-	Nelson, Nev.
DV	-	Detrital Valley, Ariz.	OV	-	Overton, Nev.
G	-	Gold Butte, Nev.	S	-	Searchlight, Nev.

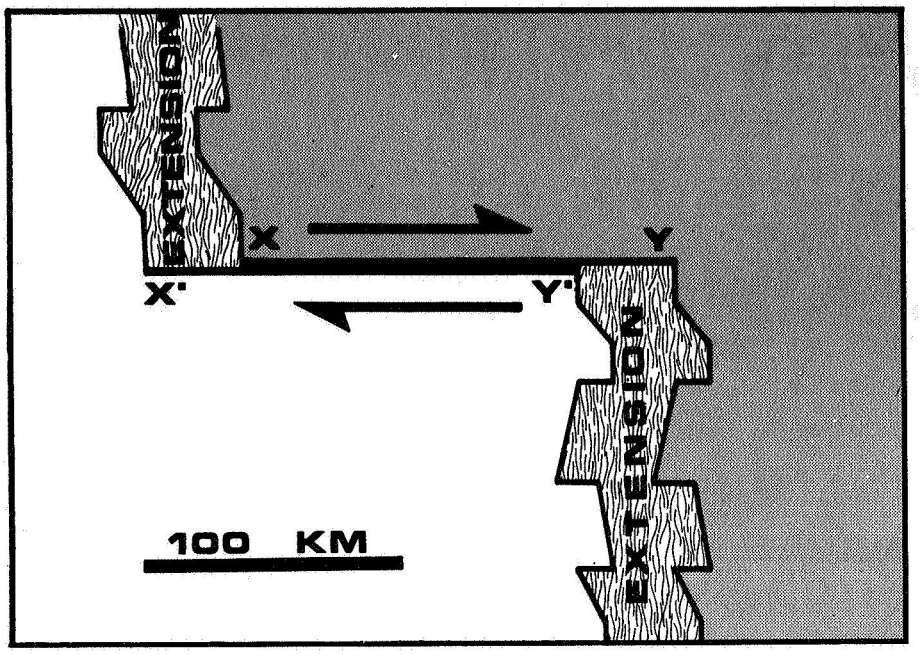


Figure 2.
Simplified tectonic diagram of a transform fault (X-Y) separating two areas of crustal extension (braided patterns). The shaded and white areas represent two crustal "plates". The Las Vegas shear zone is believed to be the transform fault which forms the northern boundary of an extensional province along the Colorado River.

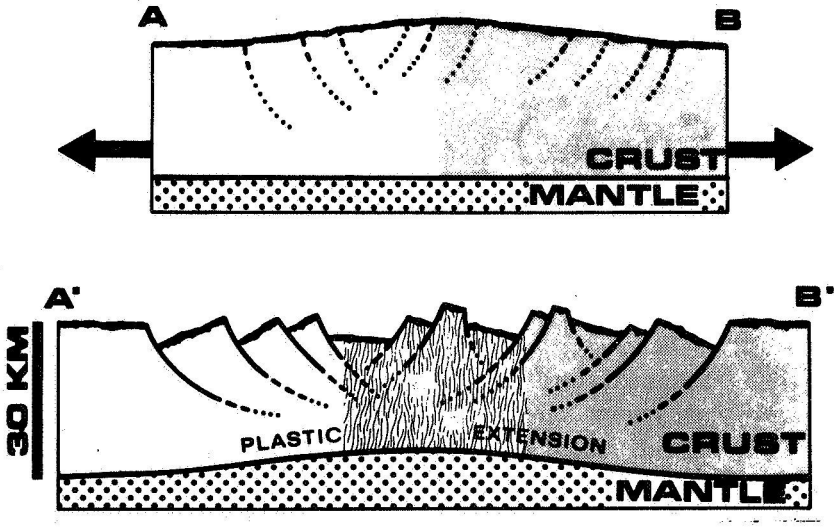


Figure 3.
Vertical sections of a region before and after crustal extension. Mechanisms of extension are normal faulting, plastic extension in the lower crust, and formation of new crust by volcanism and plutonism (braided pattern).

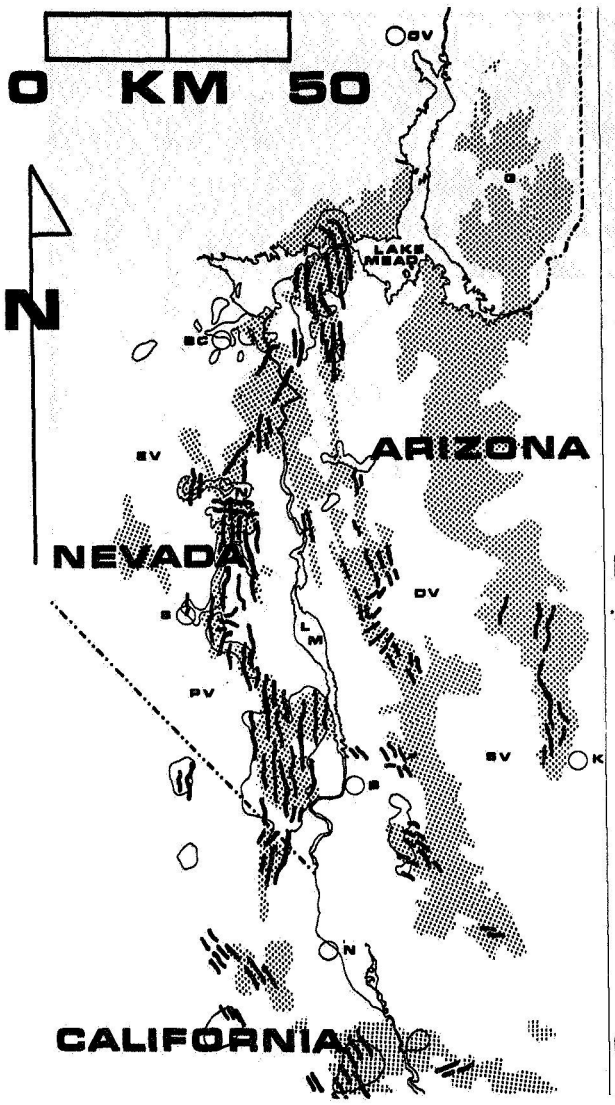


Figure 4. Distribution of Tertiary intrusive rocks, believed emplaced during crustal extension. Granitic plutons are outlined, and dike swarms are shown with heavy lines. Stippled areas are generalized bedrock exposures. Location names are as in Figures 1 and 6.

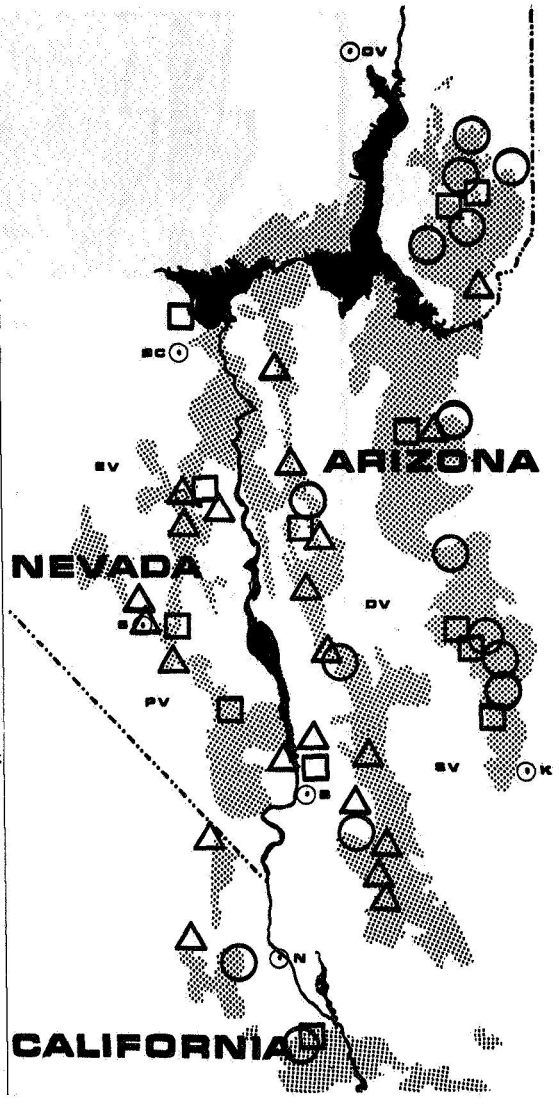


Figure 5. Distributions of known mineral deposits are indicated by triangles for gold; squares for lead, zinc, and silver; and circles for copper and molybdenum. Stippled areas are generalized bedrock exposures. Location names are as in Figures 1 and 6.

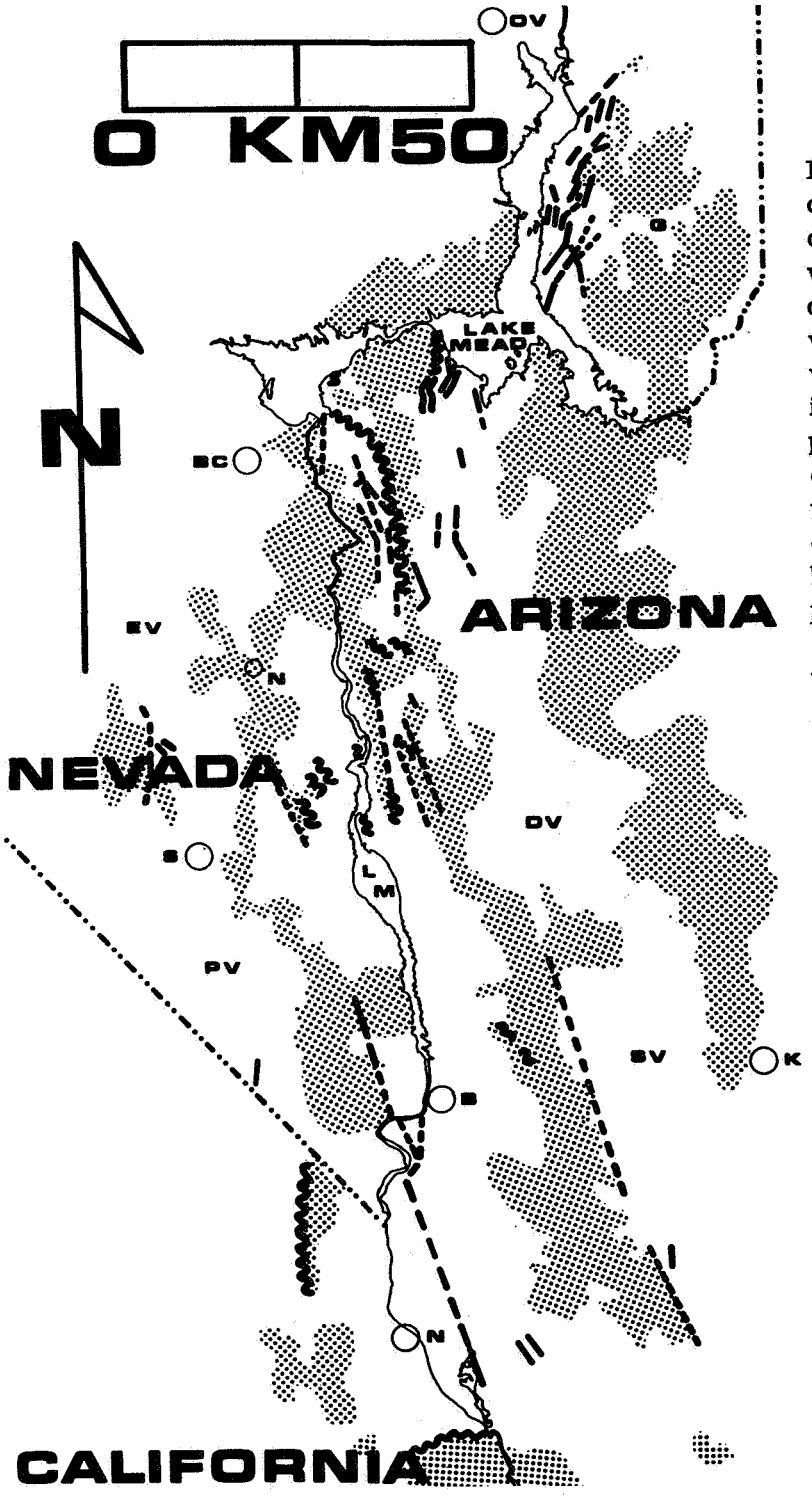


Figure 6. Newly recognized faults which cut alluvium are shown with solid lines where distinct; dashed lines where indefinite. Previously reported faults in alluvium, also apparent in ERTS imagery, are shown with wiggled lines. Faults cutting bedrock have been excluded. Stippled areas are generalized bedrock exposures. Location names are as in Figure 1, with the following additions:

EV-Eldorado Valley
K-Kingman, Ariz.
N-Needles, Calif.
PV-Piute Valley
SV-Sacramento Valley

REFERENCES

Anderson, R.E., 1971, Thin Skin Distension in Tertiary Rocks of Southeastern Nevada: Geol. Soc. America Bull., v.82, p 43-58.

Anderson, R.E., Longwell, C.R., Armstrong, R.L., and Marvin, R.F., 1972, Significance of K-Ar Ages of Tertiary Rocks from the Lake Mead region, Nevada-Arizona: Geol. Soc. America Bull., v.83, No. 2, p 273-288.

Bechtold, I.C., Liggett, M.A., and Childs, J.F., 1972, Structurally Controlled Dike Swarms Along the Colorado River, Northwestern Arizona and Southern Nevada (ABS): NASA-CR-128290, E72-10192.

Bechtold, I.C., Liggett, M.A., Childs, J.F., 1973, Remote Sensing Reconnaissance of Faulting in Alluvium, Lake Mead to Lake Havasu, California, Nevada and Arizona: NASA Report of Investigation, Goddard Space Flight Center, Greenbelt, Maryland.

Callaghan, E., 1939, Geology of the Searchlight District, Clark County, Nevada: U.S. Geological Survey Bulletin 906-D, p 165-185.

Dings, G., 1951, The Wallapai Mining District, Cerbat Mountains, Mojave County, Arizona: U.S. Geol. Survey Bull. 978-E, 39 p.

Fleck, R.J., 1970, Age and possible Origin of the Las Vegas Shear Zone, Clark and Nye Counties, Nevada: Geol. Soc., America Abs. with Programs (Rocky Mountain Sec.), v.2, No. 5, p 333.

Lausen, G., 1931, Geology and Ore Deposits of the Oatman and Katherine Districts, Arizona: Arizona Bur. Mines Bulletin 131, Geol. Ser. 6, (Univ. Bull., v 2, No. 2), 126 p.

Longwell, C.R., 1963, Reconnaissance Geology Between Lake Mead and Davis Dam, Arizona-Nevada: U.S. Geol. Survey Prof. Paper 374-E, 51 p.

Longwell, C.R., Pampeyan, E.H., Bowyer, B., and Roberts, R.J., 1965, Geology and Mineral Deposits of Clark County, Nevada: Nevada Bur. Mines Bull. 62, 218 p.

Ransome, F.L., 1923, Geology of the Oatman District, Arizona, A Preliminary Report: U.S. Geol. Survey Bull. 743, 58 p.

Stewart, J.H., 1971, Basin and Range Structure: A System of Horsts and Grabens Produced by Deep-Seated Extension: Geol. Soc. America Bull., v.82, p 1019-1044.

Thompson, G.A., Meister, L.T., Herring, A.T., Smith, T.E., Burke, D.B., Kovach, R.L., Burford, R.O., Salehi, A., and Wood, M.D., 1967, Geophysical Study of Basin-Range Structure, Dixie Valley Region, Nevada: U.S. Air Force Cambridge Research Labs. Spec. Rept. 66-848.

Volborth, A., 1972. Personal Communication. Nevada Bureau of Mines, Reno, Nevada.

Paper G 22

ERTS APPLICATIONS IN EARTHQUAKE RESEARCH AND MINERAL EXPLORATION IN CALIFORNIA

Monem Abdel-Gawad and Joel Silverstein, *Science Center, Rockwell International, Thousand Oaks, California 91360*

Abstract

We shall demonstrate with examples that ERTS imagery can be effectively utilized to identify, locate, and map faults which show geomorphic evidence of geologically recent breakage. Several important faults not previously known have been identified. By plotting epicenters of historic earthquakes in parts of California, Sonora, Mexico, Arizona, and Nevada, we found that areas known for historic seismicity are often characterized by abundant evidence of recent fault and crustal movements. We also found that the opposite is not necessarily true: There are many examples of seismically quiet areas where outstanding evidence of recent fault movements is observed. One application is clear: ERTS-1 imagery could be effectively utilized to delineate areas susceptible to earthquake recurrence which, on the basis of seismic data alone, may be misleadingly considered safe. ERTS data can also be utilized in planning new sites in the geophysical network of fault movement monitoring and strain and tilt measurements. ERTS data on transverse faults and their interaction with the San Andreas system in west central California are providing significant scientific insights into the geological history of the state. In addition, an apparent correlation was observed between the distribution of mercury deposits in the California Coast Ranges Province and transverse fault zones trending west-northwest oblique to the trend of the San Andreas system. The significance of this correlation in mineral exploration will be discussed.

In this brief paper we describe significant observations derived from our study of the fault pattern revealed in ERTS-1 imagery of the central part of the Pacific mountain system of California. The practical applications of this work relate directly to problems of earthquake hazards and mineral exploration. Space limitations do not allow but a few illustrative examples.

ACTIVE FAULTS AND SEISMICITY PATTERNS

In California the most salient geologic hazard problem is the effect of earthquake damage to areas of high population density and industrial and life-supporting facilities. Activity on the San Andreas fault system has long been recognized as a major source of earthquakes. However, when we plotted the distribution of earthquake epicenters on ERTS-1 imagery we found that the seismicity pattern alone is inadequate in defining areas susceptible to earthquakes. The recent San Fernando and Oxnard earthquakes

occurred in areas which if judged by seismic history alone would be considered relatively safe. On the other hand large segments of the San Andreas fault which are known from geologic evidence to have been recently active are now seismically quiet. Since our records of historic earthquakes span a relatively short time interval and the seismicity pattern appears to shift with time it becomes apparent that we are in need of another effective means to identify faults showing evidence of recent geologic activity and to regard such evidence as a more reliable basis for assessing the potential earthquake hazard.

Our approach to assess the application of ERTS-1 imagery to this problem is to plot the epicenters of historic earthquakes using a computer-stored list on overlays corresponding to the geometry of ERTS imagery and correlate the seismicity pattern with our observations on fault continuities, intersections, and inferred evidence of recent breakage.

Figures 1 and 2 are only examples of this approach which we applied so far to a vastly larger area of California, Utah, and Nevada.

Figure 1 is MSS image #1037-18064 showing the western part of the Transverse Ranges in California. Some of the major known faults are indicated by solid lines in the corresponding map. Several observations derived from this scene are significant. First that many bends of the San Andreas fault and other members of the system shown in the geological maps (Atlas of California) correspond to a distinct system of transverse faults trending west-northwest, oblique to the San Andreas system, which have acted to bend, offset, and otherwise distort these breaks.

The occurrence of major east-west faults in the Transverse Ranges is very well known; many of these are characterized by left-lateral shear. ERTS imagery has contributed to show that this system is not confined to the Transverse Ranges but is pervasive throughout the Coast Ranges. We suspect some of these may be major crustal breaks extending under the San Joaquin Valley and may be responsible for flextures in the configuration of the western side of the Sierra Nevada block and the Great Valley. Other transverse faults occur as distinct short segments lodged between throughgoing faults of the San Andreas system. We suspect those to be remnants of an old transverse shear fault system now largely intersected, offset, and in places incorporated within the San Andreas fault system. The geological maps of California show some of these transverse faults as conjugate or branching secondary features of the San Andreas system. ERTS-1 imagery on the other hand reveals that they belong to a separate and distinct fault system.

We are placing emphasis on this observation for profound scientific and practical considerations. The scientific significance will be subject to a more detailed treatment elsewhere (Abdel-Gawad and Silverstein, 1972). It may be useful, however, to suggest here that the immense complexity of the fault block mosaic of the crust in California and the Pacific Cordillera at large may be due to repeated and episodic interaction of two rather than one primary shear systems, which have cut and displaced one another and the process appears to be continuing at present.

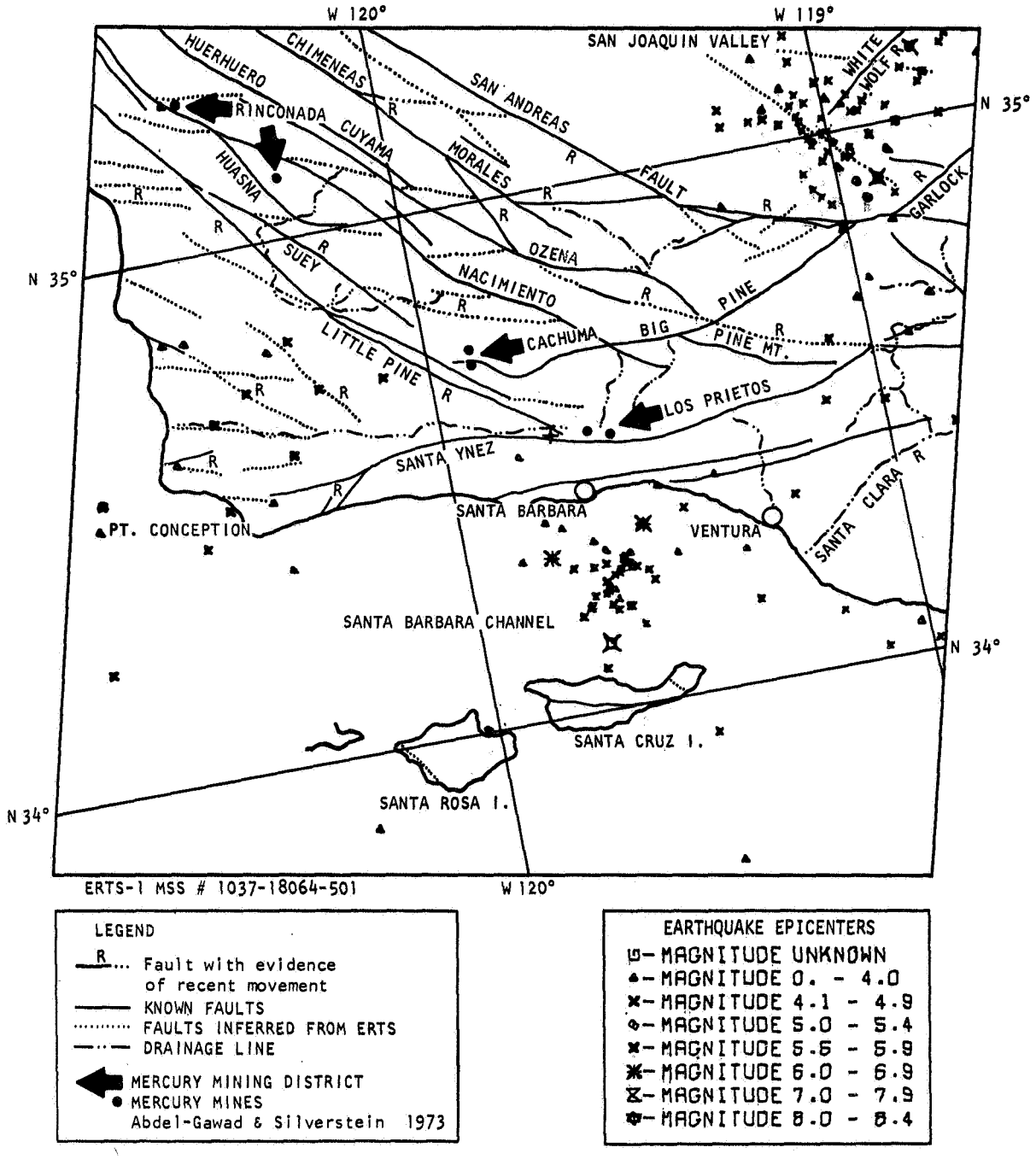

W 120°
W 119°
N 35°
N 34°
SAN JOAQUIN VALLEY
HUERHUERO
CHIMENEAS
SAN ANDREAS
FAULT
WHITE WOLF
GARLOCK
RINCONADA
CUYAMA
MORALES
HUASNA
SUEY
OZENA
NACIMIENTO
PINE
CACHUMA
BIG PINE MT.
LITTLE PINE
LOS PRIETOS
SANTA YNEZ
SANTA CLARA
PT. CONCEPTION
SANTA BARBARA
VENTURA
SANTA BARBARA CHANNEL
SANTA CRUZ I.
SANTA ROSA I.
ERTS-1 MSS # 1037-18064-501
LEGEND
Fault with evidence of recent movement
KNOWN FAULTS
FAULTS INFERRED FROM ERTS
DRAINAGE LINE
MERCURY MINING DISTRICT
MERCURY MINES
Abdel-Gawad & Silverstein 1973
EARTHQUAKE EPICENTERS
MAGNITUDE UNKNOWN
MAGNITUDE 0. - 4.0
MAGNITUDE 4.1 - 4.9
MAGNITUDE 5.0 - 5.4
MAGNITUDE 5.5 - 5.9
MAGNITUDE 6.0 - 6.9
MAGNITUDE 7.0 - 7.9
MAGNITUDE 8.0 - 8.4

Figure 1

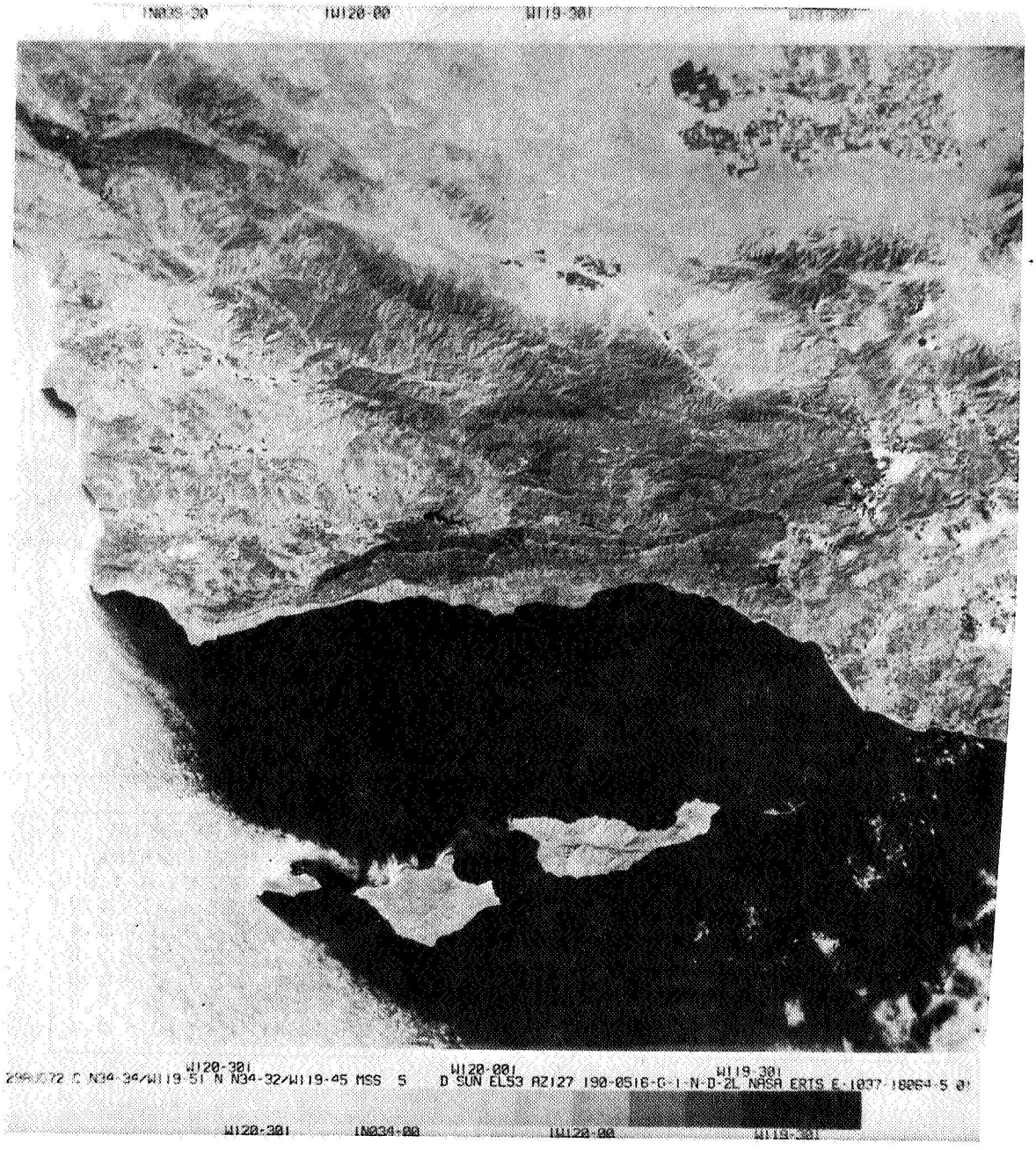

W120-30I
W120-00I
W119-30I
D SUN EL53 AZI27 190-0516-G-1-N-D-2L NASA ERTS E-1037-18064-5
W120-30I
N034-00
W120-00
W119-30I

Figure 1a

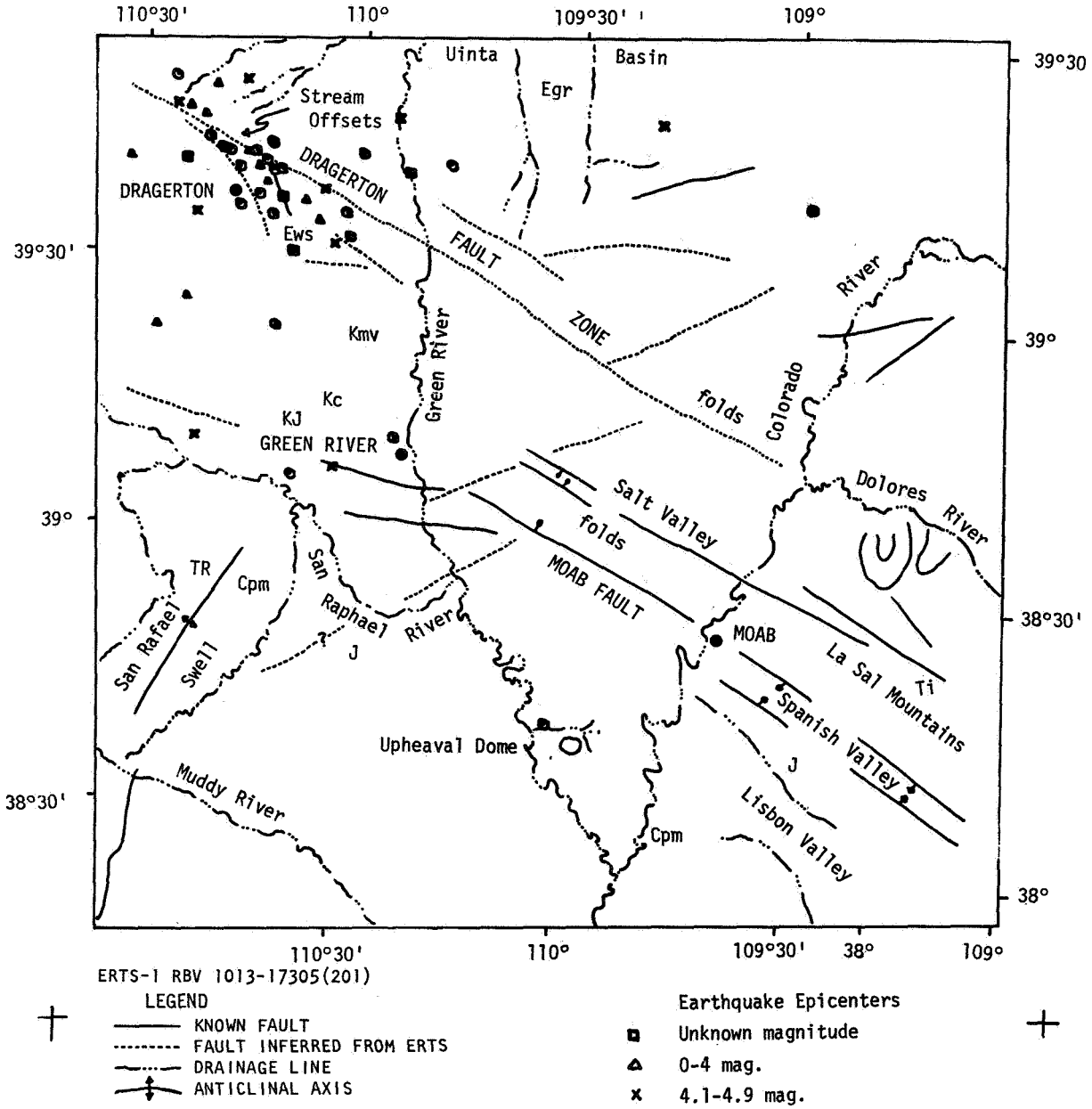

110°30'
110°
109°30'
109°
39°30
39°
38°30'
38°
Uinta
Basin
Egr
Stream
Offsets
DRAGERTON
DRAGERTON
FAULT
ZONE
Ews
Kmv
Kc
KJ
GREEN RIVER
Green River
folds
Colorado
River
Salt Valley
folds
MOAB FAULT
MOAB
Dolores River
La Sal Mountains
Ti
Spanish Valley
J
Lisbon Valley
Cpm
Upheaval Dome
TR
Cpm
San Rafael
Swell
San Raphael River
J
Muddy River
ERTS-1 RBV 1013-17305(201)
LEGEND
KNOWN FAULT
FAULT INFERRED FROM ERTS
DRAINAGE LINE
ANTICLINAL AXIS
Earthquake Epicenters
Unknown magnitude
0-4 mag.
4.1-4.9 mag.

Figure 2


W110-301
N038-001 W110-00
W109-301
05AUG72 C N38-53/W109-48 N N38-54/W109-45 RBV 1 DXHO SUN EL56 AZ123 191-0181-G-1-N-D- NASA ERTS E-1013-17305-1 01

Figure 2a

In Figures 1 & 4 we have identified by the symbol (R) examples of areas where we have inferred from the ERTS imagery evidence of Holocene (recent) activity on fault traces. Noting that in many places evidence of recent activity on transverse faults is almost as pervasive as that noted on the San Andreas fault system, it is rather difficult to escape the conclusion that transverse stresses are acting to distort, bend, and offset the San Andreas fault system, a process which inevitably lead to locked structures on which tectonic stresses are built and subsequently released by sudden breakage. Such a complex interaction between two episodically active fault systems may explain the tendency of earthquakes to cluster near fault intersections, an observation which has been known for some time (Allen et al., 1965).

The interaction of the two active fault systems suggests that in planning the geophysical networks for fault monitoring, more attention should be paid to active transverse faults than they are receiving at present.

Figure 1 shows many fault lineaments inferred from ERTS-1 imagery which were either not previously mapped or shown on maps incorporated with other faults. One particular example of interest is a fault lineament representing the southeastern extension of the Cuyama-Ozena fault, running along Hot Springs Canyon across Big Pine fault. This lineament is aligned with the middle segment of the San Gabriel fault. The intervening area in the vicinity of Lake Peru is likely to be subject to fault propagation.

Considering the relation of seismicity to the fault pattern, study of ERTS-1 imagery shows that in most areas where earthquake clusters occur, there is usually ample evidence of recent faulting. The opposite, however, is not necessarily true: there are many areas and even major fault segments characterized by geomorphic features indicating recent faulting, such as stream offsets and sharp lineaments in the alluvium, which are seismically quiet. This indicates as mentioned before, that characterization of earthquake hazardour areas largely on the basis of the present distribution of earthquake occurrences can be quite misleading and may result in unpleasant surprises. Based on our analysis of ERTS data over large areas in California, Nevada, Utah, and Sonora, it appears feasible to utilize ERTS imagery to identify many more potentially active faults than is presently known. Maps showing the location of potentially active faults could be prepared and in our opinion would be far superior to available maps and certainly will contribute to a more reliable earthquake safety planning program.

On the other hand our method of plotting the epicenters of historic earthquakes on ERTS imagery has been found to be useful in identifying previously unknown faults.

An example is shown in Figure 2, an RBV image showing the northern part of the Colorado Plateau, Utah. When historic earthquakes were plotted on an overlay a cluster was noted in the northwestern part of the image. The earthquake cluster drew attention to a northwest trending fault zone passing near the town of Dragerton through the Patmos Mountains and the southwestern side of the Tavaputs Plateau. This Dragerton fault zone runs parallel to the Salt Valley-Pardox valley fault zone and the Moab-Spanish Valley-Gypsum

Valley fault zones. The fault is not shown on the Tectonic map of North America (King, 1969), the Geological Map of the United States (Stose and Ljungstedt, 1960), nor in Shoemaker's (1954) Tectonic Map of Central Colorado Plateau. This lineament is significant for several reasons. On the southeast it projects towards the junction of the Dolores and Colorado Rivers and appears to be a northwestward extension of a major fault lineament defining the southwestern side of the Uncompahgre uplight projecting towards the Tertiary volcanic center of San Joan Mountains, Colorado.

RELATION OF MERCURY DEPOSITS TO TRANSVERSE FAULTS

There are some 100 mercury deposits in California clustered in 21 districts. Most deposits occur in the California Coast Ranges from Lake County to the north to Santa Barbara County to the south (Davis, 1966).

Mercury ore has long been known to be deposited in epithermal (low temperature hydrothermal) conditions and is often associated with Tertiary and Quaternary volcanic regions. In California Coast Ranges mercury deposits occur in host rock conditions which are generally similar but the individual deposits have often been described an erratic, with marked differences in character, size, grade, and local structural conditions.

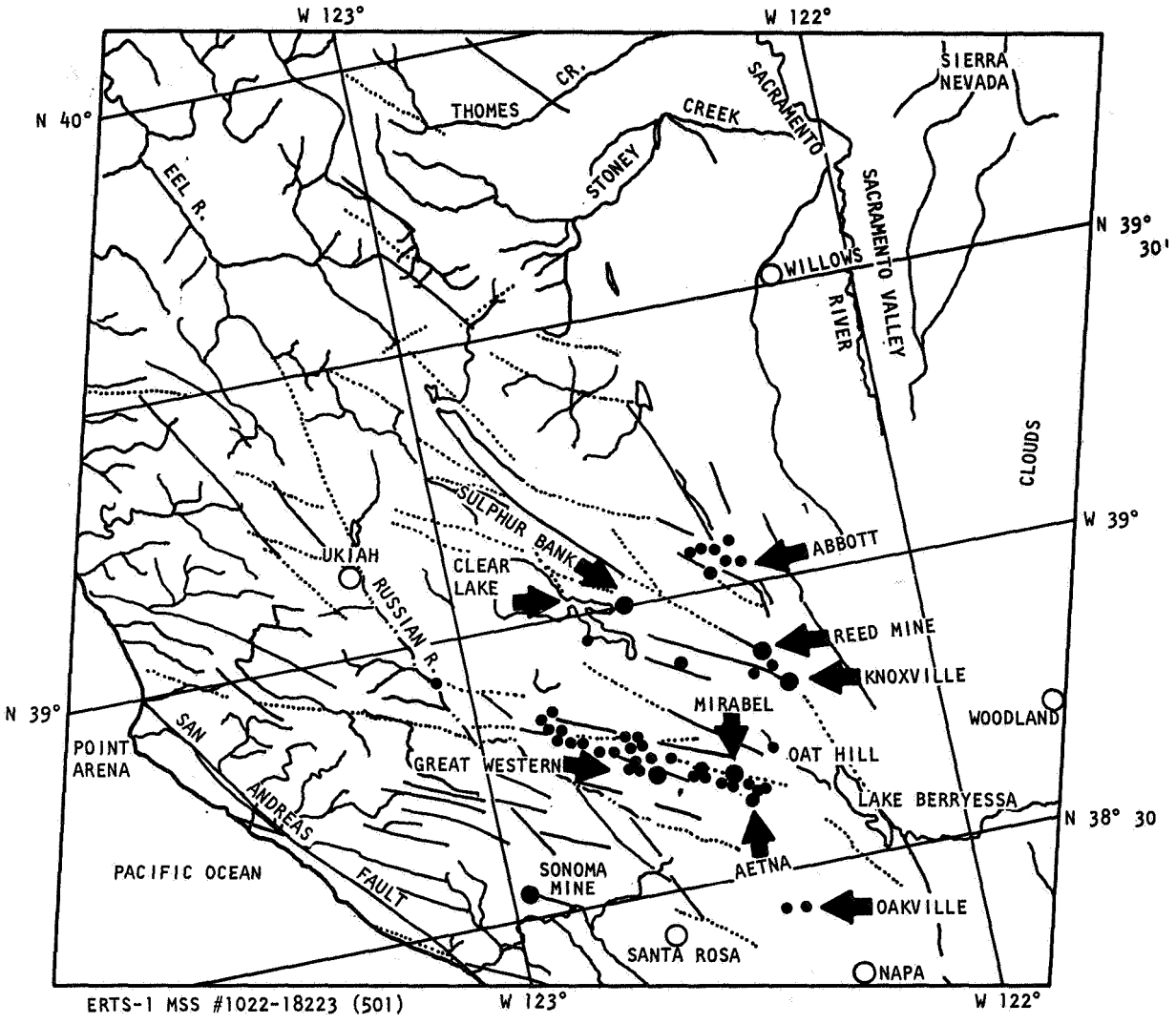
The carbonate-silica rock, an alteration product of serpentine often associated with mercury deposits, is so much more widespread than the ore itself as to be alsmost useless as an ore guide. In northern California mercury ore is found in the Clear Lake volcanic area (Figure 3). The Sulphur Bank Mine is a major hot spring-quicksilver deposit (White and Roberson, 1962).

Regionally, there has been little known regarding any specific tectonic or structural element which could be related to the regional distribution of mercury deposits even though many mines are known to occur in highly faulted, sheared, and deformed host rocks of the Franciscan Group and the overlying Upper Cretaceous strata.

That transverse faults constitute a distinct tectonic element in the deformation history of the Pacific mountain system of California appears to be economically important in addition to its profound scientific value.

Taken as an example the distribution of known mercury deposits in the California Coast and Transverse Ranges when plotted on ERTS-1 imagery shows a striking correlation with west-northwest trending shear zones, oblique to the prevalent trend of the San Andreas system.

The most striking correlation is noted in northern California in the Clear Lake and the Great Western mercury districts. Figure 3 shows an overlay map corresponding to ERTS-1 multispectral scanner scene no. 1022-18223. On this map we have plotted identifiable known faults as well as others inferred from ERTS imagery. We have also plotted as approximately as practical the most significant mercury mines as compiled by Bailey (1962). They are identified by the name of the district and some of the larger mines. The cluster of mercury mines in the Great Western, Aetna, Mirabel, and Oat Hill is the most striking in that it forms a distinct belt trending west-northwest which coincides with a zone of transverse faults. Many of these faults appear



RELATION OF MERCURY DEPOSITS TO TRANSVERSE FAULTS
COAST RANGES CALIFORNIA

LEGEND

- KNOWN FAULTS
- FAULTS INFERRED FROM ERTS
- DRAINAGE LINE
- MERCURY MINING DISTRICT
- MERCURY MINES

Abdel-Gawad & Silverstein 1973

Figure 3


W123-001
W122-381
W123-301
W123-001
W122-301
W122-001
14AUG72 C N39-13/W122-38 N N39-13/W122-33 MSS 5 D SUN EL54 AZ127 191-0307-G-1-N-D-2L NASA ERTS E-1022-18223-5 01

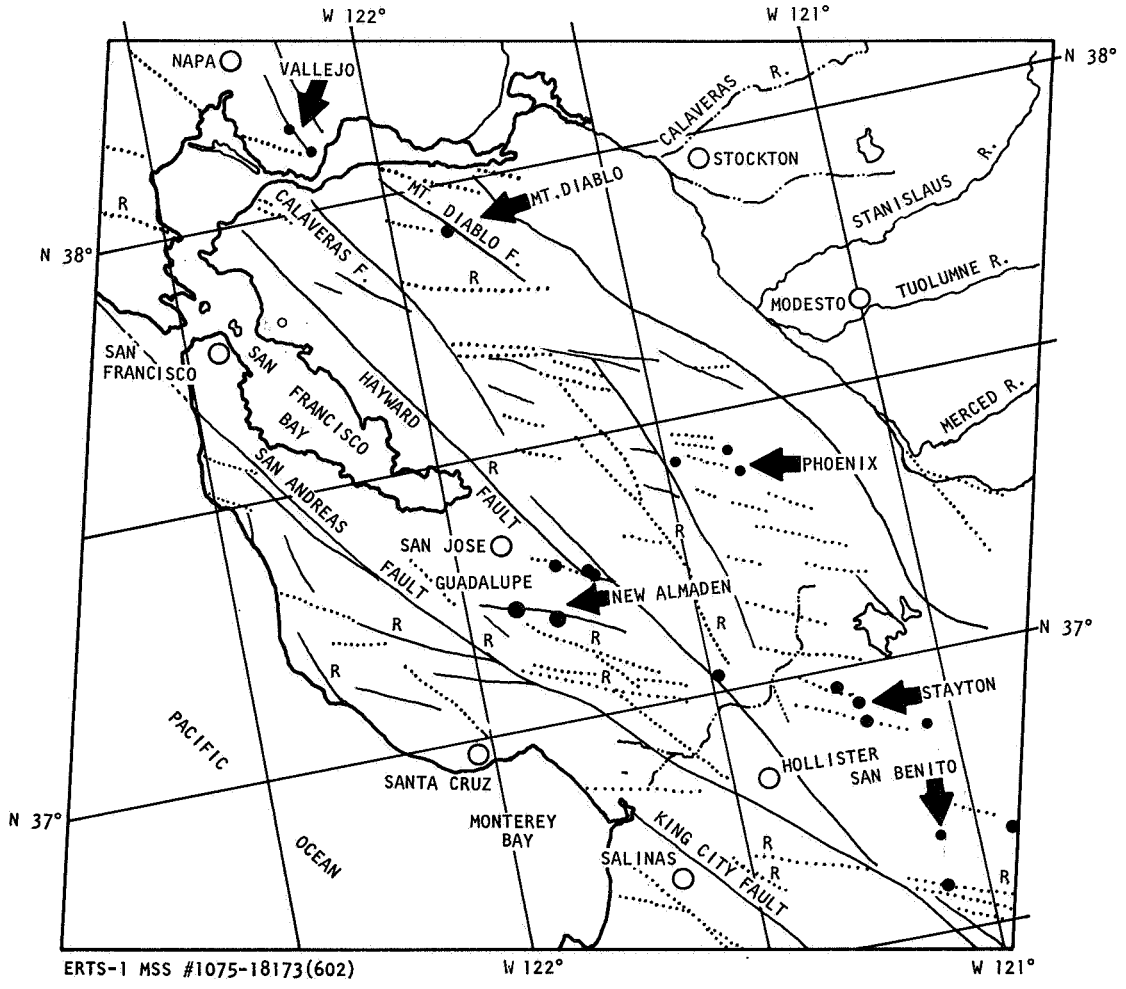
Figure 3a

on the Santa Rosa Geological Map Sheet, Atlas of California. In this specific case the relationship between mercury deposits and the transverse fault zone is rather evident from the fault pattern on the geological map. This relation, however, is not evident from the geological maps elsewhere in the Coast Ranges, because most of the known transverse faults are incorporated as bends in the northwest-trending faults of the San Andreas set and, therefore, do not stand out as a separate and significant entity. Besides, many transverse fault structures became evident from ERTS-1 imagery.

The relation between mercury mines and transverse fault zones is consequently much less apparent from the geological maps than from ERTS-1 imagery farther south in the Coast Ranges. In Figure 4 we have plotted known mercury occurrences together with transverse fault zones inferred from ERTS-1 scene 1075-18173. In this area of the Coast Ranges there are six mercury mining districts including the New Almaden, the first quicksilver mine discovered in North America and one of two most productive in California since 1846.

The New Almaden mine is typical of mercury ore associated with silica-carbonate rock underlain by graywacke, shale, greenstone, and serpentine of the Franciscan Formation. The mine is located on a "northwest trending anticline whose southwest limb is sheared and cinnabar was introduced along narrow northeast trending fractures" (Davis, 1966). Although some transverse faults are shown in the geological map (San Jose sheet) mostly as flextures in the San Andreas fault system, the position of the New Almaden, Guadalupe, and other deposits in distinct relation to transverse fault zones became readily apparent from correlation with ERTS imagery. In the Diablo Range, east of the Hayward fault four mercury districts, Vallejo, Mount Diablo, Phoenix, and Stayton are located on or near transverse fault zones identified from ERTS-1 imagery.

Figure 5 (MSS scene 1074-18121) shows the spatial relation between six mercury districts and transverse structures in the southern part of the Coast Ranges. The New Idria Mining district in San Benito County stands out as including the most productive mercury mine in the United States, which together with the New Almaden mine produced more than half a million flasks of mercury since its discovery in 1853. The New Idria cluster occurs associated with a serpentine mass which intruded through a sequence of shales and sandstones of the Upper Cretaceous Panoche formation and overlying Tertiary sedimentary rocks. Mercury ore has been described (Eckel and Myres, 1946; Davis, 1966; Linn, 1968) as localized under the New Idria thrust fault in altered Upper Cretaceous Panoche formation. A large ore shoot lies at the intersection of the New Idria thrust with a tear fault. We find it significant that the New Idria thrust has a definite transverse trend and may in fact be the surface expression of a transverse shear fault in depth. When we examine the transverse faults in this part of the Coast Ranges, particularly those which cut across the Diablo Range, east of the San Andreas fault and correlate them with the geological maps we find that they are often associated with known folds. Those have been widely regarded as drag folds and secondary faults resulting from primary right-lateral shear on the San Andreas fault. Most of the transverse faults shown on the geological maps cut the Mesozoic Franciscan formation and the overlying Upper Cretaceous sedimentary rocks, with only a few cutting rocks younger than Eocene. ERTS-1 imagery, however,



RELATION OF MERCURY DEPOSITS TO TRANSVERSE FAULTS
COAST RANGES CALIFORNIA

LEGEND

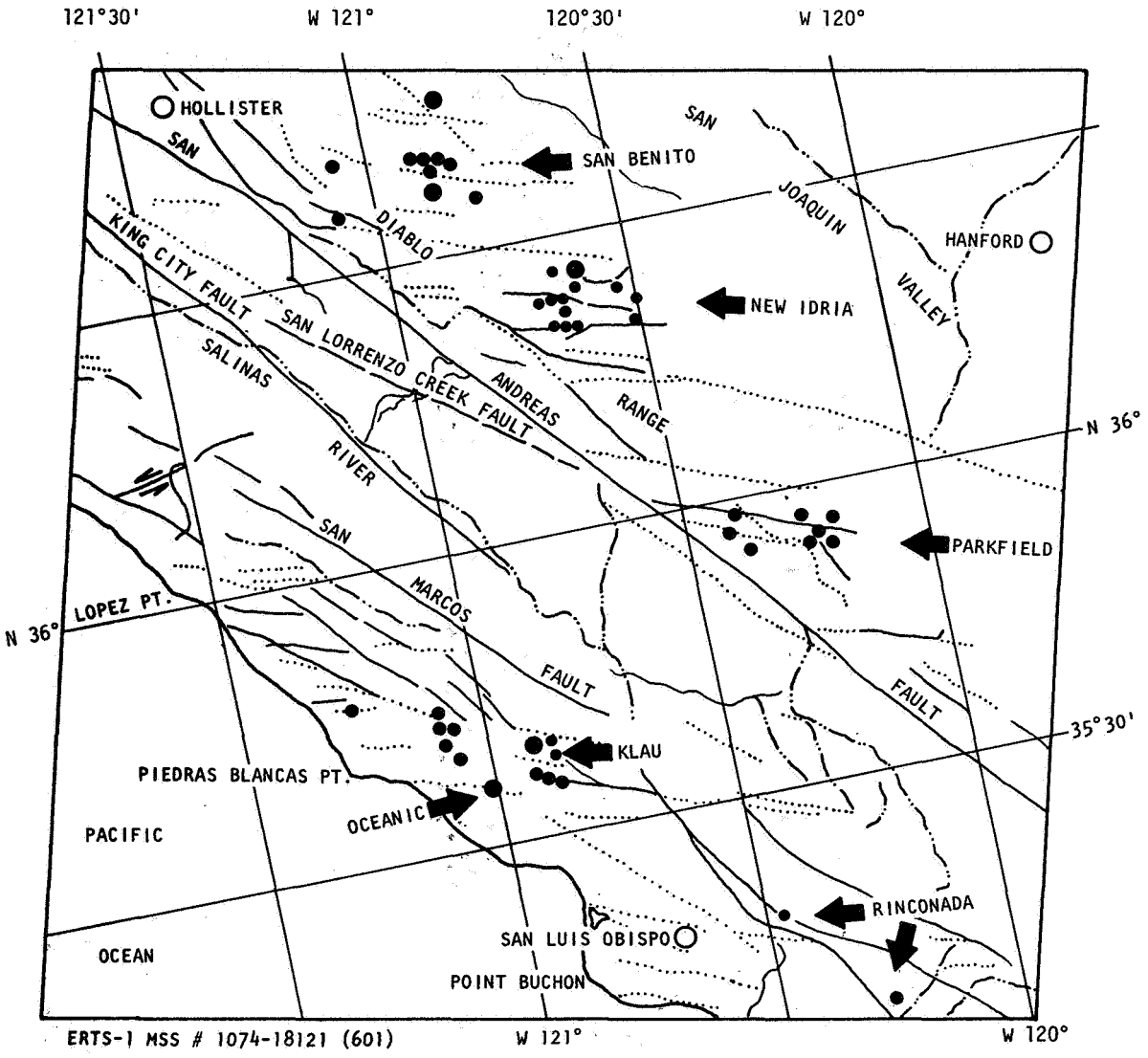
- R ..... Fault with evidence of recent movement
- ——— KNOWN FAULTS
- ..... FAULTS INFERRED FROM ERTS
- —·—·— DRAINAGE LINE
- MERCURY MINING DISTRICT
- ●●● MERCURY MINES

Abdel-Gawad & Silverstein 1973

Figure 4


W122-001
W121-301
W121-001
W122-301
W122-001
W121-301
860CT72 C N37-29/W121-44 N N37-27/W121-30 MSS 5 D SUN EL41 AZ146 190-1046-G-1-N-D-2L NASA ERTS E-1075-18173-5 02

Figure 4a



RELATION OF MERCURY DEPOSITS TO TRANSVERSE FAULTS
COAST RANGES CALIFORNIA

LEGEND

- KNOWN FAULTS
- FAULTS INFERRED FROM ERTS
- DRAINAGE LINE
- MERCURY MINING DISTRICT
- MERCURY MINES

Abdel-Gawad & Silverstein 1973

Figure 5



Figure 5a

show that a significant number of transverse faults, particularly those occurring along fold flexures on the eastern side of the Diablo Range, persist as distinct lineaments across Tertiary and Quaternary sedimentary rocks of the Great Valley. While the tectonic stresses which produced the transverse shear structures may have been initiated in pre-Tertiary times, the observation of fault lineaments across the blanket of younger rocks in the San Joaquin Valley suggests that transverse shear persisted during the deposition of Tertiary and Quaternary rocks and may very likely be still active.

Figure 1 corresponds to ERTS-1 scene 1037-18064 and shows the complex interaction of the Transverse Ranges and characteristic left-lateral wrench faults with the Coast Ranges and the San Andreas fault set. The three mercury districts, Rinconada, Cachuma, and Los Prietos indicate a relation to transverse structures. Although the Sunbird open pit mine (Los Prietos district) in Santa Barbara County has become among the large producers in the late 1960's (Mitko, F. C., 1968), it may appear surprising the mercury deposits were not found in greater abundance within the Transverse Ranges. The widespread presence of a thick blanket of Tertiary marine sedimentary rocks in this province probably accounts for the apparent scarcity of mercury deposits on the surface but there is no reason to discount the likelihood of more extensive occurrences in depth.

REFERENCES

Abdel-Gawad, M. and Silverstein, Joel, 1972: Earthquake epicenters and fault intersections in central and southern California: Type II Progress Report June-November 1972: Goddard Space Flight Center, Greenbelt, Maryland, 23 p.

Abdel-Gawad, Monem and Silverstein, Joel, The fault pattern of southern California - a model for its development (Abstract), Geological Society of America 1972 Annual Meeting, Minneapolis, Minnesota, November 13, 1972.

Allen, C. R., St. Amard, P., Richter, C. F., and Nordquist, J. M.: Relationship between seismicity and geologic structure in the southern California region: Bull. Seism. Soc. Am., V. 55, 753-797 (1965).

Bailey, E. H., 1962, Mercury in the United States-United States Geol. Survey Mineral Invest. Res. Map MR30.

Bailey, E. H. and Everhart, D. L., 1964: Geology of quicksilver deposits of the New Almaden district: U.S. Geol. Survey Prof. Paper 360, 206 p.

Bailey, E. H. and Smith, R. M., 1964, Mercury - its occurrence and economic trends: United States Geol. Survey Circ. 496, p. 1-11.

California Department of Water Resources Bulletin 116-2 Crustal Strain and Fault Movement Investigation - Faults and Earthquake Epicenters in California - January 1934 - December 1961.

Davis, F. F., 1957: Mercury in Mineral Commodities of California: Calif. Div. Mines and Geology Bull. 176, p. 341-356.

Davis, F. F., 1966: Mercury in Mineral Resources of California, Calif. Div. of Mines and Geology Bulletin 191, p. 247-254.

Eardley, A. J., Structural Geology of North America, New York, Harper and Row Publishers Inc., second edition, pp. 743 (1962).

Eckel, E. B. and Myres, W. B., 1946, Quick silver deposits of the New Idria district, San Benito and Fresno Counties, California: Calif. Div. Mines Report 42, p. 81-124.

King, P. B. (compiler), Tectonic Map of North America, Scale 1:5,000,000. United States Geological Survey (1969).

Linn, R. K., 1968, New Idria Mining District in (John D. Ridge, editor) Ore Deposits of the Unted States, 1933-1967 - The Graton-Sales Volume, The Am. Ins. Mining, Metal. and Petrol. Engineers, New York, V. 3, p. 1623-1649.

Mitko, F. C., 1968, The Mineral Industry of California in Minerals Yearbook, V. 3, U.S. Dept. of Interior Bureau of Mines, p. 127-158.

NOAA Geographic Hypocenter Data File (Magnetic Tape), January 1961 through December 1971.

NOAA Hypocenter Data Cards, January 1972 through August 1972.

Ryall, A., Slemmons, D. B., and Gedney, L. D., Seismicity, tectonism, and surface faulting in the western United States during historic time: Bull, Seism. Soc. America, V. 56, 5, 1105-1135 (1966).

Shoemaker, E. M., Structural features of southeastern Utah and adjacent parts of Colorado, New Mexico, and Arizona: Guidebook to the Geology of Utah, No. 9, Utah Geol. Soc., p. 48-69 (1954).

Stose, G. W. and Ljungstedt, O. A. (compilers), Geologic Map of the United States, scale 1:2,500,000 (1960).

White, D. E. and Roberson, C. E., 1962, Sulphur Bank, California, a major hot-spring quicksilver deposit: in Petrologic Studies: A volume in honor of A. F. Buddington: The Geological Society of America, p. 397-428.

FIGURE CAPTIONS

Figure 1. Fault pattern, seismicity, and mercury deposits in western Transverse Ranges California.

Figure 2. Fault pattern and seismicity, northern Colorado Plateau, Utah.

Figure 3. Relation of mercury deposits and transverse faults, Coast Ranges, northern California.

Figure 4. Mercury deposits and transverse faults, Coast Ranges, central California.

Figure 5. Mercury mines and transverse faults in southern Coast Ranges, California.

Paper G 23

SOME ASPECTS OF ACTIVE TECTONISM IN ALASKA AS SEEN ON ERTS-1 IMAGERY

Larry D. Gedney and James D. VanWormer
Geophysical Institute, University of Alaska, Fairbanks, Alaska 99701

ABSTRACT

ERTS-1 imagery is proving to be exceptionally useful in delineating structural features in Alaska which have never been recognized on the ground. Previously unmapped features such as seismically active faults and major structural lineaments are especially evident. Among the more significant results of this investigation is the discovery of an active strand of the Denali fault. The new fault has a history of scattered seismicity and was the scene of a magnitude 4.8 earthquake on October 1, 1972. Perhaps of greater significance is the disclosure of a large scale conjugate fracture system north of the Alaska Range. This fracture system appears to result from compressive stress radiating outward from around the outside of the great bend of the Alaska Range at Mt. McKinley. NASA aircraft data also support this assumption. One member of the fracture system was the scene of a magnitude 6.5 earthquake in 1968. The potential value of ERTS imagery to land use planning is reflected in the fact that the site of the proposed bridge and oil pipeline crossing of the Yukon River lies very near this fault.

1. INTRODUCTION

In an area as remote and inaccessible as most of Alaska, geologic mapping is, at best, hit-and-miss. Mapping in the state (if it has been done at all) is often, of necessity, the result of a few "point investigations" carried out by helicopter, with a lot of interpolation in between. For this reason, the application of ERTS imagery to a study of various aspects of the Alaskan environment takes on an importance found in few other areas.

As an example of features which may be missed by geologic field mapping in Alaska, consider that the Denali fault (which is a tectonic feature on the scale of, and perhaps more striking than the San Andreas fault) was not even named prior to 1957 (St. Amand, 1957). Since that time, it has been found to comprise an important element of the Pacific transform fault system of which the San Andreas is a member (c.g. Tobin

and Sykes, 1968). More recent studies (Richter and Matson, 1971) have revealed that much of the motion between the north Pacific plate and the continent is now probably being taken up along the Totschunda fault system connecting the active segments of the Denali and Fairweather faults. All these features are clearly visible on ERTS-1 imagery, and for some purposes, the imagery is clearly superior to even detailed ground mapping. Consider, for instance, a scene containing the intersection of the Denali and Totschunda faults (image ID No. E-1081-20275). It appears obvious that a strand of the Totschunda fault extends northwestward through Stone Creek, across the valley of the Nabesna River and into the mountains to the northwest. However, the most detailed geologic map available of this area (Richter, 1971) does not show this feature, presumably because of alluvial fill along its trace, lack of rock differentiation across it, and sheer inacessibility in the mountainous areas. This scene also shows a small unmapped fault on the northwest flank of Mt. Sanford. While this is a minor feature, it is of interest because it appears from the lighting and stream incision that it is a reverse fault. That is, the mountain has dropped with respect to the valley. The value of obtaining imagery at low sun angles is illustrated by the fact that this feature is not seen (without enhancement) on two earlier, cloud-free passes during August and September. The present scene was made on October 12 when the sun angle was 18°. Equivalent sun angles during the earlier passes were 43° and 25° (Image ID Nos. E-1010-20331 and E-1063-20273).

2. OTHER FINDINGS RELATING TO TECTONICS IN ALASKA

One of the primary objectives of this investigation was to identify seismically active faults which had been postulated on the grounds of ongoing seismicity. After several years of data accumulation, we are finding that earthquakes in central and south-central Alaska very often occur in elongated clusters where no faults are mapped. ERTS-1 imagery is being found to be extremely valuable in identifying faults in these areas. A particularly good example is found in image ID No. E-1066-20444. A seismically active strand of the Denali fault can be easily traced for at least 120 km, with end points at approximately $62^{\circ}26'$N, $149^{\circ}23'$W, and $63^{\circ}14'$N, $147^{\circ}44'$W. It forms a lineal depression along which streams flow and sag ponds form. Seismicity records dating back to 1967 reveal that earthquakes have tended to cluster along the fault in this area, particularly near the end points, and the southern end was the scene of a magnitude 4.8 earthquake on October 1, 1972. This earthquake was felt throughout the Susitna River Valley. Although it appears from the image that the Susitna River has been left-laterally offset by this feature, the fault plane solution obtained of the event of October 1 indicates right-lateral displacement, which suggests that it is a strand of the Denali fault, and not a conjugate, or tear fault. Lathram (1972) identified a linear in this approximate area on the basis of Nimbus IV imagery, although it appears offset in the Nimbus imagery in a manner which is not apparent in the higher resolution ERTS-1 imagery.

North of the Alaska Range, in the central interior, there is a broad zone of shallow seismicity which extends at least as far north as the southern Brooks Range (Gedney et al., 1972). Since 1904, eight earthquakes of magnitude greater than 6.0 (up to 7.8) have occurred in this area. Although considerable seismic data has been accumulated for this region, primarily in recent years, geologic and tectonic mapping is minimal or nonexistent. In October, 1968, an earthquake of magnitude 6.5 occurred in the Minook Creek Valley northwest of Fairbanks. Figure 1 is a mosaic composed of portions of six ERTS-1 images (Image ID Nos. E-1104-20554, E-1104-20560, E-1104-20563, E-1105-21012, E-1105-21015, and E-1105-21021). Minook Creek appears in the upper left center at approximately 65.4°N., 150.1°W. Prior to the 1968 earthquake, this feature was not recognized as a fault. Since that time, aftershock studies, fault plane solutions, and geologic field mapping have revealed that it is, indeed, a left-lateral fault. Had ERTS imagery been previously available, this conclusion would undoubtably have been reached long ago. The extreme sharpness of stream incision, the textural and tonal differences across the valley, and the series of parallel fractures in the surrounding mountains would have left little doubt. Although the left-lateral nature is not obvious on the Minook Creek fault, the fourth parallel feature to the east shows it quite well, with truncation of mountain lobes on both the north and south sides of the ridge line.

On closer inspection, one sees that the Minook Creek fault is only part of a large scale fracture system involving many other linears. Parallel features can be seen in the mountains across the Yukon River to the northwest, they can be identified on the southeast banks of the Yukon, where they affect tributary drainage, and two long lineaments are seen in the Kuskokwim Mountains to the southwest. Textural changes occur across the latter two, although they become lost in the alluvium of the Tanana River at their northern ends. Figure 2 is a key to the mosaic, pointing out these features and others mentioned in the following discussion.

An almost equally impressive set of conjugate fractures intersects the Minook Creek complex at an angle of 55°, and strikes southeast to the Alaska Range. This is roughly the dihedral angle at which most brittle substances would be expected to fail if compressive stress had been applied at an azimuth bisecting the acute angle between the two sets. In this case the direction is at an azimuth of about 345°, roughly perpendicular to the trend of the Alaska Range. The conjugate set is most apparent in the Ray Mountains, across the Yukon River from Minook Creek; but it is also visible in the mountains around Minook Creek, south of the Tanana River, and near the bottom center of Fig. 1. The latter lineament appears to truncate the small mountain near its center.

There is a strong implication that earthquakes in this area are the product of compressive stress radiating outward from around the great bend in the Alaska Range, and that this stress system has resulted in the formation of a conjugate shear system with earthquakes occurring along the individual fractures. A mechanism of this sort agrees well with the fault plane solution obtained for the 1968 earthquake, and with one obtained for a magnitude 6.0 earthquake near Fairbanks in 1967. For the

latter event, a nearly north-south azimuth of compressive stress was obtained, nearly perpendicular to the Alaska Range at this point, as was true with the Minook Creek event. The 1967 earthquake occurred on a prominent lineament extending from the town of Nenana, past Fairbanks, and into the headwaters of the Chena River to the northeast. As a suspected fault, this line was flown with a NASA aircraft (NP3A) during the summer of 1972. While conventional and reflective infrared photography failed to reveal conclusive evidence of faulting (as did side-looking radar), the IR scanner produced some unusual and unexpected results. Just south of Fairbanks, on the Chena lineament in the aftershock zone of the 1967 earthquake, there are what appear to be a series of steeply dipping folds. Their appearance virtually rules out the possibility that they are old river meanders. They are in an area which is normally regarded as being overlain by thick flood plain deposits, which makes it seem unlikely that they are a reflection of the underlying bedrock. The fold axes trend generally along the line of the Chena lineament, with an amplitude of about 7 km and a period of about 3 km. It is conceivable that they are a result of deformation of the Quaternary sediments by compressive stress in a north-south direction, although this is admittedly "reaching".

If the concept of outwardly-directed compressive stress to the north and northwest of the bend in the Alaska Range is to be taken seriously, the logical question which now arises is, "What causes the compression?". A possible explanation is that the forces which caused the Alaska Range to "buckle", forming the great 90° bight in the range at Mt. McKinley, have not yet subsided and further deformation is occurring. The primary cause is probably related to underthrusting of the north Pacific plate beneath the continental margin along Cook Inlet and the western Alaska Range (Davies, 1973). But whatever the basic energy source, it would seem plausible that further buckling of the range would result in outwardly directed compressive stress around the outside of the bend, with a resulting pattern of conjugate fractures of the type we have been discussing.

3. CONCLUSIONS

Although our discussion has dealt primarily with tectonic aspects of Alaska which can be seen on ERTS imagery, the most salient point is this: It is possible, with ERTS data, to delineate seismically active faults which may go otherwise unnoticed. Certainly the Minook Creek fault (site of the magnitude 6.5 earthquake of 1968) would have been recognized long ago, had ERTS imagery been available, and its freshness of appearance would have labeled it as being recently active. It bears pointing out that the site for the proposed Rampart bridge and oil pipeline crossing of the Yukon River is very near the Minook Creek fault if it extends to the north, and that the proposed route also crosses the two strong lineaments at the top center of Figs. 1 and 2. Particularly in Alaska, where these areas are remote and accessible only at great time and expense, ERTS imagery shows great promise as an aid in construction planning, zoning, and seismic risk evaluation.

REFERENCES

Davies, J., Crustal morphology in central Alaska, Bull. Seism. Soc. Am. 63(1), 1973 (to appear).

Gednev, L., L. Shapiro, D. VanWormer and F. Weber, Correlation of epicenters with mapped faults, east-central Alaska, 1968-1971, map with 8 pp., U.S.G.S. Open-file Report, 1972.

Lathram, E., Nimbus IV view of the major structural features of Alaska, Science, 175, 1423-1427. 1972.

Richter, D., Reconnaissance geologic map and section of the Nabesna B-4 quadrangle, Alaska, Miscellaneous Geologic Investigations, Map I-656, U.S. Geological Survey, 1971.

Richter, D., and N. Matson, Jr., Quaternary faulting in the eastern Alaska Range, Geol. Soc. Am. Bull., 82, 1529-1540, 1971.

St. Amand, P., Geological and geophysical synthesis of the tectonics of portions of British Columbia, the Yukon Territory, and Alaska, Geol. Soc. Am. Bull., 68, 1343-1370, 1957.

Tobin, D. and L. Sykes, Seismicity and tectonics of the northeast Pacific Ocean, J. Geophys. Res., 73, 3821-3845, 1968.

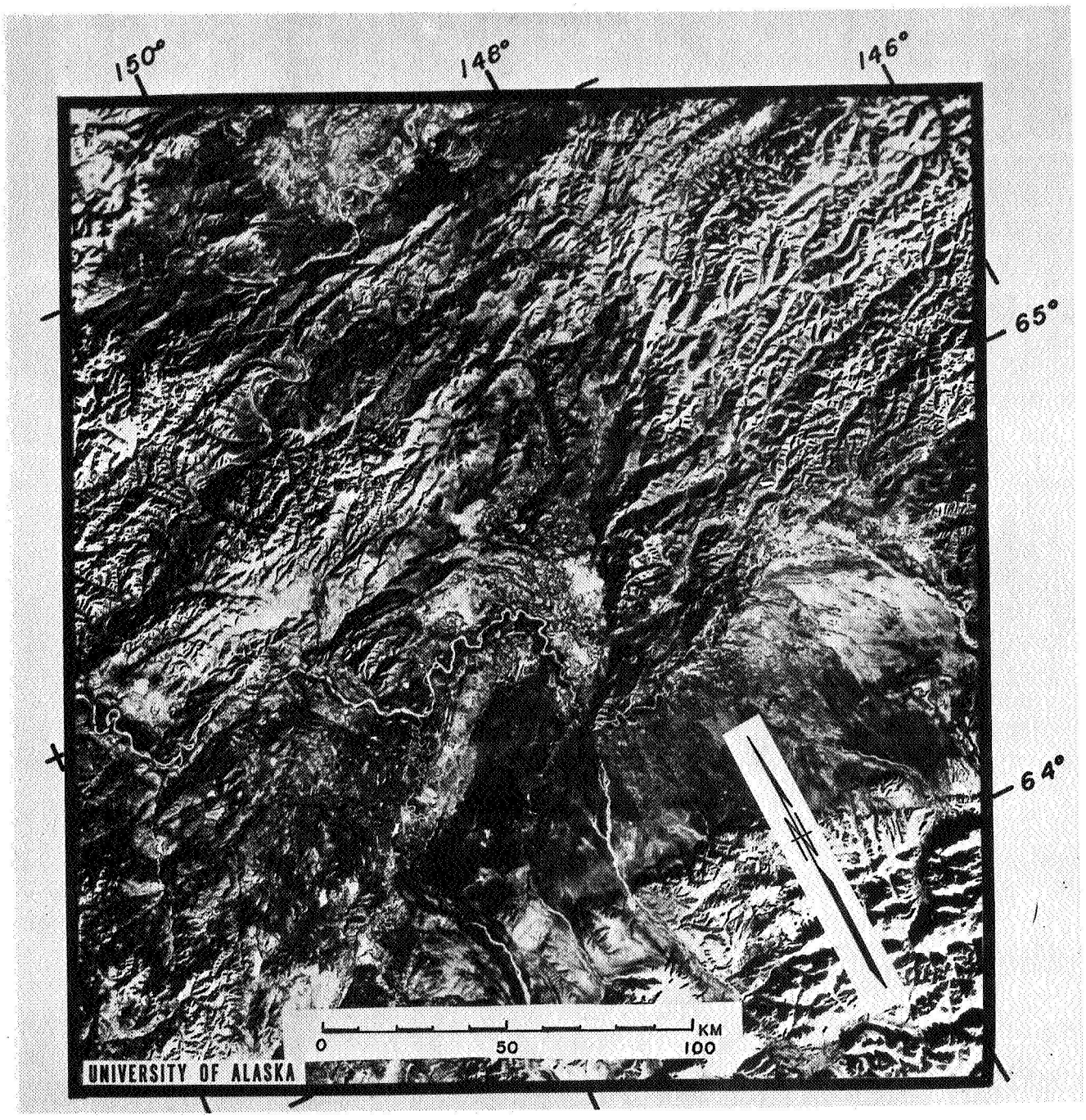


Figure 1. Mosaic of six ERTS-1 MSS images of central interior Alaska. See text for image ID Nos. and Figure 2 for key to mosaic.

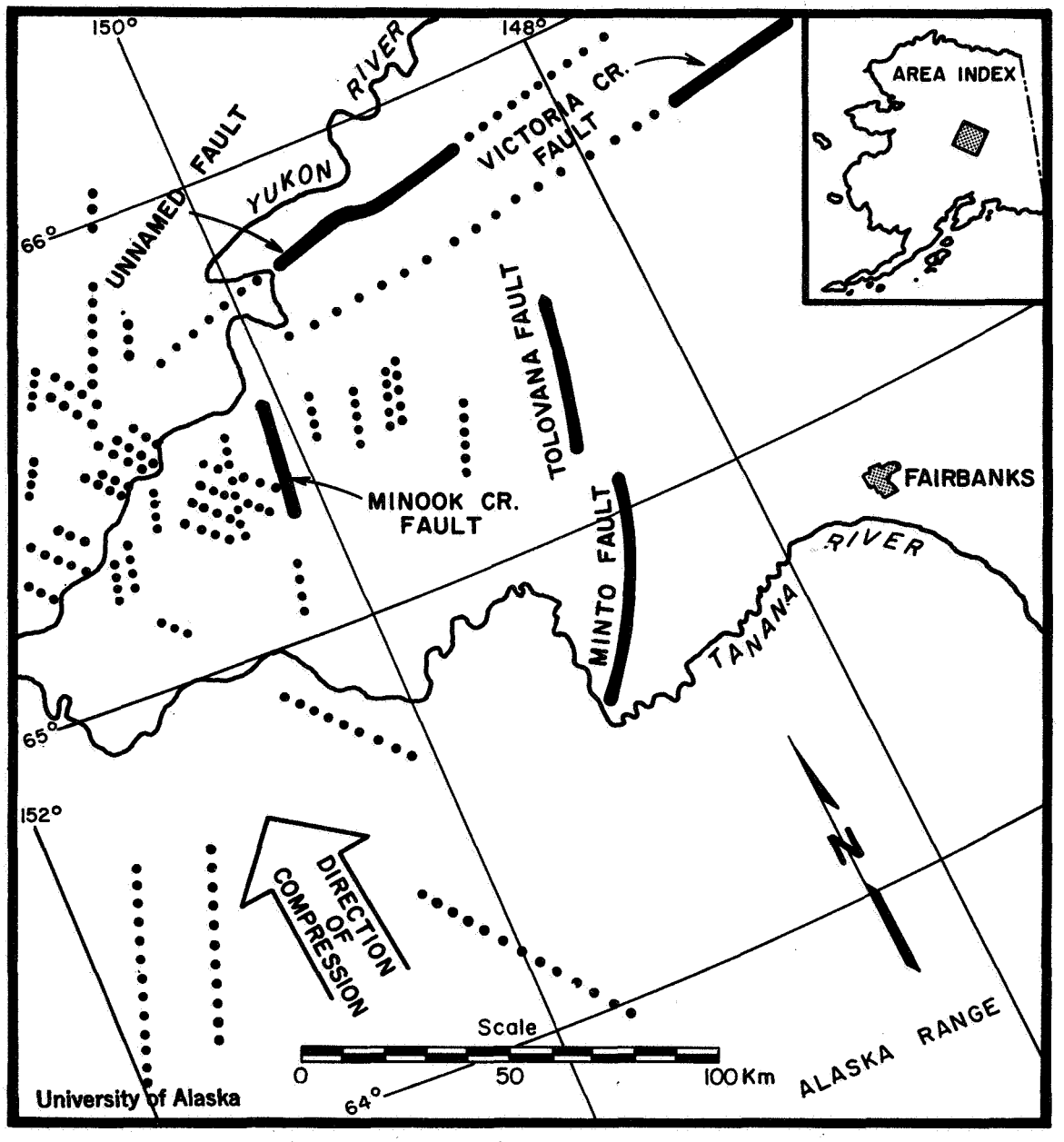


Figure 2. Key to Figure 1. Those linears shown by heavy solid lines are known faults which are identifiable in ERTS-1 imagery. Features shown in dotted lines are previously unmapped faults and lineaments recognized for the first time in the ERTS images.

Paper G 24

ERTS-1 IMAGE CONTRIBUTES TO UNDERSTANDING OF GEOLOGIC STRUCTURES RELATED TO MANAGUA EARTHQUAKE, 1972

W. D. Carter and G. P. Eaton, *U. S. Geological Survey, Washington, D. C. 20244*

ABSTRACT

ERTS-1 imaged the western portion of Nicaragua on December 24, 1972, one day after the central part of the city of Managua was devastated by a major earthquake which measured 5.6 on the Richter scale. ERTS-1 images reveal four sets of lineaments (which may reflect fault systems) along any one of which movement could have taken place. One set, trending N 50° W, includes a line of active volcanoes that parallels the coast and constitutes the southwestern edge of the Nicaraguan Depression, a regional graben which cuts obliquely across the Central American isthmus. This trend is offset approximately 10km in a right lateral geometric sense just west of the city of Managua. A parallel lineament, north of Lake Managua, marks the northeast edge of the graben. A second set, trending due N-S to N 25° W, extends northward to northwestward from the mouth of the Rio Grande (Viejo) north of Lake Managua and can be projected southward across the lake to Managua. It is this set along which geometric offset of the volcanic lineament appears to have taken place. It is paralleled by a belt of young pit craters at the west edge of the city. A third set of linears trends approximately N 50°-60° E across the Nicaraguan trench. The fourth set, which is less conspicuous, is represented by only three identified members within Nicaragua. Two others, which are subparallel, are visible on the image in the area of Honduras, to the northwest. This set is notable for the fact that it extends from the coast entirely across the Nicaraguan Depression. Its trend is N 25°-45° E. Aerial photographs and field studies in the city of Managua by other U. S. Geological Survey personnel (Brown, Ward, and Plafker, in press) indicate that this fourth set is represented by four currently active, left-lateral, strike-slip faults and a narrow belt of aftershock epicenters. Instrumental data indicate that the aftershock earthquake foci are of shallow depth (<10.0 kilometers).

Publication authorized by Director, U. S. Geological Survey.

1. INTRODUCTION

Managua, Nicaragua, was devastated by a series of 3 large earthquakes on December 23, 1972, the principal shock having a magnitude of 5.6 on the Richter scale. The loss of life has been estimated to exceed 11,000 persons and the damage to property valued at half a billion dollars (Brown, Ward and Plafker, 1973). Such destruction, as with the 1931 and 1968 earthquakes, was determined to be the result of two related causes: (1) The city of Managua is located on poorly consolidated sediments (scoria and ash) of volcanic origin; and (2) Many of the buildings are constructed of materials (masonry and tarquezal) that have little resistance to strong shaking. Direct displacement of structures situated along the course of active faults accounted for severe damage to buildings with better quake resistance (Brown and others, op. cit.).

On December 24, 1972, the Earth Resources Technology Satellite (ERTS-1), in orbit approximately 900 kilometers above the earth, acquired two multispectral images (NASA ERTS-1154-15385 and 15391) over Managua and adjacent areas to the west. These images were processed by NASA's Goddard Space Flight Center and forwarded to U. S. Geological Survey scientists for interpretation. Much of Managua was under scattered cloud cover, and therefore none of the damage could be defined. The area in the rest of the scene was cloud free, however; thus, it was possible to map a number of geologic features that may bear some relation to regional earthquake conditions and which contribute to general knowledge of the region.

The purpose of this preliminary report is to describe the evaluation of the ERTS-1 imagery and the results of rapid data interpretation (approximately 3 hours).

2. METHOD OF APPROACH

The authors have not visited Nicaragua and had access to only a very limited selection of library material when the interpretation was carried out in mid-January 1973. Positive 9" x 9" transparencies placed on a light table and an 8x magnifier were used to make mylar overlays. Diazo-foil, false color composites were made using a standard Ozalid printer.

The ERTS-1 imaging system is a 4-band multispectral scanner (MSS) in which the green (0.4-0.5μm), red (0.5-0.6μm), and two infrared bands (0.6-0.7μm and 0.8-1.1μm) can all be used to identify features. The following paragraphs attempt to explain their differences and contributions.

The green band (MSS-4) was somewhat affected by haze but clearly shows either sediment distribution or near-shore bottom features of water bodies or both (Figure 1). For example, two crater lakes on the Chiltepe peninsula of Lake Managua can be seen, but their tones are different. The lighter one is apparently more turbid than the darker. Marshland areas appear in tones lighter than water but darker than the surrounding land areas. Volcanic ash and lavas comprising volcanic cones and surrounding debris fields are darker than adjacent materials. Vegetative areas such as farmlands and cultural fields are difficult to define.

The red band is clearer in overall appearance because haze has less effect in this region of the spectrum (Figure 2). The land surface tones are dark shades of gray due to the presence of vegetation. Cultural and soil features are clearly displayed. Water penetration is minimal, but sediment plumes in estuaries are clearly visible.

The two infrared bands are very similar in that edges of water bodies are sharply defined in black (Figure 3). Marshland and levees can be clearly delineated in these bands, and they are also excellent for determining the presence of water in small rivers, streams, and arroyos.

Surface tones of land areas are brighter in the infrared bands than in the green and red bands due to higher reflectance of vegetation which appear in shades of white to light gray (Figures 3 and 4). Cultivated croplands are brightest (exclusive of clouds and snow) and can easily be defined. Natural vegetation appears as light gray. These bands are most useful in defining tectonic features, such as volcanoes and lineaments. Cultural features, such as small towns and cities, stand out as dark patches somewhat similar in tone to volcanic cinder cones. Their rectangular to irregular box-like patterns, caused by road grids and lack of radial drainage, enables one to distinguish them unambiguously.

Soil tones are subtle shades of gray and therefore are difficult to distinguish from natural vegetation in the black and white renditions of the scene. They are, however, easily distinguished in color combined renditions (Figure 5). One great advantage of these bands is the fact that one can separate natural vegetation from shadowing produced by the angle of solar illumination; in the red and green bands, however, this is more difficult.

Because of the earthquake-related destruction of Managua, a preliminary geologic structure map was made to see if such information would assist ground studies concerned with the damage. The

map (Figure 6) shows the result of about three hours of interpretation. These studies are continuing and more information is being extracted. Figure 7 was prepared in about 10 hours by Dr. J. N. Rinker.

The most obvious tectonic features visible in the scene are the Holocene volcanoes aligned parallel to the coast. This linear arrangement trends S 50° E directly toward the city of Managua. Many of the volcanoes are recognized by their dark tones and circular patterns. Many show drainage scars radiating from their central cone and lobate forms or serate edges at the termini of their flows at the margin of the volcanic debris. Several are marked by crater lakes which are seen as black spots in the near-infrared bands. Two that are clearly visible are Laguna de Apoyeque and Laguna de Jiloa on Punta Chiltepe, a peninsula on the southwest shore of Lake Managua within 10 kilometers of the city. Three other crater lakes, under clouds in the scene, lie just south of the city. One of these at the edge of the city, Laguna de Tiscapa, is a residential area which includes the Presidential Palace and the U. S. Embassy, an area where considerable damage to structures was reported.

Of next importance is a narrow belt of linear features that trends north to north-northwest (due N to N 25° W) on the north side of Lake Managua. A projection of these linears to the south, across the lake, intersects the volcano linear northwest of the city of Managua. The volcanic linear is offset approximately 10km, with the east block apparently displaced to the south. This displacement is not visible on the image, but is seen in the regional geologic map (Figure 8).

A third and fourth set of prominent linears strike north-northeastward and northeastward (N 25°-45° E and N 50°-60° E), respectively, crossing both the volcanic trend and the Nicaraguan Depression. Although it can not be seen in the ERTS-1 scene at Managua because of cloud cover, Mr. Leroy Anstead of IAGS, on duty in Managua at the time of the event, reported north-northeast trending earthcracks in the city. They were visible on the ground and in low-altitude (scale 1:5,000) aerial photography. This set has been mapped in detail by Brown, Ward, and Plafker (1973), and it is paralleled by a narrow band of earthquake aftershocks.

Strike-slip offset of a few to several tens of centimeters was measured in walls, sidewalk curbs, and roads that intersected these fractures. This trend had been mapped earlier both by Juan Kuan S. and Carlos Valle G. (written communication, undated) and on a radar mosaic of the country by Anstead (oral communication, 1973) and others for a length of over 100km. Inasmuch as this set is paralleled by three other lineaments seen on the ERTS image to the northwest, regional field investigations of this set would seem to be desirable from the standpoint of assessing regional earthquake hazards.

The authors had the opportunity to briefly study color infrared photography acquired from the NASA C-130 aircraft on or about December 28, 1972. The frame which covered the center of the city revealed the area of greatest damage to be white to light gray in tone, crudely elliptical in shape and covering about 70 blocks in area. The damage zone, trending east-west, is marked by collapsed roofs, walls, and extensive rubble in the streets. An extension of damage was seen in small areas to the north-northwest. Extensive damage also extended along this line, south of the probable epicenter of the main shock, to a small crater lake (Laguna de Tiscapa) next to which were the Presidential Palace and the U. S. Embassy. These were reported to be damaged beyond repair.

3. SUMMARY

The Managua earthquake of December 1972 constituted an early test of the ability of the ERTS-1 system to respond to a disaster situation. The alertness of the NASA satellite management team enabled the acquisition of data on the day following the event. Rapid image processing by the Goddard crew put data in the hands of geologists within 5 days of the event and copies of the initial interpretation were placed in the hands of the Nicaraguan Embassy within 2 weeks. The data obtained provided good background information on the surface geology and structure of the region.

Although cloud cover and smoke prohibited detailed studies of destruction within the city of Managua from ERTS-1, the destroyed area was large enough to have been detected in enlargements of ERTS-1 data at scales of 1:250,000 or 1:100,000 or in computer processing of the tapes. Repetitive data taken 18 days after the event would have been useful for comparative purposes. Pre-earthquake ERTS-1 imagery of Managua would also be extremely valuable in assessing changes associated with the earthquake.

4. REFERENCES

Brown, R. D., Jr., Ward, P. L., and Plafker, George, in press, Geologic and seismologic aspects of the Managua, Nicaragua, earthquakes of December 23, 1972: U. S. Geol. Survey Prof. Paper 838.

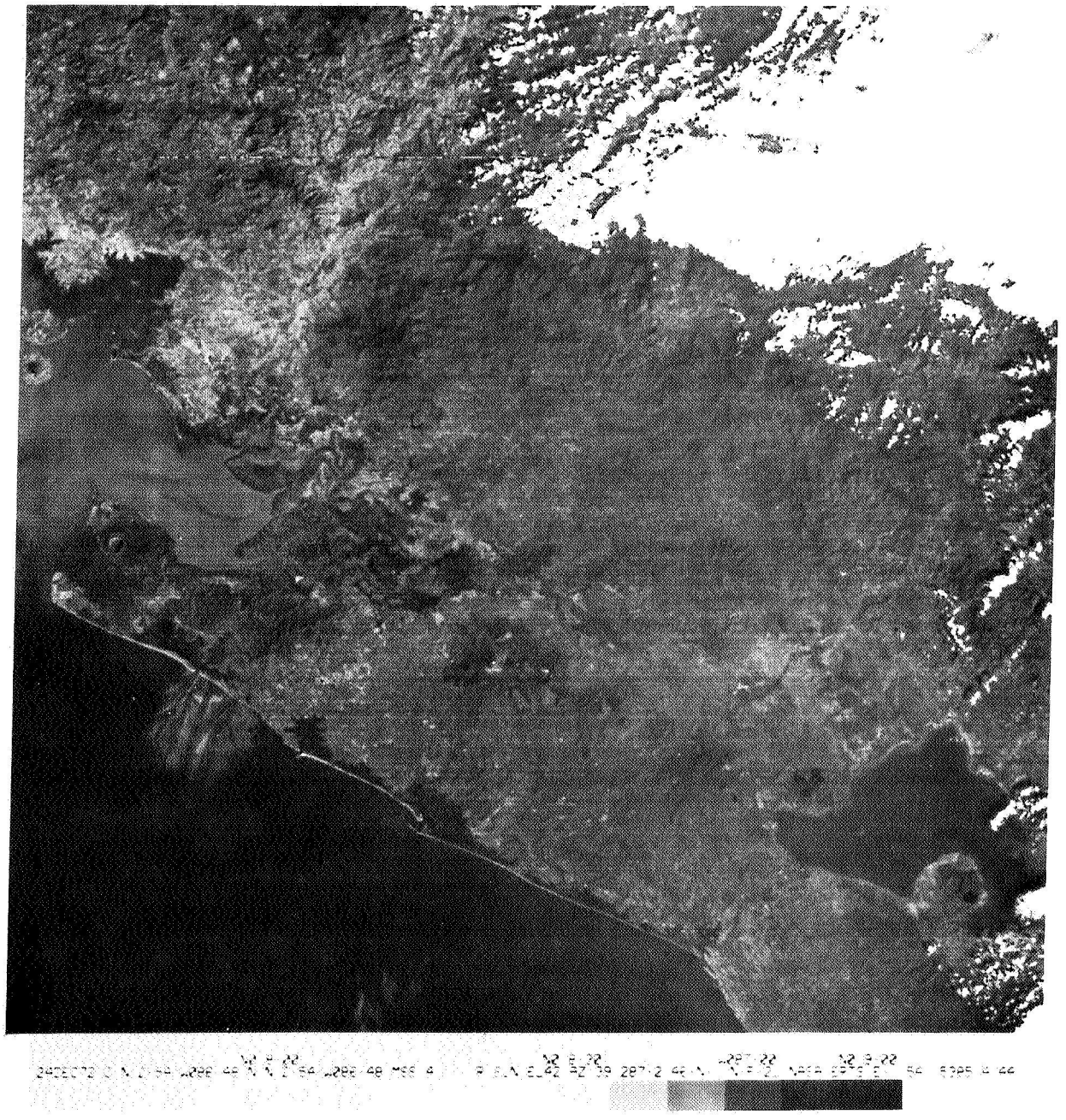


Figure 1. - Image of Nicaragua, Band 4 showing sediment plume in Bay of Fonseca



Figure 2. - ERTS-1 Image of Nicaragua, Band 5 showing cultural features

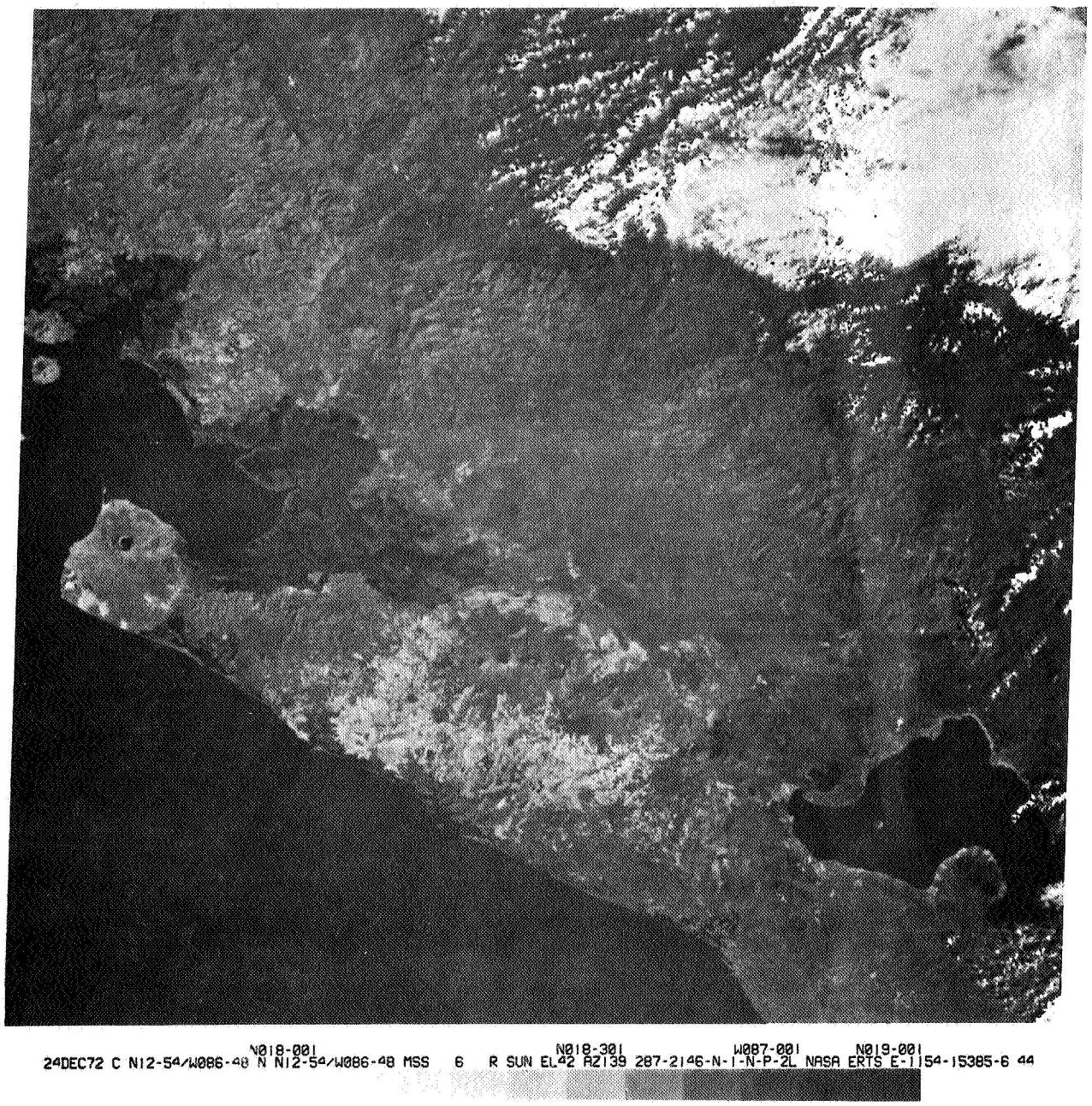


Figure 3. - ERTS-1 Image of Nicaragua, Band 6 showing distribution of volcanic centers and water bodies

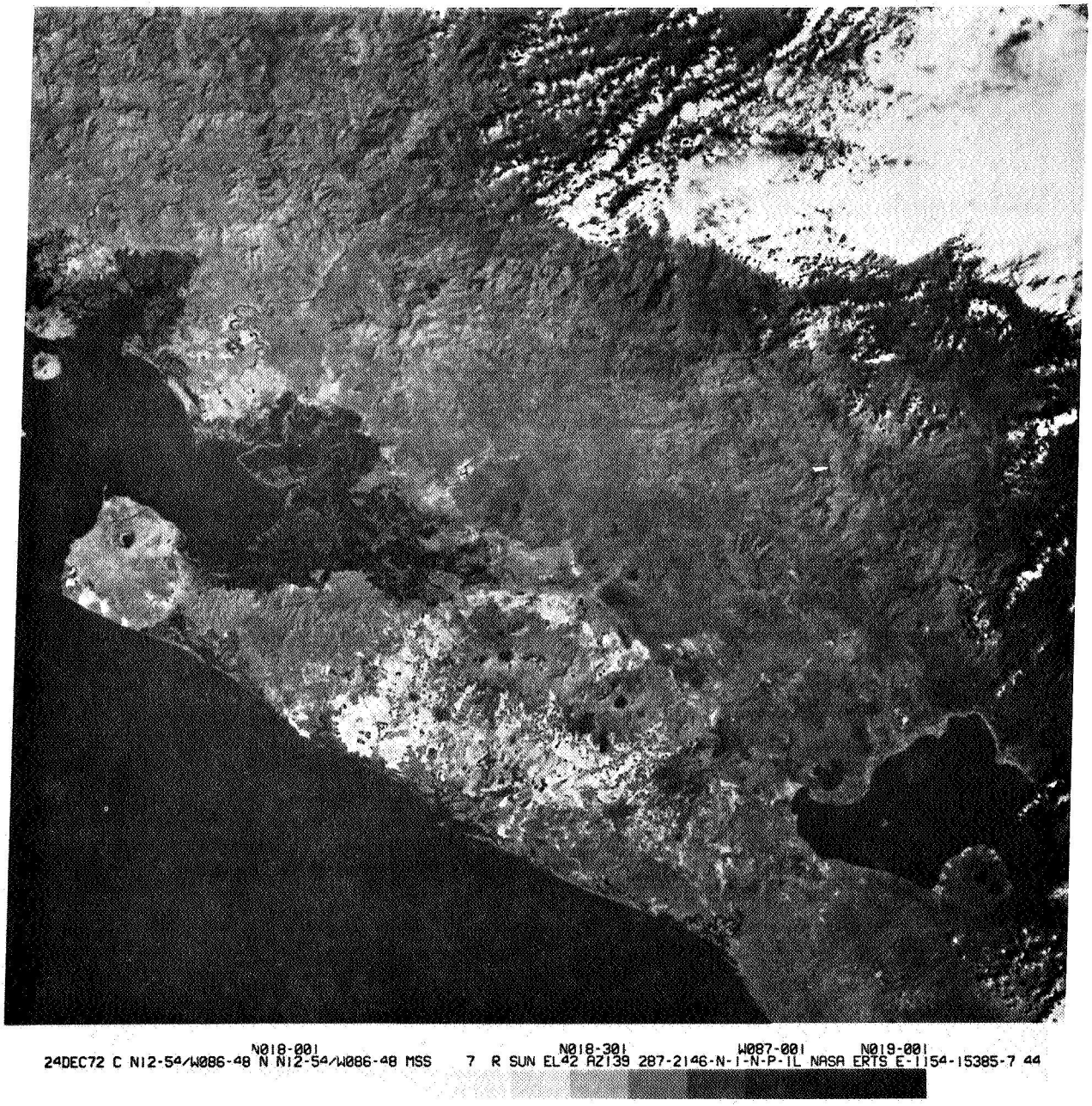
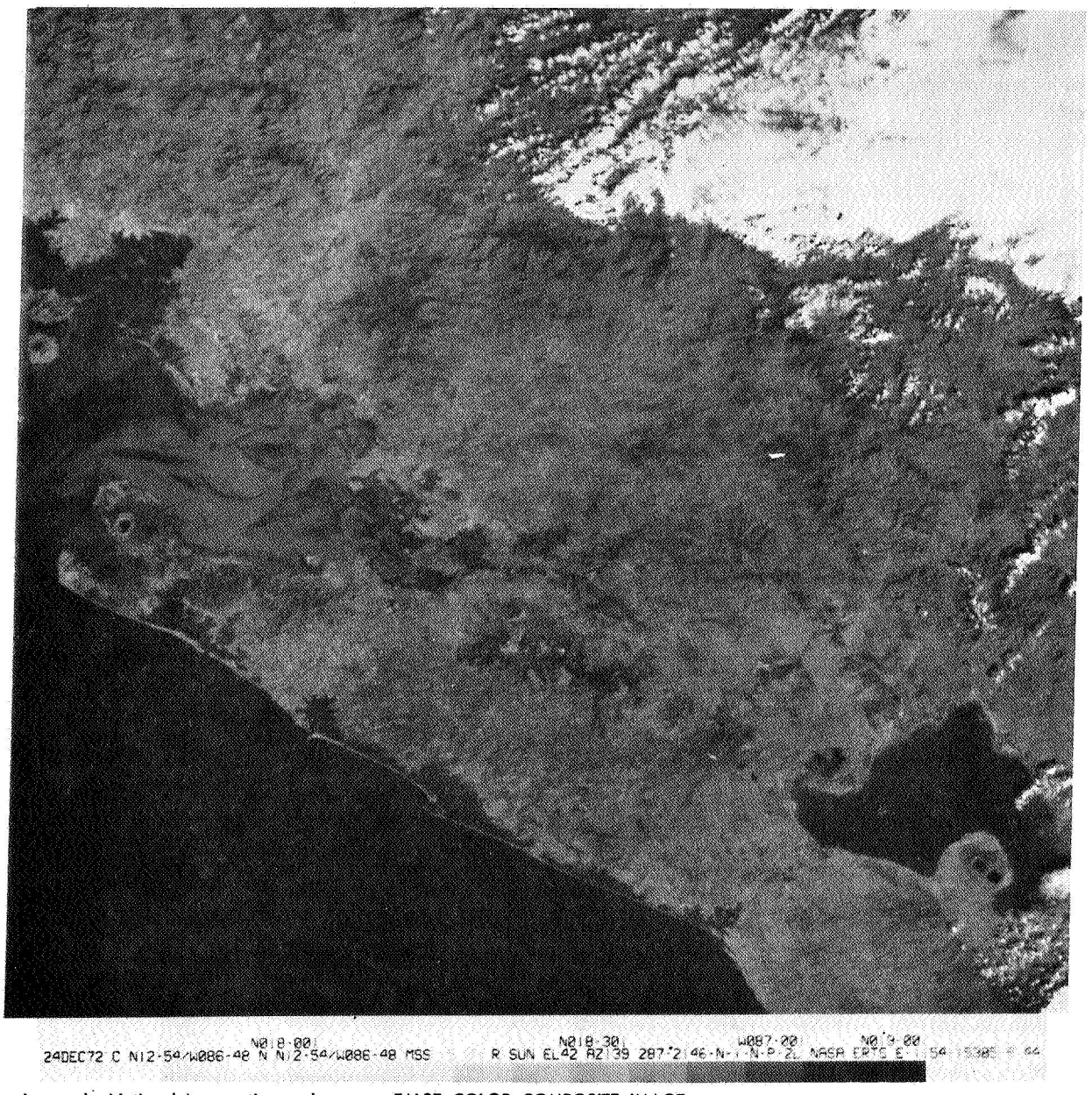


Figure 4. - ERTS-1 Image of Nicaragua, Band 7 showing features described in Figure 3 but from which interpretation was made

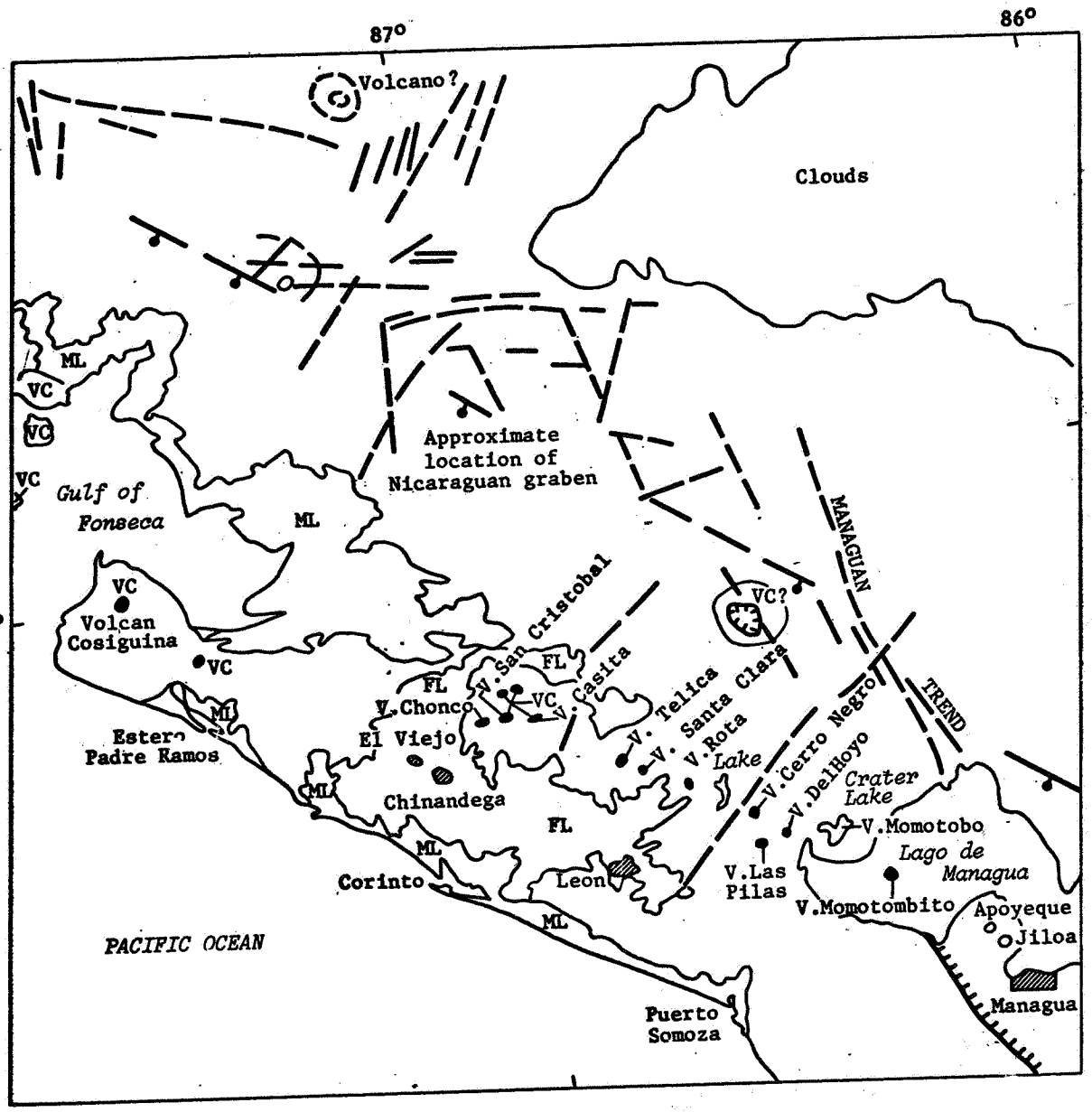
DEPARTMENT OF THE INTERIOR
UNITED STATES GEOLOGICAL SURVEY



Images by National Aeronautics and Space Administration, 1972

FALSE COLOR COMPOSITE IMAGE

Figure 5 False color composite image of Bands 4, 5, 7



EXPLANATION

ML - Marshland

FL - Farmland

VC - Volcanic crater or crater lake

City or village

Edge of caldera

Lineament; possible fractures or faults

Approximate edge of Lake Nicaragua graben; ball indicates downthrown side

PRELIMINARY SKETCH MAP OF LINEAR AND VOLCANIC FEATURES IDENTIFIED IN ERTS-1 DATA OF NICARAGUA
24 DECEMBER 1972

By
W.D.CARTER, US GEOLOGICAL SURVEY
WASHINGTON, D.C.

NASA EARTH RESOURCES TECHNOLOGY SATELLITE (ERTS–1) IMAGE
NORTHWEST OF MANAGUA, NICARAGUA—IMAGE AND FRACTURE PATTERNS, 1972

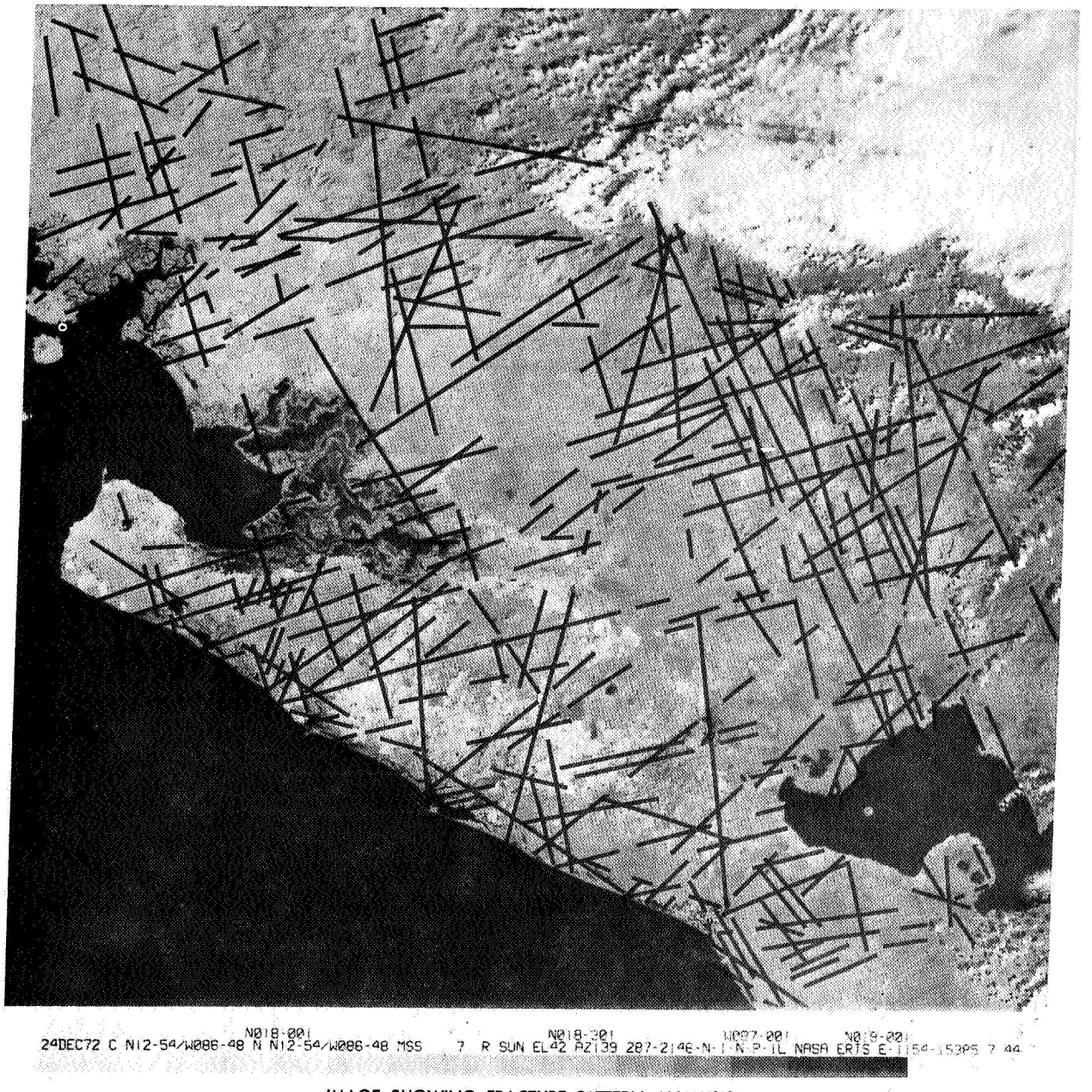


IMAGE SHOWING FRACTURE PATTERN ANALYSIS
By J. N. Rinker, Defense Mapping Agency

Figure 7

Image showing more detailed fracture pattern analysis by J. N. Rinker, DMA

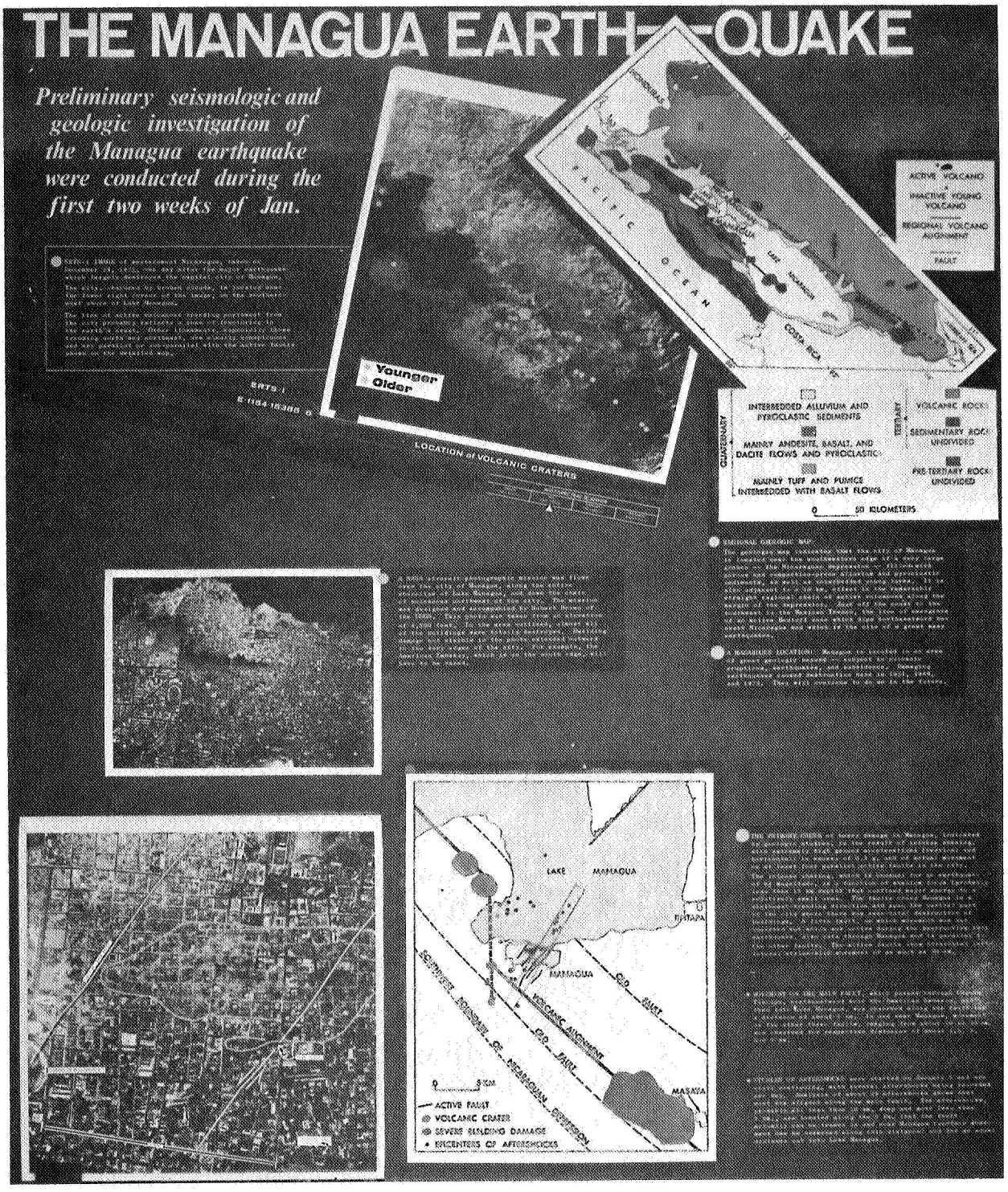


Figure 8

The Managua Earthquake summary showing preliminary seismologic and geologic investigation sources and products

Paper G 25

RECOGNITION OF SURFACE LITHOLOGIC AND TOPOGRAPHIC PATTERNS IN SOUTHWEST COLORADO WITH ADP TECHNIQUES

Wilton N. Melhorn and Scott Sinnock, *Laboratory for Applications of Remote Sensing, Purdue University, West Lafayette, Indiana 47907*

ABSTRACT

Analysis of ERTS-1 multispectral data by automatic pattern recognition procedures is applicable toward grappling with current and future resource stresses by providing a means for refining existing geologic maps. The procedures used in the current analysis already yield encouraging results toward the eventual machine recognition of extensive surface lithologic and topographic patterns. Automatic mapping of a series of hogbacks, strike valleys, and alluvial surfaces along the northwest flank of the San Juan Basin in Colorado can be obtained by minimal man-machine interaction. The determination of causes for separable spectral signatures is dependent upon extensive correlation of micro- and macro field based ground truth observations and aircraft underflight data with the satellite data.

1. INTRODUCTION

The results described in this paper pertain to automatic data processing of ERTS-1 MSS data (Scene I.D. 1119-17204, November 19, 1972) for mapping physiography and geology of an area in southwestern Colorado. A block of approximately 200 mi^2 located peripherally to the San Juan Mountain Test Site, an area defined by LARS for conducting ERTS research, was chosen for computer analysis. This area, centered around Durango, Colorado was originally chosen because it appeared as a large, cloud-free block on otherwise cloud-covered data (Scene I.D. 1029-17195, August 21, 1972). Subsequent analysis was performed on the cloud-free November data set. No correlation with aircraft underflight photography or MSS imagery has been performed for this area.

2. PHYSICAL SETTING OF AREA

The area studied near Durango ranges from 6,500 feet to about 9,000 feet MSL. Climate is relatively moderate. Mean annual precipitation at Durango is 19.54 inches but diminishes with decrease in elevation.

Winter snow accumulation of 10 to 40 feet is not uncommon, depending on altitude. Grassland or bare soil dominates below 6,000 feet, scattered piñon and juniper occur from 6,000 to 7,000 feet, and ponderosa pine and aspen become increasingly abundant above 7,000 feet. Orchards and row crops grow in the Animas River valley, and Florida Mesa southeast of Durango has been irrigated for pasture and crops since about 1900.

Geology. The San Juan Mountains are essentially an eroded, domal uplift covering about 10,000 mi^2 in southwestern Colorado. They are composed principally of volcanic rocks of Tertiary age, but older bodies of Precambrian, Paleozoic, and Mesozoic rocks are locally exposed in the mountainous core. At many places around the margin, Mesozoic rocks occur as a series of tilted strata that dip towards adjacent basins, and form a series of linear topographic highs and lows, or "hogback" ridges and strike valleys. The volcanic episode was succeeded during the Pleistocene by climatic conditions suitable for generation and vigorous activity of numerous, large valley glaciers that have recurred during at least 3 irregularly-spaced intervals of relatively short duration. Consequently, the geomorphic history of this rugged mountain and basin area is exceedingly but not abnormally complex. The regional erosion surface (late Tertiary) is in many places overlain by varying thicknesses of glacial till and outwash gravels. The area has been repeatedly, gently upwarped in recent geologic time, so that many of the glacial deposits and associated rocks are unstable under present slope conditions, and major landslides, mudflows, and rock avalanches are not uncommon anywhere in the San Juan region. The best general accounts of the topography and geology of the region are contained in Atwood and Mather (1) and Mather (2).

Immediately east of Durango the hogbacks and strike valleys, developed respectively on hard, durable sandstones and weakly resistant shales, are particularly prominent. The slopes developed on sandstone dip southeast at about 20°; thus, some strike valleys on the northwest side of hogback ridges are always in shadow at the sun-time of ERTS-1 overpass. Some of the best examples of glacially alluviated benches, cut terraces, and floodplains of the entire region exist on Florida Mesa and along the valleys of the Animas and Florida rivers. Such deposits are generally highly reflective to any sensor system.

Sandstones of the hogbacks near Durango are of terrestrial origin and contain coal beds of fairly high quality and good calorific value (14,000 BTU). Mining has been sporadic, but Zapp (3) estimated measured reserves of 42 million short tons of bituminous coal, and total recoverable reserves of 1,853 million short tons (estimating 65% recovery) within 3,000 feet of the present surface.

General stratigraphy and topographic relations of rock units in the study area are shown in Table 1.

GEOLOGIC AGE	FORMATION (MAP SYMBOL)	THICKNESS IN FEET	LITHOLOGIC AND TOPOGRAPHIC CHARACTERISTICS (TOPOGRAPHY UNDERLINED)
Quaternary	----- (Qal)	------	Low-level terrace deposits, glacial till, and outwash along Animas and Florida rivers.
	------ (Qg)	------	High-level terrace and pediment gravels, particularly on Florida Mesa.
	~~ Unconformity	~~~~~	
Upper Cretaceous	Animas formation (Ka) McDermott formation (Kmd)	250-300	Interbedded andesite breccia, volcanic conglomerates, sandy tuffs, and reddish-brown to purple clay shale. McDermott is ridge-former.
	Kirtland shale (Kk)	1200±	Interbedded greenish shale, sandy shale, sandstone; thin carbonaceous shales and coals, mostly in Farmington Sandstone member in middle of unit.
	Fruitland formation (Kf)	300-500	Non-marine, chloritic sandstone, shale, and coal beds up to 40 ft. thick.
	Pictured Cliffs sandstone (Kpc)	200-300	Light gray, marine sandstone, cliff-former, interbedded dark gray shale.
	Lewis shale (Kl)	1400-1800	Dark gray to black, calcareous, bentonitic marine shale. Wide valley-former.
	Mesa Verde Group: Cliff House sandstone (Kch)	300-350	Gray, marine sandstone, forms both scarp and dip slopes, interbedded calcareous mudstone and silty shale.
	Mesa Verde Group: Menefee formation (Kmf)	100-350	Cross-bedded gray and brown sandstone, forms ridges and scarps, with brown-black shales and bituminous coal units 4-9 feet thick.
	Mesa Verde Group: Point Lookout sandstone (Kpl)	400±	Massive, buff sandstone, cliff-former, lower part interbedded sandstone and shale.
	Mancos shale (Km)	1900-2200	Dark gray to black marine shale, valley former, sandy shale and limestone lenses (Greenhorn and Niobrara equivalents?)
	Dakota sandstone (Kd)	200±	Hard, brown sandstone, major cliff-former near Durango, interbedded carbonaceous black shale, coal lenses, and conglomeratic sandstone at base.
	~~ Unconformity	~~~~~	
Upper Jurassic	Morrison formation (Jm)	1000±	Variegated colored, bentonitic shale, mudstone, and sandstone, forms both slopes and cliffs in Durango area.

Table 1. Generalized lithologic and topographic section of the Durango, Colorado area.

3. ANALYTIC PROCEDURE

As stated above, the objectives of the continuing research are to utilize the LARSYS automatic pattern recognition procedures to obtain geologic maps which refine existing maps and to produce landform simulation maps. To map geologic materials by any remote sensing technique it is necessary to assume:

1.) That subsurface materials will manifest themselves as spectrally separable classes at the earth's surface. Lithologic types, sandstone, shale, etc., are often obscured with a veneer of soil, vegetation, water, and man-made features which reflect incident sunlight to the remote sensor. If the subsurface lithologies are to be mapped based on spectral information received by the sensor, it must be assumed that many spectrally separable surface features indicate subsurface lithologic variations.

2.) That lithologic types are naturally segregated into a limited number of discrete compositional and textural categories which can be recognized and classified by pattern recognition procedures, either machine or human. This assumption is false, but it facilitates clustering of similar lithologies into discrete classes. Transitional features which spectrally fall between two arbitrarily chosen training classes will be classified as one of the two chosen classes. The relative spatial distribution of these "misclassified" features will reflect the natural lithologic composition (e.g., an area of sandy shale may be classified as a random distribution of feature elements of the two discrete classes, sandstone and shale).

Classes Considered: Based on the information provided by Zapp (1949), it was decided to divide lithologies of the Durango area into three discrete types for analytic purposes--sandstone, shale, and alluvium. Sandstone is the subsurface rock type on the dip slopes of the hogback ridges; shale on the cret slopes and along the strike valleys; alluvium on the terraces and floodplains. Considered as a unit, these three material types are sufficient to describe the geologic materials of all erosional and depositional surfaces in the study area. Since ERTS-1 passes over the Durango area at about 10:30 hours, the west-facing cret slopes and other west-facing declivities are in shadow on the ERTS-1 data sets. Shadow areas have significantly different spectral signatures than sunlit areas and have been considered as a fourth major class.

To obtain training field coordinate numbers for the classes of interest, it was necessary to generate a coordinated graphical display of portions of the study area. The only ERTS-1 data set available for

study of the San Juan test site was an August 21 frame. Four areas within the study region were chosen for non-supervised classification (NSCLAS) and display. The coordinates of these areas were procurred from television gray scale imagery (EDIT) of the entire ERTS frame. The four chosen areas contained representatives of all the rock types and topographic forms present in the study area. The resultant NSCLAS display provided reliable visual separability of shadow patterns and alluvial areas. Application of geomorphic interpretation to the shadow patterns yielded highly probable locations for the sandstone dip slopes and shale valleys. Field coordinates were then obtained for the sandstone, shale, alluvial, and shadow areas. Training fields on each sandstone dip slope and shale valley were separated into discrete training subclasses within the major lithologic classes. Nine groups of training fields -- four sandstone, three shale, one alluvium, and one shadow -- were then exposed to the LARSYS supervised clustering algorithm (CLASS) and the entire study area classified. The resultant display map showed a much higher visual separability of the sandstone and shale areas than the NSCLAS display from which the training fields were selected. Training class performance of the features within the training fields was 63.7%. However, the results were still insufficient to meet our personal satisfaction criteria. With refinement of the coordinates of the training fields, the addition of two alluvial subclasses, one shale subclass, and two shadow subclasses, visual correlation with Zapp's geologic map improved greatly as did the training class performance (89.8%). This classification scheme of fourteen subclasses in the present degree of refinement defines the state of the art of the continuing analysis at the time of writing.

4. RESULTS

The LARSYS routines available for visual display of classified areas are: 1) PHOTO, a color or gray scale coded television image, and 2) DISPLAY, an alphanumeric coded printer image. Both modes of classification display were chosen for visual presentation of the results derived from the Durango area experiment. PHOTO images of the study region are shown in Figures 1 and 2.

Figure 1 is a physiographic simulation map displaying the four major classes. From darkest to lightest the classes are: shadow, alluvium, shale, and sandstone. The three lightest classes represent areas in sunlight and are displayed with low contrasting gray scales. The darkest class, shadow, is represented as a highly contrasting black area. This four class display produces the illusion of the third dimension in the perception of an observer familiar with vertical or low oblique remote sensing images. This effect consequently gives one a "feel" for the physiography of the study area by forcing perception to selectively focus on contrasting gray scale patterns, representing topographic variations which are surface manifestations of subsurface

lithologic variations. A color coded PHOTO display which simulates the USGS "shaded" topographic maps is also available.

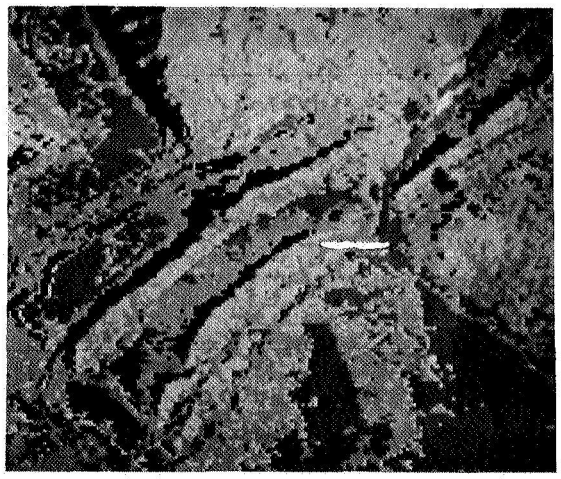
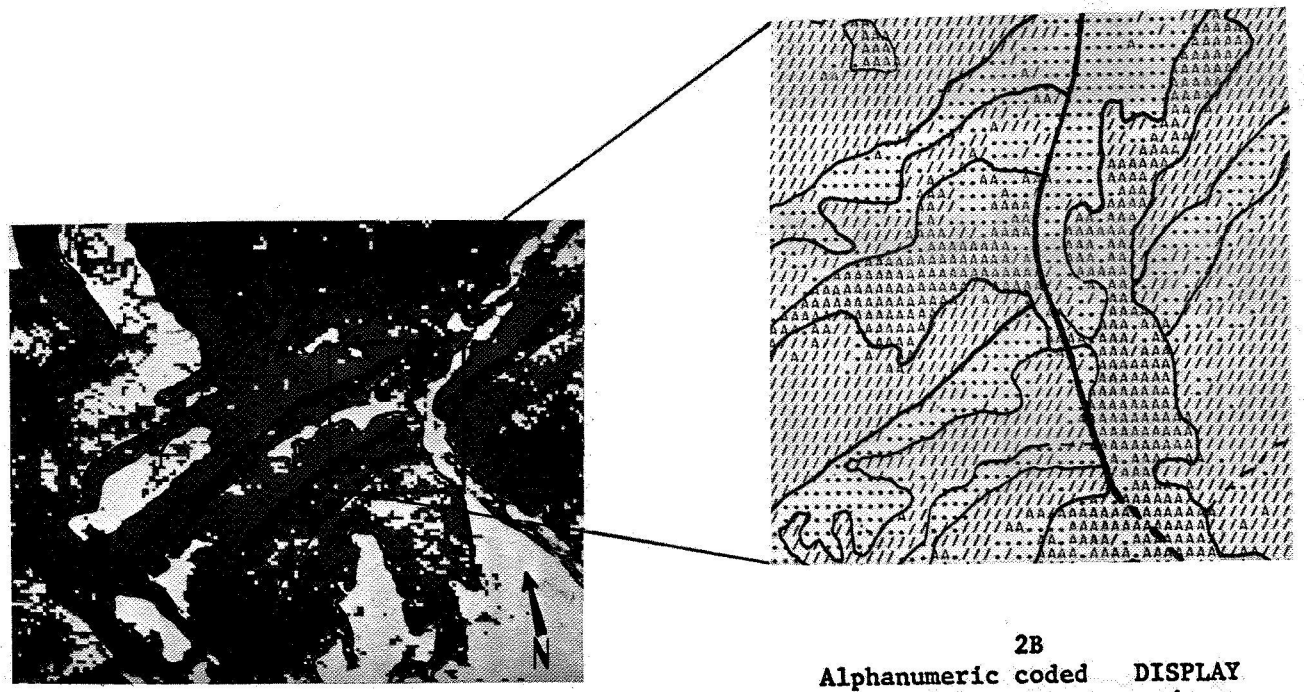


Figure 1. Computer generated physiography of the Durango, Colorado area. Approximate scale 1:150,000.

Figure 2 is a machine generated geologic map of the Durango area. The four major classes have been displayed as three classes which represent the geologic materials only. Based on geomorphic knowledge of the usual relationship between bedrock types and their topographic expression, it was assumed that the areas in shadow are underlain by shale. The shadow areas are on cret slopes that stratigraphically fall immediately below the sandstone cap rocks of the ridges. In a region of hogbacks and strike valleys developed on sandstones and shales, it may be inferred with a high degree of confidence that the surface area stratigraphically below the cap rock is underlain by shale. Proceeding on this assumption, we combined the shale and shadow classes as one displayable unit. The resultant gray scale coded map (Fig. 2A) visually correlates in general form with Zapp's map of the same area. In detail (Fig. 2B) the two maps become somewhat contradictory to one another. Based on the very scanty ground truth information other than Zapp's map, we have confidence that the automatically produced map is more reliable than the existing geologic map.

There are two reasons for this confidence. First, on the automatically produced map the pattern of alternating sandstones and shales striking northeast is seen to be abruptly offset where the Florida River is superposed across the hogbacks. The cause of this offset is inferred to be movement of the rocks along a fault in the earth's crust. The rocks on the east side have been displaced to the south relative to the rocks on the west side of the fault. Zapp's map shows no fault in this area, but a zone of weakness, such as a fault, is necessary to produce the conditions required for superposition of a stream, such as the Florida River, across resistant hogbacks. It should be emphasized that the presence of a fault is inferred from the stratigraphic patterns as recognized by LARSYS automatic pattern recognition rather than from the visual recognition of a surface lineament represented on non-classified gray scale or color imagery.

The second reason for confidence is the very high correlation between the machine map and Atwood's (1932) map of relict erosion surfaces.



2A
Gray scale coded PHOTO image. White = alluvium, gray = shale, black = sandstone. Approximate scale 1:150,000.

2B
Alphanumeric coded DISPLAY image. A = sandstone, / = shale, • = sandstone. Photographically reduced from original scale of approximately 1:24,000.

Figure 2. Computer-generated geologic map of the Durango area. Black, heavy lines representing the surface locations of lithologic contacts have been manually superimposed on the photographs.



Figure 3. Physiography of the second test area, located 30 miles east of Durango training area. Approximate scale 1:150,000.



Figure 4. Geologic map of the second test area.

Atwood shows a remnant of a Tertiary erosion surface as it exists today on the dip slope of the Pictured Cliff Sandstone just east of Durango. The boundaries of this "ancient peneplain" remnant are surprisingly similar to the boundaries of the Pictured Cliff dip slope as outlined by the computer. These two reasons, the first based on geologic inference, the second on correlation with previously mapped ground truth, indicate a high degree of accuracy and applicability of the experimental map for geologic purposes.

To test the applicability of the classification scheme to regional areas, an approximate 200 mi^2 area centered 35 miles northeast of Durango was classified by using the same statistics calculated on the experimental training fields located two to five miles east of Durango. This new test area was chosen because: 1) the lithologies were similar to those of the study area, 2) the elevations and presumably the altitude dependent vegetative cover types were different, and, 3) the reflective sun angle on the hogbacks was different. The display images of this area are presented in Figures 3 and 4. The physiographic and geologic maps of the test region "make sense" geologically, but no ground truth is available to verify our results. It is apparent that extensive field based micro- and macro-ground truth observations and aircraft underflight data of this second area are needed before any definitive statement concerning the reliability and accuracy of the machine produced maps can be demonstrated.

5. APPLICATION CONSIDERATIONS

In our opinion, the experimental method outlined above has several unique applications for improving geologic mapping capabilities. The degree of improvement depends on: 1) the character of the terrain, 2) the areal distribution of surface features, and 3) the purpose of the maps required for a particular project. Additionally:

1.) Multiple use of the same classification technique for producing alternate map types (e.g., physiographic and geologic maps) can be obtained from the same statistics.
2.) Multiple map scales, ranging from 1:24,000 to 1:1,000,000, are available to users of unaltered LARSYS displays.
3.) A high degree of accuracy is obtained.
4.) There is a regional applicability of statistics obtained from a "type section" of limited areal extent.
5.) Compact storage in magnetic data tape libraries is possible. (The Durango study area statistics necessary for display of the maps presented in this report are stored on about 15 feet of magnetic tape.)

6. REFERENCES CITED

1. Atwood, W.W., and K.F. Mather, 1932, Physiography and Quaternary geology of the San Juan Mountains, Colorado: U.S. Geological Survey, Prof. Paper 166, 176 pp.

2. Mather, K.F., 1957, Geomorphology of the San Juan mountains; New Mexico Geological Society Guidebook, 8th Field Conference, Southwestern San Juan Mountains, Colorado, pp. 102-108.

3. Zapp, A.D., 1949, Geology and coal resources of the Durango area, La Plata and Montezuma counties, Colorado: U.S. Geological Survey, Oil and Gas Investigations Preliminary Map 109, 2 sheets.

Paper G 26

ERTS-1 IMAGERY AS AN AID TO THE DEFINITION OF THE GEOTECTONIC DOMAINS OF THE SOUTHERN AFRICAN CRYSTALLINE SHIELD

Morris J. Viljoen and Richard P. Viljoen, *Geological Research Department, Johannesburg Consolidated Investment Company, Limited, P. O. Box 2, Randfontein, Republic of South Africa*

ABSTRACT

The ancient granite-greenstone cratons and the metamorphic mobile belts are two major geotectonic units of the Southern African Crystalline Shield. Each has its own distinctive structural style. The cratons are characterised by arcuate vulcano-sedimentary belts encircling or partially encircling diapirically intrusive gneissic tonalitic batholiths. These rocks, with their well defined structural imprint, are sharply transgressed by younger, more potash-rich granites. The metamorphic mobile belts, on the other hand, are characterised by paragneisses and other high grade metamorphites. Plastic flowage folding phenomena involving complex refolding and the development of basin and dome structures are the most diagnostic features.

Portions of these two geotectonic environments have been studied on ERTS-1 imagery. It was found that the broad synoptic view provided by this imagery is ideally suited to a study of the diagnostic macrostructures, and that the different geotectonic styles are clearly recorded. ERTS-1 imagery thus allows a more accurate definition than exists at present of the contact zones and internal structures of the two domains. The importance of this investigation as an aid to gaining on insight into the relevance of plate tectonics in Precambrian times is briefly discussed.

1. INTRODUCTION.

The main objective of the present study has been the identification and documentation of the important large scale features which characterise and therefore identify the major geotectonic environments of the Southern African crystalline shield. The two main geological domains recognised are the ancient, so-called granite-greenstone cratonic nuclei and the younger encircling metamorphic mobile belts. The study to date has involved the examination of ERTS.-1 colour composite imagery covering portions of these environments (Figure 1). It is hoped at a later stage to extend the study so as to define the full extent of the important contact zone between the cratonic nuclei and the metamorphic mobile belts as well as to study the internal structures and lithologies of these two environments in more detail. It is envisaged that important data relating to the relevance of plate tectonics in Precambrian times should emerge from this study.

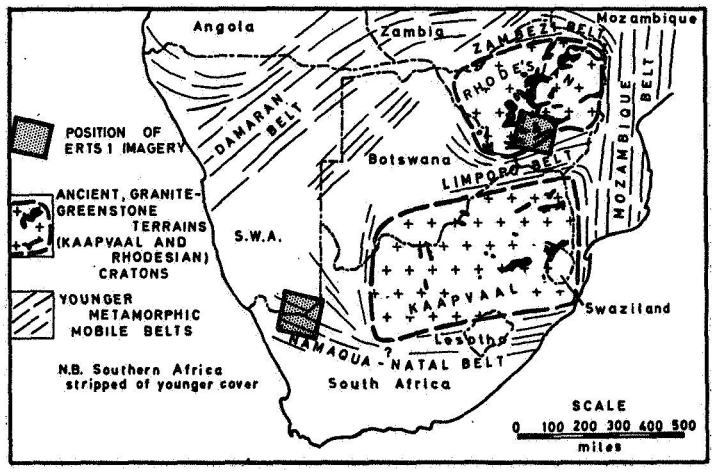


Figure 1. The Southern African Crystalline Shield showing the main geotectonic domains and the areas covered by the ERTS-1 images discussed in this paper.

2. THE GRANITE-GREENSTONE CRATONS.

Archaean granite-greenstone terrains often constitute the most ancient and stable portions of the continents and appear to be reamrkably similar in all of the better known shield areas of the world. Vulcano-sedimentary sequences known as greenstone belts are the most distinctive features of these terrains and represent the remnants of previously more extensive accumulations of volcanic and sedimentary rocks. The greenstone belts in their present form appear to "float" in the form of deformed synclinal "keels" or"rafts" in complex granite terrains.

Despite their great age such belts have not been subjected to high grades of thermal metamorphism and primary volcanic and sedimentary structures are commonly encountered. Most belts have been subjected to strong structural deformation which is responsible for their characteristic form. Narrow arcuate schist belts trending at various angles from the main belt are particularly important as are large-scale isoclinal folds with axes more or less parallel to the regional grain of the belt. The typical granite greenstone pattern showing in particular the arcuate synclinal schist slivers is depicted in figure 2.

The lowermost volcanic assemblage of most greenstone belts commences with a suite of ultramafic and related rocks, intermediate to acid tuffs and magnesium-rich basalts. Some of the ultramafics represent sub-aqueous peridotite lavas while others form part of layered intrusive ultramafic complexes. The lowermost volcanic succession is overlain largely by metatholeiitic basalts (greenstones) with narrow interlayers of acid lava and chert. Shales, greywackes and quartzites form the uppermost stratigraphic assemblages of most belts.

Several different types of granitic rock each with its own tectonic

style, petrology and chemistry are generally present. The oldest are invariably gneisses of tonalitic composition, and often intrude the lowermost volcanics in the form of diapiric domes. The arcuate schist belts tend to drape around these domes and are responsible for the distinctive greenstone pattern noted in (Fig. 2). The tonalitic gneisses often give rise to low-lying featureless country.

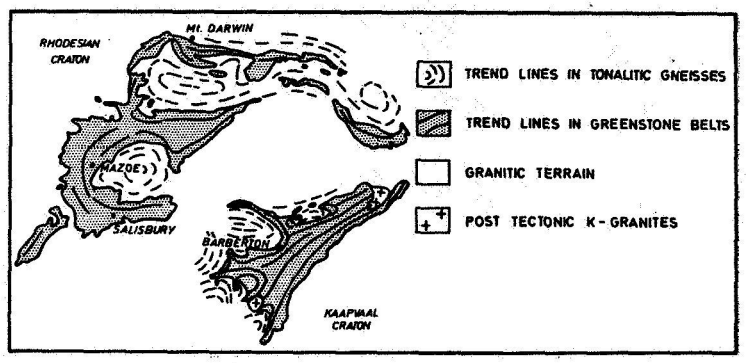


Figure 2. Typical granite-greenstone pattern showing arcuate greenstones draped around tonalitic domes. Note younger cross cutting potassium-rich granites. Examples from the Rhodesian and Kaapvaal cratons of Southern Africa.

Younger more potassium-rich granite plutons cause abrupt truncation of earlier formed structures and fabrics both in the older gneisses and in the greenstone belts. They are generally more resistant to erosion and give rise to the higher lying ground or boulder-strewn hills.

3. THE METAMORPHIC MOBILE BELT ENVIRONMENT.

Surrounding and dividing the cratonic nuclei are a series of metamorphic mobile belts. Such belts are essentially linear zones containing high grade, granitized metamorphic tectonites which show abundant evidence of rheid flow and plastic flowage folding. This can lead to the production of a complex pattern of re-folded folds in a continuous sequence of deformation as shown in figure 3 which depicts an area from the Namaqualand mobile belt of the Cape Province of South Africa. Major linear zones of transcurrent dislocation are common, particularly along the marginal zones of the mobile belts and there is usually evidence of repeated fault movement. From the above and from a comparison of figures 2 and 3 it is clear that the major structures typical of mobile belts are very different from those encountered in greenstone belts and they reflect fundamental differences in the geotectonic setting of these two environments.

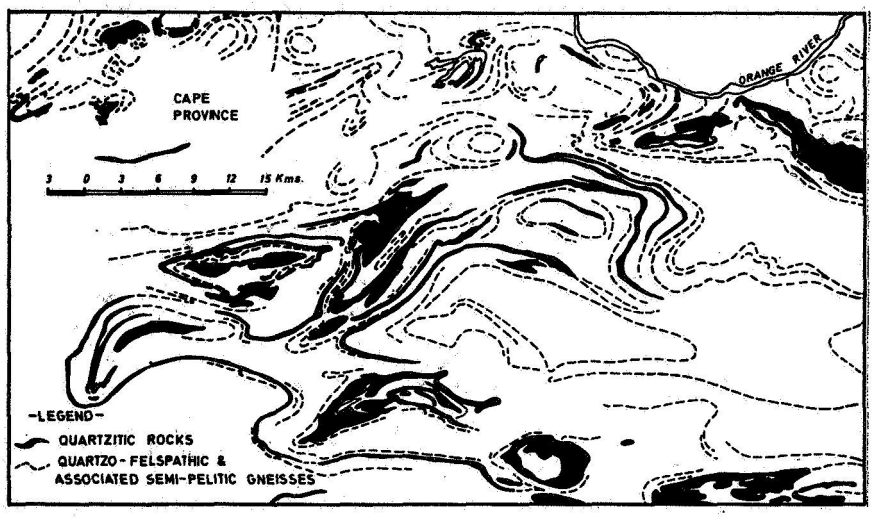


Figure 3. Typical metamorphic mobile belt pattern showing complex flowage folding phenomena of a high grade metamorphic assemblage.

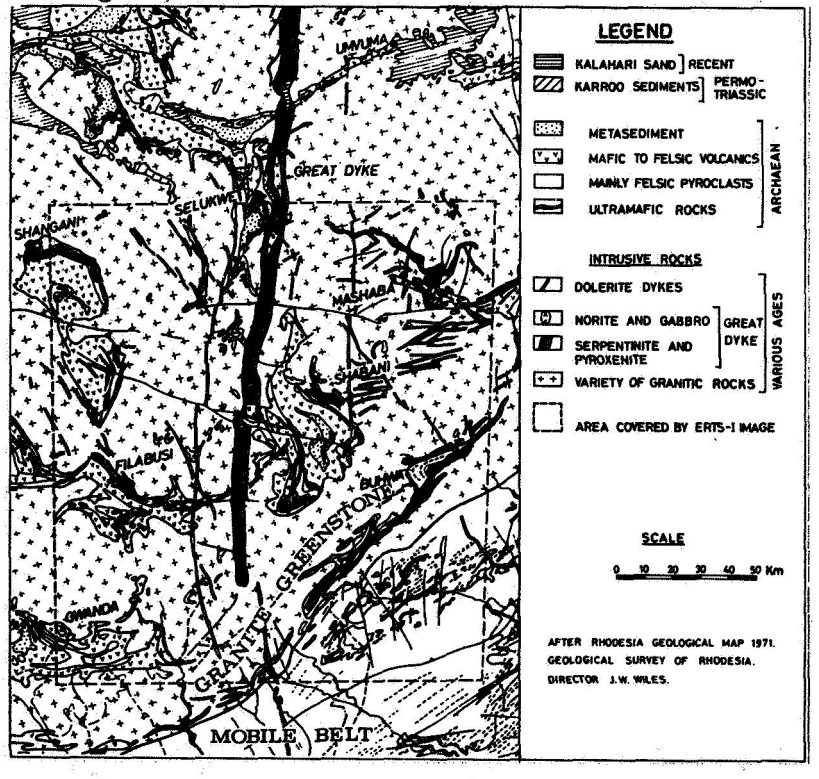


Figure 4. Geological map of part of the Rhodesian craton and the north marginal zone of the Limpopo belt.

4. ERTS-1 IMAGERY AS AN AID TO THE IDENTIFICATION OF THE DISTINCTIVE PATTERNS OF THE CRYSTALLINE SHIELD

a) THE GRANITE-GREENSTONE ENVIRONMENT.

ERTS-1 image No. 1103-07291 covers part of the southern sector of the Rhodesian craton and portion of the linear north marginal zone of the Limpopo mobile belt (Fig. 1). The available 1:1,000,000 geological survey map of this and surrounding areas is shown in figure 4. Most of the greenstone belts have been mapped but much of the granite terrain including the geology of the mobile belt is poorly understood with available data being mainly of a photogeological nature.

Figure 5 shows the ERTS image covering this area and the geological interpretation. The Great Dyke traverses the central part of the image and is the most clearly defined feature. The bulk of the Dyke is ultramafic in nature (grey blue on colour composite and dark grey on black and white prints but contains very well defined (heavily vegetated) layers and canoe shaped remnants of gabbro which give an exceptionally clear view of the internal structure of the body.

All the features of the granite-greenstone environment are clearly visible. These include the arcuate schist belt slivers which are striking features in the case of the Buhwa, Gwanda and Filabusi belts. Certain of the stratigraphic components of the greenstone belts are also distinguishable, particularly in the case of the Shangani belt where the lowermost stratigraphic assemblage comprised of resistant layered ultramafic bodies and some banded ironstones forms a resistant zone flanking the eastern margin of the belt. This zone clearly distinguished by dark grey colour tones can be traced southwards where it appears to split, one branch trending westwards and the other southeastwards where it constitutes the northern flank of the Filabusi belt. The Shabani and Mashaba ultramafic complexes are clearly visible and the waste dumps from asbestos mining operations are conspicuous. The younger intrusive nature of the Mashaba ultramafic body is clearly demonstrated by the western limb which is superimposed on a north-south stratigraphy consisting of greenstone belt slivers lying within tonalitic gneisses.

In all cases the internal structure (mainly folding)and the gross stratigraphy of the greenstone belts is discernable. In addition all the major mines in the area are clearly recognised by their waste dumps.

The distinctive geotectonic styles of the various cratonic granites are also to be seen. The generally featureless terrain which gives rise to lighter colou tones is underlain by the tonalitic gneiss assemblage. Arcuate greenstone-belt tongues protrude into this terrain and probably define or partly define individual diapiric tonalitic batholiths. Numerous cross-cutting potassium-rich granite bodies occur in the area and as a result of their somewhat more resistant and jointed nature have greater water holding properties. This has resulted in more luxuriant plant growth which clearly defines such bodies, particularly

on colour composite prints.

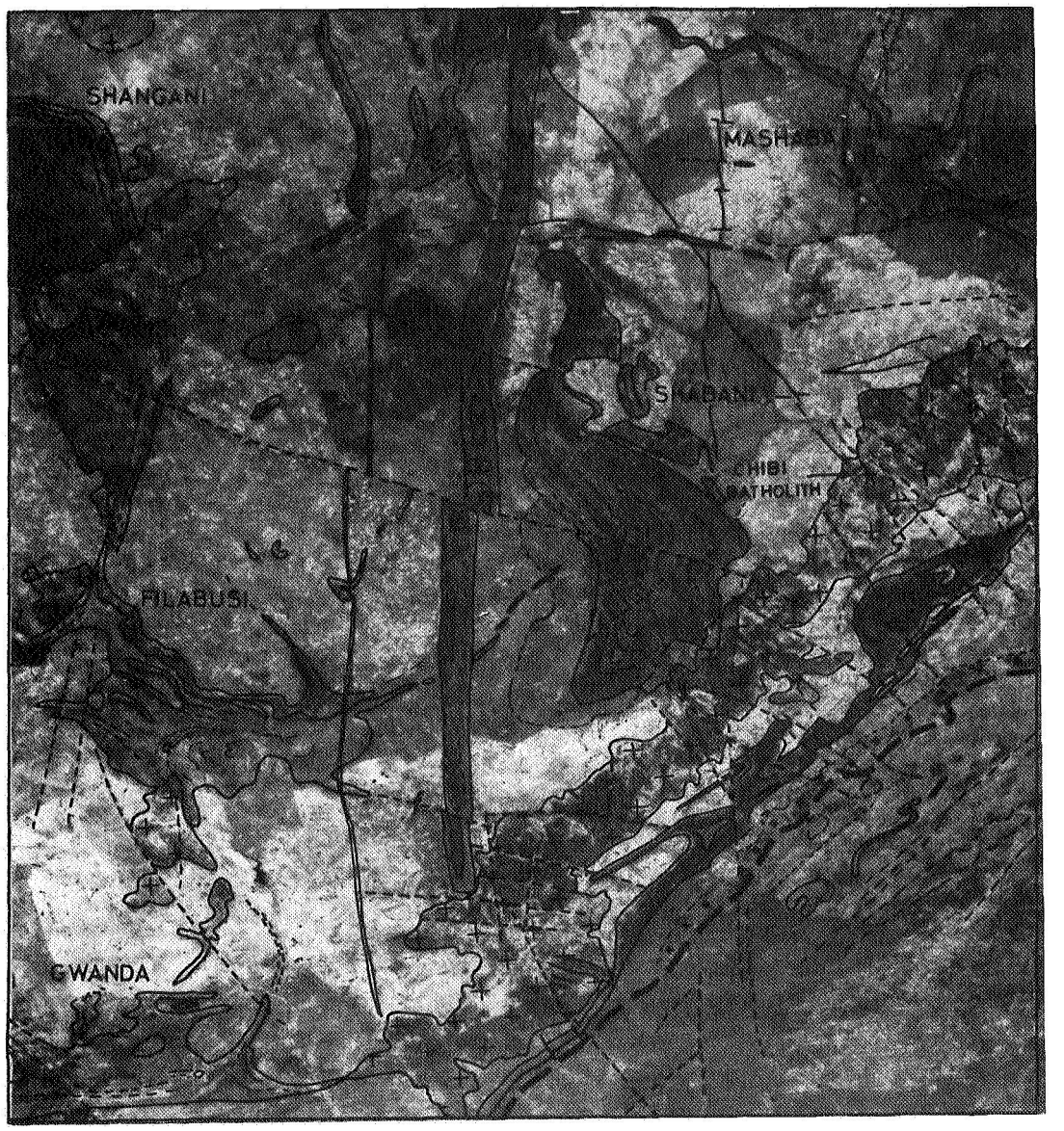


Figure 5. Photogeological interpretation of ERTS-1 image No. 1103-07291 showing part of the southern region of the Rhodesian craton and the north marginal zone of the Limpopo belt.

The most well defined of these bodies intrudes the Shangani belt causing abrupt truncation of all the stratigraphic trends. In addition several other similar but somewhat smaller bodies are also discernable in the western sector of the image. An extensive and as

yet unmapped elongated zone of potassium-rich granite has recently been identified by the Rhodesian Geological Survey in the zone between the Shabani and Buhwa greenstone belts. The contacts of this granite (termed the Chibi batholith), which might be a marginal manifestation of the Limpopo metamorphic mobile belt can be remarkable accurately mapped from the image. The body is characterised by a spectacular joint and /or fault system normal to the contact of the mobile belt. The jointing has lead to the development of numerous component granite domes which are surrounded by thick vegetation.

Besides the Great Dyke two narrow but well defined parallel satellite dykes are also conspicuous features of the image. These together with a number of other dykes which are also clearly seen give a good indication of the type and extent of faulting which has affected the entire area. All the major east-west trending faults appear to have right lateral movement.

b) THE MOBILE METAMORPHIC BELT ENVIRONMENT.

Part of the north marginal zone of the Limpopo mobile belt occupies the S.E. part of the image No. 1103-07291. Although lacking the large scale flowage folding features, present only in the central zone of the belt, the distinctive linear grain, tonal difference, and absence of arcuate forms readily distinguishes this terrain from the granite-greenstone terrain to the north.

The strong linearity of trends along the north margin is due to tectonic overprinting in the form of shearing and major transcurrent dislocation, probably just after the formation of syntectonic eutectoid granites one of which can be defined on the image.

As an example of the more typical flowage folding pattern of the mobile belts, ERTS image No. 1055-08053 covering part of the Namaqualand belt along the Orange river in the N.W. Cape Province and southern S.W.A., has been studied as part of this investigation. A few unpublished maps of a small part of this area are available and the interpretation presented in thus based largely on the ERTS image (Fig. 6).

The typical flowage folding pattern with the development of intricate fold structures in the form of cross folds, "eye" folds etc. is clearly a widespread phenomenon of the area studied. Most of the rocks are paragneisses with amphibolitic material becoming important towards the N.E. A quartzitic assemblage which splits into two ranges occurs in the southern portion of the area and is of considerable economic importance because of recent significant base metal finds. The extensions and distribution of this zone, not defined before, are readily apparent from the ERTS imagery due to the resistant nature of the quartzite ridges. In addition a major zone of dislocation with right lateral movement and not known to exist previously, is a dominant feature of the central portion of the image. Three gabbroic intrusions appear to be closely associated with this zone and nickel/copper mineralisation has been located in one of these. Tantalum-bearing pegmatites are also

present within the same zone which therefore appears to have acted as the locus for a variety of mineral deposits.

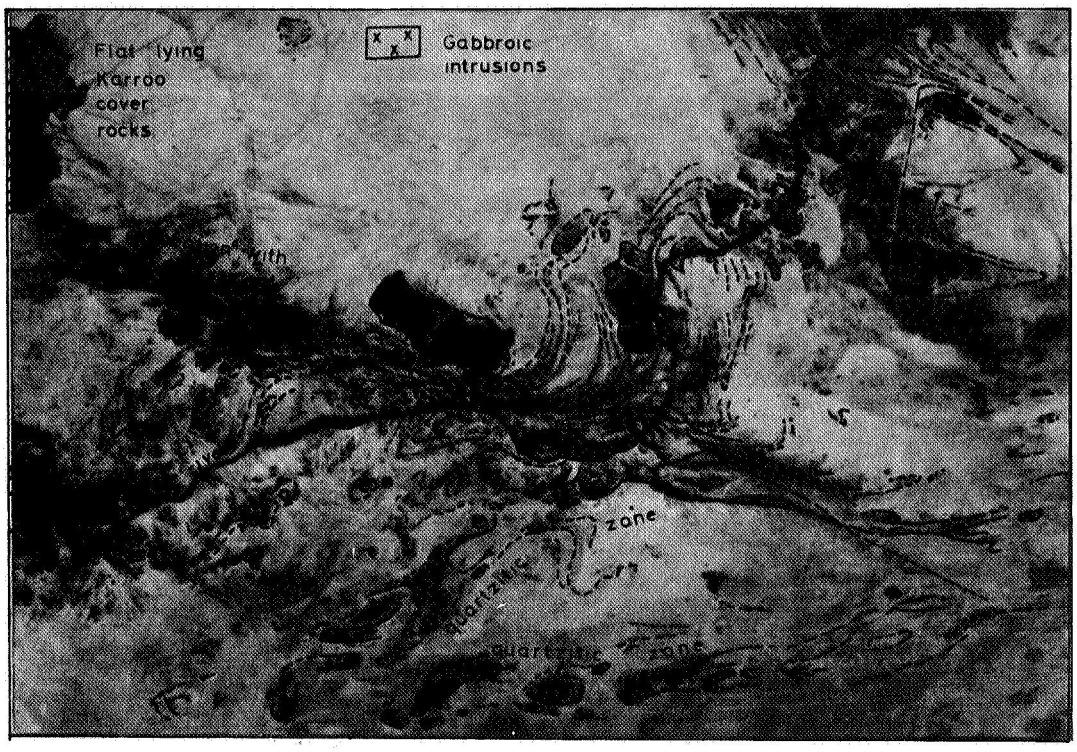


Figure 6. Portion of ERTS-1 image No. 1055-08053 of the N.W. Cape showing typical flowage folding pattern of the metamorphic mobile environment.

5. SUMMARY AND CONCLUSIONS.

It is the writer's opinion that the broad synoptic view provided by the imagery is ideally suited to a study of the diagnostic macro-structures of the two geotectonic domains considered in this paper. ERTS-1 imagery should allow for a better understanding and more accurate definition than exists at present of the contact zones of these two geologic environments. This may be of considerable economic importance, since basic/ultrabasic rocks containing some of the world's largest nickel deposits have been emplaced along similar contact regions within the Canadian Shield. These include the Thompson belt deposits at the junction of the Superior Craton with the Churchill mobile belt and the Sudbury nickel irruptive lying within the contact region of the Grenville front (mobile belt) and the Superior granite-greenstone province.

Initial results warrant a more detailed study and form the basis of proposal submitted for the ERTS-B programme. The proposal involves a study of the granite-greenstone cratons and encircling mobile belts

ith a view to gaining an insight into the relevance of plate tectonics in Precambrian times. It has been suggested that the mobile metamorphic belts could represent the root zones of mountain systems and therefore, the sites of possible subduction zones for plates of early Archaean earth crust. The greenstone belts have often been equated with island arc systems and as such could themselves represent ancient subduction zones. A study of the continuity of lithologies, gravity and magnetic data etc. from craton into the mobile belt will be an important part of the study together with a search for features which might have represented ancient transform faults.

6. ACKNOWLEDGEMENTS.

The writers would like to thank the management of the Johannesburg Consolidated Investment Co., for affording them the opportunity of undertaking the investigation on the ERTS-1 imagery and for providing the funds for one of us to attend the symposium.

Spectral Africa Ltd., are gratefully acknowledged for their co-operation and for the superb printing of the ERTS imagery which greatly aided in the geological interpretations.

aper G 27

NEW ASPECTS ON THE TECTONIC OF THE ALPS AND THE APENNINES REVEALED BY ERTS-1 DATA

J. Bodechtel and B. Lammerer, *Zentralstelle für Geo-Photogrammetrie u. Fernerkundung/München – Germany*

The alpine region is one of the most complicated and best investigated part of the world. Therefore, it is very interesting to compare the ground truth with data revealed by ERTS-1 imageries. One would expect that no new features could be detected.

Figure 1 shows the geographical situation and the main petrographical units together with the most important fractures (after TOLLMANN, 1969). One notices many diagonally crossed fractures in the northern Calcareous Alps, a few structures in the molasse and few lineaments in the crystalline central Alps revealed by geologic field work.

On the other hand fig. 2 gives a composite view of what can be detected by using ERTS-1 imageries. There are much more structures to be seen, than ever could be shown on a map with a comparative scale.

Considering the information more separately, fig. 3 shows - generalized - the largest and most striking lineaments in this area.

This kind of information, connections between shearing systems of more than regional importance, could never be revealed before. Only in one case, an European geologist (Prof. TRÜMPI, Zürich, Switzerland) supposed a connection of faults from the Loisach - Zugspitze (Germany) to the Bergell massive (Italy) by field evidence.

These large lineaments are not influenced by any nappe systems or specific rock properties. Therefore, they can be assumed to have been formed during a very late stage of the alpine orogeny. There appearence in pairs, their straight course, give strong evidence for shearing movement. The unit cube in the upper part of fig. 3 shows the sense of movement to be expected on the shear planes, assuming N - S as the direction of highest compression. The drawn directions are conform to field data. NE - SW is the main direction of left-lateral faults, NW - SE is the direction of right-lateral faults. This means that the whole Alpine body has been affected by a compressing force even after nappe transport and that the locally detected strike-slip faults belong to a huge and extended shearing system.

This system is not limited to the Alpine body, but it extends to its molasse foreland. In this foreland with its low resistent young sediments, faults and fractures are difficult to detect and they are mostly revealed by geophysical data or oil well drillings. But ERTS-1 imageries show the pattern of different lineaments very clearly. These lineaments often end at the Alpine margin or the folded part of the molasse. This folded part of the molasse probably buffered the stress down to the amount in which a shearing system could develop instead of folding or nappe overthrusts. The knowledge of the tectonic evolution and the structural pattern of the molasse may once become important for petroleum prospecting.

In the same manner, one can find faults parallel to the long axis of the Alps, which are supposed to be dip-slip faults. A good example for this type of fault is the Inn-valley fault which separates Mesozoic limestone from paleozoic rocks or from the crystalline complexes. Similar conditions occur at the Periadriatic suture which, running E-W, is limited in the West, where the NE - SW striking transverse fault "Judicarien linie" cuts it off. But on ERTS-1 images one can detect a prolongation of the suture, which goes on as a lineament for a long distance. This means, that this lineament if probably still active. Precise nivellment measurements have been testing this for some years and the first results confirm this idea.

There are some reasons, why a considerable amount of these shearing faults and lineaments could remain undetected by geologists. The first reason is their dimension. They are too extended, their course is often along broad valleys, so that the scale of the arial photographs is too large for detecting regularities. The second reason is that the displacement is mostly small and their effect is often limited to a mechanical disarrangement of zones which are scarcely exposed.

Finally the Alpine geologists are used to work in a very complicated area; the field relations between adjacent petrographical units are obscured by nappe transport, overthrusts, rapid changing in the sedimentary facies and local tectonics, so that a superregional synthesis and analysis is difficult. ERTS-1 data can, therefore, be extremely useful for supporting field work.

In fig. 4 only bedding and the distinguishable main rock units are shown together with some glacial moraines. In addition to the general strike of bedding, one can often find the direction and roughly the amount of dip when the bedding planes dissect a mountain relief.

In the crystalline series of the central Alps the parallel drainage pattern sometimes shows the direction of schistosity. New information is brought for the molasse, where even in the part which is considered to be horizontally bedded, the trace of bedding planes can be observed, but ground check has not yet been done.

In summary it can be said that ERTS-1 data make it possible to reveal new geological knowledge even in a very well investigated area. New lineaments and faults can be detected and connections between faults can be seen. In some cases tectonic hypotheses can be examined or improved, still active tectonic can be detected. Especially in the molasse, having low resistent rocks and partly covered with glacial material, an entirely still unknown tectonic pattern could be recognized.

ERTS-1 imageries can contribute to increase our knowledge of the Alps and its foreland and help for better understanding the complicated tectonics of the Alps and its relation to the molasse foredeep. Of economic importance for petroleum research, is the structure of the Molasse.

Similar to the evaluation of the tectonic of the Alps, the main structural features could also be recognized in the Apennin range of the Italian peninsula.

Locally known fault systems, predominately strike-slip faults and horst structures, could first be traced over more than a hundred kilometers. Accordinaly it was possible to supplement the known fault systems. Two main directions of lineaments may be recognized. The one striking NW-SE belongs to fold axes and to dip-slip faults, producing some horst structures. The Italian volcanoes are lined up in the same direction. The other group of lineaments strikes about E-W and represents strike-slip faults.

This work, however, has not yet been finished.

Prof. Dr. J. Bodechtel & Dr. B. Lammerer

Zentralstelle f. Geo-Photogrammetrie und Fernerkundung
Universitaet München
8 München 2, Luisenstr. 37

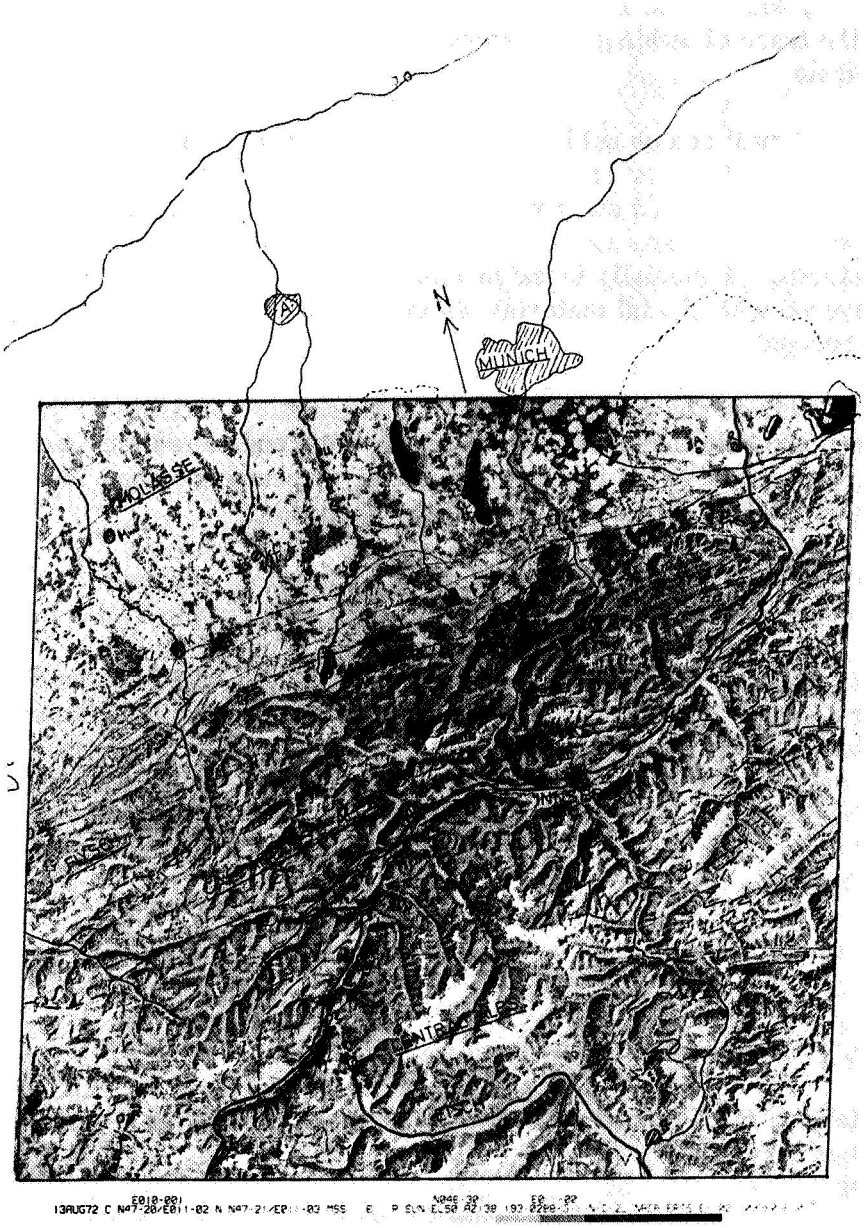


Figure 1

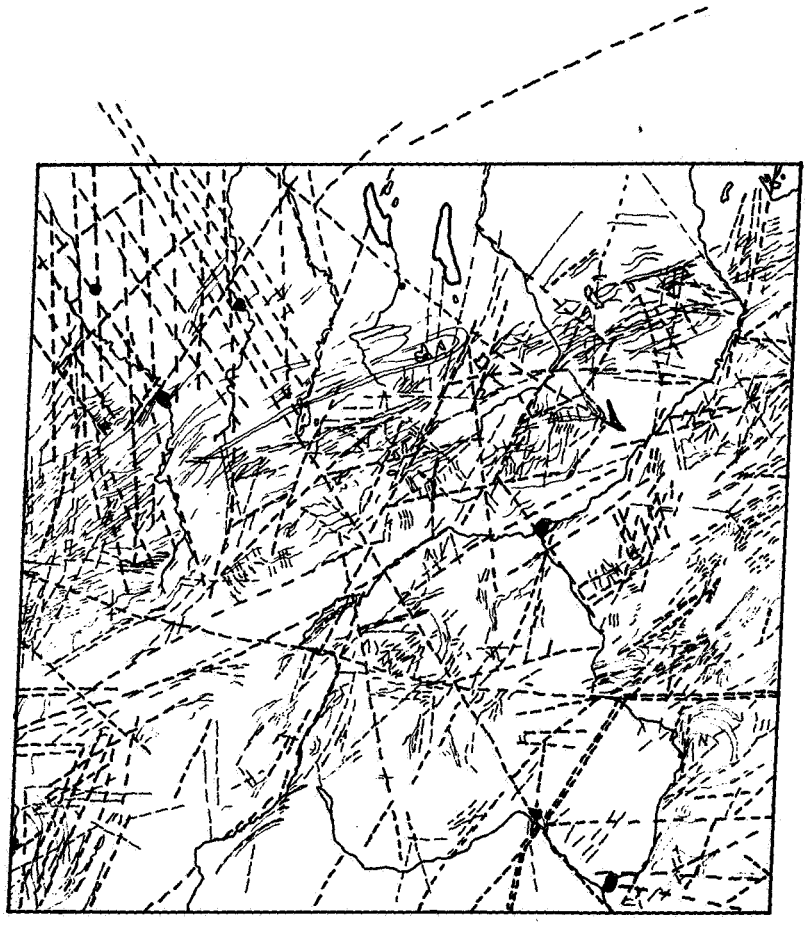


Figure 2

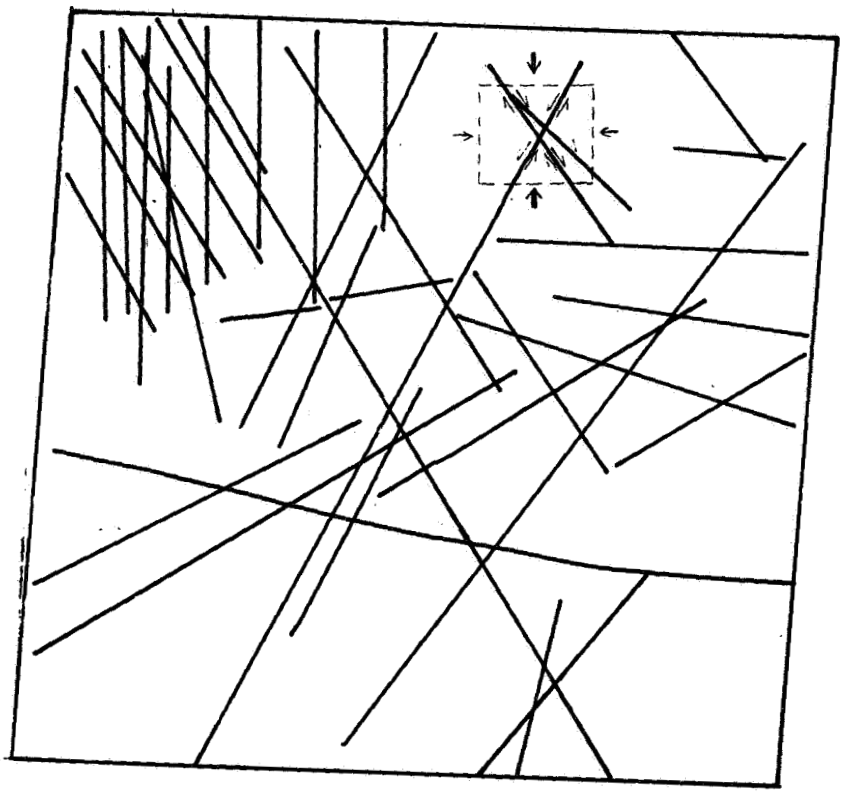


Figure 3

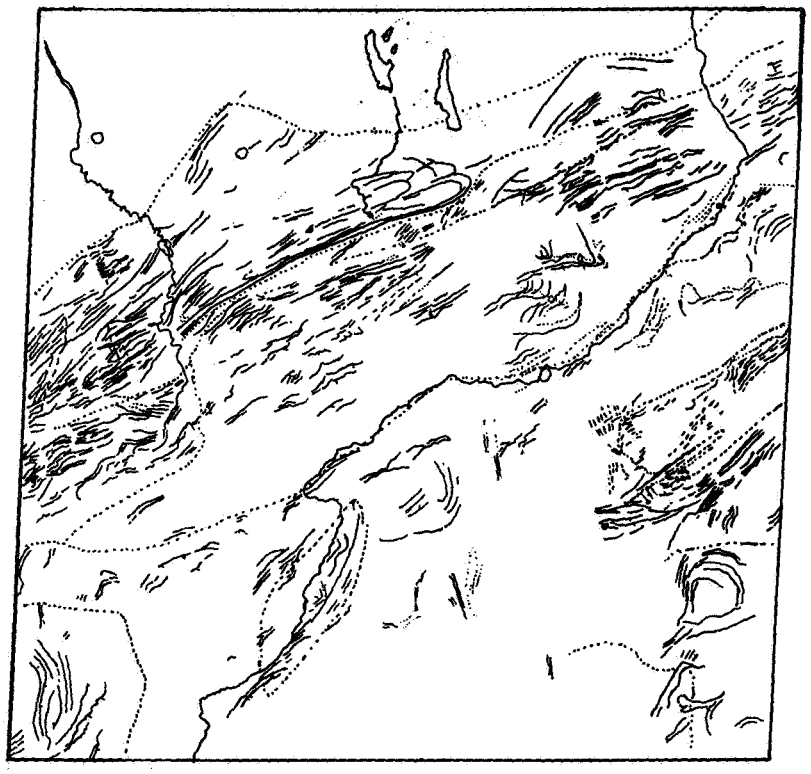


Figure 4

Paper G 28

STRUCTURAL LINEAMENTS OF GASPE FROM ERTS IMAGERY*

Roberto Steffensen, *Consultant, Interpretation Studies in Remote Sensing of Resources, 525 St. Laurent Blvd., Suite 24, Ottawa, Kik 2Z9*

ABSTRACT

A test study was conducted to assess the value of ERTS images for mapping geologic features of the Gaspé Peninsula, Quebec.

The specific objectives of the study were: 1) to ascertain the best procedure to follow in order to obtain valuable geologic data as a result of interpretation; 2) to indicate in which way these data could relate to mineral exploration.

ERTS imagery differs from aerial photography because of the technical parameters of the imaging devices employed in the satellite and because of the Earth-viewing conditions that characterize the imaging process. Sound understanding of these factors is the prerequisite for achieving satisfactory results.

Of the four spectral bands of the MultiSpectralScanner, the band from 700 to 800 nanometers, which seems to possess the best informational content for geologic study, was selected for analysis.

The original ERTS image at a scale of 1:3,700,000 was enlarged about 15 times and reproduced on film.

Geologically meaningful lines, called structural lineaments, were outlined and classified according to five categories: morpho-lithologic boundaries, morpho-lithologic lineaments, fault traces, fracture zones and undefined lineaments.

Comparison with the geologic map of Gaspé shows that morpho-lithologic boundaries correspond to contacts between regional stratigraphic units. Morpho-lithologic lineaments follow bedding trends, whereas fracture traces appear as sets of parallel lineaments, intersecting at high angles the previous category of lineaments. Fault traces mark more precisely the location of faults already mapped and spot the presence of presumable faults, not indicated on the geologic map.

*The work reported herein was supported by the Canada Centre for Remote Sensing, Dept. of Energy, Mines and Resources, under Contract Serial OGR2-0430.

As a tool for mineral exploration the structural lineaments map of Gaspé can be used:

a) to improve the understanding of the tectonic framework of the Peninsula;

b) to direct exploration efforts over specific target areas;

c) to assist in deciphering the meaning of geophysical survey data;

d) to support the delineation of trends in the distribution of regional geochemical anomalies.

INTRODUCTION

This paper describes a test study appraising the value of ERTS images in providing data helpful to the understanding of regional geologic factors. The study consists of the analysis of imagery of the Gaspé Peninsula, Quebec, obtained with the multispectral scanning instrument mounted on ERTS. The study was conducted to seek answers to the questions: What type of geologic information can be extracted from ERTS imagery? How would this information relate to standard sources of geologic data? What is the significance of the interpreted data for mineral exploration activities?

LINEAMENTS ANALYSIS

Apart from the very small scale, which carries with it an inevitable loss of detail, geologic interpretation of space imagery can be undertaken by applying the same principles that are useful in the interpretation of standard aerial photographs (Van der Meer Mohr, 1968). Of course, the scale of observations will be considerably changed, thus one would not expect to obtain the same interpreted data, as a result of photogeologic work done on the two different materials. For a photogeologist, the particular interest in analyzing space imagery lies in the expectation that the reduction in scale would compress the pictorial information in such a way that large-scale picture elements normally not associated with geologic factors are filtered out. Consequently, regional geologic features would become more apparent.

Fundamental to photo-analysis for geologic purposes is the outlining of structural lineaments, a term attributed by Allum (1966, p. 31) to "any line on an aerial photograph that is structurally controlled". By this definition, the term structural lineament embraces any alineament of topographic, vegetative

and lithologic features, or any boundary line between physiographic units, which is ascribed to the underlying geology and can be traced as a line on a photographic image. The use of the term lineament is here preferred to the term linear, also frequently used in the literature, because it refers to both straight and curved lines. This definition applies equally well to aerial photography and space imagery. However, the technique used to extract this information is not equivalent in the two cases.

Usually, with aerial photographs, the terrain is observed in stereoscopic vision, to facilitate the recognition of geomorphic features. Three-dimensional viewing of terrain considerably helps the interpreter in his endeavour to separate lines that are controlled by geologic factors from lines that are not.

The terrain stereomodel obtained by assembling two overlapping space images from adjacent orbits is characterized by reduced vertical exaggeration, because of its small base to height ratio. The diminished stereo-effect, combined with the small size of the observed landforms, limit the advantages of analyzing in stereo. The photogeologist engaged in the study of ERTS imagery will normally work without the aid of a stereoscope. The distinction between geologically controlled alineaments and alineaments resulting from natural or human causes, but unrelated to geology, becomes more difficult to him. The success in pin-pointing geologic lineaments will greatly depend on his ability and experience.

The procedure adopted for studying the ERTS imagery of Gaspé was first, to make a selection of the most appropriate spectral band and, subsequently, to enlarge the chosen original material to the format that would illustrate clearly the lineaments and at the same time provide the appropriate scale for correlation with geologic and geophysical maps.

The initial assessment of the relative informational value of the four MSS spectral bands would indicate that for Canadian terrain the band from 700 to 800 nanometers, possesses the best attributes for geologic study. On band number six, water bodies appear as very dark tones, the vegetation pattern is manifested by a wide range of photographic tones and there is a high contrast between lighted and shaded areas. The dense matrix of picture elements represented by 2,400 x 3,400 image data points per frame for the MSS system makes it possible to enlarge the original ERTS images up to about 15 times, without producing excessive visual image degradation, as would occur with standard aerial photography. It was felt that in order not to lose image quality, a film base reproducing the enlargement was required. The 1:250,000 scale of this type of enlargement matches the standard scale of compilation of regional geologic maps in Canada.

INTERPRETIVE RESULTS

The frame of orbit 793 imaged on Sept. 21, 1972, over Gaspé (Fig. 1) was the object of detailed visual analysis.

Some of the terrain on the west side of the picture is cloud-covered and consequently the resulting lineaments map of Gaspé (Fig. 2) covers mainly the eastern portion of the frame. The lineaments map shown on Figure 2 is an objective representation of imagery data, in which no attempt is made to specify the meaning of the lines in geologic terms.

This stage of interpretation can be reached with only a general knowledge of local geology. However, to classify the lines, that is, to assign lineaments to different categories, a further step is necessary, which requires a good understanding of the geology of the area, and also some inferential reasoning. The geologic setting of Gaspé is illustrated by the map prepared by McGerrigle and Skidmore (1967), and published by the Department of National Resources of Quebec. This map was the basis for the outline of the tectonic evolution of Gaspé by Béland (1969), and for the classification of mineral occurrences of Gaspé by Dugas, et. al., (1969).

The Gaspé Peninsula is a belt of Paleozoic sedimentary rocks which is a part of the Appalachian Geosyncline. It underwent successive phases of deformation with associated emplacements of igneous rocks. Greywackes and shales of Cambro-Ordovician age are predominant in a belt of slightly metamorphosed rocks, occupying Northern Gaspé, which was folded during the Taconian orogeny. Instead, in central and southern Gaspé, limestones, shales and sandstones of Ordovician, Silurian and Devonian age were folded during the later Acadian orogeny. In places, an undeformed and discordant unit of Carboniferous sediments covers the older rocks. The largest bodies of igneous rocks occur in Northern Gaspé. Mineralization in Gaspé appears to have occurred throughout a period of time, related to the successive orogenic events and normally associated with either basic or acid intrusions.

By taking into account the geologic background information, and giving consideration to the photographic appearance of the lineaments, their mutual relationship and their relation to surrounding features, a division of the structural lineaments into five categories was accomplished. The five categories are: morpho-lithologic boundaries, morpho-lithologic lineaments, fault traces, fracture traces and undefined lineaments. The corresponding map is shown in Figure 3.

Morpho-lithologic boundaries

These lineaments mark the separation of terrain units that have significantly different drainage patterns. These terrain units are sometimes enhanced by overall differences in tone. On the interpreted satellite image, the drainage pattern is expressed by its darker tone relative to the surrounding terrain. This is due both to the reduced reflectance of the water flowing in the stream channels and to the shadows associated with topographic depressions.

Comparison with the geologic map of Gaspe shows that there is correspondence between this category of lineaments and contacts of regional stratigraphic units.

The longest morpho-lithologic boundary appearing on Figure 3, coincides with the line of separation of the limestones and shales of the Matapedia group to the South from the slates and siltstones of the Fortin group to the North.

The elliptical morpho-lithologic boundary at the eastern edge of the same figure encloses the Maquerau group, an inlier of metasedimentary and metavolcanic rocks surrounded by younger Paleozoic sediments. The sharp change in terrain characteristics across a portion of Matapedia boundary and all across the Maquerau boundary suggests a fault contact.

Also distinctive is the separation of the Matapedia group from the limestones and siltstones of the Raudin group in southeastern Gaspé.

Morpho-lighologic lineaments

This category includes mainly the group of easterly trending lineaments that reflect the bedding of underlying sedimentary formations. Sills resistant to erosion might produce lineaments that would fall in this category. Some lineaments of this type originate from the influence of the strike of the strata on the drainage pattern, while others originate from differential erosion affecting the shape of terrain. At a few locations, the presence of folds is evinced by the curved outline of their closure.

Fracture zones

This category includes linear features attributable to terrain discontinuities generated by joints, minor faults and dykes. In view of the similarities in their photographic appearances, the distinction of this class from the morpho-lithologic group is not simple. Guidance in making the distinction is provided by their spatial distribution, since fracture zones are usually arranged in sets having a common orientation.

The set with orientation N 20 W, which means at right angle to the main bedding trend, seems to be the most prominent, particularly in the northwestern corner of the frame. South of the Grand Pabos fault, a set oriented N-S is well-pronounced. Also in southeastern Gaspé, it is interesting to notice a swarm of fracture lineaments, oriented N 20 E, cutting across various lithostratigraphic units.

Fault traces

In the interpreted area, there are a few lineaments that possess characteristics normally associated with large faults and were classified as such. The main fault trace corresponds to the Grand Pabos fault that on the satellite image appears as a terrain scar, which is easily recognizable over a distance of 60 miles. The continuity of the fault trace, especially at its western end, is surprising if compared with information previously acquired. On the geologic map of Gaspé (McGerrigle and Skidmore, 1967) the location of this fault is in part assumed, and shows a bend towards the south which on the basis of ERTS would be incorrect. The author undertook the photogeologic reconnaissance of the area in 1969 for the Quebec Mining Exploration Company (SOQUEM) on photographs at a scale of 1:35,000. He was not able to trace the Grand Pabos fault with the same accuracy as obtained with ERTS data.

Undefined lineaments

In this category were grouped lineaments of uncertain origin.

LINEAMENTS MAP AND MINERAL EXPLORATION

To provide a comprehensive discussion of the uses of the lineaments map in mineral exploration would exceed the scope of this publication. A few examples will be described illustrating the advantages to be derived from the application of lineaments data.

Regional tectonic framework

In recent years attention has been given to the possibility that ore deposits be related to circulation of magma and mineralized solutions along geo-crustal fractures.

Kutina and Fabbri (1972), and Kutina (1972) have compared regularities in the distribution of mineral occurrences with the presence of major morphological lineaments and major fault systems. Wertz (1972) has emphasized the role played by intersections of regional lineaments in the emplacement of intrusives, and consequently, in the regional distribution of ore deposits.

In Gaspé, where as previously noted mineralization is associated with igneous rocks, Dugas, et. al. (1969) suggested that transverse regional fractures might explain the N-S elongation of the McGerrigle batholith, and therefore, constitute the controlling factor for both the emplacement of the intrusives and the distribution of mineralized zones. He also assumed that a set of N-S aeromagnetic linears could identify such fractures. In this respect, the three sets of northerly trending fracture zones found through the study of ERTS data represent additional geologic evidence for the support of this theory. The precise significance of the fracture lineaments as to their relationship to mineralized areas warrants further investigation.

Target areas for exploration

Knowledge of the genetic type of mineralization existing in the region of interest, e.g. Gaspé, would indicate if a direct connection exists between a structural feature depicted on the lineaments map and a mineralized body. Otherwise, indications of the relationship between lineaments and mineralization can be produced by comparative analysis of the lineaments map and the regional distribution of mineral occurrences.

In Canada, data files inventories by Federal and Provincial Agencies give access to descriptive data sheets for each reported mineral occurrence, including the precise location. From these inventory data, it is an easy matter to compile a geographic map for the mineral occurrences.

The results of such a compilation for the region of Gaspé is shown on Fig. 4. In this figure, each point represents an occurrance, with the adjacent metal symbol indicating the primary mineralization. Correlations between lineaments and occurrences can be established empirically, by simply superimposing the two maps. The can also be sought by applying statistical techniques. For the region of Gaspé, the only obvious correlation between lineaments and mineralization is provided by the Grand Pabos fault, along which an alineament of occurrences is distributed. The converging evidence furnished by genetic factors, records of mineral occurrences, and structural lineaments, can direct the attention of the exploration geologist to a specific lineament, the intersection of two lineaments, or any peculiar feature appearing in the trend and pattern of the lineaments.

Interpretation of geophysical and geochemical reconnaissance data

Airborne geophysical and geochemical techniques are usually employed to localize favourable areas for follow-up field prospecting.

Positive aeromagnetic anomalies for the Gaspé region, that is, areas of the aeromagnetic contoured data where values of the magnetic field are greater than the local average, are sketched on the mineral occurrences map of Fig. 4. Data are from published aeromagnetic maps. These anomalies are originated either by various types of igneous rocks, intruded or deposited as volcanic tuffs and lavas within the sedimentary sequence, or by sedimentary rocks rich in magnetite. In Gaspé, they show close relationship to copper occurrences.

Correlation of the anomalies with the structural lineaments can be helpful in finding a satisfactory explanation for the anomalies.

The linear aeromagnetic anomaly designated by A on Figure 4 coincides with the strong lineament indicated by the same letter on Figure 3. One could assume that the anomaly is generated by a basic intrusion occurring along the lineament, which would therefore spot the location of a crustal fissure.

The letter B on Figure 4 points to two major anomalies, whose overall shape is in agreement with the curvature of the two lineaments enclosing the area indicated by Mi on Figure 3. Volcanic greywackes of the Mictaw group underlie this area.

On the New Brunswick side, the sharp rectilinear edges of a major anomaly designated by C on Figure 4 match two lineaments indicated by the same letter on Figure 3. In this case, there is no precise correspondence with the geologic map of New Brunswick, 1:500,000. (New Brunswick Dept. of Natural Resources, 1968.)

A similar procedure can be applied to interpret the regional distribution of metals, obtained as a result of geochemical stream-sediment surveys. To give an example, on Figure 5, the results of the geochemical survey for an area of southwestern Gaspé, bounded by Chaleur Bay to the south (Quebec Dept. Nat. Resources, 1971), are combined with the lineaments map. Three separate maps show the correspondence of the major lineament occurring within the area to the pattern of metal distribution for uranium, zinc and copper. Contour lines enclose areas with high concentration values. The geochemical maps were processed by computer and based on the moving average technique (rolling means), which is utilized to better outline regional trends (Gleeson and Martin, 1969).

It is evident from the figure that the major lineament marks a significant regional geochemical trend. To the north of the lineament there is, relatively speaking, a high concentration of uranium and low concentration of zinc and copper; the reverse is true for the area to the south of the lineament. If the two maps had not been combined, the trend would result much less obvious. A basic

change in lithology across the lineament, that in fact represents the contact between the Fortin group and the Matapedia group, could explain the observed trend.

CONCLUSIONS

As set forth in the introduction, the primary objective of this study was to investigate the applicability of satellite imagery for the geologic study of Canadian terrain.

The achieved results are proof that, at least for the Appalachian physiographic region, significant geologic information can be extracted from ERTS data. This information is regional in nature, and correlates well with the geologic map of the area at the scale of four miles to the inch.

Structural lineaments obtained by interpretation show interesting correlations with aeromagnetic and geochemical stream-sediment survey data. In particular, sets of transverse fracture zones, of which no indication is given by the geologic map, were observed. In the Gaspé region, these fracture zones could be related to deep-seated weakness zones in the crust, and therefore could be valuable as indicators for possible preferential locations of intrusion and mineralization.

As a plan for future work, the investigation of satellite imagery data which has been collected at various times during the year is recommended. Seasonal factors will influence both illuminating conditions and type of ground cover, resulting in the opportunity to observe different terrain aspects.

Most of the terrain features identified in Gaspé seem to have geomorphic origin and, consequently, imagery gathered during the winter season should provide an increased amount of observable geologic elements.

By studying winter imagery, and comparing the results with those achieved in this study of end-summer imagery, it is expected that a more precise definition of the specific origin of each category of structural lineaments will be reached.

ACKNOWLEDGEMENTS

Illustrations in this paper are due to the cooperation of the Geological Survey of Canada. The author wishes to acknowledge the personnel of the Geological Survey of Canada, Mineral Resources Branch, Canada Centre for Remote Sensing, and Computing Devices of Canada, for providing assistance.

Special mention is made to Dr. C. F. Gleeson, Consultant, for his advice on problems related to the mineral exploration of Gaspé.

REFERENCES

Allum, J. A. E., (1966) — "Photogeology and Regional Mapping", Pergamon Press, pp. 1-107.

Béland, J., (1969) — "The Geology of Gaspé", CIM Bulletin, Vol. 62, No. 8, pp. 811-818.

Dugas, J., Assad, R., and Marleau, R., (1969) — "Metallogenic Concepts in Gaspé", CIM Bulletin, Vol. 62, No. 8, pp. 846-853.

Gleeson, C. F., and Martin, L., (1969) — "Application of Reconnaissance Geochemistry in Gaspé", CIM Bulletin, Vol. 62, No. 8, pp. 819-823.

Hackman, Robert, J., (1967) — "Time, Shadows, Terrain, and Photointerpretation", U.S. Geol. Survey Prof. Paper 575-B, pp. B155-B160.

Kutina, Jan and Fabbri, Andrea, (1972) — "Relationship of Structural Lineaments and Mineral Occurrences in the Abitibi Area of the Canadian Shield", Geological Survey of Canada, Paper 71-9, pp. 1-36.

Kutina, Jan (1972) — "Regularities in the Distribution of Hypogene Mineralization Along Rift Structures", 24th IGC, 1972, Section 4, pp. 65-73.

Malila, William, A., (1968) — "Multispectral Techniques for Contrast Enhancement and Discrimination", Photogrammetry Engineering, Vol. 34, No. 6, pp. 566-575.

McGerrigle, H. W., and Skidmore, W. B., (1967) — Geological Map of Gaspé Peninsula, Quebec Dept. Nat. Res., Map No. 1642.

New Brunswick Dept. of Natural Resources, (1968) — Geologic map of New Brunswick, 1:500,000, Map No. N.R.1.

Quebec Dept. of Natural Resources, (1971) — Geochemistry of stream sediments, Map B-1035-A (Copper), Map B-1035-B (Zinc), Map B-1035-H (Uranium).

Van der Meer Mohr, H. E. C., (1968) — "Geological Interpretation of Hyperaltitude Photographs from Gemini Spacecraft", Proc. Eleventh Int. Soc. of Photogrammetry Congr., Lausanne, pp. 1-6.

Wertz, Jacques, B., (1972) — "Monolithic Expressions of Structure as Related to Mineralization", Western Miner, Vol. 45, No. 10, pp. 15-25.



Fig. 1- ERTS MultiSpectralScanner image of Gaspé. Orbit 793; Frame 1057-14473; Band No. 6: 700-800 nanometers.

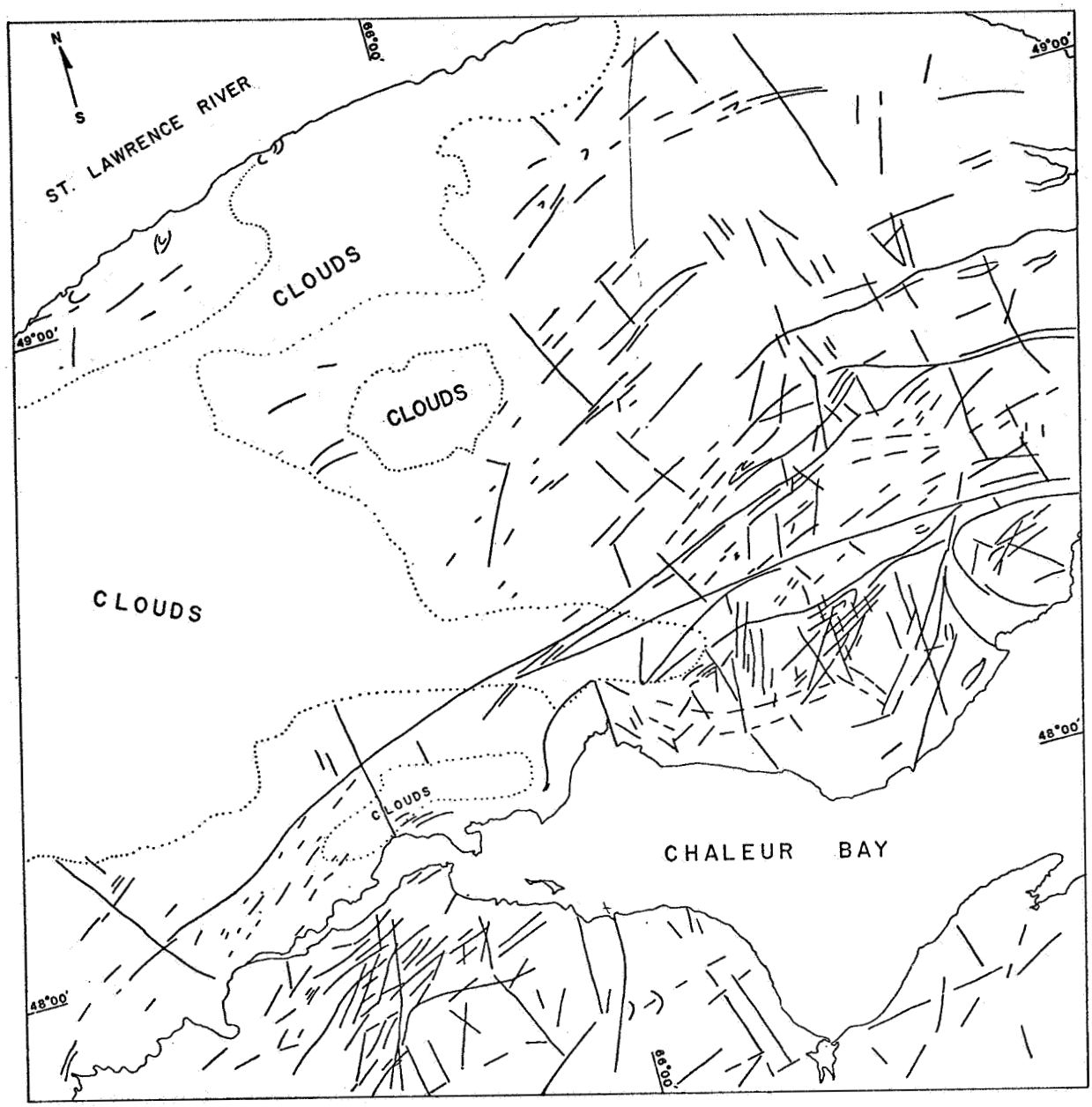


Fig. 2- Observed structural lineaments of Gaspé resulting from the interpretation of ERTS frame 1057-14473, Band No. 6.

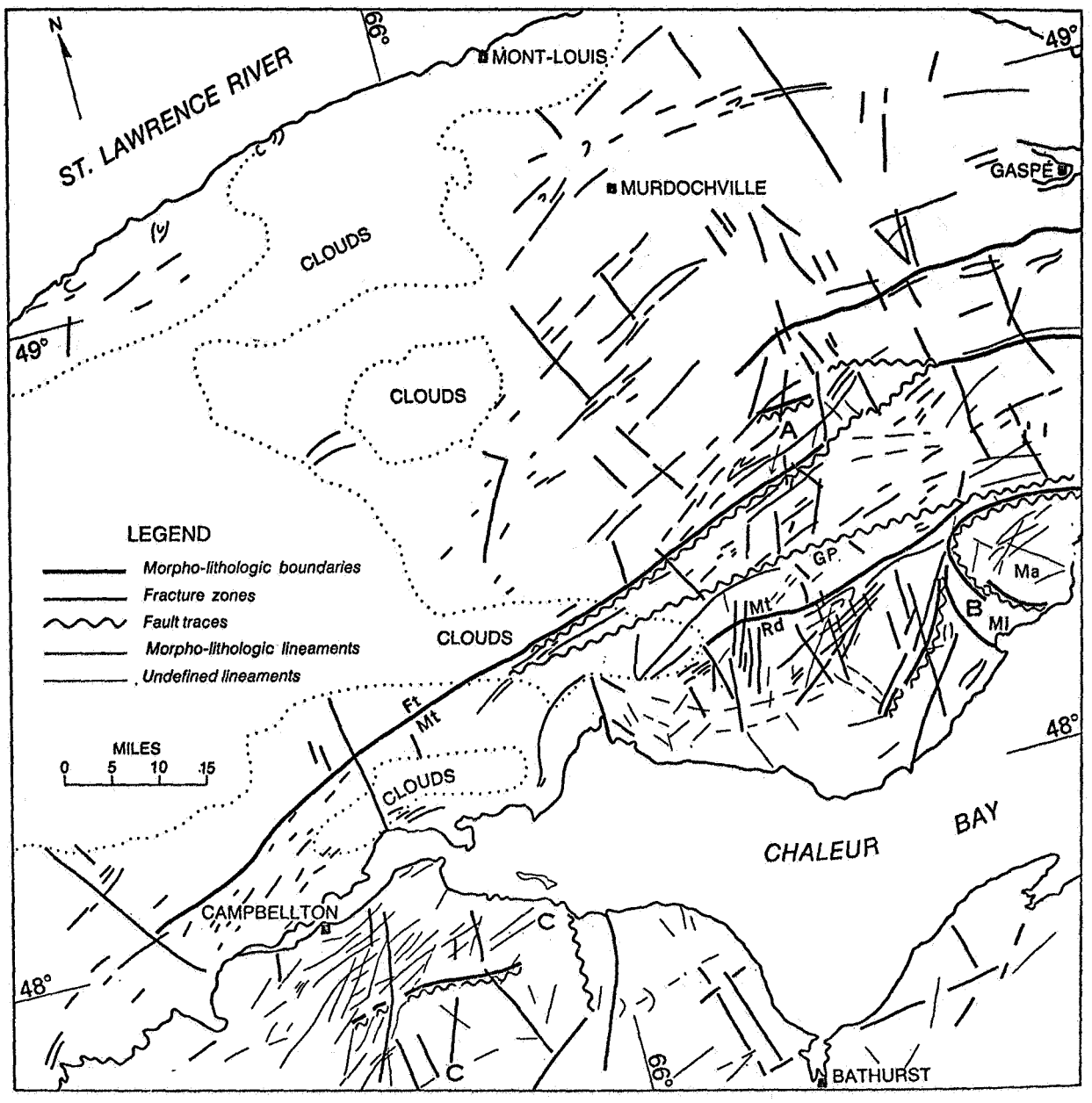


Fig. 3- Classified structural lineaments map of Gaspé

GP-Grand Pabos fault; Mi-Mictaw group; Mp-Matapedia group; Ft-Fortin group; Ma-Maquerau group; Rd-Raudin group.

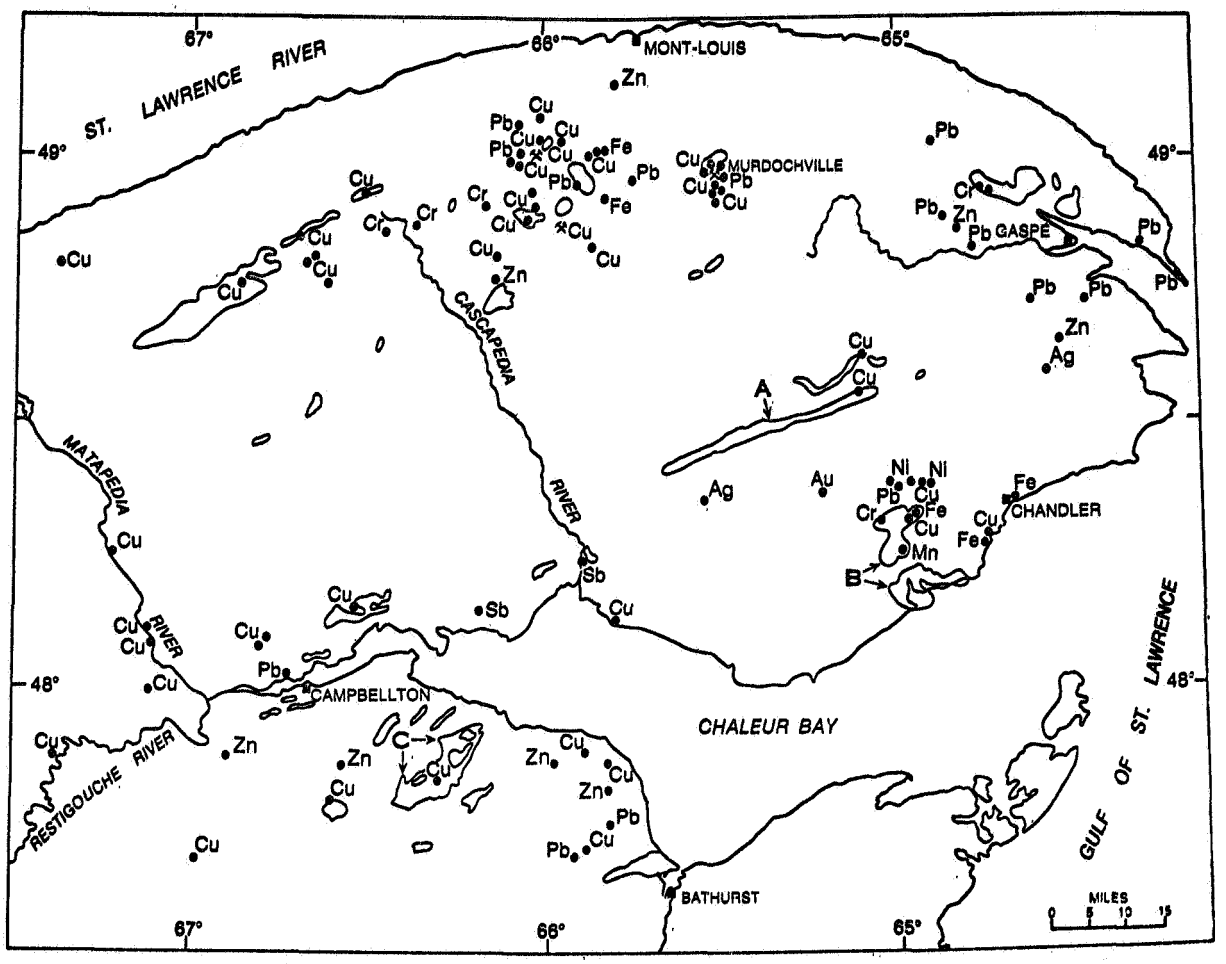


Fig. 4- Mineral occurences and contours of major aeromagnetic anomalies in Gaspé. Anomalies designated by A,B,C are correlated with lineaments of fig. 3.

Data Source: National Mineral Inventory, Mineral Resources Branch, Dept. E.M.R.; Aeromagnetic maps (1 inch to four miles series), Geological Survey of Canada, Dept. E.M.R.

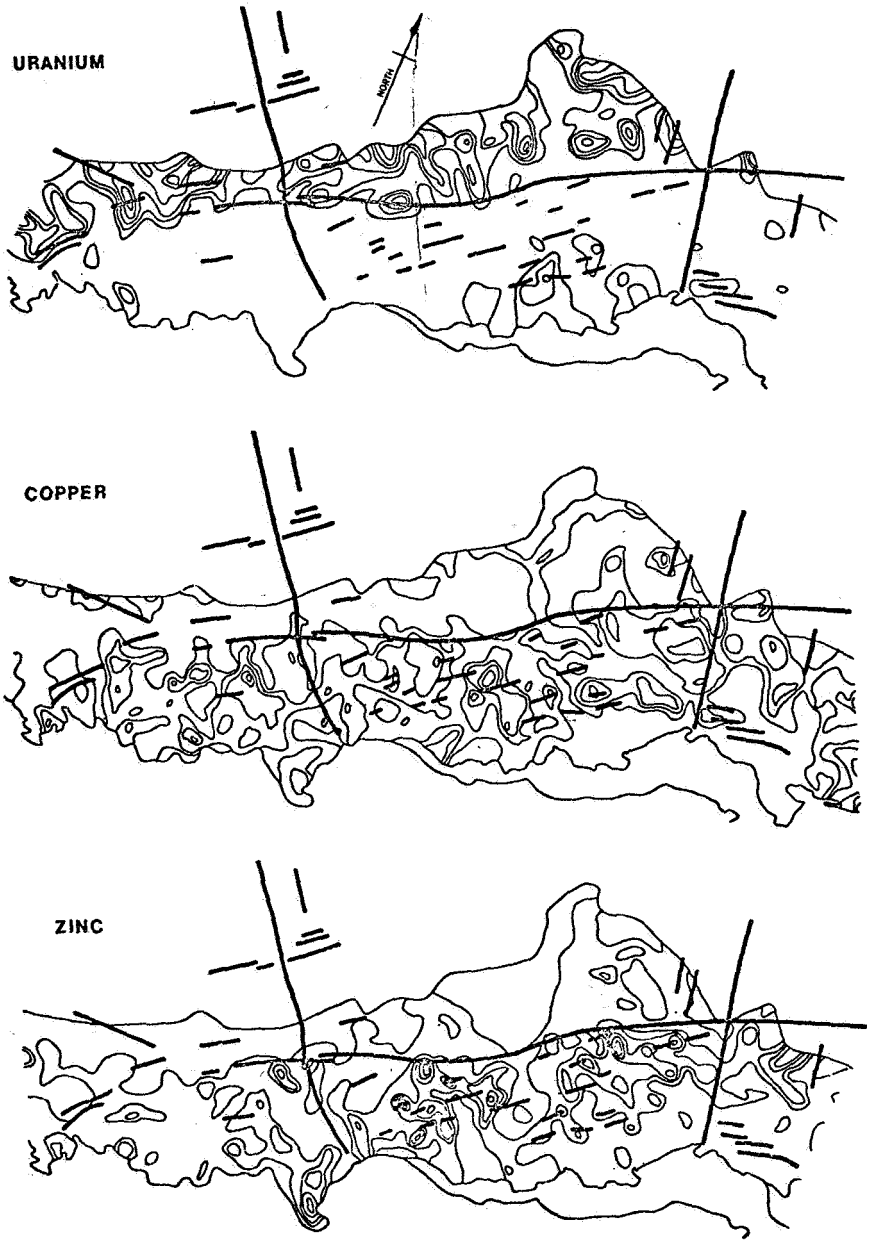


Fig. 5- Correlation of structural lineaments with geochemical stream-sediment metal distributions.

Paper G 29

LINEAMENTS IN COASTAL PLAIN SEDIMENTS AS SEEN IN ERTS IMAGERY

Charles F. Withington, *U. S. Geological Survey, EROS Program, Washington, D. C.*

ABSTRACT

Examination of satellite imagery over the Atlantic Coastal Plain near Washington, D. C. shows numerous lineaments, which cannot be accounted for by any known cultural or natural features. At least some of these lineaments represent the surface expression of faults, for one of them has been correlated with the outcrop of a fault that had been traced for several miles in southern Prince Georges County, Maryland. If a substantial number of these lineaments do indeed represent fault traces, the fact that they show on the surface suggests that the geologic history of the Coastal Plain is much more complex than has previously been recognized, and that faulting may have occurred in the Holocene, much later than has generally been recognized. The importance that such recent movements could have on future development of the Coastal Plain should be emphasized.

Earthquake prediction is becoming increasingly important in planning for the future development of the country, especially near the rapidly-growing urban centers. Even in relatively stable seismic areas, such as the Atlantic Coastal Plain, the importance of determining the potential for earthquakes is being recognized in planning for such major structures as nuclear power plants, which must be designed to withstand the earth movements that can reasonably be expected to occur. Unfortunately, the earthquake potential of much of the country is relatively unknown. Only in those areas of repeated seismic activity, such as in California, can some interpretation be made of the extent and magnitude of earthquakes. Even here, however, the location of all the active faults is not known.

The seismic potential of the Atlantic Coastal Plain is, perhaps, the least known of any area in the country, for although earthquakes have occurred here, some of them strong enough to do considerable damage, little is known of either their source, or of the location of the surface expression of the faults that caused them.

With the advent of satellite photography a new tool is available to aid in the seismic study of the country, for lineaments can be recognized that undoubtedly represent the surface traces of hitherto unmapped faults. For this paper, studies were made of the lineaments that can be seen on ERTS image 1062-15190, taken September 23, 1972, of the Atlantic Coastal Plain in the vicinity of Washington, D. C.

This image shows the area of the contact of the Coastal Plain and the Piedmont, the Fall Line, extending diagonally southwestward from the upper right center of the image to the lower left center. Two major cities, Baltimore (near the upper center) and Washington, (just left of center) lie astride the Fall Line. The Chespeake Bay, which covers much of the right side of the image lies entirely within the Coastal Plain.

To understand implications of the lineaments that can be seen on the surface of the Coastal Plain, a brief description of the area is necessary. The Atlantic Coastal Plain, extending along the coast from New Jersey southward to Florida, is underlain by poorly consolidated sediments that range in age from Cretaceous to Holocene. These sediments thicken from the western edge of the Coastal Plain where they pinch out against the crystalline rocks of the Piedmont Province, to as much as 10,000 feet at the Atlantic Ocean. The Coastal Plain has generally been considered an area of few geologic structures; those that have been reported are broad regional features such as the Cape Fear Arch and the Salisbury Embayment. Although a considerable number of minor structures have been postulated, few have been found because the poorly consolidated nature and the homogeneity of the sediments have tended to mask any surface or near surface evidence of folding or faulting.

Examination of the ERTS image shows three types of lineaments are present: those that are obviously man made, such as power lines, roads and railroads; those that are a single natural feature, such as a beach or strand line, and a third type that cannot be accounted for by any single natural or cultural feature. The latter are marked by a combination of factors, such as drainage patterns, shorelines and vegetation and other land use patterns. Only lineations of the third type are considered in the remainder of this discussion. These are

difficult to pick out on the image unless one is looking for them. The best way to see them is to hold the image at about a 45° angle away from you and look at the image from the edge. Lineations trending in the direction of the 'look' will be most easily found, so to see other lineaments, rotate the image. These alignments can best be seen on band 5 or on the color additive view, but it is anticipated that when a winter scene is available and the minor drainages better exposed, the lineations will show to good advantage also on the near infrared bands 6 and 7.

The lineations fall into three major trends: N 40° E, a direction that roughly parallels the Fall Line; N 05° W and N 35° W. Other minor trends are also seen. Each of the lineaments can be traced 30 miles or more; many disappear off the edge of the photograph, so no maximum lengths are available. Some of the lineaments can be traced at least 10 miles across the Fall Line into the Piedmont.

A significant number of these lineations may well represent the surface traces of zones of faulting that control the location of the drainages and the shorelines. Fault traces form zones of weakness in unconsolidated sediments, making them more subject to erosion. These zones of weakness are not readily apparent from examination of the surface or of topographic maps or even of high altitude photographs, indicating that a weak and discontinuous character of the alignments makes them too subtle to be seen in large scale, highly detailed view. It is a case of not being able to see the forest for the trees. When a lineament seen on the satellite image is plotted on a map, a relationship between it and some of the map features, such as anomalous drainage patterns, can be recognized. In fact, a fault system, originally described by Jacobeen, (1972), was originally found by observing anomalous drainage patterns. By study of the ERTS image it has been possible to show that this fault system extends more than 30 miles, a distance far longer than was previously recognized.

The time of movement is not certain. Jacobeen was able to tell that the movement of this one fault was intermittent from Cretaceous at least through the early Miocene. The unconsolidated nature of the Coastal Plain sediments and the homogeneity of the surface formation, however, precludes finding any evidence of movement within about 200 feet of the surface.

Numerous earthquakes in the Coastal Plain have been recorded since the coming of the Europeans some 350 years ago. The worst of these quakes are those that damaged Charleston, South Carolina in 1886. In addition, minor earth tremors occur approximately every four years in the vicinity of Richmond. A lack of visible surface evidence of faulting from these and other earthquakes had led to the general belief that the sediments were little affected by the seismic activity in the Coastal Plain. If, as it indeed seems probable, that most, if not all of the lineaments observed in ERTS data can be shown to be the surface traces of faults, a new appreciation of the importance of earth movement in the area should be made. In as much as these traces show up on the surface, movement must have taken place in comparatively recent time. This is an important factor in determining the extent of possible future faulting in the area.

To determine the extent of the faulting in the Coastal Plain, much yet needs to be done. The first step would be to plot all the lineations that can be seen on ERTS imagery for the entire Coastal Plain. The relative movements of these faults must also be determined. Only after these studies are completed can a detailed and certain knowledge of the geologic history of the Coastal Plain be understood. The results would provide information of potentially great economic and environmental importance to the planning and construction of the future development of the Coastal Plain.

Reference cited

Jacobeen, F. H., Jr., 1972, Seismic evidence for high angle reverse faulting in the Coastal Plain of Prince Georges and Charles Counties, Maryland: Md. Geol. Survey Information Circular #13, 21 p.

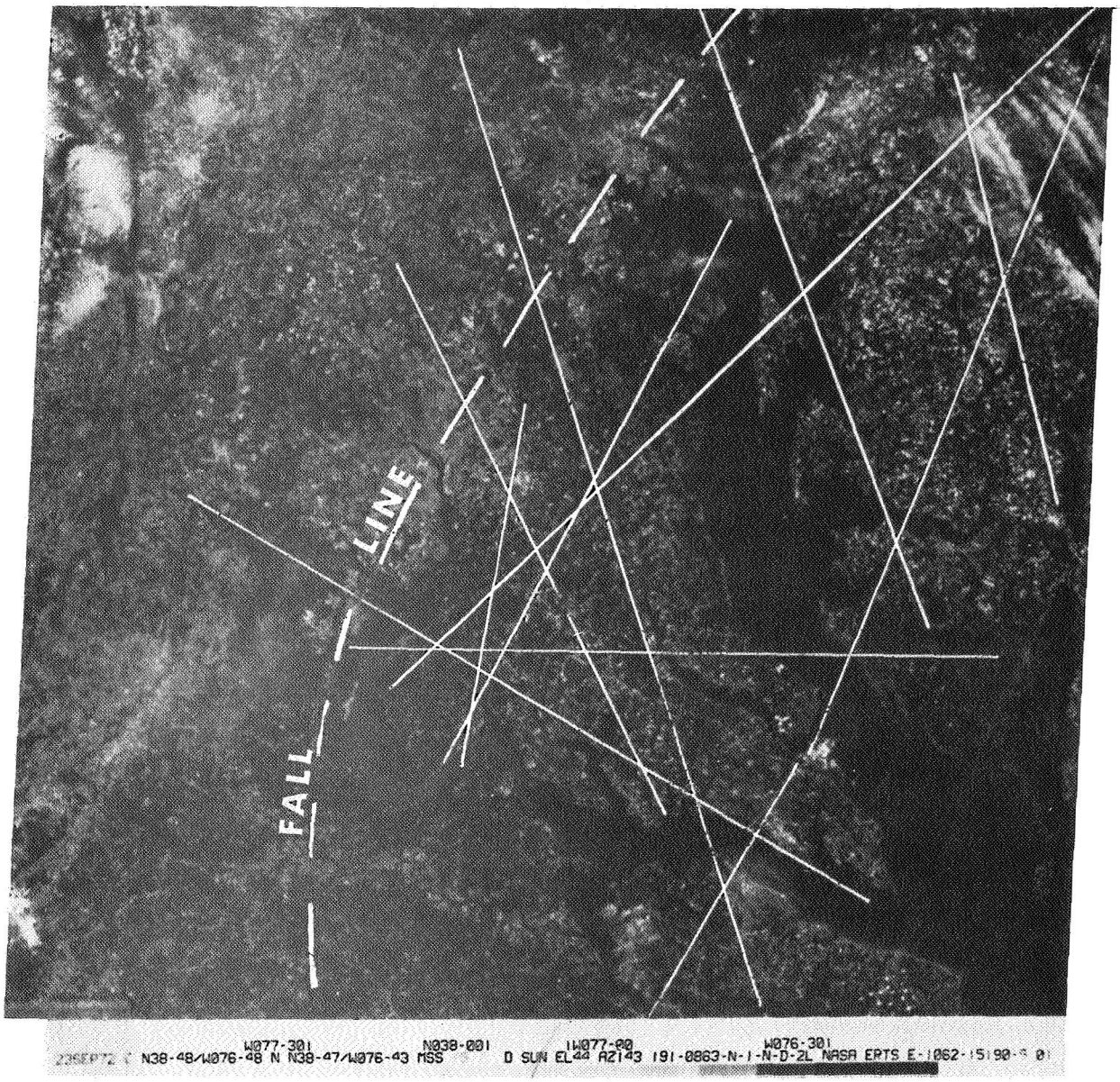


Figure 1:-- Some of the lineaments in the Coastal Plain sediments near Washington D. C. that can be seen in ERTS imagery. At least some of these lineaments are traces of faults.

Paper G 30

EVALUATION OF COMMERCIAL UTILITY OF ERTS-A IMAGERY IN STRUCTURAL RECONNAISSANCE FOR MINERALS AND PETROLEUM

Donald F. Saunders and Gilbert E. Thomas, *Texas Instruments, Incorporated, Dallas, Texas*

ABSTRACT

Five areas in North America (North Slope-Alaska, Superior Province-Canada, Williston Basin-Montana, Colorado and New Mexico-West Texas) are being studied for discernibility of geological evidence on ERTS-A imagery. Evidence mapped is compared with known mineral/hydrocarbon accumulations to determine the value of the imagery in commercial exploration programs.

Evaluation has proceeded in the New Mexico-West Texas area while awaiting imagery in the other areas. To date, results have been better than expected. Clearly discernible structural lineaments in New Mexico-West Texas are evident on the photographs. Comparison of this evidence with known major mining localities in New Mexico indicates a clear pattern of coincidence between the lineaments and mining localities.

In West Texas, lineament and geomorphological evidence obtainable from the photographs define the petroleum-productive Central Basin Platform.

Based on evaluation results in the New Mexico-West Texas area and on cursory results in the other four areas of North America, ERTS-A imagery will be extremely valuable in defining the regional and local structure in any commercial exploration program.

INTRODUCTION

Practical utilization of ERTS imagery to solve resource and environmental problems is a chief goal in the ERTS program. A strong test of practicality is provided in determining the commercial utility of the imagery in the photogeologic service business where future successful resource exploration will require innovative approaches incorporating industrial-governmental-academic cooperation and exchange of knowledge as is evident in the ERTS Program.

One such potential commercial application is the use of ERTS imagery in reconnaissance exploration for minerals and petroleum. Whether satellite imagery at a scale of 1:1,000,000 can be useful in such exploration programs is the question to be answered in this study.

STUDY AREAS AND METHODS



Fig. 1 – INDEX MAP – ERTS-A STUDY AREAS

Five areas in North America (Fig. 1) were chosen to be studied on ERTS-A imagery. These areas were picked for geologic, physiologic and climatic variations to an extent necessary to adequately evaluate the imagery.

ERTS-A imagery in the form of photo prints were mosaiced for each area and studied for geologic and geomorphic data separately by the two investigators of this study. The principle type of data discernible on the photos is in the form of fracture patterns emphasized by the drainage patterns of the areas. In many instances, the fracture patterns in conjunction with tonal alignments form lineaments that may extend for several hundred miles.

The data obtained independently by the two investigators is then compared for coincidence to establish visual validity for the mapped data. Valid data are then compared to "known" faults, fractures and lineaments in each area to establish coincidence of data. Known mining localities as well as petroleum producing sites are also compared with the mapped data to obtain any possible correlations useful to the evaluation.

STUDY BACKGROUND

Several recent papers (see References) have pointed out the ore deposits "belts" in various parts of North America and their possible association with recognized major lineaments. Other authors interested in petroleum deposits have suggested the importance of lineaments in controlling faults and folds in the stratigraphic section as well as ancient shelfs and basins. Both types of studies utilize ore or hydrocarbon production trends to define possible lineaments.

Investigators of regional fracture or lineament patterns such as Cloos (1948) and Vening Meinesz (1947) have arrived at the conclusion that these patterns are of an early Precambrian age and predate the subsequent orogenic and depositional history of the earth.

Figure 2 shows a portion of the world-wide lineament pattern of Precambrian age as defined in North America by the investigators of this study. Lineament criteria includes structural and lithologic linear zones as well as geomorphic major linear trends. Only the northeast and northwest lineaments are shown here as these are believed to represent the primordial pattern with other lineament trends being generated later during the Precambrian.

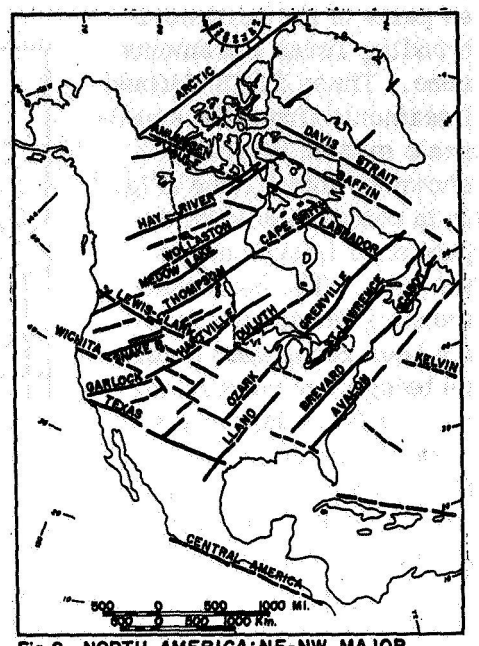


Fig. 2 - NORTH AMERICA: NE-NW MAJOR LINEAMENTS

Prior to the ERTS program, the above-mentioned lineament studies as well as that shown in Figure 2 have had to define lineaments indirectly from linear geologic-geomorphic trends. ERTS imagery now allows for the first time a visual perspective that should confirm or deny many of these previously postulated lineaments. In addition, ERTS imagery should provide a means to add a great amount of secondary fracture-lineament data that may prove useful in commercial exploration ventures.

STUDY RESULTS

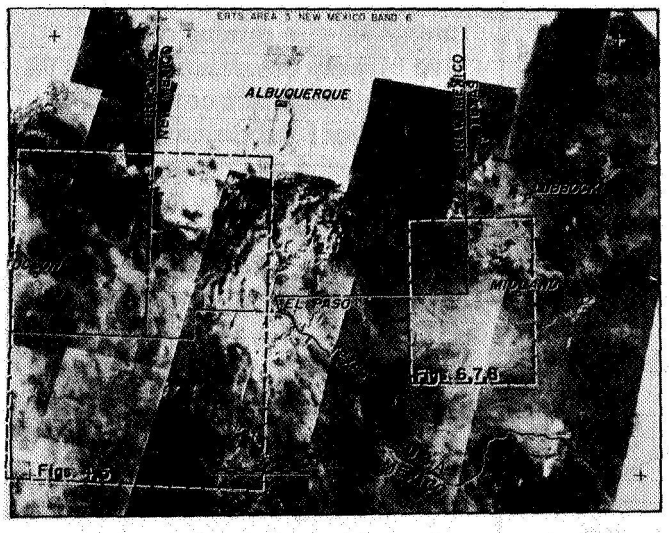


Plate 1 - Photo mosaic of ERTS-A photos in Area 3

Although five areas in North America were chosen to be studied, difficulties in receiving useable ERTS imagery in four of the five areas have limited the results as of this writing, to the Arizona, New Mexico, West Texas and Mexico area which is shown here as a small-scale, reduced mosaic of the ERTS photos in the area (Pl. 1). Results in this area have been better than expected especially in view of the rather dark tonal quality of the photo prints. Regional, northeast-trending lineaments are evident on the ERTS

photos in this area as well as parts of the northwest-trending Texas lineaments zone. These ERTS-defined lineaments (from the small-scale mosaic only) are shown as dotted lines (Fig. 3) in comparison with the published lineaments of the area. The northeast-trending lineaments have not been recognized before as being so numerous nor as clearly evident in the area. Even at the extremely small-scale mosaic of ERTS photos, it is possible to add to the data known in the area.

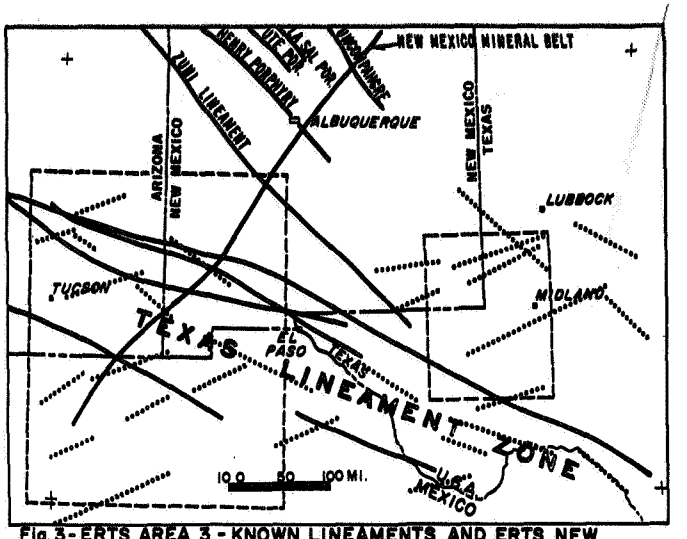


Fig. 3 - ERTS AREA 3 - KNOWN LINEAMENTS AND ERTS NEW LINEAMENTS (DOTTED LINES).

Two local areas, however, within Area 3 are especially interesting in relation to ERTS data and commercial utilization of the data. These two areas are shown by the dashed-line area outlines in Figure 3.

MINING DISTRICT: ARIZONA, NEW MEXICO, MEXICO

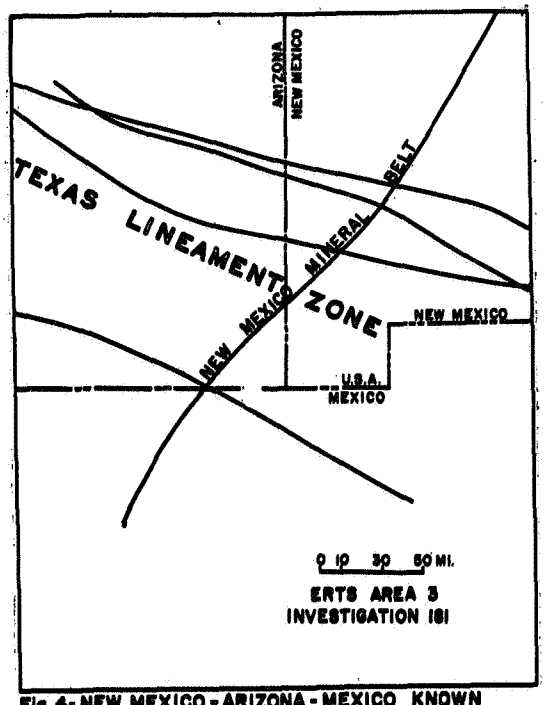


Fig. 4 - NEW MEXICO - ARIZONA - MEXICO KNOWN LINEAMENTS.

Northeast-trending lineaments in this mining district are clearly discernible on ERTS photos (lower left corner Pl. 1). In addition, subtle northwest-trending and nearly east-west lineaments are also discernible. "Known" lineaments in the area, however, are few and consist of only two major lineament trends, the New Mexico Mineral Belt (Jerome and Cook, 1967) and the various positions of the Texas Lineament zone (Kelley, 1955; Schmitt, 1966; Wertz, 1970) as shown in Figure 4.

Even with showing just the more prominent lineaments as obtained from the ERTS photos in the area (Fig. 5), there is a decided increase in data in the area thanks to the ERTS mapping medium. While this in itself could aid a commercial exploration program in the area, the plotting of the major mining districts in the area in relation to the ERTS new lineaments adds an even greater exploration perspective to the area. Invariably, the major mining districts are near coincident with the prominent northeast-trending lineaments. Secondly, the districts appear to occur along the northeast lineaments where the subtle east-west, east-southeast lineaments intersect the northeast features. Just based on this relationship for prominent new lineaments and major mining districts it is possible to postulate other prospective sites in the area where this lineament relationship occurs (Fig. 5). If this can be done using 1:1,000,000 scale photos, it is interesting to wonder just how much more accurate prospective sites could be defined if 1:250,000 scale photo enlargements were used to map even greater amounts of fracture-lineament data.

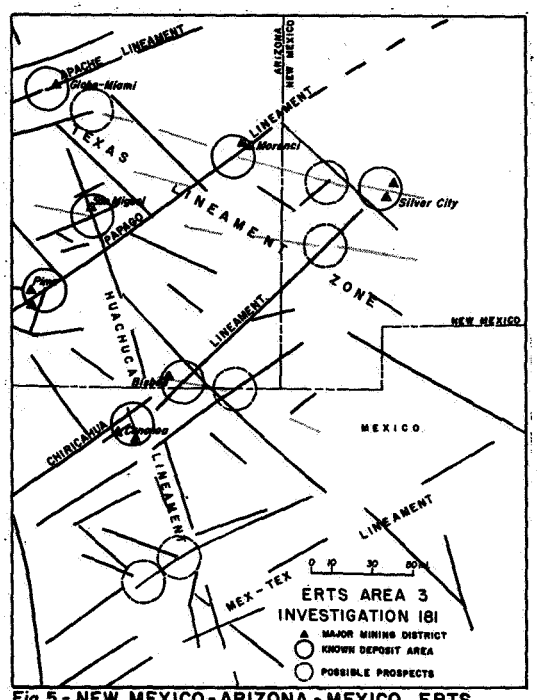


Fig 5 - NEW MEXICO-ARIZONA-MEXICO ERTS LINEAMENTS - MAJOR MINING DISTRICTS.

CENTRAL BASIN PLATFORM, WEST TEXAS

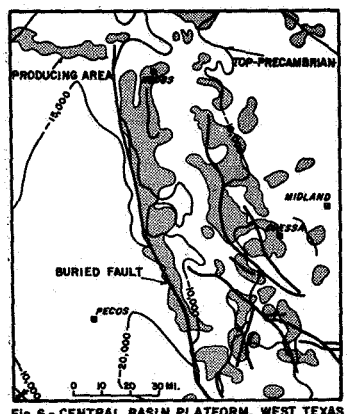


Fig. 6 - CENTRAL BASIN PLATFORM, WEST TEXAS KNOWN STRUCTURAL FEATURES

In west Texas the Tectonic Map of the U. S. (1962) defines the Central Basin platform by a series of buried flank faults that offset structural contours on the top of the Precambrian surface (Fig. 6). Hydrocarbon production localities (zip-a-tone patterns) also flank the platform. The axis of this large platform with its associated flank features trends about N 20 W. Immediately north of Hobbs, New Mexico the platform loses its identity as indicated by the structure contours, the lack of flank faults and the trend change of producing areas (Fig. 6).

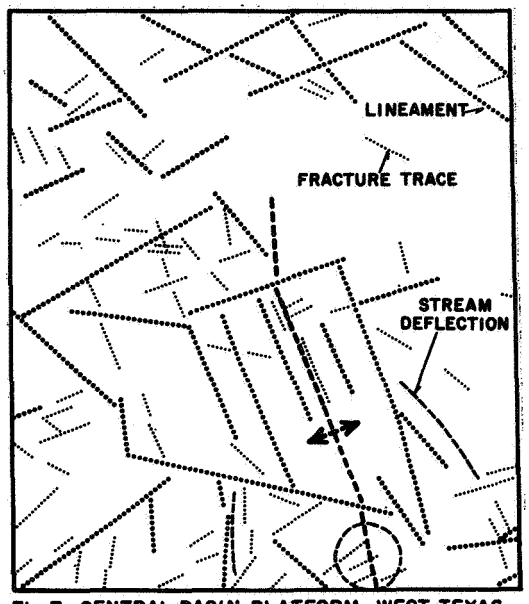


Fig. 7 - CENTRAL BASIN PLATFORM, WEST TEXAS ERTS DATA

Lineaments, fracture traces and geomorphic evidence mapped in the area on ERTS photos add a considerable amount of data in the area (Fig. 7). Combining the lineament-fracture data with the geomorphic evidence of stream deflections it is possible to infer an anticlinal axis inasmuch as the deflected stream evidence is suggestive of an anticlinal feature. The axis, however, cannot be inferred across the entire area because the lineament-fracture trace pattern changes to a northeast trend at the top of Figure 7.

Combining Figures 6 and 7 (Fig. 8) allows a direct comparison between the known data and the new data obtained from ERTS photos. In several localities the new lineaments nearly coincide with the known faults or with the flank producing areas. The inferred axis (Fig. 7) coincides with the crest of the platform as defined in Figure 6. Other more detailed comparisons can be made but an extremely interesting one is in the locality of Hobbs, New Mexico where the loss of platform identity and the change in production trend coincides well with the abrupt trend change in lineaments and fracture traces. More regional studies suggests that there may very well be a cause and effect relationship between the lineament trend change and the production trend change.

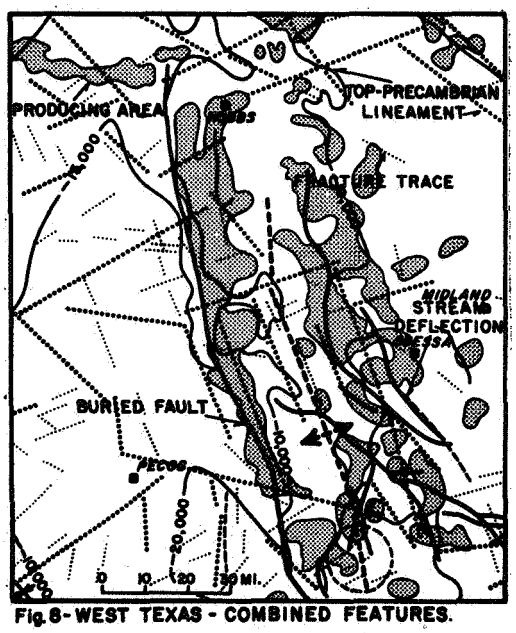


Fig. 8 - WEST TEXAS - COMBINED FEATURES.

CONCLUSIONS

The discernibility of geologic-geomorphic data on ERTS photos in west Texas that allow the surface reconnaissance mapping of a buried feature with a reasonable degree of accuracy indicates by itself the commercial value of ERTS imagery. The possibility of selecting prospective ore sites in relation to ERTS data as shown in the mining district of Arizona, New Mexico and Mexico adds to the commercial value of the imagery.

It can only be concluded from our results that ERTS-A imagery will be of tremendous value in commercial exploration programs. Regional studies of entire countries, over the worst possible terrain, will now be possible with the use of ERTS imagery. At the same time, the amount of data available should be sufficient to not only define regional basement features but also to localize more precise areas for further exploration.

REFERENCES

Brock, B. B., 1957, World patterns and lineaments: Trans. Geol. Soc. So. Africa, v. 60, p. 127 - 160.

Cloos, H., 1948, The ancient European basement blocks: Trans. Am. Geophys. Union, v. 29, no. 1, p. 99 - 103.

Hansen, A. R., 1966, Reef trends of Mississippian Ratcliff zone, northeast Montana and northwest North Dakota: Am. Assoc. Petroleum Geologists Bull., v. 50, no. 10, p. 2260 - 2268.

Hills, E. S., 1956, The tectonic style of Australia: Geotectonisches Symposium zu ehren van Hans Stille: Kommissions-Verlay von Ferdinand Enke, Stuttgart, Germany, p. 336 - 346.

Jerome, S. E., and Cook, D. R., 1967, Relation of some metal mining districts in the western United States to regional tectonic environments and igneous activity: Nevada Bur. Mines, Bull. 69.

Kelley, V. C., 1955, Regional tectonics of the Colorado Plateau and relationship to the origin and distribution of uranium: Univ. of New Mexico Pub. no. 5.

Kutina, J., 1971, The Hudson Bay paleolineament and anomalous concentration of metals along it: Econ. Geology, v. 66, p. 314 - 325.

Landwehr, W. R., 1967, Belts of major mineralization in western United States: Econ. Geology, v. 62, p. 494 - 501.

Mayo, E. B., 1958, Lineament tectonics and some ore districts of the southwest: AIME Transactions, v. 211, p. 1169 - 1175.

O'Driscoll, E. S. T., 1971, Deformational concepts in relation to some ultramafic rocks in western Australia: Special Pub. no. 3, Geol. Soc. Australia, p. 351 - 366.

Sales, J. K., 1968, Crustal mechanics of Cordilleran foreland deformation: a regional and scale model approach: Am. Assoc. Petroleum Geologists, Bull. v. 52, no. 10, p. 2016 - 2044.

Schmitt, H. A., 1966, The porphyry copper deposits in their regional setting: Geology of the Porphyry Copper Deposits, Southwestern North America; Titley, S. R. and Hicks C. L., eds.; Univ. Arizona Press, Tucson, Arizona.

Stokes, W. L., 1968, Relation of fault trends and mineralization, eastern Great Basin, Utah: Econ. Geology, v. 63, p. 751 - 759.

Tectonic Map of the United States, 1962; U. S. Geol. Survey and Am. Assoc. Petroleum Geologists; 1:2,500,000 scale.

Thomas, G. E., 1971, Continental plate tectonics: Southwest Wyoming: Wyo. Geol. Assoc. 23rd Field Conf. Guidebook, p. 103 - 123.

Vening Meinesz, F. A., 1947, Shear patterns of the Earth's crust: Trans. Am. Geophy. Union, v. 28, no. 1, p. 1 - 61.

Wertz, J. B., 1970, The Texas Lineament and its economic significance in southeast Arizona: Econ. Geology, v. 65, p. 166 - 181.

Paper G 31

STRUCTURAL INTERPRETATIONS BASED ON ERTS-1 IMAGERY, BIGHORN REGION, WYOMING-MONTANA

Richard A. Hoppin, *Department of Geology, University of Iowa, Iowa City, Iowa 52242*

ABSTRACT

Structural analysis is being carried out on bands MSS 5 and 7 of scene 1085-17294. Geologic structure is primarily revealed in the topographic relief and drainage. Topographic linears are particularly well developed in the Bighorn uplift. Many of these occur along known faults and shear zones in the Precambrian core; several have not been previously mapped. These linears, however, do not continue into the younger rocks of the flanks or do so in a much less marked manner than in the core. Linears are far less abundant in the basin or are manifested only in very subtle tonal contrasts and somewhat straight drainage segments. Some of the linears are aligned along trends previously postulated on the basis of surface mapping to be lineaments. The imagery reveals little or no evidence of strike-slip displacements along these lineaments.

Larger folds, such as the Sheep Mountain anticline, which are outlined by resistant units show up very well. Small folds or those outlined by nonresistant units or covered by Tertiary deposits are very difficult or impossible to discern.

The ERTS imagery provides especially fine detail in the uplifts. The imagery provides a basis on which targets for field checking and for supportive aircraft coverage can be efficiently chosen.

1. INTRODUCTION

This project covers an area (300 by 150 miles) extending from the eastern edge of the Black Hills to the western border of the Bighorn basin and from southern Montana to the south end of the Bighorn Basin. The principal objective is to determine the feasibility of utilizing ERTS imagery to delineate major lineaments.

Lineaments figure prominently in structural analyses and in theories regarding the tectonics of the North American Cordillera. Lineaments also are considered to be important features with regards to the occurrence of mineral deposits. Unfortunately facts relating to the existence and extent of lineaments are not always as hard or definitive as some writers seem to assume. Some lineaments are well established, but others are only provisionally located or are purely speculative. Much more work is needed to determine precisely the presence or absence of these large features and to define their characteristics.

Part of the problem of lineaments (and linears) lies in definition. Much of this appears to be due to a confusion between description and interpretation. The definition suggested here is purely descriptive. Lineaments are defined as generally rectilinear lines or zones of structural discordance of regional (100 miles or longer in length) extent. Lineaments are manifested at the surface in many diverse ways, as by single large faults or groups of faults subparallel to the lineament trend, by en-echelon oblique fault and fold belts, by large monoclines, and by juxtaposition of blocks of contrasting structures and lithologies. Other lineaments are suggested by lines of igneous bodies or alignments of ore deposits. Finally, others are revealed only by contrasting gravity and magnetic patterns related to subsurface rocks.

Linears are defined as individual straight lines a few miles or tens of miles in extent. Linears are commonly expressed in the topography and most often are structural features, but are not necessarily so. Linears can include single fault and fold-axial traces, steeply dipping dikes, hogbacks, straight drainage segments, and so on.

This paper will be restricted to a discussion of the study of a single MSS scene (1085-17294) which includes most of the Bighorn Mountains and a large portion of the Bighorn basin. Only structure will be covered here. Glacial, geomorphic, and vegetational aspects are being concurrently studied by the two co-investigators.

2. METHOD OF ANALYSIS

Geologic structure in this region is primarily revealed by topographic relief and drainage patterns. Topography in the uplift is especially emphasized in band 7 (Fig. 1) and stands out well both in mono-viewing and in stereo-viewing of side-lapping scenes.

Enlarged negative prints (Fig. 2) made from positive transparencies serve particularly well as bases for overlays. Detail can be enhanced by an optimum choice of exposure time and paper. We generally use

two different exposure times in order to bring out the detail in uplifts and, separately, in the basins. Analysis of band 7 is supplemented with similar prints of band 5 in which vegetational contrasts are more apparent. False color infrared photographs have been made from an I^2s Addcol Viewer. These have not added significantly to structural interpretation, but will provide additional input into lithologic and vegetational analysis.

Linears and fold axes are plotted on the overlay of Figure 2. Criteria used to draw linears include topographic relief, drainage, and tonal differences. Note how the linears are much more apparent and concentrated in the uplift as compared to the basin. Also shown are the recognizable folds, the outline of the uplift (dot-dash line), and the Precambrian-Paleozoic contact (dash-cross line). Figure 3 is a map showing the known structures.

One of the reasons for having chosen this area was the considerable ground truth available. However, when making an overlay, the P.I. found it difficult to be objective and ignore his knowledge of the geology. To reduce the inherent bias, several others with little or no prior background in the area were asked to do overlays. Comparisons showed a high degree of agreement. The main differences were in the individual's criteria for straightness and minimum length of linears. The resulting overlay is believed to be a fairly honest and objective first look.

U-2 photography was flown along two east-west strips; one is at the latitude of Greybull and the other at the latitude of Tensleep. In addition conventional high altitude photography has been obtained for key areas chosen on the basis of the study of the ERTS imagery.

3. DISCUSSION

The linear pattern is made up of several distinct trends; E-W, NNE-SSW, NE-SW, and NN-SE. These directions correlate well with known faults, shear zones, and monoclines in the uplift. Several "on-line" linears coincide with previously known or postulated lineaments; these are the Tensleep, Florence Pass (west of Buffalo) and Tongue River (north and west of Sheridan). These features, however, either do not continue into the younger rocks of the flanks or do so in a much less marked manner than in the core.

Two prominent linears in the core of the uplift have not been previously mapped. One trends N-S from the glaciated West Tensleep valley north across the core to a pronounced kink in the northeast flank of the range; this is to be field checked. The other, a strong NE trend correlates with a newly mapped fault in the Precambrian (in a just published USGS Bulletin on The Cloud Peak Primitive Area).

On the other hand, the Tensleep lineament is not resolvable at its east end. Though not decipherable on the ERTS imagery because of the gravel and grass cover, it can be seen on U-2 and high altitude photography. It is also well known in the subsurface in the Bighorn basin, although its delineation at the surface is poor or nil. A possible surface discordance at the west side of the basin will be investigated in the summer. The postulated lineament in Fig. 3 does not appear to be confirmed in the imagery; rather, the fault at the north end of the thrust is probably only a local tear fault associated with the overthrusting. The Tongue River lineament, long a source of controversy regarding its existence, stands out strongly.

Linears are much less evident in the basins. The folds shown in the southwest corner of the overlay are recognizable owing to the resistant hogbacks of Cretaceous Mesa Verde sandstones. The two folds to the north are marked by resistant upper Paleozoic carbonates and sandstones. Other folds cannot be deciphered either because no resistant units are exposed or they are covered by Tertiary sediments.

The prominent linears mostly occur along very old structures which have been partially reactivated during the Cenozoic. Lack of expression in the basins suggests one or a combination of the following:

1) the thick cover above the basement has masked or absorbed the later movements.

2) the later movements have been concentrated in the uplift.

Tonal contrasts in the Bighorn basin are mainly lithologic as the soil and vegetation cover is very thin. The lack of tonality contrast and the more dense drainage pattern in the Powder River Basin is related to the moister climate with a resultant heavier grass cover, and to the more widespread and thicker post-Paleocene cover.

To date, vegetation contrasts have not been too helpful in providing structural information. Conifer-bearing Cretaceous sandstones do outline a few hogbacks, as around the Black Hills. Within the Precambrian core portions of dikes greater than 150 feet wide are marked by vegetational contrast from the surrounding gneisses.

An RBV scene of the same region (1013-17291) does not show as much detail as the MSS scene. An enlarged, enhanced negative print of band 2 nevertheless provides a synoptic view that can still be of use alone.

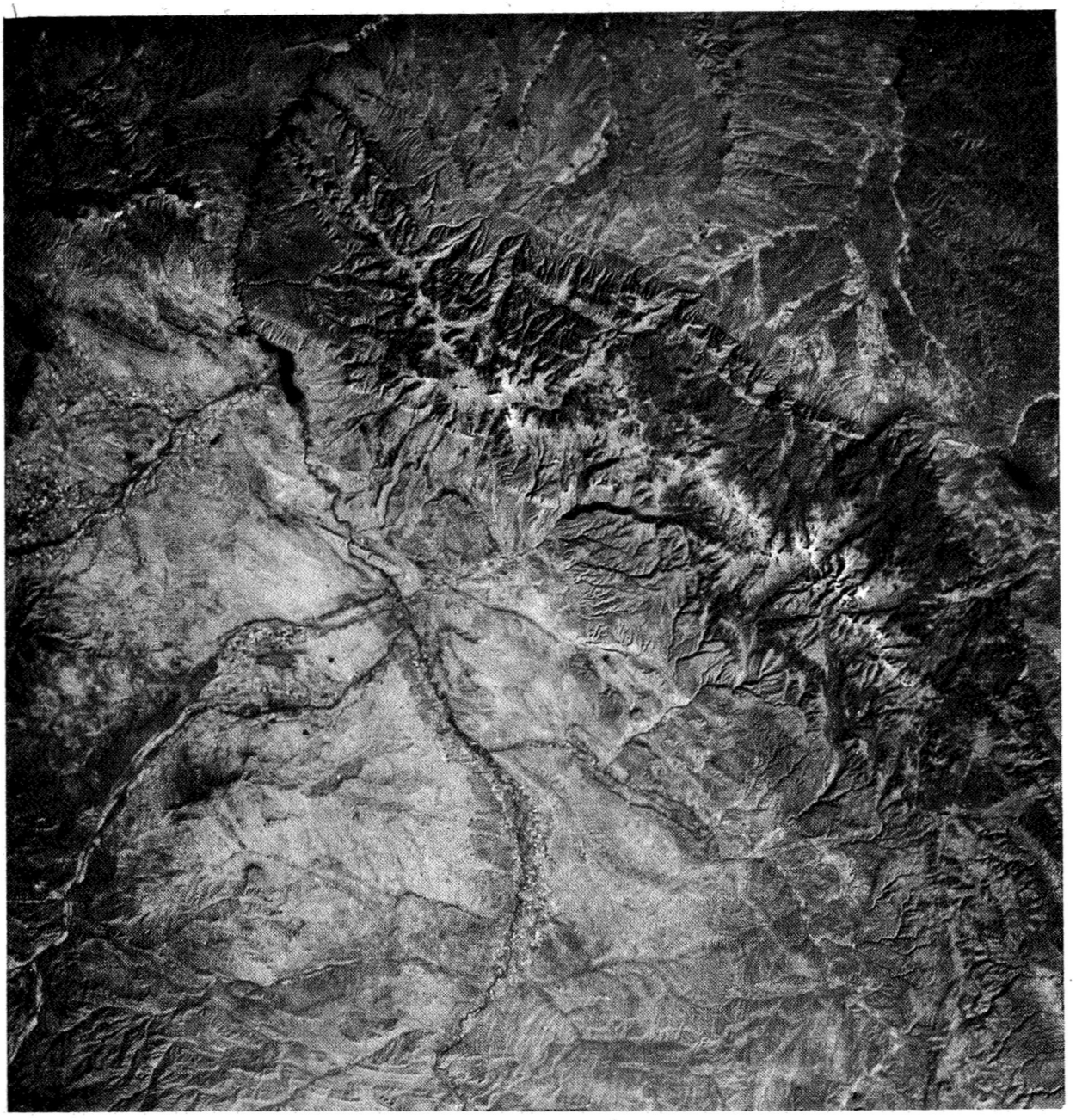


Fig. 1 - Positive print, MSS-7

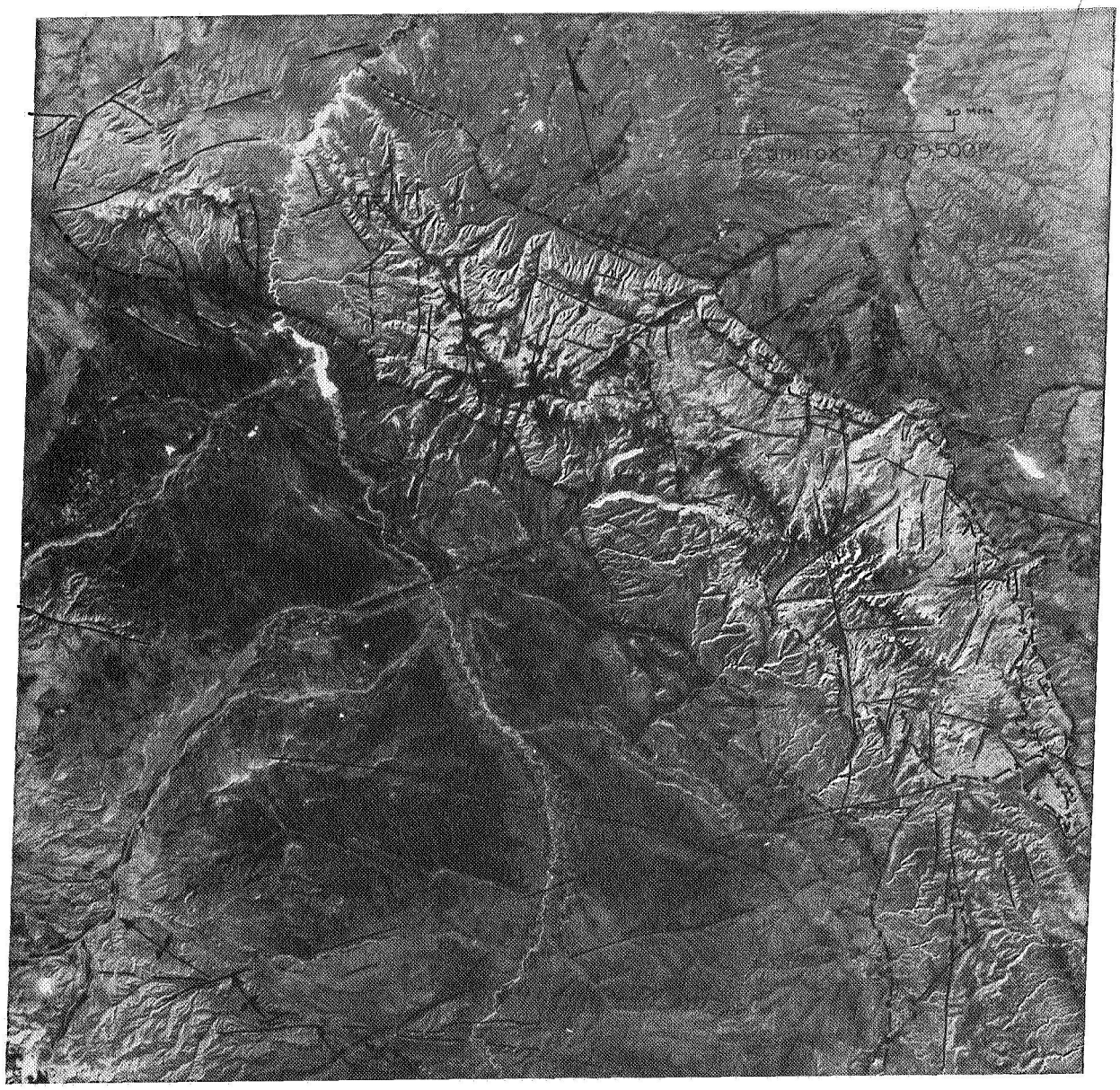


Fig. 2 - Negative print, MSS-7 with overlay. See text for annotation.

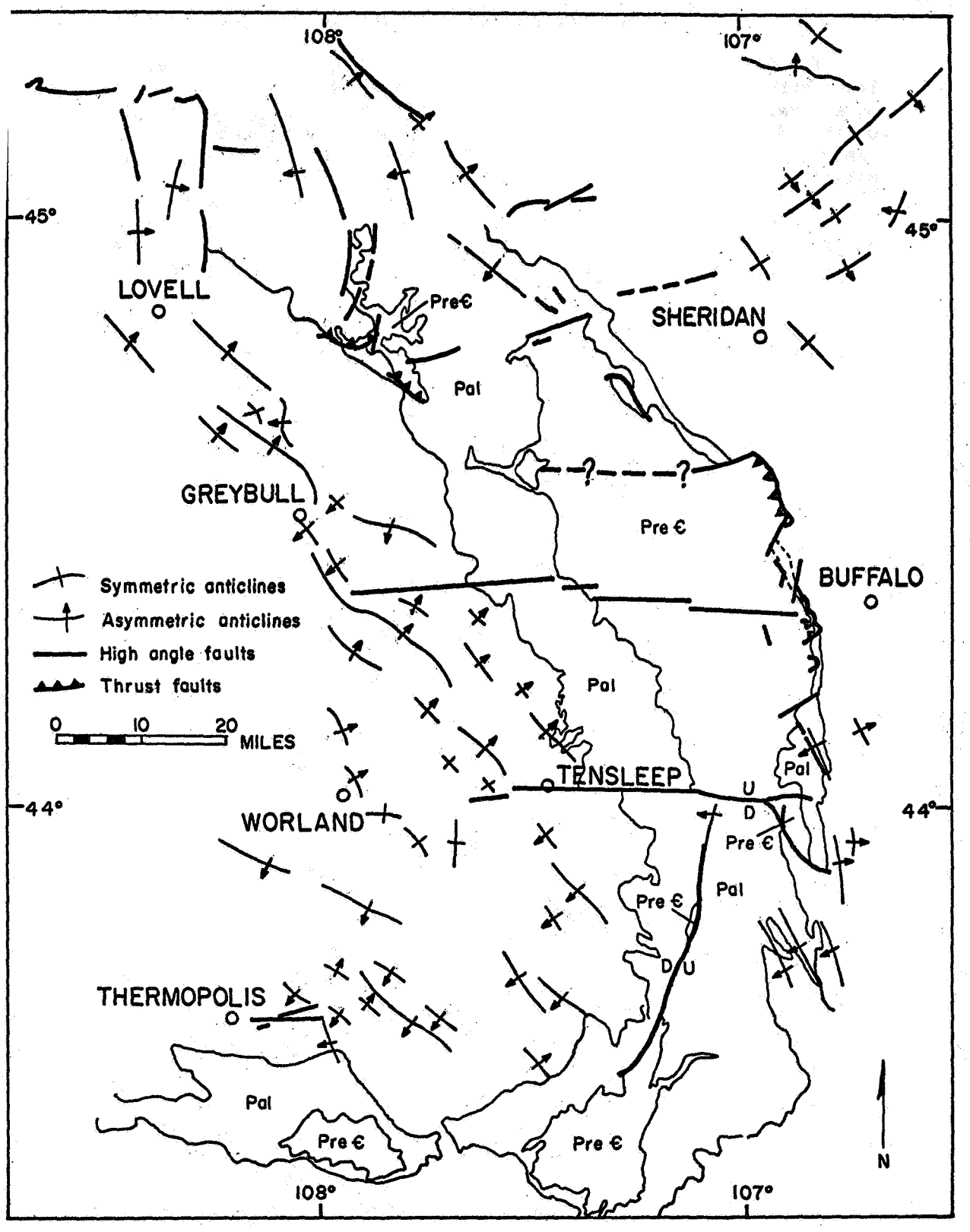


Fig. 3 - Map showing known structures

4. SUMMARY AND CONCLUSIONS

The ERTS MSS imagery, particularly band 7, provides an unparalleled structural overview unobtainable by any other means. Considerable detail is shown in the mountain uplifts and in those portions of the adjoining basins where the post-Paleocene rocks have been removed. Even though structures in the basins may be covered, extrapolation from the marginal features shown on the imagery would be warranted. In other words, in regions where far less is known of the geology as is the case here, one might predict the subsurface occurrence of folds and lineaments and hence more confidently explore the covered areas for concealed oil structures and mineral deposits.

For example, mineralization occurs along the Tensleep fault. The fault is only partly traceable on the imagery, but is known to be more extensive. The imagery allows one to more efficiently plan supporting flights (as the U-2 in this case), to select pertinent photography from available mosaics, and to plan the ground field work. Without the imagery to provide clues and to narrow the target, we would literally be feeling our way trying to verify the presence or absence of lineaments in the basins.

Finally, analysis of the imagery reveals little or no evidence of strike-slip displacement along the lineaments, a basic assumption upon which is founded a group of hypotheses invoking large scale horizontal movements along lineaments in the Cordillera.

Paper G 32

APPLICABILITY OF ERTS-1 TO LINEAMENT AND PHOTOGEOLOGIC MAPPING IN MONTANA -- PRELIMINARY REPORT

Robert M. Weidman, David D. Alt, Raymond E. Flood, Jr., Katharine T. Hawley, and Linda K. Wackwitz, *University of Montana, Missoula, Montana;* Richard B. Berg, Willis M. Johns, *Montana Bureau of Mines and Geology, Butte, Montana*

ABSTRACT

A lineament map prepared from a mosaic of western Montana shows about 85 lines not represented on the state geologic map, including elements of a northeast-trending set through central western Montana which merit ground truth checking and consideration in regional structural analysis. Experimental fold annotation resulted in a significant local correction to the state geologic map. Photogeologic mapping studies produced only limited success in identification of rock types, but they did result in the precise delineation of a late Cretaceous or early Tertiary volcanic field (Adel Mountain field) and the mapping of a connection between two granitic bodies shown on the state map. Imagery was used successfully to map clay pans associated with bentonite beds in gently dipping Bearpaw Shale. It is already apparent that ERTS imagery should be used to facilitate preparation of a much needed statewide tectonic map and that satellite imagery mapping, aided by ground calibration, provides an economical means to discover and correct errors in the state geologic map.

TECTONIC MAPPING STUDIES

A lineament map for western Montana (Fig. 1) was drawn as an overlay to a Band 7 mosaic laid directly from 9-inch prints supplied by the NASA Data Processing Facility. Most of the mapped lineaments appear to be topographic expressions of fracture (scarps and straight canyons); a few are inclined, resistant strata. They range in length from 8 to 130 km. Lineaments were checked against the geologic map of Montana (1:500,000 scale, Ross and others, 1955) and against newly-compiled test site geologic maps representing approximately one quarter of the total area covered. More than 50 of them appear to be hitherto unrecognized possible faults which will be investigated. Among some 130 lineaments annotated, lines of northeast trend are much more common than was anticipated and those of northwest trend much less so. Shadow enhancement aids significantly in recognition of lineaments trending in all directions except northwest-southeast.

Most of the important normal faults in the area are represented on the lineament map. In the area east and north of Flathead Lake these

tend to appear as scarps. In southwestern Montana they mark the boundaries between mountain blocks and Tertiary intermontane basins. Faults bounding the northeastern and northwestern sides of the Ruby Range, the west side of the Tobacco Root Mountains, and the western flanks of the Madison, Gallatin and Bridger Ranges are especially good examples. Lineaments mapped in southwestern Montana from ERTS imagery compare well with faults mapped by Burfeind (1967) with the aid of extensive geophysical work.

Low angle faults, such as the Lewis overthrust, are not readily apparent. Higher angle reverse-slip faults might be inferred from the arcuate pattern of parallel ridges in the Sawtooth Range structural salient about 75 miles west of Great Falls.

Short and medium length lineaments of northeast trend are prominent in a broad zone southeast of a line connecting Missoula and Great Falls; they appear to represent a significant fracture trend not hitherto appreciated. One such lineament defines the straight, southeast-dipping flank of the Little Belt uplift. Another, followed by the valley of the Little Boulder River, trends toward the strongly mineralized mining district at Butte.

Northwest trending faults are difficult to see because of their orientation parallel to the illumination direction. An exception is the Shroder Creek fault, clearly visible on ERTS imagery as a lineament extending 17 miles west from Flathead Lake, but mapped with considerable difficulty by LaPoint (1971), who showed that it has undergone one to two miles of right slip.

Of six prominently visible west-trending lineaments crossing the Kootenai River Canyon in extreme northwestern Montana, none are shown as faults on the state geologic map and only the southernmost two on the 1:125,000 scale geologic map (Johns, 1970). Two minor shocks recorded by the Libby Dam seismic network in August, 1972 have been referred to epicenters along these lineaments (personal communication, Gary W. Crosby, University of Montana).

Rather detailed mapping of folds in differentially eroded Paleozoic and Mesozoic strata is possible for areas of moderate relief and scanty forest cover. Study of the area between the Elkhorn and Crazy Mountains indicates that the low sun angle imagery of November (1106-17465-7) is much better for such mapping than that taken in August. Ridge patterns often allow delineation of plunging folds with wave lengths of a few kilometers; resolution of axial traces 1.6 km. apart is possible. Land form indication of dip direction allows identification of fold type at scattered locations. The most successful fold mapping utilized 1:500,000 scale enlargements under overlays and at 2x magnification under the zoom transfer scope. Annotation of a plunging fold pair suggests a significant correction

to the state geologic map for nose pattern and trend, involving a shift of an axial trace by as much as 2.6 km.

PHOTOGEOLOGIC MAPPING STUDIES

Efforts to develop criteria for photolithologic recognition of rock types and rock units from ERTS imagery have met with limited success. It is possible, with some assistance from ground truth information, to delineate the boundaries of certain major rock bodies, including those of Cenozoic basin fill, upturned Paleozoic and Mesozoic strata, and the igneous rock bodies discussed below.

Large volcanic piles are distinctive in ERTS imagery because of their tonal quality, their lack of strongly apparent internal geologic structure or structurally controlled drainage patterns, and their tendency to bury structures evident in adjacent older rocks. The Adel Mountain volcanics, of latest Cretaceous or earliest Tertiary age, were successfully delineated with only minor departures from the outlines shown on published maps, as were satellite laccoliths to the north (Fig. 2). Four topographically expressed dikes in a swarm extending northward from the main body of volcanics were recognized even though their thicknesses are well below resolution limits. Other large volcanic piles in western Montana, such as the Elkhorn Mountains and Lowland Creek fields, are less apparent, but the latter was mapped with considerable success. Outlying areas of structurally deformed Elkhorn Mountains volcanics were not recognized in imagery.

Large granitic batholiths, such as the Boulder batholith, are moderately distinctive in ERTS imagery because of their intermediate tonal quality, lack of apparent internal geologic structure, and strong tendency for control of drainage patterns by fracture sets. Smaller granitic intrusions are more readily apparent through their structural effect on the country rock than through any distinctive quality in the appearance of the intrusive rock itself. Efforts to delineate the outlines of batholithic intrusions of granite in the Pioneer Mountains led to a map (Fig.3) showing both strong correlations and major departures from the outlines shown on the state geologic map. Both the correlations and the departures are believed to be significant and this area will be examined during the coming field season.

Small granitic stocks and laccolithic intrusions of alkaline rocks are numerous in several parts of the area covered by our imagery. These tend to draw attention to themselves through their darker tonal quality, a matter of vegetative cover rather than of rock tone, but other criteria make them distinctive. Laccoliths normally exhibit circular outlines and domal form, whether or not their igneous cores are exposed. Upturned edges of sedimentary beds along the flanks of both laccoliths and granitic stocks are clearly evident in ERTS imagery.

BEARPAW SHALE BENTONITE STUDY

The possibility of recognizing Bearpaw Shale known to contain bentonite beds of economic potential was investigated for an area on the flanks of the Ingomar anticline where ground truth is well known (Berg, 1970). The area is about 130 km northeast of Billings. Using a 1/500,000 scale negative print, an overlay map (Fig.4) was drawn to show highly reflective areas of irregular pattern as well as a continuous tonal boundary thought to represent a lithologic contact. The results were compared to a ground truth map and large scale aerial photographs covering most of the bentonite deposits in the area.

Known bentonite exposures in the area are too small to be recognized directly in the ERTS imagery, but the irregular reflective patches may be a clue to their occurrence. These areas of high reflectivity are surficial clay pans, mud-filled channels and depressions, that develop on the Bearpaw Shale where dips are less than 3 degrees and bentonite beds well exposed. Further work may show that areas of high reflectivity can be used for recognition of those areas within the Bearpaw Shale where bentonite beds are exposed.

CONCLUSIONS

ERTS imagery is potentially a major tool for improving geologic knowledge of Montana. Lineament mapping has already successfully identified previously unmapped faults and emphasized the importance of northeast-trending fractures. Experimental annotation of folds has demonstrated that imagery may be used to correct errors in trend and location of axial traces inferred from the state geologic map. Satellite imagery should be used to expedite preparation of a much needed tectonic map of the entire state at a scale as large as 1:500,000. Use of imagery for tectonic mapping should result in significant saving in time and money, as well as identification of previously unmapped faults. A probable bonus would be the extension of known faults and the recognition of patterns for shorter lineaments important to regional structural analysis.

Photolithologic recognition of at least some major rock units is possible with the help of limited ground truth information. Delineation of their boundaries as expressed in ERTS imagery should lead to significant refinement of the state geologic map.

REFERENCES

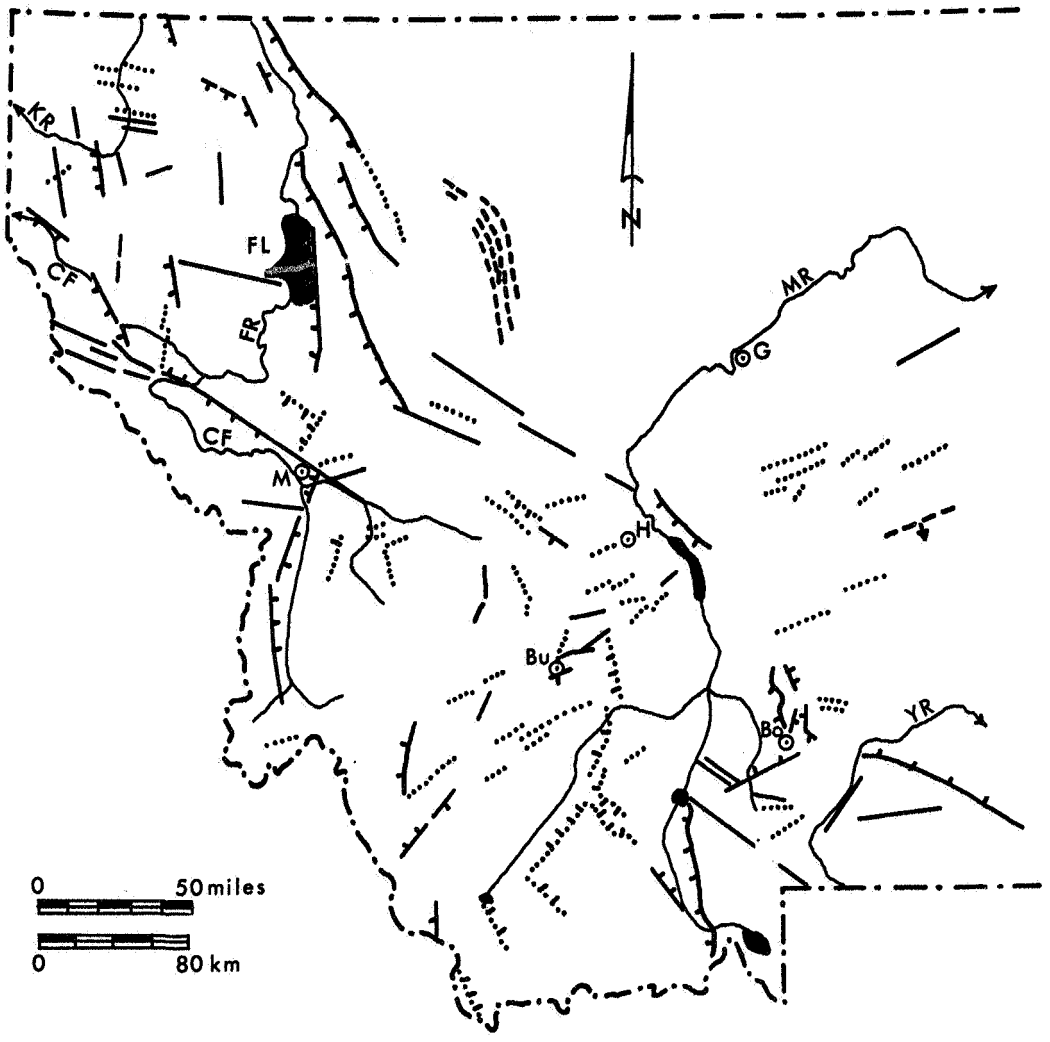
Berg, R.B., 1970, Bentonite deposits in the Ingomar-Vananda area, Treasure and Rosebud Counties, Montana: Montana Bureau of Mines and Geology Spec. Pub. 51.

Burfeind, W.J., 1967, A gravity investigation of the Tobacco Root Mountains, Jefferson Basin, Boulder batholith, and adjacent areas of southwestern Montana: unpubl. Ph.D. thesis, Dept. of Geology, Indiana Univ.

Johns, W.M., 1970, Geology and mineral deposits of Lincoln and Flathead Counties, Montana: Montana Bureau of Mines and Geology, Bull. 79.

LaPoint, D.J., 1971, Geology and geophysics of the southwestern Flathead Lake region, Montana: unpubl. Master's thesis, Dept. of Geology, Univ. of Montana.

Ross, C.P., Andrews, D.A. and Witkind, I.J., 1955, Geologic Map of Montana: U.S. Geological Survey.



Hachured lines represent scarps. Plain lines show straight canyons.

——+—+— known fault specifically recognized as imagery lineament

····'·'· lineament not represented on state or test site geologic maps

- - - - inclined, resistant strata

Fig. 1. Preliminary ERTS-1 lineament map of western Montana, drawn originally at 1:1,000,000 scale on overlay of Band 7 mosaic for late August, 1972. M - Missoula, Bu - Butte, Bo - Bozeman, H - Helena, G - Great Falls, KR - Kootenai River, CF - Clark Fork of Columbia, FR - Flathead River, FL - Flathead Lake, MR - Missouri River, YR - Yellowstone River.



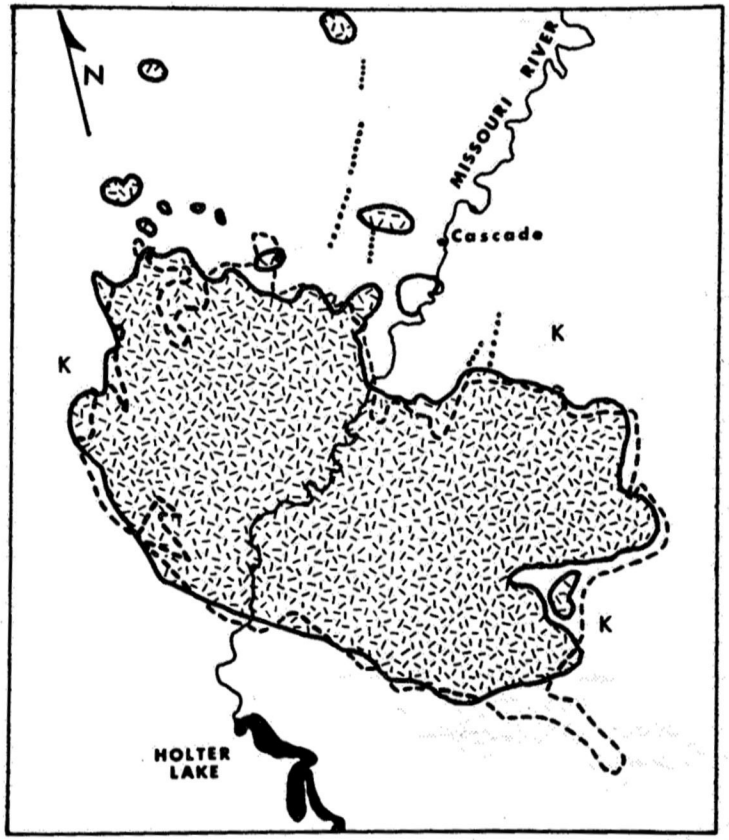


Fig. 2-1 (left). ERTS-1 detail of Adel Mountain volcanic field and Missouri River Canyon. Buttes to north are unroofed laccoliths (1089-17515-7). Fig. 2-2 (right). Contacts of Adel Mountain Volcanics drawn from Fig. 2-1 (solid lines) compared with those of state geologic map (dashed). Dotted lines are dikes. K - Cretaceous sedimentary rocks. Pattern - volcanics.

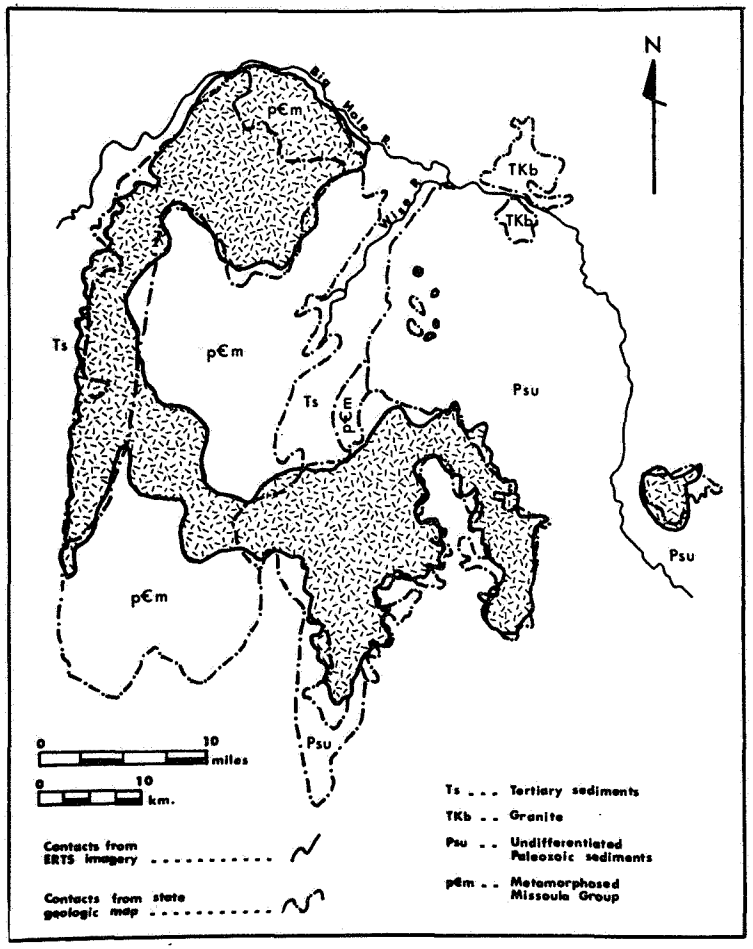


Fig. 3. Granitic contacts in Pioneer Mts. from ERTS imagery (1035-17520-7). Identity of other rock units from state geologic map. Discrepancy in west center will be field checked.

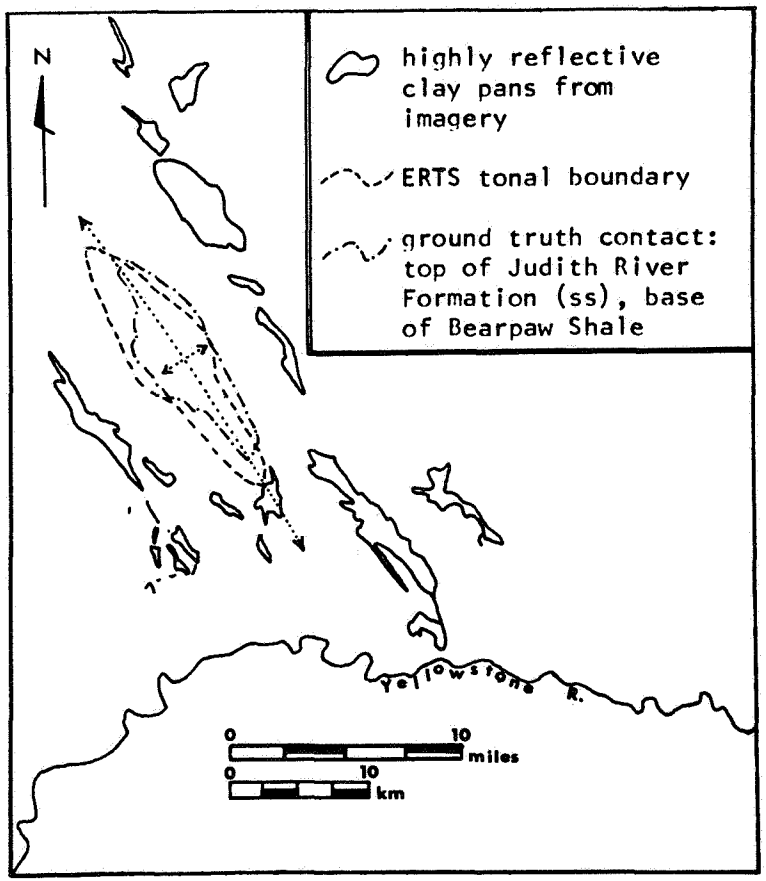


Fig. 4. Imagery map of Ingomar anticline showing sandstone core and clay pans associated with bentonite beds in Bearpaw Shale. Drawn from 1:500,000 scale enlargement (1085-17291-5).

Paper G 33

A NEW FAULT LINEAMENT IN SOUTHERN CALIFORNIA

Robert W. Pease and Claude W. Johnson, *Department of Geography, University of California, Riverside, California 92502*

ABSTRACT

ERTS-1 imagery clearly shows a 50-mile wide tectonic zone across Southern California oriented about 15° to the structures of the Transverse Ranges or with an azimuth of 70°. The zone is delineated on the imagery by terrain alignments and vegetational differences. A previously undisclosed tectonic lineament extends across the Mojave Desert and appears as a line of crustal upwarping. Pressures which would have caused this plus the occurrence of many thrust faults with the 70° azimuth indicate this to be a zone of crustal compression. Recent earthquake epicenters appear to be related to this compression zone rather than the traditional fault network of Southern California.

The Los Angeles Basin and its several sub-basins have been blocked out by the intersections of the northwest-trending Peninsular fault structures of the San Andreas system with the east-west or Transverse structures related to the Murray Fracture Zone. Local seismic interest has been focused upon faults related to the two tectonic alignments. ERTS-1 imagery of Southern California clearly indicates a third tectonic lineation which appears more closely related to recent seismic activity than the traditionally recognized structures (Figures 1 and 2).

The ERTS-recognized lineations appear as a broad zone, some 50 miles in width, which intersects the Transverse Ranges at about a 15° angle or with an azimuth of 70°. Although a limited number of landform features appear to be solely the products of the forces responsible for this sub-transverse zone, extensive evidence is also to be found in elements of the larger structures of the Transverse Ranges. Ridges that form the northwestern edge of the San Gabriel Mountains, for example, are properly oriented and in turn align with Oak Ridge which extends in a west-by-southwest direction toward the Pacific Ocean to impart the same orientation to the Santa Clara River Valley. North of the valley, the prominent ridge of the Topatopa Mountains, similarly set obliquely to the Transverse Ranges of which it is part, delineates the approximate northern edge of the zone.

The southern edge follows a line of recognized faults[1] which for the most part are buried under alluvial fill of the Los Angeles Basin. At the western end of this alignment is the Santa Monica Fault while to the east the Cucamonga Fault facets the southeastern corner of the San Gabriel Mountains near the point where the San Andreas system bisects the Transverse Ranges at Cajon Pass. It is significant to note that at this point the ERTS-recognized alignment crosses the San Andreas Fault with less than a mile of right-lateral offset which may give some clue to its age. The tectonic trend has affected the San Bernardino Mountains east of Cajon Pass by giving landform orientations that are cross-grained to the trend of the mountain range. These include a major indentation on the southern mountain front, the trend of the Big Bear-Baldwin lakes trough, and the general trend of the Santa Ana River canyon. Although the lineation just described is taken as the southern edge of the zone, ridge orientations and recognized faults in the San Jose Hills south of the San Gabriel Mountains may indicate a slightly wider zone, but evidences on ERTS imagery for this are not definitive.

The most prominent single indicator, both for the existence of the zone as well as its orientation, is a single tectonic line that extends across the Mojave Desert along the zone's northern edge and about halfway between the San Andreas and Garlock faults. On the imagery, it is particularly conspicuous along the southern edge of Rosamond Dry Lake (Figure 3) where desert-floor alluvium has been upwarped into low knolls with sufficient drainage to permit heavy stands of tree yucca (Yucca brevifolia) that form dark patches on the scans (Figures 4 and 5). To the east, the tectonic line extends along the northern edge of several low domes on the desert floor to be eventually occupied by a portion of the course of the Mojave River.

The alluvium knolls south of Rosamond playa, as well as the dome landforms, suggest that the desert tectonic line has been subject to lateral pressure from the southeast. A number of faults with the sub-transverse orientation are known to be thrust faults and the San Fernando earthquake of 1971 indicated that those buried by alluvium may well be. Recognized as thrust faults are the Santa Susanna-Santa Rosa Fault, the San Cayetano Fault, the Cucamonga Fault, and, in all probability, the Santa Monica Fault. This combination of evidence strongly suggests that the sub-transverse zone here described is a zone of active crustal compression which is absorbing much of the compressional stress being exerted by the northwestward-moving blocks of the peninsula of Baja California which intrude into Southern California.

It is of particular interest to relate the tectonics of the San Fernando earthquake of February 9, 1971, to the zone of lineations observed on ERTS imagery. Surface breaks related to the Olive View Fault[2] were thrust plates with strikes close to the 70° azimuth of the ERTS-recognized zone. Several feet of crustal compression occurred.

The compressional component of earth movement lifted the surface north of the break approximately three feet and in so doing demonstrated that forces associated with the zone may well be responsible for much of the mountain-building in and around the Los Angeles Basin. The cause of the left-lateral movement associated with the quake can also be conjectured since the wedging of the shattered crustal block against the San Andreas Fault backed by the more intact Mojave block should eject the coastal structures westward. The indication provided by the Rosamond lineation that the Mojave block is absorbing some of the crustal stress may also indicate a lessened chance that severe slippage will occur along the San Andreas Fault adjacent to the Los Angeles Basin.

An epilogue to the San Fernando movements occurred on February 21, 1973, with a sizable tremor centered near the western end of the Santa Monica Mountains (Figure 6). An extension of the Olive View Fault southwest along the Simi Hills at an azimuth of 70° joins the Sycamore Fault which is believed to have caused the recent quake. This again demonstrates that the compressional zone is active. On November 28, 1972, a swarm of small tremors centered under the alluvium near Pomona, California, a location which does not fit the traditional fault network of Southern California but which would lie on a westward extension of the Cucamonga segment of the compression-zone system.

In summary, ERTS-1 imagery in concert with previously recognized evidence delineates a zone of crustal compression across Southern California which is responsible for mountain building, landform orientations, and current seismic activity. The azimuth of the lineations that comprise the zone is intermediate between that of the San Andreas-Peninsular system and that of the Transverse structures held to be related to the oceanic Murray Fracture Zone. If pressure on Southern California is being exerted parallel to the peninsular structures, the question can rightly be asked why the compression zone is not at a perfect right angle to the pressures. One answer could be that the Transverse structures provide lines of weakness that compromise a perfect strain elipsoid. Whatever the cause for its orientation, the existence of the "Southern California Zone of Compression" may shed new light on the origin of the Transverse Ranges.

FOOTNOTES

[1] Geologic Atlas of California. California. Department of Natural Resources. Division of Mines. Scale: 1:250,000. Los Angeles, 1969; San Bernardino, 1967; Long Beach, 1962; and Santa Ana, 1965 sheets.

[2] Youd, T. L., "Landsliding in the Vicinity of Van Norman Lakes," The San Fernando, California, Earthquake of February 9, 1971. U. S. Geological Survey Professional Paper 733, U. S. Government Printing Office, Washington, D.C., 1971.

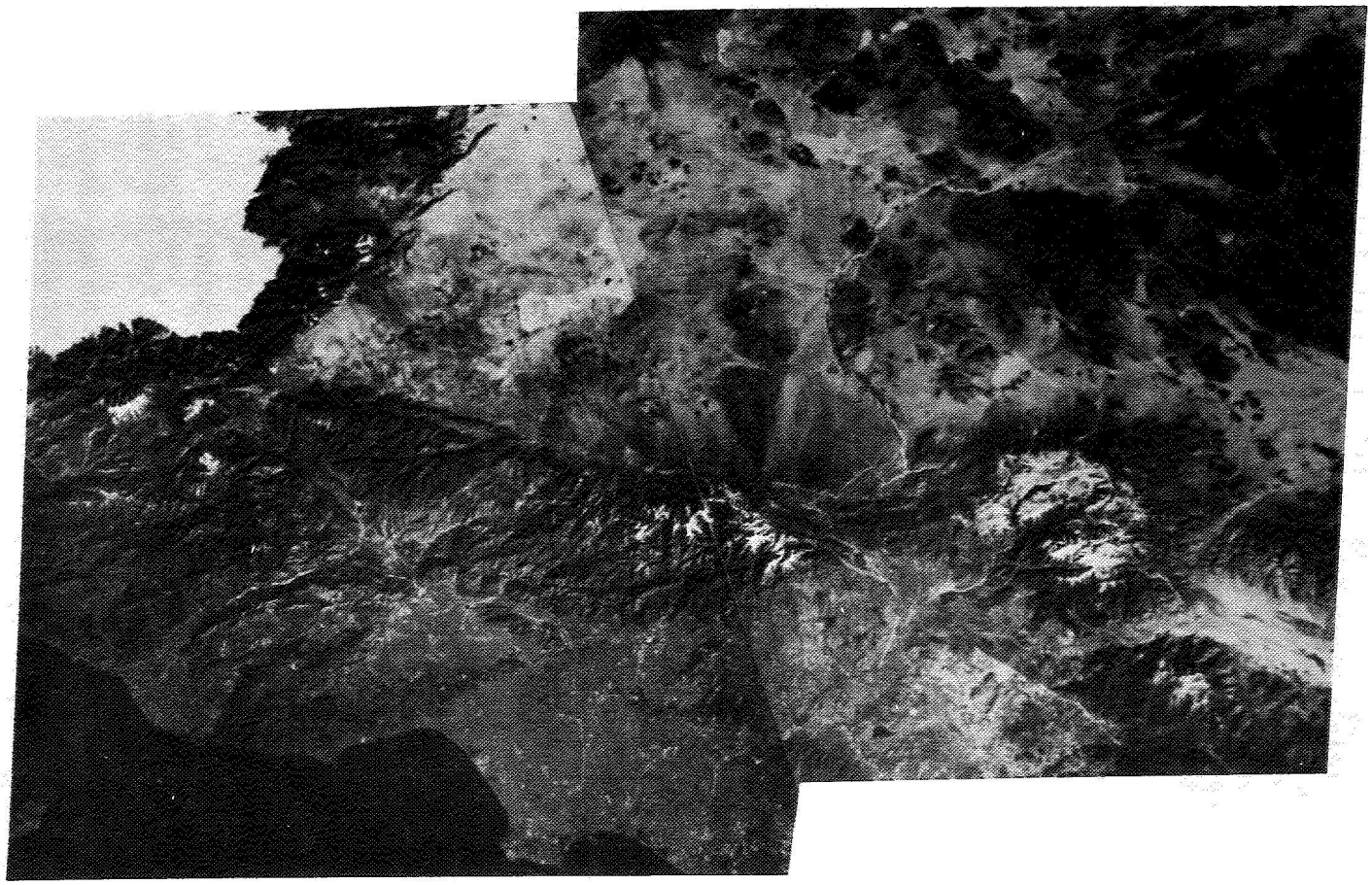


Fig. 1. A mosaic of ERTS images of 25 November (RH) and 26 November (LH) showing the Los Angeles Basin, Transverse Ranges, and Mojave Desert. The zone of tectonic lineations with the 70° azimuth is located in the accompanying map.

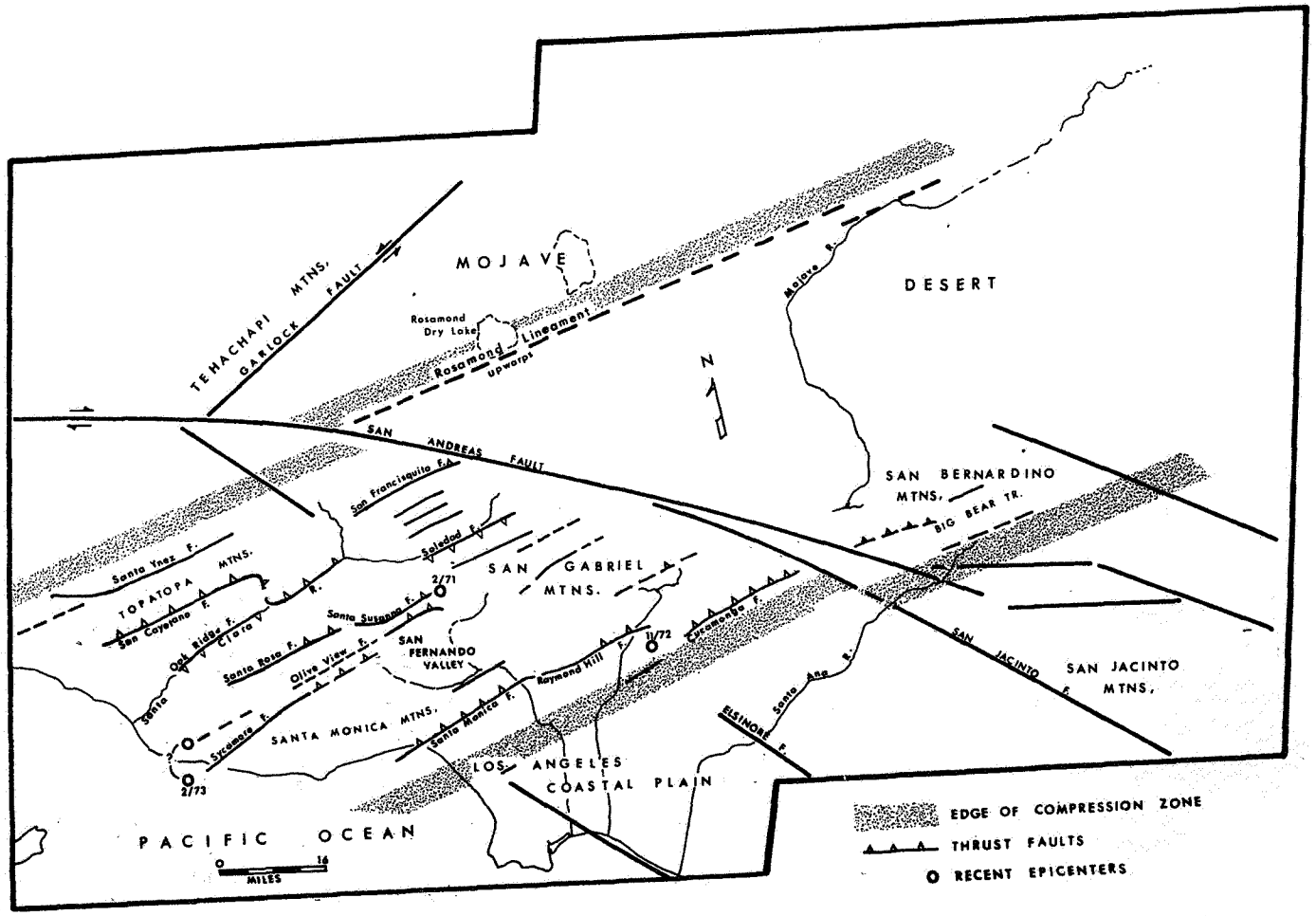


Fig. 2. A map of portions of Southern California to match Fig. 1 showing the Southern California Zone of Compression, prominent faults related to it, and place names mentioned in the text.



Fig. 3. Rosamond Dry Lake and Lineament. Band 5, November 26, 1972

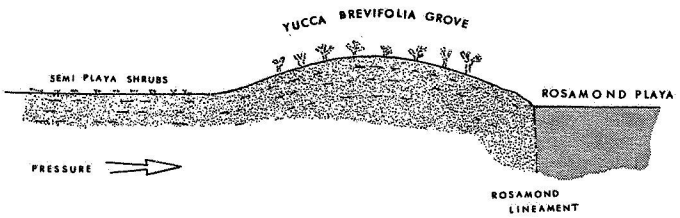


Fig. 5. Cross-section diagram of knolls along the Rosamond Lineament which appear to be upwarped from desert-floor alluvium.

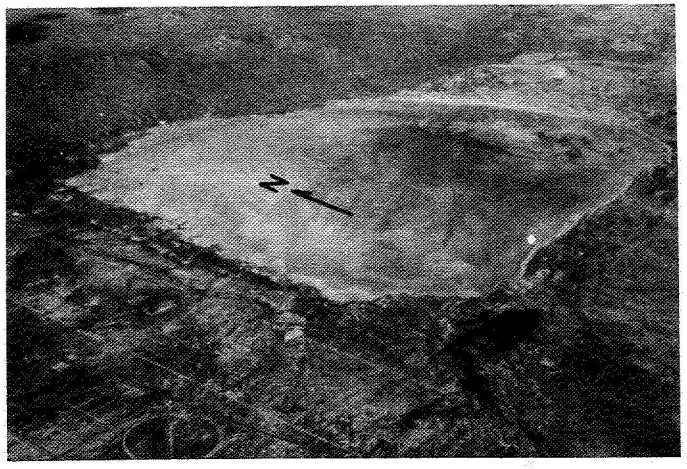


Fig. 4. An oblique view of Rosamond playa showing groves of tree yucca on knolls along lineament.



Fig. 6. The lineament of Olive View Fault connecting two recent earthquake epicenters (dots)

ENVIRONMENT SURVEYS

Paper E 1

FRACTURE MAPPING AND STRIP MINE INVENTORY IN THE MIDWEST BY USING ERTS-1 IMAGERY

Charles W. Wier, *Indiana Geological Survey, Bloomington, Indiana;* Frank J. Wobber, Orville R. Russell and Roger V. Amato, *Earth Satellite Corporation, Washington, D. C.*

ABSTRACT

Analysis of the ERTS-1 imagery and high-altitude infrared photography indicates that useful fracture data can be obtained in Indiana and Illinois despite a glacial till cover. ERTS MSS bands 5 and 7 have proven most useful for fracture mapping in coal-bearing rocks in this region. Preliminary results suggest a reasonable correlation between image-detected fractures and mine roof-fall accidents. Information related to surface mined land, such as disturbed area, water bodies, and kind of reclamation, has been derived from the analysis of ERTS imagery.

1. INTRODUCTION

Mine safety in underground coal mining has received considerable public attention because roof falls in underground mines often result in loss of life. Roof falls and rock bursts may account for only one or two fatalities in any underground mine over a period of several years, but the occurrence rate is much higher than accidents resulting from other causes. Ground truth studies in the Thunderbird Mine, Sullivan County, Indiana, showed that roof failure in the Coal VI underground workings was closely associated with zones of weakness produced by the combination of mining activity and the natural fractures in the roof rock above the coal being mined. In most cases, the mine operator cannot predict the presence and magnitude of the fractures in advance, and it is only when mining excavates such an area and roof-fall problems are caused that these fractures can be mapped. Meanwhile it is extremely hazardous to the miner and becomes expensive to the operator who must increase the required roof support and, perhaps, adjust direction of the mining entries or make other major modifications to the standard mining plan. Although the coal companies commonly do extensive core drilling before putting in a large underground mine, this drilling program does not normally record the presence of fractures because the fracture zone is usually a few inches or less in thickness. Even if the core intersects a fracture zone one could not determine the orientation of the fracture unless the

drilling method included acquiring expensive oriented cores. The authors maintain in this experiment that useful fracture data can be acquired from aircraft and ERTS-1 remote sensing records. Such imagery has not been routinely used by the mining industry for fracture mapping in coal-producing areas. Equally significant, the discrimination of fractures in areas with thick overburden has not been widely investigated. The opportunities provided by repetitive aerial and/or orbital coverage to detect subtle lineaments that are indicative of deeply buried bedrock fractures is just now being explored.

2. FRACTURE PATTERNS FROM ERTS IMAGERY

NASA's ERTS-1 program provided an opportunity to utilize repetitive synoptic coverage to develop fracture mapping techniques in areas where bedrock is obscured by thick overburden of unconsolidated deposits and to rapidly acquire such data in an area of active surface and underground coal mining. An ERTS-1 image (1070-16050-5) flown October 1, 1972, and located near the center of the Eastern Interior Coal Region (Mattoon, Illinois, to Vincennes, Indiana) shows sharply pronounced fracture trends. A predominant trend of about N 30° E is most obvious near the center of the picture (Figure 1). Fracture sets extending N 60° W also are obvious. This image on MSS band 5 (red) was acquired at the critical time interval when farmland vegetation was largely dead or plowed under and the natural vegetation along the drainage systems was still vigorous. Dead agricultural vegetation images lighter in tone than the green (dark toned) vegetation along the natural drainage systems. The contrast between the two environments reveals the structure control exerted upon the drainage systems by fractures in the underlying bedrock even though in places it is buried by more than 100 feet of glacial drift. The image immediately to the north of this area (1088-16050-5, 19 October 1972) in the vicinity of Terre Haute, Indiana, and Danville, Illinois, also shows striking fracture trends developed on the drainage pattern. Here the predominant direction of the fractures is N 10°-15° W with a secondary trend of N 70°-80° E.

The value of the repetitive coverage of ERTS imagery is obvious when one compares the imagery of the same area flown on other dates. The fracture patterns so well developed on Figure 1 are difficult to identify and trace on images of the same area acquired on 16 August (1034-16050-5), 13 September (1052-16050-5), and 6 November, 1972 (1106-16054-5).

Thus, this ERTS-1 imagery in band 5 shows a flat glacial drift-covered area which is densely cultivated except for areas that are dissected by incise drainage systems. Two major vegetal categories occur in the area: 1) short-lived cultivated crops and 2) indigenous tree and bush cover along the stream. The cultivated crops mature and die or become dormant early in the fall, whereas the other vegetation remains green and vigorous for a somewhat longer period. Reflective differences between the dead and live vegetation is pronounced at this time period. ERTS images acquired during the short duration transitional period emphasize drainage patterns which in many places are structurally controlled as evidenced by pronounced linearity or in echelon patterns.

Another aspect of seasonal influences on fracture detection is illustrated in imagery acquired on 5 November 1972 in southwestern Indiana (1105-15595-7). Indiana lies in a temperate climatic zone that receives substantial rainfall and is vegetation-covered most of the year. Band 7 (near infrared) imagery acquired during the growing season displays relatively uniform vegetative tones, and shows few surface details except for water courses and water bodies. When the vegetation has died back in early winter, band 7 provides greater detail and more nearly resembles band 5 imagery. Figure 2 reveals a lack of highly reflective vegetation which, when combined with the low sun angle of winter, emphasizes the intricate fracture pattern in limestone upland areas. The lineaments shown on this imagery reflect both straight sections of upland stream patterns and long narrow ridges. Most of the lineaments shown are in upland areas and the bedrock is not covered by glacial drift but from one to 30 feet of residual limestone soil. The preferred orientation direction of N 40°-50° E and N 60° W are also demonstrated in ground truth measurements of limestone jointing in road cuts and quarries.

Many caves have been mapped in the limestone area to the southwest of Bloomington and extending southward into Kentucky. Some of these cave maps show an elongated development along fractures that closely parallel the direction and the position of lineaments noted on Figure 2. Perhaps the best known of these caves is Wyandotte Cave that is just north of the Ohio River in Crawford County and extends for nearly two miles in a N 40° E direction. Blue Springs Cave, in southern Lawrence County, extends about two miles in a N 55° W direction.

A trace of the Mt. Carmel Fault also is shown where it cuts through the Borden siltstones to the east of Bloomington. Although the position of the Mt. Carmel Fault as shown on the imagery already had been mapped in the field, the imagery shows some indication of additional fault fractures. These are being checked in the field to ascertain whether they are related to the Mt. Carmel Fault or to the regional fracture system.

3. PHYSIOGRAPHIC UNITS FROM ERTS IMAGERY

The physiographic provinces of southwestern Indiana are readily identifiable on Figure 2. The Norman Upland, extending southward between Columbus and Bloomington, is a highly dissected and largely uncultivated area developed on the Borden siltstone. The lighter textured area extending southerly through Bloomington is predominantly pasture land and cultivated fields of the Mitchell Plain that is developed on Middle Mississippian limestones. The darker toned area to the southwest of Bloomington and extending in a southerly direction is the dissected and largely uncultivated Crawford Upland that is developed on Upper Mississippian beds of alternating shale, sandstone, and limestone. To the west the broad area occupying about the western half of the imagery is the Wabash Lowland and is developed on Pennsylvanian rocks. Except for the extreme southeastern part, the Wabash Lowland is covered with a thick mantle of unconsolidated material. More than 100 feet of glacial outwash, sands, and gravels covered by Recent alluvium occupy the major valleys. Flat

lowland areas are covered with lacustrine deposits. The upland areas are covered by several tens of feet of glacial till, overlain by a thin veneer of loess. It is in the area of the Wabash Lowland where the majority of the strip mining and underground mining of coal has occurred.

4. FRACTURE PATTERNS FROM AIRCRAFT PHOTOGRAPHY

Fracture information also is being acquired from color infrared photography at the scale of 1:120,000. This small-scale photography was flown in May, June, and August, 1971, to study the corn blight. The May flight proved of greatest utility because vegetative cover is limited and subtle soil variations indicative of buried bedrock fractures can be seen. Vegetative growth present at the time of June andAugust photographies seriously handicapped fracture analysis. This high altitude color infrared photography provides an area overview at a scale intermediate between ERTS imagery and the low altitude aircraft photography (1:20,000) that is generally available in the state. Many more sets of fractures can be delineated on this small-scale photography than has been shown on available ERTS imagery. Although fracture patterns in the exact same position on each set of imagery are not always noted, it appears that additional ERTS imagery is received and interpreted there will be a good general correlation in direction and density. Where lineaments were indicated on the high altitude color infrared photography which intercepts bedrock exposures in active and abandoned strip mines, the measured direction of fractures in the mines shows a close correspondence to the direction indicated on the photography (Figure 3B).

Studies of the relative abundance of mapped fractures in various parts of southwestern Indiana show that there are considerably more fractures that can be detected in the glaciated area than in the nonglaciated area of the coal fields. Furthermore, the area covered by the younger Wisconsinan drift to the north exhibits a greater number of fracture traces than does the area to the south which is covered only by the older Illinoian drift. This relationship has also been noted on the black and white aerial photography at the scale of 1:20,000.

Some color infrared photography at 1:20,000 scale was available. It was studied to detect short (probably secondary) fracture systems. Fracture analysis using this photography emphasized the utility of an integrated multilevel multiband approach to fracture detection, that is, lineaments identifiable using 1:20,000 scale photography are not always detectable on the 1:120,000 scale photography. Conversely, lineaments found on the small-scale photography often have a too subtle signature to be detected using large-scale photography. In general, orientation of the lineaments and relative densities are similar at the two scales.

While this study was underway one coal miner was killed and three were injured in a roof fall at the King Station Mine south of Princeton, Indiana (Nov. 8, 1972). This mine which uses the conventional room and pillar system of underground mining has been in operation for nearly 50 years. Roof-fall problems and some subsidence at the surface have occurred

intermittently in the northwestern part of the mine during the past 10 years of operation. The 1:120,000 color infrared photography of this area shows several prominent linear patterns expressed as soil (tonal) anomalies or straight stream segments. Intersecting fracture systems in the vicinity of the accident site are of particular interest as they represent probable zones of structural weakness. A preliminary analysis of the fracture data at the King Station Mine shows the major fracture trends as N 7° W and N 50° E (Figure 3A). The greatest fracture density as shown on the photography is approximately in the area of the greatest concentration of roof falls. Additional ground truth information must be obtained underground in the mine in order to better confirm these findings.

5. MINED LAND INVENTORY FROM ERTS IMAGERY

Although the main purpose of this experiment is to relate lineaments on the imagery to fractures in the roof rock over coal beds, it was obvious that one could do a creditable job in plotting the area of surface mining (strip mining) of coal (Figure 4). Seasonal conditions influence the amount of information which can be obtained; for instance, band 7 acquired during the growing season in Indiana sharply contrasts the nearly bare disturbed mine lands from the nearby undisturbed and vegetated terrane. Older strip mine areas that were ungraded and planted in trees are, in general, easy to identify but areas that have been leveled and converted to pasture land and row crops are more difficult to outline. After an inventory of a mining area has been made, the new surface mining area can readily be recognized and outlined. The repetitive ERTS coverage would provide an excellent monitoring system to map the new strip mining area on a three-months or a year basis. Isolated strip mine areas containing more than ten acres can be easily identified and mapped, but even with high contrast conditions probably isolated areas of less than five acres cannot be identified and mapped. The mined land inventory map prepared (Figure 4) was carefully checked with the strip mine maps obtained from the individual coal companies. The mapped area from ERTS imagery (1033-15591-7 and 1033-15594-7) matched closely with the ground truth mapping.

6. CONCLUSIONS

The authors conclude that repetitive ERTS-1 imagery is a useful tool for mapping regional fractures in the areas covered by thick glacial drift and for monitoring recent mined lands in coal producing areas. Seasonally dependent MSS bands 5 and 7 imagery is most useful for fracture detection. There appears to be good correlation between fractures mapped on high altitude color infrared photographs and fractures measured in the field. The likelihood of applying ERTS-derived fracture data to improve coal mine safety in the entire Eastern Interior Coal Region appears practical from the current studies being conducted in Indiana. Band 7 appears to be best for regional mined land inventories. Mapping changes of only a few acres in the configuration of large surface mined lands appear realistic with comparative analysis of time-lapse imagery.



Figure 1. ERTS-1 image (1070-16050-5, 1 October 72) of parts of Indiana and Illinois, showing fracture trends along drainage patterns.

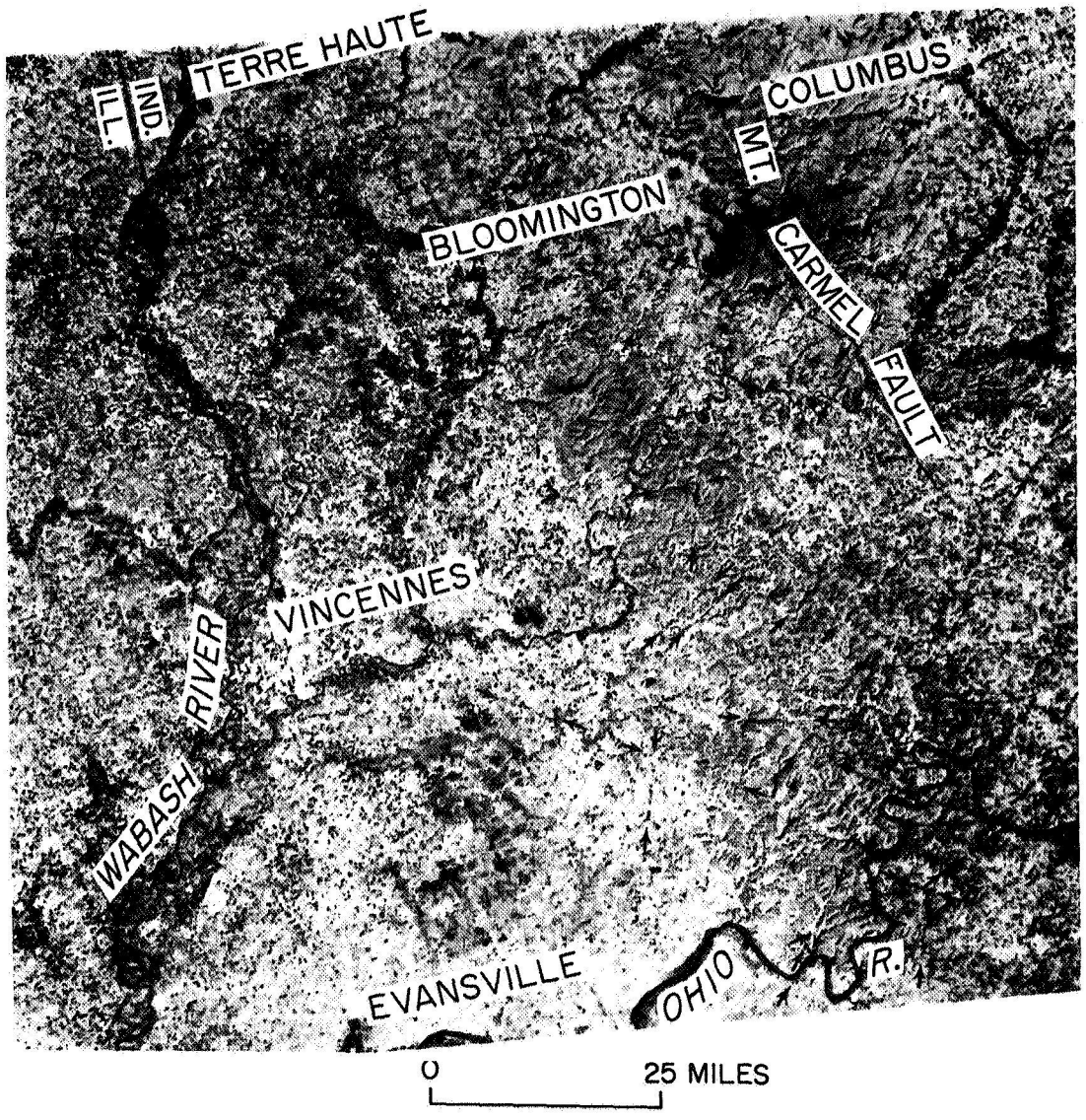


Figure 2. ERTS-1 image (1105-15595-7, 5 November 72) of southwestern Indiana, showing fracture patterns along drainageways and ridges in upland areas underlain by Mississippian limestone and siltstone.

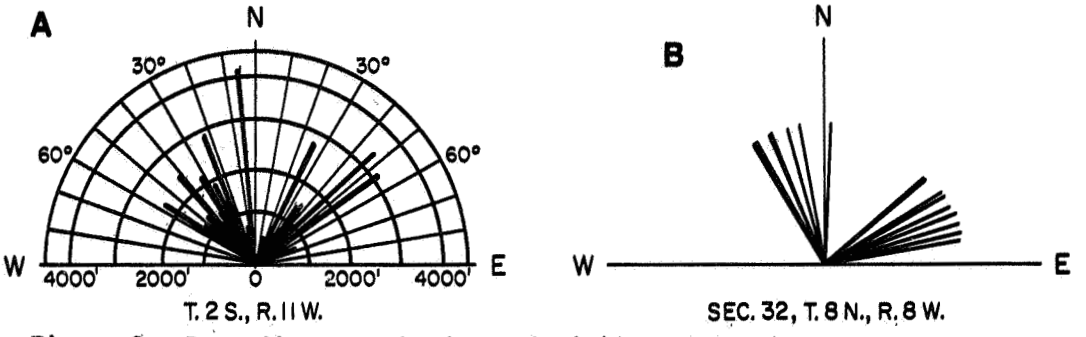


Figure 3. Rose diagrams showing orientation of fractures. A. Direction and length of fractures mapped on aerial photographs. B. Direction of fractures mapped along a strip mine highwall.

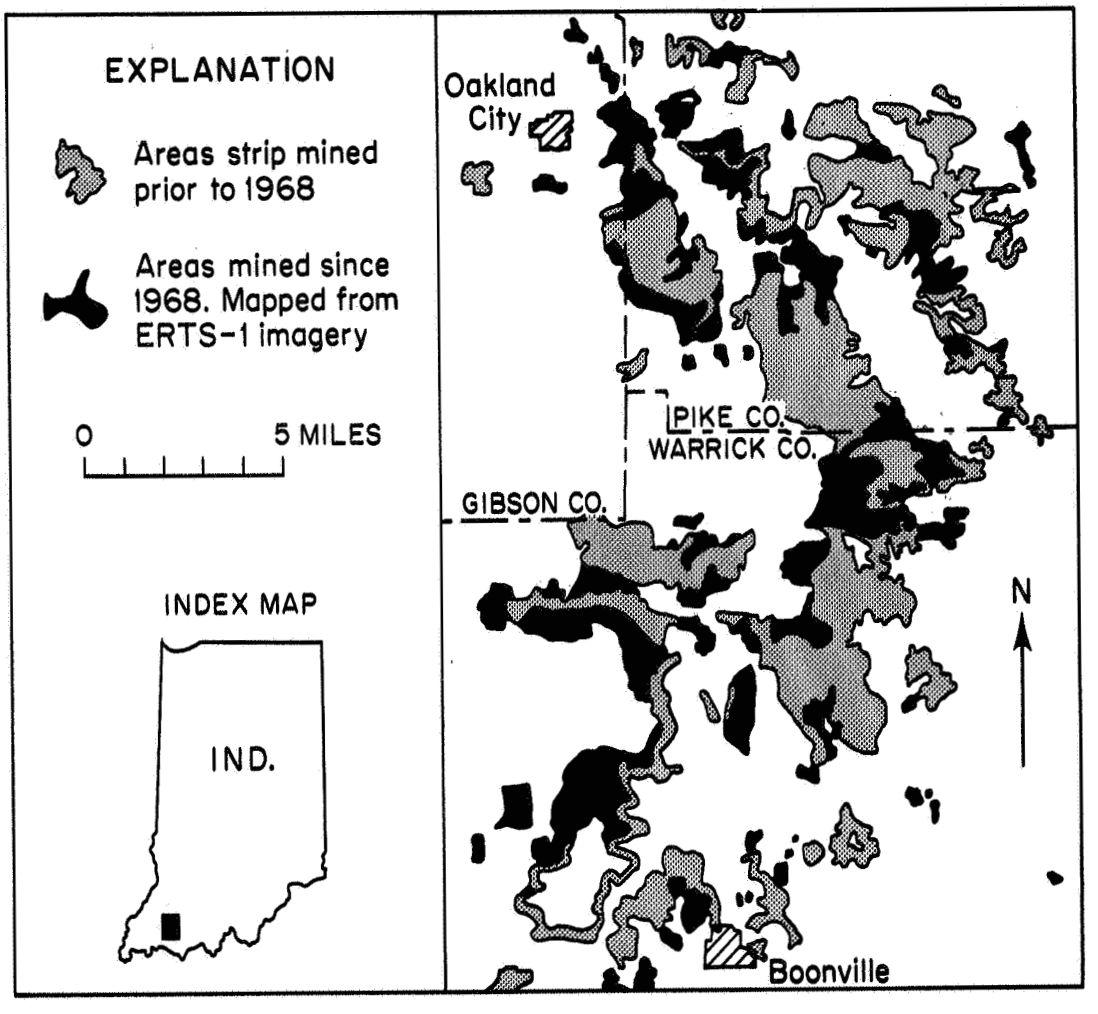


Figure 4. Map of parts of Pike and Gibson Counties in southwestern Indiana, showing strip mine areas previously mapped and that area mapped from ERTS-1 imagery.

Paper E 2

ERTS-1 INVESTIGATION OF ECOLOGICAL EFFECTS OF STRIP MINING IN EASTERN OHIO

Phillip E. Chase, *The Bendix Corporation, Ann Arbor, Michigan,*
Wayne Pettyjohn, *Ohio State University, Columbus, Ohio*

ABSTRACT

Evidence is presented of ERTS capability to detect, map and monitor the effects of strip mining. Both enlarged ERTS imagery and statistically processed outline maps and imagery of stripped earth and standing water are compared to aerial photos of a strip mine near Coshocton, Ohio. The outline maps and decision imagery are at present limited to forming a disruption map of recently mined and unreclaimed earth and the resultant standing water within the mined area. It is planned to prepare a map of the reclaimed areas (reclamation map) within the stripped area and to detect and identify ecological effects such as vegetation kills and stream sedimentation external to the stripped areas.

1. INTRODUCTION

During recent years the expansion of industry in the United States has created an increasing demand for fuel. Newspapers almost daily record grim near and long-term shortages of oil reserves and limitations in distribution and storage. Coal is a major fuel source in both Appalachia and Ohio, and the new demand for it will increase the already extensive area of underground and strip mining in the region.

Strip mining is on the increase in Appalachia. From 1940 to 1963 strip mining has increased from 9 to 34% of the Appalachian coal production (US bureau of Mines, 1963). For five states - Kentucky, Maryland, Ohio, Pennsylvania, Tennessee - strip mine production accounted for over one-third of the production, and for two - Ohio and Maryland - over 60%. The increase in stripped acreage in five counties in Ohio, as shown in Table 1, is typical. The area encompassing stripping (as well as continuing underground mining) is shown in Figure 1 (Breseckei

and George, 1966). The deposit area is approximately 50,000 square miles.

2. TEST AREA IN OHIO

The area encompassed by this investigation includes five counties in the coal mining region of the dissected Allegheny Plateau in east-central Ohio. The counties, which comprise nearly 3,000 square miles, include, from west to east, Muskingum, Coshocton, Guernsey, Tuscarwas, and Belmont. They lie in a hilly region along the western flank of Appalachia and are bounded on the east by the Ohio River. Their location within Appalachia is shown in Figure 1. A mine east of Coshocton is the example shown in this paper.

TABLE 1
COUNTY DATA OF STRIP MINING, IN ACRES*

	Coshocton	Belmont	Guernsey	Tuscarawas	Muskingum
County Total	349,000	343,000	332,000	353,000	424,000
1914-1947	622	2,254	355	4,956	1,604
1948-1971	16,818	21,042	4,014	18,039	12,280
Total Area Affected	17,440	23,296	4,369	22,995	13,884
Percentage Total Area Affected	5.00	6.79	1.31	6.51	3.27
Total Reclaimed	13,390	11,443	3,705	14,885	7,699

*Data taken from Division of Forestry and Reclamation, Ohio Department of Natural Resources (March 1, 1972).

3. GEOLOGY OF THE AREA

Although only a very small part of the area was glaciated, extensive deposits of outwash fill the valleys of the major rivers and a few of their tributaries. Elsewhere bedrock crops out, striking in a northeast-southwest direction and dipping about 25 ft/mile to the southeast.

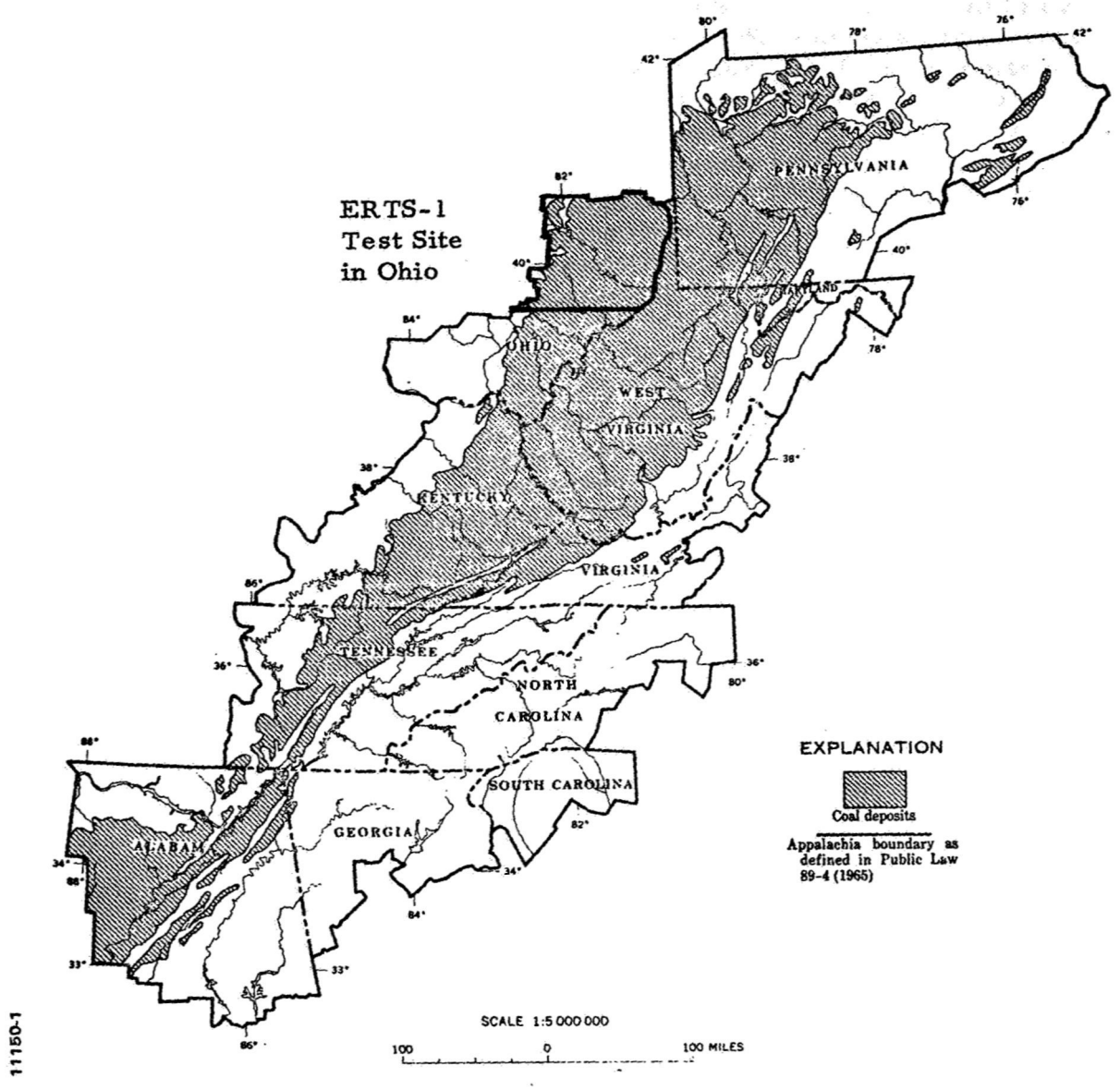


Figure 1 Location of Coal Deposits (1)

The oldest rocks crop out in the western part of Muskingum and Coshocton Counties; eastward the rocks become progressively younger. All of the exposed bedrock represent Paleozoic strata that range in age from Mississippian to Permian. They include the shale, sandstone and limestone of the Logan and Maxville units of Mississippian age; the Pottsville, Allegheny, Conemaugh and Monogahela Formations of Pennsylvania age, consisting of shale, sandstone, limestone and coal beds; and the deposits of shale, sandstone and coal forming the Dunkard Group of Permian age, which covers much of Belmont County. These exposed strata range in thickness from about 610 feet in Coshocton County to about 1100 feet in Belmont County.

4. THE STUDY PURPOSES

The primary purpose of the study is to demonstrate that ERTS-1 data can be used to prepare two types of maps. The first is the disruption map that quite simply maps stripped areas and the standing water between the spoil banks and the high wall. The second is a map of the progress of reclamation of the stripped area. Often reclamation consists only of an attempt to revegetate the stripped area.

A secondary purpose is the monitoring of strip mine impact on the land and water resources exterior to the stripped area. Two types of impact are vegetation kill and stream pollution from acid mine drainage. Another type is heavy stream sedimentation from erosion.

The accomplishment of the primary purpose would be a long step toward a major benefit of ERTS.

5. ERTS-1 IMAGERY AND DISRUPTION MAPPING

One significant result is the relative ease with which ERTS-1 will monitor new and unreclaimed stripping activities in Southeastern Ohio and in all of Appalachia. The widths of the contour strips of new or unreclaimed stripped areas are listed in Table 2 by ERTS-1 band numbers. This measurement is obtained from comparison of the ERTS-1 scene to areal photos (Figure 2).

TABLE 2
MINIMUM DIMENSION OF STRIP MINES BY BAND
(WIDTH OF A STRIPPED CONTOUR IN FEET)

Band 4	Band 5	Band 6	Band 7
400	200	250	250

The strip mines stand out well enough to be easily identified without other graphic aids (photos or maps). Since the shape is quite distinctive, detection of other areas in Appalachia without other graphic aids appears possible for a trained photo interpreter. (See Figure 3A).

Standing water within the strip mined area stands out in either bands 6 or 7. (See Figure 3B). Areas of several acres are visible. Significant increases in surface extent of water in stripped areas should be detectable on a comparative basis. However, geometric control in the change detection process would have to be carefully maintained.

An alternate approach to the preparation of disruption maps is mapping from the CCT. There are several possibilities for the preparation of automatically classified maps. The first type is the decision imagery of stripped earth and standing (or other) water as shown in Figures 4A and 4C, respectively[2]. A second possibility is probability imagery that shows earth and water each in one separate scene.[2] A third alternative is an outline map of the particular thematic classification such as earth and water in Figures 4B and 4D, respectively.

This mine east of Coshocton has features - turned earth and water - that are readily seen in the imagery and readily classified. It is neither the easiest to classify nor the most difficult and without question the capability to map strip mine disruption from ERTS is near at hand. It must be kept in mind that disruption of this nature is easiest to identify and most desirable to monitor from an ecological view point.

6. RECLAMATION MAPPING

Reclamation mapping is a monitoring task that is more complex than disruption mapping. Reclamation is the leveling of the spoils bank, removal of standing water (when necessary), and planting the area that remains. The difficulty arises from degree of success of reclamation in percentage cover and from the variety of vegetation used (vetch, pine

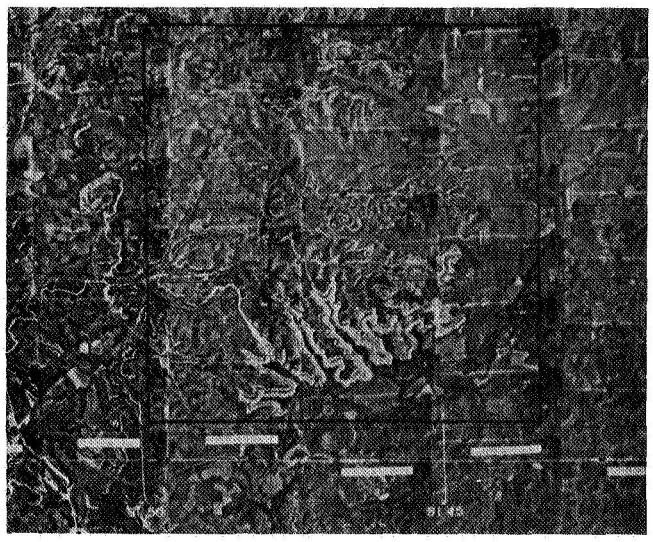
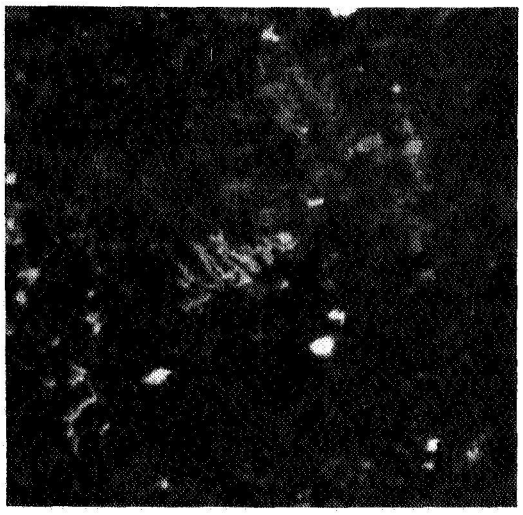


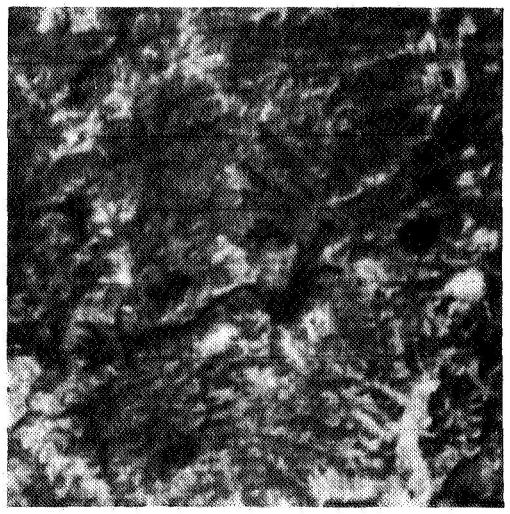
Figure 2 Aerial Photo

A.



Band 5 Bare Earth

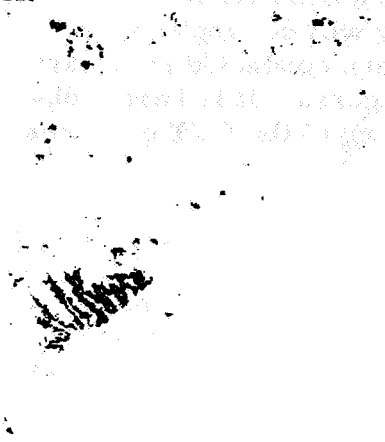
B.



Band 7 Water

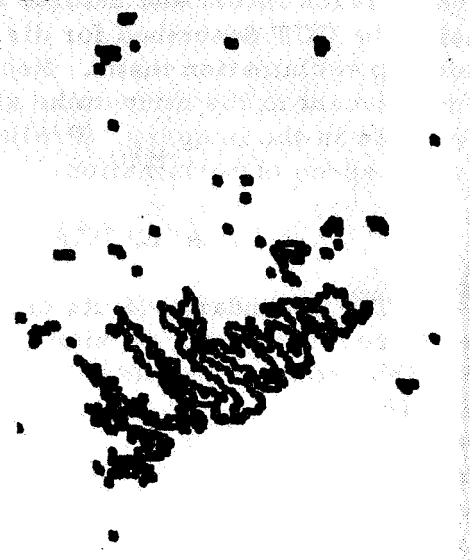
Figure 3 Scene 1084-15415

A.



Decision Imagery of Stripped Land - 4 Bands 1:500,000

B.



Cal Comp Outline of Stripped Land - 4 Bands 1:125,000

C.



Decision Imagery of Water - 4 Bands 1:500,000

D.



Cal Comp Outline of Water - 4 Bands 1:125,000

Figure 4 Decision Imagery and Cal Comp Plots of Stripped Land and Standing Water - Scene 1029-15361 August 21, 1972

trees, black locust and natural recovery). The statistical techniques using the CCT described for disruption mapping will be employed to develop reclamation maps. Reclamation has been conducted northeast and adjacent to the strip-mine shown in these figures. It is barely observable in the imagery. Preliminary processing of the CCT enhances the presence of reclamation.

7. ACID DRAINAGE & SEDIMENTATION

The secondary effects of acid mine drainage and stream sedimentation resulting from erosion is the most difficult task underway. A possible example for detailed study is the water system shown in Figures 3A, 4B and D. The apparent headwaters appear to be an area poorly vegetated and varying in extent of standing water (swamp). Ground observation and measurement and multispectral scanner data from an aircraft will be obtained and used to determine the feasibility of ERTS to detect and identify such secondary effects external to the disrupted area.

8. SIGNIFICANT RESULTS

The first significant result is that now disruption maps can be made automatically from the CCT on an operational basis at Bendix. Secondly reclamation maps will be produced in the same way in the near future. The accomplishment of these steps is a prerequisite to developing an ERTS strip mine monitoring operation.

In the course of this work it can be shown through ERTS data of the Coshocton East Mine that in the past year a dammed body of water of about 5 acres has appeared, apparently little or no stripping has occurred, and that no additional reclamation is apparent in the more recently stripped areas.

9. REFERENCES

(1) Biesecker, J. E. and J. R. George, 1966. "Stream Quality in Appalachia as related to Coal-Mine Drainage, 1965. USGS Circular 526, Washington, D. C.

(2) Chase, P. E., Conrod, A., and E. Imhoff, 1972. "Location of Sawdust in the Penobscot River by a Multispectral Scanner", Proceedings of 8th International Symposium on Remote Sensing, Ann Arbor, Michigan (To be published). Available as Bendix Report BSR 3457, Ann Arbor, Michigan.

Paper E 3

THE USE OF ERTS-1 MSS DATA FOR MAPPING STRIP MINES AND ACID MINE DRAINAGE IN PENNSYLVANIA

S. S. Alexander, J. Dein and D. P. Gold, *Office of Remote Sensing of Earth Resources, The Pennsylvania State University, University Park, Pennsylvania*

ABSTRACT

Digital processing of ERTS-I MSS data for areas around the west branch of the Susquehanna River permits identification of stripped areas including ones that are not discernible from visual analysis of ERTS imagery. Underflight data and ground-based observations are used for ground-truth and as a basis for designing more refined operators to make sub-classifications of stripped areas, particularly with regard to manifestations of acid mine drainage; because of associated diagnostic effects on vegetation, seasonal changes in classification criteria are being documented as repeated, cloud-free ERTS-I coverage of the same area becomes available. Preliminary results indicate that ERTS data can be used to moniter not only the total extent of stripping in given areas but also the effectiveness of reclamation and pollution abatement procedures.

1. INTRODUCTION

Deposits of coal in the Eastern United States represent an important natural resource for meeting immediate and future critical energy needs. While widespread strip mining has already been carried out over large areas in Western Pennsylvania and in other areas of Appalachia, there remain extensive reserves at relatively shallow depths that can be and are being extracted by strip mining. However, the actual cost involved in providing energy from these deposits significantly exceeds that of simply extracting the coal, because not only must the areas stripped be reclaimed for other productive uses, but also because severe water pollution resulting from acid mine drainage from these areas must be monitered and controlled. Even without further mining act-

ivity, solving existing environmental problems of this nature resulting from past mining activities is proving to be difficult and expensive.

Therefore, it is important to have an effective capability for monitering the areal extent of stripping, detecting the areas adversely affected by acid mine drainage, and assessing the effectiveness of reclamation and pollution abatement procedures. Because of its repeated, complete areal coverage ERTS data provides a potential means of routinely monitering and evaluating the impact of strip mining on the environment in any region of interest.

The objective of the present study is to determine the usefulness of ERTS-I data (particularly the MSS data) for this application.

2. OBSERVATIONAL RESULTS

An area along the west branch of the Susquehanna River was chosen for the initial tests of the present study because it contains old stripped areas, new stripped areas, and numerous examples of acid mine drainage and related effects associated with the mining of bituminous coal in Pennsylvania. In addition detailed ground-based geological and geophysical observations are available for one particular part of the area near Kylertown. Aircraft underflight data from U-2 and C-130 flights are available for portions of the test area as well. These additional data provide very important ground truth for evaluating the results obtained from digital processing ERTS-I MSS tapes.

The MSS digital data tape (CCT 1045-15240) for the September 6, 1972 pass over Pennsylvania was used for the computer analysis. Even though only three of the MSS channels (4,5, 7) could be used on the tape for that particular day, remarkably good results were obtained by using these three good channels simultaneously to identify the characteristic features of strip-mined areas and acid mine drainage.

The data processing consisted first of subsetting the original data tape to obtain a working digital tape covering a test area approximately 20x20 miles square in size located on the west branch of the Susquehanna River in Clearfield County and extending south from Karthus to Philipsburg. Using a series of computer programs developed by Borden and others of the Office of Remote Sensing at the Pennsylvania State University (References 1-8) the test area tape was analyzed. First we located areas of both uniformity and high spatial contrast. These data alone defined the general boundaries of some stripped areas and showed distinctive features such as the river and Interstate 80 so that unambiguous correlations with conventional map features could be made. However, we found that applying the cluster analysis programs developed by Turner (Reference 8) provided the best definition of stripped areas as well as other features in the test area. Basically these programs group the data points into clusters each of which has a characteristic spectral response. No prior knowledge about the spectral response is required in this mode of operation, although we can use training areas as another program option. Not only was it possible to identify stripped areas unambiguously, but also sub-classifications of them were found that represent real differences in conditions, such as trenched areas, recent workings, and partly vegetated peripheral zones.

Several portions of the Susquehanna River itself were classified in the same category as strip mines; while surprising at first, this finding is now believed to represent refuse from nearby stripping that was dumped along the banks in which case the classification was proper. Other areas along the river were placed in the same category as areas of dying or dead vegetation caused by acid mine drainage elsewhere in the test area. The inference that the Susquehanna in this area is highly polluted by acid mine drainage is correct as is documented in Reference 9.

Especially detailed analysis was carried out for a small area around Kylertown. Sub-divisions of the stripped areas that were distinctly classified in this test area were: trenched areas, backfills, and new stripping or areas cleared for future stripping operations. Areas of dying or dead vegetation caused by acid mine drainage from these strip mines were distinctly classified by the cluster analysis and were correctly located, including a very small one that has been studied extensively with ground-based methods.

TABLE I

Spectral Response from Cluster Analysis of the Kylertown Area

Categories	Symbol		Channels 4	5	7	Percent Area
Forests	1	-	23.43	14.29	24.42	68
Open fields	2	X	27.20	21.37	21.27	17
Trenches (strip mine)	3	+	30.50	25.72	11.00	4
Backfills (strip mine)	4	*	32.89	30.67	14.56	5
Acid mine drainage	5	0	24.67	15.67	14.33	4
New stripping	6	=	38.00	41.00	19.00	1
New or future stripping	7	Z	46.00	52.33	23.67	1

TABLE II

Distances of Separation for Categories

		1 -	2 X	3 +	4 *	5 0	6 =	7 Z
1	-	0.0	8.62	19.00	21.33	10.25	30.91	44.24
2	X	8.62	0.0	11.63	12.80	9.33	22.52	36.30
3	+	19.00	11.63	0.0	6.54	12.09	18.81	33.30
4	*	21.33	12.80	6.54	0.0	17.11	12.36	26.91
5	0	10.25	9.33	12.09	17.11	0.0	29.01	43.44
6	=	30.91	22.52	18.81	12.36	29.01	0.0	14.64
7	Z	44.24	36.30	33.30	26.91	43.44	14.64	0.0

Table I summarizes the cluster analysis results for the Kylertown test area. From examining the array of ground-based data mentioned earlier we were able to identify the categories of features found by the cluster analysis. These are listed in the first column of Table I. The degree to which these categories are separated is indicated in Table II where the distances of separation among the clusters are given. The smaller the distance between two categories the more similar they are. For example the sub-classifications 3 and 4 that differentiate trenched portions of stripped areas from backfills have a relatively small distance separation and are generally similar in spectral response as can be seen from Table I values.

The digital processing used has the further advantage that not only are features correctly classified but the total area affected by stripping can be routinely calculated from the estimates of the total area represented by each category output by the cluster analysis program. For example, we found that strip mines cover approximately 20 per cent of the test area around the Susquehanna and about 11 per cent of the area around Kylertown. The last column of Table I gives the percentage area represented by each category for Kylertown.

The spectral response was found to be quite similar for stripped areas at different locations within the test area suggesting that these characteristic signatures can be used to obtain an accurate map of existing strip mines for larger areas or perhaps the entire state or region. Also repeated application of this type of analysis will provide up to date estimates of the location and extent of new strip mining and provide current information on reclamation and acid mine drainage.

While visual examination of the ERTS-I imagery reveals the location of the larger strip mines it is not possible to distinguish the sub-classifications and details found by the digital analysis described above. The areas affected by acid mine drainage cannot be discerned and identified by visual analysis of the ERTS imagery. Therefore, digital processing is required to extract adequate information on the details of strip mining and acid mine drainage.

3. SUMMARY AND CONCLUSIONS

1. ERTS-I MSS data can be used in appropriate digital processing programs to map the extent and type of stripping that exists at the present time, including sub-classifications of each stripped area.

2. Based on the preliminary findings of this report it appears feasible to use ERTS data to moniter periodically the extent and location of current strip mining activity for large regions and to evaluate the effectiveness of reclamation and pollution abatement procedures.

3. Surface areas affected by acid mine drainage from strip mines can be located and mapped effectively through careful digital processing of the ERTS-I MSS data. They cannot be located from visual analysis of ERTS imagery.

4. Temporal coverage of stripped areas spanning different seasons supplied by repeated ERTS passes promises to provide even more powerful classification criteria because of the profound effects that strip mines and acid mine drainage have on vegetation.

4. REFERENCES

1. Borden, F. Y., 1971a; Digital Aircraft Multispectral Scanner Data Tape Format. Tech. Rept. 1-71, Office for Remote Sensing of Earth Resources, The Pennsylvania State Univ., University Park, Pa.

2. Borden, F. Y., 1971b; NMAP Program Description. Tech. Rept. 2-71, Office for Remote Sensing of Earth Resources, The Pennsylvania State Univ., University Park, Pa.

3. Borden, F. Y., 1971c; UMAP Program Description. Tech. Rept. 4-71, Office for Remote Sensing of Earth Resources, The Pennsylvania State Univ., University Park, Pa.

4. Borden, F. Y., 1972a; A digital processing and analysis system for multispectral sensor and similar data. Remote Sensing of Earth Resources, Vol. 1. Edited by F. Sharokhi. University of Tennessee Space Institute, Tulahoma, Tenn. pp. 481-507.

5. Borden, F. Y., 1972b; LMAP Program Description. Tech. Rept. 2-72, Office for Remote Sensing of Earth Resources, The Pennsylvania State Univ., University Park, Pa.

6. Borden, F. Y., and H. M. Lachowski, 1971; SUBSET Program Description. Tech. Rept. 3-71, Office for Remote Sensing of Earth Resources, The Pennsylvania State Univ., University Park, Pa.

7. Lachowski, H. M. and F. Y. Borden, 1971; STATS Program Description. Tech. Rept. 6-71, Office for Remote Sensing of Earth Resources, the Pennsylvania State Univ., University Park, Pa.

8. Turner, B. J., 1972; Cluster analysis of multispectral remote sensor data. Remote Sensing of Earth Resources, Vol. 1. Edited by F. Sharokhi. University of Tennessee Space Institute, Tulahoma, Tenn. pp. 538-549.

9. Appalachian Regional Commission, 1969; Acid Mine Drainage in Appalachia; Appalachian Regional Commission, 1666 Connecticut Avenue, Washington, D. C. 20235.

10. Deasey, G. F. and P. D.Griess, 1959; Atlas of Pennsylvania Coal and Coal Mining, Part I Bituminous Coal; Bull. of the Mineral Industries Experiment Station, No. 73, The Pennsylvania State University, University Park, Pa.

Paper E 4

MONITORING VEGETATION COVER ON MINE DUMPS WITH ERTS-1 IMAGERY: SOME INITIAL RESULTS

Brian Gilbertson, *Spectral Africa (Pty) Limited, P. O. Box 2, Randfontein, Republic of South Africa*

ABSTRACT

ERTS-1 imagery is being used in an attempt to differentiate between mine dumps having varying degrees of vegetative cover. At this stage it is clear that the various mine dumps can be located and identified. Differences in vegetative cover can be seen and measured. Patterns of vegetative growth, some characteristic to particular dumps, can also be seen. It is therefore tentatively concluded that mine dumps can be differentiated with respect to their vegetative cover on the imagery received to date. Subsequent imagery showing seasonal variations should facilitate this program.

1. INTRODUCTION

For many years the economy of South Africa was heavily dependant upon mining activities. One of the aftermaths of such activities has been the development and growth of mine tailings dumps. These dumps can be divided into two broad categories, namely sands dumps and slimes dams.

Sands dumps are mounds of crushed rock material. In time the minerals are leached out, leaving no binding properties. The resultant substance becomes similar to river sand, with no nutrient value and is left as an inert and inhospitable medium for plant growth. "Slime" residues consist of a very finely ground silicious rock. From a botanical point of view, cyanided slimes are initially noxious, but with weathering, noxious properties disappear from the dams. The ores from which these tailings are derived contain pyrite, which with weathering continuously tend to maintain acid conditions on the dump.

In recent times, attention has been directed towards mine dumps as being detrimental to the environment. For example, the Witwatersrand derives its water from one major river, the Vaal. Pollution of streams in the Witwatersrand system from mine dumps effects the Vaal because the mines are largely situated in its catchment area.

The growing concern over the problem of pollution is expressed in the Atmospheric Pollution Prevention Act (Act No. 45 of 1965). Section 32 of the act applies specifically to the mining industry. The air and

water pollution from the dumps may be largely prevented by ensuring that a vegetative growth covers the entire mine dump. In the years following the promulgation of the act, the annual expenses incurred by the Chamber of Mines of South Africa in promoting the growth of vegetation on mine dumps have grown steadily and totalled $1M for the year 1969. This amount does not include expenditures by mines which are not members of the Chamber.

The growth or decline of vegetative cover on mine dumps has to date been monitored by both aerial photography and site visits. The latter is usually preferred because of the expense of the former and the greater accuracy of the latter. On the other hand, because of the geographic separation of the mine dumps (see figure 1) site visits are inconvenient and difficult to co-ordinate.

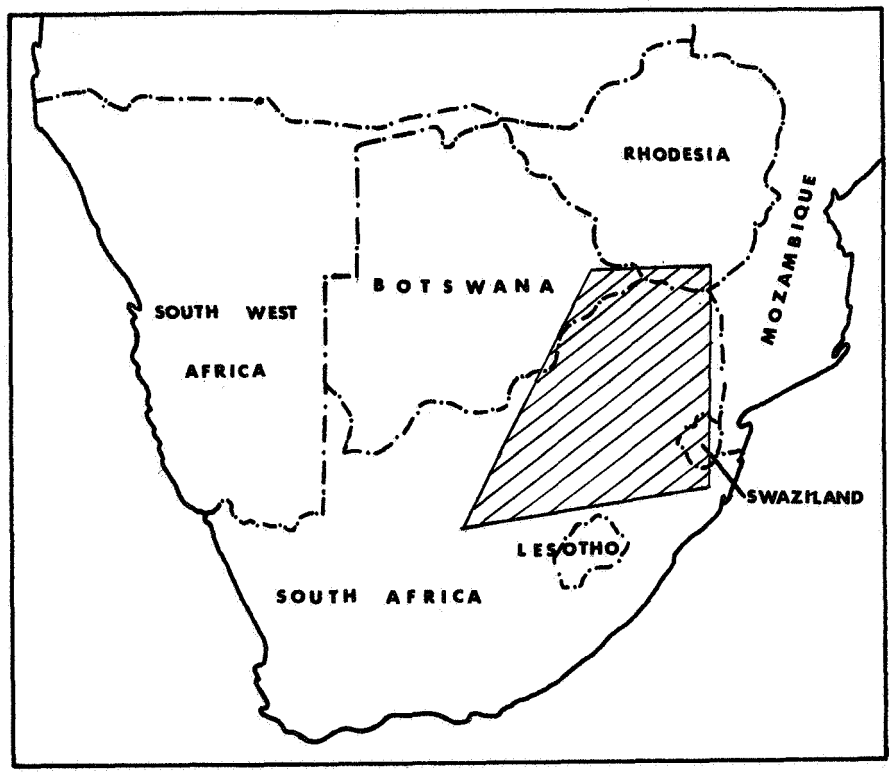


FIGURE 1

Geographical distribution of majority of mine dumps in South Africa

ERTS-1 imagery is being used in an attempt firstly to differentiate between mine dumps having varying degrees of vegetative cover, and secondly to monitor the growth or decline of this cover on any selected dump. Two ERTS-1 images (1049-07301 and 1050-07355) that include part of the main mine dump area have been received to date, and have been analysed both qualitatively and quantitatively. The results are described below.

2. CLASSIFICATION OF VEGETATIVE COVER ON MINE DUMPS

Six mine dumps were selected for intensive study. This selection was done by preparing a mosaic of the Witwatersrand Mine Dump Complex from black and white Trigonometrical Survey photography and rephotographing at a scale of 1:250 000. Part of this mosaic is shown in figure 2. A short list of dumps expected to be well resolved on the ERTS-1 imagery was compiled from this reduced mosaic. Ground observation of a selection of these dumps was then undertaken and the vegetation cover investigated.

A vegetation scale was compiled in order to classify the mine dumps into categories. This classification is shown in table 1. One "calibration" dump of each category was selected for detailed analysis on the basis of size (large as possible), homogeneity (uniformity of vegetation distribution over the top surface), and contrast (with respect to the adjacent environment). The dumps selected are listed in the last column of table 1, and are identified using the numbering system developed by the Chamber of Mines.

3. QUALITATIVE ANALYSIS

Qualitative interpretation was performed using a colour composite print prepared of image 1049-07301 with MSS bands 4,5 and 7 shown in blue, green and red respectively. A black and white positive image prepared from this colour composite is shown in figure 3. Although much detail of the colour presentation has been lost it can be seen that essentially all of the larger mine dumps present in the aerial photography mosaic of figure 2 can be detected and identified on the ERTS-1 image. This achieves the first aim of ERTS-1 proposal SR-0577.

Furthermore, there is a good qualitative relationship between the categories of table 1 and the mine dumps imaged in figure 2, with the more densely vegetated dumps (i.e. those falling in categories 4 and 5) appearing darker than the unvegetated dumps (those falling in categories 0 and 1). In addition, vegetation patterns are visible on the ERTS-1 imagery which are in good agreement with ground truth, i.e. with patterns observed on aircraft overflight photography. This can be seen by comparing figures 3 and 4.

This agreement between ERTS-1 imagery and ground truth is encouraging, particularly since ERTS-1 image 1049-07301, was gathered in

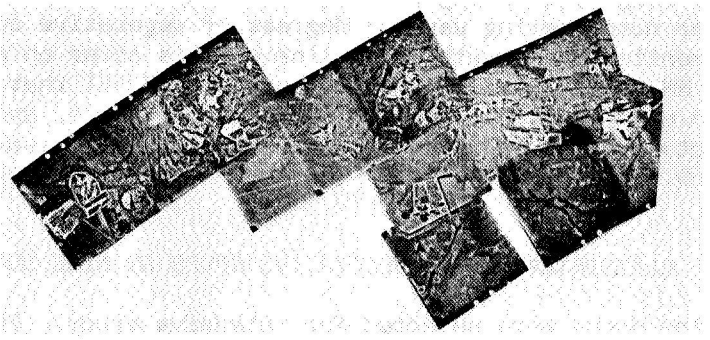


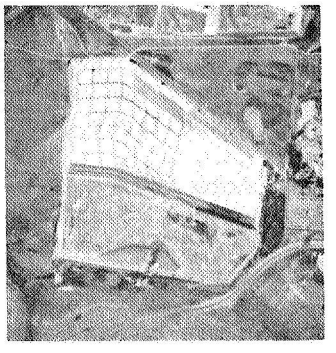
FIG. 2 : Aerial photography mosaic of West Witwatersrand area



FIG. 3 : Part of ERTS-1 image No. 1049-07301



Mine dump 1/L/38,39



Mine dump 3/L/5,6

FIGURE 4

TABLE 1

Vegetation Category	Description of Degree of Vegetative Cover	Example of dump in this Category
0	No vegetation cover	5/L/29 3/L/5 (East Side)
1	A very small plant community, usually constantly "farmed" by fertilizing, water spraying and "ploughing".	3/L/5 (West Side)
2	A poor cover of plants requiring continuous attention. Extensive "soil" exposure.	6/L/20
3	A reasonable cover of vegetation requiring occasional attention and fertilizing with a number of "soil" exposures on small areas of high acidity.	7/L/1
4	A good cover of vegetation, probably self-sustaining, with only a few "soil" exposures on small areas of locally high acidity.	1/L/40, 1/L/41
5	A probably self-sustaining plant and tree community over 100% of the dump surface.	1/A/20

September when the mine dump vegetation is, generally speaking, in poor condition. Even better agreement is anticipated for imagery gathered during the spring and summer months.

4. QUANTITATIVE ANALYSIS

Densitometric measurements were made on black and white negatives enlarged to 1:160 000 scale of various mine dumps on the ERTS-1 image. The density readings are recorded in table 2. The 95% confidence limits on the mean density readings indicate the precision of the analysis.

TABLE 2

Density readings on mine dumps imaged on 1:160 000 scale negatives

(The mean values for Band 4 show 95% confidence limits based on nine independent enlargements of a single 70 mm positive)

Vegetation Category	Mine Dump	Image Density			
		Band 4	Band 5	Band 6	Band 7
0	5/L/29	1,13 ± 0,02	1,25	1,27	1,03
	3/L/5 (East)	1,39 ± 0,05	1,51	1,61	1,28
1	3/L/5 (West)	1,30 ± 0,02	1,38	1,50	1,33
2	6/L/20	0,97 ± 0,01	0,82	1,10	0,97
3	7/L/1	0,78 ± 0,02	0,68	1,01	0,91
4	1/L/40, 41	0,84 ± 0,02	0,84	0,89	0,90
5	1/A/20	0,67 ± 0,02	0,69	0,74	0,69

Plots of image density versus wavelength (ERTS-1 band number) were prepared using the vegetation categories of table 1 and the densitometry of table 2. These plots are shown in figures 5 and 6.

Figure 5 shows a good separation between the density readings for vegetation categories 0, 1, 4 and 5. Consequently it is anticipated that mine dumps falling into these categories should be identifiable. However, a number of anomalies require further study. For example, the density readings for dump 5/L/29 (see table 2) are low compared to those for dump 3/L/5 which falls in the same vegetation category. Although this anomaly is being investigated no satisfactory explanation has yet been found.

The density readings obtained for vegetation categories 2 and 3 were at first thought to be anomalous, since their plots, which are shown in figure 6, differ considerably in shape from those of figure 5. However, investigation into the records of the Chamber of Mines Vegetation Program revealed that irrigation had been carried out on these

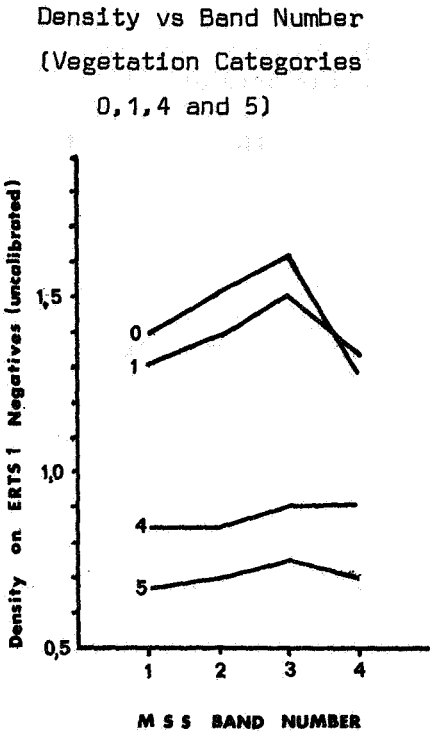


Fig. 5

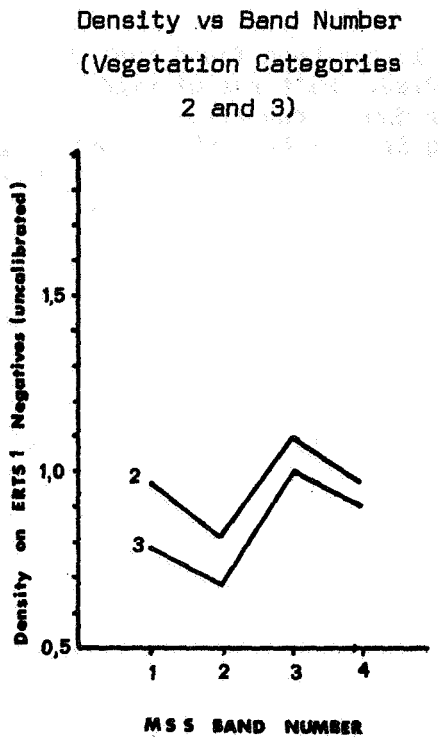


Fig. 6

dumps prior to the date on which the ERTS-1 imagery was gathered. The reflectance properties of these dumps were consequently changed quite markedly by the resulting vigorous growth of vegetation. Clearly cognisance will have to be taken of such husbandry practices during image interpretation.

A further aspect which requires investigation is the change in spectral properties of any selected mine dump with season and time. As more ERTS-1 images gathered at different times of the year become available, it may be possible to establish "signatures" which will allow the monitoring of growth or decline of vegetation on a given mine dump.

5. CONCLUSIONS

It has been found that various mine dumps can be located and identified. Patterns of vegetative growth, some characteristic of particular dumps, can also be seen. Although a number of anomalous features require further investigation, good correlation between the vegetative status of certain target mine dumps and the corresponding ERTS-1 MSS imagery has been observed.

It is therefore tentatively concluded that mine dumps can be differentiated with respect to their vegetative cover on these initial images. It is hoped that further ERTS imagery will confirm the above observations and that it will be possible to accord to all but the smallest of the mine dumps in the Witwatersrand Complex a vegetative cover category as defined in table 1. Subsequent imagery showing seasonal variations should facilitate the program.

7. ACKNOWLEDGEMENTS

The author wishes to acknowledge the contribution of co-investigators T.G. Longshaw and M.H. Kreitzer, and to express his gratitude to Messrs. W.H. Cook and J.E. Groves of the Chamber of Mines for a critical reading of this paper.

Paper E 5

REMOTE DETECTION OF AEROSOL POLLUTION BY ERTS

G. E. Copeland, A. R. Bandy, E. C. Kindle, R. N. Blais and G. M. Hilton,
Department of Geophysical Sciences, Old Dominion University, Norfolk, Virginia 23508

ABSTRACT

Photogrammetric and densitometric examination of ERTS-1 MSS imagery of Eastern Virginia coupled with extensive ground truth air quality and meteorological data has shown that the identification and surveying of fixed particulate emitters (smoke plumes) is feasible. A description of the ground truth network is included. The quantitative monitoring of smoke stacks from orbital altitudes over state size regions appears possible when tied to realistic plume models and minimal ground truth. Contrast reductions over urban areas can possibly be utilized to produce isopleths of particulates when supplemented by local measurements.

I. INTRODUCTION

Reasonably cloud free ERTS-1 MSS imagery has been obtained of Eastern Virginia since launch. To date imagery has been examined both for detailed atmospheric phenomena including contrails, urban fires and smoke plumes of fixed emission sources, and for area-wide aerosol loading manifest by image contrast reduction. The development of the method by which ERTS imagery can be applied to assessment of particulate concentrations is progressing rapidly.

II. DATA SOURCES

Data sources can be subdivided for discussion purposes into those for which data is directly available to the investigators and those for which data must be generated by the investigators.

Data sources from which information is directly available include the emission inventory and ambient air quality monitoring program of the Virginia State Air Pollution Control Board (VSAPCB), local meteorological stations, urban fire departments and the FAA Air Traffic Control Office

at local airports. VSAPCB emission inventory (partial listing in Figure 1) has been kindly made available to us so that we have a complete listing of all major industrial and governmental aerosol fixed emission sources in the area, together with an estimate of the quantity and quality of the effluent. The regular air quality monitoring of the VSAPCB also yields periodic information on concentrations of particulates and SO_2 at numerous sites (cf. Figure 2) in the test region, as well as continuous NO, NO_x, O_3, CO, and coefficient of haze (COH) and meteorological information at certain selected sites. Further meteorological information is received from the numerous weather stations (cf. Figure 3) that abound in the area because of the large number of naval installations. Aerosol plumes that are not predictable in location or character include those of urban and rural fires, and thus, fires in progress at the time of the satellite pass are reported to us by local fire departments. In addition, the pattern of contrails over the area at the time of each pass has to be verified by finding the location, direction, and altitude of all airplanes in the area capable of producing one.

Information generated by the investigators as ground truth correlation to the ERTS imagery includes much oblique and some aerial photography of selected smoke plumes, plus the data gathered and analyzed by three well-equipped laboratory facilities at Old Dominion University: an air pollution monitoring laboratory, a mobile air pollution and meteorological monitoring van, and an air pollution standards laboratory for the calibration of instruments and analysis of samples from the other two laboratories.

Photographic studies of particular smoke plumes are an essential portion of a ground truth program because they yield high resolution information, are subject to a large variety of photometric analysis techniques, and are relatively inexpensive. Typical photographs used by us in the past include NASA U-2 photos of the area, aerial photos from a local radio station weather helicopter, and photos taken by us from tall buildings during satellite passes. The U-2 high altitude photos show in higher resolution than ERTS imagery the spectral signature and dispersal of specific plumes under varying meteorological, seasonal and background conditions. Lower altitude aerial photos have been made by the helicopter of local radio station WTAR-AM during its twice daily traffic report flights. Finally, we have made horizon photos from the roofs of tall buildings using both regular and telephoto lenses, and on occasion using filters that match the band passes of ERTS MSS bands 4, 5, and 6.

The first of our three facilities at Old Dominion University devoted exclusively to air pollution studies is an air monitoring laboratory that is designated an official monitoring station of the VSAPCB, but that goes well beyond the instrumentation required for that task. The following instruments are currently in use for measuring air quality:

a continuous chemilumenescent ozone (O_3) and nitrogen oxide (NO, NO_2, NO_x) monitor; a continuous flame photometric sulfur compound (H_2S, SO_2) analyzer; a continuous flame ionization methane and total non-methane hydrocarbon analyzer; a twenty-four hour integration time SO_2 bubbler train; four high volume air samplers; and a two hour integration time coefficient of haze tape sampler. These instruments, sampling off a forty foot glass intake manifold provide information that is correlated to local meteorological variations. Such variations are monitored on the site by weather instruments mounted on a seventy foot tower giving continuous readings on analog recording devices of wind speed and direction, temperature, insolation, relative humidity, and air pressure.

The Mobile Air Pollution Laboratory is similarly equipped to monitor air quality and meteorological data at specific test sites, such as Wallops Island and Great Dismal Swamp, where month-long studies are scheduled for summer, 1973. This 8' x 18' trailer on tandem wheels can collect data with the following facilities: continuous monitors for ambient levels of O_3, NO, NO_2, NH_3, SO_2, H_2S, methane and total hydrocarbon; continuous temperature, wind speed and direction monitors at four altitudes to forty meters; ground level monitors of humidity, barometric pressure and insolation; suspended particulate monitors including millipore filters, high volume air samplers, and a single band nepthelometer; and PDP/8 Digital Acquisition System with teletype and magnetic tape units for instrumental control of the entire monitoring operation, and data manipulation and storage.

Both the mobile and fixed laboratory are supported by the Air Quality Standards Laboratory, which calibrates all instruments. Facilities include an isothermal gaseous permeation tube for providing metered flows of pollutants at known concentration levels for calibration of instruments, and devices for generating pure samples of each pollutant; milligram pan balances, microscopes, dessicators and ovens. Finally, elemental analysis of air filter samples can be done locally by x-ray fluorescence and x-ray diffraction, and additionally neutron activation analysis can be done using facilities at Virginia Polytechnic Institute.

III. CONCLUSIONS

Large amplitude high frequency variability of aerosols presents a serious problem which is beyond conventional economic resources for information sensing and processing. It has been concluded that the only hope for an adequate definition of pollution concentration would be through a judicious integration of the following four measurement, analysis and diagnostic approaches.

a. Conventional direct sensing systems, which would provide a quantitative input. (Air quality and meteorological data)
b. Remote imaging capabilities from aircraft and ERTS type satellites to provide the character of spatial resolution of the aerosols.

c. Numerical models, which combine the above and provide high temporal resolution.
d. Improved understanding of the constituents, their sources and interaction processes, which provide the basis for improved application of all the above.

In pursuit of approaches a, b, and c above the ground truth system has been developed, ERTS imagery has been analyzed and starts made on adopting numerical models for plume behavior so that the ERTS imagery may be quantified and the human intake level of aerosols determined. Smoke plumes generated by fossil fuel electrical plants are regularly detected. Numerous smaller industrial emission sources have been discovered and reported to VSAPCB. Contrails and urban fires have been detected. Detailed analysis of the characteristic plume geometries is being accomplished from ERTS imagery.

Computation of atmospheric diffusion coefficients from photometric analysis of ERTS imagery appears quite possible. This can be incorporated into numerical models to assess surface concentrations which will be verified by the mobile laboratory. This program can be solved backwards to provide estimates of stack emission rates and thus provide a great cost reduction in stack monitoring.

Figure 4 shows a drawing of a series of three plumes as observed on 23 September, 1973. Each is over 10 kilometers long. A densitometric scan perpendicular to the plumes symmetry axis is shown in Figure 5 . Although final analysis of imagery and ground truth is not yet accomplished, this plume (C) appears to closely follow standard Gaussian diffusion models. It is recognized that image spread may produce problems but this can be solved by examination of high contrast subjects and/or by incorporation of spread effects in plume models.

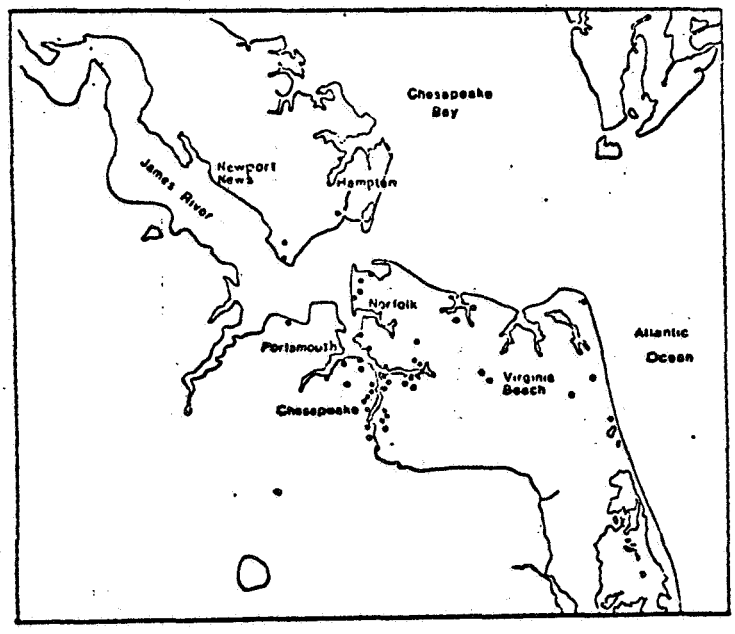


Figure 1: Locations of Major Fixed Sources of Particulate Polluters in Hampton Roads Region.

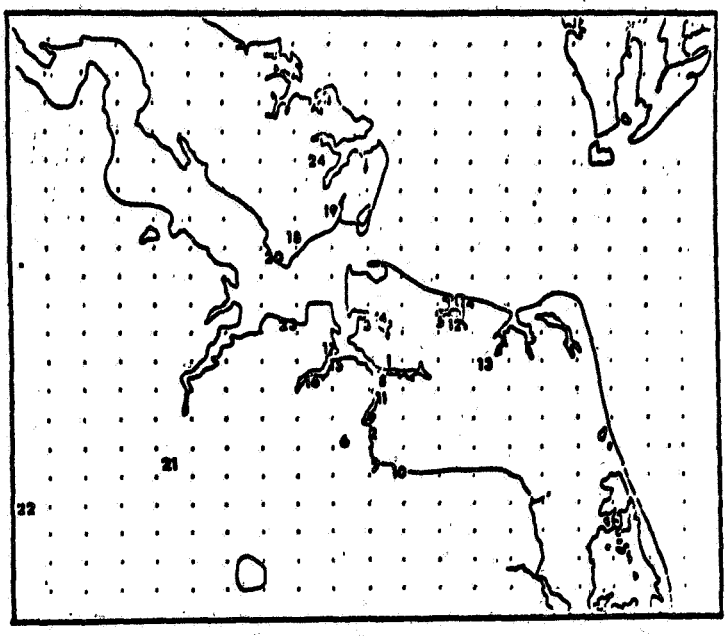


Figure 2. Locations of Major Air Quality Monitoring Sites in Hampton Roads Region (VSAPCB and ODU).

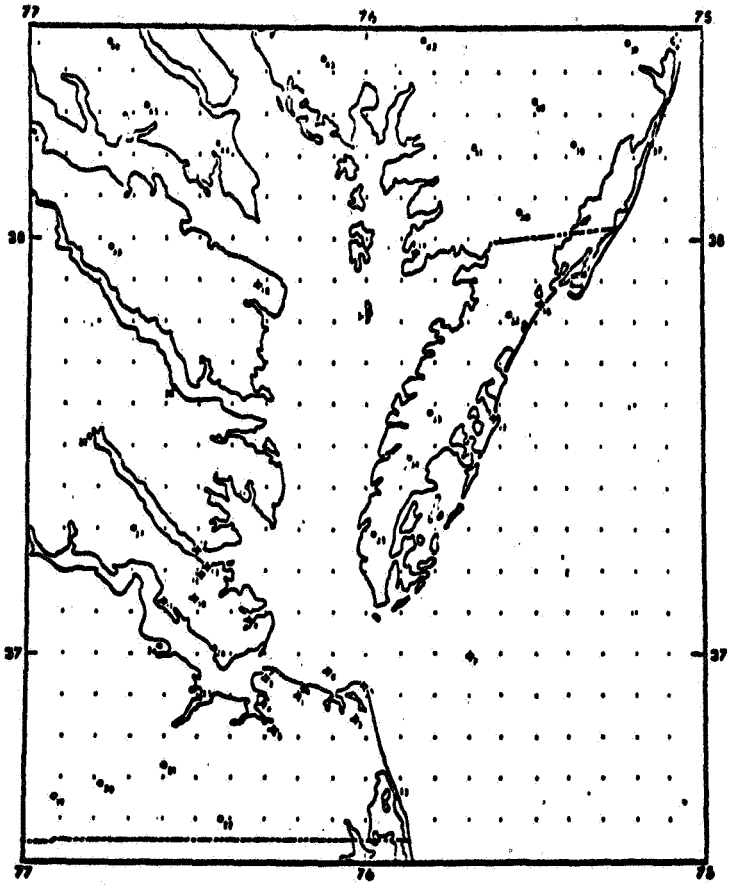


Figure 3 Locations of Meteorological Stations in the Target Area.

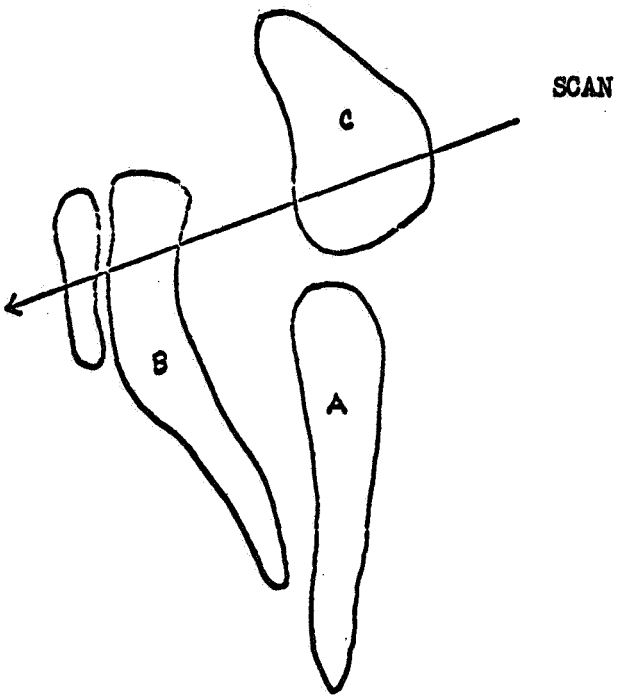


Figure 4: MSS 5 23 Sept 1972 Image I.D. 1062 15193 5
Several smoke plumes near Chester, Virginia

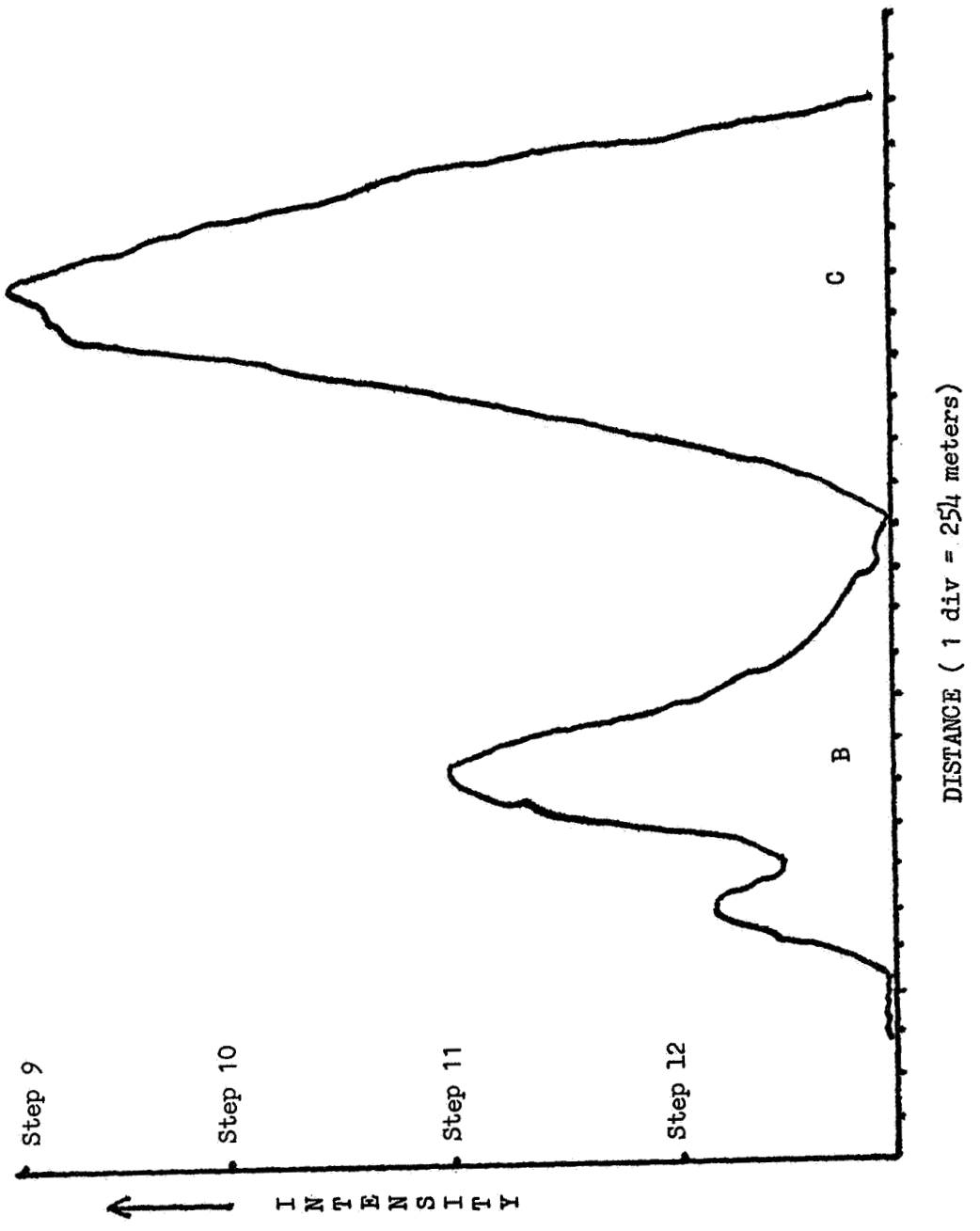


Figure 5: Densitometer Scan Perpendicular to Symmetry Axis.

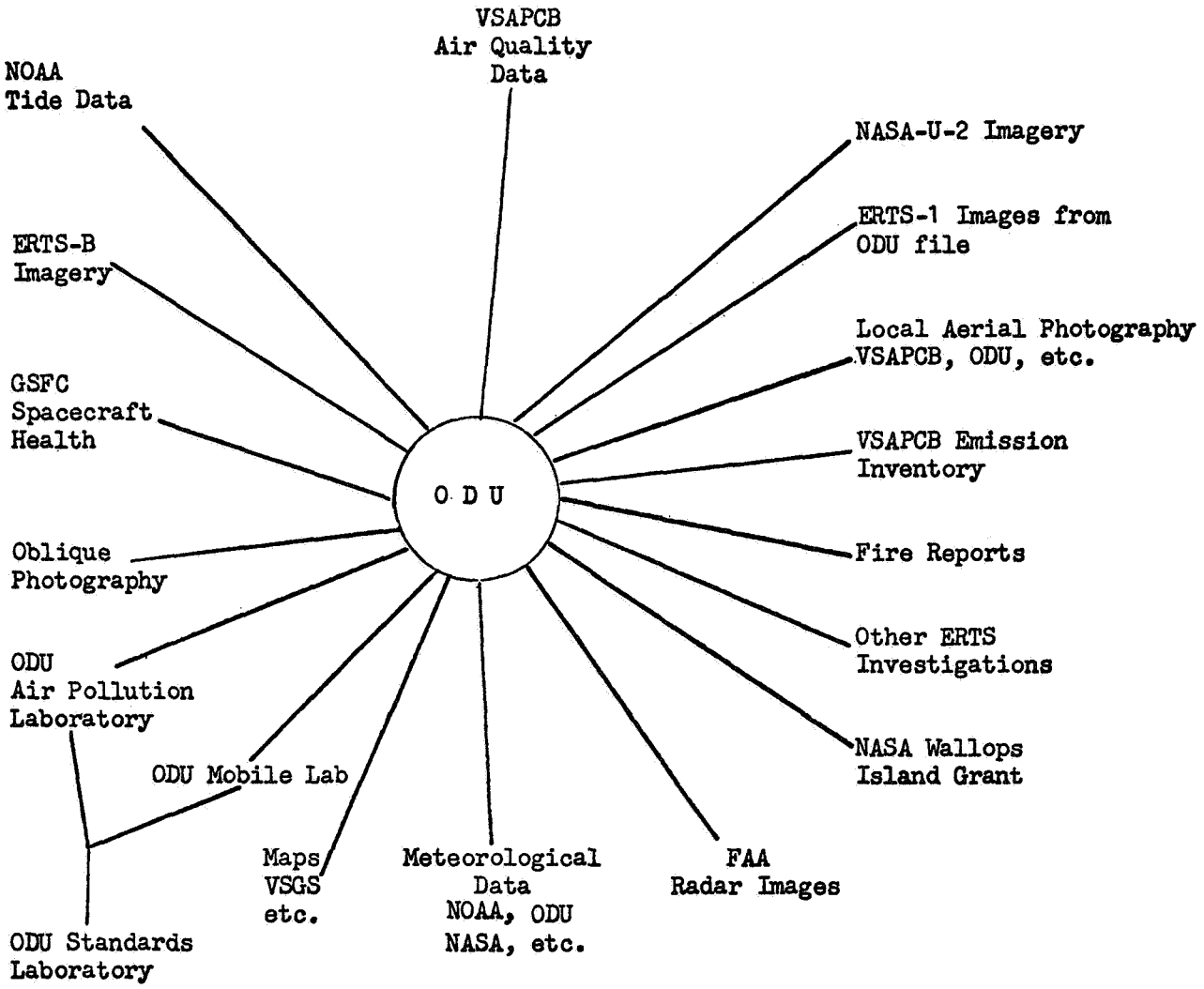


Figure 6: Data Input Sources to Earth Resources Analysis Laboratory (ODU).

Paper E 6

DETECTION, MAPPING AND ESTIMATION OF RATE OF SPREAD OF GRASS FIRES FROM SOUTHERN AFRICAN ERTS-1 IMAGERY

J. M. Wightman, *Research Officer, Forest Management Institute, Canadian Forestry Service, Ottawa, Ontario, K1A OW2*

Abstract:

Sequential band-6 imagery of the Zambesi Basin of southern Africa recorded substantial changes in burn patterns resulting from late dry season grass fires. One example from northern Botswana, indicates that a fire consumed approximately 70 square miles of grassland over a 24-hour period. Another example from western Zambia indicates increased fire activity over a 19-day period. Other examples clearly define the area of widespread grass fires in Angola, Botswana, Rhodesia and Zambia.

From the fire patterns visible on the sequential portions of the imagery, and the time intervals involved, the rates of spread of the fires are estimated and compared with estimates derived from experimental burning plots in Zambia and Canada. It is concluded that sequential ERTS-1 imagery, of the quality studied, clearly provides the information needed to detect and map grass fires and to monitor their rates of spread in this region during the late dry season.

INTRODUCTION

In the dry tropical regions of eastern and southern Africa, the traditional practice of grass burning during the winter dry season causes widespread destruction of vegetation and alteration of wildlife habitats. The burning of grass is an integral component of shifting cultivation and is therefore likely to persist. In these regions man makes use of fire for the removal of primary or secondary vegetation to initiate or continue the cultivation of subsistence crops. In more localized situations, grass is often burned off either to provide early green grazing or to drive wild animals during the hunt.

All these instances of burning are normally aimed at the removal of grass or other vegetation over very limited areas for individual requirements. However, due primarily to the optimum burning conditions which prevail (strong winds, high temperatures, and low humidity) particularly during the end of the dry season in September and October, these fires inevitably spread over vast areas.

The object of this paper is to demonstrate that ERTS-1, band-6 imagery obtained near the end of the dry season over these regions is capable of detecting and mapping this widespread and ecologically-important phenomenon. Moreover, it also demonstrates that this type of sequential imagery can be used to monitor the increase in area of fires and to estimate their rates of spread.

THE STUDY AREA

The 250,000-square-mile study area encompasses the watershed of the upper and middle portions of the Zambezi River and includes parts of the territories of Angola, Botswana, Rhodesia, South West Africa and Zambia in southern Africa (Fig. 1) The vegetation is comprised of tropical, dry, deciduous, partly-sclerophyll forest, xerophilic open woodland, spiny shrub and grassland. It is an area of low annual rainfall, ranging from 10 inches (northern Botswana) to 30 inches (central Zambia), which falls during a period rarely exceeding 5 months. The 7-month dry season normally extends from April to October during which no rain falls. Temperatures range from extremes in excess of 100°F during October just prior to the onset of the rains, to early morning frosts in the middle of the winter dry season, normally in June. During September and October, winds tend to increase and relative humidity drops to about 15 per cent.

MATERIALS AND METHODS

Normal, undodged, positive transparencies of ERTS-1, band-6 imagery (enlarged to 1:1,000,000), obtained from the EROS Data Centre, provided coverage (Fig. 2 and table 1) of the study area.

From the positive transparencies, contact internegatives were produced, from which paper prints were prepared.

During December 1972, soon after acquisition of the imagery at the end of November 1972, the author was able to visit areas on the ground covered by some of the imagery and to verify some of the interpreted phenomena.

All interpretation of the imagery was undertaken on the positive transparencies using a zoom stereoscope having a 7- to 30-times magnification capability. Stereo-viewing was possible on images from adjacent ERTS-1 swaths (Fig. 2 and Table 1) which provided about 17% image side-lap between the latitudes covered (approximately 13°00' S to 20°00'S). From the fire patterns apparent on some of the sequential portions of the imagery, and

Table 1 ERTS-1, band-6 coverage of study area.

Image Reference No.	General locality	Image centre point Lat.	Long.	Date 1972	Approximate local time of image acquisition (hours)
1	Gago Coutinho, Angola	14°31'S	21°28'E	17 Sept.	1007
2	Senanga, Zambia	15°59'S	22°32'E	16 Sept.	1001
3	Mucussu, Angola (including part of the Caprivi Strip of South West Africa)	17°24'S	22°11'E	16 Sept.	1002
4	Okavango, Swamps, Botswana	18°51'S	23°15'E	15 Sept.	0956
5	Chobe Game Park, Botswana	18°49'S	24°42'E	14 Sept.	0951
6	Wankie Game Park, Rhodesia	18°45'S	26°08'E	13 Sept.	0945
7	Lake Kariba, Zambia/Rhodesia	17°15'S	27°58'E	30 Sept.	0939
8	Kafue River, Zambia	14°30'S	25°46'E	14 Sept.	0949
9	Kabompo/Kaoma, Zambia	14°14'S	24°23'E	3 Oct.	0955

the time intervals involved, the rates of spread of the fires were estimated. These estimates were compared with rates of spread of experimental grass fires derived from burning plots in Zambia and Canada.

Some of the imagery was subsequently enhanced electronically in an attempt to accentuate the more subtle aspects of the burning patterns.

RESULTS

In general, the quality of all the imagery was excellent, and in fact all frames were ranked 8 by NASA on a 9-point scale of increasing image quality. No clouds were evident on eight of the nine images; only the Lake Kariba image (No. 7) had 10% cloud cover, and this was entirely confined to the south-west corner of the image. Some localized smoke haze resulting from active fires was evident on the Chobe Game Park image (No. 5) and the Kabompo/Kaoma image (No. 9). Portions of the area covered by image No. 9 were seen by the author from the air on 5 December, 1972, and two suspected burns were visited and confirmed on the ground on 7 December, 1972. During these visits, the entire region was experiencing an exceptionally-long dry season, as the onset of rains was then a full month overdue, and active fires were still taking place.

The most striking evidence of an active fire on the imagery was on the Chobe Game Park image (No. 5). When the image was obtained on 14 September at 0951.0 hours local time, a fire was burning and can be seen in the left centre of the image (Fig. 3, upper right). Smoke moving in a west-southwesterly direction can also be seen. On the Okavango Swamps image (No. 4), acquired from the next adjacent ERTS pass on 15 September at 0956.5 hours (exactly 24 hours, 5.5 minutes later), there can be seen a considerable areal extension in a westerly direction of patterns resulting from two lobes of the fire (Fig. 3, upper left). There was no evidence of smoke on the 15 September image, indicating that the fire had probably ceased some time during the 24-hour interval. There is portion of the westerly extension of the fire that was not imaged because at these latitudes, only about 17% image side-lap was available between adjacent ERTS-1 passes. By interpolating between the burn patterns appearing on the sequential images, it was possible to estimate the total increase in area of the two lobes (Fig. 3, lower centre). It was estimated that the northermost fire burned approximated 29 square miles, and by making the conservative assumption that it burned during the entire period between acquisition of the two images, it is estimated that this fire spread at the rate of about 13 acres per minute[1]. By similar calculations and assumptions, the southern-most fire burned approximately 45 square miles, or spread at the rate of about 20 acres per minute[2].

---

[1] $\frac{18560 \text{ acres}}{1445.5 \text{ minutes}}$

[2] $\frac{28800 \text{ acres}}{1445.5 \text{ minutes}}$

These rates of spread can be compared with those estimated from a 30-year-old experimental burning plot near Ndola, Zambia, in which each October, 11 acres burn in an average of 1 minute and 27 seconds, which is equivalent to a rate of spread of 7.6 acres per minute. Similar test-burning sites in Canada indicate that 3-to 4-foot grasses, at 4% moisture content with a 19-mile-per-hour wind, would burn along a 400-foot front at a rate of about 7 acres per minute (Pers. comm. Dr. Peter Kourtz).

The patterns resulting from many fires can be seen on much of the imagery, and in another example, the increase in area of these patterns has also been monitored. When the Kafue National Park image (No. 8) was obtained on 14 September at 0949.5 hours local time, a characteristically lobate burn pattern was clearly evident in the left centre of the image (Fig. 9, upper right). On the Kabompo/Kaoma image (No. 9) acquired from the adjacent ERTS pass on 3 October at 0955.3 hours (exactly 19 days, 5.8 minutes later) the same burn pattern had increased in size from about 7.5 square miles to about 12.5 square miles (Fig. 4, upper left). Areal increases of other burn patterns are also clearly evident in the vicinity (Fig. 4, lower centre).

DISCUSSION AND CONCLUSIONS

In the study area, the nature of the climate is such that cloud-free ERTS imagery is virtually guaranteed from late April until the end of October, and in fact, during 1972, these conditions persisted well into December. Moreover, conditions in the region are normally ideal for detecting and mapping patterns resulting from grass fires, because of the great contrast between the inherent reflectance from burned and unburned grassland and the fact that from June onwards deciduous tree species are without their impeding foliage.

With the imagery available it was unfortunately not possible to achieve complete sequential coverage of any single entire ERTS-1 frame. However, sequential coverage over a 24-hour period was obtained for some areas due to about 17% sidelap on the 13th, 14th, and 15th of September (Fig. 3), and over a 19-day period on the 14th of September and the 3rd of October (Fig. 4). However, even with the relatively small portions of the ground sequentially covered, it was possible to monitor the increase in area and direction of movement of recent and active grass fires, and to roughly estimate their rates of spread.

Given similar circumstances in terms of image quality, cloud-free conditions and sequential coverage there is no reason why ERTS-1 imagery could not be used to detect, map and monitor fires in

a variety of vegetation types in temperate latitudes. In northern Canada, for example, widespread fires occur in forest and tundra, and although the frequency of cloud-free conditions is considerably less, the greater image side-lap (57% at 60°N) would provide more opportunities for sequential coverage at 24-hour intervals.

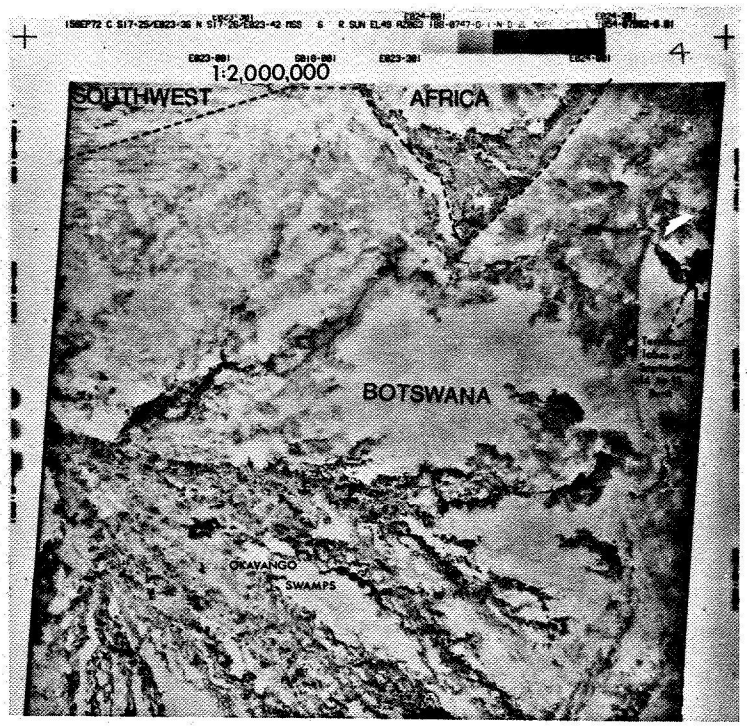
More imagery of the study area has been ordered, and it is hoped to see how fire patterns are obscured by deciduous tree foliage and cloud on imagery acquired during the rainy season. Parallel studies with imagery from northern Canada are also underway.



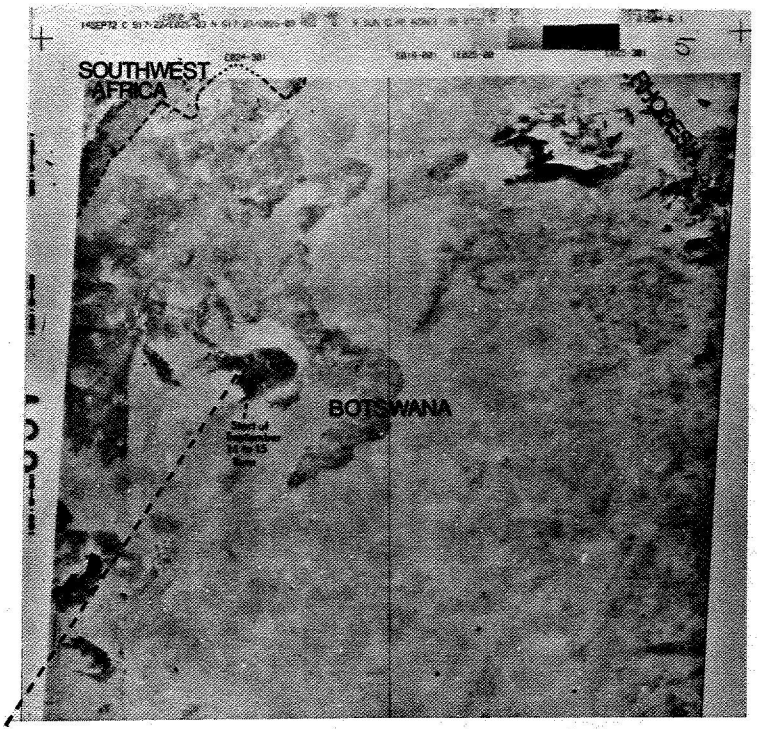
Fig. 1. Location Map of study area.



Fig. 2. ERTS-1, band-6 coverage of study area.



15 Sept. 1972
0956 hrs.



14 Sept. 1972
0950 hrs.

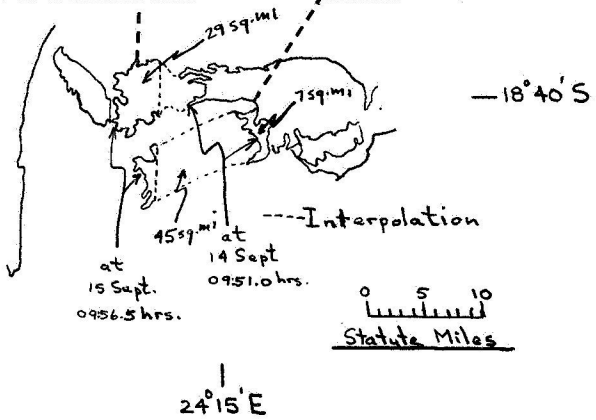


Fig. 3. ERTS-1, band-6 imagery of Botswana burn.

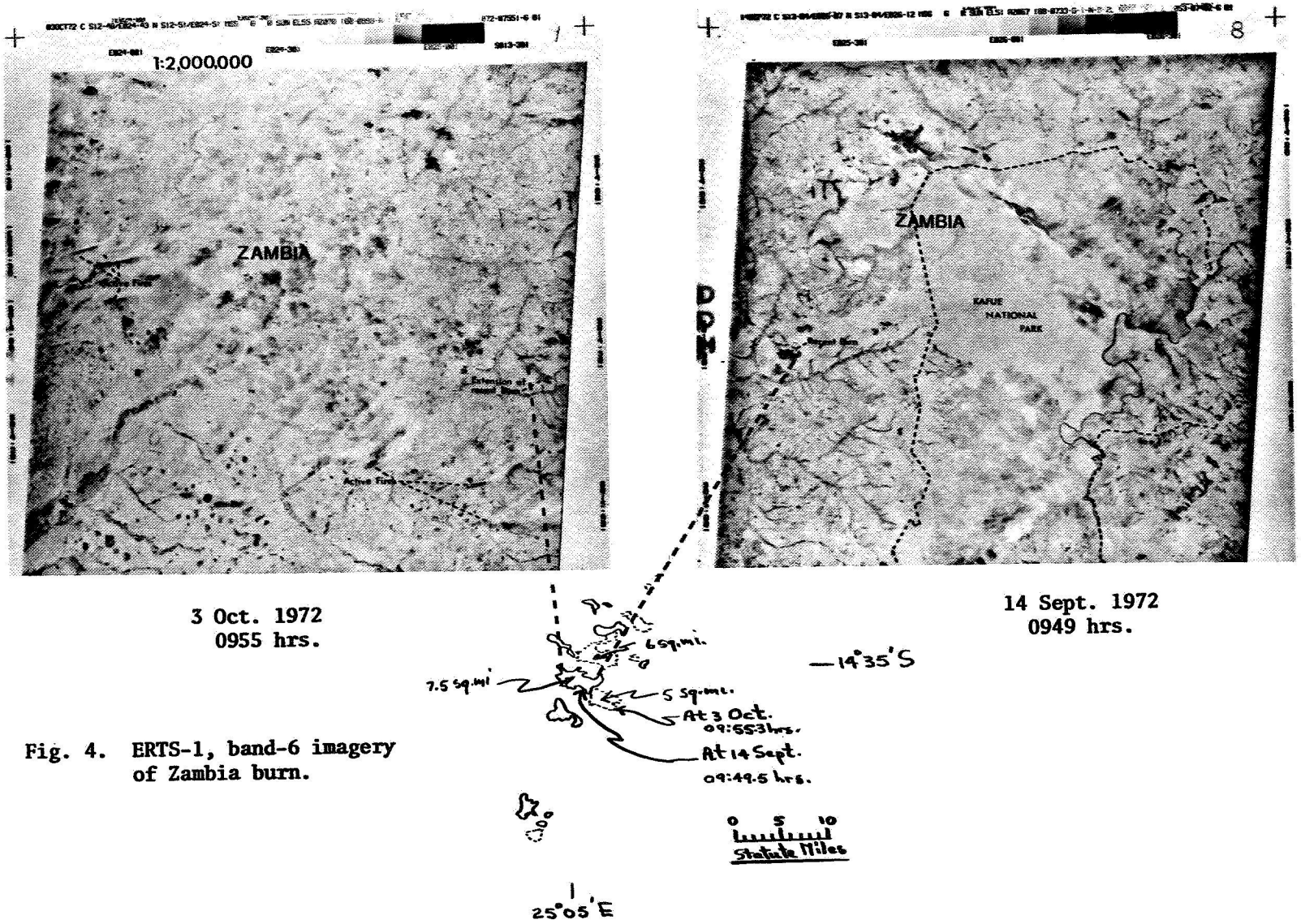


Fig. 4. ERTS-1, band-6 imagery of Zambia burn.

Paper E 7

MAPPING ATLANTIC COASTAL MARSHLANDS, MARYLAND, GEORGIA, USING ERTS-1 IMAGERY*

Richard R. Anderson, Virginia Carter and John McGinness, *Biology Department, The American University, Washington, D. C.*

ABSTRACT

Eastern coastal marshes are the most extensive and productive in the United States. A relatively low cost, moderately accurate method is needed to map these areas for management and protection. Ground-based and low-altitude aircraft methods for mapping are time-consuming and quite expensive. The launch of NASA's Earth Resources Technology Satellite has provided an opportunity to test the feasibility of mapping wetlands using small scale imagery. The test sites selected were in Chesapeake Bay, Maryland, and Ossabaw Island, Georgia. Results of the investigation indicate that the following may be ascertained from ERTS imagery, enlarged to 1:250,000: (1) upper wetland boundary; (2) drainage pattern in the wetland; (3) plant communities such as Spartina alterniflora, Spartina patens, Juncus roemerianus; (4) ditching activities associated with agriculture; (5) lagooning for water-side home development. Conclusions are that ERTS will be an excellent tool for many types of coastal wetland mapping.

INTRODUCTION

Eastern coastal areas are receiving increasing pressure from a variety of sources, mainly due to population growth. The northeastern coast is under the most pressure at the present time, but laws regulating development have been passed in several of the states. The southeastern coastline (except Florida) has had less developmental pressure, mainly from agriculture and some industry. Dredge and fill operations have altered some portions of the coastline. The prognosis is for a tremendous increase in pressure in this area during the next decade. Laws regulating development are helpful but usually require costly mapping of coastal resources. A relatively low cost and moderately accurate method for mapping these areas, including wetlands, mud flats, drainage patterns, impact of man and vegetation productivity would be very attractive to states and assure that at least a portion of this valuable ecosystem would be preserved.

*Performed under contract NAS5-21752, National Aeronautics and Space Administration. The authors appreciate the assistance of the Game and Fish Division, Department of Natural Resources, Georgia.

Investigators such as Anderson (1) and Reimold (3) have shown the reliability of using aircraft remote sensing techniques to do a variety of wetlands studies, including species mapping and vegetation productivity. Ground based ecological studies in wetlands have produced maps of relatively small areas with a high degree of accuracy. These have been valuable in developing remote sensing techniques but the process is too slow and costly for large areas. Low altitude (2,000 meters) aerial photography has been applied in New Jersey to produce wetland maps which meet national map accuracy standards. This is a relatively rapid method, but the cost may be prohibitive for some states. In order to decrease the time and cost involved in wetland mapping, it will be necessary to reduce the accuracy somewhat. It appears from this research that ERTS-1 data may be applied to rapid, relatively low cost wetland mapping on broad regional scales.

ERTS positive transparencies at a scale of 1:1,000,000 have high resolution and excellent contrast. Unfortunately, processing procedures at Goddard Space Flight Center favor the more highly reflective, upland features. Due to the high moisture content in marshlands, reflectance values are lower and are quite dark on all ERTS MSS bands. Special processing is required to bring out detail in coastal features. Detail in uplands is lost when optimum processing techniques for coastal areas are used.

The marsh-water interface and the upper wetland boundary are clearly seen on MSS bands 6 and 7. Large plant associations or communities can also be detected on either MSS band 7 or on color composites made using the Diazo subtractive color technique. In bands 4 and 5 (visible: green and red), all marsh species have a low overall average reflectance and appear very dark in tone as does the dryland vegetation. As the coastal marshes become fresher, the spectral reflectance of the species composing these marshes is higher and approaches that of dryland vegetation making the boundary less clear. It may be necessary to develop special processing techniques where wetland grades to dryland in order to clearly define this boundary.

CHARACTERISTICS OF THE TEST SITES

Figure 1 is a map of the Chesapeake Bay area showing the location of the northern test sites. The smaller areas outlined are two test areas examined in detail in the following pages. Area 1 is a salt marsh complex located at the mouth of the Chincoteague Bay in Virginia. Area 2 is a large, near-saline marsh at the mouth of the Nanticoke River in Dorchester County, Maryland. Maryland has approximately 300,000 acres of wetlands, 250,000 of which lie on the Eastern Shore, or what is commonly called the Delmarva Penninsula. Virginia has approximately 330,000 acres of wetlands, over half of which also lie on the Delmarva Penninsula.

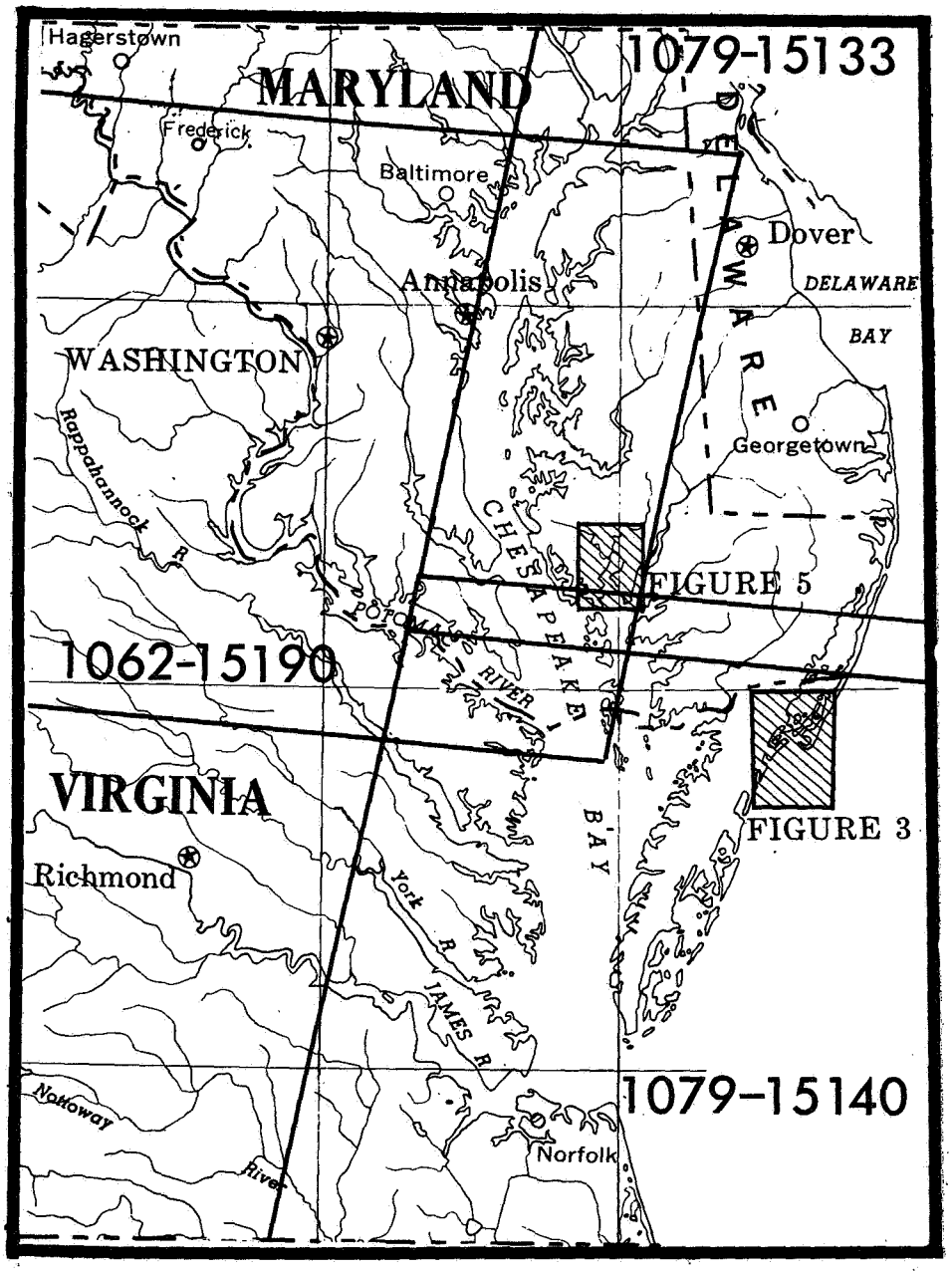


Fig. 1. Map of Chesapeake Bay area showing location of ERTS images (1079-15133, 1062-15190, 1079-15140) and smaller test areas 1 (Fig. 3 - Chincoteague marsh) and 2 (Fig. 5 - Nanticoke marsh).

The coastal marshes from North Carolina and southward represent the best development of saline marshes in the United States. Those in South Carolina and Georgia (the southern test site) are particularly well developed (Fig. 2). Cooper (2) has summarized the current knowledge of eastern coastal areas. Vegetational composition is quite similar along most of the coast but grades to mangrove swamps in Florida. Tidal amplitudes vary from two feet in some portions of North Carolina to eight feet in South Carolina and Georgia.

The two major community types which dominate the marshes of this area are Spartina alterniflora and Juncus roemerianus. These species are restricted to areas with frequent tidal inundation. S. alterniflora occurs as at least two and in some areas three growth forms. This is apparently related to tidal inundation and soil aeration. High growth (to 3 meters) is found along the banks of creeks where the substratum is very soft and tidal inundation is for the longest period of time. The next growth form (to 1 meter) grows at slightly higher elevations in a more firm substrate. The third growth type (less than 1 meter) is at the highest elevation for S. alterniflora in a firm substrate where other species may mix with it occasionally. Juncus roemerianus occurs as small to large zones mostly at the next highest elevation and where the water is somewhat fresher.

Higher, less frequently tidally inundated portions of these marshes contain several species which grow as mixed communities or in relatively small single species zones. These include Spartina patens and Spartina cynosuroides, Distichlis spicata, Baccharis halimifolia and Borrichia frutescens.

The specific southern test site was bordered on the south by Saint Catherine's Island, Georgia, and on the north by Charleston, South Carolina. The southern portion of the test site around Ossabaw Island, Georgia, was studied intensively due to the availability of good ERTS imagery.

The vegetation of this area is characteristic of the southern coastline in general. There are large zones of high and low growth S. alterniflora and J. roemerianus, and smaller zones of S. cynosuroides, B. frutescens and S. patens. There is marshland ditching in Ogeechee River related to agriculture and "lagooning" for water-side homes on the Vernon River.

RESULTS

A. Northern test site

Use of a Bausch and Lomb Transfer Scope in combination with 1:1,000,000 scale ERTS format permits enlargement of the image and

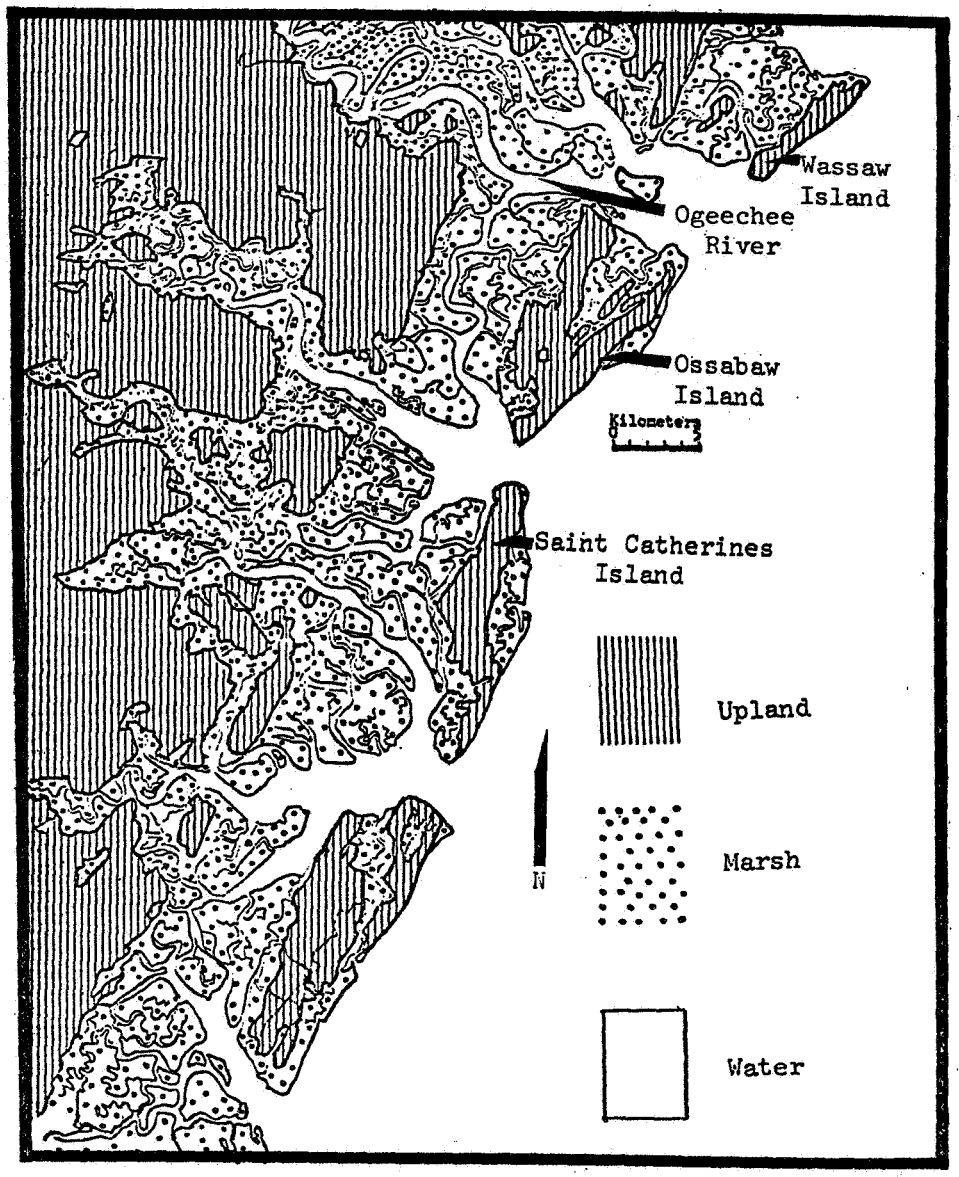


Fig. 2. Map of portion of Georgia coastline showing areas of intensive analysis.

and construction of maps and overlays to a scale of 1:250,000. Figure 3 is a 1:250,000 enlargement of an ERTS MSS 7 (1079-15140) image of the Chincoteague salt marsh complex. Figure 4 is a 1:250,000 map of the same area showing four categories; (1) upland vegetation and beach, (2) water, (3) Spartina alterniflora/Salicornia sp. association, and (4) Spartina patens/Distichlis spicata/Iva frutescens association. The spectral reflectance of the Spartina alterniflora/Salicornia sp. association is generally low, in part because of the wet mud or peat background below the vertically oriented vegetated layer which averages 7-14 inches in height. The reflectance of the mudflats and water in this band is still less. The relatively high reflectance of Spartina patens permits sufficiently large areas of the Spartina patens/Distichlis spicata/Iva frutescens association to be delineated. The upper wetland boundary is generally sharp except where broad transition zones exist. The marsh-water interface is sometimes difficult to determine in areas interlaced with numerous small tributaries or sparse patches of vegetation. Sand and marsh at the mouth of Chincoteague Bay (Figure 3: A) are not shown on the USGS 1:250,000 map published in 1966. Area C is a recent spoil fill at the tip of Chincoteague Island. Spoil areas may be easily separated from reflective vegetation by referring to bands 4 and 5 or by using a color composite since they are highly reflective in all four bands. Areas labeled D are fresh water impoundments in the Chincoteague Wildlife Refuge. The striped area at the south end of the map (B) is an area where old spoil banks are partially revegetated. It is quite distinctive in the band 7 image as a light area extending from Wallops Island to the mainland.

Figure 5 is a 1:250,000 scale enlargement of the Nanticoke marsh (MSS band 7, ERTS image 1079-15133). Species composition in this marsh is typical of a near-saline environment. The marsh area shown here is approximately 10 miles long and 5 miles wide. Figure 6 is a 1:250,000 map of the same area made by overlaying the 1:1,000,000 scale image enlarged with an overhead projector. A number of tree islands dot the marsh, the largest of which contains the small community of Elliots' Island. The marsh vegetation includes a Juncus roemarianus/Scirpus sp./Spartina alterniflora association in the lower marsh areas and a high marsh community, Spartina patens/Distichlis spicata/Iva frutescens/Baccharis halimifolia, primarily located along the edges and near the single road. Toward the northern end of the marsh, the water becomes more brackish and less saline. Stands of Spartina cynosuroides occupy the stream margins within this portion of the marsh. Isolated stands of Phragmites communis occur, but they are generally too small to be detected on the ERTS imagery. Because the signature of the dominant low marsh species Juncus roemarianus is close to that of water, it is difficult to delineate the marsh-water interface within the marsh itself.

Mapping at a scale of 1:250,000 is adequate for the general delineation of large marshes and for rather gross plant species associations. Enlargement of the imagery to a scale of 1:125,000 provides

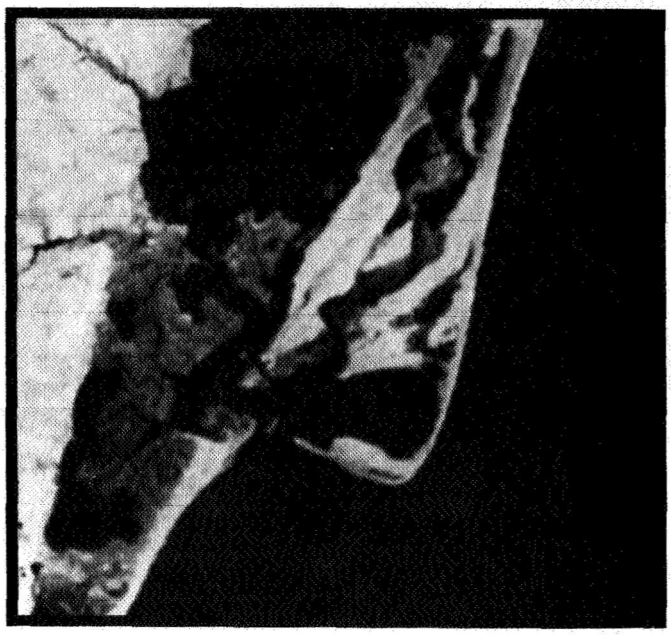


Fig. 3. 1:250,000 enlargement of Chincoteague salt marsh (1079-15140-7).

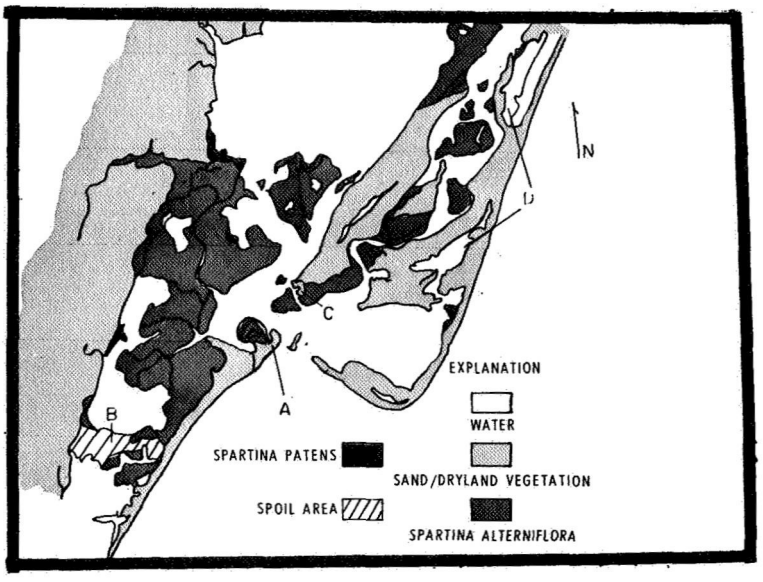


Fig. 4. 1:250,000 map of Chincoteague salt marsh. A - sand/marsh area; B - old spoil area; C - recent spoil fill; D - fresh water impoundment.



Fig. 5. 1:250,000 enlargement of Nanticoke R. salt marsh (1062-15190-7).

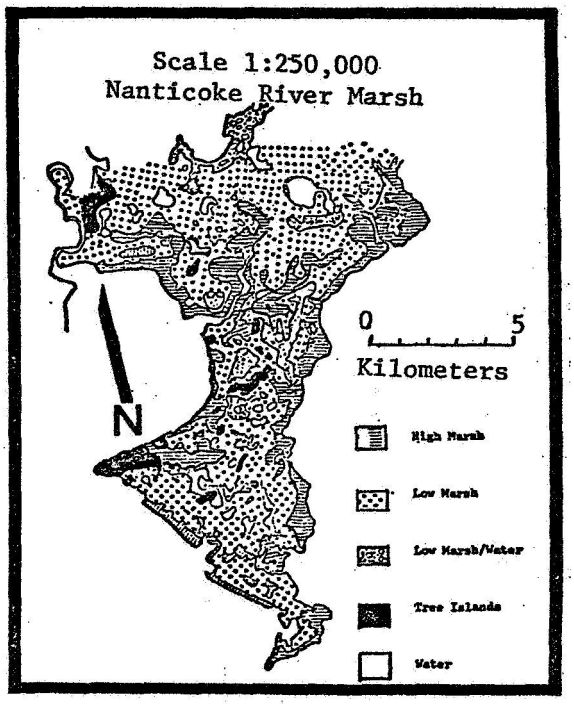


Fig. 6. 1:250,000 map of Nanticoke River marsh.

additional information when processing is done to enhance the contrast in the denser part of the image. Overlays can be made directly from the prints which show the marsh-water interface and upper wetland boundary clearly. Where broad successional zones exist, these can also be mapped. Smaller plant communities, occasionally less than 25 meters in diameter, can be identified. In addition, open and vegetated ditches dug for drainage or agriculture can be recognized and indicated on the map.

The Nanticoke marsh was experimentally enlarged from the 1:1,000,000 scale to approximately 1:24,000. All the boundaries seen in the other scales became blurred. It appears that unless the optics of the enlarging system are exceptionally good, this scale would only be useful for theme extractions such as upland, dry marsh, wetmarsh and open water where placing of boundaries is not critical.

B. Southern test site

Figure 7 is a 1:250,000 scale reprocessed enlargement of MSS band 7 (No. 1046-15324, Sept. 7, 1972) of the test site. Note good tonal differentiation in the coastal marshland but loss of detail in the upland. The upper wetland boundary is clearly seen in most of the image although patchy clouds may be mistaken for upland or tree islands in the marsh. Lagooning for water-side home development is visible near Burnside, Georgia, on the Vernon River. Of possible greater significance is the marshland ditching visible in the Fort McAllister area of the Ogeechee River. Ditching causes drying out and accelerates vegetational succession to dryland species and is therefore undesirable as currently practiced for mosquito control and agriculture in many areas. It has been assumed that the resolutional limitation of ERTS imagery would not allow definition of ditching practices. At least in this area that assumption was incorrect.

Various vegetational features are also clearly shown. Tonal characteristics of marshland vegetation in Ogeechee River are considerably different from the nearby Medway River. On the ground investigations have shown that Juncus roemerianus is the dominant vegetation in the Red Bird Creek area. The lighter tones of this species contrast nicely with the darker tones of Spartina alterniflora which makes up the bulk of the vegetation in Medway River.

Tonal structure in the Bear River marshes indicate that separation of at least two growth forms of S. alterniflora will be possible. The tall form along the creeks images lighter than the shorter forms. It appears that gross productivity estimates may be made from the imagery. The lightest tones in these marshes are at the "loop" in the Ogeechee River (Spartina cynosuroides) and off Kilkenny Creek near Belle Island (mixed populations of Borrichia frutescens and Spartina alterniflora on slightly elevated ground).

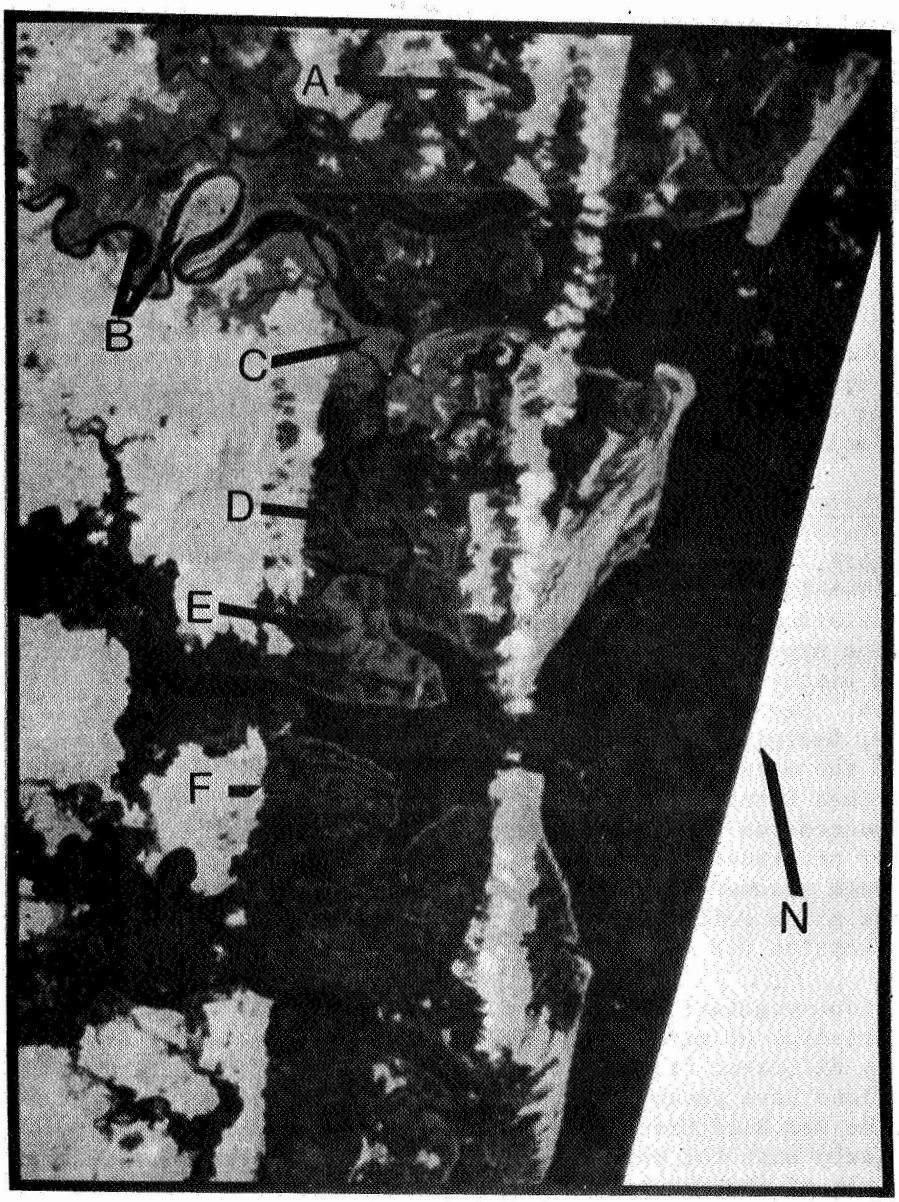


Fig. 7. ERTS image, Band 7, enlarged to 1:250,000 scale. A - "lagooning" for water-side homes; B - wetland ditching with Spartina cynosuroides; C - zone of Juncus roemerianus; D - Spartina alterniflora high growth form along creek edges (interior dark areas are low growth form of this species); E - berm with Spartina alterniflora and Borrichia frutescens; F - upland-wetland border.

CONCLUSIONS

ERTS-1 imagery (enlarged to 1:250,000) is an excellent tool by which large area coastal marshland mapping may be undertaken. If states can sacrifice some accuracy (amount unknown at this time) in placing of boundary lines, the technique may be used to do the following:

(1) Estimate extent of man's impact on marshes by ditching and lagooning.

(2) Place boundaries between wetland and upland and hence estimate amount of coastal marshland remaining in the state.

(3) Distinguish among relatively large zones of various plant species including high and low growth S. alterniflora J. roemerianus, and S. cynosuroides.

(4) Estimate marsh plant species productivity.

REFERENCES

[1]Anderson, R. R. and F. W. Wobber, "Wetlands Mapping in New Jersey," Photogrammetric Engineering (in press).

[2]Cooper, A. W., "Salt Marshes," in Coastal Ecological Systems of the United States, Environmental Protection Agency, Washington, D.C.

[3]Reimold, R. J., J. L. Gallagher, and D. E. Thompson, "Coastal Mapping with Remote Sensers," Proceedings of a Symposium on Coastal Mapping, Washington, D.C., American Society of Photogrammetry, pp. 99-112.

Paper E 8

IDENTIFICATION OF MARSH VEGETATION AND COASTAL LAND USE IN ERTS-1 IMAGERY

V. Klemas, F. Daiber and D. Bartlett, *College of Marine Studies, University of Delaware, Newark, Delaware 19711*

ABSTRACT

Coastal vegetation species appearing in the ERTS-1 images taken of Delaware Bay on August 16, and October 10, 1972 (Observation I.D. Nos. 1024-15073 and 1079-15133) have been correlated with ground truth vegetation maps and imagery obtained from high altitude RB-57 and U-2 overflights. The vegetation maps of the entire Delaware Coast were prepared during the summer of 1972 and checked out with ground truth data collected on foot, in small boats, and from low-altitude aircraft. Multispectral analysis of high altitude RB-57 and U-2 photographs indicated that five vegetation communities could be clearly discriminated from 60,000 feet altitude including, 1) salt marsh cord grass (Spartina alterniflora), 2) salt marsh hay and spike grass (Spartina patens and Distichlis spicata), 3) reed grass (Phragmites communis), 4) high tide bush and sea myrtle (Iva species Baccharis halimifolia), and 5) a group of fresh water species found in impoundments built to attract water fowl. All of these species are shown in fifteen overlay maps, covering all of Delaware's wetlands prepared to match the USGS topographic map size of 1:24,000.

Major communities of 1) Spartina alterniflora, 2) Spartina patens and Distichlis spicata, and 3) Iva frutescens and Baccharis halimifolia can be distinguished from each other and from surrounding uplands in ERTS-1 scanner bands #6 and #7. Similarly, major impounded areas, built to attract water fowl, can be identified. Mosquito control drainage ditches and plant species such as Phragmites communis which naturally occur in small, dispersed patches are impossible to discriminate within the resolution capability of the ERTS-1 scanner. In disturbed

marshes of northern Delaware Bay, Phragmites communis does occupy large enough expanses of marsh to be detected. In summary, it appears from preliminary analysis that spectral discrimination capabilities of ERTS-1 imagery compare favorably with those of aerial infrared photography and that spatial resolution is the dominant factor limiting the potential for detailed vegetation mapping using ERTS-1 imagery.

INTRODUCTION

Coastal wetlands of the type found along the entire East Coast of the United States are well suited to remote sensing techniques, particularly multispectral analysis. Use of high altitude RB-57 and U-2 color-infrared imagery in the mapping of vegetation in Delaware's saline marshes was highly successful and indicated that such mapping was possible. Some of the characteristics which make coastal marshes particularly suitable for multispectral sensing from high altitudes are:

1) The lack of topographic relief eliminates shadows and variations in sun angle across the marsh.
2) The relatively low diversity of major plant species simplifies photo-interpretation.
3) Environmental changes generally take place over large horizontal distances in the marsh; therefore, zones of relatively uniform vegetation are usually large enough to be discernible even on very high altitude imagery.
4) Each of the primary species is morphologically different enough to produce easily discriminated reflectance characteristics, particularly in the infrared portion of the spectrum.

Few natural situations afford such an opportunity to evaluate the optimum multispectral discrimination capabilities of present equipment while providing useful data on plant species distribution and land use over large areas of the coastal regime.

GROUND TRUTH

Data on the distribution of vegetation species and recent dredge-fill construction in Delaware's coastal wetlands was collected during the spring and summer of 1972. Reconnaissance on foot, in small boats, and from low altitude aircraft aided in the interpretation of high altitude RB-57 and U-2 imagery. Color and color-infrared photographs obtained by these aircraft from an altitude of 60,000 feet were analyzed by human interpreters and by automated multispectral data processing equipment. The results showed that five individual species or groups of associated species could be clearly discriminated on the basis of high altitude color-infrared imagery. In addition, construction of housing, marinas, impoundments and other alterations of the marsh were clearly discernible. The discrimination classes selected were:

1) Salt marsh cord grass (Spartina alterniflora).
2) Salt marsh hay and spike grass (Spartina patens and Distichlis spicata).
3) Reed grass (Phragmites communis).
4) High tide bush and sea myrtle (Iva frutescens and Baccharis halimifolia).
5) Fresh water impoundments built to attract water fowl.
6) Dredge fill construction since the last revision of the topographic maps.

During August of 1972, maps of all of Delaware's 115,000 acres of coastal wetlands were compiled at a scale of 1:24,000. These maps show the distribution of the six vegetation and land use classes described above (See Figure 1) and may be overlayed onto USGS topographic maps of the area. The percentage cover of each vegetation species was calculated by the GEMS computer for each of the boxed-in areas on the basis of false color enhancements made utilizing the GEMS analogue analysis capability (See Figure 2).

patches of vegetation are not distinguished from their surroundings. The tall reed grass Phragmites communis generally grows in patches too small for detection by ERTS-1 scanners and so is rarely visible in the imagery. In the industrialized northern portion of the Delaware Bay, dredge-fill operations appear to have facilitated the growth of Phragmites communis far beyond its usual limits with the result that some small marshes have become infested, often to the exclusion of other marsh plants. These marshes can be identified in ERTS-1 imagery (See Figures 3 and 8).

CONCLUSION

While ERTS-1 imagery does not appear to be applicable to detailed mapping tasks in tidal marshes due to resolution limitations, its usefulness in gross mapping and inventorying operations is evident. Complete inventories of marsh extent, dominant species distribution, and human alterations of the marsh could be performed over large areas in a very short time, making it possible to conduct such surveys frequently and at small expense.

This project is partly funded through NSF-RANN, Grant GI-33369; NOAA Office of Sea Grant, Grant No. GH-109; and NASA-ERTS-1, Contract No. NAS5-21837.

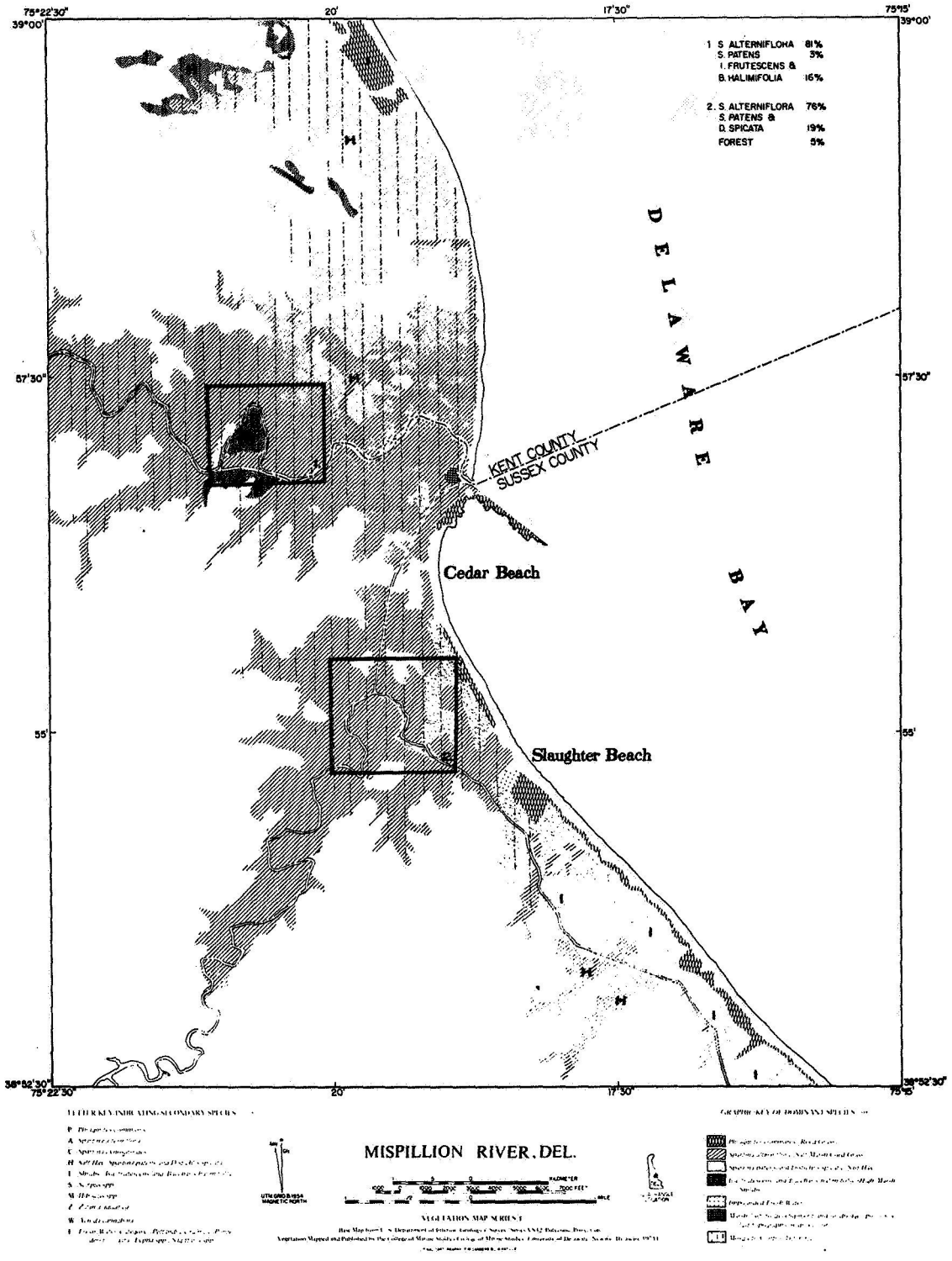


Figure 1 Overlay map of wetlands in the Mispillion River area showing four types of vegetations communities, fresh water impoundments, mosquito control ditching and marsh lost to development. Fifteen such ground truth maps were prepared, covering most of Delaware's wetlands, using NASA RB-57 imagery and multispectral analysis techniques. Note the appearance of Phragmites communis near developed areas. The boxed-in areas were analyzed to obtain computer print-outs of the percentages of minor vegetation species present.

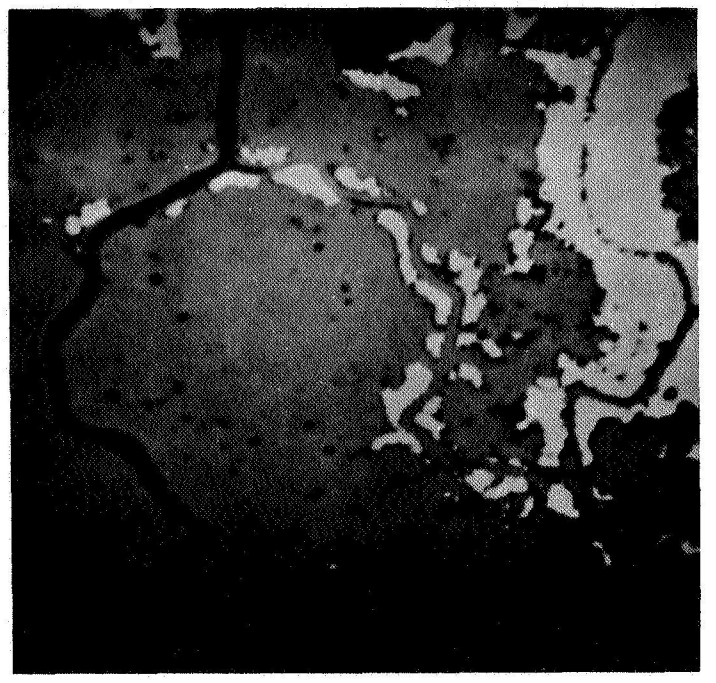


Figure 2 GEMS multispectral enhancement of area enclosed in Box #2, Figure 1. Dark grey - Spartina alterniflora
Light grey- Spartina patens and Distichlis spicata
Black - water and upland trees.

As expected, the same characteristics of coastal marshes which facilitate mapping through the use of aerial imagery and multispectral analysis also make possible the discrimination of marsh vegetation species and land use from space. ERTS-1 scanner bands 6 and 7 (.7-.8 microns and .8-1.1 microns) in images 1024-15073 and 1079-15133 (August 16 and October 10, 1973) were used to identify coastal marsh areas and to distinguish the major vegetation types within them. (See Figure 3). Areas dominated by Spartina alterniflora are clearly distinguished from those dominated by the often associated species - Spartina patens and Distichlis spicata (See Figures 3 and 4). The communities dominated by the low shrubs Iva frutescens and Baccharus halimifolia can be distinguished from adjacent communities of S. patens and D. spicata on one side and dune-beach or upland forest regimes on the other (See Figures 3 and 5). The pattern that emerges is that of the detailed topographic and tidal inundation characteristics of the marsh as seen in the horizontal zonation of those plant species sensitive to their elevation relative to mean high tide. The major tidal marsh environments and their associated plant communities may be generally identified as:

1) "Low Marsh" - Areas inundated twice daily for considerable periods of time by the high tides. Spartina alterniflora dominates in this zone.
2) "Marsh Meadow" - A transitional zone, still inundated regularly but not to as great an extent as the low marsh. In the Delaware marshes this area is dominated by Spartina patens and Distichlis spicata either individually or together.
3) "High Border" - A zone rarely reached except by the highest tides but still requiring a certain degree of salinity tolerance of its inhabitants. Thus, the name "high tide bush" given to Iva frutescens, the low shrub which, along with Baccharus halimifolia, dominates in this region. Beyond this zone is found either the beach-dune or upland forest regimes.

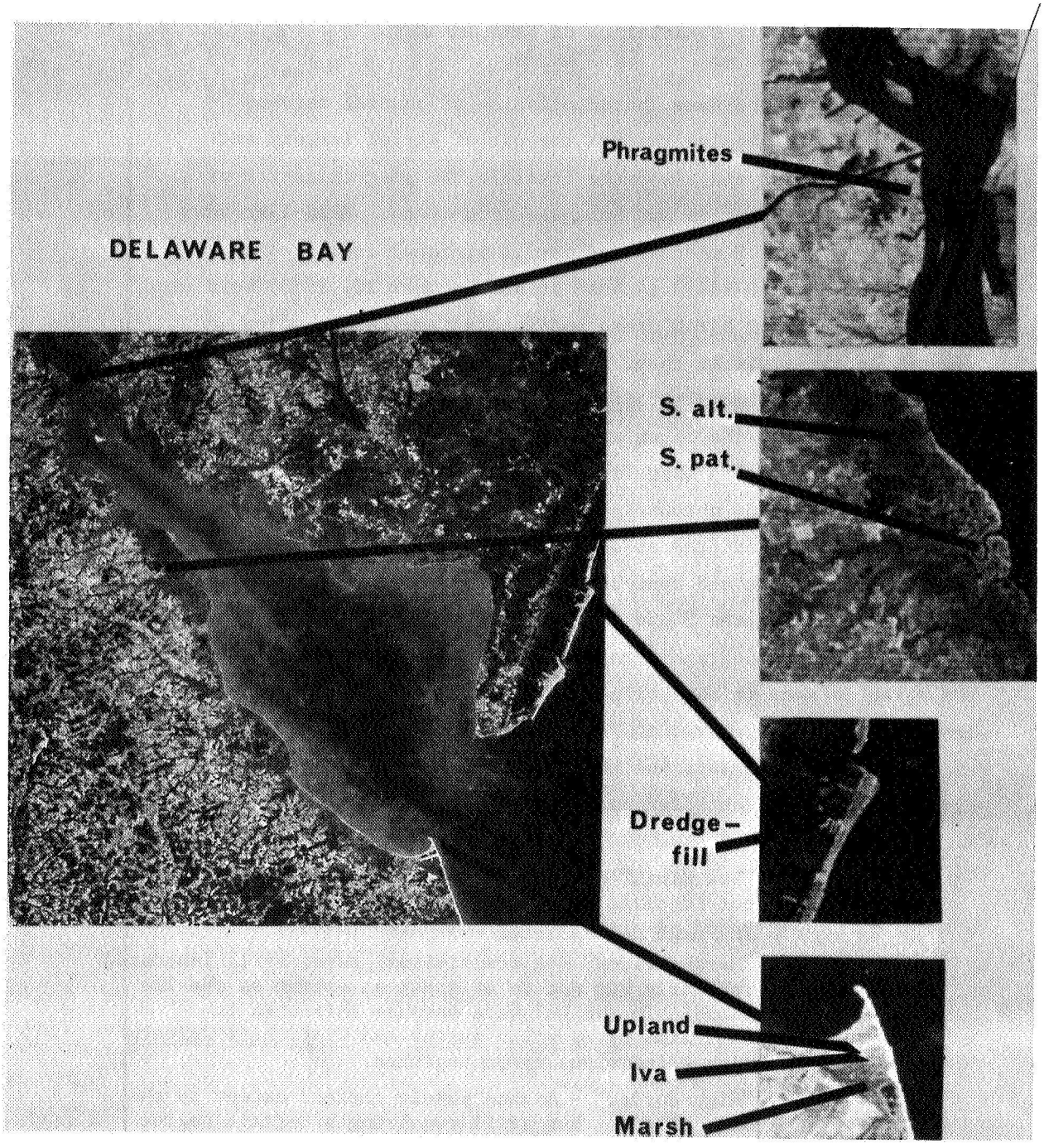

Phragmites
DELAWARE BAY
S. alt.
S. pat.
Dredge–
fill
Upland
Iva
Marsh

FIGURE 3

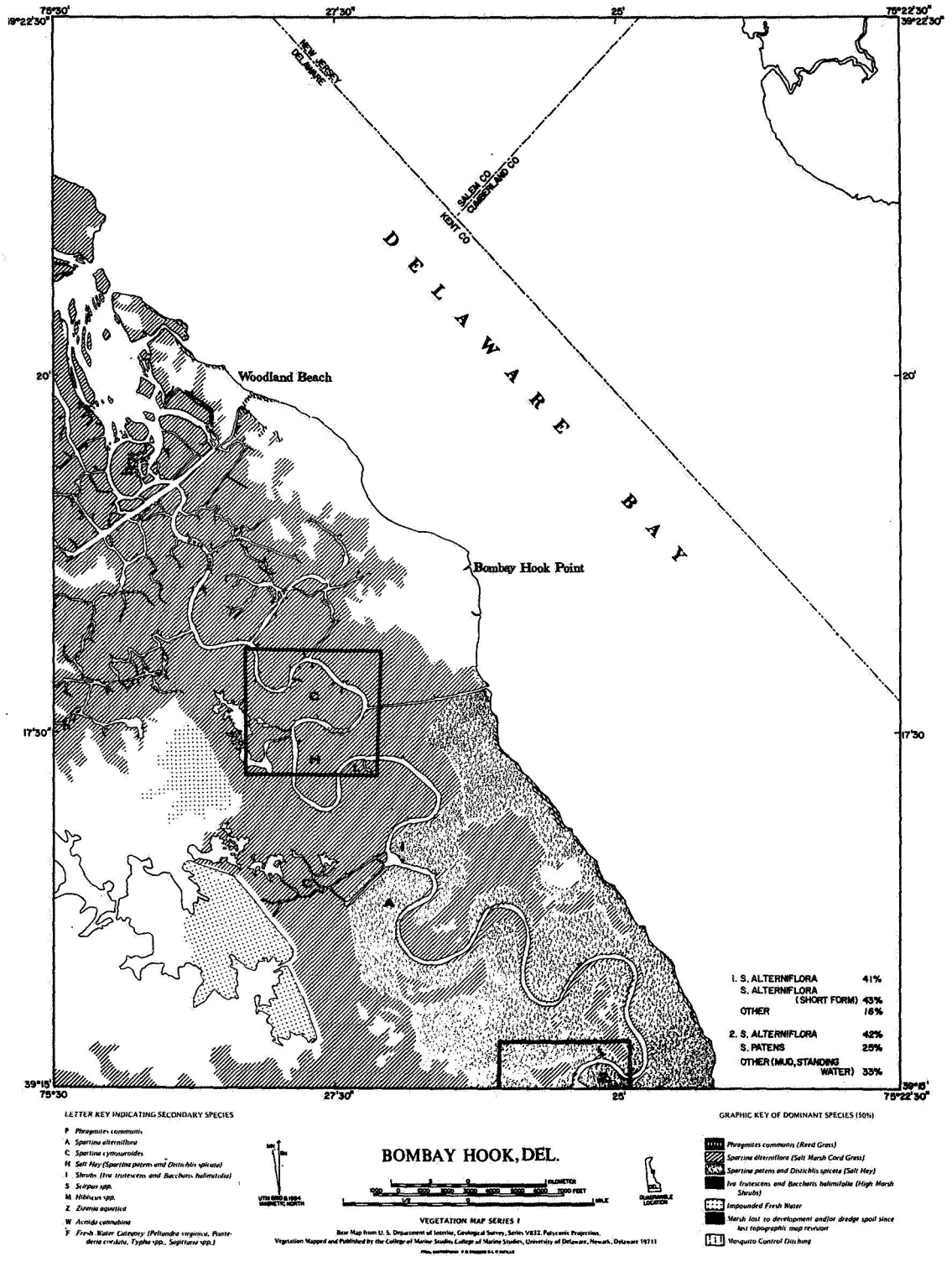


Figure 4 The large communities of Spartina alterniflora and Spartina patens shown in this map of the Bombay Hook area, can be identified in the ERTS-1 image in Figure 2.

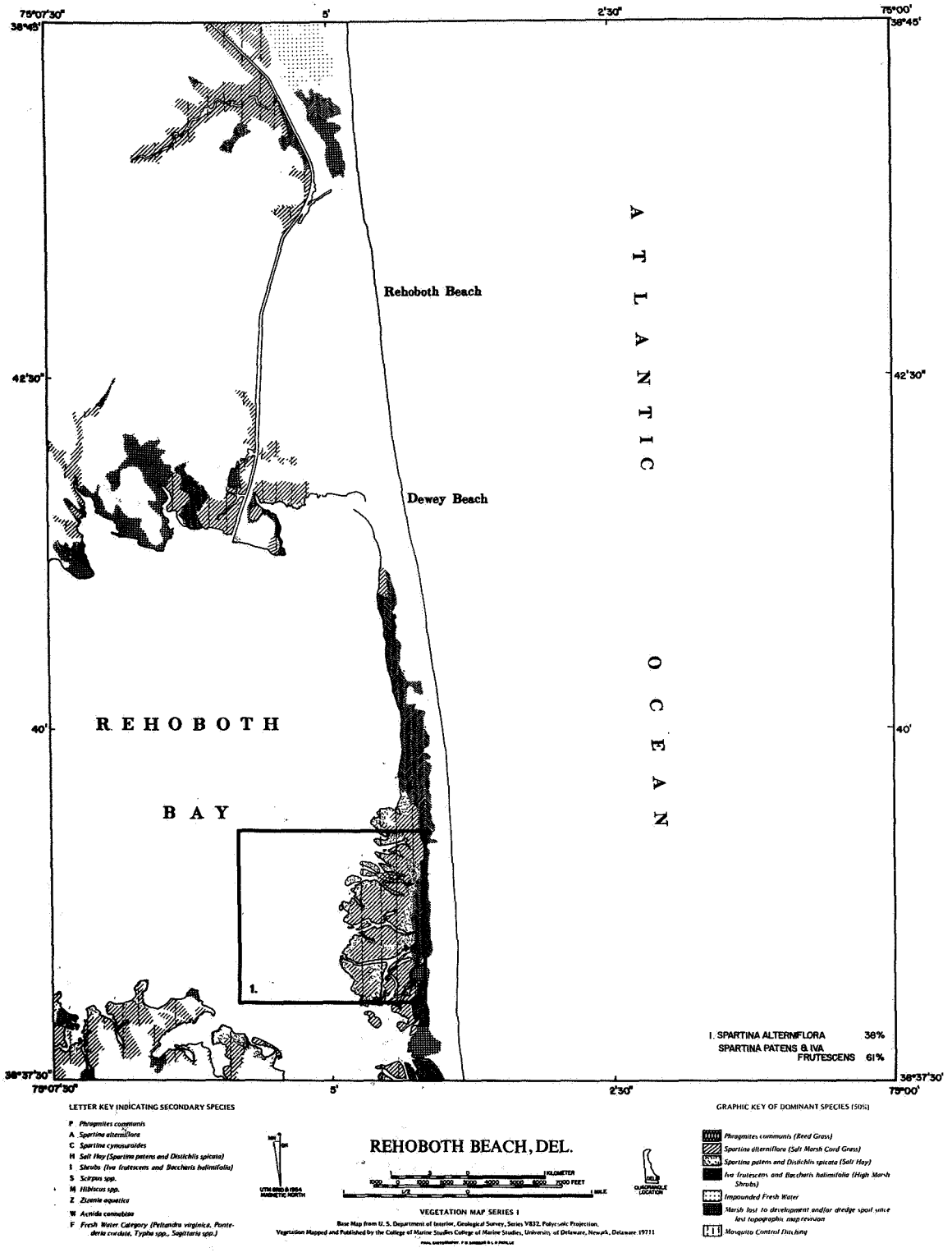


Figure 5 The strips of Iva frutescens and Baccharis halimifolia, shown in this map of the Rehoboth Beach area, can be identified in in the ERTS-1 fmage in Figure 2.

All three regimes are not necessarily always present but where any are found they are distinguishable from each other and from the non-marsh environments surrounding them. It should be noted that in all cases, spectral identification is a matter of relative reflectance properties, one species to another, and so ground truth is required. Identification of plant species through absolute spectral characteristics where no ground truth is available is difficult and unreliable due to atmospheric perturbations of the reflected light. Species identification becomes quite easy, however, if the interpreter has some general knowledge of the species distribution in the area of interest. Reconnaissance field work or even observations made from a light plane at low altitude is sufficient in most cases. Automated multispectral analysis performed using the General Electric Multispectral Data Processing System was found to be a useful tool in enhancing vegetation species and land use types on the basis of their spectral signatures. Delays in the acquisition of composite multispectral imagery have limited the application of this promising technique to date.

Large fresh water impoundments built to attract water fowl are readily identifiable as areas of standing water (no matter what the tidal stage) within the marsh, usually with straight, man-made boundaries (See Figure 3). Likewise, the straight boundaries and general lack of vegetation identify dredge-fill alteration of the marsh (See Figure 3). Multispectral enhancement of small portions of ERTS image I.D. 1024-15073 are shown in Figures 6 and 7. Note the clear discrimination between wetlands, uplands, sand and dredge-fill.

The major limitation of ERTS-1 imagery in surveying coastal marshes appears, not surprisingly, to be resolution. Objects or areas of vegetation must be of sufficient horizontal extent to be within the resolution capabilities of the ERTS-1 scanner. For this reason, small scale characteristics such as drainage ditching are not visible and small

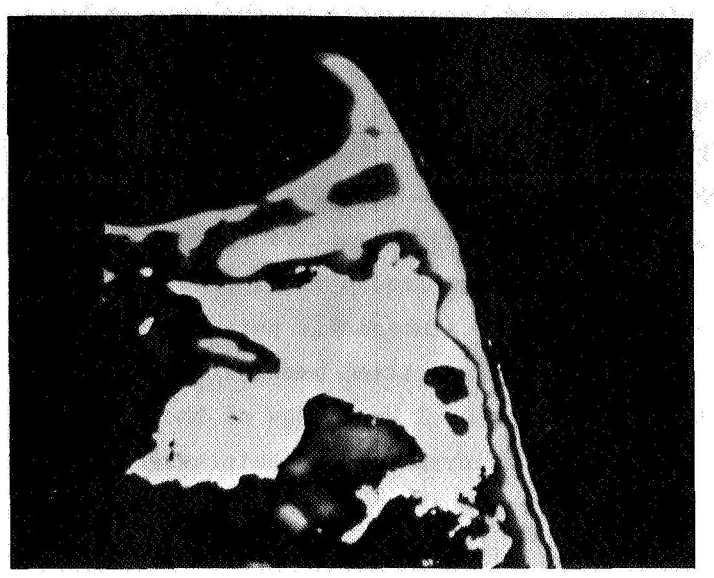


Figure 6 Multispectral enhancement of ERTS-1 image of Cape Henlopen discriminating wetlands from uplands and sand. (I.D. 1024-15073). White - wetlands dark grey - uplands light grey - sand black - water

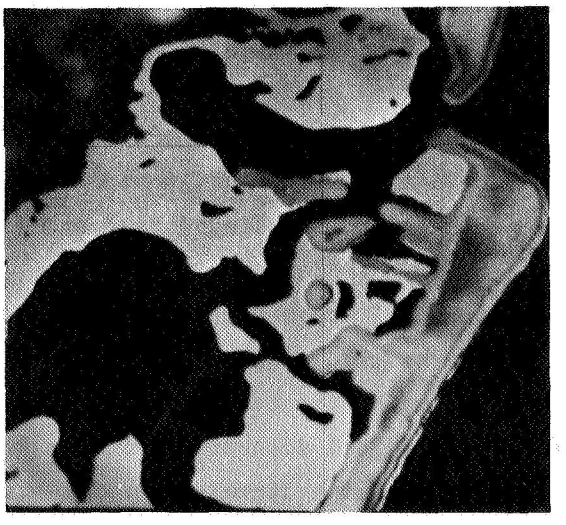


Figure 7 Multispectral enhancement of ERTS-1 image of Stone Harbor, N.J., identifying wetlands, dredge-fill and sand. white - wetlands light grey - adjacent to wetlands - dredge fill darker grey in center of island - sand black - water

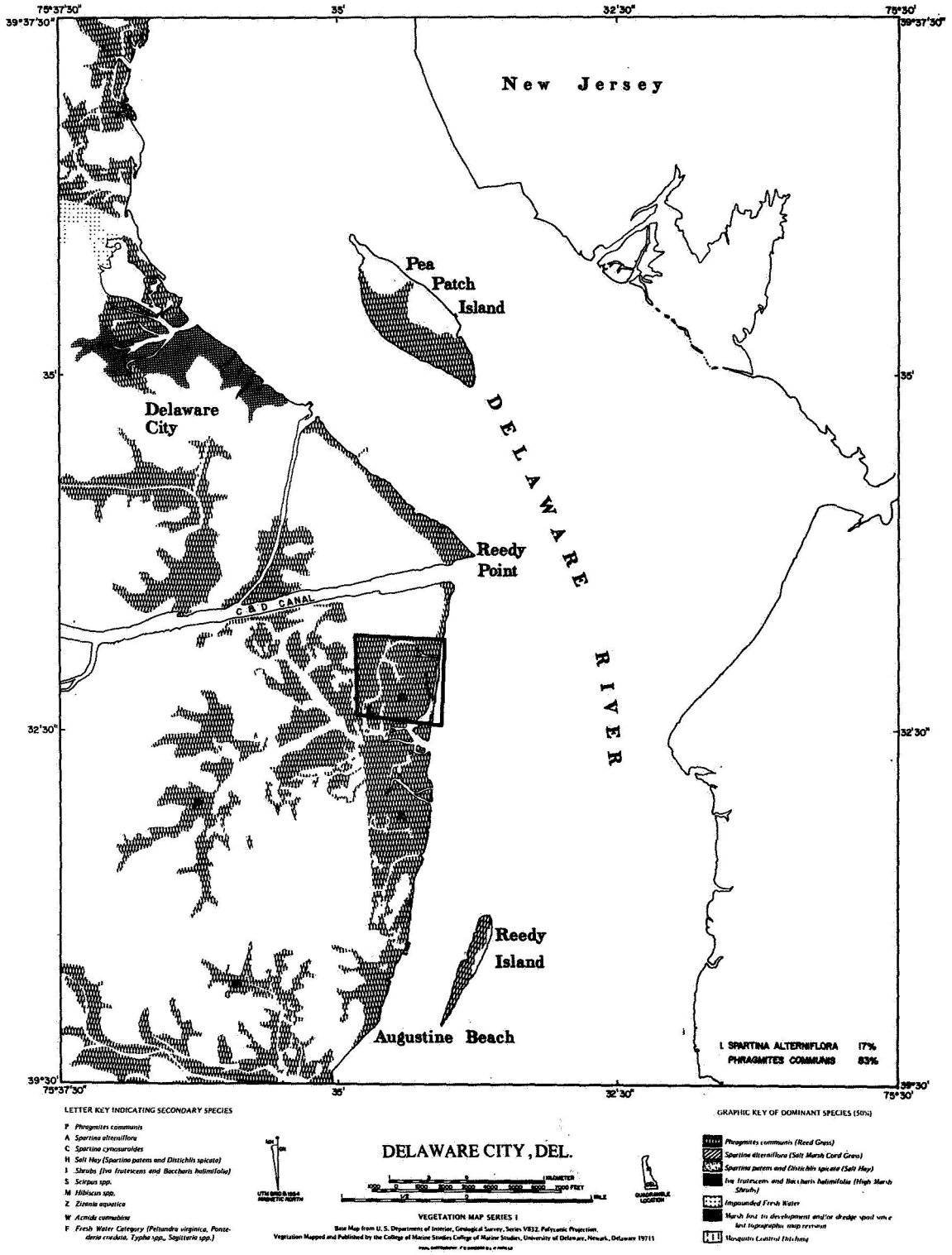


Figure 8 Heavily developed regions in northern Delaware, such as the area around Delaware City, show large concentrations of Phragmites communis and marshes lost to development.

Paper E 9

APPLICATION OF ERTS-1 DATA TO THE PROTECTION AND MANAGEMENT OF NEW JERSEY'S COASTAL ENVIRONMENT

Robert L. Mairs, Frank J. Wobber and Donald Garofalo, *Earth Satellite Corporation;* Roland Yunghans, *New Jersey Department of Environmental Protection*

ABSTRACT

ERTS-1 imagery is being used by the New Jersey Department of Environmental Protection (NJDEP) to develop information products that will assist the state in optimally managing its coastal resources and in allocating funds. Interviews with NJDEP personnel have identified significant problem areas in the coastal zone, and the types of remote sensor derived information products that can be used in real-time decision making.

Initial analyses of imagery from several successive ERTS-1 orbits have shown the extent, predominant drift, and dispersion characteristics of waste disposal in coastal New Jersey waters. Imagery (MSS Bands 4 and 5) for several orbits, shows the New-York Harbor tidal discharge extending as far south as Long Branch, New Jersey.

Within the bays, sounds, and thorofares behind the barrier islands in the southern New Jersey shore area, increased reflectance of the turbid waters has enabled the investigators to examine the effects of a large sewage effluent flow into these waters. As these waters are flushed with each tidal change, the turbid waters emanate out to the populous bathing beaches.

Analysis of early ERTS-1 data indicates that the concept of repetitive looks at coastal circulation dynamics along the New Jersey shore will provide the kinds of information necessary for more effective coastal management decision making within the New Jersey Department of Environmental Protection.

INTRODUCTION

New Jersey's coastal zone has been subjected to the demands of a growing population and the rapid industrialization which are common to states on the East and Gulf Coasts. The public has become more aware of the ecological damage that is taking place in the coastal zone while at

the same time placing more and more demands on this area for recreation. It is unlikely that any coastal area in the eastern United States will escape the influence or domination of development in the next decade. At the same time these areas must protect their recreational attractions, the most important of which is clean water. Up to the present time, man has indiscriminately used estuarine and coastal areas as an ultimate sink for the disposal of his wastes.

The capacity of coastal areas to assimilate these wastes has been reached in many areas, and a burgeoning population is threatening waters in other areas. In order to meet the problems of pollution and development, New Jersey requires additional data on coastal and estuarine environments. There is a need to know the fate of nearshore deposited wastes, the rates at which they disperse, the directions in which they travel, the rates at which an estuary can flush itself of pollutants, and the effects of an estuarine discharge on the surrounding environment.

In addition to the problem of coastal pollution, New Jersey is challenged by the continual modification of its shorelines by micro and macroscale littoral processes. The State has an active shoreline protection program which the state pays 75% of the costs of shoreline protection and the municipalities the remaining 25%. For fiscal year 1971, shore communities requested aid for projects valued at over $25,000,000 with a state share at over $19,000,000. Since the available funds are less than required for shoreline protection, there is a strong state need for ERTS-1 data, which can be used for funds-allocation. Such information is essential to the environmentally sound development of New Jersey's coastal zone.

The state of New Jersey has been a leader among states in the operational use of remote sensing techniques for resource mapping. The New Jersey Wetlands Act of 1970 and the subsequent mapping of thier entire wetlands using remote sensing techniques is an example of New Jersey's interest in protecting its coastal resources through the use of remote sensing.

Because of the information needs mentioned above, the geographical extent of these interlinking estuarine systems, the dynamics of tidal progression, and the variability of climatically controlled environmental parameters, ERTS-1 offers a significant (economic, synoptic, and logistic) complement to conventional methods of data acquisition.

OBJECTIVES

The general hypothesis upon which this investigation is based, is that useful information products can be derived from ERTS-1 monitoring of tidal and nearshore circulation dynamics in near real-time, and that

they can be applied by the State to the effective management and protection of its Coastal Zone.

The principal thrust of the program is towards results and useful products founded on sound oceanographic and environmental protection principals, while taking advantage of the synoptic and repetitive properties of ERTS-1.

APPROACH

To achieve these goals, a working interface has been established between the New Jersey Department of Environmental Protection and Earth Satellite Corporation. Initial interviews were held in the various Divisions and Bureaus of the Department to determine the kinds of problems being addressed and the information needs, i.e. what types of data are used, what additional data can be used, frequency requirements, and data accuracy requirements. During initial and follow up interviews, the major needs cited most often related to coastal engineering and pollution control. Information on nearshore circulation is one of the most important contributions that ERTS-1 can provide. Individual needs vary depending on the specific application of data. The Division of Water Resources for example, needs information that would lead to the better placement of ocean outfalls. Whereas, the Division of Marine Services needs information that would lead to better allocation of funds for shore protection structures.

Preliminary analysis and use of ERTS data have centered on these four major problem areas of importance to the State.

- OFFSHORE WASTE DISPOSAL
- ESTUARINE FLUSHING DYNAMICS
- WETLANDS BOUNDARY DISCRIMINATION
- COASTAL ZONE DELINEATION

RESULTS

New Jersey, New York, and the Federal Government are concerned over offshore dumping of waste materials into the New York Bight area. The effects of this waste disposal on future recreational use of the coastal zone, fish resources, aesthetic damage, and health; need to be understood.

There are three major dumping grounds offshore New Jersey; the acid

grounds, sewage sludge area, and the dredge spoil area. Those dumps imaged so far (Figure 1) are primarily acid and dredge spoil. The acid is the most reflective and is dumped in a characteristic hair pin pattern. The dredge spoil is loaded with particulate matter but is dumped over a much smaller area. The sewage sludge contains only 1%-3% solids and is therefore much less reflective than the other two types of dumps. The dispersion and movement of all relict dumps imaged so far has been to the west, toward the New Jersey Shoreline. Figure 1 illustrate the magnitude of the dumping itself and the radial dispersion from the designated dumping sites.

In southern New Jersey, work is centered around the Atlantic City area where an attempt is being made to forecast estuarine flushing volumes. Approximately 26 million gallons/day of domestic and industrial effluents (85% of which is only receiving primary treatment) is being emptied into the waters behind the barrier islands fronting the Atlantic City area. Analysis is underway incorporating the back-basin geometry, tidal prism, turbidity, and modeled dispersion coefficients to compare the actual volumes discharged to the normalized reflectance values in the nearshore and estuarine waters. With these data an estimate of the flushing volumes can be used by the Division of Water Resources in planning future growth.

Color composites and a mosaic of MSS Band 7 were used to delineate an upper wetland boundary for coastal New Jersey. The pink to reddish tonal signatures of the wetland vegetation, the position of the vegetation between barrier beaches and the mainland and along tidal streams, all aided in the identification and separation of wetland from upland areas. Experience gained from mapping New Jersey's upper wetland boundary using 1:12,000 color infrared aerial photography as part of the New Jersey Wetlands Mapping Program also aided in wetland vegetation identification. The tonal and textural signatures of wetland vegetation were considerably different from those of upland plant species and the boundary was drawn along a distinct tonal and textural break. Along the Delaware River tonal signatures indicative of wetland species could be identified along stream channels, but these signatures were more subtle than those seen along the coast. This map is of course a gross delineation in comparison to the 1:12,000 scale, but for illustrative purposes, this type of map is very useful.

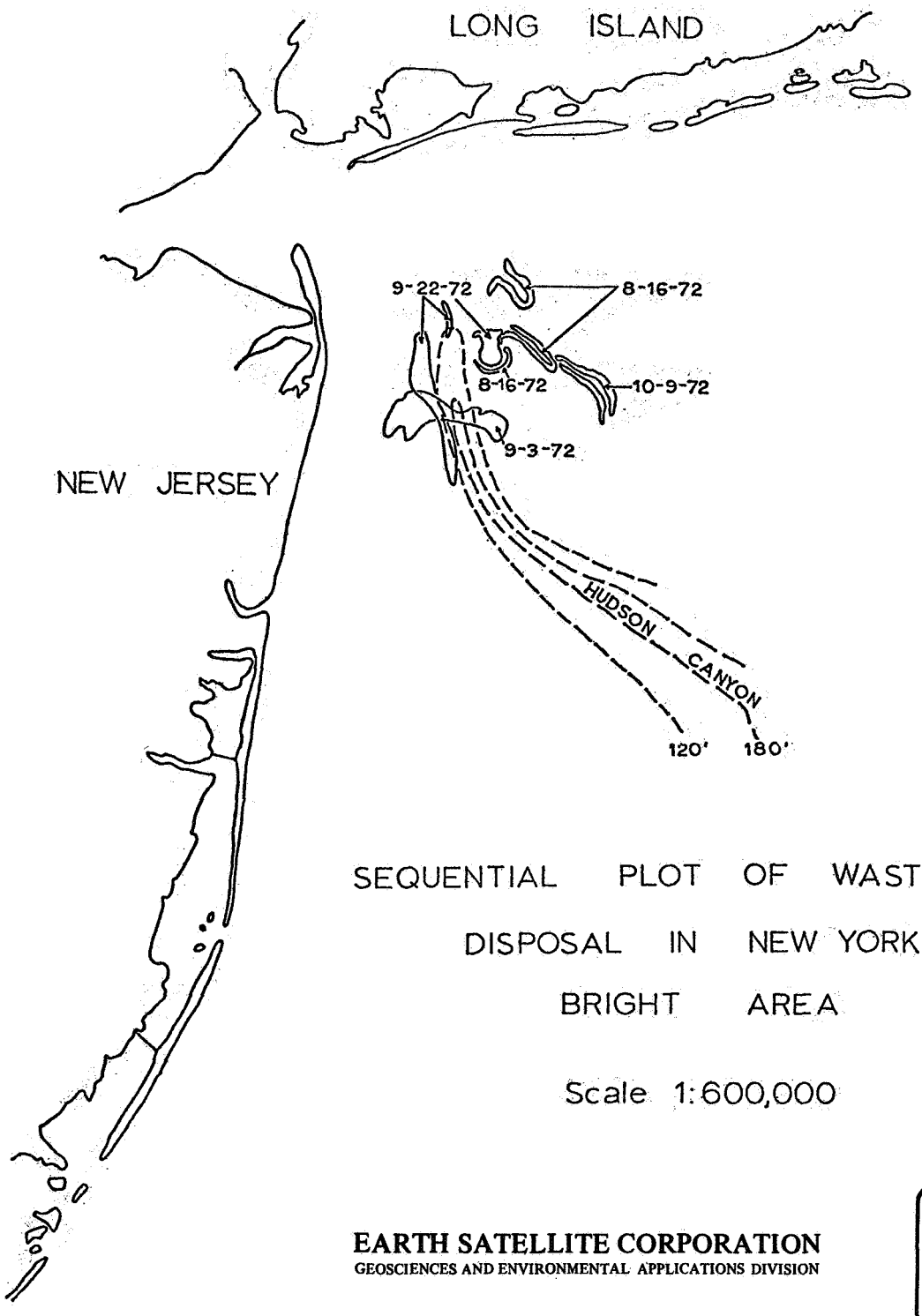
More recently, the New Jersey Department of Environmental Protection has used ERTS-1 imagery (mosaic of MSS band 5) to illustrate and explain before the State Legislature the extent of the coastal zone as defined in New Jersey's "Coastal Area Facility Review Act." New Jersey realizes that its coastal zone is a unique and irreplaceable natural resource, and that the economy of the entire State will suffer serious adverse effects if the environmental impact resulting from the

future location of major facilities is not carefully assessed. For these reasons, ERTS-1 imagery was found to be most useful in explaining the States position in regard to protecting the coastal area.

SUMMARY

These are only preliminary results of an on-going investigation of New Jersey's coastal zone. Several categories of operationally oriented products are being prepared by EARTHSAT for State use. Some of these products have been explained in the previous sections. Product development is a continuous process and is responsive to the needs of the State.

EARTHSAT and the NJDEP have recognized that ERTS-1 data and the analysis thereof can lead to the development of practical information products that can go a long way towards solving many of the near term, real world problems of the coastal environment.



SEQUENTIAL PLOT OF WASTE DISPOSAL IN NEW YORK BRIGHT AREA

Scale 1:600,000

EARTH SATELLITE CORPORATION
GEOSCIENCES AND ENVIRONMENTAL APPLICATIONS DIVISION

Paper E 10

MONITORING OCEAN DUMPING WITH ERTS-1 DATA

C. T. Wezernak and N. Roller, *Environmental Research Institute of Michigan, Ann Arbor, Michigan*

ABSTRACT

Large volumes of municipal and industrial wastes are disposed of by means of dumping at sea. Disposal of wastes by barge dumping frequently produces surface films and waste fields whose fate and effects are not adequately defined. Frequently very large areas of the marine environment are affected.

Described in this paper are the results of an analysis of ERTS-1 data for the New York Bight collected on 16 August 1972. Results are presented which show acid-iron wastes, sewage sludge, suspended solids, and major water mass boundary features in the study area. The potential of satellite remote sensing for monitoring large scale events such as ocean dumping is discussed.

1. INTRODUCTION

The volume of waste disposed of by ocean dumping is increasing rapidly. Generally, ocean dumping is viewed as a convenient mechanism for the disposal of the more objectionable waste products of contemporary society, substances which are not readily amenable to treatment by means of existing techniques, or substances which are judged to be "too expensive" to treat. In the majority of cases, waste disposal takes place not in the deep ocean but rather in nearby coastal waters. Because of numerous environmental implications associated with the practice, ocean disposal of wastes has become a matter of national and international concern.

An important element in present and future programs for managing ocean disposal of wastes is the availability of a monitoring system (or systems) which will (a) document authorized discharges to verify

compliance in terms of discharge location, (b) detect unauthorized dumps or accidental discharges, and (c) provide data regarding the movement of wastes. Monitoring systems are required not only for the detection of small spills and discharges but also for monitoring large scale events. The present report is one example of current efforts to define the potential of satellite remote sensing for large scale environmental monitoring.

2. STUDY AREA

The coastal waters adjacent to the New York Metropolitan Region are the repository for substantial quantities of sewage sludge, industrial acid-waste, construction debris, and dredge spoils [1,2].

Sewage sludge is disposed of at a location approximately 19 km. south of Long Island. At the present time, approximately 9,500 cu. m. per day are dumped at this location. In addition to nutrient enrichment of the overlying waters, the introduction of heavy metals, etc. at the immediate dump location, the practice also results in the formation of extensive surface films [3,4].

Acid-iron wastes are disposed of at a location approximately 20 km. east of New Jersey and 24 km. south of Long Island. The waste solution contains approximately 8.5% H_2SO_4, 10% $FeSO_4$, and small quantities of various metallic elements [4,5]. The wastes are dispersed by barge over a hairpin-shaped course of approximately 8 km. in length. The subsequent oxidation of the iron from the ferrous to the ferric state produces a suspension which tends to remain in a distinct pattern for long periods after dispersal.

In addition to the above substances, dredging spoils from the New York metropolitan harbor area and construction debris are dumped in the New York Bight.

3. RESULTS

Multispectral aircraft missions are included in the program in order to provide corrobative evidence for use in the analysis and interpretation of space data. The study area is large and includes low contrast phenomena of varying size and distribution. Hence aircraft data is utilized to identify features of interest in the study area and to evaluate ERTS-1 data.

A support mission was carried out by the ERIM aircraft on 16 August 1972 at a time coincident with the satellite pass over the study area. Twelve channels of data were collected over the spectral range 0.32 to 11.7 μm. A two channel display of aircraft data is shown in Figure 1. The lower spectral band (0.62-0.70 μm) corresponds to MSS 5 (0.6-0.7 μm) in the ERTS data.

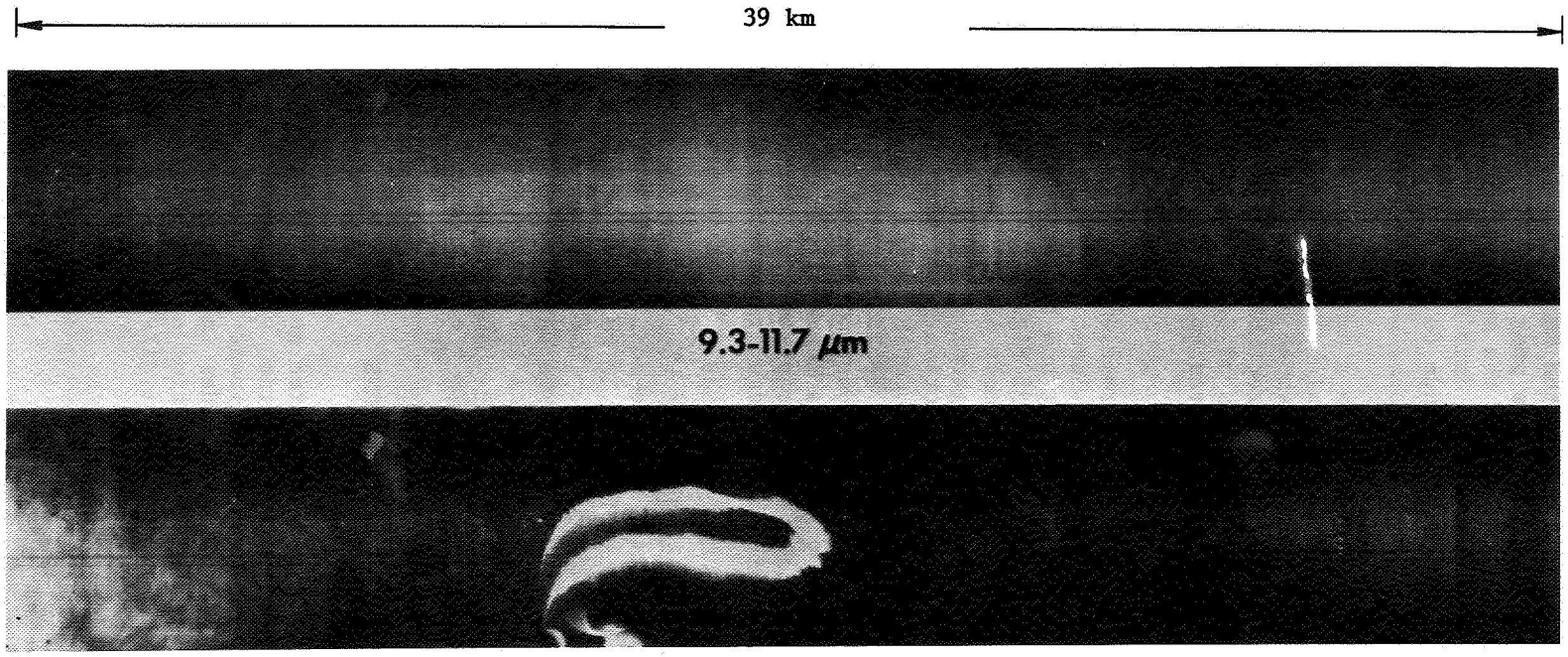
An analysis of aircraft data indicates a number of large features in the area. In addition to the acid waste (which has a reflectance peak in the 0.62-0.70 μm band), surface films, suspended solids, and water mass boundaries are evident. The latter were detectable in this case on the basis of thermal properties and on the basis of other spectral characteristics. Analysis of aircraft data was limited to those features which are within the scope of the ERTS investigation.

Figure 2 illustrates the kind of information which is obtainable by direct analysis of ERTS imagery. Clearly evident in Figure 2 (MSS 5) is the acid-waste, the sewage sludge dump area, and the suspended sediment input from the Lower Bay area. Inspection of Figure 3 (MSS 6) provides additional information regarding the area, most notably the water mass boundaries. Furthermore, an observation regarding the relative depth of the sewage sludge can be made from an inspection of Figures 2 and 3. Of the two spectral bands MSS 5 and MSS 6, greater depth detail can be expected in MSS 5 due to differences in the attenuation coefficient of the two spectral bands. As a result, in Figure 3 only that portion of the sludge which is at or very near the surface is evident, whereas the entire mass is visible in Figure 2. Finally the shape of the sediment plume, the acid-waste, and the water mass boundaries provide information regarding surface circulation patterns at the time of observation.

Shown in Figure 2A is a digital map of the acid waste. The two density levels shown represent concentration differences. The dimensions of the waste are 9.4 km. from pt. A to pt. B and 6.16 km. from pt. C to pt. D. The surface area of the waste is 1,250 hectares. The distance from the nearest point of the plume to the New Jersey coast was found to be 16.25 kilometers. This is somewhat closer to the coast than the designated acid-dump area. The sewage sludge dump is shown in Figure 2B. The center of the dump was found to be 20 km. $\pm$ south of Long Island and 20 km $\pm$ east of Sandy Hook.

4. CONCLUSIONS

An analysis of spacecraft data collected on 16 August 1972 (ERTS image ID E-1024-15071) clearly shows the distribution of an acid-waste discharge, sewage sludge dump, and major suspended sediment inputs into the study area. Additionally the data analysis provides information regarding the surface movement of the wastes and the location of major water mass boundaries. Synoptic coverage of the type available from satellite



NEW YORK BIGHT

16 August 1972

ERIM

FIGURE 1 AIRCRAFT IMAGERY

Altitude = 3048 meters

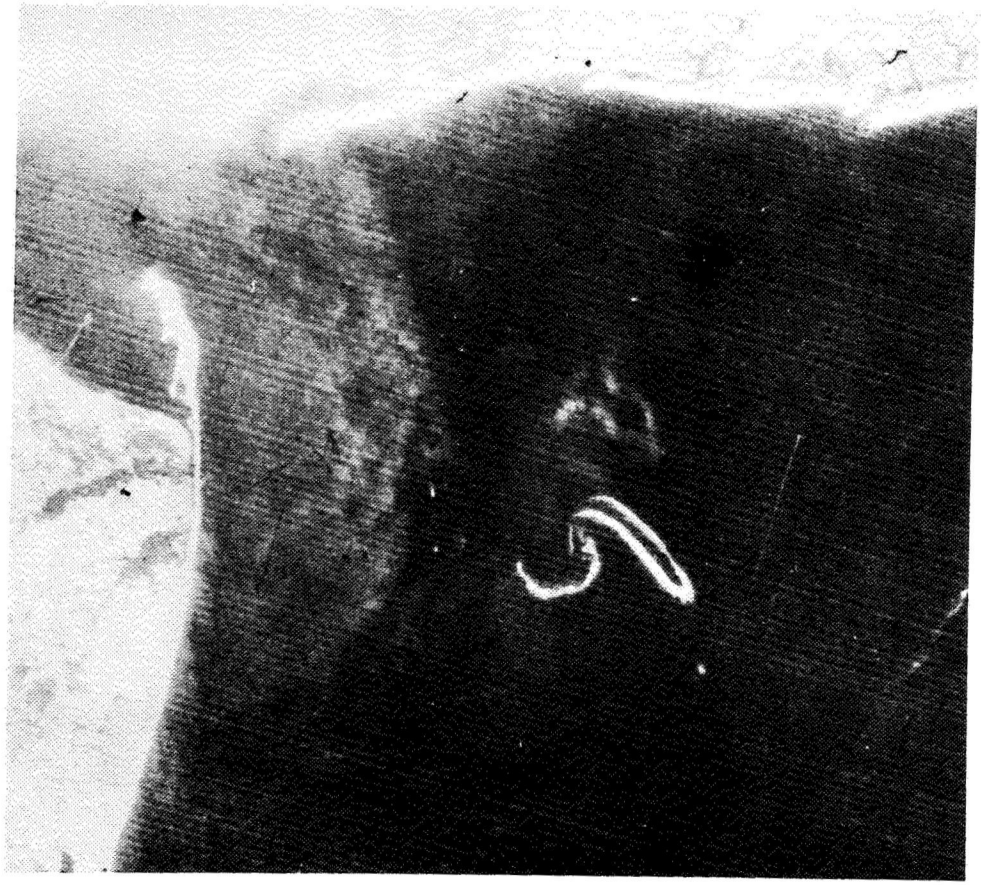


FIGURE 2 ERTS-1 IMAGE
MSS 5 0.6-0.7 μm
E 1024-15071

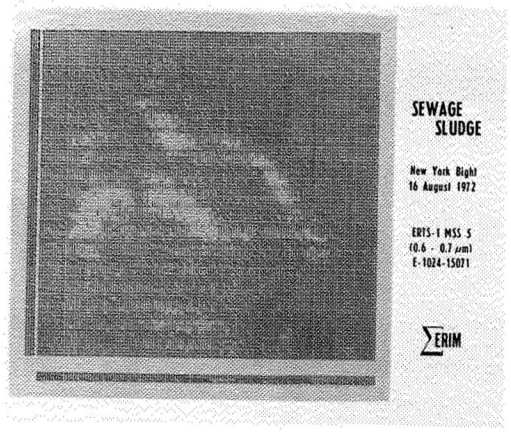


FIGURE 2B

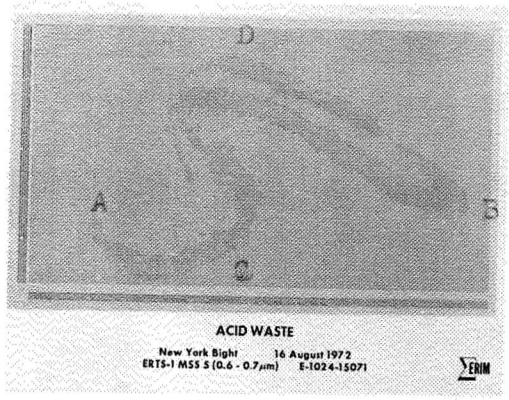


FIGURE 2A

FIGURE 3 ERTS-1 IMAGERY
MSS 6 0.7-0.8 μm
E 1024-15071

altitudes can be expected to contribute towards an understanding of surface circulation patterns in the area.

An attempt was made to differentiate waste fields and water masses using digital ratioing techniques. The results were mixed and indicate the necessity of increasing scanner gain over water areas.

A clear need exists in physical oceanography and marine pollution control for improved monitoring systems capable of providing data over large areas. Remote Sensing from space has the potential for meeting this need. Instrumental improvements in future satellites, including the addition of a high resolution thermal channel, will serve to increase the utility of satellite remote sensing.

5. REFERENCES

1. The Marine Disposal of Sewage Sludge and Dredge Spoil in the Waters of the New York Bight (Technical Memorandum 1-71, Woods Hole Oceanographic Institution, Woods Hole, Mass., Jan. 1971). (Report).

2. Survey of Marine Waste Deposits, New York Metropolitan Region (Technical Report No. 8, Marine Sciences Research Center, State University of New York, Stony Brook, New YOrk, April 1971). (Report).

3. Analyses of Dredged Wastes, Fly Ash, and Waste Chemicals -- New York Metropolitan Region, (Technical Report No. 7, Marine Sciences Research Center, State University of New York, Stony Brook, New York, October 1970). (Report).

4. The Effects of Waste Disposal in the New York Bight (Summary Final Report, National Marine Fisheries Service, Sandy Hook Laboratory, Highlands, New Jersey, April 1972). (Report).

5. R. F. Vaccaro, G. D. Grice, G. T. Rowe, and P. H. Wiebe, Water Research 6, p. 231 (1972) (Journal).

Paper E 11

ENVIRONMENTAL STUDY OF ERTS-1 IMAGERY: LAKE CHAMPLAIN AND VERMONT

Aulis O. Lind, E. Bennette Henson and James Pelton, *University of Vermont, Burlington, Vermont*

ABSTRACT

Environmental concerns of the State of Vermont currently being stressed include water quality in Lake Champlain and a state-wide land use and capability plan. Significant results obtained from ERTS-1 relate directly to the above concerns. Industrial water pollution and turbidity in Lake Champlain have been identified and mapped and the ERTS pollution data will be used in the developing court suit which Vermont has initiated against the polluters. ERTS imagery has also provided a foundation for updating and revising land use inventories which will be necessary for meeting some of the informational needs of the Land Use and Land Capability Act (Act 250) now in the process of legislative action at the state level. Major classes of land use have been identified and mapped, and substantial progress has been made toward the mapping of such land use divisions as crop and forest type, and wetlands.

I. INTRODUCTION

Among the environmental issues currently in the public spotlight in Vermont, two stand out as particularly important because they involve precedent setting resource management actions at the state level. These issues concern a) water quality in Lake Champlain, and b) land use management. This paper will attempt to address these environmental concerns in terms of some of the significant results obtained from ERTS-1 data analysis at the University of Vermont. The specific significant results forming the focus of this paper include: a) detection and monitoring of industrial water pollution, b) lake turbidity patterns, and c) land use. The general study area for which significant results

have been obtained relating to the major environmental concerns above is covered by a single ERTS scene which centers approximately on Lake Champlain (Figure 1).

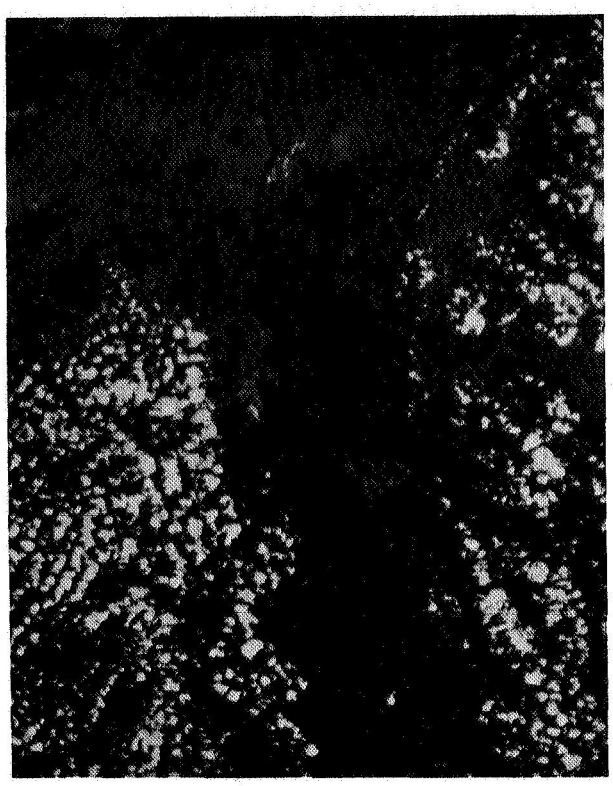


Figure 1. This RBV 2 rendition of the general study area (July 29) shows the Lake Champlain Lowland as the cloud free area around the lake. The turbid, southern arm of Lake Champlain can also be discerned.

Both RBV and MSS data were available and the range of seasonal coverage extends from late summer to midwinter. In spite of above normal cloudiness for the final quarter of 1972, about one-third of all ERTS scenes for this period were largely cloud free.

II. WATER POLLUTION

Major sources of industrial pollution are found on the New York side of Lake Champlain with major important centers of activity at Fort Ticonderoga and along the Saranac River near Plattsburgh. The bulk of the industrial pollutants being discharged into the lake stem mainly from paper manufacturing operations.

A major pollution plume from the new International Paper Company mill just north of Fort Ticonderoga was detected in the October 10th MSS scene. The plume is best seen on bands four and five (.5-.6 and .6-.7 micrometers), image number 15115. The plume appears as a darker tone in the context of the light-toned turbid water of this portion of the lake. Figure 2 shows the plume as rendered by the better contrast provided in MSS band four.

The pattern of the plume is controlled to some degree by a lake bottom diffuser pipe which extends from the treatment plant in a northeasterly direction nearly to the Vermont border. This pipe distributes the water from aeration lagoons which receive the waste products of paper digestion. The lagoons began discharging in March of 1971 at a rate of approximately 21 million gallons per day. Most of the settleable solides are removed in the treatment process, but the waste water is turbid with suspended solids. The waste water is high in sodium, conductivity and oxygen demand, and very high in phosphates. The observed color of the water is a humic, dark reddish-brown.

The State of Vermont has taken legal action against the paper company and the State of New York alleging that the new plant is reducing the water quality of the lake below Vermont standards, and that this polluted water does cross over the state boundry into Vermont. Field observations, in which the plume can be generally defined by physical and chemical parameters indicate the discharge water does cross over into Vermont (see Figure 3). The ERTS-1 imagery depicts this with exactitude, and supports the ground observations. The high phosphate concentrations in the discharge plume provide sufficient nutrients to stimulate algal blooms which contribute to the eutrophication of this part of the lake.

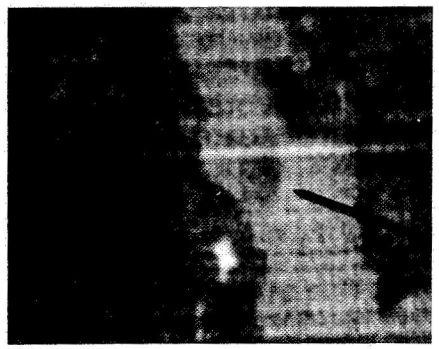


Figure 2. MSS 4 rendition of papermill pollution plume. The bright spot on the left shore is the mill site. Vermont is on the right and the boundary is approximately centered in the lake area.

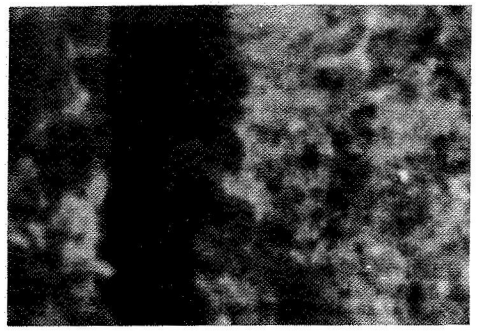


Figure 4. RBV 2 (29 July) showing turbidity boundary.



Figure 5. MSS 4 (10 October) showing extended turbidity pattern.

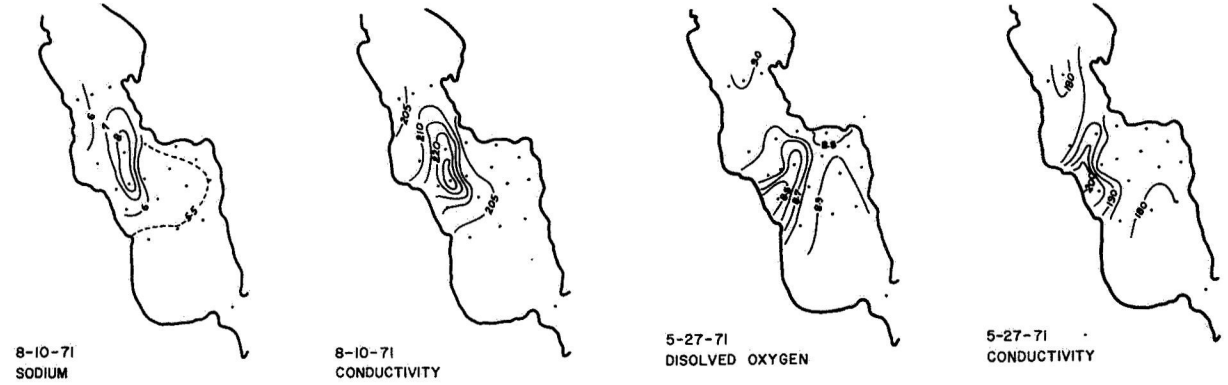


Figure 3. Pattern of chemical/physical water properties showing the plume effect similar to that in Figure 2 above.

III. TURBIDITY

It is well documented that the water in the southern end of the lake is much more turbid than the main lake, and this fact is readily seen on ERTS imagery showing the lake (see Figure 1). Transparency as measured with the Secchi disc is four to six meters in the main lake, but is less than one meter in the southern end. These contrasts are quite apparent where the two water masses meet in the vicinity of Chimney Point, Vermont, and Port Henry, New York (see Figure 4 and 5). A turbidity boundary may be identified from ERTS imagery and fluctuations in this boundary have been observed from two separate satellite coverages.

A particularly prominent extension of turbid water entering the main body of the lake was observed in the October 10 MSS scene (Bands four and five). The ERTS image shows that this turbid plume moves westerly to the western shore of the lake where it then follows the shore towards the north. The turbid water then curls back toward the east until it can no longer be detected. This indicates that the turbid, south-end water becomes part of a large clockwise circulation pattern which dominates the southern end of the main lake body. The above pattern was associated with southeasterly winds which shifted from the southwest about one-half hour before the images were generated. The turbidity patterns in this region of the lake will bear watching and although further study will be required to establish a turbidity pattern model, it is significant that at this time turbidity patterns can be observed and mapped using ERTS data.

IV. LAND USE

A second major environmental concern in Vermont focuses on land use and the development and implementation of state-wide land use regulations. A land use inventory of Vermont was conducted based on conventional aerial photography dating from the early to late 1960's, and it is this information which is being used to support the Land Use and Land Capability Plan currently under legislative review in Vermont. This legislation, known as Act 250, proposes to establish definite land use guidelines and regulations and is in itself considered

a model piece of legislation concerning land use control at the state level. Increasing pressure for land development and conversion of rural to urban land uses are changing land use patterns at a rapid rate, and therefore, it becomes necessary to update the land use inventory.

Major land use categories have been identified and mapped in several substudy areas selected as representative of Vermont land use patterns. Two strictly rural areas, one urban area, and a mountainous, forested area served as a basis for land use studies using ERTS data. All but the last area have been completely mapped at the highest classification level and progress is being made toward mapping at lower classification levels.[1] Because of the patchwork nature of land use patterns and the small unit sizes of such features as cropland, considerable scene enlargement coupled with additive color enhancements were found to be necessary ingredients of the analysis procedure.

Urban and built-up land is one of the major categories that can be mapped from ERTS imagery down to a scale of one inch equals one mile. The Burlington test area provides the best testing ground for such mapping since it constitutes the largest urban area in the state. The map of urban and built-up land (Figure 6) was made from an enlarged, color composite scene from RBV data (Bands one to three, July 29) as generated by a multispectral viewer. In addtion to the simple separation of urban or built-up vs. rural land use, it was also possible to map land use "intensities" at a lower classification level. A first-look analysis of the first Vermont winter scene (8 January) indicates that the best subject/background contrast occurs in winter with thin snow cover, and it appears that this imagery will allow for finer definition of small built-up areas including further subdivision of major built-up areas.

The rural scene in Vermont includes a mosaic of cropland, pasture land, orchards, forests, wetlands, and many streams and lakes. In the agricultural areas, separation of forest tracts from general agricultural land on ERTS imagery may be accomplished from summer or autumn imagery, however slightly better contrast is provided in autumn ERTS coverage, and a first-look at the

---

[1]The classification employed here is based on: Anderson, James; Hardy, Ernest E.; and Roach, John 1972. A Land Use Classification for Use With Remote Sensor Data, U. S. Geological Survey Circular 671, 16 pp.

Figure 6. Land use, Burlington test site.

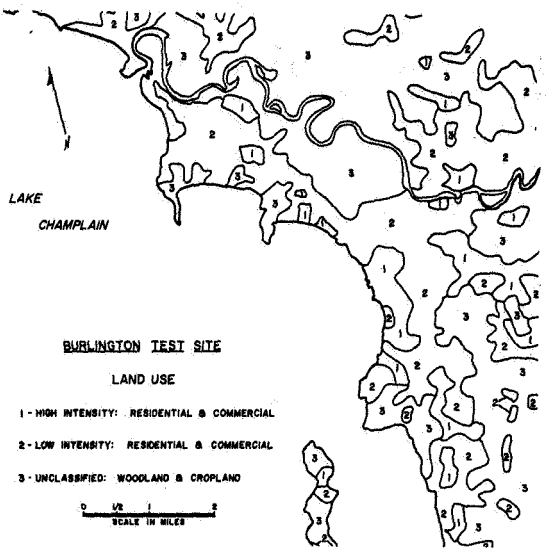


Figure 7. Land use, North Hero test site.

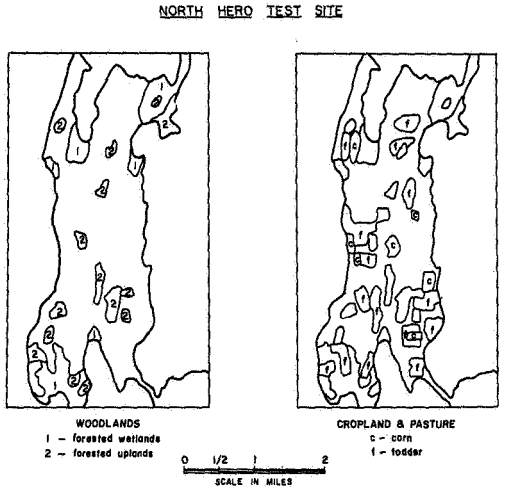
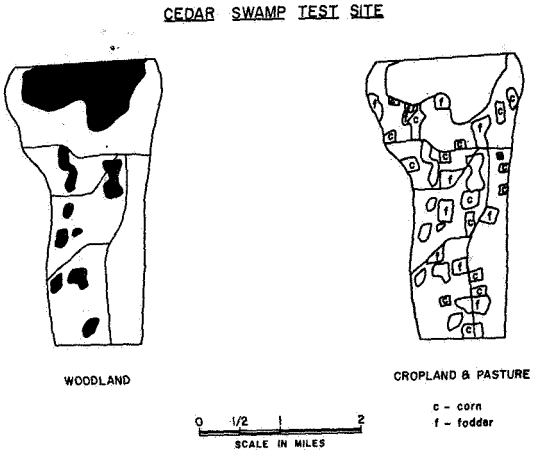


Figure 8. Land use Cedar Swamp test site. Addition of corn and fodder cropland was possible through use of autumn season coverage.



winter scenes just made available allows for very clear definition of all woodland tracts. Wooded wetlands may be differentiated on autumn coverage, and woodland/scrub units seem to be additional units for recognition and mapping from winter scenes.

Presently, it has not been possible to recognize orchards since in the available imagery they are rendered in the same tone/pattern as pastures. However, it is likely that additional seasonal coverage may bear this category out in much the same manner as for example corn fields have been identified by a unique tone produced in autumn imagery. Land use maps generated for the two rural test areas (Figures 7 and 8) are somewhat incomplete in that the cropland/pasture land distinction has not yet been fully made. It is expected that seasonal coverage will reduce the omission error as the autumn coverage did with respect to the summer coverage in the example of corn above. The autumn coverage also allowed for the identification of fields used for fodder crops.

A comparison of a test site map generated from ERTS data with a pre-existing map of land use showed that changes had occurred where woodland areas had increased at the expense of cropland or pasture land. The detail in the enlarged ERTS images was sufficient to allow for corrections in the land use information at state land use mapping scales. The ground checks confirmed these observed changes.

V. SUMMARY

ERTS-1 has provided both timely and significant environmental information for the two major state concerns regarding water quality in Lake Champlain and land use. A major paper mill discharge plume has been identified and this has become part of a precedent setting court suit involving the States of Vermont and New York. A major lake turbidity boundary has been identified and monitored, and the land use data capabilities of ERTS are substantial to the extent that pre-existing maps can be corrected.

Paper E 12

WATER TURBIDITY DETECTION USING ERTS-1 IMAGERY[1]

Harold L. Yarger, James R. McCauley, Gerard W. James and Larry M. Magnuson, *State Geological Survey, University of Kansas, Lawrence, Kansas* and G. Richard Marzolf, *Division of Biology, Kansas State University, Manhattan, Kansas*

1.0 ABSTRACT

ERTS-1 images of two federal reservoirs in Kansas exhibit good correlation with suspended load. The major reservoirs in Kansas, as well as in other Great Plains states, are playing increasingly important roles in flood control, recreation, agriculture, and urban water supply. Satellite imagery may prove useful for acquiring timely low cost water quality data required for optimum management of these fresh water resources.

2.0 INTRODUCTION

The dominant limnological feature of the Great Plains today takes the form of reservoirs constructed by the U.S. Army Corps of Engineers and the U.S. Bureau of Reclamation. The primary influence on the reservoir ecosystem is the suspended material and chemicals carried in by streams and rivers. The authors are studying ERTS images of Kansas reservoirs to determine the feasibility of monitoring these water quality indicators by satellite. The reservoirs throughout the state, which should be representative of most Great Plains reservoirs, are located in a variety of physiographic regions such as the glaciated region in the northeast, the valleys and scarps in the southeast, the dissected plateau and alluvial plains areas in central Kansas, and the high planes in the west.

Two reservoirs, Perry and Tuttle Creek, have been singled out for close study. Approximately ten water samples from each reservoir are collected during each cloud-free ERTS overpass and analyzed for concentrations of inorganic suspended and dissolved solids, organic suspended and dissolved solids, chlorophyll, potassium, phosphate, and nitrate ions. In addition, secchi disc and temperature measurements are taken at each sampling station. The two reservoirs are distinct in terms of adjacent outcropping rocks and land use. Perry drains

[1]Work supported, in part, by NASA contract NAS5-21822

a recently glaciated region in the cornbelt of eastern Kansas. Tuttle Creek drains the Flint Hills area to the west which is outcropping Cretaceous and Permian rock. The dominant land use is seasonal grazing and small grains. A later phase of this project will be to test any predictive relations derived from Perry and Tuttle Creek on other reservoirs in Kansas.

Kansas reservoirs are typically shallow and thus are susceptible to mixing by strong winds which are a characteristic climatic feature of this region. Wind generated currents are of sufficently high velocity to maintain a sizable fraction of the silts and clays in suspension and the result is turbid water (mean light extinction coefficient $\sim$ 2.5 meters^{-1}). Accordingly, reflecting energy detected by ERTS is primarily influenced by the suspended load (the predominent fraction of which is inorganic material). The determination of the secondary influence of organic material and chemicals on reflected energy must wait until the effects of inorganic suspended load are understood. The remainder of this paper is devoted to this aspect.

3.0 GROUND TRUTH ANALYSIS

The light penetration depth is primarily controlled by suspended load. The inverse secchi depth (or 1/sunlight penetration depth) is linearly related to suspended load up to $\sim$ 100 ppm (Figure 1). Least squares straight line fits to these data yield statistically equivalent slopes and intercepts. Although inconclusive, the few points beyond 100 ppm (not shown) indicate this linearity may hold up to 250 ppm. The greater point scatter in the Tuttle Creek data is due to higher average turbidity relative to Perry. This results in a smaller average light penetration depth and greater percent error in its measurement by the secchi disc method.

4.0 IMAGE ANALYSIS

Approximately 30 cloud-free and ice-free ERTS images of Tuttle Creek and Perry have been electronically sliced and displayed on our IDECS system. The color coded displays were recorded on 35 mm film for permanent storage and further analysis. The level slicing was done on the basis of equal vidicon output voltage intervals which is equivalent to equal log density intervals. The maximum number of levels/image was determined by the dynamic range of the particular band over the reservoir surface and varied from 2 to 8 levels. The equal gray levels selected by IDECS correspond to nearly equal reflected energy intervals as defined on the NASA 15 step

gray tablet. Maximum density variation (∿ 0.6 to 1.7) is usually found on the red band (MSS5) and corresponds to a power return range of 0 to ∿ 25%.

5.0 COMPARISON OF IMAGERY WITH GROUNDTRUTH

Gray level contour maps of each image were prepared for comparison with suspended load and secchi measurements (example in Figure 2). In addition, the data was examined in graphical form for each reservoir pass (examples in Figures 3 and 4). The Tuttle Creek pass 2 data exhibits a strong correlation between gray level, suspended load, and secchi depth in the green (MSS4), red (MSS5) and infrared (MSS6) bands. This data is fairly representative of other Tuttle Creek and Perry passes, except in some cases the green band correlation is poor. Bands 5 and 6 normally show strong correlation with suspended load and secchi depth with band 5 being more reliable. Band 7 is poorly correlated, but usually appears somewhat brighter at the very turbid end of the reservoir. Based on the pure water spectral attenuation coefficient, best correlation would be expected in the green band. This is probably being obscured by haze induced by atmospheric scatter. Figure 5 shows band 5 correlations for the first four passes over Perry Reservoir dating from 7-27-72 to 9-19-72. This is representative of both reservoirs, in that, the dynamic range over the reservoir surface tends to shrink as winter approaches with lower sun angle and lower average turbidity.

6.0 CONCLUSIONS

Bands 5 and 6 exhibit strong correlation with suspended load and sunlight penetration depth. In some cases band 4 also exhibits strong correlation, but is not reliable and is probably quite sensitive to atmospheric conditions. Band 7 is poorly correlated, although does show a brighter return for suspended load $\geq$ 100 ppm. The discrimination or sensitivity between gray level and suspended load is good up to 100 ppm, but appears to rapidly deteriorate above this level of turbidity. More imagery/ground truth over high turbidity water is required for further illumination of this problem. MSS imagery obtained in the high gain mode would probably be a great help in extending the discrimination. This is feasible because the power return from the reservoir surface is never more than 30% of maximum return.

In summary, the prospects for developing a reliable low cost procedure for predicting suspended load from ERTS imagery looks very good.

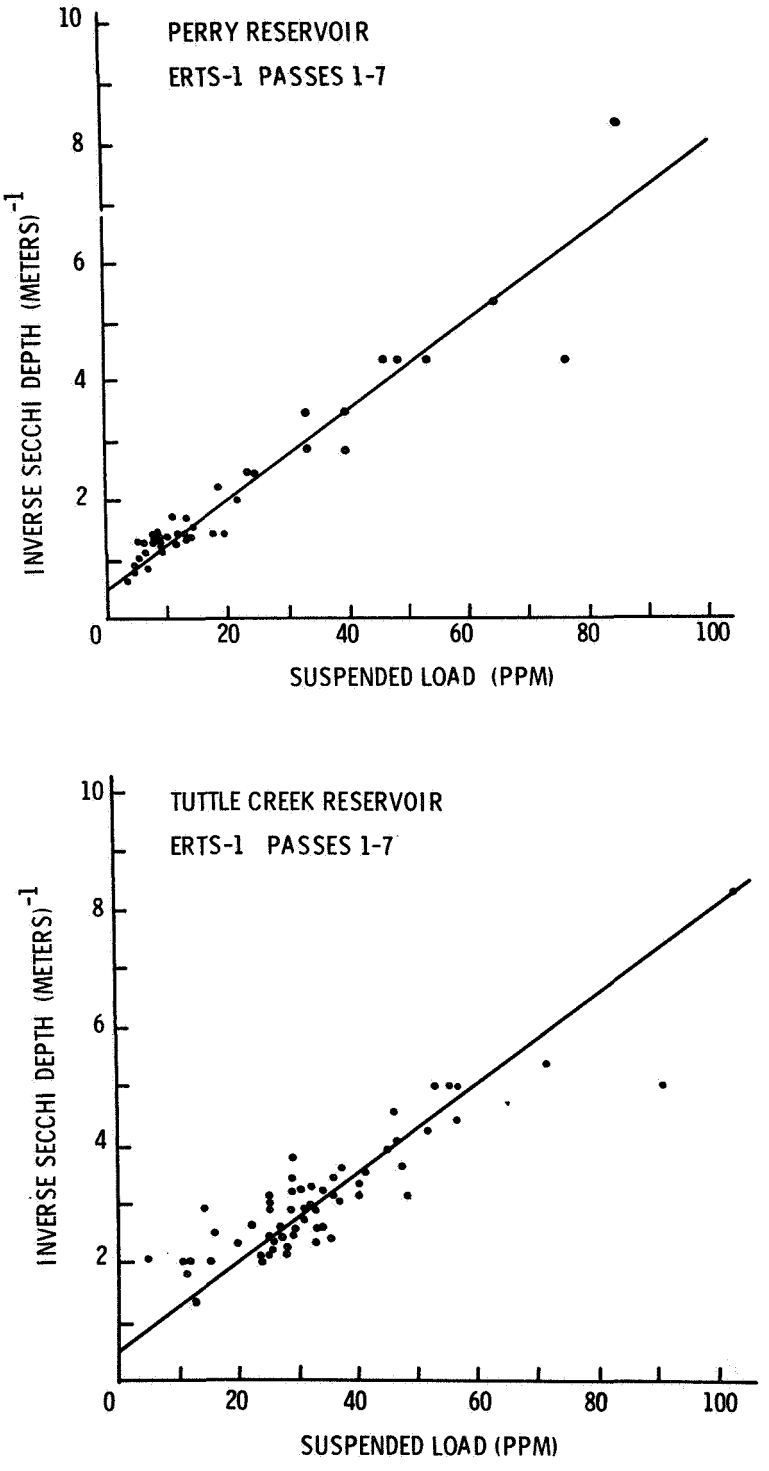


FIGURE 1. Inverse secchi depth vs. suspended load for Perry and Tuttle Creek reservoirs.

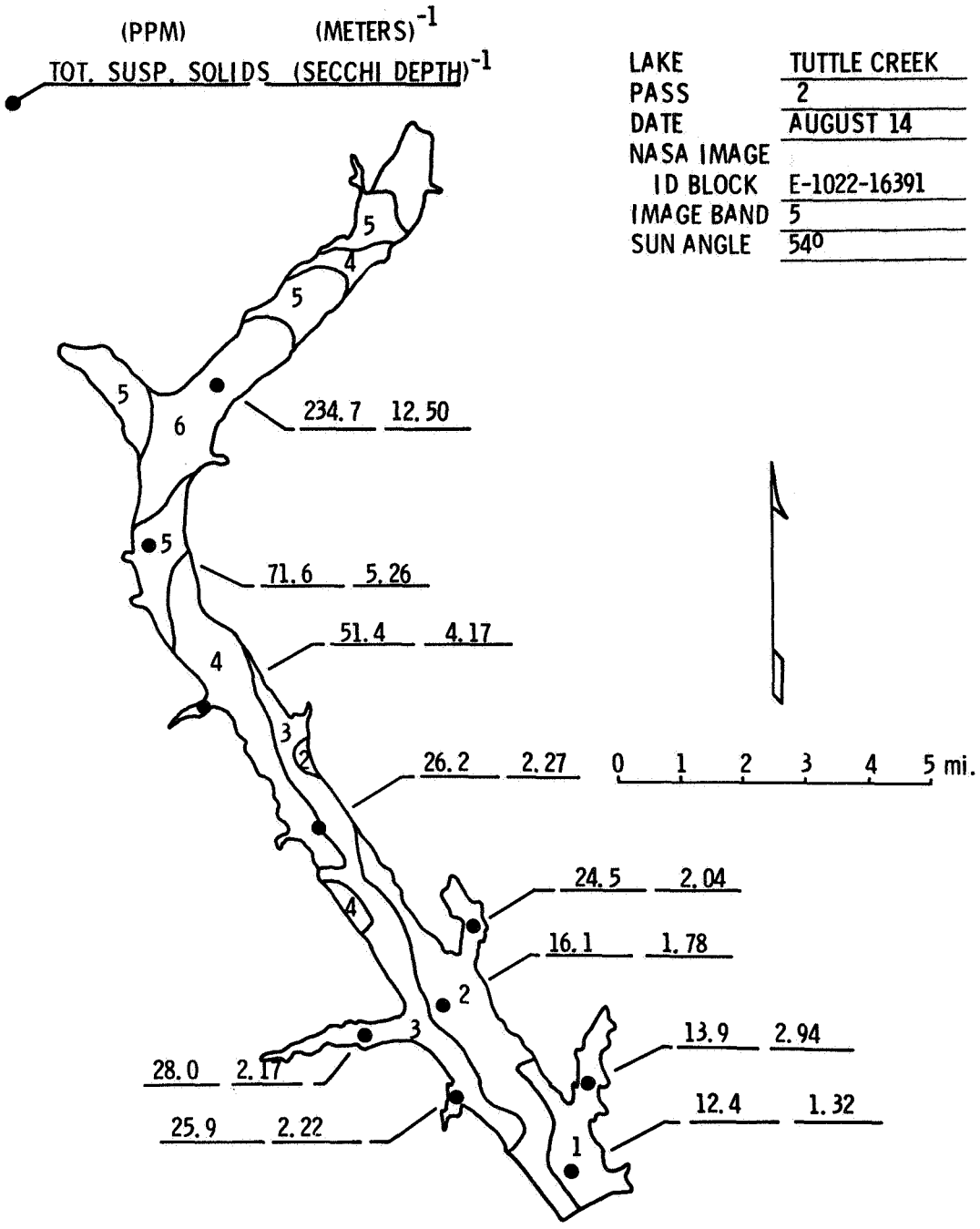


FIGURE 2. Gray level map and turbidity measurements for Tuttle Creek reservoir.

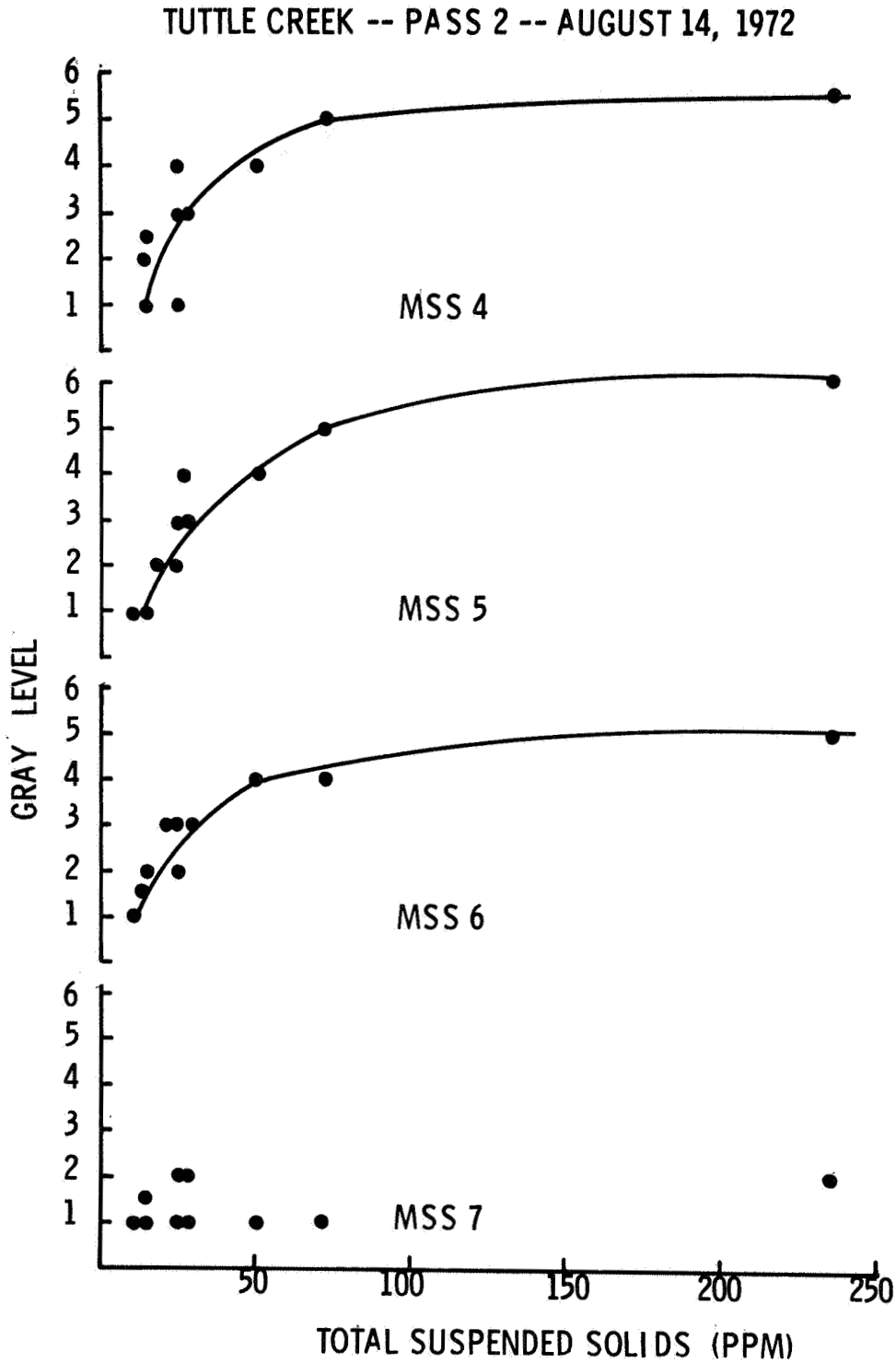


FIGURE 3. Gray level vs. suspended solids for Tuttle Creek Reservoir.

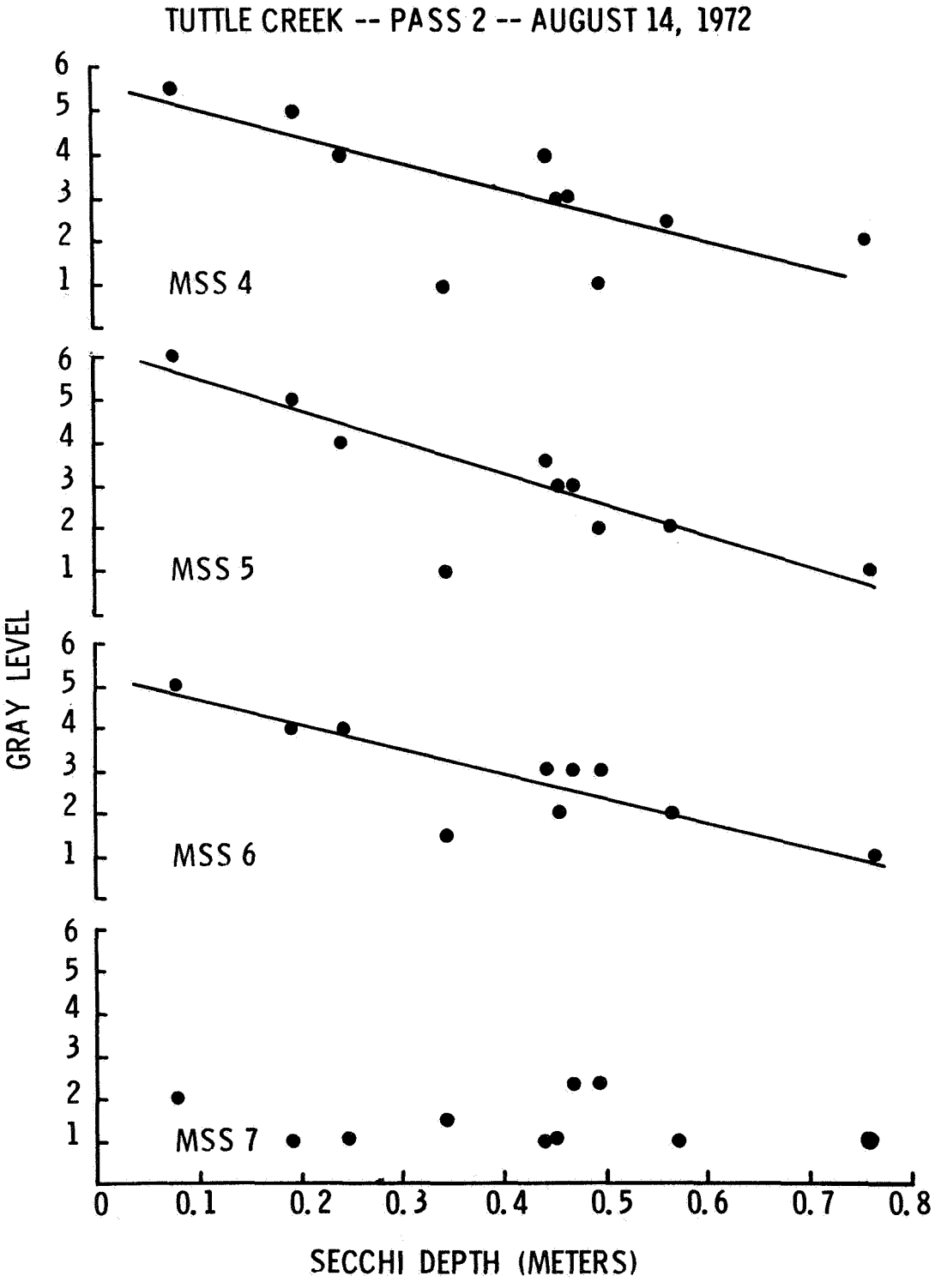


FIGURE 4. Gray level vs. secchi depth for Tuttle Creek Reservoir.

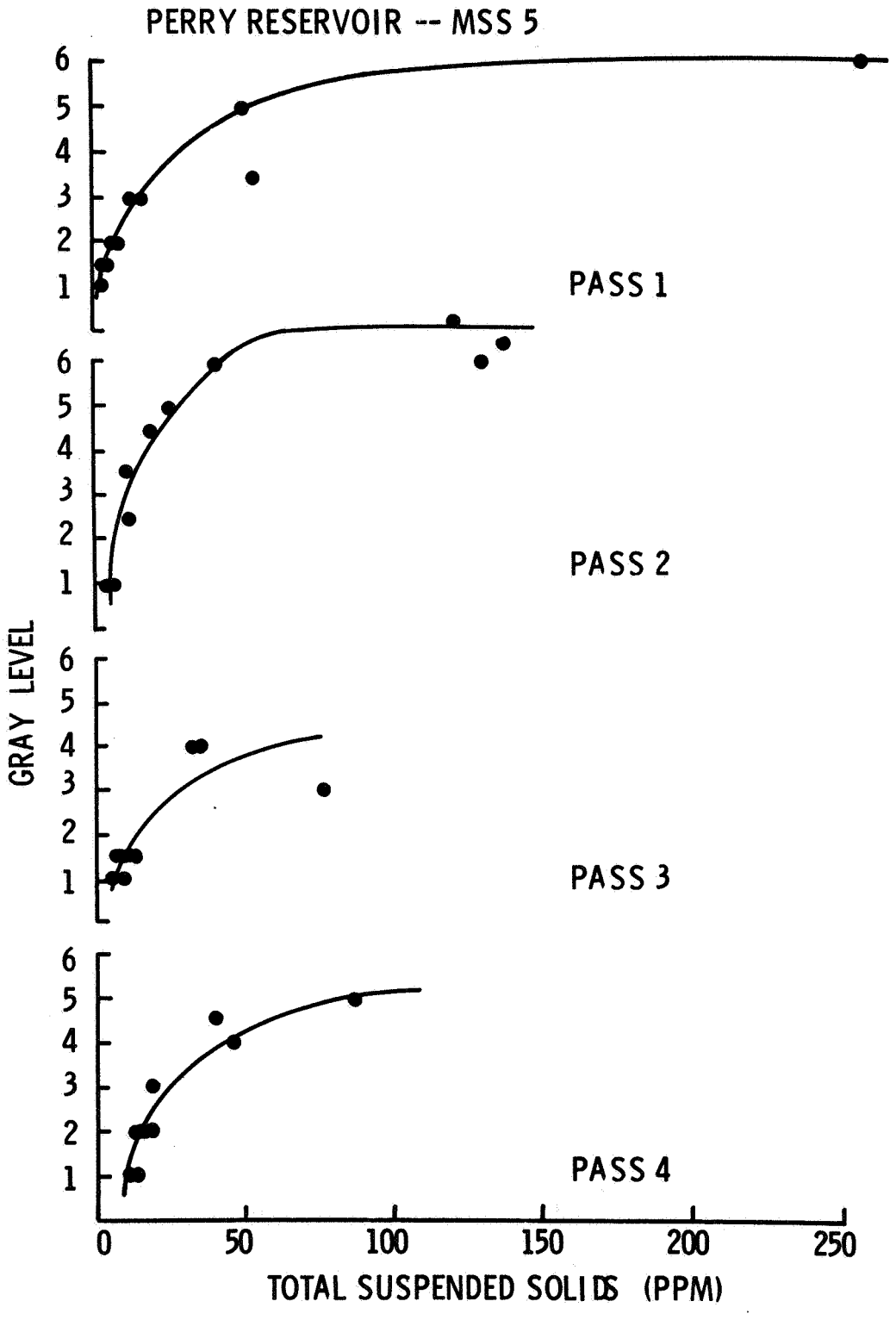


FIGURE 5. Gray level vs. suspended solids for Perry Reservoir.

Paper E 13

DIGITAL ANALYSIS OF POTOMAC RIVER BASIN ERTS IMAGERY: SEDIMENTATION LEVELS AT THE POTOMAC-ANACOSTIA CONFLUENCE AND STRIP MINING IN ALLEGHENY COUNTY, MARYLAND

J. S. Schubert and N. H. MacLeod, *Department of Biology, The American University, Washington, D. C.*

ABSTRACT

Two simple algorithms for classification of sedimentation levels in water and for delineation of active strip mines are in use as part of the development of a more general resource management information system. ERTS MSS CCT's are processed so that each pixel in each channel is geographically referenced and can be accessed individually during whole frame, multi-channel analysis or partial frame analysis.

The sedimentation analysis clearly separates classes representing the turbid Anacostia water, the less disturbed Potomac (really), and mud flats resulting from effluent of a major sewage treatment plant. Mud flats of organic or mineral origin are easily distinguished. Several classes of sedimentation are easily constructed.

Strip mines are classified as bright arcuate objects with unique reflectance and geometrical properties. In our imagery of Allegheny County, Maryland, the mines occur in rural areas where open fields are on the dissected Allegheny plateau, forests are more generally in stream channels below. The mines are cut into the horizontal contour of the valley slopes and are easily distinguished from their surroundings. Some field observations have been made, but we are not sure all mines were classified as such.

Introdution

The Earth Resources Technology Satellite offers a unique opportunity for synoptic observation of hydrological, geological and vegetational resources as they interreact within a region, such as the Potomac River Basin. This river basin, more than many others, is characterized by variation: variation in physiography which occurs as the river flows

from the Allegheny Plateau through the Ridge and Valley Province, the Blue Ridge Mountains, the Piedmont Plateau, and fianlly through the Coastal Plain into Chesapeake Bay; variation in underlying geological structure, soil type and depth, and with consequent variation in land-use, and vegetational cover; variation in climate, as illustrated by the variation in rainfall, in which the Allegheny Plateau receives more than 70 inches of rainfall annually, while the adjacent Ridge and Valley Province receives less than 40; in which the Coastal Plain is subject to heavy tropical storms as well as unpredictable thunder showers, delivering inches of rainfall in an hour. The great variation in intensity of rain across the basin coupled with the variation in soil structure and bedrock geology means that optimum development of the Basin's resources must be based on maximum understanding of the interactions of geological, vegetation, hydrological and climatic interactions occurring within the Basin if extensive damage to the environment in terms of water pollution, loss of top-soil, and sediment deposit build-up in the river channel are to be prevented. Thus, development of a data-bank based on the data from repetitive satellite coverage is imperative.

As part of the development of a data-resource bank for determining such interactions we have employed both analog multi-band imagery and digital data obtained from ERTS-A. We have developed computer analytic techniques to quantitatively evaluate changes occurring in the river in such factors as the sedimentation and organic pollution levels.

The procedure used here is one that does not require a large or dedicated computer or more than one tape drive. While the procedure is quite simple, the results appear to correlate quite well with the qualitative observations which can be made by analysis of the imagery in photographic form.

Results

The analytical technique which we have used is basically a three-step approach. The first step is to perform geographical referencing for the entire data set. This is done using a pattern-recognition technique with band 7 of the ERTS bulk-data on Computer Compatible tapes. The low reflectance of water in band seven is used to locate water features of known geographical co-ordinates. The difference between the apparent location derived from the header record on the CCT and the actual location is applied as a correction in deriving a referenced data set. The error for an individual pixel is less than 250 meters. Geographically referenced data sets have been created for several dates for the Potomac River at the Anacostia confluence and for strip mine regions in the Allegheny Plateau.

Preliminary results of the analysis of the region at the Anacostia Potomac confluence illustrate the second step of our analytical technique, multi-channel density-slicing employed in analysis of change detection. Since change detection is the significant result to be obtained from repetitive coverage by ERTS, changes in extent or presence of various classes or reflectance levels were sought rather than an absolute correlation with ground-truth quantitative sediment or organic pollution levels. A computer printer-plot map of the region for two dates in which each 50 X 80 m pixel is displayed as a printed value was generated from the geographically referenced data set at a scale of 1:20,000. The printed values correspond to nine levels of reflectance, five corresponding to a general increase in reflectance in a color composite relative to Chesapeake Bay, and three to a decrease. Values for normal reflectance level of sea, bay or unpolluted river water are in the range shown as N (normal). The algorithm used to generate these levels was derived simply by combining reflectance levels from the data tape by multiplication and assigning the product to previously determined density levels and using the density slicing techniques described.

Most of the sedimentation in the Potomac Estuary on 23 September (Fig. 1) was found either in the Anacostia River channel or down stream below the Occaquan Creek. Low values in the region below Roosevelt Island are associated with local dewage outfalls. In fact, we seem to be able to find most of the major sewage effluent sources using this analysis. Very high values of sedimentation are found in the Anacostia. These are associated with two major sources of sediment: a sand and gravel operation and run-off from open surfaces associated with construction of roads and buildings.

On 11 October, we, and of course everyone, found a very different pattern. Run-off from a heavy rainfall had carried sediment into the Potomac from West Virginia eastward. Figure 2 shows that a much different distribution of sediment is found, being heavy in the Washington area and including the region around Roosevelt Island. While levels near the previously mentioned outfall are modified by effluent, so much mineral sediment has been carried in that the outfall is obscured. The highest values are again found in the mudflats of the Blue Plains sewage plant near Wilson bridge. The mud-flat is organic, not mineral and therefore the reflectance values are very low in all channels.

A similar algorithm (addition of all four channels with subsequent density-slicing) has been developed for detection of strip-mines in the Allegheny Plateau. Normalization for this region is performed by determining the maximum, minimum and range of values over the area under investigation for each date, then using these ranges in determining the range corresponding to the composite reflectance of the strip mines.

In summary, the digital techniques developed for identification of sedimentation levels are adaptable to large or small computer installations. The results show that we can classify sedimentation levels and that it should be possible to correlate levels found in analysis with particulate levels measured in the field. In addition, organic effluents which do not contain chlorophyll were also observable, making possible the identification and monitoring of sewage and other organic inputs into riverine waters.

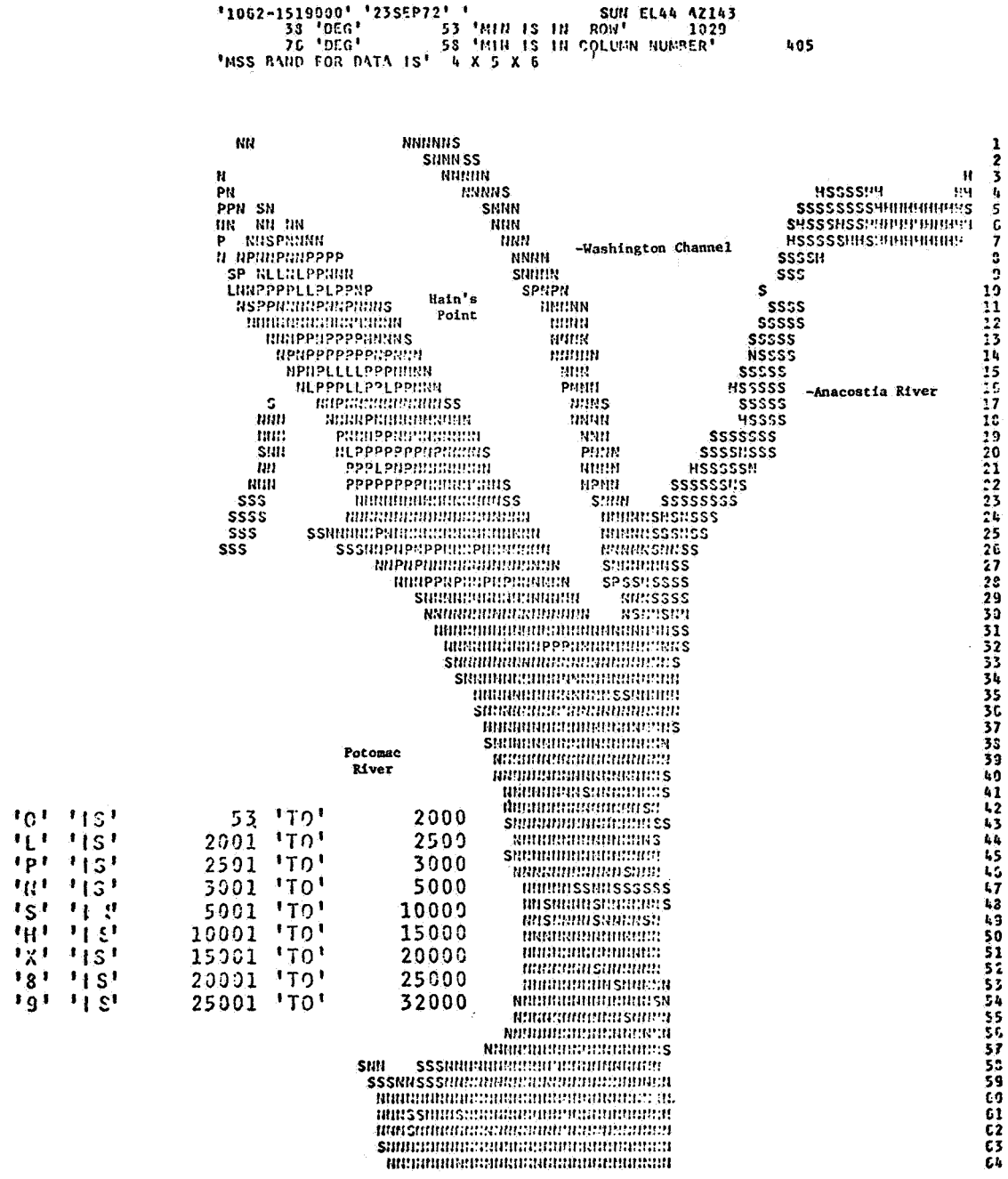
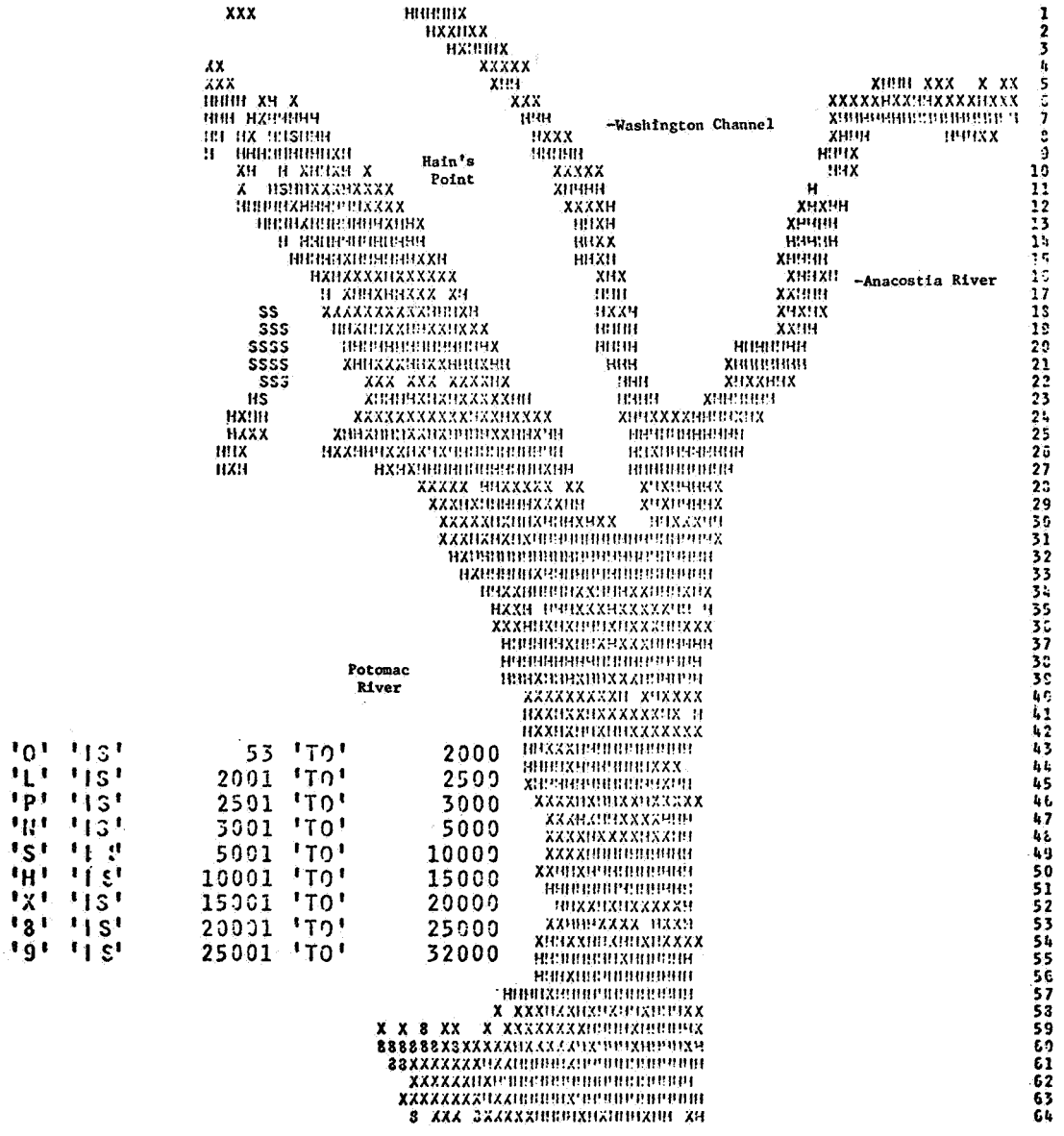


Figure 1 Digital Display of Sedimentation 23 Sep 72

```
'1080-1519201' '11OCT72' '                SUN EL38 AZ149 '
      38 'DEG'        53 'MIN IS IN  ROW'      1170
      76 'DEG'        58 'MIN IS IN COLUMN NUMBER'      485
'MSS BAND FOR DATA IS'  4 X 5 X 6
```



'O'	'IS'	53	'TO'	2000
'L'	'IS'	2001	'TO'	2500
'P'	'IS'	2501	'TO'	3000
'N'	'IS'	3001	'TO'	5000
'S'	'IS'	5001	'TO'	10000
'H'	'IS'	10001	'TO'	15000
'X'	'IS'	15001	'TO'	20000
'8'	'IS'	20001	'TO'	25000
'9'	'IS'	25001	'TO'	32000

Figure 2 Digital Display of Sedimentation 10 Oct 72

Paper E 14A

A STUDY ON THE EROSION OF NIIGATA BEACH FROM ERTS-A IMAGERY

Takakazu Maruyasu, *Institute of Industrial Science, University of Tokyo, Roppongi Minatoku, Tokyo, Japan*

ABSTRACT

One of the causes of coastal erosion is the cultural construction works such as flood control dam, short cut channel or breakwater, which reduce the transportation of river effluents such as silt and sand.

ERTS-A imagery makes clear the relations between the status of erosion, effluents pattern affected by the coastal current and the cultural construction works.

1. OBJECTIVES OF THE STUDY

Niigata alluvial plain, faced with Japan Sea, is produced by two big rivers, Shinano River and Agano River.

Niigata shore line is composed of fine sand deposits which are transported mainly by Shinano River, the third biggest river in Japan, with 12,000 square kilo meters in catchment area and 370 kilo meters in distance.

While clear water flows in Agano River at any time, water in Shinano River is rich in sand and silt, especially in the flood season and at the snow resolution time.

In the ancient time before about 80 years ago when the cultural structures such as river improvement works or flood control dams had been carried out along Shinano River, Niigata shore line had grown in the offshore direction with average rate of 30 meters to 120 meters in a year. Fig.1 shows schematic change patterns of Niigata shore line in the past.

About 70 years ago, the breakwater for the construction of Niigata Port was constructed at the outlet of Shinano River as shown in Fig. 2.

Since Ohkozu short cut channel was excavated 50 years ago to prevent Niigata City from flood, outflow of sand and silt through the outlet of Shinano River remarkably decreased.

Since then, interactions between the breakwater, the short cut channel, wind, wave and current began to attribute erosions at the both sides of the west beach and the east beach in different ways.

The shore line at the west beach has been eroded with the magnitude of 360 meters at maximum for 60 years since the completion of the breakwater, while the shoreline at the east beach, 300 meters at maximum for 40 years since the construction of the Ohkozu short cut channel.

Although a number of countermeasures such as submerged breakwater, sea walls and revetments have been constructed, erosion is still progressing.

In 1972, another short cut channel was completed against the erosion of the west beach. This new channel, however, would not be effective for improving the erosion of the east beach.

As it can be considered from the above mensioned background, the objectives of the study are as follows.

a. To investigate the distribution pattern of the sand deposit transported by Shinano River, and its behavior.
b. To study the effect of the cultural structures upon the sand sedimentation.
c. To establish the method of the preservation of coastal environment against erosion.

The use of ERTS imagery will be effective in feasibility studies of a. and b., and c. finally.

2. GROUND TRUTH SURVEYS

Following ground truth data are available from the existing surveys.

a. Change patterns of Niigata shore line.
b. Contour map of depth of Niigata beach. (Fig. 3)
c. Surveys of settlement of the beach
d. Predominant wind and its velocity.
e. Wave height.
f. Classification of the sand deposits.

3. ERTS-A IMAGERY OF NIIGATA BEACH

Following ERTS-A imagery are available for the interpretation of the erosion of Niigata beach.

Date and time;	29 August, 1972
Identified number;	032, 064, 096, 128
Format;	MSS 70mm positive
Center point;	37°20'N, 139°12'E

Cloud coverage;	about 10 percent in the mountaeneous sites
Major features included;	Niigata City, Sado Island, Shinano River, Agano River, Japan Alps, Inawashiro Lake

Fig. 4 shows contact prints of four bands made from ERTS-A.

Fig. 5 shows the enlarged print of the band MSS 4 in the scale of 1:1,000,000 with effluent pattern superposed.

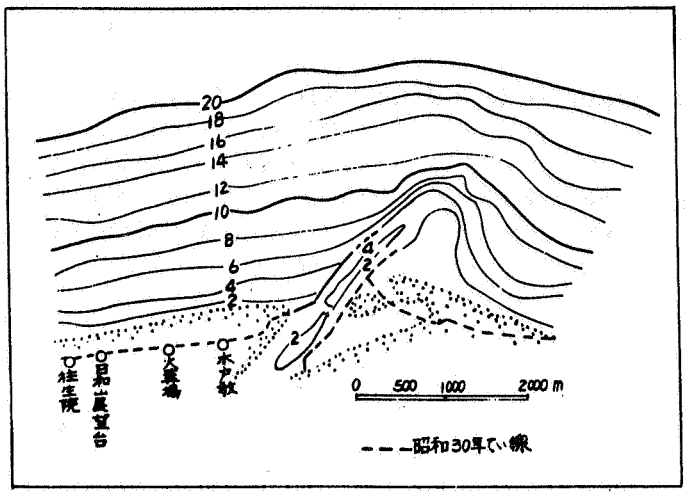
Fig. 6 shows the more enlarged print of Niigata shore line in the scale of 1:200,000 which can provide more detail information about the relations between effluents, breakwater and short cut channel, and coastal current.

Significant results are obtained from ERTS-A as follows.

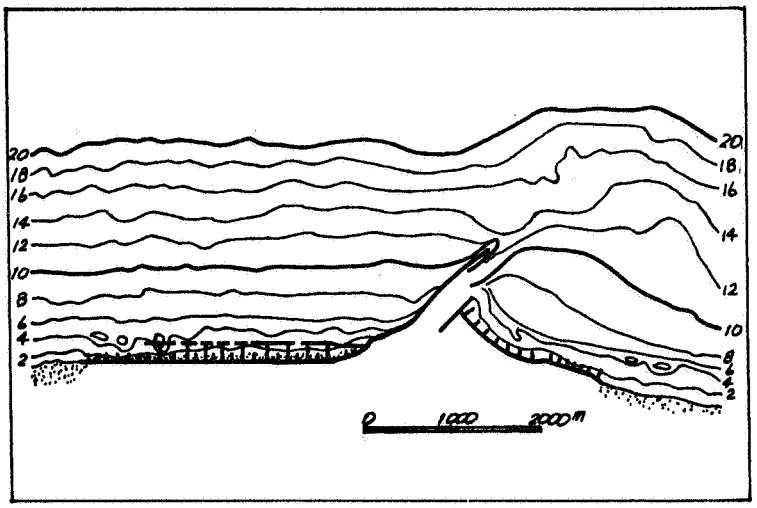
a. Effluents from Ohkozu short cut channel are refracted by the curved coast and Tsushima current, which flows in the direction of the north east. They disperse in the offshore far away from Niigata west beach and sand sedimentation is not active.
b. The new short cut channel is identified to contribute the sand deposition along the west beach as it was estimated by coastal engineers.
c. Effluents from the breakwater of Niigata port are distributed in the direction of the north east together with those from Agano River. They are also affected strongly by the coastal current.
d. The east beach has no tendency to have sand deposit from effluents. There will be increase of erosion at the east beach.

Further studies will be feasible by the use of ERTS imagery as follows.

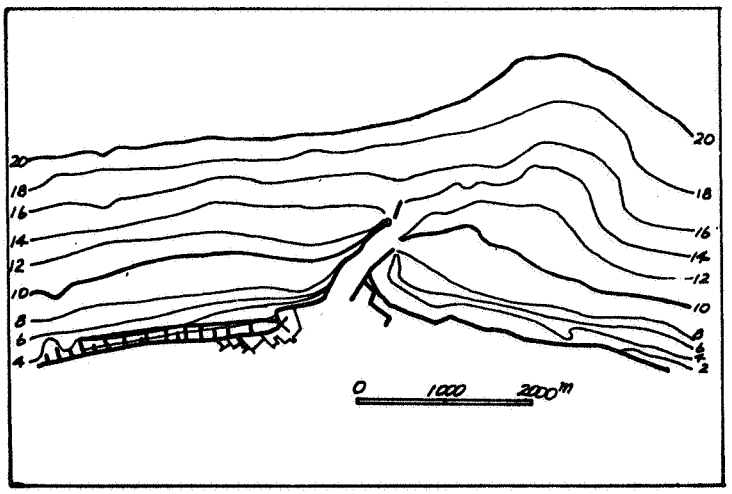
a. Estimate the volume of sand deposits discharged from Shinano River, and its ditribution, in the flood season and at the snow resolution time.
b. Surveys of the effect of the predominant winter wind on the erosion.
c. Determination of the sites of dredging and disposing sand deposit.
d. Study on the effect of the cultural works upon the coastal environment.
e. Surveys of the correlation between pomping natural gas and the settlement of the ground in Niigata coastal area.



(a) Contour map of Niigata Beach in 1905



(b) Contour map of Niigata Beach in 1960



(c) Contour map of Niigata Beach in 1970

Fig. 3 Contour map of depth of Niigata Beach

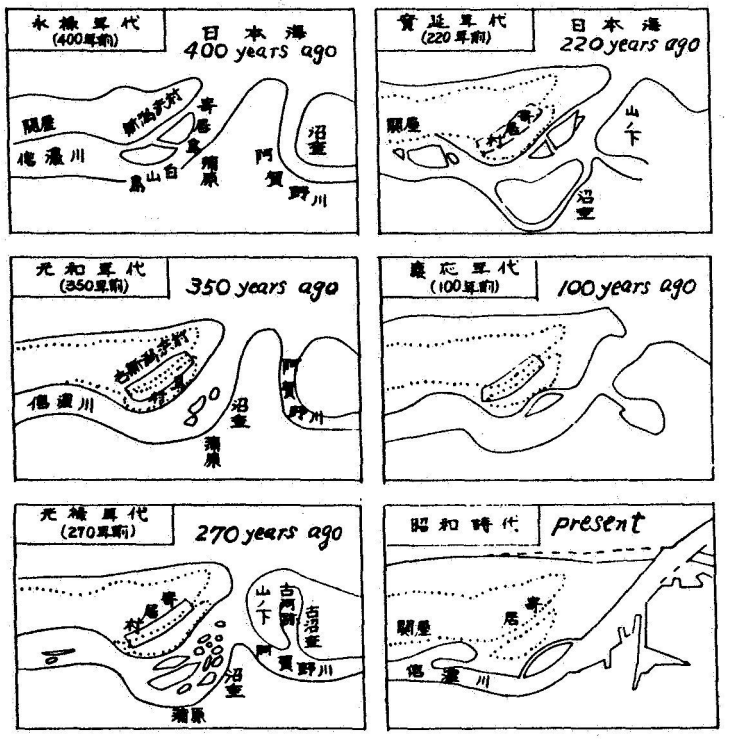


Fig. 1 Historical change pattern of Niigata Beach

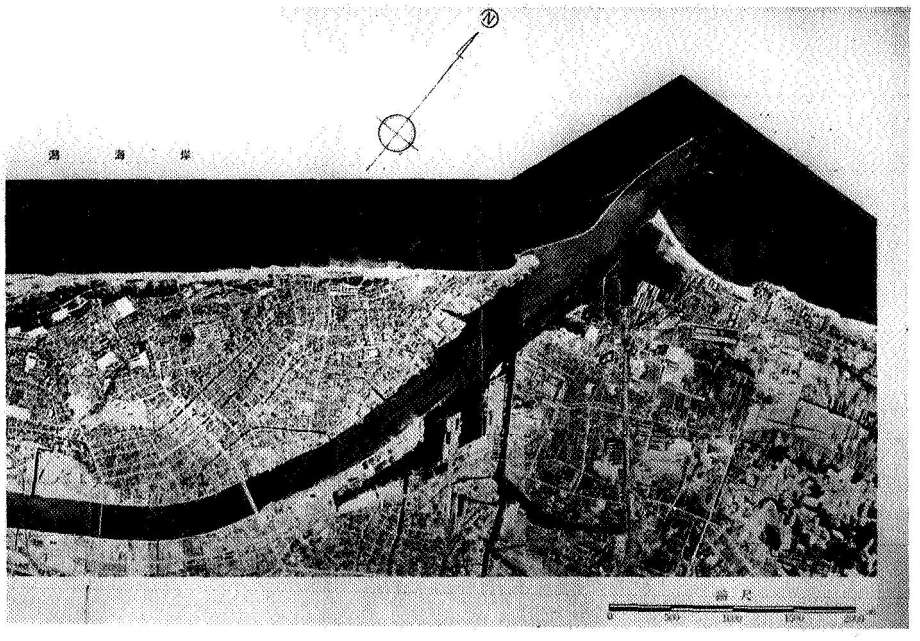


Fig. 2 Mosaic of aerial photographs of Niigata Port and its coastal environment (1958)

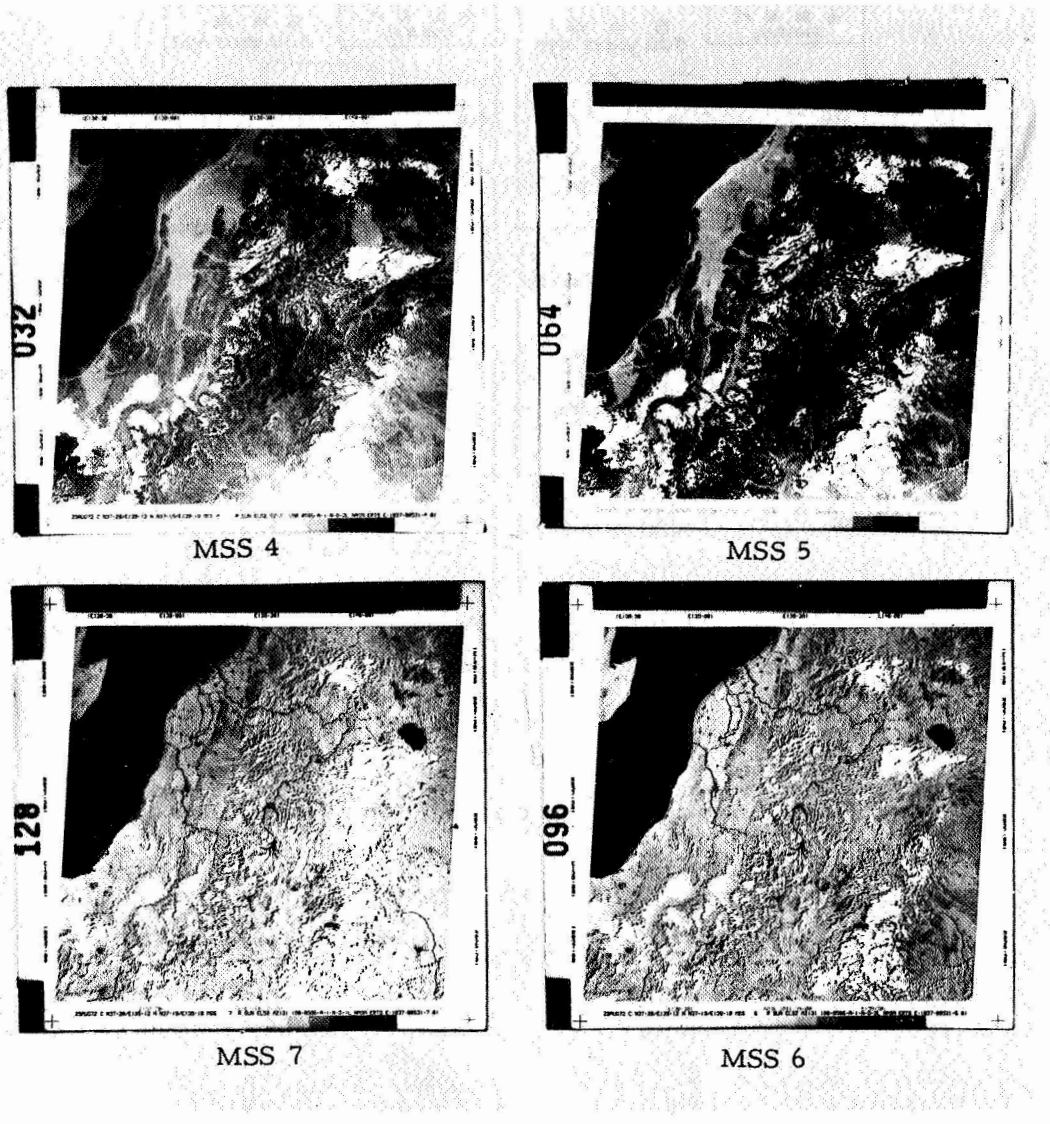


Fig. 4 Contact prints of four bands from ERTS-A

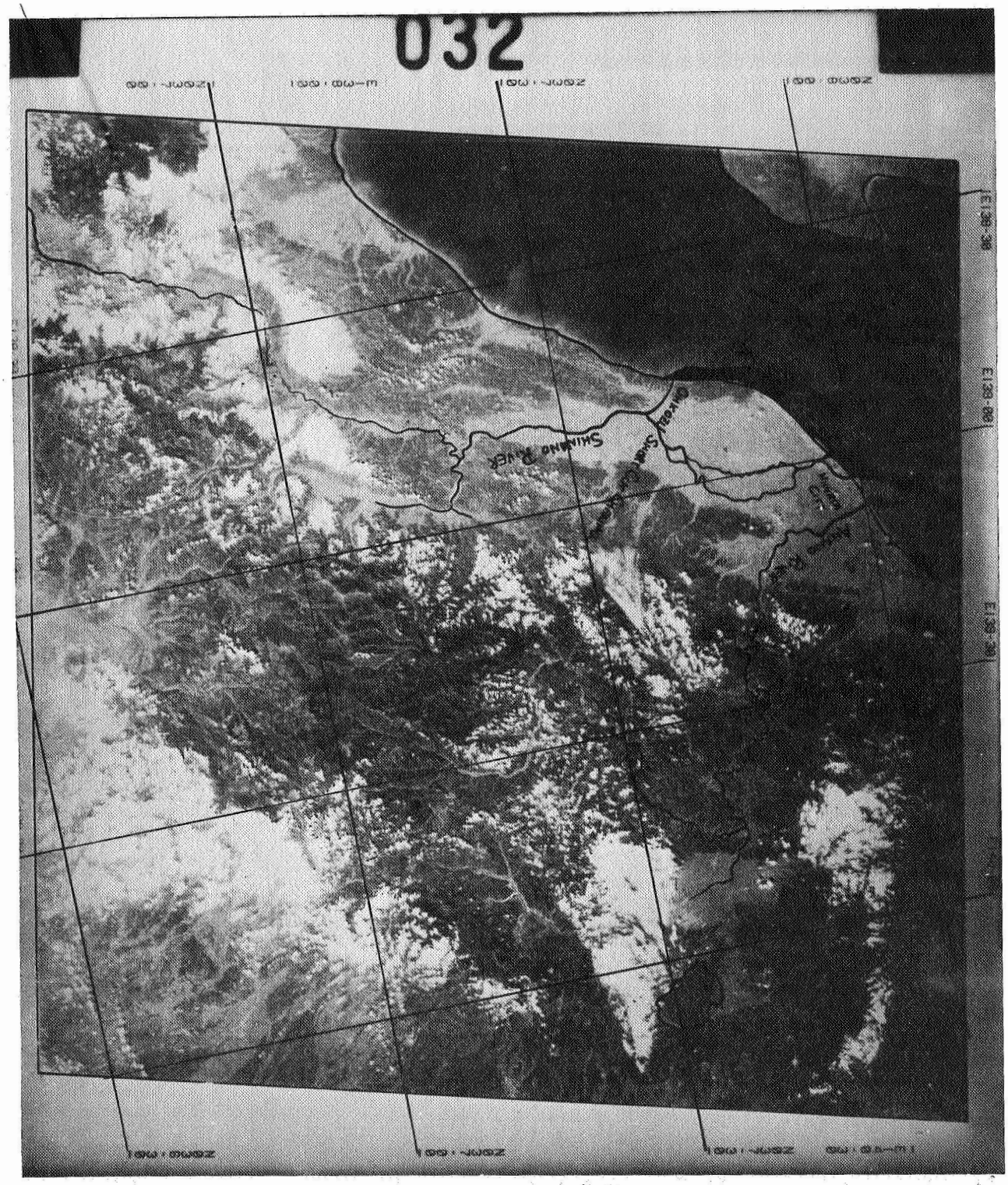


Fig. 5 Enlarged print of the band MSS 4 with effluent pattern superposed



Fig. 6 Enlarged print of ERTS Imagery

1:200,000

Paper E 14B

APPLICATION OF ERTS DATA TO THE DETECTION OF THIN CIRRUS AND CLEAR AIR TURBULENCE

Kiyoshi Tsuchiya, *Japan Meteorological Agency, Tokyo, Japan.* Toshiro Kamiko, *Tokyo International Air Weather Service, Tokyo, Japan*

ABSTRACT

The feasibility of detecting a thin cirrus and clear air turbulence from ERTS MSS data is explored. The result of analyses indicates that a thin cirrus not shown in a conventional meteorological satellite picture can be revealed in ERTS MSS picture. It is also found that the core of jet stream can be located with high accuracy from ERTS pictures and the possible area of clear air turbulence can be predicted if the data of the quality of ERTS data are available in real time.

1. INTRODUCTION

One of the most difficult problems in the interpretation of operational meteorological satellite pictures is the detection of a thin cirrus. One can hardly expect to succeed in detecting a thin cirrus in a picture taken from a meteorological satellite. The main reason is its low reflectivity.

In addition to its shortness of life time and small horizontal scale, clear air turbulence is another difficult problem to find due to invisible phenomenon. According to pilots who have encountered clear air turbulence (hereater abbreviated to be CAT) cirrus is often observed near the area of CAT.

Based on the pictures of meteorological satellites Viezee (1966) pointed out that CAT is generally found where cirrus is found near a jet stream while Ishizaki (1971) made a classification of clouds appearing in aerial photographs. Both of these studies are worthy of special attention, however the former is handicapped in its resolution and poor detectability of cirrus while the latter in the limitation of field of view and difficulty of locating the position and also measuring the horizontal extension.

ERTS has a great advantage compared with a conventional meteorological satellite in that it can respond differential reflectivity of the surface of materials in different spectrum. It has been prooved that the data of multiple spectral scanner can reveal various physical characteristics which an ordinary picture can not show in addition to its extraordinary high resolving power and accuracy in location. Taking advantage of this feature of ERTS an attempt is made to explore the feasibility of detecting cirrus and CAT from ERTS' pictures.

2. THE STUDY OF DETECTING A THIN CIRRUS FROM ERTS' PICTURE

In Fig. 1 (a), (b), (c) and (d) are shown a part of central Japan and its neighbouring sea as seen by four channels of MSS on board ERTS. It can be seen triangular wavy clouds in the pictures. Our main interest is to find the type of these clouds. Comparing four pictures one can easily find the difference in the appearance i. e. with the increase in the wave length, the clouds gradually become thinner and finally diminishes in MSS 7, or in the picture with the longest wave length. The surface weather map covering the area in the picture show the clouds as observed from the surface are mostly high cloud of cirrus as is indicated in Fig. 2. A synoptic pressure pattern is also indicated in Fig. 3 which shows a severe tropical storm with the central pressure of 990 mb is located to the south of the area.

The vertical distribution of air temperature and dew points together with the winds at Hamamatsu (47681), Shionomisaki(47778) and Hachijojima (47678) (the locations are indicated in Fig. 5) are shown in Fig. 4. Both Hamamatsu and Shionomisaki soundings show low humidity throughout the layer, which suggests that the clouds in the pictures will be fairly thin with fine structure. It is also seen from the pictures, weather maps and vertical distribution of air temperature and dewpoint at Hachijojima that the cloud becomes thicker towards south. From these analyses it can be concluded that a thin cirrus which is generally invisible in an ordinary meteorological satellite picture can be well detected in an ERTS picture.

3. THE STUDY OF CLEAR AIR TURBULENCE(CAT)

3.1 CLEAR AIR TURBULENCE OF AUG. 29, 1972

There were clear air turbulence in the northern Japan as is indicated in Fig. 6 which is made from the reports of pilots. Both B-727

and T-33 met moderate turbulence above Tsugaru Strait between 00h 45m(Z). Another T-33 encountered a weak turbulence between Niigata and Misawa, too. The same plane reported cirrus. The level of the flight was around 25,000 ft above Tsugaru Strait and around 23,000 ft between Niigata and Misawa.

3.2. ERTS PICTURES SHOWING CAT AREA

The ERTS' pictures covering the CAT area are shown in Fig. 7 (A), (B), and (C). Fig. 7 (A) is MSS 4 covering the southern Hokkaido. The small white dots over the inland area are all fair weather cumulus. The significant clouds are the larger clusters of clouds with fuzzy fibrous appearance trailing southward to the west of Tsugaru Peninsula and northward above Misawa area. It is interesting to notice that over the area to the east of Hakodate are seen very thin white cloud with wavy appearance. The surface weather observation at Hakodate (Fig. 8) indicates clear weather. If these white wavy ones are clouds, they are indication of wave motion. The area to the south of Fig. 7(A) is shown in Fig. 7 (B) and (C). Large cloud clusters are seen to the north of Ojika Peninsula with fuzzy appearance. The clouds in the inland are above the Shiragami mountain range orienting from west to east and Hachikoda mountains running from north to south. Other interesting clouds in the pictures are those located to the northwest and southwest of Ojika Peninsula with clear cut trail extending toward west. The appearance of these clouds suggest strong vertical moition embedded in strong horizontal wind with a large vertical shear. In reference with the study in the previous section, the surface weather map shown in Fig. 8, it is considered that these clouds are cirrus. However, they are different from the so called fair weather cirrus with rather uniform thickness. The fact that the clouds are fairly white even in MSS 7 (Fig. 7C) indicates that the clouds are fairly thick. The cirrus may have originated from convective acitivity and there would be large up and down draft over the area. The spacing of the clouds to the west of Tsugaru Peninsula ranges from 6.5 to 13 kms while the spacing of large clusters of clouds to the north west of Ojika Peninsula is approximately 17 kms. These fact suggest there may have been gravity wave motion with the period of Brunt-Vaisala.

3.3. METEOROLOGICAL ANALYSIS

The surface weather map of 00Z Aug. 29, 1972 is shown in Fig. 8 which indicates that the area of CAT is in the periphery of a migrating high. Most of stations in Tohoku District reported cirrus fibratus or

some indication of cirrus floccus. Towering cumulus is reported by Fukaura weather station thus static stability of the amosphere was not good in the norther Tohoku district.

In order to see the wind distribution at the flight level of the planes, 300-mb chart is made and is shown in Fig. 9 in which the contours at 60-gpm interval are drawn in broken lines while the isotachs at 20-kt inverval are drawn in solid lines. The jest stream axis is shown in a thich solid line which sharply curves cyclonically above northern Tohoku Dirstrict. The vorticity at the area of CAT reaches as large as the order of 10 sec . The cross section analysis along 140°E meridian is shown in Fig. 10. The isotherms at 5°c interval and isotachs at 20-kt interval are drawn in broken and solid lines respectively. The thick solid lines are frontal surface.

The figure indicates that the jet core is located at the level of approximately 250-mb level above Misawa area and the planes encountered CAT within the frontal layer where the vertical wind shear is the maximum. The value in this case is as large as 10 /s.

4. CONCLUDING REMARK

The previous analyses lead to the following conclusion. A thin cirrus can be successfully detected from ERTS MSS data and the features of clouds can be also known from the pictures of different spectrum. The possible CAT area can be found from the particular apperance of cirrus.

References

Ishizaki, H., 1970: Clouds. All Nippon Airways.

Viezee, W., 1966: TIROS viewed jet stream cloud pattern in relation to wind, temperature and turbulence. Stanford Research Inst.

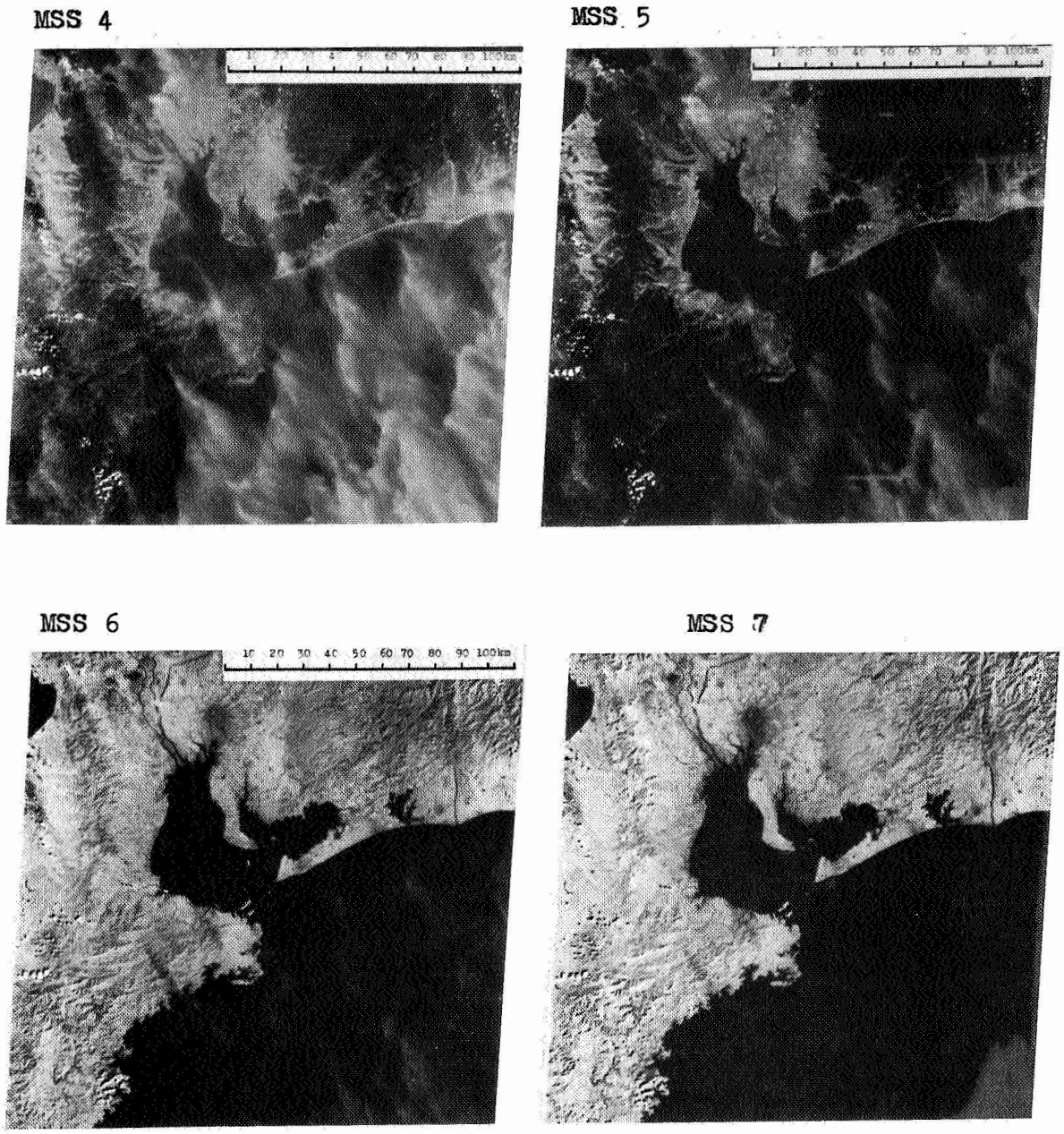


Fig. 1 Pictures of MSS, ERTS showing clouds as seen in different spectrum. 0059(Z) Oct 05, 1972.

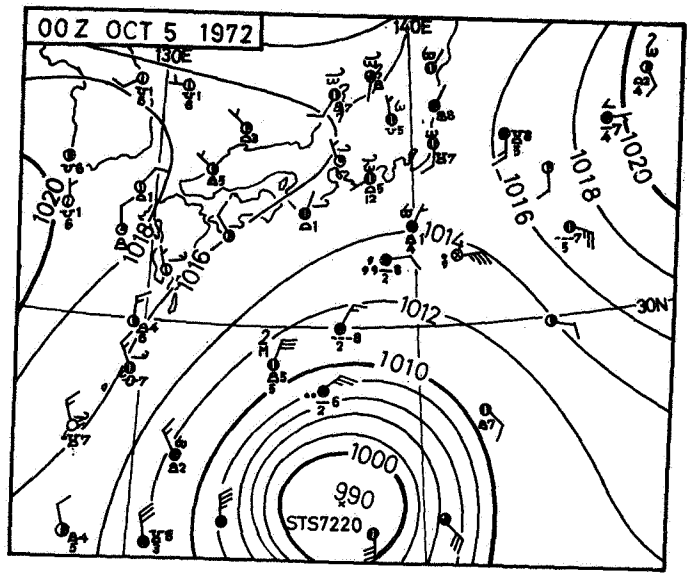


Fig. 3 The surface weather map at 00)Z) Oct 5 1972

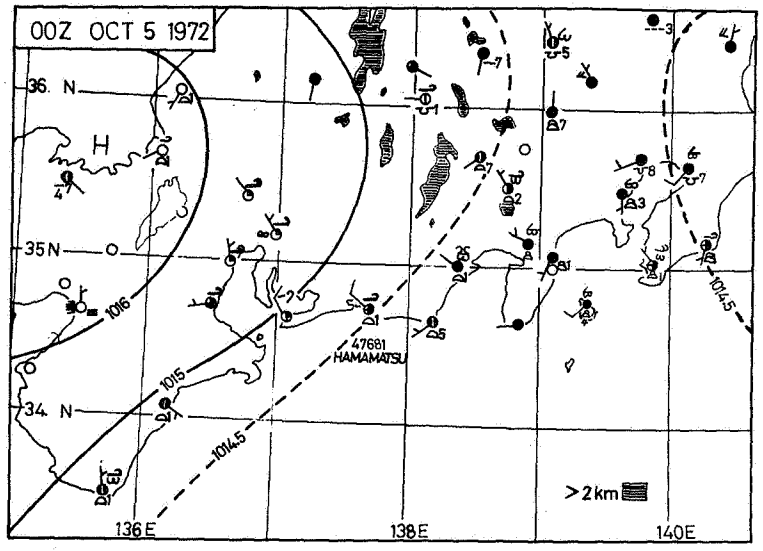


Fig. 2 The surface weather map showing cloud distribution in central part of Japan. 00(Z) Oct 5, 1972.

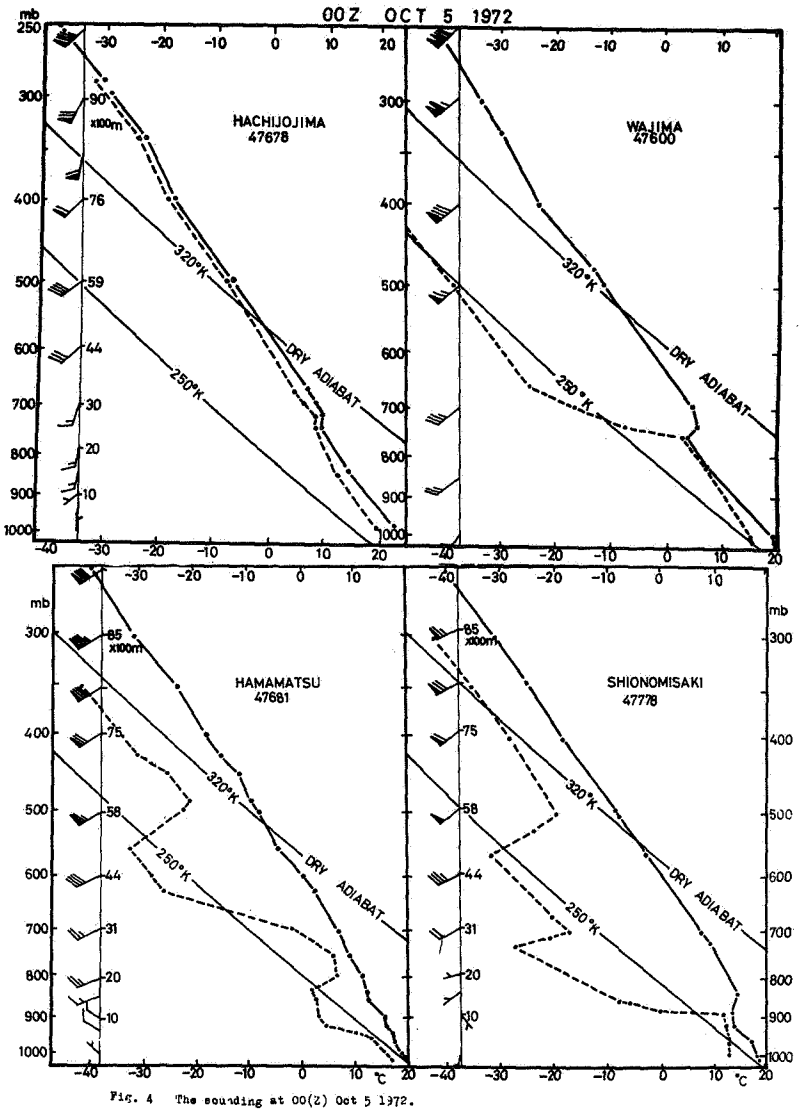


Fig. 4 The sounding at 00(Z) Oct 5 1972.

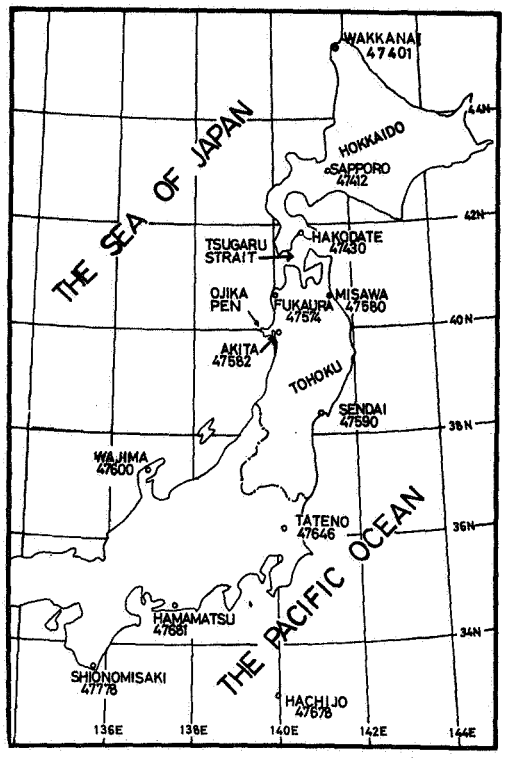


Fig.5 The map of Japan with weather stations.

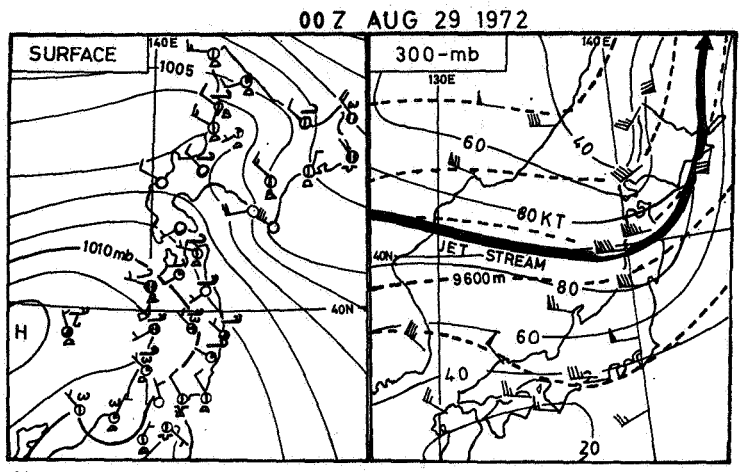


Fig. 8 The surface weather map, 00(Z) Aug 29 1972.

Fig. 9 300-mb chart at 00(Z) Aug 29 1972.

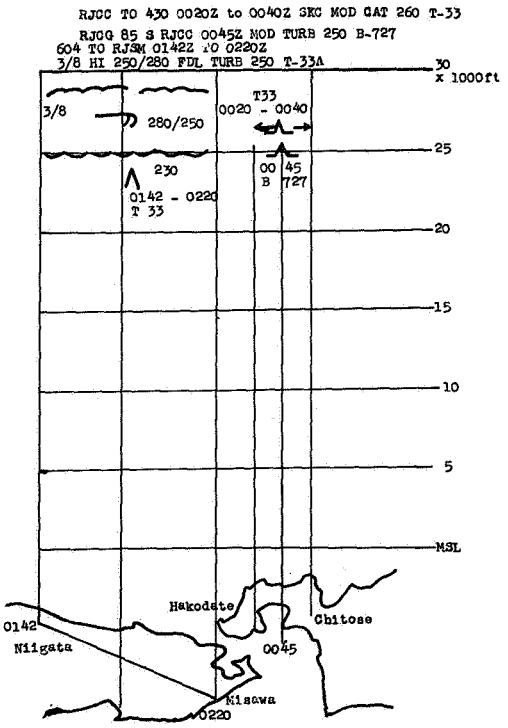


Fig.6 The flight cross section made from pilots' reports

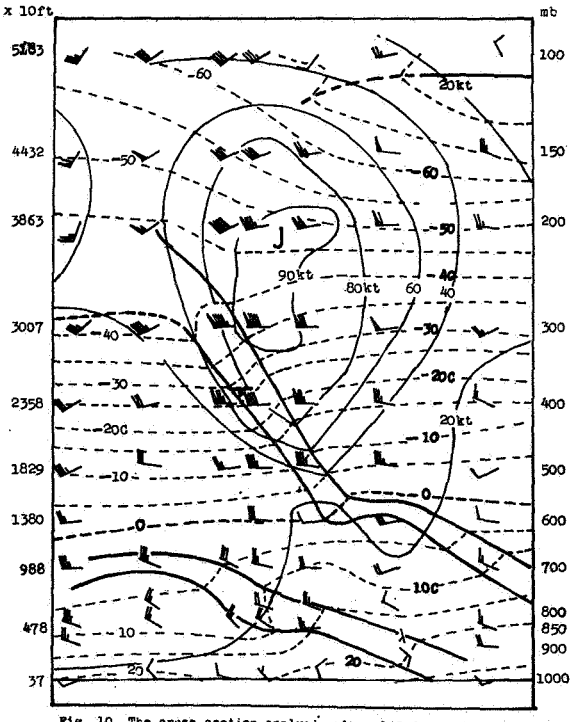
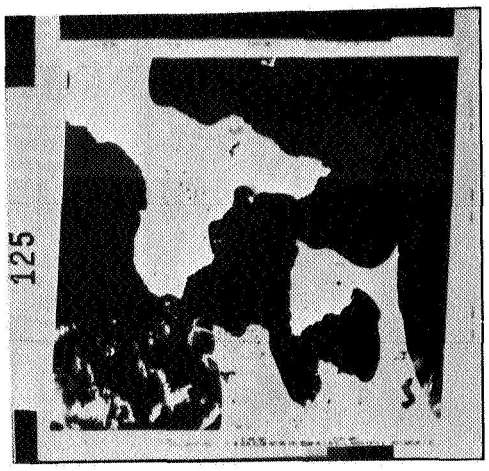


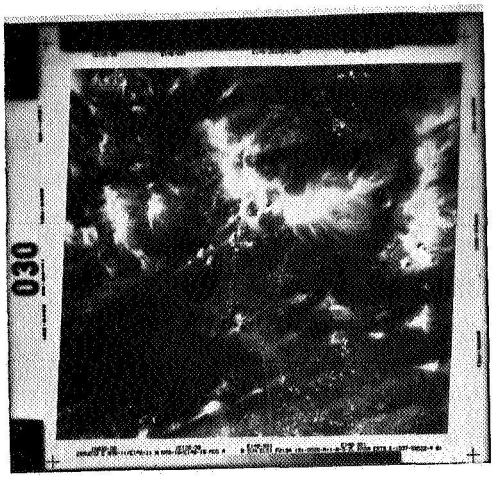
Fig. 10 The cross section analysis along 140 E meridian. The broken and solid lines are isotherms and isotachs respectively.



(A) MSS 4



(A) MSS 7



(B) MSS 4



(B) MSS 7

Fig. 7 ERTS pictures showing the clouds on the day CAT was reported
(A) 00520 (Z) Aug. 29, 1972
(B) 00522 (Z) Aug. 29, 1972

Paper E 14C

POLLUTED AND TURBID WATER MASSES IN OSAKA BAY AND ITS VICINITY REVEALED WITH ERTS-A IMAGERIES

Kantaro Watanabe, *Kyoto Gakuen University, Kyoto, Japan*

ABSTRACT

The heavy water pollution is one of the most serious problems in the Osaka Bay and its vicinity. However, the state of water pollution there has never monitored in the scale of whole Osaka Bay because the conventional point-to-point observations make it impossible to detect the periodical movement of water masses by the fairly strong tidal current.

ERTS-A took very valuable MSS imageries of Osaka Bay and its vicinity on October 24, 1972. In the MSS-4 and MSS-5 imageries a complex grey pattern of water masses can be seen. Though some of grey colored patterns seen in black and white prints of the MSS-4 and MSS-5 imageries are easily identified from their shapes as cloud covers or polluted water masses characterized by theircolor tone in longer wavelengths in the visible region, any correct distribution pattern of polluted or turbid water masses can be hardly detected separately from thin cloud covers in a quick look analysis.

In the present investigation, a simple photographic technique was applied using the fact that reflected sun light from cloud including smog and inclined water surfaces of wave have a certain component in the near infrared region, that is MSS 7, whereas the light scattered from fine materials suspended in the sea water has nearly no component in the channel of MSS 7 but has only the green and yellow component sensible in MSS 4 and MSS 5 channels. That is, combined prints were made from a positive imagery of MSS-4 or 5 together with a negative imagery of MSS-7 using a photographic enlarger. In the combined prints areas of clouds and smogs are shown as white or lighter grey, whereas polluted or turbid water masses are clearly represented with black or darker grey tone.

SIGNIFICANT RESULTS

Significant results are obtained as follows;

1) The simple method mentioned above is useful technique for detecting water masses distribution separately from cloud covers and also noise caused by the reflected sun light from wave surfaces.

2) The polluted water does not diffuse continuously into the oceanic water but forms masses of polluted water among masses of the oceanic water flown from the outer sea, that is, the Kuroshio area.

3) The polluted or turbid water mass in the just north of the Tomogashima Channel, the south outlet of the Osaka Bay, shows that the northward tidal current runs in a clockwise eddy at the tidal period when the imagery was taken. Such an eddy-like pattern of tidal current has never been revealed by the conventional oceanographic data.

4) A front between an oceanic water mass and a polluted water mass runs in the direction of NW-SE in the center part of the Osaka Bay.

5) The patterns of turbid water discharged from the Kii River and the Yoshino River show the northward tidal current in the North Kii Straits at the time of imageries taken.

6) The pattern of lighter turbid or polluted water located in the north west region of the North Kii Straits suggests the existence of a clockwise eddy in the straits.

ILLUSTRATIONS

FIG. 1 Two examples of ERTS-1 MSS imageries taken on October 24, 1972. Cloud covers, heavy smog areas and turbid water masses are represented equally by grey color in imageries of MSS-4 and -5, because they have sensible components of light in these channels. On the other hand, there is no grey-colored image of turbid or polluted water mass but are the ones of cloud cover and smog area in MSS-7 (infrared) imagery since the infrared component of light is strongly absorbed by the sea water.

FIG. 2 Using the difference of grey-colored images over sea regions in MSS-5 (or -4) and MSS-7 imageries explained in Fig.1, turbid or polluted water masses can be represented by darker images separately from cloud covers and smog areas which are represented by lighter grey images in a combined print made with a negative imagery of MSS-5 or MSS-4 together with a negative imagery of MSS-7 by a photographic enlarger.

FIG. 3 Turbid or polluted water masses distribution manually copied from the combined print (in Fig. 2). The darker is any area the heavier is the degree of turbidity or pollution in this chart. The pattern in this chart suggests that turbid or polluted waters diffuse into oceanic water masses flown from the outer sea without any continuous density variation in some short time, but form patches of turbid or polluted water masses. The major mass of polluted water is thought to locate under a cloud cover and smog areas off Osaka and Kobe ports. The putch of turbid or polluted water mass having an eddy-like pattern near the Tomogashima Channel (marked by T) is assumed to have disparted from the major mass of polluted water off Osaka and Kobe ports in a former tidal time. Effuents from the Kii and Yoshino Rivers are chearly seen.

FIG. 4 Flow pattern of tidal current inferred from the combined print of Fig. 2.

As it was at the time of tidal current shown by the inserted curve at the upper left corner, most of flowing water directed nearly north except of the ones near the Akashi and the Naruto Channels. A clockwise eddy is strikingly revealed closely north of the Tomogashima Channel. A front of two different water masses runs NW-SE nearly in the center of the Osaka Bay. These phenomena have never been observed in any point-to-point observation by ship. North of the front a clockwise eddy can be inferred in this analysis which have already been observed by ship's surveys. There are seen two small eddies, one of which is counter clockwise and another clockwise, in the mouth of the Naruto Channel which is famous by the formation of numerous eddies at the time of maximum tidal current.

Polluted and Turbid Water Masses in the Osaka Bay and its Vicinity Revealed with ERTS-1 Imageries

By Kantaro Watanabe

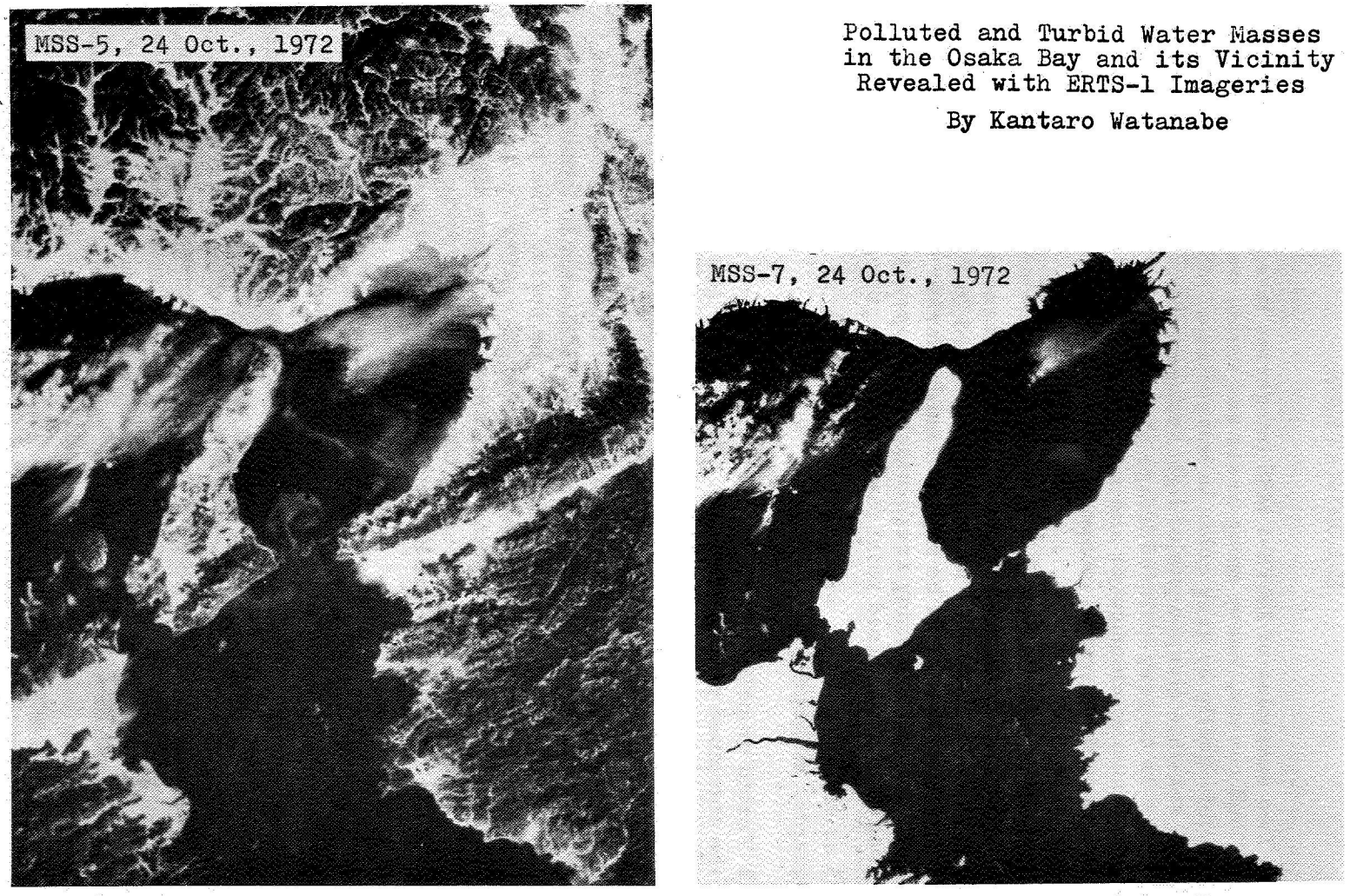


Fig. 1


Combined Print
with a Negatibe of MSS-5
and a Positive of MSS-7,
24 October, 1972

Fig. 2

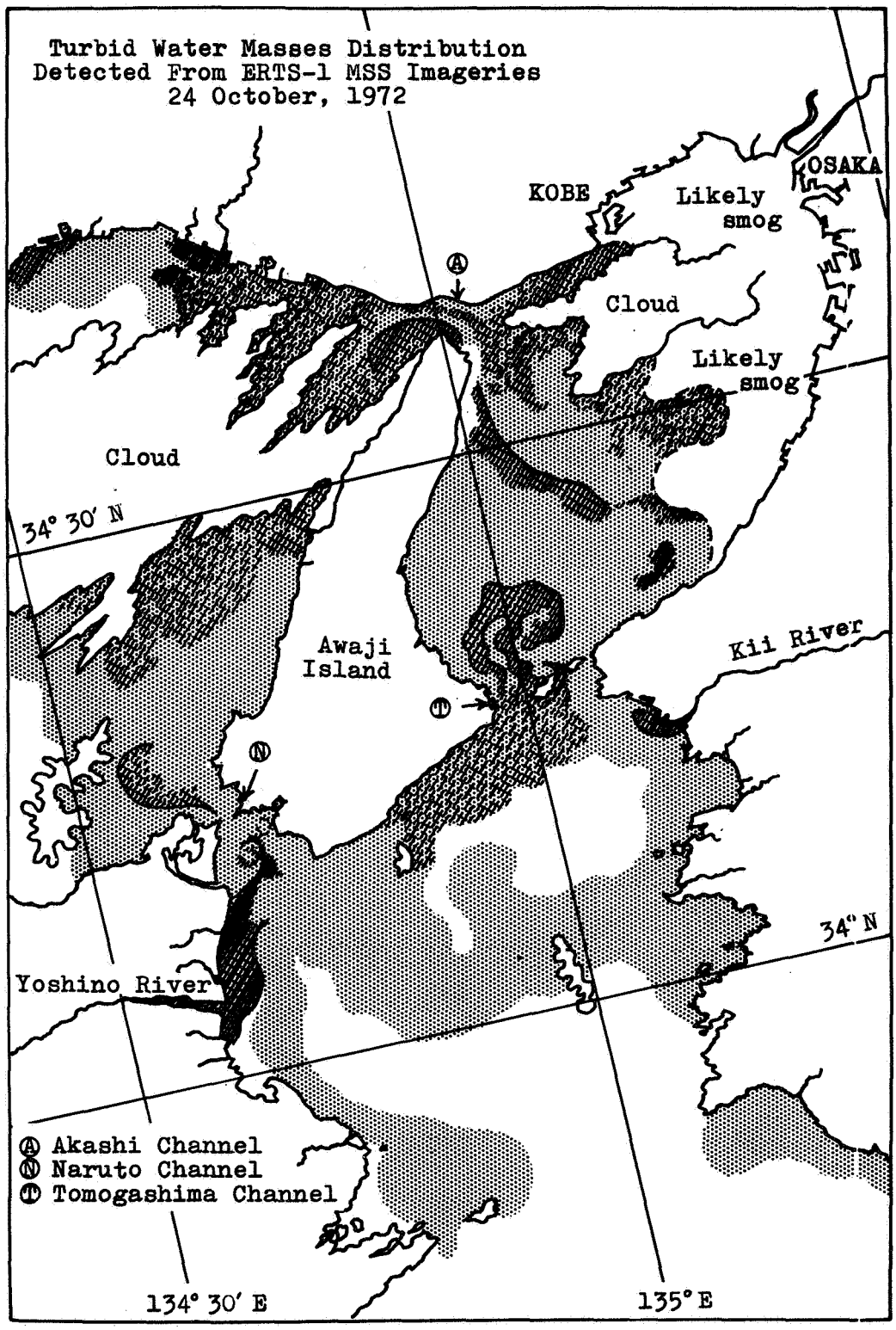

Turbid Water Masses Distribution
Detected From ERTS-1 MSS Imageries
24 October, 1972
KOBE
OSAKA
Likely smog
Cloud
Likely smog
Cloud
34° 30′ N
Awaji Island
Kii River
Yoshino River
34° N
Ⓐ Akashi Channel
Ⓝ Naruto Channel
Ⓣ Tomogashima Channel
134° 30′ E
135° E

Fig. 3

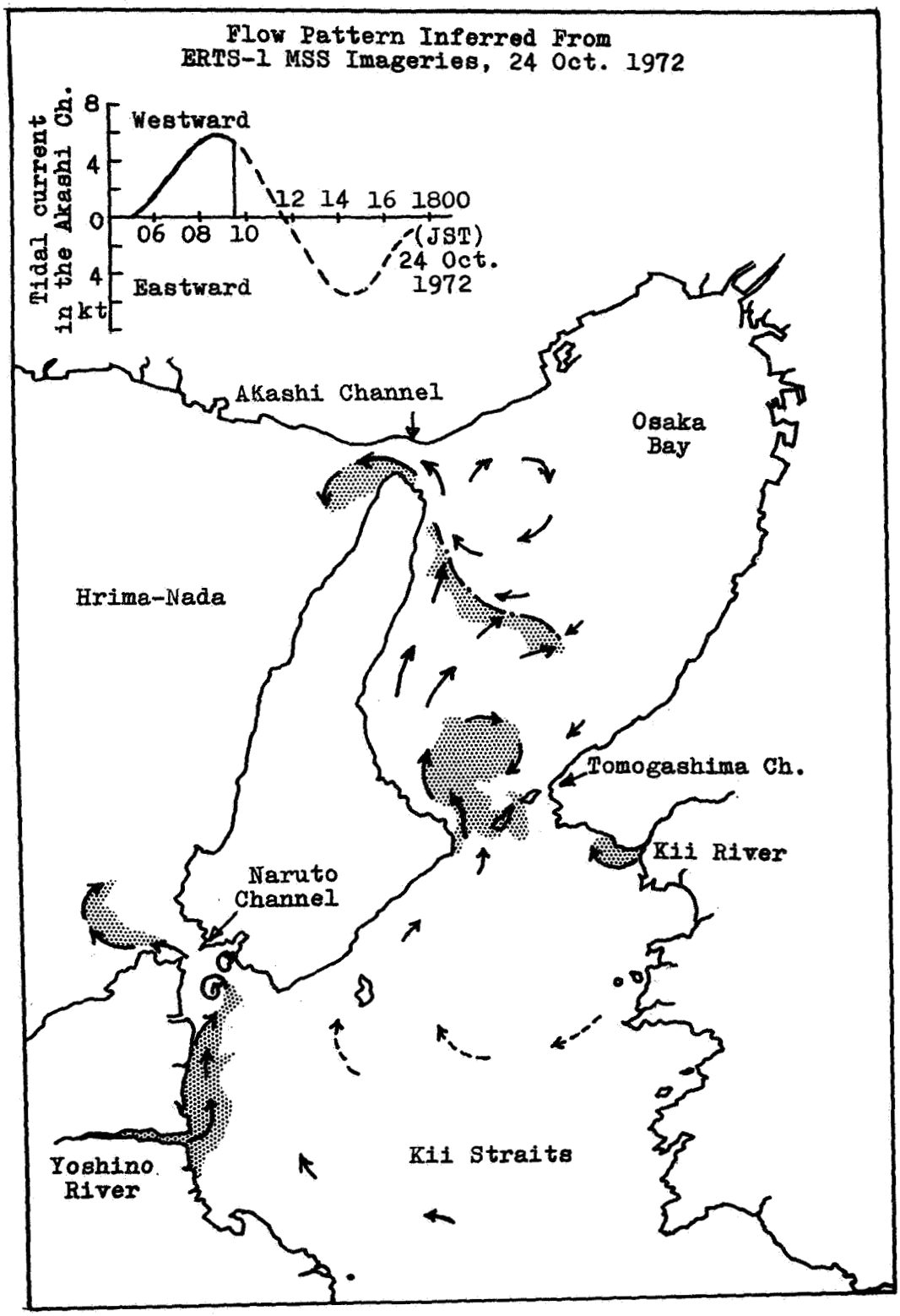

Flow Pattern Inferred From
ERTS-1 MSS Imageries, 24 Oct. 1972
Tidal current in the Akashi Ch.
8
4
0
4
kt
Westward
Eastward
06 08 10 12 14 16 1800
(JST)
24 Oct.
1972
AKashi Channel
Osaka
Bay
Hrima-Nada
Tomogashima Ch.
Kii River
Naruto
Channel
Yoshino
River
Kii Straits

Fig. 4

Paper E 14D

RED TIDE IN ISE BAY

Hiroaki Ochiai, *Toba Merchant Marine College*

ABSTRACT

From 5th to 26th of Octover, 1972, the northwestern pat of Ise Bay was seriously suffered by the dense red tide. The estimated boundery of red tide due to ship's observations were shown in Fig. 1. The area spread to eastward along the western coast of Ise Bay. However, ship's observations are sometimes not so correct because most of observation ships in Ise Bay are very samall fishing boats not equipped with efficient navigation instruments to get their position exactly.

So the author tried to find out the correct boundary of red tide as an environmental pattern using several imageries produced from ERTS-1 data. The green band with 0.50-0.60 wavelength is expected to detect the underwater circumstance where the transparency is in good condition. Where the transparency is not enough, the underwater circumstance can not be detected but only the surface circumstance.

The transparency distribution of Ise Bay as shown in Fig. 2 shows that the area along the western coast near Yokkaichi was in no good condition, while the green band imagery as shown in Fig. 3 shows the two black patterns as pointed out with arrows. They are extended to the northeastern direction and the southeastern direction respectively like as belt, which are supposed the area of red tide on Octover 5th , 1972. If additional ERTS-A imagery dated on Feb. 8th 1973 is available, the red tide spread over whole area of Ise Bay could be detected as somewhat different patterns on the basis of the groundtruth surveys.

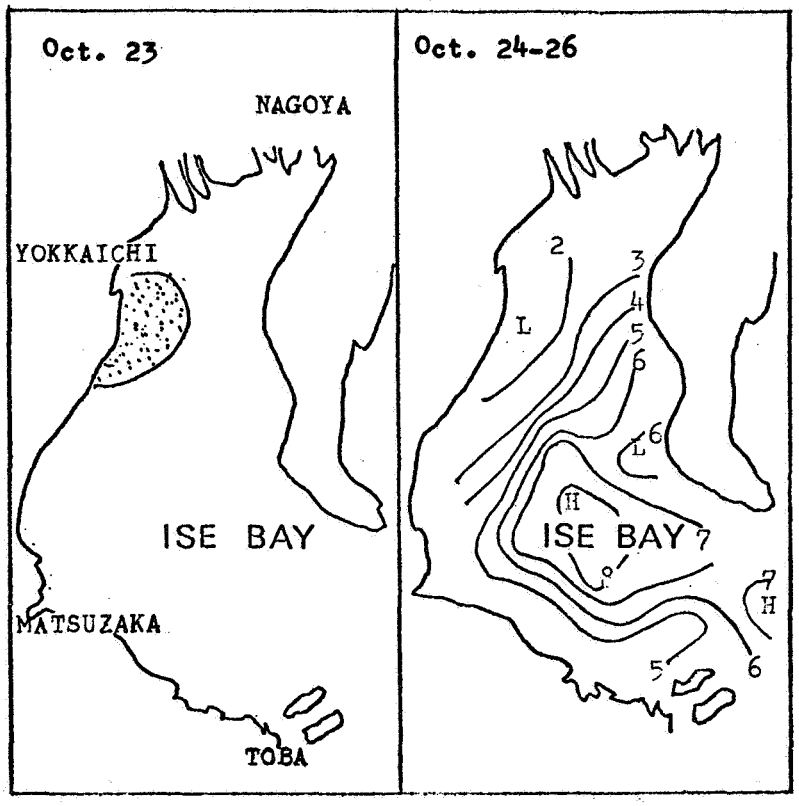


Fig. 1 Red tide area by ship's observation

Fig. 2 Transparency distribution (m)

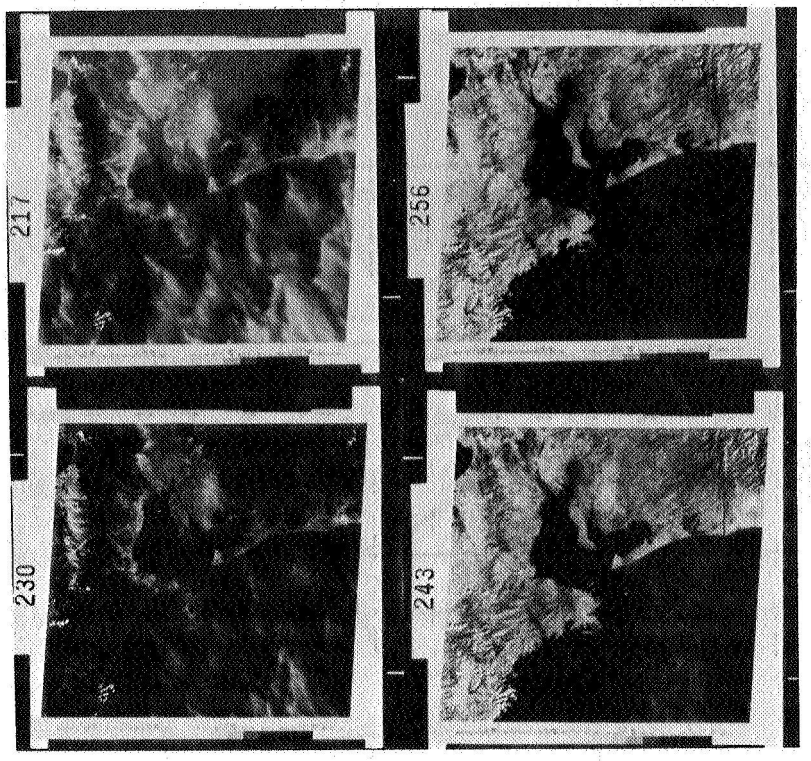


Fig. 3a ERTS-A imageries (5 Oct. 1972)



Fig. 3b Negative green band imagery

Oct. 24-26

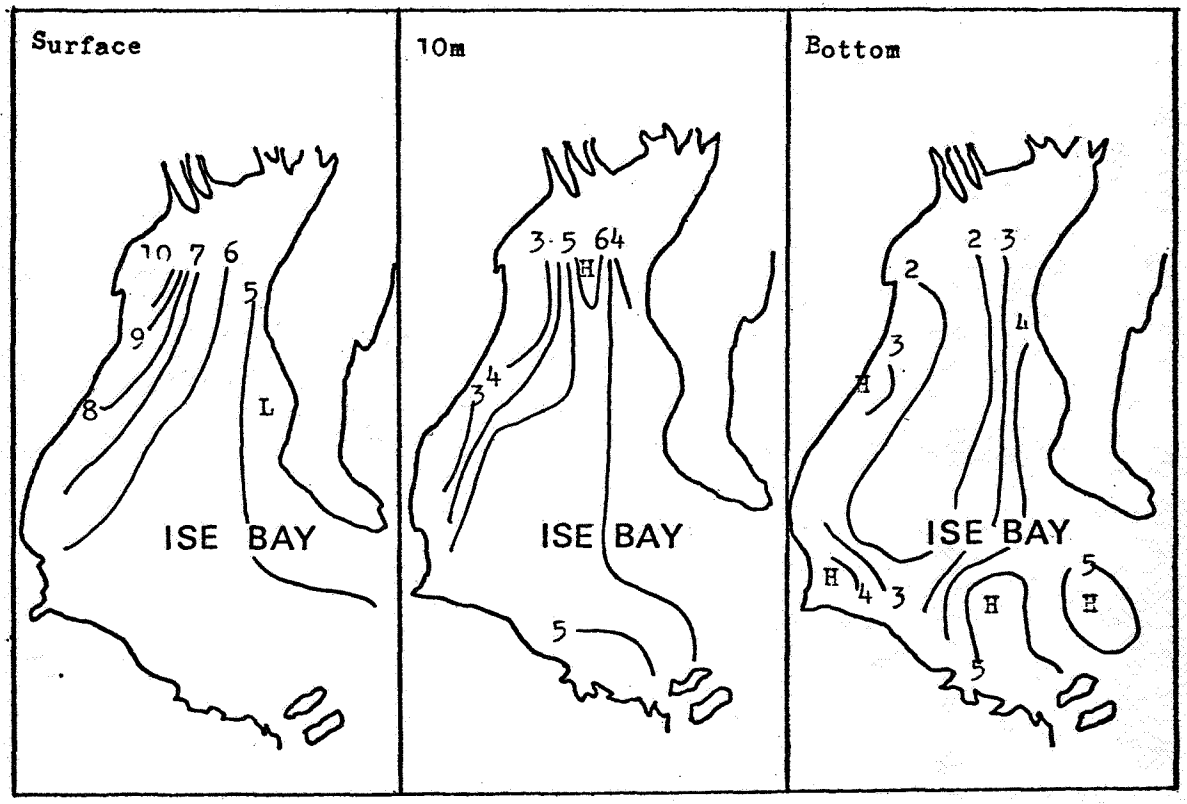


Fig. 4 D O Distribution (cc/L)

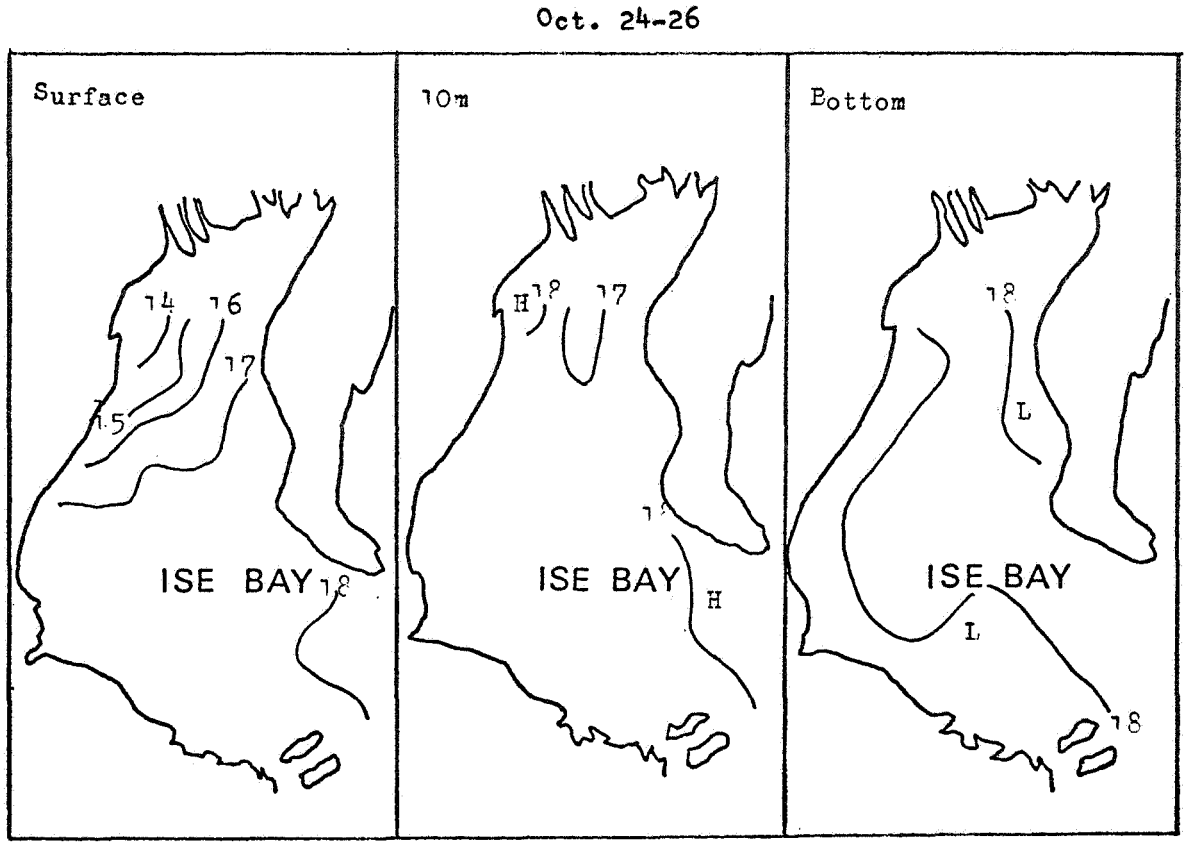


Fig. 5 Chlorinity distributions (‰)

WATER RESOURCES

Paper W 1

HYDROGEOLOGY OF CLOSED BASINS AND DESERTS OF SOUTH AMERICA, ERTS-1 INTERPRETATIONS[1]

George E. Stoertz and William D. Carter, *U. S. Geological Survey, Washington, D. C. 20244*

ABSTRACT

Images from the Earth Resources Technology Satellite (ERTS-1) contain data useful in studies of hydrogeology, geomorphology, and paleoclimatology. Sixteen Return Beam Vidicon (RBV) images and 15 Multi-Spectral Scanner (MSS) images were studied. These covered deserts and semidesert areas in southwestern Bolivia, northwestern Argentina, northern Chile, and southeastern Peru from July 30 to November 17, 1972. During the first 3 months after launching, high-quality cloud-free imagery was obtained over approximately 90 percent of the region of interior drainage, or an area of 170,000 square miles.

Hydrologic applications of ERTS imagery made evident by studies to date include: 1) mapping of salars or salt-encrusted playas, which represent water discharges from closed drainage basins; 2) mapping of drainage divides, particularly around closed basins in dry regions; 3) mapping of geologic structural data, related to origin and hydrologic closure of basins; 4) revision of geologic maps to show hydrologically important differences in surficial deposits; 5) revision of hydrologic features on topographic maps; 6) monitoring seasonal changes in floodwaters to evaluate areal and seasonal changes in weather, climate, and water resources; 7) mapping of mountain snowpack; and 8) relation of permanent drainage basin characteristics to seasonal snow cover and floodwater as an aid in estimating water resources of basins lacking meteorological or stream-gaging stations.

1. SCOPE OF THE STUDY

Cloud-free ERTS-1 coverage of the study area was approximately 90 percent complete between July 30 and October 30, 1972, comprising 16 RBV and 15 MSS images. This 3-month period represents mid-

1/ Publication authorized by the Director, U.S. Geological Survey.

winter and early spring, the period of extensive snow cover in midwinter, of heavy snowpacks in the high Andes in early spring, of extensive surface water on floodplains in closed drainage basins, of moderately high ground water levels beneath salars, and of increasing spring discharge along the periphery of salars.

The study area (Figure 1) covers most of Areas 7 and 9 in a

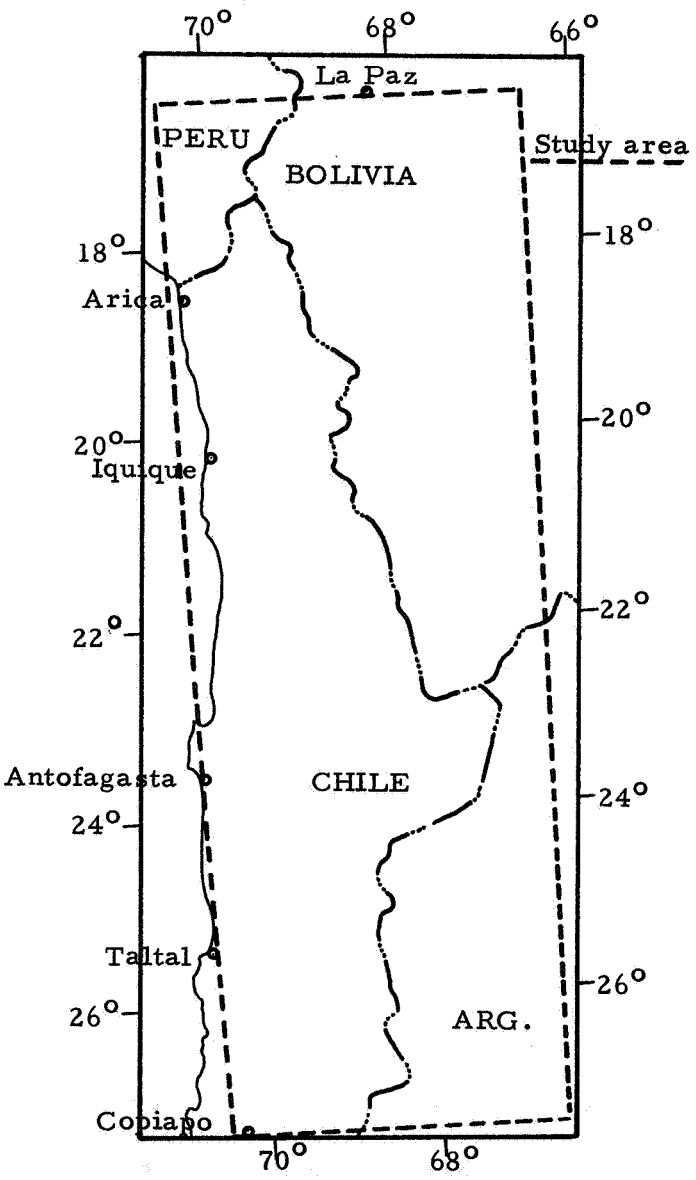


FIGURE 1. ERTS STUDY AREA

NASA-approved ERTS-1 investigation (ID IN-012); it coincides with the area of a proposed ERTS-B investigation (Proposal 22010).

Cloud-free ERTS coverage during this season prevailed except in the southwest, from latitude 25°30' to 27°30' South in Atacama Province, Chile.

2. METHOD OF STUDY

ERTS interpretations were mapped at 1:1,000,000 and later reduced to 1:2,650,000 for convenience, requiring one sheet (7 in. x 19 in.) for each subject. Page limitations prohibit their inclusion in this paper. The following have been identified on maps at 1:2,650,000: 1) 150 salars (areas of ground-water evapotranspiration); 2) 184 closed drainage basins; 3) geologic data: 681 volcanoes, faults, structural trends, diagrammatic fold axes, ancient Lake Minchin; 4) snow cover, August-October, 1972; 5) surface water, August-October, 1972: 88 seasonal lakes and floodwaters; 6) extent of 61 seasonal lakes and floodwaters, August-October, 1972; and 7) seasonal flooding versus snow cover, August-October, 1972: 40 basins having more than 40 percent snow cover, 17 basins having 20 to 40 percent snow cover, and 26 lakes larger than 1 square mile.

The basis for classification as verified, modified, or revealed by ERTS was chiefly the Operational Navigational Charts (ONC sheets P-26, Q-26, and Q-27) at 1:1,000,000, believed to be the best maps readily available in Washington, D.C. Better maps of some features are in compilation from aerial photographs for parts of the study area. In northern Chile salar borders interpreted from ERTS were compared to maps compiled from aerial photographs by the Geological Survey but not yet published.

The maps as compiled to date show corrected relative positions of features, but absolute corrections with respect to latitude and longitude have not yet been practicable. Corrections to date have been made in relation to about 250 high peaks, mostly volcanoes reaching altitudes of 14,000 to 22,000 feet, that were mapped by triangulation and are the most accurate features on existing maps. Horizontal positional discrepancies of 5 to 10 miles are common for drainage features on available published maps.

3. STUDY OF SALARS OR SALT FLATS

Salars are largely evapotranspiration troughs where most of the ground water and surface water of closed basins is discharged. Accurate delineation of salars helps in estimating the area of a desert basin from which ground water is discharged by evaporation and transpiration, and helps assess water resources in areas where water is the major limitation on development. Prior to this study, there were positional discrepancies of as much as 10 to 15 miles in the portrayal of salars and other drainage features, particularly in Bolivia and Argentina.

Salars, mapped with the aid of ERTS imagery, number 150 and cover about 10,000 square miles in the study area. Of these, 86 proved essentially correct on published and unpublished maps, but borders were refined even on well-mapped salars. Thirty-two salars were significantly modified, and 20 were mapped solely from ERTS imagery.

4. STUDY OF CLOSED DRAINAGE BASINS[2/]

Delineation of drainage divides that define the perimeter of closed basins in arid to semiarid regions is basic to water-resources appraisal and is necessary for estimating runoff or flood probability. Also, distribution of saline minerals is related to both present and former drainage divides. Saline resources include sodium chloride, sodium sulfate, calcium sulfate, potash salts, nitrates, iodates, borates, and carbonates. In several basins the overflow of divides during an ancient pluvial age has flushed salts into lower basins.

Drainage basins between latitudes 21° and 25° South are outlined on Figure 2, based on available topographic maps with ERTS-assisted revisions. Steep relief in the Andes, where most of the basins occur, helps reveal divides by erosion features and snow-capped ridges. An average profile of an Andean drainage basin would be an area of 200 square miles, a basin floor altitude of about 13,500 feet, mean basin altitude more than 14,000 feet, mean relief more than 2,000 feet, mean altitude of perimeter divides more than 15,000 feet, and average slopes of terrain more than 6 percent. These unusual characteristics will be studied further with the aid of ERTS imagery in an attempt to relate them to runoff and flooding in future seasons.

2/ Closed basins, as used here, are basins having internal surface drainage; some are hydrologically open due to subsurface leakage.

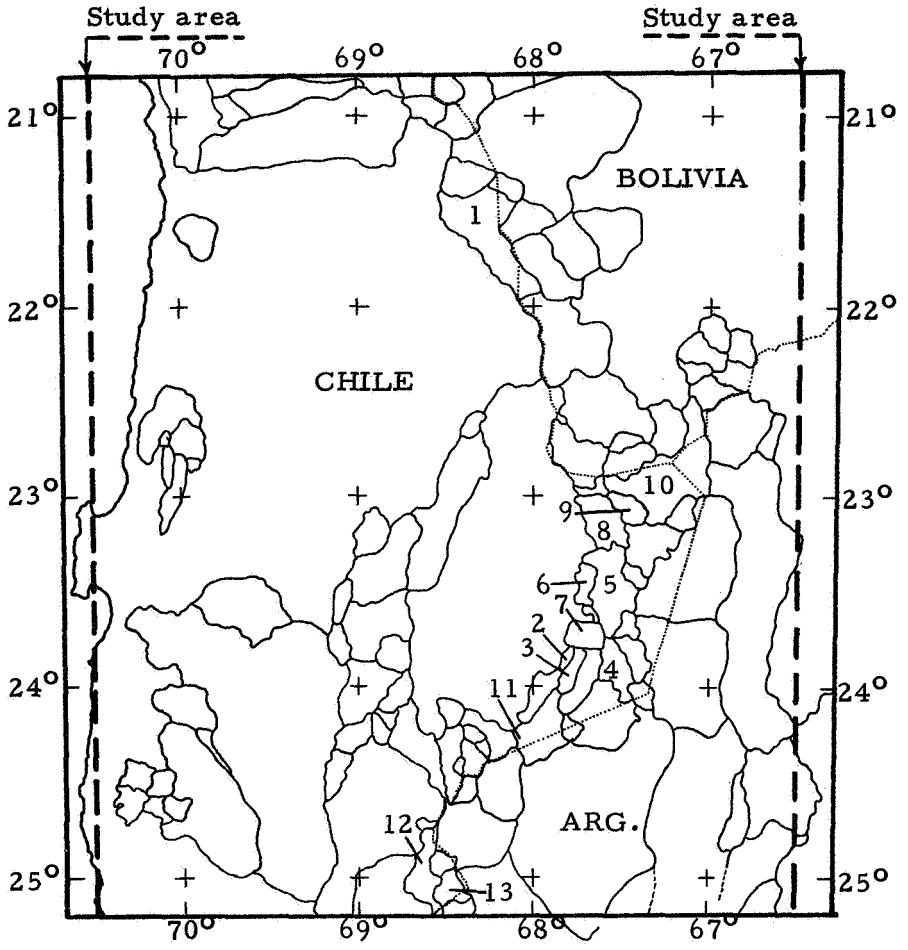


FIGURE 2. CLOSED DRAINAGE BASIN DIVIDES IN THE CENTRAL ANDES, 21° TO 25° S. Numbers refer to the 16 drainage basins summarized on Table 2; national borders shown by dotted line to distinguish from divides that coincide.

A total of 184 closed basins were mapped in the study area. ERTS images assisted in delineation of divides, particularly in the eastern half of the area, where reliable topographic maps were unavailable. However, the outlines of 47 basins are still unreliable, and future ERTS studies will be directed toward improving the reliability of these.

5. GEOLOGIC STUDIES

ERTS studies to date include delineation of volcanic craters, faults, structural trends, folds, and ancient lakebeds. Preliminary mapping covers large parts of the study area and will continue with acquisition of new imagery.

A published geologic map covering 3,600 square miles around Salar de Atacama (50 to 100 miles southeast of Chuquicamata, Chile) was experimentally evaluated using ERTS imagery. This established that refinements can be made in geologic maps with the aid of ERTS imagery, a task that could most effectively be done by geologists familiar with the areas.

Volcanic craters

Of 681 volcanoes, craters, and calderas mapped, 251 were verified, five were modified, and 171 were mapped from ERTS imagery; 230 more are shown on the Mapa Geologico de Chile (Instituto de Investigaciones Geologicas, 1968) but were unverified because of snow and cloud cover. Among nine active volcanoes, one was relocated 1.5 miles eastward; this is Volcan Parinacota (lat. 18°10' S). Fifteen calderas were mapped, 10 from previous sources and five from ERTS imagery.

Faults

Among the 5,000 linear miles of known faults in Chile between latitudes 17°30' and 25° South, about 1,500 miles could be traced on the imagery. An additional 160 linear miles of conjectural faults or realinements of known faults were mapped. The ERTS data would be most useful to geologists by delineating faults and permitting the extension of known faults as inferred or conjectural faults.

Fold axes

Major structural trends, principally fold axes, were mapped in Bolivia and Argentina, including an area of geologic interest where the Andean fold system bends around from a strike of N 40°W near La Paz, Bolivia, to N 15°E in northwestern Argentina. Detailed interpretation of geologic structures using ERTS images in an area of complex geology would require detailed knowledge of the geology. For example, in an area located 40 miles east-southeast of Uyuni a geologic map (Servicio Geologico de Bolivia, 1966, sheet 6332) shows that one straight north-

eastward traverse of 6-1/4 miles would cross 16 anticlinal axes and 16 synclinal axes, with an average spacing of one every 1,000 feet, a spacing equivalent to 32 fold axes per centimeter on ERTS imagery at 1:1,000,000.

6. STUDY OF SNOW COVER

The distribution of snow cover and surface water was studied to better understand present climate as it influences basin flooding and salt-crust morphology. This could help in understanding earlier climatic regimen, and possibly the distribution of saline resources such as the Chilean nitrate deposits. Currently the only climatic data available for most individual basins and ranges are extent of lakes or seasonal floodwaters and the distribution of snow cover. ERTS images have now made it possible to analyze both of these important parameters. These data are extremely important in understanding the water resources of mountainous areas where much of the water available to bordering lowlands originates. In the Andes, ERTS data are particularly valuable because meteorological and stream-gaging stations are scarce.

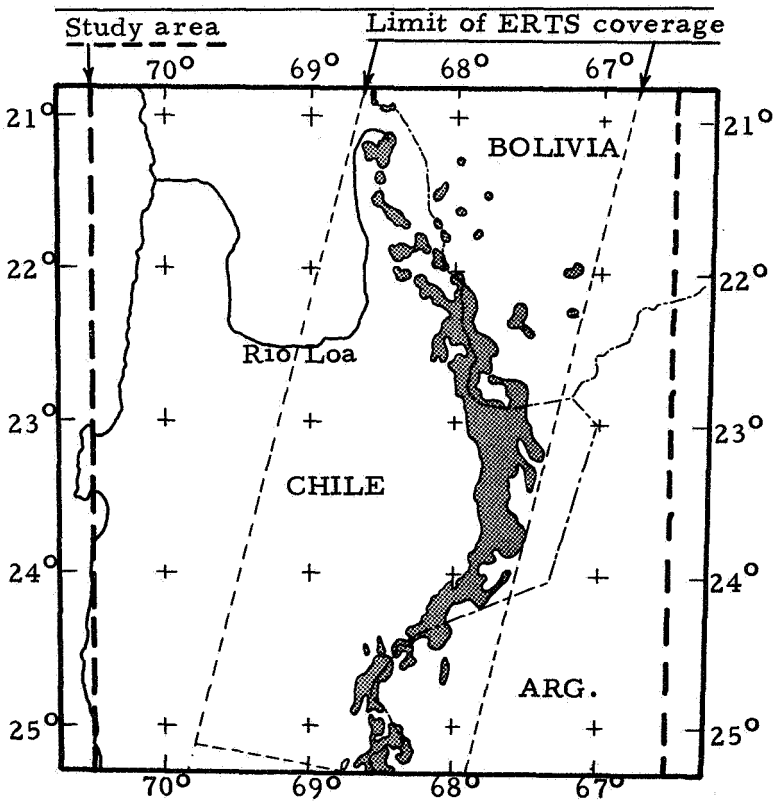


FIG. 3. ANDEAN SNOW COVER, 21° TO 25° S., OCT. 30, 1972.

Figure 3 shows the distribution of snow cover from latitude 21° to 25° South on the main Andean range on October 30, 1972. Earlier, on July 31, 1972, snow was seen to cover most of the range south of latitude 26° South, along the border between Chile and Argentina. The snow at that time covered most areas higher than 15,000 feet in the main range, while ridges extending higher than 20,000 feet 100 miles to the east were largely free of snow.

By October 30, 1972 (Fig. 3) the snow had the appearance of a heavy snowpack remaining after some melting. Snow cover was largely on the main range, extending to altitudes of about 15,000 feet on the east and to altitudes of 13,000 to 14,000 feet on the west. Additional snow cover probably lay along the border between Bolivia and Argentina but was outside the limits of ERTS coverage on October 30, 1972.

7. STUDY OF SURFACE WATER

Lakes or seasonal floodwaters were mapped at 88 places, of which 29 were lakes similar to those on existing maps, 23 were modified by ERTS data, and 36 were mapped solely from ERTS. The areas of 87 surface-water bodies are summarized in Table 1, totalling 493

Table 1. Distribution of 87 lakes and floodwaters in closed basins and deserts of South America, August-October, 1972 (excludes L. Titicaca)

Lake area, square miles	Northern one-third Lat. 16°30' - 20°S Long. 66°30'-70°30'W			Southern two-thirds Lat. 20° - 28°S Long. 66°30'-70°30'W			Whole study area Lat. 16°30'-28°S Long. 66°30'-70°30'W		
	No.	Total area	Mean area	No.	Total area	Mean area	No.	Total area	Mean area
More than 16	4	308	77	0	0	0	4	308	77
8.1 - 16	1	11	11	3	37.5	12.5	4	48.5	12.1
4.1 - 8	2	12.2	6.1	6	32.9	5.5	8	45.1	5.6
2.1 - 4	2	6.7	3.4	10	31.0	3.1	12	37.7	3.1
1.1 - 2	3	4.4	1.5	19	29.3	1.5	22	33.7	1.5
0.5 - 1	6	4.7	0.8	16	11.1	0.7	22	15.8	0.7
0.1 - 0.4	7	1.5	0.2	8	2.4	0.3	15	3.9	0.3
Totals	25	349	- -	62	144	- -	87	493	5.7

square miles. Nearly all of this surface water is saline and unfit for use, because most is on the saline floors of closed basins. However, the use of ERTS imagery to monitor seasonal changes in floodwaters on basin floors provides an opportunity to evaluate areal and seasonal changes in weather, climate, and water resources in this relatively undeveloped region that lacks both data and water.

A special study was made of the relation between seasonal flooding and snow cover in the Andes between latitudes 21° and 25°20' South during August-October, 1972. Thirty-six basins larger than 60 square miles, with the best topographic and snowpack data were studied to find which general factors favor seasonal flooding.

Three factors correlated with the extent of surface water, and in lieu of better data might help to explain and predict future surface-water conditions (for example, lakes, flooding, and runoff) in many of the 184 closed basins as well as in the more poorly known external drainage basins. The gross factors are high basin altitudes, high perimeter divides, and high percentage of snow cover. Figure 4 illustrates that the best correlation between surface water, snow cover, and altitude in August-October is given by these values: 1) mean altitude of drainage basin 13,500 feet or higher; 2) mean altitude of drainage divides 14,500 feet or higher; and 3) snowpack covering more than 10 percent of the basin on October 30. Sixteen of the 36 basins met all three criteria, and 13 of these had surface water covering more than 1 square mile or more than 0.3 percent of the drainage basin. These were the only basins having ERTS snowcover data that had water areas as large as 1 square mile or as extensive as 0.3 percent of the drainage basin.

It is concluded that these 13 basins contain the most abundant surface water resources in the region. It should be useful to extend this ERTS application and similar studies to additional areas and during other seasons, as well as to attempt analysis of ground-water resources with the aid of ERTS imagery. Further data on 16 basins containing abundant water resources are given in Table 2.

8. REFERENCES CITED

Instituto de Investigaciones Geologicas, 1968: Mapa Geologico de Chile, 1:1,000,000

Servicio Geologico de Bolivia, 1966: Mapa Geologico de Bolivia, 1:100,000

Table 2. Sixteen basins larger than 60 square miles in northern Chile, containing lakes or floodwaters larger than 1 square mile or covering more than 0.3 percent of the drainage basin, August-October, 1972.

Key no., Fig. 2	Basin area (sq mi)	Mean basin altitude (feet) [1]	Mean altitude of divides (feet)	Snow cover (percent of basin, Oct. 30)	Water area (sq. mi., Aug.-Oct.)	Water (percent of basin)
1	640	14,000	15,500	13	1.4	0.22
2	75	13,500	14,500	64	3.2	4.3
3	156	13,500	14,500	33	3.2	2.1
4	175	14,750	16,000	21	1.1	0.63
5	400	14,750	16,000	38	1.4	0.35
6	91	14,750	15,800	99	0.7	0.77
7	124	15,000	16,600	97	4.1	3.3
8	252	15,500	16,000	84	2.3	0.91
9	104	13,750	15,200	43	2.5	2.4
10	711	14,250	16,000	15 [2]	10	1.4
11	283	13,750	15,900	41	1.1	0.39
12	210	13,750	15,100	40	1.2	0.57
13	94	15,000	15,900	67	2.6	2.8
14	125	16,250	17,800	[3]	2.2	1.8
15	684	16,000	17,400	[3]	6.5	0.95
16	360	14,500	15,500	[3]	12	3.5

1/ Mean altitude of basin is defined here as $\left(\frac{A+B}{2}\right)$ where A is altitude of lowest point, and B is mean altitude of perimeter divides.

2/ Snow covered 15 percent of area imaged by ERTS on October 30.

3/ Snow cover not available for October 30, but July 31 imagery suggests high percentage of snow cover.

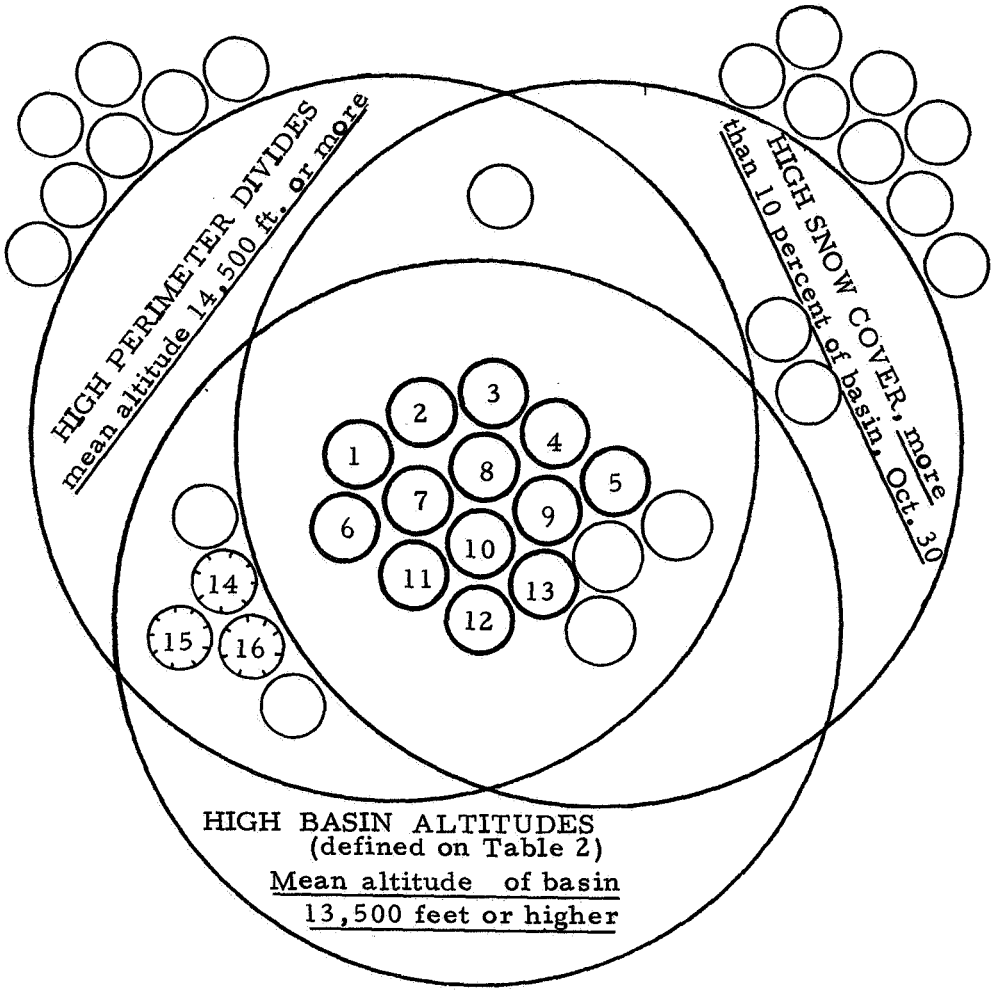


FIGURE 4. FACTORS FAVORING SEASONAL FLOODING IN 39 BASINS LARGER THAN 60 SQUARE MILES IN NORTHERN CHILE. Based on 36 basins for which snow-cover data from ERTS (Oct. 30, 1972) covers at least 30 percent of basin; includes 3 other basins known to contain perennial lakes larger than 2 square miles.

○ 23 basins without lakes or floodwaters, or where water covered less than 1 sq. mi. and less than 0.3 % of basin, Aug.-Oct. 1972

(3) 13 basins where lakes or floodwaters covered more than 1 sq. mi. or 0.3 % of basin area; basins are identified on Figure 2.

(14) 3 basins known to contain perennial lakes over 2 square miles, but snow cover data were unavailable for October 1972; basins are summarized on Table 2.

Paper W 2

DETECTION OF MAJOR RIVER BED CHANGES IN THE RIVER EBRO (NORTH-EASTERN SPAIN)

R. Espejo, J. Torrent and C. Roquero, *E. T. S. de Ingenieros Agrónomos (Universidad Politécnica de Madrid)*

ABSTRACT

The River Ebro is the most important water course in Spain crossing the Iberian Peninsula in a south-eastern direction from Central North to the Mediterranean Sea.

A study has been undertaken to evaluate major river bed changes over a distance of 30 Km. either side of the city of Zaragoza. Data, as far back as 1890 have been used showing that meanders are fairly active thus causing a noticeable repercussion on the use of nearby agricultural lands.

Results make it possible to estimate future trends in meander evolution.

1. INTRODUCTION

The River Ebro is the most important water course in Spain Along its 927 km. path from the Central-Northern part of the Iberian Peninsula to the Mediterranean Sea it collects the waters of the southern slopes of the Pyrenees and ends in a large delta of about 400 sq. km.. Mean discharge at its mouth is about 600 c.m./sec. For many centuries the delta has been building up at a quick rate thanks to an abundant supply of sediments wich have been caused by intense anthropic erosion.

The zone of the present study corresponds to the middle part of the course and and centers around the city of Zaragoza (Fig. 1). An approximate length of 60 km. has been selected leaving the city

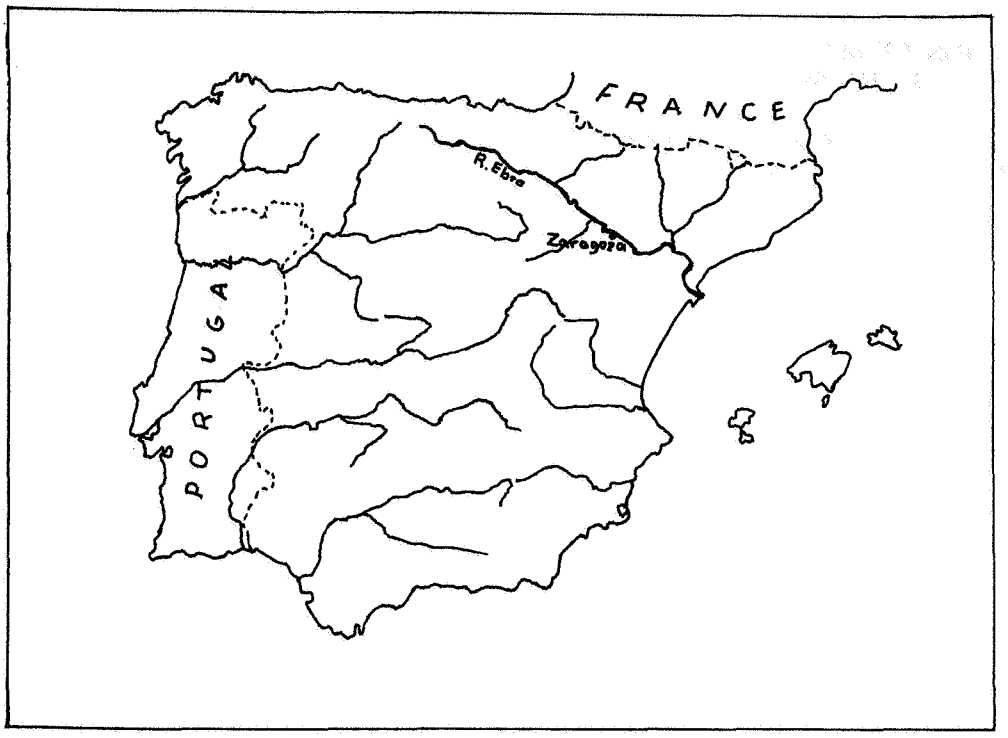


Fig. 1. Map of situation

at its center. In this area the river flows cutting a complex sequence of terraces, usually limited by Miocene sediments (gypsiferous marls)

2. MATERIALS

Selected areas that had historically showed meander activity were examined by means of topographic maps scale 1:50.000 correspondig to the years 1.892 and 1.920 (1) and aerial photographs at scales 1: 45,000 (USAF - A, 1946) and 1: 32,000 (USAF - B, 1956). Thus a clue was obtained as to the direction of river changes. Then the available ERTS-1 imagery (MSS 4, 5, 6, 7, 25th September, 1972) was used to see the evolution in the last 15 years.

Image quality was good enough to permit a clear identification of the river course and bands MSS 5 and 7 proved to be the most useful for this purpose. Reflectance for band 5 was high due to the high sediment content of the water and sufficed to identify the river. However other features like bodies of water related to old channels and depressions were only apparent in band 7.

3. MEANDER EVOLUTION

Eventual floods were a constant danger in the history of the River Ebro, but hazard has been gradually reduced thanks to a series of dams built during the last 50 years. River activity remains nevertheless intense and continuous action can be seen in meander dynamics.

Several zones of the study area have river channels that have been abandoned in the last 15 years. Figure 2 shows a typical case in which a major variation in the course of the river is observed. Mean yearly desplacements are as high as 30m., the greater activity obviously related to minor floods and seasonal peaks.

4. THE IMPACT OF RIVER DYNAMICS

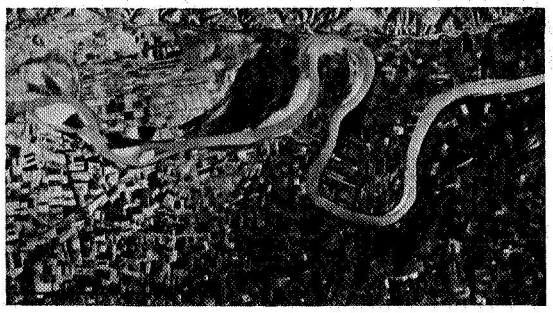
Fluvial deposits are the best agricultural lands of the area as surrounding Miocene sediments have given place to soils characterized by high salinity and shallowness. As a consequence of this, irrigation schemes were established in the area long ago and have, since then, undergone changes due to river channel displacements. These changes go, to our knowledge, as far back as the fourteenth century.

Demographic pressure adds to the good quality of alluvial deposits to cause the intense cultivation of not only terraces but recent alluvium. It has been estimated that, due to river activity, 1500 Ha. have disappeared for agricultural purposes and 900 Ha. brought under cultivation in the last 80 years.

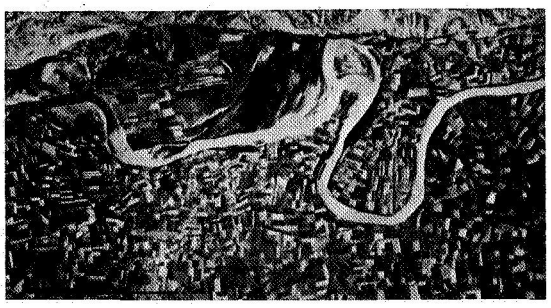
It is expected that repetitive coverage by means of satellite can help monitoring river changes in the future thus supplying valuable information to local authorities, which will be able to take primary decisions about defence works, irrigation schemes etc. Characteristics of ERTS-1 imagery will also be useful to geographers and geomorphologists so as to appraise the overall variations over a long distance of the river course.

Another point of interest arises from the possibility that band MSS 7 also shows small bodies of water. Therefore it will be feasible to detect, after flooding especially, the repartition of areas that are depressed or have a slow drainage. An example of this has been included in Figure 3 which shows small water-filled depressions in an old river channel.

FIG. 2 . AN EXAMPLE OF MEANDER EVOLUTION



a) In 1946



b) In 1956



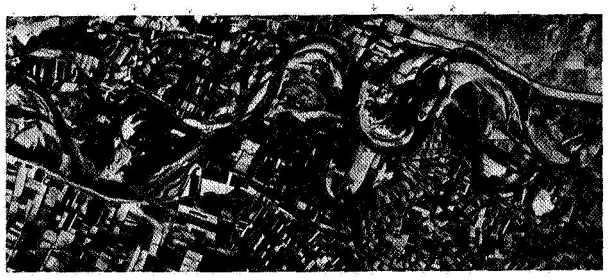
c) In 1972 (ERTS-1, MSS 5)

ERTS-1 imagery is also intended to serve as a source for the detection and selection of areas of newly deposited alluvial materials. These will be taken as pilot zones for the study of initial soil forming processes, and compared to analogous cases in other rivers were research in soil age has been undertaken.

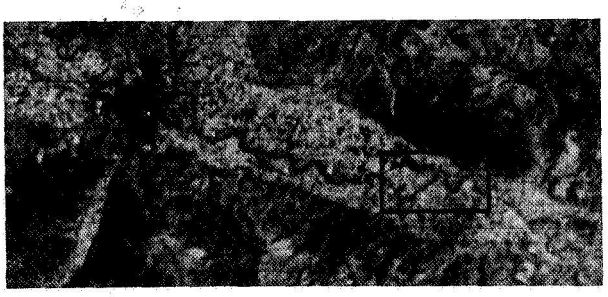
REFERENCES

(1) Mapa Agronómico Nacional. Comarca de Zaragoza. Memoria (Tomo I). Ministerio de Agricultura, Madrid, 1.950.

FIG 3. DETECTION OF A WATER-FILLED OLD RIVER CHANNEL



a) Aerial photograph



b) ERTS-1, MSS 7

Paper W 3

APPLICATIONS OF MULTISPECTRAL IMAGERY TO WATER RESOURCES DEVELOPMENT PLANNING IN THE LOWER MEKONG BASIN (KHMER REPUBLIC, LAOS, THAILAND AND VIET-NAM)

Willem J. van Liere, *Mekong Committee Secretariat, Bangkok, Thailand*

1. ABSTRACT

The use of ERTS imagery for water resources planning in the lower Mekong basin relates to three major issues:

- it complements data from areas, which have been inaccessible in the past because of security; this concerns mainly forest cover of the watersheds, and geological features.

- it refines ground surveys; this concerns mainly land forms, and soils of existing and planned irrigation perimeters.

- it provides new information, which would be almost or entirely impossible to detect with ground surveys or conventional photography; this concerns the mechanism of flooding and drainage of the delta; siltation of the Great Lake and mapping of acidity, possibly also of salinity, in the lower delta; sedimentation and fisheries in the Mekong Delta estuarine areas.

Examples are given of all these major issues (see Fig. 1, Fig. 2, Fig. 3-3 III, Fig. 4 and Fig. 5).

There are also other uses, not directly related to water resources planning, but still of prime importance to the holistic concept of river basin planning. These relate to the delimination of national reserves and to the identification of antiquities.

Examples of these are given too (see Fig. 3 and Fig. 6).

Complementary explanotory notes on ERTS images are given also directly on the different figures and images attached herewith, in conjunction with the corresponding ERTS frames.

The satellite data are particularly valuable also because their repetitive coverage gives an insight in the gradual transformation of changing features such as the extent of flooding and moisture retention in various soil types. Furthermore the availability of satellite imagery is most timely as it fills gaps in

basic data necessary for completion of development plans for the Mekong basin. These, in turn, are urgently needed, in order to finalize a realistic post-war development programme for the lower Mekong basin.

2. COMPARISON BETWEEN ERTS-1 IMAGES AND EXISTING GEOLOGICAL MAP AND FURTHER APPLICATION TO FORESTRY

2.1 Analysis (see Fig. 1, Fig. 2, in conjunction with ERTS Image 1 and Photo 1, Image 1-I and Image 2)

A comparison has been made in Fig. 1 between ERTS-1 frame No. 1111-02543 enlarged to a scale of 1 to 500,000 with an existing geological map which has been established to the same scale from a field study by J. Fromaget from 1923 to 1927 and published by the National Geographic Service of Viet-Nam 1963. This comparison leads to the following conclusions:

(i) The different gray tone scale steps found on the above ERTS-1 frame approximately correspond to the elements of regional geological structure shown on the map. As the latter is established from an old and imprecise survey, we definitely believe that ERTS imagery will help delineate more precisely the major terrain units.

(ii) With the help of both band 7 and band 5 prints, we can delineate and identify easily at least 5 major terrain units i.e. alluvium, upper Indosinias (mainly massive arenaceous group with subordinate siltstone; shale, with well-defined escarpement features); middle Indosinias (red micaceous shale, sandstone and siltstone, with basal conglomerate); calcareous series (mainly massive limestone with pronounced relief, subordinate shale and sandstone); and intrusive igneous rocks (Granite, granodiorite).

(iii) A triangular shape of fault was found east of Thakhek on the middle indosinias terrain, which is not mentioned in the existing geologic map. In addition, new lineaments were found which show rock fractures perpendicular to the NW-SW direction of the limestone outcrop north of Thakhek.

(iv) In the region of Savannakhet, the ERTS-1 image seems to demonstrate that the existing geological map allocated an exagerated area to the upper indosinias terrain, which we also find on the opposite Thai side in the form of the jurassic Phu Phan and Phra Wihan formation (max. altitude 628 m above MSL), all Indonesias formations forming a fold-belt around the Khorat cretaceous basin.

A recent spot survey by a forestry consultant with wide experience in tropical watershed management and forest conservation revealed that during the last two decades the lower Mekong basin has experienced an unprecedented destruction of

its forest resources and deterioration of its watershed conditions. He estimated that clearing of forest lands on account of shifting and semi-shifting cultivation and the clearing of trees for timber and fuel is progressing at the rate of one million hectares per year; moreover, information gathered from the satellite imagery and other sources indicates more than four million hectares of primary forests have been seriously degraded by war action. The ERTS imagery gives us for the first time a tool for periodic examination of progressive forest degradation and identification of remote areas requiring remedial action. Such an inventory is now being prepared.

2.2 Conclusions:

(i) An updated geological map of the lower Mekong basin showing new tectonic features, especially fold, fault and dome, is now feasible for the first time, thanks to the availability of ERTS imagery. The work will serve as a basis for a more detailed reconnaissance geological map, to be prepared when the whole lower Mekong basin becomes accessible for ground survey work.

(ii) Further application to forestry in remote and inaccessible areas is also possible since it is obvious that the geological structures are directly reflected by the types of forest cover. Three major vegetational cover units were identified, in Northern Laos and Thailand where the security conditions do not permit accessibility.

3. HYDROLOGICAL DATA (FLOOD PLAIN AND SEDIMENTATION OF RESERVOIRS). see also Fig. 3, Fig. 3-I, Fig. 3-II and Fig. 3-III and the corresponding images of ERTS-1 frames)

Using band 5 and band 7 positive transparencies (9.5 inch) we can delineate on an overlay and with the help of a light table, the contour of the reservoir area affected by sedimentation, since on band 5 transparency the latter area is represented by a lighter tone step than on band 7 transparency.

This comparison has identified extensive arms of two existing new tributary reservoirs which are heavy with sediment. Since no field observations had noted this phenomenon, the Mekong Secretariat is investigating to determine if siltation in these arms is beyond design forecasts and to locate excessive watershed erosion or other causes.

The flood plain and inundated areas near Phnom-Penh, Khmer Republic, or in the entire Mekong Delta, can be delineated without any difficulty. As we know the gradient of the Mekong river in this reach, through gage heights, we shall be able to follow the pattern of natural flooding as well as that of natural drainage

through the whole rainy season. This is a new and invaluable tool for flood control analysis, the Mekong Committee flood forecasting programme, and for design of agricultural polders in the flood zone. Delimiting flood areas will also serve as a guide to the zones of fish spawning in the drowned forest areas of the Khmer Republic.

4. UPDATING SOIL MAP (see Fig. 4, Image 4 and Image 4-I)

The existing general soil map of the whole lower Mekong basin (a basin of over 600,000 km^2 in size) unfortunately presents a variable degree of reliability. A high level of reliability based on systematic soil survey can be claimed only for 25% of the area; fair reliability based on reconnaissance survey can be conferred on another 25% of this area; and the data for the remaining 50% is based only on general information and can be assigned only a poor degree of reliability.

A comparison of ERTS-1 images with selected areas of the existing soil map has been made. An example of this is given in Fig. 4, which shows a comparison between the upper Nam Mun tributary basin and the corresponding ERTS-1 frame No. 1094-03303, taken on 25 October 1972.

We found that the grey tone units on the ERTS-1 frame correspond well to the different types of soil of the soil map.

Both band 7 and band 5 transparencies especially can help in delineating the soil-type units. The above finding will permit our staff to extrapolate the findings to other uncloudy ERTS-1 frames of the lower Mekong basin, and greatly improve the potential for quality mapping.

5. SEDIMENTATION AND FISHERIES AT MEKONG DELTA ESTUARINE AREAS (see Fig. 5 and Images 5-I, 5-II, 5-III)

Suspended materials at the estuaries from the various branches of the Mekong river can easily be delineated from various bands of the same ERTS-1 frame. This also leads to a knowledge the gradient of the surface of the mass of suspended silt which is entering into the sea as well as the passages through which fishes could be caught because it has been established that the density of plankton growth is directly related to the density of sediment load in any particular zone of the estuary, and the density of plankton is also directly related to the numbers and types of commercially valuable fish per square kilometer in these waters.

6. APPLICATION TO ARCHAEOLOGY (see Fig. 6, Image 6 and archaelogical Map 6-I)

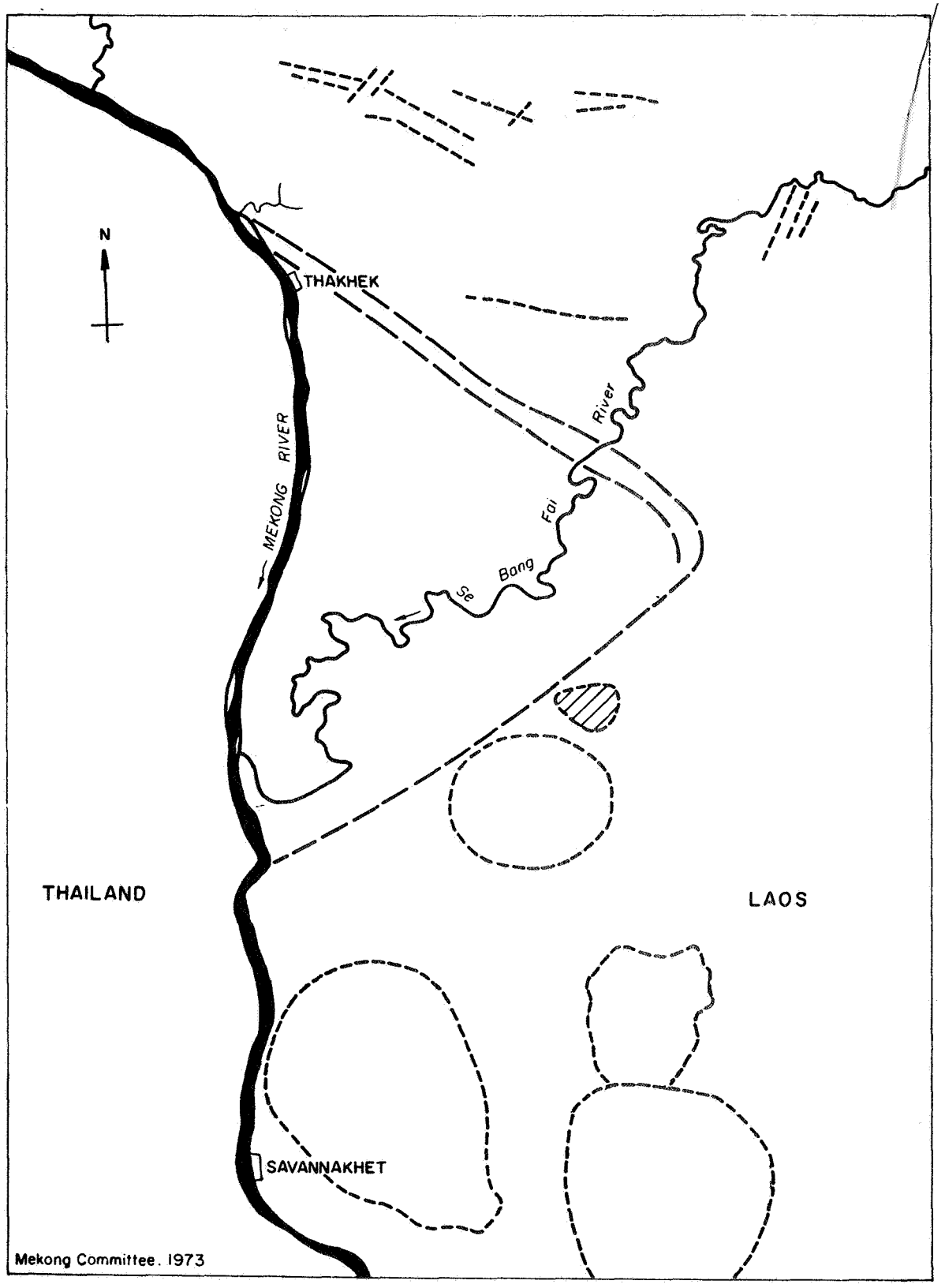
New artificial tanks and features found on the ERTS frame for the Angkor Wat region indicate interesting possibility for the delineation of archaeological sites, on the Northern shore of the Great Lake in the Khmer Republic.

The Angkhor area as it existed in the 14th century has been mapped by the French archaeologist, Bernard Groslier, after exhaustive excavation and extrapolation. To our amazement, many of the features on Groslier's reconstructed map are clearly identifiable on ERTS imagery, although ground identification is difficult (some of Groslier's locations and dimensions are also shown to be slightly in error). This raises the intriguing possibility of ERTS imagery identification of heretofore unknown ancient ruins, particularly more of the reservoir and irrigation works of the Khmers and other early civilizations in the basin which might be subject to rehabilitation.

7. CONCLUSIONS

ERTS-1 data output by its timely repetitive and multispectral aspect is of tremendous value to the planning of the integrated development of all related resources of the lower Mekong basin. Band 5, Band 6 and Band 7 multispectral images can meet nearly all our needs.

Fig. 1 GEOLOGICAL FEATURES

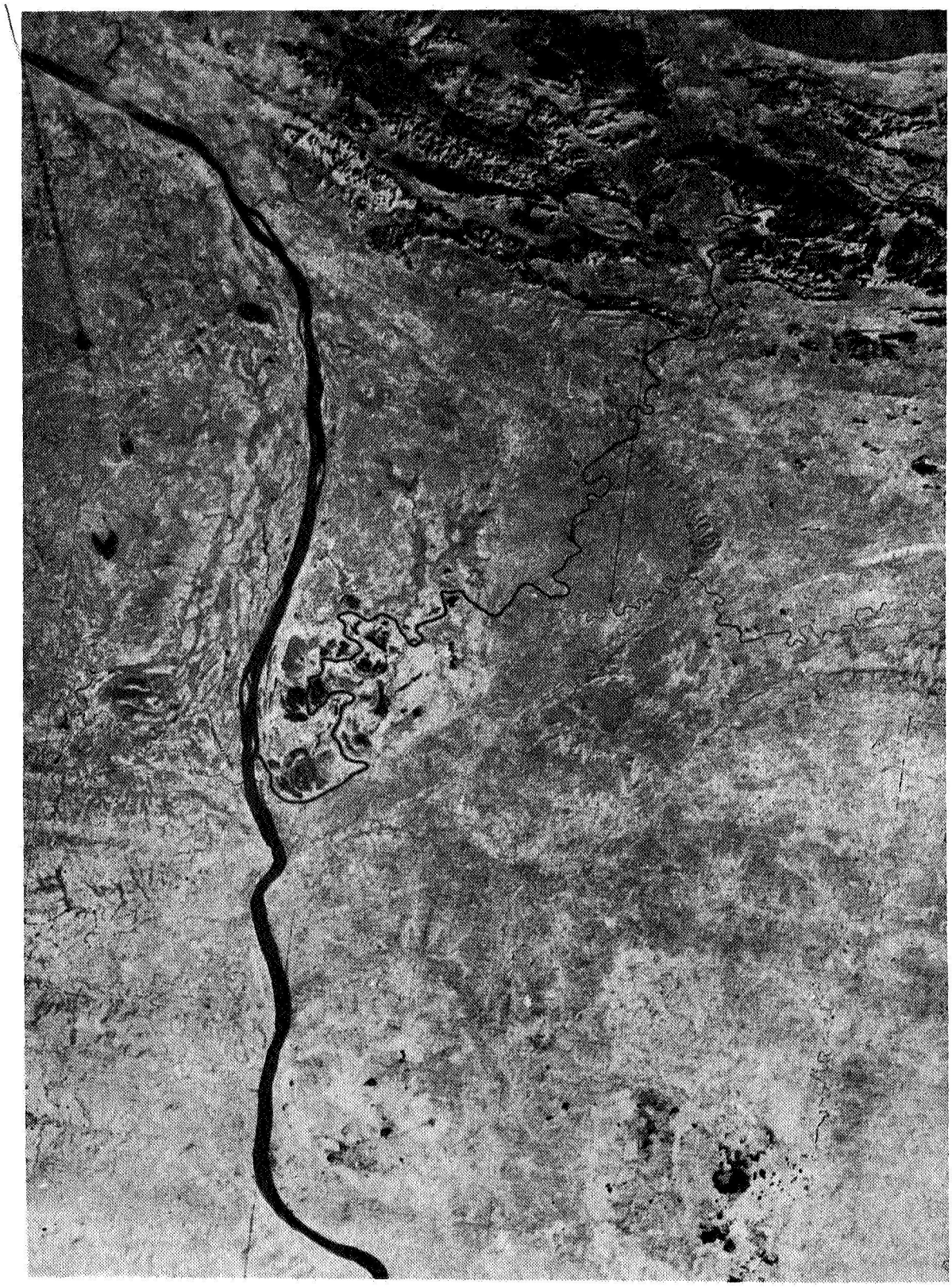


(ERTS-1 frame 1127-02451)

Fold, Fault, Fracture, Dome

N.B. Dotted lines are new features discovered

IMAGE 1



Mekong Committee 1973

(From ERTS-1 frame 1127-0245)

PHOTO - I

(EXISTING GEOLOGICAL MAP)

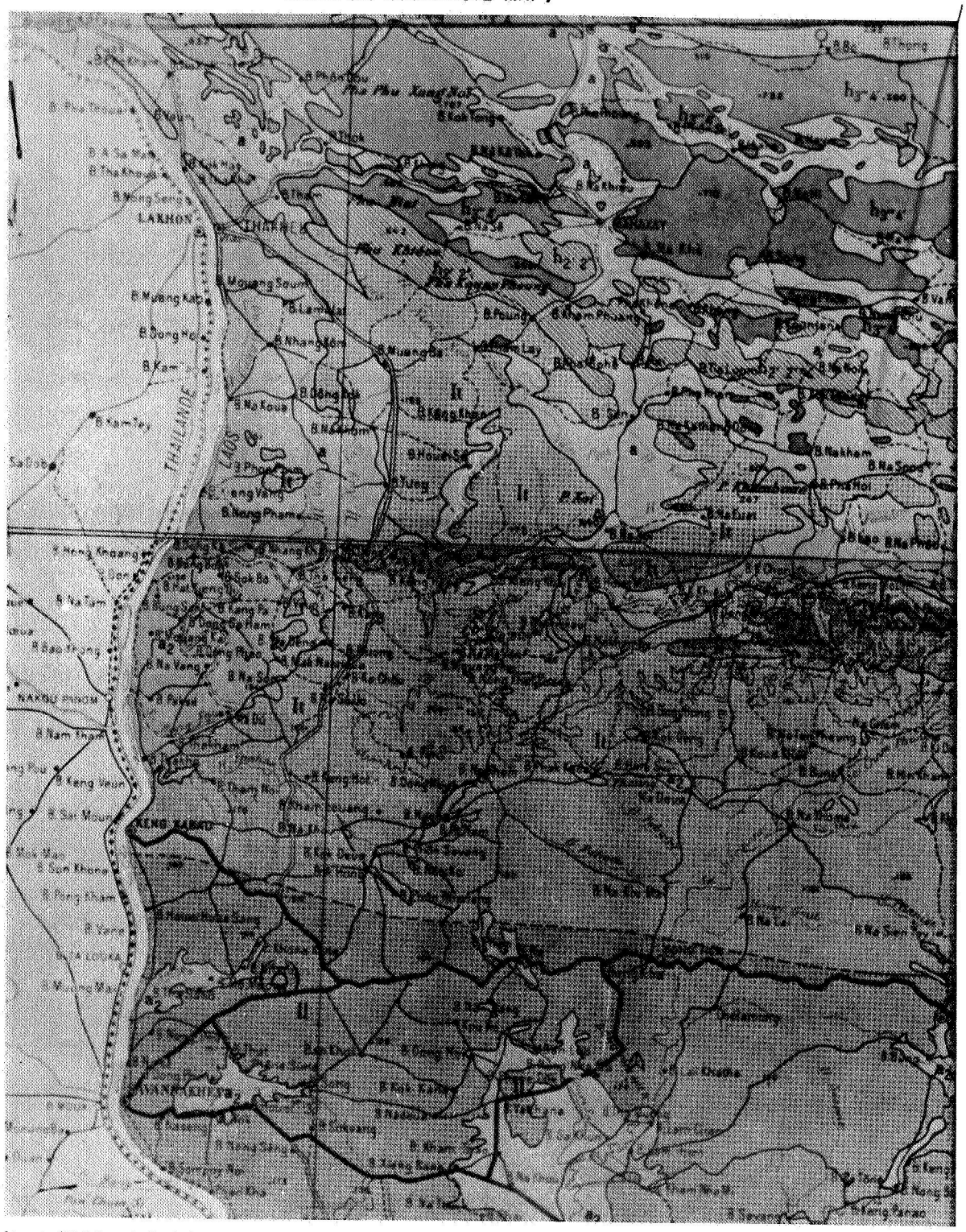
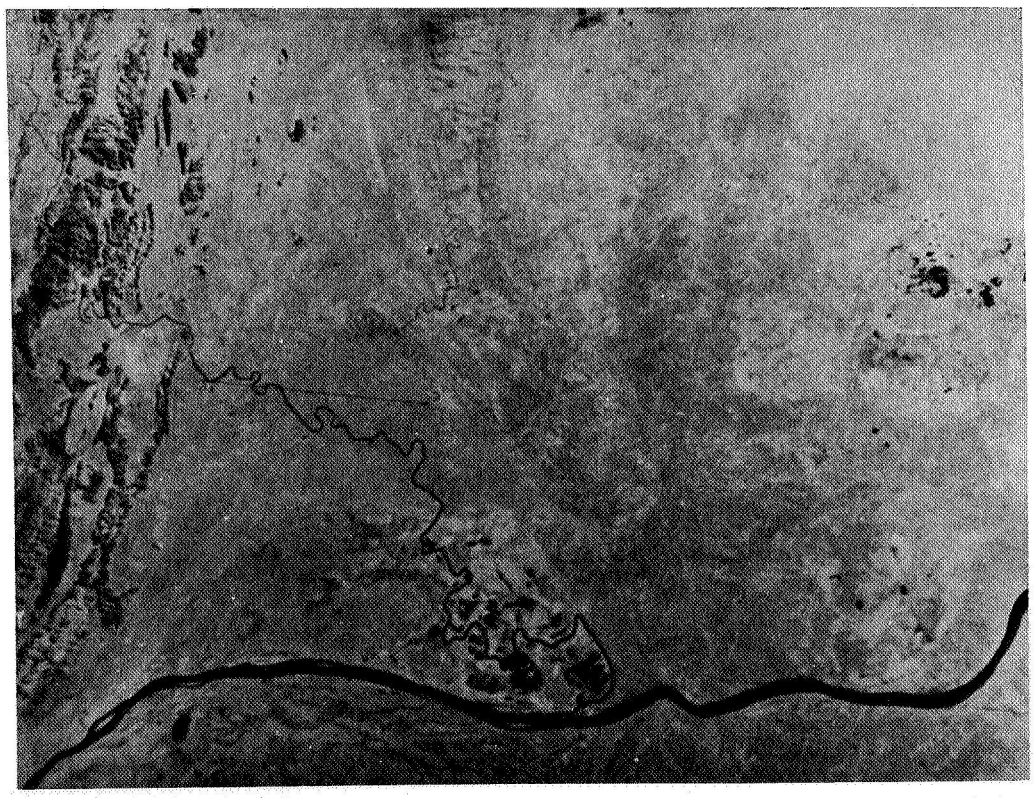

LAOS
THAILAND
LAMPHUN
Mouang Soum
Mouang Kat
Dong Hai
Kham Tay
Nam Khang
Nam Ngoua
Nam Kouse
Nam Houn
Nam Phoun
Nam Phoumi
Nam Khoang
Nam Tam
Nam Khan
Nam Pou
Nam Sai Mouan
Nam Khong
Nam Pong
Nam Yong
Nam Ma
Nam Kok
Nam Ngao
Nam Ngeun
Nam Ou
Nam Tha
Nam Ta
Nam Ha
Nam Nhiem
Nam Nhiep
Nam Nhiep Noi
Nam Nhiep Tai
Nam Nhiep Tay
Nam Nhiep Nua
Nam Nhiep Dong
Nam Nhiep Ban
Nam Nhiep Thuong
Nam Nhiep Ha
Nam Nhiep Giua
Nam Nhiep Cuoi
Nam Nhiep Moi
Nam Nhiep Cu
Nam Nhiep Tuoi
Nam Nhiep Xanh
Nam Nhiep Do
Nam Nhiep Vang
Nam Nhiep Den
Nam Nhiep Trang
Nam Nhiep Hong
Nam Nhiep Tim
Nam Nhiep Lam
Nam Nhiep Nau
Nam Nhiep Xam
Nam Nhiep Bac
Nam Nhiep Nam
Nam Nhiep Dong Bac
Nam Nhiep Dong Nam
Nam Nhiep Tay Bac
Nam Nhiep Tay Nam
Nam Nhiep Trung
Nam Nhiep Ngoai
Nam Nhiep Trong
Nam Nhiep Duoi
Nam Nhiep Tren
Nam Nhiep Giua Tren
Nam Nhiep Giua Duoi
Nam Nhiep Cuoi Tren
Nam Nhiep Cuoi Duoi
Nam Nhiep Moi Tren
Nam Nhiep Moi Duoi
Nam Nhiep Cu Tren
Nam Nhiep Cu Duoi
Nam Nhiep Tuoi Tren
Nam Nhiep Tuoi Duoi
Nam Nhiep Xanh Tren
Nam Nhiep Xanh Duoi
Nam Nhiep Do Tren
Nam Nhiep Do Duoi
Nam Nhiep Vang Tren
Nam Nhiep Vang Duoi
Nam Nhiep Den Tren
Nam Nhiep Den Duoi
Nam Nhiep Trang Tren
Nam Nhiep Trang Duoi
Nam Nhiep Hong Tren
Nam Nhiep Hong Duoi
Nam Nhiep Tim Tren
Nam Nhiep Tim Duoi
Nam Nhiep Lam Tren
Nam Nhiep Lam Duoi
Nam Nhiep Nau Tren
Nam Nhiep Nau Duoi
Nam Nhiep Xam Tren
Nam Nhiep Xam Duoi
Nam Nhiep Bac Tren
Nam Nhiep Bac Duoi
Nam Nhiep Nam Tren
Nam Nhiep Nam Duoi
Nam Nhiep Dong Bac Tren
Nam Nhiep Dong Bac Duoi
Nam Nhiep Dong Nam Tren
Nam Nhiep Dong Nam Duoi
Nam Nhiep Tay Bac Tren
Nam Nhiep Tay Bac Duoi
Nam Nhiep Tay Nam Tren
Nam Nhiep Tay Nam Duoi
Nam Nhiep Trung Tren
Nam Nhiep Trung Duoi
Nam Nhiep Ngoai Tren
Nam Nhiep Ngoai Duoi
Nam Nhiep Trong Tren
Nam Nhiep Trong Duoi
Nam Nhiep Tren Tren
Nam Nhiep Tren Duoi
Nam Nhiep Giua Tren Tren
Nam Nhiep Giua Tren Duoi
Nam Nhiep Giua Duoi Tren
Nam Nhiep Giua Duoi Duoi
Nam Nhiep Cuoi Tren Tren
Nam Nhiep Cuoi Tren Duoi
Nam Nhiep Cuoi Duoi Tren
Nam Nhiep Cuoi Duoi Duoi
Nam Nhiep Moi Tren Tren
Nam Nhiep Moi Tren Duoi
Nam Nhiep Moi Duoi Tren
Nam Nhiep Moi Duoi Duoi
Nam Nhiep Cu Tren Tren
Nam Nhiep Cu Tren Duoi
Nam Nhiep Cu Duoi Tren
Nam Nhiep Cu Duoi Duoi
Nam Nhiep Tuoi Tren Tren
Nam Nhiep Tuoi Tren Duoi
Nam Nhiep Tuoi Duoi Tren
Nam Nhiep Tuoi Duoi Duoi
Nam Nhiep Xanh Tren Tren
Nam Nhiep Xanh Tren Duoi
Nam Nhiep Xanh Duoi Tren
Nam Nhiep Xanh Duoi Duoi
Nam Nhiep Do Tren Tren
Nam Nhiep Do Tren Duoi
Nam Nhiep Do Duoi Tren
Nam Nhiep Do Duoi Duoi
Nam Nhiep Vang Tren Tren
Nam Nhiep Vang Tren Duoi
Nam Nhiep Vang Duoi Tren
Nam Nhiep Vang Duoi Duoi
Nam Nhiep Den Tren Tren
Nam Nhiep Den Tren Duoi
Nam Nhiep Den Duoi Tren
Nam Nhiep Den Duoi Duoi
Nam Nhiep Trang Tren Tren
Nam Nhiep Trang Tren Duoi
Nam Nhiep Trang Duoi Tren
Nam Nhiep Trang Duoi Duoi
Nam Nhiep Hong Tren Tren
Nam Nhiep Hong Tren Duoi
Nam Nhiep Hong Duoi Tren
Nam Nhiep Hong Duoi Duoi
Nam Nhiep Tim Tren Tren
Nam Nhiep Tim Tren Duoi
Nam Nhiep Tim Duoi Tren
Nam Nhiep Tim Duoi Duoi
Nam Nhiep Lam Tren Tren
Nam Nhiep Lam Tren Duoi
Nam Nhiep Lam Duoi Tren
Nam Nhiep Lam Duoi Duoi
Nam Nhiep Nau Tren Tren
Nam Nhiep Nau Tren Duoi
Nam Nhiep Nau Duoi Tren
Nam Nhiep Nau Duoi Duoi
Nam Nhiep Xam Tren Tren
Nam Nhiep Xam Tren Duoi
Nam Nhiep Xam Duoi Tren
Nam Nhiep Xam Duoi Duoi
Nam Nhiep Bac Tren Tren
Nam Nhiep Bac Tren Duoi
Nam Nhiep Bac Duoi Tren
Nam Nhiep Bac Duoi Duoi
Nam Nhiep Nam Tren Tren
Nam Nhiep Nam Tren Duoi
Nam Nhiep Nam Duoi Tren
Nam Nhiep Nam Duoi Duoi
Nam Nhiep Dong Bac Tren Tren
Nam Nhiep Dong Bac Tren Duoi
Nam Nhiep Dong Bac Duoi Tren
Nam Nhiep Dong Bac Duoi Duoi
Nam Nhiep Dong Nam Tren Tren
Nam Nhiep Dong Nam Tren Duoi
Nam Nhiep Dong Nam Duoi Tren
Nam Nhiep Dong Nam Duoi Duoi
Nam Nhiep Tay Bac Tren Tren
Nam Nhiep Tay Bac Tren Duoi
Nam Nhiep Tay Bac Duoi Tren
Nam Nhiep Tay Bac Duoi Duoi
Nam Nhiep Tay Nam Tren Tren
Nam Nhiep Tay Nam Tren Duoi
Nam Nhiep Tay Nam Duoi Tren
Nam Nhiep Tay Nam Duoi Duoi
Nam Nhiep Trung Tren Tren
Nam Nhiep Trung Tren Duoi
Nam Nhiep Trung Duoi Tren
Nam Nhiep Trung Duoi Duoi
Nam Nhiep Ngoai Tren Tren
Nam Nhiep Ngoai Tren Duoi
Nam Nhiep Ngoai Duoi Tren
Nam Nhiep Ngoai Duoi Duoi
Nam Nhiep Trong Tren Tren
Nam Nhiep Trong Tren Duoi
Nam Nhiep Trong Duoi Tren
Nam Nhiep Trong Duoi Duoi
Nam Nhiep Duoi Tren Tren
Nam Nhiep Duoi Tren Duoi
Nam Nhiep Duoi Duoi Tren
Nam Nhiep Duoi Duoi Duoi
Nam Nhiep Tren Tren Tren
Nam Nhiep Tren Tren Duoi
Nam Nhiep Tren Duoi Tren
Nam Nhiep Tren Duoi Duoi
Nam Nhiep Giua Tren Tren Tren
Nam Nhiep Giua Tren Tren Duoi
Nam Nhiep Giua Tren Duoi Tren
Nam Nhiep Giua Tren Duoi Duoi
Nam Nhiep Giua Duoi Tren Tren
Nam Nhiep Giua Duoi Tren Duoi
Nam Nhiep Giua Duoi Duoi Tren
Nam Nhiep Giua Duoi Duoi Duoi
Nam Nhiep Cuoi Tren Tren Tren
Nam Nhiep Cuoi Tren Tren Duoi
Nam Nhiep Cuoi Tren Duoi Tren
Nam Nhiep Cuoi Tren Duoi Duoi
Nam Nhiep Cuoi Duoi Tren Tren
Nam Nhiep Cuoi Duoi Tren Duoi
Nam Nhiep Cuoi Duoi Duoi Tren
Nam Nhiep Cuoi Duoi Duoi Duoi
Nam Nhiep Moi Tren Tren Tren
Nam Nhiep Moi Tren Tren Duoi
Nam Nhiep Moi Tren Duoi Tren
Nam Nhiep Moi Tren Duoi Duoi
Nam Nhiep Moi Duoi Tren Tren
Nam Nhiep Moi Duoi Tren Duoi
Nam Nhiep Moi Duoi Duoi Tren
Nam Nhiep Moi Duoi Duoi Duoi
Nam Nhiep Cu Tren Tren Tren
Nam Nhiep Cu Tren Tren Duoi
Nam Nhiep Cu Tren Duoi Tren
Nam Nhiep Cu Tren Duoi Duoi
Nam Nhiep Cu Duoi Tren Tren
Nam Nhiep Cu Duoi Tren Duoi
Nam Nhiep Cu Duoi Duoi Tren
Nam Nhiep Cu Duoi Duoi Duoi
Nam Nhiep Tuoi Tren Tren Tren
Nam Nhiep Tuoi Tren Tren Duoi
Nam Nhiep Tuoi Tren Duoi Tren
Nam Nhiep Tuoi Tren Duoi Duoi
Nam Nhiep Tuoi Duoi Tren Tren
Nam Nhiep Tuoi Duoi Tren Duoi
Nam Nhiep Tuoi Duoi Duoi Tren
Nam Nhiep Tuoi Duoi Duoi Duoi
Nam Nhiep Xanh Tren Tren Tren
Nam Nhiep Xanh Tren Tren Duoi
Nam Nhiep Xanh Tren Duoi Tren
Nam Nhiep Xanh Tren Duoi Duoi
Nam Nhiep Xanh Duoi Tren Tren
Nam Nhiep Xanh Duoi Tren Duoi
Nam Nhiep Xanh Duoi Duoi Tren
Nam Nhiep Xanh Duoi Duoi Duoi
Nam Nhiep Do Tren Tren Tren
Nam Nhiep Do Tren Tren Duoi
Nam Nhiep Do Tren Duoi Tren
Nam Nhiep Do Tren Duoi Duoi
Nam Nhiep Do Duoi Tren Tren
Nam Nhiep Do Duoi Tren Duoi
Nam Nhiep Do Duoi Duoi Tren
Nam Nhiep Do Duoi Duoi Duoi
Nam Nhiep Vang Tren Tren Tren
Nam Nhiep Vang Tren Tren Duoi
Nam Nhiep Vang Tren Duoi Tren
Nam Nhiep Vang Tren Duoi Duoi
Nam Nhiep Vang Duoi Tren Tren
Nam Nhiep Vang Duoi Tren Duoi
Nam Nhiep Vang Duoi Duoi Tren
Nam Nhiep Vang Duoi Duoi Duoi
Nam Nhiep Den Tren Tren Tren
Nam Nhiep Den Tren Tren Duoi
Nam Nhiep Den Tren Duoi Tren
Nam Nhiep Den Tren Duoi Duoi
Nam Nhiep Den Duoi Tren Tren
Nam Nhiep Den Duoi Tren Duoi
Nam Nhiep Den Duoi Duoi Tren
Nam Nhiep Den Duoi Duoi Duoi
Nam Nhiep Trang Tren Tren Tren
Nam Nhiep Trang Tren Tren Duoi
Nam Nhiep Trang Tren Duoi Tren
Nam Nhiep Trang Tren Duoi Duoi
Nam Nhiep Trang Duoi Tren Tren
Nam Nhiep Trang Duoi Tren Duoi
Nam Nhiep Trang Duoi Duoi Tren
Nam Nhiep Trang Duoi Duoi Duoi
Nam Nhiep Hong Tren Tren Tren
Nam Nhiep Hong Tren Tren Duoi
Nam Nhiep Hong Tren Duoi Tren
Nam Nhiep Hong Tren Duoi Duoi
Nam Nhiep Hong Duoi Tren Tren
Nam Nhiep Hong Duoi Tren Duoi
Nam Nhiep Hong Duoi Duoi Tren
Nam Nhiep Hong Duoi Duoi Duoi
Nam Nhiep Tim Tren Tren Tren
Nam Nhiep Tim Tren Tren Duoi
Nam Nhiep Tim Tren Duoi Tren
Nam Nhiep Tim Tren Duoi Duoi
Nam Nhiep Tim Duoi Tren Tren
Nam Nhiep Tim Duoi Tren Duoi
Nam Nhiep Tim Duoi Duoi Tren
Nam Nhiep Tim Duoi Duoi Duoi
Nam Nhiep Lam Tren Tren Tren
Nam Nhiep Lam Tren Tren Duoi
Nam Nhiep Lam Tren Duoi Tren
Nam Nhiep Lam Tren Duoi Duoi
Nam Nhiep Lam Duoi Tren Tren
Nam Nhiep Lam Duoi Tren Duoi
Nam Nhiep Lam Duoi Duoi Tren
Nam Nhiep Lam Duoi Duoi Duoi
Nam Nhiep Nau Tren Tren Tren
Nam Nhiep Nau Tren Tren Duoi
Nam Nhiep Nau Tren Duoi Tren
Nam Nhiep Nau Tren Duoi Duoi
Nam Nhiep Nau Duoi Tren Tren
Nam Nhiep Nau Duoi Tren Duoi
Nam Nhiep Nau Duoi Duoi Tren
Nam Nhiep Nau Duoi Duoi Duoi
Nam Nhiep Xam Tren Tren Tren
Nam Nhiep Xam Tren Tren Duoi
Nam Nhiep Xam Tren Duoi Tren
Nam Nhiep Xam Tren Duoi Duoi
Nam Nhiep Xam Duoi Tren Tren
Nam Nhiep Xam Duoi Tren Duoi
Nam Nhiep Xam Duoi Duoi Tren
Nam Nhiep Xam Duoi Duoi Duoi
Nam Nhiep Bac Tren Tren Tren
Nam Nhiep Bac Tren Tren Duoi
Nam Nhiep Bac Tren Duoi Tren
Nam Nhiep Bac Tren Duoi Duoi
Nam Nhiep Bac Duoi Tren Tren
Nam Nhiep Bac Duoi Tren Duoi
Nam Nhiep Bac Duoi Duoi Tren
Nam Nhiep Bac Duoi Duoi Duoi
Nam Nhiep Nam Tren Tren Tren
Nam Nhiep Nam Tren Tren Duoi
Nam Nhiep Nam Tren Duoi Tren
Nam Nhiep Nam Tren Duoi Duoi
Nam Nhiep Nam Duoi Tren Tren
Nam Nhiep Nam Duoi Tren Duoi
Nam Nhiep Nam Duoi Duoi Tren
Nam Nhiep Nam Duoi Duoi Duoi
Nam Nhiep Dong Bac Tren Tren Tren
Nam Nhiep Dong Bac Tren Tren Duoi
Nam Nhiep Dong Bac Tren Duoi Tren
Nam Nhiep Dong Bac Tren Duoi Duoi
Nam Nhiep Dong Bac Duoi Tren Tren
Nam Nhiep Dong Bac Duoi Tren Duoi
Nam Nhiep Dong Bac Duoi Duoi Tren
Nam Nhiep Dong Bac Duoi Duoi Duoi
Nam Nhiep Dong Nam Tren Tren Tren
Nam Nhiep Dong Nam Tren Tren Duoi
Nam Nhiep Dong Nam Tren Duoi Tren
Nam Nhiep Dong Nam Tren Duoi Duoi
Nam Nhiep Dong Nam Duoi Tren Tren
Nam Nhiep Dong Nam Duoi Tren Duoi
Nam Nhiep Dong Nam Duoi Duoi Tren
Nam Nhiep Dong Nam Duoi Duoi Duoi
Nam Nhiep Tay Bac Tren Tren Tren
Nam Nhiep Tay Bac Tren Tren Duoi
Nam Nhiep Tay Bac Tren Duoi Tren
Nam Nhiep Tay Bac Tren Duoi Duoi
Nam Nhiep Tay Bac Duoi Tren Tren
Nam Nhiep Tay Bac Duoi Tren Duoi
Nam Nhiep Tay Bac Duoi Duoi Tren
Nam Nhiep Tay Bac Duoi Duoi Duoi
Nam Nhiep Tay Nam Tren Tren Tren
Nam Nhiep Tay Nam Tren Tren Duoi
Nam Nhiep Tay Nam Tren Duoi Tren
Nam Nhiep Tay Nam Tren Duoi Duoi
Nam Nhiep Tay Nam Duoi Tren Tren
Nam Nhiep Tay Nam Duoi Tren Duoi
Nam Nhiep Tay Nam Duoi Duoi Tren
Nam Nhiep Tay Nam Duoi Duoi Duoi
Nam Nhiep Trung Tren Tren Tren
Nam Nhiep Trung Tren Tren Duoi
Nam Nhiep Trung Tren Duoi Tren
Nam Nhiep Trung Tren Duoi Duoi
Nam Nhiep Trung Duoi Tren Tren
Nam Nhiep Trung Duoi Tren Duoi
Nam Nhiep Trung Duoi Duoi Tren
Nam Nhiep Trung Duoi Duoi Duoi
Nam Nhiep Ngoai Tren Tren Tren
Nam Nhiep Ngoai Tren Tren Duoi
Nam Nhiep Ngoai Tren Duoi Tren
Nam Nhiep Ngoai Tren Duoi Duoi
Nam Nhiep Ngoai Duoi Tren Tren
Nam Nhiep Ngoai Duoi Tren Duoi
Nam Nhiep Ngoai Duoi Duoi Tren
Nam Nhiep Ngoai Duoi Duoi Duoi
Nam Nhiep Trong Tren Tren Tren
Nam Nhiep Trong Tren Tren Duoi
Nam Nhiep Trong Tren Duoi Tren
Nam Nhiep Trong Tren Duoi Duoi
Nam Nhiep Trong Duoi Tren Tren
Nam Nhiep Trong Duoi Tren Duoi
Nam Nhiep Trong Duoi Duoi Tren
Nam Nhiep Trong Duoi Duoi Duoi
Nam Nhiep Duoi Tren Tren Tren
Nam Nhiep Duoi Tren Tren Duoi
Nam Nhiep Duoi Tren Duoi Tren
Nam Nhiep Duoi Tren Duoi Duoi
Nam Nhiep Duoi Duoi Tren Tren
Nam Nhiep Duoi Duoi Tren Duoi
Nam Nhiep Duoi Duoi Duoi Tren
Nam Nhiep Duoi Duoi Duoi Duoi
Nam Nhiep Tren Tren Tren Tren
Nam Nhiep Tren Tren Tren Duoi
Nam Nhiep Tren Tren Duoi Tren
Nam Nhiep Tren Tren Duoi Duoi
Nam Nhiep Tren Duoi Tren Tren
Nam Nhiep Tren Duoi Tren Duoi
Nam Nhiep Tren Duoi Duoi Tren
Nam Nhiep Tren Duoi Duoi Duoi
Nam Nhiep Giua Tren Tren Tren Tren
Nam Nhiep Giua Tren Tren Tren Duoi
Nam Nhiep Giua Tren Tren Duoi Tren
Nam Nhiep Giua Tren Tren Duoi Duoi
Nam Nhiep Giua Tren Duoi Tren Tren
Nam Nhiep Giua Tren Duoi Tren Duoi
Nam Nhiep Giua Tren Duoi Duoi Tren
Nam Nhiep Giua Tren Duoi Duoi Duoi
Nam Nhiep Giua Duoi Tren Tren Tren
Nam Nhiep Giua Duoi Tren Tren Duoi
Nam Nhiep Giua Duoi Tren Duoi Tren
Nam Nhiep Giua Duoi Tren Duoi Duoi
Nam Nhiep Giua Duoi Duoi Tren Tren
Nam Nhiep Giua Duoi Duoi Tren Duoi
Nam Nhiep Giua Duoi Duoi Duoi Tren
Nam Nhiep Giua Duoi Duoi Duoi Duoi
Nam Nhiep Cuoi Tren Tren Tren Tren
Nam Nhiep Cuoi Tren Tren Tren Duoi
Nam Nhiep Cuoi Tren Tren Duoi Tren
Nam Nhiep Cuoi Tren Tren Duoi Duoi
Nam Nhiep Cuoi Tren Duoi Tren Tren
Nam Nhiep Cuoi Tren Duoi Tren Duoi
Nam Nhiep Cuoi Tren Duoi Duoi Tren
Nam Nhiep Cuoi Tren Duoi Duoi Duoi
Nam Nhiep Cuoi Duoi Tren Tren Tren
Nam Nhiep Cuoi Duoi Tren Tren Duoi
Nam Nhiep Cuoi Duoi Tren Duoi Tren
Nam Nhiep Cuoi Duoi Tren Duoi Duoi
Nam Nhiep Cuoi Duoi Duoi Tren Tren
Nam Nhiep Cuoi Duoi Duoi Tren Duoi
Nam Nhiep Cuoi Duoi Duoi Duoi Tren
Nam Nhiep Cuoi Duoi Duoi Duoi Duoi
Nam Nhiep Moi Tren Tren Tren Tren
Nam Nhiep Moi Tren Tren Tren Duoi
Nam Nhiep Moi Tren Tren Duoi Tren
Nam Nhiep Moi Tren Tren Duoi Duoi
Nam Nhiep Moi Tren Duoi Tren Tren
Nam Nhiep Moi Tren Duoi Tren Duoi
Nam Nhiep Moi Tren Duoi Duoi Tren
Nam Nhiep Moi Tren Duoi Duoi Duoi
Nam Nhiep Moi Duoi Tren Tren Tren
Nam Nhiep Moi Duoi Tren Tren Duoi
Nam Nhiep Moi Duoi Tren Duoi Tren
Nam Nhiep Moi Duoi Tren Duoi Duoi
Nam Nhiep Moi Duoi Duoi Tren Tren
Nam Nhiep Moi Duoi Duoi Tren Duoi
Nam Nhiep Moi Duoi Duoi Duoi Tren
Nam Nhiep Moi Duoi Duoi Duoi Duoi
Nam Nhiep Cu Tren Tren Tren Tren
Nam Nhiep Cu Tren Tren Tren Duoi
Nam Nhiep Cu Tren Tren Duoi Tren
Nam Nhiep Cu Tren Tren Duoi Duoi
Nam Nhiep Cu Tren Duoi Tren Tren
Nam Nhiep Cu Tren Duoi Tren Duoi
Nam Nhiep Cu Tren Duoi Duoi Tren
Nam Nhiep Cu Tren Duoi Duoi Duoi
Nam Nhiep Cu Duoi Tren Tren Tren
Nam Nhiep Cu Duoi Tren Tren Duoi
Nam Nhiep Cu Duoi Tren Duoi Tren
Nam Nhiep Cu Duoi Tren Duoi Duoi
Nam Nhiep Cu Duoi Duoi Tren Tren
Nam Nhiep Cu Duoi Duoi Tren Duoi
Nam Nhiep Cu Duoi Duoi Duoi Tren
Nam Nhiep Cu Duoi Duoi Duoi Duoi
Nam Nhiep Tuoi Tren Tren Tren Tren
Nam Nhiep Tuoi Tren Tren Tren Duoi
Nam Nhiep Tuoi Tren Tren Duoi Tren
Nam Nhiep Tuoi Tren Tren Duoi Duoi
Nam Nhiep Tuoi Tren Duoi Tren Tren
Nam Nhiep Tuoi Tren Duoi Tren Duoi
Nam Nhiep Tuoi Tren Duoi Duoi Tren
Nam Nhiep Tuoi Tren Duoi Duoi Duoi
Nam Nhiep Tuoi Duoi Tren Tren Tren
Nam Nhiep Tuoi Duoi Tren Tren Duoi
Nam Nhiep Tuoi Duoi Tren Duoi Tren
Nam Nhiep Tuoi Duoi Tren Duoi Duoi
Nam Nhiep Tuoi Duoi Duoi Tren Tren
Nam Nhiep Tuoi Duoi Duoi Tren Duoi
Nam Nhiep Tuoi Duoi Duoi Duoi Tren
Nam Nhiep Tuoi Duoi Duoi Duoi Duoi
Nam Nhiep Xanh Tren Tren Tren Tren
Nam Nhiep Xanh Tren Tren Tren Duoi
Nam Nhiep Xanh Tren Tren Duoi Tren
Nam Nhiep Xanh Tren Tren Duoi Duoi
Nam Nhiep Xanh Tren Duoi Tren Tren
Nam Nhiep Xanh Tren Duoi Tren Duoi
Nam Nhiep Xanh Tren Duoi Duoi Tren
Nam Nhiep Xanh Tren Duoi Duoi Duoi
Nam Nhiep Xanh Duoi Tren Tren Tren
Nam Nhiep Xanh Duoi Tren Tren Duoi
Nam Nhiep Xanh Duoi Tren Duoi Tren
Nam Nhiep Xanh Duoi Tren Duoi Duoi
Nam Nhiep Xanh Duoi Duoi Tren Tren
Nam Nhiep Xanh Duoi Duoi Tren Duoi
Nam Nhiep Xanh Duoi Duoi Duoi Tren
Nam Nhiep Xanh Duoi Duoi Duoi Duoi
Nam Nhiep Do Tren Tren Tren Tren
Nam Nhiep Do Tren Tren Tren Duoi
Nam Nhiep Do Tren Tren Duoi Tren
Nam Nhiep Do Tren Tren Duoi Duoi
Nam Nhiep Do Tren Duoi Tren Tren
Nam Nhiep Do Tren Duoi Tren Duoi
Nam Nhiep Do Tren Duoi Duoi Tren
Nam Nhiep Do Tren Duoi Duoi Duoi
Nam Nhiep Do Duoi Tren Tren Tren
Nam Nhiep Do Duoi Tren Tren Duoi
Nam Nhiep Do Duoi Tren Duoi Tren
Nam Nhiep Do Duoi Tren Duoi Duoi
Nam Nhiep Do Duoi Duoi Tren Tren
Nam Nhiep Do Duoi Duoi Tren Duoi
Nam Nhiep Do Duoi Duoi Duoi Tren
Nam Nhiep Do Duoi Duoi Duoi Duoi
Nam Nhiep Vang Tren Tren Tren Tren
Nam Nhiep Vang Tren Tren Tren Duoi
Nam Nhiep Vang Tren Tren Duoi Tren
Nam Nhiep Vang Tren Tren Duoi Duoi
Nam Nhiep Vang Tren Duoi Tren Tren
Nam Nhiep Vang Tren Duoi Tren Duoi
Nam Nhiep Vang Tren Duoi Duoi Tren
Nam Nhiep Vang Tren Duoi Duoi Duoi
Nam Nhiep Vang Duoi Tren Tren Tren
Nam Nhiep Vang Duoi Tren Tren Duoi
Nam Nhiep Vang Duoi Tren Duoi Tren
Nam Nhiep Vang Duoi Tren Duoi Duoi
Nam Nhiep Vang Duoi Duoi Tren Tren
Nam Nhiep Vang Duoi Duoi Tren Duoi
Nam Nhiep Vang Duoi Duoi Duoi Tren
Nam Nhiep Vang Duoi Duoi Duoi Duoi
Nam Nhiep Den Tren Tren Tren Tren
Nam Nhiep Den Tren Tren Tren Duoi
Nam Nhiep Den Tren Tren Duoi Tren
Nam Nhiep Den Tren Tren Duoi Duoi
Nam Nhiep Den Tren Duoi Tren Tren
Nam Nhiep Den Tren Duoi Tren Duoi
Nam Nhiep Den Tren Duoi Duoi Tren
Nam Nhiep Den Tren Duoi Duoi Duoi
Nam Nhiep Den Duoi Tren Tren Tren
Nam Nhiep Den Duoi Tren Tren Duoi
Nam Nhiep Den Duoi Tren Duoi Tren
Nam Nhiep Den Duoi Tren Duoi Duoi
Nam Nhiep Den Duoi Duoi Tren Tren
Nam Nhiep Den Duoi Duoi Tren Duoi
Nam Nhiep Den Duoi Duoi Duoi Tren
Nam Nhiep Den Duoi Duoi Duoi Duoi
Nam Nhiep Trang Tren Tren Tren Tren
Nam Nhiep Trang Tren Tren Tren Duoi
Nam Nhiep Trang Tren Tren Duoi Tren
Nam Nhiep Trang Tren Tren Duoi Duoi
Nam Nhiep Trang Tren Duoi Tren Tren
Nam Nhiep Trang Tren Duoi Tren Duoi
Nam Nhiep Trang Tren Duoi Duoi Tren
Nam Nhiep Trang Tren Duoi Duoi Duoi
Nam Nhiep Trang Duoi Tren Tren Tren
Nam Nhiep Trang Duoi Tren Tren Duoi
Nam Nhiep Trang Duoi Tren Duoi Tren
Nam Nhiep Trang Duoi Tren Duoi Duoi
Nam Nhiep Trang Duoi Duoi Tren Tren
Nam Nhiep Trang Duoi Duoi Tren Duoi
Nam Nhiep Trang Duoi Duoi Duoi Tren
Nam Nhiep Trang Duoi Duoi Duoi Duoi
Nam Nhiep Hong Tren Tren Tren Tren
Nam Nhiep Hong Tren Tren Tren Duoi
Nam Nhiep Hong Tren Tren Duoi Tren
Nam Nhiep Hong Tren Tren Duoi Duoi
Nam Nhiep Hong Tren Duoi Tren Tren
Nam Nhiep Hong Tren Duoi Tren Duoi
Nam Nhiep Hong Tren Duoi Duoi Tren
Nam Nhiep Hong Tren Duoi Duoi Duoi
Nam Nhiep Hong Duoi Tren Tren Tren
Nam Nhiep Hong Duoi Tren Tren Duoi
Nam Nhiep Hong Duoi Tren Duoi Tren
Nam Nhiep Hong Duoi Tren Duoi Duoi
Nam Nhiep Hong Duoi Duoi Tren Tren
Nam Nhiep Hong Duoi Duoi Tren Duoi
Nam Nhiep Hong Duoi Duoi Duoi Tren
Nam Nhiep Hong Duoi Duoi Duoi Duoi
Nam Nhiep Tim Tren Tren Tren Tren
Nam Nhiep Tim Tren Tren Tren Duoi
Nam Nhiep Tim Tren Tren Duoi Tren
Nam Nhiep Tim Tren Tren Duoi Duoi
Nam Nhiep Tim Tren Duoi Tren Tren
Nam Nhiep Tim Tren Duoi Tren Duoi
Nam Nhiep Tim Tren Duoi Duoi Tren
Nam Nhiep Tim Tren Duoi Duoi Duoi
Nam Nhiep Tim Duoi Tren Tren Tren
Nam Nhiep Tim Duoi Tren Tren Duoi
Nam Nhiep Tim Duoi Tren Duoi Tren
Nam Nhiep Tim Duoi Tren Duoi Duoi
Nam Nhiep Tim Duoi Duoi Tren Tren
Nam Nhiep Tim Duoi Duoi Tren Duoi
Nam Nhiep Tim Duoi Duoi Duoi Tren
Nam Nhiep Tim Duoi Duoi Duoi Duoi
Nam Nhiep Lam Tren Tren Tren Tren
Nam Nhiep Lam Tren Tren Tren Duoi
Nam Nhiep Lam Tren Tren Duoi Tren
Nam Nhiep Lam Tren Tren Duoi Duoi
Nam Nhiep Lam Tren Duoi Tren Tren
Nam Nhiep Lam Tren Duoi Tren Duoi
Nam Nhiep Lam Tren Duoi Duoi Tren
Nam Nhiep Lam Tren Duoi Duoi Duoi
Nam Nhiep Lam Duoi Tren Tren Tren
Nam Nhiep Lam Duoi Tren Tren Duoi
Nam Nhiep Lam Duoi Tren Duoi Tren
Nam Nhiep Lam Duoi Tren Duoi Duoi
Nam Nhiep Lam Duoi Duoi Tren Tren
Nam Nhiep Lam Duoi Duoi Tren Duoi
Nam Nhiep Lam Duoi Duoi Duoi Tren
Nam Nhiep Lam Duoi Duoi Duoi Duoi
Nam Nhiep Nau Tren Tren Tren Tren
Nam Nhiep Nau Tren Tren Tren Duoi
Nam Nhiep Nau Tren Tren Duoi Tren
Nam Nhiep Nau Tren Tren Duoi Duoi
Nam Nhiep Nau Tren Duoi Tren Tren
Nam Nhiep Nau Tren Duoi Tren Duoi
Nam Nhiep Nau Tren Duoi Duoi Tren
Nam Nhiep Nau Tren Duoi Duoi Duoi
Nam Nhiep Nau Duoi Tren Tren Tren
Nam Nhiep Nau Duoi Tren Tren Duoi
Nam Nhiep Nau Duoi Tren Duoi Tren
Nam Nhiep Nau Duoi Tren Duoi Duoi
Nam Nhiep Nau Duoi Duoi Tren Tren
Nam Nhiep Nau Duoi Duoi Tren Duoi
Nam Nhiep Nau Duoi Duoi Duoi Tren
Nam Nhiep Nau Duoi Duoi Duoi Duoi
Nam Nhiep Xam Tren Tren Tren Tren
Nam Nhiep Xam Tren Tren Tren Duoi
Nam Nhiep Xam Tren Tren Duoi Tren
Nam Nhiep Xam Tren Tren Duoi Duoi
Nam Nhiep Xam Tren Duoi Tren Tren
Nam Nhiep Xam Tren Duoi Tren Duoi
Nam Nhiep Xam Tren Duoi Duoi Tren
Nam Nhiep Xam Tren Duoi Duoi Duoi
Nam Nhiep Xam Duoi Tren Tren Tren
Nam Nhiep Xam Duoi Tren Tren Duoi
Nam Nhiep Xam Duoi Tren Duoi Tren
Nam Nhiep Xam Duoi Tren Duoi Duoi
Nam Nhiep Xam Duoi Duoi Tren Tren
Nam Nhiep Xam Duoi Duoi Tren Duoi
Nam Nhiep Xam Duoi Duoi Duoi Tren
Nam Nhiep Xam Duoi Duoi Duoi Duoi
Nam Nhiep Bac Tren Tren Tren Tren
Nam Nhiep Bac Tren Tren Tren Duoi
Nam Nhiep Bac Tren Tren Duoi Tren
Nam Nhiep Bac Tren Tren Duoi Duoi
Nam Nhiep Bac Tren Duoi Tren Tren
Nam Nhiep Bac Tren Duoi Tren Duoi
Nam Nhiep Bac Tren Duoi Duoi Tren
Nam Nhiep Bac Tren Duoi Duoi Duoi
Nam Nhiep Bac Duoi Tren Tren Tren
Nam Nhiep Bac Duoi Tren Tren Duoi
Nam Nhiep Bac Duoi Tren Duoi Tren
Nam Nhiep Bac Duoi Tren Duoi Duoi
Nam Nhiep Bac Duoi Duoi Tren Tren
Nam Nhiep Bac Duoi Duoi Tren Duoi
Nam Nhiep Bac Duoi Duoi Duoi Tren
Nam Nhiep Bac Duoi Duoi Duoi Duoi
Nam Nhiep Nam Tren Tren Tren Tren
Nam Nhiep Nam Tren Tren Tren Duoi
Nam Nhiep Nam Tren Tren Duoi Tren
Nam Nhiep Nam Tren Tren Duoi Duoi
Nam Nhiep Nam Tren Duoi Tren Tren
Nam Nhiep Nam Tren Duoi Tren Duoi
Nam Nhiep Nam Tren Duoi Duoi Tren
Nam Nhiep Nam Tren Duoi Duoi Duoi
Nam Nhiep Nam Duoi Tren Tren Tren
Nam Nhiep Nam Duoi Tren Tren Duoi
Nam Nhiep Nam Duoi Tren Duoi Tren
Nam Nhiep Nam Duoi Tren Duoi Duoi
Nam Nhiep Nam Duoi Duoi Tren Tren
Nam Nhiep Nam Duoi Duoi Tren Duoi
Nam Nhiep Nam Duoi Duoi Duoi Tren
Nam Nhiep Nam Duoi Duoi Duoi Duoi
Nam Nhiep Dong Bac Tren Tren Tren Tren
Nam Nhiep Dong Bac Tren Tren Tren Duoi
Nam Nhiep Dong Bac Tren Tren Duoi Tren
Nam Nhiep Dong Bac Tren Tren Duoi Duoi
Nam Nhiep Dong Bac Tren Duoi Tren Tren
Nam Nhiep Dong Bac Tren Duoi Tren Duoi
Nam Nhiep Dong Bac Tren Duoi Duoi Tren
Nam Nhiep Dong Bac Tren Duoi Duoi Duoi
Nam Nhiep Dong Bac Duoi Tren Tren Tren
Nam Nhiep Dong Bac Duoi Tren Tren Duoi
Nam Nhiep Dong Bac Duoi Tren Duoi Tren
Nam Nhiep Dong Bac Duoi Tren Duoi Duoi
Nam Nhiep Dong Bac Duoi Duoi Tren Tren
Nam Nhiep Dong Bac Duoi Duoi Tren Duoi
Nam Nhiep Dong Bac Duoi Duoi Duoi Tren
Nam Nhiep Dong Bac Duoi Du

IMAGE 1 - 1

(THAKHEK - SAVANNAKHET REGION , LAOS)

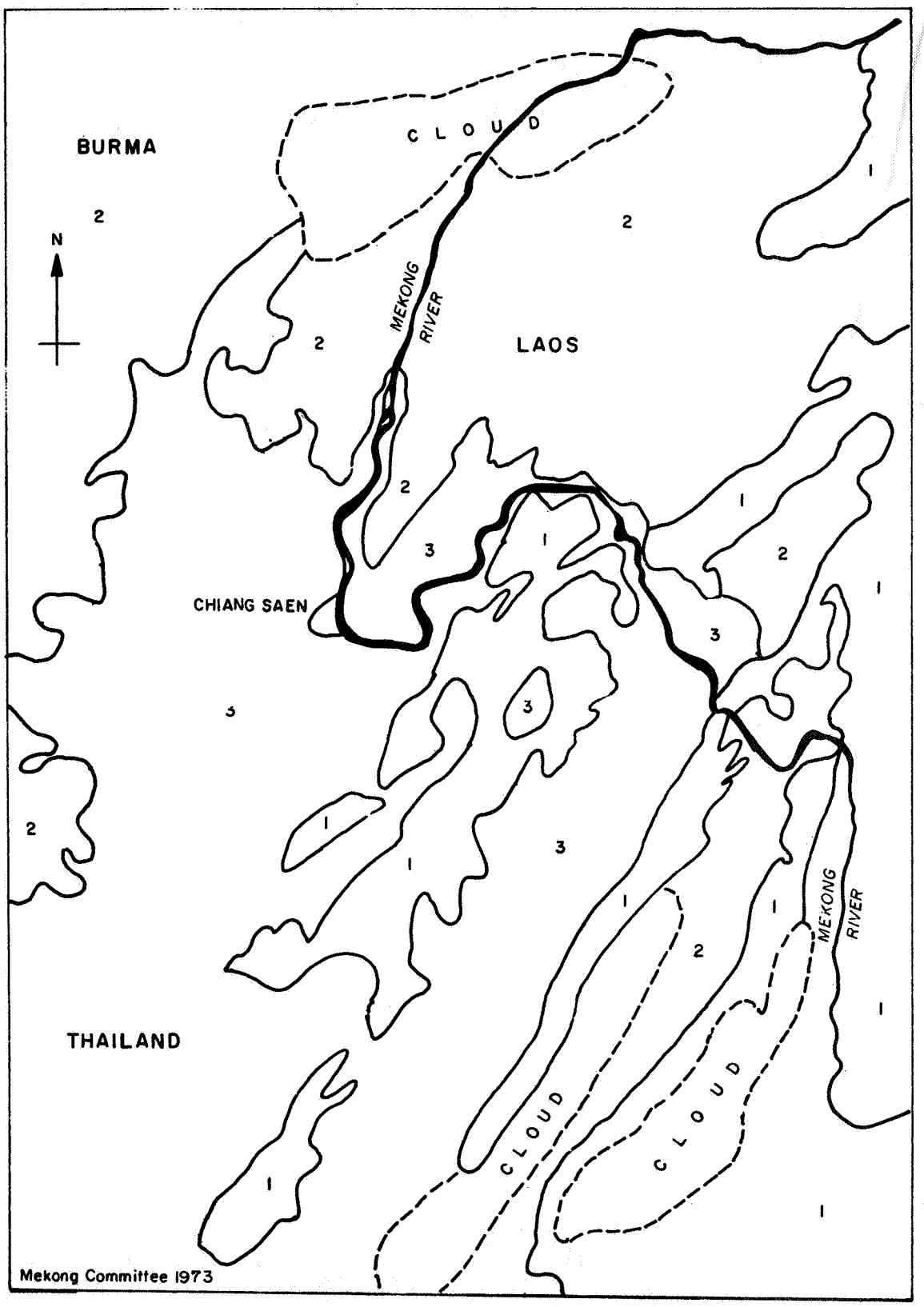




ERTS - 1 frame 1127 - 02451 &
EXISTING GEOLOGICAL MAP

Mekong Committee 1973

Fig. 2 FOREST COVER OF WATERSHED

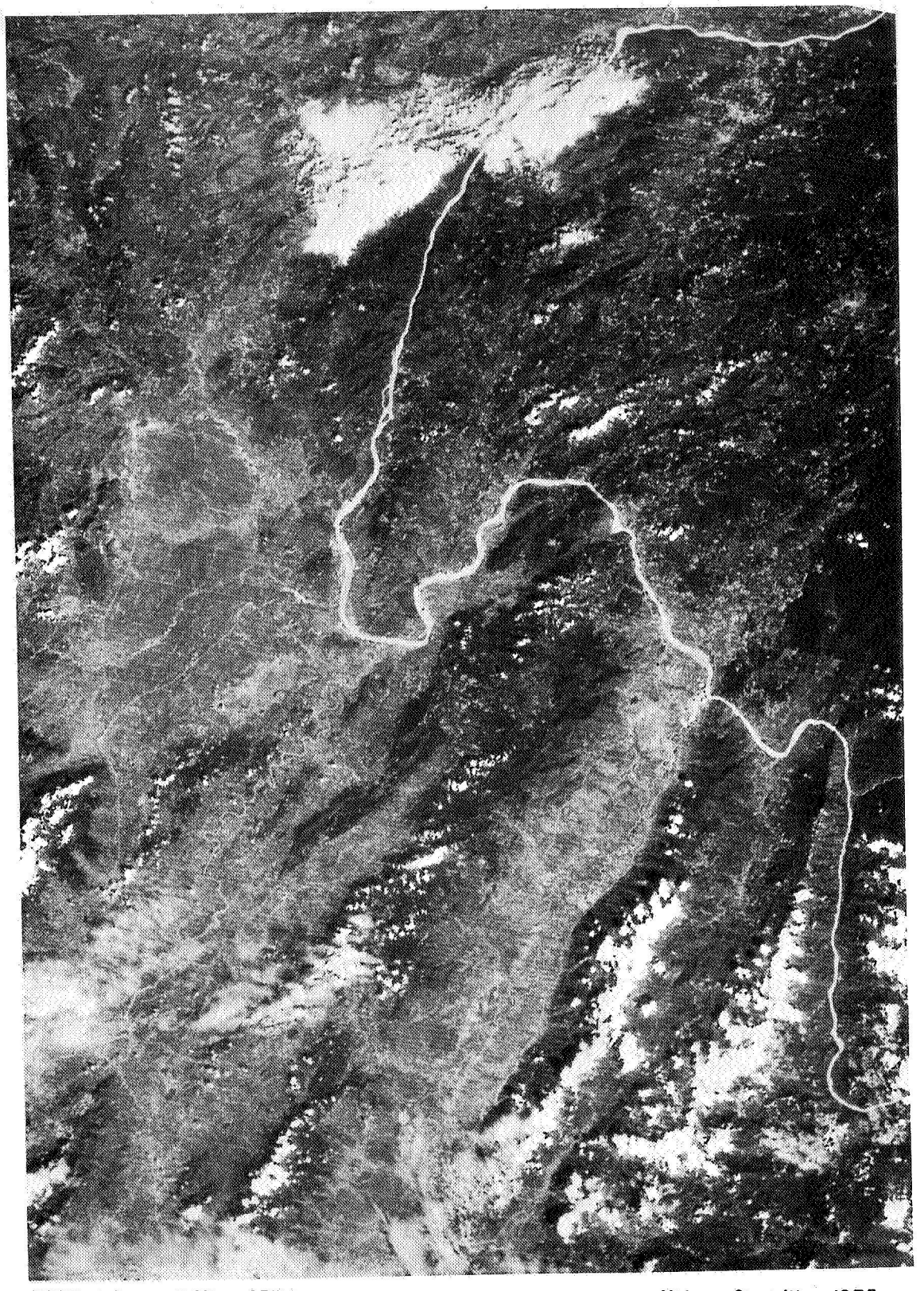


Primary forest, 2 Degraded forest, 3 Agricultural lands

(ERTS-1 frame 1097 - 03163)

IMAGE 2

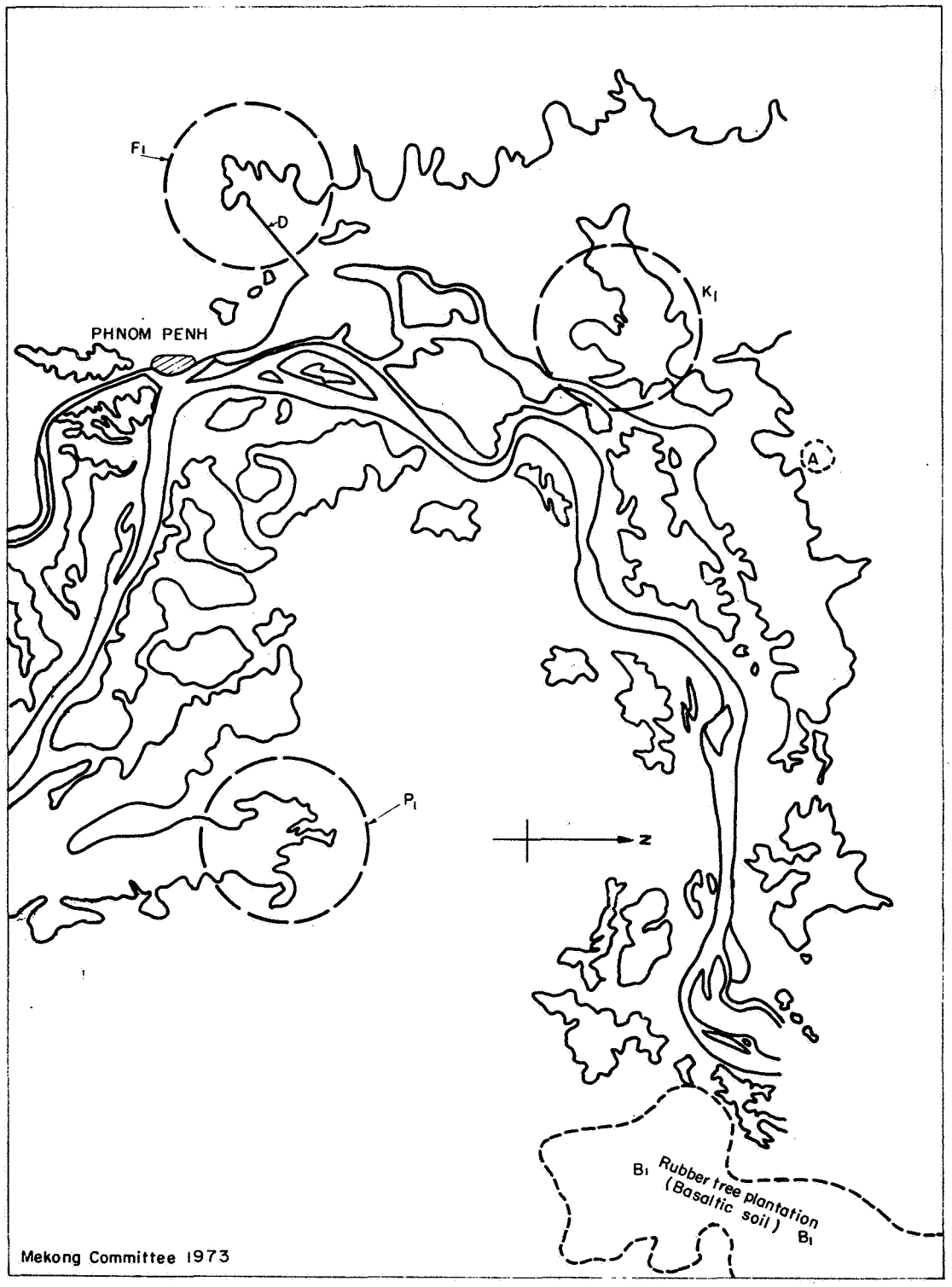
(CHIANG SEAN FORESTRY, THAILAND)



ERTS-1 frame 1097 – 03163

Mekong Committee 1973

Fig. 3 23 OCT 72 FLOOD PLAIN NEAR PHNOM - PENH KHMER REPUBLIC



N.B. Compare circled areas F1, K1 and P1 with same areas of flooding covered on 10 Nov. 72. To study drainage pattern water level recorded at Phnom Penh was 3.91 m above Mean Sea Level. (ERTS - 1 frame 1092-02501-6)

D — Flood area

(A) — Phnom Penh Polder dike

Acacias forest reserve

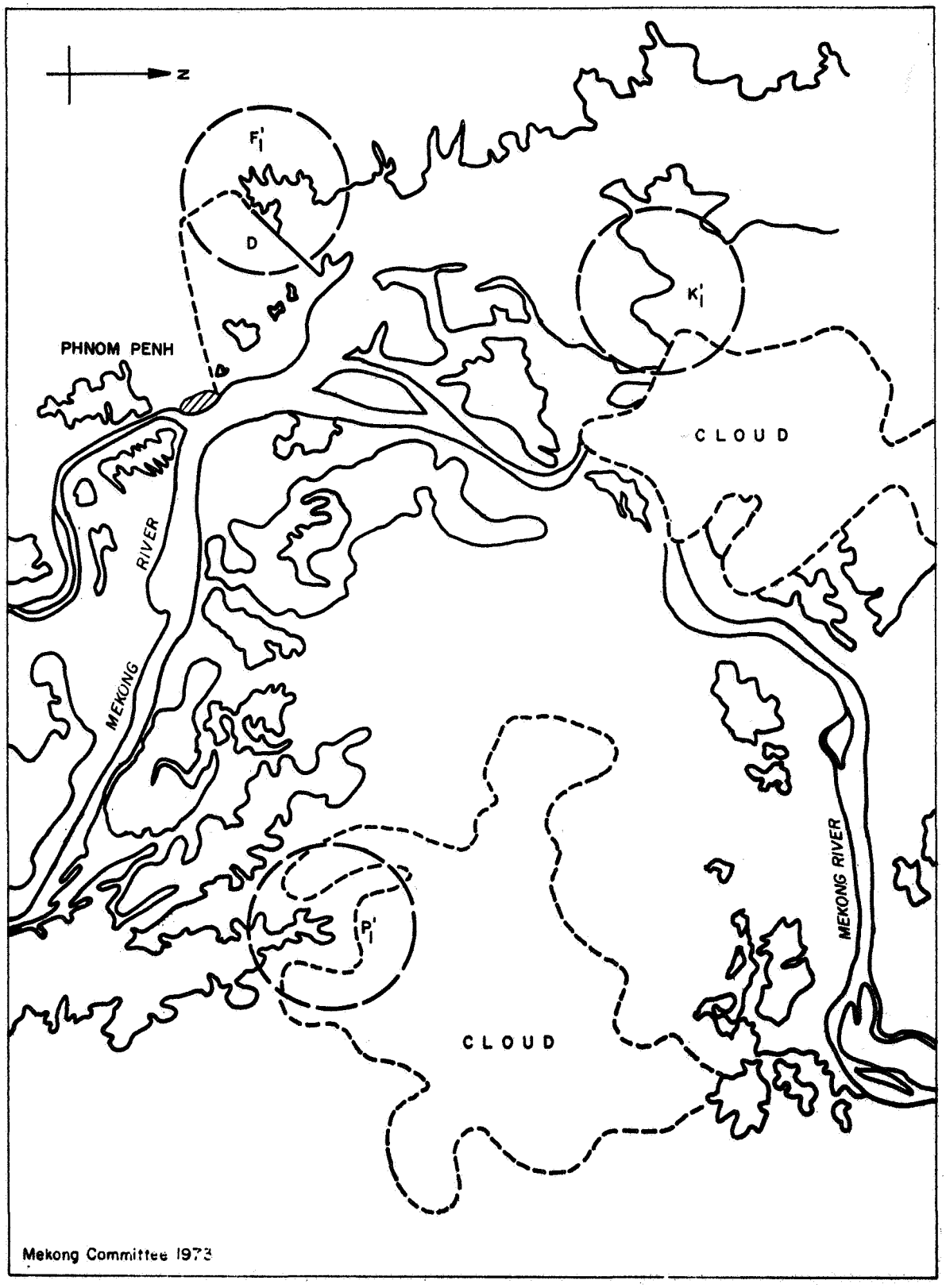
IMAGE 3



Mekong Committee 1973

(From ERTS - 1 frame 1092 - 02501-6)

Fig. 3-1 10 NOV. 72 FLOOD PLAIN NEAR PHNOM-PENH KHMER REPUBLIC



N.B. Water level recorded at Phnom Penh on 10 Nov. 72 was 3.25 m. MSL. Compare with Fig. 3

Flood area

(ERTS-1 frame 1110-02503-6)

IMAGE 3-1

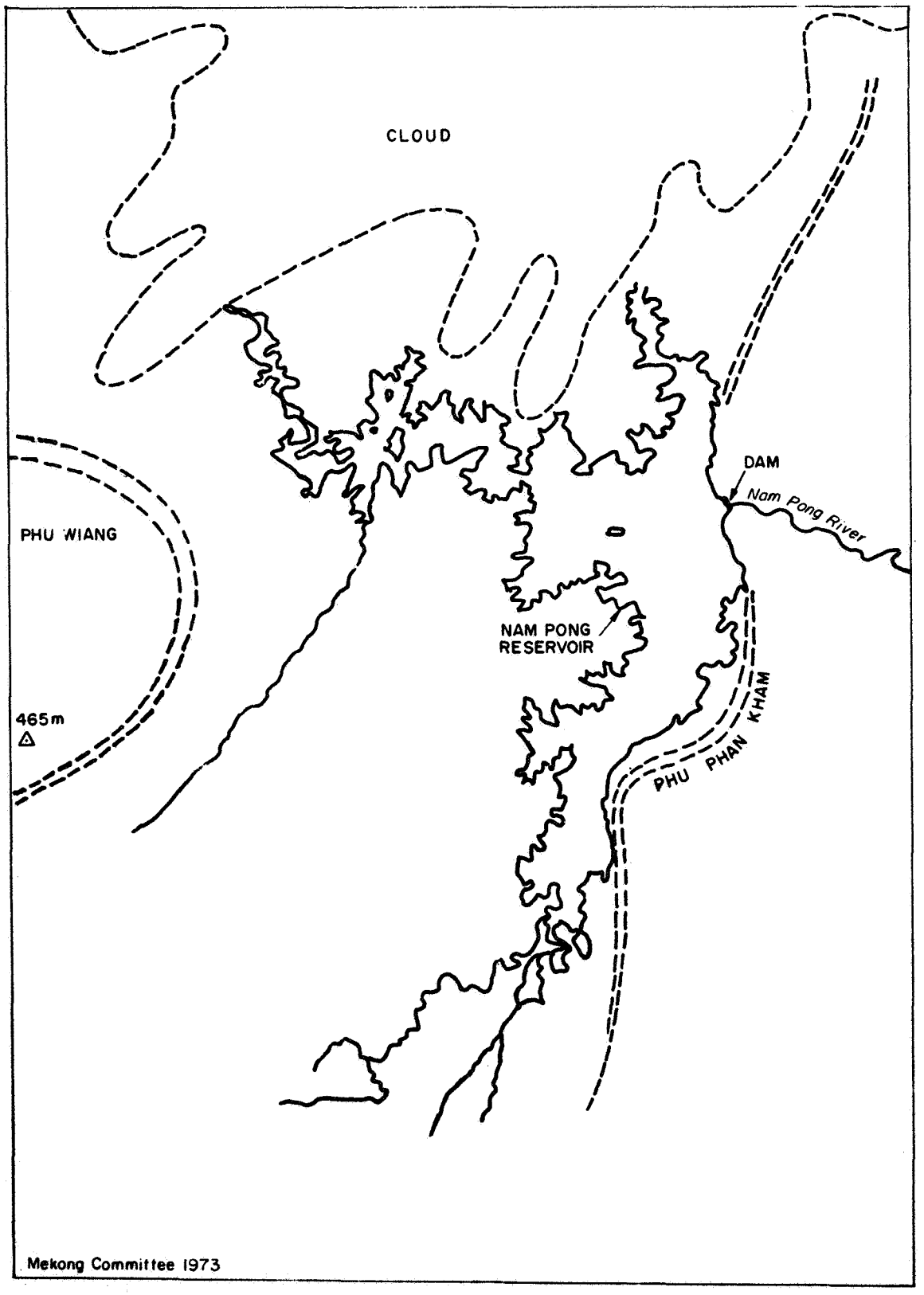


Mekong Committee 1973

(From ERTS-1 frame 1110-02503-6)

Fig. 3 - II NAM PONG RESERVOIR (NORTHEAST THAILAND)

Band 7 image



N.B. See sedimentation of Nam Pong Reservoir on Fig. 3 - III (ERTS-1 frame 1095-03055)

BAND 7, IMAGE 3

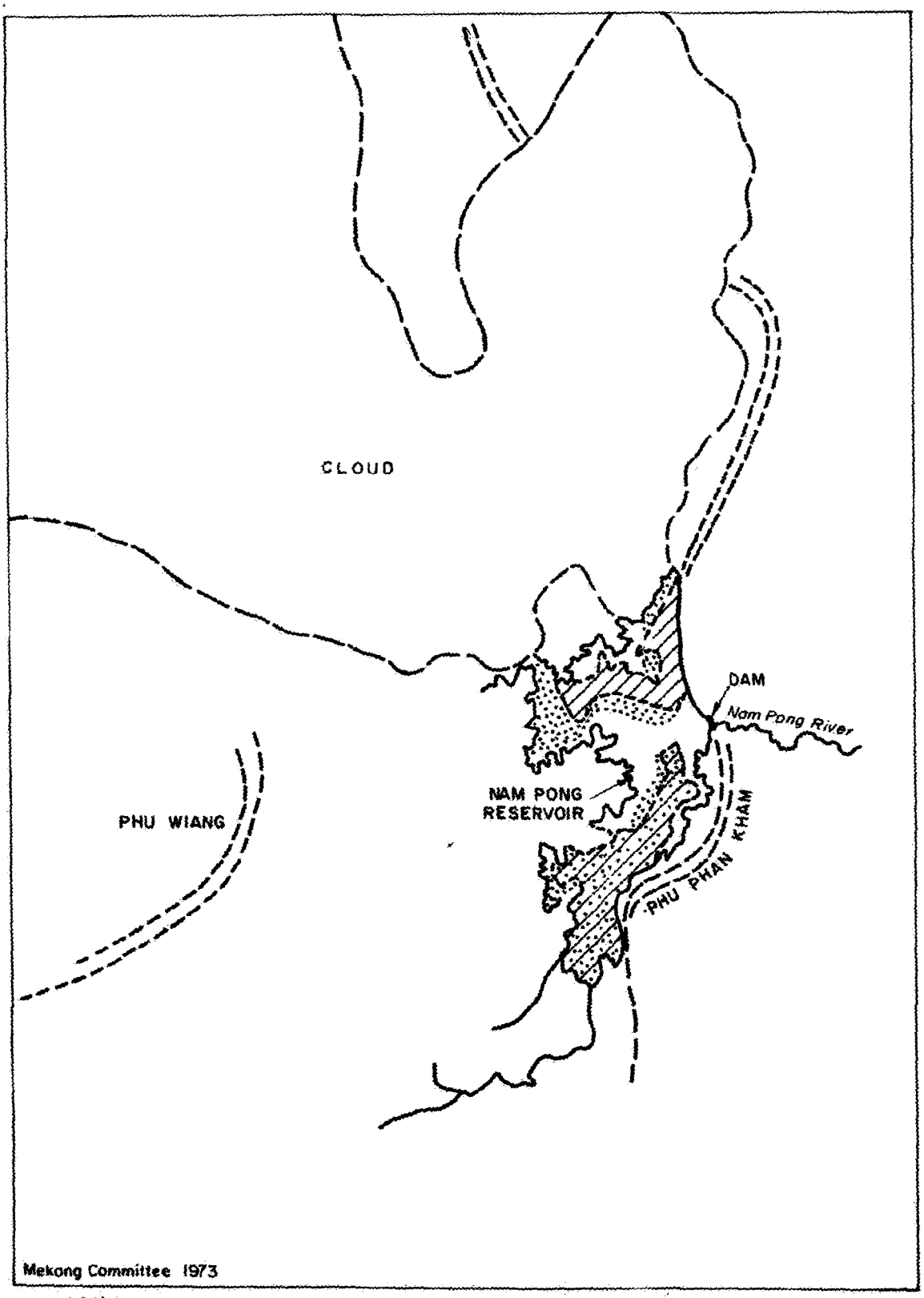
(NAM PONG RESERVOIR , THAILAND)



ERTS – 1 frame 1095 – 03055

Mekong Committee 1973

Fig. 3 - III SEDIMENTATION NAM PONG RESERVOIR



Sedimentation areas seen on Band 5 image (ERTS-1 frame 1095-03055)

BAND 5, IMAGE 3

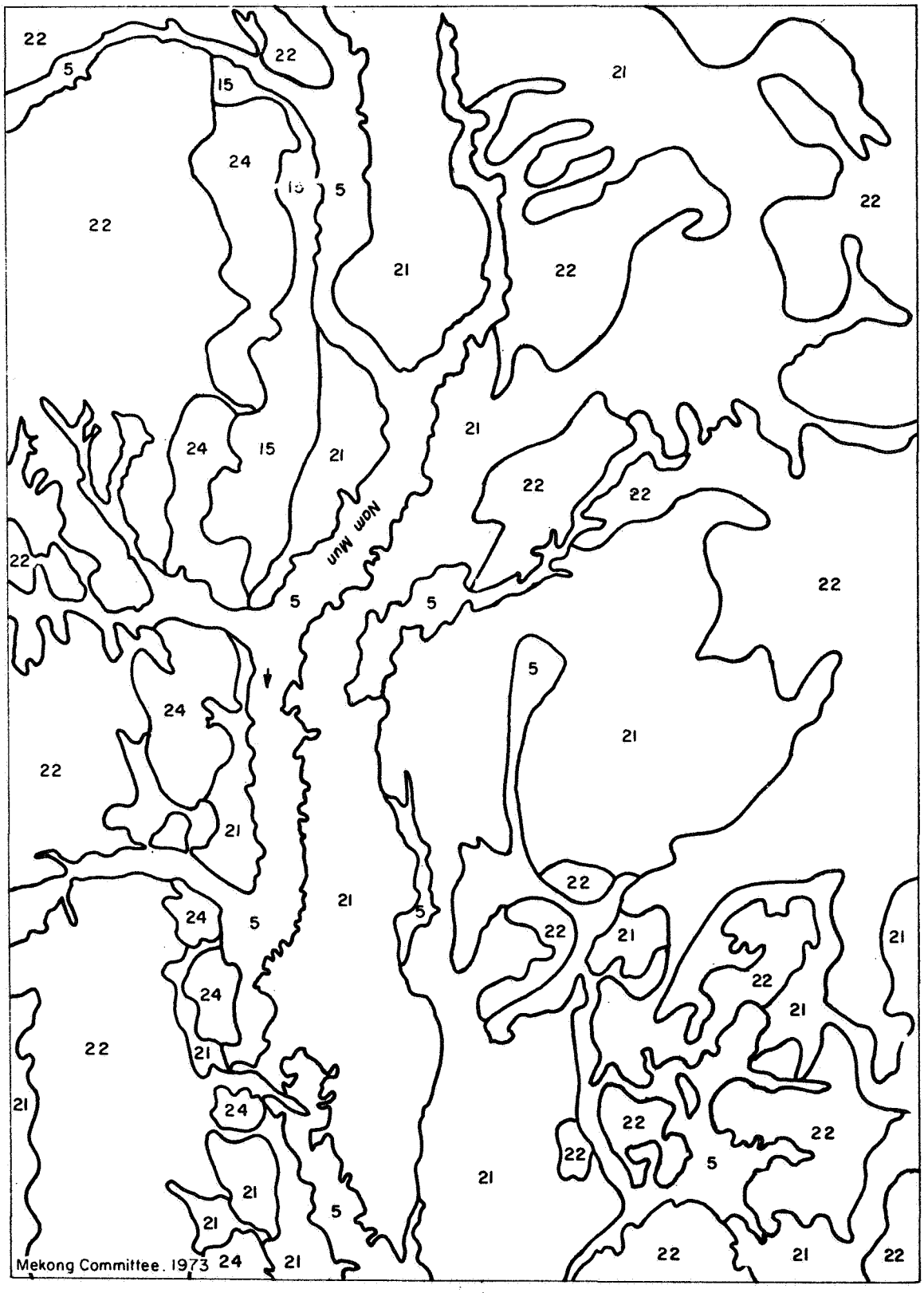
(NAM PONG RESERVOIR, THAILAND)



ERTS - 1 frame 1095 - 03055

Mekong Committee 1973

Fig. 4 UPDATED SOIL MAP



5 = Eutric gleysols (inundated areas), 15 = Ferralic cambisols, 21 = Gleyic acrisols with Ferric acrisols
22 = Gleyic acrisols, undulating slope of 0 to 8 per cent, 24 = Orthic ferralsols.

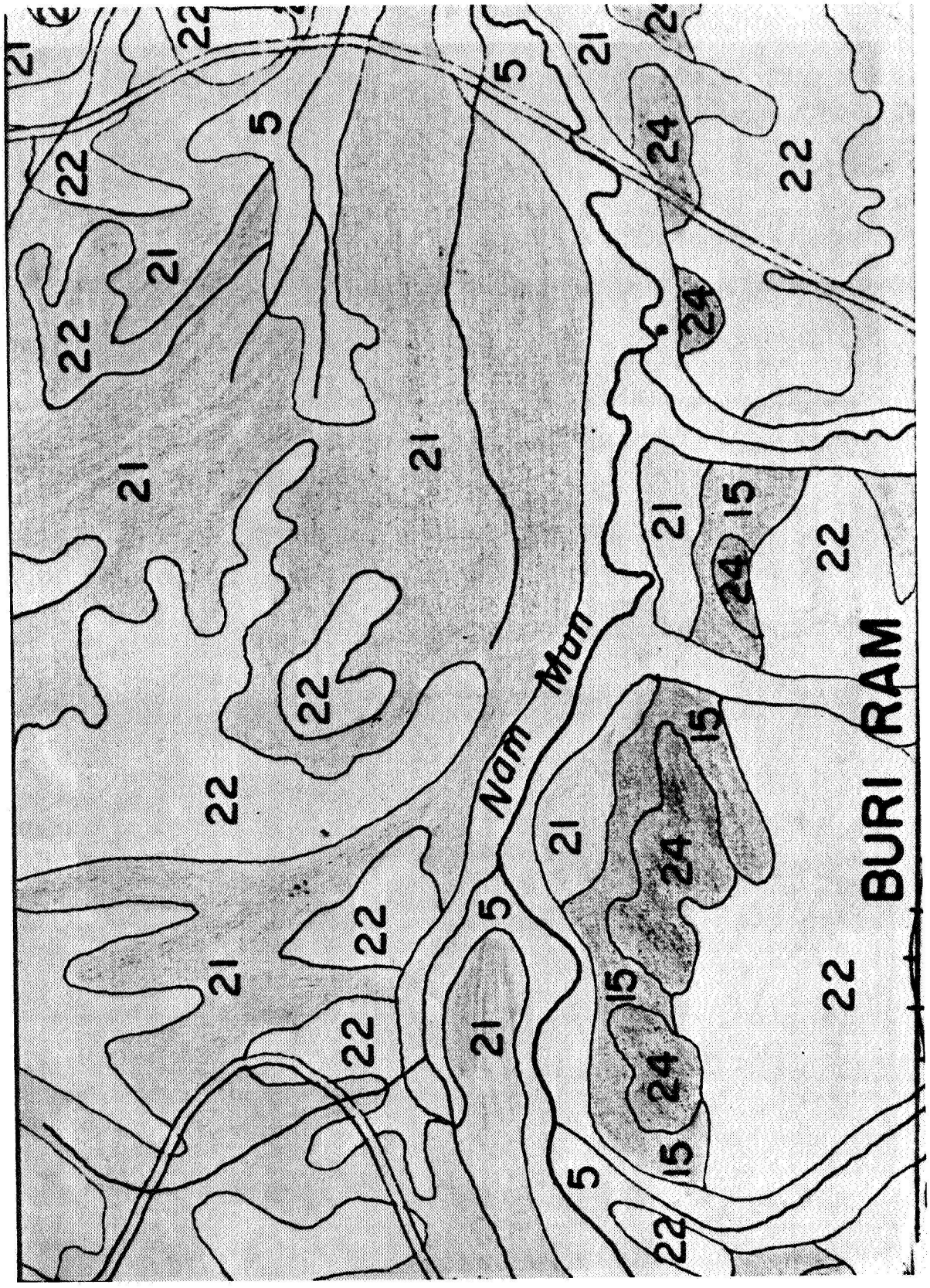
(ERTS-1 frame 1094-03003-7)

IMAGE 4



Mekong Committee 1973

(From ERTS frame No. 1094 - 03003 - 7)

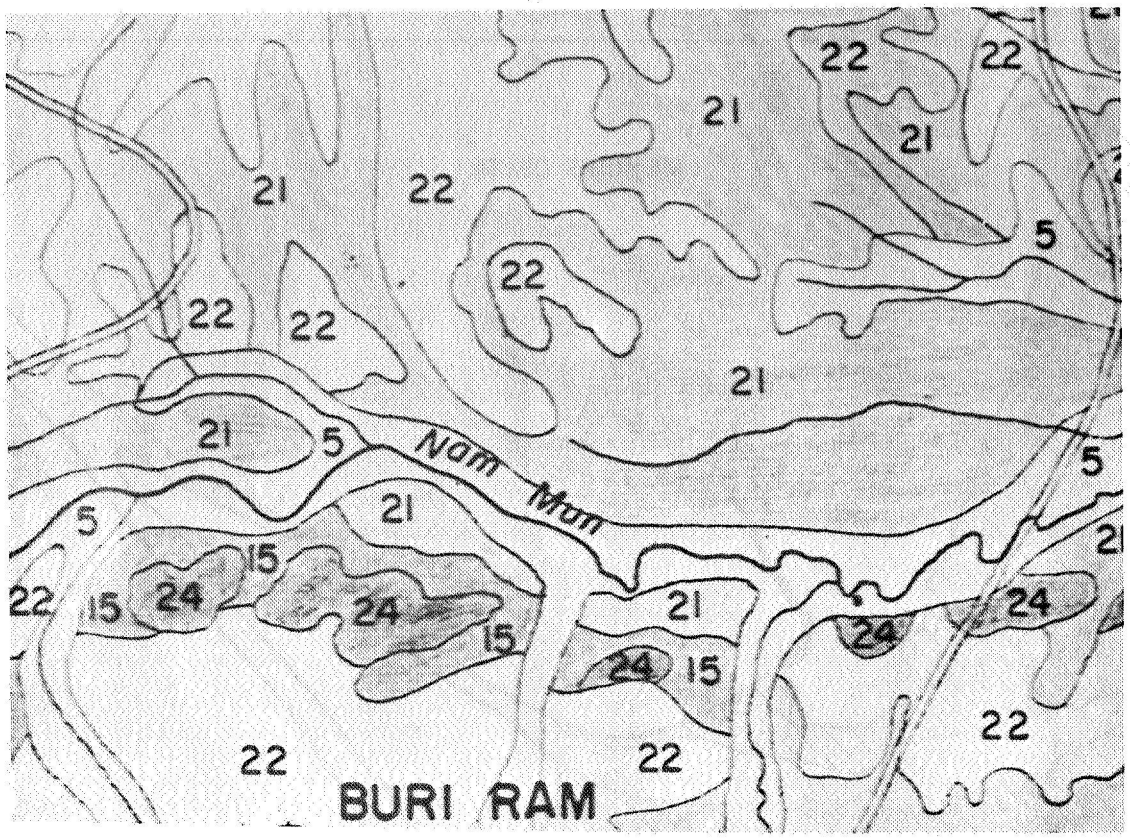


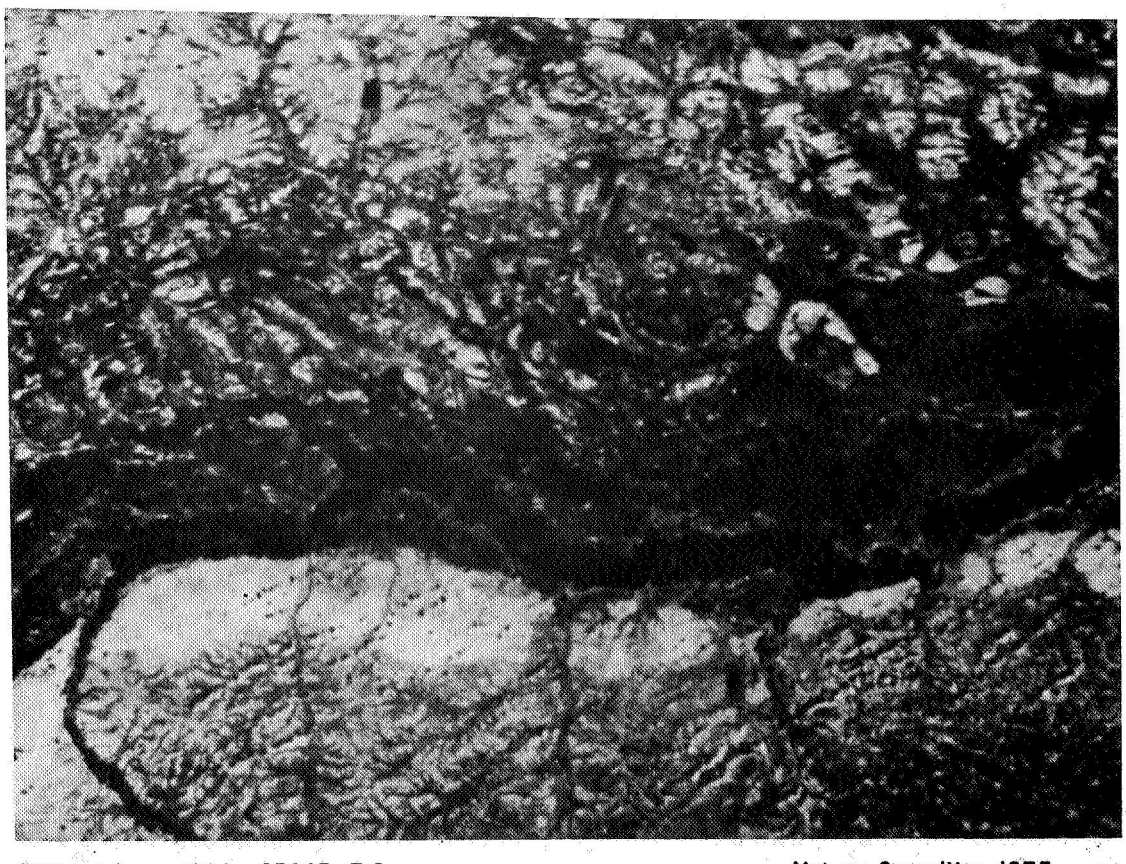
Mekong Committee 1973

(Extract from existing general soil map)

IMAGE 4-1

(UPPER NAM MUN - N.E. THAILAND)

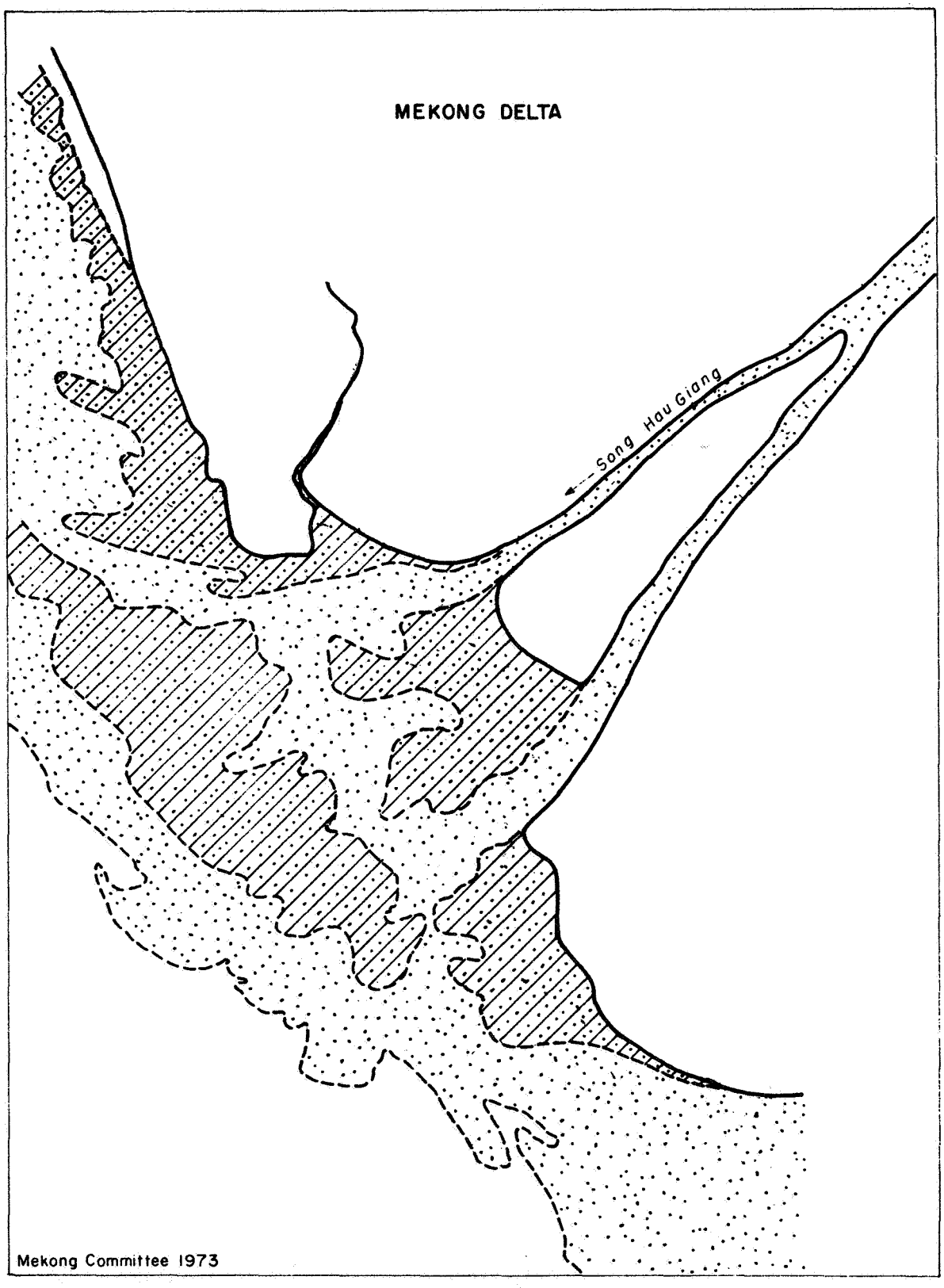




ERTS-1 frame 1094 - 03003-7 8
EXISTING SOIL MAP

Mekong Committee 1973

Fig. 5 MEKONG ESTUARIES (VIET-NAM)



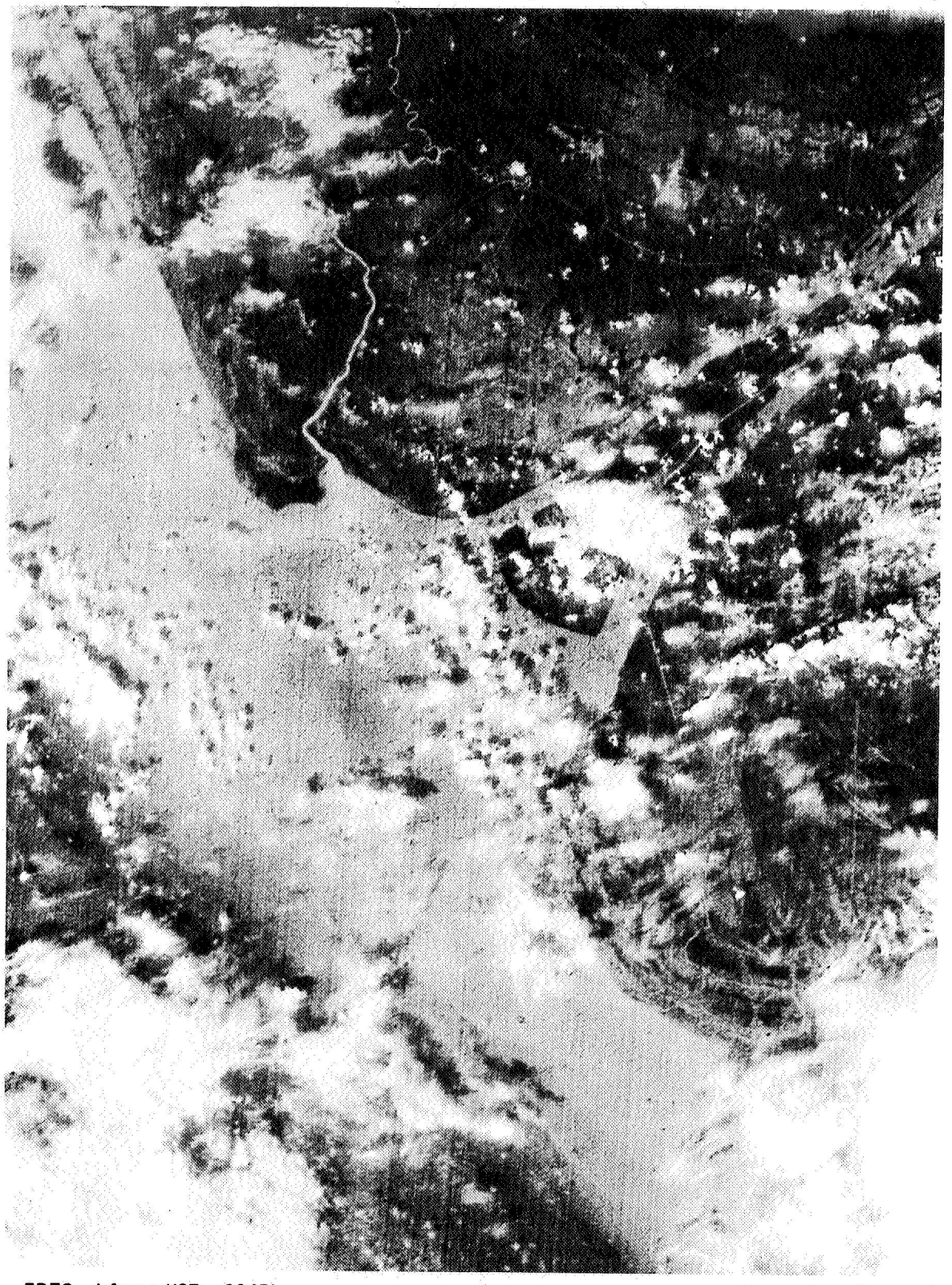
Sedimentation areas in Band 6

Sedimentation areas in Band 5

(ERTS - 1 frame 1127 - 02451)

BAND 5, IMAGE 5

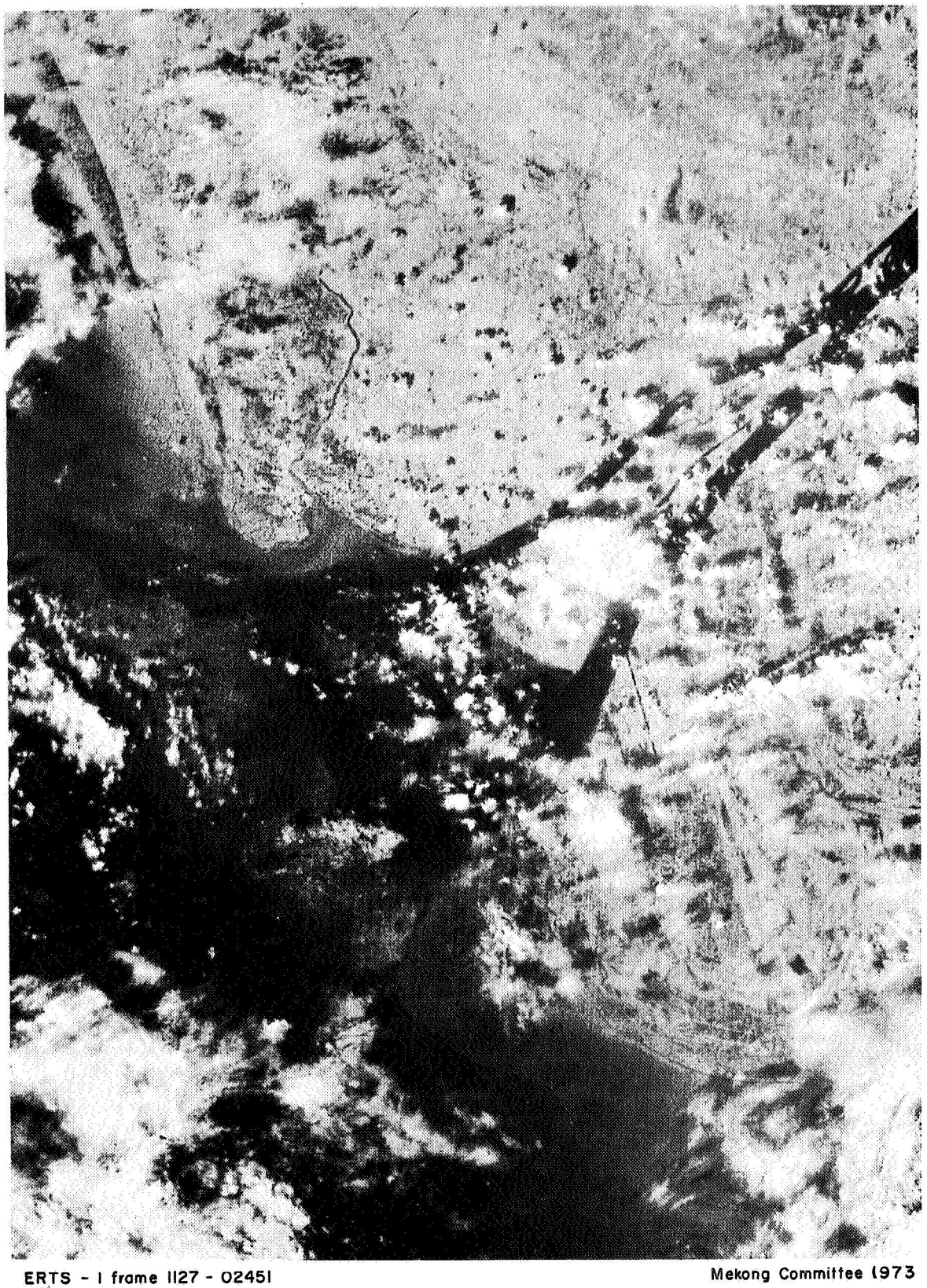
(MEKONG ESTUARIES, VIET - NAM)



ERTS - 1 frame 1127 - 02451

Mekong Committee 1973

BAND 6, IMAGE 5

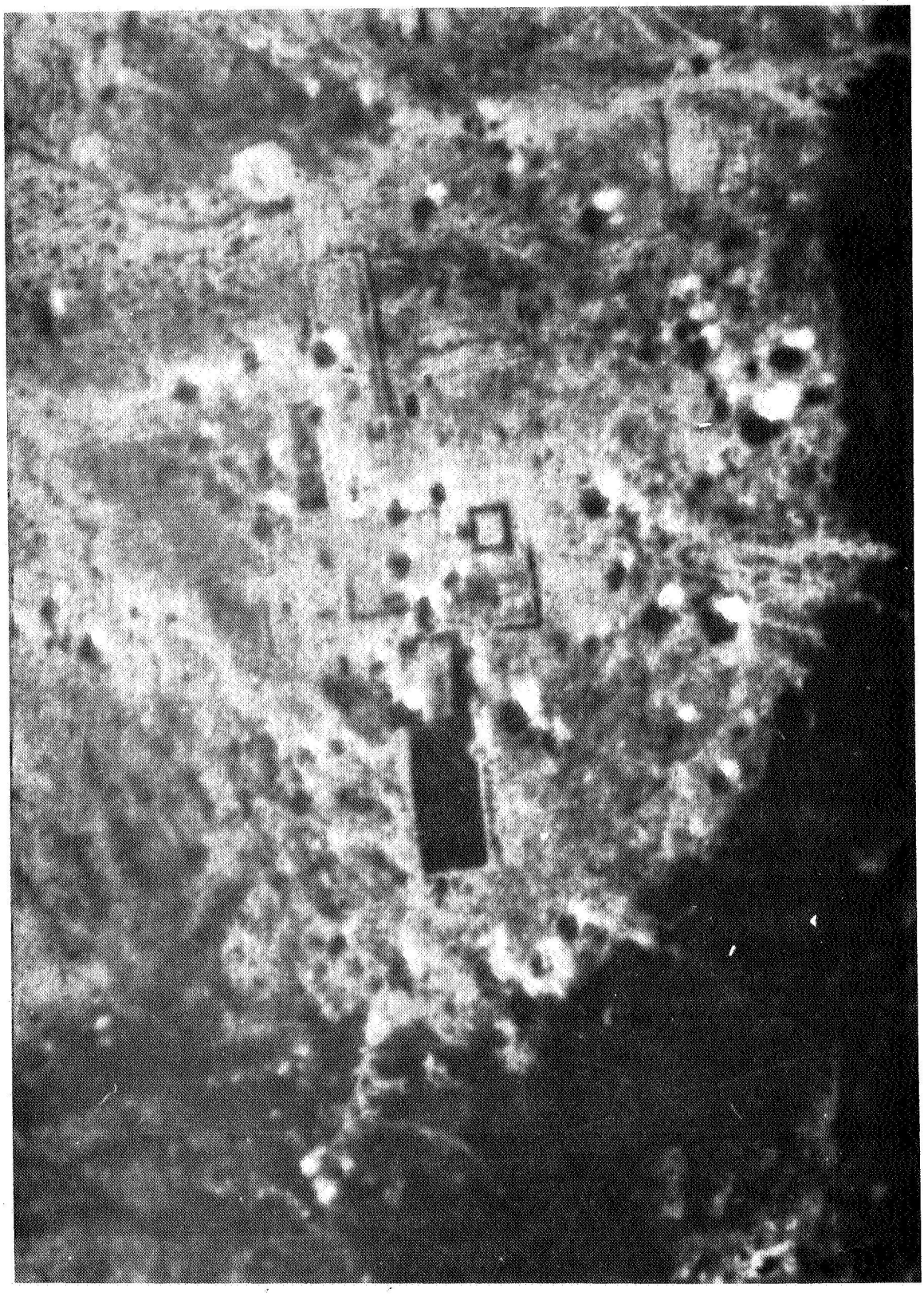


ERTS - 1 frame 1127 - 02451

Mekong Committee 1973

IMAGE 6

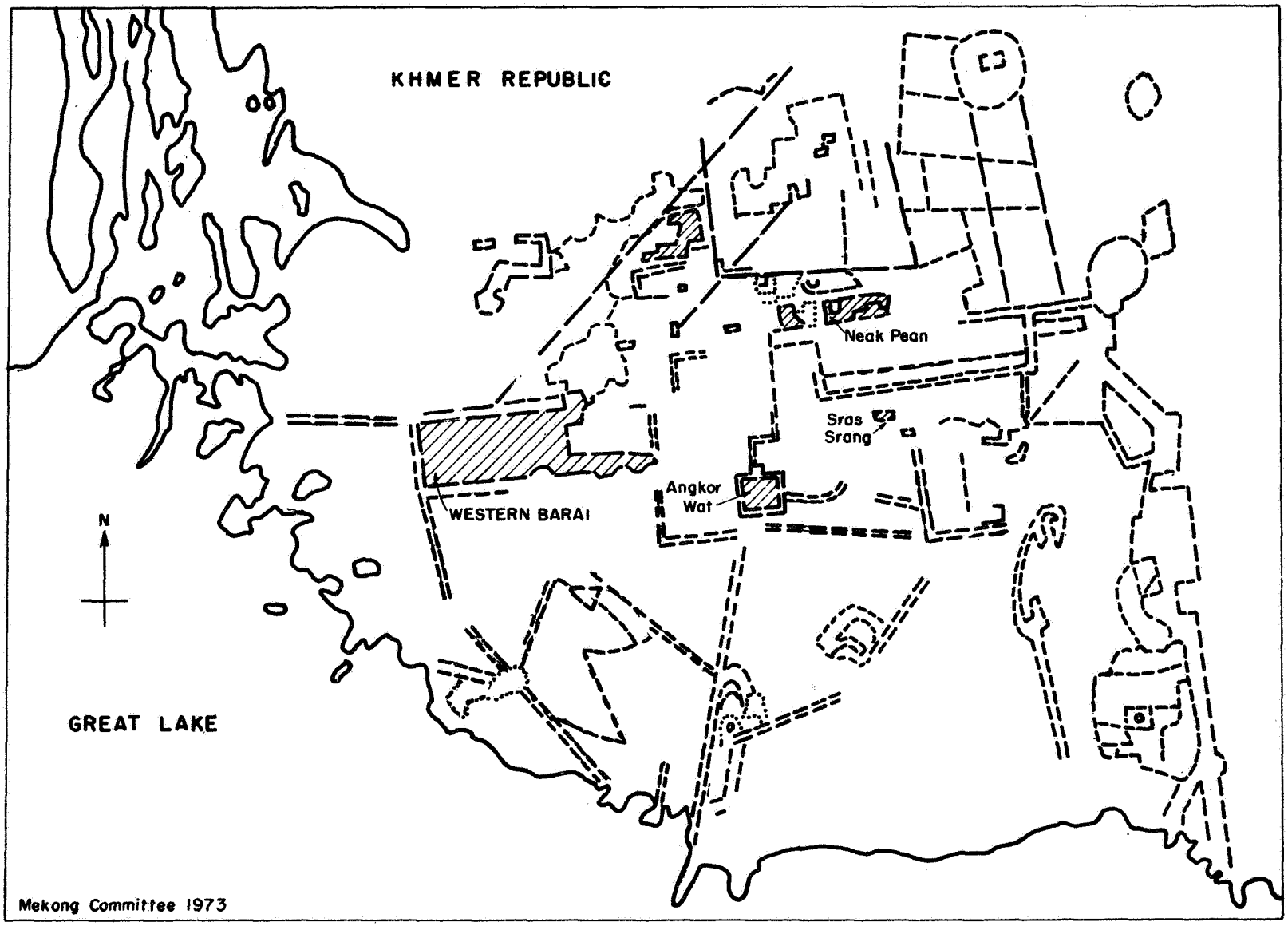
ARCHAEOLOGICAL SITES (Angkor Wat, KHMER REP.)



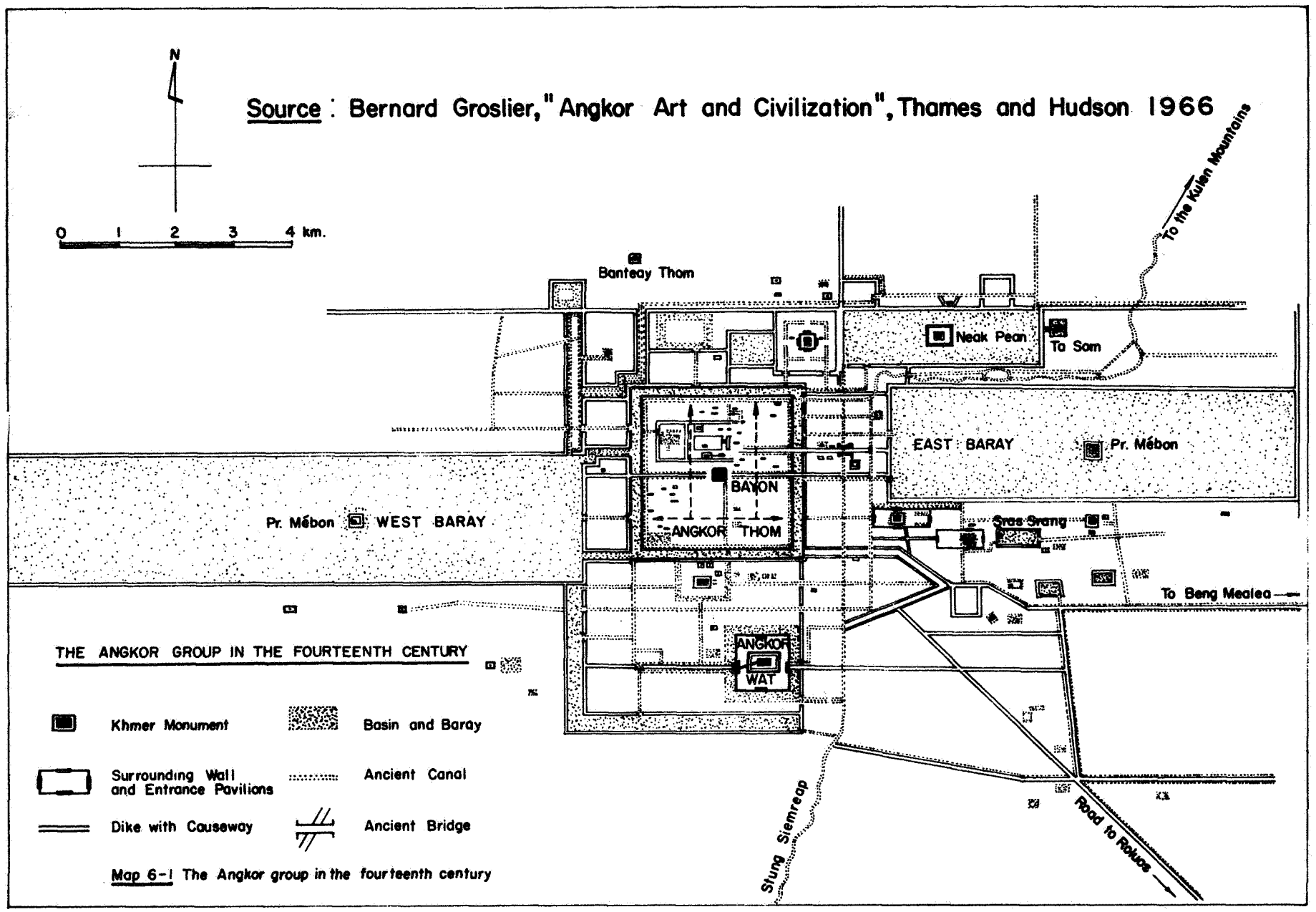
Mekong Committee 1973

(From ERTS - 1 frame 1093 - 02553 - 7)

Fig. 6 ARCHAEOLOGICAL SITES (Angkor Wat area)



(ERTS-1 frame 1093-02553-7)



Map 6-1 The Angkor group in the fourteenth century

Paper W 4

PRELIMINARY TEST OF ERTS-1 IMAGERY FOR IMPROVING DEFINITION OF NATURAL STREAMFLOW

Este F. Hollyday, *Water Resources Division, U. S. Geological Survey, Nashville, Tennessee*

ABSTRACT

Historical streamflow data, which were routinely collected at gaging stations, have been transferred to ungaged sites with varying degrees of success by relating statistical flow parameters to physiographic characteristics of a drainage basin. The basin characteristics that are most easily extracted by automated techniques from ERTS-1 imagery include open water, infrared-reflecting vegetation, snow, and massed works of man. In preliminary tests, using two small basins in the Chesapeake Bay area of Maryland and Delaware, the percent of basin areas occupied by open water and infrared-reflecting vegetation was determined from ERTS imagery and checked by aerial photography. The two basins, which were selected from a group of about 20, represent extremes in their hydrologic response to precipitation. The percent of basin areas was correlated with the residuals of multiple-regression equasions that were developed to relate streamflow characteristics to basin characteristics that, in part, were measured from topographic maps. Results of this correlation were encouraging; however, a more thorough test is needed.

(Paper not received by publication date)

Paper W 5

APPLICATION OF ERTS-1 IMAGERY TO FLOOD INUNDATION MAPPING[1]

George R. Hallberg, Bernard E. Hoyer, *Iowa Geological Survey, Remote Sensing Laboratory;* Albert Rango, *National Aeronautics and Space Administration, Goddard Space Flight Center*

ABSTRACT

In September, 1972, heavy rains initiated major flooding in southwestern Iowa, concentrated in the East and West Nishnabotna basins. The flood crest moved downstream between September 11-15. A cooperative program to evaluate the possibility of mapping flood inundation using remote sensing techniques was initiated jointly by the Iowa Geological Survey, Remote Sensing Laboratory (IGSRSL), and the U.S. Geological Survey, Water Resources Division. Ground data and a variety of low-altitude multispectral imagery was acquired for the East Nishnabotna River on September 14-15. This successful effort concluded that a near-visible infrared sensor could map inundated areas in late summer for at least three days after flood recession. ERTS-1 imagery of the area was obtained on September 18-19. Analysis of MSS imagery by IGSRSL, USGS, and NASA reinforced the conclusions of the low-altitude study while increasing the time period critical for imagery acquisition to at least seven days following flood recession. The capability of satellite imagery to map late summer flooding at a scale of 1:250,000 is exhibited by the agreement of interpreted flood boundaries obtained from ERTS-1 imagery to boundaries mapped by low-altitude imagery and ground methods. The synoptic coverage of ERTS-1 allowed extension of the flood mapping to the West Nishnabotna River. Satellite imagery allows rapid appraisal of the areal extent of flood inundation for entire river systems. This satellite flood mapping should prove valuable to federal and state agencies involved in regional floodplain management and planning.

[1] Publication authorized by the Director of the Iowa Geological Survey

Introduction

Each year the Midwest experiences flooding caused by the spring thaw and frontal rain storm activity. Annually, millions of dollars' worth of damage results to homes, businesses, public works, and crops. Current information about many physical parameters of both the river and adjoining floodplain is needed to help avert disasters.

This information must be rapidly acquired and produced in a format readily useable by many federal, state and local agencies concerned with floodplain planning and management. In Iowa, the paucity of large-scale topographic maps makes flood hazard mapping and regional flood control evaluation difficult. Last fall the Iowa Geological Survey, Remote Sensing Laboratory (IGSRSL), and the U.S. Geological Survey, Water Resources Division, began developing a remote sensing technique capable of providing data suitable to meet some of the immediate and future planning and management needs of communities located along Iowa's rivers. Low-altitude conventional and multiband photographic techniques were utilized in southwestern Iowa and resulted in an aerial photographic technique capable of fulfilling many of these data requirements. Analysis indicated that infrared sensitive film can be utilized to map Midwestern, late summer flood inundation for a minimum of three days following flood recession. Interpretation based on ERTS-1 imagery of this same region by IGSRSL, NASA, and USGS supported this conclusion. ERTS flood inundation mapping also increased the time allowable for data acquisition to a minimum of seven days following flood crest, while providing regional flood inundation data and flood control assessment.

Low-Altitude Photographic Study

A large storm system produced twenty inches of rain locally in west-central Iowa, on September 10-12, 1972 (figure 1). Flooding was recorded in the Boyer, Grand, Nodaway, and East and West Nishnabotna Rivers. Extensive overbank flooding occurred only in the Nishnabotna River Basin where record flow rates were recorded at Atlantic and Red Oak on the East Nishnabotna River and at Hancock on the West Nishnabotna River (table 1).

The Iowa Geological Survey, Remote Sensing Laboratory and the U.S. Geological Survey, Water Resources Division combined efforts to develop a method of mapping flood inundation utilizing aerial photography. Imagery was obtained on the East Nishnabotna River between Interstate 80 and Hamburg. Simultaneous field investigations were conducted to document the extent of inundation with ground data. On 14 September, color (Kodak 2445) and black and white panchromatic (Kodak 2405), vertical, stereoscopic imagery was obtained from 2400m Above Ground Level (AGL) with a Wild RC-8 camera. The black and white imagery was acquired with a minus blue filter (Wratten 12). On 15 September, multispectral imagery was obtained from 2400m AGL with an I^2S multiband camera and black and white infrared film (Kodak 2424). In addition, 35mm color (Ektachrome) and color infrared (Ektachrome infrared), oblique, stereoscopic imagery was obtained

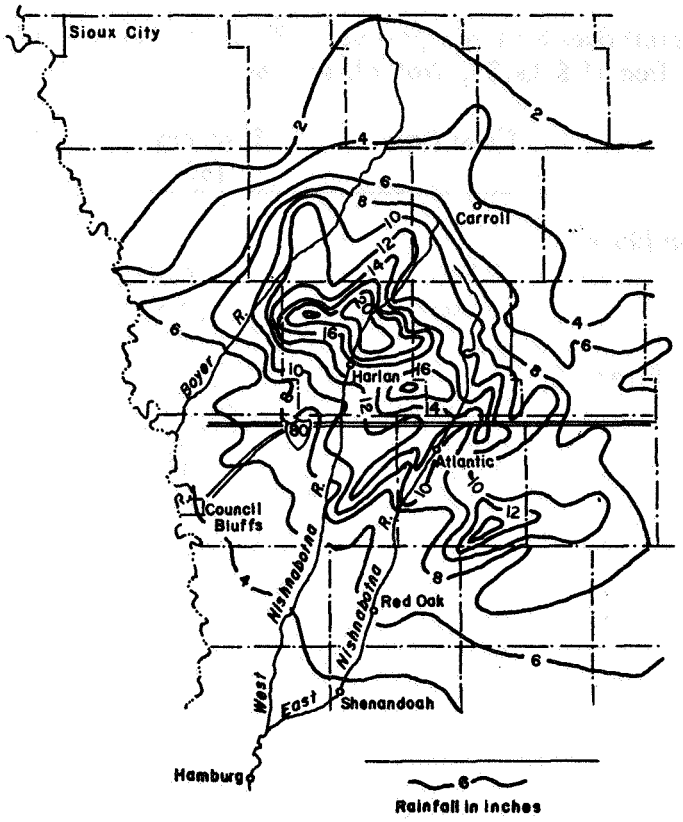


Figure 1, PRECIPITATION PATTERN
10-12 September 1972

from Climatological Data, N.O.A.H.
September, 1972

at selected locations from about 500m AGL. Conventional imagery was analyzed visually utilizing stereoscopic viewing equipment and the multispectral imagery was interpreted with the aid of an I^{2}S Mini-Addicol viewer.

Conclusions of Low-Altitude Study

The low-altitude study was successful. An aerial photographic technique was developed that can map late summer midwestern flood inundation. All known ground data agrees with this mapping. This technique should prove valuable for floodplain management and planning (Hoyer and Taranik, 1973). The basic conclusions of the study are as follows:

1. Infrared radiation (740-900nm) proved most important for flood inundation mapping (table 2). Saturated soils and standing water resulting from flooding reflect less infrared radiation than adjacent non-flooded areas. Likewise, many plants

Table 1. Flood crest data for the September, 1972, flood along the Nishnabotna Rivers, from U.S.G.S., Water Resources Division.

River	Crest Date	Discharge (cfs)	Recurrance Interval (years)
West Nishnabotna River			
at Hancock	13 Sept.	26,400	100
near Randolph	14 Sept.	18,500	7
East Nishnabotna River			
near Atlantic	12 Sept.	26,700	120
at Red Oak	13 Sept.	38,000	100
near Hamburg	15 Sept.	25,200	4

affected by the flood reflect less radiation in the infrared band than comparable plant types that were not inundated. River bottom tree species did not show this decrease in infrared reflectance.

2. Blue radiation (400-465nm) was reflected more strongly from flooded areas than from comparable surrounding areas. The green (480-570nm) and red (595-685nm) radiation bands were found to be least definitive for delineating the flooded areas.

3. Color imagery aided interpretation both in the visible and near-visible infrared portions of the spectrum. The best flood delineation was provided by multispectral color-additive viewing utilizing the blue and infrared bands. For maximum planning usage, the imagery should also be suitable for photogrammetric purposes to allow the production of topographic maps. Of commercially available films, suitable for flood mapping and photogrammetric purposes, color infrared (Kodak 2443) film was most successful.

4. Stereoscopic viewing was found to be helpful for flood interpretation. The ability to view surface relief is helpful for extrapolating the flood boundary into areas for which tones or colors are not completely definitive. This was common in very flat areas where the flood boundary may be very complex.

5. Flood inundation mapping can be accomplished in late summer for at least three days following flood cessation in the Midwest.

General Analysis of ERTS-1 Imagery

Since the launch of ERTS-1 several high quality images of southwestern Iowa have been received (table 3). Analysis of this repetitive imagery, acquired from July through October, allowed a positive determination that the Nishnabotna flood is shown on the imagery. July, August and October imagery shows that all the major perennial stream valleys in southwestern Iowa appear very similar in all spectral bands. The Nishnabotna valleys do not appear different than any other

Table 2. Suitability of low-altitude multispectral photographic images for late summer flood mapping in the Midwestern Region.

Spectral Band (s)	Appearance of Flooded Areas Versus the Appearance of Unaffected Areas	Suitability for Flood Mapping
Blue	Lighter	Fair
Green	Lighter or Darker	Very Poor
Red	Lighter or Darker	Poor
Infrared	Darker	Good
Green, red, infrared--false colored as blue, green, & red, respectively.	Darker Red, grading to Green, Blue, or Grey	Very Good
Blue, infrared--false colored as blue & red, respectively.	More Blue to Purple	Excellent

streams of comparable size.

The September 18 and 19 images were taken 6 and 7 days after the crest of the Nishnabotna flood (table 3). The major valleys in the area again have similar densities and general appearance in the green (MSS 4) and red (MSS 5) band images. However, the flooded areas in the Nishnabotna valleys and in other areas are readily apparent on the infrared bands, MSS 6 and 7. The inundated areas have sharply reduced infrared reflectance because of surface water, excessive soil moisture, and stressed plants. The flooded areas are most clearly defined on the MSS 7 image, and this was the imagery utilized for mapping the inundated area.

Analysis of the ERTS-1 imagery , by IGSRSL and NASA, reinforced the basic conclusions of the IGSRSL low-altitude, multispectral analysis: near-visible infrared sensing systems can be used to map the extent of major midwestern floods in late summer. The green and red bands were not helpful for delineation of the flood. The MSS does not have a blue channel, so no comparison can be made with the multiband camera for this band. ERTS data demonstrated that floodmapping can be accomplished one week following the recession of high water.

Flood Inundation Mapping: Comparison of Results

After initial analysis of the low-altitude imagery a map of the flooded area along the East Nishnabotna River was prepared, utilizing multispectral imagery and metric black and white panchromatic photography. Problems in interpretation of the low-altitude imagery were encountered in some areas because of the incomplete photographic coverage over the entire width of the flooded area. The accuracy of

Table 3. ERTS-1 satellite imagery of Southwestern Iowa utilized by IGSRSL. All images taken at approximately 10:30 A.M., Central Standard Time.

Date (1972)	Cloud Cover (%)	NDPF I.D. Number	Comments
26 July	20	1003-16334	Stream valleys uniform in appearance on all bands. Best defined on band 5.
	30	1003-16341	
14 August	0	1022-16382	
	0	1022-16384	
18 September	5	1057-16315	Flood inundated areas are apparent on infrared bands.
	0	1057-16332	
	10	1058-16383	
	0	1058-16390	
07 October	0	1076-16384	All floodplains apparent on infrared bands.
	0	1076-16381	

the mapping of the inundated area by low-altitude imagery was substantiated where ground observations were available. After the low-altitude analysis was completed, the interpretations of the inundated area were transferred to base maps at a scale of 1:126,720 (1 inch=2 miles). The ERTS imagery was then used to produce a map of the inundated area. The interpretation was done directly from prints, enlarged from 70mm positive transparencies to 1:250,000 scale (1 inch≈4 miles). The two maps were produced independently by the IGSRSL interpreters.

The investigators prepared a composite map at a scale of 1:250,000 to compare the low-altitude and the orbital imagery interpretations. A preliminary version of this map is shown in figure 3. The two interpretations were comparable at this scale, with 80 percent of the area mapped in complete agreement. However, small areas of discrepency exist. These areas of differences should be considered in light of certain factors. The low-altitude mapping was accomplished with incomplete photographic coverage. Multispectral imagery did not include the full width of flood inundation in many areas. At these locations the boundary had to be interpreted from stereoscopic black and white panchromatic imagery filtered to include only green and red reflected energy--the least informative spectral bands for flood mapping. Interpretive errors are possible with any imagery in flat lowland areas where the border of the flooded area is very complex. Transferring interpreted data to base maps was difficult because of the almost total lack of topographic maps along the East Nishnabotna River. A further mapping complication resulted from

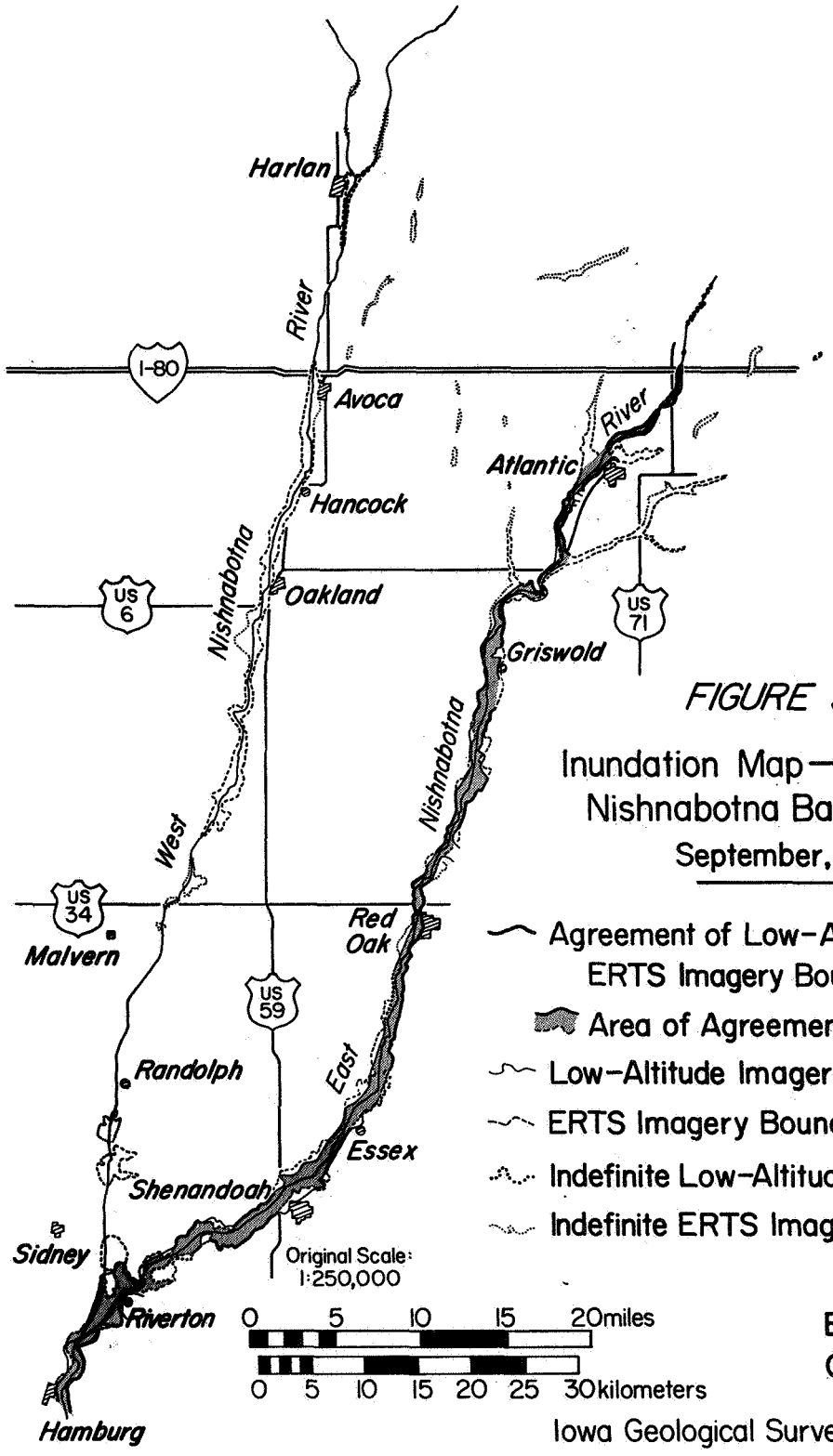


FIGURE 3.

Inundation Map—
Nishnabotna Basin Flood,
September, 1972

- Agreement of Low-Altitude and ERTS Imagery Boundaries
- Area of Agreement
- Low-Altitude Imagery Boundary
- ERTS Imagery Boundary
- Indefinite Low-Altitude Imagery Boundary
- Indefinite ERTS Imagery Boundary

B. E. Hoyer
G. R. Hallberg
Iowa Geological Survey February, 1973

the acquisition of the low-altitude imagery below Shenandoah up to 24 hours before flood crest. For this study, ERTS imagery resulted in fewer problems because it provided comprehensive coverage with an infrared sensitive system. In places the boundary was not sharply defined and was marked only by slight tonal differences on band 7 which caused some interpretive problems. Tonal differences were especially small in the upper portion of the basin (where flooding was earliest), in the broad floodplain of the West Nishnabotna River (where flooding was slight), and near urban areas (especially Red Oak). Another interpretive difficulty of ERTS imagery resulted from the large amount of infrared energy reflected from lowland tree species located within the flooded region. These trees are particularly apparent near Riverton. It is assumed that these bottomland trees were not stressed as a result of inundation. This response was not a problem for low-altitude stereoscopic imagery, but proved troublesome for ERTS imagery interpretation. Where mapping differences occur between low-altitude and satellite imagery, some refinements of one method by the other is possible based on the interpreters' judgement and re-evaluation. The map presented does not show these possible refinements, but rather indicates the total area of dispute to eliminate interpretive bias.

Flood inundation mapping was continued into the West Nishnabotna basin because of the agreement of data in the East Nishnabotna basin. The criteria used for interpretation in the East Nishnabotna basin were extended to the West Nishnabotna basin, where mapping in the northern portion was readily accomplished. However, no flooding could be interpreted throughout much of the southern portion, except in two highly questionable areas. Ground data supplied by the U.S. Geological Survey coinvestigators indicates that the West Nishnabotna did not breach its levees in the Malvern-Randolph area. Flood gaging records suggest this as well (table 1). The crest of the flood at Randolph exhibited a recurrence frequency of only seven years--indicating a very minor flood stage. The crests measured along the upper portions of the West Nishnabotna and along the East Nishnabotna indicated a 100-year flood or greater.

The 18 September ERTS imagery also revealed apparent flood inundation along other stream systems, notably in the Nodaway River and Grand River basins. U.S. Geological Survey, Water Resources Division, data indicate the flooding occurred in these areas also. Flood stages were reached on the Boyer River and in Mosquito Creek, but inundated areas are not apparent on the imagery. The flooding in Mosquito Creek was equal to a 200-year flood near Earling, but this took place in a very small localized area (drainage area of only 32 square miles). This particular area is obscured by clouds on both the September 18 and 19 ERTS images, so no assessment of the capabilities of the ERTS imagery was possible in this area. The Boyer River was imaged on 19 September. This river has been highly channelized, and the 30-year flood recorded at Logan was contained with no significant overland flooding.

A 1:250,000 scale map was prepared from the ERTS imagery by the NASA coinvestigators at Goddard Space Flight Center. General agreement existed between

the maps along the East Nishnabotna, but some gross differences occurred in the interpretation of the West Nishnabotna. The flooded area mapped by NASA was significantly larger than that mapped by the IGSRSL staff. These differences may be a function of the IGSRSL investigators' correlative low-altitude and ERTS flood-mapping experience on the East Nishnabotna. The experience gained using the East Nishnabotna flood as training allowed more confidence in their regional interpretation.

The correlation of the orbital data with ground and low-altitude data indicates the feasibility of regionally analyzing Midwestern, late summer flood inundation utilizing satellite imagery. Reasonable measurements of flood acreage seem possible for entire river systems. The total flooded area mapped in the Nishnabotna basins from the ERTS imagery was 305 km^2 or 78,000 acres (Hallberg and Hoyer, 1973). In the East Nishnabotna basin 214 km^2 or 55,000 acres were mapped, and 91 km^2 or 23,000 acres were mapped in the West Nishnabotna basin. The adequacy of existing levee systems can be evaluated on a regional basis. Interpretation of the West Nishnabotna Valley between Malvern and Randolph and the Boyer River Valley indicated that the levees were generally adequate for this flood. Evaluation of ground studies later confirmed this interpretation. The utilization of satellite imagery to assess floods could become an important tool, particularly in poorly mapped, sparsely settled, or inaccessable areas. The satellite imagery allows rapid appraisal of the areal extent of flood inundation for entire river systems. Satellite flood evaluation should prove valuable to federal and state agencies involved in regional floodplain management and planning.

References Cited:

Climatological Data: Iowa, September 1972, v.83, no.9, U.S.Dept.Comm., N.O.A.A., p.133-149.

Hallberg, G.R., and B.E. Hoyer, 1973, Flood Inundation Mapping in Southwestern Iowa, A Preliminary Report, Analysis of ERTS-1 Imagery, Iowa Geol.Sur., Remote Sens. Lab., 15p.

Hoyer, B.E., and J.V. Taranik, 1973, Aerial Flood Mapping in Southwestern Iowa, A Preliminary Report, Iowa Geol.Sur., Remote Sens. Lab., 11p.

Acknowledgements

Many people have contributed support in this flood study. Especially helpful were Sulo Wiitala, Walter Steinhilber, Ivan Burmeister and Oscar Lara, all from the U.S.Geological Survey, Water Resources Division. They arranged financial support for data acquisition, helped plan the study, supplied ground data, and provided editorial guidance. Special appreciation is extended to Morris Deutsch, EROS Project Office, U.S.G.S., for alerting us to examine the ERTS-1 imagery of the flooded area. Some of G.R.Hallberg's time and some of the ERTS imagery utilized in this project were made available via Project SR238, An Evaluation of ERTS-1 Imagery for Mapping Quaternary Deposits and Landforms in the Great Plains and Midwest.

Paper W 6

ASSESSMENT OF FLOOD DAMAGE IN ARIZONA BY MEANS OF ERTS-1 IMAGERY

Roger B. Morrison and Maurice E. Cooley, *U. S. Geological Survey, Denver, Colorado, and Tucson, Arizona*

Abstract

ERTS-1 MSS images clearly show two important effects of a large flood in southeastern Arizona - the extent of inundation and the areas affected by severe sediment deposition and erosion - although the images were made a week and a half after the flood. On October 20 and 21, 1972, the upper Gila River had its third-largest flood on record. Peak flows attained about 42,000 and 82,000 cubic feet a second at Duncan and Safford, Arizona, respectively. Two lives were lost, hundreds of people made homeless, and more than 10,000 acres of cropland inundated.

The first ERTS-1 images after the flood were made on November 1 and 2. The inundated area is best displayed on the infrared bands, particularly on band 7, where it appears as a belt along the river that is distinctly darker than adjoining parts of the flood plain. This dark belt does not appear on ERTS images that predate the flood. Presumably the low infrared reflectance of this belt is caused by still-moist soil and by flood-stressed vegetation. Inundation limits mapped from ERTS imagery agree well with those obtained by aerial photography during the flood and by ground surveys. Areas of severe sand and gravel deposition show best on band 5. By comparing before and after flood images in this band, a quick assessment can be made of the severely flood-ravaged land.

The Gila River, the third largest in Arizona, has a history of occasional large floods that result from regional storms that drop most of their rain in the high mountains in the upper parts of its watershed, near the Arizona-New Mexico line. There are no dams on the upper Gila River or its tributaries, so the floods are uncontrolled. On October 20 and 21, 1972, the upper Gila had its third-largest flood on record. Peak flows attained about 42,000 cubic feet a second at Duncan, Arizona, and about 82,000 cubic feet a second at Safford, below the confluence of the San Francisco River, which also flooded. Two lives were lost in New Mexico, hundreds of people were made temporarily homeless, and more than 10,000 acres of cropland were inundated. Figures 1, 2, and 3 are low-altitude air photographs taken during the flood crest by personnel of the Arizona Highway Department and of the U.S. Geological Survey.

Publication authorized by the Director, U.S. Geological Survey

The first post-flood ERTS images were made a week and a half after the flood, on November 1 and 2. Nevertheless, the zone that was inundated is clearly visible on infrared bands 6 and 7, particularly on band 7 (Figures 4 and 5). It shows as a belt that is distinctly darker than the adjoining parts of the river flood plain. This dark belt does not appear on the images that predate the flood. We mapped the boundary of the dark belt at 1:250,000 scale with a zoom transferscope, using the November 1 and 2 images. We also plotted at the same scale the ununda tion limit as determined from the low-altitude airphotographs taken during the flood. Figure 6 compares the results. The agreement is surprisingly good, considering the 10-day delay in the ERTS imagery and also the fact that the discrimination of the inundation limit from the ERTS images was done quite conservatively.

On subsequent infrared images the dark belt along the Gila River disappeared slowly. Unfortunately, heavy clouds completely obscured the upper Gila River area in the images taken by the second post-flood ERTS-1 pass (November 19 and 20) over the area. On the next pass (December 7 and 8) the dark belt is not quite as dark as previously (it contrasts less with the adjoining flood plain), and it is somewhat narrower. In the images from later passes (December 25 and 26 and afterward) the dark belt has disappeared. We surmise that the low infrared reflectance of the dark belt could be caused by both excess soil moisture and by flood-stressed vegetation. The slowness with which the dark belt "faded" suggests that a significant part of the lowered infrared reflectance was due to vegetation stress, because the soil surface likely dried out at a faster rate. The narrowing of the dark belt with time also favors this hypothesis, because flood stress on vegetation would tend to be greatest close to the main channel of the river.

Similar dark belts of reduced infrared reflectance were observed along the East Nishnabotna and West Nishnabotna River in Iowa, in ERTS images taken a week after a big flood last September.

We also noticed in the ERTS images taken after the Gila River flood that certain reaches of river-channel deposits had widened considerably, compared with the pre-flood images. The channel deposits, sand and gravel, show most clearly on band 5 as a very light-toned strip inside the inundated belt that appears dark on the infrared bands. The greatest widening of the channel-deposit strip is at the upper ends of two intermontane basins, the Duncan-Virden Valley and the Safford (Gila) Valley, where the Gila River debouches from narrow box canyons. Evidently these were the sites of strong sand and gravel erosion and deposition.

In conclusion, the repetitive multispectral ERTS images appear to have considerable potential for assessing two important effects of large floods -- the extent of inundation and the areas affected by severe erosion and sediment deposition -- even from images taken a week and a half after the flooding.



Figure 1. Low-altitude airphoto showing the inundation at Duncan, Arizona, near the crest of the October 20-21, 1972 flood on the upper Gila River. U. S. Geological Survey photograph.



Figure 2. Low-altitude oblique airphoto of eastern Safford (Gila) Valley, near the peak of the October 20-21, 1972 flood on the upper Gila River. U. S. Geological Survey photograph.



Figure 3. Vertical low-altitude airphoto near Safford, Arizona, taken shortly after the crest of the October 20-21, 1972 flood on the upper Gila River. Many homes in the village in lower center (Hollywood) were destroyed. Arizona Highway Department photograph.

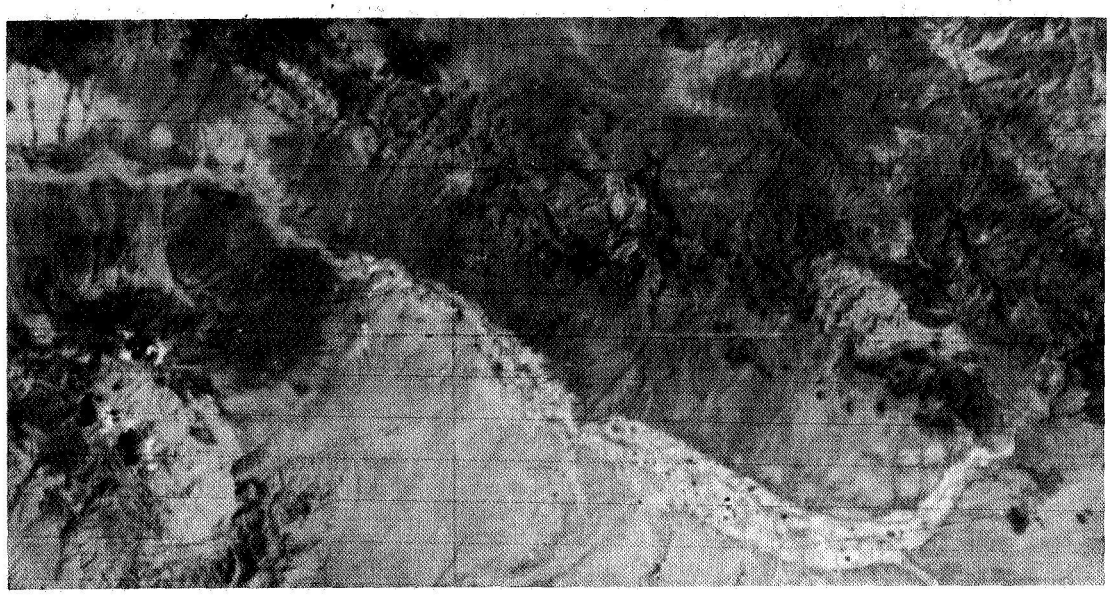


Figure 4. Conditions before the Gila River flood as shown by infrared band 7 of ERTS-1 frame 1030-17265, taken August 22, 1972. The arcuate light-toned band in the lower part of the view is the Safford (Gila) Valley, Arizona.

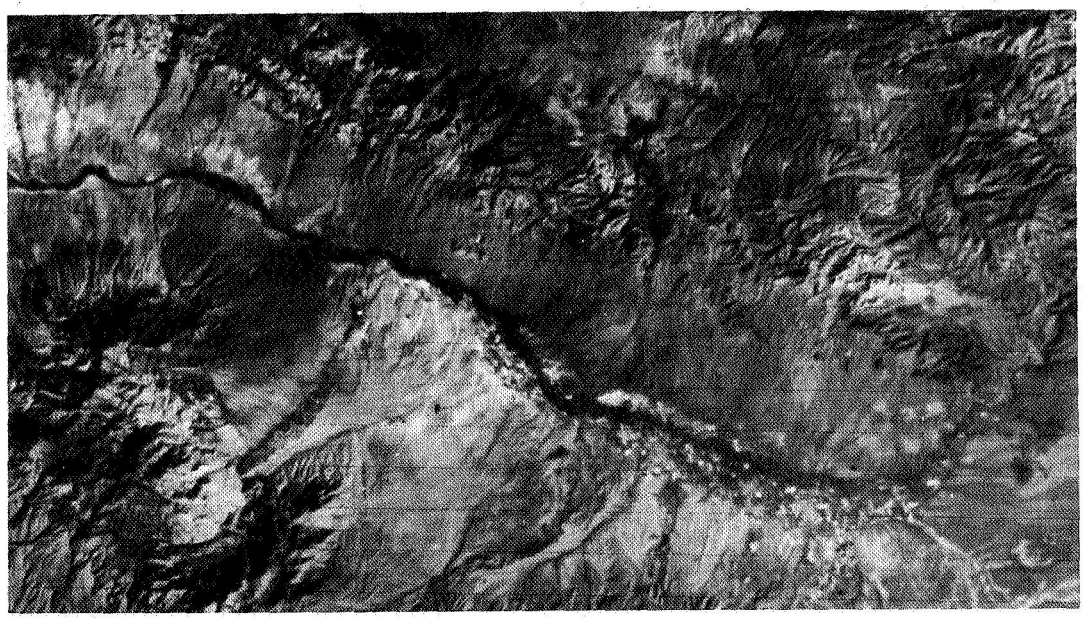


Figure 5. Conditions 1½ weeks after the Gila River flood of October 20-21, 1972, as shown by infrared band 7 of ERTS-1 frame 1102-17274, taken November 2, 1972. Note the dark belt of reduced infrared reflectance along the Gila River within the Safford Valley. This corresponds with the zone that was inundated and probably is caused by excess soil moisture and by flood-stressed vegetation.

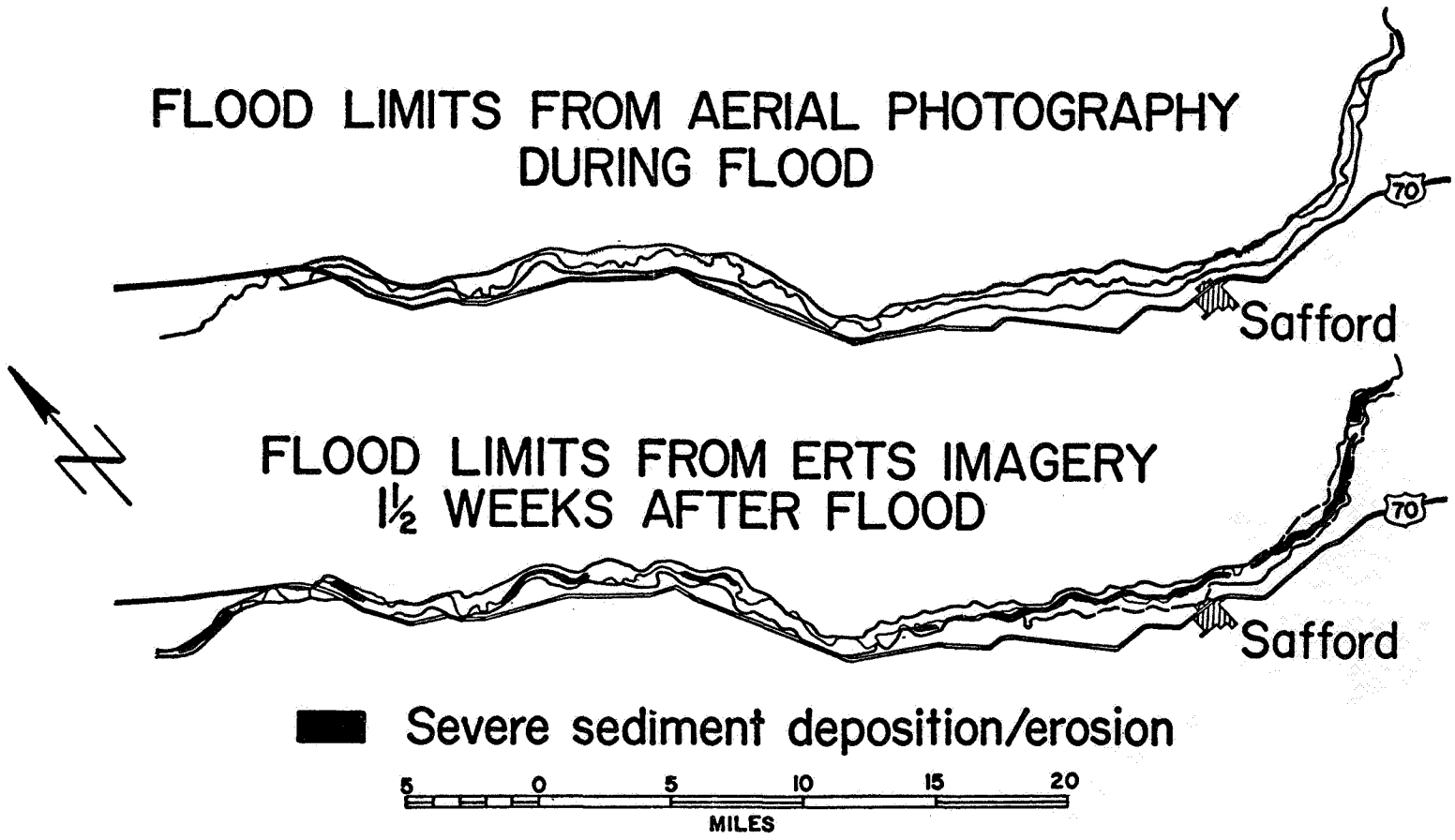


Fig. 6. Limits of October 20-21 flood on the upper Gila River in the Safford (Gila) Valley, Arizona, as determined from low-altitude aerial photography taken during the flood and from ERTS-1 imagery taken 1 1/2 weeks after the flood.

Paper W 7

USE OF THE SRI ELECTRONIC SATELLITE IMAGE ANALYSIS CONSOLE FOR MAPPING SOUTHERN ARIZONA PLANT COMMUNITIES FROM ERTS-1 IMAGERY[1]

Raymond M. Turner, *U. S. Geological Survey, Tucson, Arizona*

ABSTRACT

Cloud-free imagery covering the Tucson, Ariz., region for the period from August 22 to November 2, 1972, was used to determine the utility of ERTS-1 data for discriminating boundaries between plant communities.

The following studies were made from imagery analyzed by use of Stanford Research Institute's Electronic Satellite Image Analysis Console:

(1) Console-generated color composites from MSS-5 and MSS-6 bands were recorded photographically from the console color monitor. The color photographs were then used to compare with short-term changes in vegetative cover observed on the ground.

(2) Using the console, microdensitometric traces were made along selected traverses to quantify changes in scene irradiance across the image field. MSS-6 minus MSS-5 densitometry values were employed as a relative measure of plant cover in the wide range of vegetative zones covered by the traverses.

(3) Quantitative plant coverage data, collected at ground-truth stations along the traverses, were compared with the densitometric values.

INTRODUCTION

The U.S. Geological Survey is engaged in a program aimed at mapping southern Arizona vegetation from ERTS-1 imagery. This report describes preliminary results in which both time-lapse, color-composited imagery and microdensitometry are used to delineate and identify plant communities. The imagery was analyzed on the Electronic Satellite Image Analysis Console at Stanford Research Institute, Menlo Park, Calif., and I wish to acknowledge the important contribution of SRI scientists, especially Wm. E. Evans and S. M. Serebreny.

1/ Publication authorized by the Director, U.S. Geological Survey.

Detailed mapping of arid region vegetation using satellite imagery depends upon detecting differences in the timing of plant growth activity among the communities comprising the region's vegetative mosiac. The short-term repetitive viewing capability of the ERTS series satellites provides an especially forceful means for performing this task. In arid subtropical regions with wide elevational differences, such as southern Arizona, the varied environment gives rise to diverse plant growing regimes. Among the kinds of plants present are those that are evergreen (such as pines and live oaks at higher elevations or creosote bush at lower elevations) and those that are green only seasonally. Among the latter are winter-active species (ephemeral grasses and forbs) and summer-active species (perennial and ephemeral grasses and ephemeral forbs). At lower elevations where the dominant perennial plants tend to be widely spaced, distinguishing one open community from another would be difficult if it were not for the temporarily dense growths of the small ephemeral species that appear during seasons of favorable rainfall. Where such plants with distinctive periods of foliation grow densely enough to be detected by the relatively low-resolution systems of satellites, it should be possible to employ seasonal growth differences to map the areas they occupy.

Of basic importance to our approach is the unique manner in which green plant tissues respond to the wavelengths sensed by the ERTS-1 multispectral scanner. Our efforts to date have relied heavily on the differences in plant reflectance between the MSS band 5 and the MSS band 6. In the MSS-5 spectral range (0.6 to 0.7 micrometers) plants reflect little energy; through the MSS-6 range (0.7 to 0.8 micrometers) they irradiate strongly. Although leaf irradiance in the two bands is influenced by separate systems, one having to do with leaf pigment chemistry and the other with leaf anatomy, both systems are closely related to the quantity of foliage, the variable that we are attempting to detect.

METHODS

ERTS-1 multispectral scanner bulk imagery in 70-mm format for the Tucson, Ariz., region was used in this study. During the preliminary period covered by this report, use of MSS bands 5 and 6 was emphasized. Diapositives of cloud-free scenes were employed throughout. Use was made principally of image numbers 1030-17271-5 and 1030-17271-6 for August 22, 1972, and numbers 1102-17280-5 and 1102-17280-6 for November 2, 1972.

As one approach, microdensitometry was performed by the console across two east-west traverses (Fig. 1). Each traverse was four console TV lines wide, representing, for the magnification used, about 800 meters on the ground. Scene irradiance values along the four parallel traverses were measured and averaged for the MSS-5 and MSS-6 images. The MSS-5 values were subtracted from the MSS-6 values, and the resulting

differences as seen by the traces on the console oscilloscope were compared with an elevation profile and known vegetation patterns for the traverses. To assure image-to-image and date-to-date uniformity, densitometric readings were first made across the grey scale on each image; adjustments were then made on the console to produce comparable curves of voltage versus grey step number for all scenes. Following this adjustment, a given grey level represents the same amount of reflected energy on all scenes.

In a second analysis, plant coverage was measured at roughly 18-day intervals at five sites along two additional traverses, the Sierrita Mountain and Mile Wide Road transects (Fig. 1). The measurements, made as close to the day of the satellite's imaging overflights as feasible, were gathered from representative open communities of the desert and of the grassland bordering the desert. Changes in measured plant coverage are shown in figure 2 for the period from October 1972 through January 1973, with extrapolations made through the remainder of the twelve months. These curves show actual changes and anticipated changes in the amount of green foliage covering the soil surface. The hypothetical projected changes are shown only to illustrate how repetitive imagery may be used for identifying plant communities. The actual changes in plant cover were compared with MSS-6 minus MSS-5 densitometric traces along only the Sierrita Mountain transect. This analysis was performed on an enlarged view of part of the same images as noted above. The traverse used for densitometric analysis was four scan lines wide representing, at the magnification selected, a width of about 250 meters on the ground.

In the third analysis, additive color displays, using two primary colors, were recorded photographically from the console's color monitor. As before MSS bands 5 and 6 were employed. Cyan was paired with MSS-5 and red was paired with MSS-6, providing a partial simulation of false-color IR photography. The 35-mm full-frame images and an enlarged view of an area supporting a heavy growth of phreatophytes were analyzed for qualitative scene changes that can be used to map vegetation and to estimate the amount of plant foliage.

RESULTS

Densitometric studies.--In figure 3 may be seen the changes in scene irradiance across the Old Baldy Transect from the vicinity of the Baboquivari Mountains on the west to the Mule Mountains on the east, a distance of 170 kilometers. The oscilloscope trace gives the values obtained when MSS-5 scene irradiance is subtracted from MSS-6 scene irradiance. The images used were for August 22, 1972 (numbers 1030-17271-5 and 1030-17271-6). The difference curves resulting from this manipulation vary directly, for the most part, with changes in plant coverage. Patches of dense vegetation in moist habitats, such as valley bottoms

and high mountains, show the greatest difference values. The Santa Cruz River valley, Old Baldy (Mount Wrightson), Babocomari Creek, and the San Pedro River valley give the highest values where crossed by the transect on this image.

In figure 3, the difference trace for the Old Baldy Transect is shown for November 2, 1972 (numbers 1102-17280-5 and 1102-17280-6). Compared to the August 22 trace, there is a tendency toward a decrease in the magnitude of the difference values. The flattening of the difference curve indicated by the November trace occurs with the end of the summer rainy season and the coincident loss of foliage by the ephemeral and deciduous perennial plants as they enter the period of winter quiescence. Later, as winter annuals begin growth in response to winter rains, it is anticipated that the differences will again increase, but only for the lower elevations. At higher elevations, where evergreen oaks and pines dominate, the matrix of grasses and forbs will remain dormant during the winter resulting in values that are somewhat lower than those of summer.

In figure 4, difference traces for the Mine Transect for two dates (August 22 and November 2, 1972) are shown. A flattening of the November difference curve, as noted for the Old Baldy Transect, can also be seen here. Of particular interest is the change in the curves where the transect crosses the extensive grassland bordering upper Cienega Creek. The change is interpreted as representing a decline in green cover as the grasses enter the winter dormant condition. The low mountains along the Mine Transect have relatively low difference values in the winter because of the sparse growth of evergreen trees. Mesquites, other summer foliating shrubs, and grasses dominate the landscape at these intermediate elevations.

In figure 5, two difference traces for the Sierrita Mountain Transect for August 22 and November 2, 1972 are shown. Plant coverage is being measured at two sites (Sierrita Mountain 1 and 2, Fig. 2) along this transect for comparison with the difference traces. (Although ground-truth data are being collected at three nearby sites along the Mile Wide Road Transect, densitometry for this part of our work is incomplete and will not be reported upon at this time.) It is too early in our program to determine how closely the plant coverage values will follow fluctuations in the difference traces. As expected, the maximum difference values for November are lower than for August. At the point where the transect crosses a low area with dense phreatophyte vegetation near Brawley Wash, the values are low in November compared with August because the plants have become leafless by November. Cultivated fields, some of which are fallow and some cropped, produce characteristic sharp changes near the extreme right end of the difference curves.

Time-lapse studies of color-additive images.--Phreatophyte vegetation along a short reach of the San Pedro River near Benson, Ariz., and

in an area at the confluence of Rillito and Sabino Creeks near Tucson are being examined in detail. Changes in the enlarged, color-composite, video images will be compared with observed changes in foliation among the dominant phreatophyte or riparian species occupying the sites. It should be possible to map the vegetation of these habitats where dense, pure stands of these species occur. Identification of the species should be possible by observing the difference in timing of foliation.

Time-lapse viewing of console-generated, color-additive, full-frame ERTS images will be used to construct vegetation maps covering the main study site, an area 100 nautical miles on a side with Tucson at the center. In compiling the vegetation map, which is the final product of this project, scene changes on the multispectral images will be examined in conjunction with other analyses performed on the Electronic Satellite Image Analysis Console, such as color slicing, scene-to-scene differencing, and densitometry.

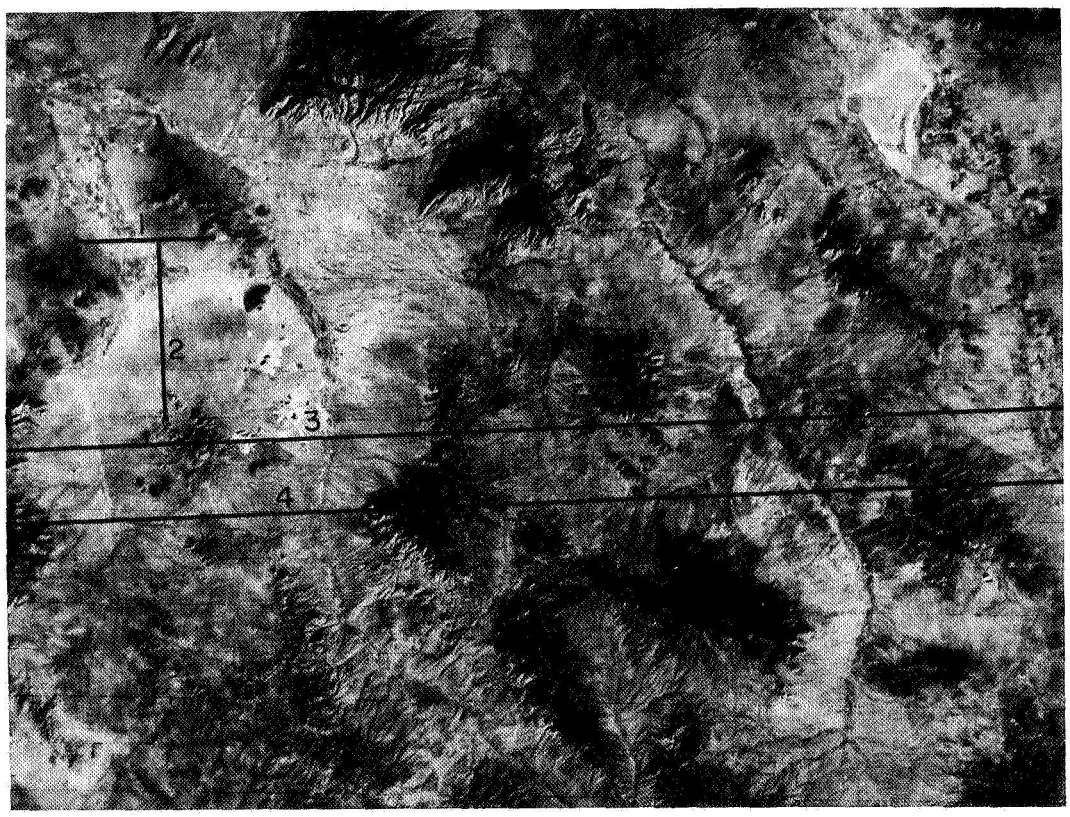


Figure 1. Part of an ERTS-1 image (1156-17280-5) showing location of transects mentioned in the text (1 = Mile Wide Road Transect, 2 = Sierrita Mountain Transect, 3 = Mine Transect, 4 = Old Baldy Transect).

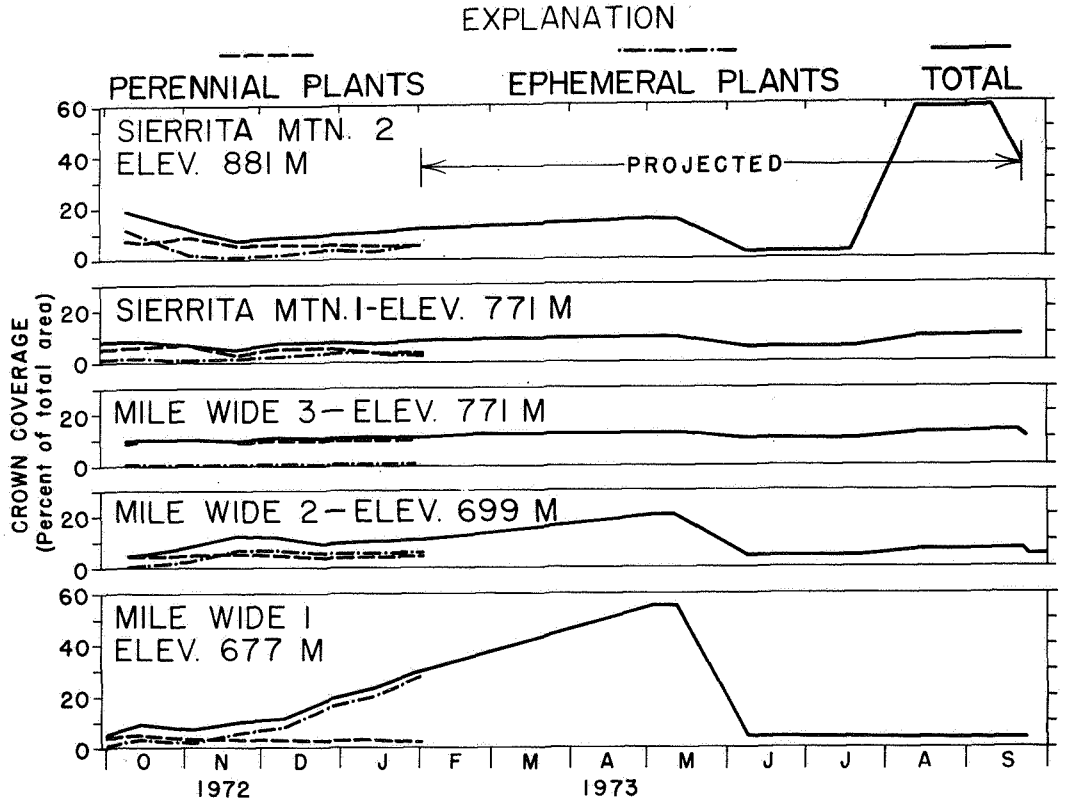


Figure 2. Actual and projected changes in plant crown coverage at five stations near Tucson Arizona. Differences in quantity and timing of foliation will be used to distinguish the plant communities as viewed on ERTS-1 imagery.

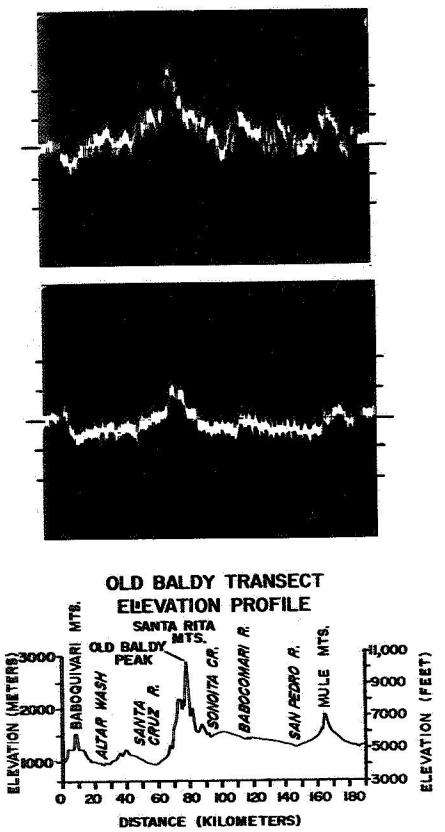


Figure 3. Elevation profile of Mount Baldy Transect and corresponding MSS-6 minus MSS-5 scene irradiance values for August 22, 1972 (upper oscilloscope trace) and November 2, 1972 (lower trace). Vertical scale = 100 millivolts/division.

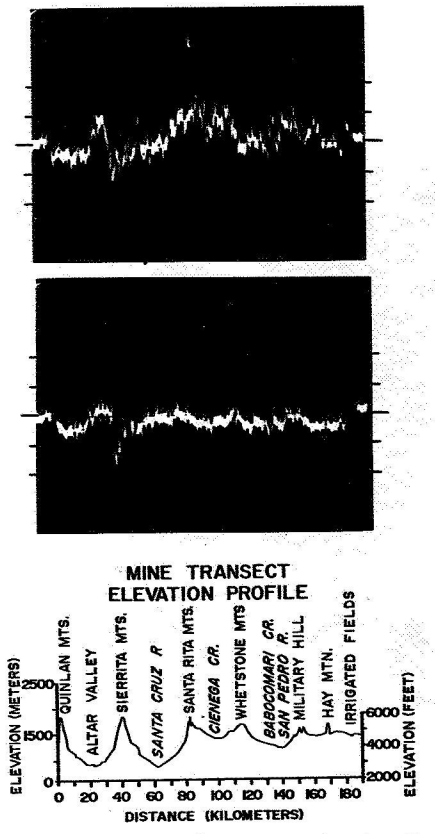
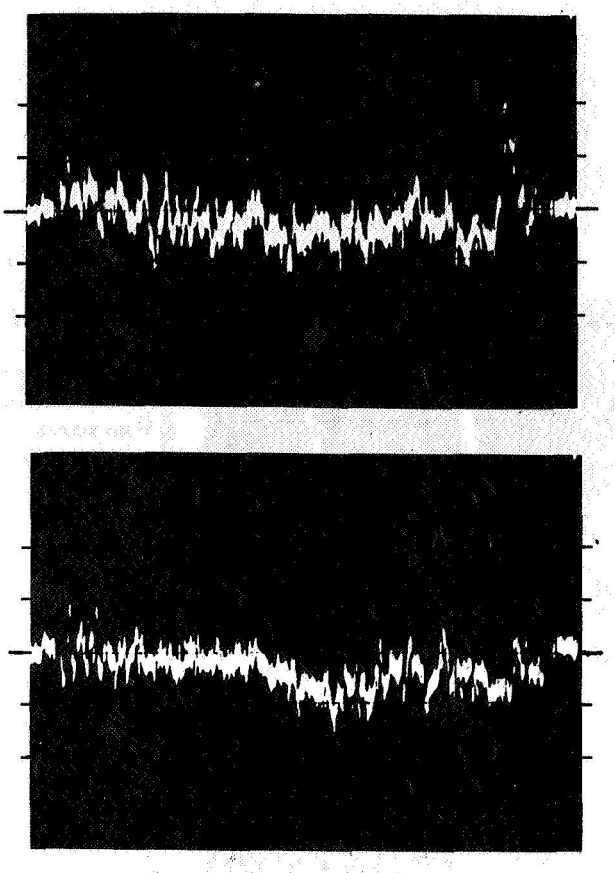


Figure 4. Elevation profile of Mine Transect and corresponding MSS-6 minus MSS-5 scene irradiance values for August 22, 1972 (upper oscilloscope trace) and November 2, 1972 (lower trace). Vertical scale = 100 millivolts/division.



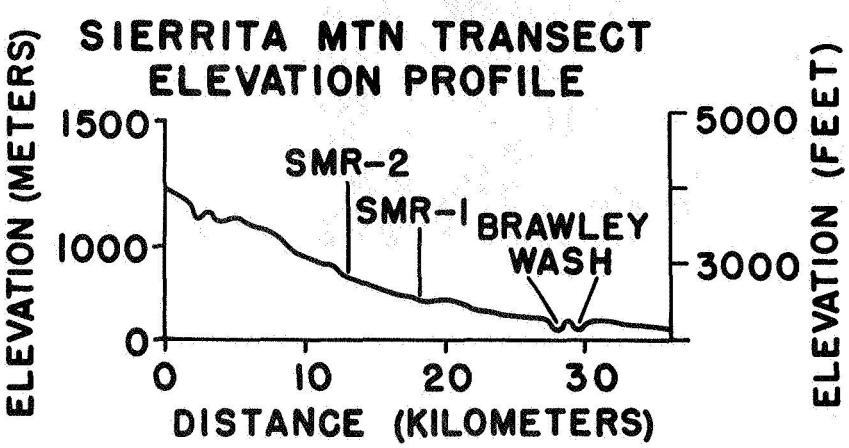


Figure 5. Elevation profile of Sierrita Mountain Transect and corresponding MSS-6 minus MSS-5 scene irradiance values for August 22, 1972 (upper oscilloscope trace) and November 2, 1972 (lower trace). Vertical scale = 100 millivolts/division.

Paper W 8

MONITORING OF STREAMFLOW IN THE VERDE RIVER BY ERTS-1 DATA COLLECTION SYSTEM (DCS)

Herbert H. Schumann, *U. S. Geological Survey, Water Resources Division, Phoenix, Arizona*

ABSTRACT

The Verde River watershed in central Arizona furnishes municipal, industrial, and agricultural water to the Salt River Valley --an area that contains more than half of Arizona's population and about one-fourth of the State's irrigated land. Water-management decisions related to the operation of large multiple-use reservoirs require accurate and continuous monitoring of moisture conditions over large remote areas.

The U.S. Geological Survey in cooperation with the Salt River Valley Water Users' Association installed a specially designed gaging station on the Verde River near the town of Camp Verde to evaluate near-real time streamflow data furnished by the ERTS-1 Data Collection System (DCS). On Nov. 3, 1972, the installation was equipped with a Stevens digital water-level recorder, modified for telemetry, and an ERTS-1 data collection platform operating in the digital-parallel mode. During the 43-day period between Nov. 3 and Dec. 15, 1972, the DCS relayed 552 transmissions during 193 data passes. The DCS system transmitted stream-stage information 4.5 times per day on the average. The amount of data received far exceeded the expected single high quality transmission rate of once per 12-hour period from the DCS system.

The digital-parallel ERTS-1 Data Collection System has furnished data sufficient to accurately compute daily mean gage heights. These, in turn, are used to compute the average daily streamflow rates during stable or slowly changing flow conditions. The digital-parallel DCS data has also furnished useful information during peak-flow periods. However, the serial-digital DCS capability, currently under development for transmitting streamflow data, should provide data of greater utility for determining times of flood peaks.

INTRODUCTION

The Salt and Verde Rivers drain approximately 13,000 square miles of central Arizona. Runoff from these rivers is stored and regulated by a series of reservoirs operated by the Salt River Valley Water Users' Association (fig. 1). These reservoirs are utilized to furnish hydroelectric power, municipal, industrial, and agricultural water to the Salt River Valley in Maricopa County, Arizona. The Salt River Valley contains more than half of Arizona's population (Phoenix metropolitan area), about one-fourth of the State's irrigated land, and is the third most important agricultural area in the United States.

The inability to accurately measure or monitor moisture conditions over large remote areas of central Arizona presents serious land and water management problems. The lack of timely information about rainfall, snow-water content, and streamflow conditions present vexing water management problems related to multiple-use reservoir operations that can and have resulted in the loss of water resources, extensive property damage, and even the loss of life.

The U.S. Geological Survey (USGS) ERTS-1 Data Collection System (DCS) experiment in Arizona includes the use of six (6) data collection platforms to relay hydrologic and meteorologic data. Data from these platforms will be used to test and evaluate the application of near real-time satellite telemetry systems to assist in the management of Arizona's land and water resources. However, because of limited time available, this presentation will be restricted to the application of the DCS to monitoring of streamflow in the Verde River.

RESERVOIRS AND STREAMFLOW

Streamflow in the Verde River is regulated by Bartlett and Horseshoe reservoirs, located northeast of Phoenix (fig. 1). These reservoirs have a combined storage capacity of 317,700 acre-feet (one acre-foot is equal to the quantity of water required to cover one acre to a depth of one foot and is equivalent to 43,560 cubic feet or 325,851 gallons). The streamflow rate in the Verde River above Horseshoe Dam has ranged from a minimum of 48 cfs (cubic feet per second) to a maximum of 81,600 cfs and has averaged 450 cfs during

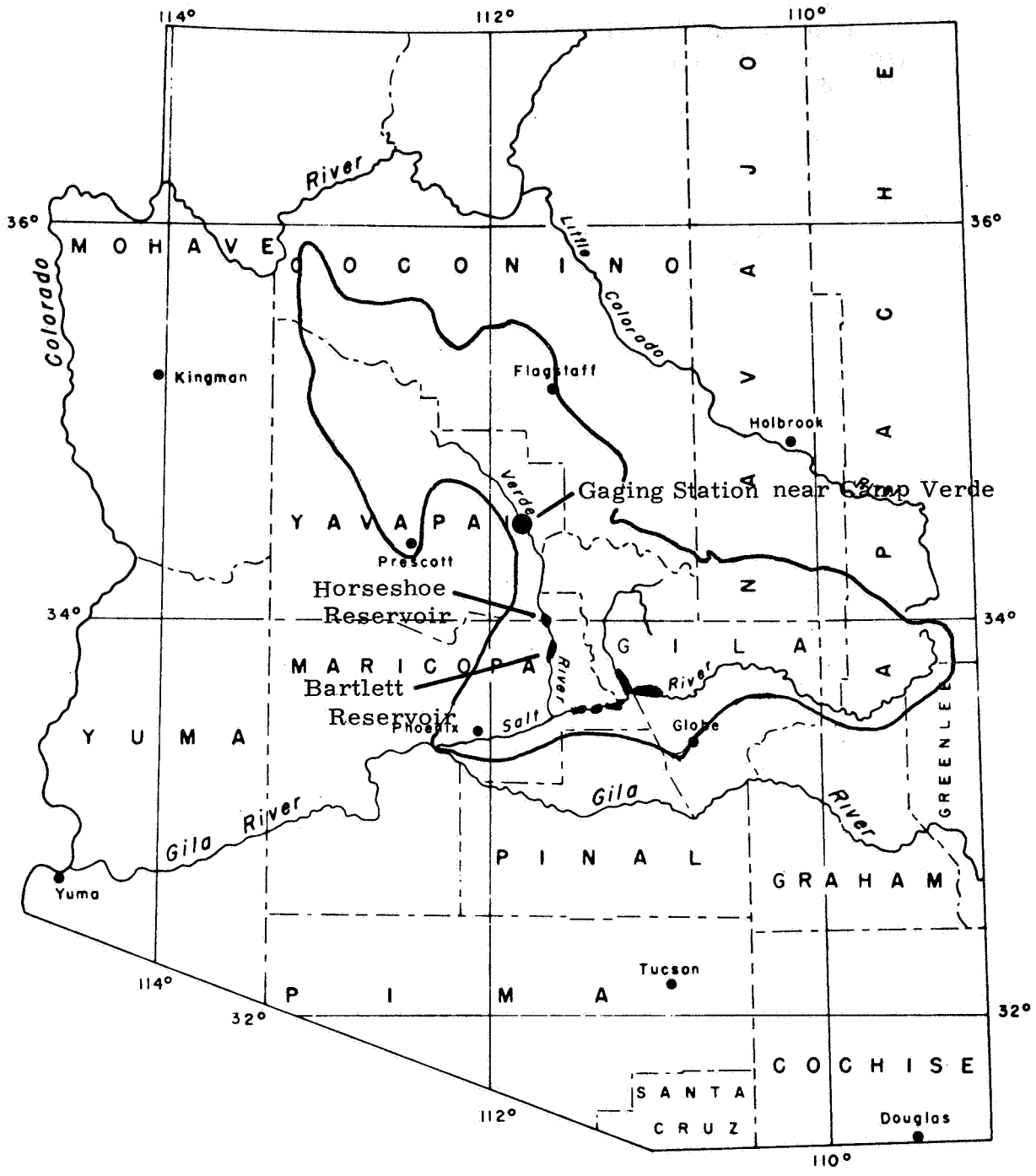


FIGURE 1. — SALT AND VERDE RIVER WATERSHEDS, ARIZONA

the 1945-1970 period of record. The U.S. Geological Survey, in cooperation with the Salt River Valley Water Users' Association, installed a specially designed gaging station on the Verde River near the town of Camp Verde to evaluate near-real time streamflow data furnished by the ERTS-1 Data Collection System (DCS) and to provide early warning of large flood flows.

STREAMFLOW INFORMATION FURNISHED BY ERTS-1 DATA COLLECTION SYSTEM

On Nov. 3, 1972, the U.S. Geological Survey gaging station near Camp Verde was equipped with a Stevens digital water-level recorder, modified for telemetry, and a ERTS-1 data collection platform operating in the digital-parallel mode. During the 43-day period between Nov. 3, and Dec. 15, 1972, the DCS relayed 552 transmissions from this installation during 193 data passes. The DCS transmitted stream stage information 4.5 times per day on the average. Stream stage or gage height is the water surface elevation referred to some arbitrary gage datum. The amount of data received from this station far exceeded the expected single high-quality transmission rate of once per 12-hour period from the DCS. This DCS data received during November and December 1972 is shown on figure 2.

The data received from the Verde River gage with the DCS system operating in digital-parallel mode furnished information sufficient to accurately compute daily mean gage heights. These data, in turn, are used to compute the daily mean streamflow rate during stable or slowly changing flow conditions. Daily mean gage heights were computed from both the digital recorder and from the DCS data. During slowly changing flow conditions daily mean gage heights determined graphically from the DCS data were within ±0.10 feet of daily mean gage heights computed from 96 readings per day supplied by the digital water-level recorder.

To obtain a preliminary estimate of the accuracy of streamflow rates as computed from the DCS data, daily mean streamflow rates were computed from both the DCS data and the digital recorder data for the period Nov. 3 through Dec. 30, 1972. The daily mean streamflow rate as determined from both data sources were compared and the differences, expressed as a percent of the flow rate computed from the digital recorder data, are shown on figure 3. During periods

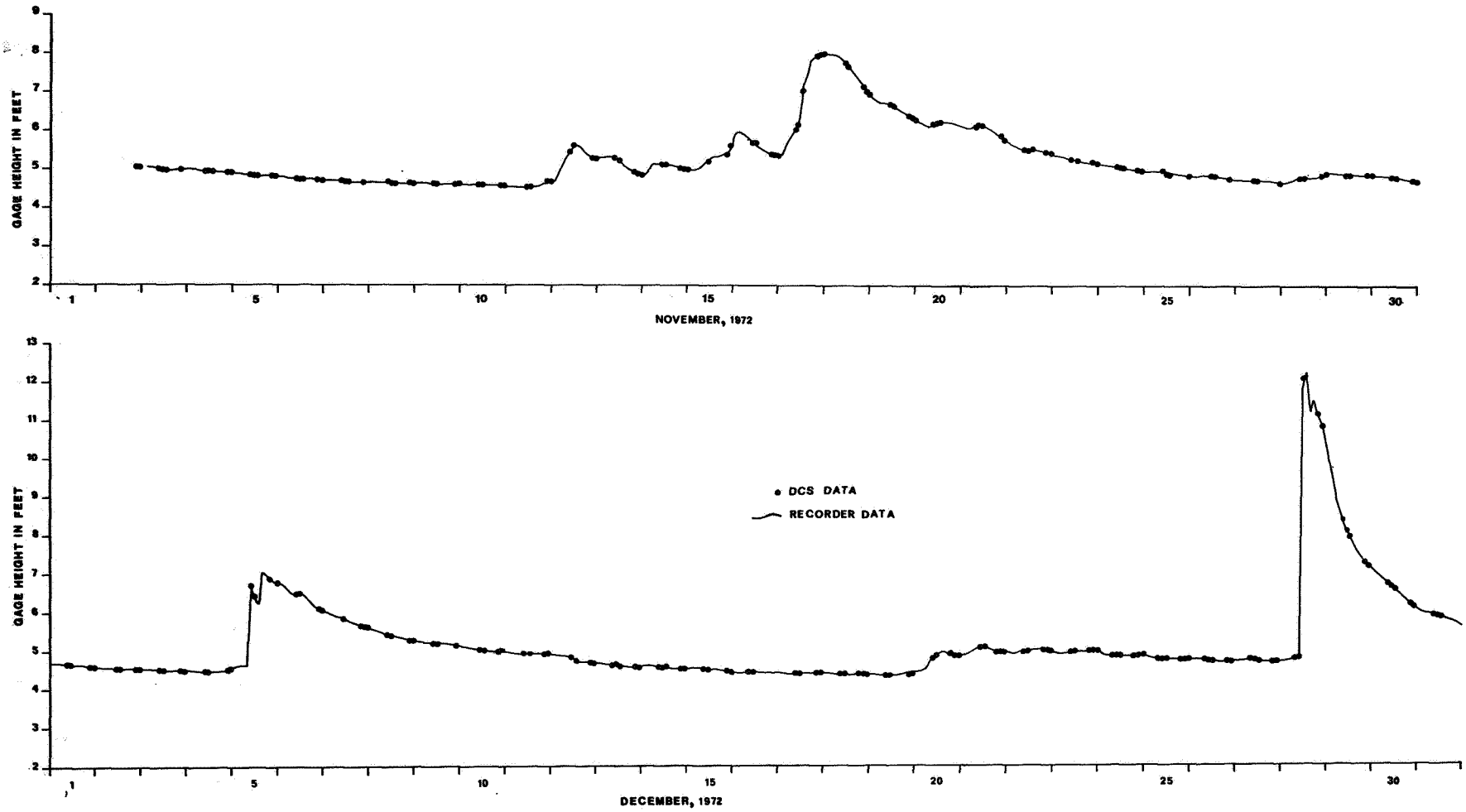


FIGURE 2.—STEAMFLOW GAGE HEIGHTS AT THE VERDE RIVER GAGE, NEAR CAMP VERDE, ARIZONA

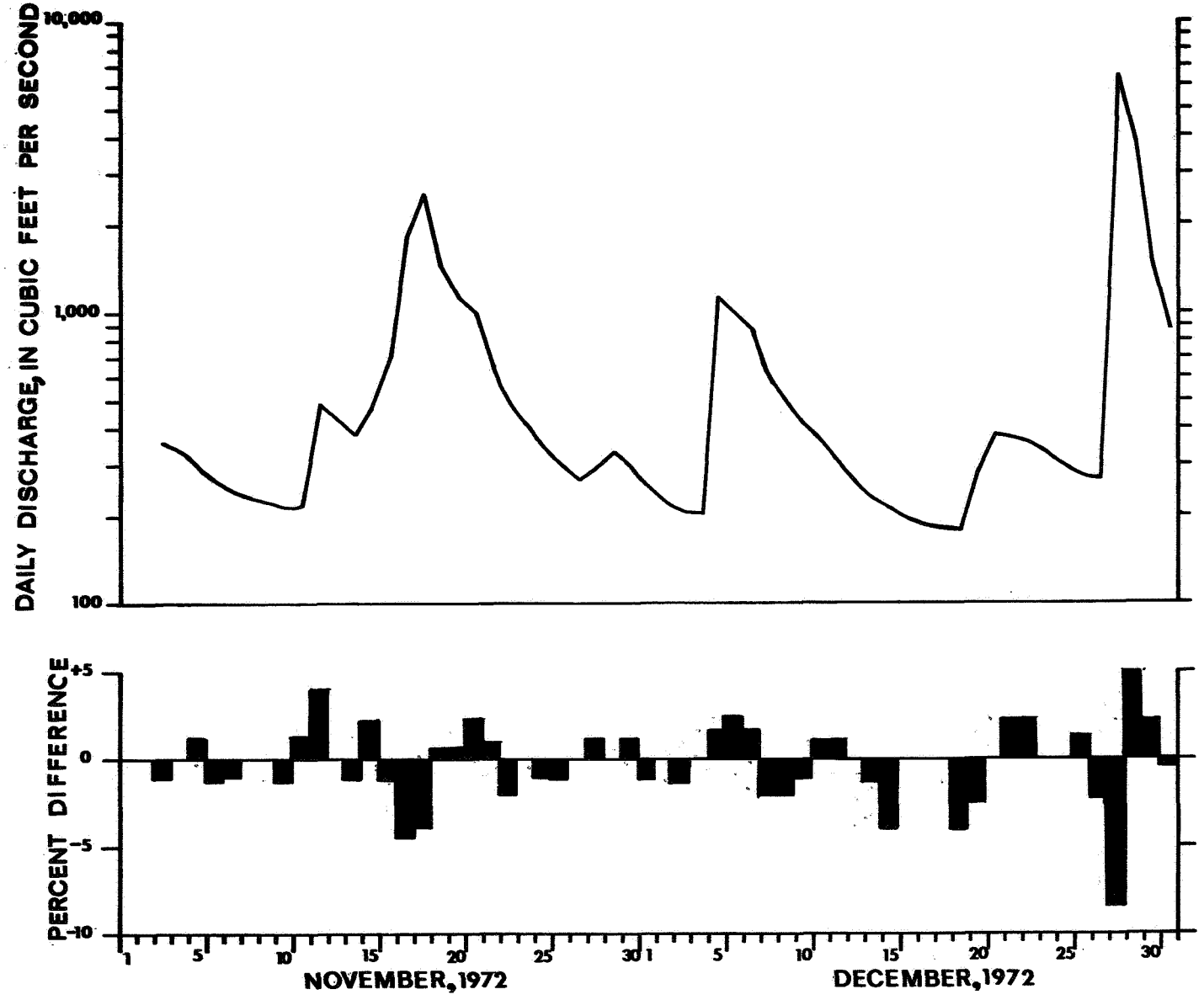


FIGURE 3.—MEAN DAILY DISCHARGE IN VERDE RIVER NEAR CAMP VERDE, ARIZONA

of stable or slowly changing flow conditions, daily mean flow rates computed from the DCS data agreed within ±5 percent of those computed from the digital recorder data. During the period of high flow in late December 1972, daily mean flow rates computed from the DCS data agreed with those computed from the digital recorder data within ±10 percent. This preliminary comparison indicates the DCS system furnished data sufficient to accurately compute daily mean streamflow rates during the first two-month period of operation at this site. However, a longer period of record is necessary to adequately evaluate the capability of the system to furnish accurate streamflow data.

The digital-parallel DCS data has furnished useful information during peak-flow conditions. Late in the afternoon of Feb. 21, 1973, the USGS was requested by the Salt River Valley Water Users' Association to furnish streamflow information on the Verde River near Camp Verde on an emergency basis. Water stored in the Verde River reservoirs had reached about 95 percent of capacity (20,000 acre-feet of available storage) as a result of runoff from a general rain over most of the watershed during the previous 24-hour period and it had become necessary to release water. The immediate problem was to determine the amount of runoff that was coming from the upper snow covered portion of the watershed in order to determine the minimum rate of release from the reservoirs that would maintain the minimum available storage capacity considered essential to provide some protection from major flood damage downstream.

The latest reading from the DCS equipped gage on the Verde River near Camp Verde was requested from the Goddard Space Flight Center (GSFC) by telephone at 1630 hours MST (Mountain Standard Time) and it indicated the flow had been approximately 400 cfs at 1227 hours MST. The next available data from this station was requested on a high priority basis by the USGS. At 2219 hours MST the next readings from the station were received by GSFC and were provided to the USGS at 2240 hours MST by telephone. These data indicated the approximate streamflow rate had increased to only about 500 cfs and this information was furnished to the Salt River Valley Water Users' Association at 2245 hours MST. The DCS had in fact furnished near-real time information - 26 minutes receipt by the satellite to delivery to the user - that indicated the snowpack was not melting at a rapid rate and releases from the reservoir could be made accordingly. DCS data received the following morning confirmed this interpretation. Although some road crossings in the Phoenix area were closed by the released water, the data

furnished the USGS by the DCS provided key information that helped water management minimize the amount of inconvenience caused by the necessary release of water while still maintaining a minimum safe margin of available reservoir storage to protect against major flooding. The serial-digital DCS capability, currently under development for transmitting streamflow data, should provide data of greater utility for determining times of flood peaks and the rate of change of streamflow.

SUMMARY AND CONCLUSIONS

The digital-parallel gage height data received from the USGS Verde River gage near Camp Verde, Arizona furnished information sufficient to accurately compute daily mean streamflow rates during the first two months of operation. However a longer period of record is necessary to adequately evaluate the capability of the DCS to furnish accurate streamflow data.

The DCS is capable of furnishing near real-time information on streamflow. On Feb. 21, 1973, the USGS was able to furnish streamflow information to aid in the operation of multiple-use reservoirs on the Verde River, within 26 minutes from the time of transmission, by means of the ERTS-1 DCS. The serial-digital capability for transmitting streamflow data by the DCS is currently under development, and should provide near real-time data of greater utility for determining time of flood peaks and rates of change of streamflow.

Paper W 9

PRELIMINARY ANALYSIS OF ERTS-RELAYED WATER-RESOURCES DATA IN THE DELAWARE RIVER BASIN[1]

Richard W. Paulson, *U. S. Geological Survey, Harrisburg, Pennsylvania 17108*

ABSTRACT

Preliminary analysis of ERTS-DCS data from water-resources stations in the Delaware River basin indicates that the Data-Collection System is performing well. Data-Collection Platforms have been successfully interfaced with five stream-gaging stations and three ground-water observation wells and are being interfaced with 12 water-quality monitors in the basin. Data are being relayed during four or five ERTS orbital passes per day, which is within the design specifications of the ERTS-DCS.

1. INTRODUCTION

This paper is a brief progress report on research being conducted for the Earth Resources Technology Satellite (ERTS) project, "Near Real Time Water Resources Data for River Basin Management," Goddard Space Flight Center identification (GSFC ID) IN 340, and on research being conducted by the Pennsylvania District, Water Resources Division (WRD), U.S. Geological Survey, to test the ERTS Data Collection System (DCS) on water resources sites in the Susquehanna River basin. A major objective of this research is to "... determine whether standard operational water resources (field) instrumentation can be interfaced successfully with DCS platforms and the data made to flow operationally to data users.", as stated in the proposal to perform the ERTS project. Real progress has been made to meet this objective; progress which indicates DCS has a great potential for managing existing field instrumented stations in the U.S. Geological Survey's Hydrologic Data Network and for monitoring water resources for management and flood warning.

The progress that has been made now permits the preparation and release, on a daily basis, of a water-resources summary of the form of the teletype release shown in Figure 1. The summary is produced from computer-processed DCS data from the Delaware River basin.

1/ Approved for publication by the Director, U. S. Geological Survey

DEL-RIV-RA-COM
TO DRBC
FM USGS HBG
ATTN: P. GOODELL

EROS-NASA
USGS DELAWARE RIVER BASIN-DATA COLLECTION SYSTEM EXPERIMENT
WATER RESOURCES SUMMARY
FEBRUARY 23, 1973

WATER QUALITY STATIONS

TIME	S.C. UMHOS	D.O. MG/L	TEMP F/C	PH
DELAWARE RIVER AT REEDY ISLAND				
12:42:55EST, FEBRUARY 22,1973	3720	12.2	35/ 1.5	6.8
20:52:36EST, FEBRUARY 22,1973	5360	12.6	35/ 1.5	7.1
21: 2: 0EST, FEBRUARY 22,1973	3120	12.6	35/ 1.5	6.9
22:39:15EST, FEBRUARY 22,1973	3400	12.5	35/ 1.5	6.9
9:27: 5EST, FEBRUARY 23,1973	5760	12.8	35/ 1.5	7.1
11: 9:26EST, FEBRUARY 23,1973	3160	12.4	36/ 2.0	7.0
DELAWARE RIVER AT CHESTER				
20:53:40EST, FEBRUARY 22,1973	260	9.2	39/ 4.0	6.8
21: 0:21EST, FEBRUARY 22,1973	264	9.4	40/ 4.5	6.8
9:25:19EST, FEBRUARY 23,1973	260	9.1	40/ 4.5	6.8
9:32: 7EST, FEBRUARY 23,1973	260	9.4	39/ 4.0	6.8
11: 6:40EST, FEBRUARY 23,1973	264	9.3	40/ 4.5	6.8

SURFACE WATER STATIONS

TIME	GAGE HEIGHT FEET	DISCHARGE CFS
DELAWARE RIVER AT MONTAGUE		
20:52:19EST, FEBRUARY 22,1973	5.61	3100
21: 0:14EST, FEBRUARY 22,1973	5.65	3190
22:40:44EST, FEBRUARY 22,1973	6.00	3980
9:24:59EST, FEBRUARY 23,1973	6.03	4060
11: 7:52EST, FEBRUARY 23,1973	5.91	3760
11:14:57EST, FEBRUARY 23,1973	5.88	3690
DELAWARE RIVER BELOW TOCKS ISLAND		
20:54:46EST, FEBRUARY 22,1973	5.92	3360
21: 1:50EST, FEBRUARY 22,1973	5.91	3330
9:24:57EST, FEBRUARY 23,1973	6.01	3630
DELAWARE RIVER AT TRENTON		
20:57:20EST, FEBRUARY 22,1973	9.69	9890
9:26:54EST, FEBRUARY 23,1973	9.77	10300
11: 7: 9EST, FEBRUARY 23,1973	9.77	10300
LEHIGH RIVER AT BETHLEHEM		
20:54:57EST, FEBRUARY 22,1973	3.20	1520
22:39:43EST, FEBRUARY 22,1973	3.20	1520
9:27:59EST, FEBRUARY 23,1973	3.19	1510
11: 7:15EST, FEBRUARY 23,1973	3.18	1500
SCHUYLKILL RIVER AT PHILA.		
20:52: 3EST, FEBRUARY 22,1973	6.40	2400
22:44:12EST, FEBRUARY 22,1973	6.40	2400
9:24:15EST, FEBRUARY 23,1973	6.40	2400
11: 7:57EST, FEBRUARY 23,1973	6.40	2400

GROUND WATER STATIONS

TIME	WELL DEPTH FEET
SALEM CITY NUMBER 1	
20:55:57EST, FEBRUARY 22,1973	23.31
20:59: 7EST, FEBRUARY 22,1973	23.33
9:26:48EST, FEBRUARY 23,1973	23.33
11: 7:36EST, FEBRUARY 23,1973	23.36
PENNS GROVE NUMBER 24	
12:43:21EST, FEBRUARY 22,1973	18.01
20:51:41EST, FEBRUARY 22,1973	18.05
22:35:28EST, FEBRUARY 22,1973	18.06
9:25:36EST, FEBRUARY 23,1973	18.10
11: 9: 6EST, FEBRUARY 23,1973	18.10
SHELL CHEM. CO. NUMBER 5	
20:54:15EST, FEBRUARY 22,1973	36.06
22:35:55EST, FEBRUARY 22,1973	36.00
22:43:12EST, FEBRUARY 22,1973	36.14
9:22:46EST, FEBRUARY 23,1973	35.89
11: 8: 0EST, FEBRUARY 23,1973	36.05

THESE DATA WERE RELAYED BY THE ERTS OBSERVATORY AND ARE PROVISIONAL.
THE SYMBOLS -- INDICATE DATA WERE SUSPECT AND WERE DELETED. THIS
SUMMARY WAS PREPARED BY THE CURRENT RECORDS CENTER IN PHILADELPHIA
USING REMOTE TERMINAL ACCESS TO THE GEOLOGICAL SURVEYS 360/65
COMPUTER IN WASHINGTON, D.C. CALL 215-597 7357 FOR FURTHER
INFORMATION.

END OF SUMMARY

DEL-RIV-RA-COM

Figure 1 - Daily water-resources summary of conditions in the Delaware River basin, compiled from ERTS Data Collection Platform data.

This processing is done in near-real time, which means that the data usually are processed and released to water-resources agencies within a few hours of the time of acquisition from an ERTS orbital pass over eastern North America. The daily summary (Figure 1) also allows the Geological Survey to monitor the performance of field instrumentation, and therefore provides the potential for more efficient management of the operation of the instruments. The summary also provides water-resources agencies with the status of water resources over a large geographical area. The research described herein is providing the Pennsylvania district with the learning experience of simulating an operational data-relay system, an experience that is a prerequisite to operational data-relay systems.

2. DELAWARE RIVER BASIN RESEARCH

Twenty Data Collection Platforms (DCP) are being installed on water-resources stations in the Delaware River basin for the project, "Near Real Time Water Resources Data for River Basin Management." These stations, and many others in the basin, are operated by the Geological Survey in cooperation with several Federal, State, and local agencies. The water-resources stations that are being instrumented with ERTS DCP's have been chosen cooperatively by members of the staff of the Delaware River Basin Commission (DRBC) and by the principal investigator. The DRBC is a regional water-resources management agency that was created by the Delaware River Basin Compact, a public law adopted by the United States of America, and the States of Pennsylvania, New York, New Jersey, and Delaware. The Compact requires the DRBC to adopt and maintain a Comprehensive Plan for the conservation and development of water resources in the basin. The water-resources stations chosen for the ERTS project include stream gages, ground-water observation wells, and water-quality monitors. DCS data from these stations can keep the DRBC, and other water-resources agencies, informed on the status of streamflow and water quality at key surface-water locations in the basin, and on the status of ground-water levels in coastal plain aquifers. The DCP locations are shown on the sketch map in Figure 2. The DCP's monitor streamflow at key points in the basin and monitor water quality in the Delaware River and in the estuary.

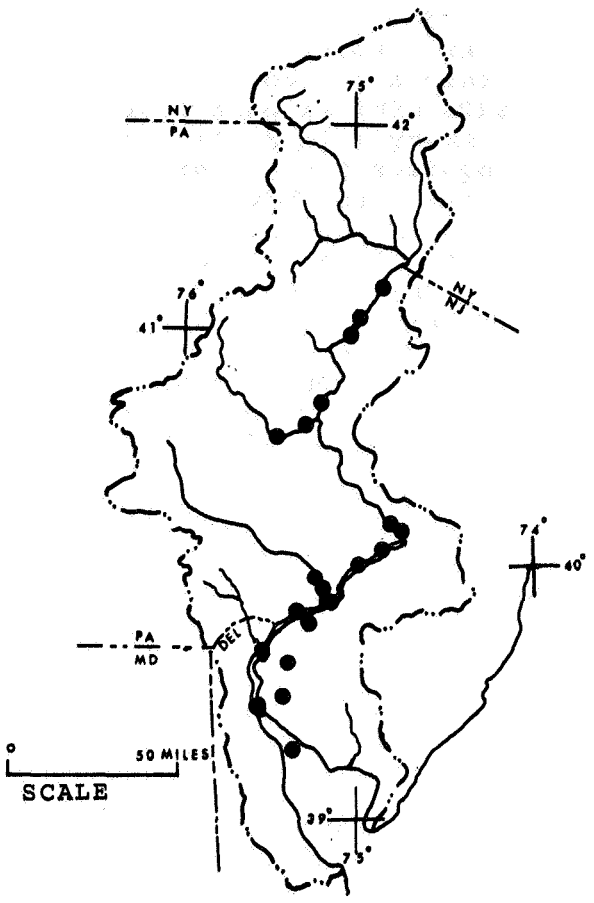


Figure 2 - Map showing locations of ERTS DCP's in the Delaware River Basin.

3. SUSQUEHANNA RIVER BASIN RESEARCH

As a reaction to the June 1972 record flood of Hurricane Agnes, which caused the loss of human life and billions of dollars in property damage, the Pennsylvania District of the Geological Survey's Water Resources Division is field installing four DCP's on stream gages in the Susquehanna River basin. The main purpose of these installations is to test DCP's ability to gather basic data that could be used for monitoring streamflow and for flood forecasing in the basin. During the flood, conventional communications with many key gaging stations were lost, although in most cases the station continued to function. Even though the ERTS-DCS only provides data during the 8-12 o'clock time frames in the morning and evening, battery operated DCP's probably would have worked well and provided very useful data from many of the stations that were out of communication.

Two of the DCP's being installed were provided to the Pennsylvania district by the ERTS project, "Susquehanna River Basin Study Using ERTS-A Data," GSFC ID UN 159. The remaining two DCP's have been provided to the district by the Department of the Interior's EROS Program. The installation, maintenance, and data processing from the platforms are being conducted by the district in cooperation with the Susquehanna River Basin Commission (SRBC), which has a role in the Susquehanna River basin analogous to the DRBS's role in the contiguous Delaware River basin. The location of the DCP's being installed in the Susquehanna River basin is shown in the map of Figure 3.

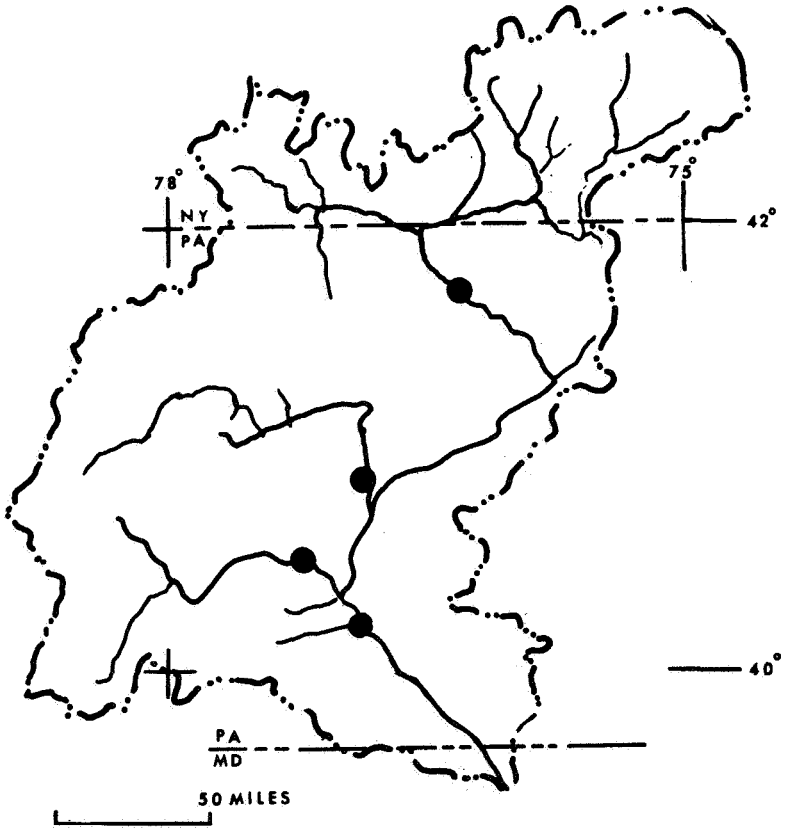


Figure 3 - Map showing locations of DCP's in the Susquehanna River basin.

4. STATUS OF DATA COLLECTION PLATFORMS

Antennas for 19 of the 20 DCP's to be installed in the Delaware River basin have been installed and the platforms successfully field tested. The 20th location has been temporarily delayed by a major renovation of the site, a Coast Guard lighthouse on an island in Delaware Bay. The DCP will be installed in the spring when construction at the site has been finished, and when the weather conditions ameliorate to make the site less hazardous to access. Three of the four DCP's have been installed on stream gages in the Susquehanna River basin. The temporary unavailability of interface equipment has prevented the fourth site from being completely instrumented. In both basins we have been very successful in installing and operating all of the stream gages and ground-water observation wells. There has been a problem in successfully interfacing many of the water-quality monitors to the DCP's. More often than not, the problems have been found to be in the water-quality monitors themselves, which always have been troublesome devices, occasionally in the interface equipment, but not in the DCP's. Several of the water-quality monitors have been successfully interfaced and operated. In particular, the DCP and water-quality monitor at Reedy Island, Delaware, an isolated island in the southern part of the Delaware River estuary, has operated almost flawlessly from early in the ERTS experiment.

The 24 DCP sites, shown in Figures 2 and 3, are providing a test of the DCP's under a wide range of environmental conditions. Two DCP's are on islands in the Delaware River estuary, where visibility of the sky is virtually unobstructed and where communication with the satellite is excellent. Another DCP is directly underneath one of the spans of the Delaware Memorial Bridge. The bridge roadway is about 150 feet above the antenna and obstructs a swath of the sky that lies directly overhead, and extends in each direction in approximately an east-west orientation. Much of the western sky also is blocked out by the support tower of one of the bridges. Yet despite these obstructions, communications with ERTS by this DCP has been excellent, although occasionally one finds a 6-minute gap between two data transmissions during a pass; the hiatus undoubtedly caused by ERTS being obscured by the bridge structure at the time of one DCP transmission. Several DCP's are located in urban environments around Philadelphia and Easton, Pennsylvania, and the DCS is working well within the one-transmission-per-12-hour period specification of the system. Several DCP's

in the more remote areas of the Pocono mountains are also working well within the specifications of the system, but because they lie in river valleys surrounded by mountains of modest elevation, some of the passes are lost when ERTS is low on the horizon. Despite these constraints, we have not had to change the transmission frequency to 90 seconds from 180 seconds to acquire the data.

The one environmental condition we will have to meet in Pennsylvania, that we have not been able to test to date, is heavy snowfall. Presumably, the DCP will become ineffective with a significant accumulation of wet snow upon the antenna. It is anticipated that we may have to place hemispherical domes over the antennas to discourage snow accumulation. However, we may have to rely on the experience of other experiments if the winter of 1972-73 continues to deny us this test.

There have been very few failures of the DCP's themselves. Three of the DCP's were returned to the U.S. Geological Survey's ERTS-DCP depot facility at the Mississippi Test Facility for maintenance when they ceased operating. They were made operational again by the replacement of either the transmitter card or the programer card. The performance of the DCP's to date has exceeded our expectations. A longer environmental test should be provided to verify this performance rate.

Approximately half of the DCP's operate in locations where there is electrical line power and at these locations, line power stepped down through a transformer, has been used to operate the platform. Characteristically there is line power at water-quality monitor locations and at some gaging stations. Ultimately, at these locations, we expect to configure the DCP's to operate on line power with standby battery power. The utility in having the platform operating, even though the water-resources monitor is not, is that we can detect the failure rapidly. The rest of the platforms are operating on four 6-volt dry cell batteries each in series. Several of the DCP's have been operating more than four months on their original set of batteries. These platforms also seem to be working well in areas where winter temperatures frequently are well below freezing, temperatures at which battery efficiency becomes low. Our plan is to allow the DCP's to operate with these batteries until they begin to fail from insufficient power, as a determination of nominal battery efficiency.

Our apprehension about the potential for vandalism at the sites, and of the antennas in particular, prompted us to go to some length in making the installations as secure and as unobtrusive as possible. In every location the DCP itself is well protected inside either a field structure, such as a 4-foot square gage house, or inside an institutional structure, such as a municipal water purification plant. In a few cases, we were able to install the antenna inside the structure too. The only constraint on this procedure is that the roof of the structure must not contain any significant amount of reinforcing steel which may ground the signal. Also, the shelter must be large enough to contain the 46-inch diameter antenna. We are considering trimming a few inches off the diameter of one of the antennas at a station, where it could not fit the gage house, as a test of the over design of the antenna relative to the actual DCP transmitter power.

Where the antenna is mounted on the exterior of the shelter, the antenna usually is painted to blend in more unobtrusively with the surroundings. To date no significant vandalism has occurred. This is due in part to measures we have taken to install the sites as securely as possible, but the suspicion that we have been lucky lingers on.

5. NEAR-REAL-TIME DATA PROCESSING

The following is a discussion of our data processing procedure for near-real-time processing of ERTS-DCS data from the Delaware River basin. The software being written for implementing the Susquehanna River basin DCP data parallels the software presently operational for the Delaware basin activities. When the software for each basin is operational, the programs will probably be concatenated to allow all the DCS data to be processed together. The timeliness of the data processing is constrained by the orbital characteristics of the ERTS satellite and by the configuration of our processing system.

ERTS-DCS specifications state that there be a very high probability that at least one message per 12-hour period will be received from each operating DCP. This specification is being met. Nominally, of the approximately 14 daily polar orbits ERTS makes each day, data are successfully relayed from Delaware River basin DCP's during four or five of the daily ERTS orbital passes.

Data are usually relayed during two or three passes between 8:00 a.m. to 12 noon eastern standard time (1300 to 1700 Greenwich Mean Time), and during two or three passes between 8:00 p.m. and 12 midnight (0100 to 0500 GMT). The opportunity for relaying data during the morning occurs as ERTS makes passes in a generally north to south direction over the western Atlantic to the central North America area. The evening opportunity occurs when ERTS passes are made in a generally south to north direction over the same area. More often than not we get two good passes, in a data relay sense, during each period; a third pass, if we get it, generally only picks up one to four of the DCP's. The third pass generally puts ERTS very close to the horizon and the period of radio visibility lasts a minute or two compared to the 10 or 15 minute-period of the better passes.

Within one ERTS orbital period (103 minutes) of the time DCP data are relayed during a pass and received at the NASA Data Processing Facility (NDPF), the data are forwarded to the Pennsylvania district by NASA teletype. Figure 4 is an example of the format of the teletyped data. The information on the teletype is in a different format than, and is a subset of, the information that is punched on cards at the NDPF, and forwarded to users at a more leisurely rate through the mail. The card format can be found in the ERTS Data Users Handbook. The only additional information found in the teletype listing that is not found in the card format is the item labeled CS at the end of a data line. It is a checksum value, which is used to verify the data in the eight octal data words labeled D1-D8. The checksum value is the units value of the octal sum of the individual octal characters in the field from the columns labeled C (message quality) to D8. It is provided to help detect teletype transmission errors which, in our experience, have been found to be very rare. Note that the data messages are being relayed by the DCS at about 3-minute intervals during a pass (Columns MM and SS specify number and seconds, respectively). Normally the data messages received from a DCP during any one period of mutual visibility are generally, but not always, the same. Our procedure is to process only one of the several identical messages, since only time is different from one message to the next.

```
CZAOOSA
PP CZAA
DE CERS 0520
25/1531Z

REF ERTS DCS
 ATT R PAULSON USGS HARRISBG PHONE  717 782 3420

 S  Y DDDHHMM SS    PID   C   D1   D2   D3   D4   D5   D6   D7   D8  CS

 N  3  2515102 19   6030  7  377  377  166  257  367  255  227  326   6
 N  3  2515105 26   6030  7  377  377  166  257  367  255  227  326   6
 N  3  2515108 33   6030  7  377  377  166  257  367  255  227  326   6
 N  3  2515111 40   6030  7  377  377  166  257  367  255  227  326   6

 N  3  2515103 24   6046  7   73  365  377  377  377  377  377  377   5
 N  3  2515106 33   6046  7   73  365  377  377  377  377  377  377   5
 N  3  2515109 42   6046  7   73  365  377  377  377  377  377  377   5
 N  3  2515112 51   6046  7   73  365  377  377  377  377  377  377   5

 N  3  2515102 32   6067  7  377  377  275  372  331  373  337  327   0
 N  3  2515109 27   6067  7  377  377  275  372  327  373  377  327   1
 N  3  2515112 41   6067  7  377  377  275  372  327  373  377  327   1

 N  3  2515103 24   6114  7  377  377  173  151  374  232  211  310   0
 N  3  2515106 28   6114  7  377  377  173  151  374  232  211  310   0
 N  3  2515109 31   6114  7  377  377  173  151  374  232  211  310   0
 N  3  2515112 35   6114  7  377  377  173  151  374  232  211  310   0

 N  3  2515102 09   6115  7  237   21  377  377  377  377  377  377   4
 N  3  2515105 36   6115  7  237   21  377  377  377  377  377  377   4
 N  3  2515109 03   6115  7  237   21  377  377  377  377  377  377   4
 N  3  2515112 30   6115  7  237   21  377  377  377  377  377  377   4

 N  3  2515103 41   6116  7   37  231  377  377  377  377  377  377   5
 N  3  2515107 15   6116  7   37  231  377  377  377  377  377  377   5
 N  3  2515110 44   6116  7   37  231  377  377  377  377  377  377   5

 NO MESSAGES        6124

 N  3  2515101 13   6215  7  373  177  377  377  377  377  377  377   1
 N  3  2515104 32   6215  7  373  177  377  377  377  377  377  377   1
 N  3  2515107 51   6215  7  373  177  377  377  377  377  377  377   1
 N  3  2515111 10   6215  7  373  177  377  377  377  377  377  377   1

 N  3  2515103 37   6223  7   37  156  377  377  377  377  377  377   3
 N  3  2515107 11   6223  7   37   36  377  377  377  377  377  377   0
 N  3  2515110 46   6223  7   37   36  377  377  377  377  377  377   0

 N  3  2515103 53   6227  7  337  333  377  377  377  377  377  377   3
 N  3  2515107 00   6227  7  337  333  377  377  377  377  377  377   3
 N  3  2515110 06   6227  7  337  333  377  377  377  377  377  377   3

 NO MESSAGES        6275

 N  3  2515105 16   6277  7  167   63  377  377  377  377  377  377   4
 N  3  2515108 29   6277  7  167   63  377  377  377  377  377  377   4
 N  3  2515111 41   6277  7  167   63  377  377  377  377  377  377   4

 N  3  2515105 09   6306  7  377  377  377  377  377  377  377  377   7
 N  3  2515108 11   6306  7  377  377  377  377  377  377  377  377   7
 N  3  2515111 13   6306  7  377  377  377  377  377  377  377  377   7

 N  3  2515103 19   6312  7  377  377  377  377  377  377  377  377   7
 N  3  2515106 29   6312  7  377  377  377  377  377  377  377  377   7
 N  3  2515109 39   6312  7  377  377  377  377  377  377  377  377   7
 N  3  2515112 50   6312  7  377  377  377  377  377  377  377  377   7

 N  3  2515104 16   6322  7  223  146  377  377  377  377  377  377   7
 N  3  2515107 52   6322  7  223  146  377  377  377  377  377  377   7
 N  3  2515111 29   6322  7  223  146  377  377  377  377  377  377   7

 N  3  2515104 41   6331  7  377  377  377  377  377  377  377  377   7
 N  3  2515107 42   6331  7  377  377  377  377  377  377  377  377   7
 N  3  2515110 43   6331  7  377  377  377  377  377  377  377  377   7

 N  3  2515102 32   6332  7  377  377  147  231  353  333  317  275   0
 N  3  2515105 54   6332  7  377  377  147  231  353  333  317  275   0
 N  3  2515109 15   6332  7  377  377  147  171  323  333  317  275   3
```

Figure 4 - Portions of teletype listing of Delaware River basin DCP data received from NASA Data Processing Facility at Goddard Space Flight Center. The data are from one ERTS pass.

These data are processed by the Pennsylvania district using remote terminal access to the Geological Survey's 360/65 computer in Washington, D.C. There is an advantage to using this system rather than a small stand-alone computer; the advantage is that computer algorithms developed by our experiment, with little or no modification, can be and have been made available to others in the USGS system. The one disadvantage is that our jobs must wait in queue to be executed. Nominally our turnaround time is under 2 hours, although, when the system goes down, it can be significantly longer. For a truly operational system, a stand-alone computer capable of remotely accessing the national system would be required.

The job output from the computer is partitioned by the software into two parts, one is for inhouse consumption and the other (see Figure 1) is for release to other agencies. The software performs several manipulations to the data. These include associating the DCP identification number with a particular water-resources station, correcting temporal information from the annual day number and Greenwich Mean Time to calendar day and Eastern Standard Time, and a rather involved manipulation of the actual platform data. For our particular application the manipulation includes breaking down the octal or hexidecimal data to 64 bits, inverting the bits (interchanging 0's to 1's), reordering the eight sets of eight bit data words, and then extracting the decimal values actually made available to the DCP's in the field by our water-resources instruments. For water-quality monitors, these values are converted to the several water-quality parameters in the proper engineering units. For stream gages, stream stage is extracted, which is used by the software to compute streamflow from rating tables, one of which is available for each station. For ground-water observation wells, well-water level is extracted.

Much of this information is put on the printed output as the data are processed and summarized. Figures 5, 6, and 7 are examples of the output provided. These summaries help field technicians monitor the performance of the platforms and help them ascertain which stations require field maintenance or repair. These summaries also help data processing personnel choose which platforms and stations are working well enough to permit the data to be processed for the summary of Figure 1.

LIST OF PARITY PASSED DATA

PRODUCT REQUEST	USER ID	PLAT ID	SAT ID	TIME YR	DAY	HR	MIN	SEC	RS ID	ERROR FLAG	MSG QUAL	DATA FORM	DATA BITS	QUALITY BITS	
SC	I340	6114	1	3	53	17	42	55	G	0	7	H	FFFF7669F6C9EFCA	FFFFFFFFFFFFFFFF	
SC	I340	6215	1	3	53	17	43	21	G	0	7	H	E77FFFFFFFFFFFFF	FFFFFFFFFFFFFFFF	
SC	I340	6030	1	3	54	1	54	27	N	0	7	H	FFFF00F2000021FF	FFFFFFFFFFFFFFFF	*
SC	I340	6046	1	3	54	1	55	57	N	0	7	H	3B73FFFFFFFFFFFF	FFFFFFFFFFFFFFFF	
SC	I340	6046	1	3	54	1	59	7	N	0	7	H	3B33FFFFFFFFFFFF	FFFFFFFFFFFFFFFF	
SC	I340	6067	1	3	54	1	51	48	N	0	7	H	FFFF8FF998F9BF9B	FFFFFFFFFFFFFFFF	*
SC	I340	6114	1	3	54	1	52	36	N	0	7	H	FFFFE6A8ECB9CBCA	FFFFFFFFFFFFFFFF	
SC	I340	6114	1	3	54	2	2	0	N	0	7	H	FFFF6DA9F879CBCA	FFFFFFFFFFFFFFFF	
SC	I340	6115	1	3	54	1	52	3	N	0	7	H	9FFDFFFFFFFFFFFF	FFFFFFFFFFFFFFFF	
SC	I340	6116	1	3	54	1	53	19	N	0	7	H	5F79FFFFFFFFFFFF	FFFFFFFFFFFFFFFF	
SC	I340	6116	1	3	54	2	0	14	N	0	7	H	5F59FFFFFFFFFFFF	FFFFFFFFFFFFFFFF	
SC	I340	6215	1	3	54	1	51	41	N	0	7	H	E75FFFFFFFFFFFFF	FFFFFFFFFFFFFFFF	
SC	I340	6223	1	3	54	1	54	46	N	0	7	H	5FB6FFFFFFFFFFFF	FFFFFFFFFFFFFFFF	
SC	I340	6223	1	3	54	2	1	50	N	0	7	H	5F76FFFFFFFFFFFF	FFFFFFFFFFFFFFFF	
SC	I340	6227	1	3	54	1	54	57	N	0	7	H	3FFBFFFFFFFFFFFF	FFFFFFFFFFFFFFFF	
SC	I340	6275	1	3	54	1	57	46	N	0	7	H	FFFF8C78DD797DC7	FFFFFFFFFFFFFFFF	*
SC	I340	6277	1	3	54	1	57	20	N	0	7	H	6F69FFFFFFFFFFFF	FFFFFFFFFFFFFFFF	
SC	I340	6306	1	3	54	1	57	29	N	0	7	H	FFFFFFFFFFFFFFFF	FFFFFFFFFFFFFFFF	*
SC	I340	6312	1	3	54	1	53	46	N	0	7	H	FFFFFFFFFFFFFFFF	FFFFFFFFFFFFFFFF	*
SC	I340	6322	1	3	54	1	54	15	N	0	7	H	939FFFFFFFFFFFFF	FFFFFFFFFFFFFFFF	
SC	I340	6331	1	3	54	1	56	54	N	0	7	H	FFFFFFFFFFFFFFFF	FFFFFFFFFFFFFFFF	*
SC	I340	6332	1	3	54	1	53	40	N	0	7	H	FFFF7B79ECFB9DC6	FFFFFFFFFFFFFFFF	
SC	I340	6332	1	3	54	2	0	21	N	0	7	H	FFFF7B99ECDB8FBF	FFFFFFFFFFFFFFFF	
SC	I340	6073	1	3	54	1	54	45	N	0	7	H	3F39FFFFFFFFFFFF	FFFFFFFFFFFFFFFF	*
SC	I340	6402	1	3	54	1	53	56	N	0	7	H	DFBEFFFFFFFFFFFF	FFFFFFFFFFFFFFFF	*

Figure 5 - Raw data converted to the standard DCS card format from the teletype format provided by NDPF.

DETAILED CHECK OF EACH PARITY PASSED MESSAGE FOLLOWS

TIME OF MESSAGE RECEPTION AT NDPF	PRODUCT REQUEST	USER ID	PLAT ID	SAT ID	TIME YR	TIME DAY	TIME HR	TIME MIN	TIME SEC	RS ID	ERROR FLAG	MSG QUAL	DATA FORM	DATA /QUALITY
12:42:55EST, FEBRUARY 22,1973	SC	I340	6114	1	3	53	17	42	55	G	0	7	H	FFFF7669F6C9EFCA ORIGINAL 0000899609361035 FFFFFFEFFFFFFFFF QUALITY
20:52:36EST, FEBRUARY 22,1973	SC	I340	6114	1	3	54	1	52	36	N	0	7	H	FFFFE6A8ECB9CBCA ORIGINAL 0000195713463435 FFFFFFFFFFFFFFFF QUALITY
21: 2: 0EST, FEBRUARY 22,1973	SC	I340	6114	1	3	54	2	2	0	N	0	7	H	FFFF6DA9F8T9CBCA ORIGINAL 0000925607863435 FFFFFFFFFFFFFFFF QUALITY
22:39:15EST, FEBRUARY 22,1973	SC	I340	6114	1	3	54	3	39	15	G	0	7	H	FFFF6EA9F7A9DACA ORIGINAL 0000915608562535 FFFFFFFFFFFFFFFF QUALITY
9:27: 5EST, FEBRUARY 23,1973	SC	I340	6114	1	3	54	14	27	5	N	0	7	H	FFFFE6F8EBB9BDCA ORIGINAL 0000190714464235 FFFFFFFFFFFFFFFF QUALITY
11: 9:26EST, FEBRUARY 23,1973	SC	I340	6114	1	3	54	16	9	26	N	0	7	H	FFFFF8C8F869DEC9 ORIGINAL 0000073707962136 FFFFFFFFFFFFFFFF QUALITY
20:51:48EST, FEBRUARY 22,1973	SC	I340	6067	1	3	54	1	51	48	N	0	7	H	FFFFBFF99BF9BF9B ORIGINAL 0000400664064064 FFFFFFFFFFFFFFFF *QUALITY
22:46:18EST, FEBRUARY 22,1973	SC	I340	6067	1	3	54	3	46	18	G	0	7	H	FFFF9FFBB9FB9FB9 ORIGINAL 0000600446046046 FFFFFFFFFFFFFFFF *QUALITY
9:22:59EST, FEBRUARY 23,1973	SC	I340	6067	1	3	54	14	22	59	N	0	7	H	FFFFBFF99BF9BF9B ORIGINAL 0000400664064064 FFFFFFFFFFFFFFFF *QUALITY
11:11:12EST, FEBRUARY 23,1973	SC	I340	6067	1	3	54	16	11	12	N	0	7	H	FFFFBFF99BF9BF9B ORIGINAL 0000400664064064 FFFFFFFFFFFFFFFF *QUALITY
20:53:40EST, FEBRUARY 22,1973	SC	I340	6332	1	3	54	1	53	40	N	0	7	H	FFFF7B79ECFB9DC6 ORIGINAL 0000848613046239 FFFFFFFFFFFFFFFF QUALITY
21: 0:21EST, FEBRUARY 22,1973	SC	I340	6332	1	3	54	2	0	21	N	0	7	H	FFFF7B99ECDB8F8F ORIGINAL 0000846613247040 FFFFFFFFFFFFFFFF QUALITY

Figure 6 - Partially reduced data, including a conversion of temporal data and a partial inversion of data bits.

EROS-NASA
USGS DELAWARE RIVER BASIN-DATA COLLECTION SYSTEM EXPERIMENT
FEBRUARY 23, 1973
RAW DATA SUMMARY

TIME	GAGE/ WELL	S.C.	D.O.	TEMP	PH
SHIP JOHN SHOAL LIGHTHOUSE					
PLATFORM ID NO.= 1					
***ERTS PLATFORM IS NOT INSTALLED AT THIS STATION ***					
DELAWARE RIVER AT REEDY ISLAND					
PLATFORM ID NO.=6114					
12:42:55EST, FEBRUARY 22,1973	0000	093	610	359	689
20:52:36EST, FEBRUARY 22,1973	0000	134	634	355	719
21: 2: 0EST, FEBRUARY 22,1973	0000	078	634	355	692
22:39:15EST, FEBRUARY 22,1973	0000	085	625	355	691
9:27: 5EST, FEBRUARY 23,1973	0000	144	642	350	719
11: 9:26EST, FEBRUARY 23,1973	0000	079	621	363	707
DELAWARE RIVER AT DEL. MEM. BR.					
PLATFORM ID NO.=6067					
20:51:48EST, FEBRUARY 22,1973	0000	640	640	640	640
22:46:18EST, FEBRUARY 22,1973	0000	460	460	460	460
9:22:59EST, FEBRUARY 23,1973	0000	640	640	640	640
11:11:12EST, FEBRUARY 23,1973	0000	640	640	640	640
DELAWARE RIVER AT CHESTER					
PLATFORM ID NO.=6332					
20:53:40EST, FEBRUARY 22,1973	0000	130	462	398	684
21: 0:21EST, FEBRUARY 22,1973	0000	132	470	406	684
9:25:19EST, FEBRUARY 23,1973	0000	130	456	400	684
9:32: 7EST, FEBRUARY 23,1973	0000	130	472	398	688
11: 6:40EST, FEBRUARY 23,1973	0000	132	468	400	686
DELAWARE RIVER AT PIER 11,PHILA.					
PLATFORM ID NO.= 5					
***ERTS PLATFORM IS NOT INSTALLED AT THIS STATION ***					
DELAWARE RIVER AT TORRESDALE					
PLATFORM ID NO.=6331					
20:56:54EST, FEBRUARY 22,1973	0000	000	000	000	000
9:27:30EST, FEBRUARY 23,1973	0000	000	000	000	000
11:12:28EST, FEBRUARY 23,1973	0000	000	000	000	000
DELAWARE RIVER AT BRISTOL					

Figure 7 - Summary of data, sorted by DCP, ID, to provide field technicians with the operational status of the DCP's.

The data that are judged to be valid are compiled, summarized and formatted into the daily externally released summary. This summary is placed in an on-line data set in the Washington computer center. Instead of returning the summary with the rest of the job output on the line printer of the batch remote terminal from which the job is submitted, the data set containing the summary is accessed

by a low speed ASR-33 teletypewriter terminal, which is also available in the Pennsylvania district office. The reason this summary is accessed by the ASR-33 is because, as it is retrieved, a punched paper tape of the summary is produced on the teletype. After the summary is retrieved, and is humanly reviewed and judged to be provisionally valid, the paper tape is used to transmit the summary to external agencies over the ASR-33, operating in the teletype mode over Western Union's TWX lines, rather than the low speed terminal mode over telephone lines.

The software we have devised to process the DCP data provides the operation of the data-relay system with important information about the operational status of the equipment in the system, and provides water-resources summaries for a large geographical area for water management purposes.

6. PRESENT ACTIVITIES

Our present activities are centered on attempting to increase the number of water-quality monitors operating in the system, and on increasing the availability of near-real-time data to water-data users. As part of the latter activity and in reaction to the devastating flood of Hurricane Agnes of June 1972, we are attempting to make DCP streamflow data available to flow forecasters in near-real time. We are revising our software to process streamflow data from both the Delaware and Susquehanna River basins and to make it available to the National Weather Service's River Forecast (RFC) Center in Harrisburg, Pennsylvania, which is responsible for flow forecasting in both basins. There is, and has been, a close working liaison between USGS hydrologists and RFC hydrologists in the operation of stream gages which provide the RFC with data for river flow forecasting. The DCS data will provide a parallel and backup system of data communications from several gaging stations and provides an excellent operational test of the DCS. We continue to work with staff members of the DRBC and, as of late, with staff members of the SRBC.

7. CONCLUSIONS

The first several months of our activities with the DCS have been rather hectic, and it has been a learning experience. We have made real progress in installing and operating DCP's on a variety of standard U.S. Geological Survey operating water-resources instruments. These instruments are a small subset of the large set of instruments that the Geological Survey operates across the United States, a growing number of which are being accessed in real time by a variety of conventional telemetry systems. Problems still remain in completing our interfacing of the DCP's with the water-quality monitors, but progress is being made now, and most of the DCP installations are performing well. We have established a computer processing system, which we have configured in a near operational mode, and it is functioning fairly well. The processing system will continue to evolve as we develop algorithms to assist us in screening the data for DCP and water-resources field instrumentation malfunctions.

From a very pragmatic and utilitarian point of view, the DCS is being demonstrated to be a viable system, which has great potential for improving the efficiency and management of field instrumentation and the earth-resources conditions which they monitor.

Paper W 10

MODELING SUBTROPICAL WATER-LEVEL DYNAMICS DISTRIBUTION

A. L. Higer, E. A. Cordes and A. E. Coker, *U. S. Geological Survey, Miami, Florida*

ABSTRACT

ERTS MSS Imagery coupled with Data Collection Platforms (DCP's) relaying virtual real time data provides the potential for optimum water-resource conservation and utilization in south Florida. Limited information gained from ERTS-1 suggests implementation of a prototype Water Resource Model capable of: (1) Disseminating data to the agencies responsible for maintaining an adequate water supply to the 2 million coastal ridge inhabitants; (2) Delineating the distribution of existing waters stored in the 1,400-square-mile Central and Southern Florida Flood Control District; (3) Quantifying the essential elements in the hydrologic cycle; and (4) Providing the basis for preserving the diverse but delicate Everglades aquatic communities.

New and existing DCP's relaying rainfall, water-levels, wind velocity and specific electrical conductance of water to the USGS via ERTS-1 will allow determination of south Florida water, and weather, and ecologic model feasibilities. Dissemination of data will provide the Central and Southern Florida Flood Control District with an opportunity for daily water-management capability decisions. Sophistication of an experimental Water Resource Management Model up to an annual prototype operational water management budget will allow Federal (National Park Service, Fish and Wildlife Service and U. S. Army Corps of Engineers), State (Central and Southern Florida Flood Control District, Fish and Game, Department of Natural Resources), and County (Dade and Broward public water supply) agencies to avert crisis negotiation for the seasonally limited water resources. A more accurate water resource model is the critical planning need in south Florida with choice of alternative storage techniques hinging on the exact quantity and duration of the seasonal surplus. Preservation of sensitive hydrobiological communities in the Everglades National Park is a primary concern.

(Paper not received by publication date)

Paper W 11

AN EVALUATION OF SPACE ACQUIRED DATA AS A TOOL FOR MANAGEMENT OF WILDLIFE HABITAT IN ALASKA

Bill J. Van Tries, *EROS Coordinator, Bureau of Sport Fisheries and Wildlife, Washington, D. C.*

It would be difficult to find, in the United States, a region which could benefit more than Alaska from improved techniques for acquisition of natural resources data.

The size of its land mass and the remoteness of large areas of the State make conventional methods of data collection difficult, expensive, very hazardous, and often inaccurate. For these reasons, information on the vegetation, hydrology, soils, and wildlife of the State is inadequate for proper management and conservation of the State's great natural resources.

The Bureau of Sport Fisheries and Wildlife, through its EROS funded Alaska ERTS-1 experiment, hopes to improve its current data collection techniques for its own internal functions, i.e. predictions of waterfowl populations in the fall migration. It also hopes to assist the State in providing certain baseline data which are essential to the State in many aspects of their land use planning functions.

The Bureau of Sport Fisheries and Wildlife ERTS experiment in Alaska attempts to yield information useful for three primary functions in the State. They are:

1. To test the feasibility of using ERTS data, in conjunction with aircraft acquired multispectral photography, to develop effective stratified sampling techniques for achieving the objectives of items 1 and 2.

2. To provide near real time assessment and evaluation of the quantity, quality, and distribution of waterfowl breeding habitat through frequent ERTS measurements of hydrologic, phenological and vegetational parameters.

3. To provide basic mapping of vegetation and terrain in certain remote areas of the State for which little or no biological data now exist.

The Bureau of Sport Fisheries and Wildlife is responsible for promulgating new waterfowl hunting laws each year because the populations of waterfowl change annually, largely as a result of habitat conditions in the Canadian and Alaskan breeding grounds.

Unlike most resident game species, waterfowl populations are influenced greatly by hunting regulations. Efficient management of this renewable resource, depends on annual adjustment of hunting regulations to insure that a sufficient number of birds remain after the hunting season to provide for production the following year.

An estimate of the size of the fall flight must be available at the time hunting regulations are set. The estimate must be reasonably accurate since, for some species, hunting is the largest cause of mortality. Regulations based on faulty estimates of current numbers of waterfowl could result in reduction of the breeding population to undesirably low levels. A need exists, therefore, to predict accurately the magnitude of the annual fall flight from the Alaska breeding grounds.

To meet this need the U.S. Bureau of Sport Fisheries and Wildlife, the Canadian Wildlife Service, and the various States have developed systematic procedures for predicting fall waterfowl populations. Aerial surveys in May and July are used to provide indices for breeding populations, habitat conditions and waterfowl production. Ground surveys made in May provide correction factors for the aerial data. However, the aerial surveys are not completed until late July, and the laws must be set in mid-August. Administrators, therefore, are hard pressed to evaluate the data and act on recommendations in time to meet this deadline.

The importance of correlating habitat conditions to waterfowl production then becomes obvious. If it can be done quickly, and with reasonable accuracy, it could be a valuable adjunctive index to determining annual waterfowl production.

The Bureau of Sport Fisheries and Wildlife ERTS-1 experiment on waterfowl habitat is based on the accepted theory that a reliable correlation exists between the "degree of wetness" (number of ponds and wetlands) existing in July and annual production of birds.

More precisely, the degree of wetness involves the dynamics of the wetlands which includes pond size, miles of edge or shoreline, water depth, related emergent and submerged aquatic vegetation and associated upland vegetation which may be used as waterfowl habitat.

The Alaska ERTS experiment attempts to test:

1. the degree to which verified (through ground or aerial surveys) ERTS vegetation data may be extrapolated to yield information on sites some distance from the points of verification

2. the utility of ERTS data in developing vegetation maps of sufficient accuracy to be useful in biological investigations and resource management

3. reliability of ERTS data in measurements of hydrologic parameters, i.e. water surface, areas, depths, miles of edge, and distribution and numbers of water bodies. These data will provide the "degree of wetness" index necessary for near real time evaluation of waterfowl habitat.

An ERTS scene dated August 30, covering the Yukon/Kuskokwim Delta was analyzed to determine the degree to which it could satisfy the needs of the experiment.

The scene was selected because it is an important waterfowl production area, it contains diverse vegetation and terrain types, has many lakes of varying size and adequate, ground surveyed, vegetation maps exist for it. Also, it is the site of a proposed navigational canal which could create a considerable biological alteration of the region.

South Dakota State University Remote Sensing Institute's SADE (Signature Analysis Dissemination Equipment) program was selected to perform the necessary analyses. Color coded density renditions of the 70 mm positive transparencies were made using a Datacolor system looking at all four MSS bands.

An area containing large lakes in MSS band 5 and an area containing small lakes in MSS band 6 were digitized using RSI's SADE. Eight gray levels were displayed, with each level having a range of 32 numbers. What appear to be significant differences in transmission levels were noted when looking at three large lakes. Interpretation of these differences must await ground or aerial surveys to be made this summer. However, from comparison with other, color coded, (Spatial Data) CRT prints and the original GSFC prints it appears that tonal differences are probably a function of a) turbidity, b) organic strain, or c) depth.

Surface area of water bodies depicted as a percentage of the total scene is immediately and directly obtainable. In the case of the Yukon/Kuskokwim frame, approximately 18.4 percent of the total frame is water area.

Measurement of pond and lake perimeters will be accomplished using a system comparable to that of the Environmental Research Institute of Michigan which is conducting another, similar, project for the Bureau of Sport Fisheries and Wildlife. Earlier studies by the BSF&W and Michigan's Willow Run Laboratories have shown this to be a feasible technique. At present the data are being studied to determine proper contracting procedures for their interpretation using a SPARC or equivalent system.

A rather simplistic approach has been adopted, and will continue to be used, for vegetation type mapping where ground verification now exists. Color coded densitometric renditions from Polaroid photography of CRT displays are compared with line, point, or quadrat transect samples traversing the area to be mapped. Areas on the conventional vegetation maps are matched to corresponding areas on the color coded densitometric displays which may or may not have identical boundaries, but agree in general with the area covered. In most cases, the conventional maps or sampled data are, and will be, from years past, therefore, exact boundaries of vegetation zones can not be expected to fit precisely the ERTS derived scenes.

As stated, vegetation maps such as the one available for the Yukon/ Kuskokwim Delta exist only for a very few areas of the State. Consequently, those that do exist will be used to test the limits of extrapolation of ERTS data for application in areas far removed from a known vegetation zone.

To apply the technique in areas for which no ground or aerial data are available, other approaches will be used. These will include aircraft acquired multispectral photography and conventional ground surveys designed to serve as sampling sites in lieu of existing vegetation maps for a given ERTS frame.

Some multispectral photography using the Bureau's I^2S camera in August, 1972, has been acquired and analyzed. Preliminary analyses indicate that it can play a vital role in substituting in part or altogether, for ground surveys in support of ERTS data. Although I^2S data were not acquired for the Yukon/ Kuskokwim Delta, coverage of areas of a similar type were analyzed and found to facilitate greatly the correlation of minimal ground data to space acquired data.

The preliminary conclusion drawn from these tests is that a stratified sampling technique using aircraft multispectral data, verified with minimal ground transect sampling, can provide near real time vegetation maps for Alaska. The maps thus produced will be of species association zones, and not detailed species maps. For the Yukon/Kuskokwim Delta the zonal coding is as follows:

1. Dense Forest

   1a. Interior High Forest - White spruce, poplar, and locally birch.

   1b. Low Forest - White spruce, poplar, aspen, and birch.

2. Open Forest - High Brush

   2a. High Brush - Principally alder, commonly mixed with willow and birch.

3. Low Vegetation

   3a. Tundra - Grass and herbs from a few inches to 3 ft. high.

   3b. Sparse Low Vegetation and Barren Areas - Chiefly sparse lichens and mosses.

4. Wet Vegetation

   4a. Marsh and Bog - Peat moss in bogs, and grasslike aquatic plants.

Paper W 12

PRELIMINARY EVALUATION OF ERTS-1 FOR DETERMINING NUMBERS AND DISTRIBUTION OF PRAIRIE PONDS AND LAKES

Edgar A. Work, Jr., *Environmental Research Institute of Michigan, Ann Arbor, Michigan;*
David S. Gilmer, A. T. Klett, *Bureau of Sport Fisheries and Wildlife, Northern Prairie Wildlife Research Center, Jamestown, North Dakota*

ABSTRACT

ERTS-1 and aircraft multispectral data collected over a North Dakota test site during July 1972, are compared to evaluate the capability of the satellite sensors to detect numbers and distribution of prairie ponds and lakes. Recognition maps using ERTS-1, MSS 7 data are generated using a level slicing technique. Surface water areas larger than two acres are recognized, but ponds in the one-to two-acre range are detected only at random. The proportion estimation technique will improve the accuracy of area determination and small pond detection.

1. INTRODUCTION

Management of migratory waterfowl is a responsibility of the Bureau of Sport Fisheries and Wildlife (BSF&W). In North America, the primary breeding areas of waterfowl are the prairies and parklands of the northern states and the prairie provinces, and extend into northern Canada and Alaska. Numbers and distributions of wetlands (natural ponds and lakes) in these regions are one of the principal criteria used in developing an index of annual waterfowl production. The BSF&W, the Canadian Wildlife Service, and various states and provinces have made annual systematic breeding-ground surveys since 1947 (1). Aerial surveys, conducted in May and July, are used with air-ground correction factors to provide indices for breeding populations, habitat conditions, and waterfowl production. Additional regional wetland surveys are made periodically to assess the long-term ecological changes due to natural and economic causes.

Canadian and U. S. wildlife biologists have suggested that a reliable production index could be derived, independent of the size of the breeding population, from an estimate of the number of ponds remaining in mid-July (2). The degree of wetness, especially changes in number of ponds, during the May-July period is now determined from established aerial transects. Biologists have speculated that these indices could be obtained more rapidly and accurately using airborne or spaceborne sensors and associated automatic data processing techniques.

To investigate the potential of remote sensing techniques, in 1968 and 1970 the Environmental Research Institute of Michigan (ERIM, prior to 1 January 1973, the Willow Run Laboratories of The University of Michigan) conducted a series of airborne multispectral scanner (MSS) data utilization and processing experiments to determine capabilities for measuring seasonal changes in waterfowl habitat. These studies were conducted 30 miles northwest of Jamestown, North Dakota at the Woodworth Station, a 6-square-mile research area operated by the BSF&W, Northern Prairie Wildlife Research Center, Jamestown. Biological interpretation and site coordination were provided by the BSF&W.

The BSF&W and ERIM are presently involved in the processing and analysis of data obtained by ERTS-1. Earlier work demonstrated the reliability of water recognition from processed aircraft multispectral scanner data (3, 4 and 5). Similar techniques are now being applied to satellite scanner data. Primary objectives of the current work are to map and generate statistics on water bodies down to the smallest size ponds detectable and to determine changes in wetness between spring and summer using ERTS-1, MSS 7 (0.8-1.1 μm) data. Coincident aircraft scanner and photographic data are being used to interpret and correlate spacecraft results. The initial ERTS-1 pass over the Woodworth test site occurred in late July, which delayed until 1973 the evaluation of satellite data for detecting seasonal change in wetlands. We anticipate that a sequence of May-July coordinated data sets will be obtained in 1973 which will permit us to continue investigations of change in seasonal wetness.

The 1972 ERTS and aircraft data have been processed to evaluate ERTS MSS data for determining numbers and distribution of prairie ponds and lakes. We have demonstrated the feasibility of pond and lake mapping using concurrent aircraft and spacecraft data and processing techniques derived from the previous aircraft program.

2. RECOGNITION TECHNIQUES

Previous investigations have tested several techniques for mapping water bodies. These include; (1) pattern recognition using multispectral data channels in the visible range, (2) thermal contrast between water and a terrain background, and (3) signal level slicing of radiation received in a single reflective infrared band. Signal level slicing is

the simplest method to implement because the reflectance of water is uniform and lower than most other scene objects. The method requires determining a signal level which separates low radiance water bodies from the other higher radiance objects in the scene. Investigators have evaluated this technique in near infrared regions (0.8-2.5 μm) and have obtained good success in all except the 2.0-2.5 μm atmospheric window, where lesser amounts of solar energy are available for scene illumination.

Implementation of the level slicing technique is accomplished by first generating a digital gray map. From this pictorial representation samples of water bodies and other known areas which exhibit low reflectance values are selected. Histograms of the distribution of reflectance levels for each training category are constructed. These distributions tend to be Gaussian, and the histogram for water will be displaced from the reflectance distributions of other objects. It is then necessary to select a decision boundary which separates surface water from all other scene objects on the basis of their reflectances.

After determining the decision boundary (i.e., slicing level), computer software is then used which generates a printed map of surface water. This program is also capable of generating various statistical summaries. However, this latter feature is not discussed in this report.

3. RESULTS

Aircraft (ERIM C-47) and satellite data were collected on 28 and 31 July 1972 respectively. The Woodworth Station is located near the nadir of the ERTS frame selected for processing. Approximately ten percent of this frame, including the Woodworth site was processed for pond recognition. Within the processed area, two physiographic regions, the Missouri Coteau and the drift plains of east-central North Dakota, are represented. Occasional shallow ponds and lakes and a partly integrated drainage system are typical of the drift plains. Numerous but less shallow ponds and lakes and a non-integrated drainage are characteristic of the Coteau. Both regions contain some of the best waterfowl breeding areas in North America. Figure 1 is a computer generated water recognition map of about three percent of the selected ERTS frame. Aircraft MSS video (1.0-1.4 μm) showing a flight line which transects the Woodworth Station is indicated. Fish Lake is located near the center of the Station. Large prairie lakes clearly discernible from ERTS data include Round (approximately 0.8 mile in diameter), Barnes, and Chase Lakes. Generally, surface water areas larger than two acres are recognized. Each character (one digital sampling element) on this map represent 1.1 acres. If a one-acre pond were divided by two adjacent digital sampling elements, it may or may not be recognized as a water body. Figure 2 compares water recognition maps of ponds and smaller lakes generated from both satellite

and aircraft data. Fish Lake has two elongated bays which are reproduced accurately in the ERTS imagery. However, some of the shoreline details of Big Lake are less accurately described. The elongated lake 1.2 miles east of Big Lake has areas of emergent vegetation and a chain of small open water areas which trail off to the southwest. These detailed features, although shown in the aircraft data are not apparent in the ERTS recognition map.

Histograms of reflectance values used to establish a decision boundary separating water and other features for the satellite and aircraft data are shown in Figures 3 and 4 respectively. In the spectral range under consideration (i.e, satellite 0.8-1.1 μm, aircraft 1.0-1.4 μm), both soils and water have low reflectance values. However, reflectance values for water are lower than those characteristic of soils, thus the two can be accurately separated (ERIM report in prep.). An examination of the satellite and aircraft recognition maps for false or omitted recognitions indicates that our decision boundaries provide accurate results. Histograms of several other scene objects are considered in the case of the aircraft data (Figure 4). During late July reflectance levels of some types of marsh vegetation are similar to soil. Shallow water which does not completely mask reflectance from bottom soil or submerged marsh vegetation may indicate reflectance values intermediate between marsh vegetation/soil and deep water. Shallow water and marsh vegetation histograms overlap because the shallow water training areas can be expected to contain some marsh vegetation and vice-versa. The location of the shallow water reflectance distribution between deep water and soil indicates the need to place a decision boundary for water recognition using ERTS data (Figure 3) nearer the soil distribution than the distribution for deep water. The ability to select shallow water training areas from satellite imagery is difficult because these areas tend to be small. Because of this the availability of aircraft imagery is important for our analysis of ERTS data.

Figure 5 is an enlarged portion of the ERTS recognition map. The dashes (omitted from the other recognition maps) represent boundary elements having reflectance values which fall within the range for soil and marsh vegetation. This condition (boundary effect) is especially prominent in the satellite recognition results. Some of these boundary elements may be attributed to marsh vegetation or bare soil margins surrounding the lakes. The boundary elements probably also contain some water. This causes the acreage of the lakes to be underestimated because the boundary elements are placed in the soil/marsh vegetation category.

4. DISCUSSION

Preliminary results demonstrate the degree to which surface water conditions can be determined using ERTS MSS data. Generally it appears

that ponds larger than two acres are recognized, while water bodies in the one-to two-acre range are detected only at random. Techniques exist which can more reliably detect small ponds and improve the size estimates of larger ones. These improvements are felt to be essential for this analysis. The proportion estimation technique determines the proportion of objects present within a resolution element using a multispectral data set and an appropriate algorithm (6). For example, boundary elements may be composed of a mixture of water, marsh vegetation, and other components. By estimating the proportion of water in the boundary elements using the proportion technique, the accuracy of lake acreage determination and the reliability of small pond detection are improved over the signal slicing technique.

With this accurate pond mapping capability (consisting of signal level slicing augmented by the proportion estimation technique) seasonal changes in surface water can be more reliably determined. The most cost-effective method for monitoring these changes on a regional basis will very likely involve joint aircraft and satellite data collection and the use of a multistage sampling design.

5. LITERATURE CITED

1. Crissey, W. F., 1957. Forecasting waterfowl harvests by flyways. Trans. N. Am. Wildl. Conf. 22:256-268.

2. Crissey, W. F., 1969. Prairie potholes from a continental viewpoint. Pages 161-169 in Saskatoon Wetlands Seminar. Canadian Wildl. Serv. Rep. Ser. No. 6, 262 pp.

3. Burge, W. G. and W. L. Brown, 1971. A study of waterfowl habitat in North Dakota using remote sensing techniques. Willow Run Labs., Inst. Sci. Technol., The Univ. of Michigan, Ann Arbor, Tech. Rep. No. 2771-7-F, 61 pp.

4. Nelson, H. K., A. T. Klett, and W. G. Burge, 1970. Monitoring migratory bird habitat by remote sensing methods. Trans. N. Am. Wildl. Nat. Resour. Conf. 35:73-84.

5. Nelson, H. F., A. T. Klett, and John E. Johnston, 1971. Application of remote sensing techniques for appraising changes in wildlife habitat. Proc. Int. Workshop on Earth Resour. Surv. Syst. Vol. II, pages 263-288. Supt. Doc., U.S.G.P.O.

6. Nalepka, R. F., H. M. Horwitz, and N. S. Thomson, 1971. Investigation of multispectral sensing of crops. Willow Run Labs., Inst. Sci. Technol., The Univ. of Michigan, Ann Arbor, Tech. Rep. No. 31650-30-T, 80 pp.

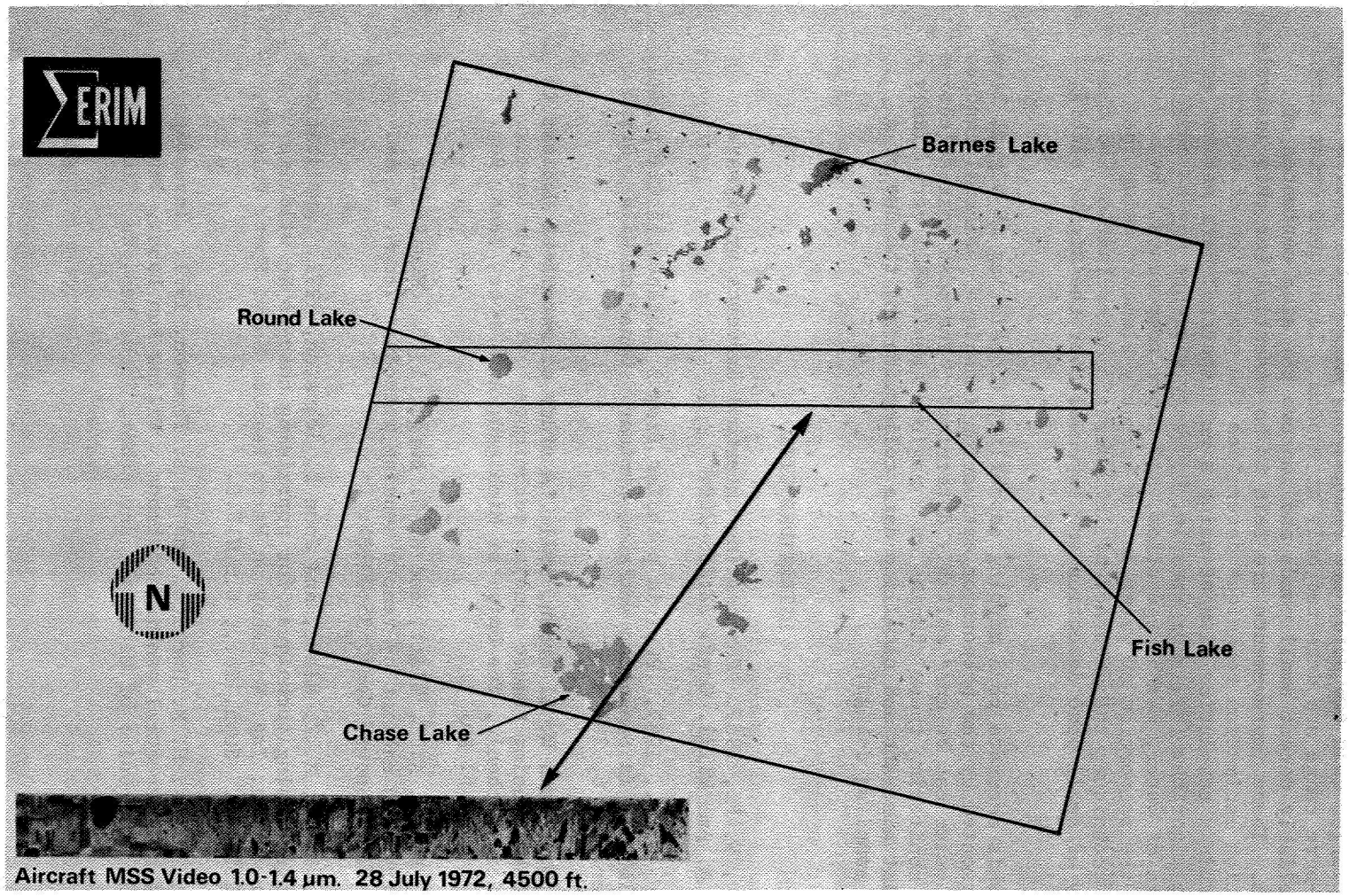
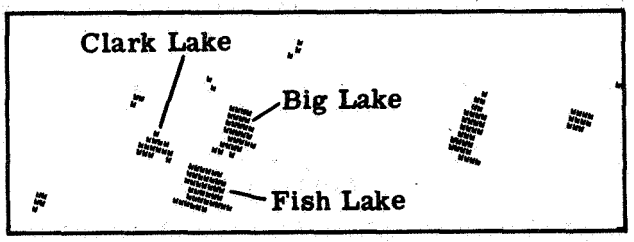


Figure 1.
DIGITAL WATER RECOGNITION MAP OF APPROXIMATELY 3% OF AN ERTS FRAME

DATA COLLECTED 31 JULY 1972 • C N45-17/W099-27 • TAPE C, LINES 1140-1540, POINTS 1-610



(a) Processed ERTS Water Recognition
(Data of 1659 G.M.T., 31 July 1973)



(b) Processed Aircraft Water Recognition from
4500 ft (Data of 1358 G.M.T., 28 July 1972)

1 statute mile

Figure 2. Comparison of details in ERTS-1 and aircraft recognition maps of ponds and lakes near Woodworth, North Dakota.

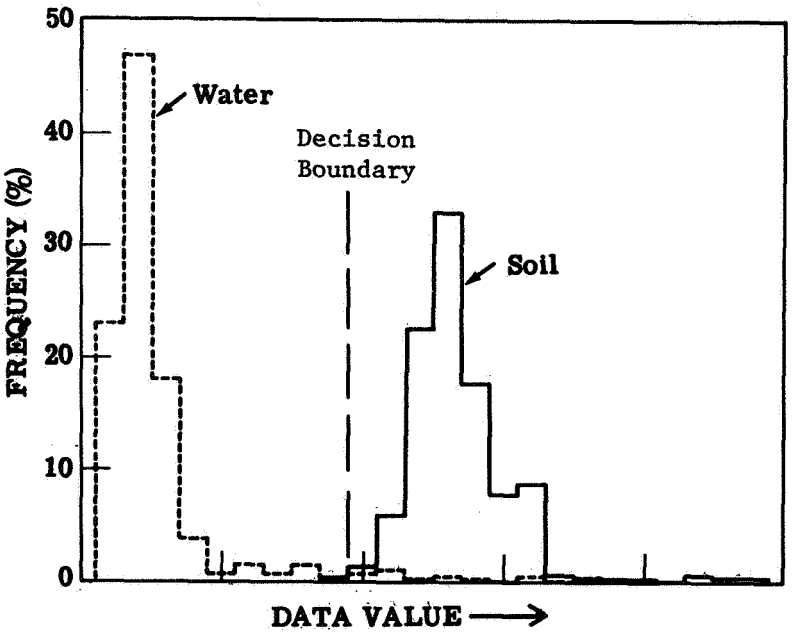


Figure 3. Histograms of reflectance values for water and soil test areas near Woodworth, North Dakota using ERTS-1 data collected at 1659 GMT, 31 July 1972.

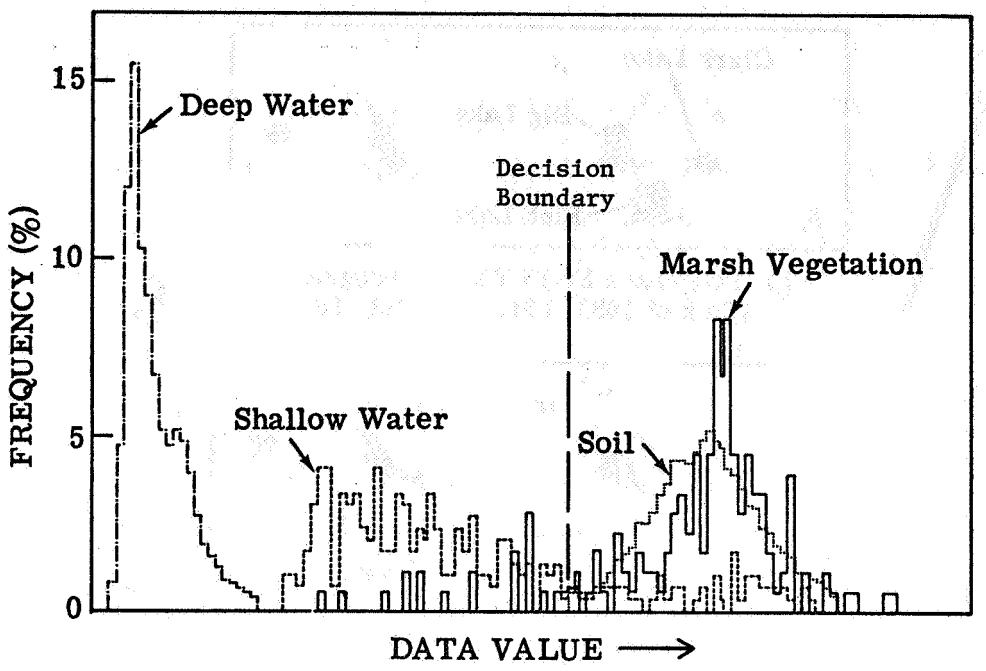


Figure 4. Histograms of reflectance values of test areas near Woodworth, North Dakota using aircraft data collected on 28 July 1972 from 4500 feet.

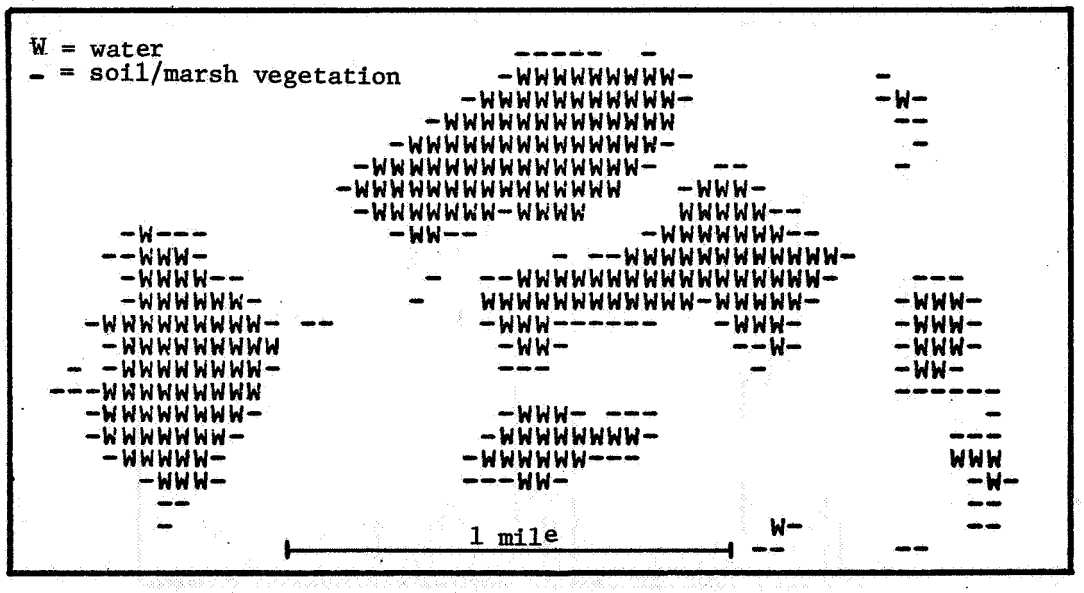


Figure 5. Example of boundary effect associated with recognition maps of ponds and lakes near Woodworth, North Dakota using ERTS-1 data collected at 1659 GMT on 31 July 1972.

Paper W 13

DYNAMICS OF PLAYA LAKES IN THE TEXAS HIGH PLAINS

C. C. Reeves, Jr., *Department of Geosciences, Texas Tech University, Lubbock, Texas*

ABSTRACT

This study shows that satellite imagery can be used for a census of the thousands of lake basins which commonly exist in semi-arid areas, and which sporadically contain water at various times of the year. Storm paths and runoff collected by such lake basins can also be closely monitored, the accuracy dependent on periodicity of the orbits and the size of the basins. Study of the relationships between spectral differences (obtained from ERTS-1 imagery) and the water balance ecosystem of the lake basins is in a preliminary stage. However, examination of ERTS-1 MSS frames show that Band 4 has the poorest tonal contrast in semi-arid West Texas, Band 5 is best for definition of vegetation, Band 6 is best for defining large water areas, and Band 7 is best for counting small lake basins with water.

Ground-truth studies reveal significant differences between the test sites, the relative importance of which will be reflected by the hydrologic balance of each lake basin.

1. INTRODUCTION

The study area covers approximately 30,000 square miles of the southern High Plains of West Texas and eastern New Mexico (Fig. 1), extending from the Canadian River Valley on the north to the Edwards Plateau on the south. East and west boundaries are marked by high caliche escarpments. In this area three small playa lake basins, considered typical of the tens-of-thousands of lake basins which pockmark the area, were originally selected as ERTS-1 study sites, a fourth larger basin complex typical of the large lake basins of the area being added after receipt of the first imagery. Objectives were: 1) to study the water budget of the lake basins, 2) to relate spectral differences obtained by ERTS satellite photography to the water balance ecosystem and geology of the basins, 3) to extrapolate these integrated

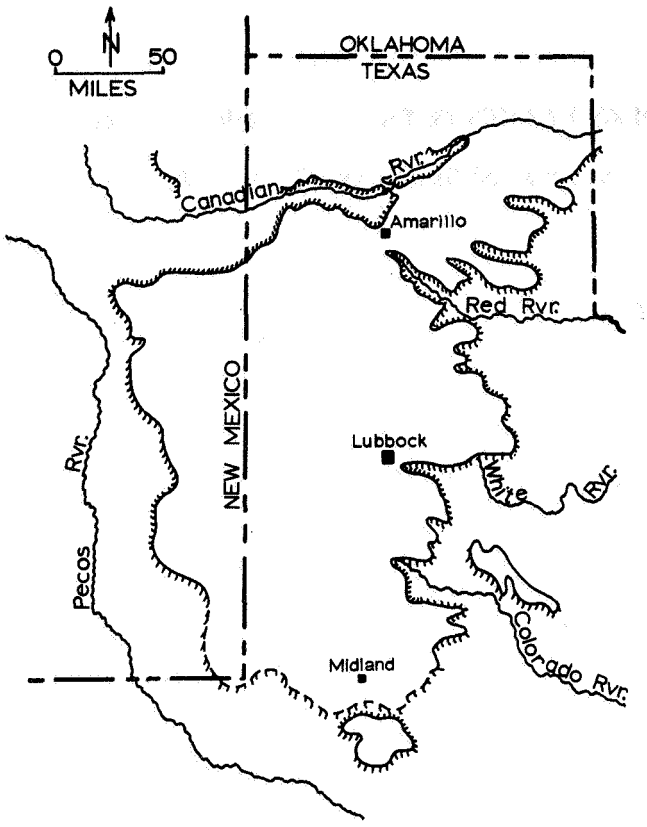


Figure 1 - Index of the southern High Plains.

data to other such lake basins on the Plains and, 4) to correlate space-acquired signatures to soils, soil moisture, geology and plants.

The original PI, Dr. W.D. Miller, was killed in a tragic accident June 22, thus, in addition to the ground truth studies and photo interpretation, I assumed responsibility of keeping up with the "intermittent" paper work. The project has also been plagued by weather. Out of 11 passes through January 1973, only 5 have been usable: we have received only 4 of those. However, the detrimental climatic events have been yielding an unusual wealth of hydrologic data.

2. APPROACH

Ground truth of the three small playa basins was secured during the summer of 1972, and ground truth studies are still underway at the large study site. This data consists of: 1) soil surveys, 2) vegetation surveys, 3) geologic surveys, and 4) water balance studies.

The three basins, each covering approximately 10,000 square meters, and the three playas each covering approximately 1000 square meters, were staked on 100 m grids. Soil scientists, using a power probe and soil auger, took cores or samples to -6 feet at each intersection. Intersections, starting in the present playas, were drilled by power flight-auger until the strand lines and thickness of the lacustrine sediments were defined. Each basin was cored in the deepest spot. Vegetation studies (contributed to the program by an outside investigator) are being conducted by 10 x 10 m grid sampling over an 800 m grid square. The large basin, (Fig. 2), consisting of a dual playa complex 5 miles long in a 9 square mile basin, is not being studied in such detail, although a geologic map, soil survey, and subsurface maps are being constructed. The water balance in one of the small basins and in the large playa complex is monitored by checking rainfall, runoff, infiltration (by tensiometers) and evaporation. Figure 3 illustrates the weather monitoring set up at small T-Bar playa, ERTS-1 test site No. 3.

3. PRELIMINARY RESULTS

No results are yet available from the vegetation or water budget studies. Soil and geologic studies are complete at the three original sites and still underway at the large Double Lakes site. Work to date, using bulk positive 9 x 9 transparencies with optical magnification and density slicing, shows that Band 4 has the poorest tonal contrast, but is best for defining cities and highways. Band 5 is best for definition of vegetation, Band 6 is best for defining large water areas and Band 7 is best for counting the small lake basins with water.

Ground-truth studies show that the three small playa basins, although similar appearing, actually have many differences, and these differences are going to affect the water balance. For example, the present playa and fringing soils at Site #1 (Heard) are underlain by up to 25 feet of



Figure 2 - Aerial view of North Double Lake, Lynn County, Texas. South Double Lake in background. Star indicates location of instrumentation.

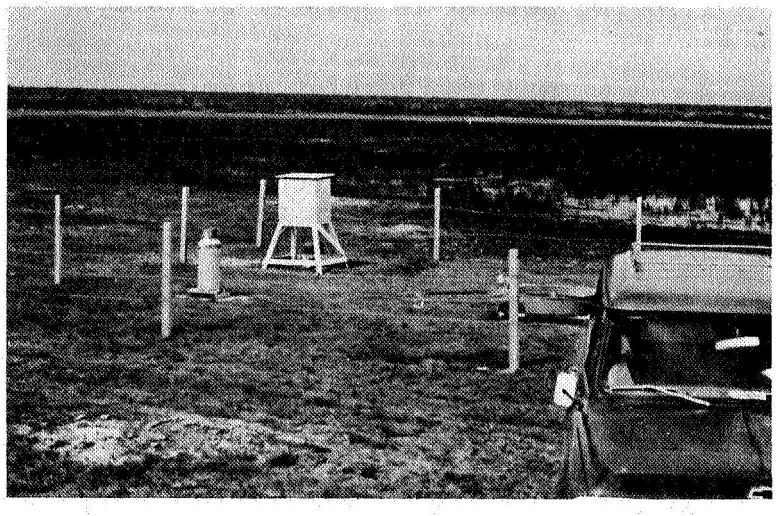


Figure 3 - T-Bar study site with weather monitoring instrumentation.

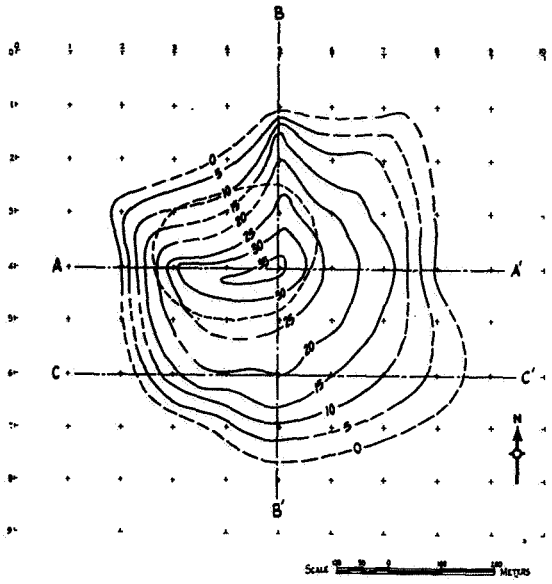


Figure 4 - Isopachous map lacustrine sediments at ERTS study site No. 1 (Heard playa). Dotted line marks present playa shape.

lacustrine clay which accumulated in a playa 4 times the size of the present playa (Fig. 4), but at Site #3 (T-Bar) the present playa marks the maximum extent of the lacustrine fill.

All of the small basins are underlain by the Pliocene caliche, the caliche exhibiting "excavations" in which the lacustrine fill collected (Fig. 5). This indicates that the basins resulted from undulations in the Pliocene surface on which the caliche formed, or that significant solution of the upper part of the caliche has occurred beneath the basins, location having nothing to do with the caliche. The former possibility appears more likely in light of other field studies of similar basins.

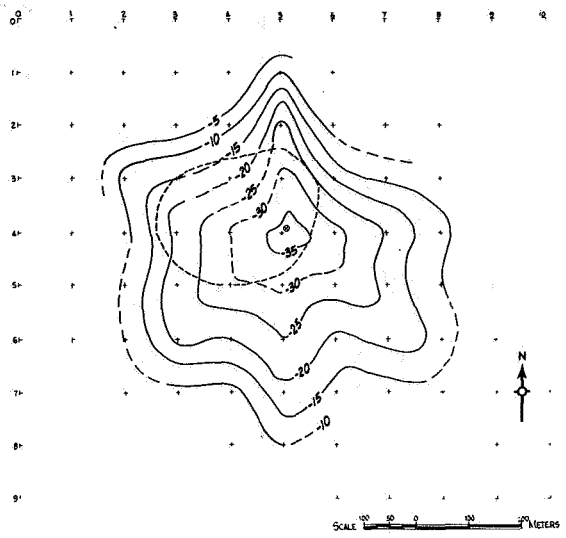


Figure 5 - Structure map on top of Pliocene caliche at ERTS-1 study site No. 1 (Heard playa).

On the other hand, preliminary ground-truth at the large Double Lakes site shows that the present playa is formed on and adjacent to a Cretaceous topographic high and that older lacustrine clays overlie permeable Ogallala sands which constitute the regional aquifer. Thus, the poor quality water area in the aquifer downdip from the Double Lakes site (and this is always the case downdip from other similar large basins in the area) is probably due to infiltration of runoff through saliferous lacustrine sediments or infiltration of saline water from the present playa. We will, hopefully, be able to pinpoint this trouble when we correlate water fluctuations measured from ERTS imagery with water balance data.

The workable resolution of the imagery has presented problems. An optical resolution of about 10 m was determined for high contrast linear objects on bands 6 and 7.

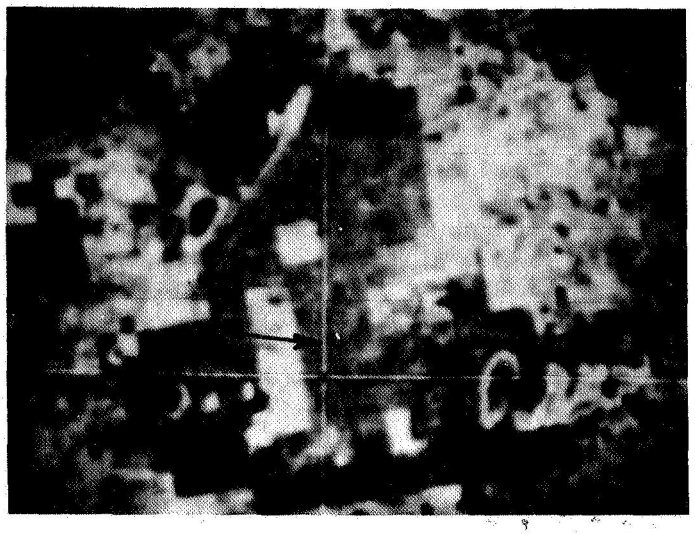


Figure 6 - Double Lakes and T-Bar ERTS-1 study sites, Lynn County, Texas. Notice resolution difficulties of measuring water extent at T-Bar site (arrow) but how water extent is imaged at North Double Lake. From SRI TV monitor.

However, vegetation surrounding the three small playas, which range from 200 to 400 m in diameter, reduces contrast between the water and vegetation in the playas. Thus, although the playas are resolvable, the measurement of changes in water area, even when magnified, have not been possible with any confidence. However, water fluctuations in both playas of the Double Lake site are easily measureable. For example, on the 29 July pass South Double Lake had a water area of 1.54 km^2 and North Double Lake a water area of 1.62 km^2. Figure 6 illustrates the water area of the Double Lake site from the 9 October pass. Notice in the north playa how the water shallows to the north, the wet mud and dry parts of the playa having signatures distinct from the flooded part.

Various soil signatures in the three small lake basins are not apparent on the imagery, although the difference in basin soils which have a higher reflectivity from surrounding eolian sands is noticeable. However, in the large

Double Lake site several soils are exhibiting spectral signatures. For example, the Drake and Porter soils have a high reflectance, the Randall is opaque to white, and the surrounding Brownfield and Amarillo range in between. Enhancement by density slicing vividly emphasizes these differences in reflectivity.

In areas of dense vegetation, such as the sorghum fields in the northern half of 1007-16575, water-filled lake basins cannot be distinguished on the transparencies on Band 5 because of lack of contrast between the vegetation and water signatures. However, on Bands 6 or 7, vegetation no longer appears opaque and the water-filled lake basins stand out.

4. BENEFITS

Regional scanning of the ERTS transparencies shows that the number of lake basins containing water on the southern High Plains, at any image time, can be counted. Offhand, this does not seem to be much of an advantage, but when you realize that we are talking about ±20,000 lake basins, it has here-to-fore been impossible from monetary, manpower, and time considerations, to take a regional "wet" census. For example, in an area of approximately 40 sq km on scene 1006-16522, 353 small playa lake basins contain water, and the count could be as high as 447. A total of 6631 playas contain water in the entire scene. Such a census is of great significance in any semi-arid area to determine how much water is available for artificial ground-water recharge, or for irrigation, at various times of the year.

Individual storm tracks can also be identified and the number of lake basins filled by such isolated storms can be counted. ERTS-1 scene 1006-16522 of 29 July, 1972, images a northwest-southeast trending storm path which skirted the southwest part of Lubbock. This isolated storm cell, with tops to 25,000 feet and a diameter of 2.4 km when spotted by radar at 1940 GMT 62 miles northwest of Lubbock, was moving to the southeast. The wetted path measures from 2 to nearly 5 km wide and extends for 38 km across the image. At least 347 small playa basins within this storm path contain water (on the image), but unfortunately antecedent conditions were not imaged. However, many dry playa basin immediately to either side of the storm path suggest that the basins containing water in the storm path were filled by the storm.

Subsidiary benefits not connected with this study are, to date, the conformation of previously observed regional lineaments, the local alignment of the playa lake basins, and the discovery of new lineaments. Crop signatures are distinctive and, I suspect, identifiable (see Marion Baumgardner's report, LARS, Purdue University). Grassland signatures are separable from cultivated land signatures.

Quantitative measurements of density profiles across the test sites and correlation of water depths with CCT data will be investigated in the next few months. During the coming summer, with a year's hydrologic data on hand, the relationships between the ERTS-1 spectral signatures, vegetation, lake level fluctuations and water balance of the test sites will be determined.

Paper W 14

STUDIES IN THE LAKE ONTARIO BASIN USING ERTS-1 AND HIGH ALTITUDE DATA

A. Falconer, S. H. Collins, W. T. Dickison and R. Protz, *University of Guelph, Guelph, Ontario;* R. P. Bukata and K. P. B. Thomson *Canada Centre for Inland Waters, P. O. Box 5050, Burlington, Ontario;* G. P. Harris and P. J. Howarth, *McMaster University, Hamilton, Ontario*

ABSTRACT

Studies in the Lake Ontario Basin are designed to provide input for models of river basin discharge and macro-scale features of lake circulation. Lake Studies appear to require high altitude imagery to record the dynamic features of Lake Ontario so that ERTS-1 data may be interpreted. Land area studies require input of soil moisture, land use and soil-sediment-geomorphology measurements some of which appear to be available, on a regional scale from ERTS-1 products.

1. INTRODUCTION

Lake Ontario is the major study area for projects undertaken as part of the International Field Year on the Great Lakes (I.F.Y.G.L.). The Western portion of the Lake Ontario Basin has within it specially designated land and lake study areas which are managed by personnel from government agencies and universities. Remote sensing data over the western portion of Lake Ontario are available from several sources. Correlation of the available remote sensing imagery with ground measurements available through I.F.Y.G.L. studies is undertaken by a team by a team of scientists whose work is co-ordinated through the Centre for Applied Research and Engineering Design (CARED) McMaster University, Hamilton, Ontario. This work is partially supported by funds from U.S.G.S. Contract No. 14-08-001-13169. Remote-sensing data available under this contract are used by Canadian government agencies which have programs in the I.F.Y.G.L and these agencies are associated with the research team co-ordinated by CARED. The individuals participating in the co-ordinated interdisciplinary research project are also involved in many other research activities funded by various agencies. The results of these other activities are, where appropriate, linked to this work in the evaluation of remote sensing imagery for I.F.Y.G.L. purposes.

The western portion of the Lake Ontario Basin (the Lake Ontario Test site see fig. 1) contains both land and lake areas. Studies over the land area are designed to provide input for models of stream basin response so that

discharge into major streams or into Lake Ontario can be predicted with greater accuracy. Over the lake the data obtained from lake study programs are evaluated alongside the remote sensing data and the purpose of the studies is to better understand the behaviour of the lake. International agreements on the control and management of Lake Ontario can only be based on the available knowledge and the continued study of the lake is of importance in all aspects so that available knowledge is as complete as possible. Both land and lake studies require a base for measurement of information. Calibration of data from sensors continues as an area of study. Some success with calibration of high altitude data has been achieved and the relationship between this and ERTS-1 data is a continuing investigation. A co-operative project between the University of Guelph and University of Michigan in the investigation of ERTS data for measurement of terrain characteristics, soils and soil moisture is examining this problem using MSS data from ERTS-1 and low altitude flights.

2. LAKE STUDIES REPORTED BY CANADA CENTRE FOR INLAND WATERS (C.C.I.W.)

In evaluating the RB-57 high altitude data, CCIW concentrated upon its potential for identifying and interpreting details of limnological phenomena occurring within inland lake systems. Obvious surficial features (many of which were the subjects of study of other investigators) such as coastal and river mouth plumes and effluents and which were felt to be readily distinguishable from ERTS and/or high altitude aerial imagery were, at least temporarily, ignored in favour of less obvious limnological data that could benefit from a high altitude overview. As is typical of all programs of remote sensing, the RB-57 data were not considered as an independent entity, but were considered in conjunction with other data collected above or below Lake Ontario during the periods of high altitude NASA overflights. These ancillary data included low altitude visible photography performed by CCIW, intermediate altitude visible photography and thermal scans performed by CCIW along with CCRS, and water quality data collected routinely via ship cruises.

Two main areas of limnological interest were explored making direct use of the RB-57 imagery; internal wave observations which have been previously reported (Boyce and Thomson, 1972) and dynamical lake processes which are about to be reported (Bukata, 1973).

1) Surface Indications of Internal Waves

The high altitude imagery clearly indicated a number of wave-like features along the north shore of Lake Ontario (2-10m wide) which are presumed to be convergence lines associated with internal waves in the lake. Figure 2 illustrates a mosaic constructed from the imagery (9 inch color infra-red film, 6 inch lens) and indicates the internal wave configurations in the area of Lake Ontario between Toronto and Oshawa. The most import information to be derived from the imagery was an estimate of the wavelength of the feature and their east-west continuity. Two main groups of waves were evident, the first group exhibiting wavelengths between 1000-1700 metres and the second group exhibiting wavelengths between 400-800 metres.

2) A Study of Lake Dynamics

Utilising those portions of the photography which display solar mirror-reflection (sun-glint) it has been shown that high altitude photography which is capable of depicting large water surfaces with good resolution is a powerful tool for evaluating relatively rapid dynamical phenomena. It has been observed that under proper conditions, photography in the visible spectral bands may delineate the dynamic interface between thermally different water masses. Extensive work is currently being performed upon the dynamics of upwelling phenomena and encouraging agreement is being obtained between the calculations of water transport rates as determined from surficial overviews of the lake and the values generally predicted from theoretical studies and ship network determinations.

3. ECOLOGICAL STUDIES OF THE NIAGARA RIVER PLUME AND AREA (reported by G. Harris)

In production ecology studies in the area of the Niagara River plume, L. Ontario, imagery from the ERTS simulation flights has been found to be useful for synoptic views of plume behaviour. In July 1972 production ecology studies were carried out from a moored barge[1] 2.8 km N of Four Mile Point Niagara-on-the-Lake, Ontario. The objective of the study was to examine the relationship between water mixing and production. Simultaneous measurements of chlorophyll (Strickland and Parsons 1968), Turbidity, Production in situ (Steemand-Nielsen 1952) and water mixing parameters were made.

On numerous occasions, peculiar chlorophyll and turbidity distributions were noted. Fig. 3 gives one such example. On July 11th the chlorophyll and turbidity distributions were rapidly reversed at 1200 hrs. in the absence of effective wind mixing in the previous few hours. The plot of chlorophyll vs. turbidity (Fig. 3) clearly shows that the water masses at 0m and 5m have reversed positions.

Examination of the imagery from the June RB57 overflight (see Fig. 4) allowed us to interpret these sorts of chlorophyll and turbidity patterns. Ground truth data gathered in June '72 showed a clear high turbidity in the plume area and a low chlorophyll concentration in the plume, presumably caused by cell destruction upriver at the falls. The plume turbidity is clearly associated with industrial effluents from the city of Buffalo as seen in the RB57 imagery from 19 October 1970. On June 7th, 1972 imagery the plumecan be seen to be spreading behind the Niagara bar and flowing out into the lake. On June 5th two sequential sets of imagery were obtained 35 mins. apart which allowed us to interpret dynamic features of the plumes from the Niagara River and the Welland Canal. Overlays of the plume outlines show changes in shape amounting to spreading rates of 600 m to 1100 m in 35 minutes (28-52 cm/sec.). These flow rates are up to 5 times the velocities that are associated with wind mixing effects and it can be seen why they have such effects on sampling in the river plume area.

---

[1]Used by courtesy of CCIW (an IFYGL project).

The thermal bar is clearly visible on the June 5th imagery marked by a large oil slick. It should be noted that on examination of sun glint areas, the surface of the water reveals many details of the river plume mixing into the lake as well as the thermal bar. Examination of such areas shows promise for further work in this study area. Surface patterns indicate a pulsing effect as the river flows over the shallows of the Niagara Bar into the lake.

Further study of this test site is in progress, but it can be seen that repeated flights over a short time period are of great value when dynamic features of the lake are being studied. Ground truth in such an area is not easy to collect because of these water velocities and only aerial photography can give the complete synoptic picture at one point in time without a large fleet of vessels and prohibitive cost. Water turbidity is very important in controlling plant production, by limiting light distribution underwater; remote sensing techniques would appear to be a promising method for detection of turbidity and suspended solids inputs.

4. STUDIES OVER THE LAND AREA

In the land area of the basin a model of either flood conditions of a stream or a model of continuous flow requires detail of the basin characteristics. Meteorological data are available or can be made available for large areas. The response of a basin can only be predicted if its characteristics can be modelled and the effect of these characteristics is primarily in storage within the basin or loss by evaporation (Dickison and Whiteley 1970, Dickinson and Douglas 1972). - Evaporation losses can be estimated from a knowledge of vegetation cover (land-use data) and stored moisture can be estimated from measurements of soil moisture. Other aspects of storage seem to be a function of terrain type and surficial geology (which may be termed geomorphology).

Vegetation cover and land-use studies over regional zones appear to be possible using ERTS imagery (see University of Michigan studies). Over small area test basins RB-57 data have been used for land-use data and the resulting correlation between image density and soil moisture status permits estimation of soil moisture values. This result has been achieved through correction of high altitude imagery (Collins 1972, MacDowall et al 1972) and a knowledge of soil types. Work by Protz and his associates (Cihlar and Protz, 1972a, 1972b, 1973, Crosson and Protz 1972, 1973a, 1973b) has shown that the characteristics of soils which can be detected by sensors are not necessarily those which are represented on published maps. This work also indicates that major soil differences can be detected. Interactions of slope type, slope class and soil properties are important, so too are interactions between parent material and soil type and all have an effect on moisture status.

For modelling of hydrologic response of river basins the knowledge of both soil type and terrain units is important. From RB-57 data the important parameters for small basins can be measured. Examination of ERTS data to date reveals that physiographic maps and soil associations maps do not appear to be directly compatable with ERTS-1 interpretation. Thus, for regional

interpretation of hydrologic parameters from ERTS we must determine the precise nature of the properties which ERTS-1 detects. It appears that useful physiographic information can be obtained from ERTS data (Bruce and Howarth 1972) and at the 1:250,000 scale ERTS provides a more accurate record of wetlands than existing maps. ERTS also permits measurement across the image so that determination of required information within the whole region appears possible.

5. CONCLUSIONS

ERTS-1 data provide a definition of the macro-scopic features within the Lake Ontario Test-site. Definition of lake features including river plumes and effluent upwelling is possible. The significance of other detail within the lake is difficult to determine because many features of the lake are dynamic features and detailed ground truth data cannot be gathered in the available time interval. High altitude (RB-57) data appear to offer the essential step in the correlation of lake behavior with ERTS data by providing keys to the time nature of the major patures.

Over the land area ERTS-1 data offer regional scale information which could yield input for models of river basin response and thus provide important data for lake level control. Maps of land-use, vegetation type soil regions and physiographic regions would provide important information and the preparation of such maps is being investigated. It is clear that ERTS-1 data offer many advantages over regional area mosaics for this purpose and the detail availabe is far greater than shown on existing maps. The ERTS-1 data also apply to the present-day situation. At the present time it appears that ERTS-1 offers hope of improving predictions of discharge from river systems. Conversely ERTS-1 also provides a basis on which to plan instrumentation and control of river systems.

ACKNOWLEDGEMENTS

University of Michigan Willow Run Laboratories for negative prints of ERTS-1 data, University of Guelph Audio Visual Department and F. Adams, D. Irvine, C. Klink for preparation of diagrams and V. Salomonson of NASA for use of ERTS imagery. Input from Ontario Ministry of the Environment and C.C.I.W. personnel during the progress of the project is greatefully acknowledged.

REFERENCES

Boyce, F.M. and K.P.B. Thomson, 1972. "Internal waves of finite amplitude in Lake Ontario". CCIW Technical Series (in press)

Bruce, W.D. and P.J. Howarth, 1972. "Geomorphic significance of surface drainage characteristics interpreted from ERTS-A simulation imagery". Proc. First Canadian Remote Sensing Symposium. Ottawa.

Bukata, R.P. and W.D. McColl, 1973. "The utilisation of sun-glint in a study of lake dynamics", to be presented at the AWRA symposium of Remote Sensing of Water Resouces, Burlington, Ontario, June 11-14, 1973.

Cihlar, J. and R. Protz, 1972a. "Tone differences preception from film transparencies" Photogrammetria 28, pp. 131-40.

Cihlar, J. and R. Protz, 1972b. "Color-film densities for Soils P.1." Photogrammetric Engineering 38, pp. 1091-1098.

Cihlar, J. and R. Protz, 1973. "Surface Characteristics of Mapping Units related to Aerial Imaging of Soils". (in preparation)

Collins, S.H. 1972. "Block Adjustment of Colour in High-Altitude photography" Proc. First Canadian Remote Sensing Symposium Ottawa.

Crosson, L.S. and R. Protz, 1972. "Use of stereoscopic orthophotos for soil-terrain analysis". Proc. First Canadian Remote Sensing Symposium. Ottawa.

Crosson, L.S. and R. Protz, 1973. "Surface characteristics of mapping units related to aerial imaging of soils". (in preparation)

Crosson, L.A. and R. Protz, 1973. "Prediction of Soil Properties from Stereorthophoto measurements of Landform properties". (in preparation)

Dickinson, W.T. and H. Whiteley, 1970. "Watershed areas contributing to runoff" Proc. I.A.S.H. Symposium Wellington, N.Z.

Dickinson, W.T. and R. Douglas, 1972. "A mathematical model of the Cam experimental catchment" Institute of Hydrology technical report, Wallingford, England.

MacDowall, J., A. Falconer and K.P.B. Thomson, 1972. "Simulation studies of ERTS-A and B data for hydrologic studies in the Lake Ontario basin". Report presented to the 4th Annual Earth Resources Program Review, Manned Spacecraft Centre, Houston, Texas, January 17-21, 1972.

Steeman-Nielsen, E., 1952. "The use of radio-active carbon (C^{14}) for measuring organic production in the sea". J. Conseil, Conseil Perm. Intern. Exploration Mer. 18, pp. 117-140.

Strickland, J.D.H. and Parsons, T.R., 1968. "A practical handbook of seawater analysis" Bulletin No. 167, Fisheries Research Board of Canada. Ottawa.

LAKE ONTARIO EXTENDED TEST SITE

NO. 239

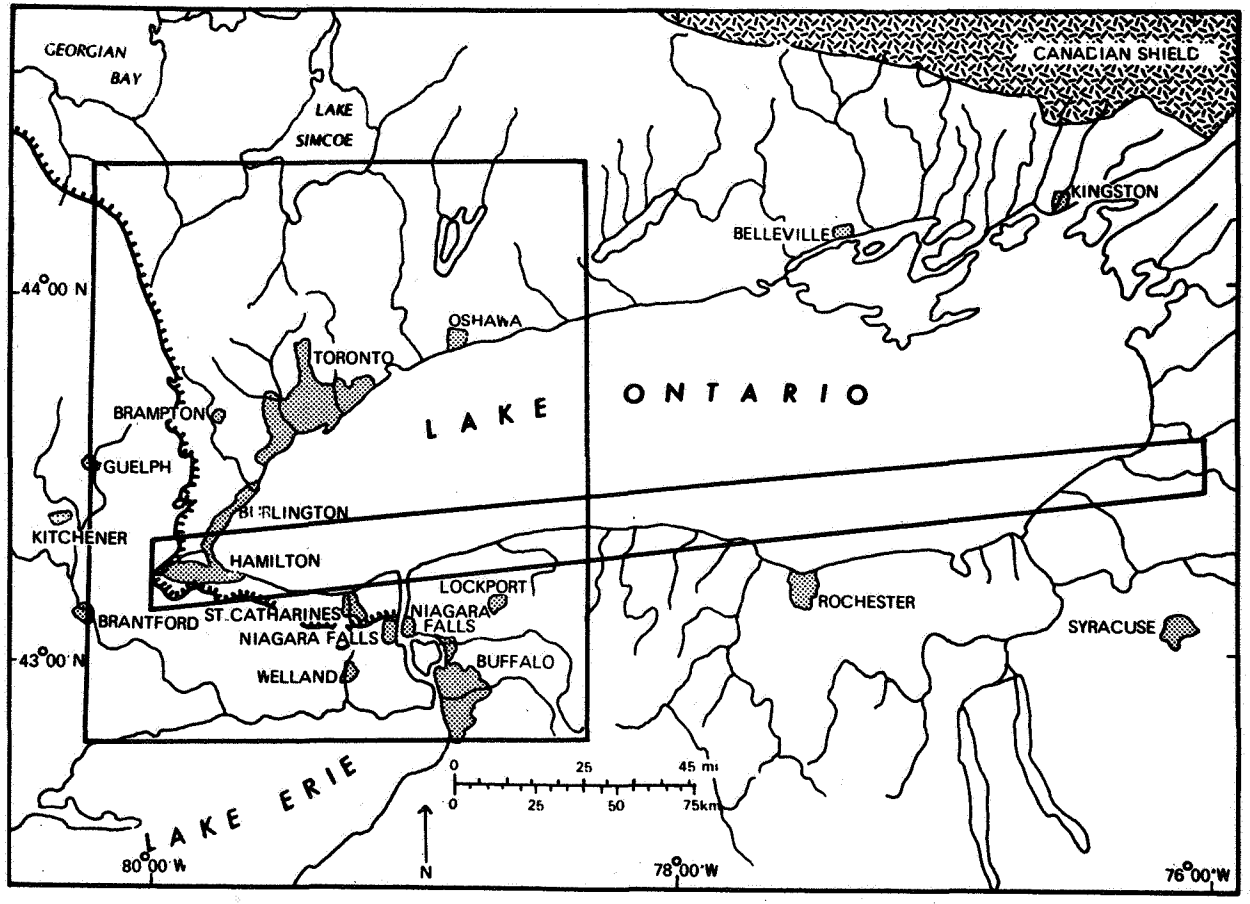
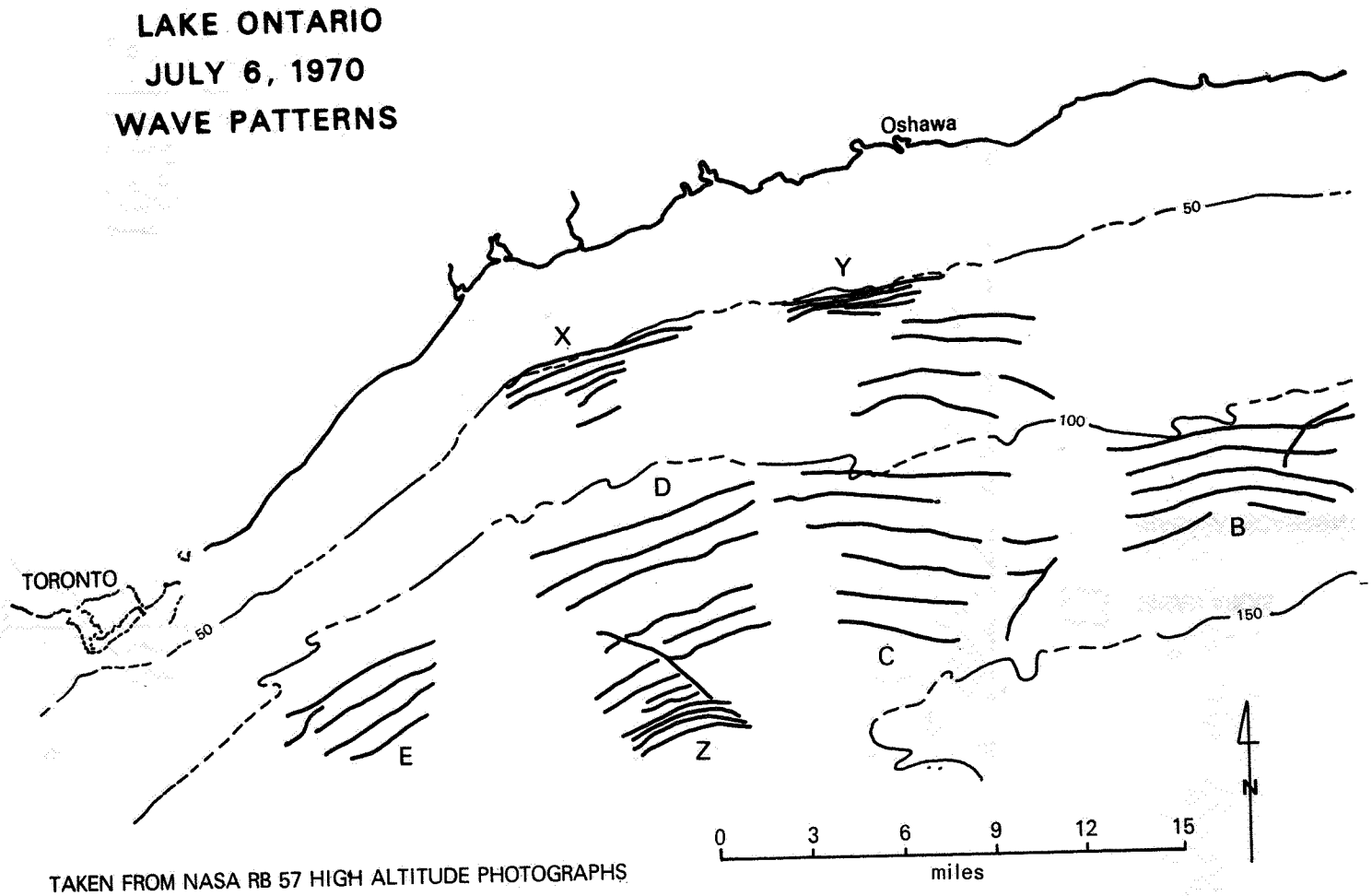


FIG 1



TAKEN FROM NASA RB 57 HIGH ALTITUDE PHOTOGRAPHS
CONTOURS IN METRES

FIG 2

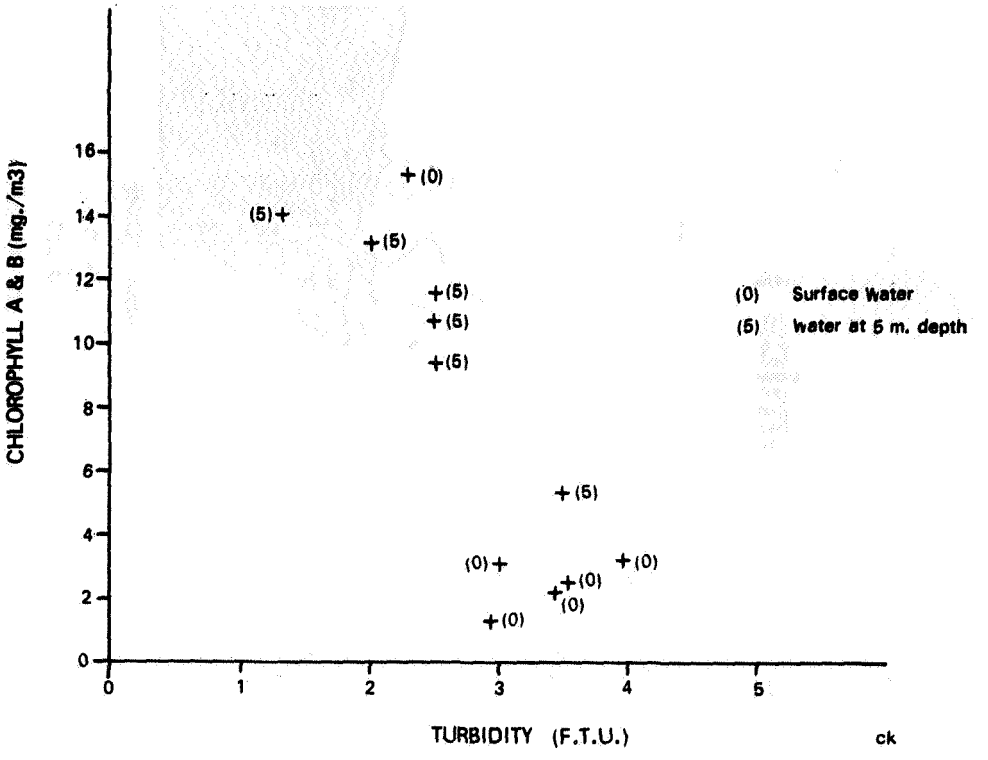


FIG 3 LAKE ONTARIO CHLOROPHYLL DATA

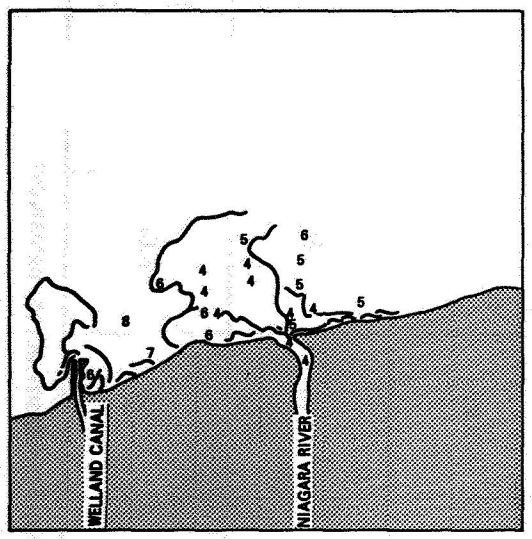
TIME IN HOURS E.S.T. / DEPTH IN METRES	CHLOROPHYLL A & B (Milligrams per cubic metre) JULY 11th, 1972.					
	0900	1000	1200	1400	1600	1800
0	3.05	1.35	15.4	2.2	2.3	3.2
5	13.9	13.09	5.54	10.8	11.6	9.4
10	9.78	7.16	5.02	5.06	3.18	4.76

CARED/ McMASTER UNIVERSITY BIOLOGY DEPARTMENT ck

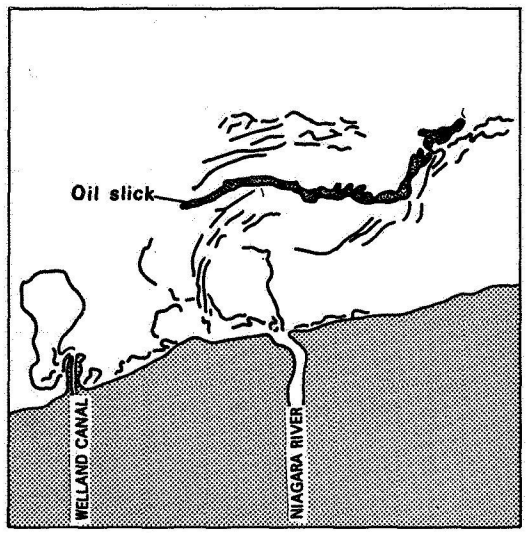
FIG 4

LAKE ONTARIO TEST SITE

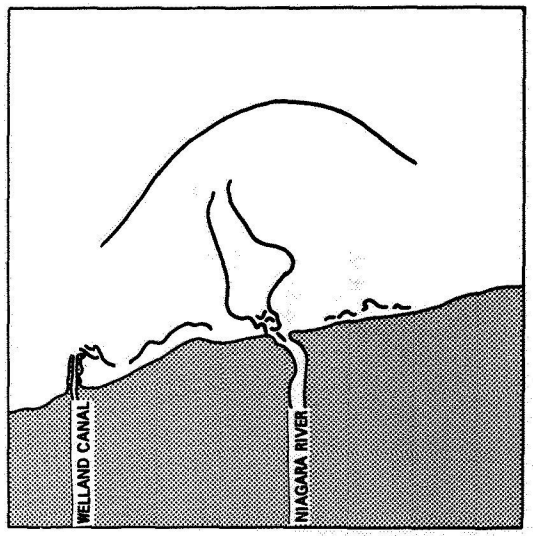
Niagara Plume (Short Term Dynamics)



NIAGARA PLUME
JUNE 5TH
SO 397
1400 HOURS



NIAGARA PLUME
JUNE 5TH
SO 397
1435 HOURS



NIAGARA PLUME
JUNE 7TH
SO 397
1550 HOURS

CARED/McMASTER UNIVERSITY

NASA RB - 57 DATA

Paper W 15

PROGRESS OF AN ERTS-1 PROGRAM FOR LAKE ONTARIO AND ITS BASIN

Thomas W. Wagner and Fabian C. Polcyn, *Environmental Research Institute of Michigan, Ann Arbor, Michigan*

ABSTRACT

The Lake Ontario drainage basin covers over 32,000 square miles of U.S. and Canadian territory. ERTS-1 data is contributing to the comprehensive study of this basin as part of the International Field Year for the Great Lakes (IFYGL). This paper details a processing approach for obtaining detailed and objective synoptic information thought to be applicable to terrestrial water balance studies of such a large area. A simple ratio algorithm was tested for minimizing daily variations in ERTS data and for allowing the discrimination of surface features and land use classes of hydrologic significance. These steps are necessary if ERTS data is to provide the quantitative information required for the study and management of areas of regional size.

1. INTRODUCTION

The Great Lakes region contains one of the most rapidly growing populations in North America - currently numbering some 35 million people. The growth of settlements from Quebec to Milwaukee is expected to continue long after other megalopolises have withered for lack of fresh water. The Great Lakes contain roughly 20% of the fresh water in all the lakes and rivers of the world and will continue to serve our transportation, energy, cultivation, domestic, industrial, and even recreational needs for many generations -- if we are intelligent in the management of this resource. Fresh water of the Great Lakes is neither inexhaustible nor unspoilable. Recent, well-publicized problems in Lake Erie, Lake Ontario, and southern Lake Michigan, have warned of a growing need for basic information and better tools for managing the Great Lakes. Clearly we must better understand the trade-offs in man's conflicting demands for fresh water and the seasonal or episodic ability of the natural drainage basin to meet these demands. With an acute awareness of these requirements to better manage

the hydrologic resources of the Great Lakes, the International Field Year for the Great Lakes (IFYGL) was launched in April, 1972.

The IFYGL is a year long synoptic study of a single Great Lake system -- the Lake Ontario basin [1]. It is a coordinated effort by U.S. and Canadian scientists from many government agencies, universities, and private concerns for the purpose of obtaining a detailed and comprehensive understanding of how such a large hydrologic systems works. The program is broken into five major research areas: (1) terrestrial water balance, (2) Lake meteorology, (3) water movements, (4) energy balance, and (5) Lake biology and chemistry.

ERTS-1 data is contributing primarily to two of these IFYGL research areas: terrestrial water balance and water quality studies related to the chemistry and biology of the Lake. This paper is concerned with the utilization of ERTS-1 data for studies of the terrestrial water balance. It represents a report of the considerations and approach being developed for this IFYGL task at this early stage in its implementation.

2. THE PROBLEM

The Lake Ontario drainage basin (including the lake) covers over 32,000 square miles of U.S. and Canadian territory (Figure 1). The problem in utilizing ERTS data to obtain information concerning the terrestrial water balance from so large an area is 1) what break-down of terrain elements observable from ERTS are hydrologically significant, and 2) how is precise quantitative information of so large an area to be obtained. We will try to answer the second question first.

3. PROCESSING APPROACH

To obtain objective and quantitative information concerning the Lake Ontario basin modern computer processing techniques must be employed. One digitized frame of ERTS-MSS data, representing an area 100 nautical miles on a side, contains nearly 10 million resolution cells in four bands -- nearly 2×10^8 individual scene samples for the entire basin. Even large digital computers have difficulty in digesting this amount of data. Unless our processing procedures and our information needs are tailored carefully, the task of processing data from portions of the required nine ERTS frames may not be economically feasible or cost-effective. Clearly a simple, processing technique performed on a rapid throughput computing facility is required [2]. Because it takes ERTS four consecutive days to obtain complete coverage of the basin, the processing technique also must be able to objectively extend feature discrimination criteria from one frame to the

next and from one day to the next.

We have just completed testing of a simple processing algorithm for a small portion of the basin on a digital computer. This algorithm is a ratio of two ERTS MSS bands. Ratioing of spectral bands has long been used as a preprocessing technique for reducing scene radiance differences due to changes in illumination or differences in the bidirectional reflectance of objects. Only recently has it been realized that the ratio of spectral bands may, in itself, provide enhancement of features not readily discerned in either of the bands individually [3].

Figure 2 compares two digital printouts in a single band for the Rochester Harbor area on two successive days. The plume from the mouth of the Genesee River may be seen along the upper right-hand edges of the images. Note, however, that the patterns for the terrain area are considerably different for the two days, even though the same digital symbols were printed for the same ERTS signal range. Figure 3 provides part of the reason for the differences in the terrain patterns; ERTS MSS signal values were systematically lower for the same areas on the second day. This may be due to differences in illumination (clouds were present in both scenes) or to ERTS MSS sensor differences from one day to the next. In any event, the extension of feature recognition criteria based on absolute signal values from one ERTS frame to the next (and perhaps from one portion of an ERTS frame to another) would net dubious classification results.

Figure 4 compares two digital printouts for a ratio of band 7 (0.8-1.1 μm) to band 5 (0.6-0.7 μm) for the same Rochester Harbor area. A minor path radiance normalization was introduced for both the images. Again the same digital symbol is used for a given signal range. The two images are nearly identical. Slight differences occur along the shoreline, where turbid shallow water looks like land, and near the bottom of the August 20th image, where two small clouds appear. This ratio technique will help to extend predetermined feature recognition criteria, based on relative differences between ERTS bands, to ERTS data of the entire Lake Ontario basin.

The approach adopted for this task is to convert digital ERTS data to an analog format and then process these data on a high-speed analog facility. The analog computer, known as "SPARC" for Spectral Analysis and Recognition Computer, can process data at a rate of 10^4 resolution cells per second (less than 2 hours is required for the entire basin). (Average operating cost for the SPARC is $50/hour.) The SPARC has an added advantage in printing the processed results as 70 mm film transparencies. A mosaic of recognition images for the entire basin will measure about 25 cm by 30 cm; an equivalent digital paper display would cover an area of approximately 25 m by 30 m.

4. DECISION CRITERIA

In stating the problem of relating ERTS data to the terrestrial water balance, we first asked the question; "what break-down of terrain elements observable from ERTS are hydrologically significant?" No final answer has yet been obtained for this important question. Indeed we are still discovering the precise nature of features which may be reliably discriminated from ERTS data. Since a concern of this IFYGL task is for rapid processing of large amounts of data, we are restricted by economics to simple decision criteria. Perhaps the simplest machine-implemented criteria is that of level-slicing, or quantizing--as it's sometimes called. In this procedure, feature classes are discriminated on the basis of the exclusiveness with which they are represented by a maximum and a minimum signal range in one band or data channel. For a variety of terrain classes signal levels were compared in each ERTS band and for the ratio of band 7 to band 5.

Spectral signatures were obtained from eight relatively large areas in the two Rochester frames discussed previously. Except for portions of Lake Ontario, these signature sample areas were by no means homogeneous, and they are only roughly identified from aerial photography as 1) agricultural, 2) wooded, 3) recreational (golf course), 4) new urban (recent residential development), 5) commercial, 6) older residential, 7) water (Lake Ontario), and 8) cloud shadow. The intent here was to obtain only a broad representation of major surface classes. It is probable that with careful signature selection each of these classes may be further subdivided.

Comparing mean values and standard deviations, it was noted which classes or groupings of classes could be separated in each ERTS band and from the ratio of band 7 to band 5. The standard deviation for the commercial area signature (downtown Rochester) spanned such a large range that it overlapped most of the other categories and had to be ignored in the ERTS band groupings (but not the ratio groupings). In general no ERTS band allowed for more than four groups of separable classes, although different combinations were evident with different bands. Of particular concern was the fact that water signatures overlapped other categories in all but band 7. The ratioed values for the same terrain classes separated neatly into five groups: 1) water, 2) wooded, 3) agricultural and recreational (golf course), 4) older residential, and 5) new urban and commercial. (Figure 5). The normalized ratio values ranged between 30 and 511 with the bulk of that range, 150-510, being represented by vegetation classes. It appears that this ratio is a sensitive indicator of vegetational differences. The decision criteria will then consist of setting maximum and minimum ratio values for those terrain classes which are considered to have significantly different hydrologic characteristics.

5. ERTS AND THE TERRESTRIAL WATER BALANCE

How does ERTS contribute to a better understanding of the water balance for Lake Ontario and what is its value in managing water resources? ERTS can provide quantitative spatial information for the entire basin. This information is useful to the extent that we know or can discover how surface features, patterns of land use or drainage, or temporal changes in these affect and are affected by the dynamics of basin hydrology. The amount of water held in storage on the land portion of the basin and rates of runoff and evapotranspiration are correlated with the area and distribution of surface features and conditions. Present models for basin hydrology depend on samples made at one or more points within the basin; there is seldom adequate knowledge of the spatial variability of a basin or of its seasonal or long term (land use) changes.

The approach for this ERTS-IFYGL task is to attempt to establish quantitative relationships between ERTS-observed features and hydrologic parameters recorded on the ground in selected watersheds of manageable size. The second step is to extrapolate these parameters from the representative watersheds to the entire basin using ERTS data. One such watershed is the Oakville Representative Basin (inset on Figure 1). Personnel from the Ontario Ministry of the Environment are actively recording in this and several other Representative Basins such parameters as precipitation, soil moisture, stream and ground water flow, and snow accumulation in the winter season. NASA and ERIM have periodically collected aircraft data from these and other study areas. These data, the ground measurements and aircraft imagery are now being used in the analysis of ERTS data by scientists at ERIM, OME, and the University of Guelph.

6. CONCLUSIONS

While the input (rainfall) to a basin is variable, man's output requirements are determ nistic [4]. Basin storage and runoff must provide consumers with energy, irrigation water, municipal supplies, and even recreation sites. Clearly, differences and changes in the surface associated with land management and water use greatly affect and are affected by surface storage, runoff, evaporation, and concomitant soil erosion and stream sedimentation rates. ERTS can help us to study and attack these problems on a truly regional scale. We believe we have developed an operationally feasible method for utilizing large amounts of ERTS data for this purpose. Preliminary studies are most encouraging [5]. A great deal now needs to be done in relating this approach to the hydrological problems which are increasingly and menacingly evident in the Great Lakes region.

7. ACKNOWLEDGEMENTS

The authors wish to acknowledge the technical assistance of D. Rebel, F. Thomson, and the staff of the ERIM Publications Department.

8. REFERENCES

1. Ludwigson, J., (1972). "International Field Year for the Great Lakes" in Geotimes, December, pp. 16-18.

2. Marshall, R. E. and F. J. Kriegler, (1971). "An Operational Multispectral Survey System," Proceedings of the 7th International Symposium on Remote Sensing of Environment, University of Michigan, Ann Arbor.

3. Vincent, R. K., (1973). "Ratio Maps of Iron Ore Deposits, Atlantic City District, Wyoming", 193301-13-S/S_a/J, to be submitted at the ERTS-1 Goddard Meeting, 5-9 March 1973.

4. Castruccio, P. A. (1972). "Remote Sensing and Data Handling - There Application to Water Resources" in Remote Sensing of Earth Resources, Committee on Science and Astronautics, U. S. Printing Office.

5. Malila, W. A. and T. W. Wagner. (in press). "Multispectral Remote Sensing of Elements of Water and Radiation Balances", in Proceedings of the 8th International Symposium on Remote Sensing of Environment, Univeraity of Michigan, Ann Arbor.

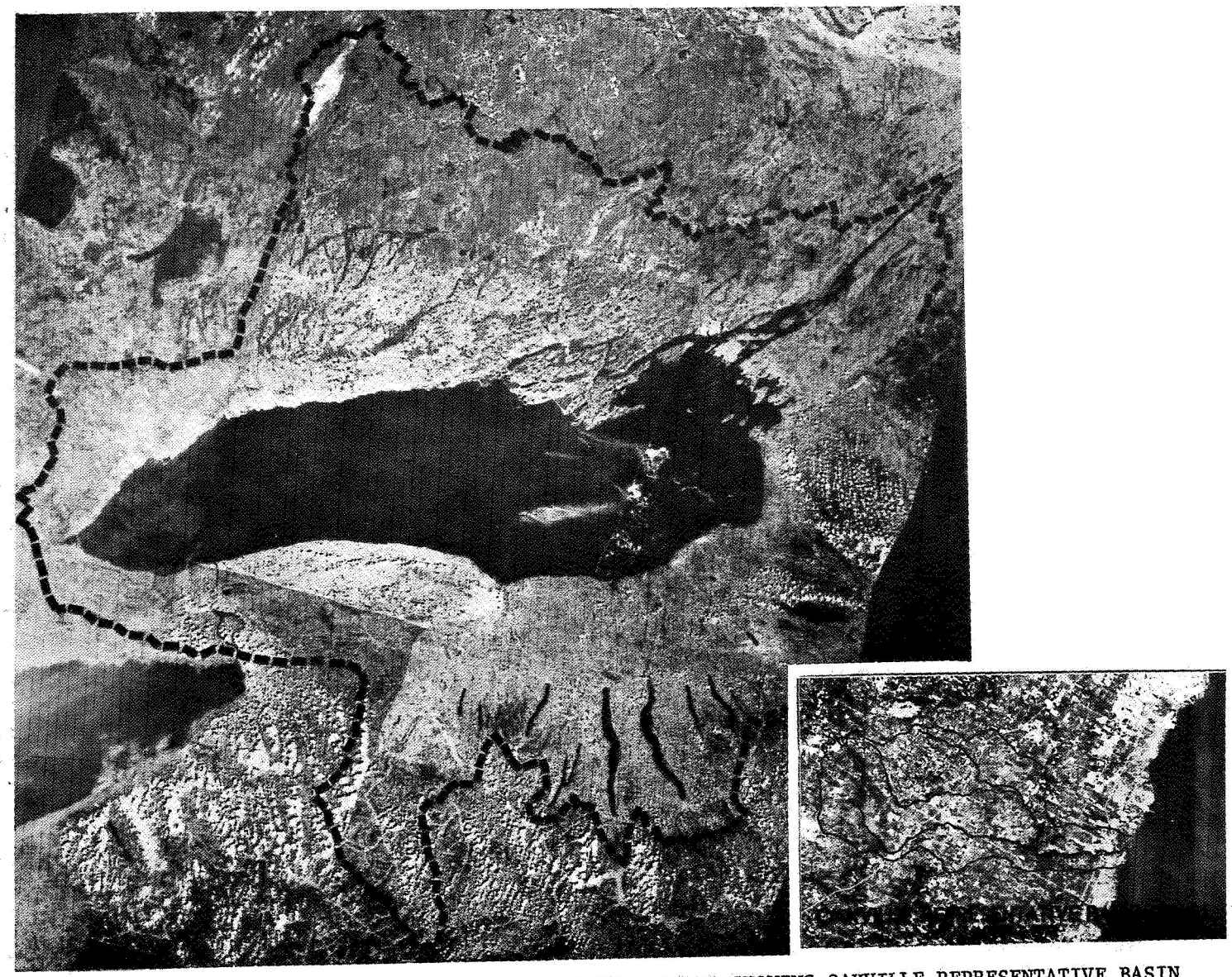


FIGURE 1. MOSAIC OF LAKE ONTARIO DRAINAGE BASIN WITH INSET SHOWING OAKVILLE REPRESENTATIVE BASIN ERTS-1 BAND 5 (0.6 - 0.7 μm). AUGUST 1972.

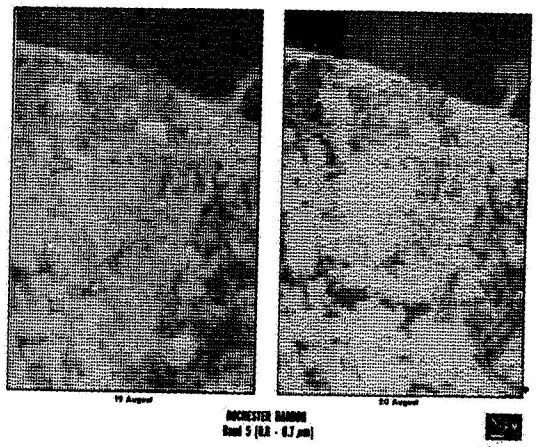


FIGURE 2. COMPARISON OF THE SAME AREA ON TWO DIFFERENT DAYS AS RECORDED BY ONE ERTS BAND.

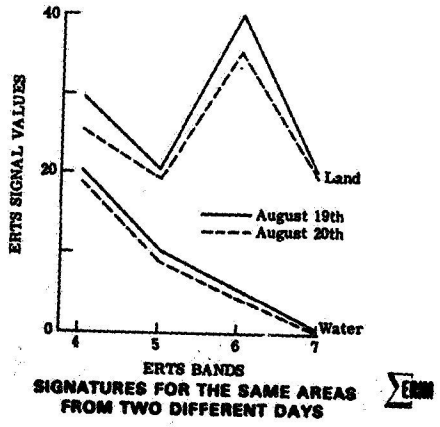


FIGURE 3. MEAN SIGNAL VALUES FOR TWO AREAS ON TWO DIFFERENT DAYS AS RECORDED IN FOUR ERTS MSS BANDS.

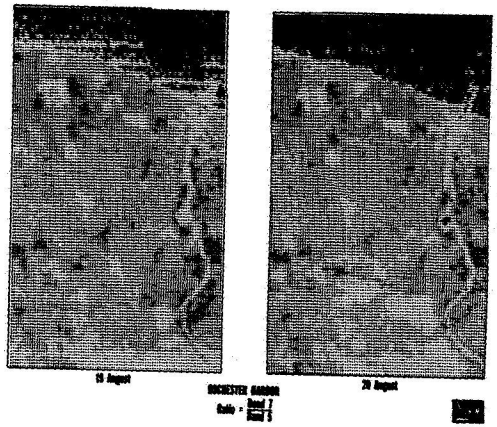


FIGURE 4. COMPARISON OF THE SAME AREA ON TWO DIFFERENT DAYS AS RECORDED BY A RATIO OF TWO ERTS BANDS.

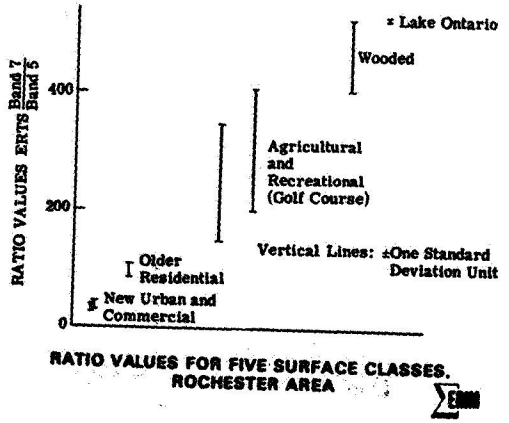


FIGURE 5. MEAN RATIO VALUES AND THEIR STANDARD DEVIATION FOR FIVE SURFACE CLASSES.

Paper W 16

REMOTE SENSING OF TURBIDITY PLUMES IN LAKE ONTARIO[1]

Edward J. Pluhowski, *U. S. Geological Survey, Arlington, Virginia*

ABSTRACT

Preliminary analyses of ERTS-1 imagery demonstrates the utility of the satellite to monitor turbidity plumes generated by the Welland Canal, and the Genesee and Oswego rivers. Although visible in high altitude photographs, the Niagara River plume is not readily identifiable from satellite imagery.

INTRODUCTION

The utility of high-altitude photography in hydrologic research has been under study in the Lake Ontario basin since July 1970. These studies, conducted by the Canada Centre for Inland Waters, McMaster University, Hamilton, Ontario, Guelph University, Guelph, Ontario, and the U.S. Geological Survey are concentrated over the western part of the basin and the southern shoreline of the lake. The research efforts focus on soil moisture and ground-water detection, water quality, and the sources, movement and fate of sediment entering the lake.

A new dimension was added to the research with the orbiting of the ERTS-1 satellite in July 1972. By way of illustration, promising results were obtained from high altitude (60,000 ft) photography with regard to monitoring the shape and area extent of turbidity* plumes entering the lake's south shore (Pluhowski, 1973). However, it was not known how effective ERTS imagery would be in detecting turbidity features greater than 100 ft in width. The purpose of this paper is to provide preliminary conclusions regarding identification of turbidity plumes in Lake Ontario from ERTS-1 imagery, and to define plume dynamics under a variety of wind stresses.

*Turbidity--the degree of opaqueness of water due principally to the amount of suspended matter.

1/ Publication authorized by Director, U.S. Geological Survey

NIAGARA RIVER AND WELLAND CANAL PLUMES

The Niagara River is, by far, the largest single source of suspended sediment entering Lake Ontario. Additionally, over 200 mgd (million gallons per day) of industrial discharge from chemical, primary metals, and paper plants in New York State enter the Niagara River (Limnos, 1972). Much of this effluent emanates in the Buffalo metropolitan area located at the eastern end of Lake Erie near the source of the Niagara River. This heavy sediment and industrial effluent loading, when combined with the very large average flow of the river (about 200,000 cfs) produces a widespread, well-defined turbidity plume in Lake Ontario in high-altitude photography.

For example, figure 1 is a high-altitude (60,000 ft) photograph of the Niagara River plume obtained on July 6,

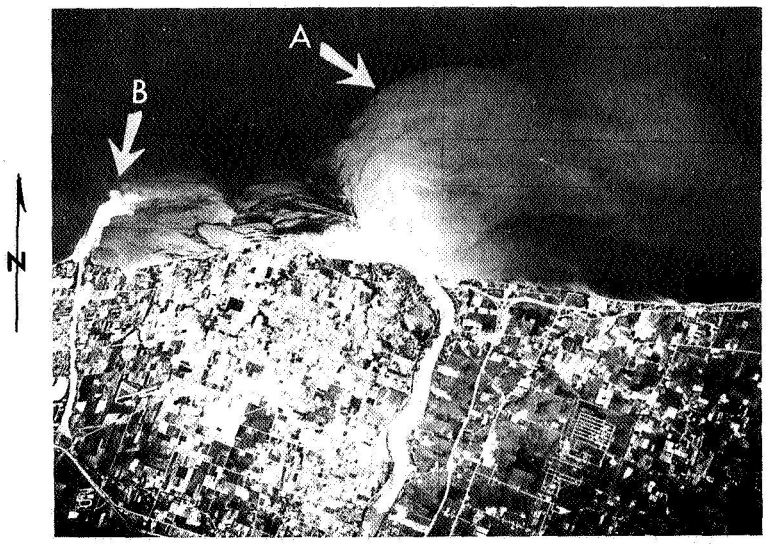


Fig. 1 -High-altitude photograph obtained July 6, 1970, showing the Niagara River plume (A) and the Welland Canal plume (B). Photography from NASA.

1972. The plume was oriented in a northwest direction at its mouth. It gradually veered to a north and finally to a east-northeast direction in response to a brisk 10-15 knot west-southwest wind. At its extreme point the plume was visible 6 miles offshore. A region of turbulent mixing is visible in the photograph along the western edge of the Niagara River plume, and in a zone within the jet itself, about 1/4 mile northwest of the river's mouth. Highly

turbid water, depicted by very bright tones, was being discharged at the entrance to the Welland Canal. The canal is affected by oil discharge and waste from cargo vessels and pleasure craft. Accordingly, the outflow from the canal, average flow, 7,000 cfs (DeCooke, 1968) appears bright in the high-altitude photography. Once beyond the canal's entrance, the Welland Canal discharge is swept to the east by prevailing west winds.

When viewed from the ERTS-1 satellite, the Welland Canal plume and a plume emanating from Port Dalhousie harbor several miles to the west are readily apparent (fig. 2).

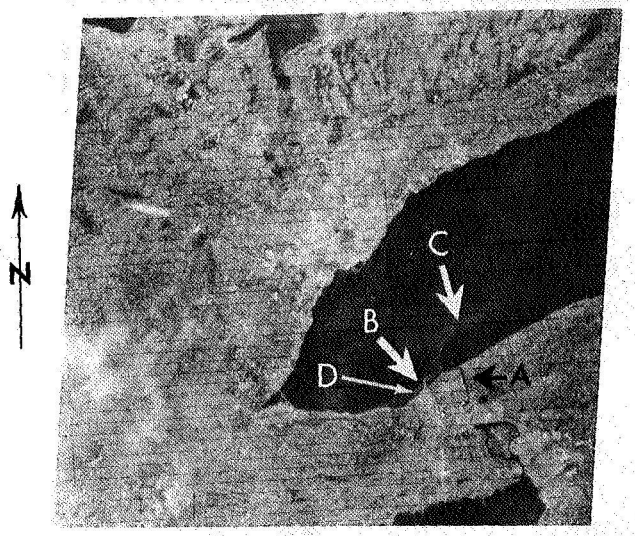


Fig. 2. - ERTS-1 imagery obtained Aug. 21, 1972 showing the Niagara River (A), Welland Canal plume (B), Port Dalhousie harbor plume (D), and the inferred boundary of the Niagara River plume (C). Imagery from NASA.

This imagery, obtained August 21, 1972, shows both plumes drifting to the east-northeast under the influence of 10- to 15-knot west-southwest winds. The Niagara River plume is not visible. Despite its large sediment load, turbidity values of the Niagara River are low--generally about 1 JTU (Jackson Turbidity Unit). By way of contrast, turbidity readings during the shipping season are high in the Welland Canal, often near 50 JTU. Accordingly, the Welland Canal plume appears much brighter in the imagery than does the Niagara River plume.

Owing to a unique combination of meteorologic and hydrologic events, the west and north boundaries of the Niagara River plume were definable in the imagery. Turbid waters from the Welland Canal and Port Dalhousie harbor plume were driven east toward the mouth of the Niagara River. The bouyant surface-spreading of the warmer and less turbid river water over the colder lake water forms a sharp tonal discontinuity along the west and north boundaries of the Niagara River plume. Thus, despite the absence of a definitive tonal signature, the areal extent and shape of the Niagara River plume can be inferred from this imagery.

The position and shape of the Niagara River plume is difficult to define in ERTS imagery whenever the surrounding lake waters are relatively clear. By way of illustration prevailing northeast winds on November 1, 1972, swept both the Welland Canal and Port Dalhousie harbor plumes away from the mouth of the Niagara River (Fig. 3). Turbidity

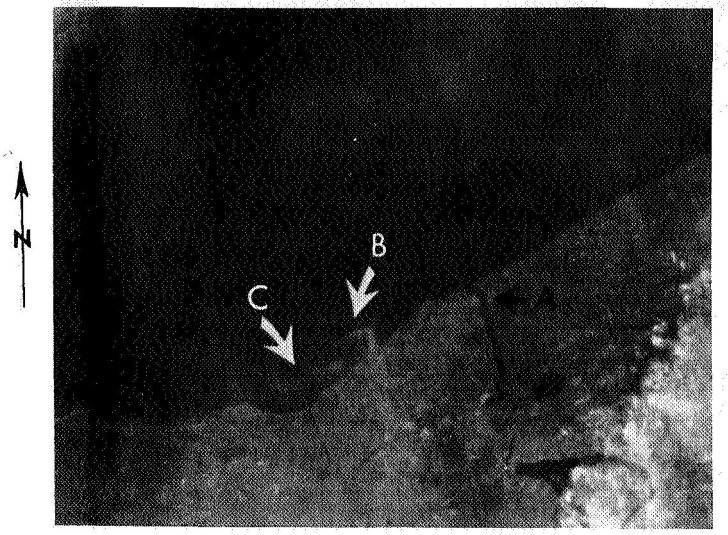


Fig. 3.- ERTS-1 imagery obtained Nov. 1, 1972, showing the Niagara River (A), the Welland Canal plume (B), and the Port Dalhousie harbor plume (C). Imagery from NASA.

levels at the time of this imagery were as follows:

Location	Turbidity (JTU)
Niagara River (at mouth)	1 to 1.5
Port Dalhousie harbor	6 to 8
Welland Canal	25

Despite the presence of a cirrostratus cloud overcast, the relative tonal intensity of each watercourse in the imagery appears to corroborate the turbidity levels shown in the above table. Because the turbid waters were moving away from, rather than toward the mouth of the Niagara River, it is difficult if not impossible to identify the Niagara River plume in this particular image.

GENESEE RIVER PLUME

Erodible soils and extensive agriculture within its basin combine to insure delivery of a large supply of sediment to the Genesee River. In addition to the sizeable sediment yield of the basin, the river receives effluents from many sources, particularly from the Rochester, New York metropolitan area. The resulting high turbidity levels at the mouth of the Genesee River impart a distinctly light color to the river when viewed on aerial photographs. Accordingly, the Genesee River plume is easily identifiable on most aerial photographs owing to the normally large tonal contrast between the plume and the surrounding, relatively clear, waters of Lake Ontario.

A well-defined counter-clockwise circulation pattern within the Genesee River plume was visible in the high-altitude photography on October 19, 1970 (fig. 4). The

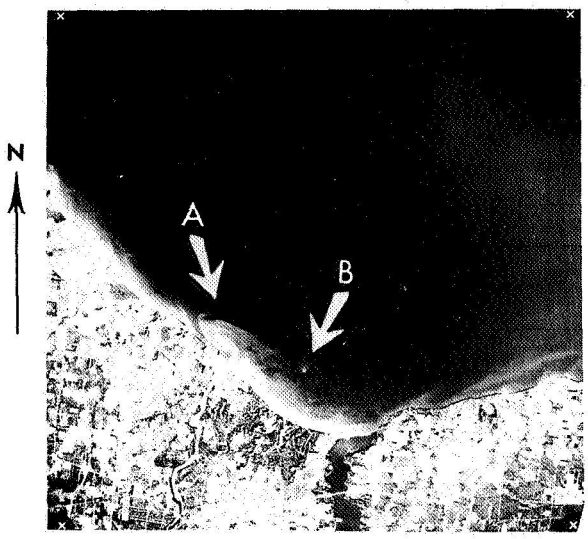
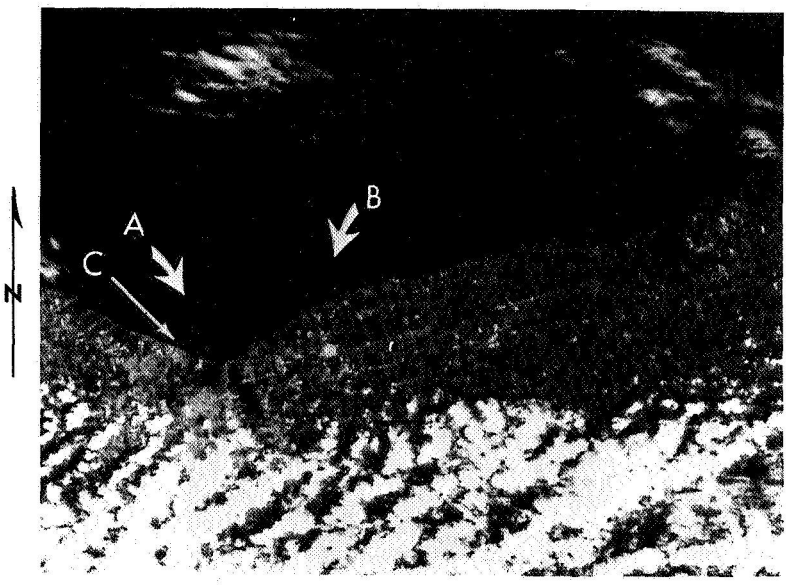


Fig. 4.- High-altitude photograph obtained Oct. 19, 1970, showing the Genesee River plume (A) and a submerged sewer outfall (B). Photography from NASA.

plume, covering about 2 sq. mi. of the lake's surface, was swept westward by prevailing 6-to 8-knot east-northeast winds. A counter-clockwise gyre, formed to the lee of the harbor breakwater, extends about one mile downwind from the mouth of the river (fig. 4). Turbidity levels ranged from 9 JTU in the Genesee River to 1 to 2 JTU in the clearer (darker) inshore waters along the base of the west breakwater. To the west of the plume, a strong northwest-trending longshore current is identifiable in the photograph. A less intense littoral current is visible east of the breakwater mixing, at that point, with flow from the Genesee River.

Effluent discharge from a submerged sewer outfall situated nearly 2 miles offshore is visible in the photograph. On October 19, 1970, pollutants from the outfall were swept westward, eventually merging with the Genesee River plume about 1 mile northeast of the river's mouth.

Two large turbidity plumes emanating from the mouth of the Genesee River were detected in the ERTS imagery obtained Spetember 6, 1972 (fig. 5). Suspended sediment



-Fig. 5.- ERTS-1 imagery obtained Sept. 6, 1972, showing the Genesee River plume (A), a longshore plume (B), and the Genesee River mouth (C). Imagery from NASA.

carried by the river initially moves to the east due to prevailing west-southwest winds. The plume abruptly divides a short distance downwind, part moving northward into Lake ontario and the remainder continued moving east along the coast line. At a point about 2 1/2 miles offshore, the northward moving plume once again abruptly changes direction, this time to the west. This anomalous pattern of motion suggests the existence of a large counterclockwise clear-water gyre between the mouth of the Genesee River and the inside boundaries of the offshore plume.

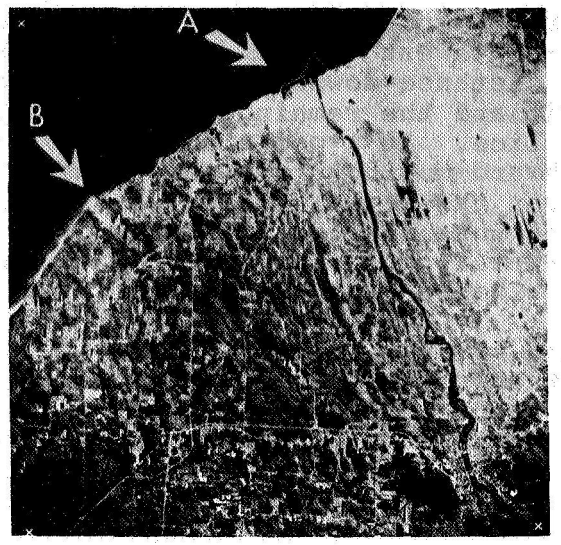
The eastward moving longshore plume is reinforced by turbidity from the previously mentioned sewer outfall, by outflow from Irondequoit Bay and shoreline erosion caused by waves approaching the shore at a large angle of incidence. The reinforced turbidity plume is clearly visible for a distance of 16 miles downwind from the Genesee River.

OSWEGO RIVER PLUME

A substantial portion of the sediment yield in the Oswego River basin is retained by numerous natural lakes and man-made impoundments found throughout the watershed. About 6 percent of the basin's 5,100 sq. mi. area represents lake surfaces (Liu and others, 1972). Extensive reaches of the Oswego River form part of the New York State Barge Canal system. Owing to these numerous man-made sediment sinks, turbidity levels at the mouth of the Oswego River are lower than might be expected. Accordingly, the Oswego River plume appears less intense in high altitude areal photography than either the Genesee River or the Niagara River plumes.

High turbidity, possibly caused by beach erosion, is evident in the high-altitude photograph obtained on October 19, 1970, adjacent to, and to the southwest of Burt Point (fig. 6). The shoreline below Burt Point is oriented on a northeast-southwest axis paralleling the the prevailing northeast winds. A strong longshore current generated by the juxtaposition of shoreline and prevailing winds resulted in a beach erosion, and the resuspension of fine-grained bottom materials.

The predominantly onshore winds on October 19, 1970, confined the Oswego River plume to the harbor and to the lee of the harbor enclosure. The area of the plume, including the harbor, was only 1.2 sq. mi. The plume was only slightly more turbid than the surrounding lake water



-Fig. 6.- High-altitude photograph obtained Oct. 19, 1970, showing the Oswego River plume (A) and Burt Point, N.Y. (B). Photography from NASA.

so that it appears just a few tones lighter than the relatively clear lake waters.

The Oswego River plume trails off to the northeast under predominantly west-northwest winds as portrayed in the ERTS imagery for August 19, 1972 (fig. 7).

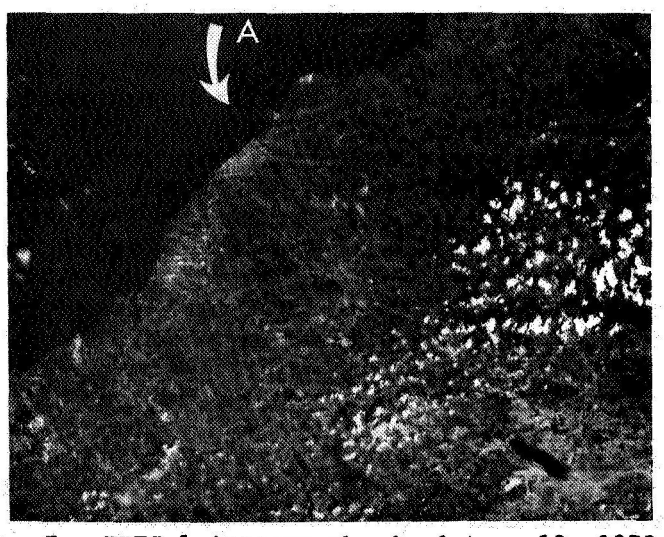


Fig. 7.- ERTS-1 imagery obtained Aug. 19, 1972, showing the Oswego River plume (A). Photography from NASA.

Turbidity levels in the clear lake waters normally average about 1 JTU whereas base flow turbidity levels of about 3 to 5 JTU are common in the Oswego River. Thus, despite the small differences in turbidity between river and lake, the Oswego River plume is identifiable from satellite imagery.

An intense zone of beach erosion over the western part of Lake Ontario was revealed by imagery obtained December 7, 1972 (fig. 8).

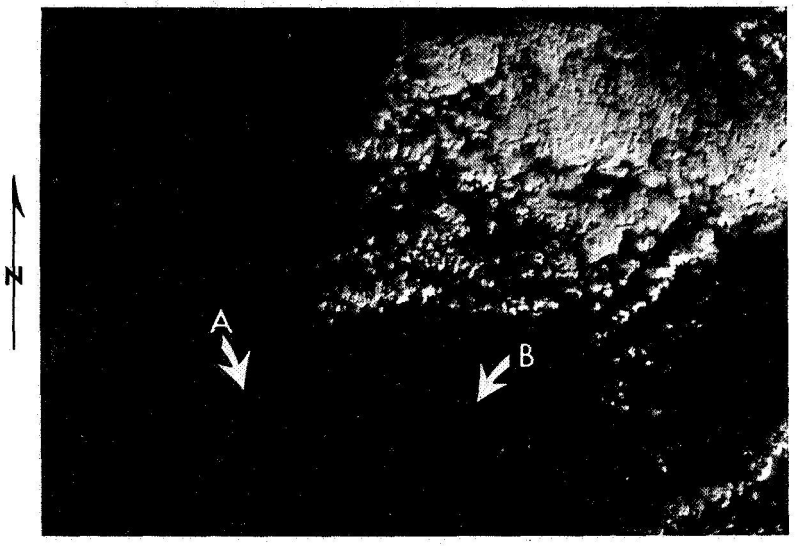


Fig. 8.- ERTS-1 imagery obtained Dec. 7, 1972, showing longshore plumes. Imagery from NASA.

Strong northwest winds on December 6 and 7 generated rough waters in Lake Ontario. The resulting wave action and higher-than-normal lake levels along the lake's south shore resulted in extensive beach erosion. This is indicated by the thin but relatively sharp tonal discontinuities in the littoral zone bordering the south shore. Another interesting feature in this imagery are the cloud formations developing over the lake and its leeward shores as the cold northwest winds gain moisture in their traverse over the lake.

CONCLUSIONS

Large turbidity plumes generated by the Welland Canal, at Port Dalhousie harbor, and the Genesee and the Oswego rivers are plainly identifiable

in ERTS-1 imagery and in high altitude photography. Although visible in high altitude photographs, the Niagara River plume could not be visually identified from the satellite imagery. Zones of intense beach erosion are visible in both aircraft photography and satellite imagery.

High altitude aircraft photography provided valuable "baseline" data which was very helpful in evaluating and interpreting ERTS-1 imagery. The high altitude photographs were small enough in scale to capture most turbidity features on a single frame and they were good enough in quality to show the fine detail in the most delicate turbidity features. With this type of background information, it is possible to assess the quality and correctly interpret the hydrologic processes causing the turbidity phenomena illustrated by satellite imagery.

Best results for detecting plumes were obtained using MSS band 5 -- little or no information could be gleaned from MSS band 7. MSS band 4 yielded generally good results, but at times appeared to be affected by haze and atmospheric moisture. MSS band 6 produced only slightly better results than band 7.

REFERENCES

DeCooke, 1968, The Great Lakes water levels problem: Limnos, v. 1, no. 1, p. 22-26.

Limnos, 1972, The situation lake by lake: v. 5, no. 1, p. 19-23.

Liu, C. S., Muralidhar, D., and Jedrov, A. C., 1972, Multipurpose operation studies of a canal-lake-river system - Oswego River system, New York: Am. Water Resources Assoc., Water Resources Bull., v. 8, no. 2, p. 349.

Pluhowski, E. J., 1973, Remote sensing of turbidity plumes in Lake Ontario: Jour. Research U.S. Geol. Survey, in press.

Paper W 17

ERTS-1 VIEWS THE GREAT LAKES

Walter A. Lyons, *Air Pollution Analysis Laboratory, College of Engineering and Applied Science, University of Wisconsin-Milwaukee, Milwaukee, Wisconsin;*
Steven R. Pease, *Department of Geography, University of Wisconsin-Milwaukee, Milwaukee, Wisconsin 53201*

ABSTRACT

The meteorological content of ERTS images, particularly mesoscale effects of the Great Lakes and air pollution dispersion is summarized. Summertime lake breeze frontal clouds and various winter lake-effect convection patterns and snow squalls are revealed in great detail. A clear-cut spiral vortex over southern Lake Michigan is related to a record early snow storm in the Chicago area. Marked cloud changes induced by orographic and frictional effects on Lake Michigan's lee shore snow squalls are seen. The most important finding, however, is a clear-cut example of alterations in cumulus convection by anthropogenic condensation and/or ice nuclei from northern Indiana steel mills during a snow squall situation. Jet aircraft condensation trails are also found with surprising frequency.

1. INTRODUCTION

With the launching of TIROS I in April, 1961, meteorologists gained a valuable tool for the study of synoptic scale weather systems. The inherent resolution characteristics of the imaging systems used, however, made it difficult to define the details of synoptic systems and failed even to detect many mesoscale processes. Atmospheric motion system peak in the mesoscale (1-100 km wavelengths). The meteorological effects induced by the Great Lakes, both upon cloud systems and air pollution dispersion, could in most cases be classified as mesoscale. ERTS-1, with its extremely high resolution as well as multispectral monitoring capability, promised to be the first satellite ideally suited to the needs of mesometeorologists, cloud physicists, and air pollution meteorologists. It appears to have more than lived up to its initial promise in this first summer and winter of monitoring the various distinctive interactions between the Lakes and the atmosphere.

2. GREAT LAKES IN SUMMER

Great Lakes surface water temperatures during spring and summer months often are as much as 30°C colder than advecting air masses. This results, under certain circumstances, in extreme supression of cumulus and thunderstorm convection over the Lakes. Moreover, lake breezes frequently push onshore, further altering convective cloud distributions.

These mesoscale cold fronts may penetrate inland from one to fifty km, typically are 500 m in depth, and have peak values of vertical motion at the leading edge of 100 to 200 cm/sec. Depending upon synoptic scale wind patterns, convective clouds near the front may either be dissipating or experiencing rapid growth (occasionally to severe thunderstorm stages). In either case, a well defined cloud line marks the inland penetration of the lake air. On 20 August 1972, conditions for a lake breeze over the lower Great Lakes were ideal. Figure 1 clearly shows the lake breeze frontal cloud band along the south shore of Lake Ontario and around both shores of Lake Erie. It is apparent that the front closely parallels the shoreline indentations, an assumption made in numerical models. The inland penetration does not seem to be affected by the presumed heat sources of major cities (Rochester and Buffalo), as is sometimes suggested. Each and every cumulus cell is easily identified. Future such images will be of great value in studying mesoscale cloud-lake interactions, and in evaluating the physical processes involved in summer precipitation deficits suspected present over the Lakes.

3. GREAT LAKES IN WINTER

During fall and winter arctic air masses, sometimes more than 30°C colder than the underlying water, move across the Lakes resulting in intense lake-effect snow squalls, dumping massive amounts of snow on lee shores. Numerous ERTS views of such events have shown the full range of patterns expected, including Bénard-like cellular patterns during weak convection, the more intense linear longitudinal bands roughly paralleling the low level winds, and the massive single-band snow squalls of the type which afflict Lakes Erie and Ontario during periods of cold, unstable southwesterly flow. Certain indications have suggested however that during situations conducive to even more intense convection than in the single-band case, a series of small mesoscale lows may propagate with the winds. Microbarograph networks at the eastern end of Lake Ontario have indicated such travelling depressions. During an intense snow burst in Chicago on 23 February 1967 (7 inches in one hour), radar revealed a spiral band echo pattern over southern Lake Michigan resembling a miniature hurricane. On 19 October 1972, a cold arctic high centered in Iowa advected air with near-freezing surface temperatures across lakes some 20°F warmer. Northeasterly flow across Lake Huron generated a multi-striated snow squall band which travelled across lower Michigan and then over Lake Michigan. The ERTS images show that the band regenerated and developed an obvious spiral cloud pattern (Fig. 2a) northeast of Chicago. Preceeding snow squalls (and perhaps mesolows) had already deposited 3-5 inches of snow over northwestern Indiana in the prior 9-12 hours, easily visible especially in the 0.5-0.6 micrometer band and in CIR composits. Snow approaching moderate intensity was falling along the Chicago shoreline at the time of ERTS overflight, and surface wind reports certainly suggest a mesoscale cyclonic circulation approaching the shore (Fig. 2b).

On 11 December 1972, cold west-southwesterly flow across southern Lake Michigan was resulting in the expected cumulus convection over the water. What is most intriguing about the cloud patterns on the lee shore-

line (Fig. 3) is the abrupt transition from scattered to nearly overcast cloud cover, the sudden formation of longitudinal bands, and a change in cloud appearance suggesting glaciation. Steep-faced 100 m high dunes at the shorelines apparently caused significant orographic lift, and combined with onshore frictional convergence within the boundary layer, the sudden increase in vertical motions produced marked changes in cloud structure, and presumably snowfall potential.

4. INADVERTANT WEATHER MODIFICATION

On 24 November 1972, cold southwesterly flow again traversed Lake Michigan. An inspection of the cumulus patterns (Fig. 4) show particulate plumes from at least seven steel mills and power plants feeding directly into the clouds. The bands emerging from these plumes, which almost certainly contain vast amounts of anthropogenic condensation and ice nuclei, form closer to the shoreline and become more intensely developed. Pollution in this area has long been suggested as the cause of the La Porte, Indiana precipitation anomaly, and this obvious incidence of inadvertant weather modification strengthens such a contention.

Man-made cirrus clouds from jet aircraft are also being considered as a potential modifying factor in the global energy balance. Figure 5a shows a broken layer of cirriform cloudiness over southeastern Wisconsin, and intermingled are contrails in various stages of diffusion, some having expanded to at least 11 km in width. In the 0.8 - 1.1 micrometer band (Fig. 5b), two things are notable: the considerable transparency of both natural and man-made cirrus in the near infrared, and the easily recognizable shadows of the jet contrails.

5. SUMMARY

As both ERTS images and supporting meteorological data become available, it is obvious that many major projects of meteorological significance should evolve. Particulate plumes visually tracked for over 50 nm from steel mills proves graphically how adjacent Air Quality Control Regions (Chicago and Southeast Wisconsin) can share common airsheds. UWM's Cessna 336 aircraft, equipped to measure total suspended particulates, will attempt to find relationships between ERTS image brightness levels and total atmospheric mass loading. Aircraft and ground all-sky time-lapse photography simultaneous with ERTS overflights will allow further investigation of ERTS resolution, cloud morphology and dynamics. A continued search for inadvertant weather modification events will be of increasing significance as large-scale cloud seeding of the Great Lakes to regulate water levels approaches operational status.

6. ACKNOWLEDGMENTS

Partial support for these studies come from NASA (NAS5-21736), NSF (Grant GA-32208) and EPA (Grant R800873) and the UWM Center for Great Lakes Studies.

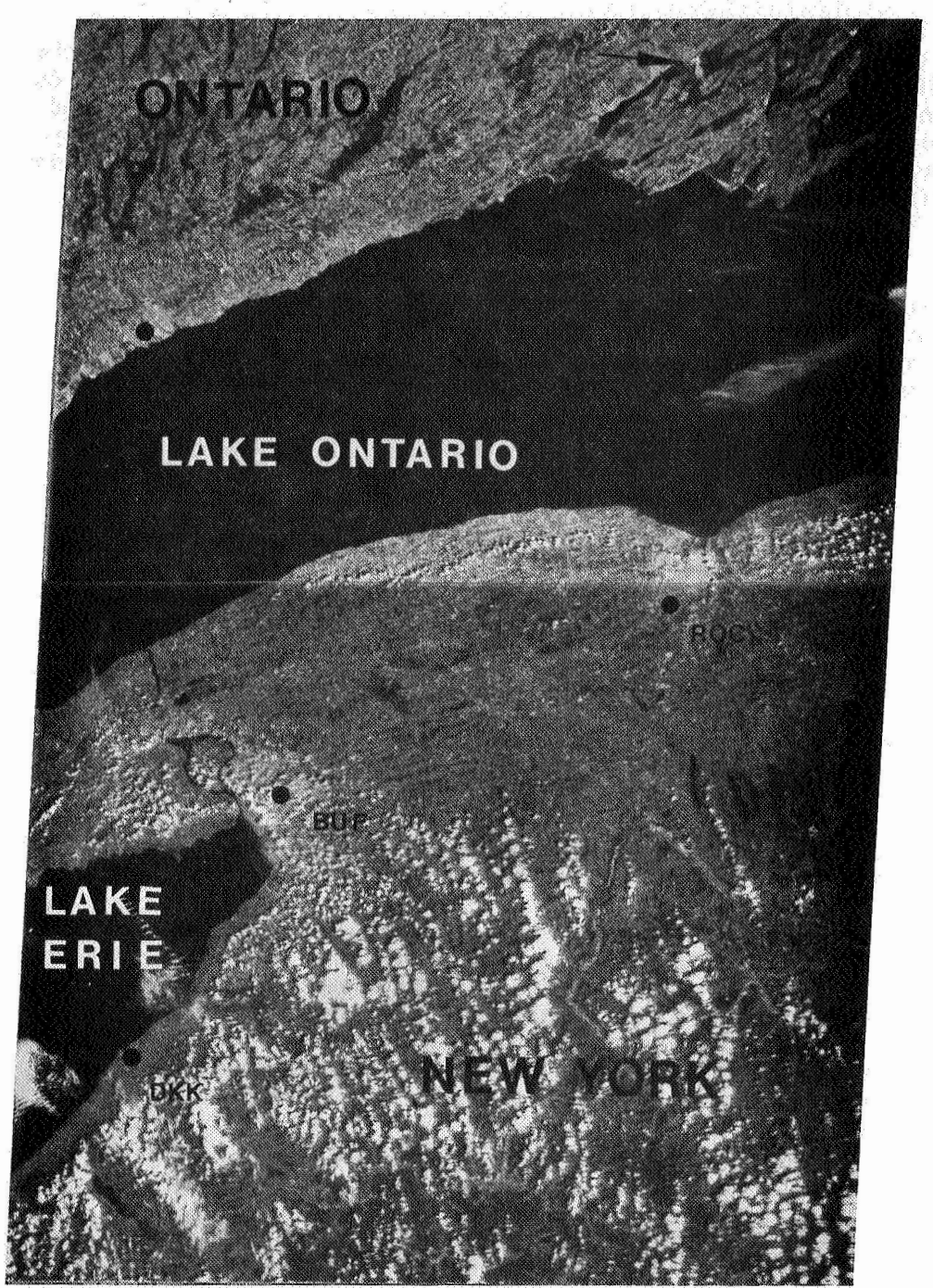


Figure 1: ERTS-1 MSS band 5 view of lower Great Lakes, 20 August 1972 showing lake breeze front cumulus clouds. Cirrus over Lake Ontario became invisible in band 7. Arrow points to apparent smoke plume. Cities noted include Toronto (YYZ), Rochester (ROC), Buffalo (BUF) and Dunkirk, N.Y. (DKK).

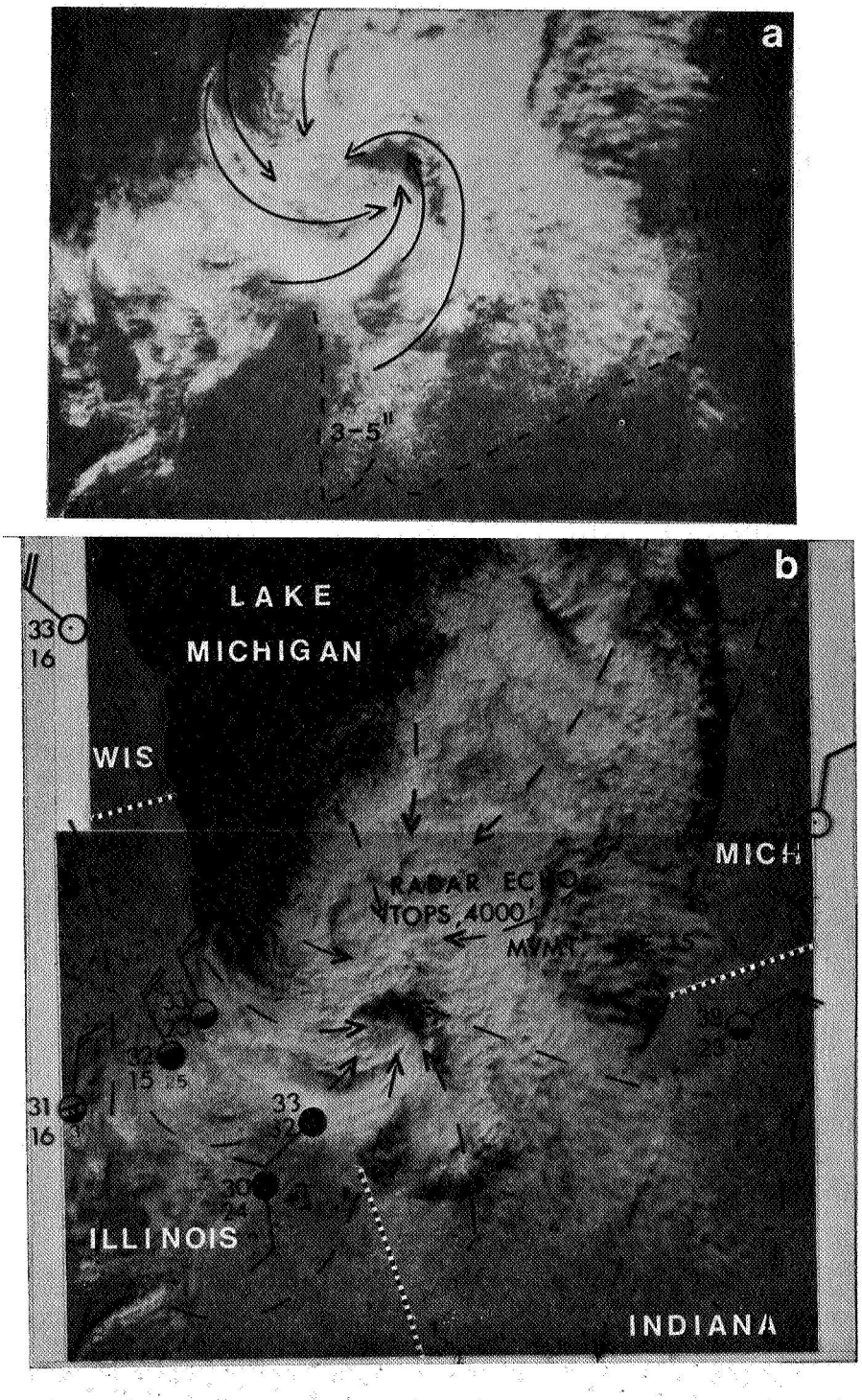


Figure 2(a): ERTS-1 MSS band 4 showing snow cover over Chicago-northwest Indiana and cyclonic cloud swirl, 19 October 1972, (b) band 7, with 1000 LST surface data and wind streamlines. One full wind barb equals 5 kts in all figures.

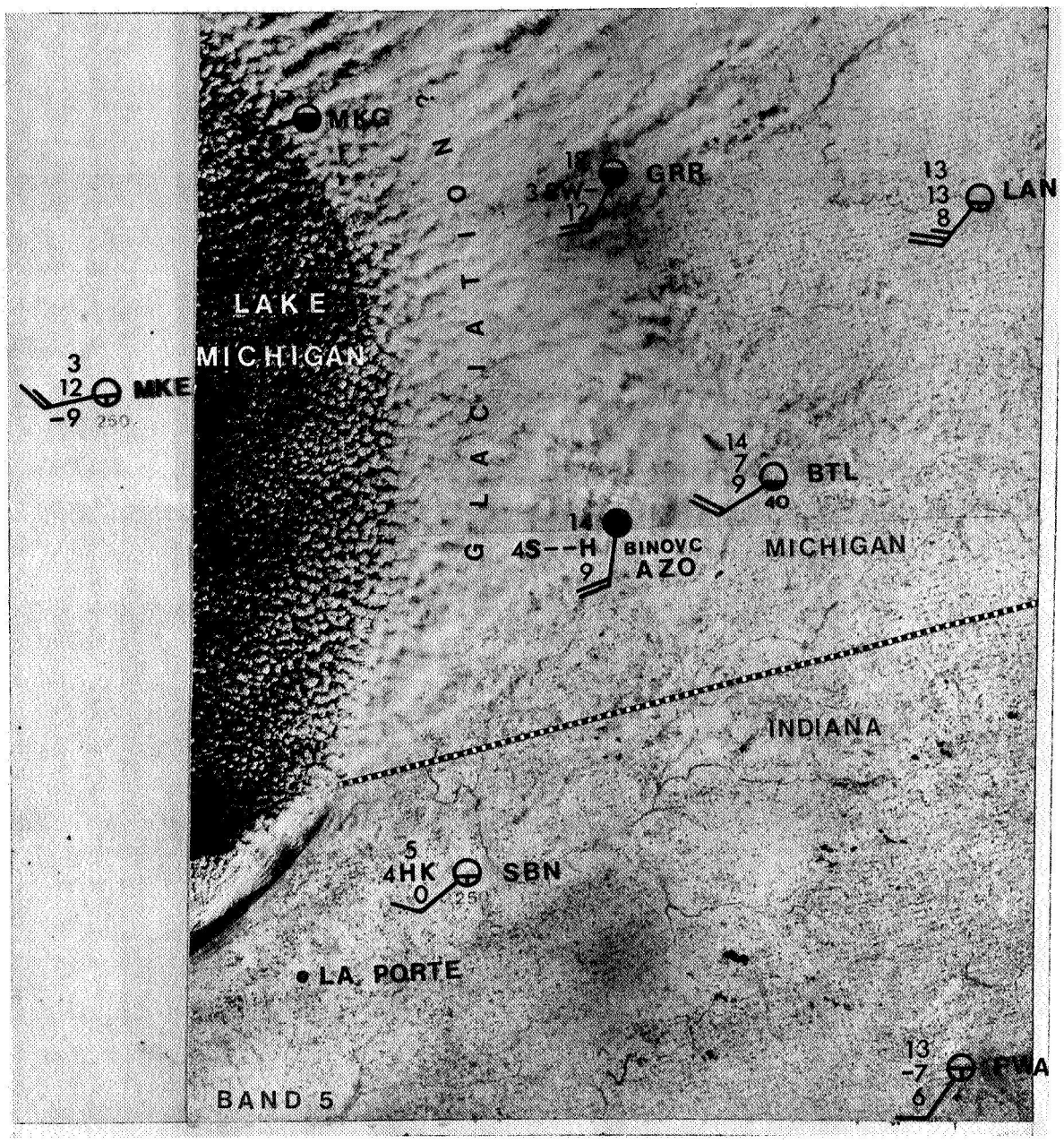


Figure 3: ERTS-1 MSS band 5 view of southeastern shore areas of Lake Michigan, 11 December 1972. Scattered and mostly random shallow cumulus convection suddenly thickens to broken to overcast as it moves inland. Orographic lift from shoreline dunes and frictional convergence, especially near Muskegon (MKG), appear likely causes. The clouds appear to rapidly glaciate about 20 nm inland. Note snow flurries at Grand Rapids (GRR) and Kalamazoo (AZO). The surface air temperatures increased from 3 to 17°F while crossing the lake.



Figure 4: ERTS-1 MSS band 6 view of southern Lake Michigan, 24 November 1972. Southwesterly flow of near freezing air over warmer lake results in cumulus convection. Plumes of suspended particulates from seven identified shoreline power plants and steel mills are causing notable effects in the shallow convective clouds. When viewing transparencies, the clouds forming out of the plumes begin noticeably closer to the shoreline and become denser and more well developed, a clear cut case of inadvertant weather modification.

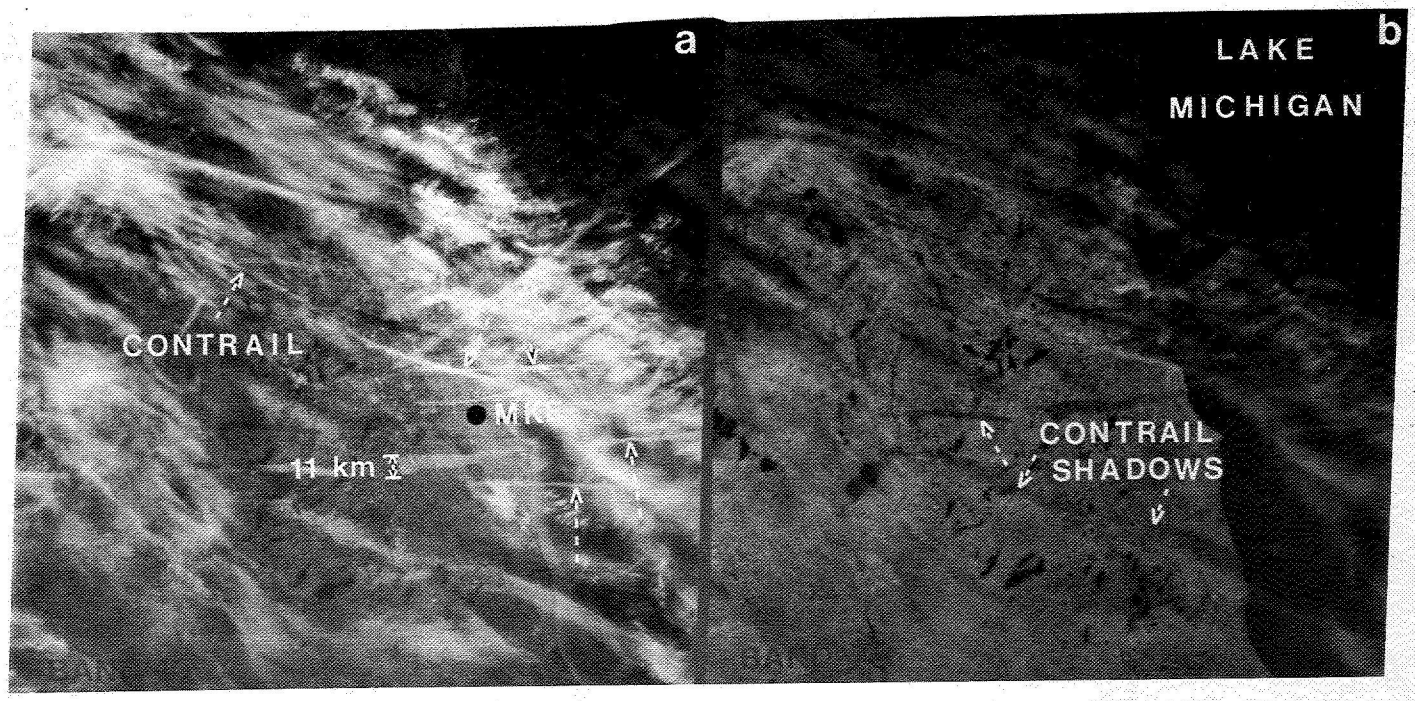


Figure 5(a): ERTS-1 MSS band 4 view of southeastern Wisconsin, 20 October 1972. The dot labled MKE is the Milwaukee National Weather Service station, reporting cirrus cloud cover at 25,000 feet. The clouds are oriented roughly with the wind at that level (310°, 60 kts). Superimposed on the natural cirrus, however, are jet condensation trails (contrails), some of which are indicated by arrows. In the moist environment at that level, some have spread to widths of at least 11 km. (b) Band 7 reveals the surprising degree of transparency of cirriform (ice) clouds in the near infrared, as well as distinct cloud contrail shadows. The spectral variations of cirrus albedo may well lend themselves to automatic detection by pattern recognition techniques.

Paper W 18

USE OF ERTS DATA FOR MAPPING SNOW COVER IN THE WESTERN UNITED STATES

James C. Barnes and Clinton J. Bowley, *Environmental Research and Technology, Inc., 429 Marrett Road, Lexington, Massachusetts 02173*

ABSTRACT

The purpose of this investigation is to evaluate the application of ERTS data for mapping snow cover, primarily in the mountainous areas of the western United States. The specific objectives are to determine the spectral interval most suitable for snow detection, to determine the accuracy with which snow lines can be mapped in comparison with the accuracies attainable from other types of measurements, and to develop techniques to differentiate reliably between snow and clouds and to understand the effects of terrain and forest cover on snow detection.

1. INTRODUCTION

The earth's snow cover is a resource that directly or indirectly affects most of the world's population. As written in a recent report on the needs for polar research (Committee on Polar Research, 1970):

> "Snow forms a transient, sedimentary veneer on much of the earth's land surfaces. The diverse economic effects of this snow layer are incalculable. It is a major and renewable hydrologic reservoir; in many areas of North America more than half of the utilized water is derived from melted winter snow. Flood damage from spring snow melt is a recurring hazard in many river basins. The obstacles and hazards to ground transportation alone are formidable ..."

In mountain areas, such as the southern Sierra Nevada in California, the hydrologic importance of snow accumulations requires accurate monitoring of the snow pack distribution. As pointed out by Anderson (1963), the annual stream flow in the areas adjacent to the southern San Joaquin Valley is the most variable of any California watershed, due mainly to a large variability in the number and intensity of the winter storms crossing the region.

In his report on the management of California's snow-zone lands for water, Anderson discusses two important characteristics of the Sierra Nevada snow pack: (a) maximum accumulation of snow, and (b) rate of melt of snow water from the pack. The first characteristic is a good indicator of total water yield, and the second of when the resulting water is delivered. Both of these characteristics may be related in some degree to the snow extent. In a study using aerial photographs, Leaf (1969) found that for each of three Colorado watersheds a functional characteristic exists between extent of snow cover during the melt season and accumulated runoff. He reports that snow-cover depletion relationships are useful for determining both the approximate timing and the magnitude of seasonal snowfall peaks.

Despite the economic and scientific implications of snow cover, existing data collection methods often cannot provide either the desired areal coverage nor observational frequency. Except in limited areas where aerial survey is used, the significant parameters are usually measured at ground stations or at widely scattered snow survey courses. Now, the capabilities of remote sensing from earth-orbiting satellites offer promise for the development of a more cost-effective means for monitoring snow cover.

2. APPLICATION OF ERTS DATA

Considerable research has been carried out in recent years to determine snow survey and other hydrologic applications of environmental satellite data (McClain, 1970). Through studies performed by Barnes and Bowley (1970, 1972) techniques to map snow cover from existing photographic and thermal infrared measurements have been developed. These studies have shown that valuable information on snow extent can be derived from spacecraft observations.

Nevertheless, limitations in the use of satellite systems designed primarily for meteorological purposes do exist. Cloud interference, which limits the number of usable satellite observations, remains a problem (for hydrologic purposes, however, daily snow observation is not normally required). Also, since mountain regions are commonly forested, vegetation effects may also influence the location of the snow line in satellite photographs. Of greater significance is that the mapping accuracy that has been attainable from the relatively poor-resolution cameras is only marginal for optimum hydrologic use. Now, ERTS-1 is providing the first opportunity to investigate the application of high-resolution multispectral data for snow survey. Through use of these data, many of the previous problems can be alleviated.

Data from some 50 ERTS passes have been received for use in the current investigation. These data cover various mountain areas in the western United States during the period from late July 1972 through early January 1973 and the relatively flatter terrain of the Upper Midwest during late November and December. Additionally, a sample of ERTS data from the Arctic has also been available.

Examination of the MSS data and the limited sample of RBV data has shown that the contrast between snow-covered and snow-free terrain is greatest in the MSS-4 (0.5 to 0.6 μm) and MSS-5 (0.6 to 0.7 μm) spectral bands. The MSS-5 data appear to be the most useful of the two bands for snow mapping, because in some instances snow-covered areas are near saturation in the MSS-4 data, causing a loss of some detail in the snow pattern. In the longer wavelengths, especially the MSS-7 near-IR band (0.8 to 1.1 μm), snow cover is more difficult to detect. However, the near-IR band may provide useful information for certain purposes such as detecting melting conditions. As discussed later in this report, MSS-7 data have been found extremely useful for studies of glaciers in the Arctic.

Snow cover can be identified in the MSS-5 data because of its greater reflectance than the surrounding snow-free terrain. Although snow and clouds have similar reflectances, mountain snow cover can be differentiated from cloud primarily because the configuration of the snow patterns is very different from cloud fields and can be instantly recognized. The snow boundaries are also sharper than typical cloud edges, and snow fields usually appear with a more uniform reflectance than do clouds, which have considerable variation in texture. Furthermore, cloud shadows are usually visible, especially with cumuliform clouds, and various terrestrial features can be recognized in cloud-free areas. In fact, in the images from the flatter terrain of the Midwest that are completely snow covered, recognition of terrestrial features is the principal means to establish cloud-free areas. Because of the high resolution of the ERTS data, numerous terrestrial features that are not visible in lower resolution meteorological satellite photographs can be recognized. In addition to natural features, such man-made features as roads, electric power lines, and cultivated fields are detectable. In the heavily forested areas of the Cascades, timber cuts are clearly visible.

3. MAPPING OF SNOW LINE ELEVATION

Mean snow line elevations have been determined for a part of the Olympic Mountains in Washington (for 29 July and 4 September), the Mt. Rainier area in Washington (28 July and 2 September), the Three Sisters Mountains in Oregon (28 July and 2 September), the White Mountains in California (16 September, 21 October, and 27 November), and the Salt-Verde Watershed area in Arizona (21 November). For each area, significant changes in snow line elevation occur during the time intervals between the ERTS observations.

For each case analyzed, the snow limit was mapped from the 9.5" prints using a transparent acetate overlay. The snow line was located at the edge of the brighter area without regard to changes in brightness within the overall area deduced to be snow covered. Although the snow-covered areas in most of the cases analyzed exhibited fairly uniform brightness, some variations in tone were observed. The relationships between these variations and factors such as terrain and forest cover will be examined

as the study progresses. Also, the accuracy of the snow line locations will be evaluated when additional correlative snow data are acquired. As the snow line elevation lowers into the more heavily forested areas as the winter progresses (in areas such as the Cascades), the snow line may not be as clearly defined as it is in the late summer and fall cases analyzed so far. To determine the snow line elevation, reference was made to charts from the National Topographic Map Series (Scale 1:250,000). Although the scale of these charts is larger than that of the 9.5" ERTS prints, charts of this scale were found to be very useful for matching the amount of detail in the ERTS data.

Olympic Mountains (Washington)

Analysis of ERTS-1 data for 29 July and 4 September 1972 reveals a 900 ft snow line retreat over the eastern two-thirds of the Olympic Mountains in northwestern Washington near 47°45'N and 123°15'W. The RBV-1 (0.475 to 0.574 μm) data for 29 July (Image ID 1006 - 18313) indicates that significant snow is still present in the eastern two-thirds of the Olympic Mountains on this date (the western third was not visible in the imagery). The snow limit mapped from the ERTS data, after being transferred to the corresponding topographic map, fits extremely well with the shape of the 5000 ft contour throughout the several narrow ridges comprising this region of the mountain range. Maximum elevation of these ridges ranges from 6000 to 7800 ft.

Analysis of MSS-5 data for 4 September (Image ID 1043 - 18372) shows that a considerable retreat of the snow line has occurred during the preceding five weeks. The mean snow line elevation measured from a considerable number of points on the contoured topographic map is at the 5900 ft level, a retreat of 900 ft from the previous observation. Actually, because the slopes in this area are not as steep as in some other areas, the 900 ft change is associated with a significant change in snow extent.

Mount Rainier (Washington)

An RBV-1 image for 28 July (Image ID 1005 - 18260) was analyzed to determine the mean snow line elevation for the Mt. Rainier area (maximum elevation 14,410 ft). The mean elevation of 65 points along the snow limit for this date is 5200 ft. Analysis of MSS-5 data for 2 September (Image ID 1041 - 18260) shows a considerable retreat in snow line elevation. The mean of 45 elevation points taken from the topographic map overlay is 6100 ft, a change of 900 ft since 28 July. This snow line retreat of 900 ft corresponds exactly to that measured for the same period over the Olympic Mountains located 100 miles to the northwest.

Three Sisters Mountains (Oregon)

ERTS observations on 28 July and 2 September indicate a 1000 ft snow line retreat on the western slope and a significantly smaller retreat of 200 ft on the eastern slope of the Three Sisters Mountains (near 44°N, 121°

45'W). On 28 July the snow line elevation mapped from the RBV-1 image (Image ID 1005 - 18265) is at 6000 ft on the western slope and at 7000 ft on the eastern slope. Five weeks later, however, the snow line mapped from the MSS-5 image (Image ID 1041 - 18265) along the western slope is 7000 ft, a change of 1000 ft from the earlier observation, whereas the mean snow line elevation on the eastern slope is 7200 ft, a change of only 200 ft.

White Mountains (California)

Analysis of three ERTS-1 passes during the period from mid-September through late November 1972 reveals broad changes in snow line elevation for the White Mountains of eastern California. This range, with peaks from 12,000 to 14,200 ft is oriented north-south just east of the Sierras between 37° and 38°N at 118°15'W. On 16 September (MSS-5, Image ID 1055 - 18055) snow cover is restricted to the higher terrain at a mean elevation of 12,800 ft. Five weeks later on 21 October 1972 (MSS-5, Image ID 1090 - 18003), a dramatic lowering of the snow line elevation has occurred, particularly along the western slopes. The snow line elevation is 7000 ft (mean of 25 points) along the western slope, and 10,500 ft (mean of 30 points) along the eastern slope.

The ERTS data on 27 November (MSS-5, Image ID 1127 - 18064) shows, however, that significant snow melt has apparently occurred during the preceding five-week period. The snow line elevation along the western slope has receded some 4000 ft to 11,000 ft (mean of 33 points), whereas measurements of the eastern slope show a retreat of only 500 ft to 11,000 ft (mean of 36 points). Of interest also is that the ERTS data show that during the period from 16 September to 27 November, the Tinemaha Reservoir, located west and just south of the White Mountains in the Owens Valley, increases significantly in size. On the earlier date, the reservoir measures 1-1/2 n.mi. north to south, whereas in late November, the length of the reservoir has increased to about 2 n.mi.

Salt-Verde Watershed (Arizona)

For the Salt-Verde Watershed area in Arizona aerial snow survey charts have been acquired for several dates, beginning 14 November (through the courtesy of the Salt River Project Office). The aerial survey procedures are described in a paper by Warskow (1971). For each aerial survey flight, which is made at approximately two-week intervals, an ocular estimate is made of the snow depth using the logs left from timber operations in the mountain areas, ground and vegetation textural characteristics, and cultural features (such as fences, road cuts) as indicators of the snow depth. Both the areal outline of the snow pack and the observed depths are recorded on a map overlay. The initial chart has been correlated with the ERTS data from a week later (21 November), and the chart of 12 January has been correlated with the ERTS data of 14 January.

Analysis of MSS-5 data from 21 November (Image ID 1121 - 17330) shows a well-defined snow boundary in the Salt-Verde Watershed, a narrow mountainous area extending from 35°30'N, 113°W southeastward to 33°45', 109°15'W. In this analysis the ERTS snow limit was transferred to the aerial snow survey map of 14 November. Although this aerial survey snow line was charted a week earlier than the satellite observation, there is good agreement between the two, especially in the region from about 35°N, 112°W to 34°15'N - 111°W. Differences showing the aerial survey snow line some 2 to 5 n.mi. broader in extent are, however, observed in the region near 34°N and 110°20'W to 111°W. As only light snow amounts (1 to 4 inches) were reported for 50% to 60% of this region on 14 November, it seems reasonable to assume that this 2 to 5 mile difference could well be the result of snow melt over the one-week period between the aerial and satellite observations. The same is undoubtedly true for differences observed along an isolated, narrow ridge just south of 34°N near 111°W, where the aerial survey indicated a trace to 1 inch above the 6200 ft level and 12 inches to 16 inches above 7000 ft. The ERTS snow line is observed close to the small area above 7000 ft in the region of significantly greater snow depth.

In the January case (Image ID 1175 - 17324), the aerial survey snow line also correlates well with the ERTS snow line. In fact, the principal difference seems to be that the ERTS snow line is more detailed, implying that the observer may smooth the snow line somewhat when compiling the aerial survey snow chart. In the areas where the snow line was estimated rather than actually observed from the flight, the differences are greater, with the snow extent mapped from the ERTS data being consistently less than that depicted on the corresponding chart.

Analysis of Arctic Data

A considerable amount of ERTS data over the Arctic has been received for use in a separate study (SR126: Evaluate the Application of ERTS-A Data for Detecting and Mapping Sea Ice). These data show the seasonal increase in snow cover in several areas such as the islands of the Canadian Archipelago and northern Alaska. For example, in late July, Banks Island in the Canadian Archipelago is completely snow-free; in late September, however, snow covers the higher elevations of the central portion of the island, and in late September the entire island is snow-covered. With snow cover, relatively small-scale terrain features, such as isolated hills, stream valleys, gullies, and ridges, are greatly enhanced. This is particularly evident in the MSS-7 band where large differences in brightness exist between sunlit features and shadows in the low-sun angle imagery.

In other Arctic data, considerable detail is evident in glaciers located along the east and west coasts of Greenland (for example, 23 September, Identifier 1062 - 16504). Detectable features include imbedded sediment trails (medial moraines), crevassed areas, and apparent limits of new snow cover over older glacial ice. Furthermore, significant

differences are apparent in the various spectral bands. Several glaciers exhibit a uniform reflectance in the MSS-4 band, whereas in the MSS-7 band the lower elevation portions appear much darker than the higher elevation portions. This difference in reflectance is believed to be due to the existence of melt-water on the surface of the glacier at the lower elevations.

4. CONCLUSIONS

The results of the analysis of the initial sample of ERTS data covering the specified test sites in the western United States indicate that the MSS-5 spectral band (0.6 to 0.7 μm) is the most useful for detecting and mapping mountain snow cover. Snow cover can be readily detected and can be distinguished from clouds because the configuration of mountain snow patterns is very different from that of clouds, snow boundaries are sharper than typical cloud edges, snow fields usually appear with a more uniform reflectance than do clouds which often have considerable variation in texture, cloud shadows are often visible, and terrestrial features can be recognized in cloud-free areas. At the ERTS resolution, numerous terrestrial features not visible in lower resolution meteorological satellite data can be detected. In addition to various natural features, man-made features such as roads, electric power lines, cultivated fields, and timber cuts are visible.

In the four mountain areas for which data have been analyzed on at least two different dates, changes in snow line elevation ranging from 200 to as much as 4000 ft have been mapped. In these analyses topographic charts of a scale of 1:250,000 have been found to be useful for measuring snow line elevation. In two cases analyzed for the Salt-Verde Watershed in Arizona good agreement is observed between the location of the snow line as mapped from the ERTS data and as depicted on aerial snow survey charts. A single ERTS frame covering much of the Salt-Verde Watershed can be analyzed in a few hours, whereas the combined flight time and time to plot the aerial survey chart is considerably longer. Thus, it does appear that snow extent can be mapped from ERTS data on a cost-effective basis.

Although a thorough investigation of the multispectral characteristics of snow has not yet been undertaken, examination of data from the Arctic has revealed that the multispectral approach can provide information on glacial conditions that cannot be ascertained from observations in a single spectral band. Several glaciers along the coasts of Greenland exhibit a uniform reflectance in the MSS-4 (0.5 to 0.6 μm) band, whereas in the MSS-7 (0.8 to 1.1 μm) band the lower elevation parts appear much darker than the higher elevations. This difference in reflectance is believed to be due to the existence of melt-water on the surface of the lower parts of the glaciers as opposed to snow cover on the upper parts.

REFERENCES

Anderson, H. W., 1963: Managing California's Snow Zone Lands for Water, U. S. Forest Service Research Paper PSW-6, Pacific SW Forest and Range Experiment Station, Berkeley, California.

Barnes, J. C., and C. J. Bowley, 1970: "Measurement of Mountain Snow Extent Using Satellite Data," paper presented at National Fall Meeting of AGU, San Francisco, California, Dec. 1970.

Barnes, J. C., and C. J. Bowley, 1972: Snow Studies Using Thermal Infrared Measurements from Earth Satellites, Final Report under subcontract No. 19334 to ARA, Inc. (NOAA/NESS Contract No. 1-35350), ERT, Inc.

Committee on Polar Research, 1970: Polar Research, A Survey, National Research Council, National Academy of Sciences, Washington, D. C.

Leaf, C. F., 1969: "Aerial Photographs for Operational Streamflow Forecasting in the Colorado Rockies," Proc. 37th Western Snow Conference, Salt Lake City, Utah.

McClain, E. P., 1970: Applications of Environmental Satellite Data to Oceanography and Hydrology, ESSA Tech. Memo. NESCTM-19, Environmental Science Services Administration.

Warskow, W. L., 1971: "Remote Sensing as a Watershed Management Tool on the Salt-Verde Watershed," paper presented at the ARETS Seminar on Applied Remote Sensing of Earth Resources in Arizona, Tucson, Arizona.

Paper W 19

EVALUATION OF ERTS IMAGERY FOR MAPPING AND DETECTION OF CHANGES OF SNOWCOVER ON LAND AND ON GLACIERS

Mark F. Meier, *U. S. Geological Survey, Tacoma, Washington*

ABSTRACT

The percentage of snowcover area on specific drainage basins was measured from ERTS imagery by video density slicing with a repeatability of 4 percent of the snowcovered area. Data from ERTS images of the melt season snowcover in the Thunder Creek drainage basin in the North Cascades were combined with existing hydrologic and meteorologic observations to enable calculation of the time distribution of the water stored in this mountain snowpack. Similar data could be used for frequent updating of expected inflow to reservoirs. Equivalent snowline altitudes were determined from area measurements. Snowline altitudes were also determined by combining enlarged ERTS images with maps with an accuracy of about 60 m under favorable conditions. Ability to map snowcover or to determine snowline altitude depends primarily on cloud cover and vegetation and secondarily on slope, terrain roughness, sun angle, radiometric fidelity, and amount of spectral information available. ERTS imagery was also used to measure glacier accumulation area ratios, detect subtle flow structures on glaciers, identify surging glaciers and monitor changes in tidal glacier termini.

No operational method now exists for monitoring the varying extent of mountain snowcover. Satellite imagery has well documented potential to do this under certain conditions; in fact snow on land is one of the most striking features to be seen on satellite images. Since it is obvious that snow can be identified and measured on satellite images this paper will explore the usefulness of ERTS-type snowcover data to scientific and operational aspects of the management of water resources. Only a few selected examples can be presented. Some interesting applications of these data to the study of glaciers will also receive mention. The data and conclusions presented here are based on a limited sample of data for calibration, measurement, and analysis. Thus these data and conclusions are considered preliminary.

1. MEASUREMENT OF SNOWCOVERED AREA

Routine measurement of snowcover on satellite imagery must be done by machine if it is to be of operational value; hand planimetering or dot-counting the highly intricate snowline is prodigiously time consuming. Also, measurement of the total snowcover shown on any certain image is of limited value; the hydrologist needs to know the snowcovered area in specific drainage basins. This requires precise registration of the imagery to a map.

We approached these problems through the use of the Stanford Research Institute electronic console ESIAC. Drainage and drainage basin outline maps of the North Cascades were superimposed and reduced to 70 mm positive transparencies. ERTS images were then registered to these maps, using the drainage pattern as a convenient guide for registration. The non-pertinent image area outside of the drainage basin was removed through use of an opaqued mask. Obvious shadows on snow were brightened with a cursor or measured separately. Image enhancement using several spectral bands to form a color presentation was used to refine the video brightness level coinciding most closely with the snow/no-snow boundary. The displayed region having a brightness higher than this level was then identified as the snowcover and a quantitative value of area of snowcover was simultaneously read out on another display. With only very general instructions operator variance was 8 percent, but after coordinating evaluation criteria operator variance reduced to 4 percent of the snowcovered area (less than 1 percent of most of the drainage basin areas).

Unfortunately, time has not allowed accurate calibration of brightness level in terms of known snow/no-snow boundaries. Thus the snow area data obtained with the ESIAC contain a small absolute error, and some slight discrepancies occur when comparing ERTS data with high-resolution aircraft data. This error will be reduced or eliminated in the next stage of the investigation when more attention will be given to calibration.

Through the study of many images, it appears that the ability to map snowcover depends primarily on cloud cover and vegetation, and secondarily on slope, terrain roughness, sun angle, radiometric fidelity of image, and amount of spectral information available. It is difficult for an experienced observer to distinguish some types of cloud or fog from snow even with all possible radiometric information, or to distinguish the snowline in forested terrain. In rough terrain, bare ground facing the sun may be lighter in tone than snow in shadow causing difficulty in identification, and this problem is intensified with low sun angle or longer wavelength sensors. Fully automatic mapping of snowcover in forested or mountainous terrain appears at this time to be impossible. Human eyes and brain control the analysis procedure, but this can be done quickly and efficiently with an interactive console such as the SRI ESIAC.

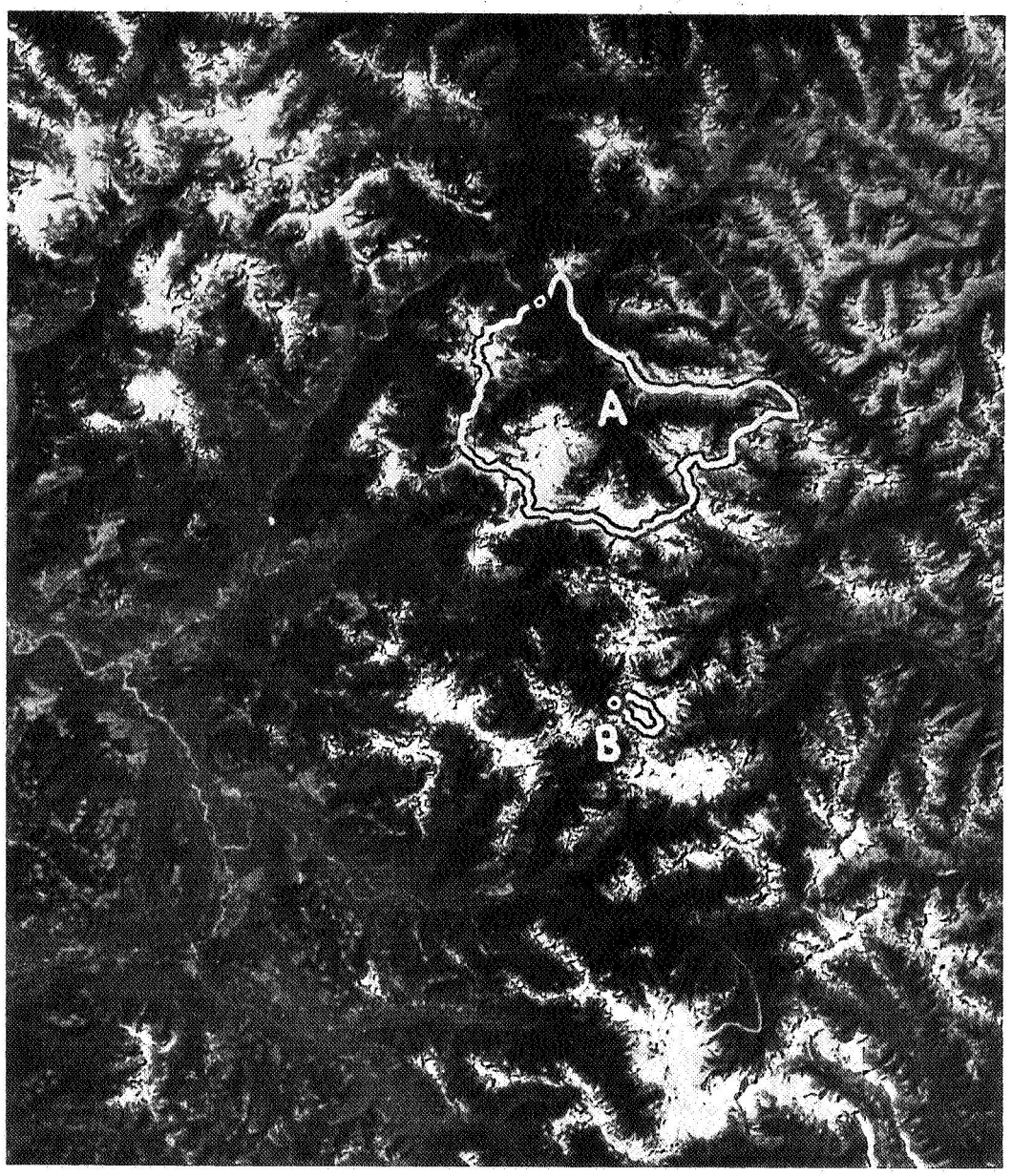


Figure 1.--2 September 1972 ERTS-1 image 1041-18253-4 of part of the North Cascades, Washington. The drainage basin Thunder Creek near Newhalem is indicated by A, *and the basin South Fork Cascade River at South Cascade Glacier is indicated by* B.

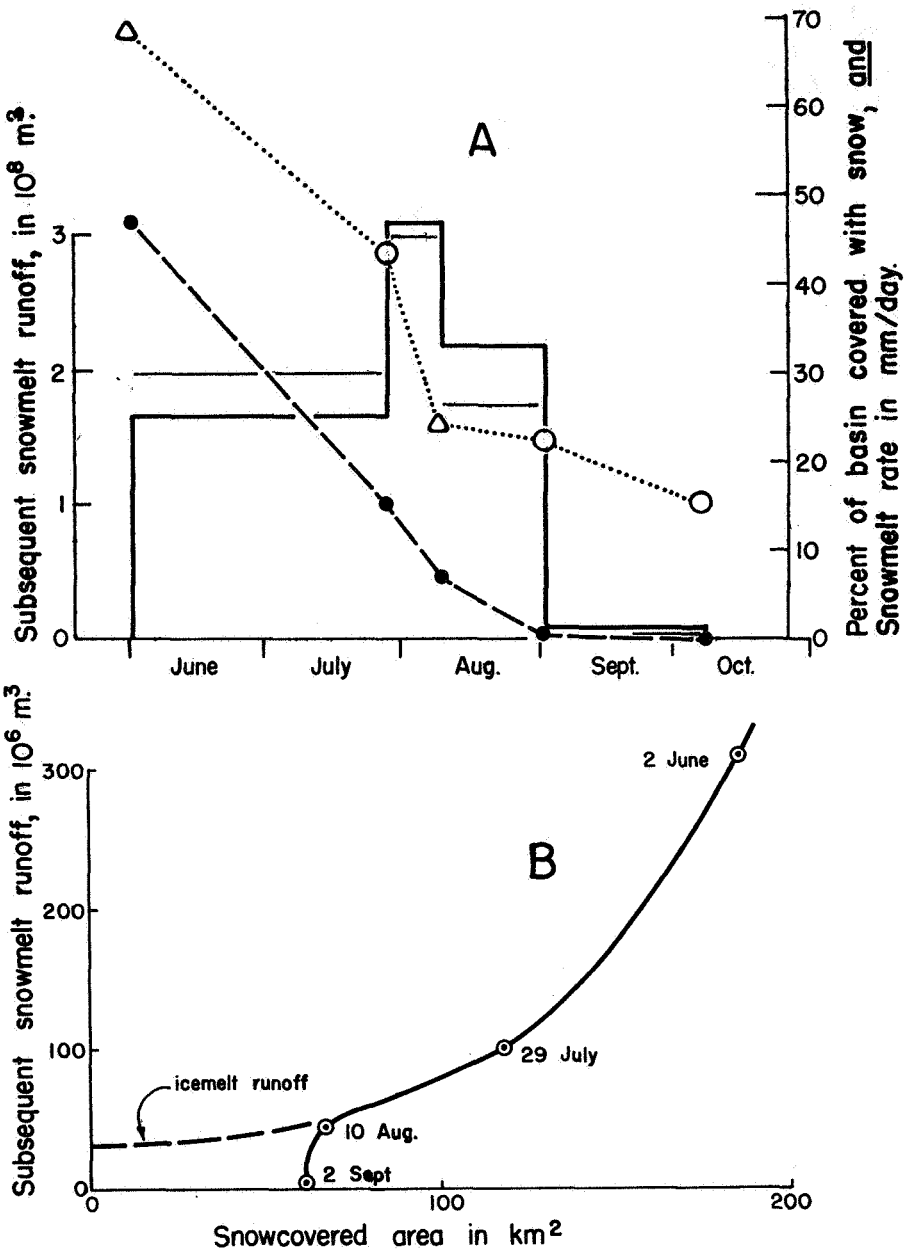


Figure 2A.--Snowcovered area (dotted line), subsequent snowmelt runoff volume (dashed line), and rate of snowmelt (heavy line) in the Thunder Creek drainage basin; thin line is average observed snowmelt rate. Triangles are data from 19.8 km altitude aerial photographs; circles are data from ERTS-1. B.*--Subsequent snowmelt runoff as a function of snowcovered area, Thunder Creek drainage basin.*

2. HYDROLOGIC ANALYSIS USING ERTS DATA

In the mountain west, most of the streamflow results from snowmelt. Therefore much effort has gone into the use of snow data in operational hydrologic procedures. Some of the newer procedures attempt to use snowcovered area as a variable or parameter. Empirical correlations between snowcover and runoff have been incorporated into computerized models for the continuous simulation of streamflow, such as the SSARR model (Rockwood, 1964; Schermerhorn and Kuehl, 1968). Snowcover data are also used to forecast subsequent runoff volumes (Parsons and Castle, 1959; Thoms and Wang, 1969; Leaf and Haeffner, 1971). These schemes, however, are strictly limited by the high cost of obtaining and analyzing aerial photographs at frequent intervals over large drainage basins. Can ERTS-type imagery fill this need?

In order to explore this problem, an analysis was made of three ERTS and two high altitude aircraft images of the drainage basin Thunder Creek near Newhalem, Washington (Fig. 1). Some results are presented in Figure 2. Snowmelt runoff from this 272 km^2 basin is utilized for the generation of electric power at Diablo and Gorge Dams on the Skagit River. Measurement of snowcovered area was done from ERTS images by SRI personnel on the ESIAC, and from high altitude aircraft photographs by USGS personnel. The snowmelt runoff and loss of snow mass were computed by a hydrologic balance procedure developed for the analysis of International Hydrological Decade glacier basins (Meier, Tangborn, Mayo, and Post, 1971; Tangborn, 1968) using hydrologic data gathered at the Thunder Creek gaging station and precipitation from nearby weather stations. These data were used with the ERTS and aircraft snowcover results to calculate the rate of snowmelt (in mm of water equivalent) in the Thunder Creek drainage basin. The calculated snowmelt rate is compared in Figure 2 with the actual melt rate observed at the index station P-1, altitude 1,890 m, on South Cascade Glacier which is 15 km south of Thunder Creek.

It is significant that the ERTS data can be used to compute other important hydrologic quantities, such as melt rate, and the results can be approximately verified by comparison with totally independent observations. Snowmelt rate is extremely difficult to measure at frequent time intervals (such as daily or weekly) at single points without very sophisticated and expensive instrumentation such as radioactive twin-probes. Snowmelt averaged over a large area is essentially impossible to measure directly with existing techniques. Yet a simple calculation using standard real-time hydrologic data combined with satellite imagery provides these results. In midsummer of 1972 the Thunder Creek snowpack changed area at a rate of about 1.6 percent per day; useful snowmelt data should be calculable for periods as short as 3-5 days if one assumes a 4 percent standard error in each area measurement.

Changes in snowcovered area in a specific drainage basin can be determined quickly with an electronic console, and Figure 2 shows that

the resulting values are consistent with laboriously planimetered aircraft data. Thus a method now exists for frequent, routine, and confident measurement of area of snowcover. The plot of snowcovered area versus subsequent runoff volume might be directly useful to continuously update reservoir inflow forecasts. Past experience using aerial photographs to measure the depletion of snowcovered areas indicates that "Snow depletion rates are highly correlated with seasonal generated runoff volumes. Furthermore, the general shapes of the curves have been fairly uniform from year to year, even though the amount of snow and weather conditions which produced runoff were not the same" (Leaf, 1967). Thus when the form of this graph is established, quick measurements of snowcovered area can be immediately converted to snowpack storage and streamflow forecasts. ERTS-type satellite imagery combined with an interactive console such as ESIAC could thus yield data on expected reservoir inflows at low cost or could be combined with other simulation or numerical modelling procedures to improve forecast accuracy. This would result in more precise regulation of reservoirs, less waste of water, the sale of additional firm power, less need to put additional ground installations in wilderness watersheds, and less damage to the valley and river environment from excessively high or low streamflows.

3. ALTITUDE OF THE SNOWLINE

The locus of lowest altitudes of a mountain snowpack often approach a plane; thus a measure of the altitude of this plane defines the extent of the snow. Furthermore, this parameter may be more useful than the total area of snowcover when making comparisons between drainage basins or mountain massifs because it is less affected by lowland area or topography. However, actual snowlines are usually intricately convoluted with some bare ground at highest altitudes and some avalanche-deposited snow at altitudes much lower than the bulk of the snowcover. Measuring the mean altitude of the snowline is usually laboriously difficult.

To avoid this problem a new parameter is here defined: the equivalent snowline altitude (ESA) is that altitude above which the drainage basin area exactly equals the area of snowcover. (The area/altitude functions for most basins of hydrologic importance are known.) In Figure 3 are plotted values of ESA as determined from ERTS and aircraft photography for different times during the summer and fall of 1972. These data are from very different types of areas--two are in the North Cascades and one is in the Middle Cascades. One is a tiny basin (South Fork Cascade River, 6 km^2) with limited altitude span, one a large area (Mount Rainier, 1,228 km^2) with altitude differences exceeding 4,000 m. Yet the absolute values and the changes in ESA with time are reasonably consistent.* Although three areas is an insufficient sample for convincing results, ESA appears to be a useful parameter for extending snowcover data.

*The 2 June value for South Fork Cascade River is anomalously high because this basin has no area below 1,613 m, and the 8 October value is low because of limited area above 2,000 m.

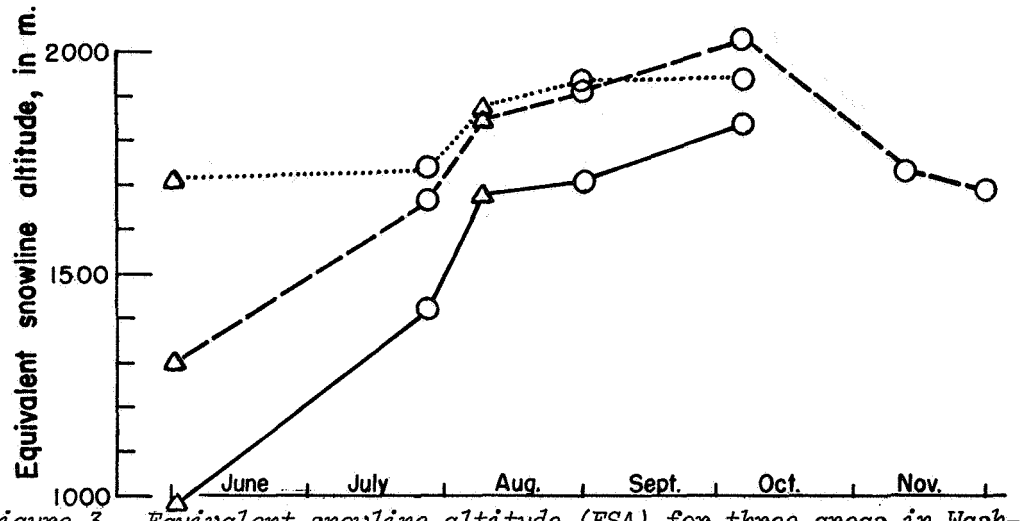


Figure 3.--Equivalent snowline altitude (ESA) for three areas in Washington: solid line, Thunder Creek drainage basin; dotted line, South Fork Cascade River at South Cascade Glacier; dashed line, Mount Rainier. Triangles are data from 19.8 km altitude aerial photographs; circles are data from ERTS-1.

Local snowline altitudes can also be obtained by superimposing a topographic map on ERTS imagery. An example of this is the following measurement of a 27 September image of the Anchorage, Alaska, vicinity, in which the snow margin is far more obvious than the snowline on the North Cascades image. This exceptionally sharp snowline was due to a storm the day before (18 mm of rain at Talkeetna) with the freezing level at 1,200 to 1,500 m above Anchorage. The snowline altitude is related to, but slightly lower than, the freezing level in the free atmosphere. Local snowline altitudes were measured by enlarging the ERTS image to 1:250,000 and using a transparent map overlay (Fig. 4). In this area the snowline altitude ranges from less than 400 m near Prince William Sound to highs of over 1,200 m west of Kenai Lake and in the higher parts of the Chugach Mountains. The freezing level was therefore lowest along the coast and highest further inland. Depressions of the freezing level parallel to the long valleys of Turnagain Arm, Port Wells, Nellie Juan River, and near Lake George are particularly striking.

Over most of the area shown in Figure 4, the altitude of the snowline could be determined with confidence to the nearest contour on the map (contour interval 200 ft = 61 m). In some local areas the snowline could not be mapped without considerable subjective decision and large variations were found between operators and between spectral bands; however, the snowline altitudes could invariably be determined to within 200 m.

Perhaps the greatest problem in understanding and monitoring mountain meteorology and hydrology is difficulty in obtaining mesoscale meteorologic information, because the mass and heat flux patterns are so complex and data gathering stations are so few in number. If mesoscale

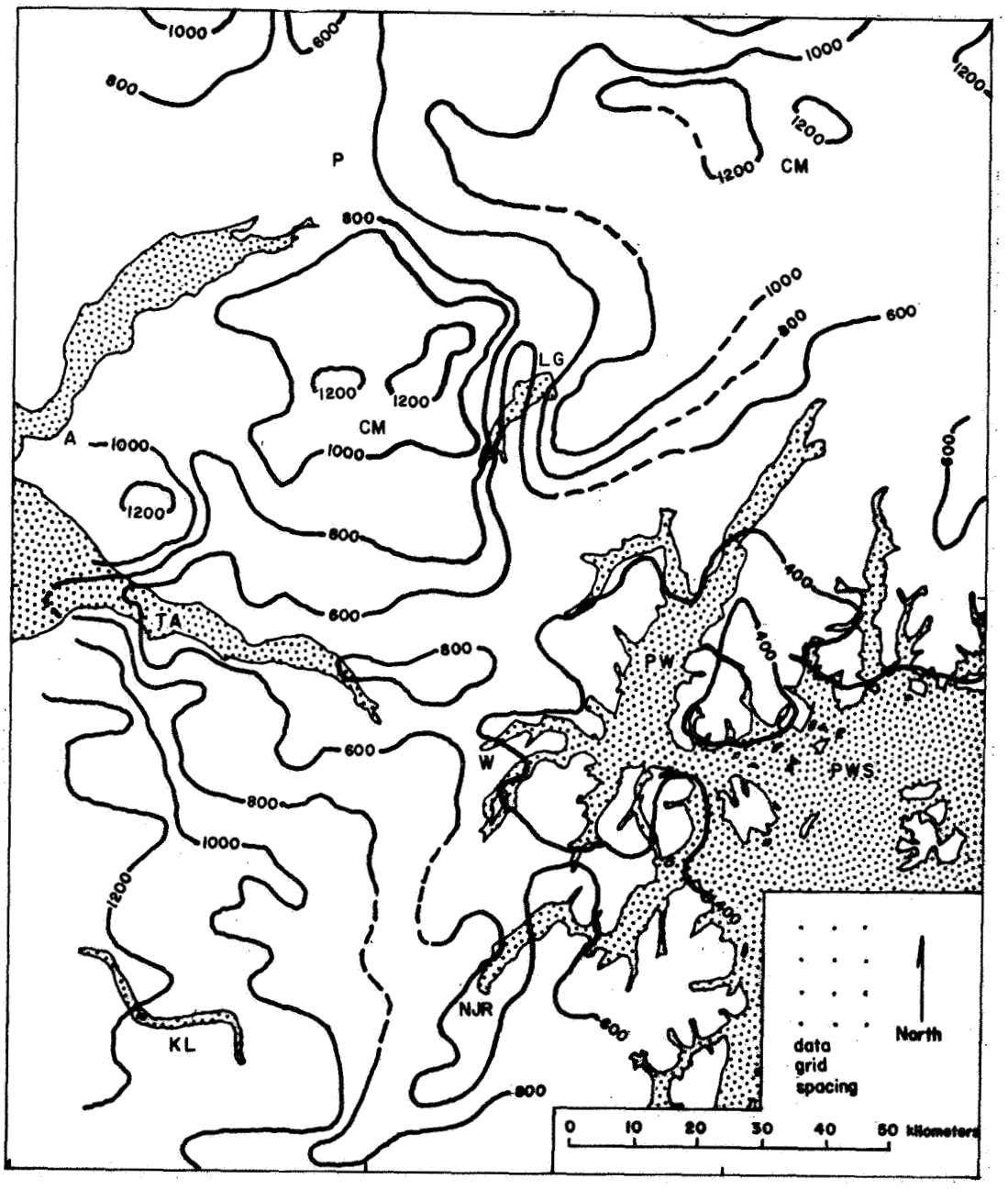


Figure 4.--Map showing the altitude of the snowline in the Anchorage area, Alaska, 27 September 1972. Data derived from ERTS images 1077-20451 and 1066-20453. Locations indicated as follows: A Anchorage, P Palmer, W Whittier, TA Turnagain Arm, CM Chugach Mountains, KL Kenai Lake, NJR Nellie Juan River, LG Lake George, PW Port Wells, PWS Prince William Sound.

variations of simple meteorological parameters could be measured, we could gain far better understanding of this problem. Thus the ability to derive synoptic mesoscale freezing level information from ERTS imagery such as Figure 4 is highly significant. A thorough analysis of the results shown in Figure 4 together with other meteorological data is now underway.

Knowledge of freezing level variations is of obvious direct importance to the utilization of the snow-water resource. In much of the mountain west, the quantity of snow produced and stored from a given precipitation event depends on the freezing level in the mountains. These data are not usually available from meteorological installations, which are generally located in lowland areas far removed from the mountains. Thus the ability to read freezing levels in the mountains from satellite imagery could be of immense operational value.

4. ACCUMULATION AREA RATIO

Snowlines on glaciers were found to be remarkably easy to identify, although alteration of the gray scale values on the bulk imagery was sometimes necessary. Thus it appears possible to rapidly determine the accumulation area ratio (AAR) from a large number of glaciers using ERTS imagery. This is important because the AAR has been proven to be a useful index to the mass balance of a glacier. By measuring the distribution of AARs at a given time in a given region and relating these to the data obtained at a glacier research station in the region, one can extend micrometeorological point measurements to meso- and even macroscale meteorological conditions. This is a necessary step in the complete understanding of glacier meteorology, a step which has been hitherto difficult to achieve.

A question arises, however, whether the resolution of ERTS imagery is sufficient to determine AARs from small glaciers (less than 10 km^2), which are most prevalent. In order to answer this problem, nine independent measurements were made for three different dates of the AAR of the small South Cascade Glacier basin (6.1 km^2) using enlarged ERTS images. The standard deviation of individual values from the means for that date was 3.4 percent. Although it has not yet been possible to check the error of the means with ground truth, AARs derived from high altitude aircraft photographs indicate that the error is less than 10 percent. Thus this powerful tool appears to be feasible even in areas where the glaciers are small.

5. OTHER GLACIER OBSERVATIONS

Other features on glacier surfaces appear in ERTS-1 imagery; some of these are surprising because they have not been observed on vertical or oblique aerial photography taken over a period of many years. One example is an interesting structure recognized for the first time on ERTS images

of Bering Glacier. Just below the firn line the ice from the two main snowfields of the Bagley Icefield merges from east and west and then bifurcates, the Bering Glacier flowing southwest and the Tana Glacier northwest (Fig. 5). This situation results in a curious flow pattern

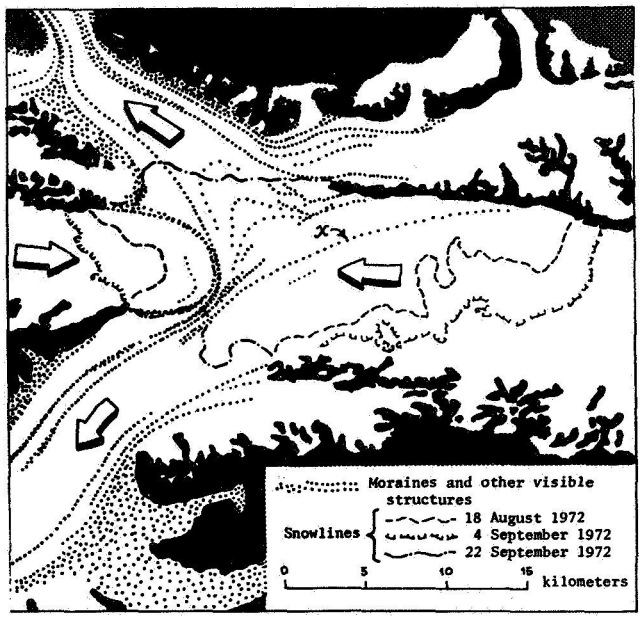


Figure 5.--Moraines, other structures, and snowlines at the juncture of the east (left) and west (right) arms of the Bagley Icefield, the Tana (upper left) and Bering (lower left) Glaciers. Arrows indicate ice flow direction. Structure labeled x is discussed in text.

which is further complicated by the fact that the Bering Glacier surges whereas the Tana evidently does not. During the surge phase additional ice must flow into the Bering lobe. The ERTS images show in remarkable detail what are probably very faint dust bands and medial moraines on the ice which, in turn, disclose directions of ice flow. A faint structure labeled x on Figure 5, probably inherited from the 1965-66 surge, suggests that during surges all of the ice from the western Bagley Icefield is channeled to Bering Glacier. When this lobe of ice begins moving into the Bering Glacier a rapid advance at the terminus, some 80 km distant, may be expected to occur three years later. Here is an example where space imagery has proven valuable to detect subtle features of such vast scale as to be unrecognizable from the ground or aircraft. There is practical importance to this: the forthcoming outburst of the large Berg Lake and other likely changes in drainage depend on the changing flow regimes of Bering Glacier, which can be understood through study of features such as this.

Surging type glaciers can be identified and large glacier surges can be monitored using ERTS imagery. For instance, the 1972 surge of the Yentna Glacier is plainly visible on ERTS imagery, and its folded moraines have been displaced more than 1,800 m down valley from their positions shown on recent maps and 1970 aerial photographs. Also visible on the ERTS image is a dark line where the rapidly flowing Yentna Glacier has sheared across the stagnant ice of the Lacuna Glacier. The causes of glacier surges--and why some glaciers surge while others do not--are questions of great scientific interest as this type of periodic sudden slippage is common to many other phenomena in nature, perhaps even to the mechanism of earthquakes. Surging glaciers may advance over large areas and cause devastating floods by blocking and suddenly releasing large quantities of meltwater; thus there is much practical interest in monitoring their behavior.

ERTS satellite images also show sequential changes in the termini of large Alaskan tidal glaciers. One particularly important example is the Hubbard Glacier. It has been advancing since first observed in 1890 and in recent years has threatened to close off Russell Fiord, which would then become a fresh-water lake and its outflow to the south would disrupt fish and game resources along the Situk River near Yakutat, Alaska. Previous to imagery from space, no scientific observations have been available in this remote area in winter. ERTS images (Fig. 6) show that a

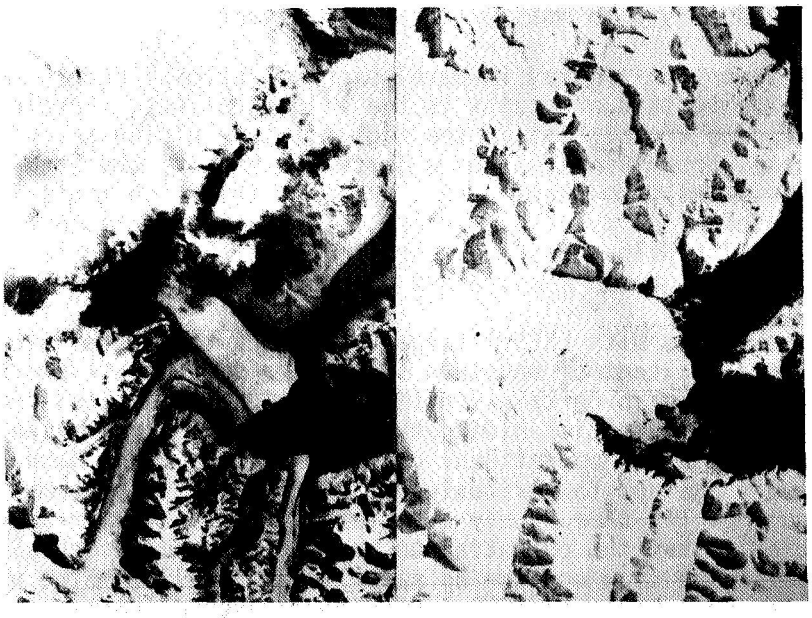


Figure 6.--Changes in terminus of Hubbard Glacier from 20 September (left) to 8 October (right). Terminus is 11 km wide. Image 1059-20052-6 (left) and 1077-21020-4.

large embayment doubled in size in only 18 days. This represents a loss of approximately 3 km^2 of the area of the terminus during this period, a loss in area greater than ever before observed in an Alaskan glacier in so short a time. ERTS imagery, by allowing glaciologists to observe sequential changes in the Hubbard's terminus, will make possible more accurate predictions as to when the Russell Fiord closure will take place.

6. CONCLUSIONS

The potential ability to map snowcover from satellites has important practical and scientific ramifications. Much of the streamflow in the mountain west originates as snowmelt. The measurement of these snowpacks provides data on spring and summer streamflow into hydroelectric, flood control or irrigation reservoirs, and efficient regulation of these reservoirs requires accurate, real-time data. The monetary value of these data is appreciable: it has been reported that the electric power utility in a single city in the Northwest realized savings of about 1M$ the first year that data from four new snow courses were incorporated in the operational program. A report on the predicted usefulness of an earth resources satellite for water management in the Columbia Basin indicates multimillion dollar yearly savings through reduction of hedge by use of satellite snow data (Planning Research Corporation, 1969). Environmental savings are also appreciable: accurate forecasts of streamflow and reservoir inflow permits minimizing damage due to excessive or deficient outflow. At the present time, snow can be accurately measured at points, but no operational means exists to monitor its areal extent.

Another reason for urgency in developing operational remote sensing techniques in the western mountains is the Wilderness Act. Precipitation rates and snowpacks are highest in the high altitude alpine areas, and here water losses are minimal. Thus a large fraction of the total streamflow originates from these areas. Most of this high mountain area is also designated or *de facto* Wilderness, either in National Forests or National Parks. The Wilderness Act specifically prohibits installations; thus there can be no ground measurement of this important water resource.

These experiments with ERTS-1 imagery indicate that satellite monitoring of the areal extent of mountain snowcover, during late summer at least, may be feasible in certain limited situations. In cloud-free conditions with little vegetation hiding the snow, an ERTS-type system will provide data of immediate operational utility. On the other hand, vegetation and clouds are apt to seriously interfere with the information transmitted much of the time. Only a system using passive (or active?) microwave radiation has the potential to monitor the snow under all conditions. An ultimate snow monitoring satellite may well combine visible light sensors such as those on ERTS-1 with microwave radiometers, in order to add occasional high resolution images to the all-weather information flow from the lower resolution radiometers.

REFERENCES

Leaf, C. F., 1967, Areal extent of snowcover in relation to streamflow in central Colorado: Proc. Internat. Hyd. Symposium, Ft. Collins, Colo., Sept. 1967, p. 157-164.

Leaf, C. F., and Haeffner, A. D., 1971, A model for updating streamflow forecasts based on areal snow cover and a precipitation index: West. Snow Conf. Proc., v. 39, p. 9-16.

Meier, M. F., Tangborn, W. V., Mayo, L. R., and Post, Austin, 1971: Combined ice and water balances of Gulkana and Wolverine Glaciers, Alaska, and South Cascade Glacier, Washington, 1965 and 1966 hydrologic years: U.S. Geol. Survey Prof. Paper 715-A, 23 p.

Parsons, W. J., and Castle, G. H., 1959, Aerial reconnaissance of mountain snow fields for maintaining up-to-date forecasts of snowmelt runoff during the melt period: Proc. West. Snow Conf., v. 27, p. 49-56.

Planning Research Corporation, 1969, A system analysis of applications of earth orbital technology to selected cases in water management and agriculture: Planning Res. Corpn., Willow Run, Mich., PRC-R-1224.

Rockwood, D. M., 1964, Program description and operating instructions "Streamflow Synthesis and Reservoir Regulation": U.S. Army Corps Engrs., North Pacific Div., Tech. Bull. 22.

Schermerhorn, V. P., and Kuehl, D. W., 1968, Operational streamflow forecasting with the SSARR model: Internat. Assoc. Sci. Hyd., Symposium on the Use of Analog and Digital Computers in Hydrology, v. 1, p. 317.328.

Tangborn, W. V., 1968, Mass balances of some North Cascade glaciers as determined by hydrologic parameters, 1920-65: Internat. Assoc. Sci. Hyd., Bern Gen. Assbly. 1967, Pub. 79, p. 267-274.

Thoms, M. E., and Wang, H. P., 1969, Compilations and use of areal snow cover observations, Columbia River Basin: Presented at Oct. 16-17, 1969 Annual Meeting, Pacific Northwest Region, Am. Geophys. Union, Portland, Oregon, 7 p.

(This page was intentionally left blank.)

NATIONAL AERONAUTICS AND SPACE ADMINISTRATION
WASHINGTON, D.C. 20546

OFFICIAL BUSINESS
PENALTY FOR PRIVATE USE $300

SPECIAL FOURTH-CLASS RATE BOOK

POSTAGE AND FEES PAID
NATIONAL AERONAUTICS AND SPACE ADMINISTRATION
451

U.S.MAIL

POSTMASTER: If Undeliverable (Section 158 Postal Manual) Do Not Return

"The aeronautical and space activities of the United States shall be conducted so as to contribute . . . to the expansion of human knowledge of phenomena in the atmosphere and space. The Administration shall provide for the widest practicable and appropriate dissemination of information concerning its activities and the results thereof."

—NATIONAL AERONAUTICS AND SPACE ACT OF 1958

NASA SCIENTIFIC AND TECHNICAL PUBLICATIONS

TECHNICAL REPORTS: Scientific and technical information considered important, complete, and a lasting contribution to existing knowledge.

TECHNICAL NOTES: Information less broad in scope but nevertheless of importance as a contribution to existing knowledge.

TECHNICAL MEMORANDUMS: Information receiving limited distribution because of preliminary data, security classification, or other reasons. Also includes conference proceedings with either limited or unlimited distribution.

CONTRACTOR REPORTS: Scientific and technical information generated under a NASA contract or grant and considered an important contribution to existing knowledge.

TECHNICAL TRANSLATIONS: Information published in a foreign language considered to merit NASA distribution in English.

SPECIAL PUBLICATIONS: Information derived from or of value to NASA activities. Publications include final reports of major projects, monographs, data compilations, handbooks, sourcebooks, and special bibliographies.

TECHNOLOGY UTILIZATION PUBLICATIONS: Information on technology used by NASA that may be of particular interest in commercial and other non-aerospace applications. Publications include Tech Briefs, Technology Utilization Reports and Technology Surveys.

Details on the availability of these publications may be obtained from:

SCIENTIFIC AND TECHNICAL INFORMATION OFFICE

NATIONAL AERONAUTICS AND SPACE ADMINISTRATION

Washington, D.C. 20546

NASA SP-327

SYMPOSIUM ON SIGNIFICANT RESULTS OBTAINED FROM THE EARTH RESOURCES TECHNOLOGY SATELLITE–1

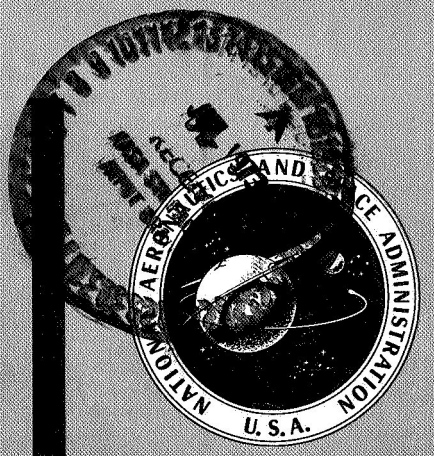
Volume I: Technical Presentations
Section B

A symposium held by

GODDARD SPACE FLIGHT CENTER

New Carrollton, Maryland

March 5–9, 1973



NATIONAL AERONAUTICS AND SPACE ADMINISTRATION

NASA SP-327

SYMPOSIUM ON SIGNIFICANT RESULTS OBTAINED FROM THE EARTH RESOURCES TECHNOLOGY SATELLITE-1

Volume I: Technical Presentations
Section B

The proceedings of a symposium held by
Goddard Space Flight Center
at New Carrollton, Maryland
on March 5–9, 1973

Compiled and Edited by

Stanley C. Freden
Enrico P. Mercanti
Laboratory for Meteorology and Earth Sciences
and
Margaret A. Becker
Technical Information Division
Goddard Space Flight Center

Original photography may be purchased from:
EROS Data Center
10th and Dakota Avenue
Sioux Falls, SD 57198

Scientific and Technical Information Office 1973
NATIONAL AERONAUTICS AND SPACE ADMINISTRATION
Washington, D.C.

This document is "made available under NASA sponsorship in the interest of early and wide dissemination of Earth Resources Survey information and without liability for any use made thereof." (NPD 8000.2A March 16, 1973)

PREFACE

The first Earth Resources Technology Satellite (ERTS-1) was launched on July 23, 1972. In the seven months since it was activated over 34,000 scenes of the earth have been obtained covering all major land masses and about 75% of the world's land area. Some areas, such as the United States, have been imaged at least twelve times. The purpose of this program is to provide an assessment of remote sensing from a satellite as a technique for inventorying and monitoring the earth's resources to provide for better management of these resources.

This Symposium provided the first open forum where the users of the ERTS data had the opportunity to present the significant accomplishments from their investigations. It also provided the first opportunity for representatives of federal, state and local organizations to present their views on how ERTS data are being used and will be used for solving operational resource management problems.

In order to provide maximum visibility for both the scientific/technological results as well as for the applications results from ERTS, and to provide these results in a relatively concise manner to those who could not be in attendance all week, the Symposium was structured into three parts:

1. The first three days, after an opening introductory session on Monday morning, were devoted to contributed papers in the various disciplines. A total of 184 papers were presented. These papers are contained in this publication as Volume I; they are numbered and presented in the order that they were listed in the Abstracts. Several papers not listed in the Abstracts are contained at the end of this Volume. A summary paper pertaining to ERTS-1 Data Product Performance, which was given as the first paper because of its general interest to all participants, is contained as the first paper in this Volume.

2. The Thursday Summary Session of the Symposium was designed to summarize the significant results presented during the first three days and also to present some typical examples of how ERTS results are being applied to solving operational resource management problems primarily at the federal and state levels. Highlighting this Summary Session were addresses by Dr. James C. Fletcher (Administrator, National Aeronautics and Space Administration), the Hon. James Symington (Representative, U. S. Congress, State of Missouri) and the Hon. Ed Reinecke (Lieutenant Governor, State of California). These were followed by a summary paper on the ERTS-1 status and then by four key papers selected from the presentations made during the first three days. On Thursday afternoon, four papers were presented which summarized the significant results from the first three days in selected disciplines. Five papers exemplifying the applications of ERTS results to meeting selected federal and state program objectives and resource management objectives in several disciplines were then presented. The proceedings of the Thursday Summary Session are contained in Volume II.

3. Volume III contains the reports of the Working Groups which were convened on Friday to summarize and critique the ERTS results in the various disciplines. These working groups were chaired by the respective discipline session chairmen and were composed of selected specialists in the disciplines. Opinions and recommendations expressed in these reports are those of the panel members and do not necessarily reflect an official position of NASA.

Stanley C. Freden
Symposium Chairman

TABLE OF CONTENTS

VOLUME I

TECHNICAL PRESENTATIONS

Paper No.		Page
	ERTS-1 DATA PRODUCT PERFORMANCE, B. T. Bachofer	1
	AGRICULTURE, FORESTRY, RANGE RESOURCES	
A 1	IDENTIFICATION OF WINTER WHEAT FROM ERTS-1 IMAGERY, Donald L. Williams, Stanley A. Morain, Bonnie Barker and Jerry C. Coiner	11
A 2	SEMI-AUTOMATIC CROP INVENTORY FROM SEQUENTIAL ERTS-1 IMAGERY, Claude W. Johnson and Virginia B. Coleman	19
A 3	CROP IDENTIFICATION USING ERTS IMAGERY, Maurice L. Horton and James L. Heilman	27
A 4	IDENTIFICATION OF LARGE MASSES OF CITRUS FRUIT AND RICE FIELDS IN EASTERN SPAIN, Fernando López de Sagredo and Francisco G. Salinas	35
A 5	ENGINEERING ANALYSIS OF ERTS DATA FOR SOUTHEAST ASIAN AGRICULTURE, Howard L. Heydt and Arthur J. McNair	37
A 6	AN INTERREGIONAL ANALYSIS OF NATURAL VEGETATION ANALOGUES USING ERTS-1 IMAGERY, Charles E. Poulton and Robin I. Welch	53
A 7	NATURAL VEGETATION INVENTORY, Barry J. Schrumpf	59
A 8	VEGETATIVE AND GEOLOGIC MAPPING OF THE WESTERN SEWARD PENINSULA, ALASKA, BASED ON ERTS-1 IMAGERY, James H. Anderson, Lewis Shapiro and Albert E. Belon	67
A 9	ERTS-1 EVALUATIONS OF NATURAL RESOURCES MANAGEMENT APPLICATIONS IN THE GREAT BASIN, Paul T. Tueller and Garwin Lorain	77
A 10	EVALUATION OF ERTS-1 IMAGERY IN MAPPING AND MANAGING SOIL AND RANGE RESOURCES IN THE SAND HILLS REGION OF NEBRASKA, Paul M. Seevers and James V. Drew	87
A 11	MONITORING CALIFORNIA'S FORAGE RESOURCE USING ERTS-1 AND SUPPORTING AIRCRAFT DATA, David M. Carneggie and Stephen D. DeGloria	91
A 12	TESTING THE USEFULNESS OF ERTS-1 IMAGERY FOR INVENTORYING WILDLAND RESOURCES IN NORTHERN CALIFORNIA, Donald T. Lauer and Paul F. Krumpe	97
A 13	INTERPRETATION OF ERTS-MSS IMAGES OF A SAVANNA AREA IN EASTERN COLUMBIA, G. W. W. Elbersen	105
A 14	DELINEATION OF MAJOR SOIL ASSOCIATIONS USING ERTS-1 IMAGERY, W. L. Parks and R. E. Bodenheimer	121

PRECEDING PAGE BLANK NOT FILMED

TABLE OF CONTENTS (Continued)

Paper No.		Page
A 15	EVALUATION OF REMOTE SENSING IN CONTROL OF PINK BOLLWORM IN COTTON, Virginia B. Coleman, Claude W. Johnson and Lowell N. Lewis	127
A 16	APPLICATION OF ERTS-1 IMAGERY & UNDERFLIGHT PHOTOGRAPHY IN THE DETECTION AND MONITORING OF FOREST INSECT INFESTATIONS IN THE SIERRA NEVADA MOUNTAINS OF CALIFORNIA, Ralph C. Hall	135
A 17	IMPACT OF ERTS IMAGES ON SURVEYS OF FOREST INSECT INFESTATIONS IN COOK INLET BASIN, ALASKA, James H. Anderson, F. Philip Weber, John M. Miller, Enzo Becia and Roy C. Beckwith	143
A 18	ERTS-1 IMAGERY AND HIGH FLIGHT PHOTOGRAPHS AS AIDS TO FIRE HAZARD APPRAISAL AT THE NASA SAN PABLO RESERVOIR TEST SITE, Robert N. Colwell	145
A 19	PHENOLOGY SATELLITE EXPERIMENT, Bernard E. Dethier, Marshall D. Ashley, Byron Blair and Richard J. Hopp	157
A 20	FOREST AND RANGE MAPPING IN THE HOUSTON AREA WITH ERTS-1 DATA, G. R. Heath and H. D. Parker	167
A 21	APPLICATION OF ERTS-1 DATA TO ANALYSIS OF AGRICULTURAL CROPS AND FORESTS IN MICHIGAN, Gene R. Safir, Wayne L. Myers, William A. Malila and James P. Morgenstern	173
A 22	CROP SPECIES RECOGNITION AND MENSURATION IN THE SACRAMENTO VALLEY, Frederick J. Thomson	181
A 23	THE RESULTS OF AN AGRICULTURAL ANALYSIS OF THE ERTS-1 MSS DATA AT THE JOHNSON SPACE CENTER, R. M. Bizzell, L. C. Wade, H. L. Prior and B. Spiers	189
A 24	AGRICULTURAL APPLICATIONS OF ERTS-1 DATA, William C. Draeger	197
A 25	IDENTIFICATION OF AGRICULTURAL CROPS BY COMPUTER PROCESSING OF ERTS MSS DATA, Marvin E. Bauer and Jan E. Cipra	205
A 26	IDENTIFICATION AND MAPPING OF SOILS, VEGETATION, AND WATER RESOURCES OF LYNN COUNTY, TEXAS BY COMPUTER ANALYSIS OF ERTS MSS DATA, Marion F. Baumgardner, Steven J. Kristof and James A. Henderson	213
	MINERAL RESOURCES, GEOLOGICAL STRUCTURE AND LANDFORM SURVEYS	
G 1	EVALUATION OF ERTS-1 IMAGERY FOR GEOLOGICAL SENSING OVER THE DIVERSE GEOLOGICAL TERRANES OF NEW YORK STATE, Yngvar W. Isachsen, Robert H. Fakundiny and Stephen W. Forster	223
G 2	ANALYSIS AND APPLICATION OF ERTS-1 DATA FOR REGIONAL GEOLOGICAL MAPPING, D. P. Gold, R. R. Parizek, and S. A. Alexander	231
G 3	GEOLOGY OF UTAH AND NEVADA BY ERTS-1 IMAGERY, Mead LeRoy Jensen	247

TABLE OF CONTENTS (Continued)

Paper No.		Page
G 4	PRELIMINARY GEOLOGIC APPLICATION OF ERTS-1 IMAGERY IN ALASKA Ernest H. Lathram, I. L. Tailleur, W. W. Patton, Jr.	257
G 5	A COMPARISON OF GEMINI AND ERTS IMAGERY OBTAINED OVER SOUTHERN MOROCCO, Herbert W. Blodget and Arthur T. Anderson	265
G 6	CAPABILITY OF ERTS-1 IMAGERY TO INVESTIGATE GEOLOGICAL AND STRUCTURAL FEATURES IN A SEDIMENTARY BASIN (BASSIN PARISIEN – FRANCE), Claude Cavelier, Jean-Yves Scanvic, Guy Weecksteen and Alain Ziserman	273
G 7	APPLICATION OF ERTS-1 MULTISPECTRAL IMAGERY TO MONITORING THE PRESENT EPISODE OF ACCELERATED EROSION IN SOUTHERN ARIZONA, Roger B. Morrison and Maurice E. Cooley	283
G 8	A STUDY OF MORPHOLOGY, PROVENANCE, AND MOVEMENT OF DESERT SAND SEAS IN AFRICA, ASIA, AND AUSTRALIA, Edwin D. McKee, Carol S. Breed and Lawrence F. Harris	291
G 9	ESTABLISHMENT, TEST, AND EVALUATION OF A PROTOTYPE VOLCANO-SURVEILLANCE SYSTEM, Peter L. Ward, Jerry P. Eaton, Elliot Endo, David Harlow, Daniel Marquez and Rex Allen	305
G 10	SATELLITE GEOLOGICAL AND GEOPHYSICAL REMOTE SENSING OF ICELAND – PRELIMINARY RESULTS FROM ANALYSIS OF MSS IMAGERY, Richard S. Williams, Jr., Agúst Bödvarsson, Sturla Fridriksson, Gudmundur Pálmason, Sigurjón Rist, Hylnur Sigtryggsson, Sigurdur Thórarinsson and Ingvi Thórsteinsson	317
G 11	PRELIMINARY ASSESSMENT OF GEOLOGICAL APPLICATIONS OF ERTS-1 IMAGERY FROM SELECTED AREAS OF THE CANADIAN ARCTIC, Alan F. Gregory	329
G 12	EXPLOITATION OF ERTS-1 IMAGERY UTILIZING SNOW ENHANCEMENT TECHNIQUES, Frank J. Wobber and Kenneth R. Martin	345
G 13	MAPPING QUATERNARY LANDFORMS AND DEPOSITS IN THE MIDWEST AND GREAT PLAINS BY MEANS OF ERTS-1 MULTISPECTRAL IMAGERY, Roger B. Morrison and George R. Hallberg	353
G 14	GLACIATION OF NORTHWESTERN WYOMING INTERPRETED FROM ERTS-1, Roy M. Breckenridge	363
G 15	FIRST-LOOK ANALYSIS OF GEOLOGIC GROUND PATTERNS ON ERTS-1 IMAGERY OF MISSOURI, William H. Allen, James A. Martin, and David L. Rath	371
G 16	RATIO MAPS OF IRON ORE DEPOSITS ATLANTIC CITY DISTRICT, WYOMING, Robert K. Vincent	379
G 17	USE OF ERTS-1 IMAGES IN THE SEARCH FOR PORPHYRY COPPER DEPOSITS IN PAKISTANI BALUCHISTAN, Robert G. Schmidt	387
G 18	RELATION OF ERTS-1 DETECTED GEOLOGIC STRUCTURE TO KNOWN ECONOMIC ORE DEPOSITS, Ernest I. Rich	395

Paper No.		Page
G 19	PRELIMINARY GEOLOGIC INVESTIGATIONS IN THE COLORADO PLATEAU USING ENHANCED ERTS IMAGES, Alexander F. H. Goetz, Fred C. Billingsley, Donald Elston, Ivo Lucchitta and Eugene M. Shoemaker	403
G 20	STRUCTURAL GEOLOGIC ANALYSIS OF NEVADA USING ERTS-1 IMAGES: A PRELIMINARY REPORT, Lawrence C. Rowan and Pamela H. Wetlaufer	413
G 21	REGIONAL TECTONIC CONTROL OF TERTIARY MINERALIZATION AND RECENT FAULTING IN THE SOUTHERN BASIN-RANGE PROVINCE, AN APPLICATION OF ERTS-1 DATA, I. C. Bechtold, M. A. Liggett and J. F. Childs	425
G 22	ERTS APPLICATIONS IN EARTHQUAKE RESEARCH AND MINERAL EXPLORATION IN CALIFORNIA, Monem Abdel-Gawad and Joel Silverstein	433
G 23	SOME ASPECTS OF ACTIVE TECTONISM IN ALASKA AS SEEN ON ERTS-1 IMAGERY, Larry D. Gedney and James D. VanWormer	451
G 24	ERTS-1 IMAGE CONTRIBUTES TO UNDERSTANDING OF GEOLOGIC STRUCTURES RELATED TO MANAGUA EARTHQUAKE, 1972, W. D. Carter and G. P. Eaton	459
G 25	RECOGNITION OF SURFACE LITHOLOGIC AND TOPOGRAPHIC PATTERNS IN SOUTHWEST COLORADO WITH ADP TECHNIQUES, Wilton N. Melhorn and Scott Sinnock	473
G 26	ERTS-1 IMAGERY AS AN AID TO THE DEFINITION OF THE GEOTECTONIC DOMAINS OF THE SOUTHERN AFRICAN CRYSTALLINE SHIELD, Morris J. Viljoen and Richard P. Viljoen	483
G 27	NEW ASPECTS ON THE TECTONIC OF THE ALPS AND THE APENNINES REVEALED BY ERTS-1 DATA, J. Bodechtel and B. Lammerer	493
G 28	STRUCTURAL LINEAMENTS OF GASPE FROM ERTS IMAGERY, Roberto Steffensen	501
G 29	LINEAMENTS IN COASTAL PLAIN SEDIMENTS AS SEEN IN ERTS IMAGERY, Charles F. Withington	517
G 30	EVALUATION OF COMMERCIAL UTILITY OF ERTS-A IMAGERY IN STRUCTURAL RECONNAISSANCE FOR MINERALS AND PETROLEUM, Donald F. Saunders and Gilbert E. Thomas	523
G 31	STRUCTURAL INTERPRETATIONS BASED ON ERTS-1 IMAGERY, BIGHORN REGION, WYOMING-MONTANA, Richard A. Hoppin	531
G 32	APPLICABILITY OF ERTS-1 TO LINEAMENT AND PHOTOGEOLOGIC MAPPING IN MONTANA – PRELIMINARY REPORT, Robert M. Weidman, David D. Alt, Raymond E. Flood, Jr., Katharine T. Hawley, Linda K. Wackwitz, Richard B. Berg and Willis M. Johns	539
G 33	A NEW FAULT LINEAMENT IN SOUTHERN CALIFORNIA, Robert W. Pease and Claude W. Johnson	547

Paper No.		Page
	ENVIRONMENT SURVEYS	
E 1	FRACTURE MAPPING AND STRIP MINE INVENTORY IN THE MIDWEST BY USING ERTS-1 IMAGERY, Charles W. Wier, Frank J. Wobber, Orville R. Russell and Roger V. Amato	553
E 2	ERTS-1 INVESTIGATION OF ECOLOGICAL EFFECTS OF STRIP MINING IN EASTERN OHIO, Phillip E. Chase and Wayne Pettyjohn	561
E 3	THE USE OF ERTS-1 MSS DATA FOR MAPPING STRIP MINES AND ACID MINE DRAINAGE IN PENNSYLVANIA, S. S. Alexander, J. Dein and D. P. Gold	569
E 4	MONITORING VEGETATION COVER ON MINE DUMPS WITH ERTS-1 IMAGERY: SOME INITIAL RESULTS, Brian Gilbertson	577
E 5	REMOTE DETECTION OF AEROSOL POLLUTION BY ERTS, G. E. Copeland, A. R. Bandy, E. C. Kindle, R. N. Blais and G. M. Hilton	585
E 6	DETECTION, MAPPING AND ESTIMATION OF RATE OF SPREAD OF GRASS FIRES FROM SOUTHERN AFRICAN ERTS-1 IMAGERY, J. M. Wightman	593
E 7	MAPPING ATLANTIC COASTAL MARSHLANDS, MARYLAND, GEORGIA, USING ERTS-1 IMAGERY, Richard R. Anderson, Virginia Carter and John McGinness	603
E 8	IDENTIFICATION OF MARSH VEGETATION AND COASTAL LAND USE IN ERTS-1 IMAGERY, V. Klemas, F. Daiber and D. Bartlett	615
E 9	APPLICATION OF ERTS-1 DATA TO THE PROTECTION AND MANAGEMENT OF NEW JERSEY'S COASTAL ENVIRONMENT, Robert L. Mairs, Frank J. Wobber, Donald Garofalo and Roland Yunghans	629
E 10	MONITORING OCEAN DUMPING WITH ERTS-1 DATA, C. T. Wezernak and N. Roller	635
E 11	ENVIRONMENTAL STUDY OF ERTS-1 IMAGERY: LAKE CHAMPLAIN AND VERMONT, Aulis O. Lind, E. Bennette Henson and James Pelton	643
E 12	WATER TURBIDITY DETECTION USING ERTS-1 IMAGERY, Harold L. Yarger, James R. McCauley, Gerard W. James, Larry M. Magnuson and G. Richard Marzolf	651
E 13	DIGITAL ANALYSIS OF POTOMAC RIVER BASIN ERTS IMAGERY: SEDIMENTATION LEVELS AT THE POTOMAC-ANACOSTIA CONFLUENCE AND STRIP MINING IN ALLEGHENY COUNTY, MARYLAND, J. S. Schubert and N. H. MacLeod	659
E 14A	A STUDY ON THE EROSION OF NIIGATA BEACH FROM ERTS-A IMAGERY, Takakazu Maruyasu	665
E 14B	APPLICATION OF ERTS DATA TO THE DETECTION OF THIN CIRRUS AND CLEAR AIR TURBULENCE, Kiyoshi Tsuchiya and Toshiro Kamiko	673

Paper No.		Page
E 14C	POLLUTED AND TURBID WATER MASSES IN OSAKA BAY AND ITS VICINITY REVEALED WITH ERTS-A IMAGERIES, Kantaro Watanabe	681
E 14 D	RED TIDE IN ISE BAY, Hiroaki Ochiai	689
	WATER RESOURCES	
W 1	HYDROGEOLOGY OF CLOSED BASINS AND DESERTS OF SOUTH AMERICA, ERTS-1 INTERPRETATIONS, George E. Stoertz and William D. Carter	695
W 2	DETECTION OF MAJOR RIVER BED CHANGES IN THE RIVER EBRO (NORTH-EASTERN SPAIN), R. Espejo, J. Torrent and C. Roquero	707
W 3	APPLICATIONS OF MULTISPECTRAL IMAGERY TO WATER RESOURCES DEVELOPMENT PLANNING IN THE LOWER MEKONG BASIN (KHMER REPUBLIC, LAOS, THAILAND AND VIET-NAM), Willem J. van Liere	713
W 4	PRELIMINARY TEST OF ERTS-1 IMAGERY FOR IMPROVING DEFINITION OF NATURAL STREAMFLOW, Este F. Hollyday	743
W 5	APPLICATION OF ERTS-1 IMAGERY TO FLOOD INUNDATION MAPPING, George R. Hallberg, Bernard E. Hoyer and Albert Rango	745
W 6	ASSESSMENT OF FLOOD DAMAGE IN ARIZONA BY MEANS OF ERTS-1 IMAGERY, Roger B. Morrison and Maurice E. Cooley	755
W 7	USE OF THE SRI ELECTRONIC SATELLITE IMAGE ANALYSIS CONSOLE FOR MAPPING SOUTHERN ARIZONA PLANT COMMUNITIES FROM ERTS-1 IMAGERY, Raymond M. Turner	761
W 8	MONITORING OF STREAMFLOW IN THE VERDE RIVER BY ERTS-1 DATA COLLECTION SYSTEM (DCS), Herbert H. Schumann	769
W 9	PRELIMINARY ANALYSIS OF ERTS-RELAYED WATER-RESOURCES DATA IN THE DELAWARE RIVER BASIN, Richard W. Paulson	777
W 10	MODELING SUBTROPICAL WATER-LEVEL DYNAMICS DISTRIBUTION, A. L. Higer, E. A. Cordes and A. E. Coker	793
W 11	AN EVALUATION OF SPACE ACQUIRED DATA AS A TOOL FOR MANAGEMENT OF WILDLIFE HABITAT IN ALASKA, Bill J. Van Tries	795
W 12	PRELIMINARY EVALUATION OF ERTS-1 FOR DETERMINING NUMBERS AND DISTRIBUTION OF PRAIRIE PONDS AND LAKES, Edgar A. Work, Jr., David S. Gilmer and A. T. Klett	801
W 13	DYNAMICS OF PLAYA LAKES IN THE TEXAS HIGH PLAINS, C. C. Reeves, Jr.	809

Paper No.		Page
W 14	STUDIES IN THE LAKE ONTARIO BASIN USING ERTS-1 AND HIGH ALTITUDE DATA, A. Falconer, S. H. Collins, W. T. Dickison, R. Protz, R. P. Bukata, K. P. B. Thomson, G. P. Harris and P. J. Howarth	819
W 15	PROGRESS OF AN ERTS-1 PROGRAM FOR LAKE ONTARIO AND ITS BASIN, Thomas W. Wagner and Fabian C. Polcyn	829
W 16	REMOTE SENSING OF TURBIDITY PLUMES IN LAKE ONTARIO, Edward J. Pluhowski	837
W 17	ERTS-1 VIEWS THE GREAT LAKES, Walter A. Lyons, Steven R. Pease	847
W 18	USE OF ERTS DATA FOR MAPPING SNOW COVER IN THE WESTERN UNITED STATES, James C. Barnes and Clinton J. Bowley	855
W 19	EVALUATION OF ERTS IMAGERY FOR MAPPING AND DETECTION OF CHANGES OF SNOWCOVER ON LAND AND ON GLACIERS, Mark F. Meier	863
W 20	DETECTION OF TURBIDITY DYNAMICS IN TAMPA BAY, FLORIDA USING MULTI-SPECTRAL IMAGERY FROM ERTS-1, A. E. Coker, Aaron Higer and Carl R. Goodwin	1715
	LAND USE AND MAPPING	
L 1	CARTOGRAPHIC QUALITY OF ERTS-1 IMAGES, R. Welch	879
L 2	PROGRESS IN CARTOGRAPHY, EROS PROGRAM, Alden P. Colvocoresses and Robert B. McEwen	887
L 3	CHANGE IN LAND USE IN THE PHOENIX (1:250,000) QUADRANGLE, ARIZONA BETWEEN 1970 AND 1972: SUCCESSFUL USE OF A PROPOSED LAND USE CLASSIFICATION SYSTEM, John L. Place	899
L 4	LAND USE INVESTIGATIONS IN THE CENTRAL VALLEY AND CENTRAL COASTAL TEST SITES, CALIFORNIA, Dr. John E. Estes	907
L 5	LAND USE IN THE NORTHERN COACHELLA VALLEY, Jack B. Bale and Leonard W. Bowden	915
L 6	LAND USE CLASSIFICATION AND CHANGE ANALYSIS USING ERTS-1 IMAGERY IN CARETS, Robert H. Alexander	923
L 7	ERTS REGIONAL-SCALE OVERVIEW LINKING LAND USE AND ENVIRONMENTAL PROCESSES IN CARETS, Robert H. Alexander	931
L 8	EVALUATION OF LAND USE MAPPING FROM ERTS IN THE SHORE ZONE OF CARETS, Robert Dolan and Linwood Vincent	939

TABLE OF CONTENTS (Continued)

Paper No.		Page
L 9	INVESTIGATIONS USING DATA FROM EARTH RESOURCES TECHNOLOGY SATELLITE IN THE FIELDS OF AGRICULTURE/GEOGRAPHY. (TIMBER INVENTORY – LAND USE) IN THE PROVINCE OF HUELVA-SPAIN, Emilio de Benito, Serafin López-Cuervo and Joaquin Rodriguez	949
L 10	GEOGRAPHIC APPLICATIONS OF ERTS-1 DATA TO LANDSCAPE CHANGE, John B. Rehder	955
L 11	IDENTIFICATION OF SOIL ASSOCIATIONS IN WESTERN SOUTH DAKOTA ON ERTS-1 IMAGERY, Frederick C. Westin and V. I. Myers	965
L 12	LAND USE OF NORTHERN MEGALOPOLIS, Robert B. Simpson and David T. Lindgren	973
L 13	REMOTE SENSING APPLIED TO LAND-USE STUDIES IN WYOMING, Roy M. Breckenridge, Ronald W. Marrs and Donald J. Murphy	981
L 14	ERTS-1 APPLICATIONS TO MINNESOTA LAND USE MAPPING, Dwight Brown, James Gamble, Steven Prestin, Dale Trippler, Merle Meyer, Joseph Ulliman and Ralph Eller	991
L 15	A MULTIDISCIPLINARY SURVEY FOR THE MANAGEMENT OF ALASKAN RESOURCES UTILIZING ERTS IMAGERY, John M. Miller and Albert E. Belon	999
L 16	THE USE OF ERTS-1 DATA FOR THE INVENTORY OF CRITICAL LAND RESOURCES FOR REGIONAL LAND USE PLANNING, J. L. Clapp, R. W. Kiefer, M. M. McCarthy and B. J. Niemann, Jr.	1007
L 17	INVESTIGATIONS OF AN URBAN AREA AND ITS LOCALE USING ERTS-1 DATA SUPPORTED BY U-"PHOTOGRAPHY," H. A. Weeden, F. Y. Borden, D. N. Applegate, and N. Bolling	1015
L 18	'FIRST LOOK' ANALYSES OF FIVE CYCLES OF ERTS-1 IMAGERY OVER COUNTY OF LOS ANGELES: ASSESSMENT OF DATA UTILITY FOR URBAN DEVELOPMENT AND REGIONAL PLANNING, S. Raje, R. Economy and J. McKnight	1023
L 19	PREPARATION OF URBAN LAND USE INVENTORIES BY MACHINE-PROCESSING OF ERTS MSS DATA, William Todd, Paul Mausel and Kenneth Wenner	1031
L 20	A COMPARISON OF LAND-USE DETERMINATIONS USING DATA FROM ERTS-1 AND HIGH ALTITUDE AIRCRAFT, M. Ann Lundelius, C. Mark Chesnutwood, Joe G. Garcia and R. Bryan Erb	1041
L 21	DIGITAL LAND USE MAPPING IN OAKLAND COUNTY, MICHIGAN, Irvin J. Sattinger and Robert D. Dillman	1047
L 22	MAPPING OF AGRICULTURAL LAND USE FROM ERTS-1 DIGITAL DATA, A. D. Wilson, G. A. May and G. W. Peterson	1055
L 23	THE USE OF THE TEMPORAL DIMENSION IN CLASSIFYING AND MAPPING ERTS-1 MSS DATA, F. Y. Borden and D. N. Applegate	1059

Paper No.		Page
L 24	IDENTIFICATION AND MAPPING OF COAL REFUSE BANKS AND OTHER TARGETS IN THE ANTHRACITE REGION, F. Y. Borden, D. N. Thompson and H. M. Lachowski	1067
L 25	AUTOMATIC INTERPRETATION OF ERTS DATA FOR FOREST MANAGEMENT, Leonard Kirvida and Greg R. Johnson	1075
L 26	LAND RESOURCES SURVEY FOR THE STATE OF MICHIGAN, Buzz Sellman	1083
L 27	TERRAIN CLASSIFICATION MAPS OF YELLOWSTONE NATIONAL PARK, Frederick J. Thomson and Normal E. G. Roller	1091
	INTERPRETATION TECHNIQUES DEVELOPMENT	
I 1	ATMOSPHERIC EFFECTS IN ERTS-1 DATA, AND ADVANCED INFORMATION EXTRACTION TECHNIQUES, William A. Malila and Richard F. Nalepka	1097
I 2	DETERMINATION OF AEROSOL CONTENT IN THE ATMOSPHERE, Michael Griggs	1105
I 3	A TECHNIQUE FOR CORRECTING ERTS DATA FOR SOLAR AND ATMOSPHERIC EFFECTS, Robert H. Rogers and Keith Peacock	1115
I 4	EXPERIMENTAL MASKING OF RBV IMAGES TO REDUCE STATIONARY RESIDUAL INACCURACIES IN RADIOMETRIC CORRECTION, Donald S. Ross	1123
I 5	GEOMETRIC QUALITY OF ERTS-1 IMAGES, Robert B. McEwen	1129
I 6	DIGITAL RECTIFICATION OF ERTS MULTISPECTRAL IMAGERY, Samuel S. Rifman	1131
I 7	RESULTS OF PRECISION PROCESSING (SCENE CORRECTION) OF ERTS-1 IMAGES USING DIGITAL IMAGE PROCESSING TECHNIQUES, Ralph Bernstein	1143
I 8	SIGNIFICANT TECHNIQUES IN THE PROCESSING AND INTERPRETATION OF ERTS-1 DATA, S. B. Cousin, A. C. Anderson, J. F. Paris and J. F. Potter	1151
I 9	COMPUTER TECHNIQUES USED FOR SOME ENHANCEMENTS OF ERTS IMAGES, Fred C. Billingsley and Alex F. H. Goetz	1159
I 10	DIGITAL ENHANCEMENT OF MULTISPECTRAL MSS DATA FOR MAXIMUM IMAGE VISIBILITY, Vidal Raphael Algazi	1169
I 11	ERTS-1 IMAGE ENHANCEMENT BY OPTICALLY COMBINING DENSITY SLICES, Gerald O. Tapper and Robert W. Pease	1179
I 12	PSEUDOCOLOR TRANSFORMATION OF ERTS IMAGERY, Jeannine Lamar and Paul M. Merifield	1187
I 13	DIGITAL INTERACTIVE IMAGE ANALYSIS BY ARRAY PROCESSING, Bruno E. Sabels and Jerry D. Jennings	1199

Paper No.		Page
I 14	COMBINING HUMAN AND COMPUTER INTERPRETATION CAPABILITIES TO ANALYZE ERTS IMAGERY, J. D. Nichols	1205
I 15	ANALYSIS OF ERTS IMAGERY USING SPECIAL ELECTRONIC VIEWING/MEASURING EQUIPMENT, Wm. E. Evans and Sidney M. Serebreny	1211
I 16	COMBINED SPECTRAL AND SPATIAL PROCESSING OF ERTS IMAGERY DATA, Robert M. Haralick and K. Sam Shanmugam	1219
I 17	TERRAIN TYPE RECOGNITION USING ERTS-1 MSS IMAGES, Nicholas Gramenopoulos	1229
I 18	CLASSIFICATION OF ERTS-1 MSS DATA BY CANONICAL ANALYSIS, H. M. Lachowski and F. Y. Borden	1243
I 19	IN SITU SPECTRORADIOMETRIC QUANTIFICATION OF ERTS DATA, Edward F. Yost	1253
	MARINE RESOURCES AND OCEAN SURVEYS	
M 1	SEASONAL CHANGES OF LITTORAL TRANSPORT AND BEACH WIDTH AND RESULTING EFFECT ON PROTECTIVE STRUCTURES, Turbit H. Slaughter,	1259
M 2	RECOGNITION OF BEACH AND NEARSHORE DEPOSITIONAL FEATURES OF CHESAPEAKE BAY, Randall T. Kerhin,	1269
M 3	APPLICABILITY OF ERTS-1 IMAGERY TO THE STUDY OF SUSPENDED SEDIMENT AND AQUATIC FRONTS, V. Klemas, R. Srna, W. Treasure and M. Otley	1275
M 4	CORRELATION OF ERTS MULTISPECTRAL IMAGERY WITH SUSPENDED MATTER AND CHLOROPHYLL IN LOWER CHESAPEAKE BAY, D. E. Bowker, P. Fleischer, T. A. Gosink, W. J. Hanna and J. Ludwick	1291
M 5	PLUME DEVELOPMENT IN LONG ISLAND SOUND OBSERVED BY REMOTE SENSING (ERTS-1), Frederick H. Ruggles, Jr.	1299
M 6	OBSERVATIONS OF SUSPENDED PARTICLE PATTERNS IN NEARSHORE NORTH-EASTERN PACIFIC OCEAN WATERS BY ERTS-1 IMAGERY, Paul R. Carlson, Richard J. Janda and T. John Conomos	1305
M 7	NEW INSIGHTS INTO THE INFLUENCE OF ICE ON THE COASTAL MARINE ENVIRONMENT OF THE BEAUFORT SEA, ALASKA, Peter W. Barnes and Erk Reimnitz	1307
M 8	ERTS-1 OBSERVATIONS OF SEA SURFACE CIRCULATION AND SEDIMENT TRANSPORT, COOK INLET, ALASKA, F. F. Wright, G. D. Sharma and D. C. Burbank	1315
M 9	SEDIMENT DISTRIBUTION AND COASTAL PROCESSES IN COOK INLET, ALASKA, Duwayne M. Anderson, Lawrence W. Gatto, Harlan L. McKim and Anthony Petrone	1323
M 10	DISTRIBUTION AND MOVEMENT OF SUSPENDED SEDIMENT IN THE GULF OF MEXICO OFF THE TEXAS COAST, Ralph E. Hunter	1341

Paper No.		Page
M 11	OCEANOGRAPHIC MAPPING OF STRUCTURE AND DYNAMICS OF THE NORTHERN GULF OF CALIFORNIA BY THE USE OF SPECTRAL MODELING AND ERTS-1, L. K. Lepley, Gustavo Calderon, and J. R. Hendrickson	1349
M 12	OCEANOGRAPHIC FEATURES IN THE LEE OF THE WINDWARD AND LEEWARD ISLANDS: ERTS AND SHIP DATA, Kirby J. Hanson, Frank Hebard and Richard Cram	1357
M 13	REMOTE SENSING OF OCEAN CURRENTS USING ERTS IMAGERY, George A. Maul	1365
M 14	USE OF ERTS DATA FOR MAPPING ARCTIC SEA ICE, James C. Barnes and Clinton J. Bowley	1377
M 15	BIOMASS IN THE UPWELLING AREAS ALONG THE NORTHWEST COAST OF AFRICA AS VIEWED WITH ERTS-1, Karl-Heinz Szekielda and Robert J. Curran	1385
M 16	ERTS IMAGERY AS AN AID TO FISHERIES MANAGEMENT IN THE NORTHERN GULF OF CALIFORNIA, J. R. Hendrickson, Alfredo Cota, Gustavo Calderon and L. K. Lepley	1403
M 17	APPLICATION OF ERTS-1 IMAGERY TO THE HARVEST MODEL OF THE U. S. MENHADEN FISHERY, Paul M. Maughan, Allan D. Marmelstein and O. Ray Temple	1405
M 18	COASTAL AND SUBMARINE FEATURES ON MSS IMAGERY OF SOUTHEASTERN MASSACHUSETTS: COMPARISON WITH CONVENTIONAL MAPS, Richard S. Williams, Jr.	1413
M 19	WATER DEPTH ESTIMATION WITH ERTS-1 IMAGERY, D. S. Ross	1423
M 20	CALCULATIONS OF WATER DEPTH FROM ERTS-MSS DATA, Fabian C. Polcyn and David R. Lyzenga	1433
	MULTIDISCIPLINARY/REGIONAL RESOURCE SURVEYS	
R 1	MULTIDISCIPLINARY APPLICATION OF ERTS-1 DATA TO NORTH CAROLINA NATURAL RESOURCE MANAGEMENT, Charles W. Welby, J. O. Lammi and Robert J. Carson	1443
R 2	NATURAL RESOURCE INVENTORY AND MONITORING IN OREGON WITH ERTS IMAGERY, G. H. Simonson, D. P. Paine, C. E. Poulton, R. D. Lawrence, J. H. Herzog, and R. J. Murray	1451
R 3	RESOURCE MANAGEMENT IMPLICATIONS OF ERTS-1 DATA TO OHIO, David C. Sweet, Terry L. Wells and George E. Wukelic	1459
R 4	ASSESSMENT OF SOUTHERN CALIFORNIA ENVIRONMENT FROM ERTS-1, Leonard W. Bowden and James H. Viellenave	1467
R 5	APPLICATIONS OF REMOTE SENSING (ERTS) TO RESOURCE MANAGEMENT AND DEVELOPMENT IN SAHELIEN AFRICA (REPUBLIC OF MALI), N. H. MacLeod	1475

PRECEDING PAGE BLANK NOT FILMED

Paper No.		Page
R 6	FIRST ERTS-1 RESULTS IN SOUTHEASTERN FRANCE: GEOLOGY, SEDIMENTOLOGY, POLLUTION AT SEA, A. Fontanel, J. Guillemot and M. Guy	1483

PAPERS NOT LISTED IN THE ABSTRACTS OF THE SYMPOSIUM

	DCP-COLLECTED ABSOLUTE TARGET REFLECTANCE SIGNATURES ASSIST ACCURATE INTERPRETATION OF ERTS-1 IMAGERY, Frederick P. Weber	1513
	UNIQUE CHARACTERISTICS OF ERTS, Alden P. Colvocoresses	1523
	ERTS-1 APPLIED FOR STRUCTURAL AND MORPHOLOGICAL INVESTIGATIONS CASE STUDIES: (1) LOS ANGELES, CALIFORNIA AND (2) COASTAL PLAIN, NEW JERSEY, Ervin Y. Kedar	1527
	A PRELIMINARY EVALUATION OF ERTS-1 IMAGES ON THE VOLCANIC AREAS OF SOUTHERN ITALY (NASA CONTRACT FO-013), R. Cassinis and G. M. Lechi	1539
	THERMAL SURVEILLANCE OF CASCADE RANGE VOLCANOES USING ERTS-1 MULTISPECTRAL SCANNER, AIRCRAFT IMAGING SYSTEMS, AND GROUND-BASED DATA COMMUNICATION PLATFORMS, Jules D. Friedman, David G. Frank, Duane Preble and J. Earle Painter	1549
	INITIAL EVALUATION OF THE GEOLOGIC APPLICATIONS OF ERTS-1 IMAGERY FOR NEW MEXICO, Karl Vonder Linden and Frank E. Kottlowski	1561
	COMPUTED ATMOSPHERIC EFFECTS ON ERTS OBSERVATIONS, Robert S. Fraser	1567
	MAPPING OF SPOIL BANKS USING ERTS-1 PICTURES, Professor Moid U. Ahmad David A. Kantner and John W. Antalovich	1575
	AIR QUALITY INDICES FROM ERTS-1 MSS INFORMATION, PR 568, Ellen L. Riley, Steven Stryker, and Edward A. Ward	1583
	SNOW COVER SURVEYS IN ALASKA FROM ERTS-1 DATA, Carl S. Benson	1593
	UTILIZATION OF ERTS-1 DATA TO MONITOR AND CLASSIFY EUTROPHICATION OF INLAND LAKES, Phillip E. Chase, Larry Reed and V. Elliott Smith	1597
	ERTS-1 OBSERVES ALGAL BLOOMS IN LAKE ERIE AND UTAH LAKE, Alan E. Strong.	1605
	USE ERTS-1 DATA FOR REGIONAL PLANNING IN THE METROPOLITAN WASHINGTON COUNCIL OF GOVERNMENTS – A SHORT BRIEF, Harry J. Mallon	1613
	LAND USE MAPPING AND CHANGE DETECTION USING ERTS IMAGERY IN MONTGOMERY COUNTY, ALABAMA, Richard Paul Wilms	1625
	DETERMINATION OF LAND USE IN MINNESOTA BY AUTOMATIC INTERPRETATION OF ERTS MSS DATA, Raymond E. Zirkle and Deborah R. Pile	1635

Page

DIGITAL DATA PROCESSING OF ERTS-1 IMAGERY OF DELAWARE BAY, Alfred C. Conrod 1641

THE USE OF PHOTOGRAPHIC METHODS IN CONTRAST ENHANCEMENT OF ERTS-1 IMAGES, Lawrence F. Harris 1649

PRECISION ANNOTATION OF PREDETERMINED PRIMARY SAMPLING UNITS ON ERTS-1 MSS IMAGES, Jan W. van Roessel and Philip G. Langley 1661

UNSUPERVISED CLASSIFICATION AND AREAL MEASUREMENT OF LAND AND WATER COASTAL FEATURES ON THE TEXAS COAST, L. M. Flores, C. A. Reeves, S. B. Hixon and J. F. Paris 1675

USE OF ERTS-1 PICTURES IN COASTAL OCEANOGRAPHY IN BRITISH COLUMBIA, J. F. R. Gower 1683

RELATIONSHIPS BETWEEN REMOTELY SENSED FISHERIES DISTRIBUTION INFORMATION AND SELECTED OCEANOGRAPHIC PARAMETERS IN THE MISSISSIPPI SOUND, Andrew J. Kemmerer and Joseph A. Benigno 1685

APPLICATION OF ERTS-1 IMAGERY IN COASTAL STUDIES, Orville T. Magoon, Dennis W. Berg and Robert J. Hallermeier 1697

APPLICATION OF ERTS-1 IMAGERY IN THE FIELDS OF GEOLOGY, AGRICULTURE, FORESTRY, AND HYDROLOGY TO SELECTED TEST SITES IN IRAN, Khosro Ebtehadj 1699

AUTHOR'S INDEX 1727

TABLE OF CONTENTS (Continued)

VOLUME II

SUMMARY SESSION

INTRODUCTION TO SUMMARY SESSION	Dr. James C. Fletcher, Administrator National Aeronautics and Space Administration
GENERAL REMARKS	Hon. James W. Symington, Representative, U. S. Congress, State of Missouri
KEYNOTE ADDRESS	Hon. Ed Reinecke, Lt. Governor State of California
REVIEW OF ERTS-1 STATUS	Dr. William Nordberg, Chief Laboratory for Meteorology and Earth Sciences NASA, Goddard Space Flight Center

KEY FINDINGS FROM SELECTED INVESTIGATIONS

IDENTIFICATION AND MAPPING OF SOILS, VEGETATION, AND WATER RESOURCES OF LYNN COUNTY, TEXAS, BY COMPUTER ANALYSIS OF ERTS MSS DATA, Marion F. Baumgardner, Steven J. Kristof and James A. Henderson, Jr.

PRELIMINARY GEOLOGIC APPLICATION OF ERTS-1 IMAGERY IN ALASKA, Ernest H. Lathram, Irvin L. Tailleur, William W. Patton, Jr. and William A. Fischer

A MULTIDISCIPLINARY SURVEY FOR THE MANAGEMENT OF ALASKAN RESOURCES UTILIZING ERTS IMAGERY, John M. Miller and Albert E. Belon

APPLICATION OF ERTS-1 IMAGERY TO FLOOD INUNDATION MAPPING, George R. Hallberg and Bernard E. Hoyer and Albert Rango

INVITED SUMMARIES IN SELECTED DISCIPLINES

AGRICULTURE, FORESTRY, RANGE RESOURCES, Charles E. Poulton

LAND USE AND MAPPING, David T. Lindgren and Robert B. Simpson

MINERAL RESOURCES, GEOLOGICAL STRUCTURE AND LANDFORM SURVEYS, Laurence H. Lattman

WATER RESOURCES, Vincent V. Salomonson and Albert Rango

INVITED PRESENTATIONS ON APPLICATIONS OF ERTS-1 RESULTS

THE EARTH RESOURCES PROGRAM OF THE CORPS OF ENGINEERS, John W. Jarman

APPLICATION OF ERTS-1 RESULTS TO USDI PROGRAMS, John M. DeNoyer

A PRELIMINARY ASSESSMENT OF ERTS IMAGERY FOR MARINE RESOURCES, Gifford C. Ewing

THE USE OF ERTS-1 DATA TO AID IN SOLVING WATER RESOURCES MANAGEMENT PROBLEMS IN THE STATE OF CALIFORNIA, Robert H. Burgy

APPLICATION OF ERTS RESULTS TO LAND AND RESOURCE MANAGEMENT IN THE STATE OF MISSISSIPPI, Preston T. Bankston

TABLE OF CONTENTS (Continued)

VOLUME III

DISCIPLINE SUMMARY REPORTS

AGRICULTURE, FORESTRY, RANGE RESOURCES, Chairman—W. J. Crea

LAND USE AND MAPPING, Chairman—D. W. Mooneyhan

MINERAL RESOURCES, GEOLOGICAL STRUCTURE AND LANDFORM SURVEYS, Chairman—N. M. Short

ENVIRONMENT SURVEYS, Chairman—L. S. Walter

WATER RESOURCES, Chairman—V. V. Salomonson

MARINE RESOURCES AND OCEAN SURVEYS, Chairman—J. R. Greaves

INTERPRETATION TECHNIQUES DEVELOPMENT, Chairman—W. L. Alford

MULTIDISCIPLINARY/REGIONAL RESOURCE SURVEYS, Chairman—G. Trafford

LAND USE AND MAPPING

PRECEDING PAGE BLANK NOT FILMED

N73-28297

Paper L 1

CARTOGRAPHIC QUALITY OF ERTS-1 IMAGES

R. Welch, *University of Georgia, Athens, Georgia 30602*

ABSTRACT

Analyses of simulated and operational ERTS images have provided initial estimates of resolution, ground resolution, detectability thresholds and other measures of image quality of interest to earth scientists and cartographers. Based on these values, including an approximate ground resolution of 250 meters for both RBV and MSS systems, the ERTS-1 images appear suited to the production and/or revision of planimetric and photo maps of 1:500,000 scale and smaller for which map accuracy standards are compatible with the imaged detail. Thematic mapping, although less constrained by map accuracy standards, will be influenced by measurement thresholds and errors which have yet to be accurately determined for ERTS images. This study also indicates the desirability of establishing a quantitative relationship between image quality values and map products which will permit both engineers and cartographers/earth scientists to contribute to the design requirements of future satellite imaging systems.

INTRODUCTION

Although the ERTS-1 imaging systems, the return-beam vidicon (RBV) and the multispectral scanner (MSS), have produced images of excellent apparent quality, the detail recorded may prove inadequate for cartographic applications at standard mapping scales. Consequently, in order to explore the cartographic potential of the ERTS images, a study was conducted in cooperation with the U.S. Geological Survey in which both simulated and operational exposures were analyzed to determine measures of image quality meaningful to cartographers and earth scientists, and which could be related to mapping requirements (Welch, 1972c). Since design parameters such as scan-lines/format and signal-to-noise ratio have limited meaning to non-engineers, an attempt was made to determine modulation transfer functions, resolution, ground resolution, and detectability and measurability thresholds for small detail, the values for which can all be related to the properties of ground objects and to cartographic tasks. These values and their relationship to topographic, photo and thematic map products are examined in this paper.

IMAGE QUALITY VALUES

The simulated imagery included several first generation film transparencies of 23 x 23 cm format on which standard Air Force collimator resolution targets had been recorded by an RBV camera linked directly to a Laser Beam Image Reproducer (LBIR). Target elements were oriented parallel and perpendicular to the scan-lines and contrasts were given as 6.5:1, 3.5:1, 1.8:1 and 1.2:1 with highlight values of between 50 and 100 percent (Weinstein, Miller, and Barletta, 1971). Although these images were not entirely representative of operational conditions in which an Electron Beam Recorder (EBR) is used to generate a 70 mm film format, the recording capabilities of the LBIR and EBR units do not differ significantly.

Using the simulated images both quantitative and visual analyses were conducted. Quantitative analyses, for example, included determinations of MTF's and measurement errors from microdensitometer and monocomparator measurements of the imaged bar groups, whereas visual analyses were performed to determine the average resolution data given in Table I.

The operational images consisted of third generation 70 mm film transparencies of Monterey Bay, California selected from ERTS orbit 28. Three RBV images representing bands 1 (0.475-0.575um), 2 (0.58-0.68um), and 3 (0.69-0.83um), and a MSS image in band 5 (0.6-0.7um) were analyzed. In contrast to the analysis procedures employed with the simulations, however, microdensitometer traces were made of the images of natural objects such as the coastline of Monterey Bay which was oriented at an angle of approximately 45 degrees to the scan-line pattern. MTF's were then derived from these edge traces using methods previously described by Welch (1971). MTF's for both simulated and operational images are given in Figure 1, and it is of interest to note the close correspondence between the MTF's for RBV bands 2 and 3 and MSS band 5, and their agreement with the MTF derived from the simulated images.

The known resolution values for the simulated images and the approximate correspondence between the MTF's for the simulated and operational images permitted estimates to be made of the operational exposure resolution. These estimates are based on a procedure in which the modulations (density differences) in the bar groups at the visually assessed resolution limit (for the simulations) were determined from the microdensitometer traces used to develop the MTF's. For the low-contrast targets these threshold modulation values averaged between 0.1 and 0.15 units. Next, the MTF's given in Figure 1 were translated vertically to the 0.23 modulation value on the ordinate which is equivalent to a linear contrast ratio of 1.6:1, a contrast ratio which is representative of the scene at the camera lens. The difference

in spatial frequency between the MTF's developed from the simulated and operational images at the 0.1 to 0.15 threshold modulation level was then noted as about 10-15 cy/mm. Since interpolation of the resolution values given in Table 1 indicated a resolution value of approximately 40 lpr/mm for a simulated image of a target having a contrast ratio of 1.6:1, the operational images can be assumed to have a resolution of 25-30 lpr/mm for the same contrast ratio. These values are based on an RBV format of 25 x 25 mm. For film formats of 70 mm and 23 cm, the equivalent resolution values are about 14 and 4 lpr/mm respectively, corresponding to a ground resolution of approximately 250 meters or an angular resolution of 0.27 mr (0.14 mr/element).

In addition to resolution values, estimates of the detectability and measurability thresholds for small detail were required. It was not possible, however, to determine these values directly from the ERTS images. Instead the comparability of these images to aerial photographs with known detectability and measurability values was established using the single-bar response functions in Figure 2. These functions, which are developed from the same microdensitometer traces used to calculate the MTF's, indicate the amplitudes generated by bars of increasing widths. From these functions it is evident that the ERTS images are comparable in quality to aerial photographs obtained with a photogrammetric mapping system such as the Wild RC8 camera and Eastman Kodak 2402 film. Detectability and measurability data for symmetric and linear objects of 1.6:1 contrast imaged on the aerial photographs are given in column 1 of Table II (Welch, 1972a). The corresponding ground object size for ERTS imagery is listed in column 2.

Although measurability estimates are given, because they are based on data derived from contact scale aerial photographs, it is difficult to relate them to ERTS images which have undergone a combination of electronic and optical enlargement. In particular, the measurement error values which indicate the differences between measured image size and the object size reduced by the correct scale factor probably do not increase linearly with the enlargement. In addition, the scan-line pattern influences measurement accuracy, causing much larger errors in measurements made perpendicular to the scan-line orientation. The relationships between scan-line width, enlargement factor, image size and measurability require further investigation.

CARTOGRAPHIC PRODUCTS

Although the image quality values which have been discussed are subject to refinement, they do provide an indication of the types and scales of maps which can be produced from the ERTS images. Three types of map products are considered: 1) topographic maps; 2) photomaps; and 3) thematic maps.

Topographic Maps

Topographic maps normally range in scale from larger than 1:24,000 to about 1:500,000, and are required by U.S. National Map Accuracy Standards to have 90 percent of the well-defined planimetric detail plotted to within 0.5 mm of its correct position, and 90 percent of the contours to within one-half the contour interval (Manual of Photogrammetry, 1966). However, since the ERTS systems are not designed to produce images from which reasonable height measurements can be extracted, we need only be concerned with planimetry. Therefore, considering map scales of 1:100,000, 1:250,000 and 1:500,000, detail must be plotted correctly to within 50, 125 and 250 meters respectively. As is readily apparent, however, the ground resolution of the ERTS images is only compatible with the accuracy requirements for maps at scales of 1:500,000 and smaller. This problem is further complicated by the fact that ground resolution values of this magnitude may not permit the drainage patterns, transportation routes and cultural features normally shown on small-scale maps to be adequately delineated. Based on these factors it appears that the ERTS imagery will prove most useful in revisions of existing small-scale aeronautical charts and maps. In addition, countries with large, unmapped areas and less rigid map accuracy standards will have the opportunity to produce preliminary planimetric maps at scales of 1:250,000 and smaller.

Photomaps

Much of the discussion on topographic mapping also applies to photomaps. In addition, however, the degree to which the ERTS images can be enlarged must also be considered. Normally, the optimum enlargement factor for the image base of a photomap is one which will result in the maximum retention of detail through the cartographic process, yet provide a product in which the images are sharp and well-defined. With small-scale imagery, such as that obtained from ERTS, an inadequate enlargement will result in the loss of considerable detail, whereas too great an enlargement will cause the image to become blurred.

Based on analytical experiments involving the use of MTF's (Welch, 1972b) an optimum enlargement factor of 7x (1:1,000,000 scale) was determined for ERTS images. Further empirical experiments by the U.S. Geological Survey have indicated a factor of as high as 14x (1:500,000 scale) can be employed while maintaining an image of acceptable quality. Enlargements of greater than 14x, although useful for direct comparisons with existing maps of equivalent scale, do not produce a photographic product of good apparent quality.

It is relevant to note that the U.S. Geological Survey has informally considered that a ground resolution equivalent to the map scale-factor multiplied by 0.1 mm is required for the production of photomaps. Consequently, for photomaps of 1:100,000, 1:250,000, 1:500,000 and

and 1:1,000,000 scale, ground resolutions of 10, 25, 50 and 100 meters respectively, would be necessary; as compared to the 250 meter capabilities of ERTS. Although the U.S.G.S. specification is probably conservative, it is evident that the resolution of ERTS images will not permit satisfactory photomaps to be produced at scales larger than approximately 1:500,000. Unfortunately, the usefulness of small-scale photomaps remains to be evaluated.

Thematic Maps

Thematic maps normally provide information concerning the distribution and areal extent of classes of objects and may be produced without concern for specific map accuracy standards. Nevertheless, thematic maps require the delineation of class boundaries and information is often extracted from the images in cell-size units. Obviously, image quality values influence both the identification of boundaries and the minimum size of data cell which can be reliably used to extract information.

In this study, the minimum size of data cell was of particular interest. It is apparent, for example, that a cell larger than the detectability threshold is required, since neither density nor area measurements of very small images indicate the properties of the corresponding ground objects. Based on data derived from the photographic measurements, it was established that a linear dimension of twice that of the detectability threshold provided the minimum size for which maximum response could be obtained, and from which the ground object's shape and area could be determined to some degree of accuracy. Measurement errors, of course, must be small in relation to the image dimensions in order to obtain accurate areas and shapes. Although the measurability estimates have been extrapolated from photographic data, it is evident that thematic information should be acquired from ERTS images using data cells with equivalent ground dimensions of several hundreds, or even thousands, of meters.

CONCLUSION

Measurements conducted on simulated and operational ERTS images indicate that the RBV and MSS systems produce ground resolutions of approximately 250 meters for low-contrast objects. Detectability and measurability thresholds for small low-contrast detail appear to be comparable to those for aerial photographs obtained with a photogrammetric camera system. However, the reliability of these threshold values is difficult to ascertain because of the differences between the optical processes used to produce the photographs and the electro-optical methods required to generate the ERTS images.

Despite the limited sample and the difficulties encountered in determining quality values, the ERTS images appear best suited to cartographic applications at scales smaller than 1:500,000, particularly for

countries which already have adequate map coverage. The study does indicate the importance of establishing a quantitative relationship between image quality values and the information requirements for different types and scales of cartographic products. If this can be accomplished, earth scientists and cartographers should be able to contribute to the design specifications of future satellite imaging systems.

ACKNOWLEDGMENTS

This report is based on work sponsored by the U.S. Department of Interior, Geological Survey, Contract No. 14-08-0001-13167, however, the conclusions are those of the author and do not necessarily represent the views of the U.S. Government. The support of Dr. R. B. McEwen of the U.S. Geological Survey is gratefully acknowledged as is the assistance provided by Mr. Masamu Aniya, University of Georgia.

REFERENCES

American Society of Photogrammetry, 1966, Manual of Photogrammetry, 105 N. Virginia Ave., Falls Church, Va. 22046.

Weinstein, O., Miller, B. P., and Barletta, J. M., 1971, "Simulations of ERTS RBV Imagery," Proceedings of the 7th International Symposium on Remote Sensing of Environment, The University of Michigan, pp. 1177-1188.

Welch, R., 1971, "Modulation Transfer Functions," Photogrammetric Engineering, V. 37, No. 3, pp. 247-259.

_____, 1972a, "Quality and Applications of Aerospace Imagery," Photogrammetric Engineering, V. 38, No. 4, pp. 379-398.

_____, 1972b, "Photomap Image Quality," The Cartographic Journal, V. 9, No. 2.

_____, 1972c, "ERTS-1 Image Quality," Proceedings of the 8th International Symposium on Remote Sensing of Environment, in press.

C11

TABLE I. AVERAGE RESOLUTION VALUES FOR THE SIMULATED IMAGES, REDUCED TO THE RBV FORMAT OF 25 x 25 mm.

Target Contrast	Resolution
6.5:1	64 lpr/mm
3.5:1	51
1.8:1	45
1.2:1	21

TABLE II. DETECTABILITY AND MEASURABILITY THRESHOLDS FOR OBJECTS OF 1.6:1 CONTRAST-RBV FORMAT OF 25 mm.

	Image Width	Ground Width
Detectability		
symmetric object	20-30um	140-210m
linear object	2-5um	14-35m
Measurability (size and shape defined for symmetric object)	40-60um	280-420m
*Measurement error	5-15um	

*Determined from measurements on the simulated RBV images (23cm format).

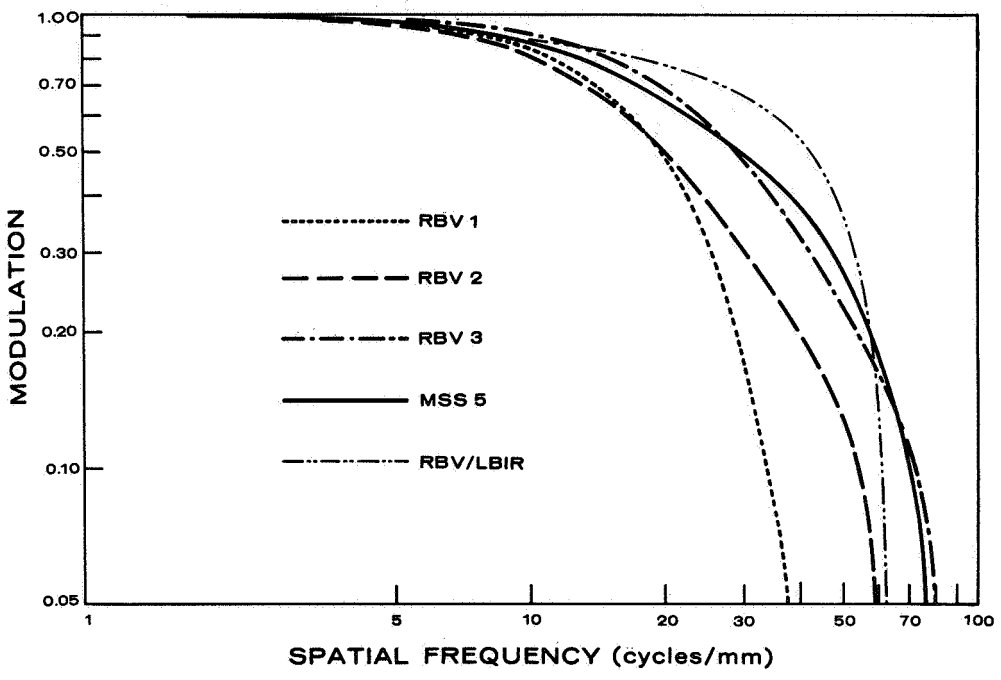


FIGURE 1. MTF'S FOR THE SIMULATED AND OPERATIONAL IMAGES.

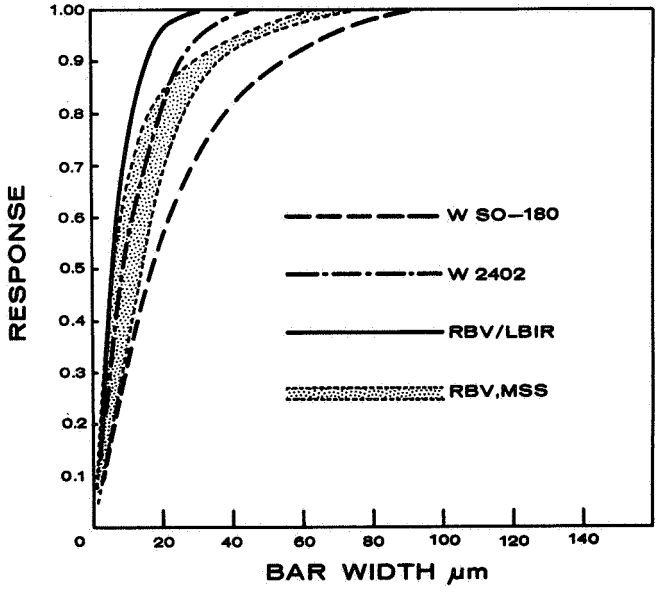


FIGURE 2. SINGLE-BAR RESPONSE FUNCTIONS FOR ERTS-1 IMAGES AND AERIAL PHOTOGRAPHS OBTAINED WITH A WILD RC8 CAMERA ON 2402 AND SO-180 FILMS. The shaded area indicates the range of single-bar response functions for the operational ERTS images.

N73-28298

Paper L 2

PROGRESS IN CARTOGRAPHY, EROS PROGRAM

Alden P. Colvocoresses and Robert B. McEwen, *U. S. Geological Survey, 1340 Old Chain Bridge Road, McLean, Virginia 22101*

INTRODUCTION

During the past 7 years the Interior Department EROS (Earth Resources Observation Systems) program with NASA sponsorship has conducted cartographic research based on high-altitude aerial and space photographs. The research has centered on the direct use of the image and its transformation into so-called photo or image maps. Today the cartographers of the Geological Survey have a real opportunity to apply themselves to making maps from data supplied by a satellite which is dedicated to remote sensing of the Earth.

On July 23, 1972, ERTS-1 (Earth Resources Technology Satellite; the figure 1 indicates the first of a series of proposed flights) was successfully launched into orbit by NASA. Within a few days its Return Beam Vidicon (RBV) cameras and Multispectral Scanner (MSS) were transmitting scenes of the Earth. The RBV cameras were turned off early in the mission because of technical problems in the control system, but the MSS continues to perform nearly flawlessly. The RBV cameras may be turned on again in the future. Two basic products are produced by NASA (Goddard Space Flight Center) from ERTS-1, which are known as bulk (system-corrected) and precision (scene-corrected) imagery. Bulk and precision processing are applied to both RBV and MSS imagery, and since there are three RBV spectral bands and four MSS bands, a variety of image forms can be produced for any one scene. NASA provides transparencies and/or prints at 1:3,369,000 and 1:1,000,000 scale to investigators and cognizant government agencies. The Interior Department, through the EROS Data Center at Sioux Falls, S. Dak., sells ERTS products to the public at nominal cost. ERTS-1 is scheduled to remain in orbit for a full year, but with good luck its effective life may be much longer.

Presented at NASA Symposium on Significant Results Obtained from ERTS-1, March 5-9, 1973.

Publication authorized by the Director, U.S. Geological Survey.

Cartographers of the Geological Survey have developed a number of ERTS-1 experiments, accepted by NASA, as follows:

Experiment	NASA Proposal
• Photomapping of the U.S.	211
• Map revision	237
• Basic thematic mapping	116
• Polar regions mapping	149
• Mapping from orbital data	150
• Overall cartographic application	233

The principal investigators for these experiments are receiving a wide variety of imagery; in addition, NASA has asked them to take a quick look at selected ERTS-1 imagery and report preliminary findings. The cartographic experiments are unique in that they apply to the development of graphics related to an accepted reference figure of the Earth to some defined degree of accuracy. However, both geometric and perceptional considerations are involved. Although the revision of line maps by means of ERTS materials is one of the more important experiments, the others concentrate on the problem of turning out maps in which the image itself provides the base.

PERCEPTIONAL CONSIDERATIONS

Maps are expected to have an informational content commensurate with their scale. For image-based products, which go under the general name of photomaps, image quality must be adequate for the map user to perceive (detect) and, within reason, identify objects that imagery of the given scale can be expected to portray. Cartographic products are normally lithographed and viewed by the unaided eye, a condition that establishes criteria for the evaluation of the perceptional quality of a photomap. Line maps, on the other hand, are highly interpreted products on which important features are shown and identified regardless of whether they can be seen or identified in imagery of the same scale. For example, major roads and railroads appear on most general-purpose maps of small scale (say 1:1,000,000), but the images of the features are not usually visible at the same scale.

The informational content of an image is based primarily on two factors, spectral and spatial response. Spectral response is measured by monochromatic tone or color differences, and the term *spectral consistency* is used here for evaluation of ERTS imaging forms in relative terms of repetitive spectral response. Line maps are normally compiled from black-and-white aerial photographs in which objects are defined by differences in density, recorded as tones of gray. As long as the density differences enable the map compiler to detect and identify the mappable object, spectral consistency is not of primary concern. But photomaps, which use the image as a base, are highly dependent on the spectral consistency of the image. Since spectral

response changes with time, sun angle, and atmospheric conditions, the production of photomaps which normally incorporate more than one image poses a real problem in attaining spectral consistency. The problem is magnified when the parameter of color is introduced, for now one must deal with three spectral responses (normally) rather than one. Automated thematic mapping--or Autographic Theme Extraction, as it is called in the Geological Survey--is based on image density slicing, and here again spectral consistency is the key.

Spatial response is measured by the minimum size of objects (of uniform response) that are uniquely recorded under certain conditions and can be identified as real scene objects rather than system noise. The term *object detectability* is used here to evaluate ERTS forms for spatial response. The term *resolution* is normally employed as a measure of spatial response for photographic products, but it relates to the minimum observable spacing between two like objects, such as stars in the sky or targets on the ground. With electro-optical systems such as TV or optical scanners, the relationship between resolution and minimum object size (detectability) is different than with photographic systems. Object detectability depends on edge sharpness or acutance as well as resolution, and the term is used in preference to resolution even though methods of quantifying detectability are not fully developed. (Rosenberg, 1971.) Both spectral consistency and object detectability are related to recorded contrast, which in turn depends on the differences in spectral response, atmospheric conditions, and image processing.

The following table evaluates the various types of ERTS imagery with respect to spectral consistency and object detectability and also indicates maximum practical printing scales for the imagery:

Perceptional Relative Image Quality

Image type	Spectral consistency	Object detectability	Maximum printing scale
RBV bulk	Poor to fair	Good	1:500,000
MSS bulk	Good	Good	1:250,000
RBV precision	Poor to fair	Fair	1:500,000-1:1,000,000
MSS precision	Poor to fair	Fair	1:500,000

We acknowledge that many ERTS-1 images have particular features that can be effectively enlarged to scales of 1:100,000 or larger; high-contrast land-water interfaces are good examples. On the other hand, objects of equal size but lower contrast become indistinguishable at the larger scales. Therefore, the maximum printing scales are rated as appropriate for maximum information content as viewed by a normal unaided eye at reading distance.

Resolution would also be a useful indicator of image quality, and the Geological Survey has asked NASA to install sizable targets on the ground for definitive resolution analysis. In the meantime, image edge analyses and similar techniques are being applied, but it is not known how well they can relate to resolution as photographically recorded in terms of target response.

The table given above is significant in that only one type, MSS bulk, exhibits image quality (perceptional) suitable for 1:250,000-scale mapping. However, conclusions about map products should not be drawn until the geometric properties have been fully examined.

GEOMETRIC CONSIDERATIONS

A major goal of the Interior Department is to map the country at various scales and with accuracy as defined by the U.S. National Map Accuracy Standards (NMAS). For planimetry the standards require, in effect, that 90% of well-defined features should be in error by no more than 0.02 inch (0.5 mm), measured on the publication scale. The 90% accuracy value is therefore ∿500 m (on the ground) at 1:1,000,000 scale, ∿250 m at 1:500,000, and ∿125 m at 1:250,000. Map errors may not be normally distributed, but for practical purposes the root mean square (rms) error of position for points tested should be less than 300 m at 1:1,000,000 scale, 150 m at 1:500,000, and 75 m at 1:250,000 scale to meet NMAS. Until recently it was considered impractical (or impossible) to make maps of scales smaller than ∿1:100,000 that met or even approached NMAS because oversize symbolization of features and other cartographic treatments require sizable positional displacement on small-scale maps. Photomaps, unless extensively annotated, do not contain displacement due to symbolization, and there is no reason why a photomap of small scale cannot meet NMAS as long as the image is geometrically sound and adequate control is available.

A prime consideration in attaining or analyzing map accuracy is the internal geometry of the imaging system. The desirable image is one that has a minimum of internal distortion. The ERTS image data processing system has unique capability, in the computer processing and electron beam recording, to system-correct many distortions. If the system were stable and if all sensor distortions and spacecraft motions were completely calibrated, the result could be an image of high internal geometric quality. At present, good calibration is available for the RBV system, and a mathematical model of the distortions has been developed (Wong, 1972). The MSS system is not suited to similar calibration, and moreover it fully incorporates (in the recorded image) the effects of small but continuous attitude changes of the spacecraft.

The available RBV frames, though limited in number, are enough for comparison of the reseau coordinates with calibrated preflight values. At ground scale the internal distortion ranges from a minimum of 42 m to a maximum of 100 m on the images evaluated. The average rms distortion

for all RBV images is 65 m and is generally a random distribution, representing images of high geometric quality and probably the practical limit for the ERTS RBV. The figures cited represent only the internal distortions of the sensor system. In practice, internal sensor distortions are combined with external distortions, such as topographic relief, earth curvature, sensor attitude, and the map projection. External distortions have been previously analyzed (Colvocoresses, 1970). When control-point image coordinates are compared with map coordinates, both external and internal distortions are effective, and the comparisons are true tests of images for mapping purposes.

Selected well-defined features on several RBV images have been compared with established Universal Transverse Mercator (UTM) coordinates. The number of points has been densified at selected sites to 15 or 20 points per image. The ability of an observer to identify and measure a ground control point varies, but for well-defined points it is between 15 and 25 m. The tested RBV frames fit the UTM coordinates with a maximum rms error of position of 150 m and a minimum of 100 m, determined by a least-squares four-parameter fit using x and y translation, rotation, and scale change. Additional adjustment allowing for tilt rectification produced a slight improvement but, as expected with a near-vertical, narrow-angle system, not enough to justify additional processing.

Many more MSS images have been measured and compared with ground control points. The MSS does not have a reseau, and preflight calibration data are not available. Since the internal and external errors cannot be separated, the only approach is to measure image points and attempt to identify and isolate specific errors. The MSS image is subject to certain microdistortions or anomalies that occur at regular intervals. In addition, some images have lines obviously omitted or displaced during processing. One anomaly is illustrated in figure 1, which is derived from a 1:100,000-scale enlargement of the Golden Gate bridge obtained from frame 1021-18172-6. The stair-step pattern is apparent; it follows a periodic cycle of 6 lines or one mirror scan. The offset is a function of the angle between the scan lines and the feature and may amount to over 100 m. The anomaly can be observed on airport runways, coastlines, and other linear features in other frames. NASA has recently indicated that the anomaly is one that they believe can be eliminated, or at least reduced, and that corrective action will be undertaken.

Early MMS images fitted to ground control had rms distortions up to 1000 m, always larger than 300 m. Best results to date were obtained with frame 1080-15192-5, showing Chesapeake Bay. Figure 2 shows a vector plot of residuals for that frame, for which rms = 192 m. Systematic error, such as changes in mirror speed and spacecraft attitude, can be corrected, so that MSS geometric quality can be further improved.

Measurements have been made on 70-mm third-generation and 24-cm (9.5-in.) fourth-generation transparencies. Some first-generation images were also measured, with results identical with

those obtained with a third-generation copy of the same scene. It does not appear that image duplication, enlargement, or processing is introducing any significant distortion even though target scales, such as 1:1,000,000, may not be exact.

Separate spectral bands of the same MSS scene have been measured and compared. The results indicate excellent register between bands, with maximum differences of only 10 to 20 m. Multispectral analysis of a single MSS scene is therefore subject to a negligible geometric error.

The bulk-image scenes are positioned by orbital data. The latitude and longitude coordinates for the midpoint of the scene given in the data block are subject to some errors, as are those for the edges of the frame. Frame 1080-15192 of Chesapeake Bay has center coordinates approximately 5 km in error. Some frames may have greater errors, but scenes processed since November 1972 are reported to be of better accuracy. However, sequential scenes cannot be registered by reference to indicated positions.

Both bulk and precision images of scene 1002-18131, Lake Tahoe, have been evaluated for geometric accuracy. The scene is available in all seven bands from the RBV and MSS and is the only one for which measurements have been made on precision-processed products. The measurements indicate an rms of 140 m for the RBV (precision) and 170 m for the MSS (precision). Since the scene was the first so processed and included unusual problems relative to terrain and control, the indicated rms values are considered to be high. The following summary contains a somewhat lower range of expected values and is based on the finding that most bulk images measured have exhibited less distortion than the Lake Tahoe scene.

Summary of expected image distortion
after best fit to ground control

Type	Error (rms, in meters)
RBV bulk	100-150
MSS bulk	200-450
RBV precision	100-150
MSS precision	100-150

Relating scales to errors through the NMAS, we might assume from the tabulated errors that maps of 1:500,000 scale could be made from RBV bulk, RBV precision, and MSS precision images whereas 1:1,000,000 would be the largest acceptable scale for MSS bulk. If the indicated errors were purely random, the deductions would probably hold, but systematic error is present and accuracy can be improved in cartographic processing. Specifically, it should be possible to improve the geometry of the bulk imagery through application of corrections determined from control-point comparison in precision processing. The procedure requires individual computations for each scene as well as a second printing with the electron beam recorder. NASA is not yet prepared to undertake

custom processing routinely, but has indicated that engineering tests of the concept will be undertaken. If the evidence indicates that custom processing will reduce distortion in bulk MSS imagery to perhaps half of present values, processing of ERTS imagery may be eventually modified to incorporate these geometric corrections.

However, it should also be noted that some types of cartographic products do not need to meet NMAS but may be useful even though their rms error is about twice the allowable NMAS error. Nevertheless, the basic conflict between perceptional and geometric qualities of the ERTS RBV and MSS images poses a real challenge to the mapmaker.

ANALYSIS OF THE MAPPING PROBLEM

With ERTS imagery, the mapping problem can be divided into two distinct categories, depending on whether identifiable ground control is or is not available. For the better mapped areas of the world, such as Europe and the United States, photoidentifiable control is readily available and permits the precise geometric evaluation and fitting of ERTS imagery to the Earth's figure. It also provides the basis for NASA's precision processing, in which the image is transformed and fitted to a recognized (UTM) map projection. In areas where ground control is not available, mapping must depend on orbital (and sensor) data by methods and techniques that are the subject of a specific ERTS investigation that is still in its early stages. The image of an RBV is a perspective projection, like the image of a conventional frame camera, and therefore mapping with RBV imagery by reference to either ground control or orbital data is a matter of well-understood, established procedures. The MSS, an optical scanner, creates a continuous image made up of a large number of independent picture elements (pixels), each representing a small segment of the Earth's surface. If printed out in raw form, the image would have such complex geometry that the mapmaker would find it all but impossible to use. To overcome the problem, NASA applies no less than 14 geometric corrections to the MSS imagery (noted on page G-18 of the ERTS Data Users Handbook prepared by General Electric for NASA). The curved Earth surface cannot be depicted on a plane without some distortion, but since the MSS image ray is always within 5.78° of the nominal vertical and the curvature of the Earth across the scene is less than 2°, the image approximates an orthographic view. The printed MSS image is a montage of sequentially produced thin projections and therefore lacks the internal geometric fidelity of the instantaneous frame image of an RBV. (See table of distortions presented earlier.)

Precision processing was defined as a system that correlates ERTS imagery to photoidentifiable ground control, rescans the image, and fits it to a specified projection. Unfortunately, precision processing involves considerable degradation of image quality that limits its application although the geometric improvement of the MSS imagery is highly significant for the mapmaker.

Regardless of availability of identifiable control and type of image used, the problem of map format is critical. The simplest format is that of a single ERTS scene whereas conventional geographic quadrilaterals or States normally require a mosaic made from several scenes. Using single scenes is relatively simple, and producing cartographic products from them is referred to as *First Phase Mapping*. Producing standard quads or State base maps is far more complex and is referred to as *Second Phase Mapping*.

FIRST PHASE MAPPING--IMAGE OR SCENE FORMAT

The first phase involves the processing of a single ERTS scene which by any of three methods has been brought to a specific scale and form and related to the figure of the Earth. Mapmakers are loath to use an image to define map boundaries, but in the case of ERTS the scenes are of sufficient size and repeatability for use in defining a series of maps. (The extent to which the system will be accepted by map users is not known.) The three methods of processing a single scene are as follows:

- Precision processing by NASA, which applies geographic (latitude and longitude) or plane coordinate (UTM) ticks to the image as transformed to the UTM projection. An agency such as USGS can then add a fine-line grid and lithograph in either black-and-white or color. The orthophotoimage of Lake Tahoe reproduced in color is a sample product; 1:1,000,000 is the only publication scale used to date, and the precision processing imposes image-quality limitations that may preclude publication at large scales. It is important to note that any ERTS image precision processed by NASA is a cartographic product. Suitable control throughout the U.S. is being identified by the U.S. Geological Survey and furnished NASA. The precision-processed images so far produced of the U.S. do meet NMAS at the 1:1,000,000 scale, and accuracy can undoubtedly be maintained wherever suitable control is available.

- A bulk ERTS MSS image can be rectified and scaled to a defined projection and a geodetic grid. At 1:1,000,000 scale the products should meet NMAS, but at 1:500,000 the error may be about twice the tolerance of NMAS. An RBV bulk image should meet NMAS at 1:500,000 and still present an image of acceptable quality in monochromatic printing.

- The third method is to bring an ERTS image as close as possible to a predetermined scale and fit a grid that has been generated from image-identified control points. The grid-fitting method is particularly applicable to bulk MSS imagery, and the products should meet NMAS at 1:500,000 scale. It should be noted that the image has not been controlled to an accepted map projection and the grid lines theoretically do not form perfect squares. However, the departure from the perfect square is so small that it is not measurable in individual grid units. At present, this procedure is the only one of the three that promises to produce a 1:500,000-scale map of good image quality at NMAS.

SECOND PHASE--QUADRANGLE OR STATE FORMAT

A 1:250,000-scale standard geographic quad extends 1° in latitude by 2° in longitude and may be covered by only 2 ERTS scenes. A 1:1,000,000-scale quad extends 4° in latitude by 6° in longitude and may contain 30 or 40 ERTS scenes. USGS 1:500,000-scale maps are now State maps rather than quadrangle maps, and therefore vary greatly in size and shape. Second phase maps at 1:250,000, 1:500,000, and 1:1,000,000 are in various stages of compilation; we hope that they will be lithographed and placed on public sale by USGS in the near future.

APPLICATIONS AND FINAL FORM

There are several cartographic applications of ERTS imagery. Revising line maps is one in which the image is not retained, but the other applications defined to date retain the image or a derivative of the image as follows:

- *Monochromatic orthophoto.*--normally derived from one spectral band and portrayed in gray tones. Colors may be assigned as a function of density, but the basic input at some stage is a single gray-tone image.

- *Polychromatic orthophoto.*--the color image application; with ERTS, normally gives a false-color rendition that includes the near-infrared.

- *Autographic theme extraction.*--a derivative application that isolates one or more basic themes, such as water, snow and ice, or infrared reflective vegetation.

Final form depends on the reproduction process used and results in photographic, diazo, or lithographic prints. The choice of final form is generally determined by the expected demand. However, diazo is now limited to a single color whereas the photo and lithographic form may be either in black-and-white or in color.

At this stage of inveatigation, it is impossible to say what combinations of the characteristics described will result in optimum products. All indications are that out of ERTS will develop one or more series of maps that will be of real value to this country and to the world as a whole.

REFERENCES

Colvocoresses, A. P., 1970, ERTS-A Satellite Imagery, *Photogrammetric Engineering*, v. 36, no. 6, p. 555-560.

Rosenberg, Paul, 1971, Resolution, Detectability and Recognizability, *Photogrammetric Engineering*, v. 37, no. 12, p. 1255-8.

Wong, K. W., 1972, Geometric Analysis of the RBV Television System (Phase II), September 1972; report available from National Technical Information Service, Springfield, Virginia 22151.

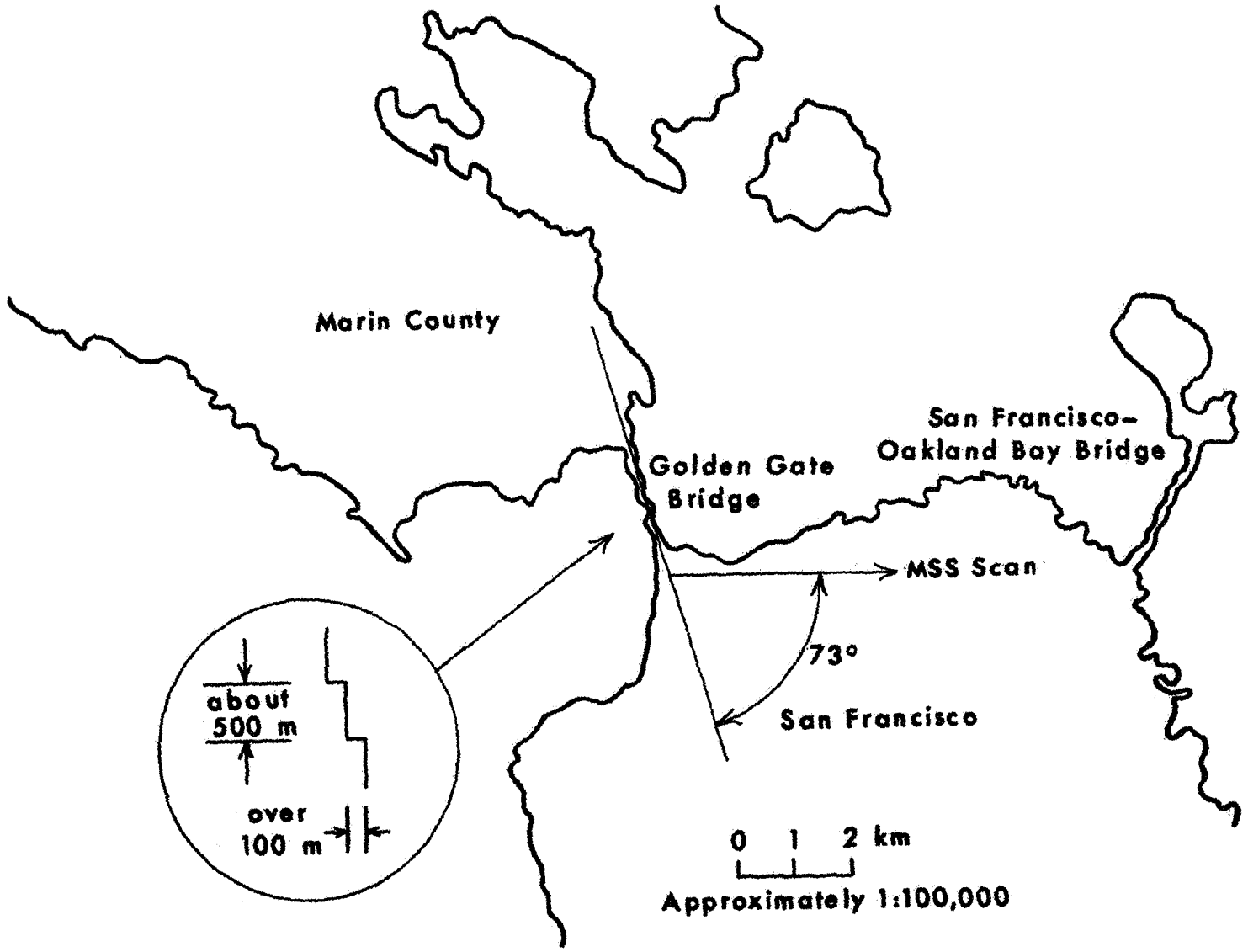
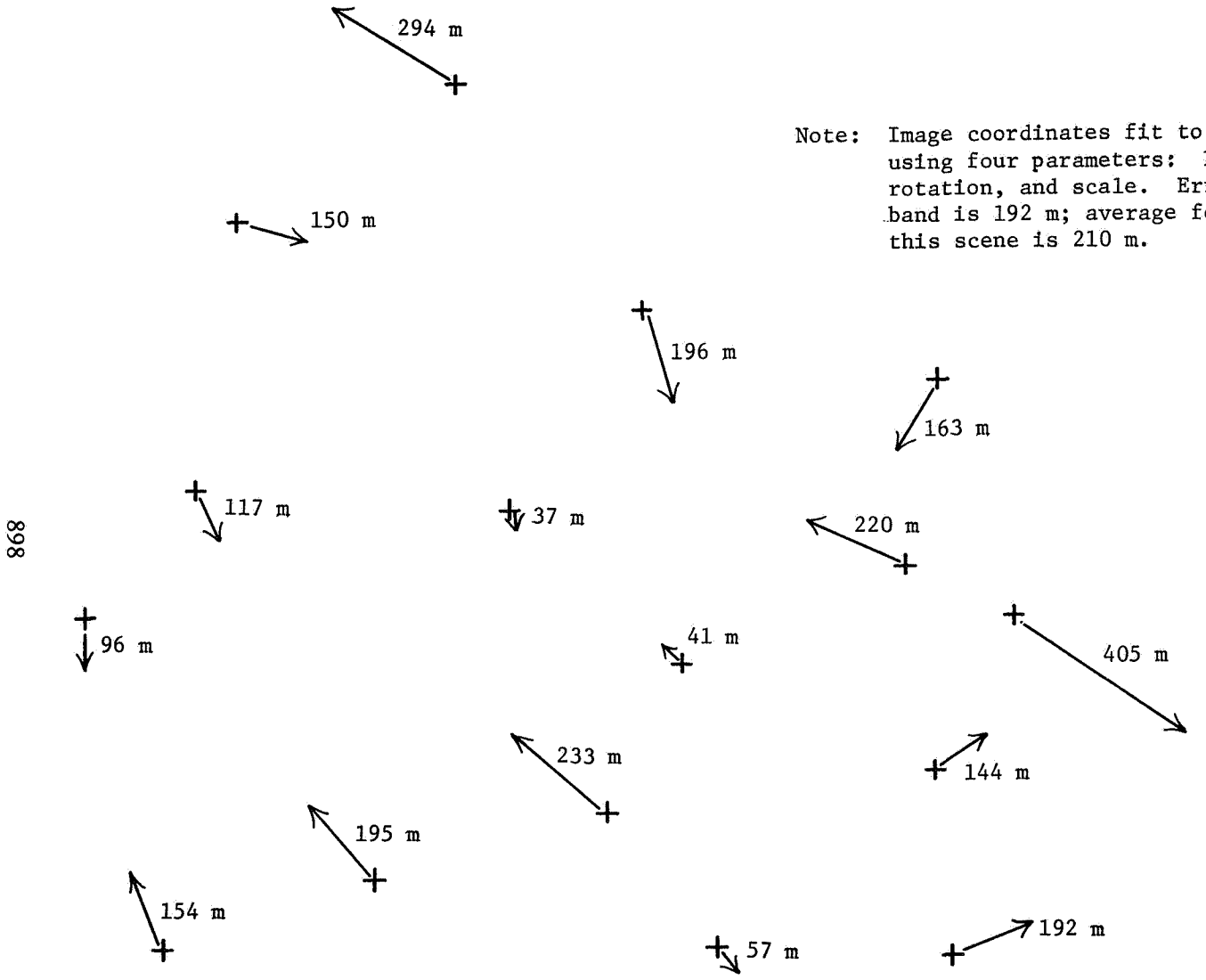


Figure 1. -- MSS line-scan anomaly.



Note: Image coordinates fit to UTM coordinates using four parameters: X and Y translation, rotation, and scale. Error (rms) for this band is 192 m; average for the 4 bands of this scene is 210 m.

Figure 2.--MSS bulk-image distortion (meters); frame 1080-15192-5, Chesapeake Bay area.

N13-28299

Paper L 3

CHANGE IN LAND USE IN THE PHOENIX (1:250,000) QUADRANGLE, ARIZONA BETWEEN 1970 AND 1972: SUCCESSFUL USE OF A PROPOSED LAND USE CLASSIFICATION SYSTEM

John L. Place, *U. S. Geological Survey, Geographic Applications Program, Washington, D. C.*

ABSTRACT

Changes in land use in the Phoenix (1:250,000 scale) Quadrangle in Arizona have been mapped using only the images from ERTS-1, tending to verify the utility of a land use classification system proposed for use with ERTS images. The period of change investigated was from November 1970 to late summer or early fall, 1972. Seasonal changes also were studied using successive ERTS images. Types of equipment used to aid interpretation included a color additive viewer, a twenty-power magnifier, a density slicer, and a diazo copy machine for making ERTS color composites in hard copy. Types of changes detected have been: a) cropland or rangeland developed for new residential areas; b) rangeland converted to new cropland; and c) possibly new areas of industrial or commercial development. A map of land use previously compiled from air photos was updated in this manner.

This information on changes can be of value to planners and resource managers at Federal, state, and regional levels, in monitoring environmental change in developing resources in broad regions of the United States. Planners need land use maps as an early step in planning both in the Governmental and private sectors. Managers utilize successive maps of land use to monitor change in the natural and man-made environment. The ERTS images focussed attention on those areas of greatest change requiring more intensive study.

Original photography may be purchased from:
EROS Data Center
10th and Dakota Avenue
Sioux Falls, SD 57198

1. INTRODUCTION

Attempts have been made in the past to map the current land use of all or most of the United States, but it took so long to compile the necessary information that some of it was obsolete before it was finally published. With the advent of earth resources satellites of the ERTS type, the potential now exists for mapping land use in very large areas of the United States and for keeping these maps relatively current. In order to utilize as much as possible of the detail available from satellite images, an intermediate scale of 1:250,000 was selected for the mapping. This is the largest standard scale for which we have nationwide coverage. Prior to the launch of ERTS, an investigation had been conducted within the USGS Geographic Applications Program with NASA and EROS sponsorship to develop procedures for mapping land use in a sample 1:250,000 quadrangle, specifically the Phoenix Quadrangle in Arizona. The land use data were read off into a computer where they were combined with information on other environmental and politico-economic factors. It was hoped that contiguous blocks of such maps and data banks could be created to cover large regions, such as the Colorado River drainage basin.

The mapping of the Phoenix Quadrangle was done primarily with the aid of high-altitude aerial photography taken by NASA in 1970. Our ERTS experiment is to determine the value of ERTS images in the updating of that 1970 map and for consequent updating of the computer data bank for the Phoenix Quadrangle. In the past few months, we have successfully mapped the changes in generalized land use between 1970 and 1972 in the test quadrangle using only the images from ERTS. We believe now that we can use the frequent passage of ERTS-type satellites to complement our map revision procedures, providing us with a capability to monitor trends in land utilization on a nearly real-time basis. Admittedly, this is still highly-generalized mapping because of the 100-meter resolution limit on the images. However, better resolution should be forthcoming from Skylab and future unmanned satellites beyond the ERTS-B era, and we are already close to the threshold for another level of detailed classification using only the ERTS-1 images. In any event, our present capabilities allow us to monitor general trends and to focus in on areas of most rapid change requiring more intensive study.

2. PROCEDURES

However, our immediate goal is to draw the most information possible from the existing ERTS images. During the past summer with

the launch of ERTS-A imminent, experimentation commenced using ERTS-simulation photographs. This procedure gave us experience in using the several spectral bands to create enhanced images on an I^{2}S Color Additive Viewer and for making land use interpretations from them. Multiband 70 mm frames were mounted in the viewer to determine the best combination of colored filters and light intensities.

With the arrival of the first ERTS images during the past five months, interpretation has been attempted using every image enhancement technique at our disposal. Experimentation has been primarily with 70 mm chips cut out of the 9 x 9 transparencies of each of the ERTS MSS bands 4, 5, and 6. The primary equipment used was (1) an I^{2}S Color Additive Viewer; (2) a Richardson Film Projection Viewer at 10-power and 20-power magnification, (3) a microfiche viewer at 12-power and 18-power magnification, and (4) a Spectral Data Systems Data Color density slicer. We have found the MSS images to be superior to the RBV images for purposes of interpreting land use.

Since it had been found previously that color infrared transparencies are generally the most useful images for land use interpretation, a search was made for the best method of creating hard copy composites from the ERTS MSS bands. Copies of color composite transparencies are being ordered retrospectively from NASA Goddard by special order form. One composite has been made by conventional photographic procedure, but this is very expensive. Diazo copying of individual bands has been done with the Diazo transparencies being overlain to form a composite. This is quite inexpensive and the quality is almost as good as the photographic product. The method demonstrated here to create briefing slides and report illustrations is the simple photographing of the display screen of the Color Additive Viewer. An example is shown in Figure 1 which is a color infrared composite of ERTS MSS bands 4, 5, and 6 taken of the eastern part of the Phoenix Quadrangle in November. Some degradation in quality occurred from the photographic step, yet this can be compared favorably with the famous Apollo-9 photo of the Phoenix area.

Almost all of the interpretation of land use change in this project was done using the Color Additive Viewer with this type of display. The most useful setting that we found showed the MSS band 4 with a blue filter and light intensity of 4, the MSS band 5 with a green filter and full light intensity, and MSS band 6 with a red filter and light intensity

of about 7. If the light intensity of the infrared band is changed rapidly up and down, it aids detection of subtle shades of red which indicate residential landscaping. The cropland with crops on it is easy to detect as bright red field plots. Fallow fields on the edge of the desert can barely be detected by the absence of faint brown brown desert shrub cover. Tree crops appeared brownish red, non-vegetated man-made features appeared bluish, and water surfaces stood out as dark blue. The 1970 map of land use was consulted and any changes discovered were plotted on an overlay upon it.

The EROS Program of the Department of the Interior has in its possession a Data Color density slicer made by Spectral Data Systems. It is housed at the Geological Survey s McLean, Virginia Office. This density slicer was tested with samples of ERTS MSS bands 5, 6, and 7. The next figure shows a photograph taken of the display screen of the density slicer which appear interesting. Although we have not yet been able to interpret these patterns to help in land use mapping, the potential is there and we seem to be getting close to something useful.

Figure 2 shows the Data Color density slicer enhancing certain gray tones of an ERTS image. Plots of land with lush, well-watered vegetation are enhanced compared to other types of surface cover, held as a duller gray background. This area is west of Phoenix in the vicinity of Sun City.

In general, of the 5, 6, and 7 bands tested, MSS band 7 gave the sharpest patterns in terms of contrast between vegetated and non-vegetated areas.

Basic to the entire investigation is the detection of change. The simplest approach was visual comparison of the 1970 map of land use with the 1972 ERTS image. An aid to this comparison would be the "quick flip" technique possible using a Bausch and Lomb Zoom Transfer Scope. Delivery of two of these instruments to our office is expected in the next few weeks. In the meantime, we have been experimenting with change detection using ERTS images taken three or more months apart. For example, field patterns in August are different from those in November. Use of the I^2S Color Additive Viewer allows both "quick flip" techniques and overlaying/registering of the August and November images.

3. FINDINGS

Nevertheless, a map of change in land use for the entire Phoenix Quadrangle was compiled by point by point visual comparison. A part of that map is shown in Figure 3, the portion around the City of Phoenix. Information already known, but recognized on the ERTS images is shown in red with solid line boundaries. New information detected by ERTS is in green with dotted boundaries. All of the changes shown here are new urban developments. New cropland was detected elsewhere in the quadrangle.

One of the goals of this experiment was to test the new standard land use classification designed for use with ERTS images and high-altitude air photos to see if it could be applied to arid areas. The proposed classification system for nationwide land use is shown in Figure 4. This classification system is described in USGS Circular 671. Basically, it consists of a first level of classification, designed for use with ERTS-type images, and a second level designed for use with high-altitude aerial photos. For the Phoenix Quadrangle, the proposed system was an apparent success. Because only satellite images were involved in the test, only the first level was used. Of the first level categories only Urban and Built-up, Agricultural Land, Rangeland, and Water existed in this quadrangle. We were particularly pleased that we came close to interpreting some of the second level categories as well, notably separating residential from other urban categories, separating out tree crops, and delimiting some mining/quarrying activities. In other areas, deciduous forests might be distinguished from evergreen forests, but surveillance over many seasons will probably be needed, and possibly use of more-advanced interpretation techniques presently being developed.

The most important test in this investigation is yet to come. When our ERTS underflight photography finally arrives--it was ordered by NASA MSC Form 192 in January 1972--we will calculate the accuracy of our ERTS interpretation. Until then, we cannot use the new discoveries to update the existing computer data bank for the Phoenix Quadrangle.

4. CONCLUSIONS

In conclusion, a map of land use change in the Phoenix 1:250,000 quadrangle has been compiled using ERTS images only. The proposed standard land use classification has been an apparent success in this test site, though not yet checked for accuracy.



Figure 1. A composite of ERTS MSS bands 4, 5, and 6 showing Phoenix and irrigated farmland November 1972, photographed from I^{2}S viewer.

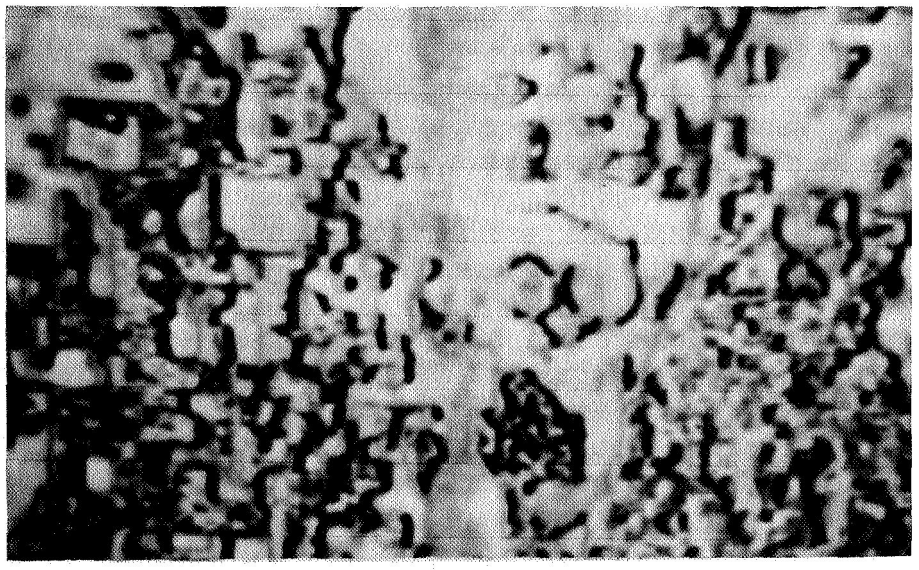


Figure 2. Data Color density slicer enhancing an ERTS image. Plots of land west of Phoenix with lush, well-watered vegetation are enhanced compared to other types of surface cover.

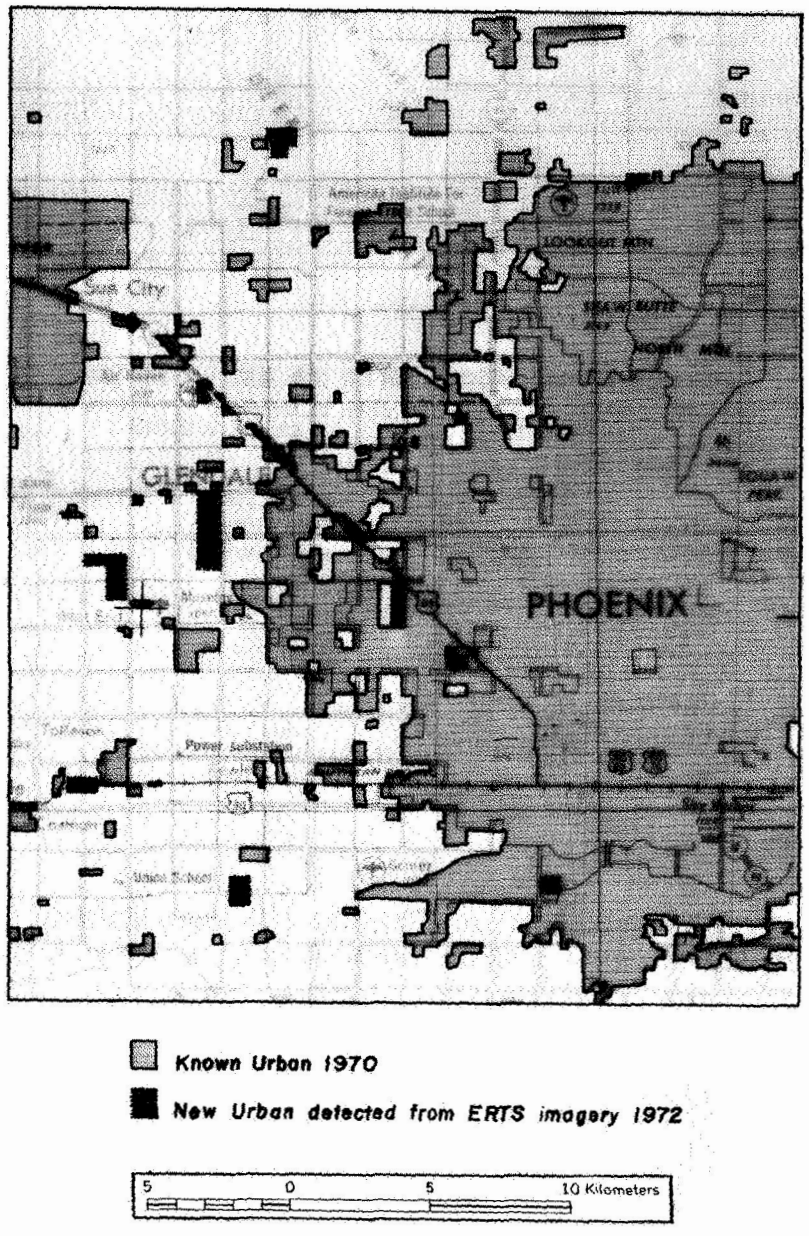


Figure 3. Map of urban and built-up land in the Phoenix metropolitan area. Areas with solid boundaries were detected in U-2 aerial photographs in 1970 and recognized in ERTS. Areas with dotted patterns are new urbanized areas detected in ERTS MSS composites. ERTS images were the only source of information used for this change detection.

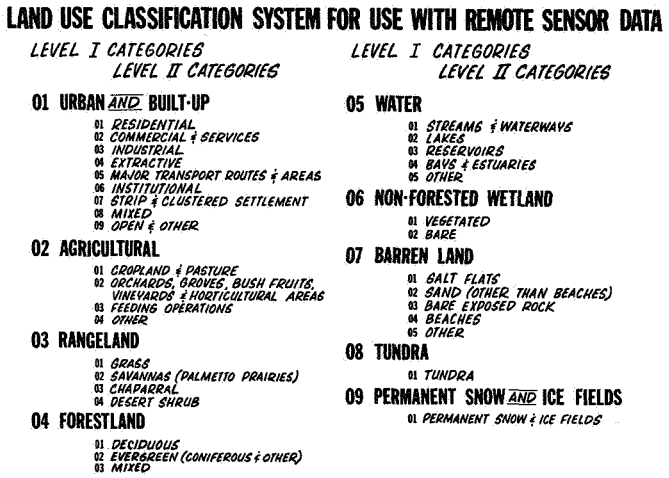


Figure 4. Proposed standard land use classification system. The first level of the classification system was designed for use with ERTS images.

N13-28300

Paper L 4

LAND USE INVESTIGATIONS IN THE CENTRAL VALLEY AND CENTRAL COASTAL TEST SITES, CALIFORNIA

Dr. John E. Estes, *Geography Remote Sensing Unit, Geography Program, University of California, Santa Barbara*

The Geography Remote Sensing Unit (GRSU) at the University of California, Santa Barbara is responsible for investigations with ERTS-1 data in the Central Coastal Zone and West Side of the San Joaquin Valley. The nature of the investigative effort involves the inventory, monitoring, and assessment of the natural and cultural resources of the two areas. Land use, agriculture, vegetation, landforms, geology, and hydrology are the principal subjects for attention. These parameters are the key indicators of the dynamically changing character of the two areas. Monitoring of these parameters with ERTS-1 data will provide the techniques and methodologies required to generate the information needed by federal, state, county, and local agencies to assess change-related phenomena and plan for management and development.

In conducting these investigations, close cooperation is being maintained with various agencies to define information requirements and establish mechanisms for information flow. Among the groups already cooperating are the Department of Water Resources, Division of Highways, Farm Advisors (Santa Barbara and Kings Counties), and the Kern County Water Agency. In the Coastal Zone, GRSU is cooperating with the Forestry Remote Sensing Laboratory (U.C. Berkeley) and the Geography Department at U.C. Riverside. The three groups are working in concert to develop resource classification schemes that are applicable along the entire California coastline. These activities will lead to the development of a relatively uniform (i.e., standardized) Coastal Zone data base from ERTS-1 imagery.

In preparation for receipt of ERTS-1 data, consierable effort was placed on establishing a solid data base for the Central Coastal Zone. Detailed classification systems were devised for the resource parameters of interest, and maps were prepared from existing RB-57 color infrared photography imaged in April, 1971 (NASA Mission 164). The data base is being used to evaluate the information content of ERTS-1 imagery. As continued ERTS-1 data is received, the classification systems will be modified to make them compatible with the information content of ERTS-1 imagery. A solid data base already exists for the West Side of the San Joaquin Valley as a result of previous research by GRSU, and it is being used in the same fashion as the Central Coastal Zone data base. The balance of this paper will deal with results obtained in the conduct of land use analysis in these test areas.

Evaluation of land use features from ERTS-1 imagery has concentrated on determining the feasibility of ERTS as a data source for identifying, delimiting and mapping various land use types. In order

to assess the capability of ERTS-1 data to provide land use information within a data base context, investigations have concentrated on identification of specific land use parameters within diverse environmental and cultural settings. More specifically, cultural features which have been under close examination are: 1) urbanized areas (extent and location: both absolute and relative); 2) transportation routes and networks; and, 3) agricultural development and extent.

Three sets of ERTS-1 MSS positive transparencies (frame numbers: #1002-18140, North Central Coastal Region; #1073-18064, South Central Coastal Region; and, #1019-18062, Central Valley Region) were used to evaluate specific land use information potential of ERTS data for diverse environments. For each of the ERTS-1 frames utilized, each of the MSS bands (Channels 4-7) was evaluated for information content and feasibility for land use studies. An example of the type of results achieved in this investigation can be seen in Table 1. In all, some ten pages of this type have been prepared indicating the relative interpretability of various land use parameters on the ERTS-1 imagery. An example of a land use map generated in this study is shown in Figure 1.

PROBLEMS ENCOUNTERED

Several problems were encountered in the overall conduct of these investigations. While major interpretation difficulties centered around the resolution levels of the various MSS bands, several other problems were encountered. For instance, where certain tone and/or texture signatures exhibited low object to background contrast ratios, it was very difficult to make basic land use categorization decisions. In the Central Valley Test Site, difficulties were encountered in feature identification in areas of idle lands (i.e., those lands not developed for agricultural or urban uses). In such areas it was difficult to identify both urban and transportation features. Problems due to low contrast ratios in the Central Coastal Test Site made it difficult to locate certain urban centers in areas of rangeland/grassland, especially in those areas where transportation features exhibited weak signatures on the imagery. Steep, mountainous topography also made certain features difficult to interpret.

ANALYSIS AND RESULTS

Central Valley Region:

In addition to a thorough evaluation of the four MSS Bands for the identification of urban, transportation and agricultural features, a basic land use map of the entire Central Valley Region from frame #1019180625 was produced on acetate. Gross scale features were identified, classified, and mapped. These included: urban areas; agricultural land; idle land; natural vegetation and land forms (selected); highways; canals; airports; and, in one case, a portion of a railroad line. Particularly significant was the ability to delineate the shapes and extents of urban area boundaries and to map agricultural land, as opposed to non-agricultural (especially idle land).

URBAN AREAS

Sixteen (16) urban areas were identified on the image. Nearly one-third were located along U.S. 99, the established transportation route

thru the valley, while the others were located on secondary transportation arteries. The major focus of the majority of cities is as a regional/local center for surrounding agricultural hinterlands.

Identification was facilitated by tracing linear highway routes, especially along U.S. 99. Here the characteristic greyish, mottled signatures of the urban areas contrasted well with the surrounding environment. Several other communities of varying sizes were also accurately identified owing to their location in areas of heavy cultivation and secondary road networks. Again, the urban signatures contrasted well with the darker tone and rectangular pattern of the agricultural hinterlands.

The only major city in the area not identified was Corcoran (1970 population 5,249), located south of Hanford and west of Tulare on California 43. Reasons for this lack of an identifiable signature are being evaluated. Also, the absence of significant urban development along Interstate 5 is a result of the relatively underdeveloped agricultural state and geographic isolation of the area. This in itself is a result of non-availability, until recently, of adequate water for irrigation (now being changed by construction of the California Aqueduct) and isolation caused by inadequate transportation access (prior to the completion of Interstate 5).

In all cases, the cities were first located and identified by their mottled grey signature, and then the boundaries were mapped by determining the areal extent of the signature. Initial results appear to be fairly accurate (both in shape and extent) as verified by comparison with NASA high flight CIR imagery (March, 1971; 1:60,000 and 1:120,000 scale) and U.S.D.C. Coast and Geodetic Survey Sectional Aeronautical Charts.

AGRICULTURE/NON-AGRICULTURE (IDLE LAND) IDENTIFICATION

Basic land use mapping indicates that the major portion of land in the San Joaquin Valley (bounded by the Coast and Temblor Ranges on the West and the Sierra Nevadas on the East) comprises Ac (agricultural, crops) and Ni (idle land). While it has not been possible thus far to identify individual crop types within the Ac classified areas (or to further sub-divide between row and orchard crops on a gross scale), it was possible to recognize agricultural land use owing to rectangular field signatures and/or the presence of extensive, regular vegetation tone/texture. Ni land was identified on the basis of the absence of field boundaries and presence of uniform vegetation/soil tonal responses. However, it should be noted that it is possible that small areas of fallow land may have been included in the Ni classification, where field boundaries blended with the similar light signature of the bare soil.

Regardless, a high degree of mapping accuracy is possible. The following specific example is an indication of the reliability of mapped data for the study area. During the Summer, 1972, an agricultural land use map of a portion of Kern County (radiating from Bakersfield N, W, & S) was constructed from 1971 NASA high flight 70mm black and white negatives (enlarged to a scale of 1:290,000), and cross-checked with 1:120,000 scale CIR imagery. This was sent to the Kern County Water Agency (K.C.W.A.) for verification of agriculture acreage estimates. When K.C.W.A. figures were received, the same area was mapped from

ERTS-1 with an estimated error for ERTS data of less than 0.5 percent: The results of these studies can be seen below:

Source	Agriculture Acreage Estimate (acres)
1. 1969 Crop Survey(Kern County)	746,104 (excluding fallow)
2. NASA High Flight (70mm)- 1971	753,369
3. ERTS-1	748,050

Central Coastal Test Site:

An evaluation of the four MSS bands was completed for the North portion Coastal test region, specifically examining the signatures of the urban, transportation, and agriculture land use categories on each band. Urban concentrations and transportation routes were located by scanning the images with a 10x magnifier to identify the typical tone/texture responses of each, and then the gross outlines and/or linear patterns interpreted from the imagery were compared with U.S.D.C. Coast and Geodetic Survey Sectional Aeronautical Charts for verification purposes. Agricultural signatures were generally quite satisfactory, with fields as small as 40 acres visible. Furthermore, tonal differences in field plots (both on the macro and micro level) were noted and their significance is being analyzed.

An examination of the four MSS bands for the South portion of the Central Coastal test region was also completed. The evaluation again examined three major categories: urban concentrations; transportation networks; and, agricultural development. Further identification was completed of gross scale features such as urban areas, agricultural land, natural vegetation, highways, airports, and military installations. Once again, the ability to identify and delineate the shape and extent of urban areas and developed agriculture from ERTS-1 imagery was found to be of particular significance. The application of this identification capability of specific features to future regional planning appears feasible.

URBAN AREAS

Nine (9) urban areas were located within the South portion of the Central Coastal Region. The majority identified were along the immediate coast or within coastal valleys. Smaller urban areas located inland were virtually unidentifiable owing to low contrast ratios between transportation arteries (highways specifically) and the areas they traversed. This made identification of urban areas using these indicators impossible. However, the characteristic greyish, mottled signatures of the urban areas along the coastal areas, which contrasted well (in most cases) with the surrounding areas of agriculture, lessened this identification problem.

In all cases, cities were first located and identified by their mottled grey signature, and then boundaries were mapped by determining the areal extent of the signature. Initial results appear to be fairly accurate (both in shape and extent) as verified by comparison with NASA high flight CIR imagery (March, 1971; 1:60,000 and 1:120,000 scale) and U.S.D.C. Coast and Geodetic Survey Sectional Aeronautical Charts. Precise, mathematical verification as to actual accuracy is planned.

AGRICULTURE LAND IDENTIFICATION

The basic land use map of this area which was constructed indicates that the majority of land in other than urban concentrations may be classified either as natural vegetation or rangeland. While the amount of cultivated land is relatively insignificant when compared to total land area, its importance should not be overlooked. Predominantly located along coastal river valleys or nestled between the coast and mountains, these areas are sites of intensive cultivation of specialized or high yield/high cash value crops. Identification of such sites of intense agricultural production was facilitated by the regularity of field patterns and tonal contrasts exhibited by areas of such activity. In addition, range and natural vegetation were identified, in the main, by their lack of regular boundaries and tonal responses and textures exhibited (light grey/mottled and dark grey/solid respectively). The existance of large areas categorized as Ar (rangeland) in the Santa Ynez Valley, Lompoc, and Santa Maria areas in the western portion of Santa Barbara County indicates the importance of the cattle industry in this region of the Central California Coastal Zone. These large areas of essentially open space, on the fringe of the greater Los Angeles metropolitan area, are also quite attractive to developers, and the ability to provide synoptic information in this dynamic environment is important.

SUMMARY AND CONCLUSIONS

Experimental results to date indicate that ERTS-1 type data can be a valuable source for environmental resource information needs. The resolution of ERTS-1 data places constraints upon the detail to which specific environmental phenomena can be investigated. Furthermore, resolution limitations create certain problems for investigation of environments in which a diversity of phenomena are localized in small areal units (e.g., as the Central Coastal Zone of California). These limitations, however, are mitigated to a large degree through the synoptic perspective afforded by ERTS-1. ERTS-1 data provides a capability to inventory resources over extensive areas, and generate data for these areas at essentially a single point in time. Although the detail of information may be insufficient for specific user requirements, the advantage of this synoptic view is that large scale environmental resource information can be: 1) obtained within a standardized format for a single date; and, 2) monitored and updated with comparative ease to reflect changing resource conditions. This is not feasible utilizing conventional data collection methods. The implications are highly significant for resource management and planning.

With respect to the specific land use studies which the Geography Remote Sensing Unit has conducted in the Central Valley and Central Coastal test sites, California, the following conclusions can be made:

1. Urban areas can be differentiated best on MSS bands 4 and 5.
2. Transportation linkages (highways, roads, airports, canals) are most readily defined from MSS band 7.
3. Agricultural field boundaries are adequately identifiable on MSS bands 4 - 7, and most clearly defined on band 7.

4. Cultivated land can be mapped accurately (under 5% error) from MSS band 5. Fallow land identification explains the majority of error.
5. Land use is difficult to map in the California coastal environment because many individual use categories occupy very small areal units; land use mapping is easier and capable of more sophisticated refinements in the arid California Central Valley.

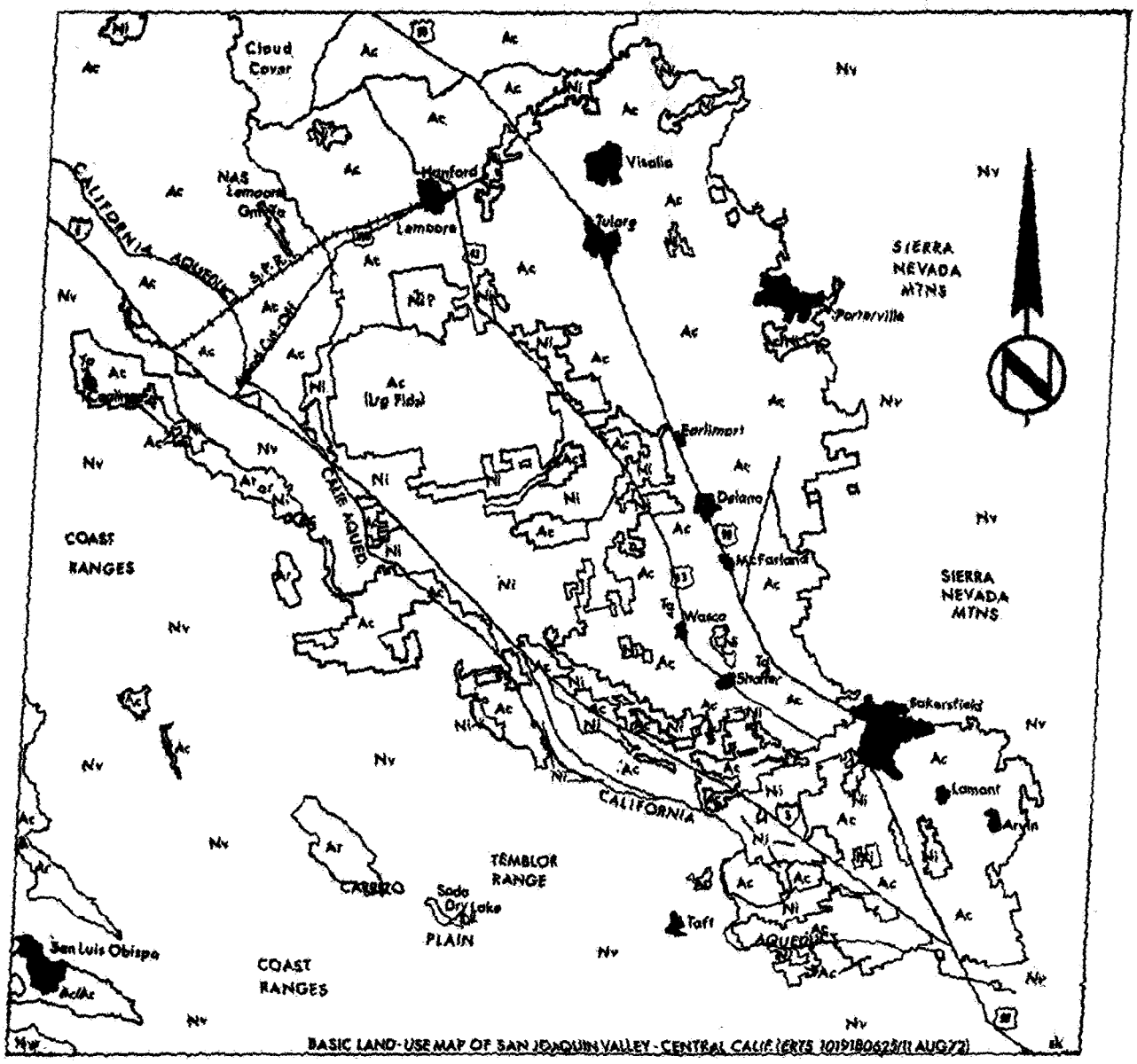


Figure 1. Example of Basic Land Use Map derived from Earth Resource Technology Satellite Data

TABLE 1. An Example of the Type of Evaluation of MSS Bands 4 - 7; Transportation Features Conducted by Personnel of the Geography Remote Sensing Unit, University of California, Santa Barbara.

LOCATION	BAND 4	BAND 5	BAND 6	BAND 7
U.S. 99-4 lane	Good response along entire route except when passing thru urban areas, where road signature blends with urban. Stands out well in areas of intensive agriculture, as well as areas of low-lying, sparse natural vegetation. Linear regularity aids in identification as does light signature.	Fair to Good. Same as for Band 4, except that signature fades to the Northwest in an area of small fields and bare soil (highway and fields both display light tone)	Poor to Fair. Road shows dark response which tends to blend very subtly with surroundings.	Fair to Good. Dark, linear response against lighter agriculture signature. Also, unlike Band 5, it is well defined along entire ERTS-1 image.
Interstate 5-4 lane	Poor to Good. Major portion of route well defined. However, as much of the surrounding land remains undeveloped, the signature tends to fade when this occurs on both sides of Interstate 5. Light response of road good against agriculture (dark), but poor against open land (also light).	Poor to Fair. Generally same as Band 4. However, more fade out in undeveloped areas.	Poor. Tends to blend with light signature of surrounding land along majority of route.	Poor. Light signature against light background--majority of route traced on Figure 1 not visible.
Calif. 43-2 lane	Poor to fair. Irregular response. Visible in areas of agriculture where regular field patterns lend good contrast. However, in several large sections (figure 2) identified as Ni areas or Ac with bare soil, the road tends to blend.	Same as Band 4.	Not visible.	Fair. Dark response is well defined against agricultural regular patterned background. Slight loss of resolution in bare soil and idle land areas.
Calif. 198-2-4 lanes	Poor. Visible thru Hanford although small field aptterns tend to disrupt signature. Contrast is poor. Cannot be traced thru the idle land east of Hanford and west of U.S. 99.	Same as Band 4.	Not visible.	Poor. Dark tone only visible against agricultural background with great difficulty.
Avenal cut-off-2 lane	Poor to Fair. Light pattern contrasts in areas of varying toned agriculture. Fades when encountering homogeneous light responses of bare soil, etc.	Same as Band 4.	Poor to Fair. Due to dark, linear pattern against lighter signature of agriculture.	Good. Dark linear response against regular agricultural patterns.

N73-28301

Paper L 5

LAND USE IN THE NORTHERN COACHELLA VALLEY

Jack B. Bale and Leonard W. Bowden, *Department of Geography, University of California, Riverside, California 92502*

ABSTRACT

ERTS-1 imagery has proved to have great utility for monitoring land use change and as a data source for regional planning. In California, open space desert resources are under severe pressure to serve as a source for recreational gratification to individuals living in the heavily populated southern coastal plain. Concern for these sensitive arid environments has been expressed by both federal and state agencies. The northern half of the Coachella Valley has historically served as a focal point for weekend recreational activity and second homes. Since demand in this area has remained high, land use change from rural to urban residential has been occurring continuously since 1968. This area of rapid change is an ideal site to illustrate the utility of satellite imagery as a data source for planning information, and has served as the areal focus of this investigation.

1. INTRODUCTION

ERTS-1 imagery has been useful for monitoring land use change and has served as a potential data source for regional planning in one Southern California test site. Open space desert resources, in California, are under severe pressure to serve as a source for recreational gratification to individuals living in the heavily populated southern coastal plain. Concern for these sensitive arid environments (the Colorado and Mojave Deserts) has been expressed by both federal and state agencies. The northern half of the Coachella Valley, part of the Colorado Desert natural province, has long served as a focal point for weekend and seasonal (winter) recreational activity.

2. AREA

The Coachella Valley is the northern most extension of the Salton-Imperial Trough (Figure 1). Land use has traditionally been a contrast between agriculture and recreation. The valley is approximately 50 miles (80.5 km) long and averages less than 15 miles (24 km) in width. As a

structural trough it is bounded on both the north and southwest by the highest mountain ranges in Southern California. It terminates in the south at the Salton Sea and narrows to the north to form San Gorgonio Pass. If one wished to delimit geographic regions solely on physical characteristics, the Coachella would qualify. Dominant land use types dictate that the valley be divided into two regions (Glend nning, 1949). The northern half of the valley possesses a recreational economic base while the southern half from Indio to the Salton Sea depends primarily on an agricultural economic base. The investigation has been limited to the northern half of the valley where recent residential and recreation oriented building occurs at rates far above county averages.

3. RESEARCH DESIGN

Research objectives involve the qualitative testing of ERTS-1 imagery as a data source for land use monitoring at the urban-rural fringe in the desert environment. Base land use data was obtained in 1966 and 1969. This information was then compared with the record obtained from ERTS-1 to produce a map of change. Analysis of the change, where it is concentrated, and how quickly it is occurring will provide insight into potential regional problems.

4. DATA SOURCES

Although ERTS-1 imagery served as the primary data source both U-2 and RB-57 photography were also used. Field surveys and the aforementioned high altitude imagery allowed the information interpreted from the ERTS-1 to be verified and more precisely located.

Two formats of ERTS-1 imagery were used with an I^2S Mini-Addcol Color Viewer to produce interpretable false color representations. 70 mm positives were used in their entirety, while only a portion of reproduced 9" x 9" (22.9 cm x 22.9 cm) positives were used. The accompanying diagram illustrates the basic workings of the color viewer. Diazochrome black and white positive transparencies were prepared from 9" x 9" (22.9 cm x 22.9 cm) ERTS positives. These were then cut to fit the 2-3/4" x 2-3/4" (6 cm x 6 cm) yoke format of the color viewer. The resulting scale as visible on the ground glass view plate of the color viewer was approximately 1:150,000. This technique provided more enlargement, but less resolution than the enlarged 70 mm positive transparencies. MSS bands 4, 5, and 7 were used in three of the four channels of the color viewer. In order to reconstruct a false color infrared image band 4 was projected through a blue filter, band 5 through a green filter and band 7 through a red filter. In order to enhance the image record of commercial activities along main thoroughfares the filters used for bands 5 and 7 were switched and a false color image with green in place of red was created.

5. MAPPING PROCEDURES

The largest portion of the mapping was accomplished from enlarged positives or projected slides taken of a portion of the reconstructed 70 mm image on the color viewer view plate. Projected images were worked at scales no larger than 1:62,500. Resolution usually extended to 80 acre 1/8 sections. Better resolution occurred where intense signatures associated with specific uses can be found in isolated parts of the valley. Linear features and land use arrays appear to be more visible than other features of equal area. Such findings were expected and not in themselves surprising.

Strict procedures were established for and followed during the mapping process. One interpreter accomplished all the mapping. Factors which influence the quality and resolution of land use information gleaned during this study include the scale of the imagery, the scale of the final map product, the availability of secondary data sources, the expertise of the interpreter, and finally, how well the interpreter knows the subject area. In evaluating the usefulness of a remote sensing system, there is no justification for faulting a mapping procedure because one interpreter, through his own knowledge of an area is more proficient at correctly identifying land use than another equally skilled individual who does not know the area.

During this study more land use information could be extracted from the imagery because the interpreter "knew" the region, than would have been possible otherwise. Familiar areas where residential and commercial urban uses are fixed, because of high capital investment, served as a base for identifying uses in less well known areas and in areas where change has taken place. Members of any regional planning organization should be as knowledgeable about areas under their jurisdiction as our interpreter in the Coachella.

Previous land use mapping in 1966 by R. Van Curen served as a base for change comparison. An intermediate set of information was obtained in 1969 through the work of J. B. Bale and W. G. Brooner for Palm Springs. The land use classification used for ERTS-1 derived information, is a modification of the one used in 1966. This, of course, is necessary to maintain consistency and allow land use change identification. In most areas, the classification scheme allows more detail to be recorded than is actually visible from the imagery--the 1966 survey was based on both a low altitude large scale photographic record and detailed field work. A less detailed classification system would inhibit interpretation processes where additional information is available on the photo.

Techniques developed in previous agricultural surveys at the University of California, Riverside and elsewhere facilitate identification of agricultural uses. Crop calendars, dependence on false color

infrared film where various shades of red facilitate interpretation, and the fact that agricultural fields usually cover large areas, allow interpreters to obtain greater detail (even to identification of specific crops) in an agricultural area than in urban areas. In the Coachella Valley, however, certain urban associated recreation uses, specifically golf courses and fairway side housing, can be easily identified (Tamarisk, Bermuda Dunes, La Quinta, Canyon Country Club, Thunderbird, etc.). This combination of residential and recreational use has its own category in the land use classification scheme.

6. "GROUND TRUTH"

All areas where positive change was mapped within the city limits of Palm Springs were ground checked February 18, 1973. In every instance some form of positive change had taken place in or adjacent to the boundaries drawn on the map. In no instance were the boundaries drawn on the map exact representations of the actual area where the change occurred. Although no attempt was made to identify the new land uses as they were being mapped, it was noted in the field that all change identified consisted of residential structures or subdivisions except for one park in section 34 at the north end of town. All areas of change 1/8 section or larger were recorded. Change did occur which was not recorded, but it was from one use other than open space to another or it occurred over an area which was too small to be recorded (Figure 2).

East of Palm Springs in the unincorporated portion of the test site, land use change was monitored with similar accuracy to that which was achieved in the more densely occupied city area. Identification of land use type as well as land use change was attempted. Boundaries again could not be placed exactly, but in only two instances were land uses misinterpreted. The first case was a locational problem involving the improper positioning of a small area of abandoned vineyards in the south central part of Figure 3. Secondly, at Thousand Palms recreational residential use involving mobile homes around a golf course was not identified. Less critical problems involved the category of agricultural abandonment (C2a in figure 3). Here, no distinction could be made between actual removal of orchards or groves, and their complete removal. The difference between active agriculture, and abandonment or disinvestment was always apparent.

7. RESULTS

From both maps and the ERTS-1 imagery, it is obvious that much of the urban development has occurred on the various alluvial fan surfaces that eminate from the San Jacinto Mountains. These areas, somewhat protected by spur ridges from the winds which are strongest along the axis

of the valley, were developed first and still contain most diversified urban uses (residential, parks, commercial). More recent residential development has occurred on the upper portion of some fans (Deep Canyon Fan for example) or along the south center axis of the valley at the expense of open space or agricultural uses. All agriculture will be gone from the north half of the valley within the next few years.

Change in the Palm Springs area consists primarily of the filling in of an already urban environment. Alternate sections within the city limits belonging to the Agua Caliente Indian Reservation are now being transformed from open spaces to urban uses. Problems were encountered while working in this more complex urban environment. With the present system of combining and projecting reconstructed imagery, land use boundaries within the city could not accurately be drawn. Furthermore, except for most single family residential areas, parks, golf courses, and some, specific commercial uses, a full range of urban uses including most commercial areas, multi-family residential, governmental, and other institutional uses were not discernible. Positive change however was visible where other forms of use have replaced open space.

Farther to the southeast, in what was originally a less complicated agricultural landscape, change occurs in the center of the valley. This area, originally a "blow-sand" environment is undergoing a transformation from open space and agriculture to recreational and residential uses. What exists is perhaps the heaviest concentration of golfing facilities in any area of this size in the world. In situations where direct conversion from agriculture does not occur, fields are abandoned, left fallow or trees (either citrus or date palm) are maintained as ornamentals to residential uses. Agricultural abandonment is one form of factor disinvestment common to the rural-urban fringe in Southern California (Goehring, 1971).

8. ANALYSIS

Although no regional planning agency with responsibilities in the Coachella Valley has yet to integrate ERTS-1 imagery into their resource management procedures, various members of the planning departments of Riverside County and Palm Springs City have made casual use of reconstructed images. Individuals from both organizations have, from other sources, already been made aware of problems illustrated by ERTS-1 imagery. Alarmed by what appears to be a loss of amenities in a primarily recreational urban environment, officials in Palm Springs have called a temporary building moratorium, and proposed revolutionary measures to maintain open space within the city (personal communication, Department of Planning and Development, City of Palm Springs and Proposed Open Space and Conservation Element, Palm Springs General Plan). County officials have expressed little concern over loss of open space but have been confronted by numerous local conservation

organizations that have expressed concern over a number of related topics ranging from loss of wildlife habitat to deteriorating ground water quality.

Perspectives available from ERTS-1 imagery allow regionwide views containing information in quantities not available from compoiste sources (maps or photo mosaics). The sequential nature of the imagery adds to potential utility although biannual collection instead of every 18 days would suffice to monitor urban land use change in the northern Coachella Valley.

Additional building and subsequent increases of human activity will jeopardize numerous specialized natural habitats in surrounding areas. Most recent land use change suggests a loss of unique natural habitats, including fan surfaces emanating from the San Jacinto Mountains, the sand dune habitat that extends along the axis of the valley, and the Bighorn sheep habitats in the mountain slopes surrounding the valley bottom. Continued residential construction has also reduced the habitat value of the valley to man. Increased environmental pollution (air pollution, noise and visual pollution) threaten the area's economic base. Amenity loss stemming from the lack of attention to concepts of environmental design and consequent impacts of continuing development can be inferred. Sequential ERTS-1 imagery has recorded the most recent chapter of the Coachella Valley's continuing environmental alteration.

9. REFERENCES

Bale, J. B. and W. G. Brooner (June 1970), "Experimental Land Use Mapping from High Altitude Panoramic Photography," Paper Presented at APCG Meeting, Santa Cruz, California.

Glendinning, Robert M. (1949), "Desert Contrasts, Illustrated by the Coachella," Geographical Review, 39: 221-228.

Goehring, Darryl R. (1971), Monitoring the Evolving Land Use Pattern on the Los Angeles Metropolitan Fringe Using Remote Sensing, Technical Report T-71-5, Contract No. N00014-69-A-0200-5001, NR 387-047 and NASA NGL 05-003-404, Department of Geography, University of California, Riverside.

Roos, Marvin (January 1973), Assistant Planner, Department of Planning and Development, Palm Springs, California, Personal Communication.

Van Curen, R. (1966), "Land Use Maps of the Coachella Valley," Unpublished, University of California, Riverside.

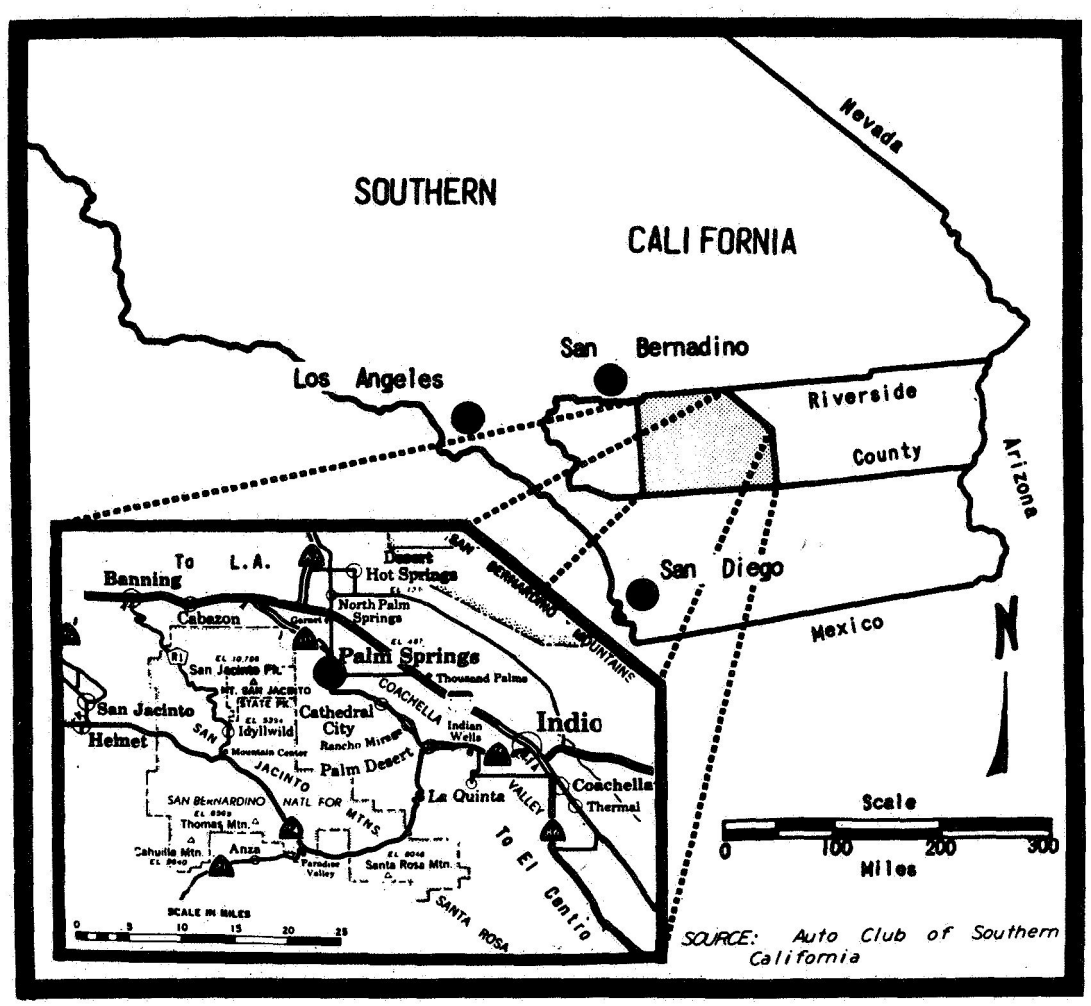


Figure 1. Location of Study Area

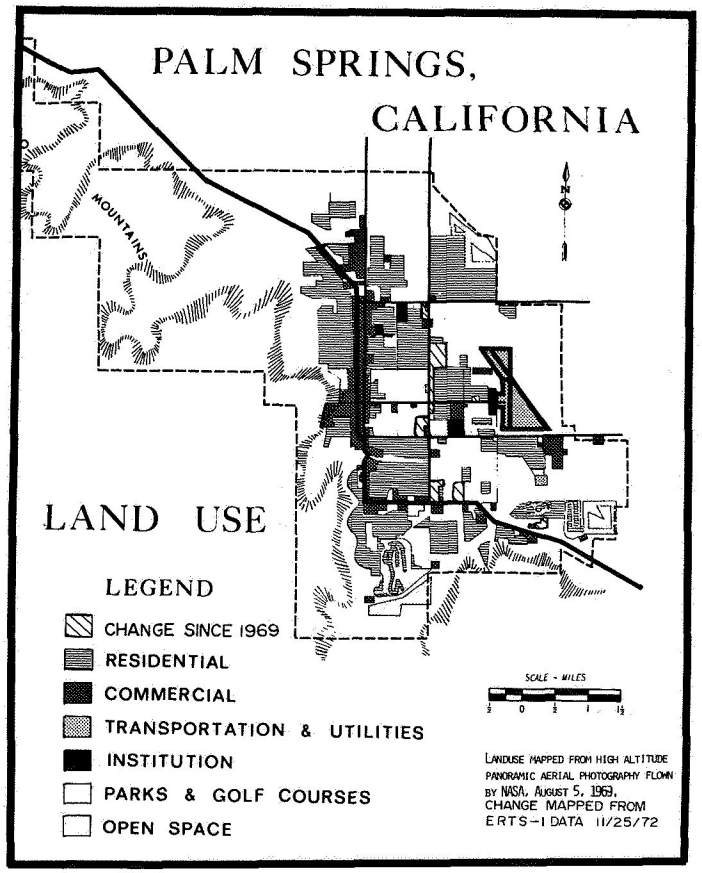


Figure 2. Change in Palm Springs

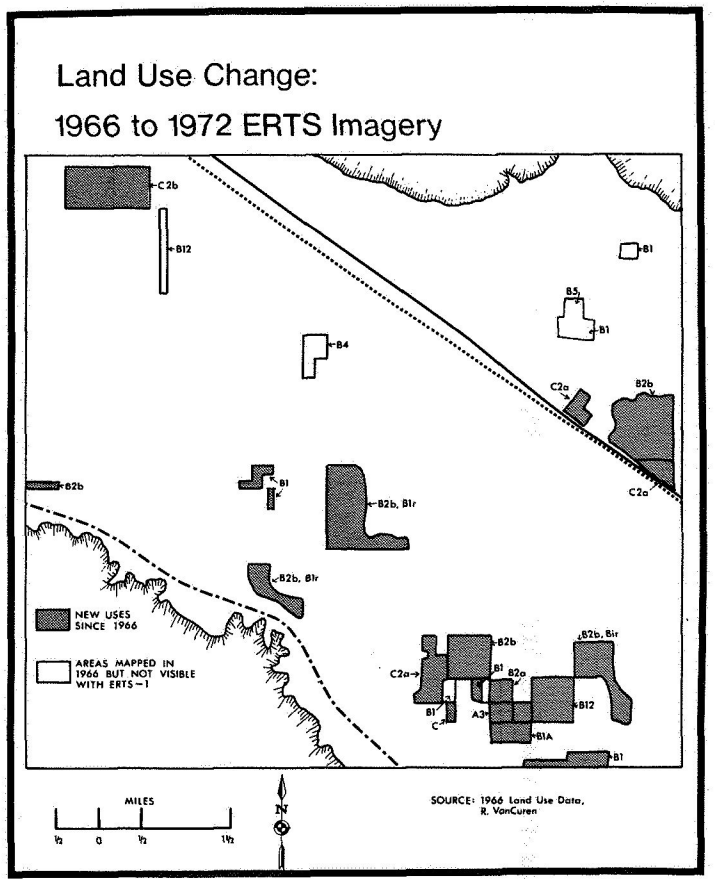


Figure 3. Change in the County

N73-28302

Paper L 6

LAND USE CLASSIFICATION AND CHANGE ANALYSIS USING ERTS-1 IMAGERY IN CARETS

Robert H. Alexander, *U. S. Geological Survey, Geographic Applications Program, Washington, D. C.*

ABSTRACT

Land use detail in the CARETS area obtainable from ERTS exceeds the expectations of the Interagency Steering Committee and the USGS proposed standardized classification, which presents Level I categories for ERTS and Level II for high-altitude aircraft data. Some Levels II and III, in addition to Level I, categories were identified on ERTS data. Significant land use changes totaling 39.2 km^2 in the Norfolk-Portsmouth SMSA were identified and mapped at Level II detail using a combination of procedures employing ERTS and high-altitude aircraft data.

INTRODUCTION

ERTS imagery in the Central Atlantic Regional Ecological Test Site (CARETS) area was examined to determine what categories of land use could be detected, and to what extent land use change could be identified and mapped. The images reported on here are from the ERTS multispectral scanner, taken over the Washington-Baltimore area (E-1080-15192, 11 Oct. 1972, color composite of bands 4, 5, and 7) and over the Norfolk, Virginia area (E-1079-15140, 10 Oct. 1972, color composite of bands 4, 5, and 7; and E-1133-15144, 3 Dec. 1972, color composite of bands 5 and 7).

1. Categories of Land Use

In the discrimination of land use types in the CARETS region, ERTS exceeds the expectations of the 1971 Interagency Steering Committee on Land Use Information and Classification. That Committee presented a two-level land use classification system for use with remote sensing data; a Level I for use with spacecraft data, and a Level II for use with high-altitude aircraft data. Land use data at Levels I and II are useful for regional and statewide land use inventories, and for the needs of

Original photography may be purchased from:
EROS Data Center
10th and Dakota Avenue
Sioux Falls, SD 57198

many federal agencies to assist in making land management decisions. Levels III and IV were anticipated as being derivable from medium and low-altitude imagery, respectively, and fulfilling more detailed needs of local agencies for information in support of land use planning, transportation forecasting, and environmental impact statements. The U.S. Geological Survey has published the two-level classification in Geological Survey Circular 671, and is urging that agencies involved with "land use" missions adopt compatible classifications so that standards for the exchange of land use data can be established and costly duplication can be avoided.

In addition to the expected Level I, several categories of Level II land use were obtainable from the ERTS imagery, and even a few from a proposed Level III. Therefore the full potential of ERTS for land use analysis will not be realized if categories for mapping are confined to Level I. Levels I, II, and III categories which were identified on ERTS imagery of the CARETS area are listed in Table 1. Some examples of Level III land use are shown in Figure 1. Proposed Level III categories are listed only for Level I "urban and built-up" lands; however, as ERTS imagery for different seasons becomes available, it is likely that extensions to Level III will be possible also in agricultural, forest, and wetland categories. During the next phases of the ERTS investigations, interaction among investigators and potential users of land use information is recommended, so that similar definitions can be applied to land use types, and exchange of data can be facilitated. The USGS CARETS team will welcome any recommendations concerning the establishment of Level III categories for this region, as determinable from further analysis of ERTS data. Such recommendations will be consolidated by the CARETS team into a proposed Level III classification for CARETS.

2. Identification and Mapping of Land Use Change

To investigate the utility of ERTS data in identifying and mapping significant land use changes, the Norfolk-Portsmouth Standard Metropolitan Statistical Area (SMSA) was selected for detailed analysis. This SMSA serves as the principal sub-region for detailed system tests of procedures for the various subtasks of the CARETS project before applying them to the remainder of the CARETS region (Figure 2).

A UTM-gridded photomosaic was used as a mapping base. Similar mosaics are available for the entire CARETS region, having been

compiled from 1970 NASA RB-57 photography. The data base from which change was to be measured is a Level II land use map at a scale 1:100,000, also compiled from the same 1970 high-altitude aerial photography, and available for the entire CARETS region. A transparency of the 1970 land use map was placed over an enlarged transparency of the color composite of the Norfolk area ERTS image, also at a scale of 1:100,000. After learning some of the principal visual signatures of the various land use types as they appeared on the enlarged ERTS image, a skilled photointerpreter examined each section of the area being mapped, and outlined with pencil all areas that appeared to have changed since 1970. Based on comparison with the data base, and his becoming familiar with the visual signatures of the major land use types as portrayed on the ERTS enlargement, the interpreter indicated the present land use, to a Level II detail if possible, and to Level I if not. Then reference was made to the 1972 ERTS underflight (U-2) photography of the area, to verify whether change had actually occurred, and whether the correct interpretation of that change had been made.

The "verified" changes were mapped on a separate overlay, along with "false"changes, or changes which the ERTS imagery suggested, but which did not actually occur. Area measurements of each of the categories of land use change were made by dot grid planimeter, and the results totaled for the SMSA. The area measurement and tabulation will be done automatically when the land use data base is digitized and change mapping extended to the remainder of CARETS. Examples of the photomosaic, Level II land use map, ERTS image, and change map for a portion of the test site (South Norfolk vicinity) are shown in Figures 4 through 7. Figure 3 depicts the location of the South Norfolk site within the Norfolk-Portsmouth SMSA.

Results of the 1970-72 change analysis are summarized as follows:

Area analyzed (SMSA total)	1911 km^2
Total aircraft-verified land use change, Level I	36.2 km^2
ERTS-identified land use change, Level I	26.5 km^2
Percent of Level I change identified with ERTS	73.2 %
Total aircraft-verified land use change, Level II	39.2 km^2
ERTS-identified land use change, Level II	22.4 km^2
Percent of Level II change identified with ERTS	57.3 %
"False" change (erroneously indicated by ERTS)	64.3 km^2

The results are consistent with a previous study, which measured Level I land use change for the Norfolk-Portsmouth SMSA averaging 16.7 km^2 per year for the period 1959-1970. The comparable figure for the 1970-1972 period is 18.1 km^2 per year. Preliminary examination by the staff of the Southeastern Virginia Planning District Commission indicates that these results might serve to satisfy portions of a U.S. Department of Transportation (DOT) requirement for 1970-1972 land use change data for revised transport demand forecasting. Conventional land use survey costs for the DOT requirement will be compared with costs using the ERTS-aircraft data analysis method: 32 photointerpreter man-hours (including learning period with ERTS imagery) plus film and drafting materials for change mapping and verification in a fast-growing metropolitan area of 1911 km^2 (739 square miles).

Almost all of the "false change" turned out to be bare fields which in the October and December ERTS imagery had a bright appearance similar to urban areas. Data from the growing seasons would surely alleviate this problem. The results of the change analysis are considered to be highly promising--even without the sophisticated signature determination which is possible with ERTS MSS data, a high proportion of Level I and II land use change was detected and identified correctly with ERTS.

SUMMARY AND ACKNOWLEDGMENT

Based on the encouraging results of this preliminary analysis, the next phases of the investigation will extend coverage to the remainder of the CARETS area. Uniform land use data sets from both ERTS and aircraft sources will be compared and tested for environmental impact applications. Formal user evaluation by key state agencies and other potential users will be obtained. This report and the entire USGS CARETS project is the result of a team effort; staff geographers who have contributed to this effort as members of the team include William B. Mitchell, Ivan Hardin, Peter DeForth, Harry F. Lins, Jr., Katherine Fitzpatrick, and Ken McGinty. Their continued support is gratefully acknowledged.

Table 1. Land Use Categories Identified on ERTS Imagery in CARETS. Numbering System From Geological Survey Circular 671.

Level I	Level II	(Proposed) Level III
1 URBAN AND BUILT UP	11 Residential	Single-family residential
	12 Commercial and services	Retail trade area
	14 Extractive	Sand and gravel pits
	15 Transportation, communication and utilities	Airports Highways Power line rights-of-way
	17 Strip and clustered settlement	
	19 Open and other	
2 AGRICULTURAL	21 Cropland and pasture	
4 FORESTLAND		
5 WATER	51 Streams and waterways	
	52 Lakes	
	53 Reservoirs	
	54 Bays and estuaries	
6 NON-FORESTED WETLAND	61 Vegetated	
	62 Bare	
7 BARREN LAND	74 Beaches	

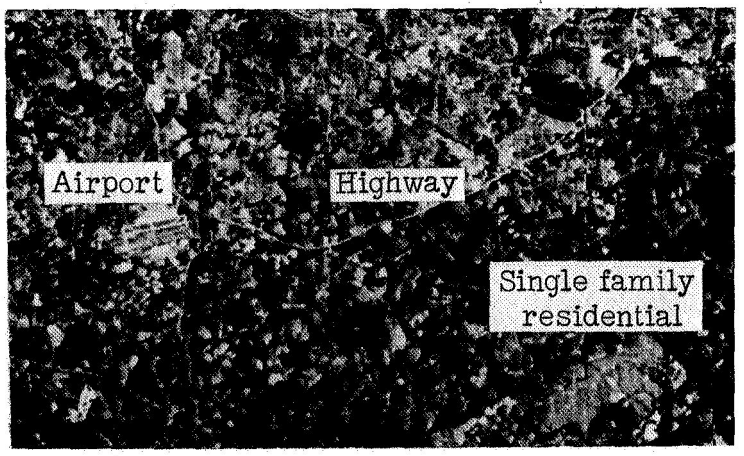


Figure 1. Examples of Level III land use from ERTS image of national capital area (E-1080-15192-5, 11 Oct. 1972).

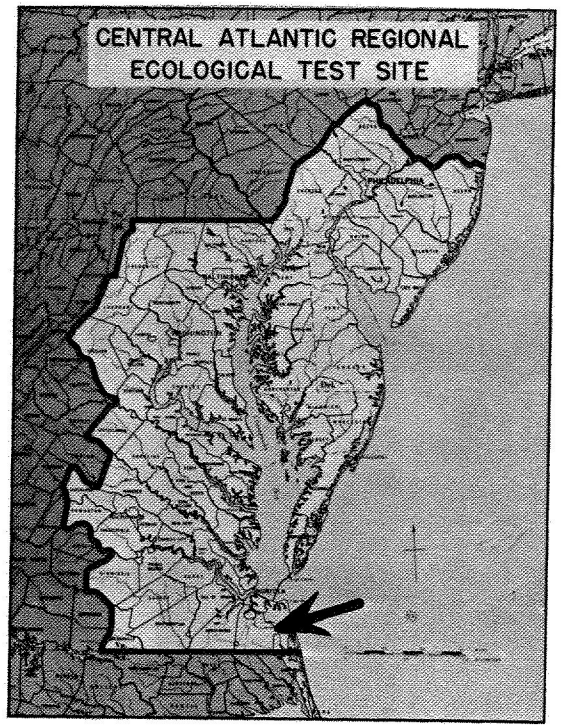


Figure 2. CARETS location map showing Norfolk-Portsmouth Standard Metropolitan Statistical Area (SMSA).

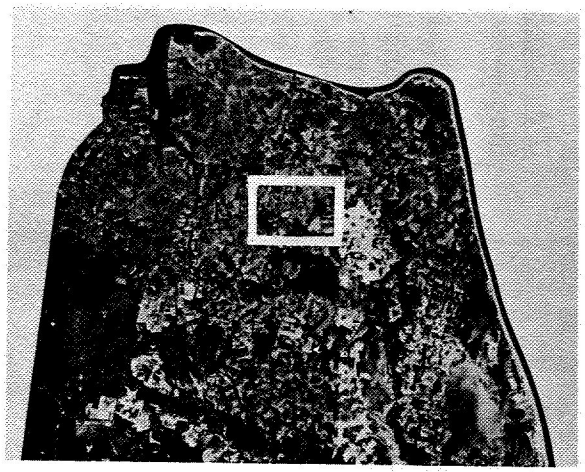


Figure 3. Norfolk-Portsmouth SMSA showing location of South Norfolk test site for ERTS-detected land use change.

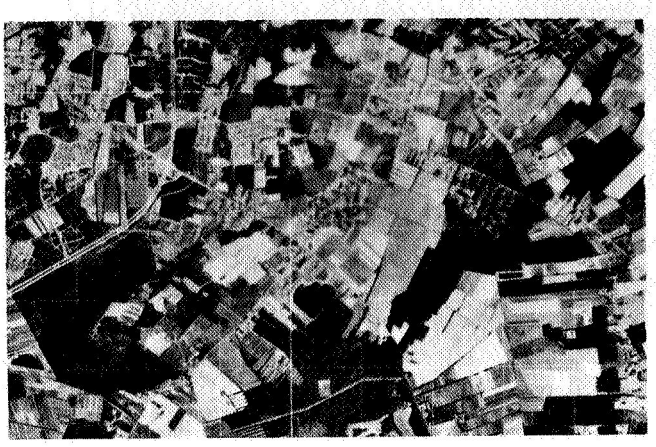


Figure 4. South Norfolk test site: 1970 Photomosaic, photography from NASA/MSC Mission 144. Scale 1:100,000.

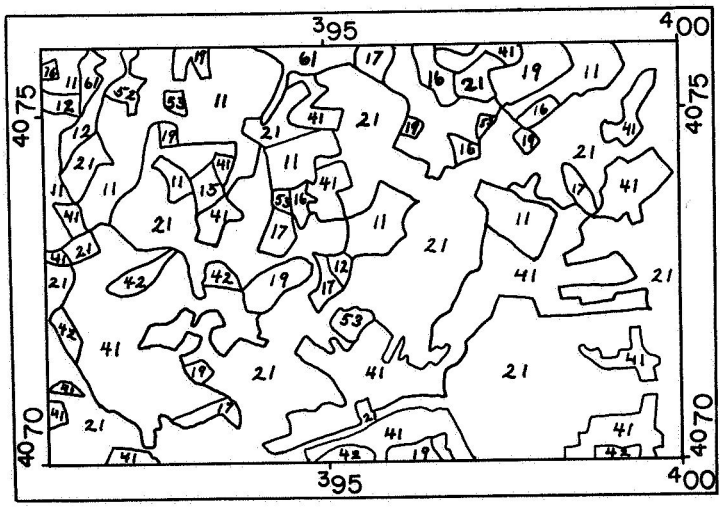


Figure 5. South Norfolk test site: 1970 Level II land use map. Land use categories numbered as in Table 1. Scale 1:100,000.



Figure 6. South Norfolk test site: portion of ERTS MSS image E-1133-15144-5, 3 Dec. 1972, enlarged to a scale of 1:100,000.

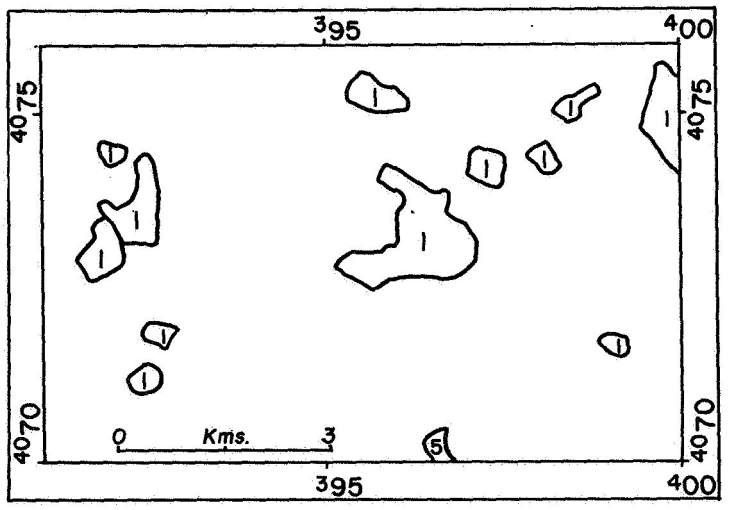


Figure 7. South Norfolk test site: land use change mapped using technique combining ERTS and high-altitude aircraft data. Scale 1:100,000.

N73-28303

Paper L 7

ERTS REGIONAL-SCALE OVERVIEW LINKING LAND USE AND ENVIRONMENTAL PROCESSES IN CARETS

Robert H. Alexander, *U. S. Geological Survey, Geographic Applications Program, Washington, D.C.*

ABSTRACT

A mosaic of ERTS images of the CARETS region has been used to partition the region into zones on the basis of similarity of tones and textures visible at a regional-scale overview. The resulting patterns were compared with existing small-scale maps of the region representing relief, land surface forms, geology, soils, vegetation, forest types, and land use. The ERTS-derived zones most closely resemble the patterns on the small-scale land use map, suggesting that, at least in a highly-developed region such as CARETS, "land use" is an indicator or resultant surface expression of several interacting environmental processes. These results lend support to the CARETS model of inter-disciplinary regional analysis, whereby remote sensor-derived data sets on land use and land use change become the basic data entry into a regional information system to serve regional planners and land managers.

ERTS images of the Central Atlantic Regional Ecological Test Site (CARETS) were examined at a variety of scales ranging from the "contact" scale of the 70 mm film chips supplied to the investigator (scale 1:3,300,000) to enlargements of more than 33 times (scale 1:100,000). There are advantages attendant upon the use of each particular scale, stemming from the hierarchy of scales of the environmental processes that have shaped the visible landscape.

One procedure found useful for a regional-scale overview is to obtain good contrast black-and-white prints of the MSS 5 band ERTS images at a scale of 1:1,000,000, piece them together into an uncontrolled mosaic, and view the whole thing at arm's length rather than with a magnifying glass. This was done for the CARETS region and some of the surrounding territory with ERTS images ranging in dates from September to

Original photography may be purchased from:
EROS Data Center
10th and Dakota Avenue
Sioux Falls, SD 57198

December 1972. The following images were used to make the mosaic:

E-1045-15243-5, 6 Sept. 72
E-1045-15245-5, 6 Sept. 72
E-1045-15252-5, 6 Sept. 72
E-1079-15131-5, 10 Oct. 72
E-1079-15133-5, 10 Oct. 72
E-1080-15185-5, 11 Oct. 72
E-1080-15192-5, 11 Oct. 72
E-1080-15194-5, 11 Oct. 72
E-1133-15144-5, 3 Dec. 72.

The ERTS mosaic displays, almost at a glance, the major geological and hydrological features of the region, extending from the folded Appalachians to the Atlantic Ocean (Figure 1). The chain of major metropolitan centers--Philadelphia, Baltimore, Washington, Richmond, and Norfolk--can be seen in relation to the hinterland mountain features, and particularly to the waterways of the Chesapeake and Delaware Bays and their tributary estuaries.

Closer examination reveals more subtle geological and hydrological controls to the land pattern such as regional outcrop trends, folds and faults, and major stream patterns. After accounting for the effects of these major geological and hydrological features, there remains a residual of landscape patterns which at this regional-scale overview are integrated by the sweep of the ERTS scanner into distinctive tones and textures. Each segment of the land surface reflects a pattern made up of forested tracts, farms, clusters of habitations, roads, and other paraphernalia of man's intensive occupance of this region.

A basic hypothesis of the model of interdisciplinary regional analysis used in the CARETS investigation is that "land use" at least in a highly-developed region, is an indicator or resultant surface expression of several interacting environmental processes; further, of all the environmental and socio-economic processes which contribute to the surface patterns, "land use" is the one with data sets most accessible to ERTS sensors.

To give this hypothesis a rudimentary test, the ERTS photomosaic of the CARETS region was visually partitioned into zones or "photomorphic regions" on the basis of similarity of tones and textures (Figure 2). This process could be made much more rigorous by employing a variety of

automatic scanning or pattern recognition techniques. The resulting patterns were compared, again visually, with the following small-scale maps in the National Atlas of the United States: relief, land surface form, tectonic features, geology, soils, vegetation, forest types, and land use.

All of these small-scale maps were compiled and prepared in final form long before ERTS became a reality. A cursory comparison indicated that the ERTS-derived patterns most closely resembled those of the National Atlas land use map (Figure 3). These results lend a measure of support to the CARETS hypothesis, and suggest further research to explore the linkages between data sets on land use as observed from ERTS and data sets on processes of the physical environment such as those affecting the geologic structure, lithology, surficial materials, hydrology, soils, vegetation, and climate. These linkages will be explored in the next phase of the CARETS project investigation, during which data sets on land use and land use change derived from both satellite and aircraft imagery will become the basic entries into an experimental regional information system to serve regional planning and land management agencies. An essential element of this information system is that user retrieval of the land use data is made compatible with correlative information on geology, topography, hydrologic factors, and population and economic data so that the land use patterns can be "calibrated" in terms of their probable environmental impact and their relationships to other factors that the planners must consider in allocating portions of the region to future land use changes. Bringing remote sensor-derived land use information together with the other data sets as required by the analytical and forecasting models of the planners calls for a computer-based geographic information system, which is being provided as part of the CARETS investigation.

The ERTS-derived zones of similarity are hypothesized to be subregions of similar land use characteristics. When land use data sets derived from ERTS imagery have been incorporated into the digital file for the region, retrieval and aggregation according to the outlines of the photomorphic regions obtained from the mosaic will make possible detailed quantitative comparisons of the land use regions with the ERTS tonal regions. In the meantime, areas assigned to each of the ERTS photomorphic regions were compared to areas from the National Atlas land use map, and the results are displayed in Table 1.

The map units of each correspond roughly as shown; more detailed mapping units were derived from the photomorphic region map. With the exception of the category where urban areas are included, the two maps show an intriguing correspondence. The similarities in pattern of the two maps are of course not shown by this crude area comparison method of map correlation.

The payoffs in regional-scale analysis of ERTS data seem to be of two major kinds. First, partitioning of ERTS data into subsets or photomorphic regions may provide a very economical sampling strategy for selecting sites for more detailed field measurements if, as is suspected, many other environmental variables turn out to be correlated with the similarity of patterns on ERTS imagery. Second, and of most importance in the long run, regional-scale sequential analysis of ERTS imagery, and that of follow-up systems capable of monitoring environmental change, may provide an increase in our basic knowledge of the complex of interwoven environmental processes which shape man's habitat.



Figure 1. Uncontrolled photomosaic of 9 ERTS MSS images covering the Central Atlantic Regional Ecological Test Site (CARETS). Polaroid reduction from mosaic scale of 1:1,000,000.

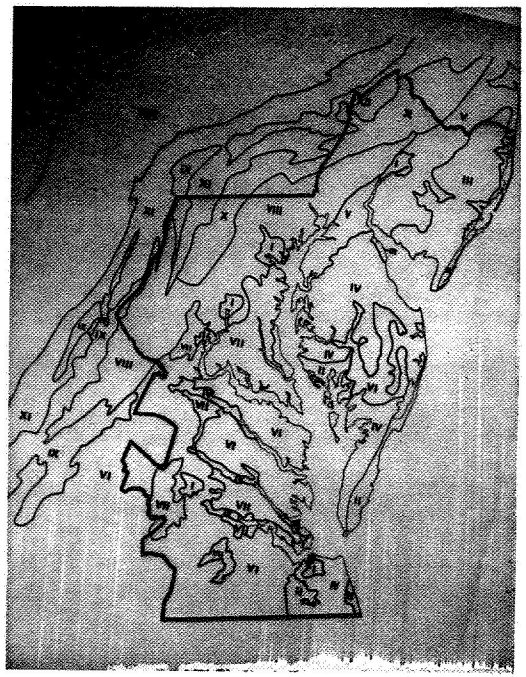


Figure 2. Photomorphic regions derived visually from ERTS photomosaic of CARETS Numerals arbitrarily assigned to units of similar tone and texture.

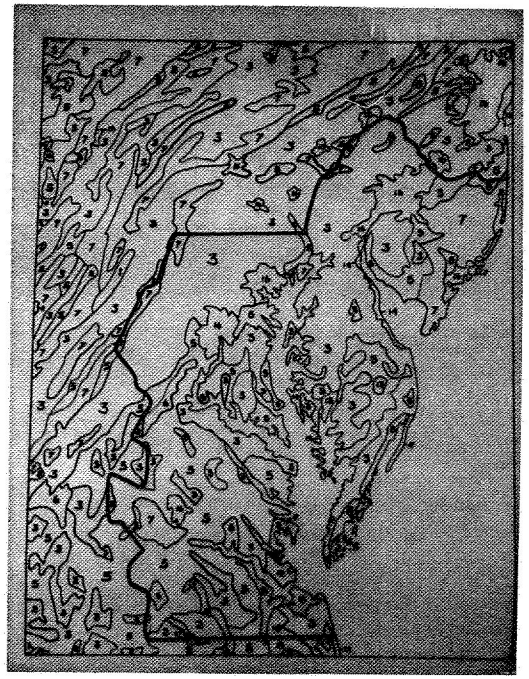


Figure 3. Land use in CARETS, from National Atlas of the United States; original Atlas scale 1:7,500,000. Key to map units in Table 1.

Table 1. Comparison of CARETS Map Units, National Atlas Land Use Map and ERTS Photomorphic Regions.

LAND USE MAP		ERTS PHOTOMORPHIC REGIONS	
MAP UNIT*	% AREA COVERED	% AREA COVERED	MAP UNIT
3	44	42	IV V VIII X XI
5	34	31	V
6 & 7	10	22	III VII IX XII
13 & 14	3	4	II
16	8	1	I

*Key to National Atlas Map Land Use Units: 3-Cropland with pasture, woodland, and forest; 5- Woodland and forest with some cropland and pasture; 6- Forest and woodland grazed; 7- Forested and woodland mostly ungrazed; 13- Swamp; 14- Marshland; 16- Urban areas as defined by U.S. Bureau of the Census.

N73-28304

Paper L 8

EVALUATION OF LAND USE MAPPING FROM ERTS IN THE SHORE ZONE OF CARETS*

Robert Dolan and Linwood Vincent, *Department of Environmental Sciences, University of Virginia, Charlottesville, Virginia*

ABSTRACT

ERTS imagery of the Atlantic shoreline zone of the Central Atlantic Regional Ecological Test Site (CARETS) was evaluated for classifying land use and land cover, employing the USGS Geographic Application Program's land use classification system (Geological Survey Circular 671). ERTS data can provide a basis for land cover and land use mapping within the shoreline zone, however because of the dynamic nature of this environment, two additional terms are considered: vulnerability of classes to storms and progressive erosion, and sensitivity of the classes to man's activities.

INTRODUCTION

ERTS-1 imagery of the CARETS region is being evaluated for use in classifying land use on the barrier islands of the mid-Atlantic Coast using the United States Geological Survey's Land Use Classification (Circular 671). Changes in this fragile environment occur on a variety of temporal and spatial scales, many of which are commensurate with the sampling possible from ERTS-1. Response of the islands to storms and long-term trends results in changes in the dimensions and distributions of the land use classes. ERTS-1 imagery offers, therefore, the possibility of monitoring the immediate and long-term response of the barrier islands to the processes, both human and natural. Since the barrier islands are subject to rapid and destructive change, the implications if this ability to monitor land cover types is potentially great.

*This research is being conducted within the CARETS Research Program, Geography Programs, United States Geological Survey.

PRECEDING PAGE BLANK NOT FILMED

Original photography may be purchased from:
EROS Data Center
10th and Dakota Avenue
Sioux Falls, SD 57198

The purposes are (1) to provide an initial evaluation of ERTS imagery for mapping land use on the barrier islands, and (2) to estimate the potential of ERTS for measuring the vulnerability and sensitivity of the land cover classes to change caused by man and nature. The area of investigation spans the coast from Atlantic City, New Jersey to Cape Lookout, North Carolina with the focus of the study centered upon landscape seaward of the Pleistocene/Recent contact.

REGIONAL DESCRIPTION

Barrier islands are biophysical complexes consisting of sand beaches, sand flats, dunes, and marshes. The islands rarely exceed one mile in width, range in length from one to twenty miles and are separated from each other by tidal inlets. The distances from the islands to the mainland may range from less than one-half mile to more than twenty miles. The principal physical processes occurring include the sand transport by tide, wind and wave generated currents, eolian transport, tidal inundation of the marshes, and storm surge overwash of the beach, dune and marsh areas. The ecology of the islands is fragile, with changes in the marsh and dune grasses rapidly masking change associated with the physical processes.

Erosion problems are critical along the CARETS coastline, especially in areas where man has intensely developed the landscape. Temporal scales of erosion include long-term trends due to eustatic sea level rise, short-term changes due to individual storms, and change associated with tidal cycles. When the dunes are breached and surges of seawater penetrate the interior of the island, damage can be inflicted upon public and private property. The flooding can disrupt transportation and communication, isolating sections of the islands. Overwash is a beneficial process, however, when it occurs in the natural landscape. It moves nutrients into the marsh, and has been suggested as the means by which the islands maintain themselves when sea level rises.

Recent research suggests that a hierarchy of shoreline landforms exists, with size ranging from beach cusps to capes (10 meters to 100 kilometers) and with the elements of this hierarchy dynamically linked to particular nearshore processes (Fig. 1). This system of landforms is important because the severity of the erosion that a locale experiences from a storm depends not only upon the intensity and duration of the storm, but also upon the position of the locale with

E

respect to the hierarchy of shoreline landforms. The presence or absence of elements of this system along the coastline can signify areas with a potential for rapid change; therefore, their appearance on the imagery can provide an indication of trouble areas.

CLASSES OF LAND COVER

The United States Geological Survey's Land Use Classification provides for two levels of classification based on two levels of remote sensing data (Table I). Level I is for use with satellite imagery and Level II is for use with satellite and high-altitude imagery combined with topographic maps. The following classes are frequently apparent on imagery of the mid-Atlantic barriers.

Forest Land--In general, the forest lands are evergreen or mixed.

Water--Streams and waterways are present, but bays and estuaries dominate.

Nonforest Wetland--All Level II elements are present.

Barren Land--The two Level II elements present are beaches and sand deposits other than beaches. Sand other than beaches will include both dunes and sand flats.

For the purpose of this report only Level I classification was mapped, although some Level II imagery was used to check the accuracy at Level I. Initial surveys indicate that color IR imagery at a scale of 1:60,000 was more than sufficient to accomplish Level II mapping with the exception of urban development classification.

ANALYSIS

Landmarks and features on the imagery that are important in delineating the land cover classes include the interfaces between sand flats and marshes, marsh and lagoon, and beach and ocean; turbidity patterns in the oceans and estuaries, and vegetation distributions. The following is an assessment of the individual ERTS-1 bands utility:

MSS-4 Sand surfaces are evident, as are sand to vegetation transitions. The band is not

Table 1

Land-Use Classification System for Use With Remote Sensor Data

Level I	*Level II*
01. Urban and Built-up Land.	
	01. Residential.
	02. Commercial and services.
	03. Industrial.
	04. Extractive.
	05. Transportation, Communications, and Utilities.
	06. Institutional.
	07. Strip and Clustered Settlement.
	08. Mixed.
	09. Open and Other.
02. Agricultural Land.	
	01. Cropland and Pasture.
	02. Orchards, Groves, Bush Fruits, Vineyards, and Horticultural Areas.
	03. Feeding Operations.
	04. Other.
03. Rangeland.	
	01. Grass.
	02. Savannas (Palmetto Prairies).
	03. Chaparral.
	04. Desert Shrub.
04. Forest Land.	
	01. Deciduous.
	02. Evergreen (Coniferous and Other).
	03. Mixed.
05. Water.	
	01. Streams and Waterways.
	02. Lakes.
	03. Reservoirs.
	04. Bays and Estuaries.
	05. Other.
06. Nonforested Wetland.	
	01. Vegetated.
	02. Bare.
07. Barren Land.	
	01. Salt Flats.
	02. Beaches.
	03. Sand Other Than Beaches.
	04. Bare Exposed Rock.
	05. Other.
08. Tundra.	
	01. Tundra.
09. Permanent Snow and Icefields.	
	01. Permanent Snow and Icefields.

good for the differentiation of marsh vegetation types, or of the beach from the surf zone (Fig. 2A).

MSS-5 The sand to marsh transition is best indicated on this band. Turbidity is easily observed. As with band MSS-4, marsh to water and shore to water transitions are not well-defined (Fig. 2B).

MSS-6 Both water to land boundaries and vegetation transitions are evident. This band is poor for sand to marsh transitions (Fig. 2C).

MSS-7 This band is the best for water to land transitions, and in particular, for discerning the shoreline. Dune ridges and vegetation patterns also show well. Similar problems as MSS-6 for sand/vegetation transitions exist (Fig. 2D).

The land cover of the mid-Atlantic barrier islands from Atlantic City, New Jersey to Assateague Island, Maryland and from the Virginia-North Carolina border to Cape Fear, North Carolina have been mapped at Level I. Examples are given in Figure 3. The problems encountered in mapping for each land cover and land use class are discussed in the following list.

Urban and Built-up Areas--These areas are difficult to distinguish on barrier islands unless the development is intense because of large areas of unvegetated sands that remain between the buildings. This problem is easily removed at Level II. Areas where marshes have been dredged and filled for development are easily recognized from ERTS-1 imagery.

Forest Lands--Areas of heavy evergreen or mixed cover are readily evident on MSS-6 or MSS-7. The only areas on the barrier islands that have this type of land cover are usually older, high-standing dunes. On the false color imagery the forests appear a brighter red than marshes. Level II imagery should be sufficient to answer any questions that arise in Level I mapping.

Water--Water/land transitions are best delineated on MSS-6 and MSS-7. No particular problems were encountered in mapping at Level I.

Nonforest Wetland--Sand to marsh transitions are best indicated on MSS-4 and MSS-5, marsh to water is best on MSS-6 and MSS-7. Some differentiation of wetland types is evident, but Level II imagery is necessary for accurate identification.

Barren Land--The barren lands of barrier islands are primarily the beaches, dunes, and sand flats. The beach areas are separable from sand flats and dunes by their lack of vegetation on Level I. Level II imagery may be necessary for accurate separation of sand flats from dunes.

EVALUATION

ERTS-1 imagery is sufficient for identifying Level I classes of land cover and land use and can be used for rapid assessment of the distribution of the land cover on a regional scale. Elements of the Level II classification are also evident, but more work is required before it will be possible to assess whether or not the majority of Level II classifications can be carried out without extensive use of high-altitude underflights. The combination of resolution, regional coverage and sampling interval makes ERTS imagery desirable when large-scale assessments of change, such as after a major storm, or longer-term changes in distribution of land cover and land use are needed.

Changes in distributions of land use classes on the barrier islands signify the response of this environment to natural and man-caused processes. Therefore, a shift in the relative distribution of vegetated dunes and sand flats may be indicative of an erosion trend, or a decrease in marsh area may represent increased dredge and fill or significant storm generated overwash.

The barrier islands are one of the most dynamic and sensitive environments inhabited by man. The interconnections among the processes and the equilibrium form of the land is such that changes in any one part of the island can be rapidly transmitted to other areas. For purposes of

of planning in this environment measures on the vulnerability and sensitivity of the different land cover classes are needed if the use of the islands is to be properly planned.

Environmental vulnerability can be defined as the possibility that a land cover class may undergo significant change. The vulnerability of a beach may, therefore, be very high when compared to a marsh area. Vulnerability can also vary between sites within a particular land cover class. For planning purposes, vulnerability indicates the risk of damage from storms or other environmental changes.

Sensitivity can be defined as the degree of possible damage to the land class from actions of man. Barrier dunes and marshes may, therefore, be more sensitive than beaches and sand flats. Sensitivity gauges the possible effect of man upon the land class.

Vulnerability and sensitivity can be estimated from repetitive coverage of long reaches of CARETS coast. ERTS imagery has sufficient resolution and adequate repetitive coverage to accomplish the task. Some high-altitude imagery and supportive field work is necessary to calibrate the interpretative decisions.

By monitoring land cover distributions on undeveloped islands, and then estimating vulnerability and sensitivity, the natural dynamics of the barrier island environment can be estimated. The information gained can then be applied to areas already developed or areas planned for development. This system of analyses can then serve to forecast where serious environmental problems will likely occur.

SUMMARY

ERTS imagery can be used to map Level I land cover and land use distributions on the barrier islands of the CARETS region. Mapping of some elements at Level II is also possible. It appears that vulnerability and sensitivity of the land cover classes can be estimated from the investigation of ERTS imagery with some supportive underflights and field work. These additional data should provide a planning base for future development of the sand beaches and barrier islands of the mid-Atlantic Coast.

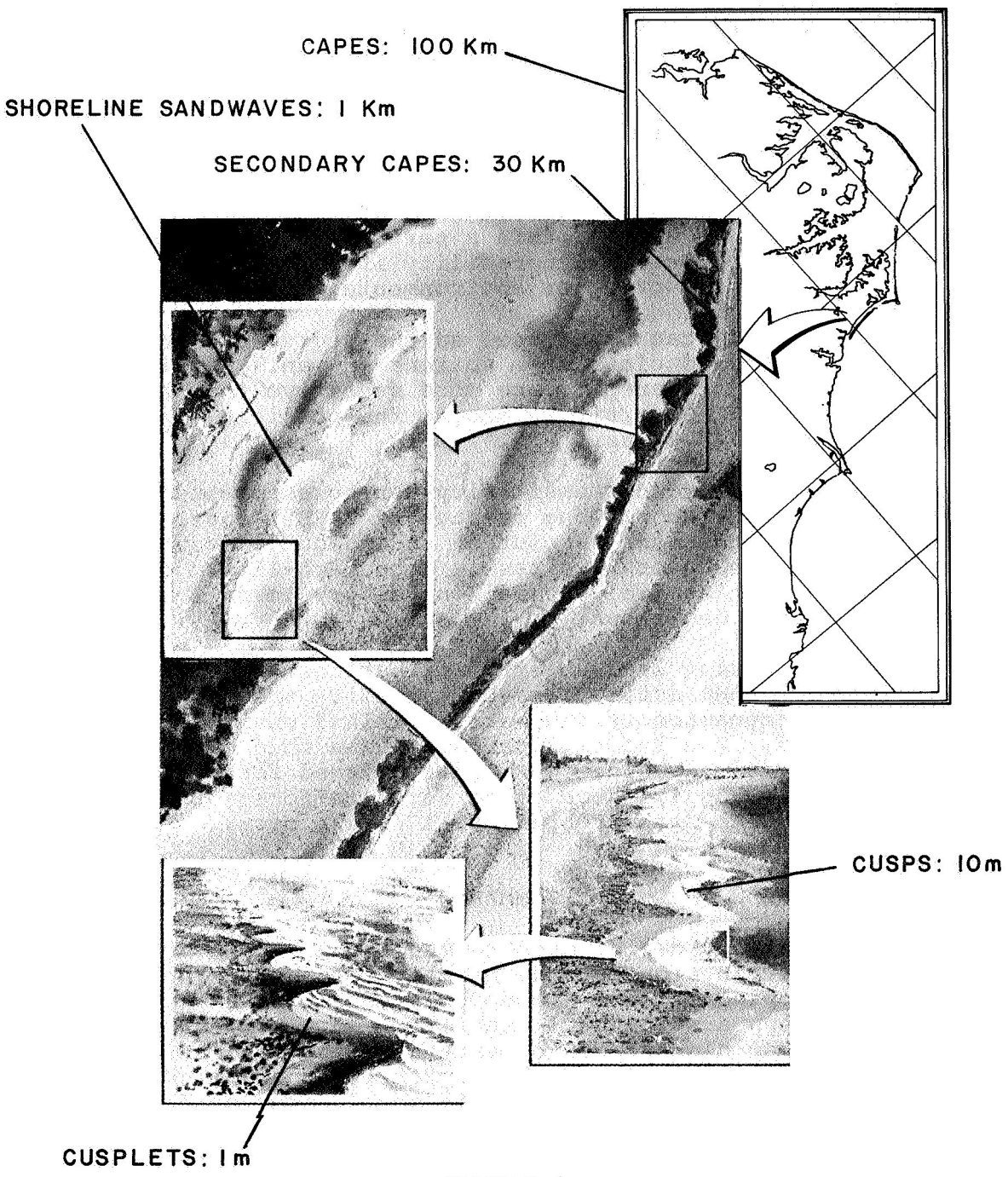


FIGURE 1

HIERARCHY OF CRESCENTIC AND RHYTHMIC COASTAL LANDFORMS

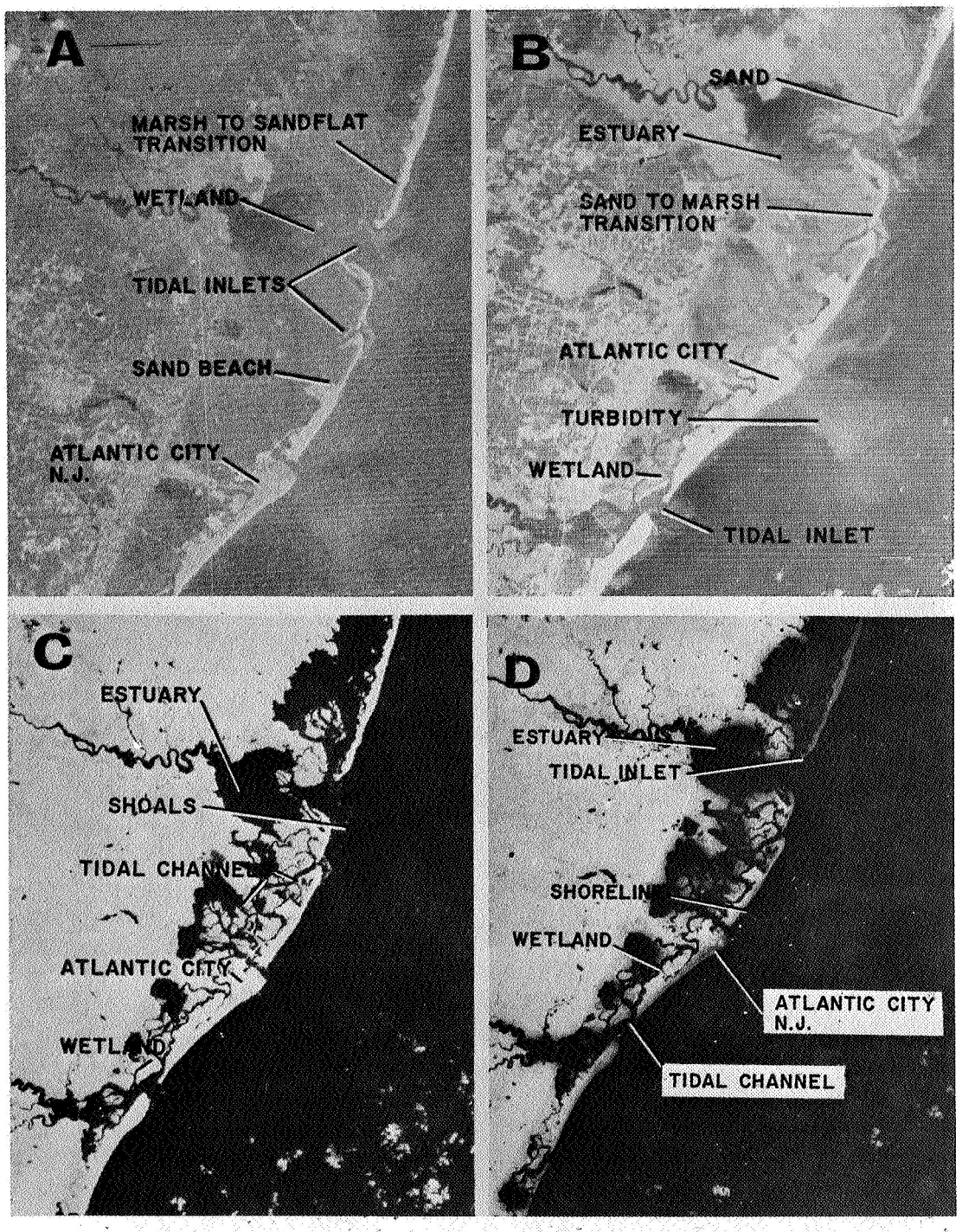


FIGURE 2
UTILITY OF MSS BANDS

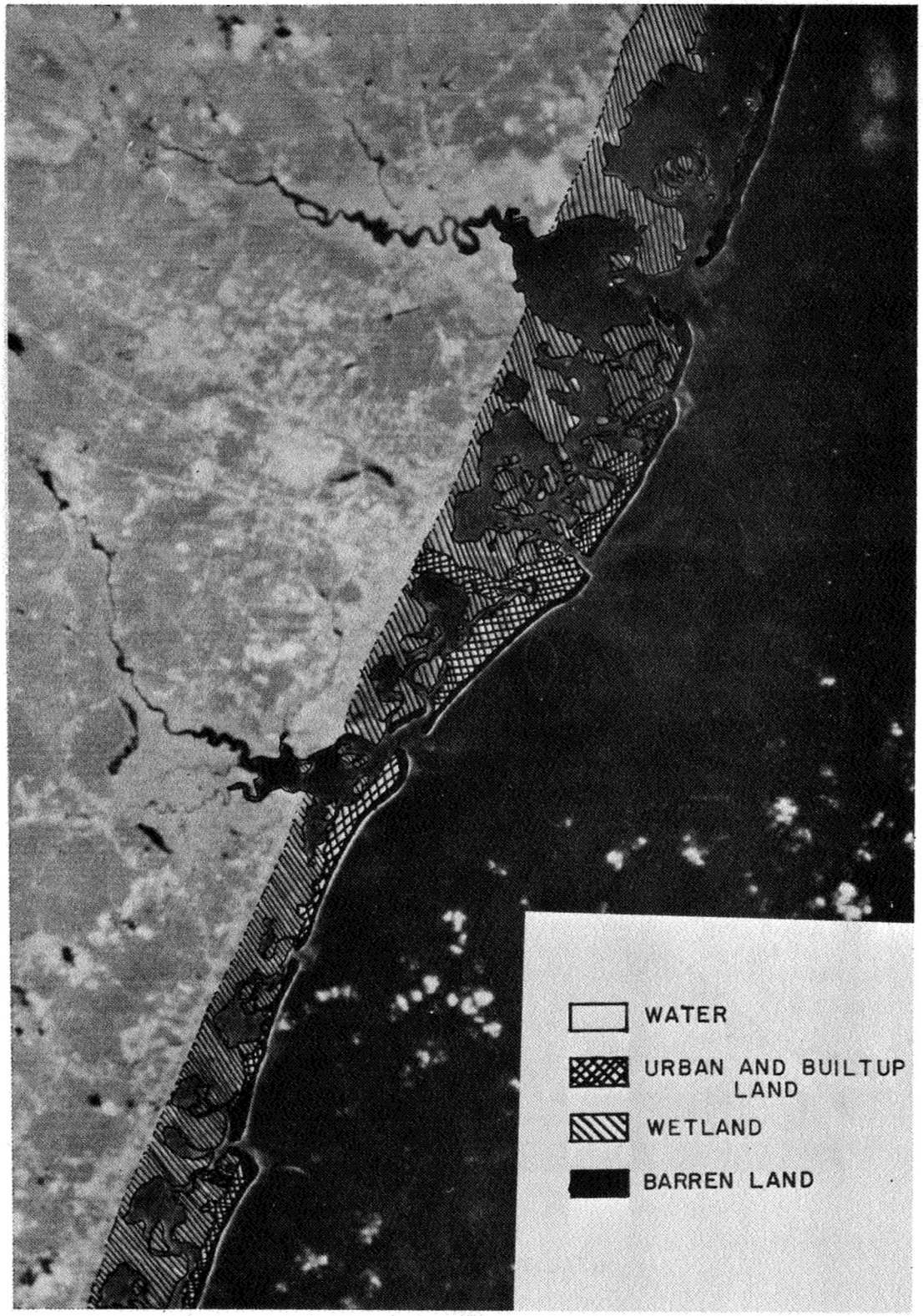


FIGURE 3
COASTAL LAND USE, ATLANTIC CITY, NEW JERSEY
(ERTS E 1024 - 15073-5, AUGUST 16, 1972)

N73-28305

Paper L 9

INVESTIGATIONS USING DATA FROM EARTH RESOURCES TECHNOLOGY SATELLITE IN THE FIELDS OF AGRICULTURE/GEOGRAPHY. (TIMBER INVENTORY - LAND USE) IN THE PROVINCE OF HUELVA-SPAIN

Emilio de Benito, Serafin López-Cuervo, Joaquin Rodriguez, *Universidad Politécnia, Escuela Técnica Superior de Ingenieros de Montes, Madrid*

ABSTRACT

A test-site was chosen in the area object of this study, with the purpose of elaborating the patterns for the future total use of the satellite photographs.

The election of the test-site was made having in mind the following criteria.

- A flat terrain for eliminating the dangers of shadows produced by a difficult topography.
- Searching of well defined natural limits for the test site.

The elaboration of a card showing the different uses of the terrain at a 1:100.000 scale, the agrarian structures of the same at a 1:100.000 scale, both purposes as a reduction of the cartography of the inventary.

The study of the remission curves of the various species and phytological associations, of the soil and the hydrography of the zone.

Due to the lack of satellite-photographs from the study-area, a number of photos from the northern area of Spain have been studied, these from the point of view of obtaining answers from the spectra of the vegetation masses.

BACKGROUND

The area purpose of this study is one of the most interesting forestal zones of Spain, this study being made more interesting due to the fact of this zone being the site of an important cellulose factory, which is of great importance for the agroeconomical structure of the province.

During the decade of the 60's a forestry inventary at a regional scale was made, in the year 1.970 an inventary at commercial scale was made with the aid of aerial photography.

The zone has been completely covered with photos of the 1:35.000 and 1:10.000 scales; pan-chromatic and infra-red emulsions.

Yearly flights have been made to control the evolution of the forests.

The above information has been used for the confection (elaboration) of a card showing the different uses of the land, special care has been had in not making generalizations for avoiding loss of information.

The eight most important structures have been studied, so that they could be of importance for answering spectra.

These were established by the genus Pinus, Quercus, Eucaliptus, characteristical vegetation of the tindeland, mold-vegetation, the water-resources of two rivers characteristically different due to the nature of their pourings, and finally by the sea-water.

The remission curves were obtained with the aid of a Beckmann DK-2 specterphotometer.

SATELLITE-PHOTOGRAPHS

The study has been made with the only photos available, those of the basin from the river Ebro.

Theoretically, and with the help of the remission curves, the idoneus filtration processing for each of the spectral bands found.

With the aid of a multispectral projection camera, the photos were obtained using the additive methods, following also the processing above described, with the help of empirical methods depending on the background of the zone.

With all these criteria all the theoretic end empirical compositions were defined, later they were developed in the laboratory.

The filtrations were made with a series of gelatin-filters from Kodak C.P.: Yellow-15; green-50; red-50; light-blue-50.

Once the working material ready as described end with the aid of eight views an interpretation was established by eight specialists in photo-interpretation, each had access to the same source of documentation.

The number 8 is the basis over which a complete comparison can be made.

The results of the interpretation were exploited having in mind the obtaining of those correlations which should have the greatest warranty, a resume is as follows.

Comparative study between the same band of the two processes described.

MSS-4
- Without filtration. Residing areas very diffuminated. Better definition of the relief as with filtration. Better definition of the grey tones as with filtration.
- With yellow - 15 filtration. Generally, less definition as without filtration.

MSS-5
- Without filtration. Generally, less definition as with filtration.
- With green - 50 filtration. Greater range of grey tones. The best definition of the vegetation of all the 4 bands.

MSS-6
- Without filtration. Better tonality of greys as with filtration.
- With light-blue - 50 filtration. Bad definition.

MSS-7
- Without filtration. Residing areas clearly defined. The best definition of the drainage of all the 4 bands. The best definition for studying the shadow areas.
- With red - 50 filtration. Mediocre definition, considerable loss of tonality.

Comparative study between the 4 bands of the two processes described.

A difficult orography presents a heavy masking due to the shadows produced. This causes a notable loss of information from the tone-factors. The orography is projected with a good hypsometric definition.

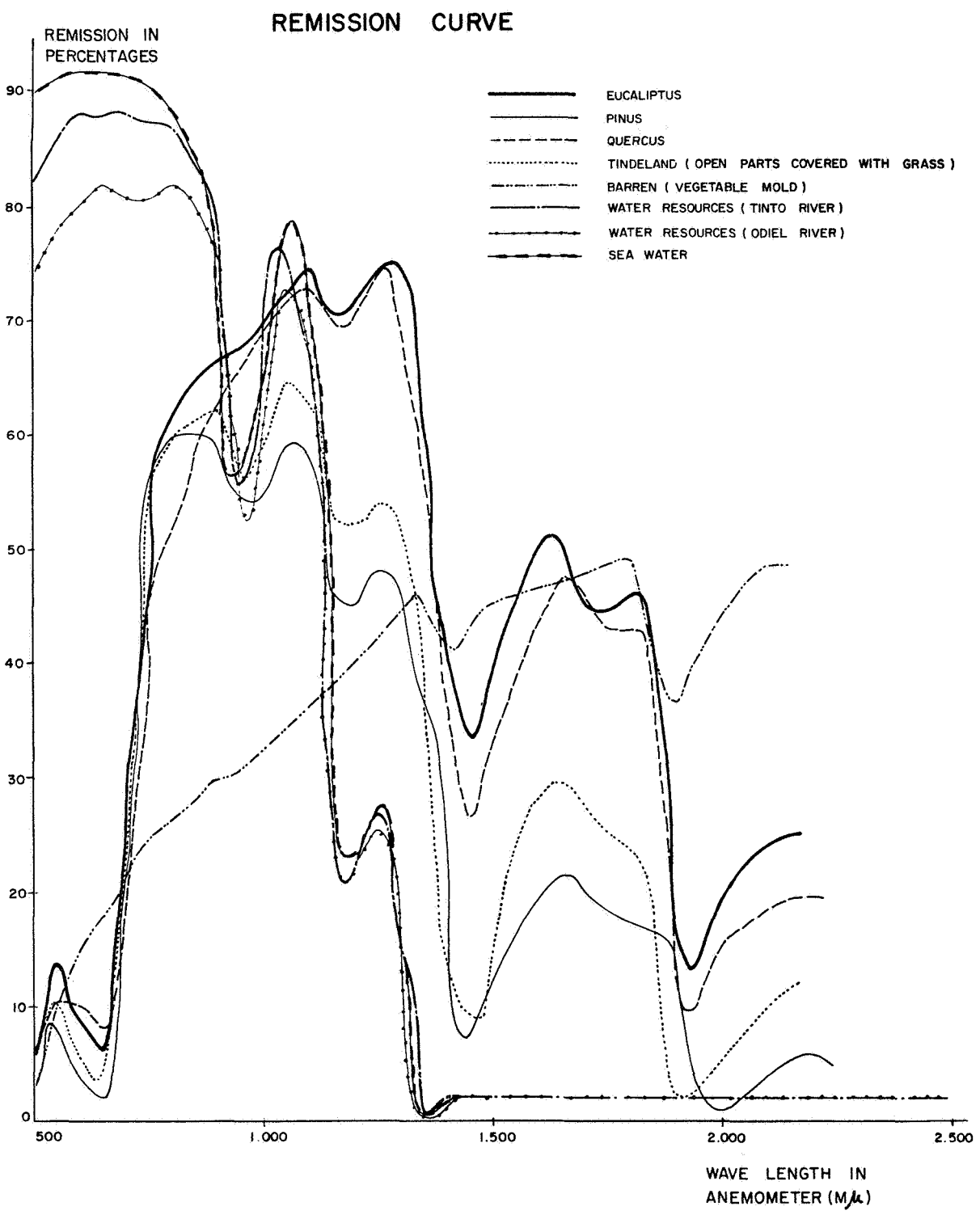
The best information is obtained with the following composition:

MSS-4 — Without filtration

MSS-5 — With green - 50 filtration.

MSS-6 — Without filtration.

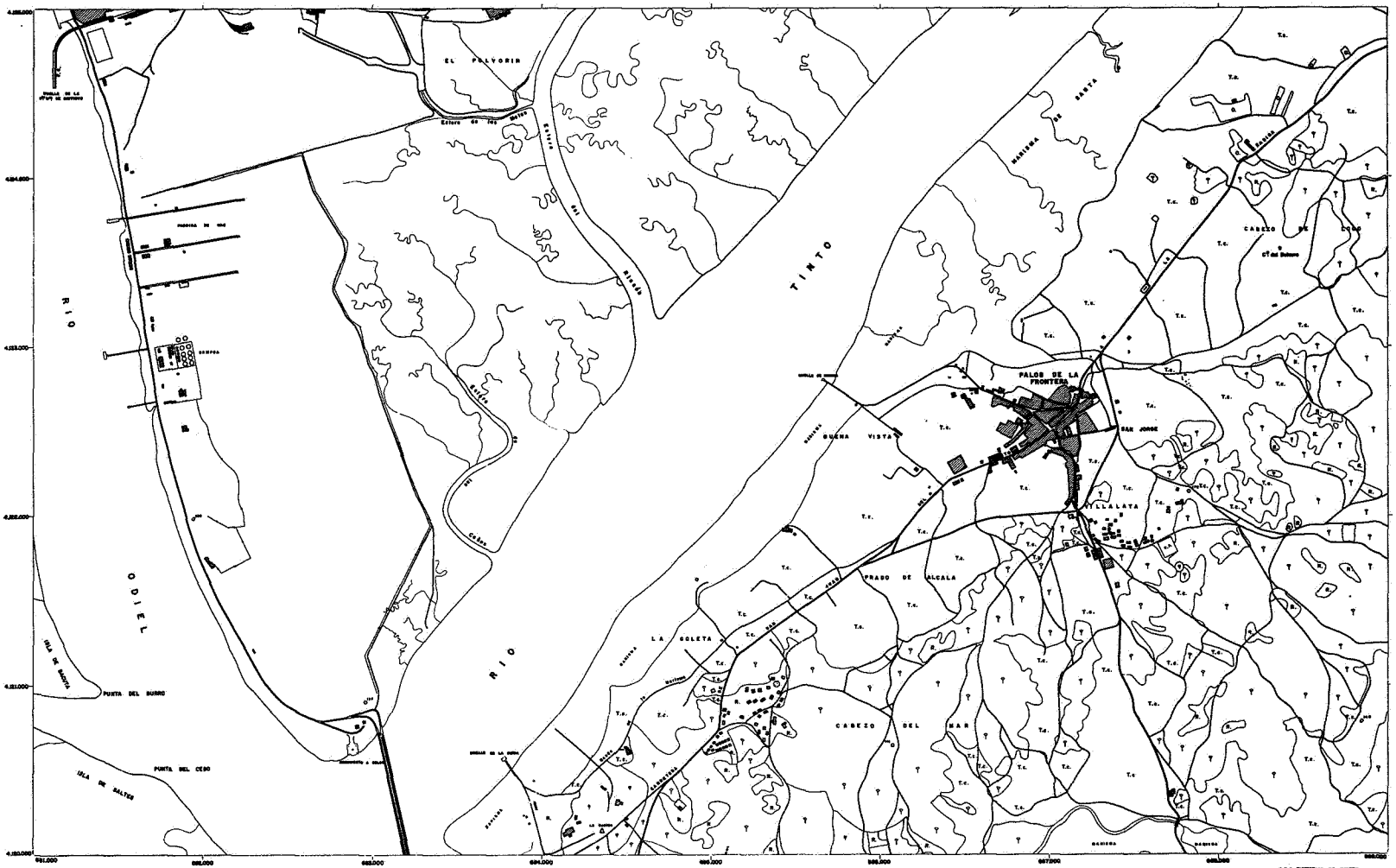
MSS-7 — Without filtration.


REMISSION CURVE
REMISSION IN PERCENTAGES
EUCALIPTUS
PINUS
QUERCUS
TINDELAND (OPEN PARTS COVERED WITH GRASS)
BARREN (VEGETABLE MOLD)
WATER RESOURCES (TINTO RIVER)
WATER RESOURCES (ODIEL RIVER)
SEA WATER
90
80
70
60
50
40
30
20
10
0
500
1.000
1.500
2.000
2.500
WAVE LENGTH IN ANEMOMETER (Mμ)

E.N.C.E.

HUELVA

INVENTARIO FORESTAL


RIO
TINTO
RIO
ODIEL
PALOS DE LA FRONTERA
SAN JOSE
VILLALATA
BUENA VISTA
PRADO DE ALCALA
LA SOLETA
CABEZO DEL MAR
EL PELVORIN
PUNTA DEL BURRO
PUNTA DEL CEBO
ISLA DE SALTES
ISLA DE SAUCINA
Cabezo
Cabezo
Cabezo

N73-28306

Paper L 10

GEOGRAPHIC APPLICATIONS OF ERTS-1 DATA TO LANDSCAPE CHANGE

John B. Rehder, *Department of Geography, University of Tennessee, Knoxville, Tennessee*

ABSTRACT

The analysis of landscape change requires large area coverage on a periodic basis in order to analyze aggregate changes over an extended period of time. To date, only the ERTS program can provide this capability. Three avenues of experimentation and analysis are being used in the investigation: (1) a multi-scale sampling procedure utilizing aircraft imagery for ground truth and control, (2) a densitometric and computer analytical experiment for the analysis of gray tone signatures, comparisons and ultimately for landscape change detection and monitoring, and (3) an ERTS image enhancement procedure for the detection and analysis of photomorphic regions.

INTRODUCTION

The ERTS-I capabilities of sensing the same geographic point every 18 days and providing a 13,225 square mile view from each image challenge us to the task of analyzing landscape change from a regional perspective. The investigation focuses on the East Tennessee Test Site, a 20,000 square mile region in which landscape change elements such as forest alterations, strip mines, highway construction, urban-suburban growth, and cyclic seasonal changes in agriculture are being analyzed (Figure 1). Two test sites of smaller dimensions are being intensively studied within the larger test region. The Knoxville Test Site, an 11 x 21 mile area which encompasses the city of Knoxville and the western portion of Knox County, is being investigated for landscape change associated with urban growth. A second smaller test site on the Cumberland Plateau is being monitored for forest alterations and landform disturbances associated with surface strip mining for coal. Unfortunately, the humid East is not the most ideal region for landscape change analysis because the high percentage of cloud cover has reduced the number of useable satellite observations to three for our study area since August.

Three avenues of experimentation and analysis are being used in the investigation: (1) a multi-stage, multi-scale sampling procedure, (2) a densitometric and computer analytical experiment, and (3) an image enhancement procedure.

PRECEDING PAGE BLANK NOT FILMED

Original photography may be purchased from:
EROS Data Center
10th and Dakota Avenue
Sioux Falls, SD 57198



F

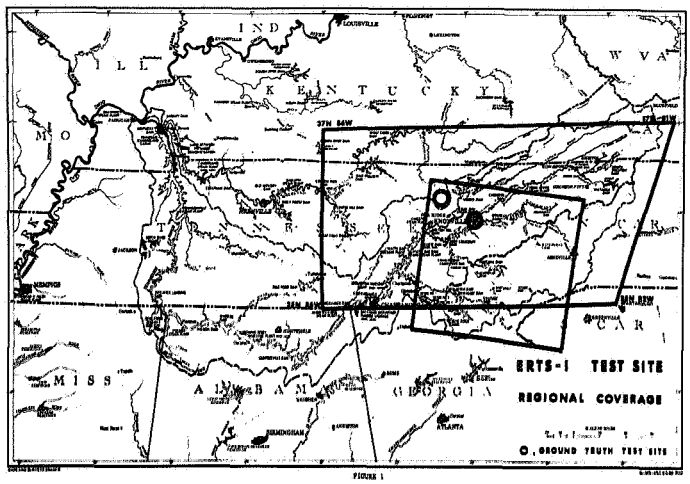


Figure 1 - The East Tennessee Test Site with a representative ERTS frame for scale.

The multi-stage sampling experiment has involved the generation and analysis of low altitude imagery flown from 10,000' in June-August, high altitude aircraft imagery from a NASA RB-57 overflight at 60,000' in April, and the ERTS-I imagery since August. Primarily designed as a source for ground truth data, the aircraft imagery has proven its value in establishing a control base for comparisons with the ERTS imagery.

The intermediate scale imagery from the April RB-57 overflight has been most useful for control. Figure 2 of the Cumberland Plateau Test Site illustrates in a negative print the nature of strip mine scars on the landscape for this area. At this scale one can see not only the modified land surface but also the internal characteristics of the surface mines. Note the extent of cleared, stripped land and the forested area at the bottom of the image for this observation in April. Now, in Figure 3 viewing the same area from an enhanced ERTS image for October 15, one can detect a distinct increase in dark tones indicating cleared land in the area that had been forested in April. This represents a significant landscape change.

Microdensitometric and computer techniques are being used to analyze the ERTS imagery for gray tone signatures, comparisons, and ultimately for landscape change detection and monitoring. Using the same strip mine example, let's observe the same patterns of surface configuration on the computerized map (Figure 4). The experiment involves the microdensity scanning of a positive band 5 image in which strip mines appear as light tones against a dark forested



Figure 2 - A portion of an RB-57 image of the Cumberland Plateau illustrating surface mining scars in April, 1972. Note the unmined area indicated by the arrow.



Figure 3 - A portion of an ERTS image of the Cumberland Plateau indicating landscape changes in surface mining scars in October, 1972. Note the mined area shown by the arrow.

background. Gray tone densities are then digitized and computer processed into a computer map and histogram (frequency distribution). By comparing such machine analyzed data from different dates of satellite observations, we can determine if the number of light tones indicating strip mined areas have increased at the expense of dark tones for the same area.

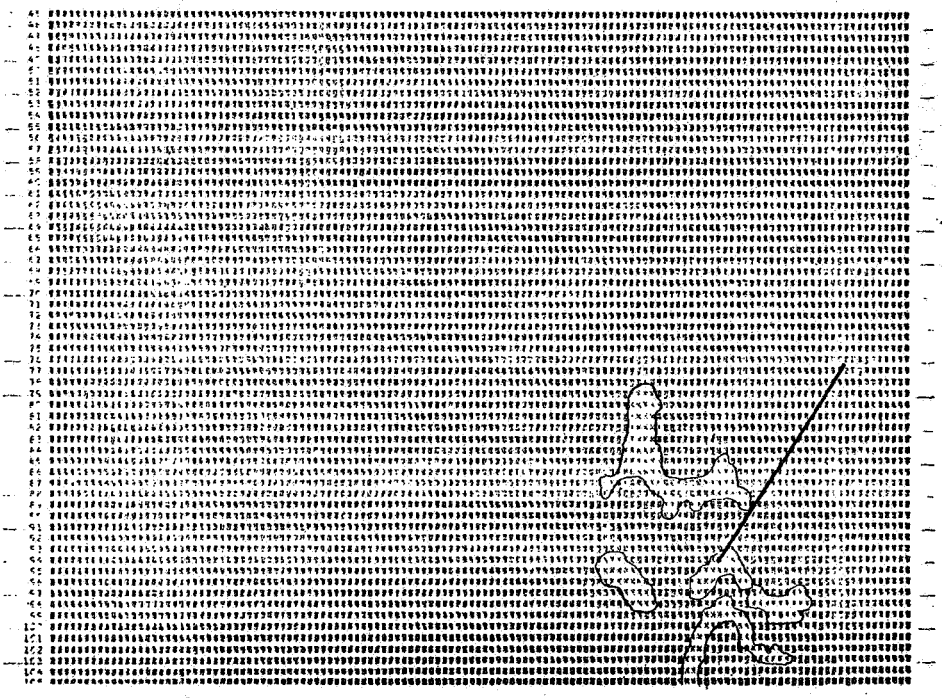


Figure 4 - Microdensity scan displayed in a computer map printout illustrating the same surface mine signatures from an ERTS band 5 image. See figure 3.

Barring extraneous signals from cloud cover, one then should be able to conclude that forest cover has been altered and strip mines have been increasing because of the increased frequency of light toned signatures.

Comparisons between the two histograms in figure 5 with the upper one representing August 22 and the lower one October 15, have resulted in the inverse from the expected. This is because only two relatively clear observations for the strip mined area have been obtained and the atmospherics on August 22 created a serious cloud

and haze problem. Given time and more but clearer observations, these problems can be rectified.

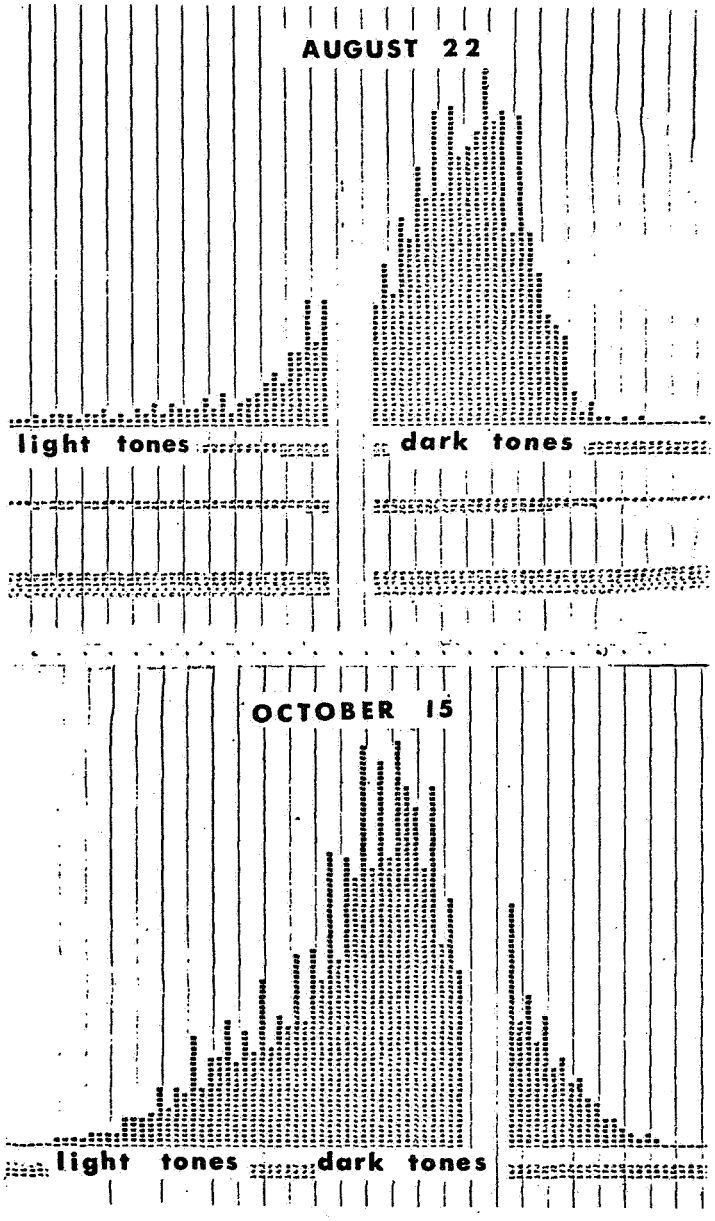


Figure 5 - Histograms of gray tone densities. ERTS band 5 images for August 22 and October 15, 1972.

In addition to this experiment, applications toward earth resources management problems involve the generation of enhanced

ERTS imagery for emphasizing areas of potential and current landscape dynamics. In this regard several photomorphic regions have been under observation.

The Great Smoky Mountains represent a region of cyclic, seasonal change for which natural and not man-made causes predominate. Figure 6, a negative print from band 7, illustrates a temporary landscape change phenomenon of a surficially wetted area on the western, windward slopes of the Smokies. The day preceding this ERTS observation, a frontal disturbance deposited approximately 2"-3" of rainfall on the windward slopes. By comparison, Knoxville, located downslope in the valley received 1.12" of precipitation. The wetted surface shown here in white tones was sufficiently wet to register in tones not unlike the surrounding streams and T.V.A. reservoirs to the north and west. The satellite monitoring of a water-shed such as this indeed has application toward water resources, flood prediction, and a host of other water management problems.

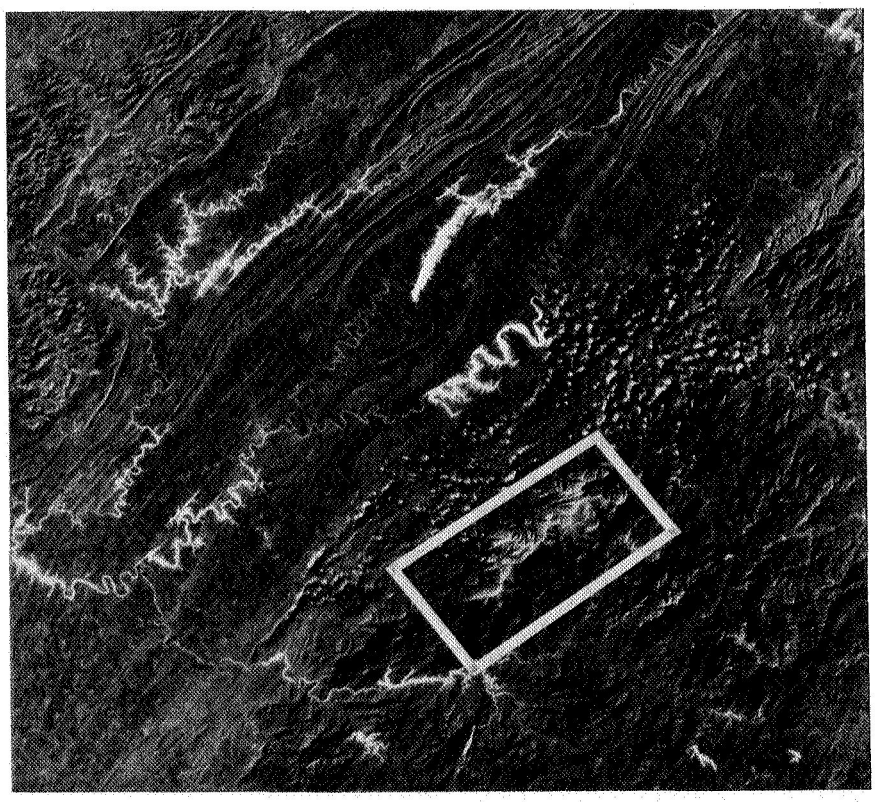


Figure 6 - ERTS band 7 negative print of the East Tennessee Test Site. Note light toned wetted surface on the Great Smoky Mountains.

One of the more humanly responsible photomorphic regions is illustrated by the enhanced band 5 image in figure 7. Using a positive transparency as a negative we have produced a negative print which enhances normally light toned cultured features into dark ones. Reading black on white, one can observe a broad agricultural area in the eastern portion of the Great Valley and the spider web effect of roads and routes leading to Knoxville. The built up area of Knoxville and suburban growth areas to its west appear much sharper on this image than on the normal black and white. The black dots and lines of deepest intensity indicate areas of highest reflectance for band 5 and generally for this area represent areas of cleared earth. Such bare red soil surfaces are best illustrated by the I-81 interstate highway construction in the northeast portion of the image. Westward one can see again the strip mines enhanced as black jagged lines on the Cumberland Plateau.

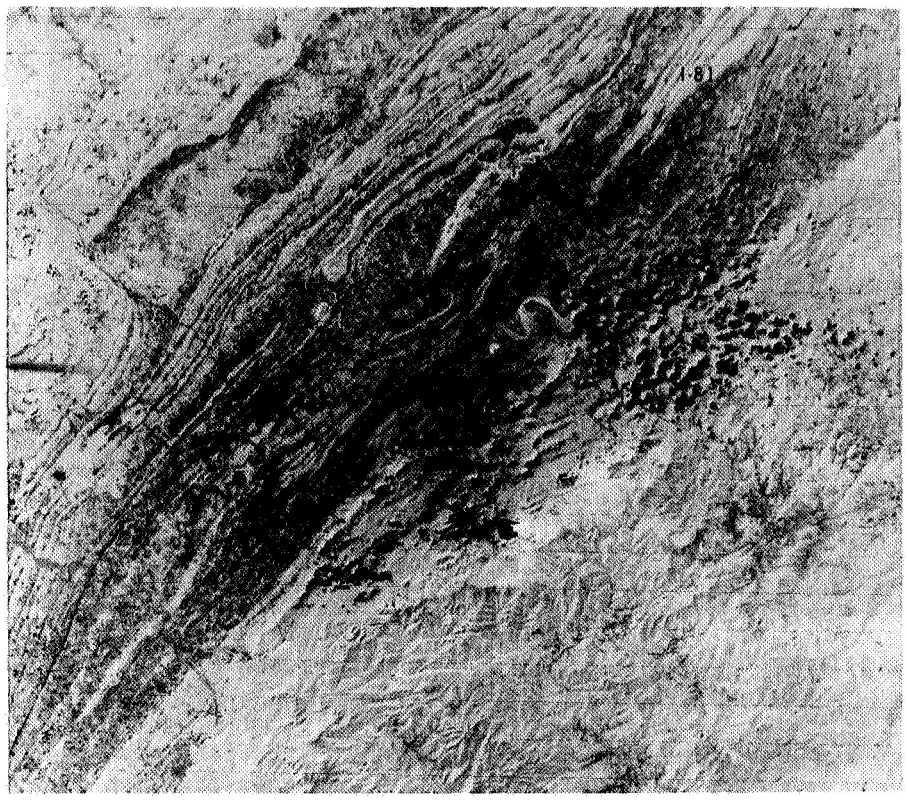


Figure 7 - ERTS band 5 negative print of the East Tennessee Test Site. Note urban and agricultural areas - man-made landscapes - shown in dark tones. Disregard clouds at right.

In each photomorphic region we can determine a certain and separate degree of tonal unity and distinctiveness. More importantly, a management and landuse distinction exists in each region. On a positive print, dark toned rough forested lands indeed represent a different tonal and landuse quality than do light toned, cleared cultural landscapes (Figure 8). Although forested vs cleared land surfaces are understood in detail here on earth, one requires the region-wide view to analyze such regional variations and to express to the general public the importance of such distinctive regions. In many ways, variations like these in tonal quality, reflect variations in earth resources and thus suggest a different set of values and management principles to be applied to each.

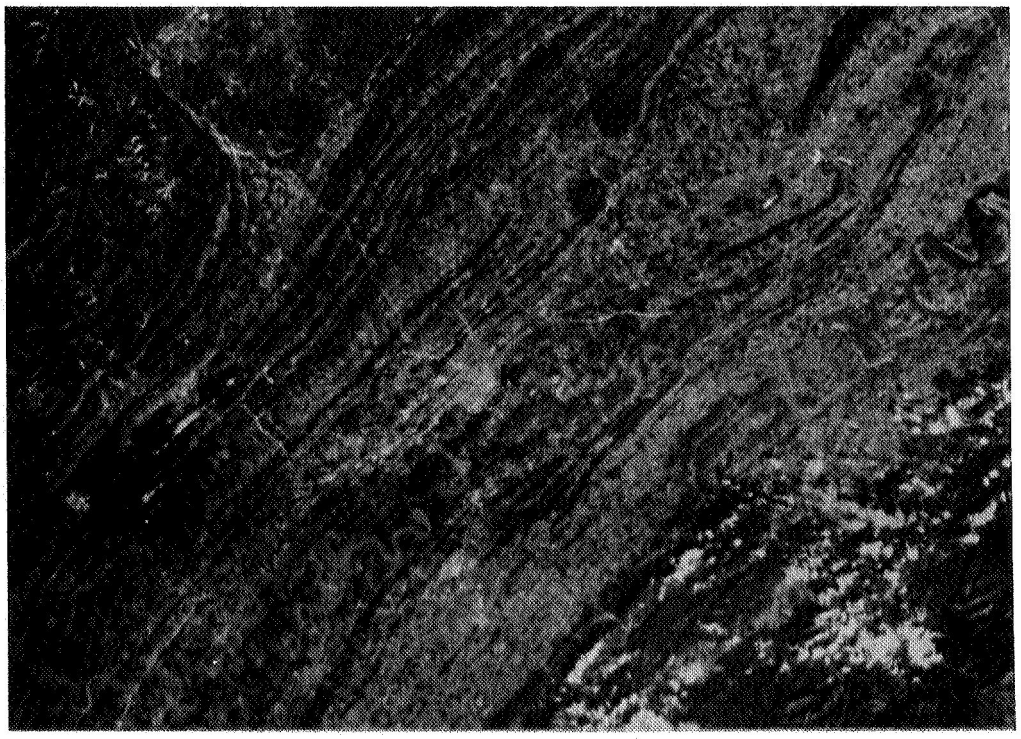


Figure 8 - ERTS band 5 positive print of a portion of the East Tennessee Test Site.

Because man's individual actions in creating landscape change are relatively small on a cell for cell basis, any investigation such as this one requires large area coverage on a periodic basis in order to observe and analyze aggregate changes over an extended period of time. To date, only the ERTS program can provide this capability. The continued analysis of data from ERTS-I and, more

importantly, from ERTS-B would insure a success in the analysis of landscape change from a geographic point of view and would be a contribution in the study of man's role in changing the face of the earth.

N73-28307

Paper L 11

IDENTIFICATION OF SOIL ASSOCIATIONS IN WESTERN SOUTH DAKOTA ON ERTS-1 IMAGERY[1]

Frederick C. Westin and V. I. Myers, *Plant Science Department and Remote Sensing Institute, South Dakota State University, Brookings, South Dakota*

ABSTRACT

Soil association maps show the spatial relationships of land units having characteristic soil depths and textures, available water capacities, permeabilities, pH characteristics, plasticity indices, liquid limits, and the like, from which broad interpretations can be made such as how the soil is suited as a source for topsoil, and as a source for sand and gravel, and how corrosive the soil is for steel and concrete, and what crop and grass yields can be expected. Film color composites of bands 4, 5, and 7 viewed over a light table with magnification show the soil associations of western South Dakota that are now recognized, and, in addition, several new soil association areas have been brought to light.

INTRODUCTION

Soil maps are an integral part of an effective agricultural research and advisory program. Soil maps are used for farm and ranch planning, for crop and grass yield estimates, for land appraisal, for guidance for prospective land buyers, for land use planning, for irrigation planning, for drainage planning, for assessing potentialities for special crops, for rural zoning, and for forest management.

Soil maps are of different scales ranging usually from 1:15,840 to 1:7,000,000. The large scale maps necessary for detailed land planning show the extent of individual soils, and are made by boring holes and walking over the land so that delineations are observed over their entire extent.

Small scale soil maps, called soil association maps, are geographic associations of one or several soils and usually are at scales of 1:500,000 to 1:1,000,000. Simonson (1971) states that each soil association consists of a set of geographic bodies that are segments of the soil mantle covering the land surface. Soil associations may include like or unlike soils and they are linked together by mode of occurrence rather than degree of similarity.

1/SDSU-RSI J-73-01. Supported in part by contract No. NAS-5-21774. Authorized for publication as Journal Series 1170, South Dakota Agricultural Experiment Station, South Dakota State University, Brookings, S. D.

PRECEDING PAGE BLANK NOT FILMED

Although soil association maps of small scale are not as precise for interpretations as detailed soil maps of large scale, they nonetheless have use for broad planning purposes and for education. A recent soil association map prepared by Westin and Bannister (1971) is published at a scale of 1:500,000. The map was prepared by using detailed soil survey data along with geologic, geomorphic, topographic, climatic and biotic information as well as aerial photographs. The map units are associations of soil series. Soil profile descriptions, laboratory data and interpretation information are available for the soil series used.

It should be emphasized that the soils on soil maps are not defined in terms of profiles alone. According to the soil survey staff of the USDA (1951), each soil unit is a particular kind of landscape and it is these landscapes of soils that are classified and shown on soil association maps. Although soil profiles cannot be seen on air or satellite imagery, soil landscapes are visible. Soil landscapes exhibit a characteristic surface geometry such as relative frequency of streams, and a characteristic surface composition such as the percentage of bare soil areas. Other features used in differentiating soil landscapes include vegetation, and hydrology.

The ERTS 1 MSS imagery brings spatial and temporal advantages for the recognition of soil landscapes. These are that each frame covers about 8,400,000 acres, is available in 4 spectral bands, and the imagery is repeated every 18 days. The purpose of this study was to determine if western South Dakota soil landscapes presently shown on the Soil Association map can be recognized by viewing ERTS 1 MSS imagery and whether new or revised soil associations are recognizable.

PROCEDURE

The ERTS imagery observed for this study in western South Dakota consisted of the 4 MSS bands with wavelengths ranging from .5-1.1 um. The study was confined to 3 frames: (1) 19 August 1972 C N 42-57, W 102-37; (2) 6 September 1972 C N 44-30, W 102-06; and (3) 12 October 1972 C N 44-35; W 102-00. The four bands were observed singly and also in color composites made from bands 4 (.5-.6 um); 5 (.6-.7 um); and 7 (.8-1.1 um). The color composites were made by projecting each black and white frame through a color filter. Using this procedure the intensity of a particular hue was governed by the gray scale value shown by each feature.

The procedure used to study the soil landscapes or associations on ERTS imagery was to view, with a binocular, each of the four bands and the color composites over a light table under 3-power magnification. A mylar overlay was placed over the ERTS frame and lines were drawn upon the overlay using a 0.2 Castell 990 pen and black Pelikan drawing ink. The inking was done when the frame was under magnification. Photo interpretation techniques were used to recognize the soil association boundaries. Use was made of colors, tones, patterns, and shapes,

as well as the drainages. The nature of the parent rock and its mode of deposition, and the climatic, biotic and physiographic factors of the environment all were considered. For comparison purposes the published soil association map of Westin and Bannister (1971), of scale 1:500,000 was reduced in scale to correspond to the 1:1,000,000 scale of the ERTS image.

RESULTS

The results of this study consist of four comparison maps, figures 1 through 4, on which a soil association from the published map is compared to the soil landscape recognized on the ERTS image. The lines from the ERTS map all were drawn from color composites. Although each of the four MSS bands were studied singly, the most useful images were produced by the color composites. Of the individual bands, the 5 band (.6-.7 um) gave the best contrast and clearest image. The 7 band (.8-1.1 um) appeared to be useful to show vegetation vigor. For example, in the semiarid rangeland of western South Dakota the less productive steep sides of the Cheyenne River valley showed appreciably different reflectance than the rolling to undulating interfluves having deeper soils and more grass.

The ERTS color composites for western South Dakota were clear and sharp. Images remained sharp under 3-power magnification but magnification greater than 3X or 4X resulted in hazy boundaries. No interpretation problems were encountered. Range lands were distinguishable and relative vigor of the grass was apparent by the intensity of the red hues. Dimensions of cropped fields and other features could be estimated by placing a metric scale under the magnified composite.

In addition to the vegetative features visible on the color composites, physical features also are apparent. The exact configuration of the South Dakota badlands is visible and can be traced on overlays from the composite. Within the badlands, the actively-eroding, barren wall is distinguishable from the badlands basins. This is a significant separation since the wall produces no vegetation while there is grass produced in the badlands basins although some areas are not accessible. Stream bottomlands can be seen and mapped by pattern and color. Irrigation areas and alfalfa fields present in the bottomland are red-hued and are recognizeable. Terraces in this area are separable from uplands, valley sides and bottomlands. The soil present on the terraces in this area are medium-textured in contrast to the clay soils of the uplands, and this, plus flat topography, results in their use to grow winter wheat. Steep-sided stream valleys having clay soils stand out in the September and October frames since they have less reflectance in the infrared bands and this results in a different hue. They also are obvious because of their closely-spaced parallel drains. Broad soil textures in general can be recognized on ERTS frames if some geologic information is available. The sandhills area with its lack of streams and its linear pattern speckled with red-hued subirrigated meadows is unique. The clayey soils in this area have a closely-spaced stream pattern.

In the upper Cretaceous area north of the Cheyenne River, the sandy soils derived from sandstones show up with a redder hue than the finer-textured adjacent soils from shales. This may be due to the more vigorous grass growth resulting from the fact that in this climatic area sandy soils have a better water-supplying ability than clayey soils.

Figures 1 through 4 show specific comparisons between the soil association map and the ERTS composites. Each figure is accompanied by an explanatory paragraph. It should be noted that there is general agreement between the two maps but that the use of ERTS composites would improve the accuracy of many of the soil associations presently recognized in South Dakota. Also several new associations are apparent on the ERTS imagery that were not shown on the Soil Association Map.

Figures 5 and 6 are examples of thematic and interpretation maps developed for a portion of western South Dakota. The delineations were drawn from ERTS imagery and the soil characteristic and interpretation information came from the data store of the South Dakota Cooperative Soil Survey.

Several conclusions seem apparent as a result of this study. First, in semiarid western South Dakota, landscape features are well defined. Steep valley sides, broad interfluves, contrasting textures all are present in this area and all are clearly visible on ERTS color composites. Therefore the general technique discussed in this paper should be applicable in other areas having well defined landscape features and information on the environmental factors affecting soils along with soil profile descriptions and data. Second, the 8 million acre scene that can be scanned on one frame allows for comparisons of soil associations usually over their entire extent. This is an advantage since anamolies immediately become apparent. Moreover each observed feature is in proprotion. Third, vegetation over the entire area is at the same instant of growth. Thus color differences on the composites are, at least in part, due to the different abilities of the soil associations to produce vegetation. These vegetative differences, then, reflected in the varying hues visible in the composite, help separate soil associations. This coupled with the comparisons possible with 4 spectral bands gives a wide range of images for the study of the soil landscape and its use.

LITERATURE CITED

Soil Survey Staff. 1951. Soil Survey Manual ARS, USDA, Wash. D. C. p. 131.

Simonson, R. W. 1971. Soil Association Maps and Proposed Nomenclature. Soil Sci. Soc. Amer. Proc. 35: pp. 959-963.

Westin, F. C. and D. L. Bannister. 1971. Soil Association of South Dakota (Map) AES Info. Series No. 3 Agr. Expt. Sta., South Dakota State University, Brookings, and USDA Soil Conservation Service, Huron, SD.

Figure 1

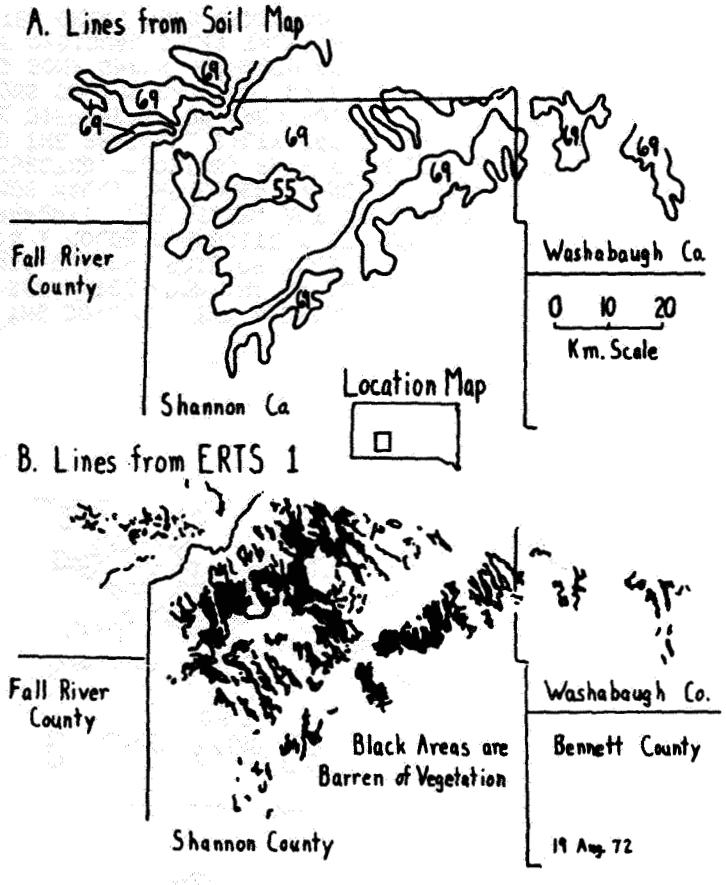
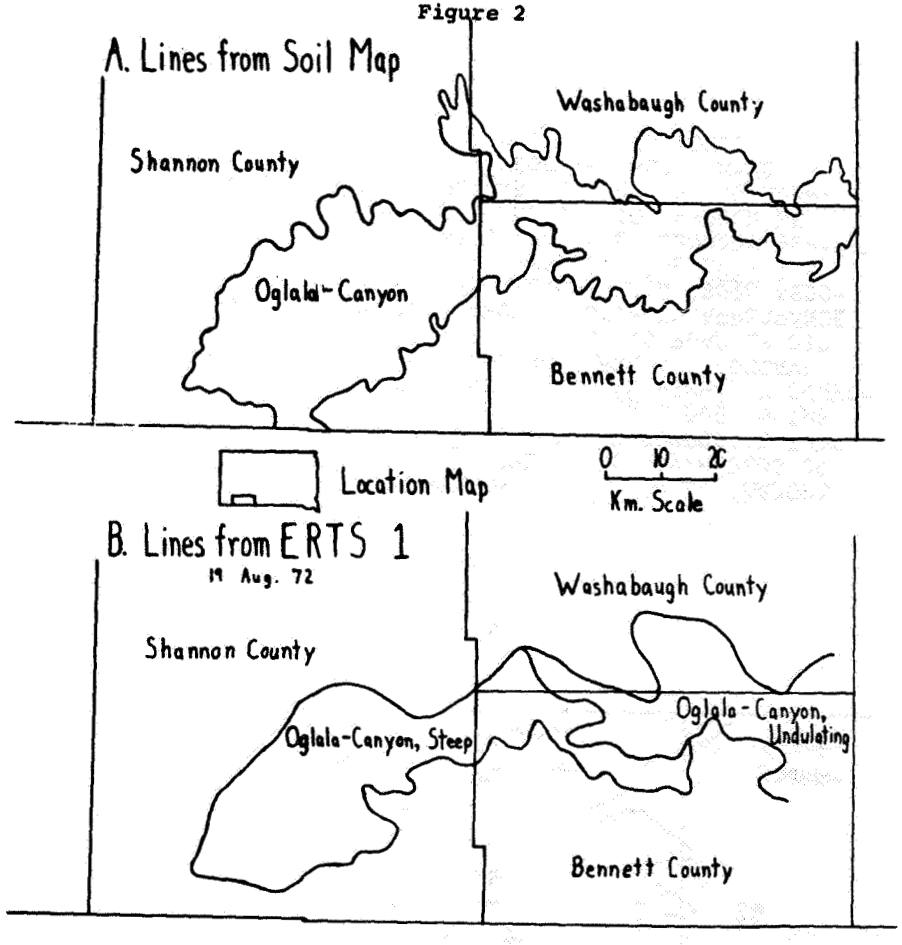


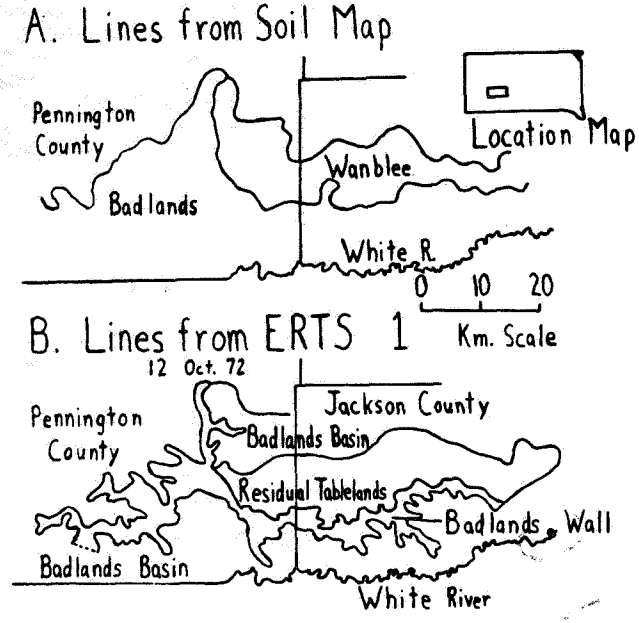
Figure 2



ON THE SOIL ASSOCIATION MAP TWO DELINEATIONS ARE SHOWN IN THIS AREA - 69 (BADLANDS) AND 55 (TUTHILL-RICHFIELD) THE 55 AREA IS A TABLELAND OF GENTLY UNDULATING SANDY LOAMS. ON THE ERTS 1 COLOR COMPOSITE THE ACTUAL BADLAND WALL OR ACTIVELY ERODING BARREN AREA SHOWS UP WHITE AND CAN BE DISTINGUISHED FROM THE ASSOCIATED AREAS WHICH HAVE VEGETATION. THIS AREA HAS BEEN MASKED OUT ON THE ERTS 1 MAP WITH BLACK INK. A COMPARISON OF THE SOIL MAP WITH THE ERTS MAP SHOWS THAT ONLY ABOUT HALF OF THE 69 AREA ON THE SOIL MAP IS IN CAPABILITY CLASS VIII - BARREN OF VEGETATION. THE REMAINING AREA HAS USEFUL VEGETATION.

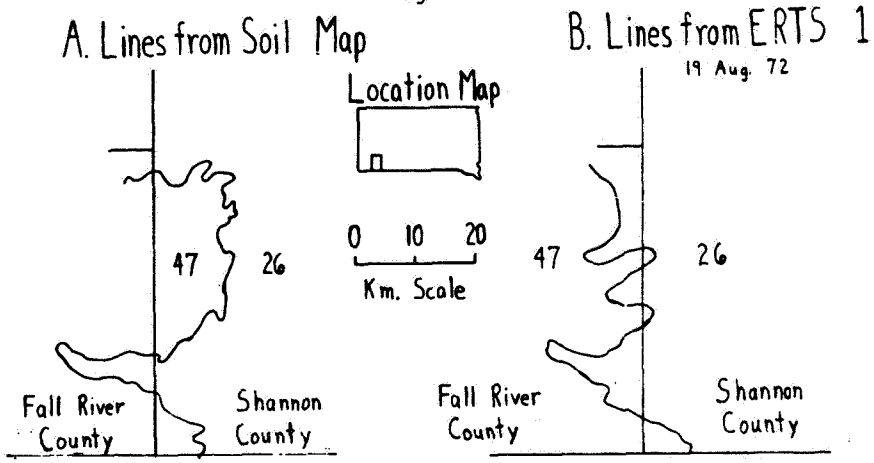
THE PINE RIDGE AREA OF THE OLIGOCENE IS SHOWN AS ONE DELINEATION ON THE SOIL MAP (OGLALA-CANYON SOIL ASSOCIATION). THE ERTS 1 COLOR COMPOSITE SHOWS THAT THE WESTERN SECTION OF THIS SOIL ASSOCIATION IS CHARACTERIZED BY CLOSELY SPACED DRAINS, SEVERAL TO THE KILOMETER, WHICH INDICATES STEEP SLOPES. THE DRAINAGE PATTERN IN THE EASTERN PORTION CONSISTS OF WIDELY SPACED DRAINS WITH BROAD INTERFLUVES, SEVERAL KILOMETERS WIDE, INDICATING MUCH LESS RELIEF. RUNOFF, EROSION HAZARD, RANGESITE, AND STOCKING RATES WOULD BE DIFFERENT FOR THE EASTERN AND WESTERN PORTIONS OF THIS AREA.

Figure 3



ON THE SOIL MAP THE BADLANDS AREA (CLASS VIII LAND) IS SEPARATED FROM THE WANBLEE SOIL ASSOCIATION (A DENSE CLAYPAN SOIL OF CLASS VI CAPABILITY). ON THE ERTS 1 COLOR COMPOSITE THREE SOIL ASSOCIATIONS ARE APPARENT: THE STEEP, ACTIVELY ERODING BARREN BADLANDS WALL, THE LOWER LYING UNDULATING IRREGULARLY DISSECTED, SLOPING, PARTLY VEGETATED BADLANDS BASINS, AND THE RESIDUAL SILTY TABLELAND. INTERPRETATIONS ARE DIFFERENT FOR EACH SOIL AREA. NO VEGETATION GROWS ON THE BADLANDS WALL WHILE THE BADLANDS BASIN HAS SOME GRASS ALTHOUGH ACCESSIBILITY IS A PROBLEM. THE RESIDUAL SILTY TABLELAND IS IN THE SILTY RANGESITE, GROWS GOOD GRASS AND IS MARGINAL CROPLAND.

Figure 4



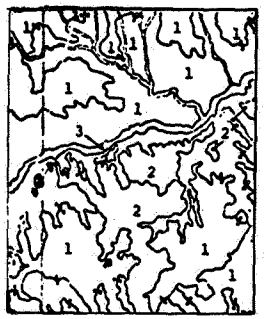
THE SILTY SOILS IN ASSOCIATION NUMBER 26 (KADOKA-EPPING) ARE DERIVED FROM THE WHITE RIVER BEDS OF TERTIARY AGE. ON THE ERTS 1 COLOR COMPOSITE THIS ASSOCIATION HAS A FRECKLED APPEARANCE DUE TO THE ASSOCIATION OF THIN BARREN SOILS (EPPING) ON CONVEX KNOBS, AND DEEPER PROFILES ON PLANE AND CONCAVE POSITIONS (KADOKA). THIS PATTERN IS READILY DISTINGUISHABLE FROM THE REGULAR, UNIFORM APPEARANCE OF THE CLAY SOILS OF THE PIERRE PLAIN (SOIL ASSOCIATION NUMBER 47 PIERRE-SAMSIL). THE ERTS 1 COLOR COMPOSITE INDICATES THAT THE BOUNDARY SEPARATING THE 26 AND 47 SOIL ASSOCIATION SHOULD BE LOCATED ABOUT 15 KILOMETERS WEST OF THE BOUNDARY SHOWN ON THE SOIL MAP. THESE TWO SOILS HAVE DIFFERENT RANGESITES AND SOIL LIMITATIONS.

FIGURE 5

ESTIMATED SOIL PROPERTIES SIGNIFICANT TO ENGINEERING

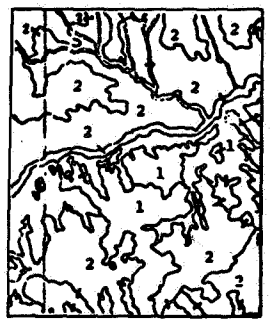


U. S. D. A. TEXTURE



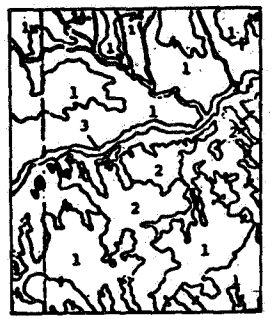
LEGEND
1. CLAY
2. LOAM
3. SANDY LOAM

REACTION (pH)



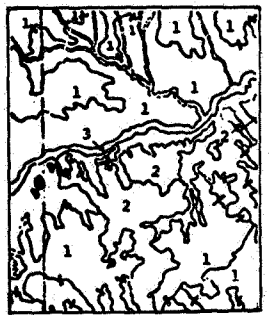
LEGEND
1. 6.6 - 7.3
2. 7.4 - 7.7

A. A. S. H. O. CLASSIFICATION



LEGEND
1. A - 7
2. A - 4 OR A - 6
3. A - 4

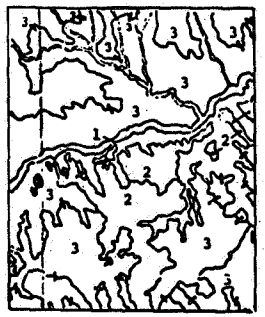
UNIFIED CLASSIFICATION



LEGEND
1. CH
2. ML OR CL
3. SM - SC

Km. SCALE 0 10 20

PERMEABILITY - (INCHES PER HOUR)



LEGEND
1. 2 - 6
2. 1.2 - .2
3. .02 - .2

AVAILABLE WATER (INCHES PER INCH)



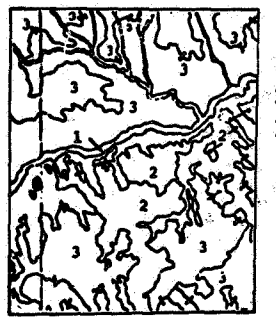
LEGEND
1. .14 - .17
2. .18 - .2
3. .08 - .14

LIQUID LIMIT



LEGEND
1. 10 - 28
2. 15 - 46
3. 45 - 80

PLASTICITY INDEX



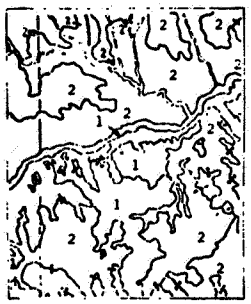
LEGEND
1. 0 - 10
2. 5 - 19
3. 22 - 65

FIGURE 6

INTERPRETATION OF SOIL ASSOCIATION MAPS



SUITABILITY OF THE SOIL AS A SOURCE OF TOPSOIL



LEGEND
1. GOOD
2. POOR

SUITABILITY OF THE SOIL AS A SOURCE OF SAND AND GRAVEL



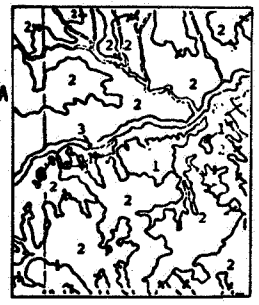
LEGEND
1. GOOD
2. POOR

POTENTIAL WINTER WHEAT YIELDS, HIGH MANAGEMENT



LEGEND
1. 32 BU/A
2. 24 - 29 BU/A
3. NOT ADAPTED

DEGREE AND KIND OF LIMITATION OF THE SOIL FOR SEWAGE LAGOONS



LEGEND
1. MODERATE (MODERATE PERMEABILITY)
2. SEVERE (LESS THAN 40" TO SHALE
3. SEVERE (RAPID PERMEABILITY)

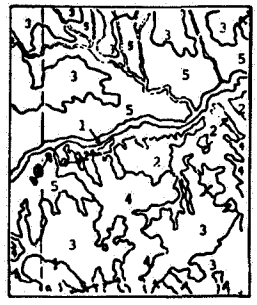
Km. SCALE 0 10 20

ESTIMATED DOMINANT RANGESITE



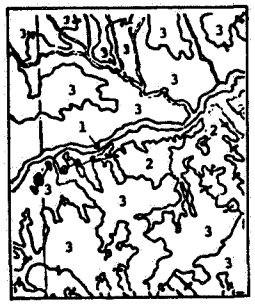
LEGEND
1. OVERFLOW
2. SILTY
3. CLAYEY
4. SHALLOW

ESTIMATED GRASS YIELDS



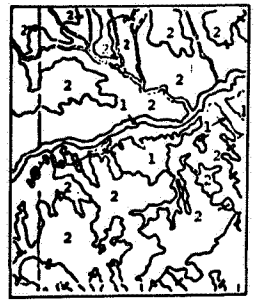
LEGEND
1. 3200 #/A/YR
2. 2500 #/A/YR
3. 2000 #/A/YR
4. 1800 #/A/YR
5. 1500 #/A/YR

CORROSIVITY - UNCOATED STEEL



LEGEND
1. LOW
2. MODERATE
3. HIGH

CORROSIVITY - CONCRETE



LEGEND
1. LOW
2. MODERATE (CORRESPONDS TO 1000-7000 PPM OF WATER-SOLUBLE SULFATES

N73-28308

Paper L 12

LAND USE OF NORTHERN MEGALOPOLIS

Robert B. Simpson, David T. Lindgren, *Dartmouth College, Hanover, New Hampshire*

1. INTRODUCTION

The major objective of our project is to map and digitize the land use of northern Megalopolis, that is the states of Massachusetts, Connecticut, and Rhode Island, and to evaluate ERTS as a planning tool for megalopolitan areas. The southern New England region provides a good test of ERTS's capabilities because of its complex landscape. Not only are there great differences in the degree of urban development, but in relief and vegetative cover as well.

At the time of the first-look seminar last September Bob Simpson presented a land-use map of Rhode Island (Figure 1) which we had compiled from a single CIR transparency. The image was the widely distributed one taken over southeastern New England on 28 July. That image suffered not only from the presence of clouds over such critical areas as downtown Providence, but from faulty rectification as well. Nevertheless, working at a scale of 1:250,000, that is a four-times magnification of the Rhode Island portion of the ERTS image, the 1200 square miles (3100 square kilometers) of Rhode Island were mapped in less than 40-manhours. The land use legend for that map consisted of eight categories including three residential categories, a combined commercial-industrial category, transportation, agriculture, woodland, and water. Our conclusion was that the objectives stated in the project proposal were feasible, providing cloud-free coverage became available.

2. PRESENT EVALUATION

In the months since the first-look seminar we have received a number of good quality, cloud-free images covering our study area, in particular those from the mid-October orbits. Those images became available to us in working form, that is as four-times enlargements (1:250,000 scale), during the first week of January. An intensive land use mapping program has been in progress since that date, and although the map-making part of our project is still incomplete we now have sufficient working experience with ERTS imagery to provide a realistic appraisal of its capabilities.

Working primarily with CIR transparencies, a decision made after a careful evaluation of the four MSS bands, and with occasional reference to MSS band 5 images, the mapping has been largely completed for Rhode Island and Massachusetts . The mapping technique consists of interpreting

Original photography may be purchased from:
EROS Data Center
10th and Dakota Avenue
Sioux Falls, SD 57198

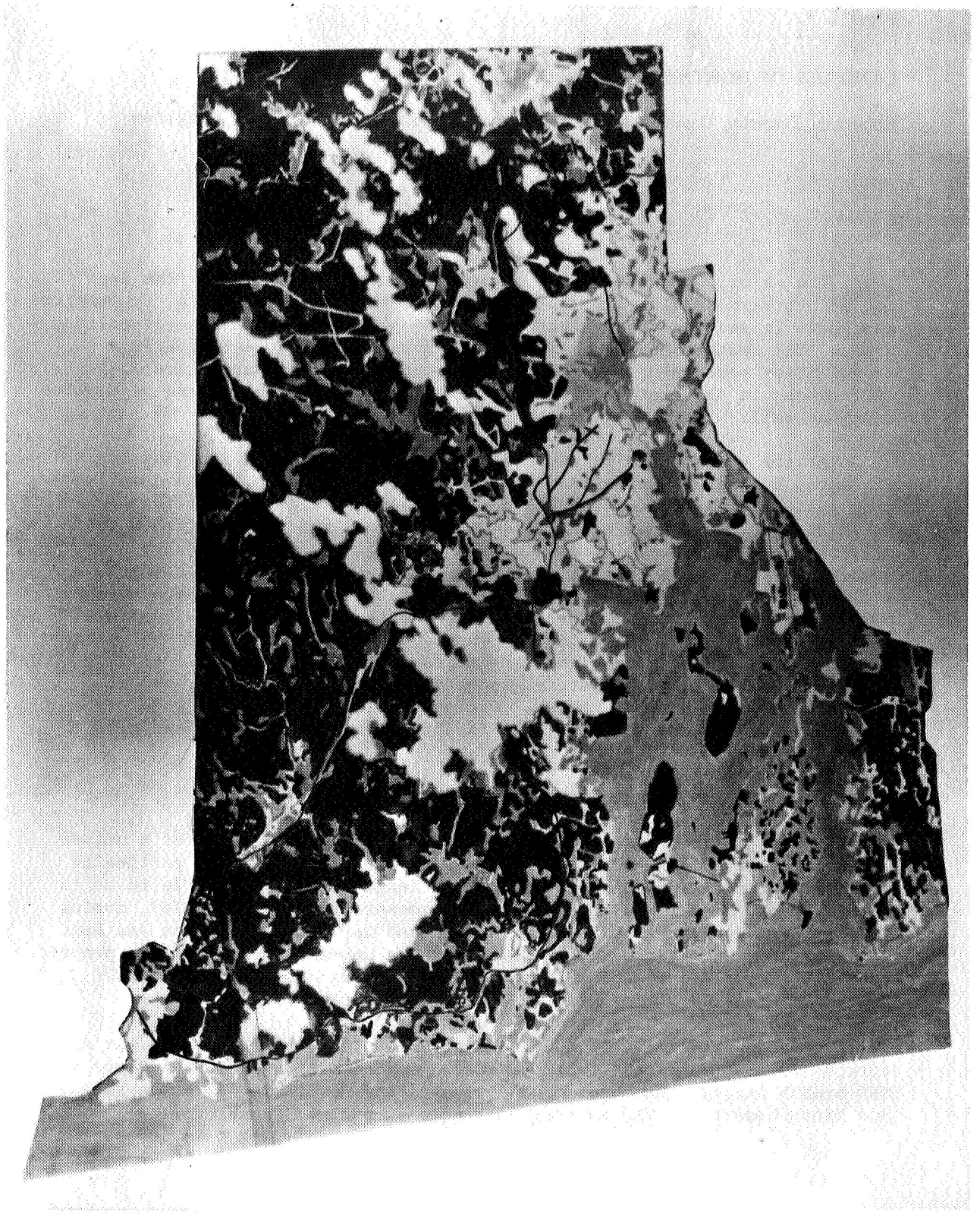


Figure 1. Land Use Map of Rhode Island (September 1972)

land use directly on mylar overlays to the 1:250,000-scale ERTS enlargements. The data are then transferred, block by block, to a more permanent mylar base. This base, which includes many control features traced from USGS 1:250,000 topographic quadrangles, provides the final land use map with considerable locational and scalar accuracy.

The present land use legend which was derived in accord with the guidelines suggested by the Department of Interior was increased from the eight categories used in the preparation of the Rhode Island map of September 1972 to eleven categories for the present map (Figure 2). The three additional categories include Marshland, Beach, and a third category called Restricted Open Space. The latter refers to such land uses as golf courses, cemeteries, and parks which on ERTS imagery are visible primarily within builtup areas where they appear salmon pink against an otherwise bluish background. Two changes were also made in the legend. The Single-Family Residential category was changed to Low-Density Residential, the Multifamily and Mixed Residential to High-Density Residential. While it is arguable the difference may only be one of semantics, the new terms do in fact better reflect what is actually being observed on the ERTS imagery.

As a means of evaluating the capacity of ERTS to provide land use data we have produced the following chart illustrating the range of land use identifications from the most simple to the most complex (Figure 4). At the most simple level, that is the delineation of water from land, ERTS is extremely effective. The CIR composite, as well as MSS bands 6 and 7, reveal the presence of water bodies as small as 300 feet (100 meters) in diameter. While some very marshy areas may appear as water bodies and therefore be included under the Water category, overall this category can be accurately applied.

Of the land categories Woodland can also be identified with great accuracy. Small patches of woodland may be lost in suburban areas, but such losses are compensated for by the inclusion of small clearings into the Woodland category.

In the non-wooded areas the Builtup categories can be easily differentiated from the Non-Builtup categories. In fact, if one were interested in builtup areas as a whole, ERTS would be the most effective medium for displaying them. The degree of accuracy at this point is very high. However, as the Builtup category is subdivided into more detailed categories, the degree of error begins to increase.

Within builtup areas the residential categories are unquestionably the most difficult to differentiate. The High-Density Residential category in effect refers to those areas of multifamily and mixed housing found primarily within the central cities and inner suburbs of metropolitan regions. As distance from the central city increases, however, housing density declines and light-density, single-family housing becomes dominant. The line separating the two is difficult to determine not only from aerial photography but in the field as well.

ERTS LAND USE CLASSIFICATIONS

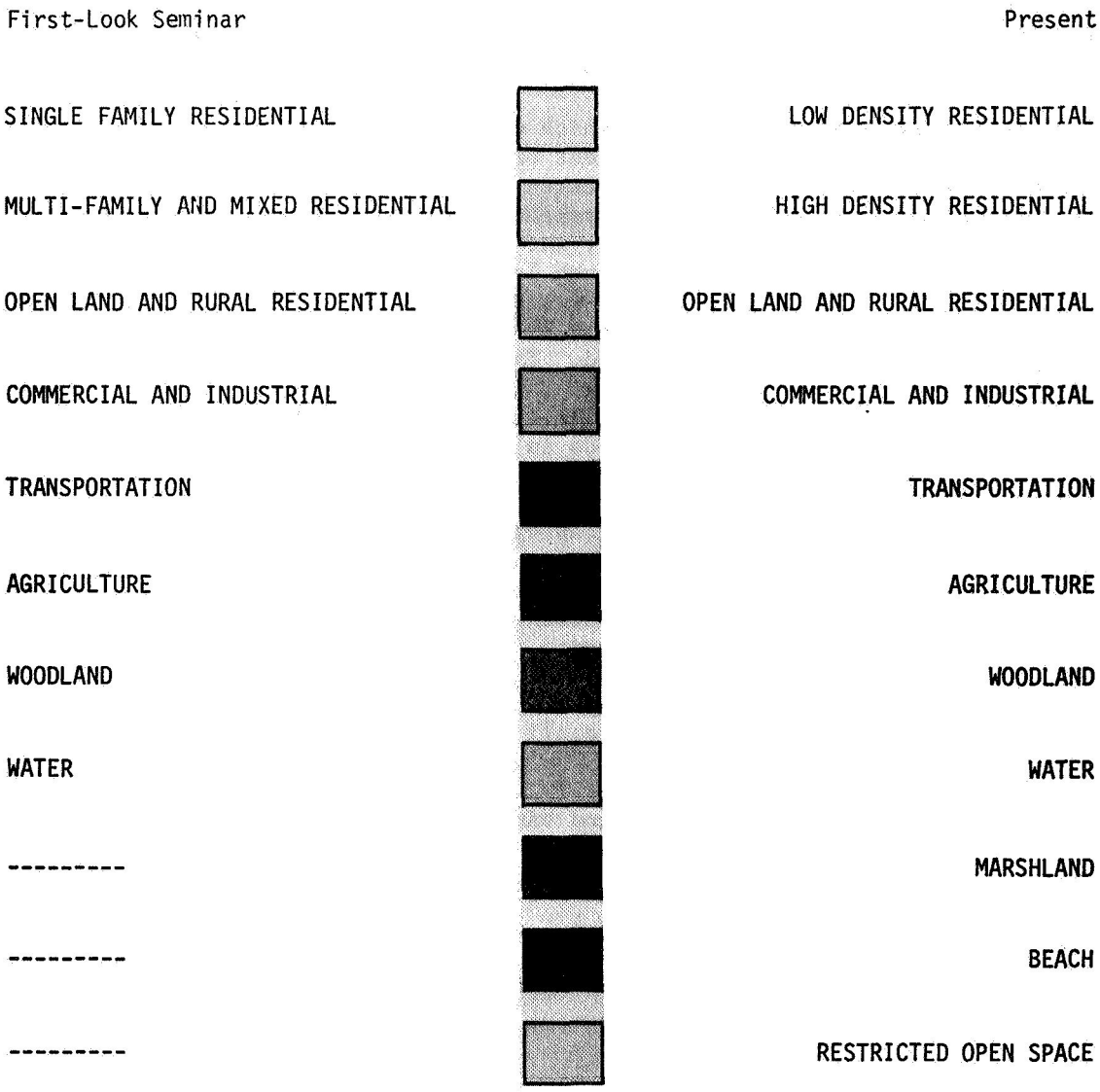


Figure 2. ERTS Land Use Classification

WATER	XXX	XXX	XXX	XXX
LAND	WOODLAND	XXX	XXX	XXX
	NON-WOODED	BUILTUP	RESIDENTIAL	LOW-DENSITY RESIDENTIAL
				HIGH-DENSITY RESIDENTIAL
			NON-RESIDENTIAL	COMMERCIAL AND INDUSTRIAL
				TRANSPORTATION
				RESTRICTED OPEN SPACE
		NON-BUILTUP	DEVELOPED	AGRICULTURE
				OPEN LAND AND RURAL RESIDENTIAL
			UNDEVELOPED	MARSHLAND
				BEACH

Figure 3. ERTS Land Use Identification Scheme

As for differentiating residential areas from the CBD, this can be done with a fair degree of accuracy. A problem arises in the delimitation of the outer edge of suburban development from surrounding open countryside just as it does in the field. Where residential areas merge with woodland October imagery is better than summer imagery because fewer leaves obscure the houses. However, where suburbs merge with open fields the July imagery is preferred because of the greater contrast between fields and housing.

Non-residential land uses within builtup areas are easier to identify than housing. For example, the urban industrial-commercial areas are consistently identified. Some transportation land uses are consistently identified. Major highways, airfields, and bridges can be identified with considerable accuracy, but railroads and powerlines can only occasionally be observed.

The category Restricted Open Space is utilized only in urbanized areas where such features as golf courses and cemeteries are identifiable. In rural areas this category cannot be applied meaningfully because such features tend to merge with open fields.

In the non-builtup areas most categories can be effectively applied. Agriculture refers exclusively to row crops and plowed fields. The only major difficulty is encountered in the Connecticut River Valley of Massachusetts where such fields are occasionally confused with commercial-industrial areas. Ultimately it was found that the commercial-industrial areas could best be identified on the July imagery when the fields were pink.

The Open Space and Rural Residential category proved to be very useful. In general it reflects a common feature of the New England landscape - rural roads bordered by open hayland and occasional dwellings.

The Undeveloped categories are relatively easy to identify. Major areas of marsh show well since CIR is a particularly useful medium for this purpose. Beaches are a minor land use but the category allows for their identification since in New England they are a popular recreational feature.

Overall the land use classification developed was applied with relatively good accuracy. Several categories, particularly the Non-Builtup ones were identified with great accuracy, while the Builtup categories have several areas of difficulty. Nevertheless, our experience to this date has been that ERTS can provide greater land use detail than we originally anticipated. And as our experience using ERTS imagery increases so too should our ability to use it effectively.

3. CONCLUDING REMARKS

When the color-coded land use map of northern Megalopolis is completed, a digital computer version will be compiled in order to permit a variety of spatial-analytical investigations. Map-to-computer conversion will be done manually by superimposing a UTM-oriented grid over the map and inputing land use data to the computer cell by cell. At present we are thinking in terms of one square-kilometer cells, subdivided into quarter kilometers in critical areas. Even on the square-kilometer basis there will be some 38,000 cells.

With the computer data bank it will be possible to explore on a quick, first-look basis the possible utility of ERTS to several land use related planning concepts. These include

(1) the delineation of the rural-urban interface, a phenomenon of interest to the Bureau of Census in defining SMSA's;

(2) the identification of sinks and sources of population "energy" in terms of a positive and negative deviation from average population densities;

(3) a look into the possibility of predicting population growth trends from ERTS imagery.

Although these investigations will be little more than "first looks", they will hopefully provide some insight into the capabilities of ERTS to solve recognized planning problems.

Finally, we have given some thought to the cost effectiveness of ERTS for making land use maps. We estimate that ERTS is less expensive by a factor of 10 than comparable mappings from aircraft. In fact it appears reasonable to say that the differences in cost of land use mapping, as between medium-altitude aircraft, high-altitude aircraft, and satellite platforms, and assuming a "state-sized" area, are similar to the differences in the scales of their imagery (Figure 4).

(LAND USE MAPPING)

ESTIMATE OF
COMPARATIVE COSTS [1]

Platform	Scale	Ratio	Minimum Cost Estimate
Medium Altitude Aircraft	1:20,000	1	$ 350,000
High Altitude Aircraft	1:100,000	1/5	70,000
ERTS-1	1:250,000	1/12.5	28,000

[1] Assuming an 11-category legend and a "state-sized" area.

Figure 4. Estimate of Comparative Costs for Land Use Mapping

N73-28304

Paper L 13

REMOTE SENSING APPLIED TO LAND-USE STUDIES IN WYOMING

Roy M. Breckenridge, Ronald W. Marrs and Donald J. Murphy, *Department of Geology, University of Wyoming, Laramie, Wyoming 82070*

ABSTRACT

Impending development of Wyoming's vast fuel resources requires a quick and efficient method of land-use inventory and evaluation. Presently, little or no land-use information or cartographic control is available for many areas of concern. Proper control of development depends upon land-use and physiographic information representing all aspects of the affected area, including agricultural and urban development, natural vegetation, hydrology geology, topography, and mineral resources development. Preliminary evaluations of ERTS-1 imagery have shown that physiographic and land-use inventory maps can be compiled by using a combination of visual and automated interpretation techniques.

Test studies in the Powder River Basin showed that ERTS image interpretations can provide much of the needed physiographic and land-use information. Water impoundments as small as one acre were detected and water bodies larger than five acres could be mapped and their acreage estimated. Flood plains and irrigated lands were successfully mapped, and some individual crops were identified and mapped. Coniferous and deciduous trees were mapped separately using color-additive analysis on the ERTS multispectral imagery. Gross soil distinctions were made with the ERTS imagery, and were found to be closely related to the bedrock geology. Several broad unstable areas were identified. These were related to specific geologic and slope conditions and generally extended through large regions. Some new oil fields and all large open-cut coal mines were mapped.

The most difficult task accomplished was that of mapping urban areas. Most Wyoming towns are surrounded by agricultural land, natural flood plains, and/or rangeland. With these widely varying settings the populated areas are often difficult or impossible to delineate by visual photointerpretation techniques. Densitometry proved to be of considerable aid in making the subtle distinctions necessary in urban mapping. Four-color isodensitracings were made for each of the four ERTS-MSS bands. Interpretation of these isodensitracings permitted accurate mapping of the populated area, and usually allowed segregation of new

and old residential, industrial, commercial and business, and open segments within the towns. Larger features such as airstrips, factories, schools, golf courses, parks, and cemeteries were mappable as individual installations but most could not be identified.

Areas of new development can usually be defined, allowing a capability for change detection and updating of obsolete maps. Snow-cover provides a considerable degree of enhancement of the urban areas by increasing the contrast between the populated areas and the surrounding country. Work in the urban areas provides a striking example of this snow-enhancement and the detail available from a snow-enhanced image.

TEXT

Land-use considerations have become critically important in Wyoming where greatly increased development of natural resources is anticipated. Of prime concern at the present is the development of coal resources in the Green River and Powder River Basins as fuel for huge generators. The direct impact of mining, the diversion of water, and the effluent from coal-fired electrical generators will be considerable, but the associated increase in population and the necessary urbanization will have far-reaching effects on the environment in Wyoming. The construction and operation of the power plants and supporting mines will result in a substantial increase in the state's population (perhaps as much as 50%). These population increases will, in turn, affect almost every aspect of land-use.

Governmental agencies have recognized the need for thorough land-use planning in order to properly control development and prevent costly or unnecessary damage to the land and its inhabitants but there is very little land-use data available for use as a basis for such planning. As is commonly the case, the problem requires an immediate solution. It is totally impractical to begin a program for gathering detailed land-use data by conventional means because 1) such a program would be too expensive, 2) insufficient time is available, 3) much of the data would be obsolete by the time the program is complete. Consequently, planners must find a rapid and efficient means of obtaining the necessary land-use information and a way to continually up-date that information.

As soon as it became apparent that the ERTS satellite program offered considerable potential for obtaining much of the needed land-use data, the state planning office of the Department of Economic Planning and Development contracted the University of Wyoming Remote Sensing Laboratory for a pilot study to determine what land-use data might be gained from the ERTS-1 imagery. The pilot program was to be a quick-look study designed to assess the ERTS-1 imagery as a tool for acquisition of land-use data. The Powder River Basin was chosen as a general

test area (Fig. 1) and suitable sub-areas within the basin were selected for testing individual applications.

Because the pilot program was time-limited, a suite of tasks was selected as a representative group of ERTS applications which might yield information necessary for land-use planning. Included in this group were:

1. Identification and mapping of water impoundments
2. Detection of potentially unstable areas
3. Mapping of flood plains, irrigated land, and crops
4. Discrimination of coniferous and deciduous trees
5. Range mapping (type and/or quality)
6. Mapping of soil types
7. Slope estimation
8. Mapping of mined areas
9. Mineral resources mapping (actual and potential)
10. Areas having potential for construction materials
11. Mapping of areas of urban and rural development

Application of standard photointerpretation, color-additive viewing, and/or isodensitometry to these tasks provides results which suggest that many of these tasks can be done routinely. Figure 2 is a land-use classification map for the Powder River Basin test area, constructed from interpretations of ERTS imagery. In addition to the broad land-use categories represented on this map, there is a great deal of other significant land-use information available from the ERTS data.

Water impoundments can be readily mapped from the infrared (band 7) ERTS imagery. Impoundments covering 5 acres or more can be mapped reliably and most impoundments larger than 1 acre can be located. However, the actual size of these smaller impoundments cannot be accurately estimated because they are represented by too few scanner resolution elements.

Although in some parts of Wyoming, local unstable areas (landslides, slumps, etc.) have been identified from the ERTS imagery none could be identified in the Powder River Basin test area. Potentially unstable areas were identified on the basis of their regional associations. The potentially unstable areas in the Powder River basin mappable from ERTS include 1) dune fields, 2) flood plains, 3) areas of potential mineral development (coal, oil, uranium), and 4) areas likely to be underlain by clay-bearing soils. Identification of these areas from the ERTS imagery required integrated interpretation of all ERTS bands. Color-additive viewing provided some enhancement of the flood plains and aided in soil and lithologic distinctions.

Color-additive viewing was of considerable utility in mapping of natural flood plain vegetation and irrigated farm land. The red and infrared bands (5 and 7) have the greatest utility in distinguishing

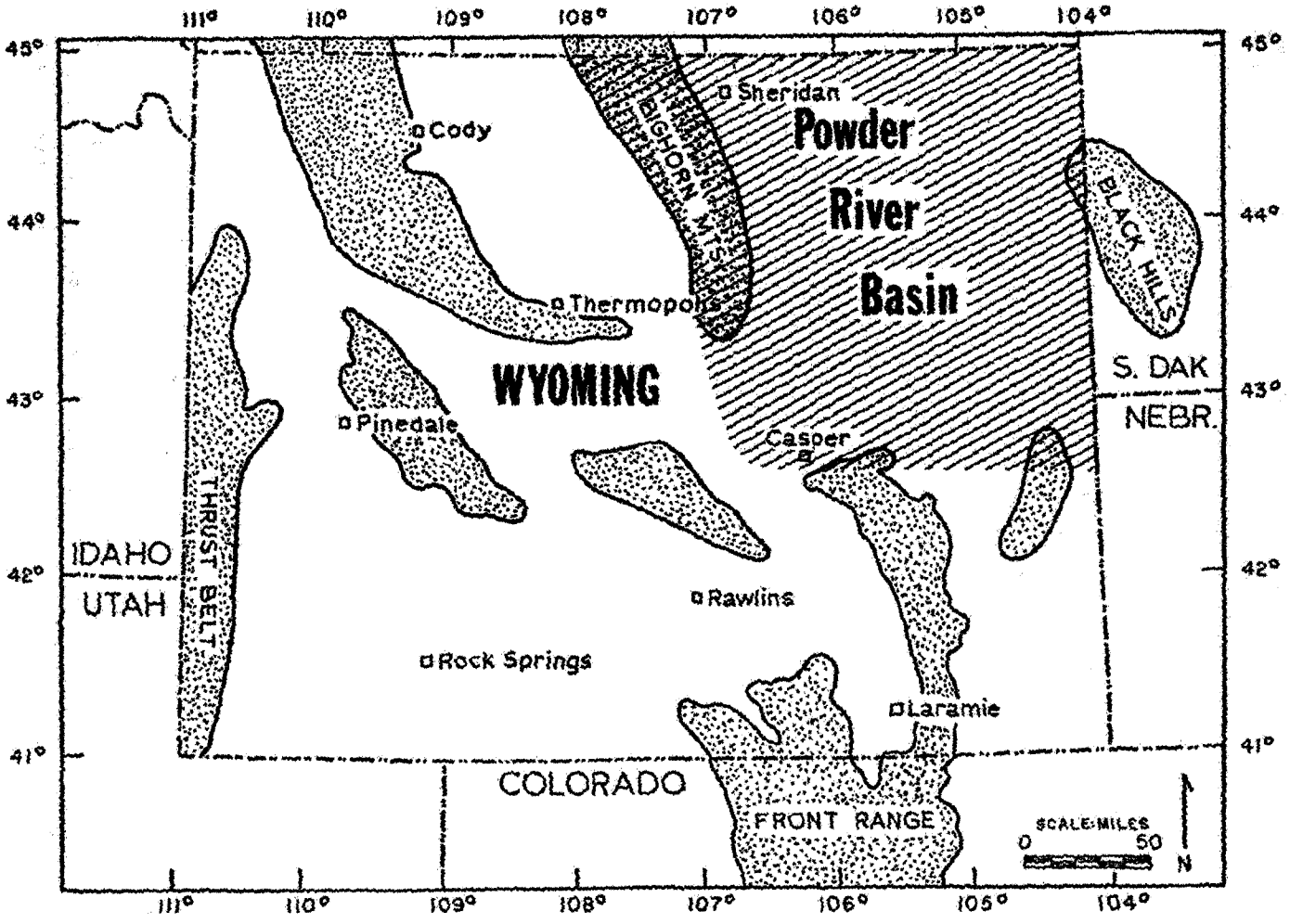


Figure 1. Index map showing the location of the Powder River Basin test area (cross-hatched).

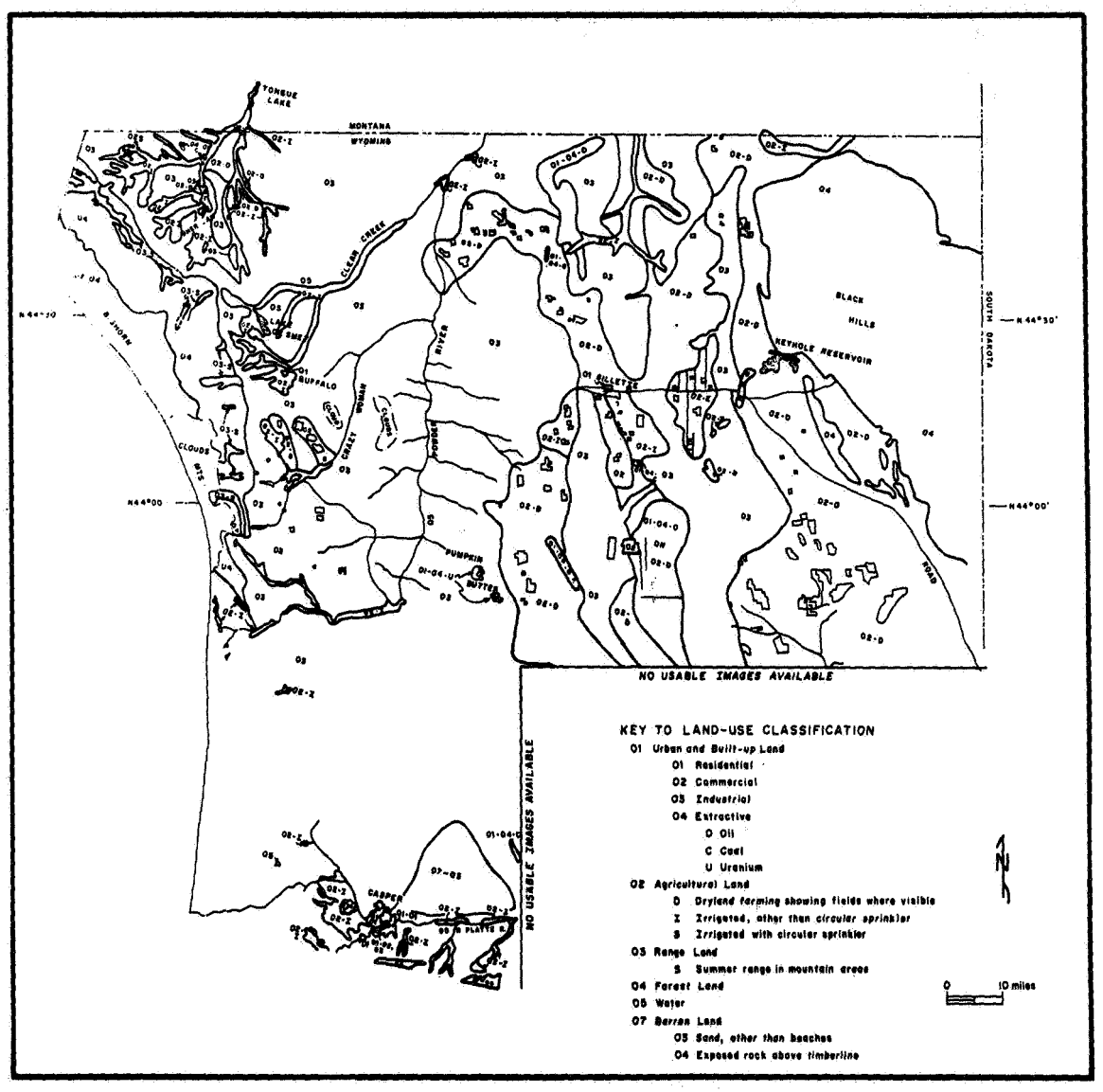


Figure 2. Land-use classification map for the Powder River Basin, Wyoming constructed from ERTS-1 image interpretations.

contrasts within the vegetation. Interpretation of the ERTS-1 imagery provided adequate detail for mapping broad-scale agricultural patterns. Some detail features were recognized in the agricultural pattern. These might allow crop identification if supplemented with other image interpretations showing seasonal variations.

Maps of distribution of conifers and deciduous vegetation were compiled from ERTS-1 interpretations for the Bighorn Mountains. These maps are necessarily generalized due to the very small scale of the ERTS images, but they yield a fairly reliable estimate of the distribution of these major forest subdivisions.

Rangeland is readily distinguishable from other agricultural lands and can be subdivided on the basis of tone and texture. The resulting map can be correlated to standing biomass at the time of the satellite overpass, but range type and quality (a time-dependent factor) cannot be established without control data and complementary interpretations from repetitive coverage.

Broad soil classifications can be interpreted from the ERTS imagery on the basis of tone, texture, and regional association. The resulting maps show excellent correspondence with the state soil map which classifies soils on the basis of composition (which relates to parent material). Very little correlation is evident between the soil interpretations derived from ERTS and the more detailed soil maps based on the newer Seventh Approximation classification, but similarities may exist between the larger soil groups and the ERTS interpretation.

Slope estimations were based on stream pattern analysis. The frequency and patterns of drainages were used as criteria for subdividing the Powder River Basin into zones of equivalent slope. The actual slope values for the various areas were then determined from the topographic maps. This application was particularly successful in the Powder River Basin which has a very intricate system of small drainages that reflect even subtle changes in regional slope.

Abandoned, producing, and developing open-cut coal mines are visible on the ERTS imagery, but small open-cut uranium, bentonite, and gypsum mines and surface evidence of underground mines in the Powder River Basin could not be seen on the ERTS imagery. However the large uranium mines in the Gas Hills district of central Wyoming can be seen on the imagery.

A map of known and potential coal resources was constructed from the combined mine locations and geologic interpretations of the Powder River Basin. This generalized map is useful for defining areas of probable or possible coal mine development for the proposed electrical power installations or other energy needs. Maps of potential areas for the development of other mineral resources were compiled with the favorable

locations defined on the basis of geologic interpretation. For example, dunes and terraces were designated as potential sources of sand and gravel, areas of limestone outcrop were mapped as possible sources of lime, and areas of structurally favorable geologic patterns were designated as areas of potential petroleum resources (although virtually all structures visible on the surface have already been tested).

Perhaps the most difficult task attempted was the mapping of urban areas. Cities and towns of Wyoming are relatively small (population 60,000 or less). Early attempts to outline the areas of urban development by standard photointerpretation techniques were unsuccessful. Although the urban areas could generally be located on the imagery, there was often insufficient contrast with the surrounding rural development to allow definition of the urban area. Color-additive viewing was useful in some instances where subtle contrasts on two or more bands could be enhanced by composite display, but it was soon discovered that the ability to discern urban areas was largely dependent on the overall contrast with the surrounding area, and that the urban areas were generally too small to exhibit a characteristic texture or pattern. Even under magnification the urban areas generally appear as fuzzy-grey areas with subtle variations in internal tone and texture. The patterns are too intricate and tonal variations too subtle for visual interpretation.

This problem was circumvented by employing the isodensitracer as a tool for enlarging the images for the urban areas (up to 50X) and enhancing subtle density contrasts. Interpretation of the resulting isodensity contour maps usually allows separation of the urban areas from the surrounding rangeland and natural vegetation but still provides little distinction between urban and agricultural land. A more powerful technique was devised to segregate urban areas from agricultural land. In this technique, four color isodensitracings are prepared for each of the multispectral images and the isodensitracings are then composited to form a color composite map.

Both isodensitracing techniques reveal patterns within the urban areas that can often be related to type or intensity of development. In some instances the industrial and/or business districts can be segregated from residential areas. New residential areas are commonly distinct from older residential areas which have mature trees. Parks or recreational areas are sometimes identifiable.

The advantages of repetitive coverage are well demonstrated in our attempts at urban mapping. We were forced to go to great lengths to accurately define urban areas and significant zones within the urban areas using the early ERTS images (taken in the summer and autum of 1972). However, when we received the first winter maps over Wyoming, it became apparent that snow-cover provides great enhancement of urban areas. Not only does the snow mask all contrasts in rural areas and increase the contrast between the urban areas and their surroundings, but it provides

means of obtaining a pseudo-thermal map that records intensity of cultural activity in remarkable detail. The urban areas and transportation routes are readily apparent on the images showing snow-cover and, with isodensity contouring, zones of increased activity (business districts, industrial facilities, etc.) are shown in patterns of increasing density which reflect the degree to which the snow-cover has been disturbed. Interpretations of the isodensity contour maps from these winter ERTS images compare very favorably with interpretations of comparable aircraft photography and provide considerable data for updating most city maps (Fig. 3).

This study demonstrates, that even though photointerpretative techniques using ERTS data cannot provide detail that many land-use applications require, it is capable of providing a great deal of broad-scale, basic land-use data on a continuing basis. This information can be derived from the ERTS data far more quickly and efficiently than by conventional techniques. Consequently, the ERTS program can supply information for land-use planning as long as there is a need for constructing or revising the broad-scale land-use data base.

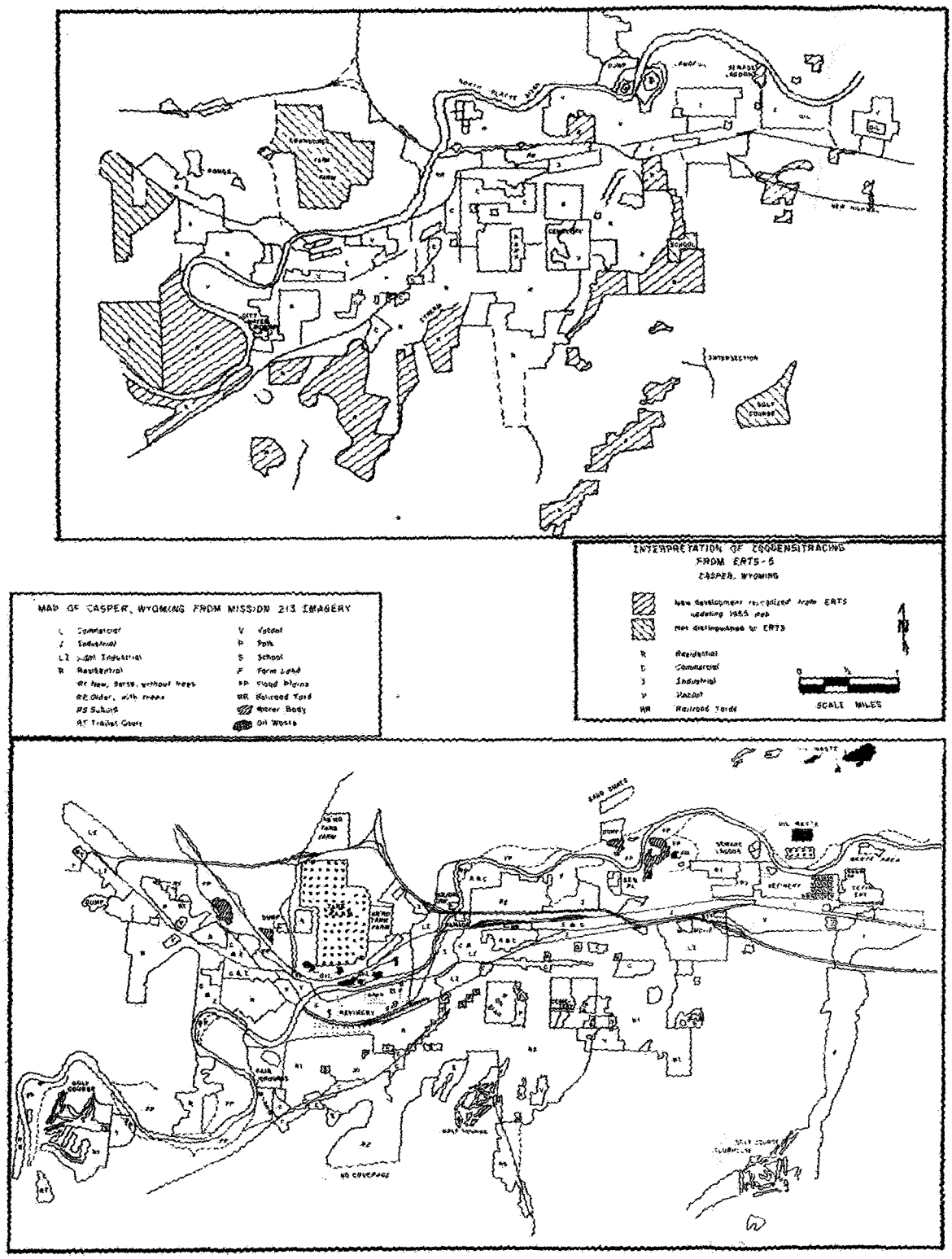


Figure 3. Comparison of interpretation of an ERTS image isodensitracing with an interpretation of a 1:30,000 scale aerial photograph. The ERTS image (1101-17185) was taken with snow on the ground.

N73-29310

Paper L 14

ERTS-1 APPLICATIONS TO MINNESOTA LAND USE MAPPING

Dwight Brown, James Gamble, Steven Prestin and Dale Trippler, *Department of Geography, The University of Minnesota, Minneapolis, Minnesota 55455;* Merle Meyer, Joseph Ulliman and Ralph Eller, *College of Forestry, The University of Minnesota, St. Paul, Minnesota 55101*

ABSTRACT

Land use class definitions that can be operationally employed with ERTS-1 imagery are being developed with the cooperation of personnel from several state, regional, and federal agencies with land management responsibilities within the state and the University of Minnesota. Investigations of urban, extractive, forest, and wetlands areas indicate that it is feasible to subdivide each of these classes into several subclasses with the use of ERTS-1 images from one or more time periods.

INTRODUCTION

A spate of recent and pending state legislation has broadened and will greatly expand the powers of various state and local government agencies in the field of land use management in Minnesota. Land management agencies, charged with policy development and implementation, will require current land use data classified in a way that allows them to be employed in day to day operations. Cooperative efforts involving personnel from the State Planning Agency (SPA), several departments at the University of Minnesota, and state and federal agencies with land management responsibilities within the state are aimed at defining appropriate classes of land use information for incorporation into the Minnesota Land Management Information System (MLMIS). The system currently contains a ninefold land use classification for the nearly 1,400,000 forty-acre data cells in the state. These data are now four to five years old and will require continual updating. Furthermore, the classes are general and do not fully satisfy the land management agencies' needs for detailed land use information.

ERTS-1 imagery is being examined as a broad-scale, seasonally repeated data collection system in order to determine the suitability of this kind of imaging system for solving some of the land use data needs of the state. The questions we are specifically asking are: 1) What classification schemes are most useful to data users and how can they be met with ERTS

PRECEDING PAGE BLANK NOT FILMED

Original photography may be purchased from
EROS Data Center
10th and Dakota Avenue
Sioux Falls, SD 57198

type data? 2) What are the appropriate times of year to collect information for these various classes of land use? 3) What is the appropriate mapping unit or data cell size for mapping land use from ERTS? 4) What methods of interpretation, spectral band(s), and data processing will extract the maximum information from the ERTS-1 system?

Cooperative involvement of data users is the key to developing a successful classification scheme. The present MLMIS land use classification includes forested, urban residential, urban non-residential or mixed residential, cultivated, pasture or open, transportation, water, marsh, and extractive. The user agencies, almost exclusively, require more detail within one of these broad classes of land use. Once classes are established, the suitability of ERTS-1 for providing appropriate data can be determined. Timing, cell size, appropriate spectral bands, and data processing procedures can then be determined.

This paper will focus on four broad areas of land use: urban, extractive, forested, and wetlands. To achieve optimum classification schemes within these categories personnel from the State Planning Agency, the State Department of Natural Resources, the Metropolitan Council, the National Forest Service, the USDI Bureau of Sport Fisheries and Wildlife, County Land Commissioners, the Department of Iron Range Resources and Rehabilitation, private forest management firms, and the Soil Conservation Service are cooperating in the development and evaluation of land use classes. It is already evident that needs of data users vary greatly, and that information needs of individual data users are not always well defined. This project is bringing the land and resource management people together to better define and make more compatible, their information needs.

INTERPRETATION

PROCEDURES. Test areas for each broad class of land use were selected on the basis of the quality of ERTS-1 imagery received to date (Fig. 1). Interpretation procedures for the work reported here are largely based on the use of bulk MSS 70 mm positive transparencies. These are either projected for interpretation of individual bands or color combined in the Institute of Agriculture Remote Sensing Laboratory's I^2S Mini-Addcol color combiner. These color combined scenes are then photographed and projected for interpretation at scales ranging from 1:30,000 to 1:250,000. Nine-inch bulk positive and negative transparencies of these ground scenes have been obtained on retrospective requests, and are now being analyzed by density level slicing with an Interpretation Systems VP-8 image analyzer.

Ground truth to support these investigations is based on field investigations and a variety of aerial photography provided by the State Planning Agency, the College of Forestry, and NASA. Preliminary interpretation results based on these materials will be discussed individually for the four broad classes of land use.

URBAN. In MLMIS, urban land is divided into two classes--urban residential and urban non-residential or mixed residential. The very low threshold of detection (five dwellings or one commercial structure per forty-acre cell), although suitable for interpretation from high altitude photography, is neither operable from high quality ERTS-1 MSS images nor does it produce a useful data set for metropolitan Twin Cities land use analysis and planning. The scheme being tested for use with ERTS imagery is a more detailed land use classification designed to maximize compatibility with the land use system developed by the Metropolitan Council. Results are very encouraging for the development of a much more useable and detailed data base.

Figure 2 shows examples of the classification scheme on color combined MSS bands 5, and 7 of October 6, 1972 ERTS coverage of the Twin Cities. This date of coverage has the maximum contrast of the four periods of coverage received to date. The threshold of detection of residential land seems to be about twenty dwellings per forty acres.

EXTRACTIVE. A 288 square mile test area in the Mesabi Range was selected to develop a classification scheme for extractive industries. A portion of this area is shown in Figure 3. Interpretation of July 6, 1972 NASA underflights provides the basis for comparison with ERTS-1 images and ground truth is supported by published maps of mining features. Bands 4, 5, and 7 are projected individually for interpretation and classification of extractive features into tailings and mine pits. ERTS-1 imagery compares very favorably with the 1:120,000 scale photography in terms of area measurements; however, accuracy is directly related to size. Class assignment was difficult for shallow pits and low tailings piles from the September 18, 1972 images. However, January 4, 1973 images (Band 7) provide sufficient snow enhancement of shadows at low sun angles to allow seperation of positive and negative mine features.

Age of abandoned pits and tailings is also a factor affecting the ease of detection. Some features not readily identified as old tailings piles on individual bands are detectable on color combined images (Fig. 3). Older, water-filled pits and active tailings ponds can also be identified. Furthermore, gravel quarries in the test area show up only on Band 5 and are thus separable from the iron extraction facilities.

FORESTED. The diversity and importance of forests in Minnesota has dictated the use of several test sites. August 12, 1972 color combined images of the Superior National Forest allow the separation of conifers and hardwoods (Fig. 4). Also evident are the logging patterns and wildfire burn. Better color contrasts are obtained on the October 7, 1972 color combined image of the Chippewa National Forest area (Fig. 7). Conifer-hardwood distinctions are easily made and in some areas lowland conifers can be separated from upland conifers.

The optimal color combinations for enhancing forest classification and interpretation is with a green filter with Band 5 and a red filter

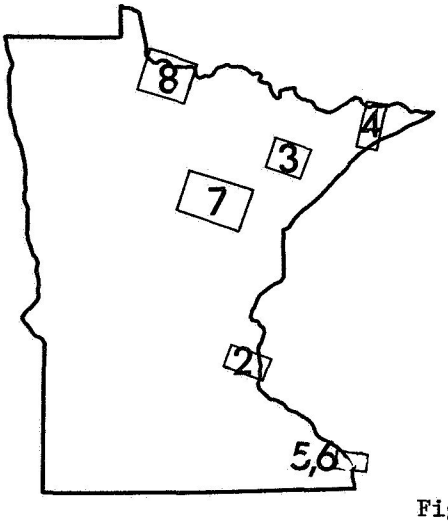


Figure 1. Location of Figures 2 through 8.



Figure 2. Color combined image, Twin Cities Metropolitan Area. Letters denote classes of urban use: A=Commercial Core; B=Industrial Core; C-Commercial/Industrial Strip; D=Multiple Dwellings; F=Older, Single Family Dwellings; G=Newer, Single Family Dwellings; H=Recreational/Open Space; I=Transportation; J=Water.

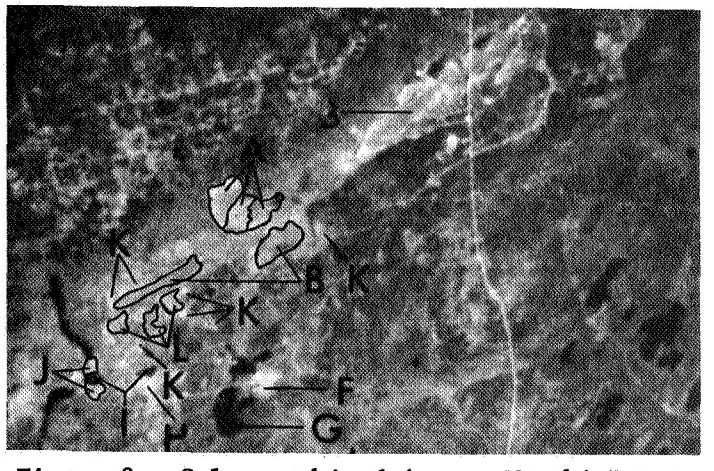


Figure 3. Color combined image, Mesabi Range. Letters represent extractive land use classes. A=Tailing Ponds; B=Deep Open Pit Mines (Iron Ore); L=Shallow Open Pit Mines (Taconite); K=Tailings Piles or Stripping; F=Hoyt Lakes (population 3,634); G=Reservoir; H=Aurora (population 2,531); I=Water filled, abandoned Iron Ore Pits; J=Old Tailings Piles.

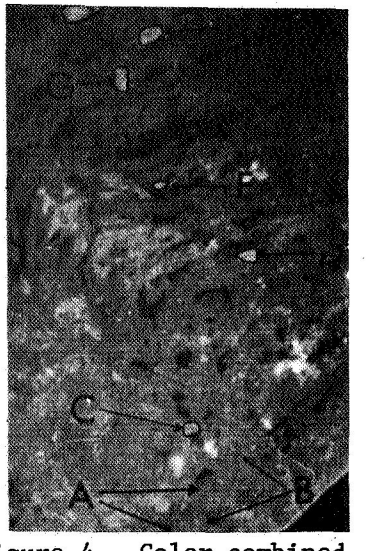


Figure 4. Color combined image, Superior National Forest. Letters denote forest types: A=Conifer; B=Conifer/Conifer-Hardwood; C,D,F,G, & H=Logged areas; I=Conifers in logged area.

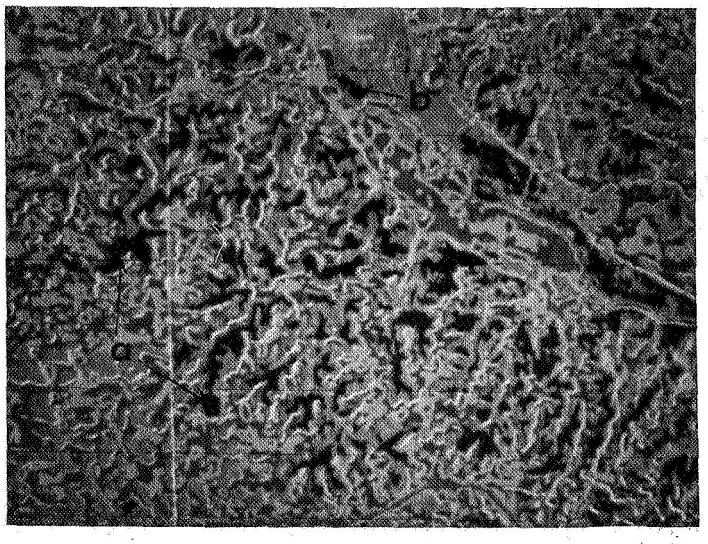


Figure 5. An image of band 7 for the area shown in Figure 6 which has been density sliced to emphasize forests: a=Upland Deciduous Forests; b=River Bottom Deciduous Forest.

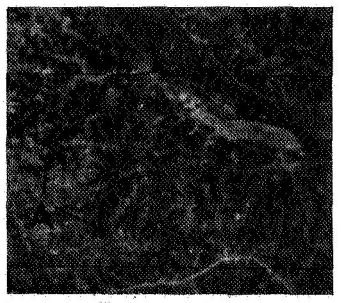


Figure 6. Color combined image of S.E. Minnesota. A and B are the same areas as on Figure 5.



Figure 7. Color combined image of the Chippewa National Forest. The letters indicate land use classes and forest types: A=Open/Pasture/Crops; B=Grand Rapids; C=Upland Conifers; D=Conifers-Hardwoods; F=Hardwoods-Open/Pasture/Crops; G=Lowland Conifers; H=Upland Hardwoods, with a narrow band of conifer and conifer-hardwood.

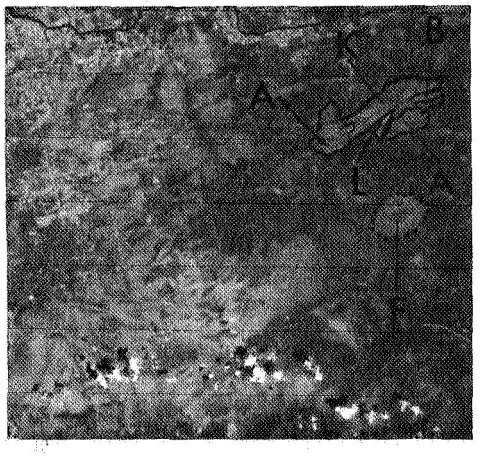


Figure 8. Color combined image of the Big Bog area of Northern Minnesota. A,B,K and L show different wetland types in a patterned bog area. F shows a similar bog that is not delineated but contains all of the features of A,B,K, and L. A=Raised Bog; B=String Bog and Patterned Fen; K=Poor Swamp Forest; L=Cedar or Larch String Bog and Fen.

B

with Band 6 or 7. Where tonal contrasts are high, forest vegetation types can be identified for plots as small as 5-10 acres. Further work holds some promise for the development of two density classes. The type, density, and site characteristics being developed are being evaluated by forest land managers for use in the field and office.

Southeastern Minnesota hardwood forests are scattered along deeply entrenched dendritic drainage systems (Fig. 5, 6). Density level slicing is being tested as a means for separating and inventorying these very irregularly-shaped hardwood stands. With some ground truth in hand it seems feasible to separate these densely forested areas from the scattered trees or non-forested areas using Band 7 of the August 12, 1972 coverage.

WETLANDS. Minnesota has extensive areas of wetlands that are important for water storage and wildlife habitat. The wide variations in size, in permanence, and in location (relative to the major ecotones in the state) multiply the dimensions of the classification and data collection problems. Small seasonal wetlands which are of particular importance to waterfowl habitat management cannot be observed until spring. Lack of cloud free summer coverage also prevents analysis of large southern perennial wetlands until spring. Fall coverage of the Glacial Lake Agassiz plain does allow analysis of patterned bogs in Minnesota's most extensive wetlands area. This area can be subdivided into several wetland types that are based on vegetation/peatland relations. Two patterned bogs that are representative of the big bog landscape are shown in Figure 8. The patterned bog features which occupy much of this part of the state are surrounded by forest lands. The classification shown here also includes the lowland/coniferous forests category. Results of interpretation of several of these patterned bog areas compares very favorably with highly detailed ground truth based on in-depth ecological studies.

CONCLUSIONS AND FURTHER WORK

The potential of ERTS-1 as a tool for mapping land use information on a state wide basis is beyond the expectations of those persons involved. Interpretation of inhouse produced 2" x 2" slides of color combined images and projected 70mm bulk images is the simplest and most fruitful data extraction technique attempted to date. Using high quality ERTS images at appropriate season(s), these techniques can yield much more detailed land use information than now exists for a state that stands as a leader in the field of land management information.

Within the last three weeks the groups working daily with imagery have observed almost an exponential growth of applications and potentials for ERTS-1 data. There is considerable value in the use of multiple

season data to increase the accuracy and detail of land use classification and further to identify those features whose presence in the landscape is transient in time.

We have begun to monitor the cultivation of land in a four township area because the identification of cultivated land from a single late summer image is virtually impossible. While this interpretation effort is time consuming it may have added benefits in the utility of the information. For example it will allow classification of cultivated land according to season; thus, making it possible for game managers to know the habitat conditions at any critical season. Further, these data will allow analysis of sediment availability and erosion potential by drainage basin by time period.

Preliminary studies on density of artifical surfaces of the Twin Cities indicate that with some training and ground truth it will be possible to make a map of impermeable surfaces from ERTS which can be coupled with storm sewer data to produce models for urban run-off management. Trained personnel are now achieving 90 percent or better accuracy of manual interpretation on training sets in the Twin Cities area.

Snow enhancement has also been of value in forest, cultivated, and extractive land use classification. It also provides a better basis for mapping urban housing densities and rural population distributions.

Results obtained thus far are very encouraging. The trade off between extent of coverage and detail is not as limiting as it originally appeared and repetitive coverage provides compensation. In summary, both cultural and vegetative landscape features have been classified and mapped from fall ERTS imagery. Urban land use reduces to nine classes; extractive land use to four. Six to twelve classes of forest vegetation can be identified, as well as five classes of northern wetlands.

IMAGE IDENTIFICATION

Figure	Image Type	Date	I. D.	Band
2	Color Combined	6 Oct. 72	1075-16321	5,7
3	Color Combined	18 Sept. 72	1057-16311	5,7
4	Color Combined	12 Aug. 72	1020-16252	5,7
5	Density Sliced	12 Aug. 72	1020-16252	7
6	Color Combined	12 Aug. 72	1020-16270	5,7
7	Color Combined	7 Oct. 72	1076-16370	5,6
8	Color Combined	2 Sept. 72	1041-16421	5,7

Paper L 15

A MULTIDISCIPLINARY SURVEY FOR THE MANAGEMENT OF ALASKAN RESOURCES UTILIZING ERTS IMAGERY

John M. Miller and Albert E. Belon, *University of Alaska, Fairbanks, Alaska 99701*

ABSTRACT

The ERTS program provides an opportunity to narrow an environmental knowledge gap which impedes planning at a critical time in one of the richest, yet most underdeveloped, regions in the United States - Alaska. ERTS-1 data have been applied to a coordinated multidisciplinary survey which has the overriding purpose to provide updated resource inventory data to land use planning groups and government agencies concerned with resource management. Of particular emphasis in this survey are vegetative, hydrological and geological analyses of the proposed trans-Alaska transportation corridor, and lands to be selected by the State of Alaska, the native corporations, and the Department of Interior. Our preliminary analyses are demonstrating that ERTS data are satisfying these objectives on a regional scale.

BACKGROUND

The most crucial problem in Alaska today is a great environmental knowledge gap which impedes planning and adversely affects the decision making process at a critical juncture in the history of Alaska's economic and social development. This problem has been recently and forcefully manifested in several ways:

1) The controversy surrounding the proposed construction of the trans-Alaska pipeline from the arctic coast to the southern port of Valdez, and the recent U.S. Appellate Court decision denying the permit for its construction.

2) The deterioration of fisheries resources in the Alaskan coastal zones and continental shelf. This results partly from a poor environmental knowledge of these regions.

3) The establishment by the Congress and the Alaska State Legislature of the Joint Federal-State Land Use Planning Commission. This Commission has the awesome task of recommending by 1975 a comprehensive land use plan for Alaska's 375 million acres, thereby assisting the State of Alaska, the federal government, and the Alaska native

PRECEDING PAGE BLANK NOT FILMED.

B

corporations with the selection of 220 million acres of public domain lands.

The basic data for informed land use research and planning in Alaska is sparse and often outdated. Therefore, even the first task of planning on a broad regional basis labors under severe handicaps. Alaska is so vast, and the arctic environment is so varied, that this environmental knowledge gap will not be bridged soon by conventional means with normal dollar resources. Thus, the ERTS program with its demonstrated capability for economical large-scale surveys afford a unique opportunity to narrow this knowledge gap.

Alaska's land mass, Figure 1, covers 586,000 square miles, encompasses 20° of north latitude, and includes four distinct climatic zones. The northern zone experiences extremely cold winters and cool summers with low precipitation. The western climatic zones have very cold winters and cool summers with moderate precipitation. The southern zone enjoys milder winters and summers with heavy precipitation, while the large climatic zone in the interior experiences extremely cold winters and hot summers with low precipitation. Seasonal temperature differences as great as 85°C are possible in the interior.

Four basic ecosystems prevail throughout Alaska:

1) Tree-dominant types cover about 40% of the southern and interior climatic zones. These include the high hemlock/spruce forests of the southern coastal regions and the mixed spruce and hardwoods of the interior flood plains, hills and valleys.

2) The shrub-dominant vegetation primarily forms transition zones north and west of the tree line, between forests and tundra.

3) Grass-dominant systems include upland moist tundra and wet coastal tundra types in the northern and western climatic zones.

4) Barren and sparse dry tundra consists chiefly of low, scattered plants in the higher elevations of central and northern Alaska.

Cultural activities are dispersed along the major river drainages as small villages and concentrations of populations occur chiefly in the southcentral Anchorage-Matanuska Valley and the Fairbanks-Tanana Valley in the interior. These two urban regions account for about half of Alaska's total population. Surface transportation includes a modern railroad from the southern coast to the interior, and a skeleton network

of paved roads from the interior to various ice free ports in the south coastal region. A prime objective of Alaskan planners is a transportation corridor from the interior rail and highway head at Fairbanks to the resource-rich northern region including, but not limited to, service to the Prudhoe Bay oil fields of the North Slope. This corridor could include a secondary highway and/or railroad and, of course, the 48-inch pipeline for shipping crude oil from Prudhoe Bay on the Arctic Coast to the southern port of Valdez.

UPDATING THE ENVIRONMENTAL DATA BASE

How to survey the environmental impact of such a transportation corridor, and particularly of the pipeline, is a matter of intense debate and controversy at the present time. It is clear that no single approach to environmental surveys will be acceptable to groups with highly divergent viewpoints upon the subject of Alaskan oil and what to do with it. In this context, ERTS-1 data forms a politically neutral base from which resource surveys can be made without necessarily arousing suspicions from groups which have mutually conflicting goals. The University of Alaska is performing multidisplicinary surveys of a north-south transect centered on the 148th meridian. Twelve ERTS projects in ten disciplines are closely coordinated with cooperating federal, state and borough government agencies to deal with an extremely wide range of environmental problems.

One area of environmental concern is the northeast Alaska caribou population with special reference to oil pipeline facilities and other natural factors that are not clearly understood. These animals may number 150,000 at present, but there have been large fluctuations in herd sizes over the past 50 years which apparently are unrelated to human activity. Migration routes and winter dispersal patterns are not well enough known to significantly improve management of the caribou resource at the present time. Snow cover has long been recognized as a major factor influencing the biology of caribou, but aerial surveys to obtain data over the vast area are prohibitively costly.

ERTS-1 images are being used in two ways to monitor herd activity. One is to map habitat favorable to caribou and the other is to locate and map environmental features that arise from large caribou aggregations. Typical winter grazing habitat includes mixed patterns of open spruce stands and treeless bogs, such as those near Anvil Lake on the low oblique aerial view of Figure 2. The caribou tend to bed down in open spruce stands for wind protection and to use the nearby treeless regions for feeding. The multiform pattern of spruce and bogs is detectable on ERTS images even by visual analysis, but digital computer techniques are being used to identify and map these habitat landforms.

Animals may winter in loose aggregations of several hundred to a thousand, and such aggregations typically remain in a drainage area and feed intensively before moving on. These feeding areas and the extensive network of trails should be identifiable on ERTS imagery acquired in April, when there is maximum snow accumulation and insignificant melt. There also is some evidence that caribou wintering areas thus disturbed melt off much sooner than other areas. Trampling activities of the herds cause early snow melt by a premature exposure of vegetation, a decrease in spectral reflectance, and a disturbance of the natural nical characteristics.

Available snow data generally do not allow sufficiently detailed mapping for many applications in research, planning and construction of civil structures and roads. The climatic differences are very pronounced along any north-south transect, and these differences are reflected in the amount, the physical characteristics, and the duration of seasonal snow cover. Snow has a great many adverse effects on man's activities in the arctic and sub-arctic because it remains on the ground for long periods. It also thermally insulates the soil-atmosphere interface and affords protection to plants and animals. From ERTS imagery, we are producing maps of snow lines across Alaska during the initiation and decay of the seasonal snow cover, cloud cover permitting.

A resource survey has been prepared from an ERTS scene of the Anaktuvuk Pass region of the Brooks Range for purposes of land use planning. Color and black and white prints were visually analyzed in cooperation with the Resource Planning Team of the Federal-State Land Use Planning Commission for Alaska. A multidisciplinary team spent only about 30 man hours in preparing a regional resource survey of a remote and undeveloped area of Alaska. The output included maps of the three predominant types of vegetation (moist tundra, low brush and high brush), Figure 3; ten watershed drainages, Figure 4; geologic features indirectly relatable to economic minerals, Figure 5. Such regional resource surveys applied to 19 regions of critical interest are primary data base objectives of the Planning Commission. These objectives can be achieved as timely inputs to the deliberation process of the Commission only by direct use of ERTS imagery. Comprehensive vegetation maps are also being prepared for much of the north-south transect of Alaska to aid the formulation of land use plans for this region which is subject to imminent development.

In particular, the Matanuska and Susitna Valleys, adjacent to metropolitan Anchorage, are presently bearing high developmental pressures because of the needs of the population heartland of Alaska. The Matanuska Valley contains the most valuable agricultural land in the state, and along with the Susitna Valley has considerable undeveloped lands. However, speculative pressures force sales of these lands at

prices that prohibit fulfillment of any agricultural potential. The limited amount of land that is suited to agriculture must be quickly identified and integrated into a long range planning structure if agriculture is to continue both its material and intangible benefits to Alaskan society. The coupling of ERTS data as a resource survey tool in these large, undeveloped areas with difficult access problems is particularly welcomed by planning agencies.

In the southern part of the transect, the type mapping has outlined the broad features of mixed woods, coniferous forest, mixed herb-shrub and sedge associations, tidal flats, subalpine shrub-grass, alpine tundra, low elevation grasslands, and agricultural croplands. Use of computer processing has also delineated silty water from clear water lakes, shallow waters from deeper waters, tidal flat vegetation from muskegs, and stands of birch-aspen.

In a joint effort with the U. S. Forest Service and the State Department of Natural Resources, we have just recently applied multispectral ERTS data to the surveillance of a 200,000 acre spruce beetle infestation near the Tyonek Indian Reservation and on the Kenai Peninsula in the Cook Inlet Basin. An estimated two billion broad feet of white spruce has been killed or damaged by the spruce beetle, but the large areal extent of the spreading infestation presents a difficult task in maintaining surveillance of the extent of the affected trees. Techniques are being implemented using ERTS data to stratify damage to white spruce into three levels - healthy stands, new killed and old kill stands.

Geologic applications of ERTS imagery also are aiding the planning for the development of Alaska. The synoptic view is particularly beneficial in mapping new tectonic features such as reported by Gedney at this symposium.

The University of Alaska is also using ERTS images to study circulation patterns and sediment transport in key estuarine environments in Alaska. The Cook Inlet has been especially well documented from ERTS, and these results are useful for designs of off-shore oil production and marine terminal facilities. The Cook Inlet study results are reported also at this symposium by Wright. Another key marine environment study involving ERTS is located in Prince William Sound and the port of Valdez, which is subject to possible intense oil terminal and shipping activities. Here the application is toward sound ecological management in the face of heavy traffic with the potential for contamination. Valdez is a deep water port, neither tide dominated nor bearing a heavy silt burden as does Cook Inlet. The continuing protection of important fisheries resources in this region is the primary goal of this University project.

SUMMARY

Broadly structured, multidisciplinary environmental surveys of Alaskan resources are underway using ERTS data as a primary input. These results are coupled to a maximum extent to various public agencies for operational applications, such as the Bureau of Land Management, Forest Service, Corps of Engineers, Bureau of Sports Fisheries and Wildlife, and the Geological Survey. Also using ERTS Alaskan data are many other agencies, including the Alaska Department of Highways, Department of Fish and Game, Department of Economic Development, Department of Natural Resources, the Joint Federal-State Land Use Planning Commission, and various borough governments. Applications of ERTS data are playing an extremely vital and timely role in planning for the imminent, and hopefully, the orderly development of Alaska.

ACKNOWLEDGMENTS

The authors appreciate the many contributions to this paper made by the ERTS Principal Investigators at the University of Alaska and by the Resource Planning Team of the Land Use Planning Commission.

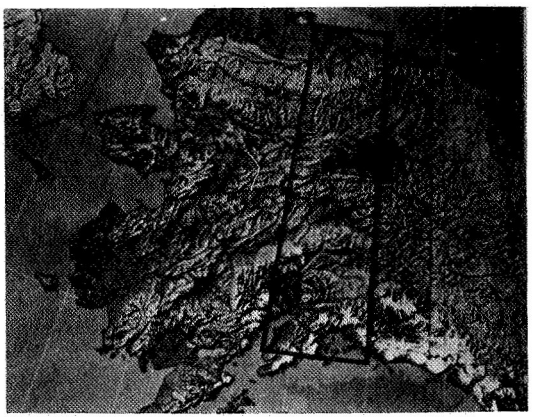


Fig. 1 Transect Survey Area

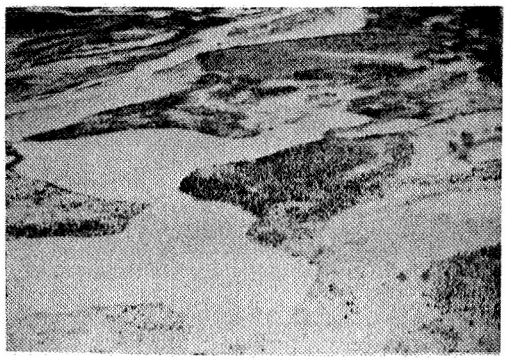


Fig. 2 Typical Caribou Habitat

(Fig. 3 Not Available)

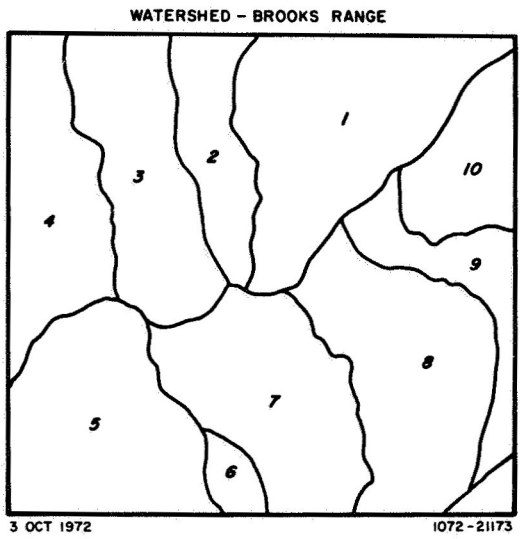


Fig. 4

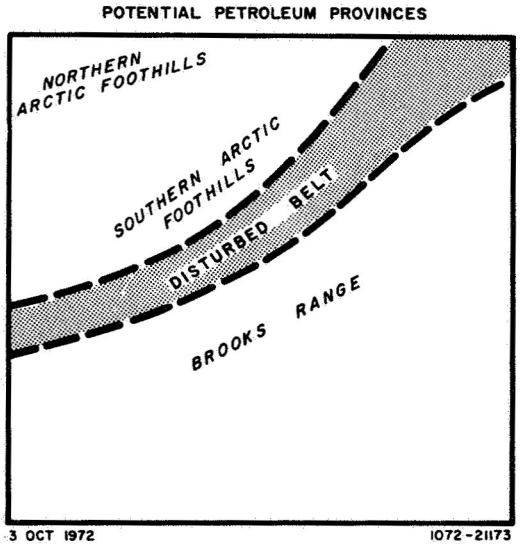


Fig. 5

N73-28311

Paper L 16

THE USE OF ERTS-1 DATA FOR THE INVENTORY OF CRITICAL LAND RESOURCES FOR REGIONAL LAND USE PLANNING

J. L. Clapp, R. W. Kiefer, M. M. McCarthy and B. J. Niemann, Jr., *The University of Wisconsin*[1], *Madison, Wisconsin*

ABSTRACT

Computer-generated spatial and statistical comparisons of critical land resource data derived from conventional sources, RB-57 photographs, and ERTS images, for an eastern Wisconsin test site, suggest that certain critical land resource data can be mapped from ERTS images on a statewide basis. This paper presents one of the biotic resources, "wetlands", as an example of the use of ERTS imagery to inventory land resources.

1. INTRODUCTION

The ERTS-1 project members at the University of Wisconsin-Madison are investigating the application and use of ERTS imagery as a data source for regional and state resource planning. A variety of resources are being evaluated and examined to determine the potential for the detection and monitoring of these resources from satellite and high altitude platforms. Resources being evaluated for detection include major biotic communities, landform configurations, land and resource areas altered by man-induced activities (e.g., farming, extraction, urbanization, and power plant construction) and the monitoring of land activity changes. This paper presents one of the biotic resources, "wetlands", as an example of the use of ERTS imagery to inventory land resources. The inventory of wetlands is especially important because the Governor's Wisconsin Land Resources Committee has concluded that "wetlands" are a critical resource, and yet, as of this date, state and regional planners do not know, in a quantitative sense, the location or extent of the State's wetland resources.

2. WETLANDS INVENTORY

To determine the effectiveness of the ERTS sensors for resource

[1]Environmental Monitoring and Data Acquisition Group, Institute for Environmental Studies; Environmental Awareness Center, Department of Landscape Architecture; and Department of Civil and Environmental Engineering.

PRECEDING PAGE BLANK NOT FILMED

Original photography may be purchased from:
EROS Data Center
10th and Dakota Avenue
Sioux Falls, SD 57198

detection and inventory, a sample site in eastern Wisconsin is being utilized. This 10 x 30 kilometer "Sheboygan Test Site", shown in Figure 1, is part of a larger (10,000 square kilometer) test site generally located between Green Bay and Milwaukee, Wisconsin. The variable "open swamp" in the 10,000 cell, computer-based REMAP I (Regional Environmental Mapping and Analysis Process) data bank can be used as a measure of "wetlands" distribution in the study area. The REMAP I data bank was developed to assist the Wisconsin Department of Transportation locate a corridor for Interstate 57 and is serving as a comparison basis for the ERTS-1 investigation. "Open Swamp" can be defined as areas of wetlands occupied by such biotic communities as those dominated by grasses, sedges, emergent aquatics, dogwoods, shrub-willows, and alders. Such communities are variously called bogs, wet meadows, marshes, or swamps.

Figure 6 is a computer-processed spatial comparison which presents quantitative information about the occurrence of "open swamp" in the Sheboygan Test Site, as derived from 3 different sources: (A) ERTS-1 multispectral imagery; (B) RB-57 high altitude color infrared photography; and (C) the REMAP I data bank. Each cell shown in this sample site is one square kilometer in size, referenced according to the UTM system. The density of the symbol printed in each cell shows the percentage of that cell occupied by "open swamp" (blank = 0%; "." = 1-9%; "," = 10-19%; etc.). Beneath each 300 square kilometer area shown on Figure 6 is given the total acres of the variable "open swamp" as determined from each of the three data sources. Numbers of occurrence and numbers of acres for each of the three types of data source (A, B and C) are presented for each level of occurrence.

The information derived from ERTS imagery was interpreted from two different dates examined concurrently - 14 September 1972 and 13 December 1972. Figure 3 shows an ERTS image (9 August 1972) of most of the REMAP I data bank area with the 10 x 30 kilometer Sheboygan Test Site outlined. Figures 4 and 5 show examples of ERTS imagery from 9 August 1972 and 13 December 1972 for this test site. In examining the four MSS bands, the images produced by Band 5 were found to present the most information for this particular variable for the dates data were available.

Information from the RB-57 photographs was interpreted from color infrared positive transparencies taken in September 1971 (September has been found to be a superior time for photo interpretation of many vegetational communities in this region). An example of RB-57 photography for the test site is shown as Figure 2.

"Open swamp" as it exists in the REMAP I data bank was obtained from two sources: (1) Borgner land cover survey maps, and (2) interpretation of small-scale panchromatic aerial photographs. The Borgner studies represent the most complete inventory of vegetational resources for the entire state of Wisconsin. They were ground studies done during the 1930's in which species types and communities identification were made.

While some areas of the state have been studied more recently (e.g., Menominee County), no other data source exists for the state as a whole. The Borgner studies were supplemented with interpretations from black and white aerial photographs in an attempt to update the Borgner maps.

Figure 6 illustrates certain differences in the spatial distribution of the variable "open swamp" as derived from the three data sources. The most conspicuous difference is in the total numbers of acres of open swamp accounted for as interpreted from each data source: 2673 acres from ERTS 1; 2248 acres from RB-57; and 5002 acres in REMAP I data bank. From preliminary investigations (ground studies and re-check of interpretations), it is our conclusion that the ERTS and RB-57 derived data are a closer approximation of the location and extent of the wetland resource in the test site than the data now stored in the REMAP I data bank. The REMAP I data represent the best existing data as derived from conventional data sources. These REMAP I data are less valid than ERTS and RB-57 data for two reasons: (1) many areas that were wetland communities in the 1930's when the Borgner maps were compiled have disappeared, and (2) the data sources used were conducive to generating errors. These errors exist in both the original Borgner studies (now generally recognized by Wisconsin ecologists as being of limited value) and in extraction and classification errors when using small-scale panchromatic photographs as a data source for interpretation. Many lowland forest areas were incorrectly coded as wetlands and account for the larger total number of acres of "wetlands" stored in the REMAP I data bank. Such classification errors were <u>not</u> made during interpretations from ERTS-1 or RB-57 data because: (1) the data were of recent vintage (1971-72), and (2) the interpreters were able to differentiate well between lowland forest and open swamp. In the case of interpretations from RB-57 color infrared photographs (September 1971), community distinctions were possible because many plants were entering dormancy. In the case of interpretations from ERTS images, these distinctions were possible by means of an examination of two dates of imagery (September and December).

In comparing the ERTS-derived data with the RB-57-derived data, both the spatial results and the numerical quantities are as expected. It appears that certain small wetland areas (e.g., less than 10% of a cell) can be recognized on RB-57 photographs but cannot be identified on the ERTS images due to resolution limitations. Resolution and edge definition characteristics appear to influence an interpreter into perceiving higher percentile levels (percents of cell classified as open swamp) on ERTS images than on RB-57 photographs.

It is important to note that the delineating of wetlands, their extent and degree of occurrence, is only the first step in a resource inventory. Eventually, questions of wetland diversity, wetland quality, amount of biotic habitat, and similar concerns must be quantified. Many of these questions can be approached with RB-57 photographic data. ERTS data offer the advantage of sequentiality and can also exist in a number of formats.

As previously mentioned, we are investigating a variety of resources to determine the potential for the detection and monitoring of these resources from satellite and high altitude platforms. Initially, 15 resource types have been mapped for the Sheboygan Test Site and another 300 square kilometer test site near Green Bay. Computer calculations and spatial printouts, such as shown in Figure 6, have been prepared for these 15 resource types. The results obtained for "Forest" and "Agriculture" have been especially promising. They show (for the Sheboygan Test Site):

	Total Acres (A) ERTS	Total Acres (B) RB-57	Total Acres (C) REMAP I
Forest	11,992	14,507	12,599
Agriculture	45,352	44,830	48,894

3. SUMMARY

Effective regional and state land resource planning are dependent upon relevant information which presently may not exist, except in inaccurate or archaic forms. Also critical, for use by state and regional planners, is resource information at varying scales, including land resource information for citizen educational purposes, large area planning (e.g., power plant sites), public facility planning (e.g., controlled access highways), and information for legislation and control of land resources. As presented in this paper, the detection, inventory and monitoring of wetland resources appears feasible for the scales of planning just described, except for legal control (which requires accurate property description). Importantly, it was shown in this paper that ERTS-interpreted information in the case of wetland resources was more descriptive and accurate than the current statewide information sources. For the detection of the wetland resources as overall patterns, the ERTS images appear comparable to RB-57 photographs as a data source.

With the coming advent of statewide planning systems, such as New York's LUNR and Minnesota's MLIS, plus the need to inventory specific resources, the extent of applicability and usefulness of satellite sensors will be tested. Definitions and data resolution levels of resource information are being established by planning and governmental agencies. In the State of Wisconsin, for example, the State is implementing a Critical Resource Information Program (CRIP) aimed at establishing definitions, units of measurement, inventory, and monitoring of critical land resources for planning and legislative purposes. The desire and need to inventory and monitor land resources during the coming decade is obvious and the extent of applicability of ERTS satellite sensors will be of utmost interest to members responsible for and interested in the land resource planning and decision processes.

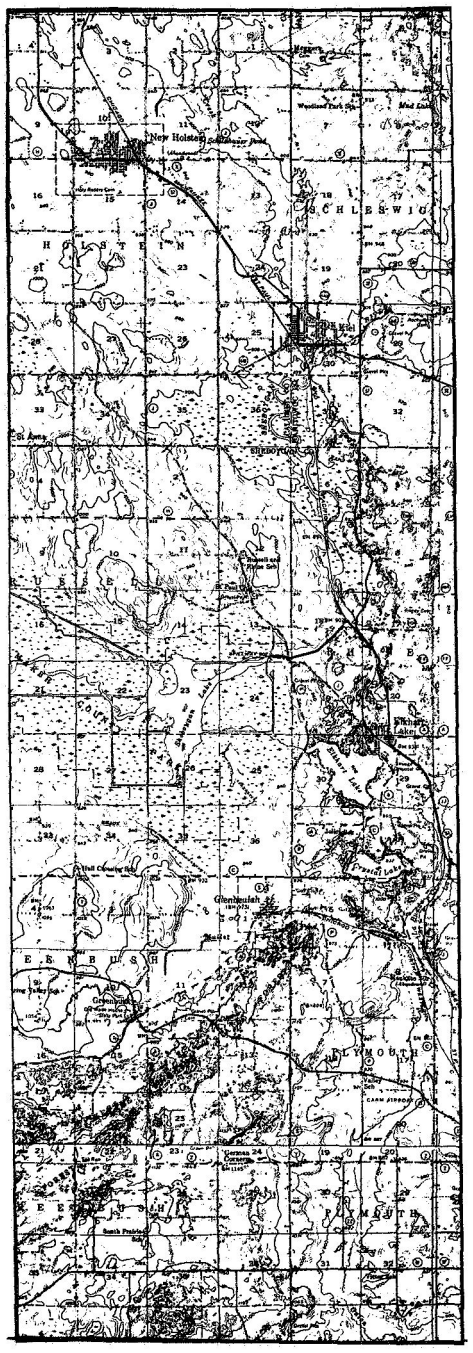


FIGURE 1

U.S.G.S. TOPOGRAPHIC MAP
10x30 km SHEBOYGAN TEST SITE



FIGURE 2

RB-57 PHOTO, 4 June 1972
Hasselblad, b/w red band



|W089-00 W088-30| W088-00| N043-00|
09AUG72 C N43-54/W087-54 N N43-54/W087-52 MSS 5 D SUN EL53 AZ132 192-0236-G-I-N-D-2L NASA E

FIGURE 3 - ERTS BAND 5 (MSS-red), August 9, 1972
GREEN BAY-MILWAUKEE REGION



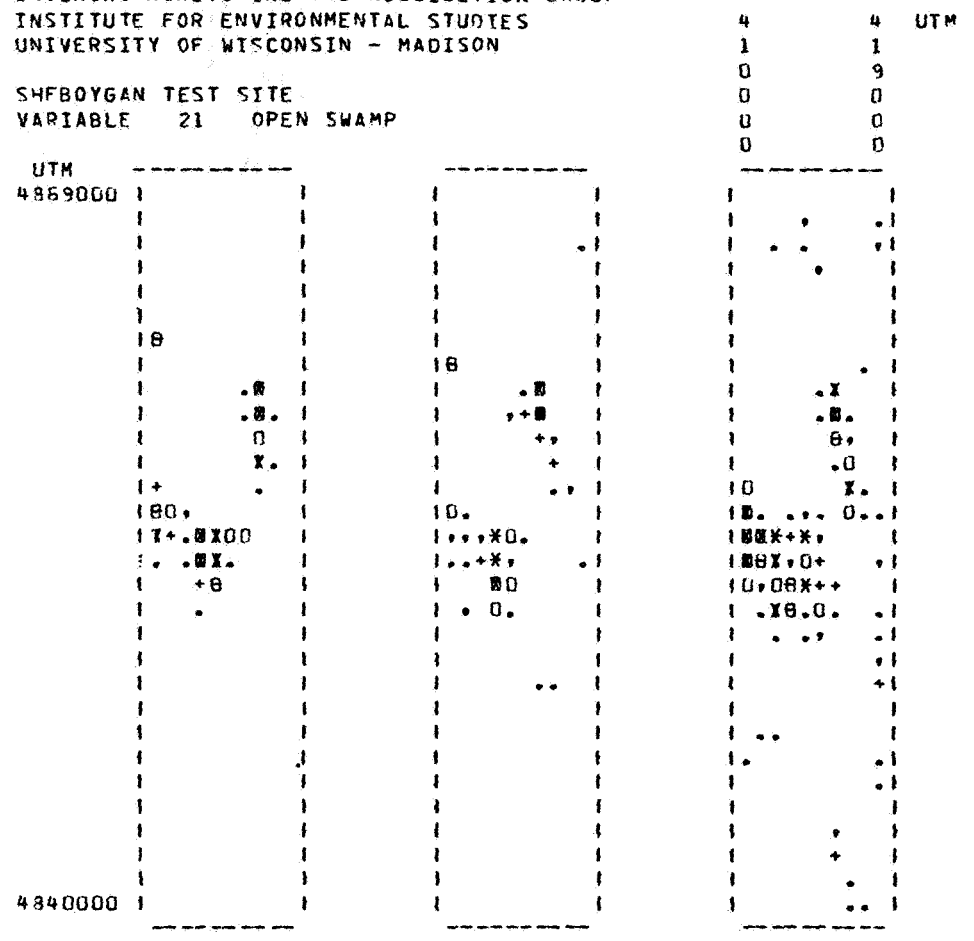
FIGURE 4

ERTS BAND 5 (MSS-red)
9 August 1972



FIGURE 5

ERTS BAND 5 (MSS-red)
13 December 1972



TOT. ACRES		2672.54			2247.70			5001.75		
LEVELS		1	2	3	4	5	6	7	8	9	10
SYMBOLS		.....	,,,,,	+++++	00000	88888	*****	XXXXX	▒▒▒▒▒	▒▒▒▒▒	▒▒▒▒▒
RANGE (%)		1-9	10-19	20-29	30-39	40-49	50-59	60-69	70-79	80-89	90-99
OCCUR	A	10	1	3	4	3	0	4	3	1	0
	B	11	8	4	4	1	2	0	2	0	1
	C	29	12	6	7	4	3	4	2	3	0
ACRES	A	222.	37.	222.	346.	351.	0.	679.	598.	217.	0.
	B	225.	358.	296.	346.	111.	296.	0.	370.	0.	245.
	C	689.	558.	435.	672.	494.	430.	674.	390.	659.	0.

FIG. 6 WETLANDS (REMAP I VARIABLE "OPEN SWAMP")
ERTS and RB-57 INTERPRETATIONS vs REMAP I DATA BANK

N73-28312

Paper L 17

INVESTIGATIONS OF AN URBAN AREA AND ITS LOCALE USING ERTS-1 DATA SUPPORTED BY U-"PHOTOGRAPHY"

H. A. Weeden, F. Y. Borden, D. N. Applegate, and N. Bolling, *Office for Remote Sensing of Earth Resources, The Pennsylvania State University, University Park, Pennsylvania*

ABSTRACT

An urban area in central Pennsylvania and the surrounding locality were investigated separately at first by photointerpretation of ERTS-1 imagery and by computer processing of MSS tapes. Each of these independent approachs had shortcomings. Next the photo-interpretation and processing were coordinated. The results of the cooperative effort of photointerpreters and computer processing analysts were much improved over independent efforts. It was found that single frames of U-2 photography could be projected onto printer output maps with little recognizable distortion in areas 10 to 25 cm square. In this way targets could be identified for use as training areas for computer processed signature identification. In addition, at any stage of category mapping, the level of success in correct classification could be assessed by this method. The results of the classification of the study area are discussed.

The state of the art of producing thematic land use maps by digital processing and analysis of multispectral scan data from ERTS-1 by the Office for Remote Sensing of Earth Resources at The Pennsylvania State University as of March 1, 1973, is the concern of this report. The geographic area of the study is a portion of East Pennsboro, Hampdon, and Lower Allen townships in Cumberland County just across the Susquehanna River from Harrisburg, Pennsylvania. The area is especially well suited for the study because it exhibits many terrain and cultural features most readily recognizable on ERTS imaging systems. The area is rapidly developing with a variety of targets including

the Susquehanna River, Conodoguinet Creek, rail marshalling yards, urban and suburban areas, industrial developments, agricultural regions, forest, as well as a newly developed system of interstate highways. Such targets, properly identified, provide fixed points of reference between which items of lesser definition can be investigated and mapped. The rapid growth in the area provides an opportunity for evaluating the temporal dimension offered by ERTS data. Initial work at Penn State exposed the limitations of machine processing alone as well as the restrictions of visual photointerpretation alone from ERTS scenes. Hence, this paper emphasizes the development of a system combining the strengths of each method.

The maps shown in Figures 2, 3, and 4 were produced on a CalComp Drum Plotter.[1] MSS bulk ERTS-1 data tapes were processed on an IBM system 370/165 using a Remote Job Entry terminal. The programs used are described in a paper by Borden (1972). Supporting ground truth used for verification came from the 7-1/2 minute quadrangle map (1:24,000 scale) of Harrisburg-West prepared by the U. S. Geological Survey from aerial photographs taken in 1961 and field checked in 1963. Culture as of 1961 required supplemental data that was provided by infrared photography taken from U-2 aircraft on July 26, 1972. The photos are of 70 mm format with a scale of 1:445,000. As character maps were produced by the high-speed printer, they were verified for accuracy by projecting the U-2 photographic transparency onto the map using a 3-1/4" x 4-1/4" Model D American Optical Company slide projector. Scale distortions of the computer-generated, character map prevented proper registration of the projected photo over the entire area of the map. This required a distribution of positively identified targets throughout the area so that adjacent portions of the scene could be sequentially brought into proper registration.

Figures 2, 3, and 4 were produced from ERTS image number 1080-15185 of October 11, 1972. As bulk MSS tapes were received from NASA, they were subset to produce working tapes for selected portions of the image with guidance for the scan line and element numbers provided by an Ozalid print from any channel of the ERTS positive transparency. Two preliminary maps are produced for review of definable

---

[1]These maps were presented in this form for the convenience of publication. The normal form of map presentation is a character map prepared on the high-speed printer.

boundaries. One shows variation in overall reflectance of the scene that is similar to gray scale maps in other systems. The second map is prepared to identify local areas of spectral uniformity. In some scenes the location of clouds and their shadows are noted to avoid misinterpretation as ground features. When these preliminary steps are completed, one is ready to proceed as indicated in the flow chart in Figure 1.

First level mapping is started by choosing training areas from the two preliminary maps. Select the most easily recognized targets from spectrally homogeneous areas with positive widely separated geographic locations. The Susquehanna River is an excellent example of such a target. Clusters of characters of lesser areal extent on the spectrally uniform map are next persued. Mean vectors are computed for the training areas using the four channels to establish spectral signatures. The euclidean distance of separation for pairs of mean vectors are computed and printed out as shown in Table 1 (to be referred later). As the character maps are produced, they are verified as described above by projecting the U-2 photos on the map. The maps may be produced in separate categories for ease of checking. Figure 2 shows such a map. Note first the easily recognized category of river in the upper right with the meandering creek entering from the left. This map shows the categories of open fields, forest, and golf course in addition to water. Areas verified by U-2 photo correlation are outlined with heavy lines. This process leads to the definition of lesser areas now geographically fixed and interpreted on the U-2 photograph. The number and variety of targets is expanded both with respect to type and extent of geographic separation. This is a cyclic operation, as indicated in the flow diagram, that continues until the mapper feels he is ready to advance to the next stage.

Second level mapping exploits a computer program using cluster analysis developed by Turner (1972). This program works where uniform training areas cannot be found because of spectral nonhomogeneity or small area. Figure 3 was greatly benefited by this technique. The signatures for some suburb, old suburb, confusion suburb, and industrial and for all parking lots and concrete were thus developed. This map was also verified by correlation with U-2 photographic projection and the targets successfully defined so marked. The category "confused suburb" comes about because of its lack of positive separation from agricultural fields. When one considers the mixed character of a suburb consisting of roofs, lawns, trees and shrubs, and streets, it is easy to see how some of these combinations might fortuitously

compare to a mix of small fields or long, narrow fields related to contour stripping. Reference to Table 1 shows that the signatures for a category of "confused suburb" (the = symbol) and that for a field (the - symbol) does not have a wide separation. This separation is the euclidean distance of separation of the vectors representing the particular target.

Categories are separated for mapping on the basis of some minimum distance. When this distance is too small, confusion may result. For example, the distance between the "confused suburb" signature and the field signature is relatively small, 1.1, thus confusion between these categories could be anticipated. In contrast, the separability of river water (the W symbol) from every other category is quite large implying no problem in classifying river water correctly. If a mixture of characters is printed in an area, it may be desirable to keep the separate signatures, but lump the area. On the other hand, the signatures may be blended to produce one character, for example, in the two industrial signatures (the + symbols) that are quite separate, 17.7, but that occur together in a mixture for many industrial areas. These separate signatures must be preserved, but would be assigned the same mapping symbol. Judgment should be used here. More work is still required on the category called highways. It comes up well in areas of high subject-to-background contrast, but is weak in urban and suburban areas. Perhaps the mapper will have to produce highway networks by the judicious connection of scattered symbols. This is not a satisfactory procedure. Other spectrally nonhomogeneous targets definable by cluster analysis that are difficult but worthy of great effort are quarries and small streams. Note again the cyclic procedure through level two.

The third and final level of mapping is now approached. It may be that too many categories have been defined and the resulting map output is too refined or too confusing to the reader. Stray symbols can be suppressed. A careful review of the map objectives should serve as a guide to the final number of categories to be mapped. When a limiting goal is established, then the final cycle can be cut off. It should be noted that the mapping program includes a percent of the area mapped for each category. This makes it easy to express the area of each category when the total area bounded is known. Figure 4 is the final presentation. This is a combination of the first two. However, in order to make the map readable, the forest area was subdued so the blank areas are forest and unclassified. The hope of

Table 1. Distances of separation for categories.

	1 W	2 =	3 -	4 +	5 +
1 W	0.0	31.8	31.5	14.2	31.4
2 =	31.8	0.0	1.1	18.3	14.2
3 -	31.5	1.1	0.0	18.0	13.8
4 +	14.2	18.3	18.0	0.0	17.7
5 +	31.4	14.2	13.8	17.7	0.0

diminishing the unclassified group may rest on the merging of data from two scenes for different seasons of the year.

Conclusions that can be reached from the work on these maps are as follows: The categories of water, forest, high density suburbs, old suburbs, industrial, parking lots and concrete are reasonably well defined. The categories of agricultural fields, highway, and low density suburbs need more study. Some items highly desirable in land use mapping may not be obtained because of size or low subject-to-background contrast. The temporal aspect of the data has not yet had sufficient opportunity to be exploited. The combined efforts of interpretation of ERTS images, aircraft underflight photographs, and computer-generated, character maps has the potential to generate land use maps of high quality.

LITERATURE CITED

Borden, F. Yates. 1972. A Digital Processing and Analysis System for Multispectral Scanner and Similar Data. In Remote Sensing of Earth Resources, Vol. I. Edited by F. Shahrokhi. The University of Tennessee, Space Institute, Tullahoma, Tennessee. pp. 481-507.

Turner, B. J. 1972. Cluster Analysis of Multispectral Scanner Remote Sensor Data. In Remote Sensing of Earth Resources, Vol. I. Edited by F. Shahrokhi. The University of Tennessee, Space Institute, Tullahoma, Tennessee. pp. 538-549.

ACKNOWLEDGEMENT

Financial support for this project was furnished by NASA on ERTS Contract NAS5-23133 and by the MITRE Corporation on Contract N 35490.

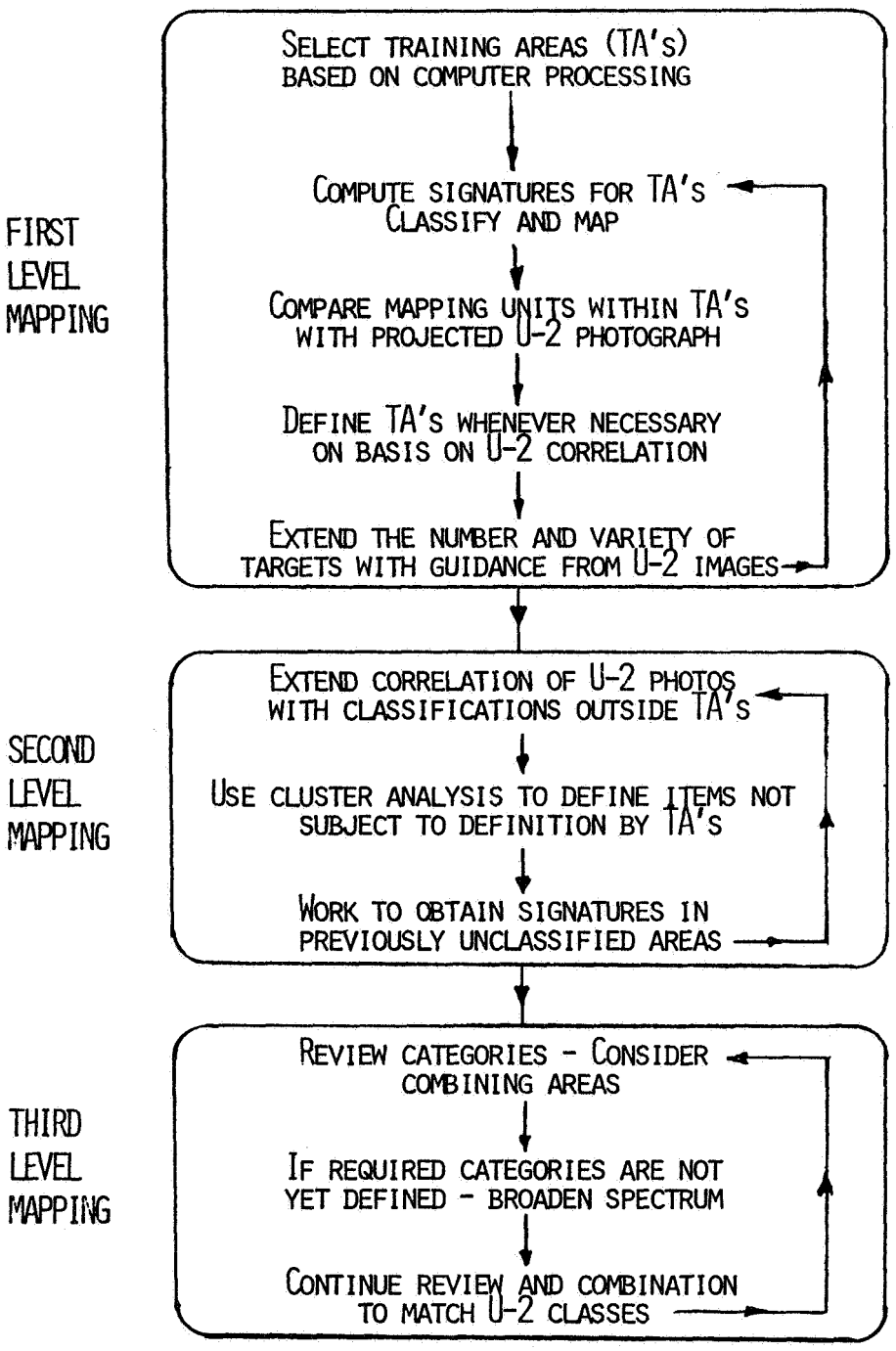


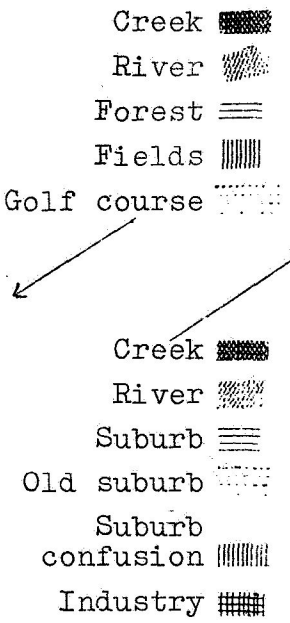
Figure 1

Mapping activity flow chart.



Figure 2

Classification map of agriculture and forest.



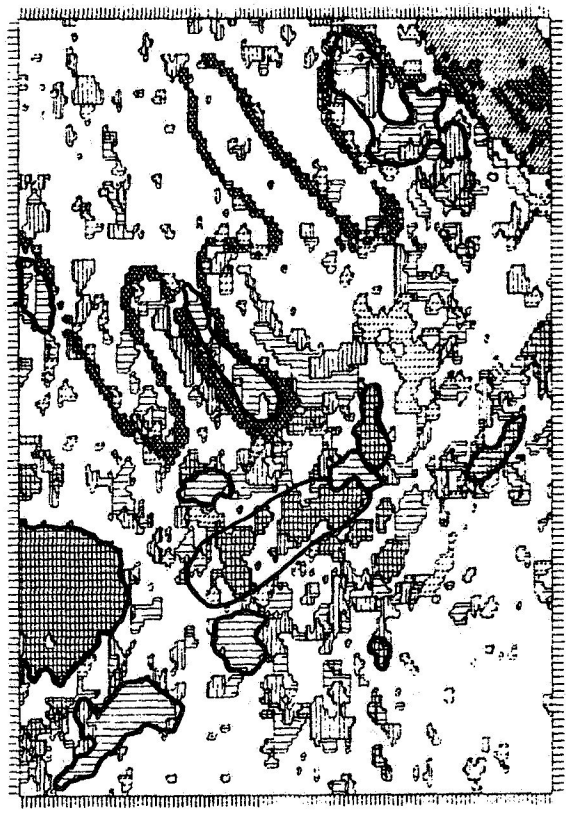


Figure 3

Classification map of suburb and industry.

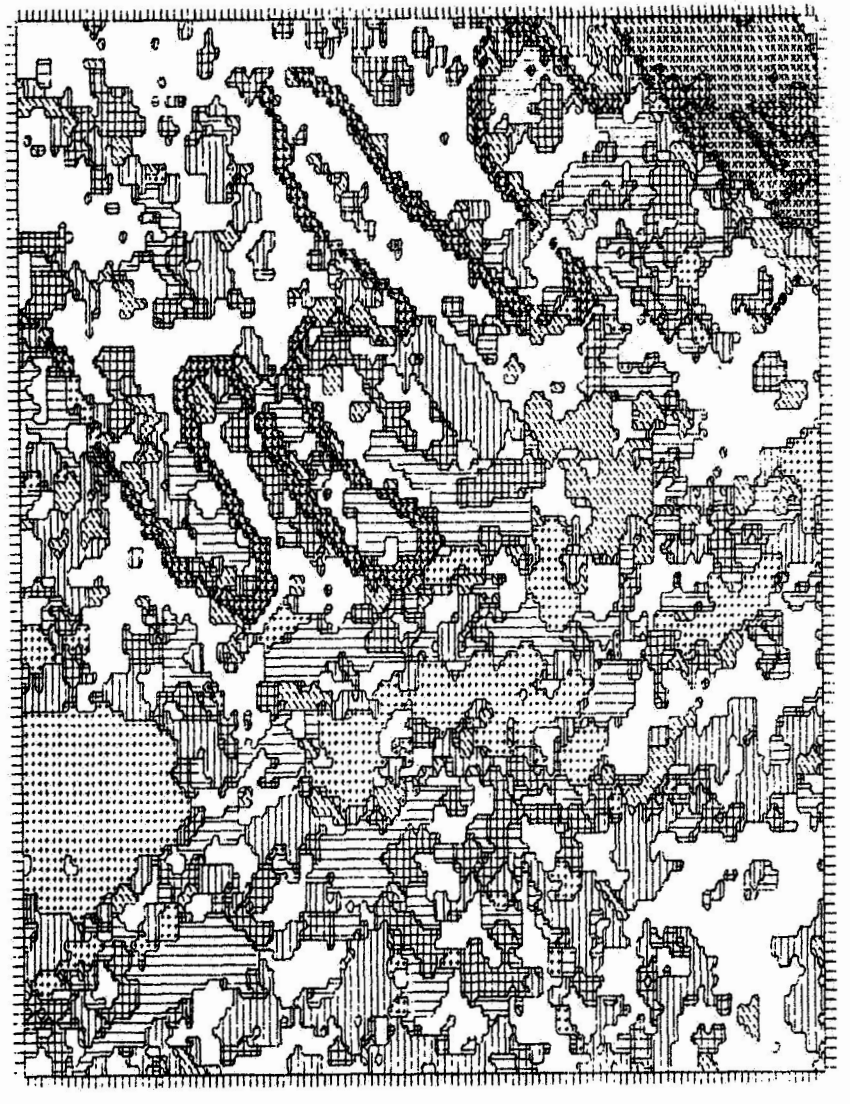


Figure 4. Classification map of all categories.

N73-28313

Paper L 18

'FIRST LOOK' ANALYSES OF FIVE CYCLES OF ERTS-1 IMAGERY OVER COUNTY OF LOS ANGELES: ASSESSMENT OF DATA UTILITY FOR URBAN DEVELOPMENT AND REGIONAL PLANNING

S. Raje and R. Economy, *General Electric Co., Space Division, Valley Forge, Penna. and* J. McKnight*, *County of Los Angeles, Regional Planning Commission*

ABSTRACT

Significant results have been obtained from the analyses of ERTS-1 imagery from five cycles over Test Site SR 124 by classical photointerpretation and by an interactive hybrid multispectral information extraction system (GEMS).

The synopticity, periodicity and multispectrality of ERTS coverage, available for the first time to LA County planners, have opened up both a new dimensionality in data and offer new capability in preparation of planning inputs.

Photointerpretation of ERTS images has produced over 25 overlays at 1:1,000,000 scale depicting regional relations and urban structure in terms of several hundred linear and areal features. To mention only one such result, a possible new fault lineament has been discovered on the northern slope of the Santa Monica mountains in the scene 1144-18015, composited of MSS bands 4, 5, 6.

GEMS analysis of the ERTS products has provided new or improved information in the following planning data categories: Urban Vegetation; Land Cover Segregation; Man-made and Natural Impact Monitoring; Urban Design; Land Suitability.

An ERTS scene, 1036-18010, analyzed by GEMS to provide spectrally-derived object class patterns was directly overlaid on a current LA County land use pattern map prepared at 1:24,000 scale. The geometric and thematic content of the GEMS-derived patterns is sufficient for routine use at the 1:24,000 standard operating scale for county and regional planning. The significant point of this converging set of results is that the internal, fine structure of the inner city has been sub-classified spectrally-spatially.

ERTS data analysis has allowed planners to establish trends that directly impact planning policies. For example, detectable grading and new construction sites quantitatively indicated the extent, direction and rate or urban expansion which enable planners to forecast demand and growth patterns on a regional scale.

This new source of information will not only assist current methods to be more efficient, but permits entirely new planning methodologies to be employed.

* Presented on 3/7/73 as paper L18 at ERTS-1 Symposium.

Original photography may be purchased from:
EROS Data Center
10th and Dakota Avenue
Sioux Falls, SD 57198

1. INTRODUCTION

The County of Los Angeles is populated by 7 million people and covers 4,083 square miles. Another 13 million people live in the adjacent counties. The Test Site SR 124 is an extremely complex environment both physically and socially. It includes a vast metropolitan area of some 1500 square miles. Its natural environment includes desert; high mountains, and two large islands. The complexity of both the urban and the natural environments of the Los Angeles region was aptly pointed out by Professor Leonard Bowden respectively in papers L5 and R4 during two sessions at this symposium.

Los Angeles County is presently involved in the preparation of a Comprehensive General Plan as required by California Law. A vast amount of data on a wide range of subjects is needed to complete this task successfully Traditional planning operations are becoming prohibitively time-consuming and expensive.. Use of ERTS data in current planning operations will provide a less expensive and more timely product, based on the findings of this investigation through the 'first look'.

The objectives of this investigation are: i) To evaluate ERTS imagery utility for its urban and regional planning applications using the complex Los Angeles area as a testing ground and ii) To ascertain the effectiveness of the General Electric Multispectral Information System (GEMS) by representative analysts/users operation.

The project involves three major parties: NASA, the General Electric Company and the County of Los Angeles. NASA gathers and preprocesses data at 1:1,000,000, 1:125,000 and 1:36 000 scales. GE - Space Division analyses the data and conducts the investigation jointly with the County Regional Planning Commission who interpret and use the data products in its planning program.

The data extraction methodology basically involves classical photo-interpretation by County members on the team and interactive electronic analyses by GE investigators. The processes are mutually strengthened by progressive interaction both by remote means and in person. Figure 1 depicts the information flow for this study.

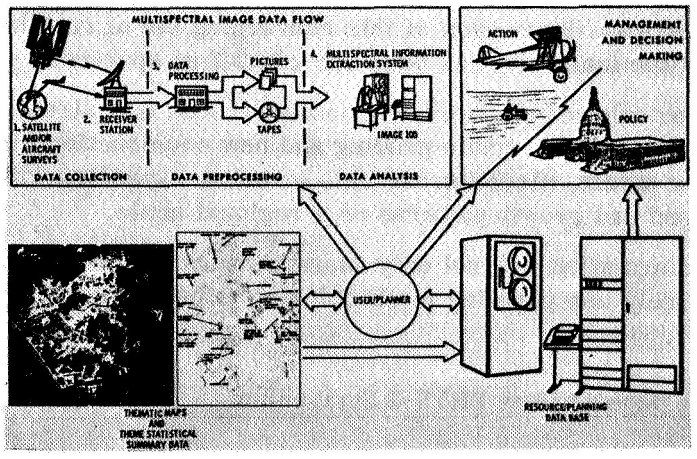


FIGURE 1 Data Analysis Flow

2. SIGNIFICANT RESULTS

The results of photointerpretation of ERTS transperancies at the 1:1,000,000 scale -both black and white as well as standard and non-standard color-composites - by the County investigators are most succintly communicated in the course of the study effort by an ever-increasing series of theme overlays/recognition maps with exhaustive annotation and commentary. Here it is appropriate to show a selected few of such overlays, as in Figure 2.

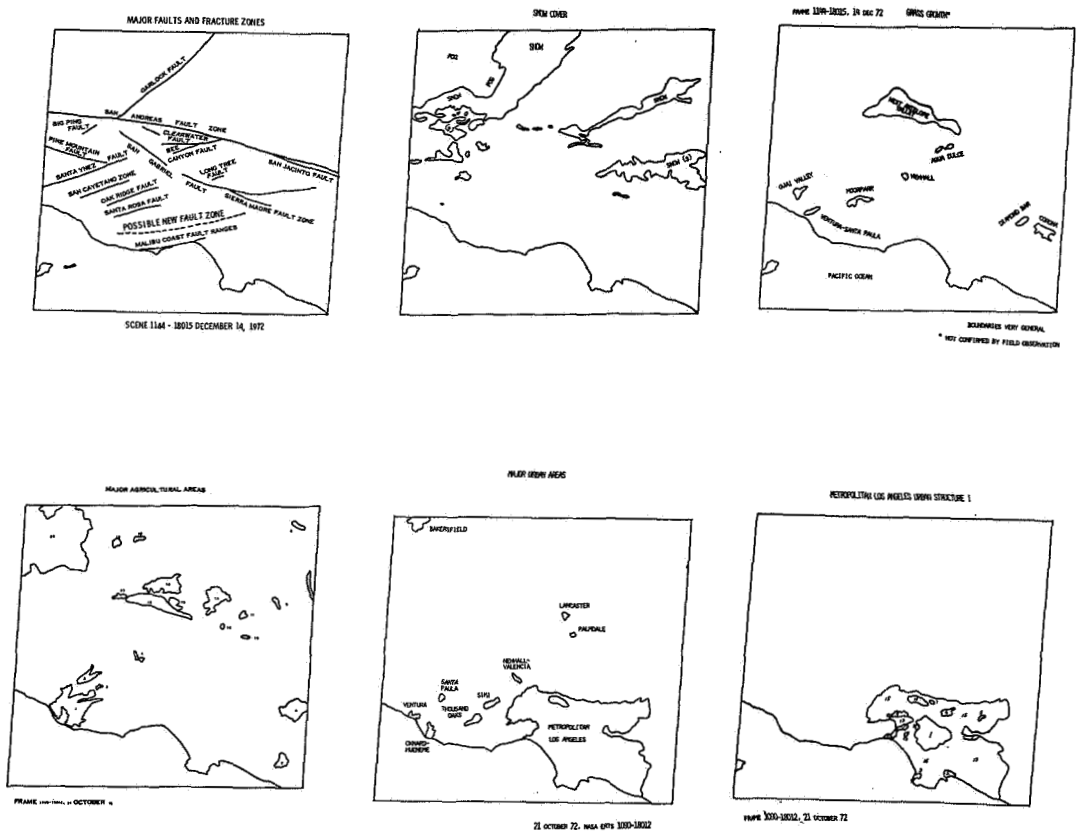


FIGURE 2 An assortment of photoreduced overlays constructed by photo-interpretation of ERTS scenes of the LA County Mainland representating regional and urban overviews of problems for further analyses.

The on-going series of overlays, inaddition to serving an orientation reference function, also gives a feel for the surprisingly vast data yield capability of the ERTS imagery. Our analysis indicates that ERTS data content exceeds the detail shown on the standard Army Map Service 1:250,000 scale plastic reflief series of maps.

Major Faults and Fracture Zones: A fairly casual visual inspection of the latest CoLA ERTS scene 1144-18015, viz. the December 14, 1972 imagery, in the non-current combination of bands (4, 5, 6) -- composited for us by the GE-Beltsville Photolab -- shows an unusually straight alignment of topographic features along the north face of the Santa Monica mountains. This suggested to the Test Site Coordinator the possibility of a major new fault zone or lineament. The County Geologist, Mr. Arthur Keene, has been assessing this possibility. The ERTS 1 Symposium Program announced a paper by Professors Pease and Johnson titled, "New Fault Lineament in Southern California". The broad pattern they presented in the paper G33 in the 3/6/73 session flanks the fault under consideration here, shown in the upper left corner o Figure 2 by the dashed line - - -. Corroboration of the existence of such a feature would indeed impact land use allocation decesion in the vicinity and its confirmed existence would have to be reflected in the mandatory Seismic Safety Element of the County General Plan. It should be pointed out too that in the imminent future, the Santa Monica Mountains will be increasingly the focus of much heated controversy with respect to their land use categorization!

Moving on to another overlay, the same December 14 print reflects major seasonal changes as compared to the previous ERTS scenes with the equivalent center point coordinates. Snow covers (upper center block in Figure 2) portions of the mountains and desert regions. Areas of new grass growth (upper right corner of Figure 2) mostly in the coastal lowlands are also seen for the first time in imagery over the Test Site. The simultaneous occurance of Spring and Winter conditions illustrate the environmental diversity of Southern California. This is new information from direct observation -- valuable to a number of local agencies concerned with water management, agriculture, recreation and transportation. It is also needed over the longer range by the planning commission to prepare an effective open space and recreation plan which takes into account also the scenic quality. This data will enable regional recreation planners identify areas of scenic quality -- a troublesome problem in scenic quality surveys otherwise made conventionally.

Brush fire burns, not shown in a figure here, show up in the August 10 NASA product E1018-18010 clearly in a four-some clump in the southeast while the October 21 scene E1090-18012 brought out very clearly the Large Sespe burn which later could be just discerned under the cloud cover in the NASA item E1036-18010 of August 28, 1972. The fire was known to have been burned during mid-August. The brush fires in Southern California form one of the major man-induced 'natural' hazards. The large areas burned in a synoptic view should impress any careless fire-bug! Incidently, data on topography, geology and fire hazard are used by planners in determining the use suitability of land. Suitability judgements are used, in turn, to allocate space for various types of land uses.

Major agricultural areas: lower left corner square in Figure 2. The very considerable variety and complexity of the introduced species of agricultural crops within the test stie are readily discernable in all the ERTS scenes on hand todate. A regional corroboration of the statement by Lt. Governor Reinecke of California - that agriculture forms the biggest industry in the State -- can be made in that County in as much as almost 10% of the County area is in agricultural use. As pointed out in the mini-paper in the Preliminary Findigs from ERTS Symposium of September 1972 dealing with Antelope Valley agriculture (area 13 in the overlay) the monitoring of

agricultural disinvestment and rural-urban conversion phenomena will be continued in what can be characterized as agricultural sub-systems study. The results of this work and the continued effort on water resources analysis from the ERTS imagery via the GEMS are reported in the study semi-annual report.

Major Urban Areas Intensive Analyses: The thrust of the effort underway in this investigation since the Preliminary Findings Symposium has been and will continue to be on the very complex urbanized regions within the Test Site (lower center, Figure 2). For the first time planners are able to directly observe the entire vast metropolitan area in a single scene on a repetitive basis. This experience is absolutely new and exciting. Again, we can directly see the shape and the general internal structure of the metropolis. An absolutely new data item is the extent and pattern of urban vegetation - a powerful clue to the physical and social segragation of the metropolitan area into subareas. (Lower right, Figure 2). It is necessary to have an accurate concept of these subareas for effective urban policy making and implementation.

Grading and New Construction Sites: Using U-2 aircraft imagery (Figure 3) for quasi-ground-truth we have been able to determine that we can identify from ERTS imagery (previous December 14 scene) all significant new grading and construction sites.

This is an emergent capability of major importance since it means we can cheaply monitor the extent and direction of new urban expansion and estimate the rate of expansion. This means we can now attack head-on a central problem of planning--trend detection. Knowledge of trend is essential for effective land use allocation and land use arrangement. The ability to identify new large construction from ERTS imagery means that it is now possible to monitor the extent, direction and rate or urban growth on a nationwide basis using only a single source data. Currently contribution to what fragmented policy in this field is made federally comes from a number of Federal Executive Departments: Commerce, Housing and Urban Development, Interior... formulated much as good deal of regional planning is done -- by abstraction, extrapolation etc. of data acquired from a multitude of sources, over a disparate time period and scale, at considerable expense. Monitoring of national urban growth could be done more cheaply by means of ERTS observation than any other on a very frequent (say, quarterly) basis. This monitoring would almost warrant a Super Cabinet charter!



FIGURE 3 One of the Vinten 70 mm frames from Ames, an area 14 X 14 naut. miles covering downtown LA - a mini-sub-site being most intensively studied using the GEMS.

Further series of 'urban' overlays, not shown again, were produced for identifying from ERTS imagery, using ground truth for discrimination as necessary, industrial and commercial districts and nodes -- shape and size factors help distinguish commercial from industrial user --; parks, cemeteries and golf courses -- these open space features are most visible on the October 21 scene composited of bands 4,5 and negative 7.

Urban Ecology: The previous overlays help sort out the urban ecology of the City. The distribution of open spaces, commercial and industrial areas above with textured difference in the urban pattern define the central city areas. Health concentration of urban vegetation defines high quality single family housing areas. These observations have been corroborated by a number of speakers during the last couple of days. Where we appear to have made more specific advance in an analysis of a complex urban area is in the further sub-classification and delineation of intra-city structural patterns of what will be characterized here as intensities of cover-use. The problem we have addressed to is that defined by Mr. James Wray during the second of his two papers -- dealing with the Washington, D. C. metropolitan area over the last decade and half.

Concurrently with the classical photointerpretation, machine analyses utilizing the GEMS have provided greatly enhanced urban analysis capability. An initial experiment involved the measurement of the intensity of red band in a color composite image (8-28-72). The results were displayed for each quartile of histogram distribution of the red intensities. Use of a 35 mm camera and projector -- in Valley Forge and Los Angeles, respectively! -- enabled us after much painstaking and patient tracking and matching to bring this ERTS-GEMS output slide to overlay onto a current land use map of scale 1:24,000 which is our operating scale for general planning work. A careful examination of the underlayed 1:24,000 scale current land use map indicates that the very exciting result is actually a measure of use intensity--a new data item directly obtainable from ERTS and highly significant in urban policy making and implementation. Moreover, these analyses have brought out areas that may be inaccurately depicted on our current land use map (scale 1:24,000).

The next series of experiments utilize the GEMS interactive multispectral signature acquisition/classification techniques to extract various land coverage classes from ERTS color transperancies. Four and seven theme analyses were performed on ERTS image 8-28-72 (scene 1036-18010), bands 4,5,7. The four and seven theme results are shown in Figures 4 and 5 respectively

The seven theme map gives a broad and meaningful ecological pattern of the most complex area of central Los Angeles. It separates areas east of the Alameda Street - San Fernando Road corridor from those to the west. It broadly separates the west side low income area from the middle income area. East of Alameda, two other middle income areas (one basically suburban) are broken out. Also major industrial and commercial districts and nodes as well as individual plants are factored out. Major open spaces are recognized as well as several dozen major street alignments defined. The texture (grain) of the urban pattern is greatly discernable. Finally, the color pattern functions like a "contour map" to give strength to edges and boundries in the ERTS scene.

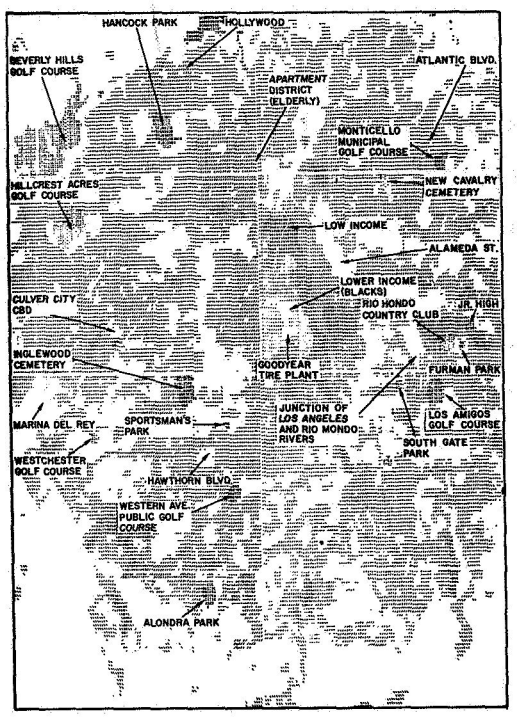


FIGURE 4 Four Theme Computer Printout from GEMS of Central Los Angeles, portion of the scene from Figure 3 above.

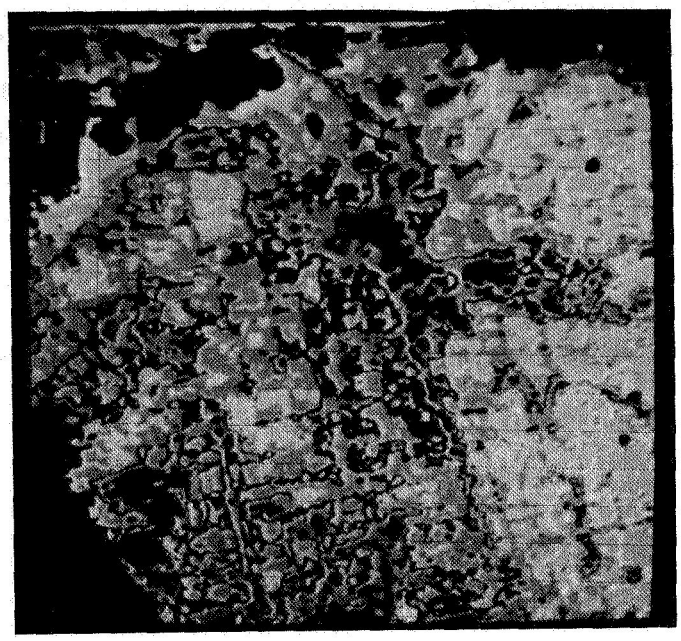


FIGURE 5 Seven Theme TV Display Picture off GEMS Screen from Scene E 1036-18010 at minimum zoom, viewing area same as in Figure 4.

This multiple theme presentation offers the potential for exciting urban design capabilities as well as providing the elements of a general design plan. This would be an absolutely new application of ERTS imagery. Even aircraft imagery is seldom applied to this use.

Preliminary GEMS histogram analyses of the Central LA Core indicates that land coverage can be segretated via GEMS into as many as 12 themes using ERTS color transperancies as inputs. With the completion of the new all digital GEMS/IMAGE 100 in July of this year, ERTS 4 channel digital data can be processed directly -- yielding significantly more land cover segregations. This better theme definition should provide even more effective information to the County of Los Angeles Regional Planning Commission.

A wide range of planning applications are presented above. There is rapidly growing interest expressed in ERTS-GEMS results being obtained by COLARPC by a variety of secondary users. The county geologist has strongly endorsed the use of ERTS for geological analysis. The county forest and fire warden has suggested establishment of a test sub-site and has made a helicopter available to project personnel on 3 occasions just since January 1, having had a first look at the ERTS imagery on hand. Personnel from the agricultural commission have verified the imagery and have repeatedly furnished ground truth. Outside the County, the Los Angeles City Depar tment of Water and Power and the California State Water Resources Board personnel have furnished the surface water acrages as ground truth based on their routine capacity curve measurements of the surface acrages.

Presentations have been made to:

1. Los Angeles County Association of Planning Officials;
2. Southern California Association of Governments (SCAG) technical staff;
3. Land Use Committee of the Citizen Planning Council;
4. Land Use Committee of the County General Plan Policy Review Board (GPPRB):
5. Conservation and Open Space Committee of GPPRB.

A presentation is scheduled on March 12 to the GPPRB - 17 major county department chiefs. Presentations have been requested by:

1. SCAG,
2. City of Los Angeles Planning Department.

The County Parks Department wants to learn if ERTS-GEMS can monitor the condition of the larger parks.

There have been several requests to use ERTS imagery in publications.

3. CONCLUSIONS

Initial results show that data from ERTS imagery can be of immense benefit in the field of urban and regional planning The impact of natural and man-made disasters can be determined timely and inexpensively.

Data on seasonal changes is available from a single source. The extent, direction and rate of urban growth can be effectively monitored. Generalized land use can be obtained at low cost and rapidly. Information on intensity of land use and urban form, neglected subects in many planning operations, are readily available from ERTS imagery.

A range of exciting opportunities are opened up in the field of comparative urban studies ERTS imagery will be widely useful in regional environmental impact analyses. Further analyses of ERTS imagery are certain to extend and deepen the benefits to primary users-investigators such as the County of Los Angeles Regional Planning Commission.

N73 -28314

Paper L 19

PREPARATION OF URBAN LAND USE INVENTORIES BY MACHINE-PROCESSING OF ERTS MSS DATA

William Todd, Paul Mausel, Kenneth Wenner, *Laboratory for Applications of Remote Sensing, Purdue University, West Lafayette, Indiana*

ABSTRACT

Spectral classes of urban phenomena identified from Earth Resources Technology Satellite (ERTS) multispectral scanner data in Milwaukee included "Suburban", "Inner City", "Industry", "Grassy" (open area), "Road", "Wooded Suburb", "Water", "Cloud", and "Shadow". The Milwaukee spectral class statistics were used to classify the Chicago area, within the same ERTS frame, and similar results were achieved. In another ERTS frame, Marion County (Indianapolis) data were classified into similar classes. The Marion County ERTS study was supported by a land use classification of an area near downtown Indianapolis that utilized 12-band MSS data collected by aircraft from 3000 feet. The results of the ERTS analyses suggest that satellite data will be a useful tool for the urban planner for monitoring urban land use.

1. GENERAL DISCUSSION

The Milwaukee County Subframe

Land use information systems are becoming increasingly important to investigators interested in large urban complexes. On August 9, 1972 ERTS passed over a large area in the Midwest, including portions of northern Illinois and southern Wisconsin. The Milwaukee County subframe was chosen to assess the utility of ERTS data for urban land use studies.

Four bands (4,5,6,7) of ERTS multispectral, digitized data were analyzed by computer programs developed at the Laboratory for Applications of Remote Sensing (LARS)[1] Initially, the data were examined on a digital imaging display (e.g. Fig. 1-A, Fig. 1-B). Significant amounts of information may be learned by studying gray scale band images but their primary purpose was for orientation. The major effort was directed toward obtaining a land use classification of the county from analysis of the four bands of ERTS MSS data.

The nonsupervised clustering algorithm ($NSCLAS) was used to disect the data into the most spectrally separable classes, using all four bands of data. Statistics were calculated for the clusters delimited, using a maximum likelihood classifier ($CLASS), and the results displayed by a line printer with different alphanumeric symbols for each class ($DISPLAY).

[1]T. L. Phillips, (Editor), LARSYS Users Manual, (West Lafayette, Indiana, Laboratory for Applications of Remote Sensing, Purdue University, 1973).

Original photography may be purchased from:
EROS Data Center
10th and Dakota Avenue
Sioux Falls, SD 57198

Most of the classes of ground cover types delineated by $NSCLAS were not adequately representative of the land use in the county. Thus, it was necessary to train the computer manually to recognize many earth surface features. Only one class chosen by $NSCLAS, representing grassy, open areas, was retained. Its field coordinate cards were combined with those chosen manually for other classes. As before, the $STAT, $CLASS, and $DISPLAY programs were used to classify the study area. Finally, the $PHOTO program was used to display and photograph the classification results from the digital display. Table 1 lists the spectral reflectance of the classes and the gray levels used for display.

In the classification results (Fig. 1-C) the white area in the central part of the study area, which contains Milwaukee's Central Business District, has a very high reflectance in the visible bands. The principal component of this class is concrete while rooftops are secondary features. This class, termed "Road", occurs also as Interstate highways and sandy beaches along Lake Michigan.

The first ring outward from the Central Business District, appearing black, is termed "Inner City". A majority of the homes in this area are the bungalow or "two-flat" type of structure, housing two or more families, and were usually built prior to 1940. Rooftops and roads are the primary constituents of this class while green vegetation is a secondary component.

The class "Industry" (dark gray) was identified only where the larger areas of heavy industry predominate. Two very large industrial regions were identified, which together form an L-shaped region located just south of the Central Business District. One region is in the Menomonee River Valley and the other in the Kinnickinnick River Valley. Rooftops are the primary, and roads are the secondary components of this class.

The ring north, west, and south of the "Inner City" is an area of complex land uses. The three primary cover types in this area are "Suburban", "Grass", and "Wooded Suburb". Most of this ring is classified as suburban (shown as white) and includes the outer areas of the City of Milwaukee, northern Wauwatosa, West Allis, and other suburbs within Milwaukee County. "Suburb" consists primarily of single-family, middle-income residences built after World War II which are characterized by a complex mixture of roads, rooftops, and green vegetation. The areas of the class "Wooded Suburb" (very light gray) are southern Wauwatosa, Fox Point, Whitefish Bay, and Shorewood which comprise the older upper income sectors of Milwaukee County. Green vegetation is the primary component of this class. Finally, the class "Grass" (very dark gray) manifests itself in this ring in the parks, golf courses, and cemeteries. Most of the outer areas of the county were classified as "Grass". A problem in the classification of this area was the misclassification of newer, upper-income areas as "Grass".

Five classes of water were identified within the study area, four of which are located almost exclusively in Lake Michigan. There is a regu-

lar succession of water classes eastward (Fig. 1-C), suggesting that the various classes of water are indicators of depth. However, reference to U.S. Geological Survey topographic quadrangles shows only slight association between the spectral classes of water and depth of water.

The fifth class of water ("Water 4") occurs in small water bodies and in the Milwaukee River. This class also appears in Milwaukee Harbor (inside the breakwater) and to the south along the coast. Factors influencing the spectral differences in water may be color, turbidity, and clarity.

Several small cumulus clouds were identified within the study area; these are located in the southern part of Milwaukee County and are displayed as white (level 16). The cloud shadows are displayed as black (level 1).

Chicago Subframe

Analysis of the Chicago subframe was undertaken to determine if the spectrally separable classes which were used to classify urban land use successfully in one metropolitan area could produce satisfactory results in another metropolitan area, within the same ERTS frame.

Images representing spectral data of Chicago from bands 5 (Fig. 2-A) and 7 (Fig. 2-B) were produced, using the same histograms generated for use in the Milwaukee area. The Chicago spectral data were analyzed by applying the $CLASS through $PHOTO sequence of computer programs, using the same $STAT deck of computer cards as used in the Milwaukee study. Chicago classification results were similar to those of Milwaukee (Fig. 2-C). The same gray levels were used for both urban classifications.

The first major ring of land use outward from the Central Business District was classified as "Inner City". This area includes most of the city of Chicago, Cicero, Berwyn, and Blue Island. Larger parks, cemeteries and large industrial areas were identified within this ring.

The next ring outward includes large areas of the classes "Suburb" and "Wooded Suburb". The larger areas of "Suburb" are found in the municipalities of Oak Lawn, Hodgkins, Norridge, Harwood Heights, and Morton Grove. Four major regions of the class "Wooded Suburb" appeared: (1) the Glencoe, Wilmette, Evanston area along Lake Michigan; (2) the suburban agglomeration south of O'Hare Airport including Oak Park, Elmhurst, Lombard, and Wheaton; (3) the suburban agglomeration to the south of the second, including Hinsdale and Downers Grove; and (4) an area in Chicago bounded by the Dan Ryan Woods on the north, 119th Street on the south, Beverly Street and Vincennes on the east, and Western Avenue on the west.

The classes "Cloud" and "Shadow" were identified in the northwestern part of the Chicago area, north of O'Hare Airport.

A problem in the Chicago classification arose in the central, older part of the urbanized area, most of which was classified as "Inner City". Too many data points within this area were classified as "Industry"

suggesting that yet another type of residential area exists in Chicago, which is not found in Milwaukee. It is speculated that such residential areas are largely void of vegetation and consist mainly of rooftops and roads.

Marion County (Indianapolis) Subframe

In another ERTS frame (pass of Sept. 30, 1972), similar spectral classes were obtained for the Indianapolis area, using the same procedures of analysis developed for the Milwaukee area. Initially, the nonsupervised ($NSCLAS) method of classification was implemented followed by the manual, or, supervised approach. Classification results are presented in Figure 3-A, and Table 2 lists the mean reflectance of classes and the gray levels used in the figure.

Whereas a class for heavy industry was obtained in the Milwaukee area, a general class of heavy industry/commerce was developed (shown as medium gray) for Indianapolis. This class includes the Central Business District. As in Milwaukee, the class "Suburban" was developed for Indianapolis. Areas in this class are located on the eastern and western flanks of Interstate 465.

In the Milwaukee study, a class "Wooded Suburb" was obtained, but a more general class "Wooded" was used in Indianapolis. Areas around the city's reservoirs and certain upper income areas near Meridian Hills and to the east were classified as "Wooded". Only one class of "Water" was developed which was represented by the primary water bodies of Geist and Eagle Creek Reservoirs. Several small cumulus clouds and their shadows were identified within the county.

A problem in the classification arose in some locations between "Suburb" and "Inner City". Areas in these classes were misclassified frequently as "Grassy" (open) or "Wooded". Apparently, the distinction between the "Suburban" and "Inner City" is not as well defined as in Milwaukee.

Supporting the Indianapolis ERTS study was an analysis of 12-band multispectral scanner data collected by aircraft from 2000 ft. over a portion of the West Fork White River near downtown Indianapolis. The same procedure of analysis was used as in Milwaukee, Chicago, and Marion County except that only four of the twelve bands (#2, .46-.49μm; #6, .55-.60μm; #10, 1.0-1.4μm; #12, 9.3-11.7μm) were used to classify the study area. Table 3 lists the mean reflectance and gray levels used in the three photos of the classification. Fig. 3-B shows the general classes of earth surface features. The classes, from darkest to lightest, are "Water", "Bare Soil", "Road", "Fine Grass", "Coarse Grass", "Trees", and "Rooftops". Fig. 3-C shows the variations in cultural features. All natural features are displayed by one gray-tone, while the two classes of "Road" and three of "Rooftop" are given varying graytones. Fig. 3-D shows the variation in natural features. All cultural features are one graytone, while "Trees", two classes of "Coarse Grass", and two classes of "Fine Grass" vary in graytone.

CONCLUSIONS

Machine processing of ERTS MSS data in urban areas has produced spectral classes which may be of value to the urban planner. Looking toward the future, timely processing of such data could result in quick updating of land use inventories. The Chicago results indicate that a careful analysis of one urban area can provide valuable information for other urban areas, with no a priori knowledge. It is not unreasonable to forecast the development of statistics, taking into account seasonal variations, which may be used to classify automatically many urban areas.

RELATIVE MEAN REFLECTANCE AND GRAY LEVELS USED FOR DISPLAY OF SPECTRAL CLASSES

Table 1. Milwaukee (ERTS)

	Bd. 4	Bd. 5	Bd. 6	Bd. 7	Level[1]
Water 1	35.20	21.41	9.94	1.49	5
Water 2	24.23	10.37	5.40	0.69	3
Water 3	19.71	9.42	5.86	1.10	1
Water 4	21.47	13.85	12.65	3.34	1
Water 5	46.83	46.50	23.83	2.83	14
Grass 1	27.01	19.88	53.16	31.35	6
Grass 2	24.03	16.25	44.18	26.59	6
Road	47.42	48.26	46.84	20.16	16
Wood Sub.	24.94	18.66	40.24	22.91	10
Inner City	30.16	25.97	34.59	16.53	1
Suburban	39.17	37.09	53.12	26.99	16
Industry	25.98	21.77	21.30	8.50	8
Cloud	71.55	69.50	89.07	44.38	16
Shadow	17.70	9.45	16.15	6.75	1

Table 2. Indianapolis (ERTS)

	Bd. 4	Bd. 5	Bd. 6	Bd. 7	Level[1]
Commerce	34.28	30.70	28.17	11.88	8
Inner City	24.01	17.04	26.18	14.09	1
Suburban	31.87	25.82	41.07	22.51	16
Grassy	23.65	17.33	34.69	20.36	5
Wooded	19.79	12.01	32.95	21.10	11
Water	22.64	13.73	8.24	1.37	1
Cloud	82.41	78.88	85.08	41.17	16
Shadow	16.49	8.46	9.46	3.31	1

Table 3. Indianapolis (2000 Feet)

	Bd. 2	Bd. 6	Bd. 10	Bd. 12	GC[2]	CC[3]	NC[4]
Rooftop 1	130.04	145.81	88.40	199.23	16	16	3
Rooftop 2	86.28	98.27	70.33	221.53	16	13	3
Rooftop 3	47.34	44.75	37.63	248.43	16	10	3
Road 1	158.67	201.79	120.61	122.80	6	6	3
Road 2	90.59	102.96	71.39	152.58	6	8	3
Fine Grass 1	50.30	72.20	150.58	132.11	8	4	9
Fine Grass 2	44.82	60.98	146.43	124.81	8	4	11
Coarse Grass 1	51.49	68.73	108.56	134.96	10	4	13
Coarse Grass 2	44.74	57.87	105.80	128.21	10	4	16
Trees	38.69	48.27	105.28	88.49	12	4	7
Bare Soil	86.93	106.52	80.57	153.01	4	4	5
Water	43.11	53.00	27.11	84.73	1	1	1
Shadow	37.82	35.70	39.24	73.98	1	1	1

[1]Gray levels used in land use classification.
[2]Gray levels used in classification: general classes.
[3]Gray levels used in classification: cultural features.
[4]Gray levels used in classification: natural features.

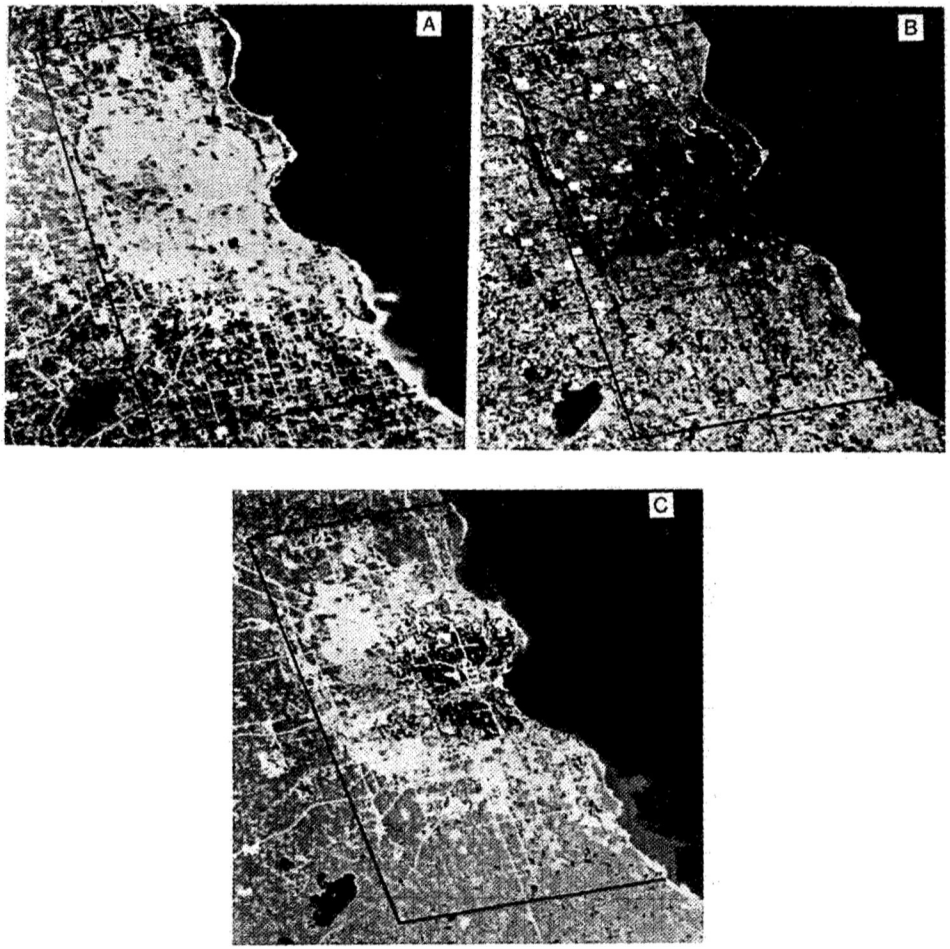


Figure 1. Photos of images from digital display. (A) is from the visible portion of the spectrum (band 5, 0.6 to 0.7 μm); (B) is from the infrared (band 7, 0.8 to 1.1 μm). (C) is a land use classification. Black line is boundary of Milwaukee County.

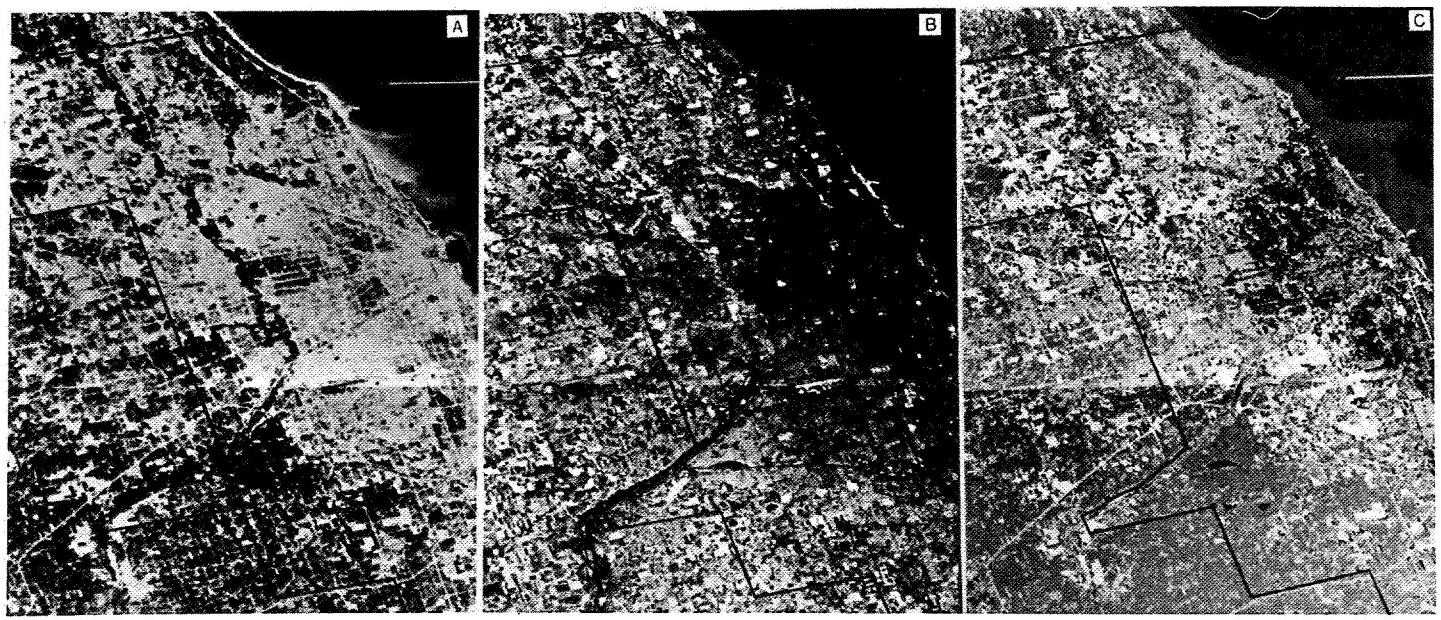


Figure 2. Photos of images from digital display. (A) is from the visible portion of the spectrum (band 5, 0.6 to 0.7 μm); (B) is from the infrared (band 7, 0.8 to 1.1 μm). (C) is a land use classification. Black line is boundary of Cook County.

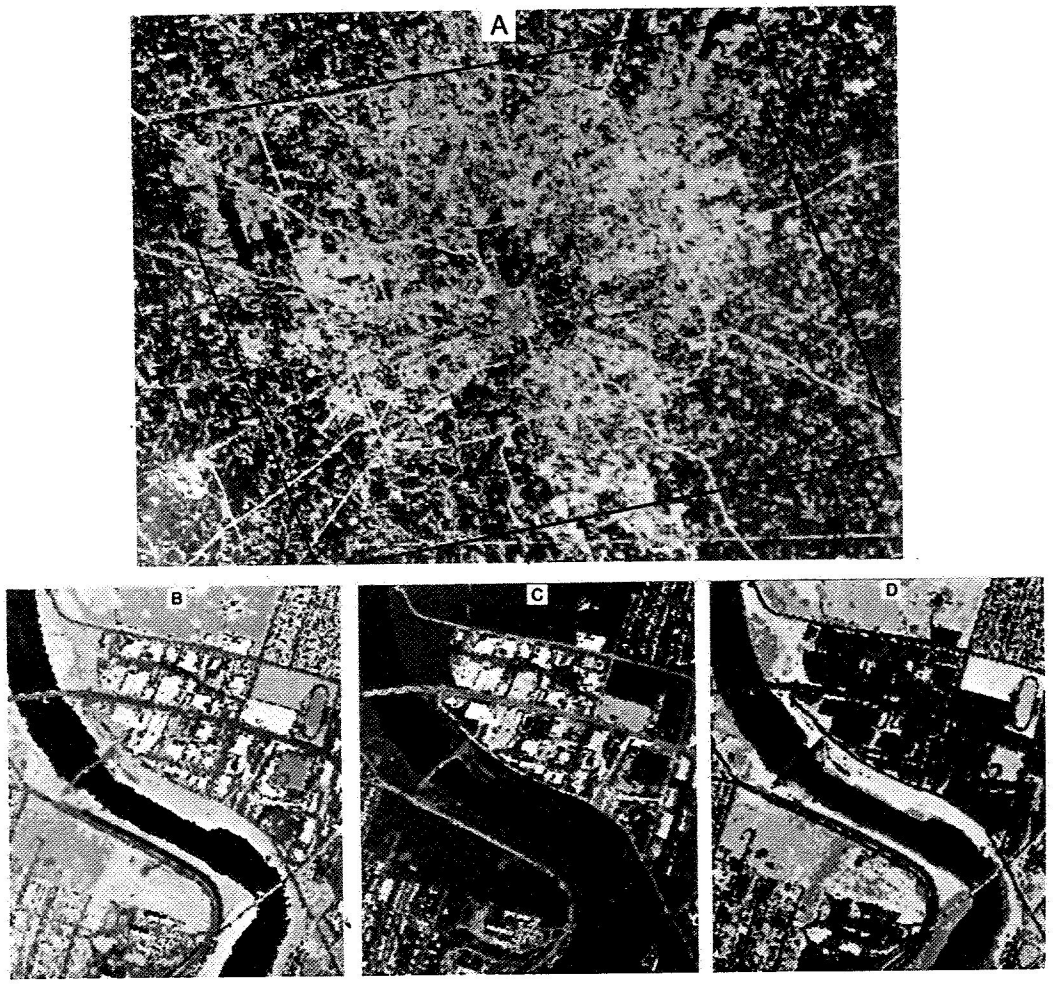


Figure 3. Photos of images from digital display. (A) is a land use classification of Marion County/Indianapolis (black line is county boundary). (B), (C), and (D) are various portrayals of a single land use classification of 2000 feet MSS data near downtown Indianapolis. (B) shows variations in general classes of surface features; (C) the variation in cultural features; (D) the variation in natural features.

N73-28315

Paper L 20

A COMPARISON OF LAND-USE DETERMINATIONS USING DATA FROM ERTS-1 AND HIGH ALTITUDE AIRCRAFT

M. Ann Lundelius,* C. Mark Chesnutwood, Joe G. Garcia and R. Bryan Erb†
Earth Observations Division, NASA Johnson Space Center, Houston, Texas

ABSTRACT

A manual interpretation of ERTS-1 MSS system corrected imagery has been performed on a study area within the Houston Area Test Site to classify land-use using the Level I categories proposed by the Department of the Interior. The two types of imagery used included: (1) black and white transparencies of each band enlarged to a scale of approximately 1:250,000 and (2) color transparencies composited from the computer compatible tapes using the film recorder on a multispectral data analysis station. The results of this interpretation have been compared with the 1970 land-use inventory of HATS which was compiled using color ektachrome imagery from high altitude aircraft (scale 1:120,000). Urban data from the same scene was also analyzed using a computer-aided (clustering) technique. The resulting clusters, representing areas of similar content, were compared with existing land-use patterns in Houston. A technique was developed to correlate the spectral clusters to specific urban features on aircraft imagery by the location of specific, high contrast objects in particular resolution elements. The surface feature composition within each picture element (pixel) could then be determined from the aircraft imagery. It was concluded that ERTS-1 data could be used to develop Level I and many Level II land-use categories for regional inventories and perhaps to some degree on a local level.

1. INTRODUCTION

The purpose of this paper is to report on the ERTS-1 investigation at the Johnson Space Center (JSC) and in particular on the use of ERTS-1 data as a source of information for compiling land-use inventories. The work of the Earth Observations Division Investigation teams and the Land-Use/Urban Analysis team in particular is acknowledged. The objectives of the overall ERTS-1 investigation at NASA/Houston are threefold: (1) To determine the categories of land-use in the Houston Area Test Site (HATS) which can be derived from ERTS-1 data and to map these for a portion of the test site; (2) To assess the utility of ERTS-1 data to detect, identify, delineate and measure features of applications interest in forest, range, coastal, agricultural and urban areas; and (3) To evaluate, with the U.S. Department of Agriculture, the utility of ERTS-1 data to detect and identify specific crop species, determine categories of land use in agricultural areas, locate field boundaries and measure crop and land-use acreages.

The investigation teams are utilizing both conventional and computer-aided interpretation techniques in working with the data. Aircraft imagery is being used as a basis for comparison with ERTS-1 data along with a land-use map of HATS derived from manual interpretation of high altitude aircraft imagery.

2. CLASSIFICATION SCHEME

The classification scheme chosen for this investigation is that described in the U.S. Department of the Interior Geological Survey Circular #671. This scheme has been proposed for possible adoption on a national basis (see Appendix I). A subsidiary objective of the investigation was to see how well this scheme fitted the Houston region and what, if any, modifications might be required to produce a meaningful classification.

---

*Lockheed Electronics Company, Inc., Houston, Texas.

†S. H. Tunnell, W. P. Bennett, V. L. Cook and D. P. McGuigan of LEC are acknowledged as contributors to this paper.

PRECEDING PAGE BLANK NOT FILMED

Original photography may be purchased from:
EROS Data Center
10th and Dakota Avenue
Sioux Falls, SD 57198

3. DATA USED

ERTS-1 data from two passes over HATS were utilized for general land-use determinations. These passes, on August 29 and October 4, 1972,[1] occurred in generally clear conditions and the satellite data appears to be excellent. On the August pass, high altitude underflights were flown over a portion of the test site. Both imagery and digital data were acquired from the NASA Data Processing Facility. The imagery was utilized in the form of black and white prints of each band enlarged from the 70 mm positive transparencies to a scale of approximately 1:250,000. The digital data was used in two ways: It was used for computer-aided classification by spectral pattern recognition, and was also used to provide color composites of 2 and 3 bands using the film recorder on a multispectral data analysis station giving essentially a first generation film product at a scale of approximately 1:250,000.

4. MANUAL IMAGE INTERPRETATION

A manual interpretation of enlarged black and white imagery, primarily bands 5 and 7, was carried out and the Level I categories were delineated for approximately one quarter of an ERTS-1 scene. The following categories were detected and identified: urban and built-up, agricultural land, rangeland, forest land, water and non-forested wetland. Of the remaining Level I categories, two do not apply to the Houston region, these being tundra and permanent snow and ice fields. In the particular area studied there was no barren land.

The combined categories of agricultural and rangeland were easily identified, but delineating the boundary between these categories was difficult. Field size and shape considerations were helpful, but the delineation is considered the least reliable of the Level I determinations. Further, the definitions were modified to the extent that pasture was grouped with rangeland. There is also a definitional issue regarding the Level I classification of oil and gas extractive areas. The land surrounding producing wells is normally grazed and thus qualifies as rangeland. However, for this effort it was designated as extractive in the urban and built-up category, holding with the original scheme. In this part of Texas it is difficult to select objectively between the rangeland and non-forested wetland categories.

The results of this classification were compared with a land-use map of HATS previously developed from small scale imagery acquired by high altitude aircraft. This map was derived from a manual interpretation of color ektachrome imagery at a scale of 1:120,000. For this previous study, carried out in 1971, a 20 category classification scheme was used.[2] To make possible a comparison with the Level I ERTS interpretation, this 20 category classification was aggregated to conform to the scheme adopted for the investigation. The agreement is generally good as can be seen by referring to Figures 1 and 2.

To make a quantitative comparison, however, a different technique was adopted. The composite color images produced at JSC from the digital data were used for a manual interpretation striving to extend beyond the Level I in the Urban and Water categories.

The conventional color composites, simulating color infrared photographs by combining bands 4, 5 and 7 were generally best for large cultural features, forest areas and extractive areas such as oil fields, but poor for small urban places and for the agricultural versus range differentiation. Using composites of bands 5, 6 and 7 the agricultural areas were more readily distinguished from rangeland. Small urban places and roads through forests were also more readily delineated on this composite. A composite of bands 5 and 7 was also studied and found most useful for cultural features.

The results of this study of color composited images from the digital data were that several Level II categories could be delineated from the ERTS-1 data. In the urban and built-up classification only three Level II categories or aggregates of categories could be identified: (1) an aggregate of commercial

---

[1]Scene ID 1036-16244 and 1073-16244

[2]Bryan Erb, "Applications Experiments in the Houston Area," Fourth Annual Resources Review, JSC 05937, vol. I (Jan 1971), p. 21-9, fig. 4.

and services, industrial and transportation, communication and utilities; (2) strip and clustered settlements and, (3) extractive areas. By deduction, the balance of the urban classifications are an aggregate of the residential and/or open and other categories. No success was expected or found with the institutional category. Thus four Level II groupings could be delineated within the urban and built-up classification. In comparison, somewhat greater detail can be derived from the high altitude aircraft data. A delineation of open land is readily obtained and the commercial-industrial-transportation grouping can be further broken down but with limited reliability. Again, the institutional category cannot be delineated with confidence.

In the water category all of the Level II categories could be delineated to include water bodies of a few acres in size. This classification compares well with that possible from the high altitude aircraft data. Another part of the investigation (carried out by the Coastal team and reported on separately in this symposium) also addressed the delineation and areal measurement of Level II features, specifically wetlands by computer-aided techniques. Good success in identification was achieved. Areal measurements were made of features a few hundred acres in size and determined accurate on the order of 90 percent based on measurements of rectified photographs from synchronous aircraft underflights.

In parallel with this investigation at JSC, a land-use determination was contracted at the Stephen F. Austin University. This effort used color infrared imagery acquired in April, 1972, by a high altitude aircraft. This determination was used as a basis for a preliminary quantitative comparison with the delineations arrived at by interpretation of the ERTS-1 data. A grid was superimposed on both interpretations and a success count made.

5. COMPUTER – AIDED CLASSIFICATION

Another major portion of this investigation has been the application of computer-aided spectral pattern recognition techniques. Both supervised and unsupervised methods have been used, however, in the land-use work only the latter method has been employed to date. The specific technique used is a clustering of the MSS data in all four channels into groups of resolution elements with like spectral content. It is then necessary, of course, to apply intelligence to the features thus clustered by correlating them to known surface characteristics derived from aircraft data or from surface observations.

ERTS-1 digital data over a portion of the Houston area was processed by the clustering method and there resulted six groups with spectrally similar features. A very preliminary comparison with the 1970 land-use maps indicates that the breakdown approximates very roughly the Level II features in the urban and built-up Level I category. It should be noted that the clusters do not correspond uniformly to actual urban patterns. One reason, of course, is that any resolution element at the ERTS-1 scale may comprise a complex conglomeration of features. It is also apparent in the data from August 29 that atmospheric haze over part of Houston perturbs the clustering results seriously. An effort being pursued as part of this investigation (by the Signature Expansion team and reported on separately in this symposium) is the correction of data for such local atmospheric effects.

The spectral content of the ERTS-1 data appears to be sufficiently high that considerable success can be obtained in computer-aided classifications at Level II. Other efforts which are part of this investigation (being carried on by the Forest team, the Range team and the Agriculture team, and also reported on separately) have shown considerable success in applying these techniques to classifications in their special areas which are at the Level II or more detailed levels.

6. CORRELATION OF ERTS DATA TO URBAN FEATURES

As mentioned in the previous section, a closer look at the results of the unsupervised classification indicated that the clusters do not correspond uniformly to actual urban patterns. Consequently an effort was made to merge this technique with conventional image interpretation to determine why distinctly different urban features were being classified as clusters of similar spectral characteristics.

The inherent spatial and spectral heterogeniety of urban features, made it desirable to examine the actual spectral composition of urban features represented by individual picture elements (pixels) in somewhat more detail than is normally necessary in analyzing homogeneous spectral responses of agricultural and forestry features. One pixel from an urban scene may comprise a very complex conglomeration of features (roofs, pavements, trees, grass, and shadows) each with its own range of spectral reflectivities integrated into an average spectral response. In order to locate and identify a specific pixel and determine its feature composition a simple technique was developed utilizing a computer printout map and aerial photographs of several scales over which transparent grids as a means of identifying points common to both media.

The clustering program was used to produce the printout in which each pixel was identified by a scan line number and an element number. In the clustering program each pixel was classified into categories of similar spectral reflectivities. Small objects of very high reflectivity (white or aluminum roofs) were often classified as individual pixels which could be readily identified on the aerial photographs. By specifically identifying and locating three or more individual pixels which lay on or near two of the printout grid lines, it became possible to construct a corresponding photo grid. A transparent grid was initially constructed to fit a 1/60,000 scale photo in which each grid cell represented 25 pixels. Successful use of this grid encouraged the construction of another transparent grid which could be used on a 1/1980 scale photo enlargement. With this large scale photo and grid it became possible to estimate the percentages of objects with different reflectivities in each pixel which made up the integrated spectral signature for that specific pixel. For the particular urban scene used in this study the clustering program classified each pixel into one of six clusters. The fraction of each pixel with certain levels of brightness found within the pixels in the six clusters are listed in the following table:

BRIGHTNESS COMPOSITION OF PIXELS IN AN URBAN SCENE

(PERCENTAGE OF AREA WITHIN A PIXEL)

PANCHROMATIC BRIGHTNESS	CLUSTER					
	1	2	3	4	5	6
High	80	20	36	4	80	56
Medium	20	80	64	8	4	
Low				88	16	44

Once specific pixels have been located the urban features comprising the pixels which constitute each cluster can be determined. For the test area (downtown Houston) shown in Figure 3, the feature composition is as follows:

Cluster 1 – Large buildings or building complexes with high-reflective roofs
Cluster 2 – Open grass-covered fields with few trees
Cluster 3 – Predominantly grass-covered areas but with a greater proportion of moderately bright objects (pavements, roads)
Cluster 4 – Predominantly tree-covered areas with small areas of roofs and streets intermixed
Cluster 5 – Predominantly paved- and roof-covered areas with many short shadows, but no trees
Cluster 6 – Complex mixture of roofs and trees or pavements and long shadows

Although the descriptions of the six clusters were purposely made quite general in order to relate as closely as possible to typical urban land-use terminology, numerous inconsistencies occurred not only within the study scene but also when these same clusters were examined in other parts of the metropolitan area. This was particularly true in the more highly built-up areas where the intermixture of very bright objects and low brightness objects was a conglomeration of bright roofs and shadows rather than bright roofs and trees as represented by cluster number six.

It is concluded from the sample detailed study of the urban area that our preliminary clustering techniques did not permit a consistent automatic classification of multispectral scanner data into categories according to usual urban land-use terminology. Although the geographical distribution of some of the clusters did coincide very well with some of the known land-use categories there was a sufficient number of classification anomalies to seriously affect the accuracies of delineations to be expected in analyzing an unfamiliar urban area. The capability of determining the spectral composition of individual pixels should be a valuable means of adjusting the clustering program parameters to provide cluster classifications more accurately. This capability should also be useful in selecting training fields for supervised data manipulations in future work.

7. CONCLUSIONS

An investigation in progress at the Johnson Space Center is exploring the utility of ERTS-1 data for land-use inventories in the Houston area. Sufficient work has been done to reach the following tentative conclusions:

(1) All applicable Level I and many Level II land-use categories can be delineated by manual interpretation of ERTS-1 images. Much better results are obtained with composites constructed directly from the digital data than with enlargements of the separate black and white material from the NDPF.
(2) Computer-aided classification can provide good results on many Level II classifications. Level I classifications may be best arrived at by aggregating more detailed determinations.
(3) The results of classifications derived by manual interpretation of ERTS-1 data compare well with those derived from high altitude aircraft data. However, aircraft data permit determination of a few more Level II categories.
(4) The USDI proposed national land-use classification scheme can be generally followed at Level I for the Houston area but a few of the definitions require some modification. Some Level II (urban) categories are difficult to determine even with aircraft data.
(5) A cooperative use of conventional manual and computer-aided techniques can be useful to correlate ERTS-1 data to specific urban features and to establish the feature composition of specific resolution elements.

A conclusion of the total investigation is that ERTS-1 appears capable of providing data with which it is possible to detect, identify, and delineate surface features of applications interest. Furthermore, it appears possible, on the basis of limited tests, to measure the areal extent of such features with good accuracy.

The overall conclusion is that ERTS-1 data can be used to study a significant array of features in several disciplinary areas and thus contribute to land-use inventory work on a regional and to some degree, on a local level.

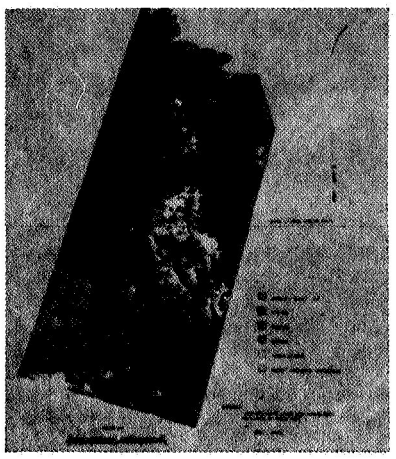


Figure 1 - Level 1 land use in HATS from high altitude aircraft data

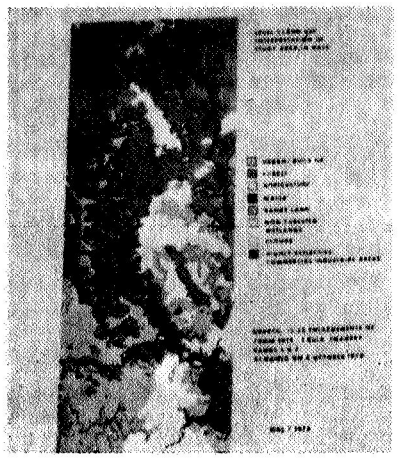


Figure 2 - Level 1 land use in HATS from ERTS-1 data

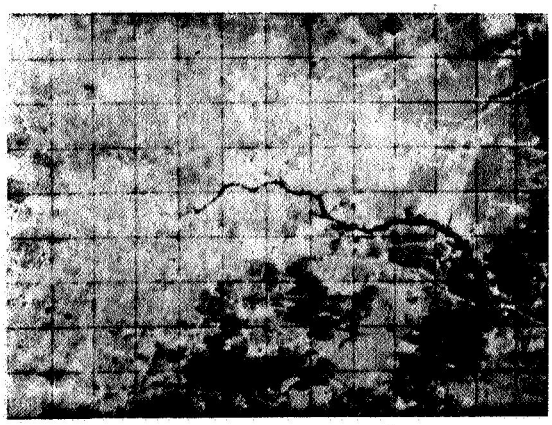


Figure 3 - Photo of downtown Houston with superimposed grid of ERTS resolution elements

APPENDIX I

LAND USE CLASSIFICATION SYSTEM FOR USE WITH REMOTE SENSOR DATA

LEVEL I	LEVEL II
URBAN AND BUILT-UP LAND	RESIDENTIAL COMMERCIAL AND SERVICES INDUSTRIAL EXTRACTIVE TRANSPORTATION, COMMUNICATIONS, AND UTILITIES INSTITUTIONAL STRIP AND CLUSTERED SETTLEMENT MIXED OPEN AND OTHER
AGRICULTURAL LAND	CROPLAND AND PASTURE ORCHARDS, GROVES, BUSH FRUITS, VINEYARDS AND HORTICULTURAL AREA FEEDING OPERATIONS OTHERS
RANGELAND	GRASS SAVANNAS (PALMETTO PRAIRIES) CHAPARRAL DESERT SHRUB
FOREST LAND	DECIDUOUS EVERGREEN (CONIFEROUS AND OTHER) MIXED
WATER	STREAMS AND WATERWAYS LAKES RESERVOIRS BAYS AND ESTUARIES OTHER
NON-FORESTED WETLAND	VEGETATED BARE
BARREN LAND	SALT FLATS BEACHES LAND OTHER THAN BEACHES BARE EXPOSED ROCK OTHER
TUNDRA	TUNDRA
PERMANENT SNOW AND ICEFIELDS	PERMANENT SNOW AND ICEFIELDS

Appendix 1 - Land use classification scheme

N73-28316

Paper L 21

DIGITAL LAND USE MAPPING IN OAKLAND COUNTY, MICHIGAN

Irvin J. Sattinger and Robert D. Dillman, *Environmental Research Institute of Michigan, Ann Arbor, Michigan*

ABSTRACT

ERTS-1 data for a portion of Oakland County, Michigan was computer processed to produce a map of water, urban areas, wooded areas, and other vegetation. Comparison with RB-57 photography of the area shows a good correspondence of the two sources of data. Preliminary evaluation indicates that this type of four-category map derived from ERTS data will be useful for conceptual studies of large geographic areas in recreational planning.

1. INTRODUCTION

The objective of this investigation is to use and evaluate ERTS data in continuing studies of land use in the seven-county area surrounding Detroit, with special emphasis on identifying and evaluating land that should be acquired and preserved for open space and recreational use and to maintain the environmental quality of the area. A major portion of the study is being concentrated on test sites in Oakland County, which is characterized by the presence of a number of lakes as well as wetland and wooded areas. Although the development of methods is concentrated on sites of limited size, it is expected that ERTS data will ultimately be used for studies of regional scope. The investigation emphasizes computer processing of ERTS-1 multispectral scanner imagery to observe and map a number of fundamental factors which determine the suitability of land for recreational use or open space. Photographic and scanner imagery from aircraft flights, ground truth, and other data sources are being used where available to supplement and evaluate the ERTS imagery.

2. DATA ANALYSIS

The only usable ERTS-1 coverage of Oakland County to date was obtained on 28 September 1972 (Observation ID 1067-15643). The usefulness of the data is limited by partial cloud cover, but at least some sections of Oakland County and adjacent areas in Southeast Michigan are cloud-free and usable (Figure 1). Since this was the only coverage of the test site obtained while foliage is visible till the spring of 1973, the data analysis has begun with usable sections of the frame.

Original photography may be purchased from:
EROS Data Center
10th and Dakota Avenue
Sioux Falls, SD 57198

Black-and-white photos of the ERTS frame in all four bands have been studied to identify major features of interest and to decide on subsequent steps for data processing. The large number of lakes in Oakland County show up well in Bands 6 and 7. Major roads, subdivisions, and wooded areas are also clearly visible in Bands 4 and 5. The southwest corner of the frame, constituting about one-sixteenth of the total frame, was printed out as a gray map by digital computer. The area printed out corresponds closely to Oakland County. This printout was studied along with existing RB-57 photography of the area and other sources of information to select a smaller area for intensive computer analysis. This area was selected at a location free of cloud cover and includes surface features of particular interest for the study objectives. The area selected is approximately nine miles northwest of Pontiac (Figures 2 and 3). It includes Big Lake, Pontiac Lake, the Pontiac Lake State Recreation Area, and the Huron Swamp, which is the site for a new 2,000 acre park, the Oakland Metropolitan Park, recently announced by the Huron-Clinton Metropolitan Authority. The park will be used to preserve a natural wild area and provide picnic areas, a trail system and an outdoor conference area.

The area supports a variety of vegetation. Figure 2, which is a vegetative map of Oakland County, indicates that vegetation in the outlined area includes mixed hardwoods, lowland hardwoods, oak-hickory stands, upland brush, grass, and crops. Continuing studies of the area will determine the capability for using ERTS data to discriminate these individual vegetation types.

The computer map in Figure 4 was prepared by using Band 5 and Band 7 data. In Band 5, certain areas, distinguished by their light tone, include residential areas with little vegetation, and bare areas, such as sand and gravel pits or major highways. Figure 4 was prepared by printing these light areas of Band 5 in red, designating them as Urban. The areas at the bottom of the map, symbolized as Urban, are actually areas of cloud cover, which also register as light in Band 5. These areas could have been separated out by level slicing of Band 5. In Band 7, water areas are consistently dark in tone, forest areas light, and other vegetated areas intermediate. For areas not printed in red, level slicing of Band 7 was performed to print out Water in blue, Forest in dark green, and Other Vegetation in light green. A comparison of Figure 3 with Figure 4 indicates that water and wooded areas are consistently mapped. The more developed residential areas with substantial tree and lawn cover tend to be mapped as Other Vegetation. This category also includes a wide variety of vegetative cover in non-urban areas. For studies which require a limited number of land use and land cover categories, this use of level slicing is a rapid and economical method for computer processing.

In verifying the accuracy of the ERTS-1 computer map, an up-to-date record of the current distribution of surface features is absolutely essential. RB-57 photography is very appropriate for this purpose, because it has adequate resolution for identifying surface features and because the use of color photography aids in the interpretation of spectral characteristics. During the initial studies reported here, RB-57 photography acquired in September 1969 and in June 1972 was available. In the 1972 photography, the test area was partially obscured by haze and clouds. Therefore, the 1969 coverage was normally used for image verification. The more recent coverage was needed, however, to study those areas where incomplete recognition occurred or where there were discrepancies between the computer map and the 1969 RB-57 photograph. Without the up-to-date coverage, no reliable determination could be made as to whether incorrect recognition was occurring or an actual change in land use had taken place.

Our original intention was to conduct the initial study over an area where we had previously acquired C-47 scanner coverage. However, this area on the ERTS frame is obscured by clouds and we are proceeding without this information, relying solely on analysis of the spectral data from the ERTS-1 tape. As soon as ERTS-1 coverage can be obtained for an area where C-47 scanner imagery is available, it will be used for diagnosis of the ERTS-1 computer mapping process. Although the C-47 flight will not be coincident in time with the ERTS-1 pass, it is expected that the comparison of data will not be seriously impaired. Because of its quantitative nature and higher resolution, scanner data will enable us to analyze and better understand the computer recognition process for known types of surface features. Direct comparison of C-47 and ERTS-1 spectral measurements will be helpful in understanding the manner in which the computer process recognizes both pure and mixed signatures, and will also indicate any modification of the spectral characteristics resulting from atmospheric effects.

The same area was also subjected to further computer processing to produce a map in which more detailed types of land use and surface cover were recognized. This work has not yet reached a stage where confirmed results can be reported; consequently, this discussion is limited to reporting the current state of this work. This effort at surface mapping used maximum likelihood-ratio processing to distinguish nine types of surface features. For this purpose, nine training sets were selected and analyzed, including two residential areas, three areas of lake surface, two forest areas, and two grass-covered areas. Using statistical data derived from spectral signatures of these areas, the four channels of ERTS data were processed to produce a computer printout.

After several preliminary maps were run, a printout was obtained in which nearly 70% of the resolution elements fell into one of the nine classes. A general examination of the results and comparison with

available RB-57 photography indicated that the areas recognized were for the most part properly classified as to general type of surface (e.g., built-up area, water, or vegetation). The areas not recognized were generally water surfaces and residential areas, indicating that the training sets for these two types of surface were too restrictive. It is clear that a broader categorization of water will produce more complete and consistent recognition. However, the training sets chosen make possible a more detailed analysis of water quality and underwater features. The results mentioned here represent only initial attempts at maximum likelihood ratio processing. It is expected that substantial improvement will be obtained with further experience.

3. APPLICATION OF ERTS-1 DATA

A preliminary evaluation of the utility of ERTS data for recreational land studies has been made from the examination of these early results by staff members of the Lake Central Region office of the Bureau of Outdoor Recreation and staff members of the Oakland County Planning Commission. It is believed that the general land use and land cover maps such as are shown in Figure 4 can be used in performing conceptual studies for large recreational developments. Examples of recent studies for which ERTS data could have been used include the Maumee Wild and Scenic River Study (in Northern Ohio and Indiana), study of the recreational potential of the Michigan shoreline of Lake Erie, and selection of corridors for an interstate scenic trail. The ERTS data can be valuable in affording a broad look in the preliminary stages of large area studies. The general patterns of land use, vegetation, and surface water are of immediate interest and provide sufficient information to identify promising sites for more detailed study. The regional office has taken steps to acquire and study ERTS imagery in its continuing evaluation of the Maumee River basin.

4. CONTINUING STUDIES

It is planned to continue with the preparation of recognition maps for this and other areas, with a view to improving the accuracy and increasing the detailed information content of these maps. The maps will be evaluated with respect to the composition and consistency of surface features recognized under a single category. Aerial photography and airborne multispectral scanner data will be used for this purpose wherever available.

In parallel with the preliminary data analysis described above, the types of information which it is hoped to derive from ERTS data are

being further defined. The investigation will concentrate on attempting to identify the specific types of surface features and conditions listed below. Distribution of emphasis on the features to be studied will depend on which are most useful for the study of recreation land and open space and on early indications of the feasibility of observing these features.

Vegetation (See Figure 2). Major categories of vegetation (e.g., deciduous forests, coniferous forests, herbaceous vegetation, cropland). Individual tree species.

Urban Areas.

Rural/Urban Boundaries.

Water Bodies. Mapping of surface extent of lakes, ponds, streams. Shallow water, sediment or pollution, aquatic vegetation.

Shorelines. Vegetation, beach, and residential development.

Wetlands. Distribution of wetlands and general classification, as described in USDI Fish and Wildlife Service Circular No. 39.

River Valleys. Water course, streamside vegetation.

As additional results are obtained, they will be reviewed with the staff of the Oakland County Planning Commission, the Bureau of Outdoor Recreation, and other interested parties to evaluate the usefulness of the resulting information for studies of recreational land and open space.



FIGURE 1. ERTS-1 PHOTOGRAPH OF OAKLAND COUNTY
(ERTS-1 Frame 1067-15643, Band 7, 28 September 1972)

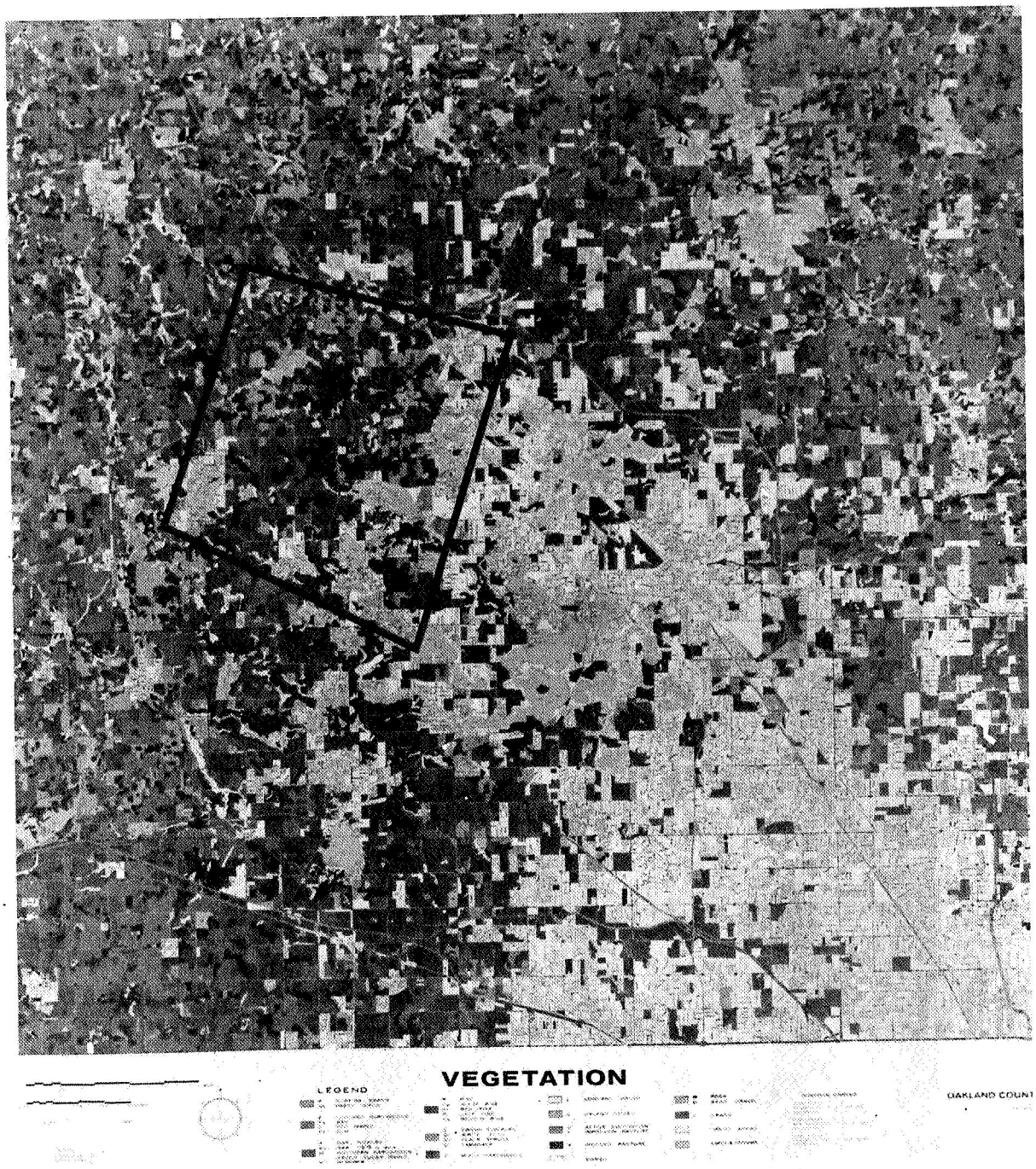
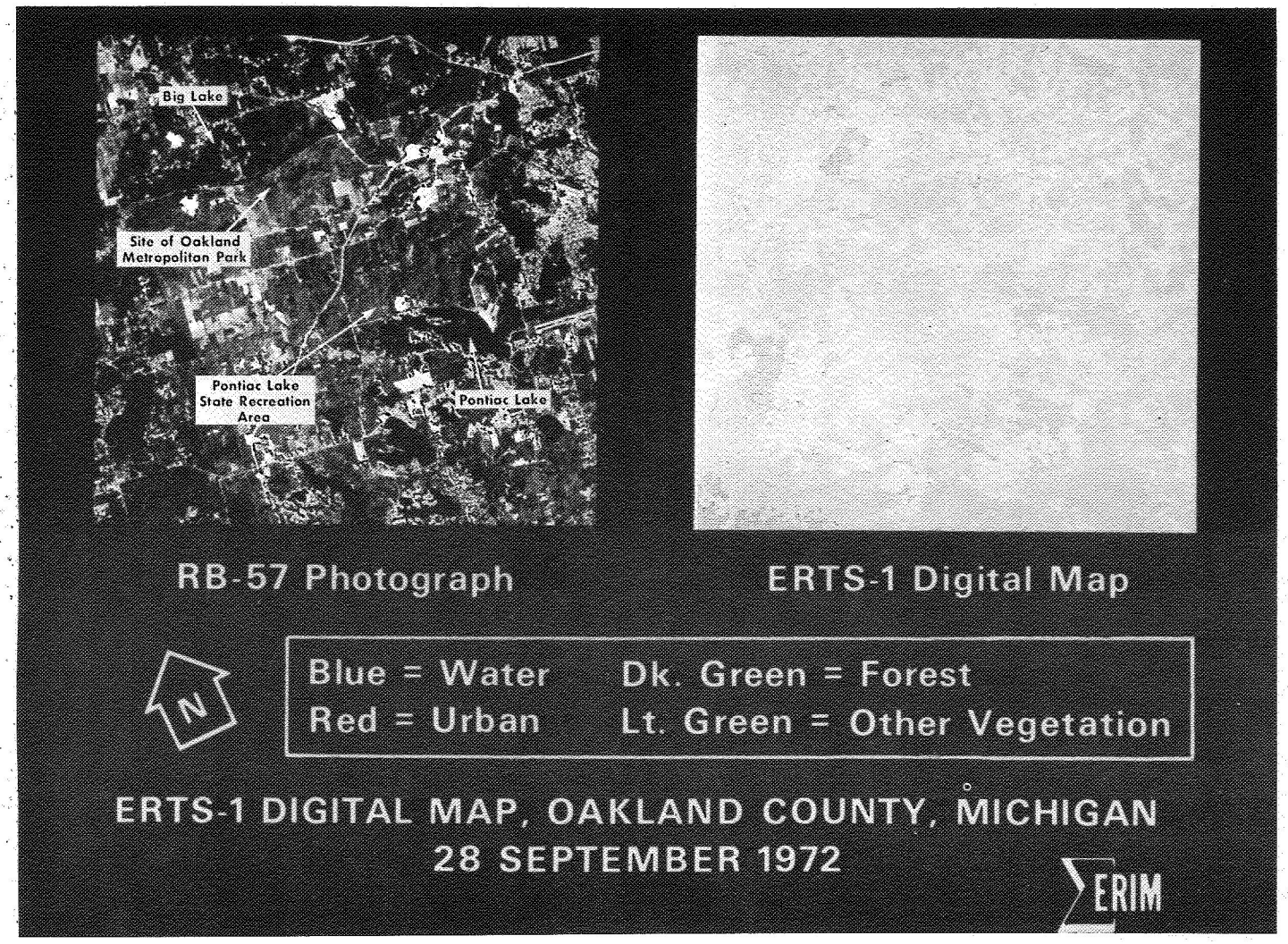


FIGURE 2. VEGETATION MAP OF OAKLAND COUNTY

FIGURE 3

FIGURE 4



N73-28317

Paper L 22

MAPPING OF AGRICULTURAL LAND USE FROM ERTS-1 DIGITAL DATA

A. D. Wilson, G. A. May and G. W. Peterson, *Office for Remote Sensing of Earth Resources, The Pennsylvania State University, University Park, Pennsylvania 16802*

ABSTRACT

A study area was selected in Lancaster and Lebanon Counties, two of the major agricultural counties in Pennsylvania. This area was delineated on positive transparencies on MSS data collected on October 11, 1972 (1080-15185). Channel seven was used to delineate general land forms, drainage patterns, water and urban areas. Channel five was used to delineate highway networks. These identifiable features were useful aids for locating areas on the computer output.

Computer generated maps were used to delineate broad land use categories, such as forest land, agricultural land, urban areas and water. These digital maps have a scale of approximately 1:24,000 thereby allowing direct comparison with U.S.G.S. 7.5 minute quadrangle sheets.

Aircraft data were used as a form of ground truth useful for the delineation of land use patterns.

I. INTRODUCTION

An area approximately 300,000 acres in size was selected for analysis within Lancaster and Lebanon Counties in southeastern Pennsylvania. This area was selected because it is one of the most important agricultural areas in Pennsylvania with a wide variety of agricultural land use. The agricultural fields are small, variable in shape, and have diverse cropping systems. Therefore, this area, with one of the most complicated agricultural land use patterns in the United States, was deemed a suitable test site to determine the abiltiy of ERTS multispectral digital data for automatic computer mapping.

II. PROCEDURES

Imagery collected on October 11, 1972 (1080-15185) was selected for analysis. Optimum conditions for the study of agricultural land use do not exist in the fall, with most of the crops harvested and the fields often littered with crop residues. However, this was one of the first good images of the area suitable for computer analysis. Three days

prior to data gathering, approximately one inch of rain was recorded and the first frost of the fall occurred on the night before the ERTS pass.

Positive transparencies were overlaid on a 1:1,000,000 scale map to locate Lancaster, Denver, Blue Ball and Lititz, Pennsylvania, on the imagery. The test site was selected using the positive transparencies and subsets were made of the NASA digital tapes. Remotely sensed units, as delineated by line and element number, were related to geographic location by means of a computer generated brightness map (1). In the computer program used to generate this map a symbol is chosen for a selected brightness range within an individual channel or for all four channels simultaneously.

A 35 mm slide of the geology of the area was projected onto the digital brightness map to relate geology to brightness patterns.

The digital data was classified using both supervised and unsupervised classifiers. The supervised classifier approach involves the use of two programs, STATS and DCLASS (1). STATS develops a variety of basic statistical values and determines signatures of selected training areas. Training areas can be irregular polygons or straight lines. A single signature can also be developed from a number of discontinuous areas. DCLASS is a mapping program that utilizes signatures developed in STATS as input. Output consists of a digital map of the selected area and/or a table of Euclidean distance between the inputed signatures. The unsupervised classifier (DCLUS) will randomly select up to 900 points and form up to 10 separable categories with a minimum critical Euclidean distance between categories chosen by the user (2.). Output is in the form of a map of the area, a table of the spectral signatures of the categories, and a table indicating the Euclidean distance between the formed categories.

III. RESULTS

Highway networks, urban areas and vegetative patterns were delineated on positive transparencies. These features were useful for relating line and element numbers to geographic area. Transparencies were also used to locate possible target areas for computer analysis.

An area representing approximately 6 percent of an ERTS image (500 lines by 585 elements) was subset from the original NASA tape. Computer generated brightness maps, using either individual channels or a combination of channels, of selected target areas were visually related to the transparencies by pattern association.

Sandstone ridges, limestone valleys, drainage patterns and some cultural features were determined from the brightness map. The ridge and valley patterns were visually related to geology maps and U.S.G.S. 7.5 minute quadrangle sheets. Bright areas were associated with bare fields and quarries and a dull area was associated with a swampy area.

For classification purposes, an area 100 lines by 240 elements in size was selected. Using an image size of 100 by 100 nautical miles, the computer output has an approximate scale of 1:18,000 across the lines and 1:22,000 down the lines. Each remotely sensed unit is approximately

1.2 acres in size.

Training areas were selected from the brightness maps in conjunction with uniformity maps. These signatures were used to map areas using a supervised classifier (DCLASS). Results of this mapping were inconclusive because of lack of any recognizable patterns. This was probably a result of using too short an Euclidean distance or the signatures were of unique features that were unidentifiable without adequate ground truth.

Because of the problems encountered with supervised classification, the data was next analyzed with an unsupervised classifier (DCLUS). Five widely separated categories were delineated using the unsupervised classifier. The first two categories were related to the forested sandstone ridges. The areas delineated agreed very closely with the vegetated areas indicated on the U.S.G.S. 7.5 minute quadrangle sheets. The third category corresponded to various bodies of water such as swamps, farm ponds and streams. The last two categories occurred in cultivated areas with one category having a high response in channels five and six and was tentatively assigned as bare soil areas. The other category in the cultivated areas was considered to be dead vegetation. Some areas did not fall into any of these categories and they were not classified.

After initial separation of these widely separated categories, additional classification within some of these categories were made using DCLUS. The water signature was further subdivided into three categories, namely, "clean water," "dirty water," and "vegetated water." Within the forested and cultivated categories many additional subcategories were delineated. At present, their identification is pending additional ground truth collection.

Various other special features were also identified. Using a known limestone quarry as a target area, three signatures were found that would adequately map quarries. Areas that were not quarries were also delineated. Some of these appear to be limestone covered parking areas.

The town of Denver was also used as a target area in an attempt to develop a signature for small communities. This was successful to only a limited extent probably due to the fact that a large percentage of Denver is vegetated.

Efforts were also made to develop signatures to map individual agricultural fields. This has been generally unsuccessful due to the small fields (generally less than five acres), most of which are on the contour and the wide variety of agricultural practices.

This study has been greatly facilitated by the aircraft program. Land use patterns on the aircraft data were related to the computer output. The aircraft data has been very useful as an interpretive aid.

IV. CONCLUSIONS

The use of ERTS digital data for the automatic mapping of land use appears very feasible. Forest land, cultivated land and water were classified within a 25,000 acre area. Additional classifications were also made within these categories and their identification is pending confirmation with ground truth.

The Pennsylvania State University programs for analyzing remote sensing

are capable of high speed operation. For example, a single run for any of the classifier programs generally takes less than 15 seconds for a 25,000 acre area and a turn around time of less than ten minutes on a remote job terminal.

The results reported here are those of a pilot study to evaluate automatic classification of the digital data. These results were obtained over a one month investigative period. It is anticipated that improvement in results will be obtained with additional study.

V. REFERENCES

1. Borden, F. Yates. 1972. A digital processing and analysis system for multispectral scanner and similar data. Remote Sensing of Earth Resources, Vol.I. The University of Tennessee, Tullahoma, Tennessee. p.481-507.
2. Turner, Brian J. 1972. Cluster analysis of multispectral scanner remote sensor data. Remote Sensing of Earth Resources, Vol. I. The University of Tennessee, Tullahoma, Tennessee. p.538-548.

N73-28318

Paper L 23

THE USE OF THE TEMPORAL DIMENSION IN CLASSIFYING AND MAPPING ERTS-1 MSS DATA

F. Y. Borden and D. N. Applegate, *Office for Remote Sensing of Earth Resources, The Pennsylvania State University, University Park, Pennsylvania*

ABSTRACT

ERTS-1 MSS data from two scenes of the same central Pennsylvania area were brought into registration by translation and then merged. The two scenes were viewed on different dates, but from adjacent ground tracks, as frequent cloud cover in Pennsylvania made it impossible to choose two scenes from the same track. Targets selected to be mapped included river water, railroad yards, creeks, urban areas, industrial areas, and vegetation. Equivalent training areas were chosen from each of the original scenes and from the merged data. Classification maps were produced for each, and a comparison was made. Scene brightness was found to have the most important effect on classification differences.

The temporal dimension of remote sensor data afforded by the ERTS-1 system is universally acknowledged to be one of the most important aspects of this satellite program. An investigation was launched to determine how well MSS bulk digital data taken at two different times for the same ground area could be merged. It was found that, at least for test areas of 100 scan lines and 100 elements, adequate registration could be obtained simply by translation; rotation was not required. Data for a test area for the two dates were merged and an investigation was begun to compare the data for the two dates and to evaluate the combination of the data. The objectives were twofold. First, by combining data it would appear possible that signature reinforcement could be achieved thus leading to improvement in classification. Emphasis was placed on this aspect. Second, temporal changes could be detected by

analysis of combined data. Less emphasis was placed on this aspect. This report presents the major initial findings.

An area in the vicinity of Harrisburg, Pennsylvania, was chosen because of the variety of targets available including such diverse ones as water, urban and suburban areas, agriculture, major transportation systems, and industrial complexes. The specific area was chosen to include as a distinctive feature, the Conodoguinet Creek that flows into the Susquehanna River directly opposite metropolitan Harrisburg. Figure 1a shows the general pattern of targets in the test area.

Because of the frequency of cloud cover in Pennsylvania, it was not possible to pick two dates separated exactly by one or more eighteen-day cycles. The clearest dates for which MSS tapes were available were August 1, 1972, and October 11, 1972. These dates are one day less than four eighteen-day cycles apart. The data were brought into registration by translation. The scan line and element translation values were found by computer processing the data for each date and then using a light table to adjust one map over the other until a match was found. The distinctive features in the test area were of most help in this task. The data were then merged accordingly onto one tape making eight channels instead of four for each observation.

Digital processing was done using a variety of programs in a system described by Borden (1972). The programs will not be discussed here except for the classifier that was used. Classification was made by using the spectral signatures obtained for the targets and by applying the following scheme:

1. Determine the class for which the euclidean distance from the unknown observation is smallest.
2. If the distance is smaller than a given critical value, assign the observation to the class.
3. If the distance is greater than the given critical value, assign the observation to the unclassified or "other" category.

Using the merged data, classification and mapping runs were made for each date separately and for the combined dates. The critical distance was in all cases the same, i.e., ten. In this algorithm a different critical value

can be set by the user for each category and this feature has had the desired effect of improving the classification in other work. However, the limit here was set at ten for all classes in order to avoid confounding the comparison between dates with different critical values.

Seventeen spectral signatures that were represented as seven mapping classes were used in the analysis. In Table 1, six signatures are presented, each of which was the dominant signature in each of six mapping categories. The seventh mapping category was forest, which, for this report, was assigned a blank as the mapping symbol; thus, for mapping purposes, combining it with the "other" category. The symbols for each of the six categories are given in the table. The six mapping categories and their symbols are railroad (:), river (W), urban (*), creek (C), suburban (-), and industrial (+). The suburban class was composed of five signatures and the industrial class contained six signatures. The two forest signatures completed the set of seventeen signatures.

The signatures were obtained by means of supervised and unsupervised analysis programs. The subareas, training areas, and cluster analysis areas, which were used for this purpose, were identical for the analysis of the two separate dates as well as the combined dates.

In addition to classification and mapping, the program that was used computes the euclidean distance between all pairs of signatures. These distances are presented in Tables 2 and 3.

A change detection program was written for the project. It compared the map symbols, element by element, between two classification maps and then output a map showing symbols which defined the outcome of the element-by-element comparisons. All character maps for this report were converted to line maps which were output on a plotter. These maps are shown in Figures 1a, 1b, 2a, and 2b.

The most important result of the investigation was that scene brightness had the greatest influence on the classification. From visual inspection of the ERTS-1 images for channel seven for each date, it appeared that the October 11th scene was brighter than the August 1st scene. This interpretation was not supported by the data. The data indicated that the August 1st scene was decidedly brighter. In Table 1, the comparison of August 1st signatures with those of October 11th shows that, for all channels and for

all signatures, the values are all substantially greater for the August 1st scene.

The scene brightness had a very definite influence on the classification by the method that was used. Because of the greater signature values in each channel for August 1, the euclidean distance of separation among classes was greater than for the October 11th date. By using a common value of ten for the critical distance, there were more observations that could not be classified August 1st as compared to October 11th. The same effect was present for the merged data, but it was more pronounced. Compare the distances of separation between the October date in Table 2 with corresponding values for the merged data given in Table 3. The distances of separation for the merged data are, overall, approximately fifty percent greater than for the October date. The August date distances were intermediate. The effect on classification was very pronounced for the merged data with 23 percent of the observations remaining unclassified as compared with only 1 percent for October 11th. The effect can be seen in the maps given in Figure 1a and Figure 1b where the greater blank area for the merged data map indicates the increased number of unclassified observations.

Because of the large difference in scene brightness, the signature for each class could not be directly compared between the two dates. Relative responses in the four channels were computed by first normalizing the signatures. After this was done, it was found that, for all of the categories except one, the normalized signatures were essentially the same for the two dates. The only one that had changed in a non-negligible way was for river water. The reason for the change will be investigated, but it is likely that a difference in turbidity, aquatic plant growth, or a similar temporal influence caused the difference.

Because of the effect of different scene brightness, the classification comparison between dates yielded only fair results. The comparison maps are presented in Figures 2a and 2b. These maps represent another level of abstraction beyond the maps of Figures 1a and 1b and the patterns are more difficult to perceive. The blank areas represent repetitive classification in the same class except for the "other" category. The dotted areas stand for repetitive "other" classification, which includes the two forest categories. The vertically lined areas represent a change from one class to another, excluding "other"; whereas the horizonally lined areas represent a change to a class from

"other" and vice versa. The vertically lined areas are of greatest interest and concern since this category would represent land use change, temporal change, or erroneous classification. Land use change in the area could only be inconsequential so the other two aspects, separately or together, must have been responsible. Upon investigation of changes for the various classes, it was found that for most classes changes were small. For three classes, however, changes were major. One forest class gained 10 percent, from 6 percent to 16 percent, from August 1 to October 11. One of the suburban classes lost 10 percent, from 15 percent to 5 percent, and another suburban class lost 4 percent, from 8 percent to 4 percent, from August 1 to October 11. The reason for this shift into forest at the expense of suburban can only be conjectured at this time. The classes were separable by distances of 15.7 or greater for both dates; therefore, there was little possibility for confusion in classification for the two classes. The training area could have been nonrepresentative; however, it appeared to be a typical suburb based on review of U-2 photography of the area. The resolution of this problem will be undertaken in continued study. However, prior to this, the difference in scene brightness will have to be rectified. A number of ways to accomplish this are possible. Before a reliable method of change detection or signature reinforcement can be developed, the effect of scene brightness will have to be accounted for or removed.

LITERATURE CITED

Borden, F. Yates. 1972. A Digital Processing and Analysis System for Multispectral Scanner and Similar Data. Remote Sensing of Earth Resources, Vol. I. Edited by F. Shahrokhi. The University of Tennessee, Space Institute, Tullahoma, Tennessee. pp. 481-507.

Table 1. Unnormalized category specifications.

	Channels							
	August 1, 1972				October 11, 1972			
	4	5	6	7	4	5	6	7
1 :	36.51	29.15	29.54	11.32	23.68	17.37	16.05	6.02
2 W	32.62	22.01	17.72	4.80	18.39	10.03	6.09	0.93
3 *	36.34	27.75	33.41	14.76	24.01	17.50	20.43	9.40
4 C	32.68	22.41	30.86	13.18	20.80	13.43	18.89	9.09
5 -	36.48	27.73	48.25	25.67	25.13	17.67	31.98	18.28
6 +	39.27	32.89	42.00	18.64	27.60	22.13	29.20	15.20

Table 2. Distances of separation for categories for October 11, 1972 data.

	1 :	2 W	3 *	4 C	5 -	6 +
1 :	0.0	14.4	5.5	6.4	20.2	17.2
2 W	14.4	0.0	19.1	15.7	32.8	31.1
3 *	5.5	19.1	0.0	5.4	14.6	12.0
4 C	6.4	15.7	5.4	0.0	17.1	16.3
5 -	20.2	32.8	14.6	17.1	0.0	6.6
6 +	17.2	31.1	12.0	16.3	6.6	0.0

Table 3. Distances of separation for categories for merged data.

	1 :	2 W	3 *	4 C	5 -	6 +
1 :	0.0	21.3	7.7	10.3	31.1	22.9
2 W	21.3	0.0	27.5	22.2	49.9	43.7
3 *	7.7	27.5	0.0	9.0	23.5	16.4
4 C	10.3	22.2	9.0	0.0	28.2	23.9
5 -	31.1	49.9	23.5	28.2	0.0	12.9
6 +	22.9	43.7	16.4	23.9	12.9	0.0

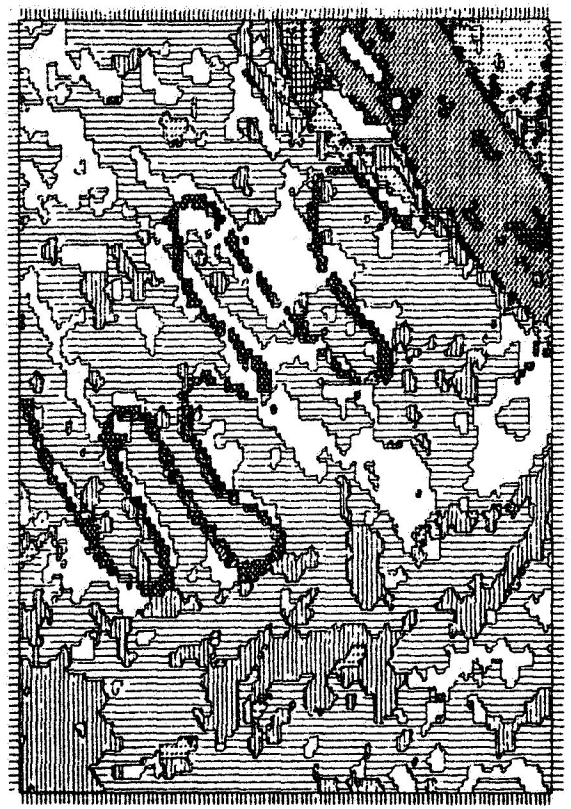
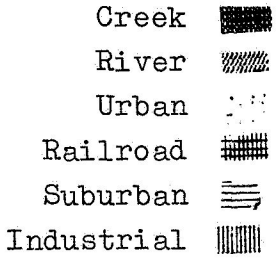


Figure 1a. October 11, 1972, classification map.



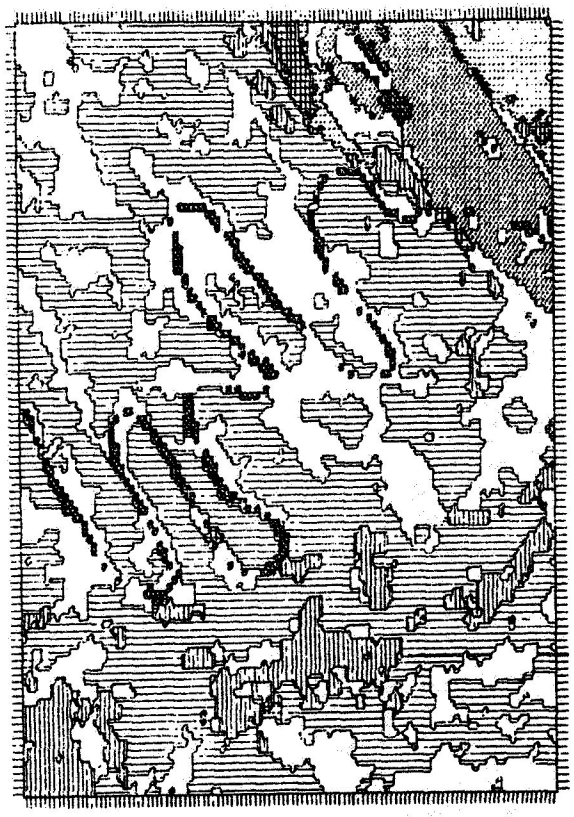
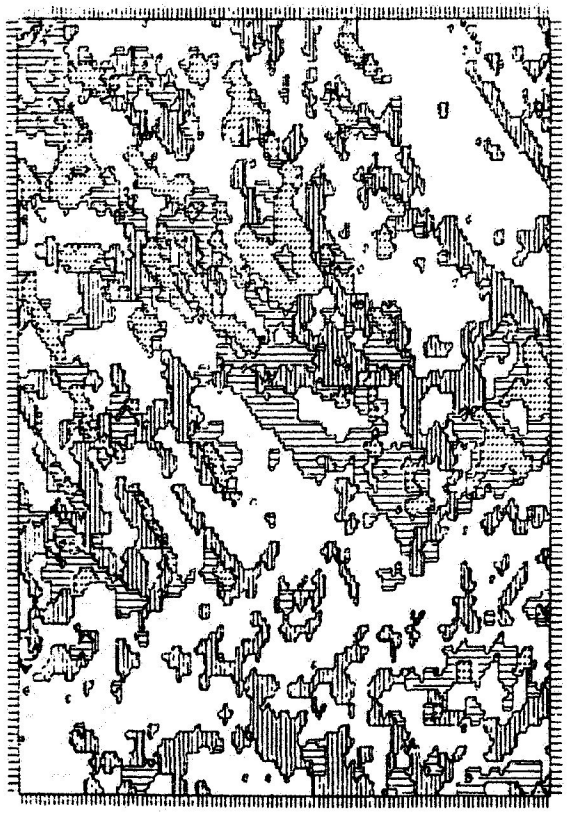
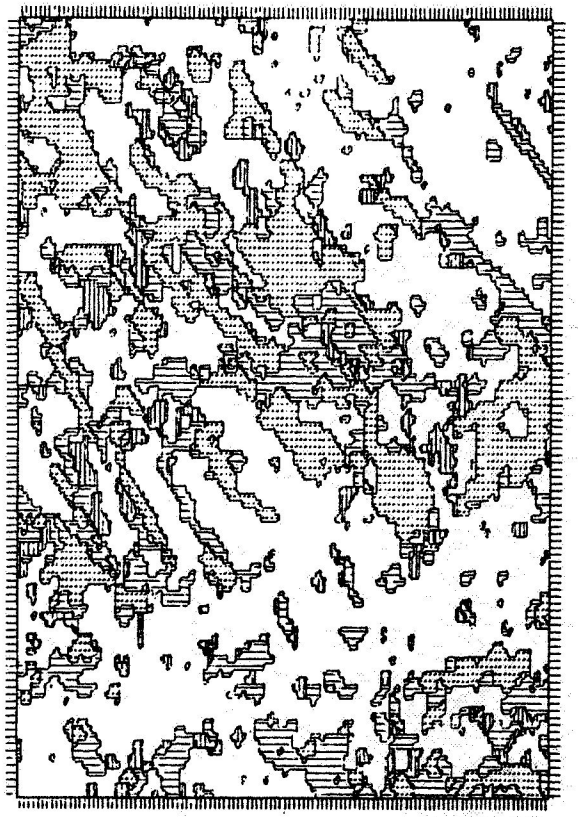


Figure 1b. August 1, 1972, merged with October 11, 1972, classification map.





Both classifications equal, but not other — blank
Both classifications different
Both classifications equal other
One symbol .EQ. other
One symbol .NE. other

Figure 2a.
Comparison map of August 1 with October 11.

Figure 2b.
Comparison map of merged data with October 11.

N73-28319

Paper L 24

IDENTIFICATION AND MAPPING OF COAL REFUSE BANKS AND OTHER TARGETS IN THE ANTHRACITE REGION

F. Y. Borden, D. N. Thompson and H. M. Lachowski, *Office for Remote Sensing of Earth Resources, The Pennsylvania State University, University Park, Pennsylvania*

ERTS-1 MSS data covering parts of Pennsylvania's Southern and Eastern Middle Anthracite Coal Fields were studied to determine how well accumulations of coal refuse could be identified and mapped by computer analysis and processing. Spectral signatures of coal refuse targets were similar to water, but had higher reflectances in all channels. Relative reflectances were in the order 4>>5>6>>7. Although no underflight photography was at hand to judge mapping success, correlation was made with 1:24,000 scale USGS maps dated 1947 and 1948. Coal refuse targets correlated well with existing maps.

A widespread and ongoing problem affecting the utilization of earth resources is the devastation of land that often accompanies the extraction and processing of mineral resources. Few areas of the world are as drastically affected by this problem as the Anthracite coal region of eastern Pennsylvania. In addition to extensive strip-mined areas, at least 16,000 acres in the region are covered by waste from coal-processing plants. Although most prominent for their barren ugliness, these immense black piles of silt, shale, and rock also pollute streams with acid and sediment and preclude more beneficial uses of the land as well.

Knowledge of the location and extent of such problem areas will be required for effective planning of corrective measures. Most assessments to date have been compilations of information from a variety of sources (Peters, Spicer, and Lovell, 1968) and, while certainly useful, have been incomplete. Furthermore, reworking of refuse and silt, extinguishing burning refuse, strip-mining, and other such activities have resulted in elimination of some banks, moving of others, and creation of new ones, in addition

to the normal increase in size of banks with continued coal production.

Thus, the capability of satellite-mounted sensors for repetitive observation of extensive areas seems to make ERTS-1 the ideal tool for routine mapping of the areas in need of reclamation. To test this supposition, an area encompassing the eastern ends of both the Southern and Middle Anthracite Fields was studied.

Bulk MSS digital data were used. The scene date was October 11, 1972, with the identification of 1080-15185. The computer processing was done within the system described by Borden (1972) for processing and analysis of MSS remote sensor data. Digital or character maps from printer output were used as working copy and for this report final maps, made from character maps, were output on a plotter.

An approximately nine-mile-square section of the study area, including the coal towns of Tamaqua, Coaldale, Lansford, Summit Hill, and Nesquehoning, was studied intensively to develop a set of spectral signatures for various targets of interest. Orientation with respect to ground locations was aided by a digital intensity map showing areas of low and high total reflectance. All of the signatures used in subsequent mapping of the entire area were obtained from this subarea.

A second digital map was produced using a program that identifies areas of relatively uniform local spectral response. Both maps were then studied to select training areas for the initial spectral signature calculations. As classification maps were produced, unclassified or confusing areas were delineated and cluster analyses were performed, establishing additional signatures in a kind of iterative process. The resulting profusion of signatures was reduced to manageable proportions by using distances of separation, such as those shown in Table 1(b), to identify groups similar enough to be represented by one mean signature. A total of 42 different signatures was used in the total mapping; the important ones relative to this report are listed in Table 1(a).

In the classification procedure used, each of the spectral signatures representing a particular target category is considered as a four-element vector. The point in four-dimensional space defined by this vector is considered the class centroid, which, together with a specified classification limit, defines the class. Each data point

can also be considered a point in four-space and is assigned to that class for which its euclidean distance from the class centroid is minimum, provided it falls within the specified limit. If it does not, then it is checked to see whether it falls within the limit for the next closest category and so on. If a point is not within the limit for any category, it is classified as other. Although 42 different categories were used, related categories were mapped using the same symbol; all four coal refuse categories, for instance, were mapped as X's. In specifying the classification limit for each category, its distances of separation from unrelated categories (i.e., those with different map symbols) were studied and the limit set at two-thirds of the smallest such distance, except for coal refuse and water, which were set equal to that minimum distance. All categories were included in the final classification, but only those listed in Table 1(a) were assigned nonblank map symbols.

No NASA underflight or other photographic coverage of the area was available. The only supporting materials used were USGS topographic maps dated 1947 and 1948, and a report by Peters, Spicer, and Lovell (1968) showing the location of most of the larger refuse banks and silt deposits in the Anthracite Region. Time limitations have thus far prevented field checking of ground truth.

With respect to the primary objective, mapping coal waste materials, the maps shown in Figures 1 and 2 speak very well for themselves. Figure 1 shows the area in the Southern Anthracite Field from which the spectral signatures were obtained. Figure 2 shows an adjacent area in the Eastern Middle Field that was mapped using the same set of signatures. In both cases, every refuse pile or silt basin that shows on either the topographic maps or the Peters, et al. (1968) map also can be identified on the ERTS map. Some of the accumulations shown on the ERTS map, however, are not on either of the others. With few exceptions, these are close to mining operations where refuse piles might logically be expected. The total area classified as refuse or silt was 6,532 acres or 6.2 percent of the overall area shown.

As anticipated from its dark gray to dull black color, the coal wastes have quite low overall reflectance. The signatures, shown in Table 1(a), are somewhat similar to those for water--relatively high in channel 4, dropping off sharply from 4 to 5, dropping only slightly or not at all from 5 to 6, and with another sharp drop between 6 and 7. The refuse reflectances are significantly higher than

three of the water signatures in every channel and consequently the distances of separation, shown in Table 1(b), are adequate for successful classification. Only muddy water has total reflectance as high as refuse and the pattern of its signature is sufficiently different to eliminate confusion.

Among the categories that were blanked out of the maps were six signatures thought to represent strip-mine spoils. Although there was virtually no problem with refuse being misclassified as strip-mine spoils, certain strip-mine spoils appear to be misclassified as refuse. One such area is a long, narrow band near the southwest corner of Figure 1 that is mapped as refuse, but shows on the topographic map as unreclaimed strip-mines. This, of course, is not surprising since some strip-mine spoils, being derived from the same geologic strata as the refuse, are closely similar to it in color. Such misclassification is, in one sense at least, not really a problem since the same environmental problems and reclamation difficulties are involved with both materials. Mapping of strip-mines will be more difficult than the coal refuse because of confusion with other targets such as roads, towns, and bare fields. The difficulties do not, however, appear insurmountable.

Other targets presented minimal problems. All water bodies that show on the topographic maps were plotted accurately. Several additional water bodies that show on the ERTS but not on the topographic maps appear to be unreclaimed stripping pits that have filled with water.

The small area near the east edge of Figure 1 that is mapped as "muddy water" is not definitely known to be that, and, as previously noted, its spectral signature is not greatly different from those of coal refuse. Although not on the topographic map, it is on the opposite side of the ridge from the coal deposits and the other mining activity. Its shape and its position astraddle Mauch Chunk Creek suggest that it is a pond, but the final determination will be made on the ground.

The signature for swamp vegetation was obtained from an upland swamp that shows on the topographic map and in the northeast corner of Figure 1. The same vegetation type also maps along the northwest side (the shaded side at 9:30 a.m.) of the ridges. This may be a direct consequence of the shading or it may indicate that the plant community is different, the shaded lower slope supporting a hemlock-rhododendron type that is similar to that of the swamp.

Again, the final interpretation must await the ground-truth determination.

Other features that were mapped more or less successfully included the four-lane highway between Hazleton and Tamaqua and a pipeline right-of-way that is apparently covered with low brush and weeds because it maps in small patches elsewhere.

What we have called on the maps an anomaly arose when one of the refuse banks, which appears on the topographic maps as almost perfectly circular, did not come out that way on the digital map. A cluster analysis gave the signature shown in Table 1(a). A glance at Table 1(b) shows that it is totally different from any other category shown and, in fact, its minimum distance of separation from any other category was 15.1 from one of the strip-mine signatures. The category has also mapped in small patches elsewhere, but we do not, at this time, know what it is. It is conjectured to be burned-out or burning refuse, known to be present in these coal fields.

In summary, use of the ERTS-1 data to map the location and areal extent of coal waste materials has been found to be feasible. It also appears that much additional useful information can be elicited from the data, particularly with regard to cultural changes over time.

LITERATURE CITED

Borden, F. Yates. 1972. A Digital Processing and Analysis System for Multispectral Scanner and Similar Data. Remote Sensing of Earth Resources, Vol. I. Edited by F. Shahrokhi. The University of Tennessee, Space Institute, Tullahoma, Tennessee. pp. 481-507.

Peters, J. W., T. S. Spicer, and H. L. Lovell. 1968. A Survey of the Location, Magnitude, Characteristics, and Potential Uses of Pennsylvania Refuse. Coal Research Admin., The Pennsylvania State University, Special Research Report No. SR-67.

G

Table 1. Specifications of map categories: (a) spectral signatures and category limits; (b) distances of separation between centroids of the categories.

(a)

Category Name	Channels 1	2	3	4	Limit
1 Refuse 1	20.88	14.43	12.34	4.42	3.6
2 Refuse 2	20.23	13.39	13.32	5.26	6.5
3 Refuse 3	21.77	15.59	14.73	5.84	4.7
4 Refuse 4	19.73	12.99	11.04	3.66	3.3
5 Wet Silt	18.49	10.79	9.79	3.26	2.1
6 Clear Water	16.79	7.57	4.79	0.69	6.7
7 Turbid Water	16.40	8.16	5.87	1.42	5.5
8 River Water	16.36	8.63	8.96	3.43	2.8
9 Muddy Water	20.12	15.67	10.10	1.98	3.3
10 Swamp Vegetation	18.39	12.72	20.56	11.94	5.5
11 Anomaly	36.00	41.33	42.50	17.00	10.0

(b)

	Category 1	2	3	4	5	6	7	8	9	10	11
1	0.0	1.8	3.1	2.4	5.2	11.6	10.5	8.2	3.6	11.5	44.9
2	1.8	0.0	3.1	2.9	5.1	11.8	10.6	7.7	5.1	10.0	44.9
3	3.1	3.1	0.0	5.4	8.1	14.6	13.5	10.8	6.3	9.5	42.0
4	2.4	2.9	5.4	0.0	2.8	9.3	8.1	5.9	3.3	12.7	47.3
5	5.2	5.1	8.1	2.8	0.0	6.7	5.5	3.1	5.3	14.0	50.0
6	11.6	11.8	14.6	9.3	6.7	0.0	1.5	5.1	10.3	20.1	56.5
7	10.5	10.6	13.5	8.1	5.5	1.5	0.0	3.7	9.4	18.7	55.4
8	8.2	7.7	10.8	5.9	3.1	5.1	3.7	0.0	8.2	15.1	52.6
9	3.6	5.1	6.3	3.3	5.3	10.3	9.4	8.2	0.0	14.8	46.8
10	11.5	10.0	9.5	12.7	14.0	20.1	18.7	15.1	14.8	0.0	40.4
11	44.9	44.9	42.0	47.3	50.0	56.5	55.4	52.6	46.8	40.4	0.0

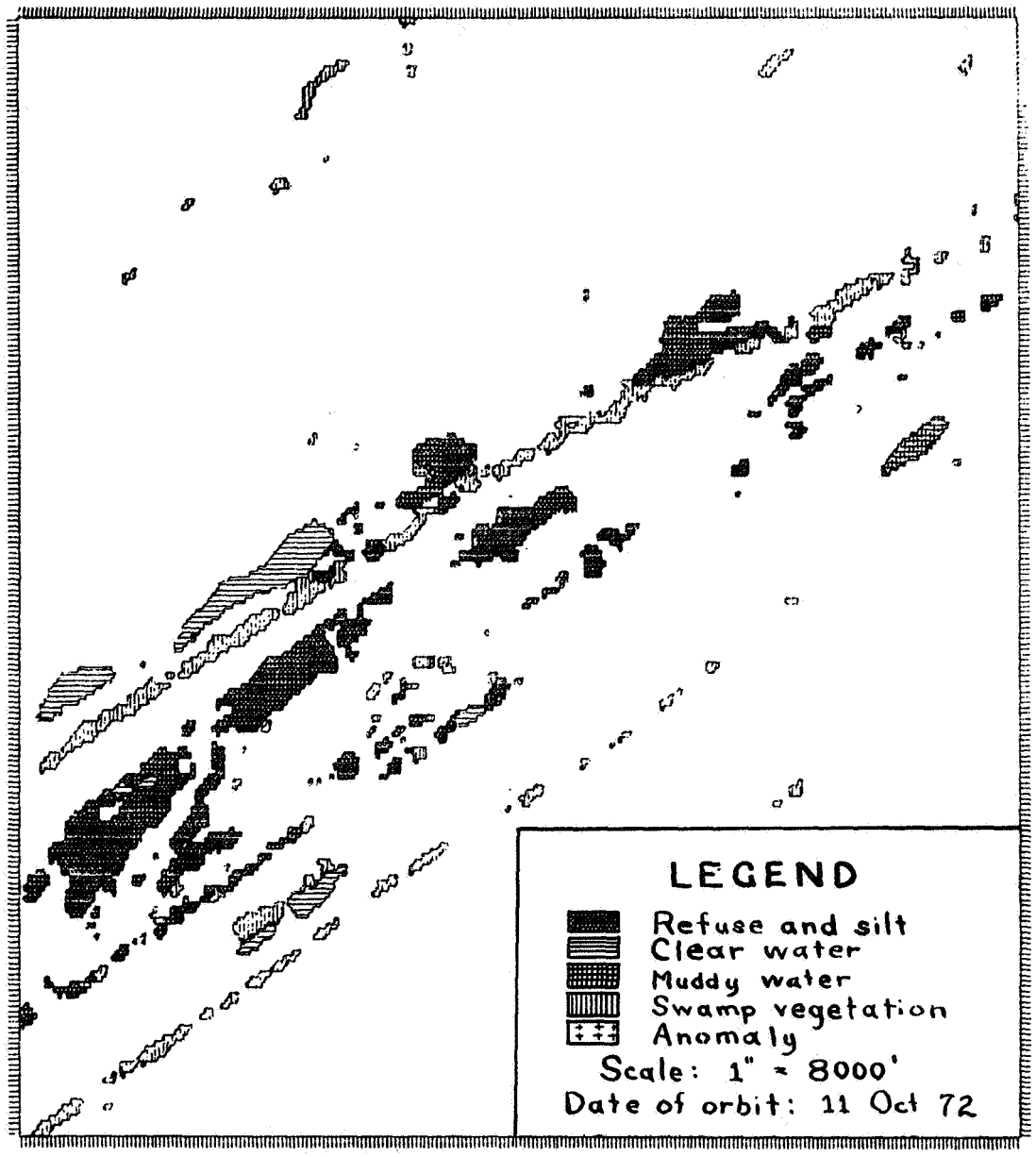


Figure 1. Computer-generated map showing coal waste accumulations in east end of Southern Anthracite Field.

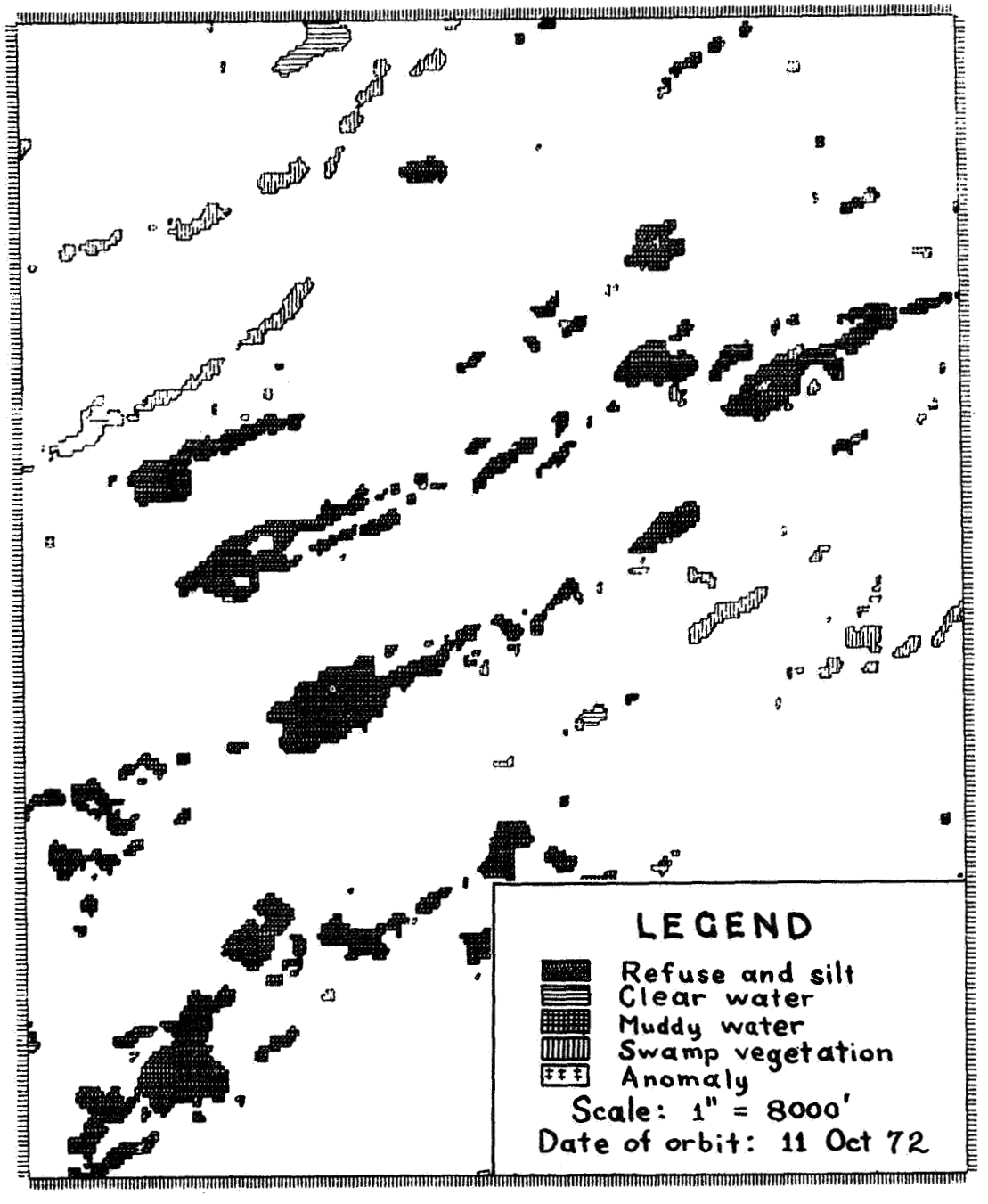


Figure 2. Computer-generated map showing coal waste accumulations in east end of Eastern Middle Anthracite Field.

N73-28320

Paper L 25

AUTOMATIC INTERPRETATION OF ERTS DATA FOR FOREST MANAGEMENT

Leonard Kirvida and Greg R. Johnson, *Systems & Research Division, Honeywell, Inc., and College of Forestry, University of Minnesota, St. Paul, Minnesota*

ABSTRACT

Automatic stratification of forested land from ERTS-A data provides a valuable tool for resource management. The results are useful for wood product yield estimates, recreation and wild life management, forest inventory and forest condition monitoring. Automatic procedures based on both multi-spectral and spatial features are evaluated. With five classes, training and testing on the same samples, classification accuracy of 74% was achieved using the MSS multi-spectral features. When adding texture computed from 8 x 8 arrays, classification accuracy of 99% was obtained.

INTRODUCTION

Managers of forest resources are faced with increasing demands for forest products as well as the needs of alternative uses for the land surface. Consideration must be given to the environmental problems associated with the removal of forest by harvesting, diseases or pests, and the effects of forest areas on the ever-increasing needs for pure water.

ERTS-A data have opened up many possibilities for effective management. However, new processing and analysis techniques will be required to exploit these data. In particular, automatic data processing appears mandatory for many interpretation and inventory functions. For example, automatic stratification by type and density class provides a common basis for multiple uses. The data are formatted for convenient insertion into a computerized data bank. Processing of repetitive coverages increases the accuracy of the inventory data and detects changes and trends.

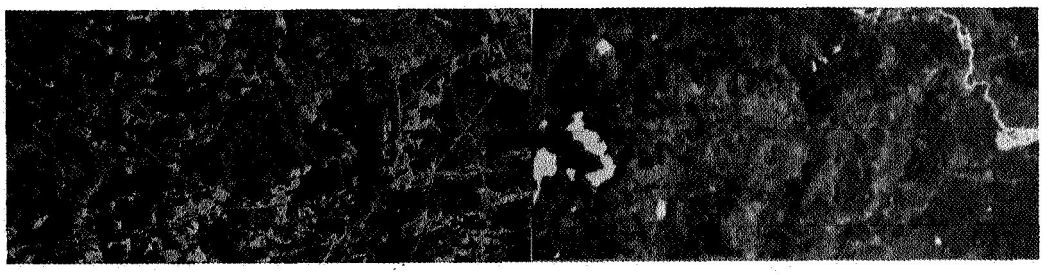
Our investigation is to determine both the feasibility of automatic interpretation from ERTS-A data and the insertion of the data into a computerized data bank. This is a cooperative effort with the

Original photography may be purchased from:
EROS Data Center
10th and Dakota Avenue
Sioux Falls, SD 57198

University of Minnesota and the Minnesota State Planning Agency. Initial results on the automatic classification of areas by forest type are described herein.

PROCEDURE

The automatic classification of forested areas to be discussed was performed for the Cloquet, Minnesota area, located 25 miles west of Duluth. An aerial photograph of the approximately 24,000 acres of forest and associated types that were stratified is shown in the left half of Figure 1. Ground truth information was obtained by using aerial photo interpreters from the University of Minnesota's Institute of Agriculture Remote Sensing Laboratory (IARSL) located in the College of Forestry. Since the College's Cloquet Forestry Center, an experimental forest, is in the midst of this area, much information was previously known about the forest types. Spring 1:90,000 panchromatic aerial photographs, numerous field checks, and previous ground experience in the study area were used by the interpreters in generating the ground truth map. The Cloquet area was delineated into five types: conifers, hardwoods, open, water, and city.



AERIAL ERTS - Band 7

Figure 1. Aerial and ERTS Images of Cloquet Study Area

The features used for classification were derived from the four MSS bands of ERTS-A image 1075-16312, an October 6, 1972 cloud free coverage of the Cloquet study area. Data from the bulk, black and white 70 mm transparencies and 7 track 800 BPI computer compatible tapes (CCT) were used as the data base. The imagery

was used for orientation and registration, and the digital data was used to perform the automatic stratification and analysis.

The ERTS digital data of the study area was then reproduced on film by writing with a digital magnetic tape to film printer for purposes of registering with ground truth information. The film output for Band 7 is shown on the right half of Figure 1. It provides an image of the study area containing grid lines corresponding to record and word on the digital magnetic data tape. Registration of ground truth with ERTS-A data was accomplished by recognition of landmarks such as water bodies in the area. Registration with ground truth maps was required for both training and evaluating the automatic classification system and for producing the stratification output.

Once ground truth and ERTS-A data were registered, type boundaries were encoded in terms of record and word numbers. From within the type boundaries, 8 x 8 arrays were isolated to serve as training samples. During training two categories of features, multi-spectral and texture, were generated for a number of 8 x 8 array samples in each class as illustrated in Figure 2.

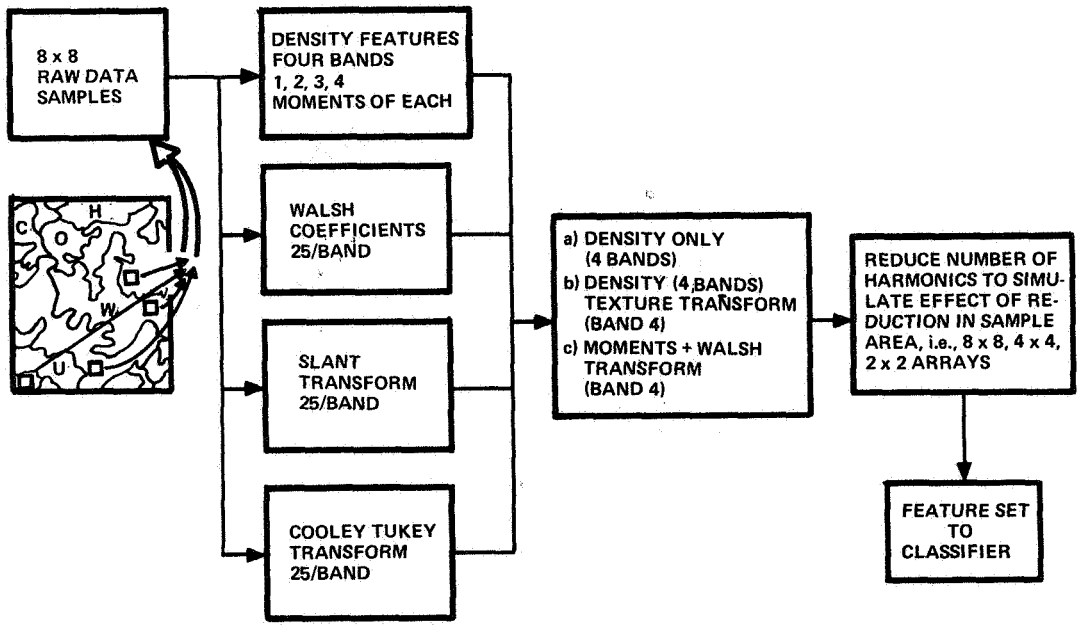


Figure 2. ERTS-A Feature Extraction Procedure

The first experiment was run using only spectral features. An illustration of the separability between the five classes is shown by the density histograms in Figure 3. The four sets of histograms were derived from each of the four MSS bands. Band 4 has a great deal of overlap between classes. Band 7 is excellent for separating water from land and was usually used for locating lakes for ground truth landmarks.

Two dimensional histograms for the five classes were also computed. These indicated high cross correlation between some pairs of bands for a few classes; however, no consistent conclusions could be drawn.

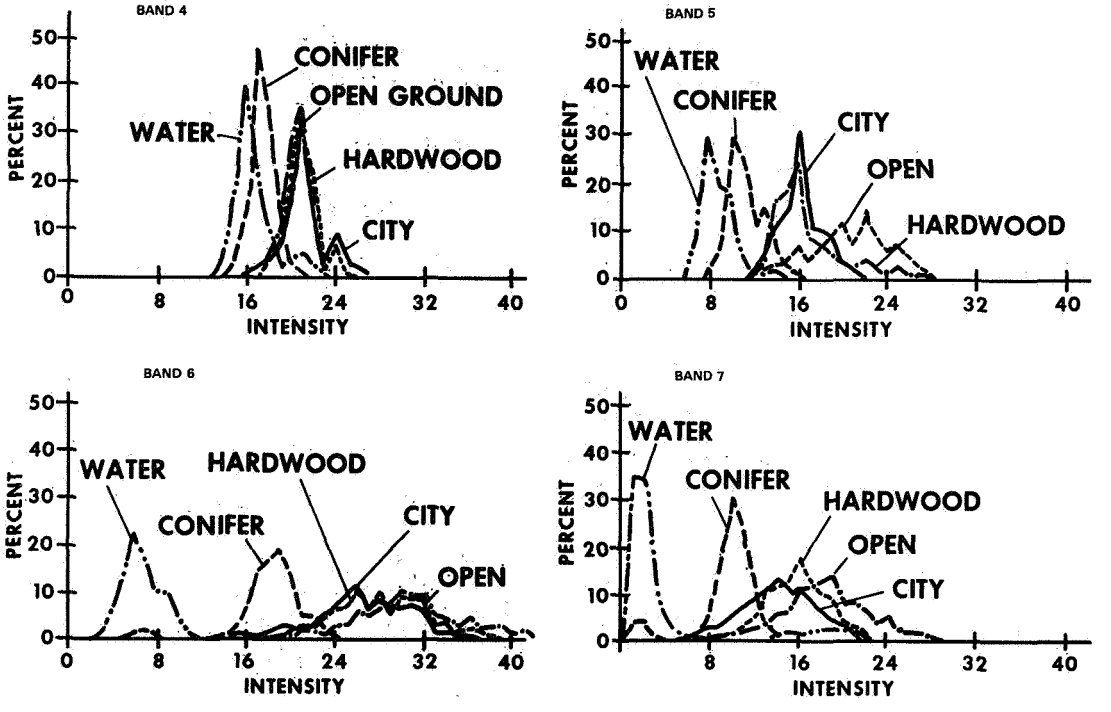


Figure 3. Histograms of Intensity Levels
ERTS 1075-16312

For texture features, two dimensional Fast Walsh, Fast Fourier and Slant Transforms were utilized. Texture features were computed from an 8 x 8 array representing approximately 70 ground acres. Texture was also computed on a 4 x 4 array to determine the effect of array size on performance. Increasing the array size increases frequency resolution which increases the classification

accuracy. However, the larger array size increases the minimum area to be classified.

Having selected the features to be used and the training set, a linear discriminant classifier is trained. Briefly, the classifier algorithm groups each of the features of the training set around an orthogonal basis vector in a least mean square sense. The "weight" matrix required to do this is computed for subsequent application to the input data during testing and during the generation of overlay maps. The class to which the input data point belongs is determined by the distance from the various orthogonal vector points. A block diagram illustrating the procedures used for automatic interpretation is shown in Figure 4.

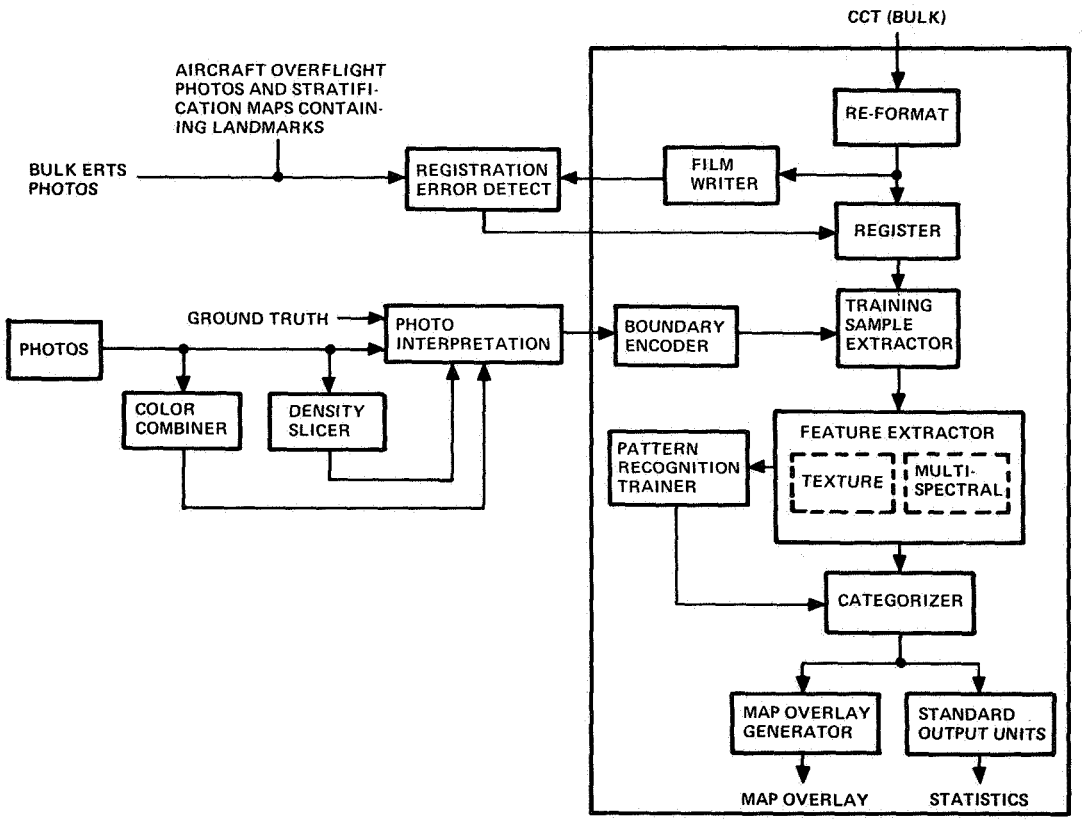
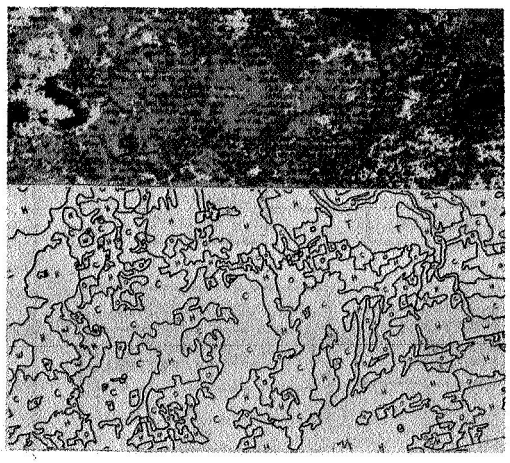


Figure 4. Data Analysis Procedures

RESULTS

Using only multi-spectral features, the classifier was trained on data derived from the 8 x 8 sample arrays from each class. The total training area was 4687 acres proportioned into five classes. Each training sample consisted of one data point, approximately one acre. After training, a delineation map was generated for the 24,000 acres including the training area. The results of the automatic classification are shown in the top half of Figure 5. Decisions were made for each acre data sample. The five classes, hardwoods, conifers, open, water, and urban, are presented as density levels increasing in density in the order listed. The performance of the automatic classification procedure can be estimated by comparing its output on the top half of Figure 5 with the photo interpreter overlay on the bottom half of Figure 5. The distortion of the classification output photo is due to the unequal spacing between ERTS samples in the x and y directions.



Key

H - Hardwood

C - Conifer

O - Open

W - Water

T - City

Figure 5. Automatic Classifier Results Based on Density and Ground Truth

When the classifier is trained and tested on the same data points, its performance is shown by the confusion matrix in Table I. Seventy-four percent of the data points are correctly classified. An indication of the types of mistakes made are shown in the confusion matrix. Notice that confusion is most common where city is called open, the next most common is open classed as hardwood and then open classed as city.

Table I. Automatic Classification Results Based on Density

Type	Sample Size	Automatic Classification Assignments in Percent Hardwood	Conifer	Open	Water	City
Hardwood	896	80.7	4.1	4.9	1.8	8.5
Conifer	1152	.5	80.9	2.3	13.9	2.4
Open	960	20.4	3.5	61.6	.6	13.9
Water	640	10.2	.0	.3	88.6	.9
City	640	8.1	6.1	24.1	6.4	55.3
Total	4288	Correct Classification Assignments = 3167				

The performance using only multi-spectral data is shown also in Figure 6. When training and testing on individual data points, the performance is 74% using the 4 MSS density bands as features.

An indication of the effect of adding texture to multi-spectral features is shown by the curve in Figure 6. Texture was computed from Band 7 using the Slant Transform. The Slant Transform is an image transform with a basis vector matched to the gradual brightness changes along an image line which compacts the image energy to as few of the transform domain samples as possible. It can be computed using a fast computational algorithm. When computed on a 4 x 4 array, the performance increases to 90% and if computed on an 8 x 8 array, the performance increases to 99%.

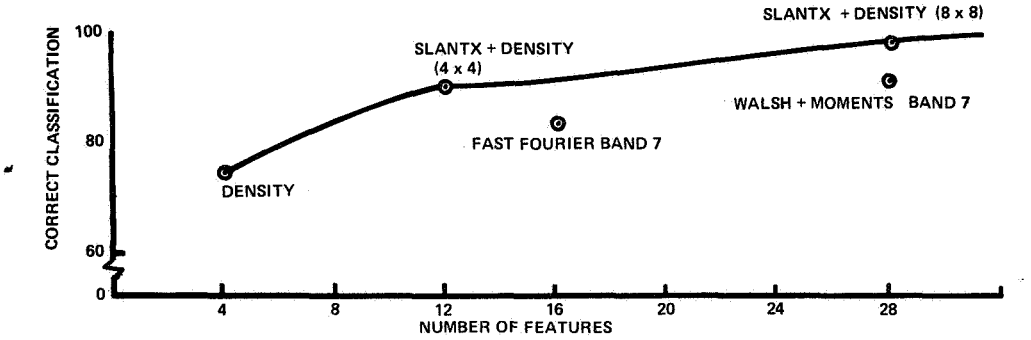


Figure 6. Performance Using Both Density and Texture

Texture was also computed using the Cooley-Tukey Fast Fourier and Walsh Transforms. The performance of these two transforms is generally very similar, the Walsh Transform utilizing a binary waveform for computational advantages. When an 8 x 8 array from Band 7

was used for calculating the Walsh coefficients and the first through the fourth moments of density from Band 7 were used for density features, the performance classification accuracy was 91%. This is an indication of the performance achievable using only Band 7 for input data.

The final point on Figure 6 was computed using the Cooley-Tukey Fast Fourier Transform on an 8 x 8 array from Band 7. Only the first four spectral components were used resulting in 16 features. The lowest frequency component contains the least amount of information and contributes 9 of the features. In the interest of minimizing features, it was deleted and a resulting performance of 89% was achieved.

DISCUSSION

Even though the results given in this paper are of a preliminary nature derived from a small test site, they indicate the feasibility of automatic stratification. In further study they will be extended in the following ways: (1) increased area of coverage to provide a larger statistical base, (2) inclusion of a finer classification by forest cover type, site, and stand density, (3) incorporation of data from multiple coverage, (4) comparison with other texture measurement techniques, and (5) application to a national forest already under an intensified management system.

The information content of the texture features may be improved by applying the Fast Fourier Transform to two MSS bands simultaneously with one band as the real input and the second as the imaginary input. The easily calculated Haar Transform may be adequate for texture, but its performance should be compared with the optimum performance achievable with the Karhunen-Lowe Transform. The latter transform is difficult to compute, but it provides the least mean square truncation error and the maximum entropy interpretation. In addition, performance of the linear classifier may be improved by cluster analysis whereby classes are generated on the basis of similarity of features.

Stratification information is useful to natural resource land managers. Our goal is to determine the capabilities of automatic classification from ERTS-A data, the maximum number of classes, and an acceptable operational data format. In addition, we seek to determine the best combination of automatic and human interpretation. We will compare automatic techniques to studies being done by IARSL on the Chippewa National Forest and the state of Minnesota Land Management Information System.

N73-28321

Paper L 26

LAND RESOURCES SURVEY FOR THE STATE OF MICHIGAN

Buzz Sellman, *Environmental Research Institute of Michigan, Ann Arbor, Michigan*

ABSTRACT

This study is designed to document the usefulness of ERTS-1 satellite imagery as an information source for a statewide inventory of Michigan's land resources. The project is currently relying on photointerpretation of MSS photography and computed processed results. The first task completed was a 1:500,000 scale land use map of the state in four classes: Urban, Forest, Water, and Agriculture and Other. This map was constructed from existing (pre-ERTS-1) information sources including federal, state and county maps, and aerial photography. An ERTS color IR photomosaic for the entire state will also be constructed at a scale of 1:250,000. The Institute is currently working on tape processed data that will include both recognition data as well as a UTM coordinate addressing capability so that the final tape can be inputed directly into computerized land use and transportation corridor analysis models.

1. INTRODUCTION

The State of Michigan, through the State Planning Division of the Bureau of Programs and Budget, has been funding a broad-based program to make it a more effective council for land use and land resource issues confronting decision makers at the state level of government. This program includes efforts at defining problems as well as alternatives to effect more positive decisions as to how we in Michigan are going to treat our land resources. The Environmental Research Institute of Michigan is participating in this program to ascertain how remote sensing systems might effectively contribute to the process of land use and land resource analysis.

Original photography may be purchased from:
EROS Data Center
10th and Dakota Avenue
Sioux Falls, SD 57198

2. CURRENT REMOTE SENSING PRODUCTS

The first of several tasks undertaken at the Institute was to map land use for the entire state at a scale of 1:500,000, using five classes: Water, Forest, Agriculture, Urban, and Other. The procedure chosen was to overlay a base map of the state with a square grid corresponding to one mile square and allocate the entire square to that class which dominated (50% +) the cell.

Heavy reliance was to have been placed on existing sources for the classification effort, especially regional and county land use maps, aerial photography and state and federal mapping sources. The plan to rely heavily upon existing information sources fell far short of expectations. Less than a quarter of Michigan's 83 counties have a generalized land use map and only half of these had sufficiently valid information to be useful for our mapping project. Other sources had to be excluded either because they were too out-of-date or because the information content could not be adequately validated as to accuracy. Thus we were forced early in this effort to map but four classes, namely, Water, Forest, Urban, and Agriculture and Other (combined).

Figures 1 and 2 show the results of this work, displaying our classification scheme for the lower and upper peninsulas respectively. The water and forest categories are direct transfers, using the one square mile cell decision procedure, of U. S. Geological Survey thematic masters produced originally at a scale of 1:250,000. This represented an acceptable compromise given that no other adequate sources was readily available for this task, especially in the case of forest cover. The areas mapped Urban were generated using aerial photography supplied by the Michigan Department of State Highways. The photography was collected over all cities in Michigan of 5000 population or greater in 1970. Thus, the map accurately depicts urban development as of that date. The extent of urban development is also being mapped for 1963, using the same procedures and data soruces. The final class, Agriculture and Other, was mapped by a process of elimination, comprising those areas not already classified as Water, Forest or Urban.

The finished map is both valuable and instructive. Its value lies in the systematic procedures used durings its construction. It is instructional in pointing out that while considerable time and resources are spent on inventories and mapping at all levels of government, no attempt has been made to structure data collection, analysis, and synthesis, so that the resulting product can serve as an input to information systems needed in the decision making process. Departments, agencies and planning groups have not yet agreed on uniform formats concerning general purpose land classification, although this process, together with a uniform base mapping program, is now underway in the State of Michigan.

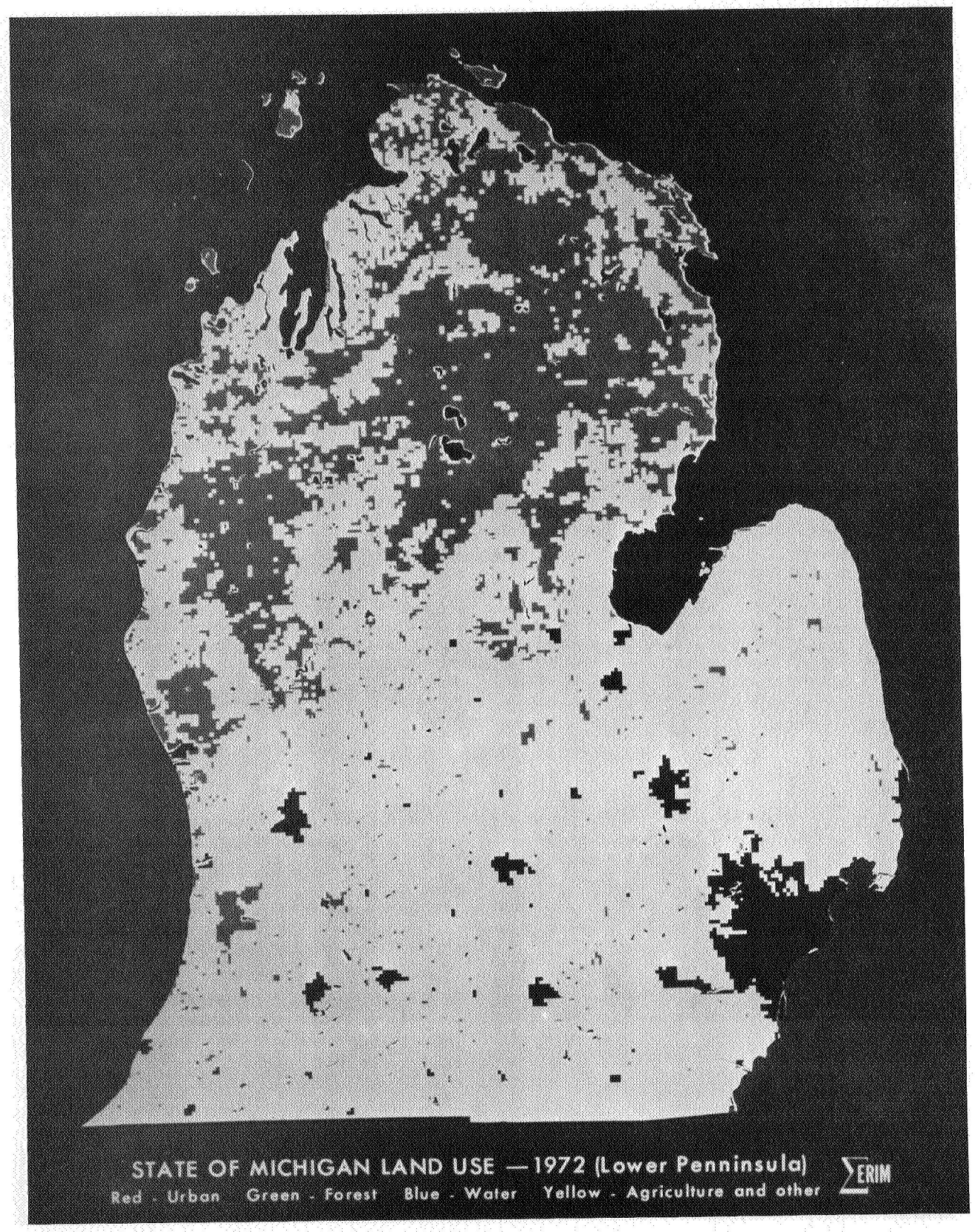
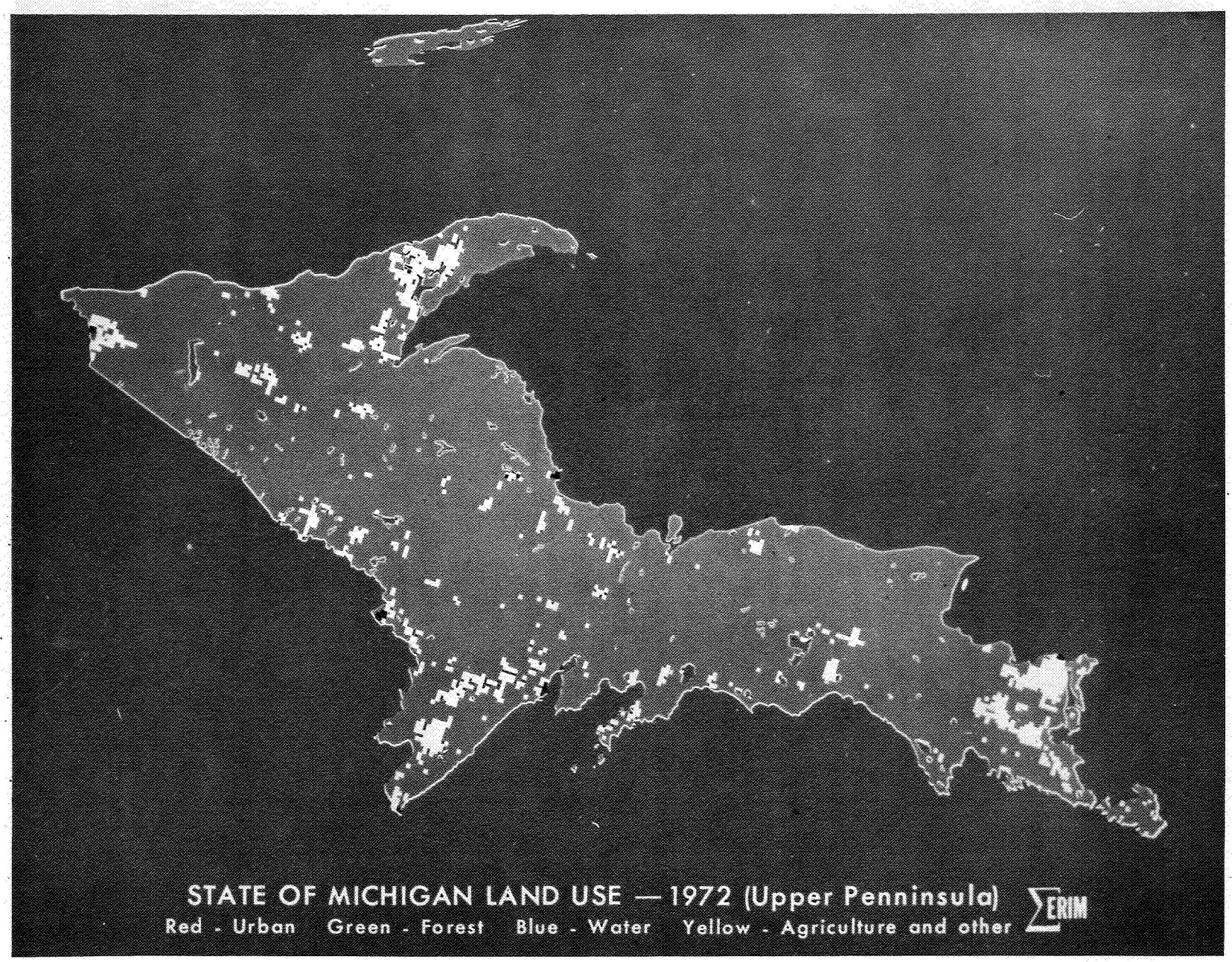

STATE OF MICHIGAN LAND USE — 1972 (Lower Penninsula)
Red - Urban Green - Forest Blue - Water Yellow - Agriculture and other
ERIM

FIGURE 1

C1.


STATE OF MICHIGAN LAND USE — 1972 (Upper Penninsula)
Red - Urban Green - Forest Blue - Water Yellow - Agriculture and other
ERIM

The Institute also plans to construct a 1:250,000 scale color IR photomosaic of the State of Michigan from ERTS-1 MSS photography (Bands 4, 5 and 7). The mosaic will be analyzed to document those classes that can be accurately mapped, against those which are discernable, from photointerpretation of the color IR mosaic. This effort is not yet complete since the collection of usable ERTS data was hampered by extremely poor weather conditions over much of Michigan this past fall. These two products, together with interpretations of RB-57 photography for more detailed inventories in urban areas, form the basis of our current products from remote sensed imagery.

3. ONGOING RESEARCH

The Institute has begun a project to make ERTS processed tape data more readily available and usable by various agencies within the state. The program involves not only the solution to data analysis and synthesis, e.g., land use inventory, but also includes the requirement that the data be addressable for computer storage, retrieval, and additional mensuration.

The Institute, together with the Michigan Department of State Highways, is cooperating on a project to use ERTS processed data tapes as a direct input to their computer-based transportation models. The goal is to produce a land use recognition tape, together with a data point addressing system based on UTM coordinates, for use in transportation land use and corridor selection analysis. This would give the Highway Department a current inventory of the location and distribution of the state's land use in a format immediately available to their information system.

The area chosen to test and refine the process centers upon Munising, located in Michigan's Upper Peninsula just north of the Hiawatha National Forest. This heavily forested region was chosen because forest cover as a class covers approximately 50% of the State, and solutions that can consistently and accurately map forest cover situations would be useful for much of the State. Further, the Highway Department will soon begin several major highway studies which must pass through the heavily wooded areas of the Upper Peninsula and the northern half of the Lower Peninsula. We are also expecting to work more closely with the U. S. Department of Agriculture's Forest Service and the State Department of Natural Resources in our analysis of forest cover situations. Thus, we are attempting to coordinate our work and results with as many users as possible.

Figure 3 shows a digital recognition map of the area, annotated with five classes or ground cover features. ERTS photography of MSS Band 5 has been included for comparison purposes. An area of approximately 356 square miles has been mapped to depict water, deciduous and coniferous

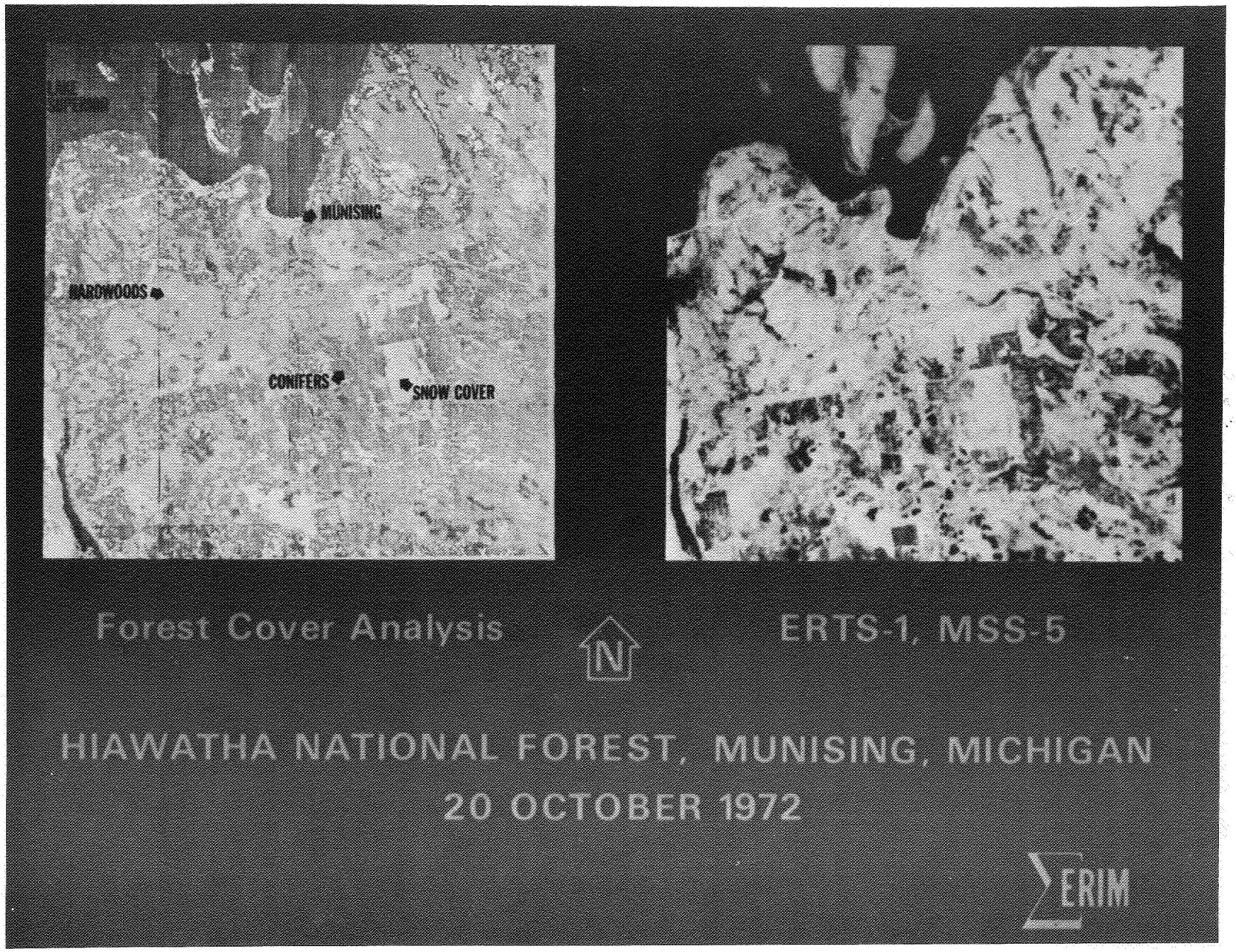

MUNISING
HARDWOODS
CONIFERS
SNOW COVER
Forest Cover Analysis
N
ERTS-1, MSS-5
HIAWATHA NATIONAL FOREST, MUNISING, MICHIGAN
20 OCTOBER 1972
ERIM

FIGURE 3

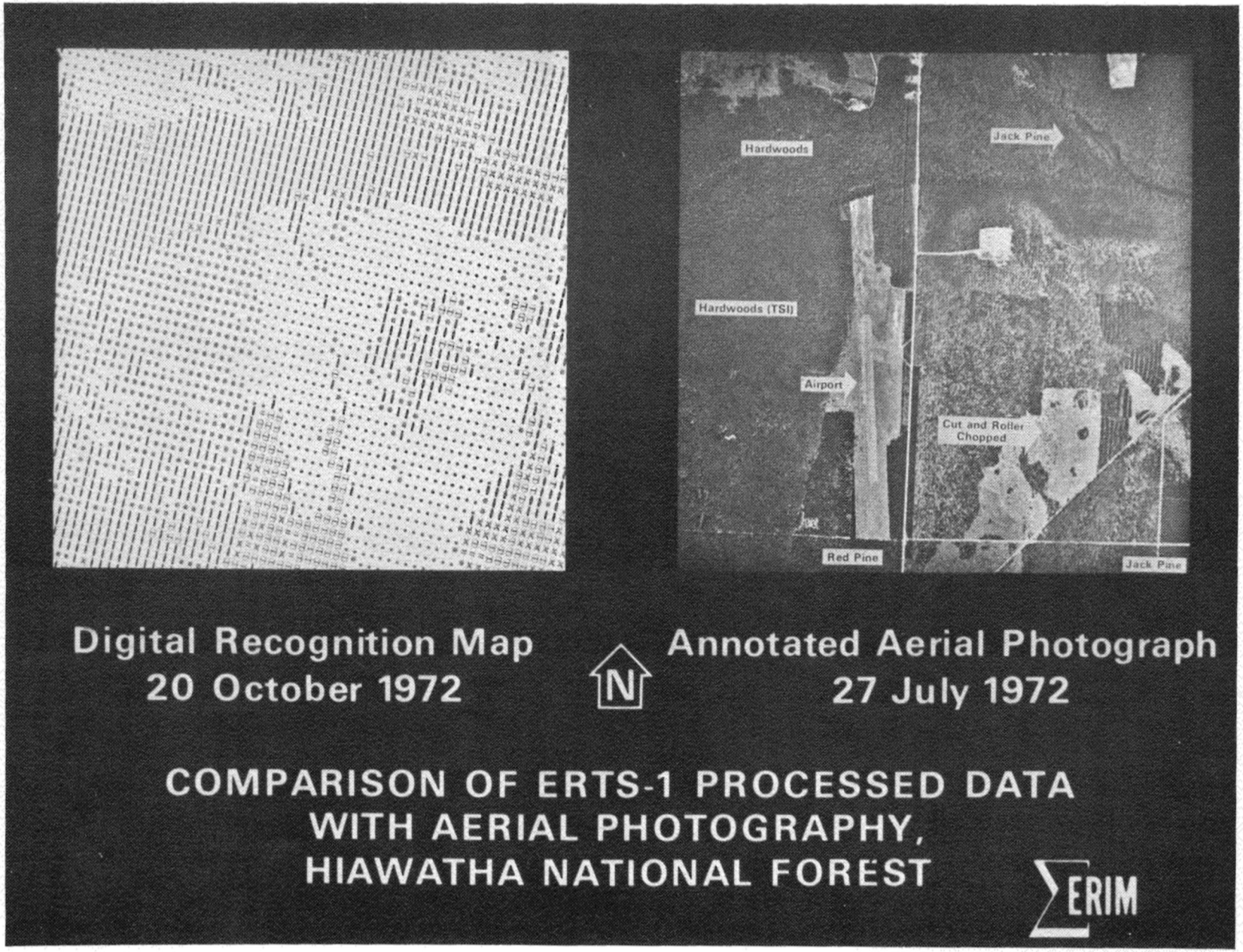

Hardwoods
Jack Pine
Hardwoods (TSI)
Airport
Cut and Roller Chopped
Red Pine
Jack Pine
Digital Recognition Map
20 October 1972
N
Annotated Aerial Photograph
27 July 1972
COMPARISON OF ERTS-1 PROCESSED DATA
WITH AERIAL PHOTOGRAPHY,
HIAWATHA NATIONAL FOREST
ERIM

FIGURE 4

tree stands, and snow cover, which represents unforested areas. The site was covered by five inches of snow and this uniform background greatly increased the accuracy of the recognition results. The map has been compared to forest type maps supplied by the U. S. Forest Service and field checked in specific areas. It is a remarkably accurate product from an initial effort at forest classification.

The area has also been mapped in seven classes, consisting of two hardwood types, mature jackpine and red pine stands, marsh, water, and snow cover. A small portion of this color coded recognition map is shown in Figure 4, together with an annotated aerial photograph taken in July of this year. This map shows the excellent correspondence of the recognition types with the annotated photograph. Of particular interest is the fact that the hardwood stand immediately west of the airport was thinned for selected individuals (TSI) this past summer and registered a distinct spectral signature from the rest of the hardwood stands in the area. It was mapped as a separate class, more by chance than calculation, and was verified as a unique hardwood stand by Forest Service personnel when field checked just a few weeks ago.

4. CONCLUSIONS

The recognition results achieved thus far are sufficiently useful, both in classification content and accuracy, for initial testing in highway modelling programs. The next step will be to address the recognition results on a point by point basis using UTM coordinates. This effort will then begin to achieve the fuller potential of ERTS data as an effective information source in land resource analysis. The mandate of present research in this area is clearly one of formatting the final product such that the users can easily and economically merge remote sensing data into their information systems.

N73-28322

Paper L 27

TERRAIN CLASSIFICATION MAPS OF YELLOWSTONE NATIONAL PARK

Frederick J. Thomson, Norman E. G. Roller, *Environmental Research Institute of Michigan, Ann Arbor, Michigan*

ABSTRACT

A cooperative ERTS-1 investigation involving U. S. Geological Survey, National Park Service, and Environmental Research Institute of Michigan (ERIM) personnel has as its goal the preparation of terrain classification maps for the entire Yellowstone National Park. Excellent coverage of the park was obtained on 6 August 1972 (Frame 1015-17404).

Preliminary terrain classification maps have been prepared at ERIM by applying multispectral pattern recognition techniques to ERTS-MSS digital taped data. Training sets for the study were selected by Dr. H. Smedes and Mr. Ralph Root (a Colorado State University student assisting Dr. Smedes). The color coded terrain maps will be presented and discussed. The discussion will include qualitative and quantitative accuracy estimates and discussion of processing techniques.

1. INTRODUCTION

Since 1967, the staff of the Environmental Research Institute of Michigan (ERIM) and Dr. Harry Smedes of U. S. G. S., Denver have explored the use of remote sensing in Yellowstone National Park. Recently, National Park Service personnel and students at Colorado State University have joined the team.

Processed aircraft multispectral scanner data showed great promise for classifying important terrain categories in Yellowstone National Park. The goal of the ERTS-1 experiment now underway was to prepare terrain

Original photography may be purchased from:
EROS Data Center
10th and Dakota Avenue
Sioux Falls, SD 57198

classification maps of the entire Yellowstone National Park using ERTS-1 MSS data. These data are to be machine processed by software currently available at ERIM. Training set selection and map verification are being done by Dr. Smedes and the students, while the National Park Service, the final users of the product, assisted in the definition of classes to be mapped.

2. PROGRESS TO DATE

Yellowstone National Park was covered in a number of ERTS-1 passes in August and September 1972. While many of the data sets were usable, the 6 August data set (frame 1015-17404) was clearly superior. No cloud cover is apparent over any portion of the park, and all channels of data (in imagery form) were free of artifacts. This data set was selected for analysis (Figure 1).

While routine digital formatting operations were carried out at ERIM, Dr. Smedes and students began an intensive ground effort to define training set categories. The training sets fall into five distinct cover classes -- 1) water, 2) exposed rock of various types, 3) grasslands of varying degrees of cover, 4) coniferous forest with different degrees of cover and different substrata, and 5) lowland/marsh vegetation areas. Several separate samples were selected for each of the cover classes. The locations of these samples were phoned to ERIM. We then performed signature extraction and analysed the signatures.

The signature analysis revealed that a number of different classes could be separated. We then decided, as a preliminary step to prepare a five category terrain classification map. The results of this map, we felt, would give us a basis for evaluating the success of more detailed mapping efforts to follow. Before preparing the recognition map, two analysis steps were performed. First, the individual signatures comprising each of the five classes were combined to yield five category inclusive, composite "super signatures", accounting for geographical and componential variability within each class. Then, optimum channels for classification were determined. The results of this step are shown in Table I below. The average probability of misclassification is an estimate of the percentage of points which will be incorrectly classified on the recognition map. Channel 2 (MSS-5) proved to be the single best channel. The combination 2, 4, 3 proved to be only slightly worse than using all four bands in the spectral classification process.

We decided to use all four bands in the spectral classification process. The recognition map was prepared on the ERIM 7094 computer. A color coded presentation was chosen portraying water in blue, rock and soil areas in red, and various vegetation classes in green (See Figure 2).

TABLE I

AVERAGE PROBABILITIES OF MISCLASSIFICATION
FOR FIVE CATEGORY RECOGNITION

Channels	Average Probability of Misclassification
2	.086
2,4	.031
2,4,3	.028
2,4,3,1	.027

3. FIVE CATEGORY RECOGNITION ANALYSIS

Recognition processing resulted in the entire scene being classified into the generalized vegetation communities and physical landscape features described elsewhere. Quantitative estimation of recognition accuracy are not yet available, but comparison of observable boundary features, e.g., lakeshore perimeters, timberline and forest-grassland ecotones, indicate high correlation with image occurrence on topographic maps and aerial photography.

Clear water bodies were effectively recognized and drainage patterns are quite evident. Occasional blue symbols marking the presence of streams or rivers aids in separating grass covered ridgetops from valleys. Further definition of drainage patterns could undoubtedly be achieved locally by mapping every digital resolution element, rather than every other element as we have done here.

Cultural features and hydrogeothermal areas dominated by stone construction, pavement and large expanses of sparse vegetation are solidly recognized in the light rock category. High density visitor use areas such as Thumb-Grant Village, Fishing Bridge and Canyon Village are easily distinguished. Additionally, well known sites of thermal activity including the upper, lower, and Norris Geyser Basins are also fully delineated. Perhaps even more significant, many of the smaller centers of hydrogeothermal activity are detectable; Sulphur, Vermillion and Pelican Springs and Brimstone Basin are all observable ringing Yellowstone Lake.

The rugged, exposed slopes of the Gallatin, Beartooth and Absaroka Ranges are appropriately identified as light rock. At lower altitudes, large exposures and rock outcrops in the Grand Canyon of the Yellowstone and Lamar and lower Yellowstone River Valleys are accurately depicted. As indication of potential future mapping detail, sand bars framing the upper Yellowstone River meanders are recognized.

Lowland meadows and wetlands characterizing the lake margins and many of the valleys also help to emphasize the drainage system, and begin to reveal the ecological structure of the non-forested landscape when their occurrence is contrasted with that of the grass-sage community.

Dominating the upper slopes of valleys up to the forest edge and again beyond timberline, the grass-sage community is most apparent in the upper Yellowstone and Lamar River Valleys and Pitchstone Plateau.

Future recognition efforts will concentrate on separating environmentally significant sub-categories within these basic cover types. Spectral analysis of data located on transects oriented along vegetation cover type and altitudinal continua is expected to reveal the feasibility of this objective. Particularly, we wish to investigate individual forest species recognition, separation of different densities of coniferous forest cover and detection of forest types on different substrates.

4. SIGNIFICANT RESULTS

Several significant results have resulted from this investigation:

1. Accurate five category terrain classification maps have been made through computer processing of ERTS-1 multispectral scanner data collected over Yellowstone National Park in August 1972.

2. The five categories recognized were exposed rock and soil, water, coniferous forest, grass-sage vegetation, and lowland grassy vegetation.

3. Further analysis is expected to yield maps with improved detail in the five general categories above.

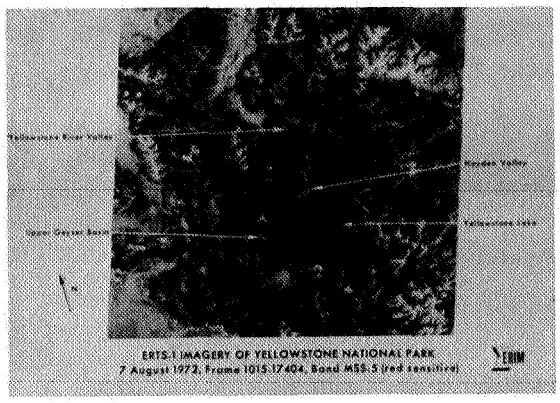


Figure 1
Yellowstone National Park Imagery

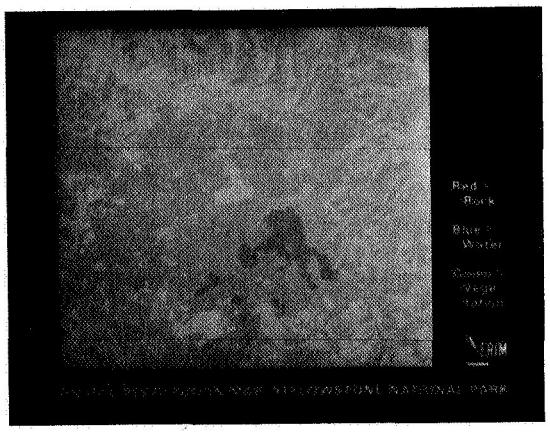


Figure 2
Yellowstone National Park Recognition Map

INTERPRETATION TECHNIQUES DEVELOPMENT

N73-28323

Paper I 1

ATMOSPHERIC EFFECTS IN ERTS-1 DATA, AND ADVANCED INFORMATION EXTRACTION TECHNIQUES

William A. Malila, Richard F. Nalepka, *Environmental Research Institute of Michigan (ERIM),* Ann Arbor, Michigan*

ABSTRACT

Atmospheric effects in satellite multispectral scanner data can influence results obtained with either manual image interpretation or computer information extraction techniques. The atmosphere attenuates radiation arriving from the surface and adds an extraneous path radiance component. Initial results of an investigation of atmospheric effects in ERTS data are presented. Empirical analyses of ERTS MSS data and simultaneous airborne MSS underflight data for one frame, along with theoretical calculations of atmospheric effects, are discussed.

The effect of limited spatial resolution on the accuracy of information extracted from ERTS data also is important. Problems occur when individual resolution elements contain two or more materials. Results from an initial application of ERIM techniques for estimating proportions of materials within individual elements are presented and discussed. Very accurate determination of surface areas of small lakes is achieved.

INTRODUCTION

This paper addresses two problems that are common to all users of ERTS-1 data, namely (1) effects of the atmosphere and (2) the relatively coarse spatial resolution of the ERTS MSS. The reported work in the first area deals with understanding and verification of atmospheric effects in ERTS-1 data while, in the second, it is on an initial application to ERTS data of ERIM processing techniques designed to estimate proportions of unresolved objects in individual resolution elements. The work is part of ERTS investigation MMC-136, entitled, Image Enhancement and Advanced Information Extraction Techniques.

ATMOSPHERIC EFFECTS

By now, all ERTS investigators must be aware of the strong influence of the atmosphere on ERTS data. For example, the lesser contrasts in ERTS Band 4 images, as compared to those in ERTS Band 5,

*Formerly Willow Run Laboratories of The University of Michigan

Original photography may be purchased from:
EROS Data Center
10th and Dakota Avenue
Sioux Falls, SD 57198

are in part due to the greater influence of the atmosphere in the shorter wavelength channel. Differences in atmospheric conditions within a given frame or between frames can change the spectrum of received radiances, thereby hampering image-interpretation efforts and degrading recognition processing and other information extraction with computers.

The major components of the radiance, L, received by a scanner are shown in the following simplified equation: $L = \frac{\rho}{\pi} ET + L_p$ where ρ is the diffuse target reflectance, E is the total (direct plus diffuse) solar irradiance on the target, T is the transmittance of the atmosphere, and L_p is the path radiance (i.e., extraneous radiation that does not emanate directly from the surface element under observation). All these quantities depend on wavelength, viewing and irradiation geometries, and atmospheric state. Both theoretical calculations and empirical studies with ERTS and underflight aircraft data have been carried out in a preliminary fashion for one ERTS frame (1033-15580, 25 Aug 72).

Theoretical Calculations

A radiative transfer model developed by Dr. R.E. Turner of ERIM* was used to compute the magnitude of atmospheric effects for a variety of conditions and to predict variations that depend on several different parameters. Fig. 1 illustrates the dependence of spectral path radiance on wavelength for a relatively clear condition (ground visual range, V = 24 km) and for a hazy condition (V = 6.4 km). Three observations can be made: (1) the amount of path radiance clearly increases as one approaches shorter wavelengths, (2) there is a strong dependence of path radiance on the albedo of the background surrounding the target, and (3) the path radiance is greater for the low-visibility case.

Nadir scan angle is another observation parameter. Large "scan-angle effects" often have been observed in airborne MSS data, where scan angles much larger than the $\pm 6°$ of ERTS are employed. These effects have both atmospheric and surface bidirectional reflectance causes. One would not necessarily expect to find them of significance in ERTS data, but Fig. 2 presents computed total radiance variations, for the atmosphere alone, that are as much as 8% of the minimum value for an 8% diffuse reflector observed through a clear atmosphere at 0.55 μm. Percentage variations in path radiance are even greater for the background albedoes shown. The scan-angle variations are reduced for longer wavelengths and, here, are negligible at 0.95 μm.

*"Importance of Atmospheric Scattering in Remote Sensing", by R. Turner, W. Malila, & R. Nalepka, Proc. of 7th Internat'l Symp. on Remote Sensing of Envir., Willow Run Labs, The Univ. of Mich., Ann Arbor, 1971.

There is, however, still an appreciable amount of path radiance at 0.95 μm, as shown in Fig. 3 for a 32% reflector. This figure illustrates directly the dependence of the total and path radiances on visual range (visual range is used as a convenient method for identifying standard atmospheric aerosol profiles used in the calculations, more exact profiles can be used, if known). Note that here the total radiance received from the target in a dark background decreases with increasing haze (shorter V) while it increases for a bright one.

Fig. 4 presents the combined effects of scan angle and visual range on spectral radiances at 0.55 μm for 8% target and background reflectances. The increase of scan angle effects for lower visual ranges is clearly shown, and path radiance is a large fraction of the total.

Empirical Studies

The ERIM multispectral scanner was flown on a series of multi-altitude passes in synchronism with the ERTS-1 pass on Aug. 25th. Reflectance panels were placed on the flight line. Airborne signals from large fields, resolvable in ERTS data, were compared to signals from the reflectance panels and equivalent reflectance values were assigned to these fields, called secondary standards. Average values then were extracted from ERTS data for each of the secondary standards the converted to radiances. (The maximum radiance values listed in Table G.2-2, pg. G-14, of the ERTS Data Users Handbook were assigned to tape levels 127, 127, 127, and 63 for ERTS Bands 4, 5, 6, and 7, respectively.)

Figs. 5-8 present plots of ERTS radiance versus target reflectance for the four ERTS bands. The dashed lines are least-squares fits to the values obtained for the secondary standards. Also on the figures are trios of lines that represent approximate calculations made with the radiative transfer model for different background albedoes.

The slopes of the theoretical lines and the empirical fits agree well, but the magnitudes differ in Bands 4 and 5 for reasonable background albedoes, especially for Band 4. The reason(s) for these differences is not known at this time, but there are several possibilities: (1) The theoretical radiance values were obtained by merely multiplying band-center spectral radiances by factors of 0.1, 0.1, 0.1, and 0.3 to approximate the ERTS spectral bandwidths; more complete and accurate calculations are desirable. (2) The reflectances assigned to the secondary standards for the empirical plots appear to be too low; higher values would improve agreement. (3) The model might be in error, although checks elsewhere of sky radiance predictions have shown good agreement with measurements and with exact calculations for a pure Rayleigh atmosphere. (4) The atmospheric profile used in the calculations might not accurately represent the true condition at the test site. (5) It is possible that the ERTS calibrations are biased or we

have misinterpreted the calibration procedures. Further study of this problem is required but, nevertheless, the strong influence of the atmosphere on ERTS data has been shown.

PROPORTION ESTIMATION

A second aspect of ERTS investigation MMC-136 is testing the applicability of advanced information extraction techniques to ERTS-1 MSS data. (These techniques have been developed at ERIM with funding provided by the Supporting Research and Technology program of NASA-JSC.) One technique addresses problems associated with accurately determining areas covered by features in the scene using scanners with limited spatial resolution, like ERTS-1 MSS. Clearly, there is a serious problem for features smaller than the instantaneous field of view of the scanner. In addition, problems exist even for larger features since many of the ERTS MSS pixels overlap the boundaries between these and adjoining features. As a result, the radiation represented in those pixels is a mixture of radiation reflected from two or more materials. Since the signals generated in such pixels are not characteristic of any one material, the pixels will generally be improperly classified. Therefore, the area assigned to each material class could seriously be in error. For example, at least 25% of the pixels covering a square field of 50 acres (20 hectares) will overlap its boundaries.

At ERIM we have developed a data processing technique* to estimate the proportions of materials contained within each pixel, by taking advantage of the fact that information is gathered in several spectral bands. This permits a more accurate determination of the area covered by each material; the greater the number of spectral bands used, the more materials can be considered. We next describe and evaluate the results of an initial test of this technique on ERTS-1 MSS data.

Test Results

For this test, we selected for processing a portion of ERTS data gathered over Southwestern Michigan on Aug. 25th. A black-and-white aerial photograph of this site is shown in Fig. 9. The primary features of this site are a number of lakes and ponds of various size surrounded by trees and agricultural fields, many of them bare soil.

The goal of this experiment was to determine the surface area of the lakes and ponds. For purposes of comparison, the data were processed using a conventional recognition algorithm in addition to the proportion estimation algorithm.

---

*"Estimating the Proportions Within a Single Resolution Element of a Multispectral Scanner", by H. Horwitz, R. Nalepka, & J. Morgenstern, Proc. of 7th Internat'l Symp. on Remote Sensing of Environ., Willow Run Labs., The Univ. of Mich., Ann Arbor, 1971.

Initially, a number of pixels containing pure samples of each of the primary scene components (water, trees, and soil) were extracted to establish training signatures for each of these materials. The same signatures were employed by both algorithms and ERTS Bands 4, 5, and 7 were used because of problems in Band 6 data for this frame.

For the conventional recognition algorithm, each pixel was assigned to one and only one class. The resulting recognition map is shown in Fig. 10; the rejection threshold was set so that 99.9% of pixels characterized by the signatures would be recognized. Portions of eleven lakes were identified, with a total area of 451,900 m^2 where an area of 4503 m^2 (79 m x 57 m) was assigned to each pixel.

We then applied the proportion estimation algorithm to the same data set and generated the lake recognition map shown in Fig. 11. In this map, the density of each symbol is proportional to the estimated proportion of water for that pixel. It is clear on comparing this map with the aerial photo that the shapes of the lakes are more accurately reproduced. Furthermore, even small lakes and ponds are detected, for a total of 19. In addition to the map, which only illustrates ranges of proportions, the exact proportions of water in each pixel were listed. It was determined, upon examining the results, that points containing small percentages of water should be ignored to eliminate false detections. From the listing we determined that the total lake area was 965,800 m^2.

Finally we used the aerial photo to determine the number and actual area of the water bodies in the scene. The total area was 1,004,000 m^2 for 20 lakes and ponds.

In Fig. 12 we present the results for comparison. Here we see that the proportion estimation technique provided significantly more accurate results than those available using the conventional processing technique.

CONCLUSIONS

The strong influence of atmospheric effects in ERTS data has been shown. Although we have not yet directly assessed the influence of these effects, we believe that they can degrade the quality of information extracted from ERTS data. Variations in atmospheric and scene parameters, both within and between frames, will be important. Techniques for reducing the influence of these effects are being investigated.

It has been demonstrated that highly accurate area estimates can be extracted from ERTS-1 data by use of an advanced information extraction technique. For the identification of areas of lakes and ponds in the test site, the 55% error of conventional recognition techniques was reduced to 3% with proportion estimation techniques. While the magnitude of improvement shown here might not be generally achievable without further development, this technique is certain to be useful for investigations in many disciplines.

SPECTRAL DEPENDENCE OF PATH RADIANCE

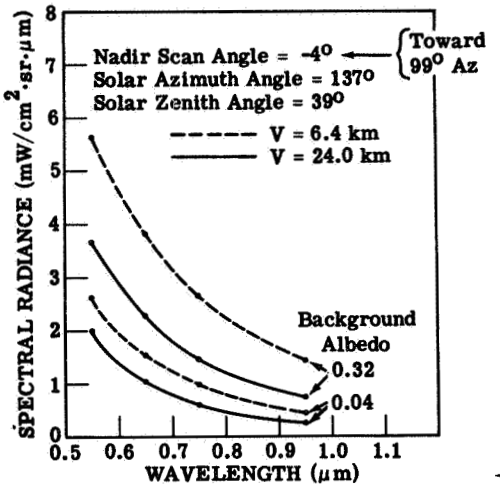


FIGURE 1

DEPENDENCE OF RADIANCE AT SATELLITE ON SCAN ANGLE, 0.55 μm

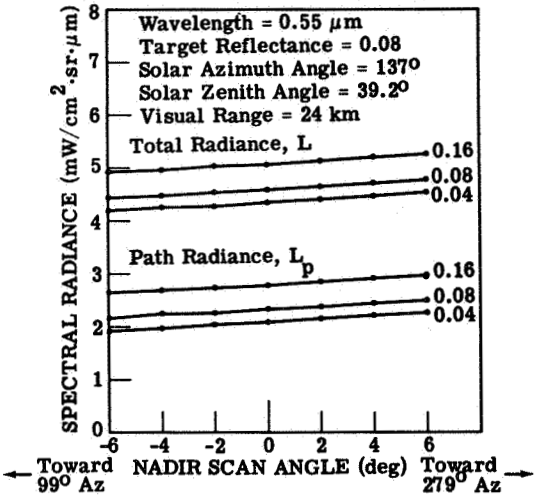


FIGURE 2

DEPENDENCE OF RADIANCE AT SATELLITE ON VISUAL RANGE, 0.95 μm

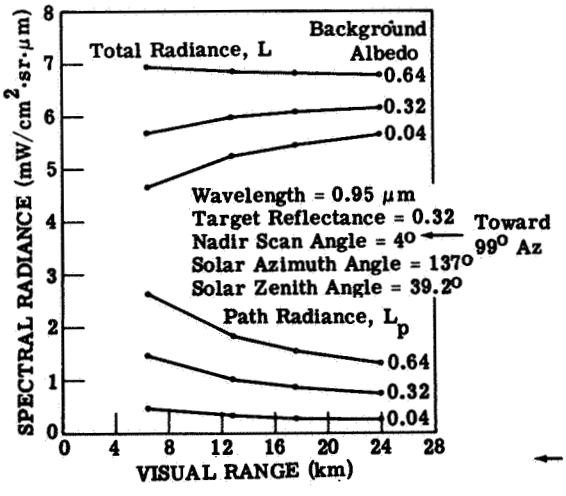


FIGURE 3

COMBINED SCAN-ANGLE AND VISUAL-RANGE EFFECTS ON RADIANCE AT SATELLITE, 0.55 μm

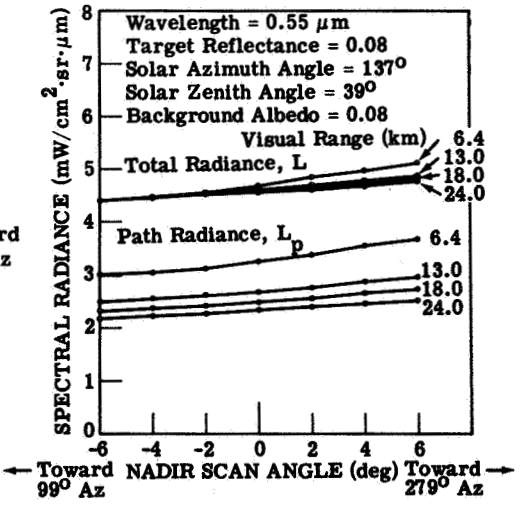
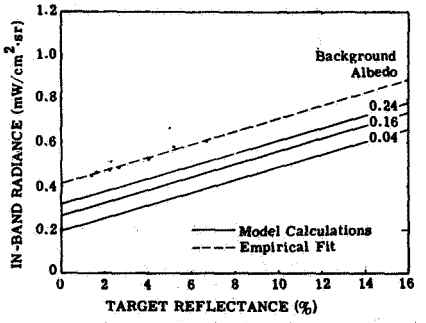
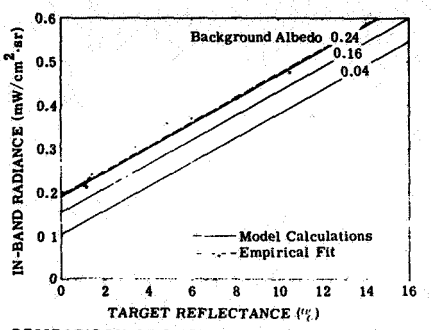


FIGURE 4



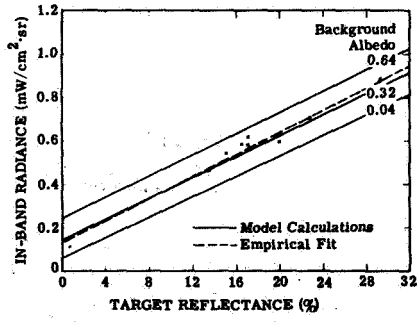
COMPARISON OF EMPIRICAL AND THEORETICAL RADIANCES FOR ERTS BAND 4 (0.5 - 0.6 μm) ERIM

FIGURE 5



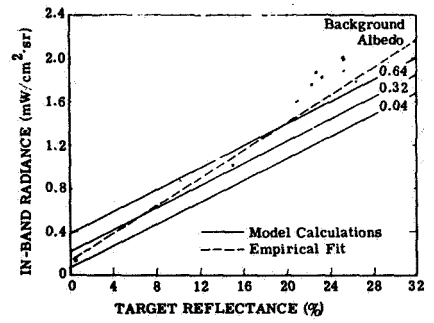
COMPARISON OF EMPIRICAL AND THEORETICAL RADIANCES FOR ERTS BAND 5 (0.6 - 0.7 μm) ERIM

FIGURE 6



COMPARISON OF EMPIRICAL AND THEORETICAL RADIANCES FOR ERTS BAND 6 (0.7 - 0.8 μm) ERIM

FIGURE 7

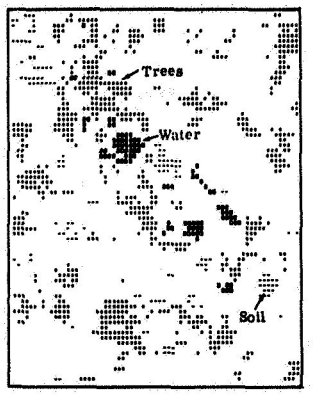


COMPARISON OF EMPIRICAL AND THEORETICAL RADIANCES FOR ERTS BAND7 (0.8 - 1.1 μm) ERIM

FIGURE 8



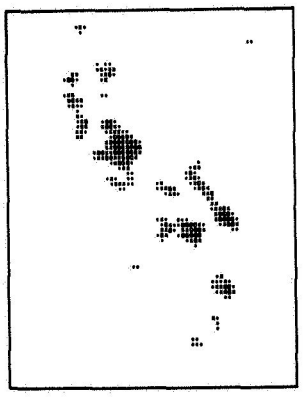
FIGURE 9



RECOGNITION PROCESSING FOR LAKES TEST AREA

ERIM

FIGURE 10



PROPORTIONS ESTIMATION *RESULTS FOR* LAKES TEST AREA (Intensity of symbol indicates proportion of lake in each resolution element)

ERIM

FIGURE 11

COMPARISON OF PROCESSING TECHNIQUES FOR ERTS MSS DATA FOR LAKES TEST AREA

(ERTS Bands 4, 5 and 7 Used)

	Ground Information	Recognition Processing	Proportions Estimation
Number of Lakes	20	11	19
Total Area (Meters^2)	1,004,200	451,900	965,800

ERIM

Figure 12

N73-28324

Paper I 2

DETERMINATION OF AEROSOL CONTENT IN THE ATMOSPHERE

Michael Griggs, *Science Applications, Inc., P. O. Box 2351, La Jolla, California 92037*

ABSTRACT

The objective of this investigation is to demonstrate the feasibility of determining the aerosol content in the atmosphere from contrast measurements of ground features, and from radiance measurements. Theoretical relationships between aerosol content and contrast reduction and radiance have been derived for ideal model atmospheres. The preliminary data analysis of the MSS transparencies has shown promising results for the contrast-aerosol content relationship in the Salton Sea/ desert region.

1. INTRODUCTION

The apparent increase of particles in the atmosphere is believed to affect the climate of the earth, and has led to the desire to monitor atmospheric aerosols on a global basis.[1,2] The ERTS-1 data present an opportunity to investigate two possible methods of measuring the aerosol content from satellite observations of contrast reduction and of radiance. Demonstration of the feasibility of these techniques will lead to routine satellite monitoring of the atmospheric aerosol content to provide information important in predicting the effect of man's activities on climate. In addition, it will provide input

parameters to atmospheric scattering models in algorithms being used to investigate surface properties of the earth's surface from space observations.

2. THEORY OF CONTRAST REDUCTION

Duntley[3] showed that the contrast reduction by the atmosphere of an object relative to the background is given by

$$\frac{C_R}{C_o} = \frac{1}{1 + \frac{B_{a(o)}}{\sigma_o B'_o}(e^{\tau} - 1)} \tag{1}$$

where

C_R is the apparent contrast,

C_o is the inherent contrast,

$B_{a(o)}/\sigma_o B'_o$ is the "sky/ground ratio", and

τ is the optical depth of the scattering atmosphere.

To further investigate this relationship, a perfectly arbitrary generalization of Eq. 1 is made:

$$\frac{C_R}{C_o} = \frac{1}{1 + g(\tau, A)} \tag{2}$$

From values published by Plass and Kattawar[4] for reflected radiance versus albedo, it is concluded that the reflected radiance is well represented by a linear function of A:

$$R_{refl}(\tau, A) = R_{refl}(\tau, 0) + A[R_{refl}(\tau, 1) - R_{refl}(\tau, 0)] . \tag{3}$$

The apparent contrast is, consequently:

$$C_R = \frac{R_{refl}(\tau, A) - R_{refl}(\tau, A')}{R_{refl}(\tau, A')}$$

$$= \frac{(A-A')[R_{refl}(\tau, 1) - R_{refl}(\tau, 0)]}{R_{refl}(\tau, 0) + A'[R_{refl}(\tau, 1) - R_{refl}(\tau, 0)]} \quad . \tag{4}$$

Since

$$C_o = \frac{A - A'}{A'} \tag{5}$$

we have

$$\frac{C_o}{C_R} = 1 + \frac{R_{refl}(\tau, 0)}{A'[R_{refl}(\tau, 1) - R_{refl}(\tau, 0)]} \tag{6}$$

By identifying with Eq. 2 we find that the unspecified function $g(\tau, A)$ may be separated into τ- and A-dependent parts:

$$g(\tau, A) = f(\tau)/A \tag{7}$$

where

$$f(\tau) = \frac{R_{refl}(\tau, 0)}{R_{refl}(\tau, 1) - R_{refl}(\tau, 0)} \tag{8}$$

Values of $f(\tau)$ using Eq. 8 have been calculated for the center wavelengths of the four MSS channels, based on interpolation of values of $R(\tau, 0)$ and $R(\tau, 1)$ calculated by Plass and Kattawar,[4, 5, 6] for the wavelengths 0.4 μm, 0.7 μm, 0.9 μm and 1.67 μm. The results, for three sun angles, for MSS 6 are shown in Fig. 1. The function $f(\tau)$ is related to the experimentally observable quantities C_o, C_R and A' by Eq. 2 and 7:

$$f(\tau) = A'(C_o/C_R - 1) \quad . \tag{9}$$

Thus, a measurement of the contrast ratio and knowledge of albedo and sun angle yields a value of $f(\tau)$ that determines

3. RELATIONSHIP OF RADIANCE AND AEROSOL CONTENT

Calculations of the radiance backscattered from the earth-atmosphere system, as seen from space have been published by Plass and Kattawar.[4,5] These calculations, using Monte Carlo techniques, consider multiple scattering of all orders, and take into account aerosol scattering and ozone absorption. Examination of the results of Plass and Kattawar shows that the outgoing radiance varies with aerosol content, and is most sensitive when the underlying surface albedo is low. The ocean, which covers much of the earth, has a low albedo at high sun angles and provides a suitable underlying surface for aerosol measurements. The calculations also indicate that the longer wavelengths ($\geq 0.7\ \mu m$) are more sensitive to aerosol changes. At shorter wavelengths the Rayleigh optical thickness is comparable to, or greater than, the aerosol optical thickness, so that changes in the aerosol content have less effect.

In order to further investigate the effect of aerosols on the upward radiance over a calm water surface, Plass and Kattawar[6] made some calculations for us for several aerosol vertical distributions, and showed a result of great importance for satellite observations of the upward radiance: the upward radiance depends strongly on the total number of aerosols, but not on their vertical distributions. Thus measurements of the upward radiance can be directly related to the total vertical aerosol content and hence the global loading.

The radiance in the MSS channel 6, centered at 0.75 μm, may be computed by interpolation of the results of Plass and Kattawar at wavelengths 0.4 μm, 0.7 μm, 0.9 μm and 1.67 μm, and by assuming a rectangular spectral response 0.1 μm wide. The results are plotted in Fig. 2 to show the relationship between the upward radiance and the aerosol content of the atmosphere for various sun angles. A simple linear relationship is shown to exist between radiance and the aerosol content. These straight lines are based on only two values of aerosol content, but a linear relationship may be established by considering the four data points for zero albedo. From these curves a knowledge of the sun angle and the absolute radiance allows the aerosol content of the atmosphere to be determined. It is seen that a 1 percent change in radiance is equivalent to about 1.5 percent change in aerosol content.

4. PROBLEM AREAS

The discussions in Sections 2 and 3 are based on theoretical calculations which use a model atmosphere, a model aerosol distribution, and assume a smooth water surface or a Lambertian surface. In practice, of course, these model conditions are never realized, so that deviations from the theoretical relationships are to be expected. Hence empirical relationships between the satellite data and the aerosol content will be investigated. However, the problem of sun glitter on the ocean still remains.

If the ocean were perfectly smooth, as assumed in the calculations, an image of the sun would be seen at the specular reflection angle, and the only upwelling surface radiation observable at other look angles from space would be the diffuse sky radiation reflected from the ocean surface and the radiation scattered up from below the ocean surface. As the smooth ocean surface is increasingly disturbed, a glitter pattern becomes increasingly larger about the specular point. At sun zenith angles greater than about 30° the glitter effect has been considered negligible (except for very rough seas) at the nadir point. However, recent measurements by Hovis (private communication from R. Fraser) suggest that this assumption is not correct, so that the ocean surface radiance at the nadir is not known accurately.

This problem might be overcome by making observations at two wavelengths, assuming that the spectral variation of the surface radiance is known. The choice of wavelengths must be made carefully since the spectral distribution of the radiance does vary due to ocean properties such as chlorophyll content, suspended matter and depth. If the ratio of reflectivities at two wavelengths remains constant for various surface conditions and sun angles, then the sun glitter problem can be eliminated.

5. PRELIMINARY RESULTS

Two test sites have been used for this investigation. One is the Salton Sea/desert region in the Borrego Desert in Southern California, and the other includes San Diego city and the ocean. Measurements of the vertical aerosol optical thickness have been made with a Volz sun photometer at the times of the satellite overpass when weather conditions permitted. The results of these measurements given, in Fig. 3, show that on all these occasions the aerosol content was lower than the Elterman 1964 model value.[7]

The ERTS-1 data received to date for these test sites have been only in the photographic format, and have been analyzed with a densitometer. Digital data have been requested and will be analyzed on a CDC 6400 computer.

The preliminary analysis of the transparency data received to date has initially shown promising results for the contrast-aerosol content relationship in the Salton Sea/desert region. The measured transparency densities were converted to radiances using the grey scale and preflight calibration data. The radiance of the water across the Salton Sea was found to be almost constant on a given frame, but, as expected, the desert surface was quite variable in radiance. The apparent contrast, C_R, was computed using the brightest portion of the adjacent desert. The inherent contrast, C_o, was calculated by assuming a reflectivity of .30 for the desert and .02 for the Salton Sea (based on albedos measured by Griggs [8]), giving a value of 14.0 for C_o. For this preliminary examination, the same value was assumed for all sets of data, neglecting the variation with wavelength and sun angle. Values of $f(\tau)$ were calculated from Eq. 9, and values of τ determined from plots of $f(\tau)$ vs τ for MSS channels 4, 5 and 6 (e.g. see Fig. 1). MSS 7 is not considered due to the influence of water vapor in this channel. These values of τ were converted to aerosol content assuming that τ is proportional to the number of aerosols.[7] The values of aerosol content in terms of N (Elterman's 1964 model value), obtained in our initial analysis, are given in Table 1. The results, except for one, are reasonable in terms of possible aerosol content, although no ground-truth data are available for comparison. The results for 10-1-72 show excellent agreement among the different channels.

TABLE 1

MSS Channel	Aerosol Content		
	4	5	6
8-26-72	2.5N	1.7N	
10-1-72	.9N	.8N	1.0N
11-6-72	1.8N	.07N*	1.1N

* Low value attributed to calibration or processing problems with this frame.

Analysis of subsequent photographic data has not been so successful due to an apparent calibration problem, at least at the low radiance end of the grey scale. The density of the transparencies for the water surfaces was found to be greater than that of the blackest step of the grey scale, which corresponds to zero radiance. Due to this problem, further analysis of the contrast-aerosol content relationship has been delayed pending the receipt of the digital data which provide more accurate radiance measurements. These tapes are also necessary to investigate the radiance-aerosol content relationship.

6. CONCLUSIONS

The preliminary analysis of the transparency data has shown promising results for the contrast-aerosol content relationship. Further analyses with the digital data, and for more satellite overpasses, are required to clearly demonstrate the feasibility of measuring the atmospheric aerosol content from ERTS measurements.

7. REFERENCES

1. "Man's Impact on the Global Environment", MIT Press, Cambridge, Mass., 1970.

2. "Remote Measurement of Pollution", NASA SP-285, 1971.

3. S. Q. Duntley, J. Opt. Soc. Am. 28, 179 (1948).

4. G. N. Plass and G. W. Kattawar, Appl. Opt. 7, 1129 (1968).

5. G. N. Plass and G. W. Kattawar, Appl. Opt. 9, 1122 (1970).

6. G. N. Plass and G. W. Kattawar, Appl. Opt. 11, 1598 (1972).

7. L. Elterman, AFCRL Report No. AFCRL-64-740 (1964).

8. M. Griggs, J. Appl. Meteor. 7, 1012 (1968).

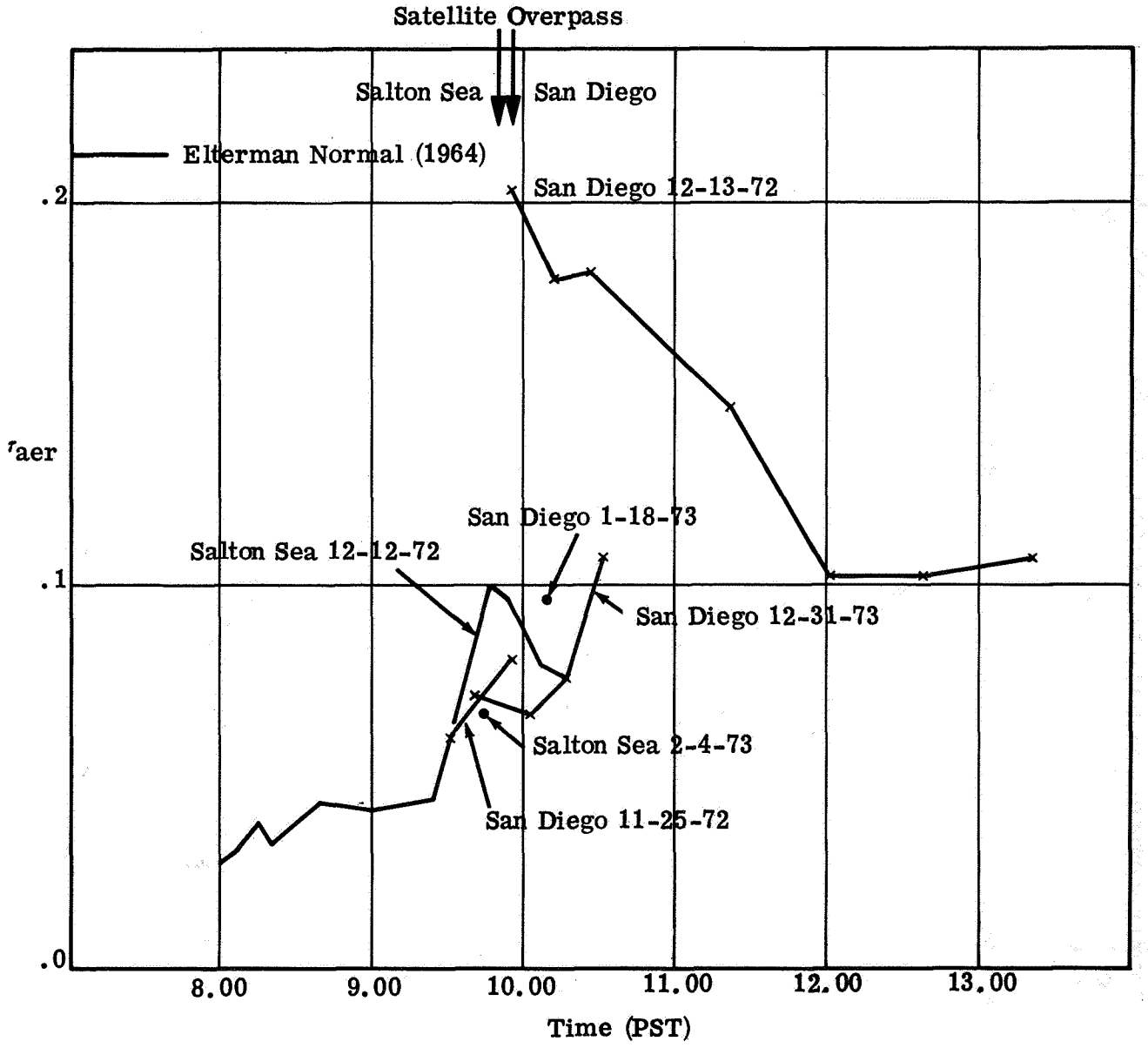


Fig. 1 Volz Data

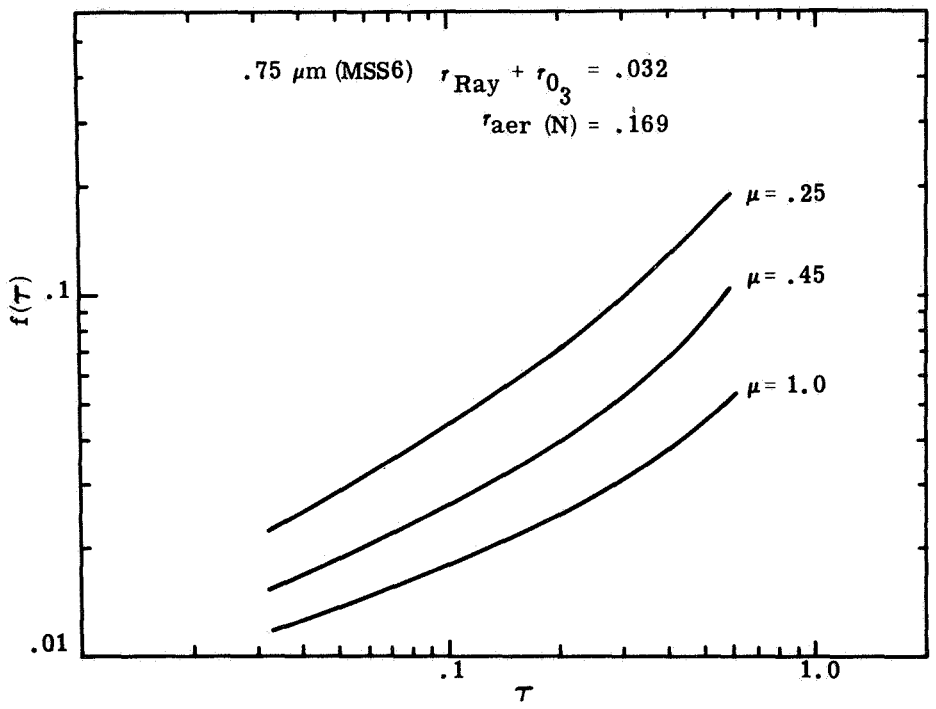


Fig. 2 $f(\tau)$ vs τ for three sun zenith angles, θ, ($\mu = \cos\theta$)

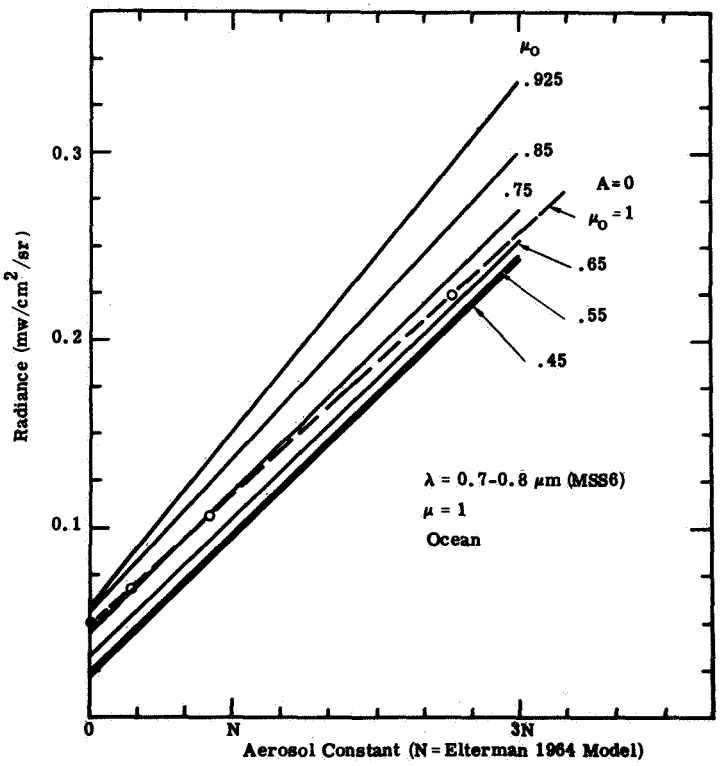


Fig. 3 Radiance vs. Aerosol Content for MSS6

N73-28325

Paper I 3

A TECHNIQUE FOR CORRECTING ERTS DATA FOR SOLAR AND ATMOSPHERIC EFFECTS

Robert H. Rogers and Keith Peacock, *Bendix Aerospace Systems Division, Ann Arbor, Michigan*

ABSTRACT

A technique is described by which an ERTS investigator can obtain absolute target reflectances by correcting spacecraft radiance measurements for variable target irradiance, atmospheric attenuation, and atmospheric backscatter. A simple measuring instrument and the necessary atmospheric measurements are discussed, and examples demonstrate the nature and magnitude of the atmospheric corrections.

1. INTRODUCTION

Measurements of atmospheric parameters and their use to transform ERTS data to absolute target reflectances are essential if the observations and reports of a large number of PIs are to be correlated and compared by NASA and other PIs in a meaningful way. ERTS-1 Experiment PR303 is evaluating the techniques for determining and removing solar and atmospheric effects that degrade the radiometric fidelity of ERTS data. This paper describes one technique, use of a Radiant Power Measuring Instrument (RPMI) to determine target irradiance, H, atmospheric transmittance for one air mass, τ, and the sky radiance seen by the spacecraft, L_{ATM}. Techniques for determining these parameters and the result of their use in transforming ERTS data to target reflectance is reported.

The total radiance, L, recorded by ERTS from a target of reflectivity, ρ, is related to these parameters by:

$$L = \frac{\rho H \tau}{\pi} + L_{ATM} \tag{1}$$

for a spacecraft looking vertically.

The target irradiance H can be further subdivided into:

$$H = H_o \tau^m \cos\theta + H_{sky} \tag{2}$$

where H_o is the solar irradiance outside the atmosphere, m is the atmospheric air mass in terms of the air mass at the zenith, θ is the solar zenith angle and H_{sky} is the sky irradiance. An Earth Resources investigator must therefore have an independent knowledge of H, τ, and L_{ATM} if he is to obtain the spectral reflectances of his target from the ERTS data.

PRECEDING PAGE BLANK NOT FILMED

2. RADIANT POWER MEASURING INSTRUMENT (RPMI)

The RPMI, developed specifically for this experiment and shown in Figure 1, provides an ERTS investigator with the capability of obtaining radiometric measurements needed to determine solar and atmospheric parameters that affect the ERTS radiance measurements.

The RPMI is a rugged, hand-carried instrument accurately calibrated to measure both downwelling and reflected radiance within each ERTS multispectral scanner (MSS) band. A foldover handle permits a quick change from wide-angle global or sky irradiance measurements to narrow-angle (6.0° circular) radiance measurements from sky and ground targets. These measurements yield ground truth site reflectance and permit calculation of additional parameters such as beam transmittance between spacecraft and ground, and path radiance (path reflectance).

12 range scales permit irradiance measurements from 0.001 to 300 W/M^2 and radiance measurements from 0.1 to 3×10^4 $W m^{-2} Sr^{-1}$. The instrument is calibrated to 5% absolute and 2.0% relative from band to band.

3. MEASUREMENT OF ATMOSPHERIC PARAMETERS

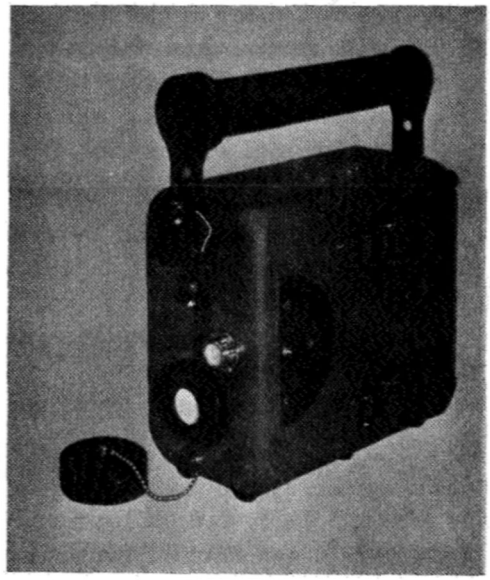
As Figure 1 shows, the RPMI is deployed in concert with ERTS overflights to obtain the direct measurements, within the four ERTS MSS bands, of: (1) global irradiance, H, (2) sky irradiance H_{sky} (i.e., by shadowing sun, and reading global minus direct beam-solar), (3) radiance from a narrow solid angle of sky $L_{meas}(\phi)$, and (4) direct beam-solar irradiance $H_{sun}(m)$. From these measurements additional solar and atmospheric parameters such as beam transmittance τ and path radiance L_{ATM} are determined, and target reflectance ρ computed using equations (1) and (2) for each spectral band.

Global Irradiance, H, is measured directly in each band as shown in Figure 1. Additional accuracy in H can be obtained by measuring the direct-beam solar irradiation, $H_{sun}(m)$ and sky irradiance, H_{sky} (direct sun shadowed out) independently and computing the total target irradiance, using:

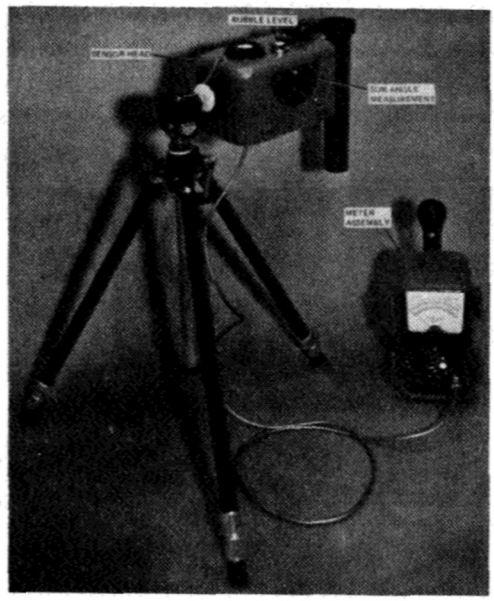
$$H = H_{sun}(m) \cos \theta + H_{sky} \qquad (3)$$

The sun angle is read from the sun dial on the side of the RPMI after leveling the instrument with its bubble level.

Beam Transmittance, τ, is determined by plotting an "extinction" curve, as shown in Figure 2. The direct-beam solar irradiation is plotted on a logarithmic scale as a function of the air mass. The

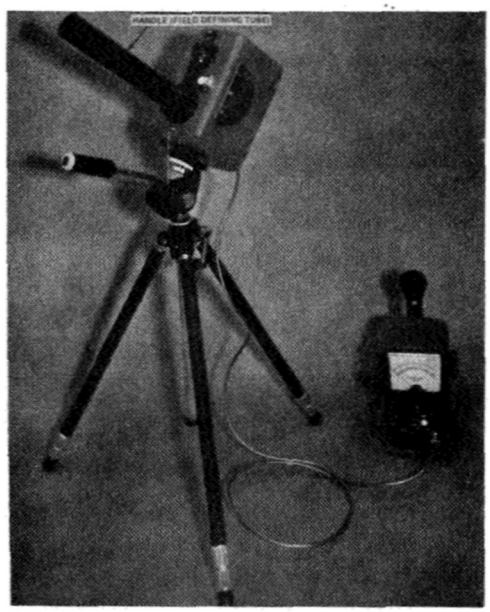


RPMI Assembled

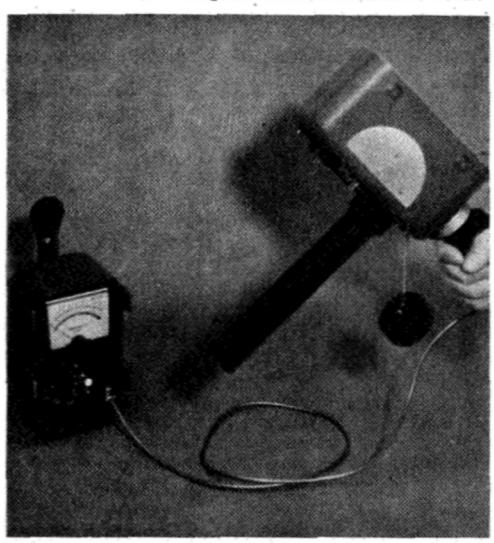


Global Irradiance (H) – 2π steradian field of view for measuring downwelling (incident) radiation ERTS MSS bands. Bubble level aids this measurement.

Sky Irradiance (H_{SKY}) – Block sun to measure global irradiance minus direct sun component, in every ERTS MSS band. Angle from zenith to sun is also measured in this mode by reading sun's shadow cast on sun dial.



Radiance from Narrow Solid Angles of Sky – Handle serving as field stop permits direct measurements through a 6.0° circular field of view. This mode is also used to measure direct beam irradiance.



Reflected Radiation – Used with small calibration panels, cards, to obtain direct measurement of truth site reflectance. Reflectance also immediately derived from ratio of reflected radiance and global irradiance.

Figure 1 Radiant Power Measuring Instrument

intercepts of the lines on the vertical axis give the solar irradiance, H_o, outside the atmosphere in each of the ERTS MSS bands, and the beam transmittance can be computed from the slope of the lines using the equation in Figure 2. Measurement of H_o can also be used for recalibration of the instrument, without the use of additional equipment, at any location in the world.

If H_o is known from prior observations, τ could be determined by making a single-point measurement of $H_{sun}(m)$. A correction can be made for the different zenith angles of the sun and spacecraft. This beam transmittance calculation assumes that the atmospheric properties in sun-to-target path are the same as in target-to-spacecraft path. Tests are being performed to determine the accuracy of this single-point measurement technique.

Path Radiance, L_{ATM}, is the energy reaching the spacecraft from Rayleigh and aerosol scattering by the atmosphere. As it cannot be measured directly, it must be derived from ground-based measurements of the backscatter. The simplest technique is to use RPMI to measure the sky radiance $L_{meas}(\phi)$ scattered at an angle, ϕ (as in Figure 3B) such that ϕ is identical to ϕ', the angle through which radiation is scattered to the spacecraft and correct the measurement for the difference in air masses between the direction of observation and the direction of the spacecraft. As this technique can only be used when $\theta > 45°$, atmospheric modeling is being performed to extrapolate from the available measurement angles to the desired angle.

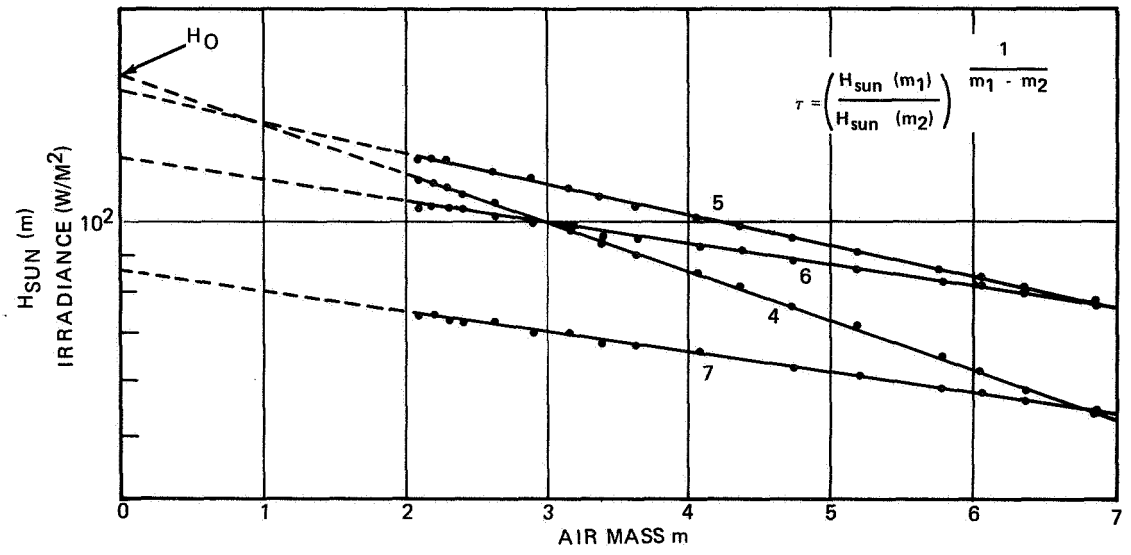


Figure 2 Atmospheric Extinction Curves

Figure 3A shows RPMI sky radiance measurements as a function of scattering angle ϕ and air mass. Each of the solid lines was obtained by pointing the RPMI at the sun and then sweeping it in azimuth, taking readings at 20° intervals for a particular elevation angle. The broken line was produced by taking readings at different elevation angles from the sun for zero azimuth. The scattering angle, ϕ, is found from:

$$\cos \phi = \sin \theta \sin \beta \cos \alpha + \cos \theta \cos \beta \qquad (4)$$

in which θ is the solar zenith angle, β is the zenith angle of the observation, and α is the azimuth measured from the sun. The air masses given in Figure 3A are the values in the direction of the observation. The air mass is continuously variable along the broken curve.

The atmospheric scattering along the line of sight should be proportional to $(1 - \tau^m)$ in which τ is the atmospheric transmission for one air mass and τ^m is the transmission of air mass m. Thus, if the RPMI radiance measurement L_{meas} is taken at a scattering angle equal to the scattering angle to the ERTS, the path radiance seen by ERTS should be related by:

$$L_{ATM} = L_{meas} \left[\frac{1 - \tau}{1 - \tau^m}\right] \qquad (5)$$

assuming the spacecraft is looking vertically through one air mass. This formula has been used by S.Q. Duntley, C.F. Edgerton, and others.

The validity of this formula was checked by multiplying the data in Figure 3A by the term containing τ in equation (5), using a value of τ determined from its extinction curve. The results are shown in Figure 3B. The radiance variation at any angle is only ±5%, which is within the measurement errors. These results can be used to give the atmospheric radiance seen by ERTS by selecting the correct scattering angle. These observations are continuing in order to determine the repeatability of the curves and the accuracy if measurements at only one or two angles are used to determine L_{ATM}.

4. EXAMPLE OF ERTS DATA CORRECTION

Since the completion of the RPMIs, local weather conditions have prevented atmospheric observations on the day of an ERTS overpass. Thus, the following comparison of atmospheric data from 12 Feb 1973 with ERTS data from 28 Sept 1972 is only to demonstrate the magnitude of the corrections and is not intended to be an accurate analysis.

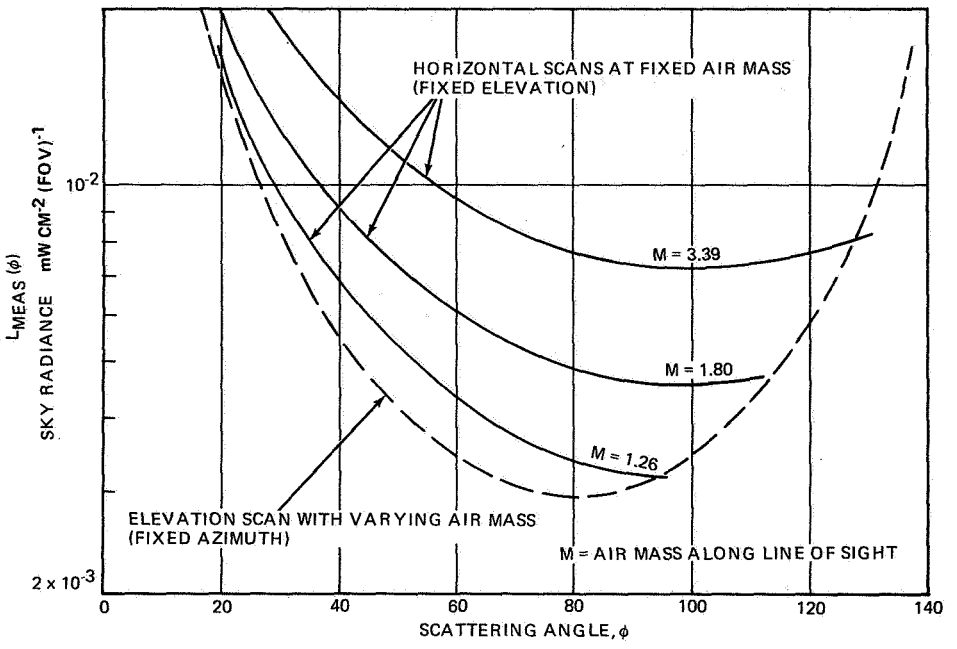


Figure 3A Atmospheric Radiance: Band 4

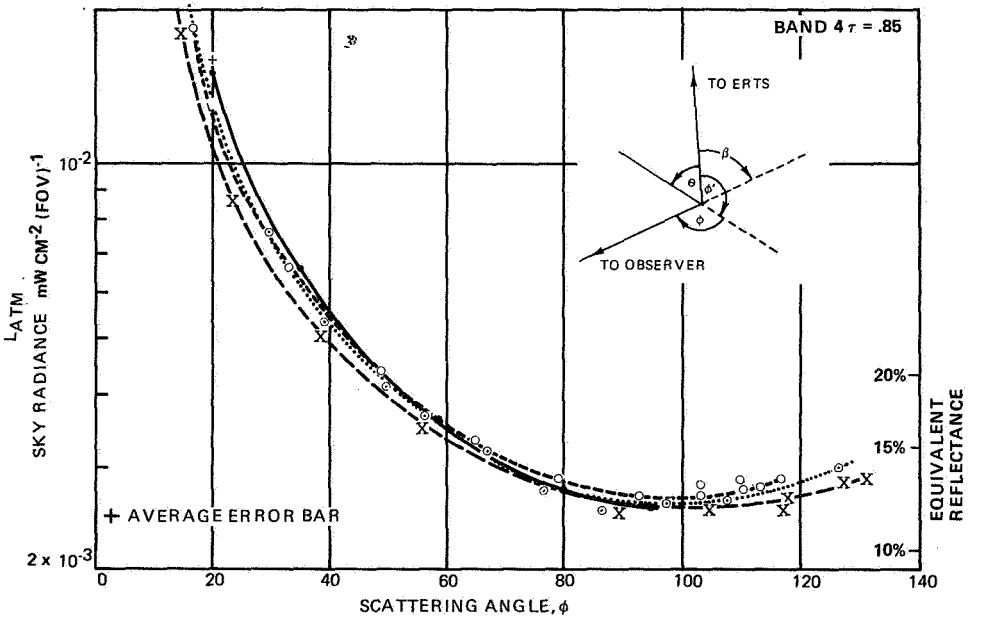


Figure 3B Scattering Data Corrected for Air Mass

Values of ERTS atmospheric path radiance were derived from data taken at Bendix in Ann Arbor, Michigan on 12 Feb 1973. Using the procedure described above, the RPMI sky radiance measurements, L_{meas}, were corrected to one air mass, and the corrected values in each of the four ERTS MSS bands were plotted as a function of the scattering angle. For a scattering angle of 131° (solar zenith angle 49°) to the ERTS, the values of L_{ATM} computed for bands 4 to 7 are listed in Table 1. These have also been converted to bit equivalents based on 7-bit levels for bands 4, 5, and 6, and a 6-bit level for band 7. The table also lists the atmospheric path radiance signal as a percentage of the full scale ERTS channel reading.

Listed in the last two columns of Table 1 are radiance values taken from ERTS data for 28 Sept 1972. The first is for water and the second is a low-lying area near the Huron River in Ann Arbor. For water, it is noted from the table that over 50% of the signal received by the spacecraft is atmospheric path radiance.

Table 2 summarizes the additional data necessary for the calculations of target reflectances. The values of H_o and τ are derived from the extinction curve as described in Section 3 using data from 12 Feb 1973. The global irradiance H is derived from the previous equation 2 using a typical measured value of sky irradiance H_{sky}. Finally, the data were used to calculate the reflectance of the target using equation (1). The results are now absolute values and are free of atmospheric and solar effects. Examples of two different targets, a small lake and a low-lying river bank, are given in Table 2.

Table 1 Atmospheric Radiance Values

Band	L_{ATM} (mW/cm^2-sr)	Bit Equivalent	% Full Scale	ERTS Data (mW/cm^2-sr)	
				Barton Pond	Bank of River
4	0.274	14	11	0.476	0.508
5	0.118	7.5	5.9	0.242	0.276
6	0.082	6	4.7	0.141	0.402
7	0.1062	1.5	2.4	0.234	1.10

Table 2 Calculation of Target Reflectivity

Band	H_o (mW/cm^2)	τ	Global Irradiance (mW/cm^2)	Target Reflectivity	
				Barton Pond (%)	River Bank (%)
4	15.05	0.81	8.41	9.3	10.8
5	13.98	0.865	8.14	5.5	7.5
6	12.00	0.909	7.38	2.8	15
7	8.57	0.913	5.02	0.9	6.8

5. SUMMARY

Solar and atmospheric parameters degrade the radiometric fidelity of ERTS data by large amounts. Without direct measurements, the unknown atmospheric transmission, target irradiance, and sky radiance prevent the measurement of absolute target reflectance. Preliminary results indicate that the RPMI will provide a straightforward, low-cost procedure that could be employed by all PIs to obtain the needed radiometric calibration of ERTS data, thus making accurate, unambiguous interpretations possible. The ERTS-1 experiment will determine the best procedures and techniques using RPMI to obtain the needed solar and atmospheric parameters, and will utilize the performance achieved by RPMI as a baseline to evaluate alternative calibration techniques.

It is hoped that the results of this investigation will support NASA in its continuing effort to identify and bring together the most cost-effective grouping of instruments and techniques to achieve radiometric calibration of ERTS data gathered on a world-wide basis.

N73-28326

Paper I 4

EXPERIMENTAL MASKING OF RBV IMAGES TO REDUCE STATIONARY RESIDUAL INACCURACIES IN RADIOMETRIC CORRECTION

Donald S. Ross, *International Imaging Systems, Mountain View, California*

ABSTRACT

RBV vidicon tube calibration data are used to correct spatially non-uniform radiance response in individual vidicons, during post-acquisition signal processing. However, examination of different ERTS-1 RBV-1, -2, and -3 image scenes showed stationary, repetitive residual inaccuracies in shading correction, large enough to affect qualitative and quantitative image analyses.

Photographic masks designed to reduce residual shading were prepared from RBV-1, -2, and -3 images of a relatively cloud-free ocean scene of uniform reflectance. When applied to other RBV scenes, the masks enabled more closely corrected RBV images to be printed. Illustrations are given of RBV-1 image before and after correction, compared with an equivalent MSS spectral image of the same scene.

1. INTRODUCTION

In an investigation where it was necessary to compare equivalent bulk-processed RBV and MSS spectral bands, a large number of local density variations were noted in RBV-1, -2, and -3 images vis-a-vis MSS-4, -5, and -6 records of the same scene. Analysis of a number of RBV scenes confirmed that many of the density variations in individual RBV spectral bands also had the same position, shape and density distribution from scene to scene.

It was necessary to correct the repetitive density variations in the RBV images before a useful comparison could be made with their MSS counterparts. The simplest method available was by photographic masking. Masking entails making a replica in opposite polarity of the image to be treated, in this case a negative mask, which when registered image-wise with the

Original photography may be purchased from:
EROS Data Center
10th and Dakota Avenue
Sioux Falls, SD 57198

original positive would have densities exactly cancelling the unwanted densities in the original scene. When the combination is reproduced, a new scene would be formed, minus the unwanted density variations.

2. THE PROBLEM

Each RBV vidicon tube in ERTS-1 is mapped during calibration for radiometric response, since the photoconducting image surfaces of vidicon tubes vary in sensitivity from point to point. Response is measured on an 18X18 matrix, and data from the 364 points are used for generating a radiometric response correction program for reducing the shading errors to about 10% during post-acquisition signal processing, before imagery is produced. In the RBV images used in this investigation, it appears that the 18X18 matrix does not provide enough correction points to sufficiently smooth out some major shading errors, and local deviations much greater than 10% persist. Spot density measurements on the RBV image cannot be related with confidence to spectral reflectances of the same scene in the equivalent MSS band.

Figure 1 is of ERTS-1 RBV-1 images of different scenes, taken several days apart, printed at high contrast to emphasize and show the correlation of stationary shading errors in the RBV-1 camera. Similar errors were found in RBV-2 and -3 images. In the three RBV bands at 1:1,000,000 scale, graduated density variations occur in circular or elliptical patches varying from a few millimeters to 15 or 20 mm in size. Linear crosshatching at 45° also was found in parts of these images, appearing as lines of graduated density 1 or 2 mm wide and up to 60 mm long; this seems to be related to the 18X18 matrix but at a 36X36 frequency.

3. MASKING

A relatively cloud-free 9.5 inch, positive transparency scene was found, E-1007-15160-1, with a uniformly-reflecting ocean surface, confirmed by examination of the MSS-4 image. The RBV-1 image showed the repetitive residual errors noted above, and was used for making the correction mask as follows:

As all ERTS-1 images are reproduced at gamma 1.0* within close tolerances, the mask would also be made at gamma 1.0. A film was selected, Kodak Commercial, polyester base, and processing was established in D-19 developer for obtaining gamma 1.0 reproduction of a calibrated

*This is not exactly correct. Reproduction of the darker areas of the bulk-processed scene (in the positive transparency) is at gamma less than 1.0, where the scene was recorded at sensor response of less than 20% full-scale. E.G., at 2% sensor output, gamma would be 0.75. In the mask, densities representing the darkest, lower gamma areas of the positive are also at a lower gamma, providing an almost perfect match for density cancellation.

step-tablet, under the contact printing exposure conditions to be used.

Bulk-processed ERTS-1 images are also controlled in density range, as well as gamma. The density range is normally adjusted to have the brightest objects in the scene such as clouds, at D 0.40±0.12 in the positive. As long as the image is on the straight line of the film reproduction material, with its density range within tolerance, and gamma 1.0 is maintained both in the mask and the image to be treated, one correction mask can be used with other images from the same spectral band.

A series of negative masks was then printed from the RBV-1 positive master, each processed to gamma 1.0. The negative mask which most completely cancelled densities in the positive master, when registered with it, was then selected for use with RBV-1 images from other scenes.

4. THE RESULT

ERTS-1 E-1002-18140, 25 Jul 72, RBV-1 was registered with the negative mask selected and reprinted through the combination. Sections of this image before and after masking are shown in Figure 2, compared with an MSS-4 image of the equivalent spectral band. The result is an obvious smoothing of residual RBV radiometric correction errors which enable the RBV-1 and MSS-4 image densities to be compared with each other for image analysis. The dark artifacts on the ocean in the lower left of the masked image are negative images of clouds, which were in the image from which the mask was made. Some scale differences exist between the reseaux of the mask and the masked image, but are not present in other RBV-1 images which have been tested. (The same procedures have been used for making radiometric correction masks of RBV-2 and -3 imagery.)

The extent to which residual shading has been reduced in the RBV-1 image is difficult to determine accurately, when comparing it with the MSS-4 image. As the RBV-1 spectral band extends further into the blue region than MSS-4, some differences might be expected from atmospheric effects, and would appear more prominently over a uniform background such as water.

However, the degree of correction exercised by the mask can be judged by measuring its density range between the lightest and darkest areas. The range is about 0.60 density units, a 4:1 difference in transmission. Density variations measured in the registered combination of the mask and the master from which it was printed do not exceed ±0.03. Maximum spatial non-uniformity of densities in the third generation 9.5 inch ERTS image is in the order of 0.10. The combined local error between the mask and the image could be in the worst case, ±0.13, or 1.35:1; a significant improvement over the original 4:1 shading error.

CONCLUSIONS

It is concluded that the 18X18 RBV correction matrix does not sufficiently eliminate radiance response inaccuracies in the bulk processed images, where densities in these images are to be related to scene radiances as viewed from the sensor position. This tends to vitiate the usefulness of an otherwise excellent sensor system.

Masking offers a relative simple means of correcting residual RBV radiometric errors, which could be applied during production of 9.5 inch enlarged images with appropriate masks on the exposure platen. RBV images made over a completely calm ocean area, undisturbed by waves and free of clouds and sun-glitter, would provide master images from which correction masks could be made for routine production work.

REFERENCE

Data Users Handbook
NASA/GSFC Document No. 71SD4249



FIGURE 1. ERTS-1 RBV-1 IMAGES SHOWING STATIONARY RESIDUAL SHADING ERRORS. LEFT, E-1004-08021-1, 27 Jul 72; RIGHT, E-1007-15160-1, 30 Jul 72.

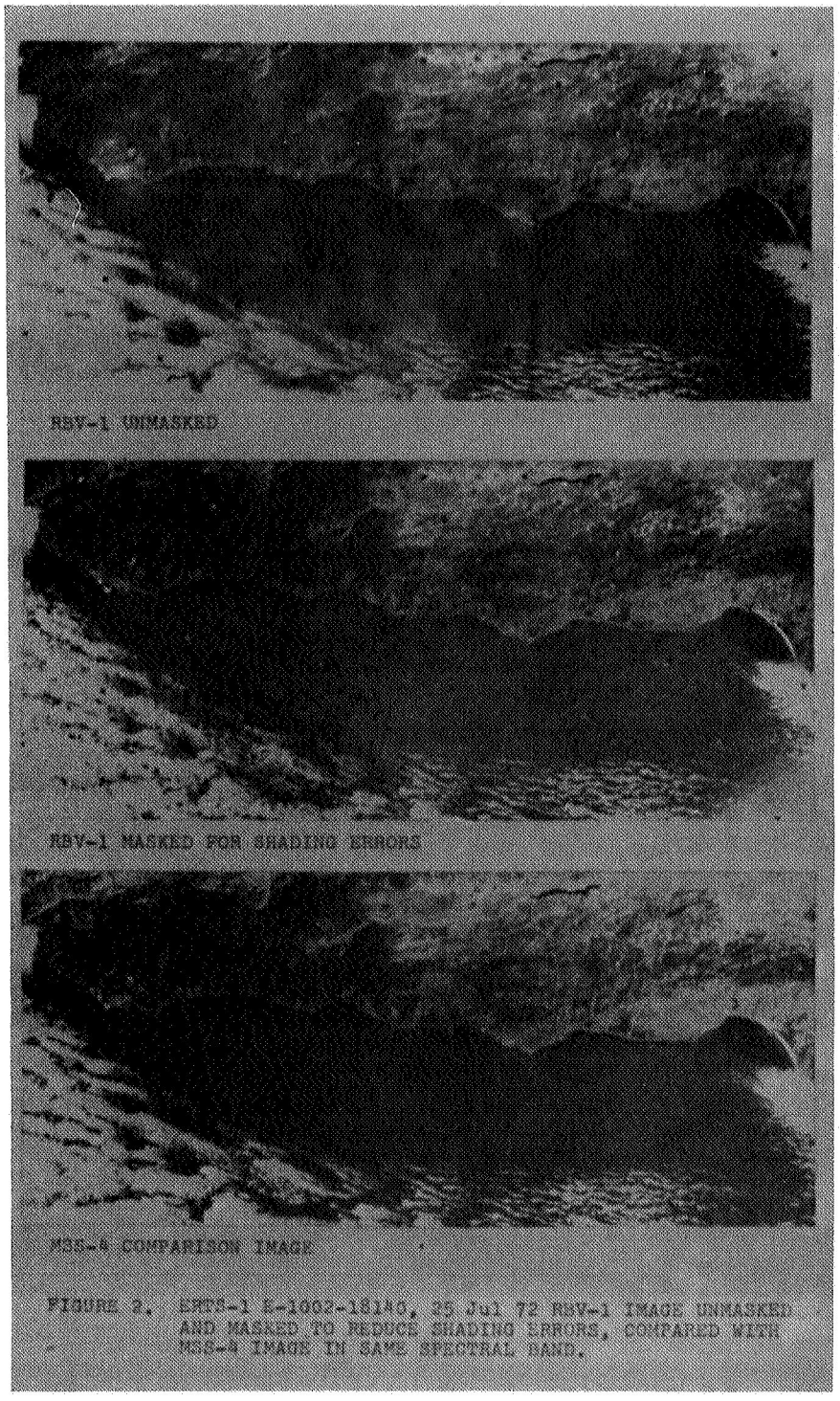


FIGURE 2. ERTS-1 E-1003-16140, 25 Jul 72 RBV-1 IMAGE UNMASKED AND MASKED TO REDUCE SHADING ERRORS, COMPARED WITH MSS-4 IMAGE IN SAME SPECTRAL BAND.

Paper I 5

GEOMETRIC QUALITY OF ERTS-1 IMAGES

Robert B. McEwen, *U. S. Geological Survey, 1340 Old Chain Bridge Road, McLean, Virginia 22101*

ABSTRACT

Geometric fidelity of an image is fundamental for referencing earth resource data to map positions. Image coordinates should register between spectral bands and between sequential images of the same scene. In addition the image coordinates should have a defined relation to map projections of the area. Selected RBV and MSS images have been precisely measured and compared with calibrated reseau and ground coordinates. The magnitude and pattern of several types of geometric distortion have been determined.

(Paper jointly presented with Alden P. Colvocoresses. See Paper L 2.)

N73-28327

Paper I 6

DIGITAL RECTIFICATION OF ERTS MULTISPECTRAL IMAGERY

Samuel S. Rifman, *TRW Systems Group, Redondo Beach, California*

ABSTRACT

Rectified ERTS multispectral imagery have been produced utilizing all digital techniques, as the first step toward producing precision corrected imagery. Errors arising from attitude and ephemeris sources have been corrected, and the resultant image is represented in a meter/meter mapping utilizing an intensity "resampling" technique. Early results from available data indicate negligible degradation of the photometric and resolution properties of the source data as a consequence of the geometric correction process. Work utilizing ground control points to produce precision rectified imagery, and including photometric corrections resulting from available sensor calibration data, is currently in progress.

I. INTRODUCTION

The production of precision processed ERTS imagery requires both precision rectification (correction of spatial distortions) of the bulk image data, as well as photometric correction of intensity values using sensor calibration data. In performing the respective corrections to the bulk imagery, it is necessary to account for a number of diverse error sources peculiar to the two sensor systems carried aboard ERTS: the three Return Beam Vidicon (RBV) cameras and the Multispectral Scanner (MSS). It is also necessary to compensate for errors external to the sensors, arising from spacecraft attitude, ephemeris and earth curvature.

In general, the problem of producing precision corrected images involves: first, the modeling of error sources that are to be corrected, and the development of techniques for accomplishing the corrections; and second, the implementation of a suitable algorithm for producing the corrected image. The emphasis of this paper will be on the second problem, with respect to some of the techniques and problems associated with the production of corrected imagery. Furthermore, because of the convenience and precision associated with the manipulation of imagery in a digital form, this paper is concerned with the problem of precision processing of imagery by purely digital techniques.

The well-known advantages of digital processing methods with respect to precision and permanence lend themselves directly to the task of generating precision digital image products for use by current and future investigators (for example, in scene/scene comparisons performed in the course of change discrimination studies). Advances in computer systems (see Reference 1 for a recent review article) have been matched recently by advances in algorithm development to make possible all-digital precision image processing, with moderate computer times. Following a

PRECEDING PAGE BLANK NOT FILMED

Original photography may be purchased from:
EROS Data Center
10th and Dakota Avenue
Sioux Falls, SD 57198

discussion of error sources, examples of ERTS-1 MSS imagery rectified by all-digital techniques at TRW Systems Group will be presented, together with a discussion of the relative merits of several algorithms utilized to produce the imagery. Extensions of these results to processing via modern mini-computers will also be indicated.

II. MSS ERROR SOURCES

Users of precision rectified ERTS imagery generally require that the products be represented in a rectangular cartesian coordinate system, i.e., that linear distance on the ground be faithfully represented in the imagery, free of errors arising within the sensor system, the spacecraft attitude and ephemeris, earth rotation and earth curvature.

Shown in Figure 1 (Reference 2), is a schematic diagram of the MSS sensor* carried aboard ERTS-1. The four band (0.5 - 1.1μm) sensor scans 185 Km wide cross-track swaths (each composed of 6 scan lines) by means of an oscillating planar mirror, which images all four bands simultaneously. The four bands are thus inherently spatially registered. The instantaneous field-of-view (IFOV) of a single sensor element is approximately 79m square on the ground from the nominal satellite altitude.

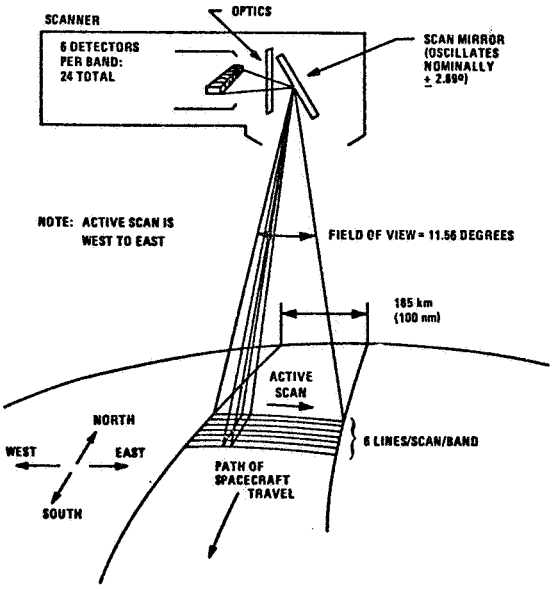


Figure 1. MSS Scanning Arrangement

* Due to the early cessation of data collection from the ERTS-1 RBV system, no discussion of error sources or correction algorithms for that sensor is included here. It is noted, however, that many algorithms developed for the MSS sensor are similar to those for the RBV sensor and have been included in the software package developed for the RBV system.

Each MSS bulk image represents 2340 individual active scan lines (scanned 6 at a time), obtained during approximately 28.6 sec. of "picture time." The mirror scan/retrace time is 73.42 ms (per 6 scan lines) and the sampling interval is 9.95 μs, so that the center/center cross-track separation of adjacent IFOV's is about 57m (nearly 30% overlap between adjacent samples).

It can now be seen that the following errors contribute in various degrees to spatial distortion in the bulk imagery: (1) scan nonlinearity, starting time jitter, repeatability, etc.; (2) change in spacecraft attitude during a picture time; (3) change in spacecraft altitude during the picture time; (4) earth curvature, a function of latitude; and (5) earth rotation, a function of latitude.

Inherent sensor errors (1) are given as $\pm$ 26m rms by Reference 2, and are therefore small and can be ignored. The bulk image data, however, have been scan length corrected to compensate for small variations in the number of samples per scan group. When this correction algorithm becomes available, it is anticipated that this small error can be corrected by means of the resampling algorithm described later.

Spacecraft attitude motion during picture scan can cause the groups of six lines to be non-parallel to each other when projected on to the ground. This effect manifests itself as a non-linear scale distortion throughout the bulk image. Change in spacecraft attitude during the picture time can also cause a small change in scale throughout the image. Earth curvature causes a scale change in the scan direction. Finally, earth rotation produces a $\sim$3° skew distortion (at $\sim$ 35-40°N latitude) in the image, essentially in the scan direction. The largest sources of error are due to the earth rotation, and the unequal number of scan lines (2340) and samples/scan ($\approx$ 3230) for a scene nominally 185 Km square.

III. IMAGE RECTIFICATION

The MSS rectification software developed by TRW currently corrects for error sources (2) - (5) using image annotation tape (BIAT or DIAT) data. In addition, a correction is made for the boresighting error, the difference between image format center (0° mirror scan) and spacecraft nadir. Provision has also been made for the inclusion of ground control points (GCP's), which are accurately measured locations of identifiable features that are used for precision image rectification. However, due to delays in obtaining the required data (bulk image tape, annotation data, and bulk imagery) for the target sites selected, it was not possible to include this refinement in the initial group of processed imagery. The ability to utilize GCP data has been verified for other scenes for which annotation data were not available.

The software developed for the precision correction of ERTS-1 imagery is shown in the functional flow diagram of Figure 2. Bulk image data is reformatted to produce a single tape with separate files containing data for each spectral band. At the same time regions called "neighborhoods" surrounding GCP locations are extracted, and are searched subsequently to precisely determine locations of GCP's within the image, using a reference library of GCP's. The GCP location data is used by a Kalman filter to refine the spacecraft attitude.

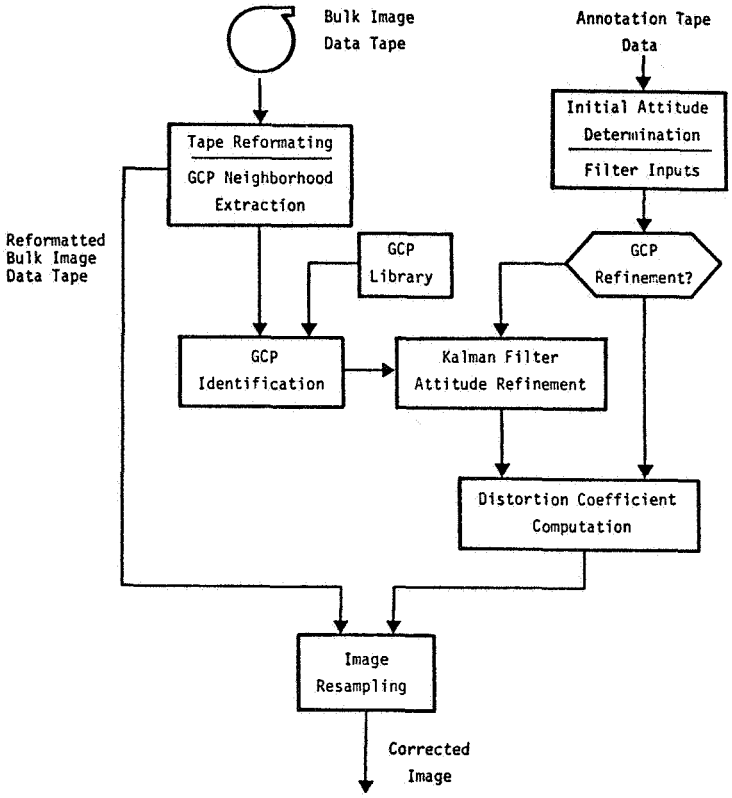


Figure 2. Precision Correction Software Schematic

Making use of the refined (or initial) attitude determination, distortion coefficients are computed which define the amounts by which the bulk image must be distorted so as to produce a rectified image, i.e., one which is linear in meter/meter coordinates. The computation of the coefficients is accomplished by mapping a small number of image locations, called "pseudo reseau points," to the final meter/meter coordinate system, taking into account the mirror scan, spacecraft attitude and ephemeris, earth rotation and earth curvature. Distortion coefficients are then defined for blocks of four pseudo reseaux, assuming a bilinear spatial distortion model (which introduces negligible errors compared to the self-consistency errors if there are enough pseudo reseaux).

The distortion coefficients thus determined are then transmitted to the resampling software, which processes the reformatted image tape so as to produce the final corrected image, including (if desired) photometric correction as well. The resampling code ensures that the output image contains the desired number of lines and samples/line, with uniform spacing of samples and lines.

An appreciation of the resampling problem may be gained by referring to Figure 3. Essentially the bulk image (array of x's) in Figure 3-a is distorted to the coordinate system of the corrected scene image (filled in zeros) of Figure 3-b, as a result of the geometric correction algorithms outlined in Figure 2. It then becomes necessary to define new values of data at the positions of the filled zeros, in terms of the given values at the position of the x's. This procedure is called interpolation.

There are several interpolation methods which provide a regular grid of lines and samples in the output corrected image, given a corrected image of unevenly spaced lines and samples. The simplest approach involves selecting the "nearest neighbor," as illustrated in Figure 4-a. In this approach, the data value of the sample (sometimes called a pixel) in the irregular array of the corrected image closest to the location of a pixel in the desired regular grid is used for the value of the regular grid point. Clearly, the intensity values resulting from this interpolation scheme correspond to true pixel locations that can be as much as $\pm$ 1/2 a spacing in error (in the regular grid). On the other hand, the computational requirements of this method are relatively modest, inasmuch as only one data value is required to determine the resampled data value. This results in relatively short running times.

An alternate method for image resampling is called bilinear interpolation (Figure 4-b), which utilizes a bilinear combination of the four closest pixel values in the irregular grid of the corrected image to compute a resampled data point. This method involves more computational time, and may result in a small loss of image resolution, due to the smoothing nature of the bilinear interpolation. On the other hand, the pixel "jitter" (one spacing offsets) at rapidly changing contours associated with the nearest neighbor scheme is avoided.

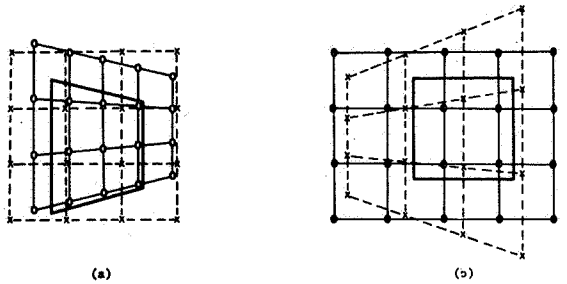
Cubic convolution resampling is an approximation to ideal sinx/x resampling. When the image content is band limited (in the spatial frequency domain), the ideal reconstruction of sampled data is of the form

$$I(x_i) = \sum_{x_K} I(x_K)\ f(x_i - x_K),$$

wherein f(x) is of the form sinx/x, and I is the function being resampled. By fitting a cubic polynomial to f (and imposing conditions for continuity, cutoff, etc.), a unique function results. Such a function is given in Figure 4-c for a cutoff at x=2, which utilizes 16 data values to compute one resampled data point. Because the convolution method most closely resembles the ideal resampling algorithm, it is expected to yield the most satisfactory results, with respect to resolution and fidelity, compared to nearest neighbor and bilinear interpolation. That is, the slope and magnitude continuity properties of cubic convolution are superior to the bilinear and nearest neighbor algorithms, by virtue of the more global nature of the data values used to produce a resampled point.

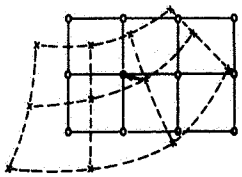
IV. RESULTS

First results of the rectification process described in Section III

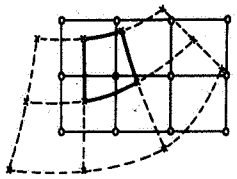


(a) (b)

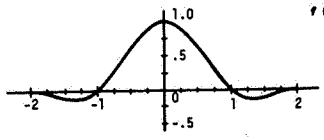
Figure 3. Resampling Problem. (a) x's denote bulk image sample locations, with respect to which the trapezoidal shaped object is imaged; (b) Filled zeros denote image sample locations in the final corrected digital image, with respect to which the rectified object is seen as a true square. The unfilled zeros in (a) represent the mapped locations of the desired image pixel locations, the values of which must be found by using an interpolation algorithm applied to the values at the x-locations. Alternatively, in the (b) system, x's denote mapped input (bulk) pixel locations in the corrected image system, which are used in conjunction with an interpolation algorithm to define the values at the filled zero locations.



(a) Nearest Neighbor Interpolation



(b) Bilinear Interpolation



$$f(x) = \begin{cases} 1 - 2|x|^2 + |x|^3 & 0 \le |x| \le 1 \\ 4 - 8|x| + 5|x|^2 - |x|^3 & 1 \le |x| \le 2 \\ 0 & 2 \le |x| \end{cases}$$

(c) Cubic Convolution Function

Figure 4. Three Possible Resampling Algorithms. Circles denote uniform pixel locations in the output, corrected image. x's denote the irregular grid of pixels (in the corrected image), derived by straightforward corrective distortions to the input bulk image. Filled in zero is a typical pixel, the value of which is to be interpolated.

were obtained for the scene 1057-18712-7 (San Francisco Bay and Monterey Bay) and involve the nearest neighbor and bilinear resampling algorithms. The convolution algorithm was developed prior to this study and converted to the ERTS data requirements. However, ERTS images were processed by means of this algorithm at too late a date to be included here.

Figure 5 shows the entire scene, reproduced from a bulk image transparency supplied by NASA/GSFC. Note that the bulk image has been corrected for the unequal number of lines and samples/line in the bulk data, as well as earth rotation. Figure 6* shows a detail taken from the upper left corner of the image, reconstructed** from the unrectified bulk image data tape supplied by NASA. The area shown is approximately 45 Km across and 120 Km long.

A rectified image corresponding to the detail in Figure 6 is given in Figure 7, utilizing the nearest neighbor interpolation algorithm. The area shown is 46.25 Km x 73.9 Km, and is aligned parallel to the spacecraft ground track. Note the steps occurring on the left edge of the image, corresponding to the successive one pixel increments associated with nearest neighbor interpolation. Careful examination of the image reveals a number of areas for which this pixel jitter is observed, and which is particularly evident for such high contrast regions as those containing a boundary between land and water. Thus, for example, note the bends in the San Antonio Creek, leading off from the WNW corner of San Pablo Bay, located in the upper middle of Figure 7 (portions of San Francisco Bay are located in the lower right of the figure, but are hidden by cloud cover).

Figure 8 shows the same scene as Figure 7, but using bilinear interpolation instead of nearest neighbor interpolation. Note the straight line appearance of the left edge of the image, in contrast to Figure 7. Note also that the bends in the San Antonio Creek are cleaner. On the other hand, note the slight resolution degradation for the complex of roads (including Interstate 80) north of Carquinez Strait, and east of Mare Island and the Napa River, compared with Figure 7. This degradation is expected by virtue of the smoothing effect of bilinear interpolation, and is absent in nearest neighbor interpolation.

It is worthwhile emphasizing here that the rectification processing was accomplished by all digital processing methods, utilizing input digital imagery. In contrast to this, bulk imagery (such as in Figure 5) is produced at the NASA Data Processing Facility by converting digital data to analogue data, and then utilizing an Electron Beam Recorder to rescan the image onto the output film.

In addition, it is useful to point out the required processing times for the production of rectified imagery. The images shown in Figures 7 and 8 were processed on a CDC 6400. Exclusive of the resampling portion, the required processing time was less than 10 seconds. In-

---

* Inasmuch as this paper is concerned with image rectification, the pictures included here have been slightly contrast-enhanced so as to bring out the image detail more clearly.

** The reconstructed images were produced from the corrected image tapes by photographing directly a high resolution CRT face, at the Jet Propulsion Laboratory's Image Processing Laboratory. The bright area in the upper left corner is a result of the reconstruction process, and is not in the corrected image data.



Figure 5. Reproduction of Scene 1057-18172-7 Bulk Image Print. The image has been corrected for the difference in the number of pixels/line and the number of lines, and has also been corrected for earth rotation (skew).



Figure 6. Reconstruction of Bulk Image Tape. This detail is taken from the upper left corner of Figure 5, and shows San Pablo Bay in the upper middle, and Port of San Francisco Bay in the right middle, partially obscured by cloud cover.

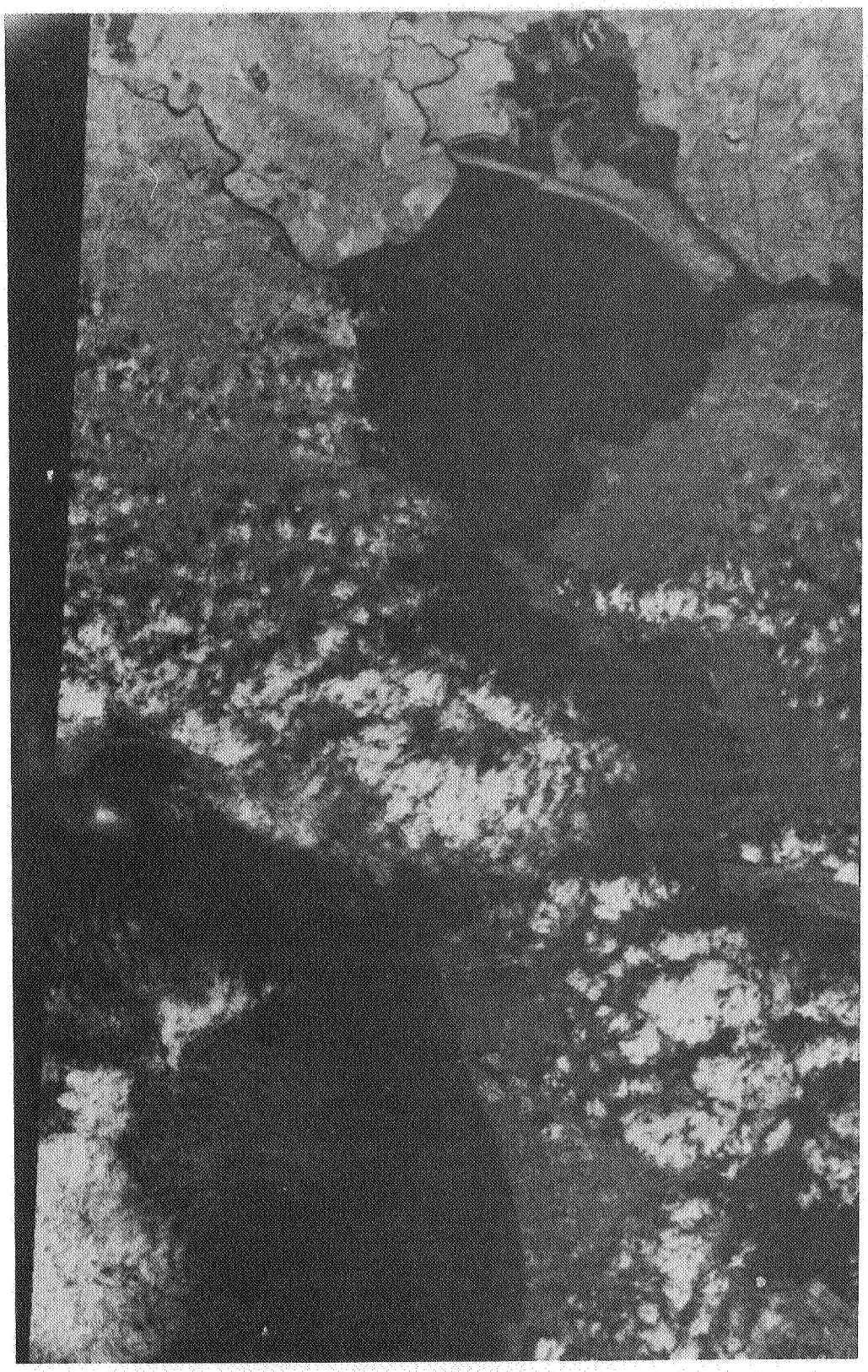


Figure 7. Reconstruction of a Portion of Figure 6 After Rectification, Using Nearest Neighbor Interpolation. Note the one pixel offsets on the left edge of the rectified image.

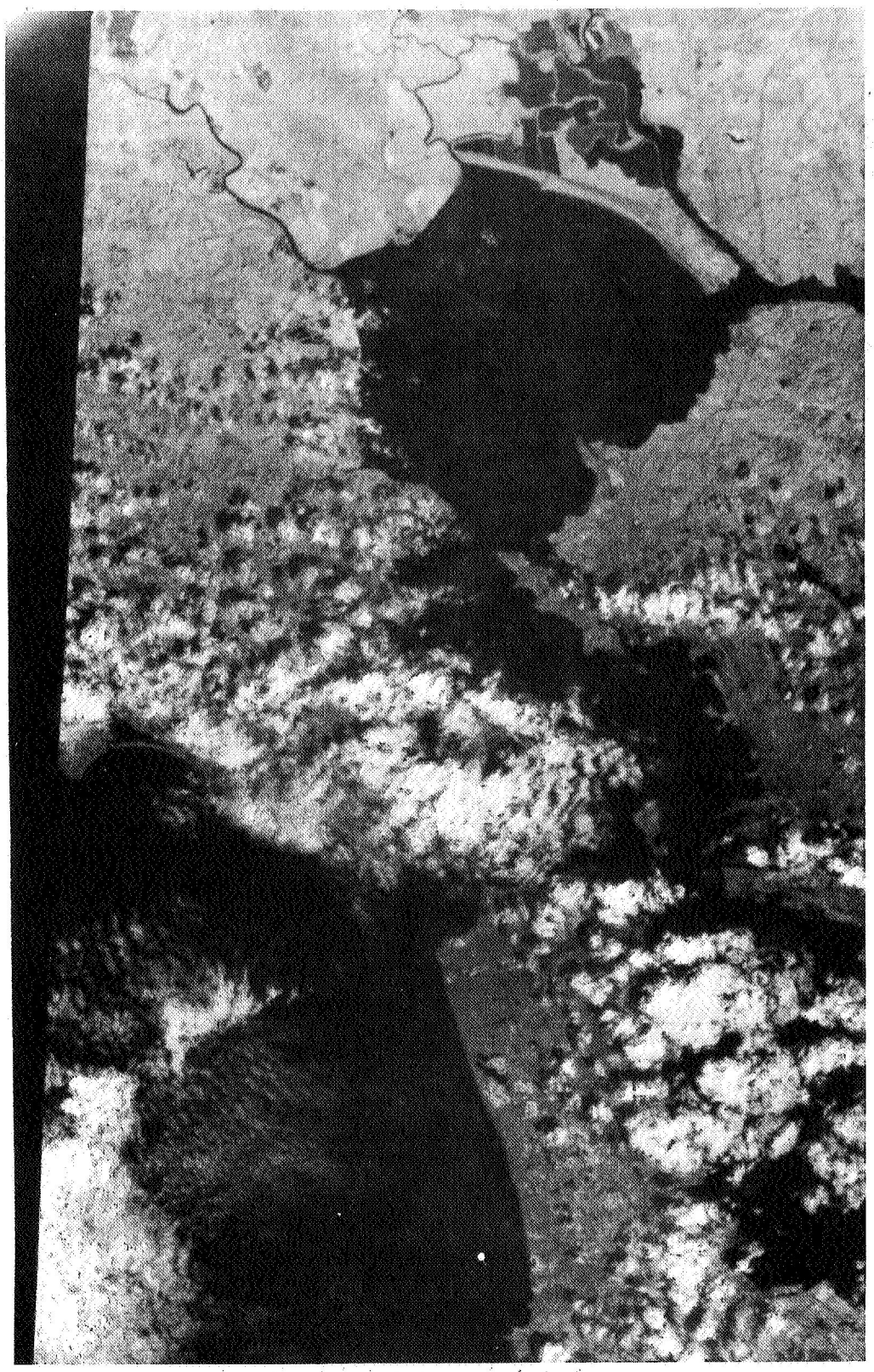


Figure 8. Reconstruction of a Portion of Figure 6 After Rectification, Using Bilinear Interpolation. Note the smooth appearance of the left edge of the rectified image, in comparison to Figure 7.

cluding GCP processing, the time required is of the order of a minute or two (depending on the number of GCP's). The most time consuming portion is the resampling algorithm, which requires approximately 52 seconds of CPU time per 10^6 pixels for bilinear interpolation. Cubic convolution requires approximately 110 seconds. In contrast, extrapolations to a PDP-11/45 minicomputer indicate 28 seconds of CPU (per 10^6 pixels) would be required for bilinear interpolation, or approximately 60 seconds of CPU for cubic convolution.

V. CONCLUSIONS

Early results have been presented for the digital rectification of ERTS imagery. Two interpolation algorithms were employed to produce the final corrected imagery included here. It was shown that small errors ($\sim$ 1 pixel, or < 60 m) result from the resampling process, for only modest CPU requirements. Nearest neighbor interpolation produces $\pm$ 1/2 pixel jitter (horizontal and vertical) which is evident in regions of high contrast. On the other hand, bilinear interpolation supplants the single pixel offsets with smooth transitions, but at the price of somewhat larger CPU times and some slight resolution degradation. It is anticipated that the cubic convolution resampling algorithm will combine the best properties of nearest neighbor and bilinear interpolation, with only modest additional CPU requirements over those for bilinear resampling. In fact, processing speeds in general have reached the point at which it is now possible to consider processing all ERTS imagery by digital methods alone.

Acknowledgement

The author gratefully acknowledges the assistance of Mr. John Morecroft of the Image Processing Laboratory of JPL in the production of negatives from our digital image tapes.

References

1. G. Nagy, "Digital Image-Processing Activities in Remote Sensing for Earth Resources," Proc. IEEE 60, 1177-1200 (October 1972). This paper is included in the Special Issue on Digital Pattern Recognition.

2. Earth Resources Technology Satellite Data Users Handbook, General Electric Document No. 71SD4249 (September 15, 1971; Revised November 17, 1972).

N73-28328

Paper I 7

RESULTS OF PRECISION PROCESSING (SCENE CORRECTION) OF ERTS-1 IMAGES USING DIGITAL IMAGE PROCESSING TECHNIQUES

Ralph Bernstein, *Federal Systems Division, IBM Corporation, Gaithersburg, Maryland, USA*

ABSTRACT

ERTS-1 MSS and RBV data recorded on Computer Compatible Tapes have been analyzed and processed, and preliminary results have been obtained. No degradation of intensity (radiance) information occurred in implementing the geometric correction. The quality and resolution of the digitally processed images are very good, due primarily to the fact that the number of film generations and conversions is reduced to a minimum. Processing times of digitally processed images are about equivalent to the NDPF electro-optical processor.

I INTRODUCTION

Investigation Objectives. This investigation deals with applying digital techniques to the processing of ERTS-1 image data, and in particular, to the Precision Processing (Scene Correction) of ERTS-1 data. The objective of the investigation is to geometrically correct an ERTS image to a UTM projection, maintain or correct the sensor radiometry (intensity), fully annotate the data, record the results on computer compatible tape (CCT) and on film, and evaluate the results.

Investigation Approach. Based upon previous analysis and experimentation (References 1 and 2), it has been felt that both good radiometry and geometry can be achieved by digital image processing, which minimizes the number of film generations and data conversions. Figure 1 shows a digital approach used to achieve Scene Correction of ERTS images. The sensor data, on computer compatible tapes (CCT's) are read into a digital computer. The geometric and radiometric corrections are implemented through software, and standard annotation data is combined with the processed image data to generate another CCT containing a scene corrected image. This tape data is then read into a film recorder, which records the data directly on 240mm (9.5 in.) film. The advantage of this approach is that the final product is a second generation photo and involves no unnecessary data conversion stages.

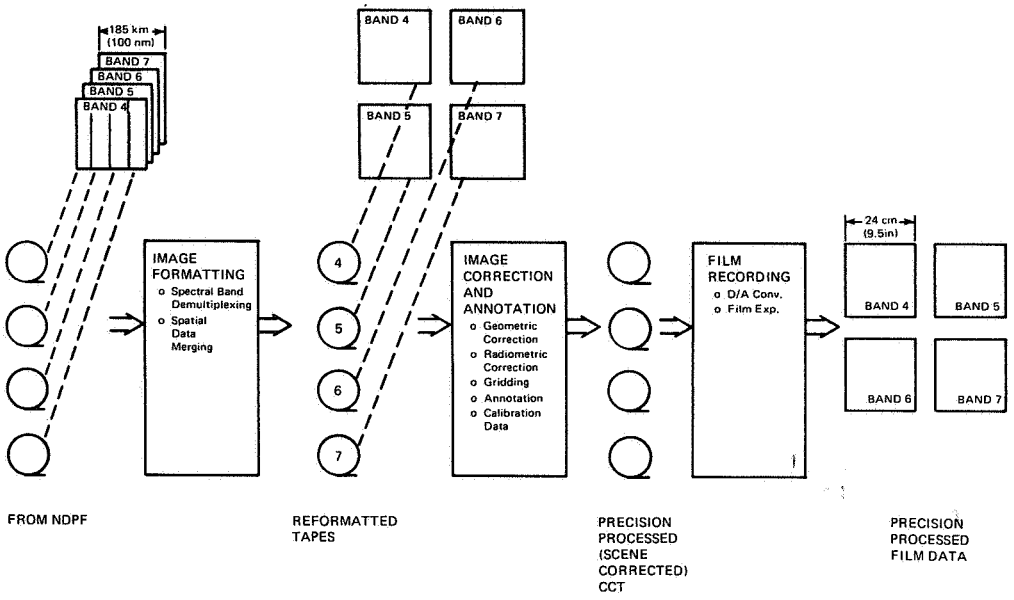


Figure 1. Digital Image Processing Approach Scene Correction

II EXPERIMENTAL APPROACH

Sensor Errors. The principal errors associated with the data received from the two ERTS sensors are listed in Table 1. These errors are fully described in Reference 3. If these errors are to be corrected, they must be either predictable or measurable. Errors due to MSS mirror velocity, panoramic distortion, scan skew, and perspective projection are constant (for all practical purposes) and can be predicted in advance. Errors due to spacecraft velocity and earth rotation can be predicted from tracking data. Attitude and altitude errors must be measured for each image. The measurement technique used here involves apparent displacement of ground control points (GCP's)—recognizable geographic features whose actual positions are well known. The image locations of the GCP's are determined by application of the Sequential Similarity Detection Algorithm (described in References 2 and 4) to appropriate areas of sensor data.

RBV scanning raster distortions are measured by observing apparent displacements of a 9 x 9 array of reseau marks etched on the faceplate of each tube. A technique has been developed to digitally locate these marks using a modified form of "shadow-casting (Reference 2). Once the reseau marks are located, the nominal and observed locations are used to evaluate the coefficients of a pair of polynomials which provide a model of the composite effect of the various scanning raster distortions.

Table 1. ERTS Sensor Data Errors

MSS	Mirror Velocity	RBV	Scanning Raster Distortions
	Panoramic Distortion		Perspective Projection
	Scan Skew		Attitude
	Earth Rotation		Altitude
	S/C Velocity		Shading
	Perspective Projection		
	Attitude		
	Altitude		
	Detector Response		

Geometric Correction. The input image is an array of digital data which represents a geometrically distorted perspective projection of some portion of the earth's surface. The output image is a geometrically correct UTM projection of the same ground area. GCP's are located in the input image, and the observed locations are corrected for all those errors which can be predicted or determined from tracking data. The nominal and observed GCP locations are then used to evaluate the coefficients of the attitude and altitude models. All of the error models are combined in a pair of bivariate polynomials which provide a composite, global mapping from output image to input image. Correct locations for only a few output image points are determined from the mapping polynomials. All other points are located by bilinear interpolation over the mapped points.

Radiometric Correction. There are a total of twenty-four detectors on the MSS, each one of which can generate only a small number (64 or 128) of distinct output values. Thus it is quite feasible to define for each detector a table which specifies the desired value corresponding to each of the possible detector output values. Radiometric correction can then be accomplished by a simple table look-up operation. Such correction tables can be used to accomplish a variety of objectives. For example, by computing average values of detector outputs in areas of approximately uniform radiance, it is possible to compute gain and bias corrections which will eliminate striping due to differing detector responses. It is also possible to generate tables which will modify the video intensities to emphasize or enhance specific types of features or to match the data values to the characteristics of the recorder and film used.

III TECHNICAL RESULTS TO DATE

Reseau Detection/Migration. The reseau detection technique was applied to all bands of images E-1002-18134 and E-1014-17375 (which have the greatest temporal separation of RBV scenes received by IBM). Search areas 50 samples square were centered on the expected locations of the 486 reseau. In all cases, as verified by examination of computer-generated shade prints, the detection technique correctly located the reseau marks. The test was then repeated on 486 image areas picked to contain no reseau. In no case was a false reseau selected.

Band 3 was selected to examine for apparent reseau migration over the twelve-day interval spanned by the two test scenes. In only one case was a migration as large as three pixels in either axis observed. This would seem to imply that RBV internal distortions are quite stationary and that the use of small reseau search areas is justified.

GCP Experimentation. The Sequential Similarity Detection Algorithm (SSDA) has been applied to a variety of targets in several image pairs. The results obtained are summarized in Table 2. Although these results must be considered preliminary, certain trends are emerging:

- Performance (i.e., ability to find the feature and average search time) varies from band to band for different types of GCP's. This suggests that in an operational system, the search for a given GCP should be conducted in that band which has exhibited the best performance on that type of target.

- Strong targets (i.e., those which present a large, distinct pattern) are located quickly. Indistinct targets require much more search time. This is what would be expected from the characteristics of the SSDA.

- When a proper combination of target and band is used, search times are acceptably small. (It should be noted that the search times given in Table 2 show the performance of an experimental FORTRAN program. An operational assembly language program can be expected to be significantly more efficient. Further, no sophistication such as hill-climbing has been added to the basic algorithm.)

Table 2. Initial SSDA Results — MSS Data

	BAND 4		BAND 5		BAND 6		BAND 7		
Target Type	No. Found/ Tried	Time (Sec)	No. Found/ Tried	Time (Sec)	No. Found/ Tried	Time (Sec)	No. Found/ Tried	Time (Sec)	Temporal Separation/ Location/
1	5/5	46	5/5	29	5/5	4	5/5	15	17 Days
2	1/1	51	1/1	47	1/1	40	1/1	45	Chesapeake
3	2/2	12	2/2	4	2/2	8	2/2	22	Search: E - 1062–15190
									Window: E–1079–15140
1	4/8	50	7/21	27	15/21	5	17/21	14	18 Days
3	0/0	–	1/2	9	2/2	11	2/2	27	Chesapeake
4	1/1	50	1/1	29	1/1	7	1/1	29	Search: E–1080–15192
5	0/0	–	16/16	9	15/16	27	14/16	50	Window: E–1062–15190
1	4/6	4	6/6	3	5/6	2	5/6	7	
2	2/8	5	6/8	12	6/8	37	6/8	20	36 Days
3	0/2	–	0/2	–	1/2	48	1/2	7	Phoenix
4	2/3	12	3/3	12	3/3	49	3/3	6	Search: E–1049–17324
6	1/2	5	2/2	6	1/2	5	2/2	52	Window: E–1085–17330
7	1/1	4	1/1	3	0/1	–	0/1	–	
1	1/2	5	2/2	3	2/2	3	2/2	6	72 Days Phoenix Search: E–1049–17324 Window: E–1121–17330

TARGET TYPE: 1 – LARGE LAND–WATER INTERFACES
2 – NON–INTERSTATE HIGHWAYS
3 – AIRPORTS
4 – SMALL LAND–WATER INTERFACES
5 – INTERSTATE–GRADE HIGHWAYS
6 – HILLS
7 – FIELDS

Note: Times are for 360/65 FORTRAN Program.

IBM

Mapping Functions and Accuracies. APL programs have been used to estimate the accuracy of several different approaches to MSS geometric correction. The first approach used the BIAT attitude and altitude data. The second approach used GCP's to evaluate cubic attitude models but took altitude data from the BIAT. The third approach added a linear altitude model which was evaluated using ground control. The fourth approach fit two 6-term polynomials to the various error models. Results for the four approaches are summarized in Table 3. They show that the use of the BIAT attitude and altitude data is inadequate for precise mapping, GCP's provide significant improvement, and the addition of an altitude model (which increases the GCP requirements by one point) further improves the mapping accuracy. The polynomial fit produces RMS errors that are comparable to the attitude/altitude model combination but maximum errors that are significantly smaller. These results show that, for the images processed, geometric distortions in MSS images are not higher than third degree.

Table 3. Predicted Geometric Correction Accuracies

Scene		Mapping Errors In Meters: BIAT For Attitude And Altitude	GCP's For Attitude Only	GCP's For Attitude And Altitude	6-Term Polynomial Fit
MONTEREY	MAX:	1517	295	115	86
E-1002-18134	RMS:	999	129	66	52
MSS 25 July 1972					
CHESAPEAKE	MAX:	1503	269	202	141
E-1062-15190	RMS:	722	111	61	68
MSS 23 Sept 1972					

Intensity Modification and Striping Removal. Several relatively simple intensity modification experiments were performed on MSS images in order to evaluate the resultant image product in terms of information content and subject quality. Cultural features, such as roads, could be more clearly seen with such an intensity change, and water pollution/sedimentation patterns were enhanced. An experiment to eliminate undesirable striping in the images was conducted, and virtually all striping was removed.

Samples of Precision Processed Images. All bands of the Chesapeake and Monterey scenes were Scene Corrected and recorded on film. Contact prints of two bands are provided at the end of this paper. It is noted that good radiometry and resolution are exhibited.

Processing Times. Table 4 shows the current estimated processing times. No attempt has yet been made to minimize processing times, and these times, although reasonable, are expected to be reduced further through the use of better image management, lower processing overhead, and higher I/O speeds. It is significant, however, that the MSS images are each processed in an average CPU time of less than 3 minutes, and an elapsed time of less than 8 minutes.

Table 4. Current Processing Times

RBV Processing

Reseau Detection — 10 seconds for 81 reseau

MSS Processing (All 4 Bands)

	CPU (Min)	Clock (Min)
Reformatting	1.7	10
GCP Detection (4 Sec/GCP)	0.8	
Geometric and Radiometric Correction	9.0	20
	11.5	30

Notes:

Computer Used — 360/65
Clock Times — Dedicated Computer (Estimated)
Geometric and Radiometric correction (CPU) — First band 3.0 minutes actual, 9.0 minutes estimated for correcting all four bands.

IV TECHNICAL PROBLEMS

Software Errors. When the Chesapeake image was geometrically corrected, some irregularities were found which were not present in the Monterey image. Vertical breaks of two pixels occurred in several Chesapeake images. To aid in finding and correcting any errors in the point shift program, an image consisting of a grid of vertical and horizontal lines was created. The grid image was geometrically corrected by the same program that corrected the Chesapeake images. The irregularities were clearly visible on this image. In addition to the two pixel vertical breaks mentioned above, some two pixel horizontal breaks were found in the horizontal lines of the grid. There were also some two pixel vertical breaks followed by one pixel vertical breaks in the opposite direction. These software problems are currently being addressed.

MSS Striping. Incomplete gain and offset compensation of MSS detector data results in a striping or banding effect when the data is recorded on film or viewed on a computer shade print. This striping is particularly noticeable in near uniform radiance regions and detracts from the image quality. Further, the banding effect has propagated in multispectral analysis programs, causing line by line misclassification errors. Some degree of success has been achieved eliminating striping by individual detector gain compensation.

V ADDITIONAL INVESTIGATION REQUIRED

Based upon the results to date, the following areas require additional investigation and analysis:

Ground Control Point Experimentation. An encouraging degree of success has been achieved in digitally detecting GCP's with temporal separation. However, more analysis is required to assess:

Seasonal Effects — How long a GCP can be used reliably.

Feature Characteristic — What type and spatial characteristics of a feature make it "best", and what are the optimum sizes of the search and window areas.

Spectral Band — What band is best for what class of GCP and least sensitive to uncontrolled variables.

Parametric Selection — What are the best values for the threshold sequence, etc.

Attitude/Altitude Effects — What is the sensitivity of the SSDA algorithm to effects which change the relative geometry of the search and window areas.

RBV Image Processing. Due to the shut-down of the RBV shortly after ERTS launch, processing priority was given to the MSS data. The only processing performed on the RBV data was reseau detection. The geometric correction of the RBV image is expected to be relatively simple. The radiometric correction of the RBV, due to the severe shading effects is expected to be challenging and will require some experimentation.

MSS Image Processing. Two different methods of determining geometric correction functions have been investigated: evaluating coefficients of various specific error models and directly fitting a polynomial function to observe GCP displacements. Polynomial fitting appears to produce more accurate results. It gives a direct compensation for the distortions present and is not subject to misconceptions about the forms of various error models. It appears to require no more ground control information than alternate methods. On the other hand, polynomial fitting can be expected to be relatively sensitive to the locations of the GCP's used. If the GCP's do not sufficiently span the image, the polynomials will be inaccurate in the regions not spanned. The error model approach, because it forces a structure on the correction functions should not be so sensitive to GCP locations. Both methods should be investigated further, particularly with regard to sensitivity to GCP number and location. It may prove that polynomial fitting with a fall-back to error modeling when the available GCP's don't span the image sufficiently is the best approach to use.

VI PRELIMINARY CONCLUSIONS

The investigation is far from complete. However, several preliminary conclusions can be made:

Preservation of Radiometric Information. Because of the elimination of unnecessary conversions and photographic generations in processing ERTS images by digital image processing techniques, radiometric information is preserved and changed only when correction or enhancement is made. Thus digitally processed images have the potential for Sensor Corrected Radiometry and Scene Corrected geometry.

Preservation of Resolution. Sensor data is maintained and is simply repositioned to achieve geometric correction. Thus, for the same reasons as above, it is likely that image resolution is not degraded by digital image processing.

Accurate Mapping. Predictive mapping computation has shown that digitally corrected images can have geometric errors of about 60 meters (RMS). Further investigation is required for a variety of scene types before this preliminary.conclusion can be confirmed.

Operational Feasibility. Digital processing provides a simple and feasible means of changing both the geometry and radiometry of a scene. Change in sensor performance and characteristics can be compensated for by computer software, and any map projections can be generated by suitable programming and parametric selection.

Throughput. Recent results have shown that four MSS bands can be precision processed in approximately 11.5 minutes of IBM 360/65 CPU time or 30 minutes clock time. This time is comparable with electro-optical processing of ERTS data. Further reduction of these times is projected when an operational system is designed and implemented.

Feasible Technology. Results generated to date suggest the feasibility of digital processing for Scene Correction of ERTS images. Long processing times in the range of hours, which have been previously predicted have not been borne out. Image quality and resolution are maintained. However, further work is necessary to address existing technical problems and refine techniques.

VII ACKNOWLEDGEMENTS

Much of this work was supported by NASA under contract NAS 5-21716. Paul Heffner, the NASA Scientific Monitor provided timely information and constructive advise. From IBM, D. G. Ferneyhough competently directed the analysis activity which was supported by Dr. H. Markarian, Dr. R. D. Depew, B. B. Clark, and M. L. Cain. S. W. Murphrey, S. R. Forrer and C. P. Colby programmed the image processing algorithms. T. F. Gaidelis provided the photographic support, and Tom Gagnon the film recording.

VIII REFERENCES

1. Bernstein, R., et al., "Experimental ERTS Image Processing", Report CESC-70-0465, May 18, 1970.

2. Bernstein, R. and Silverman, H., "Digital Techniques for Earth Resource Image Data Processing", AIAA Paper, IBM FSC 71-6017, 30 September 1971.

3. Data Users Handbook, NASA-Goddard Space Flight Center, GE Document #71SD4249.

4. Barnea, D. T. and Silverman, H. F., "A Class of Algorithms for Fast Digital Image Registration", IEEE Transactions on Computers, February 1972.

N73-28329

Paper I 8

SIGNIFICANT TECHNIQUES IN THE PROCESSING AND INTERPRETATION OF ERTS-1 DATA

S. B. Cousin, A. C. Anderson, J. F. Paris and J. F. Potter, *Lockheed Electronics Company, Inc., Houston Aerospace Systems Division*

ABSTRACT

The discipline oriented investigations underway at the Johnson Space Center (JSC) using ERTS-1 data provide an appropriate framework for the systematic evaluation of the various elements comprising a prototype multispectral data processing and analysis system. In particular such a system may be thought of as the integration of (1) a Preprocessing Subsystem, (2) a Spectral Clustering Subsystem, (3) a Correlation and Classification Subsystem, (4) Mensuration Subsystem, and (5) an Information Management Subsystem (see fig. 1). Specific elements of this system are already operational at JSC.[1]

It is in the context of this system that technique development and application is being pursued at JSC. Aircraft, ERTS and EREP data will be utilized to refine the subsystem elements for each of the data acquisition systems or system combinations that are optimally suited for a specific Earth Resources application. The techniques reported here are those that have been developed to date during the utilization of ERTS-1 data in this processing and analysis system.

1. THE PREPROCESSING SYSTEM

The Preprocessing Subsystem accepts the multispectral data from the Data Acquisition Subsystem and incorporates the measured sensor and platform characteristics (e.g., detector calibration, platform navigational parameter data, etc.) to yield absolute radiance values for each sensor resolution element. Ideally, this subsystem would include an atmospheric correction scheme to relate the sensor readings to absolute scene reflectance values. Correlation to ground control points and reference to UTM coordinates can also be accomplished at this stage. At the very least an overlay grid to allow easy reference to specific scan line and pixel numbers could be introduced by this subsystem. In the case of the ERTS-1 multispectral scanner (MSS) initial preprocessing is done by the Goddard Data Processing Facility. Since the MSS is constructed with six detectors in each of its four spectral bands, twenty-four distinct calibrations must be accounted for in this preprocessing. The detectors are swept by a calibrated source on every other retrace scan and the detector outputs are equated to the pre-measured calibration source radiance. This calibration data is continuously averaged, so that slow changes in the detectors can be calibrated out of the scene data. The success of this phase of preprocessing is dependent on (a) precise pre-measurement of the calibration source radiance, (b) accurate knowledge of the source radiance as a function of time during the calibration scan, and (c) conformance of the operating source to the prelaunch measured performance. Striping which has been observed in all four channels of the ERTS MSS data can be attributed to such correction inaccuracies. This striping is particularly evident when the scene is a large, homogeneous area such as a lake. Although the striping is due to differences in detector outputs amounting to between one and five quantum levels in the data, it is sufficient to affect sensitive spectral clustering algorithms as shown in the cluster map of figure 2.

A large rectangular area of Lake Livingston, Texas, was selected to study the statistics of the striping in the data (Frame 1037-16244) and to develop a striping removal technique. It was first established that the best available estimates for the correct average data values for water in the four ERTS channels

Original photography may be purchased from:
EROS Data Center
10th and Dakota Avenue
Sioux Falls, SD 57198

are the composite averages given by the detectors in each channel. If each detector's average output for water were moved to the composite average, the stripes would be removed and the composite average unchanged. A stripe removal procedure was therefore developed to suitably correct the recorded ERTS integer values. Twenty-four accumulator registers were established in the processing computer. Each time a new reselm was considered, the quantity $(A_T - A_i)$, representing the established difference between the ith detector average and the composite average, was added into the appropriate accumulators. Whenever an accumulator absolute value exceeded 0.5 the reselm data value for that detector was changed by the integer value closest to the current accumulator value. The accumulator was then updated by an equal but opposite amount. If the new data value was negative or greater than 127 (63 for the infrared channel) it was moved back into the allowable data range and the accumulator was corrected accordingly. In this procedure, offset correction errors are reduced using a portion of the scene itself as a calibration target. The procedure was then applied uniformly to all the data in the frame. The smoothed data was processed once more using the clustering algorithm and resulted in the cluster map shown in figure 3. The reduction in striping is clearly evident. Complete preprocessing of the data should also include a correction for gain calibration error (stripes attributable to inaccurate gain corrections have also been observed). Such a procedure, which will be important in high reflectance target scenes, is now in the process of being developed. The impact of these striping effects must be assessed by each investigator to determine if such smoothing procedures aid in his application.

The atmosphere can make a significant contribution to the apparent signature of a target viewed from space. Since the atmospheric aerosol content changes from place to place, identical targets located at different places may classify differently in automatic pattern recognition studies. The same is true for identical targets viewed at different times. Figure 4 (ERTS Frame 1038-16303 over Lake Somerville, Texas) shows an example of such unwanted atmospheric effects. The programs described here (PREPS-ROTAR) correct the sensor response data by converting the data to target reflectance, a target parameter that is independent of the atmosphere.

The atmospheric correction process in use at JSC consists of two program modules. The first module, PREPS is used to pre-calculate a family of curves relating sensor output to target reflectance. The PREPS program is based on the following assumptions: (a) the sensor is pointing in the nadir direction, (b) the target is a Lambert reflector whose reflectance is constant across a given ERTS/MSS band, and (c) the atmosphere consists of two homogeneous layers, a Rayleigh scattering molecular layer on top and a Mie scattering aerosol layer near the earth's surface. At present, calculations have been made for an aerosol layer with the characteristics of a continental type haze. Other haze models will be included in the near future.

Within the limits of the above assumptions, accurate numerical solutions to the radiative transfer problem are obtained. These solutions, which include all orders of multiple scattering, give the radiance at the sensor as a function of wavelength, target reflectance, haze level in the atmosphere and solar zenith angle. They are then normalized, multiplied by the sensor response function and integrated across the sensor bandwidth to obtain the sensor output as a function of target reflectance using the atmospheric haze level, solar zenith angle, instrument mode (compressed or linear) and instrument gain (high or low) as fixed parameters.

For any MSS frame to be corrected, the appropriate solar zenith angle, instrument mode and instrument gain are selected. A "response tape" is produced for each desired set of these parameters. The response tape contains curves (i.e., tables), which relate instrument response to target reflectance for a given haze level. The haze level is specified by giving the haze optical depth τ at wavelength 0.5 μm. The optical depth at other wavelengths is determined by the haze model. A typical set of response curves is shown in figure 5. The three curves shown correspond to $\tau = 0.0$, 0.424, and 0.848.

To correct each reselm in the MSS frame the second module (ROTAR) is used. The input to the ROTAR program consists of the appropriate response curves and the ERTS data to be corrected. The user can divide the frame into rectangular areas and assign values of τ to each area. ROTAR generates a "correction curve" for each optical depth input to the program. The curve relates the instrument output to the target reflectance for each specific value of optical depth. It is obtained by interpolating (or extrapolating) to the designated values of τ

from the input response tables. Each data point is corrected by determining the target reflectance from the appropriate correction curve. The corrected data can then be analyzed with pattern recognition programs. Figure 6 shows a LARSYS grey scale map of data from the Somerville frame corrected by ROTAR. The numbers represent the percent reflectances of the picture elements in that channel.

A capability has been developed to measure the aerosol optical thicknesses at various positions in the Houston Area Test Site (HATS) during each ERTS overpass. This is accomplished by the use of PREPS photometers whose calibrated response yield the optical thickness values. These values are then used in performing the atmospheric corrections. At this point additional effort is required to develop this capability to a reliable operational system. The PREPS/ROTAR calculations have been compared with target reflectances measured on the ground. The results, which are shown in figure 7, appear accurate to within two percent. (Note: The allowable range of target reflectance is 0 to 100 percent of the Lambert perfect reflector value.) These results are under more detailed error analysis at this time. Both the ground reflectance and the aerosol optical depth measurements are subject to known systematic errors and will require further analysis for final verification.

Additional development in this preprocessing subsystem is therefore required in correcting for the gain stripping effect, in reference grid overlaying, and in further testing of the atmospheric correction scheme.

2. THE CLUSTERING SUBSYSTEM

The preprocessed ERTS data represents a class of multivariate data for which clustering subsystems have been under development for several years. Image enhancement techniques may be used to bring out subtle spectral variations or data groupings will be clustered to aid in the selection of "training fields" for use in the classification subsystem. An example of such a technique is the ISODATA algorithm.[3] It is an iterative technique for grouping each multivariate data point with other similar data points. On each iteration, all of the data points are assigned to one of the existing clusters and each cluster is examined to determine if it should be split, left alone, or combined with some other cluster. A revised set of clusters is generated and the process is repeated until the resulting clusters stabilize or some other criterion set by the investigator has been satisfied (i.e., maximum number of iterations or clusters). The fundamental assumption in the algorithm is that the data is comprised of well separated clusters of similar points. That is, there are regions in the multivariate space where the data points are dense along with areas between those regions where the data points are spare (refer to figure 8a in this discussion). The ISODATA version in use at JSC[4,5] assigns points to the existing clusters by a "city block" distance measure. Each cluster is defined by the location of its center point. The distance from a data point to a cluster is defined as the sum of the distances parallel to each of the coordinate axes. While points are being assigned to cluster, information is accumulated for recalculating cluster centers and the standard deviations in each variable for each cluster. The splitting and combining decisions are made on the basis of these standard deviations and the inter-cluster distances. If the standard deviation in one of the variables becomes larger than a fixed input value (STDMAX), the cluster is split into two clusters with centers at plus and minus one standard deviation from the old center. If clusters are too close together, they are combined and a single center is computed.

The ERTS data, recorded as integers, are similar to the results of a Poisson process which is, typically, the counting of discrete events during a fixed time period (see figure 8b for the low reflectance target analogy). For bright targets, the ERTS data appear to be normally distributed about a mean value. For mean values above 10, however, the Poisson distribution is indistinguishable from the normal distribution. The useful features of the Poisson distribution is that once the mean value is known, everything else about the distribution is known. The probability of occurrence of each integer count is known; the standard deviation is known. There is no such relationship for normal distributions. Using these facts, the split criterion in ISODATA can be established as "splitting occurs if one of the standard deviations becomes larger than the square root of the mean for that channel in that cluster." In practice, the allowable standard deviation is made proportional to the square root of the mean

with the constant of proportionality selectable by the investigator. Values of the proportionality constant of 0.8 and 1.0 have been tested and yield reasonable clustering results. The criterion for combining clusters was also modified to be consistent with this splitting criterion. Surfaces derived from the standard deviations in each cluster were investigated by entering a t value, 1.0 for 1σ, 2.0 for 2σ, etc. The algorithm assumes that the t surface is an ellipsoid in the multivariate space and is oriented with its axes parallel to the coordinate axes. It then tests the surfaces to see if they intersect on the line joining the cluster means. If they do, the clusters are combined.

Results obtained in the testing of this algorithm to date (figs. 2, 3, and 4b are examples) indicate its flexibility and its capability to generate meaningful cluster results regardless of the range of the data values considered. Additional testing of this technique is required to assess its utility in various applications.

3. THE CORRELATION AND CLASSIFICATION SUBSYSTEM

This subsystem associates material or feature designations to each set of pixel energy responses through the use of ground information available about the scene being processed or by the comparison of these responses with predetermined material spectral signatures. This can be accomplished in either a supervised classification mode, by developing classification criteria based on the "training field concept" successfully utilized by LARS at Purdue University, or in an unsupervised classification mode, by relating spectral cluster members to known, correlatable scene features, or by associating the cluster center to historically established spectral signatures. To aid in ground correlations, techniques are under development at JSC to locate specific ERTS resolution elements accurately on aerial photographs. One technique, being developed specifically in urban scenes, consists of relating specific reselms clustered as extremely high reflectance responses to the specific ground features known to cause such a response. When several appropriately spaced objects are positvely correlated with pixels in this way, a relative scale between the aerial photography and ERTS cluster maps can be established. Such geographic correlation, also being explored using high contrast boundaries in other than urban scenes, can be used as the basis for establishing polynomial pixel translation functions to allow the direct registration of the classification or clustering maps onto rectified large-scale photography or base reference maps. Once such techniques can be refined, detailed analysis of the spectrally clustered data can yield estimates to the proportionate composition of resolution elements in heterogeneous areas. One such analysis has already been performed using a land/water interface as the correlation mechanism and the comparison of calculated water area to the true area as a measure of success.

Data collected over the Galveston Bay (Texas) area on August 29, 1972 (Scene ID's 1037-16244 and 1037-16251) were analyzed through the use of the clustering algorithm. Nineteen water bodies ranging in area from 2.8 to 607.2 acres were chosen for analysis. NASA aircraft photography of the area from 60,000 feet was used as a basis for determining the true area of each of the nineteen water bodies. An examination of the locations of the cluster/classification centers in two ERTS-1 channels (MSS bands 4 and 7) as shown for example in figure 9, revealed that the non-water classes (circled symbols) lie above a threshold of 20.0 in MSS band 7. The pure water classes (boxed symbols) lie close together near 2.8 in MSS band 7. Thus, the other classes can be assummed to be simpled mixtures of water and non-water classes such that a percentage water amount can be assigned to each mixture class based on a distance measure between the two pure classes.

By considering only those mixture classes that were spatially adjacent to pure water classes, the total number of picture elements representing each of the nineteen water bodies was determined. A linear regression analysis of the results revealed that the surface area (A, acres) of a water body was given as $A = 0.60958 + 1.09344\ \Sigma_i E_i$ where E_i is the fraction of the i*th* resolution element composed of water. The standard error of the estimate was found to be 6.7 acres. The correlation coefficient of the estimate was determined as 0.998 for the sample tested. The slope of the regression curve was 1.093 which is consistent with the value of ground coverage in acres per pixel obtained by other methods. A further analysis revealed that the absolute error (5.2 acres) was independent of the size of the water body. On the basis of this limited

analysis, this regression estimate introduces no systematic errors and can be used practically for estimating the areal extent of water bodies. The estimate can be further tested, but can be expected to give the best results in terms of percentage accuracy for larger sized water bodies.

4. THE MENSURATION SUBSYSTEM

This subsystem summarizes the classified multispectral data in terms of the mensuration parameters appropriate to a specific user application. Regression formulae of the type discussed above can be used to estimate the total geographical area directly observed to be devoted to a particular land use or a specific land feature. If the total data analysis system is based on a statistically rigorous model, extrapolation algorithms can be applied in this subsystem to infer information with known accuracy and cost function levels about the total area of interest based on the limited sample data actually processed (e.g., total estimate of crop yield based on the observed acreage within the measured geographical area and the observed crop vigor and maturity). The wide coverage of ERTS data can hopefully reduce the need for such extrapolations as the capability to efficiently process ERTS data tapes further develops. In this subsystem, additional information is normally required to relate the classified remotely sensed observations to the user desired management parameters. This may be accomplished through the use of phenomenological or mathematical models to which the classified data provides input or through the correlation of the observed data with other conventionally obtained statistical data (viz., census data, historical records on dollar yield per bushel, etc.). Techniques for this subsystem have yet to be demonstrated using ERTS data, but possible approaches are being explored at JSC in the context of the joint USDA/NASA data utilization program. Since this subsystem must be closely tailored to operational requirements, user agencies must play a significant role in selecting the techniques most appropriate in this subsystem for their application.

5. THE INFORMATION MANAGEMENT SUBSYSTEM

This subsystem stores all summary data in retrieval files, updates these files at the user's option and generates outputs in formats appropriate to specific user requirements. Such a system, with high-speed response and wide output flexibility has been developed and demonstrated at JSC. This subsystem referred to as the Regional Information Management System (RIMS)[6] is based on a one square kilometer grid and contains inventory information on land-use in the HATS area. A typical output form this system using the interpretation of aircraft data as the source is shown in figure 10. Information cells representing 100 percent forestry, water, urban and agriculture have been retrieved from the data base and displayed in this geographical format. The techniques for this subsystem must also be closely tailored to the user's specific operational requirements. User definition and documentation of such requirements is essential before meaningful techniques development for this subsystem can be developed. Indications are that ERTS data can provide useful data for the generation and update of such display information.

In summary, a systematic approach toward techniques development has been adopted at JSC. The system breakdown presented herein provides a framework against which current and future techniques development effort can be related and reported. The significant techniques refinements accomplished to date at JSC have been summarized in this context with the specific areas requiring additional development and extensive user agency activity highlighted.

REFERENCES

1. S. B. Chism, C. L. Hughes. "Screening and Data Handling Plan for ERTS-1 Computer Compatible Tape and Aircraft 24-Band Scanner Data." Lockheed Electronics Company, Inc., 640-TR-132, January 1973.
2. "ERTS Data Users' Handbook." Goddard Space Flight Center, Document 71SD4249.
3. Ball, G. H. and Hall, D. J. ISODATA, A Novel Technique for Data Analysis and Pattern Classification, Technical Report, Standard Research Institute, Menlo Park, California, May 1965.

4. Kan, E. P. F. and Holley, W. A. "More on Clustering with Final Recommendations in ISODATA," Lockheed Electronics Company, Inc., Houston, Texas, Technical Report 640-TR-112, May 1972.

5. Minter, R. T. "ISOCLS, Iterative Self-Organizing Clustering Program." Lockheed Electronics Company, Inc., Houston, Texas, CPD 202, October 1972.

6. Allison, J., Argo, W. and Shelton, M. "Users' Guide to a Regional Information Management System (RIMS)." To be published.

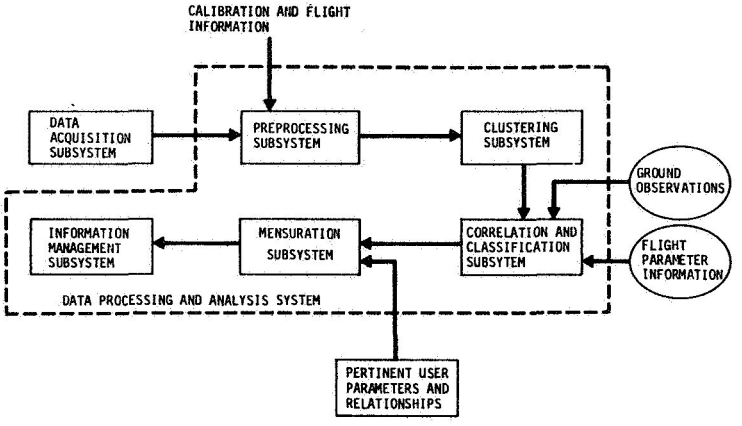


Figure 1 - Elements of a multispectral data processing and analysis system.

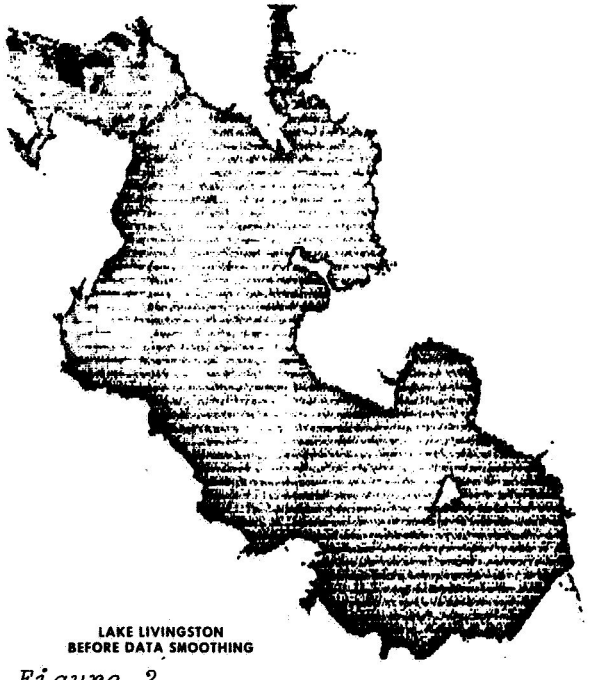


Figure 2

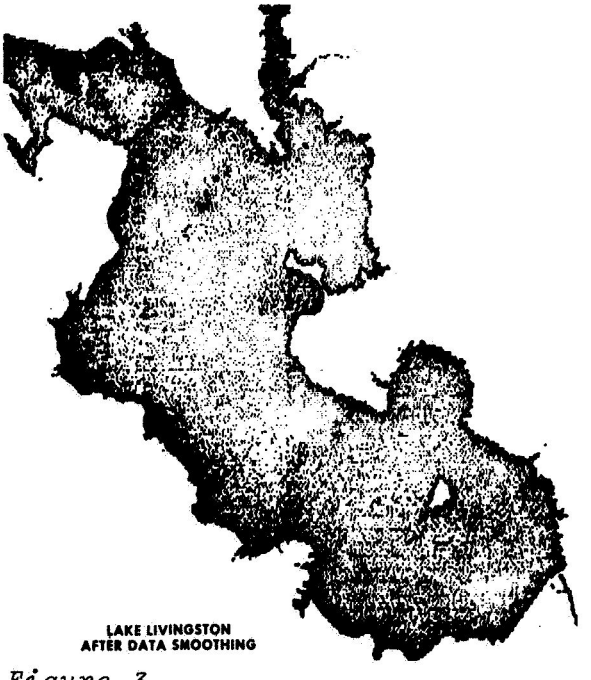


Figure 3

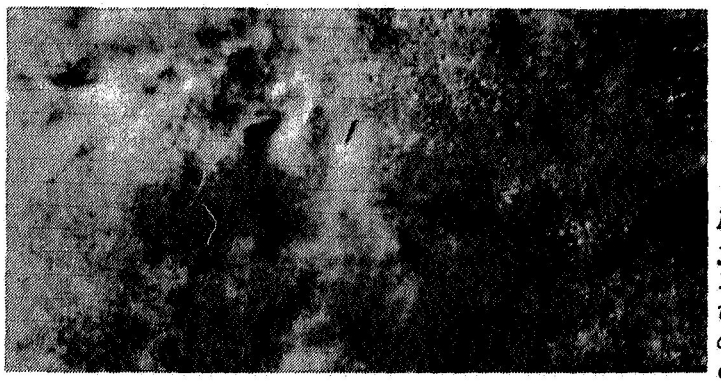


Figure 4a - ERTS MSS frame of August 30, 1973, of Lake Somerville. Thick haze over the lake is evident.

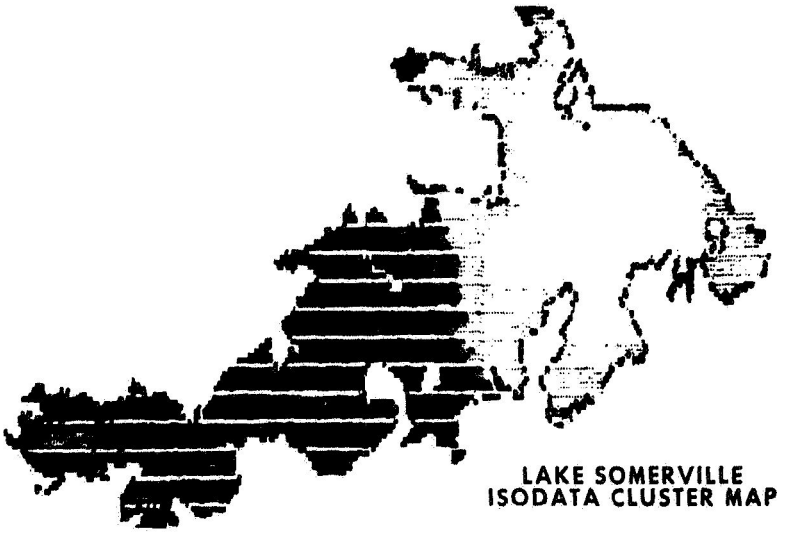


Figure 4b - ISODATA cluster map of Lake Somerville from the MSS data of August 30, 1973. Haze layer resulted in the lake being classified as several targets. On clear days the same program classifies the lake as a single target.

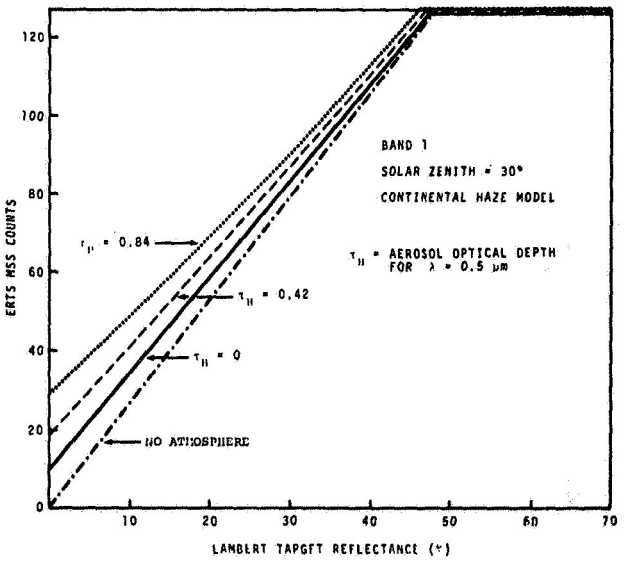


Figure 5 - Response curves for the ERTS MSS.

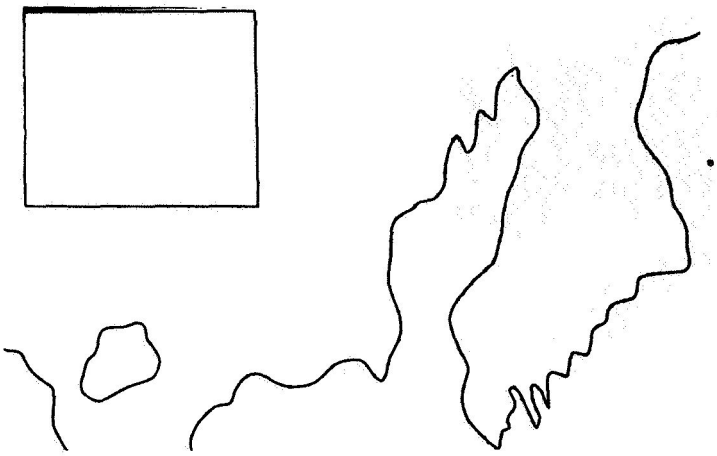


Figure 6 - Corrected gray scale map for a portion of the Somerville frame.

REFLECTANCE OF WATER, LAKE LIVINSTON, AUGUST 29, 1972

NADIR LOOK ANGLE

BAND	GROUND MEASURED VALUE (%)	MSS-ROTAR VALUE (%) $r_H = 0.5$
1	2.7	1
2	1.7	0
3	0.8	0

REFLECTANCE OF WATER, LAKE SOMERVILLE, AUGUST 30, 1972

NADIR LOOK ANGLE

BAND	GROUND MEASURED VALUE (%)	MSS-ROTAR VALUE (%) $r_H = 0.7$
1	3.5	2
2	2.5	1
3	1	0

Figure 7 - Comparison of reflectances obtained from ERTS MSS data corrected with ROTAR to ground measuring values.

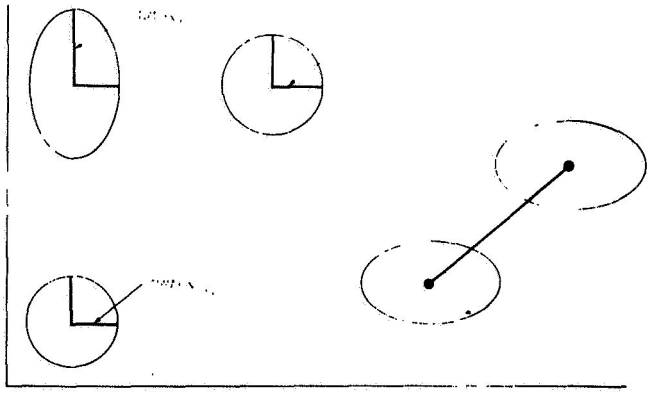


Figure 8 - Typical cluster parameters and illustration of their influence.



Figure 10 - Typical RIMS output of the HATS Area.

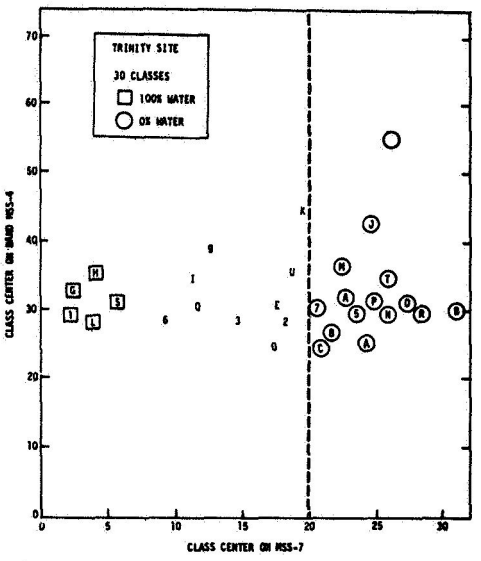


Figure 9 - Location of class centers for Trinity Delta.

N73-28330

Paper I 9

COMPUTER TECHNIQUES USED FOR SOME ENHANCEMENTS OF ERTS IMAGES

Fred C. Billingsley, Alex F. H. Goetz, *Jet Propulsion Laboratory, Pasadena, California*

ABSTRACT

The JPL VICAR Image Processing System has been used for the enhancement of images received from the ERTS for the Arizona Geology Mapping Experiment(1). This system contains flexible capabilities for reading and repairing MSS digital tape images, for geometric corrections and interpicture registration, for various enhancements and analyses of the data, and for display of the images in black and white and color.

An initial decision was made in the design of the experiment to use the ERTS MSS tapes as the prime data source in anticipation of using the VICAR System for the data reduction. This decision was made on various counts:

1. Previous experience with digital image processing at JPL for deep space missions, Apollo, and on other pictures had demonstrated the usefulness of digital processing.
2. Meaningful accurate calibration could be applied if the calibration data were available.
3. Various geometric manipulations such as map matching and overlay registration could be done without loss of photometric fidelity.
4. The multiple inaccuracies which would be suffered in attempting to use film data could be avoided.
5. Various special products such as ratio pictures could be easily produced.
6. Multispectral classifications could be obtained.
7. Various spatial filters for such as lineament emphasizing could be easily applied.
8. It was expected that the MSS would present appreciably more uniform data than would the RBV cameras.
9. The VICAR system with its extensive gamut of processing programs was available to the experimenters.

This research presents the results of one phase of research carried out at the Jet Propulsion Laboratory, California Institute of Technology, under Contract No. NAS 7-100, sponsored by the National Aeronautics and Space Administration.

Original photography may be purchased from:
EROS Data Center
10th and Dakota Avenue
Sioux Falls, SD 57198

Original photography may be purchased from:
EROS Data Center
10th and Dakota Avenue
Sioux Falls, SD 57198

ERTS PROCESSING

The early MSS tapes received from GSFC contained bad data occurring on every sixth line of the green and near IR, which appeared to be a scale factor and offset problem. To avoid loss of data, initial cleanup attempted to correct these two factors. Subsequent tapes, however, contain other types of errors which seem to be caused by random bit drop-outs for major parts of lines, and which seem to occur on random lines. Consequently, the ERTSFIX program has been modified to detect each picture line which deviates more in average value from its two neighbors than a preset tolerance. These bad lines are eliminated and the average of the neighboring lines is substituted. This produces a fairly clean picture but reduces the vertical resolution at these points. Errors over small parts of lines which are not detected by the ERTSFIX thresholding are located manually and averaged out.

The original MSS data have not been skewed to compensate for earth rotation. Although for the majority of the processing this would make no difference, skew correction for registration to maps appreciably aids the field investigator and so is routinely done. A skew correction is applied using a program which laterally shifts the data in each picture line by a progressively changing amount as required to produce the desired output skew. Following this, flexible rubber sheet stretching may be applied if desired for precise overlay matching or for registration to maps. Final adjustment for aspect ratio is accomplished by film recording at differing horizontal and vertical pixel spacings.

The images as received are relatively low contrast and it has been found useful to stretch the contrast before presenting the data for visual inspection. Stretching to the limits of the available digital number (DN) range has been used for black and white presentation (Figure 1). This produces stretches which vary for the different colors and vary between pictures. Stretching in the digital domain has the particular advantage that it is under precise control, can be linear or non-linear, and does not suffer from the toe and shoulder saturations encountered with photographic stretching. For color presentation it is desirable to have uniform color presentation throughout a series of pictures. A fixed predetermined stretch is therefore used. Comparison of the stretched pictures with the original GSFC color prints reveals considerable additional detail not visible in the original.

A second presentation which has been found useful is obtained by forming the ratios of pictures, the two most useful of which have been the ratios of each of the bands to red and each of the bands to an average of all four colors. Figure 2 shows the ratios of red and the 0.8-1.1 IR to the average. This ratioing process largely eliminates the brightness components of the original pictures and produces a color display whose color variations are more indicative of material variations than the simple pseudo color displays.

A program FUNC has been written which allows the function

$$DN_{out} = \left(\frac{Ax + By + C}{Dx + Ey + F}\right)(Gx + H)^{I} + J$$

to be performed on two pictures where x is the input DN of one picture and y is the input DN of the second. By suitable manipulation of the coefficients this program may be used to perform the ratioing, picture averaging, picture differences, offset and gain change, and exponentiating. A two dimensional table is first built up to 8 bit precision using the coefficients entered as parameters. The two input pictures are then read in parallel and an output picture assembled in synchronism by reference to the table at a location determined by the DN's of the two input pictures, pixel-by-pixel. Rapid processing speed is afforded by the table lookup method.

High frequency detail may be contrast stretched to enhance its visibility or anisotropically filtered to emphasize geologic structures with differing orientations. Spatial filtering by convolution (our normal method) has two important practical advantages: For the large pictures and the reasonable size filters used for ERTS it is faster than doing the required two-dimensional FFT, and since filtering is in the real domain the effects may be easily visualized and to some extent the filters may therefore be designed heuristically. Examples of a horizontal filter is given in Figure 3. Filtering in the Fourier domain has been advantageous primarily where the filter function in frequency space is fairly complex. This process has not been necessary for the ERTS images.

Clustering and classification is accomplished using an extension of the techniques previously described(2) for the Apollo S-158 experiment. Training samples are chosen by the analyst (Figure 4) to represent the various materials for which classification is desired, and their average value and deviation for the four bands are found by a program CLSTRN and tabulated. The four-dimensional decision volume is defined using three two-dimensional decision spaces of 128x128 locations each. Within each space rectangular areas based on the previously determined average and deviation for each material are delineated. A subsequency rule is used to eliminate the effects of overlap. Alternatively, the defined areas may be of any shape desired by manual delineation.

A two-dimensional cluster diagram in which increasing darkness represents increasing quantity of pixels at a given DN intersection may be presented to the analyst for inspection, either in image form or on a line printer. For better visualization this cluster picture may be contrast stretched and contoured with the results shown in Figure 5. The analyst manually defines in the two-dimensional cluster spaces the areas corresponding to the various materials based on the CLSTRN parameters.

Four dimensional classification using these two-dimensional spaces is done in three passes using the two-dimensional classifier HSTLOC2, first using two bands, then the output of the first pass with the third band,

and finally the output of the second pass with the fourth band. Because of the way the VICAR system is organized this multiple pass approach is quite simple to apply. While not as sophisticated as the LARS approach, it has provided a useful interim capability.

Areas containing fine detail will show a variance larger than those in which there is not much activity. Therefore, edges, lines, and fine structure will be visible in such a picture with a brightness related to the variance. Figure 6 is a variance picture of the same area as Figure 1.

Registration is normally accomplished in two steps. First, translational offsets are simply accomplished utilizing the truncating capabilities of VICAR. The required translations of small areas used for pass points are then obtained by cross correlation. One of several rubber-sheet stretching programs may then use these parameters to distort the picture to accomplish the desired overlay match. The basic operation of these programs is to systematically generate a uniform-grid output picture, obtaining the required data by weighted interpolation from the four nearest neighbors surrounding the precise calculated location in the input picture. It has not been found satisfactory to use simply the nearest neighbor to the calculated location for the output data, as this reduces the resolution. The location in the input picture is calculated from the array of distortion parameters, using linear interpolation between. We have considered higher-order generating functions for the location calculations, but have not found them necessary.

After registration, any inter-picture operation, such as DIFFPIC to detect temporal changes by picture differencing, may be applied. VICAR is designed to handle multiple input and output pictures where appropriate to the required tasks. Figure 7 is such a DIFFPIC of the Verde Valley area.

VICAR - THE JPL IMAGE PROCESSING LANGUAGE

A large amount of picture processing can be done with normal general-purpose computers and the standard Fortran batch processing software. This is not particularly efficient, however, so with large numbers of pictures to be processed, special attention must be given to reducing or by-passing the inefficient parts of the Fortran language and/or doing programming in machine language. In addition, an image processing laboratory should make available to the analyst an efficient data handling system for the development of algorithms and for the recording, processing, and display of pictures.

To facilitate the use of the system by the analyst and to enable him to rapidly call for new processes, an image processing software system based upon English language commands has been designed for the Image Processing Laboratory of the JPL. This system requires a minimum of programming knowledge and data inputs from the analyst, and performs automatically the input/output processing and routine bookkeeping. This language has been designed to allow the analyst to easily and quickly process one or a string of pictures through one or more processes automatically.

Philosophy

The fundamental philosophy of the VICAR system is that the image analyst, in accomplishing his picture processing, will call for execution one or more of a group of programs from the system library, entering parameters at the time of execution to suit his particular needs. These library programs will have been previously debugged and documented, and are available for any analyst to call on. A continually growing system is thus provided as various analysts require new processes and write the required executable programs. Over 200 executable programs are presently available.

Standard Format

A standard format has been established for both tape and disk data sets. All of the standard VICAR processing programs are designed to operate with this standard data set format.

Video samples are normally represented as 8-bit data bytes. With the Data Converter Feature of the IBM 360 tape controller, both seven and nine track tapes may be logically equivalent. The standard tape format in use at JPL is IBM-compatible seven-track tape written with ODD parity at 800 b.p.i. Each reel of tape may contain up to 99 files, determined only by the size of the files. Each file contains one video frame and is followed by a trailing file mark. The last file on a reel must be followed by two trailing file marks.

All data are recorded in an 8-bit mode, compatible with that specified in IBM SRL A22-6866. The 8-bit data samples are written in a mode where three 8-bit data bytes are recorded on tape as four 6-bit characters.

Tapes from outside sources should meet the above standards generally, but may be at other tape densities.

Vicar Summary

The primary features of VICAR as compared to separate programs are:

1. Easier to use due to standardization of procedures and formats and the reduction in the number of control cards.
2. Saves time and money in programming by providing buffering, housekeeping, label processing, and many other capabilities to the programmer.
3. Allows interaction between programs which would otherwise be difficult for a user to control.
4. Can be improved in the future without necessarily modifying all the programs.
5. Faster execution due to the elimination of returns to the operating system between tasks.

The Programs

Of the 200+ executable programs available, about half are of general purpose interest, the remainder being written around peculiarities of various projects, such as specialized programs for processing pictures from the Mariner spacecraft camera. Of the group of general interest, a moderate number have been used in ERTS processing, supplemented by some ERTS special programs such as ERTSFIX. Table I lists some of these, with typical execution times for a 1600x1700 pixel ERTS picture (i.e., two of the four strips comprising one ERTS frame). As a general rule, processing time is linearly proportional to the picture area, so small portions of the pictures - easily extracted by VICAR - are generally used for experimentation.

ERTS MSS PROCESSING TIMES
4 bands, two strips (1620x1620)

		Min.
VMSS	GSFC format to VICAR format on disk, 1 strip	6½
CONCAT	Join two strips to form 1620x1620, 4 colors	18
STRETCH	Expand to 8-bit range, 4 colors	4½
ERTSFIX	Cleanup bad lines, 1 color (depend on severity of problem)	3½-7
SKEW	Skew, 4 colors	7½
PICAVE	Average four bands	8
FUNC	Ratio band to average	5½/ratio
HISTOGRAM	Generate histograms, 4 colors	8
DIFFPIC	Difference picture, one pair	4
STRETCH	Contrast stretch, 4 colors	16
FILTER	Spatial frequency filter, 1 color	12½
AFILTER	Asymmetric filter, 1 color	31½
FASTFIL2	Suppress low frequency, 1 color	8
CLSTRN	Calculate x, σ up to 150 areas, 4 colors	3
HISTLOC2	2-dimensional classifier (1000x1200)	10
HISTLOCN	N-dimensional classifier (N=4)	30
TAPE	Generate save tape, 5 pix.	6
SAR	Read/Write 4-frames to tape	5
FOTO	Quick look Polaroid picture, 1000x1000	1½
REGISTER/ CROSS	Generate registration parameters by cross correlation	15
GEOM	Rubber sheet stretch for registration	5-20,typ

TABLE I

CONCLUSIONS

The VICAR image processing system has proven to be versatile and capable of handling the diverse array of digital processing functions required for ERTS.

Image processing for visual presentation may include such non-reversible processes as low-spatial-frequency filtering, since numerical output is not required. These must be avoided where subsequent numerical operations are required.

ACKNOWLEDGMENTS

The untiring efforts of Alan Gillespie and Mike Blackstone, of the JPL Image Processing Laboratory staff, for the digital processing, and Ron Wichelman of the JPL Photolab for the color work, are acknowledged.

REFERENCES

1. Goetz, A. F. H., Billingsley, F. C., Elston, D. P., and Shoemaker, E. M., Preliminary Geologic Investigators in the Colorado Plateau Using Enhanced ERTS Images, ERTS-A Investigator's Symposium, March 1973.
2. Billingsley, F. C., Computer-Generated Color Image Display of Lunar Spectral Reflectance Ratios, Phot. Sci. & Eng. 16 #1, 1972, p. 51-57.

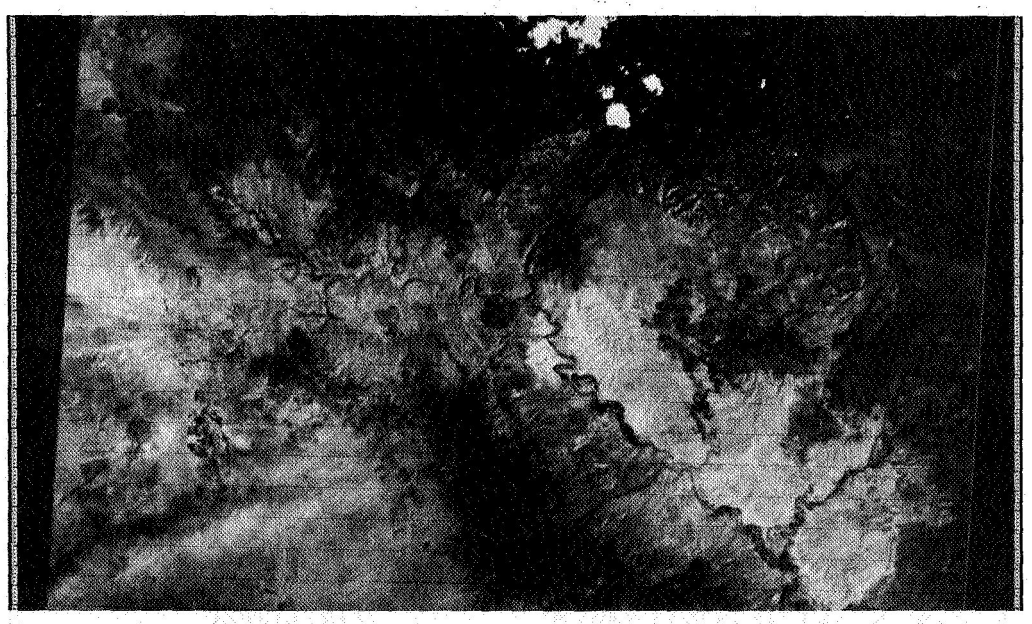


Figure 1. A section of ERTS Frame 1014-17375 (Red band), contrast stretched.

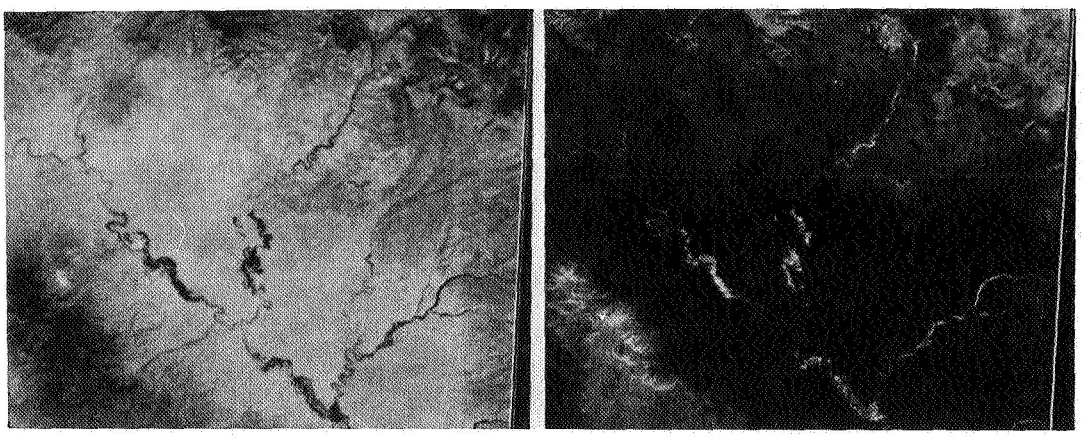


Figure 2. Ratios may be taken to emphasize variations due to color
a) Ratio of Red/Average b) Ratio of IR2/Average

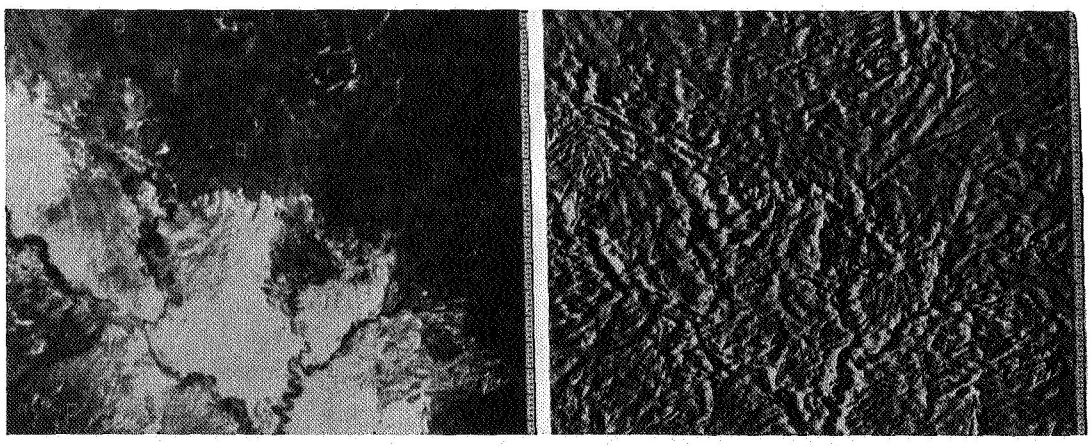


Figure 3. Spatial filters may be used to emphasize structure
a) Original b) Horizontal elimination filter

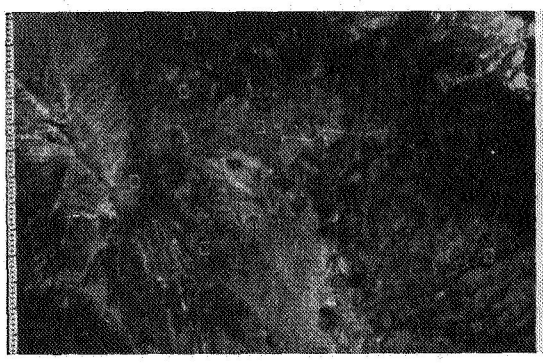


Figure 4. Portion of frame showing typical training areas

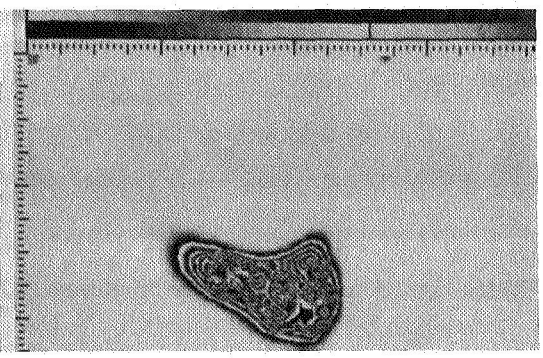


Figure 5. 2-dimensional cluster diagram

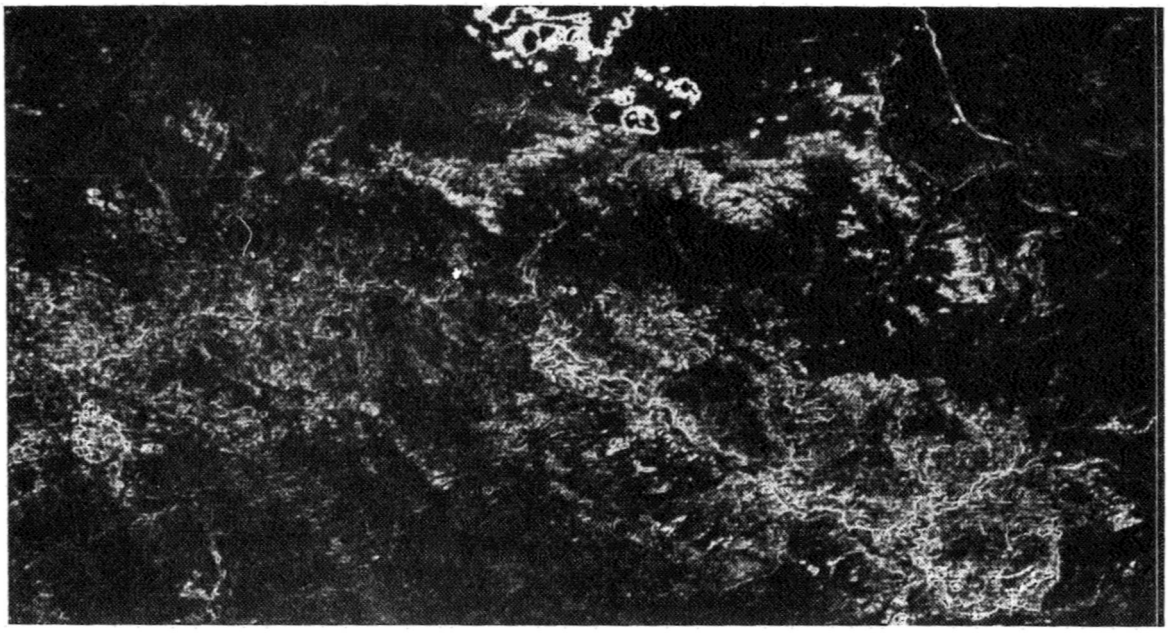


Figure 6. Variance activity picture displaying the local variance at each picture point.

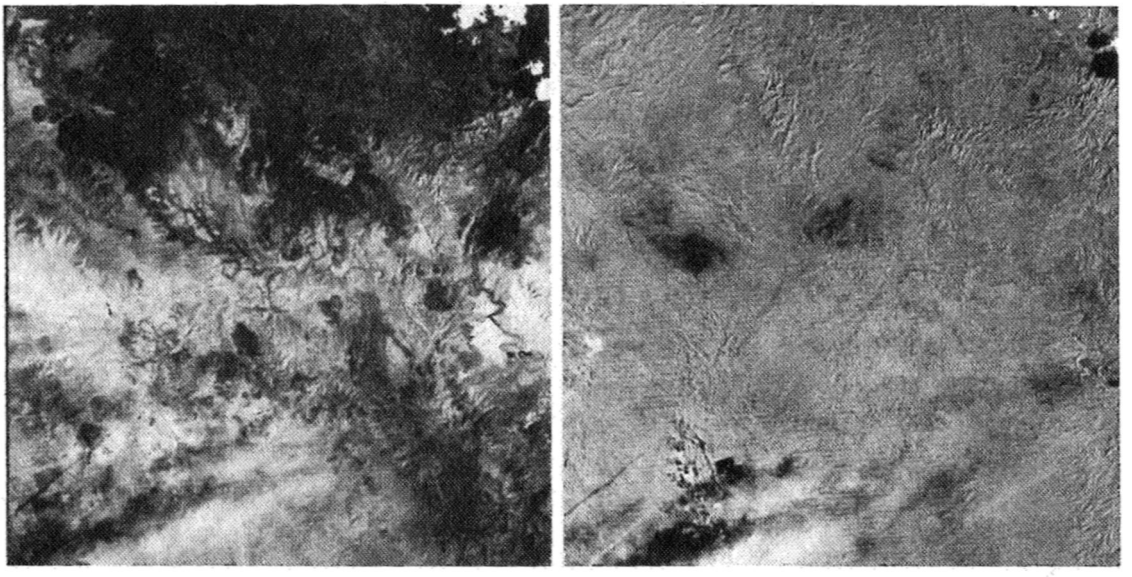


Figure 7. After registration, picture differencing, temporal changes which would otherwise require close inspection to detect show up clearly.

a) Original b) DIFFPIC, Aug. 24-Aug. 6, Red

N73-28331

Paper I 10

DIGITAL ENHANCEMENT OF MULTISPECTRAL MSS DATA FOR MAXIMUM IMAGE VISIBILITY

Vidal Raphael Algazi, *Department of Electrical Engineering, University of California, Davis, California*

ABSTRACT: A systematic approach to the enhancement of images has been developed. This approach exploits two principal features involved in the observation of images: the properties of human vision and the statistics of the images being observed. The rationale of the enhancement procedure is as follows: in the observation of some features of interest in an image, the range of objective luminance-chrominance values being displayed is generally limited and does not use the whole perceptual range of vision of the observer. The purpose of the enhancement technique is to expand and distort in a systematic way the grey scale values of each of the multispectral bands making up a color composite, to enhance the average visibility of the features being observed.

1. Introduction: The visual inspection of images of natural objects to provide qualitative or quantitative information is one of the most common uses of ERTS 1 data. With the advent of the digital computer as a useful image processing tool, black and white images with a grey scale and multispectral images, can be precisely manipulated before display to provide the viewer with an improved visibility of features of interest. The visual inspection of images to provide quantitative information is constrained by properties of human vision. The dominant properties are an excellent spatial resolution and a comparatively poor resolution to light intensity variations. For color vision an important property of the eye is the ability to distinguish a large number of color hues. This good resolution in the color dimension is exploited in pseudocolor and false color presentations in which the grey scale of images are mapped into color for improved visibility.

In this paper we consider several aspects of the enhancement of grey scale images by mapping into grey scale or color images. We are interested in the monotonic mapping of the grey scale of an image. By monotonic we mean that the order of grey scale values is preserved in the mapping into a grey scale or that the grey scale values map into a fixed and readily identifiable order of color hues.

For our defined task, elementary consideration of properties of human vision lead us to propose new enhancement methods for "optimum" image visibility. Another family of enhancement methods is then discussed which also takes into account statistical properties of the images themselves.

PRECEDING PAGE BLANK NOT FILMED

Original photography may be purchased from:
EROS Data Center
10th and Dakota Avenue
Sioux Falls, SD 57198

2. Conditions of the Study: Since we are concerned with physical attributes of light and color sensations, some terminology which differentiates objective and subjective aspects is needed. For the objective aspects we shall use the formalism of colorimetry in terms of a defined "standard observer" and color-stimulus specification in terms of tristimulus values [1]. Thus, luminance is a measure of energy while brightness will denote the corresponding sensation. The dominant wavelength in the spectrum yields a sensation of hue. The purity of the color excitation is related to the sensation of color saturation. What we hope to exploit, for the purpose of image enhancement, are some elementary aspects of the extensively studies relationship between the objective and subjective spaces. We shall assume that the techniques for the recording and display of images are not limiting the range and resolution of luminances reproduced. For the color rendition we have to refer to specific color primaries and we shall use the standard NTSC colors.

We thus consider a part of the image enhancement problem shown in the diagram below.

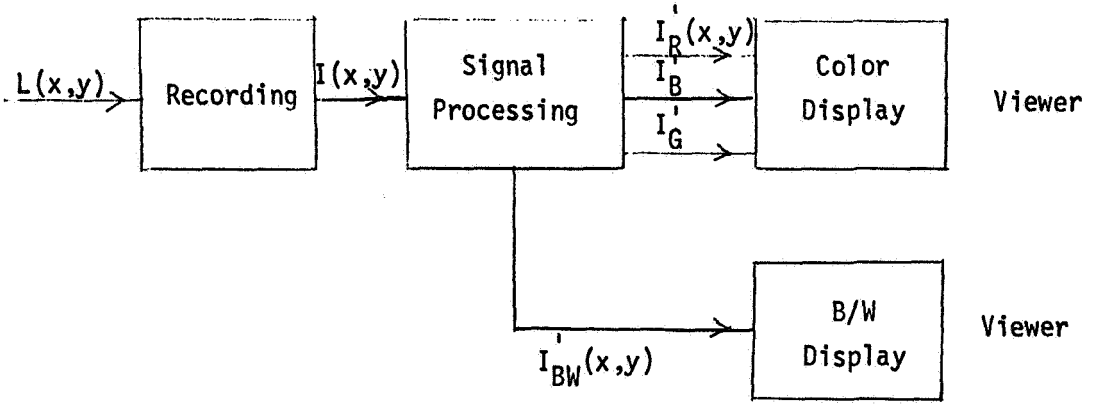


FIGURE 1

If the recording system and display introduce nonlinear effects of their own, these can be compensated to a substantial extent by signal processing, but such compensation depends on the physical devices used. Here we shall assume that the intensity variables I and the luminance variables L are proportional. Referring to Figure 1 we can now describe more precisely the problem of interest. We would like to process the signal I(x,y) in such a way that $L'_R(x,y)$, $L'_B(x,y)$, $L'_G(x,y)$, or $L'_{BW}(x,y)$ will allow the viewer a maximum discrimination of the luminance values

$L(x,y)$ at each point, without substantial degradation of the spatial resolution. This image enhancement problem has two aspects. The first one is the choice of a mapping transformation of L into L' which provides the maximum number of distinguishable levels in L. The second aspect of the problem is the rational exploitation of the statistics of the image, recognizing that for each application only a small range of intensity values is generally relevant.

3. Mapping Intensities into a Grey Scale: It is well known that human vision adapts to an extremely large range of luminance levels of more than one million to one [4,5]. However, the total range of luminance that the visual system can discriminate simultaneously is rather small and 15 to 20 grey scale steps from black to white are claimed as typical. This discrimination corresponds roughly to constant thresholds of $\frac{\Delta L}{L}$, result which matches the commonly assumed logarithmic sensitivity of the eye to luminance values [4]. Thus constant brightness steps will correspond to luminance steps spaced exponentially. Given a total range of luminance from black, L_B, to white, L_W, $L_R = L_W - L_B$, the relation

$$I'_{BW}(x,y) = [L_R + 1]^I + L_B - 1 \qquad (1)$$

in which $0 \leq I \leq 1$, will yield the desired mapping in a subjective linear scale from black to white. It will also provide maximum visual discrimination in the quantity I. In the viewing of a CRT display the available adjustment of brightness and contrast will take care of the adjustment to L_R and L_B and the signal processing has only to provide an exponential correspondence between I and I'. These theoretical results can be verified experimentally as discussed later on in this paper.

4. Pseudocolor Mappings: For black and white images (or MSS monospectral scans) it is of interest to examine pseudocolor maps which provide a color scale with improved discrimination. There are a number of aspects in this problem which have lead us to examine mappings with a constant luminance and also mappings using a luminance variation as well as a variation in hue. Because of space limitation we shall omit this discussion and refer the interested reader to reference (11).

5. Experimental Determination of Differential Visibility: In the experimental application of image enhancement, one is confronted with the limitations of the display devices, the photographic processes, etc. It is thus desirable to verify experimentally the differential sensitivity of each grey scale mapping. We have developed a simple technique to perform this measurement which is specially suitable to interactive work, using a digital computer. The table of values shown in Figure 2 is displayed using whatever grey-scale mapping techniques

and display devices are to be tested.

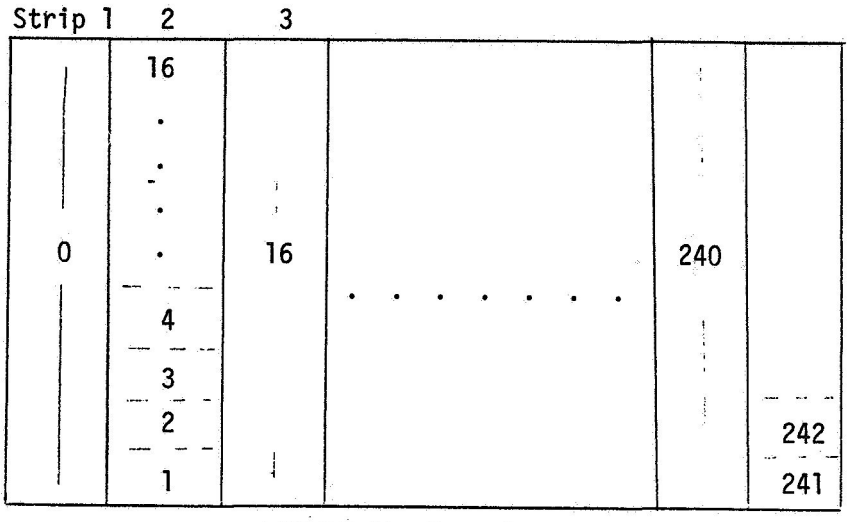


FIGURE 2: Test Image

The test table is designed so that the distance between adjacent strips is variable between 1 and 16. The total range 0 - 256 corresponds to the commonly used 8-bit integer display. An image of the test table is shown in Figure 3. We observe the vertical lines of the test table, but careful examination reveals that each line cannot be perceived vertically across the entire image. Assume that the line between strips 2 and 3 cannot be perceived for values of strip 2 between 8 and 9. That means that 16 - 8 = 8 is the threshold of visibility of the input variable for the proposed mapping in the range of input values 8 to 16. Thus by a single image one can verify the linearity of the scale and even devise a compensation table if needed.

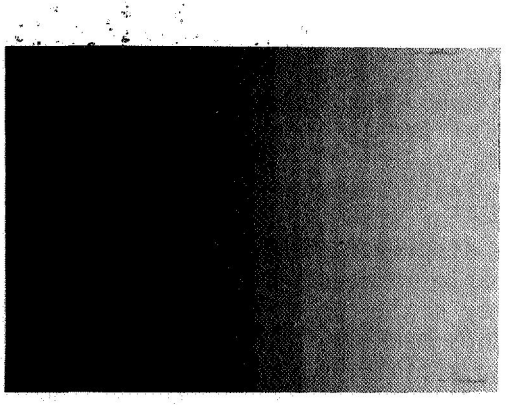
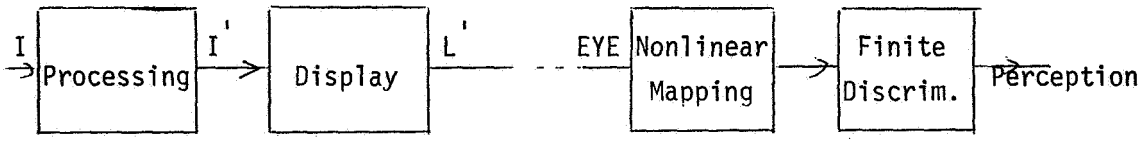


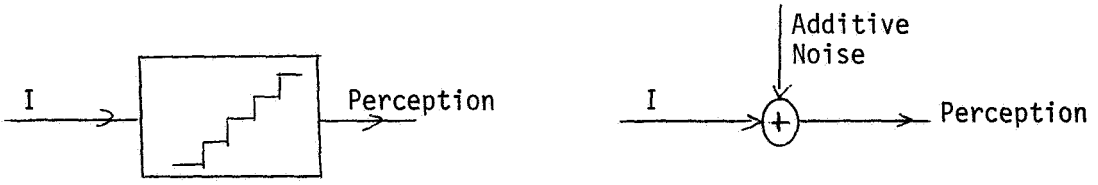
FIGURE 3: Image of the Test Table

6. Mappings Based on the Statistics of Intensity Values: In our discussion of the mapping of intensity I into a linear perceptual space we have not made any assumption about the statistical distribution of I. It is clear, however, that some consideration of the distribution of I is needed, if for nothing more than to scale the range of I so that the image enhanced covers the whole perceptual range available. Considerably more can be said by combining the concept of perceptual space with a constant differential with some previous work on quantization and estimation of the authors and others [8,9,10]. Assuming that we have still a limit on the increment ΔI which can be perceived, we can model this situation by assuming that the perceptual space is quantized, with uniform quantization steps, or by assuming that we have some additive noise which prevents the differential perception of small input increments. Figure 4 illustrates the situation.



Linear Relation

a) Linearization of Perceptual Scale



b) Models of Finite Discrimination

FIGURE 4

For both models of Figure 4b a precise mathematical optimization problem can be solved. Consider the model of Figure 5.

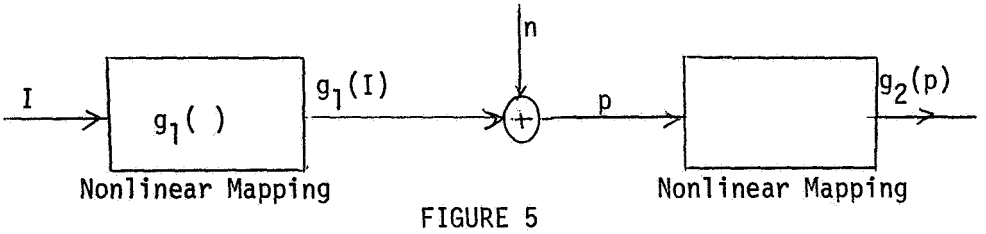


FIGURE 5

We would like to determine the nonlinear mapping $g_1(\ )$ and $g_2(\ )$ such that the distortion D is minimized

$$D = E\{W[I - g_2(p)]\} \tag{2}$$

I - g(p) is the error between the input and output variables of Figure 3, W( ) is an error weighting function, E denotes statistical expectation over the distribution of the random variable I. In a communication context the optimization problem considered corresponds to the design of nonlinear scalar transmitters and receivers [10]. If a uniform quantizer is substituted for the additive noise we are then designing a non uniform quantizer [9]. Under the conditions of small additive noise or small quantization steps the solution to both problems is the same.

Consider the class of error weighting function $W(e) = |e|^c$ and let us assume that the range of the variable $g_1(I)$ is limited. Then D of equation 2 is minimized by choosing

$$g_1(I) = K_1 \int_{-\infty}^{I} [f_I(x)]^{\frac{1}{c+1}}\, dx + K_2 \tag{3}$$

in which $f_I(x)$ is the probability density function of I and the constant K_1 and K_2 are chosen to yield the desired range for $g_1(I)$. For small noise $g_2(\ )$ is then the inverse of $g_1(\ )$. We have assumed in (3) that the range of I is limited and that $f_I(\ )$ does not have a long tail. For a discussion of the effects of the tails of $f_I(\ )$ see [9].

Let us now interpret and adapt these results to image enhancement. We can adapt the diagram of Figure 5 to the case of vision as shown in Figure 6.

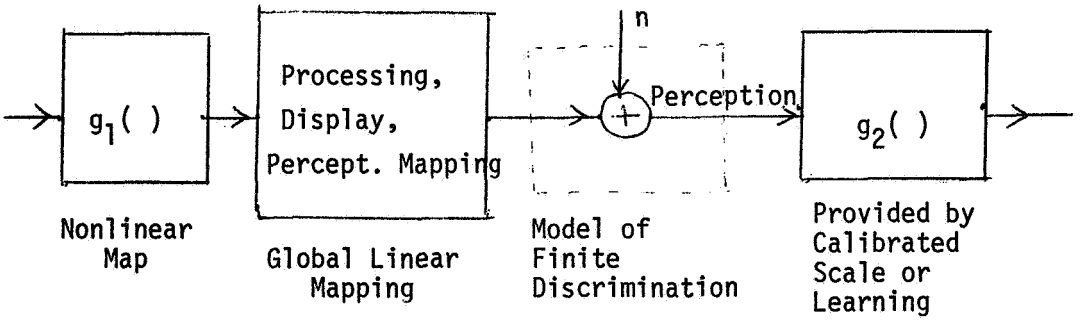


FIGURE 6

The significant part of Figure 6 is the interpretation of the nonlinear operation $g_2(\ )$ as occuring in the brain and provided by learning. For instance the display of a linear scale in I at the same time that the processed image is displayed allows the viewer to calibrate his visual scale and compensate for it. The compensation is indicated by $g_2(\ )$. What the introduction of the mapping $g_1(\ )$ has done is to reassign the intensity values I according to their frequency of occurrence so that the more frequent values are spread out farther in a perceptual scale. Thus, the mapping $g_1(\ )$ provides a global mapping from I to p with a nonlinear perceptual scale but which maximizes the total average visibility of the image.

Note that under the condition mentioned earlier $g_1(\ )$ does not depend on the specific number of quantization steps or additive noise in the model of Figure 4c and the results are applicable to all the mapping into a linear perceptual space discussed before.

A question remains open in the choice of constant c in equation 3. Recall that the class of error weighting function is $W(e) = |e|^c$. Since I is an intensity or energy variable one would expect that $c = 1$ is a good choice. Note that the choice $c = 0$ has been proposed on an ad hoc manner [6].

Another result pertinent to image enhancement is available from reference 9. It is possible to evaluate quantitatively the improvement in the visibility of the image due to the nonlinear mapping $g_1(\ )$ as a function of the probability density function $f_I(\ )$. If A and B are the range of $F_I(\ )$, then

$$F = \frac{D\ Nonlinear}{D\ Linear} = \frac{1}{[B-A]^c}\left[\int_A^B [f_I(x)]^{\frac{1}{c+1}}\, d_x\right]^{c+1} \qquad (4)$$

We find $F = 1$ as expected if $f_I(\ )$ is uniform.

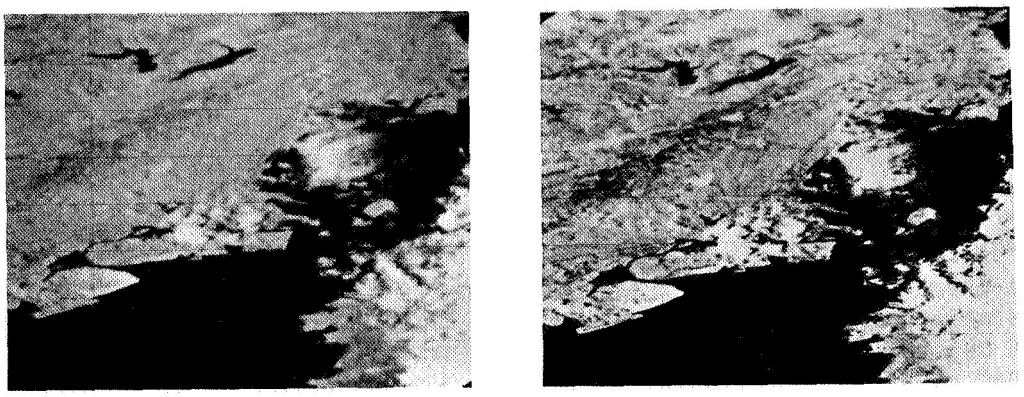
7. Implementation of the Enhancement Technique: The following steps are followed in the enhancement of MSS multispectral data:

1. Extraction of a geographic area of interest from NASA CTT.
2. Display on a color monitor of standard color composites.
3. Generate histograms of each spectral band.for subareas of the image with features of interest.
4. Generate an enhancement table for each of the spectral bands corresponding to the histogram of intensity values in that band.

5. Apply enhancement table to the spectral components and display of enhanced images.

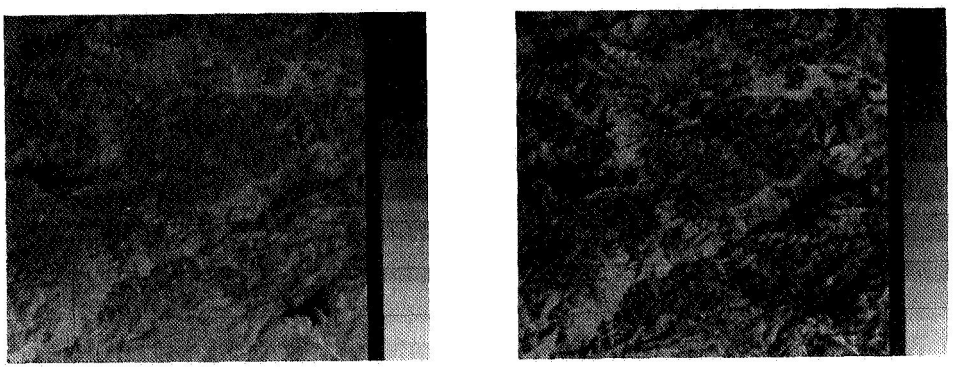
The procedure can be iterated if needed.

8. Examples: We demonstrate the technique on two examples, Figure 7a and 7b are from MSS band 6 for the East Bay region (San Francisco Bay) showing the cities of Oakland, Berkeley and Richmond. Figure 8a and 8b are from MSS band 6 for the Bucks Lake region in California, a NASA test site. The improved visibility due to enhancement (7b and 8b) is striking for water, urban areas and forestry and wildlands.



a) Original b) Enhanced

FIGURE 7: East Bay (1003-18175), MSS Band 6



a) Original b) Enhanced

FIGURE 8: Bucks Lake (1002-18125) MSS Band 6

9. Conclusions: A powerful technique for the systematic enhancement of multispectral MSS data has been presented and illustrated - the technique is specially suited for interactive work since the digital processing takes only a few minutes once the data has been reformatted. Since the method provides enhanced visibility of whatever is present in the area on which the enhancement algorithm is designed it provides a powerful experimental tool for the discovery of new patterns and relationships.

10. References:

[1] See for instance J.J. Sheppart, Jr., Human Color Perception, American Elsevler, 1968.

[2] R.W.G. Hunt, Reproduction of Color, Wiley, 1967.

[3] R.W. Burnham, R.M. Hanes, C.J. Bartleson, Color, John Wiley & Sons, 1963.

[4] T. Cornsweet, Visual Perception, Academic Press, 1970.

[5] J.J. Sheppard, Jr., R.H. Stratton and C. Gazley, Jr., "Pseudo Color as a Means of Image Enhancement," Am. J. Optom. and Arch. Am. Ac. Optom., Vol. 46, October 1969, pp. 735-754.

[6] H.C. Andrews, A.G. Tescher, R.P. Kruger, "Image Processing by Digital Computer," IEEE Spectrum, July 1972, pp. 20-32.

[7] T.G. Stockham, Jr., "Visual Processing in the Context of a Visual Model," Proc. IEEE, Vol. 60, No. 7, July 1972, pp. 828-842.

[8] P.F. Panter and W. Dite, "Quantization Distortion in Pulse Count Modulation with Non Uniform Spacing of Levels," Proc. IRE, Vol. 39, Jan. 1951, pp. 44-48.

[9] V.R. Algazi, "Useful Approximations to Optimum Quantization," IEEE Trans. on Com. Techn., Vol. Com-14, No. 3, June 1966, pp. 297-301.

[10] V.R. Algazi, "On Scalar Transmitters and Receivers," IEEE Trans. Com. Techn., Vol. Com-17, No. 2, April 1969, pp. 330-331.

[11] V.R. Algazi, "Image Enhancement by Grey Scale Mapping," Chapter 8, Appendix A. Integrated Study of Earth Resources in the State of California based on ERTS 1 data - Semi-Annual Report, January, 1973.

N73-28332

Paper I 11

ERTS-1 IMAGE ENHANCEMENT BY OPTICALLY COMBINING DENSITY SLICES

Gerald O. Tapper and Robert W. Pease, *Department of Geography, University of California, Riverside, California 92502*

ABSTRACT

The technique of density slicing using a photographic film and its application to enhancement of ERTS-1 imagery has proved to be useful for mapping varigated areal phenomena and provides a useful supplement to the I²S Mini-Addcol viewing system. The initial experiments conducted with this film were encouraging, and indicated that this technique of density slicing using readily accessible darkroom facilities and simple darkroom procedures allows rapid, accurate, and facile interpretation of certain areal phenomena to be made from the imagery. The distribution of the Tree Yucca, Yucca brevifolia Jaegeriana. In the Eastern Mojave Desert of Southern California and Southern Nevada was used as an example to test the accuracy of the technique for mapping purposes. The distribution was mapped at a relatively high level of accuracy.

1. INTRODUCTION

The technique of density slicing using a photographic film and its application for pre-enhancing ERTS-1 imagery in preliminary testing appears to be an effective tool for mapping varigated areal phenomena and provides a useful supplement to the I²S Mini-Addcol viewing system. The test involved enhancement of selected ERTS-1 imagery (November 1972), out of the Las Vegas, Nevada region and eastern Mojave desert. Early difficulties in obtaining high resolution enhanced imagery from ERTS-1 MSS imagery by use of Diazochrome composites and initial interpretation from the 70 mm MSS chips in the viewer (Figure 1) led to experimentation with an equidensity film, Agfacontour Professional, to pre-enhance selected ERTS-1 MSS bands.

2. EQUIDENSITY FILM

Briefly, Agfacontour equidensity film is a black and white copy film, which at a specific exposure and development becomes transparent, creating a band or line of isodensity.[1] Caution is required during

PRECEDING PAGE BLANK NOT FILMED

Original photography may be purchased from:
EROS Data Center
10th and Dakota Avenue
Sioux Falls, SD 57198

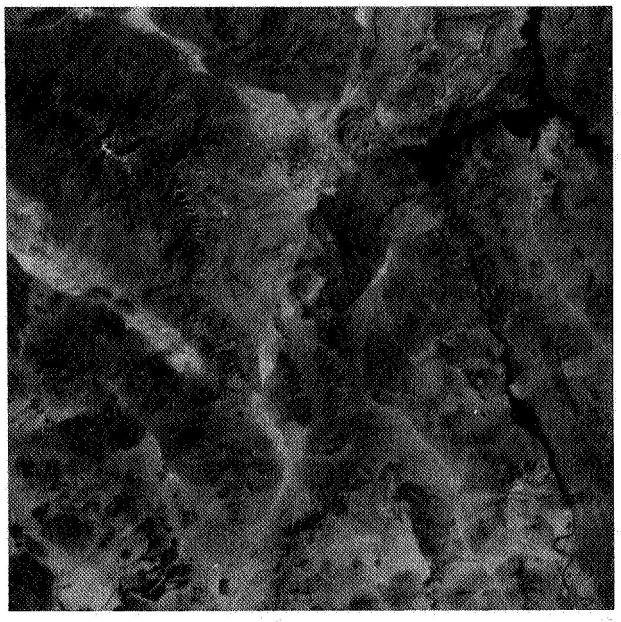


FIGURE 1: ERTS-1 Frame 1106-17495, Band 7, Eastern Mojave Desert of Southern Nevada and Southern California.



FIGURE 2: Density slice enhancement of ERTS-1 Frame 1106-17495.

exposure and development, and adequate control of both exposure and development is critical to obtain proper densities on the positive density slices. The underexposed and overexposed areas of the film adjacent to the transparent sector essentially remain black or opaque. The transparent portions of the image relate to a specific band of density on the negative and an areal representation of that density manifests itself on the positive equidensity film. The emulsion is blue sensitive, and the width of this band or thickness of the density slice can be varied by increasing or decreasing the amount of yellow filtration used during the exposure process. Only first generation equidensity of the ERTS-1 imagery were used in this study, and subsequent enhancements of the imagery should include second generation density slices. The above implies a procedure where by the first generation density slice is contacted onto a litho film and a subsequent density slice is taken from that negative. Perhaps even third generation density slices might be required to further enhance the image. Initial results indicate this technique of density slicing, using accessible darkroom facilities and procedures, allows rapid, accurate, and facile interpretation of certain areal phenomena. The distribution of the Joshua Tree or Tree Yucca, Yucca brevifolia (Jaeger variation)[2] in the Eastern Mojave Desert of Southern California, and Southern Nevada was used as an example to test the technique in terms of accurately mapping a minor element of the desert's environment.

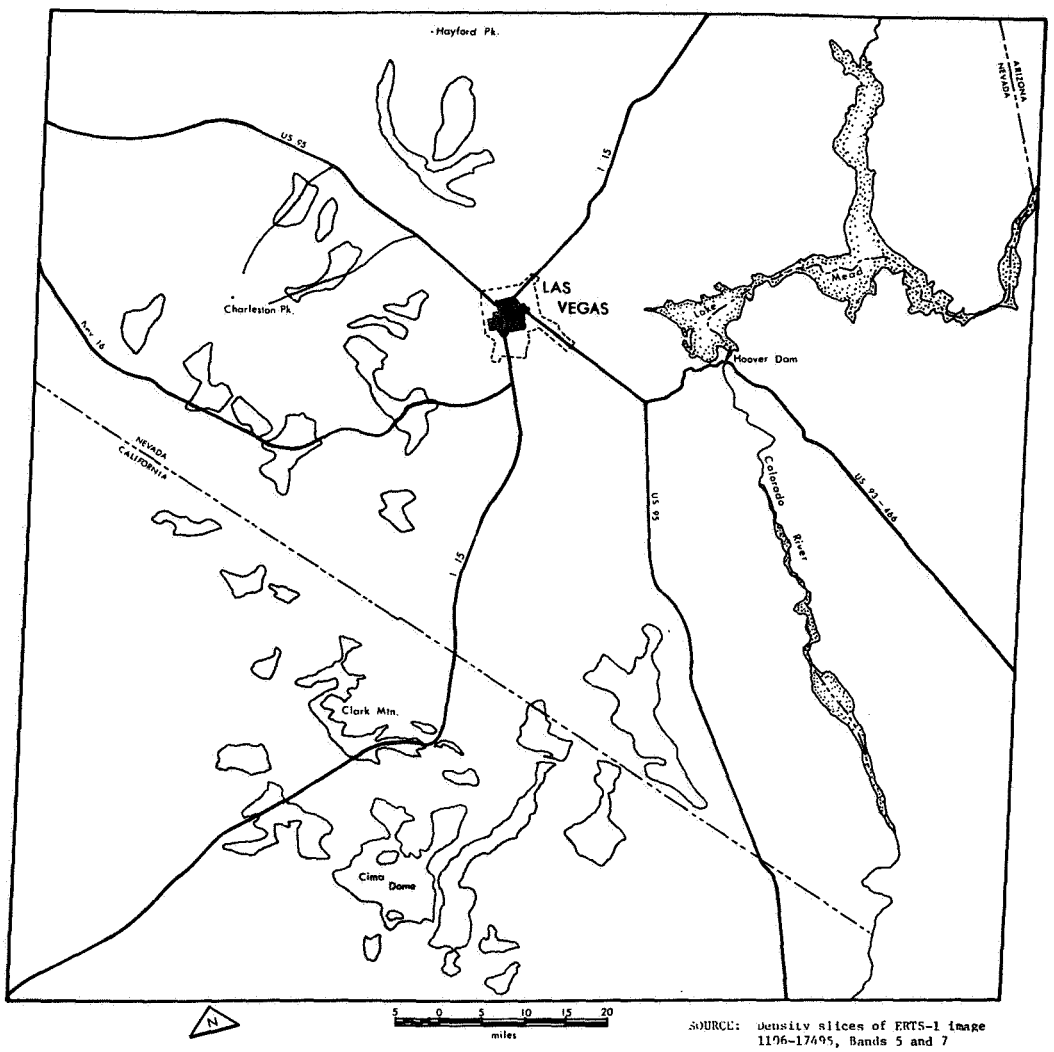
3. MAPPING OF YUCCA BREVIFOLIA JAEGERIANA[3]

The negatives of MSS Bands 5 (0.6-0.7 micrometers) and 7, (0.8-1.1 micrometers) of the Las Vegas region were used to produce various density slices on the equidensity film. The first step in this process was to determine the negative density of a predetermined concentration of Y. brevifolia Jaegeriana. Teutonia Peak or Cima Dome, a well known geomorphic feature in the Eastern Mojave, covered by a dense stand of Tree Yucca Y. brevifolia Jaegeriana, was used.[4] Once this density had been determined using a densitometer with a suitably small sensing spot, the equidensity film was exposed to isolate this preselected density. A series of different density slices were also extracted from the same negatives bracketing the above key density. The resultant density slices were than viewed in the combiner using various filter combinations. The result is an enhanced and mappable bispectral signature for an environment containing the Y. brevifolia (Figure 2). The enhanced density slice specifically depicting this environment was viewed through a green filter, the other three density slices used for the combination were projected through red, blue, and white (no filter) filters. It is felt that the green signature was most easily accommodated by the human eye for proper interpretive purposes. The areal expression of the environment containing Tree Yucca was then mapped from the combined enhanced imagery (Figure 3).

FIGURE 3

DISTRIBUTION OF

Yucca brevifolia Jaegeriana



SOURCE: Density slices of ERTS-1 image 1196-17495, Bands 5 and 7

4. FIELD CHECK OF MAPPED YUCCA BREVIFOLIA JAEGERIANA

Over a three day period the mapped distribution of Y. brevifolia Jaegeriana was field checked by the author.[5] This field check of the mapped data revealed a high correlation with the actual Yucca distribution. The field check also involved keying the vegetative community associated with it. This was done to determine more accurately the basis for the signature. With the exception of two sites, the mapped signature from the enhanced imagery was a location for the Y. brevifolia. Two exceptions were in areas where extremely high concentrations of another Yucca, Mojave Yucca or Yucca shidigera, was found in combination with an almost pure stand of Creosote Bush, Larrea divaricata. The morphology of mature Y. shidigera (which is quite similar to the Y. brevifolia in its juvenile form), when found in a vegetative community having a high density of the Creosote Bush as a similar signature on the imagery. The mapped locations were all indicative of Y. brevifolia Jaegeriana and its related community (Figure 4) but an inaccuracy was noted for the boundaries of each location. In all instances interpreter error on the boundary may result from the interaction of several related elements. Foremost of these is a change in topography from a low local relief fan surface to one of more rugged topography and high local relief. The key area for example, Cima Dome, where the initial sample density was determined, is a feature of low surface relief on the Mojave landscape. The density of the Y. brevifolia community as isolated on Cima Dome should apply only to other low relief features where the plant is present, i.e., upper portions of alluvial fans, old pediment surfaces, and some high elevation alluvial-filled valleys. These types of surfaces where the Tree Yucca community is present should provide similar physical characteristics of albedo, texture, slope, and exposure to the sensor, and thus would present a similar density on the density slice. Another group of factors influencing the determination of the boundary of the Y. brevifolia community is a change in the signature between the environment of one plant community and another.

Examination of the table (Figure 4) reveals that the signature mapped belongs to a vegetative community dominated by Y. brevifolia, Blackbush, Coleogyne ramosissima, and Burrograss, Scleropogon brevifolius. Note also that a group of minor species are nearly always found in association with the above dominants. These are Mormon Tea, Ephedra spp., certain varieties of Cactii, Opuntia spp. and Echinocerus spp., and Cheesebush, Hymenoclea salsola. Also, in certain sites, at lower elevations of +1000 meters Y. shidigera becomes a codominant and is on other sites a minor species. Further tests need to be made to determine the degree to which plant associates other than the Tree Yucca contribute to the imagery signature.

Yucca brevifolia Jaegeriana and its Associated Vegetation

Site	Elevation	Dominant Species: Joshua Tree *Yucca brevifolia Jaegeriana*	Mojave Yucca *Yucca shidigera*	Fleshy-fruited Yucca *Yucca baccata*	Creosote bush *Larrea divaricata*	Blackbush *Coleogyne ramosissima*	Western Juniper *Juniperus occidentalus*	Piñon Pine *Pinus monophylla*	Grasses including Burrograss *Scleropogon brevifolius*	Minor Species: Joshua Tree *Yucca brevifolia Jaegeriana*	Mojave Yucca *Yucca shidigera*	Fleshy-fruited Yucca *Yucca baccata*	Creosote bush *Larrea divaricata*	Blackbush *Coleogyne ramosissima*	Cactii *Opuntia spp. Echinocereus spp.*	Mormon Tea *Ephedra funera Ephedra nevadensis*	Cheesebush *Hymenoclea salsola*	Unknown species (shrubs)
Ivanpah Mountains - 1	3340'	x	x		x				x			x			x	x	x	
Ivanpah Mountains - 2	3930'	x	x						x			x	x		x	x		
Ivanpah Mountains - 3	4640'	x									x	x	x		x	x	x	
Teutonia Peak - Cima Dome	5200-4100'	x						x	x		x	x	x		x	x		
Piute Valley - 1	<3000'		x		x				x					x				
Piute Valley - 2	3000-4500'	x				x			x		x				x	x	x	
Lanfair Valley	4200'	x							x		x		x	x	x	x	x	
Halloran Summit - 1	4000'	x		x		x			x		x		x		x	x	x	x
Halloran Summit - 2	3700'	x	x		x	x			x			x			x	x	x	
New York Mountains	3200-4200'	x		x	x						x				x	x		x
Nipton	3200'	x	x		x				x			x			x	x	x	
Ivanpah - 1	<3000'		x		x				x	x				x	x			
Ivanpah - 2	>3000'	x			x				x		x	x			x	x	x	
Clark Mountains - 1	>4000'	x							x		x			x	x	x	x	x
Clark Mountains - 2	4500-3200'	x	x	x	x		x	x	x					x	x	x	x	
Cottonwood Valley - 1	<3000'		x		x				x						x			
Cottonwood Valley - 2	3000-4100'	x				x			x		x		x		x	x	x	
Cottonwood Valley - 3	>4100'		x	x		x			x						x		x	
Lovell Wash - 1	>4500'	x					x	x	x		x		x	x	x		x	x
Lovell Wash - 2	3200-4500'	x							x		x	x	x	x	x	x	x	
Lovell Wash - 3	<3200'		x		x	x			x						x	x	x	x
Wheeler Fan - 1	3100'	x	x	x	x	x			x						x	x	x	x
Wheeler Fan - 2	3760'	x							x				x		x	x	x	
Wheeler Fan - 3	6200'	x					x	x	x						x	x	x	
Kyle Canyon Fan - 1	<3000'	x	x		x				x					x	x	x	x	
Kyle Canyon Fan - 2	3000-6000'	x				x			x		x					x		
Kyle Canyon Fan - 3	<6000'	x					x	x	x		x					x		x
Yucca Forest	4500-6500'	x				x			x		x		x		x	x	x	
Las Vegas Mountains	3500-4800'	x				x			x		x		x		x	x	x	
Pine Springs - 1	3200-3400'	x	x		x				x						x	x		
Pine Springs - 2	3500-4100'	x			x				x						x	x	x	x
Red Rock Valley	3000-3600'	x	x	x					x				x		x	x		
Goodspring Valley	3200-4400'	x	x		x				x					x	x	x	x	x

FIGURE 4

5. CONCLUSIONS

To reiterate, the technique of pre-enhancing ERTS-1 MSS 70 mm chips with an equidensity film has greatly enhanced the utility and application of the imagery. The density slicing technique also provides a useful supplement to the I^2S Mini-Addcol Viewing System, especially for mapping discrete varigated phenomena. It would be almost impossible to map this specific environment from the standard ERTS-1 chips alone, although a fairly good approximation could be made by a Biogeographer familiar with the region.

The technique should not be viewed as final however, since its full potential has not yet been realized. A further test of the technique might include mapping all the various vegetation environments in the Mojave, something which, when considering the facility with which Y. brevifolia was mapped, could be done with small inputs of interpretation time.

Density slicing of ERTS-1 imagery as realized from this technique has the potential for increasing the interpretability and use of the imagery and can provide the user with environmental data not easily obtained with other technology. The technique can contribute to studying various physical and cultural environments, and can be used to map their areal signatures at a high level of confidence.

6. FOOTNOTES

[1]Ranz, E. and E. Schneider (1970), "Der Äquidensitenfilm als Hilfsmittel bei der Photointerpretation," Bildmessung und Luftbildwesen, 2: 123-134.

[2]Jaeger, Edmund C. (1968), Desert Wild Flowers. Stanford: Stanford University Press.

[3]Yucca brevifolia Jaegeriana is a smaller, shorter leafed variety of the Joshua Tree, Yucca brevifolia, Jaeger, 1968, p. 15.

[4]Huning, J. R. and R. M. Petersen (1973), "Use of Yucca brevifolia as a Surrogate for Detection of Near-Surface Moisture Retention," NASA Technical Report N-71-1, Department of Geography, University of California, Riverside.

[5]The author would like to acknowledge the able assistance of Jack B. Bale in conducting the field check and in keying the various species of vegetation at each site.

N73-28333

Paper I 12

PSEUDOCOLOR TRANSFORMATION OF ERTS IMAGERY

Jeannine Lamar, *The Rand Corporation, 1700 Main Street, Santa Monica, California;* Paul M. Merifield, *Earth Science Research Corporation, 1318 Second Street, Suite 27, Santa Monica, California*

ABSTRACT

For several years, a group at Rand has been studying human vision and the effectiveness for improving detection and recognition. In the course of this work, a number of image enhancement techniques have been developed.

One of the photographic techniques which shows great promise as an aid in interpreting ERTS imagery is pseudocolor transformation. It is a process where each shade of gray in an original black-and-white image is seen as a different color in the transformation. The well known ERTS-1 MSS image of the Monterey Bay-San Francisco area was transformed using a technique which requires only two intermediate separations. Possible faults were delineated on an overlay of the transformation before referring to geologic maps. The results were quite remarkable in that all large active or recently active faults shown on the latest geologic map of California were interpreted from the image for all, or much, of their length. Perhaps the most interesting result was the Reliz fault. The fault is shown as covered; however, a lineation corresponding to the position of the fault is visible on the image.

The usefulness of ERTS images in identifying recently active faults is demonstrable. Although the faults are also visible in the unenhanced image, they are clearly accentuated and more easily mapped on the pseudocolor transformation.

PRECEDING PAGE BLANK NOT FILMED

Original photography may be purchased from:
EROS Data Center
10th and Dakota Avenue
Sioux Falls, SD 57198

The eye can distinguish a difference in any of the three visual coordinates (hue, saturation, and luminance), and is quite sensitive in this regard even for complex images.[1] In discrimination tasks with a black-and-white image, the eye responds to differences in only one of the coordinates -- luminance -- over its gray-scale range from black to white. In a pseudocolor enhancement of a black-and-white image, a particular chromaticity/luminance combination is obtained from each shade of gray in the original black-and-white image. By thus using all three visual coordinates, one can transform a small gray-scale difference in the black-and-white original into an easily distinguished color (chromaticity/luminance) difference in the pseudocolor enhancement.

Numerous techniques, both photographic and mechanical, have been developed for creating pseudocolor transformations. Among the mechanical devices are Aerojet-General's Spectrovision,[2] which produces a video display with up to 64 colors, and Spatial Data Systems'[3] color display system with 32 colors. International Imaging Systems'[4] additive color optical viewer projects up to six images onto a rear projection screen with a variety of optical filters on each channel to create natural, false, and pseudocolor effects.

The transformation of a black-and-white image into a pseudocolor version can be effected photographically in a variety of ways. Perhaps the simplest is the transformation of shades of gray to colors in such a way that the progression of grays from white to black is transformed to successive colors in the spectrum -- white to red, light gray to orange, etc. This can be accomplished by using several black-and-white separations in which information on the intensity levels in the original image is encoded. Each separation contains information relating to a limited range of intensities. Many such high-contrast "masks" may be used, with each one encoding only a very narrow range of intensities in the original. Examples of such laborious techniques are an early effort by Gazley, Stratton, and Rieber[5] involving 64 separations and also one developed by D. S. Ross[6] a number of years ago where discrete density levels are recorded on separate sheets of film and color is produced from each separation. Such procedures are time consuming and expensive, and produce results that are more easily

obtained by computer techniques.[7] A more realistic approach to photographic transformation processes is to limit the number of separations, such as the recent example by Robert Gooding[8] in which the original is divided into four density regions, each illuminated with a different color of light, superimposed, and then photographed on a single piece of color film. Our approach to photographic transformations has been to develop a process which transforms a continuous gray scale into a continuous chromatic scale.

Two techniques have been developed at Rand, both of which employ intermediate black-and-white records or separations. One involves three separations,[9] the other only two.[10] The two-separation process relies on the following characteristics of the color material used in the final stage of the process: (1) the use of relatively broad-band "blue" and "red" filtered light sources, which affect the green-sensitive emulsion as well as the red- and blue-sensitive emulsions; (2) the overlapping spectral sensitivity of the three emulsion layers; and (3) the relation of the density to the exposure of the three emulsion layers when exposed to these light sources. Thus an exposure of a negative color material to a "blue" light source will increase the density of not only the blue-sensitive layer (yellow dye formation) but also the green-sensitive layer (magenta dye formation). Similarly, exposure to a "red" light source will increase the density of not only the red-sensitive layer (cyan dye formation) but also the green-sensitive (magenta dye formation). Furthermore, above a certain level of exposure of the red- and blue-sensitive layers to the respective red and blue light sources, the response of the green-sensitive layer can be affected with minor change to the other layers.

Although the final pseudocolor print is on color material, the intermediate separations are on black-and-white materials. In the two-separation process, the density ranges of these separations must be carefully controlled. Let us assume that our transformation will be such that the light areas in the positive form* of the original black-and-white will appear red, the medium areas green, and the dark areas blue.

Let the black-and-white separations, which are positive and negative versions of the original, be designated O_p and O_n. If O_n is contact printed onto the negative color material using the red light source, the

*The original may be in either positive or negative form.

processed image will have color steps which follow the left dashed line of Fig. 1. Similarly, if O_p is printed using the blue light source, the color steps of the processed image will follow the right dashed line of Fig. 1. With proper exposure, the image density of each will vary from no noticeable exposure at one end to a dense and highly saturated image at the other. The high-density portions of the two film images are of course at opposite ends of the gray scale. If these two film images are now sandwiched in register and illuminated from the rear, the hues of the resulting subtractive dye layers of each step will follow the dashed line of Fig. 2.

If this process is exactly repeated using a double exposure on only one sheet of color material, the resulting image will be nearly identical to that of the two individual sheets. Thus one may produce a full gamut of spectral colors by two exposures.

A schematic of the resulting two-separation process is shown in Fig. 3. The original is positive, and the light areas of the original are to be reproduced as red. If either but not both of these conditions were reversed, the red and blue exposures would be interchanged.

Figure 3 is almost self-explanatory; the process is as follows:

1. The first separation, O_n, is made from the original positive and developed. (The original is not ordinarily used as a separation because its density range and physical size are rarely compatible with the process.
2. The second separation, O_p, is contact printed (<u>not</u> emulsion to emulsion) from O_n and developed.
3. O_n is contact printed (emulsion to emulsion) on color material with a red light source.
4. O_p is contact printed (emulsion to emulsion) on the same color material with a blue light source.
5. The color material is processed.

The steps in the pseudocolor transformation of a 5-step gray scale are illustrated in Fig. 4 for the two-separation process. Shown schematically are the density levels in the original, the density levels in the

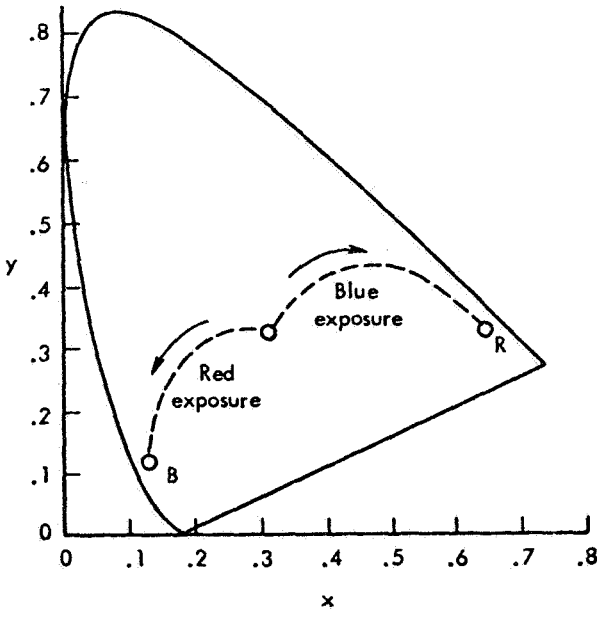


Fig. 1 -- Chromaticity changes with increasing exposure to either red or blue light sources.

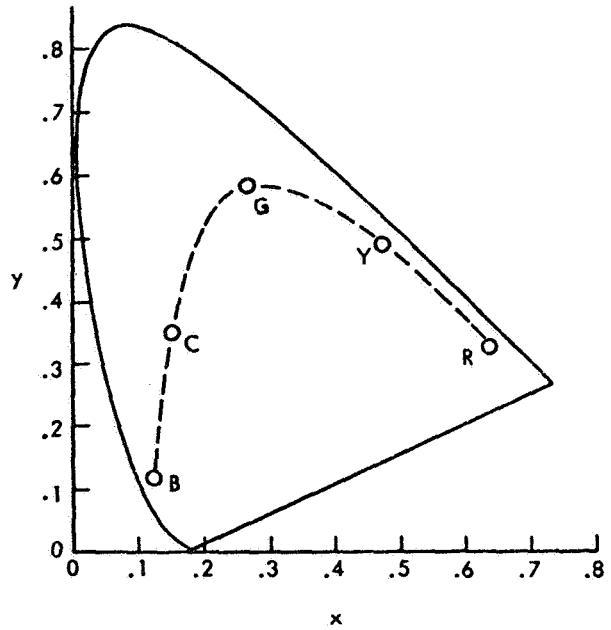


Fig. 2 -- Chromaticity gamut resulting from various double-exposure combinations of red and blue light sources.

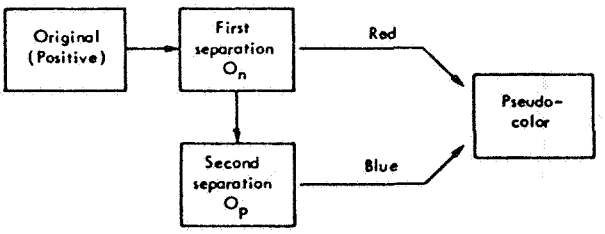


Fig. 3 -- Schematic of two-separation process.

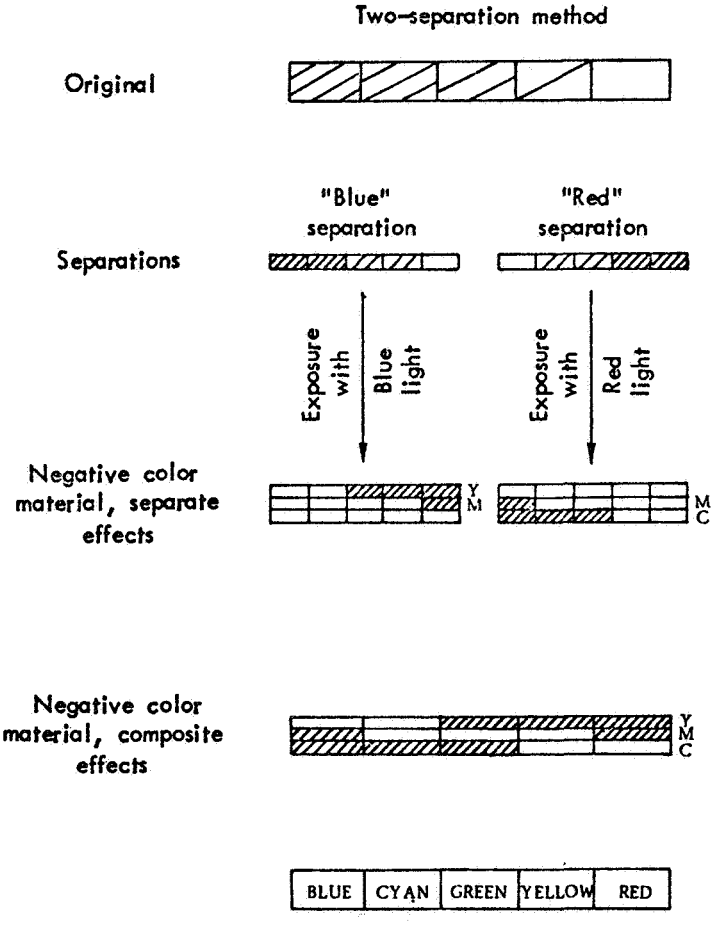


Fig. 4 -- The response of a negative color material to a 5-step gray scale for the two-separation process

black-and-white separations, the dye densities produced in the negative color material by separate filtered exposures, the composite dye effects in the negative color material, and the resulting subtractive color produced.

A trial-and-error method was used to determine a satisfactory combination of density limits for the separations O_p and O_n, the selection of red and blue filters, and the amount of exposure on color material. The color material used was Ektacolor Print Film, a negative material intended primarily for display transparencies from Kodacolor or Ektacolor negatives. This film has a speed range suitable for exposure with an ordinary photographic enlarger, and is processed with Kodak C-22 chemicals.

The light source was a No. 212 enlarging lamp (150 w) operated at 115 v. Several different red and blue filters were tried to give the approximate chromaticity traces of Fig. 1. The objectives was to select filters that pass an appropriate amount of light in the green range compared to that passed in the red or blue end of the spectrum. The results of these trials indicated the most satisfactory filters to be the Wratten 23 A (red) and 47A (blue).

Since one has no control over the form of the original, the initial task is twofold: (1) reducing or enlarging to a standard format, and (2) obtaining a density range of approximately .5 to 3.2. The latter task is one of determining exposure and development to obtain the desired density extremes. This requires a prior calibration of the black-and-white separation materials, which was done for both Commercial and Contrast Process Ortho film. Once both separations, O_n and O_p, have density ranges from .5 to 3.2, they may be successively contact printed (emulsion to emulsion) onto the color material with their respective red and blue filters. The amount of exposure should be such that the red and blue extremes of the image are highly saturated, but not so much as to cause muddy (brownish) yellows.

If the density ranges of O_n and O_p are too high, the greens and yellows will be underexposed and too light if the red and blue ends are correct. If the separations do not have enough density range, the greens and yellows will be too dark for saturated reds and blues.

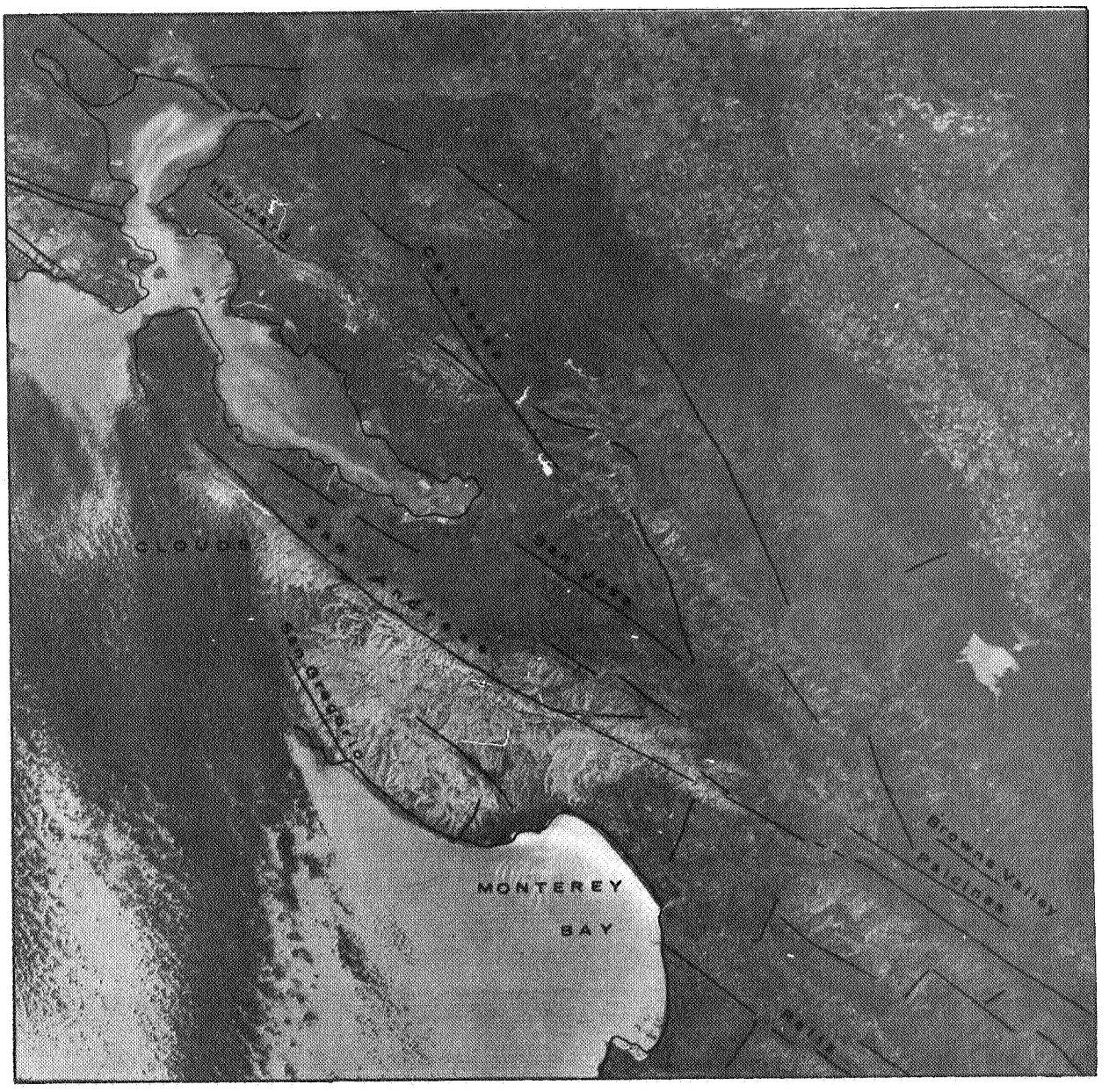
The advantage gained by presenting an image in color are quite obvious even though color films do not possess the high resolution of black-and-white films. The processes which we have developed maintain between 34 and 40 lines/mm in the final transformation.

A pseudocolor transformation of the well-known ERTS-1 image of the Monterey Bay/San Francisco area was made. Possible faults were delineated on an overlay of the transformation before referring to geologic maps of the area. Figure 5 is a black-and-white print of the ERTS image with the overlay. The results were quite remarkable in that all large active or recently active faults shown on the latest geologic map of California[11] were interpreted from the image for all, or much, of their lengths. In addition, several other lineations were readily visible. It is unlikely that they are all faults, but they have similar appearance to known faults and justify being checked against larger-scale geologic maps and in the field. The most interesting result of this investigation was detection of the Reliz fault. This fault is shown as covered, or not visible from the ground by Jennings. However, a lineation corresponding to the position of the fault was discovered on the pseudocolor image. This fault is visible on the unenhanced image when one knows where to look, but it is clearly accentuated and more easily mapped on the pseudocolor transformation.

An example of the use of a false color* transformation is in the determination of the density and temperatures of clouds. Two negatives of a hurricane, one IR, one visible, were obtained from the Air Weather Service at Offutt AFB. Two composites of these images were created, a blue record with the visible transparency, and a red record with the IR transparency. As the hue of composite one goes from white to black, the cloud temperature drops from high to low, the cloud density is high when the hue is white, yellow, or red, medium when the hue is cyan, green, or dark orange, and low when the hue is blue, dark aqua, or black.

In composite two, the visible is the red record and the IR is the blue record. As the hue progresses from white to black, the cloud density progresses from low to high, the low temperatures are seen as white, yellow, or red, the medium temperatures as cyan, green, or dark orange, and the high temperatures as blue, dark aqua, or black.

*False color differs from pseudocolor in that the color image is constructed from information from more than one spectral band.



Faults and possible faults interpreted from pseudocolor transformation of ERTS-1 image

We intend to combine the various combinations of the four spectral bands from MSS data in a similar manner in our investigation of earthquake fault detection.

If we use computer techniques to generate the separations, more sophisticated classes of transformations will become possible. As an example, color can be keyed to density gradient instead of density level. Figure 6 shows this type of transformation for a boundary region of varying

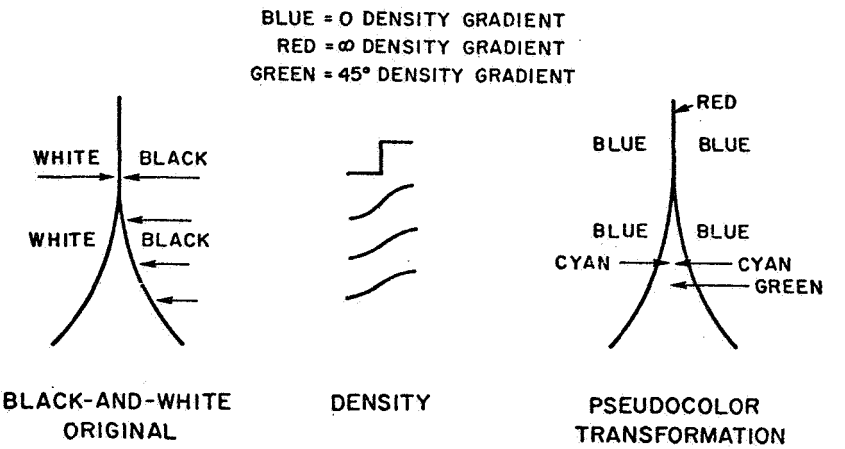


Fig. 6 -- Schematic illustration of a pseudocolor system in which color is keyed to density gradient

density gradient. The computer will also allow freedom from the restrictions of photographic emulsions so as to utilize more effectively the added perceptual dimensions of hue and saturation. For example, an effective transformation scheme may be the keying of hue to density level and brightness to density gradient. Such a transformation is illustrated schematically in Fig. 7 for the same boundary region as seen in Fig. 6.

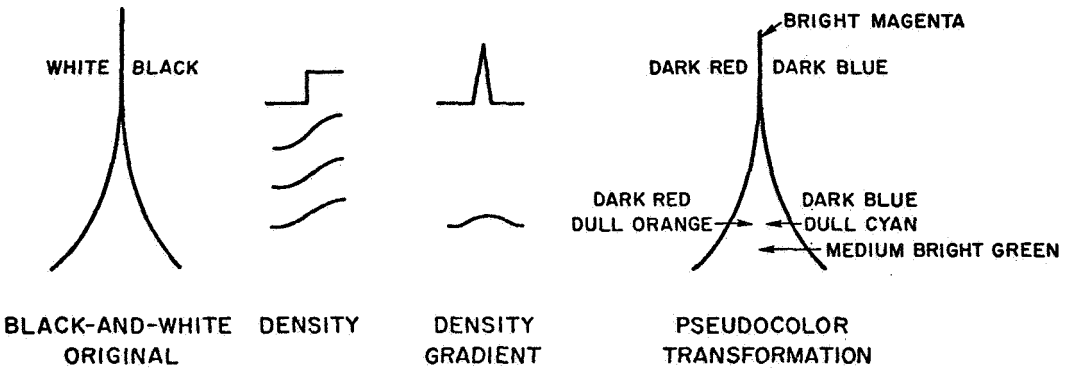


Fig. 7 -- Schematic illustration of a pseudocolor system in which hue is keyed to density level and brightness is keyed to density gradient

These computer techniques are under investigation presently and seem to show great promise for future image enhancement.

REFERENCES

1. Sheppard, J. J., Jr., H. L. Moshin, R. H. Stratton, D. Dugas, A. Madansky, *Color Discrimination in Static Displays*, The Rand Corporation, RM-5303-ARPA, November 1967.
2. *Spectrovision, Real-Time, High-Resolution Imaging Systems*, Aerojet-General, El Monte, California.
3. *System 800 Model 805 Color Display*, Spatial Data Systems, Inc., Goleta, California.
4. *New Product Information*, International Imaging Systems, Mountain View, California.
5. Gazley, C., Jr., J. E. Rieber, and R. H. Stratton, *Pseudocolor Processing of Electronic Photographs*, The Rand Corporation, RM-5297-PR, April 1967.
6. "Color This Brain Visible," *Life*, March 7, 1969, 78.
7. Lamar, J. V., *Computer Techniques for Pseudocolor Image Enhancement*, The Rand Corporation, R-787-NIH, June 1971.
8. Maas, Keith A., "Building Color Images, *Technical Photography*, Feb. 1973.
9. Stratton, R. H., and J. J. Sheppard, Jr., *A Photographic Technique for Image Enhancement: Pseudocolor Three-Separation Process*, The Rand Corporation, R-596-PR, October 1970.
10. Stratton, R. H., and C. Gazley, Jr., *A Photographic Technique for Image Enhancement: Pseudocolor Two-Separation Process*, The Rand Corporation, July 1971.
11. Jennings, C. W., Geologic Map of California, Scale: 1:750,000; California Division of Mines and Geology, preliminary unpublished edition, subject to revision, 1972.

N73-28334

Paper I 13

DIGITAL INTERACTIVE IMAGE ANALYSIS BY ARRAY PROCESSING

Bruno E. Sabels, *Tetra Tech., Inc., Houston,* Jerry D. Jennings, *Geocom, Inc., Houston*

Geophysical and ERTS Data Processing Are Similar

This paper endeavors to draw a parallel between the existing geophysical data processing service industries and the emerging earth resources data support requirements. The relationship of seismic data analysis to ERTS data analysis is natural because in either case data is digitally recorded in the same format, resulting from remotely sensed energy which has been reflected, attenuated, shifted and degraded on its path from the source to the receiver. In the seismic case the energy is acoustic, ranging in frequencies from 10 to 75 cps, for which the lithosphere appears semi-transparent. In earth survey remote sensing through the atmosphere, visible and infrared frequency bands are being used. Yet the hardware and software required to process the magnetically recorded data from the two realms of inquiry are identical and similar, respectively. The resulting data products are similar.

In several decades of evolution, the geophysical data processing industry has become application oriented and cost effective. It is driven by a very intensive competition. This is not the case at this time in earth survey data analysis, which has hardly entered the commercial sector. Therefore, it is interesting and probably beneficial to consider the potential of an existing technology with regard to a developing one.

Detailed Comparison Between ERTS and Geophysical Data

A survey of ERTS-1 investigations discloses several categories of efforts which can be compared with seismic data processing categories. First there are the optical and digital filtering and enhancement techniques,

which attempt to eliminate noise or improve contrast in the resulting display. With improved processing algorithms, these lead to classification techniques, and to hybrid selection and suppression methods. Then there are highly sophisticated spectral and spatial detection efforts, aimed at low signal-to-noise contrasts, for the detection of subtle shades of grey or the respective color, which represent differences in soils, chlorophyll, stress, infestation, or other manifestations of resources conditions. Because the dynamic range of the information which can be derived from any one recorded element is limited by the number of bits per byte, several spectral or temporal exposures are generally stacked and correlated.

Conversely, seismic processing starts with corrective programs, followed by correlative displays of features of similar reflective, attenuative and conductive properties, which in geological terms are better known as stratigraphy and structure. Over and beyond these fundamental displays, the industry has learned to isolate and enhance, even in color, any combination of variables of value to the explorationist, ranging from velocities, energies, frequency shifts, and reflection coefficients to rock type, porosity, water content, temperature, pressure, and hydrocarbon concentration. The more sophisticated analyses are based on relatively large arrays of data which have been precisely recorded, in as many as 48 channels, under rigid gain control. The reconstruction of the signal characteristics in the computer is possible within a large dynamic range, exceeding 100 db and approaching 180 db. This precision is not available for ERTS data, where acquisition and transmission limitations, and restrictions of spectral and temporal multiplicity leave room for improvement in later, more advanced eras of earth survey.

A detailed discussion of a specific enhancement of hydrocarbon content in gas and oil bearing sediments was recently published by C. I. Craft (Oil and Gas Journal, Feb. 19, 1973, pp. 122-125). Color processes for the display of geophysical parameters have been publicized by several geophysical data processing companies, both in the U. S. and abroad.

Interactive Mode and Different Service Concepts

Geophysical data services do not limit their attention and competition to a more accurate and useful information content of the final product. They have also devised new ways of meeting and involving the client, and of participating in designing the product of his choice, where and when he needs it. This service approach is today completely outside of the realm of ERTS investigations, where time and costs are still relatively secondary considerations. In geophysical processing, the usual interactive involvement of the geophysicist in the man-machine cycle has been expanded to include the client, who is generally the user of the data. Remote terminals in major user's offices--hundreds or thousands of miles away from the computer facility--allow real time display of intermediate data processing steps, and allow decisions and participation as to further iterations, choices or measures of enhancement. There are two more dimensions of service, however, which are available to the geophysical data user. Some service companies have adapted and standardized their data processing capability so that they can take advantage of existing computer centers around the world. They may, for example, use the "brand X" computer system, and they can make it work wherever a business potential and a computer location coincide, be it Chicago, Calgary, London or Singapore! And in even closer interaction with the field crews, some geophysical service companies are dispatching miniaturized computer centers into the field, wherever it may be, to work literally tied in with the field data acquisition.

Service at Low Costs - A Goal for ERTS Users

Some day, similar customer services will exist in earth survey data anlaysis as are described above. Indeed, the multi-user possibilities of ERTS data promise even cost savings over the generally specialized geophysical data utilization. A data center has quoted rates as low as \$0.02 per km^2 for image data correlation, based on two compatible frames. This low unit cost results from the use of special purpose equipment which is attached to the computer for the more efficient handling of large amounts of data. For the geophysical data industry, such equipment and the corresponding soft ware were developed by the Shell Oil Company.

Other Applications in NASA Earth Observation Programs

So far, only ERTS data were addressed. One other application of geophysical data technology is in the Skylab/EREP program. This is particularly appropriate because the data recorded in manned missions need not be restricted as much as ERTS data, as far as data intensity is concerned. From such applications of geophysical methods, changes may result in the design or performance characteristics of later generation earth survey data acquisition systems.

Mutual Technology Transfer

The parallel between geophysical and earth survey data analysis is hampered at this point by insufficient "channels" of ERTS data available to us. Therefore, most of our efforts were based on geophysical data, in the same format as ERTS CCT's. We can interchange seismic and ERTS data in government and industrial processing facilities. And we expect that this work will benefit the geophysical data industry as well, as evidenced by the introduction of false color processes in seismic data displays.

Potential of High-Speed Processes for ERTS Data

In summary, the array processor is introduced as an instrument to free the investigator from data processing chores, so that he can use his time more efficiently for the interpretation and utilization of the data. Conversely, data products are made available to users who are not investigators. The service, patterned after the commercial seismic data processing industry, will therefore increase the potential for the application and utilization of ERTS data. Further details of the two discussed data industries are being pursued.

Appendix - Array Processor Capabilities

This section describes the array processor, developed by Shell Oil Company, which is used in conjunction with a medium to large computer center. There are several brands of processors and computer systems on the market, which may have similar capabilities.

The AP, as the array processor is called for short, performs specific instructions in memory independent of the central processing unit or CPU. This makes the AP similar to a multi-processing system, except

that the AP has a hard-wired instruction set of about 21 operations which are most common in geophysical data processing. These operations need not be detailed in the programming software, step by step, but are executed instantaneously by one command.

Initially, the AP was used for multiply/add operations which it performs effectively in 250 nanoseconds. About 25% of all geophysical calculations were done in the hardware algorithm modules. Today, many other mathematical functions have been utilized or adapted, and the AP is typically employed for about 70% of the geophysical calculations. The instructions available include the following:

vector inner product	partial matrix multiply
sum of squares	sum of vector elements
scalar multiplication	vector element by element multiply
scalar add	vector element by element sum
complex vector element multiply	fast Fourier transform
convolving multiply	limits readout
interpolations	

Many of these instructions are common to image correlation, enchancement and analysis.

The single most effective instruction is the convolving multiply. The improvement realized by using the AP versus the CPU is better than 20 to 1. The instruction is used in filtering, auto-correlation and -convolution, cross-correlation, and auto-statics. These geophysically oriented processes are mathematically applicable in image correlation, correction and classification.

The interpolation instruction is another heavily engaged AP favorite. Improvements in processing time are better than 9 to 1 over the CPU. This instruction is used in fiducial and statics correction, stacking and resampling of data. Functionally, these processes correspond to the stretching or compressing of data, either linearly or in time. In image analysis of ERTS data, similar instructions become important in dealing with registration and boundary problems.

The partial matrix multiply instruction yields improvements of 4 to 1 and is used in calculating the Z transform filters by polynomial division, recursive filtering, velocity determination, and for preparatory sine and cosine function generation for the fast Fourier transform algorithm.

The fast Fourier transform is widely used to convert between the time and frequency domains, so as to expedite the processing. Savings of better than 5 are realized in using the AP versus the CPU.

N73-28335

Paper I 14

COMBINING HUMAN AND COMPUTER INTERPRETATION CAPABILITIES TO ANALYZE ERTS IMAGERY

J. D. Nichols, *Forestry Remote Sensing Laboratory, University of California, Berkeley, California 94720*

Abstract

The human photo interpreter and the computer have complementary capabilities that are exploited in a computer-based data analysis system developed at the Forestry Remote Sensing Laboratory, University of California. This system is designed to optimize the process of extracting resource information from ERTS images.

The human has the ability to quickly delineate gross differences in land classes, such as wildland, urban, and agriculture on appropriate ERTS images, and to further break these gross classes into meaningful subclasses. In agricultural areas, the subclasses can be delineated on the basis of general tone and texture differences that relate to crop type and field size. In the wildland areas, delineations can also be made, based on tone and texture, which represent general vegetation systems, such as grasslands, brush, trees, and barren areas. The computer, however, can more efficiently analyze point-by-point spectral information and localized textural information which can result in a much more detailed agricultural or wildland classification based on species composition and/or plant association.

These human and computer capabilities have been integrated through the use of an inexpensive small scale computer dedicated to the interactive preprocessing of the human inputs and the display of raw ERTS images and computer classified images. The small computer is linked to a large scale computer system wherein the bulk of the statistical work and the automatic point-by-point classification is done.

PRECEDING PAGE BLANK NOT FILMED

Introduction

When processing ERTS imagery, several factors affecting the cost and accuracy of land use classification become apparent. (1) There are numerous, irregularly shaped areas in the imagery which can be rapidly delineated into classes by the photo interpreter accurately enough to meet user requirements. (2) Some of these areas, because they are of little or no interest to the user, can be disregarded. (3) In localized areas, detailed automatic spectral pattern classification of plant species and plant communities can be done with a high degree of accuracy. (4) Computer classification costs increase rapidly with the number of classes being considered for each picture element. (5) There is a one-to-one relationship between the number of points being classified and the cost of computer classification.

With these factors in mind, a hardware-software system has been developed at the Forestry Remote Sensing Laboratory that integrates human and computer capabilities to increase classification accuracy and reduce processing costs.

The System

Because of the higher cost of tying up a large scale computer to do interactive processing, a "mini" computer with a substantial set of interactive peripherals (Figure 1) has been implemented. All of the ERTS tape reformatting, training area extraction, coordinate digitizing and image display can be done on this interactive system. This system is linked via dedicated, high speed communication lines to the CDC 6600-7600 computer complex at the University of California Lawrence Berkeley Laboratory, where the major computational tasks are performed. Although the system is used in the processing of ERTS data both manually and automatically, of greater interest here is the integration of human and computer capabilities.

Processing

Human and automatic processing of the ERTS data goes on in parallel as shown in Figure 2 to the point where the information generated by both methods is merged and the final product is output in the form of a classified image and summary statistics.

Human processing starts using the appropriate ERTS image of the study area. The interpreter quickly delineates gross differences in land use classes, such as wildland, urban and agriculture. If possible, these classes are further subdivided into meaningful subclasses. In agricultural areas, they can be delineated on the basis of general tone and texture differences that relate to crop type and field size. In

wildland areas, delineations which represent general vegetation systems such as grasslands, brush, trees, and barren areas, can also be made based on tone and texture. The boundaries of the strata are then digitized and recorded on magnetic tape, using either the comparator or coordinate digitizer, and a description of the individual stratum is entered on the tape. The image coordinates of control points are also recorded to be used to relate the image coordinate system to the ERTS tape coordinate system.

At this point in the processing, the tape coordinates of the control points obtained from the reformatted study area along with scale and skew data are input into a transform which then converts photo interpreter strata coordinates to tape data coordinates. This transformation is verified and then applied to the digitized coordinates of the strata boundaries. This produces a point-by-point overlay in which each boundary point corresponds to an ERTS picture element. Within these boundaries each point on the ERTS tape is then assigned to the corresponding photo interpreter strata. The training set for automatic classification is extracted by stratum from the ERTS image, statistics computed and test sets classified to ensure accurate classification within each stratum.

The next step is the detailed classification of each of the ERTS picture elements. A picture element and the corresponding stratification point are read. If the strata is one to be spectrally classified, the classification is done and the results put in the corresponding point of output image. If not, the photo interpreter stratum is put in the output image. This is continued point-by-point or by some sampling scheme until the processing is completed. The resultant image is a combination of photo interpretation and automatic classification with a statistical summary of the classification. As an alternative to photo interpreter delineation of strata, existing geological, geographical, or political maps can be used to stratify the ERTS data for classification or used to partition the statistical summary into meaningful reporting areas after classification.

Conclusions

Computer costs are reduced significantly by reducing the number of classes to be considered during automatic point-by-point classification. If, for example, 40 classes exist over the entire study area but through stratification only 8 classes are considered for each point using ten strata, a 4 to 1 reduction in computer costs would be realized. A second source of saving is the elimination of areas from automatic classification by interpreter delineation when the human can adequately specify the land use or that the area is not of interest to the resource manager. This saving is nearly one to one for each point eliminated,

but the saving is reduced by the computational overhead needed to determine the point-by-point strata assignment.

The classification accuracy is increased significantly by separating, through stratification, classes that have spectral signatures so similar that they cannot be separated by the discriminant analysis routine. Preliminary results indicate that this separation is important between strata in the agricultural areas and between wildland and agricultural areas.

Future Work

This interpretation technique will be tested in the wildland agricultural complex to determine the optimum mix of human and computer efforts. The next major developmental step along these lines will be the joining of adjacent images through the use of computer mapping techniques. This will allow the inventory and mapping of large geographic regions to a common base through the integration of human and computer capabilities.

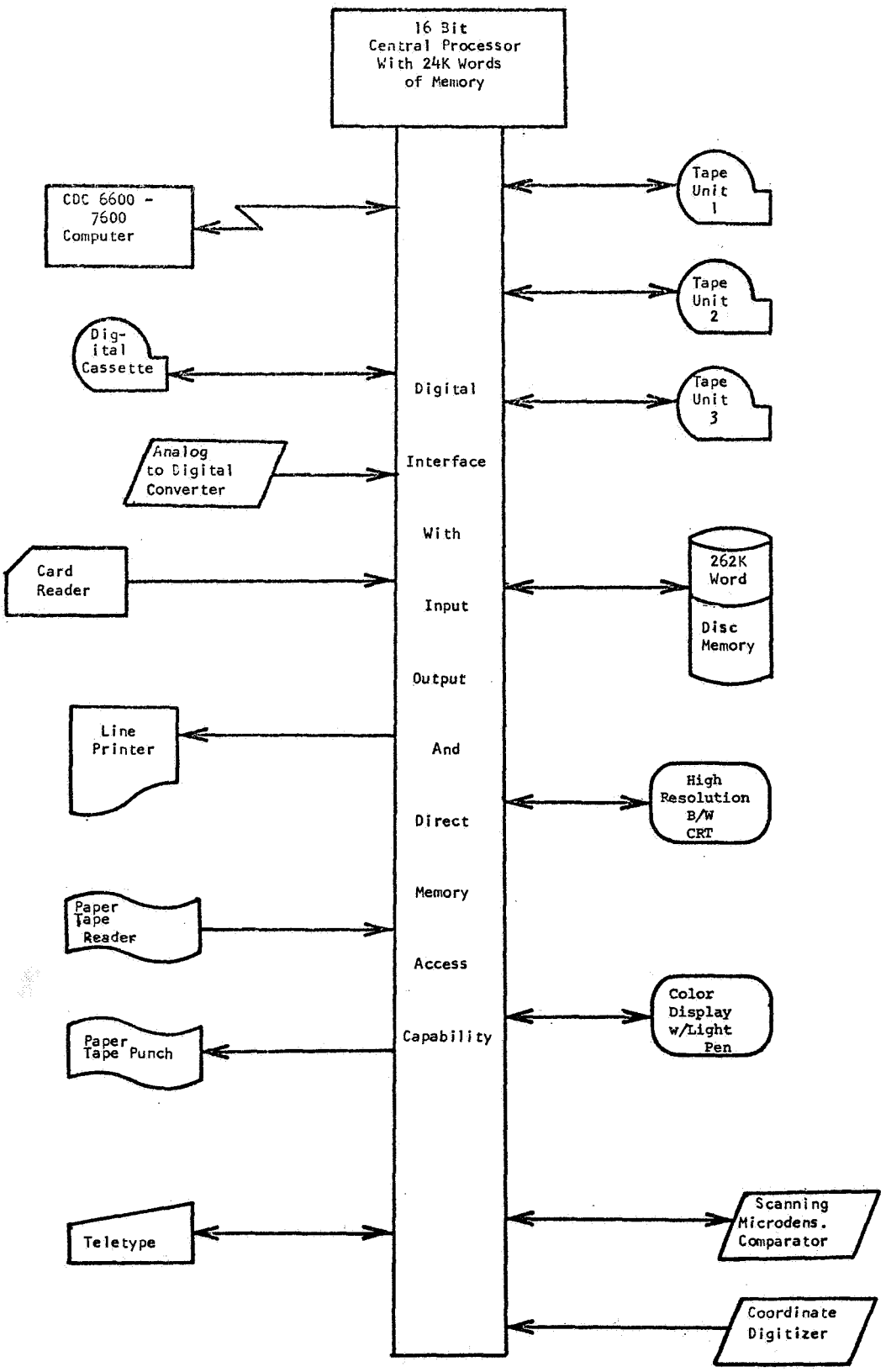


Figure 1. Forestry Remote Sensing Laboratory Computer display system.

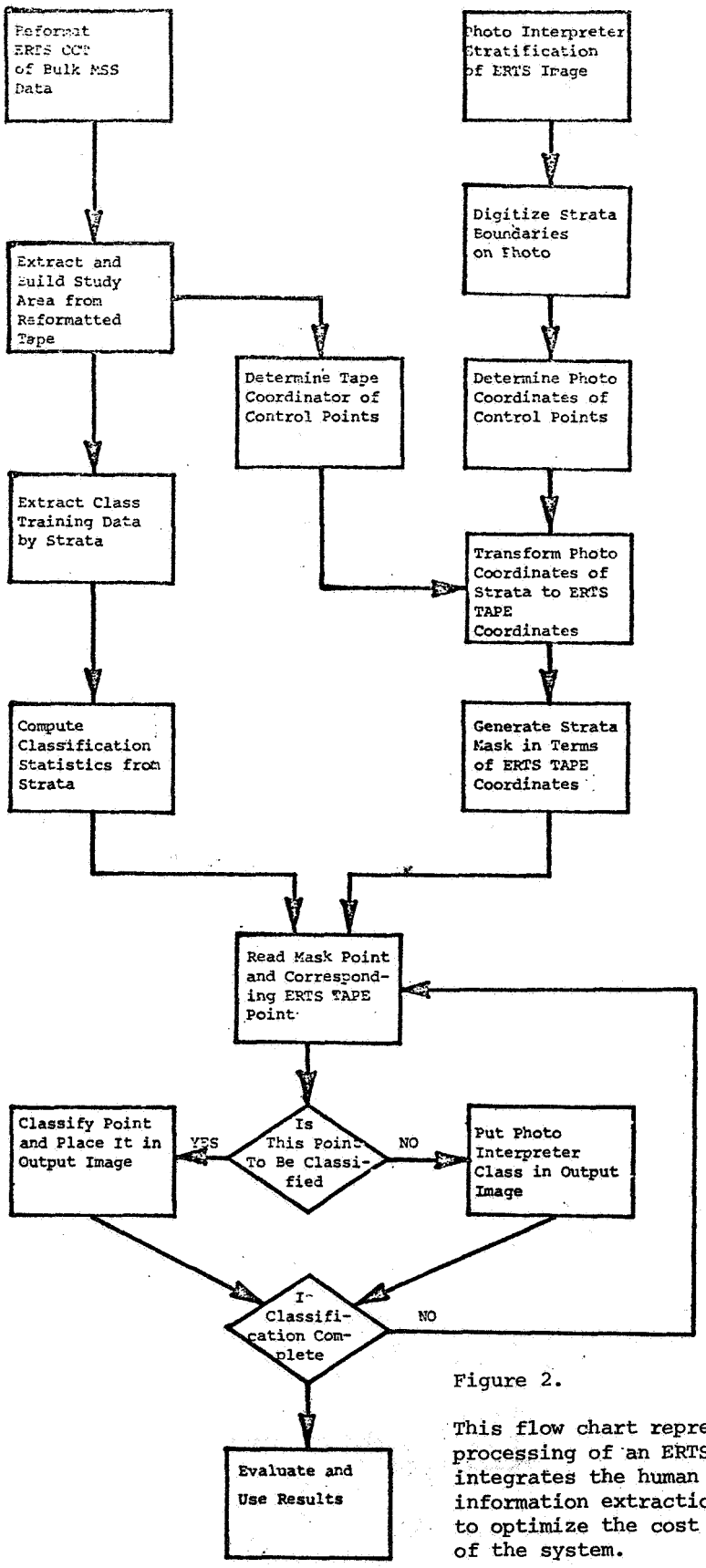


Figure 2.

This flow chart represents the basic processing of an ERTS image that integrates the human and computer information extraction capabilities to optimize the cost effectiveness of the system.

N73-28336

ANALYSIS OF ERTS IMAGERY USING SPECIAL ELECTRONIC VIEWING/ MEASURING EQUIPMENT

Wm. E. Evans and Sidney M. Serebreny, *Stanford Research Institute, Menlo Park, California 94025*

ABSTRACT

An Electronic Satellite Image Analysis Console (ESIAC) is being employed to process imagery for use by USGS investigators in several different disciplines studying dynamic hydrologic conditions. The ESIAC provides facilities for storing registered image sequences in a magnetic video disc memory for subsequent recall, enhancement, and animated display in monochrome or color. Quantitative measurements of distances, areas, and brightness profiles can be extracted digitally under operator supervision. Initial results are presented for the display and measurement of snowfield extent, glacier development, sediment plumes from estuary discharge, playa inventory, phreatophyte and other vegetative changes.

1. INTRODUCTION

An Electronic Satellite Image Analysis Console (ESIAC) providing television animation, editing and video processing capabilities has been in use by Research Meteorologists at SRI since early 1967 primarily for analysis of ATS imagery.(1) During 1972 a new console was constructed having design features specifically oriented towards the needs of ERTS. As part of the NASA ERTS-1 program this new equipment is being utilized to meet the data processing needs of a group of ERTS principal investigators within the U.S. Geological Survey (Water Resources Division) operating in widely diverse specialties but all part of the W.R.D. program in Dynamic Hydrology.*

The basic objective of this equipment is twofold: First, it attempts to present the imagery in a form that will show up, or hopefully even emphasize, the phenomena of interest. Occasionally this display function alone can contribute enough to understanding that no more is required. Frequently, however, there is also a need for a second function--that of extracting quantitative measurements from the imagery.

The principal image enhancement technique in the ESIAC, is rapid sequential presentation of registered images--time lapse series, flicker

* The work reported here is being performed under NASA Contract NAS5-21841.

Original photography may be purchased from:
EROS Data Center
10th and Dakota Avenue
Sioux Falls, SD 57198

Original photography may be purchased from:
EROS Data Center
10th and Dakota Avenue
Sioux Falls, SD 57198

comparisons, and the like. Additional image enhancement capability is provided through contrast and polarity manipulation, easy scale changes (zoom), and false-color display of multispectral imagery.

Quantitative measurements of distances, areas, and signal amplitudes are made under operator guidance and may be output in digital form.

2. HARDWARE

The equipment is illustrated photographically in Figure 1, and in block diagram form in Figure 2. Items in the block diagram are grouped by function into four principal categories: Input, Storage, Processing, and Output.

- Data input is nearly always via positive film transparencies, though other media can be accommodated. The transparency input station is fitted with a high quality Vidicon camera, ten-to-one macro-zoom optics, and a system of micropositioners and reference graticules to aid in registering new images to those previously stored. Overhead is a second Vidicon camera which is used for inputting hard copy maps or pen marks made by the operator. Another input is x, y position information for the electronic crosshairs, or cursor, whose location is controlled by a track-ball in the desk top.

- Storage memories are located in the base of the console, and the memory controls are on either side of the main display. A 16" analog magnetic video disc recorder is fitted with two moving head channels, each channel capable of storing up to 300 addressable 525-line TV frames. The heads may be stepped independently or in unison, at easily controllable rates. A third memory unit, now under construction, will be solid state and will hold one frame of binary (two level) imagery for masking functions that will be discussed later. Small 7-inch TV picture monitors (preview monitors) are permanently connected to show what images are available from the camera or memory channels.

- In the Processing section is a video mixing panel, which permits positive or negative amounts of video signals from any or all of four input channels to be merged into a composite signal to be viewed on the main black and white picture display.

  Three video level decision circuits are shown. Each of these is really a fast one-bit Analog to Digital converter having an adjustable threshold level. The binary video signal can be displayed as an image photographed, stored, superimposed onto other images, or the total number of TRUE picture elements in the frame can be counted by the digital counter.

- Output devices include the main picture monitor, a color display, a digital counter, an oscilloscope for monitoring video

waveforms (e.g., individual radiance profiles) and a teleprinter--for recording distance and area measurements made from the display.

The color display has been found to be extremely useful in analyzing ERTS images. It has separate, simultaneous inputs for red, green, and blue channels. Thus high quality three-primary false-color displays can be achieved by connecting the three inputs to registered images from the A disc, the B disc, and the camera. Alternatively, by driving both the green and the blue channels from the same source, two bands can be compared in a two-primary, red-cyan system. This is the operating mode that has been found most useful to date. A principal reason for this choice is that with the present equipment, two bands can be viewed in time lapsed color (by stepping A and B disc channels together) while three cannot. Additionally, however, two-band comparisons tend to be inherently easier to comprehend than three. For many purposes, the step from monochrome to two-band color has been found to be both dramatic and highly meaningful, while the incremental subjective value of the next step to three-band color is much more questionable.

3. APPLICATIONS

As an example of the ESIAC capability we will outline an approach to a problem of considerable practical importance--that of measurement of snow cover from ERTS imagery.* The basic procedure is to scan the image transparency for the band showing the best snow-surround contrast--perhaps MSS band 5. A video level decision circuit is then used to isolate and count all those picture elements which are brighter than some appropriately chosen threshold level.

One procedure for choosing the threshold level is to electronically superimpose the binary mask image obtained from the level decision circuit (LDC) onto the full tone scale image so that it is displayed optionally either as an excessively white highlight or as an abnormal brightness reduction. The operator then adjusts the decision threshold until he achieves a match between the TRUE portion of the binary mask and what he judges to be the snowfield.

When clouds, fog, or haze are present the problem of defining the snow cover becomes much more difficult. Identification is appreciably easier when the color display is used, but by far the most powerful device, when it can be employed is the time-lapse capability, using imagery of the same scene taken at different times. Permanent features such as snow can be read through an astonishing amount of cloud

* This example is selected from work being performed for Dr. Mark F. Meier of the USGS Water Resources in Tacoma, Washington.

clutter when the latter can be made to move while the former remains relatively fixed.

To map or measure the partially obscured areas, we are experimenting with methods of manually editing the video-derived binary thematic masks while the mask is being observed superimposed on the time-lapse display.

For one current project, an important task is to partition the snowpack into specific drainage areas. Figure 3 presents data for a portion of the North Cascade range in north central Washington. The first panel defines a specific drainage basin of interest by an electronically superimposed outline derived from a hand-drawn mask prepared with the aid of a contour map used to locate the ridges and high points surrounding the basin. The remaining panels of Figure 3 show binary masks (white) resulting from logically ANDing the outputs of two Level Decision Circuits, one used for thresholding the band 5 signal at the indicated levels, and the other used to derive a clean basin image (grey) from the hand-drawn map. The area figures shown are the ratios of picture element count in the white regions to the picture element count for the total basin. Masks of this type are being compared (by superposition) to both monochrome and color imagery and to ground truth surveys in an effort to refine the rules for specifying optimum threshold settings. It is obvious that critical registration of the drainage outline map to the ridge lines is an essential part of accurate measurement, and the console is well adapted for that task. The scaling, registration and superpositioning capabilities also permit synthesis of composite images such as that illustrated in Figure 4 which shows an ERTS image of Mt. Rainier plus 1000 foot elevation contours taken from a topographic map.

Three additional applications will be described briefly. (1) For Mr. Fred Ruggles (USGS Water Resources Division in Hartford, Connecticut), the ESIAC is being used to enhance the visibility of patterns caused by the suspended sediments in the waters of the Connecticut, Thames, and Housatonic Rivers in order to study the mixing patterns of estuarine discharges into Long Island Sound at different phases of the tidal cycle. Suspended sediments in the waters of the Sound increase the reflectivity slightly and act as tracers. The river discharge plumes are visible from space as subtle modulation of the sediment patterns. For this work, the interest is almost entirely at the lowest end of the radiance scale, and best results have been obtained by working from negative transparencies, inverting them to positive images electronically when required, and using the entire brightness gamut of the video system to enhance only the first two or three steps of the grey scale range. One objective is to assemble a time-lapse sequence from portions of scenes imaged at different times in the tidal cycle, (2) Dr. Raymond M. Turner, USGS Water Resources Division office in Tucson, Arizona is studying the distribution of phreatophytes and other Arid-Land plant communities. For him the equipment is being used as a versatile color microdensitometer to prepare radiance profiles along specific transects for individual bands (Figure 5) and for radiance differences between bands.

These profiles can then be studied in time lapse along with the imagery, (3) for Dr. C. C. Reeves, Jr. of Texas Tech. University ("Dynamics of Playa Lakes in the Texas High Plains") we are using the area-measuring capability to compile statistics on water areas within specific playas and totals for the hundreds of others within an ERTS frame. Additionally, the time lapse capability is being utilized to search for patterns in lake-fill distribution that might correlate with geographical, meteorological, or seasonal conditions.

4. CONCLUSIONS

While ERTS sequences have not yet become available in sufficient length for full exploitation of the trend-enhancing power of the time-lapse technique, a significant amount of experience with imagery already received has provided convincing proof that much of the data now being accumulated will be extremely well suited for such analysis.

Electronic viewing/measuring equipment should not be regarded as competing with photographic prints in cost, convenience, and image quality nor with computer processing of digital tapes in the precision of fully objective measurements. Although the equipment described here provides capabilities that do extend surprisingly far into the realms of both of these mutually exclusive techniques, its greatest and virtually unique utility lies in providing rapid and extremely versatile coverage of a large middle ground of analysis tasks--particularly those that can benefit from sequential or simultaneous display of numerous images, and from interactive guidance by the scientific investigator. For this purpose we have evolved a system that we believe provides reasonable trade-offs among the competing factors of operating simplicity, processing volume, accuracy, maintainability, and cost.

At the NASA ERTS-1 Symposium, March 5-9, 1973 a color movie was presented using a series of ERTS-A frames to depict the changes with time of the areal coverage of snow as well as changing coverage and color of vegetation and crops.

5. REFERENCES

1. Serebreny, S.M., E. J. Wiegman, R. G. Hadfield, and W. E. Evans, "Electronic System for Utilization of Satellite Cloud Pictures," Bull. of the Amer. Meteor. Soc., Vol. 51, No. 9, Sept. 1970, pp. 848-855.

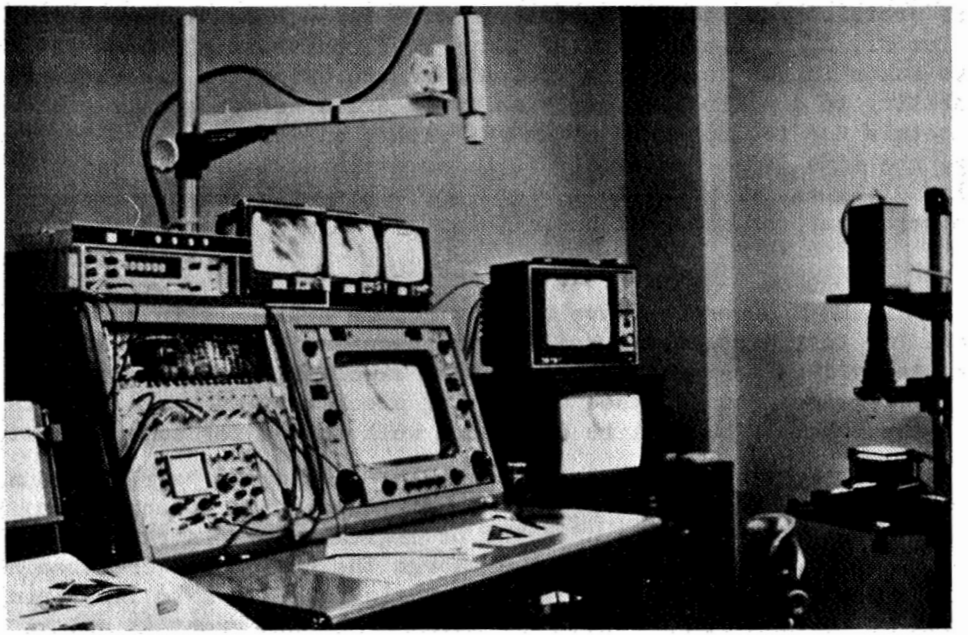


FIGURE I ELECTRONIC SATELLITE IMAGE ANALYSIS CONSOLE (ESIAC)

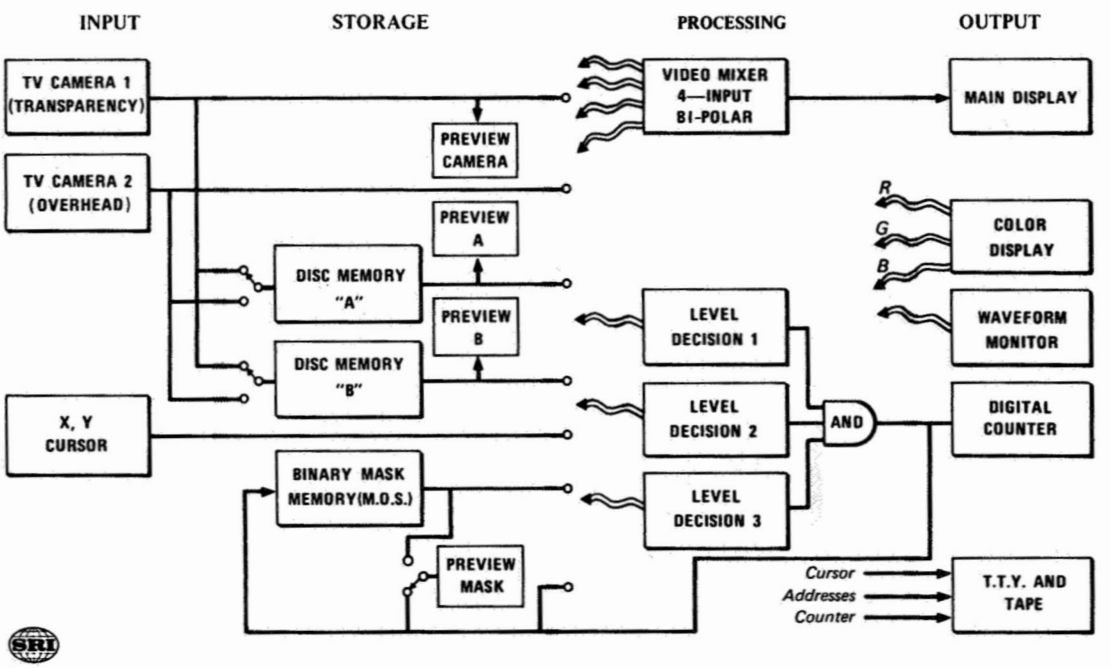


FIGURE 2 BLOCK DIAGRAM OF ESIAC

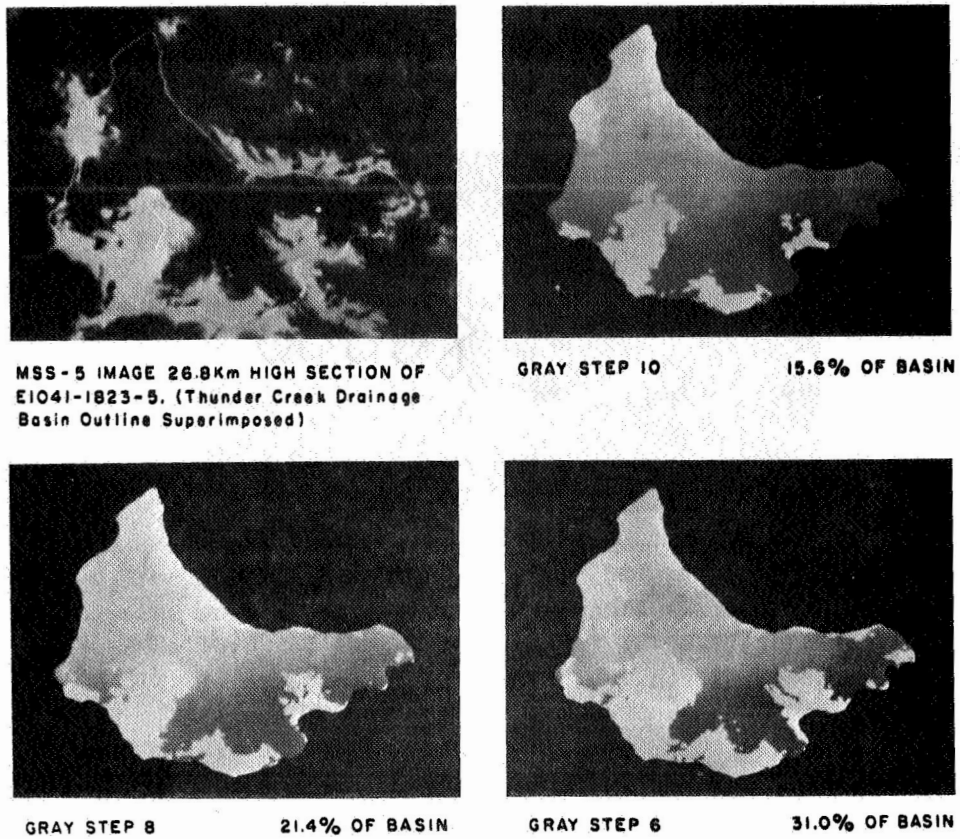


Fig. 3 Areal Distribution of Radiance above Threshold for 2 September 1972 Band 5(.6-.7μ)

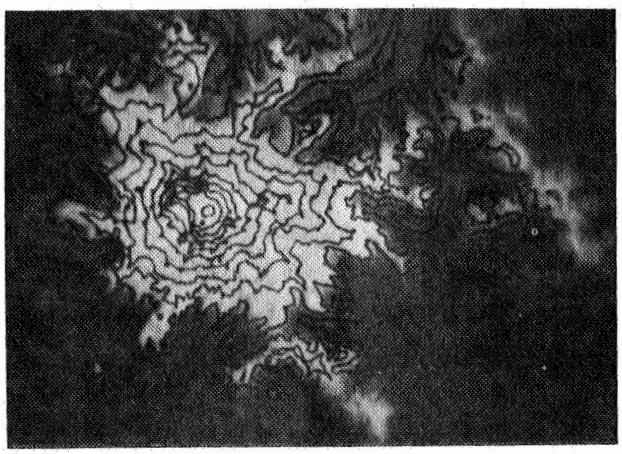


Fig. 4 ESIAC Display of Mt. Rainier, Washington for 29 July 1972 30-km High Section of ERTS Image No. 1005-18260-5.1000 ft Contours Electronically Superimposed.Center Contour is for 14,000 ft

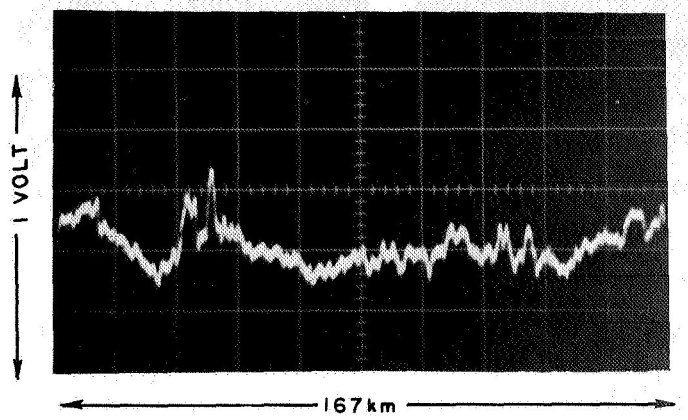


Fig. 5a Radiance Profile along MINE Transect in Arizona Desert (ERTS-1 Frame 1102-17280-5) Vertical Scale and dc Level same as for Grey Scale of Fig. 5b

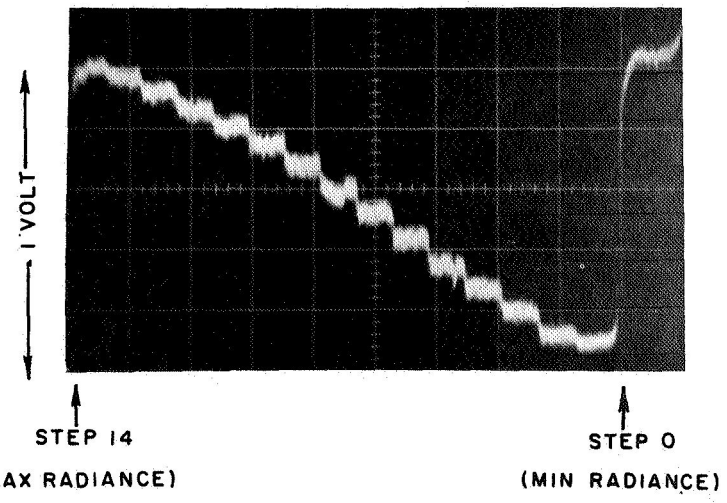


Fig. 5b Video Signal Response for Scan Across Calibration Grey Scale of Positive Transparency used for Fig. 5a

N73-28337

Paper I 16

COMBINED SPECTRAL AND SPATIAL PROCESSING OF ERTS IMAGERY DATA

Robert M. Haralick and K. Sam Shanmugam, *University of Kansas Center for Research, Inc., Space Technology Laboratories, Lawrence, Kansas*

ABSTRACT

A procedure for extracting a set of textural features for ERTS MSS data is presented. The textural features were combined with a set of spectral features and were used to develop a classification algorithm for identifying the land use categories of blocks of digital MSS data. The classification algorithm was derived from a training set of 314 blocks and tested on a set of 310 blocks. The overall accuracy of the classifier was found to be 83.5% on seven land use categories.

1. INTRODUCTION

Spectral, textural and context features are three fundamental pattern elements used in human interpretation of imagery data. Spectral features describe the average band to band tonal variations in a multiband image set where as textural features contain information about the spatial distribution of tonal values within a band. Context features contain information derived from areas surrounding the sub-image region being analyzed. When small image areas are independently processed by a machine, only the textural and spectral features are available to the machine.

In much of the automated procedures for processing image data from small areas, such as in crop classification studies, only the spectral features are used for developing a classification algorithm. Other than simple averaging of spectral values within an image area to eliminate irregularities, textural features are generally ignored. Because the areal characteristics of texture carry so much information it is important to use the textural features in automated image processing schemes, except in applications where the poor resolution of the imagery does not provide meaningful textural information.

Other than some work with Fourier, Hadamard transforms (1), (2) and auto-correlation function, there exists little or no theory to aid in establishing what the textural features should consist of. We have developed a set of quickly computable textural features for automatic analysis of MSS and other imagery. We used these features to perform a land use classification of a 5100 square mile area covered by part of an ERTS-A, MSS band 5 image consisting of over 600 blocks of size 64 x 64 resolution cells. The land use categories identified consisted of coastal forest, wood lands, annual grass lands, water bodies, urban areas, small and large irrigated fields. Up to 70% of the image blocks were identified correctly based on the textural features, compared to an accuracy of 74 to 77% for a scheme based on the spectral characteristics of the 4 band MSS image set. When the combined textural and spectral features were used as inputs to the classifier, up to 83.5% of the image blocks were identified correctly.

Original photography may be purchased from:
EROS Data Center
10th and Dakota Avenue
Sioux Falls, SD 57198

2. TEXTURAL FEATURES FOR ERTS-MSS DATA

2.1 Spatial Grey Tone Dependence Matrix

Let $L_x = \{1,2,\ldots,N_x\}$ and $L_y = \{1,2,\ldots,N_y\}$ be the x and y spatial domains and $L_y \times L_x$ be the set of resolution cells. Let $G = \{1,2,\ldots,N_g\}$ be the set of possible grey tones. Then a digital image I is a function which assigns some grey tone to each and every resolution cell; $I: L_y \times L_x \rightarrow G$.

An essential component of our conceptual framework of texture is a matrix, or more precisely, four closely related matrices from which all texture-context features are derived. These matrices are termed angular nearest neighbor grey tone spatial dependence matrices.

We assume that the texture-context information in an image I is contained in the over-all or "average" spatial relationship which the grey tones in image I have to one another. More specifically, we shall assume that this texture-context information is adequately specified by the matrix of relative frequencies P_{ij} with

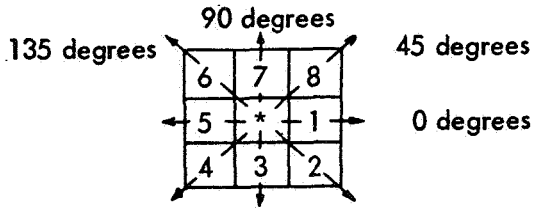


Figure 1. Resolution cells nos. 1 and 5 are the 0-degree (horizontal) nearest neighbors to resolution cell '*', resolution cells nos. 2 and 6 are the 135-degree nearest neighbors, resolution cells 3 and 7 are the 90-degree nearest neighbors, and resolution cells 4 and 8 are the 45-degree nearest neighbors to '*'. (Note that this information is purely spatial, and has nothing to do with grey tone values.)

which two neighboring resolution cells separated by distance d occur on the image, one with grey tone i and the other with grey tone j (see Figure 1). Such matrices of spatial grey tone dependence frequencies are a function of the angular relationship between the neighboring resolution cells as well as a function of the distance between them. Formally, for angles quantized to 45° intervals the unnormalized frequencies are defined by:

$$P(i,j,d,0^\circ) = \#\{((k,l),(m,n)) \in (L_y \times L_x) \times (L_y \times L_x) \mid k-m=0,\ |l-n|=d,\ I(k,l)=i,\ I(m,n)=j\}$$

$$P(i,j,d,45^\circ) = \#\{((k,l),(m,n)) \in (L_y \times L_x) \times (L_y \times L_x) \mid (k-m=d,\ l-n=-d) \text{ or } (k-m=-d,\ l-n=d),\ I(k,l)=i,\ I(m,n)=j\}$$

$$P(i,j,d,90^\circ) = \#\{((k,l),(m,n)) \in (L_y \times L_x) \times (L_y \times L_x) \mid |k-m|=d,\ l-n=0,\ I(k,l)=i,\ I(m,n)=j\}$$

$$P(i,j,d,135^\circ) = \#\{((k,l),(m,n)) \in (L_y \times L_x) \times (L_y \times L_x) \mid (k-m=d,\ l-n=d) \text{ or } (k-m=-d,\ l-n=-d),\ I(k,l)=i,\ I(m,n)=j\} \quad (1)$$

These spatial grey tone dependence matrices can be normalized by dividing each entry in the matrix by the total number of resolution cell pairs used in computing the entries. Details of the procedure used in computing the entries in the matrices may be found in (3).

2.2 Textural Features

From each of the grey tone dependency matrices we extract a set of 32 textural features. The equations which define these features are given in (4). For illustrative purposes we define three of these features:

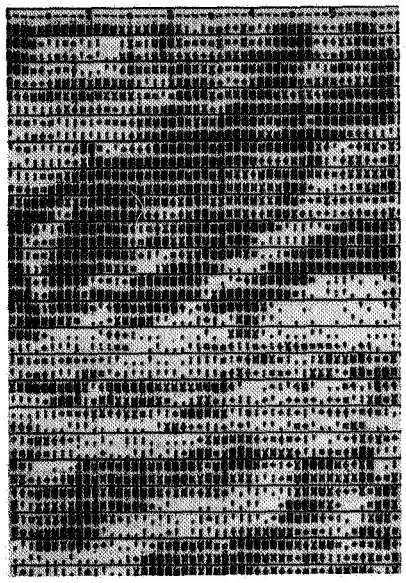
$$f_1 = \sum_{i=1}^{N_g}\sum_{j=1}^{N_g}\left(\frac{P(i,j)}{\#R}\right)^2 ; \quad f_2 = \sum_{n=0}^{N_g-1} n^2 \left\{ \sum_{|i-j|=n} \left(\frac{P(i,j)}{\#R}\right)\right\}; \quad f_3 = \frac{\sum_{i=1}^{N_g}\sum_{j=1}^{N_g} \frac{ij\,P(i,j)}{\#R} - \mu_x\mu_y}{\sigma_x\sigma_y} \tag{2}$$

where, $\#R$ is the number of resolution cells pairs, and μ_x, μ_y and σ_x, σ_y are the means and standard deviations of the marginal distribution P_y and P_x obtained by summing the rows and colums of $P(i,j)/\#R$. To explain the significance of these features, let us consider the kind of values they take on two different land use category images. Figure 2 shows the digital printout of two sub-images from the California frame. The image shown in 2(a) belongs to the grass land category and image shown in Figure 4(b) is mostly water. Values of the features f_1, f_2, and f_3 are also shown for these images in Figure 2.

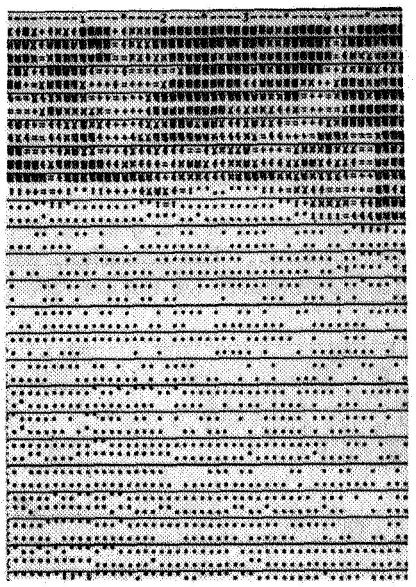
The angular second moment features (ASM), f_1, is a measure of homogeneity of the image. In a homogeneous image, such as shown in 2(b), there are very few dominant grey tone transitions. Hence, the P matrix for this image will have fewer entries of large magnitude. For an image like the one shown in Figure 2(a), the P matrix will have a large number of small entries and hence the ASM feature which is the sum of squares of the entries in the P matrix will be smaller. A comparison of the ASM values given below the images in Figure 2 shows the usefulness of the ASM feature as a measure of the homogeneity of the image.

The contrast feature f_2 is a difference moment of the P matrix and is a measure of the contrast or the amount of boundaries present in an image. Since there is a large amount of boundaries present in the image 2(a) compared to the image shown in 2(b), the contrast feature for the grassland image has consistently higher values compared to the water body image.

The correlation feature, f_3, is a measure of linear grey tone dependencies in the image. For both the images shown in Figure 2, the correlation features is somewhat higher in the horizontal (0°) direction, along the line of scan. The water body image consists mostly of a constant grey tone value for the water plus some additive noise. Since the noise samples are mostly uncorrelated, the correlation features for the water body image have lower values compared to the grassland image. Also the grassland image has a considerable amount of linear structure along 45° lines across the image and hence the value of the correlation feature is higher along this direction compared to the values for 90° and 135° directions.



a. Grassland



b. Water Body

Angle	ASM	Contrast	Correlation	ASM	Contrast	Correlation
0°	.0128	3.048	.8075	.1016	2.153	.7254
45°	.0080	4.011	.6366	.0771	3.057	.4768
90°	.0077	4.014	.5987	.0762	3.113	.4646
135°	.0064	4.709	.4610	.0741	3.129	.4650
Avg.	.0087	3.945	.6259	.0822	2.863	.5327

Figure 2. Textural Features for Two Different Land Use Category Images.

The various features which we suggest are all functions of distance and angle. The angular dependencies present a special problem. Suppose image A has features a, b, c, d for angles 0°, 45°, 90°, and 135° and image B is identical to A except that B is rotated 90° with respect to A. Then B will have features c, d, a, b for angles 0°, 45°, 90°, and 135° respectively. Since the texture context of A is the same as the texture context of B, any decision rule using the angular features a, b, c, d must produce the same results for c, d, a, b or for that matter b, c, d, a (45° rotation) and d, a, b, c (135° rotation). To guarantee this, we do not use the angularly dependent features directly. Instead, we use two symmetric functions of a, b, c, d, their average, and their range. The textural features used in our study were computed for four angles and for a distance of one.

3. SPECTRAL FEATURES

The spectral features used in our study consisted of the mean and variance of the grey tone values within each image block. These features were computed for each

of the four MSS bands, thus yielding a set of 8 spectral features for each image block. The mean and variance of the spectral data have been used extensively in the past for crop classification studies based on MSS data.

4. LAND USE CLASSIFICATION STUDIES

4.1 Data Set

All of the data used in our present study were derived from parts of the ERTS-I image frame 1002-18134. The date of the flight was July 25, 1972, and the center coordinates of the frame were 37.291N, 120.935W. The area of coverage includes the San Francisco Urban area and the Monterray Bay on the coast line of California. Of the four image strips in this frame, all of strip one and one-half of strip three were digitally processed. The second MSS band (MSS-5) image and the area processed are shown in Figure 3.

As a first step in the digital processing, the image area processed was divided into a total of 648 sub-images of size 64 x 64 resolution cells (each covering a ground area of 8.5 square miles). For each of the sub-images, the digital spectral data from the second MSS band (MSS-5) were extracted. The imagery data for each sub-image was then normalized using an equal probability quantizing algorithm and the 32 textural features for each sub-image were then computed. The spectral features for each image block were computed using the digital data from all four sensor bands.

Ground truth for each of the sub-images were obtained with the help of photointerpreters working on the MSS images and the color composite image. A total of seven land use categories could be identified reasonably well on the image and for 624 of the 648 sub-image blocks we could determine a distinct land use category. The set of 7 land use categories used in our study consist of the following:

4.2 Categories of Land Use Detectable on ERTS Image (1002-18134)

(1) Coastal Forest: This area can be typified as a dense temperatue rainforest sited on the windward side of the Coast Ranges of California. It is composed of needle-leaf and broadleaf evergreen trees which generally form a continuous cover.

(2) Woodlands: These are areas to the leeward side of the Coast Ranges. At higher elevations, these woodlands consist of oaks, mostly evergreen, with varying but less continuous cover. At lower elevations these oak woods grade into chapparal which provides decreasing cover with decreasing elevation until it gives way to annual grasslands.

(3) Annual Grasslands: This is an area of non-native annual grasses which have already completed their life cycle by the end of July (turned brown). This area is primarily, like the preceding two categories, quite mountainous. This is also the natural vegetation which would be found in the Great Valley of California except for anthropogenic vegetation.

(4) Urban: Centers of human activity are extremely important as a landscape component within this frame, they are non-randomly located in a size hierarchy of central places connected by transport links. The primary urban agglomerations within



Figure 3. Two strips whose boundaries are shown on the top were processed from this MSS image set (1002-18134).

the frame are the San Jose-Oakland segment of San Francisco, and parts of the Sacramento-Stockton urban complex. Unlike the preceding categories, one of the main image features of urban areas is non-uniformity. Both pattern and texture, as well as a variety of tones, are associated with urban complexes.

(5) Large Irrigated Fields: For practical purposes all field agriculture in the Great Valley is based on irrigation. The areas assigned to this category would most

likely contain field crops such as cotton, alfalfa, and other crops readily adaptable to high mechanization. Most tree crops and vineyards would also be in this category.

(6) Small Irrigated Fields: These areas would contain high value low mechanization crops typified by vegetables.

(7) Water: Although almost self-explanatory as a term, the category in this instance is used to include: (a) ocean, (b) lakes — natural and man-made, and (c) standing water (in fields and on flood plains).

Out of the 648 sub-images in the frame, the photointerpreters helped us to find a unique land use ground truth category for a total of 624 sub-images. Due to cloud cover and other ambiguities the ground truth for 24 sub-images could not be positively identified.

4.3 Classification Algorithm

The problem of developing an algorithm for identifying the land use categories of sub-image blocks from an ERTS MSS image set can be stated as follows. A set of N measurement pairs (X_1,θ'), $(X_2, \theta^2),\ldots (X_N, \theta^N)$ are given as learning observations. A vector measurement (pattern) X_i, where the components of X_i are the spectral and textural features of a sub-image block, comes from an image block whose land use category θ^i is known. θ^i is one of the R land use categories (R=7, in our study) $c_1, c_2,\ldots c_R$. Based on the set of learning observations, we want to develop an algorithm for identifying the land use category of a sub-image block based on the measurement (pattern) vector X it produces.

In a widely used algorithm (Fukunaga (5), Fu and Mendel (6), Miesel (7)), the pattern space is partitioned into a number of regions using a set of hyperplanes (decision boundaries) whose locations are determined by the sample patterns. Each region is dominated by sample patterns of a particular category. When a new pattern is presented for identification, it is assigned a category depending on the region in which it belongs. If the new pattern X is located in a region dominated by sample patterns of category c_j, then X is classified as coming from category c_j.

For the multicategory problem involving N_R categories, a total of $N_R(N_R-1)/2$ hyperplanes are used to partition the pattern space. These hyperplanes are defined by a set of weight vectors $W_{ij}(i = 1,2,\ldots,N_R, j = 1,2,\ldots,N_R; j > i)$ which separates the sample patterns belonging to the ith and j^{th} categories. A regression type algorithm given in Fukunaga (Chapter 4) was used to obtain the weight vectors. After the location of the hyperplanes are determined, the classification of new patterns is done as follows. For each category c_i, the number of hyperplanes, V_i, which give a positive response when the new pattern X is presented are determined using

$$V_i = \sum_{\substack{j=1 \\ j \neq i}}^{N_R} \frac{|W_{ij}^T Z| + W_{ij}^T Z;\ i = 1,2,\ldots,N_R}{2\,|W_{ij}^T Z|}$$

where Z is the augmented pattern vector obtained by adding a component of value 1 to X, i.e.,

$$Z = \begin{bmatrix} 1 \\ X \end{bmatrix} .$$

X is assigned to category c_j if $V_j = \max \{V_i\}$. If there is a tie between categories c_m and c_n, then X is assigned to c_i if $W^T_{mn} Z < 0$ or to c_n if $W^T_{mn} Z \geq 0$. Several modifications of the linear discriminant function method and a multitude of other classification procedures may be found in the references cited.

4.4 Results of Land Use Classification Experiments

The textural and spectral feature vectors for each of the 624 sub-images were divided arbitrarily into training and test sets. The classification algorithm was developed using the information contained in the training set and the samples in the test set were assigned to one of the seven possible land use categories. The accuracy of classification was obtained by comparing the category assigned by the classifier with the known ground truth category and the results are presented in the following paragraphs.

Experiment No. 1: In this experiment, a land use classification scheme was developed using only the textural features of the sub-images on MSS-5 band. Fifty per cent of the samples were arbitrarily selected and used for developing the classification algorithm and the algorithm was tested on the remaining samples. There were seven land use categories and the overall identification accuracy of the classifier on the test samples was 67.5%. With 70% of the samples used for training, the accuracy of the classifier was 70.5%.

Experiment No. 2: In this experiment the classification algorithm was developed and tested using only the spectral features. With 30% of the samples in the test set, the accuracy of the classifier was 74% on the test set and with 50% of the samples in the test set, the accuracy of the classifier was 77%.

Experiment No. 3: Eight textural features were combined with eight spectral features and the algorithm developed and tested using the combined features. The overall accuracy of the land use classification algorithm was 83.5% for test set sizes of 30% and 50%. The contingency table for the classification is shown in Table I.

5. DISCUSSION

The results of our study clearly demonstrates the need for using both the spectral and spatial (textural) characteristics of ERTS MSS data for developing classification procedures. The 83.5% accuracy we have achieved on automatic land use classification procedure is less than the accuracy of human interpreters. The difference in accuracy between the automated procedure and human interpreters can be attributed to the following factors:

TABLE I
CONTINGENCY TABLE FOR LAND USE CLASSIFICATION OF TEST SAMPLES

Assigned Category / True Category	Coastal Forest	Woodlands	Annual Grass-Lands	Urban Area	Large Irrigated Fields	Small Irrigated Fields	Water	Total
Coastal Forest	23	1	2	0	0	0	1	27
Woodlands	0	17	10	0	1	0	0	28
Annual Grasslands	1	3	109	1	1	0	0	115
Urban Area	0	3	10	13	0	0	0	26
Large Irrigated Fields	1	2	6	0	37	2	0	48
Small Irrigated Fields	0	0	4	0	3	24	0	31
Water	0	0	0	0	0	0	35	35
TOTAL	25	26	141	14	42	26	36	310

Number of Training Samples = 34 Number of Test Samples = 310
Accuracy of Classification on Training Set = 84.0%
Accuracy of Classification on Test Set = 83.5%

(1) The context information in the image, on which image interpreters rely heavily, was not taken into account by the automated procedure.

(2) The automated classification algorithm assumed unimodal distribution for the feature vectors from each category. This assumption is not valid for at least some of the categories, such as urban land use category, which consists of many sub-categories and hence a multimodal distribution.

(3) A loss in accuracy is inevitable when the training of the classifier is done using samples from one area of the image and testing on a different area due to environmental changes such as different soil and atmospheric conditions.

We believe that if some of the above deficiencies are taken care of, (we are developing procedures to take care of some of them) the accuracy of automated processing of ERTS MSS data will be quite comparable to the accuracy of human image interpreters.

REFERENCES

1. Rosenfeld, A. and E. Troy, "Visual Textural Analysis," University of Maryland Computer Science Center, TR-70-116, June, 1970.

2. Kaizer, Herbert, "A Quantification of Textures on Aerial Photographs," Boston University Research Labs, Technical Note 121, 1955, AD69484.

3. Haralick, R. M. et al., "Texture-Tone Study with Application to Digitzed Imagery," Technical Reports 182-2, 182-3, U. S. Army Engineer Topographic Laboratories, Contract DAAK02-70-C-0388, University of Kansas Center for Research, Inc., 1971, 1972.

4. Shanmugam, K., R. M. Haralick and R. Bosley, "Land Use Classification Using Texture Information in ERTS MSS Imagery," Technical Report No. 2262-1, University of Kansas Center for Research, Inc., January, 1973.

5. Fu, K. S. and J. M. Mendel, "Adaptive Learning and Pattern Recognition Systems," Academic Press, New York, 1972.

6. Miesel, W., "Computer Oriented Approaches to Pattern Recognition," Academic Press, New York, 1972.

7. Fukunaga, K., "Introduction to Statistical Pattern Recognition," Academic Press, New York, 1972.

N73-28338

Paper I 17

TERRAIN TYPE RECOGNITION USING ERTS-1 MSS IMAGES

Nicholas Gramenopoulos, *Earth Resources Data Processing, Optical Systems Division, Itek Corporation, Lexington, Massachusetts*

ABSTRACT

For the automatic recognition of earth resources from ERTS-1 digital tapes, both multispectral and spatial pattern recognition techniques are important. Recognition of terrain types is based on spatial signatures that become evident by processing small portions of an image through selected algorithms.

This paper describes an investigation of spatial signatures that are applicable to ERTS-1 MSS images. Artifacts in the spatial signatures seem to be related to the multispectral scanner. A method for suppressing such artifacts is presented. Finally, results of terrain type recognition for one ERTS-1 image are presented.

1. INTRODUCTION

The information conveyed to a human observer by a black and white MSS image is spatial. The multispectral information is contained in the brightness variations between the four spectral MSS images. It has been observed that combining the multispectral and spatial pattern recognition techniques enables more resources to be recognized at a greater accuracy.

The objects that can be recognized depend on the ground resolved distance and scale of the imagery. In the ERTS-1 images, various types of terrain can be recognized: cultivated land, urban areas, desert, mountains, bodies of water and cloud-covered terrain.

The recognition operation involves computer processing of small parts of an image to determine the presence of signatures that can be uniquely associated with terrain types. The spatial signatures are strongly dependent on image characteristics, such as scale and ground resolved distance and must be developed by analysis of the ERTS-1 MSS data.

Original photography may be purchased from:
EROS Data Center
10th and Dakota Avenue
Sioux Falls, SD 57198

This paper describes the terrain type recognition results obtained by processing a portion of the ERTS-1 MSS image no. 1049-17324-5. This image was acquired on 10 September 1972 over Arizona. The portion processed covers approximately 2,140 square nautical miles surrounding Phoenix, Arizona (see Figure 1).

Section 2 describes the preprocessing operations required to retrieve a black and white digital image suitable for spatial pattern recognition from the bulk processed computer compatible tapes delivered by the NASA Data Processing Facility.

Section 3 describes the development of spatial signatures for the various terrain types using optical diffraction patterns and digital processing algorithms.

Section 4 describes the results of the terrain classification for the ERTS-1 image discussed above, and in Section 5, conclusions are drawn.

2. PREPROCESSING OF MSS DATA

Each computer compatible tape delivered by NDPF contains one-quarter of an ERTS image. The four spectral bands (for an MSS image) are interleaved. In addition, the sampling interval (in meters) along a scan line is smaller than the sampling interval between scan lines. In other words, there are more picture elements along a kilometer on the surface of the earth parallel to a scan line (approximately East-West direction) than a kilometer normal to a scan line (approximately North-South direction). Furthermore, successive lines are slightly shifted to each other owing to the earth's rotation in relation to the satellite velocity.

The decoding and reformating program first retrieves the red band image (.6 - .7 microns) and separates it from the other spectral bands. It also selects data from the CCT's and combines them into one image covering a contiguous area of the test site. This image is then interpolated and resampled so that the sampling interval in both directions is equal and the skewness due to the earth's rotation is removed. Figure 1 shows an example of a reformated image obtained from two CCT's containing MSS data for ERTS-1 image 1049-17324. This image has 1,000 by 1,170 pixels and was formed by taking 1,000 lines from each of two adjacent CCT's. Each line in a CCT has 810 pixels. Corresponding lines in the CCT's were combined to form lines twice as long, containing 1,620 pixels each. After interpolation and resampling, the lines have only 1,170 pixels each. Skewness due to the earth's rotation has not been corrected in this image.

The red band image was selected because it carries more spatial information than the images of the other bands.

The resampling of an image to equalize the sample spacing in the two orthogonal directions is necessary to remove image distortion. If not corrected, the image distortion causes artificial variations in the spatial signatures of the terrain types. The distortion consists primarily of elongation of object dimensions in the scanning direction. Thus, a square farm would appear as a rectangle or a skewed parallelogram depending on its orientation to the scanning direction.

3. SPATIAL SIGNATURE DEVELOPMENT

Terrain types can be digitally recognized if they can be associated with spatial signatures which can be defined as unique patterns in a set of measurements involving a small area of an image. The area size that has been employed in this investigation is 32 x 32 picture elements which corresponds to about 2.5 x 2.5 kilometers on the surface of the earth.

The Fourier transform of an image is a convenient means to isolate and extract spatial signatures. Terrain signatures in the ERTS image can be efficiently analyzed using the Fourier transforming properties of lenses. Section 3.1 describes the analysis of optical diffraction patterns for the development of terrain signatures. Section 3.2 describes the signatures that were developed digitally.

3.1 Optical Diffraction Patterns

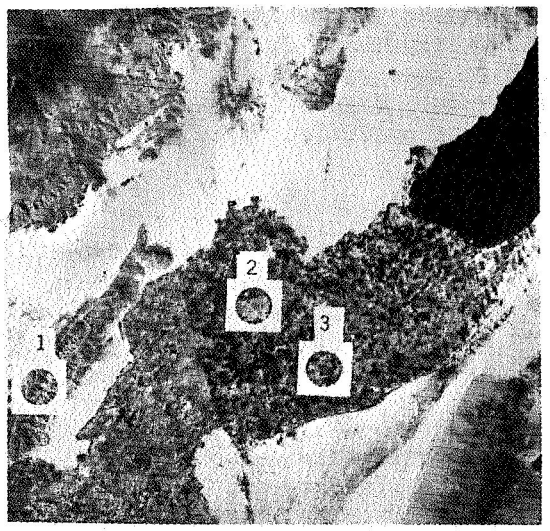
To obtain diffraction patterns of small portions of ERTS-1 images, a special optical bench is employed. To obtain good size diffraction patterns, a long focal length lens (48 inches long) is being used. The 9½-inch transparencies supplied by NDPF were reduced to a scale of 1:3,000,000 and developed to a gamma of two. The image area whose diffraction was obtained was limited by a circular aperture 2mm in diameter.

The diffraction patterns have some artifacts not related to the terrain images.

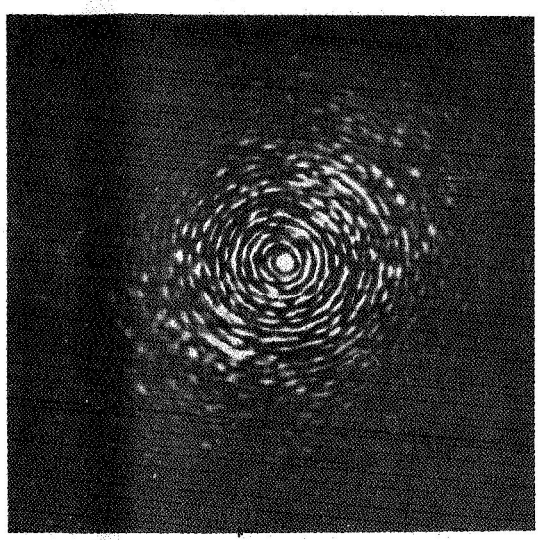
To eliminate or suppress artifacts in the diffraction patterns, a mask is employed when photographing the diffraction patterns. The mask is itself the photograph of the diffraction pattern of an image area (from ERTS images) with no detail such as areas of water from lakes or the ocean. The masks have been used with very good results. They have suppressed artifacts and eliminated overexposure of low spatial frequency components by the central order.



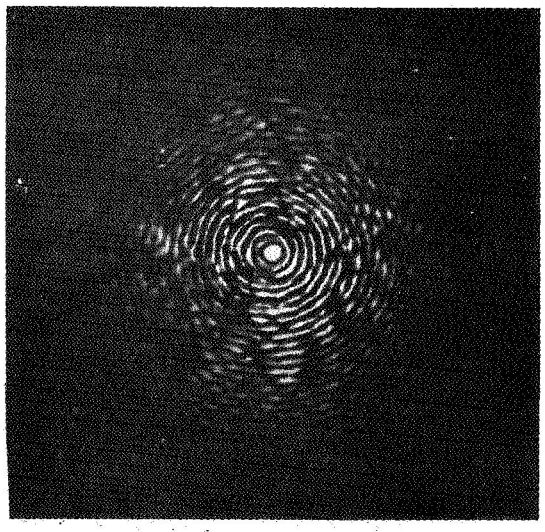
FIGURE 1. ERTS-1 Image No. 1049-17324-5
Recorded from Digital Data



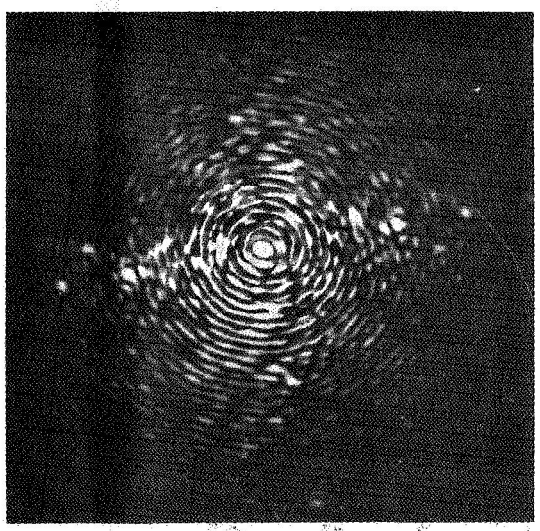
ERTS-1 image 1070-17445-5



030-1 Mountaninous



030-2 Urban



030-3 Cultivated

FIGURE 2. ERTS-1 Image and Diffraction Patterns

Diffraction patterns of terrain types from eight ERTS-1 images have been obtained and analyzed.[1] Signatures have been isolated for cultivated land in the red band image, and some urban areas in the IR2 (.8 - 1.1 microns) band. The signatures consist of orthogonal rows of frequency spots. Mountains and rivers have structured diffraction patterns. Simple spatial signatures such as rows of frequency spots have not been isolated for these terrain types. Figure 2 shows an ERTS-1 image and diffraction patterns from the encircled areas.

3.2 Digital Signatures

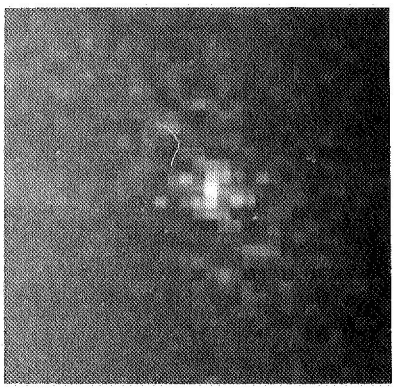
The digital recognition of terrain types is partially dependent on developing spatial signatures from the Fourier transforms of small areas of an image. Each area, otherwise known as a cell, consists of 32 x 32 picture elements. Thus, the entire image is divided into a matrix of 36 x 31 non-overlapping cells. Each cell is subjected to processing that assigns it to one terrain type.

The processing operations are divided into feature selection and classification. Feature selection preceeds classification. This is a data reduction operation. While each cell is initially characterized by 1,024 numbers, after feature selection, each cell is characterized by 8 numbers. Thus, in the feature space, each cell is described by a vector of greatly reduced number of dimensions. The selection of the features must be accomplished by analysis of the data, and there is no guarantee that the features selected convey most of the information available in the original data. The features that have been employed during this investigation are: the mean value of a cell, the histogram, a number representing a count of high derivative values within the cell, and the energies contained in specific non-overlapping sectors of the Fourier transform of a cell.

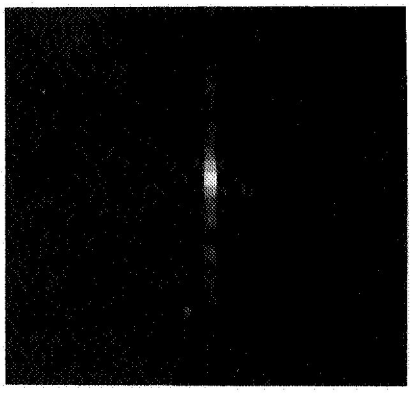
Figure 3 shows the amplitude of the Fourier transforms of four cells. The horizontal direction coincides with the scanning direction of the multispectral scanner. The frequencies represented by the squares vary from 0.39 to 5.9 cycles per kilometer. Due to the ground resolved distance of the MSS data, the street pattern of Phoenix is not resolved in the red band image. Also, the boundaries between adjacent farm plots are not resolved (see Figure 1). The farm pattern within a cell seems to be established by crops of equal brightness. If such crops exist in adjacent plots, they have the appearance of larger farms of irregular shape. Also, the farm pattern is affected by clouds and highways.

---

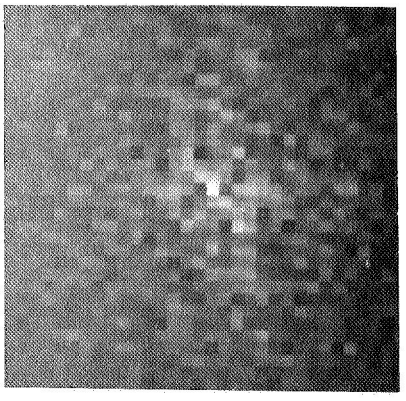
[1] Gramenopoulos, N. and Corbett, F., "Diffraction Pattern Analysis of ERTS-1 Images," Technical Report of ERTS-1 investigation.



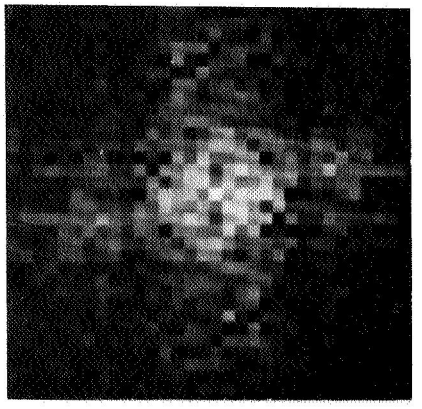
Mountain



Desert



City



Farms

FIGURE 3. Digital Fourier Transforms of Cells

Extensive analysis of the Fourier transforms has produced the following results:

1. It appears that frequencies larger than 3.5 cycles/km contain the information needed to discriminate between the terrain types. Frequencies less than 3.5 cycles/km carry significantly less information.

2. Regardless of terrain type, there is significant energy along the vertical frequency column ($f_x = 0, f_y$) where x is the horizontal direction and y the vertical. In addition, this column has local peaks at the frequencies $f_y = 2.1$, 4.2 and 6.3 cycles/km. These appear to be multiples of 1/6 the scanning rate (12.6 lines/km) of the Multispectral Scanner. Since the scanner has six detectors per spectral band, it is conceivable that these frequencies are artifacts due possibly to small errors in detector response remaining after calibration. The calibration errors may not be large enough to produce line structure in an MSS image. In any case, the frequency column mentioned and the two columns adjacent to it contain frequency components of the same order of magnitude as the components which have been related to farms. The discrimination results between the various terrain types were improved when these three columns were replaced by zeros.

Measurements of Fourier transform energy are made as follows:

a. All frequencies less than 3.5 cycles/km and larger than 5.9 cycles/km are eliminated.

b. In the remaining Fourier transform, the largest peak (or maximum) is determined.

c. The energy in a sector which is $\pi/8$ radians wide and centered on the largest peak is determined. The energy within this sector (S_1) is one of the features.

d. The energies in similar size sectors which are displaced from the first one by $\pi/4$, $\pi/2$ and $3\pi/4$ radians in a clockwise direction are also determined and constitute the features S_2, S_3 and S_4, respectively.

Upon completion of the feature selection operation, the classification operation can then be carried out using only the feature vectors. The classification involves assignment of the cells to the terrain types by partitioning the feature space. For this investigation, the division of the feature space was done manually, in order to analyze the usefulness of the features that were selected. The classification algorithm consists of logic statements containing many thresholds.

4. TERRAIN CLASSIFICATION RESULTS

In order to determine the accuracy of the classification algorithms, two assignment matrices of cells were developed by photointerpretation. One matrix represents assignments using only the ERTS-1 red band image 1049-17324-5. The other matrix represents assignments using all available information (maps, aerial photography, and a land use map*). Comparing these two matrices, one finds that the first one has about 2.5% errors, which indicates the error rate of a photointerpreter if he were to use only the red band ERTS-1 image. Most of the errors are due to isolated urban areas near cultivated land, mountains or desert.

The computer classification matrix was compared to the most accurate photointerpreter matrix. The results are tabulated in Table 1.

Many cells contain two terrain types and the computer assignment of a cell is deemed correct if one of the terrain types is correctly recognized. Clouds and cloud shadows can confuse the classification of underlying terrain. Therefore, cells that contain even a small cloud or a cloud shadow are not assigned to a terrain type. The underlying terrain can be classified from different ERTS-1 images when it is cloud free.

Whenever cells cannot be classified with reasonable confidence, they are assigned to an unidentified group. This can be justified by the fact that all the information available (the other three spectral images) is not being utilized yet and it is desirable to defer making decisions on questionable cells until the spectral information is introduced. Due to scale and resolution, only three types of natural terrain can be recognized: desert, mountains, and riverbeds or flood plains. However, in the land use map*, the following categories of terrain were classified: undissected flat land, slightly dissected flat land, rolling land, moderately dissected land, hills, mountains and flood plains. Our

* Poulton, C.E., Schrumpf, B.J., Johnson, J.R., "Ecological Resource Analysis from High-Flight Photography for Land Use Planning," Applied Remote Sensing of Earth Resources in Arizona, Proceedings 2nd ARETS Symposium, University of Arizona, November 2-4, 1971.

TABLE 1. COMPARISON OF CLASSIFICATION RESULTS

COMPUTER ASSIGNMENT	PHOTOINTERPRETER'S ASSIGNMENT 1	2	3	4	5	6	7	8	TOTAL
0	0	0	3	15	22	6	14	0	60
1	61	0	0	0	0	0	0	1	62
2	0	2	0	1	0	0	0	1	4
3	1	0	417	6	7	8	5	0	444
4	0	0	3	248	1	9	2	1	264
5	0	0	5	3	131	2	4	0	145
6	0	0	1	5	3	71	8	0	88
7	0	0	1	0	0	0	4	0	5
8	0	0	0	0	0	0	0	13	13
TOTAL	62	2	430	278	164	96	37	16	1085

CLASS IDENTIFICATION

0 = Unidentified
1 = Clouds
2 = Water
3 = Desert
4 = Farms
5 = Mountains
6 = Urban
7 = Riverbed
8 = Cloud Shadows

category of desert includes: undissected, slightly dissected, rolling and moderately dissected deserts. Our mountainous category includes hills and mountains. Our urban category includes airports and military bases.

Due to the population density of the area and man's activities, the signatures of the various terrain types vary considerably, thus increasing the probability of error. The following examples have been noted:

1. Highways and canals cutting through desert can be confused with flood plains.

2. Urban development has extended into the hills north of Phoenix and new developments farther north into the desert have been initiated. These areas are now urban, but retain some of their former desert or mountainous characteristics, thus producing some classification errors.

3. The urban areas are spreading into farmland near Glendale and farms have been noted surrounded by urban areas or in the process of being coverted to new developments. Such areas have produced classification errors or unidentified cells. Sun City, a circular urban development near Glendale, is quite different in appearance than downtown Phoenix.

4. The Salt River bed runs through Phoenix. The waters of this river have been diverted for irrigation and the river bed is now dry. The river bed is used for urban or industrial purposes, but it is thinly populated in comparison to Phoenix. Classification errors and unidentified cells were found along the river bed.

It was also noted that farms are a dominant terrain type. Most cells containing two terrain types with farms being one of them, were assigned to the farm category.

The classification results are shown in the annotated photograph of Figure 4. The letters were superimposed on the image of Figure 1, and are centered within each cell. The interpretation of the symbols is:

D = Desert	R = Riverbeds
U = Urban	C = Clouds
F = Farms	S = Cloud Shadows
M = Mountains	Blank = Unidentified

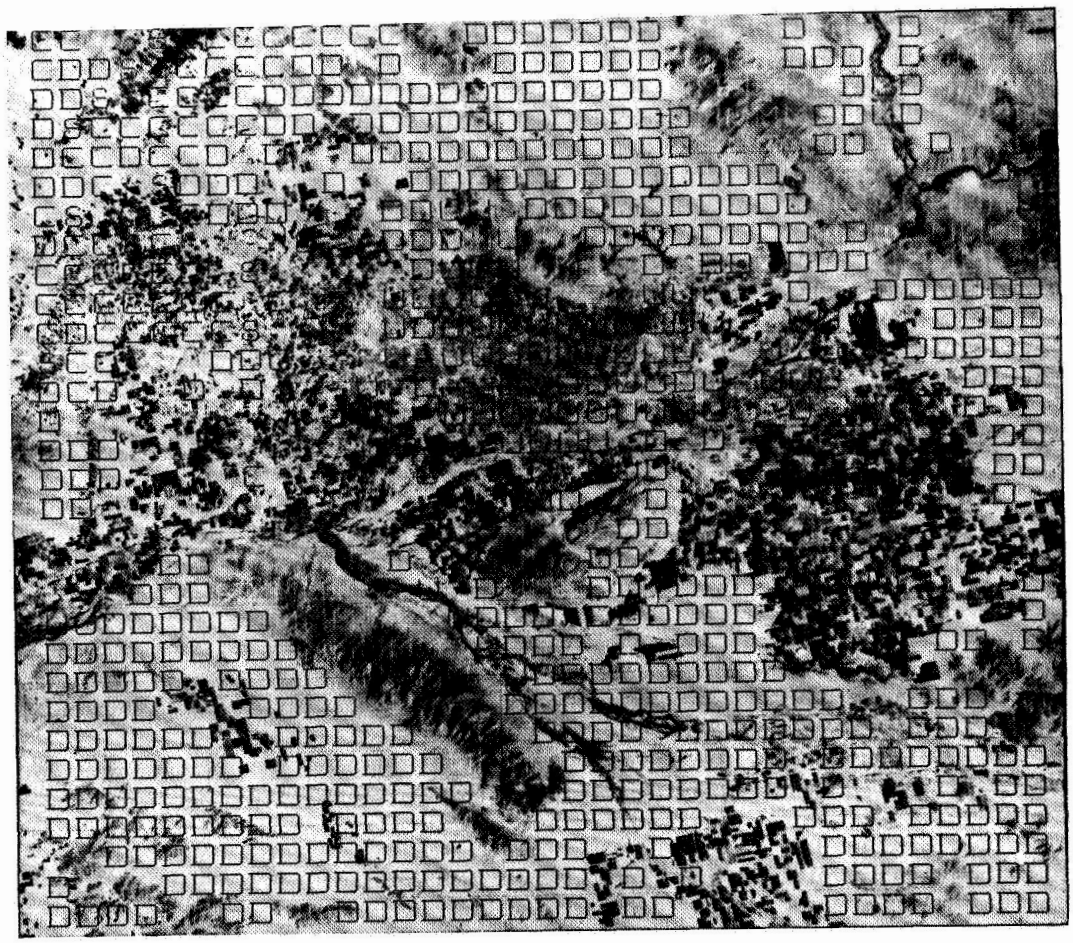


FIGURE 4. ERTS-1 Image and Terrain Classification Results

5. CONCLUSIONS

The recognition of terrain types is accurate for desert (97%), farms (89%) and mountains (80%). The accuracy for urban areas is lower (74%) and poor for riverbeds (11%). These results are indicative of what can be achieved using a single ERTS-1 image. Due to the resolution of the system, urban areas cannot be recognized with a very high degree of confidence until the information in the other spectral bands has been exploited. Most of the errors in the urban category seem to occur in thinly populated areas associated with recent urban expansion into desert, farms, riverbeds and hills.

One potential application of the technique described is in land use inventory and management. For this application, boundaries between terrain types are also required and one needs to demonstrate that the technique works accurately for other regions of the country with human adjustment of the classification algorithm kept to a minimum.

We are proceeding with the automatic boundary development which at the present time, has not been completed. The boundaries can be used to accurately define the terrain regions and, furthermore, cells containing boundaries can be eliminated, thus, further improving the accuracy of the classification.

An expansion of the classes recognized will be implemented by the introduction of the multispectral information (the other three spectral bands).

A very significant result of this investigation is that the features selected are sufficient for the purposes of classifying terrain types. The four most important features are derived from the Fourier transforms of the cells. That these features can be used to classify terrain from other test sites is strongly suggested by the similarities observed in the diffraction patterns from six test sites. On the other hand, the classification algorithm which employs the feature vectors is image-dependent. While a specific algorithm may be applicable to a small sequence of ERTS-1 images, it seems unlikely that a fixed algorithm could be used successfully on all ERTS-1 images. For this reason, the partitioning of the feature space will be done by "clustering" techniques similar to those employed by multispectral recognition algorithms. Feature space vectors will be grouped into classes that satisfy a selected criterion. By this approach, a fully automatic terrain recognition system can be evolved which consists of an image-independent selection of features followed by an image-dependent classification algorithm.

N73-28339

Paper I 18

CLASSIFICATION OF ERTS-1 MSS DATA BY CANONICAL ANALYSIS

H. M. Lachowski and F. Y. Borden, *Office for Remote Sensing of Earth Resources, The Pennsylvania State University, University Park, Pennsylvania*

ABSTRACT

The objective of canonical analysis is to obtain the maximum separability among a number of categories. The application of canonical analysis was investigated using the merged MSS ERTS-1 data for one area viewed on two dates. The effect of threshold values on classification regions and confusion regions was investigated.

INTRODUCTION

Canonical analysis, which is also known as multiple discriminant analysis, is a multivariate statistical method that has application to classification of multivariate observations into statistically defined categories. Linear combinations of the observed measurable characteristics are found that yield one or more indices that emphasize the differences among the classes. The linear combinations are then applied to data for unknowns and supply the means for classification. Canonical analysis has been used satisfactorily many times in classification problems in the biological and natural sciences. It has obvious potential advantages for a similar application in the field of remote sensing. In this research, the method was tailored for classification of remote sensor data collected by multispectral scanners (MSS) carried by airplanes and satellites.

COMPUTATIONAL METHOD

MSS digital data, having a response for each of p spectral bands or channels, are organized according to scan lines across the flight path and by elements within scan lines. The data can be considered to be multivariate of dimension p with, say, $X_{i\,j}$ being the observational vector for scan line i and element j. In the use of canonical analysis for classification of unknown data into k+1 categories (i.e., k defined categories and an "other" category), an estimate for the mean vector of each of the k classes is needed, as well as for the corresponding covariance matrix. For MSS data, these statistics can be obtained by the use of training areas, each of which is considered to be spectrally

PRECEDING PAGE BLANK NOT FILMED

homogeneous. At least one training area must be defined for each class and the training areas must be representative of the classes to be investigated. In a geometric sense, in p dimensions, each class is defined by its mean vector and its covariance matrix. The covariance matrix defines the elipsoidal dispersion pattern of points clustering around the class mean vector.

Canonical analysis accomplishes four things in a geometrical sense. First, the origin is translated to the point of the overall mean vector. Second, the original axes are rotated to new orthogonal positions. In this, the first axis is placed according to the maximum possible separability among the class mean vectors. The second axis is positioned orthogonally to the first and according to the maximum remaining class separability and so on for the other axes. The third accomplishment is scaling the axes so that the elipsoidal dispersion patterns are transformed into spherical patterns. The fourth feature is that the space dimension required for satisfactory classification is, in general, substantially reduced. This means that if there are p original variables, the canonical transformation will generally yield substantially less than p transformed new variables that still retain essentially all of the useful information for satisfactory classification. Because it will be necessary to refer to the test results in discussing the method, such discussion will be deferred until after the test data have been described.

THE TEST AREA AND PRELIMINARY COMPUTATIONS

The test area resides in the vicinity of Harrisburg, Pennsylvania, just northwest of the central metropolitan part of the city and stretches across the Susquehanna River encompassing substantial land back from both shorelines (Figure 4B). It includes a part of the river, a railroad marshalling yard, suburban areas, and areas of vegetation. ERTS-1 bulk MSS data from two dates were mapped after being brought into registration by translation and merged. Each element in the test area as a result of merging was composed of eight values, four from each of the two dates. The two dates were August 1, 1972 (scene 1009-15241), and October 11, 1972 (scene 1080-15185). The October 11th overpass was one day prior to the fourth eighteen-day cycle. These two dates were chosen because they were the only ones for which MSS tapes were in hand and for which the test area was cloud free.

The test area was chosen because it was familiar and had a variety of natural and cultural targets. The specific targets that were selected for study were river water, the railroad yard, two suburban targets, and two vegetation targets. The categories are referred to by numbers in figures and tables, therefore, category 1 stands for river, 2 for railroad yards, 3 and 4 for suburbs, and 5 and 6 for vegetation. The area was dominated by these categories.

The mean (spectral signature) and the covariance matrix were computed for selected training areas using various algorithms from the digital processing system for MSS data as described by Borden (1972). These statistics were then input to the canonical analysis program (Lachowski, 1973) where the transformation matrix was computed and transformations of the mean vectors were performed. Following this, each unknown MSS observation was transformed using the transformation matrix and classified into one of the known categories or into the "other" category.

RESULTS AND DISCUSSION

The canonical analysis of the test data showed that essentially all of the separability (99.9%) among the six categories could be recovered in four canonical axes. The four axes accounted for 88.5, 11.1, 0.2, and .06 percent, respectively, of the separability. In Figure 1 the transformed means are plotted for the first two axes as the center points of the circles. The circles represent the 94.5% contour for the transformed dispersion about each mean. The radius of each circle is 1.9, the threshold value, which corresponds to the 94.5% contour. Considering the two axes together, confusion in classification can occur only where circles overlap and, for the 1.9 threshold value, no confusion occurs. The circles have been projected onto each axis in Figure 1, thus producing classification intervals. Overlap occurs for some of these intervals on the first axis and for many on the second axis, thus indicating two axes are needed for separability using a 1.9 threshold value. In Table 1 the indicators of overlap or nonoverlap in classification intervals are presented for each axis. The map of the classification using the 1.9 threshold value is shown in Figure 3, where the vegetation and suburb classes were assigned the same mapping symbol for map clarity in this report.

To show the situation that occurs when classification regions overlap, the test data were run with a threshold value of 3.0 that corresponds to a 99.7% contour for transformed dispersion about the means. Although this would be an unrealistically high value in practice, the influence of the threshold value on confusion regions is amply demonstrated. Plots of the transformed means are presented in Figure 2. In this case, confusion regions exist for the two axes considered together for classes 4 and 5 and 5 and 6. Even with the four axes, confusion could not be entirely resolved although the confusion regions were decreased in size. The mapping results show this in Figure 4A, where the classification confusion is mapped as a separate category. If each of the two axes is considered separately, as seen by the projection of the circles onto the axes in Figure 2, there are four overlapping intervals for axis one and eight overlapping intervals for axis two. The corresponding indicators are given in Table 2.

If an observation falls in a confusion region, what can be done to resolve the confusion? The way in which this was handled was to assign the observation to the class to which it was nearest to the mean; i.e., using a minimum euclidean distance classification scheme based on the transformed data. The mapping results for this are shown in Figure 4B, where it appears that this was a reasonable path to follow. An assignment was made to the "other" category if a transformed observation fell outside every classification region. The "other" category is mapped as the blank areas in all of the figures. The threshold value not only has an influence on the sizes of the confusion regions, but also on the number of "other" classifications. As the threshold value increases, the sizes of the confusion regions increase, but the number of "other" classifications decreases and vice versa. This effect can be seen in the comparison of Figure 4 with Figure 3 where the unclassified area is greater for the smaller threshold value.

The transformation vectors for each of the four axes are presented in Table 3. The values in each vector are analogous to partial regression coefficients of multiple regression. Some interpretation can be made of these for MSS data since the data for all channels have the same order of magnitude. For the first vector, for example, the transformation is dominated by channel seven for each date. The interpretation here is that the emphasis is on the spearation of water from nonwater signatures because of the generally low reflectance of water in channel seven. The plot in Figure 1 bears this out, where the greatest separation is shown to be between the water class and the others for axis one.

FUTURE WORK

Although classification advantages have not been discussed in the report, it appears that strategies can be employed that would reduce computation time in classification by use of canonical analysis. One possibility can be seen with reference to Figure 1. Suppose the classification intervals for the classes are stored for all of the axes, then, by transformation with the first vector, followed by a table look-up, one can determine if the observation falls in any class interval or intervals. If it does not fall in any interval, it is "other." If it falls in one interval only, it is either in that class or "other." If it falls in two or more intervals, it is in a confusion region and the transformation for the next axis has to be made. Work is presently in progress to implement such a procedure, as well as to investigate other similar ones.

LITERATURE CITED

Borden, F. Y. 1972. A Digital Processing and Analysis System for Multispectral Scanner and Similar Data. Remote Sensing of Earth Resources, Vol. 1. Edited by F. Shahrokhi. University of Tennessee Space Institute, Tullahoma, Tenn. pp. 481-507.

Lachowski, H. M. 1973. Canonical Analysis Applied to the Interpretation of Multispectral Scanner Data. M.S. thesis, The Pennsylvania State University, University Park, Pa.

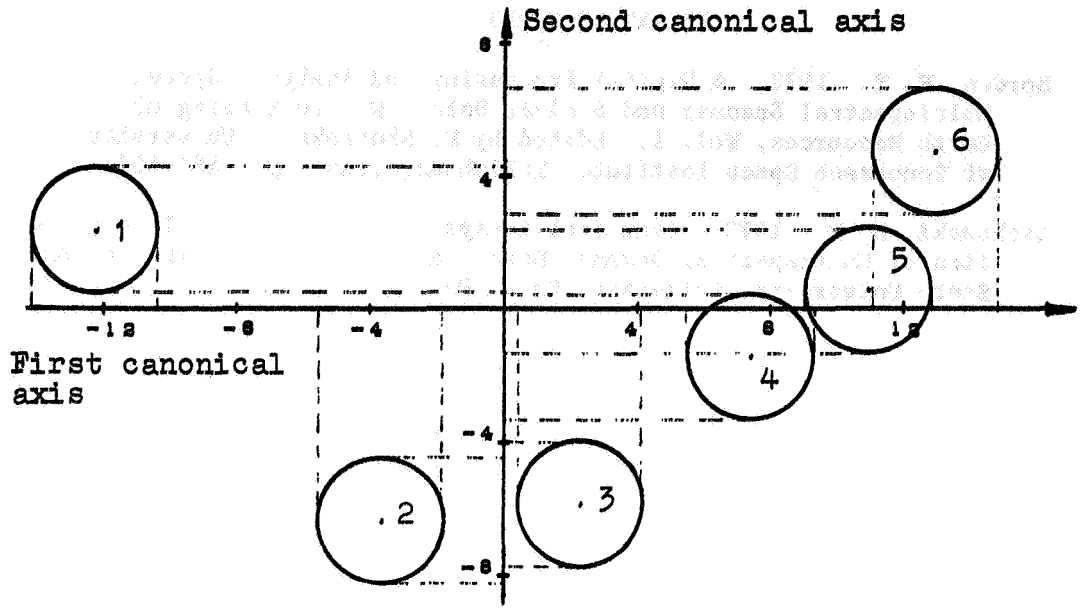


Figure 1. Geometric representation of the separation of the transformed mean estimates for all the categories and their 94.5% classification regions using the first two canonical axes.

Table 1. Matrices showing category overlaps (1's) and nonoverlaps (0's) for the 94.5% classification intervals using the first two canonical axes.

	First Canonical Axis						Second Canonical Axis					
	Category						Category					
Category	1	2	3	4	5	6	1	2	3	4	5	6
1	1						1					
2	0	1					0	1				
3	0	0	1				0	1	1			
4	0	0	0	1			0	0	0	1		
5	0	0	0	1	1		1	0	0	1	1	
6	0	0	0	0	1	1	1	0	0	0	0	1

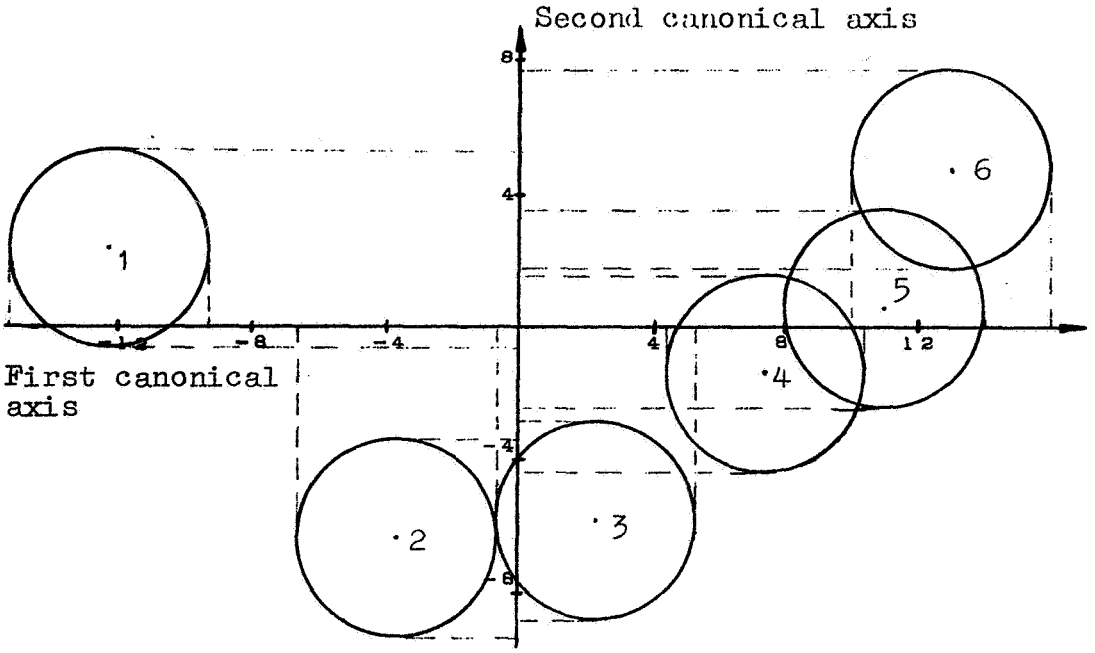


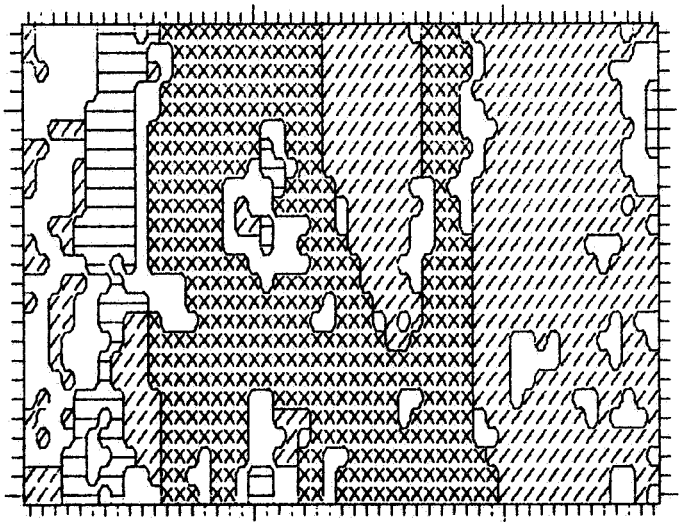
Figure 2. Geometric representation of the separation of the transformed mean estimates for all the categories and their 99.7% classification regions using the first two canonical axes.

Table 2. Matrices showing category overlaps (1's) and nonoverlaps (0's) for the 99.7% classification intervals using the first two canonical axes.

	First Canonical Axis						Second Canonical Axis					
	Category						Category					
Category	1	2	3	4	5	6	1	2	3	4	5	6
1	1						1					
2	0	1					0	1				
3	0	0	1				0	1	1			
4	0	0	1	1			1	1	1	1		
5	0	0	0	1	1		1	0	0	1	1	
6	0	0	0	1	1	1	1	0	0	0	1	1

Table 3. Transformation matrix used for transforming mean estimates (signatures) for the known categories and for transforming each unknown observation.

Channel	Canonical Axes			
	1	2	3	4
August 1				
4	0.045	-0.313	0.303	-0.112
5	0.016	-0.561	-0.686	0.227
6	0.122	0.008	0.476	-0.434
7	0.417	0.009	0.305	0.705
October 11				
4	-0.073	-0.177	0.505	0.565
5	-0.101	-0.332	0.054	-0.096
6	0.205	-0.158	-0.215	-0.370
7	0.546	0.254	-0.382	0.427



Railroad yards ——
Vegetation and suburbs /////
River xxxx
Other blank

Figure 3. Computer generated map for the test area with the threshold value set at 1.9.

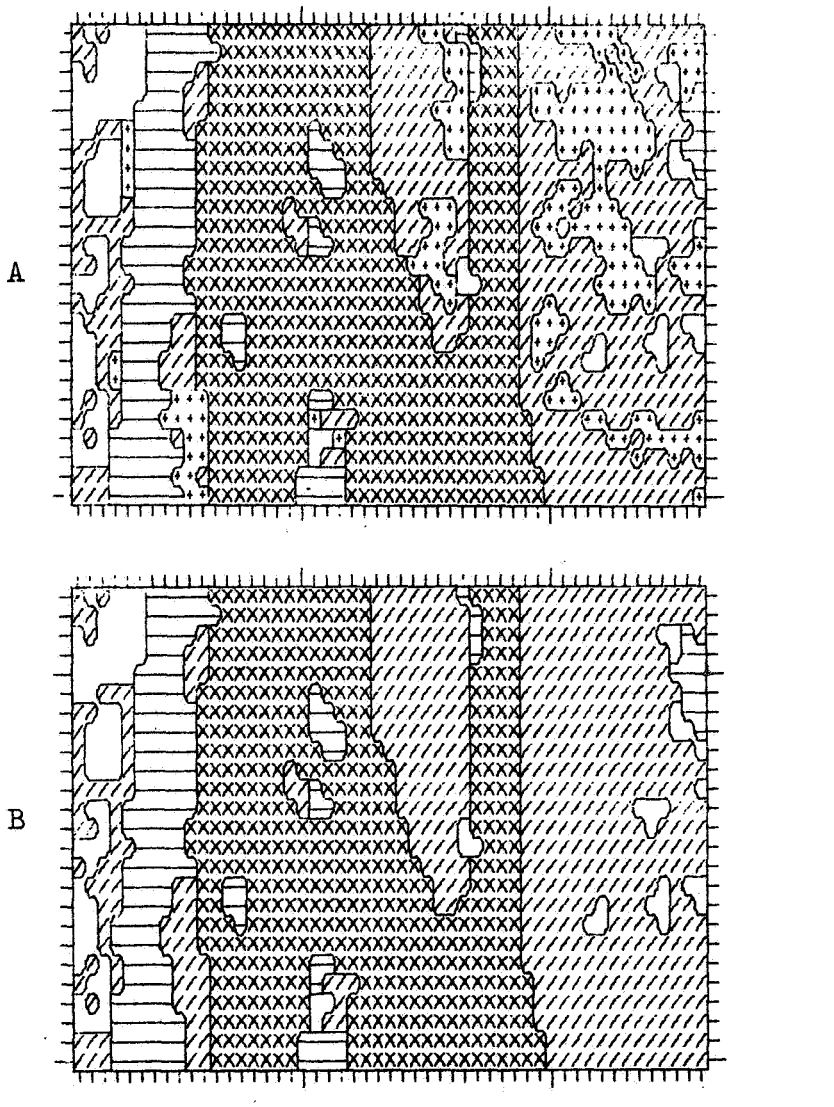


Figure 4. Computer generated maps of the test area with the threshold value set at 3.0. Map A indicates where confusion occurred. Map B shows the confused areas classified into one of the known categories.

N73-28340

Paper I 19

IN SITU SPECTRORADIOMETRIC QUANTIFICATION OF ERTS DATA

Edward F. Yost, *Science Engineering Research Group, Long Island University, Greenvale, New York 11548*

ABSTRACT

The task of correlating in situ spectral reflectance measurements with ERTS imagery has commenced. A method of additive color analysis of a single multispectral band taken on different dates indicates that ERTS-1 bulk images have sufficient spatial and spectral fidelity to show indications of the presence of soil moisture in desert playas and changes in soil moisture with time. The chain of causality between soil moisture, in situ spectral reflectance, and ERTS multispectral scanner image density remains to be established during the subsequent phases of this study.

1. INTRODUCTION

This project was undertaken by Long Island University to establish the relationship between in situ spectral reflectance measurements and the photometric characteristics of ERTS-1 multispectral scanner imagery. All imagery of the test site at Willcox Playa, Arizona, which was received was cloud free; however, clouds obscured a test site at Prescott National Forest, Arizona, where in situ spectral reflectance measurements were being obtained during the 27 September-2 November 1972 period of ERTS-1 image acquisition.

A "first look" analysis of the imagery was performed using a multispectral color viewer. The additive color analysis revealed the existence of significant spectral reflectivity differences in the Willcox Playa between 27 September and 2 November 1972. A time sequence analysis of the 600-700 nm (red) band was performed for the ERTS-1 acquisition dates of 27 September, 14 October, and 2 November 1972. This method of time sequence analysis permitted the association of differences in soil moisture over time with the color of the multispectral display. ERTS-1 bulk images were found of sufficient spatial fidelity to allow good image registration of the image of the Willcox Playa.

2.1 PRESCOTT, ARIZONA - COPPER BASIN

The Copper Basin lies to the east of Prescott and contains a wide variety of soil types and vegetation. The tree species which predominate are juniper, manzanita, and pine. They grow in regions containing pyrite,

PRECEDING PAGE BLANK NOT FILMED

Original photography may be purchased from:
EROS Data Center
10th and Dakota Avenue
Sioux Falls, SD 57198

diorite, limestone, and shale. The Spectral Data telespectroradiometer was used to measure the reflectance spectra of the pine species. A group of sixty targets was used, with each set consisting of three scans. The three scans were averaged and the envelope of all pine species reflectance is shown in Figure 1. Although the amplitude of the curves differs, the basic distribution of the data is consistent. It was anticipated that stands of these pine trees could be differentiated from the other vegetation

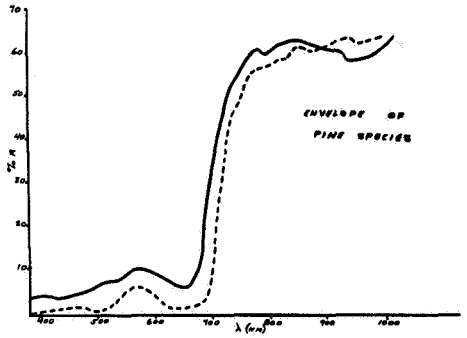


Figure 1. Envelope of spectral distribution of sixty samples pine species, in Copper Creek region, Arizona.

seen on ERTS-A imagery. However, the only frame of ERTS imagery which has been received contains a cloud directly over the test site. Simultaneous with the measurement of the spectra, a low-altitude flight was made over the Copper Basin area. Two sets of filters were used on the Spectral Data Model 10 multispectral camera: a broad band set approximating those on ERTS-A and a narrow band set consisting of two visible and two near-infrared bands. The multispectral low-altitude color composite results, which simulated true color or Ektachrome film, show no differentiation between the juniper, manzanita, and pine trees. The simulation of Ektachrome Infrared film does not discriminate between the species either. Figure 2 is a map of the pine trees (represented as dots) and the juniper-manzanita areas (represented as crossed areas) for a small region along Copper Creek. This map corresponds to the multispectral additive color imagery analyzed. Synthesizing the narrow band imagery by projecting the two visible bands as blue and red and the near-infrared band as green shows a distinct difference between pine trees and the other two species.

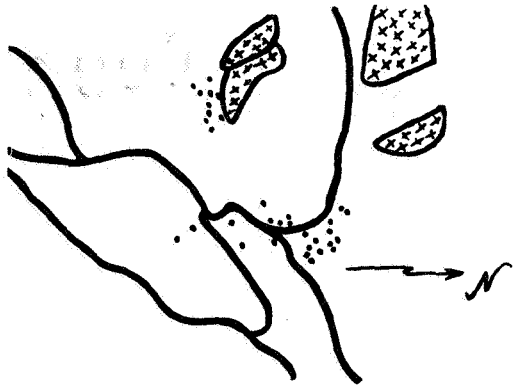


Figure 2. Ground truth of pine versus juniper-manzanita trees in Copper Basin.

Pine trees are displayed as a vivid yellow, while juniper and manzanita are green. The low-altitude imagery was analyzed using the Spectral Data Model 64 viewer; the composite imagery was photographed off the viewer screen.

2.2 WILLCOX PLAYA, ARIZONA

The Willcox dry lake consists of a flat, shallow clay type surface which much of the time is hard and cracked due to the great evaporation which occurs during the heat of the day. The Playa is subject to a wide change of environmental conditions. That is, periodic heavy rainstorms wash down soil from outlying regions, thereby flooding parts of its surface. Its boundaries alter with time; windstorms blow loose gravel and sand, depositing it in other areas which did not contain that soil base. Because of its dynamics, Willcox Playa was chosen for spectral analysis of its soils and multispectral image analysis of changes in spectral distribution within the area as a function of time. Figure 3 shows the general terrain of the dry lake bed. The area is approximately ten miles square and is surrounded by elevations up to 7500 feet; an alluvial fan exists to the west. Surface cracking appeared in the test sites which were measured. In addition to the large truck-mounted telespectroradiometer, a smaller unit measured the reflectance close to the surface. Both types of data were obtained at two stations, the averages of which are shown in Figure 4. Within the accuracy of the

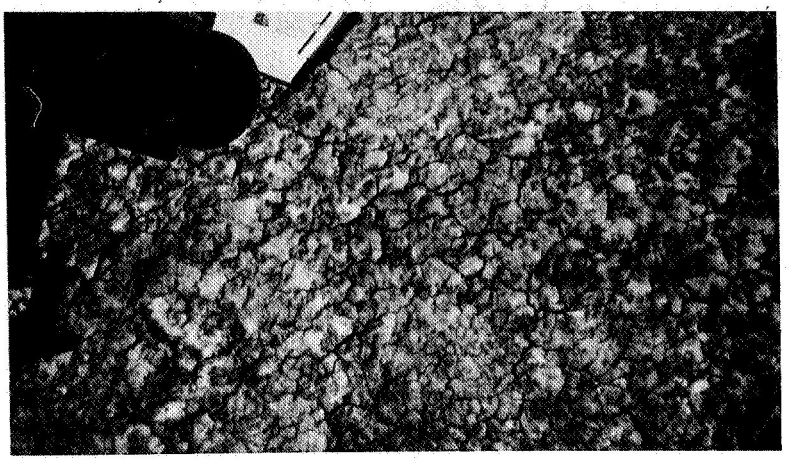


Figure 3. Close-up of the surface of the northwest portion of Willcox Playa when dry.

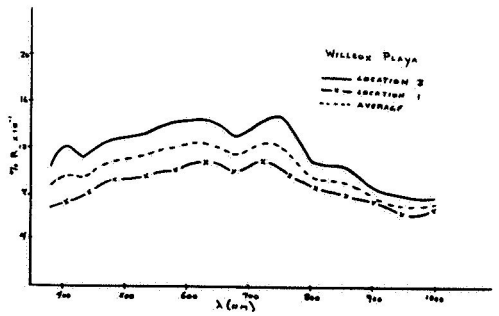


Figure 4. Soil reflectance at two locations in Willcox Playa.

telespectroradiometer (2 1/2% in the visible range and 5% in the near-infrared) it is apparent that the soil reflectance distribution is almost the same. The average is shown as the center curve. However, the brightness of the two locations differs and this has been attributed to the presence of the moisture which existed in location # at the time of measurement. Apparently this moisture did little to bias the reflectance data in the red region which had previously been suggested. Within four days of obtaining these measurements, the ERTS-A satellite made a pass over the Willcox area. Figure 5 shows a black-and-white composite of that frame with the entire portion of the dry lake achromatic or essentailly the same shade of gray. Neither the multispectral composite simulation of true color (the green band projected as cyan and the red band projected as red) nor the simulation of Ektachrome Infrared (the green band projected as blue, the red band as green, and the near-infrared band as red) showed any visible signs of reflectance change between September 27, October 14, and November 2. A distinct change in brightness did exist between the individual data, but the color remained the same. It was concluded, therefore, that changes in the soil moisture conditions were too small to be seen in a conventional multispectral composite for any given overflight. However, the dynamics of soil moisture were studied



Figure 5. Black-and-white multispectral composite of ERTS-A image over Willcox Playa, September 27, 1972.

on a temporal basis using the NASA release band 5 positives for September 27, October 14, and November 2. The Playa itself was located in a different position of the frame for each date so that only the intersect of the three images was recombined in additive color. The September 27 band 5 was projected as blue, the October 17 band 5 as green, and the November 2 band 5

as red. Ordinarily the colors in a multispectral display are indicative of reflectance differences which exist as a function of wavelength. However, the vivid color differences which were seen in the time sequential multispectral photo represented reflectance changes in the red spectral region as a function of time. The colors within and surrounding the Playa may be interpreted as follows:

-- A colorless shade of white or gray indicates no change in surface moisture content between 27 September and 2 November 1972.

-- Yellow indicates areas where a decrease in soil moisture occurred between 27 September and 14 October and little change from 14 October to 2 November.

-- Orange also indicates a decrease in soil moisture between 27 September and 14 October, coupled with a reduced rate of decrease to 2 November.

-- Cyan or red are areas where moisture changed little between 27 September and 14 October, then increased greatly by 2 November.

-- Red indicates areas where surface water did not change between 27 September and 14 October, then decreased between 14 October and 2 November.

-- Green indicates a reduction in surface moisture from 27 September to 14 October and an increase between 14 October and 2 November.

-- Blue indicates the opposite effect from those areas that appear yellow; i.e., surface moisture increases between 27 September and 14 October with no change between 14 October and 2 November.

3. CONCLUSIONS

ERTS-1 bulk multispectral scanner imagery, when recombined in a single additive color presentation, show color differences which are related to spectral reflectance changes of desert dry lakes (Playas). When the same bands acquired at different times are reconstituted in color, changes in reflectance at the same wavelengths with time are shown as colors.

MARINE RESOURCES AND OCEAN SURVEYS

N73-28341

Paper M 1

SEASONAL CHANGES OF LITTORAL TRANSPORT AND BEACH WIDTH AND RESULTING EFFECT ON PROTECTIVE STRUCTURES

Turbit H. Slaughter, Geologist, *Maryland Geological Survey, The Johns Hopkins University, Baltimore, Maryland*

ABSTRACT

The shorelines of Maryland's portion of the Chesapeake Bay exhibit seasonal changes in direction of littoral transport and resulting beach width. Observation and study of this process at selected locations emphasizes the necessity of study for a complete years seasonal cycle before stating erosion rates of an area to be protected by structures and the cyclincal presence or absence of beaches.

The purpose of this paper is to describe seasonal beach conditions at four selected sites and resulting physical changes to protective structures. The seasonal changes will be shown by 35mm slides of the sites and of ERTS-1 underflight photography of these sites. Through the use of ERTS-1 multi-spectral photography, it will be possible to make widespread predictions elsewhere in the Bay as a direct aid in protective structure design.

1. INTRODUCTION

Aerial photography is available to the public from the U. S. Department of Agriculture, Agricultural Stabilization and Conservation Service, flown generally during warm weather months. The photography is panchromatic, showing all objects in varying shades of gray. The precise line of tide on the beach is not distinguishable, however, shallow offshore structural features are discernable. Littoral transport studies must necessarily include all seasons and the position of tide along the shoreline should be mapable from photography.

Seasonal ERTS-1 underflight color IR and color positive photography has established a geologic baseline reference of the shoreline environment of the Chesapeake Bay, and the Atlantic coast.

The purpose of this paper is to discuss in some detail one discipline application of the Maryland Geological Survey's Coastal-Estuarine Geology program, relating accumulated pre and current ground truth to ERTS-1 low altitude color IR and color positive film.

The Survey has been actively gathering physical data on the Chesapeake Bay nearshore environment since 1963. As a consequence, it has become

Original photography may be purchased from
EROS Data Center
10th and Dakota Avenue
Sioux Falls, SD 57198

apparent that littoral transport direction is seasonal, with a net direction and is related directly to seasonal prevailing winds, to intense local weather occurrences, and to the geographic location of the shore to prevailing wind direction. The geology of an eroding physiographic unit is vital to the total erosion-deposition budget of the unit, however, it becomes apparent that the nearshore shallow environment must contribute a share of the total E-R budget. To comprehend fully the offshore-onshore erosional depositional relationship, Mr. Randall T. Kerhin, geologist with the Maryland Survey, is studying in detail the offshore bar and trough structure and composition. The locations of areas to be described are shown in Figure 1.

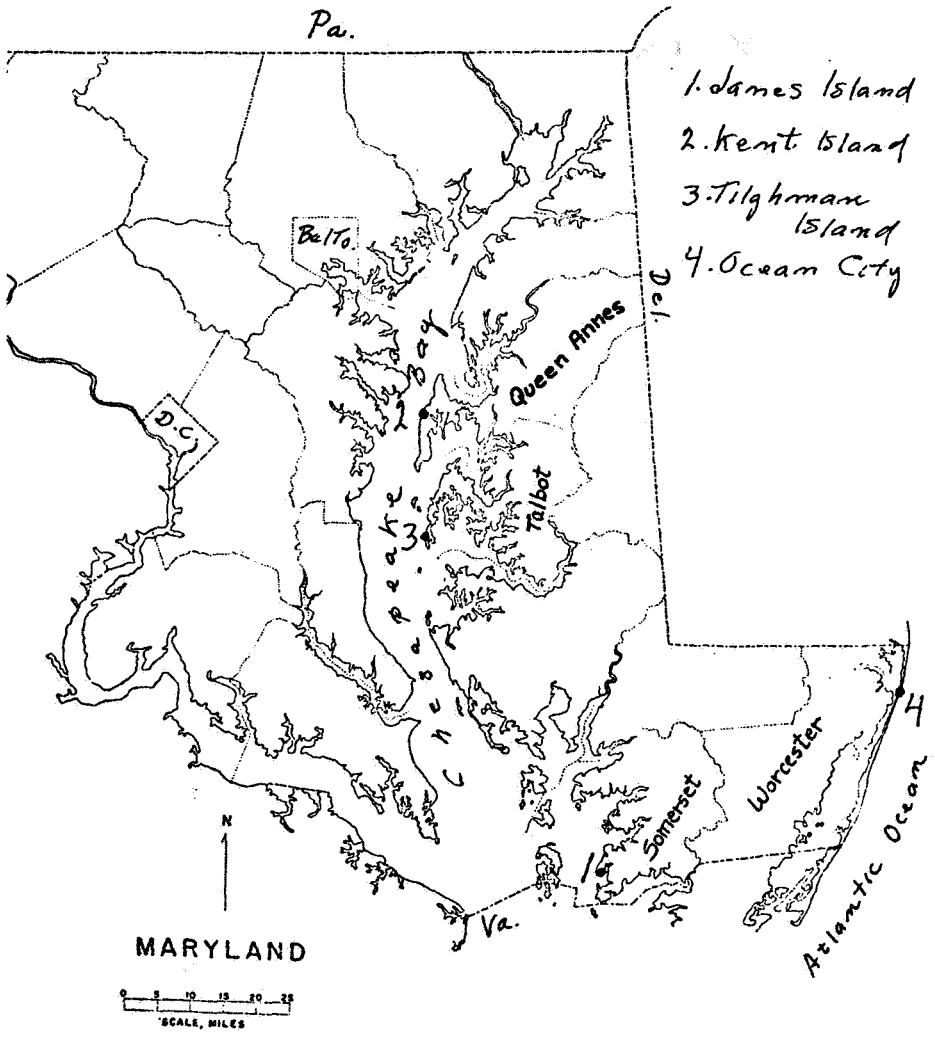


Figure 1. Locations of areas discussed

A study of the geomorphologic problem of a former spit that now serves as a barrier beach extending along the southern boundary of Janes Island State Park, Somerset County, extends slightly southeastward of Island Point a distance of 4,800 feet, disclosed two apparent but different types of littoral data. During the summer months, due to winds blowing from the southwest across Tangier Sound moved sand northward to a cove bordered by scrub size trees. There was no beach in front of the thick deep rooted organic marsh vegetation. Wave action would break chunks of the vegetation mass up and through them up on the shore. During the winter months the winds from the northwest would move the sand southward and by late spring there would be a sand beach completely covering and protecting the summertime eroding marsh shore edge. The erosion rate of this location is 1.5 feet a year, a relatively low rate, but understandably so. A time sequence of April and July, is shown by Figures 2, and 3.

Janes Island State Park - Island Point, - Looking North



Figure 2 April 29, 1971

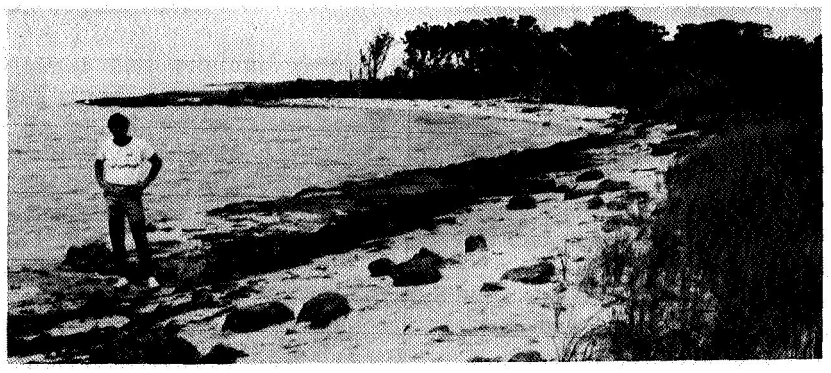


Figure 3 July 22, 1969

Through the inspection of the ERTS-1 film, these facts are documented by Figures 4 and 5, which are photo copies of ERTS-1 underflight mission 16, October 20, 1972, and mission flight 226, January 16, 1973, respectively. Unfortunately flights earlier than October are not available. The fall-winter littoral transport direction southward began before October 20, as evidenced by mission 226 flight. The color IR film definitely delineates the sand shoreline separately out the ice, while the color positive film shows the offshore bar and trough structures which the color IR does not.

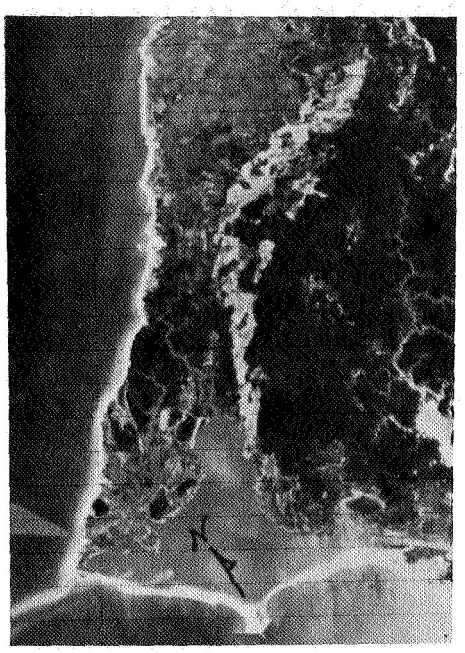


Figure 4. Janes Island
ERTS-1 Mission 16
Underflight Oct. 20, 1972

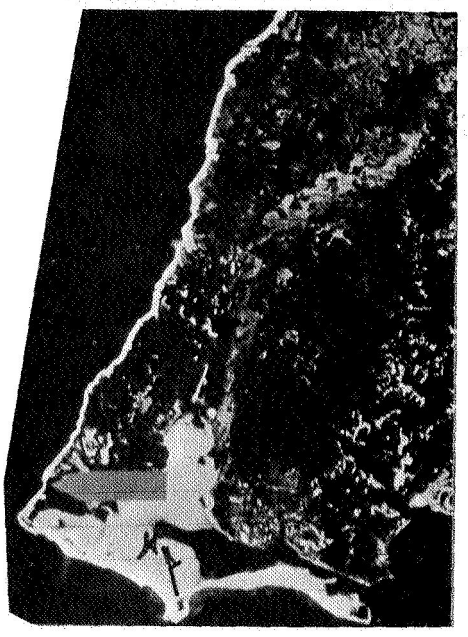


Figure 5. Janes Island
ERTS-1 Mission 226
Underflight Jan. 16, 1973

A second example area for which the Survey has pre and current ERTS-1 ground truth is the northern marker of a measured mile on Kent Island, Queen Annes County. During the summer months sand accumulates on the southern side of the groin to which the marker is attached, causing a starvation of the northern shoreline. The process is reversed in the winter; erosion rate is measured to be 5 feet a year. Figure 6 shows the summer starved condition and Figure 7 shows the winter buildup. This situation could be prevented by elimination of the groin. ERTS-1 underflight film mission 215 from an altitude of 10,000 feet dated September 23, 1972, is shown in Figure 8 and the January 16, 1973 flight is shown in Figure 9. The arrow points to the groin. The ERTS-1 film clearly shows this littoral reversal.

Figure 6. North Mile Marker - Kent Island - August 3, 1971



Figure 7. North Mile Marker - Kent Island - March 5, 1971



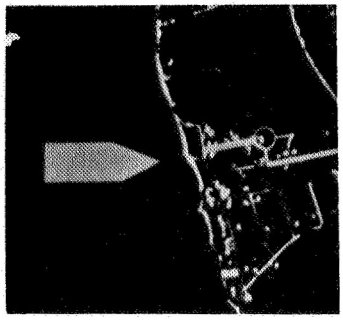


Figure 8.

Kent Island
ERTS-1 Mission 215
Underflight Sept. 23, 1972

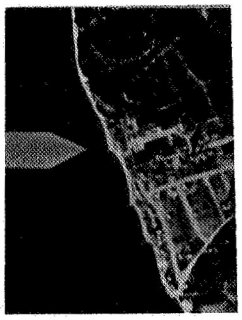


Figure 9.

Kent Island
ERTS-1 Mission 226
Underflight Jan. 16, 1973

Another area of interest is located immediately north of the U. S. Navy Research Laboratory tower, south Tilghman Island, Talbot County. Although the property is now privately owned, the State of Maryland acquired shore property having 3,800 feet of shoreline in 1963. Erosion at the rate of 16 feet per year of the area north of the protected Navy property was endangering a county road paralleling the shoreline. As a consequence the State provided in 1965, a sum of $50,000 to be used in construction of approximately 1,100 feet of protective structures which were considered as a "show case test site".

Construction was begun in April, 1966 and completed in September, 1967. The first section of structure was keyed to the northern end of the Navy steel bulkhead and consists of 270 feet of timber bulkheading, reinforced at the toe with 1/4 ton rip-rap. The remaining 730 feet was protected by a sloped revetment of interlocking concrete blocks. The use of concrete blocks in revetment design has been documented by Hall, J. V. and Jachowski, R. A. (1964) and Hall, J. V. (1967). The revetment at Tilghman has been described by Mohl, E. V. and Brown, J. D. (1967) and Slaughter, T. H. (1967).

Background knowledge of offshore and onshore conditions of the area indicated a high hydrodynamic environment, with little or no beach during most of the year. The offshore was shallow cored, indicating a predominent sandy bottom which could serve as a source of littoral material, especially during the winter months. By the spring of 1971 it was apparent that for a number of reasons, the northern 200 feet of the concrete block revetment was in trouble, the toe of the structure was being undermined. As a result of toe undermining, the structure failed along this section. (Figure 10 shows the northern end of the structure on September 26, 1967 shortly after completion. Figure 11 shows the same location on October 4, 1972.)

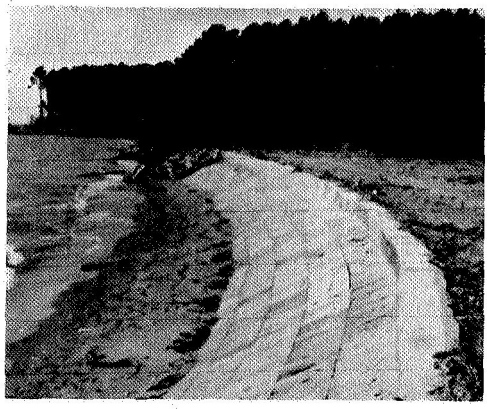


Figure 10. S. Tilghman Island
Sept. 26, 1967

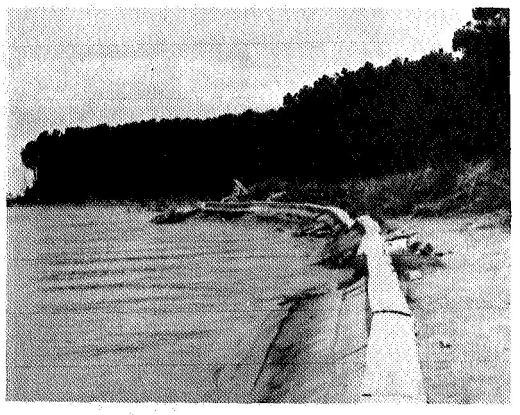


Figure 11. S. Tilghman Island
Oct. 4, 1972

Inspection of ERTS-1 low altitude flight film, Color IR of October 20, 1972, Figure 12 and January 16, 1973, Figure 13, and color positives of January 16, 1973, does not show any beach for the 3,800 feet under consideration. The lack of winter sand accumulation as shown by the January 16, 1973 flight may not be the usual situation as sometimes is the case, but it emphasizes the fact that there is very little beach sand to be counted on to protect the toe of the revetment.



Figure 12.

S. Tilghman Island
ERTS-1 Mission 16
Underflight
Oct. 20, 1972



Figure 13.

S. Tilghman Island
ERTS-1 Mission 226
Underflight
Jan. 16, 1973

The last area to be described is the beach at Ocean City, Maryland, specifically the beach between 12th and 27th Streets, and 73rd and 78th Streets. These are two areas of Ocean City beach groin field systems. The groins in the southern field were erected over the period 1938 to 1961. The northern groin field was erected in 1961.

Of concern is the effectiveness or non-effectiveness of the groin fields and individual groins. Winter northeast winds take their toll of the beach and in some cases the dune is under extreme high tide attack. (Figure 14 dated February 7, 1973, shows weak beach conditions at the 75th Street groin.

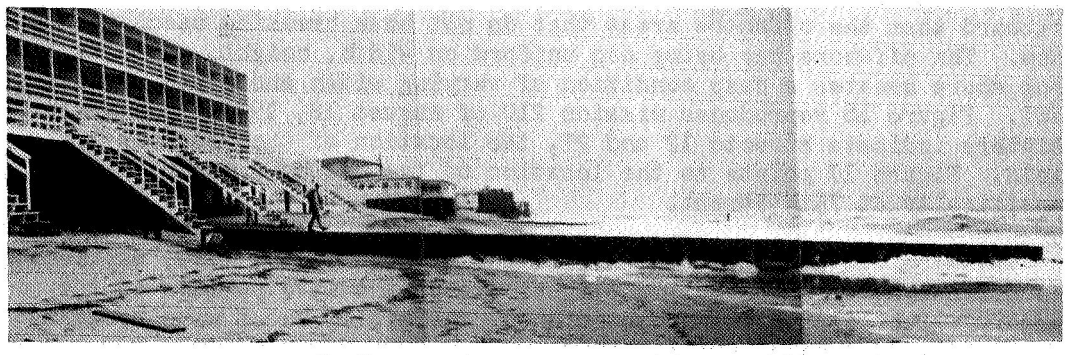


Figure 14. Ocean City, 75th Street February 7, 1973

Figure 15 shows the beach conditions at 13th Street on October 17, 1972. The groin in the foreground is completely exposed and high tide reached under the base of the boardwalk.



Figure 15. Ocean City, 13th Street October 17, 1972

Available offshore profiled data obtained by the U. S. Army Corps of Engineers along Ocean City beach show the nearshore bar to vary in width and height and distance from shore. Personal knowledge of Ocean City summer beach swimming conditions, documents the existence of rip currents, when along shore currents are increased. ERTS-1 underflight low altitude film of mission 210 on August 12, 1972, disclosed very clearly, the apparent relationship of the offshore bar to the beach. The day was a fairly normal summer day weather-wise, winds started off in the morning from the north and swung around to the southeast later in the day. Maximum wind was 6 to 10 mph. The minimal offshore wave breaking pattern of the day disclosed that where the waves break the shoreline is farther eastward than the offshore areas that do not have breaking waves facing them. The offshore bar being non uniform on width, height, and distance from shore creates a cusp condition of varying width and depth of enlargement. Figure 16 reproduces mission 210 of August 12, 1972. The numbered pointers indicate streets 12 and 27, the location of the southern groin field. Figure 17 points to the location of the northern groin field, specifically at 75th Street.

Mission 226 low altitude underflight of January 16, 1973, duplicates the essence of August 12, 1972 flight, except the wave pattern of the January flight is a little more intense, therefore, exact wave breaking patterns are not discernable.

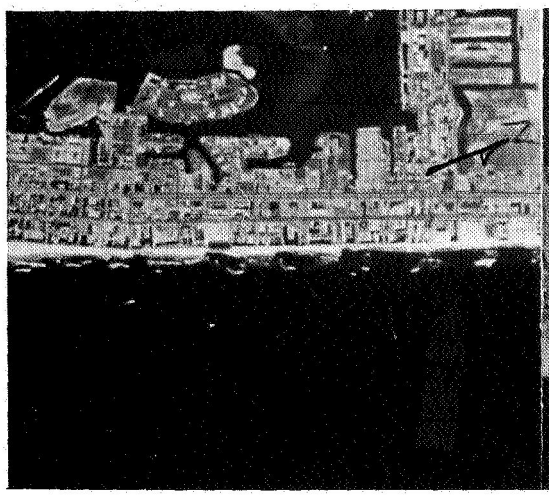


Figure 16. South Ocean City
ERTS-1 Mission 210
Underflight August 12, 1972

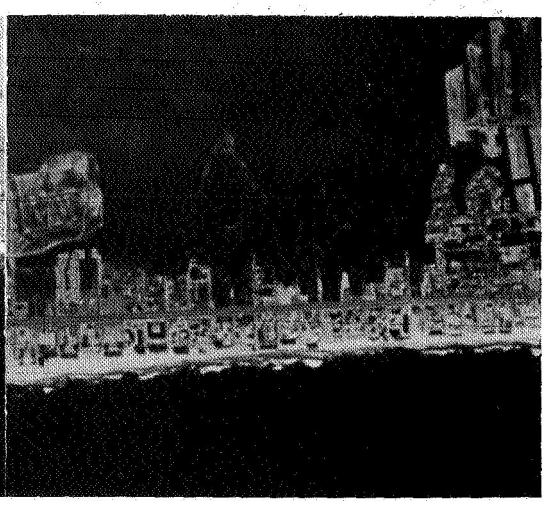


Figure 17. South Ocean City
ERTS-1 Mission 210
Underflight August 12, 1972

ERTS-1 low level underflight multi-spectral photography has proven to be a most productive aid in study of littoral transport of selected areas within the Chesapeake Bay, and of geohydrodynamic processes along Maryland's Atlantic Coast.

REFERENCES

Hall, J. V. and Jachowski, R. A. (1964), Concrete Block Revetment Near Benedict, Maryland: U. S. Army Coastal Engineering Research Center, Miscellaneous Paper No. 1-64

Hall, J. V. (1967), Wave Tests of Revetment Using Machine-Producted Interlocking Blocks: U. S. Army Coastal Engineering Research Center, Reprint

Mohl, E. V. and Brown, J. D. (1967), Flexible Revetment Using Interlocking Concrete Blocks, Tilghman Island, Maryland: Journal of the American Shore and Beach Preservation Association, Vol. 35, No. 2, October, 1967

Slaughter, T. H. (1967), Vertical Protective Structures in the Maryland Chesapeake Bay: Journal of the American Shore and Beach Preservation Association, Vol. 35, No. 2, October, 1967

N73-28342

Paper M 2

RECOGNITION OF BEACH AND NEARSHORE DEPOSITIONAL FEATURES OF CHESAPEAKE BAY

Randall T. Kerhin, Geologist, *Maryland Geological Survey, The Johns Hopkins University, Baltimore, Maryland*

ABSTRACT

Beach and nearshore depositional features are being mapped with the objectives of determining a quick-look analysis of littoral drift and sedimentation patterns in areas of little or no data. Evaluation of beach and nearshore features aid in the selection of small boat harbors, shoreline protective structures, and general coastal zone development.

Through ERTS-1 aircraft support imagery, beach depositional features mapped are cuspate forelands, welded beach ridges, and recurved spits. The nearshore depositional features exhibit a bar and trough topography with three distinct types of sedimentary structures; longshore, transverse, and reticulated bars. Synoptic coverage of beach and nearshore depositional features by ERTS-1 data help in determining the general sedimentation patterns, growth of the beach features and stability of the bar and trough topography.

1. INTRODUCTION

The Chesapeake Bay region of Maryland is an area of intense research into the physical, chemical, and biological aspects of the marine sciences. One area that has received little investigative research has been the beach and nearshore environment and related sedimentary structures. Kindle (1936) was the first to note the nearshore sand bars of Chesapeake Bay. Since Kindle's notes, the Maryland Geological Survey has conducted preliminary observations on the nearshore sand bars in a cooperative program with the Coastal Engineering Research Center at Chesapeake Bay, Maryland. With the enactment of the Coastal Zone Management Act of 1972 and a proposed House Joint Resolution by the State of Maryland, more emphasis is now being conducted into the coastal zone of Maryland. Using ERTS-1 aircraft support imagery, beach and nearshore depositional features of Chesapeake Bay are being mapped and described with the objectives of developing for the State of Maryland a geological baseline for the coastal zone (Figure 1.)

Beach Depositional Features

Beach depositional features are uncommon to Chesapeake Bay especially with the shore erosion problems that exist. The beach sedimentary structures occupy a small percentage of the total area of Chesapeake Bay and are

PRECEDING PAGE BLANK NOT FILMED

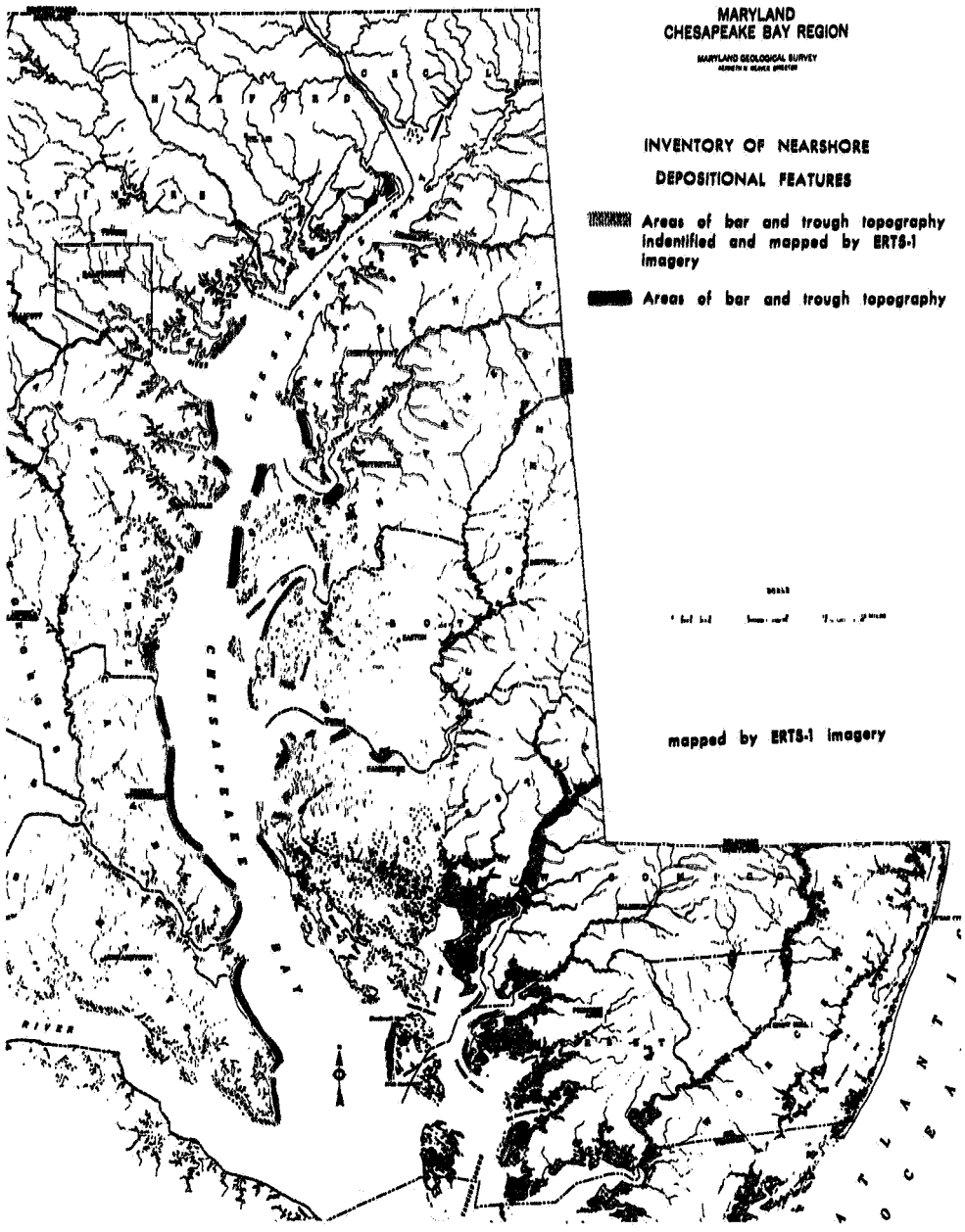


Figure 1. Preliminary distribution map of the nearshore depositional feature of Chesapeake Bay

generally localized. Features being mapped by ERTS-1 aircraft support imagery are baymouth bars, recurved spits, and cuspate forelands.

One area of interest is the Long Beach-Flag Ponds community of Calvert County. As shown by Figure 2, the depositional features are a series of beach ridges and a secondary recurved spit developed on a straight reach of coastline. Historically, the cape of Flag Ponds has migrated southward over distance of 1500 feet from 1847 to 1945 with linear recession of approximately 300 feet on the east shore (Singewald & Slaughter, 1949).

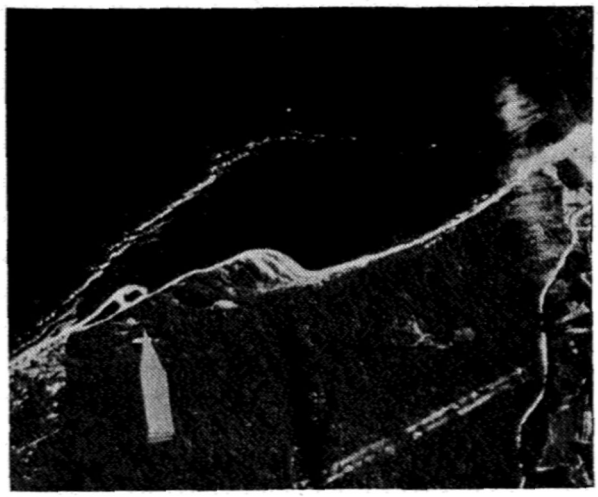


Figure 2. Aircraft support (Wallops-NASA) imagery of Flag Ponds, Oct. 1972, a cuspate foreland and recurved spit forming on a straight reach of coastline. Note breaking wave pattern

The development of the secondary beach feature, the recurved spit, first appeared in the mid-1960's. The young age of the recurved spit suggests a massive introduction of sediment into the nearshore environment, north of the Flag Ponds area. One possible explanation is that in 1949 the Long Beach harbor was dredged and disposal of the sediments was south of the harbor jetties. With a predominate southerly drift direction, the disposal sediments migrated southward. Accumulation of the sediments as a recurved spit appears related to the wave refraction pattern (Figure 2) and creation of a reverse current direction. Schubel (1972) also suggests a reverse current or eddy system for the Flag Ponds area. The migration of the nose of the spit has progressed in the southerly direction. The growth of the recurved spit has occurred in "spurts" and not as a continuous growth pattern. Each additional growth of the recurved spit appears related to the occurrence of a preceding northeast storm.

Nearshore Depositional Features

Prime prerequisites of nearshore sand bars are gradually sloping nearshore bottom and abundant sand supply (Davis and Fox, 1972). A gradually sloping nearshore bottom is evident in Chesapeake Bay as indicated by hydrographic charts. Abundant sand supply is being introduced into Chesapeake Bay from the eroding shoreline and not by the major river systems. (Schubel, et.al., 1972)

Figure 1 is a preliminary distribution map of the nearshore bottom structures. The major nearshore bottom as indicated by the darkened pattern have been previously known but ERTS-1 aircraft support imagery has supplied the capability to delineate, describe and interpret these structures.

The predominate sand bar type is the longshore bar and is confined to areas of generally straight coastlines. The length of straight coastline does not appear to influence longshore bar and trough development as seen by longshore bar development in the subestuaries where small lengths of coastline are prevalent. The longshore bars are generally parallel to the shoreline and to each other and continue along the coast until the structures are interrupted by headlands or natural tidal channels. The longshore bars are diverted in the offshore direction and diffused into a shoal area with or without a reticulated bar pattern. For example, parallel longshore bars exist along a straight coastline of Calvert County from Herring Bay to Plum Point. As the longshore bars approach Plum Point, a prominent headland, the longshore bars diffused into a shoal area without a reticulated bar pattern adjacent to Plum Point (Figure 3), whereas along Eastern Neck in Kent County, the longshore bars are diverted offshore by a tidal channel and develop a shoal area with reticulated bar pattern (Figure 4).

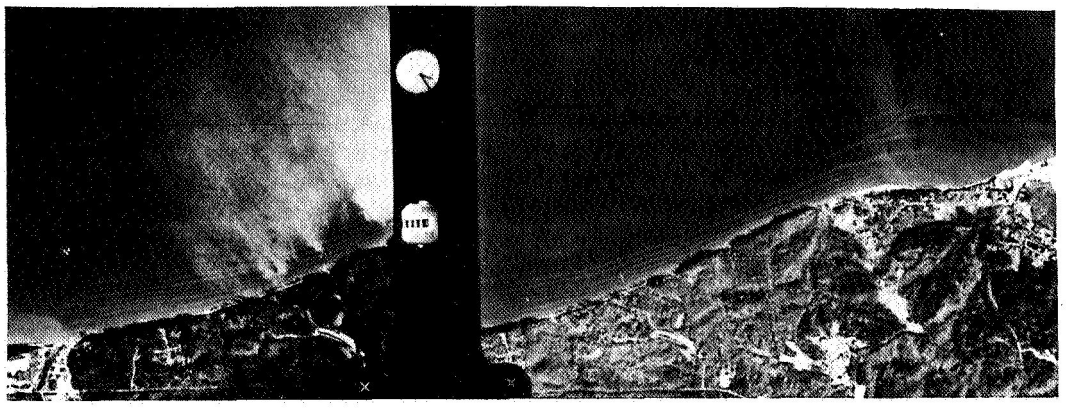


Figure 3. Aircraft support (Wallops-NASA, Oct. 1972) imagery of Longshore Bar-system diverted by prominent headlands. Plum Point at Chesapeake Beach, Maryland

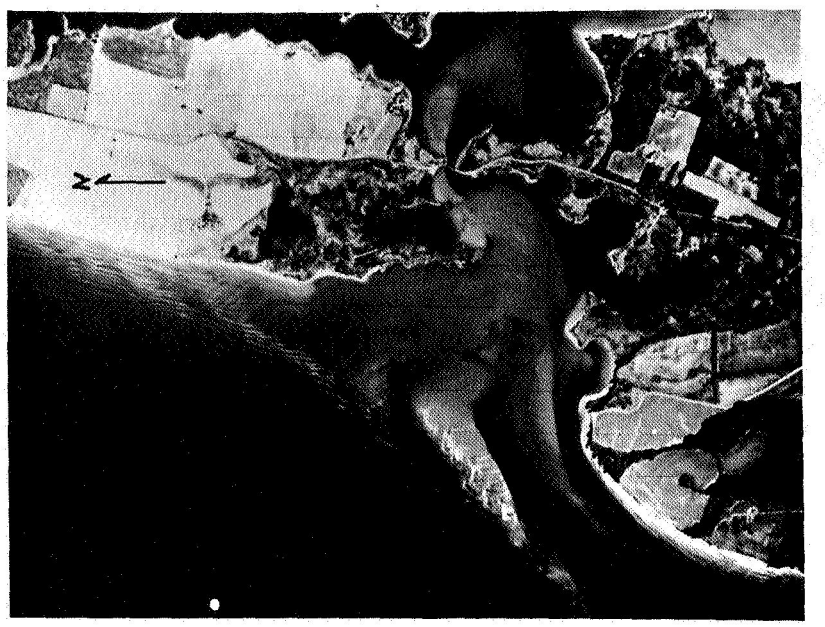


Figure 4. Aircraft support (Wallop-NASA) imagery Oct. 1972, of Longshore bar system diverted by natural tidal channel at Eastern Neck Island

The number of longshore bars may be as many as fifteen and generally increase in size and wavelength in the offshore direction (Figure 5). In some areas, two distinct sets can be delineated, an inner set of closely spaced, small amplitude bars and an outer set of widely spaced, large amplitude bars interrupted by a natural channel. The intervening channel is wider than the corresponding trough dimensions which allow for division of the bars into two sets. Bifurcation and a sinuous form are common features of the longshore bars particularly the inner nearshore longshore bars. Along a longshore bar, the bars exhibit high pockets of sand with intervening low areas or saddles and appear to be related to bifurcation of the bar form.

Summary

With the capability of the ERTS-1 aircraft support imagery, the beach and nearshore depositional of Chesapeake Bay are being mapped and a geological baseline of the coastal environment is being developed. The beach features are uncommon to Chesapeake Bay and are localized features. Baymouth bars, recurved spits, and cuspate forelands are the common features. The nearshore depositional features exhibit a longshore bar and trough topography and generally confined to straight reaches of shoreline. The longshore bars may number as many as fifteen and increase in size and wave length in the offshore direction.

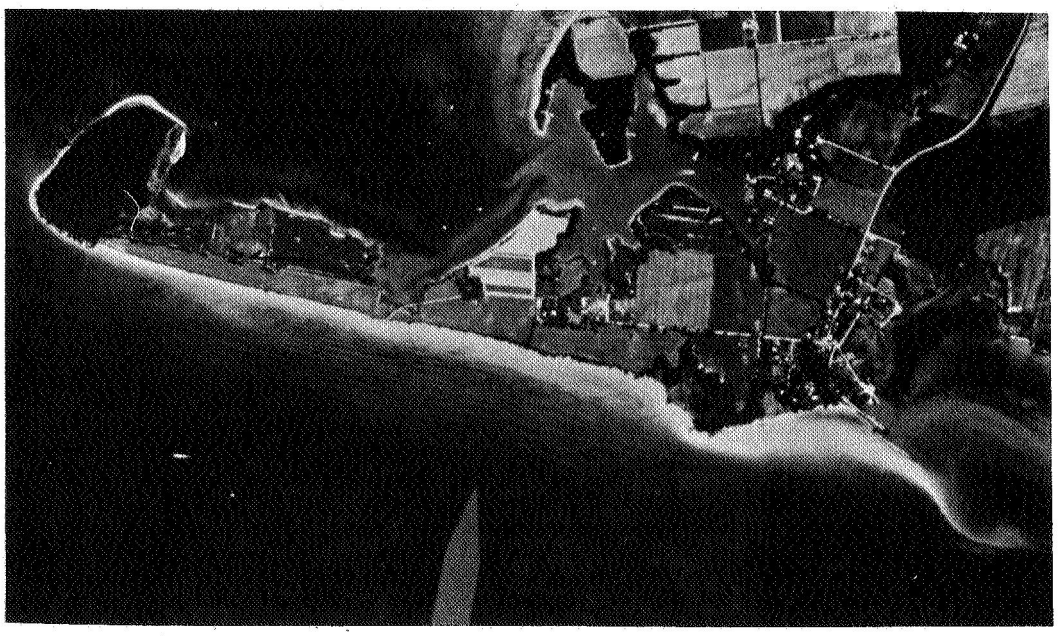


Figure 5. Aircraft support (Wallops-NASA) Oct. 1972 imagery Rich Neck exhibiting typical longshore bar and trough system of Chesapeake Bay

REFERENCES

Davis, R. A. and W. T. Fox, 1972, Coastal processes and nearshore sand bars: Jour. of Sed. Pet., vol. 43, p. 401-412

Kindle, E. M., 1936, Notes on shallow-water sand structures: Jour. Geol., vol. 44, pp 861-869

Schubel, J. R., H. H. Carter, E. W. Schiemer, and R. C. Whaley, 1972, A case study of littoral drift based on long-term patterns of erosion and deposition: Chesapeake Sci., vol. 13, p 80

Singewald, J. T. and T. H. Slaughter, 1949, Shore Erosion in Tidewater Maryland: Md. Geol. Survey, Bull. 6, pp 1-121

N73-28343

Paper M 3

APPLICABILITY OF ERTS-1 IMAGERY TO THE STUDY OF SUSPENDED SEDIMENT AND AQUATIC FRONTS

V. Klemas, R. Srna, W. Treasure, M. Otley, *College of Marine Studies, University of Delaware*

Imagery from three successful ERTS-1 passes over the Delaware Bay and Atlantic Coastal Region have been evaluated to determine visibility of aquatic features. Data gathered from ground truth teams before and during the overflights, in conjunction with aerial photographs taken at various altitudes, were used to interpret the imagery. The overpasses took place on August 16, October 10, 1972, and January 26, 1973, with cloud cover ranging from about zero to twenty percent. (I.D. Nos. 1024-15073, 1079-15133, and 1187-15140). Visual inspection, density slicing and multispectral analysis of the imagery revealed strong suspended sediment patterns and several distinct types of aquatic interfaces or frontal systems.

The interfaces are a major hydrographic feature in Delaware Bay and frequently include regions of high convergence. As shown in Figure 1, in the upper and middle bay and interfaces tend to align along the flow axis of the river or parallel to the shoreline. They are strongest during the ebb portion of the tidal cycle and seem to be associated with velocity shears induced by differences in bottom topography. Boundaries like the one shown in Figure 2 exhibit a strong change in color and turbidity, with Secci depths changing by roughly a factor of two as one crosses them. Convergence of these boundaries is illustrated in Figure 3, which shows a boundary moving across the anchored fluorescein dye pack, and capturing and holding the end of the dye streak. The displacement of portions of the wake of a ship crossing a boundary, shown in Figure 4, is an indication of shear along the boundary. Storms tend to break up the boundaries, with three dimensional patches of the more turbid water not mixing with the less turbid water, but clinging together up to one hour after the boundary itself has been destroyed.

Original photography may be purchased from:
EROS Data Center
10th and Dakota Avenue
Sioux Falls, SD 57198

Original photography may be purchased from:
EROS Data Center
10th and Dakota Avenue
Sioux Falls, SD 57198

The second type of interface, shown in Figure 5, is primarily a tidal intrusion of the shelf water during incipient flood tide, with associated discontinuities in salinity and temperature. The convergence properties of such fronts attract heavy accumulations of foam which were found to contain strong concentrations of toxic substances. The shelf water, having higher salinity and density than bay water, tends to penetrate into the bay along the deep channel, and thus establish higher salinity in the middle than near the shores of the bay. (Figure 6). Thus the apex of the frontal wedge in Figure 5 is moving along the deep channel of the bay.

Figure 7 shows ERTS-1 imagery of the mouth of Delaware Bay in band 5 obtained on August 16, 1972. Best visibility of boundaries and sediment plumes was obtained in band 5. As illustrated in Figure 8, locally suspended sediment is visible above the shoals near Cape May. One boundary is visible near the middle of the bay mouth, a second one protrudes in the southerly direction from Cape Henlopen, and a third one extends in the southeasterly direction further south, near Indian River Inlet. This boundary was moving rapidly at the time and divers operating in 18 feet of depth noted a change in visibility from two feet to six feet as the boundary passed over the tower they were working on. Figure 9 shows the boundary approaching the beach two miles north of Indian River Inlet. Figure 10 shows a similar boundary moving shoreward, as seen from an aircraft. The tide condition at the time of the ERTS-1 pass was near peak flood velocity at the mouth of the bay. Since microdensitometry traces between the Capes in Figure 7, seem to correlate with the depth profile, most of the visible suspended sediment should represent sand from local shoals and shallow areas put into temporary suspension by the flood current and waves. Sample analyses and Secci depth measurements seem to support this conclusion. This relationship becomes more complex during ebb tide when large quantities of silt and clay are also present.

Figures 11 and 12 show band 5 imagery from ERTS-1 passes over Delaware Bay on October 10th, 1972, and January 26th, 1973 respectively. Figures 13 and 14 describe the tidal conditions in the bay at the time of the respective ERTS-1 overpasses. Note that on October 10th there was high water slack at the baymouth and peak flood near the Chesapeake and Delaware Canal, in the upper portion of the bay. (Figure 13). Therefore, as illustrated in Figure 15, very strong boundaries are visible in Figure 11 in the upper portion of the bay. In contrast, according to Figure 14, on January 26th, the baymouth was flooding; near the C & D Canal the tide was ebbing; and there was a high slack in the upper half of the bay. Therefore the ERTS-1 image in Figure 12 shows considerable mixing and less boundary formation in the upper portion of the bay than the image in Figure 11.

The three transsects across the bay shown in Figure 15 are traversed by boats and low altitude aircraft during ERTS-1 overpasses to collect ground truth. Boats and aircraft were coordinated via radio, to direct the ground teams to stations. At each station, water samples were taken at the surface and/or one meter depth. Secchi depth, temperature, color and salinity were also recorded. The water samples were filtered using a Millipore filtration apparatus and 54mm Gilman glass filter pads. The filter pads were dried at 105°C, dessicated and weighed to determine the mass of the particulate matter. Carbon analyses were run on filter pads from each station to determine total percent carbon, by weight. X-ray diffraction analyses are presently being conducted on the remaining filter pads, to determine clay mineralogy. Densitometer traces and density slicing across all ERTS-1 bands are currently being correlated with suspended sediment load, sediment size, Secci depth and other parameters. (Figure 16).

Before the October 27, 1972, pass of ERTS-1, an 800 foot wide slick of Rhodamine-B dye was inserted at the proposed eight mile site for an offshore oil terminal, as shown in Figure 17. Cloud cover prevented the satellite from imaging the dye slick, however, aircraft tracking the dye patch recorded a boundary sweep across the dye patch stretch it along the boundary, and carry it about a mile towards the bay during flood tide. The stretched dye slick is shown in Figure 18, at the end of its one mile traversal, using narrowband red filters to enhance the weakened dye concentration. Coordinated experiments involving dye drops, sludge and acid disposal during ERTS-1 overpasses will be carried out during the coming six weeks.

ERTS-1 Multispectral scanner band 5 (0.6-0.7 microns) gave the sharpest definition of interfaces between waters of differing turbidity. Band 4 (0.5-0.6 microns), due to its deeper water penetration, was more sensitive to patterns having lower turbidity, yet was veiled by a uniform blanket of atmospheric scattering making identification of sediment patterns more difficult. Band 6 (0.7-0.8 microns) and band 7 (0.8-1.1 microns) clearly delineated the shore line and discriminated water from land in the marshes.

This project is partly funded through ONR Geography Programs, Contract No. N00014-69-A0407; and NASA-ERTS-1, Contract No. NAS5-21837.



Figure 1: Aquatic interfaces and frontal systems observed in Delaware Bay.

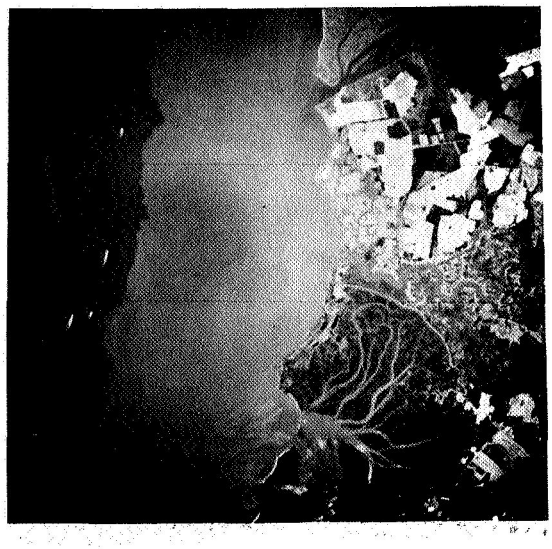


Figure 2: A shear boundary near the Delaware Coast.

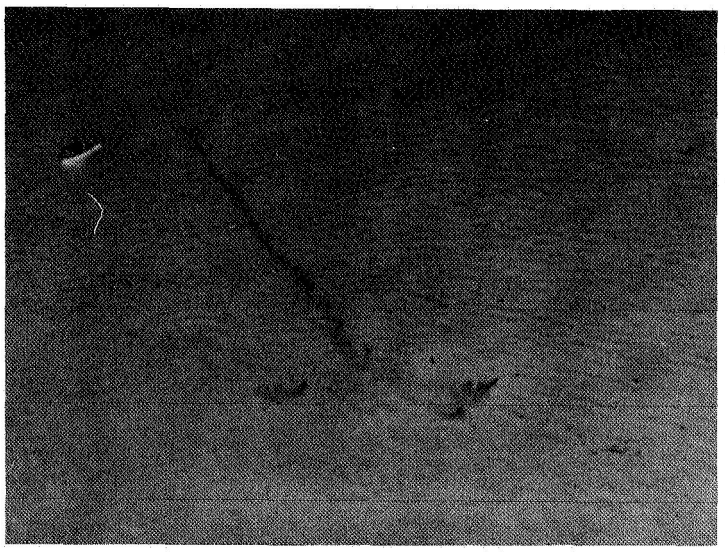


Figure 3: Dye experiment to show convergence properties of boundary.

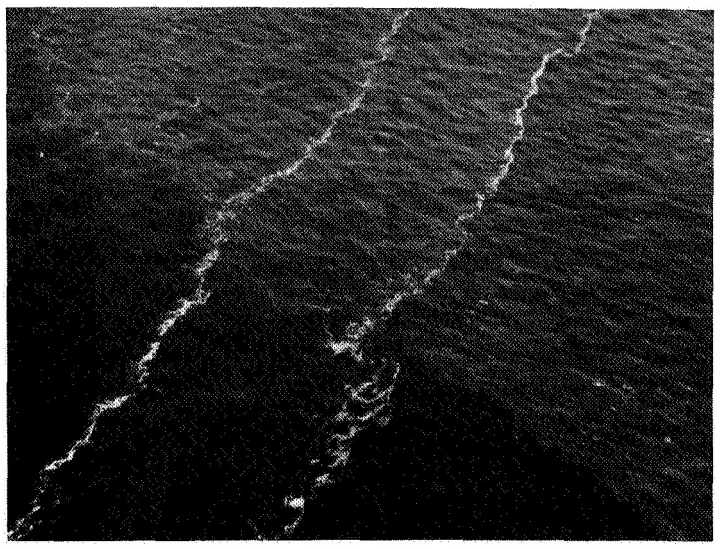


Figure 4: Shear visible in displacement of wake of ship crossing boundary.

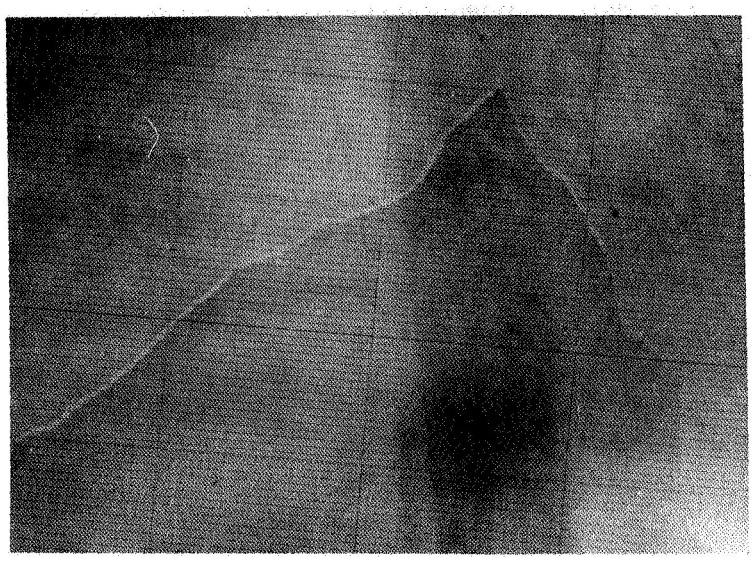


Figure 5: Frontal system due to salt water intrusion into Delaware Bay.

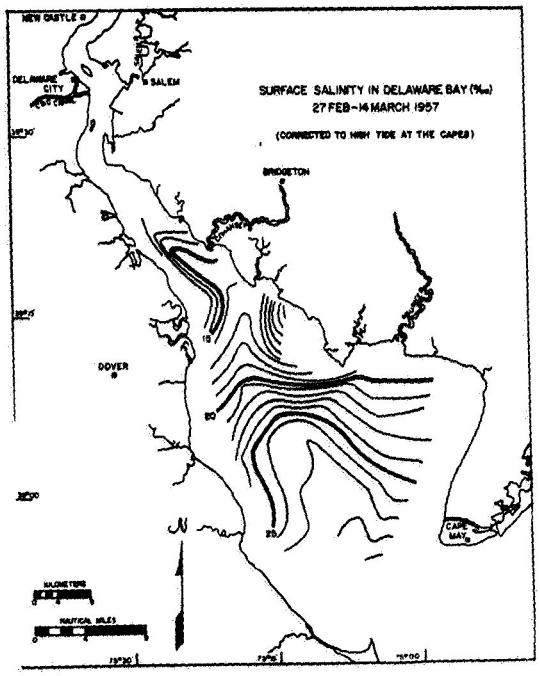


Figure 6: Salinity distribution in Delaware Bay.

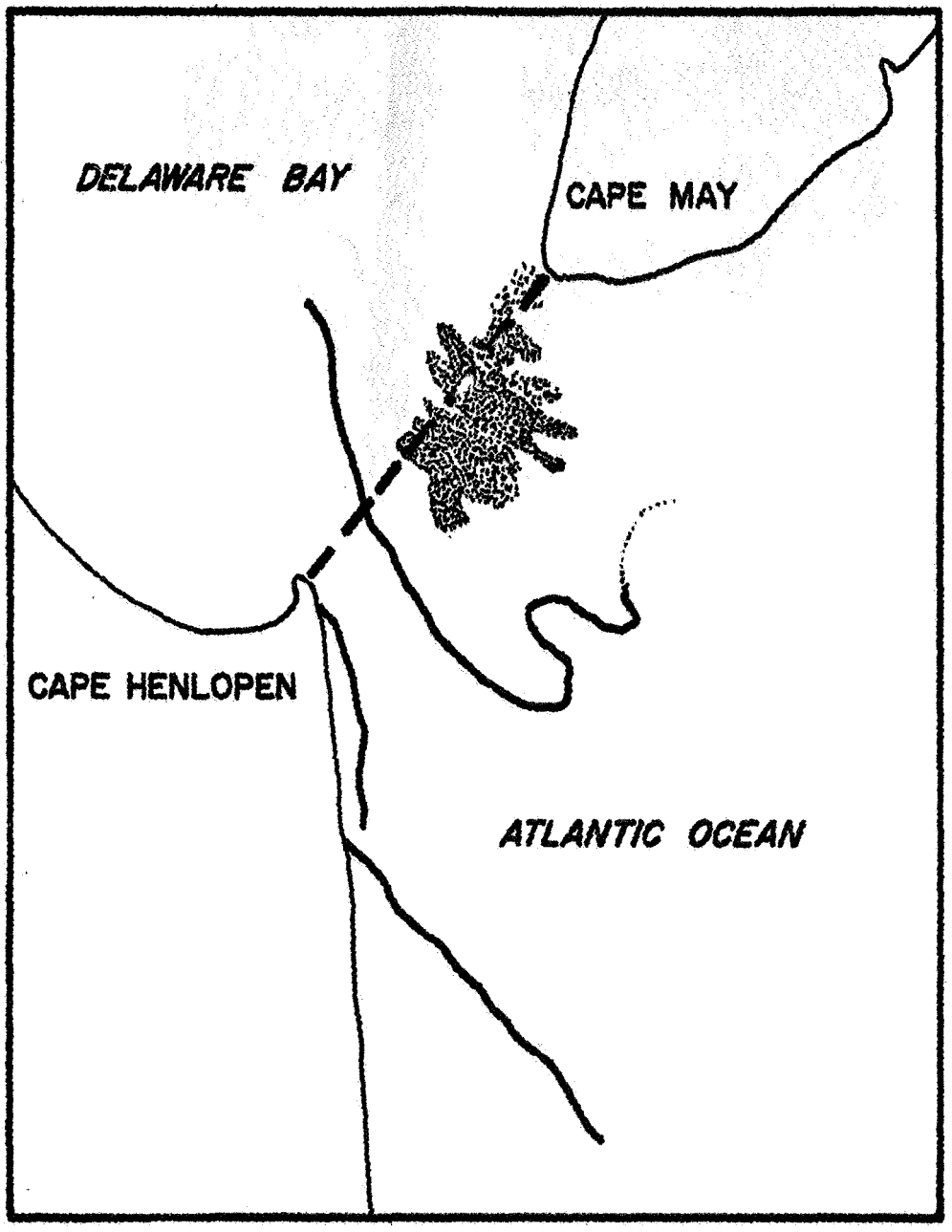


Figure 7: Aquatic boundaries and suspended sediment plumes identified in the ERTS-1 image of August 16, 1972, shown in Figure 6.

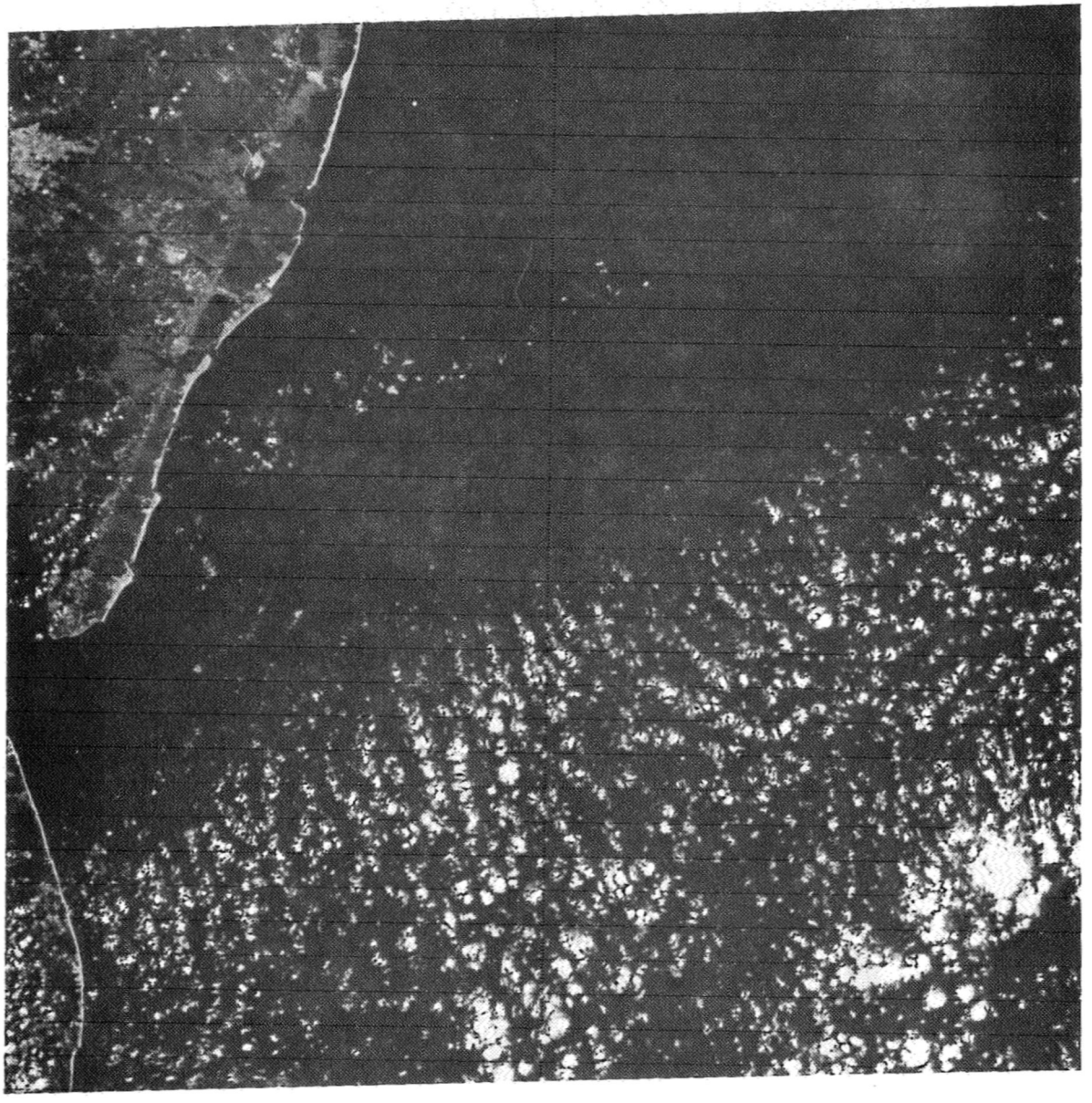


Figure 8: ERTS-1 image of the mouth of Delaware Bay (Band 5, August 16, 1972, I.D. 1024-15073).

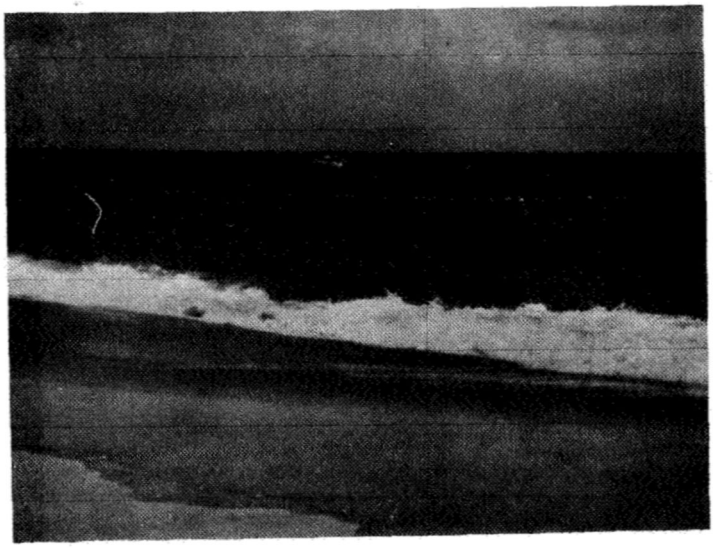


Figure 9: Boundary in ERTS-1 picture of Figure 7 seen approaching the beach.

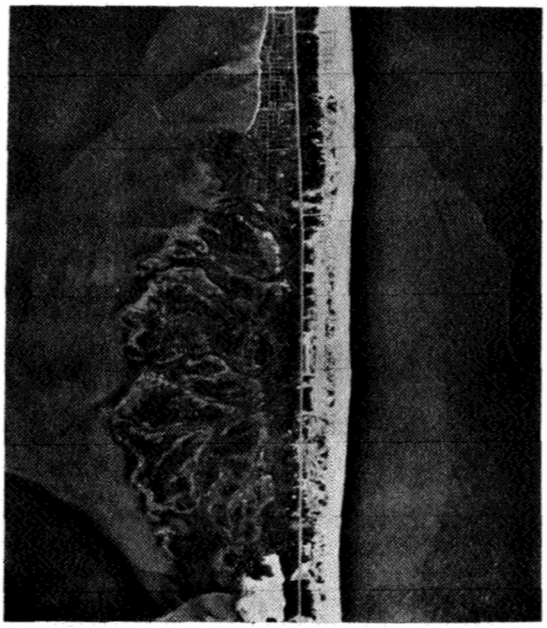


Figure 10: Aircraft picture of boundary near Indian River Inlet.



Figure 11: ERTS-1 image of Delaware Bay obtained in band 5 on October 10, 1972. (I.D. No. 1079-15133).



Figure 12: ERTS-1 image of Delaware Bay obtained in band 5 on January 26, 1973. (I.D. No. 1187-15140).

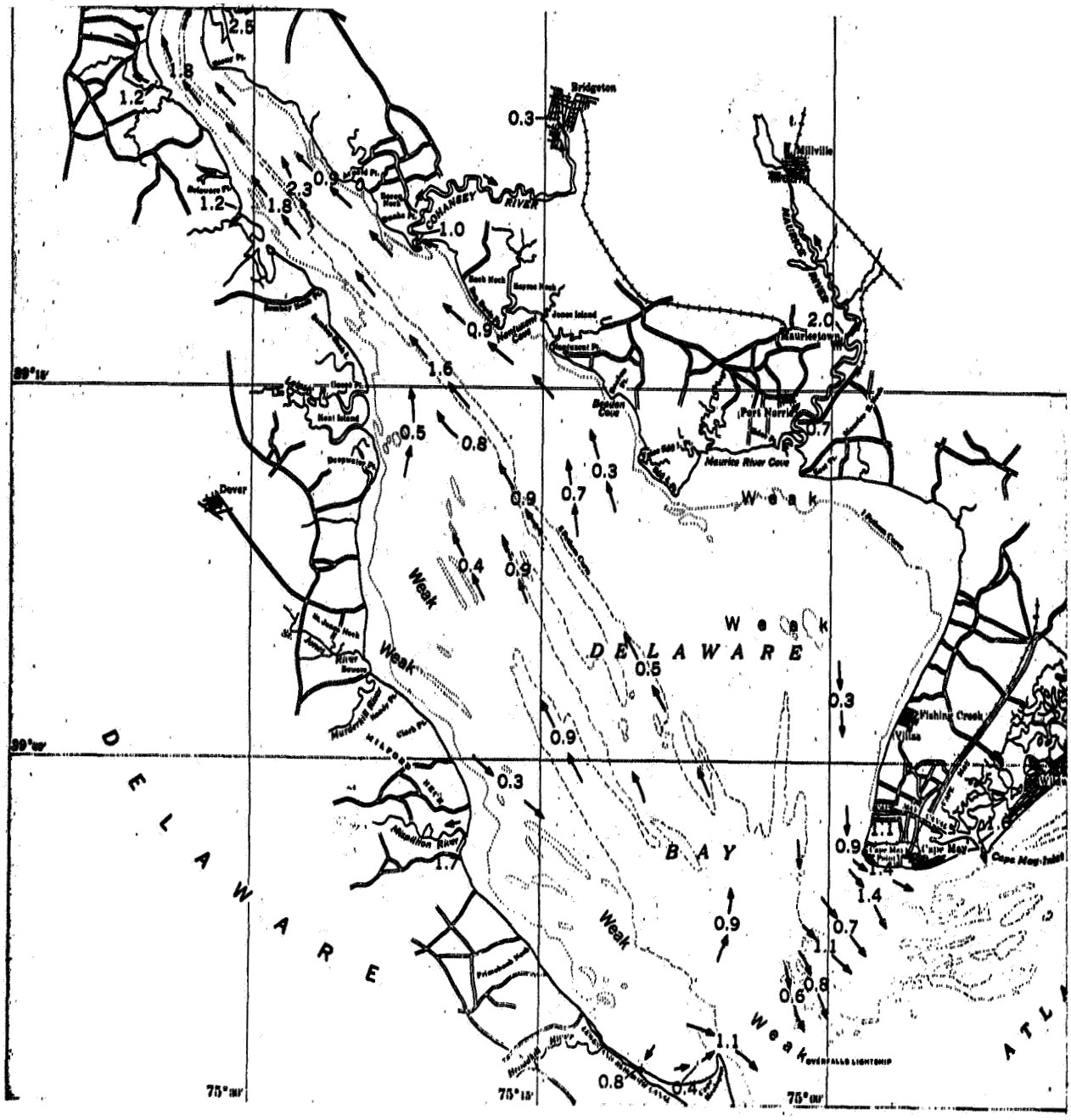
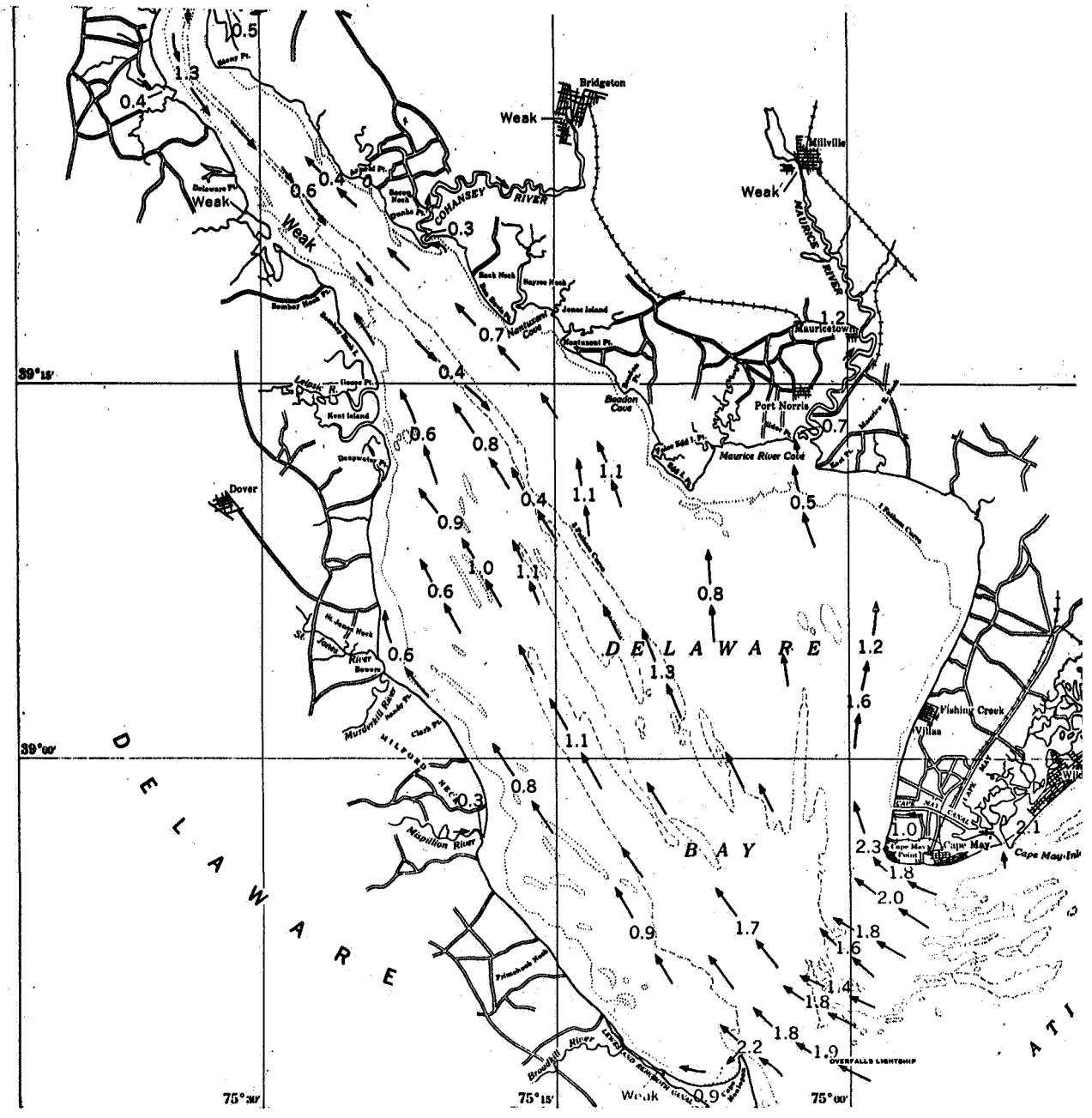


Figure 13 Tidal conditions in Delaware Bay at the time of the ERTS-1 image shown in Figure 11. The upper bay is near maximum flood, resulting in sharp shear boundaries.



ONE HOUR BEFORE MAXIMUM FLOOD AT DELAWARE BAY ENTRANCE

Figure 14 Tidal conditions in Delaware Bay at the time of the ERTS-1 image shown in Figure 12. The upper bay is near high water slack, causing boundaries to weaken and more mixing to occur.

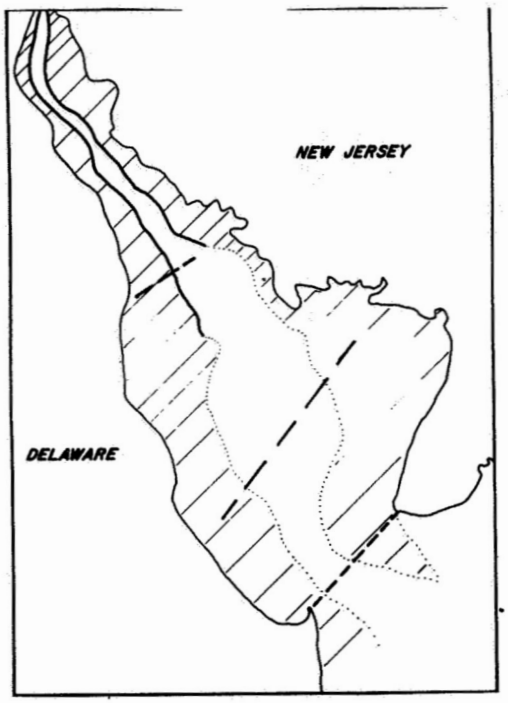


Figure 15: Aquatic boundaries and suspended sediment visible in ERTS-1 image of October 10, 1972, shown in Figure 11. Transsects of boats and aircraft collecting ground truth are shown in the upper, middle and lower Delaware Bay.

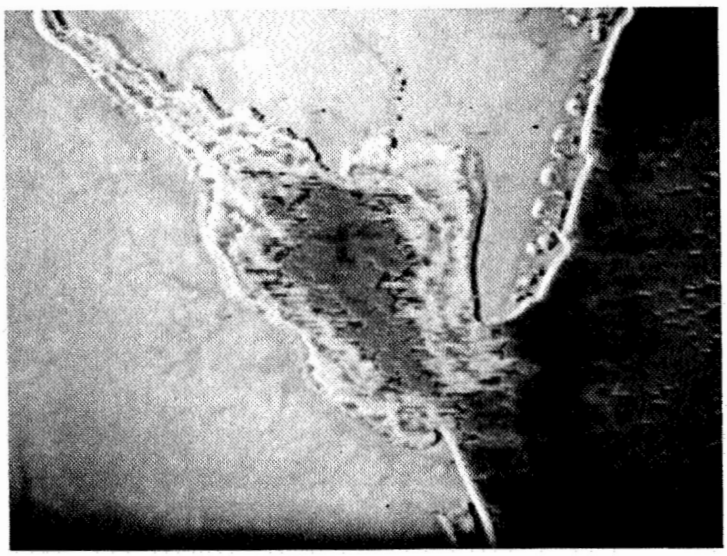


Figure 16: Result of Color Density Slicing of ERTS-1 Image of Figure 11. (October 10, 1972, pass over Delaware baymouth).

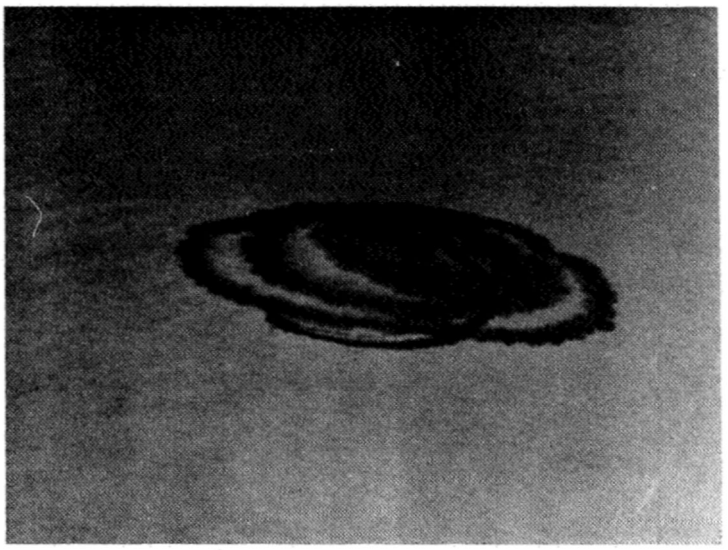


Figure 17: Rhodamine-B dye patch injected at proposed 8-mile off-shore oil terminal site. The size of the patch is about 800 feet.



Figure 18: Dye patch is captured by moving frontal systems and carried one mile towards the Bay.

N73-28344

Paper M 4

CORRELATION OF ERTS MULTISPECTRAL IMAGERY WITH SUSPENDED MATTER AND CHLOROPHYLL IN LOWER CHESAPEAKE BAY

D. E. Bowker, *NASA-Langley Research Center, Hampton, Virginia,* P. Fleischer, T. A. Gosink, W. J. Hanna and J. Ludwick, *Old Dominion University, Norfolk, Virginia*

ABSTRACT

The feasibility of using multispectral satellite imagery to monitor the characteristics of estuarine waters is being investigated in this study. Preliminary comparisons of MSS imagery with suspended matter concentrations, particle counts, chlorophyll, transmittance and bathymetry have been made. Some visual correlation of radiance with particulates and chlorophyll has been established. Effects of bathymetry are present, and their relation to transmittance and radiance is being investigated. Greatest detail in suspended matter is revealed by MSS band 5. Near-surface suspended sediment load and chlorophyll can be observed in bands 6 and 7.

Images received to data have partially defined extent and location of high suspensate concentrations. Turbid water of the James River enters Chesapeake Bay as a plume that can be traced along the southern shore and extends seaward of Cape Henry. An area of highly variable turbidity exists in the lower Bay between Hampton and Cape Charles, and may be related to strong tidal currents and large-scale bedforms found here. Net quantity of suspended matter in the lower Bay has been decreasing since the inception of the study, and represents the diminution of turbid flood waters carried into the Bay in late September, 1972. The results so far point to the utility of MSS imagery in monitoring estuarine water character for the assessment of siltation, productivity, and water types.

1. INTRODUCTION

The single most useful body of data that one could assemble concerning an estuarine system would be information from which a realistic model of water movement could be developed for the system is generally recognized. Almost all else that occurs in the system is controlled by circulation or is strongly related to it. The causes of water movement, such as tides, wind, and density gradients due to variations in salinity, sediment load and temperature have been delineated. The

Original photography may be purchased from:
EROS Data Center
10th and Dakota Avenue
Sioux Falls, SD 57198

integration and correlation of the causes of water movement in an estuarine system are complex problems which have been adequately solved for only a very few simple situations.

The lower Chesapeake Bay is a complex estuarine system. It, like many other similar systems, is undergoing continuous change. The factors influencing water circulation are not stable. Physical models of parts of this system have been constructed by the U. S. Army Corps of Engineers. These models have yielded useful results in several experiments, but the changing patterns of water circulation in the actual system cannot be duplicated in these physical models. The water circulation patterns in the lower Chesapeake Bay system remain largely unknown.

Direct measurements of water movement may bot as fully explain the dispersal of pollutants, the mixing of fresh and salt water, or the dynamics of sediment movement as measurement of the item of interest. While these and other phenomena are the results of, and are related to, water movement, their relationships to water circulation patterns are not exactly similar. Thus some measurements in addition to that of water movement may be necessary to describe the phenomena of concern. Remote sensing of suspended sediment load, bottom topography, and other parameters related to water circulation would contribute to more understanding and better management of the resources of our estuarine environments. From our measurements of chlorophyll, plankton, sediments, and bottom topography, some estimates of productivity and sediment dynamics can hopefully be derived for the test area, and by correlations with ERTS data be extended to similar interpretations for other coastal zone areas.

Suspended sediments in estuarine water play important roles in estuarine ecology, and at the same time are involved in certain key physical processes of the tidal environment. Physical processes revealed by the pattern of suspended sediment concentration in water include the elements of circulation, mixing, turbulence and dilution as well as scour or erosion of the bottom and shoreline. The importance to ecology is linked to the capacity of clay-sized sediments to absorb, and later to release, both organic and inorganic substances. Living organisms are a part of the suspended matter in estuarine waters. The chlorophyll in such waters is contained principally in these living organisms. To be assessed these have to be distingusihed from the non-living particulates.

In bay, river and near-coastal waters the suspended sediment load is several orders of magnitude higher than that found in the open ocean. Thus the determination of chlorophyll levels in coastal zone waters by remote sensing is more difficult than in the open sea.[3] Since these waters are shallower than the open sea, there is the

probability that the bottom will contribute to the remotely sensed image. Separation of the contribution of the various factors to the satellite imagery is a major part of our objectives.

The sketch map (Figure 1) shows the eighteen helicopter sampling stations and the three transects (dotted lines) in the lower Chesapeake Bay test site that have thus far been occupied. The Old Dominion Institute of Oceanography research ship, Linwood Holton, is used for bottom profiling with precision echo depth recorder on the ship and to log the attentuation coefficient, using a Bendix Transmissometer; to log surface salinity, using a Beckman in situ salinometer supplemented with periodic collection of water samples; and to log surface water temperature.

Water samples will be collected in real time from a helicopter platform and returned quickly to the laboratory for examination. Water samples are analyzed for salinity, chlorophyll content, sediment content, and optical transparency. Particulate counts and size-distribution analyses are made by means of a Millipore π Mc particle measurement counter. Inorganic sediments will be examined by microscope and x-ray diffraction.

2. SATELLITE DATA OBSERVATIONS

To date we have received only one complete set of data, namely that for the October 10, 1972 pass. We have had four additional satellite pass dates with clear weather, but only partial picture coverage for two of those dates has come to us.

All of the clear weather days on which we have had satellite coverage have been under calm wind conditions and thus a haze has affected all satellite coverage of this test site.

Figure 5 is a MSS band 5 negative print of the test site area at high tide from the October 10, 1972 pass. The enormous sediment load in the James River as well as what is assumed to be sediment structure in the Bay is obvious. The James River at the time of the pass was carrying sediment from recent floods in the Richmond area, but carries more sediment than the neighboring tributaries visible to the north, and it remained so in a picture from the December 3, 1972 pass.

It has been found that film is not a satisfactory method for micro-scale work due to the relatively poor quality of the prints, densitometer drift problems, and the "venetian blink" effect. Computer readout of the individual lines is superior, but is not without its own set of problems. For example, using the print as a first look tool, it is necessary to ascertain which line(s) of the several thousand in the scene contain the information sought. Another is, that all of the

structure visible in the bay (Figure 5) is caused chiefly by only three neighboring shades of gray on the 0-64 shading scale.

High contrast subjects such as the Bay-Bridge (along sample points 1,2,3) as well as the islands, the Hampton Roads Bridge and the James River Bridge (along sample points 13,14) are discernable in this band. The mothballed fleet (above sample site 11) is also quite visible.

Note also that the main channels seem to be evident in the detail. (The channels run close to 50 feet whereas most of the surrounding water is less than 30 feet.)

The scene is somewhat washed out in band 3, but shoal waters do show a pronounced bottom signal. If one looks progressively from band 3 to band 7, the shoal effect can be readily followed.[4,5] The expected sharp delineation between land and water masses is found in band 7, but it can be noted that the heavy sediment load around the outer peninsula (near sample sites 3 and 4) is still visible in band 7.

3. SURFACE SAMPLE DATA

There seems to be a positive correlation between particulate count and chlorophyll concentration data (Figures 3 and 4) and there appears to be a rough correlation between the sediment data and the pictures (Figure 2) but no correlation with the pictures is obvious for the chlorophyll containing portion of the load. Unfortunately, the surface truth data for this pass was collected on October 9, 1972 instead of the 10th because of an early error on our part in computing the satellite pass date.

Chlorophyll values are found to vary by factors of 2 to 3 within short horizontal distances and thus it is suggested that several samples from approximately a 1000 foot square be combined for a composite sample at sampling locations so as to better match the broad footprint of the satellite data. For this pass the chlorophyll concentrations range from about 10 to 40 mg/m^3 with some highs of 150 to 350 mg/m^3 (see Figure 4). Later passes have chlorophyll values all down in the 10-30 (or less) mg/m^3 range. We hope to obtain a continuous record of chlorophyll across the Bay this spring when an improved model of a tunable dye laser becomes available.[6]

The particulate load runs on the order of several hundred thousand particles per liter with the size range maximum occurring between 0.5 and 1.5μ for the October 10 pass. Later passes analyze for an order of magnitude less particles and with the particle size range maximum between 2 and 4μ.

References

3. Confer Report by Karl Heinz Szekielda, University of Delaware and Robert Curran, NASA-Goddard - "Chlorophyll Structure in the Ocean." E-72-10047

4. Confer Report by Robert L. Charnell and George A. Maul of the NOAA-Physical Oceanography Laboratory," Oceanographic Observation of New York Bight From ERTS-1". E72-10156

5. Confer Report by V. Klemas, University of Delaware, "Applicability of ERTS-1 Satellite Imagery to the Study of Coastal Processes." E72-10119

6. P. B. Mumola, NASA-Langley and H. H. Kim, NASA-Wallops. "Remote Sensing of Marine Plankton by Dye Laser Induced Fluorescence." Presented at the 1972 IEEE Conference on Engineering in the Ocean Environment, Newport, Rhode Island, September, 1972.

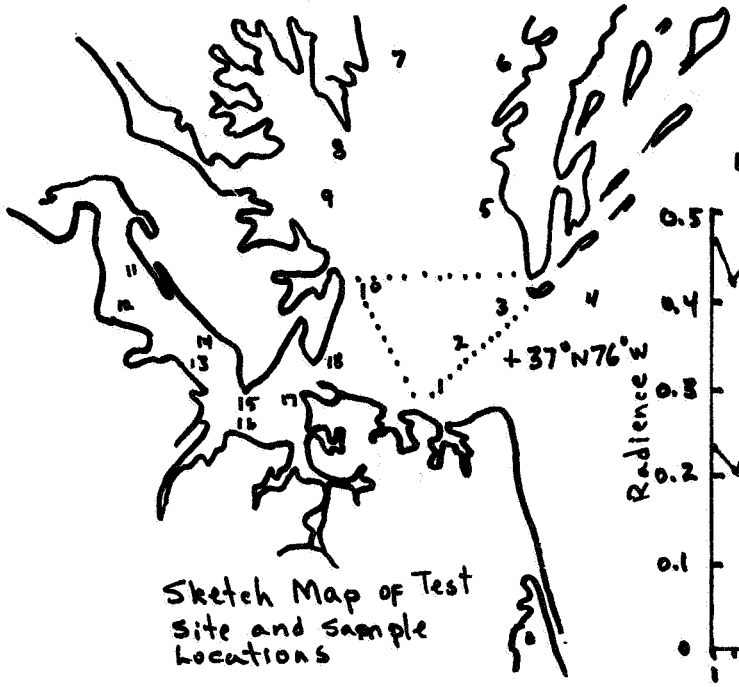


Figure 1

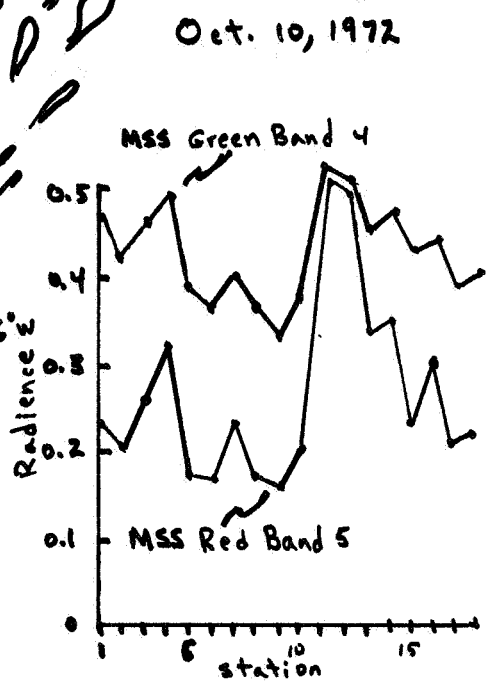


Figure 2

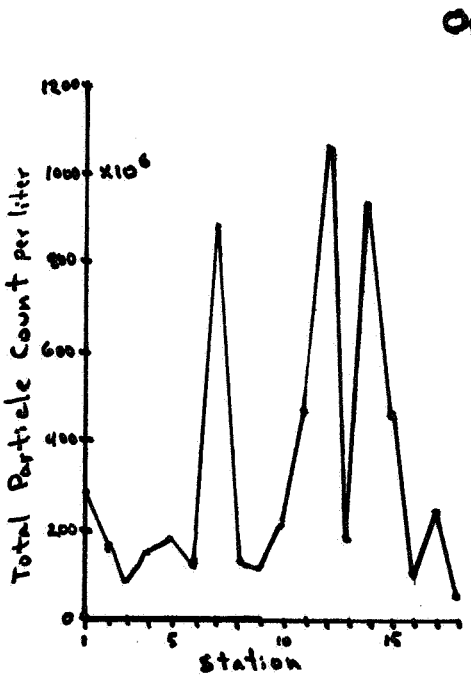


Figure 3

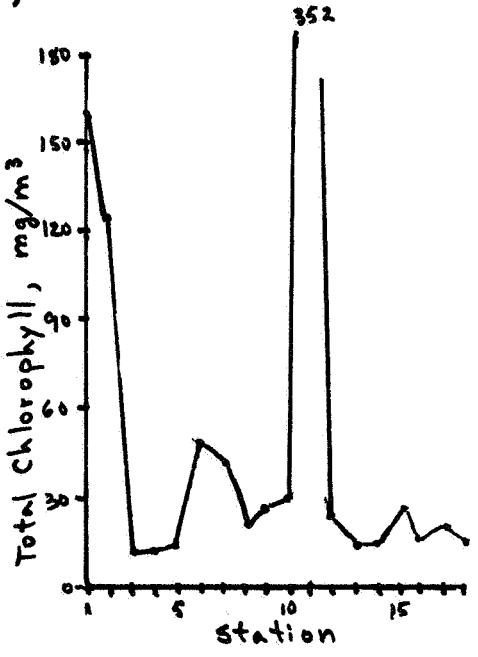


Figure 4

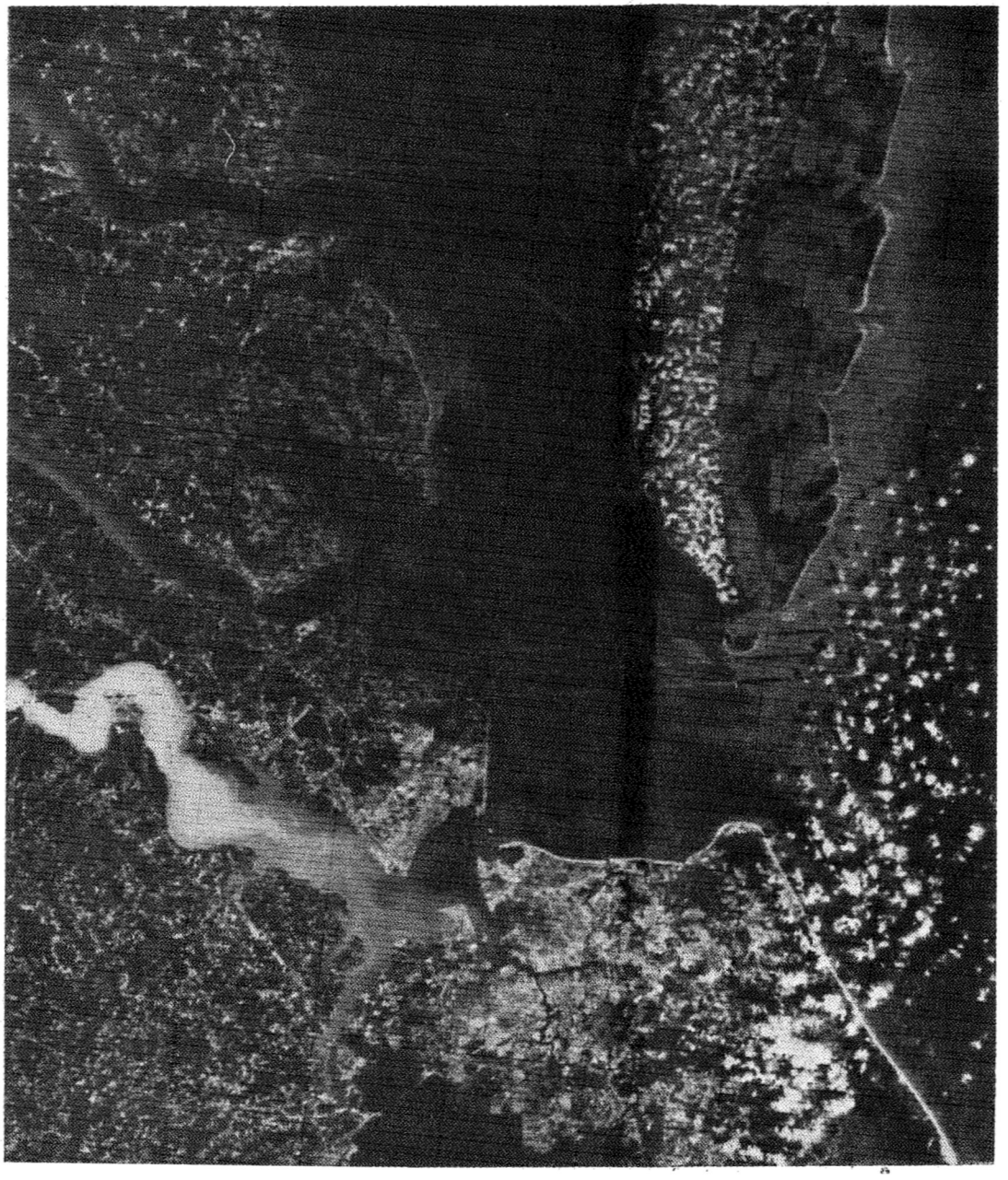


FIGURE 5
MSS Band 5. October 10, 1972. Chesapeake Bay Entrance

N73-28345

Paper M 5

PLUME DEVELOPMENT IN LONG ISLAND SOUND OBSERVED BY REMOTE SENSING (ERTS-1)

Frederick H. Ruggles, Jr., *U. S. Geological Survey, WRD, Hartford, Connecticut*

ABSTRACT

As the Connecticut River flows into Long Island Sound, large plumes are developed during the mixing of ocean and estuarine waters. Plumes were delineated for July 28, October 8, October 27, and December 2, 1972, by analyzing ERTS-1 imagery with the SRI Electronic Satellite Image Analysis Console (ESIAC). Insertion of MSS band 5 into the ESIAC produced the best result in this analysis. The four plumes that have been delineated provide the first input to a time-lapse analysis of circulation patterns at the eastern end of Long Island Sound.

INTRODUCTION

All plans for water and land resources management in Connecticut must consider the ultimate effect of these plans on the estuarine, coastal, and ocean environment of Long Island Sound. One such plan "to preserve and enhance Long Island Sound"--is under preparation by New England River Basins Commission. Basic to development of this plan is an understanding of the hydrology of Long Island Sound area. (See fig. 1.)

The non-tidal system of water movement in the study area is fairly well understood and documented; however, the movement of estuarine and ocean water is not as well documented or understood. This deficiency, combined with the relatively short study time available, dictated that new approaches be tried to achieve the knowledge necessary for proper planning. This report suggests a new technology, remote sensing, to achieve an understanding of ocean dynamics.

PRECEDING PAGE BLANK NOT FILMED

Estuaries that empty into Long Island Sound carry a relatively large volume of material in suspension that is ultimately discharged into the ocean environment. Large plumes are formed as this suspended material mixes with the ocean; this formation is a function of the hydrodynamic conditions encountered. In an effort to understand this phenomenon, delineation of the plumes by analysis of ERTS imagery is in progress, and the delineations will be displayed ultimately in time-lapse form for further analysis. For this report, only those plumes emanating from the Connecticut River are discussed.

IMAGERY DATA SELECTED

The time period covered by this report is from July 23, 1972, to December 2, 1972, and eight (8) potential scenes are available for analysis. The study procedure was to visually review the data in Hartford, Connecticut, and then subject the scenes to close scrutiny using the Stanford Research Institute (SRI), Electronic Satellite Image Analyses Console, (ESIAC), which is described in a report by Evans. Of the 8 scenes examined visually, only the scenes taken on July 28, October 8, October 27, and December 2, 1972, appear to be suitable for ESIAC analysis.

ESIAC ANALYSIS

Input to the ESIAC was in the form of 70 mm transparencies of MSS bands 4, 5, 6, and 7. Film positives were inserted into the console and fairly good results were obtained for July 28 and October 27. By utilizing film negatives and comparing with the film positives, and a color enhanced display, it was possible to obtain fair results for October 8 and December 2. The four scenes were analyzed and yield plume delineations that are compatible to hydrodynamic conditions that prevailed at the time of scanning. Figures 2a, 2b, 2c, and 2d are the plumes as traced from the imagery analysis.

Figure 2a is a tracing of the plume on July 28, 1972. This plume was delineated using a film positive of band 5 made by SRI from a NASA furnished negative. In this instance, step 1 of the gray scale was expanded to penetrate through the haze and fog.

Figure 2b is a tracing of the plume on October 8, 1972. This plume was delineated using band 5 transparencies furnished by NASA, and a color enhanced display of the band 5 transparencies.

Figure 2c is a tracing of the plume on October 27, 1972. This plume was delineated using bands 5 and 6 positive and negative transparencies furnished by NASA.

Figure 2d is a tracing of the plume on December 2, 1972. This plume was delineated from a band 5 positive transparency furnished by NASA, and a color enhanced display. This plume delineation may be suspect because band 5 negative and band 4 were not available at the time of analysis. In this case the color enhancement was the key to delineation of the plume.

SUMMARY

Plumes that have their origin in a fresh-water estuarine river system were identified in the ocean environment of Long Island Sound by using ERTS multispectral scanning data. It is not always possible to delineate these plumes using simple lantern type projection equipment, because the chemical and physical composition of the plume and ocean water are sometimes very similar. In this analysis, the ESIAC was utilized to expand the scenes and subject the transparencies to varying combinations of viewing techniques to identify and delineate the plumes. Best results were obtained when using band 5 transparencies. Indications are that when the scene being analyzed is predominantly in the first two steps of the gray scale it is best to use the negative transparencies. When the analysis is being done above the first two steps of the gray scale, it is best to use the positive transparencies.

REFERENCE

Evans, W. E., (in preparation), Time-lapse analysis of ERTS imagery using special electronic viewing/measuring equipment: Proc. 2d Annual Remote Sensing of Earth Resources Conference, University of Tenn. Space Inst., Tullahoma, Tenn.

B

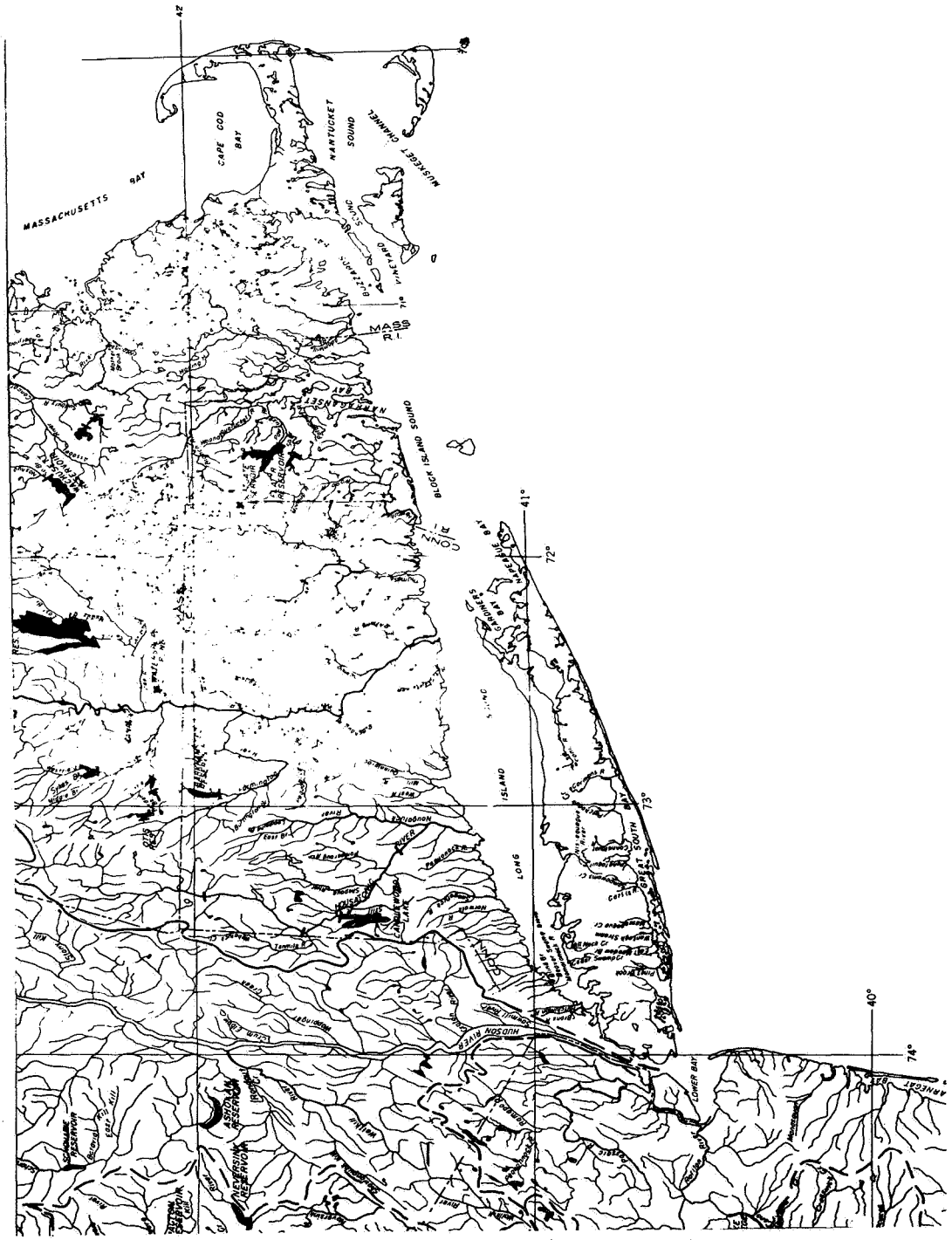


Figure 1-- Location map of Long Island Sound Area.

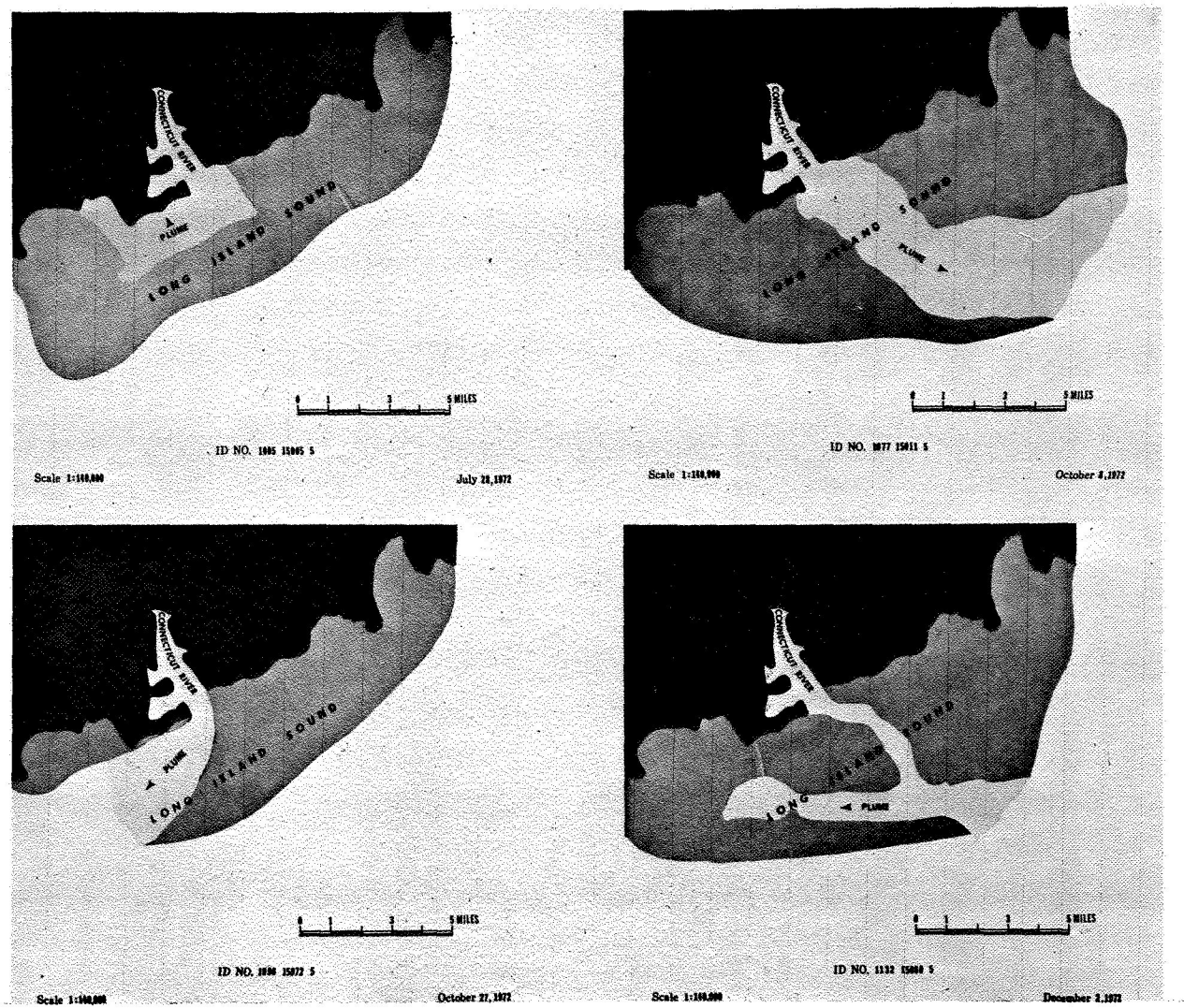


Figure 2-- Plume delineation at the mouth of the Connecticut River in Long Island Sound.

Paper M 6

OBSERVATIONS OF SUSPENDED PARTICLE PATTERNS IN NEARSHORE NORTHEASTERN PACIFIC OCEAN WATERS BY ERTS-1 IMAGERY

Paul R. Carlson, Richard J. Janda and T. John Conomos, *U. S. Geological Survey, Menlo Park, California 94025*

ABSTRACT

The principal sources of nearshore turbid water seen on ERTS multispectral scanner imagery are river effluents, actively eroding headlands and coastal landslides, production of planktonic organisms, and waste effluents. Changes in the location and configuration of turbid water masses are related to variance in river discharge, intensity of surf action, and direction of nearshore currents, as well as availability of suspended particles. The large areal coverage of ERTS images has allowed comparison of the size, distribution, and gray shade (color) of adjacent river effluent plumes such as those associated with the Eel, Klamath, and Smith Rivers of the northern California coast. Variations in plume characteristics, best seen on the green and red bands, can also be related to differences in landforms and land use within these contributing river basins observed on the same image. Different turbid nearshore water masses are shown by dissimilar spectral signatures on ERTS imagery. These signatures apparently reflect differences in the relative proportions of lithogenous and biogenous suspended particles in distinctive water masses. The 18-day observation cycle allows definition of seasonal and storm-related variations in effluent dispersal patterns. Documentation of spatial and temporal distribution of turbid nearshore surface waters observed on ERTS images, when applied to studies of coastal currents and sediment distribution patterns, can provide a better data base for planning wise use of coastal resources.

(PAPER NOT PRESENTED)

PRECEDING PAGE BLANK NOT FILMED

N73-28346

Paper M 7

NEW INSIGHTS INTO THE INFLUENCE OF ICE ON THE COASTAL MARINE ENVIRONMENT OF THE BEAUFORT SEA, ALASKA[1]

Peter W. Barnes and Erk Reimnitz, *Office of Marine Geology, U. S. Geological Survey, Menlo Park, California*

ABSTRACT

Areal patterns from field data and ERTS-1 imagery have shown a close relationship between geologic processes and the influence of sea ice along Alaska's northern coast, perhaps the nation's least known continental margin. Ice acts as (1) a bottom-gouging agent, (2) an influence on water circulation, (3) a carrier of sediments, and (4) an influence on water types.

INTRODUCTION

Problems associated with resource management are difficult to solve even when dealing with a region that is well understood. The remote, harsh and little known environment of the Arctic continental margin, coupled with the vast developmental potential that is emerging, underscores the need for an assessment of the region's natural character and the processes operating to maintain or change that character. In an effort to elucidate the geologic character of this area, an extensive series of field studies was carried out in the test site area on the coast and continental shelf of northern Alaska (Fig. 1).

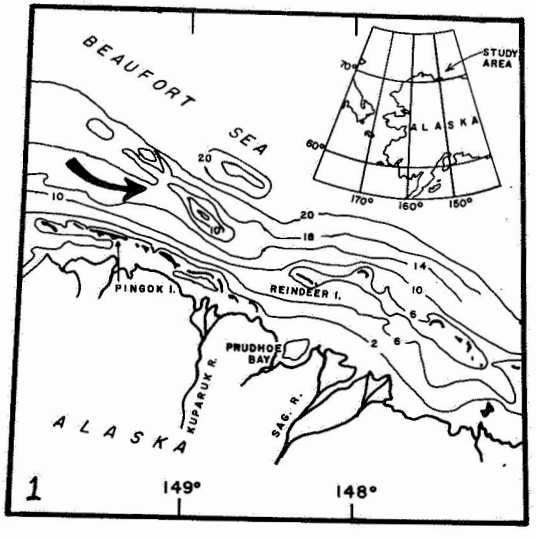
Work began during the period of overflow of Arctic rivers onto sea ice in May and June 1972. Then, during the open-water season, extending from July into September, studies were continued using the Naval Arctic Research Laboratory's research vessel NATCHIK, the Coast Guard ice-breaker GLACIER and the Geological Survey's research vessel LOON.

The primary accomplishment of these studies pertaining to the ERTS-1 program was the acquisition of data on water characteristics (temperature, salinity, turbidity, particulate matter, currents), ice characteristics (thickness, movement, sediment load), and sediment characteristics (texture, depositional history, movement) (see Barnes, and others, 1973 for a discussion of methods and equipment). The ERTS-1 sattelite has been taking high-quality Multi Spectral Scanner images (pictures) in four spectral bands from 0.5 to 1.1 micrometers of a 100-nautical-mile swath of the earth's surface since July 1972. It

[1]Authorized by the Director, U.S. Geological Survey

PRECEDING PAGE BLANK NOT FILMED

Original photography may be purchased from:
EROS Data Center
10th and Dakota Avenue
Sioux Falls, SD 57198



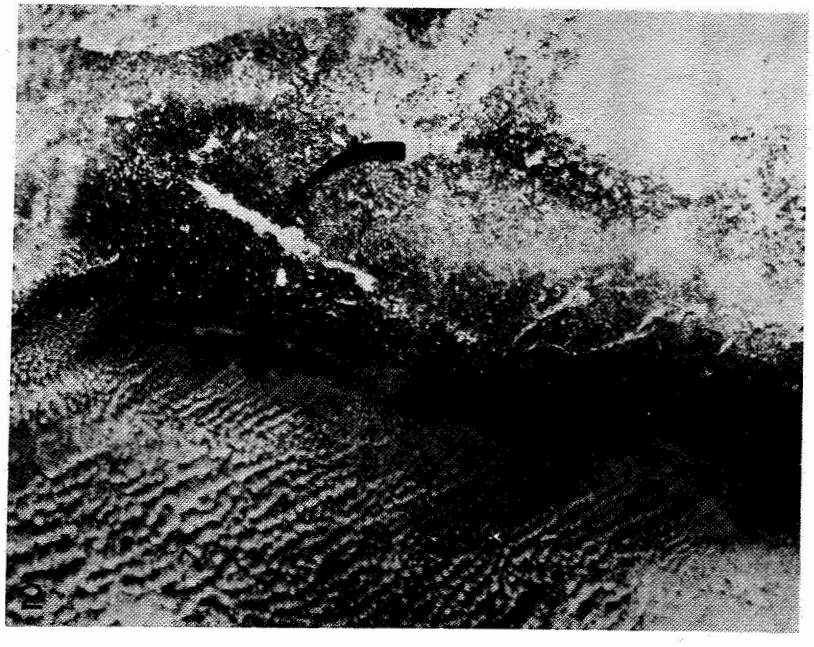


Figure 1. Location of the study area on the northern Alaska coast and continental shelf and bathymetry of a portion of the shelf off northern Alaska. Note the location of ridges northeast of Pingok Island which apparently serve as loci for ice grounding and coincide with the strip of grounded ice in Figure 2.

Figure 2. "Reef" of apparently grounded ice north of Pingok Island which coincides with a submarine ridge (see Figure 1). This ridge is extensively scoured by frequent ice contact (ERTS-1 image on 12 August 1972, 1020-21281-5).

covers the same area every 18 days. At the latitude of our study area (70°N) there is a 70% sidelap of successive orbits and images.

Preliminary analysis has been completed for all images of the test site area obtained before the spacecraft shut down due to low sun angle on 1 November. Images have been selected that (1) are coincident with and can be correlated with our field data and (2) demonstrate events within the test area. The following information has been extracted from the images in conjunction with field data:

(a) surface distribution of suspended matter, temperature and salinity along the coast.

(b) coastal current directions from grounded ice and ice-distribution patterns.

(c) determination of ice-movement patterns from successive, overlapped images.

(d) correlation of grounded ice with topographic highs.

RESULTS

Ice Scour

Although it has long been known that ice in many forms interacts with the sea floor in Arctic coastal regions (Rex, 1955; Kovacs, 1972; Pelletier and Shearer, 1972; Reimnitz, and others, 1972) the details have remained sketchy. Bathymetric, side-scan sonar, high-resolution sediment profile records, and SCUBA diving observations, coupled with imagery show ice-grounding to be dependent on bottom relief. An elongate ridge with a crest at a water depth of 8-15 meters extends from some 25 miles west of Reindeer Island (Fig. 1). The seaward flank of this ridge is extensively marred with grooves up to 1.5 meters deep, while the landward slope is essentially free of these features (Reimnitz and Barnes, 1972). Diving observations reveal the grooves to be sediments plowed up into unstable ridges. Similar relations were found on other ridges and seaward slopes of the offshore islands. Imagery from August 12, 1972, shows the ridge west of Reindeer Island to be the locus of a mass of grounded ice (Fig. 2). The congruity between the location of intensively gouged bottom and the grounded ice mass confirms the source of the grooves as grounding ice. Furthermore, it is apparent that ice is actively scouring the bottom at present.

The practical implications of these observations are twofold: (1) the safety of offshore platforms, structures, and pipelines depends on

the rate, depth, distribution and intensity of ice gouging. (2) Shipping will be guided by the presence or absence of barriers to onshore movement of ice.

Ice Dynamics

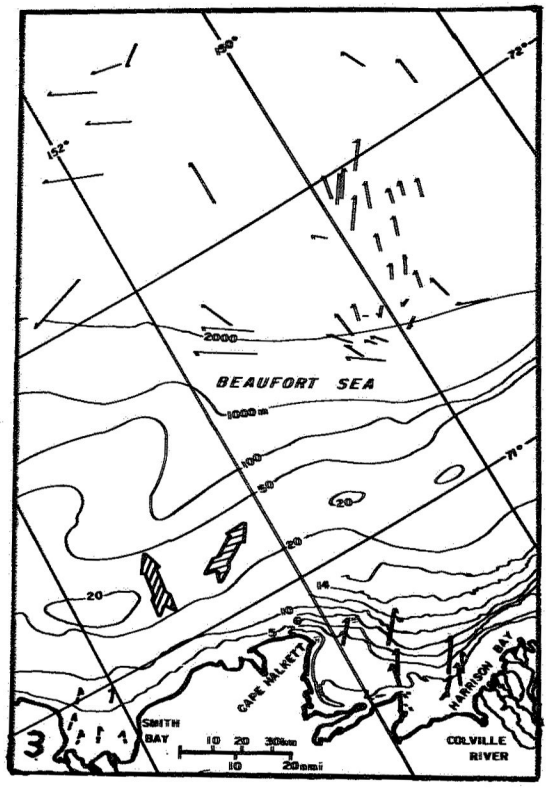
Ice movement and distribution in the Beaufort Sea play an important part in any shipping and economic development along this coast. It has been known that wind and ice-movement directions correlate well (Sverdrup, 1928; Campbell, 1965). Our summer observations confirm this. In addition a set of overlapping ERTS-1 images on October 7th and 8th, 1972, quantify the same relation (Fig. 3). However, these images also show that there is considerable variance between wind direction and ice drift, probably due to the added influence of currents and coastline shape (Nikiferov and others, 1967). These photos also show the separation of new bay ice from the coast due to wind stress (Fig. 4).

In Harrison Bay maximum drift of newly forming ice was about 0.5 km/hr in a northeasterly direction (Fig. 3). Offshore at a distance of 100 km, ice movement varied from a northwesterly direction at up to 0.8 km/hr paralleling the coast and the average current (H.O. Office, 1958), to a northeasterly direction at up to 0.4 km per hour. The winds during the 24-hour period averaged about 17 km/hr from the southwest. It appears that the movement of thin new ice in Smith and Harrison Bays more closely parallels wind directions and is affected more positively than the thicker pack ice offshore. Evidently the pack ice is influenced more by currents and/or intra-pack forces.

Water Characteristics

Coastal circulation along the Arctic shores of Alaska is poorly understood (Kinney, and others, 1972). Interpretation of oceanographic conditions is complicated by the 9-month ice cover, relatively large meterologic tides, and the paucity of data.

The surficial coastal water masses encountered during the summer reflect three major sources. The earliest to manifest itself (late June thru July) is the low-salinity (0-10 ppm), relatively warm (1-11°C), and turbid (>15 light attenuation coefficient--α) river runoff. During July river water fills the zone between the coast and the yet unmelted sheet of seasonal ice. As melting progresses (middle of July to August) a second water type develops, formed as a result of the contribution of melt water from pack ice. This water is of moderate salinity (5-15 0/00), low temperature (0-2°C), and low light attenuation ($<3\alpha$). The first two surface-water types are generally 1-2 meters thick and probably never more than about 5 meters in some of the deeper lagoons.



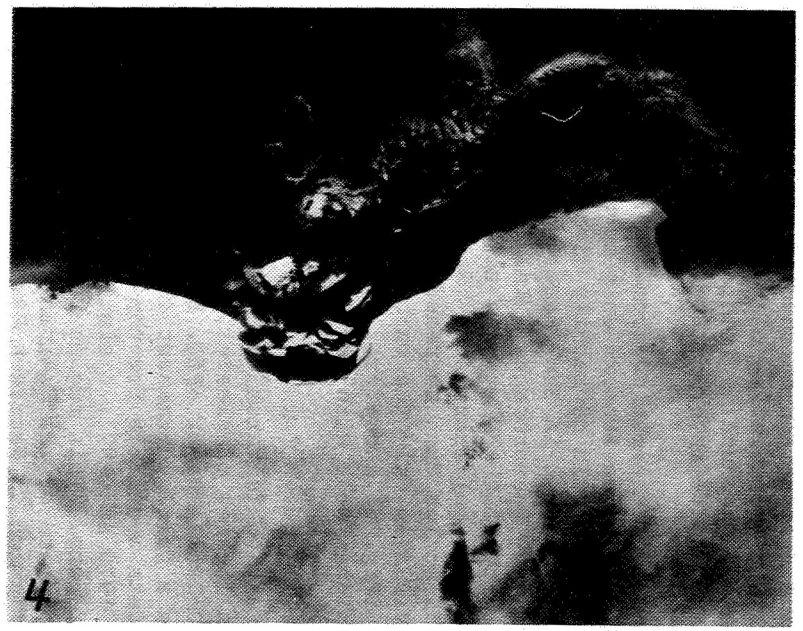


Figure 3. Ice movement vectors (small arrows) derived from overlapping ERTS images of passes on October 7 and 8. Vector scale is the same as the map scale. The large (crosshatched) arrows are average wind directions for October 7 and 8 from ground stations 250 km east and west of this area. The broken arrows in Smith Bay indicate sense of direction (see Figure 4) of movement as cloud cover precluded vector determination. (Plotted from ERTS images 1076-21392-7, 21394-7, and 1077-21451-7 and 21453-7.)

Figure 4. Smith Bay and Cape Halkett showing offshore movement of newly formed ice due to southerly and southwesterly wind stresses (ERTS image 1077-21453-7). (See also Figure 3.)

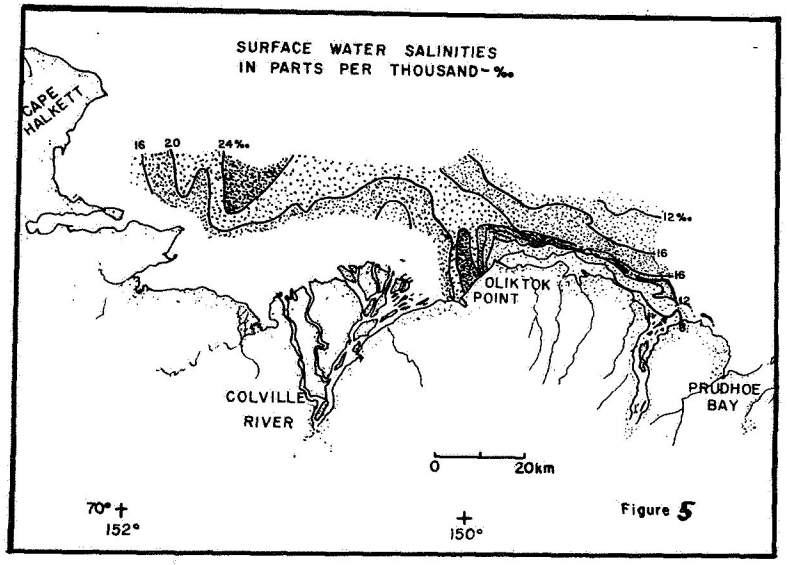
A third water type is characterized by moderate salinity (25-30 0/00), low temperature (<1°C), and relative clarity (<5 α). This "oceanic" water is seen as a background influence, interacting with the river and ice melt waters to create intermediate types.

Using field measurements of the period from the 27th through the 30th of July 1972, and ERTS-1 images from 25 July covering the same region, these three water types could be readily distinguished (Figs. 5 & 6). The circulation patterns seen in the imagery compare favorably with the turbidity and salinity measurements. In general there is an offshore decrease in turbidity as the distances to source of suspended matter (rivers and coastal erosion) increases. Salinity initially increases in an offshore direction then decreases as the offshore pack is approached (Fig. 5). Visually only the turbidity gradient is obvious in the spacecraft imagery (Fig. 6), however. The observed offshore decrease in salinity correlates well with the location of the pack ice and its melt waters.

One of the most interesting features noted in this image and confirmed by field data is an area of clearer, more saline water close inshore just east of the Colville River (Fig. 5). Apparently this influx of "oceanic" water is a fairly permanent feature. Upon comparing temperature and salinity data available for the entire 1972 summer season and the seasons of 1970 and 1971, a similar pattern of colder, more saline water is found here. This region represents either an area of upwelling under the influence of the dominant northeast winds, or reflects a clockwise circulation in Harrison Bay and an entrainment of offshore water. In any event, the image and field data strongly suggest that Colville River detritus is being carried westward towards Cape Halkett.

CONCLUSIONS

Although the coastal environment of Arctic Alaska is far from being understood, it is apparent, that ice is perhaps the most important agent affecting modern geologic processes. Ice is the source of a coastal water type, disrupts and bulldozes bottom sediments, and influences shelf-circulation patterns. ERTS-1 imagery has aided in interpreting the complex field relations. Furthermore, it will continue to be an aid in monitoring the changing geologic and oceanographic processes, as this remote area becomes exploited.



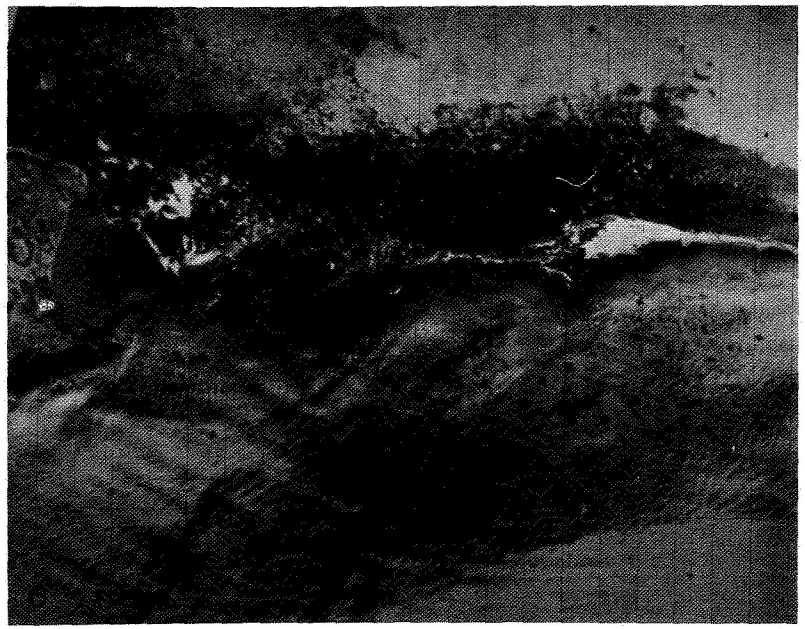


Figure 5. Salinity of surface waters in parts per thousand, mainly from values measured on July 27-31, 1972. Interpretation and contouring were aided by data obtained in August and September of 1970, 1971, and 1972. Note the high salinity water near Oliktok Point.

Figure 6. ERTS-1 image (RVB 3) of July 25 covering area of field data (Figure 5). A turbid water mass can be seen close in along the coast and off the delta of the Colville River. The large accumulation of ice fragments blocked up against the offshore islands NE of the Colville delta is "streaming" bits of ice to the west. Note the intrusion of more saline, clearer water near the coast just east of the Colville delta (from ERTS-1 image 1002-21300-3).

REFERENCES CITED

Barnes, P. W., Reimnitz, Erk, Gustafson, C. W., and Larsen, B. R., 1973, U.S.G.S. marine geologic studies in the Beaufort Sea off Northern Alaska, 1970 through 1972; location and type of data: U.S. Geol. Survey Open-File Report, 11 p.

Campbell, W. J., 1965, The wind-driven circulation of ice and water in a polar ocean: Jour. Geophysical Research, v. 70, p. 3279-3301.

Hydrographic Office, 1958, Oceanographic Atlas of the Polar Seas, Part II, Arctic: H.O. Pub. 705, U.S. Navy Hydrographic Office, Washington, D.C.

Kinney, P. J., Schell, D. M., Dygas, J., Nenahdo, R., and Hall, G. E., 1972, Baseline study of the Alaskan Arctic aquatic environment--nearshore currents: Report R-72-3 Univ. of Alaska, College, Alaska, p. 29-47.

Kovacs, A., 1972, Ice scoring marks floor of the Arctic shelf: Oil and Gas Jour., Oct. 23, 1972, p. 92-106.

Nikiferov, E. G., Geedovich, Z. M., Yefimov, Y. N., and Romanov, M. A., 1967, Principles of a method for calculating the ice redistribution under the influence of wind during the navigation period in Arctic seas: Trudy, Arkticheskii i Antarkticheskii Nauchno-inledovatel'skii Institut, Leningrad, v. 257, p. 5-25, translated in AIDJEX Bulletin 3, 1970.

Pelletier, B. R., and Shearer, J. M., 1972, Sea bottom scouring in the Beaufort Sea of the Arctic Ocean: 24th Internat. Geol. Cong., Sec. 8, Marine Geology and Geophysics, p. 251-261.

Reimnitz, Erk, and Barnes, P. W., 1972, Sea ice as a geological agent affecting the margin of the Arctic [abs.]: Trans. Am. Geophys. Union, v. 53, no. 11, p. 1008.

Reimnitz, Erk, Barnes, P. W., Forgatsch, T. C., and Rodeick, C. A., 1972, Influence of grounding ice on the Arctic shelf of Alaska: Marine Geology, v. 13, p. 323-334.

Rex, R. W., 1955, Microrelief produced by sea ice grounded in the Chukchi Sea near Barrow, Alaska: Arctic, v. 8, p. 177-186.

Sverdrup, H. O., 1928, The wind drifting the ice on the north Siberian Shelf: Norwegian North Polar Exped. with the Maud 1918-1925, Scientific Results, v. 4, no. 1, 46 p.

N73-28347

Paper M 8

ERTS-1 OBSERVATIONS OF SEA SURFACE CIRCULATION AND SEDIMENT TRANSPORT, COOK INLET, ALASKA

F. F. Wright, G. D. Sharma and D. C. Burbank, *Institute of Marine Science, University of Alaska, Fairbanks, Alaska*

ABSTRACT

Cook Inlet is a large tide-dominated estuary in southern Alaska. Highly turbid streams enter the upper inlet, providing an excellent tracer for circulation in the lower inlet. MSS 4 and 5 images both can be used in this area to plot sediment and pollutant trajectories, areas of (probable) commercial fish concentration, and the entire circulation regime.

INTRODUCTION

Cook Inlet is one of the largest estuaries in North America. It extends almost 200 nautical miles (360 Km) northeastward from the Gulf of Alaska and is over 30 nautical miles (54 Km) wide through much of its extent (Figure 1). Depths are typically less than 20 fathoms (40 m). The hinterland is predominantly mountainous and glaciation is still extensive. Deglaciation is occurring around the upper inlet and tremendous quantities of 'glacial flour' (largely silt and clay-sized mineral grains) enter the inlet. Cook Inlet lies at about latitude 60° North, and the climate could be regarded as subarctic. There is, however, strong maritime influence and temperatures are never low enough to completely inhibit runoff. Circulation of the inlet's waters is dominated by tidal effects. In the upper inlet, tidal ranges greater than 30 feet (10 m) are not uncommon, and currents in excess of eight knots (14 KPH) are often encountered. Despite its size and extreme tidal and climatic influences, Cook Inlet appears to behave as a model high latitude estuary, and an understanding of the regime here should be useful in all estuarine circulation and mixing problem areas.

ERTS imagery is particularly well suited for the study of Cook Inlet circulation. The highly turbid runoff waters can very readily be distinguished from clean sea water on both MSS Bands 4 and 5. This information, of course,

Original photography may be purchased from:
EROS Data Center
10th and Dakota Avenue
Sioux Falls, SD 57198

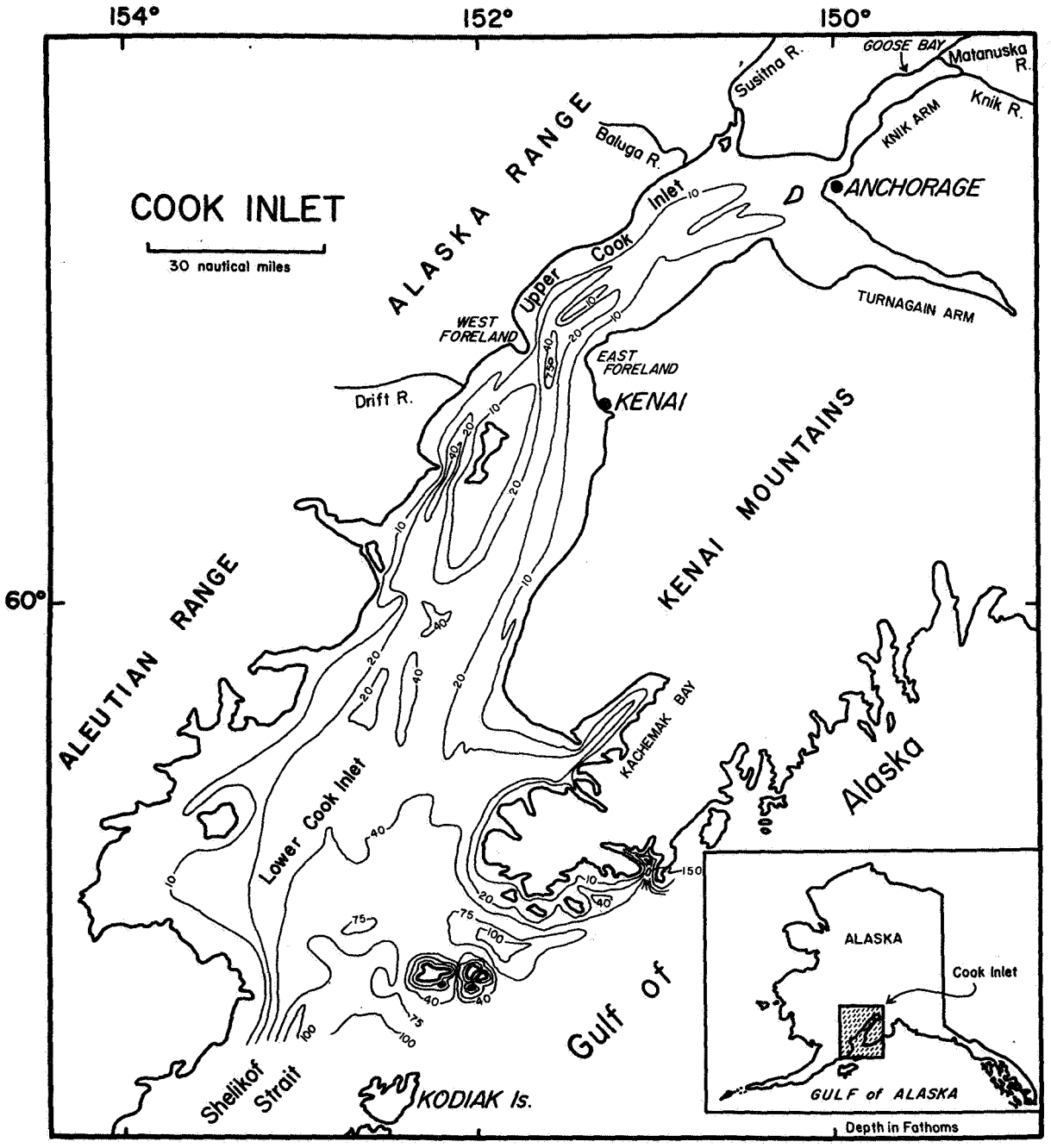


FIGURE 1. Cook Inlet, Alaska, showing bathymetry and major tributary rivers (from Sharma and Burrell, 1970).

could also be obtained from conventional aerial photography, but the size of the inlet and the speed of the tidally-controlled mixing processes make it virtually impossible to obtain a truly synoptic survey. Standard oceanographic procedures, limited by vessel and sampling speeds, are hopeless to obtain an instantaneous view of the inlet. Even ERTS requires two frames to cover the entire inlet, but these do give us a true picture, clearly defined by the turbid fresh waters, of the instantaneous circulation pattern.

Circulation in Cook Inlet is of far more than academic interest. By coincidence, the majority of the turbid waters originate from Knik Arm in the vicinity of the city of Anchorage, Alaska's population and industrial center. Offshore petroleum production also is largely confined to the upper inlet. Thus tracing the turbid waters permits us to follow in detail the trajectory of potential pollutants from these sources. As well, Cook Inlet supports a major salmon fishery. Migrations of the salmon are known to be related to water movements but little systematic study has been made of this in the inlet area. Significant fisheries for herring, shrimp, tanner and king crab are found in the normal sea waters of the lower inlet. An understanding of the circulation patterns will be important to both environmental protection and resource development and management in the entire Cook Inlet area.

DIRECT OBSERVATIONS OF COOK INLET CIRCULATION

Although Cook Inlet has been important as a gateway to the Alaskan interior since Russian times, there was relatively little navigation or systematic study of the area until quite recently. Mariners, in fact, avoided the inlet as much as possible because of its dangerous waters. The Alaska Railroad, for example, circles the head of Cook Inlet, but its major termini were at Seward and Whittier on the Gulf of Alaska. Anchorage, now the population and industrial center of the state, developed during and after World War II as a staging point between the coast and the interior. It was not until successful petroleum development in the 1950's that there was significant regular commerce in the upper inlet. Aside from basic tide height and current observations, and rather superficial bathymetric survey, oceanographic studies of Cook Inlet were non-existant until required for petroleum related engineering projects. The first large-scale studies of hydrography, sedimentation, and chemistry were conducted by the University of Alaska in the later 1960's (Kinney, Groves and Button, 1970; Sharma and Burrell, 1970). These data, with much additional biological and engineering information,have recently been compiled by Evans and others (1972).

In cooperation with the ERTS program, the University of Alaska is presently conducting an extensive series of cruises in Cook Inlet. These cruises have been scheduled to coincide with ERTS orbits over the inlet, but the only

G

useable imagery obtained to date was collected when there were no surface observations. One cruise (25-29 September 1972) was conducted with the University's major vessel, Acona. During this cruise, complete hydrographic data as well as suspended sediment values were obtained for the entire water column, in order to provide reference figures. Additional cruises have been conducted with a smaller, chartered vessel based on Homer in the lower inlet. Sampling with the small vessel is usually restricted to the surface waters, but her speed (over four times that of Acona) permits a much larger area to be covered while the satellite is actually overhead.

Sea surface observations ("ground truth") obtained during the Cook Inlet cruises have included measurement of water temperatures, salinities, and suspended sediment load (Figure 2). These data, though clearly not 'synoptic' in the normal oceanographic sense, give us an understanding of the general water types present in the inlet. It has been found that, during the active runoff season, the water types can be easily characterized. Runoff tends to be low in salinity and very, very high in suspended load. Values greater than 100 mg/l suspended material characterize the upper inlet; the highest value reported was over 1700 mg/l from the Anchorage area. Sea water, of course, tended to have salinities ranging downwards from 32 o/oo and was relatively transparent. Water temperature shows a very decided seasonal effect. Sea water tended to be 10-12°C regardless of season, while runoff ranged from warmer than the sea in later summer (12-16°C) to considerably colder in the winter and spring (4-8° C). Suspended sediment concentrations greater than 2-4 mg/l have proven to be the most reliable criterion for rapidly distinguishing the two water masses of the inlet.

ERTS - 1 IMAGERY OF COOK INLET

The normally cloudy conditions of the Alaskan coast have severely interfered with ERTS observations of Cook Inlet. Only on one occasion in 1972 were useable images collected. Fortunately, due to the high latitude compression of orbital tracks, data were obtained for the entire inlet on two successive days, 3-4 November. The transparencies of these data, particularly the MSS 4 and MSS 5 Bands, are extremely good, and several grey shades within the turbid waters can be distinguished with the naked eye. These gradations appear to be correlable with relative concentrations of suspended material in the surface water layers. There are indications that turbid waters somewhat below the actual water surface can be detected by comparison of the two bands. Unfortunately, these subtle distinctions are not found on the enlarged prints.

A comparison of the suspended load information from the September cruise and the November ERTS image (Figures 2 and 3) makes clear the utility of the ERTS observations. The hydrographic data show a somewhat confused pattern of suspended sediment distribution, reflecting the fact that it required five

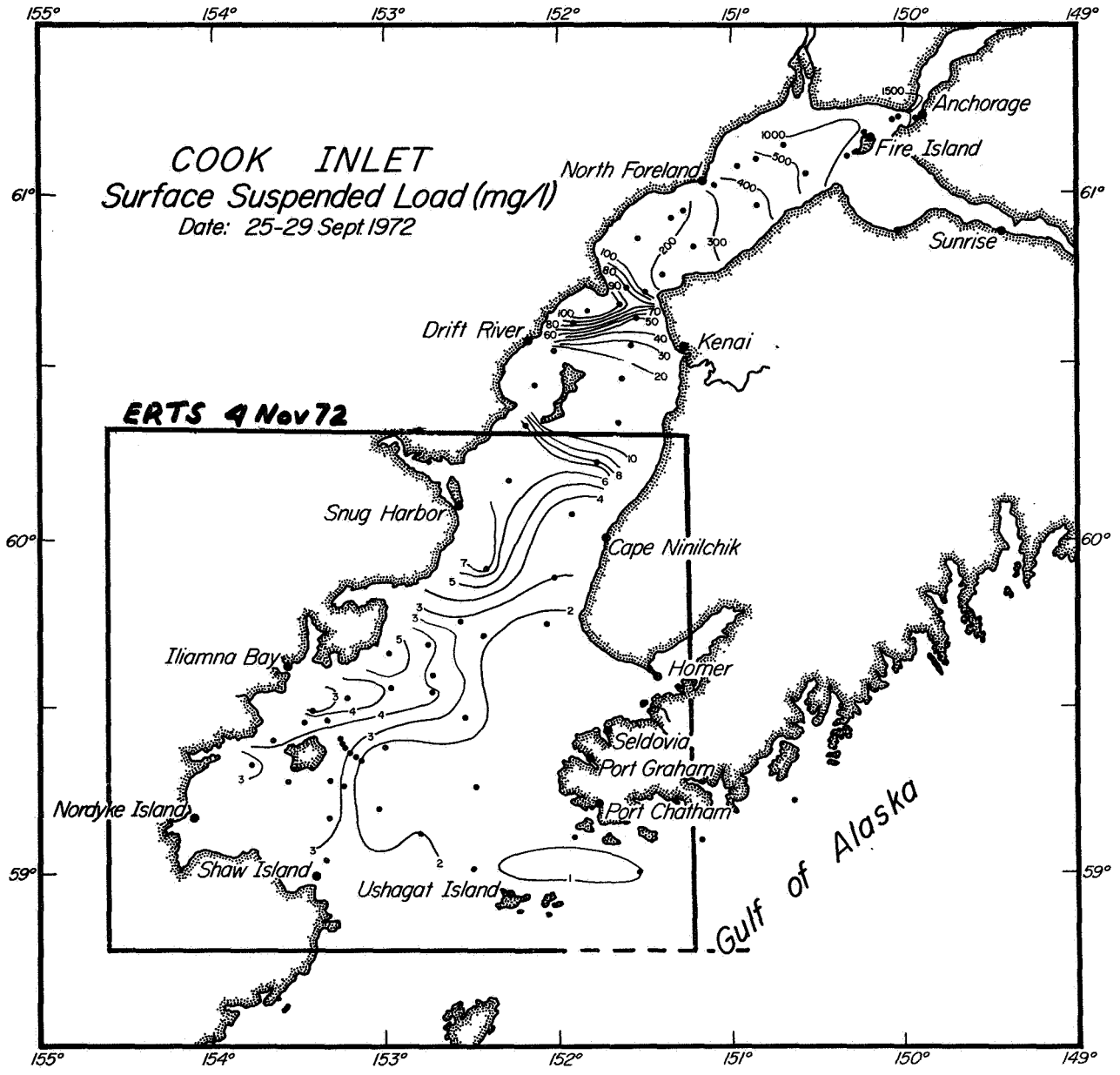


FIGURE 2. Suspended sediments in the surface waters of Cook Inlet, September 1972. Area shown in Figure 3 is outlined.

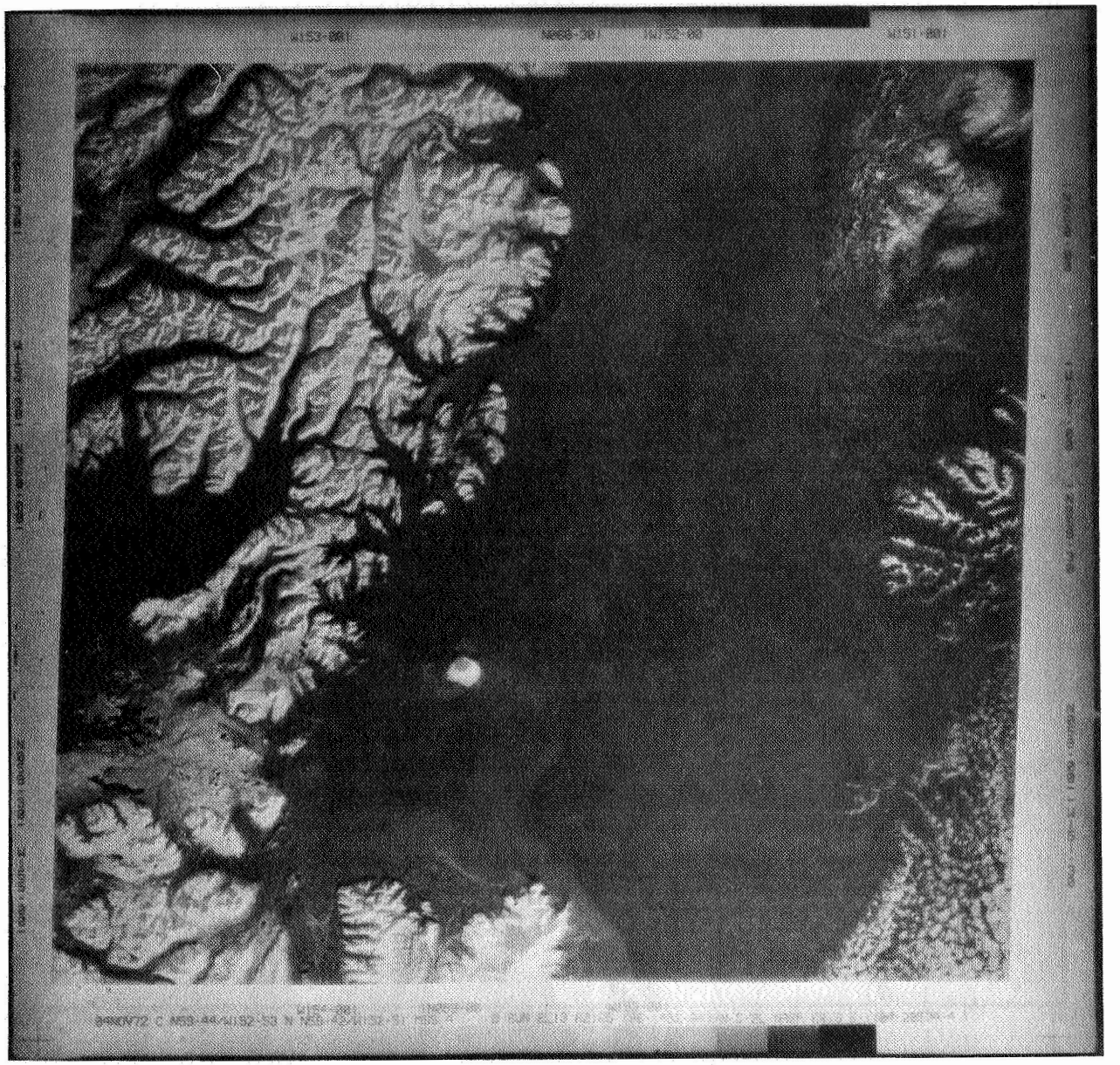


FIGURE 3. ERTS Image of Lower Cook Inlet, MSS 4 Band, November 4, 1972.

days to collect all the stations shown. The ERTS image, on the other hand, reflects accurately the conditions at one instant. It was just after low slack water in the lower inlet, and the flood is commencing. A very distinct mass of clear sea water is seen advancing up the eastern side of the inlet, extending then almost as far north as Cape Ninilchik, while turbid waters dominate the surface to the west. This pattern very clearly reflects the influence of Coriolis effect upon the circulation of Cook Inlet. This is the tendency of moving particles to be deflected by the earth's rotation toward the right in the northern hemisphere. In the ERTS image of Cook Inlet we see both the incoming and outflowing currents controlled by this effect. This picture is corroborated by numerical models of inlet circulation (Matthews and Mungall, 1972).

APPLICATION OF ERTS - 1 DATA IN COOK INLET

An understanding of the circulation regime is essential to the systematic protection and development of the resources of the Cook Inlet region. The local salmon fishery presents a good example of the relation of the fauna to the environment (Evans et al., 1972). The fish routinely enter the inlet on their spawning run and proceed with the tide, dropping to the bottom to rest when the tide sets against them. Apparently, also, they tend to mass for a time near the boundary between the clear and turbid waters before they make their final run to the spawning streams. The non-anadromous fisheries of the lower inlet -- including commercial operations for herring, shrimp, and crab, and sports fishing for halibut -- are, of course, limited by the extent of relatively normal sea water. ERTS imagery can locate the water mass boundary with precision and, with repetitive coverage, we should ultimately be able to predict its location at any stage of tide or runoff. This boundary is also important as a factor in navigation. An extensive "trash line" of floating logs and other terrestrial debris may accumulate there and create a genuine hazard to navigation. As well, emphemeral but often nasty tide rips and whirlpools may develop along the boundary.

The major input of turbid waters into the Inlet is actually from the Knik and Matanuska Rivers, both tributary to the Knik Arm above the city of Anchorage (Sharma, in progress). This coincidence permits the ERTS imagery to be used in another way. Effectively all non-solid sewage and industrial waste from the city is discharged directly into the inlet where its trajectory and sites of dispersion can easily be followed by tracing the turbid waters. Most of the current petroleum development is also limited to the upper inlet, so an understanding of the circulation will permit prediction of the behavior of any spill.

As yet, too few satellite observations of Cook Inlet circulation have been obtained to permit more than the most superficial conclusions about the regime. Both additional satellite and surface observations will be required to generate an integrated picture, however, the potential utility of the satellite system in this environment cannot be doubted. The extremely turbid inflow at the head of the inlet provides us with a unique tool to study all aspects of the circulation of Cook Inlet.

REFERENCES

Evans, Charles D., Eugene Buck, Richard Buffler, Greg Fisk, Robert Forbes, and Walt Parker, 1972, The Cook Inlet Environment, A Background Study of Available Knowledge: Report to U.S. Army Corps of Engineers, Alaska District, Contract DACW85-72-C-0052, Resource and Science Service Center, Alaska Sea Grant Program, University of Alaska, Anchorage, 128 p.

Kinney, P.J., J. Groves, and D.K. Button, 1970, Cook Inlet Environment Data: Report #70-2, Institute of Marine Science, University of Alaska, 120 p.

Matthews, J.B., and J.C.H. Mungall, 1972, A Numerical Tidal Model and its Application to Cook Inlet, Alaska: Journal of Marine Research, v. 30 (1), p. 27-38.

Sharma, G.D., and D.C. Burrell, 1970, Sedimentary Environment and Sediments of Cook Inlet, Alaska: Bulletin, American Assoc. of Petroleum Geologists, v. 54 (4), p. 647-654.

N73-28348

Paper M 9

SEDIMENT DISTRIBUTION AND COASTAL PROCESSES IN COOK INLET, ALASKA

Duwayne M. Anderson, Lawrence W. Gatto, Harlan L. McKim and Anthony Petrone,
U.S. Army Cold Regions Research and Engineering Laboratory, Hanover, New Hampshire 03755

Abstract

Regional hydrologic and oceanographic relationships in Cook Inlet, Alaska have been recognized from sequential ERTS-1 MSS imagery. Coastline configuration is well defined on bands 6 and 7 of images 1103-20513, 1103-20520, 1103-20522, 1104-20572, 1104-20574 and 1104-20581. Current patterns are visible in the inlet because of differential concentrations of suspended sediment. These patterns are most evident on bands 4 and 5. The circulation patterns within Cook Inlet are controlled primarily by the interaction between the semi-diurnal tides and the counter clockwise Alaska current. In general, heavily sediment laden water is seen to be confined to portions of the inlet north of the Forelands and west of Kalgin Island. Tongues of clear oceanic water are observed to enter the inlet through Kennedy Channel along the east shoreline in the vicinity of Cape Elizabeth. A recurring counterclockwise circulation pattern observed around Kalgin Island seems to result from the interplay of the northerly moving water along the east shore and the southerly moving, sediment laden, water along the west side of the inlet. Prominent, fresh water plumes, heavily laden with sediment are visible at the mouths of all major rivers. Relect plumes from as many as three tidal stages have been recognized. Tidal flats and a number of unmapped cultural features appear prominently in bands 5 and 6 of a number of the images.

INTRODUCTION

The Cook Inlet area of south central Alaska (Fig. 1) is a transportation, industry and population center. With pressure mounting rapidly here for extensive development, it is necessary to continue the environmental research required to increase our basic understanding of this region as soon and as vigorously as possible. Environmental disturbances caused by rapid development have potentially deleterious effects on land and water quality. One of the concerns of the Corps of Engineers is to help control and alleviate these adverse effects.

Original photography may be purchased from:
EROS Data Center
10th and Dakota Avenue
Sioux Falls, SD 57198

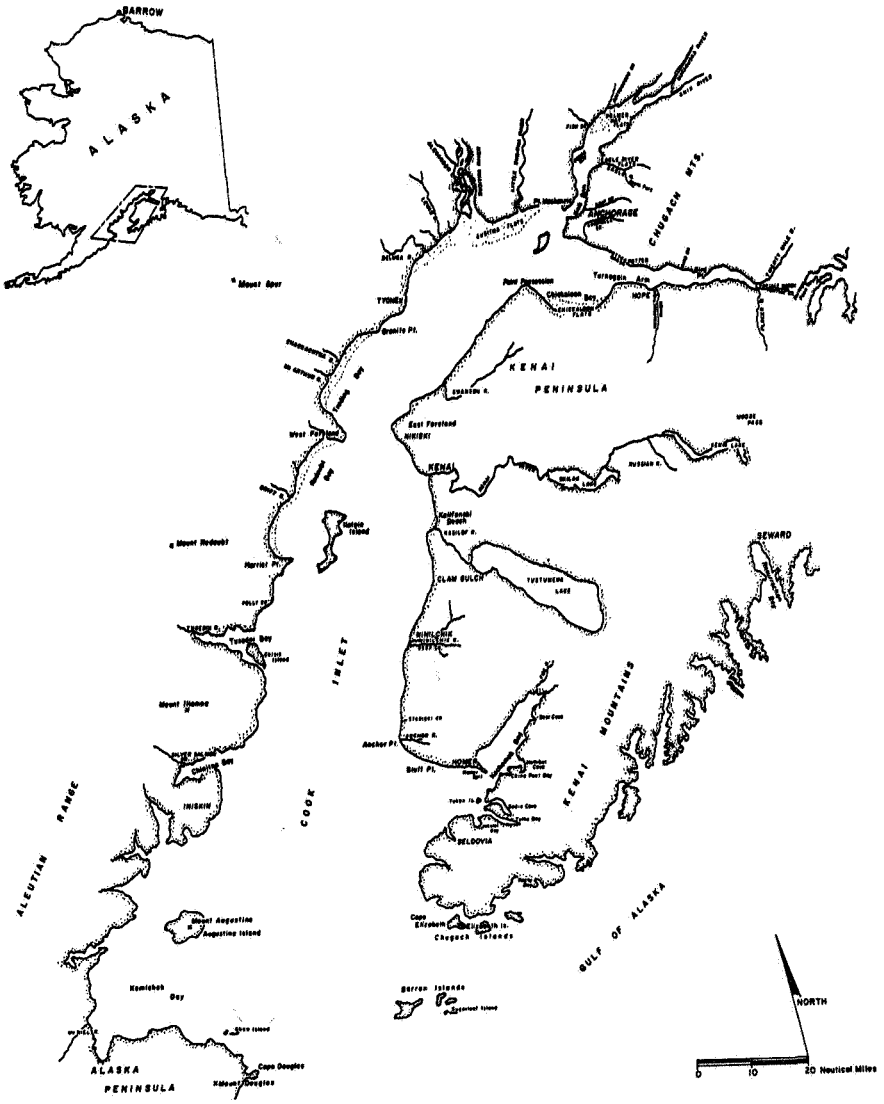


Figure 1. Regional Map of Cook Inlet

Suspended sediment currently is the most serious and detrimental pollutant in all water bodies. It is estimated that newly developing areas may produce as much as 20,000 - 30,000 times more sediment than natural undisturbed areas (Environmental Currents, 1972). High sediment loads are particularly troublesome in navigable rivers, inlets, channels and harbors where siltation is of enormous economic impact. To aid in controlling or to avoid such siltation problems, the Corps of Engineers wants to develop an improved understanding of the hydrology, sedimentation and coastal processes in cold water estuaries and inlets. Cook Inlet is a cold water estuary in which sedimentation and sediment redistribution is of continuing importance and concern. Synoptic views sequentially obtained from the ERTS-1 satellite provide data on transport-circulation processes which influence the sedimentation in Cook Inlet. The purpose of this investigation is to verify the utility and effectiveness of these data in the synoptic survey of coastal sedimentation and related processes in Cook Inlet.

BACKGROUND

In the Cook Inlet area the Corps of Engineers is particularly concerned with providing deep draft and small boat harbor improvements, maintaining deep draft berthing and maneuvering channels, controlling beach erosion and continuing harbor construction. To aid in performing these functions, data have been collected at the specific site locations: efforts directed to the collection of regional data have been minor. This approach was also followed by other investigators. Rosenberg and others (1967 and 1969) examined the oceanographic processes in the Nikiski area. Various petroleum companies active in the area investigated the oceanographic processes around the mouth of the Drift River and in Trading Bay (Marine Advisors, 1966 and 1969). However, few efforts have considered the inlet as an entity. Sharma and Burrell (1970) investigated the distribution of bottom sediments in a large portion of the inlet. Wagner and others (1969) and Evans and others (1972) compiled all available information dealing with the environmental and oceanographic aspects of the region. Although the general oceanographic relationships are beginning to emerge, it is apparent that much remains to be learned.

GEOGRAPHIC SETTING

Cook Inlet is a large tidal estuary in south central Alaska. It is oriented in a northeast-southwest direction and is approximately 180 nautical miles long and increases in width from 20 nautical miles in the north to 45 nautical miles in the south. The inlet is bordered by extensive tidal marshes, lowlands with many lakes, and mountains (Fig. 3). Tidal marshes are prevalent around the mouth of the Susitna River, in Chickaloon Bay, Trading Bay and Redoubt Bay. The Kenai Lowland

separates the inlet from the Kenai Mountains on the upper southeast side. The Susitna Lowland lies between the Talkeetna Mountains on the northeast and the southern Alaska Range on the northwest. The Kenai Mountains are adjacent to the inlet mouth on the southeast; the Alaska-Aleutian Range forms the western border.

ESTUARY CHARACTERISTICS

Coastline Characteristics

The coastal configuration of the inlet is characterized by sea cliffs extending from the head of Kachemak Bay to Turnagain Arm. Pocket beaches that occur along this coast are generally composed of sand and/or coarser sediment while finer grained material is present in lower energy locations. Along the northwest and west coasts from Point Mackenzie to Harriet Point an extensive coastal plain borders a shoreline of scattered sea cliffs and pocket beaches. From Harriet Point to Cape Douglas the steep mountains slope directly into the inlet in most locations and bayhead beaches form in many of the numerous small embayments along this coast. Sea cliffs are generally found only on the promontories along this coast.

Bathymetry

The depth of the upper inlet north of the forelands is generally less than 20 fathoms. The deepest portion, 45 fathoms, is located in Trading Bay just off the mouth of the MacArthur River (Sharma and Burrell, 1970). Turnagain and Knik Arms are the shallowest areas, with much of the bottom exposed as tidal flat at low tide. South of the forelands two channels, one between Kalgin Island and Harriet Point and another between Kalgin Island and the southeast shore, extend southward in the inlet and join in an area west of Cape Ninilchik. The deepest portion of the western channel, located between Kalgin Island and Harriet Point, is approximately 70 fathoms. The eastern channel is deepest just south of a line between the forelands. It is 75 fathoms in this area and rapidly shoals to approximately 30 fathoms until it merges with the western branch to form a single channel. South of Cape Ninilchik this channel gradually deepens to approximately 80 fathoms and widens to extend across the mouth of the inlet between Cape Douglas and Cape Elizabeth.

Tides/Tidal currents

The tides in Cook Inlet are semi-diurnal with two unequal high tides and two unequal low tides per tidal day (24 hours, 50 minutes) and high tide in Anchorage occurs 4.5 hours later than at the inlet mouth (Fig. 2). Mean diurnal tide range varies from 13.7 feet at the mouth

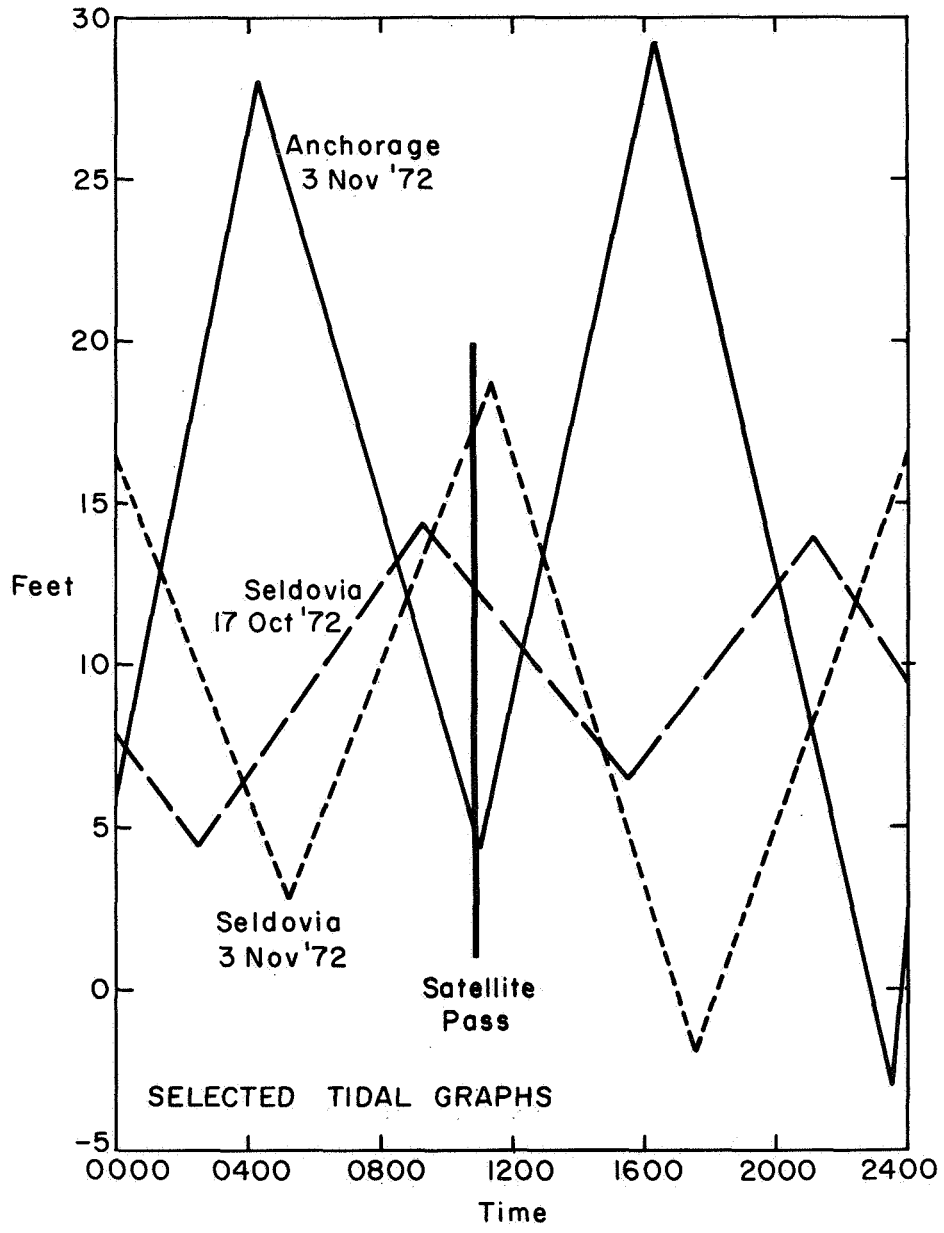


Figure 2. Selected Tidal Graphs

to 29.6 feet at Anchorage. It varies within the lower portion of the inlet from 19.1 feet on the east side to 16.6 feet on the west side (Wagner et al., 1969). The extreme tidal range produces tidal currents typically 4 knots and occasionally 6 to 8 knots (Horrer, 1967). The high Coriolis force at this latitude, the strong tidal currents and the inlet geometry produce considerable cross currents and turbulence throughout the entire water depth during both ebb and flood tides (Burrell et al., 1967). The turbulence is especially active along the eastern shore of the inlet.

Surface Circulation

The circulation of the inlet is influenced by bathymetry, morphometry and fresh water drainage (Evans et al., 1972). The water in the upper inlet is well mixed due to the large tidal fluctuations in this shallow, narrow basin. During summer when surface runoff is high there is a net outward movement of water from the upper inlet. With reduced runoff in the winter there is virtually no net outflow (Murphy et al., 1972). The middle inlet has a net inward circulation of cold, saline oceanic water up the eastern shore and a net outward flow of warmer and fresher inlet water along the western shore (Evans et al., 1972). These water types are well mixed vertically along the eastern shore but separated laterally resulting in a shear zone. In the lower inlet this lateral temperature and salinity separation is maintained but in the western portion vertical stratification occurs with colder, saline oceanic water underlying warmer, less saline inlet water. During tidal inflow the deeper oceanic water rises to the surface at the latitude of Tuxedni Bay and mixes with the inlet water (Kinney et al., 1970).

Sediment Distribution

The currents and circulation patterns are especially important in determining the distribution of suspended and bottom sediments throughout the inlet. The suspended sediment is mostly of glacial origin with the highest concentrations in the northern portion of the inlet, a well-mixed turbulent zone of strong tidal currents. Suspended sediment is nearly absent in the waters of the central and eastern portions at the inlet mouth. Bottom sediments have been grouped into three facies: a predominantly sand facies in the upper inlet, a sandy gravel with minor silt and clay facies in the middle inlet, and a gravelly sand and minor interspersed silt and clay facies in the lower inlet (Sharma and Burrell, 1970).

INTERPRETATION OF ERTS IMAGES

Coastal Configuration

The coastal landforms and cultural features along the Cook Inlet shoreline are most distinct on ERTS MSS bands 5, 6 and 7. The

D

mountainous borders of the inlet on the southeast and the lower northwest and the coastal plain border on the upper northwest and east are easily recognized (Fig. 3). Homer spit and the Susitna River delta are apparent. The major cities and towns (Anchorage, Nikiski, Kenai, Homer and Seldovia) and some previously unmapped developments south of the mouth of the Drift River (6 on Figure 5) and on the southern shore of the West Forelands are readily identifiable.

Tidal Flat Distribution

The high sediment load in glacial rivers is the main source of material found in the tidal flats throughout the inlet. MSS band 5 and 7 images are ideal for analysis of these tidal flats. Because the major portion of sediment deposited in the inlet is carried by the Susitna and Knik Rivers (Rosenberg et al., 1967) the major portion of the tidal flats is located in the inlet north of the forelands (Fig. 3). In the lower inlet the tidal flats occur as bayhead bars in the numerous embayments along the western shore and northeast of Homer in Kachemak Bay. The high current velocities and frequent changes in current directions of the inlet water produce variations in the distribution and configuration of the flats. The migration of some major tidal flat channels and the redistribution of some tide flats in Knik and Turnagain Arms can be detected on MSS frame 1103-20513-5 (compare with the National Ocean Survey Navigational Chart 8553). A knowledge of these changes is particularly important in maintaining navigation channels and harbor facilities.

River Plumes

The sediment- laden rivers that discharge into the inlet produce sediment plumes which are visible on MSS bands 4 and 5. Figure 3 shows the distribution of plumes from some of the major rivers around the inlet. Although the Knik and Matanuska Rivers at the head of Knik Arm contribute a major portion of the sediment deposited in the inlet (Wagner et al., 1969) these rivers do not have distinct sediment plumes. The river-borne sediment is dispersed so quickly in this high energy area and the sediment concentration is so high (approximately 1350 mg/l;Kinney et al., 1970) in the inlet water at that location that a distinct plume is not formed. The Susitna River, another major sediment contributor, has only a small plume because the river discharge is reduced (Rosenberg et al., 1967) during the winter months (Fig. 3). In addition, the plume is less distinct because the inlet water at the mouth of the Susitna River has a high suspended sediment concentration (approximately 1540 mg/l; Kinney et al., 1970). MSS frame 1015-21022-5 (Fig. 4), taken 7August, shows the sediment plumes from the Drift (3) and Big (4) Rivers during flood tide. The shape and location of the plumes can be used to infer the current direction along the west shore between MacArthur River (1) and Tuxedni Bay (2). Currents appear to be moving in a northerly direction. Relict sediment plumes in this area are visible far offshore and indicate the

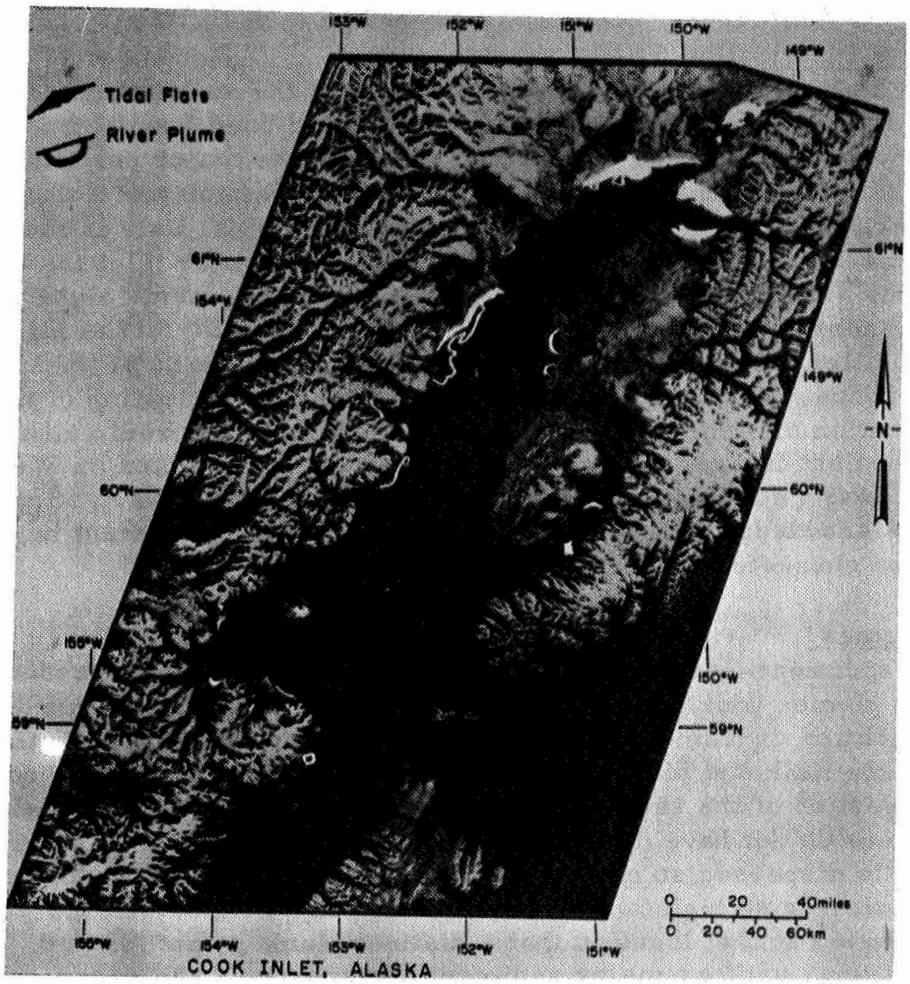


Figure 3. **Tidal flat distribution and river plumes**

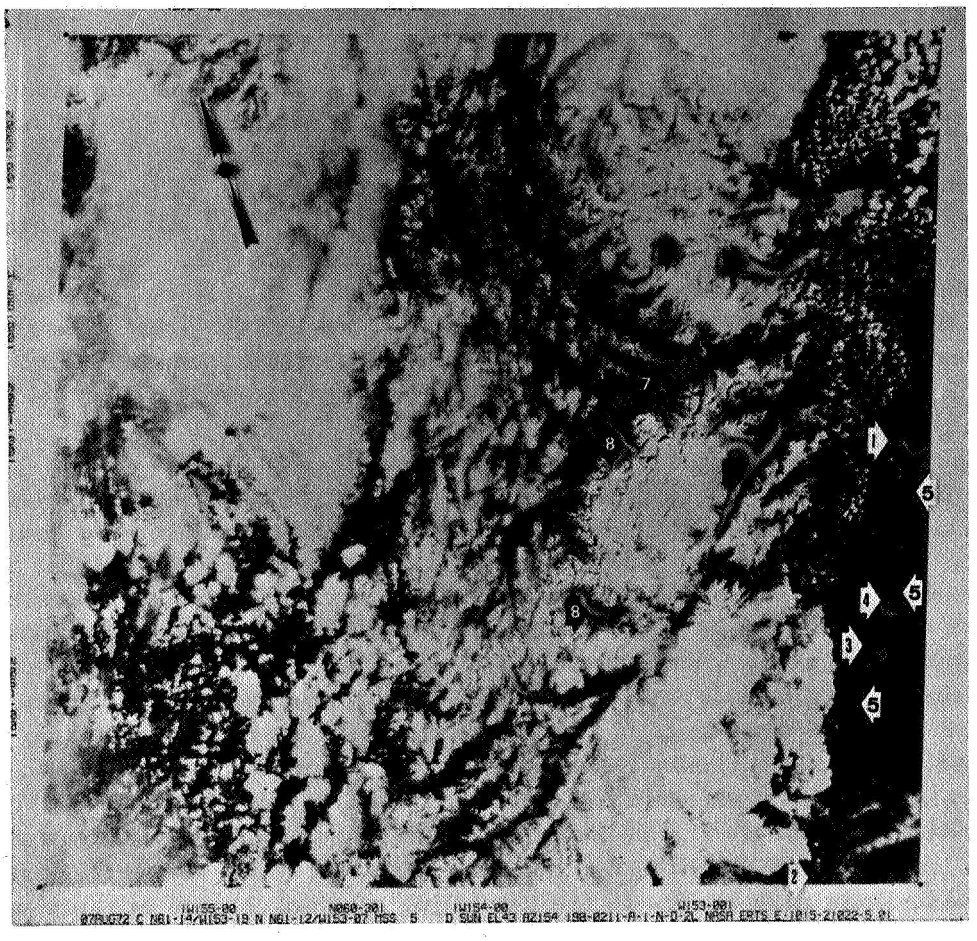


Figure 4. The west shore of Cook Inlet between MacArthur River and Tuxedni Bay

net water movement through several tide cycles. Tidal flats (5) are discernible as a gray border along the coastline. Mt. Spurr (6), one of the many volcanoes in the Chigmit Mountains, Lake Chakachamna (7) and numerous glaciers (8) are also apparent in this scene.

Tidal changes in the sediment plumes of the Big (5) and Drift (6) Rivers are shown in MSS scene 1049-20512-5 (Fig. 5) taken 10 September 1972. The southerly direction of the near-shore current during ebb flow in Redoubt Bay (7) is inferred by the shape of these river plumes. The sediment-laden water from Tuxedni River (12) is transported along the coast in a southerly direction between Chisik Island (13) and the mainland. This movement also indicates that the coastal currents were moving south along the west shore when the image was taken. The shape of the sediment plumes of the Kenai (15) and the Kasilof (14) Rivers indicate a southern current along the east shore in this location. Other features on this scene are: snowcapped Kenai Mountains (1), Kenai Lowland (2), the East (3) and the West (4) Forelands, a counterclockwise current pattern (8) around Kalgin Island (9), tidal flats (10), Harriet Point (11), and Lake Tustumena (15) with a high sediment concentration.

Water Types

Bands 4 and 5 of MSS scenes 1103-20513, 1103-20520, 1104-20572 and 1104-20574 clearly show the distinction between the more sediment-free, saline oceanic water in the southeastern portion of the inlet and the sediment-laden, fresher inlet water in the northern and southwestern parts of the inlet. Recognition of this relationship is possible because the sediment in the inflowing fresh water functions as a tracer, making sediment distribution patterns visible. Daily changes and changes that occur every 18 days in this regional sediment distribution can be detected. Figure 6a shows differences in the main boundary between the oceanic and fresh water in the southern inlet on two successive days. The boundaries separate the water types during low tide in Anchorage and high tide in Seldovia (Fig. 2). The irregularity of the western portion of these lines may be due to the upwelling of cold, saline oceanic water that occurs in the western portion of the inlet (Evans et al., 1972; Kinney et al., 1970). The northern portion of the 4 November boundary is also quite irregular, possibly due to this upwelling effect. According to Bowden (1967) some estuaries are characterized by a salt wedge that moves headward into the estuary along the bottom while the fresh water outflow moves over this wedge and out the estuary. In Cook Inlet this subsurface tongue of oceanic water progresses headward and moves up the shoaling bottom of the inlet to the latitude of Tuxedni Bay where it rises to the surface south of Kalgin Island during flood tide (Kinney et al., 1970). The upwelling waters appear as a large area of clear water surrounded by sediment-laden water. This process produces a zone

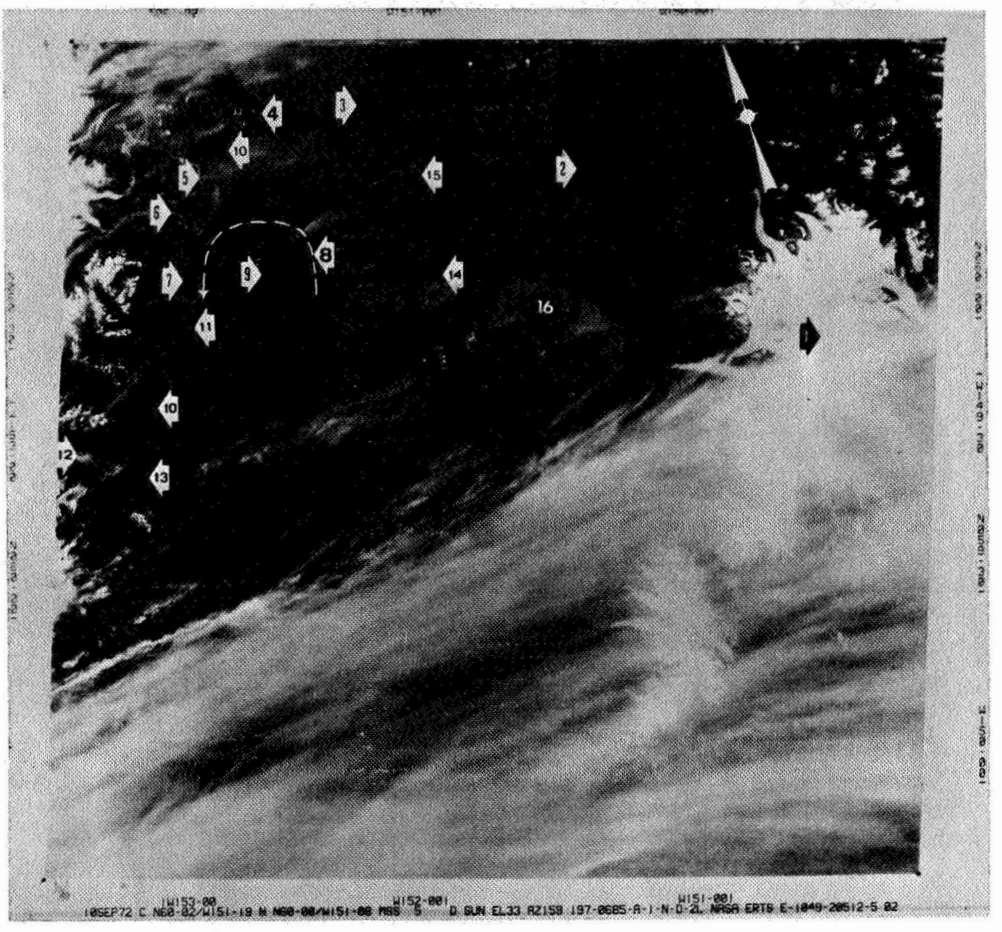


Figure 5. Central portion of Cook Inlet

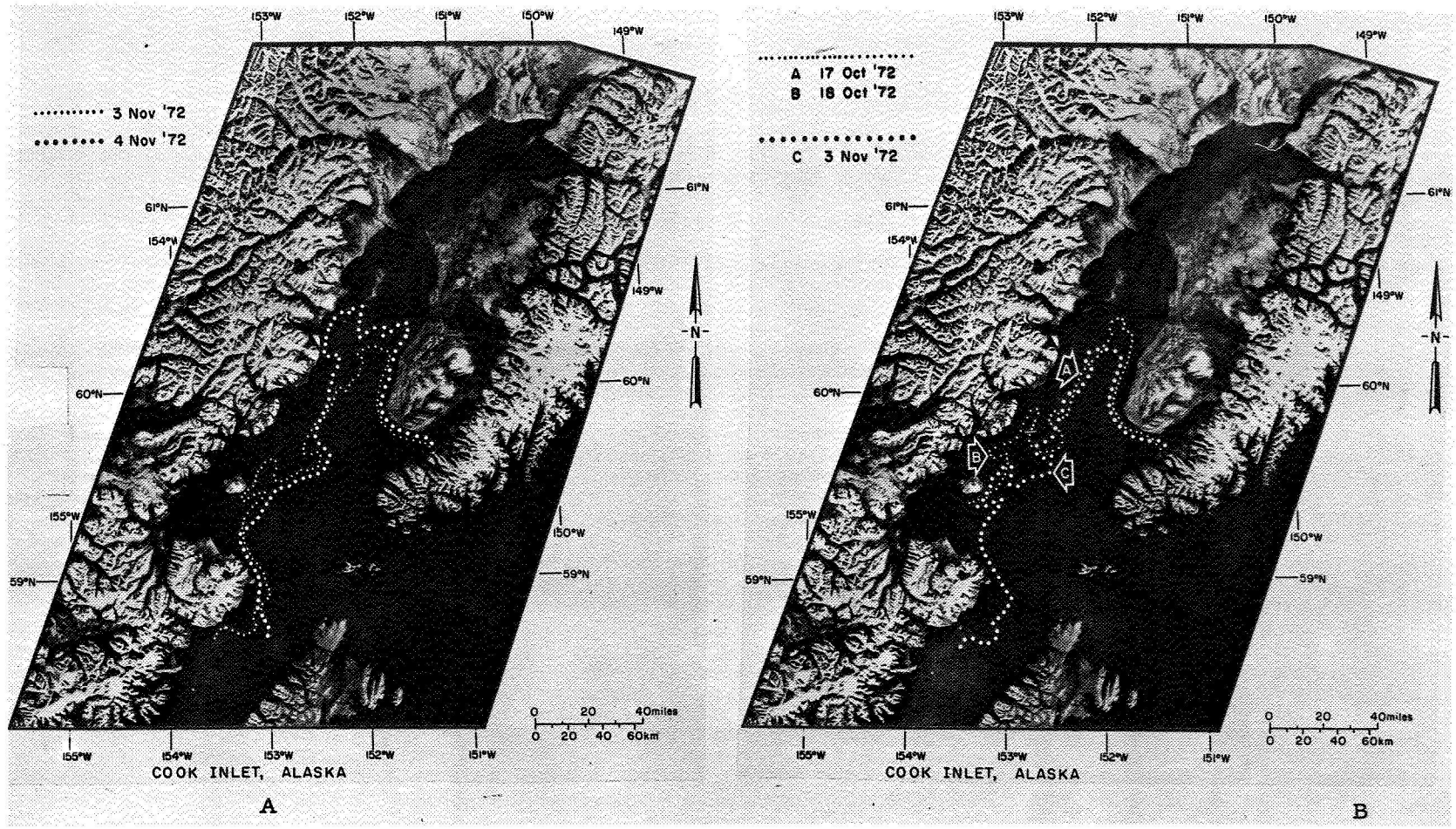


Figure 6. Boundaries separating oceanic and inlet water

of high nutrient concentration in the photic zone at this location. This may be significant to the fishing industry since certain species of fish may tend to concentrate in this high nutrient area. Changes in the boundary over an 18-day cycle are shown in Figure 6b. These boundaries are generally comparable to those in Figure 6a. Although changes in the sediment distribution and surface circulation produce some obvious minor alterations in the regional distribution of water types, the major relationships appears to remain consistent with time.

Surface Circulation

The high suspended sediment concentration in the inflowing fresh water and in the inlet water functions as a natural coloring agent by which the surface circulation of tidal and long-shore currents can be observed. The currents are most visible in MSS bands 4 and 5. Figure 7 shows the surface circulation in the inlet based on published data (Evans et al., 1972) and inferred from ERTS-1 imagery. The regional circulation of the inlet water as previously understood was observed and verified with few changes in the ERTS images. The clear oceanic water enters the inlet at flood tide along the east side around the Barren Islands. A portion of this clear water is forced into the inlet by the counterclockwise Alaska Current in the Gulf of Alaska. A distinct tongue of this oceanic water, which can be seen on MSS frames 1104-20574-5 and 1103-20520-4, occupies the southeastern portion of the inlet and becomes less distinct in a northeast direction by mixing with the sediment in the upper inlet water around Ninilchik. The tide front progresses up the inlet (nearly 150 miles) in approximately 4 1/2 hours. It moves faster along the east shore, being diverted in that direction by the Coriolis force. A back eddy not previously reported (dotted arrow) was apparent on MSS frames 1103-20513-5, 1103-20520-5 and 1104-20574-5 just offshore from Clam Gulch. The eddy forms in the slack water area northeast of Cape Ninilchik during flood tide. The tide front continues past the East Foreland, a large peninsula protruding some 10 miles into the inlet and is partially diverted across the inlet, where it abuts the West Foreland. At this point, part of the diverted front moves south of the West Foreland and the remainder moves north. This circulation pattern is repeated twice daily during the two daily flood tides. The result is a counterclockwise circulation pattern around Kalgin Island (Fig. 5). The circulation of surface water north of the forelands appears to be similar to that previously reported (Evans et al., 1972). The ebb flow in the inlet moves predominantly along the northeastern shore past the forelands. This pattern was discernible on the imagery except for a previously reported counterclockwise pattern (dashed arrow) formed north of the forelands. This pattern is formed as the ebbing waters abut the West Foreland and some are diverted across the inlet and move headward with the flood current along the east shore.

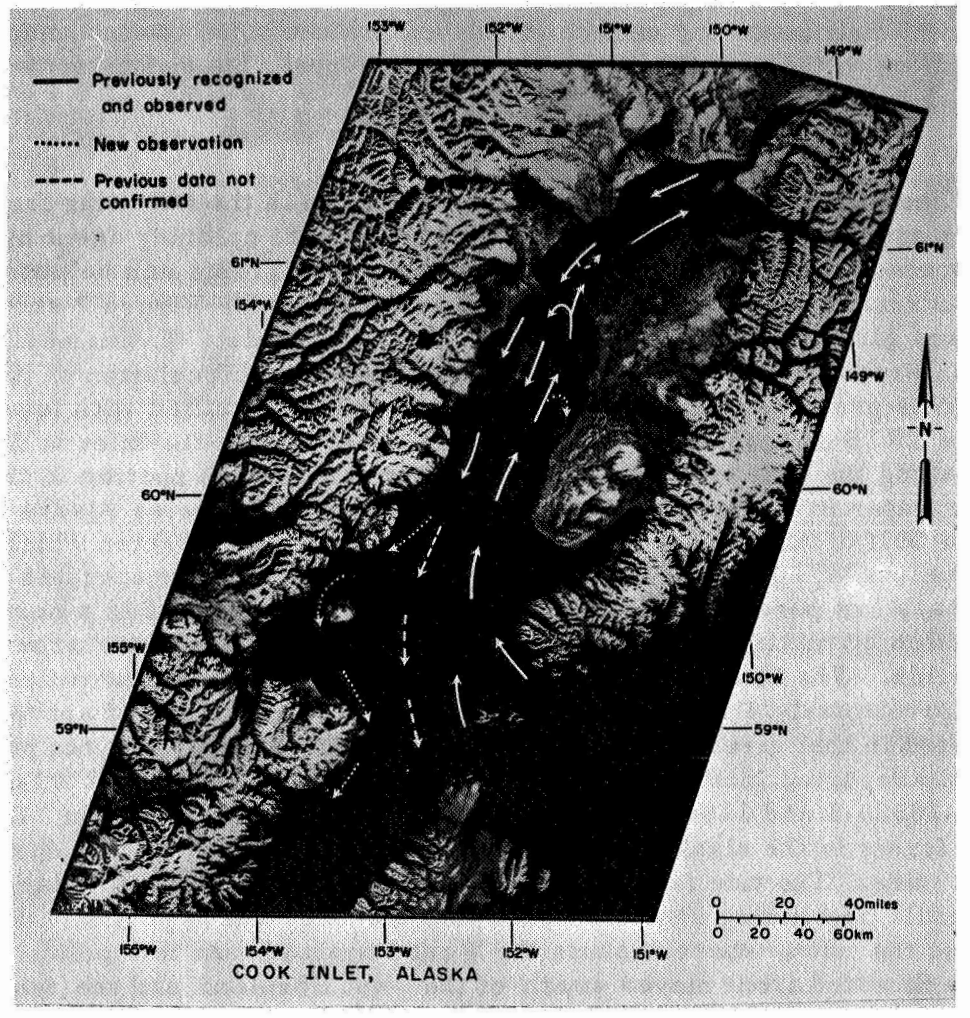


Figure 7. Surface current patterns

As the sediment-laden ebbing water moves past the area of Chinitna Bay (Fig. 1) it appears to flow along the shoreline and circulate around the west side of Angustine Island in Kamishak Bay. It continues to parallel the coast past Cape Douglas and progresses through Shelikof Strait. This circulation pattern in Kam ishak Bay was not previously reported but is clearly visible on the MSS imagery.

CONCLUSIONS

The richness of the ERTS satellite imagery in information on ocean circulation and coastal processes is clearly evident. The changes in the distribution and configuration of tidal flats can be monitored with MSS band 5 and 7 images. Knowledge of these changes is particularly important in maintaining navigation channels and harbor facilities. Upwelling, which produces a region of high nutrient concentration, can be detected on MSS bands 4 and5. This is significant to the fishing industry of Homer, Ninilchik and Kenai, since certain species of fish may tend to concentrate in this region. The distribution of sediment and the surface circulation are also visible on MSS bands 4 and 5. ERTS-1 will permit the collection of sufficient observational data on transport-circulation processes to develop an understanding of the regional relationships between river hydrology, sediment distribution and near-shore oceanography in Cook Inlet.

REFERENCES

Bowden, K. F., 1967, Circulation and diffusion: Estuaries, Amer. Assoc. for the Advancement of Science Publ. No.83, Washington, D. C. p. 15-36.

Burrell, D. C. and D. W. Hood, 1967, Clay - Inorganic and organic-inorganic association in aquatic environments, Part II: Institute of Marine Science, University of Alaska, College, Alaska.

Environmental currrents, 1972, Environmental Science and Technology, vol. 6, no. 12, p. 965.

Evans, C. D., E. Buch, R. Buffler, G. Fisk, R. Forbes and W. Parker, 1972, The Cook Inlet environment, a background study of available knowledge: Resource and Science Service Center, University of Alaska, Anchorage, Alaska.

Horrer, P. L., 1967, Methods and devices for measuring currents: Estuaries, Amer. Assoc. for the Advancement of Science Publ. No. 83, Washington, D. C. p. 80-89.

Kinney, P. J., J. Groves and D.K. Button, 1970, Cook Inlet Environmental data. R/V Acona Cruise 065- May 21-28, 1968: Institute of Marine Science Report R-70-2; University of Alaska, College, Alaska, 120p.

Marine Advisors, Inc., 1966a, Currents near the mouth of Drift River, Cook Inlet, Alaska: San Diego, California.

Marine Advisors, Inc., 1966b, Hydrographic survey in Trading Bay, Cook Inlet, Alaska: San Diego, California.

Murphy, R. S. and R. F. Carlson, 1972, Effect of waste discharges into a silt laden estuary, a case study of Cook Inlet, Alaska: Institute of Water Resources Report IWR 26, University of Alaska, College, Alaska, 42p.

Rosenberg, D.H., D. C. Burrell, K. V. Natarajan and D. W. Hood, 1967, Oceanography of Cook Inlet with special reference to the effluent from the Collier Carbon and Chemical Plant: Institute of Marine Science Report No. IMS-67-3, University of Alaska, College, Alaska, 80p.

Rosenberg, D. H., K. V. Natarajan and D. W. Hood, 1969, Summary Report on Collier Carbon and Chemical Corporation Studies in Cook Inlet, Alaska, Parts I and II, November 1968-September 1969: Institute of Marine Science Report No, 69-13, University of Alaska, College, Alaska.

Sharma, G. D. and D. C. Burrell, 1970, Sedimentary Environment and Sediments of Cook Inlet, Alaska: Amer. Assoc. Pet. Geologists, vol. 54, no. 4, 9. 647-654.

Wagner, D. G., R. S. Murphy and C. E. Behlke, 1969, A program for Cook Inlet, Alaska for the collection, storage and analysis of baseline environmental data: Institute of Water Resources, Report No. IWR-7, University of Alaska, College, Alaska, 284p.

N73-28344

Paper M 10

DISTRIBUTION AND MOVEMENT OF SUSPENDED SEDIMENT IN THE GULF OF MEXICO OFF THE TEXAS COAST*

Ralph E. Hunter, *U. S. Geological Survey, Corpus Christi, Texas*

ABSTRACT

ERTS-1 imagery has proven very useful in studies of the distribution of suspended sediment in the Gulf of Mexico off the Texas coast. Moreover, by using suspended-matter concentrations as tags on water masses, much information on water movement can be obtained. The utility of suspended sediment as a tracer is dependent on the sediment remaining in suspension long enough to travel an appreciable distance or to be visible on successive images. Although the evidence is not conclusive, it seems likely that much of the suspended sediment in Gulf of Mexico nearshore waters during normal sea-state conditions has remained in suspension since the time of its entry into the Gulf of Mexico through rivers and tidal inlets.

Superimposed on the general offshore decrease in turbidity are more complex concentrations of turbid water which may be classified as plumes or bands. A plume is attached to its source river or inlet during its growth, but at the end of an ebb tidal cycle, the plume from a tidal inlet becomes detached and drifts passively. Most bands are aligned either parallel or obliquely to shore. Water movement in some oblique bands is known to be toward shore, whereas in others it is away from shore. The bands may originate in several ways: by drift along streamlines from localized sources, such as river mouths, where suspended sediment is being continuously supplied; by the deformation of ebb-tide plumes after they have been detached from their source at a tidal inlet; or by the concentration of suspended sediment in the convergence or divergence zones between water masses, especially in the convergence or divergence zones associated with helical circulation cells.

1. INTRODUCTION

The movement of suspended fine-grained sediment, which is one facet of the sedimentological cycle involving the erosion, transport, and deposition of earth materials, is a geologic problem particularly accessible to study by repetitive remote-sensing techniques. ERTS-1 imagery has proven suitable for such studies; the imagery reveals differences of as little as 0.7 mg/l in the concentration of suspended particulate matter in surface waters of the Gulf of Mexico.

*Publication authorized by the Director, U.S. Geological Survey

PRECEDING PAGE BLANK NOT FILMED

Original photography may be purchased from
EROS Data Center
10th and Dakota Avenue
Sioux Falls, SD 57198

Suspended sediment is environmentally important from several standpoints. Its entry into suspension may constitute erosional damage, and its deposition may be damaging to channels, harbors, and biologically productive wetlands or sea floors. It may be considered a pollutant because of its detrimental effects on certain organisms; moreover, it may contain adsorbed metallic and organic compounds that are pollutants.

Under certain conditions the remote sensing of suspended particulate matter may be used as a tool for investigating physical oceanographic problems. One condition is that water masses must differ distinguishably in their content of suspended matter. If this condition is fulfilled, certain aspects of the flow system, especially current directions, may be deducible from the pattern of turbidity contrasts visible in an image; however, the capability of measuring current velocities is severely limited. A further condition is that the concentrations of suspended matter in distinct water masses must remain sufficiently close to constant long enough for the water masses to be recognizable in successive images. If this condition is fulfilled, the suspended-matter concentrations can be used as tags on water masses, by which their movement can be traced. Under favorable conditions, the Lagrangian field of motion can be determined in much greater detail by this method than is practicable by using discrete drift objects such as drogues or bottles. The first condition has usually been fulfilled in ERTS-1 imagery of the Texas coast, and the second condition has sometimes been fulfilled in the overlap areas of ERTS-1 images taken on successive days but has so far not been fulfilled in images taken during successive 18-day ERTS-1 cycles.

2. SOURCES OF SUSPENDED SEDIMENT

Most of the suspended particulate matter so abundant in coastal parts of the northwestern Gulf of Mexico is fine-grained terrigenous sediment (Manheim, Hathaway, and Uchupi, 1972). This sediment enters the Gulf of Mexico in three known ways: through river mouths, by flow of turbid bay and lagoon waters through tidal inlets, and by resuspension of sea-floor sediments during times of strong waves. The relative importances of the three sources of suspended sediment in the Gulf of Mexico are not known.

It was suspected, from the occasionally poor correlation between wave activity and nearshore turbidity, that resuspension of sea-floor sediments might not be the most important source of suspended sediment in coastal waters of the Gulf of Mexico. The ERTS-1 imagery supports this hypothesis and suggests that much of the suspended sediment in the nearshore waters at any one time has remained in suspension since the time of its entry into the Gulf of Mexico through rivers and tidal inlets. Although resuspension of shelf sediments may be significant during major storms, some evidence suggests that even during hurricanes,

resuspension may not be the most important source of suspended sediment (Hayes, 1967, p. 33-42).

The evidence from the ERTS-1 imagery concerns the behavior of river-mouth plumes and plumes from tidal inlets. When a plume from the Rio Grande is well developed, it can be traced continuously for distances of at least 75 km downdrift (south during the fall and winter of 1972-73) along the coast (Fig. 1). Ebb-tide plumes generated at tidal inlets become detached at slack water and drift with the coastwise current (Fig. 2). As many as four detached ebb-tide plumes have been seen downdrift (south during the fall and winter of 1972-73) of Aransas Pass, the most distant one having traveled about 85 km in 4 days of relatively calm weather. Evidently, suspended sediment introduced into the Gulf of Mexico through tidal inlets can remain in suspension for several days, even during relatively calm conditions, and can account for much of the turbidity in coastal waters, even at points far removed from river mouths and tidal inlets.

3. DISTRIBUTION OF SUSPENDED SEDIMENT

In general, the concentration of suspended matter in the northwest Gulf of Mexico decreases offshore (Manheim, Hathaway, and Uchupi, 1972). Superimposed on this gradient are more complex local variations in turbidity, most of which may be classified as plumes or bands.

Plumes are formed by jet flow from river mouths and tidal inlets. As the intracoastal bays and lagoons are presently less saline than sea water, plumes from the tidal inlets form surface layers like those from rivers. Coastal currents affect both types of plumes, causing their distal ends to bend in the direction of the current. The development of the two types of plumes differs, however, because river discharge continues for indefinite periods, whereas the discharge from a tidal inlet is restricted to periods of ebbing tidal currents.

If river discharge and coastal currents are steady enough, a river-mouth plume approaches a steady-state form so that its distal end drifts passively with the coastal current while the sediment disperses and settles in the water column. The Rio Grande plume has been seen to extend southward 65 km, hugging the convex shoreline, then becoming detached at a point of increased curvature and extending at least another 10 km along its previous line of movement (Fig. 1). The plume, or at least its surface part, is evidently kept pressed against the shoreline by an onshore component of surface drift. The suspended sediment may disperse seaward in a near-bottom layer as the river water mixes with sea water or as the suspended sediment falls from the less dense surface layer into an underlying layer of sea water. The plume from the Brazos River commonly extended obliquely offshore to the southwest during the winter of 1972-73, giving evidence of offshore surface

E

drift. Because of the lack of confinement, the offshore-drifting plume disperses rather rapidly and has not been traceable more than 40 km from its source.

Plumes from tidal inlets never attain a steady-state form because of their pulsing character. During or very shortly after its detachment at slack water, an ebb-tide plume is deformed in such a manner that its nearshore end lags behind its offshore end (Fig. 2). Its sharply defined updrift edge thus becomes oriented obliquely offshore in the direction of drift. The flow pattern by which an ebb-tide plume is deformed during and immediately after detachment is not yet fully understood. Later, during its drift along the coast, the direction of obliquity of the updrift edge of a plume is sometimes reversed (Fig. 2), indicating that the edge has been sheared because of a shoreward increase in longshore-current velocity. This phenomenon is restricted to a nearshore zone no more than 10 km wide and is evidently a result of the wave-driven circulation.

Most bands of turbid water are fairly straight and are oriented either parallel or obliquely to shore (Figs. 3 and 4). Occasionally, however, bands are incorporated into vortices having diameters of from 10 to 20 km; such vortices have been seen only during periods of relatively calm weather, when previously generated flow systems are presumably moving largely by inertia. The bands detectible on ERTS-1 imagery are on the order of 1 to 10 km wide and occur either singly or in series.

One of these bands was sampled at sea and photographed by a NASA aircraft from an altitude of 18,000 m coincidentally with an ERTS-1 overpass in late August 1972. The band was about 5 km wide, was centered along a line about 8 km from shore, and extended for a distance of about 120 km from Aransas Pass southward. Measured concentrations of suspended matter at the water surface were 1.0 to 1.8 mg/l within the band, compared with 0.2 to 0.8 mg/l on either side; the concentrations generally increased with depth. Horizontal and vertical salinity and temperature gradients were slight. Drift-bottle recoveries, plume orientations, and the orientations of linear slicks, which are visible in the aerial photographs are of the type produced by Langmuir circulation (Langmuir, 1938; Asaf, Gerard, and Gordon, 1971), indicated that the average current direction was southward, parallel to the axis of the band. At its southern end, the band gradually impinged against the concave shoreline. At the point of impingement, the aerial photographs showed an abundance of turbid rip-current plumes.

The direction of water movement in a band may be either toward or away from the point at which the band touches shore. Along the Texas coast north of Aransas Pass during the fall and winter of 1972-73, the bands were usually oriented obliquely to shore, diverging from

the shoreline in a southwestward direction. The direction of water movement in this area was southwestward and away from shore, though not necessarily exactly parallel to the bands.

The bands may originate in several ways. Some are simply long, relatively narrow plumes from river mouths. These bands are necessarily oriented along streamlines of the flow system. Some bands originate by the detachment and deformation of plumes from tidal inlets. In these bands, which are oriented obliquely to shore, the water movement is not necessarily parallel to the bands and may be more nearly parallel to shore.

Converging and diverging currents are probably important in shaping bands that originate from river-mouth or tidal-inlet plumes and may be solely responsible for the formation of other bands. Although direct evidence is lacking, the great lengths and uniform widths of some bands suggest that the currents are commonly organized into paired helical circulation cells of Langmuir type but much larger in scale than typical Langmuir cells. The axes of such cells, if they exist, are probably parallel to the primary or average current direction.

It is conceivable that suspended sediment could be concentrated in either the zones of surface convergence and downwelling or in the zones of surface divergence and upwelling of a system of helical circulation cells. The former distribution could occur if the suspended sediment were concentrated in a less dense water mass trapped in the zone of surface convergence between two circulation cells of denser, less turbid water. The latter distribution could occur if the concentration of suspended matter increased downward, and such a distribution could reach a steady state if the settling velocities of the particles were equaled by the velocity of upwelling. The turbid band sampled at sea during late August 1972 was probably of this latter type.

4. CONCLUSIONS

ERTS-1 imagery has furnished valuable information on the sources, distribution, and movement of suspended sediment in the northwestern Gulf of Mexico; much of this information could hardly be obtained in any other way and could certainly not be obtained over such large areas at such frequent intervals other than by satellites. Measurements of current velocity from single images have proven possible where the place and time of origin of detached plumes from tidal inlets could be inferred, and measurements by time-lapse methods have proven possible in the areas of overlap between images taken on successive days. In addition, the patterns of turbidity variation in the imagery reveal a wealth of detail on current directions and relative velocities.

5. References

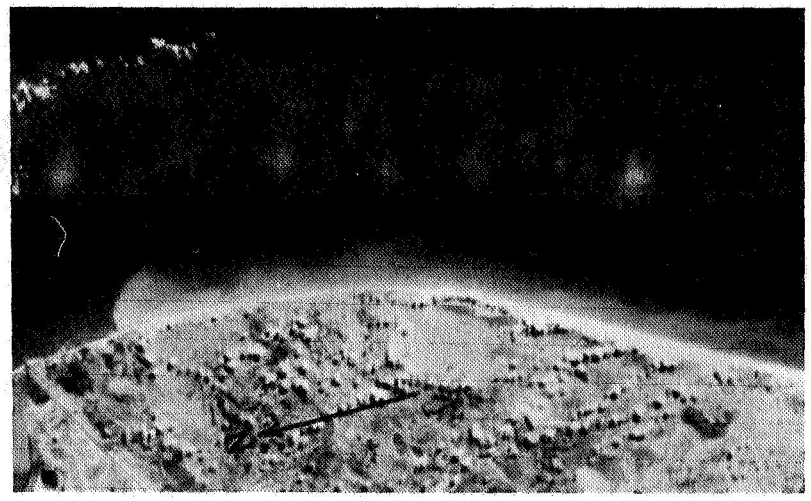
Asaf, G., Gerard, R., and Gordon, A. L., 1971, Some mechanisms of oceanic mixing revealed in aerial photographs: Jour. Geophys. Research, v. 76, no. 27, p. 6550-6572.

Hayes, M. O., 1967, Hurricanes as geological agents: Case studies of hurricanes Carla, 1961, and Cindy, 1963: Texas Univ. Bur. Econ Geol. Rept. Inv. 61, 56 p.

Langmuir, Irving, 1938, Surface motion of water induced by wind: Science, v. 87, no. 2250, p. 119-123.

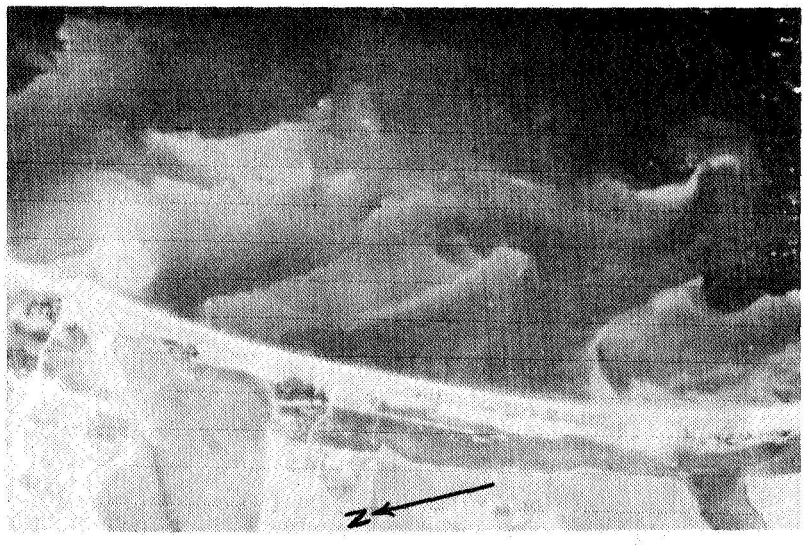
Manheim, F. T., Hathaway, J. C., and Uchupi, Elazar, 1972, Suspended matter in surface waters of the northern Gulf of Mexico: Limnology and Oceanography, v. 17, no. 1, p. 17-27.

F



0 20 40 km

Fig. 1. - Plume of turbid water from the mouth of the Rio Grande on October 4, 1972; part of image 1073-16260, band 4.



0 20 40 km

Fig. 2. - Active and detached ebb-tide plumes of turbid water from Aransas Pass, Texas, on October 23, 1972; part of image 1092-16314, band 4.

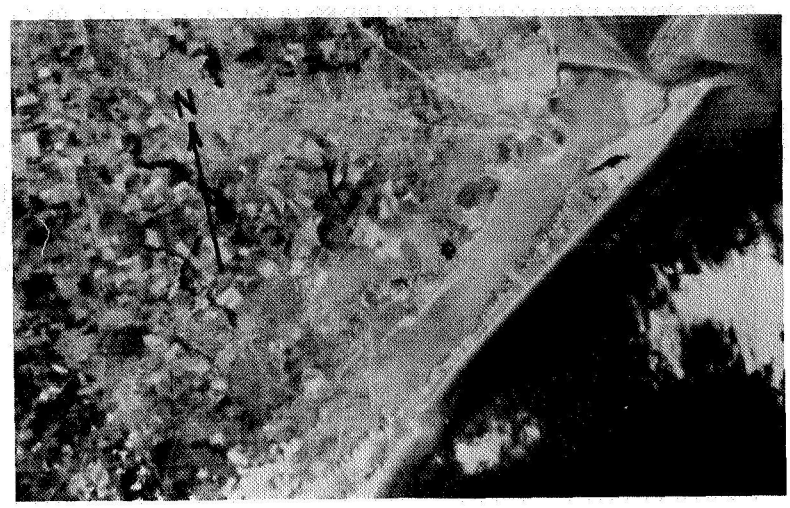


Fig. 3. - Band of turbid water oriented parallel to the shoreline of Galveston Island, Texas, on August 29, 1972; part of image 1037-16251, band 5.

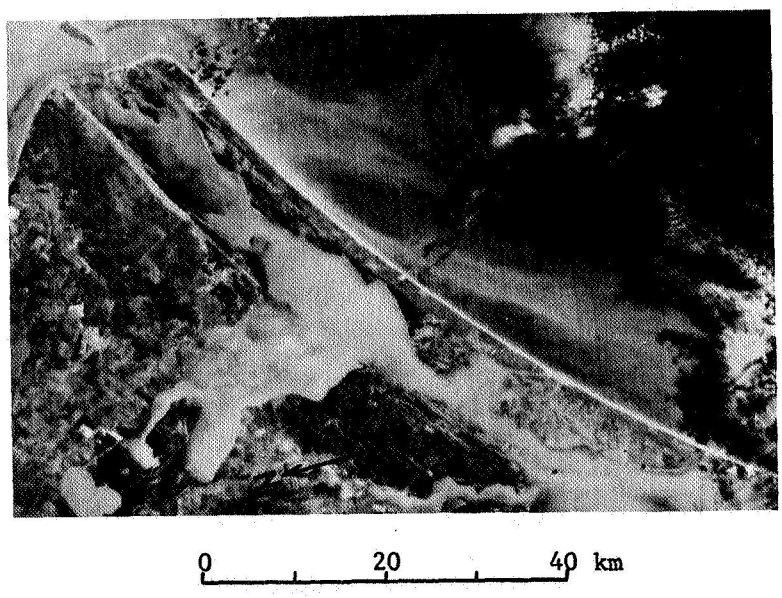


Fig. 4. - Bands of turbid water oriented obliquely to the shoreline of Matagorda Island, Texas, on November 10, 1972; part of image 1110-16313, band 5.

N73-28350

Paper M 11

OCEANOGRAPHIC MAPPING OF STRUCTURE AND DYNAMICS OF THE NORTHERN GULF OF CALIFORNIA BY THE USE OF SPECTRAL MODELING AND ERTS-1

L. K. Lepley, Gustavo Calderon, and J. R. Hendrickson, *University of Arizona , Tucson, Arizona*

ABSTRACT

Distribution and flow of water masses at four depth intervals were determined by analyzing ERTS imagery through the use of optical models of classes of vertical oceanographic profiles. Data used for these models was obtained from shipboard measurements including surface spectral radiance, and optical and more conventional oceanographic depth profiles. The spectral models obtained were applied to radiance-contoured ERTS imagery in band 4, 5, 6, and 7.

Features mapped by direct photointerpretation of ERTS imagery include submerged shoals, current streamlines, and location of possible upwellings, downwellings and submarine springs.

1. INTRODUCTION

One objective of this effort is to attempt to produce a series of oceanographic maps covering the annual range of seasonal effects and semidiurnal tidal effects in the Northern Gulf of California. Surface spectral data coupled with correlative vertical oceanographic profiles taken from ships can be used to obtain a measure of the vertical dimension to classify water masses seen in ERTS-1 imagery.

2. BACKGROUND

The known properties of sea water (Duntley, 1972; Lepley, 1968) and the results of the Scripps Institute of Oceanography's Fresnel II survey in the Gulf (Austin, 1972) were used to aid interpretation of ERTS-1 imagery obtained before the first University of the Arizona/Mexico surface truth cruises had begun (Hendrickson, 1973a).

Original photography may be purchased from:
EROS Data Center
10th and Dakota Avenue
Sioux Falls, SD 57198

The imagery of the ERTS-1 overpass corresponding to our January, 1973 surface truth cruise consisted mostly of clouds, but fortunately the previous December 29 ERTS overpass corresponded to an analogous tidal situation. Our studies of the first half-year of ERTS imagery indicate that the tidal excursions (to 7 meters) at the head of the Gulf are the most important factor in the dynamics of movement there.

3. APPROACH AND METHODS OF ANALYSIS

Reflectance measurements were taken in the discrete wavelength bands corresponding to ERTS MSS bands (.5-.6μ, .6-.7μ, .7-.8μ, .8-1.1μ) from the ship "Adventyr". Turbidometer profiles, secchi disk readings, visual observations, and analysis of water samples provided correlative data. Figure 1 shows the stations where radiometer data was acquired.

The spectroradiometric readings were taken from 2meters above the water surface with an Exotech ERTS Radiometer using a 15° field of view for upwelling radiation and a 160° field of view for downwelling radiation.

The ratio of upwelling to downwelling radiation was then plotted (figure 2) and identified with corresponding turbidometer, secchi disk, ocular, and other observations summarized in table I.

Although many more of these data will attach more (or less) validity to the apparent clustering and correlation of these spectra, the results are encouraging. Table I was constructed to show the classes of water that the spectral curves correspond to. Two assumptions were made in the analysis of the ERTS imagery and surface spectroradiometric data:

1. The transparency of clear water decreases monotonically with increase in wavelength of the four MSS bands.

2. The head of the Gulf is usually made of a wedge of clearer water which thins toward the Colorado River estuary and overlies at least one layer of very turbid water.

Surface spectroradiometric readings taken during the oceanographic cruise of January 12 to 22, 1973 (figures 1 and 3 and Table I) show a tendency to cluster according to: (a) depth of clear water over the underlying turbid layers (b) the amount of plankton in clear water and (c) clarity of the surface layer.

A technique was devised to produce maps of incremental reflectance values from ERTS imagery with the aid of an imaging densitometer. Imagery from the four ERTS channels were processed to produce density contours by the use of a Spacial Data model 704/8 video densitometer. ERTS negative transparencies were used for the analysis because more light is available for densitometry of the infrared imagery of water (very bright in negatives). The density increments were normalized so that the brightest contour corresponded to the wet tidal flats at the estuarine shoreline and the darkest contours corresponded to the darkest water in the image. Each contour corresponds to an increment of reflectance in a spectral band. These four contoured images were superimposed in register. The points of intersection of the contours corresponds to sets of incremental reflectances: spectra. We would prefer to obtain a more extensive space and time distribution of surface truth spectra coupled to imagery from syncronous overflights before attaching much significance to our results. Figure 3 is shown only to illustrate the results of this procedure (from E-1159-17451-4,5,6,7, December 29). The spectral classifications are here normalized at the brightest end to the wet tidal flats at the head of the estuary (1111) and at the darkest end in relatively clear water (3333).

4. RESULTS

We have been able, with a limited amount of surface truth data and a large amount of ERTS data, to construct a working model that relates the spectral reflectance of the Northern Gulf of California, as seen from altitudes of 2 meters and 490 nautical miles, to the thickness of the surficial clear layer, and turbidity and plankton content of the surficial layer.

Direct interpretation of ERTS imagery has yeilded some interesting possibilities (reported in Hendrickson, 1973a) including:

1. Indentification of submarine shoals by their disturbing effects on otherwise smoothly laminated layers of turbid water;
2. Establishing the direction of net rotary transport of water;
3. Identifications of bodies of semi-permanent bodies of clear water, some of which may be plumes of submarine springs.

REFERENCES

Austin, Roswell W., 1972

Surface truth measurements of optical properties of the waters in the northern Gulf of California. 4th Annual Earth Resources Program Review; Vol. IV; NASA Manned Spacecraft Center, Houston, Texas. pp. 106-1.

Duntley, Seibert Q., 1972

Detection of Ocean Chlorophyll from earth orbit. 4th Annual Earth Resources Program Review; Vol. IV; NASA Manned Spacecraft Center, Houston, Texas. pp. 102-1.

Lepley, L.K., 1968

Coastal water clarity from space photographs. Photogrammetric Engineering, Vol. 34 No. 7, July.

Hendrickson, John R.,1973a

Study of the marine environment of the Gulf of California. Type II Program Report for Period 21 June - 31 December, 1972. NASA, Goddard Space Flight Center.

Hendrickson, John R., 1973 b

Study of the marine environment of the northern Gulf of California. Type I Progress Report for Period ending February 20, 1973. NASA, Goddard Space Flight Center.

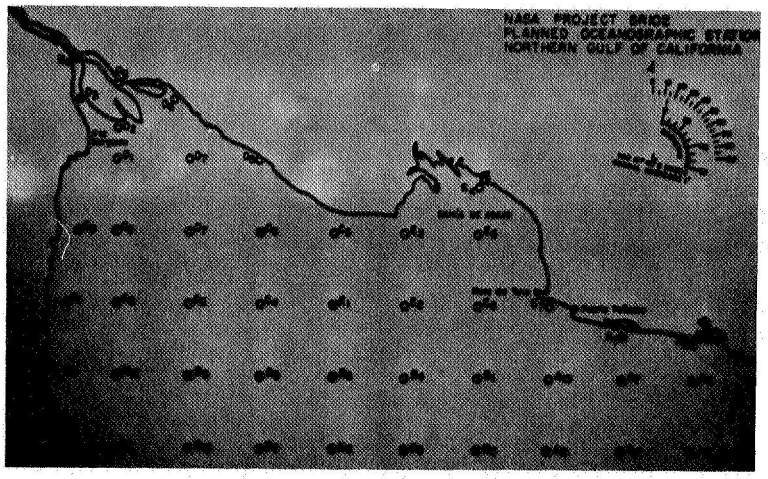


Figure 1. Oceanographic stations obtaining spectro-radiometric and correlative data (solid dots).

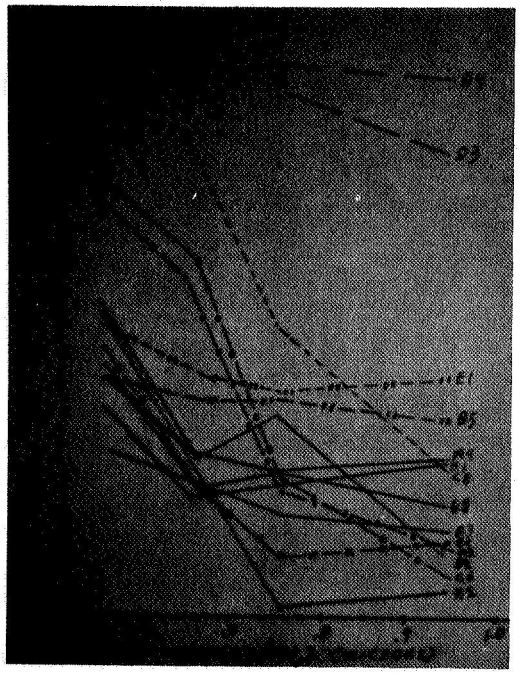


Figure 2. Relative relfectance curves, keyed to figure 1 and table I.

TABLE I

STATION NUMBER	SURFACE OBSERVATIONS
D3, D4	Water completely turbid. Depths less than 4 meters. Secchi disk visible to 15 centimeters.
C8	Thin layer of clear water over turbid water. Water deeper than 7 meters. Secchi disk visible to 1 meter.
C6, B12	Thick layer of clear water over turbid water. Depths around--18 meters. Secchi disk visible to 2 meters.
A1,A2,A9 B3,B8,B12	Very clear waters. No turbid layers. Water deeper than 30 meters. Secchi disk visible to 25 meters.
E1, B5	Clear and deep waters with suspended macro organic particles. No turbid layers. Secchi disk visible to 15 meters.
B9	Clear waters over semi turbid layers below 4 meters. Depths around 30 meters. Secchi disk visible to 5 meters.

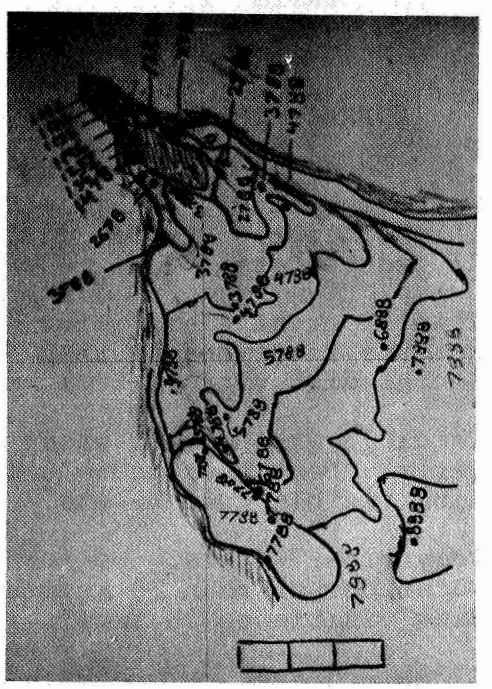


Figure 3. Classification of Gulf of California waters by normalized spectra from ERTS-1159-17451-4,5,6,7.

N73-28351

Paper M 12

OCEANOGRAPHIC FEATURES IN THE LEE OF THE WINDWARD AND LEEWARD ISLANDS: ERTS AND SHIP DATA

Kirby J. Hanson, Frank Hebard,[1] and Richard Cram,[2] *Atlantic Oceanographic and Meteorological Laboratories, National Oceanic and Atmospheric Administration, Miami, Florida*

ABSTRACT

Analysis of the ERTS data in portions of the eastern Caribbean are presented for October 1972 showing features which are, as yet, not explained.

Ground truth data obtained in that area during Nobember 1972 are presented. These include vertical temperature structure in the mixed layer and thermocline, and surface measurements of salinity, temperature, and chlorophyll.

1. INTRODUCTION

In previous work in this area, Ingham and Mahnken[3] found that tuna schools and bird flocks were concentrated in an area west of St. Vincent Island, Lesser Antilles. They also noted that plankton and primary productivity in the mixed layer were higher in this area than in the Atlantic, and that horizontal temperature differences existed in the upper thermocline in this area which suggested the presence of eddy-like features in the ocean. They suggested the possibility that the increased productivity of this area is a consequence of downstream turbulence on the Caribbean side of St. Vincent Island.

2. ERTS-1 DATA

NASA has collected ERTS-1 MSS Channel 4-7 data over portions of the eastern Caribbean on four cycles in the September-November, 1972 period. For the two ERTS cycles of best photographic coverage, the ERTS photos have been

[1] National Marine Fisheries Service, NOAA, Washington, D. C.

[2] Rosensteil School of Marine and Atmospheric Science, University of Miami, Coral Gables, Florida

[3] Turbulence and Productivity near St. Vincent Island, B.W.I., A Preliminary Report, Contribution No. 42, Tropical Atlantic Biological Laboratory, Bureau of Commercial Fisheries, Miami, Florida 33149

Original photography may be purchased from:
EROS Data Center
10th and Dakota Avenue
Sioux Falls, SD 57198

Original photography may be purchased from:
EROS Data Center
10th and Dakota Avenue
Sioux Falls, SD 57198

F

mosaicked and are shown in Figures 1 and 2. The island arc is visible in many of these ERTS photos.

In comparing Figure 1 (October 13-16, 1972) and Figure 2 (Nov. 17-21, 1972), it is clear that there are horizontal differences in the upward spectral radiance from the ocean surface during the October 13-16 period, but such differences are only slightly apparent in the November 17-21 period. These horizontal differences appear in the lee (west side) of each of the major islands of the Lesser Antilles. Figures 1 and 2 have been presented as negative prints of MSS Channel 4.

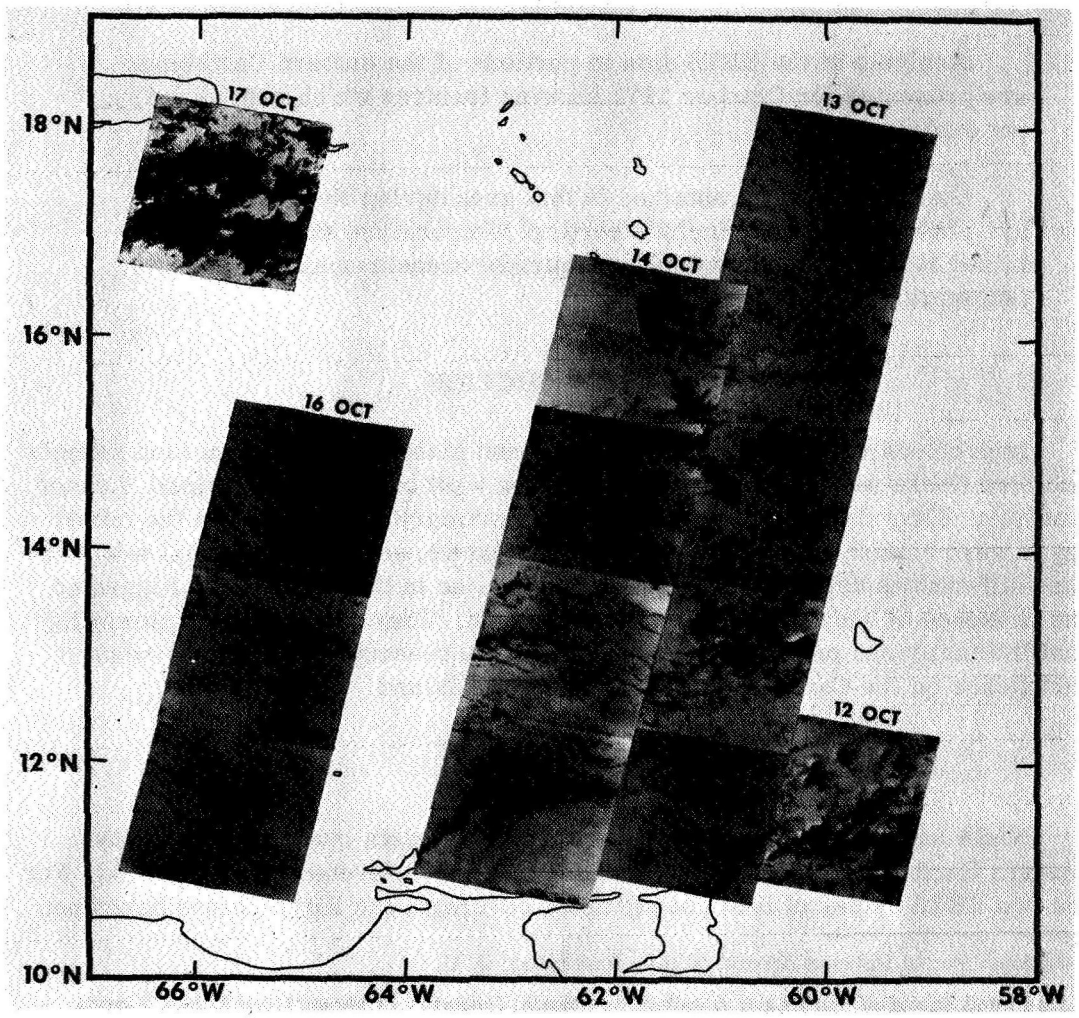


Figure 1. ERTS MSS Channel 4, 13-14, 1972

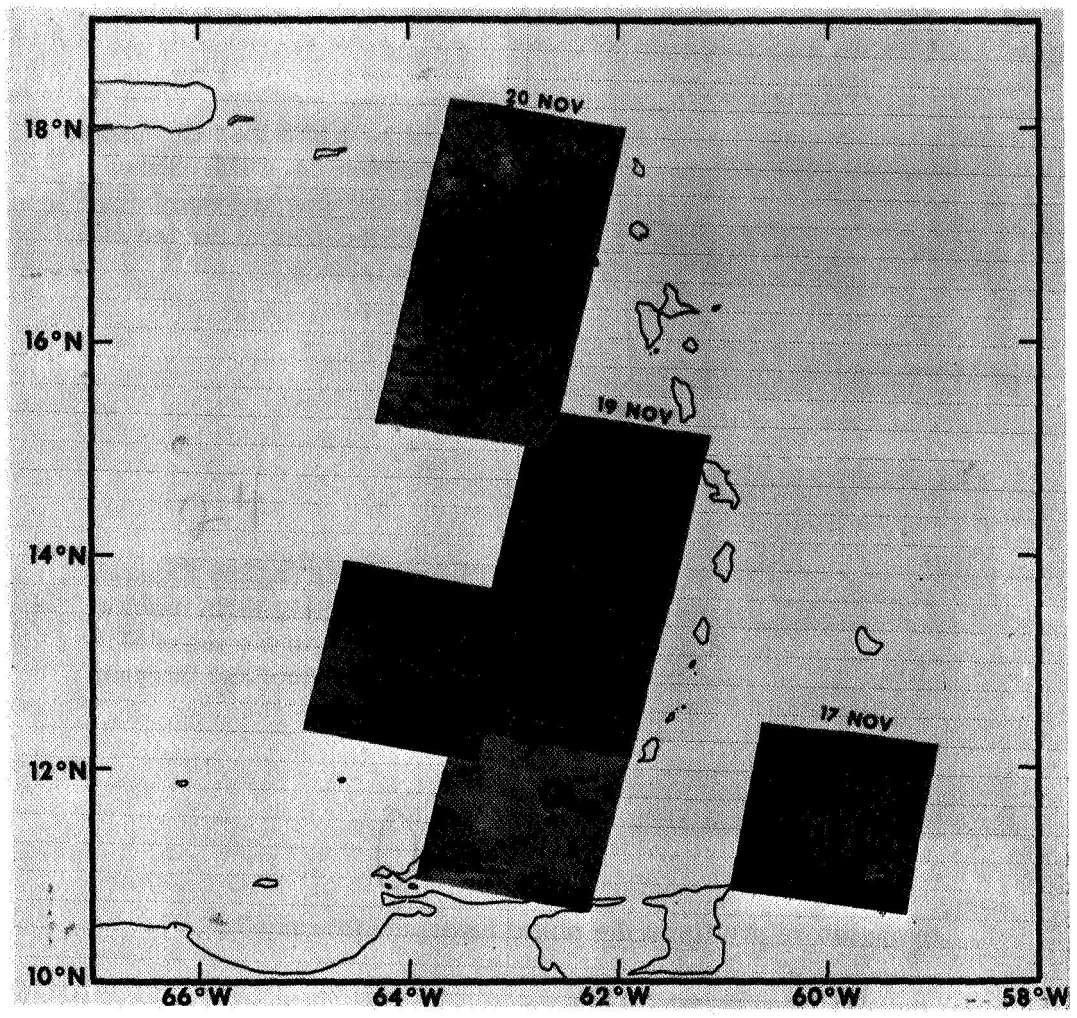


Figure 2. ERTS MSS Channel 4, Nov. 17-21, 1972

The ocean area west of Guadeloupe and Dominica is shown in more detail in Figure 3 and the ocean area west of Grenada and St. Vincent is shown in Figure 4 from the October 14, 1972, MSS Channel 5 data. These same ocean features are visible in MSS Channels 4-7.

3. GROUND TRUTH DATA (Nov. 15-16, 1972)

Ground truth information was obtained in the eastern Caribbean on the NOAA/CARIB cruise of the NOAA ship DISCOVERER. The ship track and times are shown in Figure 5; the hours are GMT. The ocean variables measured were:

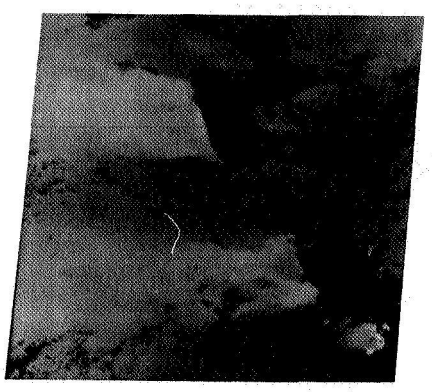


Figure 3. ERTS MSS Channel 5, October 14, 1972. Shows Guadeloupe and Dominica and features in the lee of the islands.

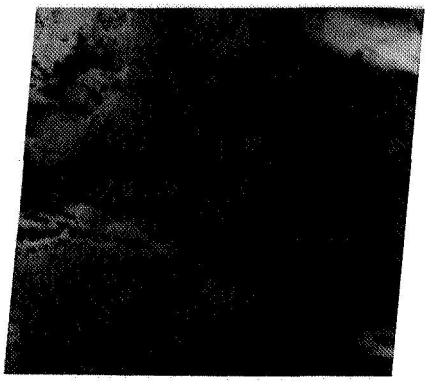


Figure 4. ERTS MSS Channel 5, October 14, 1972. Shows features in the lee of St. Vincent (top) and Grenada (bottom).

1. temperature profile in the mixed layer and thermocline,
2. surface salinity,
3. surface chlorophyll,
4. surface nutrients,
5. upward spectral radiance at the sea surface.

The first three variables have been analyzed and are presented in Figures 6 through 9.

4. DISCUSSION

At the time of collection of ground truth data in the Eastern Caribbean in mid-November, 1972, ERTS data were not yet available to give an indication of

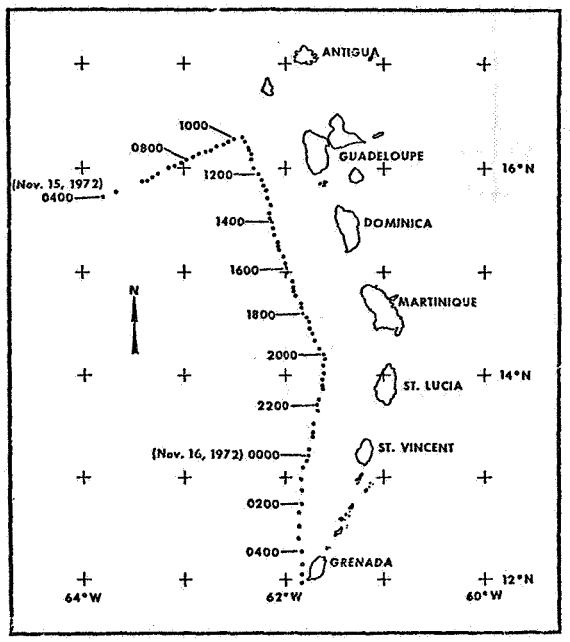


Figure 5. Cruise of DISCOVERER, Nov. 15-16, 1972

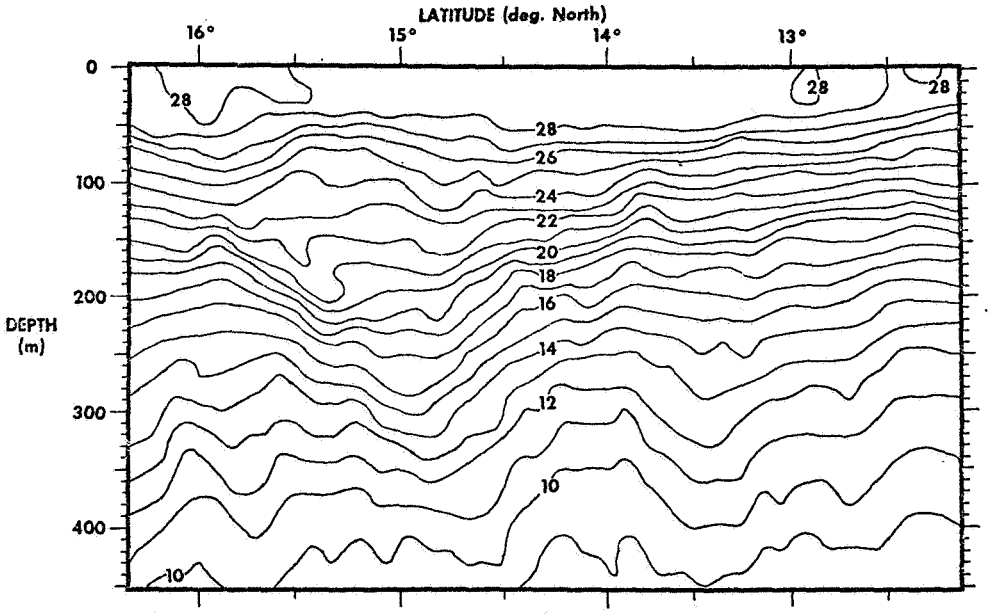


Figure 6. Temperature cross-section along ship track of Figure 5.

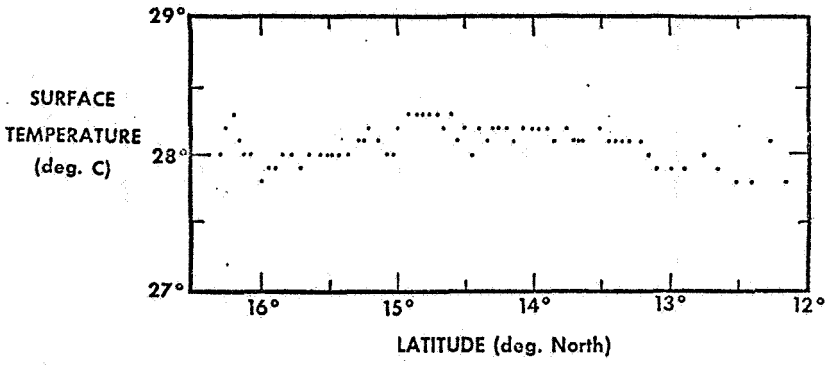


Figure 7. Surface temperature along ship track of Figure 5.

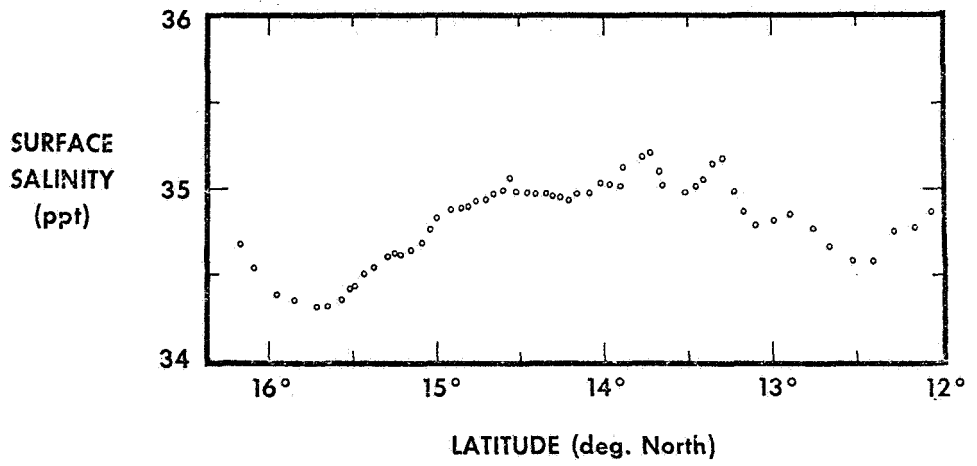


Figure 8. Surface salinity along ship track of Figure 5.

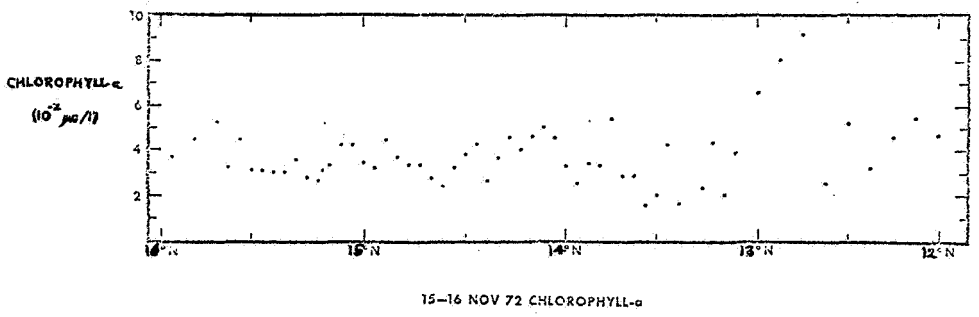


Figure 9. Surface chlorophyll along ship track of Figure 5.

the size and spatial distribution of the features which were apparent in ERTS data, occurring in the lee of each major island in the Antilles arc (Figure 1). Because of this lack of information when the ground truth were collected, only a single north-south cross section was obtained which parallelled the Antilles Island arc.

In the November 19-20, 1972 ERTS data (Figure 2), there are only very small horizontal gradients in image density in the lee of Martinique and Grenada compared to the October 13-14 period. The ground truth data (Figures 6 – 9) obtained four days earlier in that area do not reveal a pattern similar to that of the ERTS data of November 19-20, 1972.

Unfortunately, there were no ground truth taken during the October 13-14, 1972 period which is the only time these ocean features have been clearly apparent in the ERTS data. The features visible in the October 13-14, 1972 ERTS data (Figure 1) may result from one or a combination of causes associated with the atmosphere or ocean. Some possibilities are:

1. The sea state and/or swell is modified in a wind shadow of the island,
2. The run off of island rainfall carries high turbidity water in the mixed layer downstream of the island,
3. The phytoplankton in the mixed layer of the ocean has increased due to increased nutrients associated with upwelling.

We have compared the surface wind observations on the islands during the October 13-14 period with the November 17-21 period and found that the easterly winds were lighter during the October 13-14 period than the November 19-20 period. Thus, the wind observations at the island stations do not support the possible explanation in (1) above, that the sea state is modified due to wind shadow of the island.

In examining the ocean features which are visible in Figure 1, we find that the features are most apparent in channels 5 and 6, and are somewhat less apparent in channels 4 and 7.

Based on the present information, it is not possible to reach a firm conclusion about the cause of the features visible in Figure 1. It is hoped that in the future ground truth in coincidence with the ERTS data, and adequate ERTS data coverage, will resolve the question of the cause of these features.

N73-28352

Paper M 13

REMOTE SENSING OF OCEAN CURRENTS USING ERTS IMAGERY

George A. Maul, *National Oceanic and Atmospheric Administration, Atlantic Oceanographic and Meteorological Laboratories, Miami, Florida*

ABSTRACT

Major ocean currents such as the Loop Current in the eastern Gulf of Mexico have surface manifestations which can be exploited for remote sensing. A time series to study certain aspects of the surface expression of this current was begun in August 1972. Surface chlorophyll-a concentrations, which contribute to the shift in color from blue to green in the open sea, were found to have high spatial variability; significantly lower concentrations were observed in the current. The cyclonic edge of the current is an accumulation zone which causes a peak in chlorophyll concentration. The dynamics also cause surface concentrations of algae, which have a high reflectance in the near infrared. Combining these observations gives rise to an "edge effect" which can show up as a bright lineation on multispectral imagery delimiting the current's boundary under certain environmental conditions. Frequently the sea-state in the current is higher than in surrounding water due to differential shear. When high seas introduce bubbles, white caps, and foam, the reflectance is dominated by scattering rather than absorption. This has been detected in ERTS imagery and used for current location.

PRECEDING PAGE BLANK NOT FILMED

Original photography may be purchased from:
EROS Data Center
10th and Dakota Avenue
Sioux Falls, SD 57198

INTRODUCTION

The major circulation feature of the Gulf of Mexico is the so-called Loop Current. This flow enters the basin as a well formed western-boundary current through the Yucatan Straits. It penetrates into the Gulf to a varying latitude before it exits through the Straits of Florida. Transporting vast amounts of heat, salt and momentum, the current significantly affects circulation on the shelf, local fisheries, marine transportation, and is thought to be associated with hurricane intensification.

The current boundary separates two water masses. Across the boundary there is a difference in temperature, salinity, color, velocity, and biomass. These surface manifestations can be used for remote sensing in our efforts to monitor the current's variability. However, surface temperature difference, one of the best indicators, is not usable in the subtropics due to summer insolation which makes the sea surface isothermal. Other surface features, such as ocean color and evidences of horizontal current shear, probably have less seasonal variability.

This paper is a preliminary report on a time series of observations across the surface boundary layer of the Loop Current, and its detection by remote sensing, using several aspects of the surface features. The research is designed to investigate the seasonal variability of the juxtaposed water masses, both temporally and spatially, and the detection by ERTS of their boundary.

FIELD EXPERIMENTS

The field work began in June 1972 with a ship/aircraft experiment designed to detect the color boundary of the Loop Current front south of Dry Tortugas. The NASA C-130 flew over the research vessel track which was oriented in the same azimuth as ERTS suborbital track. Seven altitudes were flown, at 100 mb decrements, over the ship. Aircraft data collection included RC-8 color and color IR photography as well as multispectral photography to simulate the ERTS MSS imagery, PRT-5 sea surface temperature profiles, Bendix 24 channel scanner data, and inflight recordings of atmospheric temperature, pressure and moisture.

Prior to the aircraft overflights the scientific crew aboard R/V BELLOWS located the boundary. Measurements of

ocean temperature, chlorophyll-a, volume scattering function, and salinity were made every ten meters down to 50 meters; Forel color, and upwelling and downwelling spectral irradiance were taken at each of the five stations that bracketed the front. During the overflights on the following day, closely spaced surface measurements of the same variables (except irradiance) were taken. All measurements were made using standard oceanographic techniques or analyzed by methods detailed by Strickland and Parsons (1968).

In August 1972 a time series of the Loop Current by ship and satellite was begun. The cruise plan is to occupy the suborbital track of ERTS that crosses the west Florida shelf approximately 200 kilometers west of Tampa and terminates in the center of the Yucatan Straits. Every 36 days, the R/V VIRGINIA KEY is on the suborbital track. Continuous surface observations of radiometric temperature (in conjunction with the NOAA-2 IR sensors) and chlorophyll-a (by the fluorometric method of Lorenzen, 1966) are made; at approximately 12 kilometer intervals XBT's are taken, and samples are drawn for salinity, bulk temperature, volume scattering function, and biomass analysis. At appropriate daylight stations, measurements of upwelling and downwelling spectral radiance are made using a 1/4 meter Ebert scanning spectro-radiometer. A standard hydrographic section of the Yucatan Straits is made in order to estimate the geostrophic transport relative to 800 db. After the section, the cyclonic edge of the current is tracked by following the pathline of the 22° C isotherm at 100 meters; this pathline loops from the western edge of Yucatan to the Florida Straits south of Dry Tortugas and is in close proximity to the surface front. Finally another hydrographic section is observed along the suborbital track of ERTS that passes from Key West to Havana.

It is planned to continue the cruises to collect one year of data in order to obtain an evalutaion of the seasonal variability. The final field experiment, planned for the autumn, is a SKYLAB/EREP mission involving a ship and an aircraft.

PRELIMINARY RESULTS

The cyclonic edge of the Loop Current tends to concentrate flotsam and jetsam. Natural materials, such as surface marine algae, were seen from the June photo-

graphy to have a pinkish cast on color IR (SO 397) film; this is confirmed in black and white IR photography (type 2424 film and a 89B Wratten Filter). When these algae are present, they appear as a bright lineation marking the edge of the current in ERTS MSS-6 (0.7-0.8μm).

A second consequence of the boundary layer dynamics is to concentrate chlorophyll bearing organisms. A typical profile across the current boundary is given in figure 1. This transect is from Key West harbor, out the channel into the coastal water, and across the front. The feature of interest is the peak in chlorophyll-a concentration just at the boundary. This is a phenomenon noticed in each of the six cruises to date and occurs to a varying degree in the deep sea as well as near shore. Details of the variability will have to await further sampling because of expected seasonal and biological dependence. One would expect however that a shift towards the green would occur and enhance the boundary in MSS-4(0.5-0.6μm). This does indeed happen as will be discussed below.

A third observation is the usual change in sea state across the boundary. When winds and associated waves cross into zones of high current velocity with an opposing set, the seas generally build up rapidly. It is not uncommon for the sea state to increase from 1 to 2 meters when crossing into the current. Thus an increase of white caps, foam, and bubbles is encountered near the edge which increases the reflectance in the current. This raises the reflectance in all channels, but in a non-uniform (wavelength dependent) manner.

The term "edge effect" (Maul, 1972) was coined to describe these phenomena which can be exploited to detect the boundary of major ocean currents. Other streaming events, such as sediments being entrained by the Gulf Stream after passing source regions such as Cape Hatteras (ERTS 1132-15092), can be considered part of this edge effect. It allows a multispectral approach to recognize the boundary of these currents in the absence of sea surface temperature changes.

To understand the physics of reflection from the ocean, consider a simple model of an ocean of semi-infinite depth (Z) with spherical scattering. The spectral reflectance R(Z,-) is defined as the ratio of the

upwelling irradiance H(Z,+), i.e. that from the ocean, to the downwelling irradiance H(Z,-), i.e. that from the sky and sun:

$$R(Z,-) \equiv \frac{H(Z,+)}{H(Z,-)}$$

The reflectance is tacitly assumed to be a function of wavelength. From scattering theory the reflectance at the sea surface (Z=0) can be shown to be

$$R(0,-) = 1-H(\mu)\sqrt{1-\omega_0}$$

where ω_0 is the ratio of the scattering coefficient (b) to the attenuation coefficient (α), $H(\mu)$ is the so-called H-function for various scattering albedos (ω_0) as tabulated by Chandrasekhar (1960) and μ is the cosine of the zenith angle. It should be emphasized that this model does not include multiple scattering or the angular dependence of scattering such as the Monte Carlo calculations of Gordon and Brown (1973). Nevertheless it provides an analytic solution to the radiative transfer equation which illustrates the fundamental variables in reflectance.

An example of calculated reflectance from a plane water surface with the sun in the zenith [$H(\mu_0)$] is given in figure 2. The curves are based on scattering and attenuation coefficients given by Jerlov (1968) for natural ocean water bodies; α and b are chosen to exemplify the behavior of reflectance. Curve 1 is the spectral reflectance for pure water. Curve 2 is generated by changing the attenuation coefficient due to an increased absorption coefficient ($a=\alpha-b$) due to yellow substance. Note that the reflectance is lower and that the peak has shifted to a longer wavelength. Curve 3 is generated by increasing the scattering coefficient due to isotropic scatters whose b is twenty times the Rayleigh (molecular) scattering at 450 nm.; only the magnitude of the scattering increases, in a wavelength dependent manner, with the peak invariant. Curve 4 combines the effects of absorption and scattering. The reflectance is lower than pure scattering and the wavelength of the peak is shifted to the green.

Curves 1 and 4 can be likened to the change in reflectance encountered when crossing an ocean front. An example of an observed reflectance pair is taken from

the June aircraft experiment and given in figure 3. These are uncorrected for the immersion effect and the reflectances are approximately 20% too high. The zenith angle was $\sim 20°$ in each case. $H(Z,+)$ was measured 1 meter below the surface. The Loop Current water (marked 2) is lower in chlorophyll-a (< 0.1 mg m^{-3}) and lower in volume scattering coefficient ($\beta(45)=2.6 \times 10^{-3} m^{-1}$) than the coastal water (marked 4) with 0.4 mg m^{-3} chlorophyll-a and $\beta(45)=5.4 \times 10^{-3} m^{-1}$. If one assumes that the absorption coefficient is proportional to the chlorophyll-a concentration and the scattering coefficient is proportional to the volume scattering coefficient at 45° (Beardsley et al, 1970) then a qualitative confirmation of reflectance theory is given.

The curves further suggest that changes in ocean color will be reflected in MSS-4. Figures 4a and b are images from ERTS-1 taken over the eastern Gulf of Mexico during times of surface observations. Figure 4a is MSS-4 data showing the higher reflectance of water from Florida Bay pouring over the Keys and being entrained by the Gulf Stream. This image confirms the discussion in the previous paragraph.

Figure 4b is MSS-5 data taken north of the Yucatan Straits during a period of surface observations. The curving discontinuity in the water masses outlines the edge of the current. However, the blue waters of the current are brighter than the adjoining waters in contradiction to the results in figure 3. The explanation must come from figure 2, where we see the effect of increased scatterers. A marked increase in sea state was encountered in the current, which can account for a much higher scattering coefficient due to entrapped air.

An additional explanation of this is offered through consideration of sea state alone. Ross and Cardone (1972) observed that with 15 m s^{-1} winds, 10% of the surface of the sea is covered with white caps, and white caps reflect approximately 90%. If reflectance of the ocean is assumed to be 5% in the absence of white caps and 10% of the sea is covered with white caps, then reflectance is $R=5\%(.9) + 10\%(.9)=13.5\%$ or 270% higher than without white caps.

The spectrum of total upwelling irradiance from above the ocean $H_T(0,+) = [R(0,-) + R_S]H(0,-)$ where R_S is the

reflectance of the surface (both diffuse and direct). For the case R_s = constant and a given $H(0,-)$, H_T depends on ω_0. From figure 2 we estimate that the ratio of $R(0,-)$ at 450 nm to that at 525 nm for pure water is ∿4.5 (curve 1). The same ratio with scatterers only in the water (curve 3) is 2.0. Quantitative confirmation with realistic scattering phase functions will have to be calculated using the Monte Carlo code. Theoretically, the signal of a differential radiometer (Arvesen, 1972) is subject to such variation in ω_0. If it is fortuitous that ω_0 always varies in the ocean such that $R(0,-)_{525}$ is constant (Duntley, 1972), then a dual channel intrument will work in the absence of sea state changes.

The solar spectrum is fairly flat in the visible region ($H(0,-)_{450}/H(0,-)_{700}$∿1.3). Hence, higher sea states, which reflect high percentages of white light, proportionally add more long wavelength energy to the upwelling irradiance. In terms of a chromaticity diagram, this means that the purity changes but not the dominant wavelength. To correct for sea state a channel in a multispectral scanner near 1 μm appears useful. At this wavelength there is a maximum in the attenuation coefficient of pure water (i.e. $\omega_0 \to 0$), a maximum in atmospheric transmissivity, and the influence of chlorophyll seems low.

CONCLUSIONS

ERTS imagery has been successful in providing information on the ocean in both the nearshore and deep sea environment. As the result of an edge effect the cyclonic side of the Gulf Stream can reflect in several ERTS bands as a prominent feature paralleling the current's edge. It is found however that sea state is a significant variable that can dominate the reflectance and change the spectral signature of surface waters. The prospect is therefore raised that passive remote sensing using ERTS may be used to quantitatively estimate sea state and near surface winds in areas of homogeneous water masses. Further, the sea state problem must be considered a dominant variable in the determination of ocean color from aerospace sensors.

REFERENCES

Arvesen, J. C. (1972). Fourth Annual Earth Resources Review, Vol. IV, NASA MSC-05937, pp. 104-1 to 104-2.

Beardsley, G. F., H. Pak, K. Carder, and B. Lundgren (1970). Journal of Geophysical Research, 75 (15), pp. 2837-2845.

Chandrasekhar, S. (1960). Radiative Transfer, Dover, New York, 393 pgs.

Duntley, S. Q. (1972). Fourth Annual Earth Resources Review, Vol. IV, NASA MSC-05937, pp. 102-1 to 102-25.

Gordon, H. R. and O. B. Brown (1973). Applied Optics. (in press).

Jerlov, N. G. (1968). Optical Oceanography, Elsevier, New York, 194 pgs.

Lorenzen, C. J. (1966). Deep Sea Research, 13, pp. 223-227.

Maul, G. A., (1972). Interim Report on Remote Sensing of Ocean Currents from ERTS, NASA-CR-12907, National Technical Information Center, E72-10233.

Ross, D. B. and V. Cardone (1972). Fourth Annual Earth Resources Review, Vol. IV, NASA MSC-05937, pp. 85-1 to 85-20.

Strickland, J. D. H., and T. R. Parsons (1968). A Practical Handbook of Seawater Analysis. Fisheries Research Board of Canada, Ottawa, 311 pgs.

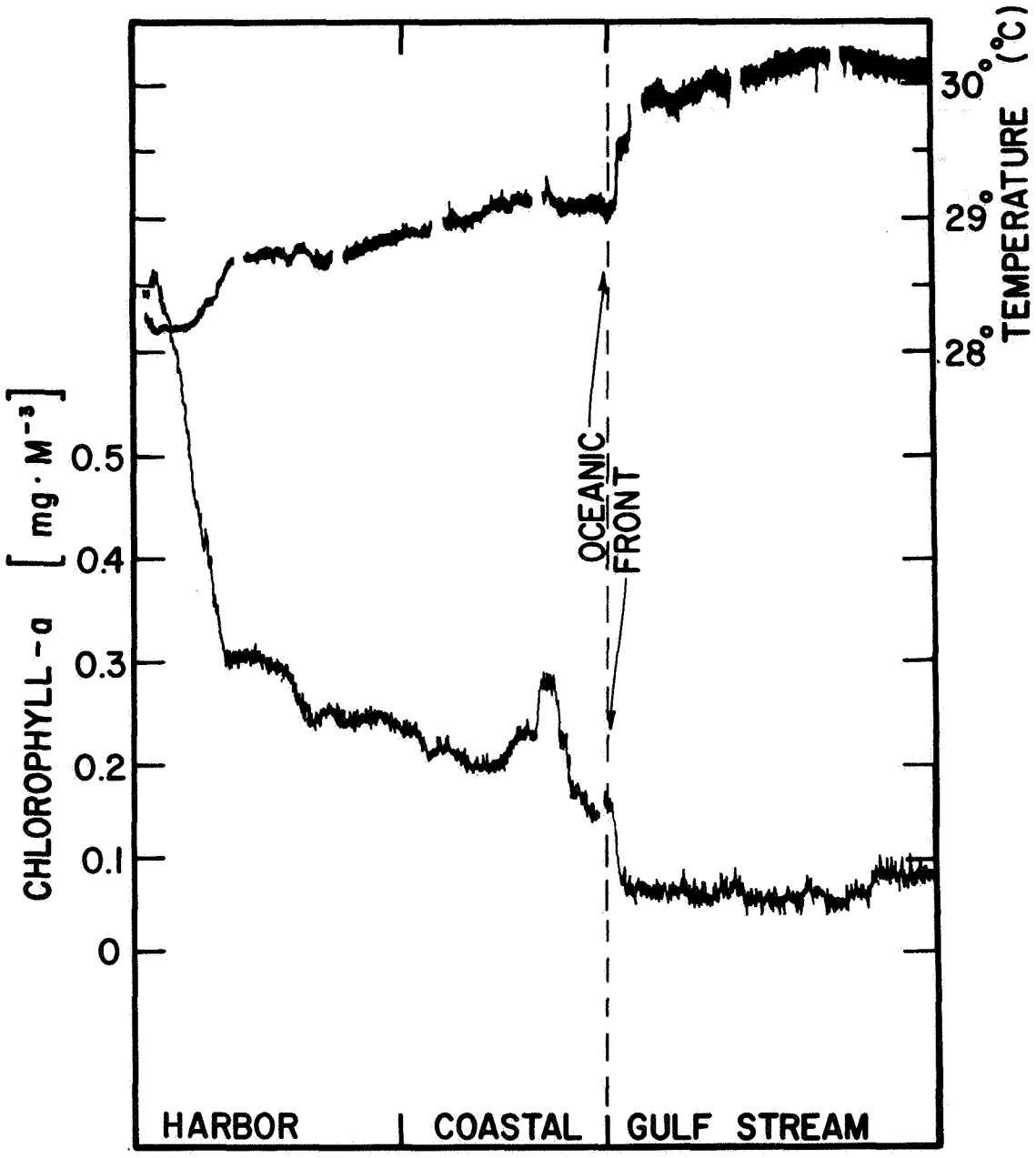


Figure 1: Surface temperature trace (upper) and surface chlorophyll-a profile (lower) across the Loop Current front and into Key West harbor. Horizontal scale across the figure is approximately 75 kilometers.

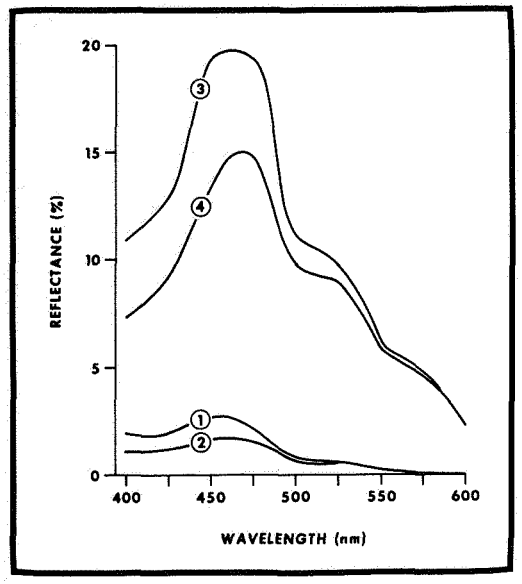


Figure 2: Results of theoretical calculations of reflectance from the water. 1 pure water, 2 pure water plus absorption due to yellow substance, 3 pure water plus isotropic scattering, 4 scattering plus absorption.

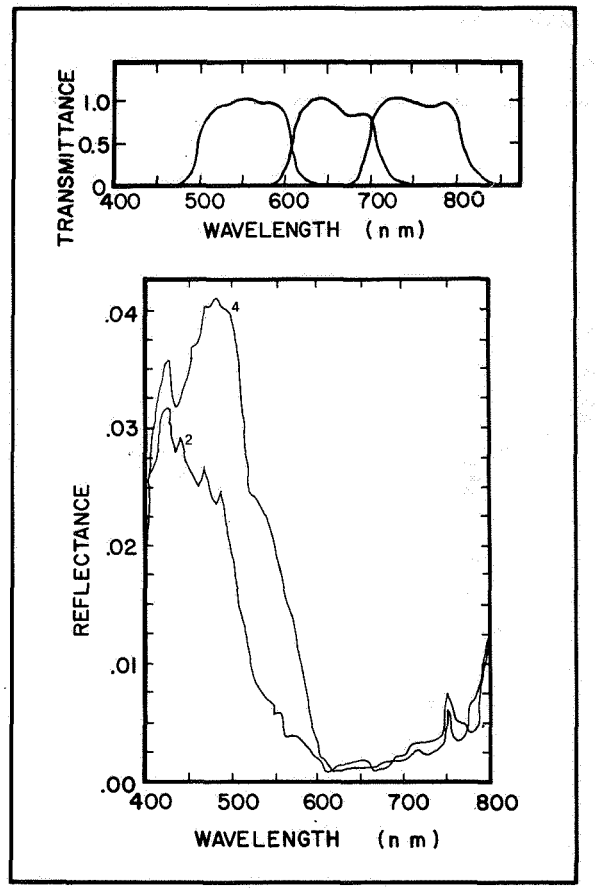


Figure 3: Observed reflectance across the Loop Current boundary. 2 current; 4 coastal water. Bottom depth exceeded 100 meters. Zenith angle about 15° in each case. The upwelling irradiance was measured at 1 meter depth. Upper panel has the spectral response of MSS 4, 5, and 6.

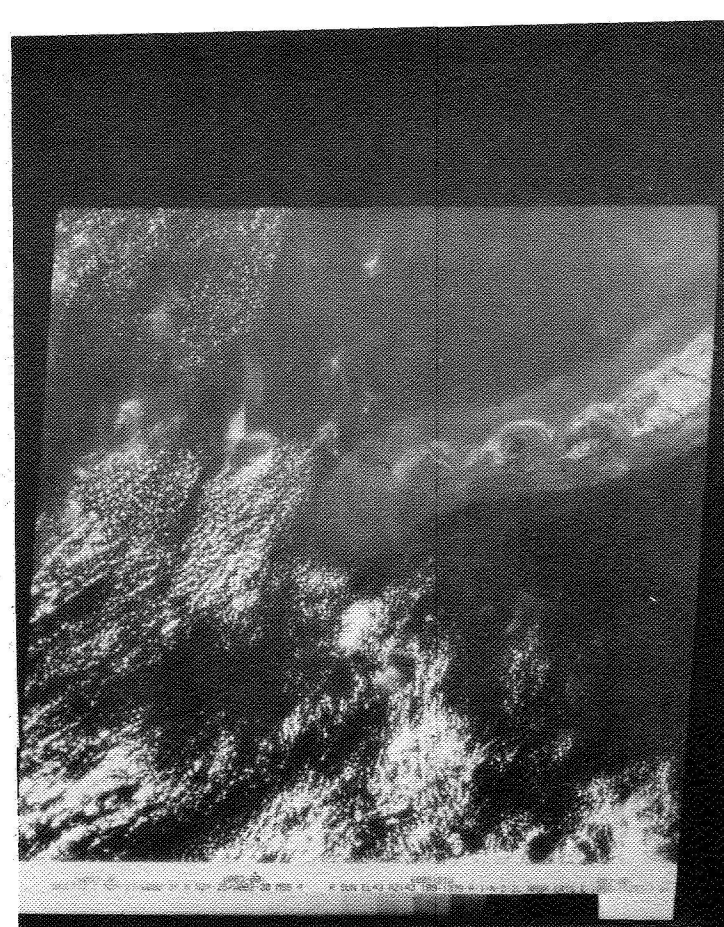


Figure 4a: MSS 4 imagery of the western Florida Keys showing water from Florida Bay being entrained by the Loop Current. The greener water from the bay appears brighter.

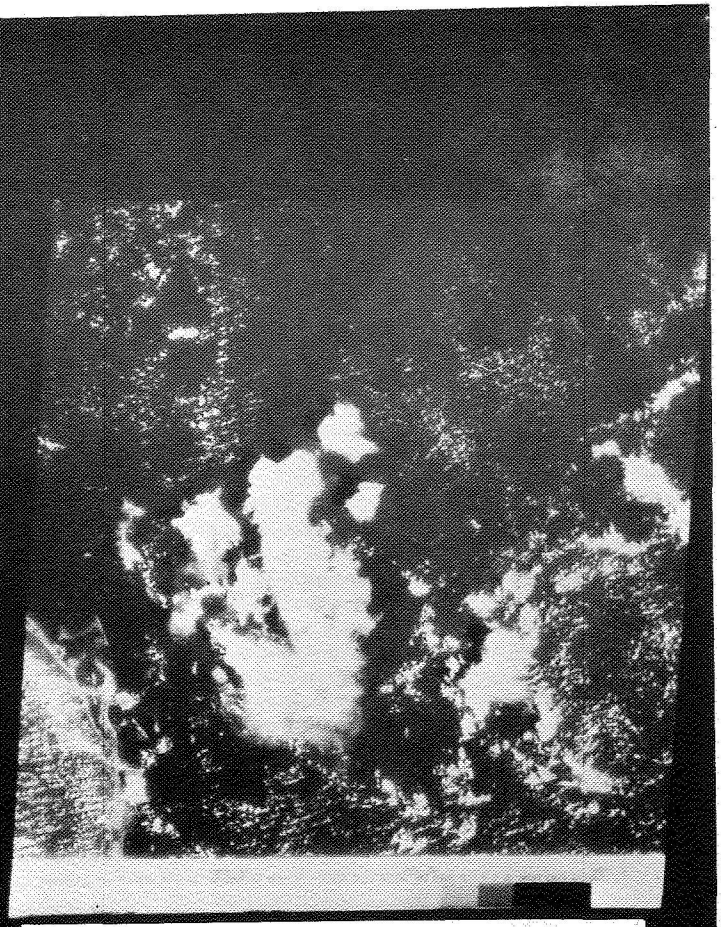


Figure 4b: MSS 5 imagery of the Loop Current exiting from the Yucatan Straits into the Gulf of Mexico. The blue water of the current appears brighter due to a higher sea state.

N73-28353

Paper M 14

USE OF ERTS DATA FOR MAPPING ARCTIC SEA ICE

James C. Barnes and Clinton J. Bowley, *Environmental Research and Technology, Inc., 429 Marrett Road, Lexington, Massachusetts 02173*

ABSTRACT

The purpose of this investigation is to evaluate the application of ERTS data for detecting and mapping Arctic sea ice. The specific objectives are to determine the spectral bands most suitable for detecting ice, to measure the scale and types of ice features that can be detected, and to develop interpretive techniques for differentiating ice from clouds and for mapping ice concentrations. The ERTS data are being analyzed primarily for three Arctic areas, the eastern Beaufort Sea, Baffin Bay, and the Greenland Sea.

1. INTRODUCTION

Extensive further study of the Arctic sea ice is essential for both economic and scientific purposes. Of particular national interest is the economic development of Arctic Alaska. Regardless of the course of this development and the eventual decision affecting oil transport, economic exploitation will require increased shipping in Arctic waters, demanding increasingly accurate ice-condition forecasts.

The increasing scientific interest in sea ice is demonstrated by the recent formation of Project AIDJEX, the Arctic Ice Dynamics Joint Experiment, the purpose of which is to gain a quantitative understanding of the interaction between the fields of motion of the atmosphere, the pack ice, and the liquid ocean (Division of Marine Resources, 1970). Several scientists have pointed out that because of the critical effect of sea ice on the heat balance of the Arctic, the amount of ice may be an important and possibly a key factor in the climate of the northern hemisphere (Fletcher, 1966; Maykut and Untersteiner, 1969; and Committee on Polar Research, 1970). In another report, Fletcher (1968) states that the seasonal patterns of surface heat exchange over oceanic regions, which are directly related to ice distribution, are the most important factors to monitor in both the Arctic and Antarctic.

Despite the importance of adequate ice information, the inaccessibility of the polar regions has required the use of slow and costly methods for data acquisition. Now, in Project AIDJEX and in other upcoming scientific endeavors in polar regions, remote sensing will play an increasingly vital

PRECEDING PAGE BLANK NOT FILMED

role. In fact, as early as 1966, Fletcher stated that the "observational barrier" in the Arctic was crumbling primarily under the impact of satellite observation systems. Clearly, the benefits that will result from the continued development of improved spacecraft ice survey techniques will be substantial.

2. APPLICATION OF ERTS DATA

Although studies such as those reported by McClain and Baliles (1971) and Barnes, Chang and Willand (1972) have demonstrated that useful sea ice information can be acquired from existing meteorological satellite systems, nevertheless, serious limitations in the use of these data do exist. In particular, the spatial resolutions of the sensors are adequate only for detecting gross ice boundaries and do not permit the mapping of small-scale features such as leads and polynyas, which may be especially critical for heat-balance considerations. Furthermore, intermediate ice concentrations cannot be mapped with the reliability desired by scientific and operational personnel, and icebergs, except for the largest Antarctic tabular bergs, cannot be detected. ERTS-1 is now providing the first opportunity to investigate the application of high-resolution, multispectral spacecraft data for ice mapping.

Analysis of ERTS-1 MSS data and a limited sample of RBV data from the Arctic during the period from late July through late October 1972 indicates that sea ice can be identified in all of the spectral bands because of its high reflectance. Moreover, considerable information on ice type and on ice surface characteristics can be derived from the joint analysis of the various spectral bands, particularly the MSS-4 (0.5 to 0.6 μm) and MSS-7 (0.8 to 1.1 μm) data. Identification of ice types and the scales of ice features can be made according to variations in reflectance and spatial patterns. Also, although ice and clouds may have similar reflectances, ice can be distinguished from clouds through the following interpretive keys:

- The brightness of ice fields and large ice floes is often more uniform than that of clouds. Furthermore, ice floes and features such as leads and cracks within an ice field can at times be detected through thin cirriform cloud cover.
- Cloud shadows can often be detected on the underlying ice surface.
- Edges of most ice features, particularly ice floes, are more distinct than edges of clouds.
- Ice cover fits coastlines and islands, permitting land features to be recognized.

- The spatial frequencies of ice features are not characteristic of cloud patterns. These features include ice floes surrounded by broken ice, narrow ice bands, and spiral patterns induced by ocean currents.

- When repetitive coverage is available, some ice features remain stable over the 24-hour interval between observations. Even at the longer periods between ERTS cycles, some large floes can still be identified.

3. MAPPING OF ICE FEATURES

The analysis of 9.5" positive prints for two passes crossing Hudson Bay in the area south of Coats and Southampton Islands during late July (Pass 41, 26 July; Pass 55, 27 July) shows a well-defined ice boundary southwest of Coats Island, with several bights and tongues apparently caused by a westerly surface wind flow. The ice along the immediate ice edge appears to consist mostly of brash or rotten ice, whereas the ice east of the edge consists of varying concentrations of vast, big, or medium category ice floes. An ice belt is visible off the south coast of Southampton Island, and fast ice together with some vast ice floes are located along and just off the north coast of Coats Island. (NOTE: Ice floes are defined in the WMO Sea Ice Nomenclature (WMO Pub. No. 259, TP. 145) as follows: Giant Floe - over 10 km (6.3 n.mi.) across; Vast Floe - 2 to 10 km across; Big Floe - 500 to 2000 m across; Medium Floe - 100 to 500 m across; Small Floe - 20 to 100 m across).

The ice features mapped from the ERTS data are in good agreement with the conditions reported in ice charts (supplied by the Canadian Ice Forecasting Central) for the last week in July. These charts indicate a sharp, irregular (bights) ice edge extending southwest of Coats Island with ice-free water to the west, and an ice belt south of Southampton Island composed of 3/10's of first year ice of which 1/10 is medium or larger size floes. The area northwest of Coats Island in Fisher Strait is shown to be comprised of 5/10's of first year ice of which 2/10's is medium or larger size floes.

Banks Island

Four ERTS passes crossing the Banks Island, Amundsen Gulf, and Franklin Bay area during late July have also been analyzed (Pass 43, 26 July; Pass 71, 28 July; Pass 85, 29 July; Pass 98, 30 July). Although much of Amundsen Gulf is open water in these passes, several isolated vast ice floes are located off the west coast of Banks Island, south of a giant ice floe (about 12 km x 50 km). A field of very close (7-8 oktas) and close (6-7 oktas) pack ice is located to the southeast of Banks Island, and areas of close, open (3-6 oktas) and very open (1-3 oktas) pack ice exist in Amundsen Gulf. Ice in Franklin Bay is composed of close, open

and very open pack ice; although one giant floe and several vast ice floes are observed in the bay, the majority of the ice consists of big, medium and small floes.

Aerial survey ice charts for the period 25-30 July indicate that a giant ice floe does exist off the southwest coast of Banks Island. A small area south of this giant ice floe is indicated as 4/10's of first year ice of which 2/10's is comprised of medium or larger size floes. The area of Amundsen Gulf south of Banks Island to about 70.5°N is indicated as open water with some loose ice strips, and several small areas of first year ice are indicated south of 71°N into Franklin Bay.

With the repetitive coverage of the Amundsen Gulf area, measurements of ice motion have also been made. Measurements of the positions of ice floes off the west coast of Banks Island during the 24-hour periods indicates a mean direction of motion toward the west-southwest at about 8 knots. Little or no movement is observed in the giant floe to the north, although some deterioration (breaking off of smaller floes) has apparently occurred. Measurements of the 24-hour motions of ice floes in western Franklin Bay off the coast of Cape Bathurst show a mean direction toward the northwest at 7 to 15 knots into Amundsen Gulf and the Beaufort Sea.

Eastern Beaufort Sea

In two ERTS passes crossing the eastern Beaufort Sea southwest of Prince Patrick Island (Pass 141, 2 August; Pass 420, 22 August) a well defined irregular ice boundary can be identified in the Beaufort Sea. For the earlier pass, the MSS-5 and MSS-7 bands were used in the analysis because ice features in the MSS-4 band appeared nearly saturated; for the later pass, the MSS-4 and MSS-7 bands were used. On 2 August, a total of 13 very large "giant floes" (10 to 35 n.mi. across) can be identified within the area from about 72° to 75°N and 132° to 138°W. These floes are surrounded by ice concentrations consisting primarily of open pack and close pack with many various sized smaller floes. Twenty days later, on 22 August, the same 13 giant floes can be identified because of their shapes and surface features. Significant deterioration has occurred in only two of the floes, where large areas (about 1/4 of the original floe size) have apparently broken off their southern edges and broken into smaller floes. As positive identification of these giant floes was possible over the 20-day period, their motions could be measured. These measurements indicate a mean direction of motion toward the southwest, with a clockwise shift in the direction of motion from north to south; in addition to moving in a more westerly direction, the southernmost floes also moved more slowly.

Visible surface features in the floes in this area include apparent leads, fractures, thaw holes, and puddles. Surface features that are brighter than the surrounding areas (in contrast to the dark fractures and leads) may be ridges or hummocks. A comparison of the surface features of individual floes over the 20-day period, primarily using the MSS-7 band,

shows that noticeable changes do occur. Both puddles (depressions in the ice filled with melt water) and thaw holes (vertical holes in the ice formed when puddles melt through to the underlying sea water) appear as small dark spots on the ice surface, making it difficult to distinguish between the two. However, since many of the smaller dark spots observed on 2 August are not visible on 22 August, it suggests that they are puddles which have refrozen. The larger dark spots which are visible on both dates are undoubtedly thaw holes. Also, the multispectral analysis of the MSS-4 (or MSS-5) and MSS-7 bands provides additional information to distinguish between puddles and thaw holes, since at the shorter wavelengths, puddles do not appear as dark as do thaw holes.

Greenland Sea (along East Coast of Greenland)

ERTS imagery covering the eastern coastal area of Greenland (Pass 890, 25 September; Pass 1057, 7 October) shows wide variations in ice types and concentrations. Several features of interest in the ice field can be detected, including compacted belts and eddies that apparently result from the combined effect of surface wind and current flow. Also, in enlargements of one scene from the 25 September pass, fast ice can be identified along the north coast of Shannon Island (located just north of 75°N at 18°W). A darker pattern within one area of the fast ice is believed to be the result of flooded ice, since a river with numerous small tributaries empties into the bay at this location. This pattern in the MSS-7 data is not as black as open water, and is light-gray in the MSS-4 band, suggesting that the melt water may have become refrozen.

Enlargements of selected areas of the MSS-4 and MSS-7 frames for 7 October show distinct ice features that are not readily detectable in the original 9.5" positive prints. In this case, the original prints, which presumably were processed through standard photographic procedures applied to all images and directed toward enhancement of land features, are too dark to depict much of the sea ice. The experimentation in producing the enlarged prints shows, however, that special processing of the 70 mm negatives to obtain desired brightness and contrast allows ice features to be brought out, although the snow-covered land areas are saturated.

In one enlargement, what appears to be bands of ice southeast of Kap Brewster in the original print (MSS-4), is seen to be actually the denser portions of a cirrus cloud band. In another enlargement of Scoresby Sund, areas of rotten or brash ice and possible icebergs not visible in the original 9.5" positive prints can be detected. For example, in the original MSS-4 print, several areas of compacted brash ice appear in a dark gray tone, while large floes or icebergs are barely visible; in the corresponding MSS-7 band, no ice is visible. In the MSS-4 enlargement, however, distinct northern and southern limits of rotten or brash ice can be detected, and the limits of the areas of compacted brash ice are clearly visible as well as additional areas of compacting with lesser concentrations. In addition, the major floes or bergs appear much brighter and are at a scale that allows measurement of their sizes.

4. MULTISPECTRAL CHARACTERISTICS OF SEA ICE

The investigation of the multispectral characteristics of sea ice has concentrated on a comparison between the MSS-4 (0.5 to 0.6 μm) and MSS-7 (0.8 to 1.1 μm) bands. The results of the initial analysis of these spectral bands are summarized below:

- Overall contrast is greater at MSS-7. Open water areas and mountain shadows appear blacker than at MSS-4.

- Some areas of sea ice that appear uniformly bright at MSS-4 are very dark at MSS-7; these are believed to be areas of melt-water on top of the ice surface. Other features that appear dark in both bands are believed to be cracks or thaw holes through the ice. Thus, through use of both spectral bands, puddles can be distinguished from cracks and thaw holes.

- Areas of apparent brash ice appear darker than areas of thicker ice at MSS-4, but can still be easily detected; these areas are difficult to distinguish from open water at MSS-7. However, ice floes that are difficult to distinguish from surrounding ice at MSS-4 because of similar reflectances, appear distinctly brighter than the surrounding ice at MSS-7.

- In areas of nearly solid ice cover, greater detail is evident at MSS-7. This is primarily because tonal differences between ice floes, brash ice, and cracks and openings are greater at MSS-7 than at MSS-4. Also, tonal variations within some ice floes are evident at MSS-7; these variations may be associated with hummocks, ridges, or refrozen leads.

- Broken cloud fields over ice are more easily distinguishable at MSS-7 because of more distinct shadows, both on the ice surface and within the cloud field itself. However, the most reliable method to distinguish between clouds and ice is to use both the MSS-4 and MSS-7; at MSS-7, cracks in the ice and cloud shadows have similar reflectances, whereas at MSS-4, the cracks appear significantly darker than do the cloud shadows.

- Glaciers on the coasts of Greenland generally have a uniform reflectance throughout their extents at the MSS-4 spectral band. The lower extents of several of these glaciers, however, appear much darker at the MSS-7 band. This difference is likely due to melt water covering the lower portion of the glacier as opposed to snow covering the higher elevation part.

5. CONCLUSIONS

Sea ice is detectable in all of the ERTS MSS spectral bands and can be distinguished from clouds through a number of interpretive keys. The photographic processing of prints from the original 70 mm negatives can be important for ice detection, however, since exposures selected to retain detail in land areas may result in the loss of significant ice features. Overall, the MSS-4 (0.5 to 0.6 μm) and MSS-5 (0.6 to 0.7 μm) bands appear to be better for mapping ice boundaries, whereas the MSS-7 (0.8 to 1.1 μm) band provides greater detail in the ice features.

Considerable information on ice type can be derived from the ERTS data. Ice types that appear to be identifiable include: ice floes of various categories, pack ice of various concentrations, ice belts, brash ice, rotten ice, fast ice, leads, fractures, cracks, puddles, thaw holes and flooded ice. Although larger icebergs can be seen, it is difficult to distinguish them from ice floes. Ice features as small as the "small floe" (20 to 100 m across) can be detected, and the sizes of features somewhat smaller than 100 m across can be measured from enlarged ERTS prints. Ice concentrations can be mapped, and the resulting concentrations are in good agreement with the limited amount of correlative data available to date. Ice features can be identified over 24-hour periods enabling their movements to be measured; some large floes can even be recognized over intervals of as long as 20 days, enabling mean ice movements over longer periods to be determined.

The multispectral analysis of the ERTS MSS-4 and MSS-7 bands provides much information on ice type and ice surface features that cannot be derived from a single spectral band. For example, thaw holes can often be distinguished from puddles because of their different appearances in the two bands. These surface features can be indicative of ice age. Furthermore, snow lines on glaciers can be reliably mapped through the joint use of the MSS-4 and MSS-7 data.

6. REFERENCES

Barnes, J. C., D. T. Chang, and J. H. Willand, 1972: "Image Enhancement Techniques for Improving Sea Ice Depiction in Satellite Infrared Data," Journal of Geophysical Research; Oceans and Atmospheres Edition, 77(3), pp. 453-462.

Committee on Polar Research, 1970: Polar Research, A Survey, National Research Council, National Academy of Sciences, Washington, D. C.

Division of Marine Resources, 1970: Arctic Ice Dynamics Joint Experiment, Report No. AIDJEX - Bull-1, University of Washington, Seattle.

Fletcher, J. O., 1966: "Forward," Proc. of the Symposium on the Arctic Heat Budget and Atmospheric Circulation, Memorandum RM-5233-NSF, The RAND Corporation.

Fletcher, J. O., 1968: "The Polar Oceans and World Climate," Proc. of the Long-Range Polar Objectives Conference, U. S. Department of Transportation, Washington, D. C.

Maykut, G. A. and N. Untersteiner, 1969: Numerical Prediction of the Thermodynamic Response of Arctic Sea Ice to Environmental Changes, Memorandum RM-6093-PR, The RAND Corporation.

McClain, E. P. and M. D. Baliles, 1971: "Sea Ice Surveillance from Earth Satellites," Mariners Weather Log, 15(1), pp. 1-4.

N73-28354

Paper M 15

BIOMASS IN THE UPWELLING AREAS ALONG THE NORTHWEST COAST OF AFRICA AS VIEWED WITH ERTS-1

Karl-Heinz Szekielda, *University of Delaware,* Robert J. Curran, *Goddard Space Flight Center*

Light penetration in water is affected by plankton, algae, and dissolved and suspended matter. As a consequence, the composition of backscattered light from below the air-sea interface is determined by the nature of the constituents in the water column. In contrast to the absorption spectrum of chemically pure chlorophyll in solution, algae suspensions absorb and scatter light more uniformly throughout the visible part of the electromagnetic spectrum. Because of their spectral absorption and scattering properties plankton concentration can be estimated by measuring the spectral backscattered radiance over water. Our experiments using this approach were performed in upwelling regions along the North-West Coast of Africa.

The North-West Coast of Africa was chosen for several reasons:

1. From the oceanographic point of view knowledge of the NW Coast of Africa is very poor.
2. We are collaborating with the CINECA program which is an international oceanographic cooperation providing access to multiship cruises for ground truth.
3. Climatological conditions favor space observations.

Original photography may be purchased from:
EROS Data Center
10th and Dakota Avenue
Sioux Falls, SD 57198

4. No river discharge appears in the upwelling area thus changes in sea color are produced by plankton organisms.

A typical analysis of wind speed and direction for the test site is shown in Fig. 1. These data were obtained during 1967 onboard the H. M. S. "Hydra".

The Alize, blowing in a northeast direction along the coast of Spanish Sahara and Mauritania is predominant the whole year. As a consequence of this wind system, the Canary Current is present during much of the year in a southwest direction. Wind stress and the geostrophic sloping of the isotherms leads to upwelling in the near coastal zone especially at Cape Sim, Cape Ghir, Cape Juby, Cape Blanc, and Cape Verde. The euthrophication of the productive layer by increased nutrient transport from the deeper layers causes extremely high concentrations of chlorophyll. Since the adjacent regions are arid, visibility through the atmosphere favor observation by satellite. Fig. 2 shows a composite of data for the reflected solar energy between 0.7-1.1 μm as collected by channel 7 of the MSS. The frames were obtained during ERTS-1 overpass of the NW Coast of Africa between 32°N and 10°N. The area covered includes Morocco, Spanish Sahara, Mauritania, Senegal, Gambia, Portuguese Guinea, and Guinea.

The following color composites of channels 4, 5, and 7 give evidence of the types of climatic conditions encountered in the test site. The northern boundary of the test site includes the region of the Anti Atlas mountains in Morocco. Figure 3 shows the coast of Morocco south of the

upwelling areas of Cape Sim and Cape Ghir. From studies made using data gathered from the satellites Nimbus 2, 3, and 4 and our recent analysis of NOAA 2 data, this slide shows the northern limit of the cloud free region of the test site. Part of the test site includes arid regions or desert. Figure 4 shows part of Senegal south of Cape Blanc with the Island Tidra included. The area shown in this figure is also part of an ongoing program to study the chemical impact of eolian dust from the Sahara on the nutrient budget of the ocean. The ERTS-1 imagery was used to determine the geographic path of the transported sand. The results of this part of the study will be discussed in thesis form.

The only important river discharge in the test site is from the Gambia River which is shown in Figure 5. The river discharge is to the south in agreement with the movement of the Canary Current. The shifting of the river mouth from north to south, in evidence by closer analysis of the figure, is probably a long term evolutionary process resulting from the Canary Current.

The chlorophyll distribution as obtained from direct measurements aboard research vessels during August 1972 is shown in Fig. 6. This area was investigated by the Spanish R. V. "Cornide de Saveedra" in the North and the British R. V. "Discovery" in the South. The concentration of chlorophyll in the outer section near the Canary Islands is representative of the open ocean with values around 0.5 $\mu g \cdot l^{-1}$. High chlorophyll concentrations were found in the upwelling area near Cape Juby with values above 8 $\mu g \cdot l^{-1}$. Thus, the chlorophyll concentration for this

test site ranges over two orders of magnitude. In plankton blooms maximum concentrations were found up to 16 $\mu g \cdot l^{-1}$. Generally speaking, the whole coastal area shows eutrophication with chlorophyll concentrations above 0.5 $\mu g \cdot l^{-1}$ which is still one order of magnitude higher than in the open ocean.

Maximum gradients of chlorophyll concentration were always found to be close to the coast with highest concentration near Cape Juby. Fig. 7 shows the display of channel 4 from the MSS during the operation of "Cornide de Saveedra" in this area. The gray scale indicates increased plankton concentration as evidence by backscattered light in the 0.5-0.6 μm region of the MSS. Channel 5, 6, and 7 showed neither cloud contamination nor sun glint. For more details, part of the encircled area was investigated with grid print maps from the digital values found on computer compatible tapes.

To derive the position of the coastline with the radiance measurements, we established the frequency histogram of all data. The total picture consisted of 585 lines with 810 samples per line with 47,380 points. An average gray level was 1.14 milliwatts/cm^2/steradian. The frequency histogram for channel 4 is shown in Fig. 8, where all data were normalized to the maximum of 100.

The two maxima in the frequency distribution indicate the different gray levels for water and the adjacent continent. The high radiance of 1.17 to about 1.56 $mw/cm^{-2}/ster.^{-1}$ (i.e., 60 to 80 digital units)

corresponds to an albedo of from 0.254 to 0.339 and shows the reflective properties of the desert region. Gray levels between 0.51 and 0.98 $mw/cm^{-2}/ster.^{-1}$ (i.e., 26 to 50 digital units) correspond to albedo levels of 0.110 to 0.213 and can be assigned to the radiance of the ocean. The frequency distribution shows that gray levels greater than 0.98 $mw/cm^{-2}/ster.^{-1}$ (albedo equals 0.213) are caused by the coastal features or the continent. Consequently we developed a threshold level for the position of the waterline to be indicated by radiances less than 0.98 $mw/cm^{-2}/ster.^{-1}$.

Fig. 9 shows a computer printout where characters were assigned to the radiance. Only every 12th line was used with a sample spacing of 12. The gradient visible by the assigned character 0 shows the positon of the coastline. The region near Cape Juby shows high radiance caused by plankton. The transportation of plankton within the Canary Current can be seen by the symbols 0 and 8. Radiance less than 0.61 $mw/cm^{-2}/ster.^{-1}$ had no assigned symbol. The offshore area in the northwest corner of the display indicated low radiance and consequently low concentration of plankton organisms.

Fig. 10 gives the analysis of the total values as obtained from the generated grid print map over an area of 30 km. The isolines of radiances were smoothed over about eight grid points. The position of the coastline was established by the maximum gradient at the interface between continent and ocean. The nearest isoline to the coast was three grid print points from the coast which corresponds to a distance

of about 300 meters. This should avoid the most important influence of the bathymetry near the coastline.

Oceanic regions with high productivity have a thin eutrophic layer and consequently the photo-penetration depth is very shallow. Readings with the Secchi disc in the upwelling area showed only five meters. This can be explained by the light attenuation of plants. Highest radiance can be found in the near coastal waters where upwelling is expected to be strongest. Repeated coverage with ERTS showed that the plankton bloom are not persistant. They change their size and their location.

Continuous recordings of chlorophyll concentrations during the ground truth program in the upwelling area along the NW Coast of Africa showed similar patterns as derived with ERTS-1.

The recordings parallel to the coast showed periodic variations in the chlorophyll concentration which showed the same spacing as the periodicity observed with ERTS-1 data. In other words, we detected the real distribution structure of plankton with ERTS-1 as it could never be investigated with the conventional method or even multiship cruises.

We were asked to stress the economical point of view in our investigations. A very simple calculation will demonstrate the advantage of satellite information for the research in upwelling regions. Dr. W. Fisher from the United States Geological Survey estimated the

cost per km^2 in the image to be less than 3 cents. The analyzed frame would cost about $324. Including computer time we can estimate the total amount for the satellite coverage to be $1,000. The information obtained with the ship was in the order of $30,000 or roughly 30 times more expensive. I think that this estimate and the presentation of data show the high potential and the inexpensive acquisition of information obtained with the satellite in our studies. It is desirable that NASA focus more on the activity in spacecraft oceanography.

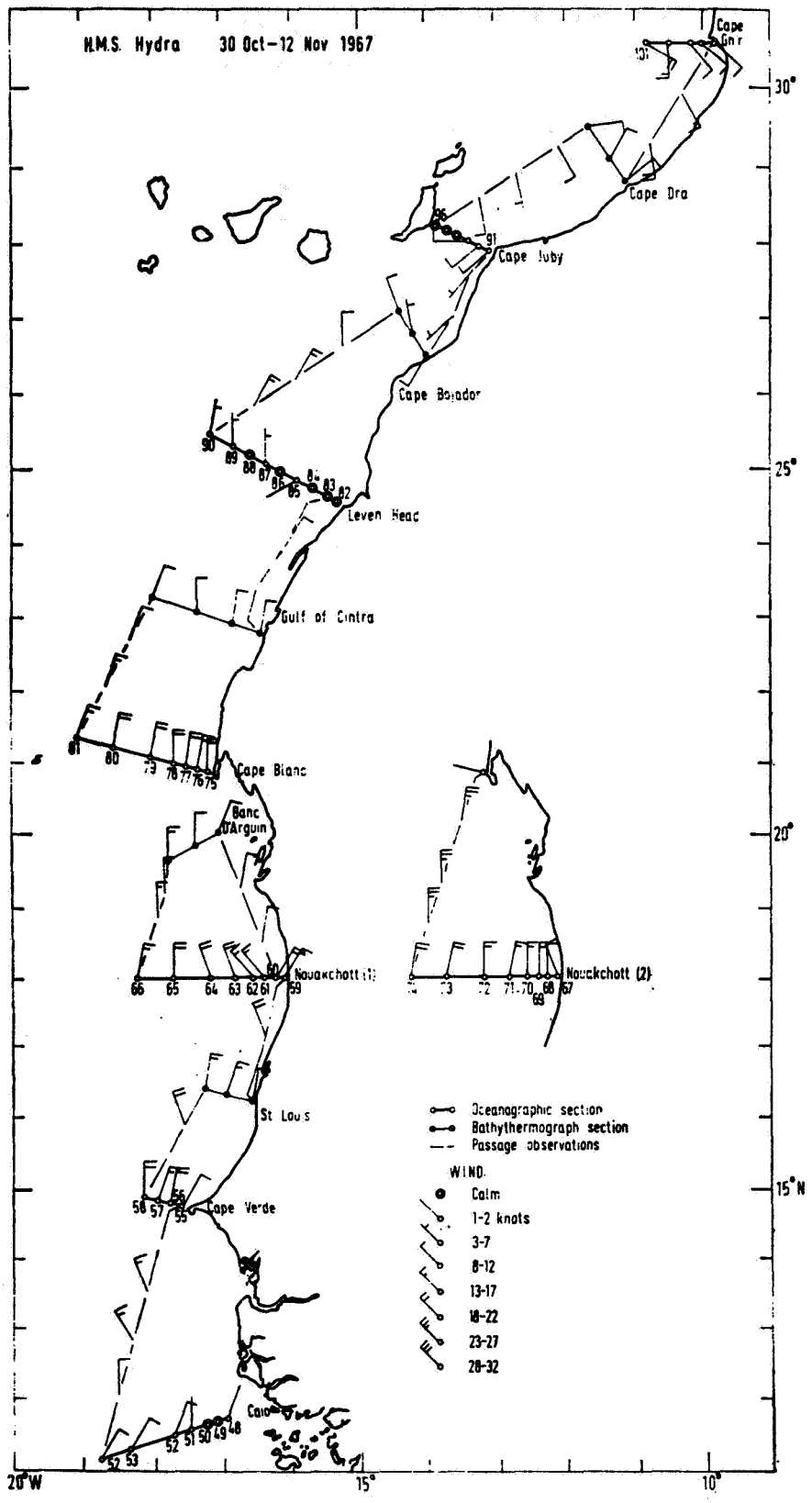

H.M.S. Hydra 30 Oct–12 Nov 1967
Cape Dra
Cape Juby
Cape Bojador
Leven Head
Gulf of Cintra
Cape Blanc
Banc d'Arguin
Nouakchott (1)
Nouckchott (2)
St Louis
Cape Verde
Oceanographic section
Bathythermograph section
Passage observations
WIND
Calm
1-2 knots
3-7
8-12
13-17
18-22
23-27
28-32
30°
25°
20°
15°N
20°W
15°
10°

Figure 1

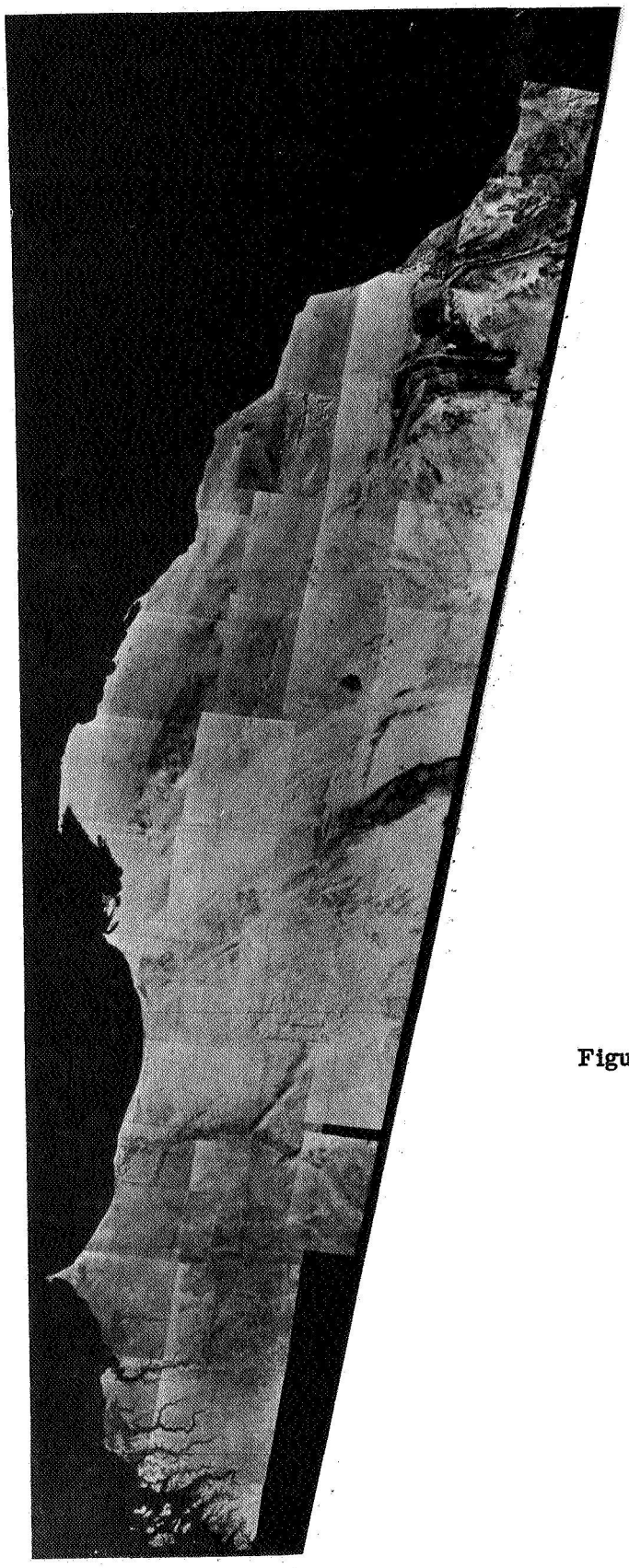


Figure 2

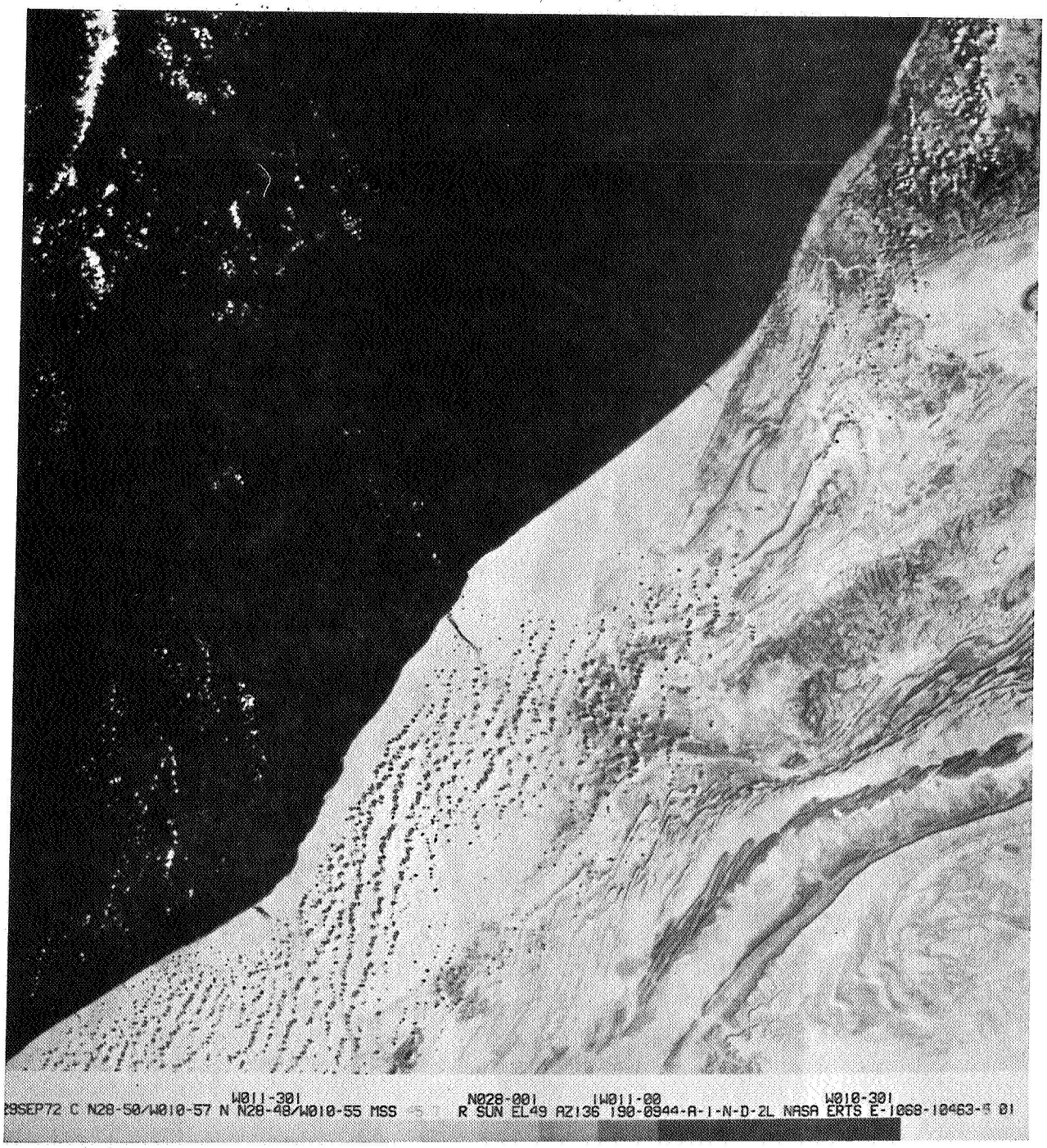

W011-301
N028-001
W011-00
W010-301
29SEP72 C N28-50/W010-57 N N28-48/W010-55 MSS
R SUN EL49 AZ136 190-0944-A-1-N-D-2L NASA ERTS E-1068-10463-5 01

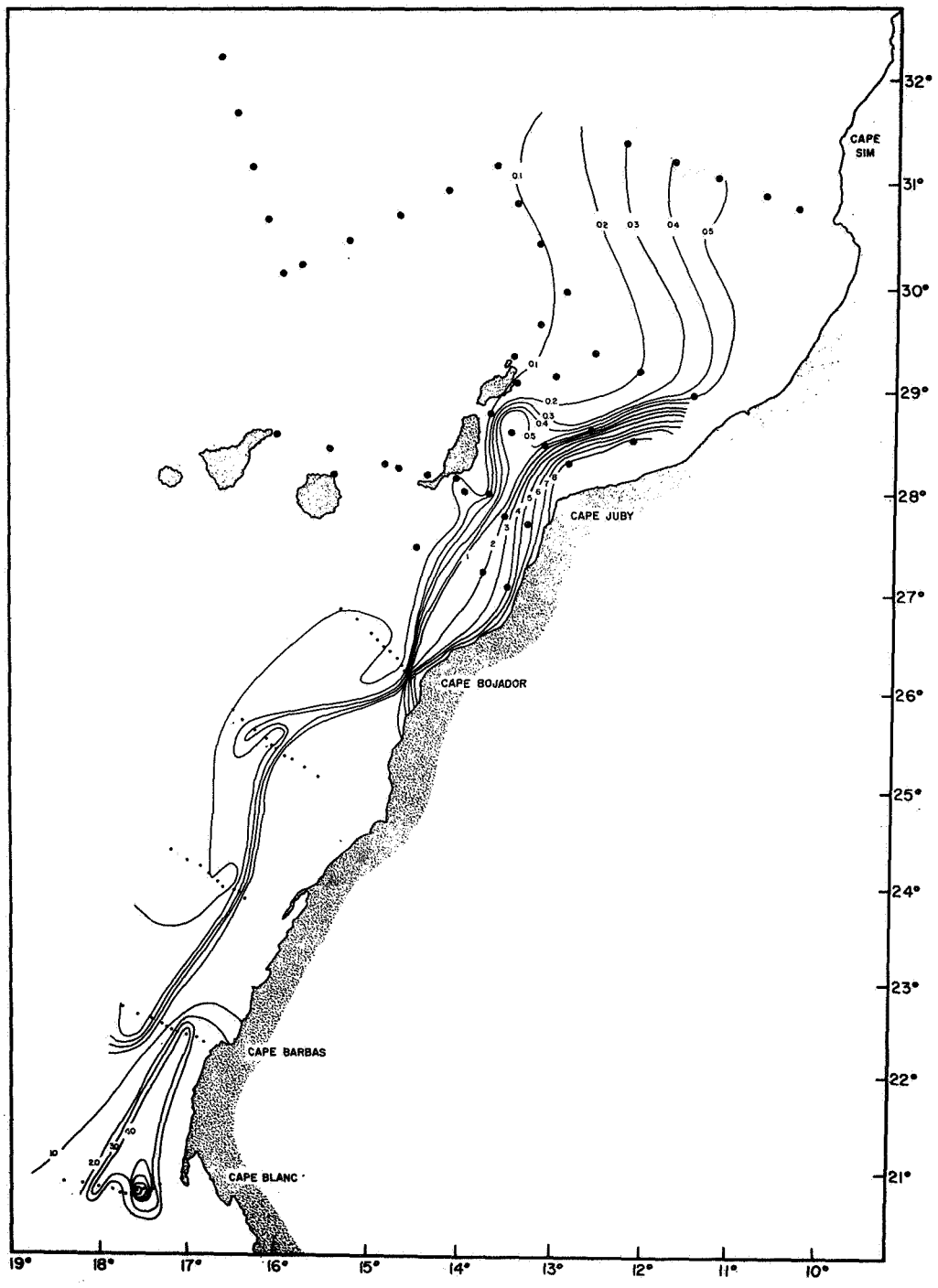
Figure 3


W017-001
W016-301
W016-001
9NOV72 C N20-05/W016-16 N N20-02/W016-14 MSS 5 R SUN EL45 AZ141 189-1474-G-1-N-D-2L NASA ERTS E-1106-110

Figure 4


1W016-30
W016-001
W015-301
SEP72 C N15-59/W015-47 N N15-57/W015-42 MSS R SUN EL55 AZ120 188-0958-A-1-N-D-2L NASA ERTS E-1069-10560-5

Figure 5


CAPE SIM
CAPE JUBY
CAPE BOJADOR
CAPE BARBAS
CAPE BLANC
32°
31°
30°
29°
28°
27°
26°
25°
24°
23°
22°
21°
19°
18°
17°
16°
15°
14°
13°
12°
11°
10°

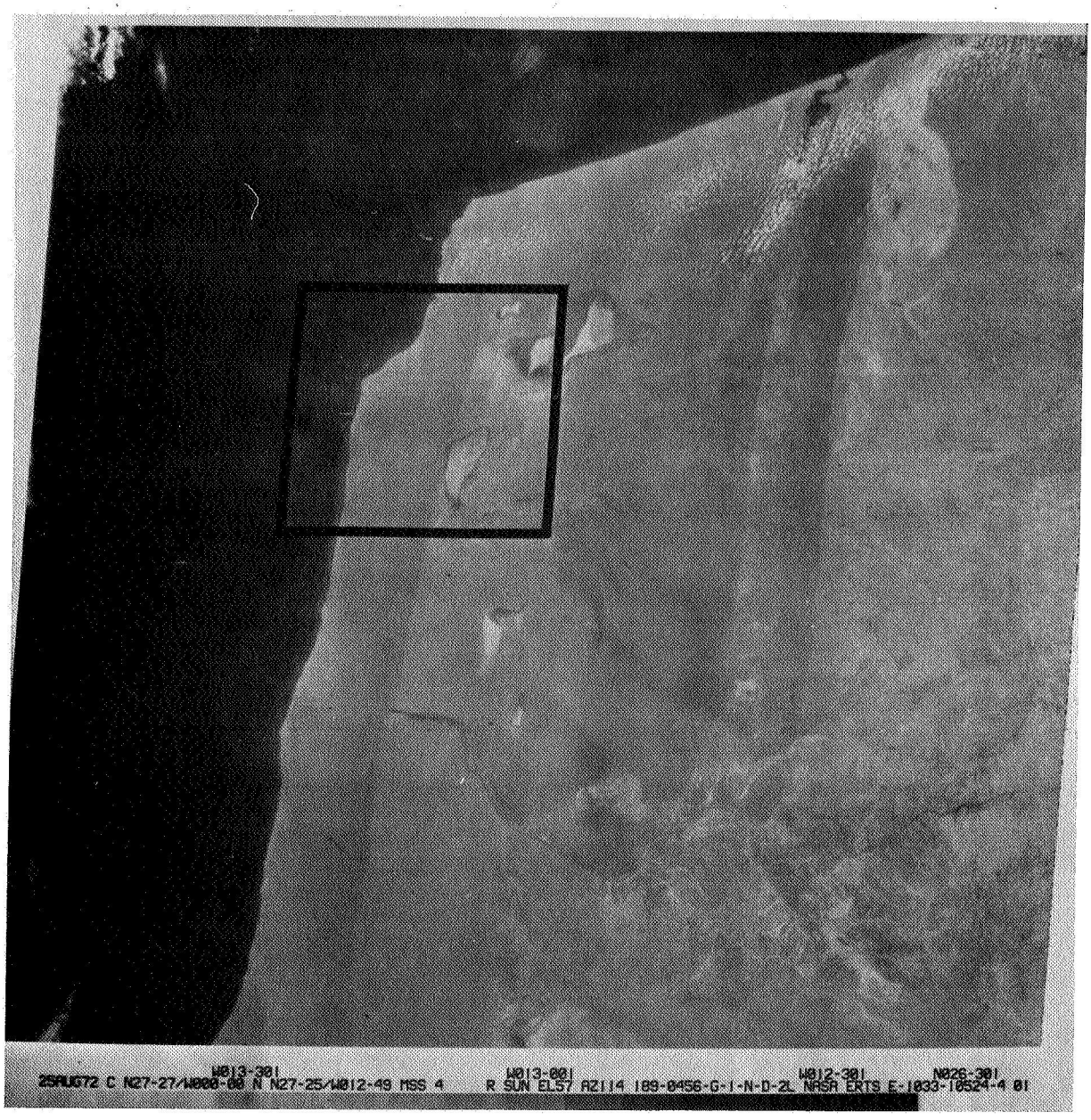

W013-301
25AUG72 C N27-27/W000-00 N N27-25/W012-49 MSS 4
W013-001
R SUN EL57 AZ114 189-0456-G-1-N-D-2L
W012-301
NASA ERTS E-1033-10524-4
N028-301
01

Figure 7

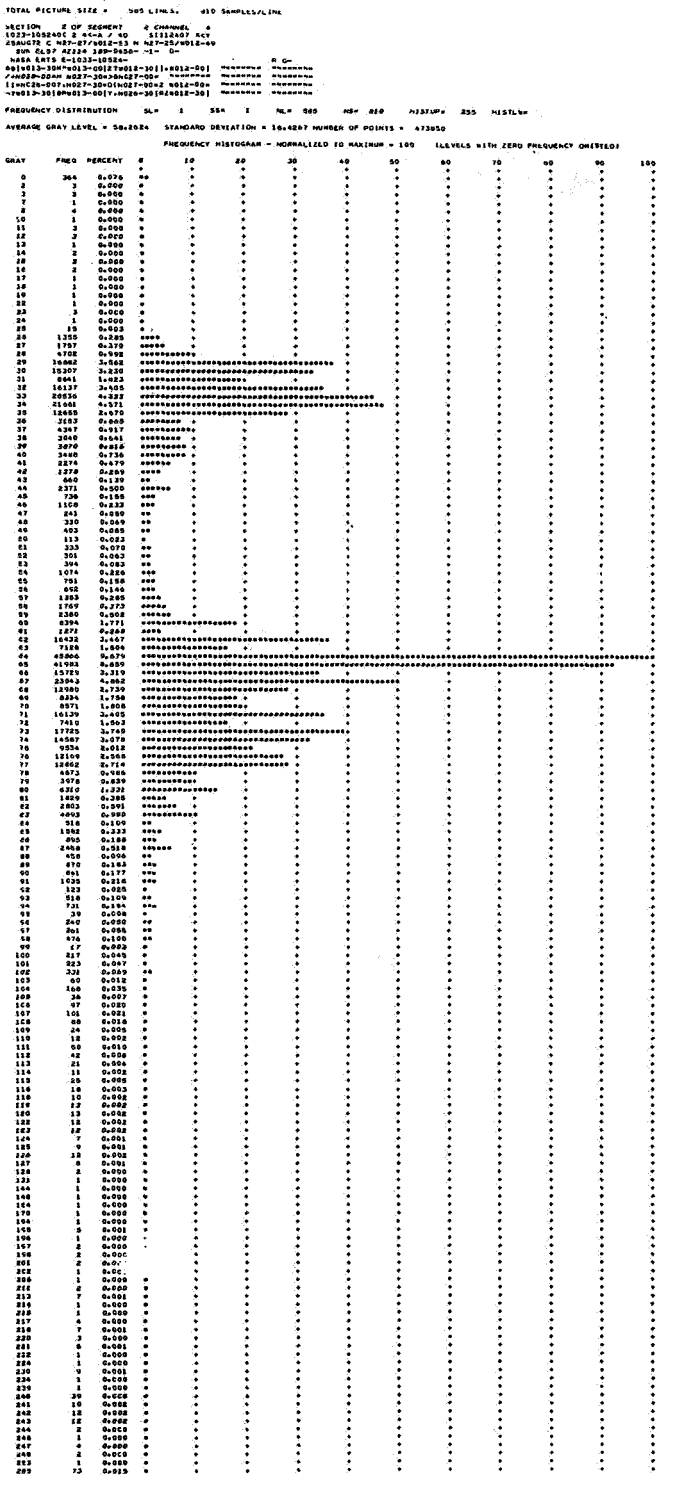


Figure 8

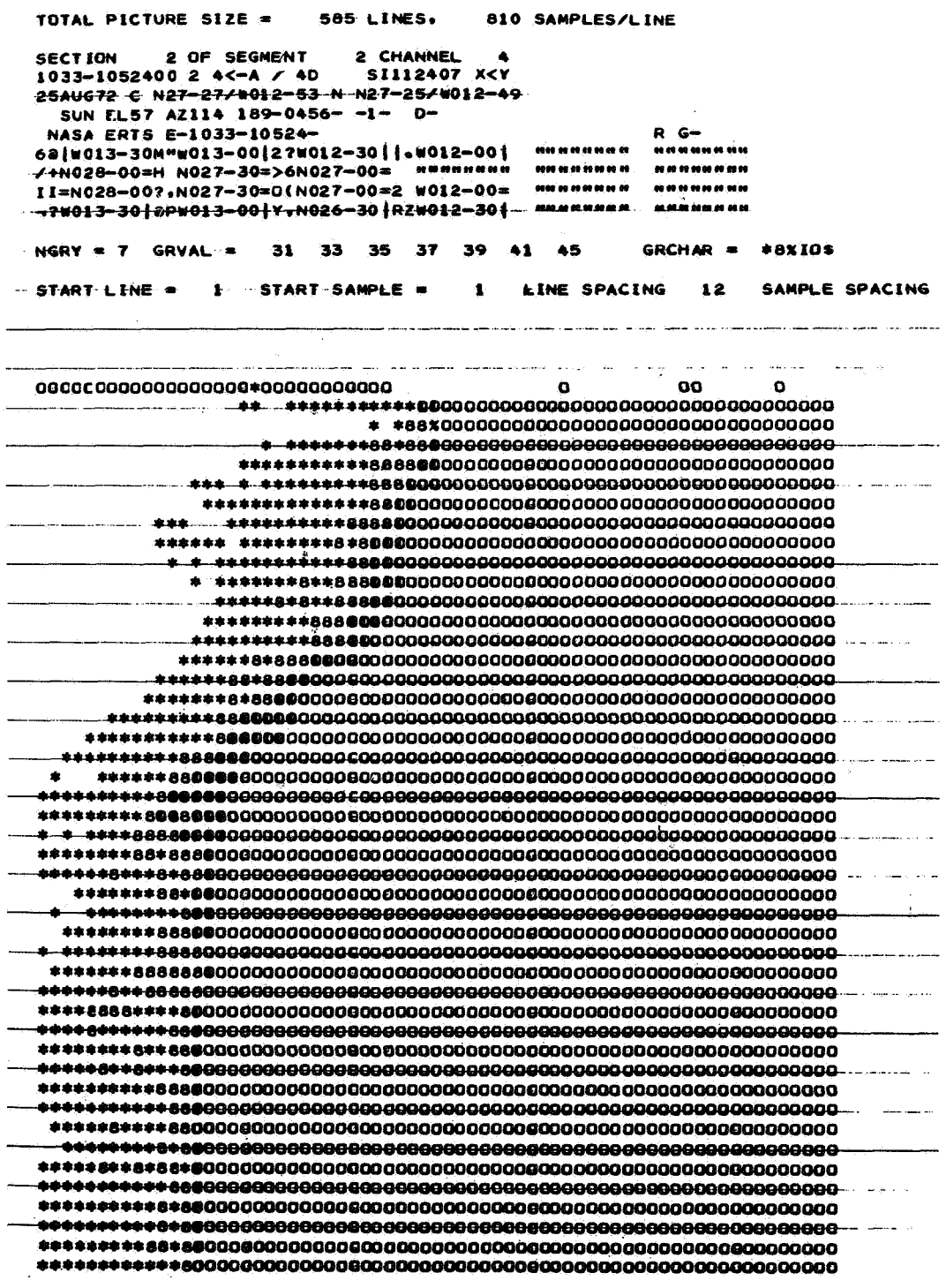

TOTAL PICTURE SIZE = 585 LINES. 810 SAMPLES/LINE
SECTION 2 OF SEGMENT 2 CHANNEL 4
1033-1052400 2 4<-A / 4D SI112407 X<Y
25AUG72 C N27-27/W012-53 N N27-25/W012-49
SUN EL57 AZ114 189-0456- -1- D-
NASA ERTS E-1033-10524-
R G-
NGRY = 7 GRVAL = 31 33 35 37 39 41 45 GRCHAR = *8XIO$
START LINE = 1 START SAMPLE = 1 LINE SPACING 12 SAMPLE SPACING

Figure 9

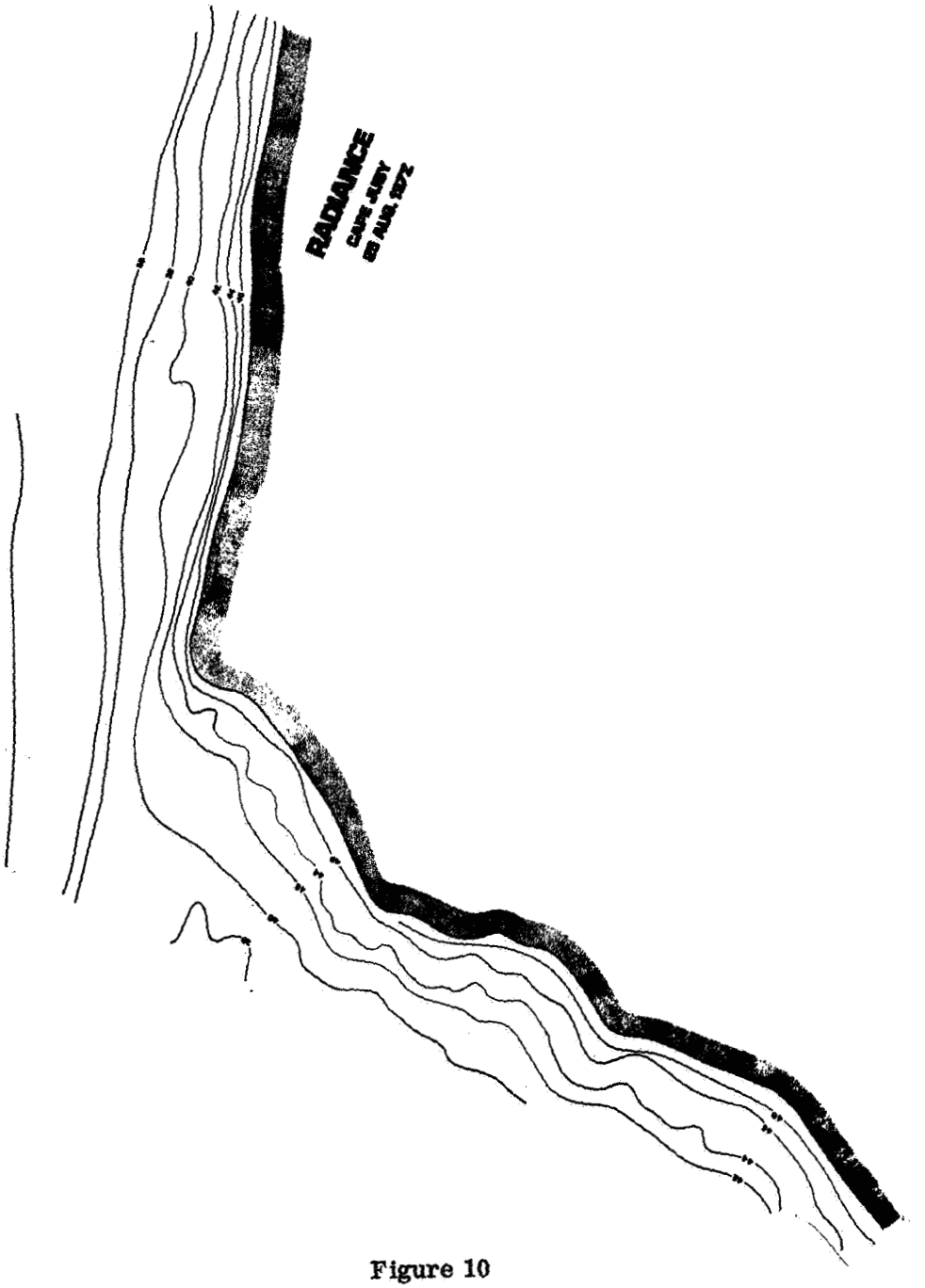


Figure 10

Paper M 16

ERTS IMAGERY AS AN AID TO FISHERIES MANAGEMENT IN THE NORTHERN GULF OF CALIFORNIA

J. R. Hendrickson, Alfredo Cota, Gustavo Calderon and L. K. Lepley, *Department of Biological Sciences, University of Arizona*

ABSTRACT

Commercial fishing activity in the northern Gulf of California is presently a trial and error process, and product often varies widely with respect to area and time of catch. Monitoring and predictive processes could be expected to optimize fishing effort and support needed management activities.

Turbidity patterns, extent of intertidal exposure, and other oceanographic phenomena detectable by ERTS imagery were studied in relation to selected fisheries in the northern Gulf. Particular attention was given to local variations in the species composition of surface plankton relative to turbidity conditions, interpretation of migratory activity of a commercial fish species through use of ERTS-1 imagery, and mapping of commerical clam beds by synoptic satellite imagery.

(PAPER NOT PRESENTED)

PRECEDING PAGE BLANK NOT FILMED

N73-28355

Paper M 17

APPLICATION OF ERTS-1 IMAGERY TO THE HARVEST MODEL OF THE U. S. MENHADEN FISHERY

Paul M. Maughan, Allan D. Marmelstein, O. Ray Temple, *Earth Satellite Corporation, 1747 Pennsylvania Avenue, N. W., Washington, D. C.*

ABSTRACT

Preliminary results of an experiment to demonstrate the utility of ERTS-1 imagery for providing significant information to the harvest model of the menhaden industry are reported. Fisheries and related environmental data were obtained discontinuously throughout the 1973 menhaden (a surface schooling, coastal species) fishing season in Mississippi Sound.

The unexpected complexity of the physical environment in Mississippi Sound precluded simplistic analysis of fish/environment relationships. Preliminary indications are that an association does exist between fish availability and differences in water transparency (turbidity) within the Sound. A clearer relationship is developing between major turbid features imaged by ERTS-1 and location of successful fishing attempts. On all occasions where relatively cloud-free ERTS-1 overflight days coincided with fishery activity, overlays of catch location on ERTS-1 images show an association of school position with interfaces between imaged turbid features. Analysis is currently underway to determine persistence of such associations in an attempt to define minimum satellite return time necessary to maintain continuity of associations.

Within the context of the menhaden harvest model, benefits which may accrue to the industry can be measured in terms of reduced dependence on spotter aircraft for generalized fish school location. The satellite repeat time is of critical importance to this application.

1. INTRODUCTION

Menhaden are small surface schooling pelagic fish which occur in the nearshore coastal waters of the Atlantic and Gulf Coasts of the United States. These herring-like fish support the largest volume fishery in this country. The fishery is divided into two regional units: one presently centered around the Chesapeake Bay and the other centered around the Mississippi River Delta

PRECEDING PAGE BLANK NOT FILMED

Original photography may be purchased from:
EROS Data Center
10th and Dakota Avenue
Sioux Falls, SD 57198



B

and the nearby areas east and west. The Chesapeake Bay fishery is the older and was formerly considerably more extensive, but lack of availability of the resource has caused a sharp decrease in the range and extent of the fishery. To the contrary, the Gulf of Mexico fishery is more recent and is considered to be an expanding, dynamic fishery.

Menhaden are fished by twin skiff, purse seine vessels assisted by spotter-pilots flying light aircraft, whose responsibility is to locate a commercially accessible aggregation of schools and guide the fishermen in their capture. The well-developed harvest technology of the menhaden fishery coupled with the inherent remote sensing aspects of the discovery and capture of the resource suggested its use as a demonstration for the applicability of remotely acquired oceanographic data as a complementary source of information for harvest and management decision processes.

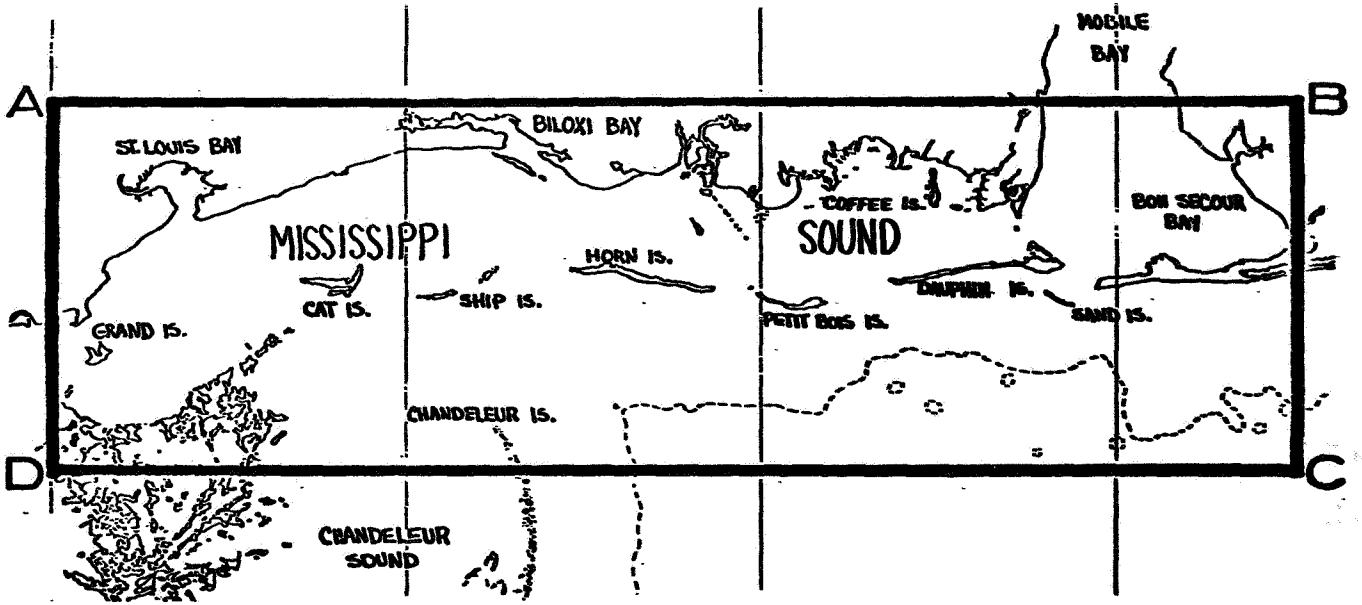
The research program reported herein represents a cooperative effort undertaken by EarthSat and the National Fish Meal and Oil Association, in conjunction with NASA Earth Resources Laboratory (ERL) and the Fisheries Engineering Laboratory (FEL) of the National Marine Fisheries Service (NMFS) colocated at the Mississippi Test Facility (MTF). Other NMFS participants included the Pascagoula Laboratory in southeastern Mississippi, the St. Petersburg Laboratory in western Florida and the Beaufort Laboratory in coastal North Carolina.

Four sub-experiments were designated which involved space applications, oceanographic applications, living marine resource applications and fishery utilization applications. Responsibility for the experiments was designated according to the individual objectives of each of the experiment participants, but acquisition and interpretation procedures were shared amongst all participants. This paper will concentrate on the fishery utilization sub-experiment.

2. EXPERIMENTAL DESIGN

The test site selected for the combined ERTS-1 experiment was an area bordering the Mississippi Gulf Coast, called Mississippi Sound (Figure 1). This approximately one hundred mile by ten mile rectangular area is a portion of the Gulf of Mexico isolated by a discontinuous series of barrier islands. It was selected as the test site for several reasons. First, it supports a large menhaden fishery which, during a typical year, produces 30% of the total Gulf of Mexico catch. Secondly, it was logistically simple in that all of the commercial fishing companies operating in the Sound utilized port facilities located at Moss Point, Mississippi. Further, the Sound is in close proximity to the Mississippi Test Facility and the NMFS Pascagoula Laboratory.

Data acquisition was to occur from a multi-platform, multi-level system, utilizing the ERTS spacecraft, medium and low altitude NASA aircraft, low altitude aircraft supplied by the National Marine Fisheries Service, spotter aircraft used by the fishing companies for locating the resource, and surface vessels of two types. Vessels chartered by NASA and NMFS occupied preselected stations on major data acquisition days. Selected commercial fishing vessels were utilized for discontinuous random data acquisition, keyed to the individual fishing efforts of the vessels chosen.



SCALE

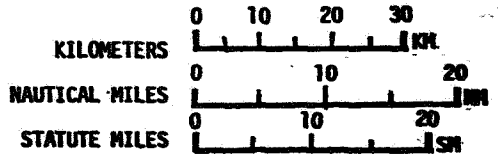


FIGURE 1: TEST SITE

Routine surface sampling for the utilization experiment proceeded from May to October 1972. EarthSat personnel occupied positions as scientific observers aboard three commercial menhaden vessels continuously during the period June through September. These individuals obtained oceanographic observations each time a capture attempt was initiated upon a school of menhaden. At the time of capture or attempted capture, observations of temperature, salinity, secchi depth (turbidity), water color and associated meteorological data were obtained to coincide with fisheries data concerning the size of the school captured, its position and the time of capture. These observations were made the first three days of each fishing week except during periods where ERTS-1 overpass or major field activity occurred later in the week -- in which case the sampling period was extended for the entire week. All sampling was achieved so as to not interfere with first priority fishing activity.

Once weekly, throughout the season, a minor field exercise was undertaken -- termed a "secondary day" -- wherein an aircraft overflight was made of the prime fishing area in order to obtain temperature distributions as mapped by a thermal scanner. These flights were directed by the Earth Resources Laboratory at MTF. Simultaneously, an aircraft was dispatched from the Pascagoula Laboratory of NMFS to acquire aerial photography of fish schools and menhaden fishing activity. During these days, several charter vessels were utilized for transect ground truth.

At several periods during the summer, selected nominally to correspond with ERTS-1 overflight, major field exercises -- termed "main days"-- were undertaken wherein vessels chartered by NMFS and ERL occupied discrete positions along transect lines which were also overflown by the NASA NP3A aircraft operating from Houston. Additionally, those aircraft observations discussed above were also undertaken. Fishing activity proceded as usual with fish sampling occuring at random locations dictated by the location of commercially accessible fish schools. Where possible, increased numbers of EarthSat personnel were utilized to enlarge the number of vessels from which fishery sampling was obtained.

All data acquired through ground sampling programs were accumulated and held in a computer-operated data management system. As possible, remotely acquired data was transferred to computer-compatible format and entered into the same common data bank accessible to all participants in the experiment.

3. DATA ANALYSIS

Analysis of ERTS-1 imagery utilized the excellent properties of turbid feature dilineation possible from the MSS images. Overlays of geographic location of individual fish sets compared to turbid features visible from images have led to several potential relationships discernable from ERTS imagery. Such analyses were combined with an examination of relationship between known bathymetric features and areas interpreted as turbidity within the Mississippi Sound. Visual comparison demonstrates that in some cases the ERTS-1 images view bottom topography whereas in other instances ERTS-1 images apparently view turbid water features. Digital image processing and statistical routines are currently being employed in an attempt to segregate these effects. An analysis of these data shows that nearly all fish catches are made between the one to two fathom bathemetric contours. Sets almost always fall in or along turbid features.

In the analysis performed to date, the data generally can be grouped into two classes. In the first class of data catches appear to associate with the interface between areas of markedly different turbidity. Such sets also associate with shallower areas leading to the speculation that this turbidity is wave-induced in the shallow water. The reason for the association is not clear. In the second class, associations centered on plumes of turbid water which occur in depths of approximately two fathoms.

The 29th of September is an example of the latter class of data. Immediately behind Dolphin Island (Figures 2 and 3), an area was observed to contain numerous fish schools centered in a turbid feature. This represented a highly atypical situation in that generally catches in the eastern Sound slightly to the north associated with a large marshy island known to the fishermen as Coffee Island. On this date no fish were observed in the vicinity of Coffee Island which was extremely unusual, and all catches were made in the turbid feature in an area where few catches had been made over the previous three months of the fishing season. On the 29th of September two million fish were taken by three vessels from this area. Examination of catch records prior to this overpass demonstrate that an increasing association with this area occurred from the 27th to the 29th of September, indicating a possible persistence of this feature. Events after the 29th were not defined due to the cessation of fishing on the 29th, the end of the fishing week.

Statistical methods are also being employed to attempt to relate environmental observations such as temperature, salinity, and turbidity to the abundance and occurrence of commercially accessible menhaden. To date, such attempts have been largely unsuccessful due, we feel, to the perturbed nature of the environment. The Mississippi Sound is a naturally complex estaurine system and is heavily trafficed by commercial and pleasure vessels. The vessel traffic introduced artificial complications into the environment which make coherent sampling extremely difficult.

4. DISCUSSION

Areas exhibiting turbidity in shoal water tended to be those areas which were previously well known as centers of fishing activity; for example, the area around Coffee Island. However, the one instance demonstrated in the September 29 image where fishing activity centered in a plume in deeper water represents a unique occurrence which when supported by repeated evidence, indicates the first instance where a satellite acquired image could be used as an input for management purposes. Persistent association of commercially accessible fish schools with such a feature provides the impetus for utilizing such interpretation as a management tool for restricting harvest efforts.

However, in general it must be said that the potential of these techniques lies more in management than in harvest in respect to the menhaden industry. The general high efficiency of search and capture exhibited by this fishery precludes a major input from remote sensing satellite systems into these activities. However, the potential for predicting on a longterm basis probable locations could greatly reduce the resource investment in search aircraft and time so employed. Further these techniques suggest a possible means of worldwide survey for potential fishing sites for similar species of Clupeoid fishes known or thought to exist in similar environments.

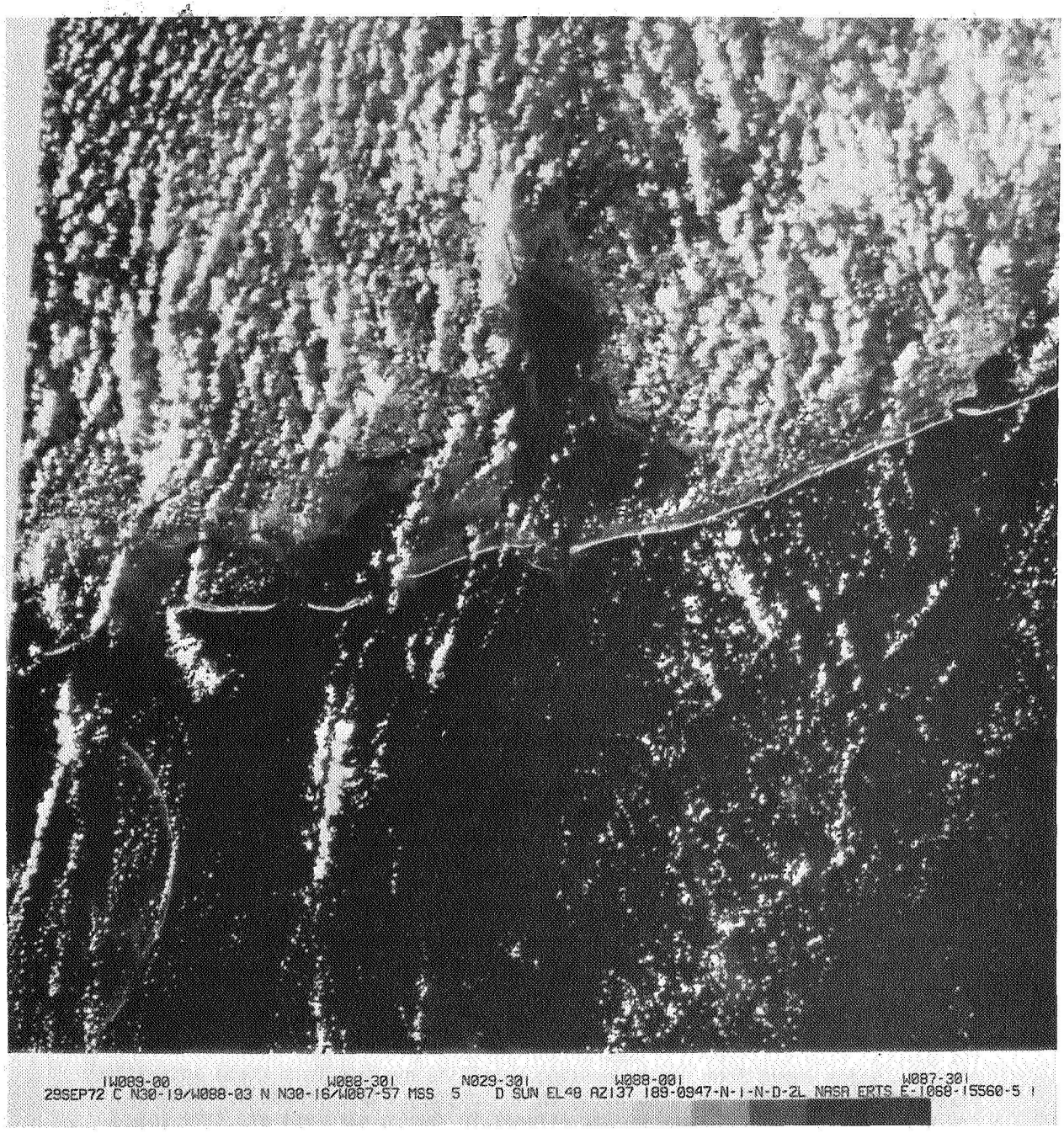
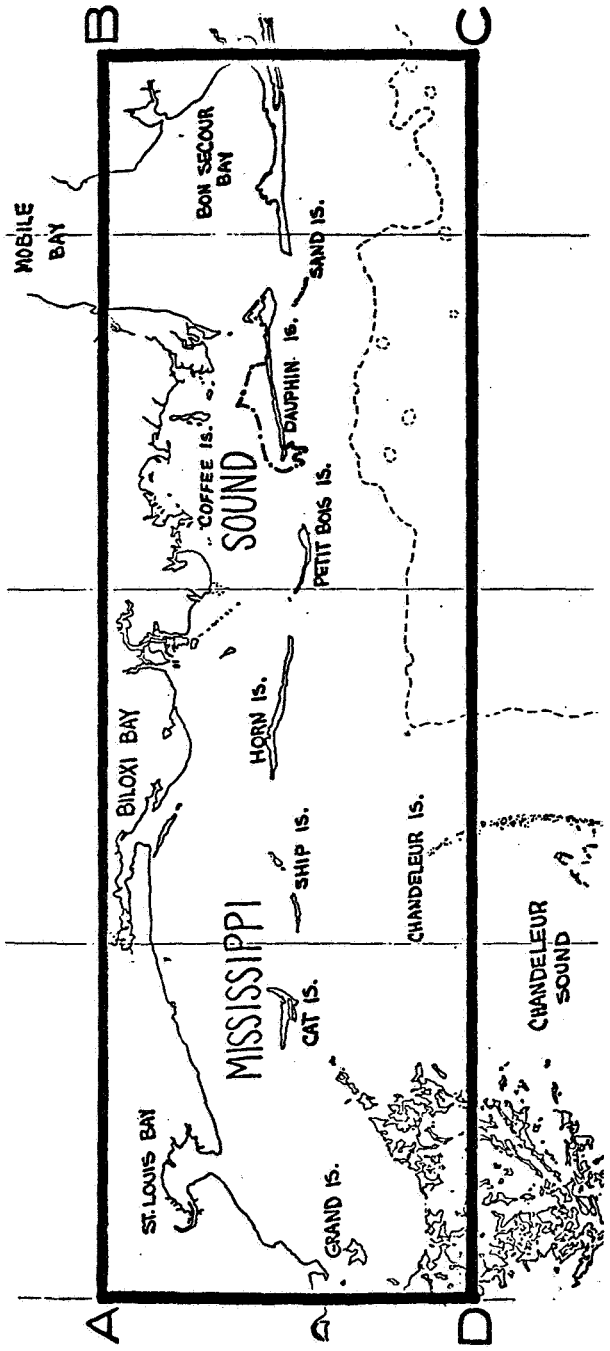


FIGURE 2: ERTS-1 MSS BAND 5 IMAGE, 29 SEPTEMBER 1972



—·—· POSITION OF TURBIDITY FEATURE

FIGURE 3: PLUME POSITION AS DERIVED FROM FIGURE 2

N73-28356

Paper M 18

COASTAL AND SUBMARINE FEATURES ON MSS IMAGERY OF SOUTHEASTERN MASSACHUSETTS: COMPARISON WITH CONVENTIONAL MAPS*

Richard S. Williams, Jr., *U.S. Geological Survey, EROS Program Office, Washington, D.C., 20244*

ABSTRACT

Three ERTS-1, MSS images (28 July 1972, 1 Sept. 1972, and 8 Oct. 1972) of southeastern Massachusetts, including Cape Cod Bay, Cape Cod, and Nantucket Sound, show a variety of dynamic geologic and hydrologic phenomena. Coastal features imaged include the coastline at different times in the tidal cycle, harbors, lakes and ponds, marshes (wetlands), and beach and dune areas; submarine features include tidal flats, shoals, dredged and natural channels, and bars. Comparison with conventional maps at 1:1,000,000 and 1:250,000 scales show many inaccuracies between the ERTS imagery and the two map scales. The discrepancies are caused by cartographic generalization from larger scale maps and, in some instances, actual changes in landforms. The marine geological information shown on the ERTS imagery is not shown on the 1:1,000,000- or 1:250,000-scale maps, nor is other mappable environmental information, necessary to effective resource management decisions, affecting the area. The ERTS-1 imagery of the southeastern Massachusetts area provides two-dimensional coastal and submarine information superior to conventional maps at 1:250,000 or smaller scales. The ERTS-1 imagery can be used to increase the accuracy of these maps, portray additional environmental information, and provide the capability for frequent updating of maps at such scales. ERTS-1 imagery provides a very cost-effective method for provision of certain types of environmental data for Cape Cod and environs.

*Publication authorized by the Director, U. S. Geological Survey

Original photography may be purchased from:
EROS Data Center
10th and Dakota Avenue
Sioux Falls, SD 57198

PRECEDING PAGE BLANK-NOT FILMED

Original photography may be purchased from:
EROS Data Center
10th and Dakota Avenue
Sioux Falls, SD 57198

1. INTRODUCTION

A preliminary analysis of ERTS-1, MSS imagery of southeastern Massachusetts, including Cape Cod, Cape Cod Bay, and Nantucket Sound, has been completed. Special emphasis has been given to a study of Plymouth and Duxbury Bays because of the availability of imagery from at least three orbital passes (Table 1). Examples of imagery of coastal and submarine features are given at scales of 1:1,000,000; 1:250,000; and 1:125,000, and compared to conventional maps at 1:1,000,000 and 1:250,000 scales, and 1:125,000-scale Ektachrome infrared aerial photography.

Table 1. - Selected ERTS-1 Imagery of Southeastern Massachusetts and Tidal Data for Time of Image Acquisition (Anonymous, 1971)

Date	Image ID No.	Local Time (hrs.)	Tidal Times (hrs.) for Plymouth Bay High	Low	Rise (m)
28 July 1972	E-1005-15005	1001	1240	0643	3
1 Sept. 1972	E-1040-14552	0955	0500	1118	3
8 Oct. 1972	E-1077-15011	1001	1138	0541	3

Coastal areas, such as Cape Cod, represent one of the most difficult areas in which to do accurate geologic mapping and in which to maintain the currency of conventional topographic maps (Williams and Friedman, 1970). The Cape Cod coastline is continually changing from a combination of natural forces (Davis, 1896) and manmade modifications. Offshore bars and shoals; sediment distribution; the water-land contact; areas of beach and dune sediments; position of tidal and river channels; vegetation assemblages; and even cultural features are in a constant state of flux. Small wonder then that our conventional maps of Cape Cod are out of date, and as can be seen by comparison of ERTS-1 MSS imagery at the 1:1,000,000 and 1:250,000 scales, such small-scale maps are inaccurate, particularly in the portrayal of the coastline and lakes.

The key to accurate and timely coastal mapping is the acquisition of optimum imagery (Stringham and Williams, 1970) for the specific purpose to which it will be employed. Optimum imagery implies frequent coverage at specific spectral bands. Aerial spectrophotography (Williams, 1971),

if available, can fulfill these requirements. In most cases, however, aerial photography of an area is infrequently scheduled, usually acquired during one season (summer), and in only one spectral band. ERTS imagery provides the needed data for maps at 1:250,000 scale or smaller. MSS band 4 or band 5 is best for showing shoals and bars on Cape Cod; band 5 is best for cultural features; and band 6 or 7 is excellent for the land-water contact (shoreline), harbors, inlets and marshes, and for lakes and ponds. The remainder of the paper will be directed at describing various coastal and submarine features on the MSS imagery of southeastern Massachusetts under different tidal conditions (different water depths) and comparison of these features with conventional maps of the area.

2. COASTAL FEATURES

Figure 1 compares three ERTS-1, MSS images from the same scene (1 Sept. 1972, E-1040-14552), bands 4, 5, and 7, with a 1:1,000,000-scale map [IMW, NK-19, Boston, North America, 1969; compiled by Army Map Service in 1955 from 1:250,000 maps (1947), 1:506,880 maps (1939), and USC&GS charts (1947 and 1949)]. The images were acquired at 0955 hrs. local time about 1 1/2 hrs. before low tide in Plymouth Bay, Wellfleet Harbor, Provincetown, and Barnstable Harbor (Beach Point) (Anonymous, 1971). In an area as large as Cape Cod, with different bottom configurations, etc., the times of high and low tide vary from place to place. For instance, low tide in Pleasant Bay was not reached until 3 hrs. later (4 hrs. after passage of the satellite) than Plymouth Bay.

Many inaccuracies are apparent when the ERTS-1, MSS images are compared to the 1:1,000,000-scale map, which shows the shoreline at time of mean sea level. How many of the discrepancies are due to actual changes in the coastline since time of mapping and how many are due to the subjective generalizations by the cartographer who drafted the original map is impossible to say. With the ERTS image, however, it is not necessary to generalize, since the original scale of the image "pre-processes" the data for the cartographer. There should also be less subjective variation between different cartographers, hence a better "fit" between different areas within a map or between different maps becomes possible. See the "fit" between the two 1:250,000-scale maps in Plymouth

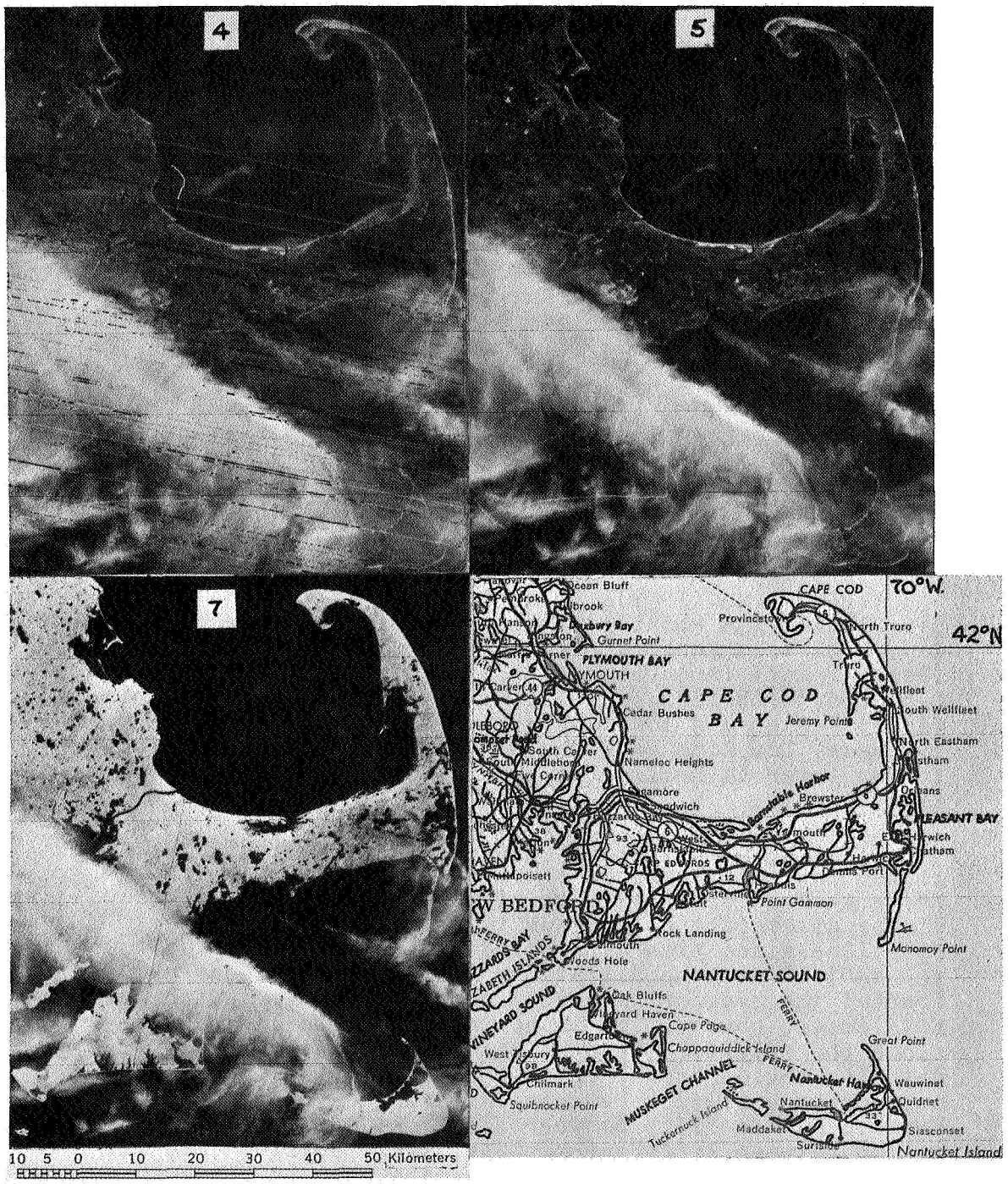


Figure 1. - Comparison of 1:1,000,000-scale ERTS-1, MSS imagery (1 Sept. 1972, E-1040-14552, MSS bands 4, 5, and 7) with 1:1,000,000-scale map (IMW, NK-19, Boston, North America, 1969) of southeastern Massachusetts, showing coastal and submarine features. Note the inaccuracies in the portrayal of the coastline and inland lakes on the map when compared with the MSS images. For much of Cape Cod Bay the tide will ebb 1 hr. 23 min. after image acquisition.

Harbor 3km east of long. 70°45'W. for a striking example of subjective inaccuracy (Figure 2). A comparison of the coastline configuration of the tip of Cape Cod (Provincetown area), Jeremy Point on the western side of Wellfleet, Point Gammon south of Hyannis, Barnstable Harbor, Great Point and the cuspate bar on Nantucket Island, Monomoy Point and Island south of Chatham (Oldale, Friedman, and Williams, 1971) between the MSS image (band 7) and the map graphically portray the differences.

The portrayal of lakes and ponds on the 1:1,000,000 map shows a decided lack of cartographic precision. Almost no lakes or ponds are portrayed on the map with their accurate shape when the map is compared with the MSS image (band 7). Although some of the lakes may have changed in size or shape the representation of most of these is grossly inaccurate. There is no question that ERTS imagery will permit a far superior 1:1,000,000 map of southeastern Massachusetts.

Figure 3 and 4 show enlargements of ERTS-1 MSS imagery of the Plymouth and Duxbury Bay areas. Discrepancies and inaccuracies are present on the 1:250,000-scale maps (NK 1904, Boston, 1956, revised 1970; and NK 19-7, Providence, 1947, revised 1969), although not to the degree of the 1:1,000,000 map. Note the shoreline around Saquish Head and the configuration of inland lakes and ponds. The 1:250,000-scale MSS images (bands 4, 5, and 7) of Figure 3 and the 1:125,000-scale MSS images of Figure 4 (bands 5 and 7) were acquired on 28 July 1972 (E-1005-15005) at 1000 hrs. local time or about 2 hrs. 40 min. before high tide.

Also of particular interest on band 5 of MSS imagery is the distinction of dune areas, particularly in the Province Lands area northeast of Provincetown and along Sandy Neck north of Barnstable Harbor. Areas of marshes (wetlands) can be delineated, particularly in western Wellfleet and around Barnstable Harbor.

3. SUBMARINE FEATURES

Figure 1 shows considerable detail of submarine features along the coastal and bay areas of southeastern Massachusetts. MSS band 4 shows the greatest submarine detail, but the wavelengths needed for water penetration

C

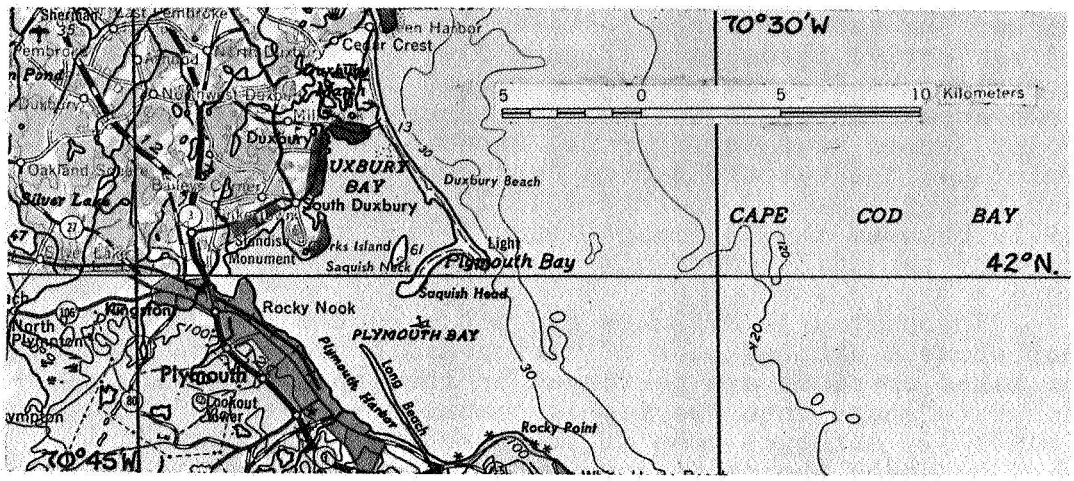


Figure 2. - 1:250,000-scale map (NK 19-4, 1956, rev. 1970; NK 19-7, 1947, rev. 1969) of the Plymouth and Duxbury Bay areas, Massachusetts. Compare with Figure 3. Datum reference is mean sea level.

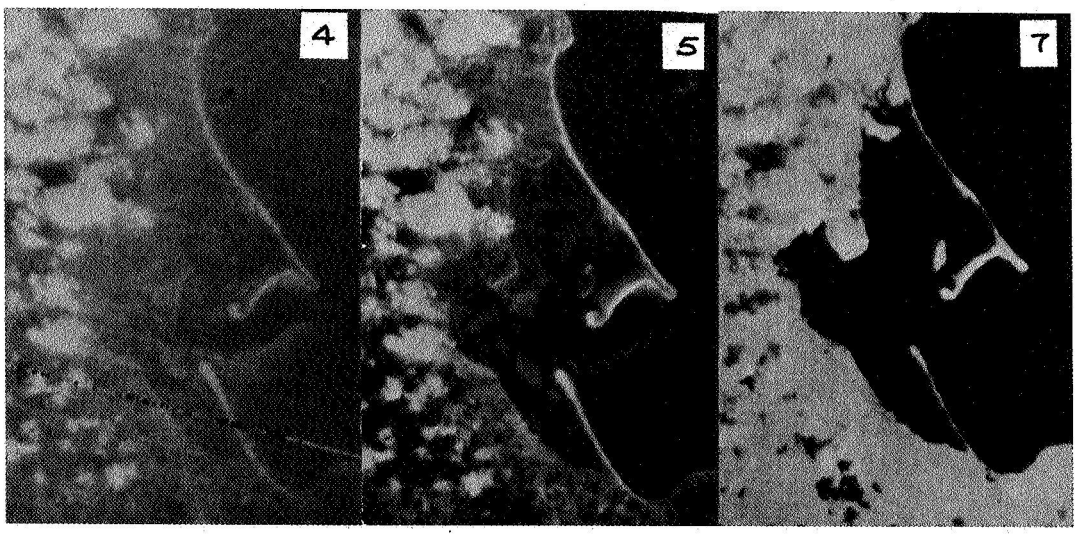


Figure 3. - Enlargement of ERTS-1, MSS imagery (28 July 1972, E-1005-15005, bands 4, 5, and 7) to 1:250,000 scale. Compare with Figure 2. Image was acquired 2 hrs. 40 min. before high tide.

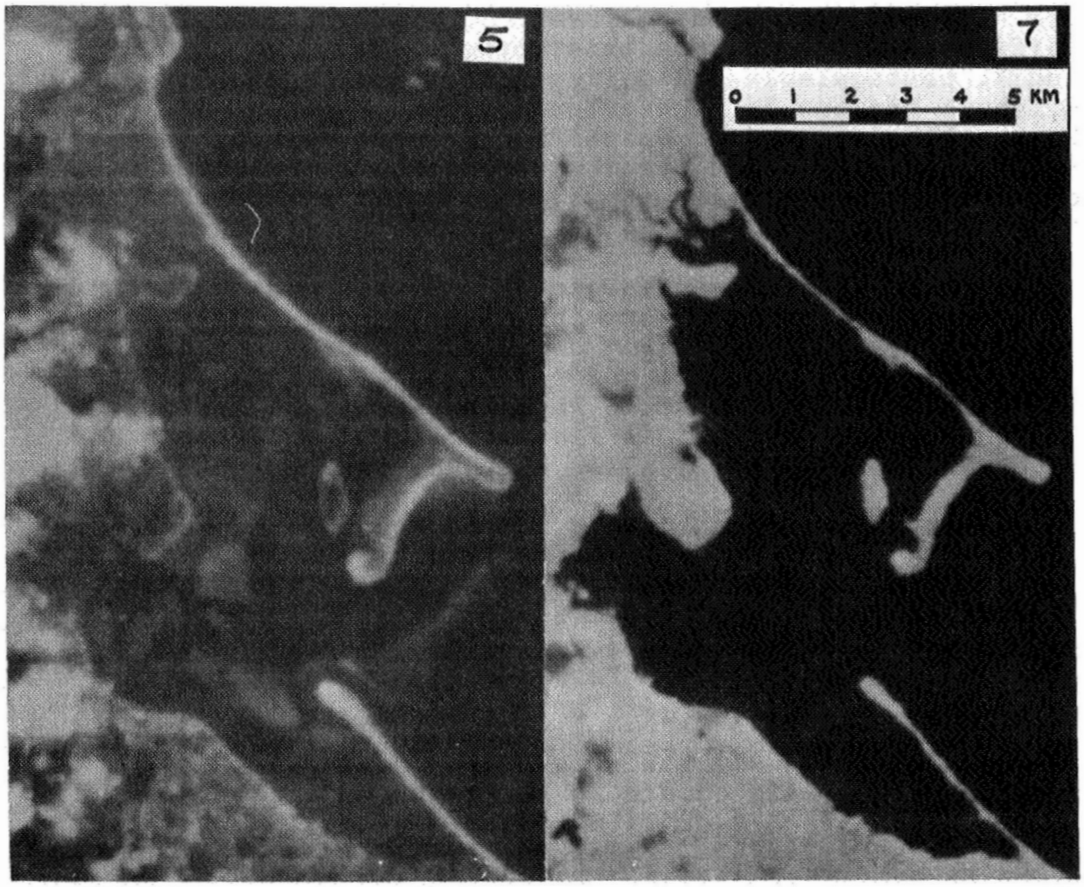


Figure 4. - Enlargement of ERTS-1, MSS imagery (28 July 1972, E-1005-15005, bands 5 and 7) to 1:125,000 scale. Image was acquired 2 hrs. 40 min. before high tide.

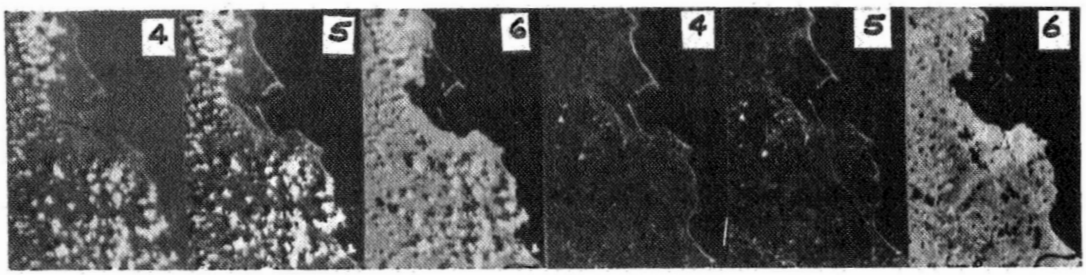


Figure 5. - ERTS-1, MSS imagery (1:1,000,000 scale) of Plymouth and Duxbury Bays, Massachusetts. Images A-F (left to right). Images A-C (28 July 1972, E-1005-15005, bands 4, 5, and 6; image acquired 2 hrs. 40 min. before high tide). Images D-F (8 Oct. 1972, E-1077-15011, bands 4, 5, and 6; image acquired 1 hr. 39 min. before high tide)

are also affected by atmospheric moisture. (Note the difference in thin cloud penetration between bands 4, 5, and 7; particularly the difference between 4 and 7.) An offshore bar can be seen extending the length of the outer Cape, all along Nauset Beach from Chatham to North Truro and Provincetown. It becomes two offshore bars northwest of North Truro. Shoals can be seen in Cape Cod Bay between Provincetown and Jeremy Point (Wellfleet). Note the extensive shoaling west of Jeremy Point and the low tide expanse of Billingsgate Island, nearly covered at high tide and once the site of a thriving fishing community. The shoal areas in Cape Cod Bay off Eastham, Orleans, and Brewster are well delineated. The channel entrances to Barnstable Harbor, Plymouth Bay, and Wellfleet Harbor, and the configuration of tidal flats in Barnstable Harbor and Plymouth and Duxbury Bays are also visible.

Tidal flats and channels can be seen in Plymouth and Duxbury Bays on three different ERTS-1, MSS frames. On Figure 1 the time of image acquisition was 1 hr. 23 min. before low tide. On Figures 3, 4 and 5A-5C, the image was recorded at 2 hrs. 40 min. before high tide. On Figure 4D-4E the image shows the harbor at 1 hr. 39 min. before high tide.

Figure 3 shows the configuration of tidal flats, channels, bars, and shoals in Plymouth and Duxbury Bays at an enlargement scale of 1:250,000. Figure 4 shows the same features at 1:125,000. These submarine features are not shown on the conventional 1:250,000-scale map even though these features can be portrayed. Comparison of the 1:125,000-scale enlargement of the ERTS-1, MSS image (band 5) with a 1:125,000-scale Ektachrome infrared aerial photograph (NASA, RB-57F photograph acquired on 13 Sept. 1969 at 1020 hrs., film type S0117; Photo No. 6293), taken 1 hr. 40 min. before high tide, showed similar features in Plymouth and Duxbury Bays.

Although the ERTS-1, MSS imagery of submarine features in harbor and coastal areas gives only the two-dimensional view, with precise depth information still to be measured by conventional means, periodic analysis of such imagery can be employed to determine when changes in position of tidal flats, bars, and shoals occur. This information could then be used in the scheduling of bathymetric surveys of specific areas when new surveys are needed.

4. CONCLUSIONS

The ERTS-1, MSS imagery of southeastern Massachusetts provides important geologic and hydrologic information necessary for the frequent and accurate updating of conventional 1:1,000,000 and 1:250,000 maps of the area, and perhaps even for map scales of 1:125,000. Because various types of maps provide an important source of environmental information for resource management decisions, it is important that such maps be current and accurate. Based on a preliminary analysis of MSS images of Cape Cod, the ERTS imagery provides environmental information not available from conventional sources (chiefly aerial photography), except at very high cost. ERTS-1 imagery provides the following advantages both from type of data acquired and low relative cost:

1. Synoptic, nearly instantaneous coverage of a large area at different times in the tidal cycle of a coastal area (over several orbital cycles).

2. Repetitive, cyclic, and frequent coverage at relatively low cost.

3. Permits the regional mapping of marshes (wetlands), tidal flats, shoals, bars, and harbor channels, not normally shown on 1:250,000 and smaller scale maps.

4. Avoids the subjective differences in cartographic representation by the same cartographer on one map or between different cartographers on separate maps caused by generalization of features by portraying the environmental data at the correct scale initially.

5. By periodically recording specific types of environmental information, and if converted to a map or other form of presentation in a timely manner, ERTS imagery provides relevant and current data to resource managers necessary to accurate decisions.

5. REFERENCES

Anonymous, 1971, Tide tables - high and low water predictions, 1972, East Coast of North and South America: Natl. Ocean Survey, Natl. Oceanic and Atmos. Admin., U. S. Dept. of Commerce, 290 p.

Davis, W. M., 1896, The outline of Cape Cod: Am. Acad. Arts and Sci. Proc., v. 31, p. 303-332; also pub. in Geographical Essays, New York, Dover Pub., p. 690-724, 1954.

Oldale, R. N., Friedman, J. D., and Williams, R. S., Jr., 1971, Changes in coastal morphology of Monomoy Island, Cape Cod, Massachusetts, in Geological Survey Research 1971: U. S. Geol. Survey Prof. Paper 750-B, p. B101-B107.

Stringham, J. A., and Williams, R. S., Jr., 1970, Applications of reconnaissance concepts to mapping problems: Proc. of the Geodetic and Research and Development Symposium, Seventh DOD Geodetic-Cartographic-Target Materials Conf., Cameron Station, Va., p. 37-105.

Williams, R. S., Jr., and Friedman, J. D., 1970, Geologic mapping applications of coastal aerial photography, Cape Cod, Massachusetts (abs.): Photogrammetric Eng., v. 36, no. 6, p. 597.

Williams, R. S., Jr., 1971, Geological applications of aerial spectrophotography: Preliminary findings from Cayo Icacos, Puerto Rico (abs.): Trans., Fifth Caribbean Geol. Conf. (1968), Geol. Bull. No. 5, Queens College Press, p. 252.

N73-28359

Paper M 19

WATER DEPTH ESTIMATION WITH ERTS-1 IMAGERY

D. S. Ross, *International Imaging Systems, Mountain View, California*

ABSTRACT

Contrast-enhanced 9.5 inch ERTS-1 images were produced for an investigation on ocean water color. Such images lend themselves to water depth estimation by photographic and electronic density contouring.

MSS-4 and -5 images of the Great Bahama Bank were density-sliced by both methods. Correlation was found between the MSS-4 image and a hydrographic chart at 1:467,000 scale, in a number of areas corresponding to water depth of less than 2 meters, 5 to 10 meters and 10 to about 20 meters. The MSS-5 image was restricted to depths of about 2 meters.

Where reflective bottom and clear water are found, ERTS-1 MSS-4 images can be used with density contouring by electronic or photographic methods for estimating depths to 5 meters within about one meter.

1. INTRODUCTION

There are about 130,000 km of world coastline commonly plied by shipping. The continental shelves have an average slope of 2 m/km. (1) The coastal ocean area up to 20 m depth is in the order of 1,300,000 km^2, while shallow seas have more than an equivalent area in this depth range. It has been estimated that 95% of the world's coastal waters permit 70% or more light transmission per meter (70% = 5 m Secchi Depth. (2) The potential area for water depth examination by ERTS is thus very large.

Natural Color Gemini and Apollo space photography proved it was possible to see the ocean bottom in clear water at depths to 30 meters or more. Although ERTS-1 is primarily designed for terrain sensing, and does not have a blue spectral band contributing image energy equivalent to that sensed by the color film in the blue region, nevertheless a number of MSS-4 images show evidence of bottom recording in depths of 10 meters or more.

Specially processed ERTS-1 images appear capable of yielding information at image scales as large as 1:100,000, which can contribute materially

Original photography may be purchased from:
EROS Data Center
10th and Dakota Avenue
Sioux Falls, SD 57198

to knowledge of changes in world coastal bathymetry. Most charts were originally hand-contoured from sometimes limited sounding data; many have not been revised for 10, 20 or even 50 years, and bottom topography has been altered in the interim by storms, currents and tidal action.

2. LIGHT TRANSMISSION IN SEAWATER

Maximum transmission of light in clear seawater is in the 470-480 nm blue-green spectral region. (3) Water acts as an optical filter, progressively absorbing radiant energy at longer wavelengths, until almost complete absorption occurs in the near-infrared. Maximum clear water transmission is found in the green ERTS-1 MSS-4 band (Figure 1). In coastal waters suspensions of sediment, biological matter and pollutants, according to types and concentrations, attenuate light transmission and shift the water window from the blue-green toward the longer wavelength green and yellow spectral regions. Heavy concentrations of suspended matter eventually restrict remote sensing to surface or near surface spatial and spectral information in all bands.

3. IMAGE ENHANCEMENT FOR WATER DEPTH ESTIMATION

ERTS-1 images require enhancement for this purpose. During an investigation on ocean water color several MSS-4 images of the shallow Bahama Banks were worked with, and areas of possible correlation between image density and chart depths were noted. Photographic and electronic density contouring processes were then applied.

Contrast Enhancement. ERTS-1 images are reproduced at gamma 1.0, exactly as the sensor saw the scene through the atmosphere. Ocean phenomena are normally of low contrast to begin with and, in the MSS-4 gamma 1.0 reproduction, may be further reduced to a half or fifth of true ground value by Rayleigh and Mie effects. Scene contrast can be partially restored by reprinting the image on high contrast photographic materials by carefully controlled, conventional processes. One of the images selected (Figure 2) was reproduced at gamma 2.55; densities in the original between the shallow water and deep ocean had a range of 0.52, increased during reproduction to 1.33. The enhanced contrast and improved density range of this image, when compared with the hydrographic chart at 1:1,000,000 scale, showed large areas of correlation with depth. However, the small differences in the continuous tone density scale made positive judgement of density boundaries difficult, and density-slicing was resorted to.

Photo-Optical Density-Slicing. Fourteen isodensity slices were made of the water area by an I^2S technique, each density contour being produced on a separate sheet of film. In the final registered false color composite, these were reduced for clarity to five 0.075 density contours and four 0.037 D steps, to represent the 0.52 density range in the input image.

Electronic Density Contouring. The image was processed in an I^2S Digicol electronic image analyzer. This method permits real-time density slicing under the control of the operator, with false color display of density

differences, the ability to make spot density measurements, cut density profiles through the image, and to do planimetry of selected areas. As the image is converted to digital form, it can be fed into storage or computer processing. Density slice-width and placement within the density range of the input image is also possible. Black and white resolution is limited to 1000 X 1000 elements, and color to 525 X 525; however, the image area viewed by the video camera lens can be reduced to match the inherent resolution of the image, thus preserving the information content.

4. RESULTS

Figure 3 (original in color) shows groupings of the photo-optical density slices for depths of less than 2 meters and approximately 5 and 10 meters. The chart, C & GS 1112, 1:466,940 (Rev. 23 Sept. 68), was reduced to 1:1,000,000 scale for overlay and slice selection. Chart depths are in fathoms for mean low water. Water less than one meter deep is clearly separated in areas to the S. and E. of Bimini, and along the Keys to the S. These areas total about 12,500 km^2. In the S. E. corner of the image where chart depths average 4 m, however, an extensive area shows as equally shallow. This may be caused by sunglitter, although the chart warns "The charted position, size, shape and orientation of the---banks in the Bahama Islands are unreliable". Other density slices representing 4-5 m depths agree well with the chart and total about 75,000 km^2 in area. The deeper water area is confused by cloud and cloud shadow, but general correlation exists for 5-10 m. The northern end of the Bank has a well-defined shelf about 18 m deep, changing abruptly to 180 m and more. Correlation was found here for an area about 8,000 km^2, but the image density was very close to the D max of the original positive and on the borderline of detectibility.

As shown in Figure 4, very similar results were obtained with electronic image digitizing, but with the advantage of "tuning in" to the minimum separate density variations in real time.

The image of the area off Key Largo (Figure 5) was enlarged 12.5X to 1:80,000 chart scale. Tide had been rising for several hours prior to image acquisition; figures which follow are for mean low water. On the untreated enlargement, light reflected from the bottom was found on linear features about 200 m wide, in shallow water. Several circular formations, both light and dark, and 200 m in diameter also correlated with the chart. Theoretically, bulk MSS can resolve 136 m with a low contrast subject. Extensive areas 8 to 10 m deep agreed with the chart, the deepest being about 12 m. Many tone reversals were found, due to marine grasses and corals at 2-3 m, which, however, followed the depth contours quite closely.

Electronic image digitization, as shown in Figure 5, was applied to contour the enlarged image. Time has not permitted photo-optical density slicing of this image, but it is evident that either technique is an essential aid for the interpretation of image density domains related to water depth.

5. BATHYMETRIC INTERPRETATION

The Bahama Banks image was from an area where the ocean bottom is largely homogeneous and composed of highly reflective calcareous materials; the Florida Reef image has very inhomogeneous bottom. Relating density information in ERTS images to water depth must be done with caution, as many factors affect apparent water luminance and bottom reflection. Bathymetric interpretation should be done by the professional hydrographer or oceanographer, familiar with the area examined. Enhanced ERTS imagery would aid him by greatly reducing the number and length of transects required to sound a large area and by identifying areas requiring close investigation. MSS bands -4, -5 and -6 are particularly useful for this work. MSS-5 is strictly limited in water penetration, but clearly delineated, in this test, areas where chart depths were less than 2 m. Bands -6 and -7 show surface detail primarily; in several cases MSS-6 images show density differences in charted depths of one-half to 2 meters; Figure 5 shows an example.

Effects of Marine Flora. Some Caribbean regions have dense beds of marine grasses, or living corals, which modify reflectance from the bottom, and could lead to false conclusions about water depth. However, many marine algae show depth zonation tendencies related to the depth at which they can satisfy photosynthetic processes. (4,5) Knowledge of algae types, location and associated depths in a region could aid interpretation. Certain algae also require specific types of bottom. Some of the kelp families require firm holdfasts, and also expose fronds of the surface, the latter being detectible in the infrared bands as surface phenomena. Several clearly defined areas in Figure 2 to the south and east of Bimini are judged to be large algael beds at depths in the order of 4 meters.

Turbid Water. Light-colored sediments in the water can give false indications of shallow water. Near-surface turbidity normally appears similar in images of different spectral bands, but is usually identifiable by distinctive eddies and flow-lines. Turbid water currents appear to follow bottom topography in some instances.

Surface Reflectance. Large bodies of wind-generated whitecaps, individually below sensor resolution limits, become integrated as light areas, and will appear about the same order of density in all spectral bands. At high sun elevations, in relatively calm seas, many wave facets may be tilted and oriented to reflect integrated sunglitter directly into the sensor. Wave angles below 20° with sun elevations of 60° can cause this. Light areas (in the positive) will appear in all bands from this effect. Swells with wavelengths in the order of 100 meters would give similar results.

ERTS-Image Densities. ERTS image density range is primarily controlled for terrain subjects, and water areas in MSS-5, -6 and -7 positive images may be very dense and appear featureless when comparing these bands, unless examined by high-intensity transmitted light, or reprinted for the water area. Very thin cloud otherwise may be concealed by high densities in these bands, and may be mistaken in MSS-4 as a variation in water luminosity and depth.

6. CONCLUSIONS

Under favorable circumstances ERTS-MSS resolution can detect subsurface detail as small as 200 m in diameter. Enhanced and density-contoured imagery appears to permit estimation of water depth to at least 5 m within a meter or so, in the regions and at the scales assessed; and would be a valuable aid to chart revision by directing the hydrographer to areas requiring closer examination. Water depth over large areas of world coastline and shallow seas can be assessed by ERTS imagery and image processing techniques.

REFERENCE

(1) Weyl, P. K. - Oceanography - John Wiley & Sons, 1970.
(2) Lepley, L. K. (then U.S. Naval Oceanographic Office), Coastal Water Clarity from Space Photographs, Photogram. Eng. XXXVI, Vol. 7, Jul. 1968.
(3) Jerlov, N. G. - Optical Oceanography, Elsevier, 1968.
(4) Polcyn, F. C. & Rollin, R. A. - Remote Sensing Techniques for Location & Measurement of Shallow-Water Features, Willow Run Laboratories, Jan. 1969.
(5) Conrad, A., Kelly, M., & Boersma, A. - Aerial Photography for Shallow Water Studies on the West Edge of the Bahama Banks, MIT Experimental Astronomy Laboratory, Nov. 1968.

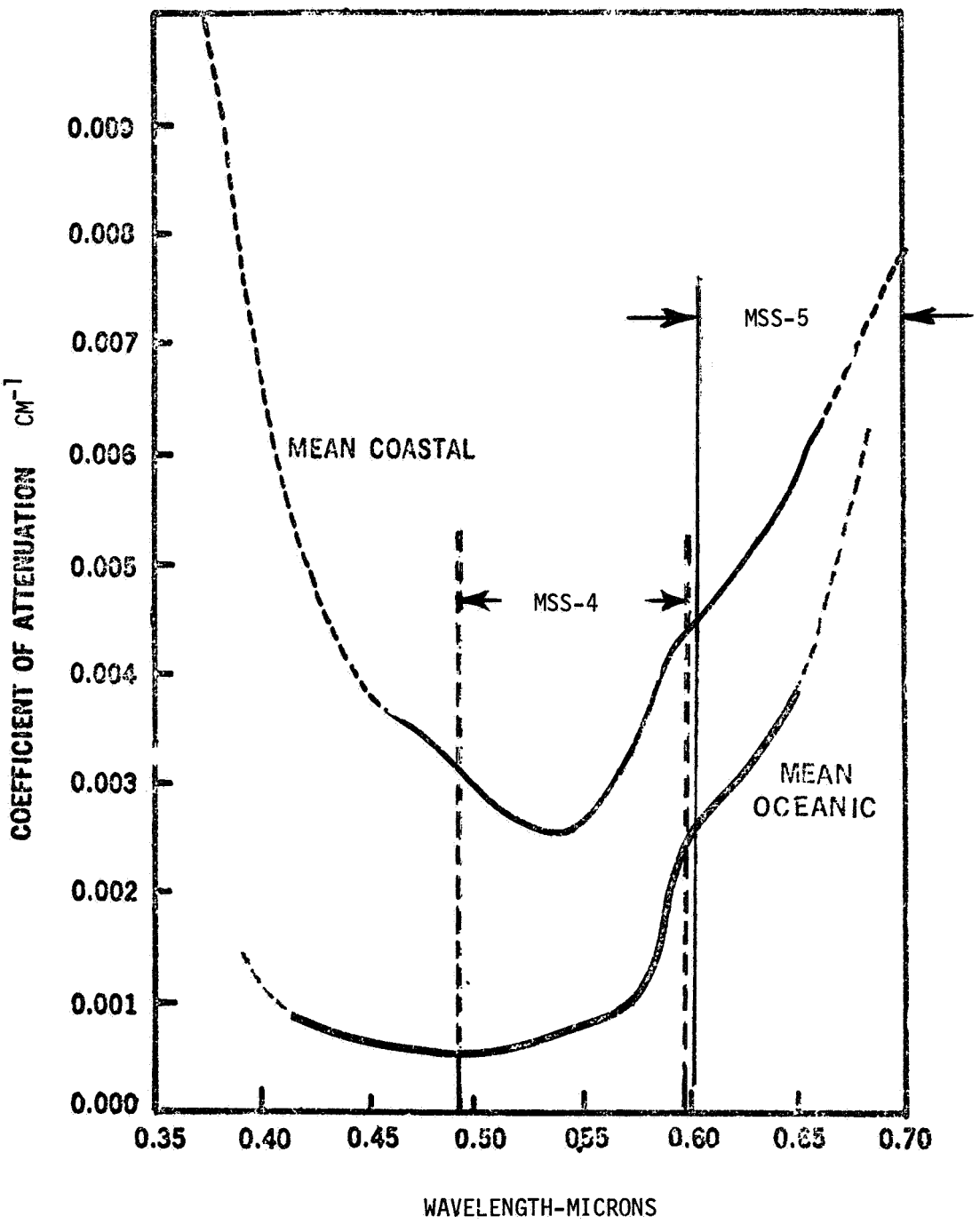


Figure 1. Light Attenuation in Ocean Water and ERTS-1 MSS-4 and MSS-5 Spectral Bands.

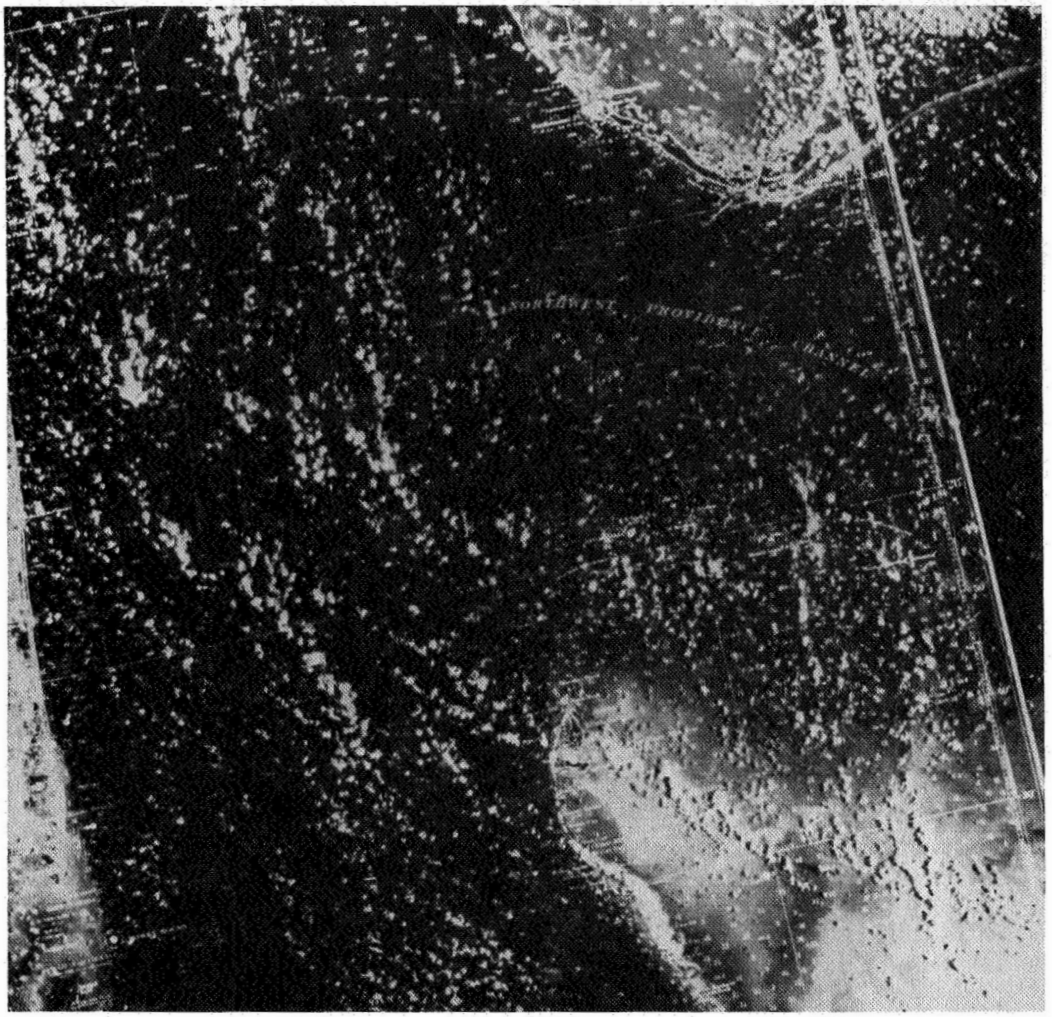


Figure 2. E-1007-15165-4. Lower Right, Great Bahama Bank with Chart Overlay. Original Scale 1:1,000,000.

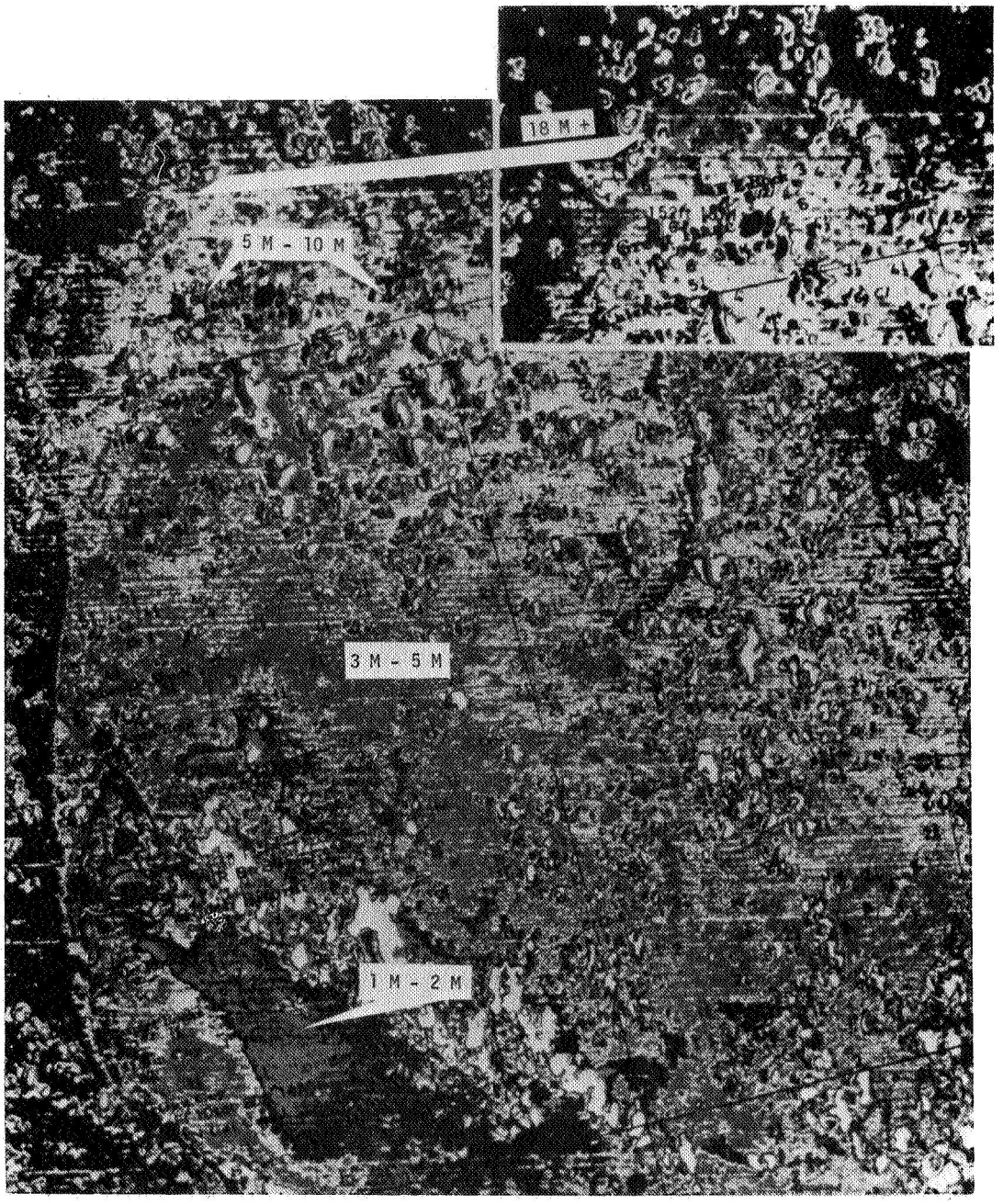


Figure 3. Photo-Optical Density Slices for Depths of 2 M or Less, 3 M – 5 M, and 5 M – 10 M. Note Enlarged Area Where Depth is 18 M or More. (Original in Color).

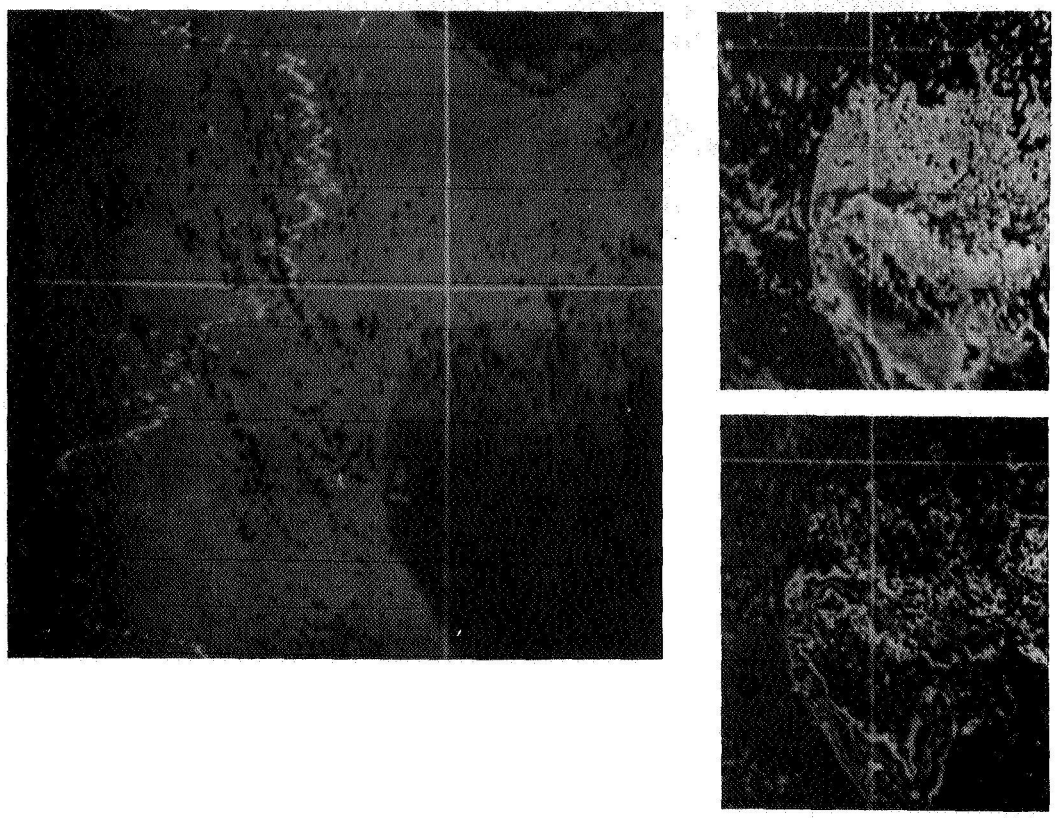


Figure 4. Electronic (Digicol) Image Density Contouring (Original in Color). The Input Image is Displayed as a Continuous Tone Negative Image on the Left. The Electronic Marker Lines Intersect Where 180 M Water Depths Begin. The Transmission Profile of the Negative Cut by the Vertical Line is Displayed to the Left as the Wavy White Curve.

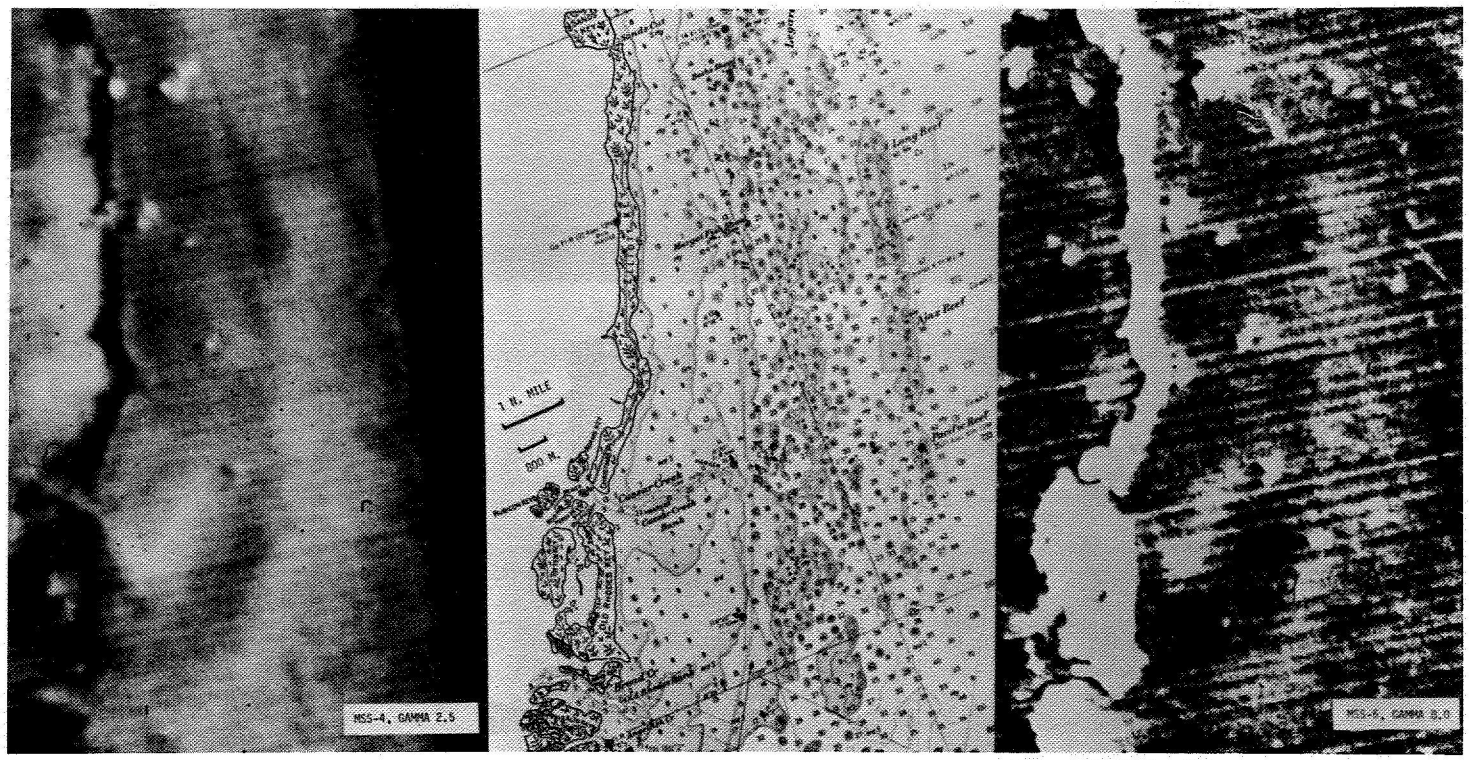


Figure 5. Section of MSS-4 and MSS-6, E-1007-15172, Enlarged 12.5X to Chart C&GS 1249, (Rev. Oct. 21, 1968) Scale 1:80,000. Area Shown is North of Key Largo Coral Reef Preserve Near Miami, Florida. White Bottom Areas in MSS-4 (Left) Near Edge of Reef Are About 200 M Wide. MSS-6 Image (Right) 700 NM-800 NM Shows Bottom on Ceasar Creek Bank, Probable Depth of 0.5 M, but Also Distinguishes Bottom Reflectance in 1 M to 2 M Depths. Chart Depths are in Feet.

N73-28358

Paper M 20

CALCULATIONS OF WATER DEPTH FROM ERTS-MSS DATA

Fabian C. Polcyn and David R. Lyzenga, *Environmental Research Institute of Michigan, Ann Arbor, Michigan*

ABSTRACT

ERTS-1 MSS data taken on October 10, 1972 of the Little Bahama Bank are being used to demonstrate the use of ERTS-1 data for mapping of shallow water features for the purpose of upgrading world navigation charts. Marked reflectance differences occur for the shallow water areas in Bands 4, 5, and 6. Digital processing of two adjacent data tapes within the ERTS frame covering an area of about 40 by 40 miles has been completed. Correlation of depth measurements to 5 meters has been successful. A mathematical model for depth measurements using ratio of voltages in Band 4 and 5 has been successfully developed and is being tested for accuracy. Additional studies for areas near Puerto Rico and in Northern Lake Michigan will be undertaken. Satellite data will also provide geographical evidence for verifying existence or nonexistence of doubtful shoal waters now appearing on world charts and considered to be hazardous to shipping.

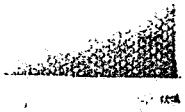
1. INTRODUCTION

The opportunity for global coverage afforded by earth orbiting satellites such as ERTS-1 makes possible for the first time to completely survey the oceans in a short time and in a common format and thus update the world's navigation charts.

The International Hydrographic Office has expressed concern over the status of shipping charts around the world, many of which cannot be updated due to lack of technical resources on the part of some countries. Meanwhile, some maps contain data based on survey records from the early 19th century, when the simplest techniques subject to a variety of errors were used for depth soundings.

Doubtful shoals occur for many reasons; positions are known only approximately. The same shoal may have been reported by two different ships with inaccurate geographical coordinates (Ref. 1). Location

Original photography may be purchased from:
EROS Data Center
10th and Dakota Avenue
Sioux Falls, SD 57198



information is one of the most frequent sources for ambiguity on the shipping charts.

Chart makers are forced to use such labels as Position Approximate, and Existence Doubtful in reference to some reported sightings. Depths measured by lead lines tend to give too large a depth because of bending of the line. Echo Sounders can give errors from suspended materials that cause depths to be too shallow. Storms bring rapid changes so that even recent maps may be in error due to shifting sand bars and coastline readjustments. If only surface ships are used for hydrographic surveys, a long slow process is involved and sampling procedures are necessarily incorporated.

Satellite remote sensing affords a solution to some of these problems. Shallow waters less than 50 feet (17 meters), the most dangerous from the point of view of ship safety, are measurable from ERTS-1. Because of the 100 mile by 100 mile format, location information referenced to well known large land masses are possible and will do much to improve maps.

All points within the 10,000 sq mile frame can be observed and shallow waters easily identified on Band 4 with Band 6 or 7 used to mark land/water boundaries. Doubtful shoals can be eliminated. Existence or non-existence of doubtful shoals can be ascertained especially in regions where water clarity permits optimum light penetration. The problem that remains is to determine the accuracy of depth measurement with satellite remote sensors.

The ERTS investigation designated UN 200 carried out for NASA by the Environmental Research Institute of Michigan is planned to answer this question.

2. THE EXPERIMENTAL TECHNIQUE

Previous work (Refs. 2,3) on remote sensing techniques identified multispectral ratio processing as a promising technique for the remote detection of water depth. The technique employs the relation shown by the equation

$$z = \frac{1}{f(\theta,\phi)(\alpha_1-\alpha_2)} \ln \frac{k_1 V_1 H_1 \rho_1}{k_2 V_2 H_2 \rho_2}$$

where z = water depth

α_1, α_2 = extinction coefficients of water at two different wavelengths

ρ_1, ρ_2 = bottom reflection in two different bands

k_1, k_2 = constants of the instrument which are known

H_1, H_2 = incoming solar radiation

V_1, V_2 = analog signals observed in the multispectral scanning of the shallow features.

For the satellite case, V_1 and V_2 are obtained from Bands 4 and 5 of the MSS digital tape. The incoming solar radiation is available from standard references. The extinction coefficient is obtainable from ground measurements, or estimated on the average for a given geographical area based on a knowledge of the conditions and adjustments to the known values for clear water. ρ_1 and ρ_2 are reflectances for the bottom materials, some types of which are known. Since the ratio for bottom reflectances appears in the equation, only relative spectral information is needed.

3. RESULTS

An ERTS-1 frame taken over the Bahama Islands was used in the initial investigation to date. The ERTS Frame 1079-15165 was taken on October 10, 1972 (79th day since launch of ERTS-A) at 15 hours, 16 minutes, 50 seconds. Principal point of image is 27.45°N, 78.82°W (Northwest of Grand Bahama Island). Solar elevation is 74.4°. Frame covers approximately 100 x 100 nautical miles, with Grand Bahama Island in the lower right-hand corner and the Little Bahama Bank covering most of the lower half of the frame. There is a 30% cloud cover for the frame as a whole, but most of the clouds are in the upper half. There is a small patch of clouds in the center of the Bank and over Grand Bahama Island.

In Figure 1, the multispectral scanner (MSS) channel 4 (.5-.6 μm) clearly shows underwater features in the bank north of Grand Bahama Island. Most of these can be identified on the Hydrographic Office depth chart, (see Fig. 2) but there are a large number of streaks in the center of the frame which are not on the published chart.

MSS channel 5 (.6-.7 μm) shows some of the shallower areas of the bank, as well as land and clouds.

MSS channels 6 and 7 (.7-.8 μm and .8-1.1 μm) show no underwater features. Water absorption is so high in these channels that the only signal received over water is due to surface reflection.

Going from channel 4 to 7, land areas become progressively brighter, shallow water areas become darker, and clouds remain at about the same brightness. Sale Cay (on the right) thus appears dark against a

light background in channel 4, is almost indistinguishable in channel 5, and stands out clearly against a dark background in channels 6 and 7.

The multispectral characteristics are evident in the comparison for the four bands from the MSS. The digital tapes were then used to produce a relative depths chart shown in Figure 3.

This density map was made from the digital output from MSS channel 4. The darkest symbol (e.g., in the lower left-hand corner) corresponds to a signal less than 24 volts (amplification arbitrary). A blank corresponds to a signal of greater than 38 volts. The interval from 24 to 38 volts was divided into 7 equal subintervals and a separate symbol assigned to each. Every 4th line and point of the data was used in making the map (each line of the original data corresponds to an east-west strip 79 meters wide, and each point along the line occupies 56 meters, so each symbol on the graymap represents an area of 216 x 316 meters).

This map gives an indication of water depth, within the range of 0-10 meters. The bottom-reflected signal is proportional to

$$e^{-\alpha(\sec\theta + \sec\phi)z}$$

where α is the attenuation coefficient, θ is the observation angle, ϕ is the solar zenith angle, and z is the depth. α is on the order of $0.2\ m^{-1}$, so the bottom-reflected signal is approximately proportional $e^{-0.27z}$, where z is the depth in meters. The bottom-reflected signal is obtained by subtracting off the deep-water signal, which is about 23 volts for channel 4.

The shallowest areas (corresponding to blanks on the map) return a signal of about 41 volts. Using this as the reference level z_o, we have

$$V_b(z_o) \equiv V(z_o) - 23 = 18 \text{ volts}$$

The bottom-reflected voltage at any other depth z is then given by the relation

$$\ln V_b(z_o) - \ln V_b(z) = 0.27\ (z-z_o)$$

From the Hydrographic Office depth chart, the depth in the white areas is about 1 fathom (6 feet). Using this value for z_o, the depths corresponding to each of the symbols on the map are given in the following table:

SYMBOL	VOLTAGE RANGE	DEPTH RANGE (Ft.)
-	37-38	7-9
•	35-36	9-11
=	33-34	11-13
*	31-32	13-16
I	29-30	16-20
θ	27-28	20-24
H	25-26	24-33
H	0-24	33-∞

The deepest areas in the north-western part of the bank are thus about 5 fathoms, which agrees with the depth chart. The white streaks in the center of the bank appear to be about a fathom below the surface.

Calculations based on two channels of information give absolute values for depth where some knowledge of bottom reflection is known. This was done only at those points where both channels 4 and 5 received bottom reflection signals.

For the sand bars (white streaks in Fig. 3), calculation of water depth was completed since the general reflection characteristic for wet sand had been previously determined. Agreement with HO chart 5990 was evident: the chart refers all depths to the mean lowest water level, so that adjustments due to tidal action need to be completed for final comparison.

4. DISCUSSION

The ERTS satellite image for the Little Bahama Bank shows features not present on the HO chart 5990 for the Northwest and Northeast Providence channels. This chart was revised in 1969 but it uses data from British surveys between 1836 and 1885 and U.S. Navy Surveys to 1963. There are indications of shifting currents being responsible for the build-up of sand shoals and the ERTS imagery supports that observation. It appears that sand build up over this bank indicates a potentially harmful condition which can eventually kill the protective coral bank to the "islands". Cutting shipping channels arbitrarily could change the sand deposition profile. This action will be investigated as part of the verification phase of the experiment.

5. SUMMARY

ERTS-1 data tapes from the MSS can be used for mapping shallow water features. It was demonstrated that depths can be calculated by ratio processing for those shallow depths that return a signal in both channels 4 and 5. By performing analysis of channel 4 data only, a more complete depth map can be made on a relative depth basis. However, if additional control points are known, and if the reflectances of bottom materials are taken into account, an absolute depth map can be made. Even without depth information, the satellite data is still useful because existence of shallow features are detectable and their geographical positions more accurately known than heretofore possible.

The economic benefits derived from the improvement of the world charts has been analyzed initially by Zissis et. al (Ref. 4). World $ losses of about one billion per year in shipping are estimated. Reduction in losses due to those factors that would be traceable to improved navigation charts amounts to several millions per year.

6. REFERENCES

1. F. C. Polcyn, W. Brown, and I. Sattinger, The Measurement of Water Depth by Remote Sensing Techniques (Final Report), Report No. 8973-26-F, Willow Run Laboratories of the Institute of Science and Technology, The University of Michigan, Ann Arbor, November 1970.
2. W. L. Brown, F. C. Polcyn, A. N. Sellman, and S. R. Stewart, Water-Depth Measurement by Wave Refraction and Multispectral Techniques, Report No. 31650-31-T, Willow Run Laboratories of the Institute of Science and Technology, The University of Michigan, Ann Arbor, August 1971.
3. O. E. Prewett, D. R. Lyzenga, F. C. Polcyn, and W. L. Brown, Techniques for Measuring Light Absorption, Scattering, and Particle Concentrations in Water, Report No. 190500-1-F, Environmental Research Institute of Michigan, Ann Arbor, March 1973.
4. G. J. Zissis, et. al, Design of a Study to Evaluate Benefits and Cost of Data from the First Earth Resources Technology Satellite (ERTS-A), Report No. 11215-1-F, Willow Run Laboratories of the Institute of Science and Technology, The University of Michigan, Ann Arbor, July 1972.

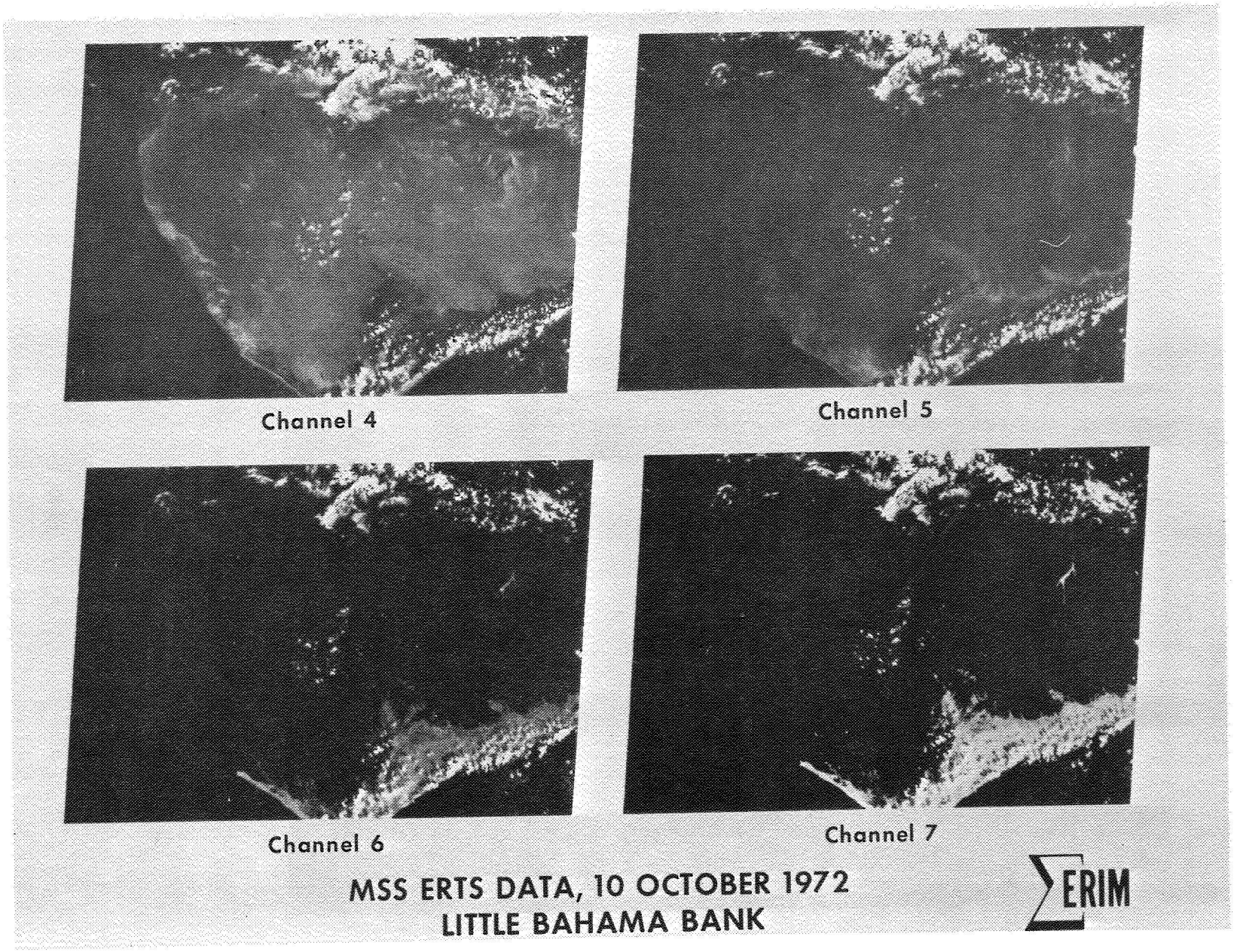

Channel 4
Channel 5
Channel 6
Channel 7
MSS ERTS DATA, 10 OCTOBER 1972
LITTLE BAHAMA BANK
ERIM

FIGURE 1

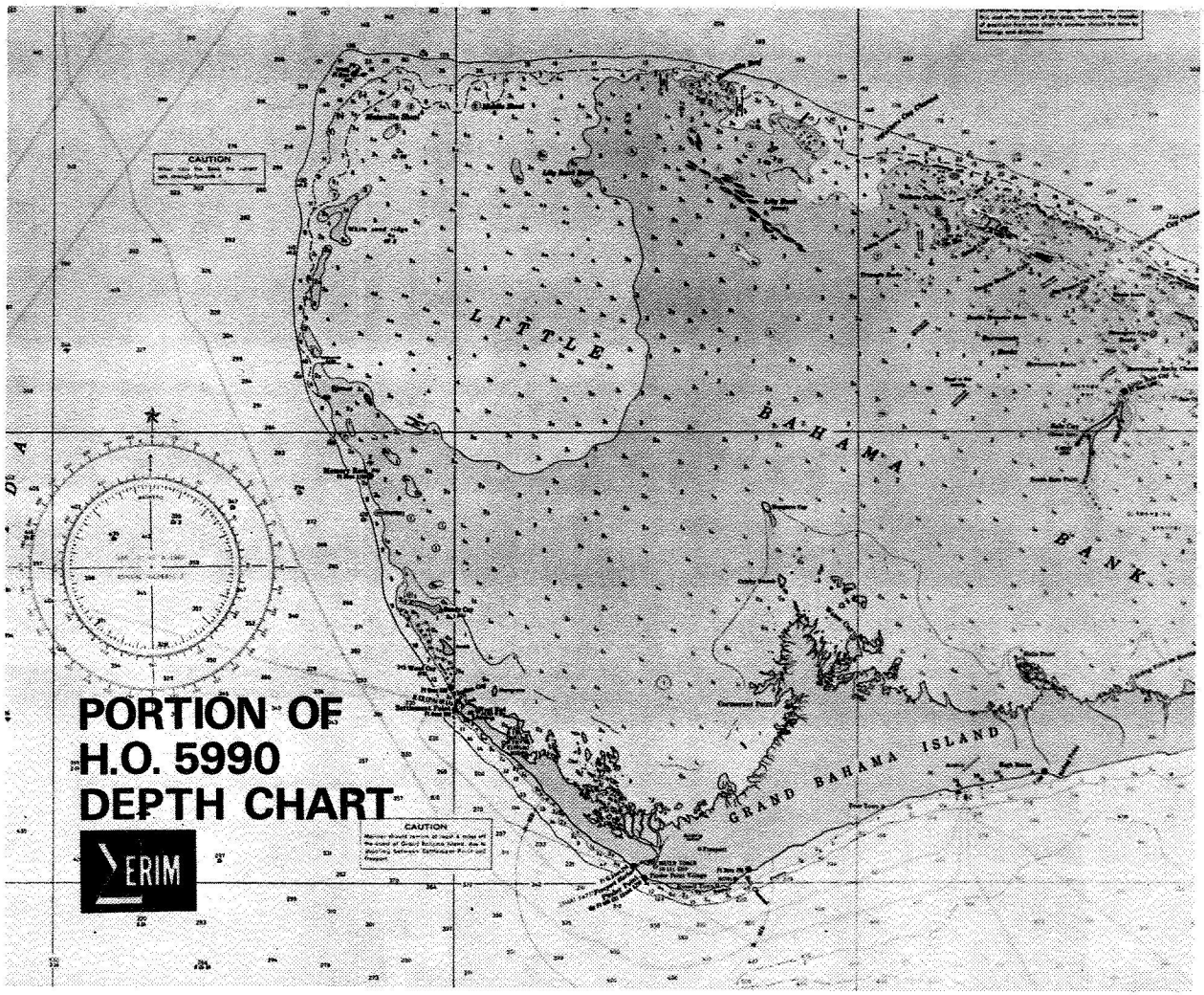

PORTION OF
H.O. 5990
DEPTH CHART
ERIM
LITTLE BAHAMA BANK
GRAND BAHAMA ISLAND
CAUTION

FIGURE 2

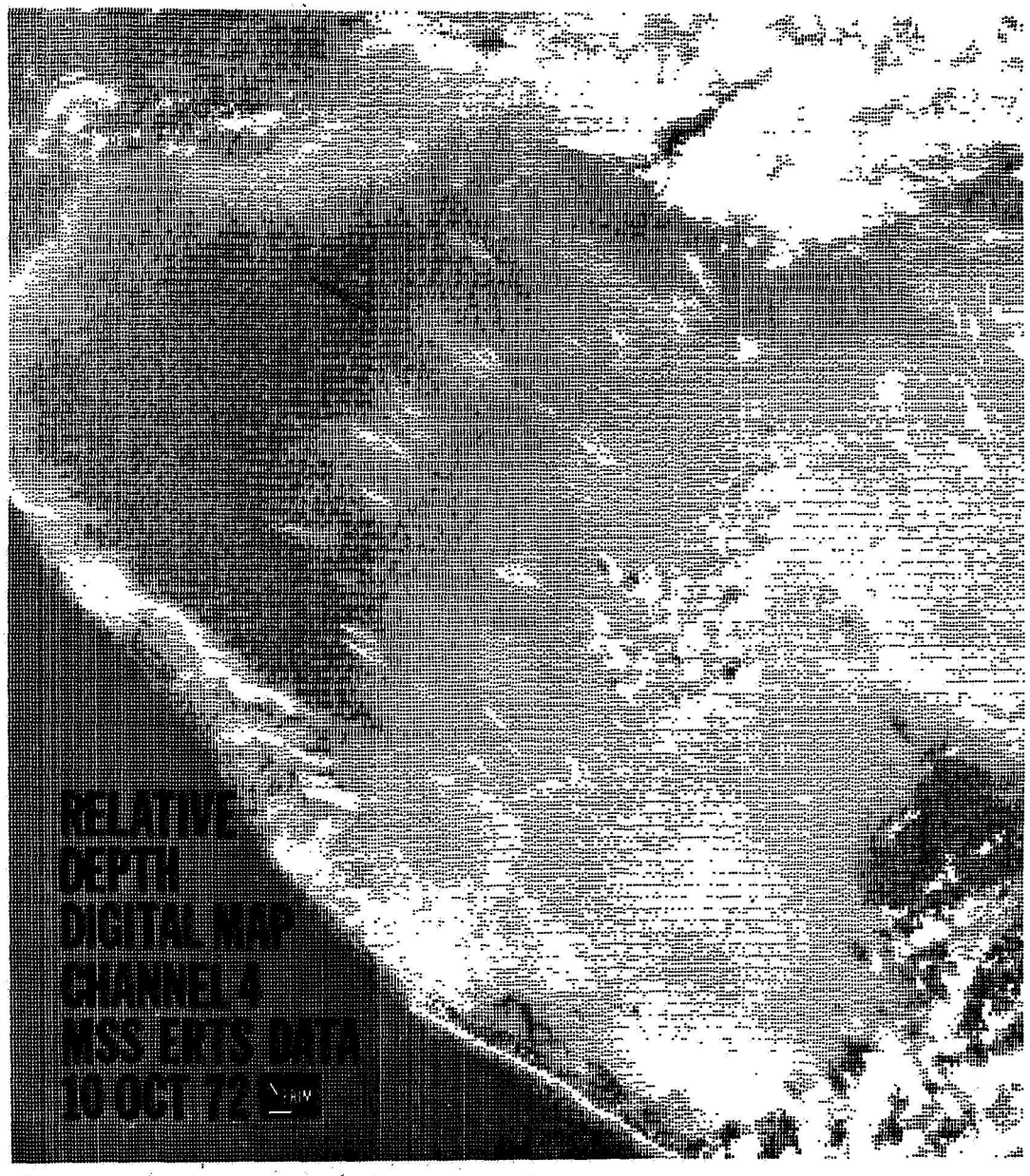


FIGURE 3

MULTIDISCIPLINARY/REGIONAL RESOURCE SURVEYS

N73-28359

Paper R 1

MULTIDISCIPLINARY APPLICATION OF ERTS-1 DATA TO NORTH CAROLINA NATURAL RESOURCE MANAGEMENT

Charles W. Welby, J. O. Lammi, Robert J. Carson, *North Carolina State University, Raleigh, North Carolina*

Introduction

That ERTS-1 imagery provides a synoptic view of a region is well understood. Conveying to planners, managers, and politicians a macroimage of the region in a dynamic mode, the imagery emphasizes the interrelations of cultural geography and physical geography together with the interdependence of many natural resource and environmental factors. Two examples of the use of ERTS-1 data are monitoring of man's activities affecting the forest resource and pinpointing sources of sediment load in streams and rivers.

Forest Resources

The forests of North Carolina provide the raw material for the state's third largest industry; planning for use and management of this natural resource requires a variety of information. It appears that ERTS-1 imagery can furnish important data about distribution of forest-cover types and about activities within the forested areas. Repetitive images from ERTS-1 allow resource managers to monitor changes in the forested areas. Examples of such changes are clear-cutting activities and expansion of urban and suburban developments into forested areas.

In North Carolina most forest harvesting is done by the clear-cutting method. Imagery enlarged to a scale of approximately 1:300,000 provides a spectacular display of bare lands and affords a method for rapidly taking inventory of the total clear-cut acreage in a given region. Furthermore, the repetitive coverage even if only at seasonal intervals, provides a method for monitoring this activity. In the absence of a permit system for cutting there is no other means of acquiring this type of information within reasonable economic and time constraints. Knowledge of the amount of clear-cutting activity going on is of great value to those concerned with forest resource management as well as to regional planners and others concerned with the broad aspects of the physical and economic well-being of North Carolina.

Original photography may be purchased from:
EROS Data Center
10th and Dakota Avenue
Sioux Falls, SD 57198

The MSS-5 imagery at an approximate scale of 1:300,000 was compared with 1:63,360 scale airphoto index sheets of the U. S. Agricultural Stabilization and Conservation Service. In the several forest areas studied openings of about five acres are clearly visible on the ERTS-1 imagery, and somewhat smaller cleared tracts can usually be recognized.

Although forests are usually regenerated either naturally or by planting immediately after harvest, many areas lie bare because of neglect or because of an intent to convert land to other uses such as agricultural or urban. Cleared areas are often subject to soil erosion and may be sources of sediment to streams, lakes and estuaries. Use of ERTS-1 imagery can help those charged with resource planning and management to keep abreast of rapid changes and to determine those places where their efforts and limited resources should be concentrated so as to accomplish their responsibilities most effectively.

Within an urban complex the expanding activities of man destroy much of the wooded area as the periphery of the city expands. In the vicinity of Raleigh, North Carolina, conversion of suburban forests to industrial, commercial, and non-wooded residential areas has been traced on ERTS-1 imagery. Within the older parts of the city the paucity of trees signifies changing land-use patterns and a general lowering of the quality of life for the residents.

Figure 1 (1045-15254-5; Sept. 7, 1972) illustrates the different types of wooded areas within the city of Raleigh and the extent of the wooded areas around the city. In the southeast quadrant (top of photograph is north) residential areas, indicated by the gray to black tones, are closely interspersed with commercial-industrial developments shown in white. In the north and northwest part of the city the residential areas are indicated by the dark tones associated with the trees. Lighter gray tones indicate less dense tree cover. Growth of the city north and northwestward is documented. The figure graphically shows the demolishing of the woodlands surrounding the city, and with a minimum of effort the major areas from which significant amounts of sediment are being eroded may be delineated. Some knowledge of cultural relationships in the area must be brought to bear in interpreting the various reflectances.

The relationship of the Uwharrie National Forest to the High Rock Lake-Badin Lake complex on the Yadkin River is shown in the lower righthand corner of Fig. 2 (Image 1046-15313-5; Sept. 7, 1972). The National Forest is represented by the dark tone near the edge of the picture and Badin Lake by the medium gray tone to the left (west) of it. Other forested areas (dark tones) and their geographical relationships to the works of man are also shown by this figure. The contrast between the open fields (light-colored) and the darker forested areas are clearly brought out. It is possible to gain a better appreciation

of the physical relationships of the various natural resources from this image than from a map and to view in perspective man's effect on the forest and water resources.

Sediment Pollution

Determination of suspended sediment load in rivers, lakes, and estuaries was early recognized as a possible use of ERTS-1 type data. The U. S. Geological Survey's network of gaging stations can provide some information about sediment load to streams and lakes; however, the synoptic view can be obtained only from high altitude photography or satellite imagery. Included in the synoptic view is the distribution of major sources of sediment. Some are point sources; others are tributaries to the major streams.

Images of two rivers and chains of reservoirs along them provide an opportunity to evaluate ERTS-1 imagery as a tool to monitor sediment sources as well as loads of sediment.

Figure 3 (1080-15201-5; Oct. 11, 1972) is part of the Buggs Island Lake-Lake Gaston-Roanoke Rapids Reservoir (west to east) chain of lakes on the Roanoke River at the North Carolina-Virginia border. Soils on the North Carolina side of the lakes are rated as moderately to severely erodible.

A three-day period of rain ending on October 6 preceded the pass of the satellite and produced the influx of sediment. The white in the lakes represent sediment plumes. Most of the sediment in the western end of Buggs Island Lake has come through the Roanoke River drainage system. Tributaries to the lake are also supplying sediment, pointing to areas where some consideration should be given to erosion control. Interestingly enough, the Nutbush Creek arm of the lake, which extends southward into North Carolina toward the city of Henderson, shows no sediment influx. This is a relationship which exists in other views of this area.

Downstream from Kerr Dam on Buggs Island Lake considerable sediment influx can be seen near the midpoint of Lake Gaston. Contributing drainage basins lie both north and south of the lake. Little or no sediment appears to have reached the Roanoke Rapids Reservoir.

Along the Yadkin River in central North Carolina a series of dams impound water for electrical power generation. An ERTS-1 image (1046-15313-5) of September 7, 1972, shows the sediment plume entering the uppermost of the lakes, High Rock Lake (Fig. 2). A three-day rain storm preceded the passage of the satellite. Suspended sediment in the Yadkin River measured at Yadkin College, about 25 miles up-

E

stream from High Rock Lake Dam, increased from 90 ppm on September 5 to 242 ppm on September 6 and decreased to 189 ppm on September 7. River discharge increased from 1,870 cfs on September 5 to 3,380 cfs on September 6 and decreased to 2,360 cfs on September 7. The plume is shown also on the band 6 imagery, although in this band it does not appear so extensive.

Along the course of the Yadkin River there are numerous light areas suggesting sediment sources. If the imagery were to be enlarged sufficiently,it might be possible to quantify the sediment input from these areas by densitometric methods. In addition the many fallow fields interspersed with the scattered wooded areas (dark) and covered fields (medium gray) are possible sources of sediments. Developed areas surrounding Winston-Salem are other possible sources.

Small light areas adjacent to Badin Lake, downstream from High Rock Lake, suggest possible sediment sources, but the areas adjacent to the lake are wooded, the east side of the lake being part of the Uwharrie National Forest, the top of which appears at the edge of the photograph.

In sharp contrast to the sediment influx into High Rock Lake is the apparent absence of a sediment load in Lake Norman, about 50 miles southeast of High Rock Lake. One part of the reason for the difference is probably the difference in land use upstream from the lake, along the Catawba River as well as adjacent to the lake. Most of the Catawba River is dammed, and immediately adjacent to the river wooded and grassed areas predominate. Along much of the Yadkin drainage the land is intensively used for both commercial and agricultural purposes.

Since many of man's major resource management activities are on a scale sufficiently large to be monitored by ERTS-type imagery, considerable cost economies over conventional data gathering seems possible. Land managers accustomed to working with large-scale air photos may belittle the utility of the ERTS imagery, both in terms of cost and available detail. However, our studies of the ERTS imagery suggest that ERTS-1 is not so much a way of acquiring detailed geological, hydrological, and biological data as a method of observing relationships between man and his natural resources. The benefit-cost evaluation is then one of the satellite system alone rather than in comparison with alternatives that do not really exist. We have attempted to show by our examples the utilitarian aspect of ERTS data in two natural resource management problems.

Conclusion

Although this paper has concentrated on only a few types of

natural resource phenomena which can be observed on the ERTS-1 imagery, the interrelationship of these with urbanization and intensity of land use can be seen. Certainly, critical areas requiring priority natural resource management action can be identified, and the updating of information about a region will prove valuable in effective planning and management of the natural resources.

Not to be lost in the concentration upon the potential usefulness of the information available on the ERTS-1 imagery for operational planning and management is the fact that the synoptic view shows to policy makers, whether elected or appointed, the possible effect of a given action or decision about one region or area upon adjacent regions or areas.

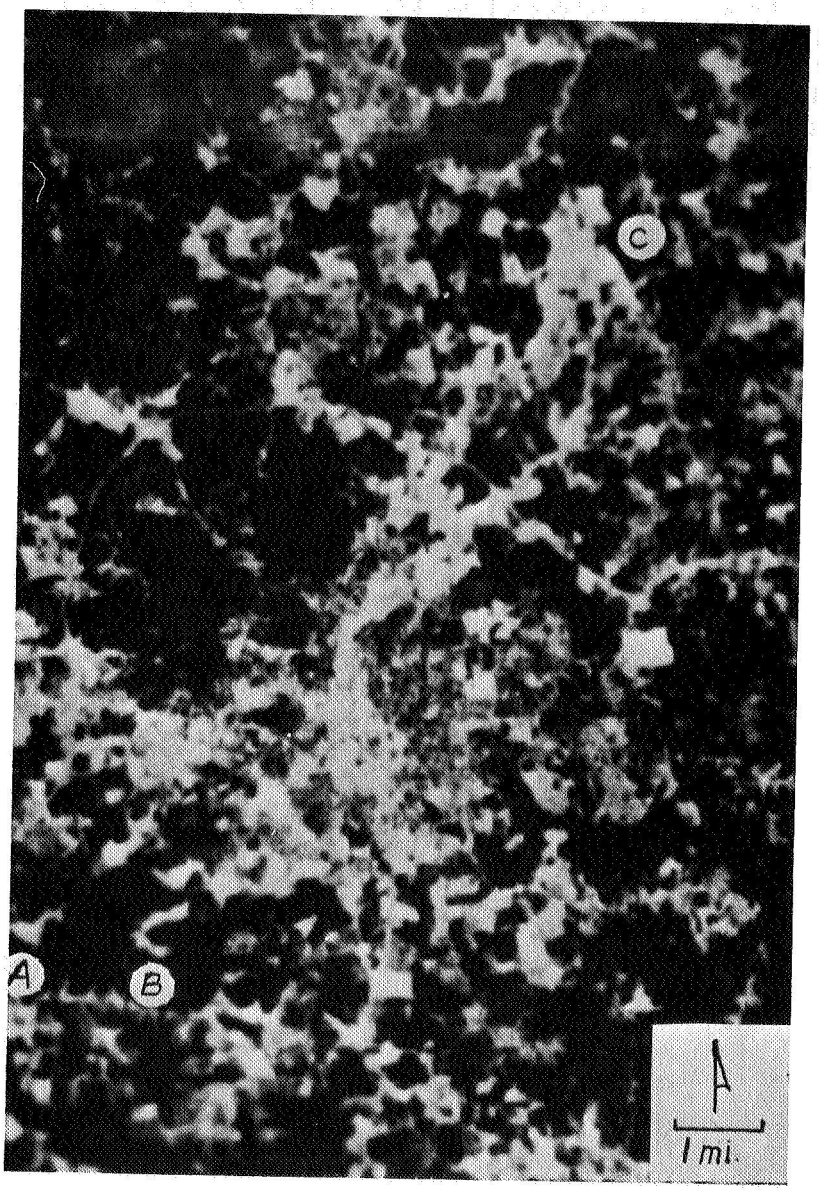


Fig. 1. Raleigh, N. C., showing the growth of the city into the surrounding wooded areas. Two highly silted water supply reservoirs (A and B) reflect in very light gray tones; developing residential-commercial area in the northeast quadrant (C). Image No. 1045-15254-5; Sept. 7, 1972

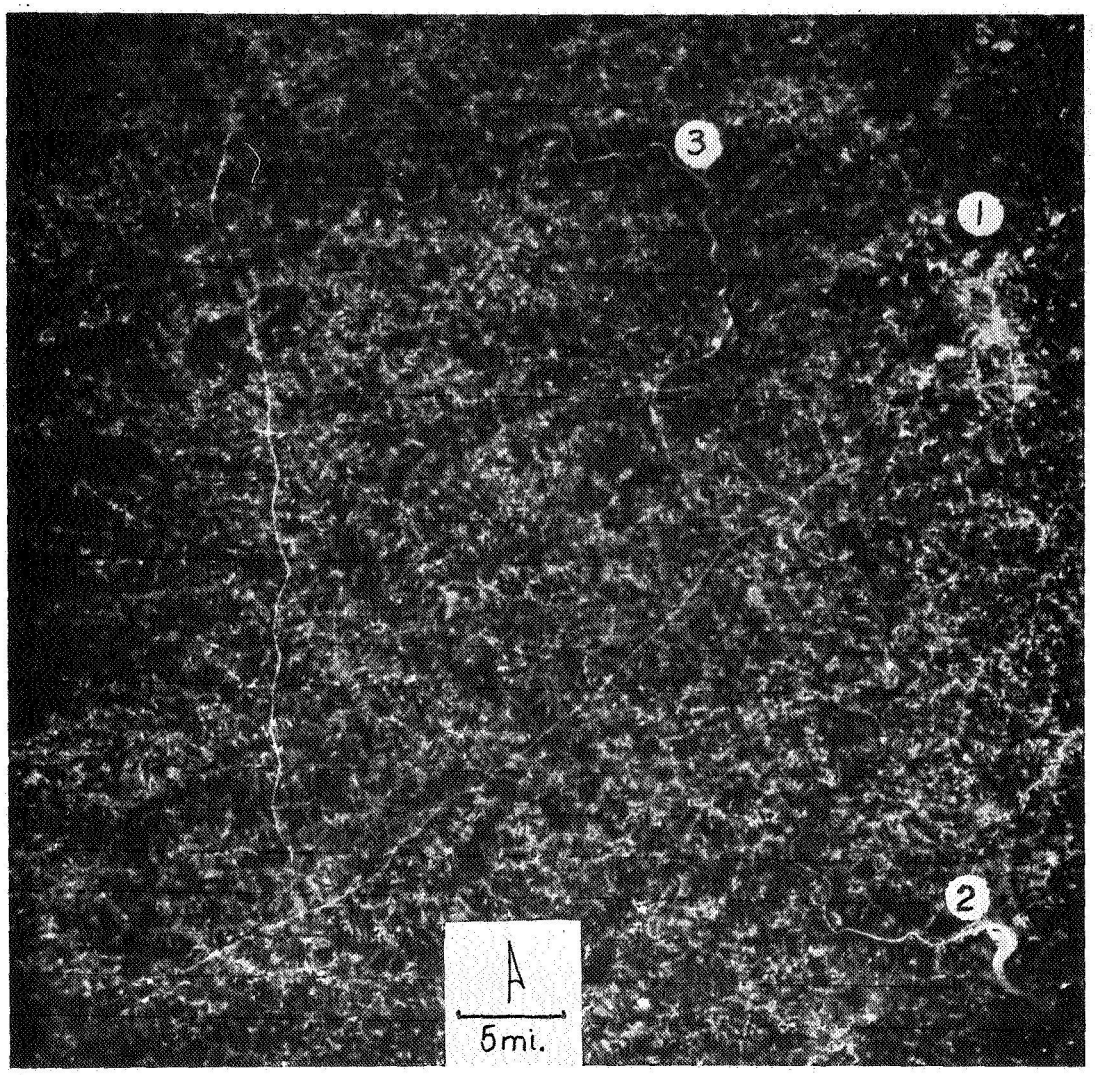


Fig. 2. Yadkin River and High Rock Dam Sediment Load. The light colored area is High Rock Lake following sediment influx from Yadkin River drainage basin. Uwharrie National Forest dark tones at edge of picture.
1. Winston-Salem 2. High Rock Lake 3. Yadkin River.
Image No. 1046-15313-5; Sept. 7, 1972

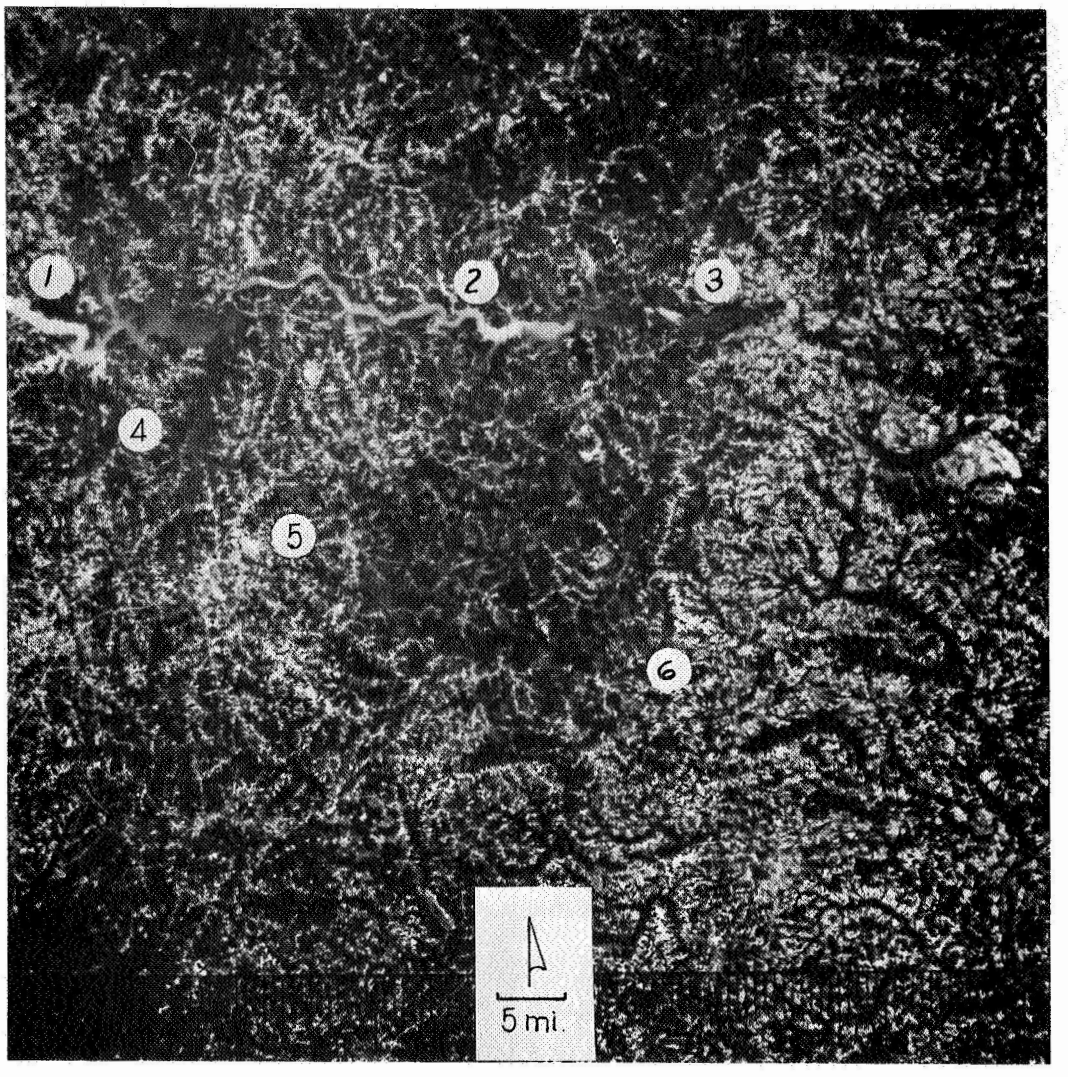


Fig. 3. Buggs Island Lake-Lake Gaston-Roanoke Rapids Lake. Sediment entering Buggs Island Lake appears as light tone.
1. Buggs Island Lake 2. Lake Gaston 3. Roanoke Rapids Reservoir 4. Nutbush Creek 5. Henderson, N. C.
6. Fall Line.
Image No. 1080-15201-5; Oct. 11, 1972

N73-28360

Paper R 2

NATURAL RESOURCE INVENTORY AND MONITORING IN OREGON WITH ERTS IMAGERY

G. H. Simonson, D. P. Paine, C. E. Poulton, R. D. Lawrence, J. H. Herzog, and R. J. Murray, *Oregon State University, Corvallis, Oregon*

ABSTRACT

Multidiscipline team interpretation of ERTS satellite and highflight imagery is providing resource and land use information needed for land use planning in Oregon. A coordinated inventory of geology, soil-landscapes, forest and range vegetation, and land use for Crook County, illustrates the value of this approach for broad area and state planning. Other applications include mapping fault zones, inventory of forest clearcut areas, location of forest insect damage, and monitoring irrigation development. Computer classification is being developed for use in conjunction with visual interpretation.

1. INTRODUCTION

Land use planning is receiving high priority attention at state and local levels in Oregon. ERTS imagery has the potential to provide much resource data urgently needed in the planning process throughout the state.

Rapid population growth and accelerating urban, industrial and recreational development are placing unprecedented demands on the fixed amount of land resources available. Conflicting land uses and speculative land conversions are leading to an increased recognition of potential problems and the need for long range planning.

Problems of growth and attendant pressures on the fixed land resource are common to some degree in most states. The situation in Oregon is similar to that of other Western states. Mountainous terrain, wide variations in climate, intermingled public and private land ownership, varied land use and highly variable population densities characterize much of the Western region. Inadequate planning for land use and urban expansion has contributed to the problems apparent in rapidly urbanizing regions such as the Los Angeles Basin, and could lead to similar problems for the Willamette Valley in Oregon. Extensive and largely uncontrolled speculative growth of recreation subdivisions in remote areas is adversely affecting open space attributes over wide areas of the West.

Oregon exemplifies much of the West in its stage of development and is an excellent test area. The very fact that much open space remains, often in attractive surroundings, is creating demands on land that threaten to diminish quality of environment and liveability in the state. Oregon citizens are becoming aware that direction and control of land development is needed to achieve a balance between economic growth and environmental quality. Land use planning in all counties is required by recent legislation and will be further strengthened through current legislative proposals for state wide standards.

Original photography may be purchased from:
EROS Data Center
10th and Dakota Avenue
Sioux Falls, SD 57198

2. PURPOSE OF THE STUDY

The Oregon ERTS project is directed toward applications in land use planning. Present planning efforts in the state although commendable, are often based on inadequate, incomplete and sometimes outdated land resource information. Our primary objective is to demonstrate the usefulness of ERTS imagery in compiling and presenting a coordinated resource and land use information base for land use planning. We are utilizing multiple-discipline team interpretation of ERTS satellite and high flight imagery, and ground truth to provide planners with a current, comprehensive inventory of range and forest vegetation, soils, geology, water areas and land use. The resource information is compiled on ERTS imagery for working with local planners to analyze and assess applications and methods of presentation for land use planning.

3. APPROACH

ERTS imagery for all of Oregon is given a quick-look analysis for information content and usefullness. However, we are doing a comprehensive pilot study of land use planning applications in only one county at present. Crook County in Central Oregon was selected for an in-depth study because land use planning there is just beginning, the county has an active interest in obtaining resource information; county boundaries largely coincide with a major watershed, and the area is representative of much of Oregon east of the Cascade Mountains. The county has a varied terrain of rangeland, forested mountains and irrigated valleys. The population is relatively low and Prineville is the major town. Ranching, forest products, farming and recreation are the major enterprises.

Most of our work to date has been in generalized mapping of the resources and land use through ERTS image interpretation, on-the-ground observations, and existing resource information. Black and white prints of MSS, band 5 imagery at 1:1,000,000 scale were initially used. Recently we have been able to start work with color-reconstituted transparencies of bands 4-5-6 and 4-5-7, and enlargements of band 5 at a scale of 1:250,000.NASA highflight photography at 1:120,000 and larger scales is being used in conjunction with ground truth observations, and will be used later in multistage sampling experiments of forest inventory and larger scale analysis of resources.

4. RESULTS

Generalized maps of Crook County showing geology, soil-landscapes, vegetation and land use, and timber density are illustrated in Figure 1 to 4. Abbreviated explanatory legends for the map symbols are appended. Figure 5 shows the geographic distribution of several land resource units defined by a high degree of similarity in resource and land use characteristics as determined from the individual resource maps. These maps are drawn on ERTS color-reconstituted, 1:1,000,000 scale imagery and constitute a broad, synoptic picture of the terrain, land uses, and resources of the country.

The individual resource maps of Crook County (Figures 1 to 4) show 12 soil-landscape units, 8 geologic divisions, 17 vegetation and land use units, and 5 classes of timber density. Surface water areas show on several of the maps. Overlaying these maps provide an ideal mechanism for informed, rational solution of specific land use problems.

The five combined land resource units delineated as examples in Figure 5 have the following general characteristics:

1. Nearly level to gently sloping alluvial flood plains and terraces with deep, well-drained medium textured soils. Minor poorly drained soils may be alkaline. Soils on terraces may be moderately deep to indurated hardpans. This land is used for irrigated cropland, meadowland, and homesites.
2. Nearly level to gently rolling, lightly dissected volcanic plains with vegetation types including low sagebrush, big sagebrush and sagebrush-juniper on shallow and very shallow, stony and very stony soils, mostly with clayey subsoils. This land is used for grazing and wildlife habitat.
3. Hilly, mixed volcanic, juniper-sagebrush uplands with moderately deep, clayey soils. This land is used for grazing, wildlife habitat and recreation.
4. Steeply sloping mountainous, mixed volcanic terrain with open Ponderosa pine and scattered occurrence of other conifers, on moderately deep, medium and fine textured soils. This land is used for commercial timber, summer grazing, wildlife habitat and recreation.
5. Strongly dissected lava plateaus with low sagebrush on scablands and open Ponderosa pine in the draws. The soils are very shallow and very stony in scabland areas, with moderately deep, medium textured soils on north slopes. This land is used for grazing, wildlife habitat and recreation.

About 12 to 15 of these land resource units are needed to adequately characterize Crook County at this level of generalization. Many of the same units would have wide extent on a state map.

Information shown at this scale and level of generalization is helpful in developing an overview and general understanding of the resources, potentials and problem areas of a county. Information presented on ERTS imagery at this small scale appears to be most appropriate for general planning at state or regional levels. County level and local area planning generally requires more detailed information but the support high-flight imagery is ideal for determining and presenting these higher levels of detail in selected problem areas. ERTS imagery enlarged to a scale of 1:250,000 is well suited for mapping resource and land use information with a degree of generalization useful for broad planning at the county level. Assessment of ERTS imagery in consultation with county planners has supported these preliminary judgments.

5. OTHER APPLICATIONS

Several significant uses of ERTS imagery in land use and resource inventory and monitoring have been demonstrated in other parts of Oregon. The alignment and distribution of faults in much of south-central Oregon has been mapped at 1:1,000,000 on ERTS, band 5 and color reconstituted bands 4,5, and 6. These are shown for the Deschutes Basin on Figure 6. Similar mapping on high flight imagery shows a slight increase in detail, but with very serious geometric fidelity loss. The area is dominated by the west end of the Brothers Fault Zone which crosses the figure just above the Newberry scarp. The juvenile character of this zone is shown by the lack of a single integrated break and by the crossing of the Green Ridge Fault by extensions of this zone. Green Ridge faulting is dated at 2 to 4 million years ago. This relation is not clear on high flight imagery.

Different MSS band combinations and a variation in intensity level in color reconsitutions of ERTS imagery show advantages in identifying delineating, and seasonal monitoring of various vegetation types. For example, bands 4,5,7 seem best for identifying juniper woodland. Bands 4,5,6 appear to be most sensitive for picking up the initial flush of green growth of annual grasses and winter grains. The contrast between dry grasslands and shrub-steppe vegetation is apparently very strongly enhanced by the combination of bands 4,5 and half power 7.

Forest clearcut areas are easily seen and mapped on 1:1,000,000 scale ERTS imagery. Examination of color reconstituted frames indicates that clearcut areas can be visually stratified by age to some degree from the ERTS imagery. Computer classification has been successful for delineating clearcut areas from digital data and will greatly increase capability to discriminate age differences. Tussock moth damage is spreading rapidly in forests of Eastern Oregon. Algoriths are in an intermediate stage of development for detecting forest areas experiencing this insect infestation from digital data.

Irrigation development is rapidly expanding along the Eastern Oregon-Washington border near the Columbia River. ERTS imagery has provided the first up to date and accurate record of this development. Satellite imagery is an excellent means of measuring the extent and rate of increase of this important change in land use.

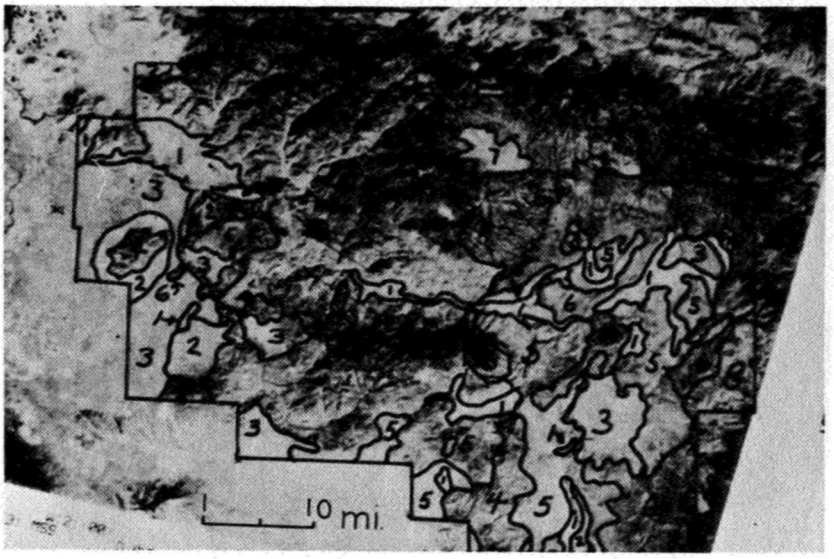


Figure 1. Geology of Crook County, Oregon, showing 8 units.
ERTS frame 1076-18211--4, 5, 6

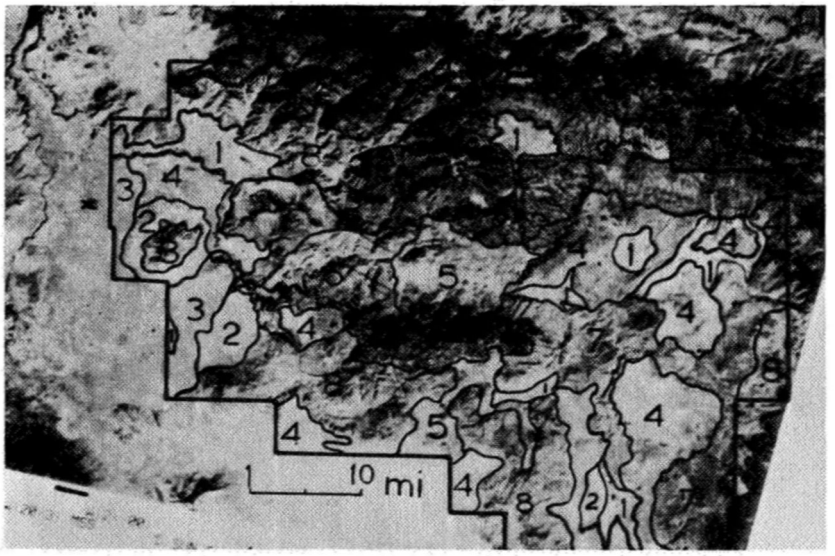


Figure 2. Soil-landscapes in Crook County, Oregon, showing 12 classes.
ERTS frame 1076-18211--4, 5, 6

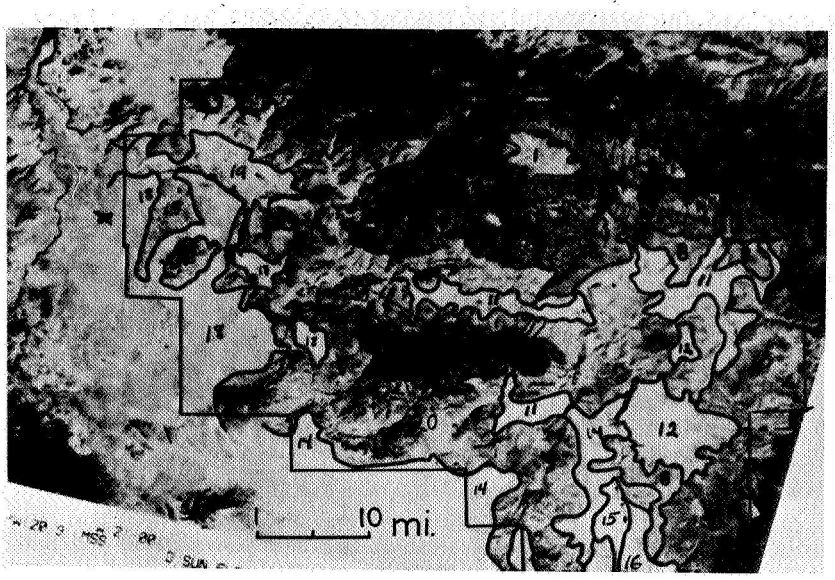


Figure 3. Vegetation and land-use in Crook County, Oregon, showing 17 classes. ERTS frame 1076-18211--4, 5, 6

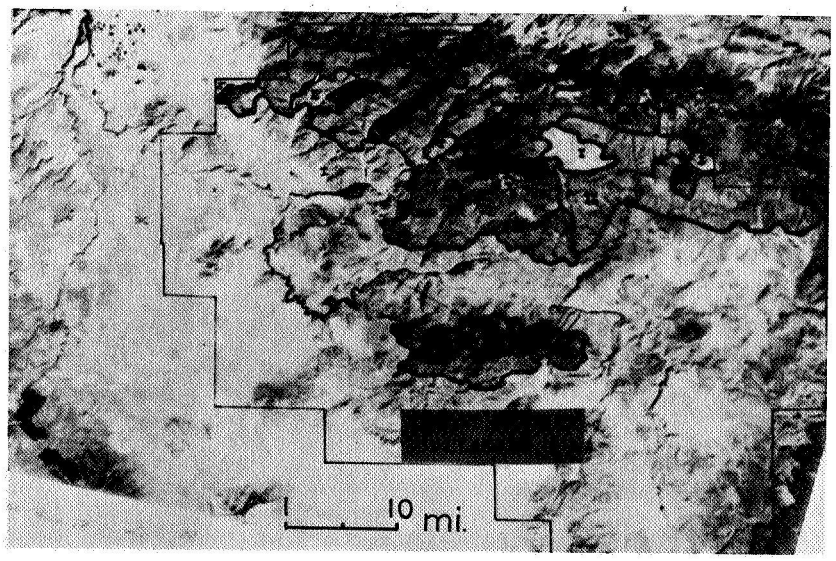


Figure 4. Forest density types in Crook County, Oregon, showing 5 classes. ERTS frame 1076-18211--4, 5, 6

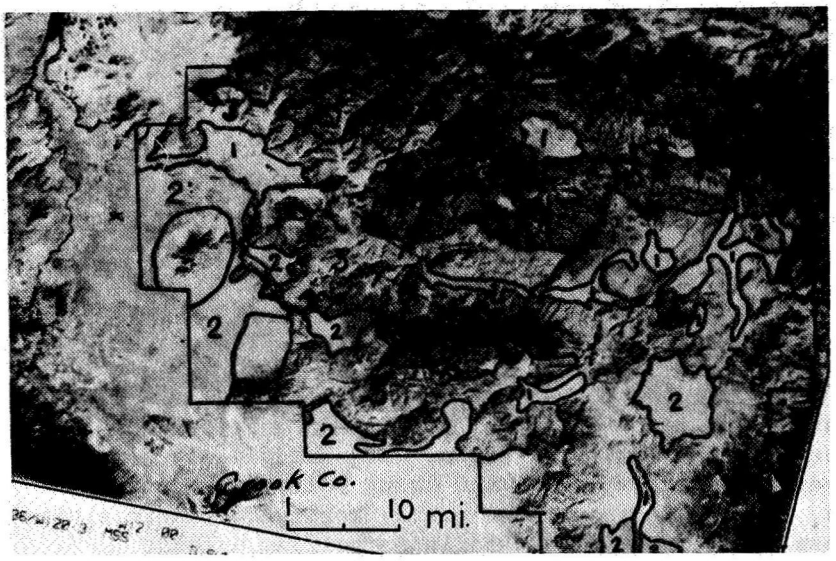


Figure 5. Land resource units for Crook County, Oregon, showing 5 classes. ERTS frame 1076-18211--4, 5, 6 (partial classification shown)

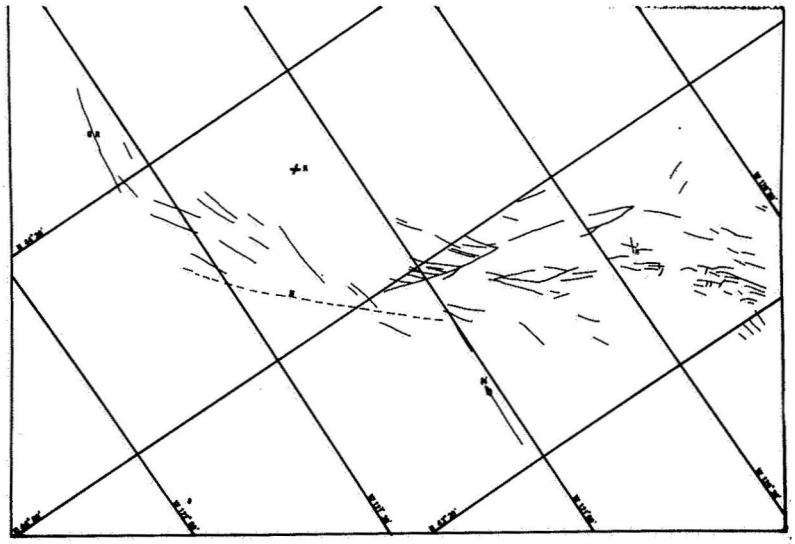


Figure 6. Fault pattern of the upper Deschutes Basin, Oregon.

APPENDIX

Abbreviated Legends for Figures 1 through 4, delineated on ERTS Imagery at 1:1,000,000 scale.

Figure 1. Geology

1. Alluvium and unconsolidated terrace materials
2. Unconsolidated fan gravels
3. Rim basalts, resistant plateau formers
4. Silicic to andesitic, shallow intrusions and domes
5. Weakly consolidated tuffs and tuffaceous sediments
6. Columbia River basalts - resistant bedrock
7. Clarno and John Day Formations, weak, easily eroded bedrock
8. Paleozoic and Mesozoic rocks, mixed bedrock types

Figure 2. Soil-Landscape Units

1. Deep, silty and loamy soils on floodplains and terraces
2. Mod. deep and shallow loamy soils, with hardpan, on alluvial fans
3. Mod. deep and shallow, sandy and loamy soils on lava flows
4. Shallow, stony, loamy soils on gently rolling volcanic plains
5. Mod. deep and shallow clayey soils in rolling uplands
6. Shallow and mod. deep clayey soils and rock, in steeply rolling upland
7. Shallow and very shallow, stony soils, in dissected, rolling uplands
8. Shallow stony soils and mod. deep loamy soils in steeply rolling upland
9. Very shallow stony soils on level to rolling lava plateaus; interspersed with mod. deep, loamy soils on north slopes
10. Mod. deep, loamy and clayey soils in steeply rolling mountains
11. Mod. deep and deep loamy soils, on north slopes, above 4500 ft. elev.
12. Shallow stony soils and cliffs, in major canyons

Figure 3. Vegetation and Land Use Classes

1. Meadows
2. Low Sagebrush/Ponderosa pine
3. Ponderosa pine/Low Sagebrush
4. Ponderosa pine
5. Meadow/Low Sagebrush/Douglas-fir
6. True Fir and Mixed Conifer Types
7. Ponderosa pine/Juniper
8. Low Sagebrush/Big Sagebrush
10. Big Sagebrush/Low Sagebrush
11. Big Sagebrush/Cover Crops
12. Low Sagebrush
14. Tall Sagebrush
15. Rangeland Seedings/Cover Crops/Greasewood
16. Tall Sagebrush
18. Western Juniper
19. Cover Crops
20. Juniper/Low Sagebrush/Tall Sagebrush

Figure 4. Forest Density-Type Classes

1. Less than 10% stocked with commercial trees, or nonstocked
2. Poorly stocked - mostly Ponderosa pine
3. Poor to medium stocked - mixed larch and Ponderosa pine
4. Medium to well stocked - Douglas-fir, larch and true fir
5. Very well stocked - mostly true fir on north facing slopes

N73-28361

Paper R 3

RESOURCE MANAGEMENT IMPLICATIONS OF ERTS-1 DATA TO OHIO

David C. Sweet and Terry L. Wells, *State of Ohio, Department of Economic and Community Development* and George E. Wukelic, *Battelle Columbus Laboratories*

ABSTRACT

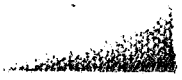
Initial experimental analysis of ERTS-1 imagery has demonstrated that remote sensing from space is a means of delineating and inventorying Ohio's strip-mined areas, detecting power-plant smoke plumes, and providing the data necessary for periodically compiling land-use maps for the entire state. This paper summarizes the nature and extent of these problems throughout Ohio, illustrates how ERTS data can contribute to their solution, and estimates the long-term significance of these initial findings to overall resource management interests in Ohio.

1. INTRODUCTION

NASA has provided the State Government of Ohio, on behalf of a number of its agencies* and assisted by Battelle Memorial Institute's Columbus Laboratories, with the opportunity to participate in the ERTS-1 program as a multidisciplinary user-investigator concerned with evaluating the state resource management implications of ERTS-1 data. This symposium has been organized to publicize significant results thus far obtained from ERTS-1. In this connection I would like to report first on what we feel is our most significant result to date. This is the swiftness with which remote sensing from space has captured the interest and confidence of potential state and local user groups, in spite of their limited previous experience in applying remote sensing technology. Moreover, significant progress toward demonstrating state-level utility has occurred. However, state needs for larger scale imagery and thermal infrared data for many applications are much in evidence. While in many cases our application findings and potential benefits are not directly translatable to other states, we nonetheless feel confident that the promise of ERTS will spread throughout the nation, insuring adequate user support for continuing orbital survey missions.

* Department of Economic and Community Development (Lead Agency)
Department of Natural Resources
Department of Transportation
Ohio Environmental Protection Agency

Original photography may be purchased from:
EROS Data Center
10th and Dakota Avenue
Sioux Falls, SD 57198



F

2. PRELIMINARY RESULTS

Although clouds have been a continuing problem, usable ERTS MSS imagery has been acquired for almost the entire state. However, the current availability of usable repetitive data is limited to portions of eastern Ohio. For imagery analysis and interpretation we are utilizing manual electro-optical image analysis techniques (multispectral and density/color viewers). These have been equally effective in visually demonstrating ERTS potentialities, accommodating real-time problem solving exercises involving technical and planning specialists, and generating sample ERTS data application products for subsequent utility assessment. The status of and state interest in our analytical program efforts are briefly summarized in Table I. Further discussion is limited to areas wherein ERTS data utility has definitely been demonstrated.

TABLE I. STATUS OF MAJOR ERTS DATA APPLICATION CANDIDATES UNDER EXAMINATION IN OHIO

Application Area	State Need	Potential State Value
	Utility Feasibility Demonstrated	
Strip mining	> 1/4 million acres affected	Help implement 1972 strip-mine law
Land use	Multiagency priority problem	Provide periodic statewide views of major land-use changes
Air quality	New Ohio EPA interest	Test computer model
Mapping	Current maps needed at all agency levels	Prepare photo base maps
	Utility Feasibility Under Study	
Sanitary land fills	> 1,400 illegal sites estimated	Detect illegal and/or new sites
Flood plains	50 % of Ohio cities subject to flood damage	Help define and enforce statewide regulatory law
Outdoor recreation	50 state parks exist--major expansion program underway	Help select new sites
Lake Erie	Unusual high water level posing severe erosion and flood hazard problems	Support Operation Foresight

A. Strip-Mine Reclamation Planning and Monitoring Implications

In April 1972, responding to overwhelming public sentiment, the Ohio Legislature passed legislation placing very stringent controls on strip mining in the state. This law places many new reclamation requirements on the operator, requires extensive preplanning of strip-mine operations, and gives the state the power to deny licenses to strip mine under certain conditions. The implementation of this law is a tremendous task which as yet hasn't been totally effected.

The state anticipates that ERTS data will prove useful in several ways in implementing the law. Initially, there is a need for an inventory and map of all strip-mined land to support reclamation planning activities, as an accurate and recent inventory in a readily available form does not exist. Information is especially scanty on land stripped before 1948, when Ohio passed its first strip-mine legislation.

As can be seen in Figure 1, ERTS photography is quite responsive to detecting surface-mining operations and reclamation efforts. This ERTS-1 scene of southeastern Ohio taken on August 21, 1972, shows an 8-mile long strip-mined area in which the Big Muskie is operating. Ground truth confirms that the dark square in the center of the stripped area was the location of the Big Muskie at the time. Figure 2 illustrates how well ERTS strip-mine imagery compares with aircraft photography. This photo shows a very small strip-mined area near Zaleski, Ohio. The satellite imagery has been magnified over 140 times to match the 1:24,000 scale routinely used in planning and map preparation.

With the ability to identify strip-mined areas established, an attempt was made to inventory and map the strip-mined areas of one Ohio county. Figures 3 and 4 show the distribution of stripped and unreclaimed land for Harrison County as displayed in an 32-color viewer enlargement of ERTS-1 MSS band 5 imagery. Area calculations correspond quite favorably to Department of Natural Resources (DNR) data. ERTS-1 data showed a total stripped acreage of 18.4 percent (or 47,472 acres) as compared to 19.01 percent (or 49,064 acres) for DNR. For unreclaimed acreage the figures were 6.2 percent for ERTS-1 and 6.8 percent for DNR. Comparison with aircraft data and on-site visitations are planned to further substantiate the accuracy of the inventory before proceeding with a 23 county survey of strip-mined areas in southeastern Ohio.

The current effort is to determine the extent to which ERTS multidate data can aid in enforcing the reclamation provisions of the strip-mine law. Under the law a strip-mine operator is required to commence backfilling, grading, and resoiling within three months after removal of overburden. Planting of vegetation must take place no later than the next appropriate season. With present ERTS resolution capabilities, it is doubtful that backfilling efforts can be monitored to the extent

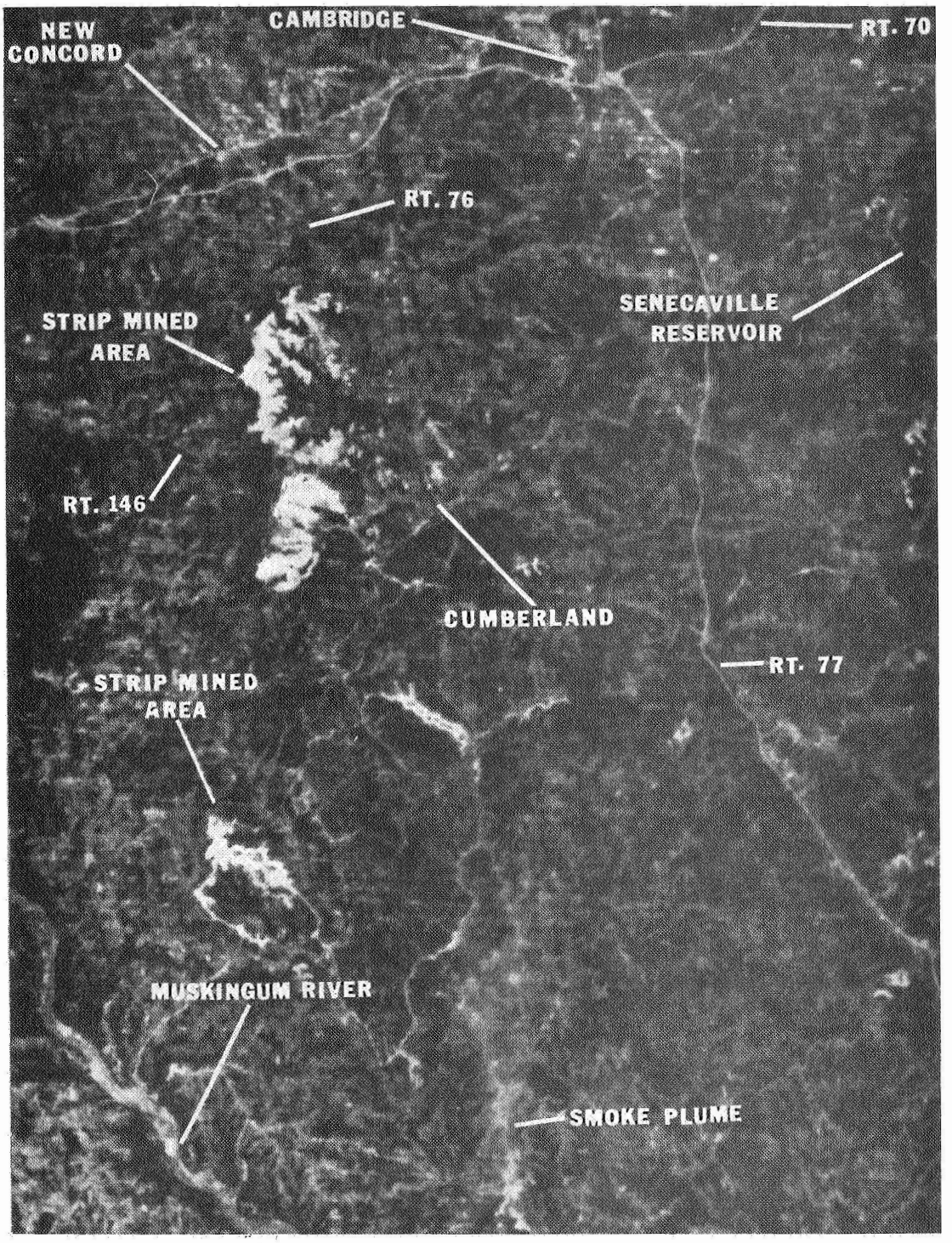


Fig. 1. Enlargement of ERTS MSS Band 5 Imagery (21 Aug 72) Showing Ohio Strip-Mine Areas.

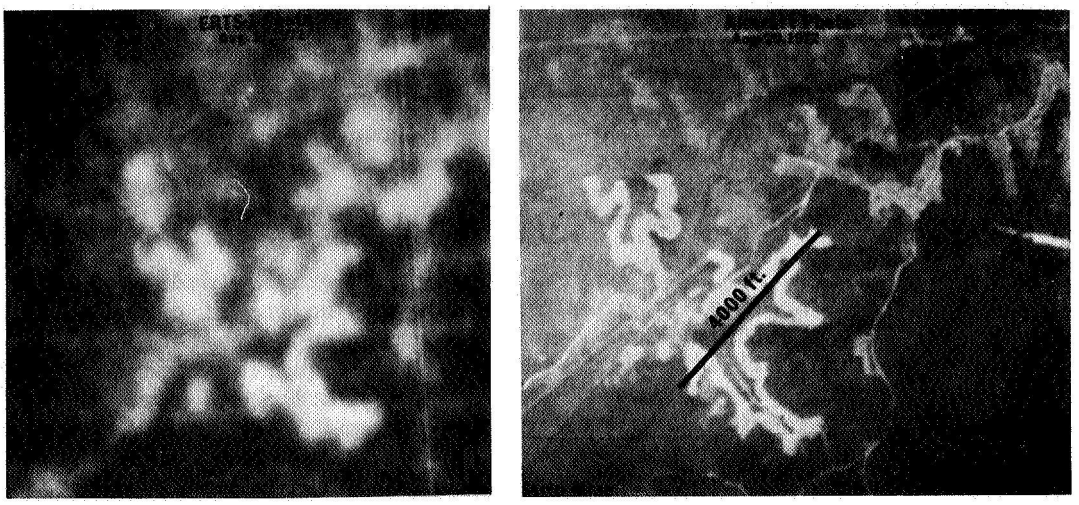


Figure 2. Comparison of ERTS-1 and Aircraft Photos of Strip-Mine Area Near Zaleski, Ohio. (Comparison Made at a Scale of 1:24,000.)

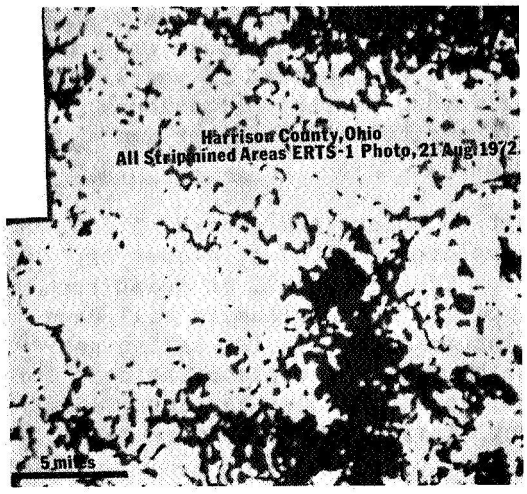


Fig. 3. Black Areas Represent Total Strip-Mined Areas of Harrison County, Ohio. (ERTS Imagery as Displayed on 32-Color Viewer.)

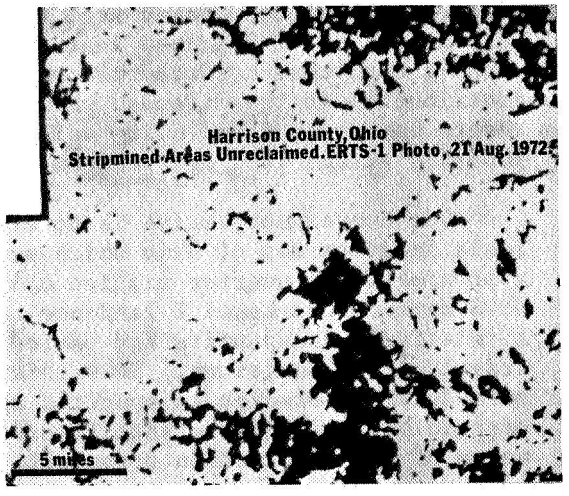


Fig. 4. Black Areas Represent Unreclaimed Strip-Mine Areas of Harrison County, Ohio. (ERTS Imagery as Displayed on 32-Color Viewer.)

necessary for regulatory purposes. However, ERTS data will be useful in determining if lasting reclamation has been accomplished. In many cases the initial vegetative cover appears healthy at first, but after several years a change in hydrologic conditions may cause acid water to reappear and destroy the vegetation. This capability will permit more accurate judgments in issuing permits and releasing bonds posted by strip-mine operators.

B. State Land-Use Planning Implications

Support for a national land-use policy has grown steadily stronger and indications are that Congress will soon act on one of the several land-use bills presently under consideration. One of the common features of these bills is that states will be required as part of their land-use planning process to include "the preparation and continuing revision of a statewide inventory of the land and natural resources of the State". This is one area in which orbital survey data will help multiagency efforts in Ohio. Specifically, ERTS imagery will provide a current and comprehensive data base illustrating the inter-relationships of static and dynamic natural and cultural surface features.

Thus far we have established that mapping of natural and cultural features from ERTS imagery can be done with confidence to scales of larger than 1:125,000. Figure 5 provides examples of our pilot land-use mapping efforts in the over 500 square mile Columbus/Franklin County area. These scenes, taken from the Spatial Data 32-color viewer, show the various major land-use features discernible: total urban coverage, urban growth that has occurred principally over the last 12 years, and distribution of tree stands, parks, and woods. Aerial photo index sheets have been found quite valuable in verifying the extent and geometry of the land-use patterns generated.

Our current objective is to attempt to update the general 1:500,000 scale land-use map of Ohio which was completed in 1967 at a cost of approximately a quarter million dollars. If successful, at least for USGS recommended Level I land-use categories, state planners will have a relatively inexpensive and periodic information base for making general land-use decisions. This information will not replace the need for more detailed studies in specific areas; and therefore, any improvement of resolution in future satellite survey missions will increase the value of the information provided.

C. Environmental Quality Implications

An Ohio Environmental Protection Agency was established in October 1972 to consolidate environmental quality protection activities in Ohio. It has prepared the implementation plan required by the Federal Clean Air Act to meet standards set by the Federal EPA. As part of this plan,

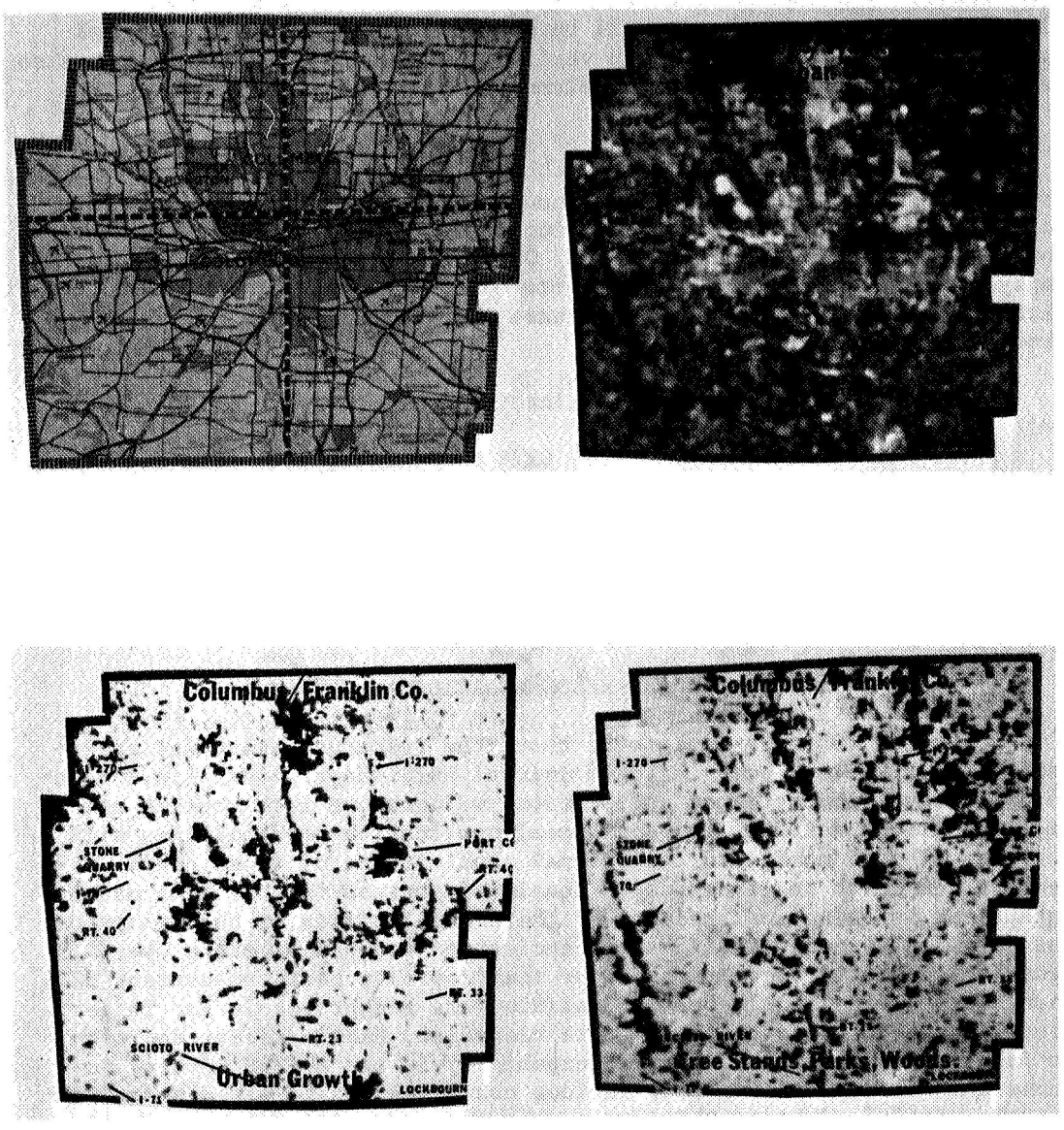


Figure 5. Illustrations of Urbanized Land-Use Features Discernible on ERTS-1 Photography.

officials are required to establish emission limitations for all significant state pollution sources. In an effort to determine the effect of pollution sources on air quality, the state has developed an air movement model. The demonstrated ability of ERTS to detect major smoke plumes on a repetitive basis will be utilized in combination with meteorological data to evaluate and verify this model. ERTS imagey may also reveal the extent to which smoke plume confluence is occurring.

Although the prime interests of state EPA personnel generally associate with thermal infrared data (unfortunately unavailable from ERTS-1), some preliminary assessments have been made as to the utility of ERTS for detecting illegal and/or selecting new sanitary landfill sites and monitoring Lake Erie sedimentation. Ohio EPA interest and confidence in applying remote sensing technology are manifest in a grant request submitted to enable the agency to purchase and operate a fully equipped remote sensing aircraft.

D. Mapping Implications

Enlargements of bulk processed ERTS MSS imagery have been found to match very closely most standard map scales in common use in Ohio. The resource management implications from the standpoint of preparing up-to-date thematic maps are obvious. Currently, 1:250,000 mosaics of Ohio in two MSS bands (5 and 7) are being prepared by the Department of Transportation. These mosaics will serve as photo base maps for state transportation research and planning.

3. SUMMARY AND RECOMMENDATIONS

Obviously, Ohio is optimistic about the resource management application opportunities emerging from initial ERTS imagery analysis. Hopefully, several demonstrated applications will mature into routine statewide planning functions, and additional application possibilities will surface. The economic and operational implications of these early results remain to be determined. Equally important is that some user enthusiasm is being lost because of the unavailability of thermal infrared data. Also, many application candidates proposed by state user agencies but found to be marginal or inappropriate based on current ERTS data capabilities, could become feasible were higher resolution imagery provided. Accordingly, from a state viewpoint, NASA's recent decision to incorporate a thermal infrared capability in the ERTS-B mission is sound and we suggest also that serious consideration be given to modifying the mostly redundant RBV into a system for providing larger scale imagery on a repetitive but longer term basis.

N73-28362

Paper R 4

ASSESSMENT OF SOUTHERN CALIFORNIA ENVIRONMENT FROM ERTS-1

Leonard W. Bowden and James H. Viellenave, *Department of Geography, University of California, Riverside, California 92502*

ABSTRACT

ERTS-1 imagery is a useful source of data for evaluation of earth resources in Southern California. The improving quality of ERTS-1 imagery, and our increasing ability to enhance the imagery has resulted in studies of a variety of phenomena in several Southern California environments. These investigations have produced several significant results of varying detail. They include the detection and identification of macro-scale tectonic and vegetational patterns, as well as detailed analysis of urban and agricultural processes. The sequential nature of ERTS-1 imagery has allowed these studies to monitor significant changes in the environment. In addition, some preliminary work has begun directed toward assessing the impacts of expanding recreation, agriculture and urbanization into the fragile desert environment. Refinement of enhancement and mapping techniques and more intensive analysis of ERTS-1 imagery should lead to a greater capability to extract detailed information for more precise evaluations and more accurate monitoring of earth resources in Southern California.

1. INTRODUCTION

The research effort at the University of California, Riverside has consisted of attempts to determine the value of ERTS-1 and similar data for analysis of environmental problems in a variety of regions in Southern California. Initial findings dealt mainly with mapping land use changes from ERTS-1 9" x 9" Diazochrome false color transparencies, but advanced methods of displaying and enhancing the imagery have made it possible to conduct more detailed studies of specific environments. In addition, the data from the U-2 flights were of significant value for detailed interpretation and verification of patterns extracted from ERTS-1 data.

The general objectives of the investigations conducted by UCR under the ERTS-1 program are listed as: (1) mapping of general land use patterns in rural and urban regions of Southern California; (2) monitoring of changes in land uses, particularly in urban and rural/

urban locations and with additional emphasis placed upon analysis of wildland areas coming under urban and/or agricultural pressures; (3) monitoring environmental pollution in Southern California basins; and, (4) developing models defining "environmental quality."

Out of these goals have grown a series of specific studies. In some cases, the concepts of these individual studies are included under more than one of the four prescribed goals, lending greater importance to the studies and demonstrating greater utility of ERTS-1 data.

There are four studies that were considered important enough to be presented as separate papers. The studies include (1) Semi-Automatic Crop Inventory From Sequential ERTS-1 Imagery by Claude W. Johnson and Virginia B. Coleman; (2) New Fault Lineaments in Southern California by Robert W. Pease and Claude W. Johnson; (3) ERTS-1 Image Enhancement by Optically Combining Density Slices by Gerald O. Tapper and Robert W. Pease; and (4) Land Use in the Northern Coachella Valley by Jack B. Bale and Leonard W. Bowden, and appear elsewhere in this volume. In addition, there are other important studies that use ERTS-1 imagery and merit description.

2. MAPPING VEGETATION IN ORANGE COUNTY FROM ERTS-1 DATA

Vegetation mapping from high flight U-2 imagery at small scales (1:131,000) can be accomplished with proper methodological procedures. These same techniques can be applied to the ERTS-1 imagery for interpretation of (generalized) vegetation patterns on the landscape. However, the greater perspective gained from ERTS-1 at greater altitudes can both aid and hinder investigation and accuracy.

Using U-2, RC-10 high flight color infrared imagery, Orange County was mapped for vegetation and wildlife patterns. Development of a functional classification scheme is of primary importance. It must be coordinated with the capability of the imagery to record information as well as with the needs of the investigation. It was felt that the best accuracy could be achieved using ten vegetation classifications (Grassland, Coastal Sage, Chaparral, Oak Woodland, Pine Woodland, Riparian, Fresh Water Marsh and Salt Water Marsh) and five wildlife associations (large animals, small animals, upland birds, waterfowl, and saltwater birds) (Figure 1).

In formulating the classification system an intensive study of ERTS-1 imagery (Band 7) and the U-2, RC-10 CIR imagery was required to determine patterns of specific tonal and texture registration. Careful attention was given to locational relationships such as slope orientation, drainage patterns, accessibility of wind systems and moisture, and elevation. Broad general patterns can be determined in the ERTS-1 photos and more specific and accurate delimitations made with the U-2 imagery.

Field checking was required to identify the specific signature pattern and determine the vegetative type characteristic of that registration. After a signature has been identified then it can be applied to the entire study to delineate the vegetation type.

In this systematic development a functional classification system can be formulated based on observable data and geared to the photography. The methodology can be applied to any region for mapping vegetation and should yield accurate, comprehensive results.

Mapping of vegetation can provide a useful data base for planning, especially when introduced into a computer format with land use, landform, and hydrological data. Digital plotting of boundaries recorded from air photos can enable quantification of, heretofore, arbitrary information and quickly provide accurate, usable data.

3. IMPACT OF OFF-ROAD VEHICLES

The recreational use of off-road vehicles, especially in the arid regions of the western United States, has become an important and rewarding leisure time activity. As a result, off-road vehicular traffic, especially motorcycle traffic, has already caused considerable damage to these delicate desert environments, and this damage will certainly become more widespread unless regulatory action is taken promptly to prevent overuse and destructive uses of the terrain.

Location of damaged areas and the study of their proliferation would aid greatly in efforts to minimize the impact of this vehicular traffic. Such a study would also provide a rational basis upon which to establish regulatory policy for off-road vehicles. In this study the utility of remote sensing techniques for the dual purposes of location and study of damaged areas is explored.

Using imagery of California's northern San Gabriel bajada spanning nearly three years from July 1968 to July 1972, all major areas of off-road vehicular damage within the study region were located (Figure 2). Growth of areas subject to damage, for the time period in question, was also mapped for specific locations.

Small scale imagery, particularly from the U-2 and NASA Mission 164, was found to be most desirable for purposes of initial location of damaged areas. Larger scale photography (1:24,000-1:30,000) was found to be more appropriate for more intensive study once damaged areas had been located. CIR imagery, particularly under a stereoscope, was found to be especially valuable in this investigation. Imagery of damaged areas from more than one date is, of course, requisite for a temporal comparison for expansion of damage.

Remote sensing techniques have direct application to the tasks of locating and studying off-road vehicle damage. Aerial survey is clearly superior to ground survey for these purposes for several reasons. First, the use of air photographs allows vast areas to be rapidly examined. Second, the perspective offered by aerial photographs allows the interpreter to easily see spatial patterns not readily visible from the ground. Finally, the number of man hours required for ground survey and mapping of damaged areas probably renders that method prohibitively expensive.

4. IMPACT OF THE BARSTOW TO LAS VEGAS MOTORCYCLE RACE

The most recent high altitude imagery, utilizing the U-2 platform, the RC-10 camera, and color infrared film, clearly shows the traces of random off-road vehicle (ORV) activity in the Mojave Desert. From this imagery, the extent of the areas of usage can easily be determined, and, with proper ground study, can reveal the types of environmental changes that have resulted. Simply stated, the premise of this study is: if patterns of random ORV usage can be detected, then surely the traces and environmental modifications resulting from intensive use in a specific area could be determined.

In communicating with the Bureau of Land Management (BLM), it was found that the annual Barstow to Las Vegas Motorcycle Race (consisting of approximately 2,600 riders and 15,000-20,000 spectators) was to be held 25 November, as part of a four day affair. The BLM was greatly concerned with this event and was engaged in setting up a preliminary study to determine the effects of the race and decide whether it should be continued. At that time, no aerial coverage was planned by the BLM, their study sites being restricted to ground transects across the route of the race, subsequently our interest was welcomed and encouraged. The proposed study would monitor environmental changes incurred by the annual Barstow to Las Vegas Motorcycle Race from high altitude aircraft and ERTS-1 imagery. Conclusions would be supported by ground checks and low altitude photo comparison. Changes could also be monitored over time, as the race is run over a course that differs only slightly from year to year.

The areas affected included the most common types of Mojave terrain; alluvial fans, playas and washes. As will be seen, these areas vary in their ability to accommodate intensive (ORV) recreational usage and the amounts and nature of damage that they incur.

Damage that was anticipated, again, varied with the type of material involved. First, the surface soil was expected to be altered. A slight cementing of stable desert surface materials is to be expected because of the net upward movement of water, that carries with it dissolved minerals which are deposited at the surface. Any weight applied to this

surface would necessarily break it, exposing the looser subsurface material. In this process, the surface material is broken, allowed to be transported, and the subsurface material is compacted. The result is a surface with high erosion hazard by both wind and water, underlain by a relatively impervious subsoil. The surface is therefore (allowed to be) denuded of its surface layer, the compacted subsurface promoting the lateral movement of water and preventing, in large part, the germination of plants that could promote erosion control.

This type of effect would be greatest upon alluvial fans. However, the degree of damage is largely dependent upon the portion of the fan that is used. This is necessarily a function of the depositional characteristics associated with stream velocity, slope, and channel width. Coarse debris is better able to withstand intensive usage, and is found at the head of the fan since it is the first deposited (a result of its greater weight). Materials increase in fineness and susceptibility to damage as slope decreases or distance from the source increases.

Desert pavement is subject to similar, though less intense, damage since it is a resistant surface but located on a relatively level area. Once the surface is broken, subsurface material is most susceptible to wind and water erosion.

Playas require a slightly different consideration. Soil textures are fine, but the area serves as the local base level, effectively eliminating water erosion hazards. The slightly structured playa surface is therefore only susceptible to wind erosion. Perimeters of playas, however, are some of the most likely archaeological sites in a desert environment, and may be subject to destruction.

Washes, in regard to usage, are blessed with instability. Sudden convectional showers that typify desert storms, and its resultant heavy runoff, greatly rework these ephemeral stream channels at frequent intervals. No desert surfaces can form and the coarseness of the sands in their beds resist compaction. Vegetation that inhabits stream courses is also adapted to frequent change.

Much of the damage that is inflicted on these areas results from the reaction of the riders to the particular surfaces over which they rise. Flat, or expansive vegetation free, firm surfaces are most attractive, because they allow greater speed. Also in these areas, trails widen dramatically, as passing is desirable. The qualities that are attractive, to the rider, are those which make it most susceptible to damage. These are, by and large, fans, playas, and pavement surfaces. Washes, those areas that can withstand heavy usage, are in slower, concentrated parts of the course. Because of its looseness, riders slow down, and tend to follow single-file.

Most of the changes observed are visible on U-2 imagery. From the ground sites that were monitored the extent of the types of change noted can be plotted and the types of change can be projected for those areas not covered in the ground survey. This change could prove to be beneficial in some respects (i.e. grazing enhancement) or detrimental in others, to surfaces, erosion potential, vegetation and possibly disease (valley fever).

In those areas that were damaged, there were alternate routes that would have resulted in diminished effects. Imagery of current U-2 scale and resolution will provide a valuable tool in planning future events in the desert that will result in a minimum amount of damage. This type of imagery will also lead to improved recreational planning of all types in areas where an environment may be so easily damaged. Most important, is that ERTS-1 imagery is as useful for planning future races as some of the U-2 data because those areas that can withstand heavy use are mappable.

5. URBAN REGIONAL LAND USE

The metropolitan area of which Riverside and San Bernardino form the core, has been selected by USGS as one of 26 sites for study of urban land use under the Urban Atlas Project. The basic data gathering system, of mapping land use information on USGS 1:24,000 sheets, is being continued until its completion. Computer maps are being prepared from the base data. Five quadrangles have been finished and are mosaiced together (Figure 3).

This large scale data base, while useful in its present condition, also allows rapid and useful correlation with ERTS-1 and ERTS-B imagery. The sequential nature of ERTS-1 imagery fits in well with the requirements of the project, those of monitoring urban and regional land use changes. The conversion of conventionally mapped data into a format for computer storage and manipulation allows quick comparisons of several dates, and thus rapid assessment and calculation of urban changes. The feasibility of such monitoring has already been established in the paper mentioned earlier (Bale and Bowden, "Land Use in the Northern Coachella Valley").

Present plans include the production of a technical report summarizing all the work of the project at UCR. It will include details on the methodology and techniques as well as analysis of data from selected sites in the study area. This paper will provide local county and city planners with quantitative data and adaptable techniques for their use in evaluating land use changes and processes occurring in the area. It also reflects the ability and intention of this research program to go beyond the limited objectives stipulated by USGS and make information available for practical, local agency utilization.

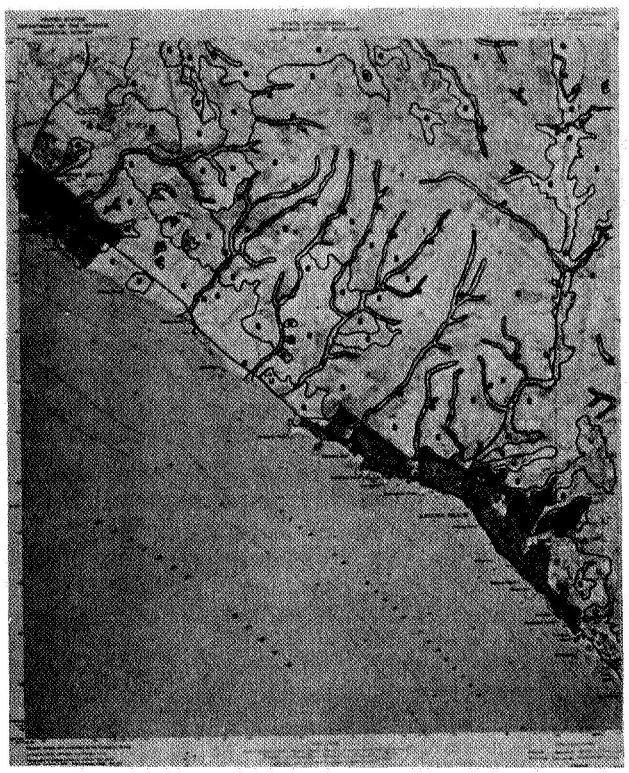


Figure 1

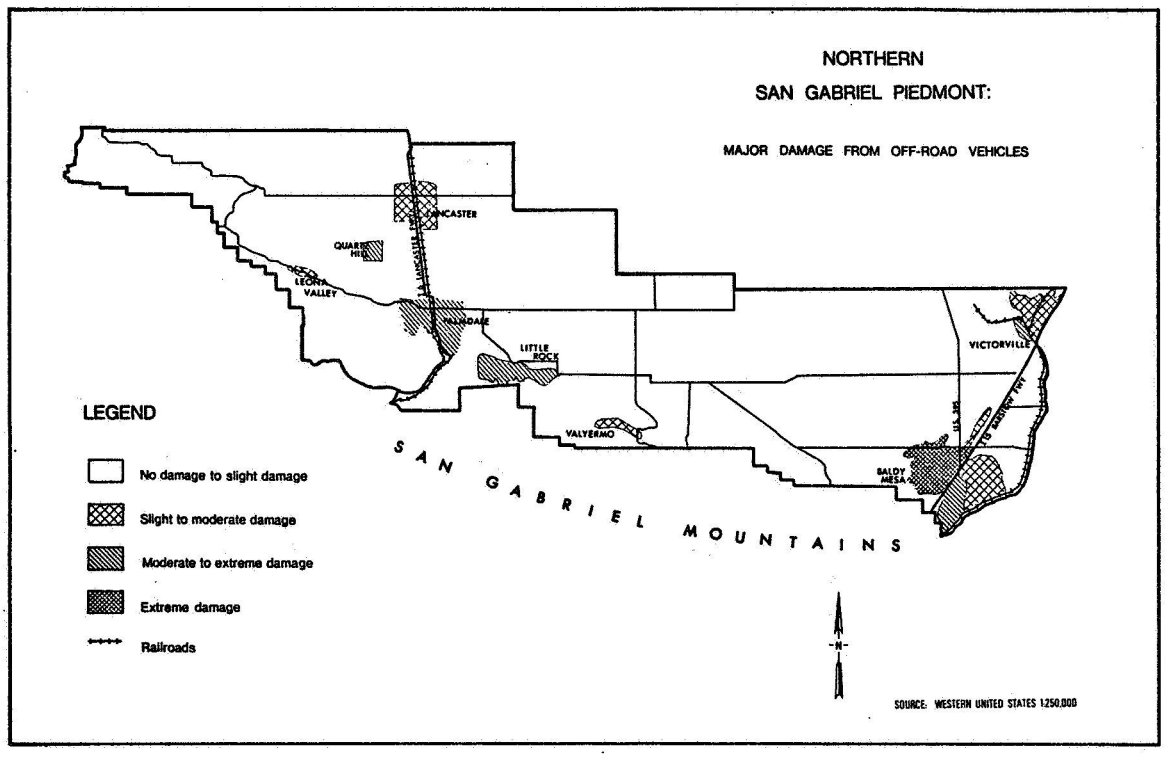


Figure 2

G

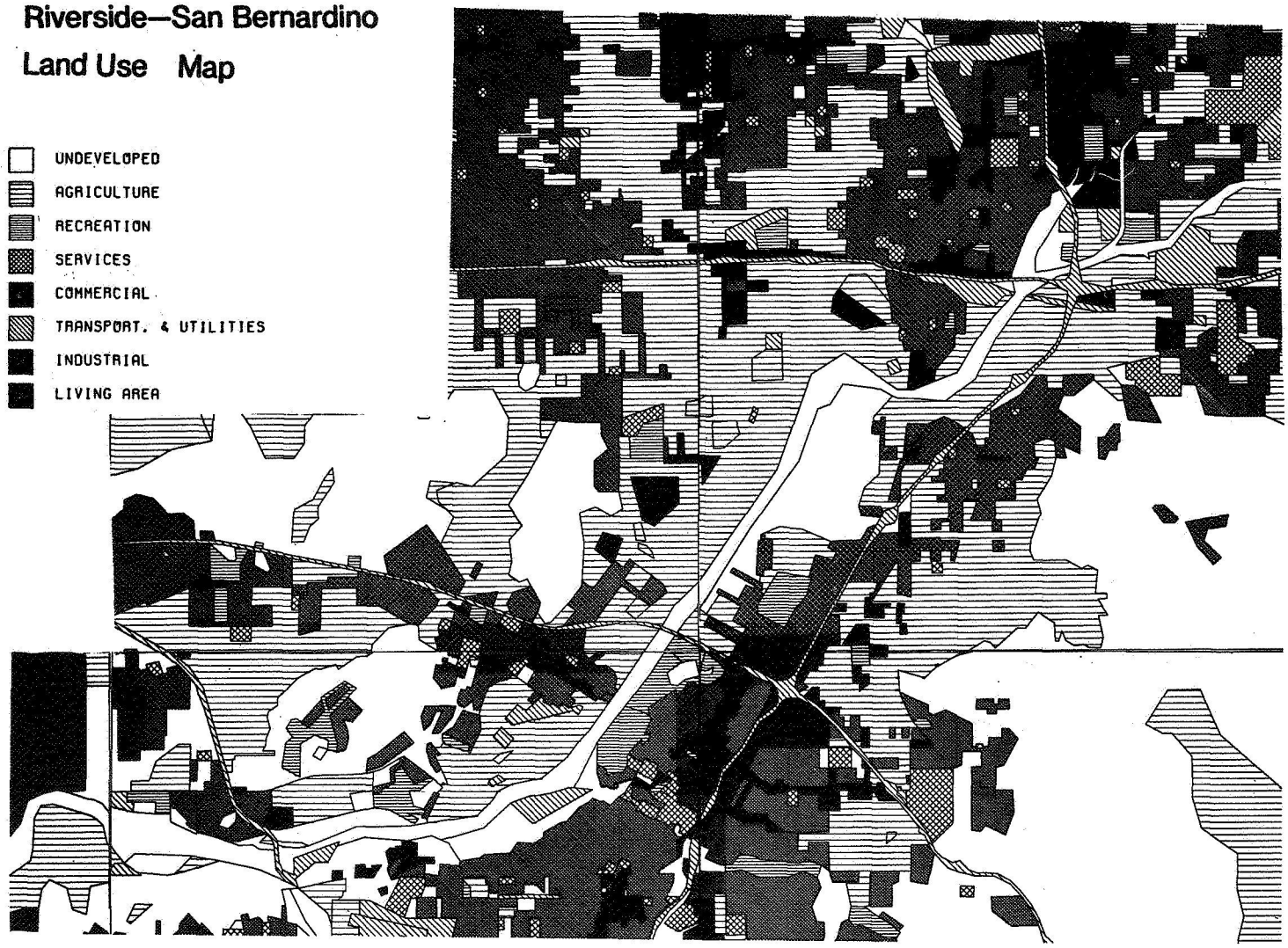

Riverside—San Bernardino
Land Use Map
UNDEVELOPED
AGRICULTURE
RECREATION
SERVICES
COMMERCIAL
TRANSPORT. & UTILITIES
INDUSTRIAL
LIVING AREA

Figure 3

N73-28363

Paper R 5

APPLICATIONS OF REMOTE SENSING (ERTS) TO RESOURCE MANAGEMENT AND DEVELOPMENT IN SAHELIEN AFRICA (REPUBLIC OF MALI)

N. H. MacLeod, *Department of Biology, The American University, Washington, D. C.*

ABSTRACT

The primary resource management problem in Sub-Saharan Africa (the Sahel) is increasing aridity or desertification. Space observations of sand streams, dune orientations, moisture and vegetation changes and other factors associated with desertification have been made. It is not yet known whether the process is caused by human activities or climatic changes or both.

A second major interest is grazing of cattle, sheep and goats which is associated with major movements of people and animals twice yearly to obtain forage -- from the savannah in fall and winter, and from huge areas of marsh (the Inland Delta) in spring and summer. These movements (transhumance) pass through more settled cultivators and into regions occupied by fishermen. The changes in available forage are being observed. The location of the cultivators is also being mapped from ERTS imagery -- for the first time. Field burning after rains is widely practiced and has been observed and the extent measured in ERTS imagery. In some areas of Mali, this measurement is an estimate of area to be planted to grain in the next season -- an unmeasured parameter heretofore.

Hydrological analysis is being carried on in the Niger and Bani River watersheds. The size, timing and areal extent of the annual flood is of particular interest. So far, good imagery of the maximum flood stage has been obtained and assessed.

Geologic information on fault zones, sand dune formations, scarps, tectonic basins and focal points of faulting (points from which fractures appear to radiate) are all visible and heretofore mapped inaccurately or not at all. The information on possible areas in which

Original photography may be purchased from:
EROS Data Center
10th and Dakota Avenue
Sioux Falls, SD 57198

mineralization has occurred are being mapped and noted for Malien officials carrying on their own ERTS investigations.

At the present time, the countries in the semi-arid zone of West Africa -- the Sahelien Zone -- are faced not only with the problems of economic development, but also with ecologic deterioration which they perceive to be a major and rapidly intensifying hazard.

The Republic of Mali in West Africa has recognized the problems of economic development and has also recognized that the data base of fund of knowledge concerning their natural resources is very meager. Maliens also recognize that the productive potential of the Sahelien Zone may bring their economy to a position of a major grain and livestock producer if they can control desertification and combine hydrologic and agronomic resources. They also recognize that their entry into world markets will be hastened by the discovery and development of mineral ores, energy sources (including geothermal), ground for crop and livestock production, water, and petroleum resources. Further, they realize their technical services, though staffed with able people, are inadequate for the performance of the necessary miracles.

Mr. Mamadou Konate, Director, Geological and Mining Services of Mali, in conjunction with U.S. AID, USGS and NASA technicians and members of the Malien technical services, is Principal Investigator of an ERTS-1 investigation through which the government of Mali (GOM) hopes to establish the necessary data base or resource inventory for long-range development planning in geology, hydrology, forestry, agriculture and grassland management. (I am speaking today both as a co-investigator in the GOM study and as a Principal Investigator for the U.S. "counterpart" ERTS investigation -- UN431). I have just returned from Mali, and I have the following report on our progress in analysis of the ERTS-1 imagery in relation to Malien development goals.

First, progress is being made in developing a detailed geologic map of the country (Figure 1). Overlays of geologic features drawn from the imagery of the Gao region are compared with recent maps drawn from French field studies. The major additions from the ERTS imagery are fault lines; more specific delineation of sand fields; and mapping of sedimentary pediments in the area. The Niger River, in this and other areas, follows lineaments apparently controlled by these. The Gao graben (a downfaulted block) is a feature of major interest because of its potential as a petroleum or water source. The western boundary of the graben has now been quite precisely mapped from the space imagery.

In the next sets of figures of the southern Inland Delta of the Niger River -- a tectonic basin (Figure 2), and the frame to the west, which contains a major irrigation scheme installed by the French (also

G.

a tectonic basin), and the so-called Delta Mort or Dead Delta -- we can point out some major advances in understanding of the hydrologic and vegetation regimes. We find that the Niger and Bani Rivers follow courses which are similar in orientation to the major lineaments -- possibly fractures found throughout southern Mali. These lineaments have been described in the Bandiagara Highland to the east, but not in the lowlands. We had thought the arrow-shaped, light-colored structures were dunes. They have been mapped as such -- dunes which are thought to be several thousand years old. An aerial reconnaissance, coupled with a ground observation at Mopti (located at the arrow in Figure 2), showed these were barren flats -- actually laterite covered by less than a meter of sand. These flats are cultivated in some villages. They are flooded each year and are thus supplied with water. Millet, rice, and cotton are the major local crops. The presence of the lineaments has an interesting relationship to ground water supplies in the region -- a resource which the Maliens wish to develop for livestock production. In years of below-normal precipitation, the flow of water out of the Inland Delta is greater than can be accounted for by precipitation alone. The excess outflow must come from ground water. The question is where is that reservoir of ground water? We feel that the fractures may be either the reservoirs themselves, or that they act as channels for the aquafers supplying the extra outflow. These hypotheses can be rather inexpensively tested by drilling into the lineaments.

The Niger River floods each year as it carries off the precipitations associated with the north and south advance and retreat of the Intertropical Convergence (ITC) each summer. The flood crest takes about six months to flow downstream. On 22 September 1972, the date of this image, the flood crest was in the southern Inland Delta, shown here, and thus its aerial extent can be measured from this image. This is an important measurement for nomadic animal husbandrymen who bring their cattle into the Delta each year to forage, for the Bozo fishermen who harvest 50,000 tons of fish from the Niger each year, and, of course, for the cultivators in the Delta.

The question of desertification can also be examined in this image. The soil is sandy in most of the area, but one would like to examine what appear as deposits of dunes or regions of sand to determine the mode and time of their origin. One particularly intriguing area is that between the Niger and Bani Rivers where an unwatered river channel can be seen. There is no vegetation or water in the channel -- it is not a wadi or channel for an ephemeral river, for it would be watered at this time of peak runoff if it were. No one knows the answers, but the stream was not previously mapped. Is there no water because of increased aridity, or has the watershed been captured by the Bani or Niger Rivers? Why is there no vegetation? The discovery of the existence of this and other such unwatered drainage systems in southern Mali pose major hydrologic problems worthy of much further study.

In the northwest corner of the image, one can see a cuspid pattern of tones. This is an area of range for the Peul, a cattle-owning people. The different tones are caused by differences in the type of vegetative cover -- the darker tones correlating with scattered trees and shrubs, the lighter with open grassland. Color additive techniques can be used on successive images to determine the cahnges in available forage during the rain-free season and the zones of highest productivity.

In Figure 3 the irrigation scheme, Office du Niger, is a prominent feature. By digital analysis we have mapped the pattern of irrigation channels, irrigated fields, and the adjacent cultivator fields. We have also mapped temporal changes in vegetative cover and soil moisture in the region.

Surface runoff patterns are peculiar in the region west of the irrigation scheme. In the imagery we find some areas devoid of surface drainage-ways. Aerial reconnaissance showed us that this is indeed the case. We feel that soils are very porous in the area and that there is some hope of finding aquafers shallow enough to be developed for livestock water-points so that the range may be better utilized by nomadic cattlemen.

We were particularly pleased to find the lineaments trending northeast and northwest from the northern part of the Office du Niger. By bringing together our data resources, we found that the northwest lineament (which has a water-formed channel in it) leads to a large circular depression -- the Hodh -- on the Mali-Mauretanian border. In 1964 the depression was so filled with water that it became a lake -- even now there is surface water detectable in the imagery. However, no one knew the source of the lake water -- it was a "gift of God." So it was, but we have found the channel -- that to the northwest of the Office du Niger. It can be filled using existing structures by controlling water flow into the Office du Niger from the Niger River during the Niger flood.

A dry-bed stream channel is located in the west-central portion of the image. Obviously, a large flow of water was required to form the channel, which continues northward to the Hodh and beyond. In the Hodh region of the channel is more than two miles wide and is located in the Sahara Desert itself. Further studies must be carried on; but the stream beds, the lake bed, and the lineaments make an intriguing combination for one interested in mapping and developing surface and ground water resources in that region.

All of the Mali images are full of interest for many disciplines. We have not fully addressed the question of desertification, but the ability to map sand from the imagery has been demonstrated. We also are able to map much of the vegetation of Mali to set a baseline condition for further development of extensive, intensive, and irrigated

agriculture.

There are still fascinating questions remaining concerning the lineaments, some of which control the course of the Niger, the Bani, the shape of the Delta and the Office du Niger, and relationship of the lineament to the former drainage channels. The answers can be sought now that a data base is becoming available to reveal the nature of the land surface.

While these comments merely brush lightly over the concerns of development, merely stating some of the discoveries without fully considering their implications for improvement and without conveying all that has been done in analysis, one may surmise that at least the inventory of resources has begun. Just this beginning has already affected the planning processes of the Malien government and of aid-donor agencies. We are also acquiring an appreciation of the dynamics of the cultivator-nomad relationships, the climate and land-use, and a more quantitative approach to the desertification problem.

A further immediate outcome is the emerging understanding by all participatns in the project -- Malien and U.S. -- of the regional nature of problems confronting Maliens in evolving a new kind of economy and the interwoven fabric of her natural resources -- geologic, hydrologic, biotic, and human -- that can be mustered for the development.



Figure 1 Republic of Mali

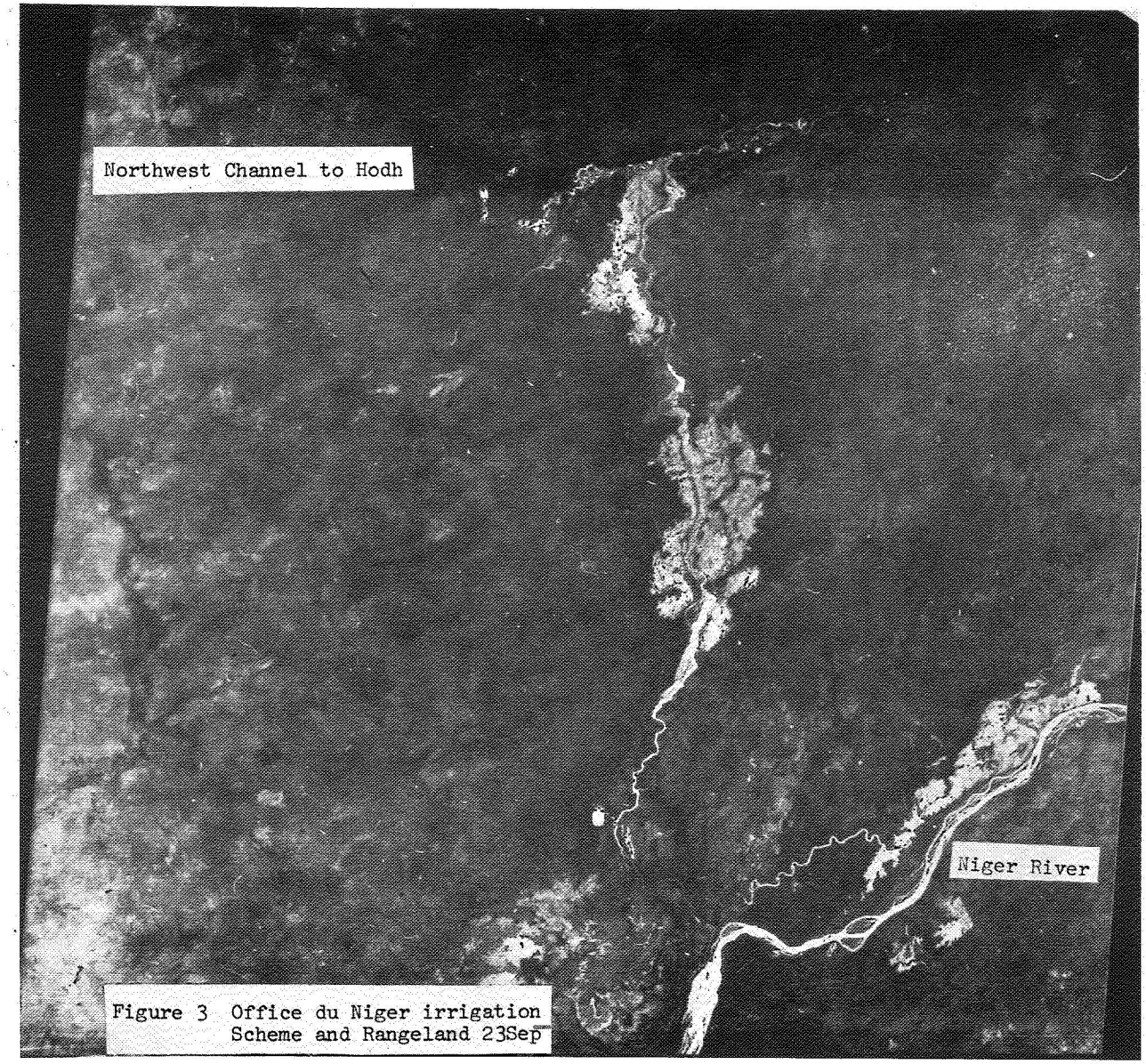


Figure 3 Office du Niger irrigation Scheme and Rangeland 23Sep

Figure 2 Inland Delta of the N
Niger River 22 Sep 72

N73-28364

Paper R 6

FIRST ERTS-1 RESULTS IN SOUTHEASTERN FRANCE: GEOLOGY, SEDIMENTOLOGY, POLLUTION AT SEA

A. Fontanel, J. Guillemot, M. Guy, *Institut Francais du Pétrole, 92502 Rueil-Malmaison, France*

ABSTRACT

This paper summarizes the results obtained by four ERTS projects in Southeastern France (MMC 009.01, 009.02, 009.03, 009.04). With regard to geology, ERTS photos of Western Alps are very useful for tectonic interpretation because large features are clearly visible on these photographs even though they are often hidden by small complicated structures if studied on large-scale documents. The 18-day repetition coverage was not obtained, and time-varying sedimentological surveys were impossible. Nevertheless, we were able to delineate the variations of the shorelines in the Rhone Delta for a period covering the last 8,000 years. Some instances of industries discharging pollutant products at sea were detected, as well as very large "anomalies" of unknown origin. Some examples of coherent optical processing have been made in order to bring out tectonic features in the Alps mountains.

I - LINEAR TRENDS OBSERVED IN THE WESTERN FRENCH ALPS

(P.I. J. Guillemot) MMC 009.03

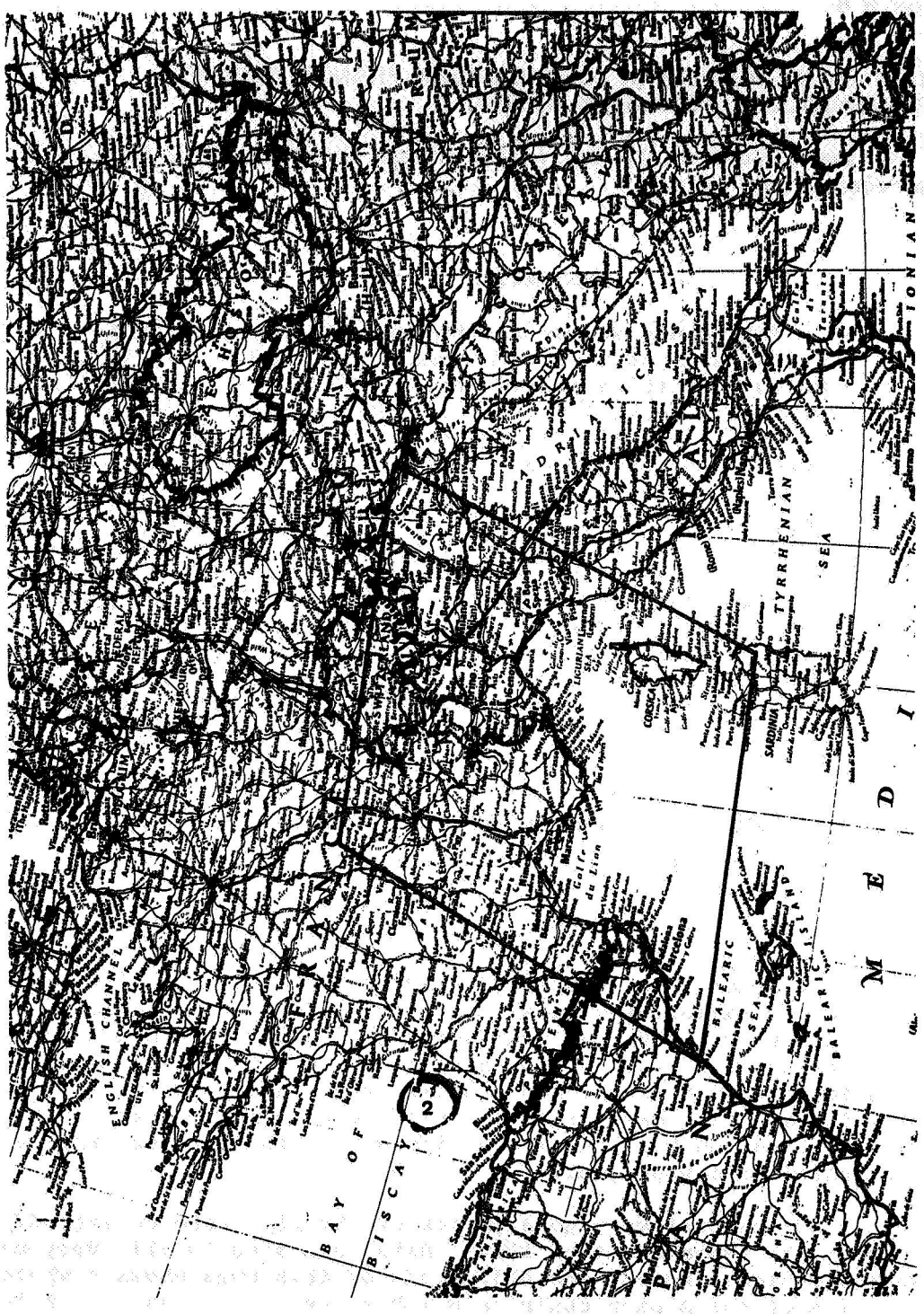
1. INTRODUCTION

The aim of the project PYRALP (009.03) was to study the tectonic relationships between the Alps and the Pyrenees and to make a survey of the fault network which separates these two mountain ranges and which is supposed to be related to the western Mediterranean collapse. Bad weather during autumn does not permit any image of the eastern Pyrenees to be obtained. Cloud cover was always much too heavy so it was impossible to carry out the main objective of the project.

But several very good photos of the Alps were delivered. They permit the improvement of ERTS 1 data in a structurally very complicated region. Indeed, one ERTS photo of this area shows a whole section of the Alpine chain in which rocks are intensively folded

PRECEDING PAGE BLANK NOT FILMED

Original photography may be purchased from:
EROS Data Center
10th and Dakota Avenue
Sioux Falls, SD 57198


ENGLISH CHANNEL
BAY OF BISCAY
TYRRHENIAN SEA
BALEARIC SEA
BALEARIC ISLANDS
SARDINIA
CORSICA
M E D I
2

and faulted. For the most part, each of the structures is less than 5 km wide and they are often hardly discernible from the photo.

However, through the various trends of the numerous small structures due to the folding of the sedimentary cover, linear features showing few preferential trends can be separated. These features, which are mainly visible when observed in a mosaic of several photos, are presented here on only one photo taken as an example.

2. GEOLOGICAL SKETCH OF THE AREA DESCRIBED

The area described in this paper, as an example of the information that the ERTS images can add to geological knowledge, is undoubtedly among one of the areas in the world more visited by geologists during the last century. The number of published papers about the geology of the western Alps is very great. It could be more than one thousand.

The selected example is part of the area shown by photo No. 1078-09562 of Oct. 9, 1972. This photo represents the valley of the lower Rhone, south of the city of Lyons and north of its Delta. There the Rhone runs from north to south and its valley, partially filled by alluvial deposits, separates the Massif Central in the west and the Alps in the east.

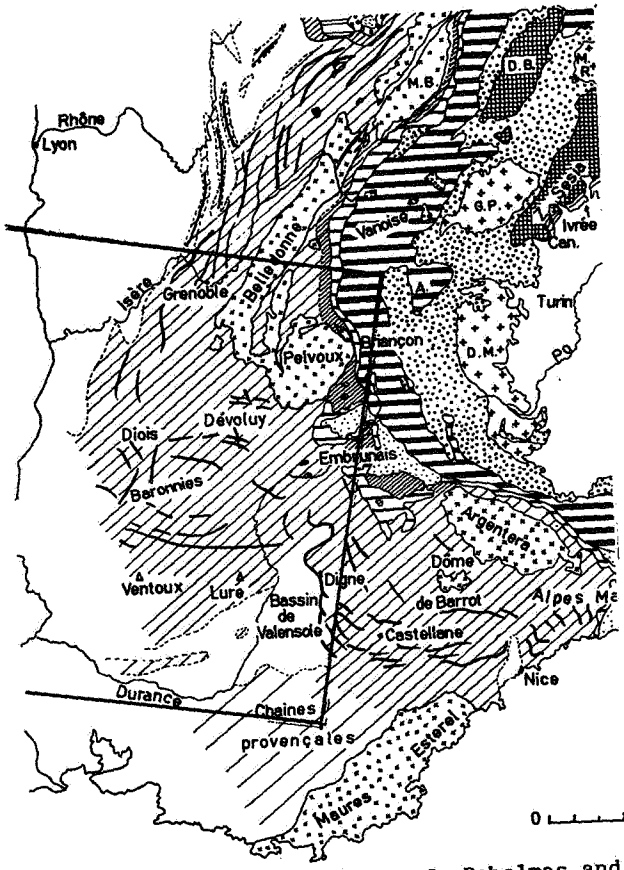
The Massif Central is a large uplift of metamorphosed rocks, mainly of Hercynian age, covered by a thin, deeply dissected layer of sedimentary rocks of Mesozoic age. The rise of the uplift was contemporaneous to the Alpine folding and accompanied by volcanism (Chaine des Puys) and formation of meridian troughs (Limagne). On its eastern border, the sedimentary rocks gently dip southeast although cut by numerous faults.

The Alps differ from the Massif Central by a thick severely-folded sedimentary sequence of Mesozoic and Cenozoic ages.

Several provinces have been separated by Alpine geologists, and, as can be seen in Figure 1, the westernmost part of the French Alps, represented by ERTS photo 1078-09562, is in the outer province (domaine externe) where are distinguished a "zone dauphinoise" in the north and a "zone provençale" in the south.

One of the outer crystalline massifs (Pelvoux, Belledonne) lies in the northeastern corner of the photo.

The "zone dauphinoise" is characterized by folds trending north-south in opposition to the "zone provençale" where the axis of the fold is east-west.



(After J. Debelmas and M. Lemoine)

Fig. 1

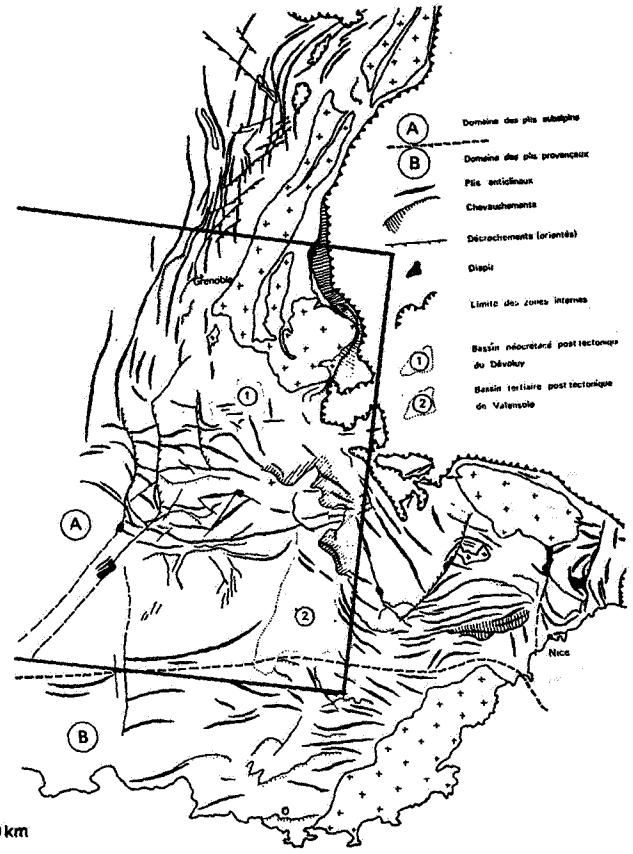


Fig. 2

Figure 1 is a structural sketch map of the western Alps published a few years ago (J. Debelmas and M. Lemoine*). On this map the area studied can easily be replaced in the general context of the Franco-Italian Alps. The sketch does not reveal any linear fracture, but several of them are drawn on Figure 2 published later by the same two geologists. The limits of ERTS photo No. 1078-09562 are drawn on both Figures 1 and 2.

DESCRIPTION OF THE AREA REPRESENTED BY ERTS PHOTO No. 1078-09562 (figs. 3 and 4)

An attentive study of the ERTS photo selected for this paper has been made. The features observed are not new features. They can be found on published geological maps (this is not very surprising in an area where so many geological surveys have been carried out). However several linear features can be pointed out more accurately than can be done from field surveys and geological maps.

West of the Rhone valley to the north of the Ardeche River are sedimentary unfolded Mesozoic series of the east flank of the Massif Central. Metamorphic rocks outcrop northwest of the Rhone-Isere junction. Dominant features are fracture lines trending mainly N 50° E to N 60° E with a few directions N 30° E to N 40° E. These faults are present both in the sedimentary and metamorphic rocks.

Southward, in the southwestern corner of the photo are gentle folds trending eastwest, cut by faults trending N 50° E to N 60° E. Some fractures trending north-south can be observed in the westward adjoining ERTS photo (1061-10015). They are only present in metamorphic rocks.

35 km north of the Ardeche River is a remnant of a quaternary basalt flow, the "Plateau des Coirons."

In the area east of the Rhone Valley the relief appears more intricate. However the two main directions of folding (dauphinoise and provençale) are quite clear from the photo (Fig. 3), i.e. N-S in the north, E-W in the south. Most structures are asymmetric, the anticline often overthrusting its syncline. On the photo some of the synclines are easily discerned owing to the reversal of relief in the Mesozoic series where thick limestone and shale formations alternate, but drawing the axis of the anticlines is almost impossible.

---

* J. Debelmas, M. Lemoine, 1964, L'Information Scientifique, Edit. Baillière et fils, Paris, p. 1-33.



Fig.3
Photo ERTS 1078 - 09562 - 6 -
Scale : 1/1 000 000
(A strip 5cm large has been cut off in the right side of the original photo)

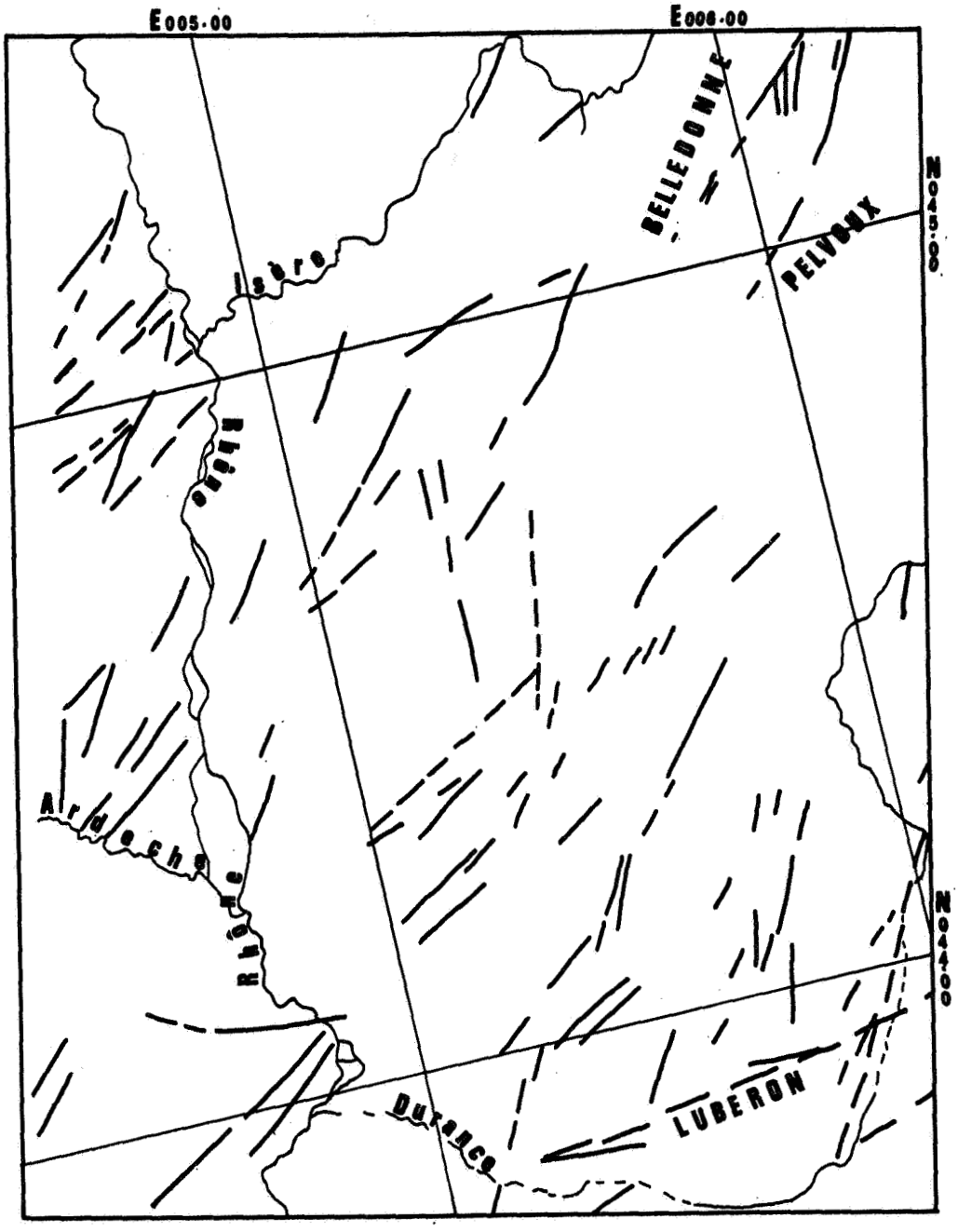


Fig. 4
Overlay of the photo fig. 3, showing the linear features pointed out.
Scale : 1/1 000 000.
Explanation in the text.

As in the border of the Massif Central, west of the Rhone, and in spite of a much more complicated tectonics it is possible to point out numerous linear features (Fig. 4). Their trends are identical, mainly N 50° E to N 60° E, and directions between N 30° E and N 40° E are also present. They are mainly traces of faults but in some places they are also flexures or geomorphological lines.

In the southeastern part of the photo a linear feature more than 100 km long trends N 80° E. This trend is also represented southward in Provence. It is not a fault line but the axis of a narrow anticline slightly faulted (Luberon anticline) prolonged by a straight line valley (Asse River) beyond a large valley (Durance) trending N 30° E.

The north-south faults (strike slip faults) which are near the center of the photo quadrangle in Figure 2 can hardly be spotted on the photo, probably because they run in a soft sedimentary formation (Upper Jurassic black shale). Likewise, the western borders of the Digne overthrusts near the central eastern limit of the photo are not visible.

COMPARISON WITH FIELD DATA

The whole area is covered by published geological maps on a 1:80,000th scale. Some of them have been revised four times, and more than half of the area is covered by published geological maps at the 1:50,000th scale. Field surveys were completed at various scales up to 1:10,000th.

A point by point comparison of field data and ERTS 1 data is beyond the scope of this report. But a simple comparison with Figure 2 which is a very interpretative tectonic sketch map is sufficient to give a fair idea of the help brought by ERTS imagery to the geological surveying of a tectonically complicated region.

The main fact which appears is the homogeneity and parallelism of trends of the linear features in the metamorphic massif as in the sedimentary folded zone. From detailed geological maps, the fault network is much more complicated. Besides SW-NE fractures, numerous faults trend SE-NW. They are hardly visible or not visible in the ERTS photos.

This leads us to think that most of the linear features trending SW-NE visible in the ERTS photos are reflections of deep-seated faults in the basement, while the SE-NW faults shown by field data are only in the sedimentary cover separated from the basement by a "decollement" in the Triassic series.

According to these features from ERTS data, the SW-NE trend is greatest in the western Alpine tectonics. It might be related to wrench faults in the basement. This idea has to be verified by a larger survey of the ERTS imagery and by a more accurate comparison with the field data.

3. CONCLUSION

Carrying on a project whose objective was to study the relationships between the Alps and the Pyrenees (Southern France), ERTS photos of the western French Alps have been carefully examined for tectonic interpretation. From this survey it appears that ERTS photos obviously show up some large features which in the field are often hidden by small complicated structures. In the example, these features trending SW-NE (N 30° E to N 60° E) are tentatively interpreted as reflections of deep-seated wrench faults in the basement of the folded sedimentary series.

C16

II - SOME RESULTS FROM THE STUDY OF THE DYNAMIC BEHAVIOR OF COASTAL SEDIMENTATION IN THE GULF OF LIONS

MMC 009.01 (P.I. M. Guy)

1. INTRODUCTION

The Gulf of Lions is a preferential area to study sedimentation problems on account of the complexity of the phenomena and of previous work.

The objectives of the project "GOLION" proposed for investigation of ERTS I data are:

i) A correlative study of the deformations in the patterns of sediment discharges at sea under various meteorological conditions.

ii) The precise mapping of the Holocene shorelines and a study of the chronology of the sediment bodies.

The short-term behavior of the coast is related to the meteorological conditions, and its study requires repeated coverage. Its long-term behavior is related to epeirogenic movements and eustatic sealevel changes, so a very small scale would be useful.

This paper relates some results obtained in the first phase of operations. Some good photographs were obtained ; but, due to very bad weather conditions, repeated coverage was not made and the coverage of the shoreline was limited to the Rhone Delta in the eastern part of the Gulf of Lions.

Nevertheless two important results were attained :

i) MSS bands 6 and 7 very clearly show the former shorelines of the Rhone Delta and enable them to be mapped directly.

ii) Recent changes in the morphology were clearly related to structural control (MSS 5).

2. MAPPING AND DATING THE FORMER SHORELINES

Figure 5 is an enlargement of part of photo 1078-09564 band 6 to a scale of 1:500,000th. Figure 6 is a sketch of the main coastal ridges or beaches and of the natural levees of the former beds of the Rhone.

They clearly show the southward accretion of the delta by numerous beaches which form an impressive beach pattern.



Fig. 5
Enlargement of the northwestern quadrangle of photo 1078-09564, Mss 6, showing the Rhône delta.

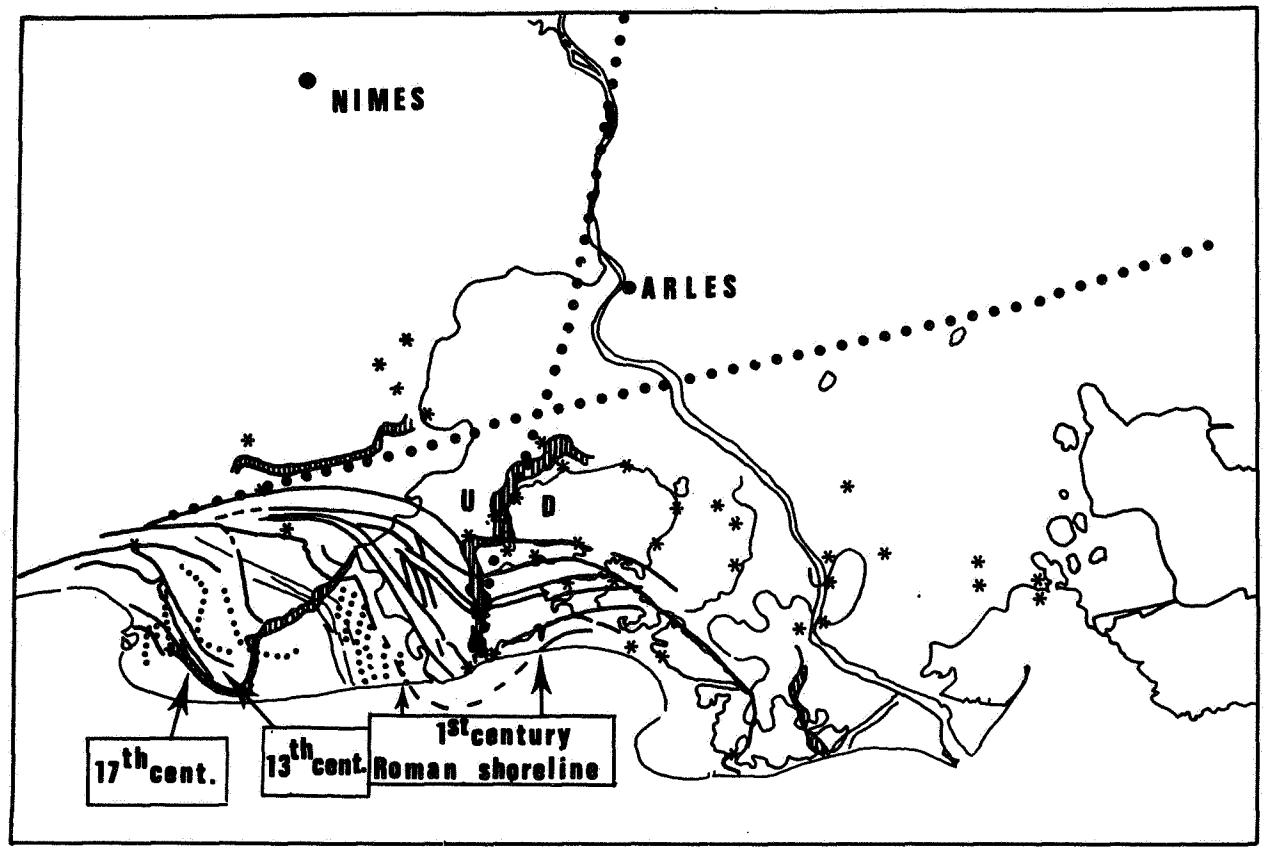


Fig. 6

* Roman built ruins

Levees of former beds of the Rhône

Already Known } Beach ridges
New }

Faults controlling Holocene Movements

Up
Down

These alluvial beaches and levees were recognized to exist in general before the ERTS I photo (Kruit*). However, it was difficult to link the ridge elements among one another so as to reconstruct the former shorelines, and so this had not been done in detail (cf. Fig. 9). In addition, unconformities between beach lines show that the accretion of the delta in the Holocene did not take place continuously. Variations in the sealevel or local tectonic phenomena are the probable causes of this jerkiness.

By using the positions of archaeological vestiges on the drawing of the ridges, the different phases can be dated with great accuracy. For example, Figure 6 shows that all the Roman vestiges are located behind a well-defined ridge line. Such a detailed analysis is now being made.

The eastern part of the delta shows a less clear-cut outline on the first ERTS I photos, although the phenomena are just as clear on the airphotos. The pictures taken in spring, and then in summer with different water levels, could be used to complete the layout of this area.

3. STRUCTURAL CONTROL OF SOME ANOMALIES

Fault control has been demonstrated by ERTS I photographs of the Rhone Delta.

On the MSS 5 and 6 photographs (Fig. 5), the eastern part of the Camargue region shows the outline of its former levees softened by the present overburden as the result of a slight downward movement. The western part is sharpened and eroded, and the clear lines of the beaches appear very detailed.

On the MSS 5 band, where slight changes in vegetation are emphasized, the boundary between these two zones is a very straight line, probably a fault trending N 30 E (Fig. 7).

Wells for petroleum exploration drilled some years ago have shown great changes in the thickness of the Tertiary sediments when crossing through this zone. But the exact position of the fault and its recent activity was not known.

The northernmost line of beaches forms, in its western end, a serie of curves asymptotic to a morphological alignments trending

---

* C. Kruit, 1955, Sediments of the Rhone Delta, Mouton, The Hague.

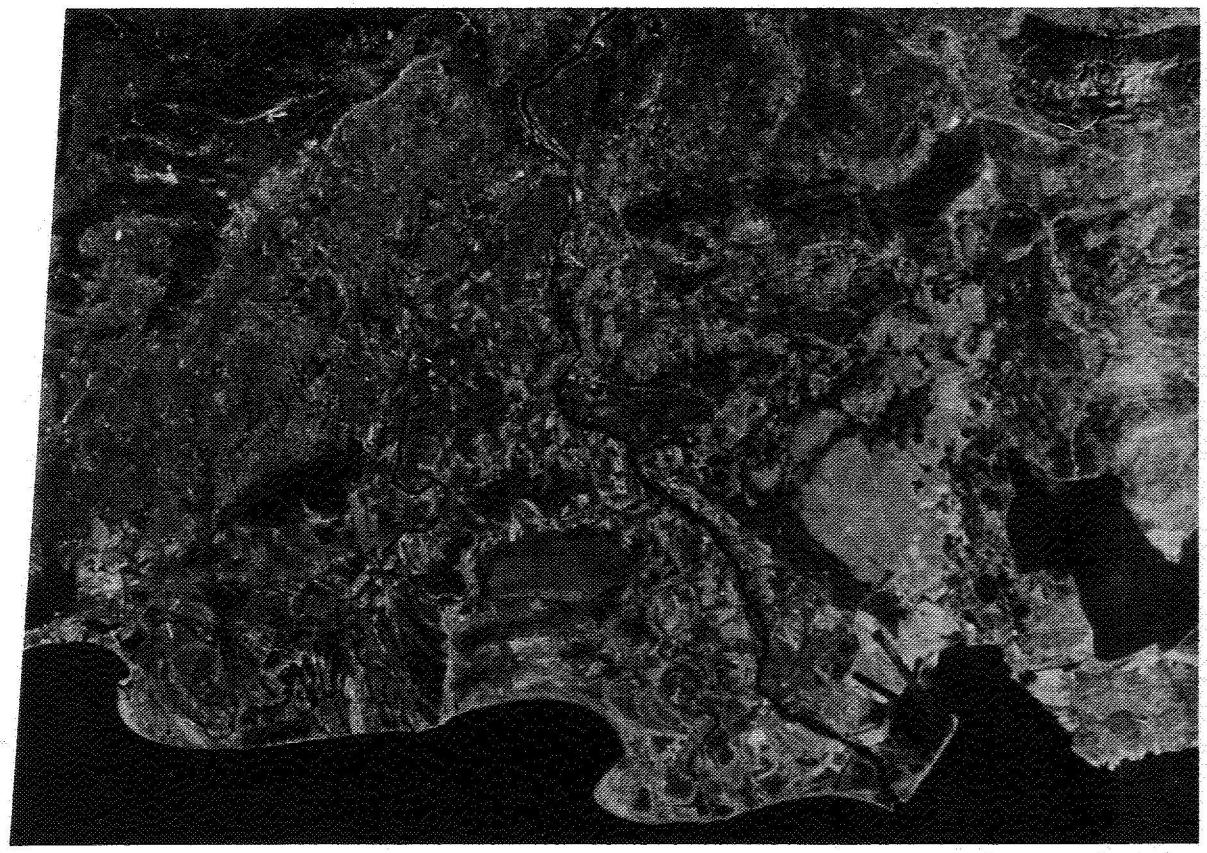


Fig. 7
Enlargement of the northwestern quadrangle of photo 1078-09564, Mss 5, where fault-alignments are perceptible by changes in the vegetation.

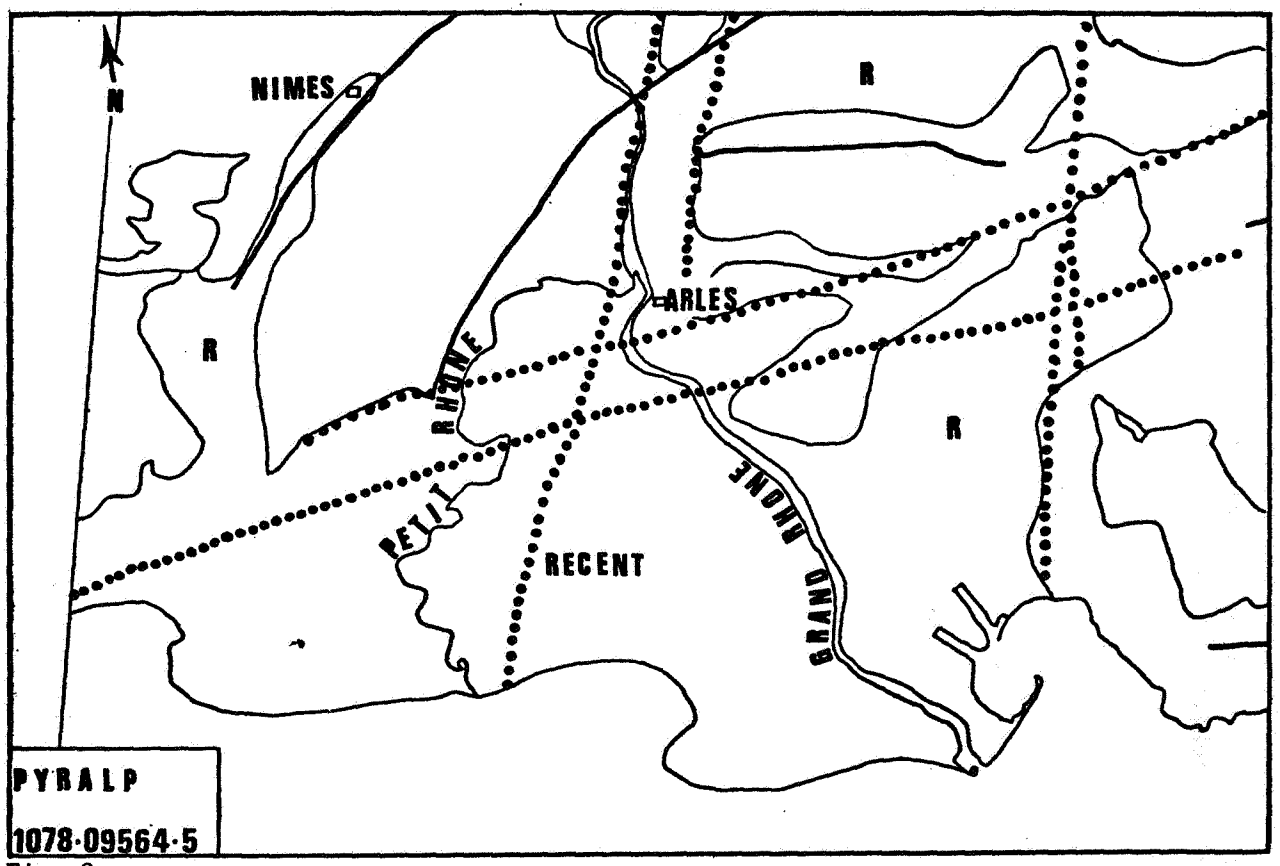


Fig. 8

These alignments are parallel to a network of faults studied by the PYRALP project.

approximatily E-W (N 70 E).

This alignment is known, in its eastern part from Secondary outcrops, as a large fault.

Study of the Alpine structure by the PYRALP project has shown the homogeneity of such a network of faults.

4. CONCLUSION

With these first observations on ERTS I photographs, a detailed study can be made of dynamic processes of the Gulf of Lions in the Holocene period.

The respective contributions of eustatic movements, climatic changes (increase in discharge) and structural control may be separated from one another by a precise study of the interrelationships of the geomorphic features, completed by ground surveys of archaeological and sedimentological remains.

Unfortunately, bad weather conditions have limited this study to the Rhone Delta, but the western part of the Gulf of Lions will probably be photographed in spring so that this study can be completed.

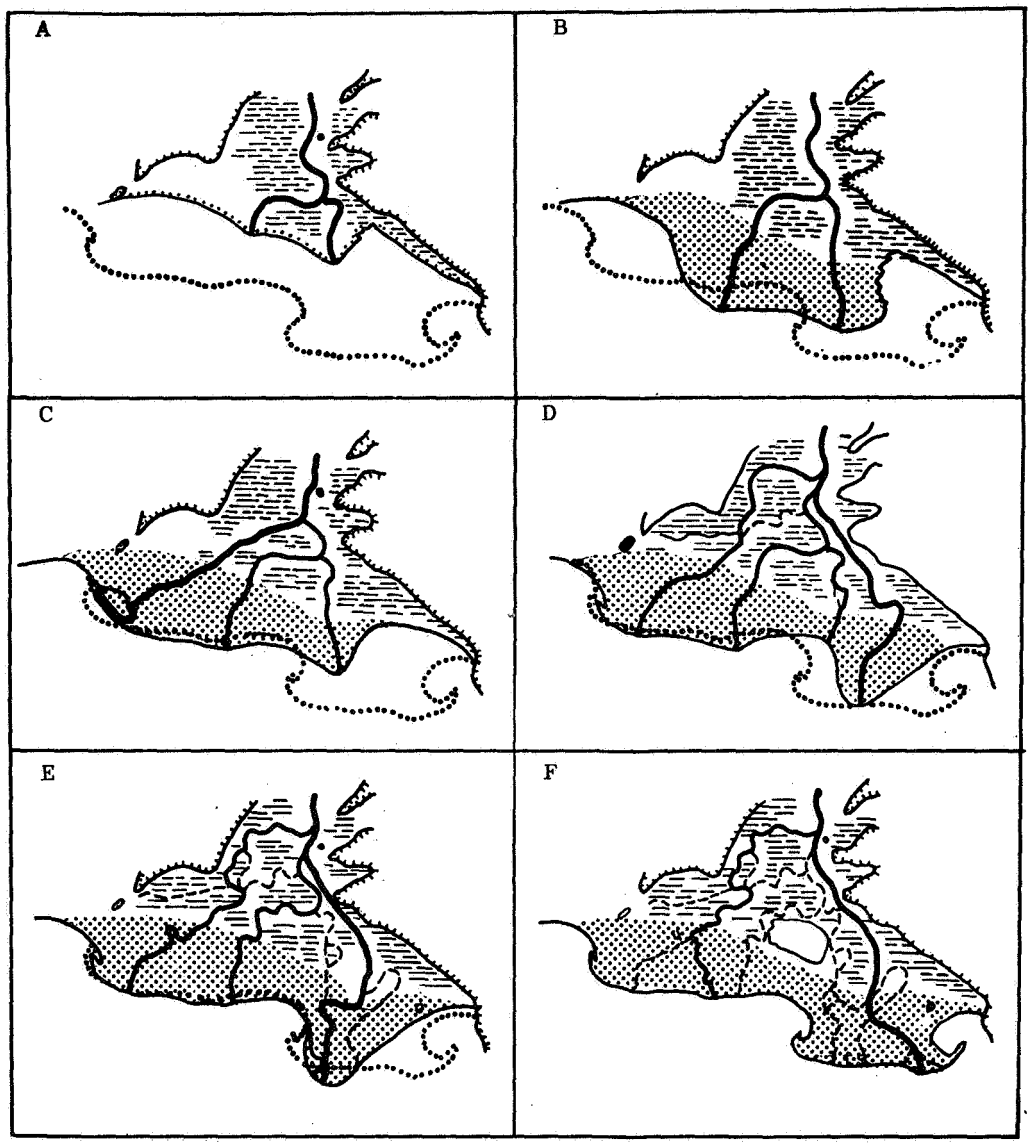


Fig. 9

Previous knowledge of the successive stages of Rhone delta advance during the last 5,500 years - (From KRUIT - 1955)

A - CLIMATIC OPTIMUM
B - PERIOD OF MAXIMAL ACCRETION
C - GREEK and ROMAN PERIOD
D - LATE ROMAN PERIOD
E - EARLY MIDDLE AGES
F - PRESENT SITUATION

Marsh
Beach and coastal lake deposits
Active channels
Abandoned channels

III - STUDY OF POLLUTION AT SEA IN THE WESTERN MEDITERRANEAN
MMC 009.02

(P.I. A. Fontanel)

1. INTRODUCTION

Our aim is to study the usefulness of ERTS imagery, associated with airborne records, to detect and perhaps identify various pollutants at sea and on coastal lakes in the southeastern part of France. Indeed the Mediterranean is almost a closed sea and pollution is a serious problem (Fig. 10).

2. RESULTS

A joint experiment was scheduled on September 19, 20 and 21 by I.F.P. (P.I. organization) and CNEXO (Co.I organization) under three different ERTS I tracks.

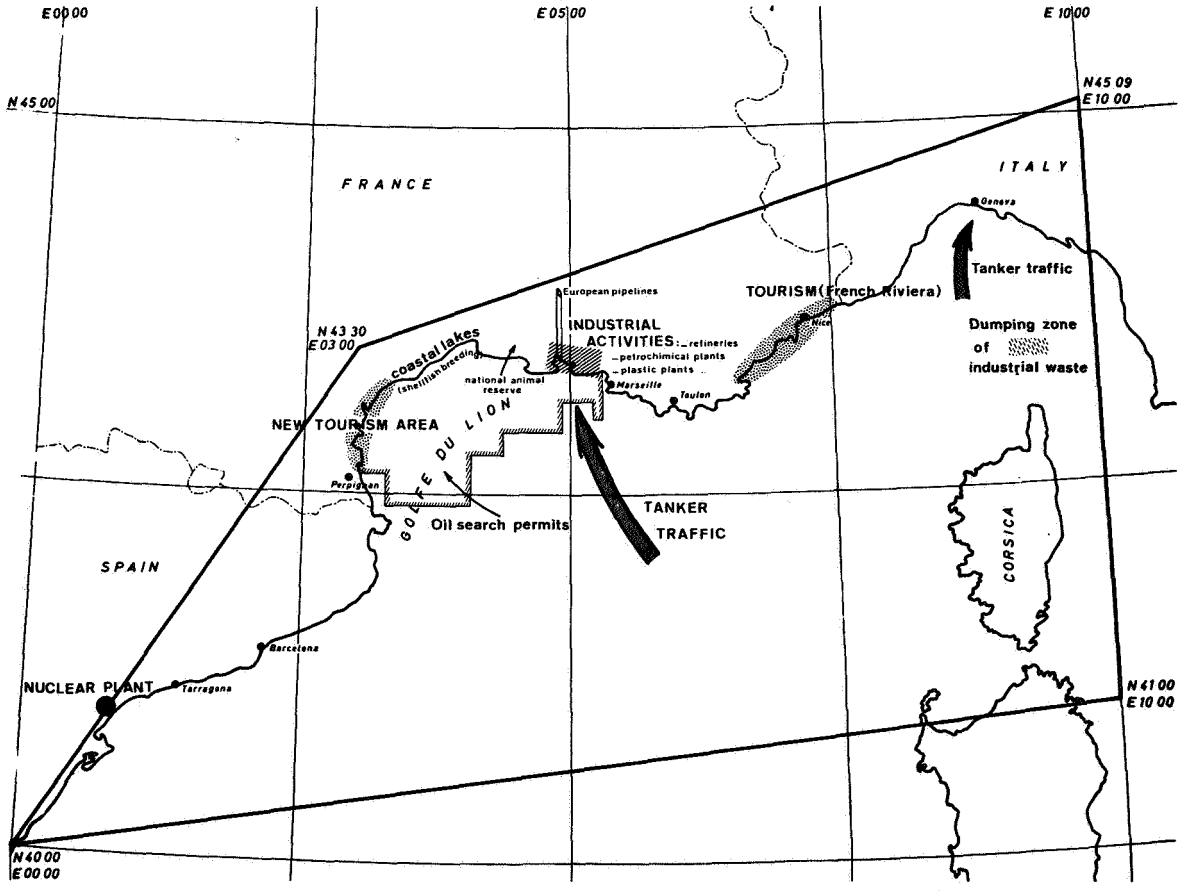


Fig. 10 Pollution problems encountered in the investigation zone

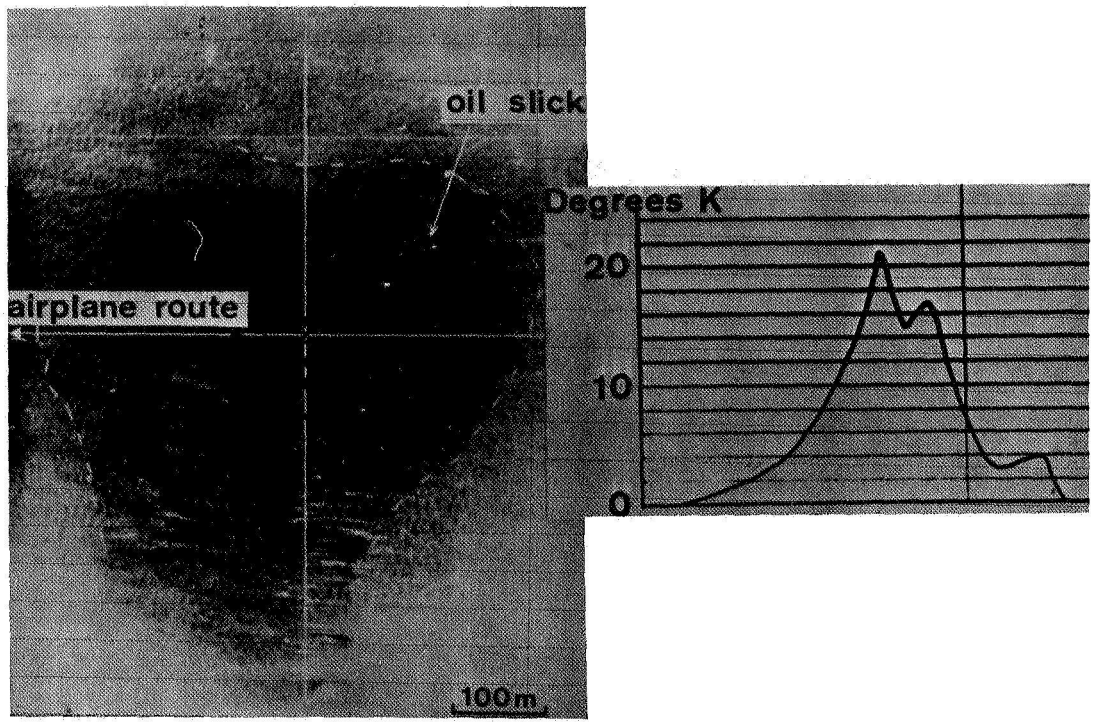


Fig. 11 Oil slick detection with a 32 GHz radiometer

Our aim was to pour various products at sea on parallel 42°30' (colza oil, crude oil, fuel oil, fresh water), to take samples of these products at different times in order to study their chemical variations, and also to track the slicks during daytime and nighttime with various airborne sensors including:

- color and infrared color photography (RC 10, Wild cameras)
- television camera for nighttime observation
- infrared scanner in the 3 to 5 micron band
- " " 8 to 14 " "
- microwave diffractometer at 32 GHz

Because of rough seas, we were only able to pour colza oil (6 m^3) at sea. Unfortunately, we did not receive ERTS imagery corresponding to the pouring point, quite certainly because cloud coverage was too great for ERTS. Furthermore, with regard to airborne records, results were obtained only with a T.V. camera, the 8-12 micron scanner and the 32 GHz diffractometer. The colza oil slick was clearly detected with these three devices, but we will give only the microwave results here. The left part of Figure 11 shows an image of the slick obtained with a vertical 35 mm camera (used solely to locate the airplane route). The right part shows the

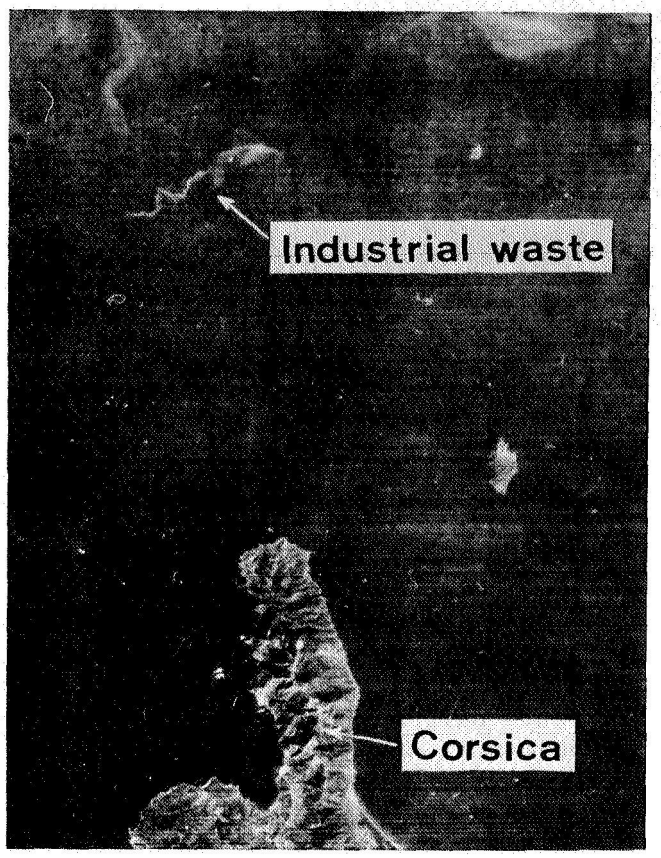


Fig. 12 Photo ERTS I - 1075-09393 - 4
scale 1:1,000,000
The arrow shows a patch of industrial waste containing ferrous oxides and sulfuric acid.

difference in brightness temperature between the slick and the surrounding water as recorded during the pass over the slick. The antenna is 0.70 m long. The beam width is about one degree. Its axis is directed behind the airplane route and is tilted 5 or 10 degrees with regard to the vertical. The temperature sensitivity is about 2° K. Fourteen passes were made after the oil was poured, from 9 a.m. to 12 a.m. The altitude was 250 m (800 feet) and the speed 75 m/sec. The polarization was horizontal at one time and vertical at another time. No noticeable difference was observed between the two polarizations. The brightness temperature differences between the oil and the surrounding water varied in the range of 10° K up to 34° K between the different passes.

Many remote sensing results have already been obtained by the P.I. and Co.I organizations in the visible and infrared bands, concerning coastal lakes and industrial zones on the southeastern coast of France, but they will not be presented here because they are not related to ERTS passes.

Up to now we have not received a complete ERTS coverage of the area (Fig. 10), and the 18-day repetition was not obtained, except with one photograph.

Nevertheless, several interesting features appeared on some ERTS photographs, but we will limit our discussion to two main examples.

Some industries have decided to dump their waste at sea off Corsica. These dumpings are not regular in time and occur at various locations. A certain concern can be felt among Corsicans about this waste which could be dangerous for the ecological balance of the region. Recently, a French oceanographic vessel went out to take samples of the polluted water in order to determine its noxiousness for marine life. This waste (called "red mud") contains ferrous oxides, other oxides such as titanium oxides, and sulfuric acid. Fig. 12 shows a patch of red mud 25 km long and two or three kilometers wide. This example proves that, under good weather conditions, satellite monitoring is possible and very useful for detecting and locating this type of dumping.

Figure 13 shows a very extensive "anomaly" in the northern part of the Ebro Delta, running for about 180 km along the Spanish shoreline and about 180 km off the coast.

Its origin is still unknown, but it is obvious that small-scale ERTS imagery is well suited for detecting such large phenomena.

---

* This photo has been received by Pr. Rey (ARNICA project).

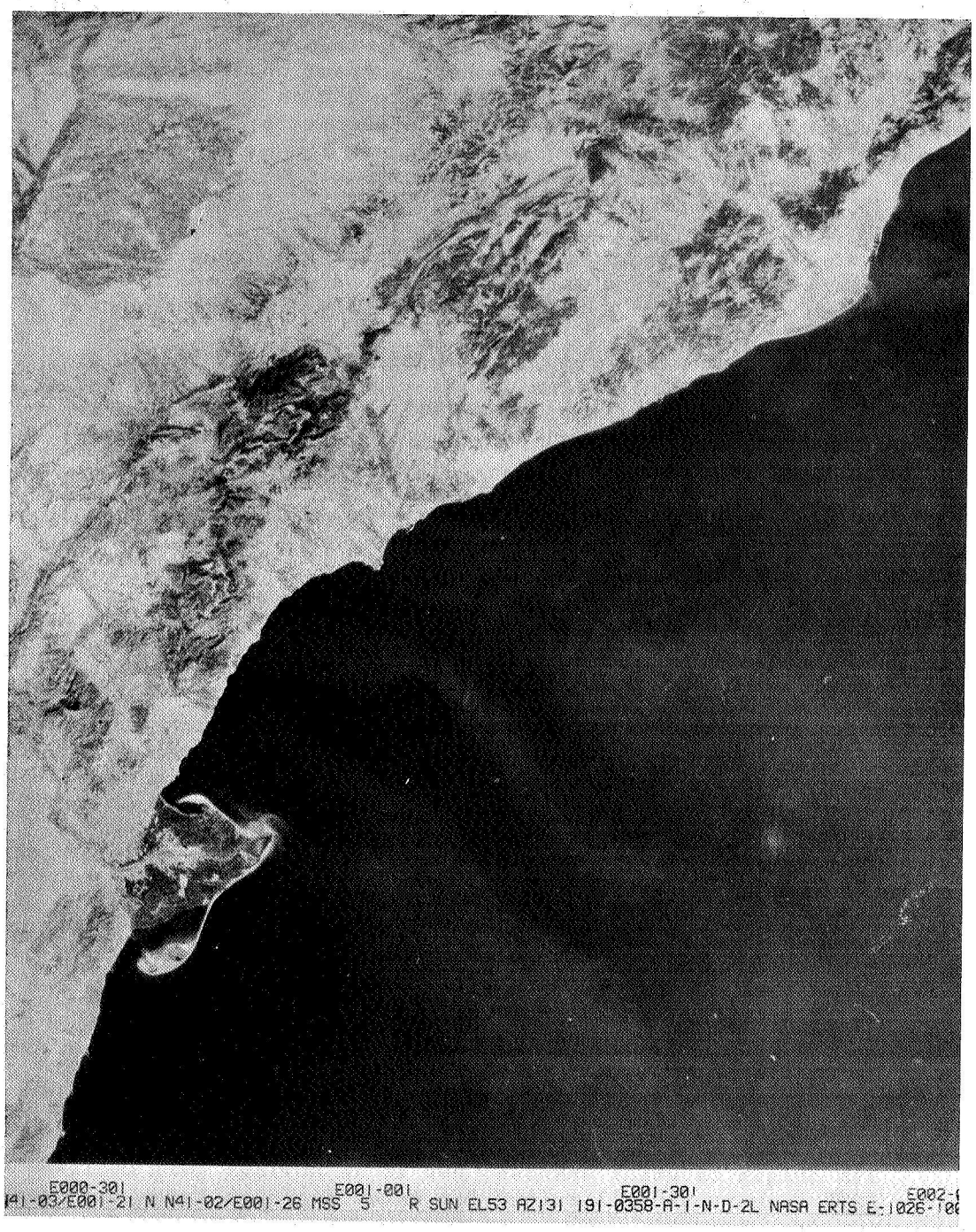


Fig. 13 · Large anomaly of unknown origin at sea

Experiments are scheduled in June 1973 to explain this "anomaly" which is, in part, situated offshore from a nuclear power plant.

3. CONCLUSION

It is obvious, from these examples, that small-scale ERTS imagery is well suited to detect such large phenomena.

IV - PROCESSING OF ERTS IMAGERY

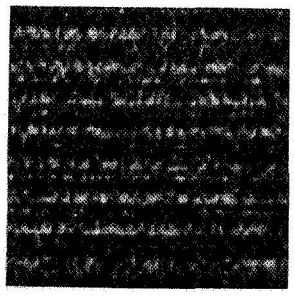
(P.I. A. Fontanel) MMC 009.04

1. INTRODUCTION

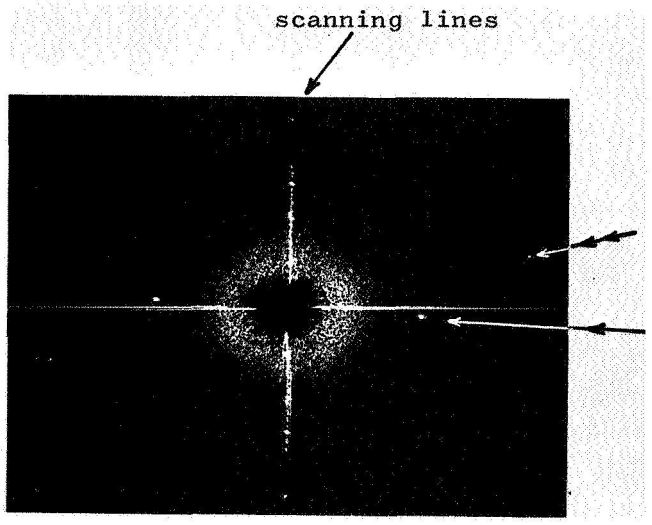
The aim of this project was to improve the quality of photographs, in order to make geological, geophysical, etc. interpretation easier and to automate some parts of this interpretation. We used optical and digital filtering techniques.

2. TWO-DIMENSIONAL SPECTRA OF MSS PHOTOGRAPHS

The optical Fourier transform of all MSS photos received shows two series of luminous dots positioned 92° and 77° with regard to the scanning lines. The spacing between these dots corresponds to a distance of 160 m and 85 m in the field. Fig. 14 shows an enlargement (approximately x 12 with respect to 1:1,000,000th scale) of an MSS photo taken at sea with its two dimensional spectrum. This phenomenon appears on each MSS spectrum but is very strong in areas with low contrast. It can hinder various kinds of studies of the MSS spectra. For example, we found this difficulty in trying to bring out the ancient Roman land partition in northern Italy.



a. Enlargement of an MSS photo



b. Two dimensional spectrum of a. The arrows (on the right side) show the directions of spurious points.

Fig. 14

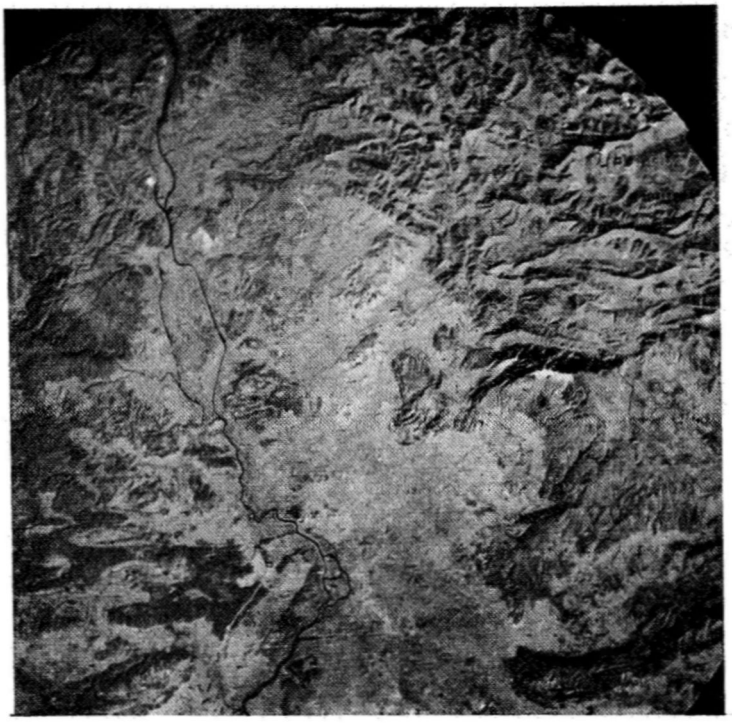


Fig. 15 a

Part of an image of an original MSS photo thru the coherent optical system
(1078-9562-6)
(scale 1:1,000,000)

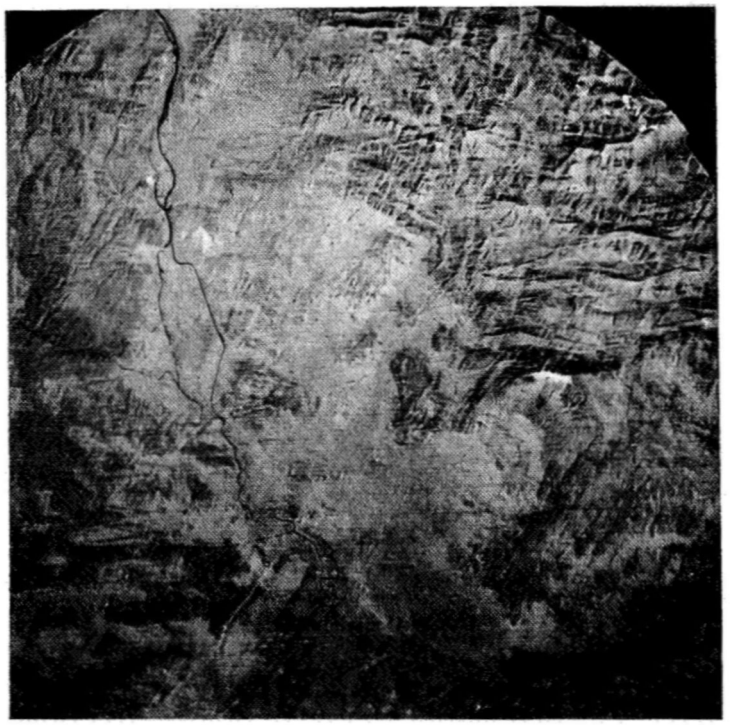


Fig. 15 b

Optical directional filtering of 15 a in order to bring out the NE-SW tectonic features



Fig. 16 a Digitized original aerial photograph (taken on test-site)



Fig. 16 b Contrast enhancement of Fig. 16 a

3. COHERENT OPTICAL FILTERING

The photos in Fig. 15 b represent the southwestern corner of an ERTS image taken as an example of the use of coherent optical filtering in order to bring out tectonic features in a complicated area (ERTS I - 1078-09562). The main trends are underlined after directional filtering (Pincus, Dobrin*, Fontanel et al. 1967**). These underlined features correspond to the main tectonic fractures described in the first part of this paper (P.I. J. Guillemot).

4. DIGITAL PROCESSING

We did not receive magnetic tapes from NASA, so we only processes digitized aerial photographs taken on test sites. Fig.16a shows a digitized original aerial photo, and Fig. 16b shows the same photograph after contrast enhancement.

We also applied numerical directional filtering techniques to aerial photographs. Some examples will be given in later reports.

GENERAL CONCLUSION

In this report we have presented the findings of four ERTS projects. However we want to point out that these different researches were carried out in close collaboration between the P.Is. even though the objectives would appear to be different at the first glance.

For example, the faults spotted in the Camargue region, and which provided an explanation for various sedimentological phenomena (GOLION project), were situated in a much wider setting, thanks to structural geology surveys carried out farther north (PYRALP project). Likewise, there is no point in emphasying the links which

---

* M.J. Pincus, M.B. Dobrin, 1966. "Geological Application of Optical Data Processing", J. Geophys. Res., 71(20), p. 4861-4869.

** A. Fontanel, G. Grau, J. Laurent, J. Montadert, 1967, Etude des photographies aériennes par diffraction de la lumière cohérente. Actes Symp. Intern. Photo-interpretation, Edit. Technip, Paris, III, p. 13-22.

exist between sedimentology and offshore pollution problems. Concerning the TRONU project which has to do with optical and numerical processing, it is being done on photos covering all four of the projects described.

PAPERS NOT LISTED IN THE ABSTRACTS OF THE SYMPOSIUM

N73-28365

DCP-COLLECTED ABSOLUTE TARGET REFLECTANCE SIGNATURES ASSIST ACCURATE INTERPRETATION OF ERTS-1 IMAGERY

Frederick P. Weber, *Pacific Southwest Forest and Range Experiment Station, Forest Service, U. S. Department of Agriculture, Berkeley, California 94701*

ABSTRACT

Data collection platforms (DCP's) are being used at a Black Hills, South Dakota, test site (MMC 226A) to record radiometric measurements needed to determine solar and atmospheric parameters that affect ERTS-1 multispectral scanner radiance measurements.

A total of 72 channels of analog data are transmitted from an unattended ground truth site via three DCP's at least six times a day. The system has operated with only minor problems since September, sending forth daily measurements of biophysical responses and atmospheric conditions. Comparisons of scene radiance data calculated from ERTS images with that measured on the ground show the image-measured values to be 35 percent higher for the green channel and 20 percent higher for the red channel for the same scene targets. Radiance values for channels 6 and 7 are nearly the same from the ground data and from the imagery.

1. INTRODUCTION

The Forest Service investigation in the Black Hills of South Dakota focuses on monitoring forest stress in the ponderosa pine (Pinus ponderosa Laws.) ecosystem using coordinated data collected from ERTS 1, aircraft, and from ground instrumentation. The cause of the stress being monitored in the Black Hills is a widespread epidemic of the mountain pine beetle (Dendroctonus ponderosae Hopk.). The bark beetle was responsible for over 10,000 infestation spots in the northern Black Hills this past year as identified on high-flight aerial photography obtained in September 1972 after the dead trees were fully discolored. The infestation spots identified ranged in size from single trees to many hundreds of trees with the greatest number of trees occurring in infestations having 11 to 25 trees.

Establishment of an ERTS 1 intensive study site was begun during May 1972 for the purpose of measuring radiometric responses of the principal components of the ecosystem in relation to changing atmospheric and environmental conditions. Our primary concern was to

Original photography may be purchased from:
EROS Data Center
10th and Dakota Avenue
Sioux Falls, SD 57198

provide closeup spectral radiometric ground truth of the relation between healthy ponderosa pine and the trees which were under stress from attack by the mountain pine beetle. Figure 1 shows the location of the intensive study site in the Black Hills. It was deemed important to monitor spectral radiometric information on two additional ecosystem components--(1) open pastures and grasslands which occupy the majority of nonforest land in the Black Hills and (2) soil and rock outcrops which provide the targets of greatest reflectance contrast with the forest. The rock outcrops provide important control points because they are easily identifiable within the forest on small-scale imagery.

2. METHODS

Many biophysical and atmospheric parameters were measured throughout the test site, but the most important was absolute target reflectance. These data were obtained in terms of scene radiance and irradiance as measured with our RS-2 ERTS-1-matched spectral radiometers shown in Figure 2. One of the 4-channel radiometers was positioned over each of four locations within the study site (over healthy pine, beetle-killed pine, grassland pasture, and rock outcroppings). Each instrument was positioned at the top of an instrument tower in a way that would provide a clear vertical (downward-looking) view of the target from a height of 7 meters (m).

In practice, the RS-2 spectral radiometers provide continuing information of importance in each of the ERTS multispectral scanner (MSS) bands for each of the ecosystem targets. Figure 3 shows the calibrated radiance output at 5 levels for each radiometer detector. Due to the slightly different spectral responsivities of each detector-filter combination, there is a different calibrated radiance for a given neutral density level. For the calibration data (Figure 4), the detector response was measured for each channel as a function of changing target exitance, with target exitance being the energy in watts per unit area of each target. Detector response levels shown in Figure 5 are for unamplified signals from Pin 10 DP detectors with a 10° field-of-view. In operation the output signals from each of the spectral radiometer channels is amplified with a UDT-101 (M) at a gain of 10 before entering the recording system.

In addition to recording target reflectances at each test site with the RS-2 radiometers, additional data collected include net all-wave radiation and upwelling shortwave radiation. At one central location, instruments measure the spectral components of downwelling radiation, atmospheric water vapor content, temperatures, and windspeeds.

Instrumentation data from all four sites are wired into a central data recording facility where sensor signals are amplified and multiplexed for broadcast over the ERTS data collection system (DCS) via

three data collection platforms (DCP's) (Figure 6). In all, 72 channels of data are multiplexed over 24 DCP channels. At the same time that instrumentation data enter the DCP buffers they are recorded in parallel on a digital data acquisition system. As the instrumentation laboratory is located within the forest, it was necessary to mount the DCP antennas at the top of a 32 m instrumentation tower, as shown in Figure 7.

Two satellite images of the Black Hills were selected for the purpose of scene correlations between ground truth data and ERTS MSS scene radiance data. Scene 1047-17175 provides clear coverage of the western Black Hills for September 8, 1972, on MSS channels 4, 5, and 7. Scene 1065-17175 provides partially open coverage of the north-central Black Hills on September 26, 1972, when all channels of the MSS were working well. Figure 8 shows a black-and-white rendition of a 4-channel color composite created on our I^2S color recombiner for the September 26 data.

For the purpose of scene radiance analysis of the ERTS image, microdensitometer scans were made of several transects on each image and all available spectral bands. Scan densities were converted to scene radiance for each 70 mm bulk data scene using calibration data taken from the 15 step wedge on each scene. Several of the scans made on the September 26 scene are shown by the white lines on Figure 1. Radiance data were correlated to scene points using proportional distances from control points which could positively be identified on both the satellite images and the RB-57 small-scale photography.

3. RESULTS

In the past we have received incomplete seasonal radiometric data for the Black Hills because of the large expense in manning test site instruments over long periods of time. It is clear that a significant benefit of ERTS is having the DCS capability for continuously monitoring field instruments and being able to send current and accurate data to our office hundreds of miles away from the remote field site. The minimum of three daytime transmissions of field data seems adequate for monitoring critical biophysical responses and environmental conditions. It seems a simple matter to add a few totalizing circuits to existing instrumentation so as to better utilize the three nighttime data transmissions.

As a result of daily monitoring of Black Hills radiometric instruments we are now beginning to get a clearer picture of spectral energy relationships in the ponderosa pine ecosystem over time. For example, Table 1 shows how albedo of the rock outcroppings was unchanged from September 8 to 26, whereas the albedo of the pasture increased 3 percent. During the same period healthy ponderosa pine showed a 1 percent decrease while bark beetle-killed pine increased by 1 percent. In

addition to knowing trends, the implication is that we now know for any satellite scene the relation of absolute reflectances between different ecosystem components.

Table 1. The relationship between albedos is shown for four Black Hills, South Dakota, ecosystem components at the time of two ERTS 1 passes in September.

Target	Percent Albedo[1] September 8	September 26
Healthy pine	11	10
Stressed pine	15	16
Pasture grass	19	22
Rock outcrop	24	24

[1] Albedo is the ratio of upwelling to downwelling shortwave radiation

Scene radiance data obtained from the September 8 imagery of the Black Hills is shown in Table 2.

Table 2. Black Hills scene radiance data for September 8, 1972, are derived from microdensitometer analysis of black-and-white 70 mm bulk data positives for scene 1047-17175.

Target	Scene Radiance (milliwatts/cm^2-SR) MSS Channel[1] 4	5	7
Healthy pine	0.333	0.188	0.847
Stressed pine	0.344	0.229	0.983
Lake	0.339	0.200	0.657
Rock outcrop	0.418	0.270	1.218
Mecadum road	0.394	0.194	0.953
Concrete highway	0.339	0.239	1.062
Mine tailings	0.354	0.249	1.170
New logging road	0.333	0.243	1.014
Tornado area	0.414	0.300	1.206

[1] Imagery received for channel 6 was unusable because of the large number of data dropouts

The 70 mm bulk imagery was fully adequate for extracting the scene radiance signatures of some ecosystem targets such as healthy ponderosa pine and rock outcroppings, using precision microdensitometry. However, even better numbers can be calculated for some of the hard-to-pinpoint targets like bark beetle infestation areas when the 9 1/2-inch black-and-white bulk imagery becomes available.

When it became apparent that we were not going to get ERTS-1 imagery of the Black Hills that was free of clouds over the entire study area during 1972, we settled on the September 26 scene for intensive analysis. We have examined color recombinations of this scene created to optimum illumination levels in our I^2S viewer. The best enhancements of the enlarged color recombination were photographed on color transparency film (Figure 8) and placed in a VARISCAN viewer for scene point correlation. Significantly, we were able to retain good quality ecosystem scene point recognition when the image was enlarged to a viewing scale of 1:32,000 on the VARISCAN screen. This was a useful step in becoming familiar with scene points before measuring the scene radiance with the microdensitometer scans. Table 3 shows the calculated scene radiance for the September 26 imagery of the Black Hills.

Table 3. Black Hills scene radiance data for September 8, 1972, are derived from microdensitometer analysis of black-and-white 70 mm bulk data positives for scene 1065-17175.

	Scene Radiance (milliwatts/cm^2-SR)			
	MSS Channel			
Target	4	5	6	7
Healthy pine	0.154	0.087	0.158	0.392
Stressed pine	0.140	0.093	0.144	0.399
Pasture grass	0.214	0.148	0.239	0.601
Mecadum road	0.213	0.105	0.173	0.440
Rock outcrop	0.316	0.204	0.353	0.920
Open pit gold mine	0.250	0.170	0.311	0.805
Golf course	0.217	0.156	0.244	0.628

The significance of scene radiance calculations on the MSS imagery is illustrated in Table 4 where they are compared to scene radiance measurements made of similar ecosystem targets on the ground which were transmitted to us by the DCS. It is noteworthy that here we are getting the first data which show the effect of atmosphere on radiance values as measured on imagery when compared to that which exists near the ground. Prior to this time we have only had predictions of what

should happen with generalized conditions. We see the greatest effect of atmosphere on MSS channel 4 where there is an overall 30 plus percent increase in scene radiance on the satellite imagery. For the infrared channel 7 there is less than 10 percent overall difference in measured values, with the ground-measured radiance being the higher.

Table 4. The relationship is shown between scene radiance data measured on ERTS-1 MSS imagery (scene 1065-17175) and that measured on the ground in the Black Hills by the RS-2 spectral radiometers.

	Scene Radiance (milliwatts/cm²-SR)							
	MSS Channel							
	4		5		6		7	
Target	ERTS	Ground	ERTS	Ground	ERTS	Ground	ERTS	Ground
Healthy pine	.154	.102	.087	.065	.158	.179	.392	.468
Stressed pine	.140	.093	.093	.101	.144	.135	.399	.506
Pasture grass	.214	.141	.148	.159	.239	.280	.601	.646
Rock outcrop	.316	.219	.204	.199	.353	.358	.920	.999

4. DISCUSSION

From preliminary work with ERTS-1 imagery we look forward with great expectations to receiving one good summertime image of the entire Black Hills test site under full sun conditions. Having already learned to analyze imagery gathered under less than optimum conditions, there is considerable reason for wanting additional good quality coverage so that we can accomplish the goals of the study. Data presented in this report were analyzed from two September ERTS-1 images. One image covered only a small portion of the study area and one MSS channel malfunctioned. The other image was obtained on a cloudy day when the atmospheric water content was high (relative humidity measured at the test site at the time of the satellite overflight was 82 percent). We anticipate few problems in the continued operation of the DCP's and the data collection system.

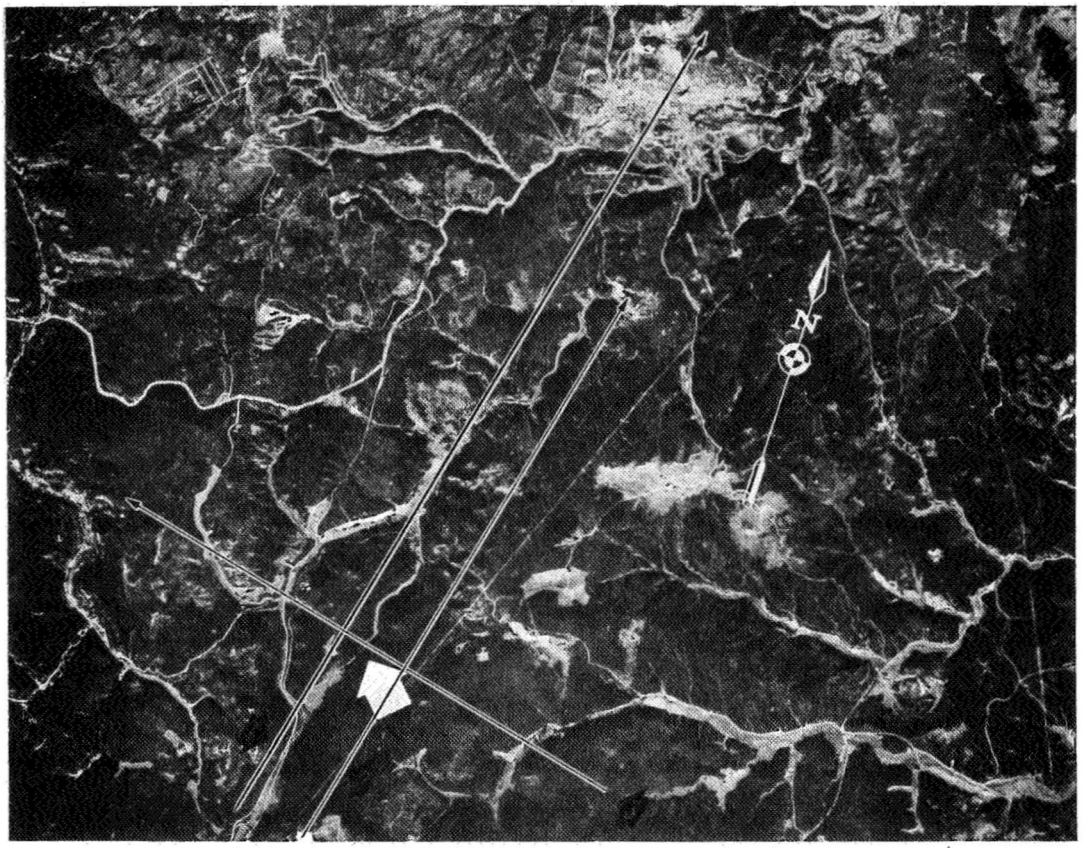


FIGURE 1. A PORTION OF THE BLACK HILLS FORESTRY TEST SITE SHOWS SOME OF THE MICRODENSITOMETER SCAN LINES

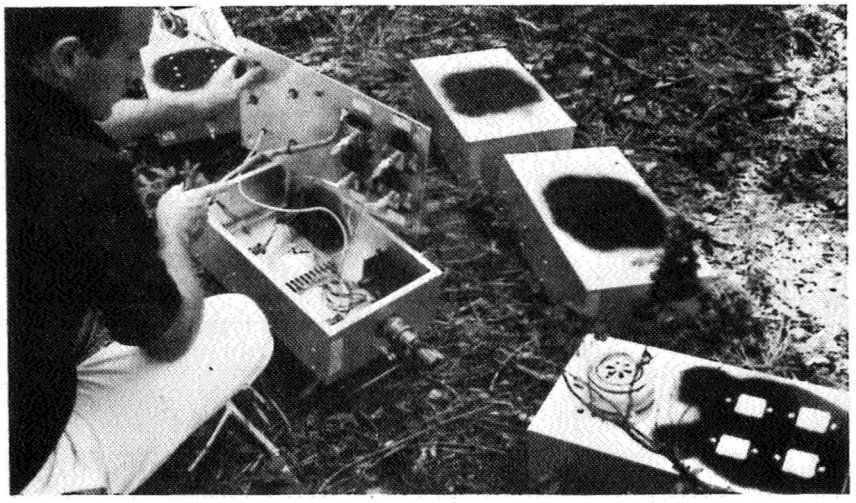


FIGURE 2. RS-2 SPECTRAL RADIOMETERS

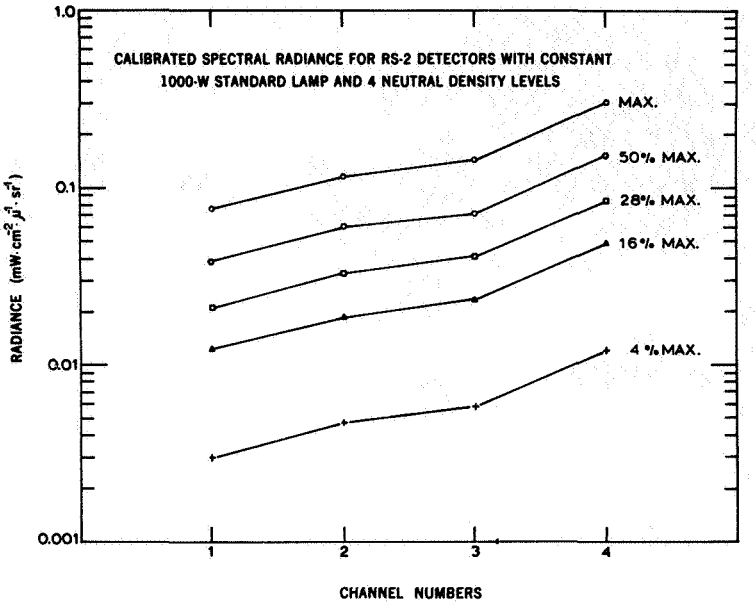


FIGURE 3. CALIBRATED SPECTRAL RADIANCE FOR RS-2 DETECTORS

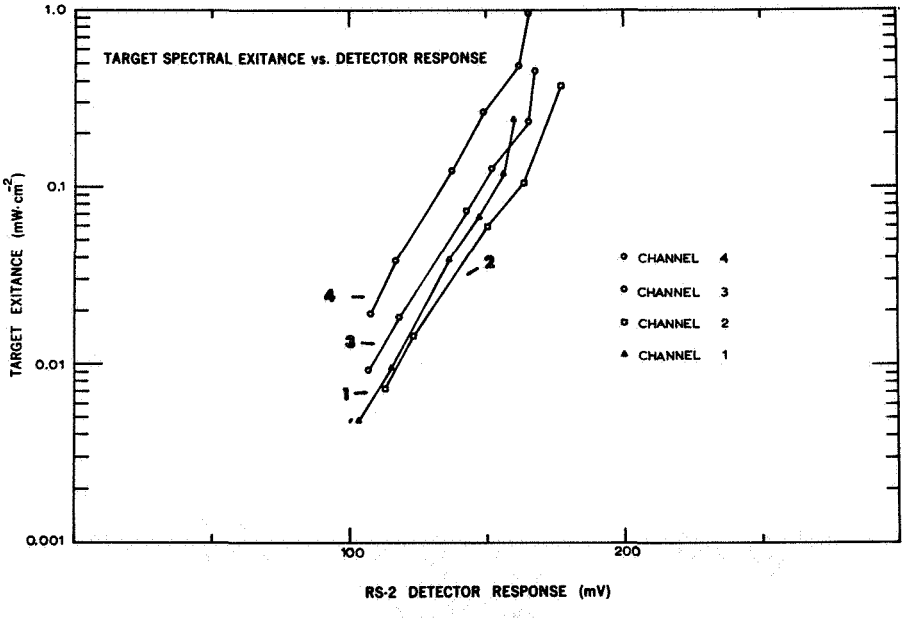


FIGURE 4. TARGET EXITANCE VERSUS DETECTOR RESPONSE FOR RS-2 RADIOMETERS

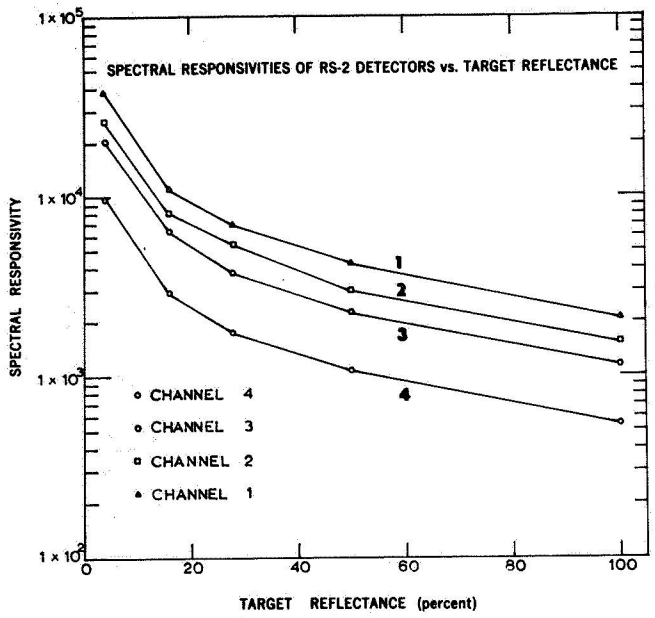


FIGURE 5. SPECTRAL RESPONSIVITIES OF THE RS-2 DETECTORS FOR FIVE LEVELS OF ABSOLUTE TARGET REFLECTANCE

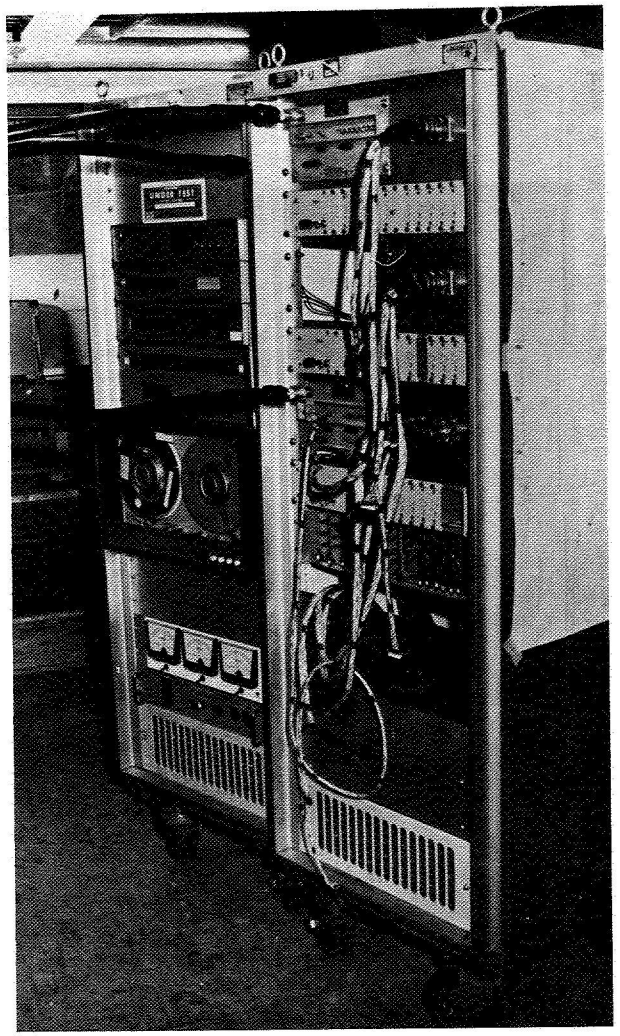


FIGURE 6. DIGITAL DATA ACQUISITION SYSTEM (left) DCP AND MULTIPLEXER CONSOLE (right)

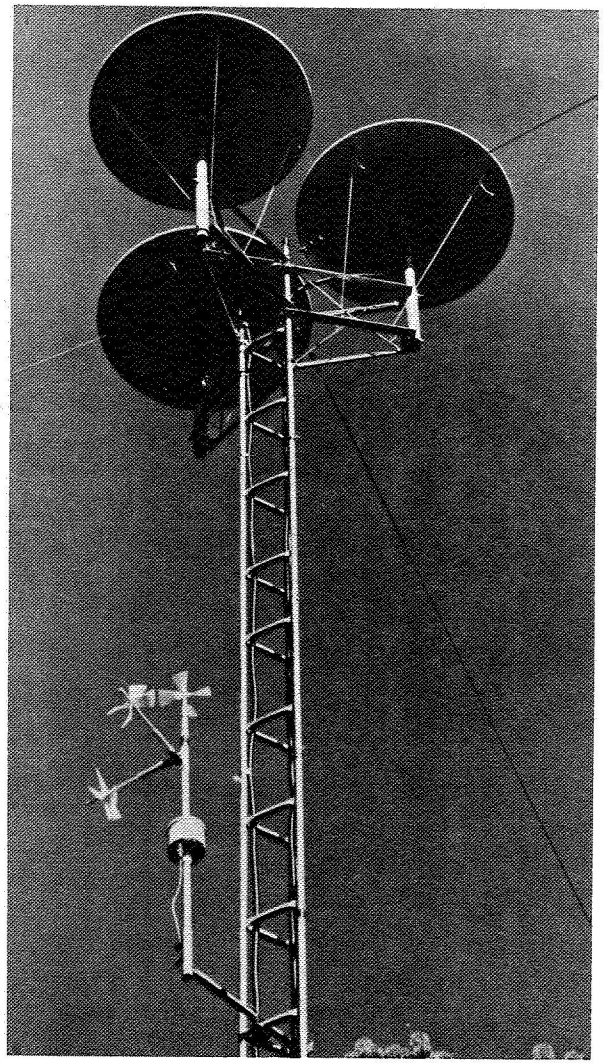


FIGURE 7. DCS/DCP TRANSMIT ANTENNA TOWER



FIGURE 8. FOUR CHANNEL COMPOSITE OF ERTS SCENE 1065-17175 AT SCALE OF 1:100,000

N73-28366

UNIQUE CHARACTERISTICS OF ERTS

Alden P. Colvocoresses, *U. S. Geological Survey, Washington, D. C. 20244*

Aerial cameras and the photographs they produce have been increasingly applied to mapping and related studies for over 50 years. The manned spaceflights have demonstrated what film cameras can do in space and they could provide a data source from which maps would be one of the principal products. ERTS was not defined with mapping as one of its principal objectives, but with ERTS-1 in orbit certain unique characteristics or advantages of the electronic transmission (TV) Earth-sensing system become apparent to the mapmaker. (Electronic transmission from geosynchronous orbit has characteristics completely different from either ERTS or film systems. This paper does not include any comparisons with geosynchronous Earth sensing.)

Six of the more obvious advantages over aircraft and satellite film systems are as follows:

1. Long life and coverage. Even after 7 months of flying, some areas of the U.S. are still not adequately covered by ERTS for cartographic purposes. Apparently a full year will be needed to complete the coverage even though the sensor is turned on for every pass over the U.S. That a single film-return satellite could be efficiently flown for such a long period, or come anywhere near complete U.S. coverage, is doubtful in the extreme. With luck ERTS-1 may survive for 2 or more years and thus provide repetitive as well as complete coverage, making the most of only one launch, spacecraft, and instrument package.

2. Near real time. The advantage of electronic transmission in near real time is obvious even though the capability of realizing the advantages has not been fully developed. For example, a cartographic product was produced within 2 weeks after scene acquisition by ERTS. Electronic transmission of imagery has, in the past, included sizable geometric distortions. ERTS is proving that imagery can be electronically transmitted without serious distortion.

3. Orthogonality. No aerial photosystem or film-return space system (as proposed by Interior) provides imagery as near orthogonal as that of ERTS. The field of view of the ERTS MSS extends only 5.76° from the nominal vertical. The near orthogonality of ERTS imagery precludes compilation of topographic (contour) maps but simplifies small-scale planimetric mapping and revision. Since topography changes little, maintaining up-to-date planimetry is the

Presented at NASA Symposium on Significant Results Obtained from ERTS-1 New Carrollton, Maryland, March 6, 1973.

major mapping problem once an area has been topographically mapped. An orthophotoquad consisting of little more than an image precisely referenced to the figure of the Earth is probably the most effective method of portraying up-to-date planimetry. ERTS imagery is ideal for small-scale orthophotoquads for two reasons. First, external errors such as relief displacement are so small that the image can be used directly, except in areas of extreme relief, without going through the complex transformation provided by an analytical plotter or an orthophotoprinter. Second, the narrow field of view means that the entire scene is being imaged with a nearly constant vertical aspect and thus provides uniform spectral response from any given element of the scene.

4. Radiometric fidelity. The ERTS signals, particularly those of the MSS, are in effect those of a focusing radiometer, recording radiated energy with a range and precision well beyond the capability of any current film system. Therefore, either on tape or as later recorded on film, the spectral image of a given scene will be more meaningful from ERTS than from any film camera. Since ERTS records four wavebands, they can be combined to provide a response optimized for particular scenes or for objects of sufficient size. Film cameras can record up to three bands on one film (color or color IR), but altering the combination for a particular scene or object is complex and imprecise. The separate band characteristic of ERTS is particularly important for mapping objects or areas that have unusual radiometric responses or that are imaged under unusual conditions of illumination, such as the polar regions.

5. Extension into the near IR wavelengths. Available aerial films cut off between 0.8 and 0.9 μm, which is about the same as for band 6 of the MSS. MSS band 7, at 0.8 to 1.1 μm, has opened a window for remote sensing for which operational film systems do not have a capability. The band is enormously powerful and has demonstrated the following unique capabilities:

a. Effective penetration of thin clouds and contrails (under certain conditions).

b. Definition of the water/land interface with high precision, enabling detection and identification of water bodies as small as 200 m diameter and determination of water stage to a fraction of a meter through boundary correlation in flat, shallow areas. The capability is particularly significant when one considers that the instantaneous field of view of the MSS (spot size) is 79 m.

c. Superior definition of vegetation patterns, largely due to the differential sensitivity of band 7 to vegetation types.

d. Superior definition of natural features. Geologists (and others) are selecting MSS 7 as the best single band for depicting the Earth's physiographic structure.

e. In some cases cultural features are best defined on band 7. For example, the pattern of major streets in Los Angeles as so far recorded by ERTS.

Aerial film systems being developed abroad cover the MSS-7 waveband.* If they become operational, the current advantage of the MSS-7 waveband will, of course, be reduced.

6. Extension into the thermal wavelengths. NIMBUS-5 and NOAA-2 are demonstrating thermal mapping with a spot size of 700 to 900 m. ERTS-B is scheduled to carry a thermal scanner of about one third this spot size, that is 240 m. Thermal mapping with a spot size of 240 m has enormous potential application and is, of course, impossible with film systems.

Today television is an accepted means of visual communications, and TV Earth sensing systems such as ERTS and its successors promise to take their place beside the film camera as essential tools for cartography.

*Information from Dr. George Zissis of the University of Michigan.

N73-28367

ERTS-1 APPLIED FOR STRUCTURAL AND MORPHOLOGICAL INVESTIGATIONS CASE STUDIES: (1) LOS ANGELES, CALIFORNIA AND (2) COASTAL PLAIN, NEW JERSEY

Ervin Y. Kedar, *Department of Geography, William Paterson College of New Jersey*

This report addresses itself to a major earth's resources management problem; namely, the application of ERTS-1 imagery for geo-morpho-tectonics, and subsequently seismic-risk, earthquake, and mineral exploration applications.

Case Study No. 1 – Los Angeles, California

ERTS-1 image (MSS color composite of August 10, 1972, E-1018-501, centered at N 34.13/w 118-27), which covers the area from South Los Angeles to the Mojave Desert and from Eastern San Gabriel Mts. to Cuyama Valley and Central Santa Ynez Mts., of the Transverse Ranges, California, was analyzed (fig. 1). This image was studied in conjunction with the following conventional sources: (1) the Los Angeles Sheet of the geologic map of California (1); (2) the map of the Geology of the Central Santa Ynez Mountains, Santa Barbara County, California (2); (3) the geologic map of Transverse Ranges, Southern California (3).

A comparison of ERTS-1 image to the conventional sources indicated the usefulness of the image in studying structural geology.

The following are aspects of the comparisons:

(1) Each conventional source failed to show the Verdugo Mts. lineament, the Simi Hills lineament and the Santa Monica Mts. lineament, all of which bound the San Fernando Valley (fig. 2). These structural lineaments which are seen readily on the ERTS-1 image are apparently the major morphotectonic features in the structural framework of the San Fernando Valley. The image also indicates that Point Dume is the seaward extension of the Simi Hills lineament across the Santa Monica Mts., and that Point Dume represents a post-Cretaceous/early Paleocene geotectonic episode.

(2) Each conventional source fails to show the oval-shaped sedimentary basin between the Simi Hills lineament in the S.E. and the Oakridge fault in the N.W. This oval-shaped unit, which has no physiographic name, since it was not seen yet, is a lithological and structural unit separated from the adjacent region. It is inferred from ERTS-1 image that the Violin Canyon watershed, the upper part of the Santa Clara River system, is the major source of sedimentation in the oval basin.

PRECEDING PAGE BLANK NOT FILMED

Original photography may be purchased from:
EROS Data Center
10th and Dakota Avenue
Sioux Falls, SD 57198

(3) Neither conventional source showed the major structural element in the Transverse Ranges; namely, the Ventura-Soledad Trough. This structural trough, which is readily seen on the ERTS-1 image, cuts across the Transverse Ranges from Antelop Valley to Santa Barbara Channel. It is believed that Ventura-Soledad Trough is the most seismic part of greater Los Angeles. Newhall, California, the epicenter of the San Fernando Valley earthquake in February 1971, is located on the intersection of the San Gabriel Fault, the Verdugo Mts. Fault, the Simi Hills Fracture Belt and the Ventura-Soledad Trough. This conclusion was derived from ERTS-1 image analysis (fig. 3).

The conventional sources do not show the above mentioned information because they are either overgeneralized or undergeneralized. The geologic map of the Transverse Range Province has only fault lines and rock age distribution and lacks drainage patterns and contour lines. The Los Angeles sheet of the geologic map of California has too much information (road system, railroads, power line, etc.) and makes no distinction between major faults and local faults. ERTS-1 image was found to be a generalized, yet selective, source of information.

Case Study No. 2 – Coastal Plain, New Jersey

ERTS-1 image (MSS color composite of August 17, 1972, E-1024-15071-501 centered at N 40-21/w 073.26), which covers the area from the Palisades, New York-New Jersey to Burlington, New Jersey, and from New Brunswick, New Jersey to the great Pecomic Bay, New York, was analyzed (fig. 4). This image was compared with: (1) the geologic map of New Jersey 1:1,000,000 (4); (2) the geologic map of New Jersey 1:250,000 (5); and (3) selected maps as published in the geology of selected areas in New Jersey and Eastern Pennsylvania (6).

In this case study, too, ERTS-1 image indicated its usefulness in studying the structural geology of the test site region.

The following are aspects of this case study:

(1) The coastal plain is underlain almost entirely by unconsolidated marine and fluviatile clay, silt, sand and gravel of Late Cretaceous and Tertiary Age. Much of this province is covered by Quarternary deposits, particularly in the inner and outer lowlands and the southern one-third of the central upland of the Coastal Plain. The difficulty of mapping the quarternary deposits was recognized a long time ago (Salisbury 1917, 7). He subdivided the Pleistocene deposits into three formations: (from the oldest to the youngest) (a) the Bridgeton; (b) Pensauken; and (c) Cape

May. The major portion of the Pensauken is confined to a 20-mile wide belt whose axis extends from Staten Island, N. Y., south westward to Salem, N. Y. This belt was first seen and traced on the ERTS-1 image. It was suggested that this belt is trough shaped. This trough was only roughly mapped (Campbell and Bascom 1933, 8). It was also concluded that the Pensauken was an alluvial deposit formed by the combined ancestral drainage system of the Hudson River (9), (fig. 5).

(2) The Coastal Plain has potential economic ilmenite sands type ore bodies and other heavy mineral deposits (10). Today several companies mine these and other minerals in the Coastal Plain. Some of the mines can be seen and identified on the ERTS-1 image, such as the mines at Lakehurst, N. J. In order to determine the location of these mineral deposits, the ancient drainage patterns have to be determined. ERTS-1 imagery can be used for the hypothetical reconstruction of ancient drainage patterns (see (1)a on previous page), (fig. 6).

Conventional sources, including field investigation, have been found to be inadequate to supply all the required structural and paleohydrographic information needed.

It is, therefore, concluded that ERTS-1 was found to be an essential supplementary source of information for geologic explorations, much like and even better than space photography from manned spacecraft, and SLR imagery (11).

REFERENCES

1. Anon: Los Angeles Sheet of the Geologic Map of California, 1:50,000, 1955.

2. T. W. Dibblee, Jr., Geology of the Central Santa Ynez Mountains, Santa Barbara County, California, Bull. 186, California Division of Mines and Geology, San Francisco, 1966.

3. Olaf P. Jenkins, Geologic Map of Transverse Range Province, Southern California, Department of Natural Resources, State of Califronia, Bull. 170, Chap. 2, Cont. 3, Plate 4, 1954.

4. Geologic Map of New Jersey, 1:1,000,000, New Jersey Geographical Press, Little Falls, N. J., 1962.

5. J. V. Lewis and H. B. Kummel, The Geology of New Jersey, Geologic Map 1:250,000, Geological Survey of New Jersey, 1915.

6. Geology of Selected Areas in New Jersey and Eastern Pennsylvania and Guidebook of Excursions, edit. by Seymour Subitzky, Rutgers University Press, New Jersey, 1969.

7. R. D. Salisbury and G. N. Knapp, The Quarternary Formations of Southern New Jersey: The Final Report Series of the State Geologist, Vol. VIII Department of Conservation and Economic Development, Trenton, New Jersey, 1917.

8. M. R. Campbell and F. Bascom, Origin and Structure of the Pensauken Gravel: Am. Your. Sci., Vol. 26, p. 300-318.

9. R. R. Jordan, Columbia Sediments of Delaware: Delaware Geological Survey, Bull. No. 12, Newark, 1964.

10. Frank J. Markewicz, Ilmenite Deposits of the New Jersey Coastal Plain, in Geology of Selected Areas in New Jersey, pp. 363-382, 1969.

11. The following are publications by E. Y. Kedar:

Side-Looking Radar (SLR) Imagery Applied to Seismic-Risk Mapping, Eighth International Symposium on Remote Sensing of Environment, October 2-6, 1972, Ann Arbor, Michigan.

Clustering Phenomena in Side-Looking Radar (SLR) Micro-Texture, Electro-Optics 1972 Conference, September 12-14, 1972, New York City.

Space Photographs of the Earth in the Study of Plate Tectonics, 22nd International Geographical Congress, Montreal, Canada, August 10-15, 1972.

Earth Photographs from Space Applied for Geomorphotectonic References presented at the Association of the American Geographers, Kansas meeting, April 1972.

Earth Photographs from Space for Plate Tectonics and Earthquake-Risk Mapping, American Society of Photogrammetry, March 12-17, 1972, Washington, D. C., Proceedings of the 38th Annual Meeting, ASP.

Application of the Discriminant Function in Automatic Pattern Recognition of Side-Looking Radar, presented to the Seminar of the Society of Photo-Optical Instrumentation Engineers, Redando Beach, California, Feb., 1972.

Plate Tectonics in the Israel-Sinai Region, The Geological Society of America, Abstracts, the 1971 Annual Meeting, Washington, D. C., November, 1971, Vol. 3, No. 7, p. 476, 619.

An Automatic Analytical System of Side-Looking Radar (SLR) Imagery and its Applications in Environmental Discrimination, Proceedings of the Technical Program, Electro-Optical Systems, N. Y., September 5-6, 1971, pp. 353-356.

Manual and Automatic-Computerized Systems of Side-Looking Radar Imagery Analysis for Crop Discrimination, in the American Society of Photogrammetry, Proceedings, ASP-ACSM, Fall Convention, San Francisco, September 1971, pp. 190-199.

Manual and Automatic-Computerized System in SLR Application for Land Use Survey, Technology, Utilization Ideas for the 70's and Beyond, American Astronautical Society, Vol. 26, Science and Technology, May 1971, pp. 239-262.

Plate Tectonics in the Red Sea Region as Inferred from Space Photography, NASA Technical Note, TN D-6261, NASA, Washington, D. C., April 1971 and presented at the Seventh International Symposium on Remote Sensing of Environment, May 1971, Ann Arbor, Michigan.

Plate Tectonics in the Red Sea Region as Inferred from Space Photography, Earth-Observation Division, Johnson Space Center, NASA, S-257.

Transverse Range: Tectonic Inferences from Earth Photographs from Space. Earth-Observation Division, Johnson Space Center, NASA, TF7-2, June 1970. NR-E9-00-000-01056.

Texas Lineament Traced on Earth Photographs Taken from Space. Earth-Observation Division, Johnson Space Center, NASA TF7-3, June 1970. NR-E9-09-998-00407.

Space Photographs of the Earth in the Study of Plate Tectonics. Earth-Observation Division, Johnson Space Center, NASA, TF7-4, June 1970. NR-E9-EJ-998-01055.

Plate-Margin Morphotectonics Case Study: The Israel-Sinai Section. Earth-Observation Division, Johnson Space Center, NASA, TF7-6, June 1970. NR-E9-00-998-01131.

Space Photographs of the Earth in the Study of Geotectonics, Science and Earth Technology, Vol. 23, American Astronautical Society 69-579, October 1969, pp. 331-332.

Application of Space Photographs for Geomorphological Study; Taurus Mountains, Turkey, Earth Observation Division, Johnson Space Center, NASA, TF7-1, August 1969, NR-E9-03-000-00634.

Geomorphotectonic Inferences from Apollo and Gemini Photographs: A Case Study of the Southwestern United States, presented at the 32nd Annual Meeting of the Association of Pacific Coast Geographers, San Fernando Valley State College, June 11-14, 1969.

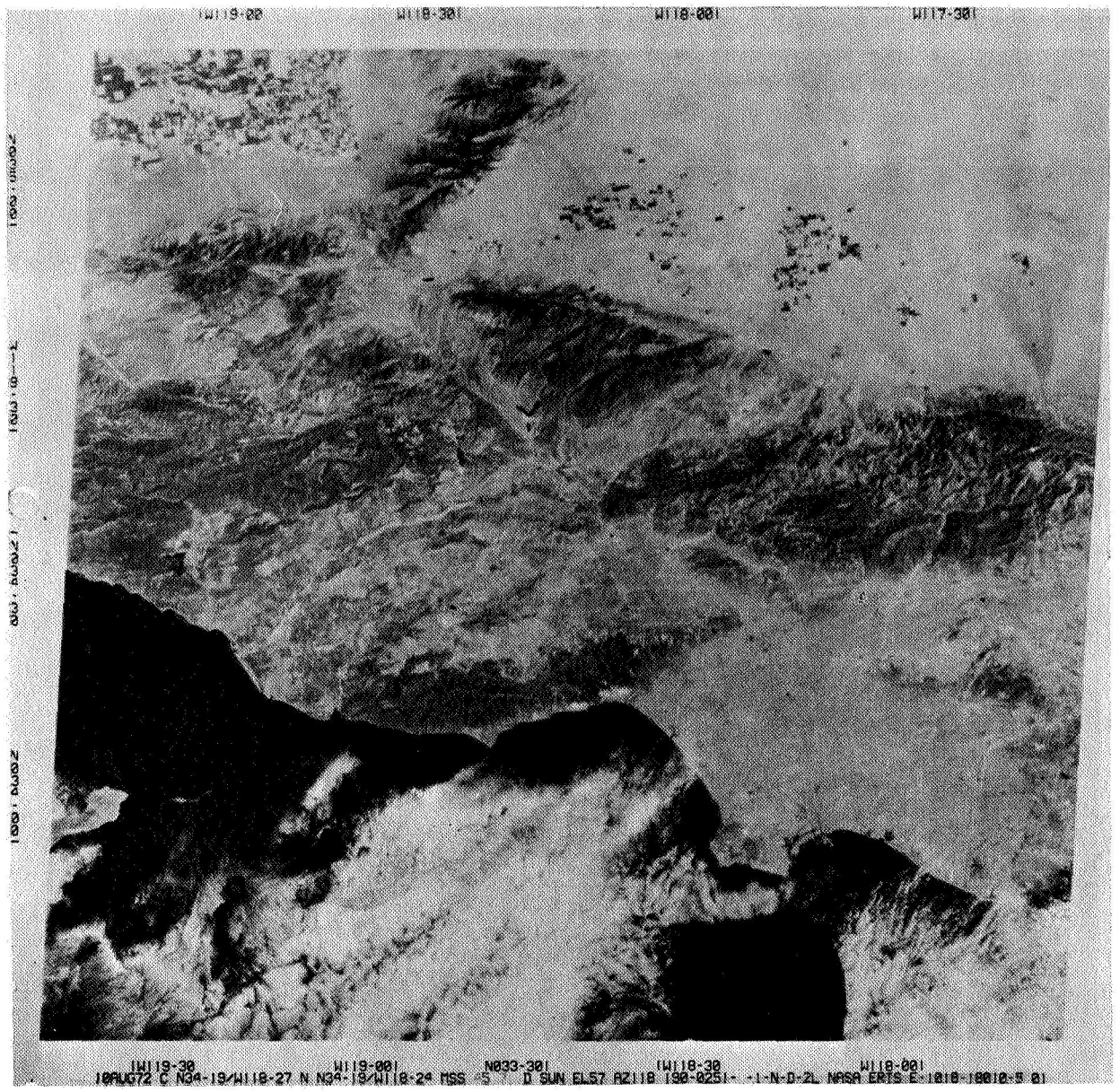


Fig. 1 ERTS MSS Color Composite of August 10, 1972
Centered at N 34.13/W 118.27.

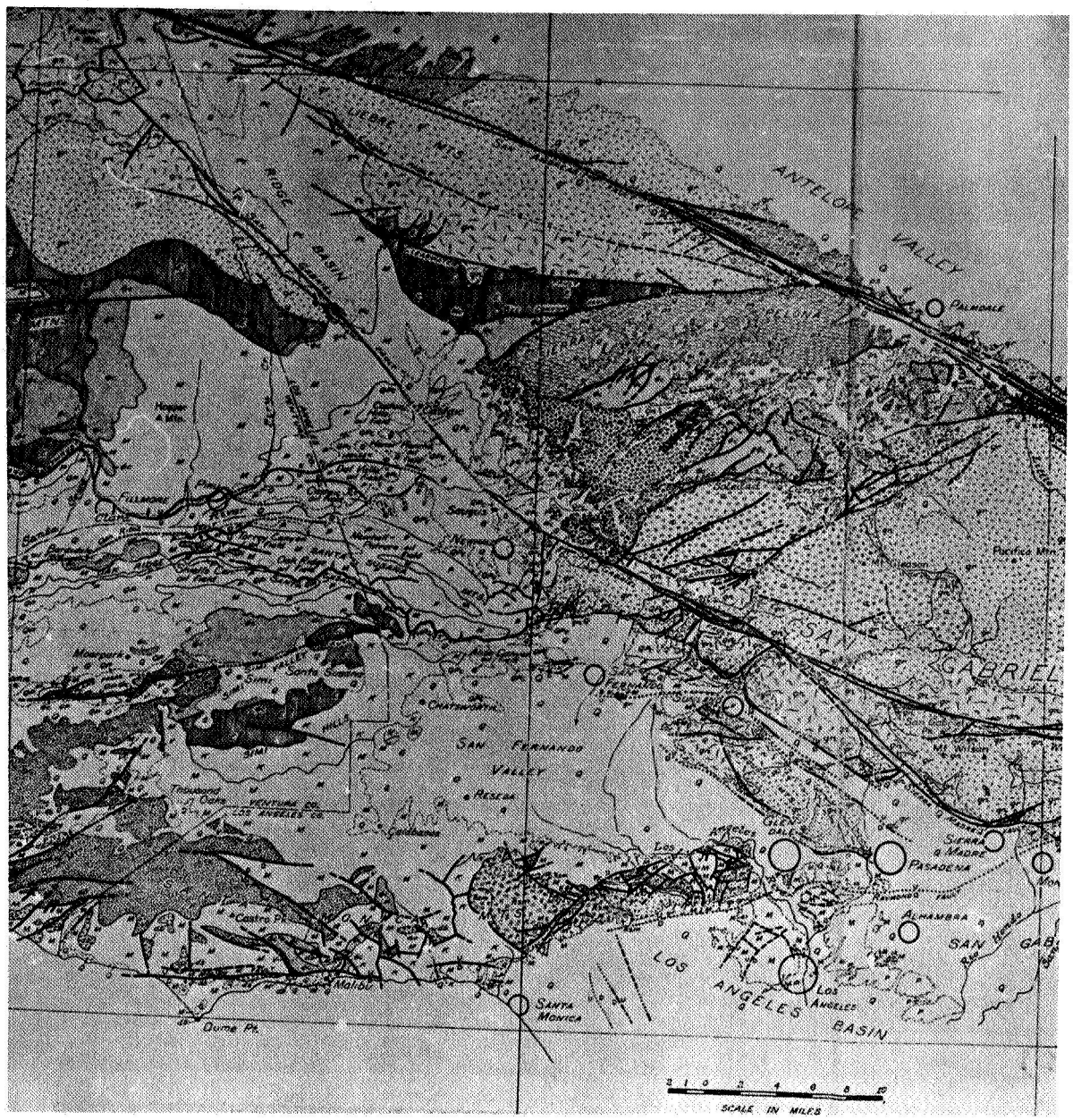


Fig. 2 Geologic Map, Transverse Range Province.

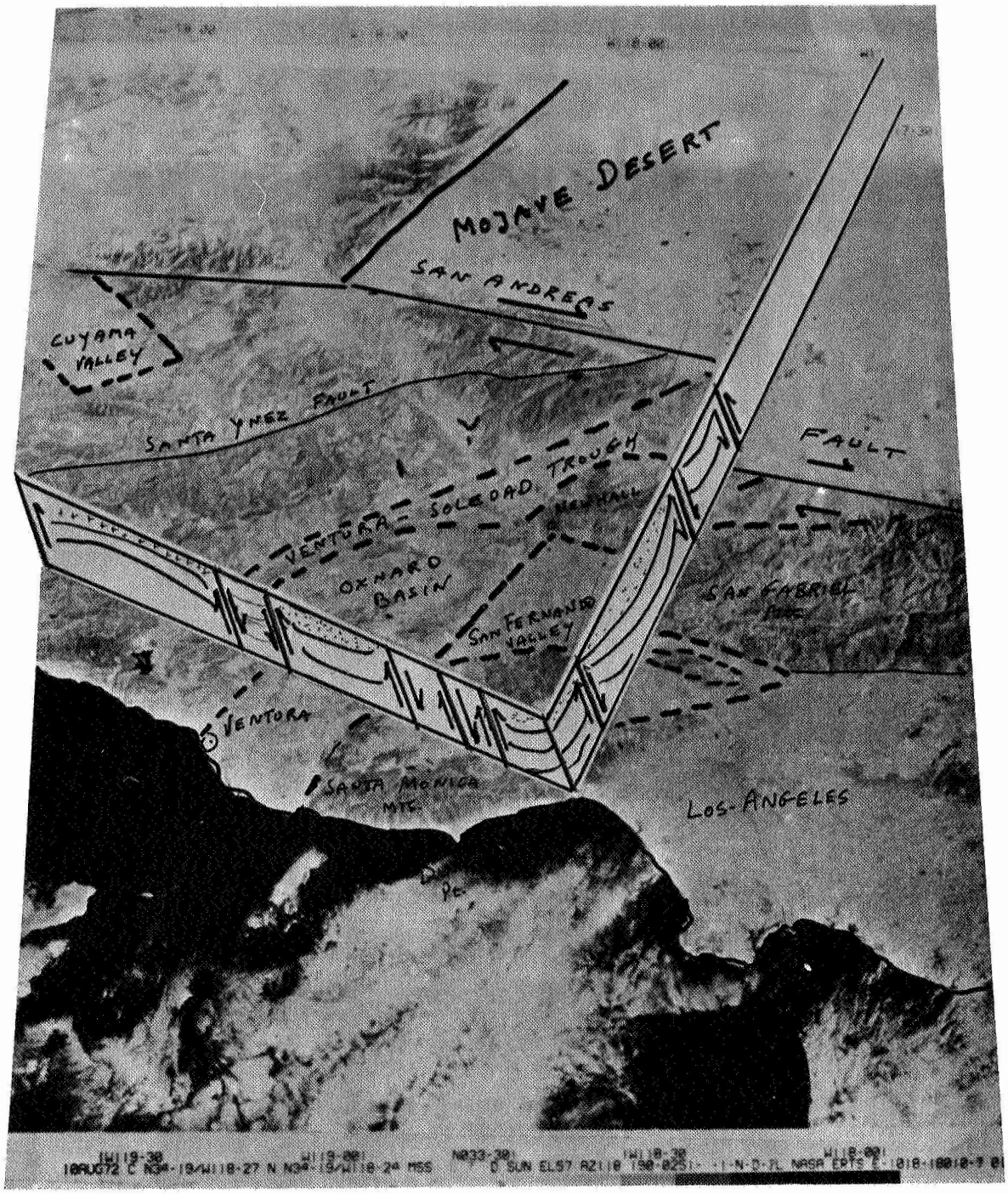


Fig. 3 ERTS-1 MSS Color Composite of August 10, 1972, Structural Analysis (See fig. 1).



Fig. 4 ERTS-1 MSS Color Composite of August 16, 1972, Centered at N 40.21/W 073.26.

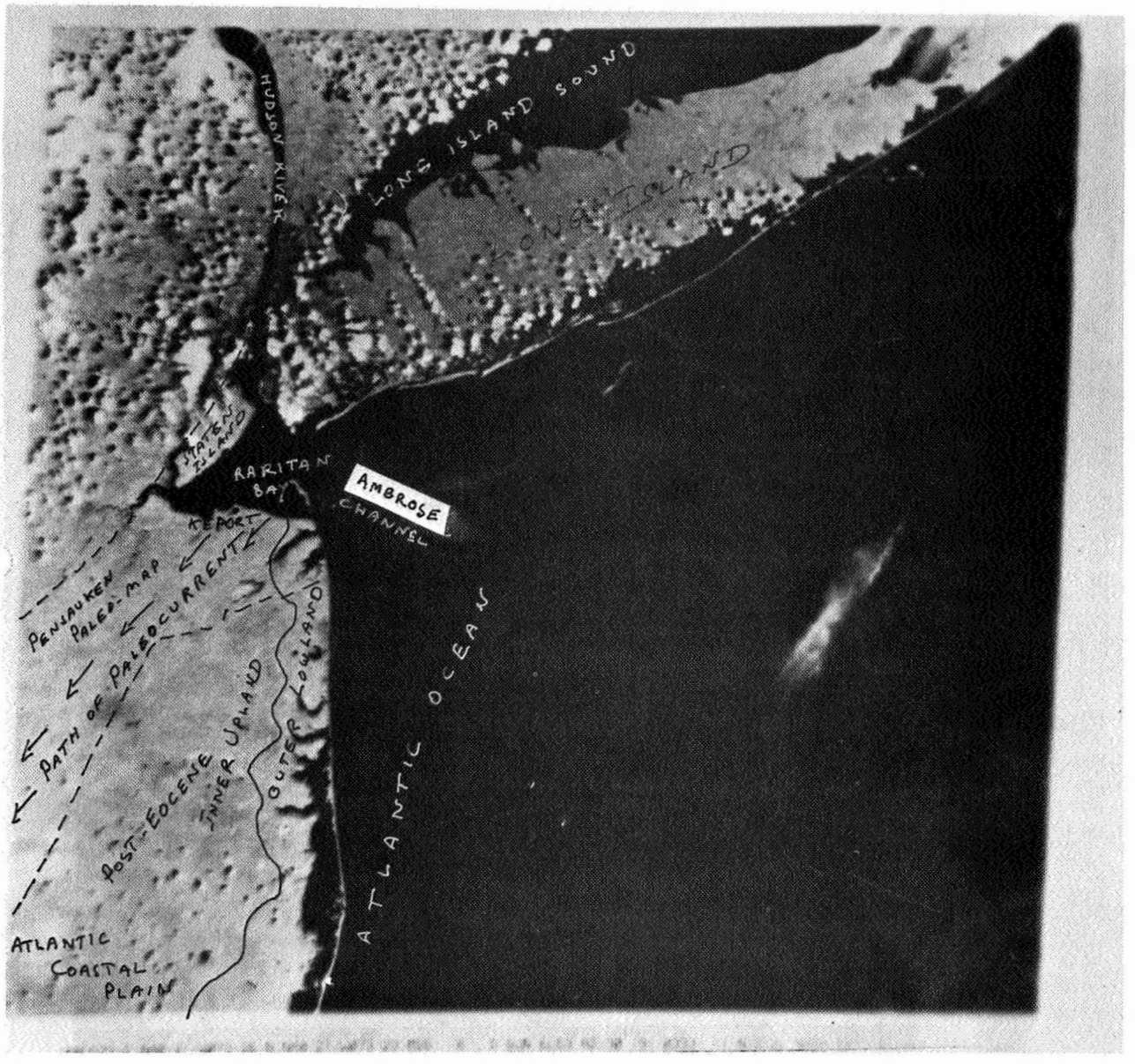
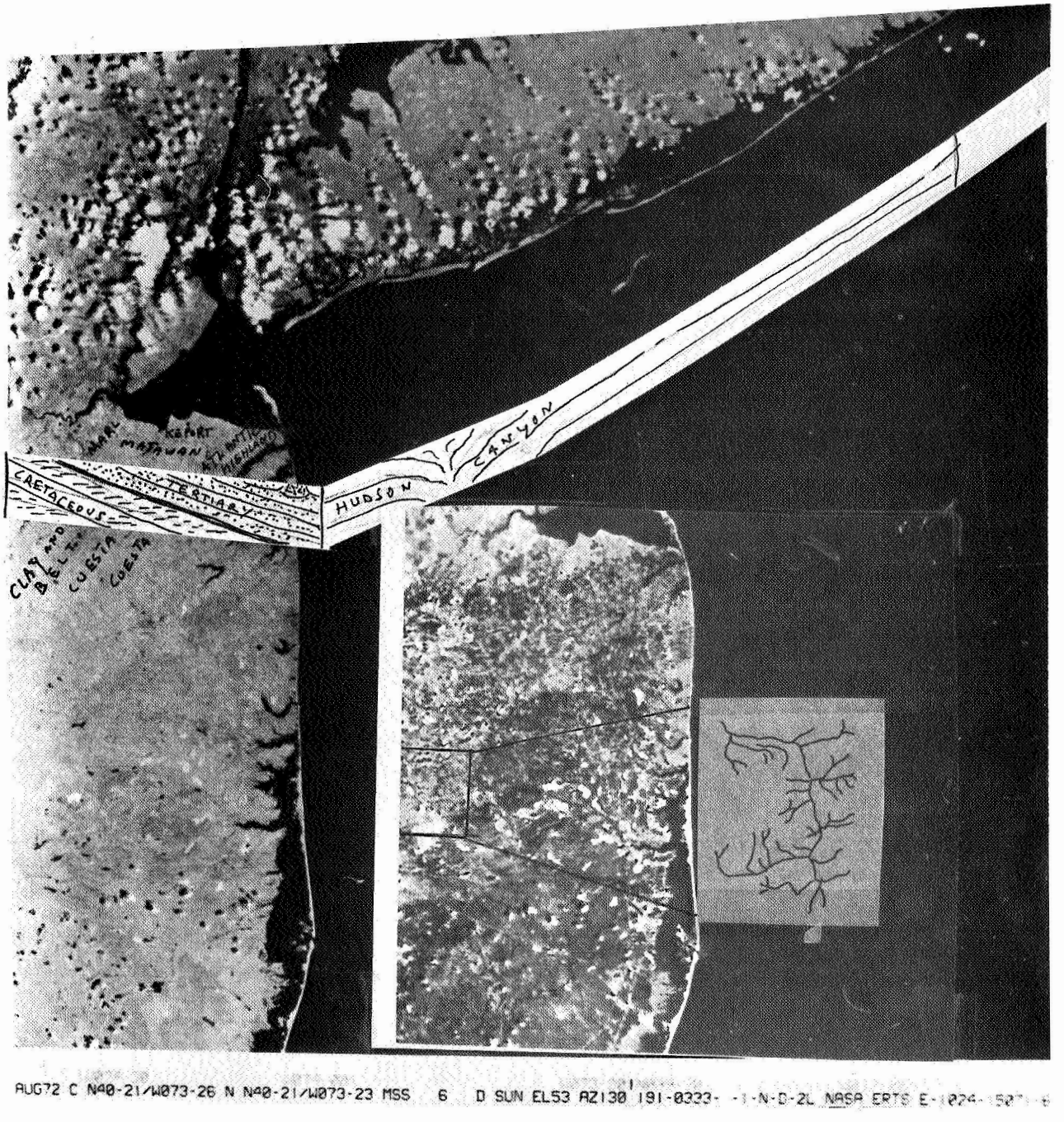


Fig. 5 ERTS-1 MSS of Eastern New Jersey Paleo-Hydrology.



AUG72 C N40-21/W073-26 N N40-21/W073-23 MSS 6 D SUN EL53 AZ130 191-0333- -1-N-D-2L NASA ERTS E-1024-52

Fig. 6 ERTS-1 MSS Structural and Hydrographic Interpretations.

N73-28368

A PRELIMINARY EVALUATION OF ERTS-1 IMAGES ON THE VOLCANIC AREAS OF SOUTHERN ITALY (NASA CONTRACT FO-013)

Cassinis R., Lechi, G. M., *National Research Council of Italy (CNR) Laboratorio per la Geofisica della Litosfera, Milano, Italy*

The test site selected for the investigation covers nearly all the regions of active and quiescent volcanism in southern Italy, i.e. the Eastern part of the island of Sicily, the Aeolian Islands and the area of Naples.

The three active European volcanoes (Etna, Stromboli and Vesuvius) are included.

The investigation is in the frame of a programme for the surveillance of active volcanoes by geophysical (including remote sensing thermal methods) and geochemical methods.

It is also in connection with the Geodynamics project for the Mediterranean-Alpine region.

By the multispectral analisys of ERTS-1 data we intend to study the spectral behaviour of the volcanic materials as well as the major geological lineaments with special reference to those associated with the volcanic region.

Secondary objectives are also the determination of the hydrographic network seasonal behaviour and the relationship between the vegetation cover and the different type of soils and rocks.

Original photography may be purchased from
EROS Data Center
10th and Dakota Avenue
Sioux Falls, SD 57198

We received the images of the first available pass over the test site (August 9 1972) only in January 1973.

However, we were able to produce a first enhancement of the images by false colour composition of two passes (August 9 and Nov. 23 1972) in order to perform a first evaluation of the seasonal effects.

In this paper only the results obtained by the Aug.9 pass over the Southern part of Sicily are discussed and illustrated.

Technical approach.

For the composition we used only the 5,6,and 7 bands because the band 4 was not shipped.

The selection of the best set of filters and light intensity was done by means of a multiple projector.

The photographic composition was accomplished by a sequential contact printer using the same filters and intensities employed in the multiple projector.

The colour composite images are performed using yellow, magenta and cyan colours in order to standardize the results.

In order to map the different steps of reflectance, an optical-fiber device was employed, scanning the selected composite transparencies.

As a second phase a "multispectral reader" will be used, scanning simultaneously different images of the same area and producing electrical signals which will be add or subtracted or divided.

This technique will be used in order to have a more quantitative interpretation.

Description of the colour enhanced images.

Fig. 1 represents an uncontrolled mosaic of three images (band 7) taken on Aug. 8 and 9 1972 over Sicily.

In that season the soil is very dry and bare except in some restricted areas.

The sun elevation was 56 degrees.

Fig 2 and 3 represent two composite colour enhancements of the Southern part of Sicily.

The enhancement of Fig. 2 is done by the subtractive method using cyan (band 5) magenta (band 6) and yellow (band 7).

The composite image of Fig. 2 is particularly suitable to see the geological lineaments (SE corner, on the Ragusan plateau) as well as the contrast between recent lava flows and the typical vegetation of Mount Etna (upper right).

The composite image of Fig. 3 was obtained by reversing colours of the bands 5 and 6; the additives used was red (band 5) green (band 6) and blue (band 7).

The vegetation is particularly enhanced by this composition.

Fig. 4 is an enlargement to the scale of 1:100.000 of Fig. 2 showing the Etna Volcano. (coord : 37,30 N; 15,00 E)

The max. elevation of the cone is of 3300 m.a.s.l.

This active strato-volcano produces basic lavas; the last great eruption occurred in May 1971.

The main eruptions normally occur from the central cone but the most dangerous lava flows erupt from secondary fissures opening on the slopes.

Our investigation, so far, is concentrated on the analysis of the spectral behaviour of lavas; several tones were observed in the areas covered by the volcanic materials, as appears on the different colour composition.

The main difficulty to establish a correlation between the tone and the lava type and/or age, lies on the vegetation cover.

However we attempted a first rough classification of the volcanic materials based on the following criteria:

1) Extention of old lavas completely covered by vegetation. In this case there is a large error in computing the spectral difference between the lavas and the vegetation cover.
2) Recent lava flows (less than 400 years about). The extention of lava flows is clear and the vegetation yelds a small error in computing the areas.
3) Very recent volcanic activity (from 1960). A relatively small area around the main crater clearly shows a reflectance quite similar to that of water; this can be explained by the total lack of vegetation and can also depend on the thin cover of pyroclastic deposition. In this case the reconnaissance is good.

A positive result is the identification of some, small areas surrounded by lava flows and of different reflectance which can be correlated with the exposures of sedimentary formations.

Fig. 5 is a map of the relative reflectivities measured around the cone by a reader employing a fiber-optic system.

Remarks.

As a preliminary correlation we remark that, though the interpretation is affected by errors, the potential discriminative power of the multispectral analysis is confirmed.

The limitation of this investigation is also given by the insufficient number of bands to be analized and by the difficulty to receive the repetitive coverages.

In fact, the repetitive observation of the same area will enable the investigators to follow the spectral behaviour of the surface under different sun angles and azimuths and in different seasons, especially taking account of the influence of the vegetation cover.

Furthermore we began to analyze the potential of ERTS imagery enhanced by the colour composition to define the main geological features in the surveyed area.

Good results were obtained particularly on the SouthEast of Sicily over the Ragusan plateau, where several faults are clearly observed.

In some cases a better pattern recognition is reached by the synoptic power of the ERTS enhanced images.

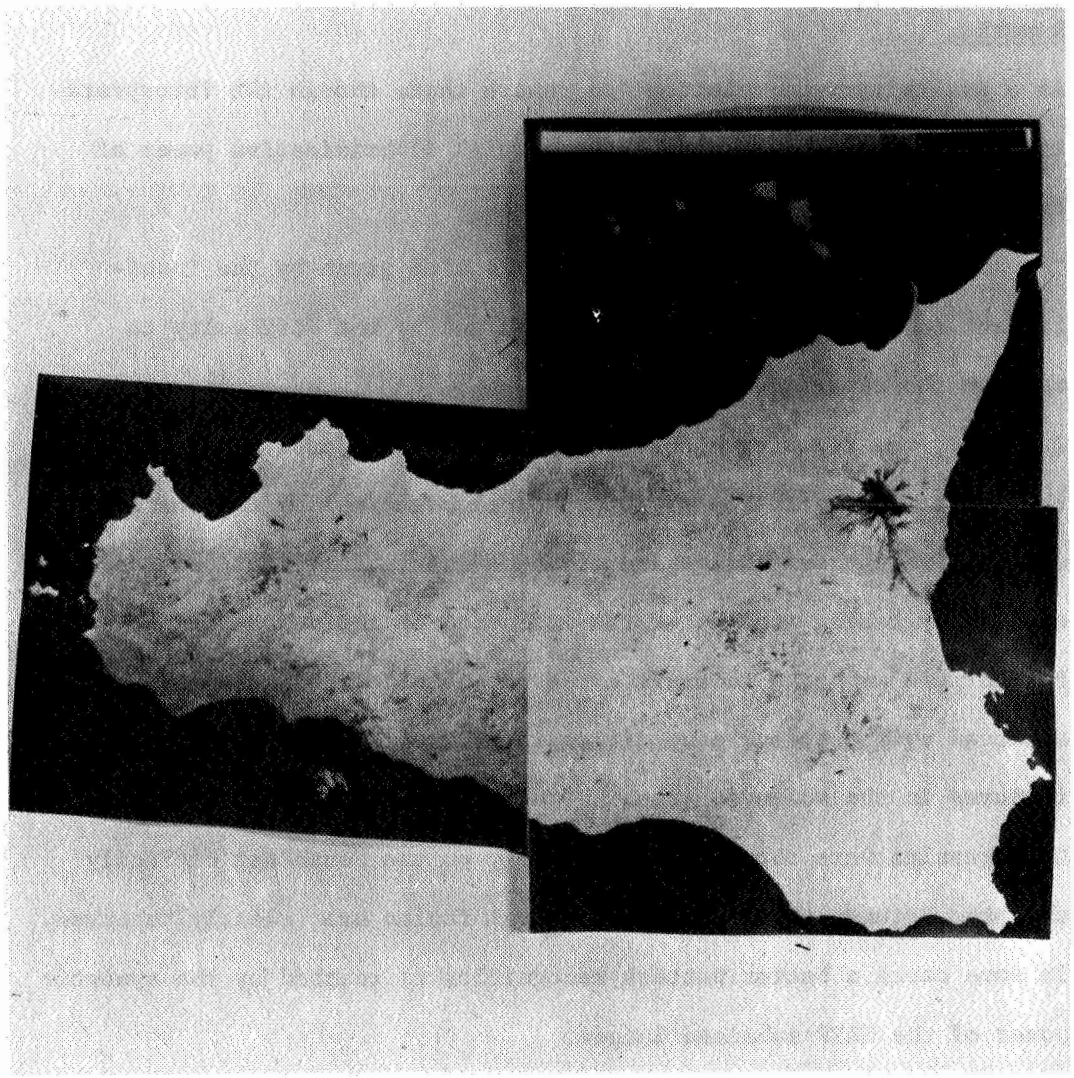


Figure 1. Assembling of Three ERTS-1 Images over Sicily (Band 7)
Orbits of August 8 and 9, 1972

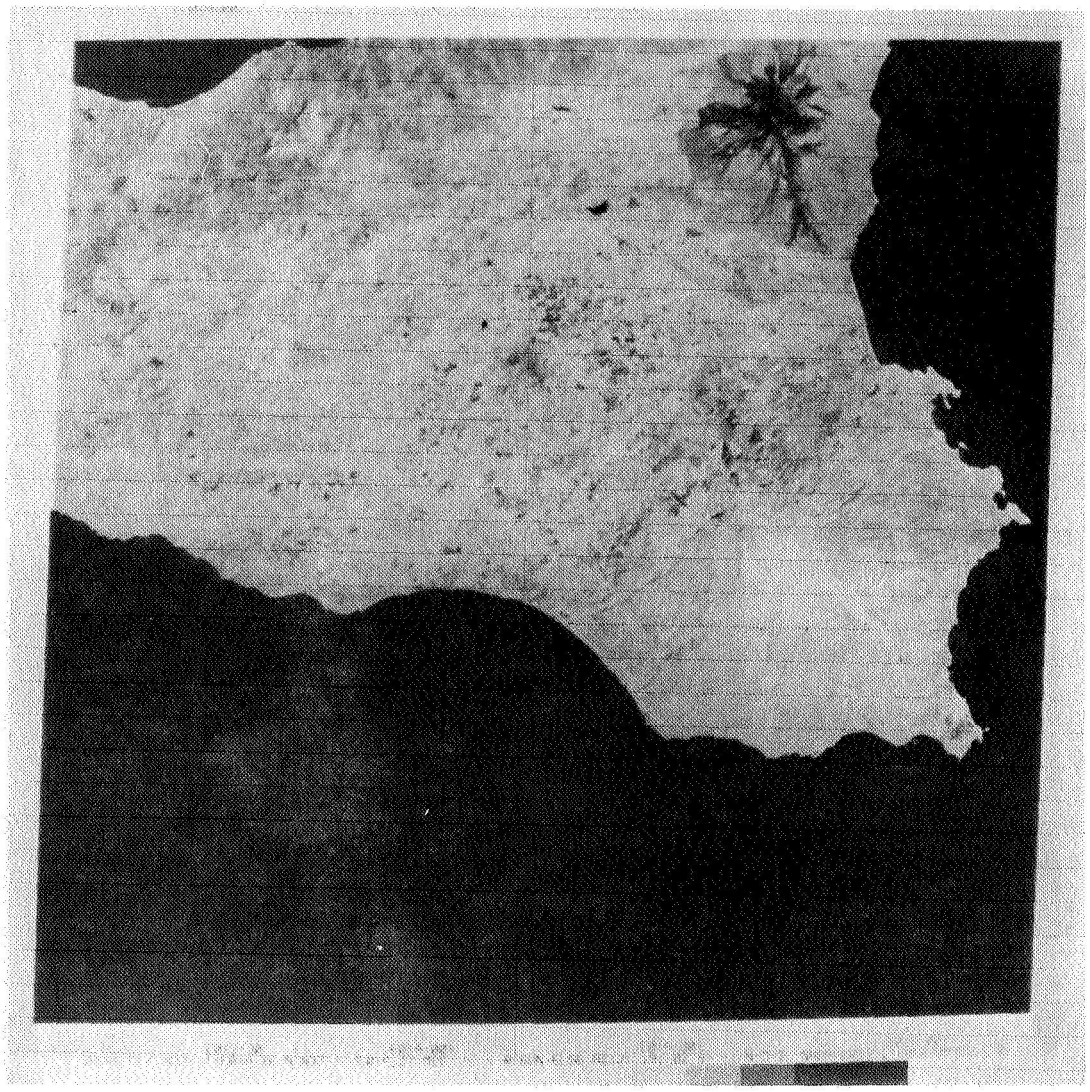


Figure 2. Composite Image of the Southeastern Sicily from Bands 5, 6, and 7, Original Colours: Cyan, Magenta and Yellow

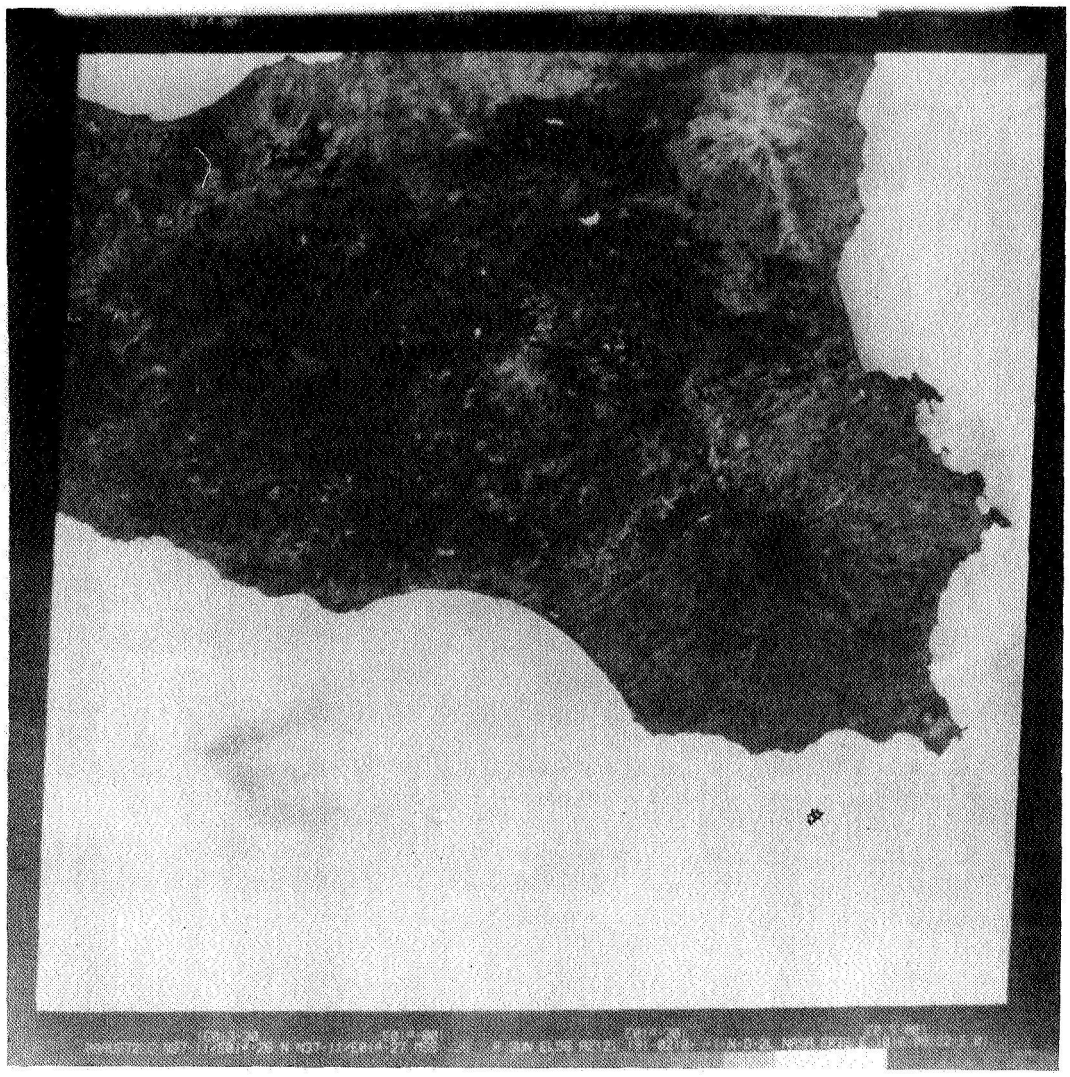


Figure 3. The Same Image Obtained by Reversing Colours of the Bands 5 and 6, Additives Used: Red, Green and Blue

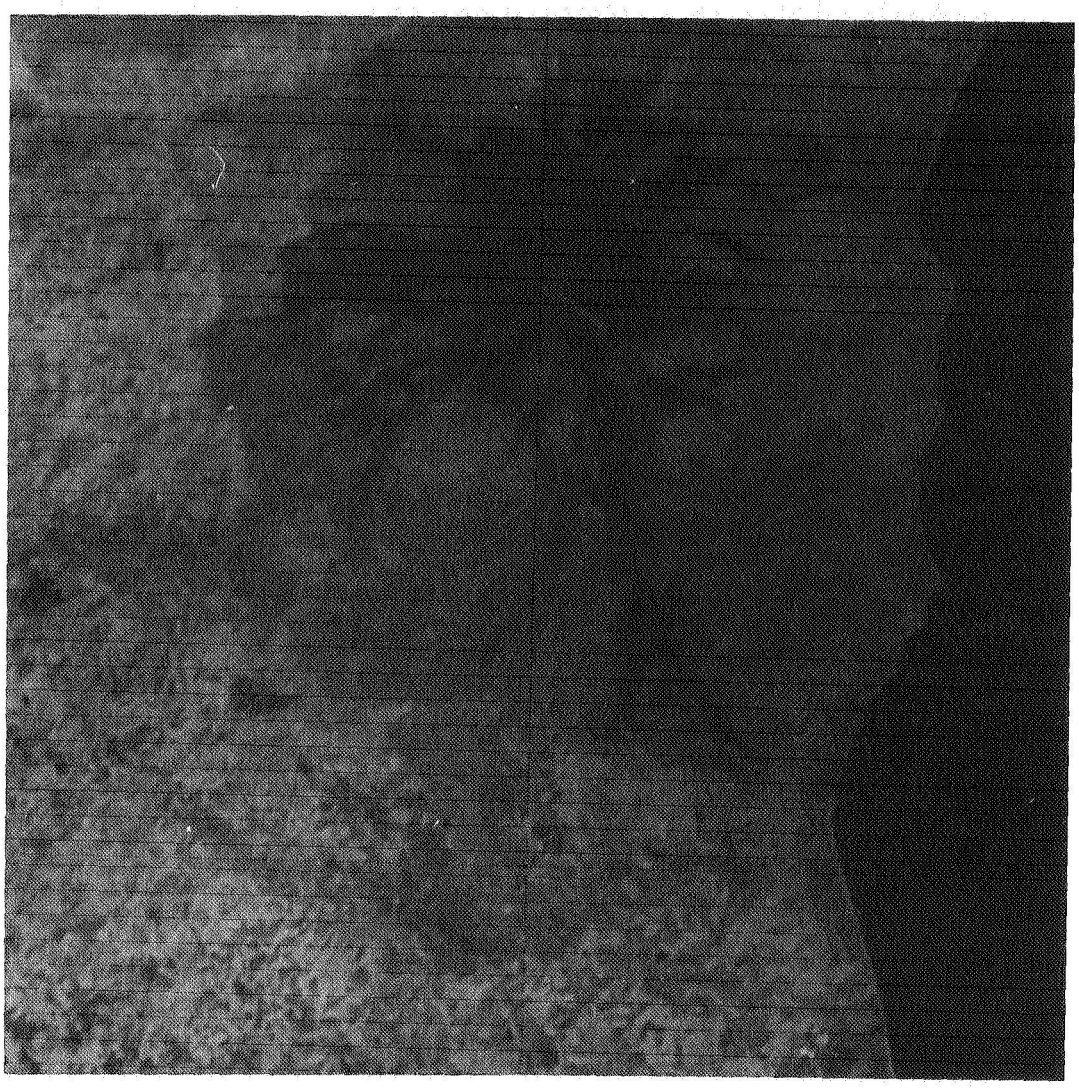


Figure 4. Enlargement from Image of Figure Showing Mount Etna and the Recent Lava Flows (Original Scale 1:100,000)

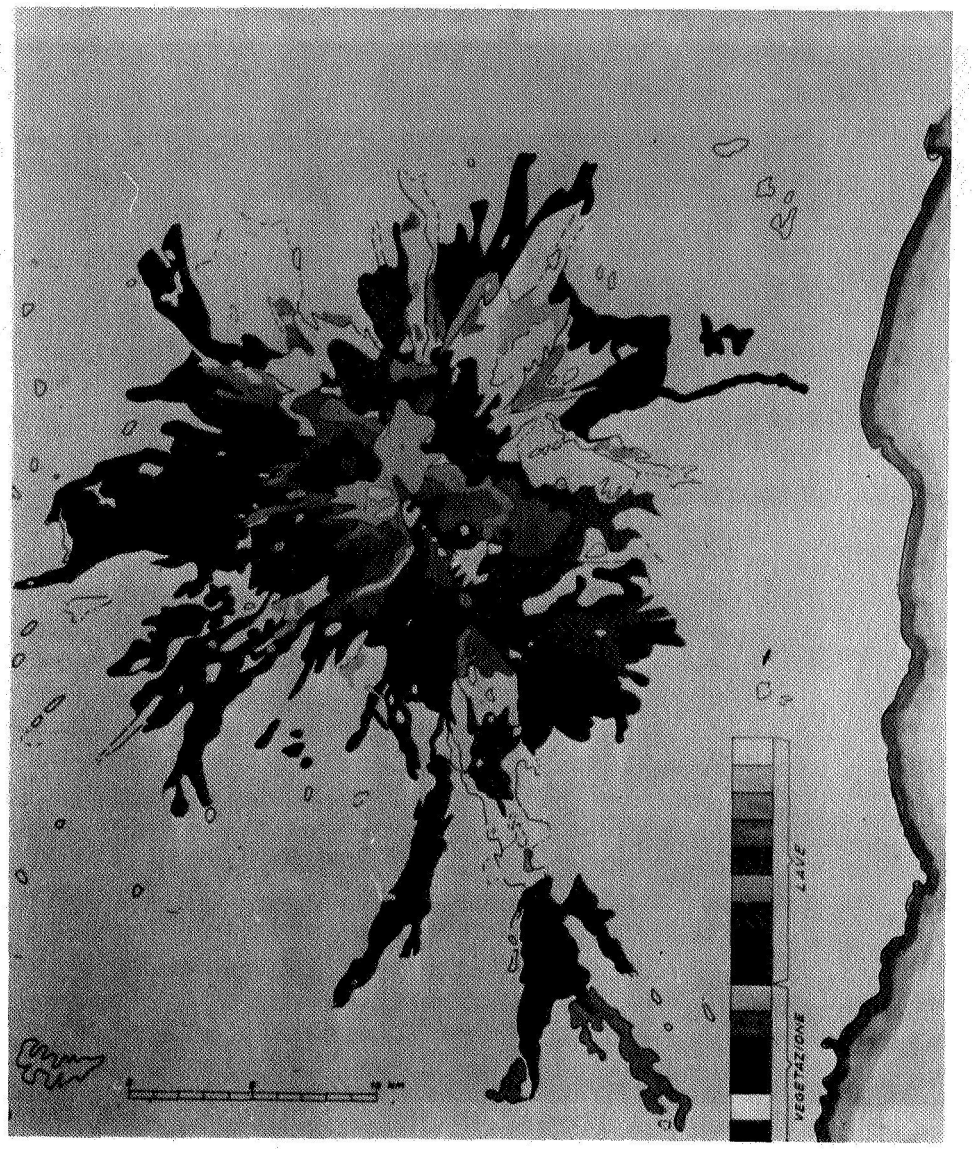


Figure 5. Map of Relative Reflectivities Measured Around the Volvanic Cone; Reflectivity Increases from Top to Bottom of the Scale

N73-28369

THERMAL SURVEILLANCE OF CASCADE RANGE VOLCANOES USING ERTS-1 MULTISPECTRAL SCANNER, AIRCRAFT IMAGING SYSTEMS, AND GROUND-BASED DATA COMMUNICATION PLATFORMS*

Jules D. Friedman, *U. S. Geological Survey, Washington, D. C.;* David G. Frank, *U. S. Geological Survey, Tacoma, Washington;* Duane Preble, *U. S. Geological Survey, Bay St. Louis, Mississippi* and J. Earle Painter, *Goddard Space Flight Center, Greenbelt, Maryland*

ABSTRACT

A combination of infrared images depicting areas of thermal emission and ground calibration points have proved to be particularly useful in plotting time-dependent changes in surface temperatures and radiance and in delimiting areas of predominantly convective heat flow to the earth's surface in the Cascade Range and on Surtsey Volcano, Iceland. In an integrated experiment group using ERTS-I Multispectral Scanner (MSS) and aircraft infrared imaging systems in conjunction with multiple thermistor arrays, volcano surface temperatures are relayed daily to Washington via Data Communication Platform (DCP) transmitters and ERTS-I. Estimates of the magnitude of radiative and convective heat flow at several surface thermal manifestations in Lassen Volcanic National Park are providing data on the energy yield at the earth's surface during Lassen's current period of repose. Repetitive aircraft infrared imaging missions have recorded the outgoing radiative flux from the terrestrial surface, which has been essential in locating, delimiting and recording changes in surface thermal anomalies at Lassen, Mt. Rainier, Mt. St. Helens, Mt. Baker, Mt. Shasta and Mt. Hood. ERTS-I MSS imagery has revealed curvilinear structures at Lassen, the full extent of which have not been previously mapped. Interestingly, the major surface thermal manifestations at Lassen are aligned along these structures, particularly in the Warner Valley. On Lassen Peak, and possibly at Mt. St. Helens, smaller thermal anomalies are controlled by the contact margins of silicic or intermediate extrusive plugs, and particularly at Lassen, may mark a line of structural weakness along Manzanita Creek Valley.

*Publication authorized by the Director, U.S. Geological Survey.

Original photography may be purchased from
EROS Data Center
10th and Dakota Avenue
Sioux Falls, SD 57198



1. INTRODUCTION AND BACKGROUND

In regions of active volcanism, during periods of repose of active volcanoes as well as during periods of eruption, a sizable heat flux reaches the surface by mass transfer. At Wairakei in New Zealand, Robertson and Dawson (1964, p. 134) have shown that in at least the Wairakei environment, conduction is the dominant mechanism of transfer when the difference between the surface temperature and that at 100 cm depth is less than 25°C. Where the temperature at 100 cm exceeds 25°C, convective transfer becomes the dominant mechanism. This transition corresponds to a heat flux of about 50 μcal cm^{-2} sec^{-1} (2.09×10^{-4} joules cm^{-2} sec^{-1}), or 33 times the mean terrestrial flux. The capability of airborne optical-mechanical infrared line-scan systems to distinguish and record changes in surface thermal anomalies corresponds to a flux of about 200 μcal cm^{-2} sec^{-1} (Pálmason et al., 1970, p. 404) well within the range of predominantly convective transfer.

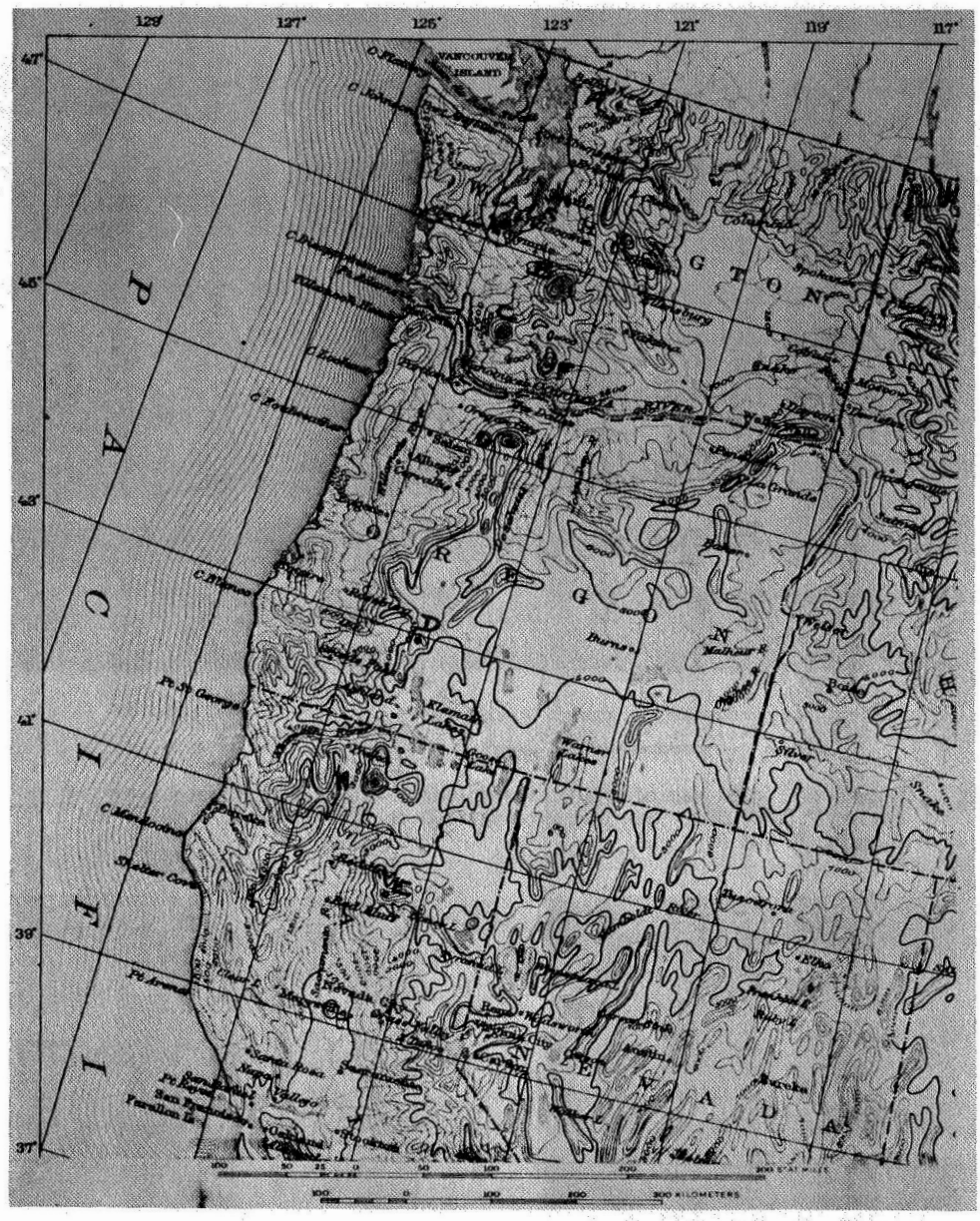
An increase in convective heat flow prior to volcanic outbreaks within areas of volcanic thermal anomalies has been documented at a number of volcanoes (Moxham, 1971, p. 103-105) including Askja, Taal, Kliuchevskoi, Surtsey, and others. The study of repose-period energy yield and of the circumstances under which thermal forerunners can be used as a predictive clue to impending volcanic activity are the subjects of this report.

It is known that vapor emission associated with convective transfer also fluctuates as a result of changes in barometric pressure and precipitation aside from that resulting from forerunning volcanic thermal emission. Consequently, systematic continuous temperature observations at a number of volcanic fumaroles by ground-based thermistor-probe recording or transmission systems, and synoptic airborne infrared line-scan surveys, are important in providing the essential geophysical data for significant thermal emission studies of volcanic systems.

The ERTS-I Data Communication System has been used in conjunction with Geological Survey-Forest Service and Manned Spacecraft Center aircraft infrared surveys of several Cascade Range volcanoes in an integrated experiment in which analysis of ERTS-I MSS images has provided useful tectonic lineament information.

2. ERTS-I MULTISPECTRAL SCANNER IMAGE ANALYSIS

Large-scale tectonic lineaments of the Cascade Range have been identified on MSS images covering the following volcanic areas (figure 1): Mt. Baker, Mt. St. Helens, Mt. Rainier, Mt. Hood, Mt. Adams, Mt. Shasta, and Lassen Volcanic National Park (figure 2). The MSS image coverage of the Lassen volcanic area is particularly interesting and merits special attention.



Contour Interval 100 feet

Figure 1. Volcanoes of the Cascade Range where thermal anomalies have been recorded. (A) Mt. Baker, (B) Mt. Rainier, (C) Mt. St. Helens, (D) Crater Lake (hydrologic anomalies), and (E) Lassen Volcanic National Park, (F) Mt. Adams, (G) Mt. Hood, and (H) Mt. Shasta. Thermistor arrays transmitting surface temperatures via DCP's and ERTS-I satellite are sited at (A), (C), and (E) (two sets). Mt. Baker, Mt. St. Helens and Lassen have been active within the last two centuries.

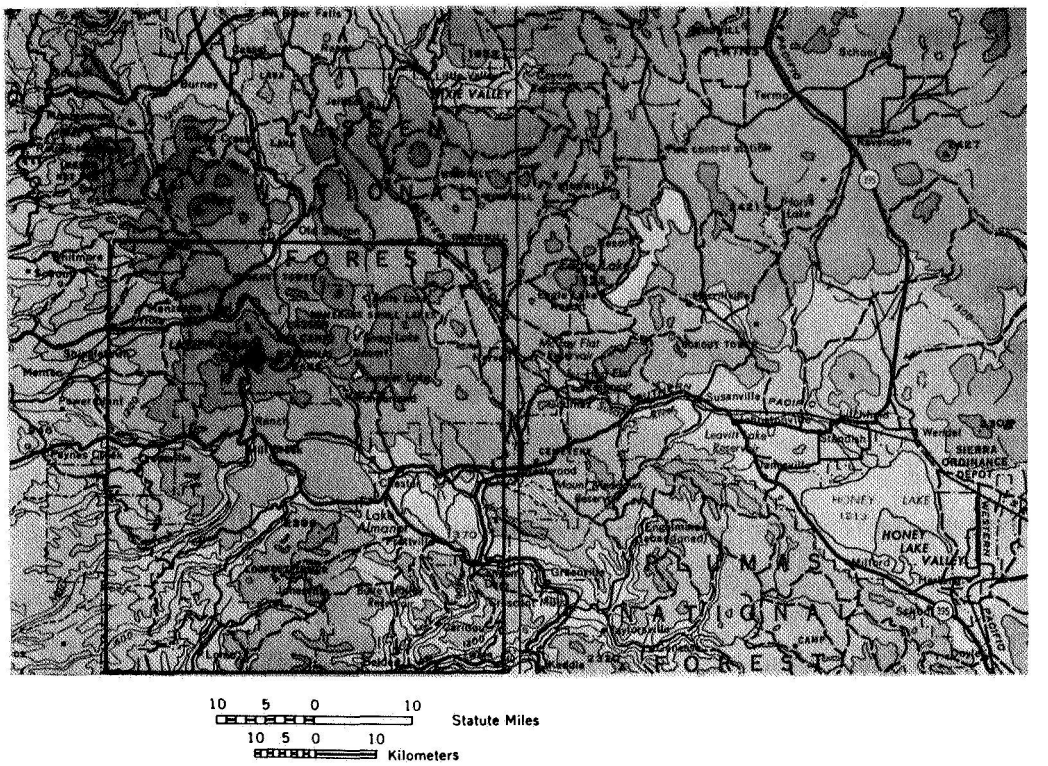
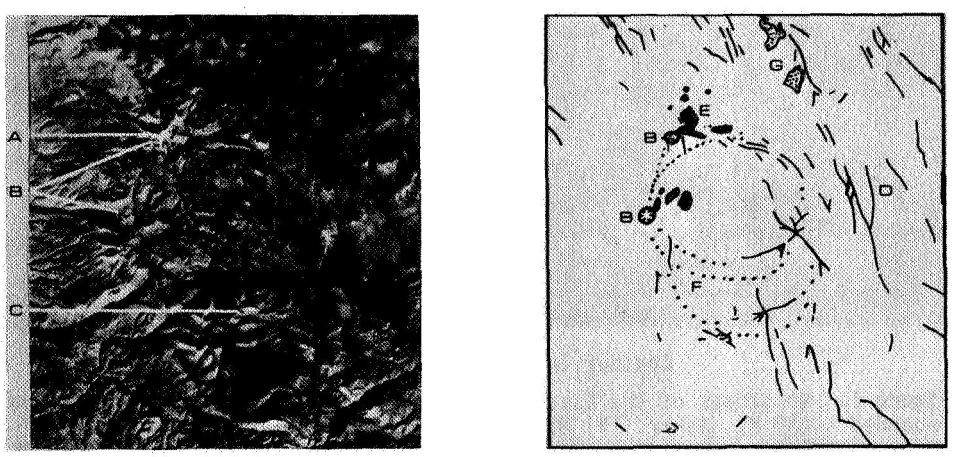


Figure 2. Index map of the Lassen Volcanic National Park area. Scale: 1:1,000,000. Contour interval 300 feet. Area in box shown in figures 3A and B.



A B

Figure 3A and B. Portion of ERTS-I, MSS image E-1075-18164, band 6, October 6, 1972: (A) Lassen Peak, (B) Brokeoff caldera, Battle Creek Meadows caldera, (C) Butt Mountain volcanic center, (D) mapped faults (solid lines), (E) dacite domes, (F) inferred lineaments (speculative), and (G) recent basalt flows. Fault and dome locations from Lydon et al. (1960).

Curvilinear features, several of which coincide with known fault lines in the southeastern part of the Lassen area are identifiable. Frames E-1075-18164, October 6, 1972, and E-1094-18224, October 25, 1972, in particular provide good stereopair coverage of the area. The synoptic effect of the images suggests a large circular feature, about 20 kilometers in diameter, centered on the North Branch, North Fork of the Feather River. Additional concentric features trend toward the south. In figures 3B and 4, previously mapped faults and other geologic features are shown with solid and dashed lines. Previously mapped fault zones, but which seem to be part of an unmapped larger pattern, extend along the Warner Valley from Lake Almanor northwest and then west toward the Brokeoff caldera of late Pliocene or Pleistocene age. Dacite domes, including Lassen Peak, are located along the northwest segment. A stratovolcano of Pliocene or Pleistocene age and related dacite domes are located along the western segment of the circular feature at Battle Creek Meadows (MacDonald and Gay, 1966). The concentric curvilineaments, shown as a dotted line, along the southern segment of the large circular feature, may encompass a large eruptive center of Miocene age near Butt Mountain. Lydon (1961) has proposed a source for volcanic tuffaceous sediments of the Tuscan Formation, of Pliocene age, in this same area near Butt Mountain.

Whether this circular pattern that appears on the ERTS-I images thus represents a large volcanotectonic collapse structure which developed in stages from Miocene time through the present is not yet clear. It is notable, however, that there appears to be structural control of the location of the Lassen dacite domes and specific structural control of the points of thermal emission along the Warner Valley faults.

3. AERIAL INFRARED SURVEYS AND THERMAL ANOMALIES

Night aerial infrared images (spectral bands 4.5-5.5μm and 8-14μm) were acquired over the Cascade Range volcanoes in 1972 expressly for this project (SR 251) by NASA's Manned Spacecraft Center's aircraft program, utilizing the RS-14 scanner operating in the NP3A earth resources aircraft, and by a U.S. Forest Service fire-detection aircraft equipped with a similar infrared scanner, operating under a cooperative agreement with the U.S. Geological Survey.

The results of the aircraft missions included plots of the major surficial thermal anomalies of the volcanoes listed below, showing the relationship of the anomalies to topography and geologic structure. Thermistor arrays transmitting temperatures of several anomalous areas via the ERTS-I Data Communications System, discussed in the next section, and related field reconnaissance investigations with a portable fixed-field PRT-10 infrared radiometer and bimetallic thermometer probes have provided temperature calibration or reference points for the infrared images.

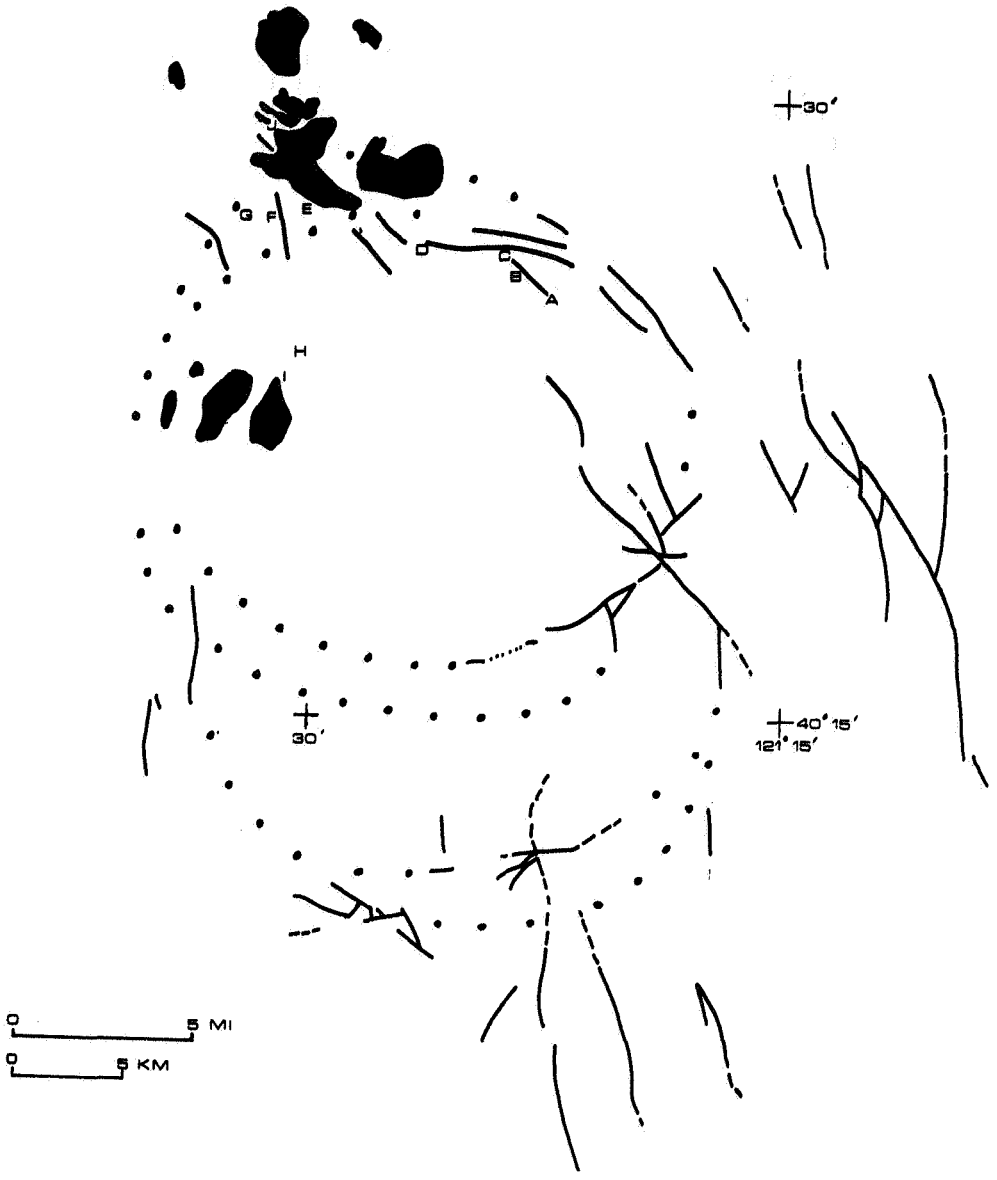


Figure 4. Structural control of geothermal manifestations and thermographic infrared anomalies in the Lassen Volcanic area, in relation to lineaments appearing in ERTS-1, MSS image E-1075-18164. Solid lines are mapped faults; dotted lines are inferred lineaments. Mapped faults and dome locations correspond to those shown by Lydon et al. (1961). Location of geothermal manifestations and infrared anomalies are shown by letters: (A) Terminal Geyser, (B) Boiling Springs Lake, (C) Drakes Springs, (D) Devils Kitchen, (E) Bumpass Hell, (F) Little Hot Springs, (G) Sulphur Works, (H) Growler Hot Springs, (I) Morgan Hot Springs, (J) Aligned NW-trending, infrared anomalies associated with Lassen Cone. Scale: 1,250,000. Thermistor arrays monitoring temperature changes are located at (B), (D), and (E). ERTS-1 satellite transmission from DCP's from (D) and (E).

Lassen Area. The major surface thermal manifestations of the Lassen volcanic area, as recorded on the aerial infrared images (figure 4, areas A-D; figure 5; figure 6), are aligned along faults depicted on the ERTS-I MSS images described above, particularly the Warner Valley fault system. One of the larger thermal manifestations here, Boiling Springs Lake, was radiating early in the afternoon of October 2, 1972 (prior to installation of a thermistor array) 1.8×10^2 watt m^2 from its surface, equivalent to an outward radiative flux of 4300 μcal cm^{-2} sec^{-1} (1.813×10^{-2} joules cm^{-2} sec^{-1}), or for the entire lake surface, a mean flux of $.713 \times 10^6$ cal sec^{-1} (2.985×10^6 joules sec^{-1}) ±3.47 percent (standard deviation based on 16 scattered radiometric temperature readings on the lake surface, from inflow area to outlet, by PRT-10 radiometer). On Lassen Peak, the positions of smaller thermal anomalies are apparently controlled by the contact margins of historical or Holocene silicic or intermediate extrusive plugs and thus may mark a line of structural weakness along the upper reaches of Manzanita Creek Valley.

Mt. Shasta. Two anomalies were recorded in 1972 in a depression about 200 feet below the summit. No change is apparent since a previous aerial survey in 1966 (Moxham, 1970). The southern anomaly corresponds to thermal springs ranging from 72°-84°C; the northern anomaly may be similar.

Mt. Hood. Several anomalies which delineate warm ground and steam vent areas around Crater Rock, the Devils Kitchen, and Steel Cliff about 700 feet below the summit, were recorded in 1972.

Mt. St. Helens. Two barely perceptible thermal anomalies on a northeast trend were recorded in 1971 and 1972. The first anomaly corresponds to warm ground having a radiometric surface temperature of 36°C, 700 feet downslope from and southwest of the summit crater, approximately equivalent to a heat flow of 700 μcal cm^{-2} sec^{-1} (2.93 joules cm^{-2} sec^{-1}) on July 17, 1972. The epicenters of well-recorded earthquakes during the summer of 1970 also form a roughly linear pattern trending northeast from the summit of Mt. St. Helens (Unger and Mills, 1973, p. 1065-1066, figure 2).

Mt. Rainier. Thermal infrared images acquired in 1971 and 1972 reveal a distribution of anomalies similar to those recorded in 1964 (Moxham et al., 1965) and 1966 (Moxham, 1970). In April 1972, a pinpoint bright anomaly north of the main crater was recorded clearly for the first time since 1964.

Mt. Baker. The inside rim of the summit crater (100 feet below the summit) is lined with thermal anomalies, recorded in 1971 and 1972, and corresponding to warm ground and fumaroles emitting vapors through melt holes in the crater firn field. Representative temperatures for July 1972, are 60°C for the warm ground surface and 90°C for the

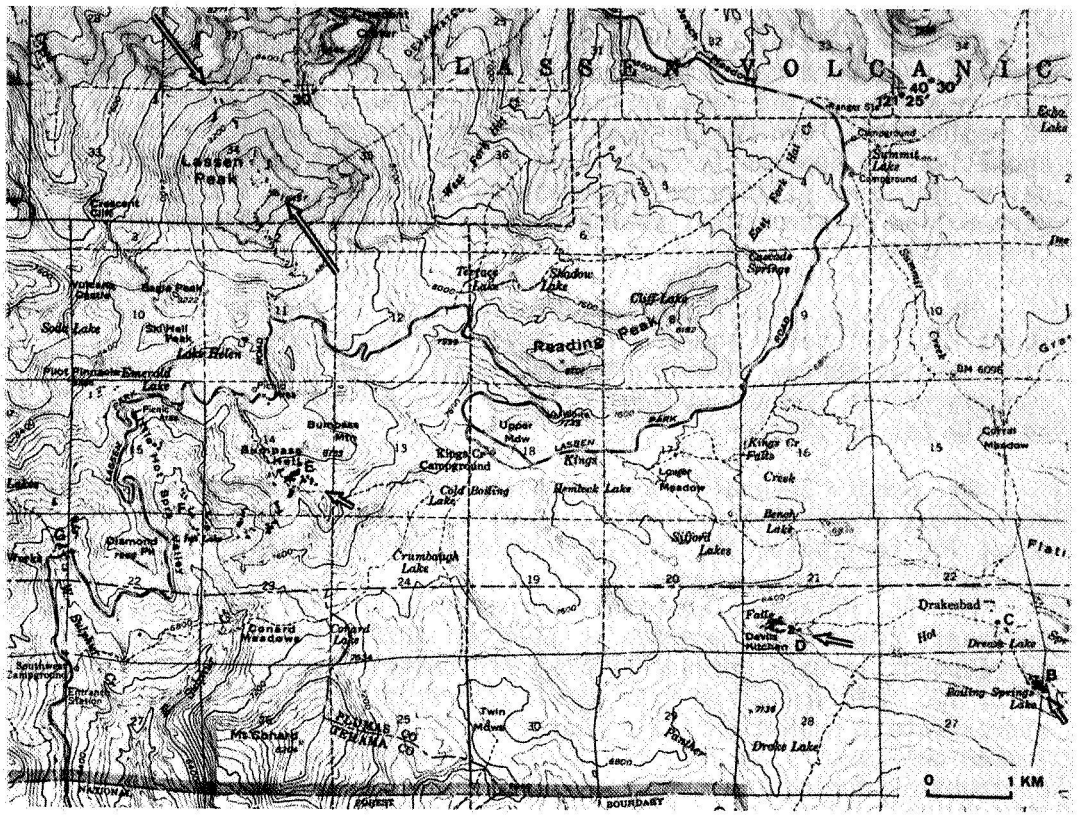


Figure 5. Thermographic infrared anomalies of April 20, 1972, 2041-2147 PDT, are as follows: (B) Boiling Springs Lake, (C) Drakes Springs, (D) Devils Kitchen, (E) Bumpass Hell, (F) Little Hot Springs Valley, (G) Sulphur Works, (J) infrared anomalies associated with the Lassen cone. Locations correspond to those in figure 4. Base from U.S. Geological Survey, Lassen Volcanic National Park and vicinity, 1957.

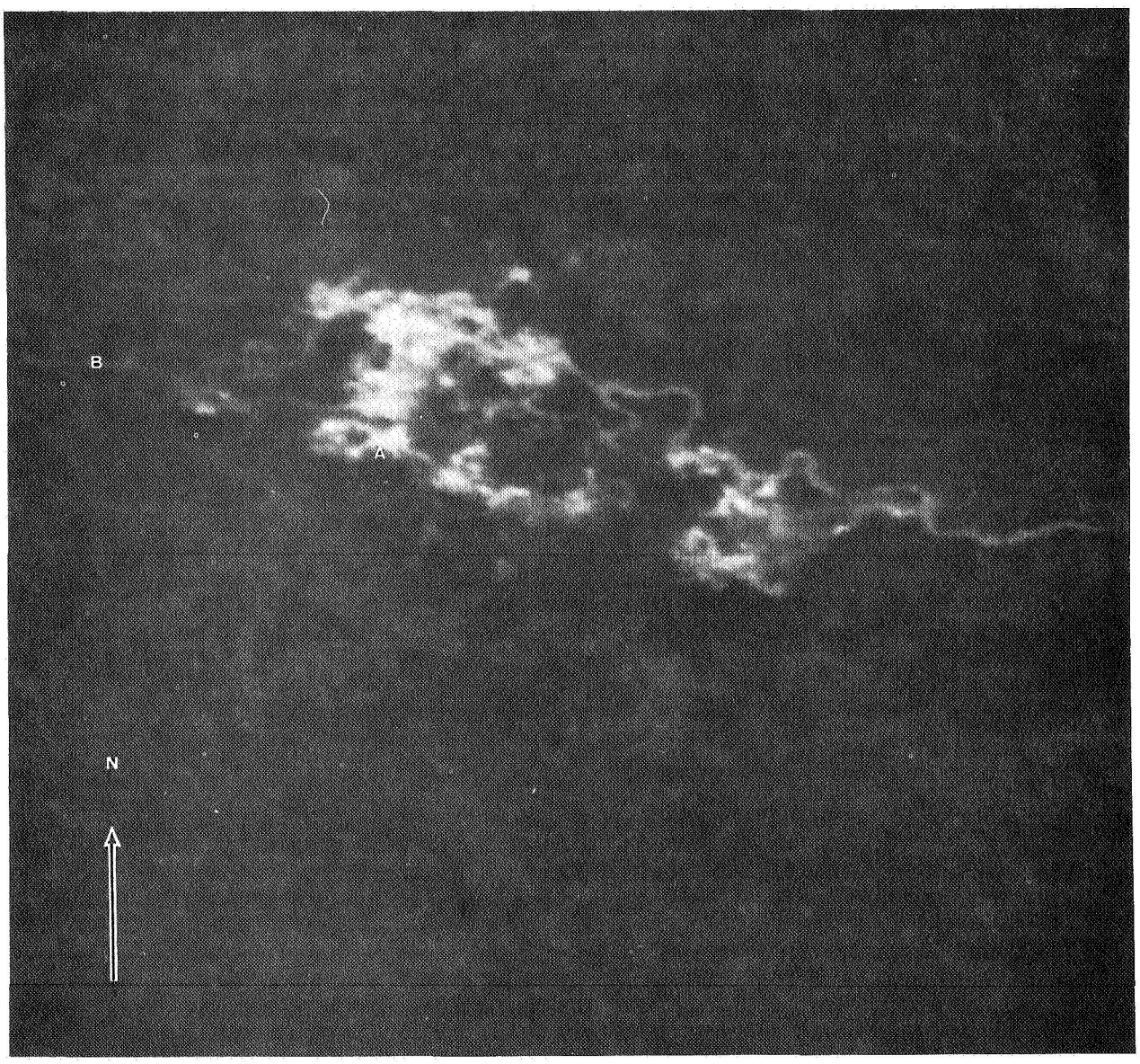


Figure 6. Aerial thermal infrared image of Devils Kitchen. April 20, 1972, 2130 PDT, flight altitude - 10,000 feet, $\frac{V}{H} = \frac{160}{3000}$. Polarity: black = cold, white = warm. (A) DCP 6104 thermal monitoring site, (B) Hot Springs Creek. Scale approximately 1:5000.

steam. A smaller thermal anomaly near the head of Mazama Glacier represents a fumarole area similar to that of the summit crater.

4. DATA COMMUNICATION PLATFORMS AND THERMISTOR ARRAYS

Four DCP's and two Fischer-Porter paper-punch tape recorders, each receiving temperature data from eight-probe thermistor arrays have been placed in operation (by February 1973) in carefully selected volcanic sites as part of ERTS-I experiment SR 251. (An additional site near the summit of Mt. St. Helens will be instrumented when weather permits in 1973.) Each site was selected to coincide with a thermal anomaly of volcanogenic or geothermal type which has been recorded on aerial thermographic infrared images. The temperature data can thus provide radiometric calibration points for the thermal radiation levels represented on the images, as well as time-dependent data showing temperature, radiation, and anomalous heat flow variations during the course of the experiment.

The following sites have been instrumented: (1) Devils Kitchen thermal area, Lassen volcanic area, California -- DCP 6104, Oct. 1972; (2) Bumpass Hell thermal area, Lassen volcanic area, California -- DCP 6020, Oct. 1972; (3) Boiling Springs Lake, Lassen volcanic area California -- Fischer-Porter paper-punch tape recorder operated by storage batteries and a servomechanism, Oct. 1972; (4) Mt. Baker, Washington, north slope fumaroles -- DCP 6251, Feb. 1973; (5) Surtsey Volcano, Iceland, thermal anomalies of tephra rim -- DCP 6056, Fischer-Porter system as above, Nov. 1972. A description of the Surtsey installation can serve as an example of a typical thermistor array-DCP site similar to those listed above.

Surtsey Thermal Instrumentation. On November 14, 1972, temperature measuring instrumentation including DCP set 6056 was installed on Surtsey volcanic island about 30 kilometers off the south coast of Iceland, and southwest of Heimaey. Eight temperatures are transmitted twice daily over the ERTS-I Data Collection System (DCS) and are recorded on paper tape every 32 hours.

The eight variables and their ranges are: air temperature (-25° to 25°C); nongeothermal ground surface (-25° to 25°C); geothermal ground surface (-25° to 25°C); and five one-meter geothermal probes (0° to 100°C). Linear thermistor networks encapsulated in stainless steel fixtures are the basic transducers. One-meter stainless steel rods were used for the geothermal depth probes, stainless steel prisms 2.5x2.5x12 cm, were used for the ground surface sensing, and a stainless tube, 1x8 cm, sheltered from the wind and sun was used as the air temperature thermistor mount. Each probe has a mating signal conditioner which, when power is applied, converts a full scale probe temperature change to a full scale range of 0 to 5.0 volts.

F

The ERTS DCP transmits data from eight analog channels every 90 seconds. During each transmission and 40 milliseconds (ms) prior to each transmission, the preamplifiers are turned on by command from the DCP. Total "on" time for the system is about 80 ms per transmission period. This low duty cycle allows a five to eight month battery life with about 16 kg of alkaline batteries. Transmissions were regularly received twice daily until December 25, 1972 when heavy winds may have blown over the antenna and interrupted data transmission. This station represents the greatest range over which the ERTS-DCS successfully communicated at the time of installation. Three steps were taken to ensure maximum possibility for transmission to the satellite: (1) maximum system voltage of 27 volts was used to give maximum rf output power (2) maximum transmission repretition rate of 90 seconds was used, and (3) antenna clearance to the southwest down to a 10 degree angle was taken into account during site selection.

A backup 16-channel paper tape recording system is operated in parallel with the DCP transmitter. Once every 32 hours the eight temperature parameters are recorded. A 32-hour cycle gives three different daily recording times spaced 8 hours apart which recur on a 3-day cycle. On command from the crystal controlled timer the preamplifiers are turned on and the parameters sequentially punched on the paper tape. After the last parameter, which is a reference voltage level used for a system check, the recording system and preamplifiers are shut off. Standby power consumption is about two milliwatts (70 μA @ $\pm$13.5 V).

The successful installation and high quality message transmission (levels 6 and 7) over the ERTS-DCS demonstrates that data of this type may be reliably gathered with a thermistor array system of this nature in difficult environments and in very remote locations over a straight-line distance from Goddard Space Flight Center of 4800 kilometers.

5. SUMMARY

ERTS-I multispectral scanner images have been proved to be useful for tectonic lineament analysis, and in the Lassen area, show that the distribution of volcanogenic thermal anomalies as recorded on aerial thermographic infrared images are fault controlled in the Warner Valley. Time-dependent changes in temperature, radiation and anomalous heat flow from these thermal manifestations are being transmitted by the ERTS-I Data Communication Systems and are being recorded and analyzed by a U.S. Geological Survey IBM 360/65 computer program. Results are expected to give estimated variations in dormant or repose period anomalous thermal energy yield at the surface in the Lassen volcanic area. Similar data are expected from several other thermally instrumented sites.

REFERENCES CITED

Lydon, P.A., Gay, T.E., and Jennings, C.W., 1960, Geologic map of California, Westwood sheet: California, Div. of Mines, scale, 1:250,000.

Lydon, P.A., 1961, Sources of the Tuscan Formation in northern California, in East-Central Sacramento Valley-Marysville (Sutter) Butte-Chico Creek-Oroville, Geol. Soc. Sacramento, Am. Field Trip 1961: Sacramento, Calif., Geol. Soc. Sacramento, p. 22-24.

MacDonald, G.A., and Gay, T.E., Jr., 1966, Geology of the southern Cascade Range, Modoc Plateau, and Great Basin areas in northeastern California, in Mineral Resources of California: U.S. Cong., 89th, 2d Sess., Comm. Interior and Insular Affairs, Comm. Print (California Div. Mines and Geology Bull. 191), p. 43-48.

Moxham, R.M., Crandell, D.R., and Marlatt, W.E., 1965, Thermal features at Mount Rainier, Washington, as revealed by infrared surveys, in Geological Survey Research 1965: U.S. Geol. Survey Prof. Paper 525-D, p. D93-D100.

Moxham, R.M., 1970, Thermal features at volcanoes in the Cascade Range as observed by aerial infrared surveys: Bull. Volcanologique, v. 34, no. 1, p. 77-106.

Moxham, R.M., 1971, Thermal surveillance of volcanoes, in T. Minikami et al., The surveillance and prediction of volcanic activity: UNESCO, Paris, p. 103-105.

Pálmason, G., Friedman, J.D., Williams, R.S., Jr., Jónsson, J., and Saemundsson, K., 1970, Aerial infrared surveys of Reykjanes and Torfajökull thermal areas, Iceland, with a section on cost of exploration surveys: Geothermics Special Issue 2, p. 399-412, U.N. Symp. on the Development and Utilization of Geothermal Resources, Pisa, 1970, v. 2, part I.

Robertson, E.I., and Dawson, G.B., 1964, Geothermal heat flow through the soil at Wairakei: New Zealand Journal Geology and Geophysics, v. 7, p. 134-143.

Unger, J.D., and Mills, KF., 1973, Earthquakes near Mount Saint Helens, Washington: Geol. Soc. America Bull., v. 84, no. 3, p. 1065-1066.

C

N73-28370

INITIAL EVALUATION OF THE GEOLOGIC APPLICATIONS OF ERTS-1 IMAGERY FOR NEW MEXICO

Karl Vonder Linden and Frank E. Kottlowski, *New Mexico State Bureau of Mines and Mineral Resources, Socorro, New Mexico*

ABSTRACT

Coverage of approximately one-third of the test site, the state of New Mexico, had been received by January 31, 1973 and all of the images received were MSS products. Images recorded during the first two months of the ERTS-1 mission are of poor quality, owing largely to high ground reflectance. Later images are of better quality and MSS bands 5 and 7 have proven to be particularly useful. Features noted during visual inspection of $9\frac{1}{2}$ x $9\frac{1}{2}$ prints include major structural forms, vegetation patterns, drainage patterns and outcrops of geologic formations having marked color contrasts. The Border Hills Structural Zone and the Y-O Structural Zone are prominently reflected in coverage of the Pecos Valley. A study of available maps and remote sensing material covering the Deming-Columbus area indicated that the limit of detection and the resolution of MSS products are not as good as those of aerial photographs, geologic maps, and manned-satellite photographs. The limit of detection of high-contrast features on MSS prints is approximately 1000 feet or 300 meters for linear features and about 18 acres for roughly circular areas.

TEXT

The New Mexico State Bureau of Mines and Mineral Resources is a state agency whose function is to provide basic information to explore, evaluate, develop and manage the State's natural resources. Over the past 20 years, bureau geologists have made considerable use of conventional aerial photographs for geologic field mapping. The staff also recognized the potential usefulness of satellite photography while studying photographs of southern New Mexico taken during the Apollo and Gemini programs. Subsequently, the Bureau submitted to NASA an ERTS-1 proposal, the objectives of which are as follows:

1. To study ERTS-1 images with emphasis on discovering and subsequently investigating previously unrecognized geologic phenomena in New Mexico.

2. To evaluate RBV and MSS imagery as a geologic tool by comparing the quality of ERTS-1 images with aerial photographs, manned-satellite photographs, geologic maps, and topographic maps of the same area.

The data forms requested from NASA were $9\frac{1}{2}$-inch by $9\frac{1}{2}$-inch black and white prints and 70-mm black and white negatives. Quarterly coverage of the entire State was requested for all MSS bands and maximum cloud cover was specified at 30 percent or less.

By late January, we had received coverage of approximately one-third of our test site, the State of New Mexico. All images received were MSS products. The quality of the earlier products was very poor; the prints appeared to be considerably overexposed. Communications with other ERTS product users indicated this problem was not uncommon to images taken in much of the southwestern U. S. and the poor quality was largely due to high ground reflectance. Fortunately, the quality of the coverage of our test site improved markedly with the arrival of imagery recorded in October and November.

Parts of New Mexico having reasonably good-quality coverage include the northwest corner, the entire Rio Grande Valley, the Estancia Valley, the southwest corner in the Lordsburg-Deming area, and the southern part of the Pecos River Valley, including the adjacent parts of the High Plains and the Guadalupe Mountains (Figure 1). We are particularly interested in the mountainous regions of the state, but we have not yet received coverage of most of the Datil-Mogollon volcanic region, in the southern, west-central part or of the Sangre de Cristo Mountains in the north-central part.

Predominant features noted during unaided visual inspection of the better quality $9\frac{1}{2}$-inch x $9\frac{1}{2}$-inch prints include major structural forms, drainage patterns, vegetation patterns and outcrops of geologic formations having marked color contrasts. MSS bands 5 and 7 have been the most useful, although bands 4 and 6 are not without value to geologic studies. In a gross sense, band 5 is probably the best available for determining lithology while band 7 appears to be best-suited to structural features. Man-made features are more readily identifiable on band 7 imagery, perhaps because of a pronounced difference in the heat-retention properties of natural and artifical materials.

Geologic contacts between bedrock and unconsolidated bolson (valley-fill) deposits are evident along the Rio Grande Valley (1010-17143, 17145, and 17152*) and in the southwestern corner of New

* Numbers refer to NDPF identification numbers of images illustrating feature(s) described.

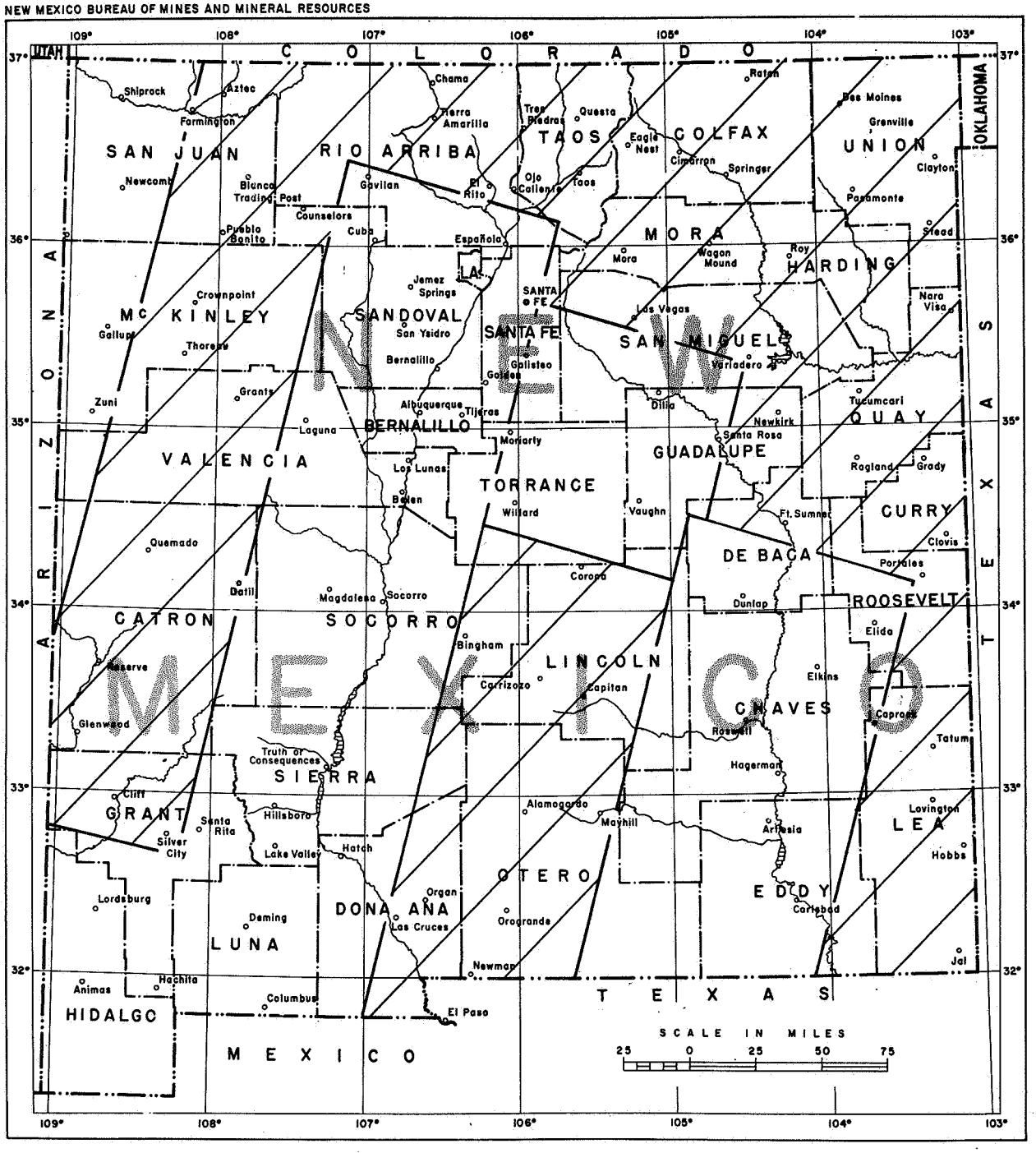


Figure I. ERTS-I Coverage of New Mexico as of January 21, 1973

Areas not hachured represent usable coverage

Mexico (1029-1713). Sedimentary contacts between grayish marine units and reddish-brown continental units also have been identified on ERTS imagery. They are particularly conspicuous east of Socorro where the continental Permian Abo Formation overlies the marine Pennsylvanian Madera Limestone (1010-17145 and 1063-17092). Unfortunately, coverage of the west-central part of the state, an area characterized by numerous Cenozoic volcanic units, has not been received, hence we cannot report on the ability to distinguish individual flow units.

Vegetation patterns of the two major types found in New Mexico are clearly shown by ERTS data. Extensive stands of forest in the more mountainous regions are visible on all MSS bands, but they are particularly prominent in color composites (1010-17143). Cultivated lands are restricted largely to major river valleys (1010-17143, 17145 and 17152 as well as 1062-17042) and the High Plains area of the eastern and southeastern parts of the state (1062-17033). The regular shapes of cultivated tracts are particularly useful features for identification.

Structural features identified on ERTS-imagery include volcanic forms, sedimentary forms, faults and areas that have undergone severe folding and shattering. The huge Jemez (or Valles) Caldera in northern New Mexico is shown with surprising detail and the outlines of the basalt-capped Mesa Prieta and Black Mesa can be readily identified (1010-17143). The mid-Tertiary volcanic complex of Mt. Taylor and its three associated peripheral flows is depicted as a classic "volcanic stereotype." The sedimentary structure of the Guadalupe Mountains in southeastern New Mexico has been recorded in marked detail (1062-17042). The 40-mile long, southeastern-facing Permian reef front is clearly shown southwest of Carlsbad as are the shallow-water marine and evaporite facies stretching northwestward from the crest of the reef.

The north-south trending Nacimiento Fault, west of the Jemez Caldera (1010-17143) had been thoroughly mapped prior to the launch of ERTS-1, but subsequent study of MSS imagery indicated a previously unreported, clearly defined lineament extending southward from the mapped portion of the fault for a distance of about 60 miles (1010-17143 and 17145).

The central Rio Grande Valley, particularly between Albuquerque and Socorro, is a seismically active structural depression. Fortunately, no significant seismic event has taken place in this area since the launch of ERTS-1, hence we cannot describe any new fault scarps. The geologically recent fault-line scarps bordering the Magdalena Mountains and Socorro Peak are visible however (1010-17145).

In the Pecos Valley of southeastern New Mexico, the Border Hills Structural Zone and the Y-O Structural Zone are prominent, even in places where these faulted and folded linear features are difficult to see on the ground surface (1062-17040).

One of the uses planned for our ERTS-1 investigation was to monitor the progress of strip mines in the state; specifically land disturbed around the active pits and revegetation programs. The large Navajo Mine, west of Farmington, is clearly visible, largely because the operators strip about 400 acres of overburden each year in a relatively level and unvegetated area. However, the visual contrast between the disturbed ground and the undisturbed, barren landscape is not too great (1030-17260).

The McKinley Mine near Gallup is located in a highly dissected and relatively vegetated area (1030-17262). Individual pits are small and the contrast between mined and unmined land is not great. The York Canyon Strip Mine has been opened on a heavily timbered plateau west of Raton. We have not received coverage of this area yet, but we anticipate that the strip pits will contrast sharply with the wooded, unmined areas.

In summation, we feel we have met with moderate success regarding the first objective of our investigation. Although our limited work with ERTS so far has not revolutionized New Mexico geology, it has pointed out some new insights on previously known features. We are optimistic that the receipt of better quality imagery and complete coverage of the state will add more geologic information.

The second phase of our investigation is a comparative evaluation of ERTS-1 imagery with aerial photographs, Apollo and Gemini photographs, and geologic maps. The most extensive coverage of these latter type data depict the southwestern part of New Mexico; the area west of El Paso, Texas, and generally south of Interstate Highway 10. Coverage of all or most of this area was obtained during the missions of Gemini IV and Apollo VI as well as by RB-57 aircraft using several sensors. Additional sources of coverage were provided by the New Mexico State Geological Map and Sheet 2 of the Apollo VI Photomap series published by the U. S. Geological Survey.

The RB-57 imagery, particularly color photography using 2448 film, provided the lowest limit of detection of any of the photographic data used. Color prints of film taken during Gemini IV was second as far as definition of geologic features was concerned. Film products from Apollo VI were far inferior to both the RB-57 and Gemini IV photographs. The sharp contrast between the Gemini and Apollo

photographs was due in no small part to the larger scale of the Gemini shots.

ERTS-1 coverage of the southwestern part of the state was recorded by the MSS only on two separate passes (1010-17154 and 1029-17213). Unfortunately, frame 1010-17154 is of extremely poor quality and all four MSS bands are far inferior to any of the comparative data. Frame 1029-17213 is one of the best we have received and it is clearly comparable, if not superior, to Apollo VI coverage of the same area. Although the limits of detection of this frame are not as low as those of Gemini IV and the RB-57 output, the larger area covered is a definite advantage in studying regional geology.

Although no RBV data have been available for our study site, we have established some quantitative values for the limits of MSS imagery. The limit of detection for high-contrast features on MSS prints is approximately 300 meters for linear features and about 18 acres for roughly circular areas.

N73-28311

COMPUTED ATMOSPHERIC EFFECTS ON ERTS OBSERVATIONS

Robert S. Fraser, *Goddard Space Flight Center, Greenbelt, Maryland 20771*

ABSTRACT

The nadir radiances of many models of the earth-atmosphere system were computed for a fixed solar zenith angle. These data indicate that the standard deviations of the Multispectral Scanner responses to changes in water vapor and aerosols would be small on a continental-wide basis.

The computed effects of the atmosphere on ERTS observations are usually not large. Data given at this symposium in other papers show that the path radiance of just the atmosphere can be strong and quite variable, which is true. However, that is not the whole story. The radiant energy that arrives at a satellite can be separated into two parts: the path radiance just mentioned and also the light transmitted from the ground directly through the atmosphere without interacting with it. The remarkable thing is that the two parts tend to change in opposite directions, thereby tending to compensate each other. For example, if the atmospheric turbidity increases, the path radiance increases but the atmospheric transmission decreases. Mother Nature is trying to help the Principle Investigators.

The light scattered by the atmosphere to ERTS-1 depends on the following variables: the solar zenith angle, the surface reflectivity, the presence of clouds even when there is a clear line-of-sight between the satellite and a surface target, water vapor, and particulates. The atmospheric models used for the computations that are presented here are free of clouds. The point that will be developed in this report is that for a fixed solar zenith angle the atmosphere would appear to cause only small variations over a large region such as the continental United States. The atmsophere can cause significant effects near strong pollution sources such as big cities; but on a continental basis the computed atmospheric effects are small.

Particulates play an important role in atmsopheric scattering. Although their sizes range over three orders of magnitude, only those particulates with radii between 0.1 and 1 μm have a significant effect on the ERTS observations. Figure 1 shows this fact for a small volume of slightly absorbing particulates. The size distribution function is

inversely proportional to the particle radius to the fourth power. Such a law applies for average conditions near the surface of continental regions (Junge, 1963). One-half of the mass of such particulates consists of those with radii less than one micrometer and the particles with the remaining mass have radii between one and 10 micrometers, as shown in Fig. 1. However, the cumulative extinction curve shows that the particles smaller than one micrometer account for 90 percent of the attenuation in a beam of light. The inset curve for the probability density function shows that the particles with 0.2 μm radius have the strongest interaction with light of wavelength 0.55 μm. Computations of the extinction characteristics of many models of atmospheric aerosols show that particles with diameter about equal to the wavelength interact more strongly with the light than other particles.

The particles that scatter sunlight most effectively towards the zenith are still smaller. If the solar zenith angle is 30° - 40°, the scattering angle towards the zenith is 150° - 140°. Figure 2 gives the probability density functions for light scattered in these directions. They are strongly peaked at a radius of 0.1 μm. Particles larger than 1 μm radius scatter essentially no light towards the zenith.

Models of the atmosphere used for computations given here are free of clouds, contain the invariant gases, 316 Dobson units of ozone, water vapor, and particulates. The mass loading of the particulates varies from none to the mean value plus two standard deviations, except in Fig. 4. The corresponding turbidity factor, which is the ratio of the total vertical optical thickness to the optical thickness of just the scattering gases, is at $\lambda = 0.55$ μm 1.3 for no particulates, 3.3 for an average continental amount, and 5.3 for two standard deviations above the mean. Shifrin and Shubova (1964) have measured the standard deviation of the turbidity factor and found it to be one-half. However, a much larger standard deviation of two is computed from values of surface extinction that were measured by Koprova (1971). Most surface extinction coefficients support the smaller value of one-half though. A standard deviation of the turbidity factor of one is assumed here. The indices of refraction of the particulates are either 1.5 or 1.5 - 0.03 i. They are assumed to be spheres, which is known to be an approximation when the particles are solid.

Water vapor absorption does not affect the first three bands of the ERTS Multispectral Scanner, but has a strong effect on the 0.8 - 1.1 μm band. The total amount of precipitable water in a vertical column varies from 1.5 cm to 4.4 cm, which applies in a warm, moist tropical atmosphere. The surface of the earth is assumed to be homogeneous and reflect light isotropically according to Lambert's law.

The numerical computations utilizing the models have an internal consistency of three significant figures. The computed nadir radiances for a model atmosphere with a mean turbidity factor of 3.3 at

λ = 0.55 μm are compared with measured values in Fig. 3. The observations were made from aircraft east of Cape Hatteras in a cloud-free region. The values of the surface reflectivity used in the calculations were those derived from measurements made at a height of 0.3 km. The measured and computed values agree fairly well. The model can be adjusted to decrease the discrepancies, but the exercise is not fruitful since the true aerosol state at the time of the measurements is not known.

The net effect of both the atmospheric transmission and path radiance on the ERTS observations is important and not just either one alone. Either factor can be large, as shown for the path radiance in Fig. 4, which gives the relative contribution of path radiance to the total radiance. The turbidity factors are 1.3, 4.3, and 13.3 for successive curves from the lowest to the highest. The middle curve represents more or less average turbidity. The path radiance decreases from 100 percent when the ground is black to a significant fraction of 37 percent when the surface reflectivity is 1.0. Also, the fraction of airlight increases significantly as the turbidity increases.

However, Fig. 5 shows that when the trade-off between path radiance and transmission are accounted for, the net change is sensor response for an atmosphere without particulates to one with average loading is less than 10 percent if the surface reflectivity is greater than 0.1. The effect of particulates is greatest over dark surfaces such as water. The effect for all the MSS channels is similar to those given by the two curves.

An estimate of the two standard deviations ranges of the ERTS MSS sensor responses are given in Fig. 6. These data are based on the computations for the many models already discussed; but the ranges are based on educated guesses concerning the atmospheric aerosols, since the statistical characteristics of the aerosol state are not known. The mean sensor response for each spectral band is nearly a linear function of the surface reflectivity, as has been noted before. The sensor response for the 0.8 - 1.1 μm is lower than those of the other bands because the sensor gain is lowest for the 0.8 - 1.1 μm band and significant water vapor absorption occurs in this band but not in the others. The ratio of the standard deviation, which is one-fourth the height of the bars on the graph, to the mean is small. For example, when the surface reflectivity is 0.2, the ratio is about 5%. This variability can be compared with the ultimate achievable accuracy in making atmospheric corrections, which is related to the National Bureau of Standards' Calibration Lamps. They have an accuracy of only 5 percent. The atmospheric variability should be measured by many high altitude observations of different surfaces whose reflectivities are constant. Such data are expensive to acquire by aircraft. The ERTS-1 MSS measurements may be satisfactory for this purpose.

The ratio of the standard deviation of the nadir radiances, which are derived from the data on Fig. 6, to the noise equivalent radiances (NER) of the MSS sensor systems are given in Fig. 7. The NER's were measured before ERTS-1 launch. The variation is appreciable in the 0.5 - 0.6 μm channel, but in the remaining bands the variations are comparable to the NER's. If the radiance variation caused by the atmosphere is comparable to the NER's of future ERTS' sensors, then no attempt need be made to correct for the atmosphere.

Future studies of atmospheric effects should be directed towards solving well-defined problems. The atmosphere does not seem to have an important effect on current ERTS-1 observations, except for water observations. The data given here indicate that the effects will be weak when considering a large region and large length of time. Operational methods to correct for atmospheric effects appear to be expensive. Such corrections would also add to the heavy burden of data reduction systems. Therefore, development of an operational system to correct for atmospheric effects should be based on need and then on the capability of making the corrections.

REFERENCES

1. Junge, C. E., "Air Chemistry and Radioactivity," Academic Press, New York.

2. Koprova, L. I., Izv., Atms. Oceanic Phys. 7, 415 (1971).

3. Shifrin, K. S. and Shubova, G. L., Izv., Geophys. Ser., 161 (1964).

FIGURE CAPTIONS

Fig. 1. The probability density of extinction (inset), the cumulative probability of extinction, and the cumulative probability of mass of atmospheric particulates as functions of their radius. The size distribution function of the number of particulates is inversely proportional to the fourth power of the radius. The index of refraction of the particulates is 1.5 - 0.03 i. The wavelength is 0.55 μm.

Fig. 2. The probability densities of the light scattered in the directions 140° or 150° as functions of radius. The parameters are given in the Fig. 1 caption.

Fig. 3. Comparison of measured and computed spectral radiances of the nadir over the ocean. Measurements were made by Hovis in July 1972.

Fig. 4. The computed ratio of the path radiance to the total radiance of the earth-atmosphere system in the nadir direction. The index of refraction of the particulates is 1.5. The solar zenith angle is 40°. The wavelength is 0.55 μm.

Fig. 5. The relative increse in the MSS sensor response to the nadir radiance when the atmospheric model without particulates adds the average amount of particulates. The size distribution function of the particulates is inversely proportional to the fourth power of the radius. The index of refraction of the particulates is 1.5. The solar zenith angle is 40°.

Fig. 6. Range of sensor responses in the 4 MSS spectral bands to the nadir radiance. The estimated variation is plus and minus two standard deviations. The number above each set bands is the surface reflectivity. The solar zenith angle is 40°.

Fig. 7. The ratio of the standard deviation of nadir radiances, which are derived from Fig. 6, to the noise equivalent radiances of the MSS sensors.

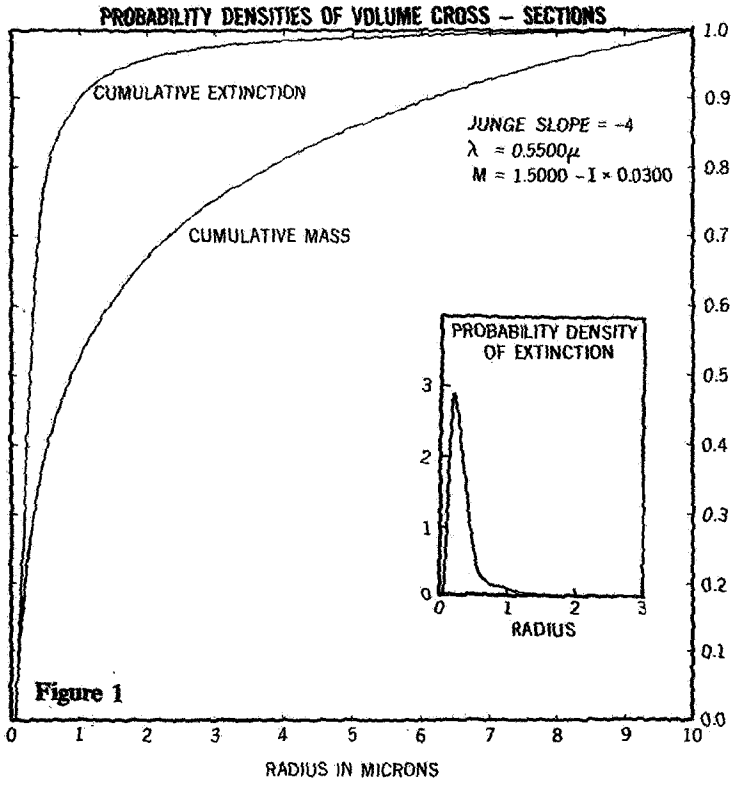


Figure 1

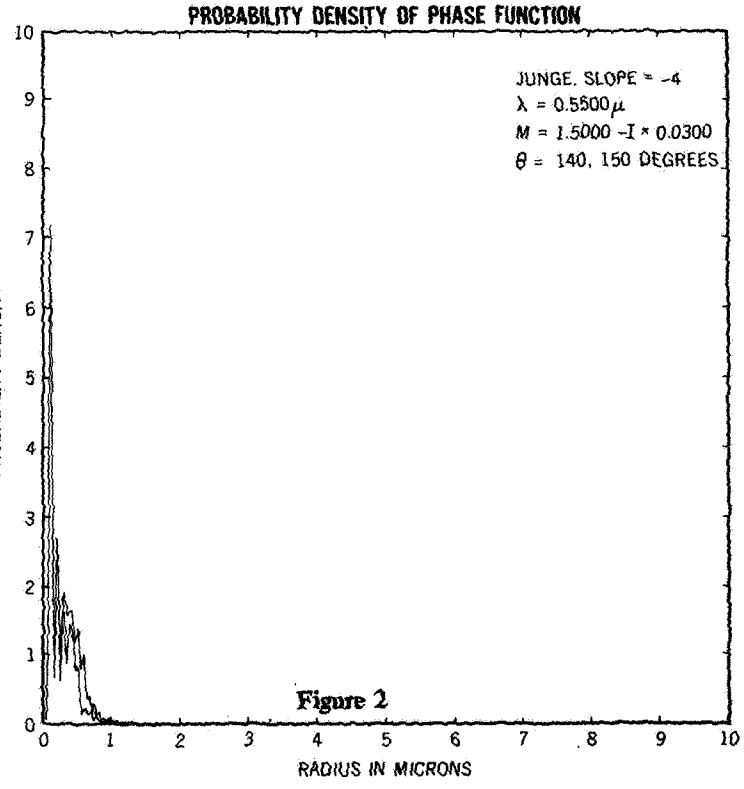


Figure 2

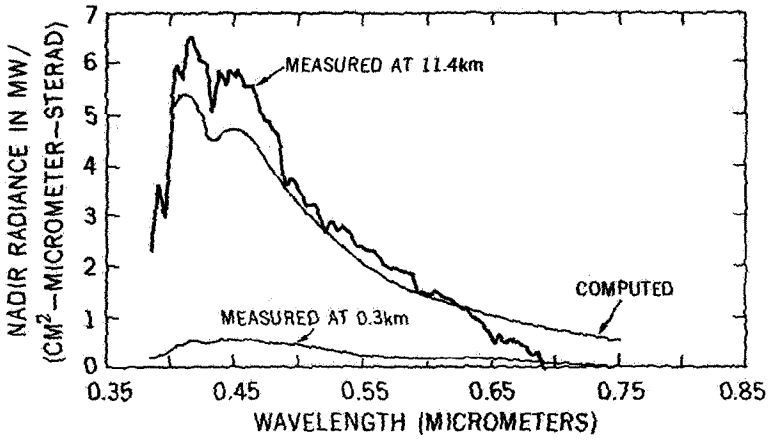


Figure 3

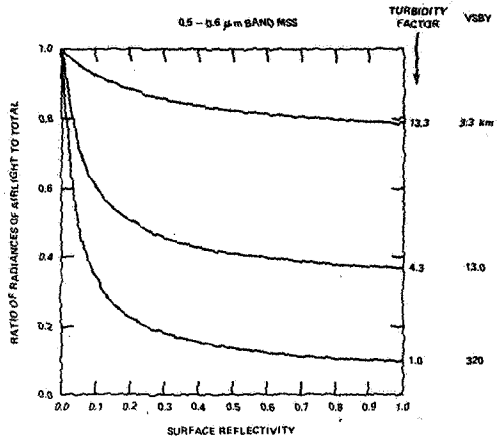


Figure 4

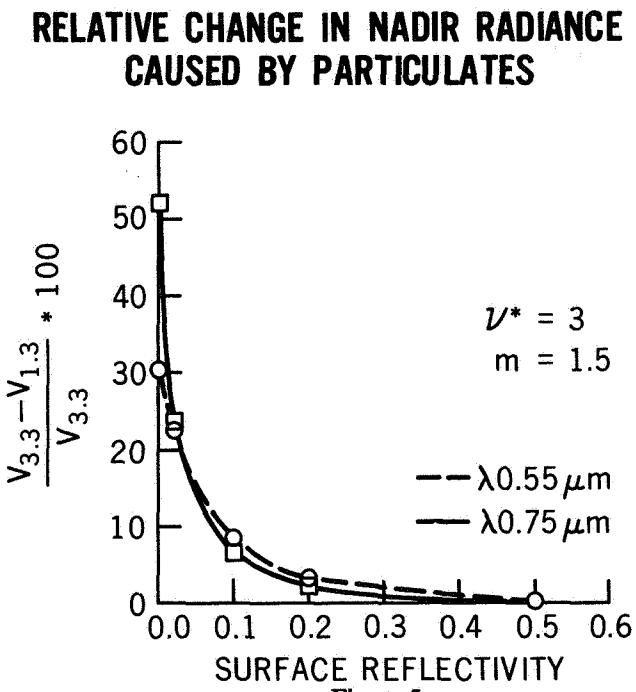


Figure 5

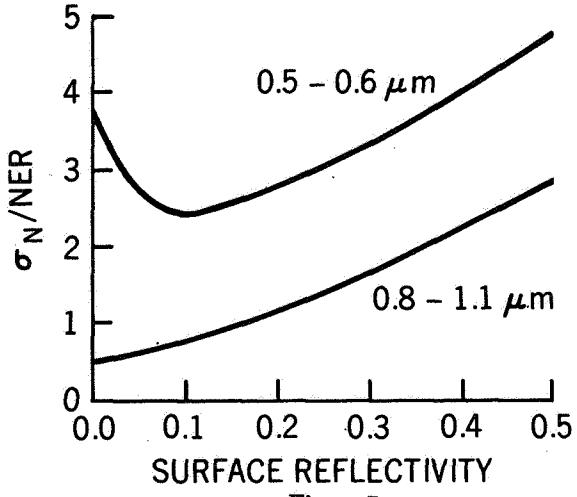


Figure 7

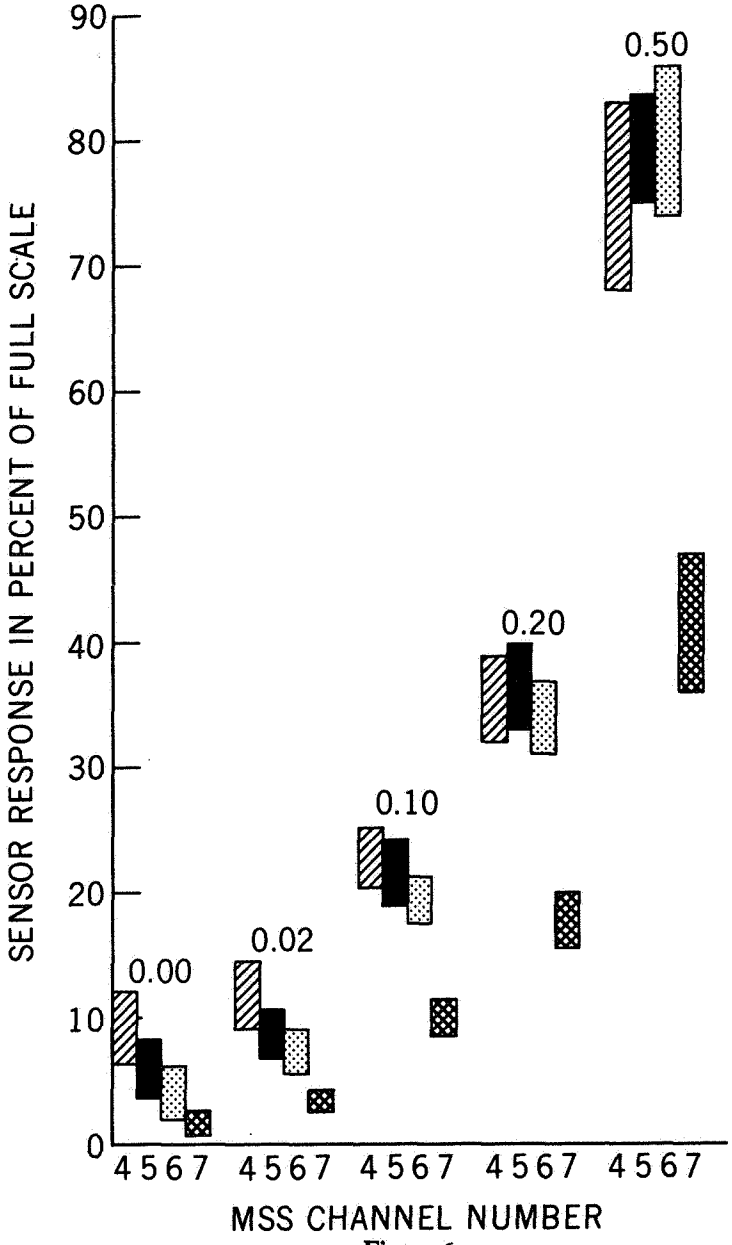


Figure 6

N73-28372

MAPPING OF SPOIL BANKS USING ERTS-1 PICTURES

Professor Moid U. Ahmad and David A. Kantner, *Geology Department, Ohio University, Athens, Ohio 45701;* John W. Antalovich, President, *Kucera and Associates, Inc., Mentor, Ohio*

Abstract

NASA's Earth Resources Technology Satellite (ERTS-1) is sending good quality pictures. Four pictures of different wave lengths (MSS 4,5,6,7) are used in the study of two strip mine areas in Southeastern Ohio. The first area is near Piedmont Lake and the second area is near New Lexington. In this study 9.5 inch prints were examined under a binocular microscope and the gray tone is correlated with the actual ground conditions at several sites. For the New Lexington area, color infrared pictures taken at an elevation of 18,000 feet were also used for correlation with the ERTS-1 imagery. The results indicate that MSS 5 and 7 are most useful in defining the stripped land and show that the hydrological and soil characteristics are remarkably different than the surrounding lands.

Method of Investigation

We have received two good sets of images of Southeastern Ohio. The rest of the images were spoiled due to the cloud cover. In this investigation we examined 9.5 inch prints under a 10-25 power binocular microscope with under and over lighting capabilities.

We were interested in the reclaimed strip mine areas, unreclaimed strip mined areas, and undisturbed land. We selected two areas for detailed work - (1) near Piedmont Lake and (2) near New Lexington. The location of these areas is shown on Fig. 1.

Strip mined areas near Piedmont Lake were identified on the ERTS-1 pictures and the gray tone described. Two methods of describing the gray tone were used, the objective numerical gray scale which is included on each ERTS-1 picture and a subjective verbal description. It was found that the verbal description seemed better for making comparisons between pictures because of inconsistencies in gray scales between pictures and the narrow range of usable tone on some of the gray scales. The strip mine areas were also located on topographic maps and the ground conditions were checked by visiting each site.

The graytone data obtained for each site for each MSS band is not included because of lack of space. We found MSS5 (Red) and MSS7 (Infrared) showed well defined features. Figures 2 and 3 are the enlargements of ERTS-1 pictures for the areas near Piedmont Lake and Table 1 (end of paper) describes the condition of each site.

PRECEDING PAGE BLANK NOT FILMED

Original photography may be purchased from:
EROS Data Center
10th and Dakota Avenue
Sioux Falls, SD 57198

G

We followed a similar procedure for New Lexington area but also used color infrared pictures (Kodak Ektachrome Infrared Aero Film 8443) supplied by the Manager of Wayne National Forest. The gray tone data obtained for each site for each MSS band is not included. Figures 4 and 5 are the enlargements of ERTS-1 pictures and Fig. 6 and 7 are the copies of color infrared. Table 1 describes the ground condition of each site.



Fig. 1 - AREA OF STUDY

No.1 - LAKE PIEDMONT STUDY AREA
No. 2 -NEW LESINGTON STUDY AREA

Discussion of Data

Highways

Certain highways were valuable reference features which were used to locate areas on the ERTS-1 pictures. Highways are best distinguished on the Red (MSS5) pictures. They are represented as light gray lines against a darker background. They show up fairly well on the Green (MSS4) pictures as light gray lines. They barely show up on the Infrared pictures as vague medium gray lines against a lighter background. Major four lane concrete highways are depicted best. Minor highways only show occasionally.

Water Bodies

Bodies of water were also used as reference features because they are prominent visible features. They are most visible on the Infrared pictures and are represented by a distinct black shade. It appears that the black areas representing bodies of water (lakes and rivers) show up larger or wider than they actually are. This may be due to water saturated areas adjacent to these bodies. The Red and especially Green pictures are poor for identifying lakes because the lake areas appear to blend in with the vegetative tone on the picture and are hard to distinguish from the picture background. The Ohio River channel, however, is better distinguished from its floodplain on these two pictures (especially Red) than on the Infrared pictures.

Coal Concentrations

Coal piles and spills are best shown on the Infrared pictures as black areas. This is why the town of Holloway and the Hanna processing plant show up so well on the ERT-1 pictures when other settlements their size do not.

Natural Vegetation

The general background tones on the ERTS-1 pictures represent the natural vegetation of the area, a combination of mainly hardwood forests and grassy areas where the trees have been removed. The background tone of the Infrared pictures is a light gray. The vegetation doesn't show well and details of the general topography of the land surface are more readily visible. The Red and Green pictures have a mottled background which seems to show the differences in vegetation, although it was not studied in detail. The darker tones in the mottled background may represent the trees covering most of the ridges and the lighter shades represent the more grassy valley bottoms. This might turn out to be a crude method to determine the topographic pattern of ridges and valleys.

Unreclaimed Strip Mined Lands

The unreclaimed areas show up as the darker grays to black on the Infrared pictures (e.g., site 5, Fig. 2) against a light gray background. They show up as white to light gray on the Red pictures (e.g., site 5, Fig. 3) against a mottled light gray to dark and black background. They show up on the Green pictures as light gray against a mottled lighter gray background. So far, specific larger strip mines have been observed on the ERTS-1 pictures and located by using their relationship to other identifiable features on the pictures and comparing the shape of the areas with mapped strip mines and the general topography.

Stripped lands show up well on all the MSS bands. Undoubtedly, the reason is that they are more or less barren of vegetation and composed of rock and soil material with different hydrologic characteristics which cause a marked difference in the reflectance as compared to vegetated land. It is possible that the stripped lands may be confused with similar barren areas such as plowed fields, but this has not yet been investigated. Strip mines do seem to have a characteristic irregular shape and are often large enough to be seen easily on this scale of picture which may aid in their identification. Very small strip mines have not yet been investigated sufficiently to determine their visibility on ERTS-1 pictures.

Reclaimed Lands

In the Piedmont Lake area, the reclamation was fairly recent (less than five years), graded first to some semblance of the original contour and planted with grass. From the small amount of data we have been able to collect at present, it appears that under these conditions the reclaimed land may show up as slightly darker than the unreclaimed stripped areas on the Green and Red pictures (e.g., sites 16 and 5, Fig. 3) and a little lighter thant the unreclaimed areas on the Infrared pictures (e.g., sites 16 and 5, Fig. 2).

The sites studied in the New Lexington area are older, and were stripped and reclaimed 20-30 years ago. The spoil was not graded at all and the land was planted with trees which have grown relatively large and dense by this time. The study sites were fairly well defined on the Infrared picture (Fig. 4) but were poorly defined on the Red (Fig. 5) and Green pictures. On the Infrared, the reclaimed areas appear to be slightly darker than the natural forest areas (e.g., sites 5b and 7, Fig. 4). More work is needed here to find out if distinction between older tree reclaimed areas and natural wooded areas is possible from the ERTS-1 pictures.

Reclaimed lands seem to be the most difficult areas to distinguish. Not enough work has been done yet to show whether this is inherent or just lack of data. Research should continue in the direction of finding some consistant method of defining reclaimed areas on the basis of the tone that represents them on the four ERTS-1 bands. One problem lies in the variety of conditions that can exist for such land. For example, the type of vegetative cover, the percentage of coverage, and the time since stripping and/or reclamation efforts might all affect the tone recorded on the pictures.

There is a need for continued research to determine if there is a measurable and consistant change visible on ERTS-1 pictures in reclaimed land from the stripped condition to grading, planting, and the establishment and growth of vegetation to a point in time when conditions may blend back into the natural vegetative background, at least as far as the ERTS-1 imagery is concerned.

Conclusions

(1) Large scale unreclaimed stripped land can be easily distinguished on all the MSS bands.

(2) It may be possible to distinguish reclaimed land from the natural vegetative background and unreclaimed land but more intensive research is required.

(3) The stripped land appears to have different soil and hydrological characteristics than the surrounding land.

Acknowledgements

We are grateful to Mr. W.D. Carter, Assistant Program Manager of the EROS Program, U.S. Geological Survey for supplying us with the ERTS-1 pictures for this study.

We are also grateful to Dean Norman S. Cohn, Director of Research at Ohio University for a grant to conduct field investigation, and Mr. Rene Elisar of Wayne National Forest who provided us with color Infrared pictures for the New Lexington area.

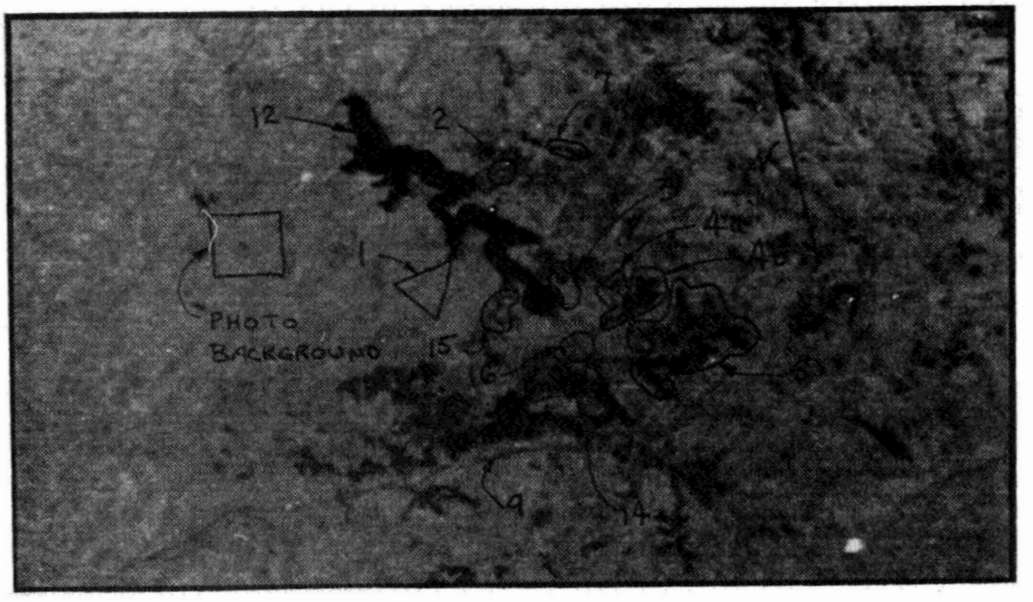


Fig. 2 - LAKE PIEDMONT STUDY AREA

Close up of Aug. 21, 1972 Infrared ERTS-1 (MSS7) (Photo ID. No. E-1029-15361-5N000) showing sites studied
Scale 1 cm. - 1.77 mile



Fig. 3 - LAKE PIEDMONT STUDY AREA

Close up of Aug. 21, 1972 Red ERTS-1 (MSS5)
(Photo ID. No. E-1029-15361-5N000) showing sites studied
Scale 1 cm + 1.77 mile

SEE TABLE NO. 1 FOR SITE DESCRIPTIONS



Fig. 4 - NEW LEXINGTON STUDY AREA

Close up of Oct. 15, 1972 Infrared ERTS-1 (MSS7) showing sites studied
Scale 1cm= .61 mile
Photo ID. No. E-1084-1545-5N000



Fig. 5 - NEW LEXINGTON STUDY AREA

Close up of Oct. 15, 1972 Red ERTS-1 (MSS5) showing sites studied
Scale 1cm.=.61 mile
Photo ID. No. E-1084-1545-5N000

SEE TABLE NO. 3 FOR SITE DESCRIPTIONS

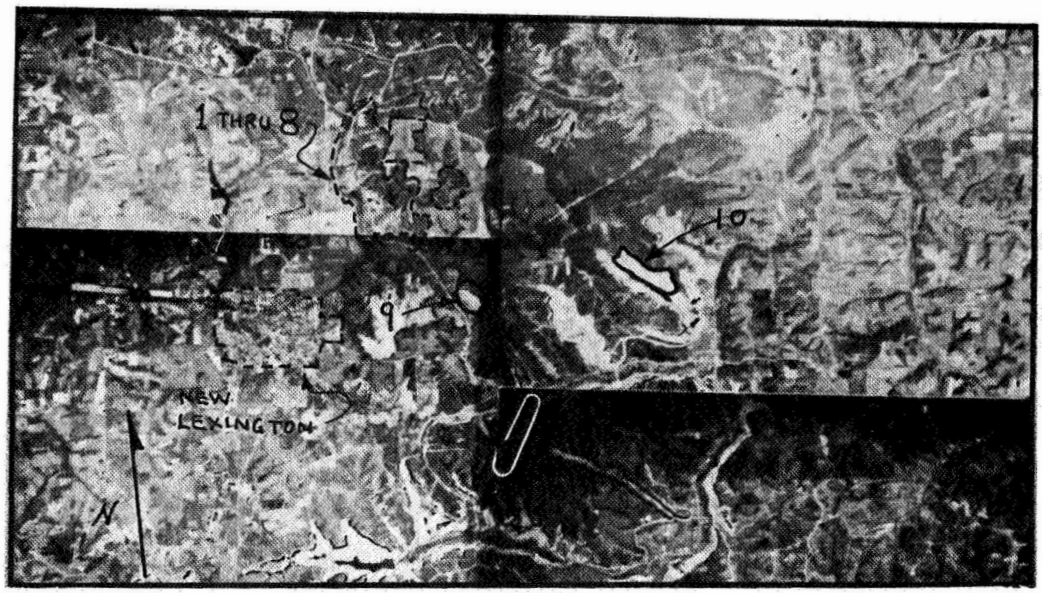


Fig. 6 - NEW LEXINGTON STUDY AREA

Color Infrared photo mosaic (courtesy Wayne National Forest) showing sites studied



Fig. 7 - NEW LEXINGTON STUDY AREA CLOSE UP

Close up of color infrared photo (courtesy Wayne National Forest Service) showing sites studied
May 11, 1972, Altitude 18,000 feet, Copy Scale 1cm.= .17 mile

SEE TABLE NO. 1 FOR SITE DESCRIPTION

TABLE 1 - SITE DESCRIPTIONS

Site Code No.	SITE DESCRIPTION (Unstudied sites omitted)
	LAKE PIEDMONT STUDY AREA
1	Natural hard wood forest area.
2	Stripped area reclaimed in 1968 according to Ohio Law. Area now has grass and brush growing on it and some small trees. Coverage somewhat sparse.
3	Grass reclaimed area, well graded. Fairly good coverage.
4a	Stripped valley which has been graded and newly grassed and what appears to be slightly restripped near the highwall.
4b	Stripped valley which had been graded but not yet grassed.
5	Large valley which has had massive stripping on both sides. Large highwalls and spoil banks. Entire valley practically devastated. No reclamation.
7	Location of the town of Holloway. Shows up because of coal piles and spills along an eight track wide railroad switch yard.
9	Rt. 70 - A four lane concrete highway.
12	Lake Piedmont Reservoir.
14	Location of Hanna's coal processing plant. An area of coal piles and spills.
15	A narrow stripped bench.
16	A predominently grass reclaimed area. Graded, some scattered trees, vegetation generally sparse and patchy.
NM	New stripping of site no. 5 found on the Oct. 15 picture which is generally obscured by clouds. Not shown on the site location picture.
	NEW LEXINGTON STUDY AREA
1a	Black shale and coal slag piles.
1b	Black shale and coal slag piles.
2	Small ponds.
3	Normal farm grass pasture land.
4	Black shale and coal slag piles in moist stream bottom areas.
5a	According to a resident, this area was stripped some time in the 1940's. It was stripped by the area method and reclaimed soon after stripping by the normal trees used at that time. The trees are now large (up to 8" - 10"). Some normal hardwoods.
6	According to a resident, this area was stripped some time in the 1940's. It was stripped by the area method and reclaimed soon after stripping by the normal trees used at that time. The trees are now large (up to 8" - 10"). Some normal hardwoods. Fairly densely grown.
7	Normal forested land. Not dense, with grassy areas.
8	Normal dense forested area.
9	A practically barren spot in a strip mine mined by the area method.
10	Barren strip mine mined by the contour method.

N73-28373

AIR QUALITY INDICES FROM ERTS-1 MSS INFORMATION, PR 568

Ellen L. Riley, Steven Stryker, and Edward A. Ward, *The MITRE Corporation, 1820 Dolley Madison Blvd., McLean, Virginia 22101*

ABSTRACT

Comparison between ground based atmospheric turbidity network measurements and the average scene grayness from MSS Channel 4 data is in progress. Correlation between these two sources is promising. If continued correlation occurs for other ERTS-1 overflight dates and ground test sites, a new operational use of ERTS-1 useful to Federal, state and international organizations will become available.

1. INTRODUCTION

Over the last decade, the need to quantify the air quality of our nation has become apparent. New organizations, Federal, state and local, have been formed to manage this environmental resource. Though air quality monitoring has been carried on for decades, the sum total of these monitoring efforts at best has been sporadic, poorly planned, and very incomplete in depicting the areal and temporal features on scales larger than 20 kilometers. Major urban areas and industrial zones have been monitored by arrays of in-situ air quality sensors in which the intent was to understand the local or microscale (<20 km) distribution of the emissions and the corresponding variations of air quality; larger - mesoscale (20 - 600 km) distributions have been studied to a much lesser degree. Two or three fragments of mesoscale air quality information come to mind which bear review in order to set the stage for describing our work to date.

During the last ten years, many air quality display computer simulations have been attempted. A large number of these simulations follow a semi-deterministic approach where the pollution emissions of an urban area are mathematically modeled both areally and temporally. Transport and diffusion simulations of these emissions are performed taking into account local weather conditions and in some cases terrain.

Displays of the air quality resulting from such simulations are then compared with measured in-situ air quality and the models are then fine tuned for more faithful representations of the quantitative value of air quality. Models for handling total particulates (settleable and suspended), oxides of sulfur, carbon monoxide, etc. exist and follow the general simulation procedure described above. Experience with total suspended particulates (TSP) has shown that there is a considerable difference between calculated and measured values in the urban area and that it is largely a constant offset which is called background TSP. This background TSP is found to vary across the United States but is generally on the order of one-half of the annual urban values monitored. Such a widely distributed TSP we have chosen to call the mesoscale air quality (MAQ). Too few non-urban air quality stations exist in this country to get a firm quantitative measure of this MAQ distribution. National Oceanic and Atmospheric Administration in conjunction with the Environmental Protection Agency and the World Meteorological Organization of the United Nations have a world array of air turbidity sensing stations (approximately 50 in the U.S.) obtaining data toward understanding this mesoscale and even the macroscale phenomena. More will be said about this turbidity network data later in this report when MITRE's MAQ index efforts are described. A paper by Flowers, McCormick and Kurfis[1] related analysis of turbidity network data to mesoscale weather movements and rainfall showing the variability of turbidity over the United States.

A second insight into the MAQ has been described by Clodman and Taggart[2] where a correlation of APT pictures from the ESSA 2 satellite was compared with synoptic weather maps of the same time period. On numerous occasions when no major frontal areas were in the eastern United States and the atmospheric water vapor was negligible, large turbid areas of air were present. Clodman correlated these data with ground observations of ceiling and visibility and concluded that the ESSA 2 satellite pictures were showing large multi-state air quality disturbances.

Thus both reported efforts[1,2] have pointed to the existence of a mesoscale air quality phenomena, and our experiences with the simulations have pointed to a need for quantitative temporal and areal measures of MAQ if we are to manage our air quality control efforts wisely. In the

---

[1] E. G. Flowers, R. A. McCormick, and K. R. Kurfis, "Atmospheric Turbidity over the United States, 1961-1966", Journal of Applied Meteorology, Vol. 8, No. 6, pp. 955-962, December 1969.

[2] J. Clodman and C. I. Taggart, "The Movement of Large-Scale Air Pollution Areas as determined by Satellite Photography", Unpublished paper for the Director, Meteorological Services Research Branch, Atmospheric Environmental Service, Downsview, Ontario, Canada.

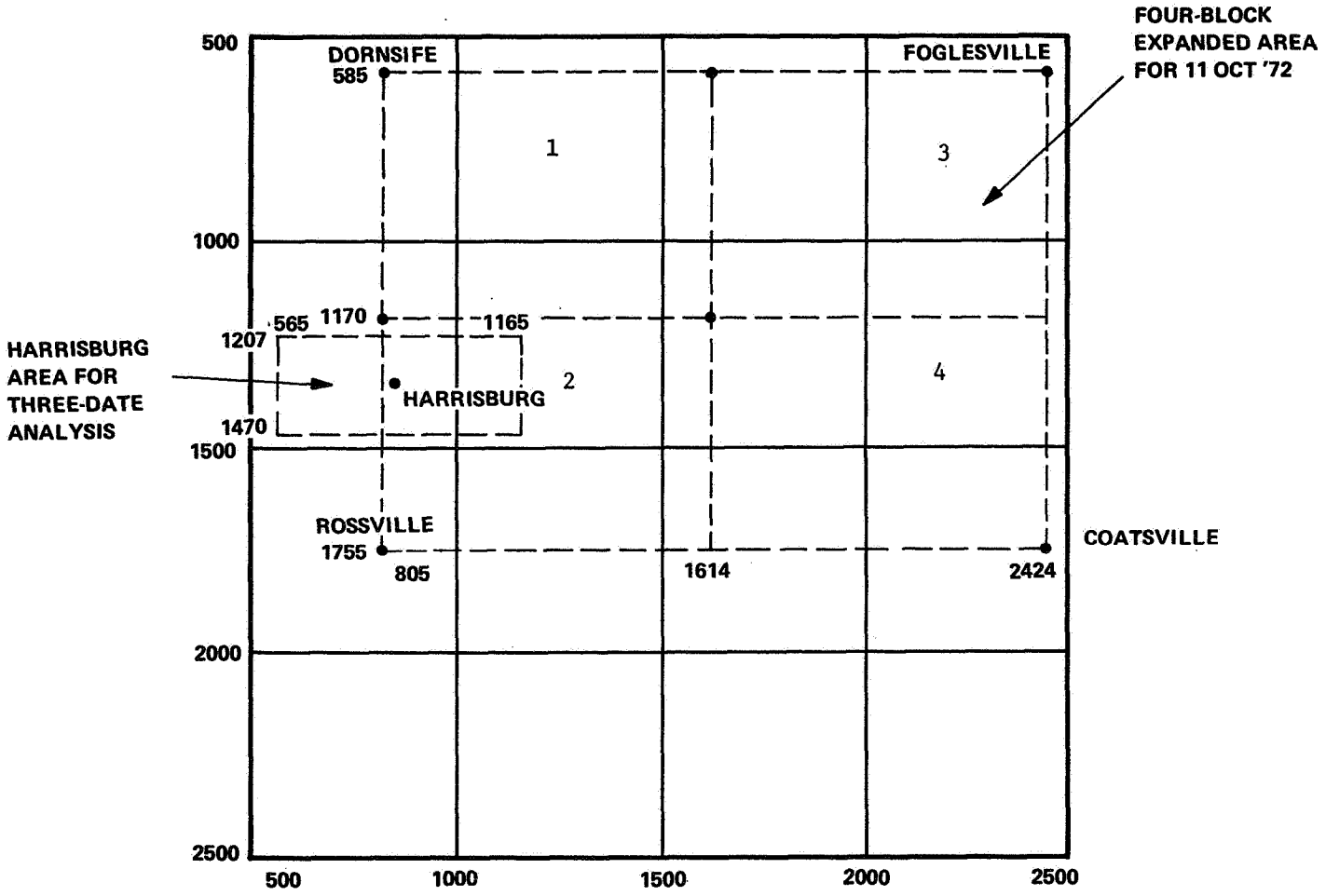
succeeding paragraphs we describe how we are attaining MAQ trends, non quantitative, areally and temporally. If continued correlations with the turbidity network and other Federal, state and local air quality assessments prove to be possible, then ERTS-1 will be a rapid means of mapping turbidity and/or MAQ. Care is required that we screen from our in-situ and turbidity network data all microscale effects. One crude measure has been to apply a population correction to the turbidity network data described below. Other corrections will be pursued in the next nine months of this investigation.

2.0 DISCUSSION

Our investigation in air quality has been in the development of an index of total air pollution burden variation (time and space); and consequently, calculation of background air quality trends from ERTS-1 data, uses two inputs. The two inputs are (1) the measure of total grayness (reflectance intensity) of one specific test area from sequential ERTS-1 overflights; and, (2) the earth observations of atmospheric turbidity (NOAA/EPA turbidity network with Rayleigh scattering and ozone absorption compensated for) over the same area on dates of ERTS-1 coverage.

The first step is to select the dates of ERTS-1 coverage in which clouds are not present over the test area. Second, compile all the turbidity network data about the test area possible. Such data are gathered on a daily (3 times per day) basis; and therefore good ERTS-1 MSS, all channels, on a relatively cloud-free day becomes the controlling factor for correlation date selection. Days in which turbidity data are not available are days of high percentage of cloud cover; thus, our ERTS data would also be of no value. On the approximately one pass over test site every 18-days schedule, we have found that 1 August 1972, 11 October 1972, and 16 November 1972 had near zero cloud cover and good ERTS imagery.

The basic analytical tool used for the ERTS-1 MSS data has been the intensity map program. The intensity map program (developed by Pennsylvania State University and called N-MAP) not only prints a thematic map of the reflectance of each channel, but also computes the average grayness statistics for the selected test site for each MSS channel. The average grayness is, of course, subject to interference by surface objects (heterogeneous nature of the test area) as well as by the total atmosphere and the sun light angle. Since both turbidity network data and the MSS data are recorded within a short time of each other (less than 35 minutes) the sunlight effect can be overlooked. Care must be taken in the test site selection for homogeneity. The Harrisburg training area boundaries are shown in Figure 1. The large, four block area shown is also being analyzed for turbidity variation on a given date.



*ELEMENT BOUNDARIES SHOWN ARE SPECIFICALLY FOR THE 11 OCTOBER 1972 MSS DATA. BOUNDARIES TEND TO CHANGE SLIGHTLY FOR DIFFERENT DATE'S COVERAGE OF THE "SAME" AREA.

FIGURE 1

AIR QUALITY TRAINING AREAS

Since the turbidity network[1,3,4] records turbidity using the Volz sunphotometer which measures a raw reflectance measure at 0.5 micrometers, we have used only ERTS-1 MSS Channel 4, which includes the 0.5 micrometer range data.

The second major input for analysis in addition to ERTS-1 intensity data, was turbidity network data. Originally operated for the National Air Pollution Control Administration (now part of EPA) by NOAA, the turbidity network reports observed and calculated readings of turbidity from sites around the world and in most states on a daily basis. The standard instrument is a Volz sunphotometer. Turbidity network data from seventeen stations about our test area (see Figure 2) for the three optimal ERTS-1 dates (1 August 1972, 11 October 1972, and 16 November 1972), and the days before and after each optimal date, have been analyzed with corresponding daily weather maps to calibrate for rainfall and frontal movement. Rainfall was found to have less than 24 hour effect, mainly lowering turbidity at a given monitoring site, and frontal movement was found to have at least a 48 hour lowering effect.[3] When analysis and calculation was completed for each of the 17 monitoring sites selected as most relevant to MITRE's Test Site 1, a fundamental vector/gradiant analysis was performed to estimate ground-measurable turbidity over Test Site 1. The figures obtained from these calculations (which essentially reflect, at a given elevation, the extinction produced by the variable amount of dust, haze, and water vapor in the atmosphere-- viz., total turbidity), have been plotted as the available ground truth information that gives an indicator of total turbidity over Test Site 1. Figure 3 and Table 1 show this information in graphical and tabular form.

Because many of the turbidity network stations are located in major metropolitan areas, a second series of calculations were made in an attempt to reduce all reporting stations to a uniform "background" standard unrelated to local sources, based mainly on the work of Larsen[5] with regard to relating total suspended particulate (TSP) to population. Larsen has shown that urban TSP approximately doubles for every order of magnitude change in population of that urban area. In our analysis all turbidity network reporting stations were scaled to a 10,000

---

[3] R. A. McCormick, "Atmospheric Turbidity", Presented at 60th Annual Meeting of the Air Pollution Control Association, Paper 67-32, June 11-16, 1967.

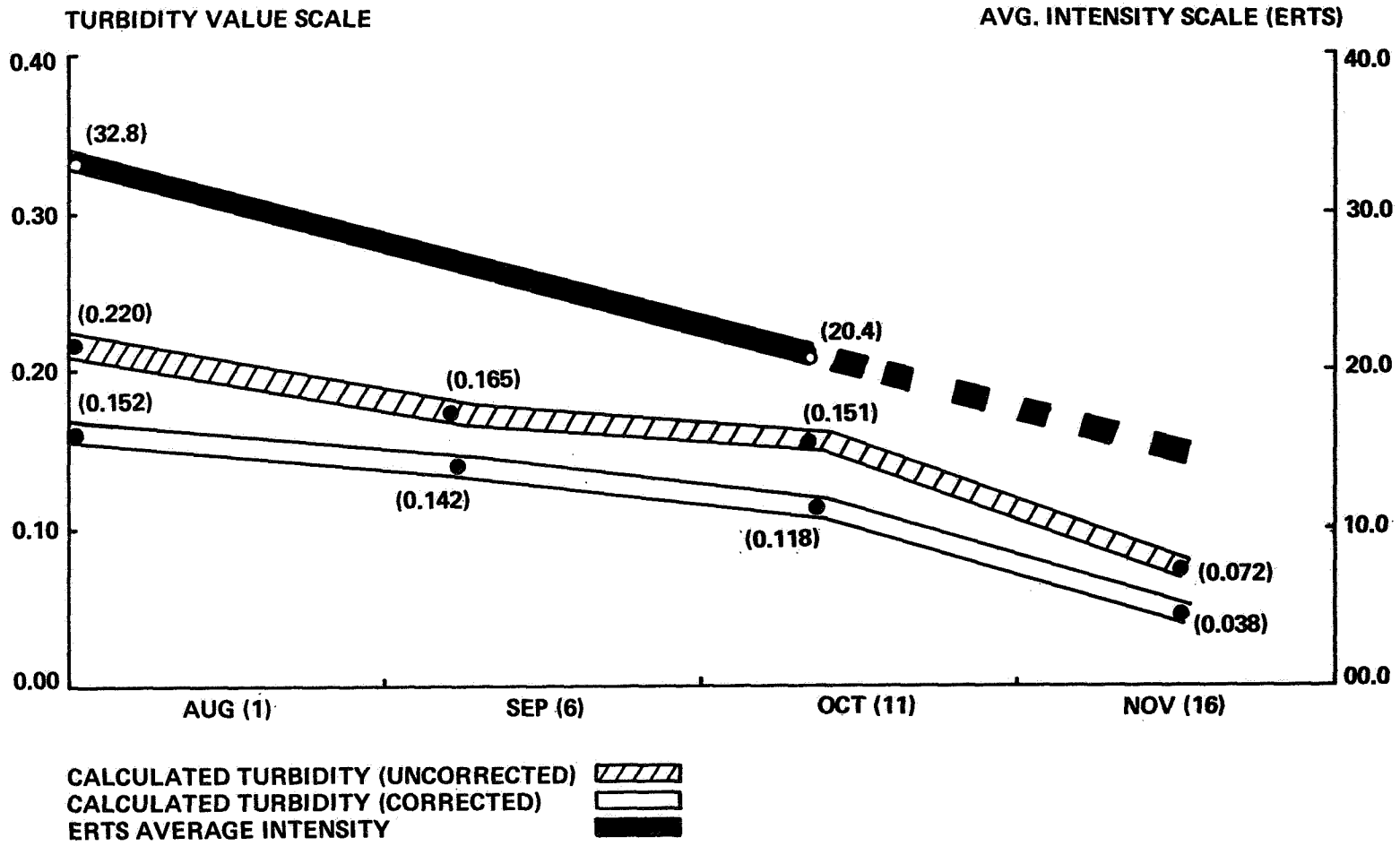
[4] "Atmospheric Turbidity Data for the World", U. S. Department of Commerce, National Oceanic and Atmospheric Administration, Environmental Data Service, Vol. 1, July - December 1971.

[5] R. I. Larsen, "United States Air Quality", Archives of Environmental Health, Vol. 8, pp. 325-333, February 1964.

C-17



FIGURE 2
TURBIDITY NETWORK STATIONS
REPORTING DATA FOR THE MITRE ERTS-1 INVESTIGATION



1589

COMPARISON OF ERTS-1 AVERAGE INTENSITY VARIATION WITH CALCULATED TURBIDITY VARIATION OVER THE HARRISBURG, PA. TEST SITE

FIGURE 3

C-12

ERTS-1 AVERAGE INTENSITY (CH. 4)

1 August 1972		32.8
11 October 1972		20.4
16 November 1972		24.9 (Corrected to 12.0)
11 October 1972	BLK 1	22.1
	BLK 2	24.4
	BLK 3	21.8
	BLK 4	26.4
	TOTAL (AVG)	94.7 (23.675)

CALCULATED TURBIDITY FOR HARRISBURG TEST AREA

	Uncorrected	Pop. Corrected
1 August 1972	0.220	0.152
6 September 1972	0.165	0.142
11 October 1972	0.151	0.118
16 November 1972	0.072	0.038

TABLE 1

CALCULATED TURBIDITY DATA

person population. Another choice would have been to scale to a rural population density more closely resembling a non-urban background. The many possibilities of introducing large specific error in this approach are well recognized, but it is nonetheless felt that, within an acceptable error range, useful correlations between in situ and satellite sensors will yield beneficial applications.

Our data presented in Figure 3 and Table 1 show such a trend. Comparison of ERTS-1 MSS Channel 4 data with ground truth turbidity network data for only three dates to this point in the MITRE investigation shows striking correlation, both in the scaled and raw data. As more data become available, and as analysis techniques are improved, ERTS-derived air indices and specifications for an optimal ERTS air quality monitoring system will be developed and presented.

N73-28374

SNOW COVER SURVEYS IN ALASKA FROM ERTS-1 DATA

Carl S. Benson, *University of Alaska, Fairbanks, Alaska 99701*

ABSTRACT

September and October ERTS scenes have been analyzed to delineate snow cover patterns in Northern Alaska's Brooks Range and on Mt. Wrangell, an active volcano in South Central Alaska.

ERTS images demonstrate that the snow on the Northern foothills of the Brooks Range are significantly more affected by katabatic wind action than are the Southern foothills. Aufeis deposits along arctic rivers also can be identified in late summer. A survey of such aufeis deposits could identify additional summertime sources of fresh water supplies.

Images of Mt. Wrangell enable us to monitor the interaction between volcanic heat and the mass balance of glaciers that exist on active volcanoes. Temporal changes in the areas of bare rock on the rim of the caldera on the summit reveal significant melting of new snow from an extensive storm on August 18. Digital analysis of data from subsequent passes over the summit on September 7, 23 and 24 reveal considerable bare rock exposed by melting, which is virtually impossible from solar heating at this altitude and date.

INTRODUCTION

This report contains a brief description of two of three University of Alaska projects dealing with ERTS applications to studies of snow and ice in Alaska. One project is titled "Survey of the seasonal snow and ice cover in Alaska", and the other is "Glaciological and volcanological studies in the Wrangell Mountains, Alaska".

The build up of the seasonal snow cover was observed on the images obtained in September and October 1972. The sharp climatic boundary of the Brooks Range was especially evident. The distribution of snow by winds can be seen in the first snowfalls. This is especially true when the snow does not cover the entire region. An excellent example is provided by the images from the arctic on 12 September 1972. The images 1051-20595 and 1051-21002 show the Brooks Range with snow on hill tops but with more snow on the North than on the South foothills. Also, the Northern foothills are significantly more affected by wind action. South of the Brooks Range the snow lies in a relatively undisturbed state on the higher ground.

PRECEDING PAGE BLANK NOT FILMED

In sharp contrast to this, the snow on the North slope of the Brooks Range is drawn out into long windswept patterns. The drainage of katabatic winds down major stream valleys is evident. The winds channeled by topography redistribute the snow and actually remove it from selected regions. The problem of determining snow line altitude is especially complicated because of winds in the Brooks Range, and also because the snow line paridly descends to sea level in early October. In the Alaska Range the Chugach Range we are beginning to employ the area integration approaches developed and reported by Mark Meier, USGS.

Aufeis deposits on arctic rivers can be identified in the late summer and early fall. This gives us the possibility of making an inventory of the aufeis deposits which persist through the summer season.

After freeze up has occurred and a continuous snow cover exists, it is still possible to identify open water reaches on streams flowing through the region. Such cases are especially identifiable on the MSS 7 images.

The purpose of the glaciological and volcanological project is to study the interaction between volcanic heat and the mass balance of glaciers existing on active volcanoes. It may also be considered as one of the first steps in the general problem of observing geothermal phenomena by satellites, but a thermal infrared channel on ERTS B is essential for future geothermal studies.

In order to monitor the interaction between volcanic heat and the ice and snow cover of Mt. Wrangell, it is necessary that changes in the area of bare rock exposed by melting at the summit be observed. Our results to date indicate that this can be done. On image 1010-20331 (2 August 19/2) areas of bare rock on the summit are clearly visible on 9½ x 9½ inch paper prints. The image 1026-20220 (18 August 19/2) shows high, thin clouds over the summit being driven by southerly winds, which usually indicates a storm developing in the area. This was verified on image 1027-20275 taken the following day (19 August 1972) when the summit was under heavy clouds. Finally, on 20 August 1972, the third day of this sequence, the summit is again clearly shown. Visual inspection of the image was sufficient to show that the summit was entirely snow covered.

Subsequent clear weather satellite passes over the summit occurred on September 7 (1046-20332), September 23 (1062-20221), September 24 (1063-20273/1063-20280), September 25 (1064-20331), and October 12 (1081-20275/1081-20281). However, the sun angle during these passes changed from 31 degrees on September 7 to 20 degrees on October 12. This caused heavy shadows in the summit area so that bare rock could not be identified with certainty. As a result, we decided to investigate enhancement techniques which could be utilized to separate snow and bare rock in areas covered by heavy shadows.

Digital tape of one of the September 23 images was processed, and printouts of density levels (by pixel) over the summit were obtained from bands 5 and 7 of this image. These were partly contoured, so that the relevant areas could be located, and the densities in these areas were then examined. The results showed clearly that a significant variation exists in the densities within the areas of heavy shadow, which could not be observed on the photographic products and further that the darker localities coincide with the bare rock outcrops which were present prior to the storm of August 19.

The possibility that melting could occur from solar heating at the summit of Mt. Wrangell during September is virtually non-existent--we know this from our previous field work at the summit. Therefore, the removal of snow from the outcrops must, of necessity, be attributed to volcanic heat.

As a result of these studies, we believe that the ERTS data are adequate to supply the information needed to study the effects of volcanic heat on the melting of snow. The applicability of ERTS data to the study of the mass balance of the Wrangell ice cap is still under investigation. However, there is no doubt that it will be possible to assign a qualitative (i.e., positive or negative) value to the mass balance of each glacier flowing off the Wrangell Mountains, based upon the relationships between snow, firn and glacier ice at the end of the yearly melt season. Boundaries between these zones are visible on the ERTS images without enhancement.

N73-28375

UTILIZATION OF ERTS-1 DATA TO MONITOR AND CLASSIFY EUTROPHICATION OF INLAND LAKES

Phillip E. Chase and Larry Reed, *The Bendix Corporation, Ann Arbor, Michigan;*
V. Elliott Smith, *Cranbrook Institute of Science, Bloomfield Hills, Michigan*

ABSTRACT

A technique is being developed for use of ERTS in estimating and monitoring trophic levels of inland lakes. Preliminary findings are that Michigan lakes and ponds of one acre or more are resolvable in bands 5, 6 and 7 of NASA MSS imagery under fair conditions (haze and 70% cloud cover). In processed imagery (CCT) smaller features, including water color patterns, are evident within some lakes of 40 acres or more. Image distortion of lake size, shape, orientation, etc. is minimal; discrimination of lakes and ponds from various wetlands is good. Subsequent ERTS and aircraft imagery will be correlated with detailed ground truth of water color and quality in eutrophic test lakes.

1. INTRODUCTION

Eutrophication or nutrient-organic enrichment is responsible for losses in water quality, property values and recreational uses of inland lakes. Lakes in urban and suburban areas are being degraded rapidly by large inputs of sewage and fertilizer nutrients. Algal blooms, macrophyte growths and high turbidity result from increasing productivity in these waters. Since the attendant discoloration of lakes is detectable by remote sensors, water color is the mediating factor between ERTS imagery and water quality.

In a study of 530 Wisconsin lakes Juday and Birge (1933) established empirical relationships between water transparency (turbidity) and its plankton content and color (platinum-cobalt scale). A similar relationship was found between water color and its organic carbon content. Thus as a lake becomes more productive (eutrophic) it undergoes a series of color changes from blue to green, yellow, brown and even red (Hutchinson, 1957). These color changes must be accounted for in terms of other trophic state indicators before color itself can be used to gauge water quality. Lake water colors also must be identified in remote imagery. Finally, repetitive monitoring is essential to recognize long-term trophic changes

PRECEDING PAGE BLANK NOT FILMED

Original photography may be purchased from
EROS Data Center
10th and Dakota Avenue
Sioux Falls, SD 57198

Original photography may be purchased from
EROS Data Center
10th and Dakota Avenue
Sioux Falls, SD 57198

as distinct from short-term or seasonal variations. ERTS provides a means for regular surveillance of lake trophic levels and rates of enrichment. The present study focusses on the practical correlation of ERTS data and water quality in lakes.

2. GROUND MONITORING AND TEST SITE AREA

Six glacial lakes (40-1280 acres), varying from mildly to highly eutrophic, are under study in Oakland County, Michigan. Biological and chemical factors in four of these have been surveyed for the previous three years. While water color has been highly variable in each lake, average differences in color and quality between lakes allow them to be ranked in order of increasing productivity. A program of in situ and laboratory measurements has been designed to characterize water and lake color and to define trophic levels at the time of ERTS passes. These measurements include: water transparency (turbidimetry), water color (platinum-cobalt and Forel-Ule scales), particulate color (reflectance spectra), particulate ash/dry weight ratios, organic carbon, nitrogen and phosphorus, chlorophyll, plankton (qualitative and surface-sky radiometry. Transient factors, such as pH, temperature and blooms, will be noted as well. Ground monitoring will begin as soon as the lakes are ice-free.

Figure 1 presents the test area and five of the test lakes (Cass, Orchard, Lower Long, Forest and Island). The map is based upon data in USGS maps (1965), aerial photos and ground observation.

3. REMOTE MONITORING

Despite unfavorable weather locally since ERTS launch, one set of usable imagery is available for the study area. In this scene (Figure 1) for September 28, 1972 five of the six study lakes are visible through 70% cloud cover within the indicated 50-square-mile area. This area includes numerous other lakes and ponds that also have been useful for analyzing ERTS resolution of small water bodies and their discrimination from various wetlands. The smallest ponds (or channels) that can be resolved are approximately 200 ft. in diameter or slightly less than one acre in area. These appear as gray spots in the B/W imagery. Elongated ponds or channels that are approximately 100 ft. in width are also evident but have no definite shape in the imagery.

Larger ponds that appear as black (full density) images are at least 550 ft. in diameter, or approximately 5 acres in area. Their greater

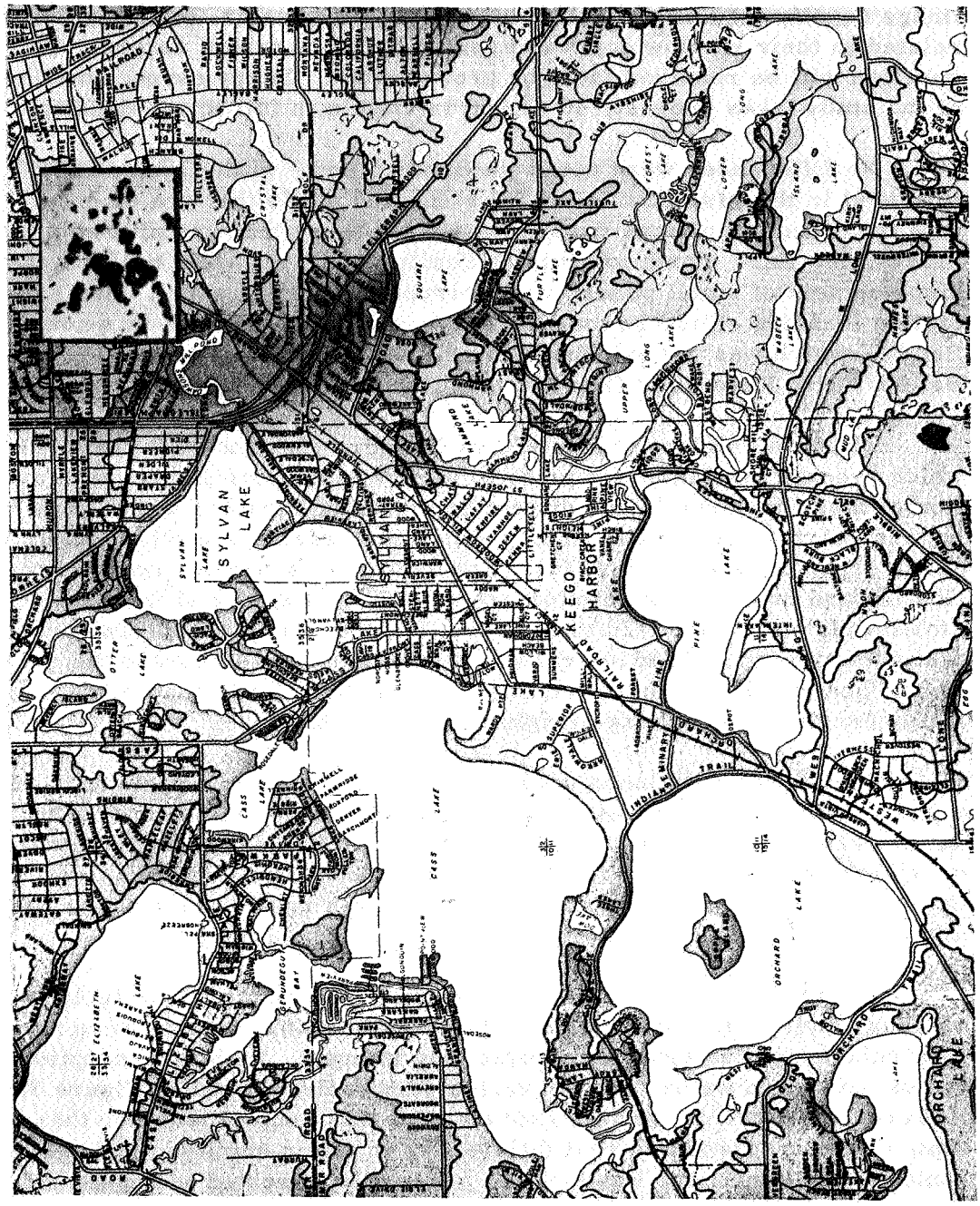


Figure 1 Oakland County Planning Commission Map of ERTS Study-Sub Area (1968) ERTS Scene 1067-15463-7 Inset Upper Left Hand Corner

image density may be a function of sensor response or, possibly, may be related to their shallow depth and generally more turbid waters. This question will be resolved later by ground truth. In any event, smallest of the study lakes (Forest, 40 acres) is visible in full image density.

No differences were noted (in Bands 6 and 7 of the NASA GSFC imagery) in the resolution of small elongated ponds that are oriented with the direction of scan (west to east) and those that are aligned normal to scan lines (north to south). Similarly, no apparent distortion or displacement of small ponds was observed in Bands 6 and 7. Some distortion (banding effect) in the imagery received from NASA was noted in Band 5, which was not evident in later imagery produced from CCT in Bendix Earth Resources Data Center (Figure 2 and Figure 3).

Electronic enlargements of this imagery (Bendix CCT imagery), which became available just prior to this report, show improved resolution of these features (some distortion exists in Figure 2 and Figure 3 because earth rotation and other geometric errors are not corrected. Such corrections are underway). For example, swamps composed of floating and emergent vegetation are readily distinguished from the smallest lakes visible. In bands 6 and 7 swamps appear as gray areas distinct from other wooded areas. Further study will resolve the question of how much floating or emergent vegetation a lake may contain and still show the image characteristics of "open water".

One of the study lakes contains a one-acre island visible in bands 6 and 7. The conclusion is that ERTS resolution is approximately the same whether it concerns a light object in a dark field (islands on water) or a dark object in a light field (ponds on land). The first key step - determining that ERTS-1 detects and separates small inland water bodies and wetlands - has been accomplished.

The image density of lake water has been examined for variations in all four bands. In certain lakes patterns of variable density were noted, particularly in the negative transparency images. With few exceptions the variations in water "color" were evident only in Band 5 (Figure 3). However, because of partial cloud cover it was unclear whether these tonal effects represented real differences in water quality. Under better atmospheric conditions Bands 4 and 5 would be expected to record differences in water color that are within the visible spectrum (blue to red). Water colors of green, green-yellow, yellow, yellow-brown, and red-brown are common occurrences among the six study lakes. Surface phenomena, such as algal blooms (of cyanophytes) that are seen occasionally on the lakes, may well be detectable in Bands 6 and 7 (near IR)



Figure 2 Enlargement of ERTS Study Sub-Area
as Shown in Figure 1
(1067-15463 Band 7)

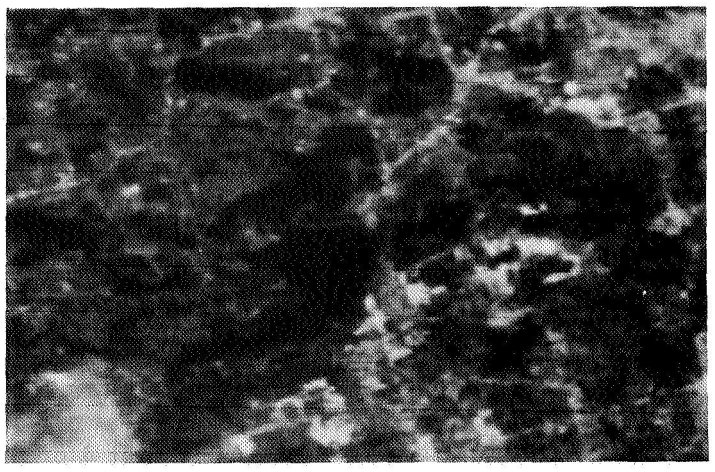


Figure 3 Enlargement of ERTS Study Sub-Area,
as Shown in Figure 1
(1067-15463, Band 5)

as well. Comparison of these images with bathymetry maps of lakes indicates that only part of the variable density is due to bottom reflection and macrophytes. Some of the variation is due to backscatter from organic and inorganic suspensions. (See Table 1) for a summary.

4. DATA PROCESSING

A series of lake water surface maps combining the CCT data of all four channels will be prepared. Preliminary statistical computer processing indicates a wide variety of color data in the four bands. The next key test now underway is the comparison (for Orchard Lake) of the bathymetry map, ERTS-1 individual band alpha numeric printouts, (CCT) ERTS-1 probability density imagery (CCT), ERTS-1 decision imagery, ERTS-1 Cal Comp water feature boundaries, and similar statistically processed imagery for an 11-channel scanner (Bendix M^2S). This study is expected to verify that ERTS-1 can detect the various causes of lake water color for smaller inland lakes - including the important backscatter from suspensions.

The final key step of correlation ERTS-1 data to trophic level and classifying lakes will be performed in the spring, summer and fall of 1973.

5. SIGNIFICANT RESULTS

ERTS-1 imagery has shown several changes (or inaccuracies) to have occurred since the Oakland County map (Figure 1) was drawn (1968). ERTS-1 and ground observation indicates the southern part of Otter Lake is a swamp. A pond was dredged to become a lake, as is now apparent in the ERTS-1 imagery[4]. Other detail corrections of the base map could be listed.[5]

More key is establishing that ERTS-1 detects lake areas of one acre and can monitor average lake colors to as small as 5 acres. In addition color features are demonstrably observable in at least 3 of the test lakes in the imagery. And of course statistical processing of the CCT is producing improved geometrical resolution and spectral separation because of the greater information present in the CCT.

B

TABLE 1. NAMED LAKES VISIBLE IN ERTS-1 IMAGERY (Sept. 28, 1972)
OF OAKLAND COUNTY (Scene 1067-15463)

Lake Name	ERTS Band Visibility				Area (Acres)	Max. Depth (Feet)	Shore Length (Miles)	Ref. Number*	Lake Shape	Shape Fit: Image/Map	Lake Islands			Var. Image Density (Band 5)
											Present/ Absence	ERTS Band Visibility		
	4	5	6	7								5	6	
Cass	+	+	+	+	1280	123	11.5	331	Elliptical	Good	No			Yes
Orchard	+	+	+	+	788	110	5.7	344	Circular	Good	1	+	+	Yes
Union	+	+	+	+	465	102	4.0	232	Elliptical	Good	No			
Sylvan	+	+	+	+	458	---	4.7	329	Triangular-	Good	No			Yes
Pine	+	+	+	+	395	90	4.3	347	Elliptical	Good	No			Yes
Elizabeth	+	+	+	+	363	90	3.3	925	Rectangular	Good	No			Yes
Upper Straits	+	+	+	+	325	96	5.5	359	Elongate	Good	No			Yes
Walnut	+	+	+	+	232	101	3.2	381	Square	Good	No			
Lower Long	+	+	+	+	178	95	3.7	411	Elongate	Good	No			Yes
Middle Straits		+	+	+	171	55	4.1	263	Elongate	Good	No			Yes
Green		+	+	+	166	---	3.0	340	Elongate	Good	No			
Upper Long	+	+	+	+	108	---	2.5	348	Elongate	Good	No			
Island	+	+	+	+	101	35	2.0	444	Triangular	Good	3	-	-	Yes
Square	+	+	+	+	94	67	1.4	405	Square	Good	No			
Crescent		+	+	+	90.4	40	2.3	918	Elongate	Fair	2	+	+	
Hammond	+	+	+	+	85	---	1.5	330	Circular	Good	No			
Otter		+	+	+	81	---	1.8	934	Elliptical	Poor	No			
Crystal	+	+	+	+	51	---	2.2	969	Elongate	Good	No			
Forest		+	+	+	40	55	0.8	410	Circular	Good	8	-	-	Yes
Turtle	+	+	+	+	37	65	1.4	406	Elliptical	Good	No			
Orange			+	+	37	---	1.1	416	Elliptical	Good	No			
Wabeek		+	+	+	25	---	0.9	447	Rectangular	Good	No			
Geneva		+	+	+	19.2	---	0.8	921	Elliptical	Good	No			
Darby		+	+	+	16.5	---	0.7	334	Square	Good	No			
Simpson			+	+	13.2	---	0.5	337	Elliptical	Fair	No			
Crawford			+	+	13.0	---	0.5	453	Elliptical	Good	No			
Morse			+	+	13.0	---	0.9	371	Rectangular	Fair	No			
Mirror		+	+	+	11.0	25	0.5	367	Elliptical	Fair	No			
Sodon			+	+	10	19	0.4	446	Circular	Fair	No			
Landers			+	+	9.6	---	0.6	342	Rectangular	Good	No			
Scotch		+	+	+	9.3	---	0.6	338	Elliptical	Good	No			
Dawson's Mill Pond			+	+	8	---	1.1	970	Elongate	Poor	No			
Fiddle			+	+	7.5	---	0.6	920	Elongate	Poor	No			
Cross			+	+	7.3	---	0.6	337	Elliptical	Good	No			
Dow			+	+	6.5	---	0.4	346	Square	Poor	No			
Mud			+	+	6.2	---	0.5	349	Rectangular	Fair	No			
Egg			+	+	5.6	---	0.3	356	Elliptical	Fair	No			
Haines			+	+	5.5	---	0.4	449	Triangular	Fair	No			

6. REFERENCES

1. Chase, P. E. & V. E. Smith, 1973. Utilization of ERTS-1 Data to Monitor and Classify Eutrophication in Inland Lakes. Interim report to NASA GSFC September 1972 - January 1973, Contract NAS 521810, Bendix Report BSR 4010.

2. Hutchinson, G. E. (ed.) 1957. A treatise on limnology. Vol. 1. Geography, physics and chemistry. John Wiley and Sons, Inc. New York. 1015p.

3. Juday, C. and E. A. Birge. 1933. The transparency, the color and the specific conductance of the lake waters of northeastern Wisconsin. Trans. Wisc. Acad. 28:205-259.

4. The new 'lake' lies on a line between Wabeek and Pine Lake in Figure 2.

5. Golf courses and cemetaries are particularly visible in Figure 2.

N73-28316

ERTS-1 OBSERVES ALGAL BLOOMS IN LAKE ERIE AND UTAH LAKE

Alan E. Strong, *National Oceanic and Atmospheric Administration, National Environmental Satellite Service, Hillcrest Heights, Maryland 20031*

ABSTRACT

During late summer when the surface waters of Lake Erie reach their maximum temperature an algal bloom is likely to develop. Such phenomena have been noticed on other shallow lakes using ERTS-1 and characterize eutrophic conditions. The concentration of the algae into long streamers provides additional information on surface circulations. To augment the ERTS-1 MSS data of Lake Erie an aircraft was flown to provide correlative thermal-IR and additional multiband photographs. The algal bloom is highly absorptive in the visible wavelengths but reverses contrast with the surrounding water in the near-IR bands. The absorption of shortwave energy heats the dark brown algal mass, providing a hot surface target for the thermal-IR scanner.

1. INTRODUCTION

As aircraft flights were being made over Lake Erie on 15 October 1972, underflying ERTS-1, a long dark streamer was observed between Kelleys and South Bass Islands and the Ohio shoreline. Although it was known the ERTS imagery would barely reach this area, the flight pattern was modified on site to provide sufficient coverage of this water-borne material.

2. OBSERVATIONS

The NOAA Buffalo DeHavilland aircraft was equipped with a Spectral Data Corporation multiband camera system, to spectrally simulate ERTS, and a Daedalus Dual-Channel Thermal Scanner. Flying at an altitude of 5.8 kilometers, the photography covered a swath beneath the aircraft of approximately 2.5 nautical miles. The IR-imagery covered a 5 nautical mile swath. Since our main surface truth operations were being conducted along the Canadian shore of the lake, no quantitative measurements have been obtained for the area in question off Port Clinton, Ohio.

Original photography may be purchased from:
EROS Data Center
10th and Dakota Avenue
Sioux Falls, SD 57198

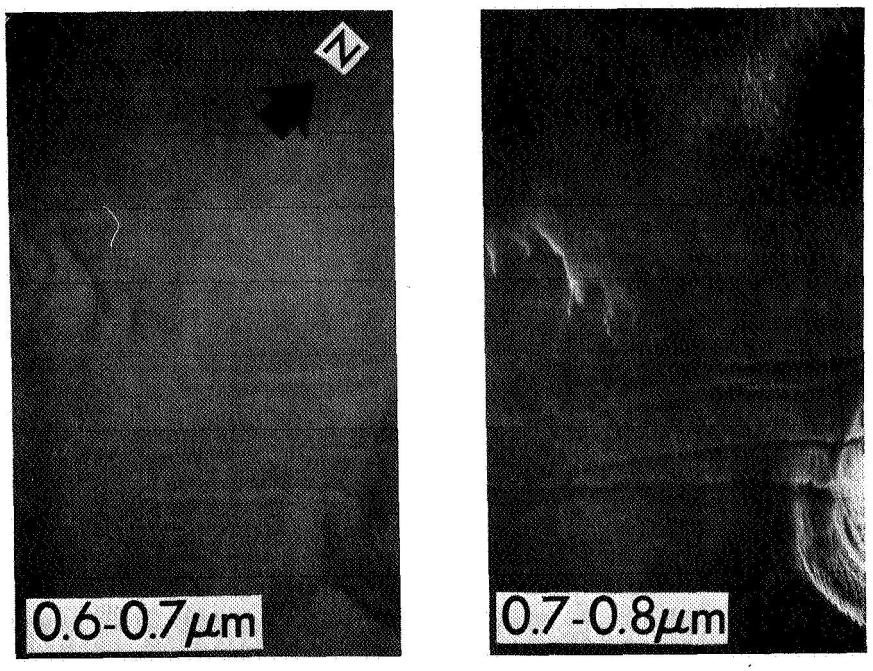


Figure 1. Multiband photography, 15 October 1972. Altitude 5.8 km; Time: 1837 GMT. See Figure 4 for chart locations.

The multiband camera observations are presented in Figure 1. An abrupt reversal in contrast is evident between the ERTS-simulated MSS bands "5" and "6". The material that absorbs shortwave energy in the visible wavelengths reflects incident radiation in the near-IR wavelengths. Due to the strong solar absorption in the visible it was not surprising to find an associated high surface temperature in the thermal-IR. This simultaneous information is presented in Figure 2. The near-surface manifestation of this material is made evident as small boat wakes normal to the streamer appear to cut both the visible, reflected-IR and thermal-IR features.

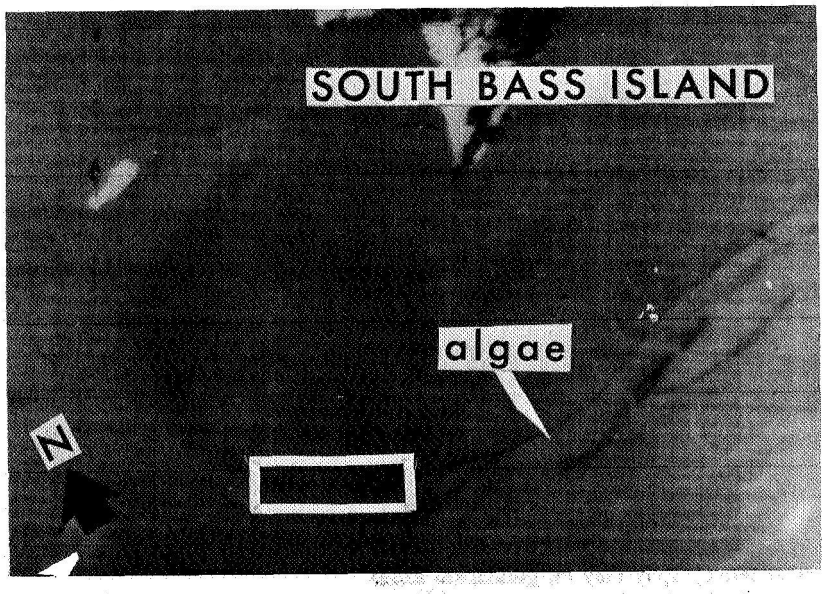


Figure 2. Thermal imagery over same area as Figure 1. Darker tones are warmer temperatures. Spectral wavelength is 9-14μm. Box locates area covered by Figure 1.

A portion of the ERTS-1 MSS data has been redisplayed on our Digital Muirhead Device (DMD) at the National Environmental Satellite Service. Use of the DMD makes it possible to enhance the lower radiances characteristic of water. It has been seen that considerable information is available from ERTS altitudes from what initially appears in the original unenhanced imagery as a uniform black tone. A reprocessed 7.2 nautical mile north-south DMD swath of the original MSS imagery is illustrated in Figure 3. The "chip" begins at Point Pelee on the north shore of Lake Erie and terminates at Marblehead, just north of Sandusky, Ohio. Although the 15 October ERTS-1 imagery barely covered the phenomenon observed in Figures 1 and 2, the high reflectance of the westernmost portion can be seen in MSS-6 (Fig. 3c) immediately west of Kelleys Island and more faintly in MSS-7 (Fig. 3d). A chart locates the information in Figure 4.

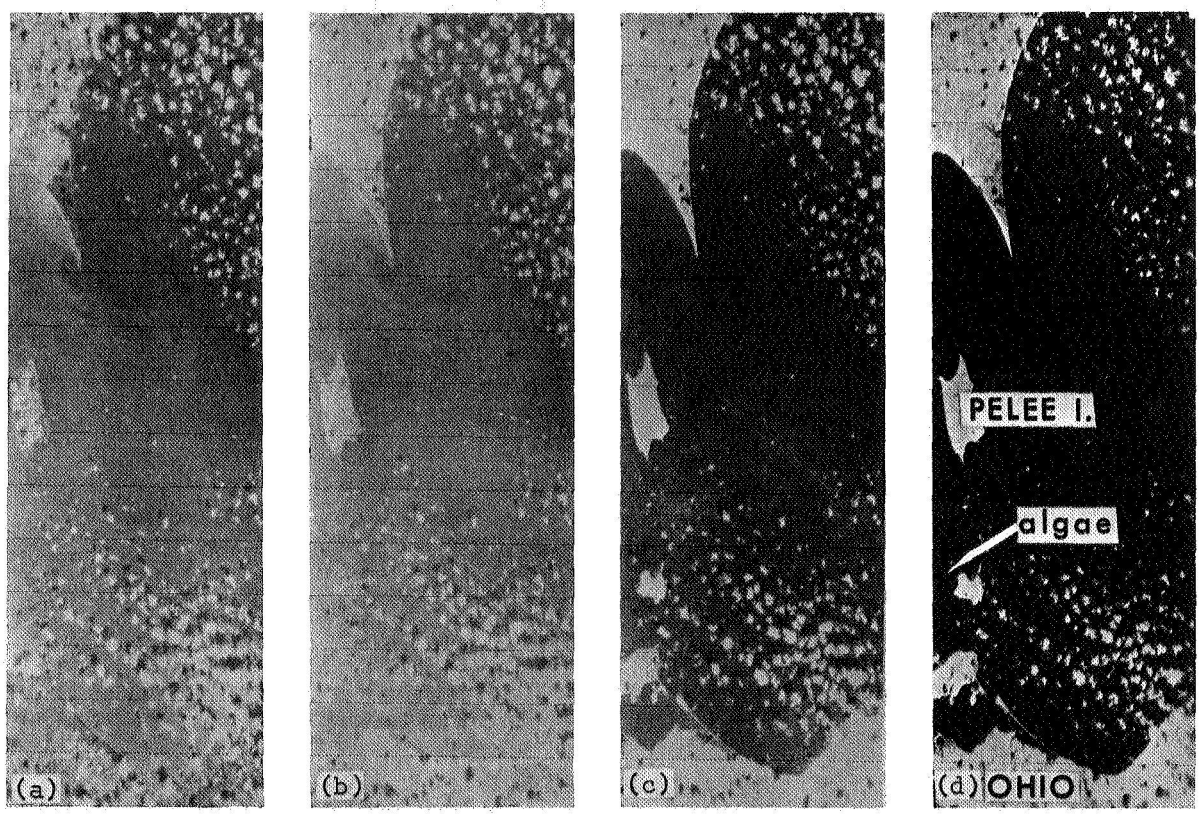


Figure 3. Digital enhancement of ERTS-1 image taken on 15 October 1972 at 1541.3 GMT. Swath is from western edge of image and covers approximately a 7.2 nautical mile width. Enhancement is greatest in the first five radiance levels (counts)-(a) MSS-4, (b) MSS-5, (c) MSS-6 and (d) MSS-7.

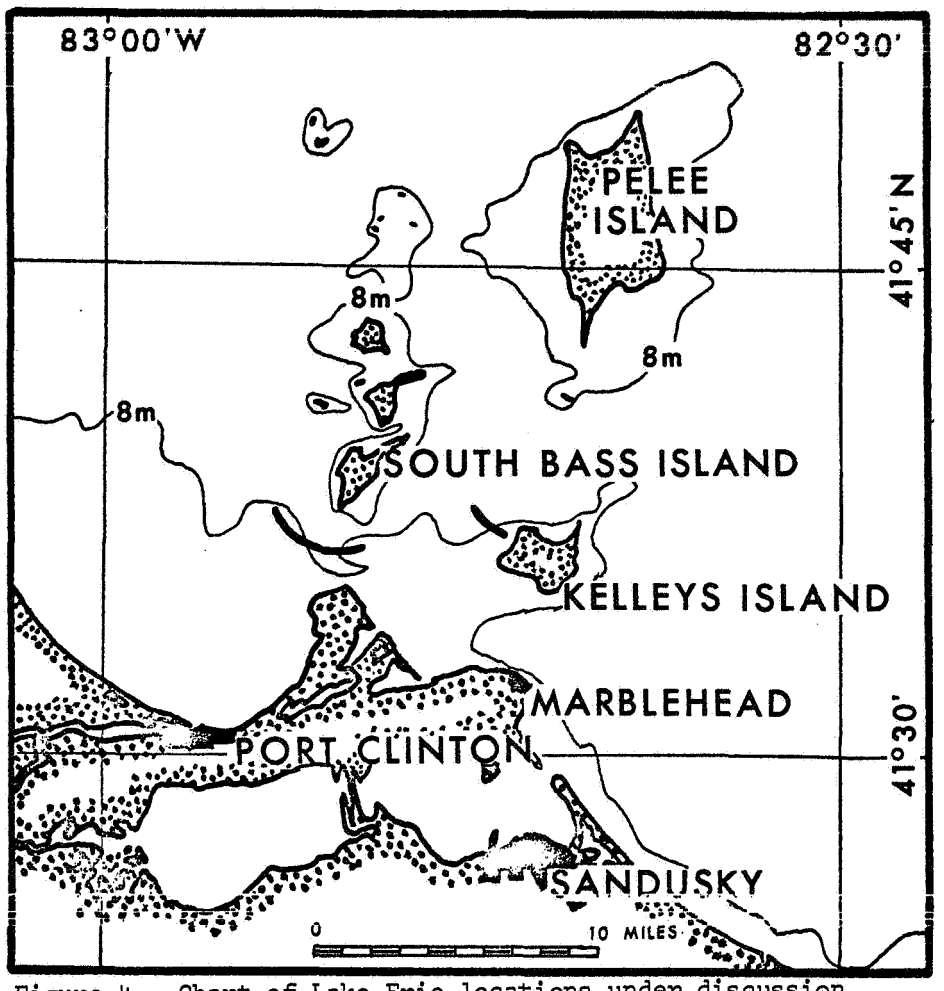


Figure 4. Chart of Lake Erie locations under discussion. Information from ERTS-1 and aircraft have been located using the Bausch and Lomb Zoom Transfer Device.

A much superior observation of an identical phenomenon has been located in the ERTS imagery. This is of Utah Lake during September 1972. Figure 5 shows anticyclonic gyre in this shallow (ca 3m) and highly eutrophic lake ($PO_4^{=}$ca. 0.5mg/l) that reverses contrast at 0.7μm and covers a large percentage of the surface of this lake (lake-surface area is ca. 375 km^2). ERTS-1 imagery acquired on both 12 and 29 September 1972 showed this feature. Utah Lake is known for its high turbidity and during summer months algae blooms frequently follow calm periods. (Dr. David White, Brigham Young University, personal communication)

3. RESULTS AND CONCLUSIONS

Based on the success of ERTS MSS to resolve a strong chlorophyll reflectance on Utah Lake, it is our contention that an algae bloom has taken place on Lake Erie. The vigorous growth of this resulting biomass is rich in chlorophyll, and provides a strong reflection of radiant energy in the near-IR bands. The dark green or brown color of this phenomenon is likely to render the algal surface darker at visible wavelengths than surrounding high turbidity coastal waters as was observed in MSS bands 4 and 5. Algae blooms can be expected to occur during periods of low surface winds, warm water conditions and substantial insolation. These conditions preceded both Lake Erie and Utah Lake observations. Although most Great Lake algae blooms can be expected to be on a scale barely resolved by ERTS resolutions, a careful interpreter and some judicious computer processing should reveal many more algae bloom situations that have previously gone unnoticed. Monitoring these blooms and their distributions not only provides information on the quality of the water that supports them but also valuable information of circulation of the water supporting this rich biomass.

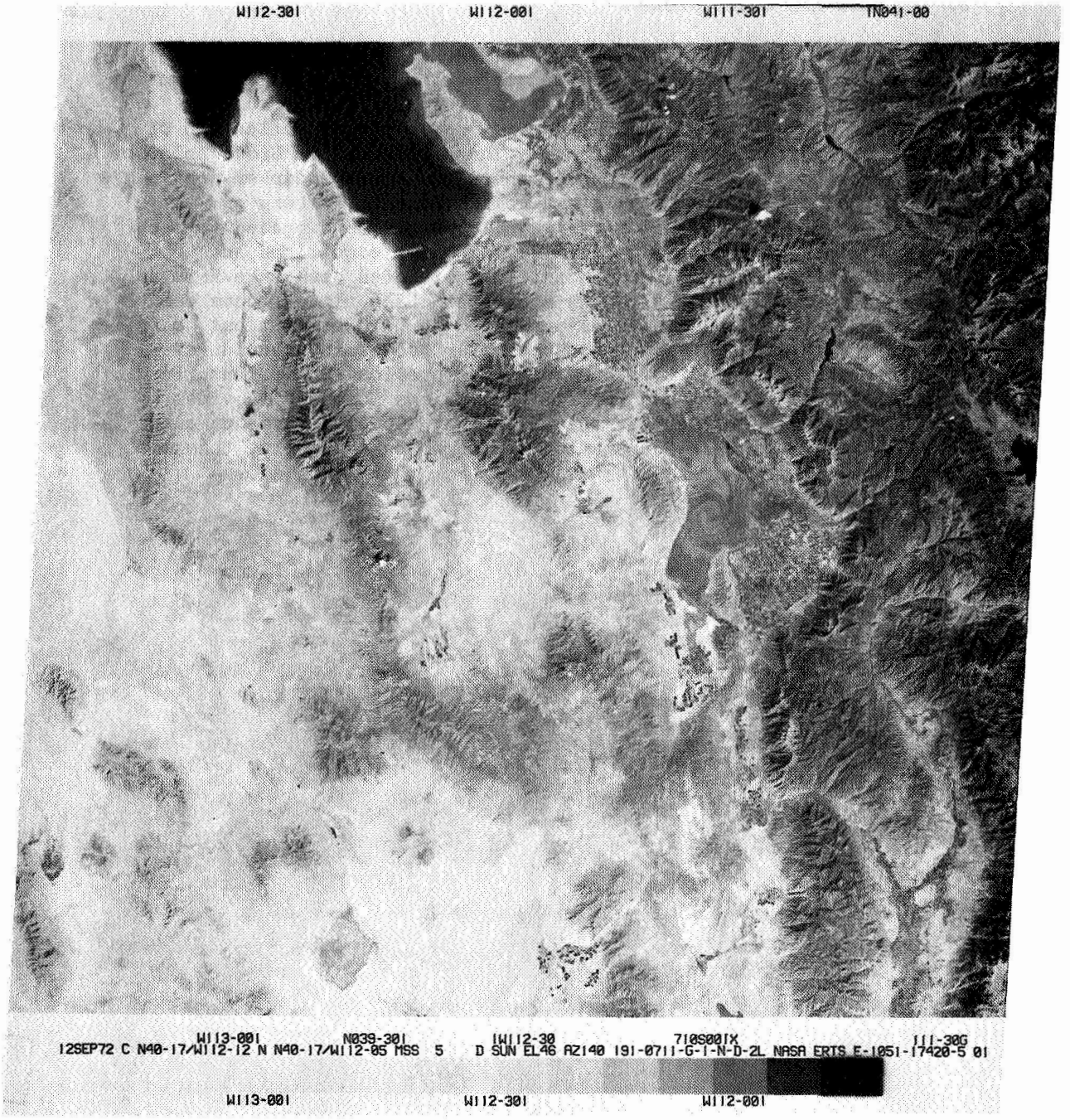


Figure 5a. Utah Lake, 12 September 1972, Time: 1742 GMT. MSS-5.

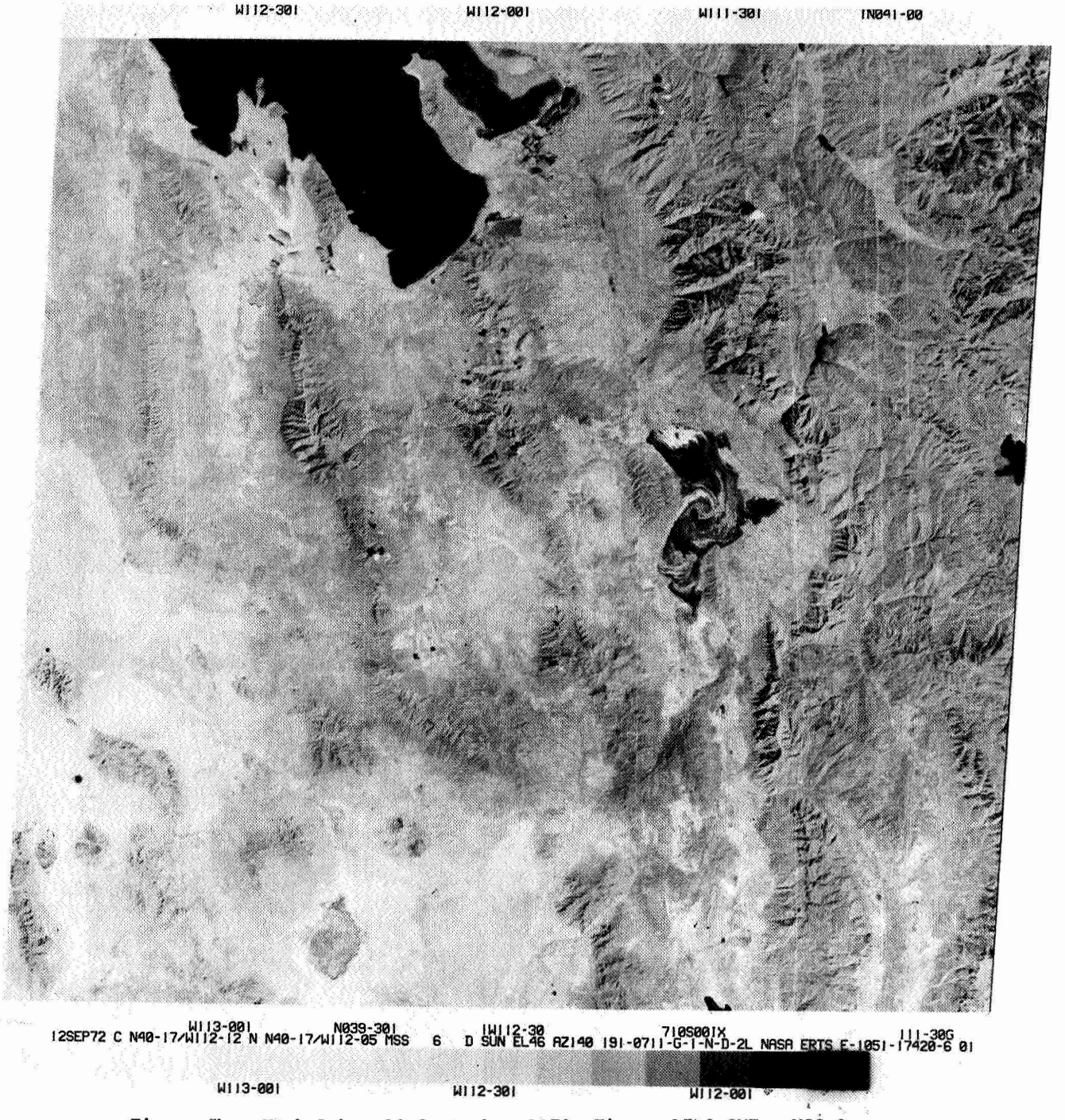


Figure 5b. Utah Lake, 12 September 1972, Time: 1742 GMT. MSS-6.

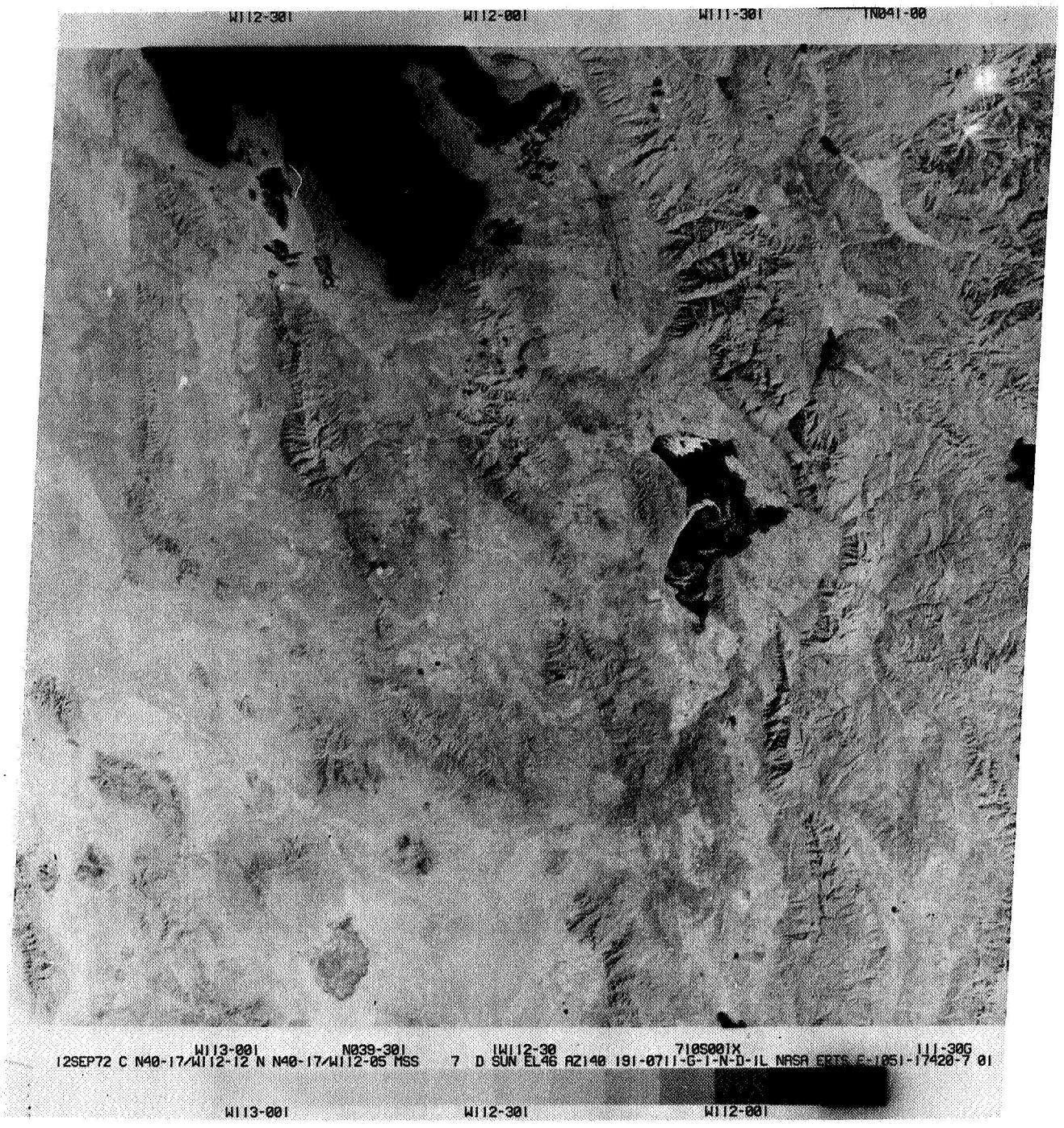


Figure 5c. Utah Lake, 12 September, Time: 1742 GMT. MSS-7.

N73-28377

USE OF ERTS-1 DATA FOR REGIONAL PLANNING IN THE METROPOLITAN WASHINGTON COUNCIL OF GOVERNMENTS – A SHORT BRIEF

Harry J. Mallon, *Director, Remote Sensing Project, Metropolitan Washington Council of Governments*

ABSTRACT

Land use and land use activity changes over discrete intervals of time represent basic data requirements in regional planning studies. This paper reports on two examples of land use analysis required by the Council of Governments' transportation planning staff. Both were undertaken utilizing remote sensing imagery analysis. One study using large scale aircraft imagery developed a high degree of analytical detail and functional identification. The other, to support further detailed data base evaluation, utilizing ERTS-1 and small scale aircraft imagery, developed data identifying in more general detail major activity changes within the metropolitan region.

Introduction.

"Urban policy planning is a complex process of analysis, intervening in and managing the political conflict that is inextricably related to urban change. Research is needed into the structure of public policy making, characteristics of urban policy formulation and implementation, strategies and techniques of change-program management. New methods, new techniques and concepts of planning must be developed. If planners are to be effective policy analysts and change managers, they must receive cognitive inputs and skills for dealing with a complex policy making system ...."[1]

It would be presumptive to claim that the substance of this brief paper would meet the requirements pointed to in the referenced quotation. However, it will address itself to one of the basic ingredients neccessary to support correct policy analysis and decision making, namely; current and uniform information on urban change, its early recognition, classification, and quantification, and will offer several examples of the introduction of imagery analysis techniques - using aircraft and ERTS-1 data - into the change analysis process.

Data Development.

An integral element of the Metropolitan Washington Council of Governments is its Transportation Department. The department functions under the Council's Director, as the staff for the metropolitan area's Transportation Planning Board and other related Council of Governments' policy and technical committees. Its principal function is to data and studies, to prepared plans, and to develop strategies for use by the Board, other planning groups, and the elected officials of the metropolitan region to assist them in dealing with the transportation problems and needs of the region.

As would be expected, certain classes of information such as residential and housing data (location and type), population densities, location of accessible employment areas, transportation routes, route densities , and changes in these with respect to existing data bases, represent critical needs for survey and study, growth projections, and planning purposes.

In November 1972, the Remote Sensing Project was requested by the Transportation Department to provide data at two distinct levels of degree and detail in support of current studies. Both tasks were required in fairly short periods of time: two to three weeks.

The first was to develop from appropriate imagery, land use and related quantified data for comparative use with an existing 1968 data base, on two rapidly growing districts in Loudoun County, Virginia. Then, as an extention of this, the analysis was to be repeated on the same districts for the years 1970 and 1972.

Specific information required included: the delineation and measurement of land use (to the second order of detail in the COG Land Use Classification Table, i.e., within a commercial classification, say, to identify offices, shopping centers, stores, filling stations, etc.; and in area, to the size, say, of a filling station); to plot these delineations on an appropriate scale map; to identify housing units by types; to estimate the numbers of corresponding dwelling units; and to determine the mileages of public rights-of-way by types (2,3,4 lane undivided and divided roads).

The second task was to prepare from imagery analysis, a generalized land use change map over the same periods of time for the entire metropolitan Washington region.

The data for the first task were developed from commercially available aerial photography using conventional stereoscopic imagery analysis supported

by field visits where needed. Photographic scales of about 1:30,000 were used, and because 1968 imagery of the region was not available (not an unusual situation) the analyses were performed only for the 1970 and 1972 periods. The land use data developed for these two periods are shown on the maps in Figures 1 and 2 respectively. Most of the developed area, it will be noted, is residential, the hatched areas of the same color representing new construction. As can be seen from the uncolored portions, these two districts are essentially rural or undeveloped in character, although in process of rapid and current change. The large residential areas in the lower central portion of the maps constitute the new communities of Sterling Park and Sugar Land Run Estates.

An interesting point of the analysis, possibly worthy of mention, is a method utilized for estimating the number of dwelling units in the garden-type, multi-family buildings in these areas. A composite floorspace figure in square feet was computed from the measured ground areas of the buildings and their heights in stories. Allowing for stair-wells and other non-residential building useage, a conversion figure of about 1500 - 1600 square feet per unit was used to convert floor space areas to corresponding numbers of dwelling units. For one garden apartment group, 370 dwelling units were estimated from the imagery, a figure which compares fairly well with the number of 380 units provided by the building management. Recognizing that wide variations are possible in the use of such factors, it was nevertheless interesting to note the fair agreement with data in other sources [2] for similar housing types.

The detailed analyses undertaken during the first of these two tasks and briefly described herein were important and necessary preliminary foundation stones for what was to be accomplished in the second task, namely; a region-wide land use activity change analysis. This task undertook to pin-point and to plot graphically those areas in the region which, during stated time periods, developed major growth/change patterns. This information would be used to provide data in support of transportation studies describing and structuring regional change, its impact, and also to evaluate the currentness of existing data from other sources on those areas experiencing the major changes.

Specifically, the task was to produce land use activity change maps at a regional scale of 1:96,000 for the periods 1970 and 1972. As stated previously, the time constraints were close: two to three weeks. This was much too short to plan for complete, new, large scale aerial photo coverage of the region's approximately 2500 square miles of area, even if the budget could have supported it (which it couldn't). What was available to the Project then for the analysis were two principal sources of imagery. For 1970, the excellent CARETS Mission of September 1970, flown in color IR by NASA for the USGS, was on hand on loan from the USGS. For the 1972 data, the ERTS-1 MSS black and white and color composited imagery of September 23rd and October 11th 1972 were available, having been recently purchased from the EROS Data Center at Sioux Falls, South Dakota.

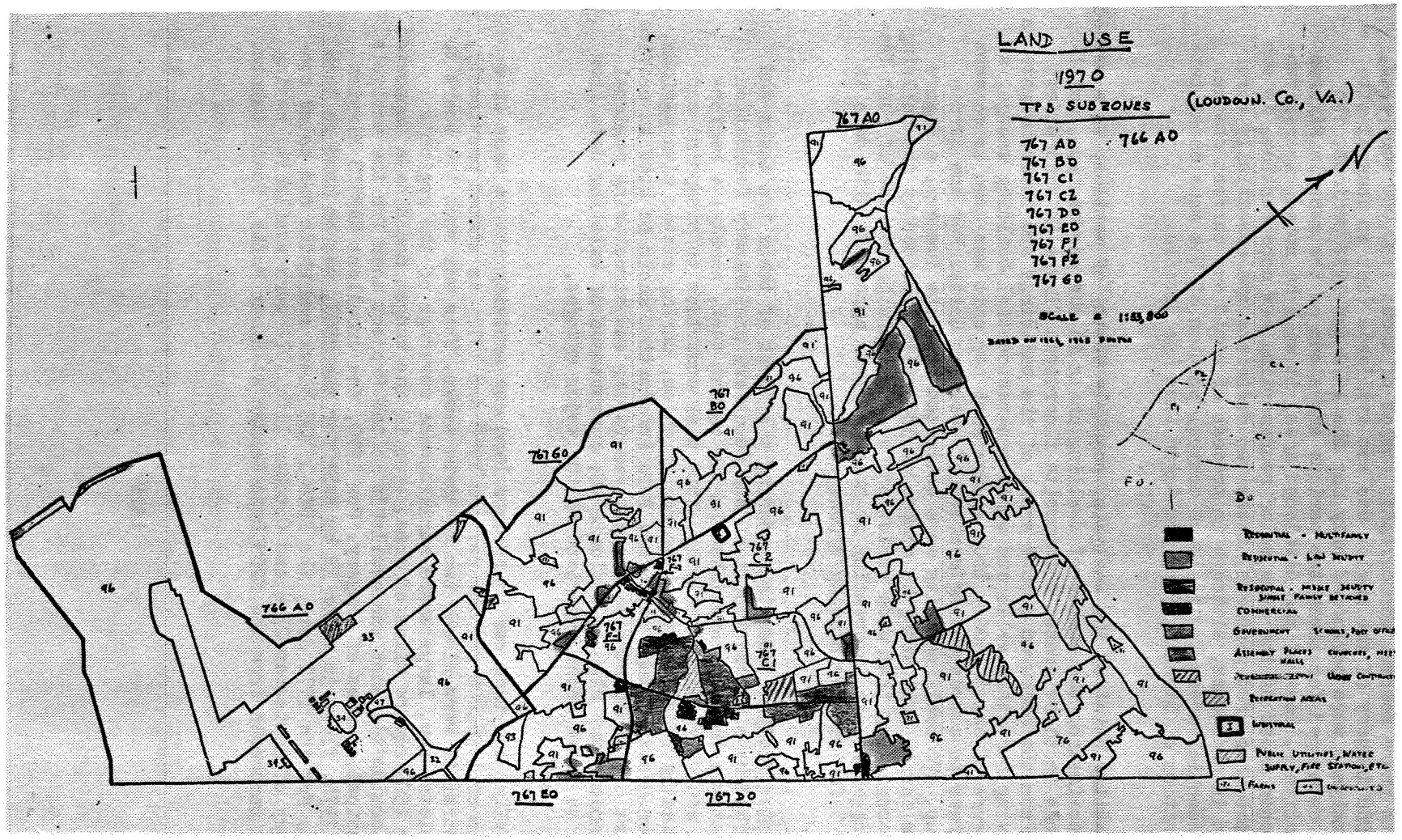


Figure 1. Land Use in TPB Districts 766 and 767, Loudoun County, Va., based upon 1970 imagery analysis.

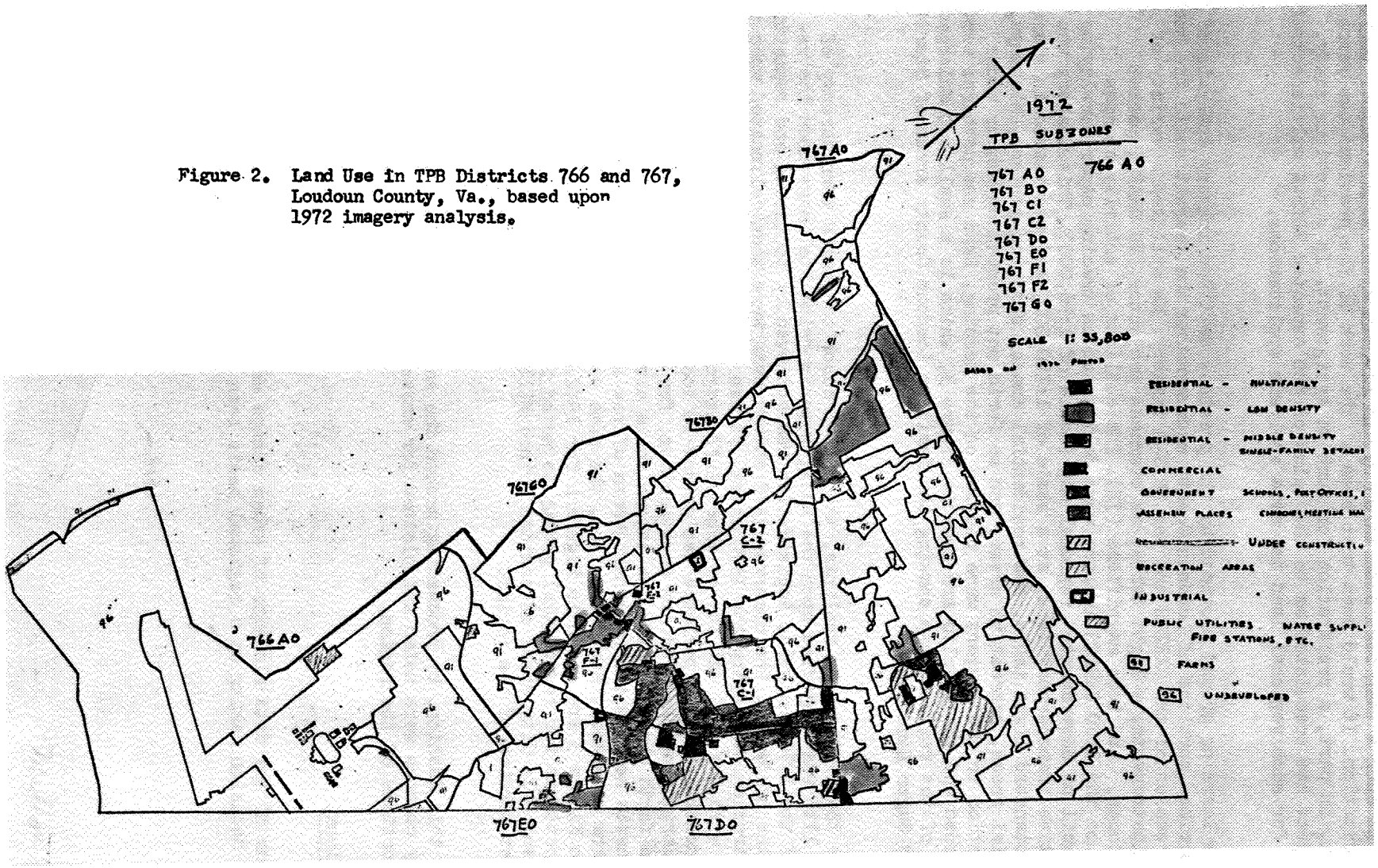


Figure 2. Land Use in TPB Districts 766 and 767, Loudoun County, Va., based upon 1972 imagery analysis.

Rarely had such a task been undertaken by the Project staff with a higher degree of anticipation. It would seem that some of the work of the previous two years had been, in part, a preparation for such an assignment. In a previous study, the Project had speculated as to the value of the expected ERTS-A multispectral returns for such regional land use data analysis applications. [3]

The learning ground provided by the previous detailed imagery analysis of the described portions of Loudoun County made smoother the transition to the much smaller scales of the CARETS and the ERTS-1 imagery. We utilized a variety of simple instruments: a light table, an overhead projector (VU GRAF), pocket stereoscopes, and tube magnifiers (7X). The outlines of activity changes visible on the 1970 CARETS imagery were delineated on tracing paper overlaying the Council of Governments' regional map (scale of 1:96,000). This imagery was in positive transparency form, at a scale of 1:120,000, and was viewed in stereo over a standard light table. New residential areas, shopping centers, highways, industrial areas, recreation areas, and so forth not present earlier or under construction in the imagery were plotted on the tracing. Land use patterns were color coded and the results are seen in Figure 3, which is a small but enlarged portion of the regional map showing the familiar Loudoun County areas of Sterling Park and Sugar Land Run.

For the 1972 change analysis, the ERTS-1 color composite transparency of October 11th was projected upon the wall, superimposing its image upon the results of the 1970 analysis. Registration was achieved by focussing and repositioning of the projector. The observed 1972 change data were then delineated upon a second tracing overlaying the 1970 sheet. It was necessary, of course, to work closely with the 1970 and the enlarged 1972 imagery to interpret cultural and other identities. As experience was gained in looking for distinctions in tonal values (bright patches for new construction, for example), and by continuous back and forth checking with the larger scale aircraft imagery, it was possible to delineate readily the prominent areas of new activity. Ground checks were made where necessary. For comparison, the same areas of Loudoun County seen above in Figure 3 are shown in Figure 4 for 1972. Figures 5 and 6 show similar change patterns for residential growth as noted for 1970 and 1972 in the Woodbridge and Dale City areas of eastern Prince William County, Virginia, in the southwest portion of the region.

In this fashion, by proceeding around the metropolitan area, similar activity changes were noted and plotted for areas in adjoining Maryland and other portions of the region.

Conclusions.

Some of the data elements of urban change necessary for planner's study and related decision making on a regional basis seem to be at hand with the data

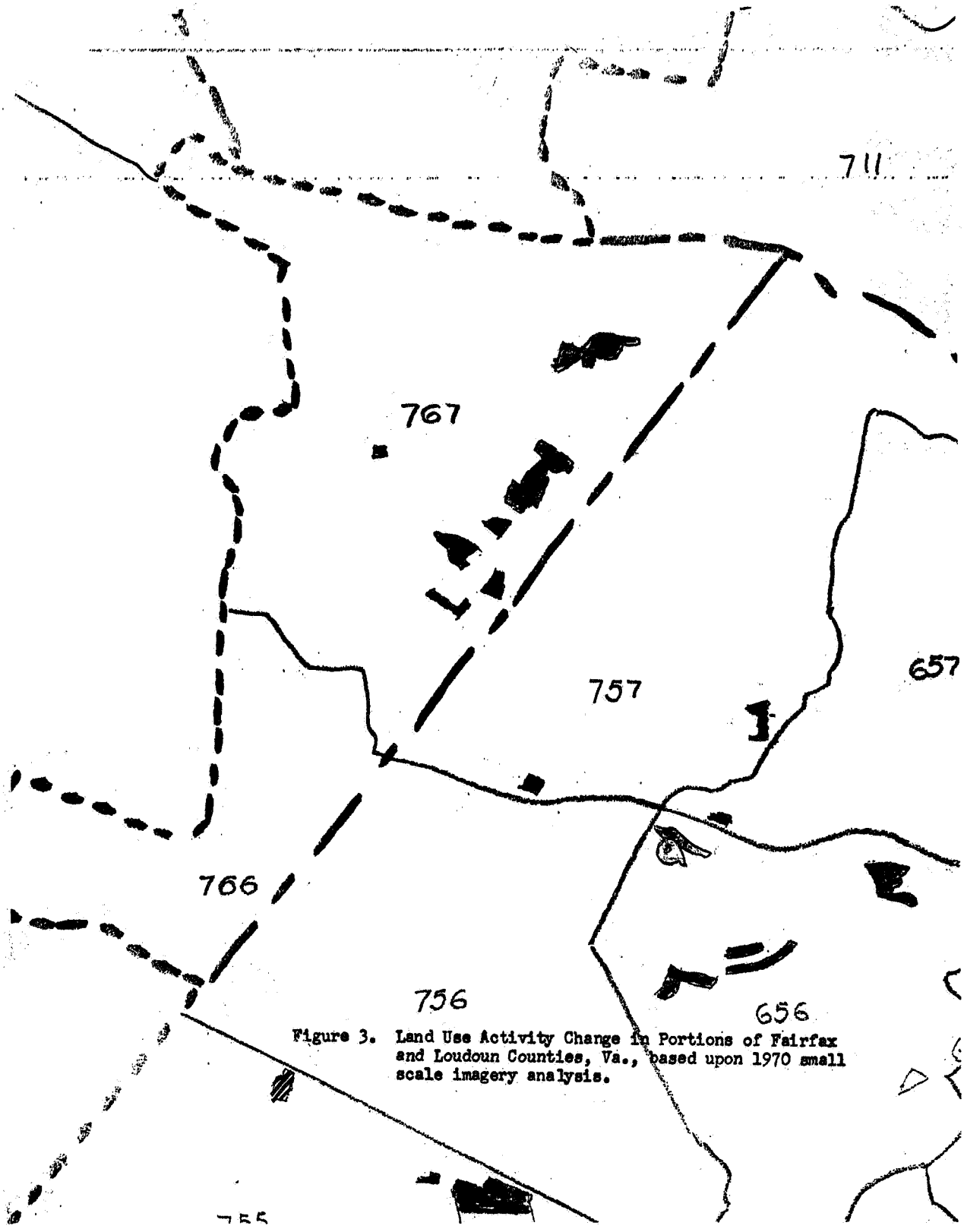


Figure 3. Land Use Activity Change in Portions of Fairfax and Loudoun Counties, Va., based upon 1970 small scale imagery analysis.

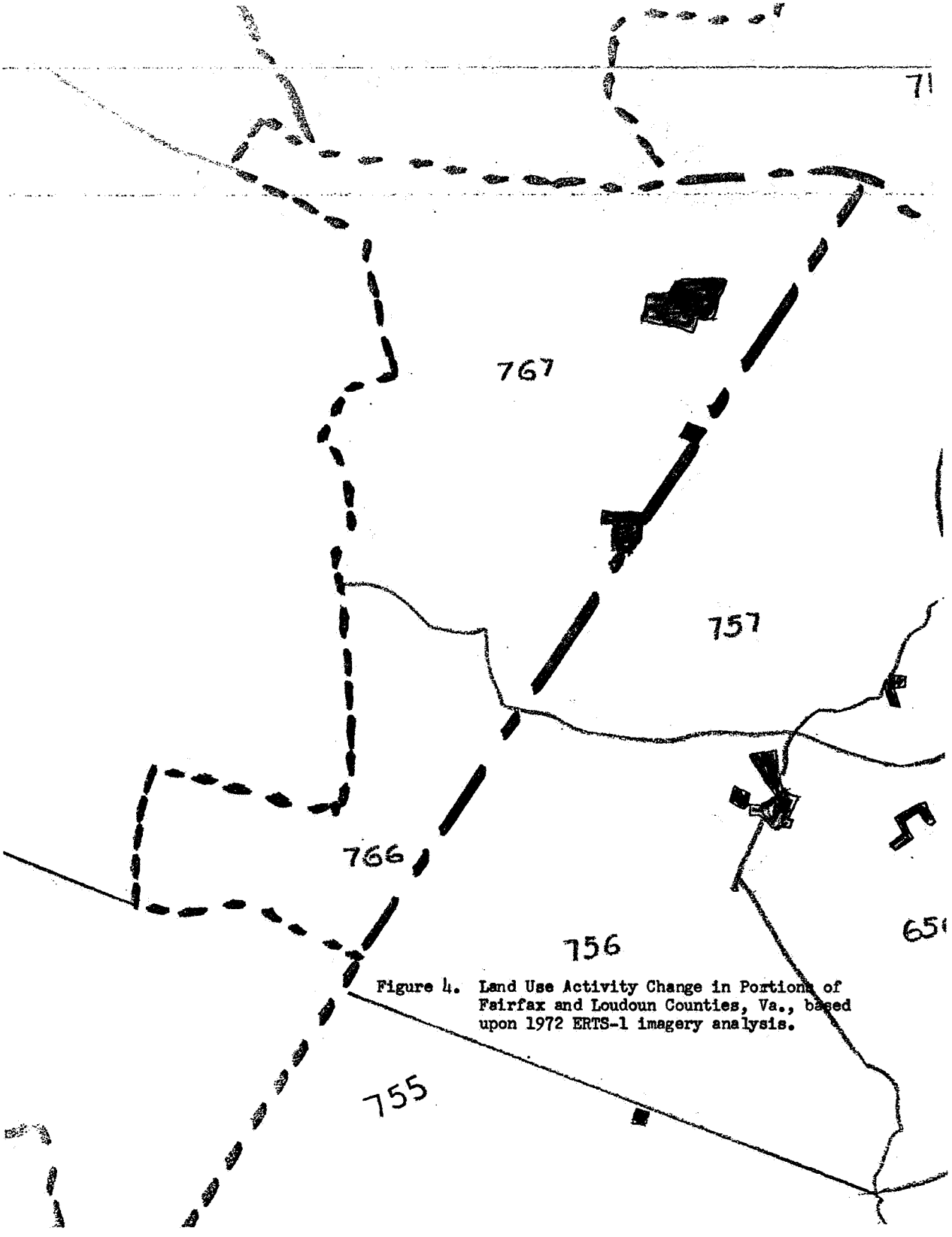


Figure 4. Land Use Activity Change in Portions of Fairfax and Loudoun Counties, Va., based upon 1972 ERTS-1 imagery analysis.

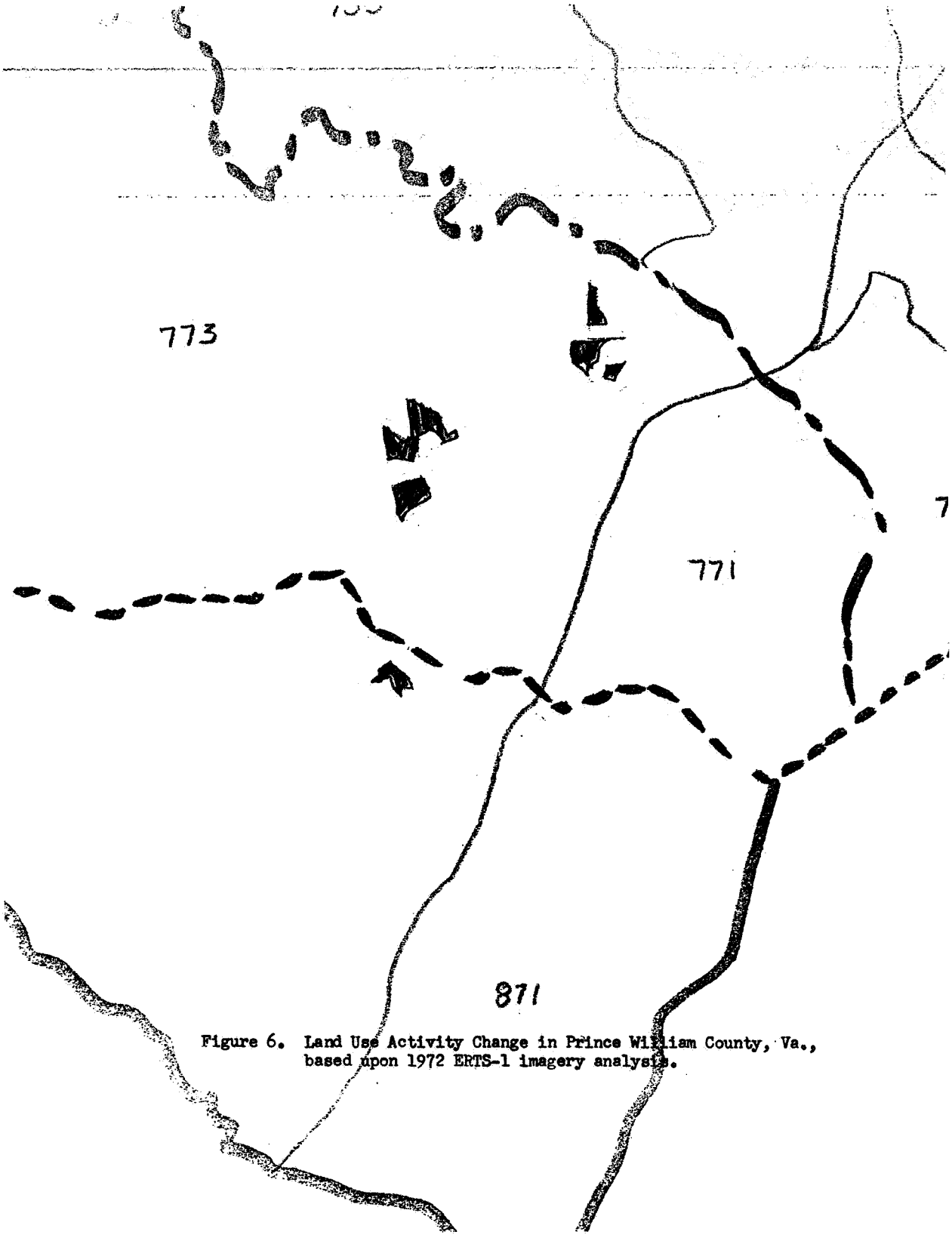


Figure 6. Land Use Activity Change in Prince William County, Va., based upon 1972 ERTS-1 imagery analysis.

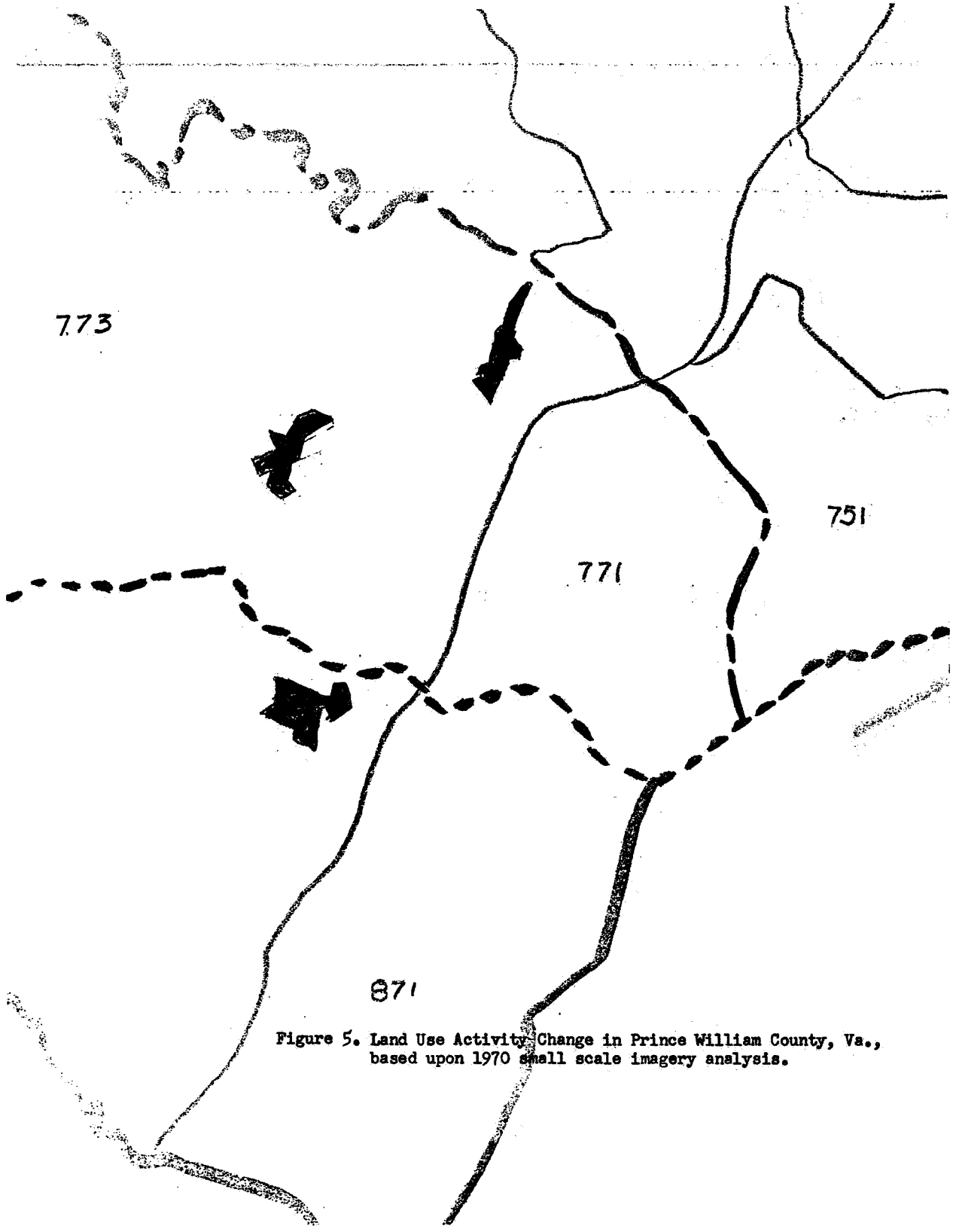


Figure 5. Land Use Activity Change in Prince William County, Va., based upon 1970 small scale imagery anslysis.

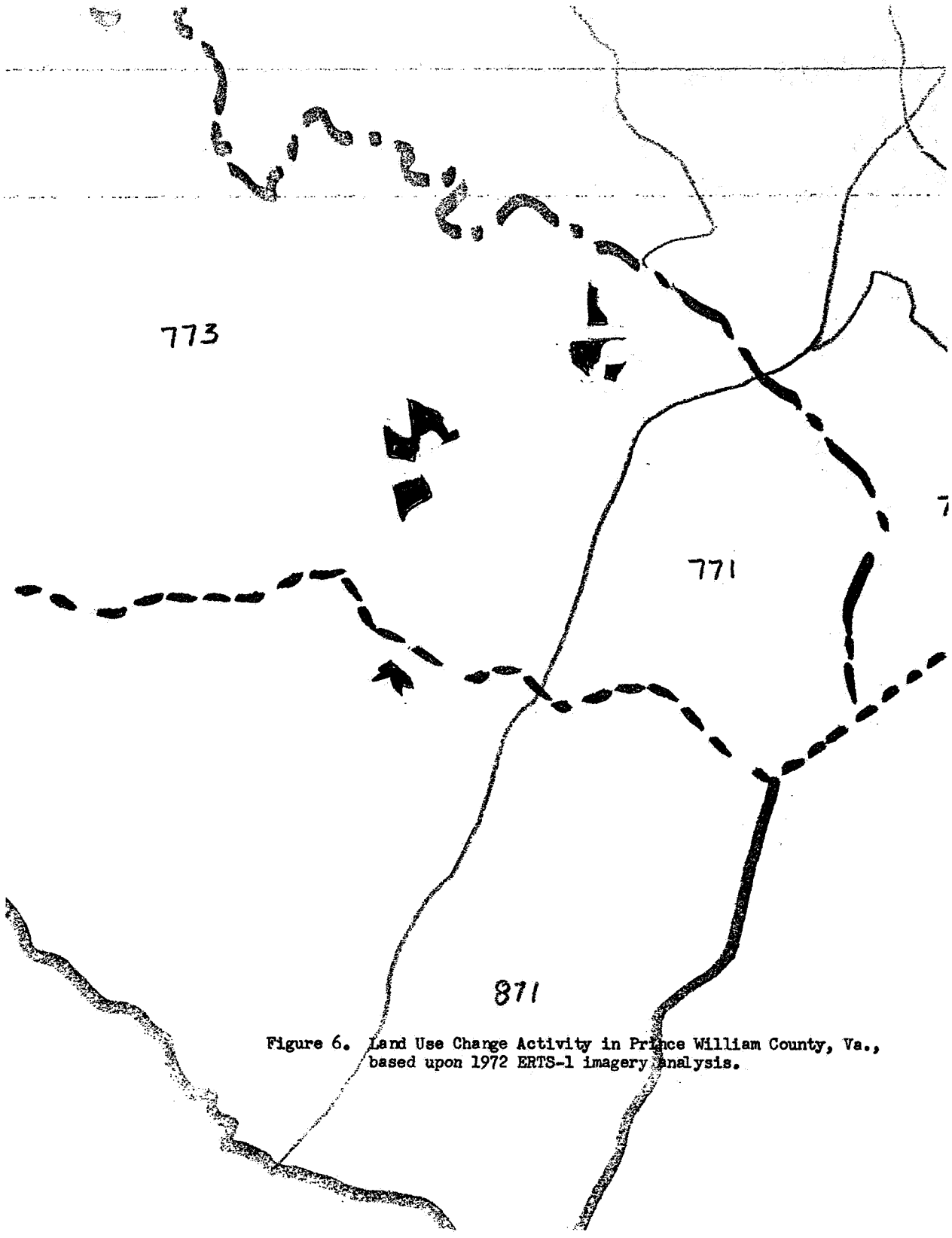


Figure 6. Land Use Change Activity in Prince William County, Va., based upon 1972 ERTS-1 imagery analysis.

made possible by manipulative analysis of the ERTS-1 imagery. It is timely, sequential , and uniform. This appears to be the case on the basis of the relatively simple and preliminary analysis described in the foregoing. It is particularly pleasant to offer this conclusion since it gives credence to several experimental designs for ERTS-A data utilization made in an earlier Project study [4], with respect to regional land use, transportation, and general overall planning studies within the metropolitan area.

References.

1. Rondinelli, D.R., 1973, Urban Planning as Policy Analysis: Management of Urban Change, Journal of the American Institute of Planners, January 1973, Vol. 39, No. 1, pp 13 - 22.

2. Community Builders Handbook, American Edition, 1968, Urban Land Institute, Washington, D.C., pp 107 - 110.

3. Mallon, H.J. and Howard, J.Y., 1972, Benefits From Remote Sensing Data Utilization in Urban Planning Processes and System Recommendations, Technical Report No. 6, January 1972; prepared under terms of Contract No. 14-08-0001-12708 for the U.S. Geological Survey.

4. Mallon, H.J. and Howard, J.Y., 1972, Proposed Experimental Programs for Testing Remote Sensing Applications in the Metropolitan Washington Area, Technical Report No. 7, February 1972; prepared under terms of Contract No. 14-08-0001-12708 for the U.S. Geological Survey.

N73-28318

LAND USE MAPPING AND CHANGE DETECTION USING ERTS IMAGERY IN MONTGOMERY COUNTY, ALABAMA

Richard Paul Wilms, *The University of Alabama, Department of Civil and Mineral Engineering*

ABSTRACT

The feasibility of using remotely sensed data from ERTS-I for mapping land use and detecting land use change was investigated. Land use information was gathered from 1964 air photo mosaics and from 1972 ERTS data. The 1964 data provided the basis for comparison with ERTS-I imagery. From this comparison, urban sprawl was quite evident for the city of Montgomery. A significant trend from forestland to agricultural was also discovered. The development of main traffic arteries between 1964 and 1972 was a vital factor in the development of some of the urban centers. Even though certain problems in interpreting and correlating land use data from ERTS imagery were encountered, it has been demonstrated that remotely sensed data from ERTS is useful for inventorying land use and detecting land use change.

INTRODUCTION

The University of Alabama, in conjunction with the Alabama Geological Survey, and the George C. Marshall Spaceflight Center, is conducting a vigorous program to determine the feasibility of using remotely sensed data from ERTS-I for (1) mapping land use and land use change, (2) the inventory and management of natural resources, and (3) the improvement of environmental quality in Alabama.

This paper documents an initial study utilizing ERTS-I imagery to determine its applicability to mapping land use and detecting land use change. Good quality, cloud-free ERTS imagery covering most of the state of Alabama was acquired October 15-18 on the satellites fifth pass over the area. Montgomery County, located in the central portion of the State was selected for the initial study primarily because of the large number of first level land use categories represented and also because of the city of Montgomery, the state capitol, which, it was expected, would demonstrate urban growth detectable by ERTS-I.

LAND USE INTERPRETATION AND MAPPING

Land use was mapped for Montgomery county from two types of imagery, conventional air photo mosaics at a scale of 1:63,360 and ERTS imagery. The process of mapping land use from photo mosaics was begun prior to receiving

Original photography may be purchased from:
EROS Data Center
10th and Dakota Avenue
Sioux Falls, SD 57198

Original photography may be purchased from:
EROS Data Center
10th and Dakota Avenue
Sioux Falls, SD 57198

ERTS data. The digital land use data was compiled for each square kilometer, based on six general land use categories considered compatible with satellite resolutions, namely: urban, agricultural, forestland, water, barren land, and non-forested wetland. These correspond to the latest classification scheme proposed by the U. S. Government Inter-Agency Steering Committee on Land Use Information and classification.

The digitized land use data for Montgomery county, compiled from 1964 air photo mosaics and termed "historic" data, provided the basis for comparison with and analysis of ERTS-I imagery. By storing the historic data in computer format, it was possible to generate maps of per cent of land use per square kilometer for a specific category or maps of dominant land use per square kilometer. The latter proved to be best suited for comparison to ERTS data to determine change; the former, however, was especially helpful in spectral analysis of ERTS imagery.

Land use information was extracted from ERTS imagery in much the same manner as from the air photo mosaics, except that instead of estimating what per cent of each square kilometer was occupied by each of the six land use categories, only dominant land use per square kilometer was recorded. An acetate mylar grid was prepared to overlay the ERTS images; the grid cell size corresponded to the image scale of 1: 1,000,000; hence, each square millimeter represented one square kilometer which facilitated rapid comparison with the historic data. Positioning the grid on the ERTS image to correspond to the correct UTM coordinates for that area and using a lighted magnifying glass and light table to view the scene, each cell was color coded as follows:

red	urban
brown	agricultural
green	forested
blue	water
black	barren land
orange	non-forrested wetland

Black and white positive prints corresponding to all four spectral bands were used as well as a color composite image of the Montgomery scene at the same scale. Spectral bands six and seven (near infrared) were first examined under the grid to determine the location of prominent lakes and streams. This initial step was necessary in order to forgo the possibility of classifying a lake or reservoir as some other form of land use when viewing bands four and five (visible bands). After color coding the appropriate cells dominated by water bodies, the grid was applied to the same scene in bands four (green) and five (red). Cultural features were especially prominent on band four even down to secondary roads inside the city of Montgomery itself. Spectral band five displayed agricultural and forestland patterns extremely well.

To aid in interpretation of ERTS-I imagery, an I^2S Mini-Addcol color additive viewer was used to produce color composites of the Montgomery scene.

Use of this instrument enabled features such as small towns, roads, and rock outcroppings that otherwise faded into the background to be distinguished. Varying the light intensity and filter combinations made it possible to highlight features of interest, whether cultural or physical.

Certain interpretation difficulties were encountered resulting from both errors in interpretation by the analyst and constraints in scale and resolution imposed by the ERTS imagery. As might be expected, large areas of homogeneous land use were easily recognized for both time periods and land use categories covering as little as 5% of a square kilometer could be readily interpreted on the 1964 air mosaics. No such detail could be extracted from the ERTS scenes however, thus dictating dominant land use per square kilometer.

Cleared land near Montgomery was recognized as such on the air photo mosaics, but could not be distinguished from the urban area on the smaller scale ERTS scenes. Familiarity with the area however, indicated that the bare land in the 1964 data had been cleared for single and multiple family dwellings and had since been developed thus corroborating that area's having been classified urban on the ERTS scene.

In addition to the I^2S viewer, additional large scale photos (1: 20,000) and U.S.G.S. topographic maps offered supplemental information as an aid in interpretation.

COMPARISON AND CHANGE DETECTION

Upon completion of land use mapping for both time periods (1964 and present), an analytical comparison program was initiated for the purpose of detecting land use change in Montgomery county.

From the computerized 1964 land use data, it was possible to generate a map denoting dominant land use per kilometer. This printout was then color coded to facilitate comparison with land use information derived from ERTS.

From Fig. 1, it is obvious that the metropolitan Montgomery area has experienced considerable growth in the past nine years. It should be mentioned that although a large number of barren land categories would be expected in an area undergoing rapid urban sprawl, barren land was not distinguishable from urban and was thus included in the urban category. This is not altogether in error, for there is usually a very short time period between clearing of land in or near a city and construction on that site.

Other cities are shown to have experienced growth also; and this growth was detectable by comparing 1964 data with that obtained from ERTS-I (Fig. 1). For example, the town of Ramer in southern Montgomery

county dominated only one square kilometer in 1964, but now dominates three square kilimeters. Likewise, the small towns of Mount Meigs and Merry in the northeastern part of the county which were not even recorded as dominant in 1964, each dominated one square kilometer in 1972 according to ERTS-I.

The construction of main highways had a marked influence on the growth of the urban areas. As can be seen on Fig. 2, in 1964, many sections of main roads were either under construction or only in the proposed stage (dashed lines). By 1972, however, imagery from ERTS indicated that these roads were in use and that other roads not proposed in 1964 had been built such as the completion of the northern portion of the ring-road around the city of Montgomery (Fig. 2). There seems to be good correlation between road construction and urban growth both in Montgomery and in the small towns of Mount Meigs and Merry, mentioned previously, which are thought to have benefited directly from the completion, by 1972, of I-85 which runs eastward from the inner Montgomery city area. I-65, proposed but not yet under construction according to 1964 air photos, runs southwesterly out of Montgomery and is now open to traffic. I-65 was very prominent on MSS-5 and is thought to have accounted for a part of the urban growth in that area. Some small urban developments were visible along the new major traffic arteries described above, but did not occupy a major portion of the grid cell in which it occurred and was thus absorbed in the more dominant use and hence, not mapped.

The dominant transition in rural land use in Montgomery county was from forest to agricultural (Fig. 1, 2). Forests still lined the Catoma Creek which flows from southeast Montgomery county to its confluence with the Alabama River in the northwest. Asthetic appeal of these forests along the Catoma may have been partly responsible for the apparent growth of the urbanized fringe of the city of Montgomery in that direction.

Two square kilometers within the bounds of the city of Montgomery were dominated by forestland.

These correspond to parks and areas of widely spaced single family dwellings.

PROBLEMS ENCOUNTERED

Besides detecting actual land use change, the comparison of 1964 data with that derived from ERTS (Fig. 1, 2) may indicate change in a cell where no change has in fact occurred. Because of the low resolution of the ERTS images, small areas of individual land use were grouped into larger homogeneous land use areas and classified according to the dominent form, thus falsely indicating that a change in land use had occurred. Dubious land use changes, such as agricultural to forestland, were probably due to just such an event. Despite the apparent misinterpretation of land

use and change detection in some instances, it has been shown that ERTS imagery is capable both of extracting land use information and monitoring land use changes in the rural and urban environment.

FUTURE PHASES OF THE STUDY

Now that the coding of "historic" land use data (from air photo mosaics, 1:63,360) has been completed for all 67 counties in Alabama and the data computerized, future efforts will concentrate on updating the information utilizing remotely sensed data from ERTS-I. The extraction of land use data from ERTS imagery will provide the information needed for change assessment and will, in itself, serve as an "historic" data base with which to compare subsequent ERTS coverage. Once the color coded land use information has been digitized and stored in a computer, timely land use maps can be generated for any category or combination of categories. Furthermore, with both "historic" and ERTS-derived land use information in computer storage, comparison of the two data bases can be performed internally, thus automating the process of change detection. Ultimately, the analysis of ERTS imagery will be extended to the rest of Alabama for comparison with existing land use information.

In conjunction with the land use phase of the Alabama ERTS project, the correlation of water quality parameters with ERTS imagery will be investigated by the establishment of four to seven data collection platforms (DCP's) within the Warrior River basin. The DCP's will telemeter information concerning water temperature, turbidity, pH, and flow rate to ERTS as it passes overhead where it will be combined with corresponding spectral data and relayed back to Earth.

Also to be investigated is the effect that subsurface geology exerts on land use patterns. The potential of this study was demonstrated in small measure by the agricultural pattern in Crenshaw county (Fig. 3). As can be seen, the amount of agricultural activity decreases sharply south of the contact between the highly eroded and fertile Midway Group Clays to the north and the more rugged and erosion-resistant Wilcox Group sandstones to the south.

CONCLUSIONS

The work thus far performed, part of which is outlined in this paper, indicates that small scale imagery from ERTS-I is a valuable tool in land use inventory and change detection. The accuracy of any interpretive effort, however, is directly proportional to the quality of the imagery being analyzed. Only of late has image quality been acceptible for analysis. If tighter and more consistent control is applied to data processing in the future, ERTS imagery should prove to be useful in a wide array of land use mapping and change detection programs.

REFERENCES

Anderson, J. R., Hardy, E. E. and Roach, J. T., 1972, "A Land-Use Classification System For Use With Remote Sensor Data, Geological Survey Circular 671, Washington, D. C.

Lins, H. F., and Milazzo, V. Z., 1972, "The Use of Small Scale Multi-Band Photography for Detecting Land-Use Change," Proceedings of The 8th International Symposium on Remote Sensing of Environment, Ann Arbor, Michigan.

D

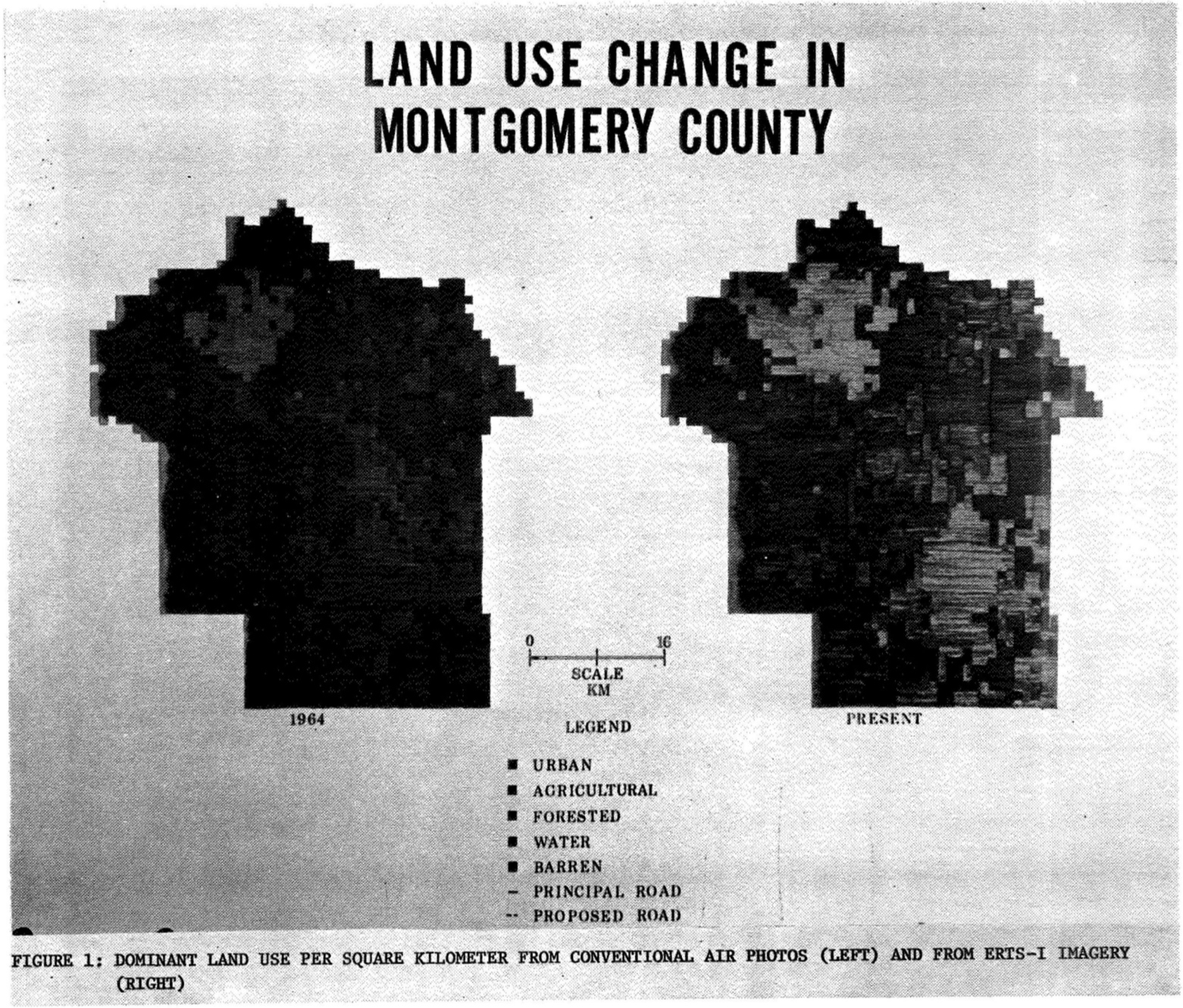


FIGURE 1: DOMINANT LAND USE PER SQUARE KILOMETER FROM CONVENTIONAL AIR PHOTOS (LEFT) AND FROM ERTS-I IMAGERY (RIGHT)



FIGURE 2: THE APPARENT EFFECT OF ROAD CONSTRUCTION ON LAND USE TRENDS

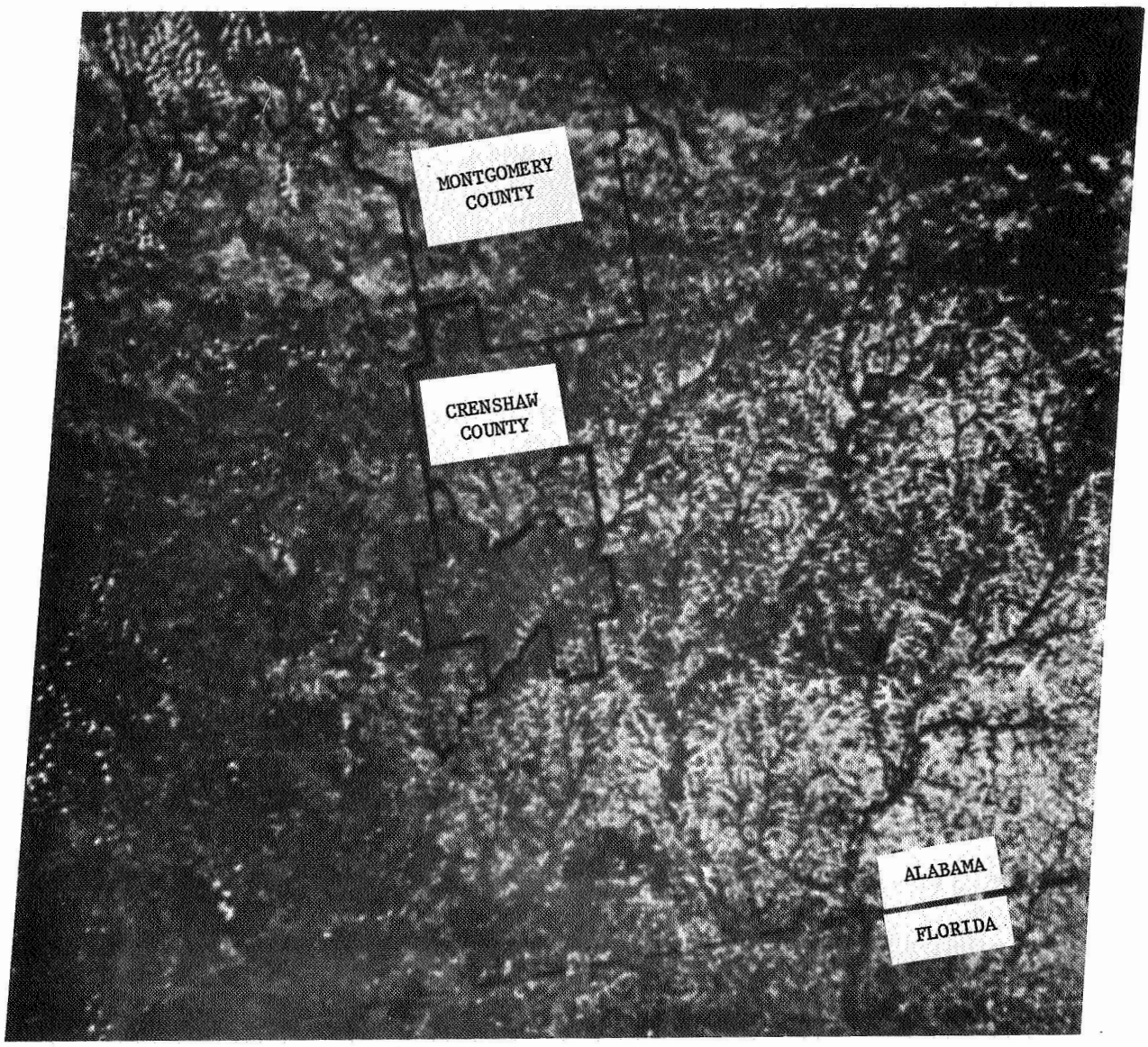


FIGURE 3: MONTGOMERY SCENE (ERTS): THE EFFECT OF SUBSURFACE GEOLOGY ON RURAL AGRICULTURAL PATTERNS AS DETECTED BY ERTS-I

N73-28374

DETERMINATION OF LAND USE IN MINNESOTA BY AUTOMATIC INTERPRETATION OF ERTS MSS DATA

Raymond E. Zirkle and Deborah R. Pile, *Systems & Research Division, Honeywell, Inc., and Department of Geography, University of Minnesota, St. Paul, Minn.*

INTRODUCTION

The aim of this program is to determine the feasibility of identifying land use in Minnesota by automatic interpretation of ERTS-MSS data. Ultimate objectives include establishment of land use delineation and quantification by computer processing with a minimum of human operator interaction. This implies not only that reflectivity as a function of calendar time can be catalogued effectively, but also that the effects of uncontrolled variables can be identified and compensated. Clouds are the major uncontrollable data pollutant, so part of our initial effort is devoted to determining their effect and the construction of a model to help correct or justifiably ignore affected data.

Other short range objectives are to identify and verify measurements giving results of importance to land managers. Lake-counting is a prominent example. Open water is easily detected in Band 7 data with some support from either Band 4 or Band 5 to remove ambiguities. Land managers and conservationists commission studies periodically to measure water bodies and total water count within specified areas.

We performed a lake count in Ramsey County and compared the ERTS-derived count with a concurrent University of Minnesota aerial photo planimetry count. The results were usually within 10 percent on individual water bodies. Consideration of reasons for the discrepancies indicates that the ERTS method should be used as the comparison reference. The feasibility of water estimation using ERTS data is established, the extension to implementation is straightforward, and at least one worker used to the frustrations and tedium of conventional methods is impressed.

PRECEDING PAGE BLANK NOT FILMED

ATMOSPHERIC EFFECTS STUDY

Reflectivity of terrain is the basis for multispectral (color) discrimination to determine land use, vegetation species and stress, water quality, etc. The multispectral scanner collects reflected sun irradiation in the visible and near infrared. Additive components contributing to the MSS output include both useful terrain reflection and useless atmospheric scatter. The terrain reflects both direct sunlight and downscattered skylight in quantities and relative proportions dependent on sun angle, local and general atmospheric conditions, and wavelength.

A cursory glance at almost any ERTS photograph shows the wide variety of situations which can occur and the futility of trying to characterize the atmosphere by an average number or by single point measurements. Throughout a 100 by 100 nmi format the clouds vary widely in density, size, shape, orientation and position. No particular situation ever repeats. A fascinating continuum exists between the extremes of no-cloud and dense cloud. The ground can be seen through tenuous cloud, and various densities of cloud shadow are cast. One question of interest is the degree of cloud allowable which will still permit land use categorization.

The ultimate data processor requirements will be shaped partly by desirability and partly on feasibility. We anticipate a need for cloud and cloud effect detection, and for data correction based on sun angle, season, and atmospheric conditions. It is assumed that inputs such as sun angle and geographic location will be available, but that atmospheric corrections should be derived from MSS data as simply as possible. Point-by-point or small-area correction is needed to reduce data storage requirements on-line because major disturbances such as cloud shadows occur in the data stream before the clouds.

Our efforts to date have included construction of a computer simulation to compute the expected apparent radiance of large easily identified surface objects for which the spectral reflectivity is reasonably well-known. Computation of the expected intrinsic radiance due to direct sun illumination is straightforward. However, the skylight component in a given situation is not so well known, and the contribution due to atmospheric scattering toward the MSS is not known. To estimate the effects, MSS data for large water bodies, for cloud shadowed terrain are used, and for dense clouds are used.

Dense, powder-pull clouds casting recognizable shadows provide one way to estimate the proportion of indirect illumination when the shadows fall on identifiable homogeneous terrain. Thus, we are comparing the appearance in MSS data of band values in and out of cloud shadows at various sun angles with the computational model.

The insertion of tenuous cloud, visible or not, changes the spectral illumination and appearance of the terrain, as well as the radiance levels. The "color diagram" coordinates of the source shift, the reflectivity of the terrain shifts, and the observed radiance coordinates move toward the source as the cloud density increases. Large bodies of water provide the most stable large area reflector, so we are using data from the Red Lakes, Lake Superior, et al, in the Minnesota area to derive correction factors. This effort supplements the forest species and land management computer classification described in a companion paper by Kirvida, et al. The classifier derived therein pertains to a small area at one time under favorable atmospheric circumstances. This work is aimed at extending the classifier to varying calendar, atmospheric and geographic conditions.

RAMSEY COUNTY LAKE STUDY

This study compares the determination of lake acreage from ERTS data with that from conventional means. The relatively low radiance values of water in ERTS Band 7 give initial geographic orientation in pilot run printouts (rivers, lakes, ponds). Lines drawn around clusters of values in the count range 0 to 5 correspond reasonably well with the map or photo locations, shapes and relative sizes. By chance a University of Minnesota graduate student was performing a planimetry survey for the Minnesota Land Management Information System at the time we received MSS tapes.

Each MSS data point corresponds nominally to about 1.5 ground acres. To account for element overlap along the scan lines, the expression $1.104N + .453L$ converts the number of elements to acres, where N is the number of elements and L is the number of scan lines involved. The signal level range 0 to 5 is arbitrary, and subsequent analysis indicates that 0 to 3 might be better. However, the results given here are for the initial 0 to 5 range, which appears adequate to discriminate open water from marsh.

Table 1 shows results for 16 of 72 map designated water areas or basins. These 16 are "fish" or "marginal-fish" lakes for which planimetry results were available. The discrepancies in apparent area vary from less than one percent to 42 percent, with seven less than 10 percent.

In comparing figures it must be remembered that the lake area includes most marsh areas around the lake, and not just the areas of open water. However, the MSS Band 7 levels appear to indicate only open water, or water with small amounts of emergent vegetation or rushes.

Results on the remaining 56 lakes indicate that the ERTS data more accurately reflect the current water orientation than do the old map data. Aerial photographs have shown that many lakes on the map have been subsequently eliminated by drainage (some map information dates back to 1949).

Water areas not designated as lakes were found in the ERTS data. These corresponded to areas of water or swamp on USGS topographic maps. Since the appearance of water appears detectable, water fluctuation in a swamp area of known contour could be used to estimate the water table variation. This information, when combined with other information dealing with inflow and outflow from a lake by surface systems would enable the determination of mass budgets for lakes.

Table I. Ramsey County Fish Lake Survey

LAKE		ACREAGE		RATIO
No.	Name	ERTS-DERIVED	MAP PLANIMETRY	PLAN./ ERTS
62-1	Silver	59	73	1.23
7	Gervais	204	206	1.01
13	Phalen	191	192	1.01
28	Sucker	55	60	1.08
39	Twin	25	35	1.42
46	Pleasant	551	627	1.14
54	McCarran	62	70	1.12
55	Como	63	72	1.14
56	Owasso	332	355	1.07
57	Josephine	112	115	1.03
61	Turtle	416	447	1.07
71	Valentine	50	60	1.19
73	Snail	138	185	1.34
78	Johanna	189	225	1.19
62-82	Wabasso	37	46	1.25
82-167	White Bear	2367	2479	1.05
16 lakes	Sums	4851	5247	1.08

One of the most important lake types in Minnesota is that in which ducks breed. These lakes are usually small and periodic, appearing in the spring and summer as lakes, but as swamps and dry spaces the rest of the year. The importance of these lakes is often not realized in time to prevent farmers from draining them. Location of these lakes by ERTS monitoring could help preserve these areas and the Minnesota duck population.

CONCLUSIONS

Progress is being made in the areas of sun angle and atmospheric effects on the data and its interpretation. The effort is aimed at correction using only navigation and calendar data needed for satellite operation and derivations from the MSS data.

Water estimation of value to land planners and conservationists has been demonstrated with verification of performance by comparison with a concurrent study involving map planimetry, aerial photos, and field-checking. The satellite will provide seasonal and annual coverage with timely information in a way not now feasible by conventional methods. For example, the reference data were obtained using the most recent files, which date back to 1949, and from most recent photography taken in 1968. The calendar time involved was three to four months, which is a reflection on priority pressure on trained manpower available. ERTS data can help relieve this problem by providing the needed information while freeing trained manpower for more appropriate parts of the effort.

ACKNOWLEDGMENT

The cooperation of Jack Flynn in making available his lake-count data is gratefully acknowledged.

N73-28380

DIGITAL DATA PROCESSING OF ERTS-1 IMAGERY OF DELAWARE BAY

Alfred C. Conrod, *Bendix Aerospace Systems Division, Ann Arbor, Michigan 48107*

ABSTRACT

A user-oriented Earth Resources Data Center is in operation at Bendix Aerospace, which is capable of automatically producing classification imagery and thematic maps from ERTS Computer Compatible Tapes. The ERDC is now being used to process ERTS-1 data under a subcontract to Bendix from the University of Delaware.

ERTS coverage of Delaware Bay has been processed to produce classification imagery of water masses in the bay, and a map of all land-water boundaries along the shoreline including wetlands and inland lakes. The paper shows and describes the imagery and the user's video monitor color display, and describes the data processing facility and methodology.

1. INTRODUCTION

Bendix Aerospace is under sub-contract to The University of Delaware to provide data processing and other support for the University's ERTS-1 investigation of Delaware's coastal resources and environmental conditions. In the conduct of its work for the University, Bendix is using its Earth Resources Data Center (ERDC) to process ERTS-1 MSS data. The ERDC is a dedicated data processing facility designed to accept ERTS CCT's, MSDS and Skylab High Bit Density Tapes (HBDT's) and Bendix Modular Multiband Scanner HBDT's and to produce video and film outputs of original imagery and enhancements and thematic maps. The ERDC has been designed to be a user-oriented facility; i.e., it is intended to be used by Earth Resources investigators and not by data processing experts. Consequently, the procedures and the underlying methodology are of interest to all of the ERTS (and Skylab) investigators who are using CCT (or HBDT) data.

The balance of the paper will briefly describe the facility and the procedures for its use, and show preliminary decision imagery and a thematic map of the Delaware Bay region.

PRECEDING PAGE BLANK NOT FILMED

Original photography may be purchased from:
EROS Data Center
10th and Dakota Avenue
Sioux Falls, SD 57198

2. BENDIX EARTH RESOURCES DATA CENTER

The nucleus of the Bendix Earth Resources Data Center (ERDC) is a Digital Equipment Corporation PDP-11/15 computer with 32K words of core memory, two 1.5M word disc packs, two 9-5rack 800 BPI tape transports, a line printer, a card reader, and a teletype unit. Other units are: an Ampex FR 2000 14-track tape recorder; bit synchronizer and tape deskew drawers which can reproduce up to 13 tape channels of multispectral data from high density tape recordings; a high speed, hard wired, special-purpose computer for processing multispectral data; a 70-mm laser film recorder for recording imagery on film; and a color, moving window, computer-refreshed display. This facility is owned by Bendix: it is the result of an evolutionary program initiated in 1967 and is dedicated to the processing of remote sensing data. Access is also available to a computer controlled, precision plotting table (which is part of a Bendix Datagrid® Digitizer system) and the corporate IBM-370-155 facility, with which the ERDC is colocated. Access to these additional facilities is available through use of computer-compatible tape (CCT) for communication.

The ERDC can accept data on CCTs, high-density tapes (10,000 bits per inch per track, 13 tracks). The color display can be used for screening and editing data or as a processed output viewing device. Typical data inputs are ERTS CCTs, NASA 24-channel scanner high-density tapes or CCTs, EREP S192 reformatted high-density tapes or CCTs, and high-density tapes from Bendix scanners such as the Modular Multiband Scanner (M^2S). The facility is used for in-house applications research, current ERTS-1 experiments in addition to the Delaware investigation, commercial and government resource management contracts, and as a commercial service at hourly rates.

Processing of the ERTS MSS data can be broken down into a sequence of three steps. The first step is screening and editing, in which samples of data are extracted from the data tape for use in subsequent analysis steps.

Screening and editing are accomplished through use of a color display. The display is the moving window type with display refresh performed by the computer. The display is 128 elements by 128 elements. Full ERTS resolution is maintained by displaying only 128 cells from an 832-element scan record on the ERTS MSS data tape. The resolution element at which the display will start can be selected by the operator. In effect, the operator can move through the tape and see any selected 1/8 segment of the scan record displayed. When the area from which it is desired to select a data sample is displayed, the display can be stopped

and the computer can be instructed to dump the data displayed from the data tape onto the disc. A line printer printout is simultaneously generated showing the data dumped. The printout contains scan line count down the left-hand side, shows the beginning resolution cell number in the header, and has resolution cell counting aids every 10 cells at the top. Using these identifiers, training sets can be selected (one resolution cell at a time if desired) and transferred from the dump area of the disc to a disc area set aside for the particular target type selected. The display and dump sequence can be repeated as many times as desired.

The second step is off-line analysis. Multivariate analysis can be performed to separate or enhance targets. We have programs to perform regression analysis, factor analysis, principal component analysis, canonical analysis, cluster analysis, and discriminant analysis. Scatter diagrams and histograms can be generated to determine expected classification or enhancement algorithm performance. For level slicing or contouring, histograms are generated to permit selection of level slicing or contour intervals. Various tabular outputs, such as covariance matrices, are also available.

The third step is the actual processing. In this case the computer acts as a process control computer, and the processing is done in a special-purpose, hardwired computer. The special-purpose computer is used to allow high throughput rates (essentially the fastest rate at which the computer tape transport can read data). Processed output can be displayed on the display, or paper or film hard copy can be generated.

3. PROCESSED ERTS-1 IMAGERY OF DELAWARE BAY

Examples of processed ERTS-1 imagery are shown in the accompanying illustrations. All of the illustrations shown were produced from CCT's of the overpass of 10 October, 1972; Number 1079-15133. Three of the possible outputs are shown here; a strip of imagery from a CCT, decision imagery, and a thematic map.

Figure 1 is a portion of the overall ERTS-1 scene, that was produced in the Bendix ERDC. The segment shown, which is a print of MSS Channel 5, contains the section of data that was processed to provide the examples in the other illustrations. The banding that is exhibited on all of the illustrations except the thematic map is an ERTS-1 detector characteristic. The use of a radiometrically corrected CCT would have eliminated that artifact.

Figure 2 shows classifications of target categories achieved by the use of decision imagery. Five categories were selected by choosing training set areas through visual examination of bulk imagery, since ground truth data was not acquired from the University. The training sets are described in the image captions. The set marked "Coastal Inlet Sediments" may be suspect, since we were recently informed by the University that it is thought that they can see bottom in the lagoon from which the training set was drawn.

It should be emphasized that the decision imagery in Figures 2 and 3 is not density sliced, but represents separation by spectral signatures. Spectral signature recognition is more precise than photographic or electronic density slicing, in that spectral signatures are not as subject to modification by variations in atmospheric or illumination effects.

Figure 3 contains two illustrations. On the left is an illustration of the simultaneous displays of all classified categories. This is similar to what one would see on the video monitor display, except that only a portion of the scene is shown on the monitor as mentioned earlier, and the monitor is of course in color. The right hand illustration is a thematic map, which in this case shown the land-water boundaries. The map agrees with the 1:250,000 scale USGS maps of the region, except where the thematic map shows changes in the New Jersey shoreline since the 1966 edition of the USGS map. (This will be covered in detail in the University's reports.) The three small areas in the bay are probably ships. Vessels of 600' to 800' are known to pass here, though visual inspection of the bulk images did not disclose any vessels.

4. SUMMARY

The results shown here were produced by personnel who are data users, and not data processing specialists. We believe we have successfully developed and demonstrated a method by which virtually any ERTS investigator can achieve precise and quantifiable results directly from CCT data.



Figure 1.

Portion of MSS Channel 5 Image, Produced on the Bendix Aerospace ERDC.

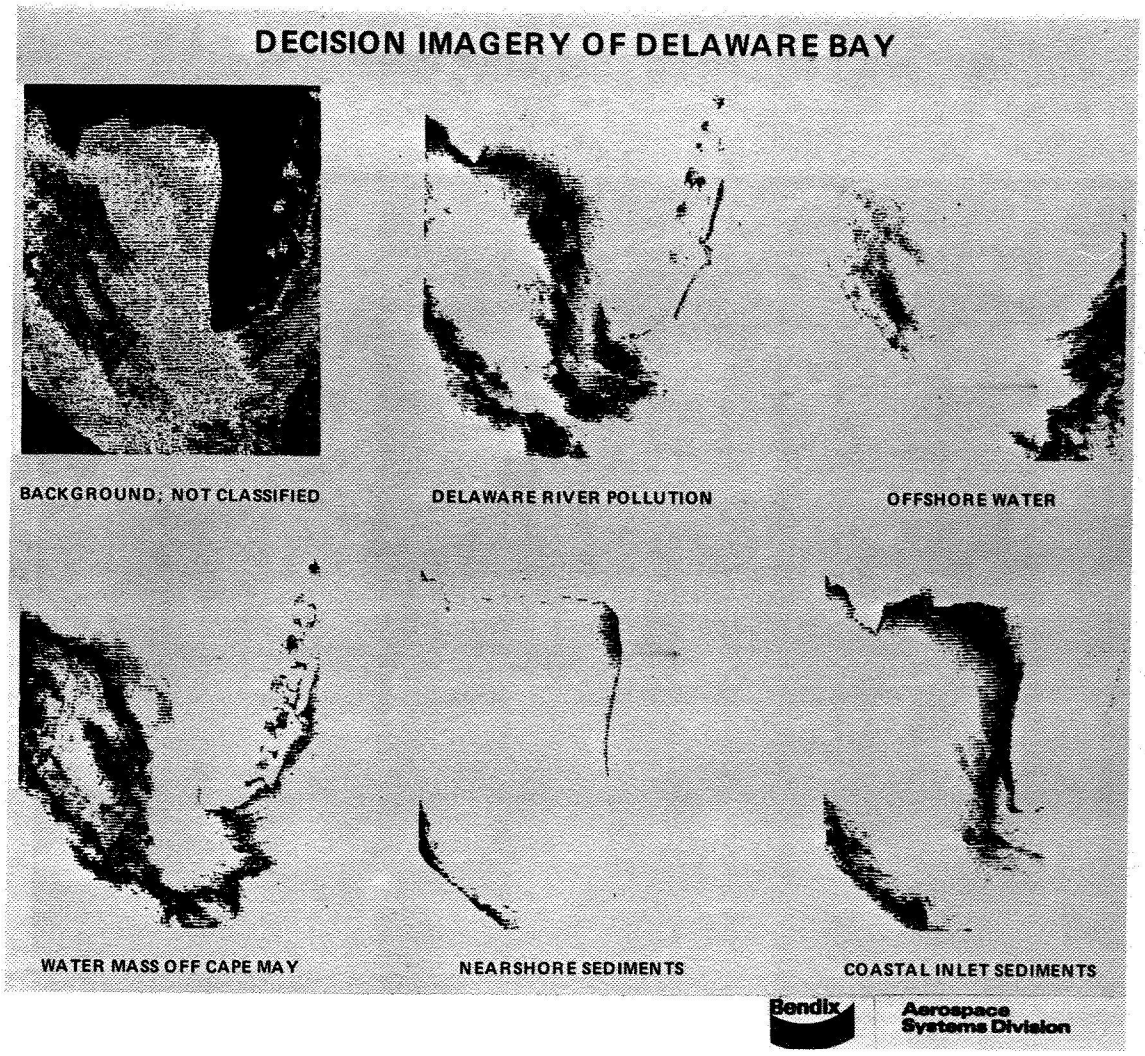

DECISION IMAGERY OF DELAWARE BAY
BACKGROUND; NOT CLASSIFIED
DELAWARE RIVER POLLUTION
OFFSHORE WATER
WATER MASS OFF CAPE MAY
NEARSHORE SEDIMENTS
COASTAL INLET SEDIMENTS
Bendix
Aerospace
Systems Division

Figure 2.

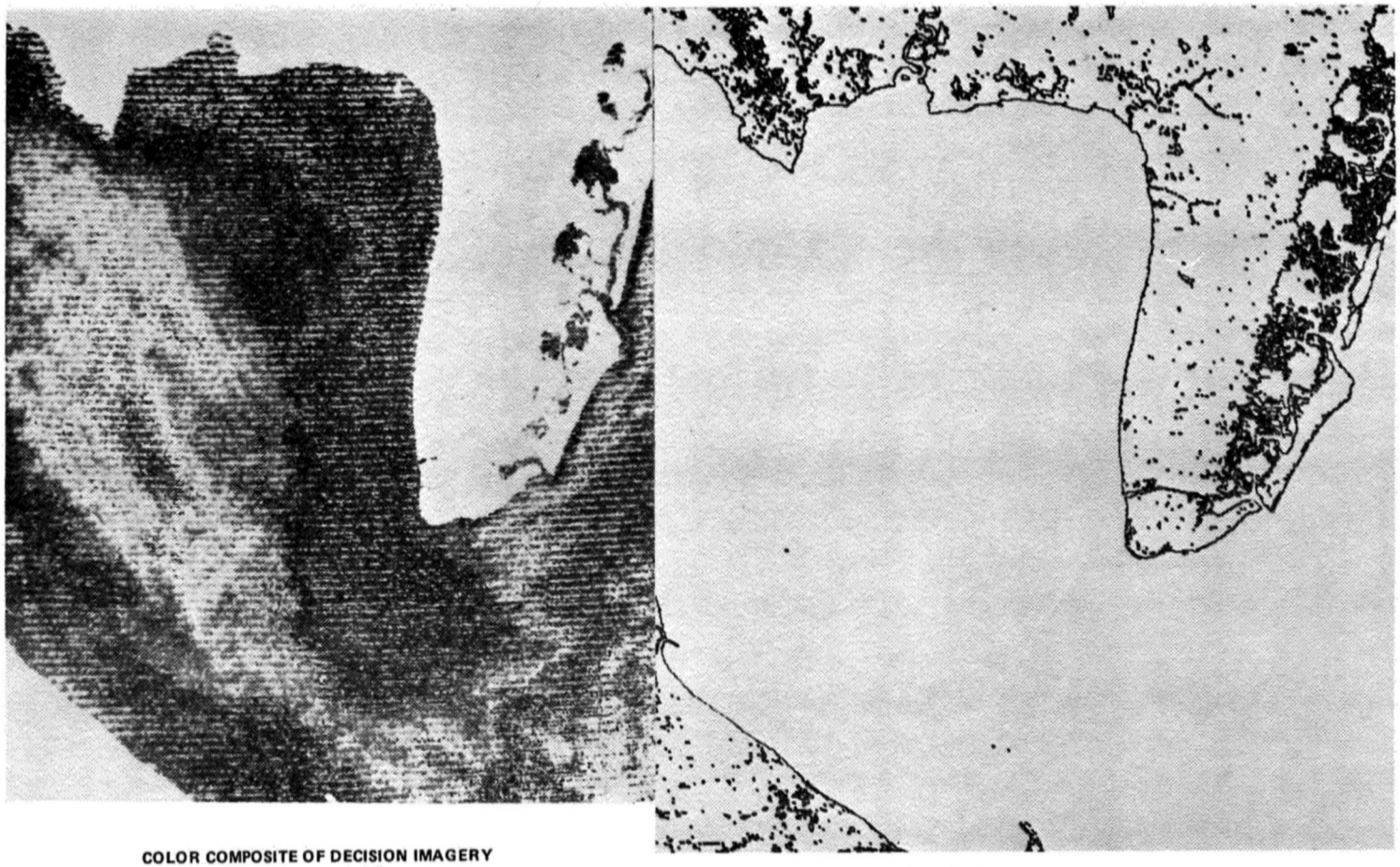


Figure 3 Processed ERTS MSS Data of Delaware Bay

N75-24381

THE USE OF PHOTOGRAPHIC METHODS IN CONTRAST ENHANCEMENT OF ERTS-1 IMAGES*

Lawrence F. Harris, *U. S. Geological Survey, Museum of Northern Arizona, Flagstaff, Arizona 86001*

ABSTRACT

The contrast of ERTS 70mm positive images can be enhanced to varying degrees by rephotographing the images with different types of negative films, and by overdeveloping the films with different developers. A combination of high-contrast copy film (Kodak 5069) and a high-energy developer (Kodak D-11) yields high contrast. Still greater contrast may be obtained by using a film of higher contrast capability and a developer of higher energy capability. Contrast can also be enhanced in the printing process with the use of high-contrast photographic papers, or with the use of polycontrast photographic paper and filters. Contrast enhancement by photocopying delineates topographic boundaries and may aid in the objective measurement of topographic parameters.

1. ACKNOWLEDGEMENTS

I thank Harry W. Smedes and Carol S. Breed, both of the U.S. Geological Survey, for comments and suggestions on the manuscript. The research was supported by the National Aeronautics and Space Administration ERTS-A Project SR-131.

2. INTRODUCTION AND PURPOSE

The ERTS-A Project SR-131 concerns the occurrence and morphology of dunes in many arid regions of the world, as interpreted from the appearance of these features on ERTS-1 imagery. Because sand features on ERTS images are sometimes "washed out" in the standard processing, dune patterns can often be more sharply delineated on contrast-enhanced prints made from contrast-enhanced negatives, which in turn are made from the standard ERTS 70mm positives. The boundaries between the lee and windward slopes of individual dunes are better defined on prints made from contrast-enhanced negatives than on the original ERTS positives. Sharper contrast aids in the recognition of eolian dunes, and it is hoped that it will also aid in the measurement of their morphologic parameters.

3. PROCEDURE

The ERTS positives were placed on a light table which transmits a light intensity constant in both space and time (A Laser Sciences Inc. light table, Model LT 630, was used in this study) and were rephotographed with negative film. An Asahi Pentax Spotmatic 35-mm single lens relfex camera was used because it fitted conveniently into the microscope holder of the light table. The camera was equipped with a 50-mm lens and helicoidal extension tubes for closeup photography.

---

* Publication authorized by the Director, U.S. Geological Survey

PRECEDING PAGE BLANK NOT FILMED

Original photography may be purchased from:
EROS Data Center
10th and Dakota Avenue
Sioux Falls, SD 57198

In order to determine the proper exposure, different types of negative films were exposed in grades ranging from underexposure to overexposure and were then overdeveloped. The combination of underexposure and overdevelopment results in an increase in contrast. If, as in this case, the ERTS positive does not cover the entire field of view of the camera, the remainder of the field must be blacked out to enable the light meter to determine accurate times of exposure. For example, on a test roll of Kodak Panatomic X (ASA-32), an ERTS 70mm positive was rephotographed at 1/15 second[1/] at the following apertures: The correct exposure as determined by the camera light meter "E" increased by 2 f-stops, "E", and "E" reduced by 1, 3, 5, and 7 f-stops respectively (as shown in tables 1 and 2). The test film was then overdeveloped by 50 percent. (Note: Information on developing times for film types is packaged with the film or developer. If actual temperature of the developer differs from that recommended, adjust the time-of-development according to the film data sheet, or by use of the developing computer on page 9 of the Kodak Darkroom Guide). After development, at least one and generally several of the contrast-enhanced exposures were useful for printing. For the same test roll, the best exposure was E reduced by 5 f-stops. This underexposure was representative of the degree of contrast-enhancement that could be obtained for this particular combination of film type and developer. Different test rolls were similarly exposed and overdeveloped with recommended developers (table 1). Panatomic X, Plus X Pan, and High Contrast Copy Film 5069 were overdeveloped with Kodak D-76, D-76, and DK-50 respectively. The results, summarized in table 1, indicate that the high-contrast copy film offers the greatest contrast when overdeveloped with the recommended type of developer, followed by Plus X Pan, and Panatomic X.

The same types of films were again given variable exposure, but were overdeveloped with a high-energy developer to further enhance contrast. These results are summarized in table 2. High-contrast copy film again offers the greatest contrast, followed by Panatomic X and Plus X Pan. Note the reversal in order of contrast between Panatomic X and Plus X Pan.

Table 3 combines the results of tables 1 and 2, and shows the relative degree of contrast that exists between each film and developer combination in the first two experiments. A printed photograph from the negatives for each combination of developer and film type is illustrated in figure 1. Note the increase in contrast from A to F. Figures 2, 3, and 4 illustrate contrast enhancement in photographs printed from the three Kodak film types overdeveloped in Kodak D-11. In each figure, A, B, and C represent prints made on contrast grade 3 paper from Plus X, Panatomic X, and high contrast copy film, respectively. "D" is also a print made from high-contrast copy film, but it was printed on polycontrast with a number 4 filter to further enhance contrast. In all figures the increase in contrast becomes greater from A to D. In figure 2 there is an increase in the visibility of the "patterned ground" (the white-splotched ground covering the left half of the photo),

---

[1/] Shutter speed must be less than 1/60 second if 60-cycle-per-second AC current is used by the light table. For films with ASA ratings of 64 or greater, it may be necessary to use filters to reduce light input, allowing for slow shutter speeds. Recommended filters are neutral density, red, or polarizing. The latter filter can reduce glare if glass is used to hold the ERTS positive in place.

Kodak Film Type (and ASA speed)	Contrast	Best Exposure (E=proper f-stop indicated by light meter)	Kodak Developer	Recomm. Time of Dev. (68°F, small tank) (minutes)	Actual time of Dev. at 68°F, small tank (minutes)	Percent of over dev.	Filter	Shutter speed (sec.)
Panatomic X (ASA 32)	low ↑ ↓ high	E+5 f-stop	D-76	7	10.5	50	none	1/15
Plus X Pan (ASA 125)		E+4, 5 f-stop	D-76	6	9.0	50	red	1/30
High-contrast copy 5069 (ASA 64)		E-1 f-stop 0 E+1 f-stop E+2 f-stop	DK-50	5	6.5	30	polarizing	1/15

Table 1. Order of contrast of three types of Kodak films overdeveloped with recommended developers and the photographic conditions under which they were exposed and developed.

Kodak Film Type	Contrast	Best Exposure (E=proper f-stop indicated by light meter)	Kodak Developer	Recomm. Time of Dev. (68°F, small tank) (minutes)	Actual Time of Dev. at 68°F, small tank (minutes)	Percent of over dev.	Filters	Shutter speed (sec.)
Plus X Pan ASA 125	low ↑ ↓ high	E+5, 7 f-stop	D-11	3.5	5.66	62	None	1/15, 1/30
Panatomic X ASA 32		E+5, 7 f-stop	D-11	3.5	5.5	57	Red	1/30
High-contrast copy 5069 ASA 64		E+3, 2, or 1 f-stop	D-11	6.0	7.5	25	Polarizing	1/15

Table 2. Order of contrast of three types of kodak films overdeveloped with a high energy developer (kodak D-11), and the photographic conditions under which they were exposed and developed. High-contrast copy film is very sensitive and several closely spaced exposures may be necessary even after a good exposure has been predetermined.

	Kodak Film Type	Developer	Percent Overdev.	Code letter in Fig. 1
Low contrast ↑	Plus X Pan	D-76	50	A
	Panatomic X	D-76	50	B
	Plus X Pan	D-11	62	C
	Panatomic X	D-11	57	D
	High-contrast copy 5069	DK-50	30	E
↓ High contrast	High-contrast copy 5069	D-11	25	F

Table 3. Order of contrast of the various combinations of film and developer types listed in tables 1 and 2. Figure 1 shows variations in contrast printed from enhanced negatives made from the combinations of film and developer above.

and in the dunes in the lower left and center, from A to D. In figures 3 and 4 increases in contrast are not limited to the size of the topographic features. Although the dunes in figure 4 are very small, enhancement techniques employed here noticeably improve their visibility. If further contrast is needed, films with a higher contrast capability, as well as developers of higher energy, are available.

Further contrast enhancement may be obtained by photocopying (on a Xerox or IBM copier) 8" X 10" or larger prints of already contrast-enhanced ERTS negatives (fig. 5). The topographic features desired to be enhanced can be somewhat controlled by a simple form of density slicing (the adjustment of the light-dark copy control on the photocopying machine being used). In many instances, this process further delineates the boundaries of topographic features and may simplify the measurement of morphologic parameters (in the case of ERTS-A SR-131, dune width, length, density, crest regularity, and others (as defined by Harris, 1972, p. 29, 48).

4. CONCLUSIONS

The contrast of ERTS positive images can be enhanced to varying degrees by rephotographing the images with different types of negative films, and by overdeveloping the films with different developers. A combination of high-contrast copy film (Kodak 5069) and high-energy developer (Kodak D-11) gave the greatest contrast among those tested. Still greater contrast is obtainable by using a film with greater contrast capability and a higher energy developer. Contrast can also be enhanced in the printing process; prints can be made on higher contrast photographic papers, (grade 5 or higher), or on polycontrast paper using the appropriate filters.

Another method of contrast enhancement is photocopying 8" X 10" prints made from contrast-enhanced negatives. This further delineates topographic boundaries and may simplify the objective measurement of morphologic parameters.

5. REFERENCES CITED

Harris, L. F., 1972, The role of climate in the morphology and evolution of Mancos Shale slopes on the Colorado Plateau: Dissertation, PhD, The Johns Hopkins University. Presented Nov. 1972 at Geol. Soc. America annual meeting, Minneapolis; Abs. published in Abstracts with Programs, v. 4, no. 7, 1972, p. 529.

Kodak Master Darkroom Dataguide, [3d ed.; (1st ed., 1970)]: Eastman Kodak Co., Rochester, N. Y.

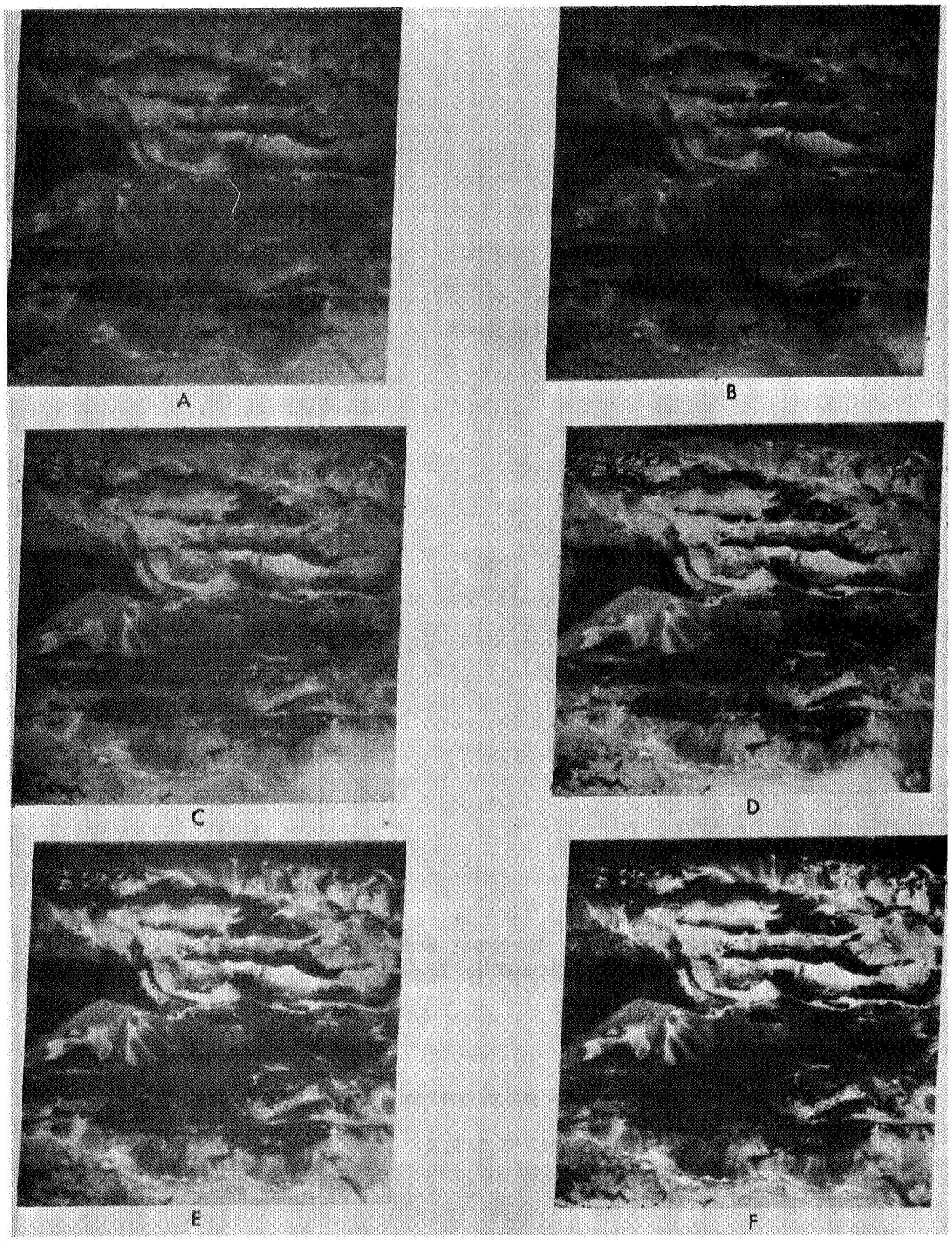


Figure 1. Illustration of the relative degree of contrast for each combination of developer and film-type used. Contrast increases from A to F. Note in particular the increase in contrast of the lakeside dunes in the left center. The photographs are of ERTS frame 1074-24242-7, the Takla Makan Desert in China. All negatives were printed on contrast grade 3 paper. A, Plus X Pan developed in Kodak D-76; B, Panatomic X developed in Kodak D-76; C, Plus X Pan developed in D-11; D, Panatomic X developed in D-11; E, High contrast copy 5069 developed in DK-50; F, High contrast copy 5069 developed in D-11.

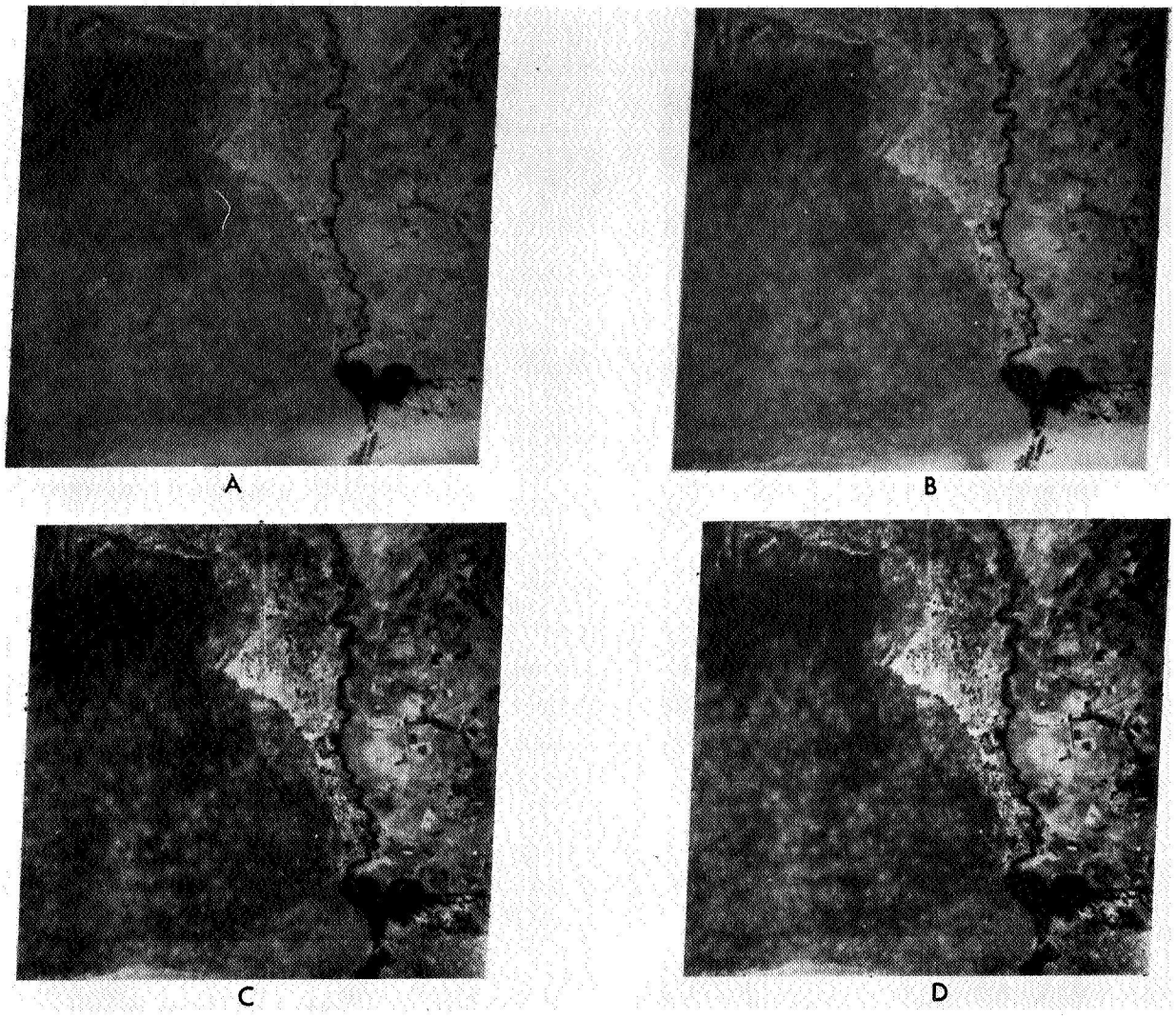


Figure 2. ERTS 1070-05443-7. Contrast enhancement of ERTS images using the three film types overdeveloped in Kodak D-11. See text for explanation.

A, Plus X
B, Pan X
C, High-contrast copy
D, High-contrast copy with polycontrast enhancement

Location: west of Tashkent, U.S.S.R.
Note the increase in contrast of the "patterned ground" and dunes in the lower left and center from A to D.

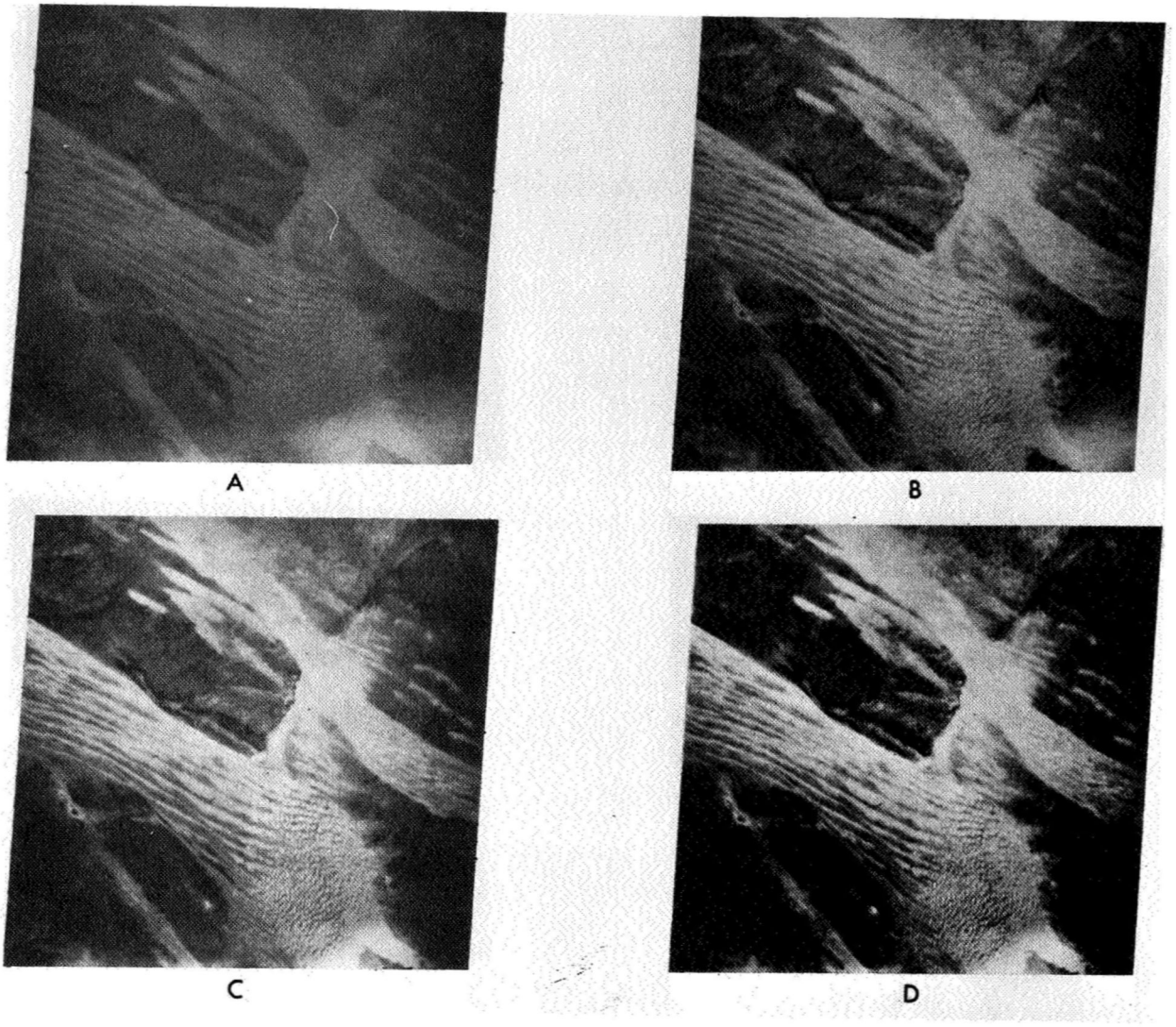


Figure 3. ERTS 1083-07033-7. Contrast enhancement of ERTS images using the three film types overdeveloped in Kodak D-11. See text for explanation.

A, Plus X
B, Pan X
C, High-contrast copy
D, High-contrast copy with polycontrast enhancement

Location: An Nafud Desert in Saudi Arabia.
Note the increase in contrast of both large and small eolian landforms.

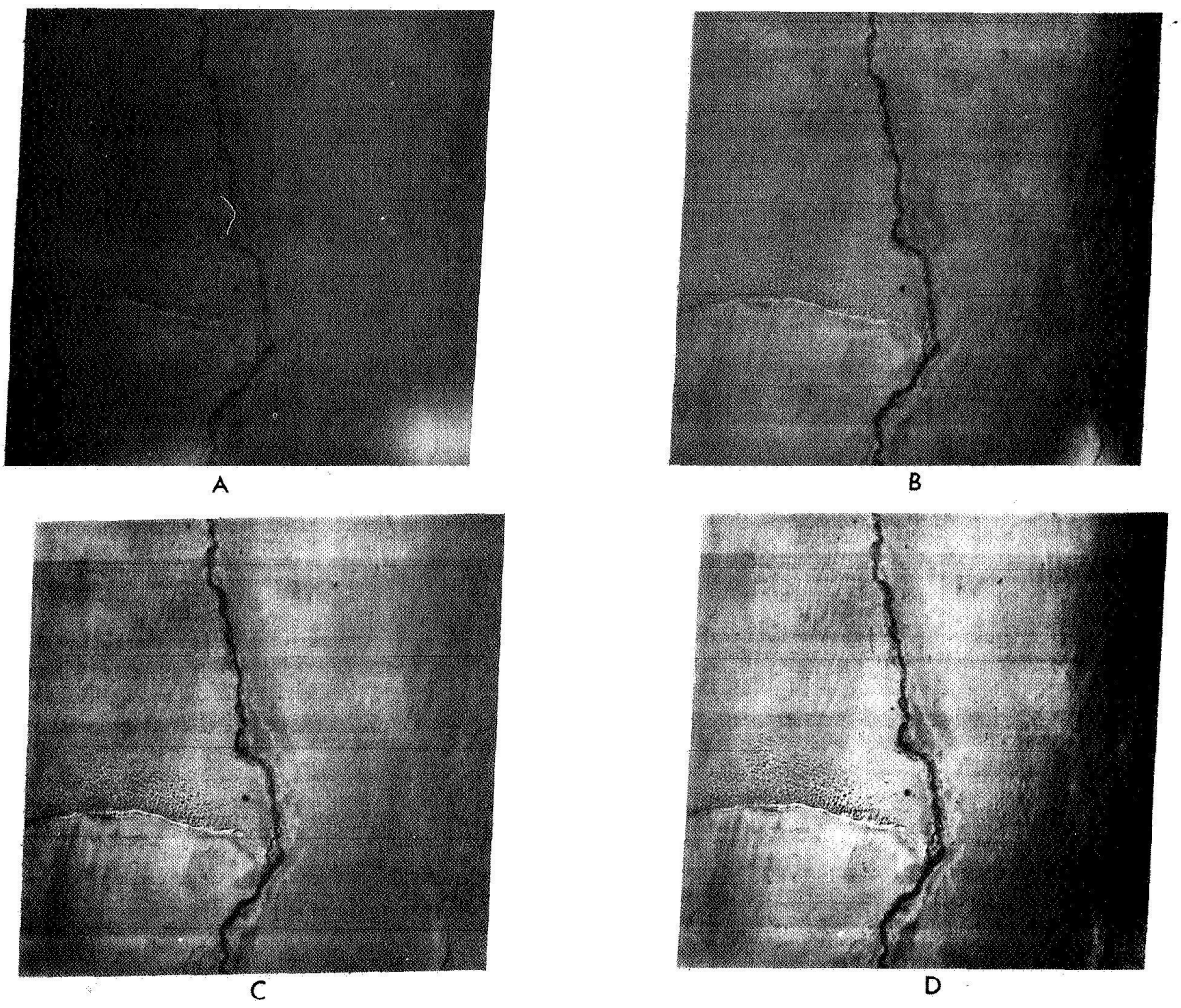


Figure 4. ERTS 1078-04481-6. Contrast enhancement of ERTS images using the three film types overdeveloped in Kodak D-11. See text for explanation.

A, Plus X
B, Pan X
C, High-contrast copy
D, High-contrast copy with polycontrast enhancement

Location: Takla Makan Desert, China.
Note the increase in contrast of the small dunes in the lower left center.

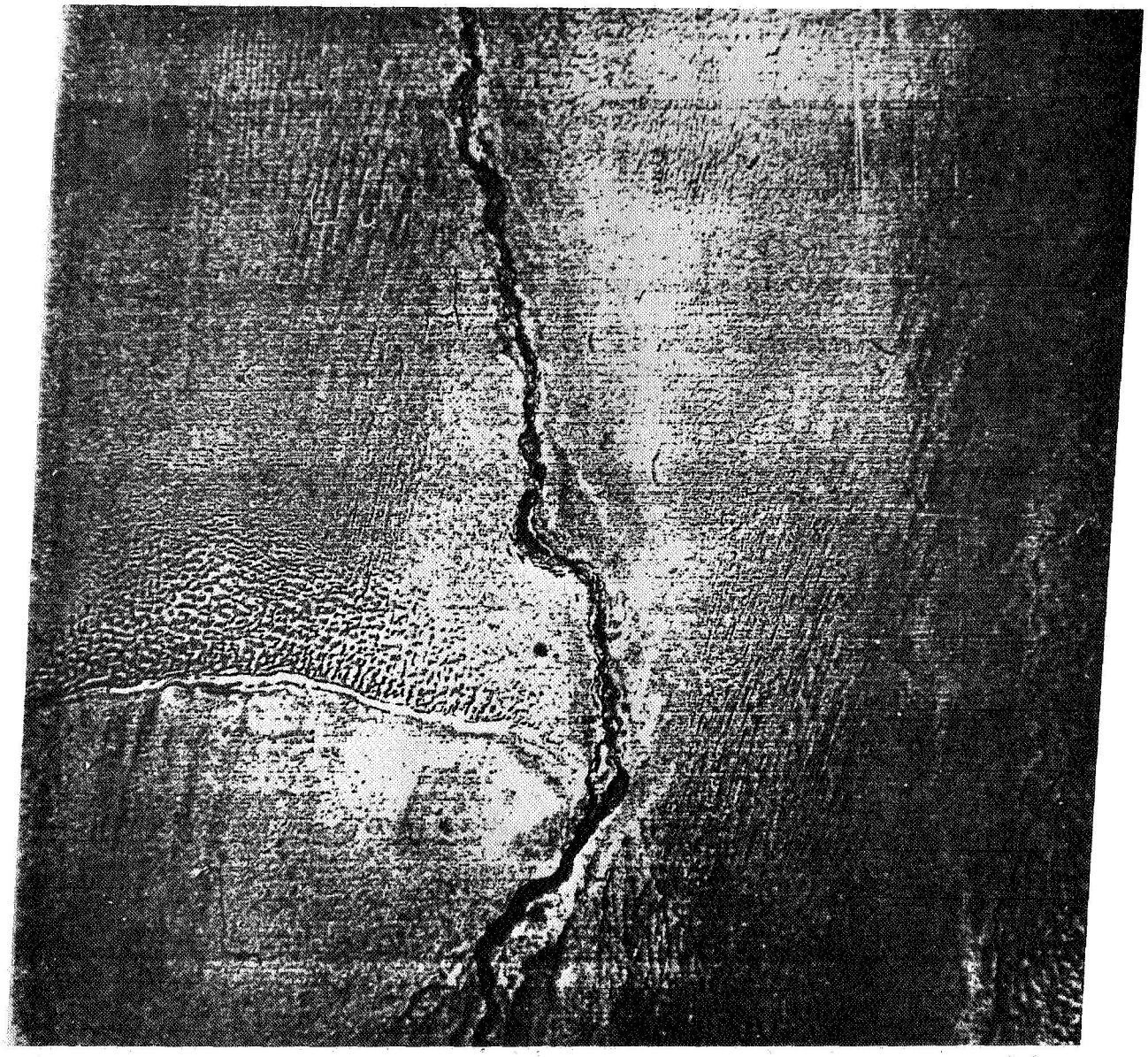


Figure 5. Contrast enhancement of ERTS 1078-04481-6 (shown in fig. 4), by photocopying on the IBM Copier II. The photocopy was made from an 8" X 10" photograph printed from a contrast-enhanced negative. This process further delineates topographic boundaries and aids in the measurement of morphologic parameters.

N73-28382

PRECISION ANNOTATION OF PREDETERMINED PRIMARY SAMPLING UNITS ON ERTS-1 MSS IMAGES

Jan W. van Roessel, and Philip G. Langley, *Earth Satellite Corporation, Berkeley, California*

ABSTRACT

Resectioning programs were developed for projecting the boundary corners of sample units, management units, and counties into U2 RC-10 and ERTS-1 MSS images. The technique used includes corrections for earth curvature, terrain elevation, and MSS distortions. The minimum standard error obtained was about 0.15 mm or 150 meters on the ground. This technique now makes it possible to include land ownership as an integral part of forest resource sampling plans using ERTS imagery.

1. INTRODUCTION

As an integral part of our ERTS-1 investigation, "The Development of a Multistage Forest Sampling Inventory System" we developed a subsystem to locate sample unit boundaries on the various stages of aerial and space imagery. The development of this subsystem was prompted by the demands for forest inventories of lands with irregular ownership patterns. These patterns defied the approach used in the early stages of multistage forest inventories using Apollo 9 photography (Langley, et al, 1969).[1] At that time, the sample units were simply defined by superimposing a grid on the satellite image. Thus, to insure greater spatial correspondence between the sample units of the various stages and to insure that the inventory would be conducted within the property limits, we developed a computational method for transferring basic sample units from ownership maps to ERTS and U2 imagery.

Also of interest was the accuracy with which a single point could be located on the ERTS images so that we could define the minimum size sample unit that could be used at the ERTS stage of a multistage resource inventory. The significant findings of the resulting investigation are presented in this paper.

Original photography may be purchased from:
EROS Data Center
10th and Dakota Avenue
Sioux Falls, SD 57198

PRECEDING PAGE BLANK NOT FILMED

Original photography may be purchased from:
EROS Data Center
10th and Dakota Avenue
Sioux Falls, SD 57198

2. BACKGROUND

Multistage variable probability sampling is a method in which the probabilities for the selection of sample units at stage n + 1 are based on criteria evaluated from the sample units at stage n. With n increasing, the total ground area sampled decreases until in the final stage a number of ground plots is visited. At the same time the expense incurred in the evaluation of a unit on the ground increases with n. The extremes are the complete evaluation of a tree on the ground on one hand and the separation of land into forest and non-forest classes on space imagery on the other. The direct combination of these extremes is not always possible. Therefore, to tie the extremes together intermediate stages, consisting of aerial imagery, are used to provide a correlation chain through which the first and the last stage are connected. If this chain had a bad link, the survey would be clearly inefficient and ineffective.

In our opinion, a fundamental requirement for a high linear correlation between sample units is a good spatial correspondence between adjacent stages of aerial or space imagery. To our knowledge, no research has yet been performed to establish the sensitivity of the sampling variance in relation to spatial mismatches between sample units at different stages. However, by using a precision annotation process, mismatches can be avoided so that this type of error can be omitted from consideration, thereby leaving fewer and more important issues for investigation at the present stage of our research.

A recent application of the multistage inventory concept to commercial property in the State of California demonstrated the need for the annotation of ownership patterns on aerial imagery. In this instance clusters of GLO sections proved to be the natural sample units for this kind of forest inventory. Unfortunately, an approximately one-square-mile land unit is by no means square on the map due to early primitive surveying techniques. In addition, the section is sometimes rather heavily subdivided.

The annotation problem for the commercial survey, in which the first stage consisted of 1:40,000 scale aerial photography was solved by performing an individual resection for each photograph, followed by a perspective projection of all the relevant corner points of the land sections onto the photographs. In the present ERTS-1 investigation, we are adding two additional stages, namely a high altitude stage of U2 RC-10 photography and a space stage of ERTS MSS imagery. Thus we were faced with the problem of also having to project the land sections or multiples thereof onto the U2 photographs and the ERTS images.

F

3. APPROACH

We obtained good results with individual spatial resections of the 1:40,000 aerial photographs, which were performed with an efficient program with semi-automatic quality control. The same resection program also worked well for the U2 RC-10 photographs. As input for the resection, a set of known identifiable ground points was needed which could be identified and measured on the photographs. These points were taken from USGS topographic maps and put into digital form with a map digitizer. For the ERTS image it was also possible to perform a space resection, but we thought it necessary to obtain a much larger number of points to make possible the evaluation of residual image distortions. As it is somewhat difficult to identify map features on ERTS imagery in rugged, mountainous terrain, we set out to identify a set of natural landmarks on the U2 RC-10 photographs that could also be readily identified on the ERTS images. We then used the U2 photographs to determine the ground coordinates of these points by executing a block adjustment. The block adjustment was also thought more desirable for the U2 stage because of its inherent greater accuracy due to simultaneous adjustments and the use of a precision MANN TA1/P monocomparator.

To minimize the programming effort, ground coordinates determined with the block adjustment, together with their measured plate coordinates, were fed into the existing resection program to perform the final transformation of the digitized section corners for the U2 stage.

The block adjustment was performed after the two strips of U2 photographs with ten photos each had been triangulated. Schuts triangulation and block adjustment programs were used for this purpose. Coordinates were expressed in a secant plane system, with its origin in the test area, to remove the influence of earth curvature. The standard errors computed with the control points and tie points used in the adjustment proved to be 12.8, 10.3 and 4.4 m, respectively, for Easting, Northing and height. The planimetric errors correspond to a point identification error of about 0.1 mm on the photographic plate. The results can be considered very good in view of the 1:126,000 scale of the RC-10 photography.

With the block adjustment completed and the coordinates of all ERTS identifiable points in hand, we then concentrated on the space resections of the ERTS MSS images.

4. RESECTION OF ERTS MSS IMAGES

Background and Theory

In contrast to the resectioning of aerial photographs, the ERTS MSS images present two problems: (1) the MSS image is produced by a multispectral scanner with a geometry different than that of aerial

cameras, and (2) there is little relief displacement in the image which is needed to determine all parameters of the resection.

The first problem is in part solved by the NASA data processing facility where the geometry of the MSS image is shaped to resemble the geometry of an aerial photograph not considering relief displacement (Forrest, 1970)[2]. As for the second problem, it can be shown that at least one parameter cannot be estimated when all the object points are in a plane. With the object points situated on a curved surface, such as the earth's surface, possibilities exist for additional ambiguities between parameters. The problem can be solved by calculating some of the resection parameters from the orbital elements with high accuracy. These values can then be inserted into the solution so that a fewer number of parameters need to be finally determined.

In the resection program for the annotation of the ERTS MSS images, we decided to take a completely general approach in which any parameter could be enforced at the value of its initial approximation by assigning appropriate weights. This approach can be implemented by using the parameter approximations in auxiliary equations in the linearized equation system:

$$\Delta p = p^{\circ\circ} - p^{\circ} + \varepsilon \qquad (1)$$

where:

Δp represents the correction to the approximation at the ith iteration

$p^{\circ\circ}$ is the approximation of the parameter value

p° denotes the parameter estimate to be enforced in the solution

ε is the difference between the least squares adjusted value of the parameter and the value to be enforced in the solution.

For the first iteration, $p^{\circ\circ}$ is taken equal to p°. Then, if we place a large weight on the auxiliary equation, ε will be close to zero, and Δp will also be close to zero, and the initial approximation, which is equal to the desired parameter value will not receive any corrections in the iterative process. Thus, the intially assigned parameter value will remain unchanged throughout the solution.

The normal equations take on the following form for n data points:

$$(\underline{X}\,\underline{W}^{-1}\,\underline{X}')^{-1}\,\Delta = \underline{X}\,\underline{W}^{-1}\,\underline{Y} \qquad (2)$$

with X' of the following form:

$$X'_{(11,9,n)} = \begin{bmatrix} a_x^1 & a_x^2 & \cdots\cdots & a_x^9 \\ a_y^1 & a_y^2 & \cdots\cdots & a_y^9 \\ 1 & 0 & \cdots\cdots & 0 \\ 0 & 1 & \cdots\cdots & 0 \\ \vdots & & & \vdots \\ 0 & \cdots\cdots & & 1 \end{bmatrix}$$

(the third dimension is not shown)

where a_x^1, a_x^2 ..., a_y^1, a_y^2 are the partial derivatives of the collinearity equations with respect to the nine resection parameters for a particular point.

The matrix has the following elements (only the first row is shown):

$$Y'_{(9 \times n)} = [\varepsilon_x \; \varepsilon_y \; (p_1^{\circ\circ} - p_1^{\circ}) \; (p_2^{\circ\circ} - p_2^{\circ}) \; \cdots\cdots \; (p_9^{\circ\circ} - p_9^{\circ})] \quad (3)$$

where ε_x and ε_y are the discrepancies resulting from an evaluation of the collinearity equations for the point under consideration with the current set of parameter approximations.

The matrix W is a diagonal 11 x 11 weight matrix with unit weights in the first two positions, zero weights for those parameters that need to be estimated, and large weights (for instance 100 unit weights) for those parameters that are to remain constant.

Thus, with the indicated solution we were free to fix or estimate parameters as needed. As the orbital path of the ERTS satellite is known quite accurately, the likely parameters to be enforced in the solution are the exposure station coordinates for the center of the image. For this purpose, the indicated latitude and longitude of the photocenters were taken from the ERTS catalog. To obtain the satellite altitude we prepared a program that computes the exposure station coordinates from orbital data furnished by NASA, given the GMT pertaining to the image center. However, we anticipated that the latitude and longitude indicated in the catalog would be more accurate than the estimates computed by our program, as we only included first-order harmonic terms. In the solution either the artificial focal length or the altitude needs to be enforced.

We selected the altitude, since we assumed that scale change would be introduced in the bulk process through the introduction of an artificial focal length.

Coordinate Systems

The same secant plane coordinate system used for the block adjustment of the U2 photographs was used for the resection of the ERTS MSS images. The conversion from the geographic coordinate system to the secant plane coordinate system yields coordinates of the control points in a cartesian coordinate system. The XY plane of this system slices through the reference ellipsoid, so that the point elevations also reflect earth curvature.

The earth curvature accounts for part of the perspective displacement encountered in the bulk processed MSS image so that the use of the collinearity equation for the along-track direction in conjunction with the secant plane elevations was therefore partly justified.

Polynomial Fitting of the Residuals

To eliminate systematic trends remaining in the point residuals after the resection had been performed, we included in the resection program a general polynomial fitting routine, with which we could fit separate trend surfaces through the x and y residuals of the plate coordinates. This part of the program could then account for the unexplained remaining systematic distortions.

For the polynomial surface fitting we used hybrid orthogonal polynomials in the x and y plate coordinates, generated with a recurrence relation. The maximum power of the polynomials is automatically determined by the program and then discounted to evaluate all possible power surface fits. For each power Root Mean Square Errors (RMSEs) were computed to assess the goodness of fit.

In the testing phase of the program we discovered that the polynomial fitting routine is general enough that, in terms of the residuals, almost identical results can be obtained by either performing a resection or by keeping all parameters fixed and then making the polynomial adjustment. Thus with the present program one can either opt for the classical resection technique or obtain the optimum polynomial fit.

Experimental Results

Two ERTS MSS images, designated 103 and 104, were resected. These images covered our Redding (Northern California) test area. The ground control points were not distributed over the entire images. Rather, we confined them to those portions covering our forest inventory test site.

In this regard, only 1/16 of image 103 was resected while the resection area for image 104 was approximately 1/6 of the total image area. A total of 18 points were used for image 103, while 30 points were used as input for the resection of image 104. In both cases we only attempted to estimate the three rotation parameters and the artificial focal length in the resection. The other parameters were held fixed as described before. The estimated values for the rotation parameters (yaw, roll and pitch) were: -11.173°, -0.156°, -0.025°, -10.984°, -0.161° and -0.019°, respectively, for images 103 and 104. To investigate the change in the rotation parameters and the exposure station coordinates in the case when the ground coordinates of the image center would be allowed to change we removed the weights from the image center coordinates and obtained the following results: the image center shifted by approximately 7.2 and 35.3 km in Easting and Northing, respectively, while roll and pitch increased to 2.056° and 0.423°, respectively. The combined RMSE for x and y remained practically unchanged. This experiment reinforced the notion that shifts of the image center can be compensated for by rotational changes, causing an ambiguity when trying to estimate both types of parameters.

The quality of the resections of images 103 and 104 is indicated in the following table.

Table I

RMSEs FOR RESECTION OF MSS IMAGES 103 AND 104
(millimeters)
(x 1000:meters on the ground)

Image	Resection Result	After polynomial adjustment		
		Power 1	Power 2	Power 3
Image 103 (18 points)				
RMSE for x	0.142	0.129	0.123	--
RMSE for y	0.146	0.138	0.116	--
Resultant	0.144	0.133	0.119	--
Image 104 (30 points)				
RMSE for x	0.233	0.225	0.217	0.187
RMSE for y	0.196	0.181	0.176	0.146
Resultant	0.215	0.204	0.198	0.167

First, we can see in Table I that the RMSEs vary from 0.119 to 0.233 mm. This variation amounts from one to two times the identification accuracy of the U2 RC-10 photography (0.1 mm), which is reasonable considering that the resolution of the MSS images in considerably less than that of the RC-10 photographs. Thus we can conclude that the point identification accuracy is the limiting factor with respect to the resection quality.

Secondly, we can see in Table I that the polynomial adjustment does not appreciably improve the RMSEs. To test this hypothesis we can compare the RMSEs before and after polynomial adjustment by combining them in the form of an F statistic. For instance, an F value of 1.29 can be computed from the resultant RMSE of image 104 before polynomial adjustment (0.215) and from the resultant value after a third-degree adjustment (0.167). At the 90% confidence level this value should be greater than 1.51 to reject the hypothesis. This is not the case and thus we cannot confirm that the polynomial adjustment contributes significantly to the overall accuracy.

An interesting result of some further experimentation was that the polynomial adjustment is useful when, for instance, all the parameters but yaw (azimuth) are held fixed. In this case we would have to compare an RMSE of 0.575 with one of 0.199 after a third-degree polynomial adjustment, giving rise to an F statistic of 6.49. In this particular case a first-power adjustment (fitting of a plane) still gave an RMSE of 0.232 indicating that a scale change in the form of an adjustable focal length was the most important adjustment mechanism that was not allowed to function when held constant.

With the resection results in the form of the covariance matrix of the estimated parameters, it should be possible to propagate the variances to determine the accuracy of individual projected points. However, we know that the accuracy of the individual point is bounded by the RMSEs for x and y obtained from the resection. Thus, it seems reasonable to assume a maximum standard error of 220 meters on the ground for any point projected on the MSS image within the resection area. Had we only made a scale change and used the image directly as a map, the error would have been in the neighborhood of 743 meters according to the data users handbook.

5. THE PRODUCTION OF IMAGE OVERLAYS

After the resectioning of the space images was completed, the results were stored for subsequent use in the production of the image overlays. We decided to use the second-degree residual estimation in both cases even though the benefits of this estimation were not clear-cut, but we were convinced that the accuracy would not be degraded because of it.

Three types of points needed to be annotated on the space image, namely: the primary sample unit corner, the county line points, and the management unit boundaries. For the primary sample units we decided to take blocks of 4 x 4 GLO land sections. Thus, one primary unit would cover approximately 16 square miles. All points were digitized from three maps at a scale of 1/2-inch to the mile. Geographic coordinates were then assigned to each point by means of an interpolation method using a set of map control points with known coordinates. The geographic coordinates were subsequently converted to secant plane coordinates. At this point no elevations had as yet been assigned to the digitized map points.

To produce elevations for the digitized points we developed a digital terrain model of which a hypsocline chart is shown in Figure 1. This model covers an area of 125 x 125 km of our Redding test area and includes part of the central valley, the Trinity Alps and the Mount Shasta area. In this area the maximum terrain variation is 14,000 ft. Elevations for the model were obtained by sampling an aeronautical chart with an 18 x 18 grid.

A test of the model showed that the RMSE of the actual terrain around the model surface amounted to 330 m. Under the assumption that the space image has a perspective geometry (including relief displacement), it can be shown that elevation errors in the order of 330 m would induce plate position errors of 37 micrometers whereas errors of 111 micrometers would be incurred by assuming a mean terrain elevation. However, the MSS image is formed by perspective projection (including terrain relief) in the cross-track direction only, while in the along-track direction after bulk processing the perspective projection would only be valid for general earth curvature. Thus, one would actually need two different terrain models to account for both types of perspective variation. At the present stage we used the one model shown in Figure 1 which accounts both for relief displacement and earth curvature since the elevations were transformed to the secant plane system.

After the elevations were assigned to the digitized points they were processed through a program that sorts the points by image and projects them onto the image in a rectangular coordinate system defined by the registration marks at the four corners of the image. These coordinates were then plotted on stable transparent material with a Hewlett Packard 9125A calculator-plotter at an enlargement ratio calculated by measuring a set of known distances on the enlargement.

The resultant overlay is shown in Figure 2a. In this figure the county line is indicated by A, the management unit boundary by B, and a primary sample unit corner by B. Note how the county line follows a set of mountain ridges extremely well.

At D in Figure 2a we have indicated a clear-cut GLO land section, which in terms of the primary 4 x 4 section sample unit occupies the second row, third position, counted from the upper left corner. The same cut-over section is indicated by D in Figure 2b. Figure 2a shows a section of a U2 RC-10 1:126,000 scale photograph with a computer-produced overlay of the second stage sampling units, which in this case are the land sections and their subdivisions.

6. SUMMARY AND CONCLUSIONS

As a part of our investigation, "The Development of a Multistage Forest Sampling Inventory System Using ERTS-1 Imagery," we developed a system to provide precision annotation of predetermined primary sampling units on the ERTS-1 MSS images. In the development of this system we aimed for accurate results, but we realized there is a certain limit beyond which further refinement was not justified for a particular application; in our case, a forest inventory.

Therefore, we applied generalized resection theory for the development of the system realizing that the geometry of the MSS imagery after bulk processing is not entirely commensurate with this theory. However, the results obtained with the investigation showed that at present the limiting factor with respect to overall accuracy is not the basic model but the accuracy with which known points can be identified on the MSS image. In any case entirely satisfactory results were obtained for the purpose of annotating sample units for a forest inventory. The maximum position error of 220 meters indicates that the delination of the one-square-mile land section itself on ERTS-1 MSS imagery would be technically feasible.

7. REFERENCES

1. Langley, P.G., "New Multi-Stage Sampling Techniques Using Space and Aircraft Imagery for Forest Inventory," Proc. Sixth Int. Symposium on Remote Sensing of Environment, University of Michigan, Ann Arbor, Michigan, 1969(2).

2. Forrest, R.B., "Geometric Processing of ERTS Images," Bendix Research Laboratories, Southfield, Michigan 48076.

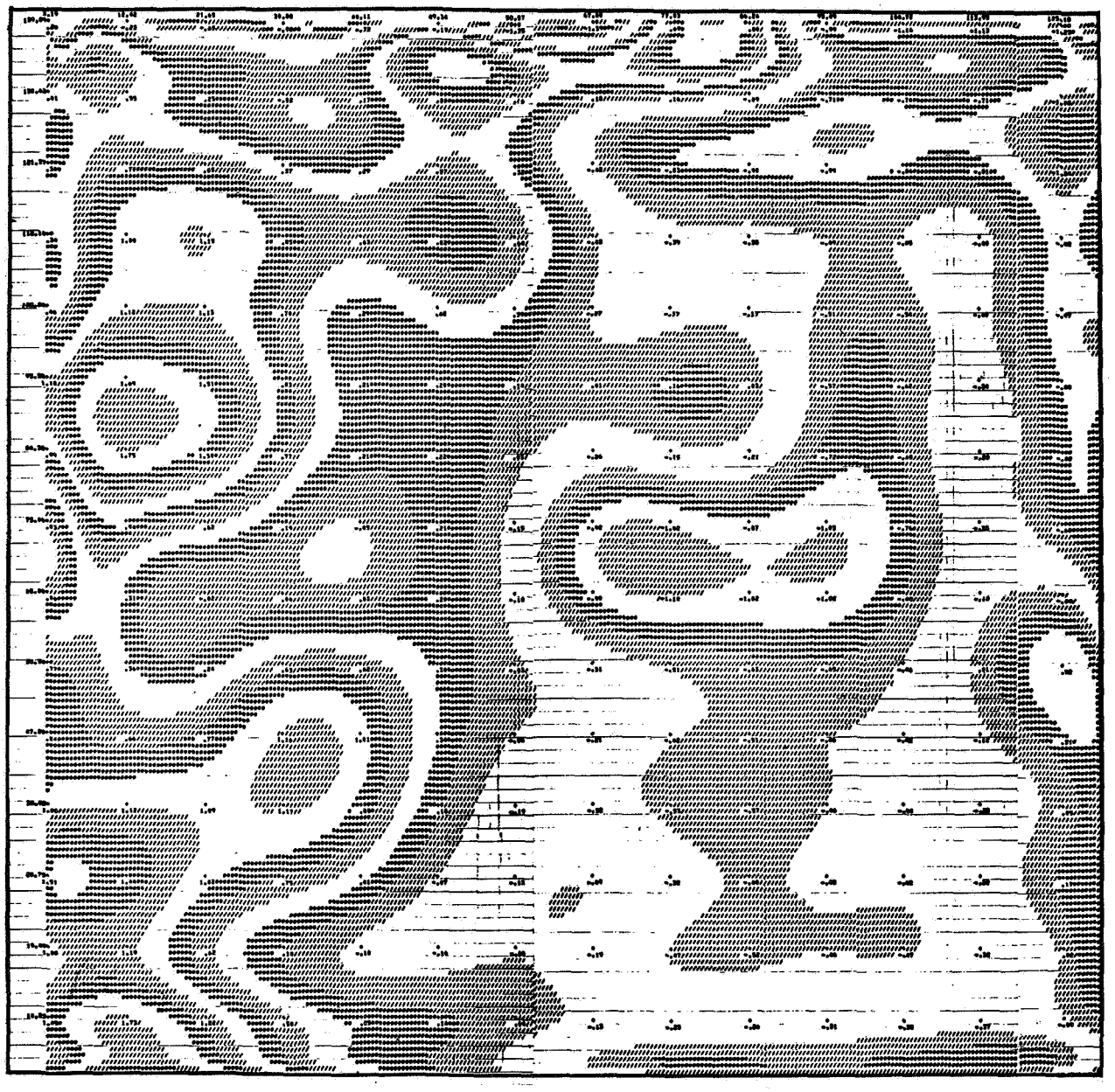


Figure 1

The digital terrain model illustrated by the hypsocline chart was used to assign elevations to digitized map points for subsequent correction of the boundary corners in the ERTS image overlay. The model covers an 125 x 125 km area, and includes a correction for earth curvature.



Figure 2a

U2 RC-10 photograph, scale 1:126,000 with second stage sample unit boundaries annotated by means of analytical resectioning. The light toned square indicated by "D" is a clear cut section which is also shown on the ERTS image of Figure 2b.

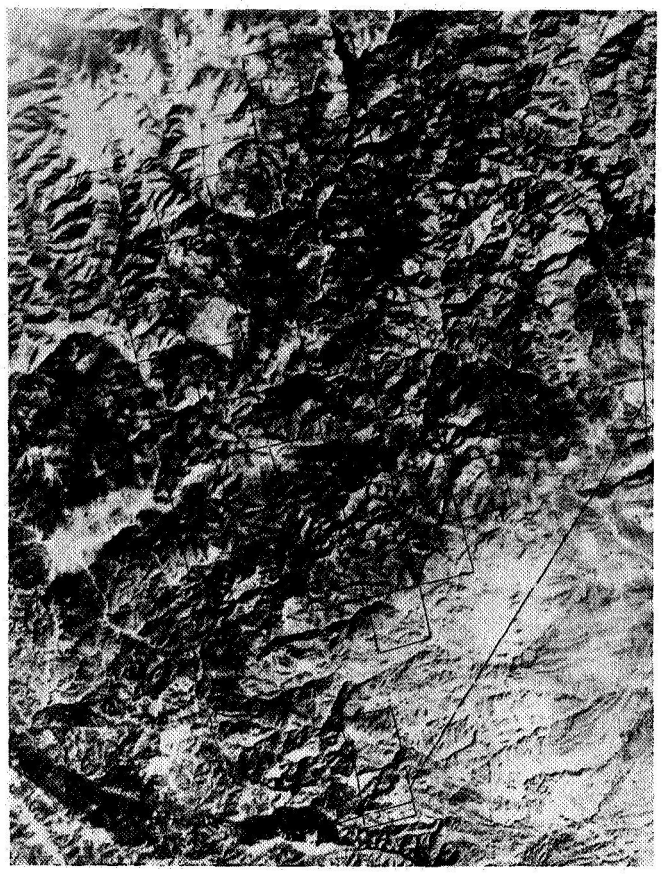


Figure 2b

ERTS-1 MSS band 5 image, with primary sample unit boundaries annotated by means of analytical resectioning. County lines are indicated by "A", management boundaries by "B", and sample unit boundaries by "C". "D" indicates the one square mile clear cut area shown in Figure 2a.

N73-28383

UNSUPERVISED CLASSIFICATION AND AREAL MEASUREMENT OF LAND AND WATER COASTAL FEATURES ON THE TEXAS COAST

L. M. Flores, C. A. Reeves, S. B. Hixon and J. F. Paris, *Lockheed Electronics Company, Inc., Houston Aerospace Systems Division*

ABSTRACT

ERTS-1 multispectral scanner (MSS) digital data was used to delineate coastal land, vegetative, and water features in two portions of the Texas Coastal Zone. ERTS-1 MSS data (Scene ID's 1037-16244 and 1037-16251) acquired on August 29, 1972, were analyzed on NASA Johnson Space Center systems through the use of two clustering algorithms. Seventeen to 30 spectrally homogeneous classes were so defined. Many classes were identified as being pure features such as water masses, salt marsh, beaches, pine, hardwoods, and exposed soil or construction materials. Most classes were identified to be mixtures of the pure class types. Using an objective technique for measuring the percentage of wetland along salt marsh boundaries, an analysis was made of the accuracy of areal measurement of salt marshes. Accuracies ranged from 89 to 99 percent. NASA aircraft photography was used as the basis for determining the true areal size of salt marshes in the study sites.

1. INTRODUCTION

The purpose of this paper is to report on the application of two classification algorithms to ERTS-1 multispectral scanner (MSS) system corrected data acquired over the Galveston Bay (Texas) area on August 29, 1972 (Scene ID's 1037-16244 and 1037-16251). Specifically, two algorithms (ISOCLS and NSCLAS) available at the NASA Johnson Space Center (JSC) were used to produce classification symbol maps of portions of the Texas coastal zone. The resulting classes then were related to an information hierarchy selected for the MSC ERTS-1 coastal estuarine investigation.

HIERARCHY OF COASTAL FEATURES

Level 1	Level 2	Level 3
Water	Water Mass Features	Turbid water Productive water Nonproductive water
	Bottom Features	Vegetated Nonvegetated
Nonwater	Sand (beaches, spoil)	
	Wetland	Vegetated Open water Nonvegetated
	Other	

Photography obtained by the NASA WB-57 aircraft on August 30, 1972, was used to aid in the identification of the classes defined by the algorithms and to provide a basis for the measurement of the true area of selected features such as water bodies and marsh.

PRECEDING PAGE BLANK NOT FILMED

Original photography may be purchased from:
EROS Data Center
10th and Dakota Avenue
Sioux Falls, SD 57198

2. METHOD OF ANALYSIS

Two study sites were edited from ERTS-1 MSS system corrected data contained in frames 1037-16244 and 1037-16251. These sites covered (1) Trinity River Delta area including salt, brackish, and fresh water marshes, and (2) Galveston Island, West Bay, Pelican Island, and offshore Gulf waters.

One computer compatible tape (CCT) containing the Galveston data was sent to Purdue University. This data set could then be analyzed through the use of the remote terminal at JSC. Both sets could be analyzed by JSC systems.

Since the two study sites exhibited natural features of complex configuration and unknown spatial extent, it was decided to use classification algorithms to produce classification symbol maps of the sites. Each of the two algorithms (ISOCLS and NSCLAS) attempts to partition the data into spectrally homogeneous groups. They then generate classification maps to display the geographical regions in which these homogeneous groups of data occur. A detailed description of ISOCLS can be found in references 1 through 5. A description of NSCLAS is given in reference 6.

Photography (film 2443, color IR) of the study sites was obtained by the NASA WB-57 aircraft from 60,000 feet (MSL) on August 30, 1972, one day after the subject ERTS-1 data. The photography was rectified and enlarged to a scale of 1:41,200. Then, wetland areas were delineated by coastal analysis team members. The area of each delineation was determined through the use of a photographic data quantizer (planimeter). Field trips into the sites were made to aid in the identification of classes defined by ISOCLS in that site. Photo interpreters identified classes in both sites through the use of the aircraft photography.

In the case of the areal measurement of the wetland areas in the Galveston site, an objective technique described in reference 7 in this symposium was used to count picture elements and partial picture elements on the boundary of the marsh.

3. RESULTS

Space does not permit the inclusion of all of the color coded classification maps produced during the present analysis effort. Examples of level two maps in each site are shown in figures 1 and 2 (originals are in color). In figure 2, four classes are shown: water, forested areas, vegetation including marsh, and bare soil/beach/asphalt/concrete. In figure 3, three classes are shown: water, wetland (marsh), and other.

4. WETLAND ANALYSIS

Using the objective technique described in reference 7 (this symposium), the areas of three wetlands were determined. The results are given in table I.

TABLE I.– RESULTS OF DETERMINING AREA OF WETLANDS FROM ERTS-1 DATA THROUGH AN OBJECTIVE TECHNIQUE

WETLAND NUMBER	ESTIMATED AREA (ACRES) ISOCLS	ESTIMATED AREA (ACRES) NSCLAS	TRUE AREA (ACRES)	PERCENT ACCURACY ISOCLS	PERCENT ACCURACY NSCLAS
1	864.13	871.56	866.0	99.6	99.4
2	197.97	193.77	191.3	96.5	98.7
3	150.86	165.94	149.6	99.2	89.1

The accuracies in wetland (marsh) area measurement are quite high. Both algorithms accurately define wetland features and boundary classes. It is not possible at this time to determine the more superior algorithm; however, ISOCLS on the UNIVAC 1108 was able to handle a larger number of data points than NSCLAS on the IBM 360/67 at Purdue University.

5. MIXTURE PROBLEM

A graph depicting the position of cluster means in the first and fourth channels of the ERTS-1 MSS is shown for the Trinity site in figure 4 for a

30-cluster case, which will be the subject for the remainder of this discussion. This figure is a good representation of the data and of the results of the cluster analysis. With few exceptions the second and third channels of the MSS add little new information.

The clusters obtained here are, for the most part, mixtures of some of the major classes that exist on the surface. The remaining clusters can be uniquely related to these major classes. The following table shows those clusters that can be so related:

Cluster Identification	Class
B,R,D,N,S	Vegetation excluding trees
C	Pine Trees
4	Hardwoods
F	Beach/asphalt/concrete
U,K	Bare soil
1,G,H,L,S	Water

The clusters have been identified by assigning to them consecutive arbitrary symbols 1, 2, ..., 9, A, B, ...

Up to five clusters can be identified as belonging to water bodies. No quantitative relationship can be assigned to these clusters at this time because there was no concurrent water survey on the date of the ERTS pass, The following is a general description of the type of water clusters and where they occur:

Cluster Identification	Class or Description
1	Bay water (probably slightly turbid)
G	Turbid (fresh or saline) water
H	Highly turbid water, very shallow water, or under-water spoil banks
L	Fresh water that occurs in lakes
S	Turbid fresh water or turbid water with a small amount of vegetation (less than 10 percent).

The clustering analysis differentiates forested areas from other types of vegetation. Within the forested areas, pine trees and hardwoods can also be differentiated and assigned to separate clusters. Vegetation types other than trees cannot be separated. Specifically, the same combination of clusters occur over vegetated areas which are known to contain different classes such as Phragmites communes, Spartina spartinae, and pasture land.

One conspicuous fact that this investigation has brought forth is that a good part of the data can be related to a mixture of two or more classes found on the surface. In the case of wetlands area, the proportion of classes contributing to a particular mixture varies in a continuous fashion over the possible range. Under these circumstances there are no natural groupings of the data; so the clustering program tends to partition the data at arbitrary places.

It may be noted that data assigned to clusters which represent a mixture of classes, can be obtained by linearly combining data assigned to clusters identified with one of the major classes. This fact may be easily seen by inspecting figure 4 where, for example, data points in cluster 8 can be obtained by linearly combining data points in clusters 5 and C. In this manner, a range of ratios of a particular mixture can be extracted from the data. The following table represents this range for the water/vegetation mixture. These numbers represent an estimate only and are not the result of a statistical study.

G

Cluster Identification	Ratio of Water
6	.6-.95
Q	.5-.8
3	.3-.7
E	.2-.6
2	.1-.5
7	0-.35
5	0-.20
N	0-.10
R	0-.05

Other mixtures could consist of almost any possible combination of the major classes that have been identified. The following table presents a list of possible mixutres that have been verified:

Cluster Identification	Mixture
4	Hardwoods; pines and vegetation (excl. trees)
C	Pines; hardwoods and water
0	Dense pines; trees and water
8	Pines and vegetation (excl. trees); hardwoods vegetation (excl. water) and water
6,Q,3,2,7	Marsh; vegetation and water
I,9	Water and bare soil/beach/asphalt in increasing proportion of bare soil/beach/asphalt
P, A, T, M, J	Vegetation and bare soil/beach/asphalt/concrete in increasing proportion of bare soil/beach/asphalt/concrete
E,U,K	Vegetation, water, and bare soil/beach/asphalt/concrete in increasing proportion of bare soil/beach/asphalt/concrete

6. CONCLUSION

Two clustering algorithms were used to produce classification maps of the Trinity River delta area (Scene ID 1037-16244) and the Galveston area (scene ID 1037-16251) from data obtained on August 29, 1972. Seventeen to thirty classes were defined. Most of these classes represented mixtures of land, water, and vegetation including forest. Through the use of a cluster diagram, ranges of percent of water and wetland were assigned to some classes. Improvements would result if a statistical approach were used for the mixture problem.

7. RECOMMENDATIONS

Further analysis is needed to determine whether the position of cluster centers in the cluster diagram can be used to identify the cluster as representing a certain class of coastal features.

REFERENCES

1. Ball, G. H., and Hall, D. J.: A Clustering Technique for Summarizing Multivariate Data, Behavioral Science, Volume 12, 1967.

2. Ball, G. H., and Hall, D. J.: ISODATA, A Novel Technique for Data Analysis and Pattern Classification. Technical Report, Menlo Park, California, Standard Research Institute, May 1965.

3. Kan, E. P. F.: "The Latest Version of ISODATA(A)/ISOCLS", Lockheed Electronics Company, Inc., HASD, Houston, Texas, Technical Memorandum TM642-570, September 1972.

4. Kan, E. P. F.; and Holley, W. A. : "More on Clustering With Final Recommendations on ISODATA," Lockheed Electronics Company, Inc., Houston, Texas, Technical Rep. 640-TR-112, May 1972.

5. Minter, R. T.: "ISOCLS, Iterative Self-Organizing Glustering Program", Lockheed Electronics Company, Inc., HASD, Houston, Texas, Computer Program Documentation CPD202, October 1972.

6. Swain, Pitt.: "Pattern Recognition: A Basis for Remote Sensing Data Analysis", LARS Information Note 11572, West Lafayette, Purdue University.

7. Cousin, S. B., Anderson, A. C., Paris, J. F., Potter, J. F.: "Significant Techniques in the Processing and Interpretation of ERTS-1 Data", Lockheed Electronics Company, Inc., HASD, Houston, Texas.

G

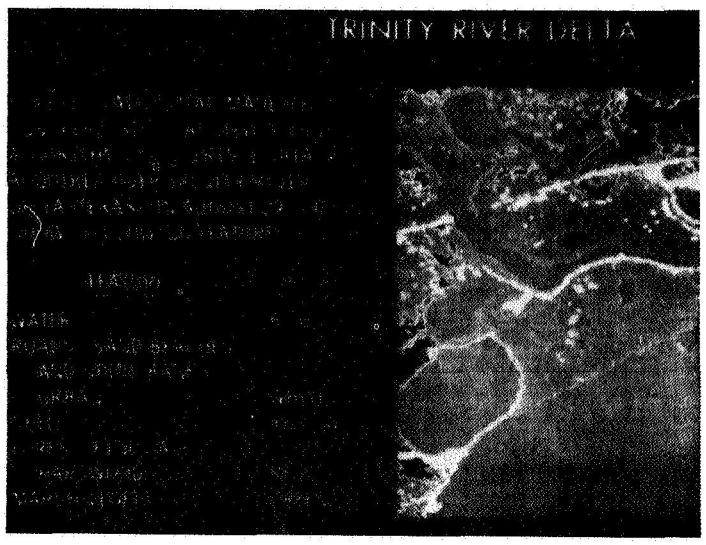
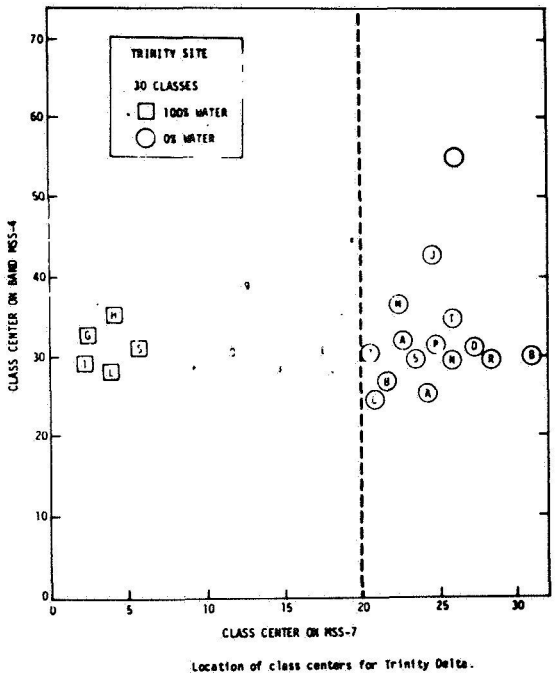


Figure 1



Location of class centers for Trinity Delta.

Figure 2



Figure 3

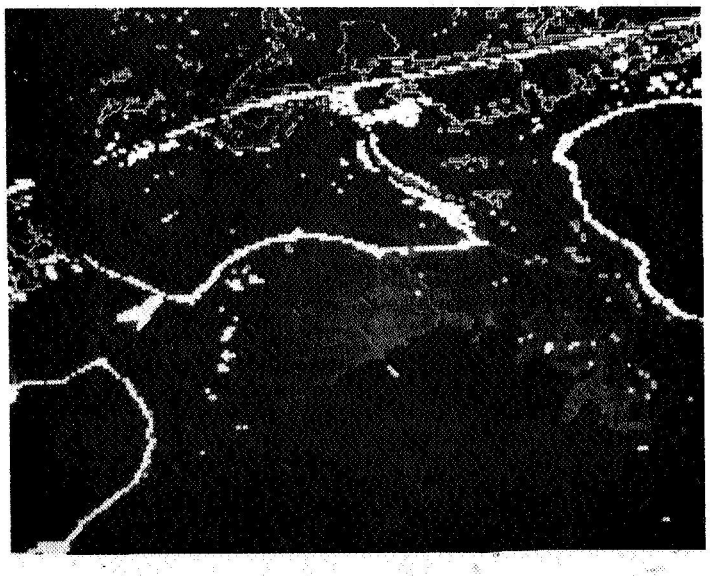


Figure 4

N73-28384

USE OF ERTS-1 PICTURES IN COASTAL OCEANOGRAPHY IN BRITISH COLUMBIA

J. F. R. Gower, *Marine Sciences Directorate, Environment Canada, 1230 Government Street, Victoria, B. C.*

The ERTS-1 colour composite picture of the Vancouver-Victoria region 1007-18365 illustrates very beautifully the value of ERTS data for coastal oceanography. The water of the Fraser River plume which is so clearly visible in the centre of the scene has been of interest to oceanographers on the west coast of Canada for a long time as an easily visible tracer of surface water circulation in the Strait of Georgia. Maps of the plume at different states of the tide and with different river flow and weather were compiled from oblique aerial photographs in 1950 and used in the siting of sewage and other outfalls in the Vancouver area. More recently high level aerial photomosaics have been used to map the plume area, but the plume can spread over distances of 30 to 40 miles and many photographs, with the uneven illumination inherent in wide angle coverage, are needed for the mosaic.

The ERTS satellite gives the first complete view of the plume area. Electronic enhancement of the images shows that the satellite's narrow angle coverage allows very weak surface turbidity features to be made visible to give information on surface currents over a wide area.

Canada, as you know, has its own ground station at Prince Albert and processing centre at Ottawa run by the Canada Centre for Remote Sensing. From the examples I have seen the Canadian colour composites allow coastal features to be more easily distinguished. Ships delayed by a dock strike in Vancouver on September 4, 1972 are clearly visible at anchor in English Bay, and the British Columbia ferries can be seen crossing the Strait of Georgia. Comparing imagery from two dates, in which the ferries show at the same position, verifies that both the ferries and the ERTS-1 satellite are "sun-synchronous".

Although our evaluation has not advanced very far yet, it does seem that ERTS-1 pictures will be extremely useful for the environmental studies that are becoming increasingly important, as well as for some of our continuing oceanographic programs.

PRECEDING PAGE BLANK NOT FILMED

N73-28385

RELATIONSHIPS BETWEEN REMOTELY SENSED FISHERIES DISTRIBUTION INFORMATION AND SELECTED OCEANOGRAPHIC PARAMETERS IN THE MISSISSIPPI SOUND

Andrew J. Kemmerer and Joseph A. Benigno, *Southeast Fisheries Center, Pascagoula Laboratory, Pascagoula, Mississippi 39567*

ABSTRACT

A feasibility study to demonstrate the potential of satellites for providing fisheries significant information was conducted in the Mississippi Sound and adjacent offshore waters. Attempts were made to relate satellite acquired imagery to selected oceanographic parameters and then to relate these parameters to aircraft remotely sensed distribution patterns of resident surface schooling fishes. Initial results suggest that this approach is valid and that the satellite acquired imagery may have important fisheries resource assessment implications.

INTRODUCTION

A basic need of fishery resource managers and resource users is timely synoptic information about the resource. Resource managers need this information for effective management and use allocation, while users need it to guide their fishing and investment strategies. The tremendous costs involved in gathering adequate resource information through classical approaches, however, has hampered fulfillment of this need. All too often, resource managers are forced to base decisions on little or no information, while users must be content to base their decisions on intuition and often biased personal knowledge. In response to this need, the NMFS is attempting to identify, develop, and evaluate new resource assessment methods so that managers and users alike can be relieved of many resource related uncertainties. As a means to this end, aerial and satellite remote sensing techniques are being examined to determine if they can be utilized to provide pertinent fisheries resource information.

A 15-month study was initiated in July 1972 under NASA Projects 240 and 258 to establish the feasibility of using ERTS-1 imagery to assess, monitor, and predict the distribution and availability of a living marine resource. The study represents a combined Federal Government and private industry effort and stressed acquisition of data to:

PRECEDING PAGE BLANK NOT FILMED

Original photography may be purchased from:
EROS Data Center
10th and Dakota Avenue
Sioux Falls, SD 57198

Original photography may be purchased from:
EROS Data Center
10th and Dakota Avenue
Sioux Falls, SD 57198

- Determine the effectiveness and reliability of ERTS-1 and high-level aircraft sensors to provide fisheries significant data about coastal waters.

- Demonstrate the feasibility of using remotely-sensed oceanographic data to predict the availability and distribution of adult menhaden in the Mississippi Sound and adjacent waters.

- Evaluate the usefulness of remotely-acquired oceanographic, environmental, and resource information for improving the harvest and management of the menhaden resource.

This paper presents a summary of some of the early study results with emphasis given to statistical relationships between the fishery resource and selected oceanographic parameters. Data analyses are far from complete and as such, none are considered conclusive.

SUMMARY OF EXPERIMENTAL DETAIL

The experimental approach employed is to convert satellite and aircraft remotely sensed data into oceanographic parameters, relate these parameters to the fishery resource, and then determine if the relationships have meaning in terms of the commercial fisheries and its management. At present, only a small amount of remotely sensed oceanographic data are available; consequently, the reported resource related analyses depend primarily upon sea-truth information collected with standard techniques to calibrate remote sensors.

Study Area

This study area is a 8,685 square kilometer rectangle in the north central Gulf of Mexico (Fig. 1). It encompasses all of the Mississippi Sound, the lower portion of Mobile Bay, and extends offshore to approximately the 10-fathom curve (i.e., approximately 50 kilometers offshore). The study area was selected because of the Mississippi Sound, which is a shallow (mean depth 3 meters) and turbid (secchi disc visibility varies from about 1 to 2 meters) body of water. The Sound supports a substantial commercially important menhaden population, which generally is fished from about mid-April to October.

Data Acquisition

Data acquisition activities were divided into four categories: main day, secondary and special purpose missions, and commercial fishing. Main-day missions occurred at the time of selected ERTS-1 overpasses (7 August, 25 August, and 28 September 1972) and included an intensive sea-truth sampling effort--up to 144 stations were occupied (95 stations in the Sound). Only a few sea-truth stations were occupied during secondary missions, which were conducted weekly to record temporal environmental and fishery changes. Special purpose missions were

designed to meet specific limited objectives and as such, did not necessarily follow set schedules. Oceanographic and fisheries data were obtained from commercial fishing vessels in fishing areas Monday through Friday throughout most of the experimental period.

Data considered in this paper were collected during the main-day missions. Remotely sensed oceanographic data are not included, nor is much attention given to the offshore portion of the study area.

Oceanographic Data: Oceanographic or sea-truth data were collected from about 25 surface vessels, usually within a few hours of the satellite overpass. Oceanographic parameters measured included surface temperature, water transparency (secchi disc), sea state, surface current (float and impeller-type current meters), salinity (induction salinometer), surface chlorophyll-a (acetone extraction), water color (Forel-Ule color comparator), and water depth. Complete descriptions of methods and results can be found in NASA-ERL/MTF special reports numbers 025, 032, and 034.

Fisheries Data: Aerial photography provided all fisheries data used in this paper. Menhaden are particularly susceptible to photographic sensing because of their characteristic surface or near-surface schooling behavior. (For discussions on aerial photography as a pelagic fisheries assessment tool, see Bullis, 1967; Benigno, 1970; and Drennan, 1969.) Photographic fish sensing missions were flown to provide approximately 95 percent coverage of the study area at an altitude of 2,469 meters. A 6-inch lens and 9-inch film format aerial mapping camera, supplied with GAF blue insensitive film, constituted the sensor. Missions over the Sound were flown in the morning (0700-1000 hours) to correspond as closely as possible to ERTS-1 overpasses. Processed film was interpreted at 3X to 33X magnification and data recorded included position, number, and size (surface area) of fish schools.

DATA ANALYSIS AND DISCUSSION

Oceanographic Parameter and Fish Distribution Relationships

Initial attempts to describe relationships between menhaden school distribution and available oceanographic parameter measurements (surface sea-truth) produced interesting results. Four parameters repeatedly stood out as significantly defining fish distribution patterns (Table 1). Chlorophyll-a, surface current, temperature, and sea state appeared to have little influence on menhaden. The lack of significance with respect to chlorophyll-a was surprising in that menhaden are primarily plankton feeders; one might expect a priori that these fish would tend to be distributed according to phytoplankton

biomass. The significant correlation between fish distribution and water color cannot be explained at this time, although presumably color served as an indicator of a condition influencing the fish--perhaps zooplankton. Secchi disc visibility did not correlate as well as was expected; commercial fish spotter pilots generally regard turbid waters as "fishy" areas. Literature sources suggest a menhaden preference for low salinity waters, which was borne out here by the significant negative correlation. Depth also appeared to be an important parameter, with menhaden apparently preferring shallow waters.

Table 1.--Simple linear correlations between the distribution of menhaden schools during the three main-day missions and selected oceanographic parameters (the dependent variable was time normalized by dividing the number of fish schools at any given location by the total population of detected schools).

Parameter	Degrees of Freedom	Correlation Coefficient	Level of Significance
Salinity	195	-0.257	99%
Color	113*	-0.283	99%
Secchi disc	195	-0.100	75%
Depth	195	-0.216	99%

* Color was not measured on the 7 August main-day mission

The lack of precise correlations between fish distribution and oceanographic parameters, as indicated by the correlation coefficients, was not discouraging; rather, the fact that the correlations had statistical significance was quite encouraging. The way the data were handled probably contributed significantly to the lack of precision. Water conditions at fish school locations generally had to be estimated based on conditions at sea-truth stations located several kilometers away. The Mississippi Sound is an extremely dynamic aquatic environment, and as such little reliance can be placed on interpolated or extrapolated values. There were other obvious sources of experimental error. The fish sensor (aerial photography) had certain limitations such as water penetration depth (roughly estimated to be about 1.5 times the secchi disc visibility depth), minimum detectable school size (about 40 square meters surface area) and minimum detectable school density (unknown). There was also doubt as to whether or not all fish schools detected were menhaden and how much commercial fishing activities influenced the distribution of schools. And finally, because aquatic organisms are influenced directly or indirectly by all

conditions of their environment, there is little reason to expect that any single parameter would explain all of the experimental variation.

Multiple regression techniques were employed to determine if significantly more experimental variation could be explained by combining the parameters listed in Table 1. Data used in this analysis were taken from the last two main-day missions (25 August and 28 September), as no water truth color information was obtained on 7 August. The dependent variable was number of fish schools (normalized for time) and the independent variables were salinity, secchi disc visibility, color, and the two factor interactions between these variables (i.e., salinity x secchi disc visibility, salinity x color, and secchi disc visibility x color). The resultant equation (Table 2) was highly significant (99.95 percent) and explained about 30 percent of the experimental variation (Table 3). Water depth erroneously was not included in the analysis; subsequent analyses suggest that this parameter might have significantly increased its precision.

Table 2.--Components of a multiple regression equation where the normalized number of menhaden fish schools is predicted based on oceanographic parameters.

Parameter	Coefficient	Standard Error of Coefficient
Salinity (S)	-0.04565	0.01087
Secchi disc (D)	-0.06599	0.02785
Color (C)	-0.07368	0.01664
S x D	0.00207	0.00079
S x C	0.00237	0.00065
D x C	0.00004	0.00091

Constant = 1.42682
Standard error of Y = 0.03881

Table 3.--Analysis of variance for a multiple regression analysis of menhaden distribution versus selected oceanographic parameters (Table 2).

Source Variation	Degrees of Freedom	Mean Square	F-Value
Total	114	0.00200	
Regression	6	0.01086	7.192***
Error	108	0.00151	

Correlation coefficient = 0.535

A tentative conclusion from the foregoing analyses is that menhaden appear to be distributed according to environmental conditions in the water mass. Notably, all of the parameters significantly correlated with fish distribution, except for depth, can be measured remotely. Future analyses will emphasize remote, synoptically acquired oceanographic parameter information which should substantially increase experimental precision.

ERTS-1 Imagery and Fish Distribution Relationships

A preliminary analysis of the 7 August ERTS-1 multispectral scanner (MSS) imagery was performed to determine if the imagery contained readily apparent fisheries significant information. August 7 was selected because it was the only day where four MSS channels (i.e., 4, 5, 6, and 7) were available and there was no significant cloud coverage over the study area. Channels 6 and 7, representing spectral ranges 0.7 to 0.8 and 0.8 to 1.1 microns, respectively, appeared to have little water mass information (e.g., boundaries, turbid areas, etc.), while channel 4, covering a spectral range of 0.5 to 0.6 microns, appeared to have too much density detail for this type of analysis. Channel 5, representing 0.6 to 0.7 microns, for reasons not clearly understood at this time, did appear to provide fisheries significant information.

Figure 2a shows a portion of the ERTS-1, channel 5 imagery for the west end of the Mississippi Sound and adjacent offshore waters as displayed on a I^2S DIGICOL video screen. Superimposed on the image are locations of 23 photographically-detected fish schools (the four closely grouped fish school locations shown in the middle left portion of the photograph actually should be 10 positions). The water imagery densities were divided into two density ranges and color enhanced. All of the fish school locations were found to lie in the less dense range

of the two ranges (Fig. 2b). The characteristics of the I^2S permitted further division of the density range containing the fish schools into four narrower discrete ranges. When this was done, all of the fish school locations were found to either lie in or immediately adjacent to a single narrow image density range (Fig. 2c).

Although it may be too soon to draw conclusions from the foregoing analysis, it does suggest that ERTS-1 remotely sensed data may have significant fisheries meaning.

ERTS-1 Imagery and Oceanographic Parameter Relationships

A preliminary analysis was performed on the ERTS-1, MSS, channel 5 imagery for 7 August to determine if image densities could be explained based on selected oceanographic parameter information. An isodensity tracing was made of the image as a first step to provide quantitative density data. The tracing was not particularly satisfactory because of instrument limitations which caused more than one density to be represented by the same color trace. Nevertheless, the density measurements probably were reasonably accurate.

Water depth, secchi disc visibility, and the interaction between these two parameters, were regressed against image density (Tables 4 and 5). These particular parameters were selected because of their significant correlation with fish distribution (Table 1) and because the ERTS-1 image seemed to describe turbidity and depth patterns in the water. The analysis was highly significant (99.95 percent) and explained 59 percent of the experimental variation. Unfortunately, color data were not available for 7 August and as such, there is no way to determine if color would have significantly reduced the error term.

Table 4.--Analysis of variance for the relationship between ERTS-1 image density and two oceanographic parameters.

Variation	Degrees of Freedom	Mean Square	F-Value
Total	47	0.00508	
Regression	3	0.04692	21.040***
Error	44	0.00223	

Correlation coefficient = 0.768

Table 5.--Components of a multiple regression equation where levels of ERTS-1, MSS, channel 5, image density are predicted.

Parameter	Coefficient	Standard Error of Coefficient
Water depth	0.00677	0.00294
Secchi disc visibility	0.02324	0.00677
Interaction	-0.00047	0.00036

Constant = 0.57763
Standard error of Y = 0.04717

TENTATIVE CONCLUSIONS

1. The distribution of photographically detected adult menhaden in the Mississippi Sound was significantly correlated with secchi disc visibility, surface salinity, water color, and water depth.

2. ERTS-1, 7 August, channel 5 imagery appeared to contain fishery significant information; all detected menhaden schools were located in areas of lowest image density.

3. Image density patterns could be explained statistically with good precision based on water depth and secchi disc visibility measurements, parameters which correlated significantly with the distribution of menhaden.

LITERATURE CITED

Benigno, Joseph A. 1970. Fish detection through aerial surveillance. Technical Conference on Fish Finding, Purse Seining, and Aimed Trawling; Reykjavik, May 1970, FAO, FII:FF 70/78, 13 pp.

Bullis, Jr., Harvey R. 1967. A program to develop aerial photo technology for assessment of surface fish schools. Proceedings of the Gulf and Caribbean Fisheries Institute, 20th Annual Session: 40-43.

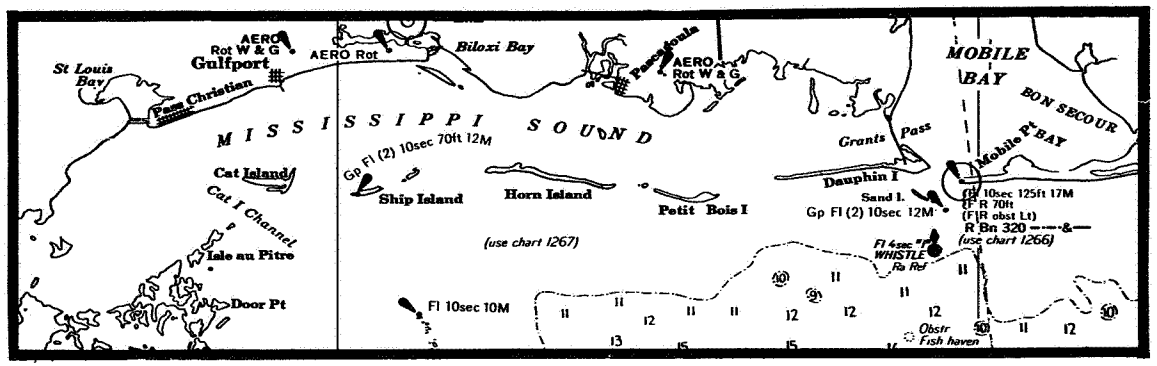
Drennan, Kirby L. 1969. Fishery oceanography from space. Proceedings of the Sixth Space Congress; Space, Technology, and Society. Canaveral Council of Technical Societies, Cocoa Beach, Florida: 9.1-9.6.

NASA-ERL/MTF. 1972. Sea remote sensing program, Mississippi Sound remote sensing study, August 7, 1972. Report No. 025; 18 October 1972.

_____. 1972. Sea remote sensing program, Mississippi Sound remote sensing study, August 25, 1972. Report No. 032; 30 November 1972.

_____. 1973. Sea remote sensing program, Mississippi Sound remote sensing study, September 28, 1972. Report No. 034; 9 January 1973.

C-18



TEST SITE COORDINATES

	LATITUDE	LONGITUDE
A)	30°27'N	89°30'W
B)	30°27'N	87°45'W
C)	30°00'N	87°45'W
D)	30°00'N	89°30'W

SCALE 1:875,000

N.MI. 10 20

KM. 10 20 30 40

TEST SITE DIMENSIONS

LENGTH: 170 KM.

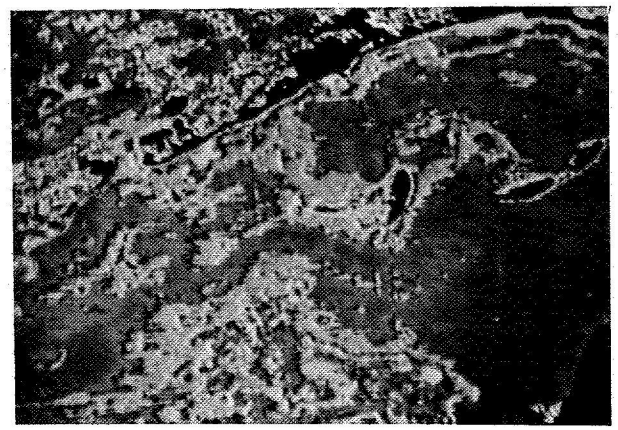
WIDTH: 51 KM.

AREA: 8685 SQ.KM.

Figure 1.--ERTS-1 study area



a



c



b

Figure 2. ERTS-1, channel 5, August 7 image of western portion of study area (Fish school locations are shown as black dots):

a. I^2S DIGICOL television screen image.

b. Image water densities divided into two ranges and enhanced. Instability of the television image caused fish locations on the extreme left of the figure to appear on the beach.

c. Enhancement of a narrow density range within the range containing the fish school locations--note how the fish schools either fall adjacent to or within this narrow range.

N73-28386

APPLICATION OF ERTS-1 IMAGERY IN COASTAL STUDIES

Orville T. Magoon,[1] Dennis W. Berg[2] and Robert J. Hallermeier[3]

The basic ERTS output is four black-and-white photographs presenting the same scene recorded in each multi-spectral scanner band. Mosaics covering large regions at a 1:250,000 scale can be compiled from these photographs. Office study of the image of each band separately, in combination with other bands, and in conjunction with other available data (navigation charts, tide tables, etc.) permits extraction of data useful in coastal engineering planning and coastal processes studies. Specific examples are listed below in which significant information on regional shoreline configuration or nearshore water movements has been obtained from unenhanced ERTS imagery.

Tidal Inlet Configuration. An MSS 5 image of 16 Aug 72 clearly defines the configuration of Indian River Inlet, Del. The offset between the barrier islands north and south of the inlet gives an indication of predominant south-to-north longshore littoral transport at the inlet. In general, sediment plumes emanating from an inlet may be discernable on MSS 4 or MSS 5 and may give some indication of longshore transport direction at the time of the image. This type of information is important in coastal engineering planning.

Navigation Information. Timely information useful for navigation is shown in ERTS imagery of the Sangi Islands obtained on 27 Jul 72. These islands are in the tropical Pacific between the Celebes Islands and the island of Mindanao. Data from the ERTS images is a valuable supplement to available navigation charts, which are based on data collected in March 1939 and updated in June 1966.

The particular islands in this vicinity selected for detailed examination are Pulau Tahulandang, Pulau Ruang and Pulau Pasige. MSS 7 shows a narrow, incised body of water on the eastern shore of Pulau Ruang not indicated on available charts. This may indicate a recent change

---

1. Coastal Engineering Branch, U.S. Army Engineer Division, South Pacific, 630 Sansome Street, Room 1212, San Francisco, CA 94111.
2. Chief, Evaluation Branch, U.S. Army Coastal Engineering Research Center, 5201 Little Falls Road, N.W., Washington, D. C. 20016
3. Coastal Processes Branch, U.S. Army Coastal Engineering Research Center.

PRECEDING PAGE BLANK NOT FILMED

in the land mass, which may have been caused by volcanic action or major erosion of the island. The uncharted bay has a different tone on MSS 5, and exhibits a deltaic feature, possibly indicating deposition of eroded sediments in the nearshore area.

The full extent of coral reefs fringing these islands is shown in MSS 4, while comparison of MSS 4, MSS 5 and MSS 6 gives an indication of the relative depths of these reefs. The absence of coral reef development on the northern and eastern shores of Pulau Taulandang may be interpreted as indicating the direction of predominant wave action.

Nearshore Water Movement. Nearshore flow patterns may be traced using the recorded suspended sediment patterns in ERTS imagery. An ERTS image of Lituya Bay, Alaska, obtained on 18 Sep 72, shows a well-defined plume of turbid water associated with the Alsek River. Water flow to the northwest may be inferred from this plume's shape.

ERTS imagery of the Laptev Sea coastline on the northern shore of Siberia on 16 Sep 72 shows important fluid mixing phenomena. A mosaic of MSS 4 images displays a convoluted interface between waters of markedly different turbidities. A narrow surface streak (of ice, probably) extends from the center of the Laptev Strait indicating flow of the sediment-laden water towards the west into the Laptev Sea. Well-defined counter-clockwise gyres are prominent in the mixing interface; Coriolis effects would favor formation of such gyres.

A mosaic of MSS 4 images of the mouth of the Colorado River (30 Sep 72) slightly overlaps a mosaic of MSS 4 images of a region slightly further south in the Gulf of California (29 Sep 72). The structure of the complex suspended sediment pattern in the overlap area is quite different on the two days. The existence and lifetime of such fluid mixing features can be of great importance in the design of nearshore oceanographic measurement programs.

This analysis and report are a part of the research program of the U.S. Army Coastal Engineering Research Center of the U.S. Army Corps of Engineers. The full report, including the descriptive photography, is being published as Technical Memorandum No. 40 of the Coastal Engineering Research Center.

N73-28387

APPLICATION OF ERTS-1 IMAGERY IN THE FIELDS OF GEOLOGY, AGRICULTURE, FORESTRY, AND HYDROLOGY TO SELECTED TEST SITES IN IRAN

Khosro Ebtehadj, *Plan Organization, Imperial Government of Iran, Tehran, Iran*

ABSTRACT

The preliminary study of the ERTS-1 imagery coverage of Iran, commenced on October 26, 1972, upon receipt of the data. All of the images were carefully examined, and a photomosaic covering approximately ninety-five per cent of the country was prepared. A number of images, of selected areas were studied in detail.

In the field of geology, a number of large scale faults were identified, which do not figure on geological maps. Furthermore, a preliminary study was carried out on the recent sediments, their possible sources, and origin. A limited number of geological work maps were prepared as well.

In the fields of agriculture and forestry, studies based on color composite prints of certain areas were undertaken, with a purpose of identifying potential arable areas.

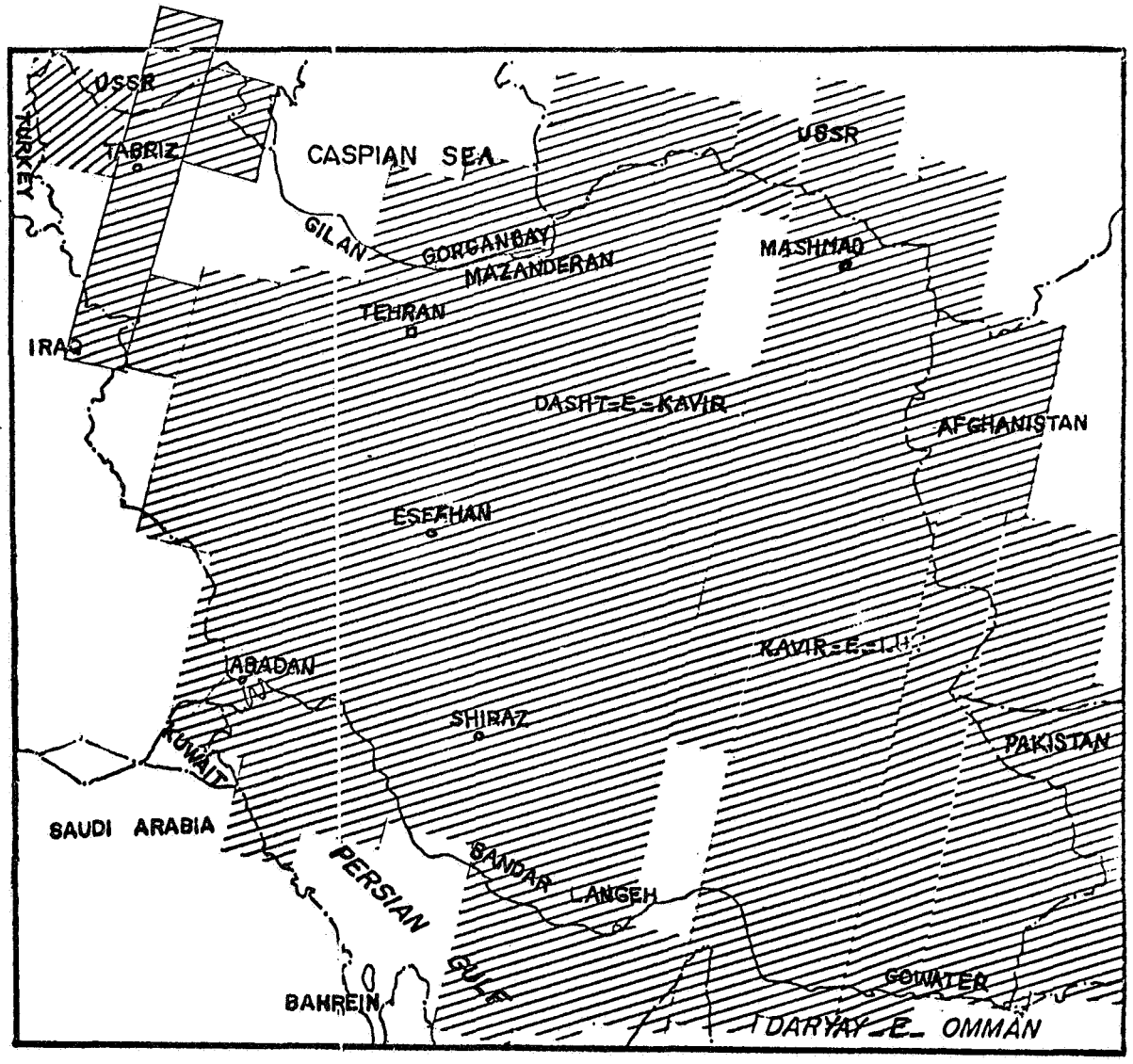
Investigations in the field of water resources resulted in the discovery of a number of small lakes, and streams. Furthermore, fluctuations of the water level in some lakes were observed.

INTRODUCTION

The first series of ERTS-1 imagery coverage of Iran were studied in a number of disciplines, i.e., agriculture, forestry, geology and hydrology. A general preliminary study in the above mentioned fields was undertaken, and particular emphasis was given to certain selected test sites. These results of the investigations and observations were accomplished with conventional photographic interpretation techniques which could be considerably expanded if multispectral imaging equipment permitted additive color techniques to be used.

Notwithstanding these constraints, some interesting observations were made which demonstrate the usefulness of the ERTS-1 data as a means of mapping and defining the natural resources of Iran.

Original photography may be purchased from:
EROS Data Center
10th and Dakota Avenue
Sioux Falls, SD 57198



Areal extent of ERTS-1 imagery coverage of Iran up to this date (coverage shown by shaded areas).

GEOLOGY

All of the ERTS-1 imagery were carefully examined, and a number of them were selected for detailed geological study. These images were compared with the 1:2,500,000 Geological Map of Iran, and the 1:1,000,000 Geological Map of SW Iran, compiled by the Iranian Oil Operating Companies.

Particular emphasis was given to the tectonics, and the lithology of different test sites. A preliminary study was also carried out on the recent sediments, especially in regard to evaporitic deposits in playas.

1. Tectonics

The major physiographic features of Iran are:

- The Alborz range: Located in the northern part of the country, with an E-W trend.

- The Zagros range: Situated in the central part of the country, with a NW-SE trend.

- Dasht-e-Kavir (Kavir desert): An area covered with alluvial and aeolian sediments, in the central part of Iran.

- Dasht-e-Loot (Loot desert): An area in the SE of the country, covered with alluvial and aeolian deposits.

By studying the mosaic of the ERTS-1 imagery, a major fault, several hundred kilometers in length, and more or less parallel to the Zagros Thrust Fault was identified. This fault was not previously recorded, and thus does not appear on geological maps.

Preliminary study of the imagery taken by ERTS-1 of the SE corner of Iran, denotes the presence of a larger number of faults than what appears on our geological maps.

Numerous anticlines, synclines, and salt domes which characterize the SE part of the Zagros range, are clearly visible on the image taken of the Bandar Lengeh area (part of test site A). Thus a regional map of the area was prepared to complement existing large scale maps.

Two fairly large faults with a NW-SE trend were identified on the ERTS-1 images taken of the Isfahan area. These faults do not appear on any of our geological maps.

2. Lithology

A relatively detailed study of the consolidated, as well as the unconsolidated sediments, was carried out on the imagery taken of Isfahan. As a result, different types of recent unconsolidated sediments; i.e., lake evaporitic deposits,

river deposits, and talus, were differentiated using tonal changes. Areas covered by the weathered, and eroded by-products of nearby igneous and metamorphic source rocks (Protores), are visible by dark-grey to black shades. Whereas, by-products of the weathering, and erosion of sedimentary rocks, appear as grey patches. Finally, sediments (mostly evaporites) present in playas, and river channels, are visible as white patches.

On the imagery taken from the extreme SE region of Iran (near the Pakistan border), a number of igneous bodies were identified which are not present on our geological maps. In order to determine their nature, as far as being lava flows, or intrusions, it is planned to study thoroughly this area in the near future.

In general, it can be stated that where geological maps of Iran do not differentiate alluvial deposits, and classify them into different lithological categories, it is possible with a fair degree of certainty, by using tonal changes which different recent sediments exhibit, to further refine their lithological nature, and thus discern differences and subtle facies changes.

Conclusion

It appears that notwithstanding the relatively short time, and the very limited hardware available, some encouraging results were obtained in the application of the ERTS-1 imagery to the field of geology. Hence, it is assumed that by embarking on a detailed field geological investigation program, more fruitful results will be achieved.

AGRICULTURE AND FORESTRY

Investigations in the fields of agriculture and forestry were subject to constraints, for lack of adequate hardware, and especially insufficient repetitive ERTS-1 imagery coverage of Iran. Nevertheless, a few noteworthy observations were made, which demonstrate the usefulness of the satellite imagery for natural resources inventory, and planning in these disciplines.

1. Agricultural and Forestry Survey of the Isfahan Area

Study of the ERTS-1 false color composite prints (MSS bands 4, 5 and 7), of the greater Isfahan area (in central Iran) was undertaken, in order to determine the nature, and distribution pattern of the cultivated fields, as well as the natural vegetation.

As stated above, due to the lack of the required hardware, a definite distinction between different types of cultivated fields and/or crops was not

possible. Nevertheless, cultivated areas were identified, and distinguished from the forested regions. It was possible to delineate cultivated lands around the Zayandeh-Rood river and its tributaries, and also identify potential arable regions.

These regions appear capable of sustaining plant life, and their absence could presumably be due to one, or a combination of the following factors:

- Chemical nature of soil; i.e., too alkaline.
- Physical nature of soil; i.e., texture, permeability, porosity, etc.
- Topography; e.g., steep gorges, or slopes which are being continuously washed by running surface waters.
- Geographical isolation; too distant from the nearest inhabited areas, therefore at the present uneconomical.

Thus, it is planned to start a program of field investigations, with a purpose of collecting adequate ground truth data, in order to identify what is (are) the limiting factor(s), and define possible remedy(ies).

2. Mazandaran-Damavand Region

On the color composite prints (MSS 4, 5 and 7) of the Mazandaran province (including the Damavand volcano), areas covered with vegetation are readily observable. Although at the present with inadequate hardware, and insufficient field data, no attempt was made to distinguish different types of crops or genera of trees, yet different tones of red and pink were believed to be linked to the following phenomena:

- Diversity of tree genera and species.
- Forest distribution and density.
- Presence of areas covered with shrub.
- Deforestation, and timber cutting.
- Possible conversion of forested regions into cultivated or pasture land.

Conclusion

It is firmly believed, that with sufficient ERTS-1 imagery coverage of Iran a resource inventory covering forested regions as well as farmlands can be established. The first order priority will be given to the Mazanderan, Gilan, and Azerbaijan provinces, which are rich in vegetation cover.

WATER RESOURCES

This phase of the investigations consisted of a general study of the ERTS-1 imagery coverage of the Fars province, the SE corner of the Caspian Sea, the Hozsultan salt lake, and the NW region of the Persian Gulf.

The following observations are of significance:

1. Lakes: their location, areal extent, seasonal fluctuations, as well as water quality may be assessed.

2. Rivers: river channel, drainage pattern, and their sources in relation to the snow melt or springs, can be determined.

3. Alluvial Deposits: it is possible to differentiate, and map alluvial deposits, and estimate the areal extent of alluvial plains, and alluvial fans.

4. Marine Phenomena: study of the discharge of stream sediments into the Persian Gulf, the Caspian Sea, and finally the nature and directions of the offshore currents, may be determined.

1. Lakes

The nature, distribution, and location of water bodies, as observed on the photo-mosaic of the ERTS-1 images, were compared with the 1971 Hydrological Map of Iran, with the following results:

a. Three new lakes were identified on the ERTS-1 imagery coverage of the Fars province, which do not appear on hydrological maps of this region. These lakes are:

   - The Dariush Kabir dam and reservoir built on the Kor river in 1972.
   - A small lake, North of the Parishan lake, in the Kazeroon area.
   - A small lake, in the Sivand river basin.

The absence of these lakes on hydrological maps may possibly be explained by the following reasons:

- The Hydrological Map of Iran was published in 1971, and at that time construction of the Dariush Kabir dam, and its associated reservoir was not completed yet.

- The amount of precipitation during the year 1971-1972, exceeded that of the previous years. Hence, topographic depressions were filled with water, and thereby new lakes were formed.

b. Another interesting feature was observed while studying the ERTS-1 images taken of the Fars province. It was noticed that water bodies exhibit tonal differences. This phenomenon presumably is due to one, or a combination of the following factors:

   - Depth of water.
   - Chemical composition of water.
   - Presence of organic material, i.e., algal growth.
   - Industrial pollution of water (although rare).

c. An important observation was recorded, relevant to the fluctuations of the water-level in the Hozsultan salt lake. The image taken by ERTS-1 on September 4, 1972, shows a small body of water, about 18 km^2 in size, present in the western part of this salt lake. But on the following series of images taken 18 days later, the areal extent of this body of water had significantly decreased, to the point of being barely discernible. This phenomenon is probably due to extensive evaporation, and very little surface or subsurface, replenishment.

2. Rivers

River channels, and their drainage pattern, are easily observable on the ERTS-1 imagery. Thus, after ascertaining the area of each watershed, with future repetitive imagery coverage, it may be possible to initiate seasonal yield forecasting for particular streams, taking into account snow coverage, and quality of each particular stream.

An interesting finding was made by studying the imagery taken of the Gowater Bay (near the Pakistan border), in the extreme south-eastern region of Iran. On the image taken of this area, four streams can be readily seen with a N-S direction, terminating into the Gowater Bay, whereas the Hydrological shows only three streams.

3. Alluvial Deposits

The areal extent, and boundary between different types of unconsolidated sediments are easily observable on the ERTS-1 images. Since most wells and Ghanats* in Iran are drilled or dug in alluvial deposits, the distribution and differentiation of the latter is of great significance for hydrogeological investigations, and artificial recharge in a country like Iran, where water is scarce.

4. Marine Phenomena

The following observations were made:

a. Gorgan Bay (Caspian Sea): a comparison between the ERTS-1 imagery taken of this region, with maps based on aerial photographs taken in 1955, indicates that the shape of this bay has significantly changed. It can be seen that the form of the barrier bar has increased eastward towards the mainland. Thus with time the entrance to the bay might eventually become obstructed. This phenomenon is presumably due to the lowering of the sea-level, and also to the accumulation of stream sediments which are being transported, and deposited by offshore currents.

b. On the ERTS-1 images covering the NW portion of the Persian Gulf, extensive delta formation and sedimentary deposition may be observed. In addition to the foregoing, the direction of some of the offshore currents are readily visible. The prevailing direction being from the northwest of the Persian Gulf, southeastward into the Oman Sea.

Conclusion

The preliminary observations, and results obtained, from the ERTS-1 imagery application to the field of hydrology were of significance. Hence, it is firmly believed that by complementing data derived from the interpretation of the satellite imagery, with field observations, a substantial as well as useful volume of data will become available for water resources planning in different regions of the country.

*Ghanat, is a horizontal interceptor to the ground water table, which is linked through a series of interconnected wells. The flow from the intercepted water table is thus directed through the underground channel to the population center.

SUMMARY AND CONCLUSIONS

The preliminary analysis of a number of selected ERTS-1 images was undertaken in the fields of geology, agriculture, forestry, and hydrology, with a purpose of testing its applicability and usefulness for mapping the natural resources of Iran. As a result, a number of phenomena, such as faults, streams, lakes, and potential arable lands were identified.

It must be pointed out, that due to a number of limiting factors, the results of this study is by no means conclusive. Notwithstanding, the relatively short time available, lack of sufficient hardware, and inadequate repetitive imagery coverage, yet, some encouraging results were obtained, which demonstrate the importance of satellite imagery application for multidisciplinary purposes.

FUTURE PLANS

The ERTS-1 program, according to NASA's definition, is a research and development type of project. Thus, rightfully, the Plan Organization of the Imperial Government of Iran approach to this project has been conservative. But in light of the encouraging results obtained thus far, we believe that a more detailed and thorough program of study may now be undertaken. To this effect, the next phase of the investigations will consist of the following:

- Purchase of the necessary color additive and enhancement hardware.
- Ground truth data collection program, in a number of selected test sites throughout the country.
- Formation of a larger multidisciplinary cadre of specialists.

A major project entitled: "Geological Mapping and Mining Exploration in Eastern Iran," will be shortly undertaken. The area is approximately 340,000 km^2, and covers nearly all of the geology test site B. This region will be the subject of detailed field geological investigations, and possibly airborne geophysics in a number of selected areas.

It is also planned to undertake a fixed-wing remote sensing study, as well as, detailed field investigations, in few selected test sites, for multidisciplinary purposes.

It is evident, that the above mentioned activities will be most helpful, and complementary to the volume of information derived from the ERTS-1 imagery interpretation.

B

REFERENCES

Geological Map of Iran, Scale 1:2,500,000. Compiled by the Geological Staff of the Iran Oil Co., 1959.

Geological Map of SW Iran, Scale 1:1,000,000. Compiled by the Geological and Exploration Division, IOOC, 1969.

Hydrological Map of Iran, Scale 1:1,000,000. Compiled by the Ministry of Water and Power, 1971.

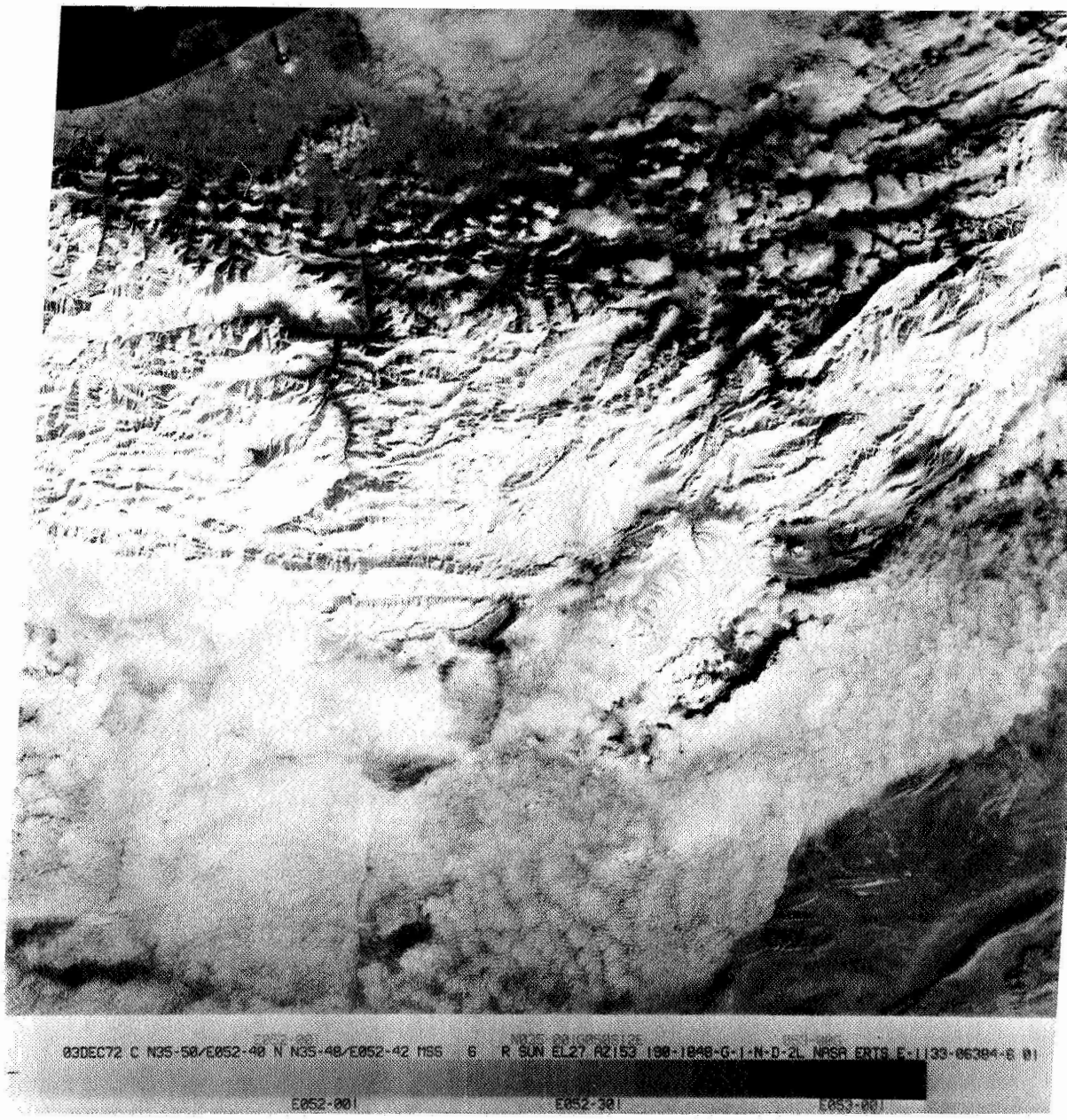


Plate I Damavand Volcano and Alborz Mountains in Mazandaran Province

B



Plate II Northeastern Dasht-e-Kavit (Kavir Desert)



Plate III Isfahan, Central Iran



Plate IV Gowater Bay near Pakistan Border

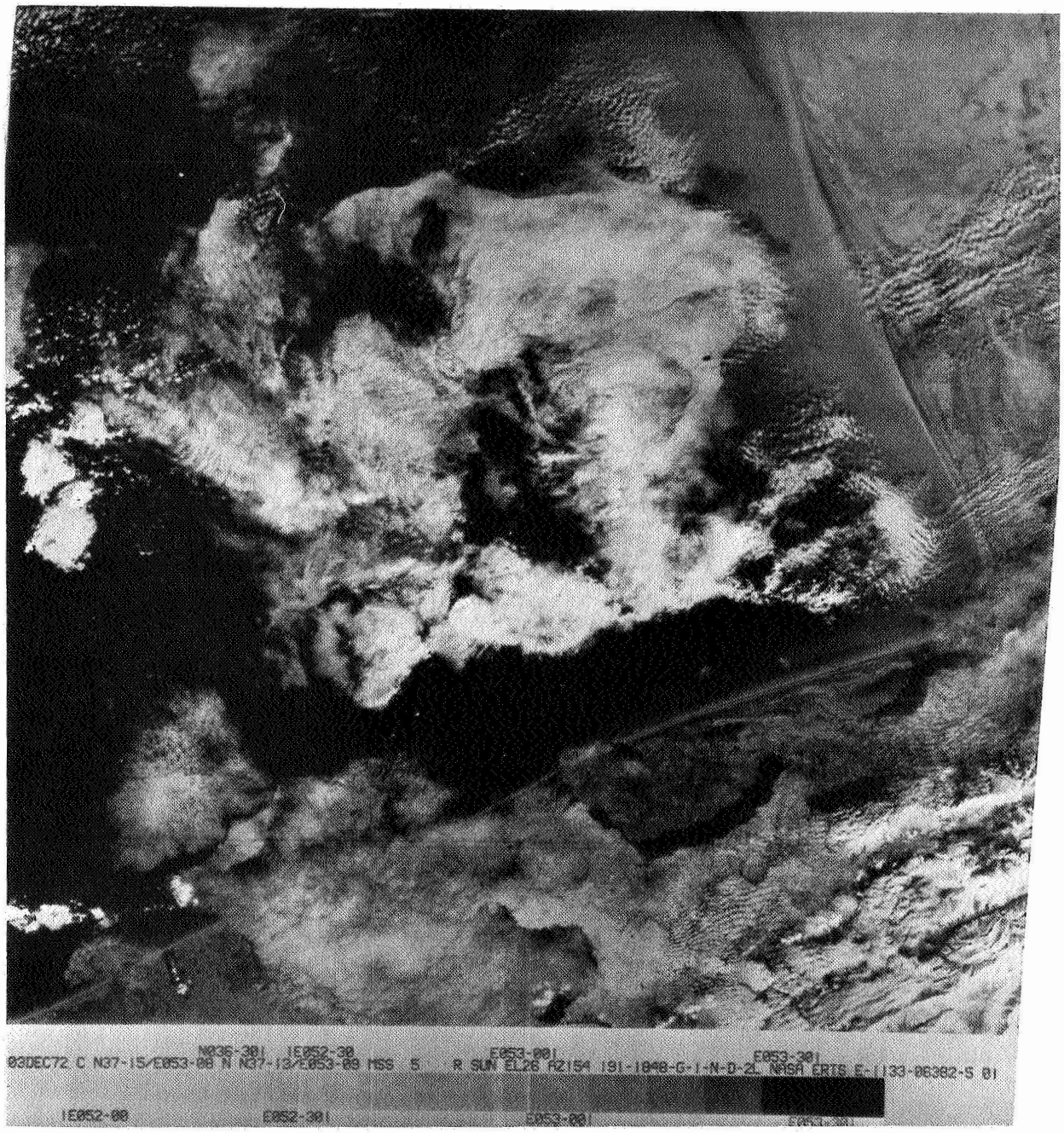


Plate V Gorgan Bay in Southeastern Caspian Sea

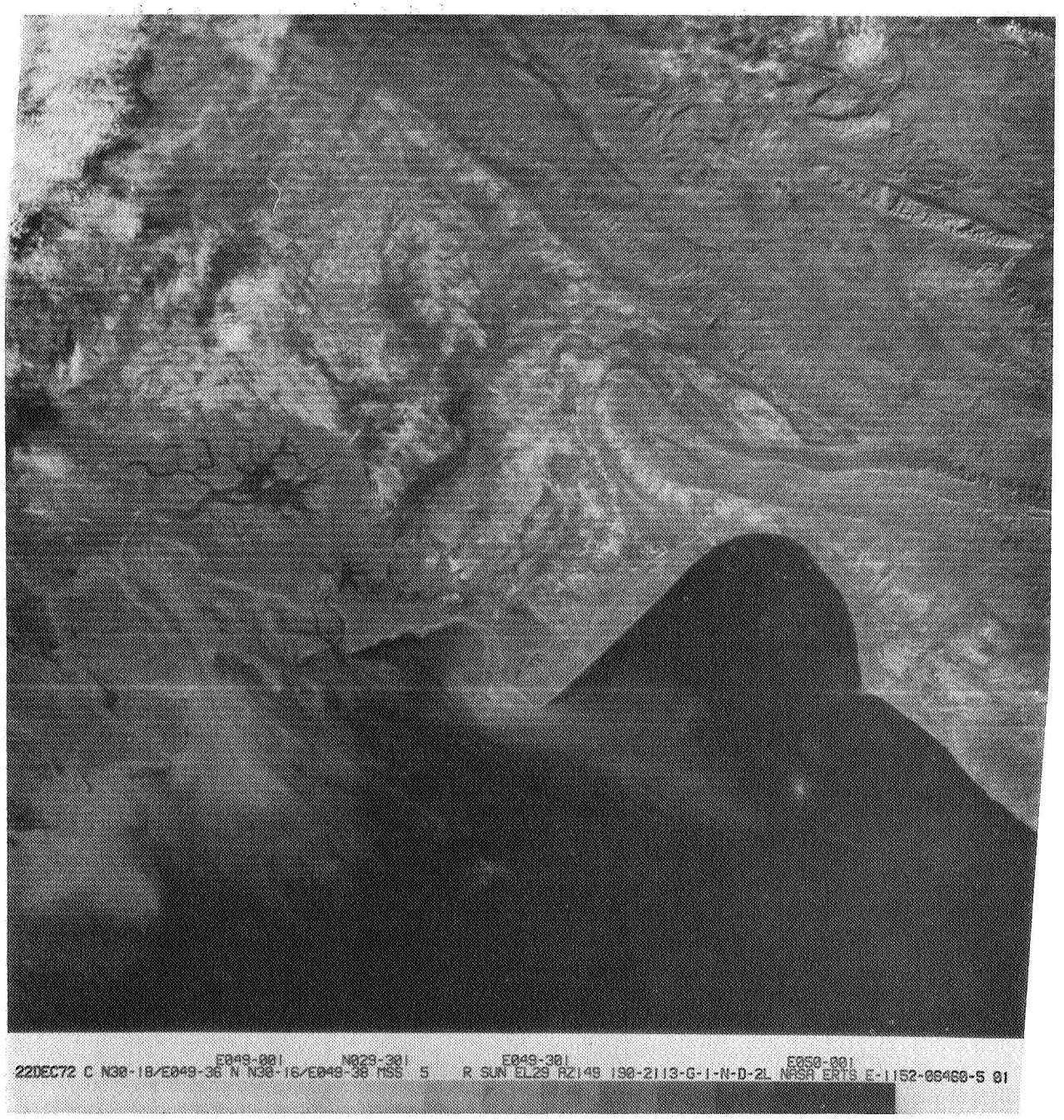


Plate VI Northern Part of Persian Gulf near Tigris/Euphrates Delta

N73-28388

DETECTION OF TURBIDITY DYNAMICS IN TAMPA BAY, FLORIDA USING MULTISPECTRAL IMAGERY FROM ERTS-1

A. E. Coker, Aaron Higer and Carl R. Goodwin[1]

ABSTRACT

In 1970, Congress authorized the deepening of the Tampa Bay channel (Rivers and Harbors Act of 1970) from 34 to 44 feet. In order to determine the effects of this deepening on circulation, water quality, and biota, during and after the construction, the U.S. Geological Survey, in cooperation with the Tampa Port Authority, has collected data and developed a digital simulation model of the bay.

In addition to data collected using conventional tools, use is being made of data collected from ERTS-1. Return-Beam Vidicon (RBV) multispectral data were collected, while a shell dredging barge was operating in the bay, and used for turbidity recognition and unique spectral signatures representative of type and amount of material in suspension. The processed data integrated with other modeled parameters provide an overview of the dynamics of turbid material during dredging periods. A three-dimensional concept of the dynamics of the plume was achieved by superimposing the parts of the plume recognized in each RBV band. This provides a background for automatic computer processing of ERTS data and three-dimensional modeling of turbidity plumes.

1/ Messrs. Coker and Goodwin are Hydrologists, U.S. Geological Survey, Tampa, Florida, and Mr. Higer is a Hydrologist with the U.S. Geological Survey, Miami, Florida

Original photography may be purchased from:
EROS Data Center
10th and Dakota Avenue
Sioux Falls, SD 57198

Original photography may be purchased from:
EROS Data Center
10th and Dakota Avenue
Sioux Falls, SD 57198

DETECTION OF TURBIDITY DYNAMICS IN TAMPA BAY, FLORIDA USING MULTISPECTRAL IMAGERY FROM ERTS-1

Background to Ongoing Estuarine Modeling in Tampa Bay

The Port of Tampa is the 8th largest in the nation with 36 million tons of total cargo handled annually. In terms of export tonnage, the port is 4th in the country with 11 million tons annually. Through this one port passes 50 percent of all the cargo tonnage in the State of Florida. This commerce provides 200 million dollars per year of wages and salaries to workers in the Tampa area, 15-18 million dollars per year to the U.S. Government in the form of customs receipts and, in addition, 50 million dollars per year to the positive side of the important balance of payments ledger.

In 1970, the Congress of the United States authorized the deepening of the channel (Rivers and Harbors Act of 1970) to 44 feet, mean low water (Figure 1). It is estimated that this harbor deepening will continue for 8 to 10 years before completion. Before engineering or construction can begin on such a long term project, however, public opinion and legislation require that the effect of the project on the environment must be predicted in advance to insure that adequate precautions will be taken to limit any adverse ecological effect and provide a means to evaluate alternative construction methods. To obtain this predictive ability and other necessary information, the Tampa Port Authority entered into a cooperative program with the U.S. Geological Survey to collect necessary physical, hydrodynamic, biochemical and other data to develop a sophisticated digital simulation model of Tampa Bay. This modeling program is underway and will be useful in predicting the effect of harbor deepening on circulation, water quality and biota during and after the construction period.

An extensive data collection program has been in operation for over a year to verify a model of this type. Time synchronous tidal elevations are being recorded every 5 minutes at 14 locations around the bay. Wind data from eight stations and water velocity data at 12 points are also being collected.

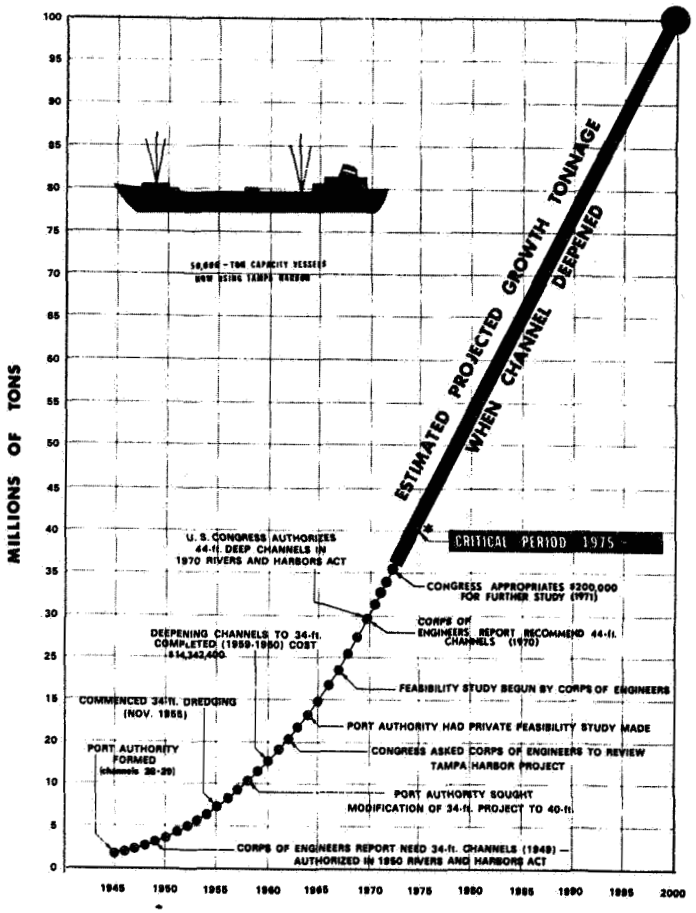


Figure 1. Projected growth for shipping tonnage and critical period of 1975 for Tampa Bay

Other data collection phases of the investigation included intensive biochemical analyses, analyses of sediment from the bay bottom, 32 water quality parameters, and definition of the bathymetry of the bay bottom by both water-borne, automated, depth-sounding equipment and aerial stereo compilation. Seismic surveys of the ship channel to locate sub-bottom strata have been run in conjunction with a test drilling program necessary for strata identification.

This background information and the carefully verified simulation model will permit predictions that will materially aid the wise management of Tampa Bay. To illustrate the output of the model, a frame from a preliminary time-lapse movie output generated by the simulation model is presented (Figure 2).

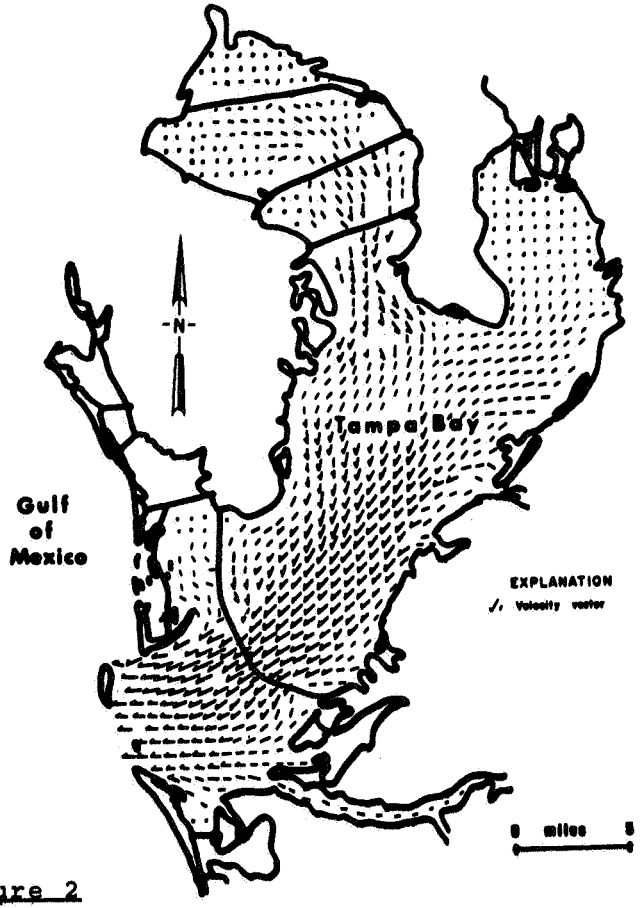


Figure 2

SIMULATED VELOCITY VECTOR GRID OF TAMPA BAY SHOWING OUTGOING TIDE WHEN CONDITIONS WERE SIMILAR TO ERTS OVERPASS ON AUGUST 2, 1972

This diagram delineates velocity patterns during a hypothetical ebb-flow condition similar to the time of Earth Resources Technology Satellite (ERTS) overpass made on August 2, 1972. The use of data from high-flying aircraft and spaceships provides a unique opportunity to monitor selected parameters using remote-sensing techniques that will aid the overall goal of environmental protection and enhancement while the main channel of Tampa Harbor is being deepened. The control of the concentration, dispersion and ultimate location of the fine-grained material introduced into the water by the dredging process, commonly called turbidity, is of utmost importance to the survival of many biological communities existing in Tampa Bay.

Objectives

A target of opporutnity was provided when ERTS imagery was recorded over Tampa Bay on August 2, 1972. The imagery was processed for turbidity recognition and integrated with the estuarine model to provide a method for synoptically observing and predicting the movement and distribution of turbid material caused by dredging operations.

Approach

Tidal stage data and wind measurements were acquired during a time when conditions were similar to the ERTS overpass of August 2, 1972. These data were edited, formalized and put into the digital model of Tampa Bay to produce the simulated velocity vector grid of the bay (Figure 2). At the same time a shell-dredging barge was operating in the bay. This dredging simulated turbid conditions that would be caused by channel dredging and the effects of tidal action on the movement and distribution of a turbidity plume (See Figure 3). Sampling for turbidity of bay water and near the shell dredging barge was acquired for ground-truth information and the analyses plotted (See Figure 4).

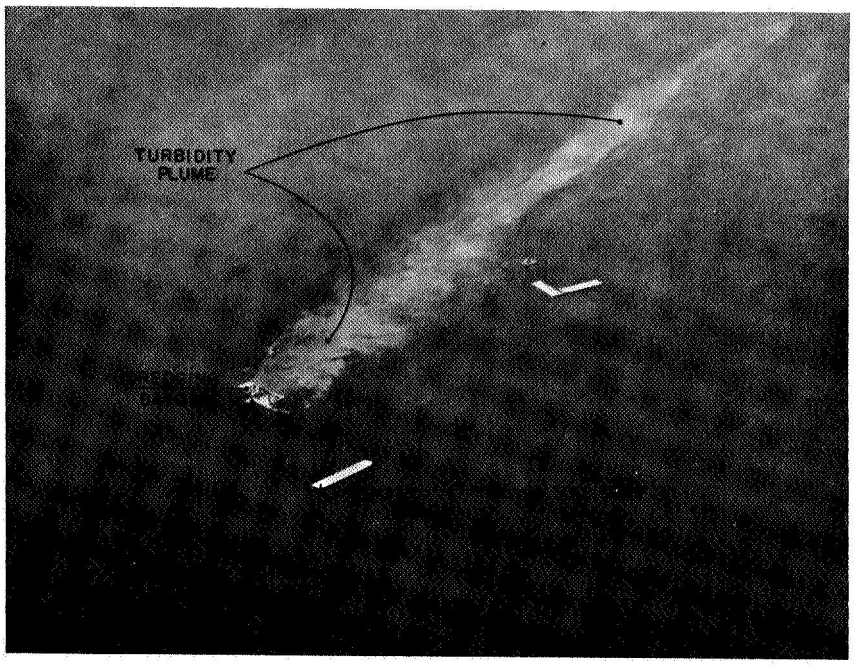


Figure 3 PHOTOGRAPH OF SHELL DREDGING OPERATION AND TURBIDITY PLUME

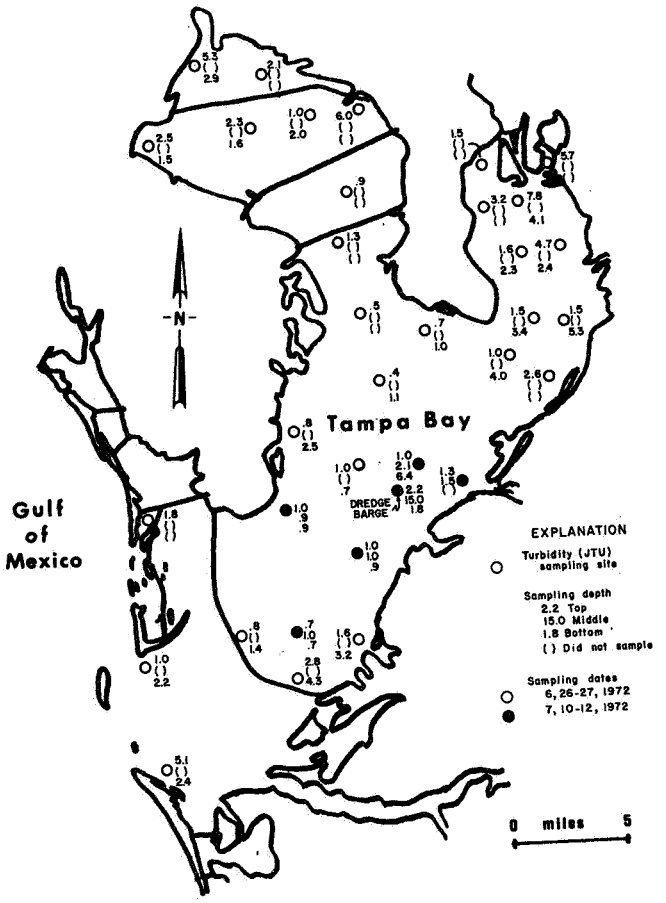


Figure 4. Sampling sites showing quality (turbidity) of Tampa Bay water and near a shell dredging barge

Black and white imagery transparencies from the ERTS Return-Beam Vidicon (RBV) multispectral three-camera system were taken over Tampa Bay on August 2, 1972. ERTS Image ID's are E-1010-15333-1, E-1010-15333-2 and E-1010-15333-3. This system operates in three different spectral regions, the green band 475 to 575 millimicrons; the red band 580 to 680 millimicrons; and the near infrared band 690 to 830 millimicrons.

Photo identification was made by comparing the transparencies, aerial photographs, maps and ground-truth information (Figure 4) of the bay with the velocity vector grid (Figure 2) and the imagery. The relative size and shape of the turbidity plume as recognized in each RBV band is illustrated in Figure 5. An appraisal of selectively singular bands for photo interpretation purposes to recognize and delineate selected estuarine features is presented in Table 1.

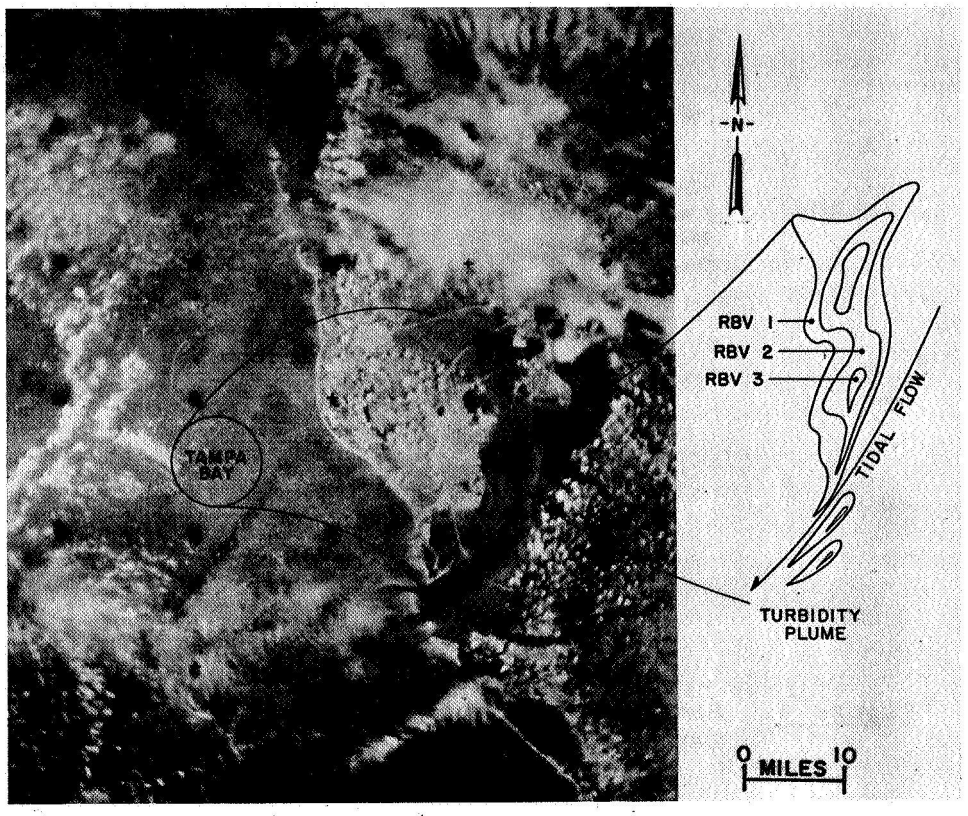


Figure 5 COLOR ADDITIVE ENHANCEMENT OF RBV IMAGES 1,2 AND 3 AND SKETCH OF TURBIDITY PLUME

ERTS Image ID E-1010-15333-1, E-1010-15333-2 and E-1010-15333-3.

Table 1. Estuarine Features That are Recognizable in the Imagery of ERTS RBV 1, 2, and 3 Bands

	RBV 1 Green	RBV 2 Red	RBV 3 Near Infrared
Differentiation of land from water features			
Maximum			X
Moderate		X	
Minimum	X		
Presence or absence of shoreline vegetation			
Maximum			X
Moderate		X	
Minimum	X		
Presence or absence of underwater features such as scour channels, vegetation and turbid flow (varies with turbidity)			
Maximum	X		
Moderate		X	
None			X
Aerial distribution of turbidity plume			
Maximum	X		
Moderate		X	
Minimum (at surface only)			X
Water penetration (varies with turbidity)			
Maximum	X		
Moderate		X	
None			X

An International Imaging Systems viewer was used to prepare a color additive enhancement of the turbidity plume from the three RBV black and white image separates. Colors were assigned as follows: RBV band 1 = blue, RBV band 2 = green and RBV band 3 = red. These images were simultaneously displayed on the viewer while color intensities were adjusted to produce a color composite enhancement of the turbidity plume. A black and white photograph of this enhancement is illustrated on Figure 5.

Analysis

Organic detritus and clay particles make up the major part of suspended particulate matter (turbidity) that results from dredging operations in the waters of Tampa Bay. The water absorbs and reflects sunlight so that the RBV imagery depicts a signature indicative of the turbid condition of the water. The intensity of reflection registered in the imagery will be modified by quantity and type of material in suspension, stratification and settling depth, type of bottom material and water surface roughness. If the water is clear or slightly turbid, the sun's energy that spans RBV-3 (longer wavelengths) is mostly absorbed at the surface, and that of RBV-2 and 1 will penetrate to progressively greater depths before being absorbed. For this water the resulting tones on positive black and white images will be almost black for band 3 with progressively lighter, but still dark, tones for bands 2 and 1. The lighter tones are caused by the greater penetration and scattering (less absorption) of light from suspended particulate matter in the water and atmosphere at the shorter wavelengths of bands 2 and 1. Depending upon the span of energy (RBV band), type of particulate matter, stratification, depth of settling and bottom conditions, the more turbid waters will be more reflective than the less turbid waters and will appear as lighter gray tones on the imagery.

On both RBV-1 and 2 positive images, the sediment plume is depicted by lighter gray tones near the center and darker tones of lower reflectance at the outer edges of plume. The turbidity plume boundaries in RBV-1 extend beyond those in RBV-2 or 3 and may be areas of deeper settling depths and/or contain less particulate matter in suspension (Figure 5).

The energy span of RBV-3 is mostly absorbed by water at the surface, and only the particulate matter at the surface reflects light. The part of the plume at the surface may be delineated by lighter gray tones in the imagery of this band. This part of the plume may also contain recently suspended material that may be more highly concentrated.

Assuming that the bay water is slightly turbid (Figure 4), a three-dimensional concept of the shape of the more turbid plume may be demonstrated by superimposing those parts of the plume observed in all three bands (Figure 5). The outer boundaries observed in band 1 may be at deeper settling depths than those of band 2 and/or contain less particulate matter in suspension. That part delineated by band 3 is near the surface, and the movement of the plume toward the mouth of the bay is in response to ebb tide conditions at the time of ERTS overpass (Figures 3 and 5).

Conclusions

Spectral signatures of gray scale tones indicative of turbid conditions of type, concentration, stratification, settling depth and area of dispersion were observed in the RBV imagery of Tampa Bay. The observed current patterns indicate that the plume moved toward the mouth of the bay in response to ebb tide conditions at the time of the ERTS overpass.

Preliminary studies indicate that ERTS imagery and computer-compatible tapes may be automatically processed in conjunction with associated ground information for quantifying these spectral signatures. The processed data may then be used as a tool for synoptically mapping and monitoring spatial and temporal conditions of turbidity and for comparing natural with manmade turbidity for appraising the resources of Tampa Bay and other estuaries. Furthermore, the processed data used in conjunction with the Tampa Bay digital simulation model may provide the basis for developing a three-dimensional concept to model the dynamics of turbidity plumes.

Prior to ERTS the extent of dispersion of dredging silt plumes in an area as extensive as Tampa Bay (over 300 square miles) could only be made by connecting stations of equal percent turbidity derived from a massive sampling program. However, the positions and number of transects for turbidity sampling did not usually allow complete synoptic coverage showing the dynamic distribution of the turbidity plume. Furthermore, compared with ordinary massive sampling programs, the associated ground-truth information needed for purposes of correlation with the ERTS imagery may be considerably reduced in number of transects and samples across the bay.

The channel deepening in Tampa Bay, as estimated, is scheduled to continue for 8 to 10 years. Comprehensive environmental appraisal studies are underway and programmed to continue during the construction period to continuously evaluate, monitor and guide the effects of dredging and disposal operations on the bay. The digital simulation modeling program of Tampa Bay is a part of these environmental studies. The synoptic and repetitive coverage of Tampa Bay by ERTS offers a timely opportunity to apply products of the space program to monitor and to help solve environmental problems such as those in Tampa Bay and other estuaries.

AUTHOR INDEX

A

Abdel-Gawad, Monem, 433
Ahmad, Moid U., 1575
Alexander, Robert H., 932, 931
Alexander, S. A., 231
Alexander, S. S., 569
Algazi, Vidal Raphael, 1169
Allen, Rex, 305
Allen, William H., 371
Alt, David D., 539
Amato, Roger V., 553
Anderson, A. C., 1151
Anderson, Arthur T., 265
Anderson, Duwayne M., 1323
Anderson, James H., 67, 143
Anderson, Richard R., 603
Antalovich, John W., 1575
Applegate, D. N., 1015, 1059
Ashley, Marshall D., 157

B

Bachofer, B. T., 1
Bale, Jack B., 915
Bandy, A. R., 585
Barker, Bonnie, 11
Barnes, James C., 855, 1377
Barnes, Peter W., 1307
Bartlett, D., 615
Bauer, Marvin E., 205
Baumgardner, Marion F., 213
Bechtold, I. C., 425
Becia, Enzo, 143
Beckwith, Roy C., 143
Belon, Albert E., 67, 999
Benigno, Joseph A., 1685
Benson, Carl S., 1593
Berg, Dennis W., 1697
Berg, Richard B., 539
Bernstein, Ralph, 1143
Billingsley, Fred, C., 403, 1159
Bizzell, R. M., 189
Blair, Byron, 157
Blais, R. N., 585
Blodget, Herbert W., 265
Bodechtel, J., 493
Bodenheimer, R. E., 121
Bödvarsson, Ágúst, 317
Bolling, N., 1015
Borden, F. Y., 1015, 1059, 1067, 1243
Bowden, Leonard W., 915, 1467
Bowker, D. E., 1291
Bowley, Clinton J., 855, 1377
Breckenridge, Roy M., 363, 981
Breed, Carol S., 291
Brown, Dwight, 991
Bukata, R. P., 819
Burbank, D. C., 1315

C

Calderon, Gustavo, 1349, 1403
Carlson, Paul R., 1305
Carneggie, David M., 91
Carson, Robert J., 1443
Carter, Virginia, 603
Carter, William D., 459, 695
Cassinis, R., 1539
Cavelier, Claude, 273
Chase, Phillip E., 561, 1597
Chesnutwood, C. Mark, 1041
Childs, J. F., 425
Cipra, Jan E., 205
Clapp, J. L., 1007
Coiner, Jerry C., 11
Coker, A. E., 793, 1715
Coleman, Virginia B., 19, 127
Collins, S. H., 819
Colvocoresses, Alden P., 887, 1523
Colwell, Robert N., 145
Conomos, T. John, 1305
Conrod, Alfred C., 1641
Cooley, Maurice E., 283, 755
Copeland, G. E., 585
Cordes, E. A., 793
Cota, Alfredo, 1403
Cousin, S. B., 1151
Cram, Richard, 1357
Curran, Robert J., 1385

D

Daiber, F., 615
de Benito, Emilio, 949
DeGloria, Stephen D., 91
Dein, J., 569
de Sagredo, Fernando López, 35
Dethier, Bernard E., 157
Dickison, W. T., 819
Dillman, Robert D., 1047
Dolan, Robert, 939
Draeger, William C., 197
Drew, James V, 87

E

Eaton, Jerry P., 305, 459
Ebtehadj, Khosro, 1699
Economy, R., 1023
Elbersen, G. W. W., 105
Eller, Ralph, 991
Elston, Donald, 403
Endo, Elliot, 305
Erb, R. Bryan, 1041
Espejo, R., 707
Estes, John E., 907
Evans, Wm. E., 1211

F

Fakundiny, Robert H., 223
Falconer, A., 819
Fleischer, P., 1291
Flood, Raymond E., Jr., 539
Flores, L. M., 1675
Fontanel, A., 1483
Forster, Stephen W., 223
Frank, David G., 1549
Fraser, Robert S., 1567
Fridriksson, Sturla, 317
Friedman, Jules D., 1549

G

Gamble, James, 991
Garcia, Joe G., 1041
Garofalo, Donald, 629
Gatto, Lawrence W., 1323
Gedney, Larry D., 451
Gilbertson, Brian, 577
Gilmer, David S., 801
Goetz, Alexander F. H., 403, 1159
Gold, D. P., 231, 569
Goodwin, Carl R., 877, 1715
Gosink, T. A., 1291
Gower, J. F. R., 1683
Gramenopoulos, Nicholas, 1229
Gregory, Alan F., 329
Griggs, Michael, 1105
Guillemot, M. Guy, 1483
Guy, M., 1483

H

Hall, Ralph C., 135
Hallberg, George R., 353, 745
Hallermeier, Robert J., 1697
Hanna, W. J., 1291
Hanson, Kirby J., 1357
Haralick, Robert M., 1219
Harlow, David, 305
Harris, G. P., 819
Harris, Lawrence F., 291, 1649
Hawley, Katharine T., 539
Heath, G. R., 167
Hebarb, Frank, 1357
Heilman, James L., 27
Henderson, James A., 213
Hendrickson, J. R., 1349, 1403
Henson, E. Bennette, 643
Herzog, J. H., 1451
Heydt, Howard L., 37
Higer, Aaron, 877, 1715
Hilton, G. M., 585
Hixon, S. B., 1675
Hollyday, Este F., 743
Hopp, Richard J., 157
Hoppin, Richard A., 531
Horton, Maurice L., 27
Howarth, P. J., 819
Hoyer, Bernard E., 745
Hunter, Ralph E., 1341

I

Isachsen, Yngvar W., 223

J

Janda, Richard J., 1305
James, Gerard W., 651
Jennings, Jerry D., 1199
Jensen, Mead LeRoy, 247
Johns, Willis M., 539
Johnson, Claude W., 19, 127, 547
Johnson, Greg R., 1075

K

Kamiko, Toshiro, 673
Kantner, David A., 1575
Kedar, Ervin Y., 1527
Kemmerer, Andrew J., 1685
Kerhin, Randall T., 1269
Kiefer, R. W., 1007
Kindle, E. C., 585
Kirvida, Leonard, 1075
Klemas, V., 615, 1275
Klett, A. T., 801
Kottlowski, Frank E., 1561
Kristof, Steven J., 213
Krumpe, Paul F., 97

L

Lachowski, H. M., 1067, 1243
Lamar, Jeannine, 1187
Lammerer, B., 493
Lammi, J. O., 1443
Langley, Philip G., 1661
Lathram, Ernest H., 257
Lauer, Donald T., 97
Lawrence, R. D., 1451
Lechi, G. M., 1539
Lepley, L. K., 1349, 1403
Lewis, Lowell N., 127
Liggett, M. A., 425
Lind, Aulis O., 643
Lingren, David T., 973
López-Cuervo, Serafin, 949
Lorain, Garwin, 77
Lucchitta, Ivo, 403
Ludwick, J., 1291
Lundelius, M. Ann, 1041
Lyons, Walter A., 847
Lyzenga, David R., 1433

Mc

McCarthy, M. M., 1007
McCauley, James R., 651
McEwen, Robert B., 887, 1129
McGinness, John, 603
McKee, Edwin D., 291
McKim, Harlan L., 1323
McKnight, J., 1023
McNair, Arthur J., 37

M

MacLeod, N. H., 659, 1475
Magnuson, Larry M., 651
Magoon, Orville T., 1697
Mairs, Robert L., 629
Malila, William A., 173, 1097
Mallon, Harry J., 1613
Marmelstein, Allan D., 1405
Marquez, Daniel, 305
Marrs, Ronald W., 981
Martin, James A., 371
Martin, Kenneth R., 345
Maruyasu, Takakazu, 665
Marzolf, G. Richard, 651
Maughan, Paul M., 1405
Maul, George A., 1365
Mausel, Paul, 1031
May, G. A., 1055
Meier, Mark F., 863
Melhorn, Wilton N., 473
Merifield, Paul M., 1187
Meyer, Merle, 991
Miller, John M., 143, 999
Morain, Stanley A., 11
Morrison, Roger B., 283, 353, 755

Morgenstern, James P., 173
Murphy, Donald J., 981
Murray, R. J., 1451
Myers, V. I., 965
Myers, Wayne L., 173

N

Nalepka, Richard F., 1097
Nichols, J. D., 1205
Niemann, B. J., Jr., 1007

O

Ochiai, Hiroaki, 689
Otley, M., 1275

P

Paine, D. P., 1451
Painter, J. Earle, 1549
Pálmason, Gudmundur, 317
Paris, J. F., 1151, 1675
Parizek, R. R., 231
Parker, H. D., 167
Parks, W. L., 121
Patton, W. W., Jr., 257
Paulson, Richard W., 777
Peacock, Keith, 1115
Pease, Robert W., 547, 1179
Pease, Steven R., 847
Pelton, James, 643
Peterson, G. W., 1055
Petrone, Anthony, 1323
Pettyjohn, Wayne, 561
Pile, Deborah R., 1635
Place, John L., 899
Pluhowski, Edward J., 837
Polcyn, Fabian, 829, 1433
Potter, J. F., 1151
Poulton, Charles E., 53, 1451
Preble, Duane, 1549
Prestin, Steven, 991
Prior, H. L., 189
Protz, R., 819

R

Raje, S., 1023
Range, Albert, 745
Rath, David L., 371
Reed, Larry, 1597
Reeves, C. A., 809, 1675
Rehder, John B., 955
Reimnitz, Erk, 1307
Rich, Ernest I., 395
Rifman, Samuel S., 1131
Riley, Ellen L., 1583
Rist, Sigurjón, 317
Rodriguez, Joaquin, 949
Rogers, Robert H., 1115
Roller, Norman E. G., 635
1091
Roquero, C., 707
Ross, Donald S., 1123, 1423
Rowan, Lawrence C., 413
Ruggles, Frederick H., Jr.,
1299
Russell, Orville R., 553

S

Sabels, Bruno E., 1199
Safir, Gene R., 173
Salinas, Francisco G., 35
Sattinger, Irvin J., 1047
Saunders, Donald F., 523
Scanvic, Jean-Yves, 273
Schmidt, Robert G., 387
Schrumpf, Barry J., 59
Schubert, J. S., 659
Schumann, Herbert H., 769
Seevers, Paul M., 87
Sellman, Buzz, 1083
Serebreny, Sidney M., 1211
Shanmugam, K. Sam, 1219
Shapiro, Lewis, 67
Sharma, G. D., 1315
Shoemaker, Eugene M., 403
Sigtryggsson, Hlynur, 317
Silverstein, Joel, 433
Simonson, G. H., 1451
Simpson, Robert B., 973
Sinnock, Scott, 473
Slaughter, Turbit H., 1259
Smith, V. Elliott, 1597
Spiers, B., 189
Srna, R., 1275
Steffensen, Roberto, 501
Stoertz, George E., 695
Strong, Alan E., 1605
Stryker, Steven 1583
Szekielda, Karl-Heinz, 1385

T

Tailleur, I. L., 257
Tapper, Gerald O., 1179
Temple, O. Ray, 1405
Thomas, Gilbert E., 523
Thompson, D. N., 1067
Thomson, Frederick J., 181,
1091
Thomson, K. P. B., 819
Thórarinsson, Sigurdur, 317
Thórsteinsson, Ingvi, 317
Todd, William, 1031
Torrent, J., 707
Treasure, W., 1275
Trippler, Dale, 991
Tsuchiya, Kiyoshi, 673
Tueller, Paul T., 77
Turner, Raymond M., 761

U

Ulliman, Joseph, 991

V

van Liere, Willem, 713
van Roessel, Jan W., 1661
Van Tries, Bill J., 795
VanWormer, James D., 451
Viellenave, James H., 1467
Viljoen, Morris J., 483
Viljoen, Richard P., 483
Vincent, Linwood, 939
Vincent, Robert K., 379
Vonder Linden, Karl, 1561

W

Wackwitz, Linda K., 539
Wade, L. C., 189
Wagner, Thomas W., 829
Ward, Edward A., 1583
Ward, Peter L., 305
Watanabe, Kantaro, 681
Weber, Frederick P., 143, 1513
Weecksteen, Guy, 273
Weeden, H. A., 1015
Weidman, Robert M., 539
Welby, Charles W., 1443
Welch, Robin I., 53, 879
Wells, Terry L., 1459
Wenner, Kenneth, 1031
Westin, Frederick C., 965
Wetlaufer, Pamela H., 413
Wezernak, C. T., 635
Wier, Charles E., 553
Wightman, J. M. 593
Williams, Donald L., 11
Williams, Richard S., Jr. 317, 1413
Wilms, Richard Paul, 1625
Wilson, A. D., 1055
Withington, Charles F., 517
Wobber, Frank, J., 345, 553, 629
Work, Edgar A., Jr., 801
Wright, F. F., 1315
Wukelic, George E., 1459
Yarger, Harold L., 651
Yost, Edward F., 1253
Yunghans, Roland, 629
Zirkle, Raymond E., 1635
Ziserman, Alain, 273

☆ U. S. GOVERNMENT PRINTING OFFICE : 1973 727-486/579